



# THEORY OF GEARING

Kinematics, Geometry, and Synthesis

**Third Edition**

Stephen P. Radzevich



**CRC Press**  
Taylor & Francis Group



# Theory of Gearing

Updated throughout for the third edition, *Theory of Gearing: Kinematics, Geometry, and Synthesis* is an essential resource for engineers in the field of gearing. Detailing gear design, production, inspection, and application, the book covers cutting-edge gear types to enable the reader to fully keep track of modern gear developments.

Demonstrating the rigorous scientific theory behind optimal gear design, manufacture, and performance, a key focus of the new edition is on aiding engineers in designing low noise transmissions in smaller sizes, improving fuel consumption and reducing emissions. Chapters included will discuss key features of Split-Power-Transmission-Systems (SPTS) with equal (almost equal) power share, and Uniform Rotary Motion. Entirely new chapters for the third edition include: Parallel-Axes involute gearing of specific design and gear, and Novikov/Conformal and High-Conformal gearing.

The book will be of interest to engineers and researchers in the gearing industry. It will also have relevance to those working in tribology, metallurgy, and materials processing, alongside engineers working in precision manufacturing.





# Taylor & Francis

Taylor & Francis Group

<http://taylorandfrancis.com>



# Theory of Gearing

## Kinematics, Geometry, and Synthesis

Third Edition

Stephen P. Radzevich



CRC Press

Taylor & Francis Group

Boca Raton London New York

---

CRC Press is an imprint of the  
Taylor & Francis Group, an **informa** business



Third edition published 2023  
by CRC Press  
6000 Broken Sound Parkway NW, Suite 300, Boca Raton, FL 33487-2742

and by CRC Press  
4 Park Square, Milton Park, Abingdon, Oxon, OX14 4RN

*CRC Press is an imprint of Taylor & Francis Group, LLC*

© 2023 Stephen P. Radzevich

First edition published by CRC Press 2012

Second edition published by CRC Press 2018

Reasonable efforts have been made to publish reliable data and information, but the author and publisher cannot assume responsibility for the validity of all materials or the consequences of their use. The authors and publishers have attempted to trace the copyright holders of all material reproduced in this publication and apologize to copyright holders if permission to publish in this form has not been obtained. If any copyright material has not been acknowledged please write and let us know so we may rectify in any future reprint.

Except as permitted under U.S. Copyright Law, no part of this book may be reprinted, reproduced, transmitted, or utilized in any form by any electronic, mechanical, or other means, now known or hereafter invented, including photocopying, microfilming, and recording, or in any information storage or retrieval system, without written permission from the publishers.

For permission to photocopy or use material electronically from this work, access [www.copyright.com](http://www.copyright.com) or contact the Copyright Clearance Center, Inc. (CCC), 222 Rosewood Drive, Danvers, MA 01923, 978-750-8400. For works that are not available on CCC please contact [mpkbookspermissions@tandf.co.uk](mailto:mpkbookspermissions@tandf.co.uk)

*Trademark notice:* Product or corporate names may be trademarks or registered trademarks and are used only for identification and explanation without intent to infringe.

ISBN: 9781032318578 (hbk)  
ISBN: 9781032318585 (pbk)  
ISBN: 9781003311744 (ebk)

DOI: 10.1201/9781003311744

Typeset in Times  
by codeMantra



---

# Contents

Preface.....	xxi
Acknowledgments.....	xxiii
Author .....	xxv
Introduction.....	xxvii

<b>Chapter 1</b>	<b>Non-Involute Gearing.....</b>	<b>1</b>
1.1	Spur Non-Involute Gear Pairs .....	1
1.1.1	Pin Gearing .....	2
1.1.2	Lantern Gearing .....	2
1.1.3	Cycloid Gearing .....	3
1.1.4	Clock-Type Gearing.....	6
1.1.5	Special-Purpose Gearing .....	6
1.1.5.1	Roots Blower.....	7
1.1.5.2	Spur Rotors of Oil Pump .....	10
1.2	Peculiarities of Transmission of Rotary Motion by Means of Non-Involute Gears .....	11
1.2.1	On Violation of the Conjugate Action Law in Non-Involute Gearing.....	11
1.2.2	Interaction of Non-Involute Gear with Rack.....	14
1.3	Helical Non-Involute Gearing .....	18
1.3.1	Helical Rotors for <i>Roots Blower</i> .....	18
1.3.2	On Infeasibility of Dr. <i>Wildhaber Helical Gearing</i> (US Pat. No. 1,601,750) .....	19

## ***PART I Fundamentals***

<b>Chapter 2</b>	<b>Kinematics of Gear Pair.....</b>	<b>25</b>
2.1	Transmission of Motion by Means of Gears .....	25
2.2	Gear Vector Diagram .....	27
2.2.1	Concept of Gear Vector Diagram.....	27
2.2.2	Kinds of Gear Vector Diagrams.....	32
2.2.2.1	Gear Vector Diagrams of Rotary-Negative Crossed-Axes Gear Pair .....	34
2.2.2.2	Gear Vector Diagrams of Rotary-Positive Crossed-Axes Gear Pair .....	39
2.2.2.3	Gear Vector Diagram of Rotary-Zero Crossed-Axes Gear Pair.....	41
2.2.2.4	Analytical Criterion of the Kind of Crossed-Axes Gear Pair.....	43
2.3	Classification of Possible Kinds of Gear Vector Diagrams.....	43
2.4	Complimentary Vectors of Gear Vector Diagrams.....	54
2.4.1	Centerline Vectors Associated with Gear Pair.....	54
2.4.2	Axial Vectors Associated with Gear Pair .....	55
2.4.3	Useful Kinematic and Geometric Formulas .....	57



<b>Chapter 3</b>	Principal Planes and Main Reference Systems Associated with Gear Pair.....	61
3.1	Principal Planes Associated with Gear Pair.....	61
3.1.1	Intersected-Axes Gearing.....	63
3.1.2	Parallel-Axes Gearing.....	64
3.2	Plane of Action in Gear Pair .....	65
3.2.1	Plane of Action in Intersected-Axes Gearing .....	67
3.2.2	Plane of Action in Parallel-Axes Gearing.....	68
3.3	Main Reference Systems Associated with Gear Pair.....	68
3.4	Transformation of the Main Coordinate Systems .....	72
3.4.1	Transition from the Gear Reference System to the Main Reference System .....	73
3.4.2	Transition from the Pinion Reference System to the Main Reference System .....	75
3.4.3	Transition from the Plane-of-Action Reference System to the Main Reference System.....	77
<b>Chapter 4</b>	Smooth Transmission of Uniform Rotary Motion: Three Fundamental Laws of Gearing.....	79
4.1	Transmission of Rotary Motion: The Present-Day Practice.....	79
4.2	The Law of Contact: <i>The First Fundamental Law of Gearing</i> .....	81
4.3	The Conjugate Action Law: The Second Fundamental Law of Gearing .....	86
4.3.1	Equivalent Pulley-and-Belt Transmission .....	86
4.3.2	Camus-Euler-Savary Theorem.....	88
4.3.3	Euler-Savary Equation .....	95
4.3.4	Peculiarities of Contact Geometry in Conjugate Gear Pairs .....	98
4.3.5	Brief Comments on Envelope Surfaces of the First and of the Second Kind .....	99
4.4	The Equal Base Pitches Law: The Third Fundamental Law of Gearing .....	101
4.5	On the Correlation of the Discussed Results with the Earlier Obtained Results .....	107
<b>Chapter 5</b>	Permissible Variation of the Design Parameters in <i>Equivalent Pulley-and-Belt Transmission</i> .....	109

## ***PART II Geometrically Accurate Gearing***

### ***SECTION II-A Geometrically Accurate Gearing: Parallel-Axes Gearing***

<b>Chapter 6</b>	Involute Gearing: Kinematics and Geometry .....	121
6.1	Principal Features of Parallel-Axes Gearing .....	121
6.1.1	Kinematics of Parallel-Axes Gearing .....	121
6.1.2	Gear Ratio in Parallel-Axes Gearing .....	124
6.1.3	Permissible Variation of Transverse Pressure Angle .....	129

6.2	Tooth Flank Generation.....	136
6.2.1	Desirable Line of Contact in a Gear Pair.....	136
6.2.2	Line of Action and Path of Contact in Parallel-Axes Gearing.....	138
6.2.3	Operating Base Pitch.....	142
6.2.4	Gear Tooth Flank of Favorable Geometry: General Approach.....	145
<b>Chapter 7</b>	<b>Simplified Approach to Generation of Involute Gear Tooth Flank.....</b>	<b>153</b>
7.1	Generation of Involute Tooth Profile.....	153
7.1.1	Involute Gear Tooth Profile.....	157
7.1.2	Gear Tooth Flank in the Lengthwise Direction of the Gear Tooth.....	159
7.1.2.1	Tooth Flank in Spur Involute Gear.....	159
7.1.2.2	Tooth Flank in Helical Involute Gear.....	161
7.1.2.3	Tooth Flank in Gear with Circular-Arc Teeth in the Lengthwise Direction.....	167
7.1.3	Tooth Flank Geometry in the Lengthwise Direction of Gear Tooth.....	171
7.1.4	Adopted Gear Terminology.....	172
7.2	Alternative Approach for Derivation of Equation of Involute Tooth Flank.....	174
7.2.1	Generation of Spur Gear Tooth Profile by Means of Straight Line.....	174
7.2.2	Generating Auxiliary Rack (Basic Rack) in Spur Gear.....	180
7.2.3	Alternative Approach for Derivation of Equation of Helical Involute Gear Tooth Flank.....	182
7.2.4	Generating Basic Rack of Helical Gear.....	186
7.2.5	Descriptive-Geometry-Based Approach for Determination of Straight Generating Line.....	187
7.2.5.1	Gear Base Helix Angle $\psi_{b,g}$ : General Approach.....	187
7.2.5.2	Base Diameter $d_{b,g}$ in Involute Gear.....	188
7.3	Comments to Peculiarities of Geometry of Involute Gear Tooth Flank.....	189
7.3.1	Characteristics of the Generating Basic Rack.....	189
7.3.2	Gears with Low Tooth Count.....	193
7.3.3	Length of Involute Tooth Profile.....	198
<b>Chapter 8</b>	<b>Parallel-Axes Involute Gearing of Specific Design.....</b>	<b>201</b>
8.1	Conical Involute Gearing.....	201
8.1.1	Kinematics of Conical Involute Gearing.....	201
8.1.2	Geometry of Tooth Flanks of Spur Conical Involute Gear.....	202
8.1.3	Geometry of Tooth Flanks of Conical Involute Gear with Helical Teeth.....	210
8.2	Internal Involute Gearing: Features of Kinematics and Geometry of Tooth Flanks.....	212
8.2.1	Features of Tooth Flank Geometry and Gear Design.....	213
8.2.2	Gear Coupling as a Reduced Case of Internal Parallel-Axes Gearing.....	217
8.2.3	On Commonality between Internal Gearing and Strain Wave Gearing (Harmonic Drive).....	218



8.3	<i>Pinion Gear-to-Rack Mesh</i> as Reduced Case of Parallel-Axes Involute Gear Pair.....	222
<b>Chapter 9</b>	<b>Gear Tooth Profile Modification: Generating Rack Shift .....</b>	<b>227</b>
9.1	Addendum Modification (Tooth Profile Shift) .....	227
9.2	Profile Shift Coefficient.....	230
9.3	Gear Tooth Flank Geometry Depending on Profile Shift Coefficient .....	232
9.4	Basic Equations for Gear Pair with Addendum Modification.....	233
9.4.1	Principle of Addendum Modification.....	234
9.4.2	External Spur and Helical Gear Pairs .....	234
9.5	Determination of Profile Shift Coefficients: Geometric Blocking Contours.....	236
<b>Chapter 10</b>	<b>Interaction of Tooth Flanks in Parallel-Axes Involute Gearing.....</b>	<b>241</b>
10.1	Interaction of Tooth Flanks in Spur Involute Gearing .....	241
10.2	Interaction of Tooth Flanks in Helical Involute Gearing .....	246
10.3	Transmission of Uniform Rotary Motion by Gear Teeth in Parallel-Axes Involute Gearing .....	248
10.4	Contact Ratio in Parallel-Axes Gearing.....	248
10.4.1	Length of Zone of Action in Parallel-Axes Gearing.....	250
10.4.1.1	Preliminary Remarks.....	250
10.4.1.2	Length of Zone of Action in External Gearing .....	254
10.4.1.3	Length of Zone of Action in <i>Low-Tooth-Count Gearing</i> .....	255
10.4.1.4	Length of Zone of Action in Internal Gearing .....	256
10.4.1.5	Length of Zone of Action in <i>Pinion Gear-to-Rack Mesh</i> .....	258
10.4.1.6	Face Advance (In Design of Helical and Other Non-Spur Gearing) .....	260
10.4.1.7	Highest and Lowest Points of Single-Tooth Contact .....	264
10.4.2	Contact Ratio: Generalized Approach .....	265
10.4.3	Impact of Tooth Flanks Elastic Deformation into Contact Ratio in Gear Pair.....	268
10.5	External Involute Gear Pair.....	269
10.5.1	Main Design Parameters .....	269
10.5.2	Variation of Parameters of Tooth Flank Geometry .....	274
10.5.2.1	Normal Curvature at Point of Gear Tooth Flank .....	274
10.5.2.2	Variation of Gear Tooth Profile Angle and Helix Angle.....	278
10.5.3	Special Point of Meshing .....	278
10.6	Contact Motion Characteristics .....	282
10.6.1	Sliding Conditions.....	282
10.6.2	Specific Sliding .....	287
10.7	Elements of Dynamics in Geometrically Accurate Parallel-Axes Gearing .....	288
10.7.1	Forces Acting in Plane of Action .....	289

10.7.2	Forces Acting in Transverse Section of Geometrically Accurate Parallel-Axes Gear Pair .....	298
<b>Chapter 11</b>	<b><i>Novikov/Conformal and High-Conformal Gearing</i> .....</b>	<b>301</b>
11.1	Introductory Remarks.....	301
11.1.1	A Brief Overview on Conformal Gearing: State-of-the-Art.....	301
11.1.1.1	An Assumed Origination of Conformal Gearing .....	301
11.1.1.2	The Power Density.....	303
11.1.1.3	Design Features of Conformal Gearing .....	304
11.1.2	Variety of Potential Designs of Conformal Gearing.....	305
11.2	Conformal Gearing ( <i>Novikov Gearing</i> ) .....	305
11.2.1	The Essence of <i>Novikov Gearing</i> .....	305
11.2.2	Kinematics of Parallel-Axes Gearing .....	311
11.2.3	Plane of Action.....	312
11.2.4	Operating Base Pitch.....	313
11.2.5	Boundary Novikov Circle in Novikov/Conformal Gearing .....	316
11.2.6	<i>Novikov/Conformal Gearing</i> as a Reduced Kind of Involute Gearing .....	318
11.2.7	Constraints onto the Design Parameters of Tooth Geometries in <i>Novikov/Conformal Gearing</i> .....	324
11.2.8	Fundamental Design Parameters in <i>Novikov/Conformal Gearing</i> .....	330
11.2.9	Tooth Flank Geometry in <i>Novikov/Conformal Gearing</i> .....	331
11.2.10	Configuration of Interacting Tooth Flanks at Point of Culmination.....	334
11.2.11	Design of <i>Novikov/Conformal Gear Pair</i> .....	335
11.2.12	Elements of Kinematics and Geometry of <i>Novikov/Conformal Gearing</i> .....	339
11.2.13	Line of Action and Path of Contact in <i>Novikov/Conformal Gearing</i> .....	340
11.2.14	Contact Ratio in Parallel-Axes <i>Novikov/Conformal Gear Pair</i> .....	342
11.2.15	Tooth Profile Sliding in <i>Novikov/Conformal Gearing</i> .....	343
11.2.16	Novikov/Conformal Gearing with Two Pseudo-Paths of Contact ...	345
11.2.17	Local and Global Contact Geometry of Interacting Tooth Flanks.....	348
11.2.18	The Power Density in <i>Novikov/Conformal Gearing</i> .....	351
11.3	High-Conformal Gearing .....	352
11.3.1	Contact Geometry in <i>High-Conformal Gearing</i> .....	352
11.3.2	High-Conformal Parallel-Axes Gearing .....	355
11.3.3	On the Accuracy Requirements for High-Conformal Parallel-Axes Gearing .....	359
11.4	On the Impossibility of Generating-Finishing of Gears for <i>Novikov/Conformal Gearing</i> and <i>High-Conformal Gearing</i> .....	364
11.4.1	Peculiarities of the <i>Gear-Machining Mesh</i> .....	364
11.4.2	Inevitable Violation of the Fundamental Laws of Gearing in the <i>Gear-Machining Mesh</i> .....	365
11.4.3	On the Inconsistency in Tooth Profile Curvatures .....	367

## SECTION II-B Geometrically Accurate Gearing: Intersected-Axes Gear Pairs

<b>Chapter 12</b>	Geometrically Accurate Intersected-Axes Gear Pairs .....	371
12.1	Earliest Designs of Intersected-Axes Gear Pairs .....	371
12.2	Kinematics of Intersected-Axes Gearing .....	372
12.3	Base Cones in Intersected-Axes Gearsets .....	378
12.3.1	Path of Contact, and Instantaneous Line of Action .....	383
12.3.2	Operating Base Pitch Calculation .....	384
12.4	Tooth Flanks in Gear for Geometrically Accurate Intersected-Axes Gearset .....	385
12.4.1	Applied Coordinate Systems and Linear Transformations .....	385
12.4.1.1	Main Reference Systems .....	385
12.4.1.2	Operators of Rolling .....	387
12.4.1.3	Operators of Linear Transformations Associated with the Gear Housing .....	389
12.4.2	Tooth Flank of a Gear in Intersected-Axes Gear Pair .....	390
12.4.3	Path of Contact Point .....	399
12.4.4	Intersected-Axes Gearing with Variable Pressure Angle .....	401
12.5	Analytical Representation of Conjugate Action Law in Intersected-Axes Gearing .....	402
12.6	Favorable Tooth Proportions in Intersected-Axes Gears .....	404
12.6.1	Angular Base Pitch .....	405
12.6.2	Transverse Pressure Angle .....	408
12.6.3	Angular Pitch .....	412
12.6.4	Angular Tooth Thickness, and Angular Space Width .....	414
12.6.5	Angular Backlash .....	415
12.6.6	<i>Gear Tooth-Line</i> and <i>Gear Space-Line</i> in Intersected-Axes Gears .....	418
12.6.7	Angular Addendum and Angular Dedendum .....	420
12.6.8	Specification of Design Parameters in Intersected-Axes Gearing .....	423
12.7	<i>Tredgold Approximation</i> .....	425
12.8	Principal Features of Geometrically Accurate <i>Novikov/Conformal</i> and <i>High-Conformal</i> Intersected-Axes Gearing .....	427
12.8.1	Path of Contact in <i>Novikov Conformal/high-Conformal</i> Intersected-Axes Gearing .....	427
12.8.2	Boundary Cone .....	428
12.8.3	Bearing Capacity of <i>High-Conformal Gearing</i> .....	430
12.9	Design Parameters in <i>Novikov conformal/High-Conformal</i> Intersected-Axes Gearsets .....	431
<b>Chapter 13</b>	Interaction of Tooth Flanks in Geometrically Accurate Intersected-Axes Gearing .....	437
13.1	Kinematic and Geometric Elements of Interaction in Geometrically Accurate Intersected-Axes Gearset .....	437
13.1.1	<i>Equivalent Pulley-and-Belt Transmission</i> for Intersected-Axes Gearset .....	438
13.1.2	Path of Contact .....	438



13.1.3	Zone (Field) of Action in Intersected-Axes Gearing .....	439
13.2	Transmission of Uniform Rotary Motion in Intersected-Axes Gearing .....	442
13.3	Contact Ratio in Intersected-Axes Gearing .....	445
13.3.1	Transverse Contact Ratio .....	446
13.3.2	Face Contact Ratio .....	449
13.3.3	Total Contact Ratio.....	450
13.4	Contact Motion Characteristics in Intersected-Axes Gearing .....	450
13.4.1	Sliding in Geometrically Accurate Intersected-Axes Gearing .....	451
13.4.1.1	Descriptive Geometry-Based Solution to the Problem of Determination of Sliding in Geometrically Accurate Intersected-Axes Gearing .....	451
13.4.1.2	Analytical Solution to the Problem of Determination of Sliding in Geometrically Accurate Intersected-Axes Gearing.....	456
13.4.1.3	Specific Sliding in Geometrically Accurate Intersected-Axes Gearing.....	463
13.4.1.4	Features of Specific Sliding in Geometrically Accurate Intersected-Axes Gearing .....	464
13.5	Elements of Dynamics of Geometrically Accurate Intersected-Axes Gearing.....	464
13.5.1	Principal Assumption Adopted in Load Analysis of Geometrically Accurate Intersected-Axes Gearing.....	465
13.5.2	Forces of interaction in Geometrically Accurate Intersected-Axes Gearing.....	467
13.5.2.1	Resultant Force Acting in Geometrically Accurate Intersected-Axes Gearing.....	468
13.5.2.2	Forces Acting on Gear and Pinion in Geometrically Accurate Intersected-Axes Gearing .....	470
13.5.2.3	Normal Force Acting on gear in Geometrically Accurate Intersected-Axes Gearing .....	473
13.6	Testing of Geometrically Accurate Spiral Bevel Gears: Contact Pattern .....	474
13.6.1	Testing Conditions.....	474
13.6.2	Predicting Contact Geometry in Geometrically Accurate Spiral Bevel Gearing .....	475

## **SECTION II-C    *Geometrically Accurate Gears: Crossed-Axes Gearing***

<b>Chapter 14</b>	Geometrically Accurate Crossed-Axes Gear Pairs: R-Gearing.....	481
14.1	Kinematics of Crossed-Axes Gearing .....	481
14.2	Pressure Angle in Crossed-Axes Gearing .....	486
14.2.1	Crossed-Axes Gearing with Transverse Pressure Angle of a <i>Constant</i> Value.....	486
14.2.2	Crossed-Axes Gearing with Transverse Pressure Angle of a <i>Variable</i> Value.....	487
14.3	Base Cones in Crossed-Axes Gear Pair .....	488
14.4	Tooth Flank of a Gear in Geometrically Accurate Crossed-Axes Gear .....	493
14.4.1	Applied Coordinate Systems and Linear Transformations .....	494

14.4.1.1	Main Reference Systems .....	494
14.4.1.2	Operators of Rolling/Sliding .....	495
14.4.1.3	Operators Associated with Gear Housing .....	498
14.4.2	Gear Tooth Flank in Crossed-Axes Gearing.....	499
14.5	Fulfillment of Conjugate Action Law in <i>R – Gearing</i> .....	510
14.6	Desirable Tooth Proportions in Crossed-Axes Gear Pair.....	513
14.6.1	Operating Angular Base Pitch .....	514
14.6.2	Low-Tooth-Count Crossed-Axes Gears .....	518
14.6.3	Transverse Pressure Angle .....	518
14.6.4	Angular Pitch .....	522
14.6.5	Angular Tooth Thickness, and Angular Space Width, in the Round Basic Rack .....	523
14.6.6	Angular Addendum, and Angular Dedendum, in Round Basic Rack .....	524
14.6.7	Specification of the Design Parameters in Crossed-Axes Gearing.....	529
14.7	Backlash in Crossed-Axes Gearing.....	530
14.8	Possible Analogy of <i>Tredgold Approximation</i> for Crossed-Axes Gearing ...	532
14.9	Main Features of Geometrically Accurate <i>Novikov/Conformal</i> and <i>High-Conformal</i> Crossed-Axes Gearing.....	533
14.9.1	Path of Contact in <i>Novikov/Conformal</i> and <i>High-Conformal</i> Crossed-Axes Gearing .....	533
14.9.2	Boundary N-Cone in <i>Novikov/Conformal</i> , and <i>High-Conformal</i> Crossed-Axes Gearing .....	534
14.9.3	Bearing Capacity of Crossed-Axes <i>Novikov/Conformal</i> , and <i>High-Conformal</i> Gearing.....	536
14.10	Design Parameters of <i>Novikov/Conformal</i> , and <i>High-Conformal</i> Crossed-Axes Gearing.....	536
<b>Chapter 15</b>	<b>Interaction of Gears in Geometrically Accurate Crossed-Axes Gearing .....</b>	<b>543</b>
15.1	Interaction between Tooth Flanks in Geometrically Accurate Crossed-Axes Gearing.....	543
15.1.1	<i>Equivalent Pulley-and-Belt Transmission</i> of Crossed-Axes Gear Pair.....	543
15.1.2	Path of Contact, and Instantaneous Line of Action .....	544
15.1.3	Zone of Action (Field of Action) in Crossed-Axes Gearing .....	545
15.2	Transmission of Uniform Rotary Motion by Means of Crossed-Axes Gearing .....	546
15.3	Contact Ratio in Crossed-Axes Gearing .....	550
15.4	Contact Motion Characteristics in Crossed-Axes Gearing .....	552
15.4.1	Sliding in Geometrically Accurate Crossed-Axes Gearing .....	553
15.4.2	Analytical Solution to the Problem of Determination of Sliding Velocity in Geometrically Accurate Crossed-Axes Gearing .....	553
15.4.3	Specific Sliding in Geometrically Accurate Crossed-Axes Gearing .....	559
15.4.4	Features of Specific Sliding in Geometrically Accurate Crossed-Axes Gearing .....	561
15.5	Elements of Dynamics of Geometrically Accurate Crossed-Axes Gearing.....	562

15.5.1	Principal Assumption Adopted in the Load Analysis of Geometrically Accurate Crossed-Axes Gearing.....	562
15.5.2	Forces of Interaction in Geometrically Accurate Crossed-Axes Gearing .....	565
<b>Chapter 16</b>	<b>Geometrically Accurate Worm-Gearing: Peculiarities of Kinematics and Geometry .....</b>	<b>573</b>
16.1	Worm-Gearing: Accomplishments from the Ancient Times till Now .....	573
16.1.1	Early Designs of Worm-Gearing .....	573
16.1.2	Worm-Gearing of Conventional Designs.....	577
16.1.3	<i>Spiroid</i> Gearing .....	583
16.1.4	<i>Helicon</i> Gearing .....	586
16.1.5	Internal Worm-Gearing.....	588
16.1.6	Worm-Gearing with Rolling Elements .....	589
16.2	Fundamentals of Worm-Gearing with Line Contact between Worm Threads and Worm-Gear Tooth Flanks .....	590
16.2.1	Kinematics of Geometrically Accurate Worm-Gearing .....	590
16.2.2	Base Cones in Geometrically Accurate Worm-Gearing.....	590
16.2.3	Peculiarities of Sliding in Plane-of-Action Apex in Geometrically Accurate Worm-Gearing.....	593
16.3	Criterion to Distinguish Worm from Gear .....	593
16.4	Analysis of Design of Worm-Gear-Drive [Pat. No. 257,246, USSR, 1968].....	598

### ***PART III Real Gears: Kinematics, Geometry, and Application***

<b>Chapter 17</b>	<b>Geometrically Accurate Real Gearing: <math>S_{pr}</math> – Gear System.....</b>	<b>605</b>
17.1	Preliminary Considerations.....	605
17.1.1	Root Causes for Real Gears Differ from Geometrically Accurate Gears.....	605
17.1.2	Applied Coordinate Systems.....	607
17.1.3	Displacements of Gear Axis of Rotation from its Desirable Configuration.....	608
17.1.4	Closest Distance of Approach between Gear and Mating Pinion Axes of Rotation.....	613
17.2	Tooth Flank Geometry in Geometrically Accurate Real Gearing: $S_{pr}$ – Gear System .....	619
17.2.1	Tooth Flank Geometry in Geometrically Accurate Real Gearing... ..	620
17.2.1.1	The Adopted Concept for Tooth Flank Generation of Gears for $S_{pr}$ – Gear System .....	620
17.2.1.2	Preferred Reference Systems .....	622
17.2.1.3	Derivation of Equation of Tooth Flank in $S_{pr}$ – Gearing....	624
17.2.1.4	Angular Base Pitch in $S_{pr}$ – Gearing .....	629
17.2.1.5	Features of Interaction of Tooth Flanks in $S_{pr}$ – Gearing ...	631
17.2.2	Possible Improvement in Specification of Tooth Flank Geometry in $S_{pr}$ – Gearing.....	632
17.3	Redundant Parameter Elimination .....	633
17.3.1	Possible Correlation between Displacements in $S_{pr}$ – Gearing .....	633



17.3.2	Account for the Normal Distribution of Manufacturing Errors onto the Geometry of Tooth Flanks .....	635
17.4	Possibility of Implementation of the Concept of $S_{pr}$ – Gearing in Design of Gear Coupling.....	636
17.5	Possibility of Implementation of the Concept of $S_{pr}$ – Gearing in Point Contact Gear Systems .....	638
17.6	Correlation among the Gear Systems of Different Kinds .....	639

## ***PART IV CΣu – Variable Gearing***

<b>Chapter 18</b>	<i>CΣu–var Gears: Kinematics, Geometry, and Novel Concept to Design Geometrically Accurate Gears.....</i>	<i>645</i>
18.1	Preamble: Permissible Variation of Design Parameters in <i>Equivalent Pulley-and-Belt Transmission</i> .....	646
18.2	Fundamentals of Geometrically Accurate <i>CΣu–var Gearing</i> .....	649
18.3	Classification of Gear Vector Diagrams of <i>CΣu–var Gear Pair</i> .....	650
18.4	Tooth Flank Generation in Geometrically Accurate <i>CΣu–var Gearing</i> .....	657
18.5	A Key Mistake in Known Methods of Machining Gears for Geometrically Accurate <i>CΣu–var Gearing</i> .....	662
18.6	Examples of Application of <i>CΣu–var Gearing</i> .....	663
18.7	Possibility of Implementation of the Concept of $S_{pr}$ – Gearing in Design of $\Sigma$ –var Gearing .....	665

## ***PART V On Synthesizing of Favorable Geometrically Accurate Gear Pairs***

<b>Chapter 19</b>	Features of Contact Geometry .....	671
19.1	On the Meaning of the Term <i>Synthesis of Favorable Gear Pair</i> .....	671
19.2	<i>Dupin Indicatrix</i> .....	673
19.3	Indicatrix of Conformity at Point of Contact of a Gear and a mating Pinion Tooth Flanks .....	674
19.4	Concept of Synthesizing of Favorable Geometrically Accurate Gear Pair...	675

## ***PART VI Real Gears and Their Application***

<b>Chapter 20</b>	Generic Gear Surfaces .....	681
20.1	Origination of Generic Gear Surface .....	681
20.2	Examples of Gear Pairs Composed of Gears with Generic Gear Surfaces Various Geometries .....	682
20.3	Evaluation of the Total Number of Possible Generic Gear Surfaces .....	683
20.3.1	Possible Profiles of Generic Gear Surface Constructed in Axial Section of Gear.....	684

20.3.2	Profile of Generic Gear Surface Constructed in Section by Plane at an Angle to Gear Axis.....	694
20.4	Possibility of Classification of Gear Pairs .....	697
20.5	Examples of Implementation of Classification of Gear Pairs .....	698
20.6	Auxiliary Generating Racks of Possible Geometries.....	701
<b>Chapter 21</b>	<b>Approximate Real Gearing .....</b>	<b>711</b>
21.1	Approximate Real Parallel-Axes Gearing.....	712
21.2	Approximate Real Intersected-Axes Gearing .....	713
21.2.1	Root Causes for Inaccuracies in Real Intersected-Axes Gears .....	714
21.2.2	Approximate Real Intersected-Axes Gears.....	715
21.2.2.1	Straight Tooth Bevel Gears.....	715
21.2.2.2	Spiral Bevel Gears .....	717
21.2.2.3	Face Gears .....	719
21.2.3	Generation of Tooth Flanks of Gears for Intersected-Axes Gearing.....	720
21.2.3.1	Generation of Tooth Flanks of Straight Bevel Gears .....	720
21.2.3.2	Generation of Tooth Flanks of Spiral Bevel Gears .....	724
21.2.3.3	Tooth Flanks of Bevel Gears Cut Using Continuous-Indexing Method of Gear Machining.....	728
21.2.4	Examples of Approximate Real Intersected-Axes Gear Pairs .....	728
21.3	Approximate Real Crossed-Axes Gearing .....	732
21.4	Worm Gearing .....	736
21.5	Tooth Flank Modification.....	739
21.5.1	Brief Historical Overview on Gear Tooth Flank Modification .....	740
21.5.2	Requirements to Design Parameters of Modified Portions of Tooth Flanks.....	740
21.5.3	Kinds of Tooth Flank Modifications .....	742
21.5.3.1	Tooth Flank Modifications Which Restrict the Usable Flank .....	742
21.5.3.2	Transverse Profile Modifications .....	742
21.5.3.3	Flank Line (Helix) Modifications .....	743
21.5.3.4	Flank Face Modifications .....	744
21.5.4	Description of Modifications by Functions .....	744
21.5.5	On the Most Favorable Modification of Gear Tooth Flanks .....	744
<b>Chapter 22</b>	<b>Local Geometry of Interacting Gear Tooth Flanks .....</b>	<b>747</b>
22.1	Local Geometry of Interacting Tooth Flanks in Parallel-Axes Gearing .....	747
22.1.1	Kinematics of Interaction of Gear Tooth Flanks .....	747
22.1.2	Local Geometry of Interacting Tooth Flanks .....	748
22.2	Local Geometry of Interacting Tooth Flanks in Intersected-Axes Gearing.....	752
22.2.1	Kinematics of Interaction of Tooth Flanks .....	753
22.2.2	Local Geometry of Interacting Tooth Flanks .....	754
22.3	Local Geometry of Interacting Tooth Flanks in Crossed-Axes Gearing .....	756
22.3.1	Kinematics of Interaction of Tooth Flanks .....	756
22.3.2	Local Geometry of Interacting Tooth Flanks .....	758
22.4	Local Geometry of Interacting Tooth Flanks in <i>Novikov/Conformal and in High-Conformal Gearing</i> .....	760

22.4.1	Kinematics of Interacting Tooth Flanks .....	760
22.4.2	Geometry of Interacting Tooth Flanks.....	763
<b>Chapter 23</b>	<b>Strength of Gear Teeth .....</b>	<b>767</b>
23.1	Contact Strength of Gear Tooth in <i>Low-Tooth-Count Gearing</i> .....	767
23.1.1	Adopted Principal Assumptions.....	768
23.1.1.1	Comments on Analytical Description of Local Geometry of Contacting Surfaces Loaded by Normal Force: <i>Hertz Proportional Assumption</i> .....	768
23.1.1.2	Assumption of Even Torque Share .....	771
23.1.2	Principal Features of <i>Low-Tooth-Count Gears</i> .....	772
23.1.3	Analytical Model for Calculation Contact Stress.....	773
23.1.4	Formula for Calculation <i>Hertz Contact Stress</i> .....	777
23.1.5	Specific Pressure Factor .....	777
23.1.6	Combined Compressive-Shear Stress in <i>Low-Tooth-Count Gearing</i> .....	778
23.2	Bending Strength of Gear Teeth.....	780
23.2.1	Comments on <i>Lewis' Formula</i> .....	780
23.2.1.1	Cantilever Beam of Equal Strength.....	781
23.2.1.2	<i>Lewis' Formula</i> for the Calculation of Bending Strength of Gear Teeth.....	782
23.3	Effective Length of Line of Contact.....	786
23.3.1	Length of Single Line of Contact in Parallel-Axes Gearing.....	786
23.3.2	Effective Length of Lines of Contact in Parallel-Axes Gearing .....	791
23.3.2.1	Effective Length of Lines of Contact in Spur Parallel-Axes Gearing .....	792
23.3.2.2	Effective Length of Lines of Contact in Helical Parallel-Axes Gearing .....	795
23.4	Loading of Gear Teeth.....	799
23.5	Method for Simulation of Interaction of Gear and Mating Pinion Tooth Flanks.....	802
<b>Chapter 24</b>	<b><i>SPTS</i> – Split Power Transmission Systems .....</b>	<b>809</b>
24.1	Root Cause for Unequal Torque Sharing in a Split Torque Transmission.....	813
24.2	Mobility of Split Power Transmission Systems.....	814
24.3	<i>Power Density</i> of Gear Transmission Systems .....	815
24.4	Epicyclic Gear Drives.....	816
24.5	Structural Formula for Planetary Gear Drives.....	818
24.6	Correspondence among Angular Velocities of All the Members in Planetary Gear Drive.....	819
24.7	Formulating the Problem of Equal Load Sharing in Planetary Gear Drives: State-of-the-Art.....	820
24.7.1	Ordinary Planetary Gear Drives .....	820
24.7.2	Planetary Gear Drives with Flexible Pins.....	821
24.8	Alternative Approach for Equal Torque Sharing in Split Power Transmission.....	826
24.8.1	Planetary Gear Drive with Elastomeric Load-Sharing Device.....	827
24.8.2	Elastic Load-Sharing Device .....	828
24.8.2.1	Elastic Properties of Elastic Load-Sharing Device .....	828

24.8.2.2	Examples of Implementation of Elastic Load-Sharing Device .....	831
24.9	Main Features of Split Power Transmission Systems with Preloaded Elastic Load-Sharing Devices .....	838
<b>Chapter 25</b>	<b>Vector Approach in Kinematic and Dynamic Analysis of Complex Gear Transmission Systems .....</b>	<b>839</b>
25.1	Possible Kinds of Graphical Representation of Rotating Gear .....	839
25.2	Vector Diagrams of Complex Gear Transmission Systems .....	841
25.3	Features of Vector Diagrams of Complex Gear Transmission Systems with Intersected-Axes and Crossed-Axes Gear Pairs .....	844
25.3.1	Elementary Gear Vector Diagram of Intersected-Axes Gear Pair....	845
25.3.2	Elementary Gear Vector Diagram of Crossed-Axes Gear Pair .....	846
<b>Chapter 26</b>	<b>Gear Ratio of Multistage Gear Transmission System .....</b>	<b>849</b>
26.1	Principal Kinematic Relationships in Multistage Gear Transmission System .....	850
26.1.1	Range ratio of Speed Variation of Gear Transmission System .....	851
26.1.2	Characteristics of Transmission Group .....	851
26.2	Analytical Method for Determining Transmission Ratios .....	852
26.3	Rotational Speed Chart .....	852
26.4	Broken Geometric Series.....	853
26.5	Minimum Number of Gear Pairs .....	854
26.6	Determining Tooth Number of Gears of Group Transmissions.....	855
<b>Chapter 27</b>	<b>Gear Accuracy.....</b>	<b>857</b>
27.1	Inspection of Gears for Parallel-Axes Gear Pairs .....	857
27.1.1	Concept of Inspection of Involute Gear Tooth Profile .....	857
27.1.2	Span Measurement .....	859
27.1.3	Constant Chord Tooth Thickness .....	864
27.1.4	Tooth Thickness Measurement in Internal Gear.....	866
27.2	Inspection of Gears for Intersected-Axes Gear Pairs.....	866
27.2.1	Concept of Inspection of Bevel Gear Tooth Profile .....	867
27.2.2	Concept of Inspection of Bevel Gear in Lengthwise Direction of Gear Teeth.....	868
27.3	Inspection of Gears for Crossed-Axes Gear Pairs .....	868
27.3.1	Concept of Inspection of Gear Tooth Profile .....	869
27.3.2	Concept of Inspection of Gear in Lengthwise Direction of Gear Teeth.....	870
27.4	Mounting Distance: Accuracy of Axial Location of Gears in the Gear Housing.....	870
27.4.1	On the Correlation between the Tooth Flank Geometry and the Mounting Distance .....	871
27.4.2	Mounting Distance in Intersected-Axes Gearing .....	873
27.4.2.1	Relative Disposition of Base Cones in Intersected-Axes Gearing.....	873
27.4.2.2	Edge Contact in Misaligned Intersected-Axes Gearing...	874



27.4.2.3	Disposition of Base Cone of a Gear in Relation to the Plane of Action in Intersected-Axes Gearing.....	874
27.4.2.4	Mounting of Gears in Intersected-Axes Gear Housing.....	876
27.4.2.5	Tolerance for the Accuracy of the Mounting Distance in Intersected-Axes Gearing.....	878
27.4.3	Mounting Distance in Crossed-Axes Gearing .....	880
27.4.3.1	Relative Disposition of Base Cones in Crossed-Axes Gearing .....	881
27.4.3.2	Disposition of Base Cone of a Gear in Relation to the Plane of Action in Crossed-Axes Gearing.....	882
27.4.3.3	Mounting of Gears in Crossed-Axes Gear Housing.....	883
27.4.3.4	Tolerance for the Accuracy of the Mounting Distance in Crossed-Axes Gearing .....	884
27.5	Contact Pattern .....	886
27.6	Permissible Alteration to Bevel Gear Tooth Flank Geometry .....	888
<b>Chapter 28</b>	<b>Gear Noise and Vibration.....</b>	<b>889</b>
28.1	Root Causes for Vibration Generation and Noise Excitation .....	889
28.1.1	Root Cause for Vibration Generation and Noise Excitation in Geometrically Accurate Gearing .....	889
28.1.2	Root Cause for Vibration Generation and Noise Excitation in Approximate Gear Pairs.....	890
28.1.2.1	Violation of the <i>Law of Contact</i> .....	890
28.1.2.2	Violation of the <i>Conjugate Action Law</i> .....	890
28.1.2.3	Violation of the Equality of Base Pitches.....	892
28.2	Transmission Error .....	896
28.2.1	On the Nature of Transmission Error.....	896
28.2.2	Determination of Transmission Error .....	898
28.2.3	Base Pitch Variation of Rotation Vector .....	901
28.3	Variation of Axial and Radial Forces.....	902
28.4	Alternative Causes of Noise Excitation in Gear Pair .....	903
28.4.1	Influence of Contact Ratio.....	903
28.4.2	Influence of Location of the Point at Which the Resultant Load Is Applied .....	903
28.5	On a Possibility of Prediction of Gear Noise Excitation .....	906
<b>Chapter 29</b>	<b>Design Peculiarities of Geometrically Accurate and Almost Geometrically Accurate Gears.....</b>	<b>909</b>
29.1	Design Peculiarities of Gears for $R$ – Gearing.....	909
29.1.1	Essence of Kinematics in Crossed-Axes Gearing.....	909
29.1.2	Base Cones .....	910
29.1.3	Tooth Flanks in Geometrically Accurate Crossed-Axes Gears.....	912
29.2	Permissible Simplification: Design Peculiarities of Gears for $R_{sp}$ – Gearing.....	915
<b>Chapter 30</b>	<b>A Brief Overview on Evolution of the <i>Scientific Theory of Gearing</i> .....</b>	<b>919</b>
30.1	Preliminary Remarks .....	925
30.2	Three Main Periods in the Evolution of the Gear Art and Gear Science .....	925

30.2.1	Pre-Eulerian Period of Evolution of the Gear Art .....	926
30.2.2	The Time When the Fundamental Contribution by <i>Leonhard Euler</i> has been Done – the Origin of the <i>Scientific Theory of Gearing</i> .....	936
30.2.2.1	Involute Tooth Profile for Parallel-Axes Gearing.....	937
30.2.2.2	The Euler-Savary Formula .....	939
30.2.2.3	<i>Leonhard Euler</i> and the <i>Euler-Savary Formula</i> .....	941
30.2.2.4	Equivalent Pulley-and-Belt Transmission .....	945
30.2.3	Post-Eulerian Period of Evolution of the Theory of Gearing .....	946
30.2.3.1	Robert Willis and the Fundamental Theorem of Parallel-Axes Gearing .....	946
30.2.3.2	A Mistake (1842) Committed by <i>Theodore Olivier</i> .....	948
30.2.3.3	Miscellaneous Improvements to the Gear Art .....	951
30.2.3.4	The Research Carried Out by <i>Chaim Gochman</i> .....	951
30.2.3.5	Equality of Base Pitches in Geometrically Accurate Parallel-Axes Gearing .....	953
30.2.3.6	Geometrically Accurate Worm Gearing .....	954
30.2.3.7	<i>Shishkov Equation of Contact</i> , $n_g \cdot V_\Sigma = 0$ .....	954
30.2.3.8	Diagram of Screw (by Professor <i>A.F. Nikolayev</i> ) and its Application in Gearing.....	956
30.2.3.9	Principal Planes, and Reference Systems Associated with Gear Pair.....	956
30.2.3.10	Contact Geometry: Indicatrix of Conformity at Point of Contact of Tooth Flanks.....	958
30.2.3.11	Condition of Conjugacy of Interacting Tooth Flanks (General Case: for Gears of all Kinds) .....	960
30.2.3.12	Angular Base Pitches: Operating Angular Base Pitch in Gear Pair.....	961
30.2.3.13	Crossed-Axes Gearing with Line Contact between the Tooth Flanks ( <i>R-Gearing</i> ).....	962
30.2.3.14	Scientific Classification of Gearing .....	962
30.2.3.15	Geometrically Accurate Real Gearing .....	962
30.2.3.16	Generalized Equation of Conjugacy of Interacting Tooth Flanks: for Gearing of All Kinds .....	963
30.3	Other Contributions to the Field of Geometrically Accurate Gearing.....	964
30.3.1	Tooth Flank Geometry in Geometrically Accurate Intersected-Axes Gearing.....	964
30.3.2	Contribution by Prof. <i>N.I. Kolchin</i> .....	966
30.3.3	Contribution by Prof. <i>V.L. Novikov</i> .....	967
30.3.4	Contribution by Prof. <i>V.A. Gavrilenko</i> .....	969
30.3.5	Contribution by Prof. <i>E.B. Vulgakov</i> .....	969
30.3.6	Contribution by the Other Gear Theoreticians .....	969
30.3.7	Contribution by <i>Walton Musser</i> .....	973
30.4	Developments in the Field of Geometrically Inaccurate Gearing.....	974
30.4.1	<i>Samuel Cone</i> Double-Enveloping Worm Gearing.....	974
30.4.2	Approximate (Geometrically Inaccurate) Bevel Gearing .....	975
30.4.3	Approximate (Geometrically Inaccurate) Crossed-Axes Gearing... ..	976
30.4.4	Approximate (Geometrically Inaccurate) Crossed-Axes Gearing: Face Gearing .....	978
30.5	Theory of Gearing at the Beginning of the Twenty-First Century: State-of-the-Art .....	979

30.6	Favorable Approximate Gearing .....	979
30.7	Accomplishments in the Field of <i>Non-Circular</i> Gearing.....	979
30.8	Tentative Chronology of Evolution of the Theory of Gearing .....	980
30.9	On the Other Efforts that Pertain to Evolution of Scientific Theory of Gearing.....	983
<b>Chapter 31</b>	<b>On the Lack of Understanding of the <i>Scientific Theory of Gearing</i> by the Majority of Gear Scientists and Engineers .....</b>	<b>985</b>
<b>Appendix A:</b>	<b>Elements of Vector Calculus .....</b>	<b>1007</b>
<b>Appendix B:</b>	<b>Elements of Differential Geometry of Surfaces.....</b>	<b>1013</b>
<b>Appendix C:</b>	<b>Change of Surface Parameters .....</b>	<b>1029</b>
<b>Appendix D:</b>	<b>Applied Coordinate Systems and Linear Transformations.....</b>	<b>1031</b>
<b>Appendix E:</b>	<b>Contact Geometry of a Gear and a Mating Pinion Tooth Flanks.....</b>	<b>1059</b>
<b>Appendix F:</b>	<b>The Closest Distance of Approach of Tooth Flanks of a Gear, and a Mating Pinion .....</b>	<b>1083</b>
<b>Appendix G:</b>	<b>Engineering Formulae for Specification of Gear Tooth Flank.....</b>	<b>1089</b>
<b>Appendix H:</b>	<b>On the Inadequacy of the Terms Wildhaber-Novikov Gearing, and W-N Gearing .....</b>	<b>1093</b>
<b>Conclusion</b>	<b>.....</b>	<b>1103</b>
<b>Notation</b>	<b>.....</b>	<b>1107</b>
<b>Glossary</b>	<b>.....</b>	<b>1111</b>
<b>References</b>	<b>.....</b>	<b>1121</b>
<b>Bibliography</b>	<b>.....</b>	<b>1131</b>
<b>Index</b>	<b>.....</b>	<b>1143</b>

---

# Preface

Gearing plays a role, usually unseen, in the lives of everyone in the civilized world. Few people know anything about gears and even fewer understand them. Even practicing engineers, except those who are gear specialists, know little except the rudiments about gears.

A couple dozen of more or less serious books have been written on gearing during the last five decades. Numerous books titled *Theory of Gearing* have been published. Most texts on the theory of gearing target the compilation and systematization of known achievements in the field of gearing. No effort has been undertaken to this end to develop a theory of gearing that covers all known achievements, as well as making possible the development of novel kinds of gearing that feature the desirable performance (predictive capabilities). A solution to this problem is disclosed by the author in this book.

It is likely that *Theodore Olivier's Theory of Gearing* (1842) was the first book ever published in the field [95]. To be honest, the book by *Th. Olivier* [95], as well as all other books published to this end, is not a *scientific* book in nature. Practical and theoretical experience is compiled in the published books. A scientific theory should be based on a set of postulates, from which the entire theory is derived. No definitive book of this sort in the field of gearing is published to this end.

Initially, the working title *Theory of Gearing: Anti-Litvin* was adopted for this book when the first edition (2012) of this book was under preparation. This was done mainly for two reasons. Firstly, none of the books on gearing published in the past deserve to be titled *Theory of Gearing*, since no scientific theory of gearing had been developed until approximately 2010. Secondly, many aggressive statements have been made about the priority of *F. Litvin* in the development of the theory of gearing. This theory is outlined in his book *Theory of Gearing*, editions of 1960, 1968, 1994, and 2004. All of these claims are wrong. The listed books are not among the first ones ever to be titled *Theory of Gearing*, and *F. Litvin* did not develop a theory of gearing in the scientific understanding of this term. The aforementioned books by *F. Litvin* are a kind of collection of the earlier accomplishments in the field of gearing, which mislead the professionals in the field of gear kinematics and gear geometry.

Previous treatments of the kinematics and geometry of gears use numerous approximations and introduce errors when they are applied to gears with a significant profile mismatch, such as those that have been developed in recent practice. It is therefore timely to reconsider the basic theory of the kinematics and geometry of gears so, as to provide a sound basis for the evaluation and development of future designs.

This book is written for engineers and researchers, those who work in the field of gear design, gear production, and application of gears. One of the main goals (purpose) of this book is to focus the attention of gear researchers on the development of a *scientific theory of gearing*, and to stimulate them to undertake extensive research in this particular field of mechanical engineering. The term *scientific* in this context is understood in the following manner. A concept is postulated and then the entire *theory of gearing* is derived from the postulated concept. The concept adopted in this book incorporates a prespecified configuration of rotation vectors of a gear and its mating pinion, as well as an input torque. The rest of the design parameters of a desirable (favorable) gear pair can be derived from the postulated concept. To draw up the maximum possible output from what *kinematics* and *geometry* of gearing are capable of providing us with, is among the goals of this book.

The *Theory of Gearing* is a kind of *scientific* theories, as all known designs of gearing are covered by the theory, and, moreover, all potentially possible gear designs are predicted by the theory. Any scientific theory is a self-consistent system of interconnected knowledge, capable of, on the one hand, to describe all known facts and phenomena, and, on the other hand, to predict yet unknown facts and phenomena covered by the theory. The scientific classification of the facts and phenomena covered by the theory is an integral part of the scientific theory.



With that said, the term *Scientific Theory of Gearing* is defined in the following way:

**Definition:** *The “Scientific Theory of Gearing” is a self-consistent system of interconnected knowledge, scientific methods of and means for, that is capable of, on the one hand, describing all known facts and phenomena, and, on the other hand, to predict yet unknown facts and phenomena covered by the theory; it is based on, and derived from (or can be derived from) an adopted set of axioms (the fundamental facts that are assumed evident, and do not require to get proven).*

The *adopted set of axioms* includes:

- a. a rotation vector of the driving shaft
- b. a rotation vector of the driven shaft (i.e., a configuration of the two rotation vectors is required to be pre-specified)
- c. an input/output torque
- d. a criterion to meet when synthesizing a gear pair with a desirable performance

Here and below the kinematics of a gear pair is of prime input component, as the geometry of the interacting tooth flanks of a gear and of a mating pinion can be derived on the premise of a given kinematics of a gear pair. Therefore, the discussed below theory can be referred to as the *kinematic* theory of gearing.

All known gear designs are covered by proposed the *scientific theory of gearing*. Numerous novel designs of gears can be derived using the disclosed theory. For the first time ever, a problem of synthesis of a gear pair with a desirable performance gets an analytical solution in this book.

---

# Acknowledgments

I would like to share the credit for any research success with my numerous doctoral students with whom I have tested the proposed ideas and applied them in the industry. The contributions of many friends, colleagues, and students are overwhelming in number and cannot be acknowledged individually, and as much as my benefactors have contributed, their kindness and help must go unrecorded.

My thanks also go to those at CRC Press who took over the final stages of preparing this book and coped with the marketing and sales of the fruit of my efforts.



# Taylor & Francis

Taylor & Francis Group

<http://taylorandfrancis.com>

---

# Author



**Dr. Stephen P. Radzevich** is a Professor of Mechanical Engineering, and a Professor of Manufacturing Engineering. He received the M.Sc. (1976), the Ph.D. (1982), and the Dr.(Eng)Sc. (1991) – all in mechanical engineering. Dr. Radzevich has extensive industrial experience in gear design and manufacture. He has developed numerous software packages dealing with *CAD* and *CAM* of precise gear finishing for a variety of industrial sponsors. His main research interest is *Kinematic Geometry of Surface Generation*, particularly with the focus on (a) precision gear design, (b)

high power density gear trains, (c) torque share in multi-flow gear trains, (d) design of special-purpose gear cutting/finishing tools, (e) design and machining (finishing) of precision gears for low-noise/noiseless transmissions of cars, light trucks, etc. Dr. Radzevich has spent about 40 years developing software, hardware, and other processes for gear design and optimization. Besides his work for industry, he trains engineering students at universities and gear engineers in companies. He authored and co-authored more than 30 monographs, handbooks, and textbooks. The monographs entitled *Generation of Surfaces* (2001), *Kinematic Geometry of Surface Machining* (CRC Press, 2008), *CAD/CAM of Sculptured Surfaces on Multi-Axis NC Machine: The DG/K-Based Approach* (M&C Publishers, 2008), *Gear Cutting Tools: Fundamentals of Design and Computation* (CRC Press, 2010, second edition 2017), *Precision Gear Shaving* (Nova Science Publishers, 2010), *Dudley's Handbook of Practical Gear Design and Manufacture* (CRC Press, 2012, second edition 2016), *Theory of Gearing: Kinematics, Geometry, and Synthesis* (CRC Press, 2012, second edition 2018), *Geometry of Surfaces: A Practical Guide for Mechanical Engineers* (Wiley, 2013, second edition Springer, 2019), *Advances in Gear Design and Manufacture* (CRC Press, 2019), *High-Conformal Gearing: Kinematics and Geometry* (CRC Press, 2015, second edition Elsevier, 2020), *Recent Advances in Gearing – Scientific Theory and Applications* (Springer, 2021), are among the recently published volumes. He also authored and co-authored about 350 scientific papers, and holds more than 260 patents on invention in the field, both, USA patents and international patents.



# Taylor & Francis

Taylor & Francis Group

<http://taylorandfrancis.com>



---

# Introduction

There is nothing more practical than a good theory

James C. Maxwell<sup>1</sup> (1831–1879)

This book is written for the engineers and researchers who work in the field of gear design, gear production, and application of gears.

There are many practical guides for the calculation of the design parameters of gears and gear pairs. This issue is more or less successfully covered in the books listed in the *References* and *Bibliography* sections of this book. Readers who are interested in performing the calculations of a gear are referred to these sources.

This book aims mostly to outline a possible solution to the problem of synthesis of a gear pair with the most favorable performance. The creation of a gear pair that is capable of reproducing a given motion of a driven member when a motion of a driving member is known, is the main goal of the synthesis of gearing. Therefore, in this book, a given pair of the rotation vectors,  $\boldsymbol{\omega}_g$  and  $\boldsymbol{\omega}_p$ , and the torque on the input shaft,  $\mathbf{T}_m$ , are the main inputs for synthesizing gear pairs<sup>2</sup>.

In the developed scientific theory of gearing the following fundamental postulate<sup>3</sup> is adopted:

**Fundamental postulate:** *All the design parameters of a favorable gear pair for a particular application can be derived from a given configuration of the rotation vectors of the driving and of the driven shafts, and on the power being transmitted by the gear pair.*

The kinematics of a gear pair is the starting point for solving the problem of synthesis of a gear pair with the desirable performance. The geometry of tooth flanks of the driving member and that of the driven member, can be derived on the premises of kinematics of the gear pair. (It is realized here that the kinematics of a gear pair is given.) Ultimately, the best possible set of the design parameters of the gear, and the pinion can be derived from the kinematics, and geometry of the tooth flanks of the mating gears.

The main portion of the input information for the purpose of synthesizing of a desirable gear pair is limited to the following:

- Input rotation (and torque)
- Configuration of a driven shaft in relation to a driving shaft
- Desirable output rotation and torque

The rest of the data (between the driving shaft and the driven shaft) should be calculated to ensure the favorable design of the gear pair.

The approach disclosed in this book makes possible a solution to the problem of synthesizing a gear pair in compliance with the aforementioned formulation.

---

<sup>1</sup> James Clerk Maxwell (June 13, 1831–November 5, 1879) – is a famous Scottish theoretical physicist.

<sup>2</sup> It should be stressed here that the rotation vectors,  $\boldsymbol{\omega}_g$  and  $\boldsymbol{\omega}_p$ , as well as others rotations to be introduced below, are not vectors by nature. However, when special care is undertaken, rotation vectors,  $\boldsymbol{\omega}_g$  and  $\boldsymbol{\omega}_p$ , can be treated like ordinary vectors are treated.

<sup>3</sup> It is instructive to point out here on the similarity between the proposed *scientific Theory of Gearing*, and the *Euclidean geometry*. The entire *Euclidean geometry* is derived from the postulated set of a several axioms (the total number of the postulated axioms in the *Euclidean geometry* is still disputed). Any and all scientific theories should possess this property, as the *Euclidean geometry* possesses. The proposed *scientific Theory of Gearing* meets this requirement, as it is derived from a set of postulates, outlined in the *Fundamental postulate*.

Harmonic gear drives are not considered in this book, as harmonic drives are not gear pairs at all. Harmonic gear drives are mechanisms of another nature rather than gearing.

I try to refer the reader to related sections of this book in both directions, forward, as well, as backward.

## HISTORICAL BACKGROUND

Primitive gears and gear transmissions are used by human being for many centuries. An experience accumulated in the gear design, manufacture, and application, was needed to be generalized. The necessity of the theory of gearing for the needs of gear practitioners is realized for a long while. In a certain sense, the theory of gearing can be viewed as a kind of *road map* that helps one traveling *from one location* (i.e., from a problem that one currently is encountered with) to *another location* (i.e., to a desirable solution to the aforementioned problem).

It is likely the 1842 book by *Theodore Olivier Theory of Gearing* [95] is the first book ever dedicated to gear science, and titled *Theory of Gearing*. Since the publication of this book by *Th. Olivier*, numerous attempts have been undertaken to develop a *scientific theory of gearing*: The book<sup>4</sup> by *Th. Olivier* is followed by 1852 book<sup>5</sup> by *E. Sang*, and then by 1886 master thesis<sup>6</sup> by *H.I. Gochman*, as well, as by numerous other books on the topic, published later on. Unfortunately, all the books published under the title *Theory of Gearing* (published by the year of ~2010) consist of no scientific theory of gearing. These books cannot be referred to as books on *theory of gearing*, rather they are collections of know achievements in the field of gear science and arts, having no ability to predict novel unknown yet designs of gears and gearing. Despite dozens of books being published in the field to this end, the problem remains unresolved, and no *scientific theory of gearing* is developed so far.

A more in-detail historical overview of the developments in this field can be found in Chapter 1: “A Brief Overview on the Evolution of the Scientific Theory of Gearing.”

This book is the first (and the only so far) attempt to outline systematically the theory of gearing starting from very simple signs like rotations of the gear and that of the pinion and ending with the calculation of the design parameters of the desirable gear, which best fits the prescribed conditions of functioning.

## IMPORTANCE OF THE SUBJECT

Gears are used in most mechanisms and machines. Transmitting and transformation of an input rotation is the main purpose of gearing. As gearing is extensively used in present-day practice, even a small improvement to a gear pair is capable of returning significant benefits to the user. This is, first of all, due to the total number of gears in use being enormous.

## UNIQUENESS OF THIS PUBLICATION

This book is unique for many reasons. Without going into detail, it is sufficient just to say that a *scientific Theory of Gearing* is developed in the book for the first time ever. The reader who becomes familiarized with the book should be able to design the best possible gear pairs for any given application.

---

<sup>4</sup> Olivier, T., *Théorie Géométrique des Engrenages destinés*, Bachelier, Paris 1842, 118 pages.

<sup>5</sup> Sang, E., *New General Theory of the Teeth of Wheels*, Edinburgh, 1852.

<sup>6</sup> Gochman, H.I., *Theory of Gearing Generalized and Developed Analytically*, Odessa, 1886, 229 pages.

INTENDED AUDIENCE

This book is intended to gear experts both from academia and industry. This book is of critical importance to university students, particularly those studying mechanical and manufacturing engineering. The book could also be interesting to engineers and researchers from other areas of mechanical engineering: aerospace engineering, automobile engineering, etc.

ORGANIZATION OF THIS BOOK

This book consists of a large number of sections, including, but not limited to 31 chapters, appendices, and so forth. In order to make reading of this book easier, its structure is schematically illustrated by means of the organization chart, shown in Figure 0.1.

The main portion of this book is organized into six parts: Part I–VI. Where necessary, the separate chapters are put together to form sections: II-A, II-B, and II-C. The acronym “G.-A.” in Figure 0.1 stands for “geometrically-accurate.”

Chapter 1, is titled “Non-Involute Gearing.” This chapter is considered separate, as it does not belong to any part, or to a section of this book. Considering the evolution of gear designs chronologically, the discussion in this chapter begins with ancient gears. This is natural, as the oldest designs of gears were, of course, of non-involute tooth profile.

This is followed by the discussion on spur and helical non-involute parallel-axes gear pairs. Pin gearing, cycloid gearing, lobes of *Roots blower*, and oil pump rotors, are covered in the discussion on *spur non-involute* parallel-axes gear pairs. Helical rotors in the design of the lobes of *Roots blower* rotors, along with an analysis and a proof of infeasibility of *Helical Gearing* by Dr. E. Wildhaber (US Pat. No. 1,601,750), are covered in the discussion on *helical non-involute* parallel-axes gear pairs.

Peculiarities of transmission of a rotary motion by means of non-involute gearing are discussed. This discussion includes, but not limited to the discussion of conditions of transmission of rotation by means of non-involute gearing, and of the interaction of non-involute gear with a rack.

The rest of the main body of the book is comprised of six parts: Part I–VI.

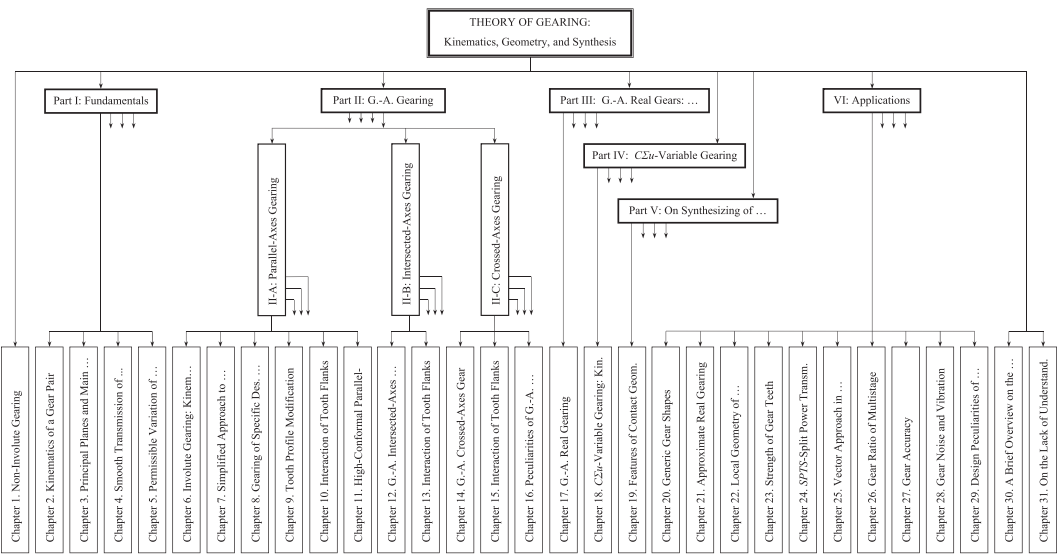


FIGURE 0.1 The organization chart of this book.

The first part of this book is titled “Part I. Fundamentals.” Four chapters: Chapters 2–5 comprise this part of this book.

Chapter 2 of this book is titled “Kinematics of a Gear Pair.” The principal kinematics of a gear pair is discussed to the best possible extent in this chapter. An analysis of transmission of motion by means of gear teeth is covered in this chapter. Vector representation of a gear pair kinematics in the form of gear vector diagram is extensively used for this purpose. For convenience, the gear vector diagrams of three different types are discussed in detail, namely:

- a. gear vector diagrams of rotary-negative crossed-axes gear pairs
- b. gear vector diagrams of rotary-positive crossed-axes gear pairs
- c. gear vector diagrams of rotary-zero crossed-axes gear pairs

In all three aforementioned cases, the conditions of both, of pure rolling, and of pure sliding, are analyzed. Ultimately, an analytical criterion of each type of crossed-axes gear pair is proposed.

The use of the gear vector diagrams makes possible a scientific classification of all possible kinds of the gear vector diagrams. Upon the classification was developed, a set of complimentary vectors to the gear vector diagrams is introduced. They include both, the centerline vectors, and the axial vectors of a gear pair. The consideration ends with a set of useful kinematic and geometric formulas.

Possible future developments in the theory of gearing are an important output from the analysis undertaken in Chapter 2 of this book.

Chapter 3 of this book is titled “Principal Planes and Main Reference Systems Associated with Gear Pair.” In this chapter, three principal planes, and a set of the main reference systems associated with a gear pair are established. Usage of the principal planes, and of the main reference systems is convenient in the further analysis.

Along with a general case of crossed-axes gearing, the reduced cases of intersected-axes gearing, and of parallel-axes gearing, both, are used to illustrate details of the approach. The discussion on the main reference systems associated with a gear pair is complemented with the corresponding analytical description of the coordinate systems transformations. Transition from the gear reference system, and from the pinion reference system to the main reference system, both, are described analytically.

In Chapter 4, titled “Smooth Transmission of Uniform Rotary Motion: Three Fundamental Laws of Gearing,” three fundamental laws of gearing are formulated.

To transmit a uniform rotary motion smoothly from a driving shaft to a driven shaft, all three fundamental laws of gearing must be fulfilled.

To obey the *first fundamental law of gearing*, proper contact between tooth flanks,  $\mathcal{G}$  and  $\mathcal{P}$ , of a gear, and its mating pinion must be ensured. *Shishkov equation of contact*,  $\mathbf{n} \cdot \mathbf{V}_{\Sigma} = 0$  is extensively used for analytical description of the required condition of contact between the tooth flanks,  $\mathcal{G}$  and  $\mathcal{P}$ .

The conjugate action law is the *second fundamental law of gearing*. *Equivalent pulley-and-belt transmission* is used for the derivation of this fundamental law of gearing. Ultimately, the *equation of conjugacy*,  $\mathbf{p}_{in} \times \mathbf{V}_m \cdot \mathbf{n}_g = 0$ , of the tooth flanks,  $\mathcal{G}$  and  $\mathcal{P}$ , is derived. The performed analysis of parallel-axes gearing makes possible to formulate the *Camus-Euler-Savary theorem*. The *Camus-Euler-Savary theorem* (or just *CES – theorem*, for simplicity) can be viewed as a reduced case of the *second fundamental law of gearing*. The *CES – theorem* is valid only for parallel-axes gearing. This theorem is not generalized yet to more general cases of gearing, namely, neither to intersected-axes gearing nor to crossed-axes gearing.

Finally, the condition of equal base pitches of a gear and of a mating pinion is discussed with respect to parallel-axes gearing. The equality of base pitches is valid only in the case of parallel-axes gearing, and is said to be a reduced case of the *third fundamental law of gearing*. To fulfill the *third fundamental law of gearing*, both base pitch of a gear and base pitch of a mating pinion must be equal to the operating base pitch of the gear pair.

The permissible variation of the center-distance in a parallel-axes gear pair, and in the actual value of the transverse pressure angle, are briefly outlined in Chapter 5 of this book. This chapter is titled “Permissible Variation of the Design Parameters in *Equivalent Pulley-and-Belt Transmission*.” Despite of this analysis was executed by means of *equivalent pulley-and-belt transmission*, the obtained results are valid for parallel-axes involute gearing.

Here, in Figure 0.1, the short arrows are shown next to the box labeled “Part I. Fundamentals,” as well, as next to numerous other boxes, indicate a potential possibility of additional boxes of a lower level, those detailing the corresponding box of a higher level.

Part I of this book is followed by Part II. The second part of this book is titled as “Geometrically-Accurate Gearing.” Part II is composed of three sections, namely, of Sections II-A–II-C. In these sections, fundamentals of geometrically accurate gearing of various designs are analyzed.

In Section II-A, the geometry and kinematics of geometrically accurate gear pairs those operating on parallel axes of rotation of a gear and its mating pinion are considered. This section of this book is titled as “Geometrically-Accurate Gearing: Parallel-Axes Gearing.” Six chapters comprise the second section of this book. They are Chapters 6–11.

The discussion in Section II-A begins with in-detail analysis of the kinematics and geometry of parallel-axes gear pairs. The corresponding Chapter 6 that is titled as “Involute Gearing: Kinematics and Geometry.”

Two principal problems are covered in this chapter. The first of two aforementioned problems pertain to principal features of the kinematics and geometry in parallel-axes gearing. The discussion of the first problem includes, but not limited to the analysis of the kinematics, the gear ratio, and the permissible transverse pressure angle variation, in parallel-axes gearing. Tooth flank generation is the second problem discussed in this chapter. The following issues are covered in the consideration: of (a) a desirable line of contact between the tooth flanks of a gear and a mating pinion, (b) the line of action, and path of contact in a gear pair, (c) operating base pitch in a gear pair, and (d) general approach to gear tooth flank of a favorable geometry. The discussion on these two principal problems forms the foundation of geometrically accurate parallel-axes gearing.

On the premise of the obtained results in the kinematics and geometry of tooth flanks, a simplified approach for the generation of involute gear tooth flank is developed. This approach is disclosed in Chapter 7. This chapter is titled as “Simplified Approach to Generation of Involute Gear Tooth Flank.” Here, more in-detail analysis of tooth flank generation is performed. A simplified approach for involute gear tooth flank generation is disclosed. For this purpose, generation of involute tooth profile in geometrically accurate parallel-axes gear pair is considered. The involute gear tooth profile, and the tooth flanks of a gear and its mating pinion in spur, helical, and circular-arc (in the lengthwise direction gear) tooth flanks are investigated. Then, possible forms of a gear tooth in the lengthwise direction are considered, and the adopted gear terminology is outlined. Ultimately, derivation of the *Euler-Savary equation* is provided.

An alternative approach for the derivation of equation of the involute tooth flank is discussed. The generating straight line of a spur gear, the length of involute tooth profile, and generating basic rack of a spur gear are covered in this discussion. Both the methods, that is, an analytical approach, as well as the descriptive-geometry-based determination of the straight generating line are discussed.

Conical involute gears are considered with a focus on the kinematics of conical involute gearing, and on the geometry of the tooth flanks of a spur, and a helical conical involute gear. At the end of the chapter, a set of conditions to be fulfilled by a pair of mating gears is formulated in engineering terms.

The kinematics and geometry of parallel-axes involute gearing of specific design are discussed in Chapter 8. This chapter is titled as “Parallel-Axes Involute Gearing of Specific Design.” The discussion begins with the kinematics of conical involute gearing and is followed by the geometry of tooth flanks in spur, and in helical conical involute gears. Then, the kinematics and geometry of tooth flanks in internal involute gearing are outlined, including some features of tooth flank geometry and the gear design. Gear coupling in this book is construed as a reduced case of internal parallel-axes



gearing. The performed analysis is followed by a discussion on the commonality between internal gearing, and strain wave gearing (harmonic drive). The chapter ends with a brief consideration of *pinion gear-to-rack mesh*, which is interpreted as a reduced case of parallel-axes involute gear pair.

In Chapter 9, titled “Gear Tooth Profile Modification: Generating Rack Shift,” generation of modified tooth flanks in involute gear is discussed. The addendum modification (namely, the tooth profile shift), profile shift coefficient, along with the gear tooth flank geometry depending on the profile shift coefficient, are covered in this discussion. The basic equations for a gear pair with addendum modification are listed in this chapter of this book. This section ends with the usage of the geometric blocking contours for the determination of the profile shift coefficients.

The discussion in Chapter 10 “Interaction of Tooth Flanks in Parallel-Axes Involute Gearing” is focused mainly on the interaction between the tooth flanks of gears in parallel-axes spur gearing, as well, as in helical involute gearing that are capable of transmitting an input uniform rotation smoothly. Special attention is given to the analysis of contact ratio in parallel-axes involute gearing. This issue is discussed to the best possible extent. In particular, transverse contact ration in a *low-tooth-count gearing* got in-detail consideration. The impact of elastic deformation of the gear teeth onto the total contact ratio in gear pair is briefly outlined.

Principal design parameters and their variation within the tooth flank in external involute gear pair are discussed. In particular, the variation of the normal curvature of the gear tooth flank, and of the tooth profile angle and helix angle got in-detail investigation. The special point of meshing is discovered, and the location of this point in relation to a gear and a mating pinion is determined.

Sliding conditions and specific sliding between a gear and a mating pinion tooth flanks are discussed in the sub-section on contact motion characteristics. In the discussion on elements of dynamics of perfect parallel-axes gearing, the forces acting in the plane of action, and in a transverse section of a geometrically accurate parallel-axes involute gear pair are analyzed.

In Chapter 11 titled as “Novikov/Conformal and High-Conformal Gearing,” the kinematics, and geometry of tooth flanks in *Novikov/conformal* and *high-conformal* parallel-axes gearing are discussed. The consideration begins with a brief overview of conformal gearing with focus on the origin of *Novikov/conformal* and *high-conformal* gearing, and on the power density in *high-conformal* gearing. It is shown that, by nature, *Novikov/conformal* and *high-conformal*, are reduced cases of helical involute gearing with zero length of field of action, and with zero transverse contact ratio. The essence of gearing of this kind is briefly outlined, and the fundamental design parameters of *conformal gearing* are discussed. This analysis follows by a discussion on transition from involute gearing to conformal parallel-axes gearing (*Novikov gearing*). For this purpose, the boundary  $N$  – circle in conformal gearing is introduced, and possible tooth geometries are analyzed. Tooth profile sliding, along with the tooth profile rolling in *Novikov/conformal* and *high-conformal* gearing, are covered in the sub-section on tooth profile rolling/sliding. The consideration of the elements of the kinematics and geometry in *Novikov/conformal* and *high-conformal* gearing is followed by the analysis of design of conformal gear pair.

A possible way of evolution of conventional conformal gearing to conformal gearing with two pseudo-paths of contact is discussed. The consideration of tooth flank geometry in conformal gearing includes an analysis of the configuration of interacting tooth flanks at the culminating point along with the local and global contact geometry of interacting tooth flanks.

Principal features of high-conformal gearing are outlined, and the difference between *conformal gearing* and *high-conformal gearing* is shown. This discussion follows by the consideration of contact geometry, as well as of the accuracy requirements for high-conformal parallel-axes gearing. The chapter ends with a brief discussion on the impossibility of finish-cutting of gears for conformal, and for high-conformal gearing in generating (continuous-indexing) machining processes.

Geometrically accurate intersected-axes gearing is discussed in Section II-B: “Geometrically-Accurate Gearing: Intersected-Axes Gear Pairs.” This section of the book is composed of two chapters: Chapters 12 and 13.

Geometrically accurate intersected-axes gear pairs are discussed in Chapter 12, “Geometrically-Accurate Intersected-Axes Gear Pairs.” The discussion begins with the consideration of the earliest designs of intersected-axes gearing and follows by the analysis of the kinematics, and of the base cones in intersected-axes gearing. The path of contact and the instantaneous line of action are considered here. Then, the tooth flanks of geometrically accurate intersected-axes gear pairs are discussed. For this purpose, a set of reference systems is introduced and discussed in detail, including, but not limited to intersected-axes gearing with variable pressure angle. This discussion is followed by an analysis of the desirable tooth proportions in intersected-axes gears: angular base pitch, transverse pressure angle, angular pitch, angular tooth thickness, and angular space width, angular backlash, angular addendum and angular dedendum, and specification of the design parameters in intersected-axes gearing are discussed as well. The concept of the *Tredgold approximation* is briefly outlined here.

Geometrically accurate *Novikov/conformal*, and *high-conformal* intersected-axes gearing got special attention in Section 12.8 of the book. The discussion begins with the analysis of the main features of gearing of this particular kind and follows by a discussion of the path of contact, pseudo-path of contact, boundary cones, and bearing capacity of high-conformal gearing. This discussion ends with the consideration of the design parameters in *Novikov/conformal*, and *high-conformal* intersected-axes gearing.

In Chapter 13, “Interaction of Tooth Flanks in Geometrically-Accurate Intersected-Axes Gearing,” the discussion begins with the analysis of the *equivalent pulley-and-belt transmission* for intersected-axes gear pair, and follows by the analysis of the path of contact and zone (field) of action in intersected-axes gearing. Then, the transmission of a uniform rotary motion by means of gear teeth in intersected-axes gearing is discussed. The analysis of the contact ratio is performed in this section to the best possible extent. Then, the contact motion characteristics are investigated. For this purpose, sliding in geometrically accurate intersected-axes gearing, and elements of dynamics of the gearing are discussed.

The discussion on sliding between the interacting tooth flanks of a gear and its mating pinion includes a descriptive geometry-based solution to this problem as well as analytical solution to the problem of determining sliding in geometrically accurate intersected-axes gearing. Specific sliding and its features are also discussed.

In the discussion on dynamics of gearing, the principal assumption that is adopted in the load analysis of geometrically accurate intersected-axes gearing is formulated. Forces of the interaction between the gear teeth are considered.

This chapter ends with the consideration of preliminary testing of geometrically accurate spiral bevel gears with a focus on the contact pattern. Conditions of the preliminary testing are outlined, and the parameters of contact geometry in the tested spiral bevel gearing are predicted. The predicted contact geometry is in extremely good correlation with the results of the testing.

Various kinds of geometrically accurate crossed-axes gearing are discussed in Section II-C, titled “Geometrically-Accurate Gears: Crossed-Axes Gearing.” Three chapters, namely, Chapters 14–16, comprise this section of the book.

This section of the book opens with Chapter 14, titled “Geometrically-Accurate Crossed-Axes Gear Pairs: R-Gearing.” The discussion begins with the analysis of the kinematics of crossed-axes gearing. The pressure angle in crossed-axes gearing is specified, and gearing with a *constant* transverse pressure angle, as well as with variable transverse pressure angle are considered. Then the base cones in crossed-axes gear pair are constructed.

Numerous reference systems are introduced aiming at the investigation of the tooth flank geometry in geometrically accurate crossed-axes gear. Transition from a reference system to another one is described analytically in the form of the operators of linear transformations. This results in an expression for the gear tooth flank in crossed-axes gearing. Gearing of this design is referred to as *R – gearing*. *R – gearing* is the only kind of geometrically accurate gearing with line contact

between the tooth flanks of a gear and its mating pinion. The conjugate action law in  $R$  – gearing crossed-axes is described analytically.

The desirable tooth proportions in crossed-axes gear pairs are specified. This includes, but is not limited to: (a) Operating angular base pitch; (b) Low-tooth-count crossed-axes gears; (c) Transverse pressure angle; (d) Angular pitch; (e) Angular tooth thickness, and angular space width in the round basic rack; and (f) Angular addendum and angular dedendum of the round basic rack.

A possible evolution of *Tredgold approximation* towards crossed-axes gearing is briefly outlined.

Special consideration in this chapter of the book is given to the analysis of the main features of geometrically accurate *Novikov/conformal*, and *high-conformal* crossed-axes gearing. Path of contact, *boundary N-cone*, and bearing capacity of crossed-axes *Novikov/conformal*, and *high-conformal* gearing are covered in this discussion. At the end of the chapter, calculation of the design parameters of *Novikov/conformal*, and *high-conformal* crossed-axes gearing is considered.

Chapter 15 is titled “Interaction of Gears in Geometrically-Accurate Crossed-Axes Gearing.” In this chapter, the interaction of tooth flanks of a gear and its mating pinion in crossed-axes gearing is discussed. The *equivalent pulley-and-belt transmission* of crossed-axes gear pair is extensively used in this analysis. The path of contact, and the zone (field) of action, are investigated. This analysis is followed by the consideration of the conditions for transmitting a uniform rotary motion by means of gear teeth in crossed-axes gearing. Then, contact ratio in crossed-axes gearing is discussed to the best possible extent.

Special attention is given to the investigation of contact motion characteristics in crossed-axes gearing. Sliding, specific sliding, and features of specific sliding between the teeth flanks in geometrically accurate crossed-axes gearing got in-detail consideration.

This chapter of the book ends with the discussion of elements of dynamics of geometrically accurate crossed-axes gearing. A principal assumption, adopted in load analysis of geometrically accurate crossed-axes gearing, is formulated here, and forces of interaction of the gear teeth are analyzed. The latter analysis includes, but is not limited to the forces that act in geometrically accurate crossed-axes gearing: (a) the resultant force, (b) the forces acting on the gear and the pinion, as well as (c) the normal force acting on the gear.

Peculiarities of geometrically accurate worm gearing are discussed in Chapter 16. This chapter is titled “Geometrically-Accurate Worm-Gearing: Peculiarities of Kinematics and Geometry.” The discussion in this chapter is focused on the features of worm gearing with line contact between the worm threads and the worm-gear tooth flanks. This is a novel kind of worm gearing not known in the past. The kinematics, base cones, and the peculiarities of sliding at around the plane-of-action apex in geometrically accurate worm gearing are covered in this chapter. An analytical criterion to distinguish a worm from a helical gear with a low tooth count is proposed. The chapter ends with an analysis of a particular design of worm gear-drive [Pat. No. 257,246, USSR, 1968], which is used to demonstrate the importance of the theory of gearing for gear experts.

The kinematics, geometry, and application of real gears are discussed in Part III of this book. This part is titled “Real Gears: Kinematics, Geometry, and Application.” It consists of one Chapter: 17 that is titled “Geometrically-Accurate Real Gearing:  $S_{pr}$  – Gear System.”

In this chapter, geometrically accurate real gearing is considered. A novel design of geometrically accurate real gearing is proposed. The proposed design of gearing is referred to as  $S_{pr}$  – gear system.

The discussion begins with the preliminary considerations. The following topics: (a) the root causes for the real gears differ from geometrically accurate gears, (b) applied coordinate systems, (c) displacements of a gear axis of rotation from its desirable configuration, and (d) determination of the closest distance of approach between a gear and its mating pinion axes of rotation, are covered in this chapter. This analysis follows by the discussion of tooth flank geometry in geometrically accurate real gearing, that is, in gears for  $S_{pr}$  – Gear System. The adopted concept for tooth flank generation of gears for  $S_{pr}$  – gear system, preferred reference systems, derivation of equation for

tooth flank in  $S_{pr}$  – *gearing*, angular base pitch in  $S_{pr}$  – *gearing*, and features of interaction of the tooth flanks in  $S_{pr}$  – *gearing*, are covered in this section of the book.

Then, possibilities of implementation of the concept of  $S_{pr}$  – *gearing* in design of two-degrees-of-freedom gearing, and in design of gear coupling are analyzed.

It is shown that normal distribution of manufacturing errors onto geometry of tooth flanks can be taken into account when designing gears for  $S_{pr}$  – *gear System*. It is also demonstrated that the concept of  $S_{pr}$  – *gearing* cannot be used in gear systems with point contact between the tooth flanks of a gear and a mating pinion, such as in design of gears for Novikov/conformal gearing, and for high-conformal gearing.

The consideration in this section of the book ends with the analysis of correlation among the gear systems of various types.

Part III has a huge potential for the evolution (to be considered in a few more chapters in the future editions of this book).

The kinematics and geometry of gearing with variable the center-distance,  $C$ , the shaft angle,  $\Sigma$ , and the gear ratio,  $u$  (the so-called  $C\Sigma u$  – variable gearing), are discussed in Part IV, titled “ $C\Sigma u$  – Variable Gearing.” This part of the book consists of a single Chapter 18, that is titled “ $C\Sigma u$  – Variable Gears: Kinematics, Geometry, and Novel Concept to Design Geometrically-Accurate Gears.” In this chapter, the discussion begins with the analysis of fundamentals of geometrically accurate non-circular gearing. Then the tooth flank generation in geometrically accurate non-circular gear pair is discussed. The chapter ends with an analysis of inconsistency of known methods of machining gears for perfect non-circular gear pairs.

Part IV has a huge potential for further evolution (to be discussed in a few more chapters in the future editions of this book).

A concept of synthesizing favorable geometrically accurate gear pairs of all kinds (namely, parallel-axes gear pairs, intersected-axes gear pairs, and crossed-axes gear pairs) is proposed in Part V. This part of the book is titled “On Synthesizing of Favorable Geometrically-Accurate Gear Pairs.” It is comprised of a single Chapter 19 that deals with gear pairs with favorable performance. Chapter 19 is titled “Features of Contact Geometry.” The contact geometry between the tooth flanks of a gear and that of a mating pinion is analyzed in this chapter. The meaning of the term *synthesis of the favorable gear pair* is clarified. It is shown how *Dupin indicatrix* at point of contact of a gear, and its mating pinion tooth flank, as well as indicatrix of conformity at point of contact of a gear and a mating pinion tooth flanks can be employed for solving the problem of synthesizing of favorable gear pair.

Part V has a huge potential for evolution to be outlined in a few more chapters in the future editions of this book.

The last part of this book, Part VI: “Real Gears and Their Application” is comprised of ten chapters (Chapters 20–29).

Generic gear shapes are discussed in Chapter 20: “Generic Gear Shapes.” The origination of the generic gear shape, and examples of gear pairs composed of gears with generic shapes of various geometry are covered in this discussion. The total number of possible generic gear shapes is estimated. The possible profiles of generic gear shape constructed in axial section of a gear, as well as the profile of generic gear surface constructed in section by plane at an angle to the gear axis of rotation, are taken into account in this analysis. A possibility of classification of gear pairs is discussed, and examples of implementation of the classification of gear pairs are provided.

Chapter 21 is titled “Approximate Real Gearing,” and deals with approximate real gearing. Approximate real parallel-axes gearing, approximate real intersected-axes gearing, as well as approximate real crossed-axes gearing, including worm gearing, are covered in this discussion. The root causes for the inaccuracies of real approximate gears along with the generation of their tooth flanks are analyzed. Numerous examples of the gear designs, and of the applied methods for tooth flank generation are provided.

Special attention is given to the analysis of gear tooth flank modification. This discussion begins with a brief historical overview on gear tooth flank modification. Then, it is followed by consideration of the requirements to design parameters of modified portions of tooth flanks. Numerous kinds of tooth flank modifications are analyzed. The description of gear tooth flank modifications by functions is briefly outlined.

In Chapter 22 is titled “Local Geometry of Interacting Gear Tooth Flanks.” The local geometry of interacting tooth flanks of a gear and its mating pinion is considered in this chapter. The discussion is followed by the analysis of local geometry of the interacting tooth flanks in intersected-axes gearing. The kinematics and the local geometry of the interacting tooth flanks are considered. Then, the local geometry of interacting tooth flanks in crossed-axes gearing is investigated. The kinematics and the local geometry of the interacting tooth flanks in crossed-axes gearing are covered in this discussion. The chapter ends with an analysis of the local geometry of interacting tooth flanks in *Novikov/conformal*, and in *high-conformal* gearing. Again, the discussion is focused mainly on the kinematics, and the geometry of interacting tooth flanks in *Novikov/conformal*, and in *high-conformal* gearing.

Strength of gear teeth is discussed in Chapter 23 titled “Strength of Gear Teeth.” The discussion begins with the adopted principal assumptions. The *Hertz proportional assumption* and the *assumption of equal torque share* are the two adopted chapter assumptions. This discussion is followed by the analysis of the principal features of *low-tooth-count gears*, and by the development of an analytical model for calculating contact stress. Formula for the calculation of *Hertz contact stress* is introduced, and the specific pressure factor is discussed. The discussion of the gear contact strength ends with the calculation of the combined compressive-shear stress in *low-tooth-count gearing*.

Then, the bending strength of gear teeth is discussed. For this purpose, the inconsistency of *Lewis’ formula* for the calculation of gear teeth bending strength is explained.

The effective length of line of contact in a gear pair is considered in detail, including, but not limited to the length of a single line of contact, as well as the effective length of lines of contact in spur and helical parallel-axes gearing. This discussion is followed by the analysis of loading of the gear teeth.

A method of simulation of the interaction of a gear and its mating pinion tooth flanks is disclosed at the end of Chapter 23 of the book.

Titled “SPTS – Split Power Transmission Systems,” Chapter 24 is devoted to gear transmissions that feature split power flow. The root cause for non-uniform torque sharing in split power transmission system, mobility of split power transmission systems, and the *power density* of gear transmission systems are covered in this chapter. The discussion is followed by the analysis of epicyclic gear drives, and a structural formula for planetary gear drives is considered. Then, a correspondence among angular velocities of all the members in a planetary gear drive is discussed. Further discussion is focused mainly on formulating the problem of equal load sharing in planetary gear drives, along with the consideration of the state-of-the-art in this particular area of gear design. Ordinary planetary gear drives and planetary gear drives with flexible pins are analyzed.

Ultimately, an alternative approach for uniform torque sharing in split power transmission system is proposed. This includes, but is not limited to the planetary gear drive with elastomeric load sharing device, and examples of implementation of elastic load sharing device. The chapter ends with the discussion of the main features of split power transmission systems with preloaded elastic load sharing devices.

Chapter 25 is titled “Vector Approach in Kinematic and Dynamic Analysis of Complex Gear Transmission Systems,” and deals with a vector approach for kinematic and dynamic analysis of complex gear transmission systems. Possible kinds of images for a rotating gear, along with the gear vector diagrams for complex gear transmission systems are covered in this discussion. Features of gear vector diagrams for complex gear transmission systems with intersected-axes, and with



crossed-axes gear pairs, are disclosed. For the first time ever, elementary gear vector diagram for intersected-axes gear pairs, and for crossed-axes gear pairs are discussed in particular.

In Chapter 26 “Gear Ratio of Multistage Gear Transmission System,” the discussion begins with the consideration of principal kinematic relationships in a multistage gear drive. The range for the ratio of speed variation for gear drive, and the characteristic of transmission group are covered in this discussion. Further, an analytical method for determination of transmission ratios is disclosed. The rotational speed chart, broken geometric series, and a minimum required number of gear pairs are considered. The chapter ends with the determination of tooth number of gears of group transmissions.

In Chapter 27 “Gear Accuracy” a few novel methods for inspection accuracy of the gears are briefly discussed. A perfect datum surface is used in every of the considered methods of gear inspection. These makes the methods of gear inspection more accurate, and more reliable.

There are many sources for the vibration generation, and an excessive noise excitation in a real gear pair. The most critical of them are analyzed in Chapter 28, titled “Gear Noise and Vibration.” Kinematic and geometric factors that affect the noise excitation are briefly discussed. Some physical factors, like a variation of the loading in a gear pair, that allow for a kinematic/geometric interpretation are also outlined here.

Section VI “Applications” ends with the consideration of the design peculiarities of geometrically accurate, and almost geometrically accurate gears. This analysis is performed in Chapter 29 titled “Design Peculiarities of Geometrically-Accurate and Almost Geometrically-Accurate Gears.” Features of the design of gears for  $R$  – gearing, as well as for  $R_{sp}$  – gearing, are considered as examples.

Chapter 30 is titled “A Brief Overview on Evolution of the Scientific Theory of Gearing.” In this chapter the milestone accomplishments that comprise the foundation of the scientific theory of gearing are briefly outlined. The discussion begins with the consideration of the earliest designs of gears.

The evolution of the gear art falls into three periods, namely, into pre-*Eulerian*, *Eulerian*, and post-*Eulerian* periods of evolution of the gear science and art. The scientific theory of gearing is originated in the *Eulerian* period of the gear art. Then, the developments in the field of geometrically accurate gearing are considered. The contributions by *G. Grant*, Prof. *N. Kolchin*, Prof. *M. Novikov*, Prof. *V. Gavrilenko*, and others are covered in this discussion. Ultimately, a tentative chronology of the evolution of the theory of gearing is established.

The developments in the field of approximate gearing are another consideration in Chapter 30 of the book. Here *S. Cone* double-enveloping worm gearing, approximate bevel gearing, approximate crossed-axes gearing, as well as face gearing are briefly discussed.

A brief summary of the milestone accomplishments in the theory of gearing achieved by the beginning of the twenty-first century is provided. Condition of contact of the interacting tooth flanks of a gear and its mating pinion, condition of conjugacy of the interacting tooth flanks of a gear and that of a pinion, and condition of equal base pitches of the interacting tooth flanks of a gear and of a pinion are covered in this discussion. The chapter ends with the concluding remarks.

In Chapter 31 titled “On the Lack of Understanding of the Scientific Theory of Gearing by the Majority of Gear Scientists and Engineers,” the most common mistakes that result in misunderstanding of the scientific theory of gearing are briefly discussed.

There are several appendices in the book. The appendices are as follow: (a) Elements of vector calculus, (b) Elements of differential geometry of surfaces, (c) Change of surface parameters, (d) Applied coordinate systems and linear transformations, (e) Contact geometry of a gear and a mating pinion tooth flanks, (f) Closest distance of approach between a gear, and a mating pinion tooth flanks, (g) Engineering formulae for the specification of gear tooth flank, and (h) On inadequacy of the terms *Wildhaber-Novikov Gearing*, and *W-N Gearing*. The provided list of titles of the appendices makes clear what the appendices deal with.



This book ends with the “Conclusion.” Here, the principal accomplishments are systematically outlined.

This book, which starts with the basics and steadily moves toward advanced scientific theory of gearing, may help both to refute ill-informed and prejudiced views on the topic, which sometimes even verge on ridicule, and to broaden interest in the science of mechanisms so that its place in our educational institutions and mechanical engineering practice is better recognized.

Much as I wish otherwise, I can hardly hope that this book is entirely free from omissions, or mistakes; or that it is as clear and ambiguous, as it should be. If you have any constructive suggestions, please communicate them to me via e-mail: [radzevich@usa.com](mailto:radzevich@usa.com).

**Stephen P. Radzevich**  
*Sterling Heights, Michigan, USA*  
*February 19, 2022*

---

# 1 Non-Involute Gearing

Non-involute gearing is a kind of gearing that the practical application of gears began with. The term *non-involute gear* was proposed a long time ago for gears with non-involute tooth profile that are used in the design of parallel-axes gearing. Numerous known designs of non-involute gearing are approximate gearing, as all of them, by nature, are not capable of transmitting a steady input rotary motion from the input shaft to the output shaft. Later on, approximate intersected-axes gearing, as well as crossed-axes gearing, was also referred to as *non-involute gear* despite that the gear tooth profiles in geometrically accurate intersected-axes gearing and in geometrically accurate crossed-axes gearing are also of non-involute geometry.

In ancient times, smart men were able to produce gears only with non-involute tooth profiles. Non-involute gearing is geometrically inaccurate by nature. Involute gears were invented much later than the gears with non-involute tooth profiles. The kinematics and the geometry of non-involute gearing are of scientific interest and of practical importance for gear engineers, as gears of these designs are still extensively used in the industry, especially when slow rotations and low torque are required to be transmitted.

Just a few kinds of non-involute gearing are recognized in present-day practice<sup>1</sup>:

- pin gearing
- lantern gearing
- cycloid gearing
- clock-type gearing
- special-purpose gearing

Before discussing the kinematics of non-involute gear pairs and the geometry of tooth flanks in non-involute gears in detail, let us discuss a brief overview of known designs of non-involute gearing. The overview begins with consideration of spur non-involute gear pairs and is followed by a discussion on helical non-involute pairs.

## 1.1 SPUR NON-INVOLUTE GEAR PAIRS

Various practical applications of spur non-involute gear pairs are well known. They are used to transmit a rotation from a driving shaft to a driven shaft in various designs of oil pumps, air blowers, and so forth. The tooth profiles of such gears are shaped in a form of cycloids, extended epicycloids, round pins, and special-purpose profiles.

In spur non-involute gear pairs, only one pair of teeth is engaged in mesh at every instant of time. Because it is clear from further discussion in this section, it does not mean that the transverse contact ratio in non-involute gear pair equals to one ( $m_p = 1$ ). No, this is incorrect, as the transverse contact ratio,  $m_p$ , can be specified only in involute gearing and cannot be specified in gearing with other tooth profile geometry. The face contact ratio,  $m_F$ , in spur non-involute gear pairs is zero, that is, an equality  $m_F = 0$  is always valid.

---

<sup>1</sup> It is right time to point out here that *Novikov gearing* (or, in other words, *conformal gearing*) is a reduced kind of involute gearing (i.e., *Novikov gearing* is not a kind of non-involute gearing). Therefore, *Novikov gearing* is discussed below in this book in Chapters 6, 7, 8, and 10 where involute gearing is also discussed.



**FIGURE 1.1** Old-style pin gearing with intersected axes of rotation of a gear and of a mating pinion.

### 1.1.1 PIN GEARING

Pin gearing is probably the first kind of gearing ever used by smart men. Initially, a small pinion was designed so as to have pins either parallel to the pinion axis of rotation (in parallel-axes gearing) or radially, as shown in Figure 1.1, for intersected-axes gearing. The pins were evenly spaced circumferentially and assembled either between two or in a single disc. The discs were rigidly connected to the driving shaft. A large gear had a disc rigidly connected to the driven shaft. The pins were mounted radially around the periphery of the disk with equal space between adjacent pins. A few more modifications of the initial design of pin gearing are also well known. Present days, pin gearing has very limited applications in the industry.

This discussion allows for an intermediate conclusion:

**Conclusion 1.1.** *No smooth (with a constant angular velocity ratio) transmission of a uniform rotary motion is possible by means of pin gearing, as the mating tooth profiles do not conjugate to one another.*

Pin gearing cannot be geometrically accurate gearing by nature.

### 1.1.2 LANTERN GEARING

Eventually, pin gearing, shown in Figure 1.1, was replaced with lantern gearing. An example of old-style lantern gears made out of wood is illustrated in Figure 1.2. In lantern gearing, the pinion teeth are cylindrical pins with axes parallel to the axis of the gear, so the teeth profile is a circle. The pinion is designed as an assembly of pins placed between two discs (see Figure 1.3). Such a design does not require the profile generation of the pinion teeth, which is an important advantage of gearing of this particular design. Moreover, in huge size pin gearing, the pins can rotate either around journals or around bearings. This allows for reduction (a) of friction between interacting tooth surfaces, (b) of tooth wear, and ultimately, and (c) power losses in the gear pair. The mating gear teeth are of cycloid profile.

Lantern gearing was investigated by Prof. *E. Buckingham*. In particular, he proposed [15] a construction of path of contact,  $P_c$ , for lantern gearing (see Figure 1.4).



**FIGURE 1.2** Old-style lantern gears made out of wood.

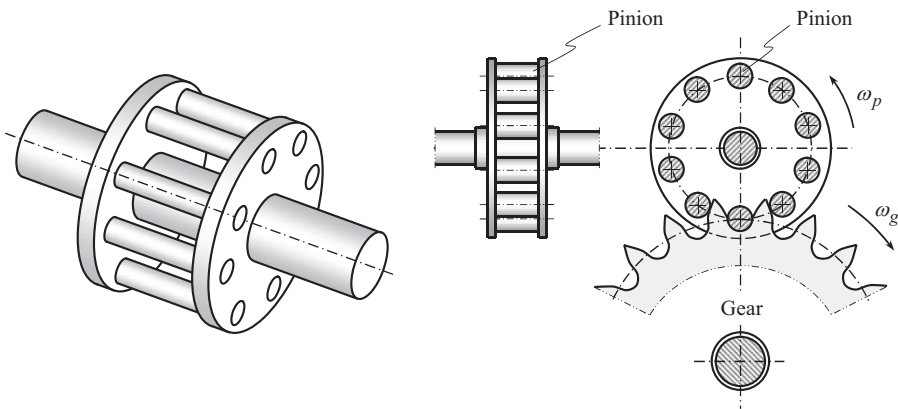


**FIGURE 1.3** Schematic of external lantern gearing.

Lantern gearing is used in the design of huge size construction and transportation machinery. In these applications, pins are rotated in bearings about their axes of rotation, and a larger amount of power is transmitted under a very slow rotation of the driving and driven shafts.

### 1.1.3 CYCLOID GEARING

Before involute gearing was invented (~1760) by *Leonhard Euler*, cycloid gearing was the main type of gearing used by practical men. It received an extensive application, first of all, in design of clock gearing.

In cycloid gearing, cycloid of a circle is used as a tooth profile. A cycloid curve is generated as the trajectory of point of a circle that rolls with no sliding over another circle (or over a straight line

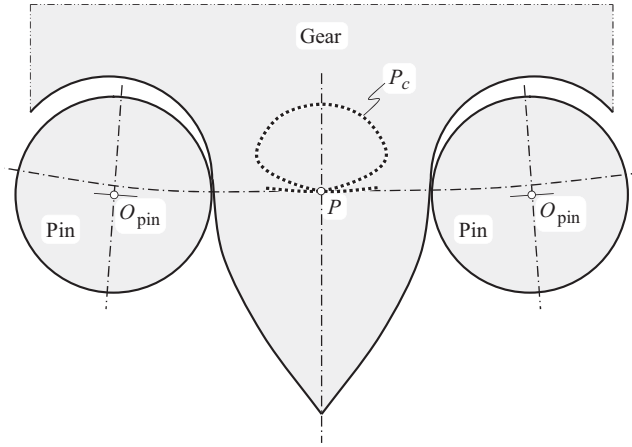


**FIGURE 1.4** Path of contact,  $P_c$ , in pin gearing. (Adapted from: Buckingham, E., 1988, *Analytical Mechanics of Gears*, New York: Dover Publications, Inc., First published 1949.)

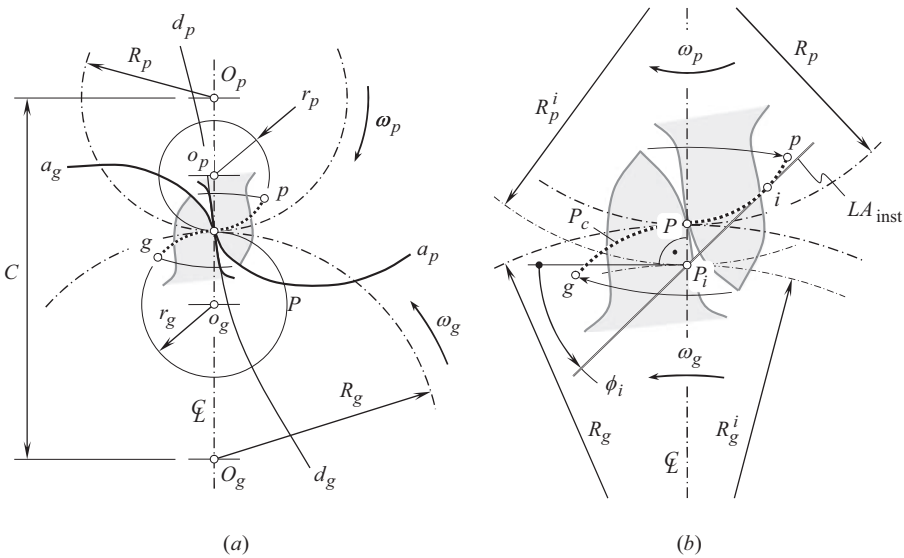


**FIGURE 1.5** Schematic of cycloid gearing: (a) cycloid tooth profile, and (b) path of contact,  $P_c$ , and the instantaneous line of action,  $LA_{inst}$ , in cycloid gearing.

in a reduced case of cycloid gearing). Henceforth, the difference between ordinary, extended, and shortened cycloids has to be made.

An example of cycloid gearing is schematically shown in Figure 1.5a.

In Figure 1.5a, the center of rotation,  $O_g$ , of the gear, and that,  $O_p$ , of the pin, are at certain center-distance,  $C$ . The rotations of the gear and of the pin are denoted by  $\omega_g$  and  $\omega_p$ , correspondingly. The pitch radius of the gear is designated as  $R_g$ , and that of the pin is designated as  $R_p$ . The pitch point is denoted by  $P$ .

Two auxiliary centrodes of radii  $r_g$  and  $r_p$  that have centers at  $o_g$  and  $o_p$  are used to generate the addendum and the dedendum of the tooth profile of the gear and of the pin.

The generation of the gear tooth profile can be executed in two steps:

**First**, to generate a gear tooth addendum, consider rolling with no sliding of an auxiliary axode (of a radius,  $r_p$ ) over the gear pitch circle (of a radius,  $R_g$ ). The circles of radii  $r_p$  and  $R_g$  are in external tangency in relation to one another. The pitch circle of the gear is considered stationary. In such a relative motion, point of the circle of a radius,  $r_p$ , traces the epicycloid,  $Pa_g$ , within the transverse plane rigidly connected to the gear. A portion of the arc,  $Pa_g$ , is used as the profile of the addendum of the gear tooth.

**Second**, to generate the gear tooth dedendum, consider rolling with no sliding of an auxiliary axode of a radius,  $r_g$ , over the gear pitch circle of a radius,  $R_g$ . The circles of radii  $r_g$  and  $R_g$  are in internal tangency in relation to one another. The pitch circle of the gear is considered stationary. In such a relative motion, point of the circle of a radius,  $r_g$ , traces the hypocycloid,  $Pd_g$ , within the transverse plane rigidly connected to the gear. A portion of the arc,  $Pd_g$ , is used as the profile of the dedendum of the gear tooth.

Similar to the generation of the gear tooth profile, the generation of the pinion tooth profile can be executed in two steps as follows:

**First**, to generate the pinion tooth addendum, consider rolling without sliding of the auxiliary axode of a radius,  $r_g$ , over the pinion pitch circle of a radius,  $R_p$ . The circles of radii  $r_g$  and  $R_p$  are in external tangency in relation to one another. The pitch circle of the pinion is considered stationary. In such a relative motion, point of the circle of a radius,  $r_g$ , traces the epicycloid,  $Pa_p$ , within the transverse plane rigidly connected to the pinion. A portion of the arc,  $Pa_p$ , is used as the profile of the addendum of the pinion tooth.

**Second**, to generate the pinion tooth dedendum, consider rolling with no sliding of the auxiliary axode of a radius,  $r_p$ , over the gear pitch circle of a radius  $R_p$ . The circles of radii  $r_p$  and  $R_p$  are in internal tangency in relation to one another. The pitch circle of the pinion is considered stationary. In such a relative motion, point of the circle of a radius,  $r_p$ , traces the hypocycloid,  $Pd_p$ , within the transverse plane rigidly connected to the gear. A portion of the arc,  $Pd_p$ , is used as the profile of the dedendum of the gear tooth.

The path of contact,  $P_c$ , in cycloid gearing<sup>2</sup> is a smooth, piecewise curve, composed of two circular arcs of the radii  $r_g$  and  $r_p$ . These two arcs,  $gP$  and  $pP$ , comprise the path of contact,  $gPp$  (see Figure 1.5a).

An enlarged view of two teeth in contact in cycloid gearing is shown in Figure 1.5b. For the driving pinion and the driven gear, the tooth flanks are engaged in contact at the starting point,  $p$ , of the path of contact,  $P_c$ . As the pinion rotates,  $\omega_p$ , contact point between the tooth flanks travels along the path of contact,  $P_c$ , from point,  $p$ , to point,  $g$ . Point,  $g$ , is the end point of contact of the tooth flanks. While traveling along the path of contact,  $P_c$ , at certain configuration of the gears, the contact point through the pitch point,  $P$ . At every instant of time, the pinion tooth flank acts over the gear tooth flank along the instantaneous line of action,  $LA_{inst}$ , namely, in the direction tangential to the path of contact,  $P_c$ , at current point,  $i$ , within the path of contact,  $P_c$ . A straight line that is tangent at  $i$  to the path of contact,  $P_c$ , is referred to as the *instantaneous line of action*,  $LA_{inst}$ .

As the path of contact,  $P_c$ , in cycloid gearing is composed of two circular arcs, a straight line through current point  $i$  tangential to the  $P_c$  forms a different transverse pressure angle,  $\phi_{i,i}$ , with the

<sup>2</sup> The path of contact,  $P_c$ , in Figure 1.5 is shown assuming that only one pair of teeth makes contact, and the contact point traces the entire path of contact,  $P_c$ , from point  $p$  to point  $g$ . In reality, in cycloid gear pair as well as in non-involute gear pairs of other designs, at certain instant of time, the contact between one pair of teeth is terminated by the next pair of teeth that is entered in mesh. The interruption of the contact commonly happens long before the first contact point traces the entire path of contact,  $P_c$  (from point  $p$  to point  $g$ ). This statement is also valid with respect to every transverse section in helical non-involute gear pair.



perpendicular to the centerline,  $\mathfrak{L}$ . Moreover, the location of the current pitch point,  $P_i$ , within the centerline,  $\mathfrak{L}$ , can be determined: current pitch point,  $P_i$ , is the point of intersection of the centerline,  $\mathfrak{L}$ , by the instantaneous line of action,  $LA_{\text{inst}}$ . The instantaneous line action is commonly designated as  $LA_{\text{inst}}$ .

Due to the migration of the instantaneous pitch point,  $P_i$ , back and forth along the centerline,  $\mathfrak{L}$ , the current values of the pitch radii of the gear,  $R_g^i$ , and of the pinion,  $R_p^i$ , differ from their nominal values (the inequalities  $R_g^i \neq R_g$  and  $R_p^i \neq R_p$  are valid). Under a uniform rotation of the driving pinion (when  $\omega_p = \text{const}$ ), and at a constant center-distance,  $C$ , the alteration to the pitch radii  $R_g^i$  and  $R_p^i$  of the gear and of the pinion causes a corresponding variation in the rotation,  $\omega_g$ , of the driven gear. Ultimately, the rotation,  $\omega_g$ , of the gear depends on the actual value of the angle,  $\varphi_p$ , through which the pinion turns about its axis at a time,  $t$ , that is, certain functionality  $\omega_g = \omega_g(\varphi_p)$  is observed in cycloidal gearing. Here, the angle  $\varphi_p$  equals to  $\varphi_p = \omega_p t$ .

This consideration allows for an intermediate conclusion:

**Conclusion 1.2.** *No smooth (with a constant angular velocity ratio) transmission of a uniform rotary motion is possible by means of cycloid gearing, as the mating tooth profiles do not conjugate to one another.*

Under a uniform rotation of the driving shaft, the rotation of the driven shaft is not uniform. As a result, cycloid gearing is used to transmit only slow rotations at low loads. When a transmitting rotation is slow, and when the tooth numbers of the gear and of the pinion are large enough, the impact of the fluctuation of rotation of the driven shaft becomes reasonably small.

It should be mentioned here that cycloid gear pairs are sensitive to any alteration in center-distance,  $C$ .

#### 1.1.4 CLOCK-TYPE GEARING

In the design of gears for clock-type gearing, arc segments of cycloid of tooth addendum are approximated by circular arcs. For the gear, the tooth profile is approximated by a circular arc that the best fits the cycloid tooth profile. For the pinion (i.e., for the trib), significantly larger deviations are permissible.

In clock-type gears, the addendum is formed by a circular arc of a radius  $r_{pr}$ . Practically, the radius,  $r_{pr}$ , equals either  $r_{pr} = \frac{2}{3}S_g$ , or  $r_{pr} = \frac{5}{6}S_g$  (as illustrated in Figure 1.6a), or  $r_{pr} = S_g$  (see Figure 1.6b), where  $S_g$  is the gear tooth thickness.<sup>3</sup> Other proportions for the gear tooth profile are also permissible.

Gear tooth profile dedendum is formed by straight lines through the axis of rotation of the gear (by radial straight lines), as shown in Figure 1.6. The fillet is commonly rounded. The backlash in the clock-type gearing is in the range of  $c_n = (0.3 \div 0.5)m$ . Radial clearance equals  $\sim 0.4m$ .

The clock-type gearing is in the design of not-reversible gear transmissions. Under such a scenario, the backlash does not influence the accuracy of the mechanism. Clock-type gearing is also used in the design of clocks and watches, in small size units, and so forth. Mechanical watches are perhaps the most important area of application of clock-type gearing.

#### 1.1.5 SPECIAL-PURPOSE GEARING

Meshing of other non-involute profiles is also extensively used in the present-day industry. A few examples in this regard are considered immediately in the following section.

<sup>3</sup> See GOST 13678-73 for details.

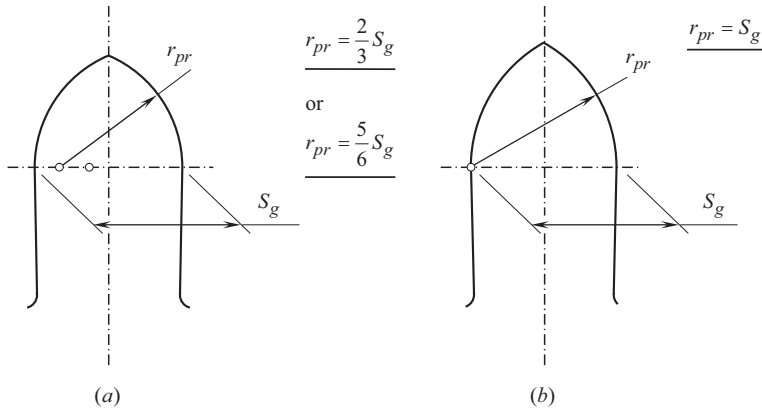


**FIGURE 1.6** Clock-type gear tooth profiles: (a) general case, and (b) simplified design of the gear tooth profile.

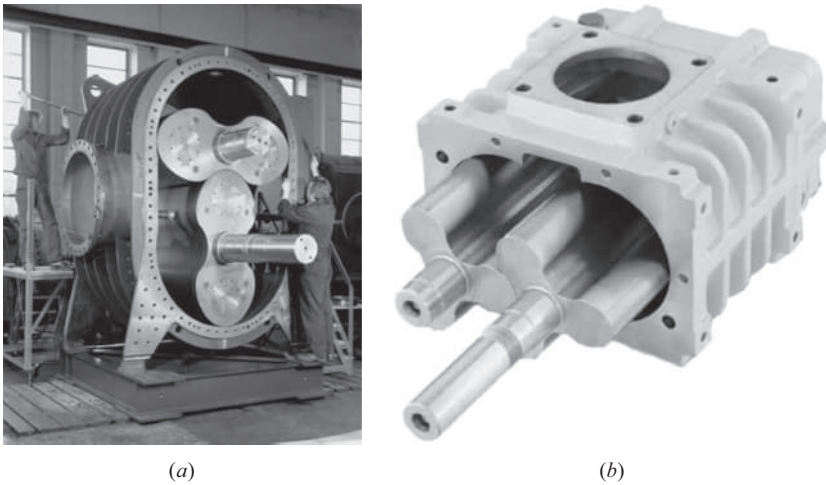


**FIGURE 1.7** Roots blowers: (a) two-lobe blower and (b) three-lobe blower.

### 1.1.5.1 Roots Blower

*Roots blower*<sup>4</sup> can be viewed as an example of spur gearing of non-involute tooth profile (Figure 1.7).

Referring to Figure 1.8a, a *Roots blower* is composed of two rotors. Each rotor is either of two or of three lobes. The rotors are mounted on the shafts and are assembled in a housing. The rotors are rotated with angular velocities  $\omega_1$  and  $\omega_2$  about their axis of rotation,  $O_1$  and  $O_2$ . Two driving gears are implemented to synchronize the rotations of the rotors about their axes. The tooth ratio of the driving gear pair is equal to one ( $u = 1$ ). The nominal pitch radius,  $R_w$ , of each rotor is equal to the pitch radius of the driving gear.

The transverse cross section of the rotors is shaped in the form of four circular arcs of a radius,  $r_l$ , tangential to one another, as shown in Figure 1.8b.

<sup>4</sup> It is named for American inventors and brothers *Philander Roots* and *Francis Marion Roots*, founders of the *Roots Blower Company*, Connersville, Indiana, who first patented the basic design in 1860 as an air pump for use in blast furnaces and other industrial applications. In 1900, *Gottlieb Daimler* included a *Roots*-style supercharger in a patented engine design, making the *Roots*-type supercharger the oldest of the various designs now available. *Roots blower* are commonly referred to as air blowers or positive displacement (PD) blowers.

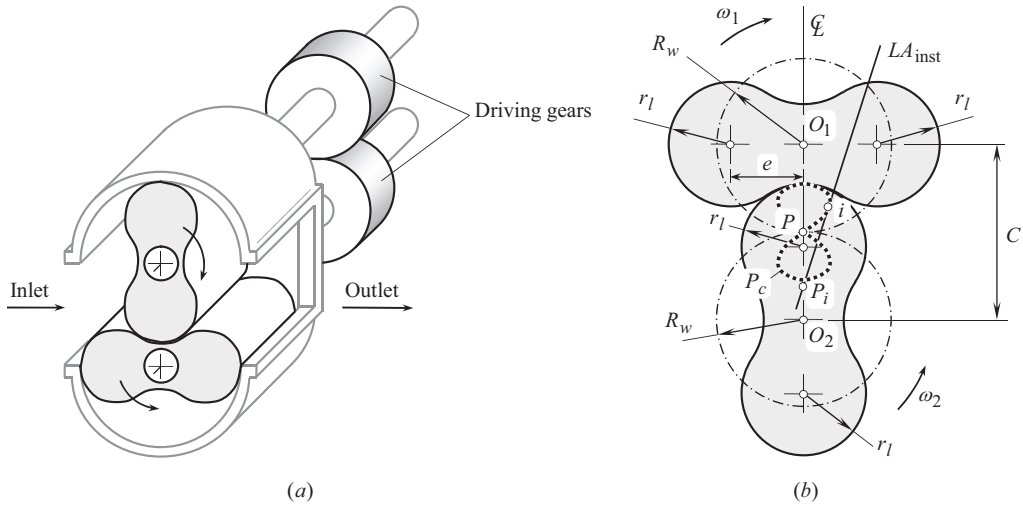


**FIGURE 1.8** Two-lobe *Roots blower*: (a) close-up and (b) interacting profiles of the lobes.

Air discharger for diesel engines is a good example of practical application of *Roots blower*.

Two different modes of meshing should be distinguished regarding the *Roots blower* lobe profiles.

In the first mode, it is assumed that the rotors (see Figure 1.8) are capable of transmitting a rotation from one shaft to another one, or, in other words, let us assume that one of the rotors is the driving member and the other one is the driven member of a pair of non-involute profiles represented by two rotors.

The transverse lobe profile of the rotor addendum is a circular arc of a radius,  $r_l$ , centered at a distance,  $e$ , from the axis of rotation of the rotor. The addendum angle of a rotor is equal to  $90^\circ$  for a two-lobe rotor and  $60^\circ$  for a three-lobe rotor.

Following the established practice of designing of *Roots blower* rotors, the following expression:

$$R_w^2 + e^2 - 2R_w e \cos v = r_l^2 \quad (1.1)$$

has to be fulfilled.

In Eq. (1.1), angle  $v$  is equal to  $45^\circ$  for two-lobe rotors, and  $v$  is equal  $30^\circ$  for three-lobe rotors. The distance of the center of the circular lobe profile from the axis of rotation of the lobe is designated as “ $e$ ” (see Figure 1.8b).

The position vector of point,  $\mathbf{r}_l$ , of the rotor addendum can be analytically expressed by the following matrix equation:

$$\mathbf{r}_l(\theta) = \begin{bmatrix} r_l \sin \theta \\ r_l \cos \theta \\ 1 \end{bmatrix} \quad (1.2)$$

For two-lobe rotors, the angular parameter,  $\theta$ , is within an interval:

$$-2 \tan^{-1} \left( \frac{(e + r_l)^2 - R_w}{\sqrt{2} e R_w} \right) \leq \theta \leq 2 \tan^{-1} \left( \frac{(e + r_l)^2 - R_w}{\sqrt{2} e R_w} \right) \quad (1.3)$$

The dedendum of one of the rotors is generated by the addendum of the other one. Equation (1.2) of the lobe addendum allows the equation:

$$\mathbf{r}_2(\theta) = \begin{bmatrix} r_l \sin(\theta - 2\varphi) - e \sin 2\varphi + 2R_w \sin \varphi \\ r_l \sin(\theta - 2\varphi) + e \cos 2\varphi - 2R_w \cos \varphi \\ 1 \end{bmatrix} \quad (1.4)$$

for position vector of point,  $\mathbf{r}_2$ , of the rotor dedendum.

In Eq. (1.4), the current value of the angle of rotation of the rotor,  $\varphi$ , is calculated as the root of the equation of contact:

$$R_w \sin(\theta - \varphi) - e \sin \theta = 0 \quad (1.5)$$

The position vector of point of the line of action,  $\mathbf{r}_{la}$ , can be expressed in the form of a column matrix:

$$\mathbf{r}_{la}(\theta) = \begin{bmatrix} r_l \sin(\theta - \varphi) - e \sin \varphi \\ r_l \sin(\theta - \varphi) + e \cos \varphi \\ 1 \end{bmatrix} \quad (1.6)$$

The equation for the path of contact,  $P_c$ , can be represented in the following form:

$$R_w \sin(\theta - \varphi) - e \sin \theta = 0 \quad (1.7)$$

It should be stressed here that when the equalities  $e = R_w$  and  $\varphi = 0$  are valid, that is, when the circular arc of a radius,  $R_w$ , is centered at the instantaneous center of rotation,  $P$ , all the perpendiculars to the lobe profile pass through the pitch point,  $P$ , under any value of the angular parameter,  $\theta$ . Therefore, the relation  $e = R_w$  should be avoided when designing rotors for *Roots blower*.

The path of contact in Figure 1.8b is labeled as  $P_c$ . For an arbitrary point,  $i$ , within the path of contact, an instantaneous line of action,  $LA_{inst}$ , that is tangential at  $i$  to the path of contact,  $P_c$ , is constructed. The instantaneous line of action,  $LA_{inst}$ , and the centerline,  $\Phi$ , intersect each other at an instantaneous pitch point,  $P_i$ . In general, instantaneous pitch point,  $P_i$ , is not coincident with the nominal pitch point,  $P$ . Therefore, under a constant center-distance,  $C$ , and a uniform input rotation,  $\omega_1$ , of the driving rotor, the rotation of the driven rotor,  $\omega_2$ , is not uniform. Moreover, for certain locations of point  $i$  within the path of contact,  $P_c$  (i.e., when the instantaneous line of action,  $LA_{inst}$ , is parallel to the centerline,  $\Phi$ ), conditions for the transmission of rotation are especially unfavorable.

In the second mode, two gears are used to drive the rotors. As each of the rotors is driven by the individual gear, the rotors are rotated smoothly. However, when driven individually, a gap between the lobe profiles is always observed. A *Roots blower* is not workable without a minimum permissible gap between the lobe profiles. The minimum permissible width of the gap is not of a constant value and depends on the actual value of the angle of rotation of the rotors. Once a gap always occurs between the lobes of the rotors, no meshing (no interaction) of lobe profiles is observed at all (see Figure 1.8b).

It should be mentioned here that the closest distance of approach,  $\delta_{cda}$ , between the working surfaces of the rotors can be calculated. This distance,  $\delta_{cda}$ , depends on the angular configuration of the rotors. As the rotors rotate, the closest distance of approach,  $\delta_{cda}$ , alters from its minimum value,  $\delta_{cda}^{\min}$ , to its maximum value,  $\delta_{cda}^{\max}$ . The inequality  $\delta_{cda}^{\min} \leq \delta_{cda} \leq \delta_{cda}^{\max}$  is valid for *Roots blower* that has spur rotors.

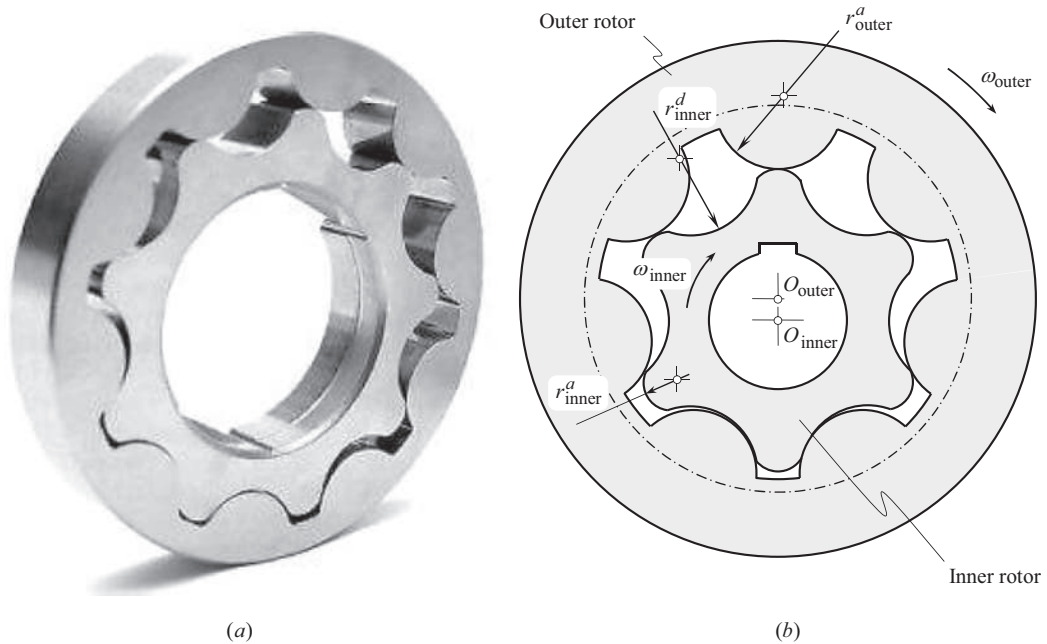


**FIGURE 1.9** Oil pump: (a) close-up and (b) the main design parameters: radius of the convex circular-arc profile of the inner rotor,  $r_{outer}^a$ , and radius of the concave circular arc profile of the outer rotor,  $r_{inner}^d$ .

This consideration allows for an intermediate conclusion:

**Conclusion 1.3.** *No smooth transmission of a uniform rotary motion is possible by means of rotors of Roots blower, as the mating rotors do not conjugate to one another.*

Individual rotation of each of the rotors is required for *Roots blower*.

### 1.1.5.2 Spur Rotors of Oil Pump

Non-involute rotors are used in the design of oil pump [50]. The pumping mechanism consists of two elements: inner rotor and outer rotor. Both the rotors are schematically shown in Figure 1.9a. The inner element always has one less tooth than the outer one. The inner rotor is located off center, and both rotors rotate about their axes of rotation.

During one part of the assembly's rotation cycle, the area between the inner and the outer rotors increases, which creates a vacuum. This vacuum creates suction, and this is where the intake is located. When the area between the rotors decreases, compression occurs. Fluid is pumped during this compression period of time.

A synchronizing involute gear pair axially adjacent to its corresponding rotors, usually carries the rotary load, so that the pair of rotors is used solely to create and maintain the typically high-pressure differentials between the inlet and outlet ports.

The wheel profiles are either epicycloidal or hypocycloidal. In particular applications, circular arcs are used to shape the lobe profile of the rotors (see Figure 1.9b). Minimum tooth clearances are required for handling gases, but curve-linear approximations to epicycloids or hypocycloids usually suffice for handling fluids.

In principle, the interaction on internal non-involute spur gears (see Figure 1.9) is the same as that for external spur gears. Any of the basic rack forms used for spur gears may be used also for internal gears as well. In present-day practice, the form of the basic rack usually is known.

There are more possible limitations to an internal gear drive than there are for an external gear drive, particularly, when the difference between the number of teeth in the internal gear and the number of teeth in the spur pinion is small. Hence, the design of the tooth forms for internal gear drives is more critical and more exacting than that for external gear or spur gear drives.

A secondary action between the teeth of an internal gear drive [15] becomes possible. The most general practical application of an internal gear drive is in pump rotors where the tooth profile of one or both of the two members is formed by continuous curves and where the internal gear has one more tooth than its mating pinion. This secondary action exists mostly between the addendum of the mating gear teeth, whereas the primary action exists between the addendum of one gear tooth and the dedendum of the mating gear tooth.

It can be shown that neither circular arc tooth profile nor epi- or hypotrochoidal tooth profiles allow smooth transmission of a uniform rotation from the driving shaft to a driven shaft. Because the pitch point for (a) circular arc tooth profile, (b) epitrochoidal tooth profile, and (c) hypotrochoidal tooth profile, as well as for many other tooth profile geometries, migrate within a certain portion of the centerline,  $\Phi$ , rotation of the driven shaft cannot be uniform.

In spur non-involute gearing of all designs, no base pitch of a gear and a mating pinion can be defined. This is because in spur non-involute gearing, the desirable plane of action,  $PA$ , intersects the tooth flanks,  $\mathcal{G}$  and  $\mathcal{P}$ , of a gear and a mating pinion not at a right angle. Once no base pitch exists, the transverse contact ratio in spur non-involute gearings cannot be defined, and only one pair of teeth is always engaged in mesh.

This consideration allows an intermediate conclusion:

**Conclusion 1.4.** *No smooth transmission of a uniform rotary motion is possible by means of spur gears of non-involute tooth profile, as the mating rotors do not conjugate to one another.*

## 1.2 PECULIARITIES OF TRANSMISSION OF ROTARY MOTION BY MEANS OF NON-INVOLUTE GEARS

Transmission of rotary motion by means of non-involute gearing features certain peculiarities. These peculiarities are mainly due to the tooth profiles in non-involute gears do not conjugate to one another.

### 1.2.1 ON VIOLATION OF THE CONJUGATE ACTION LAW IN NON-INVOLUTE GEARING

To transmit smoothly a uniform rotation from a driving shaft to a driven shaft by means of gear teeth, the pitch diameters of the driving member and that of the driven member must be of constant values, and they must be independent of the actual value of the angle of rotation of the driving shaft. In such a scenario, the pitch point,  $P$ , within the centerline is stationary: The pitch point coincides with the point of tangency of the pitch circles of the gear (of a diameter,  $d_g$ ), and that of the pinion (of a diameter,  $d_p$ ). When rotation of a driving shaft is steady, and when a rotation of the driven shaft with a constant speed is required, no migration of the pitch point within the centerline is allowed.

The path of contact,  $P_c$ , in non-involute gear pair is a planar curve. At every instant of time, a tooth flank of the driving member acts against a tooth flank of the driven member along an instantaneous line of action,  $LA_{inst}$ . The instantaneous line of action,  $LA_{inst}$ , is tangential to the path of contact,  $P_c$ , at a current contact point of the interacting tooth profiles. In order to ensure uniform rotation of the driven shaft, the instantaneous line of action,  $LA_{inst}$ , has to pass through the stationary pitch point,  $P$ . To meet this requirement, it can be assumed that in order to generate a non-involute tooth profile, a rotation about the pitch point,  $P$ , through a certain angle is the only permissible motion to the instantaneous line of action,  $LA_{inst}$ , to be performed when the contact point,  $K$ , travels along the path of contact,  $P_c$ .

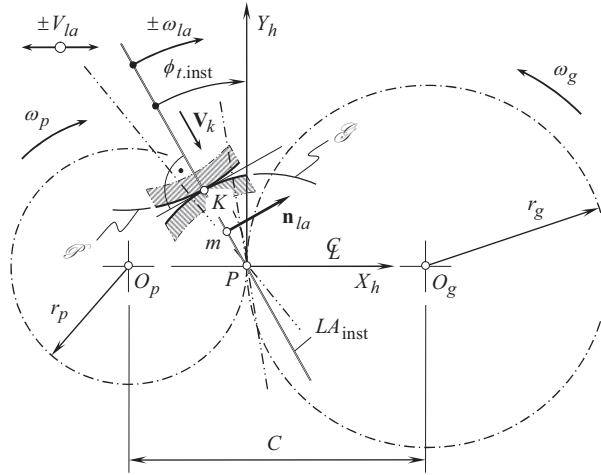


**FIGURE 1.10** Permissible kinematics of instantaneous line of action,  $LA_{inst}$ .

In Figure 1.10, the pitch circle of a gear (of a diameter,  $d_g = 2r_g$ ), and that of a mating pinion (of a diameter,  $d_p = 2r_p$ ) share a common point, which the pitch point,  $P$ , is coincident with. The axis of rotation of the gear,  $O_g$ , and that of the pinion,  $O_p$ , are at certain center-distance,  $C$ , apart from one another. The rotations of the gear,  $\omega_g$ , and of the pinion,  $\omega_p$ , are synchronized with one another in timely manner.

At current instant of time, the tooth flank of the gear,  $\mathcal{S}$ , and that of its mating pinion,  $\mathcal{P}$ , contact each other at contact point,  $K$ . The contact point,  $K$ , travels (with a linear velocity vector,  $V_k$ ) along the instantaneous line of action,  $LA_{inst}$ , when the gears rotate. The magnitude,  $V_k$ , of the linear velocity vector,  $V_k$ , can be either of a constant value or it can be of time-dependent value. The instantaneous line of action,  $LA_{inst}$ , forms transverse pressure angle,  $\phi_{t,inst}$ , in relation to the perpendicular to the centerline,  $\Phi$ . When the gears rotate, the instantaneous line of action,  $LA_{inst}$ , is free to turn (with an angular velocity,  $\pm\omega_{la}$ ) about the pitch point,  $P$ . No additional straight motion,  $\pm V_{la}$ , of the instantaneous line of action,  $LA_{inst}$ , is permissible in the case under consideration.

When the gears rotate, the contact point,  $K$ , traces:

- The path of contact,  $P_c$ , in a stationary reference system associated with the gear pair housing
- The gear tooth profile,  $\mathcal{S}$ , in a reference system associated with the gear
- The pinion tooth profile,  $\mathcal{P}$ , in a reference system associated with the pinion

Therefore, it is anticipated that once the path of contact,  $P_c$ , in a non-involute gear pair is specified, the rest of the design parameters (namely, the tooth profiles,  $\mathcal{S}$  and  $\mathcal{P}$ ) of the gear pair can be derived following routing procedures.

Because the instantaneous line of action,  $LA_{inst}$ , is tangential to the path of contact,  $P_c$ , it can be viewed as an envelope to a family of consecutive positions of the  $LA_{inst}$  in its motion in relation to a motionless reference system.

A *Cartesian* coordinate system,  $X_h Y_h$ , is associated with the gear pair housing. The pitch point,  $P$ , is the origin of the reference system  $X_h Y_h$ .

In the coordinate system  $X_h Y_h$ , the following expression:

$$Y_h = X_h \tan(90^\circ + \phi_{t,inst}) = -X_h \cot \phi_{t,inst} \quad (1.8)$$

can be used for the analytical description of the instantaneous line of action,  $LA_{inst}$ .



Current configuration of the instantaneous line of action,  $LA_{\text{inst}}$ , depends on the current value of the transverse pressure angle,  $\phi_{t,\text{inst}}$ . Once the parameter  $\phi_{t,\text{inst}}$  is eliminated from Eq. (1.8), this equation represents the line of action,  $LA$ , itself. *Shishkov equation of contact*,  $\mathbf{n} \cdot \mathbf{V}_\Sigma = 0$  [197,198], is commonly used in order to eliminate of the angular parameter,  $\phi_{t,\text{inst}}$ , from Eq. (11.8).

The unit normal vector,  $\mathbf{n}_{la}$ , at current point,  $m$ , within the instantaneous line of action,  $LA_{\text{inst}}$ , can be analytically described as follows:

$$\mathbf{n}_{la} = \mathbf{i} \cos \phi_{t,\text{inst}} + \mathbf{j} \sin \phi_{t,\text{inst}} \quad (1.9)$$

The linear velocity vector,  $\mathbf{V}_m$ , of point  $m$  equals:

$$\mathbf{V}_m = \boldsymbol{\omega}_{la} \cdot \mathbf{r}_m \quad (1.10)$$

where the position vector of the point  $m$  is denoted by  $\mathbf{r}_m$ .

The following expression:

$$\mathbf{V}_m = \boldsymbol{\omega}_{la} \cdot \mathbf{r}_m = \boldsymbol{\omega}_{la} \cdot (-\mathbf{i} X_m + \mathbf{j} Y_m) \quad (1.11)$$

can be composed for the linear velocity vector,  $\mathbf{V}_m$ . The velocity vector,  $\mathbf{V}_m$  (not shown in Figure 1.10), is aligned with the unit normal vector,  $\mathbf{n}_{la}$ .

The vectors,  $\mathbf{n}_{la}$  and  $\mathbf{V}_m$ , from Eqs. (1.9) to (1.11) are substituted into *Shishkov equation of contact*,  $\mathbf{n} \cdot \mathbf{V}_\Sigma = 0$  [197,198]:

$$\mathbf{n}_{la} \cdot \mathbf{V}_m = \boldsymbol{\omega}_{la} \cdot (-X_m \cos \phi_{t,\text{inst}} + Y_m \sin \phi_{t,\text{inst}}) = 0 \quad (1.12)$$

This returns a formula for the function “ $-\cot \phi_{t,\text{inst}}$ ”:

$$-\cot \phi_{t,\text{inst}} = \frac{Y_h}{X_h} \quad (1.13)$$

After  $1 \equiv 1$  the function “ $-\cot \phi_{t,\text{inst}}$ ” from Eq. (1.13) is substituted into Eq. (1.8), the latter is reduced to identity,  $1 \equiv 1$ . The identity does not depend on the enveloping parameter,  $\phi_{t,\text{inst}}$ . This means that no envelope to a family of consecutive positions of the moving instantaneous line of action,  $LA_{\text{inst}}$ , is physically possible by nature. Therefore, no path of contact,  $P_c$ , as well as no corresponding tooth profiles,  $\mathcal{S}$  and  $\mathcal{P}$ , of a gear and that of a mating pinion can physically exist, for which a non-involute gear pair is capable of transmitting an input rotation smoothly.

This consideration allows for a conclusion:

**Conclusion 1.5.** *No smooth transmission of a uniform rotary motion is possible by means of spur gears of non-involute tooth profile, as the mating rotors do not conjugate to one another.*

*Conclusion 1.5* is of importance for further analysis of helical non-involute gearing. It is also of critical importance for gear finishing (gear generating) operations, particularly for rotary shaving process of spur gears that have non-involute tooth profiles (e.g., gears for *Novikov/conformal gearing*). Despite the axes of rotation of the work gear and of the shaving cutter in rotary shaving process being skewed, the performed two-dimensional analysis makes it clear that non-involute tooth profiles of spur gears cannot be accurately shaved by nature.

### 1.2.2 INTERACTION OF NON-INVOLUTE GEAR WITH RACK

One more example of the interaction of non-involute tooth profiles can be found when designing a hob for machining straight-sided splines. The hob design is based on an auxiliary rack (or *basic rack*, in other words), the teeth of which are engaged in mesh with the splines of the spline shaft. The tooth profile of the rack is commonly generated as an envelope to a family of consecutive positions of the spline profile when the pitch circle of the spline rolls with no sliding over the pitch line associated with the rack.

The determination of the coordinates of points of the tooth profile of a rack conjugate to a spline shaft commonly is executed using the *method of common perpendiculars*. An example of how this kind of problem can be solved is illustrated in Figure 1.11 (This schematic can be traced back to the 1875 *F. Reuleaux* book: Reuleaux, F., *Lehrbuch der Kinematik*, Braunschweig, 1875).

The spline profile is associated with a pitch circle of a radius,  $r_{w.sp}$ . The pitch line of the rack to be determined is tangent to the pitch circle of the spline shaft. Point of tangency of the pitch line and of the pitch circle,  $r_{w.sp}$ , is the pitch point in the rolling motion of the spline shaft and the rack. The pitch point is designated as  $P$ .

The spline shaft is rotated about its axis of rotation,  $O_{sp}$ . The angular velocity of this rotation is designated as  $\omega_{sp}$ . The rack is associated with the pitch line. The rack travels straightforward together with the pitch line. The linear velocity of the rack is designated as  $V_{rc}$ .

Let us assume that at the initial configuration of the pitch circle and the pitch line, the profile of the spline passes through the pitch point,  $P$ . This profile is at a distance,  $r_{sp}$ , from the axis of rotation,  $O_{sp}$ , of the spline shaft. Practically, the straight-line profile is tangential to a circle of the radius  $r_{sp}$ . The radius,  $r_{sp}$ , is equal to one-half the spline thickness of the spline shaft.

When the spline shaft rotates, the lateral spline profile is rotated together with the spline shaft. Consequently, the spline shaft lateral profile passes through points 1, 2, ...,  $(i-1)$ ,  $i$ . Point 1 is coincident with the pitch point,  $P$ . The pitch line travels straightforward. In this motion, the pitch point consequently occupies positions  $1^*$ ,  $2^*$ ,  $3^*$ , .... The distance  $1^*-2^*$ ,  $2^*-3^*$ , ... between consequent locations of the pitch point is equal to the lengths of the arcs  $\curvearrowright 1-2$ ,  $\curvearrowright 2-3$ , ... of the pitch circle of the spline shaft. This is because the pitch line of the rack is rolling with no sliding over the pitch circle of the spline shaft.

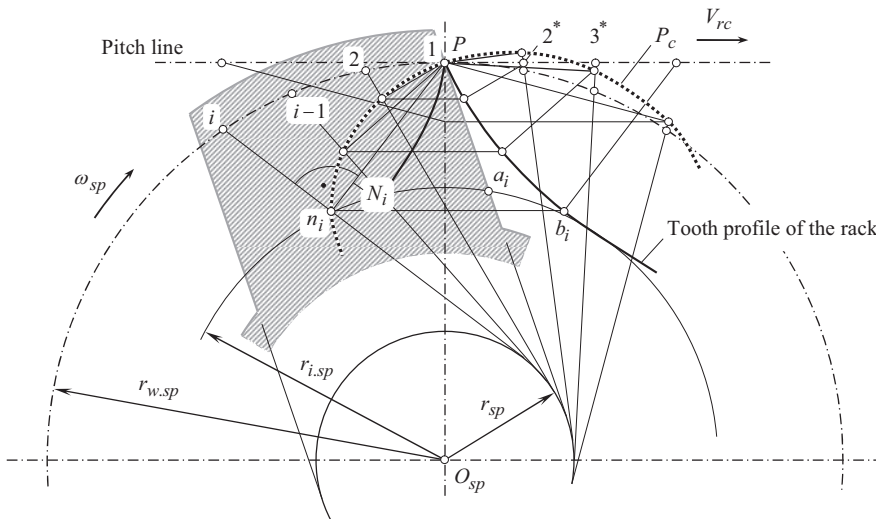


**FIGURE 1.11** Generation of a rack tooth profile as an envelope to a family of consecutive positions of the lateral profile of a spline in a straight-sided spline shaft. (This schematic was originally published in the 1875 *Reuleaux* book: Reuleaux, F., *Lehrbuch der Kinematik*, Braunschweig, 1875.)

At every chosen location of the spline lateral profile, perpendiculars to the profile are constructed so as to pass through the pitch point,  $P$ . For example, a perpendicular,  $N_i$ , is normal to the spline profile at its  $i$  – th location (see Figure 1.11). Point  $n_i$  is the point of tangency of the lateral profile of the spline and the rack tooth profile.

Constructed in this way, plurality of points for various configurations of the lateral spline profile are located within the path of contact,  $P_c$ . In a transverse section by a plane, the path of contact,  $P_c$ , is traced by contact point in rolling motion of the given spline shaft and the rack to be determined. The path of contact is determined in a stationary reference system.

In a reference system associated with the spline shaft, all the points are located within the lateral spline profile of the spline shaft.

When the spline shaft rotates, points of the lateral profile consequently cross the path of contact,  $P_c$ . At these instants of time, the points coincide with the corresponding points of the rack tooth profile. An arbitrary point,  $n_i$ , within the path of contact,  $P_c$ , corresponds to the point of contact in  $i$  – th location of the lateral profile of the spline. If point,  $n_i$ , returns to the initial position of the spline by means of rotation through the angle of the arc  $\widehat{Pi}$ , then this point occupies the position of the point  $a_i$ .

Similarly, in a reference system associated with the rack, contact points are located within tooth profile of the rack, which has to be determined.

Let us assume that an arbitrary point,  $n_i$ , within the path of contact,  $P_c$ , is associated with the pitch line,  $P_{in}$ . To determine the location of this point in the initial instant of time, the pitch line together with the point  $n_i$  travels through a distance that is equal to the arc length  $\widehat{Pi}$  in a direction opposite to the direction of straight motion of the rack tooth in its rolling motion. After this transition is complete, point  $n_i$  occupies the position of point  $b_i$ . Point  $b_i$  is located on the tooth profile of the rack. All points of the rack tooth profile are constructed similar to that the point  $b_i$  is constructed. By connecting the constructed points by a smooth curve, the rack tooth profile can be determined.

The aforementioned approach for the determination of tooth profile of a rack that is enveloping to a family of a spline shaft profile is commonly adopted. However, this method is inaccurate by nature – it can be used only for approximate generation of the rack tooth profile. It is assumed here that the generated tooth profile of the rack can generate the spline profile of the straight-sided spline shaft when a problem that is inverse to the original problem is considered. This is not correct. As these enveloping profiles do not conjugate to one another, no straight-sided spline profile can be generated in the inverse rolling of the rack in relation to spline shafts. In practice, instead of a straight-sided spline profile, a curved profile of the splines is generated (see Figure 1.12).

This discussion reveals that the use of *method of common perpendiculars* returns a tooth profile of the rack that is an envelope to a family of consecutive positions of the spline shaft profile, but not conjugate to it.

The analytical description of a gear tooth flank of appropriate geometry, and that for a mating pinion tooth flank, can be derived solely on the bases of *Shishkov equation of contact*,  $\mathbf{n}_g \cdot \mathbf{V}_\Sigma = 0$ . A schematic for the derivation is illustrated in Figure 1.13.

For the discussion that follows, a configuration of the axis of rotation of the gear,  $O_g$ , of the axis of rotation of the pinion,  $O_p$ , and of the pitch point,  $P$ , is shown in Figure 1.13. Arbitrary contact point,  $K_i$ , of the tooth profiles of the gear and of the pinion is located within a transverse section by a plane that is perpendicular to the axes of rotations,  $O_g$  and  $O_p$ . For arbitrary contact point,  $K_i$ , the linear velocity vectors,  $\mathbf{V}_g$  and  $\mathbf{V}_p$ , are constructed. These two linear velocity vectors make possible the construction of the linear velocity vector of sliding,  $\mathbf{V}_{rl}$ , of the tooth flanks in relation to one another. As the gears in mesh have to meet the *Shishkov equation of contact*,  $\mathbf{n}_g \cdot \mathbf{V}_\Sigma = 0$ , the linear velocity vector,  $\mathbf{V}_{Ki}$ , of contact point has to be perpendicular to the linear velocity vector of sliding,  $\mathbf{V}_{rl}$ . The direction of the linear velocity vector,  $\mathbf{V}_{Ki}$ , is through the pitch point,  $P$ . If the linear velocity vector,  $\mathbf{V}_{Ki}$ , is not perpendicular to the linear velocity vector of sliding,  $\mathbf{V}_{rl}$ , then a component  $\mathbf{V}_{mi}$  of

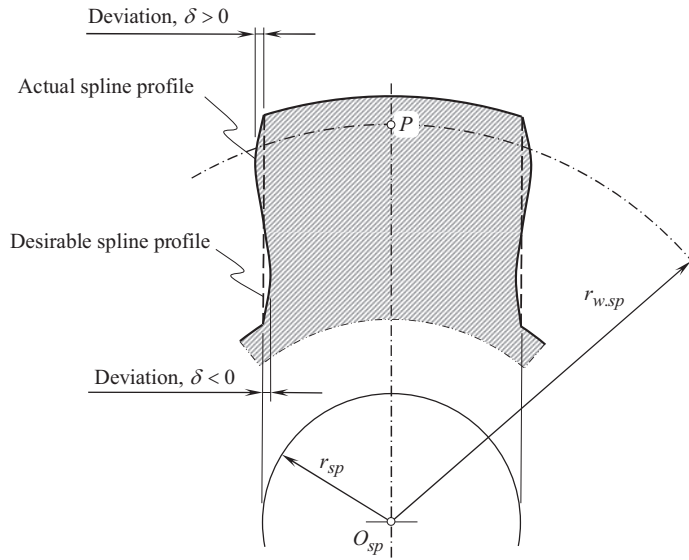


**FIGURE 1.12** Deviation,  $\delta$ , of the actual lateral profile of a spline shaft from its desirable profile.

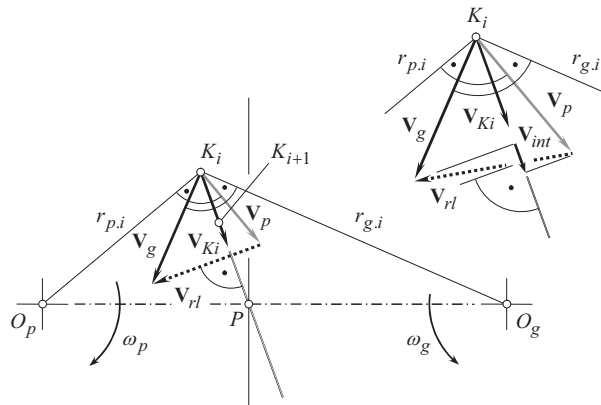


**FIGURE 1.13** Instantaneous parameters of the kinematics of contact point in a pair of interacting tooth profiles.

the linear velocity vector,  $\mathbf{V}_{Ki}$ , will cause either interference of the tooth profiles of the mating tooth flanks, or the tooth flanks will depart from one another. Neither interference of the tooth flanks nor their separation is permissible. Moreover, if the linear velocity vector,  $\mathbf{V}_{Ki}$ , is not perpendicular to the vector of sliding, this causes the pitch point,  $P$ , to migrate within the centerline,  $\Phi$ , of the gear pair. This is not permissible, as it causes variation in the angular velocity of the driven shaft.

Once the direction of the linear velocity vector,  $\mathbf{V}_{Ki}$ , is predetermined on the premise of the *Shishkov equation of contact*,  $\mathbf{n}_g \cdot \mathbf{V}_\Sigma = 0$ , the next position of the contact point,  $K_{i+1}$ , is within the straight line through the point,  $P$ , along the linear velocity vector,  $\mathbf{V}_{Ki}$ . Point  $K_{i+1}$  is located at an infinitesimally small distance from point  $K_i$ . Constructed in this way, all the points  $K_i, K_{i+1}, \dots$  are within the straight line of action,  $LA$ .

Finally, the use of *Shishkov equation of contact*,  $\mathbf{n}_g \cdot \mathbf{V}_\Sigma = 0$  makes possible the determination of the desirable line of action,  $LA$ , for a parallel-axes gear pair that is capable of transmitting smoothly

a uniform rotation from the driving shaft to the driven shaft. The line of action is represented by the set of contact points  $K_i, K_{i+1}, \dots$  considered in a motionless reference system associated with the gear housing (this line should be a straight line through the pitch point,  $P$ ). That same set of contact points  $K_i, K_{i+1}, \dots$  considered in a reference system associated with the gear,  $X_g Y_g Z_g$ , represents the gear tooth flank,  $\mathcal{G}$ . Similarly, that same set of contact points  $K_i, K_{i+1}, \dots$  considered in a reference system associated with the pinion,  $X_p Y_p Z_p$ , represents the pinion tooth flank,  $\mathcal{P}$ . Only involute tooth profiles meet the requirements imposed by *Shishkov equation of contact*,  $\mathbf{n}_g \cdot \mathbf{V}_\Sigma = 0$ , for spur gearing, and only screw involute tooth flanks meet the requirements imposed by *Shishkov equation of contact*,  $\mathbf{n}_g \cdot \mathbf{V}_\Sigma = 0$ , for helical parallel-axes gears. This statement can be proved analytically. The equation of involute tooth profile can be derived based solely on the premise of the equation of contact,  $\mathbf{n}_g \cdot \mathbf{V}_\Sigma = 0$ . Gears of no other geometry are capable of smoothly transmitting a uniform rotation from a driving shaft to the driven shaft.

Envelope profiles and envelope surfaces not of all geometries are suitable for smooth transmission of an input rotation with a constant angular velocity of the driving shaft. The only profiles/surfaces that envelope to one another in both directions of the generating motion, namely, in the direct direction (in the first case, the moving profile/surface is generating the generated profile/surface) as well as in the reverse direction of the generating motion (in the second case, the generated profile/surface when moving inversely generates the originally given profile/surface). This makes it possible to formulate a theorem:

### Theorem 1.1

The only gears capable of smoothly transmitting a uniform rotary motion from a driving shaft to a driven shaft, are those for which the tooth flanks envelope each other in both directions of relative motion, namely, in the direct and in the reverse direction of the gear and of the pinion rotation.

All conjugate profiles/surfaces meet the theorem, and vice versa, if profiles/surfaces meet the theorem, they conjugate to one another. *Theorem 1.1* is an equivalent of the conjugate action law – of the second fundamental law of gearing.

In parallel-axes gearing, only involute tooth profiles (for spur gears) and screw involute surfaces (for helical gearing) are capable of transmitting a uniform input rotation smoothly. Tooth flanks of no other geometries are capable of transmitting a uniform rotation smoothly.

Consider parallel-axes gearing when a tooth profile,  $\mathcal{P}_1$ , is generated as an envelope to a family of consecutive positions of an arbitrary smooth regular tooth profile,  $\mathcal{G}_1$ . When the moving profile,  $\mathcal{G}_1$ , is not of involute shape, and the rotations of the driving and driven shafts are at uniform angular velocities,  $\omega_g$  and  $\omega_p$ , correspondingly, then in the reversed rotation the tooth profile  $\mathcal{P}_1$  will not generate the initial tooth profile  $\mathcal{G}_1$  but, instead, it will generate a tooth profile  $\mathcal{G}_2$  of another geometry. This process can be continued: The tooth profile  $\mathcal{P}_{i+1}$  is generated by the tooth profile,  $\mathcal{G}_i$ . Then the tooth profile  $\mathcal{G}_{i+1}$  is generated by the tooth profile  $\mathcal{P}_{i+1}$ , and so on. This process could be endless as the initial tooth profile  $\mathcal{G}_1$  is not involute.

One more important result can be drawn up from *Theorem 1.1*. When a gear tooth flank deviates at a certain value,  $\delta_{o,g}$  (either under the operating load or due to manufacturing errors), from the desirable involute shape, it is a wrong way to compensate for this deviation by a corresponding deviation,  $\delta_{l,p}$ , of the pinion tooth flank, as schematically illustrated in Figure 1.14. Ease-off diagrams should be used separately for a gear, and for a mating pinion.

Although it was used to illustrate for the case of parallel-axes gearing, *Theorem 1.1* can be enhanced to illustrate the cases of intersected-axes gearing, and of crossed-axes gearing, as well.

The present discussion relates just to one pair of gear teeth engaged in mesh. Further, the requirement of equal base pitches of a gear, and of a mating pinion, to operating base pitch in the gear pair, ( $p_{b,g} = p_{b,op}$ , and  $p_{b,p} = p_{b,op}$ ), allows proceeding to real gearing that have certain number of the tooth flanks engaged in mesh simultaneously. This means that *Shishkov equation of contact*,

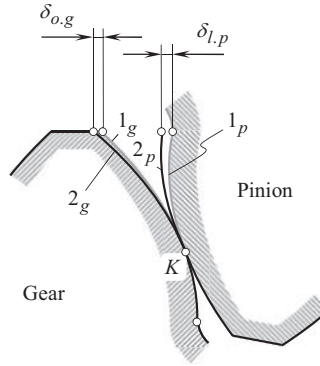


**FIGURE 1.14** Deviations of the actual gear,  $2_g$ , and pinion,  $2_p$ , tooth profiles from the corresponding desirable involute forms  $1_g$  and  $1_p$ , correspondingly.

$\mathbf{n} \cdot \mathbf{V}_\Sigma = 0$ , is the first condition to be considered in gear kinematics and gear geometry. Ultimately, the entire geometric theory of gearing can be derived based on just three laws:

1. The law of contact (*Shishkov equation of contact*,  $\mathbf{n} \cdot \mathbf{V}_\Sigma = 0$ )
2. The conjugate action law
3. The equal base pitches law,  $p_{b,g} = p_{b.op}$  and  $p_{b,p} = p_{b.op}$

The above discussion can be enhanced to other kinds of fit gearing, namely, to intersected-axes gears as well as to crossed-axes gearing.

### 1.3 HELICAL NON-INVOLUTE GEARING

Helical gear pairs those composed of gears of non-involute tooth profiles deserve a particular consideration. Below, a brief discussion on helical non-involute gear pairs begins with the practical implementation of non-involute gear pairs.

#### 1.3.1 HELICAL ROTORS FOR *ROOTS BLOWER*

Not many applications of non-involute helical gear pairs can be found in the industry. Helical rotors in *Roots blower* are one such rare application.

From Figure 1.15, a *Roots blower* is composed of two helical rotors. Each rotor is of three lobes. The rotors are mounted on the shafts and are assembled in a housing. The rotors are rotated with angular velocities,  $\omega_1$  and  $\omega_2$ , about their axis of rotation,  $O_1$  and  $O_2$ , correspondingly. The axes of rotation,  $O_1$  and  $O_2$ , are at a center-distance,  $C$ , apart from one another. Two driving gears are used to rotate the rotors about their axes. The tooth ratio of the driving gear pair equals to one ( $u = 1$ ). The nominal pitch radius of each rotor is equal to the pitch radius of the driving gear.

It should be mentioned here that the closest distance of approach,  $\Delta_{cda}$ , between the interacting surfaces of the helical rotors can be calculated. The actual value of the distance,  $\Delta_{cda}$ , depends on the current angular configuration of the rotors. As the rotors rotate, the distance,  $\Delta_{cda}$ , in every transverse section of the lobes changes from a minimum value,  $\Delta_{cda}^{\min}$ , to a maximum value,  $\Delta_{cda}^{\max}$ . The inequality  $\Delta_{cda}^{\min} \leq \Delta_{cda} \leq \Delta_{cda}^{\max}$  is valid for *Roots blowers* that feature helical rotors.

The closest distance of approach,  $\delta_{cda}^{\min}$ , between the interacting surfaces of spur rotors, and the largest distance,  $\delta_{cda}^{\max}$ , between helical rotors of a *Roots blower* that have helical rotors, relate to one another in such a way that the inequality  $\Delta_{cda}^{\min} \geq \delta_{cda}^{\max}$  is observed.

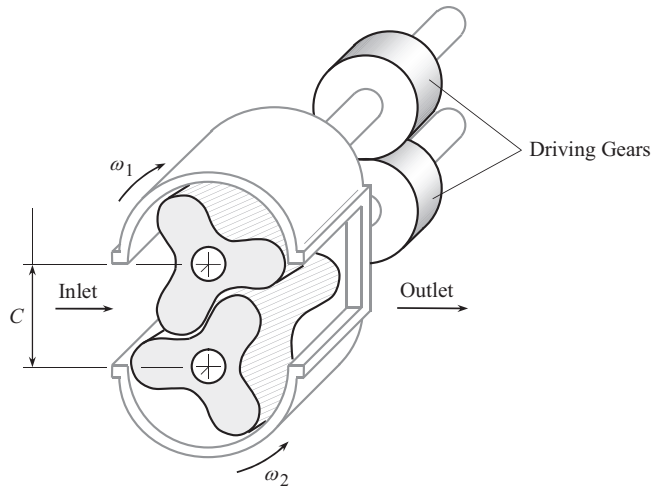


**FIGURE 1.15** Three-lobe *Roots blower* (helical non-involute rotors).



**FIGURE 1.16** Close-up of two helical non-involute rotors in mesh.

The following statement is proved:

**Conclusion 1.6.** *As only one pair of lobes is always in contact, helical rotors of Roots blower are not capable of transmitting a uniform input rotation.*

Individual rotation of the rotors is a must for *Roots blowers* with helical rotors.

That same statement is valid with respect to helical rotors of axial pumps that have a non-involute profile of the lobes (see Figure 1.16) as well as with other helical surfaces that have non-involute profiles. Therefore, modern designs of blower rotors feature working surfaces in the form of helical involute surfaces, as in the design of a blower depicted in Figure 1.17.

### 1.3.2 ON INFEASIBILITY OF DR. WILDHABER *HELICAL GEARING* (US PAT. NO. 1,601,750)

The proven infeasibility of helical gearing with a non-involute tooth profile for smooth transmission of a uniform rotation makes it reasonable to perform an analysis of the feasibility of the well-known *Helical Gearing* proposed in 1923 by a famous inventor, Dr. E. Wildhaber [101]. *Helical Gearing* by Dr. E. Wildhaber [101] is a perfect example of helical gearing with a non-involute tooth profile. The necessity of such an analysis is important because of the following:



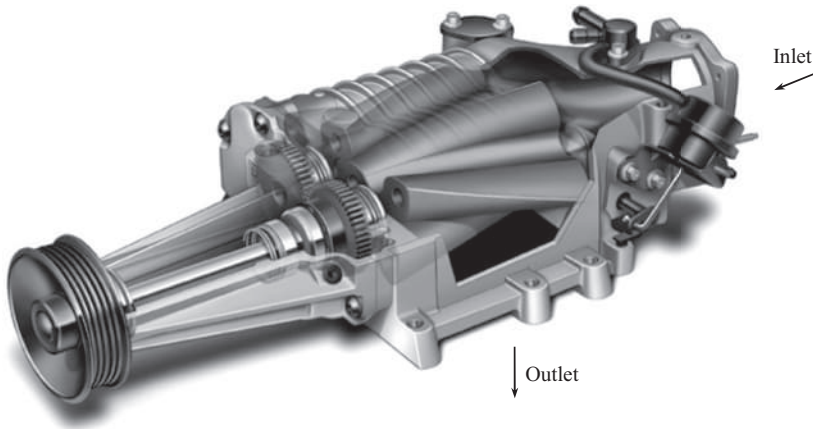


**FIGURE 1.17** Example of a blower (super-charger) with screw involute interacting surfaces of the rotors

1. The analysis can clearly show that *Helical Gearing* by Dr. E. Wildhaber [101] is infeasible at all. This analysis is helpful to less experienced gear experts, those who loosely combine the *Helical Gearing* proposed by Dr. E. Wildhaber, with conformal gearing later proposed by Dr. M.L. Novikov [123]. Such a combination of two completely different gear systems results in absolutely meaningless (stupid) terminology, like *Wildhaber-Novikov gearing* and/or *W-N gearing*
2. Incorrect interpretation of the kinematics and the geometry of *Helical Gearing* by Dr. E. Wildhaber [101] (along with that with respect to *Novikov gearing*) has caused huge confusion in designing, and, especially, in the production of gears for *Novikov gearing* (as gears for *Novikov gearing* cannot be finish-cut in continuous-indexing process of gear machining)

A few more reasons for the necessity of such an analysis can be mentioned in addition.

*Helical Gearing* by Dr. E. Wildhaber [101] is illustrated in Figure 1.18 (for more details, refer to Appendix H).

Wildhaber's invention is related to the tooth shape of gears, which run on parallel axes, and may be applied to helical gears, such as single helical gears, double helical gears, or herringbone gears. Providing accurate gearing of circular arc profile is one of the purposes of helical gearing [101]. No other tooth profiles except the circular arc profile are proposed in this invention.

In Figure 1.18, 1 denotes a helical gear that has teeth, 2, in contact with the teeth, 3, of a mating pinion, 4. As is customary, the helical gearing is analyzed with reference to a normal section, *that is*, line 2–2 in the upper part in Figure 1.18, which is normal to the helix of the pitch circle. The lower part in Figure 1.18 illustrates the said normal section 2–2 for both the pinion, 4, and gear, 1.

As an example, it has been assumed that the tooth profiles, 6, of the gear, 1, are circular arcs of radii, 7, and centers, 8, in the shown normal section. The centers, 8, are situated close to the pitch circle, 9, of the gear. The location of the centers, 8, in relation to the line of action, *LA*, is not specified in the invention. The corresponding teeth of the pinion, 4, are so shaped as to allow rolling of the pitch circles, 9 and 10, on each other, which is well-known to those skilled in the art. So, no freedom in choosing the pinion tooth profile is allowed in the invention.

When the gear tooth, 2, is in the position shown in Figure 1.18 and its center at 8, then it contacts with tooth, 3, at a point, 11, which may be determined by a perpendicular to the tooth, 2, through the point, 12. Point, 12, is the contact point between the two pitch circles, 9 and 10. Point 12 is commonly referred to as the *pitch point*. The said perpendicular is in the present case the connecting line between the pitch point, 12, and the center, 8, of the tooth profile.

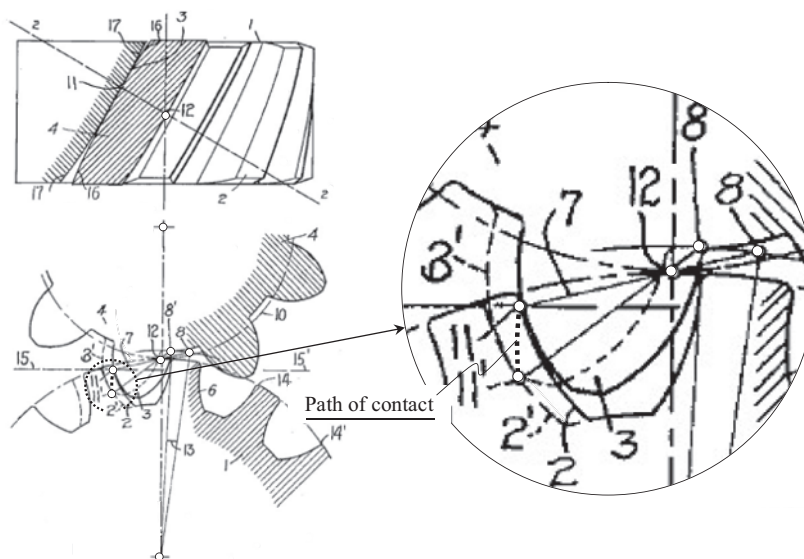


**FIGURE 1.18** Schematic of *Helical Gearing* by E. Wildhaber (U.S. Pat. No. 1,601,750, 1926.)

Another position, 2', of the gear tooth and 3' of the corresponding pinion tooth are shown in dotted lines in Figure 1.18. The tooth profiles contact here at a point, 11', which can be determined similar to point 11. It is noted that *the contact point has traveled from 11 to 11'* during a small angular motion of the gears.<sup>5</sup> A certain path of contact,  $P_c$ , is a curved line through points 11 and 11'. *The contact point has passed practically over the whole active profile* during a turning angle, 13, of the gear; this angle corresponds only to a fraction of the normal pitch, 14, that is, 14'. The said normal pitch equals the circular pitch of the shown normal section.

Omitting numerous inconsistencies and discrepancies between the design parameters of the gear pair, it is of critical importance to stress here that traveling of the contact point within a transverse section<sup>6</sup> of the gear pair indicates that *Helical Gearing* [101] features a path of contact,  $P_c$ , of a certain length,  $L_{pc}$  (i.e.,  $L_{pc} > 0$ ). If the length,  $L_{pc}$ , of the path of contact,  $P_c$ , is not of a zero value, and the teeth are of a circular arc shape, then the vital requirement of equal base pitches of the gear and of the pinion in *Helical Gearing* [101] is not fulfilled.

In the invented gearing [101], the contact point between two normal profiles passes over the whole active profile during a turning angle, which corresponds to less than one-half the normal pitch; usually, it is much less than that.

It is then claimed that *Wildhaber's Helical Gearing* [101] is capable of ensuring better contact between the teeth of the gear and of the pinion in a direction perpendicular to the *contact line between two mating teeth*. Therefore, it is expected that the proposed helical gearing features *line contact* (and not *point contact*) between the tooth flanks of the gear and that of the pinion.

The gearing according to the invention [101] is strictly a gearing for helical teeth. It is not advisable on straight teeth, on account of the explained *short duration of contact between the tooth profiles*. It should be pointed out here that in the invention [101], a short duration of contact and not instantaneous contact between the tooth profiles is anticipated.

<sup>5</sup> The ability of the contact point to travel over a tooth profile has been mentioned for several times in the patent description (see Appendix H for more details).

<sup>6</sup> If the contact point travels within the normal section, 2 – 2, then the projection of the contact point onto the transverse section travels within the transverse section, as well.

The interacting profiles of the gear teeth are concave and circular, and their *centers are substantially situated on the pitch circle of the gear*. The convex working profiles of the pinion are also of a circular shape. Their radii are substantially the same as the radii of the mate tooth profiles. *The centers of these profiles are similarly situated on pitch circle of the pinion*. Because the centers of the tooth profiles are situated within the corresponding pitch circles, the centers cannot be situated within the line of action,  $LA$  (or the instant line of action,  $LA_{inst}$ ).

More details on inconsistency, and discrepancy between the design parameters of *Wildhaber's Helical Gearing* and *Novikov gearing* are outlined in Appendix H.

The performed analysis reveals that the *Helical Gearing* proposed by *Wildhaber* [101] is a kind of helical gearing that has a non-involute tooth profile, and features the path of contact,  $P_c$ , of certain length,  $L_{pc}$  (i.e.,  $L_{pc} > 0$ ). As it is shown in this chapter of the book, gear pairs of this particular type are not capable of transmitting a uniform rotation smoothly.<sup>7</sup>

The infeasibility of *Wildhaber's Helical Gearing* [101], and the principal features of *Novikov gearing* make it possible to conclude that these two gear systems cannot be combined into a common design of gearing that is often loosely referred to as *Wildhaber-Novikov gearing*, or *WN-gearing*. These two gear systems must be considered individually and separately from one another.

The consideration in this section of the book can be summarized as follows: Neither spur non-involute gear pairs nor helical non-involute gear pairs of all known designs (as well as of all designs, those to be developed in the future) are capable of transmitting a uniform rotation smoothly. This is mainly because three fundamental laws of gearing are not fulfilled in *Wildhaber's Helical Gearing* [101], and, thus, base pitches of the gear,  $p_{b,g}$ , and that of the pinion,  $p_{b,p}$ , do not equal to operating base pitch of the gear pair,  $p_{b,op}$ , as the first two ( $p_{b,g}$  and  $p_{b,p}$ ) cannot be specified at all.

---

<sup>7</sup> It should be noted here that the *Wildhaber's Helical Gearing* [101] is a kind of mistake. Unfortunately, this invention attracted widespread interest within the gear engineering community. It should be clearly realized that this invention is a huge mistake. No doubt, this mistake should be forgiven, as we all are mistaking from time to time. Dr. *E. Wildhaber* is credited with smart solutions to so many complex engineering problems, and his contributions on gear engineering are invaluable.

# *Part I*

---

## *Fundamentals*

Gears are extensively used in the design of many mechanisms and machines in the present-day industry. As an example, a gearbox with double-helical gears is depicted in Figure 1. Transmission of an input power (of an input torque and of an input rotation) is one of the main goals of gearing of all designs: the output power equals to the input power subtract the power losses.

Transformation of an input rotary motion from a driving shaft to a driven shaft is the second main goal of the use of gear pairs: the output rotation can be either slower compared to the input rotation (as it is observed in gear reducers) or it can be higher compared to the input rotation (as it

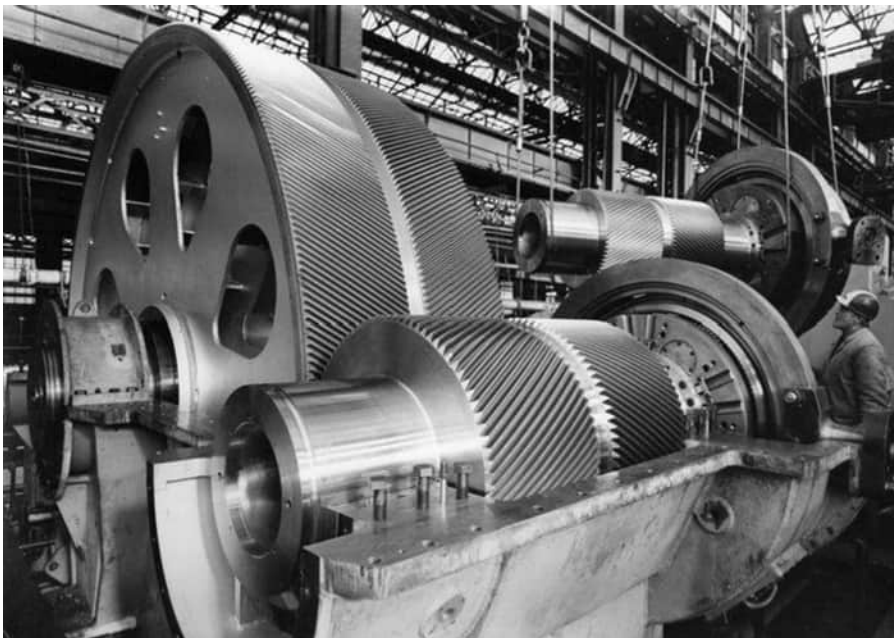


**FIGURE 1** Gearbox with double-helical gears.

is observed in gear multipliers). Change of the direction of rotation is also a kind of transformation of an input rotation: the output rotation can be changed either to a rotation in the opposite direction, or it can remain the same, or the axes of an input rotation and of an output rotation can form an angle of a certain value.

As of today, the enormous amount of practical experience has been accumulated in the realm of design and manufacture of gears and gear transmissions. Based on the accumulated experience, it is now possible to design and manufacture gears and gear trains in a wide range of power transmitting applications, rotations of the input and output shafts, and so forth.

In today's design practice, the desirable kind of a gear pair commonly is given. The design of an actual gear pair goes through a well-established industry routing procedure.

The procedure of designing a gear pair begins with an analysis of kinematics of the gear pair to be designed. This means that the actual position and orientation of the output shaft in relation to that of the input shaft have to be specified. Then, a rotation of the input shaft, and a rotation of the output shaft must also be given. A configuration of the input and of the output shafts in relation to one another, together with a given rotation of the input shaft and of desirable rotation of the output shaft comprise the so-called *principal kinematics* of gear pair<sup>1</sup>. Analysis of the kinematics of a gear pair is always complemented with the analysis of power being transmitted by the gear pair. For this purpose, the input torque also has to be specified.

Based on a given *principal kinematics* of a gear pair, the desirable geometry of the tooth flanks of gears for the gear pair to be designed can be determined. In later phases of the design procedure, physical phenomena in the gear tooth mesh are taken into account. This includes friction between the tooth flanks of mating gears, lubrication of the gear mesh, tooth strength issues, manufacturing errors, and the axes misalignment, displacements of tooth flanks of the gear under the applied load, and so forth.

Summarizing, one can conclude that the input and output rotations, along with the input torque is the most critical portion of the input information that is required to design a gear pair with desirable performance. Profound investigation of the kinematics of gear pairs is vital for the gear designer.

Here and below in this chapter of the book, only geometrically accurate gears and gear pairs are discussed.

This part of the book comprises four chapters (Chapters 2–5).

The discussion below begins with the analysis of *principal kinematics* of gear pair.

---

<sup>1</sup> Sliding between the tooth flanks of mating gears, specific sliding, and so forth, all are covered by the term *kinematics* of gear pair.

---

# 2 Kinematics of Gear Pair

Transmission and transformation of motion from an input shaft to an output shaft are two main purposes of the use of gearing. Kinematics of gearing includes rotations of the driving and the driven gears about their axes, the instantaneous rotations of the driving and the driven gears in relation to each other, and sliding of the tooth flanks of the mating gears. Kinematics of a gear pair along with the input torque is the starting point for solving the problem of synthesizing a gear pair with favorable performance.

## 2.1 TRANSMISSION OF MOTION BY MEANS OF GEARS

Gear pair is commonly composed of two mating gears that are assembled in a housing, and that move in relation to each other when a rotation is transmitted from a driving shaft to a driven shaft.<sup>1</sup> Although other designs are feasible, it is common practice to mount mating gears on shafts. Examples of commonly used gear pairs are illustrated in Figure 2.1. In Figure 2.1, the input rotation is denoted by  $\omega_{in}$ , and the output rotation is designated as  $\omega_{out}$ .

In this book, the following definition is adopted to the term *gear pair*:

### Definition 2.1

Gear pair is an elementary mechanism that is composed of two mating gears mounted in a housing, which is used to transmit and transform a rotary motion from an input shaft to an output shaft.

In a gear pair, the mating gears perform an instantaneous rotation in relation to one another. This makes possible construction: (a) of the plane of action, (b) of the path of contact, as well as of other elements of the gear pair.

Two examples in this regard are given below.

**First**, consider a *bolt-and-nut* pair. Threads of the bolt and that of the nut make *surface-to-surface* contact with each other. With an appropriate value of the helix angle, a rotation of the bolt can be transformed and transmitted to a straight motion of the nut, and vice versa, that is, a rotation of the nut can be transformed and transmitted to a straight motion of the bolt. When the helix angle is zero, then a rotation cannot be transmitted and cannot be transformed; when the helix angle is a right angle (as in gear coupling), then the rotation can be transmitted, but cannot be transformed.

**Second**, consider a *rack-to-rack* pair. Tooth flanks of the racks make *surface-to-surface* contact with each other. When one of the racks travels straightforward at an angle in relation to another rack, the second one also travels straightforward at an angle in relation to the first rack. In this way, a transformation of the direction of the straight motion is observed. If the first rack travels in a direction parallel to a direction of teeth of the second rack, then the tooth flanks of the racks *slide over one another* – no translation of motion is possible in such a scenario. If the first rack travels in a direction perpendicular to a direction of tooth of the second rack, then no transformation of the motion is possible in this case.

---

<sup>1</sup> It is right point to stress here that in contrast to gear pair, harmonic drive is composed of more than three components (it is composed of a stator-gear, a flexible gear, and a wave generator, that are assembled in the housing). All the components are vital for the design of harmonic drive. In this book, harmonic drive is not considered, as this is not a kind of gearing (*harmonic drive* is a mechanism of another nature).



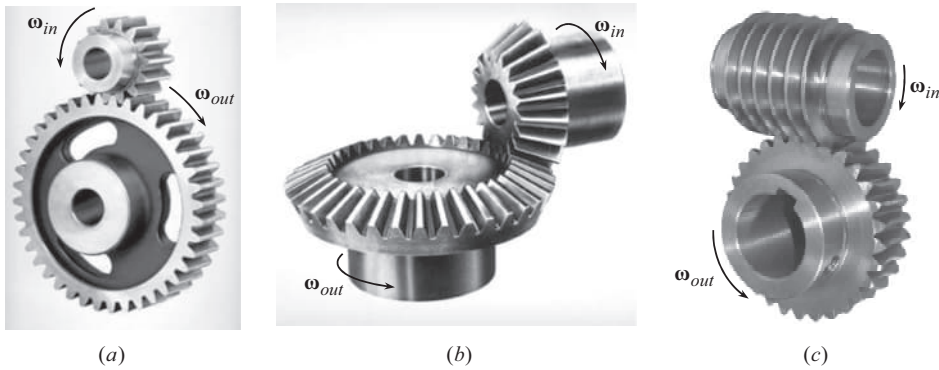


**FIGURE 2.1** Examples of various kinds of gear pairs: (a) parallel-axes gear pair ( $P_a$  – gearing), (b) intersected-axes gear pair ( $I_a$  – gearing), and (c) crossed-axes gear pair ( $C_a$  – gearing).

In these examples, namely, in *bolt-and-nut* pair, and in *rack-to-rack* pair, both the kinematic pairs can be construed as a reduced case of a gear pair. However, neither plane of action nor path of contact, and so forth, can be constructed for the considered kinematic pairs. The relative motion of the components, in both cases, cannot be construed as a kind of instantaneous rotation. Therefore, special care is required to be undertaken when treating reduced cases of gear pairs, as they often possess not all the properties that regular gear pair does.

The purpose of a gear pair is twofold:

1. The use of a gear pair makes possible transmission of rotary motion from an input shaft to an output shaft, and
2. Motion transformation is always occurred when a motion is transmitted (when a motion is transmitted, either the rotation and its direction, or just rotation, of the input shaft, or just direction of rotation of the output shaft, is altered)

Rotation transformation of another nature can also be observed when transmitting a motion by means of a gear pair, that is, a rotation can be transformed into a translation and vice versa. Transformation of this kind is observed when a gear is engaged in mesh with a rack. When the rack is driven, the transformation of the rotation into translation is occurred; otherwise, when the gear is driven, the translation of the rack is transformed into the rotation of the gear.

One of three configurations of the axes of rotation of a gear and that of a mating pinion are possible when rotary motion is transmitted between two shafts:

- the axes of rotation are parallel to each other, as in parallel-axes gearing (as in  $P_a$  – gearing, for simplicity)
- the axes of rotation intersect each other, as in intersected-axes gearing (as in  $I_a$  – gearing, for simplicity)
- the axes of rotation cross each other, as in crossed-axes gearing (as in  $C_a$  – gearing, for simplicity)

The third configuration of crossing axes of rotation of a driving shaft and of a driven shaft (namely,  $C_a$  – gearing) should be construed as the most general one. When the closest distance of approach of the crossing axes is zero, the third case is reduced to the second one, namely, it is reduced to the case of intersecting axes of rotation ( $I_a$  – gearing). On the other hand, if the crossed-axes angle is either zero, or equal to either  $0^\circ$ , or  $180^\circ$ , then the third case of crossing axes of rotation is reduced to the first case, that is, it is reduced to the case of parallel axes of rotation ( $P_a$  – gearing).



**FIGURE 2.2** A gear rotation vector,  $\omega_g$ , may be associated with a rotating gear.

## 2.2 GEAR VECTOR DIAGRAM

The principal kinematics of a gear pair is based on two rotations. They are:

1. Rotation of a gear about the gear axis of rotation,  $O_g$ , with an angular velocity  $\omega_g$ , and
2. Rotation of a mating pinion about the pinion axis of rotation,  $O_p$ , with an angular velocity  $\omega_p$ .

The angular velocities,  $\omega_g$  and  $\omega_p$ , are synchronized with one another (commonly, in reduction gear pairs,  $\omega_p/\omega_g = u$ , where  $u$  is the gear ratio. In increasing gear pairs,  $u = \omega_g/\omega_p$ . More generally,  $u = \omega_{\text{input}}/\omega_{\text{output}}$ ).

Consider a gear as an example. When the gear rotates about its axis of rotation,  $O_g$ , a circular-arc arrow is often used to depict this rotation. The angular velocity of this rotation is of certain value,  $\omega_g$ . A rotation vector<sup>2</sup>  $\omega_g$  can be used to illustrate rotation of a gear about its axis of rotation,  $O_g$ , as illustrated in Figure 2.2.

Similar to the gear rotation vector,  $\omega_g$ , rotation of a mating pinion can also be represented by a pinion rotation vector,  $\omega_p$ . The rotation vectors  $\omega_g$  and  $\omega_p$  are of magnitudes  $|\omega_g| = \omega_g$ , and  $|\omega_p| = \omega_p$ , correspondingly. The right-hand screw rule is used for the determining a direction of rotation vectors,  $\omega_g$  and  $\omega_p$ .

### 2.2.1 CONCEPT OF GEAR VECTOR DIAGRAM

The instantaneous motion of a gear in relation to a mating pinion, as well as the instantaneous motion of the pinion in relation to the gear, can be determined based on the rotation vectors  $\omega_g$  and  $\omega_p$ , and the actual configuration of the axes of rotation,  $O_g$  and  $O_p$ . It is a routing procedure to

<sup>2</sup> Angular velocity is considered in this book as a vector along the axis of rotation that is pointed in a direction defined by the right-hand screw rule. It is realized here and below that rotations,  $\omega_g$  and  $\omega_p$ , are not vectors by nature. Therefore, special care is required to be undertaken when treating rotations as vectors. In particular, when coordinate systems transformation is analytically described by means of matrices, the order of the matrices in the matrix product is predetermined by the order of the elementary coordinate system transformations, that is, it is not permissible to change the order of the matrices in the matrix product. This is of critical importance when rotation vectors,  $\omega_g$  and  $\omega_p$ , are represented in matrix form.

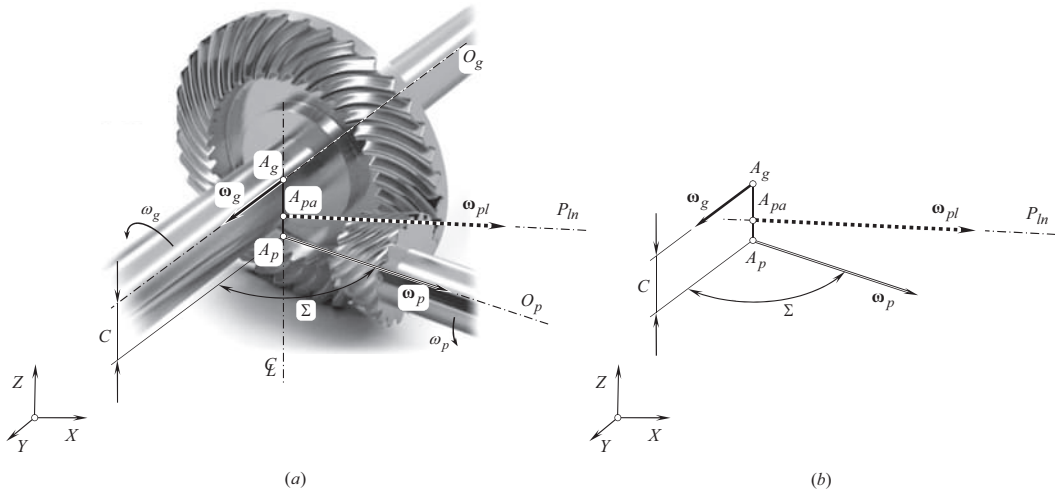


**FIGURE 2.3** Kinematics of gearing with a constant gear ratio,  $u$  : (a) schematic of a crossed-axes gear pair and (b) an equivalent *gear vector diagram*; The rotation vectors,  $\omega_g$  and  $\omega_p$ , of the  $C_a$  – gearing are at a center-distance,  $C$ , apart from one another, and form a crossed-axes angle,  $\Sigma$ .

determine the center-distance,  $C$  (the center-distance,  $C$ , is, the closest distance of approach of the axes of rotation,  $O_g$  and  $O_p$ ), the shaft angle,  $\Sigma$  (i.e., the angle that the axes of rotation,  $O_g$  and  $O_p$ , form with one another), and the gear ratio,  $u$  (i.e., equal to the ratio  $u = |\omega_{input}|/|\omega_{output}|$ ). Due to this, a pair of rotation vectors,  $\omega_g$  and  $\omega_p$  (along with the design parameters  $C$ ,  $\Sigma$ , and  $u$ ), is referred to as *gear vector diagram*. For a given transverse pressure angle,  $\phi_{\omega.t}$ , base cones for the gear pair can be determined uniquely by means of the corresponding *gear vector diagram*. *Gear vector diagram* can be construed as a first step of evolution of the so-called *screw diagram*, which was investigated by Prof. A.F. Nikolayev [88,89] in the late 1940s and early 1950s. More examples in this regard can be found in the public domain. The *screw diagram* is the first iteration in the development of the *gear vector diagram*.

Making use of the rotation vectors,  $\omega_g$  and  $\omega_p$ , allows one for the determination of sliding of tooth flanks of mating gears. Ultimately, the kinematics of a gear pair can be entirely expressed in terms of two rotation vectors,  $\omega_g$  and  $\omega_p$  [179,180].

Referring to Figure 2.3a, consider a crossed-axes gear pair ( $C_a$  – gearing) together with the associated rotation vectors  $\omega_g$  and  $\omega_p$ . A *Cartesian* coordinate system,  $XYZ$ , is associated with the crossed-axes gear pair. The rotation vectors,  $\omega_g$  and  $\omega_p$ , of a gear and its mating pinion are at a center-distance,  $C$ . The center-distance,  $C$ , is a straight-line segment that is measured along the centerline,  $\mathfrak{L}$ , and equals to the closest distance of approach between the axes of rotation,  $O_g$  and  $O_p$ , of the gear and its mating pinion, correspondingly. In the particular case under consideration, the crossed-axes angle,  $\Sigma$ , equals to  $90^\circ$ . The crossed-axes angle,  $\Sigma$ , can also be either acute ( $\Sigma < 90^\circ$ ), or it can be obtuse ( $\Sigma > 90^\circ$ ).

The rotation vectors of a gear,  $\omega_g$ , and its mating pinion,  $\omega_p$ , are in fact sliding vectors (see Figure 2.3b). They can be applied at any point within the gear axis,  $O_g$ , and the pinion axis,  $O_p$ , correspondingly. It is convenient to apply the rotation vectors,  $\omega_g$  and  $\omega_p$ , at points of intersection,  $A_g$  and  $A_p$ , of the corresponding axes of rotation,  $O_g$  and  $O_p$ , by the centerline,  $\mathfrak{L}$  (i.e., by a line along which the center-distance,  $C$ , is measured). As it will be shown later on in this book, points  $A_g$  and  $A_p$  are in nature the apexes of the base cones of the gear and its mating pinion, correspondingly. In a case when the axes of rotation,  $O_g$  and  $O_p$ , intersect one another (namely, when  $C = 0$ ), it is convenient to apply the rotation vectors,  $\omega_g$  and  $\omega_p$ , at point of intersection of these axes [179,180].

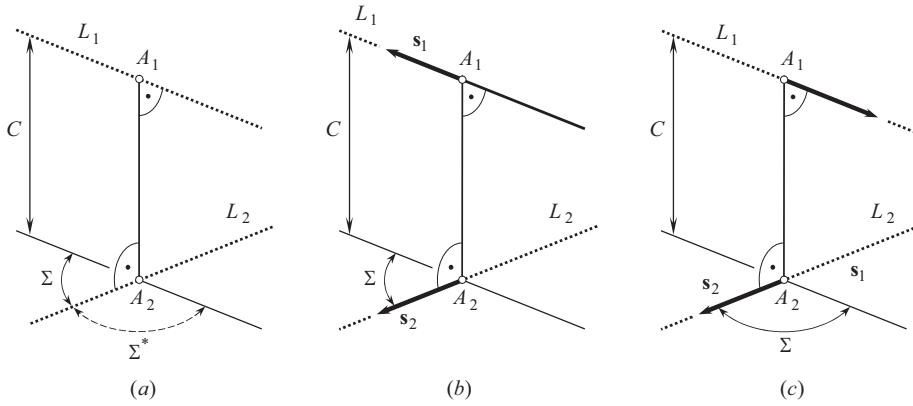


**FIGURE 2.4** On the definition of crossed-axes angle,  $\Sigma$ , in a gear pair: the directions of the straight lines,  $L_1$  and  $L_2$ , (a) are not specified, (b) are specified ( $\Sigma < 0^\circ$ ), and (c) are specified ( $\Sigma > 0^\circ$ ).

The magnitude,  $\omega_g$ , of the rotation vector of the gear is  $\omega_g = |\omega_g|$ , whereas the magnitude,  $\omega_p$ , of the rotation vector of the mating pinion is  $\omega_p = |\omega_p|$ . The magnitudes,  $\omega_g$  and  $\omega_p$ , of the rotation vectors,  $\omega_g$  and  $\omega_p$ , are synchronized with one another.

The crossed-axes angle,  $\Sigma$ , is measured between the rotation vectors,  $\omega_g$  and  $\omega_p$ . Therefore, an equality<sup>3</sup>:

$$\Sigma = \angle(\omega_g, \omega_p) \quad (2.1)$$

is valid.

Equation (2.1) immediately yields a formula:

$$\Sigma = \tan^{-1} \frac{|\omega_g \times \omega_p|}{\omega_g \cdot \omega_p} \quad (2.2)$$

for the calculation of the actual value of the crossed-axes angle,  $\Sigma$ .

A more in-detail explanation is required in order to make clear the concept of the crossed-axes angle,  $\Sigma$ .

Consider two crossing straight lines,  $L_1$  and  $L_2$ , the directions of which are not specified (see Figure 2.4a). In the case under consideration, the straight-line segment  $A_1A_2$  is the closest distance of approach of the straight lines,  $L_1$  and  $L_2$ , and, therefore, the length of the straight-line segment  $A_1A_2$  equals to the center-distance,  $C$ , for the straight lines  $L_1$  and  $L_2$ . The angular configuration of the straight lines,  $L_1$  and  $L_2$ , can be specified either by the acute angle,  $\Sigma$ , or by the obtuse angle,  $\Sigma^*$ . The specifications of the crossed-axes angle of the straight lines,  $L_1$  and  $L_2$ , by means of the angles  $\Sigma$  and  $\Sigma^*$  are equivalent to one another, as long, as the directions of the straight lines  $L_1$  and  $L_2$  are not taken into account.

Consider two crossing straight lines,  $L_1$  and  $L_2$ , the directions of which are specified (see Figure 2.4b and c). Once the directions of the straight lines  $L_1$  and  $L_2$  are specified (e.g., the directions are specified by the unit vectors,  $s_1$  and  $s_2$ , pointed along the straight lines,  $L_1$  and  $L_2$ ), it becomes clear when the crossed-axes angle,  $\Sigma$ , is acute (see Figure 2.4b), and when it is obtuse (see Figure 2.4c). Thus, no duality in the specification of the crossed-axes angle,  $\Sigma$ , is observed for the straight lines,  $L_1$  and  $L_2$ , with specified directions. The similar is valid with respect to the rotation

<sup>3</sup> For the reader's convenience, elements of vector calculus are concisely summarized in Appendix A.

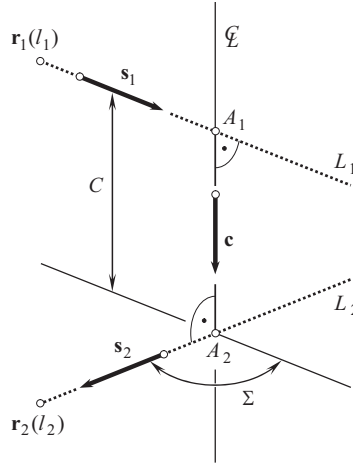


**FIGURE 2.5** Determination of the center-distance,  $C$ , in a gear pair.

vectors,  $\omega_g$  and  $\omega_p$ , in a gear pair. Based on this discussion, the following formula can be used for the calculation of the crossed-axes angle,  $\Sigma$ :

$$\Sigma = \tan^{-1} \frac{\omega_g \times \omega_p}{\omega_g \cdot \omega_p} \quad (2.3)$$

For a specified pair of rotation vectors,  $\omega_g$  and  $\omega_p$ , the closest distance of approach,  $C$ , between the straight lines,  $L_1$  and  $L_2$ , can be calculated based on the following approach.

To calculate the length of the common perpendicular,  $C = A_1A_2$ , to the straight lines  $L_1$  and  $L_2$  (see Figure 2.5), the directions of the lines,  $L_1$  and  $L_2$ , are denoted by the unit vectors  $\mathbf{s}_1$  and  $\mathbf{s}_2$ ; the position vectors of current points  $l_1$  and  $l_2$  are denoted by  $\mathbf{r}_1(l_1)$  and  $\mathbf{r}_2(l_2)$ ; and the direction of the centerline,  $\Phi$ , is denoted by the unit vector  $\mathbf{c}$  (still unknown yet). The magnitude of a vector  $\mathbf{C}$  that is pointed along the centerline,  $\Phi$ , equals to the center-distance,  $C$ .

Then, the following expression can be composed for the calculation of the center-distance,  $C$ :

$$\mathbf{C} = \mathbf{r}_1 + l_1 A_1 \mathbf{s}_1 = \mathbf{r}_2 + l_2 A_2 \mathbf{s}_2 - C \mathbf{c} \quad (2.4)$$

On taking the scalar product of this equation with  $\mathbf{c}$ , we obtain:

$$\mathbf{r}_1 \cdot \mathbf{c} + l_1 A_1 \mathbf{s}_1 \cdot \mathbf{c} = \mathbf{r}_2 \cdot \mathbf{c} + l_2 A_2 \mathbf{s}_2 \cdot \mathbf{c} - C \quad (2.5)$$

However, since the direction  $\mathbf{C}$  is perpendicular to the lines  $L_1$  and  $L_2$ , the products  $\mathbf{s}_1 \cdot \mathbf{c}$  and  $\mathbf{s}_2 \cdot \mathbf{c}$  are zero, so that:

$$C = (\mathbf{r}_2 - \mathbf{r}_1) \cdot \mathbf{c} \quad (2.6)$$

Moreover, since  $\mathbf{c}$  is perpendicular to the unit vectors  $\mathbf{s}_1$  and  $\mathbf{s}_2$ , it is proportional to  $\mathbf{s}_1 \times \mathbf{s}_2$ . As the center-distance  $C$  is to be a length, it must be of a positive value, so that finally:

$$C = \left| \frac{(\mathbf{r}_2 - \mathbf{r}_1) \cdot (\mathbf{s}_1 \times \mathbf{s}_2)}{|\mathbf{s}_1 \times \mathbf{s}_2|} \right| \quad (2.7)$$

The use of the rotation vectors,  $\omega_g$  and  $\omega_p$ , makes possible construction of the vector of instantaneous rotation,  $\omega_{pl}$  (see Figure 2.3b), of the pinion in relation to the gear (or vice versa, namely, the vector of instantaneous rotation of the gear in relation to the pinion). The point of interception of the line of action of the vector of instantaneous rotation,  $\omega_{pl}$ , by the centerline,  $\mathfrak{k}$ , is designated as  $A_{pa}$ . As it is shown later on in this book, point  $A_{pa}$  is, by nature, the apex of the plane of action in the gear pair.

For the further analysis below, principle of inversion<sup>4</sup> of rotations is used. Two different options have to be distinguished in this regard:

**First**, the gear pair can be rotated about the pinion axis of rotation,  $O_p$ , with the rotation,  $-\omega_p$ .

In this scenario, the pinion becomes stationary [as:  $\omega_p + (-\omega_p) = 0$ ], and the resultant instantaneous rotation of the gear is equal to the following:

$$\omega_{gp} = (\omega_g - \omega_p) \quad (2.8)$$

Such a situation corresponds to the case of rotation of the gear in relation to the pinion, when the latter is supposed to be motionless.

**Second**, the gear pair can be rotated about the gear axis of rotation,  $O_g$ , with the rotation,  $-\omega_g$ . In this scenario, the gear becomes motionless [as:  $\omega_g + (-\omega_g) = 0$ ], and the resultant instantaneous rotation of the pinion is equal to the following:

$$\omega_{pg} = (\omega_p - \omega_g) \quad (2.9)$$

Such a situation corresponds to the case of rotation of the pinion in relation to the gear, when the latter is supposed to be stationary.

Evidently, the rotation vectors,  $\omega_{gp}$  and  $\omega_{pg}$ , are of equal magnitudes, and of opposite directions to one another ( $\omega_{gp} = -\omega_{pg}$ ). Below, the rotation vector of a pinion in relation to the motionless gear,  $\omega_{pg}$ , is referred to as the vector of instantaneous rotation,  $\omega_{pl}$  [an equality  $\omega_{pl} = \omega_{pg} = (\omega_p - \omega_g)$  is valid; for the rotation vector of a pinion in relation to the motionless gear,  $\omega_{gp}$ , an equality  $\omega_{pl} = -\omega_{gp} = -(\omega_g - \omega_p) = -\omega_g + \omega_p$  is valid].

The just considered *gear vector diagrams* are vital for the scientific theory of gearing.

In addition to the gear vector diagrams constructed on the premise of the rotation vectors,  $\omega_g$  and  $\omega_p$ , corresponding vector diagrams can be constructed on the premise of the torque vectors.

The torque applied at a gear shaft is denoted by  $\mathbf{T}_g$ , while the torque applied at a mating pinion shaft is designated as  $\mathbf{T}_p$ . One of the torques (usually the torque,  $\mathbf{T}_p$ ) is the input torque, while another one (usually the torque,  $\mathbf{T}_g$ ) is the output torque.

An example of gear vector diagrams for the input and output torques,  $\mathbf{T}_g$  and  $\mathbf{T}_p$ , is schematically illustrated in Figure 2.6. In Figure 2.6a, a gear vector diagram for the rotation vectors  $\omega_g$  and  $\omega_p$  is shown. Then a corresponding gear vector diagram for the input and output torques,  $\mathbf{T}_g$  and  $\mathbf{T}_p$ , is constructed for the case in which the pinion is driving and the gear is driven (see Figure 2.6b). This configuration corresponds to a case of reduction gears. Figure 2.6c, a gear vector diagram for the input and output torques,  $\mathbf{T}_g$  and  $\mathbf{T}_p$ , which is constructed for that case when the gear is driving and the pinion is driven, is shown. This configuration corresponds to a case of increasing gears.

The input torque vector is always pointed in that same direction as the input rotation vector does. The output torque vector is always pointed oppositely to the direction of the output rotation vector.

Torque diagrams can be constructed for all types of gearing, namely, for gearing that feature crossing axes of rotation as well as when the axes of rotation of the driving and the driven shafts are either parallel or intersect one another.

<sup>4</sup> The process of holding stationary different links of a kinematic chain is known as *principle of inversion*.



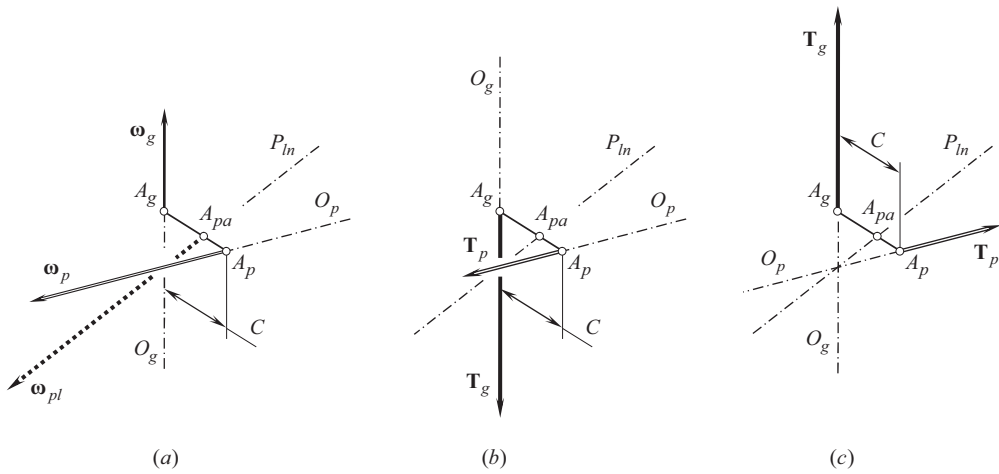


**FIGURE 2.6** Gear vector diagram for the rotations, and two gear vector diagrams for the torques in a gear pair: (a), gear vector diagram for rotations in a crossed-axes gear pair, and two vector diagrams for the torques in that same gear pair corresponding to (b) the case of reduction gearing, when the pinion is driving and the gear is driven, and (c) the case of increasing gearing, when the gear is driving and the pinion is driven.

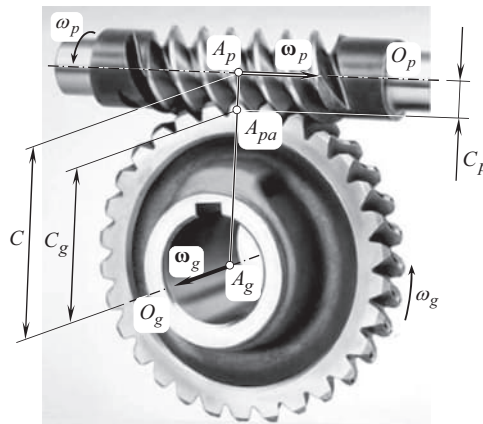


**FIGURE 2.7** An example of crossed-axes gear pair, and an associate gear vector diagram.

### 2.2.2 KINDS OF GEAR VECTOR DIAGRAMS

Let us suppose that two axes of rotation,  $O_g$  and  $O_p$ , are somehow positioned in space in relation to one another, and the aim is to transmit a rotation and torque between the axes using for this purpose gears of a certain design. Two points,  $A_g$  and  $A_p$ , are the points of intersection of the axes of rotation,  $O_g$  and  $O_p$ , by the centerline  $\mathfrak{L}$ . Then, the straight-line segment,  $A_gA_p$ , is the center-distance,  $C$ . Gear vector diagrams of various kinds can be distinguished based on the actual configuration of two axes of rotation,  $O_g$  and  $O_p$ , along with a pair of rotation vectors,  $\omega_g$  and  $\omega_p$ . In this discussion, it is convenient to refer to worm gear pair and an associate gear vector diagram (Figure 2.7). Worm gearing represents a perfect example of crossed-axes gear pair.

Shown in Figure 2.7, the *gear pair center-distance*,  $C$  is the closest distance of approach between the gear axis of rotation,  $O_g$ , and the pinion axis of rotation,  $O_p$  (i.e.,  $O_g / O_p$ ); the *gear center-distance*,  $C_g$  is the closest distance of approach between the gear axis of rotation,  $O_g$ , and the axis

of instantaneous rotation,  $P_{ln}$  (i.e.,  $O_g/P_{ln}$ ); the *pinion center-distance*,  $C_p$ , is the closest distance of approach between the pinion axis of rotation,  $O_p$ , and the axis of instantaneous rotation,  $P_{ln}$  (i.e.,  $O_p/P_{ln}$ ).

The actual position of point,  $A_{pa}$ , within the centerline,  $\Phi$ , can be expressed in terms of the rotation vectors,  $\omega_g$  and  $\omega_p$ . A ratio of the actual length of the straight-line segments,  $C_g = A_{pa}A_g$  and  $C_p = A_{pa}A_p$ , is taken into account aiming to distinguish gear pairs of different kinds. Depending on the actual location of the point,  $A_{pa}$ , in relation to the end-points,  $A_g$  and  $A_p$  (see Figure 2.7), only three different kinds of crossed-axes gear pairs can be distinguished. They are as follows:

- *Rotary-negative gear pairs* – in this kind of gear pairs, the point,  $A_{pa}$ , is located in between the end-points,  $A_g$  and  $A_p$ , of the center-distance,  $C$ . The center-distances,  $C_g$  and  $C_p$ , are measured in opposite directions from the point,  $A_{pa}$ . Therefore, these center-distances are of the opposite signs. The term *rotary-negative gear pair* is due to that in the case under consideration, the ratio of magnitudes of the center-distances,  $C_g$  and  $C_p$ , is of a negative value (namely,  $C_g/C_p < 0$ ). [Comment: The terms *rotary-negative gear pair* and *external gear pair* are not equivalent to one another];
- *Rotary-positive gear pairs* – in this kind of gear pairs, the point,  $A_{pa}$ , is located beyond the end-point,  $A_p$ , of the center-distance,  $C$ . The center-distances,  $C_g$  and  $C_p$ , are measured in the same direction from the point,  $A_{pa}$ . Therefore, these center-distances are of the same sign. The term *rotary-positive gear pair* is due to that in the case under consideration, the ratio of magnitudes of the center-distances,  $C_g$  and  $C_p$ , is of a positive value (namely,  $C_g/C_p > 0$ ). [Comment: The terms *rotary-negative gear pair* and *internal gear pair* are not equivalent to one another];
- *Rotary-zero gear pairs* – in this kind of gear pairs, the *pinion center-distance*,  $C_p$ , is of a zero value ( $C_p = 0$ , while the center-distances  $C_g \neq 0$  and  $C \neq 0$  are not equal to zero). When the equality  $C_p = 0$  is valid, the pinion axis of rotation,  $O_p$ , is aligned with the axis of instantaneous rotation,  $P_{ln}$ , in the gear pair. Therefore, the point,  $A_{pa}$ , is coincident with the end-point,  $A_p$ , of the center-distance,  $C$ . The term *rotary-zero gear pair* is due to that in the case under consideration, the ratio of magnitudes of the pinion, and of the gear center-distances,  $C_p$  and  $C_g$ , is zero (namely,  $C_p/C_g = 0$ ). [An alternative terminology is possible, as well. An inverse ratio  $C_g/C_p$  of the center-distances can be considered instead of the ratio  $C_p/C_g$ . In *rotary-zero gear pair*, the ratio  $C_p/C_g$  approaches an infinity,  $C_g/C_p \rightarrow \pm \infty$ . Following this approach, the term *rotary-infinite gear pair* can be derived. This term is equivalent to the term *rotary-zero gear pair*. Despite these terms being equivalent to one another, the preference (by convention) is given to the first one, namely, to the term *rotary-zero gear pair*].

No other kinds of crossed-axes gear pairs are possible, and any known or newly designed in the future gear pair falls into one of three kinds of gear pairs, listed above.

Here and below, the newly introduced terms *rotary-negative gear pairs*, *rotary-positive gear pairs*, and *rotary-zero gear pairs*, are used in parallel with the conventional terms *external gear pairs*, *internal gear pairs*, and *rack-type gear pairs*. It is important to keep in mind that there is a difference between the newly introduced terms, and the conventional terms used in the present-day practice.

For example, in the case of  $C_a$  – gearing, there exists a corresponding *round rack* (or a *crown gear*, in other terminology). The round rack is the limit case for gearing that either (a) alters the direction of rotation of the driving member (commonly referred to as *external* gearing), or (b) doesn't alter the direction of rotation of the driving member (commonly referred to as *internal* gearing). However, in the first case, the gear may be *internal* as well, similar to that the gear may be *external* in the second case.

Moreover, the terminology listed immediately below:

1.  $u$  – positive gearing (or just  $u^+$  – gearing) [in which the gear ratio,  $u$ , is of a positive value,  $u > 0$ ]
2.  $u$  – zero gearing (or just  $u^0$  – gearing) in rack-type spatial gear pair [*Comment:* in general, the gear ratio,  $u$ , in  $u$  – zero gearing is not mandatorily equal to zero]
3.  $u$  – negative gearing (or just  $u^-$  – gearing) [in which the gear ratio,  $u$ , is of a negative value,  $u < 0$ ]  
 may also be used in the theory of gearing. Here the gear ratio,  $u$ , equals to the ratio of an input rotation to an output rotation in the gear pair.

Summarizing the discussion, one may conclude that the actual kind of gear vector diagram (whether rotary-positive, or rotary-negative, or rotary-zero gear pair), depends on:

- a. magnitudes,  $\omega_g$  and  $\omega_p$ , of the rotations of a gear and its mating pinion, correspondingly
- b. actual value of the crossed-axes angle,  $\Sigma$ , between the rotation vectors  $\omega_g$  and  $\omega_p$
- c. actual value of the center-distance,  $C$

Scientific classification of gear vector diagrams of all kinds can be developed based on the actual values of the parameters ( $\omega_g$  and  $\omega_p$ ,  $\Sigma$ , and  $C$ ) in gear pairs.

It is the right point to stress here that no ultimate decision can be made on whether a gear pair is external or internal based only on vector diagram of the gear pair. Additional information is required in order to make a final decision in this regard.

### 2.2.2.1 Gear Vector Diagrams of Rotary-Negative Crossed-Axes Gear Pair

A gear vector diagram is constructed on the premise of certain combination of the rotation vectors,  $\omega_g$  and  $\omega_p$ , crossed-axes angle,  $\Sigma$ , and center-distance,  $C$  (Figure 2.7).

Having two rotation vectors,  $\omega_g$  and  $\omega_p$ , specified, the corresponding vector of instantaneous rotation,  $\omega_{pl}$ , of the pinion in relation to the gear ( $\omega_{pl} \equiv \omega_{pg} = -\omega_{gp}$ ) can be constructed. The instantaneous rotation,  $\omega_{pl}$ , is performed about a straight line,  $P_{ln}$ , which is the axis of instantaneous rotation.<sup>5</sup>

The vector of instantaneous rotation,  $\omega_{pl}$ , and all other kinematic parameters of a rotary-negative gear pair can be determined graphically by implementing, for this purpose, the methods developed in descriptive geometry. An example of such a construction is illustrated in Figure 2.8.

For the purposes of construction of a gear vector diagram, a reference system  $\pi_1\pi_2$  of two orthogonal planes of projection,  $\pi_1$  and  $\pi_2$ , is implemented (see Figure 2.8a). Following a convention adopted in descriptive geometry, the subscript “1” is assigned to projections of all points, lines, and so forth, onto the plane  $\pi_1$ . Similarly, the subscript “2” is assigned to projections of all of those same points, lines, and so forth, onto the plane  $\pi_2$ .

The actual location and orientation of a pair of rotation vectors,  $\omega_g$  and  $\omega_p$ , within the reference system  $\pi_1\pi_2$  can be arbitrary. However, for convenience, the rotation vectors,  $\omega_g$  and  $\omega_p$ , are

<sup>5</sup> It is a right point to explain here the reason for why the axis of instantaneous rotation of a pinion in relation to its mating gear is designated as  $P_{ln}$ . In the simplest cases of spur or helical gearing, it is a commonly adopted practice to consider an instantaneous motion of a pinion in relation to its mating gear as an instantaneous rotation about *pitch point*,  $P$ . The instantaneous rotation of the pinion occurs not about the *pitch point*,  $P$ , but, instead, it is occurred about a straight line through the pitch point,  $P$ . This straight line is parallel to the axes of rotation of the gear and the mating pinion. Therefore, it is natural to refer to the axis of instantaneous rotation as to the *pitch line*, and to designate such a straight line as  $P_{ln}$ , as it is convenient. However, under such a scenario, the term *pitch line*,  $P_{ln}$ , commonly is used in the gear kinematics, needs to be distinguished from a similar term *pitch line* that is used, for example, with respect to a rack-gear. Here and below through the rest of this book, the term *pitch line*,  $P_{ln}$  is understood in the sense of the *axis of instantaneous rotation* of a pinion in relation to its mating gear.

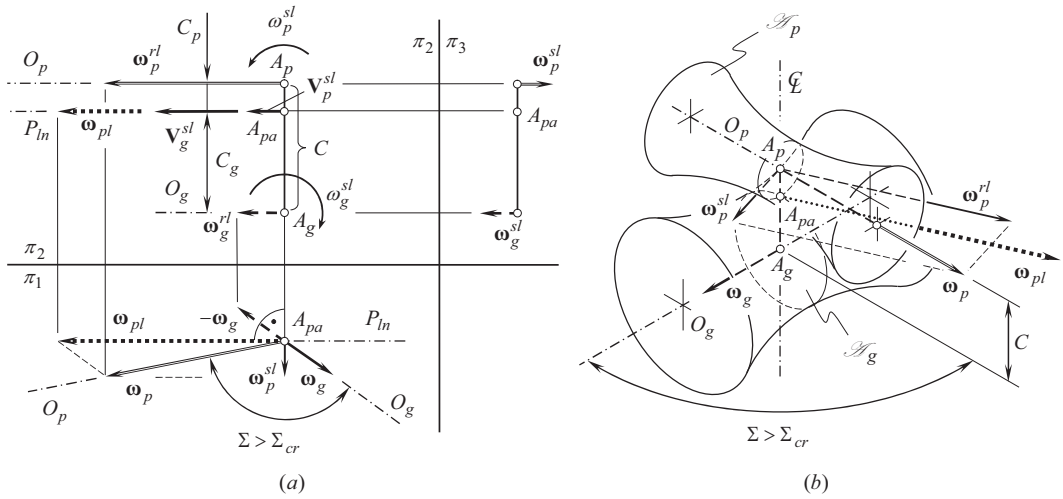


**FIGURE 2.8** Gear vector diagram of a rotary-negative (commonly external) crossed-axes gear pair (*rotary-negative  $C_a$  – gearing*) (a); and obsolete representation (by means of axodes) of the kinematics of a gear pair of that same kind (b).

depicted in the reference system  $\pi_1\pi_2$  parallel to the horizontal plane of projection  $\pi_1$ . In this scenario, the crossed-axes angle,  $\Sigma$ , is projected onto plane  $\pi_1$  with no distortion. The centerline,  $\mathcal{C}$ , is projected onto plane  $\pi_1$  into point. This point is denoted by  $A_{pa}$ .

The principle of inversion of rotations is again used here. Let us assume that a rotation,  $-\omega_g$ , is applied to a gear pair, that is, to the pinion, to the gear, and to the housing. The rotation  $-\omega_g$  does not affect the relative motion of the gear and the pinion.

Under the additional rotation,  $-\omega_g$ , the gear becomes stationary [ $\omega_g + (-\omega_g) = 0$ ]. The rotation of the gear pair housing (denoted by the rotation vector,  $-\omega_g$ ) is opposite to the rotation vector of the gear (denoted by  $-\omega_g$ ). Ultimately, the rotation of the pinion is the superposition of two rotations, namely, of the rotations  $\omega_p$  and  $-\omega_g$ . The resultant of two rotations,  $\omega_p$  and  $-\omega_g$ , is the instantaneous rotation  $\omega_{pl} = (\omega_p - \omega_g)$  of the pinion about the axis of instantaneous rotation,  $P_{ln}$ .

Within the horizontal plane of projection,  $\pi_1$ , the vector of instantaneous rotation,  $\omega_{pl}$ , can be determined as the vector difference of the rotation vectors,  $\omega_g$  and  $\omega_p$ . As the rotation vectors  $\omega_g$  and  $\omega_p$  are parallel to the plane  $\pi_1$ , the vector  $\omega_{pl}$  is projected onto the plane of projection  $\pi_1$  with no distortion. The rotation vector  $\omega_{pl}$  is applied at point  $A_{pa}$  within the centerline  $\mathcal{C}$ .

Immediately upon the rotation vector  $\omega_{pl}$  is determined, the axis of projections  $\pi_1/\pi_2$  can be constructed so as to be parallel to the vector of instantaneous rotation,  $\omega_{pl}$ . Such a configuration of the axis  $\pi_1/\pi_2$  is not a must; the configuration of the axis  $\pi_1/\pi_2$  can be arbitrary. Convenience is the only reason for selecting this particular orientation of the axis of projections  $\pi_1/\pi_2$  in relation to the rotation vector,  $\omega_{pl}$ .

#### 2.2.2.1.1 Condition of Pure Rolling in Rotary-Negative Crossed-Axes Gear Pair: General Consideration

The gear vector diagram is helpful to investigate the conditions of pure rolling (and sliding) in various kinds of gearing (Figure 2.8a).

The projections of the rotation vectors,  $\omega_g$  and  $\omega_p$ , onto the frontal plane of projections  $\pi_2$  are designated as  $\omega_g^{rl}$  and  $\omega_p^{rl}$ , correspondingly. The components,  $\omega_g^{rl}$  and  $\omega_p^{rl}$ , of the rotation vectors,  $\omega_g$  and  $\omega_p$ , are parallel to the axis of instantaneous rotation,  $P_{ln}$ . These components cause transmission of a rotation from the input shaft to the output shaft. The following equality can be directly derived from the analysis of Figure 2.8a, [179,180]:

$$C_p \cdot \omega_p \cdot \cos \Sigma_p = C_g \cdot \omega_g \cdot \cos \Sigma_g \quad (2.10)$$

This equation is valid for the magnitudes  $\omega_p$ ,  $\omega_g$ , and  $\omega_{pl}$  of the rotation vectors  $\omega_g$ ,  $\omega_p$ , and  $\omega_{pl}$ . Here and below the gear cone-angle and the pinion cone-angle are designated as  $\Sigma_g$  and  $\Sigma_p$ , correspondingly. The ratios  $C_g/C_p$ ,  $\omega_p/\omega_g$ , along with a few more formulas, can be directly extracted from Eq. (2.10).

Similarly, two more equalities can be directly derived from the analysis of Figure 2.8a, [179,180]:

$$C_p \cdot \omega_{pl} = (C_g + C_p) \cdot \omega_g \cdot \cos \Sigma_g \quad (2.11)$$

$$C_g \cdot \omega_{pl} = (C_g + C_p) \cdot \omega_p \cdot \cos \Sigma_p \quad (2.12)$$

In Eqs. (2.10)–(2.12), the distance between the apex,  $A_{pa}$ , and the gear axis of rotation,  $O_g$ , is the gear center-distance,  $C_g$ , (therefore,  $C_g = A_g A_{pa}$ ). The distance of the same point  $A_{pa}$  from the pinion axis of rotation,  $O_p$ , is the pinion center-distance,  $C_p$ , (therefore,  $C_p = A_p A_{pa}$ ). The center-distances  $C_g$  and  $C_p$  are signed values. For a negative gear pair, both of them are of positive values (i.e.,  $C_g > 0$  and  $C_p > 0$ ).

Evidently, the equality:

$$C_g + C_p = C \quad (2.13)$$

is valid in a rotary-negative external spatial gear pair of any design.

The angles,  $\Sigma_g$  and  $\Sigma_p$ , are the gear and the pinion cone-angles, correspondingly.

By definition, the cone-angles,  $\Sigma_g$  and  $\Sigma_p$ , are specified by the following expressions:

$$\Sigma_g = \angle(\omega_g, \omega_{pl}) \quad (2.14)$$

$$\Sigma_p = \angle(\omega_p, \omega_{pl}) \quad (2.15)$$

Equations (2.14) and (2.15) immediately yield the formulas:

$$\Sigma_g = \tan^{-1} \frac{|\omega_g \times \omega_{pl}|}{\omega_g \cdot \omega_{pl}} \quad (2.16)$$

$$\Sigma_p = \tan^{-1} \frac{|\omega_p \times \omega_{pl}|}{\omega_p \cdot \omega_{pl}} \quad (2.17)$$

for the calculation of the actual values of the gear cone-angle,  $\Sigma_g$ , and the pinion cone-angle,  $\Sigma_p$ .

Once the rotation vectors,  $\omega_g$  and  $\omega_p$ , and the crossed-axes angle,  $\Sigma$ , are specified, then it can be easily shown that the gear cone-angle,  $\Sigma_g$ , is calculated from the formula:

$$\sin \Sigma_g = \frac{\omega_p}{\omega_{pl}} \sin \Sigma \quad (2.18)$$

and the pinion cone-angle,  $\Sigma_p$ , can be calculated from the formula:

$$\sin \Sigma_p = \frac{\omega_g}{\omega_{pl}} \sin \Sigma \quad (2.19)$$

where the magnitude,  $\omega_{pl}$ , of the relative rotation vector,  $\omega_{pl}$ , equals to:

$$\omega_{pl} = \sqrt{\omega_g^2 + \omega_p^2 - 2\omega_g\omega_p \cos \Sigma} \quad (2.20)$$

The condition of pure rolling can be employed for the determination of location of the plane of action apex,  $A_{pa}$ , within the centerline,  $\mathfrak{L}$ . In compliance with this condition, the following ratio:

$$\frac{C_g}{C_p} = \frac{\omega_p^{rl}}{\omega_g^{rl}} \quad (2.21)$$

has to be fulfilled. Perfect correlation between Eqs. (2.21) and (2.10) is evident.

In Eq. (2.20), the following designations  $\omega_g^{rl} = |\omega_g^{rl}|$  and  $\omega_p^{rl} = |\omega_p^{rl}|$  are used (the components  $\omega_g^{rl}$  and  $\omega_p^{rl}$  of the rotation vectors  $\omega_g$  and  $\omega_p$  cause pure rolling in a gear pair).

In general, the magnitudes,  $\omega_g^{rl}$  and  $\omega_p^{rl}$ , of the vectors of pure rolling,  $\omega_g^{rl}$  and  $\omega_p^{rl}$ , are not equal to each other. The inequality  $\omega_g^{rl} < \omega_p^{rl}$  is commonly observed. The equality  $\omega_g^{rl} = \omega_p^{rl}$  is observed only in particular cases when the tooth number of a gear,  $N_g$ , and the tooth number of its mating pinion,  $N_p$ , are equal to one another (namely, when the equality  $N_g = N_p$  is valid).

From Eq. (2.13), the gear center-distance,  $C_g$ , can be expressed in terms of the center-distance,  $C$ , and the pinion center-distance  $C_p$ :

$$C_g = C - C_p \quad (2.22)$$

Substituting this expression for the gear center-distance,  $C_g$ , into Eq. (2.21), a formula:

$$C_p = \frac{\omega_g^{rl}}{\omega_p^{rl} + \omega_g^{rl}} \cdot C \quad (2.23)$$

for calculating the gear center-distance,  $C_p$ , can be derived.

Further, Eq. (2.22) can be used for the calculation of the gear center-distance,  $C_g$ . After substituting Eq. (2.23) in Eq. (2.22), the equality  $C_g = C - C_p$  can be transformed as follows:

$$C_g = \frac{\omega_p^{rl}}{\omega_p^{rl} + \omega_g^{rl}} \cdot C \quad (2.24)$$

For rotary-negative (commonly external) crossed-axes gear pairs, the plane of action apex,  $A_{pa}$ , is located within the centerline between the gear apex,  $A_g$ , and the pinion apex,  $A_p$ .

#### 2.2.2.1.2 Conditions of Pure Sliding in Rotary-Negative Crossed-Axes Gear Pair: General Consideration

A gear vector diagram is helpful to investigate the conditions of pure sliding in various kinds of gearing (Figure 2.8).

In Figure 2.8a, the components,  $\omega_g^{sl}$  and  $\omega_p^{sl}$ , of the rotation vectors  $\omega_g$  and  $\omega_p$  are perpendicular to the axis of instantaneous rotation,  $P_{ln}$ . With no distortion, these components are projected onto the frontal plane of projections,  $\pi_3$ . The plane of projections,  $\pi_3$ , is perpendicular to the axis of projections,  $\pi_1/\pi_2$ .

The rotations,  $\omega_g^{sl}$  and  $\omega_p^{sl}$ , cause pure sliding in the direction of the axis of instantaneous rotation,  $P_{ln}$ . The magnitudes  $\omega_g^{sl} = |\omega_g^{sl}|$  and  $\omega_p^{sl} = |\omega_p^{sl}|$  of the angular velocities of sliding are equal to one another ( $\omega_g^{sl} = \omega_p^{sl}$ ). The rotation vectors of sliding,  $\omega_g^{sl}$  and  $\omega_p^{sl}$ , are pointed in the opposite directions (i.e.,  $\omega_p^{sl} = -\omega_g^{sl}$ ).

Relative sliding in the direction of the axis of instantaneous rotation,  $P_{ln}$ , is created by both gear and mating pinion.

The vector of linear velocity of sliding,  $\mathbf{V}_g^{sl}$  (the component, that is created by the gear), equals to:

$$\mathbf{V}_g^{sl} = C_g \cdot \omega_g^{sl} \quad (2.25)$$

Similarly, the vector of linear velocity of sliding,  $\mathbf{V}_p^{sl}$  (the component, that is created by the pinion) is equal to:

$$\mathbf{V}_p^{sl} = C_p \cdot \boldsymbol{\omega}_p^{sl} \quad (2.26)$$

The expressions  $|\boldsymbol{\omega}_g^{sl}| = |\boldsymbol{\omega}_p^{sl}|$  and  $C_g \geq C_p$  are valid for rotary-negative (usually external) crossed-axes gear pairs; then, the component of sliding velocity,  $\mathbf{V}_g^{sl}$  (the component, that is caused by the gear), exceeds or equal to the component of sliding velocity,  $\mathbf{V}_p^{sl}$  (the component, that is caused by the pinion), namely, the inequality  $|\mathbf{V}_g^{sl}| \geq |\mathbf{V}_p^{sl}|$  is always observed.

The directions of the sliding velocities vectors,  $\mathbf{V}_g^{sl}$  and  $\mathbf{V}_p^{sl}$ , in rotary-negative gear pair are always opposite to one another. The resultant sliding velocity vector,  $\mathbf{V}_{g-p}^{sl}$ , of the gear in relation to the pinion is equal to the difference:

$$\mathbf{V}_{g-p}^{sl} = \mathbf{V}_g^{sl} - \mathbf{V}_p^{sl} \quad (2.27)$$

The resultant sliding velocity vector,  $\mathbf{V}_{p-g}^{sl}$ , of the pinion in relation to the gear is opposite to the sliding velocity vector  $\mathbf{V}_{g-p}^{sl}$ :

$$\mathbf{V}_{p-g}^{sl} = -\mathbf{V}_{g-p}^{sl} = \mathbf{V}_p^{sl} - \mathbf{V}_g^{sl} \quad (2.28)$$

The magnitude of speed of the resultant sliding in a rotary-negative crossed-axes gear pair can be calculated from the following formula:

$$V_{sc} = V_g^{sl} + V_p^{sl} \quad (2.29)$$

If the component vectors,  $\boldsymbol{\omega}_g^{sl}$  and  $\boldsymbol{\omega}_p^{sl}$ , are of the same magnitude, and are opposite to one another, then they comprise a *pair of rotation*. An equivalent velocity vector of the translation motion,  $\mathbf{V}_{sc}$ , can be constructed for a given pair of rotation. The velocity vector,  $\mathbf{V}_{sc}$ , is parallel to the vector of instantaneous rotation,  $\boldsymbol{\omega}_{pl}$ . The following formula:

$$V_{sc} = |\mathbf{V}_{sc}| = C \cdot \omega_p \cdot \sin \Sigma_p = C \cdot \omega_g \cdot \sin \Sigma_g \quad (2.30)$$

can be used for the calculation of the magnitude of the velocity vector  $\mathbf{V}_{sc}$ .

Ultimately, the resultant instantaneous relative motion of a gear and of a mating pinion is composed of:

- the instantaneous rotation,  $\boldsymbol{\omega}_{pl}$ , about the axis of instantaneous rotation,  $P_{ln}$ , and
- the instantaneous translation,  $\mathbf{V}_{sc}$ , along the axis of instantaneous rotation,  $P_{ln}$ .

Superposition of the rotation,  $\boldsymbol{\omega}_{pl}$ , and the translation,  $\mathbf{V}_{sc}$ , results in a screw motion. The parameter of the screw motion is designated as  $p_{sc}$ . The screw parameter,  $p_{sc}$ , is commonly referred to as *reduced pitch*.

For the calculation of the reduced pitch,  $p_{sc}$ , the following formula is applied [179], [180]:

$$p_{sc} = \frac{V_{sc}}{\omega_{pl}} = \frac{C \cdot \omega_p \cdot \sin \Sigma_p}{\omega_{pl}} = \frac{C \cdot \omega_g \cdot \sin \Sigma_g}{\omega_{pl}} \quad (2.31)$$

An expression:

$$\omega_{pl} = \frac{C \cdot \omega_p \cdot \cos \Sigma_p}{C_g} = \frac{C \cdot \omega_g \cdot \cos \Sigma_g}{C_p} \quad (2.32)$$



for the calculation of the magnitude of the instantaneous rotation can be derived from Eqs. (2.10) to (2.12).

Therefore, the parameter of a screw motion can be calculated from the following formula:

$$p_{sc} = C_p \cdot \tan \Sigma_g = C_g \cdot \tan \Sigma_p \quad (2.33)$$

This immediately returns the following proportion:<sup>6</sup>

$$\frac{C_p}{C_g} = \frac{\tan \Sigma_g}{\tan \Sigma_p} \quad (2.34)$$

The resultant instantaneous motion of the gear and the pinion can be construed as rolling with sliding of two *hyperboloids-of-one-sheet* over each other as illustrated in Figure 2.8b. (obsolete approach is known in the literature on gearing, see Figure 2.8b). One of the hyperboloids,  $\mathcal{A}_g$ , is associated with the gear, while the other one,  $\mathcal{A}_p$ , is associated with the pinion. In a particular case, the gear hyperboloid,  $\mathcal{A}_g$ , can be considered stationary. In such a scenario, the instantaneous rotation is performed by the pinion hyperboloid,  $\mathcal{A}_p$ .

The association with the gear hyperboloid  $\mathcal{A}_g$  is generated by the axis of instantaneous rotation,  $P_{in}$ , when this axis is rotated about the gear axis  $O_g$ . Similarly, the association with the pinion hyperboloid  $\mathcal{A}_p$  is generated by the axis of instantaneous rotation,  $P_{in}$ , when this axis is rotated about the pinion axis,  $O_p$ . The instantaneous rotation occurs about the axis of instantaneous rotation,  $P_{in}$ . The instantaneous translation is observed along the axis of instantaneous rotation,  $P_{in}$ .

As schematically shown in Figure 2.8b, two axodes,  $\mathcal{A}_g$  and  $\mathcal{A}_p$ , contact each other along the axis of instantaneous rotation,  $P_{in}$ . The vectors, those used for the description of the kinematics of rotary-negative spatial gear pair, are also depicted in Figure 2.8b. It should be stressed here that the axodes,  $\mathcal{A}_g$  and  $\mathcal{A}_p$ , are shown just for illustrative purposes. The use of axodes for the investigation of kinematics of gearing is known in the literature on gearing, and is out of date, and obsolete technic. The use of axodes for the analysis of kinematics of gear pairs has been proven to be inconvenient because axodes cannot be drawn easily and are less informative compared to gear vector diagrams. More reasons against the application of axodes in analysis of rotary-negative gear pairs can be mentioned. Because of this, axodes of a gear and a mating pinion have very limited use in this book. In all possible cases, gear vector diagrams are used instead of the corresponding axodes, as gear vector diagrams are more informative, and can be easily drawn.

### 2.2.2.2 Gear Vector Diagrams of Rotary-Positive Crossed-Axes Gear Pair

The gear vector diagram for a rotary-positive intersected-axes gear pair (commonly, an internal gear pair) is constructed similar to that a corresponding gear vector diagram for rotary-negative intersected-axes gear pair (see Figure 2.8) was constructed. The similarity allows one to focus attention primarily on the peculiarities of the gear vector diagrams for rotary-positive intersected-axes gear pairs [179,180].

Consider a rotary-positive intersected-axes gear pair with a specified set of the design parameters ( $\omega_g$ ,  $\omega_p$ ,  $\Sigma$ , and  $C$ ). An example of gear vector diagram for a rotary-positive intersected-axes gear pair is shown in Figure 2.9.

The gear vector diagram (see Figure 2.9a) is referred to a system of two orthogonal planes of projections,  $\pi_1$  and  $\pi_2$ . The vector of instantaneous rotation,  $\omega_{pl}$ , is constructed as the difference of the rotation vectors  $\omega_g$  and  $\omega_p$ . In the case under consideration, the equality  $\omega_{pl} = \omega_p - \omega_g$  is valid.

The vector of instantaneous rotation,  $\omega_{pl}$ , is constructed parallel to the plane of projections  $\pi_1$ . Therefore, the rotation vector,  $\omega_{pl}$ , is projected onto the reference plane  $\pi_1$  with no distortions.

<sup>6</sup> Reminder: The center-distances,  $C_g$  and  $C_p$ , are measured along the center-line,  $\mathfrak{t}$ , and not in two different planes perpendicular to the axes of rotation,  $O_g$  and  $O_p$ , of a gear and of a mating pinion.

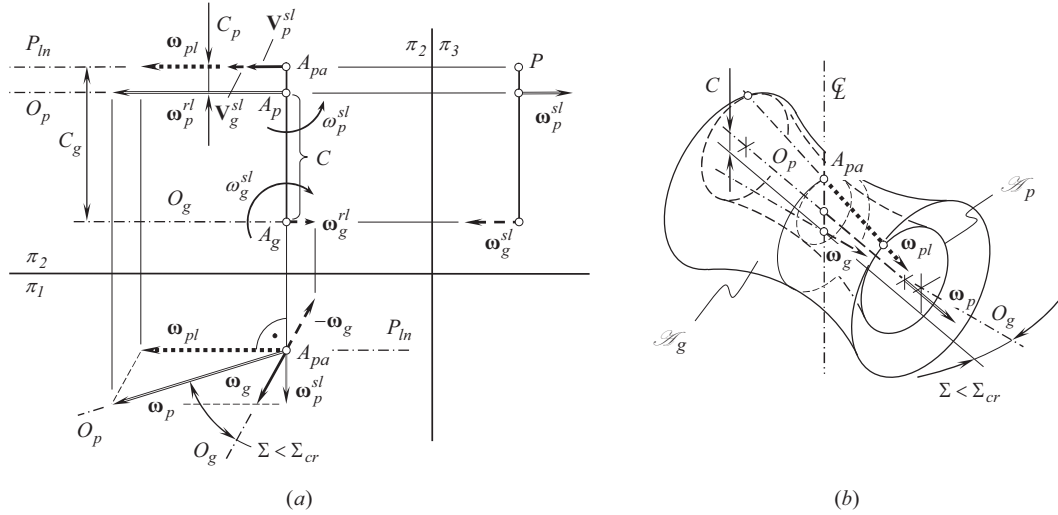


**FIGURE 2.9** Gear vector diagram of a rotary-positive (commonly internal) crossed-axes gear pair (*rotary-positive  $C_a$  – gearing*) (a); and obsolete representation (by means of axodes) of the kinematics of a gear pair of that same kind (b).

Similar to that above (see Figure 2.8), those components of the rotation vectors,  $\omega_g$  and  $\omega_p$ , that cause pure rolling of the axodes are designated as  $\omega_g^{rl}$  and  $\omega_p^{rl}$  correspondingly.

#### 2.2.2.2.1 Condition of Pure Rolling in Rotary-Positive Crossed-Axes Gear Pair: General Consideration

For a rotary-positive crossed-axes gear pair, the plane-of-action apex,  $A_{pa}$ , is located outside the center-distance,  $C$ . Instead, the pinion axis of rotation,  $O_p$ , intersects the centerline,  $\mathcal{C}$ , at point that is located between the plane-of-action apex,  $A_{pa}$ , and the point of intersection of the centerline,  $\mathcal{C}$ , by the gear axis of rotation,  $O_g$ . Hence, the following equality:

$$-C_p + C_g = C \quad (2.35)$$

is valid for a rotary-positive (commonly an internal) crossed-axes gear pair.

Equation (2.35) allows an expression  $C_g = C + C_p$ . Making use of this equality, and taking into account the conditions of pure rolling of the axodes, the following formulas:

$$C_g = \frac{\omega_p^{rl}}{\omega_p^{rl} - \omega_g^{rl}} \cdot C \quad (2.36)$$

$$C_p = \frac{\omega_g^{rl}}{\omega_p^{rl} - \omega_g^{rl}} \cdot C \quad (2.37)$$

for the calculation of the center-distances  $C_g$  and  $C_p$  were derived.

#### 2.2.2.2.2 Condition of Pure Sliding in Rotary-Positive Crossed-Axes Gear Pair: General Consideration

Two other components,  $\omega_g^{sl}$  and  $\omega_p^{sl}$ , of the rotation vectors,  $\omega_g$  and  $\omega_p$ , cause pure sliding along the axis of instantaneous rotation,  $P_{ln}$ . With no distortion, these components are projected onto the frontal plane of projections,  $\pi_3$ . As it is already shown with respect to a rotary-negative crossed-axes

gear pair, that the sliding components,  $\omega_g^{sl}$  and  $\omega_p^{sl}$ , of the rotation vectors,  $\omega_g$  and  $\omega_p$ , are of equal magnitude and are opposite to each other (i.e.,  $\omega_g^{sl} = -\omega_p^{sl}$ ).

Created by the rotated gear, the component of the linear velocity vector of sliding is equal:

$$\mathbf{V}_g^{sl} = r_g \cdot \omega_g^{sl} \quad (2.38)$$

Similarly, created by the rotated pinion, the component of the linear velocity vector of sliding is equal:

$$\mathbf{V}_p^{sl} = r_p \cdot \omega_p^{sl} \quad (2.39)$$

The following expressions:  $|\omega_g^{sl}| = |\omega_p^{sl}|$  and  $r_g \geq r_p$  are valid for a rotary-positive crossed-axes gear pair. Thus, the magnitude of the component  $\mathbf{V}_g^{sl}$  of sliding velocity vector, caused by the rotated gear, exceeds or equal to the magnitude of the component,  $\mathbf{V}_p^{sl}$ , of sliding velocity vector caused by the rotated pinion; that is, the inequality  $|\mathbf{V}_g^{sl}| \geq |\mathbf{V}_p^{sl}|$  is always observed.

The sliding velocity vectors,  $\mathbf{V}_g^{sl}$  and  $\mathbf{V}_p^{sl}$ , are always of the same directions. The resultant sliding velocity vector,  $\mathbf{V}_{g-p}^{sl}$ , of the gear in relation to the pinion is equal to the difference:

$$\mathbf{V}_{p-g}^{sl} = -\mathbf{V}_{g-p}^{sl} = \mathbf{V}_g^{sl} - \mathbf{V}_p^{sl} \quad (2.40)$$

The resultant sliding velocity vector,  $\mathbf{V}_{g-p}^{sl}$ , of the pinion in relation to the gear is opposite to the sliding velocity vector  $\mathbf{V}_{p-g}^{sl}$ :

$$\mathbf{V}_{g-p}^{sl} = -\mathbf{V}_{p-g}^{sl} = \mathbf{V}_g^{sl} - \mathbf{V}_p^{sl} \quad (2.41)$$

The magnitude of the speed of the resultant sliding in a rotary-positive spatial gear pair (commonly, an internal gear pair) is calculated from the following formula:

$$V_{sc} = V_g^{sl} + V_p^{sl} \quad (2.42)$$

Similar to that in a rotary-negative crossed-axes gear pair, the components,  $\omega_g^{sl}$  and  $\omega_p^{sl}$ , of the rotation vectors,  $\omega_g$  and  $\omega_p$ , comprise a pair of rotation for a rotary-positive crossed-axes gear pair. The pair of rotation is equivalent to a straight motion. Similar to Eq. (2.30), this allows for a formula for the calculation of the magnitude  $V_{sc}$  of speed of the resultant sliding.

Two axodes,  $\mathbf{A}_g$  and  $\mathbf{A}_p$ , of a gear and its mating pinion, along with the corresponding rotation vectors,  $\omega_g$  and  $\omega_p$ , are schematically illustrated in Figure 2.9b (This obsolete approach is known in the literature on gearing). Again, the axodes,  $\mathbf{A}_g$  and  $\mathbf{A}_p$ , are significantly less informative in comparison with the corresponding vector diagrams. It is inconvenient to draw the axodes for illustrative purposes. More reasons against the application of axodes in the analysis of rotary-positive spatial gear pairs can be mentioned. Because of this, axodes of a gear and a mating pinion have very limited use in this book. In all possible cases, gear vector diagrams are used instead of the corresponding axodes, as gear vector diagrams are more informative, and can be easily drawn.

### 2.2.2.3 Gear Vector Diagram of Rotary-Zero Crossed-Axes Gear Pair

The performed analysis of *rotary-negative* and of *rotary-positive* crossed-axes gear pairs makes reasonable a question: What is in between the *rotary-positive* and the *rotary-negative* crossed-axes gear pairs? It is reasonable to assume that gear pairs with intermediate kinematics, namely, *rotary-zero* crossed-axes gear pairs may exist. This is similar in much to that the *gear-to-rack* pair is for a parallel-axes external and internal gear pairs. Crossed-axes gear pair of this nature is referred to as the *rotary-zero crossed-axes gear pair*.

A rotary-zero crossed-axes gear pair can be construed as a reduced case (as a degenerate case) either of a rotary-positive or a rotary-negative crossed-axes gear pair, when the gear cone-angle is equal to its critical value. In other words, there must exist a rotary-zero crossed-axes gear pair as the limit case either of a rotary-negative (see Figure 2.7) or a rotary-positive (see Figure 2.9) crossed-axes gear pair.

Without going into in-detail analysis of the gear vector diagram depicted in Figure 2.7, it can be said that for a rotary-negative crossed-axes gear pair, the gear cone-angle,  $\Sigma_g$ :

$$\Sigma_g = \angle(\omega_g, \omega_{pl}) > 90^\circ \quad (2.43)$$

is an obtuse angle (see Figure 2.8).

For a rotary-positive crossed-axes gear pair, the gear cone-angle,  $\Sigma_g$ :

$$\Sigma_g = \angle(\omega_g, \omega_{pl}) < 90^\circ \quad (2.44)$$

is an acute angle (see Figure 2.9).

It is reasonable to question the case when the gear cone-angle,  $\Sigma_g$ , is a right angle (i.e., the rotation vectors,  $\omega_g$  and  $\omega_{pl}$ , are perpendicular to each other:  $\omega_g \perp \omega_{pl}$ )?

The gear vector diagram of a crossed-axes gear pair that fulfills the equality:

$$\Sigma_g = \angle(\omega_g, \omega_{pl}) = 90^\circ \quad (2.45)$$

is valid, is shown in Figure 2.10a.

In the case under consideration, axode of the gear,  $A_g$ , (a hyperboloid-of-one-sheet), is reduced to a plane that is rotated about an axis perpendicular to the plane. Axode of the pinion,  $A_p$ , (also a hyperboloid-of-one-sheet) is reduced to a cone of revolution. Kinematics of a gear pair, that features the gear vector diagram, shown in Figure 2.10a, can be interpreted as the case of rolling of the cone of revolution over the rotating plane. The latter is illustrated in Figure 2.10b. A spatial gear pair that features kinematics of this kind is referred to as the *rotary-zero crossed-axes gear pair*.

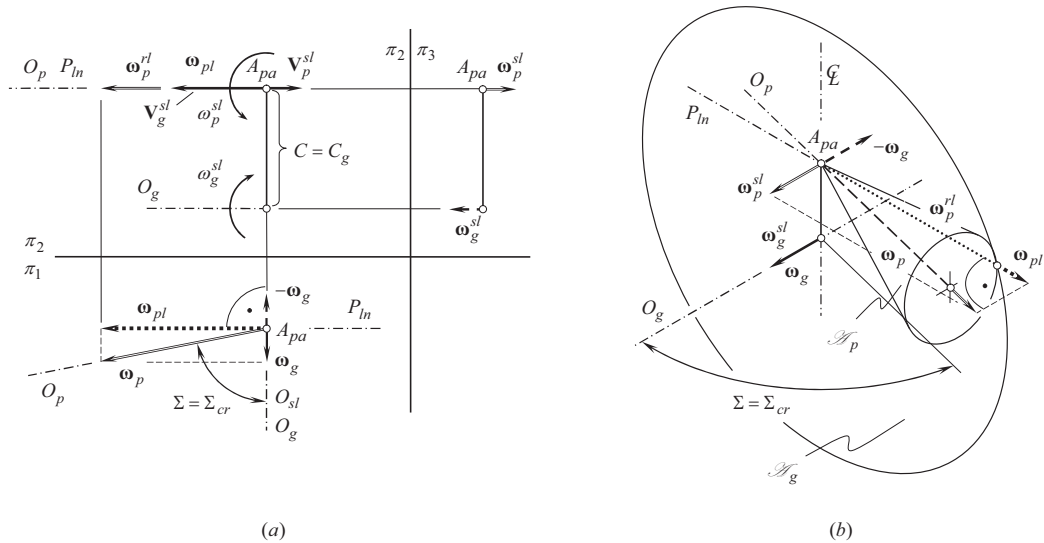


**FIGURE 2.10** Gear vector diagram of a rotary-zero (rack-type) crossed-axes gear pair (*rotary-zero  $C_a$  – gearing*) (a); and an obsolete representation (by means of the axodes) of the kinematics of gear pair of this type (b).

A critical value,  $\Sigma_{cr}$ , of the crossed-axes angle,  $\Sigma$ , corresponds to a rotary-zero crossed-axes gear pair. In other words, if the condition in Eq. (2.45) is fulfilled then the equality  $\Sigma = \Sigma_{cr}$  is observed, and vice versa.

Within the pitch-line-plane (this plane is a plane through the centerline,  $\mathfrak{t}$ , and the axis of instantaneous rotation,  $P_{ln}$ ) the linear velocity vector of sliding,  $\mathbf{V}_g^{sl}$ , in the direction of the axis of instantaneous rotation,  $P_{ln}$ , is created by the component  $\omega_g^{sl}$  of the rotation vector,  $\omega_g$ , of the gear. This rotation vector,  $\omega_g^{sl}$ , is contributed by the rotating gear. Although the component  $\omega_p^{sl}$  of the rotation vector,  $\omega_p$ , is not equal to zero (i.e.,  $\omega_p^{sl} \neq 0$ ), the linear velocity,  $\mathbf{V}_p^{sl}$ , is equal to zero ( $\mathbf{V}_p^{sl} = 0$ ). The latter equality is due to the equality  $C_g = C$  is valid for rotary-zero crossed-axes gear pair. As the equality  $C_g = C$  is observed, then the equality  $C_p = 0$  is valid, as well. Ultimately, in the case under consideration, the resultant linear velocity,  $V_{sc}$ , of sliding in the direction of the axis of instantaneous rotation,  $P_{ln}$ , equals:

$$V_{sc} = V_g^{sl} \quad (2.46)$$

It must be stressed here that not every case of rolling of a cone of revolution over the rotating plane corresponds to a rotary-zero crossed-axes gear pair. In order to be referred to as a rotary-zero crossed-axes gear pair, it is critical to fulfill the condition specified by Eq. (2.45).

The gear vector diagrams of rotary-zero crossed-axes gear pairs are of particular interest in the designing of gear cutting tools for machining gears for crossed-axes gear pairs [151,152].

#### 2.2.2.4 Analytical Criterion of the Kind of Crossed-Axes Gear Pair

Different kinds of crossed-axes gear pairs are known. The angle that is formed by the rotation vector of a gear,  $\omega_g$ , with the vector,  $\omega_{pl}$ , of instantaneous rotation of the mating pinion in relation to the gear, is the root cause for the principal difference between crossed-axes gear pairs of different kinds, namely, between rotary-negative, rotary-positive, and rotary-zero crossed-axes gear pairs. These differences are analytically described by Eqs. (2.44) and (2.45). As shown in Section 2.2.1, the equality:

$$\omega_{pl} = \omega_p - \omega_g \quad (2.47)$$

is observed for a crossed-axes gear pair.

Equations (2.44), (2.45), and (2.47), make possible the representation of the analytical criteria of the kind of a crossed-axes gear pair as shown in Table 2.1.

Analytical expressions that specify the criteria for the crossed-axes gear pair are composed on the premise of well-known properties of dot product of two vectors.

### 2.3 CLASSIFICATION OF POSSIBLE KINDS OF GEAR VECTOR DIAGRAMS

Possible kinds of gear pairs can be classified based on the vector representation of gear pair kinematics discussed in Section 2.2. Such a classification is important and is beneficial for many reasons. The development of all possible kinds of gears, and then of all possible kinds of gear pairs, is one of the reasons for the development of this classification.

**TABLE 2.1**

**Analytical Criteria of the Kind of Crossed-Axes Gear Pairs**

Type of Crossed-Axes Gear Pairs	Analytical Criterion
Rotary-Negative Gearing: ( <i>External</i> and <i>Internal</i> ) Crossed-Axes Gear Pairs	$\omega_g \cdot (\omega_p - \omega_g) < 0$
Rotary-Zero Gearing: Generalized Rack-Type Crossed-Axes Gear Pairs	$\omega_g \cdot (\omega_p - \omega_g) = 0$
Rotary-Positive Gearing: ( <i>Internal</i> and <i>External</i> ) Crossed-Axes Gear Pairs	$\omega_g \cdot (\omega_p - \omega_g) > 0$

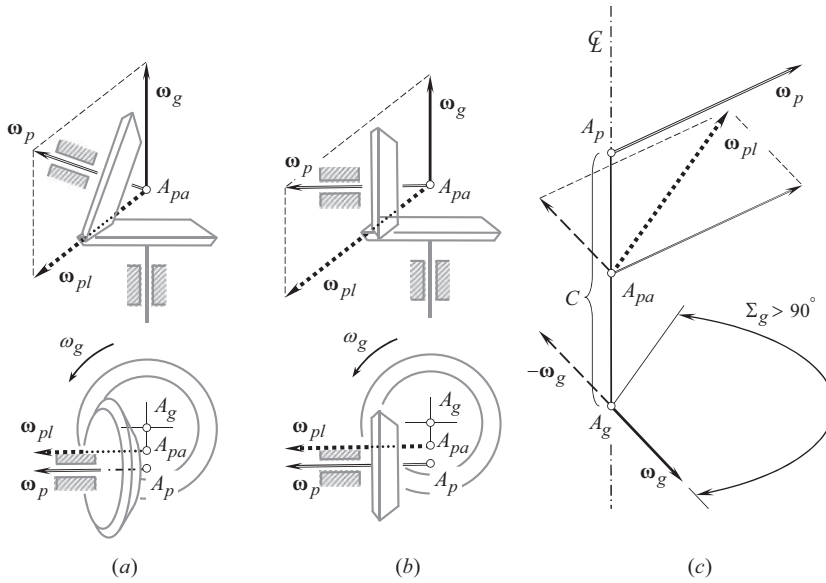


**FIGURE 2.11** Examples of rotary-negative crossed-axes gear pairs (commonly, external gear pairs) in case of (a) an obtuse,  $\Sigma > 90^\circ$ , and (b) a right,  $\Sigma = 90^\circ$ , crossed-axes angle,  $\Sigma$ , and (c) their gear vector diagram.

Crossed-axes gear pairs are considered in this book as the most general kind of gearing. The remaining possible kinds of gear pairs can be construed as a reduction (simplification) of the corresponding kind of the crossed-axes gear pairs.

As stated in Section 2.2, there are only three different kinds of vector diagrams of gear pairs with crossing axes of rotation of a gear and a mating pinion:

- *Rotary-negative crossed-axes gear pairs*, in which the inequality  $\omega_g \cdot (\omega_p - \omega_g) < 0$  is valid
- *Rotary-positive crossed-axes gear pairs*, in which the inequality  $\omega_g \cdot (\omega_p - \omega_g) > 0$  is valid
- *Rotary-zero crossed-axes gear pairs*, in which the equality  $\omega_g \cdot (\omega_p - \omega_g) = 0$  is valid

No other kinds of gear vector diagram of crossed-axes gear pairs are possible.

Examples of rotary-negative external crossed-axes gear pairs and their vector representation are schematically illustrated in Figure 2.11. For all kinds of rotary-negative spatial gear pairs (commonly, external gear pairs), the inequality  $\omega_g \cdot (\omega_p - \omega_g) < 0$  is observed (see Table 2.1). The component  $\Sigma_g$  of the crossed-axes angle,  $\Sigma$ , exceeds a right angle (i.e.,  $\Sigma_g > 90^\circ$ ) as illustrated in Figure 2.11. A rotary-negative crossed-axes gear pair can feature crossed-axes angle,  $\Sigma$ , of various values. In particular, the crossed-axes angle,  $\Sigma$ , can be either acute (i.e.,  $0^\circ < \Sigma < 90^\circ$ ) as shown in Figure 2.11a) or it can be equal to a right angle,  $\Sigma = 90^\circ$  (see Figure 2.11b), or obtuse (i.e.,  $90^\circ < \Sigma < 180^\circ$ ). Gear vector diagrams for each of three kinds of rotary-negative crossed-axes gear pairs allow them to be construed as particular cases of the gear vector diagram shown in Figure 2.11c. In Figure 2.12, a helical gear pair with crossed-axes is shown. A helical gear pair is a perfect example of rotary-negative crossed-axes gear pairs.

An example of rotary-zero crossed-axes gear pair, and its vector representation is depicted in Figure 2.13. For this kind of gear pairs, the equality  $\omega_g \cdot (\omega_p - \omega_g) = 0$  is always observed (see Table 2.1). The component  $\Sigma_g$  of the crossed-axes angle,  $\Sigma$ , is a right angle (i.e.,  $\Sigma_g = 90^\circ$ ) as illustrated in Figure 2.13a. A rotary-zero crossed-axes gear pair can feature crossed-axes angles of various values. Vector diagram of this particular type of gear pairs is shown in Figure 2.13b.

A rotary-negative crossed-axes gear pair (commonly, an internal gear pair) and its gear vector diagram are shown in Figure 2.14. For all kinds of rotary-negative crossed-axes gear pairs,

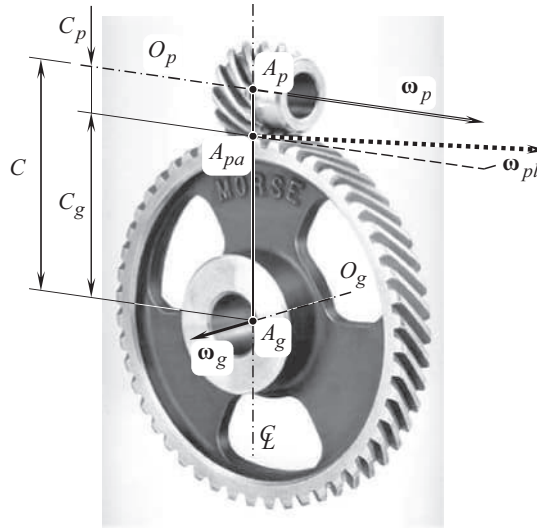


**FIGURE 2.12** The rotation vectors,  $\omega_g$ ,  $\omega_p$ , and  $\omega_{pl}$ , associated with a rotary-negative (usually, external) crossed-axes gear pair.

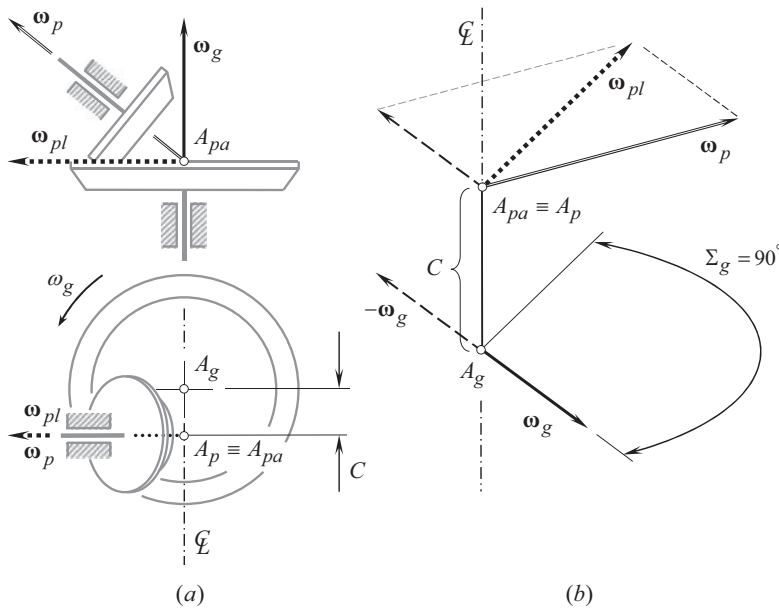


**FIGURE 2.13** An example of (a) rotary-zero crossed-axes gear pair (i.e., of a round-rack-type gear pair), and (b) its gear vector diagram.

the inequality  $\omega_g \cdot (\omega_p - \omega_g) > 0$  is valid (see Table 2.1). The component  $\Sigma_g$  of the crossed-axes angle,  $\Sigma$ , is less than  $90^\circ$  (i.e.,  $\Sigma_g < 90^\circ$ ) as illustrated in Figure 2.14a. A rotary-negative crossed-axes gear pair can feature crossed-axes angles of various values. Vector diagram for a rotary-negative crossed-axes gear pair is shown in Figure 2.14b.

The proposed classification of possible kinds of gear vector diagrams is based on an in-detail analysis of kinematics of gearing, including extremal values of the parameters  $\omega_g$ ,  $\omega_p$ , and  $\Sigma$ .



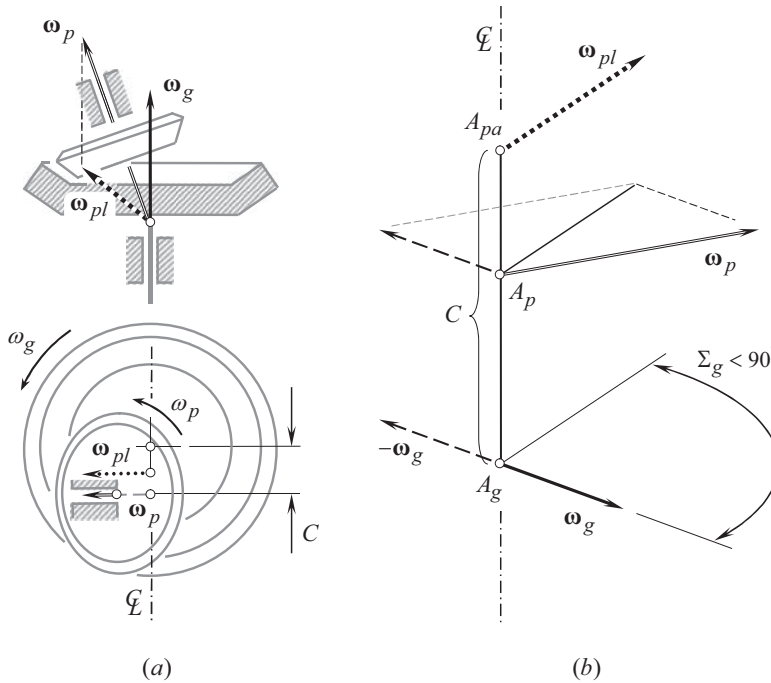


**FIGURE 2.14** An example of rotary-positive (usually, internal) crossed-axes gear pair (a), and its gear vector diagram (b).

Three different kinds of crossed-axes gear pairs comprise the first stratum of the classification of possible kinds of gear vector diagrams (see Figure 2.15):

- Rotary-negative crossed-axes gear pairs (see Figure 2.11),
- Rotary-zero crossed-axes gear pairs (see Figure 2.13), and
- Rotary-positive crossed-axes gear pairs (see Figure 2.14).

Labels 1.1, 1.2, and 1.3 are assigned to the spatial gear pairs that comprise the first stratum of the classification. The first number in each label indicates that a corresponding gear vector diagram belongs to the first stratum in the classification.

Crossed-axes gear pairs can be reduced to gear pairs of a simpler design. There are two possible ways for this kind of reduction:

**First**, the center-distance,  $C$ , can be set of a zero value, and

**Second**, the axes of rotation,  $O_g$  and  $O_p$ , of a gear and its mating pinion can be set parallel to one another.

In the second case, the crossed-axes angle,  $\Sigma$ , is equal either to  $\Sigma = 0^\circ$ , or to  $\Sigma = 180^\circ$ .

Let us begin the analysis from the first case when the center-distance,  $C$ , in a rotary-negative intersected-axes gear pair is reduced to zero.

When the equality  $C = 0$  is observed, the gear and the pinion axes of rotation,  $O_g$  and  $O_p$ , intersect one another at point,  $A_{pa}$ . The rotation vectors,  $\omega_g$  and  $\omega_p$ , are two vectors through the common point,  $A_{pa}$ . These vectors are pointed along the axes of rotation,  $O_g$  and  $O_p$ , correspondingly.

For gear pairs of this type, a sphere that is centered at the point  $A_{pa}$ , is convenient to be used for the investigation of engagement of the gear teeth. Because of this, intersected-axes gear pairs

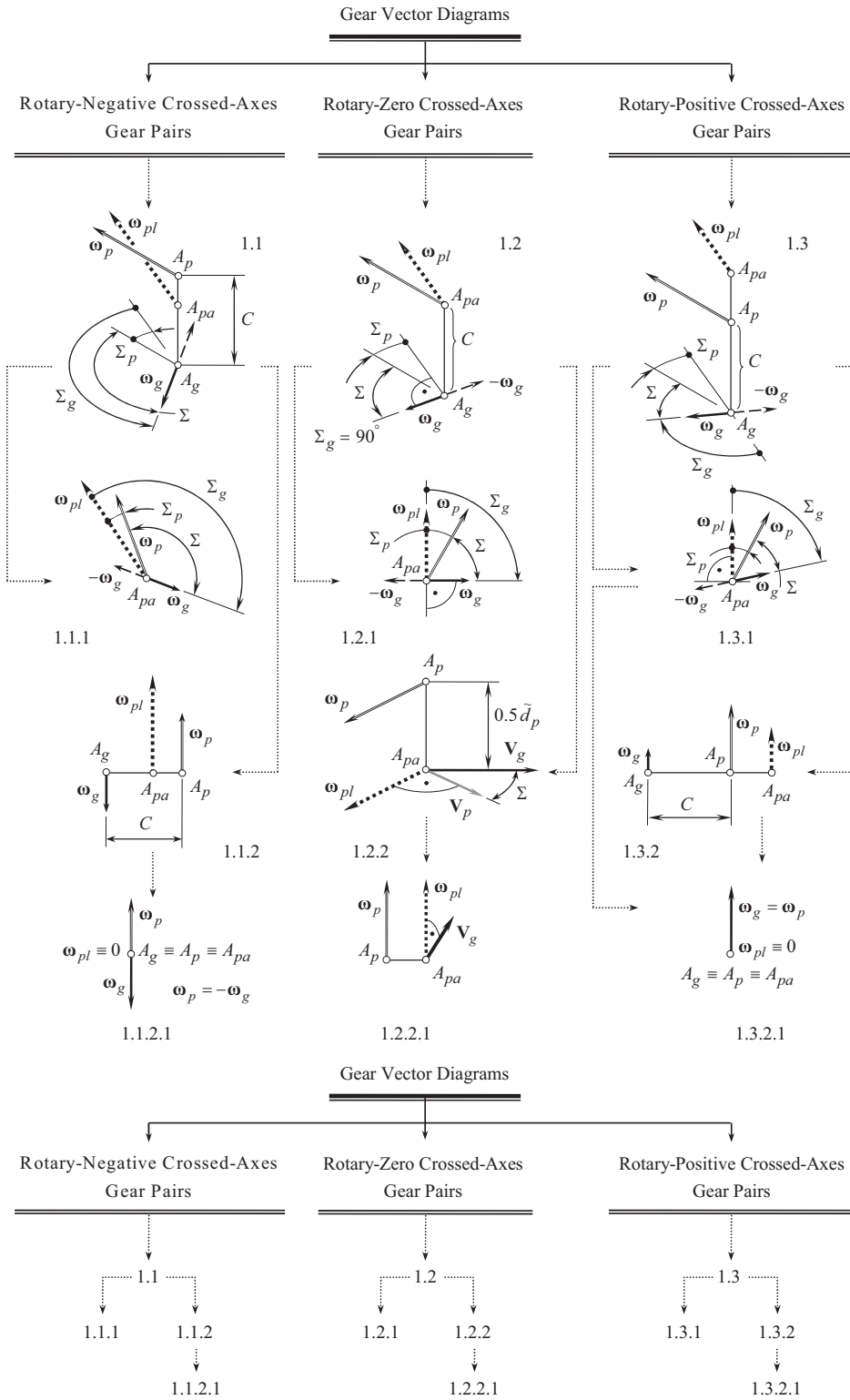
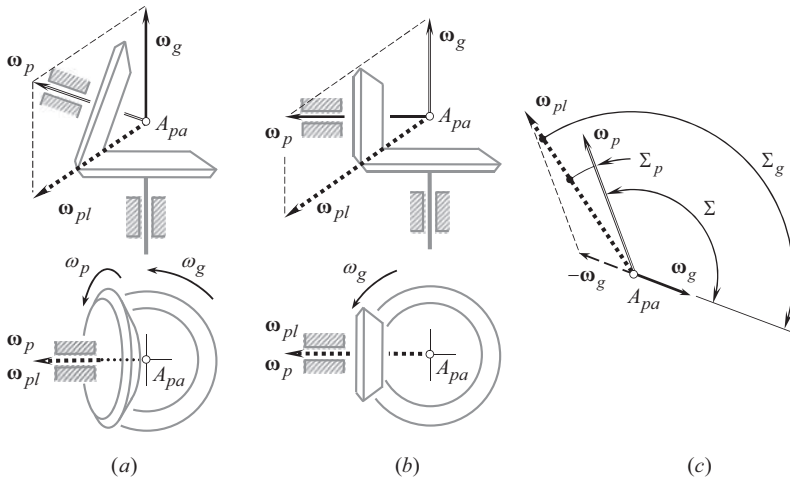
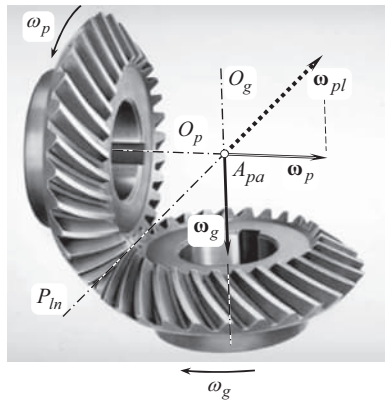


FIGURE 2.15 Classification of possible kinds of gear vector diagrams.



**FIGURE 2.16** Examples of rotary-negative intersected-axes gear pairs (commonly, external gear pairs) and their gear vector diagrams: (a) an obtuse,  $\Sigma > 90^\circ$ , and (b) a right,  $\Sigma = 90^\circ$ , crossed-axes angle,  $\Sigma$ ; and (c) is the gear vector diagram of gear pairs of this kind.



**FIGURE 2.17** The rotation vectors,  $\omega_g$ ,  $\omega_p$ , and  $\omega_{pl}$ , associated with a rotary-zero external intersected-axes gear pair.

are loosely referred to as *spherical gear pairs*. The term *spherical gear pair* is due to the tooth profiles of a gear and of its mating pinion in this case are generated on spheres.<sup>7</sup> A rotary-negative external intersected-axes gear pair and its gear vector diagram are schematically shown in Figure 2.16. For all rotary-negative intersected-axes gear pairs, the inequality  $\omega_g \cdot (\omega_p - \omega_g) < 0$  is valid (see Table 2.1). The component  $\Sigma_g$  of the crossed-axes angle,  $\Sigma$ , exceeds  $90^\circ$  (i.e.,  $\Sigma_g > 90^\circ$ ), as illustrated in Figure 2.16a. Rotary-negative intersected-axes gear pairs can feature crossed-axes angles of various values. In particular, the crossed-axes angle,  $\Sigma$ , can be chosen so as to fulfill the equality  $\Sigma_g = 90^\circ$  as shown in Figure 2.16b.

The gear vector diagram for rotary-negative intersected-axes gear pair is shown in Figure 2.16c. In Figure 2.17, a gear pair with intersected-axes of rotation of a gear,  $O_g$ , and of a mating pinion,  $O_p$ ,

<sup>7</sup> The term *spherical gear pair* is incorrect, as gears of other types, for example, crossed-axes gear pairs, are also engaged in mesh on a sphere. Therefore, replacement of the obsolete and intensively used term *conical gear pair* with the term *spherical gear pair* is not valid. In order to avoid ambiguities in further discussions, gearing of this type is referred to as *intersected-axes gearing*, or just as *I<sub>a</sub>-gearing*, for simplicity.

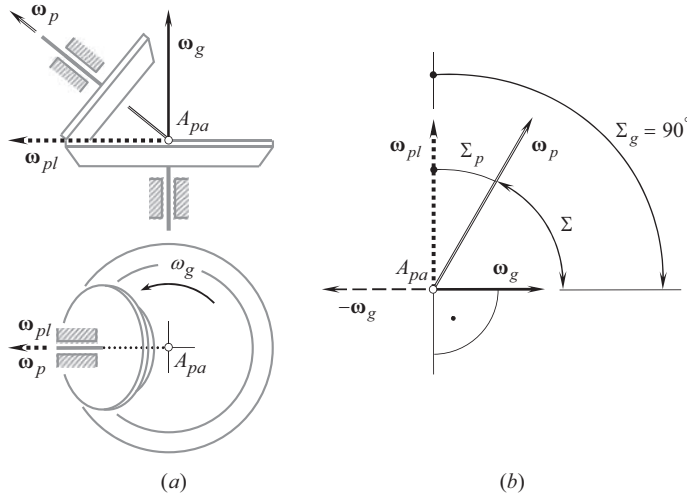


**FIGURE 2.18** An example of (a) rotary-zero intersected-axes gear pair, and (b) gear vector diagram for gearing of this kind.

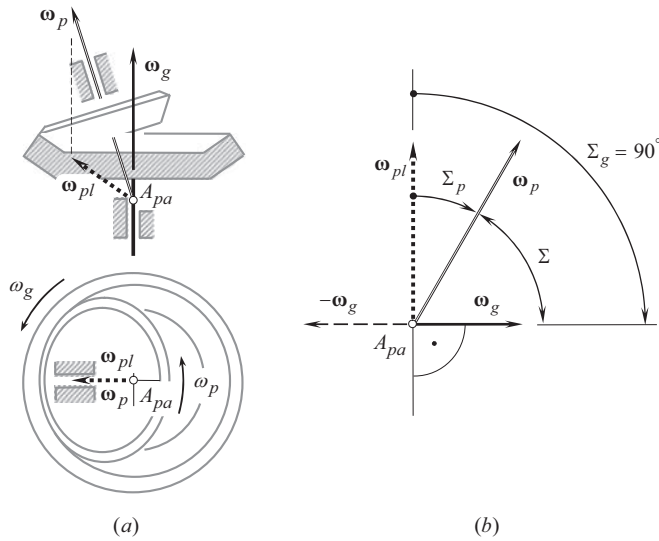


**FIGURE 2.19** An example of (a) rotary-positive intersected-axes gear pair, and (b) gear vector diagram for gearing of this kind.

is shown. Gear pair is a perfect example of rotary-negative gear pairs (usually, external gear pairs) of this particular design (Figure 2.17).

An example of rotary-zero intersected-axes gear pair and its vector diagram are depicted in Figure 2.18. For gear pairs of this type, the equality  $\omega_g \cdot (\omega_p - \omega_g) = 0$  is always observed (see Table 2.1). The component,  $\Sigma_g$ , of the crossed-axes angle,  $\Sigma$ , is equal to  $90^\circ$  (i.e.,  $\Sigma_g = 90^\circ$ ), as illustrated in Figure 2.18a. A rack-type intersected-axes gear pair can have a crossed-axes angle of various values. An example of vector diagram of gear pairs of this kind is depicted in Figure 2.18b.

A rotary-positive intersected-axes gear pair and gear vector diagram for gearing of this kind are schematically shown in Figure 2.19. For all rotary-positive intersected-axes gear pairs, the



**FIGURE 2.20** An example of internal straight bevel gear pair.

inequality  $\omega_g \cdot (\omega_p - \omega_g) > 0$  is observed (see Table 2.1). The component  $\Sigma_g$  of the crossed-axes angle,  $\Sigma$ , is less than  $90^\circ$  (i.e.,  $\Sigma_g < 90^\circ$ ), as illustrated in Figure 2.19a. A rotary-positive intersected-axes gear pair can have a crossed-axes angle of various values. A gear vector diagram for an internal intersected-axes gear pair is shown in Figure 2.19b. Figure 2.20 illustrates a perfect example of internal intersected-axis gear pair.

Three different kinds of intersected-axes gear pairs, namely,

1. Rotary-negative intersected-axes gear pairs (see Figure 2.16),
2. Rotary-zero intersected-axes gear pairs (see Figure 2.18), and
3. Rotary-positive intersected-axes gear pairs (see Figure 2.19),

comprise the first row of the second stratum of the classification of all possible kinds of gear vector diagrams (see Figure 2.15). Numbers 1.1.1, 1.2.1, and 1.3.1 are assigned to intersected-axes gear pairs of the first row of the second stratum of the classification of gear vector diagrams.

This is followed by the second case in which the axes of rotation of a gear and its mating pinion are parallel to each other. The shaft angle in these cases is either  $\Sigma = 0^\circ$  or  $\Sigma = 180^\circ$ .

When the equality  $\Sigma = 180^\circ$  is observed, the rotation vectors,  $\omega_g$  and  $\omega_p$ , are pointed in the opposite directions. Gear pairs of this kind are referred to as *parallel-axes gear pairs*. (Sometimes the term *planar gear pair* is used with respect to gearing of this kind. The term *planar gear pair* is used due to the tooth profiles of the gear and its mating pinion in this case being generated within a plane. The term *parallel-axes gear pair* is preferred and is recommended for use in scientific publications on the theory of gearing).

A rotary-negative parallel-axes gear pair and its vector diagram are schematically shown in Figure 2.21. For all rotary-negative parallel-axes gear pairs, the inequality  $\omega_g \cdot (\omega_p - \omega_g) < 0$  is valid (see Table 2.1). The vector diagram for a rotary-negative parallel-axes gear pair is shown in Figure 2.21b. In Figure 2.22, an external gear pair with parallel axes of rotation of the gear,  $O_g$ , and the pinion,  $O_p$ , is depicted. This is a perfect example of a type of external parallel-axes gear pair (i.e., rotary-negative gear pair).

On the other hand, when the equality  $\Sigma = 0^\circ$  is valid in a parallel-axes gear pair, the rotation vectors,  $\omega_g$  and  $\omega_p$ , are pointed in the same direction, which corresponds to a rotary-positive parallel-axes gear pair. A rotary-positive internal parallel-axes gear pair and its vector diagram are schematically shown in Figure 2.23a. For all negative parallel-axes gear pairs the inequality,  $\omega_g \cdot (\omega_p - \omega_g) > 0$  is observed (see Table 2.1). A gear vector diagram for rotary-negative parallel-axes gear pair is shown in Figure 2.23b.

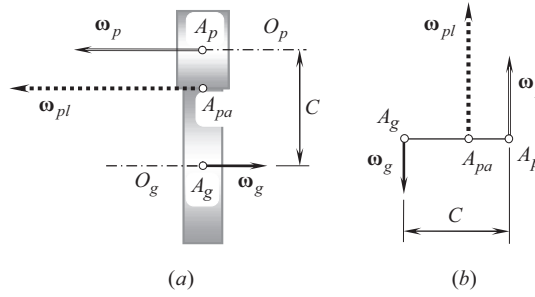


**FIGURE 2.21** An example of (a) rotary-negative parallel-axes gear pair, and (b) gear vector diagram for gear pairs of this kind.

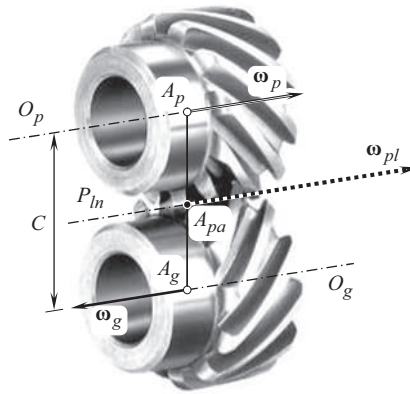


**FIGURE 2.22** Rotation vectors,  $\omega_g$ ,  $\omega_p$ , and  $\omega_{pl}$ , associated with a rotary-negative external parallel-axis gear pair.

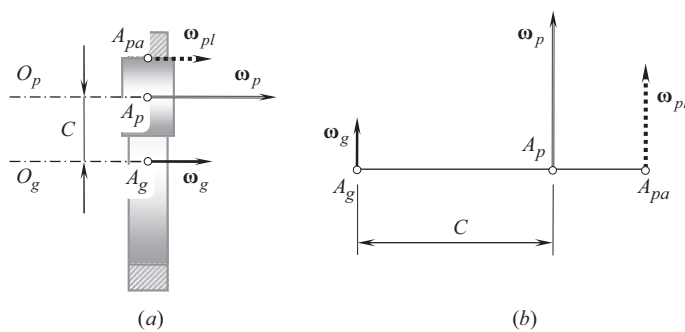


**FIGURE 2.23** Example of (a) rotary-positive parallel-axes gear pair and (b) gear vector diagram for gearing of this kind.

Two kinds of parallel-axes gear pairs, namely, rotary-negative gear pairs (see Figure 2.21), and rotary-positive parallel-axes gear pairs (see Figure 2.23), comprise the second row of the second stratum of the classification of possible kinds of gear vector diagrams (see Figure 2.15). The numbers 1.1.2 and 1.3.2 are assigned to the gear vector diagrams of parallel-axes gear pairs comprising the second row of the second stratum of the classification.

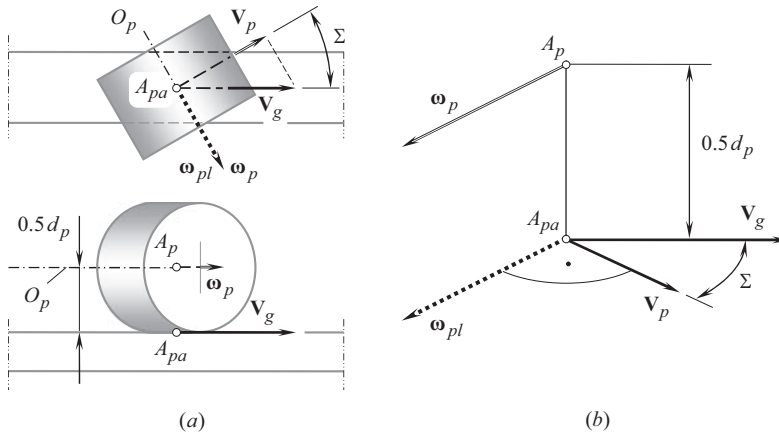


**FIGURE 2.24** A rotary-zero crossed-axes rack-type gear pair (a), and gear vector diagram for gearing of this kind (b).

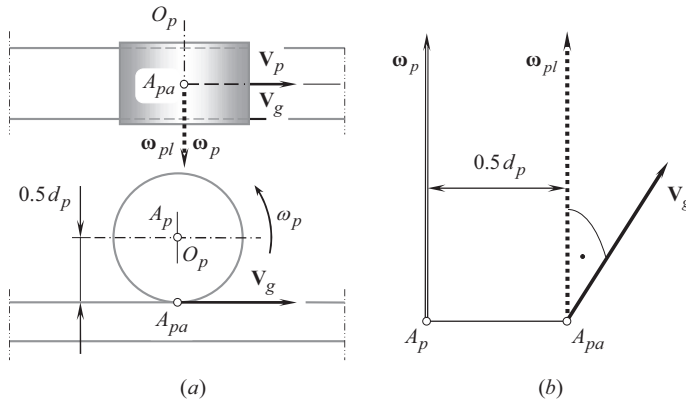


**FIGURE 2.25** A rotary-zero parallel-axes gear pair (a), and gear vector diagram of gearing of this kind (b).

Ultimately, consider a simplified case of rotary-zero crossed-axes gear pair (see Figure 2.13). In extreme cases, the tooth number of the gear can approach infinity. Infinite radius of a gear (of a gear sector) is the only way to reduce the rotary-zero crossed-axes gear pair when the center-distance is not equal to zero (i.e.,  $C \neq 0$ ). In Figure 2.24, a straight rotary-zero crossed-axes gear pair is shown, which corresponds to such a condition. The vectors of linear velocities,  $\mathbf{V}_g$  and  $\mathbf{V}_p$ , are at a crossed-axes angle,  $\Sigma$ , in relation to each other.

Rotary-zero crossed-axes gear pairs of this kind (see Figure 2.24) comprise the third row of the second stratum of the classification of all possible kinds of gear vector diagrams (Figure 2.15). The number 1.2.2 is assigned to the gear pair that comprises the third row of the second stratum of the classification.

In a particular case, say, when the crossed-axes angle equals to zero ( $\Sigma = 0^\circ$ ), a rotary-zero crossed-axes gear pair reduces to a conventional rotary-zero parallel-axes gear-to-rack gear pair. A gear-to-rack gear pair of this kind is schematically shown in Figure 2.25a. The gear vector diagram for gear pair of this design is depicted in Figure 2.25b.

Number 1.2.2.1 is assigned to parallel-axes gear-to-rack gear pair.

Gear-to-rack gear pair is a perfect example of rotary-zero parallel-axes gear pairs of this kind (Figure 2.26).



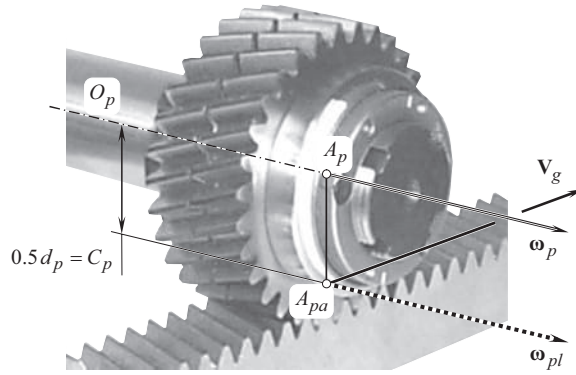


FIGURE 2.26 Rotation vectors,  $\omega_g$ ,  $\omega_p$ , and  $\omega_{pl}$ , associated with a rotary-zero parallel-axes rack-type gear pair.

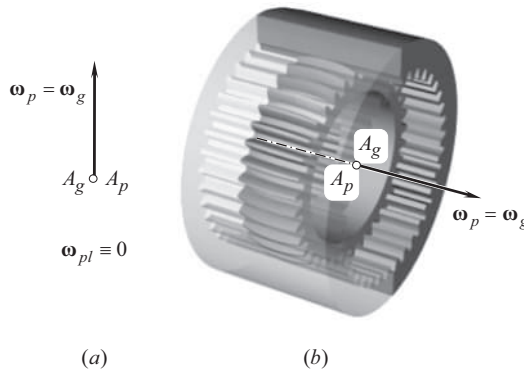


FIGURE 2.27 Gear vector diagram for gear coupling (a), and gear coupling: closeup (b).

It is instructive to note here that a rotary-zero parallel-axes rack-type gear pair can be obtained as an extreme case of either a rotary-negative parallel-axes gear pair (i.e., of the gear pair 1.1.2), or a rotary-positive parallel-axes gear pair (i.e., of the gear pair 1.3.2) under the condition that the radius of the gear approaches infinity.<sup>8</sup> In this case, the corresponding vector diagrams 1.1.2.1 or 1.3.2.1 are formally possible. Gear pairs that correspond to the vector diagrams 1.1.2.1 and 1.3.2.1 are not profoundly investigated yet.<sup>9</sup>

Finally, another extreme case needs to be mentioned here. In a particular case when the rotation vectors,  $\omega_g$  and  $\omega_p$ , are equal one another (i.e.,  $\omega_g \equiv \omega_p$ ), the rotary-positive parallel-axes gear pair 1.3.2 (see Figure 2.23) reduces to a gear coupling (see Figure 2.27). For a gear coupling, the rotation

<sup>8</sup> More accurately, the radius of a *gear sector*, and not of a *gear*, approaches infinity.

<sup>9</sup> The gear vector diagrams 1.1.2.1 and 1.3.2.1 correspond to the deeply degenerate designs of gear pairs. Because of this, significant features could be observed when developing tooth flanks for gearing that correspond to the gear vector diagrams of the kinds 1.1.2.1 and 1.3.2.1. When friction between the interacting tooth flanks of a gear,  $\mathcal{G}$ , and its mating pinion,  $\mathcal{P}$ , is not taken into account, the tangential force by means of which the torque is transmitted from the driving shaft to the driven shaft acts along the common perpendicular,  $\mathbf{n}_g$ , to the interacting tooth flanks,  $\mathcal{G}$  and  $\mathcal{P}$ . The common perpendicular,  $\mathbf{n}_g$ , intersects the axis of instantaneous rotation,  $P_{in}$ , that is, it intersects the line of action of the vector of instantaneous rotation,  $\omega_{pl}$ . In gear pairs that correspond to the gear vector diagrams 1.1.2.1 and 1.3.2.1, all three rotation vectors, namely,  $\omega_g$ ,  $\omega_p$ , and  $\omega_{pl}$ , are pointed along a common straight line,  $P_{in}$ . Once the line of action of the vector  $\mathbf{n}_g$  intersects the line of action of the velocity vector,  $\omega_{pl}$ , the arm of tangential force in the gear pair becomes zero. This means that no torque can be transmitted by a gear pair of these particular kinds. Gear coupling is not a kind of gearing (no plane of action can be constructed; no contact ratio can be defined). This discrepancy needs to be thoroughly investigated. In reality, a gear axis and its mating pinion axis are slightly misaligned. Under such a scenario, no discrepancy is observed, and gear pairs can be designed in accordance to the vector diagrams 1.1.2.1 and 1.3.2.1.

vector,  $\omega_{pl}$ , is equal to zero ( $\omega_{pl} \equiv 0$ ). The base cone apexes,  $A_g$  and  $A_p$ , are coincident with one another. Because the identity  $\omega_g \equiv \omega_p$  is valid, the center-distances,  $C_g$  and  $C_p$  (the pitch radii,  $\tilde{d}_g/2$  and  $\tilde{d}_p/2$ ), are both equal to zero (i.e.,  $C_g \equiv C_p \equiv 0$ ). Due to this, the plane-of-action-apex,  $A_{pa}$ , is coincident with the base cone apexes,  $A_g$  and  $A_p$  ( $A_g \equiv A_p \equiv A_{pa}$ ).

This particular case can also be construed as a reduced case of internal intersected-axes gear pair featuring a zero intersected-axes angle ( $\Sigma = 0^\circ$ ).

The gear vector diagram for a gear coupling is depicted in Figure 2.27a. The coupling can be composed of an internal and external spur gears with equal tooth numbers, as schematically shown in Figure 2.27b, or of a pair of similar bevel gears, or of two face gears. The number 1.3.2.1 is assigned to a degenerate gear pair of this kind.

The third stratum of the classification of all possible kinds of gear vector diagrams (see Figure 2.15) is represented by two kinds of parallel-axes gear pairs: (a) the rotary-zero gear pair 1.2.2.1 (see Figure 2.25) and (b) the gear coupling 1.3.2.1 (see Figure 2.27).

The total number of gear vector diagrams is limited just to 11 different kinds of them. Gear vector diagrams of all possible kinds are covered by the classification (see Figure 2.15). No gear vector diagrams that are not covered by the classification are possible. This allows to conclude that the classification shown in Figure 2.15 is complete and self-consistent.

This classification can be used for investigation of the kinematics, and the geometry of gearing of all kinds, namely, of all known kinds of gearing, as well as of all kinds of gearing not known yet, and that will be developed in the future.

## 2.4 COMPLIMENTARY VECTORS OF GEAR VECTOR DIAGRAMS

To simplify the analytical description of a gear pair, it is convenient to introduce a few more vectors to the gear vector diagrams. Vectors that are pointed along the centerline, as well as those pointed along the gear and the pinion axes of rotation, are of prime importance in this regard.

### 2.4.1 CENTERLINE VECTORS ASSOCIATED WITH GEAR PAIR

Referring to Figure 2.28, consider gear vector diagram of a gear pair.<sup>10</sup> The rotation vectors,  $\omega_g$  and  $\omega_p$ , are apart from one another by a center-distance  $C$ .

Two vectors,  $C_g$  and  $C_p$ , are pointed along the centerline,  $\mathfrak{k}$ . These vectors specify the distances of the axes of rotation of the gear,  $O_g$ , and its mating pinion,  $O_p$ , from the plane-of-action apex,  $A_{pa}$ . The gear centerline vector,  $C_g$ , is calculated from the following equation:

$$C_g = -C_g \cdot \mathbf{c} \quad (2.48)$$

The pinion centerline vector,  $C_p$ , is specified as follows:

$$C_p = C_p \cdot \mathbf{c} \quad (2.49)$$

<sup>10</sup> For the gear pairs with varying tooth ratios, for example, for gear pairs composed of non-circular gears, the parameters of gear vector diagram,  $\omega_g$ ,  $\omega_p$ ,  $\omega_{pl}$ ,  $C$ ,  $C_g$ ,  $C_p$ ,  $\Sigma$ ,  $\Sigma_g$ ,  $\Sigma_p$ , and others should be considered as corresponding functions of time  $t$ , or (the same) as corresponding functions of the angle of rotation of the input shaft, namely, of the angle of rotation either of the gear,  $\varphi_g$ , or of the pinion,  $\varphi_p$ . Ultimately, these functions can be represented in a generalized way as  $\omega_g(t)$ ,  $\omega_p(t)$ ,  $\omega_{pl}(t)$ ,  $C(t)$ ,  $C_g(t)$ ,  $C_p(t)$ ,  $\Sigma(t)$ ,  $\Sigma_g(t)$ ,  $\Sigma_p(t)$ . All the parameters are synchronized with one another.





Once a gear is assumed stationary (when determining the vector of instantaneous rotation,  $\omega_{pl}$ ), then the rotation vectors,  $\omega_p$  and  $\omega_{pl}$ , always form an acute angle. The multiplier  $\text{sgn}(\omega_p \cdot \omega_{pl})$  is always of a positive value and, thus, it is not necessary to implement it in Eq. (2.52).

An angle formed by the rotation vectors,  $\omega_g$  and  $\omega_{pl}$ , is obtuse for a rotary-negative gear pair, and it is acute for a rotary-positive gear pair. Because of this, the gear and the pinion in a gear pair are located at the same side of the centerline,  $\mathfrak{L}$ , so the axial vectors,  $\mathbf{A}_g$  and  $\mathbf{A}_p$ , should always be acute. This is accounted by the multiplier,  $\text{sgn}(\omega_g \cdot \omega_{pl})$ .

If magnitude,  $A_g$ , of the vector  $\mathbf{A}_g$  is known, then the following formula:

$$d_g = 2\sqrt{C_g^2 + A_g^2 \cdot \tan^2 \Sigma_g} \quad (2.53)$$

can be used for the calculation of pitch diameter,  $d_g$ , of the gear.

Conversely, if the pitch radius of the gear,  $r_g$ , is given, then for the calculation of the axial shift of the gear the formula

$$A_g = \frac{\sqrt{r_g^2 - C_g^2}}{\tan \Sigma_g} \quad (2.54)$$

can be used.

Similar to Eqs. (2.53) and (2.54), the following expressions:

$$r_p = \sqrt{C_p^2 + A_p^2 \cdot \tan^2 \Sigma_p} \quad (2.55)$$

and

$$A_p = \frac{\sqrt{r_p^2 - C_p^2}}{\tan \Sigma_p} \quad (2.56)$$

are valid for the calculation of the axial shift,  $A_p$ , and of the pitch radius,  $r_p$ , of the pinion.

It can be easily shown that the magnitude,  $A_p$ , of the pinion axial vector,  $\mathbf{A}_p$ , can be expressed in terms of the magnitude  $A_g$  of the gear axial vector,  $\mathbf{A}_g$ :

$$A_p = A_g \frac{\cos \Sigma_p}{\cos \Sigma_g} \quad (2.57)$$

The magnitudes,  $A_g$  and  $A_p$ , of the axial vectors,  $\mathbf{A}_g$  and  $\mathbf{A}_p$ , are of the same sign. Both are positive (i.e.,  $A_g > 0$ ,  $A_p > 0$ ), have zero value (i.e.,  $A_g = 0$ ,  $A_p = 0$ ), or are negative (i.e.,  $A_g < 0$ ,  $A_p < 0$ ). Consequently, three different locations of a gear in relation to the centerline are distinguished.

### 2.4.3 USEFUL KINEMATIC AND GEOMETRIC FORMULAS

The proposed vector diagrams of gear pairs (namely, vector diagrams for rotations/torques) make possible derivation of numerous auxiliary formulas for the calculation of the kinematic and geometric parameters of gear pairs.

For calculation of the center-distances,  $C_g$  and  $C_p$ , of a gear axis of rotation,  $O_g$ , and a mating pinion axis of rotation,  $O_p$ , from the axis of instantaneous rotation,  $P_{ln}$ , the following approach can be applied: Let us project the rotation vectors,  $\omega_g$ ,  $\omega_p$ , and  $\omega_{pl}$ , onto the  $N_{ln}$  – plane (*Reminder*: the normal plane,  $N_{ln}$ , is a plane perpendicular to the centerline  $\mathfrak{L}$ , illustrated in Figure 2.28). The components,  $\omega_g^{rl}$  and  $\omega_g^{sl}$ , of the rotation vector of the gear,  $\omega_g$ , and the components,  $\omega_p^{rl}$  and  $\omega_p^{sl}$ , of the

rotation vector of the mating pinion,  $\omega_p$ , are also depicted here. The rolling components,  $\omega_g^{rl}$  and  $\omega_p^{rl}$ , of the rotation vectors,  $\omega_g$  and  $\omega_p$ , are within a plane through the centerline,  $\mathfrak{L}$ .

The following expression can be derived on the premise of pure rolling in the gear pair:

$$\omega_g^{rl} \cdot C_g = \omega_p^{rl} \cdot C_p \quad (2.58)$$

For the center-distances,  $C_g$  and  $C_p$ , the following equality is valid:

$$C_g + C_p = C \quad (2.59)$$

If the center-distances,  $C_g$  and  $C_p$ , are considered the signed values, then Eq. (2.59) is valid for both, for negative and positive gear pairs.

The center-distance,  $C_p$ , can be expressed in terms of the center-distance,  $C_g$ , and the center-distance,  $C$ , as:

$$C_p = C - C_g \quad (2.60)$$

Equation (2.60) yields the representation of Eq. (2.58) in the following form:

$$\omega_g^{rl} \cdot C_g = \omega_p^{rl} \cdot (C - C_g) \quad (2.61)$$

This immediately returns a formula for the calculation of the center-distance,  $C_g$ :

$$C_g = \frac{1 + \omega_p - \omega_g}{1 + \omega_p} \cdot C \quad (2.62)$$

Once the center-distance  $C_g$  is determined, for the calculation of the center-distance  $C_p$ , Eq. (2.60) can be used. In the case under consideration, Eq. (2.60) allows the following formula:

$$C_p = \frac{1 + \omega_g - \omega_p}{1 + \omega_g} \cdot C \quad (2.63)$$

It is the right point to discuss here a few more formulas for the calculation of kinematic and geometric parameters in a gear pair, which directly follow from the analysis of Figure 2.28.

The magnitude,  $\omega_{pl}$ , of the vector of instantaneous rotation,  $\omega_{pl}$ , is calculated from the following equation:

$$\omega_{pl} = \sqrt{(\omega_g^{rl})^2 + (\omega_p^{rl})^2 - 2 \cdot \omega_g^{rl} \cdot \omega_p^{rl} \cdot \cos \Sigma} \quad (2.64)$$

For the calculation of the gear angle,  $\Sigma_g$ , that is formed by the vectors,  $\omega_g^{rl}$  and  $\omega_{pl}$ , the following equation is used:

$$\Sigma_g = \frac{1 + \omega_p - \omega_g}{1 + \omega_p} \cdot \Sigma \quad (2.65)$$

Similarly, the pinion angle  $\Sigma_p$  that is formed by the vectors,  $\omega_p^{rl}$  and  $\omega_{pl}$ , can be calculated from the equation:

$$\Sigma_p = \frac{1 + \omega_g - \omega_p}{1 + \omega_g} \cdot \Sigma \quad (2.66)$$

If the angle  $\Sigma_g = 90^\circ$  is entered into Eq. (2.65), then the expression:

$$\Sigma_{cr} = \frac{1 + \omega_g}{1 + \omega_g - \omega_p} \cdot \frac{\pi}{2} \quad (2.67)$$

for the calculation of a critical value  $\Sigma_{cr}$  of the crossed-axes angle  $\Sigma$  can be derived.

The kinematics of gearing with variable principal design parameters, namely, the center-distance,  $C(t)$ , the crossed-axes angle,  $\Sigma(t)$ , and the gear ratio,  $u(t)$  (the so-called  $C\Sigma u$  – gearing, for simplicity), is discussed below in Chapter 18.





# Taylor & Francis

Taylor & Francis Group

<http://taylorandfrancis.com>

---

# 3 Principal Planes and Main Reference Systems Associated with Gear Pair

For a gear pair with a specified set of the design parameters, a corresponding gear vector diagram for the rotation vectors (as well as for the torques) can be constructed. Several principal directions are associated with a gear pair. These directions are defined by:

- a. the rotation vector of the gear
- b. the rotation vector of the mating pinion
- c. the vector of instantaneous rotation, and
- d. the center-line

The use of the principal directions allows for the construction of a set of principal planes, and a set of main reference systems, associated with a gear pair. An analysis of all kinds of gearing is significantly simplified when the principal planes and the main reference systems are used.

Let us begin the analysis with consideration of the principal planes associated with a gear pair.

## 3.1 PRINCIPAL PLANES ASSOCIATED WITH GEAR PAIR

Consider an arbitrary crossed-axes gear pair, and construct for it the axes of instantaneous rotation,  $P_{in}$ , and the center-line,  $\mathfrak{L}$ .

A set of three principal planes can be associated with the gear pair.

The *pitch-line plane* (or just  $P_{in} - plane$ , for simplicity) is the first of three principal planes associated with crossed-axes gear pair.

### Definition 3.1

Pitch-line plane is the plane through the axis of instantaneous rotation,  $P_{in}$ , and the center-line,  $\mathfrak{L}$ , in the gear pair.

An example of possible configuration of the pitch-line plane in relation to the axes of instantaneous rotation,  $P_{in}$ , and the center-line,  $\mathfrak{L}$ , in a crossed-axes gear pair is schematically shown in Figure 3.1.

The *center-line plane* (or just  $C_{in} - plane$ , for simplicity) is the second principal plane associated with crossed-axes gear pair.

### Definition 3.2

Center-line plane is the plane through the center-line,  $\mathfrak{L}$ , in the gear pair perpendicular to the axis of instantaneous rotation,  $P_{in}$ .

An example of possible configuration of the center-line plane in relation to the axis of instantaneous rotation,  $P_{in}$ , and the center-line,  $\mathfrak{L}$ , in a crossed-axis gear pair is schematically shown in Figure 3.2.

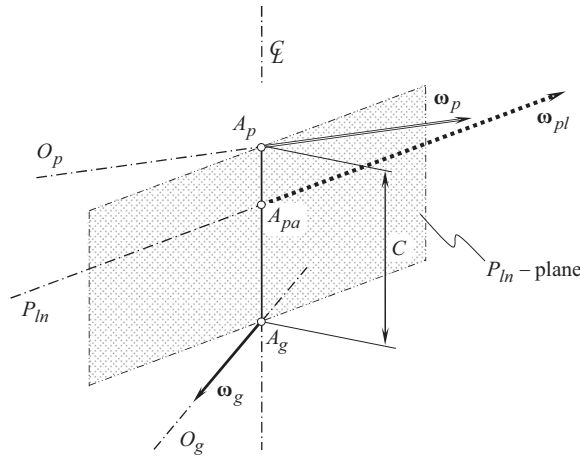


**FIGURE 3.1** Principal planes associated with gear pair: the *pitch-line plane* (the  $P_{ln}$ -plane, for simplicity).

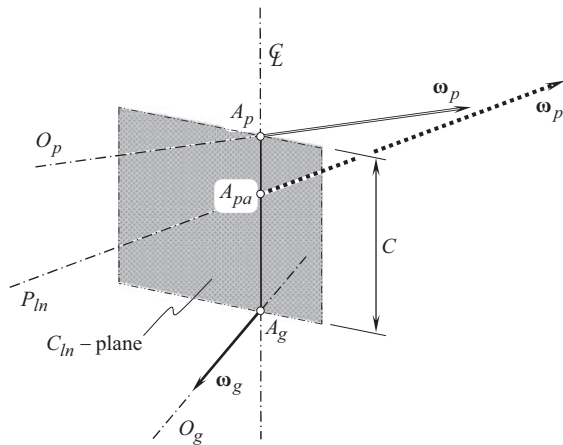


**FIGURE 3.2** Principal planes associated with a gear pair: the *center-line plane* (the  $C_{ln}$ -plane, for simplicity).

Finally, the *normal plane* (or just  $N_{ln}$ -plane, for simplicity) is the third of three principal planes associated with crossed-axes gear pair.

### Definition 3.3

Normal plane is the plane through the plane-of-action-apex,  $A_{pa}$ , perpendicular to the center-line,  $\mathcal{L}$ , in the gear pair.

An example of possible configuration of the normal plane in relation to the axis of instantaneous rotation,  $P_{ln}$ , and the center-line,  $\mathcal{L}$ , in a crossed-axis gear pair is schematically shown in Figure 3.3.

Altogether, three planes, namely,  $P_{ln}$ -plane,  $C_{ln}$ -plane, and  $N_{ln}$ -plane, form a set of principal planes associated with a gear pair. An illustrative example of a set of principal planes associated with a gear pair is schematically shown in Figure 3.4.

Here, in Figure 3.4 (as well as in Figures 3.1–3.3), the principal planes:  $P_{ln}$ -plane,  $C_{ln}$ -plane, and  $N_{ln}$ -plane, are constructed for the most general case of crossed-axes gearing. The provided definitions for the principal planes are also valid for the reduced cases of gearing, that is, for

intersected-axes gearing and for parallel-axes gearing as well. However, for the reduced cases of the vector diagrams, simpler specifications of the principal planes can be formulated.

### 3.1.1 INTERSECTED-AXES GEARING

As shown in Figure 3.4, the center-line,  $\mathfrak{L}$ , is perpendicular to the axes of rotation of the gear,  $O_g$ , and that of the pinion,  $O_p$ . This feature is helpful to specify the actual configuration of the principal planes in intersected-axes gearing.

In intersected-axes gearing, definitions of the principal planes can be reduced to:

- $P_{ln}$  – plane is the plane through the axis of instantaneous rotation,  $P_{ln}$ , and the perpendicular to the plane through the axes of rotation,  $O_g$  and  $O_p$ , of the gear and the pinion, as shown in Figure 3.5
- $C_{ln}$  – plane is the plane perpendicular to the axis of instantaneous rotation,  $P_{ln}$ . The center-line plane is also perpendicular to the plane through the axes of rotation,  $O_g$  and  $O_p$ , of the gear and the pinion (see Figure 3.6)
- $N_{ln}$  – plane is the plane through the axes of rotation,  $O_g$  and  $O_p$ , of the gear and the pinion. This is illustrated in Figure 3.7.

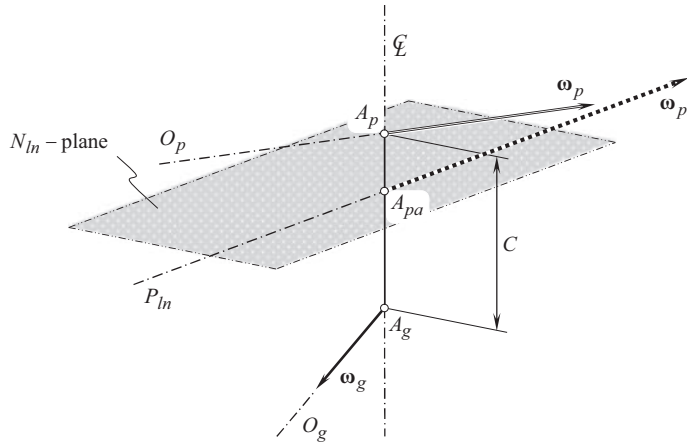


FIGURE 3.3 Principal planes associated with a gear pair: the normal plane (the  $N_{ln}$  – plane, for simplicity).

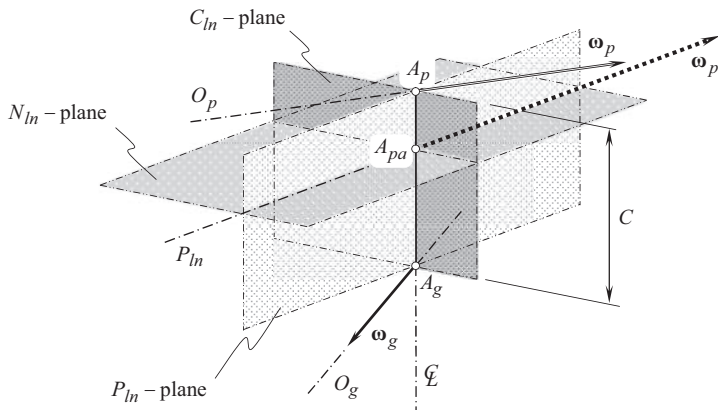
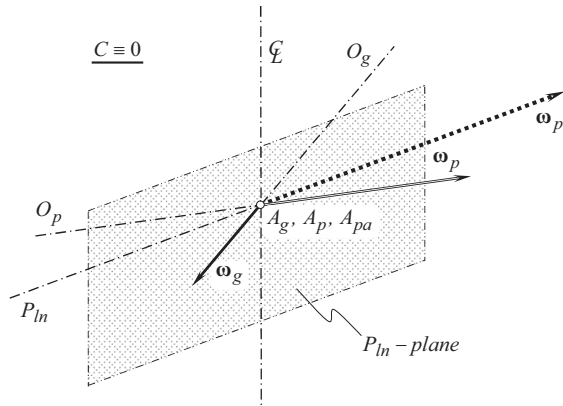
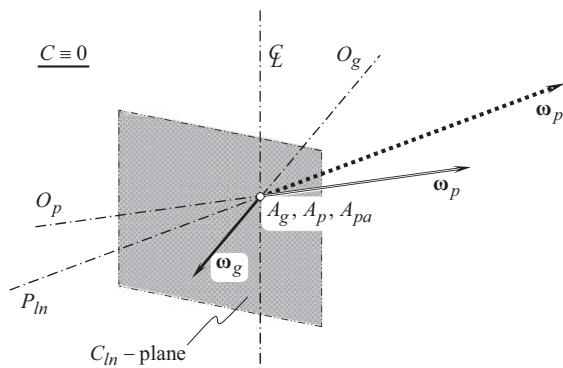


FIGURE 3.4 A set of principal planes associated with a gear pair: the pitch-line plane (the  $P_{ln}$  – plane), the center-line plane (the  $C_{ln}$  – plane), and the normal plane (the  $N_{ln}$  – plane).



**FIGURE 3.5** A set of principal planes associated with intersected-axes gear pair: the *pitch-line plane* (the  $P_{in} - plane$ ).



**FIGURE 3.6** A set of principal planes associated with intersected-axes gear pair: the *center-line plane* (the  $C_{in} - plane$ ).

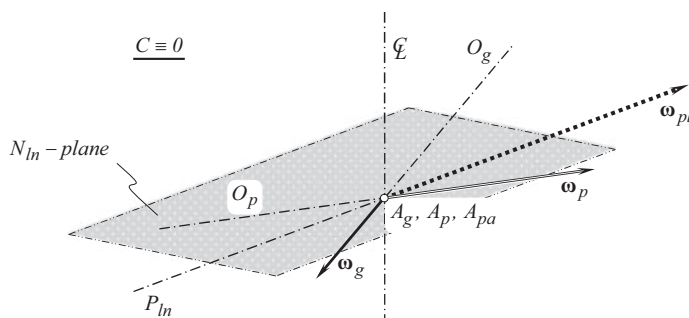


**FIGURE 3.7** A set of principal planes associated with intersected-axes gear pair: the *normal plane* (the  $N_{in} - plane$ ).

Altogether, the principal planes in intersected-axes gearing are schematically shown in Figure 3.8.

### 3.1.2 PARALLEL-AXES GEARING

For parallel-axes gearing, the principal planes can be specified in a simplified manner:

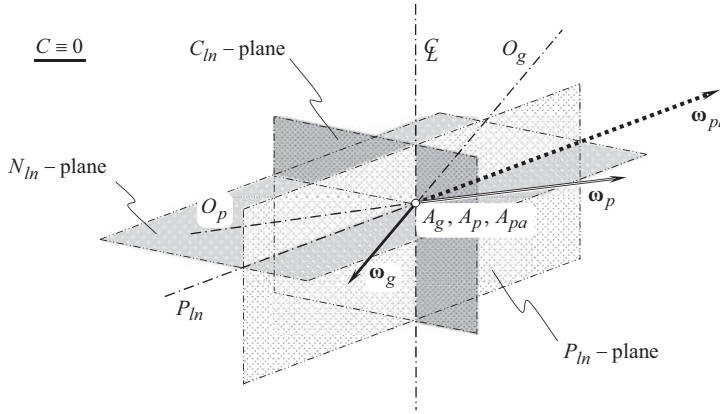


**FIGURE 3.8** A set of principal planes associated with intersected-axes gear pair: the *pitch-line plane* (the  $P_{ln}$  - plane), the *center-line plane* (the  $C_{ln}$  - plane), and the *normal plane* (the  $N_{ln}$  - plane).

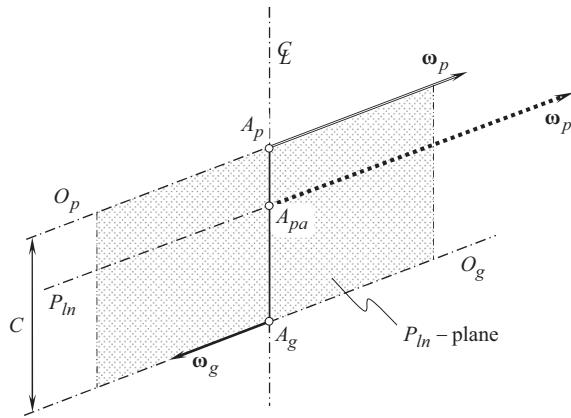


**FIGURE 3.9** A set of principal planes associated with parallel-axes gear pair: the *pitch-line plane* (the  $P_{ln}$  - plane).

- $P_{ln}$ -plane is the plane through the axis of instantaneous rotation,  $P_{ln}$ , and through the axes of rotation,  $O_g$  and  $O_p$ , of the gear and the mating pinion, as shown in Figure 3.9
- $C_{ln}$ -plane is the plane through the center-line,  $\mathfrak{L}$ , of the gear pair perpendicular to the axis of instantaneous rotation,  $P_{ln}$ , as illustrated in Figure 3.10
- $N_{ln}$ -plane is the plane perpendicular to the center-line,  $\mathfrak{L}$ , in the gear pair. The normal plane is also perpendicular to the plane through the axes of rotation,  $O_g$  and  $O_p$ , of the gear and the mating pinion (see Figure 3.11)

Altogether, the principal planes in parallel-axes gearing are schematically shown in Figure 3.12.

The use of the principal planes significantly simplifies analysis of gearing of parallel-axes gearing.

## 3.2 PLANE OF ACTION IN GEAR PAIR

Once a set of principal planes in a gear pair is determined, this makes possible an introduction of the plane of action,  $PA$ , in a gear pair.

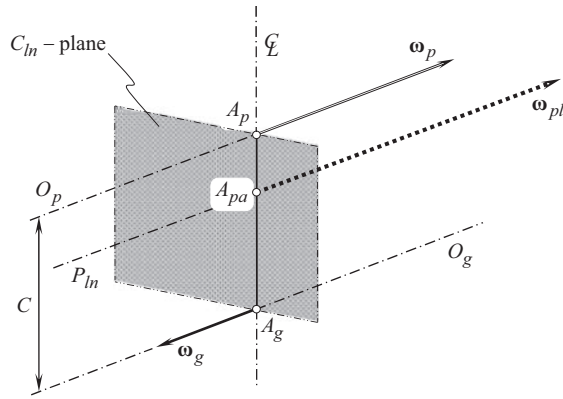


**FIGURE 3.10** A set of principal planes associated with parallel-axes gear pair: the *center-line plane* (the  $C_{ln}$ -plane).

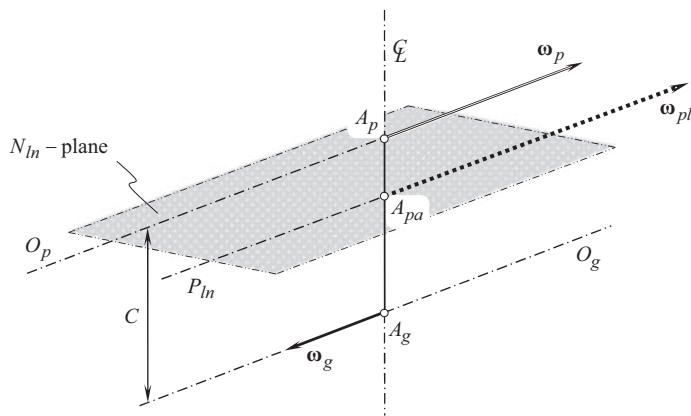


**FIGURE 3.11** A set of principal planes associated with parallel-axes gear pair: the *normal plane* (the  $N_{ln}$ -plane).

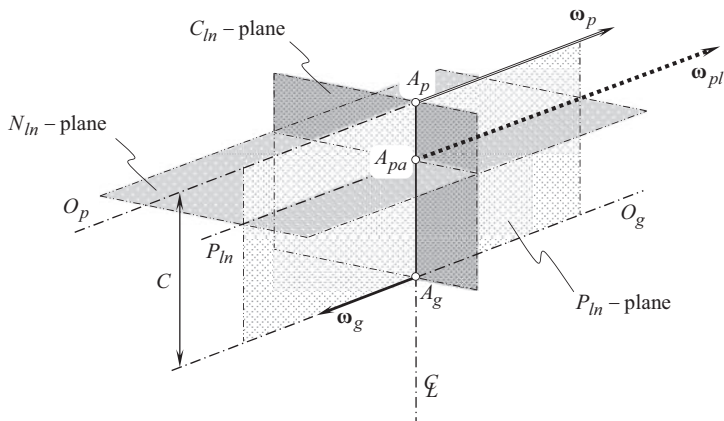


**FIGURE 3.12** A set of principal planes associated with parallel-axes gear pair: the *pitch-line plane* (the  $P_{ln}$ -plane), the *center-line plane* (the  $C_{ln}$ -plane), and the *normal plane* (the  $N_{ln}$ -plane).



**Definition 3.4**

Plane of action in a gear pair is the plane through the axis of instantaneous rotation,  $P_{ln}$ , at a transverse pressure angle,  $\phi_{t,\omega}$ , relative to perpendicular to the center-line,  $\mathcal{L}$ , of the gear pair that is constructed within the center-line plane.

The plane of action,  $PA$ , forms a transverse pressure angle,  $\phi_{t,\omega}$ , with the normal plane,  $N_{ln}$  – plane.

Configuration of the plane of action,  $PA$ , in relation to the set of principal planes in a gear pair is schematically shown in Figure 3.13.

The provided definition for the plane of action,  $PA$ , is also valid for the reduced cases of gearing, namely, for intersected-axes gearing, and for parallel-axes gearing, as well. However, for the reduced cases of the gear vector diagrams, simpler specifications of the plane of action can be formulated.

**3.2.1 PLANE OF ACTION IN INTERSECTED-AXES GEARING**

In intersected-axes gearing, the plane of action,  $PA$ , is a plane through the axis of instantaneous rotation,  $P_{ln}$ , that forms a transverse pressure angle,  $\phi_{t,\omega}$ , with the normal plane, as illustrated in Figure 3.14.

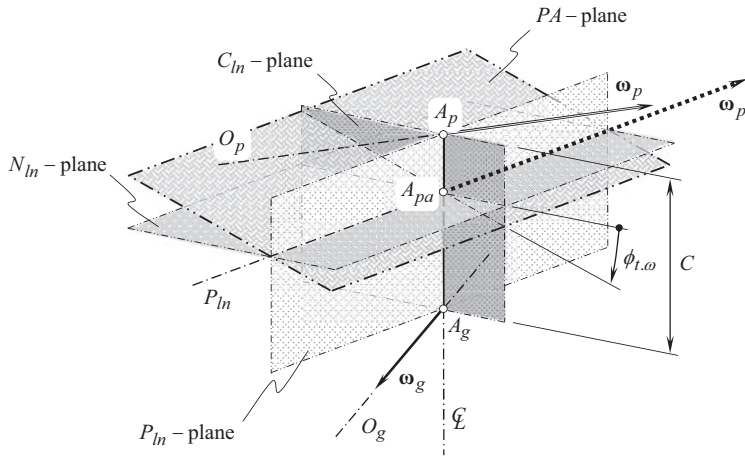


**FIGURE 3.13** Plane of action,  $PA$ , in crossed-axes gear pair.

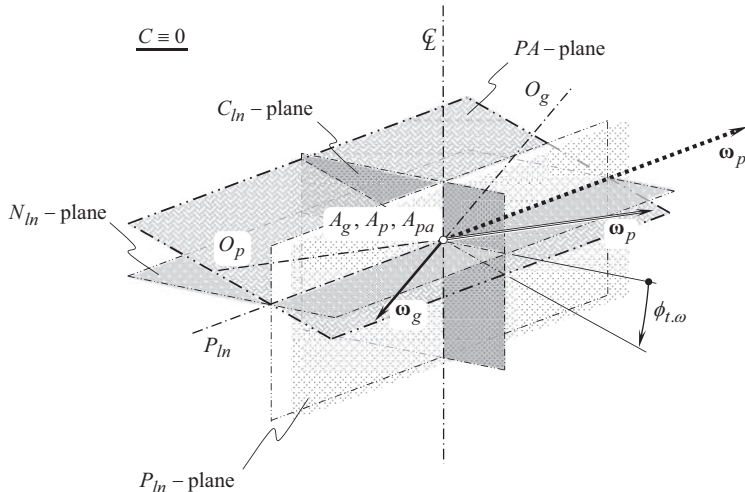


**FIGURE 3.14** Plane of action,  $PA$ , in intersected-axes gear pair.

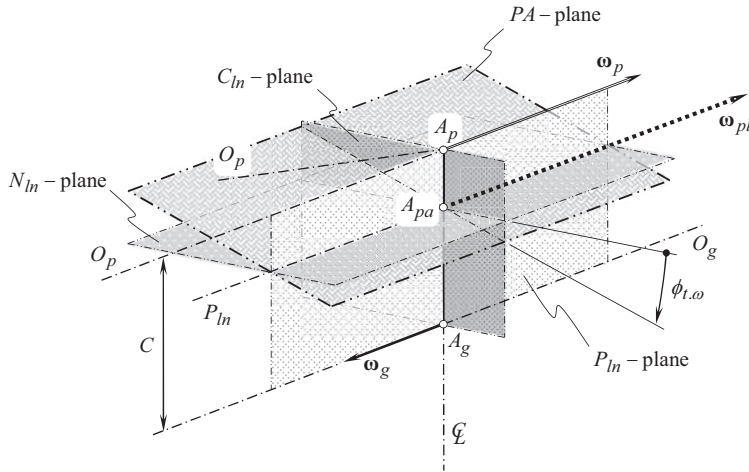


FIGURE 3.15 Plane of action,  $PA$ , in parallel-axes gear pair.

### 3.2.2 PLANE OF ACTION IN PARALLEL-AXES GEARING

In parallel-axes gearing, the plane of action,  $PA$ , is a plane through the axis of instantaneous rotation,  $P_{ln}$ , that forms a transverse pressure angle  $\phi_{t,\omega}$  with the normal plane, as shown in Figure 3.15.

## 3.3 MAIN REFERENCE SYSTEMS ASSOCIATED WITH GEAR PAIR

For the analytical description and investigation of the kinematics of gear pairs, and the geometry of interacting tooth flanks of a gear and that of a mating pinion, corresponding reference systems are associated with the gear, with the pinion, and with the gear pair. Orthogonal *Cartesian* coordinate systems are extensively used for these purposes.

Both the kinematics of gearing and the geometry of tooth flanks of a gear and of a mating pinion can be analytically described in an arbitrary reference system. However, it is convenient to choose reference systems so as to simplify analytical expressions for all the elements of the gear pair.

The simplest possible analytical representation of an element of a gear pair can be derived from specific reference systems. These reference systems are associated with the gear pair in a specific manner. Reference systems of these types are referred to as *main reference systems*.

To determine a set of main reference systems, consider gear vector diagram for an arbitrary gear pair given in Figure 3.16. The rotation vectors,  $\omega_g$  and  $\omega_p$ , of the gear and of the pinion are at a center-distance,  $C$ , and they cross one another. Points  $A_g$  and  $A_p$  are the points of intersection of the center-line,  $\mathfrak{L}$ , by the gear axis of rotation,  $O_g$ , and the pinion axis of rotation,  $O_p$ , correspondingly. The point  $A_g$  is referred to as the *gear base cone apex*, and the point  $A_p$  is referred to as the *pinion base cone apex*.

The vector of instantaneous rotation,  $\omega_{pl}$ , of theca vector through the point  $A_{pa}$ . This point is located within the center-line,  $\mathfrak{L}$ . The point  $A_{pa}$  is referred to as the *plane-of-action-apex*.

The *axis of instantaneous rotation*,  $P_{ln}$ , is the straight line through the *plane-of-action-apex*,  $A_{pa}$ , that is pointed along the vector of instantaneous rotation,  $\omega_{pl}$ .

Two straight lines through a common point uniquely specify a plane through this point. In the case under consideration, this is the plane through the axis of instantaneous rotation,  $P_{ln}$ , and through the center-line,  $\mathfrak{L}$ .

The origin of the main reference system,  $X_{ln}Y_{ln}Z_{ln}$ , is coincident with the plane-of-action-apex,  $A_{pa}$ . The axes  $X_{ln}$ ,  $Y_{ln}$ , and  $Z_{ln}$  are pointed along the lines of intersection of the principal planes, as illustrated in Figure 3.16: the axis  $Z_{ln}$  is along the vector of instantaneous rotation,  $\omega_{pl}$ ; the axis  $Y_{ln}$  is along the center-line,  $\mathfrak{L}$ ; and the  $X_{ln}$  – axis complements the axes  $Y_{ln}$  and  $Z_{ln}$  to a left-hand-oriented *Cartesian* coordinate system  $X_{ln}Y_{ln}Z_{ln}$ .

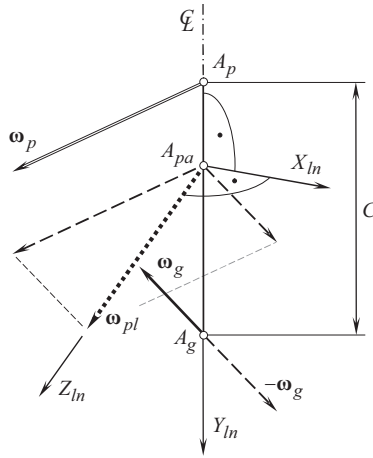


FIGURE 3.16 Main reference system,  $X_{ln}Y_{ln}Z_{ln}$ , associated with crossed-axes gear pair.

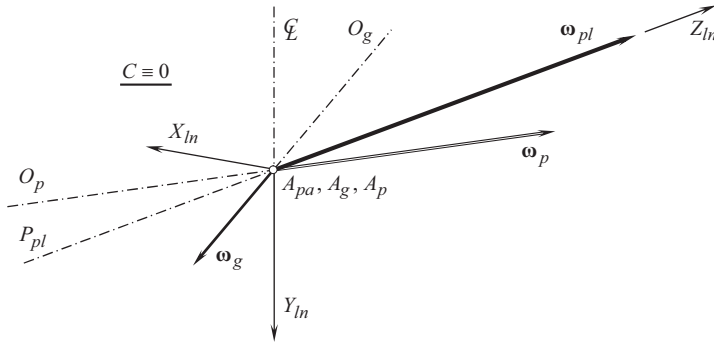


FIGURE 3.17 Main reference system,  $X_{ln}Y_{ln}Z_{ln}$ , associated with intersected-axes gear pair.

(For the reduced cases of intersected-axes gearing, and of parallel-axes gearing, the main reference system,  $X_{ln}Y_{ln}Z_{ln}$ , is shown in Figures 3.17 and 3.18 correspondingly).

The stationary gear reference system,  $X_{g,s}Y_{g,s}Z_{g,s}$ , is the second reference system associated with gear pair. The origin of the reference system,  $X_{g,s}Y_{g,s}Z_{g,s}$ , is coincident with the gear base cone apex,  $A_g$ , as shown in Figure 3.19. The axis  $Z_{g,s}$  is pointed along the rotation vector of the gear,  $\omega_g$ ; the axis  $Y_{g,s}$  is along the center-line,  $\mathfrak{L}$ ; and the  $X_{g,s}$  – axis complements the axes  $Y_{g,s}$  and  $Z_{g,s}$  to a left-hand-oriented *Cartesian* coordinate system  $X_{g,s}Y_{g,s}Z_{g,s}$ . The stationary gear reference system,  $X_{g,s}Y_{g,s}Z_{g,s}$ , is turned through the gear cone angle,  $\Sigma_g$ , about  $Z_{ln}$  – axis of the reference system  $X_{ln}Y_{ln}Z_{ln}$  associated with a gear pair as illustrated in Figure 3.20.

The gear reference system,  $X_gY_gZ_g$ , is the third reference system associated with the gear pair. The reference system,  $X_gY_gZ_g$ , is rigidly associated with the gear, and is rotated together with the gear about its axis of rotation,  $O_g$ . As illustrated in Figure 3.21, the reference systems  $X_gY_gZ_g$  and  $X_{g,s}Y_{g,s}Z_{g,s}$  share the common axis  $Z_g \equiv Z_{g,s}$ , and is turned about the  $Z_{g,s}$  – axis through a gear rotation angle,  $\phi_g$ .

The stationary pinion reference system,  $X_{p,s}Y_{p,s}Z_{p,s}$ , is the fourth reference system associated with the gear pair. The origin of the reference system,  $X_{p,s}Y_{p,s}Z_{p,s}$ , is coincident with the pinion apex,  $A_p$ , as shown in Figure 3.22. The axis  $Z_{p,s}$  is pointed along the rotation vector of the pinion,  $\omega_p$ ; the axis  $Y_{p,s}$  is along the center-line,  $\mathfrak{L}$ ; and the  $X_{p,s}$  – axis complements the axes  $Y_{p,s}$  and  $Z_{p,s}$  to a left-hand-oriented *Cartesian* coordinate system,  $X_{p,s}Y_{p,s}Z_{p,s}$ . The stationary pinion reference system,

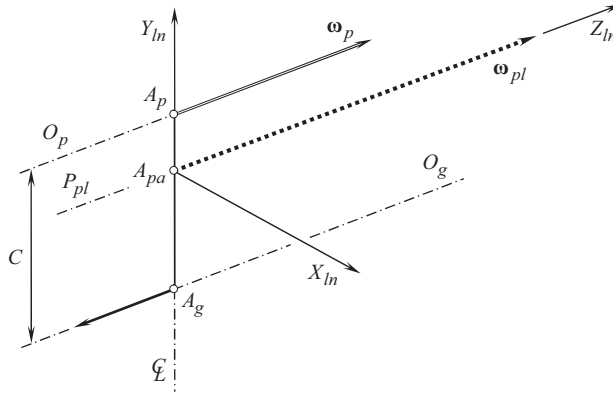


**FIGURE 3.18** Main reference system,  $X_{ln}Y_{ln}Z_{ln}$ , associated with parallel-axes gear pair.

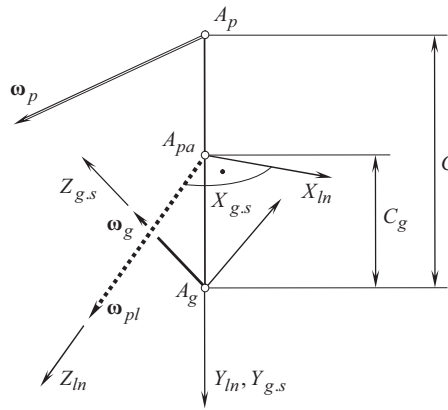


**FIGURE 3.19** Configuration of the motionless gear reference systems,  $X_{g,s}Y_{g,s}Z_{g,s}$ , in relation to the main reference system,  $X_{ln}Y_{ln}Z_{ln}$ , associated with the gear pair.

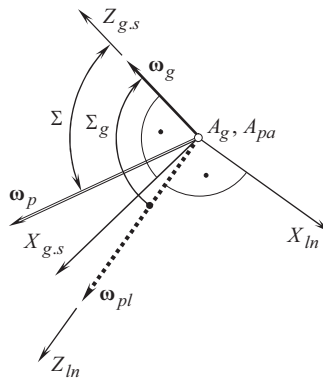


**FIGURE 3.20** The motionless reference systems,  $X_{g,s}Y_{g,s}Z_{g,s}$ , of the gear is turned through the gear cone angle,  $\Sigma_g$ , about  $Z_{ln}$  - axis of the main reference system,  $X_{ln}Y_{ln}Z_{ln}$ , associated with the gear pair.

$X_{p,s}Y_{p,s}Z_{p,s}$ , is turned through the pinion cone angle,  $\Sigma_p$ , about  $Z_{ln}$  - axis of the principal reference system,  $X_{ln}Y_{ln}Z_{ln}$ , associated with a gear pair as illustrated in Figure 3.23.

The pinion reference system,  $X_pY_pZ_p$ , is the fifth principal reference system associated with the gear pair. The reference system,  $X_pY_pZ_p$ , is rigidly associated with the pinion and is rotated together

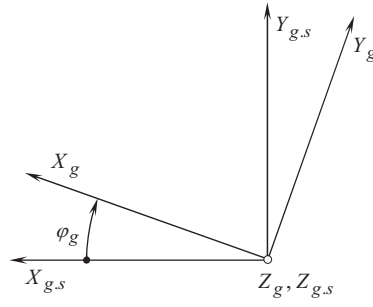


**FIGURE 3.21** Current configuration of a gear reference systems,  $X_g Y_g Z_g$ , in relation to the motionless gear reference systems,  $X_{g.s} Y_{g.s} Z_{g.s}$ .

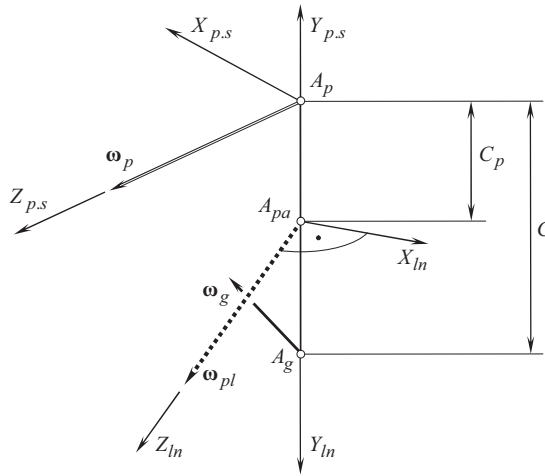


**FIGURE 3.22** Current configuration of the motionless pinion reference systems,  $X_{p.s} Y_{p.s} Z_{p.s}$ , in relation to the main reference system,  $X_{ln} Y_{ln} Z_{ln}$ , associated with the gear pair.

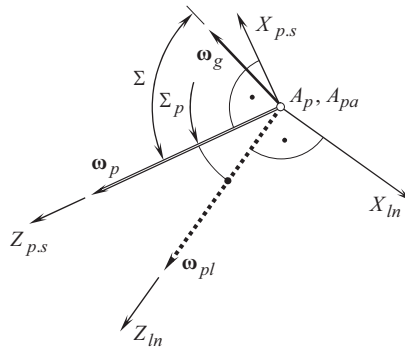


**FIGURE 3.23** The motionless reference systems,  $X_{p.s} Y_{p.s} Z_{p.s}$ , of the pinion is turned through the pinion cone angle,  $\Sigma_p$ , about  $Z_{ln}$  - axis of the main reference system,  $X_{ln} Y_{ln} Z_{ln}$ , associated with the gear pair.

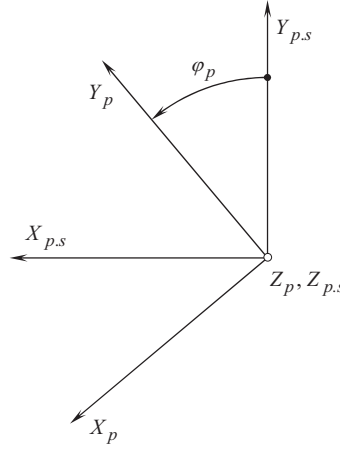


**FIGURE 3.24** Current configuration of the pinion reference systems,  $X_p Y_p Z_p$ , in relation to the motionless pinion reference systems  $X_{p.s} Y_{p.s} Z_{p.s}$ .

with the pinion about its axis of rotation,  $O_p$ . As illustrated in Figure 3.24, the reference systems  $X_p Y_p Z_p$  and  $X_{p.s} Y_{p.s} Z_{p.s}$  share the common axis  $Z_p \equiv Z_{p.s}$  and are turned in relation to one another about the  $Z_{p.s}$  – axis through a pinion rotation angle,  $\varphi_p$ .

A gear rotation angle,  $\varphi_g$ , in Figure 3.21, and a pinion rotation angle,  $\varphi_p$ , in Figure 3.24, correlate to one another in the following manner:  $\varphi_p = u \varphi_g$ , where  $u$  is the gear ratio of the gear pair.

The introduced five reference systems, namely:

1. The main reference system,  $X_{ln} Y_{ln} Z_{ln}$
2. The stationary gear reference system,  $X_{g.s} Y_{g.s} Z_{g.s}$
3. The gear reference system,  $X_g Y_g Z_g$
4. The stationary pinion reference system,  $X_{p.s} Y_{p.s} Z_{p.s}$
5. The pinion reference system,  $X_p Y_p Z_p$

form a set of the so-called *main reference systems*, associated with a gear pair.

Two more reference systems have to be considered here. They are:

1. the stationary plane-of-action reference system,  $X_{pa.s} Y_{pa.s} Z_{pa.s}$ , and
2. the plane-of-action reference system,  $X_{pa} Y_{pa} Z_{pa}$ .

A current configuration of the stationary plane-of-action reference system,  $X_{pa.s} Y_{pa.s} Z_{pa.s}$ , in relation to the main reference system,  $X_{ln} Y_{ln} Z_{ln}$ , associated with a gear pair, is illustrated in Figure 3.25. The  $Z_{pa.s}$  – axis is pointed along the vector of instantaneous rotation,  $\omega_{pl}$ ; the  $X_{pa.s}$  – axis forms the transverse pressure angle,  $\phi_{t,\omega}$ , with the axis  $X_{ln}$  of the main reference system  $X_{ln} Y_{ln} Z_{ln}$ ; and  $Y_{pa.s}$  – axis complements the axes  $X_{pa.s}$  and  $Z_{pa.s}$  to a left-hand oriented *Cartesian* reference system  $X_{pa.s} Y_{pa.s} Z_{pa.s}$ .

The configuration of the plane-of-action reference system,  $X_{pa} Y_{pa} Z_{pa}$ , in relation to the stationary plane-of-action reference system,  $X_{pa.s} Y_{pa.s} Z_{pa.s}$ , associated with a gear pair is illustrated in Figure 3.26. The reference system,  $X_{pa} Y_{pa} Z_{pa}$ , is turned about the coordinate axis  $Z_{pa.s}$  in relation to the references system  $X_{pa.s} Y_{pa.s} Z_{pa.s}$  through an angle of rotation,  $\varphi_{pa}$ , of the plane of action, *PA*.

A few more auxiliary reference systems are commonly used when a gear pair is investigated.

### 3.4 TRANSFORMATION OF THE MAIN COORDINATE SYSTEMS

Multiple reference systems are commonly applied when investigating gear pairs. It is common practice that one of the coordinate systems is associated with the gear, another one is associated with the

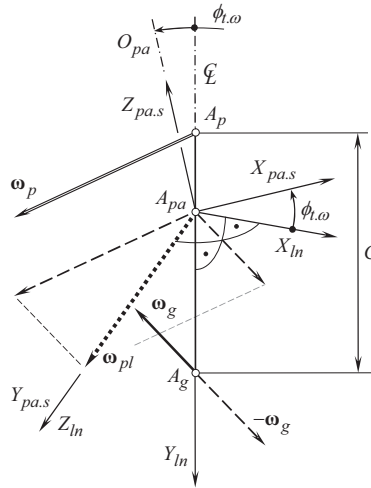


**FIGURE 3.25** Configuration of the stationary plane-of-action reference system,  $X_{pa.s}Y_{pa.s}Z_{pa.s}$ , in relation to the main reference system,  $X_{ln}Y_{ln}Z_{ln}$ , associated with a gear pair.

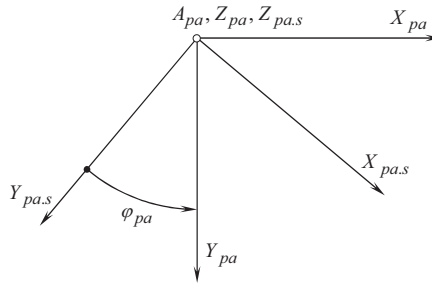


**FIGURE 3.26** Current configuration of the plane-of-action reference system,  $X_{pa}Y_{pa}Z_{pa}$ , in relation to the stationary plane-of-action reference system,  $X_{pa.s}Y_{pa.s}Z_{pa.s}$ , associated with a gear pair.

pinion, and the third reference system is associated with the gear pair housing. In addition, numerous auxiliary (intermediate) reference systems are extensively used as well.

To investigate the kinematics, and the geometry of a gear pair, all the components have to be analytically described in a common reference system. As every component of a gear pair is convenient to be represented in a specific reference system, coordinate system transformations are implemented with a goal to represent the entire gearing in a common coordinate system. For this purpose, the operators of elementary coordinate transformations are used (see Appendix D for details).

### 3.4.1 TRANSITION FROM THE GEAR REFERENCE SYSTEM TO THE MAIN REFERENCE SYSTEM

The transition from the gear coordinate system,  $X_gY_gZ_g$ , to the main reference system,  $X_{ln}Y_{ln}Z_{ln}$ , can be performed in three steps.

At the beginning, the gear coordinate system  $X_gY_gZ_g$  is turned about its axis  $Z_g$  in the counter-clockwise direction through a gear rotation angle,  $\varphi_g$  (see Figure 3.21). This elementary coordinate system transformation is analytically described by the operator of rotation,  $\mathbf{Rt}(\varphi_g, Z_g)$ :

$$\mathbf{Rt}(\varphi_g, Z_g) = \begin{bmatrix} \cos \varphi_g & \sin \varphi_g & 0 & 0 \\ -\sin \varphi_g & \cos \varphi_g & 0 & 0 \\ 0 & 0 & 1 & 0 \\ 0 & 0 & 0 & 1 \end{bmatrix} \quad (3.1)$$



Second, the stationary gear coordinate system,  $X_{g,s}Y_{g,s}Z_{g,s}$ , is translated at the gear center-distance  $C_g$  along the axis  $Y_g$ . In this intermediate position, the coordinate system  $X_{g,s}Y_{g,s}Z_{g,s}$  is labeled as  $X_{g,s}^*Y_{g,s}^*Z_{g,s}^*$ . For analytical description of the transition from the stationary gear coordinate system,  $X_{g,s}Y_{g,s}Z_{g,s}$ , to the intermediate auxiliary coordinate system  $X_{g,s}^*Y_{g,s}^*Z_{g,s}^*$ , the operator of translation,  $\mathbf{Tr}(C_g, Y_{g,s}^*)$ , is used:

$$\mathbf{Tr}(C_g, Y_{g,s}^*) = \begin{bmatrix} 1 & 0 & 0 & 0 \\ 0 & 1 & 0 & C_g \\ 0 & 0 & 1 & 0 \\ 0 & 0 & 0 & 1 \end{bmatrix} \quad (3.2)$$

Then, the transition from the auxiliary reference system,  $X_{g,s}^*Y_{g,s}^*Z_{g,s}^*$ , to the main reference system,  $X_{ln}Y_{ln}Z_{ln}$ , is analytically described by the operator of rotation,  $\mathbf{Rt}(\Sigma_g, Y_{g,s})$ , of the coordinate system  $X_{g,s}Y_{g,s}Z_{g,s}$  about its axis  $Y_{g,s}$  in the counterclockwise direction through the gear cone angle,  $\Sigma_g$  (see Figure 3.20):

$$\mathbf{Rt}(\Sigma_g, Y_{g,s}) = \begin{bmatrix} \cos \Sigma_g & 0 & \sin \Sigma_g & 0 \\ 0 & 1 & 0 & 0 \\ -\sin \Sigma_g & 0 & \cos \Sigma_g & 0 \\ 0 & 0 & 0 & 1 \end{bmatrix} \quad (3.3)$$

The resultant transition from the gear coordinate system,  $X_gY_gZ_g$ , to the main reference system,  $X_{ln}Y_{ln}Z_{ln}$ , is analytically described by the operator of the resultant coordinate system transformation,  $\mathbf{Rs}(g \mapsto ln)$ :

$$\mathbf{Rs}(g \mapsto ln) = \mathbf{Rt}(\Sigma_g, Y_{g,s}) \cdot \mathbf{Tr}(C_g, Y_{ln}) \cdot \mathbf{Rt}(\phi_g, Z_g) \quad (3.4)$$

For the inverse coordinate system transformation, that is, for transition from the main reference system,  $X_{ln}Y_{ln}Z_{ln}$ , to the gear coordinate system,  $X_gY_gZ_g$ , the operator of the resultant coordinate system transformation,  $\mathbf{Rs}(ln \mapsto g)$ , can be used:

$$\mathbf{Rs}(ln \mapsto g) = \mathbf{Rs}^{-1}(g \mapsto ln) \quad (3.5)$$

Coupled linear transformations [151,153] can be effectively used to derive the operators  $\mathbf{Rs}(g \mapsto ln)$  and  $\mathbf{Rs}(ln \mapsto g)$  of the resultant coordinate system transformations. Coupled linear transformations combine translation along and rotation about a coordinate axis.<sup>1</sup>

Only rotation is observed in the first step of the coordinate system transformation, that is, the translation is zero. Therefore (see Figure 3.22), in the case under consideration, the coupled operator of the linear transformation,  $\mathbf{Cp}_z(\phi_g, 0)$ , is identical to the operator of rotation  $\mathbf{Rt}(\phi_g, Z_g)$ :

<sup>1</sup> It is instructive to note here that only the initial and the final configurations of a reference system are accounted by the coupled linear transformations operators. No intermediate configurations of the reference system are described by the coupled linear transformations operators. Aiming an analytical description of all intermediate configurations of the reference system, an operator of screw motion,  $\mathbf{Sc}_x[a_x(t), \phi_x(t)]$ , is used instead of the coupled operator of the linear transformation,  $\mathbf{Cp}_x(a_x, \phi_x)$  (see Appendix D).

$$\mathbf{Cp}_z(\varphi_g, 0) = \begin{bmatrix} \cos \varphi_g & \sin \varphi_g & 0 & 0 \\ -\sin \varphi_g & \cos \varphi_g & 0 & 0 \\ 0 & 0 & 1 & 0 \\ 0 & 0 & 0 & 1 \end{bmatrix} \quad (3.6)$$

The next two separate linear transformations, that is,  $\mathbf{Tr}(C_g, Y_{ln})$  and  $\mathbf{Rt}(\Sigma_g, Y_{g.s})$ , can be analytically described by the coupled operator of the linear transformation,  $\mathbf{Cp}_y(\Sigma_g, C_g)$ . This operator equals:

$$\mathbf{Cp}_y(\Sigma_g, C_g) = \begin{bmatrix} \cos \Sigma_g & 0 & \sin \Sigma_g & 0 \\ 0 & 1 & 0 & C_g \\ -\sin \Sigma_g & 0 & \cos \Sigma_g & 0 \\ 0 & 0 & 0 & 1 \end{bmatrix} \quad (3.7)$$

Ultimately, the resultant transition from the gear coordinate system,  $X_g Y_g Z_g$ , to the main reference system,  $X_{ln} Y_{ln} Z_{ln}$ , is analytically described by the operator of the resultant coordinate system transformation,  $\mathbf{Rs}(g \mapsto ln)$ :

$$\mathbf{Rs}(g \mapsto ln) = \mathbf{Cp}_y(\Sigma_g, C_g) \cdot \mathbf{Cp}_z(\varphi_g, 0) \quad (3.8)$$

The use of the operators of coupled linear transformations allows a reduction in a total number of the operators of elementary coordinate system transformations that makes sense when long chains of consequent coordinate system transformations are necessary to describe analytically.

### 3.4.2 TRANSITION FROM THE PINION REFERENCE SYSTEM TO THE MAIN REFERENCE SYSTEM

The transition from the pinion coordinate system,  $X_p Y_p Z_p$ , to the main reference system,  $X_{ln} Y_{ln} Z_{ln}$ , can be performed in the following manner.

At the beginning, the pinion coordinate system  $X_p Y_p Z_p$  is turned about its axis  $Z_p$  in the clockwise direction through a pinion rotation angle,  $\varphi_p$  (see Figure 3.24) to the position of the stationary pinion coordinate system,  $X_{g.s} Y_{g.s} Z_{g.s}$ . This elementary coordinate system transformation is analytically described by the operator of rotation,  $\mathbf{Rt}(\varphi_p, Z_p)$ :

$$\mathbf{Rt}(\varphi_p, Z_p) = \begin{bmatrix} \cos \varphi_p & -\sin \varphi_p & 0 & 0 \\ \sin \varphi_p & \cos \varphi_p & 0 & 0 \\ 0 & 0 & 1 & 0 \\ 0 & 0 & 0 & 1 \end{bmatrix} \quad (3.9)$$

Afterward, the stationary pinion coordinate system,  $X_{p.s} Y_{p.s} Z_{p.s}$ , is turned about the coordinate axis  $X_{p.s}$  through an angle of  $180^\circ$  to a position of the reference system  $X_{p.s}^* Y_{p.s}^* Z_{p.s}^*$  (see Figure 3.23). This linear transformation is analytically described by means of the operator  $\mathbf{Rt}(180^\circ, X_{p.s})$ :

$$\mathbf{Rt}(180^\circ, X_{p.s}) = \begin{bmatrix} 1 & 0 & 0 & 0 \\ 0 & -1 & 0 & 0 \\ 0 & 0 & -1 & 0 \\ 0 & 0 & 0 & 1 \end{bmatrix} \quad (3.10)$$

Then, the intermediate pinion coordinate system,  $X_{p,s}^* Y_{p,s}^* Z_{p,s}^*$ , is translated at the pinion center-distance  $-C_p$  along the axis  $Y_{p,s}^*$ . In this intermediate position, the coordinate system  $X_{p,s}^* Y_{p,s}^* Z_{p,s}^*$  is labeled as  $X_{p,s}^{**} Y_{p,s}^{**} Z_{p,s}^{**}$ . For analytical description of the transition from the stationary pinion coordinate system,  $X_{p,s}^* Y_{p,s}^* Z_{p,s}^*$ , to the intermediate auxiliary coordinate system  $X_{p,s}^{**} Y_{p,s}^{**} Z_{p,s}^{**}$ , the operator of translation,  $\mathbf{Tr}(C_p, Y_{p,s}^*)$ , can be used:

$$\mathbf{Tr}(C_p, Y_{p,s}^*) = \begin{bmatrix} 1 & 0 & 0 & 0 \\ 0 & 1 & 0 & -C_p \\ 0 & 0 & 1 & 0 \\ 0 & 0 & 0 & 1 \end{bmatrix} \quad (3.11)$$

Finally, the transition from the auxiliary reference system,  $X_{p,s}^{**} Y_{p,s}^{**} Z_{p,s}^{**}$ , to the main reference system,  $X_{ln} Y_{ln} Z_{ln}$ , can be analytically described by the operator of rotation,  $\mathbf{Rt}(\Sigma_p, Y_{p,s}^{**})$ , of the coordinate system  $X_{p,s}^{**} Y_{p,s}^{**} Z_{p,s}^{**}$  about its axis  $Y_{g,s}$  in the counterclockwise direction through the angle that equals to  $(180^\circ - \Sigma_p)$  (see Figure 3.23):

$$\mathbf{Rt}(\Sigma_p, Y_{p,s}^{**}) = \begin{bmatrix} \cos(180^\circ - \Sigma_p) & 0 & \sin(180^\circ - \Sigma_p) & 0 \\ 0 & 1 & 0 & 0 \\ -\sin(180^\circ - \Sigma_p) & 0 & \cos(180^\circ - \Sigma_p) & 0 \\ 0 & 0 & 0 & 1 \end{bmatrix} \quad (3.12)$$

With that said, the resultant transition from the pinion coordinate system,  $X_p Y_p Z_p$ , to the main reference system,  $X_{ln} Y_{ln} Z_{ln}$ , is analytically described by the operator of the resultant coordinate system transformation,  $\mathbf{Rs}(p \mapsto ln)$  :

$$\mathbf{Rs}(p \mapsto ln) = \mathbf{Rt}(\Sigma_p, Y_{p,s}^{**}) \cdot \mathbf{Tr}(C_p, Y_{p,s}^*) \cdot \mathbf{Rt}(180^\circ, X_{p,s}) \cdot \mathbf{Rt}(\varphi_p, Z_p) \quad (3.13)$$

For the inverse coordinate system transformation, that is, for the transition from the main reference system,  $X_{ln} Y_{ln} Z_{ln}$ , to the pinion coordinate system,  $X_p Y_p Z_p$ , the operator of the resultant coordinate system transformation,  $\mathbf{Rs}(ln \mapsto p)$ , can be used:

$$\mathbf{Rs}(ln \mapsto p) = \mathbf{Rs}^{-1}(p \mapsto ln) \quad (3.14)$$

Again, coupled linear transformations [151,153] can be used to derive the operators  $\mathbf{Rs}(p \mapsto ln)$  and  $\mathbf{Rs}(ln \mapsto p)$  of resultant coordinate system transformations.

Only rotation is observed in the first step of the coordinate system transformation, namely, the translation is zero. Therefore, in the case under consideration, the coupled operator of the linear transformation,  $\mathbf{Cp}_z(\varphi_p, 0)$ , is identical to the operator of rotation  $\mathbf{Rt}(\varphi_p, Z_p)$ :

$$\mathbf{Cp}_z(\varphi_p, 0) = \begin{bmatrix} \cos \varphi_p & -\sin \varphi_p & 0 & 0 \\ \sin \varphi_p & \cos \varphi_p & 0 & 0 \\ 0 & 0 & 1 & 0 \\ 0 & 0 & 0 & 1 \end{bmatrix} \quad (3.15)$$

The transition from the stationary pinion coordinate system  $X_{p,s} Y_{p,s} Z_{p,s}$  to a position of the reference system  $X_{p,s}^* Y_{p,s}^* Z_{p,s}^*$  (see Figure 3.23) can be analytically described by means of the operator  $\mathbf{Cp}_x(180^\circ, 0)$ :

$$\mathbf{Cp}_x(180^\circ, 0) = \begin{bmatrix} 1 & 0 & 0 & 0 \\ 0 & -1 & 0 & 0 \\ 0 & 0 & -1 & 0 \\ 0 & 0 & 0 & 1 \end{bmatrix} \quad (3.16)$$

The next two separate linear transformations [these linear transformations are analytically described by the operators  $\mathbf{Tr}(r_p, Y_{p.s}^*)$  and  $\mathbf{Rt}(\Sigma_p, Y_{p.s}^{**})$ ] can be analytically described by the coupled operator of the linear transformation,  $\mathbf{Cp}_y[(180^\circ - \Sigma_p), -C_p]$ . This operator is equal:

$$\mathbf{Cp}_y[(180^\circ - \Sigma_p), -C_p] = \begin{bmatrix} \cos(180^\circ - \Sigma_p) & 0 & -\sin(180^\circ - \Sigma_p) & 0 \\ 0 & 1 & 0 & -C_p \\ \sin(180^\circ - \Sigma_p) & 0 & \cos(180^\circ - \Sigma_p) & 0 \\ 0 & 0 & 0 & 1 \end{bmatrix} \quad (3.17)$$

Ultimately, the resultant transition from the pinion coordinate system,  $X_p Y_p Z_p$ , to the main reference system,  $X_{ln} Y_{ln} Z_{ln}$ , is analytically described by the operator of the resultant coordinate system transformation,  $\mathbf{Rs}(p \mapsto ln)$ :

$$\mathbf{Rs}(p \mapsto ln) = \mathbf{Cp}_y[(180^\circ - \Sigma_p), -C_p] \cdot \mathbf{Cp}_x(180^\circ, 0) \cdot \mathbf{Cp}_z(\varphi_p, 0) \quad (3.18)$$

The use of the operators of coupled linear transformations allows a considerable reduction in the total number of the operators of elementary coordinate system transformations. This is reasonable, especially in cases when long chains of consequent coordinate system transformations are required to be described analytically.

The derived operators of coordinate system transformations are also valid for the reduced cases of gearing, namely, for intersected-axes gearing, and parallel-axes gearing, as well.

As in intersected-axes gearing, the center-distance is zero ( $C = 0$ ), then zero values of the design parameters  $C_g = 0$  and  $C_p = 0$  of the gear and of the pinion should be entered into corresponding formula for a coordinate system transformation.

In parallel-axes gearing, the crossed-axes angle,  $\Sigma$ , is either zero ( $\Sigma = 0^\circ$ ) or it is equal to  $\Sigma = \pm 180^\circ$ . The actual value of the gear cone angle,  $\Sigma_g$ , and the pinion cone angle,  $\Sigma_p$  (either zero or  $180^\circ$ ), depends on the actual value of the crossed-axes angle  $\Sigma$ , and equals either zero ( $\Sigma = 0^\circ$ ) or  $\Sigma = 180^\circ$ .

In a similar manner, any and all coordinate system transformations can be analytically described by means either of the operators of elementary coordinate system transformations, that is, by means of operators of translations,  $\mathbf{Tr}(x_i, X_i)$ , and operators of rotations,  $\mathbf{Rt}(\varphi_{x_i}, X_i)$ , or by means just of operators of coupled coordinate system transformations,  $\mathbf{Cp}_{x_i}(\varphi_{x_i}, x_i)$ . The latter is more practical.

### 3.4.3 TRANSITION FROM THE PLANE-OF-ACTION REFERENCE SYSTEM TO THE MAIN REFERENCE SYSTEM

The plane-of-action reference system,  $X_{pa} Y_{pa} Z_{pa}$ , is rigidly connected to the plane of action,  $PA$ , and is rotated with the  $PA$ . At a current instant of time, the plane-of-action reference system,  $X_{pa} Y_{pa} Z_{pa}$ , is turned about the  $Z_{pa.s}$  – axis in relation to the stationary plane-of-action reference system,  $X_{pa.s} Y_{pa.s} Z_{pa.s}$ , associated with a gear pair, through an angle,  $\varphi_{pa}$  (see Figure 3.26). For the analytical description of transition from the reference system  $X_{pa} Y_{pa} Z_{pa}$  to the reference system  $X_{pa.s} Y_{pa.s} Z_{pa.s}$  the following equation is used:

$$\mathbf{Rt}(\varphi_{pa}, Z_{pa.s}) = \begin{bmatrix} \cos \varphi_{pa} & -\sin \varphi_{pa} & 0 & 0 \\ \sin \varphi_{pa} & \cos \varphi_{pa} & 0 & 0 \\ 0 & 0 & 1 & 0 \\ 0 & 0 & 0 & 1 \end{bmatrix} \quad (3.19)$$

The transition from the stationary plane-of-action reference system,  $X_{pa.s}Y_{pa.s}Z_{pa.s}$ , to the main reference system,  $X_{ln}Y_{ln}Z_{ln}$ , associated with a gear pair, can be performed in two steps, as illustrated in Figure 3.25.

**First**, the reference system,  $X_{pa.s}Y_{pa.s}Z_{pa.s}$ , has to be turned counterclockwise about the axis  $X_{pa.s}$  through a right angle to a position  $X_{pa.s}^*Y_{pa.s}^*Z_{pa.s}^*$  (not shown in Figure 3.25). For analytical description of this kind of transition, an operator of rotation:

$$\mathbf{Rt}(90^\circ, X_{pa.s}) = \begin{bmatrix} 1 & 0 & 0 & 0 \\ 0 & 0 & -1 & 0 \\ 0 & 1 & 0 & 0 \\ 0 & 0 & 0 & 1 \end{bmatrix} \quad (3.20)$$

is commonly used.

**Second**, the reference system,  $X_{pa.s}^*Y_{pa.s}^*Z_{pa.s}^*$ , has to be turned counterclockwise about the axis  $Z_{pa.s}^*$  through a transverse pressure angle,  $\phi_{t,\omega}$ . For analytical description of this kind of transition, an operator of rotation:

$$\mathbf{Rt}(\phi_{t,\omega}, Z_{pa.s}^*) = \begin{bmatrix} \cos \phi_{t,\omega} & -\sin \phi_{t,\omega} & 0 & 0 \\ \sin \phi_{t,\omega} & \cos \phi_{t,\omega} & 0 & 0 \\ 0 & 0 & 1 & 0 \\ 0 & 0 & 0 & 1 \end{bmatrix} \quad (3.21)$$

can be used.

The resultant coordinate system transformation is analytically described by the operator of the resultant transformation,  $\mathbf{Rs}(pa.s \mapsto ln)$ :

$$\mathbf{Rs}(pa.s \mapsto ln) = \mathbf{Rt}(\phi_{t,\omega}, Z_{pa.s}^*) \cdot \mathbf{Rt}(90^\circ, X_{pa.s}) \quad (3.22)$$

For the inverse coordinate system transformation, the operator of the coordinate system transformation:

$$\mathbf{Rs}(ln \mapsto pa.s) = \mathbf{Rs}^{-1}(pa.s \mapsto ln) \quad (3.23)$$

is used.

Additional reference systems associated with a gear pair can be introduced when it is necessary.

---

# 4 Smooth Transmission of Uniform Rotary Motion

## *Three Fundamental Laws of Gearing*

An input uniform rotary motion from a driving shaft to a driven shaft can be transmitted by various means. If an angular velocity ratio,  $u_\varphi$ , in a gear pair is of a constant value ( $u_\varphi = \omega_{\text{input}}/\omega_{\text{output}} = \text{const}$ ), it is said that the rotation from a driving shaft to a driven shaft is transmitted smoothly. Here, the rotation of the input shaft (namely, rotation of the driving shaft) is designated as  $\omega_{\text{input}}$ , and the rotation of the output shaft (that is, rotation of the driven shaft) is designated as  $\omega_{\text{output}}$ . The angular velocity ratio,  $u_\varphi$ , in geometrically accurate gearing is of a constant value.

Geometrically accurate gears rotate smoothly, they produce almost no vibration and almost zero noise excitation. Approximate gears feature variable in time angular velocity ratio, that is,  $u_\varphi = u_\varphi(t)$ : when the input shaft is rotated steadily, the output shaft rotates with oscillations. Variation of the angular velocity ratio causes vibration generation, an excessive noise excitation, an excessive tooth flank wear, and so forth.

The actual value of angular velocity ratio in a gear pair strongly depends on tooth flank geometry of the mating gears, of the design features of a particular gear pair, of the actual configuration of the mating gears in relation to one another under an operating load, and so forth. It is important to identify a set of requirements under which the angular velocity ratio in a gear pair is of a constant value, namely, a set of requirements under which the equality  $u_\varphi = \text{const}$  is ensured. Immediately below these requirements are discussed from a general perspective – regardless of the actual kind of gearing (and only partly with focus on parallel-axes gearing). Later on, in the Chapters 6, 12, and 14, of the book, the equivalent requirements for transmitting a rotary motion smoothly are discussed (more in detail) for parallel-axes gearing ( $P_a$  – gearing), for intersected-axes gearing ( $I_a$  – gearing), and for crossed-axes gearings ( $C_a$  – gearing).

To be capable of transmitting rotary motion smoothly, gearing of all kinds has to fulfil three *fundamental laws of gearing*. This set of *fundamental laws of gearing* is discussed immediately below.

### 4.1 TRANSMISSION OF ROTARY MOTION: THE PRESENT-DAY PRACTICE

To make the engagement of two gears in mesh possible, certain kinematical and geometrical conditions have to be fulfilled. The relationships for mating external spur and helical gears are considered<sup>1</sup> here as an example.

When designing gears, in order to get two involute gears in mesh, it is practical to fulfil the following five geometrical and kinematical conditions.

- *The first condition* – The first condition governing mating involute gears immediately follows from the rope drive analogy (or from the *equivalent pulley-and-belt transmission*, in other terminology). This condition is formulated as follows:

---

<sup>1</sup> Relationships similar to those considered in this section of the book apply to mating internal gear pairs as well.

The ratio of the gear and pinion base diameters must be equal to the gear ratio:

$$\frac{d_{b,g}}{d_{b,p}} = \frac{N_g}{N_p} = u \quad (4.1)$$

Hence:

$$\frac{d_{b,g}}{N_g} = \frac{d_{b,p}}{N_p} \quad \therefore \quad \frac{p_{bt,g}}{\pi} = \frac{p_{bt,p}}{\pi} \quad \therefore \quad p_{bt,g} = p_{bt,p} \quad (4.2)$$

This means that the transverse base pitches of mating gears must be equal.

- *The second condition* – For line contact, the base helix angles of a gear and of its mating pinion must be equal:

$$\psi_{b,g} = \psi_{b,p} \quad (4.3)$$

Hence, the second condition can be formulated as follows:

*The normal base pitches of the gear and pinion must be equal:*

$$p_{b,g} \equiv p_{b,p} \quad (4.4)$$

Two involute gears having the same base pitch can be engaged in mesh with one another. To make the mesh possible, equality of base pitches of a gear and its mating pinion is the must.

- *The third condition* – For a smooth transition of tooth contact from one pair of teeth to another, there must be, theoretically, at least one point of contact in the zone of action. Because of strength conditions, there is a further requirement in the case of mating helical gears, namely:

*All points of contact along the minimum required path of contact should be correspondingly in contact along the contact line over the face width.*

By definition, the transverse contact ratio,  $m_p$ , of a gear pair is equal to:

$$m_p = \frac{\text{length of path of contact}}{\text{transverse base pitch } p_t} \quad (4.5)$$

The face contact ratio,  $m_F$  (overlap ratio), of a gear pair is defined as:

$$m_F = \frac{F_{pa} \tan \psi_b}{p_{bt}} \quad (4.6)$$

In Eq. (4.6), the active portion of the face width of mating gears is denoted by  $F_{pa}$ .

The total contact ratio,  $m_t$ , of a gear pair is equal to the sum of both:

$$m_t = m_p + m_F \quad (4.7)$$

For any and all gear pairs, fulfillment of the inequality  $m_t > 1$  is a must.

For spur gear pairs,  $m_F = 0$ . Therefore, the inequality  $m_t = m_p > 1$  must be fulfilled for spur gear pairs.

Fog helical gear pairs,  $m_p > 0$ , and  $m_F > 0$ . Therefore, the inequality  $m_t = m_p + m_F > 1$  must be fulfilled for helical gear pairs.

In order to ensure satisfactory running and loading conditions, it is recommended that [81]:



1. transverse contact ratio is somewhat greater than 1, and
  2. on helical gears, an overlap ratio that exceeds or equal to 1 is chosen.
- *The fourth condition* – Commonly, the tooth flank geometry is calculated for a zero back-lash gear pair. At the gear and pinion working pitch cylinders, therefore, the sum of the theoretical transverse tooth thicknesses of the gear  $t'_{t,g}$  and pinion  $t'_{t,p}$  must be equal to the transverse working pitch  $p'$  :

$$t'_{t,g} + t'_{t,p} = p' = \pi \frac{2C}{N_g + N_p} \quad (4.8)$$

- *The fifth condition* – The gear and pinion root cylinders must provide an adequate bottom clearance beyond the tip cylinder of the mating gears to avoid interference [81]:

$$d_{o,g} + d_{f,p} + 2C = 2c \quad (4.9)$$

$$d_{o,p} + d_{f,g} + 2C = 2c \quad (4.10)$$

Bottom clearance is denoted here by  $c$ .

To enable two gears to mesh correctly, therefore, the following design parameters of basic tooth data:

Number of Teeth	$N_g, N_p$
Base Diameter	$d_{b,g}, d_{b,p}$
Base Helix Angle	$\psi_{b,g}, \psi_{b,p}$
Base Tooth Thickness	$t_{b,g}, t_{b,p}$
Outer Diameter	$d_{o,g}, d_{o,p}$
Root Diameter	$d_{f,g}, d_{f,p}$

for both individual gears must jointly meet the set of the above conditions.

As it is clear from the discussion below in this chapter of the book, the present-day practice is primitive, and is far too from the challenges and needs of the present-day gear technology, and, moreover, of the gear technology in the future.

## 4.2 THE LAW OF CONTACT: THE FIRST FUNDAMENTAL LAW OF GEARING

In this section of the book, a constraint onto the contact geometry of tooth flanks of a gear and of a mating pinion, that is imposed by the first fundamental law of gearing, is discussed. The first fundamental law of gearing has to be fulfilled in gear pairs of all kinds: in parallel-axes gearing, in intersected-axes gearing, and in crossed-axes gearing, as well.

To fulfil the first fundamental law of gearing, the resultant velocity vector,  $\mathbf{V}_\Sigma$ , of the relative motion of tooth flanks,  $\mathcal{G}$  and  $\mathcal{P}$ , of a gear and a mating pinion has to be entirely located in a common tangent plane through contact point,  $K$ , of the interacting tooth flanks,  $\mathcal{G}$  and  $\mathcal{P}$ . The necessity of such a configuration of the resultant velocity vector,  $\mathbf{V}_\Sigma$ , with respect to the common tangent plane is illustrated by the following example.

Consider relative motion of the tooth flanks,  $\mathcal{G}$  and  $\mathcal{P}$ , of a gear and its mating pinion, as illustrated in Figure 4.1. For simplicity, but without loss of generality, normal sections through the contact point of the gear and the mating pinion are depicted there. It is also assumed that the gear tooth



The depicted in Figure 4.1 schematics illustrate the necessity of proper configuration of the linear velocity vector,  $\mathbf{V}_\Sigma$ , in relation to the common tangent plane to the tooth flanks,  $\mathcal{G}$  and  $\mathcal{P}$ , at every point of their contact. This requirement is referred to as the *first fundamental law of gearing*. The first fundamental law of gearing is formulated as follows:<sup>2</sup>

**The first fundamental law of gearing:** *At every point of contact of tooth flanks of a gear and of a mating pinion a vector of their instant relative motion has to be perpendicular to the common perpendicular at every instant of time.*

Occasionally, the first fundamental law of gearing is referred to as *condition of contact of interacting tooth flanks*, for simplicity.

Various forms of analytical representation of the *first fundamental law of gearing* are known.

To derive a convenient analytical expression that describes the first fundamental law of gearing, let's turn our attention to the following. As shown in Figure 4.1, dot product of the vectors  $\mathbf{n}_g$  and  $\mathbf{V}_\Sigma$  is:

- either of a positive value ( $\mathbf{n}_p^a \cdot \mathbf{V}_\Sigma^a > 0$ ) in the first scenario (see Figure 4.1a)
- or equals zero ( $\mathbf{n}_p^b \cdot \mathbf{V}_\Sigma^b = 0$ ) in the second scenario (see Figure 4.1b)
- or of a negative value ( $\mathbf{n}_p^c \cdot \mathbf{V}_\Sigma^c < 0$ ) in the third scenario (see Figure 4.1c)

The law of contact of two interacting tooth flanks of mating gear teeth can be expressed in the form of dot product:

$$\mathbf{n}_g \cdot \mathbf{V}_\Sigma = 0 \quad (4.11)$$

where  $\mathbf{n}_g$  is the unit vector of common perpendicular through the contact point of the tooth flanks,  $\mathcal{G}$  and  $\mathcal{P}$ , and  $\mathbf{V}_\Sigma$  is the linear velocity vector of the resultant instant relative motion of the tooth flanks,  $\mathcal{G}$  and  $\mathcal{P}$ , at contact point  $K$ .

Equation (4.11) reveals that a component of the linear velocity vector,  $\mathbf{V}_\Sigma$ , that is pointed along the common perpendicular,  $\mathbf{n}_g$ , equals to zero. Otherwise, either interference, or separation of the tooth flanks,  $\mathcal{G}$  and  $\mathcal{P}$ , in the gear pair is observed. Neither separation, nor interference of the tooth flanks,  $\mathcal{G}$  and  $\mathcal{P}$ , is permissible. Therefore, the linear velocity vector,  $\mathbf{V}_\Sigma$ , is either located in a common tangent plane, or it is of a zero value.

Prof. V.A. Shishkov was the first to propose Eq. (4.11) (as early, as in 1948, or even earlier [197,198]). Because of this, equation of contact in the form of dot product [see Eq. (4.11)] is commonly referred to as *Shishkov equation of contact*,  $\mathbf{n}_g \cdot \mathbf{V}_\Sigma = 0$ . An in-detail analysis of the reasons for why Prof. V.A. Shishkov is credited with the discovery of the equation of contact in the form  $\mathbf{n}_g \cdot \mathbf{V}_\Sigma = 0$ , is discussed in Ref. [145].

Equation of contact in the form  $\mathbf{n}_g \cdot \mathbf{V}_\Sigma = 0$  is practical in cases when the interacting surfaces are of a simple geometry, and when the resultant relative motion is also simple. The first makes possible determination the unit normal vector,  $\mathbf{n}_g$ , without derivation of the expressions for the derivatives of the equations of the contacting surface with respect to the surface parameters. The second allows the determination of the linear velocity vector,  $\mathbf{V}_\Sigma$ , without derivation of the equation of the traveling surface with respect to the parameter of motion. Solution to many gear-related problems is significantly simplified when the *Shishkov equation of contact*  $\mathbf{n}_g \cdot \mathbf{V}_\Sigma = 0$  is used. If derivation of the equations of the derivatives for the purposes of determination of the

<sup>2</sup> This was Franz Reuleaux who in the second half of the nineteenth century, has proposed the so-called *method of common perpendiculars* [188,189]. Despite of the property of common perpendiculars was used earlier by numerous researchers, including, but not limited to R. Willis [see Section 12 in Ch. Gochman 1886 book: Gochman, H.I., *Theory of Gearing Generalized and Developed Analytically*, Odessa, 1986, 229 pages, 23 Figures, pages I-X (appendix) – equations], Reuleaux deserves to be credited with the *Law of Contact*, as since his accomplishment, this law got an extensive use in the *Mechanism and Machine Science*.

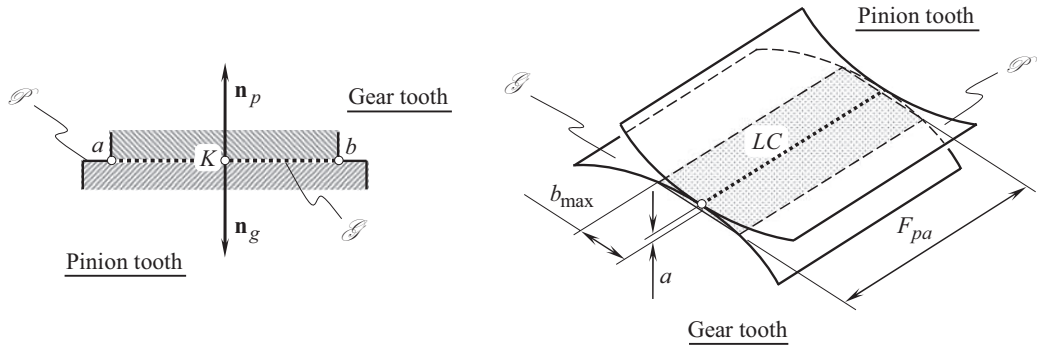


**FIGURE 4.2** Schematic of interaction of tooth flanks of a gear and of a mating pinion,  $\mathcal{S}$  and  $\mathcal{P}$ , in aligned gears.

vectors,  $\mathbf{n}_g$  and  $\mathbf{V}_\Sigma$ , cannot be avoided, the use of the *Shishkov equation of contact*  $\mathbf{n}_g \cdot \mathbf{V}_\Sigma = 0$  is less beneficial.

The condition of contact between a gear tooth flank,  $\mathcal{S}$ , and a mating pinion tooth flank,  $\mathcal{P}$ , is violated in misaligned parallel-axes gear pair when the tooth flanks,  $\mathcal{S}$  and  $\mathcal{P}$ , are displaced in relation to one another. In the aligned gear pair, the tooth flanks,  $\mathcal{S}$  and  $\mathcal{P}$ , make line contact: see dotted line in Figure 4.2. Under the applied load, the line of contact,  $LC$ , spreads over a contact patch. The contact patch length equals to the effective face width,  $F_{pa}$ , in the gear pair. The contact patch width,  $2b_{\max}$ , depends on the actual value of the distance of approach,  $a$ , of the tooth flanks,  $\mathcal{S}$  and  $\mathcal{P}$ , under operating load.

In the misaligned gears tooth flanks,  $\mathcal{S}$  and  $\mathcal{P}$ , are displaced in relation to one another. The unit normals vectors,  $\mathbf{n}_g$  and  $\mathbf{n}_p$ , form an angle that equals  $(180^\circ - \theta)$ , as shown in Figure 4.3. In this particular case, edge contact between the tooth flanks,  $\mathcal{S}$  and  $\mathcal{P}$ , is observed. The contact patch is shaped in a form of a portion of an ellipse-like curve. The contact patch length is less than the effective face width,  $F_{pa}$ , in the gear pair. The maximum contact patch width,  $2b_{\max}$ , depends on the actual value of the distance of approach,  $a$ , of the tooth flanks,  $\mathcal{S}$  and  $\mathcal{P}$ , under operating load.

This discussion can be summarized as follows.

Permissible instantaneous relative motions of tooth flanks,  $\mathcal{S}$  and  $\mathcal{P}$ , in a gear pair are shown in Figure 4.4. Relative motion of the tooth flanks,  $\mathcal{S}$  and  $\mathcal{P}$ , along the common perpendicular,  $\mathbf{n}_g$ , is not permissible; and the instantaneous relative motion is permissible in any direction within the common tangent plane through contact point,  $K$ . It should be pointed out here that a swivel relative motion,  $\pm\varphi_n$ , of the tooth flanks,  $\mathcal{S}$  and  $\mathcal{P}$ , around the axis along the common perpendicular,  $\mathbf{n}_g$ , also meets the requirement specified by Eq. (4.11). However, not all kinds of the swivel motion of the tooth flanks in Figure 4.4 are permissible. For example, no swivel relative motion is permissible about an axis that either intersects or crosses a straight line along the common perpendicular,  $\mathbf{n}_g$ , as the condition of contact,  $\mathbf{n}_g \cdot \mathbf{V}_\Sigma = 0$ , in these cases is violated. The swivel motion,  $\pm\varphi_n$ , of the tooth flanks is not necessary to transmit a rotation from a driving shaft to a driven shaft.<sup>3</sup> However,

<sup>3</sup> In the mid of 1980th Prof. *S.P. Radzevich* has introduced into consideration a permissible relative rotation,  $\pm\varphi_n$ , about contact perpendicular,  $\mathbf{n}_g$ , [148,161,172,189]. A permissible relative rotation,  $\pm\varphi_n$ , can be either intentionally introduced (for example, in NC machining of sculptured part surfaces, etc.) into the kinematics of machining, or it can be inherited to the kinematics of a real interaction of part surfaces (in  $C_n$ -gearing, etc.). In the second case, a rotation,  $\pm\varphi_n$  (or  $\omega_n$ ), is just a component of the resultant relative motion of two surfaces,  $\mathcal{S}$  and  $\mathcal{P}$ , that interact with one another. A vector of the resultant relative motion can be dissolved into a few components, and the rotation,  $\pm\varphi_n$  (or  $\omega_n t$ ) is one of the components.

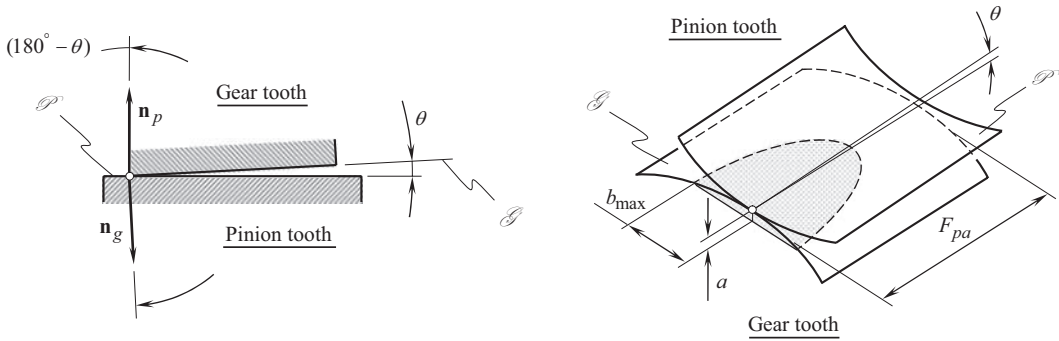


**FIGURE 4.3** Schematic of interaction of tooth flanks of a gear and of a mating pinion,  $\mathcal{G}$  and  $\mathcal{P}$ , in misaligned gears.

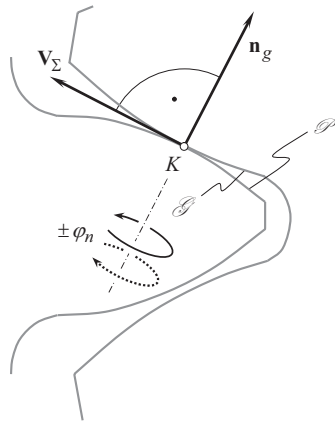


**FIGURE 4.4** Permissible instantaneous relative motions in geometrically accurate gearing.

motion of this nature,  $\omega_n$ , is observed in spatial gearing, namely, in  $C_a$  – gearing (see Figure 4.5) [148, 151, 153, 161, 167].

For a specified gear pair, the vector of swivel relative motion,  $\omega_n$ , can be expressed in terms of the rotation,  $\omega_g$ , of the gear and that,  $\omega_p$ , of the mating pinion, and the design parameters of the gear pair.

It is important to stress the readers' attention here on the following. Equation of contact,  $\mathbf{n}_g \cdot \mathbf{V}_\Sigma = 0$ , was proposed by Prof. V.A. Shishkov in the mid of the twentieth century [see Eq. (4.11)]. However, the nature of the condition of contact (but not the equation of contact itself) was properly understood by smart people in the time of *da Vinci* [23] and even in earlier times.

Fulfillment of the first fundamental law of gearing is necessary but not sufficient for transmitting a uniform rotary motion smoothly from a driving shaft to a driven shaft.

Geometrically accurate gears of all designs meet the *first fundamental law of gearing* – as this is a must.

Tooth flanks,  $\mathcal{G}$  and  $\mathcal{P}$ , of a gear and of a mating pinion that meet the requirements imposed by the *first fundamental law of gearing*, are enveloping to one another. Envelope surfaces of this geometry are referred to as the *envelope surfaces of the first kind*<sup>4</sup> [138].

<sup>4</sup> The necessity of differentiation between *envelope surfaces of the first* and *of the second kind* is due to the following. In order to generate an envelope surface to a family of surfaces, enveloping motion of a traveling surface must be independent, and can be expressed solely in terms of the geometry of the surface to be generated. In case of rolling motion, an enveloping motion is not independent. Therefore, the envelope surface can be generated not for any surface, but only for a unique surface that is conjugate to the envelope surface to be generated. Conjugate pairs of surfaces are always envelope to one another, and not vice versa.

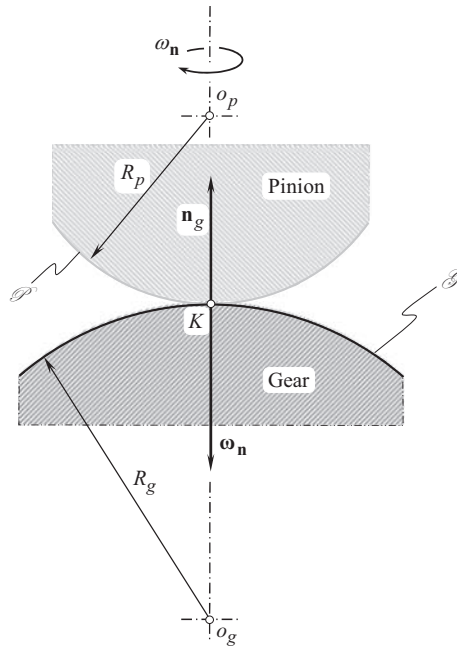


FIGURE 4.5 Swivel relative motion of tooth flanks,  $\mathcal{S}$  and  $\mathcal{P}$ , in crossed-axes gearing.

### 4.3 THE CONJUGATE ACTION LAW: THE SECOND FUNDAMENTAL LAW OF GEARING

The *conjugate action law* is the second fundamental law of gearing. Conjugacy is a specific property of a gear and a mating pinion tooth flanks (as well as tooth profiles) that roll over one another.

The conjugate action law in mesh of tooth flanks of a gear and of a mating pinion,  $\mathcal{S}$  and  $\mathcal{P}$ , is the law to be fulfilled in geometrically accurate gearing of all kinds. Below in this section of the book, the second fundamental law of gearing is discussed primarily in relation to geometrically accurate gearing with no focus on a particular kind of gearing. Then, the second fundamental law of gearing is enhanced to particular kinds of gearing: (a) to parallel-axes gearing, (b) to intersected-axes gearing as well as (c) to crossed-axes gearing.

#### 4.3.1 EQUIVALENT PULLEY-AND-BELT TRANSMISSION

Let us begin the discussion with a trivial case of transmission of rotary motion between two shafts that are parallel to one another. In the simplest case, a rotation from a driving shaft is transmitted to a driven shaft by means of two pulleys connected by means of a belt, as schematically illustrated in Figure 4.6.

Two pulleys of diameters  $d_1$  (driving) and  $d_2$  (driven) are rotated about their axes,  $O_1$  and  $O_2$ , correspondingly. The axes,  $O_1$  and  $O_2$ , are at a center-distance,  $C$ , apart from one another. The pulleys are connected to each other by a belt. The belt is tangent to the pulleys at points  $a$  and  $b$ .

The rotations,  $\omega_1$  and  $\omega_2$ , of the driving and the driven pulleys are synchronized with each other so as to meet the ratio:

$$\frac{\omega_1}{\omega_2} = \frac{d_2}{d_1} \quad (4.12)$$

The linear velocity of arbitrary point,  $m$ , of the belt,  $V_m$ , is calculated from the formula:

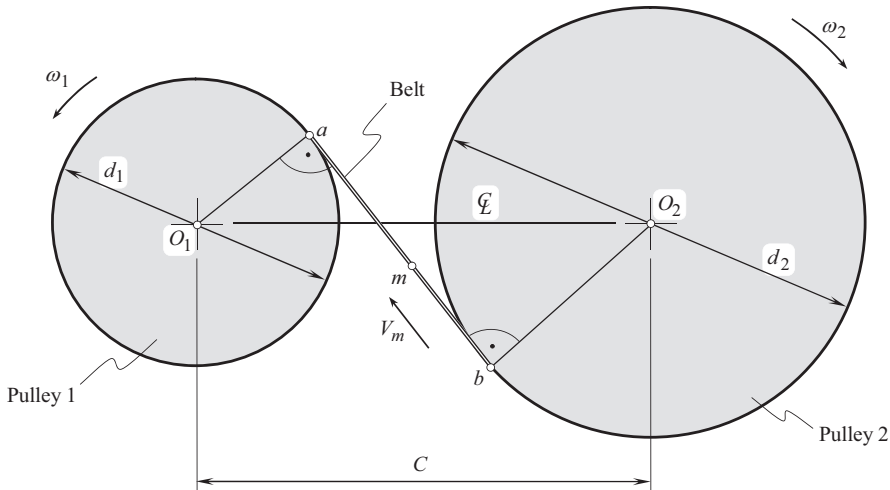


**FIGURE 4.6** Schematic of pulley-and-belt transmission.

$$V_m = 0.5 \cdot \omega_1 \cdot d_1 \equiv 0.5 \cdot \omega_2 \cdot d_2 \quad (4.13)$$

Shown in Figure 4.6, the *equivalent pulley-and-belt transmission* is capable of transmitting a uniform rotation smoothly.

In certain sense, the pulley-and-belt mechanism may be viewed as an equivalent to parallel-axes involute gear pair, namely, as an *equivalent pulley-and-belt transmission*.

It is the right point to stress the readers' attention here on three important features of the *equivalent pulley-and-belt transmission*.

**First**, when the pulleys rotate, an arbitrary point,  $m$ , within the portion,  $ab$ , of the belt traces a *straight line* in a motionless reference system associated with the transmission housing. This straight line is the path of point  $m$ . Therefore, in *equivalent pulley-and-belt transmission* every point of the belt travels straight forward.<sup>5</sup>

**Second**, when a uniform rotation is transmitted from the driving pulley 1 to the driven pulley 2, the torque is transmitted by a force that acts along the belt, namely, along the straight line,  $ab$ : in *equivalent pulley-and-belt transmission* a force is transmitted only along the belt. A force acts only along a straight line, and it can not be transmitted along a curve. Therefore, in *equivalent pulley-and-belt transmission* the straight-line segment,  $ab$ , is an equivalent of the *line of action*, along which a force that is exerted in the driving pulley is transmitted to the driven pulley.

**Third**, in *equivalent pulley-and-belt transmission* a straight path of arbitrary point,  $m$ , in the belt is aligned with the straight line of action. The line of action here is the line, along which a force, that is exerted in the driving pulley, is transmitted to the driven pulley.

It is instructive to note here that the straight-line segment,  $ab$ , at that same time serves both, namely, it serves the path of point of interest,  $m$ , and it serves the line of action in the *equivalent pulley-and-belt transmission* (see Figure 4.6). Only in parallel-axes gearing the path of contact, and the line of action, both, are straight lines that align to one another. It is also critical to distinguish the *path of contact* from the *line of action*, and never mix these two different entities.

<sup>5</sup> This statement is valid only for parallel-axes gearing, and it is not valid for intersected-axes, and for crossed-axes gearing.



To the best of the author's knowledge, it is not known who has to be credited for the invention of the *equivalent pulley-and-belt transmission* (or, in other words, the *equivalent pulley-and-belt model*) of a gear pair in *parallel-axes gearing*.

It was *G.B. Grant* who was the first to introduce (1887) the concept of the base cone in *intersected-axes gearing* [99]. He considered base cone of a gear, and a plane, tangent to the base cone. It was not realized at that time that the tangent plane is by nature the plane of action. Moreover, only one base cone, and NOT two base cones of interacting tooth flanks in bevel gears were considered by *G.B. Grant*.

For the first time ever, the *equivalent pulley-and-belt transmission* of a gear pair in intersected-axes gearing was proposed (~2008) by Prof. *S.P. Radzevich* [174]. Two base cones in tangency with the plane of action were considered [174]. Then, this model was evolved (~2008) by Prof. *S.P. Radzevich* to crossed-axes gearing [174].

#### 4.3.2 CAMUS-EULER-SAVARY THEOREM

The performed analysis of transmission of a rotary motion by the *equivalent pulley-and-belt transmission* is helpful for understanding the requirements that the tooth flank geometry in parallel-axes gearing has to meet.

A smooth transmission of a uniform rotary motion from one shaft to another shaft by means of gear teeth is possible only if interacting tooth flanks,  $\mathcal{G}$  and  $\mathcal{P}$ , are conjugate to one another.

The necessity of conjugacy of tooth flanks of a gear,  $\mathcal{G}$ , and of a mating pinion,  $\mathcal{P}$ , to one another is constituted by the *second fundamental law of gearing* and is discussed in detail immediately below in this section of the book.

In parallel-axes gearing, the *second fundamental law of gearing* is often referred to as *Camus-Euler-Savary* fundamental theorem of gearing (or just as *CES – fundamental theorem of gearing*, for simplicity). This theorem is extensively known mainly due to the 1841 book by Dr. *R. Willis*<sup>6</sup> (see Figure 4.7). In Europe, the *second fundamental law of gearing* is often referred to as the *fundamental (main) theorem of parallel-axes gearing*, or just as *Willis' theorem* [222].

The fundamental requirements governing the shapes that any pair of conjugate tooth profiles may have in parallel-axes gearing<sup>7</sup> states:

**The second fundamental law of (parallel-axes) gearing:** In parallel-axes gearing, in order to transmit a uniform rotary motion from a driving shaft to a driven shaft by means of gear teeth, perpendiculars to the tooth flanks of the interacting teeth at all points of their contact must pass through a stationary point located on the line of centers, namely, the pitch point  $P$ ; the pitch point subdivides the center-distance reciprocal to the angular velocities of the gear and the pinion. (Robert Willis, 1841 [222]).

In other words, two planar curves are said to be conjugate to one another<sup>8</sup> if common perpendicular at point of their contact is pointed along a straight line through the pitch point,  $P$ . The center of the instant rotary motion is coincident with the pitch point,  $P$ .

Tooth flanks of a gear,  $\mathcal{G}$ , and its mating pinion,  $\mathcal{P}$ , must be shaped so as to fulfil the second fundamental law of gearing. This statement is also often called the *conjugate action law*.

<sup>6</sup> Robert Willis (27 February 1800–28 February 1875), a British engineer; a major contributor to the theory of gear teeth in the nineteenth century.

<sup>7</sup> In intersected-axes gearing, and in crossed-axes gearing, in-detail, this concept is discussed in Ref. [174].

<sup>8</sup> It is wrong practice to define conjugate shapes in the following manner:

**Definition:** "A pair of transverse gear tooth profiles is said to be conjugate if a constant angular velocity of one profile produces a constant angular velocity in the meshing profile." Constant output rotation is a consequence of conjugacy of the interacting tooth profiles. The property of *conjugacy* must to be expressed in terms of the kinematics and the geometry of the interacting tooth flanks,  $\mathcal{G}$  and  $\mathcal{P}$ , of a gear and a mating pinion.

38. If the line of direction of the link in link-work, of the common normal to the curves in contact motion, and of the connector in wrapping motion, be severally termed the line of action, we can express the separate propositions which relate to the Velocity Ratio, by saying that the angular velocities of the two pieces are to each other inversely as the segments into which the *line of action* divides the line of centers, or inversely as the perpendiculars from the centers of motion upon the line of action.

I have confined these investigations, for the present,

**FIGURE 4.7** The main theorem of parallel-axes gearing (the Willis' theorem) as it is formulated by Robert Willis on page 38 in his 1841 book: Willis, R., *Principles of Mechanisms, Designed for the Use of Students in the Universities and for Engineering Students Generally*, London, John W. Parker, West Stand, Cambridge: J. & J.J. Deighton, 1841, 446p.

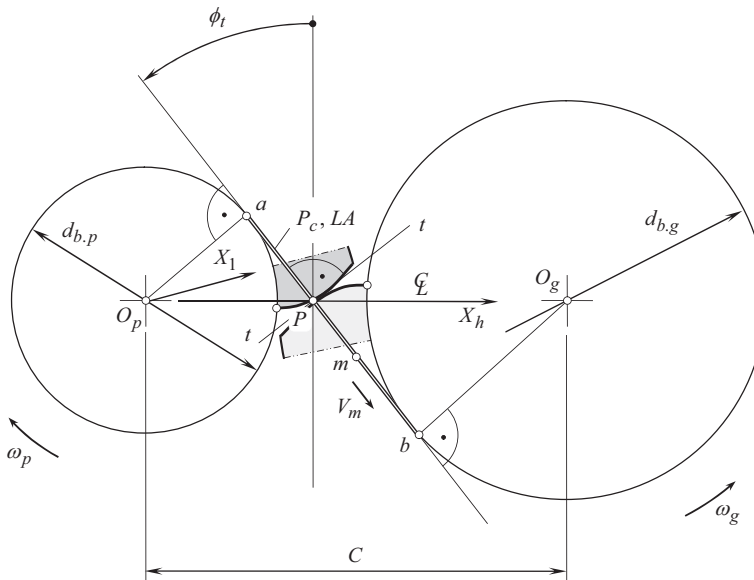


**FIGURE 4.8** Second fundamental law of gearing (*conjugate action law*): Generation of natural form of a gear tooth profile in geometrically accurate parallel-axes gearing.

One more consideration needs to be taken into account in the discussion of conjugate tooth profiles. At contact point,  $K$ , tooth flanks,  $\mathcal{G}$  and  $\mathcal{P}$ , roll and slide over one another. Because of the sliding, the instantaneous rotation can be performed only about the pitch point,  $P$ , and not about any other point – otherwise the tooth flanks interfere into each other. When the *second fundamental law of gearing* is violated, interference of the tooth flanks,  $\mathcal{G}$  and  $\mathcal{P}$ , of a gear and a mating pinion is always observed. The farther contact point,  $K$ , is situated from the pitch point,  $P$ , the more sliding motion is observed, and vice versa.

Refer to Figure 4.8 for more in-detail analysis of the *conjugate action law*. Here, the directions of rotation of the driving and of the driven gears are reversed compared to that shown in Figure 4.6, as the driven pulley is *pulled* by the belt, while the driven gear is *pushed* by the driving gear.

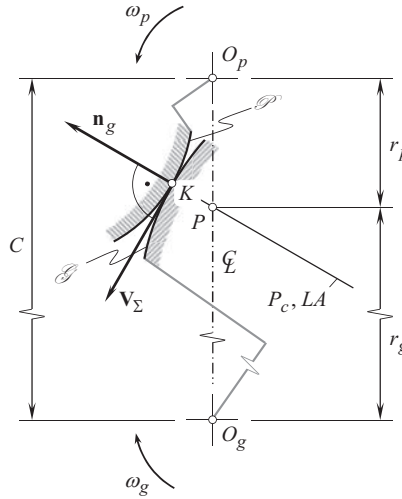


**FIGURE 4.9** Conjugate tooth profiles of a gear,  $\mathcal{S}$ , and its mating pinion,  $\mathcal{P}$ , that fulfill the *CES – fundamental theorem of parallel-axes gearing*.

For correctly designed tooth flanks of a gear and a mating pinion, contact point between the tooth flanks,  $\mathcal{S}$  and  $\mathcal{P}$ , traces a straight path of contact,  $P_c$ . When the friction is not taken into consideration, the force acts perpendicular to the common tangent plane,  $t-t$ , to the tooth flanks,  $\mathcal{S}$  and  $\mathcal{P}$ , through  $P$ . As long as the friction is not accounted for, the acting force is always perpendicular to the tooth flanks,  $\mathcal{S}$  and  $\mathcal{P}$ , at current point of their contact. The straight line of action,  $LA$ , is aligned with the straight path of contact,  $P_c$ , namely: in geometrically accurate parallel axes gearing the straight lines,  $LA$  and  $P_c$ , are congruent to one another at every instant of time when the gears rotate. It is critical to bear in mind that in the theory of gearing the *path of contact*,  $P_c$ , and the *line of action*,  $LA$ , are the two completely different entities. Therefore, the difference between the line of action,  $LA$ , and the path of contact,  $P_c$ , in parallel-axes gearing needs to be firmly realized.

One more example is illustrated in Figure 4.9.

Consider two tooth profiles,  $\mathcal{S}$  and  $\mathcal{P}$ , that contact one another at point,  $K$ , as shown in Figure 4.9. The tooth profiles,  $\mathcal{S}$  and  $\mathcal{P}$ , are designed so as to transmit a rotation from the pinion axis of rotation,  $O_p$ , to the gear axis of rotation,  $O_g$ . The axes,  $O_g$  and  $O_p$ , are at a center-distance,  $C$ . The common unit normal vector to the contacting profiles at contact point,  $K$ , is designated as  $\mathbf{n}_g$ . A straight line that is aligned with the unit normal vector,  $\mathbf{n}_g$ , is referred to as the *line of action*,  $LA$ . The line of action,  $LA$ , intersects the center line,  $\mathcal{C}$ , at the pitch point,  $P$ . According to the *second fundamental law of parallel-axes gearing* (or, in other words, according to the *CES – fundamental theorem of gearing*), the center-distance,  $C$ , is divided by the pitch point,  $P$ , onto two segments,  $O_gP = r_g$  and  $O_pP = r_p$ , so that a proportion:

$$\frac{O_gP}{O_pP} = \frac{r_g}{r_p} = \frac{\omega_p}{\omega_g} = u \quad (4.14)$$

is valid.

Contact point within the gear tooth profile,  $\mathcal{S}$ , is denoted by  $K_g$ . Similarly, contact point,  $K_p$ , within the pinion tooth profile,  $\mathcal{P}$ , is specified. At the point of tangency of the tooth profiles the points,  $K_g$  and  $K_p$ , coincide with one another, and, thus, the common contact point is designated as  $K$ .

The linear velocity vector,  $\mathbf{V}_{K_g}$ , of the point,  $K_g$ , can be expressed in terms of the rotation vector,  $\omega_g$ , of the gear, and the position vector,  $\mathbf{r}_{K_g}$ , of the point  $K_g$ , that is, an equality:

$$\mathbf{V}_{K_g} = \omega_g \times \mathbf{r}_{K_g} \quad (4.15)$$

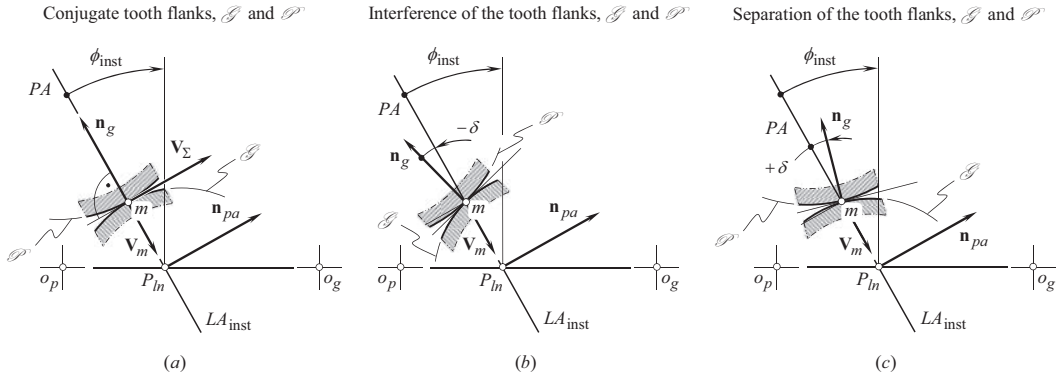


**FIGURE 4.10** To the derivation of equation of conjugacy,  $\mathbf{p}_{ln} \times \mathbf{V}_m \cdot \mathbf{n}_g = 0$ , of interacting tooth flanks,  $\mathcal{S}$  and  $\mathcal{P}$ , of a gear and its mating pinion: (a) the conjugate action law is fulfilled, (b) the conjugate action law is violated: the tooth flanks interfere into one another, and (c) the condition of conjugacy is violated: the tooth flanks separate from one another.

is valid. Similarly, the linear velocity vector,  $\mathbf{V}_{K_p}$ , of the point  $K_p$  can be expressed in terms of the rotation vector,  $\boldsymbol{\omega}_p$ , of the pinion and the position vector,  $\mathbf{r}_{K_p}$ , of the point  $K_p$ , that is, an equality:

$$\mathbf{V}_{K_p} = \boldsymbol{\omega}_p \times \mathbf{r}_{K_p} \quad (4.16)$$

is valid as well.

The linear velocity vector,  $\mathbf{V}_\Sigma$ , of the resultant motion of the tooth profiles,  $\mathcal{S}$  and  $\mathcal{P}$ , in relation to one another must be aligned with a common tangent to the tooth profiles at  $K$ , or, in other words, it should be perpendicular to the unit normal vector,  $\mathbf{n}_g$ . Because of this, the radius of instantaneous rotation,  $PK$ , is aligned with the common perpendicular vector,  $\mathbf{n}_g$ .

Therefore, when conjugate tooth profiles are in contact, the common perpendiculars at every point of the line of contact,  $LC$ , between the tooth flanks,  $\mathcal{S}$  and  $\mathcal{P}$ , must pass through the axis of instantaneous rotation of the surfaces at every instant of time, namely, for any and all possible configurations of the surfaces relative each other.

The provided verbal description of the *second fundamental law of gearing* can be complemented with an analytical expression that makes possible a conclusion whether two interacting tooth flanks are conjugate or not.

Consider a gear pair with an arbitrary configuration of the axes of rotation,  $O_g$  and  $O_p$ , of a gear and of a mating pinion, as depicted in Figure 4.10. In Figure 4.10a section of the gear pair by a plane is shown. The section plane is perpendicular to the axis of instantaneous rotation,  $P_{ln}$ . A unit vector,  $\mathbf{p}_{ln}$ , is pointed along the axis of instantaneous rotation,  $P_{ln}$ . The axes of rotation,  $O_g$  and  $O_p$ , are intersected by the section plane at points,  $o_g$  and  $o_p$ . Point  $m$  is a point of the plane of action,  $PA$ , coincident with the contact point,  $K$ . Point  $m$ , travels together with the plane of action, thus, the linear velocity vector,  $\mathbf{V}_m$ , is located within the plane of action,  $PA$ . Therefore, the plane of action can be specified in terms of two vectors, namely: of the vectors  $\mathbf{p}_{ln}$  and  $\mathbf{V}_m$ .

The actual configuration of the unit vector of a common perpendicular,  $\mathbf{n}_g$ , depends on the *actual* geometry of the interacting tooth flanks,  $\mathcal{S}$  and  $\mathcal{P}$ . In geometrically accurate gears, the unit normal vector,  $\mathbf{n}_g$ , is entirely located within the plane of action,  $PA$  (see Figure 4.10a). In approximate gears, the unit normal vector,  $\mathbf{n}_g$ , does not located in the plane of action,  $PA$ , and forms an angle,  $\delta$ , with the plane of action (only one pair of teeth is always engaged in mesh in approximate gearing). Depending on the actual value of the angle,  $\delta$  (depending on the actual displacement of the unit normal vector,  $\mathbf{n}_g$ , in relation to the plane of action,  $PA$ ), the gear and the pinion tooth flanks,  $\mathcal{S}$  and  $\mathcal{P}$ , either interfere with each other (see Figure 4.10b), or they separate from one another (see Figure 4.10c).

If the common perpendicular,  $\mathbf{n}_g$ , intersects the axis of instantaneous rotation,  $P_m$ , for any and all angular configurations of a gear and a mating pinion, then all the centers of curvature of the gear and the mating pinion tooth flanks in all transverse sections are located within the axis of instant rotation,  $P_m$ .

Not all tooth flank geometries feature conjugate mating gear.<sup>9</sup>

**Conclusion 4.1.** *Only gears with tooth flank geometry, for which all the perpendiculars to the tooth flank can be located in a plane that is tangent either to the gear base cylinder (in parallel-axes gearing), or to the base cone (in intersected-axes, and crossed-axes gearing) may feature a conjugate mating gear.*

In ordinary enveloping process, an instantaneous enveloping motion of a traveling surface in relation to a reference system associated with the desirable envelope to be determined is governed solely by a current value of the radius of curvature of the desirable envelope, that is, by the surface geometry. No specific constraints on the enveloping motion of the traveling surface are imposed in this case.

In generating enveloping process, an instantaneous enveloping motion of a traveling surface in relation to a reference system associated with the desirable envelope to be determined is governed by both:

- by a current value of the radius of curvature of the desirable envelope (that is, by the surface geometry), and
- by the parameters of the rolling relative motion.

These two reasons (a) and (b) should produce the same governing of the enveloping process, otherwise no self-enveloping surface can be generated.

In Figure 4.11, an example of interaction of local patches of tooth flanks,  $\mathcal{S}$  and  $\mathcal{P}$ , is schematically depicted. The tooth flanks,  $\mathcal{S}$  and  $\mathcal{P}$ , make contact at point,  $K$ . The radii of curvature of the interacting tooth flanks at contact point,  $K$ , equal to  $R_g$  and  $R_p$ , correspondingly (see Figure 4.11a). The centers of curvature of the tooth profiles,  $\mathcal{S}$  and  $\mathcal{P}$ , are denoted by  $O_g$  and  $O_p$ , correspondingly. In the instantaneous motion of the pinion,  $\mathcal{P}$ , in relation to the gear,  $\mathcal{S}$ , the pinion performs an instantaneous rotation,  $\omega_{p/g}$ , about the point  $O_g$ . The radius of curvature of the generated actual gear tooth flank,  $\mathcal{S}_{act}$ , equals to  $R_{p/g} \equiv R_g$ . In this scenario, the second fundamental law of gear is fulfilled, and the actual tooth flank,  $\mathcal{S}_{act}$ , is identical to the desirable gear tooth flank,  $\mathcal{S}$ , as shown in Figure 4.11a.

**Note:** Here, in Figure 4.11, a rotation,  $\omega_n$ , of the pinion,  $\mathcal{P}$ , in relation to the gear,  $\mathcal{S}$ , about the contact perpendicular,  $\mathbf{n}_g$ , is not prohibited by the second fundamental law of gearing.

When the instantaneous rotation is performed either about the center  $O_{p/g}$  (when  $R_{p/g} < R_g$ , see Figure 4.11b), or about the center  $O_{p/g}$  (when  $R_{p/g} > R_g$ , see Figure 4.11c), the second fundamental law of gear is violated, and the actual tooth flank,  $\mathcal{S}_{act}$ , differs from the desirable gear tooth flank,  $\mathcal{S}$ .

**Reminder:** The *first fundamental law of gearing* (as well as the *Shishkov equation of contact*,  $\mathbf{n}_g \cdot \mathbf{V}_\Sigma = 0$ ) is fulfilled in all three cases shown in Figure 4.11, while the second fundamental law of gearing is fulfilled only in the first case illustrated in Figure 4.11a, and is violated in the second and the third cases (see Figure 4.11b and c). The schematic in Figure 4.11 is helpful for understanding the difference between the first and the second fundamental laws of gearing and prevents the reader from making stupid conclusions in this regard.

<sup>9</sup> If no constraints are imposed onto relative motion of two interacting surfaces, a conjugate surface can be determined for any smooth regular surface. In the theory of gearing, only a pair of rotations, or a rotational motion and translational motion, are considered. With such a constraint onto relative motion (rotations and translations), a conjugate surface can be defined not for every smooth regular surface. This means that the total number of kinds of surfaces suitable for gear tooth flanks is limited [174].

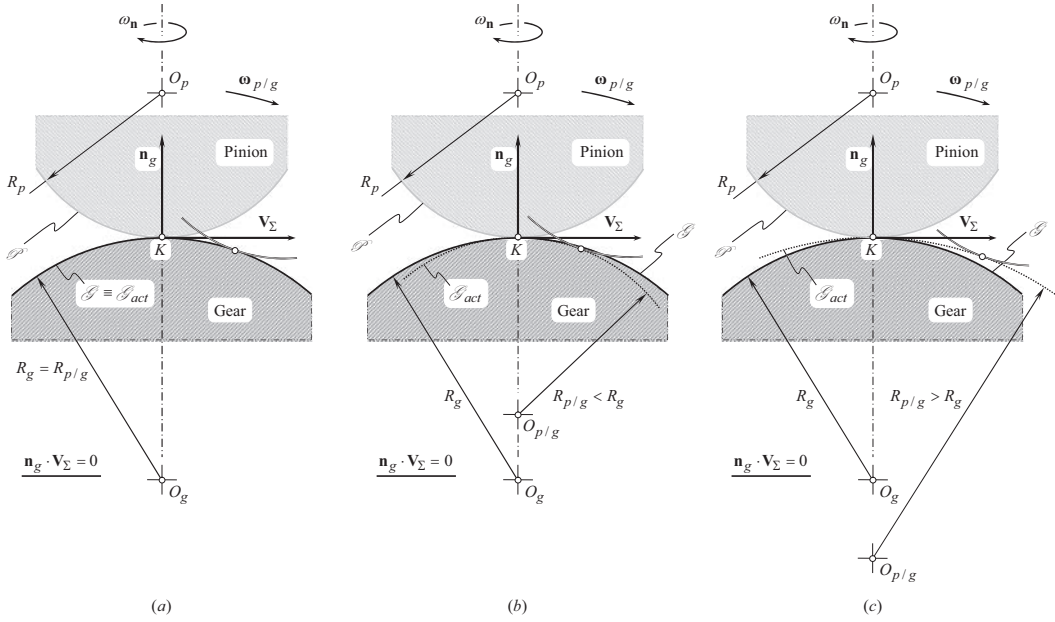


**FIGURE 4.11** Examples of (a) fulfillment, and violation: (b) interference, and (c) separation, of a gear,  $\mathcal{G}$ , and its mating pinion,  $\mathcal{P}$ , tooth flanks: the *Shishkov equation of contact*,  $\mathbf{n}_g \cdot \mathbf{V}_\Sigma = 0$  is fulfilled in all three cases (a) through (c), while the conjugate action law is violated in the cases (b) and (c).

**Important:** When the second fundamental law of gearing is fulfilled, the first fundamental law of gearing is always fulfilled, and not vice versa.

The relative motion of the tooth flanks,  $\mathcal{G}$  and  $\mathcal{P}$ , in a conjugate gear pair can be described analytically.

The elementary motions of the pinion tooth flank,  $\mathcal{P}$ , relative to the stationary gear tooth flank,  $\mathcal{G}$ , are synchronized with one another so as to keep the common perpendicular through a point within the axis of instantaneous rotation,  $P_{in}$ , as illustrated in Figure 4.12. Here, in Figure 4.12, section of the tooth flanks,  $\mathcal{G}$  and  $\mathcal{P}$ , by a normal plane through the vector of linear velocity,  $\mathbf{V}_\Sigma$ , is shown.

An equation:

$$|\mathbf{V}_\Sigma| = |\omega_{p/g}| \cdot R_g \quad (4.17)$$

can be composed based on the analysis of the instantaneous kinematics of gearing [148, 151, 153, 161, 167].

Here,  $\omega_{p/g}$  is the vector of instantaneous rotation of the pinion tooth flanks,  $\mathcal{P}$ , in relation to the motionless gear tooth flank,  $\mathcal{G}$ .

The considered examples reveal, that two tooth flanks,  $\mathcal{G}$  and  $\mathcal{P}$ , are conjugate<sup>10</sup> if and only if the unit normal vector,  $\mathbf{n}_g$ , is located within the plane of action,  $PA$ . The two vectors, namely, the vectors  $\mathbf{p}_{in}$  and  $\mathbf{V}_m$ , define the plane of action,  $PA$  (as well as the unit normal vector,  $\mathbf{n}_{pa}$ , to the plane of action,  $PA$ :  $\mathbf{n}_{pa} = \mathbf{p}_{in} \times \mathbf{V}_m$ ). The unit normal vectors,  $\mathbf{n}_g$  and  $\mathbf{n}_{pa}$ , must be perpendicular to one another. Therefore, the equality,  $\mathbf{n}_g \cdot \mathbf{n}_{pa} = 0$ , must be valid in geometrically accurate gear pairs. The required orthogonality of the unit vector  $\mathbf{n}_g$  to the plane  $PA$  (or, the same, the required coplanarity of three vectors,  $\mathbf{p}_{in}$ ,  $\mathbf{V}_m$ , and  $\mathbf{n}_g$ ) can be expressed in the form of triple scalar product:

<sup>10</sup> Two (spatial) curves within two smooth regular surfaces, that travel in relation to one another, are said to be *conjugate curves* if and only if the curves are always in (point) contact, and the common perpendicular through contact point intersects the axis of instant rotation of the surfaces.



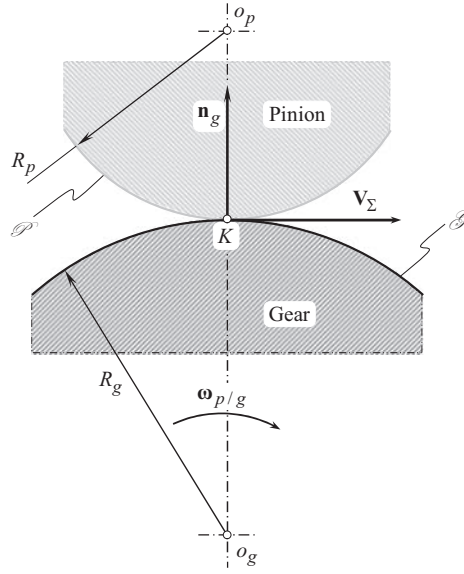


**FIGURE 4.12** Synchronization of the elementary relative motions of the tooth flanks,  $\mathcal{S}$  and  $\mathcal{P}$ , in conjugate gear pair.

$$\mathbf{p}_{ln} \times \mathbf{V}_m \cdot \mathbf{n}_g = 0 \quad (4.18)$$

As the unit vector,  $\mathbf{p}_{ln}$ , is aligned with the angular velocity vector,  $\omega_{pl}$ , Eq. (4.18) can also be represented in the form:

$$\omega_{pl} \times \mathbf{V}_m \cdot \mathbf{n}_g = 0 \quad (4.19)$$

Equation (4.18) represents an analytical expression of the *second fundamental law of gearing*. This equation is also referred to as the *equation of conjugacy* of two tooth flanks.

Here, in Eq. (4.18), is designated:

$\mathbf{p}_{ln}$  is the unit vector along the axis of instantaneous rotation,  $P_{ln}$ .

$\mathbf{V}_m$  is the linear velocity vector of point of interest,  $m$ , taken within the instantaneous line of contact,  $LC_{inst}$ , between the interacting tooth flanks,  $\mathcal{S}$  and  $\mathcal{P}$ , of a gear and a mating pinion.

$\mathbf{n}_g$  is the unit normal vector (common perpendicular) to the gear tooth flank,  $\mathcal{S}$  (to the pinion tooth flank,  $\mathcal{P}$ ), that passes through the point of interest,  $m$ .

Finally, the *second fundamental law of gearing* can be analytically represented as a set of two expressions:<sup>11</sup>

$$\begin{cases} \omega_{pl} \times \mathbf{V}_m \cdot \mathbf{n}_g = 0 \\ \mathbf{p}_{ln} \times \mathbf{n}_g \neq 0 \end{cases} \quad (4.20)$$

<sup>11</sup> The *conjugate action law (second fundamental law of gearing)* in general form (in intersected-axes gearing, and in crossed-axes gearing) was discovered in around 2008, and was published in 2010 [152]. An analytical expression [see Eq. (4.18)] for the *second fundamental law of gearing* is derived in 2017, and published in Refs. [174] and [176].



In the most general case of *crossed-axes gearing*, the *second fundamental law of gearing* is formulated as follows:

**The second fundamental law of gearing (general case):** In order to smoothly transmit a uniform rotary motion from a driving shaft to a driven shaft by means of gear teeth, perpendicular to the tooth flanks of the interacting teeth at all points of their contact must intersect the axis of instantaneous rotation in the gear pair.

A case when an instantaneous line of contact,  $LC_{\text{inst}}$ , is perpendicular to the axis of instantaneous rotation,  $P_{\text{ln}}$ , is eliminated by the second equation:  $\mathbf{p}_{\text{ln}} \times \mathbf{n}_g \neq 0$  in the set of expressions Eq. (4.20).

A line of action of the unit normal vector,  $\mathbf{n}_g$ , intersects the axis of instantaneous rotation,  $P_{\text{ln}}$ , if the expression:  $\mathbf{p}_{\text{ln}} \times \mathbf{V}_m \cdot \mathbf{n}_g = 0$ , is fulfilled.

In a geometrically accurate gear pair, an instantaneous line of action,  $LA_{\text{inst}}$  (a straight line pointed along the unit normal vector,  $\mathbf{n}_g$ ), always intersects the axis of instantaneous rotation,  $P_{\text{ln}}$ . At every point of the path of contact,  $P_c$ , an instantaneous line of action,  $LA_{\text{inst}}$ , is tangent to the path of contact,  $P_c$ . Therefore, the path of contact,  $P_c$  (which, in general, is a planar curve), is an envelope of a family of instantaneous lines of action,  $LA_{\text{inst}}$ . The path of contact,  $P_c$ , always intersects the axis of instant rotation,  $P_{\text{ln}}$ , in gearing of all kinds.

The second fundamental law of gearing is helpful, for example, when it is necessary to clarify whether or not a particular gear pair is geometrically accurate. A point within a gear tooth flank,  $\mathcal{G}$ , can be a *contact* point when the interacting tooth flanks are conjugate. For a corresponding angular configuration of a gear and a mating pinion, point of a pinion tooth flank,  $\mathcal{P}$ , that is anticipated to be in contact with the gear tooth flank,  $\mathcal{G}$ , can really be a *contact* point when the second fundamental law of gearing is fulfilled. A possibility of contact of the tooth flanks,  $\mathcal{G}$  and  $\mathcal{P}$ , in approximate gearing can be verified by means of comparison of coordinates of the *contact* point on the gear tooth flank,  $\mathcal{G}$ , and that on the pinion tooth flank,  $\mathcal{P}$ . If the coordinates of the points are identical to one another, then the point is *contact* point. Otherwise, no contact of the tooth flanks,  $\mathcal{G}$  and  $\mathcal{P}$ , at these points is possible at all.

In geometrically accurate gears, the perpendiculars,  $\mathbf{n}_g$  and  $\mathbf{n}_p$ , align with the common perpendicular,  $\mathbf{n}_{g/p}$ . In approximate gears the alignment of three perpendiculars,  $\mathbf{n}_g$ ,  $\mathbf{n}_p$ , and  $\mathbf{n}_{g/p}$ , is violated. Determination of which one of two mating gears is inaccurate, and how large are the actual values of the deviations of the gear/pinion tooth flank from the desirable gear/pinion tooth flank, becomes possible if this feature of geometrically accurate gears is taken into account.

The *second fundamental law of gearing* in its general form was verbally formulated in around 2008, and later on it was published in 2010 [152,163]. An analytical expression [see Eq. (4.20)] for the *second fundamental law of gearing* is derived in 2017, and published in [174,176].

### 4.3.3 EULER-SAVARY EQUATION

A relation between the radii of curvature of the interacting tooth profiles, and the radii of curvature of the corresponding centrodes in parallel-axes gearing is specified by the *Euler-Savary*<sup>12</sup> *theorem*.

#### Theorem 4.1

Straight lines through the centers of curvature of the conjugate tooth profiles and through the centers of curvature of the corresponding centrodes intersect each other at point within the line through the pitch point that is orthogonal to the common perpendicular to the conjugate tooth profiles.

<sup>12</sup>Felix Savary (4 October 1797–15 July 1841), a French physicist and mathematician.

The theorem can be proved by means of an equivalent three-bar mechanism that is superposed over the gear pair under consideration.

Referring to Figure 4.13, the axis of rotation of a gear,  $O_g$ , and the axis of rotation of its mating pinion,  $O_p$ , are at a center distance,  $C$ , apart from one another. The pitch point,  $P$ , is located within the centerline,  $\Phi$ . The pitch point,  $P$ , is motionless in gear pairs that feature tooth ratio,  $u$ , of a constant value, and the pitch point,  $P$ , travels back and forth along the centerline,  $\Phi$ , in gear pairs that have a variable tooth ratio,  $u$ .

A straight line,  $t_p$ , through the pitch point,  $P$ , is perpendicular to the centerline,  $\Phi$ . A straight line,  $n$ , through the pitch point,  $P$ , is perpendicular to the interacting tooth profiles at the contact point,  $K$ . A straight line,  $t_K$ , represents the common tangent at  $K$  to the interacting tooth profiles (namely,  $t_K \perp n$ ). The angle between the straight lines  $t_p$  and  $n$  is denoted by  $\phi$ .

An equivalent three-bar mechanism,  $O_pABO_g$ , is superposed over the gear pair under consideration.<sup>13</sup> The radii of curvature,  $r_g$  and  $r_p$ , of the centrodes of the three-bar mechanism are equal  $r_g = O_gP$  and  $r_p = O_pP$ . The radii of curvature,  $\rho_g$  and  $\rho_p$ , of the conjugate tooth profiles are equal  $\rho_g = KB$  and  $\rho_p = KA$  correspondingly.

In relative motion of the gear and the pinion, the pitch circle of the gear and the pitch circle of the pinion roll without sliding over one another. This relative motion in the gear pair is equivalent to the instantaneous relative motion in the three-bar mechanism when the ratio:

$$\frac{\omega_p}{\omega_g} = \frac{O_gP}{O_pP} \quad (4.21)$$

is observed.

The triangles,  $\triangle APE$  and  $\triangle ACO_p$ , are similar to one another. The similarity of the triangles yields an expression for  $PE$ :

$$PE = O_pC \cdot \frac{AP}{AC} \quad (4.22)$$

Another expression for  $PE$ :

$$PE = O_gD \cdot \frac{BP}{BD} \quad (4.23)$$

can be drawn up from similarity of the triangles  $\triangle BPE$  and  $\triangle BDO_g$ .

|||||The length of the straight-line segment,  $O_gP$ , is equal to the pitch radius,  $r_g$ , of the gear ( $O_gP = r_g$ ). The length of the straight-line segment,  $O_pP$ , is equal to the pitch radius,  $r_p$ , of the pinion ( $O_pP = r_p$ ). The lengths of the straight-line segments  $AP$  and  $BP$  is equal to certain values  $l_1$  and  $l_2$ .

The following equalities:

$$O_gD = r_g \cos \phi_t \quad (4.24)$$

$$O_pC = r_p \cos \phi_t \quad (4.25)$$

$$AC = l_1 - r_p \sin \phi_t \quad (4.26)$$

$$BD = r_g \sin \phi_t - l_2 \quad (4.27)$$

<sup>13</sup> As cited in Rosenauer and Willis [191].

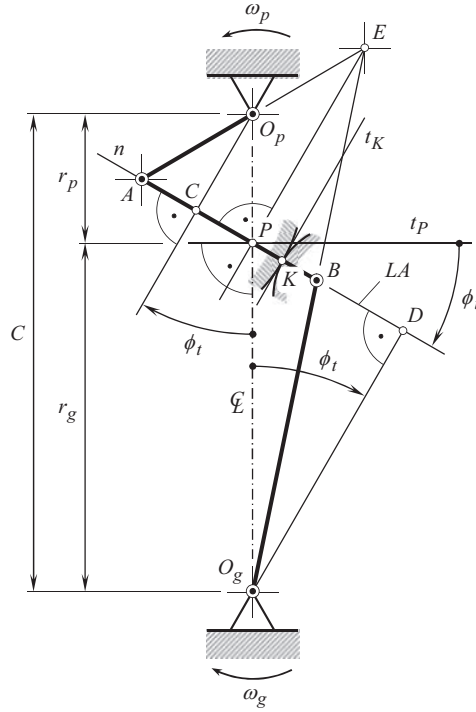


**FIGURE 4.13** To the derivation of the *Euler-Savary equation* (general case:  $u = \text{var}$ ).

immediately follow from the consideration of the schematic in Figure 4.13. These expressions for  $O_gD$ ,  $O_pC$ ,  $AC$ , and  $BD$ , can be substituted into Eqs. (4.22) and (4.23):

$$r_p \cdot \frac{l_1}{l_1 - r_p \sin \phi_t} \cos \phi_t = r_g \cdot \frac{l_2}{r_g \sin \phi_t - l_2} \cos \phi_t \quad (4.28)$$

The expression:

$$\frac{1}{r_g} + \frac{1}{r_p} = \left( \frac{1}{l_1} + \frac{1}{l_2} \right) \cdot \sin \phi_t \quad (4.29)$$

immediately follows from Eq. (4.28).

The lengths  $l_1$  and  $l_2$  are equal to the distances from the centers of curvature of the tooth profiles,  $\mathcal{G}$  and  $\mathcal{P}$ , to the pitch point,  $P$ . As it follows from Figure 4.13, these lengths are equal to:

$$l_1 = AK - KP = \rho_p - x \quad (4.30)$$

$$l_2 = BK + KP = \rho_g + x \quad (4.31)$$

correspondingly.

In Eqs. (4.30) and (4.31), the distance between the point of contact of the conjugate profiles to the pitch point is denoted by  $x$ . This distance is measured along the straight line  $n$  that is aligned with the common perpendicular to the gear,  $\mathcal{G}$ , and the pinion,  $\mathcal{P}$ , tooth profiles.

The *Euler-Savary equation*:

$$\frac{1}{r_g} + \frac{1}{r_p} = \left( \frac{1}{\rho_g + x} + \frac{1}{\rho_p - x} \right) \cdot \sin \phi_t \quad (4.32)$$

immediately follows from Eq. (4.28).

For internal gear pairs, the pitch radius of the gear,  $r_g$ , and the radius,  $\rho_g$ , of curvature of the gear tooth profile are of negative values as they are considered concave.

It is important to mention here that for the purpose of contact stress analysis, the so-called *relative curvature*,  $\rho_{rel}$ , of the contacting tooth profiles is used. A formula:

$$\rho_{rel} = \frac{1}{\frac{1}{\rho_g} + \frac{1}{\rho_p}} = \frac{\rho_g \rho_p}{\rho_g + \rho_p} \quad (4.33)$$

can be used for the calculation of relative curvature.

In the pitch point,  $P$ , that is, when  $x = 0$ , Eq. (4.32) returns:

$$\rho_{rel} = \frac{\rho_g \rho_p}{\rho_g + \rho_p} \cdot \sin \phi_t \quad (4.34)$$

This means, that for a gear pair with a specified center distance,  $C$ , and tooth ratio,  $u$  (when the radii,  $r_g$  and  $r_p$ , of the pitch circles are known), the radius of relative curvature,  $\rho_{rel}$ , as well as the rate of contact stress, is predetermined by pressure angle,  $\phi_t$ .

The shown in Figure 4.13 schematic corresponds to a general case of the *Euler-Savary theorem* (Theorem 4.1), for which the angular velocity ratio  $u = \text{var}$ . A similar schematic in a case of constant angular velocity ratio ( $u = \text{const}$ ) is depicted in Figure 4.14. This later one corresponds to a parallel-axes gearing with angular velocity ratio of a constant value.

Wrong practice is commonly adopted when analyzing whether two tooth flanks,  $\mathcal{S}$  and  $\mathcal{P}$ , of a gear and a mating pinion are conjugate, or they are not. In most cases, the performed analysis of gears and gear pairs is limited to fulfillment only of the *first fundamental law of gearing*, that is, loosely only *Shishkov equation of contact*,  $\mathbf{n}_g \cdot \mathbf{V}_\Sigma = 0$ , is used for this purpose. In the present-days practice, both, in gear science, as well as in gear engineering, fulfillment of the *second fundamental law of gearing* (of the *conjugate action law*) in a gear pair in most cases is ignored. Neither *F. Litvin* [74,76], nor *D. Dooner* [28], nor *H. Stachel* [205–207], nor their followers, pay sufficient attention to the fulfillment of the *second fundamental law of gearing* (may be except of the simplest case of geometrically accurate involute parallel-axes gearing). The condition of contact of tooth flanks,  $\mathcal{S}$  and  $\mathcal{P}$ , and not the condition of conjugacy of the interacting tooth flanks of a gear and its mating pinion, is analytically described by *Shishkov equation of contact*. All conjugate surfaces are enveloping to one another, and not vice versa. Unfortunately, this difference is often not realized at all by most of gear researchers.

Fulfillment or violation of the *second fundamental law of gearing* for gears with another (non-involute) tooth flank geometry is not discussed at all. Examples can be readily found for gears that feature cycloidal tooth profile, circular-arc tooth profile as well as tooth profiles of other geometries (those differ from the involute of a circle), where the *second fundamental law of gearing* is always violated. Moreover, the *second fundamental law of gearing* is not taken into account for gears that operate on intersected axes of rotation as well as for gears that operate on crossed axes of rotation.

#### 4.3.4 PECULIARITIES OF CONTACT GEOMETRY IN CONJUGATE GEAR PAIRS

Tooth flanks of gears for conjugate gearing are generated by means of a desirable line of contact. Therefore, line contact between the tooth flanks,  $\mathcal{S}$  and  $\mathcal{P}$ , always occurs. In approximate gearing, the interacting tooth flanks,  $\mathcal{S}$  and  $\mathcal{P}$ , are not conjugate to one another. Due to this, they may penetrate

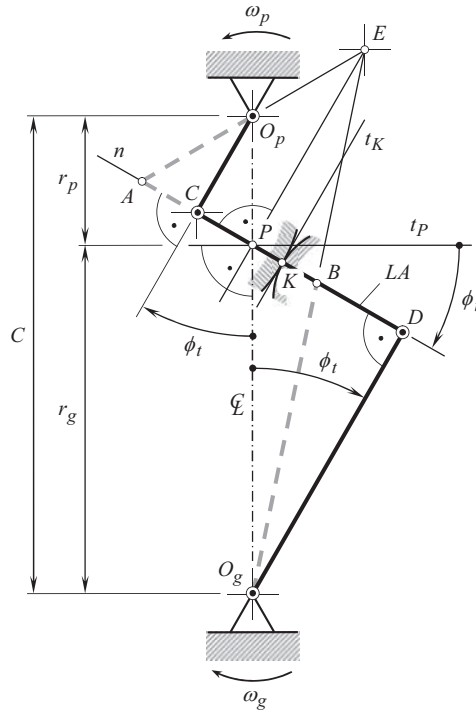


**FIGURE 4.14** An equivalent three-bar mechanism for a case of a constant gear ratio,  $u = \text{const}$ .

into one another even when the *Shishkov equation of contact*,  $\mathbf{n}_g \cdot \mathbf{V}_\Sigma = 0$  is met. The said is illustrated by an example shown in Figure 4.15. Here, in Figure 4.15, a local concave local patch of elliptic kind of the gear tooth flank,  $\mathcal{G}$ , interacts with a convex local patch of elliptic kind of the pinion tooth flank,  $\mathcal{P}$ . Such a scenario can be observed in approximate *Novikov/conformal* parallel-axes gear pairs.

As shown in Figure 4.15a, in a section by a plane through the common perpendicular,  $\mathbf{n}_g$ , the radius of curvature,  $R_g$  of the section of the gear tooth flank,  $\mathcal{G}$ , can be smaller compared to that,  $R_p$ , of the section of the pinion tooth flank,  $\mathcal{P}$ . The inequality,  $R_g > R_p$ , if any, is observed in normal plane sections within certain angle (see Figure 4.15b). In such a scenario, the characteristic curve called *indicatrix of conformity*,  $\text{Cnf}_R(\mathcal{G} \mid \mathcal{P})$ , at contact point,  $K$ , of the tooth flanks,  $\mathcal{G}$  and  $\mathcal{P}$  (see Figure 4.15c), is an effective mean for the analysis of contact geometry of interacting functional surfaces at point of their contact [see Appendix E for details on the *indicatrix of conformity*,  $\text{Cnf}_R(\mathcal{G} \mid \mathcal{P})$ ].

#### 4.3.5 BRIEF COMMENTS ON ENVELOPE SURFACES OF THE FIRST AND OF THE SECOND KIND

Tooth flanks,  $\mathcal{G}$  and  $\mathcal{P}$ , of a gear and a mating pinion that fulfil the *second fundamental law of gearing*, are enveloping to one another. Envelope surfaces of this kind are referred to as the *envelope surfaces of the second kind* [138].

The ordinary process of generation of envelope surfaces is profoundly investigated in differential geometry. Here, an instantaneous enveloping motion of a traveling surface in relation to a reference system associated with the desirable envelope to be determined is governed solely by current value of radius of curvature of the envelope. No constraints onto the enveloping motion of the traveling surface are imposed in this case.

In generation enveloping process (when two axodes roll over one another), the instantaneous enveloping motion of a traveling surface in relation to a reference system associated with the desirable envelope to be determined is governed by both:

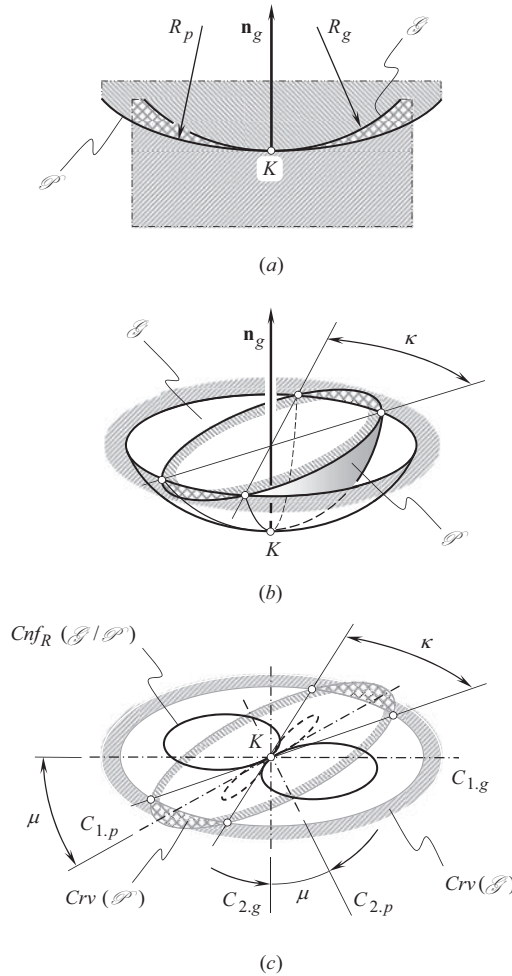


**FIGURE 4.15** Example of penetration of a pinion tooth flank,  $\mathcal{P}$ , into a gear tooth flank,  $\mathcal{G}$ , in differential vicinity of contact point  $K$  in approximate gearing: (a) normal section of a convex-to-concave contact of the tooth flanks,  $\mathcal{G}$  and  $\mathcal{P}$ ; (b) close-up of a convex-to-concave contact of the tooth flanks,  $\mathcal{G}$  and  $\mathcal{P}$ , and (c) indicatrix of conformity,  $Cnf_R(\mathcal{G}/\mathcal{P})$  at point of contact of a convex-to-concave contact of the tooth flanks,  $\mathcal{G}$  and  $\mathcal{P}$ .

- a. by current value of radius of curvature of the desirable envelope, and
- b. by the parameters of the rolling motion.

Each of these two factors (a) and (b) should produce the same governing of the enveloping process, otherwise no self-enveloping surface can be generated.

The foregoing confirms the previously made conclusion [138] that envelope surfaces,  $\mathcal{G}$  and  $\mathcal{P}$ , of two kinds are possible: *envelope surfaces of the first kind* and *envelope surfaces of the second kind*. The *envelope surfaces of the second kind* are also referred to as *reversibly enveloping surfaces*, or just as  $R_e$  – surfaces, for simplicity [155].

For a specified kinematics of gearing, not every smooth regular surface can form an *envelope surface of the second kind* [138]. When the condition of existence of the *envelope surface of the second kind* is fulfilled, the condition of existence of the *envelope surface of the first kind* is always met, but not vice versa [138].

In order to generate an envelope surface to a family of surfaces, enveloping motion of a traveling surface must be independent, and can be expressed solely in terms of the geometry of the surface to be generated.

In rolling motion, an enveloping motion is not independent. Therefore, the envelope surface can be generated not for any surface, but only for a unique surface that is conjugate to the envelope surface to be generated.

Conjugate pairs of surfaces are always envelope to one another, and not vice versa.

Fulfillment of the *second fundamental law of gearing* is necessary but not sufficient to design geometrically accurate gears, that are capable of transmitting smoothly a rotary motion from a driving shaft to a driven shaft by means of gear teeth.

#### 4.4 THE EQUAL BASE PITCHES LAW: THE THIRD FUNDAMENTAL LAW OF GEARING

The last (but not the least) is related to base pitches<sup>14</sup> of a gear and its mating pinion teeth.

Gear teeth can be viewed as series of cam surfaces that act on similar surfaces of the mating gear to impart a driving motion. An additional requirement caused by multiple interacting tooth surfaces in gears is required to be fulfilled in this regard.

The height and the lengthwise shape of the active tooth flanks of the teeth (cam surfaces) must be of such a geometry that, before one pair of teeth goes out of contact during mesh, a next pair will have picked up its share of the load. This is called *continuity of action*.

As a general rule, gearing designed in accordance with the scientific theory of gearing, will not have problems of continuity of action.

In order to provide a smooth continuous flow of power, at least one pair of teeth must be in contact at all times. This means that during a part of the meshing cycle, two pairs of teeth will be sharing the load. Any gearing must be designed such that the second pair of teeth will pick up their share of the load and be prepared to assume the full load before the first pair of teeth goes out of action.

As it is adopted in common practice, equality of base pitches of a gear and its mating pinion is considered only in a simplest case of geometrically accurate (with zero axes misalignment) parallel-axes gears. The necessity of equal base pitches of the interacting tooth flanks  $\mathcal{S}$  and  $\mathcal{P}$  got no attention with respect to gears that operate on intersected axes of rotation as well as to gears that operate on crossed axes of rotation.

The *third fundamental law of gearing* discussed below in this section of the book, requires equality of the angular base pitches of a gear and a mating pinion. For the most general case of crossed-axes gearing, the concept of equal base pitches of a gear and its mating pinion has been developed only in the recent years.

The discussion immediately below begins with a relatively simple case of parallel-axes gearing.

In Figure 4.16, local patches of adjacent gear tooth flanks,  $\mathcal{S}$ , and of mating pinion tooth flanks,  $\mathcal{P}$ , are shown. The gear and the pinion tooth flank themselves are not defined yet. Therefore, only small (local) portions of the tooth flanks,  $\mathcal{S}$ , are depicted in Figure 4.16a. All these portions of the tooth flanks of a gear are located in the differential vicinity of points, which will be the points of intersection,  $K_g$ , of the tooth flanks,  $\mathcal{S}$ , by the line of action,  $LA$ . Each tooth flank,  $\mathcal{S}$ , is perpendicular to the line of action,  $LA$ , at points  $K_g$ . All the points  $K_g$  are evenly spaced along the line of action. The distance between each pair of neighboring points  $K_g$  is said to be the gear base pitch,  $p_{b,g}$ .

A similar is valid with respect to the pinion tooth flank,  $\mathcal{P}$ , shown in Figure 4.16b. All these portions of the tooth flanks of a pinion are located in the differential vicinity of points, which will be the points of intersection,  $K_p$ , of the tooth flanks,  $\mathcal{P}$ , by the line of action,  $LA$ . Each tooth flank,  $\mathcal{P}$ , is perpendicular to the line of action,  $LA$ , at points  $K_p$ . All the points  $K_p$  are evenly spaced along the line of action. The distance between each pair of adjacent points  $K_p$  is said to be the pinion base pitch,  $p_{b,p}$ .

<sup>14</sup>Remember, that base pitch can be specified only in geometrically accurate gears; no base pitch can be specified in approximate gears, as well as in non-involute gears of all kinds.



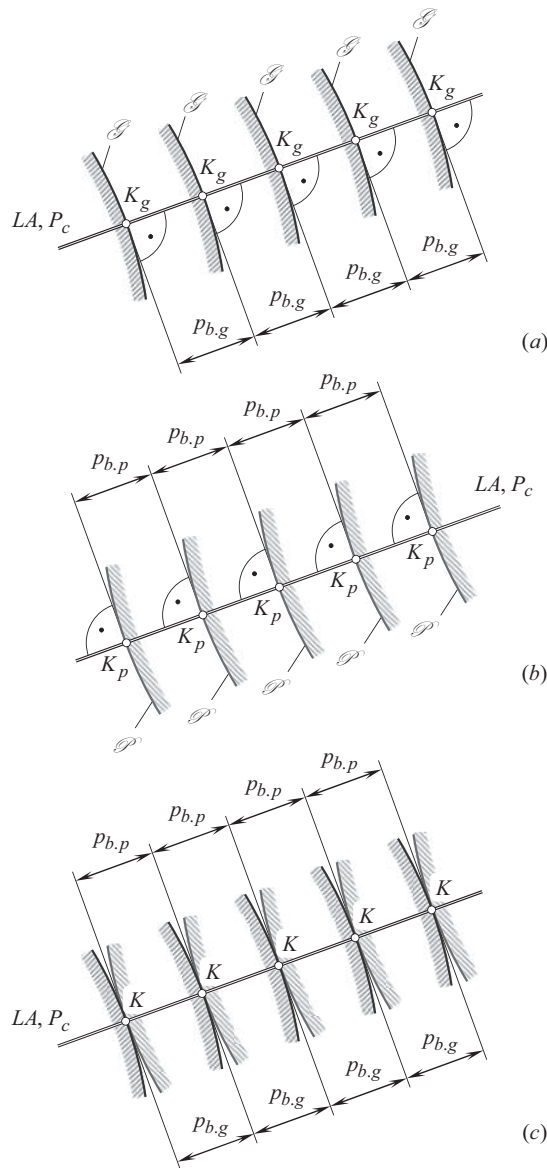


**FIGURE 4.16** On the concept of equal base pitches of a gear and its mating pinion: (a) the base pitch in a gear,  $p_{b,g}$ , (b) the base pitch in a pinion,  $p_{b,p}$ , and (c) equal base pitches in a gear pair,  $p_{b,g} \equiv p_{b,p}$ .

When the gear base pitch,  $p_{b,g}$ , and the mating pinion base pitch,  $p_{b,p}$ , are equal to one another (that is, when the identity  $p_{b,g} \equiv p_{b,p}$  is fulfilled), then the gear and the pinion can be engaged in mesh, as illustrated in Figure 4.16c. Only in such a case the load to be transmitted can be evenly shared between two (or more) pairs of interacting tooth flanks,  $\mathcal{S}$  and  $\mathcal{P}$ . Each gear point,  $K_g$ , coincides with corresponding pinion point,  $K_p$ . Because of this, the gear and the pinion points,  $K_g$  and  $K_p$ , further are designated as contact point,  $K$ .

As it follows from the analysis in Figure 4.16c, it is not a must to keep all the base pitches of a gear,  $p_{b,g}$ , equal to one another as well as to keep all the base pitches of a mating pinion,  $p_{b,p}$ , also equal to one another. It is critical to keep equality of a gear base pitch to a corresponding pinion base pitch for each pair of teeth engaged in mesh. Physically this is possible, but limits the gear ratio in a

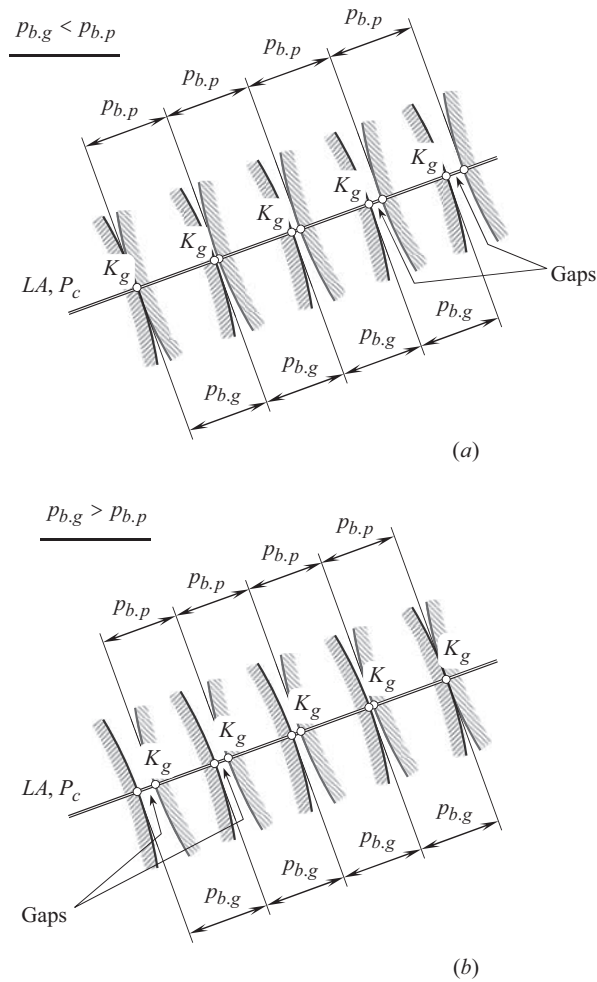


**FIGURE 4.17** Examples of violation of the *equal base pitches law*: (a) the base pitch of a gear,  $p_{b,g}$ , is smaller compared to the base pitch,  $p_{b,p}$ , of a mating pinion ( $p_{b,g} < p_{b,p}$ ), and (b) the base pitch of a gear,  $p_{b,g}$ , is larger compared to the base pitch,  $p_{b,p}$ , of a mating pinion ( $p_{b,g} > p_{b,p}$ ); in both cases the gaps are inevitable.

gear pair to an integer number, namely, to 1, 2, 3, and so forth. Such a design of gearing is impractical and is not considered in this text.

When the base pitches of a gear and of a mating pinion are not equal to one another ( $p_{b,g} \neq p_{b,p}$ ), for example, the gear base pitch,  $p_{b,g}$ , is smaller compared to the mating pinion base pitch,  $p_{b,p}$ , and, thus, the inequality  $p_{b,g} < p_{b,p}$  is valid (as shown in Figure 4.17a), only one pair of teeth is engaged in mesh at all times. A gap between the rest pairs of teeth is observed. No gaps of this sort are permissible in geometrically accurate parallel-axes gearing.

In another example illustrated in Figure 4.17b, the gear base pitch,  $p_{b,g}$ , is greater compared to the mating pinion base pitch,  $p_{b,p}$ , and the inequality  $p_{b,g} > p_{b,p}$  is valid (as shown in Figure 4.17b). Again, only one pair of teeth is engaged in mesh at all times. A gap between the rest pairs of teeth of the gear,  $\mathcal{G}$ , and the pinion,  $\mathcal{P}$ , is observed. No gaps of this sort are permissible in geometrically accurate parallel-axes gearing.

In this second example (see Figure 4.17b), the distribution of the gaps is inverse to that shown in Figure 4.17a. This is because the gear and the mating pinion are rigid bodies that physically cannot interfere into one another.

With that said, the *third fundamental law of gearing* can be formulated as follows<sup>15</sup>:

**The third fundamental law of gearing (in parallel-axes gearing):** *In parallel-axes gearing, in order to transmit a uniform rotary motion from a driving shaft to a driven shaft by means of gear teeth, the base pitch of a gear and that of a mating pinion must be equal to one another at every instant of time.*

Here, the base pitches in transverse section of the gear teeth are discussed.

If a discussion is limited just to geometrically accurate parallel-axes gearing, the concept of *base pitch* is applicable only to gears with involute tooth profile, namely, for spur, helical, herring-bone, double-helical, and so forth involute gears. No *base pitch* can be specified in gears with cycloid as well as in others non-involute tooth profiles. Ultimately, when base pitches in a gear and in a mating pinion are equal ( $p_{b,g} \equiv p_{b,p}$ ), the *third fundamental law of gearing* is always fulfilled.

In general, every gear pair features the, so-called, *operating base pitch*. The concept of *operating base pitch* in gear pair for the first time ever was introduced (~2008) by Prof. S.P. Radzevich [174]. The angular distance between two adjacent desirable lines of contact,  $LC_{des}^i$  and  $LC_{des}^{i\pm 1}$ , in a gear pair is specified by the *operating angular base pitch*,  $\varphi_{b,op}$ .

The operating base pitch is a *calculated* design parameter of a gear pair. This design parameter can not be directly measured in a gear pair, and can only be expressed in terms of other design parameters of the gear pair.

In the most general case of gearing, the third fundamental law of gearing (the angular base pitch of a gear, and that of a mating pinion, must be equal to the operating base pitch in a gear pair) for the first time ever was introduced (~2008) by Prof. S.P. Radzevich [174].

**The third fundamental law of gearing (general case):** *In geometrically accurate gearing of all kinds, the angular base pitch of a gear,  $\varphi_{b,g}$ , and that,  $\varphi_{b,p}$ , of a mating pinion, both, must be equal to operating angular base pitch,  $\varphi_{b,op}$ , of the gear pair.*

The above considered equality,  $p_{b,g} \equiv p_{b,p}$ , of the base pitches of the tooth flanks,  $\mathcal{S}$  and  $\mathcal{P}$ , of a gear and of a mating pinion is said to be a reduced case of the third fundamental law of gearing that all geometrically accurate gearing fulfil.

When the third fundamental law of gearing is fulfilled, the following set of identities is valid:

$$\begin{cases} \varphi_{b,g} \equiv \varphi_{b,op} \\ \varphi_{b,p} \equiv \varphi_{b,op} \end{cases} \quad (4.35)$$

Gearing that met the conditions specified by Eq. (4.35), are referred to as *geometrically accurate gears*.

A simplified representation of the *third fundamental law of gearing* is convenient in certain applications of geometrically accurate gears:

$$\left. \begin{aligned} \varphi_{b,g} &= \varphi_{b,op} \\ \varphi_{b,p} &= \varphi_{b,op} \end{aligned} \right\} \Rightarrow \varphi_{b,g} = \varphi_{b,p} \quad (4.36)$$

<sup>15</sup> The condition of equal base pitches of interacting tooth flanks of a gear and of a mating pinion is known at list since the beginning of the twentieth century (or even earlier). Unfortunately, it is still not known who has to be credited with this fundamental discovery in the scientific theory of gearing.

In geometrically accurate parallel-axes gearing, Eq. (4.35) reduce to:

$$\begin{cases} p_{b.g} \equiv p_{b.op} \\ p_{b.p} \equiv p_{b.op} \end{cases} \quad (4.37)$$

or simply  $p_{b.g} \equiv p_{b.p} \equiv p_{b.op}$ .

When equality of the angular base pitches (of the  $\varphi_{b.g}$ ,  $\varphi_{b.p}$ , and  $\varphi_{b.op}$ ) is discussed, it is assumed by default that tooth flanks,  $\mathcal{S}$  and  $\mathcal{P}$ , of a gear, and that of a mating pinion, both, are generated by that same desirable line of contact,  $LC_{des}$ , and with the identical configuration of the  $LC_{des}$  in relation to the plane of action,  $PA$ , for the gear and for the pinion. When the equalities  $\varphi_{b.g} = \varphi_{b.op}$  and  $\varphi_{b.p} = \varphi_{b.op}$  are valid, for example, for a helical gear and for a gear having a circular-arc profile in the lengthwise direction, these gears cannot be engaged in mesh with one another, as the gear tooth flank,  $\mathcal{S}$ , and the mating pinion tooth flank,  $\mathcal{P}$ , are generated by different desirable lines of contact,  $LC_{des}$ . A spur gear and a helical gear with the same value of the transverse base pitch, and two helical gears with different helix angle, are perfect examples in this regard.

The equality of the angular base pitches of a gear,  $\varphi_{b.g}$ , and its mating pinion,  $\varphi_{b.p}$ , to operating angular base pitch of the gear pair,  $\varphi_{b.op}$ , is a necessary and sufficient condition for gear pairs to be referred to the *geometrically accurate gears*.

In general, the *third fundamental law of gearing* is the most general one.

Taking into account that:

- The *first fundamental law of gearing* is always fulfilled when the *second fundamental law of gearing* is fulfilled (and not vice versa), and
- The *second fundamental law of gearing* is always fulfilled when the *third fundamental law of gearing* is fulfilled (and not vice versa),

The set of three fundamental laws of gearing can be substituted with the only fundamental law of gearing, namely, with the *third fundamental law of gearing*. In such a scenario, the first and the second fundamental laws of gearing are viewed as a precondition to the *third fundamental law of gearing*.

In other words, in order to fulfil the *third fundamental law of gearing*, the *second fundamental law of gearing* has to be fulfilled, as the base pitches can be defined only for conjugate tooth flanks, and not for any others. Then, in order to fulfil the *second fundamental law of gearing*, the *first fundamental law of gearing* has to be fulfilled, as conjugate surfaces exist if and only if two interacting tooth flanks meet the *first fundamental law of gearing*.

There is no need to verify whether or not either the *first fundamental law of gearing*, or the *second fundamental law of gearing*, are fulfilled, if it is known for sure that the *third fundamental law of gearing* is fulfilled.

**Conclusion 4.2:** *The equal base pitches law is the most robust law to be fulfilled in a gear pair compared to the law of contact, and the conjugate action law.*

In-depth understanding of the core of the kinematics, and the geometry of interacting of tooth flanks,  $\mathcal{S}$  and  $\mathcal{P}$  (three fundamental laws of gearing), is vital for geometric modeling of the tooth flank generation by means of CAD systems (Catia, Unigraphics, and others). Otherwise, numerous inconsistencies with the output in modeling become inevitable.

Taking into account the importance of the *third fundamental law of gearing*, this law of gearing is represented diagrammatically in Figure 4.18.

The actual value of one or more design parameters in a gear pair may deviate from its nominal (favorable) value. This immediately leads to the gear pair cannot be referred to *geometrically accurate gear pair*. These gears are referred to as *approximate gear pairs*. Possible examples of approximate gearing are listed immediately below, and are illustrated in Figure 4.19.

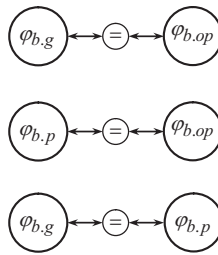


**FIGURE 4.18** Diagrammatic representation of the *third fundamental law of gearing*.

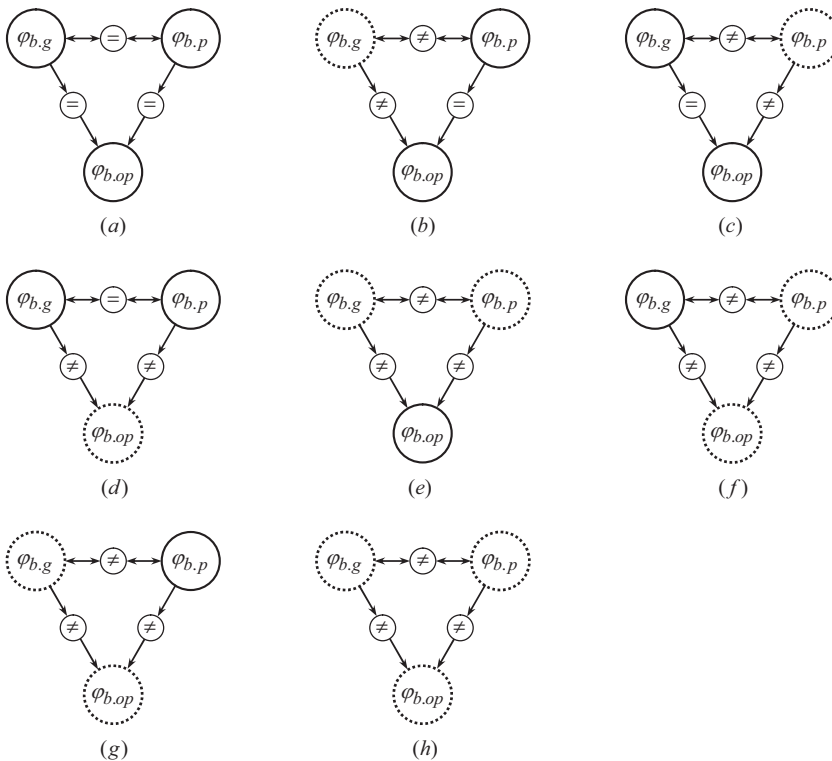


**FIGURE 4.19** Diagrammatic representation of possible deviations of the design parameters in approximate gear pairs: (a) no deviations in the angular base pitches  $\varphi_{b,g}$ ,  $\varphi_{b,p}$ , and  $\varphi_{b,op}$ , are observed; (b) angular base pitch of a gear,  $\varphi_{b,g}$ , deviates from its nominal value (no deviations in the angular base pitches  $\varphi_{b,p}$ , and  $\varphi_{b,op}$ , are observed); (c) angular base pitch of a pinion,  $\varphi_{b,p}$ , deviates from its nominal value (no deviations in the angular base pitches  $\varphi_{b,g}$ , and  $\varphi_{b,op}$ , are observed); (d) angular operating base pitch,  $\varphi_{b,op}$ , deviates from its nominal value (no deviations in the angular base pitches  $\varphi_{b,g}$  and  $\varphi_{b,p}$ , are observed); (e) angular base pitches of a gear,  $\varphi_{b,g}$ , and of a mating pinion,  $\varphi_{b,p}$ , deviate from their nominal values (no deviation in the operating angular base pitches, of a gear,  $\varphi_{b,g}$ , is observed); (g) angular base pitches of a gear,  $\varphi_{b,g}$ , and the operating angular base pitch,  $\varphi_{b,op}$ , deviate from their nominal values (no deviation in the angular base pitch of a pinion,  $\varphi_{b,p}$ , is observed); and (h) all three angular base pitches,  $\varphi_{b,g}$ ,  $\varphi_{b,p}$ , and  $\varphi_{b,op}$ , deviate from their nominal values.

1. Accurate gear, accurate pinion, and zero-displacements gear mesh – a *geometrically accurate gear pair* (see Figure 4.19a)
2. Inaccurate gear, accurate pinion, and zero-displacements gear mesh – a *approximate gear pair* (see Figure 4.19b)

3. Accurate gear, inaccurate pinion, and zero-displacements gear mesh (see Figure 4.19c)
4. Accurate gear, accurate pinion, and non-zero-displacements gear mesh (see Figure 4.19d)
5. Inaccurate gear, inaccurate pinion, and zero-displacements gear mesh (see Figure 4.19e)
6. Accurate gear, inaccurate pinion, and non-zero-displacements gear mesh (only the gear is perfect) (see Figure 4.19f)
7. Inaccurate gear, accurate pinion, and non-zero-displacements gear mesh (only the pinion is perfect) (see Figure 4.19g)
8. Inaccurate gear, inaccurate pinion, and non-zero-displacements gear mesh (see Figure 4.19h)

This subject is not profoundly investigated yet.

## 4.5 ON THE CORRELATION OF THE DISCUSSED RESULTS WITH THE EARLIER OBTAINED RESULTS

The origin of the research reported in this chapter can be traced back to the studies carried out by *Charles Camus* [16,17] and to the fundamental publications by *Leonhard Euler* (1760) [35,36].

*Camus* was close to understand the nature of the concept of *envelope surfaces of the second kind* in rolling motion of two surfaces over one another, but he did not make the last step to get the problem solved.

In the XVIIIs papers [35,36], *Euler* investigated the simplest case of transmission of a rotary motion by a gear pair with *parallel* axes, and pointed out the obligatory passage of the *line of action* (the *contact normal*, in other words) through the stationary pitch point.

Later on (~1835–1836) and independently of *Euler*, *Félix Savary* came up with the equivalent results of the research.

The so-called *main theorem of the theory of parallel-axes gearing* is the ultimate achievement of *Camus*, *Euler*, and *Savary*, in this area. This theorem is commonly called now the *Camus-Euler-Savary theorem* (or simply the *CES – theorem* of theory of gearing). In Europe, the *CES – theorem* became widely known after the publication of the 1841 book by *Robert Willis* [222]. As a consequence, the main theorem of the theory of gearing in Europe is called *Willis theorem*, which is incorrect. *Willis* himself did not derive/prove this theorem and has no direct relation to it. He only contributed to the dissemination of information on this theorem.

No criterion for the existence of an envelope curve on a plane was considered by *Euler*, and by *Willis*. Wherever it is acceptable and unacceptable, the *kinematic method* and the *Shishkov equation*,  $\mathbf{n}_g \cdot \mathbf{V}_\Sigma = 0$  are used to find the envelope curve or surface. Previously, the *kinematic method* for finding the envelope surface was used without using the *Shishkov equation*,  $\mathbf{n}_g \cdot \mathbf{V}_\Sigma = 0$ , which, of course, is less convenient. This practice has been observed since the days of *Franz Reuleaux* [188,189] who was probably the first to extensively apply the *kinematic method* in mechanism and machine science.

*George B. Grant* [99] came close to understanding of the peculiarities of the formation of the envelope surfaces during the rotational motion of the initial and envelope surfaces around the intersecting axes (the so-called *intersected-axes gearing*, or simply *I<sub>a</sub> – gearing*). However, in his valuable 1887 patent [99], challenging problems in the kinematics of gearing and geometry of the tooth flanks of a gear and a mating pinion got no solution.

From the point of view of the kinematics of gearing, and the geometry of tooth flanks of a gear and a mating pinion, finding the envelope surface in the general case of rotation, namely, when the original surface and envelope surface rotate around *crossing* axes, was not previously considered [138].



# Taylor & Francis

Taylor & Francis Group

<http://taylorandfrancis.com>



---

# 5 Permissible Variation of the Design Parameters in *Equivalent Pulley-and-Belt Transmission*

*Equivalent pulley-and-belt transmission* is a possible analogy of parallel-axes gear pair that is convenient to perform an analysis of geometrically accurate parallel-axes gearing. There are many similarities in transmitting a rotary motion by pulley-and-belt mechanism and a corresponding gearing.<sup>1</sup> Therefore, it is important to know to what extent this analogy is applicable for the purpose of analysis of gearing.

As it is already discussed in this book (see Figures 4.6 and 4.8), an *equivalent pulley-and-belt transmission* can be specified in terms of diameters of the pulleys,  $d_1$  and  $d_2$ , and the center-distance,  $C$ . Also, the ratio,  $d_2/d_1$ , of diameters of the pulleys is needed to be taken into account. A ratio of the diameters,  $d_2/d_1$ , is equal to the angular velocity ratio,  $\omega_1/\omega_2$ , of the pulleys. By convention, the ratio  $\omega_1/\omega_2$  is designated as  $u$  ( $\omega_1/\omega_2 = u$ ).

Several examples of possible configurations of two pulleys are briefly outlined immediately below.

An *equivalent pulley-and-belt transmission* is depicted in Figure 5.1. Here, point of intersection of the belt by the centerline,  $\mathfrak{c}$ , is denoted by  $P$ . The point  $P$  is a motionless point that does not travel along the centerline,  $\mathfrak{c}$ . The center-distance,  $C$ , is of a constant value. The belt forms an angle,  $\phi_t$ , with the perpendicular through  $P$  to the centerline,  $\mathfrak{c}$ . The actual value of the angle,  $\phi_t$ , can be expressed in terms of the center-distance,  $C$ , and the diameters  $d_1$  and  $d_2$  of the pulleys:

$$\phi_t = \cos^{-1} \left( \frac{d_1 + d_2}{2 \cdot C} \right) \quad (5.1)$$

As illustrated in Figure 5.2a, when the center-distance increases ( $C^* > C$ ), the angle  $\phi_t^*$  also increases ( $\phi_t^* > \phi_t$ ), and vice versa. Reduction of the center-distance results in a corresponding reduction of the angle  $\phi_t$ . Finally, when the center-distance equals to zero [ $C^{**} = (d_1 + d_2)/2$ ], the angle,  $\phi_t$ , becomes of a zero value (that is,  $\phi_t^{**} = 0^\circ$ ). The latter is schematically illustrated in Figure 5.2b.

Transmission of a rotary motion from a driving shaft to a driven shaft with parallel axes of rotation,  $O_1$  and  $O_2$ , is also possible when the center-distance,  $C$ , is of a negative value (that is,  $C < 0$ ). This particular case is schematically illustrated in Figure 5.3. Despite the pulleys do not physically exist in this scenario, the kinematics of transmission of rotary motion can be investigated assuming that the pulleys are imaginary (phantom).

The influence of the diameters,  $d_1$  and  $d_2$ , of pulleys onto the actual value of the angle,  $\phi_t$ , can be demonstrated similar to that the influence of the center-distance,  $d_1$ , on the actual value of this angle was discussed.

For all of these configurations, an equivalent geometrically accurate parallel-axes gear pair can be designed. This is possible due to the following.

---

<sup>1</sup> The only principal difference between *equivalent pulley-and-belt transmission*, and between the gear pair itself, that needs to be taken into consideration at this point is the different direction of the force by means of which the rotary motion is transmitted. In *equivalent pulley-and-belt transmission*, the driving pulley *pulls* the driven pulley, while in the gear pair, the driving gear *pushes* the driven gear.

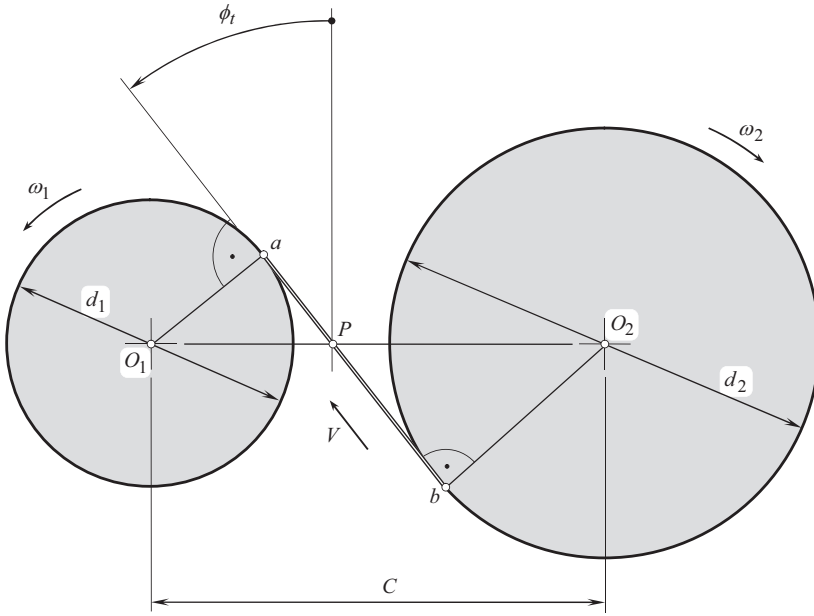


**FIGURE 5.1** On transition from *equivalent pulley-and-belt transmission* to geometrically accurate parallel-axes gear pair.

**First**, each of the pulleys of diameters  $d_1$  and  $d_2$  can be construed as envelopes to a family of consecutive positions of a line pointed along the straight-line segment,  $ab$ . As it is shown below in the further discussion, a line along the straight-line segment,  $ab$ , by nature, is the line of action,  $LA$ , in the equivalent gear pair. The pulley can be construed as an envelope to a family of consecutive positions of the line of action,  $LA$ , in their motion in relation to a reference associated with the pulley.

**Second**, consider an arbitrary point within the straight portion  $ab$  of the belt. When the *equivalent pulley-and-belt transmission* operates, this point traces in a motionless reference system a corresponding path of contact,  $P_c$ . Evidently that in parallel-axes gearing, the path of contact,  $P_c$ , is a straight line that is aligned to the line of action,  $LA$ . This makes it possible to interpret the path of contact,  $P_c$ , as an envelope (i.e., a reduced case of envelope) to a family of the lines of action,  $LA$ , when the pulleys rotate.

Another scenario is observed when a rotary motion from a driving shaft to a driven shaft is transmitted by means of two pulleys diameters of which  $d_1$  and  $d_2$  are time-dependent, namely:  $d_1 = d_1(t)$  and  $d_2 = d_2(t)$ . The functions,  $d_1 = d_1(t)$  and  $d_2 = d_2(t)$ , can also be interpreted as  $d_1 = d_1(\varphi_1)$  and  $d_2 = d_2(\varphi_2)$ , where  $\varphi_1$  and  $\varphi_2$  are the angles of rotation of the pulleys of diameters  $d_1$  and  $d_2$ , and  $\varphi_2 = \varphi_1 \cdot (d_2/d_1)$  ].

Shown in Figure 5.4 schematic corresponds to a case when the belt (the line of action,  $LA$ ) travels back and forth along the centerline,  $\mathbb{E}$ . No gear pair equivalent to the pulley-and-belt mechanism (see Figure 5.4) can be designed.

Let us assume that the angle  $\phi_t$  is of a constant value ( $\phi_t = \text{const}$ ), while the pitch point,  $P$ , is migrating within the line of centers,  $\mathbb{E}$ , depending on a current value of the rotation angle,  $\varphi_p$ , of the pinion (or, the same, of the rotation angle,  $\varphi_g$ , of the gear) as schematically illustrated in Figure 5.4. In such a scenario, for any instantaneous line of action,  $LA_i$ , instantaneous radii of the pulleys,  $r_{b,g}^{(i)}$  and  $r_{b,p}^{(i)}$  (which, by nature, are the base circles, for the gear and the pinion) can be constructed. The profile of the transverse section of the pulleys (i.e., the profile of the base curve for the gearing) can

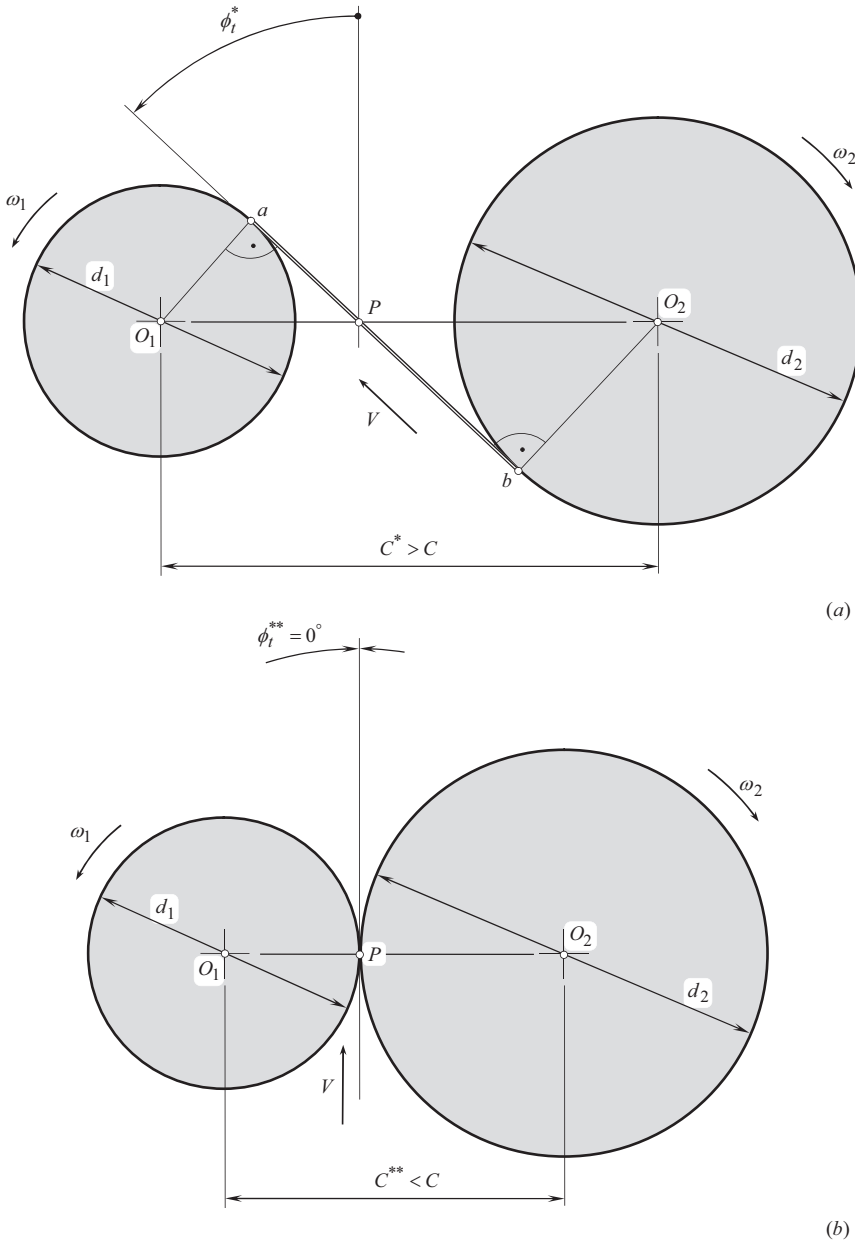


**FIGURE 5.2** Influence of variation of the center-distance,  $C$ , onto the actual value of the angle,  $\phi_1$ , in the cases when: (a) the actual center-distance,  $C^*$ , is greater than the nominal center-distance,  $C$ , and  $C^* > C$ ; (b) the actual center-distance,  $C^{**}$ , is smaller than the nominal center-distance,  $C$ , and  $C^{**} < C$ .

be specified in terms of the instantaneous lines of action  $LA_{(i-1)}$ ,  $LA_i$ , and  $LA_{(i+1)}$ , and of radii the  $r_{b,p}^{(i-1)}$ ,  $r_{b,p}^{(i)}$ , and  $r_{b,p}^{(i+1)}$  [and  $r_{b,g}^{(i-1)}$ ,  $r_{b,g}^{(i)}$ , and  $r_{b,g}^{(i+1)}$ ] of the instantaneous base circles. Such a profile does not exist, as no envelope curve can be constructed to a family of circles of different radii, and with a common center. No path of contact,  $P_c$ , is possible in the case under consideration. Ultimately, no gear tooth profile that is capable of transmitting a rotary motion from a driving shaft to a driven shaft is possible at all (no gearing equivalent to the pulley-and-belt mechanism, shown in Figure 5.4).

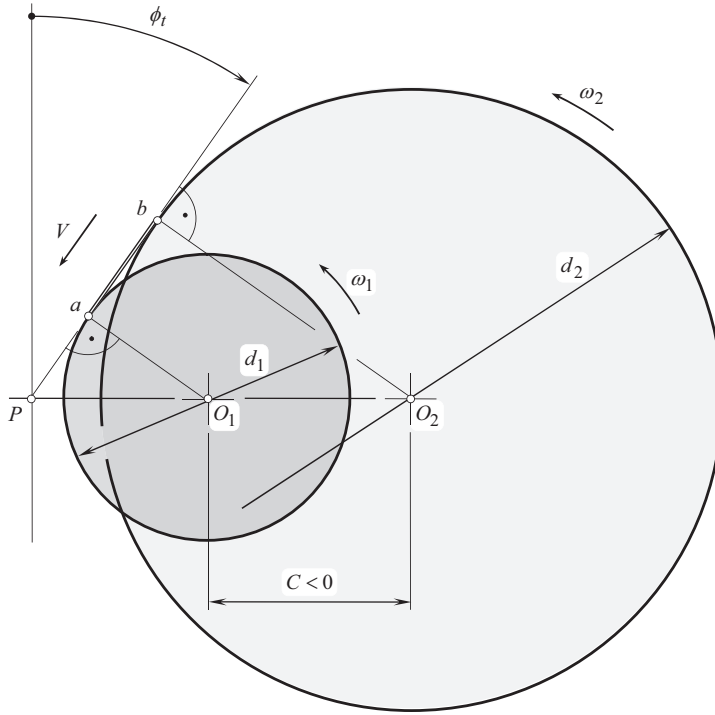


**FIGURE 5.3** Schematic of transmission of rotary motion between two parallel axes when the center-distance in the *equivalent pulley-and-belt transmission* is of a negative value ( $C < 0$ ).

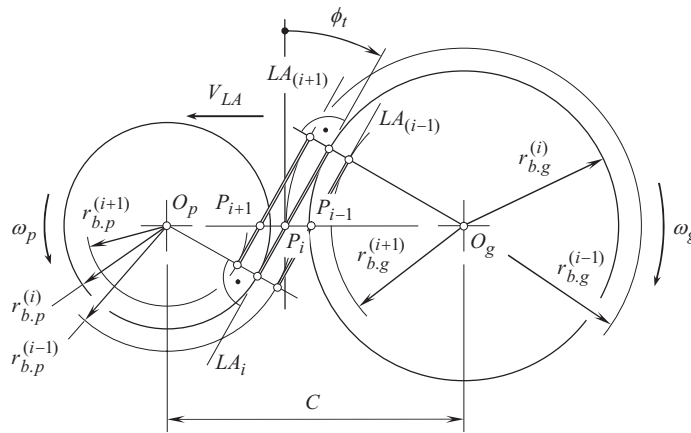


**FIGURE 5.4** In *equivalent pulley-and-belt transmission*, no transmission of rotary motion is possible when the pitch point,  $P$ , continuously travels back and forth along the centerline,  $\mathfrak{L}$ :  $\phi_t = \text{const}$ ,  $\phi_t, r_{b,p} = r_{b,p}(\varphi_g)$ .

The considered translation of the instantaneous line of action along the centerline,  $\mathfrak{L}$ , is not permissible.

A scenario when an instantaneous line of action,  $LA_{\text{inst}}$ , turns about the pitch point,  $P$ , when the gears rotate, is illustrated in Figure 5.5. Shown in Figure 5.5 situation is similar to that just considered in Figure 5.4. When the pulleys rotate, the angle between the belt and a perpendicular to the centerline (i.e., the transverse pressure angle,  $\phi_t$ ) is continuously altering (and the line of action,  $LA$ , always is a straight line through the pitch point,  $P$ ). Once the pressure angle is continuously altered,

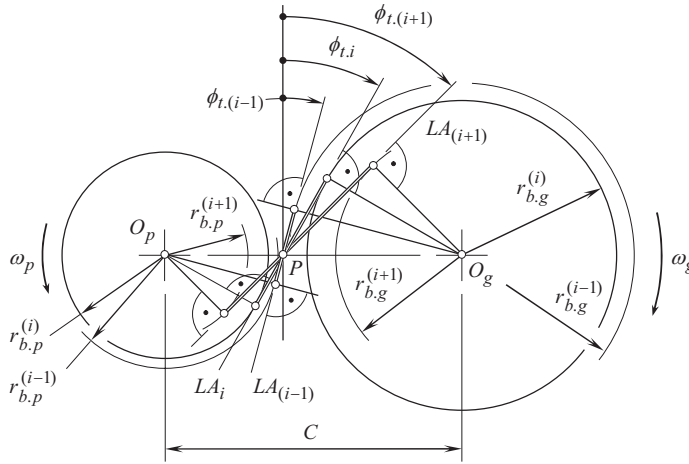


**FIGURE 5.5** In *equivalent pulley-and-belt transmission*, no transmission of rotary motion is possible when the pressure angle continuously alters its magnitude: [ $\phi_t = \phi_t(\varphi_g)$ ,  $r_{b,g} = r_{b,g}(\varphi_g)$ , and  $r_{b,p} = r_{b,p}(\varphi_g)$ ].

then an instantaneous line of action,  $LA_{\text{inst}}$ , is observed at every instant of time. Considered in a stationary reference system, no envelope to a family of consecutive positions of the instantaneous lines of action,  $LA_{\text{inst}}$ , can be constructed. This means that no path of contact,  $P_c$ , exists. No tooth profile exists for such a configuration of the line of action in relation to the pitch point. When the gears rotate, the instantaneous line of action turns about the pitch point; the common tangent (to the tooth profiles) is perpendicular to the line of action, and travels along the line of action. No envelope, in this particular case, can be generated (similar to no envelop exists for a family of circles of different diameters that feature a common center).

Ultimately, no gear tooth profile that is capable of transmitting a rotation from a driving shaft to a driven shaft can be designed at all. No pure rotation of the instantaneous line of action,  $LA_i$ , about the pitch point,  $P$ , is permissible.

However, when both the motions, namely, a translation of the instantaneous line of action,  $LA_{\text{inst}}$ , along the centerline,  $\Phi$ , and a rotation of the instantaneous line of action,  $LA_{\text{inst}}$ , about the pitch point,  $P$ , are performed simultaneously, gear teeth of a complex geometry can be generated (see Figure 5.6). In this case, the path of contact,  $P_c$ , is a planar curve that is an envelope to a family of the instantaneous lines of action,  $LA_i$ . Gear ratio,  $u$ , in the gearing shown in Figure 5.6, is time-dependent, that is, an equality  $u = u(t)$  is valid [or  $u = u(\varphi_1)$ ].

The just mentioned path of contact,  $P_c$ , (a planar curve that is an envelope to a family of the instantaneous lines of action,  $LA_i$ ), is shown in Figure 5.7. The path of contact,  $P_c$ , is traced by contact point,  $K$ . At every point of the path of contact,  $P_c$ , a corresponding *instantaneous line of action*,  $LA_{\text{inst}}$ , can be constructed. All the instantaneous lines of action,  $LA_i$ , are tangent to the path of contact,  $P_c$ , at a corresponding point.

An arbitrary contact point within the path of contact,  $P_c$ , is labeled as  $K^i$ . When the gear and the mating pinion make contact at point  $K^i$ , the instantaneous line of action,  $LA_{\text{inst}}^i$ , is in tangency to the path of contact,  $P_c$ , at  $K^i$ . This is due to the force exerted from the driving pinion is pointed along the common perpendicular to the interacting tooth flanks considered in a transverse section of a gear pair, or, the same, the force is pointed along a straight-line tangent at contact point  $K^i$  to the path of contact,<sup>2</sup>  $P_c$ .

<sup>2</sup> It is right point to stress here that in non-spur gear pairs, it is incorrect to interpret the line of action,  $LA$ , as a straight line perpendicular to the tooth flanks,  $\mathcal{S}$  and  $\mathcal{P}$ , of a gear and of a mating pinion at contact point,  $K$ . The line of action,  $LA$ , should be considered as a line within the transverse section plane that, in  $P_o$ -gearing, is perpendicular to the axes of rotation,  $O_g$  and  $O_p$ , of the gear and the pinion.

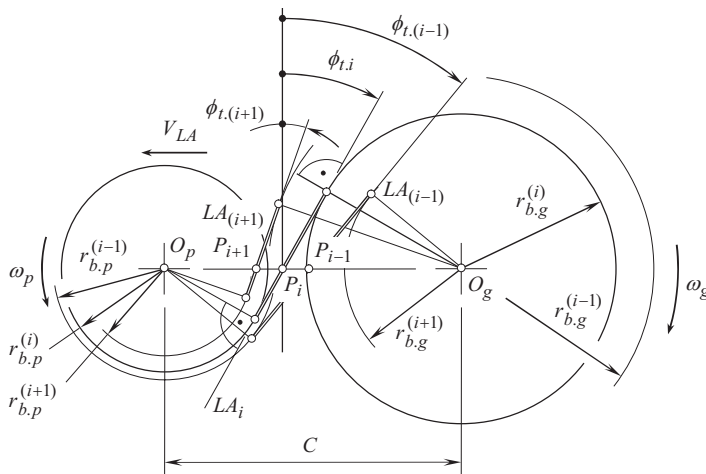


**FIGURE 5.6** Transmission of rotary motion is possible when the belt (the instantaneous line of action,  $LA$ ), travels back and forth along the centerline,  $\mathfrak{L}$ , and turns about the pitch point,  $P$ :  $\phi_t = \text{Const}, \phi_t, r_{b,p} = r_{b,p}(\phi_g)$ .

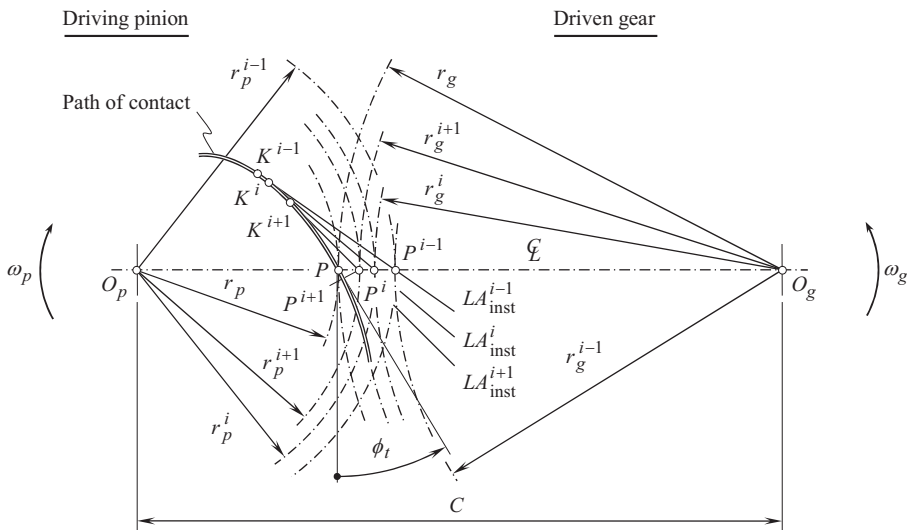


**FIGURE 5.7** Schematic of parallel-axes gearing with curved (not straight) path of contact,  $P_c$ .

Gears of the just considered kind allow for variation of the tangential component of the resultant force of interaction of the teeth in a gear pair.<sup>3</sup>

The schematics, shown in Figures 5.6 and 5.7, are useful for the investigation and the development of non-circular gearing that feature variable gear ratio,  $u = u(t)$ .

The above discussion can be summarized as follows.

<sup>3</sup> This concept is used, for example, in the design of a gear pair for fluctuating limited slip automobile differentials (see: U.S. Pat. No. 8,070,640, *Fluctuating Gear Ratio Limited Slip Differential*, S.P. Radzevich, Date: December 6, 2011, Filed: March 12, 2009, Int. Cl. F16H 48/06, F16H 48/20, F16H 57/08, F16H 57/17, U.S. Cl. 475/230).

**First**, formally, diameters of the pulley as well as gear pitch diameters can vary from zero value to plus or minus infinity. However, neither a pulley nor a gear of zero diameter is physically possible. For a particular application, an external pinion of a minimal diameter,  $d_p^{\min}$ , can be manufactured and implemented in design of a gear transmission (here  $d_p^{\min}$  is of a positive value). Similarly, for a particular application, an internal gear of a minimal diameter,  $d_g^{\min}$ , can be manufactured and implemented in design of a gear transmission (here  $d_g^{\min}$  is of a negative value). The maximal diameter of a gear approaches an infinity,  $d_g^{\min} \rightarrow \infty$ , as it is observed in a rack gear. Ultimately, pitch diameter of a gear,  $d_g$ , can vary within the interval:

$$d_p^{\min} \leq d_g \leq +\infty \quad (5.2)$$

$$-\infty \leq d_g \leq d_g^{\max} \quad (5.3)$$

The interval for gear pitch diameter:  $d_g^{\min} \leq d_g \leq d_g^{\max}$  is not possible for gears.

**Second**, formally, the center-distance,  $C$ , can vary from  $+\infty$  to  $-\infty$  including a zero value of  $C$ . Physically, no center-distance,  $C$ , of a zero value is possible.

In external gearing, the shortest permissible center-distance is of a positive value and is limited to  $C = 2 \cdot d_p^{\min} / 2 = d_p^{\min}$ . Therefore, a permissible interval for positive values of the center-distance is as follows:

$$d_p^{\min} \leq C \leq +\infty \quad (5.4)$$

In internal gearing, the shortest permissible center-distance is of a negative value and is limited to  $C = (d_g^{\min} - d_p^{\min}) / 2$ . Therefore, a permissible interval for positive values of the center-distance is as follows:

$$-\infty \leq C \leq \frac{d_g^{\min} - d_p^{\min}}{2} \quad (5.5)$$

The interval for the center-distance:

$$(d_g^{\min} - d_p^{\min}) / 2 \leq C \leq d_p^{\min} \quad (5.6)$$

is not permissible for gear pairs.

**Third**, formally, an actual value of the transverse pressure angle,  $\phi_t$ , can vary from  $+90^\circ$  to  $-90^\circ$ . Physically, no gear pair is possible when the pressure angle,  $\phi_t$ , approaches either  $+90^\circ$ , or  $-90^\circ$  value. Therefore, there exists a maximal permissible value of the positive pressure angle,  $\phi_t^{\max}$ , and for the negative pressure angle,  $\phi_t^{\min}$ . A positive pressure angle,  $\phi_t^{\max}$ , is close to  $+90^\circ$ , and a negative pressure angle,  $\phi_t^{\min}$ , is close to  $-90^\circ$ . Ultimately, a permissible interval for the pressure angle,  $\phi_t$ , can be represented in the form:

$$\phi_t^{\min} \leq \phi_t \leq \phi_t^{\max} \quad (5.7)$$

The intervals:  $-90^\circ \leq \phi_t \leq \phi_t^{\min}$  and  $\phi_t^{\max} \leq \phi_t \leq +90^\circ$  are not permissible in gearing.



The performed brief analysis of permissible variation of the design parameters of the *equivalent pulley-and-belt transmission*, and of parallel-axes gearing, is helpful for better understanding of parallel-axes gearing, and later on to enhance this experience to gearing of other designs. Ultimately, this analysis will be followed up below by novel kinds of gearing that do not allow for an *equivalent pulley-and-belt transmission*.

To the best of the author's knowledge, it is not known yet who has to be credited for the invention of the *equivalent pulley-and-belt transmission* of a ***parallel-axes*** gear pair. More research in this regard is required to be undertaken.

Regarding intersected-axes gearing, it was *G.B. Grant* who was the first to introduce (1887) the concept of the base cone in ***intersected-axes*** gearing [99]. *Grant* considered the base cone of a gear, and a plane, tangent to the gear base cone. It was not realized at the time of *Grant* that, by nature, the tangent plane is the plane of action in the gear pair. Moreover, only one base cone, and NOT two base cones of interacting bevel gears, was considered by *G.B. Grant*.

For the first time ever, the *equivalent pulley-and-belt transmission* of an ***intersected-axes*** gear pair was proposed (~2008) by Prof. *S.P. Radzevich* [174]. Two base cones in tangency with the plane of action were considered [174].

For the first time ever, the *equivalent pulley-and-belt transmission* of a ***crossed-axes*** gear pair was proposed (~2008) by Prof. *S.P. Radzevich* [174]. Two base cones in tangency with the plane of action in crossed-axes gearing were considered by Prof. *S.P. Radzevich* [174].

# Part II

---

## Geometrically Accurate Gearing

Various types of gears are extensively used in the industry to transmit and transform a rotary motion from a driving shaft to a driven shaft. Transmission and transformation of a rotary motion are the main purposes of early designs of gears. As the rotations in the past were low, and the power density was also low, no special care was taken about the accuracy of the transmitted rotation: neither the input rotation nor the output rotation often were uniform. Because of this, for a long while, no special efforts were undertaken to improve the gear tooth flank geometry: in early designs of gears, the gear teeth were shaped based mainly on common sense, and on experience gained by the gear manufacturer. Eventually, it was realized that a special gear tooth flank geometry is required in order to transmit a uniform rotary motion smoothly from a driving shaft to a driven shaft. Gears that feature an appropriate gear tooth flank geometry are capable of transmitting a rotation smoothly, that is, under a uniform rotation of the driving shaft the driven shaft rotates also uniformly. This property of gearing can be ignored when the input and output rotary motions are low, and the power density through the gear pair is also low. However, this property of gearing becomes more and more vital when the input and output rotations are getting higher, and more power is transmitted by a gear pair. The *geometrically accurate gears* are capable of transmitting a rotation smoothly. This is due to:

- The tooth flanks of a gear and its mating pinion feature geometry that meets three fundamental laws of gearing outlined above in Chapter 4 (this chapter is titled “Smooth Transmission of Uniform Rotary Motion: *Three Fundamental Laws of Gearing*”), and more in-detail is discussed below in this section of the book
- The axes of rotation of a gear and of its mating pinion are perfectly aligned to one another (the axes displacements, both, the angular and linear axes displacements are of a zero value)

Ultimately, these two features result in that transmission error in *geometrically accurate gearing* is always zero.

The analysis of all three types of *geometrically accurate gears*, namely, of:

1. parallel-axes gearing,
2. intersected-axes gearing, and
3. crossed-axes gearing,

is covered in this part of the book.

Geometrically accurate parallel-axes gear pairs are discussed in the first portion of this section of the book (Chapters 6–11). This discussion is followed by the analysis of geometrically accurate intersected-axes gear pairs in the second portion of this section of the book (Chapters 13 and 14). Ultimately, geometrically accurate crossed-axes gear pairs are discussed in the third portion of this section of the book (Chapters 15 and 16).

Design of a geometrically accurate gear pair begins with an analysis of the kinematics of the gear pair to be designed. The essence of the approach can be stated as follows:

**Essence of the approach:** *Given a pair of rotary motions specified, for example, in terms (a) of an input torque,  $T_{\text{input}}$  (b) of rotation vector of a gear,  $\omega_g$ , and (c) of rotation vector of a mating pinion,  $\omega_p$ ; the rotation vectors,  $\omega_g$  and  $\omega_p$ , are somehow configured in relation to one another. It is required to determine the most favorable geometry of the interacting tooth flanks of the gear and of the mating pinion.*

Commonly, this problem has to be solved under a certain set of constraints, such as those imposed by specific requirements for a particular gear application. The necessity to meet the kinematic and geometric requirements by means of ensuring conjugate action of the interacting tooth flanks of the gear and the pinion is of prime importance.

Physical phenomena that occur when two gears are engaged in mesh with one another are taken into account in later stages of the design process. Ultimately,

1. the kinematics of meshing,
2. the geometry of conjugate tooth flanks, and
3. physical phenomena that occur between the contacting surfaces,

all three of them comprise the discussed approach to the problem of designing the most favorable gear pair. The use of the approach enables one to solve the challenging problem of synthesizing the most favorable gear pair for a specified application.

Only the kinematic and geometric aspects of the problem of designing geometrically accurate gear pairs are discussed below in this book.

# Section II-A

---

## Geometrically Accurate Gearing

### Parallel-Axes Gearing

Gear pairs that operate on parallel axes of rotation of a driving and of driven shafts comprise a separate group of gearing that is commonly referred to as *parallel-axes gearing*. Parallel-axes gearing is also often referred to as  $P_a$  – gearing, for simplicity. Parallel axes of rotation of a gear and its mating pinion (namely, when centerlines of the shafts are parallel to one another) is the principal feature of gearing of this particular kind. Spur gearing, helical gearing, herring-bone gearing, and so forth, represent perfect examples of parallel-axe gearing.

A variety of known designs of gear pairs feature parallel axes of rotation of the driven and the driving shafts. Parallel-axes gear pairs of each kind can be specified by a corresponding gear vector diagram. *Gear vector diagram* is the key for understanding the kinematics as well as the geometry of conjugate tooth flanks of a gear and its mating pinion in parallel-axes gearing. The most favorable geometry of the tooth flanks of mating gears follows a given kinematics of gearing, and not vice versa.

The kinematics of a gear pair (specified in terms of a corresponding gear vector diagram) is the start point for solving the problem of designing the most favorable gear pair for a given application, that is, designing a gear pair with the desirable performance. First of all, configuration of the input shaft in relation to the output shaft has to be given. Then, the input torque must be specified. Finally, the rotation of the driving shaft, as well as the desirable rotation of the driven shaft, must be known. This set of input information for solving the problem of designing a desirable gear pair is self-consistent and is the shortest possible. None of the aforementioned items can be eliminated from the above-listed set of input information.

In the discussion below in this part of the book, the readers' attention is focused on the correspondence between the given parameters of the kinematics of a gear pair and the desirable tooth flank geometry of mating gears.

This section of the book is comprised of Chapters 6–11.



# Taylor & Francis

Taylor & Francis Group

<http://taylorandfrancis.com>

---

# 6 Involute Gearing

## *Kinematics and Geometry*

About 80% of gears in total operate on parallel axes of rotation. Involute gearing is the most broadly used kind of parallel-axes gearing. An example of the application of involute parallel-axes gearing is shown in Figure 6.1.

The discussion on involute gearing in this chapter begins with an analysis of specified kinematics of relative motion of a gear and its mating pinion.

Although this book is written mostly for readers who are proficient in the field of gearing, and less for the beginners in the field, for the readers' convenience some elementary concepts of basics of the theory of transmission of rotation from an input shaft to an output shaft are briefly considered in this chapter.

### 6.1 PRINCIPAL FEATURES OF PARALLEL-AXES GEARING

Various kinds of parallel-axes gearing feature common fundamental components. It is convenient to begin the discussion from the analysis of kinematics of parallel-axes gearing and to implement for this purpose earlier introduced *gear vector diagrams* (see Chapter 2).

#### 6.1.1 KINEMATICS OF PARALLEL-AXES GEARING

*gear vector diagram* is a convenient means for the investigation of the kinematics of parallel-axes gearing. A *gear vector diagram* is composed of two rotation vectors.<sup>1</sup> One of the vectors is the rotation vector of the gear. This vector is denoted by  $\omega_g$ . The other one is the rotation vector of the pinion. This vector is designated as  $\omega_p$ . The rotation vector of the gear,  $\omega_g$ , and that of the pinion,  $\omega_p$ , are located apart from each other at a certain distance. This distance is referred to as the *centre-distance* and is designated as  $C$ .

When the rotation vectors,  $\omega_g$  and  $\omega_p$ , are known, the vector of instantaneous relative rotary motion,  $\omega_{pl}$ , can be constructed. By convention, the vector of instantaneous rotation,  $\omega_{pl}$ , indicates the instant rotation of the pinion in relation to the gear. Under such a scenario, the latter is considered motionless. Instant rotation of the gear relative to the motionless pinion can also be considered.

The rotation vectors,  $\omega_g$  and  $\omega_p$ , feature directions and certain magnitudes. Magnitudes of the rotation vectors,  $\omega_g$  and  $\omega_p$ , are equal  $\omega_g = |\omega_g|$  and  $\omega_p = |\omega_p|$ , correspondingly. In parallel-axes gearing, orientation of the rotation vectors in relation to one another is restricted so as to keep the vectors parallel to one another (see Chapter 2, the first line in Table 2.1). However, the center-distance,  $C$ , can be of different values, including both positive and negative values.

When the rotation vectors,  $\omega_g$  and  $\omega_p$ , are parallel, they can be configured in relation to one another in a different manner. Examples are schematically shown in Figure 6.2.

---

<sup>1</sup> Angular velocity is considered in this book as a vector pointed along the axis of rotation in the direction defined by the right-hand screw rule. It is understood here and below that by nature, the rotations,  $\omega_g$  and  $\omega_p$ , are not vectors. Therefore, special care is required to be undertaken when treating rotations as vectors. In particular, when coordinate systems transformation is analytically described by means of matrices, the order of the matrices in the matrix product is predetermined by the order of the elementary coordinate system transformations, that is, the order of the matrices in the matrix product cannot be altered.



**FIGURE 6.1** Parallel-axes gear pair composed of spur involute gears.

In the simple case, shown in Figure 6.2a, the rotation vectors,  $\omega_g$  and  $\omega_p$ , are of the same magnitude (i.e.,  $\omega_g = \omega_p$ ), and are pointed in the opposite directions. The gear ratio<sup>2</sup> in this gear pair equals to:

$$u = \frac{\omega_p}{\omega_g} = -1 \quad (6.1)$$

The inequality  $\omega_g \leq \omega_p$  is always observed.

The sign “−” in Eq. (6.1) is due to in external gearing of conventional design the direction of rotation of the driving shaft is altered to the opposite direction of the driven shaft. This is the reason for why parallel-axes gearing of this kind is referred to as *rotationally negative parallel-axes gearing*. However, as it is shown below, numerous designs of external parallel-axes gearing can also be *rotationally positive*, namely, be a kind of external parallel-axes gearing with a positive angular velocity ratio,  $\omega_g > \omega_p$ .

The magnitude of the vector of instantaneous rotation,  $\omega_{pl}$ , is double that of the rotation vector of the gear,  $\omega_g$  (or, similarly, of the rotation vector of the pinion,  $\omega_p$ ). The rotation vector,  $\omega_{pl}$ , is parallel to the rotation vectors,  $\omega_g$  and  $\omega_p$ , and passes through the pitch point,  $P$ , at the middle of the center-distance,  $C$ .

In another example, shown in Figure 6.2b, an inequality  $\omega_g < \omega_p$  is observed. The gear ratio in this particular case is of a negative value ( $u < 0$ ). Magnitude of the vector of instantaneous rotation,  $\omega_{pl}$ , is equal to the summa of magnitudes of the rotation vectors of the gear,  $\omega_g$ , and the pinion,  $\omega_p$ , that is, an equality  $\omega_{pl} = \omega_g + \omega_p$  is valid. The rotation vector,  $\omega_{pl}$ , is parallel to the rotation vectors,  $\omega_g$  and  $\omega_p$ . The vector  $\omega_{pl}$  passes through the pitch point,  $P$ , within the center-distance,  $C$ . The pitch point,  $P$ , is located closer to the rotation vector of the pinion,  $\omega_p$ .

The gear vector diagrams (see Figure 6.2a and b) correspond to external gearing of conventional design.

<sup>2</sup> Commonly, the *gear ratio*,  $u$ , is the ratio of the larger to the smaller number of teeth in a pair of gears, namely,  $u = N_g/N_p$ , where  $N_g$  and  $N_p$  are tooth numbers of the gear and the pinion, correspondingly ( $N_g \geq N_p$ ). In the *Imperial* system of symbols, the gear ratio is denoted by  $m_G$ . The gear ratio,  $u$ , can be also expressed in terms of the rotations,  $\omega_g$  and  $\omega_p$ . A formula  $u = \omega_p/\omega_g$  can be used for this purpose. Definition of the gear ratio in terms of rotations, that is, of the input rotation,  $\omega_{\text{input}}$ , to the output,  $\omega_{\text{output}}$ , ( $u = \omega_{\text{input}}/\omega_{\text{output}}$ ), is preferred, and is adopted in this book.



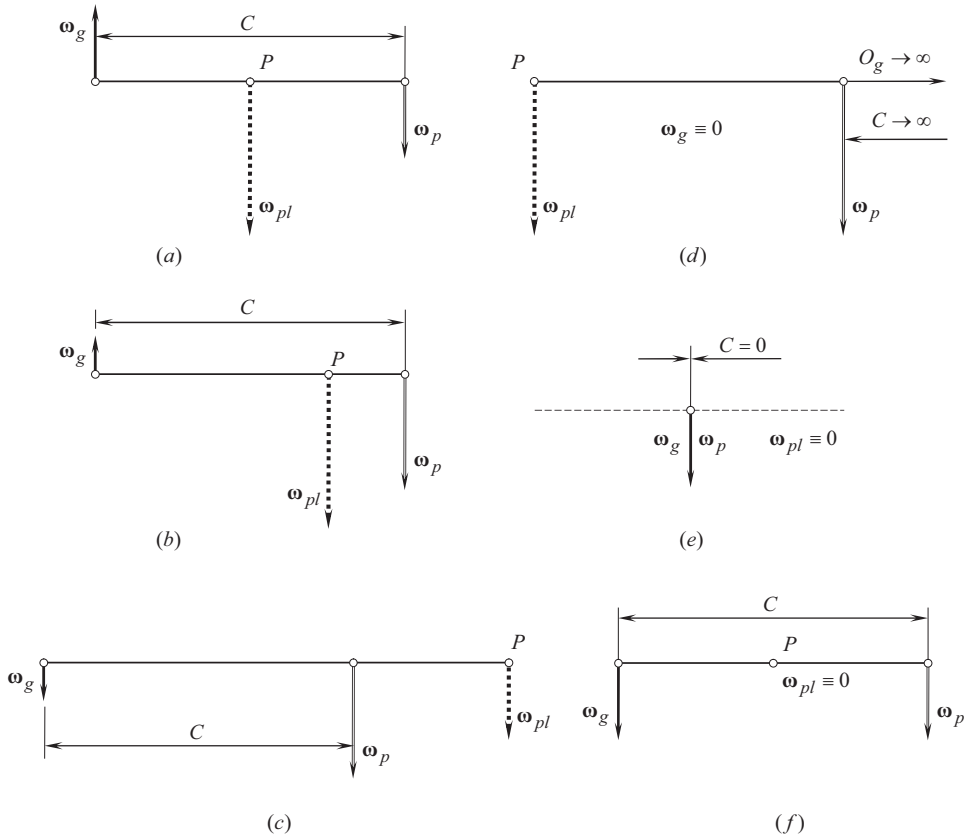


**FIGURE 6.2** Possible kinds of *gear vector diagrams* for parallel-axes gear pairs of conventional design: (a) external rotary-negative gearing with the gear ratio,  $u = -1$ ; (b) external rotary-negative gearing with a negative gear ratio  $u < 0$ ; (c) internal rotary-positive gearing with a positive gear ratio  $u > 0$ ; (d) rotary-zero *gear-to-rack* pair with the gear ratio  $u = 0$ ; (e) gear coupling with gear the ratio  $u = +1$ ; (f) hypothetical internal rotary-positive gearing with a positive gear ratio  $u > 0$ .

For the same center-distance,  $C$ , the rotation vectors,  $\omega_g$  and  $\omega_p$ , of a gear and that of a mating pinion can be pointed in the same direction, as shown in Figure 6.2c. Because the rotation vectors are in the same direction, the gear ratio in a gear pair of this kind is of a positive value ( $u > 0$ ). The magnitude,  $\omega_p$ , of rotation vector of the pinion always exceeds the magnitude,  $\omega_g$ , of rotation of its mating gear.

The gear vector diagram shown in Figure 6.2c corresponds to an internal gearing of conventional design.

The magnitude of the vector of instantaneous rotation,  $\omega_{pl}$ , is equal to the difference between the magnitudes of the rotation vectors  $\omega_g$  and  $\omega_p$ , that is, an equality  $\omega_{pl} = -\omega_g + \omega_p$  is valid. The rotation vector,  $\omega_{pl}$ , is parallel to the rotation vectors,  $\omega_g$  and  $\omega_p$ , of the gear and the pinion. The rotation vector  $\omega_{pl}$  passes through the pitch point,  $P$ , which is located outside the center-distance,  $C$ . In internal gearing of conventional design, the pitch point,  $P$ , is located outside the center-distance,  $C$ , but still within the centerline,  $\Phi$ .

The actual configuration of the rotation vectors in a gear vector diagram also depends on the length of the center-distance,  $C$ . In the above considered examples, the center-distance is of a finite length. There are no physical constraints to set the center-distance of an infinite length ( $C \rightarrow \infty$ ). An example of gear vector diagram of this particular kind is schematically depicted in Figure 6.2d. Gear vector diagram of this particular kind corresponds to a *pinion gear-to-rack gearing*. Because

the center-distance for *pinion gear-to-rack* pair is of an infinite length, the gear axis of rotation,  $O_g$ , is remote to an infinity. In this scenario, location of the vector of instantaneous rotation,  $\omega_{pl}$ , is specified in terms of the vectors  $\mathbf{V}_g$  and  $\omega_p$ , and not in terms of the rotation vectors,  $\omega_g$  and  $\omega_p$ , instead. Here, the linear velocity vector of the rack is denoted by  $\mathbf{V}_g$ . The vectors,  $\mathbf{V}_g$  and  $\omega_p$ , are synchronized with one another. Gear ratio in the pinion gear-to-rack pair (see Figure 6.2d) is of an infinite value ( $u \rightarrow \infty$ ).

The linear velocity vector,  $\mathbf{V}_g$ , is pointed perpendicular to both, to the rotation vector,  $\omega_p$ , of the pinion, and to the centerline,  $\mathbf{t}$ .

The gear vector diagram for a *pinion gear-to-rack* gear pair can be considered either as a reduced case of the gear vector diagram of external gear pair (see Figure 6.2b), or as a reduced case of the vector diagram of internal gear pair (see Figure 6.2c).

In the case under consideration, the rotation vector of the gear,  $\omega_g$ , is zero ( $\omega_g = 0$ ). Formally, a zero vector can not be parallel to another vector. However, when the center-distance approaches infinity, magnitude of the rotation vector,  $\omega_g$ , becomes smaller and smaller, and, ultimately, it approaches zero. The direction of the rotation vector,  $\omega_g$ , retains the same. It is assumed here that the direction of the zero vector,  $\omega_g$ , is remained parallel to the rotation vector,  $\omega_p$ .

Theoretically, the length of the center-distance,  $C$ , can be set equal to zero. This case is illustrated in Figure 6.2e. A gear vector diagram of this type corresponds to gear coupling. Gear ratio in gear coupling (see Figure 6.2e) equals  $u = +1$ .

Gear vector diagram for a hypothetical internal rotationally positive gearing with gear ratio  $u = +1$  is shown in Figure 6.2f. A possibility of gearing that feature gear vector diagram of this particular kind is considered below in this section of the book.

### 6.1.2 GEAR RATIO IN PARALLEL-AXES GEARING

The actual kind of a gear pair depends, to a great extent, on the magnitude and sign of the angular velocity ratio,  $u$ . The angular velocity ratio in parallel-axes gear pair is defined as the ratio of the input rotation,  $\omega_{\text{input}}$ , to the output rotation,  $\omega_{\text{output}}$ :

$$u = \frac{\omega_{\text{input}}}{\omega_{\text{output}}} \quad (6.2)$$

In reduction gears (i.e., in *gear reducers*), gear ratio equals:

$$u = \frac{\omega_p}{\omega_g} \quad (6.3)$$

In increasing gears (i.e., in *gear increasers*, or *gear multipliers*), the gear ratio equals to:

$$u = \frac{\omega_g}{\omega_p} \quad (6.4)$$

An external gear pair that is composed of gears with the same tooth count, features the gear ratio of  $u = -1$ . A gear ratio in an arbitrary external gear pair of conventional design falls into the interval  $-\infty < u < -1$ . In a *pinion gear-to-rack pair*, the gear ratio approaches an infinite value (i.e.,  $u \rightarrow -\infty$ ).

Similarly, in an arbitrary internal gear pair, that is composed of gears with the same tooth count, a gear ratio equals  $u = +1$ . A gear ratio within the interval  $+1 < u < +\infty$  corresponds to internal gear pairs of conventional design. Ultimately, in a *pinion gear-to-rack pair*, gear ratio approaches an infinite value (i.e.,  $u \rightarrow +\infty$ ).

When a discussion is limited only to rotationally negative parallel-axes gearing, the following expressions are valid for the center-distance,  $C$  (see Chapter 2, Figure 2.29):

$$C = C_g + C_p \quad (6.5)$$

and for the gear ratio,  $u$ :

$$u = \frac{C_g}{C_p} \quad (6.6)$$

here, the distance from the gear axis of rotation,  $O_g$ , to point  $P$  is designated as  $C_g$  (the gear center-distance,  $C_g$ ), and that for the pinion is designated as  $C_p$  (the pinion center-distance,  $C_p$ ). The gear center-distance,  $C_g$ , is a signed value: it is of a positive value,  $C_g > 0$ , in external gearing, and it is of a negative value,  $C_g < 0$ , in internal parallel-axes gearing. The pinion center-distance,  $C_p$ , is always of a positive value,  $C_p > 0$ . Magnitude,  $|C_g|$ , of the gear center-distance  $C_g$  is always larger, or equal to the pinion center-distance,  $C_p$ , that is, an inequality  $|C_g| \geq C_p$  is observed. As it becomes clear later, the center-distances,  $C_g$  and  $C_p$ , by nature, are the pitch radii of a gear and a mating pinion in a gear pair. With these limitations on the center-distances,  $C_g$  and  $C_p$ , the interval for the center-distance,  $C$ , is as follows:

$$0.2 \cdot C_p \leq C \leq +\infty \quad (6.7)$$

in external gearing, and

$$-\infty \leq C \leq 0 \quad (6.8)$$

in internal parallel-axes gearing.

The discussion on the angular velocity ratio [see Eqs. (6.2)–(6.6)], yields a generalized formula for the gear ratio,  $u$ :

$$u = \frac{\omega_p}{\omega_g} = \frac{C_g}{C_p} = \frac{r_{b,g}}{r_{b,p}} \quad (6.9)$$

Here, in Eq. (6.9), radii of base circles of a gear and of a mating pinion are designated as,  $r_{b,g}$  and  $r_{b,p}$ , correspondingly (for details, see below in this chapter of the book).

Based on the two expressions [Eqs. (6.5) and (6.6)], the following formulas are valid:

$$C_p = C - C_g \quad (6.10)$$

$$u = \frac{C_g}{C - C_g} \quad (6.11)$$

$$u = \frac{\bar{C}_g}{1 - \bar{C}_g} \quad (6.12)$$

where  $\bar{C}_g = C_g / C$ . Ultimately, a formula for the normalized (i.e., normalized<sup>3</sup> by the center-distance,  $C$ ) pitch radius of the gear,  $\bar{C}_g$ , in rotationally negative parallel-axes gearing can be derived:

<sup>3</sup> Here and below, when treating *normalized* parameters, it is a must to bear in mind that the original values, namely, a linear velocity vector,  $\mathbf{V}$ , a tangent force vector,  $\mathbf{T}$ , a displacement,  $\delta$ , and so forth, are the vectors with dimensions, and, therefore, they can not be added to one another (as they are of different dimensions). Normalized vectors (a unit linear velocity vector,  $\mathbf{v} = \mathbf{V} / |\mathbf{V}|$ , a unit tangent force vector,  $\mathbf{t} = \mathbf{T} / |\mathbf{T}|$ , and so forth) formally can be added to one another. However, such an operation is meaningless.

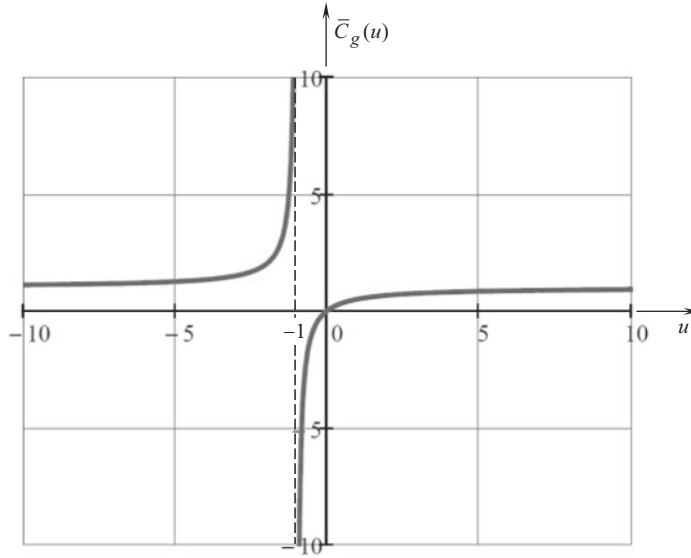


**FIGURE 6.3** A function  $\bar{C}_g(u)$  for rotationally negative parallel-axes gearing ( $\bar{C}_g = C_g / C$ ).

$$\bar{C}_g(u) = \frac{u}{u+1} \quad (6.13)$$

The function “ $\bar{C}_g$  vs.  $u$ ” is plotted in Figure 6.3. A gear pair with the gear ratio  $u = -1$  is not permissible in the case under consideration.

The performed analysis of Eq. (6.13) reveals that there are two points of special interest in the plot of the function  $\bar{C}_g(u)$ , shown in Figure 6.3. In rotationally negative parallel-axes gearings, the angular velocity ratio at these points equals  $u = -1$  and  $u = 0$ . As shown in Figure 6.4, these two points are labeled as  $A_n$  and  $B_n$ , correspondingly. In the first case, the normalized gear center-distance,  $\bar{C}_g$ , in the gear pair is of an infinite length ( $\bar{C}_g = \pm\infty$ ). In the second case, the normalized gear center-distance,  $\bar{C}_g$ , in the gear pair is of a zero length ( $\bar{C}_g = 0$ ).

Similarly, when a discussion is limited only to rotationally positive parallel-axes gearing, the following expressions are valid for the center-distance,  $C$ , and for the angular velocity ratio,  $u$ :

$$C = C_g - C_p \quad (6.14)$$

$$u = \frac{C_g}{C_p} \quad (6.15)$$

These two expressions yield a formula for the normalized pitch radius of the gear,  $\bar{r}_g$ , in rotationally positive parallel-axes gearing:

$$\bar{r}_g(u) = \frac{u}{u-1} \quad (6.16)$$

The function “ $\bar{C}_g$  vs.  $u$ ” is plotted in Figure 6.5. A gear pair with the gear ratio  $u = +1$  is not permissible in the case under consideration.

The performed analysis of Eq. (6.16) reveals that there are two points of special interest in the plot of the function  $\bar{C}_g(u)$ , shown in Figure 6.5. In rotationally positive parallel-axes gearings, the angular velocity ratio at these points equals  $u = 0$  and  $u = +1$ . As shown in Figure 6.4, these two points are labeled as  $B_p$  and  $C_p$ , correspondingly.

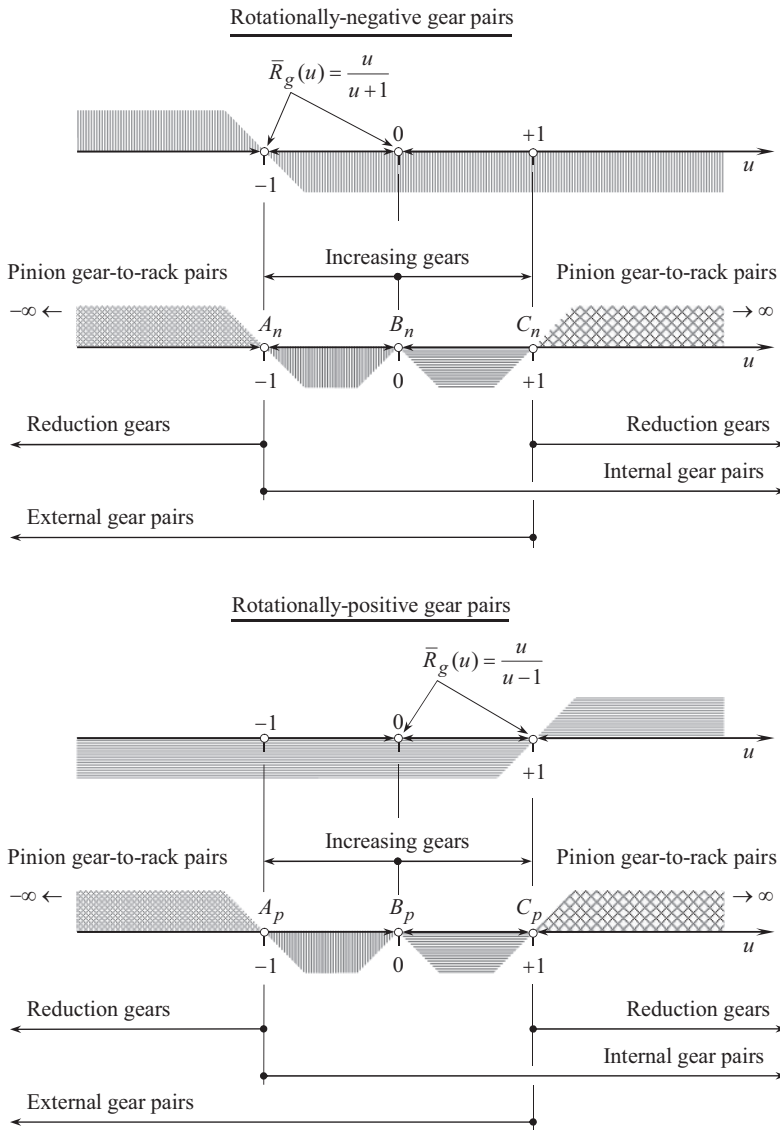


**FIGURE 6.4** Kind of a gear pair depending on gear ratio  $u$ .

Ultimately, in both cases, in rotationally negative as well as in rotationally positive parallel-axes gearing, the points  $A_n$ ,  $B_n$ , and  $B_p$ ,  $C_p$ , can be specified in terms of three values of the angular velocity ratio:  $u = -1$ ,  $u = 0$ , and  $u = +1$ . Only the point  $B_n \equiv B_p$  (where  $u = 0$ ) corresponds to an angular velocity for which no gear pair is possible at all (no gear pair that does not transmit a rotary motion can be designed at all). A gear pair can be designed for the rest of the values of the gear ratio:  $-\infty \leq u < 0$  and  $0 < u \leq +\infty$ .

The correlation between the signed value of the angular velocity ratio,  $u$ , and the actual kind of gearing is schematically illustrated in Figure 6.4.

The shown in Figure 6.4 schematic is constructed in strict formal compliance with Eqs. (6.13) and (6.16), as well as with the results that are illustrated in Figures 6.3 and 6.5. It should be stressed here that the asymptote  $u = -1$  in Figure 6.3, as well as the asymptote in Figure 6.5, correlate to points  $A_n$  and  $C_p$ , in Figure 6.4. Therefore, it is instructive to consider Figures 6.3–6.5, together, aligning (in a common schematic) the points  $A_n$  and  $C_p$ , with the corresponding asymptotes.

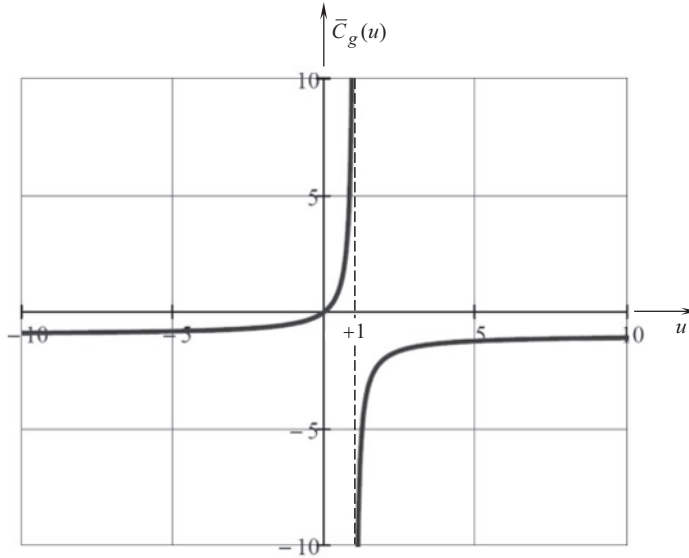


**FIGURE 6.5** A function  $\bar{C}_g(u)$  for rotationally positive parallel-axes gearing ( $\bar{C}_g = C_g / C$ ).

In a rotationally negative gearing, the direction of the input rotation is altered to the opposite direction. Therefore, in rotationally negative gearing (see Figure 6.4), gear ratios of reduction gears of conventional design correspond to the section at left of the point  $A_n$  (and the point  $A_p$ ). Gear ratios for increasing gears of conventional design correspond to the section  $A_n - B_n$ . Gear pairs with gear ratios that correspond to the section  $B_n - C_n$ , and those that correspond to the section at right of the point  $C_n$ , are not known yet. A possibility of corresponding novel designs of gear pairs in these sections of the  $u$  – axis needs to be thoroughly investigated. Also, the point  $A_n$  corresponds to conventional gearing in which tooth count of the gear and the pinion are equal to one another. Gearing that corresponds to the point,  $C_n$ , is not known yet.

The angular velocity ratio  $u \rightarrow -\infty$  corresponds to a *pinion gear-to-rack* pair that is construed as a reduced case of an external gearing when the gear tooth count approaches infinity.

In rotationally positive gearing, the direction of the output rotation is the same as the input rotation. Therefore, in rotationally positive gearing (see Figure 6.4), angular velocity ratio of reduction gears of a conventional design corresponds to the section at right of the point  $C_p$ . Angular velocity ratios for increasing gears of a conventional design correspond to the section  $B_p - C_p$ . Gear pairs with gear ratio that corresponds to the section  $A_p - B_p$ , and those that correspond to the section at left of the point  $A_p$ , are not known yet. A possibility of corresponding novel designs of gear pairs in these sections of the  $u$  – axis has to be investigated. Also, gearing that corresponds to the point  $C_p$  is not known yet.

The case of  $u = +1$  corresponds to gear couplings.<sup>4</sup>

<sup>4</sup> It should be noted again that the case of  $u = +1$  corresponds to deeply reduced design of gear pairs. Because of this, significant features could be observed when developing tooth flanks for gearing with the gear ratio  $u = +1$ . When the friction between the interacting tooth flanks of a gear,  $\mathcal{G}$ , and its mating pinion,  $\mathcal{P}$ , is ignored, the tangential force that transmits the torque from the driving shaft to the driven shaft acts along the common perpendicular,  $\mathbf{n}_g$ , to the interacting tooth flanks,  $\mathcal{G}$  and  $\mathcal{P}$ . The common perpendicular,  $\mathbf{n}_g$ , intersect the axis of instantaneous rotation,  $P_m$ , namely, it intersects the line along which the vector of instantaneous rotation,  $\boldsymbol{\omega}_{pi}$ , acts. In gear pairs with the gear ratio  $u = +1$ , all three rotation vectors, namely,  $\boldsymbol{\omega}_g$ ,  $\boldsymbol{\omega}_p$ , and  $\boldsymbol{\omega}_{pi}$ , are pointed along a common straight line,  $P_m$ . Once the line of action of the unit normal vector,  $\mathbf{n}_g$ , intersects the line of action of the angular velocity vector,  $\boldsymbol{\omega}_{pi}$ , the arm of tangential force in the gear pair becomes zero. This means that no torque can be transmitted by a gear pair of these particular kind of gearing. This discrepancy needs to be thoroughly investigated. However, when in a real gear coupling the axes misalignment is taken into account, the gear coupling can be considered as a reduced case of a gear pair.

The angular velocity ratio  $u \rightarrow +\infty$  corresponds to pinion gear-to-rack gear pair that is construed as reduced case of an internal gearing when the gear tooth count approaches infinity.

All the gear designs that are formally possible, and are outlined in Figure 6.4, need to be investigated to the best possible extent.

### 6.1.3 PERMISSIBLE VARIATION OF TRANSVERSE PRESSURE ANGLE

In the *equivalent pulley-and-belt transmission*, the angle that the belt forms with the perpendicular to the centerline,  $\Phi$ , is of critical importance. In parallel-axes gearing, this angle is commonly referred to as the *transverse pressure angle*, and is designated as  $\phi_t$ .

Commonly, for a particular gear, the transverse pressure angle,  $\phi_t$ , is of a constant value. As it is discussed in Chapter 5, theoretically, this angle,  $\phi_t$ , can be set within the interval  $0^\circ \leq \phi_t \leq 90^\circ$ .

When the transverse pressure angle equals  $\phi_t = 0^\circ$ , then the radius of curvature of the gear tooth profile is zero ( $R_g = 0$ ). As the involute tooth profile cannot be extended inward the base circle of a gear, spur gearing is impossible. Spur gear tooth flanks reduce to straight lines on the base cylinder. Helical gear tooth flanks reduce to helices on the base cylinder. Thus, helical gearing that features zero transverse pressure angle,  $\phi_t = 0^\circ$ , is impractical. Therefore, the lowest limit of  $\phi_t = 0^\circ$  for the transverse pressure angle,  $\phi_t$ , should be replaced with a certain reasonably small limit,  $[\phi_t]_{\min}$ . Actually, an inequality  $\phi_t \geq [\phi_t]_{\min}$  is observed.

When the transverse pressure angle equals to a right angle,  $\phi_t = 90^\circ$ , there is no tangential force to transmit a torque. Therefore, the highest limit  $\phi_t = 90^\circ$  for the transverse pressure angle,  $\phi_t$ , should be replaced with a certain reasonably large limit,  $[\phi_t]_{\max}$ . An inequality  $\phi_t \leq [\phi_t]_{\max}$  is observed.

Ultimately, a permissible interval:

$$[\phi_t]_{\min} \leq \phi_t \leq [\phi_t]_{\max} \quad (6.17)$$

can be set for the transverse pressure angle,  $\phi_t$ .

Referring to Figure 6.6, consider schematic of an external parallel-axes *gear-to-pinion mesh* with transverse pressure angle,  $\phi_t$ , of an arbitrary value. The gear and the pinion rotate about their axis of rotation,  $O_g$  and  $O_p$ , with angular velocities,  $\omega_g$  and  $\omega_p$ , correspondingly. The axes of rotations,  $O_g$  and  $O_p$ , are apart from one another at a center-distance,  $C$ . The pitch point,  $P$ , is located within

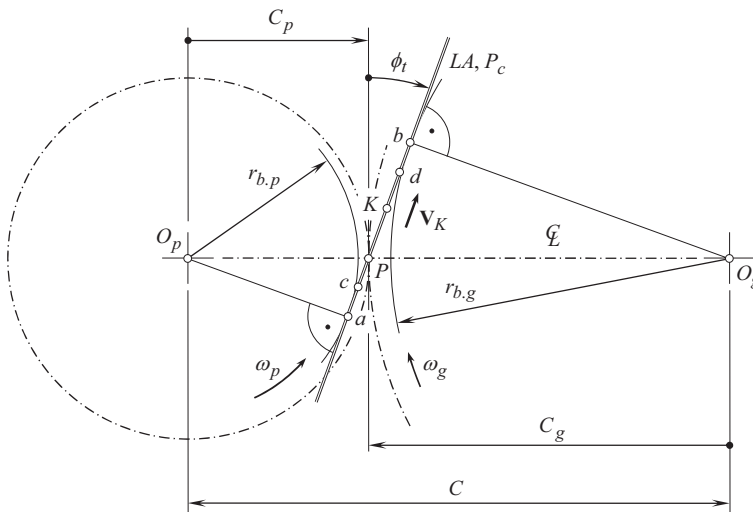


**FIGURE 6.6** Schematic of external *gear-to-pinion mesh* with transverse pressure angle,  $\phi_t$ , of an arbitrary value.



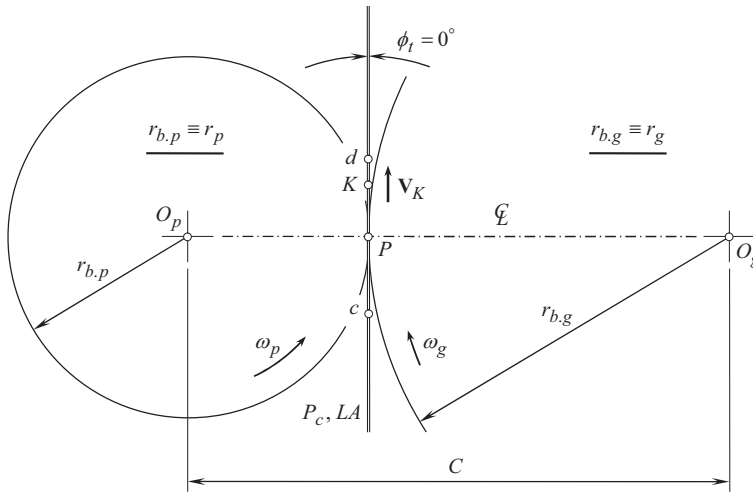


FIGURE 6.7 Schematic of an external gear-to-pinion mesh with a zero transverse pressure angle,  $\phi_t = 0^\circ$ .

the centerline,  $\mathfrak{L}$ . The ratio  $C_g / C_p$  of the center-distances,  $C_g$  and  $C_p$ , equals to the angular velocity ratio,  $u$  (here, the equality  $C_g / C_p = u = \omega_p / \omega_g$  is valid). In geometrically accurate parallel-axes gearing, the line of action,  $LA$  (and the path of contact,  $P_c$ ), forms a transverse pressure angle,  $\phi_t$ , with the perpendicular to the centerline,  $\mathfrak{L}$ , at the pitch point,  $P$ . It is worthy to stress here that the line of action,  $LA$ , and the path of contact,  $P_c$ , are two different lines, both through the pitch point,  $P$ . In a reduced case of parallel-axes gearing, these two lines,  $LA$  and  $P_c$ , align to one another (or, in other words, they are congruent to each other). The latter is not observed in more general cases of intersected-axes gearing, as well as in crosses-axes gearing.

The portion  $ab$  of the line of action,  $LA$ , is an equivalent of the free brunch of the belt in the equivalent pulley-and-belt transmission. The active portion,  $cd$ , of the line of action,  $LA$ , commonly is located within the portion  $ab$ . However, this is not a constraint, and a gear pair can be designed so as to have a contact point  $K$  that travels beyond the points  $a$  and  $b$ . At this point, the actual positions of points  $c$  and  $d$  are not constrained by the location of points  $a$  and  $b$ . Points  $c$  and  $d$  must be located within the line of action,  $LA$  – this is the only constraint taken into account at this point.

When the gears rotate, the contact point,  $K$ , between the tooth flanks of the gear,<sup>5</sup>  $\mathcal{G}$ , and of the pinion,  $\mathcal{P}$ , travels along the path of contact,  $P_c$ , with a constant linear velocity,  $\mathbf{V}_K$ , similar to that, as in a corresponding equivalent pulley-and-belt transmission.<sup>6</sup>

The transverse pressure angle,  $\phi_t$ , in a gear pair can be smaller than that shown in Figure 6.6. Pressure angle of a zero value (see Figure 6.7) is the smallest physically possible value of the transverse pressure angle. When the transverse pressure angle is zero,  $\phi_t = 0^\circ$ , in this particular case the following equalities are valid:  $d_{b,g} = d_g$  and  $d_{b,p} = d_p$ .

If the pressure angle,  $\phi_t$ , is of a large value, significant alterations to the design parameters of a parallel-axes gear pair are observed.

<sup>5</sup> It is instructive to point out here that tooth flanks of a gear,  $\mathcal{G}$ , and that of a mating pinion,  $\mathcal{P}$ , are not constructed yet.

<sup>6</sup> Operating mode of a gear pair is commonly specified in terms of the linear velocity,  $V_{K,pc}$ , of the gear's rotation on the pitch circle. It is common practice to specify the linear velocity,  $V_{K,pc}$ , of the gear rotation on the pitch circle as a product of the gear rotation,  $\omega_g$  (or  $\omega_p$ ), times the pitch radius,  $r_g$  (or  $r_p$ ), of the gear, that is,  $V_{K,pc} = \omega_g \cdot r_g = \omega_p \cdot r_p$ . Instead of this, it makes sense to specify the linear velocity,  $V_{K,bc}$ , of the gear rotation on the base circle (the linear velocity of the plane of action) as a product of the rotation,  $\omega_g$  (or  $\omega_p$ ), times the base radius,  $r_{b,g}$  (or  $r_{b,p}$ ), that is,  $V_{K,bc} = \omega_g \cdot r_{b,g} = \omega_p \cdot r_{b,p}$  (in this scenario, the magnitudes of the linear velocities correlate to one another as  $V_{K,bc} = V_{K,pc} \cdot \cos \phi_t$ ). After such an alteration, actual value of the linear velocity,  $V_{K,bc}$ , does not depend on the transverse pressure angle,  $\phi_t$ , that is more practical.

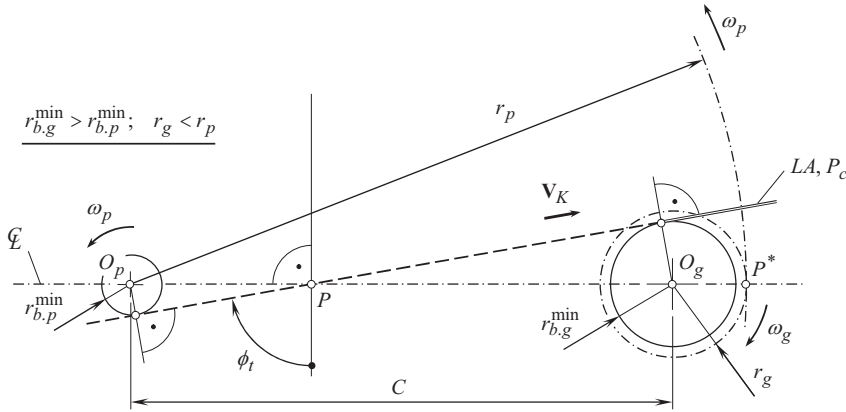


**FIGURE 6.8** Schematic of external gear-to-pinion mesh with the transverse pressure angle,  $\phi_t$ , of a large value.

**First**, radii,  $r_{b,g}$  and  $r_{b,p}$ , of the base circles of a gear and that of a mating pinion are getting smaller as the transverse pressure angle,  $\phi_t$ , becomes larger. Ultimately, at a certain value of the transverse pressure angle,  $\phi_t$ , the base radii,  $r_{b,g}$  and  $r_{b,p}$ , reach their minimum values,  $r_{b,g}^{\min}$  and  $r_{b,p}^{\min}$ , correspondingly. The minimum values,  $r_{b,g}^{\min}$  and  $r_{b,p}^{\min}$ , of the base radii,  $r_{b,g}$  and  $r_{b,p}$ , are the smallest physically possible.

**Second**, assume, that base radius of the gear,  $r_{b,g}$ , and that of the mating pinion,  $r_{b,p}$ , equal to their critical values,  $r_{b,g}^{\min}$  and  $r_{b,p}^{\min}$ , or slightly greater compared to,  $r_{b,g}^{\min}$  and  $r_{b,p}^{\min}$ . As shown in Figure 6.8, pitch radii,  $r_g = C_g$  and  $r_p = C_p$ , of the gear and the mating pinion relate to each other as  $r_g < r_p$  (or  $C_g < C_p$ ), that is, they relate to one another inversely to that, that is observed in parallel-axes gearing of conventional design ( $r_g > r_p$ ).

**Third**, the pitch circles of radii,  $r_g$  (or  $C_g$ ) and  $r_p$  (or  $C_p$ ), correspondingly, contact one another at point,  $P^*$ , and not at the pitch point,  $P$ .

Ultimately, in the internal gear pair, shown in Figure 6.8, the rotations,  $\omega_g$  and  $\omega_p$ , of the gear and that of the mating pinion are pointed oppositely to one another.

The gear and the pinion tooth flanks interact with one another out of the pitch point, that is, contact point never gets coincident with the pitch point. Because of this, the gearing under consideration is referred to as the *out-of-pitch-point-mesh gearing* (or just *OPPM* – gearing, for simplicity).

The just listed conditions are necessary, and not sufficient for transmission of a uniform rotary motion smoothly. These conditions must be complemented by a sufficient total contact ratio in the gear pair. This can be achieved by making teeth of the gear and of the mating pinion helical.<sup>7</sup>

The transverse pressure angle,  $\phi_t$ , in a gear pair can be of a larger value compared to that shown in Figure 6.6. In Figure 6.9, a schematic of a gear pair with a large pressure angle ( $\phi_t \rightarrow 90^\circ$ ) is depicted. When the transverse pressure angle is of a large enough value, the pinion can be engaged in mesh either with an external, or with an internal gear, having that same center-distance,  $C$ , in the gear pair. In the first case, the portion  $c^*d^*$  of the line of action,  $LA^*$ , is effective. In the second case, the portion  $e^*f^*$  of the line of action,  $LA^*$ , is effective. In both cases contact point,  $K$ , travels uniformly,  $V_K$ , along the line of action  $LA^*$ . This means that an internal gear pair could be a

<sup>7</sup> An effective portion of the line of action,  $LA$ , becomes insufficiently short in gearing of the design under consideration. Therefore, no spur gearing of this type is possible at all. No *pinion-gear-to-rack* gearing of this type is possible. Most of the equations, those derived for involute gearing, are valid for *OPPM* – gearing, as *OPPM* – gearing is a reduced case of involute gearing. The concept of *OPPM* – gearing can be enhanced to intersected-axes gearing, as well as to crossed-axes gearing.

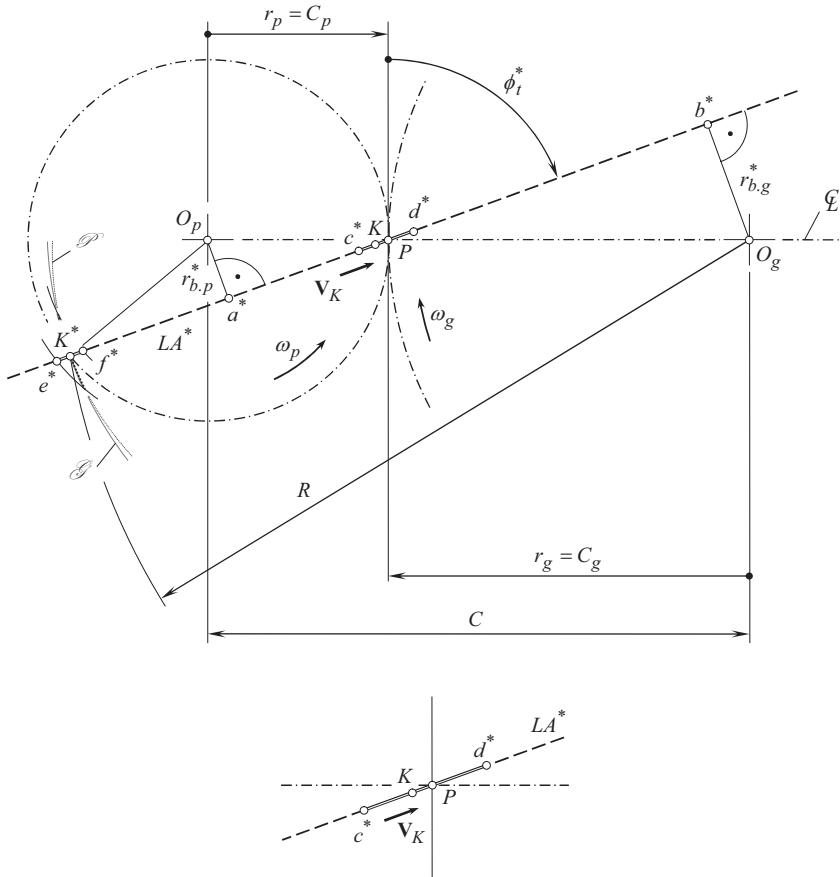


**FIGURE 6.9** A schematic of *gear-to-pinion mesh* with a large transverse pressure angle,  $\phi_t > :$  an **external** *gear-to-pinion mesh* within the active portion  $c^*d^*$ , and an **internal** *gear-to-pinion mesh* within the active portion  $e^*f^*$  of the line of action,  $LA^*$  (the directions of the rotations  $\omega_g$  and  $\omega_p$  are not altered).

*rotationally negative gear pair*. In other words, a change of the direction of rotation to the opposite direction can be observed not only in external gear pairs, but in internal gear pairs, as well.<sup>8</sup>

Point,  $K^*$ , in Figure 6.9 is another point of interception of the line of action,  $LA$ , with the pitch circle of the pinion.<sup>9</sup> Interaction of the gear,  $\mathcal{G}$ , and of the pinion,  $\mathcal{P}$ , tooth flanks can occur at point,  $K^*$ , and in its vicinity. Point,  $K^*$ , is at a distance,  $R$ , from the gear axis of rotation,  $O_g$ . The radius,  $R$ , can be expressed in terms of the design parameters of the gear pair as:

$$R = \sqrt{(r_g + r_p)^2 + r_p^2 - 2r_p(r_g + r_p)\cos 2\phi_t} \quad (6.18)$$

<sup>8</sup> A 1963 gear pair proposed by Bayazitov and Shitikov (Pat. No. 163857, USSR, *A Helical Gearing*/B.V. Shitikov, N.A. Bayazitov, Int. Cl. F06h, Filed: February 25, 1963, Published: July 22, 1964 [124] – see *Bibliography* section of the book), and 1964 PhD Thesis by Bayazitov (Bayazitov, N., *Helical Gears with a New Type of Gearing*, Ph.D. Thesis, Kazan' Technological & Chemical Institute, Kazan', 1964 [8] – see *Bibliography* section of the book), need to be mentioned in this regard. An internal gear pair of this type can be rotationally-negative, and an external gear pair of this type can be rotationally-positive. However, neither the kinematics of the gear pair, nor the geometry of gear tooth flanks is correctly specified in these sources. The discussion of a gearing of similar design can also be found out in the 2008 book by Golovin and Tarabarin (Golovin, A.A., Tarabarin, V.B., *Russian Models from the Mechanisms Collection of Bauman University*, History of Mechanism and Machine Science 5, Springer, 2008, 238 pages, [45] – see *Bibliography* section of the book).

<sup>9</sup> Besides the contact point,  $K^*$ , is located far from the contact point,  $K$ , the pitch circles of the gear and its mating pinion are remained the same even in cases of large values of the transverse pressure angle,  $\phi_t$ .

As it follows from the analysis of the schematic depicted in Figure 6.9, the inequality  $R < C + r_p$  has to be valid in any and all rotationally positive parallel-axes external gear pairs. Otherwise, if the inequality  $R < C + r_p$  is violated, no transmission of a rotation is possible by means of the gear pair. The largest permissible value of the difference:

$$[\Delta_R] = (C + r_p) - R \quad (6.19)$$

is limited by the condition in compliance to which there must be no interference between the pinion and the internal gear in the vicinity of point,  $K^*$ , that is, there must be enough room for the pinion in the interior of the internal gear. Roughly, the largest permissible value of the difference,  $[\Delta_R]_{\max}$ , does not exceed the pinion dedendum,  $b_p$ , that is, an inequality:

$$[\Delta_R]_{\max} \leq b_p \quad (6.20)$$

is valid.

The smallest value of the transverse pressure angle,  $\phi_t$ , occurs when the difference,  $[\Delta_R]$ , is of the largest permissible value,  $[\Delta_R]_{\max}$ . With this value of the difference,  $[\Delta_R]_{\max}$ , the minimal permissible value of the transverse pressure angle is calculated from:

$$[\phi_t]_{\min} = \frac{1}{2} \cos^{-1} \frac{(r_g + r_p)^2 + r_p^2 - (C + r_p - [\Delta_R]_{\max})^2}{2r_p(r_g + r_p)} \quad (6.21)$$

This equation casts into the formula for  $[\phi_t]_{\min} > :$

$$[\phi_t]_{\min} = \frac{1}{2} \cos^{-1} \frac{(u+1)^2 + 1 - \left(1 + \frac{C}{r_p} - \frac{[\Delta_R]_{\max}}{r_p}\right)^2}{2(u+1)} \quad (6.22)$$

where  $u = r_g/r_p$  is the gear ratio in the gear pair.

Under an assumption that the difference,  $[\Delta_R]$ , equals to the pinion module,  $m$ , Eq. (6.22) casts into the formula:

$$\phi_{t,m} = \frac{1}{2} \cos^{-1} \frac{(u+1)^2 + 1 - \left(1 + \frac{C}{r_p} - \frac{m}{r_p}\right)^2}{2(u+1)} \quad (6.23)$$

This formula is helpful for the determination of favorable values of the angular velocity ratio,  $u$ , at which the rest of the design parameters of the gear pair (especially the transverse pressure angle,  $\phi_t$ ) are also of favorable values.

The determination of the maximum permissible value,  $[\phi_t]_{\max}$ , of the transverse pressure angle,  $\phi_t$ , is already discussed in this chapter of the book. Ultimately, the actual value of the transverse pressure angle,  $\phi_t$ , falls into the interval:

$$[\phi_t]_{\min} \leq \phi_t \leq [\phi_t]_{\max} \quad (6.24)$$

As it is clear from the analysis of Eq. (6.22), rotationally negative internal gearing is possible only when the transverse pressure angle,  $\phi_t$ , is of a large enough value.

An example of rotationally positive parallel-axes external gear pair is depicted in Figure 6.10. As shown in Figure 6.10, the actual value of the transverse pressure angle,  $\phi_t$ , in this particular design is close to  $\sim 90^\circ$ . An *equivalent four-bar mechanism* can be constructed for the gear pair (see Figure 6.10) similar to that constructed for parallel-axes gear pairs of all other designs (see Figure 4.14).

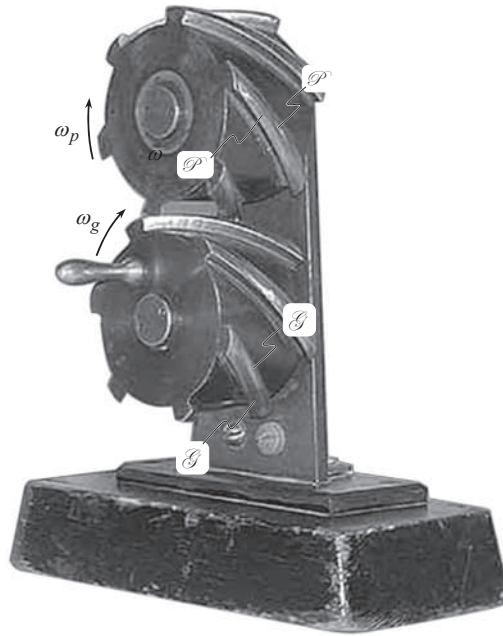


**FIGURE 6.10** Close-up of rotationally positive external parallel-axes gear pair.

After external rotationally positive, and internal rotationally negative gearings are incorporated into the analysis, then a corresponding gear pair can be associated with every point of the  $u$  – axis in Figure 6.4 (except of point  $u = 0$ ). Gear ratio of gear pairs of all possible designs falls into two intervals:  $-\infty \leq u < 0$  and  $0 < u \leq +\infty$ .

External rotationally positive, as well as internal rotationally negative gear pairs, can be also designed for the cases of gearing that operate on intersected-axes, and crossed-axes of rotation of a gear and of a mating pinion.

As both, external rotationally positive, and internal rotationally negative gear pairs, got no extensive application in the present-day industry, further in this book, the attention is mostly focused on external rotationally negative, and internal rotationally positive gear pairs. The first is commonly referred to as *external gear pairs*, while the second – as *internal gear pairs*.<sup>10</sup>

In addition to the established intervals for the angular velocity ratio ( $-\infty \leq u < 0$  and  $0 < u \leq +\infty$ ), a possibility of variation of the transverse pressure angle,  $\phi_t$ , needs to be considered here. This is especially of importance in order to avoid any confusion with conclusions drawn up from the analysis of Figure 5.6.

The illustration below (see Figure 6.11) makes clear the possibility of variation of transverse pressure angle,  $\phi_t = \text{var}$ , in parallel-axes gearing.

Three parallel-axes gear pairs 1, 2, and 3 with the same angular velocity ratio,  $u$ , and the equal center-distance,  $C$ , but with different radii of base cylinders,  $r_{b,g}^{(1)}$  and  $r_{b,p}^{(1)}$  [  $r_{b,g}^{(2)}$  and  $r_{b,p}^{(2)}$ ;  $r_{b,g}^{(3)}$  and  $r_{b,p}^{(3)}$  ], of a gear and its mating pinion rotate about the common axes,  $O_g$  and  $O_p$ , with constant angular velocities,  $\omega_g$  and  $\omega_p$  (where  $u = \omega_p / \omega_g$ ). The face widths of the gears are equal to  $F_{pa}^{(1)}$ ,  $F_{pa}^{(2)}$ , and

<sup>10</sup> Another equivalent terminology is also occasionally used in parallel to just mentioned terminology: *external gear pairs* are referred to as  *$u$  – negative gearing* (or just  *$u^-$  – gearing*, for simplicity), and *internal gear pairs* are referred to as  *$u$  – positive gearing* (or just  *$u^+$  – gearing*, for simplicity). This is mainly due to the direction of rotation of an input shaft alters to the opposite in the first case, while in the second case it remains the same. *Gear-to-rack* gearing is referred to as  *$u^0$  – gearing*. The later is due to the input rotation is transformed into the straight motion (no output rotation is observed as it is vanished).

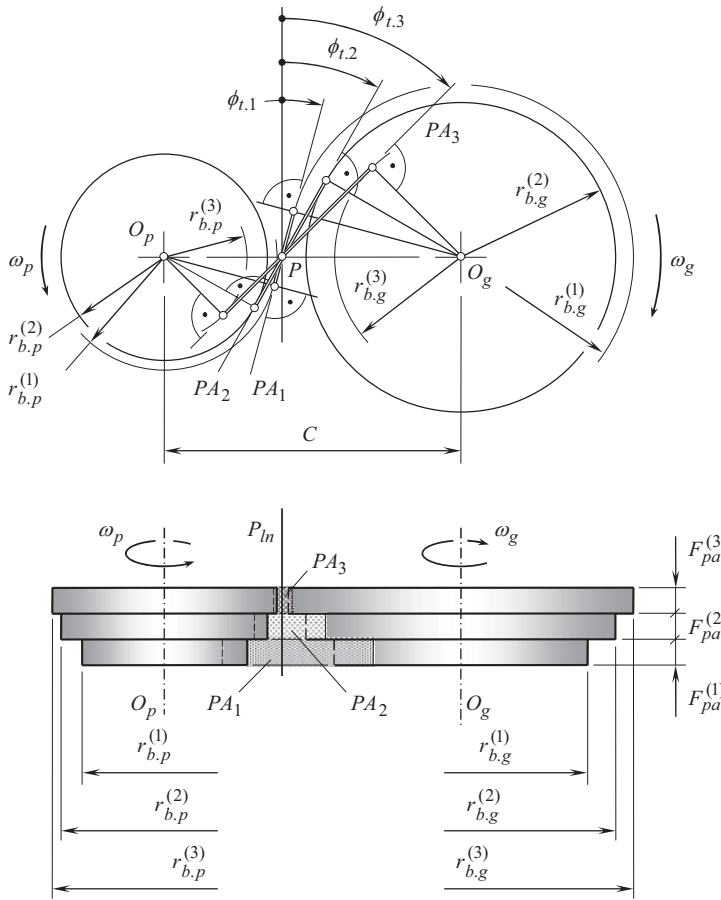


**FIGURE 6.11** On a possibility of continuous alteration of transverse pressure angle,  $\phi_t$ , along the axis of instantaneous rotation,  $P_{ln}$ , in parallel-axes gearing with a constant angular velocity ratio,  $u$ .

$F_{pa}^{(3)}$ , correspondingly. As the radii of the base cylinders  $r_{b,g}^{(i)}$  and  $r_{b,p}^{(i)}$  in each pair of gears are different (here,  $i = 1, 2, 3$ ), thus, each pair of gears features a specific value of the transverse pressure angle,  $\phi_{t,1}$ ,  $\phi_{t,2}$ , and  $\phi_{t,3}$ , correspondingly. All the planes of action  $PA_1$ ,  $PA_2$ , and  $PA_3$ , are the planes through the axis of instantaneous rotation,  $P_{ln}$ . All the planes of action  $PA_1$ ,  $PA_2$ , and  $PA_3$ , form a corresponding transverse pressure angle,  $\phi_{t,i}$ , with a perpendicular to the centerline,  $\mathfrak{L}$ , to through the pitch point,  $P$ . In the upper portion of Figure 6.11, the planes of action  $PA_1$ ,  $PA_2$ , and  $PA_3$  are projected into the corresponding lines of action  $LA_1$ ,  $LA_2$ , and  $LA_3$ .

When the gears rotate, the gears in each of the gear pairs 1, 2, and 3 are motionless in relation to one another, as each of the gear pairs feature equal angular velocity ratio,  $u$ .

The just discussed approach can be evolved: a transition from the gearing with three planes of action to a gearing with an infinite number of the planes of action. Each of the gears can be sliced onto an infinite number of infinitesimally narrow ( $dF_{pa} \rightarrow 0$ ) round strips. The transverse pressure angle,  $\phi_t$ , can be set of a different value for each of the strips. In this way, a gear pair with a variable (along the axis of instantaneous rotation,  $P_{ln}$ ) value of the transverse pressure angle,  $\phi_t$ , can be designed.<sup>11</sup>

<sup>11</sup> This analysis is helpful for understanding of a possibility of a variable (along the axis of instantaneous rotation,  $P_{ln}$ ) transverse pressure angle,  $\phi_t$ , in intersected-axes gearing, as well as in crossed-axes gearing.

## 6.2 TOOTH FLANK GENERATION

In parallel-axes gearing, tooth flanks of a gear and in its mating pinion,  $\mathcal{G}$  and  $\mathcal{P}$ , interact with one another similar to that the working surfaces in a cam mechanism do. In order to transmit a uniform rotary motion smoothly by means of gear teeth, an appropriate geometry of the tooth flanks,  $\mathcal{G}$  and  $\mathcal{P}$ , is required to be reproduced in the gear and in the mating pinion. This is because there is no freedom in selecting an arbitrary kind of tooth flank geometry in parallel-axes gearing (as well as in intersected-axes gearing, and in crossed-axes gearing).

To generate the tooth flanks,  $\mathcal{G}$  and  $\mathcal{P}$ , in a *geometrically accurate gear pair*, the discussed in the previous sections of the book *equivalent pulley-and-belt transmission* is used. The difference between the transmission of rotary motion by a *gear pair* and by *equivalent pulley-and-belt transmission* is just in the following: in an *equivalent pulley-and-belt transmission* the driving pulley *pulls* the driven pulley, while in a gear pair the driving gear *pushes* the driven gear. With that said, a *desirable line of contact* between the tooth flanks in the gear pair can be used for the generation of tooth flanks,  $\mathcal{G}$  and  $\mathcal{P}$ , of a gear and its mating pinion. The desirable line of contact is a planar curve that is entirely situated within the plane of action of the gear pair (which is equivalent to the plane of the belt in a corresponding *equivalent pulley-and-belt transmission*<sup>12</sup>).

### 6.2.1 DESIRABLE LINE OF CONTACT IN A GEAR PAIR

It is assumed that for generating tooth flanks of a gear and its mating pinion a corresponding gear vector diagram is constructed. This is followed by the construction of a plane of action,  $PA$  :

#### Definition 6.1

Plane of action,  $PA$ , in a parallel-axes gear pair is a plane through the axis of instantaneous rotation,  $P_{in}$  (or, the same, through a line along the vector of instantaneous rotation,  $\boldsymbol{\omega}_p$ ), that forms a transverse pressure angle,  $\phi_t$ , with the normal plane ( $N_{in}$  – plane).

In parallel-axes gearing, configuration of the  $N_{in}$  – plane in relation to other elements of the gear vector diagram is illustrated in Figure 3.11.

#### Definition 6.2

Line of action,  $LA$ , in parallel-axes gearing is a straight line of intersection of the plane of action,  $PA$ , by a transverse plane in the gear pair.

It is instructive to stress here that the line of action,  $LA$ , is always a straight line, as a force vector of interaction between the gear tooth flanks,  $\mathcal{G}$  and  $\mathcal{P}$ , is always pointed along a straight line through contact point perpendicular to the interacting tooth flanks. A force can not act along other curve than a straight line.

other curve than a straight line.

The plane of action,  $PA$ , can be construed as a family of all the lines of action considered in all possible transverse sections of the gear pair.<sup>13</sup> In parallel-axes gearing, the plane of action can also be construed as a plane that is generated by the line of action,  $LA$ , that travels along the axis of instantaneous rotation,  $P_{in}$ , and remains parallel to itself.

<sup>12</sup> This discussion makes clear why that much attention has been paid in the previous sections of the book to the in-detail consideration of the *equivalent pulley-and-belt transmission*.

<sup>13</sup> In a more general case of parallel-axes gearing (see Figure 6.11), not a plane of action,  $PA$ , but a so-called *surface of action*,  $SA$  is observed instead. The surface of action,  $SA$ , is a kind of ruled surface through the axis of instant rotation,  $P_{in}$  (see Figure 6.11).



The plane of action,  $PA$ , is tangent to base cylinders<sup>14</sup> of a gear and a mating pinion.

### Definition 6.3

Base cylinder of a gear is a cylinder of revolution that is generated as an envelope to a family of consecutive positions of the plane of action,  $PA$ , in its rotary motion in relation to a reference system associated with the gear when the gears rotate.

### Definition 6.4

Base cylinder of a pinion is a cylinder of revolution that is generated as an envelope to a family of consecutive positions of the plane of action,  $PA$ , in its rotary motion in relation to a reference system associated with the pinion when the gears rotate.

For the generation of tooth flanks of a gear,  $\mathcal{G}$ , and its mating pinion,  $\mathcal{P}$ , a desirable line of contact,  $LC_{des}$ , between the tooth flanks,  $\mathcal{G}$  and  $\mathcal{P}$ , is used.

**Important note:** no gear, and no pinion tooth flanks,  $\mathcal{G}$  and  $\mathcal{P}$ , are generated yet, but a desirable line of their contact,  $LC_{des}$ , is already introduced (and is used for the generation of the tooth flanks,  $\mathcal{G}$  and  $\mathcal{P}$ ).

### Definition 6.5

Desirable line of contact,  $LC_{des}$ , between tooth flanks,  $\mathcal{G}$  and  $\mathcal{P}$ , of a gear and its mating pinion is a planar curve that is entirely located within the plane of action,  $PA$ , and possesses desirable geometry that makes possible a favorable design of the gear pair.

A straight line is commonly used as a desirable line of contact,  $LC_{des}$ , between interacting tooth flanks of a gear,  $\mathcal{G}$ , and that of a mating pinion,  $\mathcal{P}$ . The desirable line of contact,  $LC_{des}$ , (or simply *line of contact*,  $LC$ ), is located within the plane of action,  $PA$ . The line of contact is associated with the plane of action. When the plane of action,  $PA$ , unwraps from the base cylinder of the driving member, and wraps over the base cylinder of the driven member in the gear pair, the line of contact travels together with the plane of action (and is stationary in relation to the plane of action,  $PA$ ).

The straight line of contact can be parallel to the axis of instantaneous rotation,  $P_{in}$  (or, the same, parallel to the axes of rotation of both, of the gear, and the mating pinion). Under such a scenario, tooth flanks of a spur gear, and of a spur pinion are generated by the line of contact,  $LC_{spur}$ , as illustrated in Figure 6.12. When the line of contact,  $LC_{helical}$ , is at an angle in relation to the axis of instantaneous rotation,  $P_{in}$ , tooth flanks of a helical gear, and of a helical pinion are generated. Actually, any planar curve,  $LC_{arbitr}$ , of a reasonable geometry can be used as a line of contact,  $LC$ , in parallel-axes gearing.

Among other planar curves, a circular arc,  $LC_{circ}$ , can be used as a desirable line of contact in a gear pair that operates on parallel axes of rotation of the gear and the mating pinion. The tooth flanks of the gear and the pinion of such a geometry can be machined either by means of the face-mill cutter or by means of the face hob. In both cases, the gear cutting tool to be implemented must have a zero profile angle of their teeth. Otherwise (when the profile angle,  $\phi_t$ , of the gear cutting tool is not equal to zero,  $\phi_t \neq 0$ ), the gear pair cannot be geometrically accurate. The main reason for that is discussed immediately below.

<sup>14</sup> Schematically illustrated in Figure 6.11 parallel-axes gearing, features *base surfaces* associated with the gear and its mating pinion, and not base cylinders. The base surface in the case under consideration is a kind of surface of revolution. Gearing with base surfaces of a gear and its mating pinion are not considered in this book.

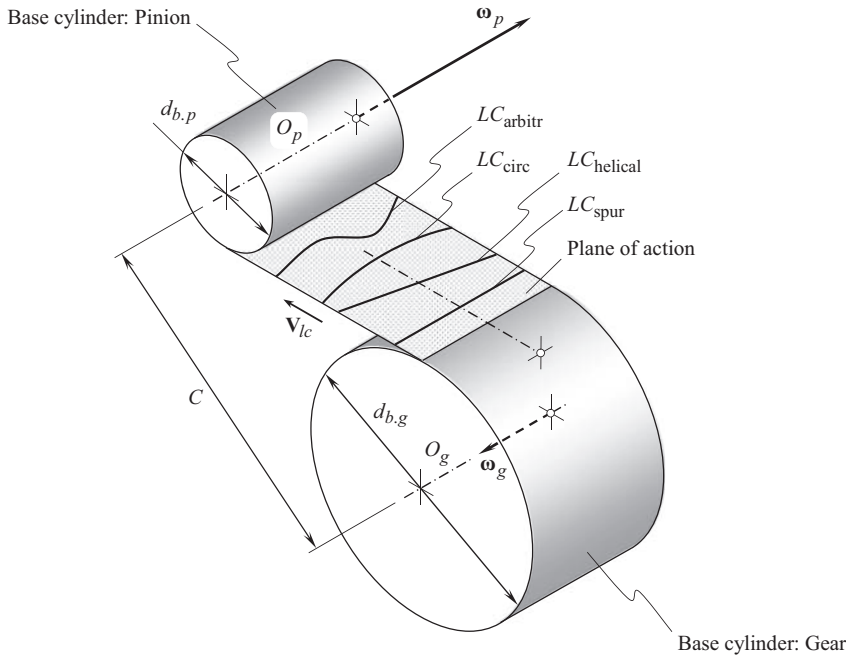


**FIGURE 6.12** Generation of tooth flank of an involute gear with an arbitrary tooth shape in its lengthwise direction.

It is important to stress here that neither geometry of the desirable line of contact,  $LC_{des}$ , nor its configuration in relation to the plane of action,  $PA$ , are allowed to be altered when a gear,  $\mathcal{G}$ , and a mating pinion,  $\mathcal{P}$ , tooth flanks are generated. This feature of the line of contact,  $LC_{des}$ , needs to be taken into account when developing novel methods of gear cutting, of gear inspection, and so forth.

The most favorable geometry of the desirable line of contact,  $LC_{des}$ , can be calculated based on output from the contact geometry in the gear pair (see Appendix E). However, in present-day practice, the geometry of the desirable line of contact,  $LC_{des}$ , is selected, and commonly, practicality is the main criterion when selecting the geometry of the desirable line of contact,  $LC_{des}$ , between the tooth flanks,  $\mathcal{G}$  and  $\mathcal{P}$ , of a gear and its mating pinion.

### 6.2.2 LINE OF ACTION AND PATH OF CONTACT IN PARALLEL-AXES GEARING

A parallel-axes gearing is schematically shown in Figure 6.13. The gear and the mating pinion rotate about their axes of rotation,  $O_g$  and  $O_p$ , with angular velocities,  $\omega_g$  and  $\omega_p$ , correspondingly. The axes rotation,  $O_g$  and  $O_p$ , are at a center-distance,  $C$ , apart from one another. Base diameter of the gear is designated as  $d_{b,g}$ , and base diameter of the pinion is designated as  $d_{b,p}$ . Outer diameters of the gear and the pinion are designated as  $d_{o,g}$  and  $d_{o,p}$ , correspondingly. In compliance to the *equivalent pulley-and-belt transmission*, the line of action,  $LA$ , between the tooth flanks,  $\mathcal{G}$  and  $\mathcal{P}$ , of a gear and a mating pinion is in tangency to both, to the base cylinder of the gear, and to the base cylinder of the pinion. Points of tangency are denoted by  $N_g$  and  $N_p$ , correspondingly.

The line of action,  $LA$ , intersects the centerline,  $\Phi$ , at the pitch point,  $P$ . (The center-distance,  $C$ , is a straight-line segment – just a portion of the centerline,  $\Phi$ ).

Points of intersection,  $P_g$  and  $P_p$ , of the line of action,  $LA$ , by the circles of the outer diameters,  $d_{o,g}$  and  $d_{o,p}$ , are the extreme points of the active portion,  $Z_{pa}$ , of the line of action,  $LA$  (i.e.,  $P_g P_p = Z_{pa}$ ).

A perpendicular through the pitch point,  $P$ , to the centerline,  $\Phi$ , forms a transverse pressure angle,  $\phi_t$ , with the line of action,  $LA$ .

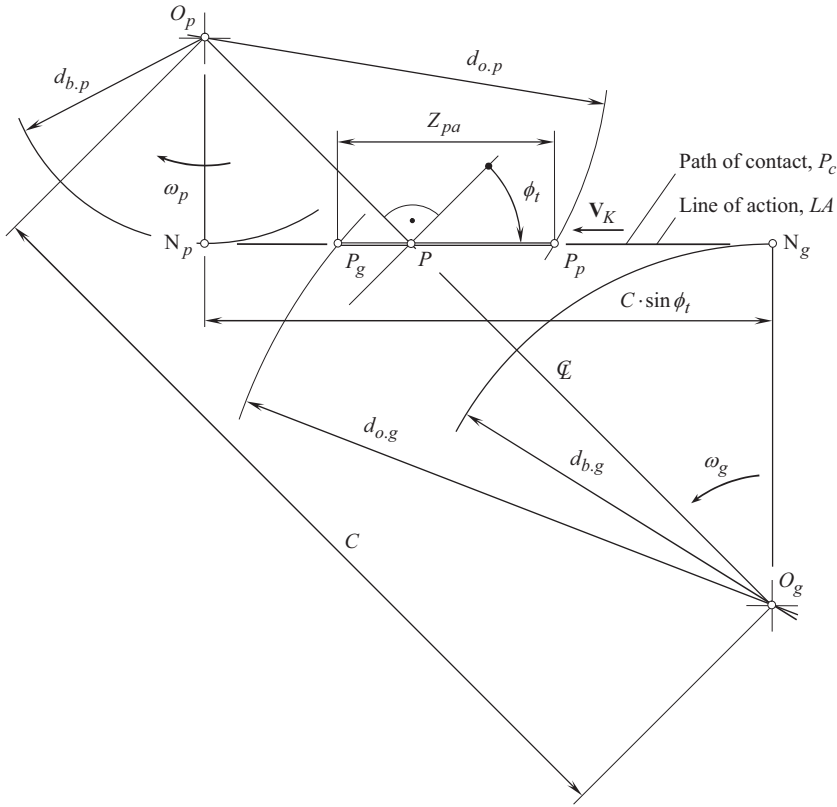


**FIGURE 6.13** In involute gearing, line of action,  $LA$ , and path of contact,  $P_c$ , are two straight lines that align to one another.

When the gears rotate, the transverse pressure angle,  $\phi_t$ , is of a constant value at every instant of time, that is, it is of a constant value for all angular configurations of the gear and the pinion in their rotation relation to one another. Therefore, when the gears uniformly rotate with rotations,  $\omega_g$  and  $\omega_p$ , contact point,  $K$ , between the tooth flanks,  $\mathcal{F}$  and  $\mathcal{P}$ , travels along the straight path of contact,  $P_c$ , with a constant linear velocity,  $\mathbf{V}_K$ . When one of the motions (either the rotations,  $\omega_g$  and  $\omega_p$ , or the translation  $\mathbf{V}_K$ ), or both is not uniform, the contact point traces a path of contact,  $P_c$ , in a form of planar curve of certain geometry. This curve,  $P_c$ , is entirely located in a transverse section of the gear pair. In the latter case, no transmission of a smooth rotation is possible.

### Definition 6.6

Path of contact,  $P_c$ , in geometrically accurate parallel-axes gearing is a straight line traced by contact point in a motionless transverse section of the gear pair.

Path of contact,  $P_c$ , is entirely located in a corresponding transverse section of the gear pair.

A family of all paths of contact,  $P_c$ , in a particular gear pair form a *path-of-contact surface*,  $S_c$  (or just *PCS*, for simplicity). When the transverse pressure angle,  $\phi_t$ , varies within the plane-of-action face,  $F_{pa}$ , a continuous set of the straight-line paths of contact,  $P_c$ , at different transverse pressure angle,  $\phi_t$ , each, form the *path-of-contact surface*, in a form of a right angle *helicoid*. When transverse pressure angle,  $\phi_t$ , is of a constant value ( $\phi_t = \text{const}$ ) within the plane-of-action face,  $F_{pa}$ , the *path-of-contact surface*, is shaped in a form of a plane through the axis of instantaneous rotation,  $P_{in}$ .

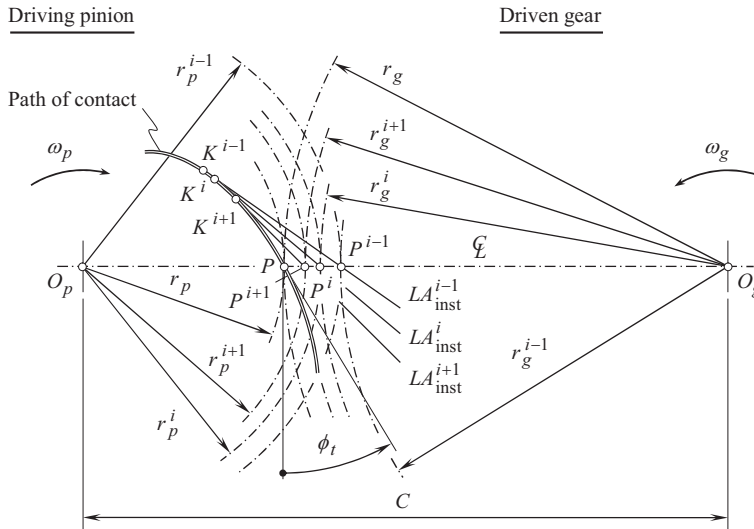


**FIGURE 6.14** Schematic diagram of parallel-axes gearing that features a curved path of contact,  $P_c$ .

When the path of contact is aligned with the line of action,  $LA$ , the tooth flank geometry generated in this manner is a unique one. Tooth profiles generated in other manners than that just mentioned are not capable of transmitting a uniform rotation smoothly.

Consider a schematic diagram of parallel-axes gearing that features a curved path of contact,  $P_c$ , as shown in Figure 6.14. The gear and the mating pinion rotate about their axes of rotation,  $O_g$  and  $O_p$ , with angular velocities,  $\omega_g$  and  $\omega_p$ , correspondingly. The axes,  $O_g$  and  $O_p$ , are at certain center-distance,  $C$ , apart from each other. The pitch point,  $P$ , is at a distance,  $r_g$  (here  $r_g = C_g$ ), apart from the gear axis of rotation,  $O_g$ , and at a distance,  $r_p$  (here  $r_p = C_p$ ), apart from the pinion axis of rotation,  $O_p$ . The transverse pressure angle at the pitch point,  $P$ , is denoted by  $\phi_t$ .

Let us assume that the gear and its mating pinion rotate so that a curved path of contact,  $P_c$ , is traced by contact point,  $K$ . At every point of the path of contact,  $P_c$ , a corresponding *instantaneous line of action*,  $LA_{inst}$ , can be constructed.

An arbitrary contact point within the path of contact,  $P_c$ , is labeled as  $K^{(i)}$ . When the gear and the mating pinion make contact at point  $K^{(i)}$ , the instantaneous line of action,  $LA_{inst}^{(i)}$ , is in tangency to the path of contact,  $P_c$ , at  $K^{(i)}$ . This is because the force of interaction between the tooth flanks of the driving and the driven gears is pointed along the common perpendicular to the interacting tooth profiles considered in a transverse section of a gear pair, or, the same, the force is pointed along a straight line that is tangent at contact point  $K^{(i)}$  to the path of contact,  $P_c$ .

A few definitions can be drawn up from the above discussion:

### Definition 6.7

Instantaneous line of action,  $LA_{inst}$ , is a straight line pointed along the common perpendicular,  $\mathbf{n}_g$ , to the tooth flanks,  $\mathcal{S}$  and  $\mathcal{P}$ , of a gear and a mating pinion at contact point  $K$ , considered in a section of the gear pair by a transverse plane.

### Definition 6.8

Instantaneous pitch point,  $P_{inst}$ , is a point of intersection of the centerline,  $\mathcal{C}$ , by the instantaneous line of action,  $LA_{inst}$ .

**Definition 6.9**

Path of contact surface,  $PCS$ , is a ruled surface composed as a locus of consecutive positions of the instantaneous lines of action,  $LA_{\text{inst}}$ .

The line of action,  $LA$ , and the path of contact,  $P_c$ , align with each other only in geometrically accurate parallel-axes gearing.<sup>15</sup>

As the instantaneous line of action,  $LA_{\text{inst}}^{(i)}$ , intersects the centerline,  $\Phi$ , at the instantaneous pitch point,  $P^{(i)}$ , the instant gear ratio,  $u_{\text{inst}}^{(i)}$ , at the corresponding instant of time, can be expressed in terms of the instantaneous radii,  $r_g^{(i)}$  and  $r_p^{(i)}$ , of the gear and the mating pinion:

$$u_{\text{inst}}^{(i)} = \frac{r_g^{(i)}}{r_p^{(i)}} \quad (6.25)$$

Because of the path of contact,  $P_c$ , is not a straight line, then the instantaneous pitch point,  $P^{(i)}$ , does not coincide with the nominal pitch point,  $P$ . Therefore, the instantaneous angular velocity ratio,  $u_{\text{inst}}^{(i)}$ , differs from the nominal gear ratio:

$$u_{\text{inst}}^{(i)} \neq u = \frac{r_g}{r_p} \quad (6.26)$$

A similar analysis can be performed with respect to other contact points,  $K^{(i-1)}$  and  $K^{(i+1)}$ , within the path of contact,  $P_c$ . Without going into details of the analysis, it can be stated that in all contact points under consideration,  $K^{(i-1)}$ ,  $K^{(i)}$ , and  $K^{(i+1)}$ , the following inequality/equality is valid:

$$u_{\text{inst}}^{(i-1)} \neq u_{\text{inst}}^{(i)} \neq u_{\text{inst}}^{(i+1)} \neq u, \quad \text{where} \quad u = \frac{r_g}{r_p} \quad (6.27)$$

It is clear from the above-performed analysis that no smooth transmission of a uniform input rotary motion is possible by means of parallel-axes gearing that features a curved path of contact,  $P_c$ .

A conclusion is drawn up from the analysis given in Figure 6.14.

**Theorem 6.1**

To transmit a uniform rotary motion from a driving shaft to a driven shaft by means of gear teeth, the tooth flank perpendiculars (in every transverse section) at all points of contact of the interacting tooth flanks must pass through a stationary point within the centerline of the two shafts.

This conclusion, in nature, is the *conjugate action law in parallel-axes gearing* (or the *CES – fundamental theorem of parallel-axes gearing*).

*Theorem 6.1* immediately follows from the second fundamental law of gearing, and obey the analytical expression:

$$\mathbf{p}_m \times \mathbf{V}_m \cdot \mathbf{n}_g = 0 \quad (6.28)$$

As it is shown below in this section of the book, only involute gearing features a straight line of action,  $LA$ , and a straight path of contact,  $P_c$ , that align to one another. In other gear systems, (a) the line of action,  $LA$ , does not exist, (b) the numerous instantaneous lines of action,  $LA_{\text{inst}}$  (that are still straight lines), and (c) the path of contact,  $P_c$  (that could be a planar curve) need to be distinguished from one another.

<sup>15</sup> In the rest of cases of  $P_a$ -gearing (cycloid gear pair, and so forth), as well as in all cases of  $I_a$ -gearing, as well as of  $C_a$ -gearing, (a) the line of action,  $LA$ , does not exist, and (b) the instantaneous line of action,  $LA_{\text{inst}}$ , and the path of contact,  $P_c$ , do not align to one another.

### 6.2.3 OPERATING BASE PITCH

The main reason for to introduced the concept of *base pitch* in geometrically accurate parallel-axes gearing is as follows.

When the gears rotate, two (or even more) pairs of teeth are engaged in mesh simultaneously. In order to keep all the gear pairs in contact, the gear teeth, as well as the pinion teeth, must be located at certain distances from one another. Otherwise, only one pair of teeth is engaged in mesh, while a gap would be observed in the other pairs of teeth. This distance is specified by:

- the *operating base pitch* in a gear pair
- the *gear base pitch* (in a gear)
- the *pinion base pitch* (in a mating pinion)

Let us consider a desirable line of contact,  $LC_{des}$ , in a parallel-axes gear pair. The line of contact,  $LC_{des}$ , occupies two adjacent positions labeled,  $LC_{des}^i$  and  $LC_{des}^{i+1}$ , as illustrated in Figure 6.15. The axis of rotation of the gear,  $O_g$ , and that of the pinion,  $O_p$ , are parallel to one another, and are at a center-distance,  $C$ , apart from each other. The base cylinder of a diameter  $d_{b,g}$  is associated with the gear. Similarly, the base cylinder of a diameter  $d_{b,p}$  is associated with the pinion. The plane of action,  $PA$ , in external parallel-axes gear pair is tangent to the base cylinders from the opposite sides. The gear and the pinion rotate,  $\omega_g$  and  $\omega_p$ , about their axes of rotation. The magnitudes,  $\omega_g$  and  $\omega_p$ , of the rotation vectors,  $\omega_g$  and  $\omega_p$ , are synchronized with one another reciprocal to the tooth count,  $N_g$  and  $N_p$ , of the gear and the pinion, that is, the ratio:

$$\frac{\omega_g}{\omega_p} = \frac{N_p}{N_g} \quad (6.29)$$

is valid in geometrically accurate parallel-axes gearing.

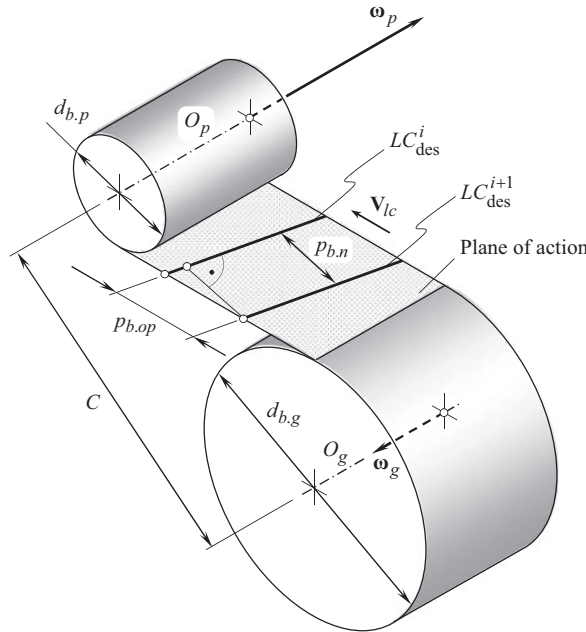


**FIGURE 6.15** Definition to the term *operating base pitch*,  $p_{b,op}$  in geometrically accurate parallel-axes gearing.

When the gears rotate, the plane of action,  $PA$ , is considered as a zero-thickness film that unwraps from the base cylinder of the gear, and wraps onto the base cylinder of the pinion, or vice versa. In such a motion, the plane of action,  $PA$ , travels with a linear velocity,  $\mathbf{V}_{lc}$ . The magnitude,  $V_{lc}$ , of the linear velocity,  $\mathbf{V}_{lc}$ , is timed with the rotations,  $\omega_g$  and  $\omega_p$ , so as to ensure rolling with no slippage of the plane of action,  $PA$ , over the base cylinders of the gear and the pinion.

A desirable line of contact,  $LC_{des}^i$ , of the  $i$ -th pair of teeth of the gear and the pinion is drawn within the plane of action,  $PA$ . As an example, the desirable line of contact,  $LC_{des}^i$ , is shown for helical involute gearing. In the case under consideration, this straight line segment forms the base helix angle,  $\psi_b$ , with the axis of instantaneous rotation,  $P_{ln}$ , or, the same, with the axes  $O_g$  and  $O_p$  (the base helix angle,  $\psi_b$ , is not shown in Figure 6.15).

The desirable line of contact,  $LC_{des}^{i+1}$ , of the adjacent  $(i+1)$ -th pair of teeth is parallel to the straight line,  $LC_{des}^i$ , (i.e.,  $LC_{des}^{i+1} \parallel LC_{des}^i$ ), and is also located within the plane of action,  $PA$ .

Measured in a common transverse section of the gear pair, the distance,  $p_{b,op}$ , between two adjacent desirable lines of contact,  $LC_{des}^i$  and  $LC_{des}^{i+1}$ , is referred to as the *operating base pitch* of a gear pair.<sup>16</sup> Here, in Figure 6.15, *normal base pitch*,  $p_{b,n}$  in a gear pair is shown for reference purposes only.

### Definition 6.10

Operating base pitch,  $p_{b,op}$ , in parallel-axes gear pair is a linear distance between every two adjacent desirable lines of contact,  $LC_{des}^i$  and  $LC_{des}^{i+1}$ , measured in a section of the plane of action by a transverse plane.

Only *conjugate* gear tooth profiles (gear tooth flanks) feature the base pitch. The base pitch can not be specified for non-conjugate gear tooth profiles (gear tooth flanks): that is, base pitch can not be specified for pin gearing, cycloidal gearing, and so forth.

The operating base pitch<sup>17</sup> in a gear pair is a calculated design parameter. It can not be measured directly in a gear pair. In parallel-axes gearing, the operating base pitch of a gear pair equals to:

$$p_{b,op} = \frac{\pi d_{b,g}}{N_g} \quad (6.30)$$

where:  $d_{b,g}$  is the gear base diameter, and  $N_g$  is the number of gear teeth.

*Note*, that *operating base pitch* in parallel-axes gear pair is introduced *prior to* (!) tooth flanks,  $\mathcal{G}$  and  $\mathcal{P}$ , of a gear and a mating pinion are constructed.

The operating base pitch in a gear pair can be also expressed in terms of the pinion base diameter,  $d_{b,p}$ , and the pinion tooth count,  $N_p$ , that is:

$$p_{b,op} = \frac{\pi d_{b,p}}{N_p} \quad (6.31)$$

<sup>16</sup> It is also important to stress here that the operating base pitch in a gear pair,  $p_{b,op}$ , is measured in linear units only in parallel-axes gear pairs. In intersected-axes gearing, and in crossed-axes gearing, the angular operating base pitch of a gear pair,  $\phi_{b,op}$ , is measured in angular units. Moreover, if the axes misalignment is taken into account, then the angular operating base pitch in a gear pair,  $\phi_{b,op}$ , is measured in angular units, namely, in parallel-axes gearing, intersected-axes gearing, as well as crossed-axes gearing.

<sup>17</sup> It is known that in parallel-axes gearing, base pitch of a gear and that of a mating pinion must be equal to one another. However, nothing is said so far about *operating base pitch* in geometrically-accurate parallel-axes gearing (the concept of *operating base pitch* in parallel-axes gear pair is introduced in around ~2008 by Prof. S.P. Radzevich [174]). Further, neither the concept of the base pitch of the gear and the pinion in intersected-axes gearing, as well as in crossed-axes gearing is discussed so far in the public domain. Moreover, the concept of *operating base pitch* in intersected-axes, as well as in crossed-axes gearing is not discussed so far in the public domain. Again, the concept of *operating base pitch* in intersected-axes, and crossed-axes gearing is introduced (~2008) for the first time by Prof. S.P. Radzevich [174].



In a geometrically accurate parallel-axes gear pair, the following three identities are observed:

- base pitch of a gear,  $p_{b,g}$ , is identical to operating base pitch,  $p_{b,op}$ , of the gear pair (i.e., an identity  $p_{b,g} \equiv p_{b,op}$  is valid);
- base pitch of a mating pinion,  $p_{b,p}$ , is identical to operating base pitch,  $p_{b,op}$ , of the gear pair (i.e., an identity  $p_{b,p} \equiv p_{b,op}$  is valid);
- ultimately, base pitch of the gear,  $p_{b,g}$ , is identical to base pitch of the pinion,  $p_{b,p}$ , and both of them are identical to operating base pitch,  $p_{b,op}$ , of the gear pair (i.e., the identity  $p_{b,g} \equiv p_{b,p} \equiv p_{b,op}$  is valid).

Therefore, the discussed above in this section of the book the condition of equal base pitches in geometrically accurate parallel-axes gearing now can be enhanced, and can be formulated as follows:

**Equal base pitches law (in geometrically accurate parallel-axes gearing):** In order to transmit a uniform rotary motion from a driving shaft to a driven shaft by means of gear teeth, the following three identities must be fulfilled at every instant of time:

- base pitch of a gear,  $p_{b,g}$ , must be identical to operating base pitch,  $p_{b,op}$ , of the gear pair ( $p_{b,g} \equiv p_{b,op}$ );
- base pitch of a mating pinion,  $p_{b,p}$ , must be identical to operating base pitch,  $p_{b,op}$ , of the gear pair ( $p_{b,p} \equiv p_{b,op}$ ); and
- both of the base pitches, namely,  $p_{b,g}$  and  $p_{b,p}$ , must be identical to the operating base pitch,  $p_{b,op}$ , of the gear pair ( $p_{b,g} \equiv p_{b,p} \equiv p_{b,op}$ ).

It is critical to note here that operating base pitch,  $p_{b,op}$ , of the gear pair is constructed (and specified) *prior to* the interacting tooth flanks,  $\mathcal{S}$  and  $\mathcal{P}$ , of the gear and the mating pinion are generated. Use of such an approach gives an opportunity to design gear with favorable geometry of the tooth flanks. For this purpose, the desirable line of contact,  $LC_{des}$ , between the tooth flanks,  $\mathcal{S}$  and  $\mathcal{P}$ , is used to generate a gear and a mating pinion tooth flanks,  $\mathcal{S}$  and  $\mathcal{P}$ .

In parallel-axes gearing that feature a straight desirable line of contact, the distance between every two adjacent lines of contact,  $LC_{des}$ , can also be specified by the *normal base pitch*,  $p_{b,n}$  (see Figure 6.15). The normal base pitch is measured within the plane of action,  $PA$ , perpendicular to the desirable lines of contact,  $LC_{des}^i$  and  $LC_{des}^{i\pm 1}$ . It is evident that normal base pitch,  $p_{b,n}$ , can be specified only for parallel-axes gear pairs with straight desirable line of contact,  $LC_{des}$ . Normal base pitch,  $p_{b,n}$ , is an auxiliary design parameter of a gear pair, which is complimentary to the base pitch,  $p_{b,g}$ , measured in a transverse plane section of the gear pair. It can be expressed in terms of the *operating base pitch*,  $p_{b,op}$  of the gear pair, and the base helix angle,  $\psi_b$ :

$$p_{b,n} = p_{b,op} \cos \psi_b \quad (6.32)$$

In this book, normal base pitch,  $p_{b,n}$ , is used for reference purposes only.

As long as a desirable line of contact,  $LC_{des}$ , is rigidly connected to the plane of action,  $PA$ , base pitch of the gear, and base pitch of the mating pinion are equal to one another. Therefore, when two equalities,  $p_{b,g} = p_{b,op}$  and  $p_{b,p} = p_{b,op}$ , are fulfilled, a gear pair of such a design is geometrically accurate. In parallel-axes gearing, the identities  $p_{b,g} \equiv p_{b,op}$  and  $p_{b,p} \equiv p_{b,op}$  (or simply  $p_{b,g} \equiv p_{b,p} \equiv p_{b,op}$ ) are met only in *geometrically accurate gearing*, that is, in involute gearing. For non-involute gearing of any and all kinds, the identity can not be fulfilled, and, moreover, base pitch of the gear and the pinion can not be specified in non-involute gearings, while the operating base pitch of the gear pair can be easily determined.

### 6.2.4 GEAR TOOTH FLANK OF FAVORABLE GEOMETRY: GENERAL APPROACH

When a pair of gears rotate in mesh, a desirable line of contact,  $LC_{des}$ , travels straight together with the plane of action,  $\cdot$ . Then, when the plane of action rolls over the base pitch of the gear, the gear tooth flank,  $\mathcal{G}$ , is generated as a family of consecutive positions of the desirable line of contact,  $\cdot$ , in its motion in relation to a reference system associated with the gear. Similarly, when the plane of action rolls over the base pitch of the pinion, the pinion tooth flank,  $\mathcal{P}$ , is generated as a family of consecutive positions of the desirable line of contact,  $LC_{des}$ , in its motion in relation to a reference system associated with the pinion. In such a scenario, the actual line of contact,  $LC$ , between tooth flanks,  $\mathcal{G}$  and  $\mathcal{P}$ , of a gear and a mating pinion is congruent to the desirable line of contact,  $LC_{des}$ , of these surfaces ( $LC \equiv LC_{des}$ ). As an example, generation of a gear and a mating pinion tooth flanks,  $\mathcal{G}$  and  $\mathcal{P}$ , is illustrated in Figure 6.16 in the case when the desirable line of contact,  $LC_{des}$ , is a straight line segment rigidly associated with the  $PA$ .

The general approach for generation of tooth flanks,  $\mathcal{G}$  and  $\mathcal{P}$ , of a favorable geometry of a gear pair is based on the consideration of a current configuration of the desirable line of contact,  $LC_{des}$ , in two reference systems, one of which is associated with the gear, and another one is associated with its mating pinion. The earlier discussed results are helpful in this analysis. Let's begin the consideration with the generation of tooth flanks of a gear and a mating pinion that are generated by a line of contact,  $LC_{arbitr}$ , of an arbitrary geometry.

In a *Cartesian* coordinate system  $X_{lc}Y_{lc}Z_{lc}$  associated with the plane of action,  $PA$ , as shown in Figure 6.17, a point of interest,  $m$ , is chosen within the pre-specified line of contact,  $LC_{arbitr}$ , of an arbitrary geometry. The position vector of point of interest,  $\mathbf{r}_{lc.arbitr}$ , allows for matrix representation in matrix form:

$$\mathbf{r}_{lc.arbitr}(v) = \begin{bmatrix} r_{lc}(v) \cdot \sin v \\ r_{lc}(v) \cdot \cos v \\ 0 \\ 1 \end{bmatrix} \quad (6.33)$$

In Eq. (6.33), distance of point  $m$  from the origin of the coordinate system  $X_{lc}Y_{lc}Z_{lc}$  is denoted by  $r_{lc.arbitr} = |\mathbf{r}_{lc.arbitr}|$ , and  $v$  is the angle that the position vector  $\mathbf{r}_{lc.arbitr}$  forms with the  $X_{lc}$  - axis. The actual value of the distance  $r_{lc.arbitr}$  is a function of the angle,  $v$ , that is, the equality  $r_{lc.arbitr} = r_{lc.arbitr}(v)$  is valid.

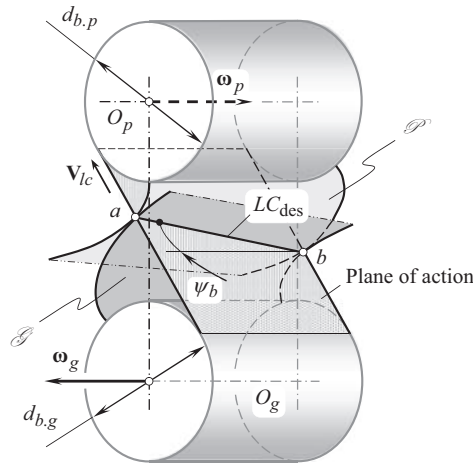
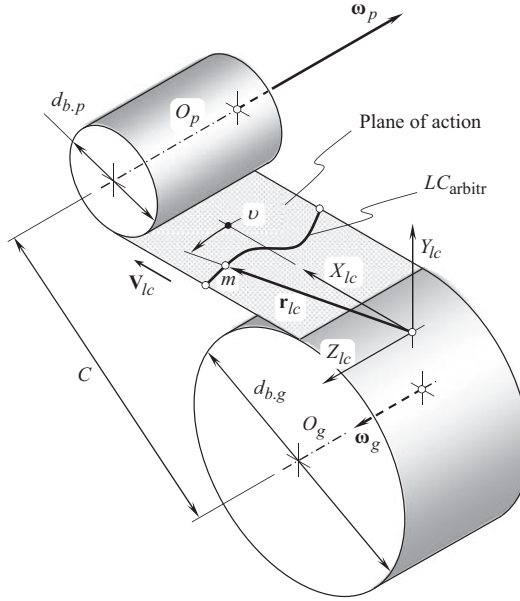


FIGURE 6.16 Generation of screw involute surfaces of tooth flanks,  $\mathcal{G}$  and  $\mathcal{P}$ , in a pair of helical gears.



**FIGURE 6.17** Schematic of generation of tooth flank of geometrically accurate gear for parallel-axes gearing: general approach.

The line of contact,  $LC_{arbitr}$ , travels together with the reference system,  $X_{lc}Y_{lc}Z_{lc}$ , in relation to the stationary *Cartesian* coordinate system  $X_{lc}^sY_{lc}^sZ_{lc}^s$  (see Figure 6.17). The vector,  $\mathbf{V}_{lc}$ , is the linear velocity vector of this motion. The distance,  $t$ , that is covered by the reference system,  $X_{lc}Y_{lc}Z_{lc}$ , in its motion with the plane of action,  $PA$ , is measured from the stationary reference system,  $X_{lc}^0Y_{lc}^0Z_{lc}^0$ .

Two more coordinate systems are used for the specification of the tooth flank,  $\mathcal{G}$ , of the gear. The *Cartesian* coordinate system,  $X_g^sY_g^sZ_g^s$ , is the stationary coordinate system associated with the gear housing. Ultimately, the *Cartesian* coordinate system,  $X_gY_gZ_g$ , is associated with the gear itself. This reference system rotates together with the gear.

The tooth flank of the gear,  $\mathcal{S}$ , can be construed as a locus of consecutive positions of lines of contact,  $LC_{arbitr}$ , that are represented in the reference system,  $X_gY_gZ_g$ . In order to represent Eq. (6.33) in the coordinate system,  $X_gY_gZ_g$ , an operator of the resultant coordinate system transformation,  $\mathbf{Rs}(lc \mapsto g)$ , is required. The operator,  $\mathbf{Rs}(lc \mapsto g)$ , can be calculated as a product of three corresponding operators of elementary coordinate system transformations (for details, see Appendix D):

- The operator of translation,  $\mathbf{Tr}[t(\varphi_g), X_{lc}]$ , from the coordinate system,  $X_{lc}Y_{lc}Z_{lc}$ , to the coordinate system,  $X_{lc}^0Y_{lc}^0Z_{lc}^0$
- The operator of translation,  $\mathbf{Tr}(r_{b,g}, Y_{lc}^0)$ , from the coordinate system,  $X_{lc}^0Y_{lc}^0Z_{lc}^0$ , to the coordinate system,  $X_g^sY_g^sZ_g^s$
- The operator of rotation,  $\mathbf{Rt}(\varphi_g, Z_g)$ , of the coordinate system,  $X_gY_gZ_g$ , in relation to the stationary coordinate system,  $X_g^sY_g^sZ_g^s$

The operator of translation,  $\mathbf{Tr}[t(\varphi_g), X_{lc}]$ , is calculated as:

$$\mathbf{Tr}[t(\varphi_g), X_{lc}] = \begin{bmatrix} 1 & 0 & 0 & 0.5d_{b,g}\varphi_g \\ 0 & 1 & 0 & 0 \\ 0 & 0 & 1 & 0 \\ 0 & 0 & 0 & 1 \end{bmatrix} \quad (6.34)$$

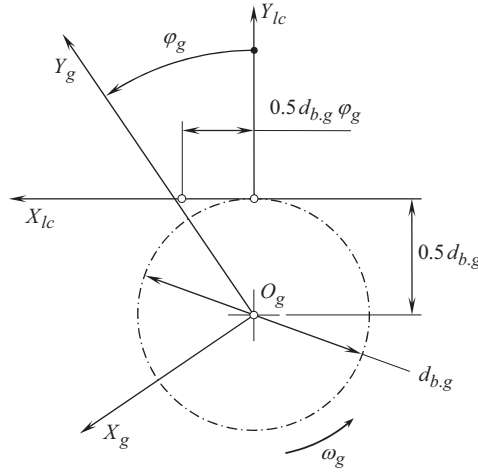


**FIGURE 6.18** Schematic of the applied coordinate systems transformations (in parallel-axes gearing).

The operator of translation,  $\mathbf{Tr}(r_{b,g}, Y_{lc}^0)$  equals to (see Figure 6.18):

$$\mathbf{Tr}(r_{b,g}, Y_{lc}^0) = \begin{bmatrix} 1 & 0 & 0 & 0 \\ 0 & 1 & 0 & 0.5d_{b,g} \\ 0 & 0 & 1 & 0 \\ 0 & 0 & 0 & 1 \end{bmatrix} \quad (6.35)$$

Ultimately, the following expression can be used for the calculation of the operator of rotation,  $\mathbf{Rt}(\varphi_g, Z_g) >$ :

$$\mathbf{Rt}(\varphi_g, Z_g) = \begin{bmatrix} \cos \varphi_g & \sin \varphi_g & 0 & 0 \\ -\sin \varphi_g & \cos \varphi_g & 0 & 0 \\ 0 & 0 & 1 & 0 \\ 0 & 0 & 0 & 1 \end{bmatrix} \quad (6.36)$$

Calculation of operators of translation and rotation is discussed more in detail in Appendix D.

These operators of elementary coordinate system transformations make possible calculation of the operator,  $\mathbf{Rs}(lc \mapsto g)$ , of the resultant coordinate system transformation:

$$\mathbf{Rs}(lc \mapsto g) = \mathbf{Rt}(\varphi_g, Z_g) \cdot \mathbf{Tr}(r_{b,g}, Y_{lc}^0) \cdot \mathbf{Tr}[t(\varphi_g), X_{lc}] \quad (6.37)$$

Equation (6.37) together with Eqs. (6.34)–(6.36) yield an expression for the calculation of the operator,  $\mathbf{Rs}(lc \mapsto g)$ , of the resultant coordinate system transformation:

$$\mathbf{Rs}(lc \mapsto g) = \begin{bmatrix} \cos \varphi_g & \sin \varphi_g & 0 & 0.5d_{b,g} \varphi_g \\ -\sin \varphi_g & \cos \varphi_g & 0 & 0.5d_{b,g} \\ 0 & 0 & 1 & 0 \\ 0 & 0 & 0 & 1 \end{bmatrix} \quad (6.38)$$

Rolling of a plane over a cylinder of revolution is analytically described by the operators of the resultant coordinate system transformation of the sort [see Eq. (6.37)]. Because of this they are commonly

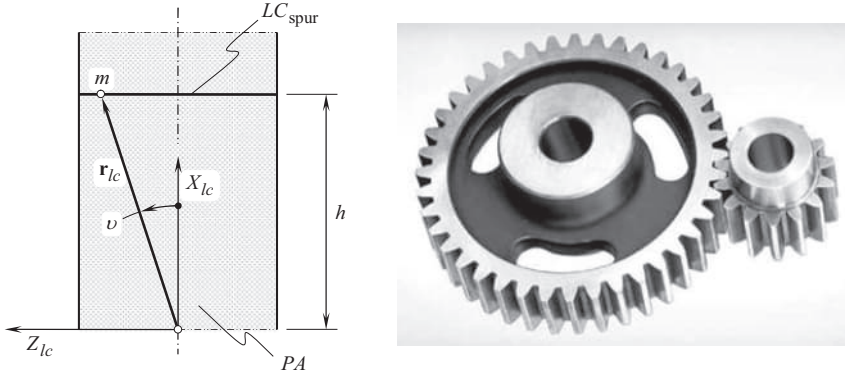


**FIGURE 6.19** Geometry of the line of contact,  $LC_{\text{spur}}$ , of tooth flanks,  $\mathcal{S}$  and  $\mathcal{P}$ , in parallel-axes spur involute gearing.

referred to as the operators of rolling. The operators of rolling are designated as  $\mathbf{Rl}_x(\varphi_g, Z)$ , namely, in the case under consideration, the equality,  $\mathbf{Rl}_x(\varphi_g, Z) = \mathbf{Rs}(lc \mapsto g)$ , is observed (see Appendix D on details of the operator of rolling).

Once the operator,  $\mathbf{Rs}(lc \mapsto g)$ , of the resultant coordinate system transformation is calculated, the following expression:

$$\mathbf{r}_{g.\text{arbitr}}(v, \varphi_g) = \mathbf{Rl}_x(\varphi_g, Z) \cdot \mathbf{r}_{lc.\text{arbitr}}(v) \quad (6.39)$$

can be used for the analytical description of the position vector of point,  $\mathbf{r}_{g.\text{arbitr}}$ , of the gear tooth flank,  $\mathcal{S}$ , that features the line of contact,  $LC_{\text{arbitr}}$ , of an arbitrary geometry. Equation (6.39) is valid for parallel-axes gearings of all types:

- for external (rotationally positive and rotationally negative) gearing
- for internal (rotationally positive and rotationally negative) gearing
- for *pinion-gear-to-rack* gear pair

As an example, consider spur parallel-axes gearing that features straight desirable line of contact,  $LC_{\text{spur}}$ , pointed parallel to the axis of rotation of the gear,  $O_g$ . For the straight line of contact,  $LC_{\text{spur}}$ , position vector of point,  $\mathbf{r}_{lc.\text{spur}}(v)$ , of the line of contact,  $LC_{\text{spur}}$ , is analytically described by a column matrix (see Figure 6.19):

$$\mathbf{r}_{lc.\text{spur}}(v) = \begin{bmatrix} h \\ 0 \\ h \cdot \tan v \\ 1 \end{bmatrix} \quad (6.40)$$

Again, Eq. (6.40) together with Eq. (6.39) yields an expression for the position vector of point,  $\mathbf{r}_{lc.\text{spur}}$ , of the gear tooth flank,  $\mathcal{S}$ , that features the line of contact,  $LC_{\text{spur}}$ , in the form of an inclined straight line, that is, of a spur gear (see Figure 6.20a):

$$\mathbf{r}_{g.\text{spur}}(v, \varphi_g) = \mathbf{Rl}_x(\varphi_g, Z) \cdot \begin{bmatrix} h \\ 0 \\ h \cdot \tan v \\ 1 \end{bmatrix} = h \cdot \begin{bmatrix} \cos \varphi_g + 0.5 d_{b.g} \varphi_g \\ -\sin \varphi_g + 0.5 d_{b.g} \\ \tan v \\ 1 \end{bmatrix} \quad (6.41)$$

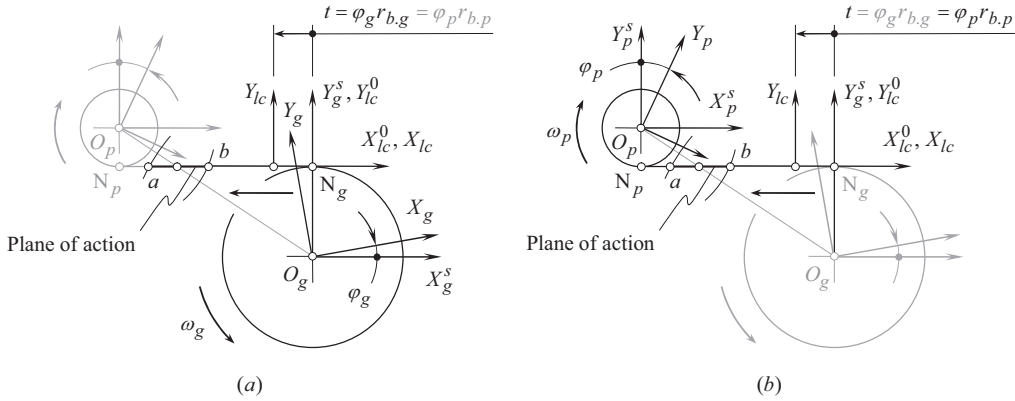


**FIGURE 6.20** The coordinate systems applied for the generation of tooth flank of involute gear with an arbitrary tooth shape in the lengthwise direction in Figure 6.17: (a) the coordinate systems associated with the gear, and (b) the coordinate systems associated with the mating pinion.

For an inclined line of contact,  $LC_{\text{helical}}$ , position vector of point,  $\mathbf{r}_{lc,\text{helical}}(\nu)$ , of the line of contact,  $LC_{\text{helical}}$ , in this particular case can be analytically described (see Figure 6.21) by a column matrix:

$$\mathbf{r}_{lc,\text{helical}}(\nu) = \begin{bmatrix} \frac{h}{\cos(\psi_b + \nu)} \cdot \cos \nu \\ 0 \\ \frac{h}{\cos(\psi_b + \nu)} \cdot \sin \nu \\ 1 \end{bmatrix} \quad (6.42)$$

Here, the base helix angle of the gear is designated as  $\psi_b$ , and  $h$  is the distance of the line of contact,  $LC_{\text{helical}}$ , from the origin of the reference system  $X_{lc}Y_{lc}Z_{lc}$ .

Again, Eq. (6.42) together with Eq. (6.39) yields an expression for the position vector of point,  $\mathbf{r}_{g,\text{helical}}$ , of the gear tooth flank,  $\mathcal{S}$ , that features the line of contact,  $LC_{\text{helical}}$ , in the form of an inclined straight line, namely, of a helical gear:

$$\mathbf{r}_{g,\text{helical}}(\nu, \phi_g) = \mathbf{R}\mathbf{I}_x(\phi_g, Z) \cdot \begin{bmatrix} \frac{h}{\cos(\psi_b + \nu)} \cdot \cos \nu \\ 0 \\ \frac{h}{\cos(\psi_b + \nu)} \cdot \sin \nu \\ 1 \end{bmatrix} = \frac{h}{\cos(\psi_b + \nu)} \begin{bmatrix} \cos \nu \cdot \cos \phi_g + 0.5 d_{b,g} \phi_g \\ -\cos \nu \cdot \sin \phi_g + 0.5 d_{b,g} \\ \sin \nu \\ 1 \end{bmatrix} \quad (6.43)$$

Ultimately, consider a line of contact that is shaped in the form of a circular arc,<sup>18</sup>  $LC_{\text{circ}}$ . In a reference system  $X_{lc}Z_{lc}$  (see Figure 6.22), position vector of point,  $\mathbf{r}_{lc,\text{circ}}(\nu)$ , of the line of contact,  $LC_{\text{circ}}$ , in this particular case allows for matrix representation in the form:

<sup>18</sup> It is likely A.C. Semple is the first who suggested the curved tooth configuration (U.S. Patent No. 5,647, *Rack and Pinion*, Amzi C. Semple, June 27, 1848 [98]). Proposed in the first half of the nineteenth century, the curved tooth configuration captured the interest of many mechanical engineers and inventors.

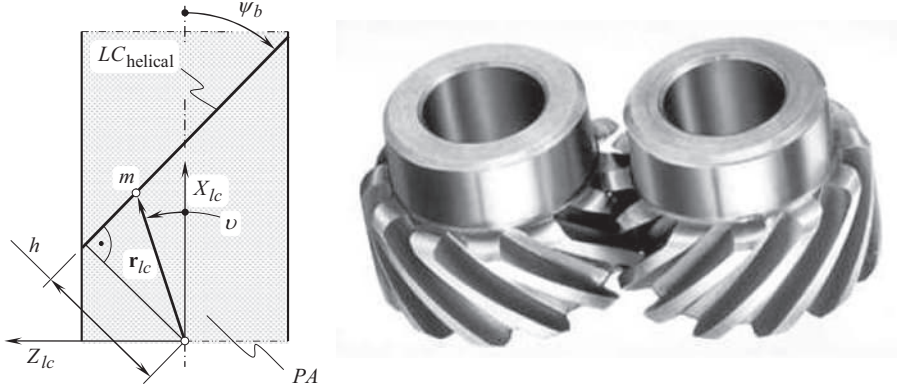


**FIGURE 6.21** Geometry of the line of contact,  $LC_{\text{helical}}$ , of tooth flanks,  $\mathcal{S}$  and  $\mathcal{P}$ , in parallel-axes helical involute gearing.

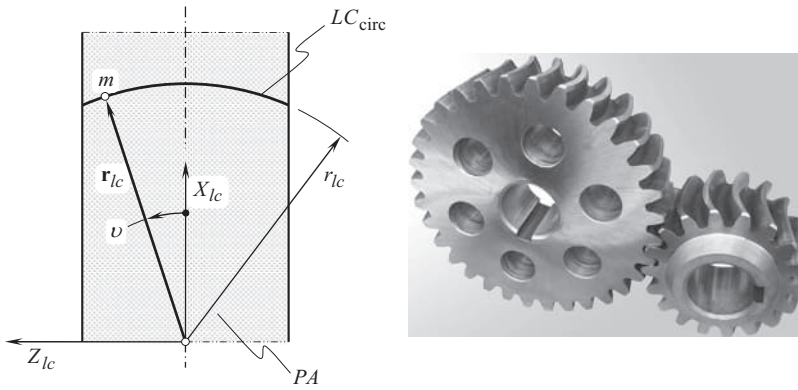


**FIGURE 6.22** Geometry of the line of contact,  $LC_{\text{circ}}$ , of tooth flanks,  $\mathcal{S}$  and  $\mathcal{P}$ , in parallel-axes involute gearing with circular-arc tooth flank geometry in its lengthwise direction.

$$\mathbf{r}_{lc, \text{circ}}(v) = \begin{bmatrix} r_{lc} \cdot \sin v \\ 0 \\ r_{lc} \cdot \cos v \\ 1 \end{bmatrix} \quad (6.44)$$

Equation (6.44) together with Eq. (6.39) yields an expression for the position vector of point,  $\mathbf{r}_{g, \text{circ}}$ , of the gear tooth flank,  $\mathcal{S}$ , that features the line of contact,  $LC_{\text{circ}}$ , in the form of a circular arc:<sup>19</sup>

$$\mathbf{r}_{g, \text{circ}}(v, \varphi_g) = \mathbf{R}\mathbf{l}_x(\varphi_g, Z) \cdot \begin{bmatrix} r_{lc} \cdot \sin v \\ 0 \\ r_{lc} \cdot \cos v \\ 1 \end{bmatrix} = \begin{bmatrix} r_{lc} \cdot \sin v \cdot \cos \varphi_g + 0.5 d_{b, g} \varphi_g \\ -r_{lc} \cdot \sin v \cdot \sin \varphi_g + 0.5 d_{b, g} \\ r_{lc} \cdot \cos v \\ 1 \end{bmatrix} \quad (6.45)$$

<sup>19</sup> If a gear with tooth flanks generated by a circular arc line of contact,  $LC_{\text{circ}}$ , is cut by a gear cutting tool with a non-zero transverse pressure angle ( $\phi_t \neq 0$ ), the condition of equal base pitches is violated.



In a similar manner, an expression for the position vector of point,  $\mathbf{r}_p$ , of the pinion tooth flank,  $\mathcal{P}$ , can be derived. For this purpose, Eq. (6.33) should be considered together with the operator,  $\mathbf{Rs}(lc \mapsto p)$ , of the resultant coordinate transformation from the coordinate system,  $X_{lc}Y_{lc}Z_{lc}$ , to the pinion coordinate system,  $X_pY_pZ_p$  (see Figure 6.20b). The operator,  $\mathbf{Rs}(lc \mapsto p)$ , can be calculated as a product of the operators of elementary coordinate system transformations. For this purpose, a stationary *Cartesian* coordinate system  $X_p^sY_p^sZ_p^s$  and the coordinate system  $X_pY_pZ_p$  that is associated with the pinion are used.

An expression for the position vector of point,  $\mathbf{r}_p$ , of the pinion tooth flank,  $\mathcal{P}$ , can be represented in a form:

$$\mathbf{r}_p(v, \varphi_p) = \mathbf{Rs}(lc \mapsto p) \cdot \mathbf{r}_{lc}(v) \quad (6.46)$$

Gears with tooth flanks,  $\mathcal{G}$  and  $\mathcal{P}$ , designed so as to fulfill Eq. (6.41), are referred to as *involute* gears for parallel-axes gear pairs. This is due to transverse section of the gear tooth flank is an involute of a circle, namely, the involute tooth profile is developed from the base circles of diameters,  $d_{b,g}$  and  $d_{b,p}$ , correspondingly.

An interval of variation of the parameter  $v$  in Eqs. (6.41) and (6.46) depends on the face width,  $F_{pa}$ , of the gear, and on the geometry of the line of contact,  $LC_{\text{arbitr}}$ . The interval of variation of the parameter  $\varphi_g$  in Eq. (6.41) and the parameter  $\varphi_p$  in Eq. (6.46) can be expressed in terms of length,  $Z$ , of the tooth height of the gear, and on the geometry of the line of contact,  $LC_{\text{arbitr}}$ .

It is evident that there is no need to implement elements of the theory of envelope surfaces for the derivation of an equation of the gear tooth flank,  $\mathcal{G}$ , as tooth flank of a gear,  $\mathcal{G}$ , is generated by a moving line of contact,  $LC$ . This is a significant advantage of the discussed approach for the generation of tooth flanks of a gear,  $\mathcal{G}$ , and that,  $\mathcal{P}$ , of a mating pinion.

Gear pairs that feature one of the following lines of contact, namely, either  $LC_{\text{spur}}$ , or  $LC_{\text{helical}}$ , or  $LC_{\text{circ}}$ , or  $LC_{\text{arbitr}}$ , retain operating base pitch,  $p_{b,op}$ , of a constant value. Therefore, these kinds of gear pairs are capable of transmitting a smooth rotation from the driving shaft to the driven shaft.



# Taylor & Francis

Taylor & Francis Group

<http://taylorandfrancis.com>

---

# 7 Simplified Approach to Generation of Involute Gear Tooth Flank

Tooth flank of a gear in a geometrically accurate parallel-axes gearing is a kind of involute surface. Gears with tooth flanks,  $\mathcal{S}$  and  $\mathcal{P}$ , designed so as to fulfill Eq. (6.39), are referred to as *involute* gears. The term *involute* that is due to the transverse section of the gear tooth flank is an involute of a circle, namely, involute tooth profile is developed from the base circle of a diameter,  $d_{b,g}$ , for a gear, and from the base circle of a diameter,  $d_{b,p}$ , for a mating pinion, correspondingly.

Once the geometry of transverse section of a gear tooth flank is known (this is an involute of a circle), simplified approaches can be used for generation, and for further analysis of tooth flank geometry of involute gears.

## 7.1 GENERATION OF INVOLUTE TOOTH PROFILE

Numerous kinds of parallel-axes involute gear pairs are extensively used in the present-day industry. Any possible kind of parallel-axes gear pair can be specified by one of five possible types of gear vector diagrams, as illustrated in Figure 6.2. Once a gear vector diagram is constructed, determination of the involute profile of a gear tooth is the next step in the analysis and design of parallel-axes gear pair.

In an *equivalent pulley-and-belt transmission*, a uniform rotation of a driving pulley 1 in Figure 7.1 causes a corresponding uniform rotation of a driven pulley 2. This schematic of transmission of a uniform rotary motion is employed for the derivation of an equation of the *natural form of gear tooth profile*: Tooth flanks of a gear and that of a mating pinion need to be designed so as to meet the following requirements:

- Contact point between the tooth flanks,  $\mathcal{S}$  and  $\mathcal{P}$ , of a gear and of a mating pinion must trace a straight-line segment  $ab$ . By nature, the straight-line segment,  $ab$ , is the path of contact,  $P_c$ , (this is illustrated by the *equivalent pulley-and-belt transmission* where the belt is tightened over the pulleys, it is always straight, and it cannot be curved). The straight-line segment,  $P_c$ , is aligned with a straight line that intersects the centerline,  $\mathfrak{t}$ , at the pitch point,  $P$ . This straight line forms a transverse pressure angle,  $\phi$ , with the perpendicular to the centerline,  $\mathfrak{t}$ , through  $P$
- Common perpendicular,  $\mathbf{n}_g$ , to the tooth flanks,  $\mathcal{S}$  and  $\mathcal{P}$ , at every contact point  $K$  is pointed along a straight line through the point,  $P$ , that, by nature, is a line of action,  $LA$  (this is because the tooth flanks,  $\mathcal{S}$  and  $\mathcal{P}$ , interact with one another like the working surfaces in a cam mechanism; if friction is not taken into account, the force of interaction is pointed along the common perpendicular,  $\mathbf{n}_g$ ). In parallel-axes involute gearing, the line of action,  $LA$ , and the path of contact,  $P_c$ , are two straight lines that align with one another
- The pitch point,  $P$ , is motionless, that is, it does not travel along the centerline,  $\mathfrak{t}$ , when the gears rotate
- The distance between contact points for every two adjacent pairs of teeth must be of the same value.

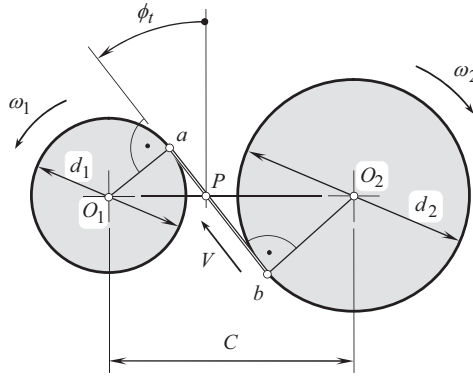


**FIGURE 7.1** On the concept of the natural form of gear tooth profile in geometrically accurate parallel-axes gearing.

With that said, let us investigate a desirable geometry of interacting tooth flanks,  $\mathcal{G}$  and  $\mathcal{P}$ , more in detail. Often, the tooth flank geometry of this kind is referred to as the *natural form of a gear/pinion tooth flank*.

Gears in a gear pair have to have the teeth of a particular geometry, for which a uniform rotation of the input shaft can be smoothly transmitted to the output shaft (i.e., the angular velocity ratio in the gear pair is of a constant value,  $\omega_{\text{input}} / \omega_{\text{output}} = \text{const}$ ). The axes of rotation of a gear and that of a mating pinion in a geometrically accurate gear pair are parallel to one another: no shafts deflections or displacements of the gear axes in relation to one another are permissible.

This discussion reveals why a rotation is transmitted *naturally* by means of geometrically accurate gearing.

Consider three *Cartesian* coordinate systems,  $X_1Y_1Z_1$ ,  $X_2Y_2Z_2$ , and  $X_hY_hZ_h$ , as shown in Figure 7.2. The first reference system,  $X_1Y_1Z_1$ , is associated with the first pulley, shown (see Figure 7.2). This coordinate system rotates with the first pulley. The second reference system,  $X_2Y_2Z_2$ , is associated with the second pulley, and it rotates with the second pulley. The third reference system,  $X_hY_hZ_h$ , is associated with the housing of the transmission. This coordinate system is a stationary one.

The axis,  $Z_1$ , is aligned with the axis of rotation of the first pulley. This axis is designated as  $O_p$ . The axis,  $Z_2$ , is aligned with the axis of rotation of the second pulley. This axis is designated as  $O_g$ . Finally, the axis,  $Z_h$ , of the stationary reference system,  $X_hY_hZ_h$ , is the axis through the pitch point,  $P$ . In parallel-axes gearing, this axis is parallel to the axes,  $O_p$  and  $O_g$ , and, thus, it is perpendicular to the plane of drawing in Figure 7.2. The axes,  $Z_1$ ,  $Z_2$ , and  $Z_h$ , are not shown in Figure 7.2.

When the pulleys rotate about their axes,  $O_p$  and  $O_g$ , the coordinate systems,  $X_1Y_1Z_1$  and  $X_2Y_2Z_2$ , turn through corresponding angles,  $\varphi_p$  and  $\varphi_g$ . Once a smooth transmission of a rotary motion is considered, then the angles,  $\varphi_p$  and  $\varphi_g$ , fulfill the following ratio:

$$\varphi_p \cdot r_p = \varphi_g \cdot r_g \quad (7.1)$$

where radii of the first and of the second pulleys are denoted as  $r_p$ , and  $r_g$ , correspondingly (for these radii, the equalities  $r_p = 0.5d_p$  and  $r_g = 0.5d_g$  are valid).

A located within the belt arbitrary point,  $m$ , travels together with the belt. A velocity of the straight motion of point,  $m$ , is equal to the linear velocity of the belt,  $V_m$ . In this motion, a straight line is traced by point,  $m$ , in the stationary reference system,  $X_hY_hZ_h$ . The straight line forms an angle,  $\phi_t$ , with the perpendicular to the centerline,  $\mathfrak{L}$ . The straight line is also tangent to the pulleys. The points of tangency are designated as  $a$  and  $b$  for the first and the second pulleys, correspondingly. The straight-line,  $P_c$ , rolls with no slippage over the pulleys of diameters,  $d_{b,g}$  and  $d_{b,p}$ . The point of intersection of the straight line,  $P_c$ , with the centerline,  $\mathfrak{L}$ , is designated as  $P$ . This point is commonly referred to as the *pitch point* in a gear pair.

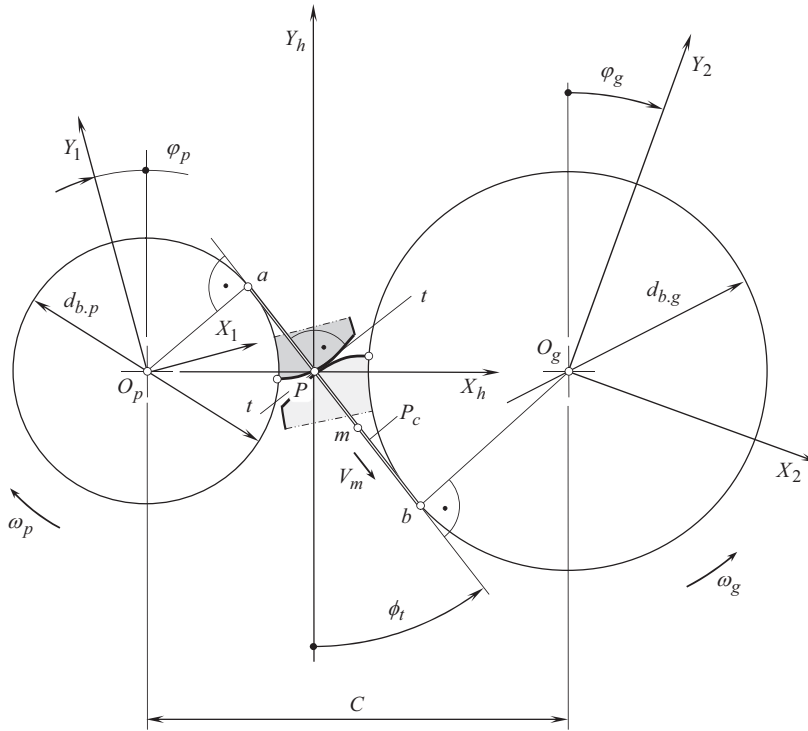


**FIGURE 7.2** Conjugate action law: Generation of the natural form of a gear tooth profile in geometrically accurate parallel-axes gearing.

The motion of point,  $m$ , can also be observed in the reference system,  $X_1Y_1Z_1$ . With respect to this coordinate system, the relative motion of point,  $m$ , can be construed as a superposition of a translation with linear velocity,  $V_m$  (see Figure 7.2), and a rotation,  $\omega_1$ . An involute of a circle is traced by point,  $m$ , in the coordinate plane,  $X_1Y_1$ .

Similarly, the motion of point,  $m$ , can also be observed in the reference system  $X_2Y_2Z_2$ . With respect to this coordinate system,  $X_2Y_2Z_2$ , the relative motion of point,  $m$ , can be interpreted as a superposition of a translation with the linear velocity,  $V_m$ , and a rotation  $\omega_2$ . Another involute of a circle is traced by point,  $m$ , in the coordinate plane,  $X_2Y_2$ .

Point,  $m$ , travels with the belt in the direction predetermined by the straight motion of the belt. No motion of point,  $m$ , is permissible in any other direction. In a stationary reference system,  $X_hY_hZ_h$ , the straight path is traced by point,  $m$ . In geometrically accurate gear pair, tooth flanks of a gear and that of a mating pinion must be designed so as to ensure that the path of contact point is aligned (is congruent) with that same straight path of point,  $m$ , in the *equivalent pulley-and-belt transmission*. In parallel-axes gearing, this line is commonly referred to as *path of contact*,  $P_c$ .

In the *equivalent pulley-and-belt transmission*, the force is transmitted along the belt. No other direction of the force is permissible. When the friction is not taken into account, the tooth flanks of the gear and of the pinion must be designed so as to ensure the line of action is aligned with that same straight line along which the force is transmitted in the *equivalent pulley-and-belt transmission*, namely, the line of action must be pointed along the straight portion of the belt. In parallel-axes gearing, this line is commonly referred to as the *line of action*,  $LA$ . The line of action,  $LA$ , is always a straight line as no force can be transmitted along a curve.

These two lines, namely, the path of contact,  $P_c$ , and the line of action,  $LA$ , are two different entities. In *geometrically accurate* parallel-axes gearing, these two lines align with one another. The latter often causes a confusion. In parallel-axes gearing of other designs (e.g., in cycloid parallel-axes gearing), the path of contact,  $P_c$ , and the line of action,  $LA$ , do not align to one another, as

the path of contact,  $P_c$ , is a planar curve, while the line of action,  $LA$ , is represented by an infinite number of instantaneous lines of action,  $LA_{inst}$ .

It is the right point to stress here the difference between *equivalent pulley-and-belt transmission*, and between *geometrically accurate parallel-axes gearing*. In an *equivalent pulley-and-belt transmission*, the straight portion of the belt is terminated by points of tangency,  $a$  and  $b$ , of the belt with the pulleys. In geometrically accurate parallel-axes gearing, neither the path of contact,  $P_c$ , nor the line of action,  $LA$ , are terminated by these points. Both the lines,  $P_c$  and  $LA$ , can be extended in both directions beyond the points  $a$  and  $b$ .

When the gears rotate, the involute profiles, that are traced within the planes,  $X_1Y_1$  and  $X_2Y_2$ , roll over one another. It can be shown that no slippage of the involute profiles is observed when the contact point is coincident with the pitch point,  $P$ . However, sliding occurs at all the rest contact points located before and beyond the pitch point,  $P$ .

This is a kinematic requirement for one tooth profile to drive the other tooth profile at a constant angular velocity ratio (remember that  $\omega_{input}/\omega_{output} = const$ ). It can also be readily understood that a pair of gear profiles contact each other at different positions as the gears rotate. The locus of all possible contact points for a given pair of tooth profiles, namely, the *path of contact*,  $P_c$ , is a straight-line segment, terminated by the extremities of the gear and the pinion teeth.

Three curves involved in the most fundamental part of gear design are as follows:

1. Path of contact,
2. Profile of the gear tooth, and
3. Profile of the pinion tooth

A basic geometric fact<sup>1</sup> of great significance is that *given a fixed center distance and speed ratio, any of these curves completely determines the other two*. It is understood here that the necessary conditions of contact of the interacting tooth flanks (the first fundamental law of gearing), as well as the condition of conjugacy of the tooth flanks,  $\mathcal{S}$  and  $\mathcal{P}$  (the second fundamental law of gearing), are met.

Therefore, *the three traces obtained in the reference systems,  $X_hY_hZ_h$ ,  $X_1Y_1Z_1$ , and  $X_2Y_2Z_2$ , are interdependent*. If a trace in one of three coordinate systems is known, then the remaining two traces can be found and can be expressed in terms of the known one. This means that the specifications of the traces in the coordinate systems,  $X_hY_hZ_h$ ,  $X_1Y_1Z_1$  and  $X_2Y_2Z_2$ , are equivalent to one another. If necessary, the two tooth profiles of the gear and that of the mating pinion can be investigated individually, or the geometry of the path of contact,  $P_c$ , can be investigated instead. Once the path of contact,  $P_c$ , is known, conjugate tooth profiles can be easily derived. The latter is a routine procedure.

The following three statements can be adopted as a rule:

- The path of contact,  $P_c$ , can be interpreted as the locus of contact points considered in the stationary coordinate system,  $X_hY_hZ_h$ , associated with the gear housing
- A gear tooth profile can be construed as the locus of contact points considered in the coordinate system,  $X_gY_gZ_g$ , associated with a gear
- A pinion tooth profile can be interpreted as the locus of contact points considered in the coordinate system,  $X_pY_pZ_p$ , associated with a pinion

It is instructive to stress here that in *geometrically accurate parallel-axes gearing*, the path of contact,  $P_c$ , and the line of action,  $LA$ , are congruent to each other. However, it is of critical importance to realize that these two lines are of completely different nature.

<sup>1</sup> It should be stressed here on that this basic geometric fact is valid **only** in a case of *geometrically-accurate gearing* (where the interacting tooth flanks are conjugate to one another), and it is **not** applicable in cases of parallel-axes gearings with other geometries of tooth flanks (where the interacting tooth flanks are not conjugate to one another), for instance, the basic geometry fact is not applicable in cases of parallel-axes gearings with a cycloid tooth profile, and others.

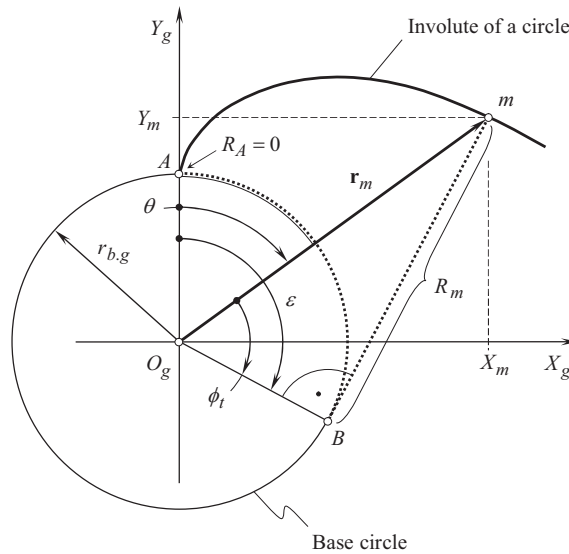


**FIGURE 7.3** Involute of a circle.

Often, specification of a gear pair in terms of geometry of the path of contact,  $P_c$ , and not in terms of the tooth profiles of the gear and that of the mating the pinion is proven to be convenient.

Two traces of point of interest,  $m$ , which are obtained within the coordinate planes,  $X_1Y_1$  and  $X_2Y_2$ , are commonly used for designing tooth profiles in gear pairs. *Leonhard Euler*<sup>2</sup> (1760) is credited with the development of the involute tooth profile for *geometrically accurate* parallel-axes gearing. Involute of a circle, which was proposed by *Euler* for gear teeth, best fits all cases of parallel-axes gearing with zero axis displacements.

The discussed interpretation of the generation of involute tooth profiles is based on the similarity between two rotating pulleys (see Figure 7.1) and between a gear pair (see Figure 7.2). The said allows for an intermediate conclusion:

**Intermediate conclusion 7.1:** *Involute of a circle can be viewed as a planar curve traced by point on a taut cord being unwound from the circumference of a stationary circle.*

Alternatively, involute of a circle is also the locus of point on a straight line that rolls with no slip-page around the circumference of a stationary circle.

Thus, the interpretation reveals that this method for generating involute tooth profiles can be referred to as the *natural* way for tooth profile generation.

### 7.1.1 INVOLUTE GEAR TOOTH PROFILE

Once the kinematics of generation of involute curve is understood, an analytical description of this curve can be easily derived.

An equation of involute of a circle is derived below in the following manner (refer to Figure 7.3).

The involute of a circle starts at a point,  $A$ , within the base circle of a radius,  $r_{b.g}$ . Magnitude of the position vector,  $\mathbf{r}_m$ , of an arbitrary point,  $m$ , of the involute curve can be expressed in terms of the base radius,  $r_{b.g}$ , and the central angle  $\varepsilon = \angle(AO_gM)$ . The length of the circular arc,  $\widehat{AB}$ , is equal

<sup>2</sup> Leonhard Eule (April 15, 1707–September 18, 1783), a pioneering Swiss mathematician and physicist, spent most of his life in Russia and Germany.



to the length of the straight-line segment,  $AB$ . This is due to the straight line rolls with no slippage over the base circle. From the  $\triangle BO_gM$ , the following equation can be composed:

$$R_m = r_{b.g} \tan \phi_t \quad (7.2)$$

In Eq. (7.2), the profile angle<sup>3</sup> of the involute curve is designated as  $\phi_t$ .

Due to an equality  $R_m = \widehat{AB}$  is valid, the following equality is valid:

$$R_m = r_{b.g} \cdot \varepsilon \text{ (rad)} \quad (7.3)$$

The central angle,  $\varepsilon$ , can be represented in the form of the sum:  $\varepsilon = \phi_t + \theta$ . This yields the following formula for the radius,  $R_m$ :

$$R_m = r_{b.g} \cdot (\phi_t + \theta) \quad (7.4)$$

Equation (7.2) considered in conjunction with Eq. (7.3) results in the following equality:

$$r_{b.g} \tan \phi_t = r_{b.g} \cdot (\phi_t + \theta) \quad (7.5)$$

Ultimately, Eq. (7.5) casts into the equation for the involute function:

$$\theta = \text{inv } \phi_t = \tan \phi_t - \phi_t \text{ (rad)} \quad (7.6)$$

The involute function,  $\text{inv } \phi_t$ , is significant in the theory of gearing as well as in applications of the theory.

The projection,  $X_m$ , of the position vector,  $\mathbf{r}_m$ , of point,  $m$ , onto the  $X_g$  – axis can be interpreted as the sum of projections onto the  $X_g$  – axis of the straight line segment,  $O_gB$ , and the straight line segment,  $R_m$  :

$$X_m = r_{b.g} \cos(\varepsilon - 90^\circ) + R_m \sin(\varepsilon - 90^\circ) \quad (7.7)$$

Similarly, the projection,  $Y_m$ , of the position vector,  $\mathbf{r}_m$ , of point,  $m$ , onto  $Y_g$  – axis can be interpreted as the sum of projections onto the  $Y_g$  – axis of the same straight line segments,  $O_gB$  and  $R_m$  :

$$Y_m = -r_{b.g} \sin(\varepsilon - 90^\circ) + R_m \cos(\varepsilon - 90^\circ) \quad (7.8)$$

Then, Eqs. (7.7) and (7.8) are rewritten in the form:

$$\begin{aligned} \mathbf{r}_m(\phi_t) = & \mathbf{i} \cdot [-r_{b.g} \sin(\phi_t + \text{inv } \phi_t) + r_{b.g}(\phi_t + \text{inv } \phi_t) \cos(\phi_t + \text{inv } \phi_t)] + \\ & + \mathbf{j} \cdot [-r_{b.g} \cos(\phi_t + \text{inv } \phi_t) - r_{b.g}(\phi_t + \text{inv } \phi_t) \sin(\phi_t + \text{inv } \phi_t)] \end{aligned} \quad (7.9)$$

Equation (7.9) describes an involute curve in terms of just two parameters, namely, of a radius of the base cylinder,  $r_{b.g}$ , and of the profile angle,  $\phi_t$ .

Equation (7.9) can also be represented in matrix form:

<sup>3</sup> Profile angle,  $\phi_t$ , is often referred to as *pressure angle*. It is incorrect to use the term *pressure angle* with respect to a curve. The term *pressure* means a kind of interaction between two curves/surfaces. As long as just one involute curve is considered, the term *profile angle* is preferred. The term *pressure angle* is applicable when an interaction of two involute curves is discussed.

$$\mathbf{r}_m(\phi_t) = \begin{bmatrix} -r_{b,g} \sin(\phi_t + \text{inv } \phi_t) + r_{b,g}(\phi_t + \text{inv } \phi_t) \cos(\phi_t + \text{inv } \phi_t) \\ -r_{b,g} \cos(\phi_t + \text{inv } \phi_t) - r_{b,g}(\phi_t + \text{inv } \phi_t) \sin(\phi_t + \text{inv } \phi_t) \\ 0 \\ 1 \end{bmatrix} \quad (7.10)$$

The representation of an involute curve in the form [see Eq. (7.10)] is preferred in many applications. In particular, matrix representation of equation of the involute curve is preferred when multiple coordinate system transformations are required to be performed.

The discussed method of generation of involute of a circle is commonly referred to as the *tracing method for generation of involute of a circle*.

The involute of a circle has an extensive application in the theory of gearing.

## 7.1.2 GEAR TOOTH FLANK IN THE LENGTHWISE DIRECTION OF THE GEAR TOOTH

A variety of practical shapes that are possible for gear tooth flanks is limited. Although the physically possible variety of gear tooth geometries is large enough, commonly used gear tooth forms in their lengthwise direction are limited to just a few forms. Straight, helical, herring-bone and double helical, circular, and cycloid, are among them.

The use of modern numerically control (NC) machines makes possible the machining of any desirable shape of gear tooth flank; application of NC machining is purposely limited to those shapes for which kinematics of machining can be represented as either a single translation/rotation or a superposition of a finite number of translations and rotations (or just a few of them).

An accurate description of the gear tooth flank is of critical importance for many applications. An analytical description of gear tooth flanks is preferred from many standpoints.

It is convenient to begin the discussion of gear tooth flank geometry from the geometry of tooth flank of spur involute gears.

### 7.1.2.1 Tooth Flank in Spur Involute Gear

Consider a spur gear with an involute tooth profile as shown in Figure 7.4a. The geometry of the tooth flank of the gear is illustrated in Figure 7.4b. The transverse section of gear tooth flanks is schematically shown in Figure 7.4c.

A coordinate system  $X_g Y_g$  is associated with the gear. In the coordinate system  $X_g Y_g$ , the position vector,  $\mathbf{r}_{inv}(V_g)$ , of point of an involute tooth profile is represented in matrix form:

$$\mathbf{r}_{inv}(V_g) = \begin{bmatrix} r_{b,g} \cdot (\sin V_g - V_g \cdot \cos V_g) \\ r_{b,g} \cdot (\cos V_g + V_g \cdot \sin V_g) \\ 0 \\ 1 \end{bmatrix}, V_g^{(l)} \leq V_g \leq V_g^{(a)} \quad (7.11)$$

In this equation, actual values of the parameter,  $V_g$ , that corresponds to  $SAP^4$  point of the tooth profile, and point of the tooth profile that is located on the major diameter ( $EAP$ ) of the gear, are designated as,  $V_g^{(l)}$  and  $V_g^{(a)}$ , correspondingly.

Once the equation of the transverse section of a gear tooth flank is derived [see Eq. (7.11)], then the gear tooth flank,  $\mathcal{S}$ , can be generated by means of a *generator line*, and a *director line*, as schematically illustrated in Figure 7.5. When a generator line travels along a corresponding director line, the gear tooth flank,  $\mathcal{S}$ , is generated as a kind of swept surface. In parallel-axes gearing, the *generator line* is often referred to as the *tooth profile*. In common practice, the terms *tooth profile*

<sup>4</sup>  $SAP$  stands for *Start of Active Profile* of the gear tooth;  $EAP$  stands for *End of Active Profile*.

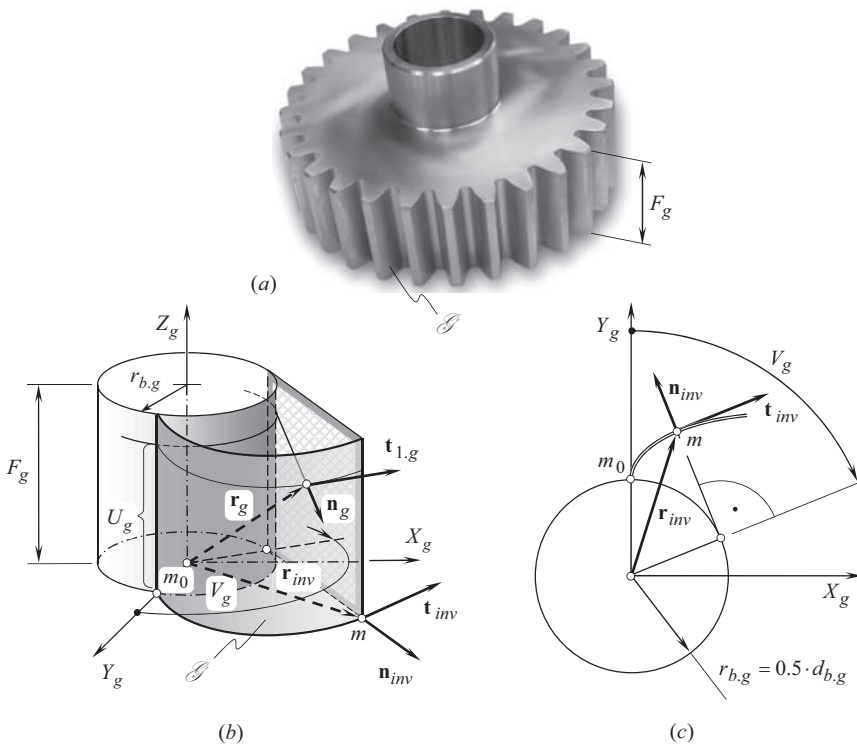


**FIGURE 7.4** Geometry of tooth flank of spur involute gear: (a) spur gear, (b) gear tooth flank,  $\mathcal{S}$ , geometry, and (c) transverse section of the gear tooth flank,  $\mathcal{S}$ .

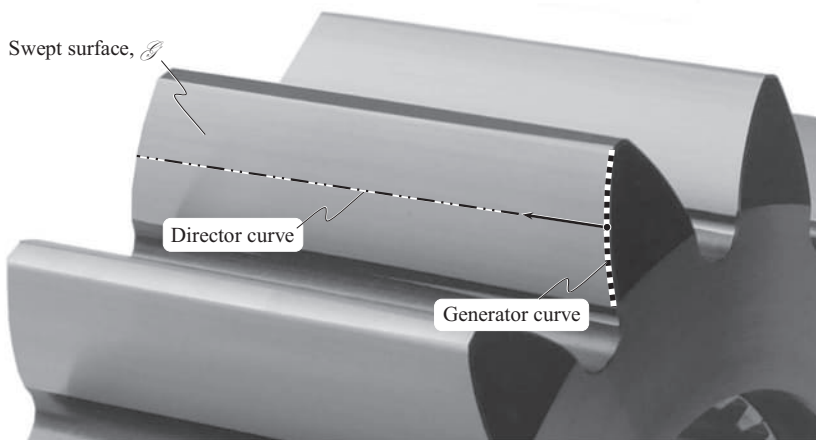


**FIGURE 7.5** Tooth flank,  $\mathcal{S}$ , of a spur involute gear generated by means of a *generator curve* and *director curve*.

(a curve) and *tooth flank* (a surface) are interchangeable. However, this *equivalency* is valid only in parallel-axes gearing. The use of the term *tooth flank* is preferred.

The use of the approach, illustrated in Figure 7.5, enables one designing a spur gear. A spur involute gear of  $N_g$  teeth (see Figure 7.6) has  $N_g$  left-hand-side tooth flanks and  $N_g$  right-hand-side tooth



**FIGURE 7.6** Spur involute gear.

flanks. All the tooth flanks of a spur gear are terminated by the outer diameter of the gear and by the *SAP* diameter. Tooth flanks of every two adjacent teeth are connected to one another by means of a fillet and by a bottom land. Occasionally, the fillets in a common tooth space can overlap the bottom land.

In general, such an approach of generation of a gear tooth flank,  $\mathcal{S}$ , is applicable only for parallel-axes gearing. In intersected-axes gearing, as well as in crossed-axes gearing, such an approach is not applicable, as the tooth flank of a gear does not allow for *sliding over itself* (excluding gears of special design, for example, for approximate gearing). This approach of generation of gear tooth flank,  $\mathcal{S}$ , is discussed more in detail immediately below.

The tooth flank of a spur involute gear,  $\mathcal{S}$ , can be represented as the locus of consecutive positions of the involute tooth profile,  $\mathbf{r}_{inv}(V_g)$ , that travels straight in the direction of the gear axis,  $Z_g$ . Let us designate the parameter of this motion of the tooth profile as  $U_g$ . Equation (7.11) immediately yields an expression for the position vector,  $\mathbf{r}_g(U_g, V_g)$ , of a point of the tooth flank of a spur involute gear:

$$\mathbf{r}_g(U_g, V_g) = \begin{bmatrix} r_{b,g} \cdot (\sin V_g - V_g \cdot \cos V_g) \\ r_{b,g} \cdot (\cos V_g + V_g \cdot \sin V_g) \\ U_g \\ 1 \end{bmatrix}, \quad \begin{matrix} V_g^{(l)} \leq V_g \leq V_g^{(a)} \\ 0 \leq U_g \leq B_g \end{matrix} \quad (7.12)$$

Current value of the parameter  $U_g$  falls within the gear face width  $F_g$ , that is,  $0 \leq U_g \leq F_g$ .

It is easy to see that for the chosen kind of parameterization of the tooth flank,  $\mathcal{S}$ , of a spur involute gear, the identity  $U_g \equiv Z_g$  is observed.

### 7.1.2.2 Tooth Flank in Helical Involute Gear

Tooth flanks of helical gears with involute tooth profile are shaped in the form of a screw involute surface. A possible method for the generation of a screw involute surface by a straight line,  $\mathcal{E}_g$ , that

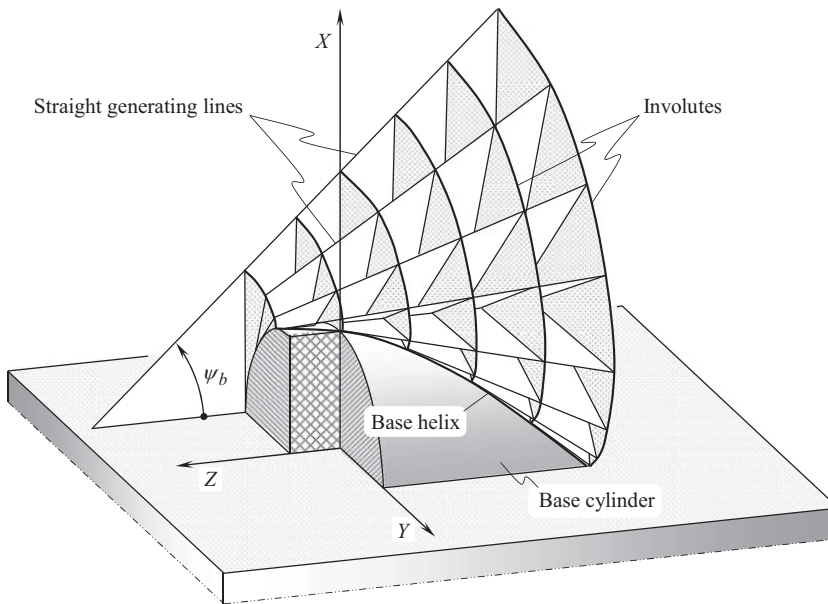


**FIGURE 7.7** The involute helicoid. (After W.F. Vogel, W.F., *Involutometry and Trigonometry*, Detroit, MI: Michigan Tool Company. Book production by Denham & Co. With permission.)

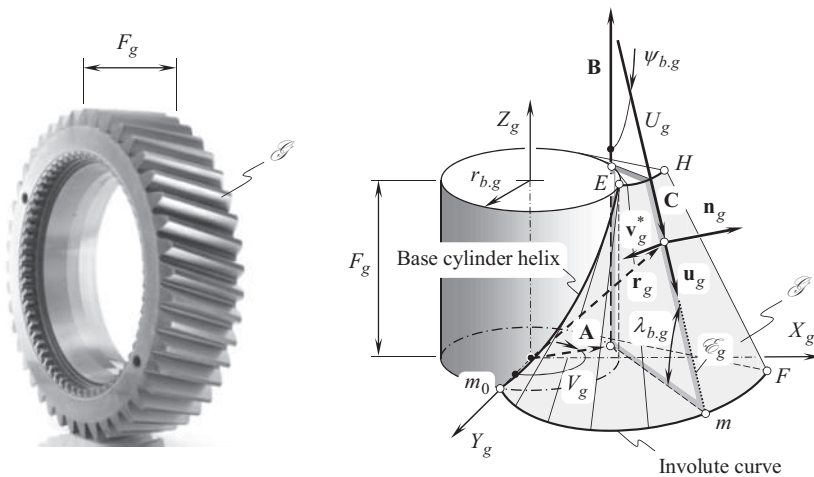


**FIGURE 7.8** Geometry of tooth flank,  $\mathcal{S}$ , of helical involute gear. (After Radzevich, S.P., *Differential-Geometric Method of Part Surface Generation*, DrSc(Eng) Thesis. Tula: Tula Polytechnic Institute, 1991, 300 pages.)

rolls with no slippage over the base cylinder of a gear is illustrated in Figure 7.7 [214]. The surface  $\mathcal{S}$  is generated as a locus of successive positions of the straight line,  $\mathcal{E}_g$ , which, by nature, is the characteristic line of the tooth flank,  $\mathcal{S}$ .

A screw involute surface,  $\mathcal{S}$ , is generated by a straight line that performs a screw motion in relation to the gear axis,  $O_g$  (see Figure 7.8). The generating line is tangent to the helix on the base cylinder of a radius,  $r_{b,g}$ . The helix in question is traced on the base cylinder using the point of tangency of the generating straight line,  $\mathcal{E}_g$ , with the cylinder. The helix is referred to as the *base helix*. The generating line,  $\mathcal{E}_g$ , of the surface  $\mathcal{S}$  forms a base lead angle,  $\lambda_{b,g}$ , with the plane perpendicular

to the  $Z_g$  – axis of the *Cartesian* coordinate system  $X_gY_gZ_g$ . It has to be mentioned here that for the tooth alignment of the mating gears to agree, their *base lead angles must be equal*. A similar statement is valid for base helix angle, that is, for the tooth alignment of the mating gears to agree, the *base helix angles of the mating gears must be equal*.

The position vector,  $\mathbf{r}_g$ , of point of the screw involute surface is represented in the form of a sum of three vectors (see Figure 7.8):

$$\mathbf{r}_g = \mathbf{A} + \mathbf{B} + \mathbf{C} \quad (7.13)$$

Here,  $|\mathbf{A}|$  equals to the base cylinder radius (i.e., the equality  $|\mathbf{A}| = r_{b,g}$  is observed). The vector,  $\mathbf{A}$ , makes a roll angle,  $V_g$ , with the  $Y_g$  – axis. The axial displacement in the screw motion is given by  $|\mathbf{B}| = p_g \cdot V_g$ , which corresponds to the rotation angle,  $V_g$ ;  $p_g$  designates the *screw parameter* (or the *reduced pitch*, in other terminology) of the tooth flank,  $\mathcal{S}$ . Finally,  $|\mathbf{C}| = U_g$  is the segment of the generating straight line,  $\mathcal{E}_g$ , measured from the tangency point on the base cylinder to the current point on the screw involute surface,  $\mathcal{S}$ .

By projecting three vectors,  $\mathbf{A}$ ,  $\mathbf{B}$ , and  $\mathbf{C}$ , onto the axes of the coordinate system  $X_gY_gZ_g$ , an equation for the screw involute surface of the gear tooth flank,  $\mathcal{S}$ , becomes possible. After rearranging components and transforming formulas, the equation of the screw involute surface,  $\mathcal{S}$ , can be represented in matrix form [81,142,151–153]:

$$\mathbf{r}_g(U_g, V_g) = \begin{bmatrix} r_{b,g} \cos V_g + U_g \cos \lambda_{b,g} \sin V_g \\ r_{b,g} \sin V_g - U_g \sin \lambda_{b,g} \sin V_g \\ r_{b,g} \tan \lambda_{b,g} - U_g \sin \lambda_{b,g} \\ 1 \end{bmatrix} \quad \begin{matrix} V_g^{(l)} \leq V_g \leq V_g^{(a)} \\ 0 \leq U_g \leq [U_g] \end{matrix} \quad (7.14)$$

Here, the maximum permissible value of the parameter  $U_g$  is designated as  $[U_g]$ . The value of the parameter  $[U_g]$  can be expressed in terms of the base diameter,  $d_{b,g} = 2r_{b,g}$ , of the gear, base lead angle,  $\lambda_{b,g}$ , and gear face width  $F_g$ .

The use of the approach, illustrated in Figure 7.5, enables the design of a helical gear. A helical involute gear of  $N_g$  teeth (see Figure 7.9) has  $N_g$  left-hand-side tooth flanks and  $N_g$  right-hand-side



FIGURE 7.9 Helical involute gear.

tooth flanks. All the tooth flanks of a helical gear are terminated by the outside diameter of the gear, and by the *SAP* diameter. Tooth flanks of every two adjacent teeth are connected to one another by means of a fillet and a bottom land. Occasionally, the fillets in a common tooth space can overlap the bottom land.

It can be shown that Eq. (7.12) is a reduced case of Eq. (7.14), and the second one can be simplified to the first one under the assumption that base lead angle is of a zero value (i.e.,  $\lambda_{b.g} = 0^\circ$ ).

Having the equation of the gear tooth flank derived [see Eq. (7.14)], further analysis of the local geometry of the screw involute surface,  $\mathcal{S}$ , of the helical involute gear can be undertaken. Derivation of expressions for the first,  $\Phi_{1.g}$ , and for the second,  $\Phi_{2.g}$ , fundamental forms at point of screw involute surface,  $\mathcal{S}$ , is required to perform this analysis.

Equation (7.14) yields the calculation of two tangent vectors,  $\mathbf{U}_g(U_g, V_g)$  and  $\mathbf{V}_g(U_g, V_g)$ , which are tangential to the  $U_g$  – and  $V_g$  – coordinate lines at point on the surface,  $\mathcal{S}$ . These vectors are correspondingly equal to:

$$\mathbf{U}_g(U_g, V_g) = \frac{\partial \mathbf{r}_g}{\partial U_g}(U_g, V_g) = \begin{bmatrix} \cos \lambda_{b.g} \sin V_g \\ -\cos \lambda_{b.g} \cos V_g \\ -\sin \lambda_{b.g} \\ 1 \end{bmatrix} \quad (7.15)$$

$$\mathbf{V}_g(U_g, V_g) = \frac{\partial \mathbf{r}_g}{\partial V_g}(U_g, V_g) = \begin{bmatrix} -r_{b.g} \sin V_g + U_g \cos \lambda_{b.g} \cos V_g \\ r_{b.g} \cos V_g + U_g \cos \lambda_{b.g} \sin V_g \\ r_{b.g} \tan \lambda_{b.g} \\ 1 \end{bmatrix} \quad (7.16)$$

Accordingly, the corresponding unit tangent vectors,  $\mathbf{u}_g$  and  $\mathbf{v}_g$ , are equal to:

$$\mathbf{u}_g(U_g, V_g) = \frac{\mathbf{U}_g}{|\mathbf{U}_g|} \quad (7.17)$$

$$\mathbf{v}_g(U_g, V_g) = \frac{\mathbf{V}_g}{|\mathbf{V}_g|} \quad (7.18)$$

The direction of the tangent vector,  $\mathbf{U}_g$ , at given point on the gear tooth flank,  $\mathcal{S}$ , is specified by the unit vector  $\mathbf{u}_g$ . Similarly, the direction of the tangent vector,  $\mathbf{V}_g$ , through the same point on the gear tooth surface,  $\mathcal{G}$ , is specified by the unit vector  $\mathbf{v}_g$ .

The calculated vectors,  $\mathbf{U}_g$  and  $\mathbf{V}_g$ , can be used for the calculation of the fundamental magnitudes of the first order of the gear tooth flank,  $\mathcal{S}$ :

$$E_g = \mathbf{U}_g \cdot \mathbf{U}_g, \quad (7.19)$$

$$F_g = \mathbf{U}_g \cdot \mathbf{V}_g \quad (7.20)$$

$$G_g = \mathbf{V}_g \cdot \mathbf{V}_g \quad (7.21)$$

$$H_g = |\mathbf{U}_g \times \mathbf{V}_g| = \sqrt{E_g G_g - F_g^2}, \quad (7.22)$$

For a screw involute surface,  $\mathcal{S}$ , Eqs. (7.18)–(7.21) return the following expressions:

$$E_g = 1, \quad (7.23)$$

$$F_g = -\frac{r_{b.g}}{\cos \lambda_{b.g}} \quad (7.24)$$

$$G_g = \frac{U_g^2 \cos^4 \lambda_{b.g} + r_{b.g}^2}{\cos^2 \lambda_{b.g}} \quad (7.25)$$

These equations yield an expression for the first fundamental form,  $\Phi_{1.g}$ , of the gear tooth flank,  $\mathcal{S}$ :

$$\Phi_{1.g} \Rightarrow dU_g^2 - 2\frac{r_{b.g}}{\cos \lambda_{b.g}} dU_g dV_g + \frac{U_g^2 \cos^4 \lambda_{b.g} + r_{b.g}^2}{\cos^2 \lambda_{b.g}} dV_g^2 \quad (7.26)$$

The discriminant,  $H_g$  [see Eq. (7.22)], of the first fundamental form,  $\Phi_{1.g}$ , at point of the gear tooth flank,  $\mathcal{S}$ , is calculated from the following formula:

$$H_g = U_g \cos \lambda_{b.g} \quad (7.27)$$

In order to derive an equation for the second fundamental form,  $\Phi_{2.g}$ , of the gear tooth surface,  $\mathcal{S}$ , the second derivatives of the position vector  $\mathbf{r}_g(U_g, V_g)$  with respect to  $U_g$ –, and  $V_g$ – parameters are required. Equations (7.15) and (7.16) for the tangent vectors,  $\mathbf{U}_g$  and  $\mathbf{V}_g$ , correspondingly, yield expressions for the derivatives of  $\mathbf{r}_g$  with respect  $U_g$ – and  $V_g$ – parameters:

$$\frac{\partial \mathbf{U}_g}{\partial U_g}(U_g, V_g) = \begin{bmatrix} 0 \\ 0 \\ 0 \\ 1 \end{bmatrix} \quad (7.28)$$

$$\frac{\partial \mathbf{U}_g}{\partial V_g}(U_g, V_g) \equiv \frac{\partial \mathbf{V}_g}{\partial U_g}(U_g, V_g) = \begin{bmatrix} \cos \lambda_{b.g} \cos V_g \\ \cos \lambda_{b.g} \sin V_g \\ 0 \\ 1 \end{bmatrix} \quad (7.29)$$

$$\frac{\partial \mathbf{V}_g}{\partial V_g}(U_g, V_g) = \begin{bmatrix} -r_{b.g} \cos V_g - U_g \cos \lambda_{b.g} \sin V_g \\ -r_{b.g} \sin V_g + U_g \cos \lambda_{b.g} \cos V_g \\ 0 \\ 1 \end{bmatrix} \quad (7.30)$$

By definition, the fundamental magnitudes of the second order can be represented in the following form:

$$L_g = \frac{\frac{\partial \mathbf{U}_g}{\partial U_g} \times \mathbf{U}_g \cdot \mathbf{V}_g}{H_g} \quad (7.31)$$



$$M_g = \frac{\frac{\partial \mathbf{U}_g}{\partial V_g} \times \mathbf{U}_g \cdot \mathbf{V}_g}{H_g} \quad (7.32)$$

$$N_g = \frac{\frac{\partial \mathbf{V}_g}{\partial V_g} \times \mathbf{U}_g \cdot \mathbf{V}_g}{H_g} \quad (7.33)$$

Equations (7.31)–(7.33) allow for the calculation of the set of formulas for the calculation of the second fundamental magnitudes at point of the helical gear tooth flank,  $\mathcal{S}$ :

$$L_g = 0 \quad (7.34)$$

$$M_g = 0 \quad (7.35)$$

$$N_g = -U_g \sin \lambda_{b,g} \cos \lambda_{b,g} \quad (7.36)$$

Finally, the equation of the second fundamental form of the tooth flank,  $\mathcal{S}$ , is derived in the form:

$$\Phi_{2,g} \Rightarrow -d\mathbf{r}_g \cdot d\mathbf{N}_g = -U_g \sin \lambda_{b,g} \cos \tau \lambda_{b,g} dV_g^2 \quad (7.37)$$

The discriminant,  $T_g$ , of the second fundamental form,  $\Phi_{2,g}$ , of the gear tooth flank,  $\mathcal{S}$ , equals:

$$T_g = \sqrt{L_g M_g - N_g^2} = 0 \quad (7.38)$$

Equations (7.26) and (7.37) are utilized when solving a wide variety of geometrical problems pertaining to gear design. For example, these equations are used for the calculation of the actual value of the radius,  $R_g$ , of normal curvature of the gear tooth flank,  $\mathcal{S}$ . For this purpose, a simple expression:

$$R_g = \frac{\Phi_{1,g}}{\Phi_{2,g}} \quad (7.39)$$

is used. Many others parameters of local geometry at point of the gear tooth flank can be expressed in terms of the first, and of the second fundamental forms,  $\Phi_{1,g}$  and  $\Phi_{2,g}$ , of the gear tooth surface,  $\mathcal{G}$ .

According to the *Bonnet<sup>5</sup> theorem*, the specification of the first and the second fundamental forms,  $\Phi_{1,g}$  and  $\Phi_{2,g}$ , determines a unique surface  $\mathcal{S}$ , and those two surfaces that have identical first and second fundamental forms must be congruent. Six fundamental magnitudes uniquely specify a surface, except its position and orientation in space.<sup>6</sup> This is often called the *main theorem in surface theory*.

The specification of a gear tooth flank,  $\mathcal{S}$ , by means of a set of six equations for the calculation of fundamental magnitudes of the first,  $\Phi_{1,g}$ , and of the second,  $\Phi_{2,g}$ , order (see Table 7.1) is commonly referred to as the *natural parameterization*, of the gear tooth flank,  $\mathcal{S}$ .

The following statements immediately follow from the analysis of Eq. (7.14):

- The curvature of the involute profile of the gear tooth flank,  $\mathcal{S}$ , at all points at the base cylinder (i.e., at the start points of the screw involute surface) is equal to an infinity, and it is equal to a zero value at infinity

<sup>5</sup> Pierre Ossian Bonnet (November 22, 1819–June 22, 1892), a French mathematician.

<sup>6</sup> It should be borne in mind here that symmetrical surfaces also feature identical fundamental forms.

**TABLE 7.1**  
**Fundamental Magnitudes of a Screw Involute Surface,  $G$**

Of the First Order, $\Phi_{1,g}$	Of the Second Order, $\Phi_{2,g}$
$E_g = 1$	$L_g = 0$
$F_g = -\frac{r_{b,g}}{\cos \lambda_{b,g}}$	$M_g = 0$
$G_g = \frac{U_g^2 \cos^4 \lambda_{b,g} + r_{b,g}^2}{\cos^2 \lambda_{b,g}}$	$N_g = -U_g \sin \lambda_{b,g} \cos \lambda_{b,g}$

- The principal curvatures of the gear tooth flank,  $\mathcal{S}$ , at points within the base helix are equal to  $k_{1,g} \rightarrow \infty$ , and  $k_{2,g} = 0$ , correspondingly
- There are an infinite number of points at which the expressions  $k_{1,g} \rightarrow \infty$  and  $k_{2,g} = 0$  are valid
- At points within the straight generating line,  $\mathcal{E}$ , the first principal curvature of the gear tooth flank,  $V$ , is equal to zero ( $k_{1,g} = 0$ ), whereas the second principal curvature is equal to infinity ( $k_{2,g} \rightarrow \infty$ )
- The straight generating line (i.e., the straight-line element of the involute surface of the gear tooth flank,  $\mathcal{S}$ ) is tangential to the helix on the base cylinder. Normal vectors to the involute surface – those along the straight-line element of the gear tooth flank,  $\mathcal{S}$ , – do not change their orientation; they are located within a common plane

The aforementioned statements are based on the implementation of formulas [see Eqs. (7.23)–(7.25), and Eqs. (7.34)–(7.36)] for the calculation of the fundamental magnitudes of the first order,  $\Phi_{1,g}$ , and second order,  $\Phi_{2,g}$ , of the gear tooth flank,  $\mathcal{S}$ .

### 7.1.2.3 Tooth Flank in Gear with Circular-Arc Teeth in the Lengthwise Direction

A desirable line of contact,  $LC_{\text{circ}}$ , between tooth flanks,  $\mathcal{S}$  and  $\mathcal{P}$ , of a gear and that of a mating pinion can be shaped in the form of a circular arc of a radius,  $R_{lc}$ . The desirable line of contact,  $LC_{\text{circ}}$ , is entirely located within the plane of action,  $PA$ , that rolls with no slippage over the base cylinder of the gear (see Figure 6.22).

The position vector of point,  $\mathbf{r}_g$ , of a gear tooth flank,  $\mathcal{S}$ , with circular-arc teeth in their lengthwise direction can be generated as a locus of consecutive positions of the desirable line of contact,  $LC_{\text{circ}}$ , in its motion (together with the plane of action,  $PA$ ) in relation to a reference system associated with the gear as schematically illustrated in Figure 7.10. In such a scenario, the position vector of point,  $\mathbf{r}_g$ , of a gear tooth flank,  $\mathcal{S}$ , is construed as summa of three vectors:

$$\mathbf{r}_g = \mathbf{A} + \mathbf{B} + \mathbf{C} \quad (7.40)$$

Here, the magnitude  $|\mathbf{A}|$  equals to the base cylinder radius (i.e., the equality  $|\mathbf{A}| = r_{b,g}$  is observed). The vector  $\mathbf{A}$  forms a roll angle,  $V_g$ , with the  $Y_g$  – axis. Magnitude of the vector  $\mathbf{C}$  equals to the radius of the desirable line of contact,  $LC_{\text{circ}}$ ,  $|\mathbf{C}| = R_{lc}$ ;  $U_g$  is the angle that the vector  $\mathbf{C}$  forms with the centerline of the plane of action,  $PA$ , as shown in Figure 7.10; finally, the axial displacement of the center of the circular-arc,  $LC_{\text{circ}}$ , in the rolling motion of the plane of action,  $PA$ , is given by  $|\mathbf{B}| = r_{b,g} \cdot V_g$ , which corresponds to the rotation angle  $V_g$ .

By projecting three vectors,  $\mathbf{A}$ ,  $\mathbf{B}$ , and  $\mathbf{C}$ , onto the axes of the coordinate system,  $X_g Y_g Z_g$ , an expression for the circular-arc involute surface of the gear tooth flank,  $G$ , becomes possible. After rearranging the components and transforming formulas, the equation of the circular-arc involute surface,  $G$ , can be represented in the following matrix form as:



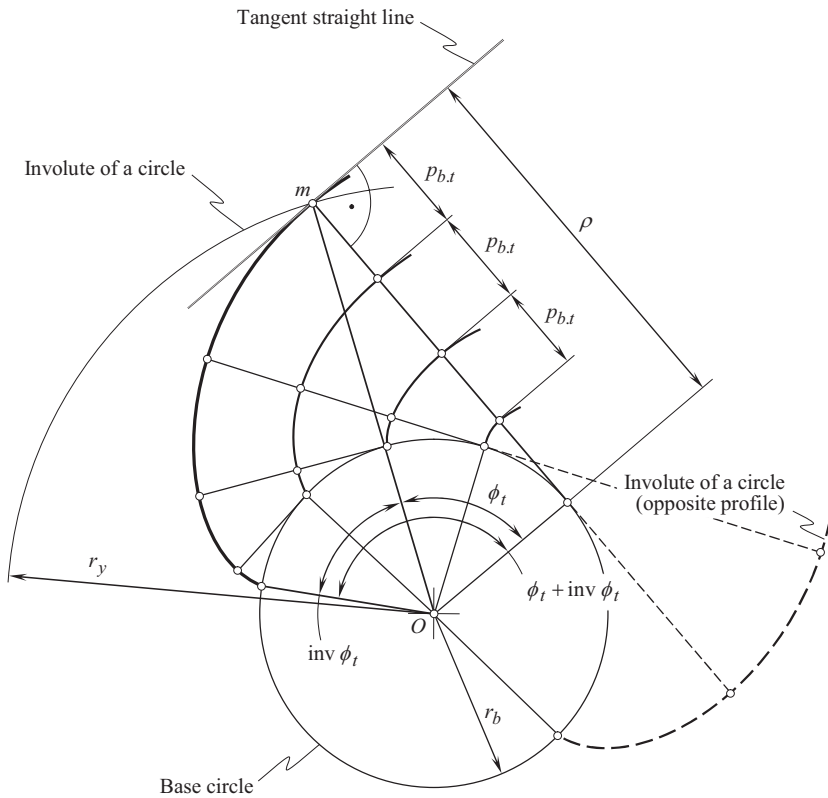


**FIGURE 7.12** Transverse base pitch,  $p_{b,t}$ , in parallel-axes involute gearing.

Prior to proceeding with a discussion on correct and incorrect approaches used to design a gear with a curved tooth shape in the lengthwise direction, it is convenient to explain the concept of *transverse base pitch* in parallel-axes gearing. Figure 7.12 is helpful to illustrate this concept. The distance between two adjacent involute tooth profiles in a section by a transverse plane is specified by the gear *transverse base pitch*,  $p_{b,t}$ . This distance is measured along a common tangent to base cylinder of the gear. Here, in Figure 7.12,  $\rho$  is the radius of curvature at point of interest,  $m$ , of the involute of a circle.

The correct and incorrect approaches used to design a gear with a curved tooth shape in their lengthwise direction are schematically depicted in Figure 7.13.

It should be stressed here that a spur gear can be sliced by a family of planes perpendicular to the gear axis of rotation (namely, by a family of transverse planes), as illustrated in Figure 7.13a. In this scenario, tooth profile for all the slices is the same, and the base pitch in every transverse slice is also of the same value.

If the planes of a family are not perpendicular to the gear axis of rotation but, instead, they have another configuration, the approach under consideration is not suitable for designing gear pairs. For example, a family of radial planes as shown in Figure 7.13b cannot be used for transformation of a spur gear into a gear with a circular arc shape in the lengthwise direction of their teeth. Because the family of planes (see Figure 7.13b) is not perpendicular to the gear axis of rotation, the base pitch in each slice of the gear differs from that in another slice. This consideration reveals that gear pairs with face-milled teeth are inconsistent from a geometrical, as well as from a kinematic standpoint. Under any circumstances, any and all changes to the geometry of the tooth flanks of a gear and of its mating pinion must be *base-pitch preserving* (no exclusion permissible!).

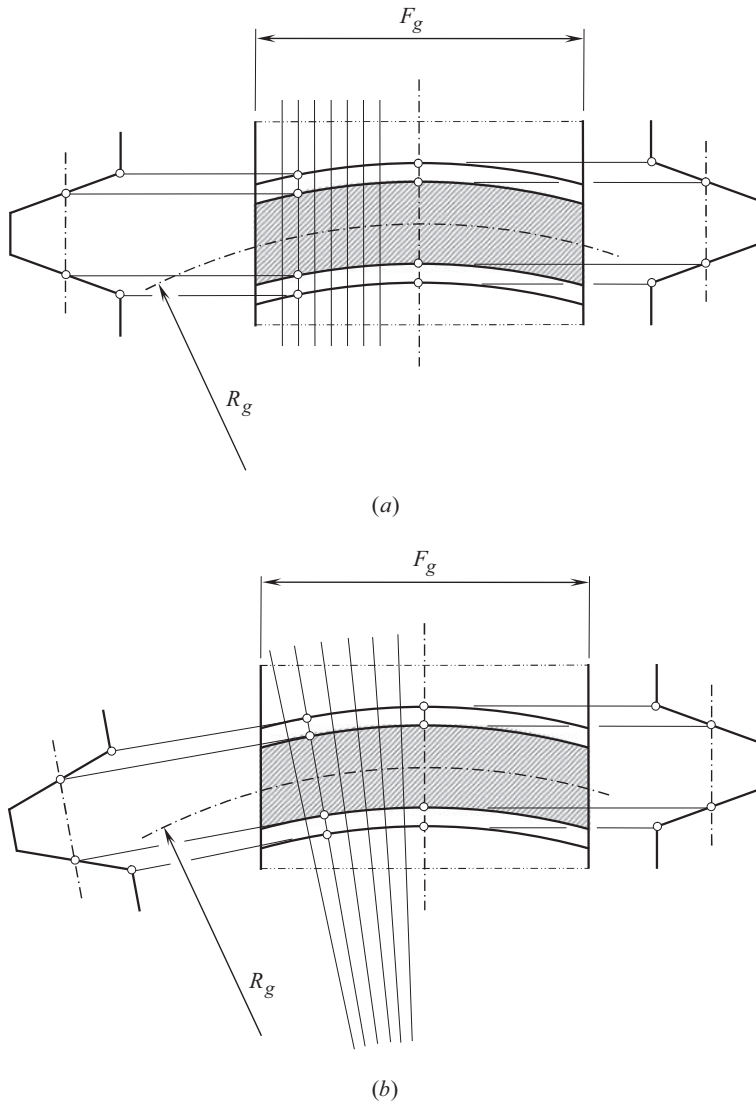


**FIGURE 7.13** Approaches for designing involute gear with curved tooth geometry in their lengthwise direction: (a) correct approach and (b) incorrect approach.

Surfaces of various geometries, that is, surfaces specified by Eqs. (7.12), (7.14), and (7.41) as well as others are used in the design of involute gears for parallel-axes gearing. These surfaces are also used as reference surfaces for gears with modified tooth flanks. Here, the term *modification* should be understood in a wide sense: *It is not just a tooth profile modification, or just a longitudinal modification (crowning) of a gear tooth flank, but it is any predesigned deviation of the actual tooth flank from its nominal geometry, which is desirable for a particular application.* Topological modification of a gear tooth flank is a perfect example in this regard.

In a way similar much to the aforementioned one, an equation for the tooth flank surface can be derived for gear of any and all designs.

It should be stressed here on the following. For the purpose of transmission of rotation between two parallel shafts, a gear and a mating pinion tooth should be shaped in the form of involutes of corresponding base circles/cylinders.

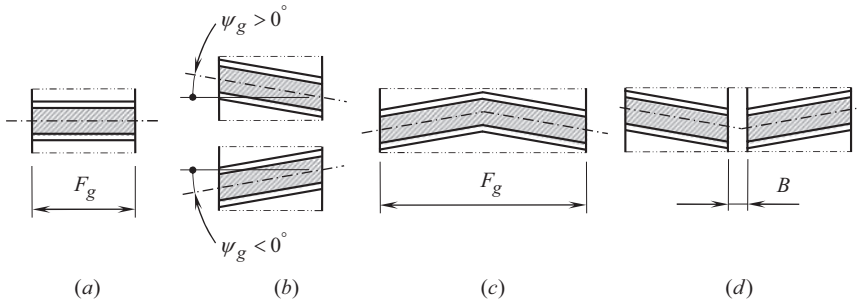


**FIGURE 7.14** Possible forms of gear teeth in their lengthwise direction: (a) spur gear, (b) helical gear, (c) herring-bone gear, and (d) double-helical gear.

### 7.1.3 TOOTH FLANK GEOMETRY IN THE LENGTHWISE DIRECTION OF GEAR TOOTH

Gears can be designed of various tooth forms in the lengthwise direction. Certain requirements should be fulfilled in order to a particular gear tooth form can be permissible, and applicable.

In the simplest case of spur involute gear, the gear teeth are straight and are parallel to the gear axis of rotation, as illustrated in Figure 7.14a. A spur gear can be sliced into an infinite number of infinitesimally thin slices by planes perpendicular to the gear axis (by transverse planes). The base pitch of the gear teeth in each slice is remained of the same value. Because of this, a spur gear can be properly meshed with another spur gear that features the base pitch of that same value.

No alteration to the base pitch of each slice of the gear occurs if the slices are turned angularly with respect to one another through a certain angular increment. Depending on the direction of the turnoff of the slices, the spur gear is transformed into a *helical gear* with either a positive, or negative helix angle. Right-handed ( $\psi_g > 0^\circ$ ), and left-handed ( $\psi_g < 0^\circ$ ), helical gear teeth are shown in Figure 7.14b. In order to balance the axial thrust, two helical gears of opposite hands can be clustered into a *herring-bone gear*, as shown in Figure 7.14c. For manufacturing purposes, a gap of certain width,  $B$ , can be designed between the helical halves of the herring-bone gear. Gears of this design are commonly referred to as *double-helical gears* (see Figure 7.14d).

The concept of transformation of spur gear teeth into helical, or herring-bone, or double-helical gear teeth can be enhanced to crossed-axis gear pairs as well.<sup>7</sup>

No constraints are imposed on the actual value of the shift of the infinitesimally thin slices of a gear, as well as on the equality of the shifts to one another. In the case of different shifts of adjacent slices, a gear with a circular arc shape in the lengthwise direction can be designed. In Figure 7.15, a few possible designs of gear tooth are shown. The circular arc tooth of a radius,  $R_g$ , can be configured either symmetrically (see Figure 7.15a), or asymmetrically. The asymmetry in two opposite directions is possible (see Figure 7.15b and c). The case shown in Figure 7.15b resembles a right-handed helical gear ( $\psi_g > 0^\circ$ ), whereas that shown in Figure 7.15c gear resembles a left-handed helical gear ( $\psi_g < 0^\circ$ ).

<sup>7</sup> In straight bevel gear for an intersected-axis gear pair, the gear tooth profile remains similar (but not identical) in all sections of the gear tooth by a sphere that has its center at the apex of the base cone of the bevel gear. The smaller radius of the spherical section, the smaller the gear tooth size, and vice versa. However, all proportions of the gear tooth do not depend on the radius of the section by a sphere, and all the proportions remain unchanged. This property allows for the slicing of a bevel gear into an infinite number of infinitesimally thin spherical slices and then shifting the slices in relation to one another. Under a corresponding shift increment, the bevel gear with straight teeth is transformed into a bevel gear with skew teeth. Similar to helical gears, bevel gears can be designed with right-handed ( $\psi_g > 0^\circ$ ) or with left-handed ( $\psi_g < 0^\circ$ ) skew teeth. Bevel gears either with herringbone or with double-helical teeth are also possible. That same approach is valid with respect to gears with circular-arc teeth in their lengthwise direction as well as with other reasonable geometries.

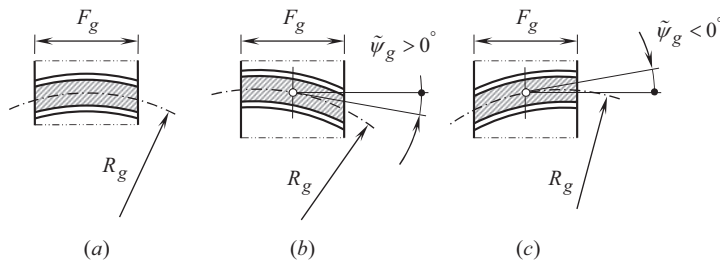


**FIGURE 7.15** Possible forms of gear teeth with a circular arc shape in their lengthwise direction: (a) symmetric, (b) asymmetric, left-shifted, and (c) asymmetric, right-shifted.

A term *line of gear tooth* can be implemented to differentiate possible forms of gear teeth in their lengthwise direction: *straight zero-inclined* (see Figure 7.14a), *straight positively inclined* (see Figure 7.14b – upper image), *straight negatively inclined* (see Figure 7.14b – lower image), *straight double-inclined* (see Figure 7.14c), *straight double-inclined separated* (see Figure 7.14d), *circular-arc zero-inclined* (see Figure 7.15a), *circular-arc positively inclined* (see Figure 7.15b), *circular-arc negatively inclined* (see Figure 7.15c), and so forth. As it follows from the listed schematics (see Figures 7.15a–7.15c), the *line of gear tooth* (or the *gear tooth line*, in other words) is a line considered in the unfolded onto a plane the pitch surface of the gear. The *gear tooth line* is equidistant to the lines of intersection of the opposite tooth flanks of the gear tooth.

Not only spur, or helical, or circular arc gear teeth in their lengthwise direction can be designed in this way. The combination of either a straight motion with a rotation, or of two rotations, makes possible designing gears with the following gear teeth geometries in the lengthwise direction: cycloid, epicycloid, hypocycloid, trochoid, epitrochoid, hypotrochoid,<sup>8</sup> and involute of a circle. Parallel-axes gear pairs and intersected-axis gear pairs, as well as crossed-axis gear pairs, can be designed this way.

Making changes to the design parameters of the auxiliary rack (to *basic rack*, in other terminology) is the easiest way to design gears with teeth curved in their lengthwise direction. Once the auxiliary rack is designed, the teeth of the gear, and that of the mating pinion, can be generated as envelopes to corresponding families of a consecutive position of the auxiliary rack (either a straight rack, or a round rack) in its motion in relation to a reference system associated either with the gear or with the pinion.

### 7.1.4 ADOPTED GEAR TERMINOLOGY

The terminology commonly adapted to the elements that make up a tooth profile (in the transverse section of parallel-axes gearing), is illustrated in Figure 7.16. Commonly (but not necessarily), the gear teeth are disposed partly above and partly below the pitch line. The complement profile is made up of the following:

- The *crest*, which is what, is remains of the original outer surface of the *blank* in which the teeth are cut
- The *flanks*, which can loosely be described as the part of the profile, are formed either by involute or by another specified curve. The opposed flanks are, for a given direction of drive, *leading flank* and *trailing flank*, correspondingly
- The *root curve*, which joins the facing flanks at the bottom of the tooth space
- The *tips* are the junctions between the crests and flanks and lie in the *tip circle*, whence *tip diameter*

<sup>8</sup> Extended cycloids (hypocycloid and hypo-trochoid) are also referred to as *prolate cycloids*. The term *curtate trochoid* is often applied to epicycloids and epitrochoids.



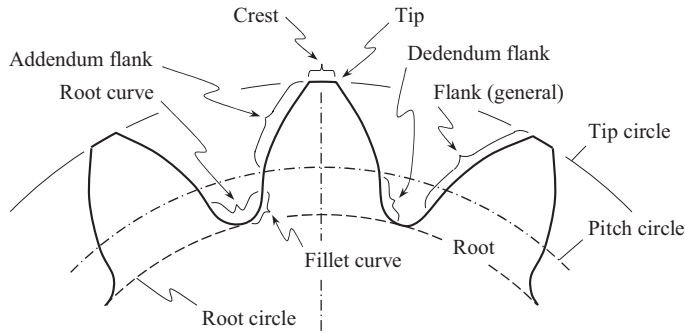


**FIGURE 7.16** Tooth profile elements. (Adapted from: Merrit, H.E., 1971, *Gear Engineering*, London: Putman Publishers.)

- The terms *addendum* and *dedendum* are used descriptively to refer to those portions of the flank that lie outside, and inside the pitch circle, respectively, in a phrase such as “pitted over the dedendum.” They can also mean, dimensionally, the radial distance of the crest above the pitch circle, and the radial distance of the bottom of the tooth space below the pitch circle, correspondingly
- The *active profile* is the portion of the flank profile that makes contact with the profile of a particular mating gear
- The flanks, described more particularly, have a *nominal profile* defined by the geometrical basis of the tooth design, for example, involute, cycloid, circular-arc, and others. The active profile may, as designed, depart from the nominal profile by the application of *tip-easing* or *profile modification*
- The *fillet curve* is the curve that is the prolongation of the flank down to the root. It is of complex form and depends on the form of the cutting or finishing tools
- The *root* is a term that sometimes means the combined fillet curves that outline the bottom of a tooth space, as in the phrases “pre-formed roots” (produced by a separate operation) and “black roots” left untouched during a profile-grinding operation. But when discussing the strength of gear teeth, it means the material of a tooth where it joins the body of the gear
- *Tip radius* is, obviously enough, a radius replacing an otherwise sharp-cornered tip, as applied to a rack cutter or hob
- *Tip chamfer* is a chamfer applied to the tip of a tooth, while the tooth is being cut, in order to prevent a burr from being formed during a subsequent shaving operation

The disposition of the addendum and dedendum relative to the pitch circle may be varied. This has long been and is still widely termed *correction*. *Addendum modification* and *profile shift* are other terminologies in this regard.

Lengthwise tooth elements are depicted in Figure 7.17.

- The *face* of a tooth, as a descriptive term, indicates the whole length of the tooth surface, as in the phrase “pitted across the entire face”
- The *face width* is the length of the teeth as seen in an axial section. In workshop parlance, it is sometimes shortened to *face*, when abbreviating the specified particulars of a gear to, for example, “10 teeth, 4 pitch, 2 in. face”
- The ends of teeth may be finished with an *end radius*, or *end chamfer*. If they slide axially into engagement, *tooth-rounding*, or *tooth-chamfering* is applied

In a spur gear, the nominal tooth surface can be regarded as swept out by a specified profile moved axially. The line of intersection of the profile with the pitch cylinder is referred to, descriptively, as



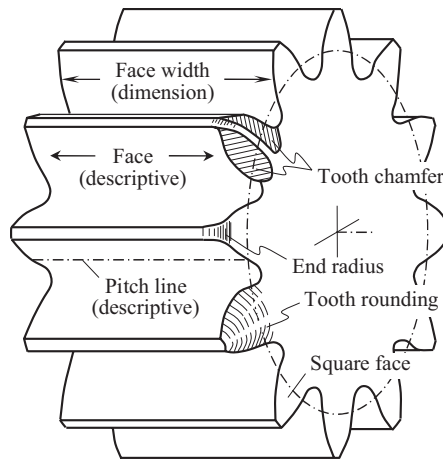


**FIGURE 7.17** Lengthwise tooth elements of spur gear. (Adapted from: Merrit, H.E., 1971, *Gear Engineering*, London: Putman Publishers.)

the *pitch line*. In actual manufacture, this straight line may be departed from deliberately, by *crowning*. An accidental departure is a *tooth alignment error*.

In a helical gear, the tooth surface is swept out by a specified profile moved along a helical path. The intersection of the flank with the pitch cylinder is commonly referred to as the *tooth helix*. Deliberate departure from this helix is described as *crowning* in automotive-type gears, and as *helix modification* in large, for example, marine turbine reduction gearing.

In spiral bevel gears, the term corresponding to tooth helix is *tooth spiral*, and corresponding to *combined deliberate departure*, in a mating pair, is *mismatch*.

In the *British Standard Glossary*, the geometrical curve that defines the lengthwise configuration of a tooth on the pitch surface has been named the *tooth trace*. It is a logical omnibus term covering the straight line of spur gears, the helix of helical gears, and the arbitrary curve in spiral bevel gears; but it has not yet become part of general drawing office and workshop vocabulary.

Two methods of generation of the involute profile of a gear tooth are considered. According to the first method, an involute tooth profile is traced by a point within a straight line when the line is rolling with no sliding over base circle of the gear (see Figure 7.3). In the second method, an involute tooth profile is generated as an envelope to a family of consecutive positions of a straight line that is associated with the pitch line when the pitch line is rolling with no sliding over the pitch circle of the gear. Both methods are used in practice. However, the second method is preferred, which is chiefly due to manufacturing issues. Gear cutting tools of most practical designs are designed on the premises of the generating rack [82].

## 7.2 ALTERNATIVE APPROACH FOR DERIVATION OF EQUATION OF INVOLUTE TOOTH FLANK

An alternative approach for the derivation of an equation of the involute gear tooth profile can be used. The relative motion of a straight line (of an auxiliary rack tooth profile) that is tangent to the involute profile at certain point is utilized in this method. For better understanding of the approach, a schematic shown in Figure 7.3 is helpful.

### 7.2.1 GENERATION OF SPUR GEAR TOOTH PROFILE BY MEANS OF STRAIGHT LINE

Consider a base circle of a radius,  $r_{b,g}$ , centering at the point  $O_g$ , as shown in Figure 7.18. Point,  $P$ , is chosen at a distance,  $r_g$ , from the center,  $O_g$ . The distance,  $r_g$ , is greater than the radius,  $r_{b,g}$ , of the

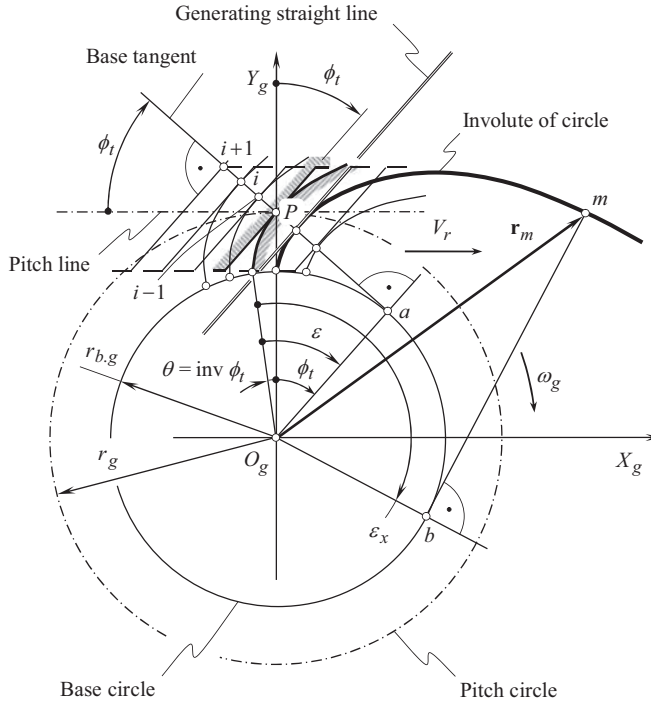


**FIGURE 7.18** Generation of the involute profile of an involute gear tooth by straight line.

base circle (i.e., the inequality  $r_g \geq r_{b.g}$  is valid). The equality of the radii  $r_g = r_{b.g}$  can be observed only in a reduced case.

The circle of the radius,  $r_g$ , that centers at the point  $O_g$ , is referred to as the *pitch circle*. A straight line that is tangent to the pitch circle is referred to as the *pitch line*. The pitch line is drawn up passing through the point,  $P$ . Thus,  $P$  is referred to as the *pitch point*.

At the pitch point,  $P$ , the base tangent and the pitch line form certain angle,  $\phi_t$ . The angle,  $\phi_t$ , is referred to as the *profile angle* of the involute curve when solely involute of a circle is considered. The angle,  $\phi_t$ , is referred to as the *pressure angle* when two conjugate profiles are considered.

When the pitch line rolls with no slippage over the pitch circle, the motion of the straight line in relation to the pitch circle can be viewed as superposition of two motions. The straight motion of the pitch line with a linear velocity,  $V_r$ , is one of these two motions. The rotation,  $\omega_g$ , of the pitch circle is the second motion. The linear velocity,  $V_r$ , of the translation and the rotation,  $\omega_g$ , are synchronized with one another so as to meet the requirement of rolling with no slippage. The requirement of rolling with no slippage is expressed analytically as:

$$\frac{V_r}{\omega_g} = r_g \quad (7.42)$$

When the gear rotates, and when the pitch line rolls with no slippage over the pitch circle, the straight line travels straight together with the pitch line. The motion of the straight line together with the pitch line is equivalent to the motion of the contact point along the base tangent, that is, it is equivalent to the motion along the line of action,  $LA$ , as it follows from the analysis of Figure 7.18. As the angle that the straight lines form with the perpendicular to the pitch line, is of a constant value,  $\phi_t$ , the straight line is further referred to as the *generating straight line*. This property of the generating straight line is employed below with the aim to generate an involute tooth profile.

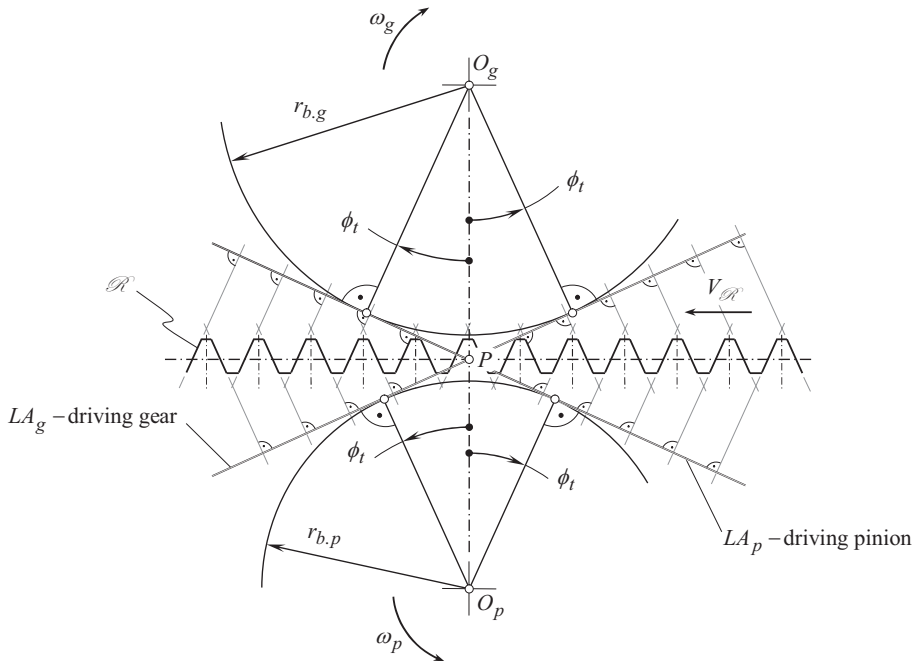


**FIGURE 7.19** Configuration of the auxiliary generating rack,  $\mathcal{R}$  (the basic rack,  $\mathcal{R}$ ), in relation to a gear and its mating pinion.

The generating straight line travels together with the pitch line as these two straight lines are rigidly connected to each other. When traveling, the generating straight line occupies numerous consecutive positions in relation to the pitch circle. At every configuration of the generating straight line, the profile angle,  $\phi_t$ , retains that same value. The involute tooth profile can be interpreted as an envelope to a family of consecutive positions of the generating straight line in its motion in relation to the pitch circle. The possibility of generating an involute of a circle as an envelope to a family of consecutive positions of generating straight line is illustrated below.

Several points,  $i$ , can be chosen within the generating line (base tangent), as it is depicted in Figure 7.18 (here  $i$  is an integer number). When the generating line rolls over the base circle of a radius  $r_{b,g}$ , each point traces a corresponding involute of the circle. All the involutes are offset with respect to one another, or, in other words, the involutes are parallel to each other. The angle that the generating straight line (base tangent) forms with the rolling pitch line is of the same value in all the positions of the generating line. This angle equals to  $(90^\circ - \phi_t)$ , where  $\phi_t$  is the profile angle of the involute curve at the pitch point,  $P$ .

The discussed straight lines (see Figure 7.18), constructed for the opposite sides of a gear tooth, form the *auxiliary generating rack*,  $\mathcal{R}$  (or, in other words, they form the *basic rack*,  $\mathcal{R}$ ). The configuration of the auxiliary generating rack,  $\mathcal{R}$ , in relation to a gear and its mating pinion is shown in Figure 7.19. When the gears rotate, the straight-sided generating rack,  $\mathcal{R}$ , travels straight with a linear velocity,  $V_R$ . The linear velocity,  $V_R$ , is timed with the rotations,  $\omega_g$  and  $\omega_p$ , of the gear and the pinion, correspondingly.

**Asymmetric gears.** Gear teeth for parallel-axes gearing can be generated by a straight-sided generating rack,  $\mathcal{R}$ , with asymmetric tooth profile. In such a scenario, a gear with a corresponding asymmetric tooth profile is generated. It is well-known that the opposite gear tooth flanks are functionally different for the majority of gear drives, where the load and duration of its application are much greater for one tooth flank than for the opposite one. Such gear drives are often called *unidirectional gear drives*. It makes sense to consider



**FIGURE 7.20** Unidirectional parallel-axes gear pair with asymmetric tooth profile of the mating gears.

the possibility of application of gears with asymmetric tooth profile (see Figure 7.20) in gearsets of this particular design. The geometry and design of gears with asymmetric tooth profiles are considered in [57].

The performed descriptive analysis can be complemented by an analytical proof of the possibility of generation of an involute of a circle by means of the moving straight generating line (by the base tangent) when the straight line is associated with the pitch line. The use of the kinematic method for the determination of an involute profile as an envelope to a family of the consecutive position of a moving straight line is helpful for this purpose.

An important mean of the kinematic method is *Shishkov equation of contact*:

$$\mathbf{n}_g \cdot \mathbf{V}_\Sigma = 0 \quad (7.43)$$

In Eq. (7.43), the common perpendicular to the contacting profiles is designated as  $\mathbf{n}_g$ , and the vector of linear velocity of the resultant relative motion of the moving curves is denoted by  $\mathbf{V}_\Sigma$ .

Originally proposed by *Franz Reuleaux* in the second half of the nineteenth century [189], the kinematic method for the determination of enveloping curves and surfaces was significantly contributed by Prof. *Shishkov*, V.A. in the late 1940s, and at the beginning of the 1950s [197,198]. *Shishkov equation of contact*,  $\mathbf{n}_g \cdot \mathbf{V}_\Sigma = 0$ , is the principal contribution by Prof. *Shishkov*, V.A. to the kinematic method. It is preferred to use *Shishkov equation of contact*,  $\mathbf{n}_g \cdot \mathbf{V}_\Sigma = 0$  in cases when both:

- a. the unit common perpendicular,  $\mathbf{n}_g$ , as well as
- b. the linear velocity vector,  $\mathbf{V}_\Sigma$ , of the resultant relative motion,

can be determined with no use of derivatives of the equation of the moving curve with respect to the parameter, which specifies a point within the curve (when the vector,  $\mathbf{n}_g$ , is determining), and with respect to the parameter of motion (when the linear velocity vector,  $\mathbf{V}_\Sigma$ , is determining).

Consider a given involute profile associated with the base circle of a radius  $r_{b,g}$ , as depicted in Figure 7.18. An equation of a profile that is associated with the pitch line when the pitch line rolls with no slippage over the pitch circle of a radius  $r_g$ , is required to be derived.

Referring to Figure 7.18, the position vector of point,  $\mathbf{r}_m$ , of the involute profile can be described by an equation in vector representation:

$$\mathbf{r}_m(\varepsilon_x) = \mathbf{i} \cdot r_{b,g} [\sin(\varepsilon_x - \theta) - \varepsilon_x \cos(\varepsilon_x - \theta)] + \mathbf{j} \cdot r_{b,g} [\cos(\varepsilon_x - \theta) + \varepsilon_x \sin(\varepsilon_x - \theta)] \quad (7.44)$$

or in a form of column matrix:

$$\mathbf{r}_m(\varepsilon_x) = r_{b,g} \cdot \begin{bmatrix} \sin(\varepsilon_x - \theta) - \varepsilon_x \cos(\varepsilon_x - \theta) \\ \cos(\varepsilon_x - \theta) + \varepsilon_x \sin(\varepsilon_x - \theta) \\ 0 \\ 1 \end{bmatrix} \quad (7.45)$$

The parameter,  $\varepsilon_x$ , of the involute curve is shown in Figure 7.18.

When the pitch line rolls with no slippage over the pitch circle, the involute curve occupies various positions in relation to the pitch line. To specify a point within the involute curve in its current configuration with respect to the pitch line, it is convenient to compose the operator  $\mathbf{Rs}(g \mapsto r)$  of the resultant coordinate system transformation. In the particular case under consideration, the operator  $\mathbf{Rs}(g \mapsto r)$  can be represented in the form:

$$\mathbf{Rs}(g \mapsto r) = \begin{bmatrix} -\sin \vartheta & \cos \vartheta & 0 & r_g \vartheta \\ \cos \vartheta & \sin \vartheta & 0 & -r_g \vartheta \\ 0 & 0 & 1 & 0 \\ 0 & 0 & 0 & 1 \end{bmatrix} \quad (7.46)$$

In Eq. (7.46), the angular configuration of the involute curve in its current location with respect to the initial location is specified by the  $\vartheta$ .

It should be stressed here that as long as a two-dimensional problem is considered, the third row and the third column in Eq. (7.46) can be eliminated. In this way, the  $4 \times 4$  matrix [see Eq. (7.46)] can be reduced to a corresponding  $3 \times 3$  matrix. The operator of the resultant coordinate system transformation,  $\mathbf{Rs}(g \mapsto r)$ , is written in the form of  $4 \times 4$  matrix solely with the goal to maintain the uniform style of the coordinate system transformations for two-dimensional cases as well as for three-dimensional (spatial) cases of gear pairs throughout the entire book.

For the calculation of the position vector of point,  $\mathbf{r}_m^r$ , within the involute curve in its current configuration with respect to the pitch line, an expression:

$$\mathbf{r}_m^r(\varepsilon_x, \vartheta) = \mathbf{Rs}(g \mapsto r) \cdot \mathbf{r}_m(\varepsilon_x) \quad (7.47)$$

is used.

Points that are specified by position vector  $\mathbf{r}_m^r$ , include points of the enveloping profile to be determined. The position vector of point of the enveloping profile fulfills both, namely, they fulfill Eq. (7.47), as well as they fulfill the equation of contact,  $\mathbf{n}_g \cdot \mathbf{V}_\Sigma = 0$ . The latter equation is used to eliminate the parameter  $\vartheta$  from Eq. (7.47).

Consider an arbitrary tooth profile,  $\mathcal{S}$ , associated with a reference system,  $X_g Y_g$ , as shown in Figure 7.21. In a coordinate system  $X_g Y_g$ , associated with pitch circle, the unit normal vector,  $\mathbf{n}_g$ , at a point of the tooth profile,  $\mathcal{S}$ , can be described by the following equation:

$$\mathbf{n}_g = \mathbf{i} \cdot \tan(\phi_{t,x} + \vartheta) - \mathbf{j} \quad (7.48)$$

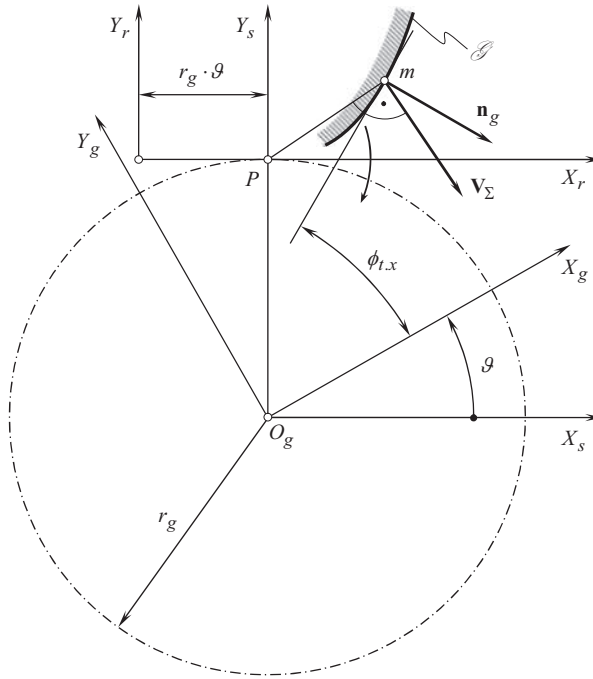


FIGURE 7.21 Derivation of equation of tooth flank,  $\mathcal{S}$ , of a spur involute gear.

The instantaneous motion of point of interest,  $m$ , within the tooth profile,  $\mathcal{S}$ , is the instantaneous rotation about the pitch point,  $P$ . This immediately yields for an expression for the unit vector,  $\mathbf{v}_\Sigma$ , that is pointe along the vector of linear velocity,  $\mathbf{V}_\Sigma$ , of the resultant relative motion:

$$\mathbf{v}_\Sigma = \mathbf{i} \cdot X_m - \mathbf{j} \cdot Y_m \quad (7.49)$$

In Eq. (7.49),  $X_m$  and  $Y_m$  designate the coordinates of point of interest,  $m$ .

Transition from the coordinate system,  $X_g Y_g$ , associated with pitch circle, to the coordinate system,  $X_r Y_r$ , embedded to the pitch line, is analytically expressed by the operator,  $\mathbf{R}_s(g \mapsto r)$ , of the resultant coordinate system transformation [see Eq. (7.46)].

According to [190], the *Shishkov equation of contact*,  $\mathbf{n}_g \cdot \mathbf{V}_\Sigma = 0$ , in a case of parallel-axes gearing, can be represented in the form:

$$\sin(\phi_{t,x} + \vartheta) = \frac{X_g \cos \phi_{t,x} + Y_g \sin \phi_{t,x}}{r_g} \quad (7.50)$$

In a particular case of the involute tooth profile, the equality  $\phi_{t,x} = 90^\circ - (\varepsilon_x - \theta)$  is valid. This expression, considered together with the equation of the involute profile [see Eq. (7.44)], yields a reduction of the equation of contact in the form of Eq. (7.50) as:

$$\sin(\phi_{t,x} + \vartheta) = \frac{r_{b,g}}{r_g} = \cos \phi_t \quad (7.51)$$

[Derived for an *arbitrary* gear tooth profile, Eq. (7.50), unfortunately is valid only for *involute* gear tooth profile, as for gear tooth profiles of other geometries the conjugate action law is violated].

The latter expression immediately returns a formula:

$$\vartheta = \varepsilon_x - \varepsilon_0 = \tan \phi_{t,x} - \tan \phi_t \quad (7.52)$$

for the calculation of the parameter  $\vartheta$ .

Considered together, the derived equation for the calculation of the angle,  $\vartheta$ , and Eq. (7.47), yields for the expression for the position vector of point of the envelope:

$$\mathbf{r}_m^r(Y_r) = \mathbf{i} \cdot Y_r \cot \phi_t + \mathbf{j} \cdot Y_r \quad (7.53)$$

or in matrix representation:

$$\mathbf{r}_m^r(Y_r) = \begin{bmatrix} Y_r \cot \phi_t \\ Y_r \\ 0 \\ 1 \end{bmatrix} \quad (7.54)$$

Formally, the position vector of point,  $\mathbf{r}_m^r$ , of the enveloping profile is a function of the rotation angle,  $\varepsilon_x$ . However, the right side in Eq. (7.53) does not depend on  $\varepsilon_x$ . This reveals that rolling of the generating line (of the base tangent) over the **base circle**, and rolling of the pitch line over the **pitch circle**, are equivalent to one another. Ultimately, an involute profile can be generated by a straight line at a constant angle with respect to the pitch line which it is associated with.<sup>9</sup>

### 7.2.2 GENERATING AUXILIARY RACK (BASIC RACK) IN SPUR GEAR

Generating auxiliary rack in a spur gear can be constructed using the straight tooth profile that is specified by Eqs. (7.53) and (7.54).

Auxiliary rack,  $\mathcal{R}$ , of a spur gear (a generating rack,  $\mathcal{R}$ ), is developed on the premise of the generating straight line (base tangent) [see Eq. (7.53)]. The generating rack,  $\mathcal{R}$ , is shaped in the form, shown in Figure 7.22, and it is conjugate to the gear tooth profile.

The transverse profile angle,  $\phi_t$ , of the generating rack tooth is equal to the profile angle of the gear tooth measured on the pitch diameter. In the most of standards issued in the industrially developed countries, the specified profile angle equals to  $\phi_t = 20^\circ$ . Gears that have profile angle of  $\phi_t = 14^\circ$  are used in the design of low noise transmissions. Gears that have profile angle  $\phi_t = 28^\circ$  are used in the design of heavily loaded gear trains. Gears with profile angle of other values are used as well.

It is common practice to specify the auxiliary generating rack,  $\mathcal{R}$ , either in terms of module,  $m$ , or in terms of diametral pitch,  $P$ , of the generating rack.<sup>10</sup> For the calculation of the rest of the design parameters of the auxiliary rack (see Figure 7.22a), standard formulas are used. These formulas are summarized in Table 7.2.

The formula  $m = 25.4 / P$  is commonly used for the purpose of conversion of diametral pitch,  $P$ , to module,<sup>11</sup>  $m$ .

The specified width,  $F_{pa}$ , of a generating rack (see Figure 7.22b) equals to the overlap of a gear face width,  $F_g$ , and a corresponding pinion face width,  $F_p$ .

<sup>9</sup> This conclusion is valid only for parallel-axes gearing, and is not valid for intersected-axes, as well as for crossed-axes gearing. A crown rack with a straight-sided tooth profile for intersected-axes gearing, and crossed-axes gearing is not more than a kind of approximation.

<sup>10</sup> Both, module  $m$ , as well as diametral pitch  $P$ , by nature, are artificially introduced scale factors. Another approach is proposed by Prof. *E.B. Vulgakov*. According to Prof. *E.B. Vulgakov* [216], the base diameter,  $d_b$ , is used as a scale factor in gearing (instead of either module,  $m$ , or diametral pitch,  $P$ ). Evidently, if either module,  $m$ , or diametral pitch,  $P$ , or base diameter,  $d_b$ , is known, the rest of them can be easily expressed in terms of the known one.

<sup>11</sup> Curiously, module and diametral pitch are size dimensions which cannot be directly measured on a gear. They are really reference values used to calculate other size dimensions which are measurable.

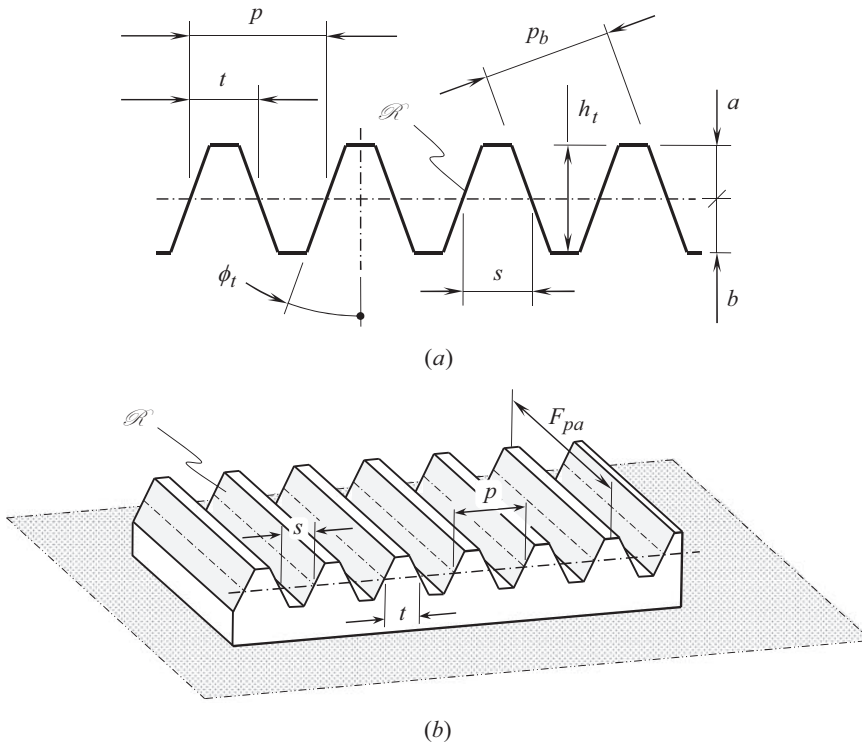


**FIGURE 7.22** Generating rack,  $\mathcal{R}$ , of spur involute gear: (a) the rack profile, and (b) 3D schematic of the rack.

**TABLE 7.2**  
**Design Parameters of Spur Generating Rack**

Design Parameter of the Rack	Metric	English
Normal Pitch (mm)	$p = \pi \cdot m$	$p = \frac{\pi}{P}$
Base Pitch (mm)	$p_b = \pi \cdot m \cdot \cos \phi$	$p_b = \frac{\pi}{P} \cdot \cos \phi$
Addendum (mm)	$a = m$	$a = \frac{1}{P}$
Dedendum <sup>a</sup> (mm)	$b = 1.25m$	$b = \frac{1.25}{P}$
Tooth Height (mm)	$h_t = a + b = 2.25m$	$h_t = \frac{2.25}{P}$
Tooth Thickness (mm)	$t = \frac{\pi m}{2}$	$t = \frac{\pi}{2P}$
Space Width (mm)	$s = \frac{\pi m}{2}$	$s = \frac{\pi}{2P}$

<sup>a</sup> For the calculation of dedendum  $b$  of a small module gear (of a fine pitch gear) the formula  $b = 1.35m$  (or the equivalent formula  $b = \frac{1.35}{P}$ ) is often used.



The auxiliary generating rack profile is *fundamental* to the specification of involute gears. The tooth profile on the gear, the generating rack profile, and the associate rack by means of which gear cutting tools are shaped, can all be determined in terms of the auxiliary generating rack. The relationship between these is discussed below.

As with a standard rack profile, the tooth thickness is equal to the tooth space width at the profile datum line and hence to half the pitch. Therefore, a gear and a mating pinion can be cut with the same gear cutting tool.

The entire dimensions for defining the auxiliary generating rack profile must be contained in the tooth data.

*The auxiliary generating rack profile can be viewed as the normal section through the teeth of a basic rack, which corresponds to a gear with number of teeth  $N_g \rightarrow \infty$ , and, thus, of pitch diameter  $d_g \rightarrow \infty$ .*

### 7.2.3 ALTERNATIVE APPROACH FOR DERIVATION OF EQUATION OF HELICAL INVOLUTE GEAR TOOTH FLANK

The discussed approach for the generation of the tooth flank in a spur involute gear by means of plane that is tangent to the base cylinder can be enhanced to generation of tooth flank in a helical gear. In the alternative approach for the derivation of equation of a helical involute gear tooth flank, the tooth flank is generated as an envelope to a family of consecutive positions of a plane that performs a screw motion about the gear axis of rotation.

A gear tooth flank,  $\mathcal{F}$ , can be generated by a plane,<sup>12</sup>  $\mathcal{R}$ , that performs a screw motion about the gear axis. The plane,  $\mathcal{R}$ , forms an angle with the gear axis of rotation,  $O_g$ . This angle can be specified in terms of the gear transverse profile angle,  $\phi_t$ , and of the plane inclination angle,  $\psi_r$ . It is proven that the angle that the plane,  $\mathcal{R}$ , forms with the gear axis of rotation,  $O_g$ , is equal to the base helix angle,  $\psi_{b,g}$ , of the gear. The angle,  $\psi_{b,g}$ , can be calculated from the formula [146]:

$$\psi_{b,g} = \cos^{-1}(\cos \phi_t \cdot \sin \psi_r) \quad (7.55)$$

The expression [see below Eq. (7.90)] can be represented in the form:

$$\psi_{b,g} = \cot^{-1} \left( \frac{\cos \phi_t}{\sqrt{\sin^2 \phi_t + \cot^2 \psi_r}} \right) \quad (7.56)$$

that is known from other sources, and that can be convenient in certain applications.

Once the angle between the lateral plane of the rack,  $\mathcal{R}$ , and between the gear axis of rotation,  $O_g$ , is known, the tooth flank of a helical gear can be determined.

Consider a plane,  $\mathcal{R}$ , that is performing a screw motion, as shown in Figure 7.23. The plane,  $\mathcal{R}$ , forms a certain angle,  $\psi_{b,g}$ , with  $X_0$  – axis of a *Cartesian* coordinate system  $X_0Y_0Z_0$ . The reduced pitch,  $p$ , of the screw motion is given. The axis  $X_0$  is the axis of the screw motion.

The auxiliary coordinate system  $X_1Y_1$  is rigidly associated with the plane,  $\mathcal{R}$ .

The equation of the plane  $\mathcal{R}$  can be represented in the form:

$$Y_1 = X_1 \cdot \tan \psi_{b,g} \quad (7.57)$$

The auxiliary *Cartesian* coordinate system  $X_1Y_1Z_1$  performs a screw motion together with the plane,  $\mathcal{R}$ , in relation to the motionless coordinate system  $X_0Y_0Z_0$ . In the coordinate system  $X_1Y_1Z_1$ , the unit normal vector,  $\mathbf{n}_r$ , to the plane,  $\mathcal{R}$ , can be analytically expressed as:

<sup>12</sup> This statement is valid only for parallel-axes gearing and is not valid in intersected-axes gearing, as well as in crossed-axes gearings. A crown rack with a straight-sided tooth profile in intersected-axes gearing, and in crossed-axes gearing, is a kind of approximation, and cannot be used for generation of tooth flanks in geometrically-accurate gearings.

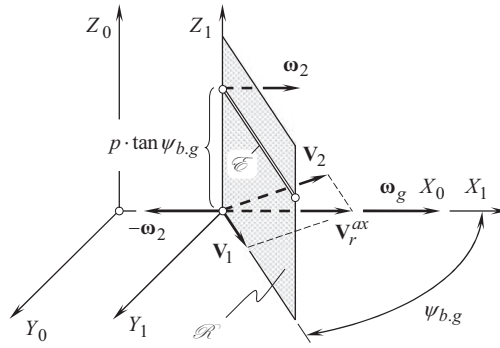


**FIGURE 7.23** Generation of screw involute surface,  $\mathcal{S}$ , as an envelope to a family of consecutive positions of lateral plane of generating rack,  $\mathcal{R}$ , that performs a screw motion.

$$\mathbf{n}_r = \begin{bmatrix} 1 \\ -\tan \psi_{b.g} \\ 0 \\ 1 \end{bmatrix} \quad (7.58)$$

The position vector,  $\mathbf{r}_r$ , of point  $m$  within the plane,  $\mathcal{R}$ , can be expressed by:

$$\mathbf{r}_r = \begin{bmatrix} X_r \\ Y_r \\ Z_r \\ 1 \end{bmatrix} \quad (7.59)$$

where  $X_r$ ,  $Y_r$ , and  $Z_r$  are the *Cartesian* coordinates of a point of the plane,  $\mathcal{R}$ .

The resultant velocity of the point of interest,  $m$ , in the screw motion of the plane,  $\mathcal{R}$ , can be analytically expressed by the vector  $\mathbf{v}_m$ :

$$\mathbf{v}_m = \mathbf{v} + [\omega_g \times \mathbf{R}] \quad (7.60)$$

where:

$\mathbf{v}$  is the linear velocity vector of the translation

$\omega_g$  is the angular velocity of the rotation

$\mathbf{R}$  is the position vector of point of interest,  $m$ , with respect to the axis of the screw motion (magnitude of the vector  $\mathbf{R}$  equals to the distance of point,  $m$ , from the  $X_0$  - axis, and the vector,  $\mathbf{R}$ , is pointed from the axis  $X_0$  to point  $m$ )

The envelope surface to consecutive positions of the plane,  $\mathcal{R}$ , in its screw motion is identical to the surface that is represented by the locus of consecutive positions of the characteristic line,  $\mathcal{S}$ , that performs that same screw motion, as the plane does. The derivation of an equation of the envelope surface,  $\mathcal{S}$ , to consecutive positions of the plane,  $\mathcal{R}$ , can be significantly simplified if rather than the screw motion of the plane,  $\mathcal{R}$ , being considered, but the screw motion of the characteristic line,  $\mathcal{S}$ , is considered instead.

The direction of the unit vector  $\mathbf{v}_m$  is of importance for the determination of the characteristic line,  $\mathcal{S}$ , while the magnitude of the vector  $\mathbf{v}_m$  is not of interest in this particular analysis. Because of this, it can be assumed that the magnitude of the rotation vector,  $\omega_g$ , is equal  $|\omega_g| = 1$ . Therefore:<sup>13</sup>

<sup>13</sup> In reality, the value of the reduced pitch,  $p$ , is given. In this way, the ratio  $|\mathbf{v}|/|\omega| = p$  is specified.

$$\omega_g = \mathbf{i}, \quad (7.61)$$

$$\mathbf{v} = \mathbf{i} \cdot p \quad (7.62)$$

These yields:

$$\mathbf{v}_m = \mathbf{i} \cdot p + \begin{vmatrix} \mathbf{i} & \mathbf{j} & \mathbf{k} \\ 1 & 0 & 0 \\ X_1 & Y_1 & Z_1 \end{vmatrix} \quad (7.63)$$

and

$$\mathbf{v}_m = \mathbf{i} \cdot p - \mathbf{j} \cdot Y_1 + \mathbf{k} \cdot Z_1 \quad (7.64)$$

At any point within the characteristic line,  $\mathcal{E}$ , dot product of the unit normal vector,  $\mathbf{n}_r$ , and of the linear velocity vector,  $\mathbf{v}_m$ , equals:

$$\mathbf{n}_r \cdot \mathbf{v}_m = p \cdot \tan \psi_{b,g} - Z_1 = 0 \quad (7.65)$$

Thus, the *Shishkov equation of contact* in this particular case can be represented in the form:

$$Z_1 = p \cdot \tan \psi_{b,g} \quad (7.66)$$

The equation for the position vector of point,  $\mathbf{r}_e(t)$ , of the characteristic line,  $\mathcal{E}$ ,

$$\mathbf{r}_e(t) = \begin{bmatrix} y \\ t \cdot \tan \psi_{b,g} \\ p \cdot \tan \psi_{b,g} \\ 1 \end{bmatrix} \quad (7.67)$$

is derived on the premise of consideration of the equation of contact together with the equation that describes the plane,  $\mathcal{R}$ , in its current configuration with respect to the axis of the screw motion.

In Eq. (7.67),  $\mathbf{r}_e(t)$  designates the position vector of point of the characteristic line,  $\mathcal{E}$ , and the parameter of motion of the characteristic line,  $\mathcal{E}$ , is denoted by  $t$ .

In the case under consideration, the characteristic line,  $\mathcal{E}$ , is a straight line. This straight line can be viewed as the line of intersection of two planes. The plane,  $\mathcal{R}$ , is the first of two planes. Another plane is parallel to the coordinate plane  $X_1Z_1$  and is remote at the distance  $p \cdot \tan \psi_{b,g}$ .

For a specified screw motion, location of the characteristic line,  $\mathcal{E}$ , within the plane,  $\mathcal{R}$ , in the initial coordinate system  $X_0Y_0Z_0$  is remained the same.

The angle of rotation of the coordinate system  $X_1Y_1Z_1$  about  $X_0$  – axis is designated as  $\varepsilon$ . The translation of the coordinate system  $X_1Y_1Z_1$  in relation to  $X_0Y_0Z_0$  that corresponds to the angle  $\varepsilon$  equals to  $p \cdot \varepsilon$ . This makes possible composing the operator  $\mathbf{Rs}(1 \rightarrow 0)$  of the resultant coordinate system transformation:

$$\mathbf{Rs}(1 \rightarrow 0) = \begin{bmatrix} 1 & 0 & 0 & p \cdot \varepsilon \\ 0 & \cos \varepsilon & \sin \varepsilon & 0 \\ 0 & -\sin \varepsilon & \cos \varepsilon & 0 \\ 0 & 0 & 0 & 1 \end{bmatrix} \quad (7.68)$$

In order to represent analytically the envelope surface,  $\mathcal{S}$ , the equation for the position vector  $\mathbf{r}_e(t)$  of the characteristic line,  $\mathcal{E}$ , is considered together with the operator  $\mathbf{Rs}(1 \rightarrow 0)$  of the resultant coordinate system transformation:

$$\mathbf{r}_g(X_1, \varepsilon) = \mathbf{Rs}(1 \rightarrow 0) \cdot \mathbf{r}_e(t) = \begin{bmatrix} X_1 + p \cdot \varepsilon \\ X_1 \cdot \tan \psi_{b,g} \cdot \cos \varepsilon + p \cdot \tan \psi_{b,g} \cdot \sin \varepsilon \\ -X_1 \cdot \tan \psi_{b,g} \cdot \sin \varepsilon + p \cdot \tan \psi_{b,g} \cdot \cos \varepsilon \\ 1 \end{bmatrix} \quad (7.69)$$

Consider the intersection of the envelope surface,  $\mathcal{S}$ , by the plane  $X_0 = X_1 + p \cdot \varepsilon = 0$ . The latter equation allows for an expression  $X_1 = -p \cdot \varepsilon$ . Therefore,

$$\mathbf{r}_{X_0}(\varepsilon) = \begin{bmatrix} 0 \\ p \cdot \tan \psi_{b,g} \cdot (\sin \varepsilon - \varepsilon \cdot \cos \varepsilon) \\ p \cdot \tan \psi_{b,g} \cdot (\cos \varepsilon + p \cdot \varepsilon \cdot \sin \varepsilon) \\ 1 \end{bmatrix} \quad (7.70)$$

The involute of a circle is analytically described by the latter equation.

The radius of the base circle of the involute curve can be expressed by:

$$r_{b,g} = p \cdot \tan \psi_{b,g} \quad (7.71)$$

Therefore, a screw involute surface, namely, a helical involute gear tooth flank,  $\mathcal{S}$ , allows for interpretation in the form of the envelope surface to a family of consecutive positions of a plane,  $\mathcal{B}$ , that performs a screw motion. The reduced pitch of the screw involute surface equals to  $p$ , and the radius of the base cylinder is equal to  $r_{b,g} = p \cdot \tan \omega_b$ . The involute screw surface shares common points with the base cylinder. The common points are within a helix. The tangent to the helix forms the angle,  $\omega_b$ , with the axis of screw motion [2,3]:

$$\tan \omega_b = \frac{r_{b,g}}{p} \quad (7.72)$$

From this, one may conclude that the following two equations  $\tan \omega_b = \tan \psi_{b,g}$  and  $\omega_b = \psi_{b,g}$  are valid. The straight characteristic line,  $\mathcal{E}$ , is tangential to the base helix of the enveloping surface,  $\mathcal{S}$ . This means that:

- if a plane  $A$  is tangential to the base cylinder, then
- a straight line,  $\mathcal{E}$ , within the plane  $A$  forms the angle  $\psi_{b,g}$  with the axis of the screw motion, and
- if the plane  $A$  rolls without slippage over the base cylinder, then the envelope surface,  $\mathcal{S}$ , can be represented as a locus of consecutive positions of the straight line,  $\mathcal{E}$ , that rolls without sliding over the base cylinder together with the plane  $A$ . The envelope surface is a screw involute surface.

The obtained screw involute surface,  $\mathcal{S}$  (see Figure 7.23), is identical to that shown in Figure 7.8, and is analytically described by Eq. (7.14).

The above discussion can be summarized with the following theorem:

### Theorem 7.1

If we screw, with pitch,  $p$ , a plane about an axis fixed in space, which axis makes an angle,  $\alpha$ , with the said plane, we describe in space a continuum of planes that successively intersect one another in a continuum of straight lines. These lines sweep out the involute helicoid,  $(a, \alpha)$ , where  $a = p \tan \alpha$ .

It might be correspondingly said that the screw of the plane *sweeps* in the same involute helicoid. The involute helicoid is, in any event, the so-called *envelope* of the continuum of planes.

This is a well-known theorem that is not found in most books about gearing. It may however be found in some books about kinematics 0 [133]. (See also page 335 in the book by Dr. J. Phillips [101,130]).

Another solution to the problem of the determining envelope of a plane that performs a screw motion is given by P. Cormac [16,21].

#### 7.2.4 GENERATING BASIC RACK OF HELICAL GEAR

When the basic rack of a helical gear is generated, the rack,  $\mathcal{R}$ , is tilted at a certain angle,  $\psi_{b.g}$ , in relation to the axis of rotation of the gear as shown in Figure 7.24. The generating rack,  $\mathcal{R}$ , travels in the direction that is specified by the linear velocity vector,  $\mathbf{V}_r$ . The magnitude,  $V_r$ , of the vector,  $\mathbf{V}_r$ , is synchronized with a rotation,  $\omega_g$ , of the gear.

The vector of linear velocity,  $\mathbf{V}_r$ , of the translational motion can be resolved into two components:

$$\mathbf{V}_r = \mathbf{V}_r^t + \mathbf{V}_r^{ax}. \quad (7.73)$$

One of the components,  $\mathbf{V}_r^t$ , of the linear velocity vector,  $\mathbf{V}_r$ , is pointed in the tangential direction to the pitch cylinder of the gear. This component causes rolling with no sliding of the pitch plane of the rack,  $\mathcal{R}$ , over the pitch cylinder of diameter,  $d_g$ , of the gear.

The other component,  $\mathbf{V}_r^{ax}$ , of the velocity vector,  $\mathbf{V}_r$ , is pointed in the axial direction of the gear. This component together with the component  $\mathbf{V}_r^t$  results in the screw motion of the lateral tooth plane of the rack,  $\mathcal{R}$ . The gear axis,  $O_g$ , is the axis of the screw motion of the plane.

The gear tooth flank,  $\mathcal{F}$ , is an envelope surface to a family of consecutive positions of the lateral plane when the rack,  $\mathcal{R}$ , performs a screw motion about the axis,  $O_g$ .

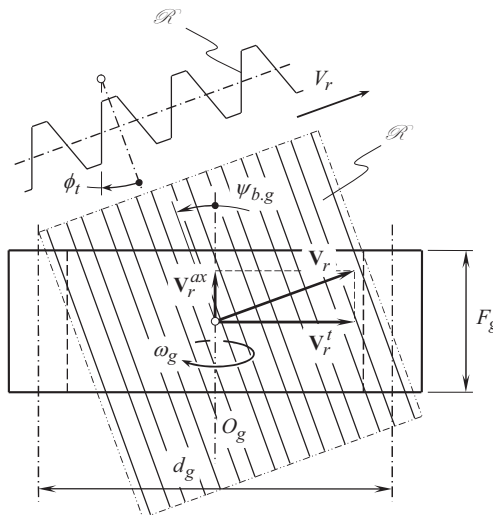


FIGURE 7.24 Generation of tooth flank,  $\mathcal{F}$ , of a helical gear by means of a helical rack,  $\mathcal{R}$ .

### 7.2.5 DESCRIPTIVE-GEOMETRY-BASED APPROACH FOR DETERMINATION OF STRAIGHT GENERATING LINE

The methods developed in descriptive geometry can be used for the determination of the straight generating line,  $\mathcal{E}$ , as well as the principal design parameters of an involute gear. A descriptive-geometry-based solution to a problem is not as accurate as that derived using analytical methods for solving engineering problems. The main advantage of descriptive-geometry-based methods is that they are helpful to eliminate rough errors in the analysis. It is strongly recommended to use descriptive-geometry-based methods along with analytical methods (and computer-based methods) for solving engineering problems, and problems in gearing in particular.

#### 7.2.5.1 Gear Base Helix Angle $\psi_{b,g}$ : General Approach

In order to determine the gear base helix angle,  $\psi_{b,g}$ , an actual value of the normal profile angle,  $\phi_n$ , as well as of setting angle,  $\zeta_r$ , of the gear rack,  $\mathcal{R}_g$ , are required to be specified. A solution to this problem derived from the premise of descriptive-geometry-based methods is discussed immediately below.

The base helix angle,  $\psi_{b,g}$ , can be constructed in a standard system of planes of projections  $\pi_1\pi_2\pi_3$ . If necessary, additional auxiliary plane(s) of projections can be constructed as well.

In the beginning, it is necessary to construct the lateral tooth surface of the auxiliary generating rack  $\mathcal{R}_g$ . A possible way for the construction of the lateral plane of the auxiliary generating rack  $\mathcal{R}_g$  is as follows.

Consider an arbitrary plane  $A$  that is perpendicular to the axis of projections  $\pi_1/\pi_2$  (see Figure 7.25). The plane  $A$  is specified by the traces  $A_1$  and  $A_2$  onto the horizontal  $\pi_1$ , and the vertical  $\pi_2$  planes of projections. Next, turn the plane  $A$  about the trace  $A_2$  through the setting angle,  $\zeta_r$ , of the gear rack to the position  $Q$ . The plane  $Q$  is specified by the traces  $Q_1$  and  $Q_2$ , the second of which is aligned with the trace  $A_2$  of the plane  $A$ . After that, the plane  $Q$  is turned about the trace  $Q_1$  through the normal profile angle,  $\phi_n$ , of the gear rack. In this final configuration, the plane is designated as  $\mathcal{R}_g$ . It is specified by the traces  $\mathcal{R}_{g,1}$  and  $\mathcal{R}_{g,2}$ , correspondingly.

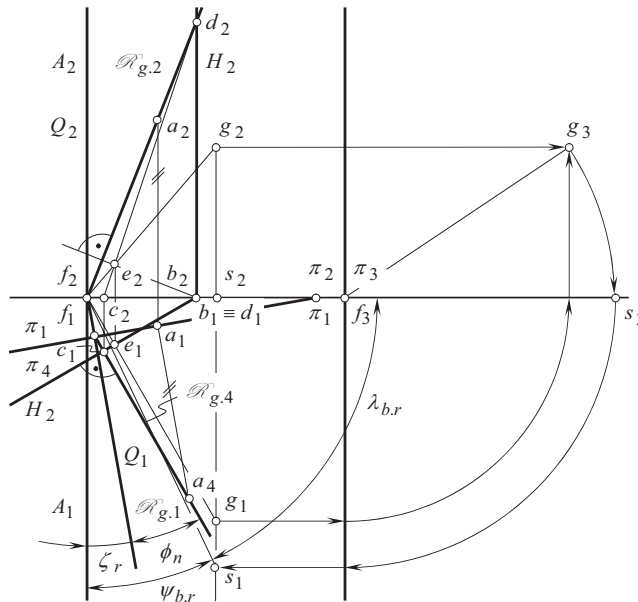


FIGURE 7.25 Determination of base helix angle,  $\psi_{b,r}$ , in gear rack.

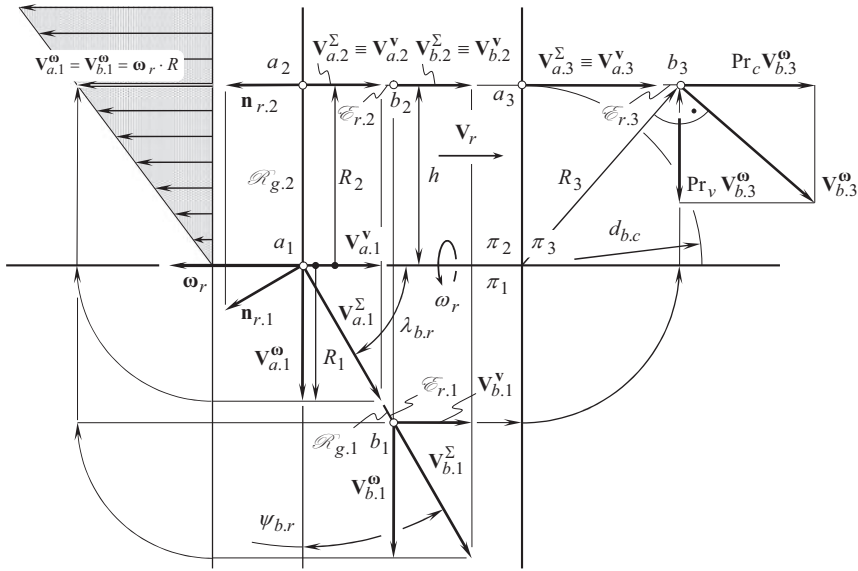


FIGURE 7.26 Determination of base diameter  $d_{b,g}$  in involute gear.

In order to construct the base helix angle,  $\psi_{b,c}$ , for this particular configuration (location and orientation) of the plane  $\mathcal{R}_g$ , an auxiliary plane of projections  $\pi_4$  is constructed so as to keep the axis of projections  $\pi_1 / \pi_4$  perpendicular to the trace  $\mathcal{R}_{g,1}$ .

The base helix angle,  $\psi_{b,c}$ , of the gear rack is the angle that the lateral rack surface  $\mathcal{R}_g$  forms with a plane, which is (a) orthogonal to the horizontal plane of projections  $\pi_1$ , and (b) orthogonal to the trace  $\mathcal{R}_{g,4}$ . The use of conventional rules – those developed in descriptive geometry – makes it possible to construct the base helix angle,  $\psi_{b,r}$ , of the gear rack, as well as of the base lead angle,  $\lambda_{b,r}$ , of the generating surface of the gear rack. The latter complements the base helix angle  $\psi_{b,r}$  to the right angle (see Figure 7.25).

The derived descriptive-geometry-based solution to the problem of determination of the base helix angle,  $\psi_{b,r}$ , gives an insight into how expressions for calculation of the actual value of this angle can be derived analytically. It also serves as a perfect tool for verification of the results of the analytical solution to the problem.

### 7.2.5.2 Base Diameter $d_{b,g}$ in Involute Gear

Let us again begin with the analysis of the property in compliance to which an involute gear tooth flank,  $\mathcal{L}$ , can be represented as an envelope surface to a family of consecutive positions of the lateral plane of the tooth of the auxiliary generating surface  $\mathcal{R}_g$ .

Consider a plane  $\mathcal{R}_g$ , configuration of which (location and orientation) is specified in a standard system of planes of projections  $\pi_1\pi_2\pi_3$ , as shown in Figure 7.26. The plane  $\mathcal{R}_g$  performs a translation along the  $\pi_1 / \pi_2$  – axis of projections. The linear velocity of the translation is designated as  $\mathbf{V}_r$ . Simultaneously, the plane  $\mathcal{R}_g$  rotates about that same axis  $\pi_1/\pi_2$  with an angular velocity  $\omega_r$ .

The base diameter,  $d_{b,g}$ , of the gear is equal to the shortest distance of approach between the characteristic line,  $\mathcal{E}_r$ , and the axis  $\pi_1/\pi_2$  of the screw motion. In order to determine the characteristic line,  $\mathcal{E}_r$ , it is necessary to select those points within the plane  $\mathcal{R}_g$ , the resultant velocity of which is pointed perpendicular to the normal vector  $\mathbf{n}_r$  to the plane  $\mathcal{R}_g$  itself. In order to do that, the velocity vector,  $\mathbf{V}_r$ , of the translation needs to be considered together with the linear velocity of the rotation  $\omega_r$ . Those points within the plane  $\mathcal{R}_g$ , the resultant velocity,  $\mathbf{V}^\Sigma$ , of which is perpendicular to the normal vector  $\mathbf{n}_r$ , are points that belong to the characteristic line  $\mathcal{E}_r$ . In the case under

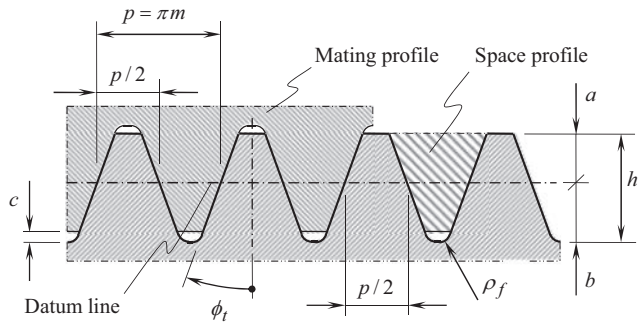


**FIGURE 7.27** Correspondence between generating rack,  $\mathcal{R}$ , and mating rack profiles.

consideration, the characteristic line,  $\mathcal{E}_r$ , is the straight line at a distance  $d_{b,g}/2$  from the axis of rotation  $\pi_1/\pi_2$  of the gear. The characteristic line,  $\mathcal{E}_r$ , crosses the axis  $\pi_1/\pi_2$  at the base helix angle,  $\psi_{b,r}$ .

The descriptive-geometry-based solution to the problem of determination of the base diameter  $d_{b,g}$  is represented in Figure 7.26. The derived solution to the problem of determining the base diameter,  $d_{b,g}$ , of the gear is insightful for the derivation of equations for the calculation of the actual value of this diameter.

In both cases (see Figures 7.25 and 7.26), the characteristic straight line,  $\mathcal{E}_r$ , is constructed. An involute gear/pinion tooth flank can be generated by means of the straight line,  $\mathcal{E}_r$ .

### 7.3 COMMENTS TO PECULIARITIES OF GEOMETRY OF INVOLUTE GEAR TOOTH FLANK

Involute gear tooth flank is shaped in the form of screw involute surface. In particular applications (spur gear) screw involute surface reduces to involute cylinder. Peculiarities in the geometry of involute gear tooth flank can be used to improve the design and manufacture of gears.

#### 7.3.1 CHARACTERISTICS OF THE GENERATING BASIC RACK

The basic rack tooth profile is bounded by the tip line at the top, and by the parallel root line at the bottom. The fillet between the straight tooth flank and the root line is usually of circular arc form, as shown in Figures 7.27 and 7.28.

The characteristics of the generating basic rack are as follows:

- The generating basic rack profile with module  $m$  has a diametral pitch  $P = \pi m$
- The datum line is the line drawn parallel to the tip and root lines where the tooth thickness is equal to the tooth space width and is equal to half the diametral pitch  $P/2$
- The dimensions of the generating basic rack profile are given relative to the datum line and are quoted as a multiple of the module  $m$ . Dimensions relating to module  $m = 1.0$  are commonly identified by asterisk (\*), that is,  $a^*$
- The mating rack profile is symmetrical to the generating basic rack profile about the datum line and is displaced by half a pitch in relation to it
- The usable parts of the flank are inclined at the profile angle,  $\phi_t$ , to a line normal to the datum line. This angle is the same as the pressure angle,  $\phi_t$  (or  $\phi_n$ ), at the reference cylinder of the gear
- The tooth depth,  $h_t$ , is divided by the datum line into the addendum,  $a$ , and the dedendum,  $b$
- The dedendum,  $b$ , is equal to the summa of the addendum,  $a$ , and the bottom clearance,  $c$



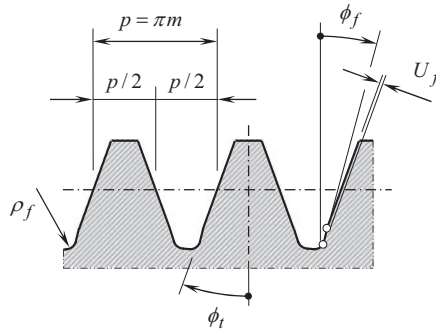


**FIGURE 7.28** Basic rack profile with (intentional) fillet undercut.

- The greatest possible fillet radius,  $\rho_f$ , is determined by the bottom clearance,  $c$ . The condition for this is [81]:

$$\rho_f \leq \left( \frac{\pi m}{4} - b \tan \phi_t \right) \cdot \tan \left( \frac{90^\circ + \phi_t}{2} \right) \quad (7.74)$$

This issue is discussed more in detail in the book by Prof. *S.P. Radzevich* [153].

- The generating basic rack profile with an (intentional) fillet undercut
- with depth,  $U_f$ , and the profile angle,  $\phi_f$ , which is schematically depicted in Figure 7.28, is used for gears cut by a protuberance gear cutting tool and finished by grinding
- The generating basic rack profile for generating external spur and helical gears is the counterpart of the basic rack profile, that is, the space profile. The true shape of the fillet produced on the gear is a trochoid generated by the tip of the generating rack profile

Apart from the standard profile angle  $\phi_t = 20^\circ$ , other profile angles are employed for special applications:

- $\phi_t = 15$  for certain printing machinery and kinematically exacting gear drives, such as for the movement of telescopes, or radar reflectors
- $\phi_t = 17\ 30'$  for marine gears with deep teeth where particularly quiet running is required
- $\phi_t = 20\ 33'$  and  $\phi_t = 25^\circ$  for cases where the flanks are subjected to extremely high contact stresses.

Addenda other than the standard  $a = 1 \cdot m$  are used for certain applications:

- $a = 0.75 \cdot m$  for stub teeth for gear of couplings
- $a = 1.25 \cdot m$  for marine gears with deep teeth.

Requirements for root forms with an increased bending strength can also be met by:

- $a = 4/3 \cdot m$  for teeth with full fillet root finished by planning with a rack type cutter
- $a = 7/5 \cdot m$  for teeth with full fillet root and intentional fillet undercut (protuberance tool) at the run-out of the grinding allowance finished by grinding (see Figure 7.28).

Having calculated the design parameters of a spur generating rack,  $\mathcal{R}$ , the corresponding design parameters of a spur gear with a given tooth number,  $N_g$ , can be calculated, as well.

**TABLE 7.3**  
**Design Parameters of Spur Gear**

Design Parameter of the Gear	Metric	Imperial
Pitch Diameter (mm)	$d = m N_g$	$d = \frac{N_g}{P}$
Base Diameter (mm)		$d_{b,g} = d_g \cos \phi_t = m N_g \cos \phi_t$
Base Pitch (mm)		$p_b = \frac{\pi d_g}{N_g} \cos \phi_t = p \cos \phi_t$
Normal Tooth Thickness (mm)	$t = m \left( \frac{\pi}{2} + 2 \cdot \xi \cdot \tan \phi_t \right)$	$t = \frac{1}{P} \left( \frac{\pi}{2} + 2 \cdot \xi \cdot \tan \phi_t \right)$
Tooth Thickness at an Arbitrary Diameter $d_y$ (mm)	$t_y = d_{g,y} \left( \frac{t}{m N_g} + \text{inv } \phi_t - \text{inv } \phi_{t,y} \right)$	$t_y = d_{g,y} \left( \frac{tP}{N_g} + \text{inv } \phi_t - \text{inv } \phi_{t,y} \right)$
Tooth Crest Width <sup>a</sup> , mm	$t_o = d_{o,g} \left( \frac{t}{m N_g} + \text{inv } \phi_t - \text{inv } \phi_{t,o} \right)$	$t_o = d_{o,g} \left( \frac{tP}{N_g} + \text{inv } \phi_t - \text{inv } \phi_{t,o} \right)$
Standard Outside Diameter (mm)	$d_{o,g} = d_g + 2m$	$d_{o,g} = d_g + 2a$
Root Diameter (mm)		$d_{f,g} = d_g - 2h_t$
Circular Pitch (mm)		$p = \frac{\pi d_g}{N}$
Average Backlash Per Gear Pair (mm)	$B = 0.040m$	$B = \frac{0.040}{P}$

<sup>a</sup> Here, tooth profile angle at outer diameter,  $d_{o,g}$ , of the gear is designated as  $\phi_{t,o}$ .

Standard equations are used for the calculation of the design parameters of a spur gear. These equations are summarized in Table 7.3.

Involute function,  $\text{inv } \phi_t$ , is used for the calculation of the tooth crest width,  $t_o$ , in Table 7.3. Involute function is defined as:

$$\text{inv } \phi_t = \tan \phi_t - \phi_t \text{ (rad)} \quad (7.75)$$

For the calculation of profile angle,  $\phi_t$ , expressed in radians, well-known formula:

$$\phi_t \text{ (rad)} = \frac{\pi}{180} \cdot \phi_t^\circ \quad (7.76)$$

is commonly used.

Normal tooth thickness,  $t$ , is expressed in terms of profile shift correction coefficient,  $\xi$ . The profile shift correction coefficient,  $\xi$ , is defined by the formula

$$\xi = \frac{\Delta x}{m} \quad (7.77)$$

The actual value of the tooth profile shift in Eq. (7.77) is denoted by  $\Delta x$ .

The helical generating rack,  $\mathcal{R}$ , is commonly specified either in terms of module,  $m$ , or in terms of diametral pitch,  $P$ , of the rack.<sup>14</sup> The helix angle,  $\psi$ , of the rack is known. For the calculation of

<sup>14</sup> The helical generating rack,  $\mathcal{R}$ , can also be specified either in terms of base diameter,  $d_b$ , of the gear.

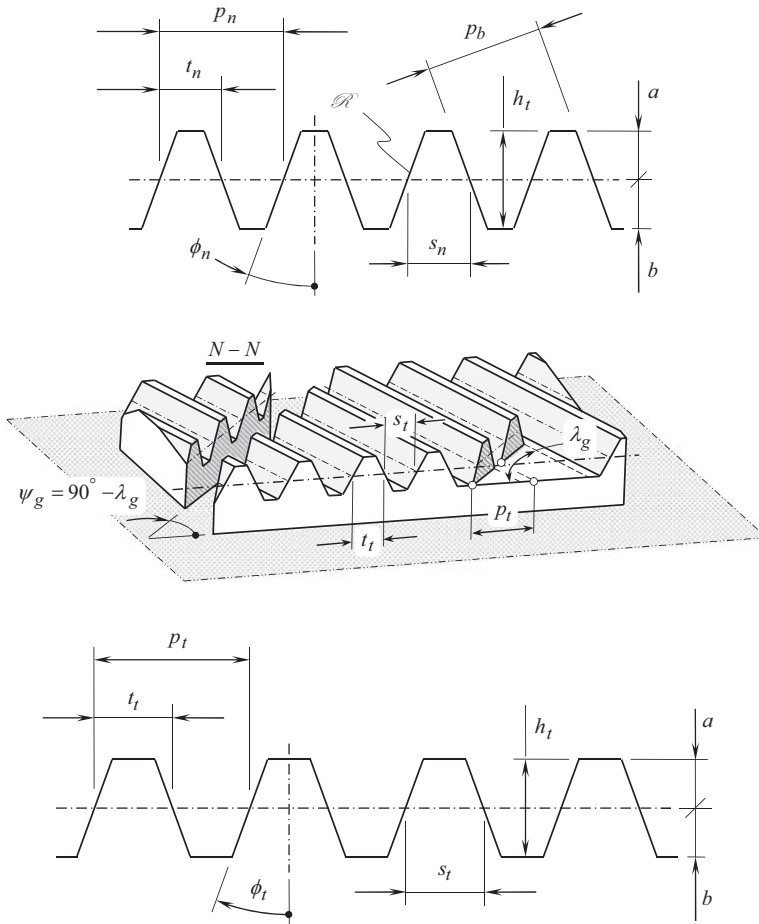


**FIGURE 7.29** Design parameters of generating rack,  $\mathcal{R}$ , of helical involute gear.

the rest of the design parameters (see Figure 7.29), standard formulas are used. The formulas are summarized in Table 7.4.

A gear can be generated by specifying only four elements, namely:

1. The reference cylinder
2. The basic rack profile (in normal section)
3. The helix angle, and
4. A position of the basic rack in relation to the generating pitch line, that is, the addendum modification (profile shift).

Having calculated the design parameters of a helical rack, the corresponding design parameters of a helical gear with a given tooth number,  $N_g$ , can be calculated, as well. Standard equations are used for the calculation of the design parameters of a helical gear. These equations are summarized in Table 7.5.

Miscellaneous formulas that are useful for calculating gear design parameters are given in Table 7.6.

The circular pitch,  $p$ , and normal circular pitch,  $p_n$ , correlate to diametral pitch,  $P$ , and the normal diametral pitch,  $P_n$ , as:

$$p_n P_n = p P \quad (7.78)$$

**TABLE 7.4**  
**Design Parameters of Helical Generating Rack**

Design Parameter of the Rack	Metric	English
Normal Pitch of the Rack Teeth	$p_n = \pi \cdot m$	$p_n = \frac{\pi}{P}$
Transverse Module (mm)	$m_t = \frac{m}{\cos \psi}$	—
Transverse Pitch	—	$p_t = \pi \cdot m_t = \frac{\pi m}{\cos \psi}$
Base Pitch (mm)	$p_{b,g} = \pi m \cos \phi_t$	$p_{b,g} = \frac{\pi \cos \phi_t}{P}$
Addendum (mm)	$a = m$	$a = \frac{1}{P}$
Dedendum <sup>a</sup> (mm)	$b = 1.25m$	$b = \frac{1.25}{P}$
Tooth Height (mm)	$h_t = a + b = 2.25m$	$h_t = \frac{2.25}{P}$
Base Pitch (mm)	$p_{b,g} = \pi \cdot m \cdot \cos \phi_t$	$p_{b,g} = \frac{\pi}{P} \cdot \cos \phi_t$
Transverse Tooth Thickness (mm)	$t_t = \frac{\pi m}{2}$	$t_t = \frac{\pi}{2P}$
Normal Tooth Thickness (mm)	$t_n = t_t \cos \psi_g$	$t_n = t_t \cos \psi_g$
Transverse Space Width (mm)	$s_t = \frac{\pi m}{2}$	$s_t = \frac{\pi}{2P}$
Normal Space Width (mm)	$s_n = s_t \cos \psi_g$	$s_n = s_t \cos \psi_g$
Normal Profile Angle (°)	$\phi_n = \tan^{-1}(\tan \phi_t \cdot \cos \psi_g)$ $\phi_n = \cos^{-1}(\sin \psi_{b,g} \cdot \csc \psi_g)$	

<sup>a</sup> For the calculation of dedendum,  $b$ , of a small module gear (of a fine pitch gear) the formula  $b = 1.35m$  (or the equivalent formula  $b = \frac{1.35}{P}$ ) is often used.

Figure 7.30 shows the development of tooth helices, which then become straight lines. The spacing of these helices on the normal, transverse, and axial planes are the normal,  $p_n$ , transverse,  $p_t$ , and axial,  $p_x$ , pitches correspondingly. The diametral pitches corresponding to the normal and transverse measures of linear spacing become the *normal diametral pitch* and *transverse diametral pitch*.

The reciprocals of the normal diametral pitch and the transverse diametral pitch are the normal module  $m$  (or  $m_n$ ) and the transverse module,  $m_t$ , correspondingly, expressed in the same unit of length.

### 7.3.2 GEARS WITH LOW TOOTH COUNT

A gear design with a low tooth count is required to be recognized. It is common that in involute gears the gear root diameter,  $d_{f,g}$ , is greater compared to the base diameter of the gear,  $d_{b,g}$ , and an inequality  $d_{b,g} < d_{f,g}$  is valid.

**TABLE 7.5**  
**Design Parameters of Helical Gear**

Design Parameter of the Gear	Metric	English
Pitch Diameter (mm)	$d_g = m N_g$	$d_g = \frac{N_g}{P_t}$
Outer Diameter (mm)	$d_{o,g} = d_g + 2a$	
Reference Diameter (mm)	$d_\psi = \frac{m N_g}{\cos \psi_g} = m_t N_g$	$d_\psi = \frac{N_g}{P \cdot \cos \psi_g}$
Standard Outside Diameter (mm)	$d_{o,g} = d_g + 2m$	$d_{o,g} = d_g + 2a$
Base Helix Angle ( $^\circ$ )		$\sin \psi_b = \sin \psi_g \cos \phi_t$ $\tan \psi_b = \tan \psi_g \cos \phi_t$
Transverse Profile Angle ( $^\circ$ )		$\tan \phi_t = \frac{\tan \phi_n}{\cos \psi_g}$ $\sin \phi_t = \frac{\sin \phi_n}{\cos \psi_b}$ $\cos \phi_t = \frac{\cos \phi_n \cos \psi_{\partial g}}{\cos \psi_b}$
Diametral Pitch (in)		$P = \frac{N_g}{d_g} = \frac{\pi}{p_t}$
Normal Diametral Pitch (in)		$P_n = \frac{N_g}{d_g \cos \psi_g}$
Transverse Diametral Pitch (mm)		$P_t = P_n \cos \psi_g$
Normal Circular Pitch (mm)		$p_n = \frac{\pi d_g}{N_g} \cos \psi_g$
Base Pitch (mm)		$p_b = \frac{\pi d_g}{N_g} \cos \phi_t = p \cos \phi_t$
Transverse Base Pitch (mm)	$p_{bt} = \pi m \frac{\cos \phi_t}{\cos \psi_b}$	$p_{bt} = \frac{\pi}{P} \frac{\cos \phi_t}{\cos \psi_b}$
Base Diameter (mm)	$d_{b,g} = m N_g \frac{\cos \phi_n}{\cos \psi_b} = d_g \cos \phi_t$	$d_{b,g} = \frac{N_g}{P} \frac{\cos \phi}{\cos \psi_b} = d_g \cos \phi_t$
Lead (mm)	$L = \pi d_g \cot \psi = \frac{\pi d_g}{\tan \psi_g}$	
Transverse Profile Angle at Tooth Tip ( $^\circ$ )	$\cos \phi_{o,g} = \frac{d_{b,g}}{d_{o,g}}$	
Axial Pitch (mm)	$p_x = \frac{\pi d_g}{N_g} \cos \phi_t \cot \psi_b =$ $= p_b \cot \psi_b = p \cos \psi_g$	$p_x = \frac{\pi}{P_n \sin \psi} = \frac{p_n}{\sin \psi_g} = \frac{L_g}{N_g}$

(Continued)

**TABLE 7.5 (Continued)**  
**Design Parameters of Helical Gear**

Design Parameter of the Gear	Metric	English
Transverse Circular Pitch (mm)		$p_t = \frac{\pi}{P_t} = \frac{p_n}{\cos \psi_g}$
Virtual Number of Teeth		$N_n = \frac{N_g}{\cos^2 \psi_b \cos \psi_g}$
Normal Tooth Thickness On Reference Cylinder (mm)	$t_n = \frac{p_n}{2}$ $t_n = m \left( \frac{\pi}{2} + 2 \cdot \xi \cdot \tan \phi_t \right)$	$t_n = \frac{p_n}{2}$ $t_n = \frac{1}{P} \left( \frac{\pi}{2} + 2 \cdot \xi \cdot \tan \phi_t \right)$
Transverse Tooth Thickness On Reference Cylinder (mm)	$t_t = \frac{m}{\cos \psi_g} \left( \frac{\pi}{2} + 2 \cdot \xi \cdot \tan \phi_t \right)$	$t_n = \frac{1}{P \cos \psi_g} \left( \frac{\pi}{2} + 2 \cdot \xi \cdot \tan \phi_t \right)$
Normal Base Tooth Thickness (mm)	$t_{bn} = m N_g \left( \frac{t_n}{m N_g} + \text{inv } \phi_t \right) \cos \phi_t$	$t_{bn} = \frac{N_g}{P} \left( \frac{P t_n}{N_g} + \text{inv } \phi_t \right) \cos \phi_t$
Transverse Base Tooth Thickness (mm)	$t_{bt} = m N_{\partial g} \left( \frac{t_n}{m N_{\partial g}} + \text{inv } \phi_t \right) \frac{\cos \phi_t}{\cos \psi_b}$	$t_{bt} = \frac{N_g}{P} \left( \frac{t_n P}{N_g} + \text{inv } \phi_t \right) \frac{\cos \phi}{\cos \psi_b}$
Transverse Tooth Crest Width (mm)	$t_{ot} = d_{o,g} \left( \frac{t_n}{m N_g} + \text{inv } \phi_t - \text{inv } \phi_o \right)$	$t_{ot} = d_o \left( \frac{t_n P}{N_g} + \text{inv } \phi_t - \text{inv } \phi_o \right)$
Root Diameter (mm)		$d_{f,g} = d_g - 2h_t$
Normal Profile Angle (°)		$\phi_n = \sin^{-1} (\sin \phi \cdot \cos \psi_b)$
Circular Pitch (mm)		$p_t = \frac{\pi d_g}{N_g}$
Base Tangent Length <sup>a</sup> (mm)	$W_k = m \left[ (k - 0.5) \pi \cos \phi + N_g \cdot \text{inv } \phi_t \cos \phi + 2 \xi \sin \phi \right]$  or $W_k = t_{bn} + p_b (k - 1)$	
Average Backlash Per Gear Pair (mm)	$B = 0.040 m$	$B = \frac{0.040}{P}$

<sup>a</sup> Tooth number in the span is denoted by  $k$ .

### Definition 7.1

In parallel-axes gearing, a gear of base diameter,  $d_b$ , which equals to, or greater than the root diameter,  $d_{f,g}$ , is referred to as the low-tooth-count gear.

In a design of a low-tooth-count gear, the inequality  $d_b \geq d_{f,g}$  is valid.

When base diameter of a gear,  $d_{b,g}$ , equals to, or greater than the gear root diameter,  $d_{f,g}$  (in this case the inequality,  $d_{b,g} \geq d_{f,g}$ , is valid), the gear is said to be a *low-tooth-count gear*, or just *LTC – gear*, for simplicity (see Figure 7.31). The use of the inequality  $d_{b,g} \geq d_{f,g}$  yields derivation of an expression for the *critical* tooth count,  $N_{lc}$ , in *low-tooth-count gear*. For a gear of a specified module,  $m$ , and a given tooth count,  $N_g$ , the pitch diameter,  $d_g$ , equals  $d_g = m \cdot N_g$ , and the root diameter

**TABLE 7.6****Miscellaneous Formulas for the Calculation of Design Parameters of a Gear**Helix Angle at Pitch Diameter ( $^{\circ}$ )

$$\cos \psi_g = \frac{N_g}{P_n d_g}$$

$$\sin \psi_g = \frac{\pi N_g}{P_n L_g}$$

Helix Angle at Any Diameter,  $d_{y,g}$  ( $^{\circ}$ )

$$\tan \psi_{y,g} = \frac{d_{y,g} \tan \psi_g}{d_g}$$

Transverse Circular Pitch at Any Diameter,  $d_{y,g}$  (mm)

$$p_{ty} = \frac{\pi d_{y,g}}{N_g}$$

Normal Profile Angle ( $^{\circ}$ )

$$\phi_n = \sin^{-1}(\sin \phi \cos \psi_b)$$

$$\phi_n = \cos^{-1}(\sin \psi_b \csc \psi_g)$$

$$\phi_n = \tan^{-1}(\tan \phi_t \cos \psi_g)$$

Transverse Profile Angle at Any Diameter,  $d_{y,g}$  ( $^{\circ}$ )

$$\phi_{ty} = \cos^{-1} \left( \frac{d_{b,g}}{d_{y,g}} \right)$$

Base Helix Angle ( $^{\circ}$ )

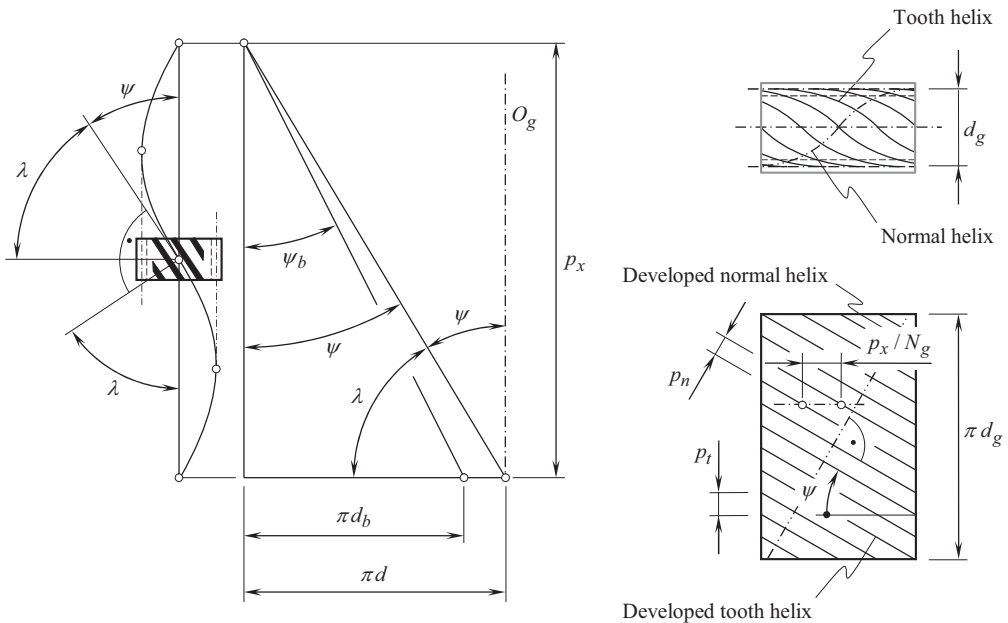
$$\sin \psi_b = \sin \psi_g \cos \phi_n$$

$$\cos \psi_b = \frac{\cos \psi_g \cos \phi_n}{\cos \phi_t} = \frac{\sin \phi_n}{\sin \phi_t}$$

$$\tan \psi_b = \tan \psi_g \cos \phi_t$$

Base Pitch (mm)

$$p_b = \frac{\pi d_{b,g}}{N_g} = p \cos \phi_t$$

**FIGURE 7.30** To the definitions of normal,  $p_n$ , transverse,  $p_t$ , and axial,  $p_x$ , pitches in helical gear.

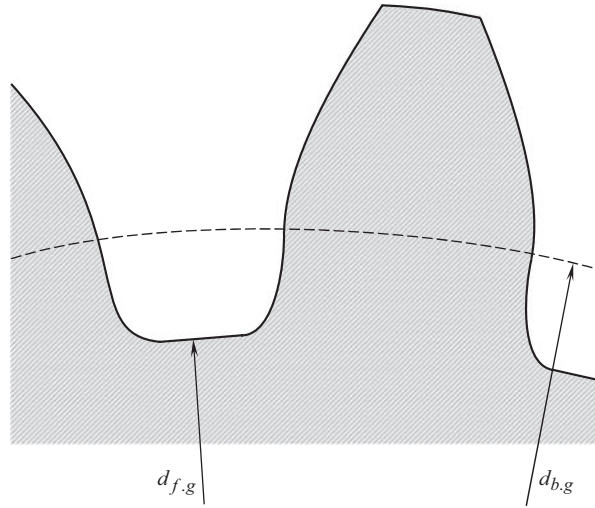


**FIGURE 7.31** The main feature of low-tooth-count parallel-axes gears (*LTC* – gears):  $d_{b,g} > d_g$ .

equals  $d_{f,g} = d_g - 2 \cdot 1.25 \cdot m$ . When the gear transverse tooth profile angle,  $\phi_t$ , is specified, then the gear base diameter,  $d_{b,g}$ , is calculated from an expression:  $d_{b,g} = d_g \cos \phi_t$ . Under an assumption  $d_{b,g} = d_{f,g}$ , the equality

$$d_g - 2 \cdot 1.25 \cdot m = d_g \cos \phi_t \quad (7.79)$$

is valid.

Let's solve this equation with respect to the pitch diameter,  $d_g$ . One can derive that:

$$d_g = \frac{2.5m}{1 - \sin \phi_t} \quad (7.80)$$

As  $d_g = m \cdot N_g$ , the *critical* tooth count,  $N_{lc}$ , equals to:

$$N_{lc} = \frac{2.5}{1 - \cos \phi_t} \quad (7.81)$$

For gears with a standard tooth profile angle  $\phi_t = 20^\circ$ , Eq. (7.81) returns for  $N_{lc} \approx 41.454$ . This means that a gear with the tooth count  $N_g = 41$  and a fewer are referred to as the *low-tooth-count gear*. In reality, a gear with 18 teeth (and not with a 42 and larger) and a fewer is referred to as the *low-tooth-count gear*. Because of this, Eq. (7.81) is modified and is represented in a form:

$$N_{lc} = k_{lc} \cdot \frac{2.5}{1 - \cos \phi_t} \quad (7.82)$$

where the factor  $k_{lc}$  equals  $k_{lc} = (0.50 \div 0.75)$ .

*Low-tooth-count gears* possess a huge potential for application in the design of *high-power-density gear drives* (or just *HPD – gear drives*, for simplicity), and, therefore, it is reasonable to anticipate that they will be extensively used in the future designs of gearsets. An alternative terminology is used with regards to *high-power-density gear drives*: they are also called as the





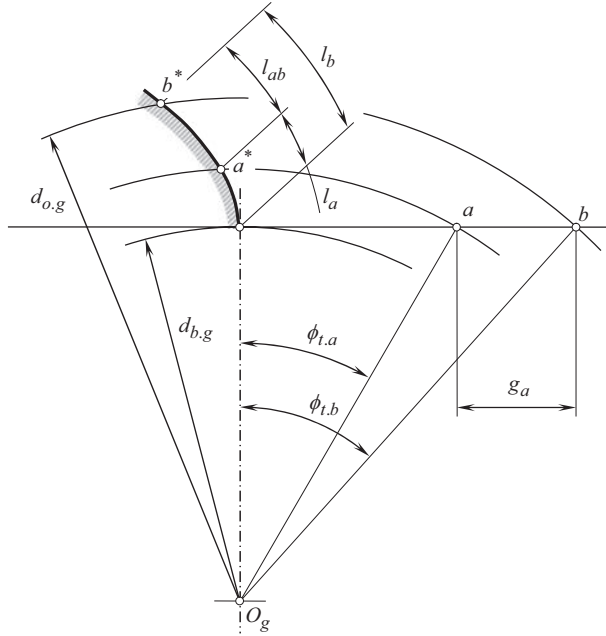


**FIGURE 7.33** Relationship between the length of path of contact,  $g_a$ , and the corresponding (effective) length of the involute profile,  $l_{ab}$ .

The following expressions are valid:

$$dl_y = r_{b,g} \tan \phi_{t,y} d\phi_y \quad (7.83)$$

$$\tan \phi_{t,y} = \phi_y \quad (7.84)$$

Hence,

$$dl_y = r_{b,g} \phi_y d\phi_y \quad (7.85)$$

The total length of the involute from the base circle to current point,  $m$ , equals to  $l_y$ . This length can be obtained by integration between the limits of 0 and  $\phi_y$  :

$$l_y = \int_0^{\phi_y} dl_y = r_{b,g} \int_0^{\phi_y} \phi_y d\phi_y = r_{b,g} \frac{\phi_y^2}{2} \quad (7.86)$$

The length,  $l_{ab}$ , of the involute profile, which is active during the path of contact,  $g_a$ , as shown in Figure 7.33, is obtained below from Figure 7.32.

The length,  $l_{ab}$ , equals to the difference between the total profile lengths,  $l_a$  and  $l_b$ , at the corresponding points  $a^*$  and  $b^*$  :

$$l_{ab} = l_a - l_b \quad (7.87)$$

$$l_{ab} = \frac{r_{b,g}}{2} (\tan^2 \phi_{t,a} - \tan^2 \phi_{t,b}) \quad (7.88)$$

where:

$$\tan \phi_{t,b} = \tan \phi_{t,a} - \frac{g_a}{r_{b,g}} \quad (7.89)$$

$$\cos \phi_{t,a} = \frac{d_{b,g}}{d_{o,g}} \quad (7.90)$$

and

$$l_{ab} = g_a \left( \tan \phi_{t,a} - \frac{g_a}{d_{b,g}} \right) \quad (7.91)$$

Investigation of gear tooth sliding is one of the possible applications for the above-derived Eqs. (7.86) and (7.91).

# 8 Parallel-Axes Involute Gearing of Specific Design

Numerous specific designs of parallel-axes involute gearing are developed and are used in the present-day industry. All the gear designs meet all three fundamental laws of gearing, and, thus, all of them are geometrically accurate gearing.

## 8.1 CONICAL INVOLUTE GEARING

Cylindrical involute gears are not the only type of gears used in the design of parallel-axes gear pairs. Conical involute gears are frequently used in anti-backlash schemes.

Apart from being frequently used in anti-backlash schemes, conical involute gears are also used as reduction gears, timing gears, and differential gears. *Beveloid gear* is another term for conical parallel-axes involute gears. A gear of this type can be viewed as an involute gear with tapered tooth thickness, tapered root, and, in most cases, tapered outside diameter.

### 8.1.1 KINEMATICS OF CONICAL INVOLUTE GEARING

A close-up of generation of tooth flanks,  $\mathcal{S}$ , of a conical involute gear by means of a generating rack,  $\mathcal{R}$ , is schematically illustrated in Figure 8.1. This is very similar to generation of tooth flanks of spur involute gears. However, instead of being parallel to the axis of rotation,  $O_g$ , of the gear, the generating rack,  $\mathcal{R}$ , is inclined to the gear axis,  $O_g$ , at an angle  $\theta$ . The angle,  $\theta$ , is commonly referred to as the *cone angle*.

The gear is rotated about the axis,  $O_g$ , with an angular velocity,  $\omega_g$ . The inclined generating rack,  $\mathcal{R}$ , travels straight tangentially in relation to the gear with a linear velocity,  $V_r$ . Magnitudes,  $\omega_g$  and  $V_r$ , of the angular velocity vector,  $\omega_g$ , and the linear velocity vector,  $V_r$ , correspondingly, are synchronized with one another ( $V_r = 0.5\omega_g d_g$ ; here the pitch diameter of the gear is denoted by  $d_g$ ).

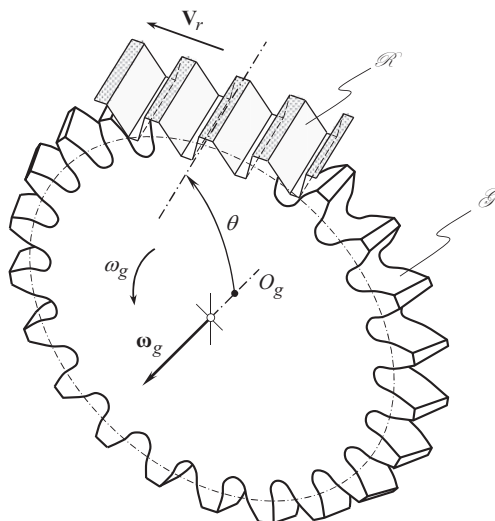


**FIGURE 8.1** Straight-sided generating rack,  $\mathcal{R}$ , in mesh with geometrically accurate conical involute gear,  $\mathcal{S}$ .

### 8.1.2 GEOMETRY OF TOOTH FLANKS OF SPUR CONICAL INVOLUTE GEAR

For the derivation of an equation for the position vector of point of the tooth flank,  $\mathcal{S}$ , of a spur conical involute gear, the following reference systems are applied (see Figure 8.2).

A *Cartesian* coordinate system,  $X_n Y_n Z_n$ , is associated with the generating rack,  $\mathcal{R}$ , as shown in Figure 8.2. Another *Cartesian* coordinate system,  $X_p Y_p Z_p$ , shares with the coordinate system,  $X_n Y_n Z_n$ , the axis  $X_p \equiv X_n$ . These two reference systems are turned in relation to one another about the  $X_p$  – axis through the angle  $\theta$ .

For the analytical description of a transition from the reference system,  $X_n Y_n Z_n$ , to the reference system,  $X_p Y_p Z_p$ , an operator of rotation,  $\mathbf{Rt}(-\theta, Z_n)$ , is used. The operator,  $\mathbf{Rt}(-\theta, Z_n)$ , can be represented in matrix form:

$$\mathbf{Rt}(-\theta, Z_n) = \begin{bmatrix} 1 & 0 & 0 & 0 \\ 0 & \cos \theta & -\sin \theta & 0 \\ 0 & \sin \theta & \cos \theta & 0 \\ 0 & 0 & 0 & 1 \end{bmatrix} \quad (8.1)$$

Ultimately, a *Cartesian* coordinate system,  $X_g Y_g Z_g$ , is associated with the gear itself.

For the analytical description of a transition from the reference system,  $X_p Y_p Z_p$ , to the reference system,  $X_g Y_g Z_g$ , an operator of translation,  $\mathbf{Tr}(0.5d_g, Y_p)$ , is used. The operator,  $\mathbf{Tr}(-0.5d_g, Y_p)$ , can be represented in matrix form:

$$\mathbf{Tr}(0.5d_g, Y_p) = \begin{bmatrix} 1 & 0 & 0 & 0 \\ 0 & 1 & 0 & 0.5d_g \\ 0 & 0 & 1 & 0 \\ 0 & 0 & 0 & 1 \end{bmatrix} \quad (8.2)$$

An operator of the resultant coordinate system transformation, that is, the operator,  $\mathbf{Rs}(n \mapsto g)$ , of the transition from the reference system,  $X_n Y_n Z_n$ , to the reference system,  $X_g Y_g Z_g$ , can be expressed in terms of the operators,  $\mathbf{Rt}(-\theta, Z_n)$  and  $\mathbf{Tr}(0.5d_g, Y_p)$ , of elementary coordinate system transformations:

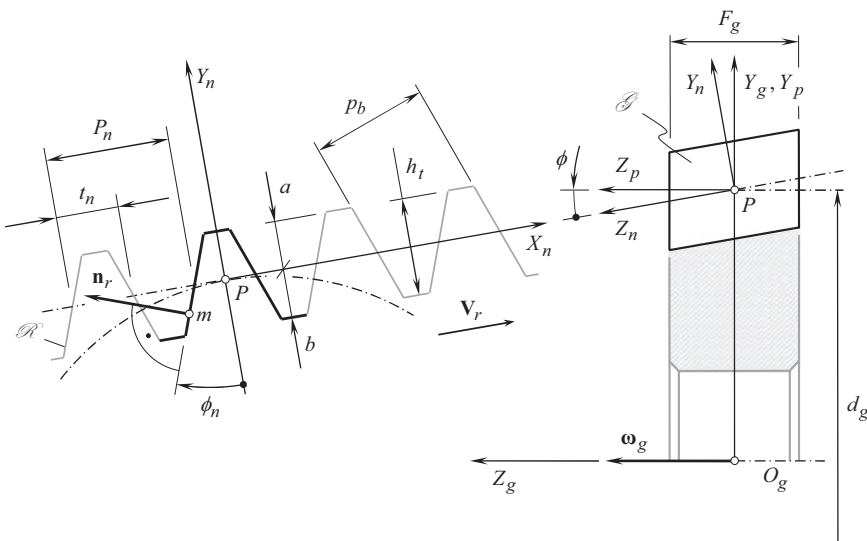


**FIGURE 8.2** Applied coordinate systems for the derivation of equation for the position vector of point of tooth flank,  $\mathcal{S}$ , of spur conical involute gear.

$$\mathbf{Rs}(n \mapsto g) = \mathbf{Tr}(0.5d_g, Y_p) \cdot \mathbf{Rt}(-\theta, Z_n) = \begin{bmatrix} 1 & 0 & 0 & 0 \\ 0 & \cos \theta & -\sin \theta & 0.5d_g \\ 0 & \sin \theta & \cos \theta & 0 \\ 0 & 0 & 0 & 1 \end{bmatrix} \quad (8.3)$$

In the reference system,  $X_n Y_n Z_n$ , the position vector of point,  $\mathbf{r}_r^{(n)}$ , of the left-hand tooth flank of the generating rack,  $\mathbf{R}$ , can be analytically described by the expression:

$$\mathbf{r}_r^{(n)} = -\mathbf{i} \cdot \frac{t_n}{2} + \mathbf{u}_n \cdot U_n = \begin{bmatrix} -\frac{t_n}{2} + U_n \sin \phi_n \\ U_n \cos \phi_n \\ V_n \\ 1 \end{bmatrix} \quad (8.4)$$

where

$t_n$  is the normal tooth thickness of the generating rack,  $\mathcal{R}$ .

$\mathbf{u}_n$  is the unit vector pointed along the left-hand tooth profile within the coordinate plane,  $X_n Y_n$ .

$U_n$  is the distance to a current point of the tooth flank,  $\mathcal{R}$ , measured along the unit vector,  $\mathbf{u}_n$ ; this is the first curvilinear (*Gaussian*) coordinate of point within the tooth flank,  $\mathcal{R}$ .

$\phi_n$  is the normal profile angle of the generating rack,  $\mathcal{R}$ .

$V_n$  is the second curvilinear (*Gaussian*) coordinate of point within the tooth flank,  $\mathcal{R}$ , ( $V_n \equiv Z_n$ ).

The aforementioned expressions for the operator of the resultant coordinate system transformation,  $\mathbf{Rs}(n \mapsto g)$  [see Eq. (8.3)], and for the position vector,  $\mathbf{r}_r^{(n)}$  [see Eq. (8.4)], allow for the representation of the position vector of point,  $\mathbf{r}_r^{(g)}$ , of the left-hand tooth flank of the generating rack,  $\mathbf{R}$ , in the coordinate system  $X_g Y_g Z_g$  associated with the gear:

$$\mathbf{r}_r^{(g)} = \mathbf{Rs}(n \mapsto g) \cdot \mathbf{r}_r^{(n)} \quad (8.5)$$

For the derivation of equation of the tooth flank,  $\mathcal{F}$ , of a spur conical involute gear, a few more intermediate coordinate systems are used. These auxiliary coordinate systems are shown in Figure 8.3.

Tooth flank in a spur conical involute gear can be determined as an envelope to a family of consecutive positions of tooth flank of the generating rack,  $\mathcal{R}$ , when the pitch plane of the rack rolls without sliding over the pitch cylinder,  $d_g$ , of the gear.

In order to determine the envelope surface, it is necessary to derive an equation of the generating rack,  $\mathcal{R}$ , when the rack occupies an arbitrary configuration in relation to the gear. The position vector of point of the generating rack,  $\mathcal{R}$ , in such an arbitrary configuration is a function of the angle of rotation,  $\varphi_g$ , of the gear about its axis,  $O_g$ . Then *Shishkov equation of contact*,  $\mathbf{n}_r \cdot \mathbf{v} = 0$ , is used to eliminate the enveloping parameter,  $\varphi_g$ , from the aforementioned equation of the generating rack,  $\mathcal{R}$  (here, the unit normal vector to the tooth flank of the generating rack,  $\mathcal{R}$ , is designated as  $\mathbf{n}_r$ , and the unit linear velocity vector of the relative motion of the rack,  $\mathcal{R}$ , in relation to the coordinate system  $X_g Y_g Z_g$  is denoted by  $\mathbf{v}$ ).

The generating rack,  $\mathcal{R}$ , in its current configuration, as well as the unit vectors,  $\mathbf{n}_r$  and  $\mathbf{v}$ , are necessarily represented in a common reference system associated with the gear, for example, the *Cartesian* coordinate system  $X_g Y_g Z_g$ . The auxiliary coordinate systems used for this purpose are depicted in Figure 8.3. Product of the corresponding operators of elementary coordinate system transformations makes possible calculation of the operator,  $\mathbf{Rs}(n \mapsto g_r)$ , of the resultant coordinate system transformation. In the particular case under consideration, the operator,  $\mathbf{Rs}(n \mapsto g_r)$ ,



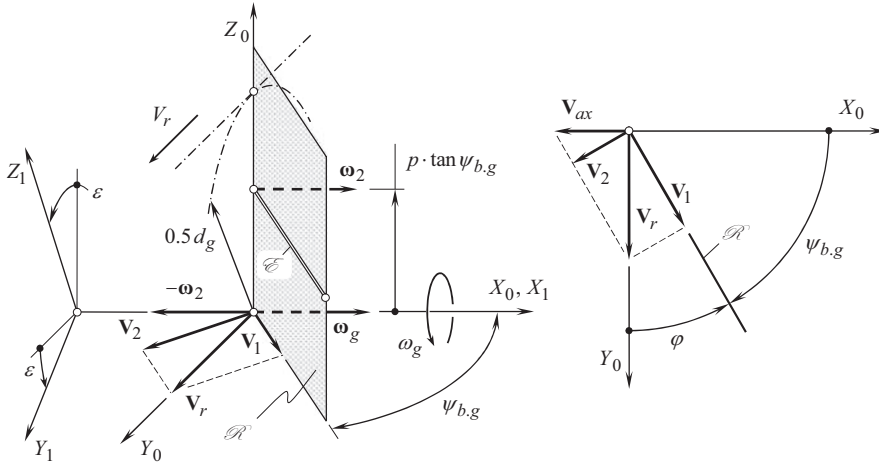


**FIGURE 8.4** Generation of screw involute surface,  $\mathcal{S}$ , as an envelope to a family of consecutive positions of the lateral plane of the rack,  $\mathcal{R}$ , that performs a screw motion.

the gear. The angle,  $\psi_{b,g}$ , can be expressed in terms of the normal profile angle,  $\phi_n$ , and cone angle,  $\theta$ , of the conical involute gear.

In the beginning, let us express the base helix angle,  $\psi_{b,g}$ , in the form:

$$\tan \psi_{b,g} = \frac{\mathbf{n}_r^{(g)} \cdot \mathbf{k}_g}{|\mathbf{n}_r^{(g)} \times \mathbf{k}_g|} \quad (8.8)$$

where

$\mathbf{n}_r^{(g)}$  is the unit normal vector to a tooth flank of the generating rack,  $\mathcal{R}$ , that is expressed in the reference system,  $X_g Y_g Z_g$ , associated with the conical involute gear.

$\mathbf{k}_g$  is the unit vector that is pointed along  $Z_g$  – axis of the reference system,  $X_g Y_g Z_g$ .

The unit normal vector,  $\mathbf{n}_r^{(g)}$  (see Figure 8.2), can be analytically expressed by the following equation:

$$\mathbf{n}_r = \mathbf{Rs}(n \mapsto g) \cdot \mathbf{n}_r^{(g)} = \mathbf{Rs}(n \mapsto g) \cdot \begin{bmatrix} -\cos \phi_n \\ \sin \phi_n \\ 0 \\ 1 \end{bmatrix} = \begin{bmatrix} -\cos \phi_n \\ \sin \phi_n \cos \theta + 0.5 d_g \\ \sin \phi_n \sin \theta \\ 1 \end{bmatrix} \quad (8.9)$$

In Eq. (8.9), the operator  $\mathbf{Rs}(n \mapsto g)$  of the resultant coordinate system transformation is specified by Eq. (7.104).

Substituting Eq. (8.9) and  $\mathbf{k}_g$  into Eq. (8.8), an expression for the base helix angle,  $\psi_{b,g}$ , of a conical involute hob can be derived:

$$\tan \psi_{b,g} = \frac{\sin \phi_n \sin \theta}{\sqrt{1 - \sin^2 \phi_n \sin^2 \theta}} \quad (8.10)$$

Once the actual value of the angle  $\psi_{b,g}$  is calculated, the tooth flank of a conical involute gear can be analytically described using the following approach: Consider a plane,  $\mathcal{R}$ , that performs a screw motion, as it is illustrated in Figure 8.4. The plane,  $\mathcal{R}$ , forms a certain angle  $\psi_{b,g}$  with  $X_0$  – axis of the *Cartesian* coordinate system,  $X_0 Y_0 Z_0$ . The axis,  $X_0$ , is the axis of the screw motion.



The screw motion of the plane,  $\mathcal{R}$ , is composed of two elementary motions: (a) of a rotation with an angular velocity,  $\omega_g$ , about the  $X_0$  – axis and (b) of a translation,  $\mathbf{V}_r$ , along the  $X_0$  – axis is another motion. The magnitudes,  $\omega_g$  and  $V_r$ , of the rotation vector,  $\omega_g$ , and the linear velocity vector,  $\mathbf{V}_r$ , correspondingly, are synchronized with one another:

$$V_r = 0.5 \omega_g d_g \quad (8.11)$$

Here, the pitch diameter of the gear is denoted by  $d_g$ .

The linear velocity vector,  $\mathbf{V}_r$ , can be expressed as the sum of two vectors:

$$\mathbf{V}_r = \mathbf{V}_1 + \mathbf{V}_2 \quad (8.12)$$

The component  $\mathbf{V}_1$  of the translatory vector,  $\mathbf{V}_r$ , is entirely located within the plane,  $\mathcal{R}$ . This component does not affect the geometry of the enveloping surface,  $\mathcal{S}$ , and, thus, the component  $\mathbf{V}_1$  can be omitted from the further analysis. The component  $\mathbf{V}_2$  of the linear velocity vector,  $\mathbf{V}_r$ , is pointed perpendicular to the plane,  $\mathcal{R}$ . The geometry of the gear tooth flank strongly depends on the magnitude ( $V_2 = V_r \sin \psi_{b.g}$ ) and the direction of this component.

When the plane,  $\mathcal{R}$ , travels straight with the linear velocity,  $\mathbf{V}_2$ , the speed of the translation  $V_{ax}$  of the plane in the direction of the  $X_0$  – axis is given by  $V_{ax} = V_r \tan \psi_{b.g}$ . Therefore, the screw motion of the plane about the  $X_0$  – axis is equivalent to a corresponding screw motion of the characteristic straight line,  $\mathcal{S}$ , about the same  $X_0$  – axis. The reduced pitch,  $p_{rl}$ , of the screw motion of the plane is calculated from the formula:

$$p_{rl} = \frac{V_{ax}}{\omega_g} = \frac{V_r \tan \psi_{b.g}}{\omega_g} \quad (8.13)$$

Consider an auxiliary reference system,  $X_1Y_1Z_1$ , that is rigidly associated with the plane,  $\mathcal{R}$ .

In the *Cartesian* coordinate system,  $X_1Y_1Z_1$ , an equation of the plane,  $\mathcal{R}$ , can be represented in an explicit form:

$$Y_1 = X_1 \cdot \tan \psi_{b.g} \quad (8.14)$$

The reference system,  $X_1Y_1Z_1$ , performs the screw motion together with the plane,  $\mathcal{R}$ , in relation to the stationary coordinate system,  $X_0Y_0Z_0$ . In the coordinate system,  $X_1Y_1Z_1$ , the unit normal vector,  $\mathbf{n}_r$ , at point of the plane,  $\mathcal{R}$ , can be analytically expressed by a column matrix:

$$\mathbf{n}_r = \begin{bmatrix} 1 \\ -\tan \psi_{b.g} \\ 0 \\ 1 \end{bmatrix} \quad (8.15)$$

The position vector,  $\mathbf{r}_r$ , of an arbitrary point,  $m$ , within the plane,  $\mathcal{R}$ , can be expressed by a column matrix:

$$\mathbf{r}_r = \begin{bmatrix} X_r \\ Y_r \\ Z_r \\ 1 \end{bmatrix} \quad (8.16)$$

The linear velocity of point,  $m$ , in the screw motion of the plane,  $\mathcal{R}$ , can be specified by the vector:

$$\mathbf{v}_m = \mathbf{V}_{ax} + [\boldsymbol{\omega}_g \times \mathbf{R}] \quad (8.17)$$

where

$\mathbf{V}_{ax}$  is the linear velocity vector of the translatory motion.

$\boldsymbol{\omega}_g$  is the angular velocity vector of the rotation.

$\mathcal{R}$  is the position vector of point,  $m$ , with respect to the axis of the screw motion (the magnitude of vector,  $\mathcal{R}$ , is equal to the distance of point,  $m$ , from the  $X_0$  – axis, and vector,  $\mathcal{R}$ , points from the axis  $X_0$  to point  $m$ ).

The envelope to a family of consecutive positions of the plane,  $\mathcal{R}$ , that performs a screw motion, is identical to the surface represented by the locus of consecutive positions of the characteristic line,  $\mathcal{E}$ , that performs that same screw motion as the plane,  $\mathcal{R}$ , does. The derivation of an equation of the envelope,  $\mathcal{E}$ , to a family of consecutive positions of the plane,  $\mathcal{R}$ , can be significantly simplified if the screw motion of the characteristic line,  $\mathcal{E}$ , is considered instead of consideration of the screw motion of the plane,  $\mathcal{R}$ .

The direction of the linear velocity vector,  $\mathbf{v}_m$ , is of importance when determining the characteristic line,  $\mathcal{E}$ , whereas the magnitude of the vector,  $\mathbf{v}_m$ , is of no interest in this particular analysis. Hence, it can be assumed that the magnitude of the rotation vector,  $\boldsymbol{\omega}_g$ , is equal  $|\boldsymbol{\omega}_g| = 1$ . Therefore,

$$\boldsymbol{\omega}_g = \mathbf{i} \quad (8.18)$$

$$\mathbf{V}_{ax} = \mathbf{i} \cdot p_{rl} \quad (8.19)$$

Equations (8.18) and (8.19) yield:

$$\mathbf{v}_m = \mathbf{i} \cdot p_{rl} + \begin{vmatrix} \mathbf{i} & \mathbf{j} & \mathbf{k} \\ 1 & 0 & 0 \\ X_1 & Y_1 & Z_1 \end{vmatrix} \quad (8.20)$$

and

$$\mathbf{v}_m = \mathbf{i} \cdot p_{rl} - \mathbf{j} \cdot Y_1 + \mathbf{k} \cdot Z_1 \quad (8.21)$$

At any point within the characteristic line,  $\mathcal{E}$ , dot product of the unit normal vector,  $\mathbf{n}_r$ , by the linear velocity vector,  $\mathbf{v}_m$ , is analytically described by the following equation:

$$\mathbf{n}_r \cdot \mathbf{v}_m = p_{rl} \cdot \tan \psi_{b,g} - Z_1 = 0 \quad (8.22)$$

Thus, in this particular case, the equation of contact,  $\mathbf{n}_r \cdot \mathbf{v}_m = 0$ , can be represented in the following form:

$$Z_1 = p_{rl} \cdot \tan \psi_{b,g} \quad (8.23)$$

The equation for the position vector of a point,  $\mathbf{r}_e(t)$ , of the characteristic line,  $\mathcal{E}$ ,

$$\mathbf{r}_e(t) = \begin{bmatrix} y \\ t \cdot \tan \psi_{b.g} \\ p_{rl} \cdot \tan \psi_{b.g} \\ 1 \end{bmatrix} \quad (8.24)$$

is derived by considering together the *Shishkov equation of contact*,  $\mathbf{n}_r \cdot \mathbf{v}_m = 0$ , and the equation that describes the plane,  $\mathcal{R}$ , in its current configuration with respect to the axis of screw motion.

In Eq. (8.24),  $\mathbf{r}_e(t)$  designates the position vector of point of the characteristic line,  $\mathcal{E}$ . The parameter of the characteristic line,  $\mathcal{E}$ , is denoted by  $t$ .

The characteristic line,  $\mathcal{E}$ , is a straight line of intersection of two planes. The plane,  $\mathcal{R}$ , is the first one of two planes. The second plane is parallel to the coordinate plane,  $X_1Z_1$ , and is at the distance,  $p_{rl} \cdot \tan \psi_{b.g}$ , from the axis of the screw motion.

For a given screw motion, the location of the characteristic line,  $\mathcal{E}$ , within the plane,  $\mathcal{R}$ , in the initial coordinate system,  $X_0Y_0Z_0$ , is remained the same.

The angle of rotation of the coordinate system,  $X_1Y_1Z_1$ , about the  $X_0$  – axis is designated as  $\varepsilon$  (see Figure 8.4). The translation of the coordinate system,  $X_1Y_1Z_1$ , in relation to the reference system,  $X_0Y_0Z_0$ , that corresponds to the rotation angle,  $\varepsilon$ , is equal to  $p_{rl} \cdot \varepsilon$ . This makes possible finding the operator,  $\mathbf{Rs}(1 \rightarrow 0)$ , of the resultant coordinate system transformation, namely, the operator of the transition from the coordinate system,  $X_1Y_1Z_1$ , to the coordinate system,  $X_0Y_0Z_0$ :

$$\mathbf{Rs}(1 \rightarrow 0) = \begin{bmatrix} 1 & 0 & 0 & p_{rl} \cdot \varepsilon \\ 0 & \cos \varepsilon & \sin \varepsilon & 0 \\ 0 & -\sin \varepsilon & \cos \varepsilon & 0 \\ 0 & 0 & 0 & 1 \end{bmatrix} \quad (8.25)$$

Equation (8.25) for the position vector of point,  $\mathbf{r}_e(t)$ , of the characteristic line,  $\mathcal{E}$ , considered together with the operator,  $\mathbf{Rs}(1 \rightarrow 0)$ , of the resultant coordinate system transformation, allows an analytical expression for the position vector,  $\mathbf{r}_g$ , of point of the enveloping surface,  $\mathcal{S}$ :

$$\mathbf{r}_g(X_1, \varepsilon) = \begin{bmatrix} X_1 + p_{rl} \cdot \varepsilon \\ X_1 \cdot \tan \psi_{b.g} \cdot \cos \varepsilon + p_{rl} \cdot \tan \psi_{b.g} \cdot \sin \varepsilon \\ -X_1 \cdot \tan \psi_{b.g} \cdot \sin \varepsilon + p_{rl} \cdot \tan \psi_{b.g} \cdot \cos \varepsilon \\ 1 \end{bmatrix} \quad (8.26)$$

Consider a case when the envelope surface,  $\mathcal{S}$ , is intersected by the plane:

$$X_0 = X_1 + p_{rl} \cdot \varepsilon = 0 \quad (8.27)$$

Equation (8.26) allows the expression  $X_1 = -p \cdot \varepsilon$ . Therefore,

$$\mathbf{r}_{X_0}(\varepsilon) = \begin{bmatrix} 0 \\ p \cdot \tan \psi_{b.g} \cdot (\sin \varepsilon - p \cdot \varepsilon \cdot \cos \varepsilon) \\ p \cdot \tan \psi_{b.g} \cdot (\cos \varepsilon + p \cdot \varepsilon \cdot \sin \varepsilon) \\ 1 \end{bmatrix} \quad (8.28)$$

The involute of a circle is analytically described by Eq. (8.28).

The radius of the base circle of the involute curve is as follows:

$$r_{b.g} = p_{rl} \cdot \tan \psi_{b.g} \quad (8.29)$$

Therefore, a screw involute surface allows for interpretation in the form of an envelope to a family of consecutive positions of the plane,  $\mathcal{R}$ , that performs a screw motion. The reduced pitch of the screw involute surface equals to  $p_{rl}$ , and the radius of the base cylinder is  $r_{b,g} = p_{rl} \cdot \tan \omega_b$ . The involute screw surface shares common points with the base cylinder. These points are within a helix. The tangent to the helix makes an angle,  $\omega_b$ , with the axis of the screw motion [146,153]:

$$\tan \omega_b = \frac{r_{b,g}}{p_{rl}} \quad (8.30)$$

One may conclude from this analysis that  $\tan \omega_b = \tan \psi_{b,g}$  and  $\omega_b = \psi_{b,g}$ . The straight characteristic line,  $\mathcal{E}$ , is tangential to the base helix of the enveloping surface,  $\mathcal{S}$ . This means that if the following conditions are fulfilled:

- a. a plane,  $A$ , is tangential to the base cylinder
- b. a straight line,  $\mathcal{E}$ , within the plane  $A$  makes an angle,  $\psi_{b,g}$ , with the axis of screw motion, and
- c. the plane,  $A$ , rolls with no sliding over the base cylinder.

Then the envelope surface,  $\mathcal{S}$ , can be represented as the locus of consecutive positions of the straight line,  $\mathcal{E}$ , that rolls without sliding over the base cylinder together with the plane,  $A$ . The envelope surface is a screw involute surface.

The tooth flanks of opposite sides of the tooth profile of a spur conical involute gear are two screw involute surfaces having the axial pitches are of the same magnitude and of the opposite hand.

An example of conical involute gear that has straight teeth is illustrated in Figure 8.5.

The line of contact,  $LC$ , between tooth flanks of two spur conical involute gears is a straight line [see Eq. (8.24)] that is not parallel to the axes of rotations of the gears. The line of contact,  $LC$ , forms a base helix angle,  $\psi_{b,g}$  [see Eq. (8.10)], with the axis of rotation of the gear, and that of the pinion. Although conical involute gears are of spur kind, the interaction between the tooth flanks of the gear,  $\mathcal{G}$ , and the pinion,  $\mathcal{P}$ , is of the same nature, as that of helical gears.

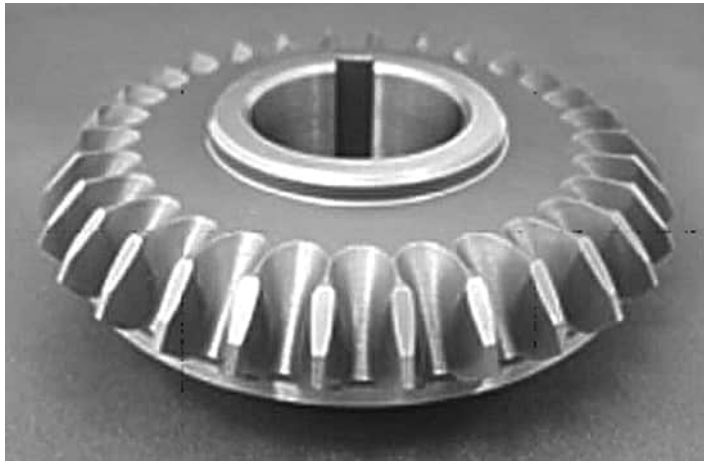


**FIGURE 8.5** Conical involute gear with straight teeth.



where

$\mathbf{n}_r^{(g)}$  is the unit normal vector to tooth flank of the generating rack,  $\mathcal{R}$ , which is analytically described in the reference system,  $X_g Y_g Z_g$ , associated with the conical involute gear.

$\mathbf{k}_g$  is the unit vector pointed along the  $Z_g$  – axis of the reference system,  $X_g Y_g Z_g$ .

The unit normal vector,  $\mathbf{n}_r^{(g)}$ , can be expressed in terms of unit the normal vector,  $\mathbf{n}_n^{(g)}$ , and the operator,  $\mathbf{Rs}(n \mapsto g)$ , of the resultant coordinate system transformation.

The unit normal vector,  $\mathbf{n}_n^{(g)}$ , is given in the normal reference system  $X_n Y_n Z_n$  [see Eq. (8.9)]

$$\mathbf{n}_n^{(g)} = \begin{bmatrix} -\cos\phi_n \\ \sin\phi_n \\ 0 \\ 1 \end{bmatrix} \quad (8.32)$$

The operator,  $\mathbf{Rs}(n \mapsto g)$ , of the resultant coordinate system transformation can be expressed in terms of operators of elementary coordinate system transformations:

$$\mathbf{Rs}(n \mapsto g) = \mathbf{Tr}(0.5d_g, Y_p) \cdot \mathbf{Rt}(-\theta, Z_t) \cdot \mathbf{Rt}(\psi_{b,g}, Y_n) \quad (8.33)$$

The operator of translation,  $\mathbf{Tr}(0.5d_g, Y_p)$ , is determined in Eq. (8.33). The operator of rotation,  $\mathbf{Rt}(-\theta, Z_t)$ , equals to the operator of rotation,  $\mathbf{Rt}(-\theta, Z_n)$ , given by Eq. (8.1):

$$\mathbf{Rt}(-\theta, Z_t) = \begin{bmatrix} 1 & 0 & 0 & 0 \\ 0 & \cos\theta & -\sin\theta & 0 \\ 0 & \sin\theta & \cos\theta & 0 \\ 0 & 0 & 0 & 1 \end{bmatrix} \quad (8.34)$$

Finally, the operator of rotation,  $\mathbf{Rt}(\psi_{b,g}, Y_n)$ , is analytically described as follows:

$$\mathbf{Rt}(\psi_{b,g}, Y_n) = \begin{bmatrix} \cos\psi_{b,g} & 0 & \sin\psi_{b,g} & 0 \\ 0 & 1 & 0 & 0 \\ -\sin\psi_{b,g} & 0 & \cos\psi_{b,g} & 0 \\ 0 & 0 & 0 & 1 \end{bmatrix} \quad (8.35)$$

The aforementioned expressions for operators of elementary coordinate system transformations,  $\mathbf{Tr}(0.5d_g, Y_p)$ ,  $\mathbf{Rt}(-\theta, Z_n)$ , and  $\mathbf{Rt}(\psi_{b,g}, Y_n)$ , yield for an expression:

$$\mathbf{Rs}(n \mapsto g) = \begin{bmatrix} \cos\psi_{b,g} & 0 & \sin\psi_{b,g} & 0 \\ \sin\theta \sin\psi_{b,g} & \cos\theta & -\sin\theta \cos\psi_{b,g} & 0.5d_g \\ -\cos\theta \sin\psi_{b,g} & \sin\theta & \cos\theta \cos\psi_{b,g} & 0 \\ 0 & 0 & 0 & 1 \end{bmatrix} \quad (8.36)$$

for the operator,  $\mathbf{Rs}(n \mapsto g)$ , of the resultant coordinate system transformation for a conical involute gear with helical teeth.

Equation (8.36) allows an expression for the unit normal vector,  $\mathbf{n}_r^{(g)}$ :

$$\mathbf{n}_r^{(g)} = \mathbf{R}s(n \mapsto g) \cdot \mathbf{n}_n^{(g)} = \begin{bmatrix} -\cos\phi_n \cos\psi_{b,g} \\ \sin\phi_n \cos\theta + 0.5d_{w,g} - \cos\phi_n \sin\theta \sin\psi_{b,g} \\ \sin\phi_n \sin\theta + \cos\phi_n \cos\theta \sin\psi_{b,g} \\ 1 \end{bmatrix} \quad (8.37)$$

In the normal reference system,  $X_n Y_n Z_n$ , the unit vector,  $\mathbf{k}_g$ , along the gear axis of rotation,  $O_g$ , can be expressed in the form of a column matrix:

$$\mathbf{k}_g = \begin{bmatrix} 0 \\ 0 \\ 1 \\ 1 \end{bmatrix} \quad (8.38)$$

Expressions for the unit normal vector,  $\mathbf{n}_r^{(g)}$ , and the unit vector,  $\mathbf{k}_g$ , are substituted in Eq. (8.31). After the necessary formula transformations are completed, an expression for the calculation of the base helix angle,  $\psi_{b,g}$ , is derived:

$$\tan\psi_{b,g} = \frac{\sin\phi_n \sin\theta + \cos\phi_n \cos\theta \sin\psi_{b,g}}{\sqrt{\cos^2\phi_n \cos^2\psi_{b,g} + (\sin\phi_n \cos\theta - \cos\phi_n \sin\theta \sin\psi_{b,g})^2}} \quad (8.39)$$

Once the base helix angle,  $\psi_{b,g}$ , is calculated, an expression for the position vector of point,  $\mathbf{r}_g$ , of the tooth flank of a conical involute gear with helical teeth can be represented in matrix form:

$$\mathbf{r}_g(U_g, V_g) = \begin{bmatrix} r_{b,g} \cos V_g + U_g \cos\lambda_{b,g} \sin V_g \\ r_{b,g} \sin V_g - U_g \sin\lambda_{b,g} \sin V_g \\ r_{b,g} \tan\lambda_{b,g} - U_g \sin\lambda_{b,g} \\ 1 \end{bmatrix} \quad \begin{matrix} V_g^{(l)} \leq V_g \leq V_g^{(a)} \\ 0 \leq U_g \leq [U_g] \end{matrix} \quad (8.40)$$

In Eq. (8.32), the base lead angle,  $\lambda_{b,g}$ , is the angle that complements the base pitch angle,  $\psi_{b,g}$ , to  $90^\circ$ , that is, the equality  $\lambda_{b,g} = 90^\circ - \psi_{b,g}$  is valid.

Tooth flanks of the opposite sides of tooth profile of a conical involute gear that has helical teeth are two screw involute surfaces of different axial pitches. The hand of the axial pitch is commonly the same. However, in particular cases, the pitches can be of opposite hands, and the axial pitch of one of the two flanks can be equal to an infinity.

The line of contact,  $LC$ , between the tooth flanks of two conical involute gears that have helical teeth is a straight line that is not parallel to the axes of rotations of the gears. The line of contact,  $LC$ , makes the base pitch angle,  $\psi_{b,g}$  [see Eq. (8.39)], with the axes of the rotation of the gear and the pinion. Interaction between tooth flanks of the gear,  $\mathcal{G}$ , and the pinion,  $\mathcal{P}$ , is of the same nature as that for helical gears of a conventional design.

## 8.2 INTERNAL INVOLUTE GEARING: FEATURES OF KINEMATICS AND GEOMETRY OF TOOTH FLANKS

Internal involute gears are used to transmit rotary motion from a drive shaft to a driven shaft when the axes of rotation are parallel to one another, and both are located on the same side relative to the axis of instantaneous rotation. The gear vector diagram of an internal gear pair is

illustrated in Figure 6.2c. No change to the direction of rotation is observed in gearing of this kind. Due to this, internal parallel-axes gearing of conventional design can be referred to as *rotary-positive parallel-axes gearing*.

### 8.2.1 FEATURES OF TOOTH FLANK GEOMETRY AND GEAR DESIGN

An internal gear pair is composed of an external pinion and of a mating internal gear (or, in other words, a ring-gear). Either a spur or helical pinion is engaged in mesh with an internal gear.

The geometry of the tooth flank of a pinion (see Figure 8.4a) is identical to that for an external gear pair.

An example of internal spur involute gear is illustrated in Figure 8.7. The analytical description of the tooth flanks of an internal gear (see Figure 8.7) is the same as in an external gear. The main difference between an internal gear and an external gear is in the location of the bodily side and the void side of the gear tooth body. Certain similarities between external and internal involute gears are illustrated<sup>1</sup> in Figure 8.8. In this discussion (see Figure 8.8) both gears are considered as designed so as to have zero backlash. In such a scenario, the tooth flanks of the internal involute gear are congruent to the corresponding tooth flanks of the external involute gear having the same tooth count, profile angle, profile shift coefficient, etc.



**FIGURE 8.7** Internal spur involute gear (ring-gear).

<sup>1</sup> In certain sense, the schematic depicted in Figure 8.8, resembles gear coupling. However, geometrically accurate gear coupling is NOT a kind of gearing, as the tooth flanks feature surface-to-surface contact, no line of action,  $LA$ , no path of contact,  $P_c$ , and no pitch point,  $P$ , can be specified in gear coupling. However, when the linear and the angular displacements of the axes of rotation,  $O_1$  and  $O_2$ , of the coupling components are taken into account, a *real* gear coupling can be considered as a kind of gearing.



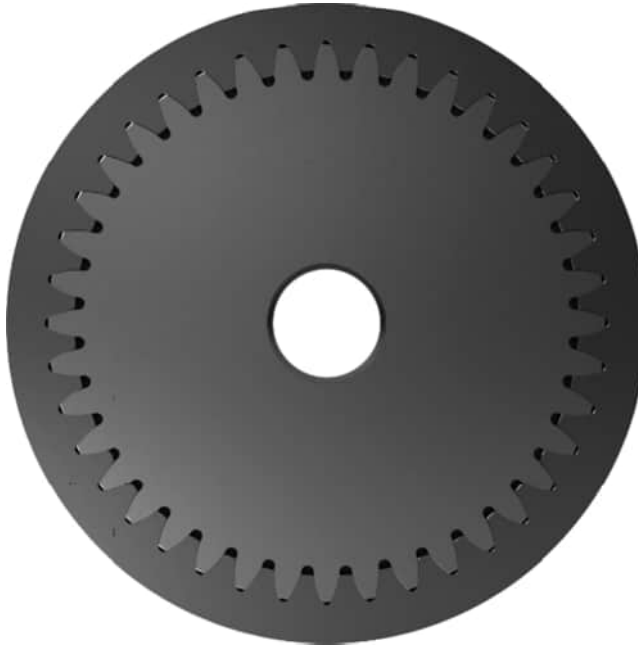


**FIGURE 8.8** Cylindrical internal and external toothing comparison. (Adopted from: <https://www.tec-science.com/mechanical-power-transmission/gear-types/cylindrical-gears/>)

The tooth flank geometry of an internal gear, including but not limited to:

- normal curvature
- profile angle
- helix angle

as well as of the others, are similar to that in the corresponding external gear.

An internal parallel-axes gear pair is composed of spur involute gears is depicted in Figure 8.9. Internal parallel-axes gear pair composed of helical involute gears are also used in the nowadays industry. For special applications, internal parallel-axes gear pair is composed of herring-bone involute gears are designed (see Figure 8.10). Another example (see Figure 8.11) illustrates the application of herring-bone internal gearing in the design of planetary gearset.

Tooth flanks in internal parallel-axes spur as well as in helical gears, interact with one another similar to that external gear pairs of a corresponding design interact. In order to transmit a uniform input rotary motion by means of internal parallel-axes gear pair, three fundamental laws of gearing are required to be fulfilled (see Chapter 4). These laws are as follows:

- *The law of contact* of the interacting tooth flanks of a gear,  $\mathcal{G}$ , and that of its mating pinion,  $\mathcal{P}$  (*Shishkov equation of contact*,  $\mathbf{n}_g \cdot \mathbf{V}_\Sigma = 0$  is commonly employed to analytically describe this law of gearing
- *The conjugate action law* of the interacting tooth flanks of a gear,  $\mathcal{G}$ , and its mating pinion [in a particular case of parallel-axes gearing, the *conjugate action law* is commonly referred to as the *Camus-Euler-Savary theorem* (or just as *CES – theorem*, for simplicity)]
- *The law of equal base pitches* of a gear and a mating pinion to operating base pitch of the gear pair.

Interference between the pinion teeth and the gear teeth is of critical importance in internal gearing. No interference is permissible in both cases, namely, in the gear design as well as when the ring-gear



**FIGURE 8.9** An internal parallel-axes gear pair composed of spur involute gears.



**FIGURE 8.10** An internal parallel-axes gear pair composed of herring-bone involute gears.

is cut by the shaper cutter. On top of that, the pinion must be assemblable with the mating ring-gear. Two different cases are distinguished in this regard. First, in a simple case, the pinion can be moved either radially, or axially to be put in mesh with the ring-gear; second, only axial assembling is permissible. The interference avoidance requires special care in internal gearing.

Example of the application of internal gear pair is illustrated in Figure 8.12. The design parameters of the internal gear pair are schematically shown in Figure 8.13.

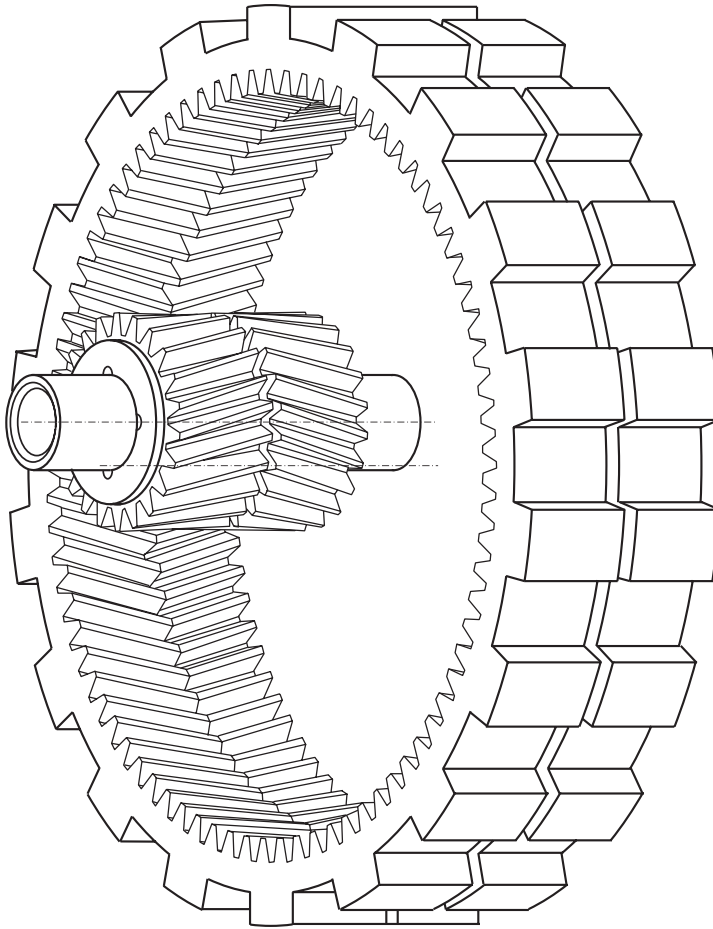


**FIGURE 8.11** Internal herring-bone involute gearing in the design of planetary gearset. (After: USA Pat. No. 6,117,036, *Split Helical Planetary Assembly*, J.L. Lanson, R. Mizon, R.C. Williams, Int. Cl<sup>7</sup>. F16H 37/08, Filed: July 29, 1999, Patented: September 12, 2000), [121].)

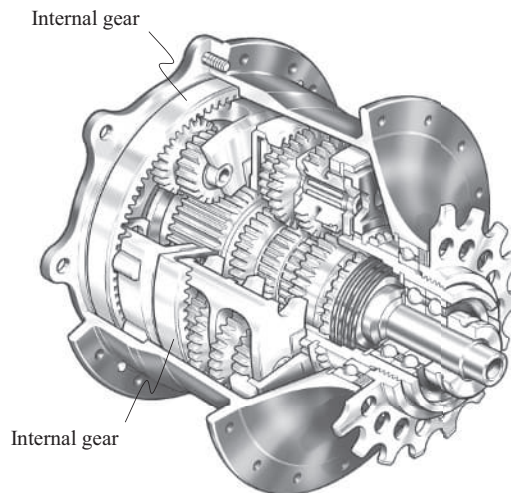


**FIGURE 8.12** An example of the application of internal gears.

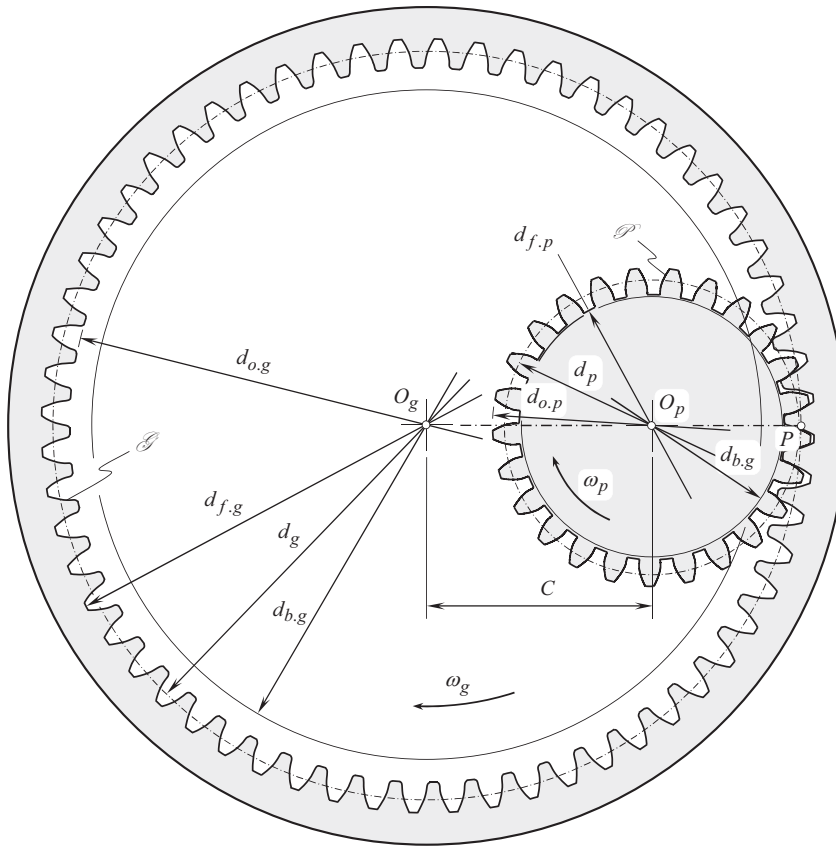


**FIGURE 8.13** Design parameters of internal gear pair.

The issues that are required to be taken into account when designing and manufacturing internal parallel-axes gear pairs are outlined immediately below:

- An interference can be observed in improperly designed internal parallel-axes gear pairs; therefore, special calculations for the lowest permissible tooth count in the ring-gear are required to be executed; the minimum difference between the tooth count of a ring-gear and a mating pinion is required to be determined
- In order to avoid undercut when shaping ring-gear, the shaper cutter tooth count has to correspond to tooth count of the ring-gear.

The consideration in this section of the book is focused mainly on the features of internal gearing, while the similarities between internal and external gear pairs are omitted.

### 8.2.2 GEAR COUPLING AS A REDUCED CASE OF INTERNAL PARALLEL-AXES GEARING

Gear coupling is commonly construed as a reduced case of internal parallel-axes gearing (Figure 8.14). This is mainly due to gear coupling being composed of an external and of internal gears with equal tooth counts ( $N_a = N_p$ ). One of the gears is connected to the input shaft, while the other one is connected to the output shaft. To accommodate for a larger angular displacement of the input and of the output shafts, both the input shaft and the output shaft are connected to external gears. In this particular design, these external gears are engaged with a common internal gear (see Figure 8.14). It is common practice to modify the teeth of the external gear(s) in their lengthwise direction.

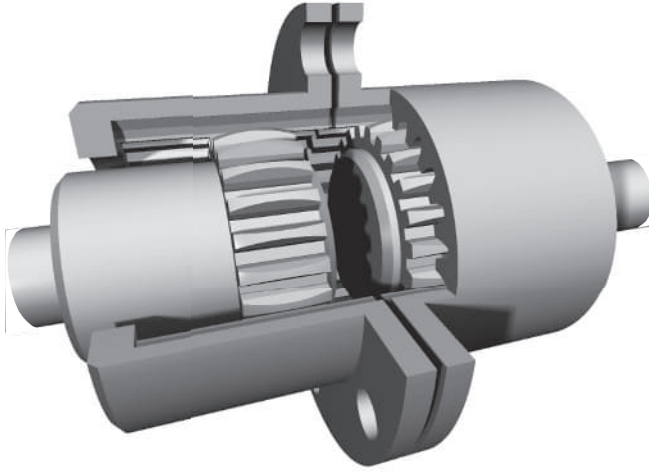


**FIGURE 8.14** Gear coupling.

Gear vector diagram of gear coupling is shown in Figure 6.2e.

In general, geometrically accurate gear coupling is not a kind of gearing at all. This is because of:

- pitch diameters of the gears,  $d_g$  and  $d_p$ , are identical to one another (the identity  $d_g \equiv d_p$  is valid)
- gear teeth are in surface-to-surface contact
- pitch point,  $P$ , is not specified
- The line of action cannot be constructed, and, therefore, the path of contact cannot be constructed, as well

A few more differences between gear coupling, and conventional gearing, can be added.

However, if the axes displacements are taken into account (see Chapter 19, Figure 19.21), all three laws of gearing, along with the equations, those derived for gear pairs, become valid for gear coupling, as well.

### 8.2.3 ON COMMONALITY BETWEEN INTERNAL GEARING AND STRAIN WAVE GEARING (HARMONIC DRIVE)

Similar to gearing, *strain wave gearing* (also known as *harmonic drive*) is a mechanism to transmit and to transform a rotary motion from a driving shaft to a driven shaft.<sup>2</sup> *Harmonic drive* was invented in 1955 by *Walton Musser*.<sup>3</sup> Here, in this mechanism, a flexible spline with external teeth, which is deformed by a rotating plug to engage with the internal gear teeth of an outer spline is used for this purpose. As illustrated in Figure 8.15, there are three basic components in the *harmonic drive*: (a) a wave generator, (b) a flex-spline, and (c) a ring-gear – all of them are put together in a housing. It is evident from that that *harmonic drive* is not a kind of gearing at all, first of all because gearing of conventional design is composed of two basic components: a gear and a mating pinion, which are put together in a housing.

<sup>2</sup> The basic concept of strain wave gearing was introduced by C.W. Musser in a 1957 patent: Pat. No. 2,906,143 (USA), *Strain Wave Gearing*, C.W. Musser, Filed: March 21, 1955, Patented: September 29, 1959, [112].

<sup>3</sup> Clarence Walton Musser (1909–June 8, 1998) inventor of *strain wave gearing*, and also credited with over 250 major inventions and discoveries.

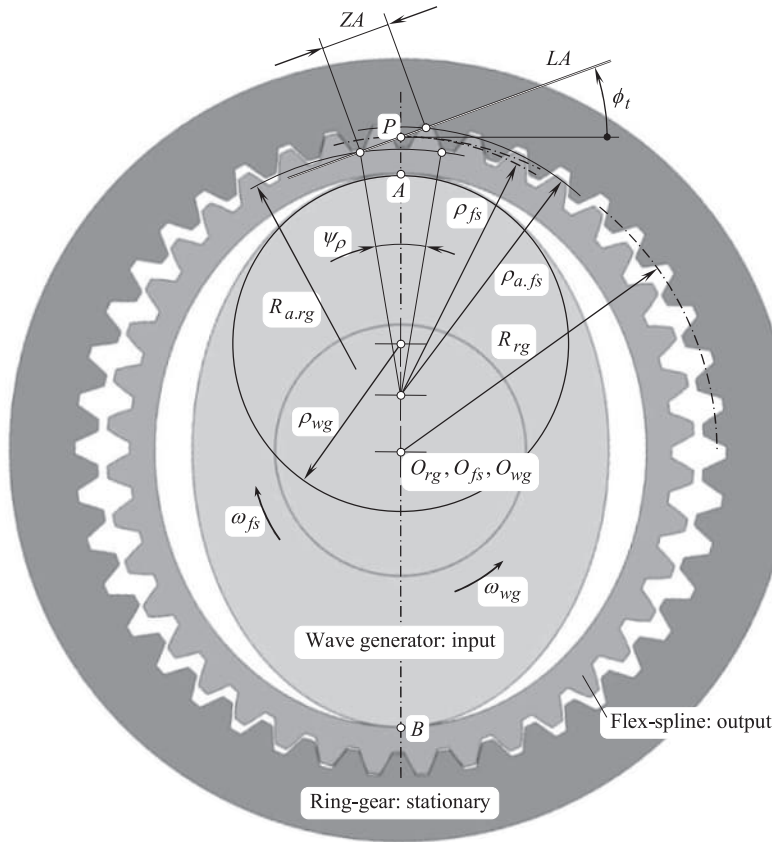


**FIGURE 8.15** Strain wave gearing (harmonic drive).

In the *harmonic drive*, a ring-gear is stationary, and it is associated with the housing (the housing is not shown in Figure 8.15). An input shaft is connected with the wave generator. When rotated, the flex-spline is deformed by the wave generator. Due to a small difference in tooth count in the ring-gear, and in the flex-spline (just one tooth, or a few teeth), the flex-spline rolls over the ring-gear. An output shaft is connected to the flex-spline. *Harmonic drive* features a huge gear ratio.

In *harmonic drive*, meshing of the flex-spline and the ring-gear can be reasonably approximated by a corresponding parallel-axes gear pair. In order to identify what is common between *harmonic drive* and internal gearing, consider a ring-gear in mesh with a mating flex-spline.

In design of the ring-gear, the pitch radius,  $R_{rg}$ , and the outer radius (top-land radius),  $R_{a,rg}$ , are identical to that in design of conventional ring-gear. These two circles are centered at the *harmonic drive* centerline,  $O_{rg}$ .

The flex-spline is considered in two states: in non-deformed (free) state and in deformed state.

In non-deformed state, the flex-spline resembles an external gear, the pitch radius, and the outer radius of which (these radii are not labeled in Figure 8.15) are identical to that in design of conventional external gear. These two circles are centered at the flex-spline centerline,  $O_{fs}$ . The latter is aligned with the *harmonic drive* centerline,  $O_{rg}$ . No reduction of the input rotation,  $\omega_{wg}$ , is observed when the flex-spline is in non-deformed state.

To engage the ring-gear in mesh with the flex-spline, the latter is deformed by means of the wave generator. The wave generator contacts the ring-gear at points A and B. The curvature of the wave generator profile at the points A and B equals to a certain value,  $\rho_{wg}$ . Correspondingly, the curvature of the pitch curve of the flex-spline at the pitch point, P, is designated as  $\rho_{fs}$ , while the curvature of the outer curve of the flex-spline at the corresponding point is denoted by  $\rho_{a,fs}$ .

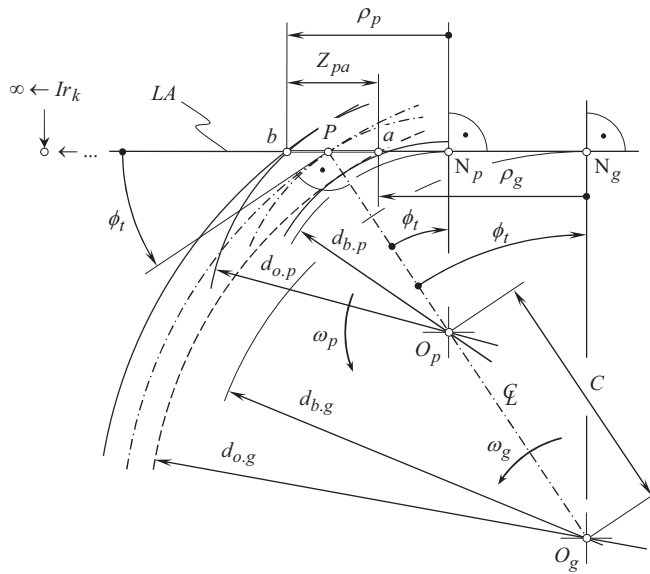


FIGURE 8.16 Basic elements of internal parallel-axes involute gear pair.

With that said, the flex-spline can be locally approximated by a sector of an external gear. This sector,  $\psi_p$ , spans over the active portion,  $ZA$ , of the line of action,  $LA$ , constructed for the rotation in both directions of the wave generator.

In order to generate the tooth profile of a *geometrically accurate* ring-gear, and that of flex-spline in a *harmonic drive*, consider the wave generator stationary, and the ring-gear, and the flex-spline, traveling in relation to the motionless wave generator. In the vicinity of pitch point,  $P$ , the motion of the flex-spline can be viewed as an instantaneous rotation about the center of curvature of the flex-spline pitch line. Under such a scenario, an involute ring-gear is meshing with locally deformed flex-spline: in the deformed state (that is, in the area of meshing) tooth profile of the deformed flex-spline is also of involute geometry and is conjugate to the ring-gear tooth profile.

Designed this way, the ring-gear for *harmonic drive* resembles much a gear for internal parallel-axes gearing. As it follows from the analysis presented in Figure 8.16, within the central angle,  $\psi_p$ , the pre-deformed ring-gear obeys all three laws of gearing.

It is clear that the tooth profile in the deformed state of the ring-gear differs from that in non-deformed state of it. This inevitably entails additional problems in machining of the ring-gear teeth. Some of the problems of this sort can be eliminated if the teeth are machined in deformed state of the ring-gear. A novel method of shaping the preloaded ring-gear is developed for this purpose.<sup>4</sup>

An intentional elastic deformation of the work is proposed to be implemented when shaping thing-wall ring-gears used in the design of *harmonic drive*, planetary gearboxes, etc. This novel method of gear shaping is schematically illustrated in Figure 8.17. Before discussing the proposed method of machining of thing-wall ring-gears, the following consideration has to be taken into account.

When operating in the gearbox, a thing-wall ring-gear is deformed by the operating load. When the deformation is large enough, the operating base pitch  $p_{b,op}$  of the ring-gear differs from that in the mating planet pinion – the latter is not permissible. Base pitch of two mating gear must be equal under any circumstances. In order to resolve this issue, the ring-gear can be cut in a deformed state. The latter could be possible, as the ring-gear is flexible enough.

<sup>4</sup> Patent pending.



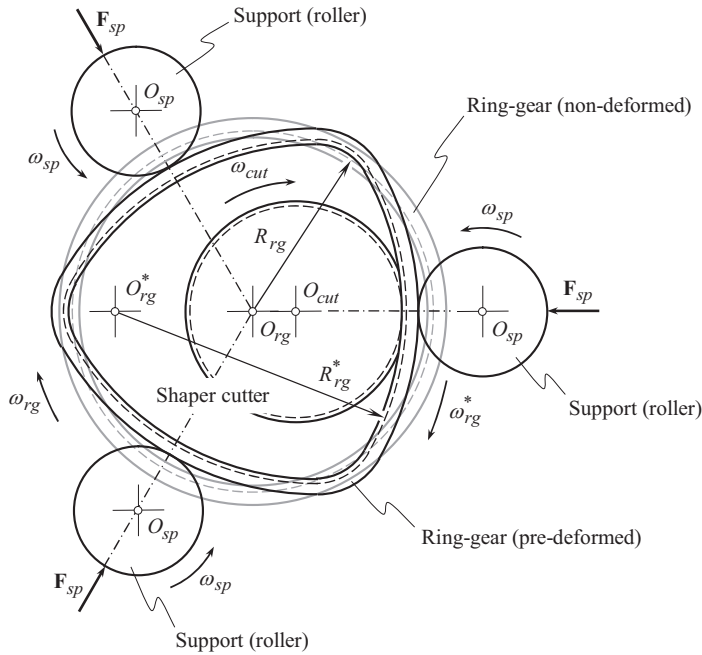


**FIGURE 8.17** Schematics of shaping of a thin-wall ring-gear in elastically deformed state.

The method<sup>5</sup> of shaping of ring-gear is illustrated in Figure 8.17. A ring-gear of pitch radius  $R_{rg}$  is cut by the shaper cutter. When being machining, the ring-gear is rotated about its axis of rotation,  $O_{rg}$ , at a constant angular velocity  $\omega_{rg}$ . The shaper cutter is rotated about its axis of rotation,  $O_{cut}$ , at certain angular velocity  $\omega_{cut}$ . The rotations  $\omega_{rg}$  and  $\omega_{cut}$  are timed with one another. When being machining, the ring-gear is intentionally deformed to that same state, at which it is deformed when operating in the gearbox. Rollers can be used for the elastic deformation of the ring-gear. The supporting rollers are rotated about their axis of rotation,  $O_{sp}$ , at an angular velocity  $\omega_{sp}$ . The supporting rollers are pushed into the ring-gear by radial forces  $F_{sp}$ . Because of the applied forces  $F_{sp}$ , the ring-gear is elastically deformed to a state when the operating pitch radius is  $R_{rg}^*$ . The operating pitch radius  $R_{rg}^*$  is always larger compared to that  $R_{rg}$  of non-deformed ring-gear (that is, the inequality  $R_{rg}^* > R_{rg}$  is always observed). It could be imagined that a phantom ring-gear of a pitch radius  $R_{rg}^*$  is rotated about a phantom axis of rotation  $O_{rg}^*$  with a certain fake angular velocity  $\omega_{rg}^*$ . The rotations of the ring-gear and of the shaper cutter are timed with one another so as to ensure equal linear velocities at the contact point of the circle of radii  $R_{rg}^*$  and the pitch circle of the shaper cutter.

In the deformed state of the ring-gear, the shaper cutter generates the gear teeth having the desirable value of base pitch equal to that of the mating pinion.

When certain intentional elastic deformation of the work is used for manufacturing purposes, the law of contact must be fulfilled in the deformed state of the part surface being machined. Other methods of machining of thin-wall (flexible) ring-gears can be proposed based on the disclosed concept.

<sup>5</sup> This method of shaping of thin-wall (flexible) ring-gears is proposed by Prof. S.P. Radzevich (~2012).



### 8.3 PINION GEAR-TO-RACK MESH AS REDUCED CASE OF PARALLEL-AXES INVOLUTE GEAR PAIR

Tooth count in a gear depends on a particular application of a gear pair. There is no physical constraint to design a gear with an infinite number of teeth. A gear with an infinite tooth count is referred as *rack-gear*, or just *rack*. Mesh of a rack-gear with a pinion gear is commonly referred to as *pinion gear-to-rack mesh*.

An example of vector diagram for *pinion gear-to-rack* gear pair is shown in Figure 6.2d. The rotation of the gear equals to zero ( $\omega_g = 0$ ), as the gear is of an infinite tooth count. The rotation of the pinion equals to a certain finite value,  $\omega_p$ . The kinematics of *pinion gear-to-rack* gear pair can be specified in terms of the linear velocity of the rack,  $V_r$ , and of the rotation of the pinion,  $\omega_p$ .

An involute *pinion gear-to-rack* gear pair can be construed as a limit case of an external gear pair when the tooth number of the gear approaches infinity ( $N_g \rightarrow \infty$ ). Under such a scenario, the pinion remains the same, while the gear (to be more exact: a gear sector) is transformed to a rack.

An example of *pinion gear-to-rack* gear pair is depicted in Figure 8.18. In a rack, the pitch circle is straightened to a straight pitch line. The same is true with respect to the radius of the outer circle,  $r_{o,g}$  as well as with respect to the radius of the root circle,  $r_f$ . Both of these radii approach infinity, and in design of a rack, they are straightened to two straight lines, parallel to the pitch line.

Tooth profile of the auxiliary generating rack,  $\mathcal{R}$  (of the basic rack,  $\mathcal{R}$ ), is bounded by the tip line at the top, and by the parallel root line at the bottom. The basic design parameters in a transverse section of a *pinion gear-to-rack* gear pair are illustrated in Figure 8.19.

The fillet between the straight tooth flank and the root line is usually rounded by a circular arc. The characteristics of the generating basic rack are as follows:

- The generating basic rack profile with module  $m$  has a pitch  $P = \pi m$
- The datum line is the line drawn parallel to the tip and root lines where the tooth thickness is equal to the tooth space width and is equal to half the pitch  $P/2$
- The dimensions of the generating basic rack profile are given relative to the datum line and are quoted as a multiple of the module  $m$ . Dimensions relating to module  $m = 1.0$  are commonly identified by asterisk (\*), that is,  $a^*$
- The mating rack profile is symmetrical to the generating basic rack profile about the datum line and is displaced by half a pitch in relation to it
- The usable parts of the flank are inclined at the profile angle,  $\phi_s$ , to a line normal to the datum line. This angle is the same as the pressure angle,  $\phi_t$  (or  $\phi_n$ ), at the reference cylinder of the gear
- The tooth depth,  $h_t$ , is divided by the datum line into the addendum,  $a$ , and the dedendum,  $b$

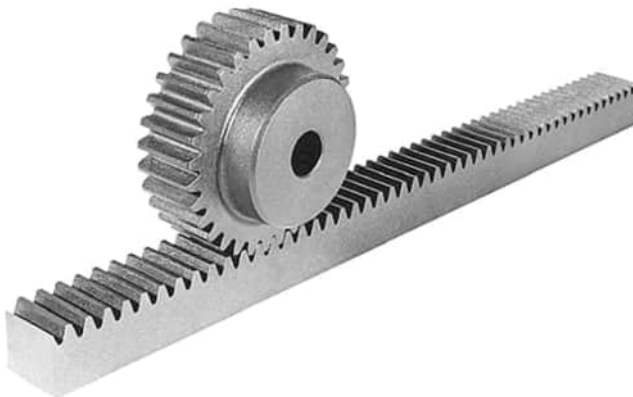
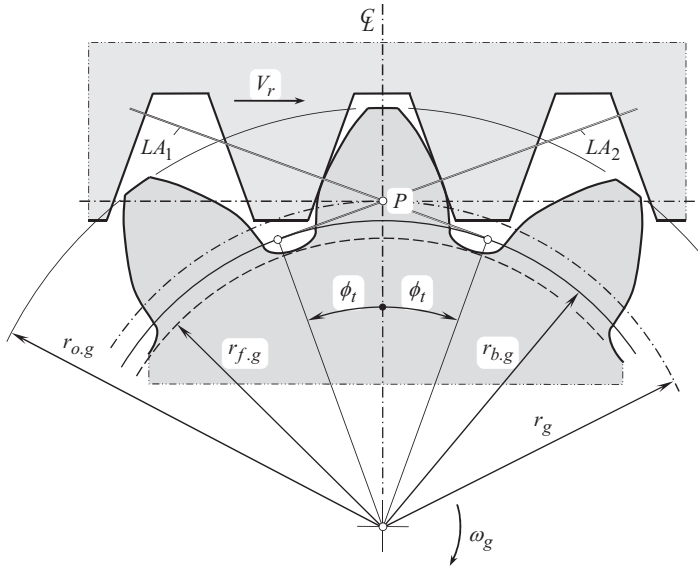


FIGURE 8.18 Pinion gear-to-rack gear pair.



**FIGURE 8.19** The basic design parameters of *pinion gear-to-rack* gear pair.

- The dedendum,  $b$ , is equal to the summa of the addendum,  $a$ , and the bottom clearance,  $c$
- The greatest possible fillet radius,  $\rho_f$ , is determined by the bottom clearance,  $c$ . The condition for this is [81]:

$$\rho_f \leq \left( \frac{\pi m}{4} - b \tan \phi_t \right) \cdot \tan \left( \frac{90^\circ + \phi_t}{2} \right) \quad (8.41)$$

More in detail, this issue is discussed in the monograph by Prof. *S.P. Radzevich* [152].

- The generating basic rack profile for generation of external spur and helical gears is the counterpart of the basic rack profile, that is, the space profile. The true shape of the fillet produced on the gear is a trochoid generated by the tip of the generating rack profile

Apart from the standard profile angle  $\phi_t = 20^\circ$ , other profile angles are employed for special applications:

- $\phi_t = 15$  for certain printing machinery and kinematically exacting gear drives, such as for the movement of telescopes or radar reflectors
- $\phi_t = 17\ 30'$  for marine gears with deep teeth where particularly quiet running is required
- $\phi_t = 20\ 33'$  and  $\phi_t = 25^\circ$  for cases where the flanks are subjected to externally high contact stresses.

Addenda other than the standard  $a = 1 \cdot m$  are used for certain applications:

- $a = 0.75 \cdot m$  for stub teeth for gear of couplings
- $a = 1.25 \cdot m$  for marine gears with deep teeth.

Requirements for root forms with an increased bending strength can also be met by:

- $a = 4/3 \cdot m$  for teeth with full fillet root finished by planing with a rack type cutter
- $a = 7/5 \cdot m$  for teeth with full fillet root and intentional fillet undercut (protuberance tool) at the run-out of the grinding allowance finished by grinding.

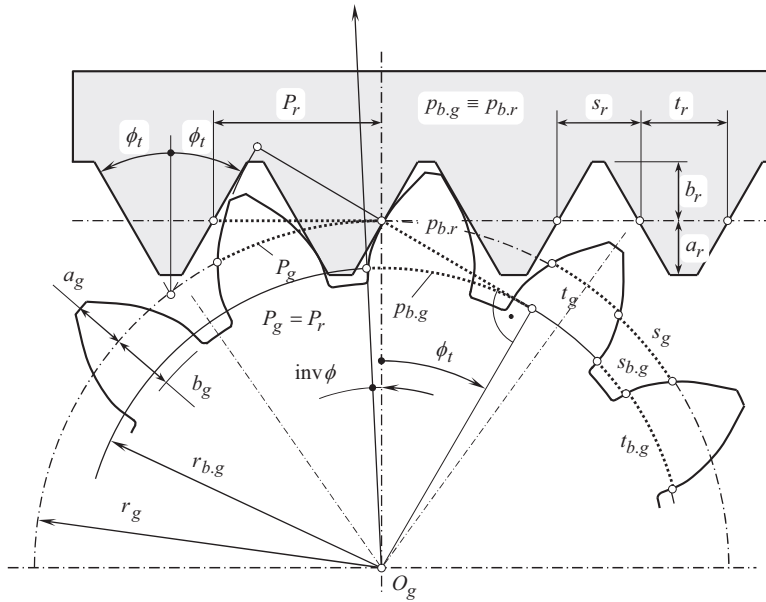


**FIGURE 8.20** A spur rack in zero-backlash mesh with a gear.

*Pinion gear-to-rack* gear pairs of two kinds are commonly recognized. They are spur and helical *pinion gear-to-rack* gear pairs. The geometry and kinematics of a spur *pinion gear-to-rack* pair is schematically illustrated in Figure 8.20.

With that said, all the above-discussed results on parallel-axes involute gearing are still valid for *pinion gear-to-rack* mesh.<sup>6</sup>

It is the right point to mention here about a paradox in *pinion gear-to-rack* mesh. The applied technique requires answering the question: *How a base line can be constructed for a rack?* in an involute *pinion gear-to-rack* gear pair. The paradox can be formulated in the other way: How to construct an *equivalent pulley-and-belt transmission* for *pinion gear-to-rack* gearset?

Consider a parallel-axes gear pair with a given diametral pitch,  $P$  (or, the same, with a specified module,  $m$ ). As an example, an involute gear sector of a gear of  $N_g = 25$  as illustrated in Figure 8.21a. The gear sector features ten teeth ( $N_{gs} = 10$ ). When the gear sector tooth number approaches infinity (that is, when  $N_{gs} \rightarrow \infty$ ), the radius of the pitch circle of the gear,  $r_g$ , approaches infinity as well ( $r_g \rightarrow \infty$ ), and the involute tooth profiles get straiten as shown in Figure 8.21b. In this way, the gear sector transforms into a rack gear.

It is natural to assume that the same is valid with respect to the base circle of the gear, namely, when  $N_g \rightarrow \infty$ , then the radius of base circle of the gear,  $r_{b,g}$ , also approaches infinity ( $r_{b,g} \rightarrow \infty$ ). Under such a scenario, the base circle straightens to a corresponding straight base line.

On the other hand, the base circle of a gear is tangent to two straight lines of action,  $LA_1$  and  $LA_2$ , through the pitch point,  $P$ . These two straight lines are perpendicular to opposite sides of the tooth profile of the gear. When the tooth number of the gear approaches infinity ( $N_g \rightarrow \infty$ ), the involute tooth profile of the gear straightens. Therefore, the two aforementioned straight lines of action,  $LA_1$  and  $LA_2$ , are perpendicular to straight tooth flanks of the rack, as illustrated in Figure 8.22.

In a rack, the center of the gear,  $O_g$ , approaches infinity ( $O_g \rightarrow \infty$ ). However, the configuration of the straight lines of action,  $LA_1$  and  $LA_2$ , is remained the same. Therefore, the straight base line

<sup>6</sup> Generation of a straight-sided rack tooth profile as a reduced case of involute tooth profile developed from the rack *base circle* is not considered in-detail here. The interested reader may wish to go into the problem on his/her own.

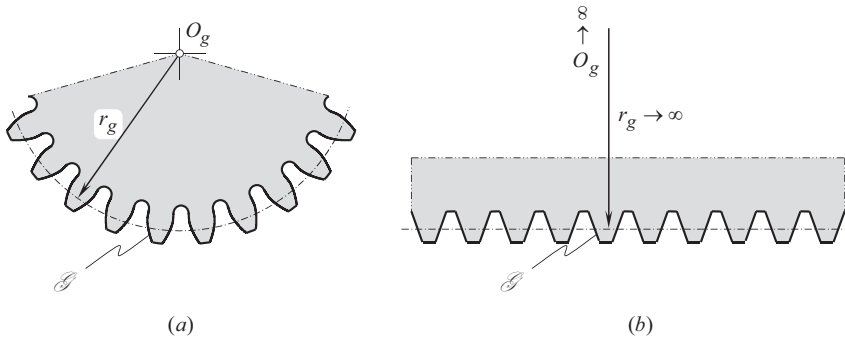


**FIGURE 8.21** On the interpretation of rack-gear as a limit case of an external gear: (a) gear with a certain tooth count,  $N_g$ , and (b) gear with an infinite tooth count,  $N_g \rightarrow \infty$ .

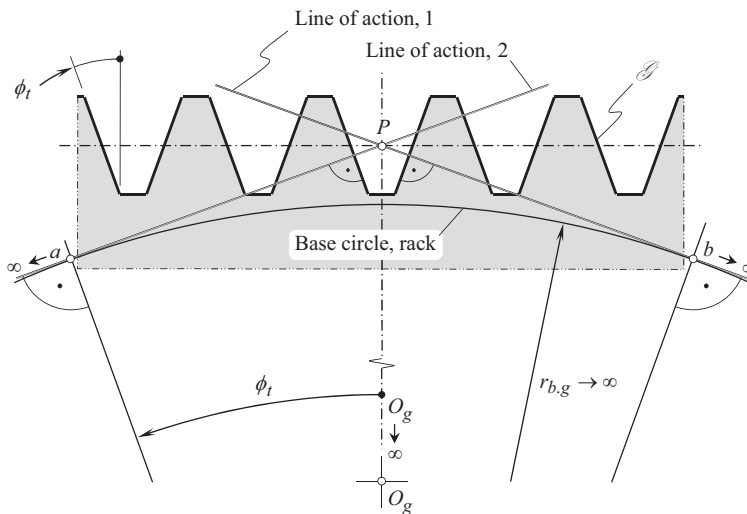


**FIGURE 8.22** Straight-sided rack-gear as a reduced case of involute gear.

intersects the straight lines of action,  $LA_1$  and  $LA_2$ , regardless of how far the center of the gear,  $O_g$ , is remote from the pitch point,  $P$ .

Ultimately, for a rack, we have, from one side, a straight base line that is parallel to the pitch line, and, from another side, this line must be in tangency to two straight lines of action,  $LA_1$  and  $LA_2$ . No straight line fulfills these two contradicting conditions at the same time. These two requirements conflict with each other. Therefore, the interpretation of *rack-gear* as a reduced case of a gear that features an infinite tooth count is ambiguous. Thus, a more in-detail analysis in this regard is required to be undertaken.

The variation intervals for the tooth flank geometry in a *pinion gear-to-rack* gear pair are within a smaller range compared to that in external gear pairs, but exceed that in internal gear pairs.



# Taylor & Francis

Taylor & Francis Group

<http://taylorandfrancis.com>

---

# 9 Gear Tooth Profile Modification

## *Generating Rack Shift*

It is common practice to generate tooth flanks in spur and helical involute gears by means of a straight-sided *generating rack* (or *basic rack*, in other words). The interaction of the basic rack and the gear is observed when the gears are cut on gear hobbers, on gear shaping machines, in generating grinding by means of worm grinding wheel and so forth.

When cutting spur and helical gears, the basic rack can be set up either to a nominal position in relation to the gear or it can be shifted from the nominal configuration. In the second case, the displacement of the basic rack can be pointed either inward or outward relative to the gear to be generated. Commonly the amount of the basic rack shift is specified by *profile shift coefficient*.

### 9.1 ADDENDUM MODIFICATION (TOOTH PROFILE SHIFT)

When gears are produced by a generating process, the datum line of the basic rack profile needs not necessarily form a tangent to the reference circle. The gear tooth form can be altered by shifting the datum line from the tangential position. The involute shape of the tooth profile is retained, and the effect is merely to use parts further from or nearer to the origin of the same involute. The radial displacement from the tangential position is termed the *addendum modification*. The displacement is considered positive when in the direction outward from the center of the gear, and it is considered negative when in the direction toward the center of the gear (applies also to internal spur and helical gears). The effect of addendum modification on the tooth form is shown in Figure 9.1.

The load-carrying capacity of the teeth without addendum modification in Figure 9.1a can be improved by the positive addendum modification, as shown in Figure 9.1b.

The positive/negative displacement of the basic rack makes possible:

- An increase in contact strength of gear/pinion teeth
- An increase in bending strength of gear/pinion teeth
- A reduction of profile sliding
- To inscribe a gear pair into a specified center-distance
- To eliminate (or to reduce) a gear/pinion undercut
- To increase contact ratio

An extremely large addendum modification results in an unsuitable tooth form with pointed teeth.

The tooth form is affected by the addendum modification. The following characteristics of a generated tooth form are particularly significant for its load capacity:

- The transverse profile angle,  $\phi_t$ , because of the relationship between the mean radius of curvature of the tooth flanks and the contact load capacity
- The tooth root thickness, because of the relationship between the modulus of the section and the bending strength at the root of the tooth

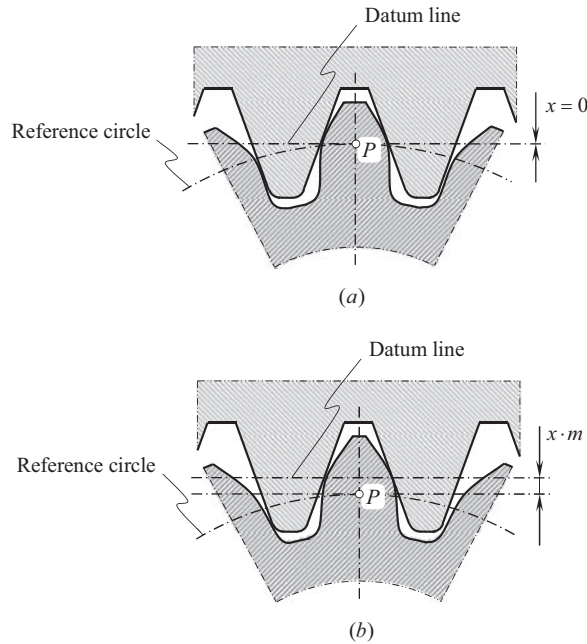


**FIGURE 9.1** Effect of addendum modification on the generated gear tooth profile: (a) zero profile shift, and (b) positive profile shift.

- The fillet radius at the critical point for bending, as at this point a rapid change in the cross-section results in stress concentration
- The crest width, as excessive shear stress at the tip is undesirable, particularly in surface hardened gears.

Two tooth profile zones have to be distinguished: the involute zone and the root fillet. The fillet form is affected greatly by the choice of the basic rack profile. While the tooth depth has to be increased slightly where the fillet forms a continuous, semi-circular area, the tooth root thickness and the fillet radius are improved significantly; thereby, the bending strength can be affected greatly by addendum modification.

Some simplifying assumptions have to be made in the mathematical analysis of the effect of addendum modification on the tooth root thickness:

1. The normal tooth form of a helical gear is deemed to be equivalent to that of a spur gear with a virtual number of teeth,  $N_{eq}$ , where:

$$N_{eq} = \frac{N}{\cos^2 \psi_b \cos \psi} \quad (9.1)$$

2. The tooth root thickness is taken to be the length,  $\bar{l}_f$ , of the chord on the root circle between the points of intersection with the tangents to the lowest points on the left- and right-hand involute flank profiles, as shown in Figure 9.2.

A generating rack profile and a tooth generated thereby are shown in Figure 9.2. The pitch point when machining the gear is denoted by  $P_m$ . When in the course of generating the tooth, the generating rack profile rolls to the right on reference circle,  $d$ , from the position shown and the gear being cut carries out a corresponding clockwise rotation, the right point  $R''$  on the line of action will be reached where the lowest point,  $R$ , of the straight generating rack flanks comes into engagement and

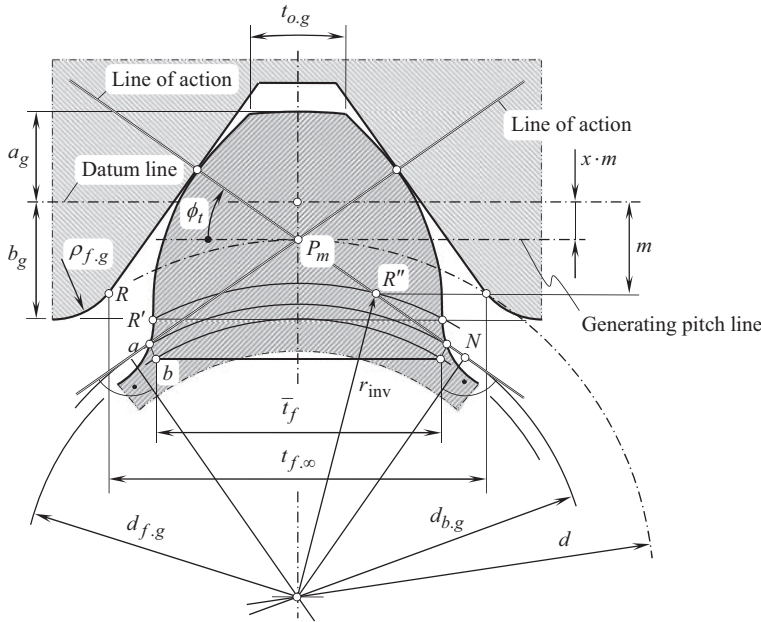


**FIGURE 9.2** Involute gear tooth form generated by the rack.

cuts the bottom point,  $R'$ , on the involute. This point at the beginning of the involute profile has the radius,  $r_{inv}$ . The fillet begins at this point on the gear and is in the form of trochoids.

For the trochoidal fillet to blend tangentially with the involute, the point  $R''$  on the line of action must lie above point,  $N$ . The point,  $N$ , here is the point of intersection between the line of action and a line drawn normal to it through the fillet trochoids that no longer blends tangentially with the involute, but intersects and shortens it.

The chord,  $\bar{t}_f$ , at the root of the tooth shown in Figure 9.2 is governed by the geometry of the involute and is related to the number of teeth,  $N_{eq}$ , and the addendum modification,  $x$ . To measure the chord,  $\bar{t}_f$ , the hypothetical straight line root profile through the points  $a$  and  $b$  is constructed. The largest possible chord dimension,  $t_{f,\infty}$ , is obtained with a rack tooth.

The performed analysis is used for determining a favorable value of the profile shift for a specified gear pair. To enable tooth forms to be compared, curves for various root thickness ratio,  $K_f$ :

$$K_f = \frac{\bar{t}_f}{t_{f,\infty}} \quad (9.2)$$

can be constructed. The root thickness ratio,  $K_f$ , curves are plotted in relation to the number of teeth and their addendum modification coefficient (Figure 9.3).

This is the first method for the determining favorable value of the generating profile shift.

The curves  $K_f = K_f(N_g)$  correlate to those shown in Figure 10.9 (see page 239 in Ref. [152] in the first edition) and in Figure 10.11 (see page 183 in Ref. [152] in the second edition).

Diagrams similar to that shown in Figure 9.3 can be constructed for various values of the transverse profile angle,  $\phi_t$ .

The bottom left region of the diagram is the cutter interference zone. The region of greater specific tooth thickness is reached rapidly by positive addendum modification. As a rough guideline, it can be assumed that below the root thickness ratio  $K_f \approx 0.7$ , poor tooth forms are obtained, which may even lead to meshing interference [81]. With extreme profile modifications, the limit of the feasible crest width of the tooth is reached;  $t_o^*$  is the crest width for a unit module.



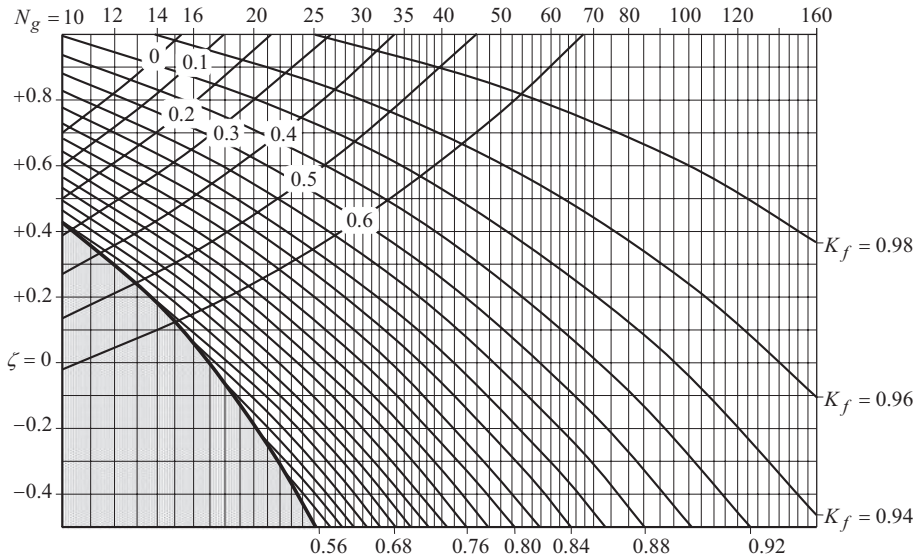


**FIGURE 9.3** Effect of the addendum modification coefficient,  $x$ , on the root thickness ratio,  $K_f$ , and the crest width,  $t_o^*$ , for  $\phi_t = 20^\circ$ ,  $a_a^* = 1.0$ ,  $b_f^* = 1.25$  and  $\rho_{f,\max}^*$ .

## 9.2 PROFILE SHIFT COEFFICIENT

Meshing of the gear-cutting tool with the gear to be machined in the process of the gear machining is commonly referred to as the *gear machining mesh*.

Three different types of gear generating processes are distinguished depending on the configuration of the gear-cutting tool in relation to the work (see Figure 9.4):

1. The pitch line of the gear cutting tool is tangent to the pitch circle of the gear being machining (see Figure 9.4a);
2. The pitch line of the gear cutting tool has no common points with the pitch circle of the gear being machining (see Figure 9.4b);
3. The pitch line of the gear-cutting tool intersects the pitch circle of the gear being machining (see Figure 9.4c).

In the first case (see Figure 9.4a), the so-called *zero setup* of the gear cutting tool is observed. The gear is generated with no profile shift (or, in other words, with zero profile shift):

$$\chi = xm = 0 \quad (9.3)$$

$$x = 0 \quad (9.4)$$

Here,  $\chi$  is the total profile shift,  $x$  is the profile shift coefficient, and  $m$  is module of the gear to be machined.

The gear tooth thickness,  $s$ , is equal to the space width,  $w$ :

$$s = 0.5\pi m \quad (9.5)$$



Therefore, tooth thickness in a gear with a positive profile shift is greater compared to that in a gear with zero profile shift. It is also clear that in a gear with a positive profile, shift tooth thickness is greater compared to the space width.

In the third case (see Figure 9.4c), the so-called *negative setup* of the gear cutting tool is observed. The gear is generated with a negative profile shift:

$$\chi = xm < 0 \quad (9.9)$$

$$x < 0 \quad (9.10)$$

The gear tooth thickness,  $s$ , is smaller compared to the space width,  $w$ , Figure 9.4c:

$$s = 0.5\pi m - 2xm \tan \phi_t \quad (9.11)$$

Therefore, tooth thickness in a gear with a negative profile shift is smaller compared to that in a gear with zero profile shift. It is also clear that in a gear with a negative profile shift tooth thickness is smaller compared to the space width.

Under any circumstances, regardless of the actual value of the gear tooth profile shift, the tooth flanks of gears that have an equal module and equal pressure angle remain conjugate to one another. The radii of the base circles (cylinders) are remained of the same value. According to Figure 9.4, they can be calculated from the formulas:

$$r_b = r \cos \phi_t \quad (9.12)$$

$$r_b = 0.5mz \cos \phi_t \quad (9.13)$$

A performed analysis of Eqs. (9.12) and (9.13) reveals that only the tooth thickness (as well as the space width) is affected by the tooth profile shift. Also, an active portion of the tooth profile depends on the actual value of gear tooth profile shift.

For the calculation of the profile shift factor, the formulae proposed by *Robert Errichello* are known:

$$x_1 = \frac{x_\Sigma}{u+1} + \frac{u-1}{3u} \quad (\text{for speed reducers}) \quad (9.14)$$

$$x_1 = \frac{x_\Sigma}{u+1} \quad (\text{for speed increasers}) \quad (9.15)$$

This is the second method for the determination of favorable value of the generating profile shift.

The use of gears with an appropriate profile shift coefficient allows for designing gearboxes with an improved performance.

### 9.3 GEAR TOOTH FLANK GEOMETRY DEPENDING ON PROFILE SHIFT COEFFICIENT

The profiles of three teeth of a gear with the same tooth count, and with different gear tooth profile shift coefficient are shown in Figure 9.5a. As it follows from the analysis of Figure 9.5a, the gear tooth profile shift coefficients  $x_1$ ,  $x_2$ , and  $x_3$ , relate to one another in the following manner:

$$x_3 > x_2 > x_1 \quad (9.16)$$

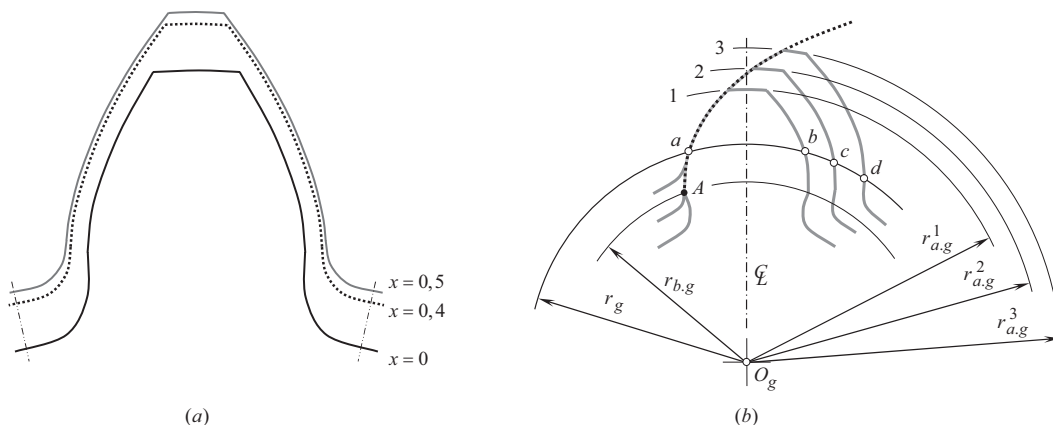


**FIGURE 9.5** Involute tooth profile geometry depending on an actual value of the profile shift coefficient,  $x$  (a), and alignment of the modified tooth profiles with a common involute curve (b).

As the pitch radii, in all the cases, under consideration are of the same value, then, an increase in the gear tooth profile shift coefficient results in a corresponding increase of the gear tooth thickness, namely, the inequalities  $s_3 > s_2 > s_1$  are valid, where  $s_1 = \widehat{ab}$ ,  $s_2 = \widehat{ac}$ , and  $s_3 = \widehat{ad}$  (see Figure 9.5a). The outer radii as well as the fillet radii of the gear also become larger in size. The gear teeth are getting thicker at the fillet diameter, and thinner at the outer diameter. Ultimately, the gear teeth bending strength is improved.

On the other hand, base circles of a gear are remained of those same radii. Therefore, that same involute profile is used as an operating profile of the gear teeth. However, depending on the actual value of the gear tooth profile shift coefficient, different portions of that same involute are used to form the gear tooth profile. Referring to Figure 9.5b, the larger the actual value of the gear tooth profile shift coefficient, the more the working portion of the involute tooth profile is remote from the base (that is, from point A). This immediately entails a corresponding increase in the radius of curvature of the gear tooth profile, and in a corresponding decrease of the contact stress (*Hertz equation*).

The use of gear tooth profile shift makes possible designing gears with various arc segments of that same involute curve: The actual portion of the involute tooth profile of that same involute curve depends on the actual value of the profile shift coefficient, either  $x_1$ , or  $x_2$ .

Finally, tooth profile shift coefficient in a gear and its mating pinion is a powerful tool that can be used in designing gear pairs with a favorable performance.

## 9.4 BASIC EQUATIONS FOR GEAR PAIR WITH ADDENDUM MODIFICATION

For a long while, simple rules of thumb were applied to the gear design geometry, before it was realized that more latitude could be applied to the tooth form. Although the basic rack profile still usually forms the basis because of gear cutter standardization, it was already recognized in the pioneering days of gear generation that the reference circle only has significance in gear production, but not for the running geometry of mating gears.

Dr. *Max Maag*<sup>1</sup> contributed significantly to this development by systematically working out guidelines for obtaining strong tooth forms from a multitude of gear designs for various gear ratios, giving rise to a system now known as the *MAAG-Tooth System* [81].

<sup>1</sup> Max Maag (7 February 1883–16 February 1960), a Swiss engineer; Doctor of engineering, h.c.; inventor; and founder of the MAAG Company.

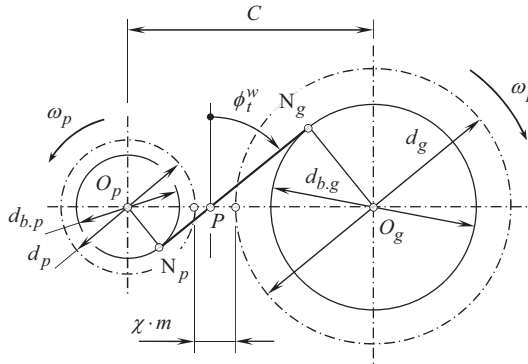


**FIGURE 9.6** An external involute gear pair with a center-distance modification,  $\chi \cdot m$ .

### 9.4.1 PRINCIPLE OF ADDENDUM MODIFICATION

If the sum of the addendum modification coefficients ( $\xi_g + \xi_p$ ) is not zero, then the center-distance does not equal the sum of radii of the reference circle. The working (operating) pressure angle,  $\phi_t^w$ , then differs from the generating transverse pressure angle,  $\phi_t$ . The amount by which the center-distance deviates from the sum of radii of the reference circles is known as the center-distance modification,  $\chi \cdot m$ . The working pressure angle,  $\phi_t^w$  (see Figure 9.6), is given by the formula [81]:

$$\chi \cdot m = C - \frac{d_g + d_p}{2} = \frac{d_g + d_p}{2} \left( \frac{\cos \phi_t}{\cos \phi_t^w} - 1 \right) \quad (9.17)$$

For mating external spur and helical gears, the center-distance modification is always smaller than the sum of the addendum modifications. An addendum shortening of  $k \cdot m$  is therefore necessary to maintain the basic rack profile bottom clearance,  $c_p$  [81]:

$$k \cdot m = \frac{m(N_g + N_p)}{2} \left[ \frac{\text{inv} \phi_t^w - \text{inv} \phi_t}{\tan \phi} - \frac{1}{\cos \psi} \left( \frac{\cos \phi_t}{\cos \phi_t^w} - 1 \right) \right] \quad (9.18)$$

This is the third method for determining the favorable value of the generating profile shift.

The geometric relationship of involute teeth was exploited in the MAAG-Tooth System by choosing relatively large addendum modifications with consequent addendum shortening large enough to avoid excessively pointed teeth. This has resulted in tooth forms with typically high bending strength.

### 9.4.2 EXTERNAL SPUR AND HELICAL GEAR PAIRS

Once the design parameters of each of the two mating gears are given (see Table 9.1), there still remains the choice of the center-distance,  $C$ , which need not necessarily be equal to the reference center-distance,  $C_d = (d_g + d_p) / 2$ , but can be modified by addendum modification subject to the dimensional criteria.

Two of the following three variables must always be specified to fix the tooth geometry. The third variable then follows from the other two (see Table 9.2).

An unconstrained choice of the center-distance,  $C$  (that is, rounded off-center-distance for standardized gear boxes) within the aforementioned dimensional criteria for the sum of the addendum modification coefficients becomes possible with a closely graduated series of formulas.

**TABLE 9.1**  
**Given Design Parameters of a Gear Pair**

Design Parameters	Designation
Pressure Angle (Transverse)	$\phi_t$
Module	$m$
Number of the Gear Teeth	$N_g$
Number of the Pinion Teeth	$N_p$
Addendum of Basic Rack Profile Per Unit Module, $m = 1$	$h_{ap}^*$
Dedendum of Basic Rack Profile Per Unit Module, $m = 1$	$h_{fp}^*$
Pitch Helix Angle	$\psi$

**TABLE 9.2**  
**Design Parameters of a Gear Pair to be Determined**

Design Parameters	Designation
Addendum Modification Coefficient of the Gear	$\xi_g$
Addendum Modification Coefficient of the Pinion	$\xi_p$
Center-Distance (Hence Indirectly $\xi_g + \xi_p$ )	$C$

**First**, when the pinion addendum modification coefficient,  $\xi_p$ , and the center-distance,  $C$ , are given, the gear addendum modification coefficient,  $\xi_g$ , can be calculated using the following formulas [81]:

$$\cos \phi_t^w = \frac{d_{b,g} + d_{b,p}}{2C} \quad (9.19)$$

$$\xi_g + \xi_p = \frac{N_g + N_p}{2} \cdot \frac{\text{inv} \phi_t^w - \text{inv} \phi_t}{\tan \phi} \quad (9.20)$$

$$\xi_g = (\xi_g + \xi_p) - \xi_p \quad (9.21)$$

**Second**, when the pinion and the gear addendum modification coefficients ( $\xi_g$  and  $\xi_p$ ) are given, the center-distance,  $C$ , can be calculated using the following formulas [81]:

$$\text{inv} \phi_t^w = \text{inv} \phi_t + \frac{2(\xi_g + \xi_p) \tan \phi}{N_g + N_p} \quad (9.22)$$

$$C = \frac{d_{b,g} + d_{b,p}}{2 \cos \phi_t^w} \quad (9.23)$$

**TABLE 9.3**  
**Gear Diameters**

Diameters	Equation for the calculation
Gear Reference Diameter	$d_g = \frac{m N_g}{\cos \psi}$
Theoretical Gear Root Diameter	$d_{f.g}^* = d_g - 2m(h_{fp}^* - \xi_g)$
Outside Diameter of the Gear <sup>a</sup>	$d_{C.g} = d_g + 2m(h_{ap}^* + \xi_g) - 2k m$
Pinion Reference Diameter	$d_p = \frac{m N_p}{\cos \psi}$
Theoretical Pinion Root Diameter (Neglecting the Backlash)	$d_{f.p}^* = d_p - 2m(h_{fp}^* - \xi_p)$
Outside Diameter of the Gear <sup>a</sup>	$d_{C.p} = d_p + 2m(h_{ap}^* + \xi_p) - 2k m$

<sup>a</sup> Here  $k \cdot m$  is the addendum shortening.

**Third**, when the gear addendum modification coefficient,  $\xi_g$ , and the center-distance,  $C$ , are given, the pinion addendum modification coefficient,  $\xi_p$ , can be calculated using the following formulas [81]:

$$\cos \phi_t^w = \frac{d_{b.g} + d_{b.p}}{2C} \quad (9.24)$$

$$\xi_g + \xi_p = \frac{N_g + N_p}{2} \cdot \frac{\text{inv } \phi_t^w - \text{inv } \phi_t}{\tan \phi} \quad (9.25)$$

$$\xi_p = (\xi_g + \xi_p) - \xi_g \quad (9.26)$$

Miscellaneous formulas are summarized in Table 9.3.

The formulas above allow for the calculation of the design parameters of spur and helical gears as well as the design parameters of parallel-axis gear pairs.

## 9.5 DETERMINATION OF PROFILE SHIFT COEFFICIENTS: GEOMETRIC BLOCKING CONTOURS

The determination of the gear tooth profile shift coefficients is targeting to ensure:

- Absence of gear tooth undercutting ( $x_1 \geq x_{1,\min}$ ,  $x_2 \geq x_{2,\min}$ );
- Absence of gear tooth pointing ( $x_1 \leq x_{1,\max}$ ,  $x_2 \leq x_{2,\max}$ );
- Continuous engagement of the gear teeth in mesh ( $m_p \geq m_{p,\min}$ ).

This means that there exists a certain permissible interval for the tooth profile shift coefficients of a gear and its mating pinion:

$$x_{1,\min} \leq x_1 \leq x_{1,\max} \quad (9.27)$$

$$x_{2,\min} \leq x_2 \leq x_{2,\max} \quad (9.28)$$

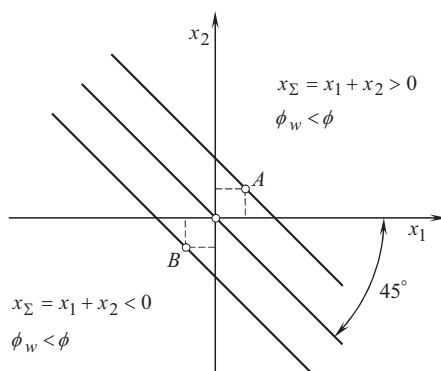


**FIGURE 9.7** Cartesian  $x_1x_2$  coordinate plane.

The relationship between the design parameters of a gear pair and its performance, and between the actual values of the profile shift coefficients  $x_1$  and  $x_2$  can be graphically illustrated in a *Cartesian* coordinate system  $x_1x_2$  (see Figure 9.7) by means of planar curves constructed for every combination of the tooth count in the gear,  $N_g$ , and its mating pinion,  $N_p$ . Every point of the *Cartesian* coordinate plane,  $x_1x_2$ , corresponds to a gear pair with a certain value of the profile shift coefficients,  $x_1$  and  $x_2$ . The origin of the coordinate system,  $x_1x_2$ , corresponds to a so-called *gear pair* that features the profile shift coefficients,  $x_1$  and  $x_2$ , of a zero value, that is,  $x_1 = 0$  and  $x_2 = 0$ . Point A corresponds to a *positive gear pair* for which  $x_1 > 0$  and  $x_2 > 0$ . Point B corresponds to a *negative gear pair* for which  $x_1 < 0$  and  $x_2 < 0$ .

A straight line that forms a  $45^\circ$  angle with the  $x_1$  - axis corresponds to a certain value of the total profile shift coefficient  $x_\Sigma = x_1 + x_2$ , and, thus, with a specific value of pressure angle,  $\phi_w$ . A straight line through the origin of the coordinate system  $x_1x_2$  corresponds to the so-called *equally shifted gear pairs* that feature a zero total profile shift coefficient  $x_\Sigma = 0$ . Gear pairs with a positive  $x_\Sigma > 0$  (and, thus, with an increased pressure angle,  $\phi_w > \phi$ ), correspond to points of the coordinate system  $x_1x_2$  that are located above the straight line  $x_\Sigma = 0$ . Gear pairs with a negative  $x_\Sigma < 0$  (and, thus, with a reduced pressure angle,  $\phi_w < \phi$ ), correspond to points of the coordinate plane  $x_1x_2$  that are located below the straight line  $x_\Sigma = 0$ .

Not all the points of the coordinate plane,  $x_1x_2$ , correspond to a workable gear pair. Tooth profile interference, reduction of the total contact ratio ( $m_t < 1$ ), tooth pointing, tooth profile undercut, and so forth, can be observed for a certain combination of the profile shift coefficients,  $x_1$  and  $x_2$ . In the coordinate system,  $x_1x_2$ , the limit values of each of these factors can be graphically interpreted by means of a corresponding planar curve. The area of permissible, and the area of not permissible values of the profile shift coefficients,  $x_1$  and  $x_2$ , are separated from one another by such a curve. A permissible area of the profile shift coefficients,  $x_1$  and  $x_2$ , is bounded within the coordinate plane,  $x_1x_2$ , by a set of graphs constructed for the limit values of the design parameters of a gear pair. The contour constructed in this manner is commonly referred to as the *geometric blocking contour* of a gear pair.<sup>2</sup> An example of a blocking contour for a gear pair with the tooth counts  $N_g = 28$  and  $N_p = 20$  is depicted in Figure 9.8. The hatching lines indicate the not permissible area for the profile shift coefficients,  $x_1$  and  $x_2$ .

In Figure 9.8, the geometric blocking contour is bounded by the following lines:

1. The line of zero interference within the gear tooth dedendum
2. The line of undercut of the pinion tooth profile

<sup>2</sup> Engineer M.B. Groman, of the USSR is credited for the idea of the, so-called, *geometric blocking contours*. He was the first to propose the concept of the geometric blocking contours in his 1952 and 1955 papers:

Groman, M.B., "On Blocking Contours for Involute Gearing," *Vestnik Mashinostroyeniya*, 1952, No. 12, pages 12–17.

Groman, M.B., "On Selection of Profile Corrections for Gear Transmissions," *Vestnik Mashinostroyeniya*, 1955, No. 2, pages 3–13.



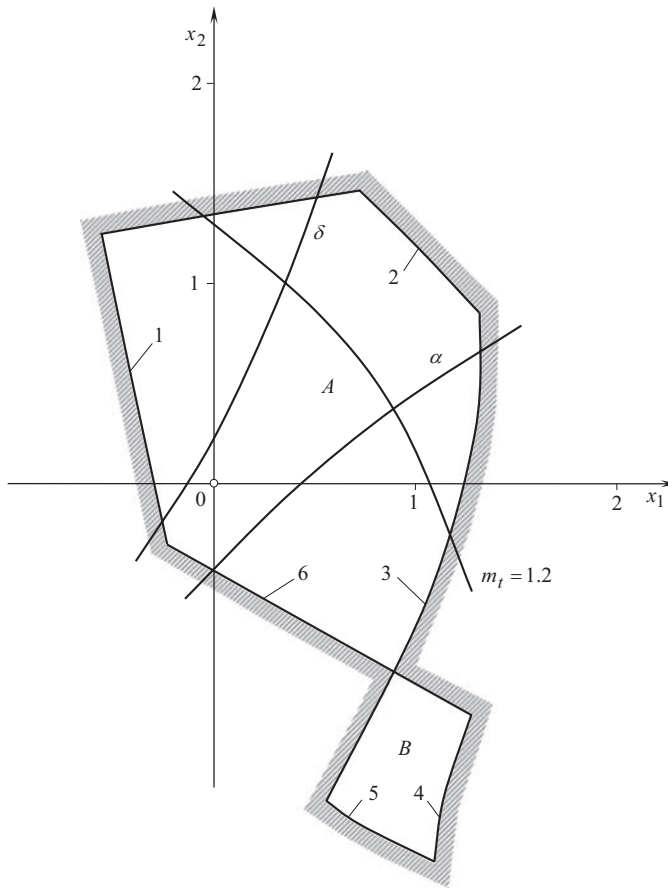


**FIGURE 9.8** An example of geometric blocking contour constructed for a gear pair with the tooth count  $N_g = 28$  and  $N_p = 20$ .

3. The line of the limit contact ratio
4. The line of zero interference within the pinion tooth dedendum
5. The line of undercut of the gear tooth profile
6. The line of pointing of the pinion tooth profile

Gear pairs that correspond to zone *A* in Figure 9.8, feature the interaction of the gear and the mating pinion tooth profiles from both sides of the pitch point; gear pairs that correspond to zone *B* in Figure 9.8, feature the interaction of the gear and the pinion tooth profiles only from one side of the pitch point.

The lines that form a blocking contour are the undisputable boundaries of an area within the coordinate plane,  $x_1x_2$ , outside of which no workable gear pair is feasible. Additional lines can be traced inside a blocking contour, that is, the lines that correspond to certain values of parameters of a gear pair:

- a.  $\alpha$  and  $\delta$  are the lines of equal tooth bending strength ( $\alpha$  – when the pinion is driving, and  $\delta$  – when the gear is driving)
- b.  $m_t = 1,2$  is the recommended value of the tooth contact ratio

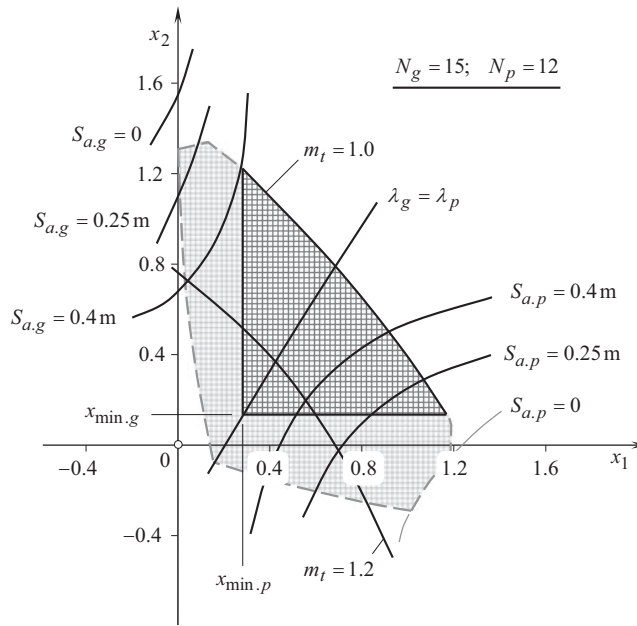


**FIGURE 9.9** An example of geometric blocking contour constructed for a gear pair with the tooth count  $N_g = 15$  and  $N_p = 12$  ( $\lambda_g$  and  $\lambda_p$  are the specific sliding of the gear and the pinion).

A geometric blocking contour can be constructed for any parallel-axes gear pair. In Figure 9.9, a geometric blocking contour for a spur gear pair with the tooth counts  $N_g = 15$  and  $N_p = 12$  is shown.

An area of the permissible values of the profile shift coefficients,  $x_1$  and  $x_2$ , is shown in dark black color. On the left side and at the bottom, this area is bounded by the condition of absence of undercut of the gear teeth ( $x_1 = x_{1,\min}$  and  $x_2 = x_{2,\min}$ ). On the right side, this area is bounded by the condition of continuous engagement of the gear teeth in mesh ( $m_p \geq m_{p,\min}$ ). An analysis of Figure 9.9 shows that the conditions of the gear and the mating pinion tooth pointing ( $s_{a,1} = 0$  and  $s_{a,2} = 0$ ) are out of the permissible area of variation of the profile shift coefficients,  $x_1$  and  $x_2$ . This reveals that for a spur gear pair with the tooth count,  $N_g = 15$  and  $N_p = 12$ , the limitation on  $m_p \geq m_{p,\min}$  is more severe compared to that on gear/pinion tooth pointing.

In gray color dashed lines (see Figure 9.9), an enhanced area for the permissible values of the profile shift coefficients,  $x_1$  and  $x_2$ , is shown. An enhanced area for the coefficients  $x_1$  and  $x_2$  has limited applications.

A set of iso-lines of a favorable value of the parameters of performance of the gear pair are traced within the area of the permissible values of the profile shift coefficients,  $x_1$  and  $x_2$ . The iso-lines are helpful for the proper selection of the coefficients  $x_1$  and  $x_2$ .

The method that is based on the application of geometric blocking contours is the fourth method for the determination of favorable value of the generating profile shift.

Geometric blocking contours are a powerful tool for designing perfect parallel-axes gear pairs. The concept of geometric blocking contours can be enhanced to the area of intersected-axes gear pairs as well as to the area of crossed-axes gear pair.



# Taylor & Francis

Taylor & Francis Group

<http://taylorandfrancis.com>

# 10 Interaction of Tooth Flanks in Parallel-Axes Involute Gearing

In parallel-axes gearing power from a driving shaft (from a pinion in gear reducers or from a gear in gear increasers) is transmitted to a driven shaft (to a gear in gear reducers or to a pinion in gear increasers) by means of two gears engaged in mesh with one another, as illustrated in Figure 10.1. When a rotary motion is transmitted by means of gearing, involute tooth flanks of a gear and that of a mating pinion interact with one another. The power from a driving shaft to a driven shaft is transmitted through a line of contact between the interacting tooth flanks. A gear tooth flank,  $\mathcal{S}$ , can be generated by means of a desirable line of contact,  $LC_{des.g}$ . Similarly, a mating pinion tooth flank,  $\mathcal{P}$ , can be generated by means of a desirable line of contact,  $LC_{des.p}$ . The desirable lines of contact,  $LC_{des.g}$  and  $LC_{des.p}$ , of a gear and of a mating pinion align with the actual line of contact,  $LC$ , in the gear pair (i.e., the lines  $LC_{des.g}$ ,  $LC_{des.p}$ , and  $LC_{des}$ , are congruent to one another).

It is convenient to begin the analysis of the interaction of tooth flanks in parallel-axes involute gearing with the analysis of spur parallel-axes involute gearing.

## 10.1 INTERACTION OF TOOTH FLANKS IN SPUR INVOLUTE GEARING

An example of spur parallel-axes gear pair is shown in Figure 10.2.

A schematic that illustrates the interaction of the tooth flanks,  $\mathcal{S}$  and  $\mathcal{P}$ , of a spur gear and its mating pinion in parallel-axes involute gearing is depicted in Figure 10.3. The interaction of tooth flanks,  $\mathcal{S}$  and  $\mathcal{P}$ , in a spur gear pair is still considered in a tight connection with an *equivalent pulley-and-belt transmission*, constructed for a considered parallel-axes gear pair.

In Figure 10.3, the axes of rotation,  $O_g$  and  $O_p$ , are parallel to each other and are positioned at a center-distance,  $C$ , from one another. The gear is rotated about its axis of rotation,  $O_g$ . The rotation



**FIGURE 10.1** Example of application of parallel-axes helical involute gear pair.



**FIGURE 10.2** Spur involute gear pair.

of the gear is specified by a rotation vector,  $\omega_p$ . A mating pinion is rotated about its axis of rotation,  $O_p$ . The rotation of the pinion is specified by a rotation vector,  $\omega_p$ .

The axis of instantaneous rotation,  $P_{ln}$ , is a straight line that is entirely located within a plane through the axes of rotation,  $O_g$  and  $O_p$ , of a gear and its a mating pinion. The axis of instantaneous rotation,  $P_{ln}$ , is parallel to the axes of rotation,  $O_g$  and  $O_p$ .

The line of contact,  $LC$ , in a parallel-axes spur involute gear pair is a straight line parallel to the axis of instantaneous rotation,  $P_{ln}$ . In a particular configuration of the gears, shown in Figure 10.3, the line of contact,  $LC$ , is aligned with the axis of instantaneous rotation,  $P_{ln}$ .

The plane of action,  $PA$ , in parallel-axes spur involute gear pair is a plane through the axis of instantaneous rotation,  $P_{ln}$ . The plane of action,  $PA$ , and a perpendicular to the centerline,  $C$ , form a transverse pressure angle,  $\phi_t$ . The plane of action,  $PA$ , is tangent to both the gear base cylinder of a radius,  $r_{b,g}$ , and the pinion base cylinder of a radius,  $r_{b,p}$ . When the gears rotate, the plane of action travels straight with a linear velocity,  $V_{pa}$ , as shown in Figure 10.3.

Analysis of interaction of tooth flanks,  $\mathcal{S}$  and  $\mathcal{P}$ , of a gear and a mating pinion is commonly performed in transverse section of parallel-axes gear pair, as illustrated in Figure 10.4.

The straight-line segments  $N_g N_g$  and  $N_p N_p$  are the lines of tangency of the plane of action,  $PA$ , and the base cylinders of a gear and a mating pinion, correspondingly.

The tooth flanks of an involute gear,  $\mathcal{S}$ , and that of a mating pinion,  $\mathcal{P}$ , interact with one another within the effective face-width,  $F_{pa}$ , of the plane of action,  $PA$ . Commonly, a gear is designed so as to make the gear face-width,  $F_g$ , smaller compared to the pinion face-width,  $F_p$  (i.e., an inequality  $F_g < F_p$  is commonly valid). Under such a scenario, the effective face-width,  $F_{pa}$ , of the plane of action,  $PA$ , equals to the gear face-width, thus, an equality  $F_{pa} = F_g$  is observed (see Figure 10.5a). Otherwise, when a gear face-width,  $F_g$ , is larger than the pinion face-width,  $F_p$  (i.e., an inequality  $F_g > F_p$  is valid), then the effective face-width,  $F_{pa}$ , of the plane of action,  $PA$ , equals to the pinion face-width, thus, and an equality  $F_{pa} = F_p$  is observed. In the case of improperly aligned gears, the effective face-width,  $F_{pa}$ , of the plane of action,  $PA$ , equals to the corresponding overlap of the face-widths,  $F_g$  and  $F_p$ , of the gear and a mating pinion as is illustrated in Figure 10.5b.

With that said, the term *effective face-width*,  $F_{pa}$ , can be defined as follows:

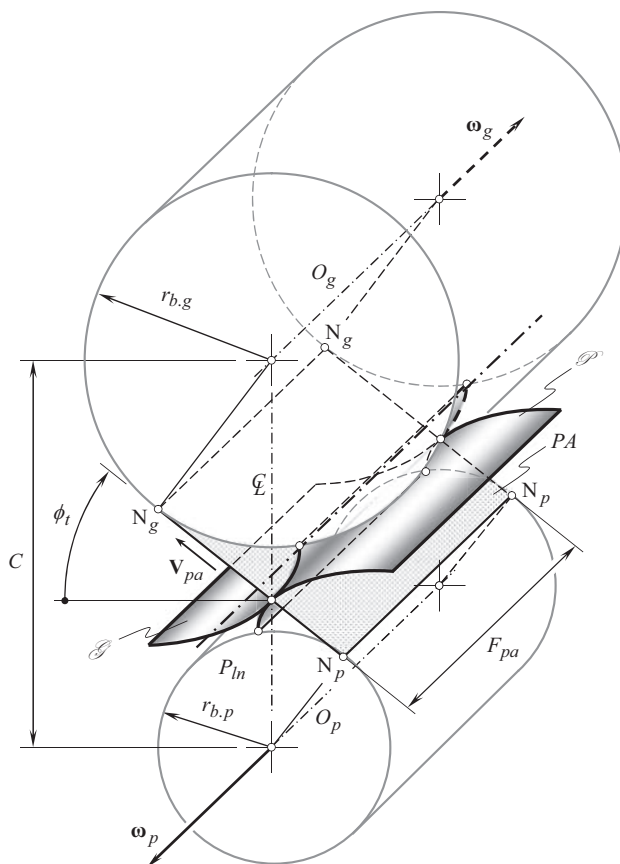


**FIGURE 10.3** Interaction of tooth flanks,  $\mathcal{S}$  and  $\mathcal{P}$ , of a gear and a mating pinion in parallel-axes gear pair composed of spur involute gears.

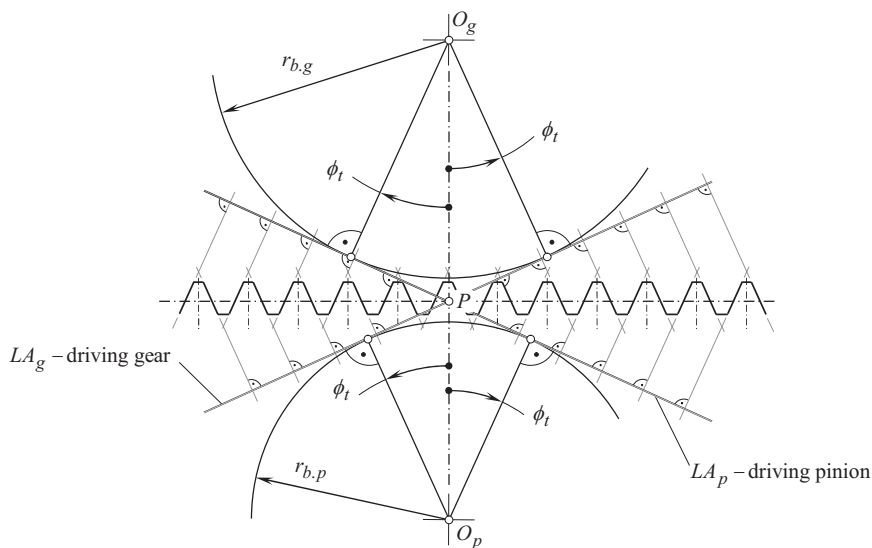


**FIGURE 10.4** Interaction of tooth flanks,  $\mathcal{S}$  and  $\mathcal{P}$ , of a gear and of a mating pinion in transverse section of parallel-axes gear pair.

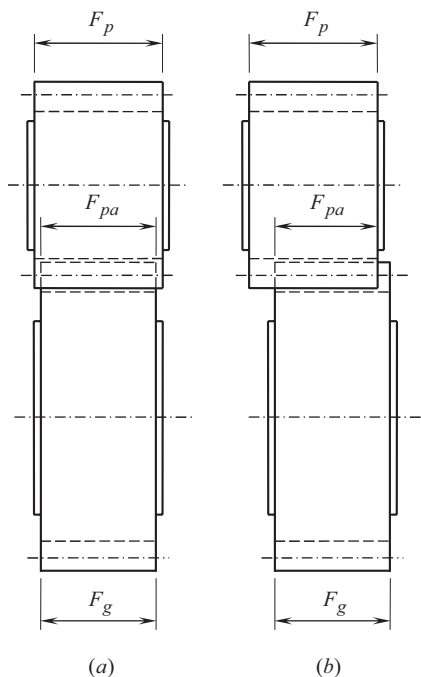


**FIGURE 10.5** Gear face-width,  $F_g$ , pinion face-width,  $F_p$ , and effective face-width,  $F_{pa}$ , in (a) properly, and (b) improperly aligned gears in the gear pair.

### Definition 10.1

Effective face-width,  $F_{pa}$ , in a parallel-axes gear pair is the width of the portion of the plane of action,  $PA$ , within which a gear and its mating pinion tooth flanks,  $\mathcal{S}$  and  $\mathcal{P}$ , interact with one another; the effective face-width is measured parallel to the axis of instantaneous rotation,  $P_{ln}$ .

A problem of the determination of the effective face-width,  $F_{pa}$  (see Figure 10.5), which commonly is simple, becomes more complex in special cases of parallel-axes gearing, for example, in a case of swash plate gear pair depicted in Figure 10.6. The effective face-width,  $F_{pa}$ , in swash plate gearing is time-dependent, and depends on the actual angular configuration of the mating gears.

Another example of time-dependent face-width in a gear is illustrated in Figure 10.7. Simple from the first glimpse, this case features the plane of action,  $PA$ , of a complex geometry with variable face-width,  $F_g$ : when the gear rotates about its axis of rotation, the effective face-width alters in time in accordance with a current configuration of the gear in relation to the plane of action,  $PA$ . Considered together with a face-width of a mating pinion, the gear face-width returns the ultimate effective face-width of the gear pair,  $F_{pa}$ .

Improper mounting of the gears in parallel-axes gear sets as well as large chamfers can affect the actual value of the effective face-width of the gear pair,  $F_{pa}$ . Figure 10.8 illustrates a significant reduction of the effective face-width,  $F_{pa}$ , caused by improper mounting of the gears, and due to large chamfers on the ends of the gears' teeth with a regular tooth count (see Figure 10.8a), and in a low-tooth-count gearing (see Figure 10.8b). A variation of the effective face-width becomes more severe in gears with a narrow face-width,  $F_{pa}$ .

The aforementioned *Definition 10.1* can be adjusted to the cases of variable in time instantaneous effective face-width,  $F_{pa}^{\text{inst}}$ .

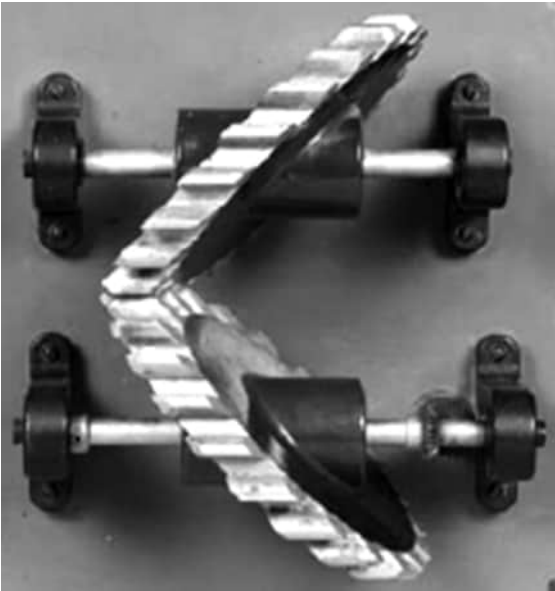


**FIGURE 10.6** A swash plate gear pair features plane of action of a complex geometry with a variable in time configuration of the effective face-width,  $F_{pa}$ .

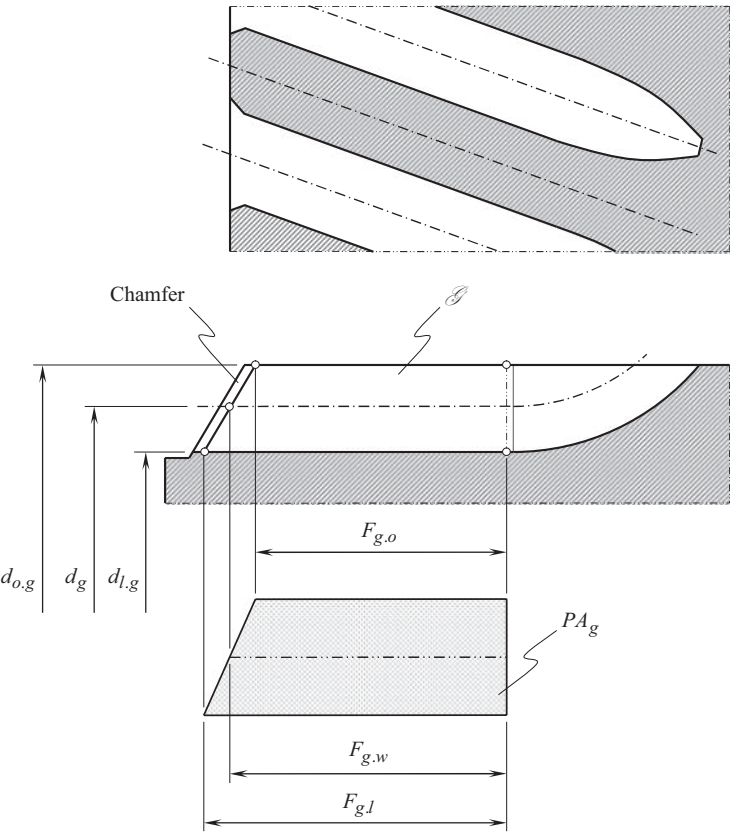


**FIGURE 10.7** Variable face-width,  $F_g$ , in a helical gear with chafer at one end.



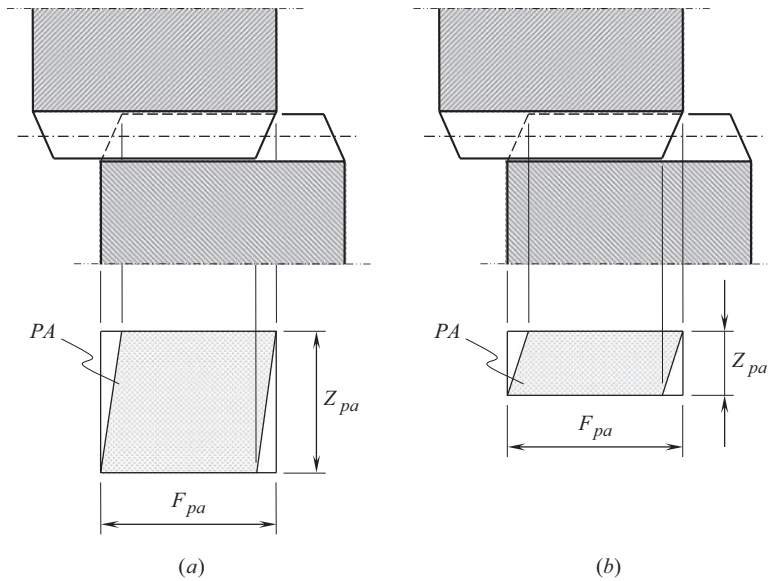


**FIGURE 10.8** Effective face-width,  $F_{pa}$ , in improperly mounted parallel-axes gears having large chamfer: (a) gears with a regular tooth count, and (b) gears with a low-tooth-count.

## 10.2 INTERACTION OF TOOTH FLANKS IN HELICAL INVOLUTE GEARING

An example of helical parallel-axes gear pair is shown in Figure 10.9. A schematic that illustrates the interaction of the tooth flanks,  $\mathcal{S}$  and  $\mathcal{P}$ , of a helical gear and its mating pinion in parallel-axes involute gearing is illustrated in Figure 10.10. The interaction of the tooth flanks,  $\mathcal{S}$  and  $\mathcal{P}$ , in a helical gear pair is still considered in tight connection with the corresponding *equivalent pulley-and-belt transmission*.

In Figure 10.10, a helical gear is rotated about its axis of rotation,  $O_g$ . The rotation of the gear is specified by a rotation vector,  $\omega_g$ , of the gear. A mating helical pinion is rotated about its axis of rotation,  $O_p$ . The rotation of the pinion is specified by a rotation vector,  $\omega_p$ , of the pinion. The axes of rotation,  $O_g$  and  $O_p$ , are parallel to one another and are positioned at a center-distance,  $C$ , from each other.

The axis of instantaneous rotation,  $P_{ln}$ , is a straight line that is entirely located within a plane through the axes of rotation,  $O_g$  and  $O_p$ , of a gear and a mating pinion. The axis of instantaneous rotation,  $P_{ln}$ , is parallel to the axes of rotation,  $O_g$  and  $O_p$ .



**FIGURE 10.9** A gear pair composed of two helical involute gears.

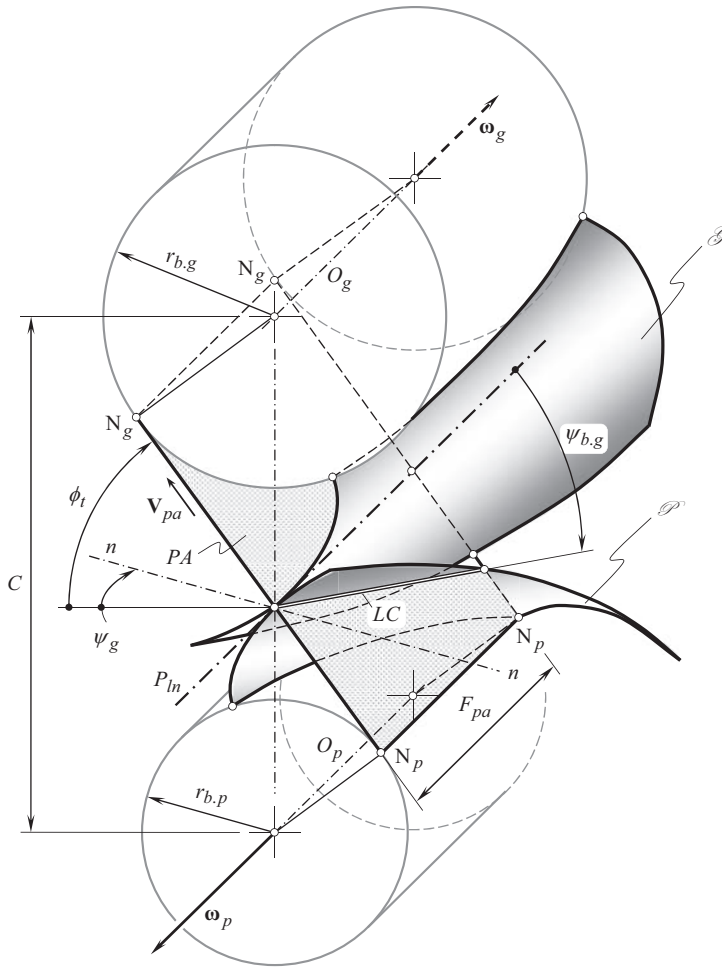


**FIGURE 10.10** Interaction of tooth flanks,  $\mathcal{S}$  and  $\mathcal{P}$ , of a gear and of a mating pinion in parallel-axes helical involute gearing.

The line of contact,  $LC$ , is a straight line. This straight line and the axis of instantaneous rotation,  $P_{ln}$ , form an angle. This angle is commonly referred to as the *base helix angle*,  $\psi_{b.g}$ . An example of straight line of contact,  $LC$ , in parallel-axes helical involute gear pair is shown in Figure 10.10. Helix angle of a gear on the pitch cylinder,  $\psi_g$ , is measured within a common plane. This plane, by nature, is the pitch plane in the gear pair. It goes through the axis of instantaneous rotation,  $P_{ln}$ , perpendicular to the centerline,  $\mathfrak{L}$ . The perpendicular,  $n-n$ , to the axis of instantaneous rotation,  $P_{ln}$ , is entirely located within the pitch plane.

The plane of action,  $PA$ , in parallel-axes helical involute gear pair is a plane through the axis of instantaneous rotation,  $P_{ln}$ . The plane of action,  $PA$ , forms the transverse pressure angle,  $\phi_t$ , with a perpendicular to the centerline,  $\mathfrak{L}$ . The plane of action,  $PA$ , is tangent to both the gear base cylinder of a radius,  $r_{b.g}$ , and the pinion base cylinder of a radius,  $r_{b.p}$ . When the gears rotate, the plane of action travels steadily with a linear velocity,  $V_{pa}$ , as illustrated in Figure 10.10.

The straight-line segments  $N_g N_g$  and  $N_p N_p$  are the lines of tangency of the plane of action,  $PA$ , and the base cylinders of a gear, and of a mating pinion, correspondingly.

Involute tooth flanks of a gear,  $\mathcal{S}$ , and of its mating pinion,  $\mathcal{P}$ , interact with one another within the effective face-width,  $F_{pa}$ , of the plane of action,  $PA$ .

### 10.3 TRANSMISSION OF UNIFORM ROTARY MOTION BY GEAR TEETH IN PARALLEL-AXES INVOLUTE GEARING

A uniform rotary motion can be transmitted smoothly by means of gear teeth of parallel-axes involute gearing. A schematic of parallel-axes gear pair associated with a corresponding *equivalent pulley-and-belt transmission* (Figure 10.11). The belt that is stretched between the two pulleys, corresponds to the line of action,  $a_g c_p$ , in Figure 10.11. A distance traveled by point,  $i$ , on the belt, corresponds with the one, described by the point of contact between the tooth flanks along the line of action. The angle formed by the perpendicular to the centerline,  $\phi$ , with the line of action is the transverse pressure angle,  $\phi_t$ .

For smooth engagement of successive teeth, the arc length along the base circle between the origins of the involutes for successive corresponding tooth flanks, namely, the base pitch, must be uniform for each gear, and identical to that of the mating gear: *Base pitches of mating gears must be equal to one another*. By definition of involute of a circle, the distance on the line of action between the points of contact of successive tooth flanks of the same hand is equal to the base pitch.

The analogy between involute gears and the *equivalent pulley-and-belt transmission* extends even further. Neither system is tied to a fixed center-distance so that the center-distance can be increased or decreased for either system without impairing its function (see Figure 5.2, in Chapter 5). Similarly, the gear ratio (or transmission ratio) is given by the base circles, or the pulley diameters, ratio in each case. The possibility of extending the center-distance gives the involute gear an appreciable advantage over the gears with other tooth profiles. The extent of the modification of the center-distance is restricted in practice by the limits imposed on the tip and root circles of the involute profile. The minimum and the maximum center-distances are determined by two conditions: On the one hand, meshing interference must not occur at the root of the tooth; on the other hand, the next tooth must have already entered into engagement prior to the previous tooth leaving the engagement, that is, the transverse contact ratio must be greater than 1.

An increase in the center-distance immediately entails a corresponding increase in the pressure angle,  $\phi$ , in a gear pair. If, for example, the center-distance increases/decreases from  $C$  (as in Figure 10.11) to  $C \pm \Delta C$  (as in Figure 10.12), then the pressure angle also increases/decreases, namely from a value of  $\phi$ , as schematically shown in Figure 10.11, to a value of  $\phi_t \pm \Delta \phi_t$  (see Figure 10.12).

Uniform motion transmission between two parallel axes is possible only if the line of action at any and all configurations of the mating gears passes through a fixed point known as the *pitch point*,  $P$ :

*Two tooth profiles in parallel-axes gearing are said to be conjugate if the line of action, LA, passes through a desirable pitch point, P, for each angular position of the driving gear at any and all configurations of the mating gears.*

### 10.4 CONTACT RATIO IN PARALLEL-AXES GEARING

Interaction between tooth flanks of a gear and a mating pinion resembles that in a cam mechanism. In both cases, the working surfaces of a driving member push over the working surfaces of the driven member. The key difference between parallel-axes gearing and cam mechanism is that in a gear pair at certain instants of time two or even more pairs of teeth make contact at that same time.<sup>1</sup> The latter is required by a continuous rotation transmission. In order to provide a smooth continuous flow of power, at least one pair of teeth must be in contact at all times. This means that during a part of the meshing cycle, two pairs of teeth will be sharing the load. The second pair of teeth must be designed such that they will pick up their share of the load and be prepared to assume the full load before the first pair of teeth goes out of action.

To ensure continuity of action, base pitch of a gear, and that of a mating pinion must be equal to operating base pitch of the gear pair.

<sup>1</sup> To a certain extent, gearing may be construed as a cam mechanism that features a plurality of simultaneously operating cams.

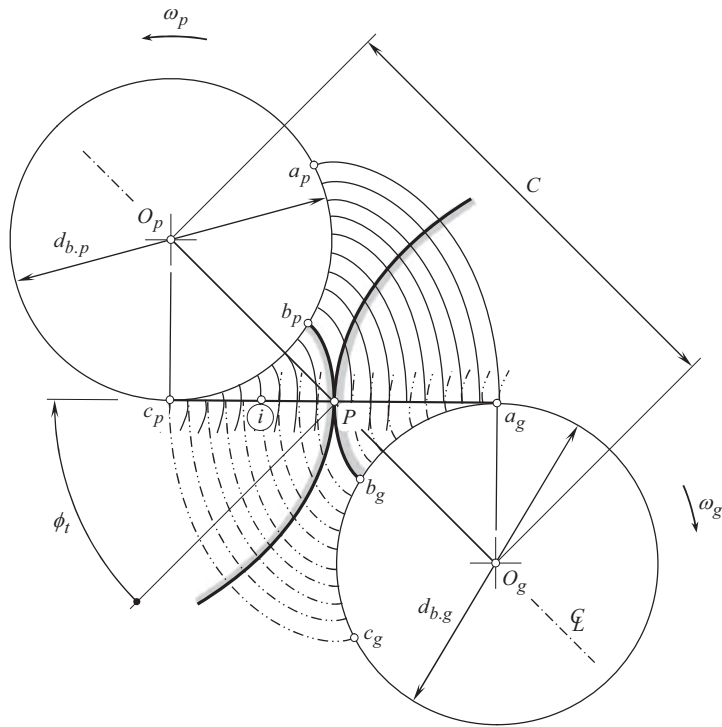


FIGURE 10.11 Interaction of involute profiles in transverse section of parallel-axes gearing.

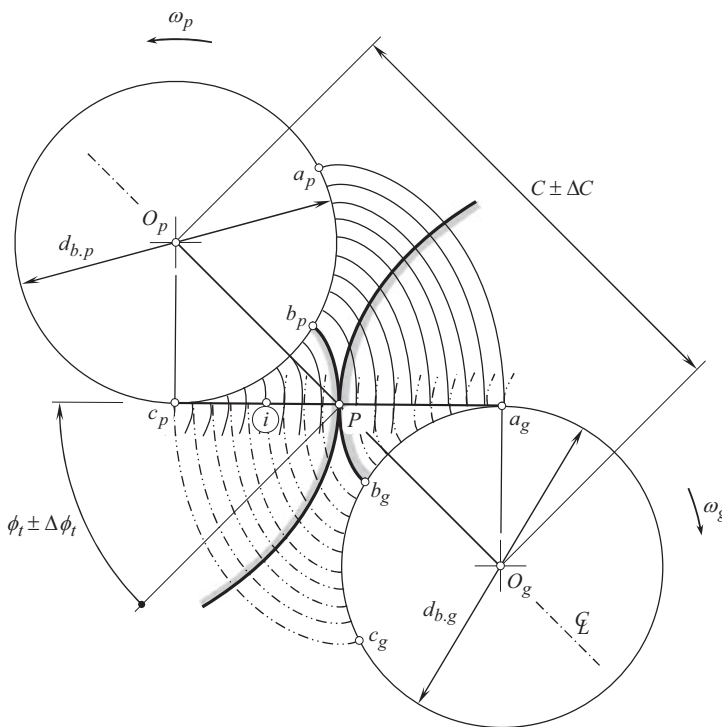


FIGURE 10.12 Schematic that illustrates insensitivity of involute gearing to alteration of the center-distance.

**Reminder:** *All three base pitches in a gear pair are measured within a plane of action of the gear pair; if no plane of action can be constructed for a particular gear pair, such a gear pair cannot be referred to “geometrically accurate gear pair”; only one pair of teeth is in contact at every instant of time in gearing having no plane of action.*

It is clear now that only involute gears feature the contact ratio greater than one. No gear ratio can be specified in gear systems of other designs, namely, in cycloid gears, and so forth. In all non-involute gears, only one pair of teeth makes contact at all times. However, this does not mean that the contact ratio in non-involute gears equals to one – in non-involute of all designs the contact ratio cannot be specified at all.

For smooth transition of tooth contact from one pair of teeth to another pair, there must be one or more pairs of teeth in contact at every instant of time. To transmit a continuous rotation from a driving shaft to a driven shaft, at least one pair of teeth must be engaged in mesh at every instant of time. The transmission of rotation is interrupted when this condition is violated. The average number of pairs of teeth of a gear and a mating pinion that are engaged in mesh at that same time is specified by the *contact ratio*. Commonly, the contact ratio is designated as  $\bar{m}$ .

In addition to the already considered three fundamental laws of gearing, the following inequality is required to be fulfilled:

$$\bar{m} \geq 1 \quad (10.1)$$

when transmission of uniform rotary motion from a driving shaft to a driven shaft by means of gear teeth<sup>2</sup> is required.

The contact ratio,  $\bar{m}$ , in a parallel-axes gear pair, can be expressed in terms of the actual length of the zone of action,  $Z_{pa}$ , and a transverse base pitch,  $p_{b,g}$ , of the gear pair. Therefore, in order to calculate the contact ratio,  $\bar{m}$ , length of the zone of action,  $Z_{pa}$  (or, in other words, the length of active portion of the line of action,  $LA$ ) is required to be calculated.

#### 10.4.1 LENGTH OF ZONE OF ACTION IN PARALLEL-AXES GEARING

The kinematics and elements of the geometry of parallel-axes gearing are involved when the actual length of the zone of action is required to be calculated. One of two possible configurations of the plane of action,  $PA$ , in parallel-axes gear pair can be used for this purpose (see Figure 10.13).

##### 10.4.1.1 Preliminary Remarks

It is convenient to begin the discussion on the length of zone of action in parallel-axes gearing referring to a schematic of parallel-axes gear pair associated with a corresponding *equivalent pulley-and-belt transmission*, shown in Figure 10.14.

The axis of rotation of the gear,  $O_g$ , and that of the mating pinion,  $O_p$ , are parallel to each other and are positioned at a center-distance,  $C$ , from one another. The base cylinder of a diameter  $d_{b,g}$  is associated with the gear. Similarly, the base cylinder of a diameter  $d_{b,p}$  is associated with the pinion. The transverse pressure angle in the gear pair is  $\phi_t$ . The plane of action,  $PA$ , in external parallel-axes gear pair is tangent to the base cylinders from their opposite sides. The gear and the pinion rotate,  $\omega_g$  and  $\omega_p$ , about their axes of rotation,  $O_g$  and  $O_p$ . The magnitudes,  $\omega_g$  and  $\omega_p$ , of the rotation vectors,  $\omega_g$  and  $\omega_p$ , are synchronized with one another reciprocal to the tooth count,  $N_g$  and  $N_p$ , of the gear<sup>3</sup> and the pinion, that is, the ratio:

<sup>2</sup> Note that in parallel-axes gearing, the *contact ratio* can be specified only for involute gearing. No *contact ratio* can be specified in gearing that features other tooth flank geometry, as neither a plane of action,  $PA$ , nor transverse base pitch,  $p_{b,t}$ , can be defined in parallel-axes non-involute gearing.

<sup>3</sup> In internal gearing, tooth count of the gear,  $N_g$ , is of a negative value,  $N_g < 0$ .

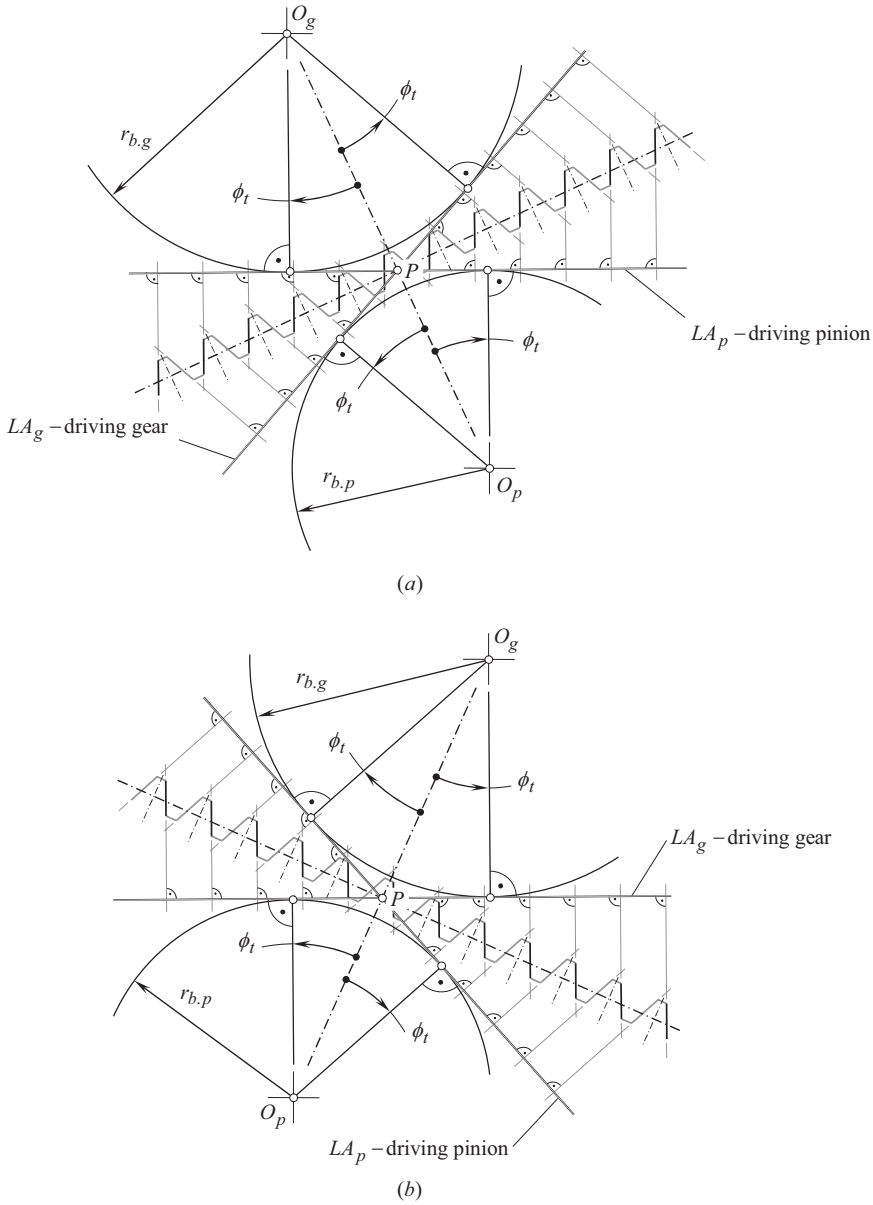


**FIGURE 10.13** Two possible configurations of the plane of action, *PA*, in parallel-axes gear pair: (a) having the pinion driving, and (b) having the gear driving.

$$\frac{\omega_g}{\omega_p} = \frac{N_p}{N_g} \quad (10.2)$$

is valid in *geometrically accurate* parallel-axes gearing.

When the gears rotate, the plane of action can be construed as a zero-thickness film that is unwrapping from the base cylinder of the driven (of the gear) and is wrapping on the base cylinder of the driver (of the pinion). In such a motion, the plane of action travels straight with a linear velocity,  $\mathbf{V}_{pa}$ . The magnitude,  $V_{pa}$ , of the linear velocity vector,  $\mathbf{V}_{pa}$ , is timed with the rotations,  $\omega_g$  and  $\omega_p$ , so as to ensure rolling with no slippage of the plane of action, *PA*, over the base cylinders of the gear and the mating pinion.



end-points  $G_{cap}$  and  $P_{cap}$ , as illustrated in Figure 10.14. These two lines form an effective portion of the plane of action in the form of a rectangle. The length of the effective portion of the plane of action is the so-called the *length of zone of action*,  $Z_{pa}$ .

### Definition 10.2

The active portion of the plane of action is a portion of the plane of action,  $PA$ , that is located within the effective face-width,  $F_{pa}$ , of a gear pair, and is bounded by the lines of intersection of the  $PA$  by the outer surfaces of a gear and that of its mating pinion.

Sometimes, the active portion of the plane of action is called zone of action, or field of action, or contact zone.

The zone of action in involute parallel-axes gears either with spur or with helical teeth is a rectangular area in the plane of action bounded by the active portion of the line of action and by the active face-width. Here and below, the active face-width is understood in sense of the face-width common for both, for the gear and for the pinion.

Graphical interpretation of the transverse contact ratio is illustrated in Figure 10.15.

The length of action,  $Z_{pa}$ , (shown in Figure 10.15) corresponds to the arc of action, shown in Figure 10.16.

In parallel-axes gearing ( $P_a$  – gearing), the actual length of effective/active portion of the line of action,  $LA$ , can be expressed in terms of: (a) the outer diameter of a gear,  $d_{o,g}$ , (b) that of a mating pinion,  $d_{o,p}$ , (c) the center-distance,  $C$ , and (d) the transverse pressure angle,  $\phi_t$ . Elementary analysis of the schematic in Figure 10.14 reveals how the length of action,  $Z_{pa}$ , can be expressed in terms of the design parameters of the gear pair.

The following approach can be utilized for the calculation of the length of zone action,  $Z_{pa}$ .

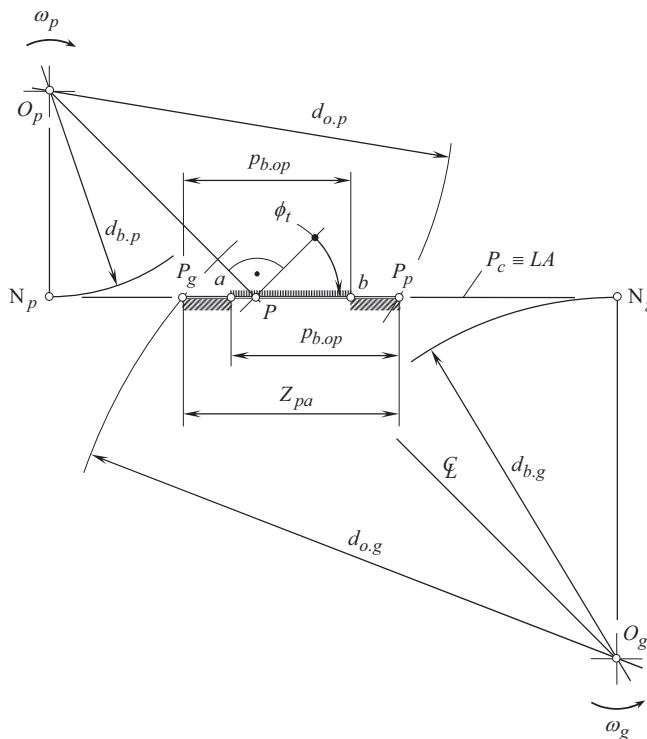


FIGURE 10.15 Graphical interpretation of transverse contact ratio.



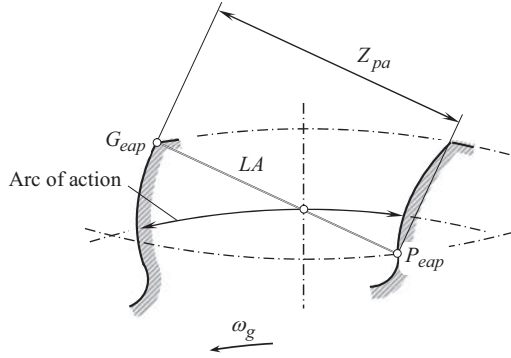


FIGURE 10.16 Arc of action in parallel-axes gearing.

#### 10.4.1.2 Length of Zone of Action in External Gearing

When two gears are engaged in mesh with center-distance,  $C$ , as shown in Figure 10.17, the line tangent to both base circles is defined as the *line of action*. When the gears rotate, the contact starts at point  $G_{eap}$ , where the end-of-active-profile diameter circle of the gear (commonly, this is the outside diameter circle of the gear, that is, an equality,  $r_{eap.g} = r_{o.g}$ , is commonly valid) intersects the line of action, passes through pitch point,  $P$ , and ends at point  $P_{eap}$ , where the end-of-active-profile diameter of the pinion (commonly, this is the outside diameter circle of the pinion, that is, an equality,  $r_{eap.p} = r_{o.p}$ , is commonly valid) intersects the line of action. The total length of active portion,  $Z_{pa}$ , of the line of action can be specified as:

$$Z_{pa} = \rho_g + \rho_p - N_g N_p \quad (10.3)$$

In Eq. (10.3),  $\rho_g$  is the radius of curvature of the gear tooth profile,  $\mathcal{G}$ , at the end-of-active-profile diameter circle of the gear;  $\rho_p$  is the radius of curvature of the pinion tooth profile,  $\mathcal{P}$ , at the end-of-active-profile diameter circle of the pinion; and  $N_g N_p$  is the projection of the center-distance,  $C$ , onto the line of action,  $LA$ .

A performed analysis of Figure 10.17 reveals that in external parallel-axes gearing the following equalities take place:

$$\rho_g = \sqrt{r_{eap.g}^2 - r_{b.g}^2} \quad (10.4)$$

$$\rho_p = \sqrt{r_{eap.p}^2 - r_{b.p}^2} \quad (10.5)$$

$$N_g N_p = C \sin \phi_t \quad (10.6)$$

Substituting Eqs. (10.4)–(10.6) into Eq. (10.3), one can come up with a formula for calculation of the total length of active portion,  $Z_{pa}$ , of the line of action in external parallel-axes gear pair:

$$Z_{pa} = \rho_g + \rho_p - C \sin \phi_t = \sqrt{r_{eap.g}^2 - r_{b.g}^2} + \sqrt{r_{eap.p}^2 - r_{b.p}^2} - C \cos \phi_t \quad (10.7)$$

The active portion of the line of action,  $Z_{pa}$ , can be expressed in terms of two components,  $Z_g$  and  $Z_p$ , namely, as the sum the  $Z_{pa} = Z_g + Z_p$ . The component  $Z_g$  (here,  $Z_g = G_{eap}P$ ) is due to the addendum



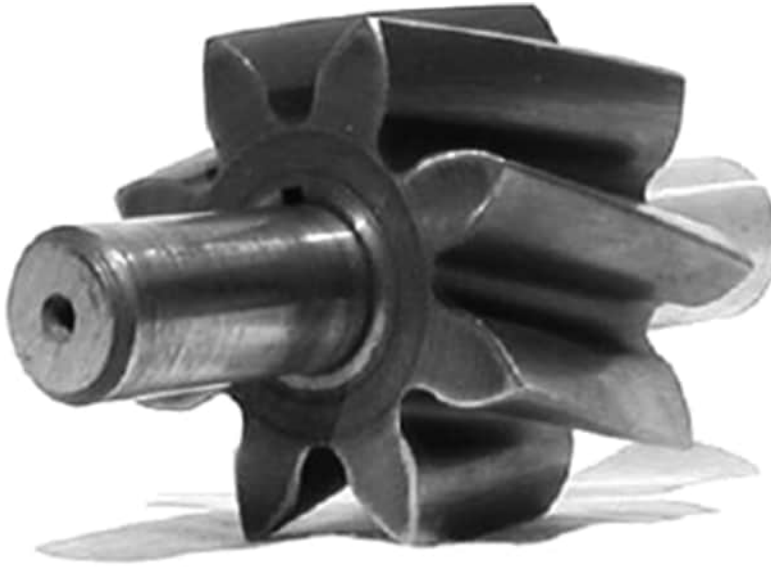


**FIGURE 10.18** A low-tooth-count helical involute gear.

1. The coordinates of point,  $m$ , are determined from the standpoint that this point is located on the involute tooth profile of the gear/pinion, and, therefore, the location of the point can be specified by the position vector  $\mathbf{r}_m^{inv}$
2. The coordinates of point,  $m$ , are also determined from the standpoint that the point is located on the undercut curve of the gear/pinion, and, therefore, the location of the point can be specified by the position vector  $\mathbf{r}_m^{uc}$

As the coordinates of point,  $m$ , in a common reference system are specified in terms of two different position vectors,  $\mathbf{r}_m^{inv}$  and  $\mathbf{r}_m^{uc}$ , these position vectors are identical to one another. Therefore, in this particular case, an identity,  $\mathbf{r}_m^{inv} \equiv \mathbf{r}_m^{uc}$ , is valid. By solving this identity, all the design parameters of the undercut gear tooth profile can be determined.

#### 10.4.1.4 Length of Zone of Action in Internal Gearing

A schematic of an internal parallel-axes gear pair is shown in Figure 10.21. A performed analysis of this schematic reveals that in internal parallel-axes gearing the following equalities take place:

$$\rho_g = \sqrt{r_{eap.g}^2 - r_{b.g}^2} \quad (10.8)$$

$$\rho_p = \sqrt{r_{eap.p}^2 - r_{b.p}^2} \quad (10.9)$$

$$N_g N_p = C \sin \phi_t \quad (10.10)$$

With the radii of curvature,  $\rho_g$  and  $\rho_p$ , calculated, the length,  $Z_{pa}$ , of the active portion of the line of action in internal gearing can be calculated by the formula (see Figure 10.21):

$$Z_{pa} = \rho_g - \rho_p + C \sin \phi_t = \sqrt{r_{eap.g}^2 - r_{b.g}^2} - \sqrt{r_{eap.p}^2 - r_{b.p}^2} + C \cos \phi_t \quad (10.11)$$

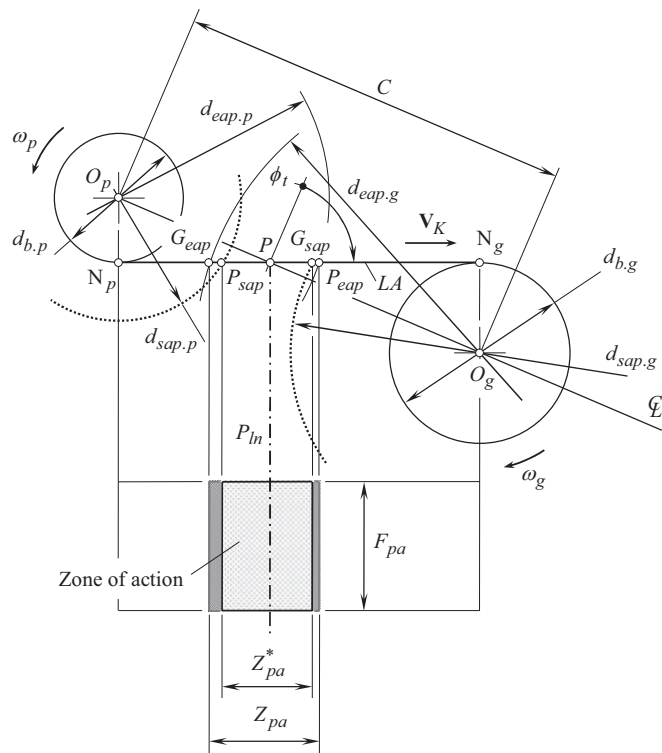


FIGURE 10.19 Zone of action in parallel-axes involute *low-tooth-count* gearing.

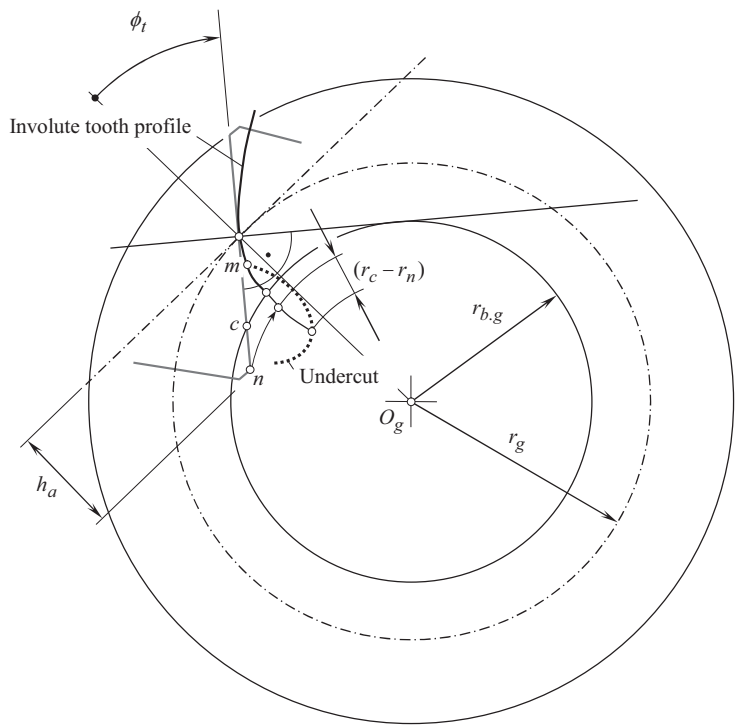
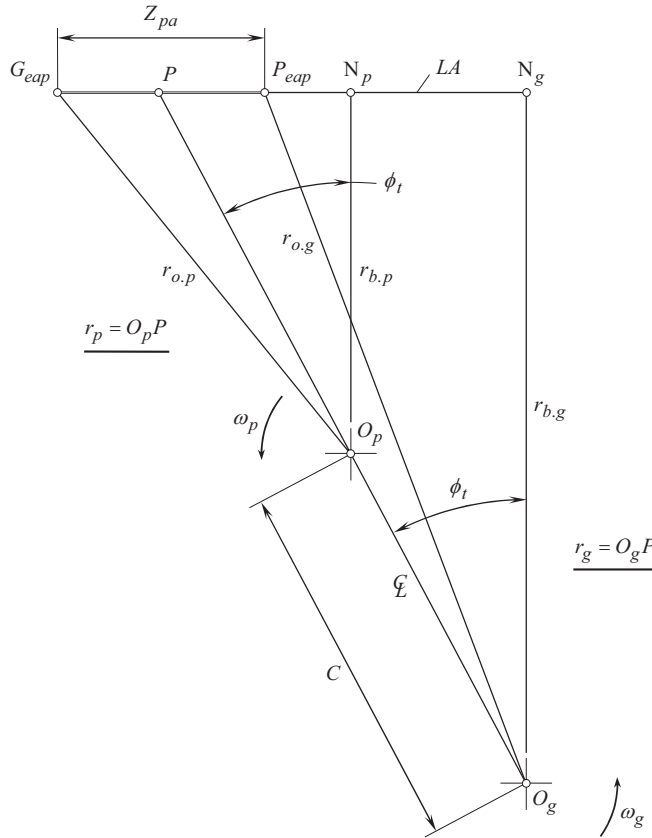


FIGURE 10.20 Generation of undercut in parallel-axes involute *low-tooth-count* gear.



**FIGURE 10.21** Length of zone action,  $Z_{pa}$ , in internal gearing.

The active portion of the line of action,  $Z_{pa}$ , can be expressed in terms of two components,  $Z_g$  and  $Z_p$ , that is, as the sum  $Z_{pa} = Z_g - Z_p$ . The component  $Z_g$  is due to the addendum of the gear,  $a_g$ , and the component  $Z_p$  is due to the addendum of the pinion,  $a_p$ .

#### 10.4.1.5 Length of Zone of Action in Pinion Gear-to-Rack Mesh

Calculation of contact ratio in *pinion gear-to-rack mesh* is a bit different compared to that in external, and in internal parallel-axes gearing. This is chiefly because of the center-distance,  $C$ , in *pinion gear-to-rack mesh* approaches an infinity ( $C \rightarrow \infty$ ), and the radius of curvature of the gear tooth profile,  $\rho_g$ , also approaches an infinity ( $\rho_g \rightarrow \infty$ ).

Refer to Figure 10.22 for the calculation of the length,  $Z_{pa}$ , in *pinion gear-to-rack mesh*. By definition, the length of active portion,  $Z_{pa}$ , of the line of action,  $LA$ , can be expressed in terms of the lengths of two straight-line segments  $Z_{pa,g}$  and  $Z_{pa,p}$ :

$$Z_{pa} = Z_{pa,g} + Z_{pa,p} = G_{eap}P + P_{eap}P \quad (10.12)$$

Here, the length of the straight-line segment,  $Z_{pa,g}$ , depends on the design parameters of the rack, and equals to  $Z_{pa,g} = G_{eap}P$  (see Figure 10.22). Similarly, the length of the straight-line segment,  $Z_{pa,p}$ , depends on the design parameters of a mating pinion and equals to  $Z_{pa,p} = P_{eap}P$  (see Figure 10.22).

The portion,  $Z_{pa,g}$ , is of the length:

$$Z_{pa,g} = \frac{a_g}{\sin \phi_t} \quad (10.13)$$

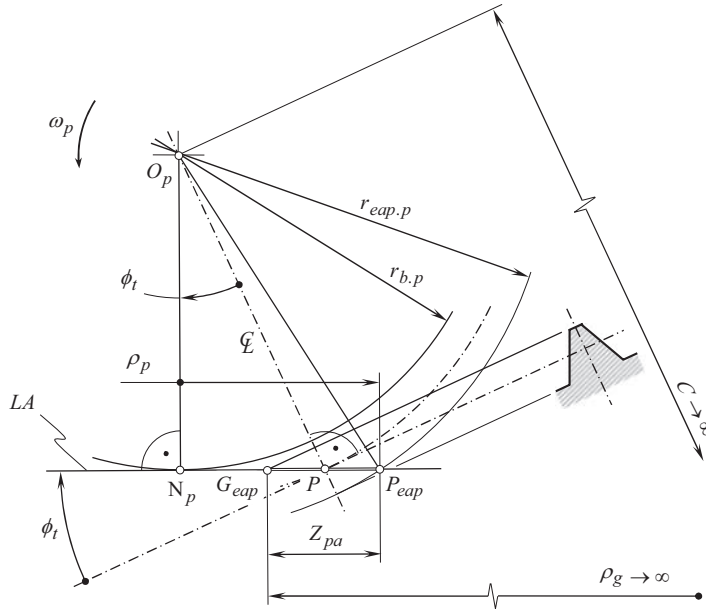


**FIGURE 10.22** Schematic for calculation the length of active portion,  $Z_{pa}$ , of the line of action,  $LA$ , in *pinion gear-to-rack mesh* (when  $C \rightarrow \infty$ , and  $\rho_g \rightarrow \infty$ ).

Here,  $a_g$  is the addendum of the gear (of the rack), and  $\phi_t$  is the transverse profile angle of the rack teeth.

The length of the portion,  $Z_{pa,p}$ , can be determined in the following way.

From the  $\triangle P_{eap}PO_p$  in Figure 10.22, cosines law can be interpreted as:

$$(O_pP_{eap})^2 = (O_pP)^2 + (P_{eap}P)^2 - 2 \cdot O_pP \cdot P_{eap}P \cdot \cos(90^\circ + \phi_t) \quad (10.14)$$

Taking into account that the following equalities are valid in *pinion gear-to-rack mesh*:  $O_pP = r_p$ ,  $O_pP_{eap} = r_{o,p} = r_p + a_p$ ,  $\angle P_{eap}PO_p = (90^\circ + \phi_t)$ , and  $\cos(90^\circ + \phi_t) = -\sin\phi_t$ , an expression:

$$Z_{pa,p} = -r_p \cdot \sin\phi_t + \sqrt{(-r_p \cdot \sin\phi_t)^2 + (r_p + a_p)^2} \quad (10.15)$$

for the calculation of the length of the straight-line segment,  $Z_{pa,p}$ , can be derived (here,  $a_p$  is the addendum of the pinion).

Considered together, Eqs. (10.13) and (10.15), yield a formula for the calculation of the length,  $Z_{pa}$ , in *pinion gear-to-rack mesh*:

$$Z_{pa} = \frac{a_g}{\sin\phi_t} - r_p \cdot \sin\phi_t + \sqrt{r_p^2 \cdot (1 + \sin^2\phi_t) + 2 \cdot r_p \cdot a_p + a_p^2} \quad (10.16)$$

A significant simplification of Eq. (10.16) is possible when both the addendums,  $a_g$  and  $a_p$ , are equal to module of the gear pair:  $a_g = m$  and  $a_p = m$ . In certain cases, the pinion pitch radius,  $r_p$ , can be expressed in terms of the pinion base radius,  $r_{b,p}$ , and the pinion transverse profile angle,  $\phi_t$ :

$$r_p = \frac{r_{b,p}}{\cos\phi_t} \quad (10.17)$$

The active portion of the line of action,  $Z_{pa}$ , can be expressed in terms of two components,  $Z_g$  and  $Z_p$ , namely, as the sum  $Z_{pa} = Z_g + Z_p$ . The component  $Z_g$  is due to the addendum of the gear,  $a_g$ , and the component  $Z_p$  is due to the addendum of the pinion,  $a_p$ . Usually, the inequality  $Z_g > Z_p$  is valid.

#### 10.4.1.6 Face Advance (In Design of Helical and Other Non-Spur Gearing)

Spur gears are extensively used in the design of parallel-axes gearing. In addition, gears of other design are also used in the design of parallel-axes gearing. These are helical gears, gears with either circular-arc, or cycloid-arc, or sine-arc profile in the lengthwise direction of gear teeth. Gears of all these kinds are referred to as *non-spur gears*. The length of *zone of action* in non-spur gearing is different compared to that in spur gears. This is chiefly due to the features of the geometry of the line of contact,  $LC$ , in non-spur gearing, that under no circumstances align with the axis of instantaneous rotation,  $P_{in}$ , when the gears rotate. As a result, the so-called *face advance*,  $Z_{adv.lc}$  is recognized in non-spur gears.

In non-spur gearing of all designs, the *face advance*,  $Z_{adv.lc}$ , has to be taken into account when determining contact ratio in a gear pair. The actual value of the *face advance*,  $Z_{adv.lc}$ , can be calculated for gearing with line of contact,  $LC$ , of any reasonable geometry. As an illustrative example, consider the determination of the *face advance*,  $Z_{adv.lc}$ , in a parallel-axes involute gear pair composed of two helical gears.

A performed analysis in Figure 10.23 reveals that the *face advance*,  $Z_{adv.lc}$ , in helical involute gearing can be expressed either in terms of the effective face-width,  $F_{pa}$ , and the base helix angle,  $\psi_b$ :

$$Z_{adv.lc} = F_{pa} \cdot \tan \psi_b \quad (10.18)$$

or in terms of the effective face-width,  $F_{pa}$ , the axial pitch of the gear teeth, the length of *zone of action*,  $Z_{pa}$ , and tooth count of the gear,  $N_g$ :

$$Z_{adv.lc} = F_{pa} \cdot \frac{Z_{pa} \cdot N_g}{p_x} \quad (10.19)$$

Another illustrative example relates to the determination of the *face advance*,  $Z_{adv.lc}$ , in a parallel-axes gear pair composed of two gears with circular-arc teeth in their lengthwise direction.

Referring to Figure 10.24, the following equation can be derived for the calculation of the *face advance*,  $Z_{adv.lc}$ , in a parallel-axes gear pair composed of two gears with circular-arc teeth in their lengthwise direction:

$$Z_{adv.lc} = R_{lc} - \sqrt{R_{lc}^2 - 0.25F_{pa}^2} \quad (10.20)$$

Here, the radius of the desirable line of contact,  $LC$ , is designated as  $R_{lc}$ .

Similarly, the face advance,  $Z_{adv.lc}$ , can be calculated for non-spur gears of other designs.

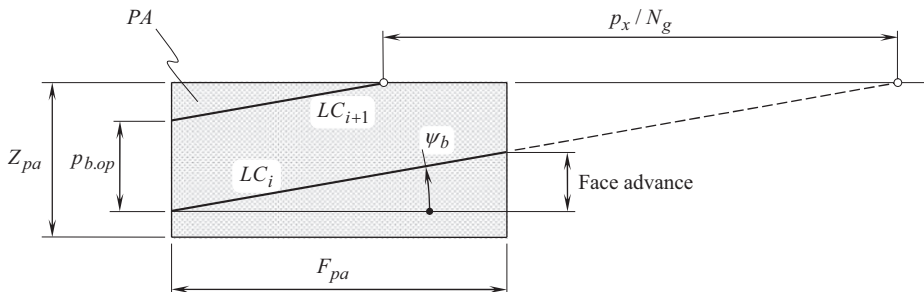
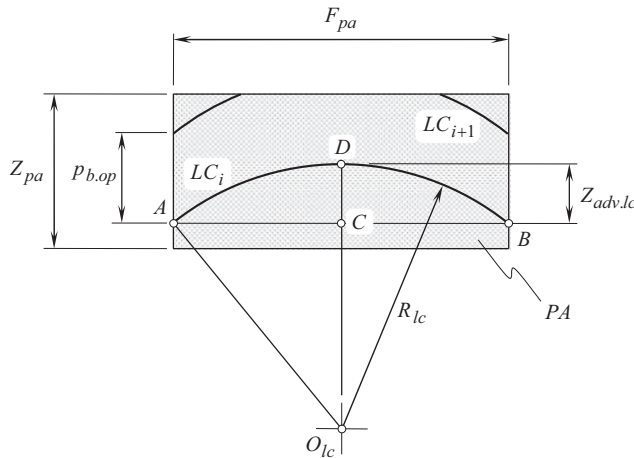


FIGURE 10.23 Face advance,  $Z_{adv.lc}$ , in helical parallel-axes involute gearing.



**FIGURE 10.24** Face advance,  $Z_{adv,lc}$ , in circular-arc parallel-axes involute gearing.

Generally speaking, face advance,  $Z_{adv}$ , is measured between the point of a line of contact,  $LC$ , that is the first to enter the plane of action,  $PA$ , and between another point of that same line of contact,  $LC$ , that is the last to enter the plane of action,  $PA$ , when the gears rotate. In the case of parallel-axes helical gear pair, the face advance,  $Z_{adv}$ , equal to  $Z_{adv} = F_{pa} \tan \psi_b$ . In a more general case, for example, for gears with curved teeth in their lengthwise direction (see Figure 10.25), the face advance can also be calculated.

With the rotation of the gears, the line of contact,  $LC$ , sweeps out the *zone of action* (see Figure 10.26). Alternatively, the *zone of action* can be regarded as the plane in which contact takes place, and the *line of contact* can be regarded at any instant of time as the common intersection between the zone of contact and the tooth surface. Commonly, a *zone of action* can be visualized as a rectangle, one side of which is the active portion of the zone of action,  $Z_{pa}$ , with the effective face-width,  $F_{pa}$ , being the other side. The active portion of the zone of action,  $Z_{pa}$ , can be viewed as a summa of the two components, namely, of  $Z_{pa,g}$ , that is due to addendum of the gear, and of  $Z_{pa,p}$ , that is due to addendum of the mating pinion.

Shown in Figure 10.26 zones  $Z_{pa,g}$  and  $Z_{pa,p}$  correspond to the arc of approach, and the arc of recess in parallel-axes gearing (see Figure 10.27).

It is instructive to note that some modifications of the design parameters of the gear, or of the mating pinion, or both, can affect the actual values of the design parameters of the zone of action,  $Z_{pa}$ . Large end chamfers/rounding can be mentioned as an example.

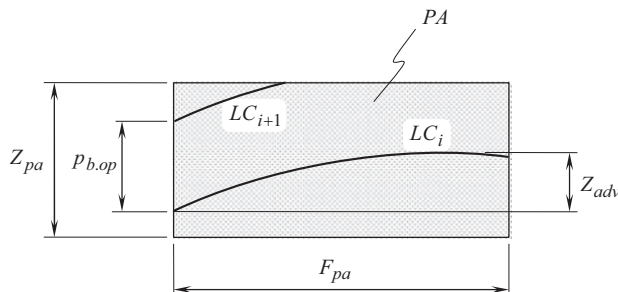


**FIGURE 10.25** To the definition of the term face advance,  $Z_{adv}$ , in geometrically accurate parallel-axes gearing.



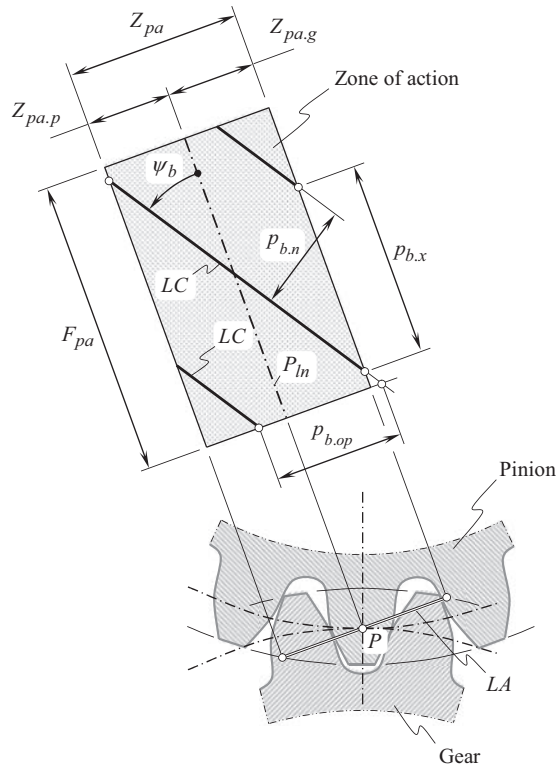


**FIGURE 10.26** Zone of action in helical involute gearing.

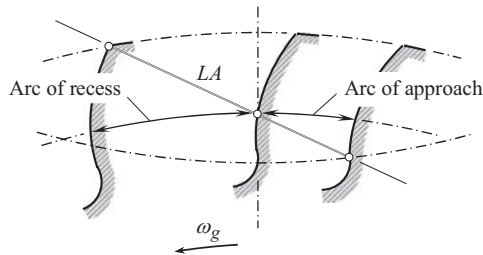


**FIGURE 10.27** Arc of approach, and arc of recess in parallel-axes gearing.

Commonly, in a parallel-axes gear pair (see Figure 10.28a), the plane of action,  $PA$ , is shaped in the form of a rectangle of  $Z_{pa}$  length, and  $F_{pa}$  width, as shown in Figure 10.28b. Because of the end chamfers/rounding, the plane of action features a more complex geometry illustrated in Figure 10.28c. In the case under consideration, at every instant of time, the plane of action features a certain instantaneous value of the effective face-width,  $F_{pa}^*$ , that is  $F_{pa}^* \leq F_{pa}$ . Similar alterations to the shape and design parameters of the zone of action are observed when the  $SAP$  – point, and/or  $EAP$  – point are displaced from their nominal positions, as illustrated in Figure 10.28d. The displacements of this sort can be caused by tooth rounding, tooth chamfering, and so forth (see Figure 10.28e).

Tooth profile undercut, or changes to the geometry of the outside surface of a gear, can significantly affect the shape and design parameters of the zone of action.

The just mentioned alterations to the design of a gear and its mating pinion could be critical, especially for low-tooth-count gears (for  $LTC$  – gears).

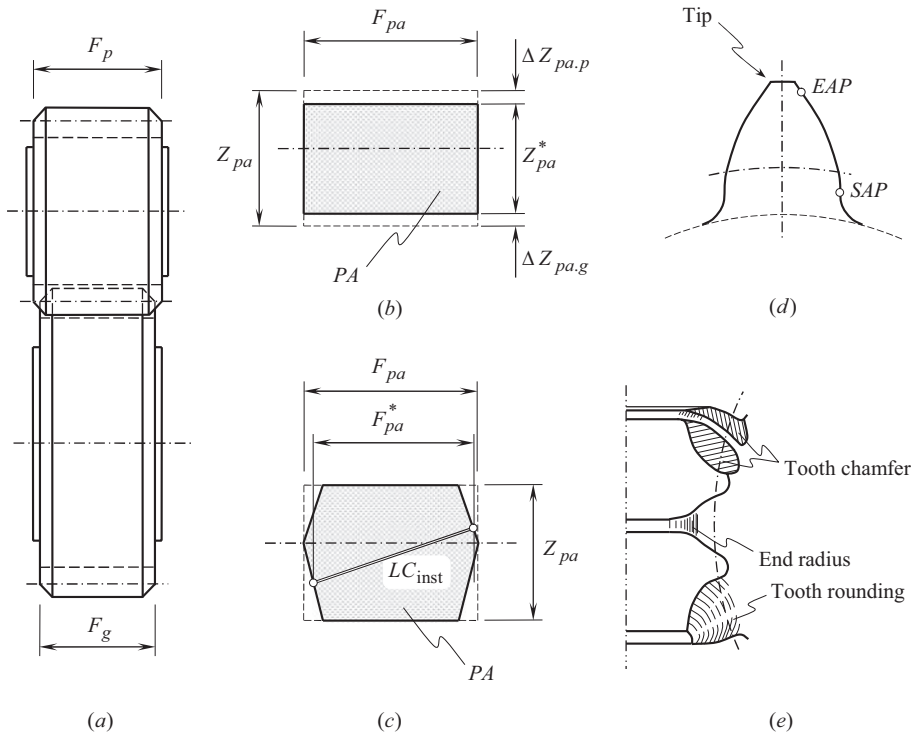


**FIGURE 10.28** Influence of the parameters of modified plane of action,  $PA$ , onto the length of the instantaneous line of contact,  $LC_{inst}$ : (a) parallel-axes gears in mesh, (b) shortened length,  $Z_{pa}^*$ , of the plane of action,  $PA$ , (c)  $SAP$  – point, and  $EAP$  – point on the gear tooth profile, (d) shortened width,  $F_{pa}^*$ , of the plane of action,  $PA$ , and (e) corresponding modifications to the gear design.

In order to put the alterations to the design of a gear and its mating pinion into account, two more components are introduced. The *gear addendum advance*,  $Z_{adv.g}$ , and the *pinion addendum advance*,  $Z_{adv.p}$ , are these two components. Figure 10.29 illustrates an example of how the components  $Z_{adv.g}$  and  $Z_{adv.p}$  can be specified in involute parallel-axes gearing that features conical outer surfaces.

All the discussed components are required to be taken into account when determining the design and parameters of the geometry of the zone of action.

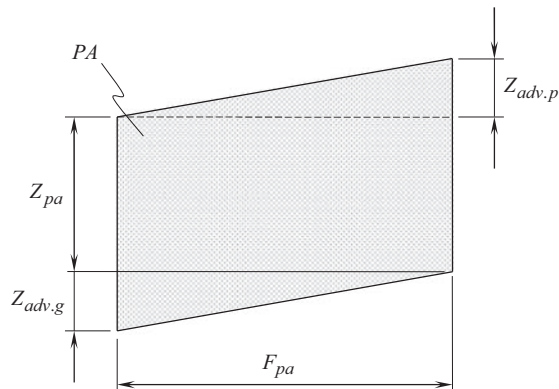


**FIGURE 10.29** Gear face advance,  $Z_{adv.g}$ , and pinion face advance,  $Z_{adv.p}$ , in parallel-axes involute gearing.

Taken together, the components  $Z_{adv.g}$ , and  $Z_{adv.p}$ , form the so-called *plane-of-action advance*,  $Z_{adv.pa}$ :

$$Z_{adv.pa} = Z_{adv.g} + Z_{adv.p} \quad (10.21)$$

It should be mentioned here, that the components are signed values.

A contribution of the *face advance*,  $Z_{adv.lc}$  to the *total face advance*,  $Z_{adv.\Sigma}$  is always considered individually, as there is no generalized equation helpful to incorporate this component into the analysis:

$$Z_{adv.\Sigma} = Z_{adv.\Sigma}(Z_{adv.pa}, Z_{adv.lc}) \quad (10.22)$$

The total length of the zone of action,  $Z_{pa.\Sigma}$ , equals:

$$Z_{pa.\Sigma} = Z_{pa} + Z_{adv.\Sigma} \quad (10.23)$$

An approach, similar to that just discussed, can be evolved to intersected-axes, as well as to crossed-axes geometrically accurate gearing.

#### 10.4.1.7 Highest and Lowest Points of Single-Tooth Contact

The performed analysis reveals two more design parameters in geometrically accurate involute gearing (Figure 10.14).

In most of the spur gear designs used in the gear trade, two pairs of teeth are in contact when a tooth enters mesh and two pairs will be in contact when a tooth leaves mesh. In the tooth contact area, though, only one pair of teeth will be in mesh. It is only when the calculated contact ratio exceeds 2.0 that two pairs of teeth can be mesh in the middle of the tooth contact area.

Since normal spur gear designs have a contact ratio over 1.0 but less than 2.0, the locations where contact shifts from one pair of teeth to two pairs of teeth have been of much interest to those rating spur gears. It can be anticipated that the most critical bending stress should come at the highest point on the tooth at which the tooth has to carry the full transmitted load. It can also be anticipated that the most critical contact stress should come at the lowest point on the tooth at which one tooth has to carry the full transmitted load.

The changeover points from one pair to two pairs of teeth are critical.

Figure 10.30 shows the basic definitions of where the highest and lowest points of single-tooth (single-pair) contact occurs. If the pinion drives, the highest point of single-tooth contact is one base

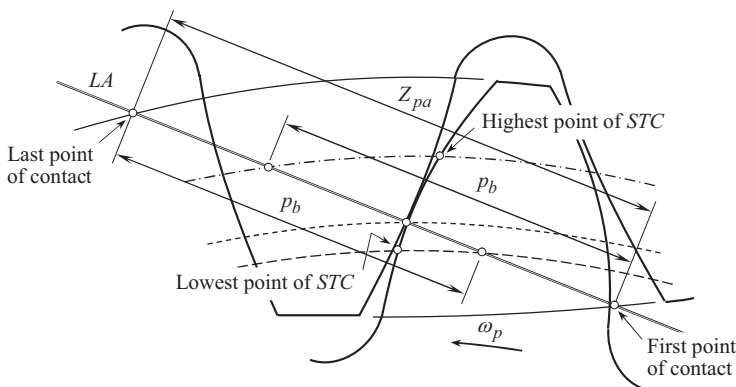


FIGURE 10.30 Definition of the highest and lowest points of single-tooth contact for involute gears.

pitch from the first point of contact. (If the pinion is driven, the *first* point of contact becomes the *last* point of contact, and the highest point of single-tooth contact is still at the same place – now one base pitch away from the last point of contact).

The lowest point of single-tooth contact is one base pitch away from the last point of contact, with the pinion driving.

In Figure 10.30, point 1 is the highest point on the pinion at which single-tooth contact is carried. This position is often referred to in gear writings as *HPSTC*.

The lowest point of single-tooth contact in Figure 10.30 is at point 2. This point is often referred to as *LPSTC*.

#### 10.4.2 CONTACT RATIO: GENERALIZED APPROACH

When two gears rotate, contacts travel from point  $P_{eap}$  to point  $G_{eap}$ . An average number of pairs of teeth moving across the total length of the zone of action,  $Z_{pa,\Sigma}$ , is defined as the *contact ratio*,  $\bar{m}$ . The contact ratio,  $\bar{m}$ , in parallel-axes involute gearing is the ratio of the total length of the zone of action,  $Z_{pa,\Sigma}$ , to operating base pitch,  $p_{b,op}$ , in the gear pair:<sup>4</sup>

$$\bar{m} = \frac{Z_{pa,\Sigma}}{p_{b,op}} \quad (10.24)$$

In spur gearing, Eq. (10.24) for the calculation of the contact ratio,  $\bar{m}$ , reduces to:

$$\bar{m} = \frac{Z_{pa}}{p_{b,op}} \quad (10.25)$$

Here, in Eqs. (10.24) and (10.25), the actual value of the operating base pitch,  $p_{b,op}$ , is calculated from the expression:

$$p_b = p \cos \phi_t = \pi m \cos \phi_t = \frac{\pi \cos \phi_t}{P_d} \quad (10.26)$$

where:

- $p$  is the circular pitch of gear.
- $\phi_t$  is the transverse pressure angle of gear.
- $m$  is the module of gear.
- $P_d$  is the diametral pitch.

For spur gears, it is common practice to keep the contact ratio not less than  $\bar{m} \geq 1.2$ . Commonly, the transverse contact ratio falls into the interval  $\bar{m} = 1.6 \div 1.8$ .

Sometimes, the ratio  $Z_{pa}/p_{b,op}$  Eq. (10.25) is loosely referred to as the *transverse contact ratio*,  $m_p$ . The term *transverse contact ratio* is outdated.

In helical gearing, Eq. (10.24) for the calculation of the contact ratio,  $\bar{m}$ , reduces to:

$$\bar{m} = \frac{Z_{pa} + F_{pa} \tan \psi_b}{p_{b,op}} \quad (10.27)$$

<sup>4</sup> In parallel to the designation  $\bar{m}$  for the contact ratio, it makes sense to introduce the designations  $\bar{m}_{pa}$  for parallel-axes gearing,  $\bar{m}_{ia}$  for intersected-axes gearing, and  $\bar{m}_{ca}$  for crossed-axes gearing.

Contact ratio,  $\bar{m}$ , for external spur gearing, can be expressed in terms of the design parameters of a gear and of a mating pinion:

$$\bar{m} = \frac{\sqrt{\left(\frac{d_{o,p}}{2}\right)^2 - \left(\frac{d_{b,p}}{2}\right)^2} + \sqrt{\left(\frac{d_{o,g}}{2}\right)^2 - \left(\frac{d_{b,p}}{2}\right)^2} - C \sin \phi_t}{p_b} \quad (10.28)$$

Similarly, contact ratio,  $\bar{m}$ , for internal spur gearing, can be expressed in terms of design parameters of a gear and of a mating pinion:

$$\bar{m} = \frac{\sqrt{\left(\frac{d_{o,p}}{2}\right)^2 - \left(\frac{d_{b,p}}{2}\right)^2} - \sqrt{\left(\frac{d_{i,g}}{2}\right)^2 - \left(\frac{d_{b,g}}{2}\right)^2} + C \sin \phi_t}{p_b} \quad (10.29)$$

Here, in Eqs. (10.28) and (10.29) is designated:

$d_{o,p}$  is the outside diameter (effective) of pinion.

$d_{o,g}$  is the outside diameter of gear (diameter to intersection of tip round and active profile).

$d_{i,g}$  is the inside diameter (effective), internal gear.

$d_{b,p}$  is the base diameter of pinion.

$d_{b,g}$  is the base diameter of gear.

$d_{b,g}$  is the base diameter of internal gear.

$C$  is the center-distance of pair.

$\phi_t$  is the transverse pressure angle.

$p$  is the circular pitch.

$p_b$  is the base pitch.

$F_{pa}$  is the effective face-width.

$\psi_b$  is the base helix angle of helical gears.

In *Novikov/conformal gearing*, an equality  $Z_{pa} = 0$  is valid. Therefore, a formula:

$$\bar{m} = \frac{F_{pa} \tan \psi_b}{p_{b.op}} \quad (10.30)$$

is used for the calculation of the contact ratio,  $\bar{m}$ , in *Novikov/conformal gearing*.

Sometimes, the component,  $F_{pa} \tan \psi_b / p_{b.op}$ , in Eq. (10.27) is loosely referred to as the *face contact ratio*,  $m_F$ . The term *transverse contact ratio*,  $m_F$ , is outdated.<sup>5</sup>

In other cases, Eq. (10.24) is used for the calculation of the contact ratio,  $\bar{m}$ .

An actual value of contact ratio,  $\bar{m}$ , in a parallel-axes gear pair falls into the range:

$$1 < \bar{m} \leq \infty \quad (10.31)$$

Under any and all circumstances, fulfillment of the inequality  $\bar{m} \geq 1$  is a must.

The contact ratio,  $\bar{m}$ , is an important design parameter of a gear pair for many reasons. As an example, this parameter is used for calculating contact stresses between the gear and the pinion tooth flanks. In this latter case, the *total length of the line of contact* (or *TLLC*, for simplicity)

<sup>5</sup> The term *face contact ratio* is incorrect, as no rotation is transmitted across the face of the plane of action, *PA*, in a gear pair. Instead, a rotation is transmitted only in transverse section of the plane of action, *PA*. Helical teeth of a gear and of a mating pinion extend *transverse contact ratio*. This is one more reason for to use the term *contact ratio*,  $\bar{m}$ , instead of the obsolete terms *transverse contact ratio*,  $m_p$ , *face contact ratio*,  $m_F$ , and *total contact ratio*,  $m_t$ .

should be taken into account. The total length of the line of contact depends on the actual value of the total contact ratio, and is of critical importance, especially for gearing having a low tooth count of the pinion.

Standard gears have a typical contact ratio of 1.2 to 1.6. The gears of this design feature double-tooth contact regions, as shown in Figure 10.31. Gear pairs that feature contact ratio greater than 2.0 (see Figure 10.32) are commonly referred to as *high-contact-ratio gears*, or just *HCR-gears*, for simplicity. In their most basic form, gears are designed to transmit power, and *HCR-gears* perform especially well. They are stronger, quieter, and smoother, and they have significantly lower stresses. Also, they normally have lower pressure angles and a greater number of teeth than standard gears.

*High-contact-ratio gears* necessitate<sup>6</sup> higher quality levels due to the required accuracy of the multiple sets of teeth in contact. They are typically more sensitive to manufacturing errors and gear tooth profile modifications.

It can be shown that helical gear pairs with non-involute tooth profile are not capable of transmitting a uniform rotation smoothly.<sup>7</sup>

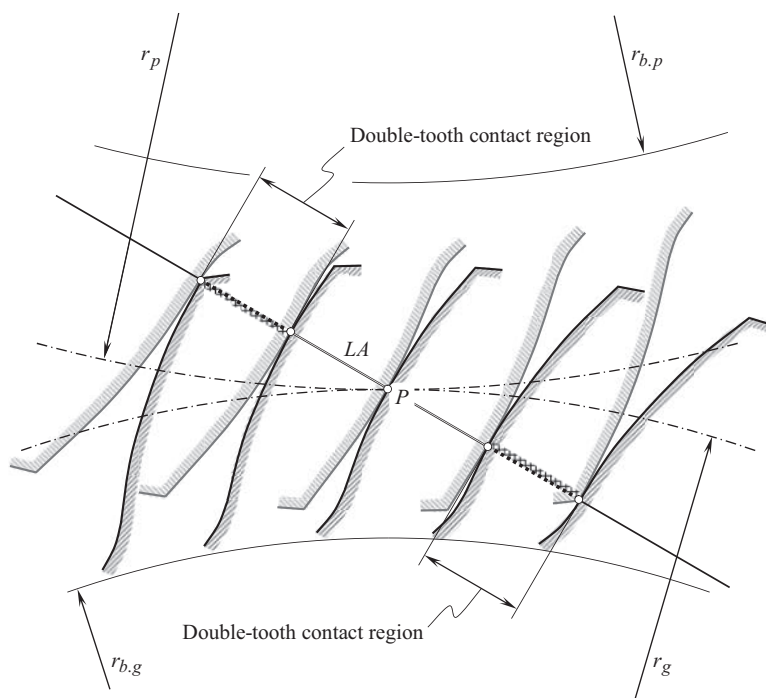


**FIGURE 10.31** Double-tooth contact regions in spur parallel-axes involute gear pair.

<sup>6</sup> It is wrong practice to define the term *transverse contact ratio*,  $m_p$ , as the ratio of the angle of action to the angular pitch. Such a definition tends to be applied to gears with non-involute tooth profile. However, this is also incorrect, as in non-involute gears, only one pair of teeth makes contact at every instant of time, and the term *transverse contact ratio*,  $m_p$ , cannot be specified in non-involute gears of all designs.

<sup>7</sup> As follows from the analysis of Fig. 2 in the U.S. patent No. 1.601.750 (E. Wildhaber, Filed: November 2, 1923, issued in October 5, 1926), the contact point travels within the transverse section from a position 11 to a position 11'. If the contact point travels within the transverse cross section, then the transverse contact ratio is greater than zero (that is,  $m_p > 0$ ). It can be concluded from the said that kinematically and geometrically *Helical Gearing* (U.S. Pat. No. 1.601.750) is not workable at all (a proof of that statement had been obtained by Dr. E. Wildhaber himself).

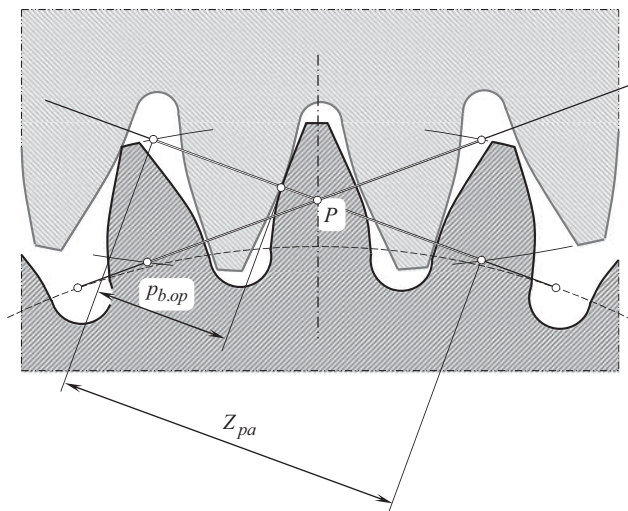


FIGURE 10.32 Schematic of *high-contact-ratio* parallel-axes gear pair.

### 10.4.3 IMPACT OF TOOTH FLANKS ELASTIC DEFORMATION INTO CONTACT RATIO IN GEAR PAIR

It is right point to stress here that the aforementioned consideration of contact ratio is based on just kinematical and geometrical analysis of gearing. When two gears rotate, tooth flanks come in contact at point, *a* (see Figure 10.33a). Then, the contact point travels along the path of contact occupying an intermediate position, *b*. The contacting tooth flanks come out of contact at point, *c*. The contact ratio depends on the length of the path of contact: the longer the path of contact, the greater the contact ratio, and vice versa. No mechanical properties of the material, which the mating gears are made up with are incorporated into this analysis.

In reality, under operating load, contact point spreads over an elliptically shaped area of contact. Hence, the tooth flanks get in contact before reaching the point, *a*, and they come out of contact beyond the point, *c* (see Figure 10.33b). The time of meshing of the tooth flanks is increased here due to the elasticity of the gears' material. Ultimately, the actual contact ratio of the gear pair becomes a bit greater.

The significance of an increase in the contact ratio due to the elasticity of the gear material increases in high-conformal gear pairs, as in gears of this system of gearing, the size of the area of contact is greater.

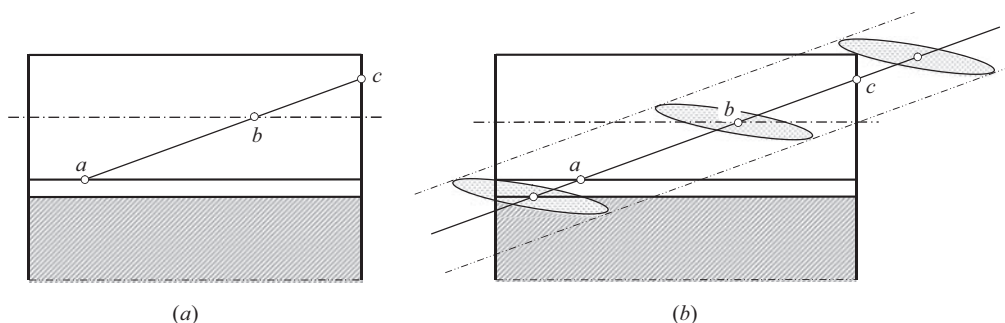


FIGURE 10.33 Impact of the elasticity of gear material on the actual value of contact ratio of a gear pair: (a) no elastic properties of a gear material are taken into account, and (b) elastic properties of a gear material are taken into account.



## 10.5 EXTERNAL INVOLUTE GEAR PAIR

An external gear pair is composed of two involute gears with the same actual value of base pitch,  $p_b$ . Close-up of an external gear pair along with the main design parameters is illustrated in Figure 10.34a and b correspondingly.

### 10.5.1 MAIN DESIGN PARAMETERS

An external gear pair can be specified by two rotation vectors, namely, by a rotation vector of a gear,  $\omega_g$ , and that of a mating pinion,  $\omega_p$ . The rotation vectors,  $\omega_g$  and  $\omega_p$ , are parallel to one another and are pointed in the opposite directions, as schematically shown in Figure 6.2a and b.

The listed below, shown in Figure 10.34b, are the main design parameters of an involute gear pair:

$d_{b,g}$ ,  $d_{b,p}$  are the base diameters of a gear and of a mating pinion.

$d_g$ ,  $d_p$  are the pitch diameters of a gear and of a mating pinion.

$d_{f,g}$ ,  $d_{f,p}$  are the root diameters of a gear and of a mating pinion.

$d_{sap,g}$ ,  $d_{sap,p}$  are the *start-of-active-profile* diameters of a gear and of a mating pinion.

$p_{b,op}$  is the operating base pitch of the gear pair.

$\phi_t$  is the transverse pressure angle of the gear pair.

$Z_{pa}$  is the length of action of the gear pair.

$C$  is the center-distance in the gear pair.

$B$  is the backlash.

$c$  is the radial clearance in the gear pair.

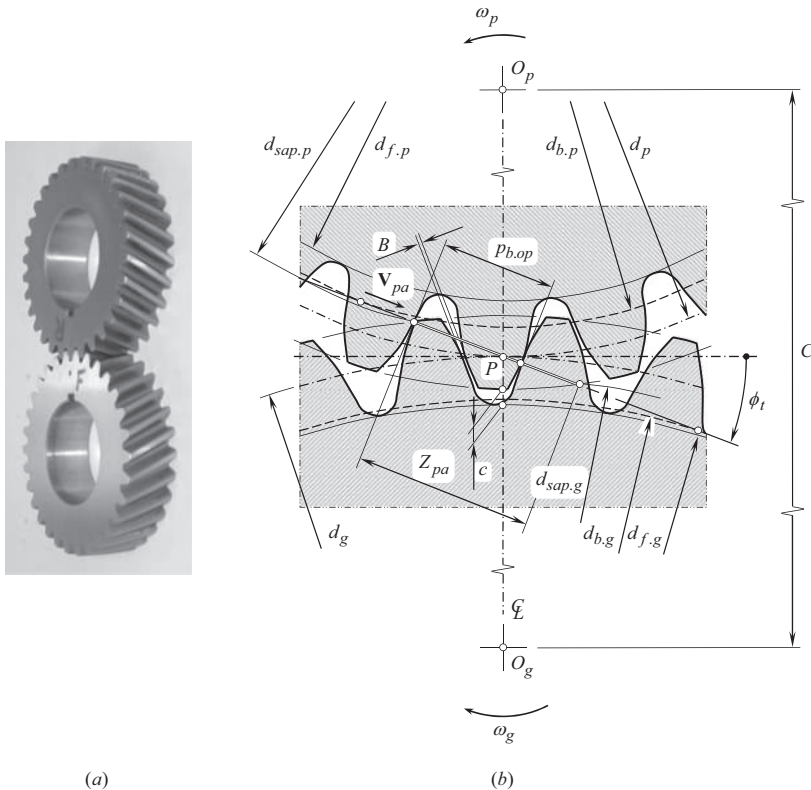


FIGURE 10.34 Close-up view (a), and the main design parameters (b) of external involute gear pair.



It is assumed here that the gears are designed with backlash of a sufficient value. Backlash is the clearance between the non-working flanks of teeth of a gear pair when the working flanks are in contact. Backlash is required to gear pair operates properly: to compensate for the heat extension, and so forth. There is a distinction between the normal backlash, circumferential backlash, and radial backlash.

The effective backlash,  $B$ , is specified within the pitch plane,  $PP$ . Therefore, in order to stress on that, backlash sometimes is denoted by  $B_{pp}$ .

### Definition 10.3

Effective backlash,  $B_{pp}$ , in parallel-axes gearing is the distance between a non-interacting tooth flank of a driving member, and that of a driven member, measured within the pitch plane in the gear pair.

Normal backlash is the shortest distance between the non-working flanks of teeth of a gear pair when the working flanks are in contact with zero force (Figure 10.35).

It is also anticipated that the gears are designed with the gear radial clearance,  $c_g$ , and the pinion radial clearance,  $c_p$ , of sufficient values, as illustrated in Figure 10.36. Commonly, the radial clearances,  $c_g$  and  $c_p$ , are equal to one another (namely, an equality  $c_g = c_p$  is valid). In such a scenario, the radial clearance is designated as  $c$ . The actual value of the radial clearance correlates with the other design parameters of gear pair according to the formula:

$$c = C - r_{f.g} - r_{o.p} = C - r_{f.p} - r_{o.g} \quad (10.32)$$

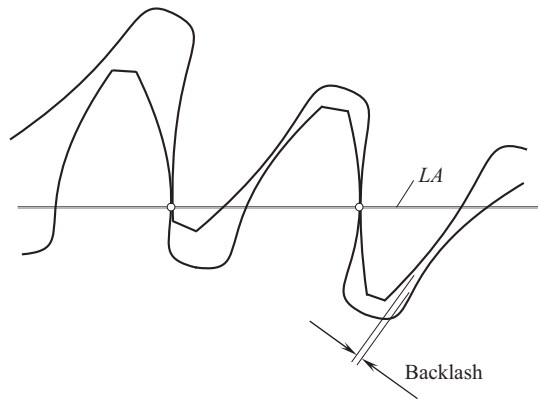


FIGURE 10.35 Normal backlash in parallel-axes involute gear pair.

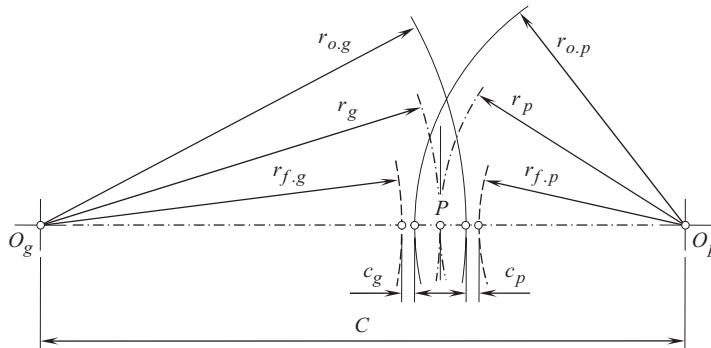


FIGURE 10.36 Radial clearance in parallel-axes involute gear pair.

It is proven to be practical to set the radial clearance equal to a quarter of module,  $m$ , in the gear pair ( $c = 0.25m$ ). In fine pitch gearing, radial clearance is increased to  $c = 0.35m$ .

In geometrically accurate parallel-axes gearing, the gears interact with one another along a line of contact,  $LC$ . The line of contact, between screw involute surface,  $\mathcal{S}$ , of a gear tooth, and screw involute surface,  $\mathcal{P}$ , of a mating pinion tooth is a straight line,  $LC$ .

The actual configuration of the line of contact,  $LC$ , in relation to the rotation vectors,  $\omega_g$  and  $\omega_p$ , is illustrated in Figure 10.37. The line of contact is entirely located within the plane of action,  $PA$ . The plane of action,  $PA$ , is tangent to the base cylinders of the gear and that of the pinion. In Figure 10.37, the diameter of the base cylinder of the gear is designated as  $d_{b,g}$ , while the diameter of the base cylinder of the pinion is designated as  $d_{b,p}$ . The line of contact,  $LC$ , crosses the axes of rotations of the gear,  $O_g$ , and the pinion,  $O_p$ , at *base helix angle*,  $\psi_b$ . In a spur gear pair, the base helix angle,  $\psi_b$ , is zero, and, hence, the line of contact is parallel to the axes of rotation of the gear,  $O_g$ , and the pinion,  $O_p$ .

An in-detail analysis of the schematic of parallel-axes gearing, shown in Figure 10.37, inspires the introduction of a novel design parameter in a gear pair.

Consider the active portion of the plane of action,  $PA$ , for parallel-axes gearing, as shown in Figure 10.38. The active portion of the plane of action is shaped in the form of a rectangle. The width of the rectangle is equal to the effective face-width,  $F_{pa}$ , of the gear set, and the height of the plane of action is equal to the length,  $Z_{pa}$ , of the active portion of the line of action,  $LA$ .

When the driving gear rotates, the line of contact,  $LC$ , travels together with the plane of action,  $PA$ . The linear velocity vector of the line of contact motion is denoted by  $\mathbf{V}_{pa}$ .

In spur parallel-axes involute gearing (see Figure 10.38a), an arbitrary configuration of the line of contact is designated as  $LC_i$ . Assume that the driving gear is rotated through one tooth. During this time, the line of contact travels at certain distance,  $p_{b,op}$ . In a new position, the line of contact is designated as  $LC_{i+1}$ . Measured in a common transverse section of the gear pair, the distance,  $p_{b,op}$ , between two adjacent desirable lines of contact,  $LC_{des}^i$  and  $LC_{des}^{i+1}$ , is referred to as the *operating base pitch* in the gear pair.<sup>8</sup>

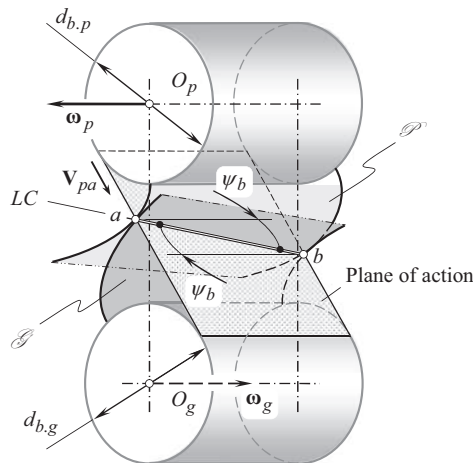


**FIGURE 10.37** Interaction of screw involute surfaces,  $\mathcal{S}$  and  $\mathcal{P}$ , of tooth flanks in a pair of involute helical gears.

<sup>8</sup> It is also important to stress here that the *operating base pitch* in a gear pair,  $p_{b,op}$ , is measured in linear units only in *geometrically-accurate* parallel-axes gearing. In intersected-axes as well as in crossed-axes *geometrically accurate* gearing, the operating base pitch in a gear pair,  $\phi_{b,op}$ , is measured in angular units. Moreover, if the axes misalignment is taken into account, then the operating base pitch of a gear pair,  $\phi_{b,op}$ , is measured in angular units in all cases, namely, in  $P_a$  – gearing, in  $I_a$  – gearing as well as in  $C_a$  – gearing.

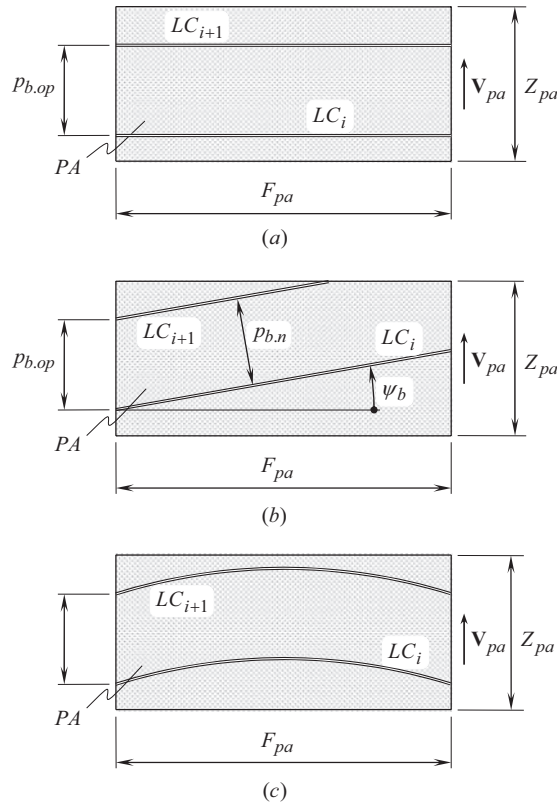


**FIGURE 10.38** Operating base pitch,  $p_{b,op}$ , in parallel-axes gearing with (a) straight teeth, (b) helical teeth, and (c) the teeth curved in their lengthwise direction.

#### Definition 10.4

Operating base pitch in parallel-axes gearing is a distance measured between points of intersection of two lines of contact of two adjacent pairs of gear teeth by a transverse plane.

*Operating base pitch* in the gear pair is a *calculated design parameter*, as this design parameter cannot be directly measured.

It is important to note here that the operating base pitch,  $p_{b,op}$ , in a gear pair is determined *before* the interacting tooth flanks,  $\mathcal{S}$  and  $\mathcal{P}$ , of the gear and of the mating pinion are determined. The use of such an approach gives an opportunity to design gear with correct geometry of the tooth flanks. For this purpose, the desirable line of contact,  $LC_{des}$ , between the tooth flanks,  $\mathcal{S}$  and  $\mathcal{P}$ , is used to generate the gear and the mating pinion tooth flanks,  $\mathcal{S}$  and  $\mathcal{P}$ .

When the gears rotate, the desirable line of contact,  $LC_{des}$ , travels together with the plane of action,  $PA$ . This is due to the straight-line segment,  $LC_{des}$ , which is rigidly associated with the  $PA$ . When the plane of action rolls over the base cylinder of the gear, the gear tooth flank,  $\mathcal{S}$ , is generated as a family of consecutive positions of the desirable line of contact,  $LC_{des}$ , in its motion in relation to a reference system associated with the gear (see Figure 10.39). The gear tooth flank,  $\mathcal{S}$ , is swept by the straight-line segment,  $LC_{des}$ . Similarly, when the plane of action rolls over the base cylinder of the pinion, the pinion tooth flank,  $\mathcal{P}$ , is generated as a family of consecutive positions of the desirable line of contact,  $LC_{des}$ , in its motion in relation to a reference system associated with the gear, as shown in Figure 10.39. The pinion tooth flank,  $\mathcal{P}$ , is swept by the straight-line segment,

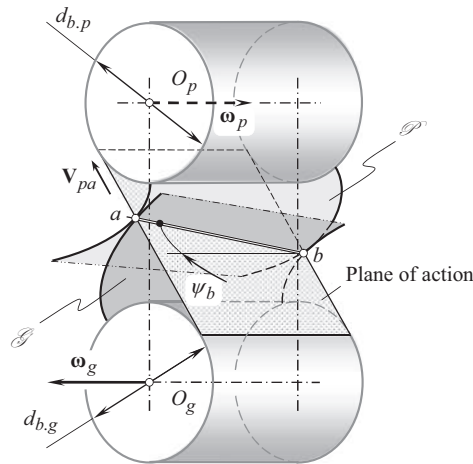


**FIGURE 10.39** Generation of screw involute surfaces,  $\mathcal{S}$  and  $\mathcal{P}$ , of tooth flanks in a pair of helical involute gears.

$LC_{des}$ . Under such a scenario, the actual line of contact,  $LC$ , between the tooth flanks,  $\mathcal{S}$  and  $\mathcal{P}$ , is congruent to the desirable line of contact,  $LC_{des}$ , of these surfaces ( $LC \equiv LC_{des}$ ). This enables equality of the base pitches of the gear and of the pinion to the operating base pitch of the gear pair (namely, the identities  $p_{b,g} \equiv p_{b,op}$  and  $p_{b,p} \equiv p_{b,op}$ , or simply  $p_{b,g} \equiv p_{b,p} \equiv p_{b,op}$  are valid), as illustrated in Figure 10.40.

In  $P_a$  – gearing, the identities  $p_{b,g} \equiv p_{b,op}$  and  $p_{b,p} \equiv p_{b,op}$  (or simply  $p_{b,g} \equiv p_{b,p} \equiv p_{b,op}$ ) are met only in geometrically accurate involute gearing. For any and all kinds of non-involute gearing, the identity is not fulfilled. Moreover, in non-involute gearing of all designs (with no exclusion), base pitch of a gear and that of a mating pinion cannot be constructed at all (while the operating base pitch of the gear pair can be easily calculated in gearing of any and all designs, with no exception).

The concept of operating base pitch,  $p_{b,op}$ , can be easily enhanced to helical involute parallel-axes gearing, as illustrated in Figure 10.38b. In this particular case, the normal base pitch,  $p_{b,n}$ , of

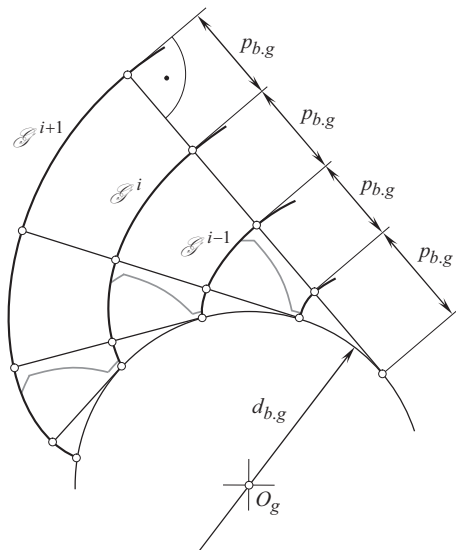


**FIGURE 10.40** Transverse base pitch of a gear,  $p_{b,g}$ , (of a pinion,  $p_{b,p}$ ) in geometrically accurate involute gear pair.

the gear pair, as well as the axial pitch,  $p_x$ , can be expressed in terms of the operating base pitch,  $p_{b.op}$ , and of the base helix angle,  $\psi_b$ .

Ultimately, parallel-axes involute gearing with teeth curved in their lengthwise direction can also be specified in terms of the operating base pitch,  $p_{b.op}$ . This latter case is schematically depicted in Figure 10.38c.

In all three cases shown in Figure 10.38, the operating base pitch in parallel-axes gearing can be expressed in terms of the base diameters of the gear,  $d_{b.g}$ , and of the pinion,  $d_{b.p}$ , and in terms of the tooth count of the gear,  $N_g$ , and of the pinion,  $N_p$ :

$$p_{b.op} = \frac{\pi d_{b.g}}{N_g} = \frac{\pi d_{b.p}}{N_p} \quad (10.33)$$

The operating base pitch,  $p_{b.op}$ , is measured along the path of contact (in section of a gear pair by a transverse plane). The operating base pitch can be calculated for a gear pair independently of the design parameters of the gear and pinion.

For parallel-axes gearing to be operated properly, all three base pitches, namely:

- the transverse base pitch of a gear,  $p_{b.g}$
- the transverse base pitch of a mating pinion,  $p_{b.p}$
- the operating base pitch of the gear pair,  $p_{b.op}$

have to be of the same value (i.e., the equality  $p_{b.g} = p_{b.p} = p_{b.op}$  has to be observed). Any and all alterations to the geometry of the line of contact, and to the motion of the line of contact together with the plane of action,  $PA$ , have to be *base pitch preserved* alterations.

## 10.5.2 VARIATION OF PARAMETERS OF TOOTH FLANK GEOMETRY

The geometry of tooth flanks plays an important role for gear pairs. Commonly, tooth flank geometry is specified at the pitch point of a gear pair. The actual values of the parameters of geometry of tooth flanks vary within the tooth height of a gear and of its mating pinion. The variation can be negligibly small for gears with a large tooth count. However, the variation becomes more significant in low-tooth-count gears. The lower the tooth count, the more significant the variation is observed, and vice versa.

This discussion necessitates an investigation into the variation of the actual values of parameters of the geometry of tooth flanks within the tooth height of a gear and that of a pinion.

The tooth flank geometry can be specified in terms of (a) radii of normal curvature, or in terms of normal curvatures as the reciprocals to them, (b) profile angle, and (c) helix angle.

### 10.5.2.1 Normal Curvature at Point of Gear Tooth Flank

The principal curvatures,  $k_{1.g}$  and  $k_{2.g}$ , at point of a gear tooth flank,  $\mathcal{S}$ , is calculated as roots of the quadratic equation:

$$\begin{vmatrix} L_g - E_g k_g & M_g - F_g k_g \\ M_g - F_g k_g & N_g - G_g k_g \end{vmatrix} = 0 \quad (10.34)$$

where

$E_g, F_g, G_g$  are the fundamental magnitudes of the first order calculated at point of the gear tooth flank,  $\mathcal{S}$ .

$L_g, M_g, N_g$  are the fundamental magnitudes of the second order calculated at point of the gear tooth flank,  $\mathcal{S}$ .

$k_g$  is the normal curvature at point of the gear tooth flank,  $\mathcal{S}$ .

$R_g$  is the radius of normal curvature at point of the gear tooth flank,  $\mathcal{S}$  (the equality  $R_g = k_g^{-1}$  is always observed).

For a gear involute screw surface,  $\mathcal{S}$ , the first principal curvature,  $k_{1,g}$ , is always of a positive value ( $k_{1,g} > 0$ ), while the second principal curvature,  $k_{2,g}$ , is always of a zero value ( $k_{2,g} \equiv 0$ ). This immediately yields a conclusion that all points within a screw involute tooth flank,  $\mathcal{S}$ , are points of parabolic kind. Local geometry of a screw involute tooth flank,  $\mathcal{S}$ , of a gear can also be expressed in terms of the first,  $R_{1,g} = k_{1,g}^{-1}$ , and of the second,  $R_{2,g} = k_{2,g}^{-1}$ , principal radii of curvature at point of the surface,  $\mathcal{S}$ .

The first principal radius of curvature,  $R_{1,g}$ , at point within the gear tooth flank,  $\mathcal{S}$ , can be calculated from the known formula [183]:

$$R_{1,p} = \frac{1}{2} \cdot \sqrt{\frac{d_{y,p}^2 - d_{b,p}^2}{1 - \sin^2 \psi \cdot \cos^2 \phi_n}} \quad (10.35)$$

At any point within the screw involute surface,  $\mathcal{S}$ , the second principal radius of curvature,  $R_{2,g}$ , approaches an infinity ( $R_{2,p} \rightarrow \infty$ ).

Consider an arbitrary point within the line action<sup>9</sup>  $N_p N_g$  (see Figure 10.41). The location of this point can be specified in terms of a variable parameter,  $z$ . In external involute gearing of conventional design, the actual value of the parameter,  $z$ , is equal to a portion of the total length,  $Z$ , of the path of contact,  $N_p N_g$ :

$$0 \leq z \leq Z \quad (10.36)$$

The parameter  $z$  is equal to  $z = 0$  at the point  $N_p$ , and it is equal to  $z = Z$  at the point  $N_g$  of the path of contact,  $P_c$ .

The smaller the tooth count in the gear,  $N_g$ , the smaller the difference:

$$(C \cdot \sin \phi_t - Z) \Big|_{N_g \rightarrow 0} \rightarrow 0 \quad (10.37)$$

Here, the center-distance in the gear pair is denoted by  $C$ . The transverse pressure angle,  $\phi_t$ , can be expressed in terms of the design parameters of the gear:

$$\phi_t = \tan^{-1} \left( \frac{\tan \phi_n}{\cos \psi} \right) \quad (10.38)$$

The first principal radius of curvature,  $R_{1,g}$ , at point of the gear tooth flank,  $\mathcal{S}$ , and the first principal radius of curvature,  $R_{1,p}$ , at that same point of the pinion tooth flank,  $\mathcal{P}$ , can be expressed in terms of the parameter,  $z$ , namely, in the form of functions  $R_{1,g} = R_{1,g}(z)$  and  $R_{1,p} = R_{1,p}(z)$ . Substituting the functions  $R_{1,g}(z)$  and  $R_{1,p}(z)$  into the formula for the relative curvature:

$$k_r(z) = \frac{1}{R_{1,g}(z)} + \frac{1}{R_{1,p}(z)} \quad (10.39)$$

yields one the equation:

$$k_r(z) = \frac{\sqrt{1 - \sin^2 \psi \cdot \cos^2 \phi_n}}{z \cdot \left( 1 - \frac{z}{C} \cdot \sqrt{1 + \frac{\cos^2 \psi}{\tan^2 \phi_n}} \right)} \quad (10.40)$$

<sup>9</sup> In parallel-axes gearing, the line of action,  $LA$ , is aligned with the *path of contact*,  $P_c$ .

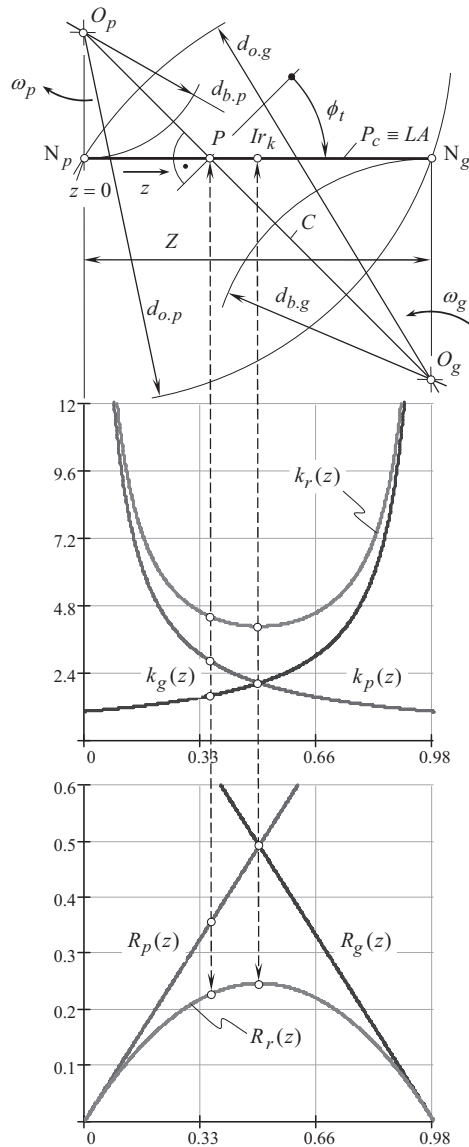


**FIGURE 10.41** Change of the elements of local geometry of the interacting tooth flanks of a gear,  $\mathcal{S}$ , and of a mating pinion,  $\mathcal{P}$ , within the path of contact,  $P_c$ .

for the calculation of the relative curvature,  $k_r(z)$ , at current point within the path of contact of the tooth flanks,  $\mathcal{S}$  and  $\mathcal{P}$ .

The radius of relative curvature,  $R_r(z)$ , equals  $R_r(z) = [k_r(z)]^{-1}$ .

For spur involute gears, the curvatures  $k_g$ ,  $k_p$ , and  $k_r$  (or the corresponding radii of curvature  $R_g$ ,  $R_p$ , and  $R_r$ ) are those of the involute tooth profile in the transverse section of the gear tooth flank,  $\mathcal{S}$ .

The alteration of the curvatures  $k_g \equiv k_g(z)$ ,  $k_p \equiv k_p(z)$ , and  $k_r \equiv k_r(z)$ , within the path of contact,  $N_p N_g$ , as well as of the corresponding radii of curvatures  $R_g \equiv R_g(z)$ ,  $R_p \equiv R_p(z)$ ,  $R_r \equiv R_r(z)$  are plotted in Figure 10.41. For the computation, the design parameters of the gear pair for an automobile differential (Table 10.1) are used.

The main reason for the variation of the radii of curvature,  $\rho_g$  and  $\rho_p$ , of tooth flanks,  $\mathcal{S}$  and  $\mathcal{P}$ , of a gear and that of a mating pinion is illustrated in Figure 10.42. A section of a gear pair by

**TABLE 10.1**  
**Design Parameters of a Gear Pair for the Automobile Differential**

Name of the Parameter	Gear	Pinion
Number of Teeth	15	6
Normal Profile Angle (°)	30°	30°
Helix Angle (°)	40.5526°, RH	40.5526°, LH
Pitch Diameter (in)	1.9194	0.7897
Center-Distance (in)	1.5650	

a transverse plane is considered as an example. At the pitch point,  $P$ , at the  $Ir_k$  – point, and at an arbitrary point,  $m$  (all three are located within the path of contact,  $P_c$ ), the radii of curvature,  $\rho_g$  and  $\rho_p$ , are constructed for the gear,  $\rho_{g.P}$ ,  $\rho_{g.Ir}$ , and  $\rho_{g.m}$ , and for the pinion,  $\rho_{p.P}$ ,  $\rho_{p.Ir}$ , and  $\rho_{p.m}$ . The gear tooth profile radii of curvature,  $\rho_g$ , are centered at point  $N_g$  on the gear base cylinder of a diameter,  $d_{b.g}$ . The pinion tooth profile radii of curvature,  $\rho_p$ , are centered at point  $N_p$  on the pinion base cylinder of a diameter,  $d_{b.p}$ . Circular arcs are passing through the points  $P$ ,  $Ir_k$ , and  $m$  for the gear (centered at  $N_g$ ), and for the pinion (centered at  $N_p$ ).

The radii of normal curvature,  $R_g$ , at point of the gear tooth flank,  $\mathcal{G}$ , and the radii of normal curvature,  $R_p$ , at point of the pinion tooth flank,  $\mathcal{P}$ , alter linearly within the active portion of the path of contact,  $P_c$ . The alteration of normal curvatures,  $k_g$  and  $k_p$ , at point of the gear and the pinion tooth flanks follow hyperbolic function. The relative normal curvature,  $k_r$ , is minimal at a special point of meshing. This point is referred to as the  $Ir_k$  – point of a gear tooth flank (see Section 10.5.3

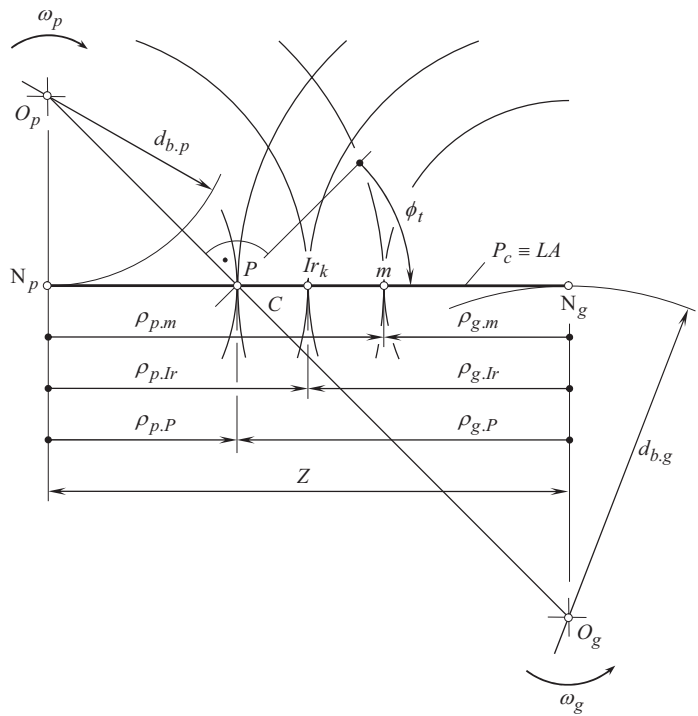


**FIGURE 10.42** Variation of the radii of curvature in a transverse section of interacting tooth flanks of a gear,  $\mathcal{G}$ , and of a mating pinion,  $\mathcal{P}$ , within the path of contact,  $P_c$ .



below for details). The location of the  $Ir_k$  – point corresponds to the middle of the center-distance,  $C$ . The value of the relative normal curvature,  $k_r$ , increases from the  $Ir_k$  – point in both directions, namely, it increases toward the gear axis of rotation,  $O_g$ , and toward the pinion axis of rotation,  $O_p$ .

It is necessary to point out here that the maximum value of the relative curvature,  $k_r^{\max}$ , occurs at the point of intersection of the outer diameter of a gear,  $d_{o,g}$ , and of the limit diameter of a mating pinion,  $d_{l,p}$ . Similarly, the relative curvature,  $\tilde{k}_r^{\max}$ , reaches its maximum value at the opposite side of the active length of the path of contact, that is, at the point of intersection of the outside diameter of the pinion,  $d_{o,p}$ , and the limit diameter of the gear,  $d_{l,g}$ . However, the inequality  $k_r^{\max} > \tilde{k}_r^{\max}$  is always observed [the equality  $k_r^{\max} = \tilde{k}_r^{\max}$  is observed only in the case when tooth count in the gear is equal to tooth count in the pinion and, thus, the equality  $N_g = N_p$  is valid].

The alteration of the actual value of the radius of relative curvature in a gear pair composed of spur involute gears is illustrated in Figure 10.43. The semi-circle constructed with the path of contact,  $N_g N_p$ , as the diameter can be shown to represent, to an appropriate scale, the term  $\sqrt{(R_g + R_p) \cdot R_r}$  (below, the square root  $\sqrt{R_g + R_p}$  is designated as  $a$ ). This is the term by means of which the change in surface stress at point of contact on the path of contact is specified while the contact moves from  $P_g$  to  $P_p$ . Near the point  $N_g$ , the product  $a \cdot \sqrt{R_r}$  approaches zero. The variation of the relative curvature,  $R_r$ , itself is constructed on the premise of change of the parameter  $a \cdot \sqrt{R_r}$  within the straight-line segment  $P_g P_p$ . The function  $R_r = R_r(z)$  is plotted in Figure 10.43. Points of the plot  $R_r = R_r(z)$  are constructed using well-known properties of similar right triangles. For arbitrary point,  $m$ , within the path of contact,  $N_g N_p$ , the sequence of points, those used for the construction, is denoted by 1, 2, 3, 4 and, ultimately, by 5 for the point on the plot of the function  $R_r = R_r(z)$ .

The relative curvature,  $R_r$ , reaches its maximum value at the  $Ir_k$  – point. The significance of the  $Ir_k$  – point is getting clear now.

A graph of the function  $R_r = R_r(z)$  similar to that shown in Figure 10.43 for a spur gear pair, can be constructed for a gear pair that is composed of helical gears. An example of the function  $R_r = R_r(z)$  of a helical gear pair is depicted in Figure 10.44. For the construction of the plot of the function  $R_r = R_r(z)$ , a straight-line segment perpendicular to the lines of contact,  $LC$ , is used. A semi-circle is constructed on this straight-line segment as on the diameter. Further construction is identical to that shown in Figure 10.43 for a spur gear pair.

Variation of *Hertz contact stress* at contact points within the line of action is strongly correlated with the function  $k_r \equiv k_r(z)$ .

### 10.5.2.2 Variation of Gear Tooth Profile Angle and Helix Angle

Alteration of the tooth profile angle,  $\phi_{n,g}(z)$ , and of the helix angle,  $\psi_{y,g}(z)$ , within the active portion of the line of action commonly is negligibly small. However, this change becomes significant in low-tooth-count gears.

For illustrative purposes the functions of variation of (a) the normal profile angle,  $\phi_{n,g}(z)$ , (b) the transverse profile angle,  $\phi_{t,g}(z)$ , and (c) the helix angle,  $\psi_{y,g}(z)$ , are plotted in Figure 10.45.

### 10.5.3 SPECIAL POINT OF MESHING

It is instructive to point out here that the minimum normal relative curvature,  $k_r^{\min}$  (and, correspondingly, the maximum radius of normal curvature,  $R_r^{\max}$ ), is observed at the special point of meshing,  $Ir_k$ , that is situated within the path of contact,  $P_c$ . The relative curvature is of a minimal value at this point of meshing, and, consequently, contact stresses reach their minimum value.

The path of contact,  $N_g N_p$ , is subdivided by the point  $Ir_k$  on two equal straight-line segments,  $Ir_k N_g$  and  $Ir_k N_p$ , as illustrated in Figure 10.46. Due to this, the equality  $Ir_k N_g = Ir_k N_p$  is valid.

The following equations for the calculation of coordinates of the  $Ir_k$  – point immediately follow from the analysis of Figure 10.46:

$$r_{Ir,g} = \frac{1}{2} \cdot \sqrt{d_{b,g}^2 + C^2 \cdot \sin^2 \phi_t} \quad (10.41)$$

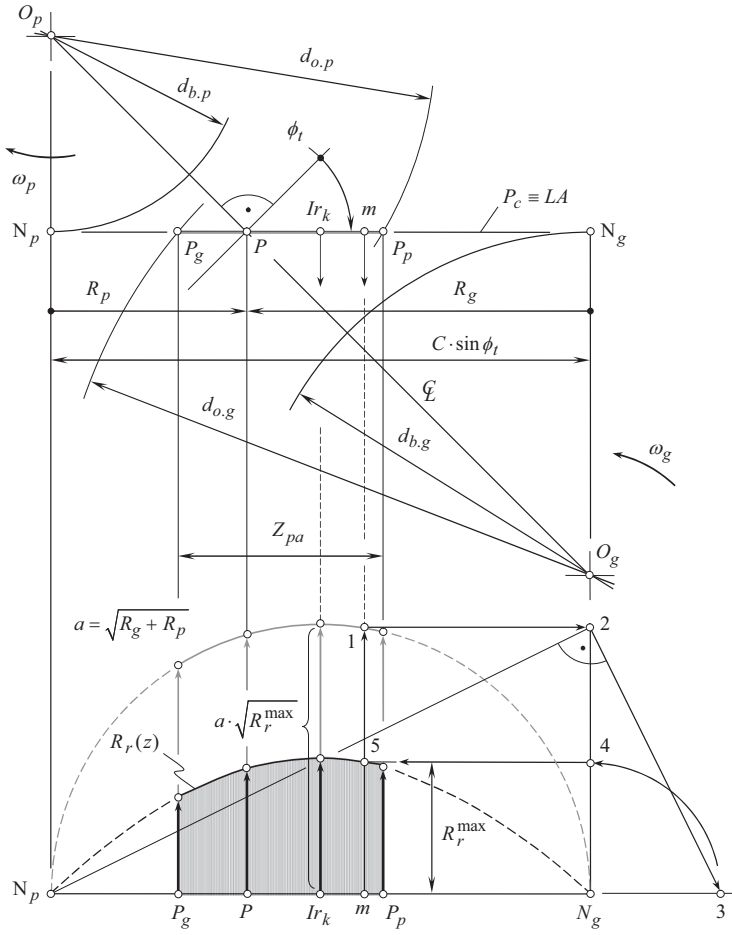


**FIGURE 10.43** An example of distribution of the relative radii of normal curvature,  $R_r(z)$ , at contact point of tooth flanks,  $\mathcal{S}$  and  $\mathcal{P}$ , within the path of contact,  $P_c$ , in a pair of spur involute gears.

$$r_{I_r.p} = \frac{1}{2} \cdot \sqrt{d_{b,p}^2 + C^2 \cdot \sin^2 \phi_t} \quad (10.42)$$

$$\cos v_g = \frac{r_{I_r.g}^2 + C^2 - r_{I_r.p}^2}{2 \cdot r_{I_r.g} \cdot C} \quad (10.43)$$

$$\cos v_p = \frac{r_{I_r.p}^2 + C^2 - r_{I_r.g}^2}{2 \cdot r_{I_r.p} \cdot C} \quad (10.44)$$

$$E_g = r_{I_r.g} \cdot \cos v_g \quad (10.45)$$

$$E_p = r_{I_r.p} \cdot \cos v_p \quad (10.46)$$

Equations (10.41)–(10.46) can be expressed in terms of the design parameters of a gear and of its mating pinion.



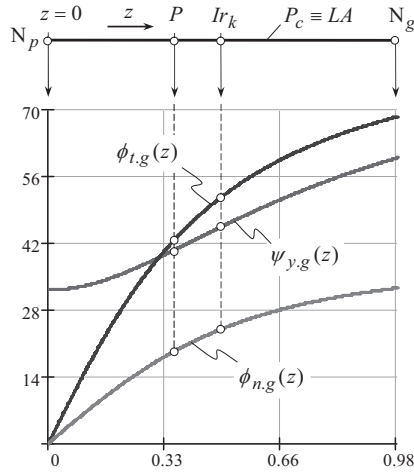


**FIGURE 10.45** Variation of the gear tooth normal pressure angle,  $\phi_{n,g}$ , transverse pressure angle,  $\phi_{t,g}$ , and helix angle,  $\psi_{y,g}$ , within the active portion of the path of contact,  $P_c$ .

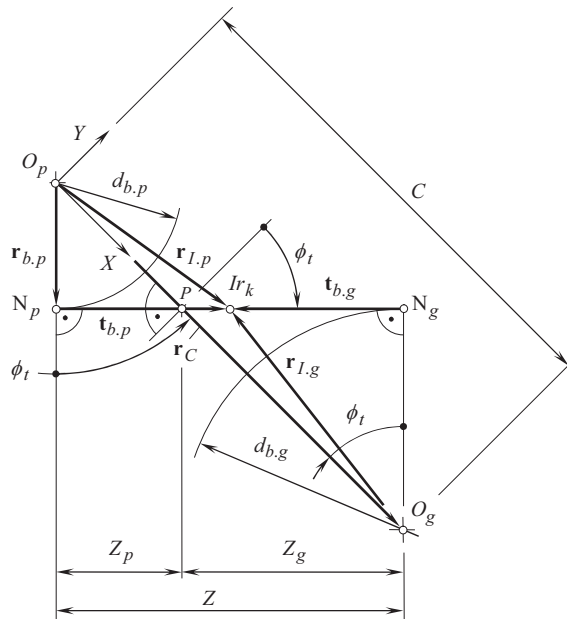


**FIGURE 10.46** On derivation of coordinates of  $Ir_k$  – point in parallel-axes external involute gear pair.

The concept of the special point of meshing,  $Ir_k$ , can be enhanced to gear pairs of other kinds, namely, for (a) helical gear pairs, (b) intersected-axes gear pairs, and (c) crossed-axes gear pairs, and so forth. For spatial gearing, a three-dimensional  $Ir_k$  – curve is can be constructed instead of the  $Ir_k$  point [166].

It should be mentioned here that for the current point within the line of action,  $LA$ , the difference  $(\rho_g - \rho_p)$  is of a constant value, as it is equal to the center-distance,  $C$ . Therefore, for an internal gear pair, the point,  $Ir_k$ , at which the relative curvature is of a minimum value, is located far beyond the outer diameter of the pinion ( $Ir_k \rightarrow \infty$ ).

## 10.6 CONTACT MOTION CHARACTERISTICS

Rolling and sliding between the tooth flanks of two mating gears occur simultaneously when transmitting a rotary motion by an external involute parallel-axes gearing (see Figure 10.47). Rolling and sliding is observed at any point of contact within the active portion of the line of contact. Pitch point is the only exception: pure rolling and no sliding occurs in the pitch point. Investigation and analysis into sliding and rolling in a gear pair is of importance from an engineering perspective. It enables, for example, determining and reducing losses due to friction between mating gears.

Figure 10.47 shows the directions of the rolling,  $RI$ , and sliding,  $SI$ , velocities on the driving and driven gear teeth. Contact on the driver tooth starts near the root of the tooth, rolls up the tooth, and ends at the tooth tip. Sliding is away from the driving gear pitch line. Contact on the driven tooth starts at the tooth tip, rolls down the tooth, and ends near the tooth root. Sliding is toward the driven gear pitch line. Like micropitting, micropitting cracks grow opposite the direction of sliding at the gear tooth surface. Consequently, the cracks converge near the pitch line of the driver, and diverge near the pitch line of the driven gear.

### 10.6.1 SLIDING CONDITIONS

The velocity vectors at point of contact between a gear and a mating pinion tooth flanks are schematically shown in Figure 10.48. Contact point,  $K$ , is an arbitrary point within the path of contact,  $P_c$ , (or within the active portion of the line of action,  $LA$ ). The contact point,  $m$ , is an arbitrary point within the line of action,  $LA$ .

At contact point,  $K$ , between the tooth flanks,  $\mathcal{G}$  and  $\mathcal{P}$ , the velocity vector,  $\mathbf{V}_{K,g}$ , of the point  $K$  on the gear tooth flank,  $\mathcal{G}$ , is pointed perpendicular to the straight-line segment,  $O_g K$ . Similarly, the velocity vector,  $\mathbf{V}_{K,p}$ , of the point  $K$  on the pinion tooth flank,  $\mathcal{P}$ , is pointed perpendicular to the straight-line segment,  $O_p K$ .

As contact point  $K$  travels along the path of contact,  $P_c$ , neither a gap between the interacting tooth flanks,  $\mathcal{G}$  and  $\mathcal{P}$ , nor interference of the tooth flanks occur. Due to this fact, the projections of the velocity vectors,  $\mathbf{V}_{K,g}$  and  $\mathbf{V}_{K,p}$ , onto the line of action are equal to each other. The projections are designated as  $\mathbf{V}_K^{tr}$ . This velocity vector is referred to as the *trailing velocity vector*, as it causes transmission of the rotation from the driving shaft to the driven shaft in the gear pair. The *trailing velocity vector* results in pure rolling of the gear and of the pinion tooth profiles over one another.

The component  $\mathbf{V}_{K,g}^{sl}$  of the velocity vector  $\mathbf{V}_{K,g}$  is pointed perpendicular to the path of contact,  $P_c$ , (to the line of action,  $LA$ ). The component  $\mathbf{V}_{K,p}^{sl}$  of the velocity vector  $\mathbf{V}_{K,p}$  is pointed also perpendicular to the line of action,  $LA$ . Both the velocity vectors,  $\mathbf{V}_{K,g}^{sl}$  and  $\mathbf{V}_{K,p}^{sl}$ , are tangent to the gear tooth profiles at the contact point  $K$ .

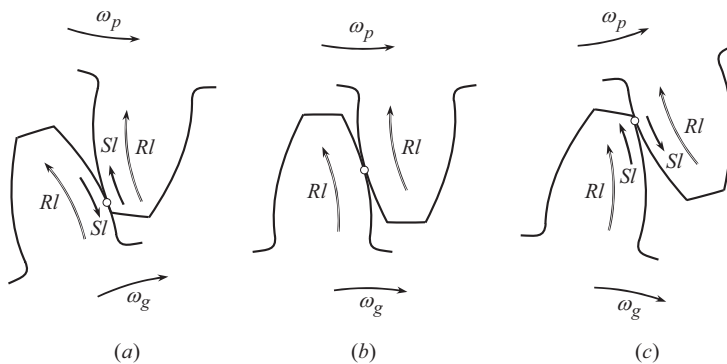


**FIGURE 10.47** Rolling motion,  $RI$ , and sliding motion,  $SI$ , in involute gearing: (a) at the beginning of meshing of the tooth flanks,  $\mathcal{G}$  and  $\mathcal{P}$ ; (b) at the pitch point,  $P$ , and (c) at the end of meshing of the tooth flanks,  $\mathcal{G}$  and  $\mathcal{P}$ .

The components  $\mathbf{V}_{K,g}^{sl}$  and  $\mathbf{V}_{K,p}^{sl}$  of the velocity vectors,  $\mathbf{V}_{K,g}$  and  $\mathbf{V}_{K,p}$ , are of different magnitudes ( $|\mathbf{V}_{K,g}| \neq |\mathbf{V}_{K,p}|$ ). The sliding velocity vector  $\mathbf{V}_K^{sl}$  equals to the difference:

$$\mathbf{V}_K^{sl} = \mathbf{V}_{K,g}^{sl} - \mathbf{V}_{K,p}^{sl} \quad (10.47)$$

The relationships between the velocities in involute gears are governed by the condition that is occurred at every contact point,  $K$ , within the path of contact,  $P_c$ . The components  $\mathbf{V}_{K,g}^{tr}$  and  $\mathbf{V}_{K,p}^{tr}$  are equal to the velocity,  $\mathbf{V}_K^{tr}$ , of the contact point along the path of contact ( $\mathbf{V}_{K,g}^{tr} = \mathbf{V}_K^{tr}$  and  $\mathbf{V}_{K,p}^{tr} = \mathbf{V}_K^{tr}$ ). Otherwise, either separation, or interference between the tooth flanks,  $\mathcal{G}$  and  $\mathcal{P}$ , becomes inevitable.

For the magnitudes,  $V_{K,g}^{sl}$  and  $V_{K,p}^{sl}$ , of the velocity vectors,  $\mathbf{V}_{K,g}$  and  $\mathbf{V}_{K,p}$ , similarity of the triangles in Figure 10.48 yields for the following expressions:

$$V_{K,g}^{sl} = |\mathbf{V}_{K,g}^{sl}| = V_K^{sl} \frac{KN_g}{O_g N_g} \quad (10.48)$$

$$V_{K,p}^{sl} = |\mathbf{V}_{K,p}^{sl}| = V_K^{sl} \frac{KN_p}{O_p N_p} \quad (10.49)$$

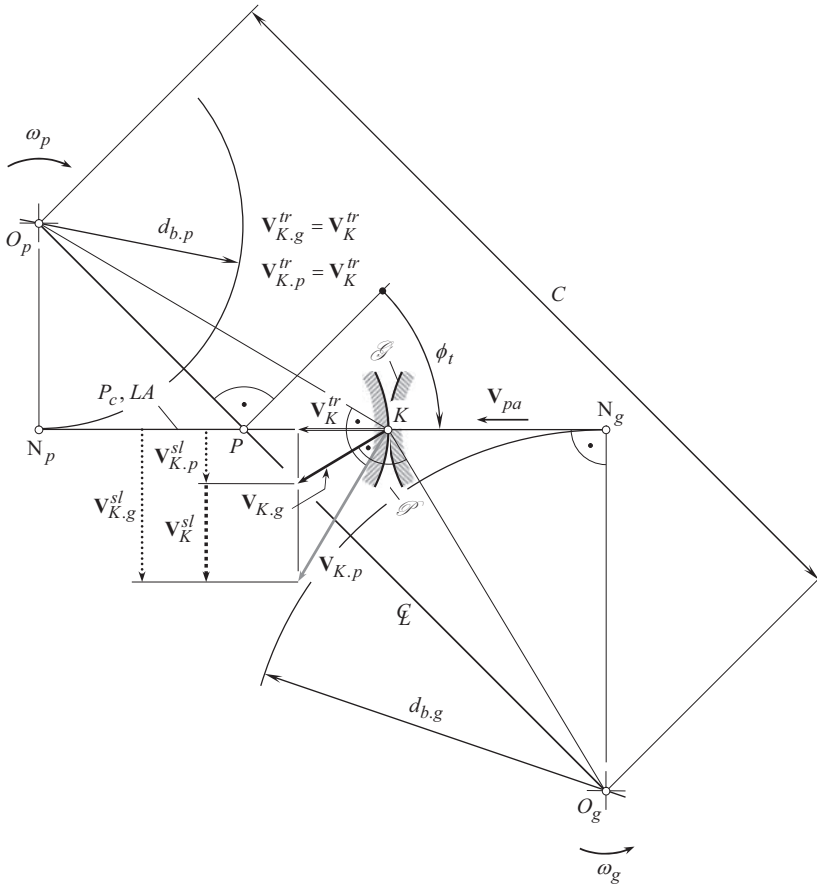


**FIGURE 10.48** Tooth profile sliding,  $\mathbf{V}_K^{sl}$ , at arbitrary point within the path of contact,  $P_c$ , in parallel-axes involute gear pair.

At the pitch point,  $P$ , the ratio:

$$\frac{KN_g}{O_g N_g} = \frac{KN_p}{O_p N_p} \quad (10.50)$$

is valid. Due to this, the equality  $V_{K.g}^{sl} = V_{K.p}^{sl}$  is valid at pitch point,  $P$ . This makes evident that no profile sliding between the tooth flanks,  $\mathcal{S}$  and  $\mathcal{P}$ , occurs at pitch point,  $P$ .

The magnitude,  $V_K^{sl}$ , of the sliding velocity vector,  $\mathbf{V}_K^{sl}$ , equals to the difference:

$$V_K^{sl} = V_{K.g}^{sl} - V_{K.p}^{sl} \quad (10.51)$$

During an infinitesimally small interval of time, the ratio of the length of the gear and of the pinion tooth profiles in contact is equal to the ratio of the velocity components,  $V_{K.g}^{sl}$  and  $V_{K.p}^{sl}$ . Due to this, at pitch point,  $P$ , the equality  $V_{K.g}^{sl} = V_{K.p}^{sl}$  is valid, and the lengths of the tooth profiles in contact are equal to each other. This corresponds to pure rolling without sliding, which takes place at this point.

Consider kinematics of the relative motion in an external parallel-axes involute gear pair, as illustrated in Figure 10.49. In an arbitrary instant of time, the trailing velocity vector,  $\mathbf{V}_K^{tr} (= \mathbf{V}_{pa})$ , of contact point,  $K$ , of the gear tooth flank,  $\mathcal{S}$ , is pointed perpendicular to the corresponding radius at which the point is located. The velocity vector,  $\mathbf{V}_{A.g}$ , of the point  $A$  of the gear tooth flank is orthogonal to the radius,  $O_g A$ . The velocity vector,  $\mathbf{V}_{A.p}$ , of the point  $A$  of the pinion tooth flank is orthogonal to the radius,  $O_p A$ . The projections of the velocities of all linear motions of rotation onto the line of action,  $LA$ , are equal to [166]:

$$|\mathbf{V}^{tr}| = 0.5 \cdot d_{b,p} \cdot \omega_p = 0.5 \cdot d_{b,g} \cdot \omega_g \quad (10.52)$$

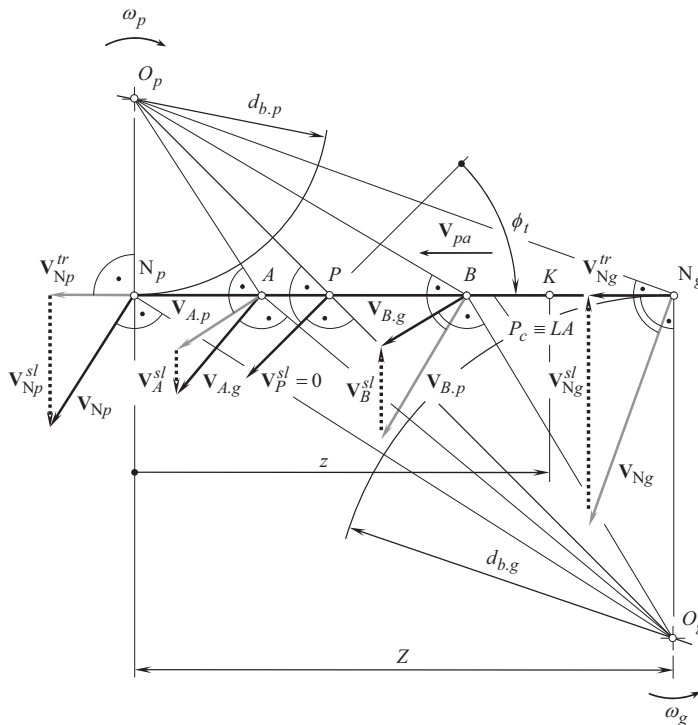


FIGURE 10.49 Kinematics of relative motion in external parallel-axes involute gear pair.

At an arbitrary contact point, the sliding velocity vector,  $\mathbf{V}_m^{sl}$ , of the gear tooth flank,  $\mathcal{S}$ , in relation to the pinion tooth flank,  $\mathcal{P}$ , equals:

$$\mathbf{V}_K^{sl} = \mathbf{V}_{K.g}^{sl} - \mathbf{V}_{K.p}^{sl} \quad (10.53)$$

At arbitrary contact point, the sliding velocity vector,  $\mathbf{V}_i^{sl}$ , of the gear tooth flank,  $\mathcal{S}$ , in relation to the pinion tooth flank,  $\mathcal{P}$ , equals  $\mathbf{V}_i^{sl} = \mathbf{V}_i^g - \mathbf{V}_i^p$ . At various points within the path of contact,  $P_c$ , the relative sliding of the tooth flanks,  $\mathcal{S}$  and  $\mathcal{P}$ , is of a different value. The magnitude,  $V_K^{sl}$ , of the sliding velocity vector,  $\mathbf{V}_K^{sl}$ , is a function of  $z$ :  $V_K^{sl}(z) = |\mathbf{V}_K^{sl}(z)|$ . The linear velocity vector,  $\mathbf{V}_K^{sl}$ , of relative sliding is always pointed perpendicularly to the line of action. The equality  $\mathbf{V}_K^{sl} = \mathbf{V}_{K.g}^{sl} - \mathbf{V}_{K.p}^{sl}$  yields for the following formula for the calculation of the magnitude of the sliding velocity vector:

$$V_K^{sl}(z) = [Z - (1 - u) \cdot z] \cdot \omega_p \quad (10.54)$$

Here,  $u$  designates the tooth ratio ( $u = d_{b.g} / d_{b.p}$ ).

Variation of the tooth flank sliding is illustrated in Figure 10.50. The sliding is of a maximum value at the base cylinders, and it is greater for the gear tooth flank, compared to that for the pinion tooth flank. No sliding is observed at pitch point,  $P$ . The sliding is in opposite direction from different sides of pitch point,  $P$ . For a driving pinion, the sliding is pointed away of the pitch point,  $P$ , while for the driven gear, the sliding is pointed toward pitch point,  $P$ .

The performed theoretical analysis of gear tooth sliding is in perfect correlation with the results of experimental research into pitting in gearing. Metallurgical sections cut transversely through micropits that (see Figure 10.51) show cracks start at or near the gear tooth surface and grow at a shallow angle (typically  $10-30^\circ$ , but sometimes as steep as  $45^\circ$ ) to the surface [34]. The results of the analysis represented in Figures 10.47–10.50, are in a good correlation with the metallurgical experiments discussed in Figure 10.51.

Features of rolling/sliding in internal gearing are discussed in Figure 10.52. As the projections  $\mathbf{V}_{sl.g}^m$  and  $\mathbf{V}_{sl.p}^m$  are of the same direction, the sliding velocity,  $\mathbf{V}_{sl}^m$ , is significantly smaller compared to that in external involute gearing. Moreover, the tooth sliding is unidirectional along the whole involute tooth profile, that is, no point with zero sliding is observed within the tooth profile in involute gearing.

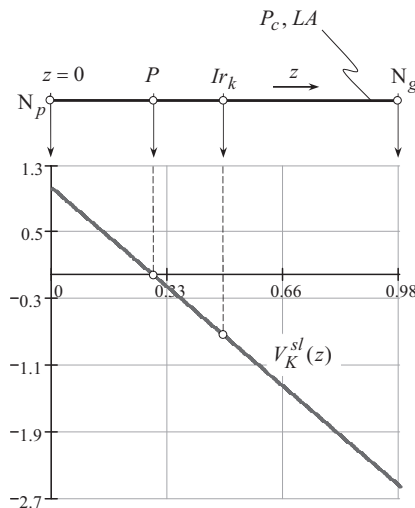
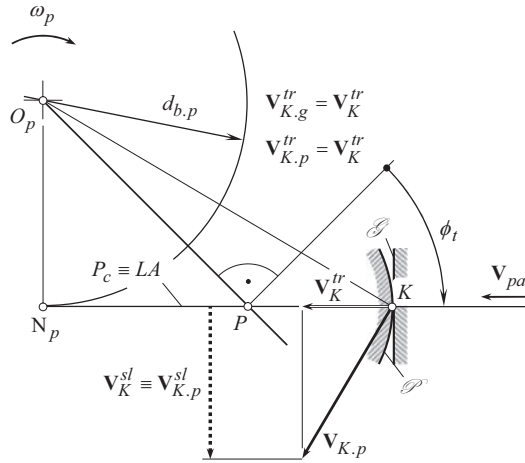


FIGURE 10.50 An example of the plot *tooth flank sliding vs.  $z$ -parameter*.







**FIGURE 10.53** Tooth profile sliding,  $\mathbf{V}_K^{sl}$ , at arbitrary point within the path of contact,  $P_c$ , in *pinion gear-to-rack* gearing.

### 10.6.2 SPECIFIC SLIDING

The impact of the design parameters of a gear and of its mating pinion onto the sliding conditions is specified by coefficients of specific sliding. For the specification of profile sliding of tooth flanks,  $\mathcal{S}$  and  $\mathcal{P}$ , a unitless parameter is used. This parameter is commonly referred to as *specific sliding*, and is denoted by  $\gamma$ . Two different parameters,  $\gamma$ , are distinguished.

**First**, the slide/roll ratio for the tooth flank,  $\mathcal{S}$ , of a gear:

$$\gamma_g = \frac{V_{K.g}^{sl} - V_{K.p}^{sl}}{V_{K.g}^{sl}} \quad (10.55)$$

The coefficient  $\gamma_g$  is commonly referred to as *specific sliding coefficient of the first order*.

**Second**, the slide/roll ratio for the tooth flank,  $\mathcal{P}$ , of a pinion:

$$\gamma_p = \frac{V_{K.p}^{sl} - V_{K.g}^{sl}}{V_{K.p}^{sl}} \quad (10.56)$$

The coefficient  $\gamma_p$  is commonly referred to as *specific sliding coefficient of the second order*.

Examples of functions,  $\gamma_g$  and  $\gamma_p$ , of specific sliding are plotted in Figure 10.54.

The equations [see Eqs. (10.55) and (10.56)] can be expressed in terms of the design parameters of a gear pair:

$$\gamma_g = \left(1 + \frac{1}{u}\right) \frac{Z_{pa.K}}{Z_{pa.K} - Z_{pa.g}} \quad (10.57)$$

$$\gamma_p = \left(1 + \frac{1}{u}\right) \frac{Z_{pa.K}}{Z_{pa.K} + Z_{pa.p}} \quad (10.58)$$

where:

$u$  is the gear ratio in the gear pair.

$Z_{pa.K}$  is the distance of contact point,  $K$ , from pitch point,  $P$  (see Figure 10.54).

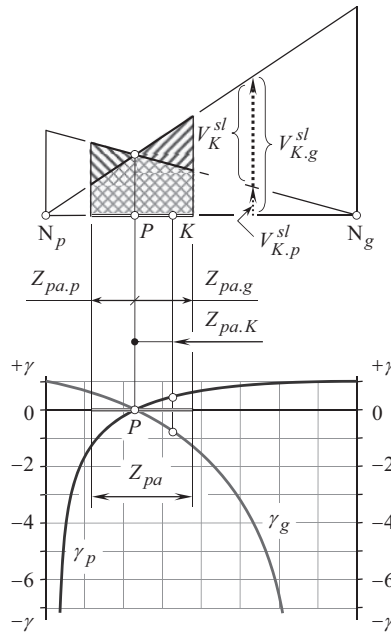


**FIGURE 10.54** Specific sliding,  $\gamma$ , in external involute gear pair.

$Z_{pa,g}$  is the portion of the active part of the plane of action,  $Z_{pa}$ , viewed from the gear side (see Figure 10.54).

$Z_{pa,p}$  is the portion of the active part of the plane of action,  $Z_{pa}$ , viewed from the pinion side (see Figure 10.54).

The impact of only the design parameters of the gear pair is reflected by specific sliding coefficients,  $\gamma_g$  and  $\gamma_p$ , of the first and of the second order, when the influence of a gear and a mating pinion rotations,  $\omega_g$  and  $\omega_p$ , is eliminated.

It should be taken into account here that the pinion teeth are engaged in mesh  $u$  times more often than the gear teeth do.

The specific sliding,  $\gamma$  (namely,  $\gamma_g$  and  $\gamma_p$ ), is of a positive value on the addendum portions of the tooth flanks. The parameter,  $\gamma$ , does not exceed 1. At the pitch point,  $P$ , it is equal to zero, and it is equal to 1 at the base circle of the mating gear.

The specific sliding on the dedendum portion of the tooth flanks is of a negative value. It is equal to zero at pitch point,  $P$ , and it is approaching minus infinity at the base circle.

Commonly, the specific sliding,  $\gamma$ , is plotted along the path of contact,  $P_c$ , as depicted in Figure 10.54. Only the region,  $Z_{pa}$ , within the path of contact,  $P_c$ , comes into effect when investigating the engagement of the gear teeth.

Because of the greater number of teeth, a *pinion gear-to-rack* gear pair features lower profile sliding compared to that in an external gear pair. However, the profile sliding in a *pinion gear-to-rack* gear pair exceeds that in an internal gear pair.

## 10.7 ELEMENTS OF DYNAMICS IN GEOMETRICALLY ACCURATE PARALLEL-AXES GEARING

Transmission and transformation of a rotary motion is the main purpose of gearing of all kinds. In parallel-axes gearing, a rotation and torque are transmitted from a driving shaft to a driven shaft. Alteration of the rotation and torque is commonly observed when transmitting a rotation.

At point within the line of action,  $LA$ , in a *pinion gear-to-rack* gear pair, the difference ( $\rho_g - \rho_p$ ) between the radii of curvature is of a constant value, as it is equal to the center-distance,  $C$ . Therefore, for a *pinion gear-to-rack* gear pair, point  $Ir_k$ , at which the relative curvature is of a minimum value, is located far beyond the outer diameter of the pinion ( $Ir_k \rightarrow \infty$ ).

### 10.7.1 FORCES ACTING IN PLANE OF ACTION

In parallel-axes gearing, an input rotation, and input torque are transmitted from a driving shaft to a driven shaft by forces that act within the plane of action. No other forces are involved in transmission of rotation and torque in parallel-axes gearing. Friction forces are taken into account in later stages of the analysis.

In a parallel-axes gear pair, an input rotation, and input torque are designated as  $\omega_{\text{input}}$  and  $\mathbf{T}_{\text{input}}$ , and an output rotation, and output torque are designated as  $\omega_{\text{output}}$  and  $\mathbf{T}_{\text{output}}$ , correspondingly. The input rotation and torque are in the same direction, while the output rotation and torque are pointed oppositely to one another. In reduction gears, a pinion is a driver and the gear is a driven element. Therefore, in this particular configuration, the input and output rotations and torques are designated as  $\omega_p$ ,  $\mathbf{T}_p$ , and  $\omega_g$ ,  $\mathbf{T}_g$  correspondingly.

Transmission of a rotation by means of a geometrically accurate parallel-axes involute gear pair is schematically illustrated in Figure 10.55. Consider a case when an input rotation,  $\omega_p$ , input torque,  $\mathbf{T}_p$ , and a gear ratio,  $u$ , of the gear pair are specified. An input rotation,  $\omega_p = |\omega_p|$ , and input torque,  $T_p = |\mathbf{T}_p|$ , from a driving shaft are transmitted and transformed to corresponding output rotation,  $\omega_g = |\omega_g|$ , and torque,  $T_g = |\mathbf{T}_g|$ , of an output shaft. Magnitude of the input torque,  $T_p$ , and magnitude of the output torque,  $T_g$ , correspond to one another as  $T_p = u T_g$ .

When transmitting rotation by means of gear teeth, the gear and pinion teeth are loaded by a distributed load. The interaction between the tooth flanks,  $\mathcal{G}$  and  $\mathcal{P}$ , of the driving and the driven gears is observed along the line(s) of contact,  $LC$ . The following approach can be utilized for the determination of the distributed force,  $f_i$ .

In Figure 10.55, the input rotation,  $\omega_p$ , is transformed to a corresponding output rotation,  $\omega_g$ . The correlation between the input rotation, and the output rotation is expressed by the formula:

$$\omega_g = \frac{\omega_p}{\mu} \quad (10.59)$$

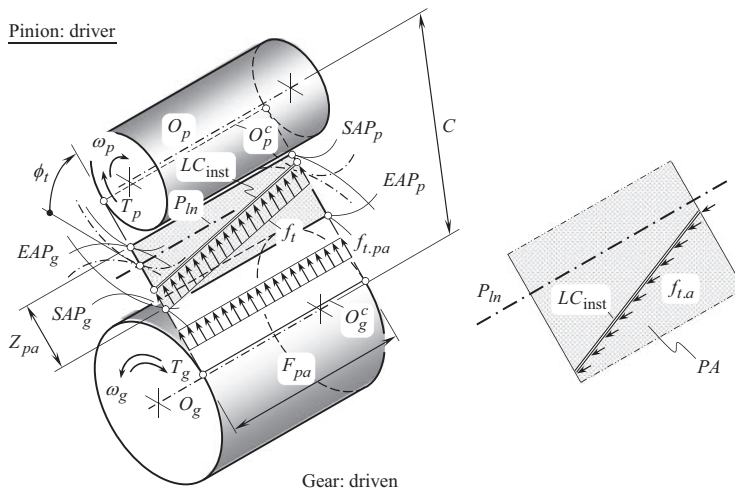


**FIGURE 10.55** Load distribution along instantaneous line of contact,  $LC_{\text{inst}}$ , in helical parallel-axes gear pair.

The magnitude,  $F_t = |\mathbf{F}_t|$ , of the acting tangential force,  $\mathbf{F}_t$ , equals:

$$F_t = \frac{2T_p}{d_{b,g}} \quad (10.60)$$

where base diameter of the driving pinion is denoted by  $d_{b,p}$ .

It is commonly assumed that the acting tangential force,  $\mathbf{F}_t$ , is evenly distributed,  $f_{t,pa}$ , along the face-width,  $F_{pa}$ , of the gear pair. An equation:

$$f_{t,pa} = \frac{F_t}{F_{pa}} \quad (10.61)$$

can be used for the calculation of the distributed load,  $f_{t,pa}$ .

Equation (10.60) is valid for the calculation of a distributed load in spur parallel-axes gear pairs. In helical parallel-axes gearing the distributed load,  $f_t$ , equals:

$$f_t = \frac{F_t}{F_{pa}} \cos \psi_b \quad (10.62)$$

where  $\psi_b$  is the base helix angle.

At every point of the line of contact,  $LC$ , the distributed load,  $f_t$ , is pointed along a line of action,  $LA$ , through the corresponding point of interest.

For the calculation of a gear contact strength, and bending strength, the distributed normal load,  $f_{t,n}$ , is commonly used:

$$f_{t,n} = \frac{F_t}{F_{pa}} \quad (10.63)$$

The lines of action of the distributed normal load,  $f_{t,n}$ , are also entirely located within the plane of action,  $PA$ .

The axial component,  $f_{t,a}$ , of the distributed load causes the axial thrust that is withhold by bearings. For calculation of the axial component,  $f_{t,a}$ , of the distributed load the following equation is used:

$$f_{t,a} = \frac{F_t}{2F_{pa}} \sin 2\psi_b \quad (10.64)$$

The axial component,  $f_{t,a}$ , does not transmit the rotation.

Equation (10.61)–(10.64) are valid in cases when the tooth flanks,  $\mathcal{S}$  and  $\mathcal{P}$ , of a gear and a mating pinion contact each other along the only line of contact,  $LC$ . As the total contact ratio,  $\bar{m}$ , in a gear pair is always greater than one ( $\bar{m} > 1$ ), in reality, two, or even more lines of contact,  $LC_i$ , are observed. Let's consider the load transmission for the cases when the plane of action,  $PA$ , is shaped in the form of a rectangle.

Commonly, in geometrically accurate spur parallel-axes gearing either one or two lines of contact,  $LC_i$ , are observed. Cases when a gear pair features three and/or more lines of contact,  $LC_i$ , are possible but they are not common.

When only one pair of the teeth is engaged in mesh, as illustrated in Figure 10.56a, the applied load is evenly distributed along a single line of contact,  $LC$ . The distributed load,  $f_t$ , is calculated from the equation:

$$f_t = \frac{F_t}{F_{pa}} \quad (10.65)$$

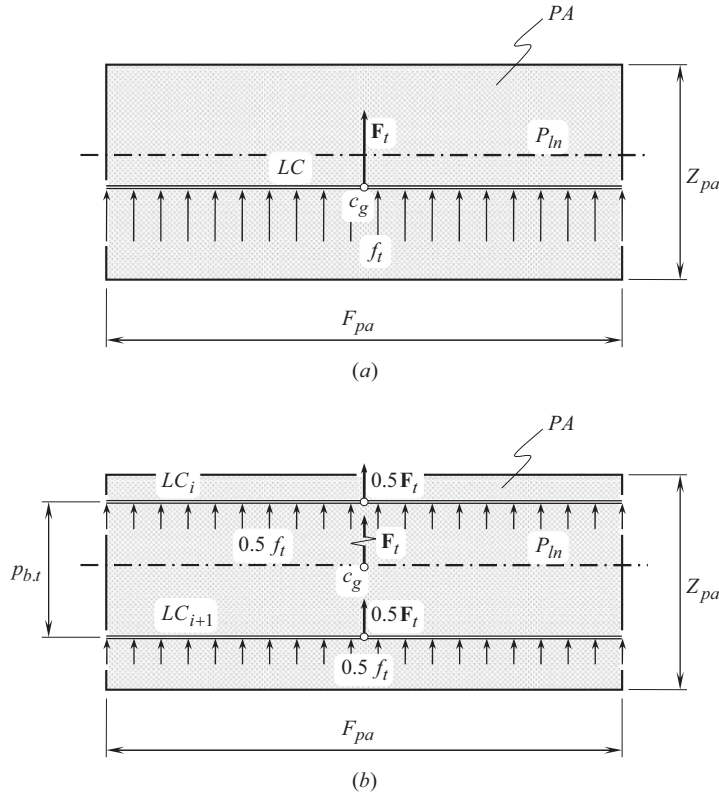


**FIGURE 10.56** Lines of contact,  $LC_i$ , in geometrically-accurate spur parallel-axes gear pair: (a) single-tooth contact of the gear teeth, and (b) double-tooth contact of the gear teeth.

The resultant (or the equivalent) force,  $\mathbf{F}_t$ , is applied at point,  $c_g$ , at the middle of a single line of contact,  $LC$ . The force  $\mathbf{F}_t$  is pointed along a line of action,  $LA$ , through the point  $c_g$ .

The distributed load,  $f_t$  [see Eq. (10.65)], is used for the calculation of contact stress as well as bending stress in spur parallel-axes gearing for such a mating gears configuration when a single pair of teeth is engaged in mesh. This mode of the gear teeth loading is the most critical one, as the entire load is withheld by a single pair of interacting teeth of a gear and a mating pinion.

When two (or more) pairs of the teeth are engaged in mesh at that same time, as illustrated in Figure 10.56b, the applied load is evenly distributed along the corresponding number of the lines of contact,  $LC_i$ . The distributed load,  $f_t$ , is shared among  $n_\phi$  pairs of teeth engaged in mesh at that same time. The distributed load per a pair of teeth,  $f_{t,n\phi}$ , equals:

$$f_{t,n\phi} = \frac{f_t}{n_\phi} = \frac{\mathbf{F}_t}{n_\phi F_{pa}} \quad (10.66)$$

The resultant force,  $\mathbf{F}_t$ , is shared among all the lines of contact,  $LC_i$ . The resultant force per a pair of teeth,  $\mathbf{F}_{t,n\phi}$ , equals:

$$\mathbf{F}_{t,n\phi} = \frac{\mathbf{F}_t}{n_\phi} \quad (10.67)$$

All the forces,  $\mathbf{F}_{t,n\phi}$ , are pointed along a line of action,  $LA$ , through the middle of the lines of contact,  $LC_i$ .

The distributed load,  $f_t$  [see Eq. (10.67)], is used for the calculation of the contact stress, as well as the bending stress in spur parallel-axes gearing for such a mating gears configuration when two (or more) pairs of teeth are engaged in mesh.

The resultant (or the equivalent) force,  $\mathbf{F}_t$ , is applied at point  $c_g$ . Point  $c_g$  corresponds to the middle of the lines of contact,  $LC_i$ , and between the first,  $LC_i$ , and the last,  $LC_j$ , lines of simultaneous contact. When two lines of contact are observed, point  $c_g$  is located at the middle in between the lines of contact. When three lines of contact are observed, point  $c_g$  is located at the center of the second line of contact, and so forth.

Similar to a single line of contact, in cases of multiple lines of contact, the force  $\mathbf{F}_t$  is pointed along a line of action,  $LA$ , through the point  $c_g$ .

When the gear rotates,  $\omega_g$ , the plane of action,  $PA$ , travels straight,  $\mathbf{V}_{pa}$  (see Figure 10.57). The leverage,  $\mathbf{R}_{cg}$ , of the resultant (or the equivalent) force,  $\mathbf{F}_t$ , with respect to the bearing support is remained the same and equals:

$$|\mathbf{R}_{cg}| = \sqrt{r_{b,g}^2 + a^2} \quad (10.68)$$

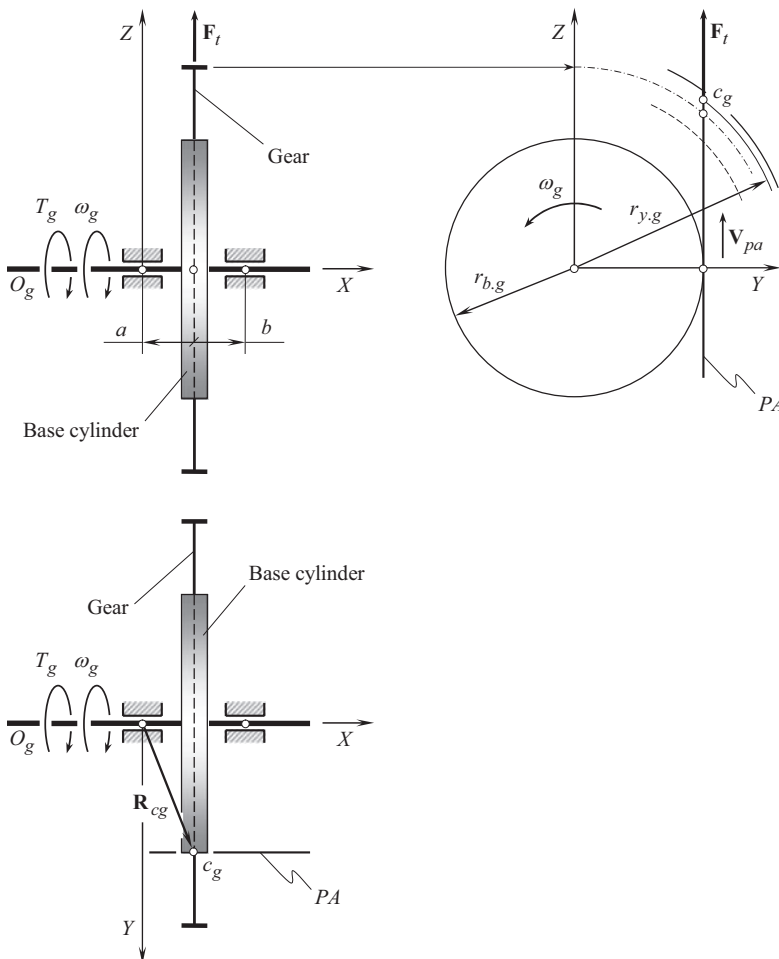


FIGURE 10.57 Bending torque in geometrically accurate spur parallel-axes gearing.

where:

$r_{b,g}$  is the base radius of the gear.

$a$  is the distance of the gear from the bearing support (see Figure 10.57).

The location of point  $c_g$  in the axial direction of the gear is not altered. Thus, the bending moment of the force,  $\mathbf{F}_t$ , with respect to the bearing support also is remained of the same value.

Geometrically accurate helical parallel-axes gearing represents a more general case of contact between tooth flanks,  $\mathcal{S}$  and  $\mathcal{P}$ , of a gear and a mating pinion, compared to that in spur gearing.

In geometrically accurate helical parallel-axes gearing either one, or two lines of contact,  $LC_i$ , are commonly observed. Cases when a gear pair features three and/or more lines of contact,  $LC_i$ , are possible, but not common in the present-day practice. In helical gearing, it is convenient to distinguish two different cases, namely, a case (a) when all the lines of contact,  $LC_i$ , are of full length, and (b) when one or more line(s) of contact is of a reduced length.

When a single pair of teeth is engaged in the mesh as illustrated in Figure 10.58a, the applied load is evenly distributed along a single line of contact,  $LC$ . The distributed tangential load,  $f_t$ , is calculated from equation:

$$f_t = \frac{F_t}{l_{LC}} = \frac{F_t}{F_{pa}} \cos \psi_b \quad (10.69)$$

where  $l_{LC}$  is the length of the line of contact:  $l_{LC} = F_{pa} / \cos \psi_b$ .

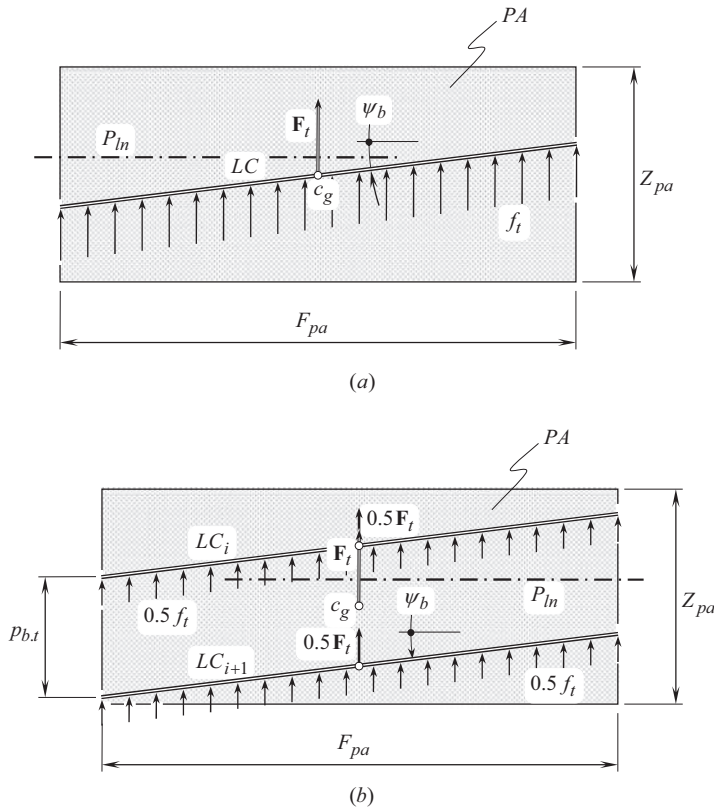


**FIGURE 10.58** Lines of contact,  $LC_i$ , of full length in geometrically accurate helical parallel-axes gear pair – tangential forces.



The resultant (or the equivalent) force,  $\mathbf{F}_t$ , is applied at point  $c_g$  at the middle of a single line of contact,  $LC$ . The force  $\mathbf{F}_t$  is pointed along a line of action,  $LA$ , through the point  $c_g$ .

The location of point,  $c_g$ , where the load,  $\mathbf{F}_t$ , is applied, is not altered in the axial direction of the gear. Thus, bending moment of the force,  $\mathbf{F}_t$ , with respect to the bearing support also is remained of the same value.

The normal force,  $\mathbf{F}_{t,n}$ , is perpendicular to the line of contact,  $LC$ . The component  $\mathbf{F}_{t,n}$  of the resultant (the equivalent) force,  $\mathbf{F}_t$ , is applied at that same point,  $c_g$ , as the load  $\mathbf{F}_t$  is applied. The magnitude,  $F_{t,n}$ , of the component  $\mathbf{F}_{t,n}$  of the resultant (or the equivalent) force,  $\mathbf{F}_t$ , equals to:

$$F_{t,n} = F_t \cos \psi_b \quad (10.70)$$

The distributed normal load,  $f_{t,n}$ , is calculated from the expression (see Figure 10.59a):

$$f_{t,n} = \frac{F_{t,n}}{l_{LC}} = \frac{F_t}{F_{pa}} \cos^2 \psi_b \quad (10.71)$$

The distributed normal load,  $f_{t,n}$  [see Eq. (10.69)], is used for the calculation of the contact stress as well as the bending stress in helical parallel-axes gearing for mating gears configuration when one pair of teeth is engaged in mesh. This mode of the gear teeth loading is the most critical one as the entire load is withhold by a single pair of interacting teeth of a gear and its mating pinion.

When two (or more) pairs of the teeth are engaged in mesh, as illustrated in Figure 10.58b, the applied load is evenly distributed along the corresponding number of the lines of contact,  $LC_i$ .

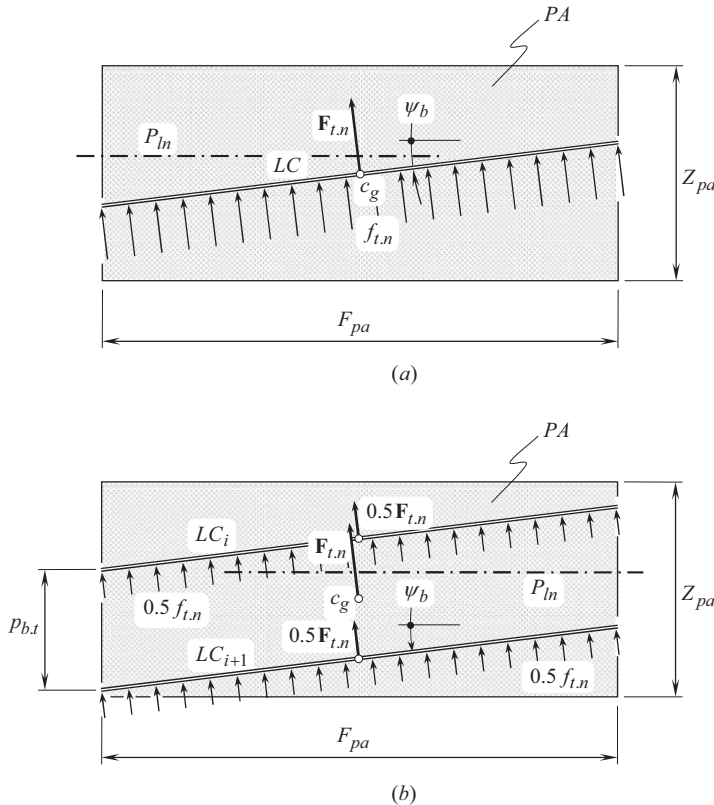


**FIGURE 10.59** Lines of contact,  $LC_i$ , of full length in geometrically accurate helical parallel-axes gear pair – normal forces.

The distributed tangential load,  $f_t$ , is shared among  $n_\phi$  pairs of teeth engaged in mesh at that same time. The distributed load per a pair of teeth,  $f_{t,n\phi}$ , equals:

$$f_{t,n\phi} = \frac{f_t}{n_\phi} = \frac{F_t}{n_\phi F_{pa}} \quad (10.72)$$

The resultant force,  $\mathbf{F}_t$ , is shared among all the lines of contact,  $LC_i$ . The resultant force per a pair of teeth,  $\mathbf{F}_{t,n\phi}$ , equals:

$$\mathbf{F}_{t,n\phi} = \frac{\mathbf{F}_t}{n_\phi} \quad (10.73)$$

The resultant (or the equivalent) force,  $\mathbf{F}_t$  [as well as the resultant (or the equivalent) normal force,  $\mathbf{F}_{t,n}$ ], is applied at point  $c_g$  (see Figures 10.58b and 10.59b). Point  $c_g$  corresponds to the middle of the lines of contact,  $LC_i$ , and between the first,  $LC_i$ , and the last,  $LC_j$ , lines of simultaneous contact. When two lines of contact are observed, point  $c_g$  is located in the middle in between the lines of contact. When three lines of contact are observed, point  $c_g$  is located at the center of the second line of contact, and so forth.

Similar to a single line of contact, in cases of multiple lines of contact, the force  $\mathbf{F}_t$  is pointed along a line of action,  $LA$ , through the point  $c_g$ .

The distributed normal load,  $f_{t,n}$ , is calculated from the expression:

$$f_{t,n} = \frac{F_t}{F_{pa}} \cos \psi_b \quad (10.74)$$

The distributed normal load,  $f_{t,n}$  [see Eq. (10.65)], is used for the calculation of contact stress, as well as bending stress in helical parallel-axes gearing when two (or more) pairs of teeth are engaged in mesh.

The resultant (or the equivalent) force,  $\mathbf{F}_t$ , is applied at point  $c_g$ . Point  $c_g$  corresponds to the middle of the lines of contact,  $LC_i$ , and between the first,  $LC_i$ , and the last,  $LC_j$ , lines of simultaneous contact. When two lines of contact are observed, then point  $c_g$  is located in the middle in between the lines of contact. When three lines of contact are observed, point  $c_g$  is located at the center of the second line of contact, and so forth.

The location of point  $c_g$ , at which the load  $\mathbf{F}_t$  is applied, is not altered in the axial direction of the gear. Thus, bending moment of the force,  $\mathbf{F}_t$ , with respect to the bearing support also is remained of the same value.

Similar to a single line of contact, in cases of multiple lines of contact, the force  $\mathbf{F}_t$  is pointed along a line of action,  $LA$ , through point  $c_g$ .

The location of point  $c_g$  in the axial direction of the gear is not altered. Thus, bending moment of the force,  $\mathbf{F}_t$ , with respect to the bearing support also is remained the same.

Ultimately, one or more lines of contact,  $LC_i$ , can be truncated, and, thus, they are not of a full length.

As illustrated in Figure 10.60a, the line of contact,  $LC_i$ , is truncated (it is not of a full length), while the next line of contact,  $LC_{i+1}$ , is of a full length (i.e., the inequality  $LC_i < LC_{i+1}$  is observed). In the example under consideration, the tangential load,  $\mathbf{F}_t$ , is shared between the lines of contact,  $LC_i$  and  $LC_{i+1}$ . The load ( $|\mathbf{F}_{t,1}| + |\mathbf{F}_{t,2}|$ ) equals (see Figure 10.60a):

$$|\mathbf{F}_{t,1}| + |\mathbf{F}_{t,2}| = |\mathbf{F}_t| \cdot \frac{F_{pa,1}}{F_{pa}} \quad (10.75)$$

where:

$$|\mathbf{F}_{t,1}| = |\mathbf{F}_{t,2}| = |\mathbf{F}_t| \cdot \frac{F_{pa,1}}{2 \cdot F_{pa}} \quad (10.76)$$

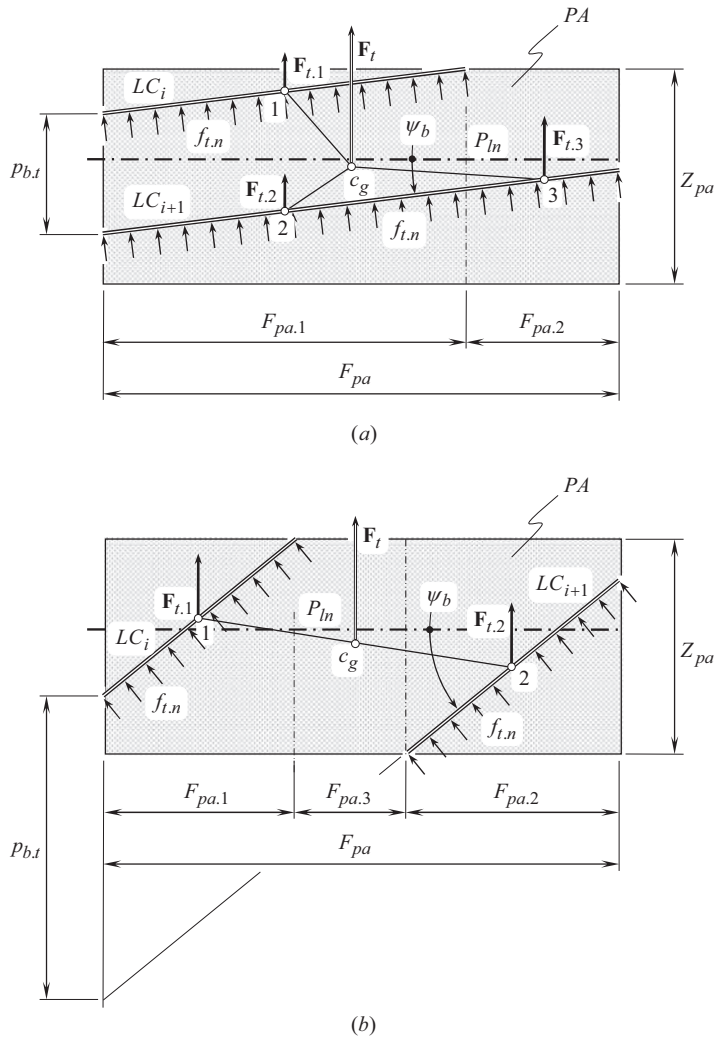


**FIGURE 10.60** Truncated lines of contact,  $LC_i$ , in geometrically accurate helical parallel-axes gear pair.

The loads,  $\mathbf{F}_{t,1}$  and  $\mathbf{F}_{t,2}$ , are applied at points 1 and 2 within the lines of contact. The points 1 and 2 correspond to points within the lines of contact,  $LC_i$  and  $LC_{i+1}$ , at the middle of the portion  $F_{pa,1}$  of the face-width  $F_{pa}$ .

The load  $|\mathbf{F}_{t,3}|$  equals (see Figure 10.60a):

$$|\mathbf{F}_{t,3}| = |\mathbf{F}_t| \cdot \frac{F_{pa,2}}{F_{pa}} \quad (10.77)$$

The load  $\mathbf{F}_{t,3}$  is applied at point 3 within the line of contact,  $LC_{i+1}$ . The point 3 corresponds to point within the line of contact,  $LC_{i+1}$ , at the middle of the portion  $F_{pa,2}$  of the face-width  $F_{pa}$ .

The resultant load,  $\mathbf{F}_t$ , is applied at point  $c_g$ . The coordinates of point  $c_g$  can be determined using the principle of the *center of gravity*, namely, point  $c_g$  is the *center of gravity* of the points 1, 2, and 3 having the *weights*  $\mathbf{F}_{t,1}$ ,  $\mathbf{F}_{t,2}$ , and  $\mathbf{F}_{t,3}$ , correspondingly.

As the gears rotate, the lines of contact,  $LC_i$  and  $LC_{i+1}$ , travel straight together with the plane of action,  $PA$ , in a transverse direction in the gear pair. The points 1, 2, and 3 as well as the point  $c_g$  migrate within the plane of action,  $PA$ . The migration of point  $c_g$  with a linear velocity,  $\mathbf{V}_{cg}$ , in

the axial direction of the gear pair results in a corresponding alteration of the arm,  $\mathbf{R}_{cg}$ , of the resultant force,  $\mathbf{F}_t$ , in relation to the bearing support of the gear shaft as schematically illustrated in Figure 10.60. When the point  $c_g$  migrates between points  $c_g^*$  and  $c_g^{**}$ , the arm  $|\mathbf{R}_{cg}|$  of the resultant force,  $\mathbf{F}_t$ , changes in the range of:

$$|\mathbf{R}_{cg}^*| \leq |\mathbf{R}_{cg}| \leq |\mathbf{R}_{cg}^{**}| \quad (10.78)$$

The variation of the magnitude,  $|\Delta \mathbf{R}_{cg}|$ , of the arm,  $\mathbf{R}_{cg}$ , causes a variable in time torque that bends the gear shaft and deforms the gear housing. The variation of the magnitude,  $|\Delta \mathbf{R}_{cg}|$ , of the arm,  $\mathbf{R}_{cg}$ , can cause an extensive unfavorable vibration of the gear housing, and an extensive noise excitation.

Another configuration of the lines of contact,  $LC_i$  and  $LC_{i+1}$ , is illustrated in Figure 10.60b.

As shown in Figure 10.60b, the lines of contact,  $LC_i$  and  $LC_{i+1}$ , are truncated (therefore, an inequality  $LC_i \neq LC_{i+1}$  is observed). In the example under consideration, the tangential load,  $\mathbf{F}_t$ , is shared between the lines of contact,  $LC_i$  and  $LC_{i+1}$ . The load  $\mathbf{F}_{t,1}$  equals (see Figure 10.60b):

$$|\mathbf{F}_{t,1}| = |\mathbf{F}_t| \cdot \frac{F_{pa,1}}{F_{pa,1} + F_{pa,2}} \quad (10.79)$$

The load  $\mathbf{F}_{t,1}$  is applied at point 1 within the line of contact,  $LC_i$ . Point 1 is in the middle of the line of contact,  $LC_i$ .

The load  $|\mathbf{F}_{t,2}|$  equals (see Figure 10.60b):

$$|\mathbf{F}_{t,2}| = |\mathbf{F}_t| \cdot \frac{F_{pa,2}}{F_{pa,1} + F_{pa,2}} \quad (10.80)$$

The load  $\mathbf{F}_{t,2}$  is applied at point 2 within the line of contact,  $LC_{i+1}$ . Point 2 is in the middle of the line of contact,  $LC_{i+1}$ .

No load is transmitted by the portion  $F_{pa,3}$  of the face-width,  $F_{pa}$ , as no lines of contact are located here. This portion of the gear face is excluded from the analysis.

When calculating contact stress in a parallel-axes gear pair, the use of the so-called *Total length of the lines of contact* (or just *TLLC*, for simplicity) is often helpful. *Total length of the lines of contact* equals to summa of the length of all the lines of contact that occur at a specified instant of time.<sup>10</sup> When two or more lines of contact do not overlap one another, the importance of the total length of lines of contact is vital: In such a case an applied load is equally distributed along the *TLLC*.

The resultant load,  $\mathbf{F}_t$ , is applied at point  $c_g$ . The coordinates of point  $c_g$  can be determined using the principle of the center of gravity, that is, point  $c_g$  coincides with the center of *gravity* of points 1, and 2, having the *weights*  $\mathbf{F}_{t,1}$ , and  $\mathbf{F}_{t,2}$ , correspondingly.

As the gears rotate, the lines of contact,  $LC_i$  and  $LC_{i+1}$ , travel together with the plane of action, *PA*. Points 1 and 2, as well as the point  $c_g$ , migrate within the plane of action, *PA*. The migration of the point  $c_g$  with a linear velocity  $\mathbf{V}_{cg}$  in the axial direction of the gear pair causes a corresponding alteration to the arm,  $\mathbf{R}_{cg}$ , of the resultant force,  $\mathbf{F}_t$ , in relation to the bearing support of the gear shaft, as schematically illustrated in Figure 10.60.

To minimize the noise excitation in helical involute gearing (and to minimize the variation of the axial force), the gears have to be designed so as to minimize the travel distance of the point  $c_g$  (see Figure 10.60). In the best-case scenario, the travel distance of a zero length is desirable.

<sup>10</sup> It is right point to stress here that actual loading of the gear teeth strongly depends on the total length of the line of contact (*TLLC*) as well as of the contact ratio in the gear pair. The influence of the total length of the line of contact, and of the contact ratio, on the gear teeth loading is complex: It could happen that when the pitch helix angle of a gear,  $\psi_g$ , increases, the total length of the lines of contact decreases, that is, the contact ratio can be greater in this case, but the total length of the line of contact can be shorter. The latter results in a higher contact stress, and in a higher bending stress in the gear teeth.

When the point  $c_g$  migrates between the points  $c_g^*$  and  $c_g^{**}$ , the arm  $|\mathbf{R}_{cg}|$  of the resultant force,  $\mathbf{F}_t$ , changes in the range of  $|\mathbf{R}_{cg}^*| \leq |\mathbf{R}_{cg}| \leq |\mathbf{R}_{cg}^{**}|$  (see Figure 10.61).

The variation of the magnitude,  $|\Delta \mathbf{R}_{cg}|$ , of the arm,  $\mathbf{R}_{cg}$ , causes a variable in time of torque that bends the gear shaft, and deforms the gear housing. The variation of the magnitude,  $|\Delta \mathbf{R}_{cg}|$ , of the arm,  $\mathbf{R}_{cg}$ , can cause an extensive undesirable vibration of the gear housing, and an extensive noise excitation.

The disclosed approach for the determination of the loads acting in every pair of teeth in geometrically accurate spur, and helical parallel-axes gearing can be enhanced to gear pairs with lines of contact of an arbitrary geometry, namely, to gear pairs with lines of contact in the form of arcs of a circle, of a spiral curve, and so forth. Generally speaking, for this purpose the plane-of-action face-width,  $F_{pa}$ , is subdivided into several segments within each of which either zero, or one, or two, and so forth lines of contact occur. If the line of contact is shaped a form of a planar curve, the corresponding portion of the plane-of-action face-width,  $F_{pa}$ , is sliced into infinite number of infinitesimally narrow slices. Portion of a line(s) of contact within each infinitesimally narrow slice is considered straight-line segment. In such a manner loading in geometrically accurate parallel-axes gear pairs with the lines of contact of an arbitrary geometry can be determined.

### 10.7.2 FORCES ACTING IN TRANSVERSE SECTION OF GEOMETRICALLY ACCURATE PARALLEL-AXES GEAR PAIR

In addition to the forces that act in the plane of action of a geometrically accurate parallel-axes gear pair, friction forces act in a transverse section of the gear pair, as schematically illustrated in Figure 10.62.

At an instant of time when two contact points,  $K_1$  and  $K_2$ , are observed, the resultant tangential force,  $\mathbf{F}_t$ , is equally shared between the points,  $K_1$  and  $K_2$ , that is, the forces  $\mathbf{F}_{t,1}$  and  $\mathbf{F}_{t,2}$  are equal to one another. The forces,  $\mathbf{F}_{t,1}$  and  $\mathbf{F}_{t,2}$ , create the input torque,  $T_p$ .

The friction forces,  $\mathbf{F}_{f,1}$  and  $\mathbf{F}_{f,2}$ , act perpendicular to the line of action,  $LA$ . As the instantaneous relative motion of the driving gear and the driven pinion is an instantaneous rotation about pitch

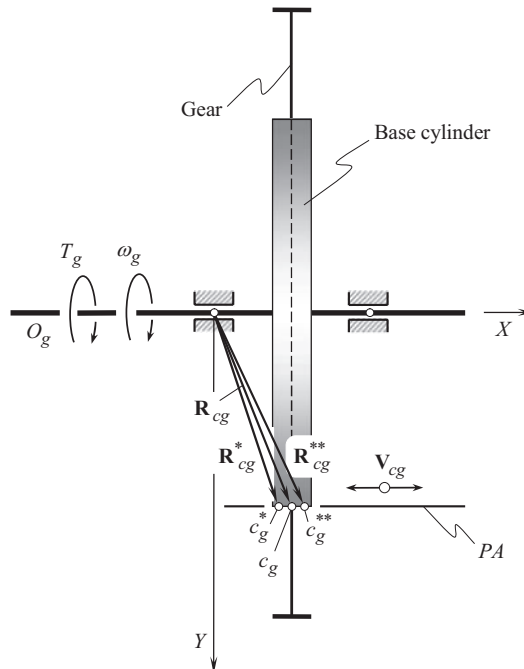
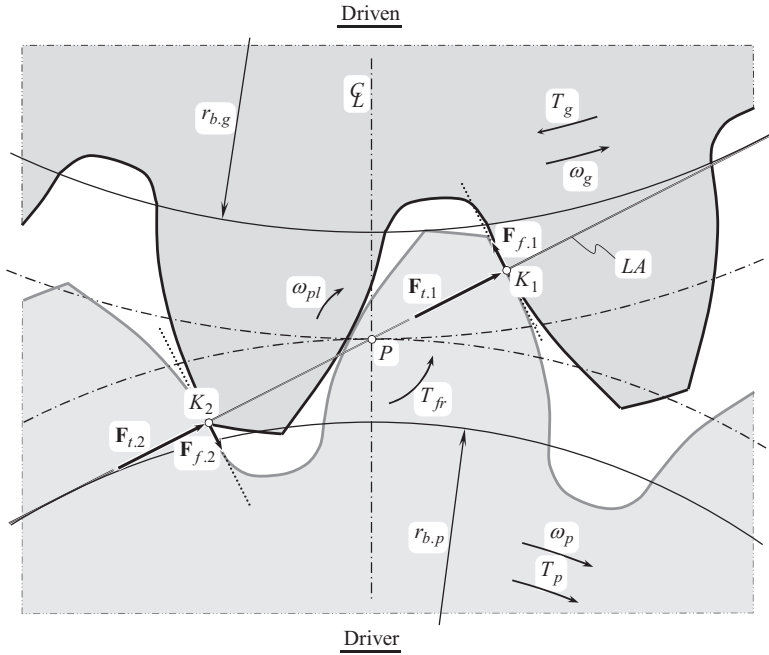


FIGURE 10.61 Variation of bending torque in geometrically accurate parallel-axes helical gearing.



**FIGURE 10.62** Forces acting in transverse section of geometrically accurate parallel-axes gear pair.

point,  $P$ , and the contact points,  $K_1$  and  $K_2$ , are located from the opposite sides of the pitch point, the friction forces,  $\mathbf{F}_{f,1}$  and  $\mathbf{F}_{f,2}$ , are pointed oppositely to one another. The friction forces,  $\mathbf{F}_{f,1}$  and  $\mathbf{F}_{f,2}$ , are equal:

$$\mathbf{F}_{f,1} = \mu \cdot \mathbf{F}_{t,1} \quad (10.81)$$

$$\mathbf{F}_{f,2} = \mu \cdot \mathbf{F}_{t,2} \quad (10.82)$$

Here, the friction coefficient is denoted by  $\mu$ .

The friction forces,  $\mathbf{F}_{f,1}$  and  $\mathbf{F}_{f,2}$ , create the friction torque,  $T_{fr}$ . The friction torque,  $T_{fr}$ , is calculated from the formula:

$$T_{fr} = F_{f,1} \cdot K_1P + F_{f,2} \cdot K_2P \quad (10.83)$$

The friction torque,  $T_{fr}$ , is pointed oppositely in relation to the input torque,  $T_p$ .

When the gears rotate, the distances,  $K_1P$  and  $K_2P$ , alter. However, summa ( $K_1P + K_2P$ ) is remained of a constant value. Therefore, in geometrically accurate parallel-axes gearing, the friction torque,  $T_{fr}$ , also is of a constant value.



# Taylor & Francis

Taylor & Francis Group

<http://taylorandfrancis.com>

---

# 11 Novikov/Conformal and High-Conformal Gearing

For a long while, many industries are facing the problem of increasing the power density being transmitted by means of gear teeth. The problem of transmitting a rotary motion from a driving shaft to a driven shaft with the highest possible power density is a challenging one. A solution to such an engineering problem requires the application of gear boxes of the smallest possible size that are capable of transmitting as much power as possible. Conformal gearing, especially high-conformal gearing, perfectly suits this requirement. To the best possible extent, both gear systems, *Novikov/conformal gearing* and *high-conformal gearing*, are discussed in the monograph by the author [157]. A problem to design *Novikov/conformal gearing* as well as *high-conformal gearing* with rolling balls is also addressed in Refs. [140, 157]. The interested reader is referred to this monograph [157] for details on *Novikov/conformal gearing* as well as *high-conformal gearing*. Here, in this section of the book, the essence and principal features of *Novikov/conformal gearing* and *high-conformal gearing* are briefly discussed.

## 11.1 INTRODUCTORY REMARKS

Despite the fact that it was invented as early as in the mid of 1950s, *Novikov/conformal* gear system is still relatively a novel gear system. This gear system is poorly investigated and got limited application in the industry. However, *Novikov/conformal* gearsets can be designed so as to ensure the extremely high density of the power. High power density is the principal advantage of *Novikov/conformal* gear system over gear systems of other designs.

### 11.1.1 A BRIEF OVERVIEW ON CONFORMAL GEARING: STATE-OF-THE-ART

Conformal and high-conformal gearing feature *convex-to-concave* contact between the tooth flanks of a gear and a mating pinion. This is with respect to both to external gearing and to internal gearing.

#### 11.1.1.1 An Assumed Origination of Conformal Gearing

The concept of *convex-to-concave* contact of the tooth flanks of a gear and its mating pinion can be traced back to the fifteenth century (1493) when the famous book by *Leonardo da Vinci* was published [23]. Initially, long time ago, an increased contact strength of the gear teeth was the main reason that initiated the developments in the field of conformal gearing.

Conventional (involute) external gearing features a *convex-to-convex* contact of the interacting tooth flanks of a gear, and of its mating pinion. In conformal gearing, the *convex-to-convex* contact of the tooth flanks is substituted with a *convex-to-concave* their contact. Due to such a substitution, the contact strength of the gear teeth can be increased proportionally to the increase of the degree of conformity of the interacting gear tooth flanks. It is natural to assume that a decision for the replacement of a *convex-to-convex* contact with *convex-to-concave* contact of the gear teeth is based on observations in nature. For instance, all joints in a human skeleton feature *convex-to-concave* contact of the bones (see Figure 11.1). None of the bones makes *convex-to-convex* contact.

The earliest known to the author design of a gearing with *convex-to-concave* tooth contact is discussed in the famous book by *da Vinci* [23]. The addendum of the gear teeth features convex geometry, while the dedendum is concave [23]. In the pinion, the addendum features convex tooth profile, and dedendum is also concave. There are a few more illustrations of gearing with *convex-to-concave* contact of the tooth flanks.



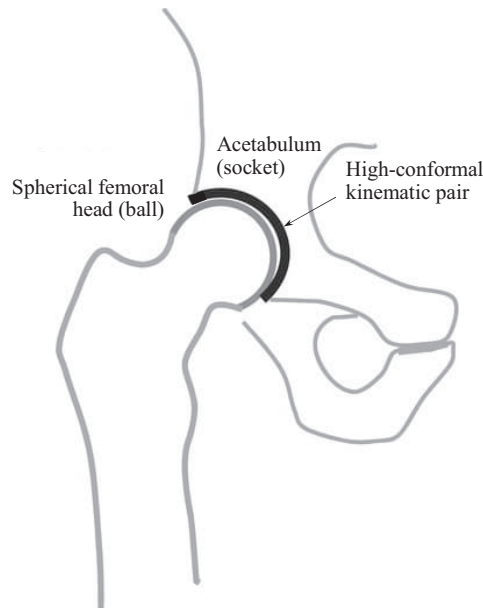


**FIGURE 11.1** *Convex-to-concave* contact of bones in human skeleton.

It is not mentioned in Ref. [221] whether the gearing is spur or helical. However, the gearing is supposed to be a spur gearing, as helical gearing was invented much later, and is credited to *Robert Hooke*.<sup>1</sup>

Because of very limited information on the design of the gearing [23], it is almost impossible to accurately evaluate the advantages and disadvantages of this particular ancient design of conformal gearing.

The *Bramley-Moore gearing* (otherwise known as the *Vickers, Bostock, and Bramley gearing* or just *V.B.B. gearing*, for simplicity) is another well-known example of gearing with *convex-to-concave* contact of the gear teeth [97].

Toothed gearing of the design proposed by *F.J. Bostock, S. Bramley-Moore, and H.J. Schmick* [96], relates to the shape and arrangement of the working faces of intermeshing teeth for spur gears for connecting rotating or oscillating bodies.

Helical gearing with circular-arc tooth profile was invented by Dr. *E. Wildhaber* [101] in the early 1920s. The invention targets an improved power capacity of the gear pair. This gear system is commonly referred to as *Wildhaber helical gearing*. *Wildhaber helical gearing* is a kind of approximate gearing, as it is not capable of transmitting a uniform rotation smoothly.

As early as in 1956 Dr. *M.L. Novikov* proposed conformal helical gearing [123] that later got the name *Novikov gearing*.<sup>2</sup> *Novikov gearing* is a kind of geometrically accurate gearing, as all three fundamental laws of gearing are fulfilled by gearing of this design. Thus, gearing of this kind is capable of transmitting an input uniform rotary motion smoothly.

*Novikov gearing* and *Wildhaber helical gearing* are the most widely known designs of gearing with *convex-to-concave* contact of the tooth flanks. In Appendix H, the author's comments on the concept of *Novikov gearing*, and on the inadequacy of the terms *Wildhaber-Novikov Gearing* and *W-N Gearing* are presented.

<sup>1</sup> Robert Hooke (28 July [O.S. 18 July] 1635–3 March 1703) – was an English natural philosopher, architect, and polymath.

<sup>2</sup> The *Novikov gear system* is named after Colonel *M.L. Novikov*, Dr. Eng. Sc., who was the head of the department at *Zhoukovskii Air Force Engineering Academy* in Moscow. After his death in 1958, his colleagues have published his work [91] under the name of *Novikov*.

An in-depth analysis of the research carried out on *Novikov gear system* is performed by the author. The results of these research studies are available in the public domain and can be found in Ref. [157]. The undertaken research reveals that gear experts all around the globe (including, but not limited to Russia, the USA, China, as well as of the rest of the world) demonstrate the absence of in-depth understanding of kinematics and the geometry of *Novikov/conformal* gearing. As a consequence, the kinematics and the geometry of *high-conformal gearing*<sup>3</sup> (or just  $H_c$  – gearing, for simplicity) are also not understood at all. It is nonsense that a gear system (*Novikov gear system*) that was proposed about 75 years ago (in the early 1950s) is still not understood by the gear community all around the world. (*Novikov gear system*, and especially the proposed later (~2008) *high-conformal gear system*, both of these unique gear systems possess great potential for the industry.

Not all the gear systems that feature *convex-to-concave* contact of the tooth flanks are capable of transmitting an input rotary motion smoothly. It is critical to stress here from the very beginning that only conformal *Novikov gearing* is a geometrically accurate kind of gearing, and, thus, it is capable of transmitting an input rotary motion smoothly. Conformal gearing of all other kinds cannot be referred to as geometrically accurate gearing (all of them are kinds of approximate gearing), and, thus, they are not capable of transmitting a uniform rotary motion smoothly.

#### 11.1.1.2 The Power Density

The *power density*<sup>4</sup> is an important consideration in gearing of many designs and applications. The higher the power density of a gear pair, the lighter the gear transmission, and vice versa. A helicopter transmission is a good example of gearing where the highest possible power density is strongly desirable. However, the aerospace industry is not the only industry that needs in application of a small size and high torque capacity gear transmissions. A gearbox for electric wind power stations is another good example in this regard. Gas consumption of trucks, cars, tractors, and other vehicles strongly depends on the weight of the vehicle, that is, the lighter the vehicle, the less the gas consumption, and vice versa. Therefore, the use of lighter gearboxes in the automotive industry is also desirable. More examples of the desirable application of lighter gearboxes with higher performance can be found in many industries. *High-power-density gearing*<sup>5</sup> (further, *HPD* – gearing, for simplicity) is the global target for future developments in the field of gearing.

An increase of the power density transmitted through a gear pair is the main goal for the development of *conformal* gearing, and later on of *high-conformal gearing* (further,  $H_c$  – gearing, for simplicity).

Two different ways to increase the power density in a gear pair are distinguished.

**First**, the power density in a gear pair can be increased by means of an increased rotation of the driving member (commonly, of the pinion). In such a scenario, the torque applied to the driving member is remained of the same value.

**Second**, the power density in a gear pair can be increased by means of an increased torque applied to the driving member (commonly, to the pinion). The rotation of the driving member is remained of the same value in such a scenario.

A combination of the first and of the second approaches is possible as well.

<sup>3</sup> *High-conformal gearing* was proposed by Prof. S.P. Radzevich in around ~2008 [174].

<sup>4</sup> Here and in the following, the *power density* is understood as the ratio of the power being transmitted through a gear pair to the volume occupied by this gear pair. The *power density* also can be specified as a ratio of a power being transmitted by a gear pair to the gear pair weight. In this latter case, the term *power-to-mass ratio* is also used.

<sup>5</sup> It is instructive to note here that broader application of *high-power-density gearing* in the future will result in the broader use of gears with a low tooth count (*LTC* –gearing, in other words). *Low-tooth-count gears* are the gears whose base diameter,  $d_b$ , is equal to, or greater than the root diameter,  $d_f$ , and for which the inequality  $d_b \geq d_f$  is valid. Commonly, *LTC* –gears are viewed in a narrower sense, that is, *LTC* –gears are the gears, whose tooth count is equal to  $N_g = 12$  or a fewer. To accommodate for that, the inequality  $d_b \geq d_f$  is represented in a form:  $d_b \geq k_{lic} \cdot d_f$ , where  $k_{lic}$  is a factor of a constant value.

### 11.1.1.3 Design Features of Conformal Gearing

Conformal gearing features, first of all, *convex-to-concave* contact between the tooth flanks of a gear and that of a mating pinion. This particular type of contact of the tooth flanks enables an increase in contact strength of the gear and the pinion teeth. It is known that *concave-to-convex* contact of machine elements is always stronger compared to *concave-to-convex* their contact. Because of this, numerous efforts were undertaken in the past to design gears with *convex-to-concave* contact between the tooth flanks of a gear and that of a mating pinion.

In most applications, especially when the input,  $\omega_{in}$ , and the output,  $\omega_{out}$ , rotations are high, the use of gearing with a constant angular velocity ratio,<sup>6</sup>  $u_{\omega} = \omega_{in} / \omega_{out} = \text{Const}$ , is preferred. Only *geometrically accurate gearing* features a constant angular velocity ratio. Gearing of the rest of designs, whose angular velocity ratio is not constant (i.e.,  $u_{\omega} = \text{var}$ , and  $u = \text{Const}$ ), is not capable of transmitting a rotary motion smoothly. These kinds of gearing are referred to as *approximate gearing*. Considered below in this chapter of the book, conformal gearing is capable of transmitting a uniform input rotation smoothly. This is because conformal gearing is a kind of *geometrically accurate gearing*. This means that conformal gearing meets all three fundamental laws of gearing:

1. The *law of contact* of tooth flanks of a gear,  $\mathcal{G}$ , and that of a mating pinion,  $\mathcal{P}$ , is fulfilled. It is common practice to specify the law of contact of two smooth regular surfaces by means of *Shishkov equation of contact*,<sup>7</sup>  $\mathbf{n} \cdot \mathbf{V}_{\Sigma} = 0$ , where  $\mathbf{n}$  designates unit normal vector of a common perpendicular through point of contact,  $K$ , of the tooth flanks,  $\mathcal{G}$  and  $\mathcal{P}$  (this vector is pointed along the line of action,  $LA$ , of the gear pair), and  $\mathbf{V}_{\Sigma}$  designates vector of the resultant relative motion of the tooth flanks  $\mathcal{G}$  and  $\mathcal{P}$  at  $K$  [174].
2. At every instant of time, the line of action,  $LA$ , passes through a point within the instantaneous axis of rotation,  $P_{in}$ , of the pinion relative to the gear (or of the gear relative to the pinion). In parallel-axes gearing, this requirement is specified by *Camus-Euler-Savary theorem* (or, more generally, by the *conjugate action law*).
3. The *law of equal base pitches* is fulfilled. At every instant of time, base pitch of a gear is equal to an operating base pitch in the gear pair, and base pitch of a mating pinion is also equal to the operating base pitch in the gear pair, that is, both of the base pitches (base pitch of the gear, and that of the mating pinion) are equal to the operating base pitch of the gear pair [174].

As per the author's opinion, the efforts undertaken in the past to develop conformal gearing, need to be discussed more in detail in order to properly evaluate the results obtained in the field to this end, and to separate the potentially useful accomplishments of the research in the field from others, that are either useless or mistake. Many ambiguities are observed in interpreting conformal gearing just because of misunderstanding of the kinematics and the geometry of gearing of this particular design.

<sup>6</sup> It should be stressed here on the difference between the *angular velocity ratio*,  $u_{\omega}$ , and between the *gear ratio*,  $u$ . The angular velocity ratio is specified as  $u_{\omega} = \omega_{in} / \omega_{out}$ . The angular velocity ratio is of a constant value for geometrically accurate gear pairs and is variable for approximate gear pairs. The gear ratio is specified in terms of tooth count of the input,  $N_{in}$ , and of the output,  $N_{out}$ , members in the gear pair  $u = N_{in} / N_{out}$ . The gear ratio is always of a constant value in geometrically accurate, as well, as in approximate gearing (of course, except of noncircular gearing).

<sup>7</sup> This equation was proposed by Prof. V.A. Shishkov as early as in 1948 (or even earlier) in his paper: Shishkov, V.A., "Elements of Kinematics of Generating and Conjugating in Gearing," in: *Theory and Calculation of Gears*, Vol. 6, Leningrad: LONITOMASH, 1948, p. 123, [197]. More in-detail, this equation is also addressed in the monograph: Shishkov, V.A., *Generation of Surfaces in Continuous-indexing Methods of Surface Machining*, Moscow, Mashgiz, 1951, 152 pages.

### 11.1.2 VARIETY OF POTENTIAL DESIGNS OF CONFORMAL GEARING

*Novikov gearing* [123] is developed for, but not limited to, parallel-axes gear trains. However, gear pairs that feature intersected axes, and gear pairs that have crossed axes of rotations of the gears can be designed in accordance with the concept proposed by Prof. *M.L. Novikov*. External and internal gearing of the proposed system of meshing is possible. The tooth ratio of the proposed gearing can be of either constant or a variable value as well as it can be time-dependent.

Moreover, conformal and high-conformal gearing represents a good platform for the development of corresponding (conformal, and high-conformal) gearing with rolling elements: balls, rollers, and so forth.

## 11.2 CONFORMAL GEARING (NOVIKOV GEARING)

A scientific approach to the design and analysis of parallel-axes *Novikov/conformal gearing* is based on the kinematics of parallel-axes gearing. The fundamental principles of gearing recently developed in the scientific theory of gearing [174] are also valid with respect to *Novikov/conformal gearing*. With that said, one can proceed with the analysis of the concept of *Novikov/conformal gearing* (or just *N – gearing*, for simplicity), and later on to evolve the concept of *Novikov/conformal gearing* to the concept of *high-conformal gearing* (further, *H<sub>c</sub> – gearing*, for simplicity).

It should be noticed from the very beginning that *Novikov/conformal gearing* as well as *high-conformal gearing* can be viewed as a kind of involute gearing. Both *Novikov/conformal gearing* and *high-conformal gearing* meet all three fundamental laws of gearing. Therefore, these two gear systems represent geometrically accurate gearing.

Let us proceed with the discussion and in-depth analysis of the main design features of *Novikov gearing*.

### 11.2.1 THE ESSENCE OF NOVIKOV GEARING

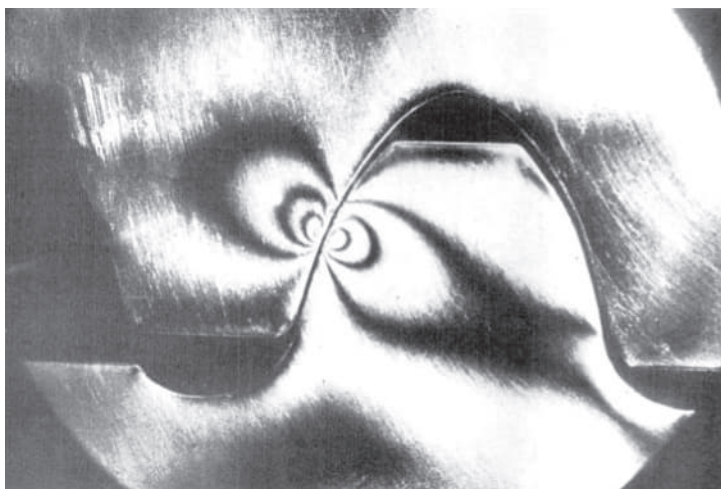
*Novikov gearing* was developed with the intent to increase the contact strength of gear teeth. Gearing of this design features higher contact strength due to the favorable curvatures of the interacting tooth flanks. Under equivalent contact stress, similar dimensions, comparable values of the rest of the design parameters, the greater circular forces, are permitted in *Novikov gearing*. (The discussion in this section of the book follows in much publication [123] Dr. *M.L. Novikov*.)

Another factor that contributes to the higher load-carrying capacity of conformal gears is that they sustain a thicker film of lubricant, owing to the rapid rolling of the areas of contact along the helix, which provides a vigorous hydrodynamic action.

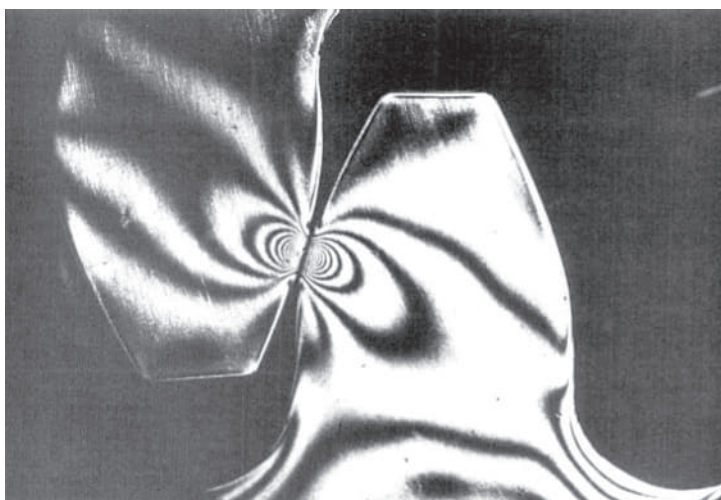
The shape of the gear teeth designed to transmit power is traditionally based on the involute curve, and all (external) gear tooth profiles in the past have been convex. However, if mating teeth are *conformal*, namely, one of them is convex while the mating one concave, the stress for a given load can be reduced; alternatively, a heavier load can be carried for the same amount of stress. This point is made clear by the photographs of photoelastic models shown in Figure 11.2.

Possible geometries of tooth profiles of the *Novikov gearing* are schematically shown in Figure 11.3. In this figure, a section of a gear and a mating pinion tooth flanks by a plane perpendicular to the axis of instantaneous rotation of the mating gears is shown. The axis passes through the current point of contact of the tooth flanks.

In Figure 11.3, the point of intersection of the planar section by the axis of instantaneous rotation is denoted by *P*. The points of intersection of the planar section by the axes of the gear and the pinion are designated as *O<sub>1</sub>* and *O<sub>2</sub>*, correspondingly. Point, *A*, is the point of meshing (in its current location). The instantaneous line of action, *LA<sub>inst</sub>*, is a straight line through the point of meshing, *A*. Ultimately, an arc *ΔAΔ* (the notations in Figure 11.3 are mainly due to Prof. *M.L. Novikov*) is a



(a)



(b)

**FIGURE 11.2** Comparison of the distribution of contact stress in: (a) *Novikov gearing* and (b) *equivalent involute gearing*.

circle<sup>8</sup> centering at the pitch point,  $P$ . In the limit case (namely, when in a transverse section of the gearset the tooth profiles make line contact with one another), the tooth profile of a gear and that of a mating pinion are congruent with an arc of this circle.

Multiple curves denoted by  $BAB$  illustrate examples of possible geometries of the tooth profile of one of two mating gears. All the curves denoted by  $BAB$  are arbitrary smooth regular curves, which are entirely located within the interior of the limit circular arc,  $\mathcal{D}A\mathcal{D}$  (i.e., all the arcs  $BAB$  are located within the bodily side of the limit tooth flank of one of the gears). All the tooth profiles,  $BAB$ , feature a high degree of conformity to the limit circular arc,  $\mathcal{D}A\mathcal{D}$ .

<sup>8</sup> The circle of a radius,  $r_N$ , centered at the pitch point,  $P$ , was introduced (circa ~2008) by Prof. *S.P. Radzevich*. He proposed to refer to this circle as to the *boundary Novikov circle*, or just as to the *boundary  $N$ -circle* in honor of Prof. *M.L. Novikov*, the principal inventor of *Novikov gearing*. The concept of the *boundary  $N$ -circle* was not known in the time of Prof. *M.L. Novikov*.



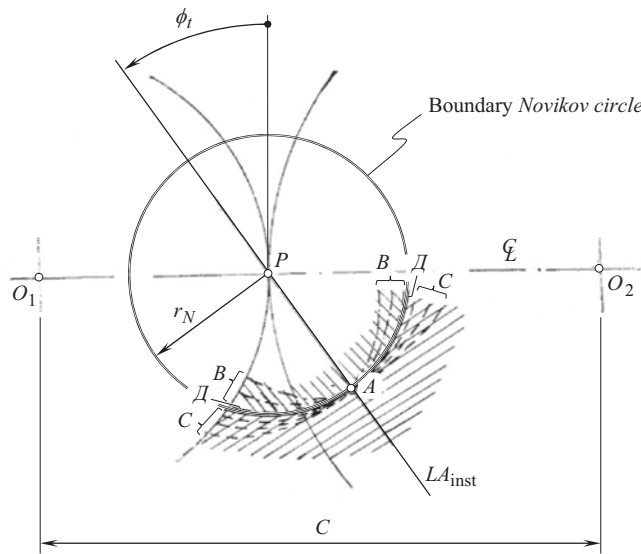


**FIGURE 11.3** Concept of Novikov gearing (after M.L. Novikov; Pat. No. 109,113, (USSR). *Gear Pairs and Cam Mechanisms Having Point System of Meshing*/M.L. Novikov, National Classification 47h, 6; Filed: April 19, 1956, published in Bull. of Inventions No.10, 1957 [123]. The *boundary Novikov circle* of a radius,  $r_N$ , was introduced later on by Prof. S.P. Radzevich).

Multiple curves, those denoted by  $CAC$ , illustrate examples of possible geometries of the tooth profile of the second of two mating gears. All the curves denoted by  $CAC$  are arbitrary smooth regular curves, which are entirely located within the exterior of the limit circular arc,  $\overline{AA\overline{A}}$  (namely, all the arcs denoted by  $CAC$ , are situated within the bodily side of the limit tooth flank of the second of two gears). All the curves  $CAC$  feature a high degree of conformity to the circular arc,  $\overline{AA\overline{A}}$ .

The configuration of either the straight pseudo-path of contact, or a smooth curved pseudo-path of contact, is specified in space, in which the actual configuration of the axis of rotation of the gear, and that of the mating pinion are given. The pseudo-path of contact is located reasonably close to the axis of instantaneous rotation of the gears. Either a constant, or time-dependent (smoothly varying in time) speed of motion of the point of contact along the pseudo-path of contact can be set up. A coordinate system is associated with the gear, and a corresponding coordinate system is associated with the mating pinion. The moving contact point traces contact lines in each of the coordinate systems. One of the contact lines is associated with the gear, and another one is associated with the pinion. Certain smooth regular surfaces through these lines are used as tooth flanks of the gear and that of the mating pinion. The following conditions should be fulfilled to make the surfaces suitable for tooth flanks in *Novikov gearing*:

- When the gears rotate, at every location of contact point, the tooth flanks must have a common perpendicular and, moreover, the condition of conjugacy of the mating tooth profiles must be fulfilled
- The curvatures of the interacting tooth profiles must correspond to each other
- No tooth flank interference is allowed within the working portions of the surfaces

If one surface is generated by a traveling curve of the family of curves,  $BAB$ , and the other surface is generated by a traveling curve of the family of curves,  $CAC$ , then the aforementioned conditions are fulfilled, and the generated in this way surfaces can be employed as tooth flanks in *Novikov gearing*.

Consider a plane through the current contact point. The plane is perpendicular to the axis of instantaneous rotation. Construct two circular arcs centered at points within the straight line through

the pitch point and the contact point. The arc centers are located within the line of action and are close to the pitch point. The constructed circular arcs can be considered as examples of tooth profiles of a gear and a mating pinion. Each of two tooth flanks is generated as a locus of tooth profiles constructed for all possible locations of the contact point. The working portion of one of two tooth flanks is convex, whereas that of the other tooth flank is concave (in the direction toward the axis of instantaneous rotation). In a particular case, the radii of the tooth profiles can be of the same magnitude, and equal to the distance from the contact point to the axis of instantaneous rotation. The centers of both profiles in this particular case are situated at the axis of instantaneous rotation. In such a scenario, the point contact is substituted by a special type of *line contact*. This requires the center-distance to be extremely accurate and independent of the operational conditions, which is impractical. *point contact* of the tooth flanks is preferred when designing favorable tooth profiles. A small difference between the radii of curvature of the tooth profiles is desirable. It should be borne in mind that during the run-in period of time, *point contact* of gear teeth transforms to the aforementioned *line contact* of the tooth profiles. However, the theoretical *point contact* of the tooth flanks is retained.

Generally speaking, it is not mandatory for the tooth profiles to be of circular-arc shapes. Tooth profiles of another geometries (those always passing through the contact point) should be situated (for one gear) within the interior of the aforementioned circular-arc profile,  $\Delta A\Delta$ , which centers at a point within the axis of instantaneous rotation as shown in Figure 11.3. For another (mating) gear, the tooth profile should be located outside the circular arc,  $\Delta A\Delta$ . Under any and all circumstances, the centers of curvature of both of convex and of concave tooth profiles are located within the instantaneous line of action,  $LA_{\text{inst}}$ .

The law of motion of contact point (i.e., the speed of contact point and its trajectory) should be chosen so as to minimize losses caused by friction of the tooth flanks, and their wear. The friction losses and wear are proportional to the relative sliding velocity in the gear mesh. Therefore, it is desirable to reduce the sliding velocity as much, as possible. For this purpose, the path of contact should be remote not too far from the axis of instantaneous rotation. On the other hand, it is also desirable to have the path of contact<sup>9</sup> situated not too close to the axis of instantaneous rotation, as this reduces contact strength of the gear tooth flanks. In addition, it is recommended to ensure favorable angles between the common perpendicular (along which the tooth flanks of one of the gears acts against the tooth flanks of the other gear) and the axes of rotations of the gears.

The opposite sides of the tooth profiles are designed in a manner similar to that just discussed. Tooth thicknesses and tooth pitch are set up so as to ensure the required bending strength of the gear teeth.

The face-width of the gear, or the length of the gear teeth, should correlate with their pitch so as to ensure the required value of the face contact ratio,  $m_F$ . Gear pairs can feature either one point of contact (when working portions of the tooth flank contact each other at just one point, excluding the phases of the teeth re-engagement), or multiple contact points (when tooth flanks contact each other at several points simultaneously).

For parallel-axes gear pairs, it is preferred to implement a straight line as the path of contact (i.e., the *pseudo-path of contact*). The straight line is parallel to the axes of rotations of the gear and that of the pinion. The speed of the contact point as it travels (i.e., *pseudo-travels*) along the straight path of contact (i.e., *pseudo-path of contact*) can be of a constant value. In this particular case, the radii of curvature of the tooth profiles in all sections of the tooth flank by planes are equal to one another. Generated this way, tooth flanks are a kind of screw surfaces. Gears featuring tooth flanks of such a geometry are easier to manufacture, and they can be cut on conventional machine tools available on the market.

<sup>9</sup> The line that was called by Dr. *M.L. Novikov* as the *path of contact*, in the present-day terminology is commonly referred to as the *pseudo-path of contact*,  $P_{pc}$ .

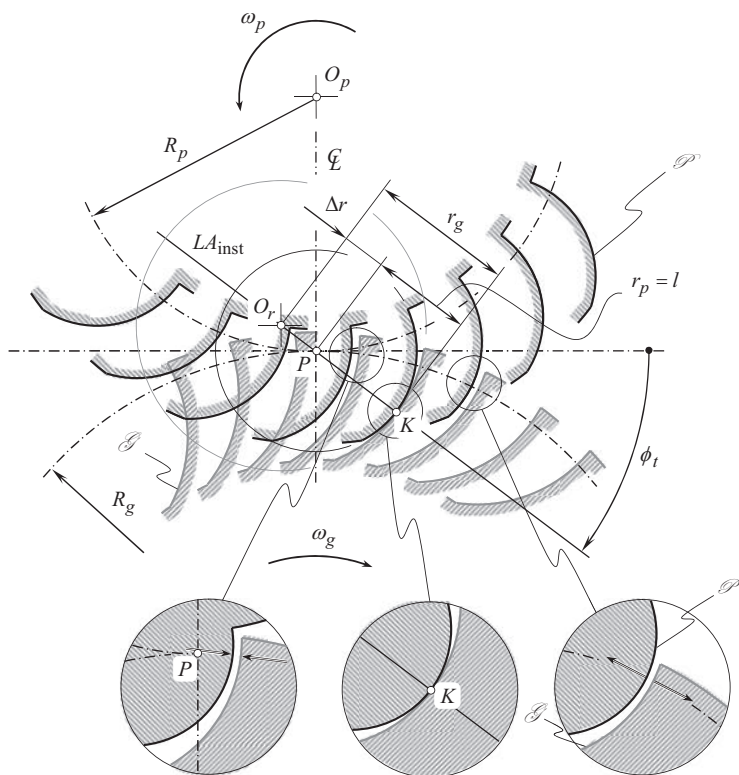


**FIGURE 11.4** Interaction between tooth flank of a gear,  $\mathcal{G}$ , and that of a mating pinion,  $\mathcal{P}$ , in Novikov gear pair.

In parallel-axes gearing with a limit geometry of the tooth profiles, *point contact* between the mating tooth flanks is transformed to their *true-line contact*. The curved contact line is situated across the tooth profile. When the axial thrust in the gear pair is strongly undesirable, herring-bone gears can be used in the design of the gearset.

A more in detail explanation of the early concept of *Novikov gearing* can be found in the book by Krasnoschokov, N.N. et al. [66], and in the monograph by Prof. S.P. Radzevich [157].

Tooth flanks contact each other only at an instant of time when the tooth profiles of both of the gear,  $\mathcal{G}$ , and of the mating pinion,  $\mathcal{P}$ , intersect the instantaneous line of action,  $LA_{inst}$ , in a common transverse section. At no time before, and after this instant of time, the tooth profiles,  $\mathcal{G}$  and  $\mathcal{P}$ , interact with one another<sup>10</sup> (see Figure 11.4). To ensure continuous contact between the tooth flanks,  $\mathcal{G}$  and  $\mathcal{P}$ , the teeth of the gear and that of the pinion are of a helical shape. The path of contact (i.e., *pseudo-path of contact*) can be situated either before, or beyond the pitch point,  $P$ . *Novikov gears* of the first type are commonly referred to as  $N_{by}$  – *gears*, whereas those of the second type are referred to as  $N_{bf}$  – *gears*.

The proposed by Prof. M.L. Novikov method for the generation of tooth flanks is based on the trajectories of the points of contact between the tooth flanks. Prof. M.L. Novikov used to refer to these trajectories as to *contact lines*. It makes sense to refer to the method of generation of tooth flanks proposed by Prof. M.L. Novikov as to the *contact lines method*. In *Novikov gearing*, contact point,  $K$ , between the tooth flanks,  $\mathcal{G}$  and  $\mathcal{P}$ , is often referred to as the *point of culmination*.

<sup>10</sup> Owing to this, M.J. French has proposed [42] to refer to this point as to *culmination*.



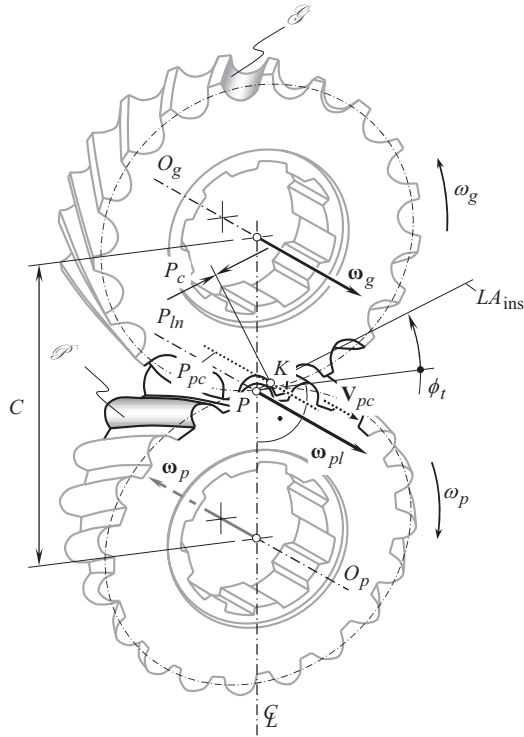


**FIGURE 11.5** Configuration of the pseudo-path of contact,  $P_{pc}$ , in relation to the path of contact,  $P_c$  (the length of the path of contact,  $P_c$ , is zero,  $l_{pc} = 0$ ), and the instantaneous line of action,  $LA_{inst}$ , in *Novikov gear pair*.

Both the gear and the mating pinion are helical. The helices are of opposite hands, namely, one of them is right-handed, and the other one is left-handed. No spur *Novikov gearing* is permissible at all. Because of the gears are helical and the helices are of opposite hands, it appears like point of contact travels (*pseudo-travels*) axially<sup>11</sup> along the gears, while remaining at the same radial position on both gear and pinion teeth,  $\mathcal{G}$  and  $\mathcal{P}$ . It is therefore fundamental to the operation of the gears that contact occurs nominally at a point and the point of contact *travels (pseudo-travels)* axially across the full width of the gears face during a rotation. It should be stated as a condition of operation of *Novikov gearing* that tooth surfaces should not interfere before or after culmination when rotated at angular speeds that are in the gear ratio.

Transverses contact ratio,  $m_p$ , in *Novikov gearing* is zero, ( $m_p \equiv 0$ ). The face contact ratio,  $m_F$ , of the gear pair is equal to the total contact ratio ( $m_F = m_t = \bar{m}$ ) and is always greater than one, ( $m_F > 1$ ).

In every transverse section of the gear pair, contact point,  $K$ , is motionless, as the length of the path of contact,  $P_c$ , is zero,  $l_{pc} = 0$ . For parallel-axes configuration, the pseudo-path of contact,  $P_{pc}$ , is a straight line through the contact point,  $K$ . The pseudo-path of contact,  $P_{pc}$ , is parallel to the axes of rotation,  $O_g$  and  $O_p$ , of the gear and the pinion, as illustrated in Figure 11.5.

When a rotation is transmitted from a driving shaft to a driven shaft, the contact point,  $K$ , *pseudo-travels* with a linear velocity,  $\mathbf{V}_{pc}$ , along the pseudo-path of contact,  $P_{pc}$ , namely, parallel to the axes of rotation,  $O_g$  and  $O_p$ , of the gear and the pinion, correspondingly (and it does not travel within the transverse cross section of the gear pair, as the length of the path of contact,  $P_c$ , is of a

<sup>11</sup> Actually, when the gears rotate, contact point,  $K$ , travels not in the axial direction of the gear pair, but, instead, it travels in a transverse section of the gear pair, along the line of action,  $LA_{inst}$ . The length,  $l_{pc}$ , of this path of contact,  $P_c$ , is zero,  $l_{pc} = 0$ . The motion of contact point,  $K$ , in the axial direction of the gear pair is a kind of illusion. Therefore, the *trajectory* of this *motion* of contact point,  $K$ , is referred to as the *pseudo-path of contact*,  $P_{pc}$ .

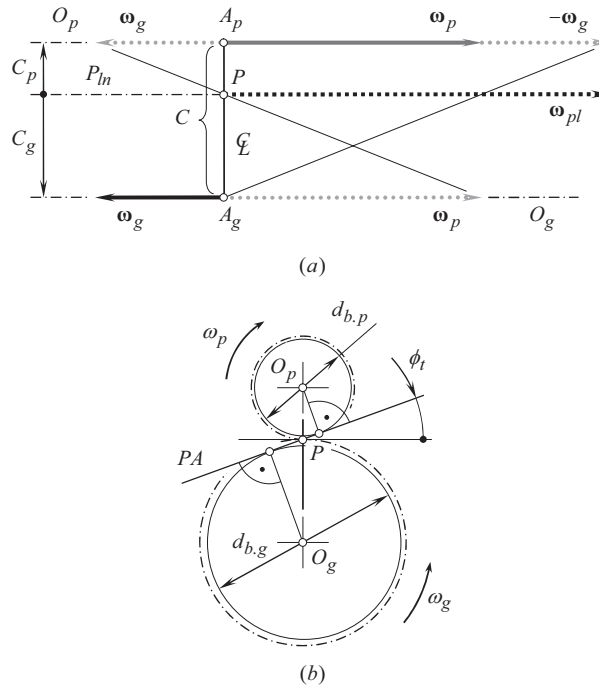


FIGURE 11.6 Gear vector diagram (a) can be constructed for parallel-axes gearing of any design (b).

zero value,  $l_{pc} = 0$ ). This is because in *Novikov gearing* the transverse contact ratio is zero ( $m_p \equiv 0$ ), and the face contact ratio is greater than one ( $m_f > 1$ ), as it was mentioned earlier in this section<sup>12</sup> of the book.

### 11.2.2 KINEMATICS OF PARALLEL-AXES GEARING

A gear vector diagram can be constructed for parallel-axes gearing of any design. As shown in Figure 11.6 gear vector diagram, the rotation vector<sup>13</sup> of a gear,  $\omega_g$ , is pointed along the gear axis of rotation,  $O_g$ . The magnitude,  $\omega_g$ , of the rotation vector,  $\omega_g$ , equals to  $\omega_g = |\omega_g|$ . The rotation vector of the mating pinion,  $\omega_p$ , is pointed along the pinion axis of rotation,  $O_p$ . The axes of rotation,  $O_g$  and  $O_p$ , are apart from one another at a center-distance  $C$ . The magnitude,  $\omega_p$ , of the rotation vector,  $\omega_p$ , is  $\omega_p = |\omega_p|$ . The magnitudes,  $\omega_g$  and  $\omega_p$ , relate to one another according to the ratio:

$$u = \frac{\omega_p}{\omega_g} \quad (11.1)$$

<sup>12</sup> Many gear engineers around the world loosely refer to *Novikov gearing* as to *Wildhaber-Novikov gearing*, or simply to as *W-N gearing*, which is incorrect. *Helical Gearing* according to the patent by E. Wildhaber [101] should be referred to as *Wildhaber helical gearing*. *Gearing with Point System of Meshing* by Prof. M.L. Novikov [90], [101] and [123] must be referred to as *Novikov gearing*. Finally, the terms *Wildhaber-Novikov gearing*, as well, as *W-N gearing*, both, must be recognized as meaningless terms; both of these terms need to be eliminated from engineering literature on gearing. The comparison of *Wildhaber helical gearing* and *Novikov gearing* (see Appendix H for details) makes it possible to understand that the conclusion made by N. Chironis: “Novikov-type gears are similar to those developed by E. Wildhaber in the early 1920s (see p. 135)” [20] is incorrect; further, the *Wildhaber’s* statement “all the characteristics of the Novikov gearing are anticipated by my patent. My gearing never had a real test here, although a pair of gears was made in the 1920’s,” as quoted in the work by Chironis [20], is also incorrect.

<sup>13</sup> It should be stressed here that by nature rotation is **not** a vector at all. However, if special care is undertaken, rotations can be treated like vectors.

The rotation vectors,  $\omega_g$  and  $\omega_p$ , form an angle  $\Sigma$  :

$$\Sigma = \angle(\omega_g; \omega_p) \quad (11.2)$$

The angle,  $\Sigma$ , is referred to as *crossed-axes angle*. In *external* parallel-axes gearing of all designs, the angle,  $\Sigma$ , always equals  $\Sigma = 180^\circ$  (and the angle,  $\Sigma$ , always equals  $\Sigma = 0^\circ$  in *internal* parallel-axes gearing of all designs).

The principle of inversion of rotations can be implemented in a parallel-axes gear pair. Let us assume that both the axes of the rotation,  $O_g$  and  $O_p$ , are rotated together with the rotation vector  $-\omega_g$ . Because the identity  $\omega_g + (-\omega_g) \equiv 0$  is valid, the gear gets stationary under the additional rotation,  $-\omega_g$ . The pinion is rotated with the rotation:

$$\omega_{pl} = (\omega_p - \omega_g) \quad (11.3)$$

The vector of instantaneous rotation,  $\omega_{pl}$ , of the pinion in relation to the gear is pointed along the axis of instantaneous rotation,<sup>14</sup>  $P_{ln}$ .

Shown in Figure 11.6a, is the gear vector diagram of a parallel-axes gear pair that is composed on the premise of the rotation vectors  $\omega_g$ ,  $\omega_p$ , and  $\omega_{pl}$ .

The axis  $P_{ln}$  intersects the centerline,  $\Phi$ , at the pitch point,  $P$ . The pitch point,  $P$ , is at a gear center-distance,  $C_g$ , from the axis of rotation,  $O_g$ , of the gear, and the pitch point  $P$  is at a pinion center-distance  $C_p$  from the axis of rotation,  $O_p$ , of the pinion. The summa of the distances,  $C_g$  and  $C_p$ , equals to the center-distance,  $C$ :

$$C_g + C_p = C \quad (11.4)$$

The center-distances,  $C_g$  and  $C_p$ , are signed values. They are of positive values in external gearing of all designs, and the distance,  $C_g$ , is of a negative value in internal gearing<sup>15</sup> of all designs [82].

As the ratio  $u = \omega_p / \omega_g$  is valid in parallel-axes gearing, the ratio of the center-distances,  $C_g$  and  $C_p$ , is reciprocal to the ratio of the angular velocities in the gear pair, that is:

$$\frac{C_g}{C_p} = \frac{\omega_p}{\omega_g} \quad (11.5)$$

The said allows proceeding to the construction of the plane of action,  $PA$ , in the parallel-axes gear pair as illustrated in Figure 11.6b.

### 11.2.3 PLANE OF ACTION

The plane of action,  $PA$ , in parallel-axes gearing is a plane through the axis of instantaneous rotation,  $P_{ln}$ , as shown in Figure 11.6b. This plane forms a transverse pressure angle,  $\phi_t$ , with a perpendicular to the plane through the axes of rotation,  $O_g$  and  $O_p$ , of the gear and of the mating pinion, correspondingly. The base diameter of the gear,  $d_{b,g}$ , and that of the pinion,  $d_{b,p}$ , can be expressed in terms of the distances,  $C_g$  and  $C_p$ , and of the transverse pressure angle,  $\phi_t$ :

$$d_{b,g} = 2C_g \cos \phi_t \quad (11.6)$$

$$d_{b,p} = 2C_p \cos \phi_t \quad (11.7)$$

<sup>14</sup> Sometimes the axis of instantaneous rotation is also referred to as the *pitch line*,  $P_{ln}$ , the later term is not recommended to use with respect to gears (see subsection 1.11 on page 5 in [82]).

<sup>15</sup> To be more exact, the center distances  $C_g$  and  $C_p$  are of positive values in rotary-positive gear pairs, and the distance  $C_g$  is of a negative value in rotary-negative gear pairs.

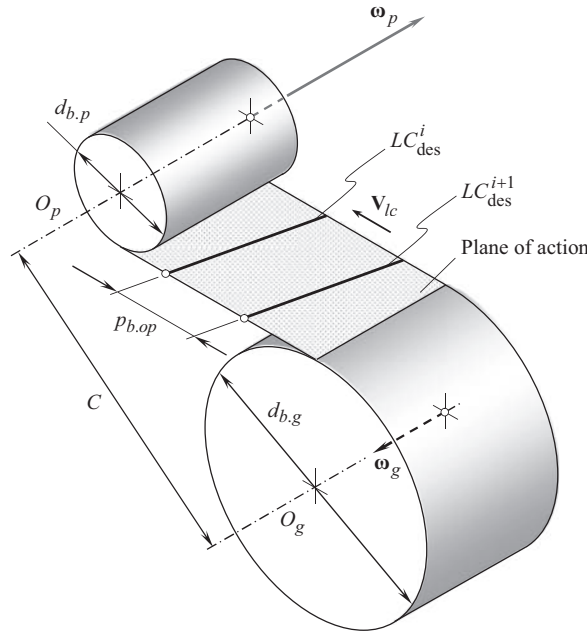


**FIGURE 11.7** Definition of the term *operating base pitch*,  $p_{b,op}$ , in geometrically accurate parallel-axes gearing.

In parallel-axes gearing, the plane of action is commonly shaped in a form of rectangle. In the lengthwise direction, the rectangle is bounded by two straight lines of tangency of the plane of action with each of two base cylinders<sup>16</sup> of diameters,  $d_{b,g}$  and  $d_{b,p}$ . The width,  $F_{pa}$ , of the rectangle equals to the length within which the face-width of the gear,  $F_g$ , and the face-width of the pinion,  $F_p$ , overlap each other.

Once the base cylinders are determined, the transmission of a rotation from the driving member to the driven member in the gear pair can be interpreted by means of the *equivalent pulley-and-belt transmission*. Either of equations [see Eqs. (11.6) and (11.7)] can be used for the derivation of an expression for the calculation of the base pitch,  $p_b$ , in a transverse cross-section of the gear pair:

$$p_b = \frac{\pi d_{b,g}}{N_g} = \frac{\pi d_{b,p}}{N_p} \quad (11.8)$$

Here, the tooth count of the gear, and that of the pinion, are designated as  $N_g$  and  $N_p$ , correspondingly.

Equation (11.8) is valid for parallel-axes gearing of all designs, those capable of transmitting a uniform input rotation smoothly.

#### 11.2.4 OPERATING BASE PITCH

It is convenient to begin the consideration of the base pitches in a gear pair with the *equivalent pulley-and-belt transmission* of parallel-axes gearing. Shown in Figure 11.7, is a schematic of the *equivalent pulley-and-belt transmission*. The axis of rotation of the gear,  $O_g$ , and that of the mating pinion,  $O_p$ , are parallel to one another, and are positioned at a center-distance,  $C$ , from each other. The base cylinder of a diameter,  $d_{b,g}$ , is associated with the gear. Similarly, the base cylinder

<sup>16</sup> In special cases, the rectangle,  $PA$ , can be extended far beyond the lines of tangency of the plane of action with the base cylinders.

of a diameter,  $d_{b,p}$ , is associated with the pinion. In an external parallel-axes gear pair the plane of action,  $PA$ , is tangent to the base cylinders from the opposite sides. The gear and the pinion rotate,  $\omega_g$  and  $\omega_p$ , about their axes of rotation. The magnitudes,  $\omega_g$  and  $\omega_p$ , of the rotations,  $\omega_g$  and  $\omega_p$ , are synchronized with one another reciprocal to the tooth count,  $N_g$  and  $N_p$ , of the gear and the pinion, that is, the ratio:

$$\frac{\omega_g}{\omega_p} = \frac{N_p}{N_g} \quad (11.9)$$

is valid in perfect parallel-axes gearing.

When the gears rotate, the plane of action may be viewed as a zero-thickness film that is unwrapping from the driven (from the base cylinder of the gear) and is wrapping over the driver (on the base cylinder of the pinion). In such a motion, the plane of action travels straight with a linear velocity,  $V_{lc}$ . The magnitude,  $V_{lc}$ , of the linear velocity vector,  $V_{lc}$ , is timed with the rotations,  $\omega_g$  and  $\omega_p$ , so as to retain rolling with no slippage of the plane of action,  $PA$ , over the base cylinders of the gear and the pinion.<sup>17</sup>

A desirable line of contact,  $LC_{des}^i$ , of the  $i$  – th pair of teeth in mesh of the gear and of the pinion is drawn within the plane of action (see Figure 11.7). As an example, the desirable line of contact,  $LC_{des}^i$ , is shown for a case of helical involute gearing. In the case under consideration, this straight-line segment forms the base helix angle,  $\psi_b$ , with the axes,  $O_g$  and  $O_p$ , of rotation of the gear and of the pinion, correspondingly (the base helix angle,  $\psi_b$ , is not shown in Figure 11.7).

The desirable line of contact,  $LC_{des}^{i+1}$ , of the adjacent  $(i + 1)$  – th pair of teeth of the gear and of the mating pinion is parallel to the straight line,  $LC_{des}^i$ , (i.e.,  $LC_{des}^{i+1} \parallel LC_{des}^i$ ), and is also entirely located within the plane of action,  $PA$ .

Measured in a common transverse section of the gear pair, the distance,  $p_{b,op}$ , between any two adjacent desirable lines of contact,  $LC_{des}^i$  and  $LC_{des}^{i+1}$ , is referred to as the *operating base pitch of the gear pair*.<sup>18</sup> It is important to notice here that the operating base pitch,  $p_{b,op}$ , of the gear pair is constructed *before* the interacting tooth flanks,  $\mathcal{F}$  and  $\mathcal{P}$ , of the gear and of the mating pinion are generated: No tooth flanks,  $\mathcal{F}$  and  $\mathcal{P}$ , of the mating gears are generated yet, but the operating base pitch,  $p_{b,op}$ , of the gear pair is already determined. The use of such an approach gives the gear engineer an opportunity to design a gear with accurate geometry of the tooth flanks. For this purpose, the desirable line of contact,  $LC_{des}$ , between the tooth flanks,  $\mathcal{F}$  and  $\mathcal{P}$ , is used to generate the gear,  $\mathcal{F}$ , and the mating pinion,  $\mathcal{P}$ , tooth flanks. Both the gear and its mating pinion have to be designed so as to retain equality of a base pitch of the gear,  $p_{b,g}$ , and that of the mating pinion,  $p_{b,p}$ , to the operating base pitch,  $p_{b,op}$ , of the gear pairs ( $p_{b,g} \equiv p_{b,op}$  and  $p_{b,p} \equiv p_{b,op}$ ).

When the gears rotate, the desirable line of contact,  $LC_{des}$ , travels together with the plane of action,  $PA$ , as this straight-line segment,  $LC_{des}$ , is rigidly associated with the  $PA$ . When the plane of action rolls over the base cylinder of the gear, the gear tooth flank  $\mathcal{F}$  is generated as a family of consecutive positions of the desirable line of contact,  $LC_{des}$ , in its motion in relation to a reference system associated with the gear (see Figure 11.8). Similarly, when the plane of action rolls over the base cylinder of the pinion, the pinion tooth flank  $\mathcal{P}$  is generated as a family of consecutive positions of the desirable line of contact,  $LC_{des}$ , in its motion in relation to a reference system associated

<sup>17</sup> It is important to point out here that in a such motion of the plane of action,  $PA$ , all the points of the *belt* travel in a section of the gear pair by a transverse plane: There is NO motion of the points of the *belt* in the axial direction (along the axis of instantaneous rotation,  $P_m$ ) of the gear pair.

<sup>18</sup> It is also important to stress here that the operating base pitch in a gear pair,  $p_{b,op}$ , is measured in linear units only in *parallel-axes gear pairs*. In intersected-axes, as well, as in crossed-axes gearing, the operating base pitch of a gear pair,  $\phi_{b,op}$ , is measured in angular units. Moreover, if the axes misalignment is taken into account, then the operating base pitch of a gear pair,  $\phi_{b,op}$ , is measured in angular units in gearing of all designs, namely, in  $P_a$  –gearing, in  $I_a$  –gearing, as well, as in  $C_a$  –gearing.

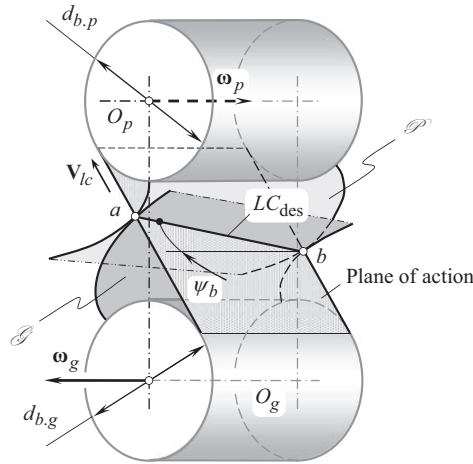


**FIGURE 11.8** Generation of screw involute surfaces,  $\mathcal{S}$  and  $\mathcal{P}$ , of tooth flanks in a pair of helical gears.

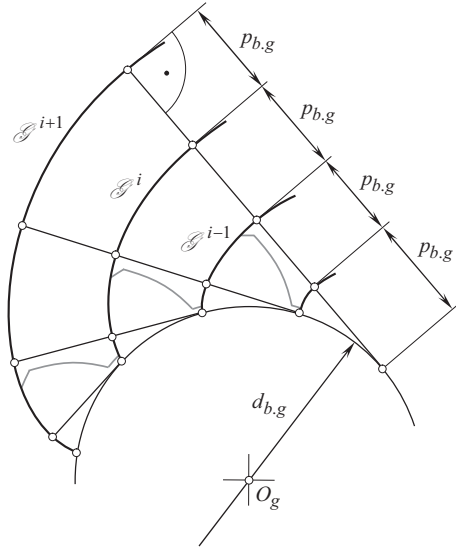


**FIGURE 11.9** Transverse base pitch of a gear,  $p_{b,g}$ , (of a pinion,  $p_{b,p}$ ) in geometrically accurate involute gear pair.

with the gear, as shown in Figure 11.8. In such a scenario, the actual line of contact,  $LC$ , between the tooth flanks,  $\mathcal{S}$  and  $\mathcal{P}$ , is congruent to the desirable line of contact,  $LC_{des}$ , of these surfaces ( $LC \equiv LC_{des}$ ). This enables equality of base pitch of a gear, and that of a mating pinion, both to the operating base pitch of the gear pair, that is:

$$\begin{cases} p_{b,g} \equiv p_{b.op} \\ p_{b,p} \equiv p_{b.op} \end{cases} \quad (11.10)$$

(or, simply  $p_{b,g} \equiv p_{b,p} \equiv p_{b.op}$ ), as shown in Figure 11.9.

In parallel-axes gearing, the identities [see Eqs. (11.10)] are met only in geometrically accurate involute gearing. For any and all kinds of non-involute gearing, the identities [see Eqs. (11.10)]

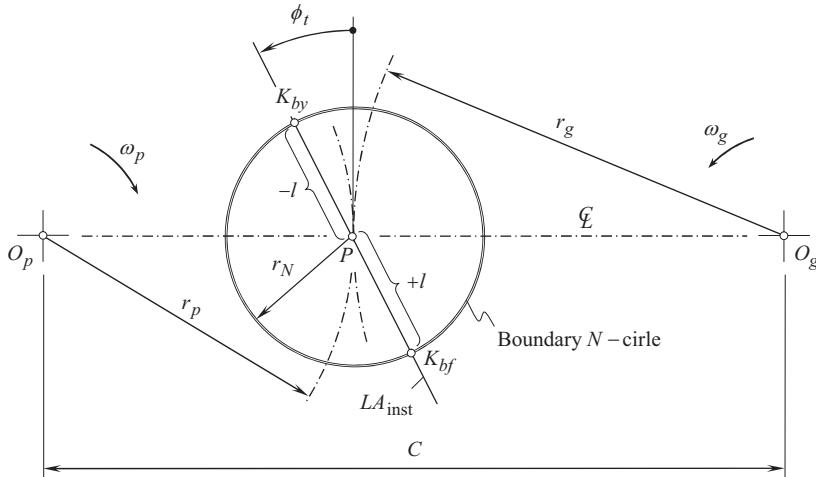


FIGURE 11.10 Boundary  $N$  – circle in Novikov/conformal parallel-axes gear pair.

cannot be fulfilled, and, moreover, base pitch neither of a gear, nor of a mating pinion can be constructed (while the operating base pitch of the gear pair can be easily determined).

### 11.2.5 BOUNDARY NOVIKOV CIRCLE IN NOVIKOV/CONFORMAL GEARING

A performed analysis of the vector diagram for a parallel-axes gearing (see Figure 11.6) reveals that a motion of a pinion in relation of the motionless mating gear is an instant rotation of the pinion about the axis of instantaneous rotation,  $P_{in}$ . Similarly, a motion of the gear in relation of the motionless pinion is an instant rotation of the gear about the axis of instantaneous rotation,  $P_{in}$ . It can therefore be drawn up from that every point of contact,  $K$ , between the tooth flanks of the gear and the pinion,  $\mathcal{G}$  and  $\mathcal{P}$ , traces a circular arc that is centered at the pitch point,  $P$ . One of the circular arcs is associated with the gear, and another one is associated with the mating pinion. Based on this consideration, the concept of the so-called *boundary Novikov circle* was introduced (~2008) [174] by Prof. *S.P. Radzevich*. The *boundary Novikov circle* is commonly referred to as the *boundary  $N$  – circle*, for convenience. The procedure of constructing the *boundary  $N$  – circle* for Novikov/conformal gear pair is briefly outlined next.

Consider the axis of rotations of a gear,  $O_g$ , and that of a mating pinion,  $O_p$ , in design of a parallel-axes Novikov/conformal gear pair, as illustrated in Figure 11.10. The axes of rotation,  $O_g$  and  $O_p$ , are at a center-distance,  $C$ , apart from one another. The gear and the pinion are rotated about the axes  $O_g$  and  $O_p$ . These rotations are labeled  $\omega_g$  and  $\omega_p$ , correspondingly. The gear ratio in Novikov/conformal gear pair equals to  $u = \omega_p / \omega_g$ .

The center-distance,  $C$ , is subdivided by point,  $P$ , into two straight-line segments,  $O_gP$  and  $O_pP$ . The ratio of lengths of the center-distances,  $C_g = O_gP$  and  $C_p = O_pP$ , is reciprocal to the gear ratio,  $u$ , in the Novikov/conformal gear pair. If the straight-line segments,  $O_gP$  and  $O_pP$ , are the pitch radii ( $O_gP = r_g$  and  $O_pP = r_p$ ) in the Novikov/conformal gear pair, then the equality  $r_g / r_p = u$  is observed. The point,  $P$ , is the *pitch point* in the conformal gear pair.

The instantaneous line of action,<sup>19</sup>  $LA_{inst}$ , is a straight line through the pitch point,  $P$ . The instantaneous line of action forms a transverse pressure angle,  $\phi_t$ , with the perpendicular to the centerline,  $\mathcal{L}$ .

<sup>19</sup> The line of action,  $LA$ , in Novikov/conformal gearing, as well, as in high-conformal gearing (or  $H_c$  – gearing, for simplicity) is referred to as the *instantaneous line of action*,  $LA_{inst}$ . The projection of the instantaneous line of action onto the transverse plane remains stationary, as the transverse component of the contact ratio,  $\bar{m}$ , in conformal gearing, and in  $H_c$  – gearing, is zero.



Two points, denoted by  $K_{bf}$  and  $K_{by}$ , are situated within the straight line,  $LA_{\text{inst}}$ , and are displaced at a distance,  $\pm l$ , from the pitch point,  $P$ . The pseudo-paths of contact,  $P_{pc}$ , are the two straight lines through the points  $K_{bf}$  and  $K_{by}$ , parallel to the axis of instantaneous rotation,  $P_m$ , in the gearing. The displacement,  $l$ , of the pseudo-paths of contact,  $P_{pc}$ , from the pitch point  $P$ , is one of the important design parameters in *Novikov/conformal gearing*. The strength of the gear teeth, and the performance of the *Novikov/conformal gearing*, both, strongly depend on the actual value of the design parameter,  $l$ .

The pseudo-path of contact that is situated beyond the pitch point,  $P$ , (in the direction of rotation of the gears) features a positive displacement, and, thus, it is labeled as  $+l$ . A *Novikov/conformal* gear mesh of this type is referred to as the  $N_{by}$  – mesh of *Novikov/conformal* gear pair. The path of contact that is situated before the pitch point (in the direction of the rotation of the gears) features a negative displacement, and, thus, it is labeled as  $-l$ . A conformal gear mesh of this type is referred to as the  $N_{bf}$  – mesh of *Novikov/conformal* gear pair.

In order to avoid violation of three fundamental laws of gearing as well as targeting the wear reduction, and reduction of the friction losses, the pseudo-paths of contact are displaced at a reasonably short distance from the axis of instantaneous rotation,  $P_m$ .

Let us imagine that the pinion is motionless; then, the contact point,  $K$  (either the point  $K_{bf}$  or the point  $K_{by}$ ), traces a circle within the corresponding transverse section of the gear pair. The circle is centered at the pitch point,  $P$ . Similarly, the gear can be assumed stationary; then, the contact point,  $K$  (either the point  $K_{bf}$  or the point  $K_{by}$ ), traces a circle within that same transverse section of the gear pair. This circle is also centered at the pitch point,  $P$ . This consideration reveals how the *boundary N – circle* of a radius  $l$  is constructed.

A transverse section of a *Novikov/conformal* gear pair is subdivided by a *Novikov circle* of a radius  $r_N = |l|$  into two areas.<sup>20</sup> The area within the interior of the boundary circle of a radius  $r_N$  (including points within the boundary circle itself) represents the area of possible shapes of the tooth profiles of one of the mating gears, and the area within the exterior of the boundary circle of the radius  $r_N$  (including points within the circle itself) represents the area of possible shapes of tooth profiles of the second mating gear.

### Definition 11.1

Boundary Novikov circle (or, boundary *N – circle*, for simplicity) is a circle centered at the pitch point in a parallel-axes Novikov/conformal gearing, the radius of which is equal to the distance of the point of contact of the tooth flanks of the gear and of the mating pinion from the pitch point of the gear pair.

It is the right point to stress here that the concept of the *boundary N – circle* is helpful for understanding of the possibility of *Novikov/conformal gearing* that features *locally line contact* between the tooth flanks of a gear and a mating pinion. In the ideal case, when all the deviations and displacements in a gear pair are of a zero value, the tooth flank of the gear,  $\mathcal{S}$ , as well as the tooth flank of the mating pinion,  $\mathcal{P}$ , can be generated by that same arc of the *boundary N – circle*. In other words, an arc of the *boundary N – circle* can be used as the tooth profile of the gear, as well as the tooth profile of the mating pinion.

In practice, a corresponding *N – cylinder* can be assigned to any and all parallel-axes *Novikov/conformal* gear pair. The axis of rotation of the *N – cylinder* is aligned with the axis of instantaneous rotation,  $P_m$ , of a gear and a mating pinion in *Novikov/conformal* gearing.

Ultimately: what is the purpose to introduce the *boundary N – circle*?

<sup>20</sup> The radius of a *Novikov circle* is designated as  $r_N$ . The obsolete designation,  $l$ , for the radius of the *Novikov circle* was used by Prof. *M.L. Novikov* for the displacement of the contact point,  $K$ , from the axis of instantaneous rotation,  $P_m$ . In reality, the equality  $r_N = |l|$  is always observed.



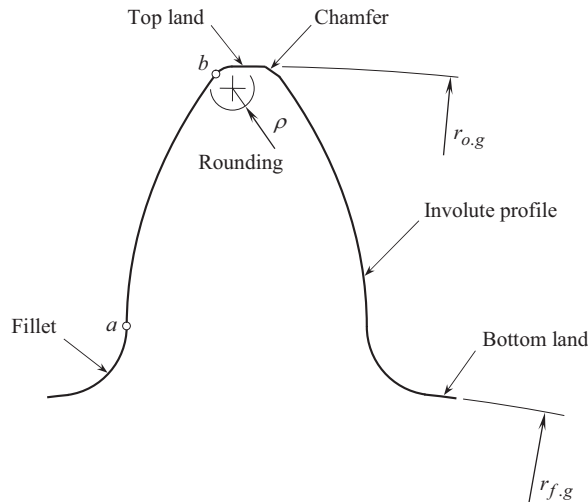


**FIGURE 11.11** Profile of a whole tooth in an involute gear.

In all kinds of gearing, three fundamental laws of gearing cover the kinematics and the geometry of functional portions of the tooth flanks, and they do not cover that for the rest portions of the tooth profile.

In *Novikov/conformal gearing*, the functional portion of the tooth profile is shrunk to the *involute point*. Therefore, in *Novikov/conformal gearing* three fundamental laws of gearing cover **only** *involute point*, and they do not cover the rest of the tooth profile. The *boundary N – circle* relates to the *rest of the tooth profile*, and not relate to the *functional portion* of the tooth profile!!

Only *instantaneous* relative rotation is considered here in *Novikov/conformal gearing*. When the constraints imposed by the *boundary N – circle* are violated, no rotation of the gears through an infinitesimally small angle is permissible, as the gear and the pinion teeth interfere with each other.

### 11.2.6 NOVIKOV/CONFORMAL GEARING AS A REDUCED KIND OF INVOLUTE GEARING

The main goal of this section of the book is to demonstrate that *Novikov/conformal gearing* is a kind of geometrically accurate parallel-axes involute gearing.

In the beginning, it is important to clarify what the term *involute gearing* stands for? Consider a section of an involute gear tooth by a normal plane as illustrated in Figure 11.11. The gear tooth profile is formed by a set of arcs, namely, by:

- a. an arc of involute of a circle
- b. a top land that is shaped in a form of a circular arc
- c. a bottom land that is shaped in a form of a circular arc
- d. a fillet – this portion of an involute gear tooth profile is shaped in a form of cycloid
- e. a chamfer/rounding

It is clear now that the involute gear tooth profile is composed of numerous portions, and the involute of a circle is the only working portion of the involute gear tooth profile. It is instructive to note here how gear pairs are commonly named. Conventional parallel-axes involute gearing is commonly referred to as *involute gearing*, as the functional portion of the gear tooth profile is shaped in a form of an involute of a circle. The rest portions of the gear tooth profile (or of the tooth space), namely: the root curve, the fillet curve, the crest, the tip chamfers, the tip rounding, and so forth are not of involute geometry (see Figures 7.16 and 11.11), and they are not taken into account when the

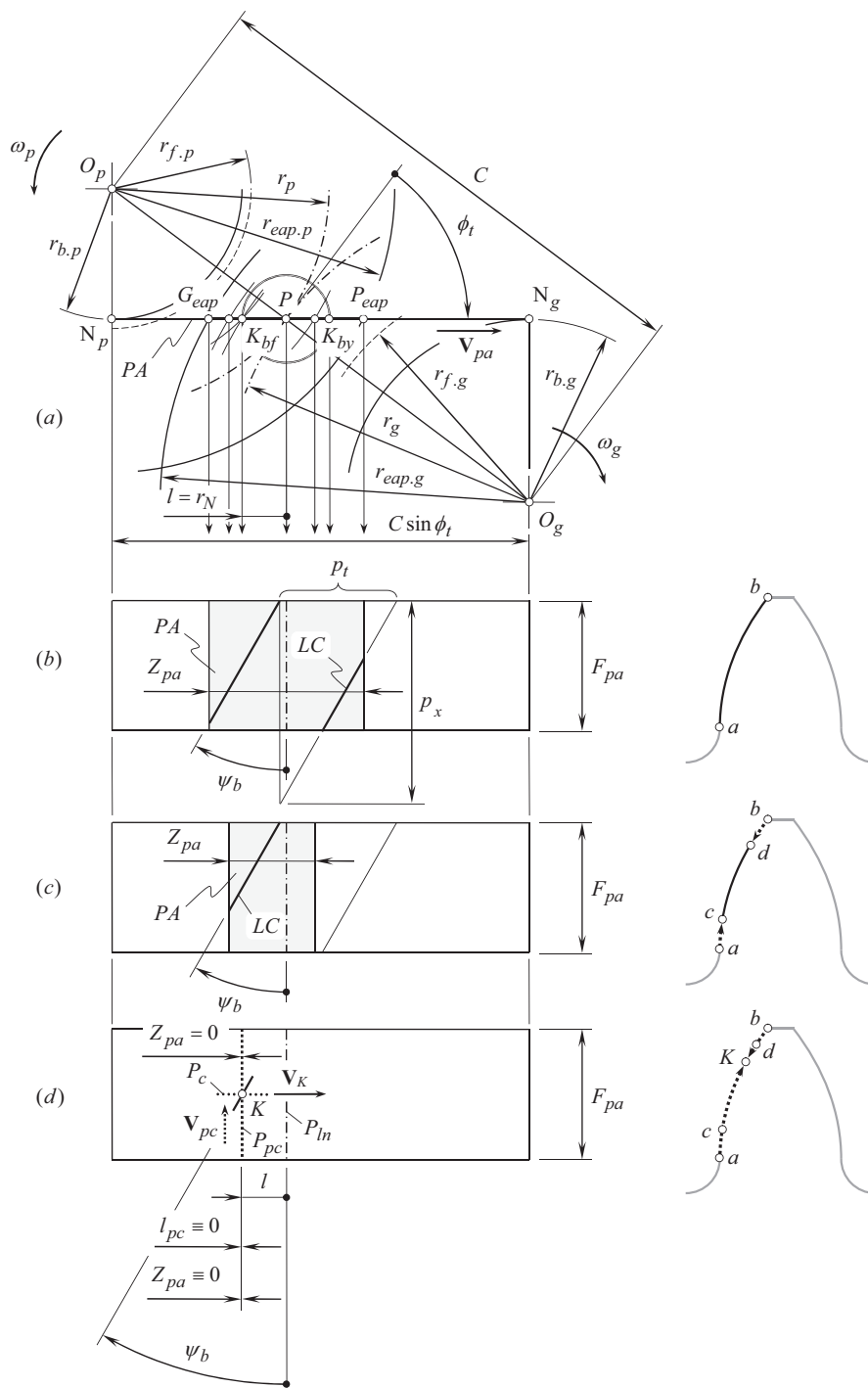


**FIGURE 11.12** Elements of parallel-axes gear pair with transverse contact ratio of a zero value (): (a) a diagram of meshing of two involute tooth profiles, (b) a full involute tooth profile, (c) a partly truncated involute tooth profile, (d) a fully truncated involute tooth profile, (e) an enlarged view of the portion (b), (f) an enlarged view of the portion (c), (g) an enlarged view of the portion (d), and (h) an example of local approximation of the involute tooth point by a circular art.

(Continued)

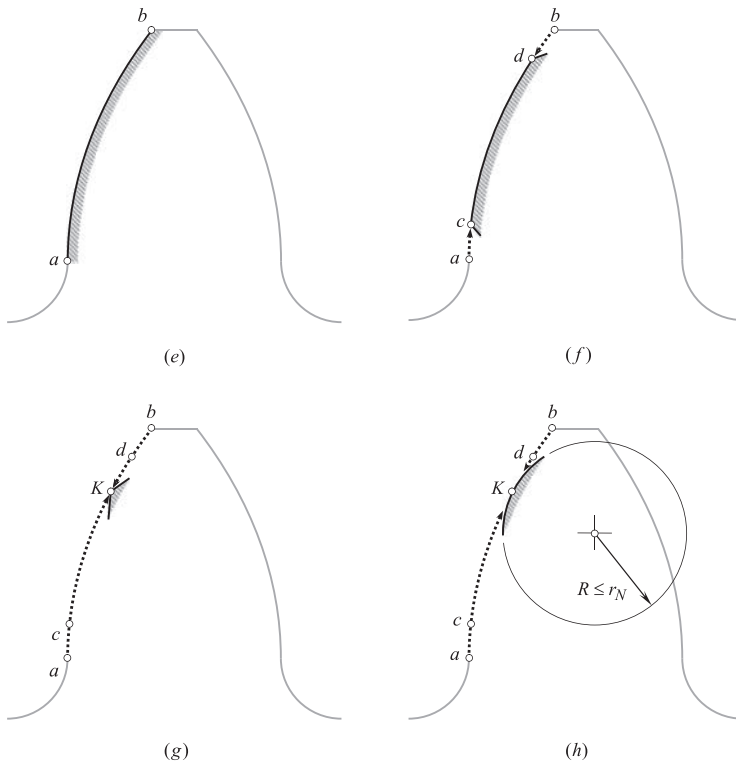


**FIGURE 11.12 (CONTINUED)** Elements of parallel-axes gear pair with transverse contact ratio of a zero value (): (a) a diagram of meshing of two involute tooth profiles, (b) a full involute tooth profile, (c) a partly truncated involute tooth profile, (d) a fully truncated involute tooth profile, (e) an enlarged view of the portion (b), (f) an enlarged view of the portion (c), (g) an enlarged view of the portion (d), and (h) an example of local approximation of the *involute tooth point* by a circular art.

name for the gearing was derived, as none of them influences correctness of meshing tooth flanks of an involute gear and of a mating pinion. It is critical: a particular name for a particular gearing is specified in terms of geometry only of the functional portion of the gear tooth profile, while the rest portions of the tooth profile are ignored in such a consideration.

In geometrically accurate parallel-axes involute gearing, tooth flank of a gear,  $\mathcal{G}$ , and that of a mating pinion,  $\mathcal{P}$ , make contact along a line of contact,  $LC$ . The line of contact is a planar curve of a reasonable geometry that is entirely located within the plane of action,  $PA$ . In *Novikov/conformal gearing*, a straight line that forms a base helix angle  $\psi_b$  with the axis of instantaneous rotation,  $P_{ln}$ , is used as the desirable line of contact.

The tooth flanks,  $\mathcal{G}$  and  $\mathcal{P}$ , of the gear and of the mating pinion interact with one another only within the active portion of the plane of action,  $PA$ . For illustrative purposes, an example of the active portion of the plane of action is depicted in Figure 11.12.

Referring to Figure 11.12a,  $N_g N_p$  is the length of portion of the plane of action measured in between the lines of tangency of the plane of action and the base cylinder of a gear and that of its mating pinion. The active portion of the plane of action,  $PA$ , is of a shorter length,  $Z_{pa}$ , compared to  $N_g N_p$  (see Figure 11.12b). The length,  $Z_{pa}$ , equals to the straight-line segment  $G_{eap} P_{eap}$ . Points  $G_{eap}$  and  $P_{eap}$  are the points of intersection of the straight line  $N_g N_p$  by the *end-of-active-profile circle* of the pinion of a radius  $r_{eap,p}$ , and by the *end-of-active-profile circle* of the gear of a radius  $r_{eap,g}$ , correspondingly. Ultimately, the active portion of the plane of action is shaped in the form of a rectangle of the size  $Z_{pa} \times F_{pa}$ , where  $F_{pa}$  is the effective width of the plane of action,  $PA$ .

In geometrically accurate helical involute gearing, the desirable line of contact,  $LC$ , between the tooth flanks of the gear  $\mathcal{G}$  and of the pinion  $\mathcal{P}$  (note, that the tooth flanks,  $\mathcal{G}$  and  $\mathcal{P}$ , are not constructed yet!!) is a straight-line segment that forms a base helix angle,  $\psi_b$ , with the axis of instantaneous rotation,  $P_{in}$  (the desirable lines of contact of other geometries are not discussed here). As the contact ratio in a gear pair is always greater than one (this is a must), at every instant of time, there must be at least one portion of the desirable line of contact,  $LC$ , within the active portion of the plane of action. This makes possible a definition for the axial pitch,  $p_x$ , of a tooth flank in a helical  $P_a$  – gearing:

### Definition 11.2

Axial pitch,  $p_x$ , in geometrically accurate parallel-axes gear pair is equal to the distance between points of intersection of two adjacent desirable lines of contact,  $LC$ , by a straight line parallel to the axis of instantaneous rotation  $P_{in}$ .

The actual value of axial pitch,  $p_x$ , can be calculated from the following expression:

$$p_x = \frac{P_t}{\tan \psi_b} \quad (11.11)$$

Equation (11.11) is valid for parallel-axes gearing of all designs capable of transmitting a rotary motion smoothly.

When the base cylinders of diameters  $d_{b,g}$  and  $d_{b,p}$  rotate, the desirable line of contact,  $LC$ , travels<sup>21</sup> (together with the plane of action,  $PA$ ) in relation to two reference systems. One of the reference systems is associated with the gear, and another one is associated with the pinion. In such a motion, tooth flank of the gear,  $\mathcal{G}$  (as well as tooth flank of the pinion,  $\mathcal{P}$ ) can be construed as a family of consecutive positions of the desirable line of contact,  $LC$ , in the corresponding reference system.

In the example illustrated in Figure 11.12b (as well as in Figure 11.12e), the active portion,  $ab$ , of the involute tooth profile is specified in terms of the radii of the *end-of-active-profile point* cylinder of the gear,  $r_{eap,g}$ , and that of the mating pinion,  $r_{eap,p}$ , correspondingly. Point  $a$  corresponds to the *start-of-active-profile point* (or just *SAP* – point, for simplicity), while point  $b$  corresponds to the *end-of-active-profile point* (or just *EAP* – point, for simplicity).

For both members of a gear pair, that is, for the gear and for the pinion, the radii,  $r_{eap,g}$  and  $r_{eap,p}$ , of the *EAP* – circle (i.e., *end-of-active-profile-circle*) can be smaller compared to the outer radius of the gear  $r_{o,g}$  (or compared to the outer radius of the pinion  $r_{o,p}$ ), for example, due to either the chamfering, or the corner rounding. In such a scenario [i.e., illustrated in Figure 11.12c and f; the radii,  $r_{eap,g}$  and  $r_{eap,p}$ , in the gear and the pinion are not labeled there], the active portion of the plane of action gets narrower. The *SAP* – point  $c$  and the *EAP* – point  $d$  become closer to one another: The active portion,  $cd$ , of the involute tooth profile is shorter compared to the active portion,  $ab$ , in the case illustrated in Figure 11.12b (and Figure 11.12e). This gives certain freedom when selecting the geometry of non-active portions,  $ac$  and  $bd$ , of the tooth profile. As these portions of the tooth profile do not interact with one another, the geometry of the segments,  $ac$  and  $bd$ , is not restricted by the conditions of meshing of the tooth profiles (which is the must for the active portion,  $cd$ ). The gear designer is free to ignore all three fundamental laws of gearing along with the requirement  $m_t \geq 1$  when designing non-active portions of the tooth profile of the gear,  $\mathcal{G}$ , and of the pinion,  $\mathcal{P}$ .

<sup>21</sup> Note, that there is no motion of the desirable line of contact,  $LC$ , in the axial direction of the gear pair, as the line of contact travels together with the plane of action,  $PA$ .

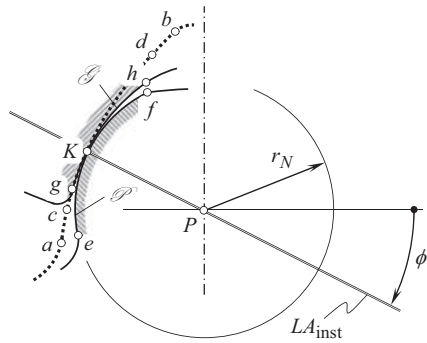


FIGURE 11.13 *Involute tooth point in parallel-axes Novikov/conformal gearing.*

In the extreme case, the *EAP* – circles of the gear and the pinion can pass through point,  $K$ , within the straight-line segment  $G_{eap}P_{eap}$ . Because of this, the length,  $Z_{pa}$ , of the active portion of the plane of action gets zero ( $Z_{pa} = 0$ ), and the active portion of the involute tooth profile shrinks to the point  $K$  (a proper selection of the distance  $PK = l$  is considered below). The non-active portions,  $aK$  and  $bK$ , of the tooth profile meet each other at the point  $K$ . The portions,  $aK$  and  $bK$ , are not subject to conditions of meshing of the tooth profiles, thus this gives an additional freedom to the gear designer when selecting the geometry of non-active portions  $aK$  and  $bK$  of the tooth profile. This particular case of parallel-axes gearing is illustrated in Figure 11.12d (and Figure 11.12g and h).

The transition from involute tooth profile in involute gearing to *involute tooth point* in *Novikov/conformal gearing* deserves a more in-detail consideration. Shown in Figure 11.13, is an involute tooth profile  $ab$ , overlapped by a gear,  $\mathcal{G}$ , and a mating pinion,  $\mathcal{P}$ , tooth profiles in *Novikov/conformal gearing*. The contact point  $K$  is the only point of the tooth profiles,  $\mathcal{G}$  and  $\mathcal{P}$ , that remains active: the tooth profiles,  $\mathcal{G}$  and  $\mathcal{P}$ , make contact only in a stationary point  $K$ , while the arcs,  $gK$  and  $hK$ , in the gear, and the arcs,  $eK$  and  $fK$ , in the pinion, are not the working portions of the gear and the pinion tooth profiles in *Novikov/conformal gearing*. Due to that, the remaining active portion of the tooth profiles is referred to as the *involute tooth point*.

As the gear tooth profile in *Novikov/conformal gearing* is still of involute geometry (namely, *involute tooth point*), then the *Euler-Savary equation* is still valid at this point of the tooth profile (and is not valid even in the differential vicinity of the *involute tooth point*). No exclusion of the validity of *Euler-Savary equation* is required in this regard aiming designing concave and convex non-involute tooth profiles (as it is often claimed in the literature on *Novikov/conformal gearing*).

As the width of the active portion of the plane of action is zero ( $Z_{pa} = 0$ ), and the involute tooth profile is shrunk to a point, the transverse component of the contact ratio,  $m_p$ , gets equal zero. To meet the inequality  $m_t \geq 1$ , the following inequality must be fulfilled:

$$\bar{m} = m_p + m_F = 0 + m_F = m_F > 0 \quad (11.12)$$

The point-type system of meshing in parallel-axes gearing that is illustrated in Figure 11.12d (as well as in Figure 11.12g and h, and in Figure 11.13), gives lots of freedom to the gear designer when designing non-active portions of the tooth profiles of a gear and its mating pinion, as the geometry of these portions is free of constraints imposed by conditions of meshing of two conjugate tooth profiles. In *Novikov/conformal gearing*, this feature is used to increase the contact strength of the gear and the pinion.

After being truncated to point  $K$ , the involute gear/pinion tooth profile can be viewed as a reduced case of involute tooth profile – in *Novikov/conformal gearing* the involute tooth profile is

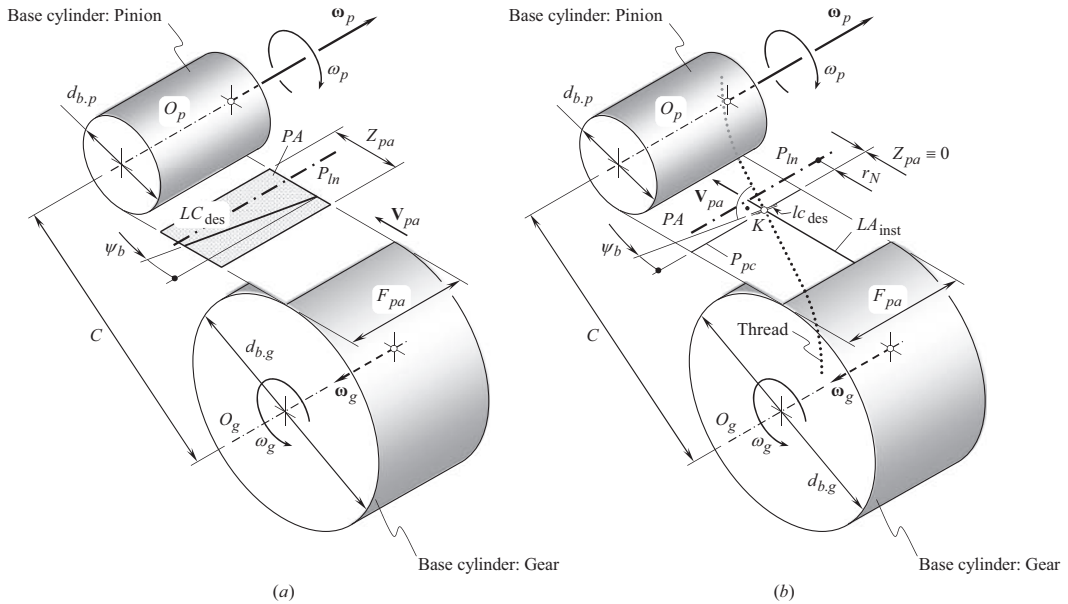


**FIGURE 11.14** On the similarity between involute gearing, and between Novikov/conformal gearing: The plane of action,  $PA$ , (a) in involute gearing, and (b) in Novikov/conformal gearing.

reduced to the *involute tooth point*. The remaining portion of the tooth profile is inactive and, thus, it can be designed independently of three fundamental laws of gearing that govern the interaction of the active tooth profiles.<sup>22</sup>

Shown in Figure 11.14 schematic provides more evidence on similarity between Novikov/conformal gearing and between involute gearing. The principal parameters of the kinematics and geometry of parallel-axes involute gearing are illustrated in Figure 11.14a. They are as follows:

- the base diameter,  $d_g$ , of a gear and that,  $d_p$ , of a mating pinion
- the plane of action,  $PA$
- length,  $Z_{pa}$ , of the zone of action
- effective face-width,  $F_{pa}$ , (effective width of the zone of action); the desirable line of contact,  $LC_{des}$
- the base helix angle,  $\psi_b$

When the gears rotate, the plane of action is viewed as a zero-thickness film that unwraps from the driven and wraps over the driver. The linear velocity vector of straight motion of the plane of action is designated as  $V_{pa}$ .

A similar *equivalent pulley-and-belt transmission* can be constructed for Novikov/conformal gearing (see Figure 11.14b). The principal parameters of the kinematics and geometry in parallel-axes Novikov/conformal gearing, namely:

- the base diameter,  $d_g$ , of a gear and that,  $d_p$ , of a mating pinion
- the plane of action,  $PA$  (c) effective face-width,  $F_{pa}$ , (effective width of the zone of action)
- the base helix angle,  $\psi_b$ ,

<sup>22</sup> The above discussion reveals that no tooth flank modification is permissible in Novikov/conformal gearing. Neither profile modification nor crowning is allowed at all in Novikov/conformal gearing.

are identical to that in involute gearing. *Novikov/conformal gearing* features a zero length of the zone of action ( $Z_{pa} \equiv 0$ ). As a consequence, the desirable line of contact,  $LC_{des}$ , in involute gearing of conventional design is substituted by the infinitesimally short desirable line of contact,  $lc_{des}$ , in *Novikov/conformal gearing*. Ultimately, the plane of action,  $PA$ , in involute gearing of conventional design is substituted by a thread in *Novikov/conformal gearing*. The thread is perpendicular to the desirable line of contact,  $lc_{des}$ . When the gears rotate, the thread unwraps from the driven and wraps over the driver. In such a motion, the thread is permanently situated within the plane of action,  $PA$ .

**Retrospective remark:** In the time, when Prof. *M.L. Novikov* has carried out his research in the field of conformal gearing, he loosely assumed that in order to transmit a uniform rotary motion with a constant angular velocity ratio, the gear teeth do not need to have a special shape, such as the involute of a circle. He meant that, if a gear is made helical then the helix itself can ensure uniform angular motion and tooth profiles can then be chosen with a view to minimizing contact stresses. This is incorrect: in order to transmit a uniform input rotation smoothly, the mating tooth profiles must feature the involute geometry. A reduced case of the tooth profile geometry (i.e., the *involute tooth point*) is also permissible. Gear tooth profiles of no other geometries are capable of transmitting a uniform rotation smoothly, that is, with a constant angular velocity ratio.

The equality of base pitch of a gear and that of a mating pinion to operating base pitch in the gear pair is inherited to *Novikov/conformal gearing*, as the gearing of this particular type is a kind of involute gearing.

### 11.2.7 CONSTRAINTS ONTO THE DESIGN PARAMETERS OF TOOTH GEOMETRIES IN *NOVIKOV/CONFORMAL GEARING*

Designing of interacting tooth profiles in a *Novikov/conformal* gear pair begins with the construction of the gear vector diagram, and is followed by the construction of the plane of action, and then – by the construction of the *boundary N – circle*. In Figure 11.15, the *boundary N – circle* of a radius  $r_N$  is constructed for a pinion tooth profile (see Figure 11.15a) and for a mating gear tooth profile (see Figure 11.15b) of a *Novikov/conformal* gear pair.

The displacement,  $l$ , is of a positive value ( $l > 0$ ) for the pinion addendum. The tooth profile<sup>23</sup> of the pinion addendum is a convex segment of a smooth regular curve,  $P_i^a$  ( $i = 1, 2, \dots$ ) through the contact point,  $K_{by}$ . The radius of curvature,  $R_P$ , of the addendum profile is equal to or less than the radius,  $r_N$ , of the *boundary N – circle* ( $R_P \leq r_N$ ). The case of equality,  $R_P = r_N$ , is the limit case, which is mainly of a theoretical interest. Geometrically, the profile of the pinion addendum can be shaped in the form of a circular arc of a radius  $r_N$ . This case of the pinion addendum profile is the limit one, which is also of theoretical interest.

It should be stressed here that none of the possible profiles,  $P_i^a$ , of the pinion addendum intersects the *boundary N – circle*. The pinion addendum profile is entirely located within the interior of the *boundary N – circle*. Therefore, not any arc of a smooth regular planar curve can be used to form the tooth profile of the pinion addendum. A circular arc, an arc of an ellipse (taken at one of its apexes), and cycloidal profile containing its apex, are examples of applicable curves for the addendum tooth profiles. Spiral curves (involute of a circle, *Archimedean spiral*, logarithmic spiral, and so forth) are examples of smooth regular planar curves no arc of which can be used in design of a pinion tooth addendum. This is because the radius of curvature of a spiral curve (as well as of many others curves) alters unidirectionally when a point travels along the curve. This alteration is

<sup>23</sup> Recall that the functional portion of the tooth profile in *Novikov/conformal gearing* is reduced to the so-called *involute point*. The rest of the gear and of the pinion tooth profiles are not functional, that is, they do not interact with each other. Due to this, there is an additional freedom for the gear designer in selecting the geometry of the non-functional portions of the tooth flanks of the gear and of the pinion.



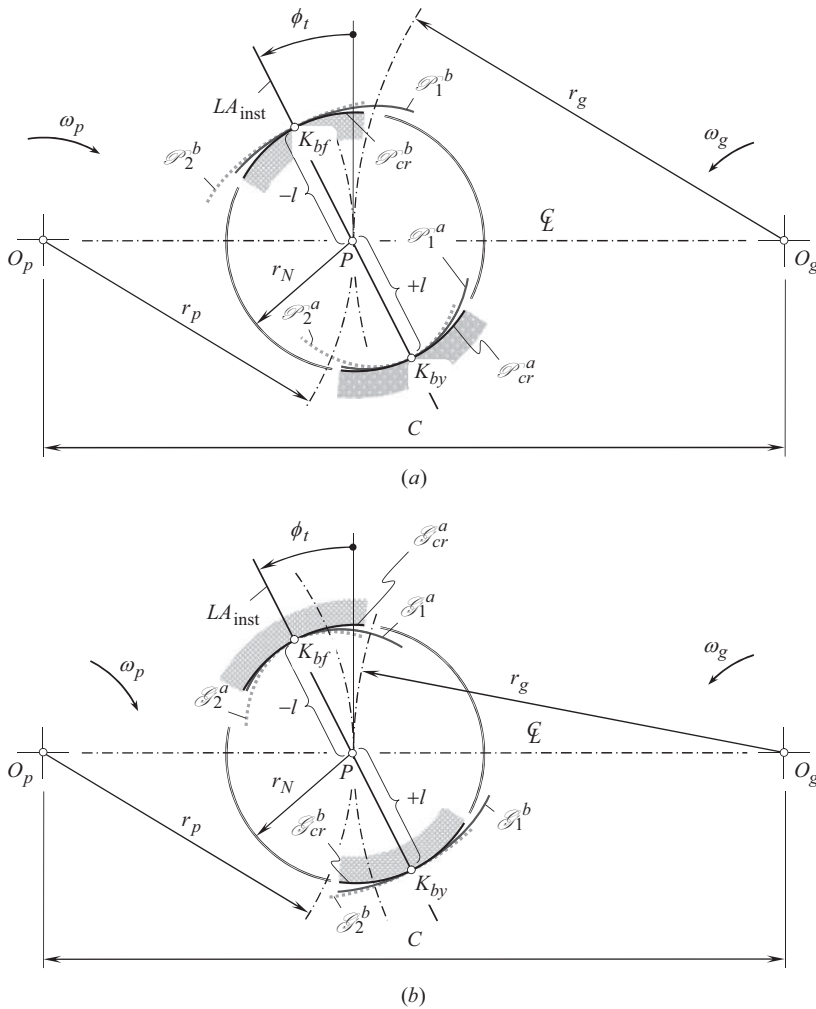


**FIGURE 11.15** Examples of possible tooth flank geometries in *Novikov/conformal* gear pair: possible shapes of the tooth flank of (a) a pinion  $\mathcal{P}$  and of (b) the mating gear  $\mathcal{G}$ .

schematically illustrated in Figure 11.16. An ellipse-arc,  $ab$ , is shown in Figure 11.16a. This ellipse-arc is entirely located within the interior of the *boundary N – circle*. The ellipse-arc,  $ab$ , can be chosen as the tooth addendum profile of a *Novikov/conformal* gear pair. An ellipse-arc,  $cd$  (see Figure 11.16a), is entirely located in the exterior of the *boundary N – circle*. The ellipse-arc,  $cd$ , can also be chosen as the tooth dedendum profile of a *Novikov/conformal* gear pair. Finally, an ellipse-arc,  $ef$  (see Figure 11.16b), intersects the *boundary N – circle*. The ellipse-arc,  $ef$ , cannot be used as the tooth profile in a *Novikov/conformal* gear pair. The same is valid with respect to all spiral curves.

The active portion,  $ef$ , of the gear/pinion tooth profile in Figure 11.16b must be *symmetrical* with respect to the axis of symmetry,  $PK$ , similar to the active portions,  $ab$  and  $cd$ , of the gear/pinion tooth profile shown in Figure 11.16a.

Therefore, at point of tangency,  $K$ , spiral curves intersect the corresponding *boundary N – circle* that is prohibited. Ultimately, it should be clear that a variety of smooth regular planar curves can be used in the design of the tooth profile of a *Novikov/conformal* gearing. The variety of the curves is not limited only to circular arcs.



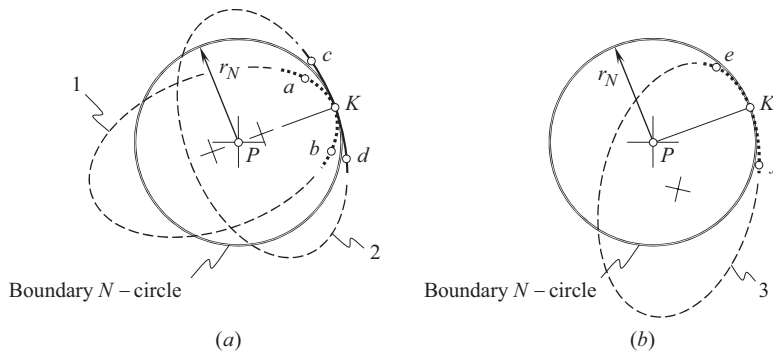


**FIGURE 11.16** Examples of ellipse-arc tooth profiles in *Novikov/conformal* gear pair: (a) permissible, and (b) not permissible.

The displacement,  $l$ , is of a negative value ( $l < 0$ ) for the pinion dedendum (see Figure 11.15a). The non-functional portion of tooth profile of the pinion dedendum is a concave segment of a smooth regular curve,  $\mathcal{P}_i^b$  ( $i = 1, 2, \dots$ ), through the contact point  $K_{bf}$ . The radius of curvature,  $R_{\mathcal{P}}$ , of the dedendum profile is equal to, or greater than the radius,  $r_N$ , of the *boundary N - circle* ( $R_{\mathcal{P}} \geq r_N$ ). The equality  $R_{\mathcal{P}} = r_N$  is observed in a limit case. Geometrically, profile of the pinion addendum can be shaped in the form of a circular arc of the radius,  $r_N$ . The pinion addendum profile of this geometry is only of theoretical interest.

The constraints imposed on the geometry of the non-functional portion of tooth profile of the pinion dedendum are similar to those imposed on the geometry of the tooth profile of the pinion addendum. The dedendum profile: (a) is entirely located within the exterior of the *boundary N - circle*, (b) shares a point with the *N - circle* (the contact point,  $K_{bf}$ ), and (c) does not intersect the *boundary N - circle*. Smooth regular curves not of all geometries can be used in the design of the pinion tooth dedendum.

An analysis that is similar to the aforementioned one regarding the pinion tooth profile, can be performed for the gear tooth profile as well. The analysis is illustrated in Figure 11.15b. The gear tooth addendum,  $\mathcal{G}_i^a$ , is entirely located within the interior of the *boundary N - circle*, whereas the gear tooth dedendum,  $\mathcal{G}_i^b$ , is entirely located in the exterior of the *boundary N - circle*. Both the profile of the gear tooth addendum,  $\mathcal{G}_i^a$ , and the profile of the gear tooth dedendum,  $\mathcal{G}_i^b$ , share a common point with the *boundary N - circle* [This point is: either the point  $K_{by}$  (in the first case), or the point  $K_{bf}$  (in the second case)]. No intersection of the tooth profiles,  $\mathcal{G}_i^a$  and  $\mathcal{G}_i^b$ , within tooth height of the gear and the pinion is allowed.

The importance of the concept of the *boundary N - circle* for the gear engineers is as follows: A *boundary N - circle* in *Novikov/conformal* gear pairs is a constraint that is imposed onto the geometry and curvature of the active portion of the tooth profile, as well as onto the geometry of the inactive portion of the tooth profile in the gear and in the pinion. The gear engineer is free to select an arc of any smooth regular curve to shape the tooth addendum profile if the arc is entirely located within the *boundary N - circle*. The gear engineer is also free to select an arc of any smooth regular curve to shape the tooth dedendum profile if the arc is entirely located outside the *boundary N - circle*.<sup>24</sup>

The concept of the *boundary N - circle* is proven to be helpful in the theory of *Novikov/conformal* gearing. As an example, Figure 11.17 illustrates a schematic of transverse section of a *Novikov/conformal* gear pair. In the case under consideration, the tooth flank of a gear,  $\mathcal{G}$ , makes contact

<sup>24</sup> At around 2008, the concept of *boundary N - circle* was introduced by Prof. S.P. Radzevich. Before 2008, no information about application of the concept of the *boundary circle* is available in the public domain.

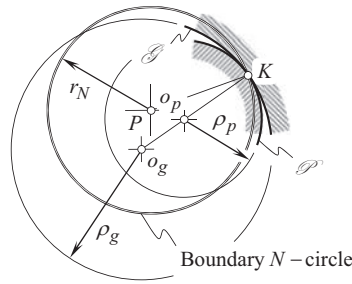


**FIGURE 11.17** Use of the concept of the *boundary N – circle* has proved to be helpful to distinguish whether a circular-arc profile is permissible for *Novikov/conformal gearing*, or not.

Involute gear with involute profile of the teeth

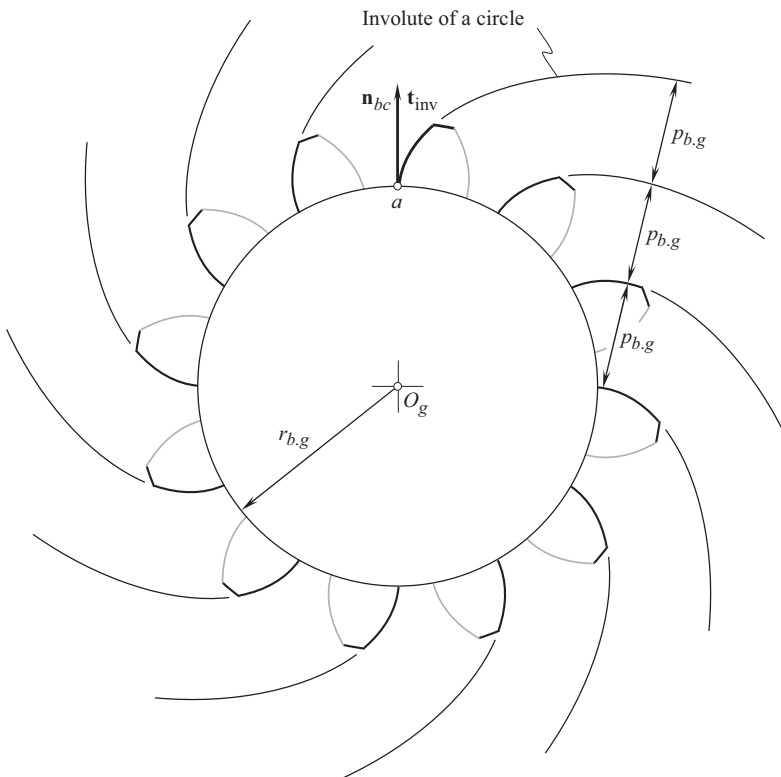


**FIGURE 11.18** Example of the *correct* configuration of involute tooth profile in relation to the base circle in the gear.

with the tooth flank of a mating pinion,  $\mathcal{P}$ , at point,  $K$ . The non-functional portion of the circular-arc tooth profiles,  $\mathcal{S}$  and  $\mathcal{P}$ , are centered at points  $o_g$  and  $o_p$ , correspondingly. The centers,  $o_g$  and  $o_p$ , are chosen so as to fulfill the necessary condition for the magnitudes,  $\rho_g$  and  $\rho_p$ , of the radii of curvature of the tooth profiles,  $\mathcal{S}$  and  $\mathcal{P}$ , at the point of tangency,  $K$  (an inequality  $\rho_g > \rho_p$  is observed). However, as the circular arcs,  $\mathcal{S}$  and  $\mathcal{P}$ , intersect the *boundary N – circle*, the gearing of this particular design is not permissible.

Referring to Figure 11.18, consider a gear that features an involute tooth profile. Gears that feature teeth of involute profile are commonly referred to as *involute gear*. Point  $a$  within the base

Non-involute gear with involute profile of the teeth

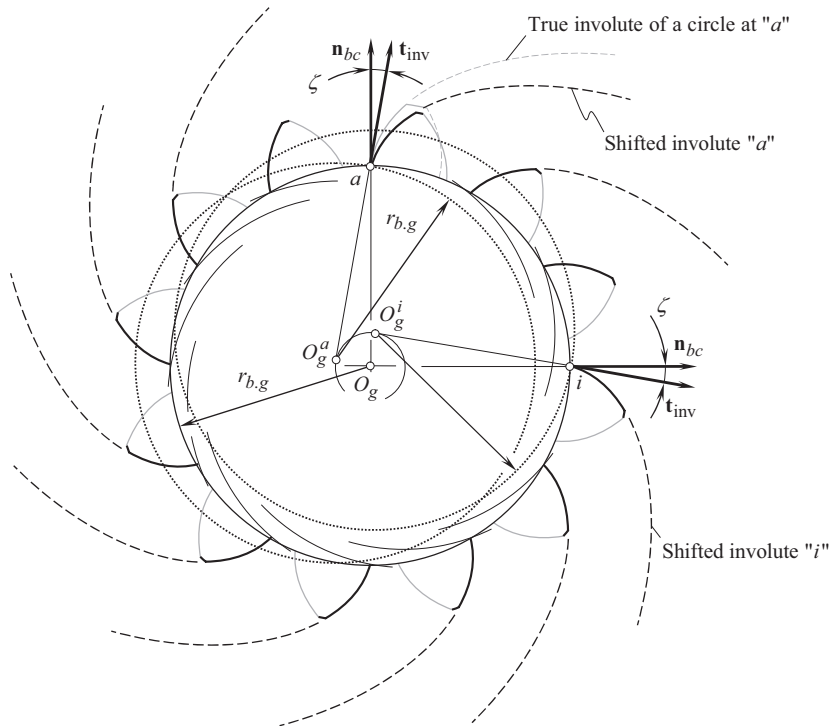


**FIGURE 11.19** Example of *incorrect* configuration of involute tooth profiles in relation to the base circle in the gear.

circle is the starting point of the involute tooth profile. All the involutes are developed from the base circle of a radius  $r_{b,g}$ . Hence, the unit normal vector,  $\mathbf{n}_{bc}$ , to the base circle at point  $a$ , and the unit tangent vector,  $\mathbf{t}_{inv}$ , to the involute curve at that same point  $a$  align with one another. As a result, at any point of interest within an involute curve, the base pitch of the gear,  $p_{b,g}$ , is of a constant value for any two adjacent tooth profiles. In other words, base pitch in the involute gear,  $p_{b,g}$ , in Figure 11.18 is preserved, as all the involutes are developed from a common base circle.

Another example is illustrated in Figure 11.19. In this particular case, the gear teeth are shaped in the form of that same involute curve, as in the case shown in Figure 11.18. However, the gear (see Figure 11.19) cannot be referred to as the *involute gear*, regardless of it features the teeth of an involute geometry. The involute curve in the gear (see Figure 11.19) is turned through an angle,  $\xi$ , about its corresponding starting point of the involute curve. All the angular-shifted involutes are constructed from different base circles of that same radius,  $r_{b,g}$ , each. However, each base circle is centered at the point,  $O_g^i$ , that is not coincident with the gear axis,  $O_g$ . Hence, the unit normal vector,  $\mathbf{n}_{bc}$ , to the base circle of the true involute profile at point  $a$ , and the unit tangent vector,  $\mathbf{t}_{inv}$ , to the angular-shifted involute curve at that same point,  $a$ , form an angle,  $\xi$ . As a result, in the gear shown in Figure 11.19, the base pitch cannot be specified at all. Once the base pitch in the gear cannot be specified, this immediately results in the fact that the fundamental equality of base pitch of a gear to an operating base pitch of the gear pair cannot be fulfilled. Ultimately, the gear (see Figure 11.19) cannot be referred to as *involute gear*.

In *Novikov/conformal gearing* [123], the circular-arc tooth profile,  $ab$ , is centered at point that is situated within the instantaneous line of action,  $LA_{inst}$ , as illustrated in Figure 11.20. In a particular

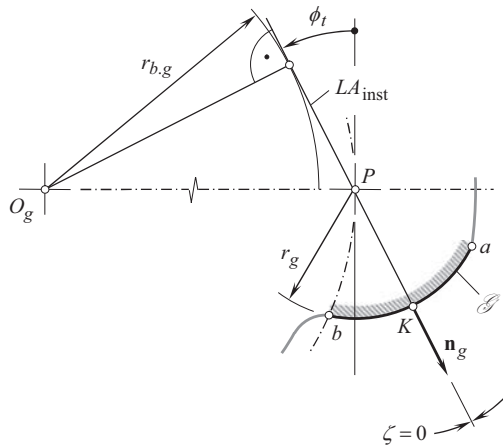


**FIGURE 11.20** Circular-arc tooth profile in parallel-axes *Novikov/conformal gearing*: Pat. No. 109,113, (USSR). *Gear Pairs and Cam Mechanisms Having Point System of Meshing*. /M.L. Novikov, National Classification 47h, 6; Filed: April 19, 1956. (After Prof. S.P.Radzevich.)

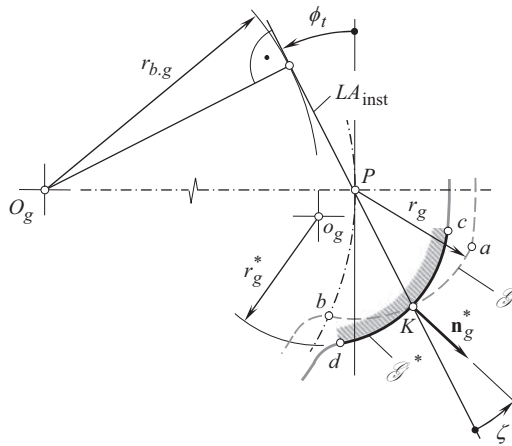


**FIGURE 11.21** Circular-arc tooth profile in *Helical Gearing* by Ernst Wildhaber: *Helical Gearing*, US Patent 1,601,750, E. Wildhaber, Filed: November 2, 1923, Patented: October 5, 1926. (After Prof. S.P.Radzevich.)

case, the center of the circular-arc tooth profile,  $ab$ , is coincident with the pitch point,  $P$ . Due to that, the unit normal vector,  $\mathbf{n}_g$ , to the gear tooth profile at the point of culmination,  $K$ , is aligned with the instantaneous line of action,  $LA_{inst}$ . The angle,  $\xi$ , that the unit normal vector,  $\mathbf{n}_g$ , forms with the instantaneous line of action,  $LA_{inst}$ , is of a zero value (i.e.,  $\xi = 0^\circ$ ). This is a necessary condition that all conformal gearing have to comply with, and, ultimately, fulfillment of this condition ( $\xi = 0^\circ$ ) makes *Novikov/conformal gearing* workable. The base pitch,  $p_{b,g}$ , in a *Novikov/conformal gearing* is measured along the instantaneous line of action,  $LA_{inst}$ . As the unit normal,  $\mathbf{n}_g$ , is aligned with the instantaneous line of action,  $LA_{inst}$ , the base pitch can be specified in *Novikov/conformal gearing*.

In *Helical Gearing* with circular-arc tooth profile proposed by Dr. E. Wildhaber [101], the circular-arc tooth profile,  $cd$ , of a radius  $r_g^*$  is centered at point,  $o_g$ , that is situated outside the instantaneous line of action,  $LA_{inst}$ , as illustrated in Figure 11.21. Because of this, the unit normal vector,  $\mathbf{n}_g$ , to the gear tooth profile,  $\mathcal{G}^*$ , at the point,  $K$ , does not align with the instantaneous line of action,



The pitch diameter of a gear,  $d_g$ , and that of a mating pinion,  $d_p$ , can be expressed in terms of a given center-distance,  $C$ , and the tooth ratio,  $u$  [174]:

$$d_g = 2u \frac{C}{u+1} \quad (11.13)$$

$$d_p = 2 \frac{C}{u+1} \quad (11.14)$$

Then, the actual values calculation of the base diameters  $d_{b,g}$  and  $d_{b,p}$  of the gear and of the mating pinion, are calculated from the equations:

$$d_{b,g} = d_g \cos \phi_t \quad (11.15)$$

$$d_{b,p} = d_p \cos \phi_t \quad (11.16)$$

correspondingly.

In Eqs. (11.15) and (11.16), the base diameters,  $d_{b,g}$  and  $d_{b,p}$ , are expressed in terms of the transverse pressure angle,  $\phi_t$ . In *Novikov/conformal gearing* parallel-axes gearing, the pressure angle,  $\phi_t$ , is identical to the pressure angle in involute parallel-axes gearing.

As *Novikov/conformal gearing* gears features zero length of the field of action ( $Z_{pa} = 0$ ), the length of the path of contact,  $l_{pc}$ , of their tooth flanks shrinks to zero ( $l_{pc} = 0$ ). Although the length of the path of contact is zero, the direction of the path of contact is remained the same.

The base pitch helix angle,  $\psi_b$ , is calculated from the following formula:

$$\psi_b = \tan^{-1}(\tan \psi \cos \phi_t) \quad (11.17)$$

In Eq. (11.17), the pitch helix angle is denoted by  $\psi$ .

Base pitch,  $p_b$ , in the case under consideration is given by:

$$p_b = p_x \sin \psi_b \quad (11.18)$$

where  $p_x$  is the axial pitch of the teeth in *Novikov/conformal gearing*.

Finally, the operating base pitch,  $p_{b,op}$ , in *Novikov/conformal gearing* is calculated from the following formula:

$$p_{b,op} = p_x \tan \psi_b \quad (11.19)$$

The similarities between Eqs. (11.13) and (11.19) and the corresponding set of equations for parallel-axes involute gearing reveal that both gear systems originate from a common concept.

### 11.2.9 TOOTH FLANK GEOMETRY IN *NOVIKOV/CONFORMAL GEARING*

A following approach is used to determine the radii of curvature of interacting tooth flanks of a gear and of a mating pinion in *Novikov/conformal gearing*.

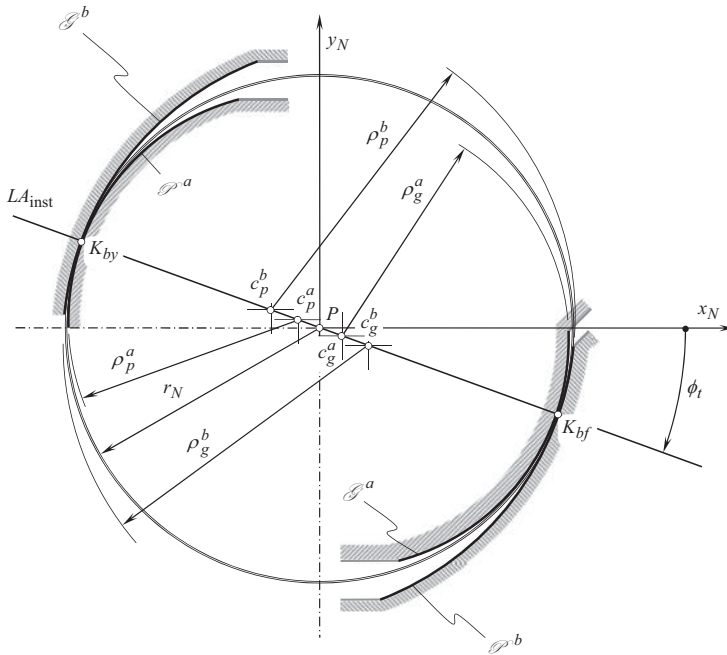


**FIGURE 11.23** Tooth profiles  $G^a$  – to –  $P^b$  and  $G^b$  – to –  $P^a$  in Novikov/conformal gearing that has two pseudo-paths of contact through contact points,  $K_{by}$  and  $K_{bf}$ , correspondingly.

A *boundary N – circle* of a radius,  $r_N$ , is centered at the pitch point,  $P$ , as illustrated in Figure 11.23. In a local reference system,  $x_N y_N$ , that has the pitch point,  $P$ , as the origin, the position vector,  $\mathbf{r}_N$ , of point of the *boundary N – circle* can be expressed in matrix form as follows:

$$\mathbf{r}_N(\varphi_N) = \begin{bmatrix} r_N \cos \varphi_N \\ r_N \sin \varphi_N \\ 0 \\ 1 \end{bmatrix} \quad (11.20)$$

where  $\varphi_N$  is the angular parameters of the *boundary N – circle* of a radius  $r_N$ .

The instantaneous line of action,  $LA_{inst}$ , is a straight line through the pitch point,  $P$ . The instantaneous line of action,  $LA_{inst}$ , forms a transverse pressure angle,  $\phi_t$ , with a perpendicular to the centerline through the pitch point,  $P$ .

In the particular case under consideration, the addendum of the pinion,  $\mathcal{P}^a$ , is shaped in the form of a circular arc of a radius  $\rho_p^a$ . This circular arc is centered at point,  $c_p^a$ , within the instantaneous line of action,  $LA_{inst}$ . The radius of curvature,  $\rho_p^a$ , is smaller compared to the radius,  $r_N$ , of the *boundary N – circle* (i.e., the inequality  $\rho_p^a < r_N$  is valid). In the local reference system,  $x_N y_N$ , the position vector,  $\mathbf{r}_p^a$ , of point of the pinion addendum profile can be expressed in matrix form as follows:

$$\mathbf{r}_p^a(\varphi_p^a) = \begin{bmatrix} \rho_p^a \cos \varphi_p^a + (r_N - \rho_p^a) \cos \phi_t \\ \rho_p^a \sin \varphi_p^a - (r_N - \rho_p^a) \sin \phi_t \\ 0 \\ 1 \end{bmatrix} \quad (11.21)$$

In Eq. (11.21), the angular parameter of the pinion addendum profile is denoted by  $\varphi_p^a$ .

In the particular case under consideration, the dedendum of the gear,  $\mathcal{S}^b$ , is also shaped in the form of a circular arc, the radius of which is  $\rho_g^b$ . This circular arc is centered at point,  $c_g^b$ , within the line of action,  $LA$ . The radius of curvature,  $\rho_g^b$ , is larger compared to the radius,  $r_N$ , of the *boundary*  $N$  – *circle* (i.e., the inequality  $\rho_g^b > r_N$  is observed). In the local reference system,  $x_N y_N$ , the position vector,  $\mathbf{r}_g^b$ , of a point of the gear dedendum profile can be expressed in matrix form as follows:

$$\mathbf{r}_g^b(\varphi_g^b) = \begin{bmatrix} \rho_g^b \cos \varphi_g^b + (r_N - \rho_g^b) \cos \phi_t \\ \rho_g^b \sin \varphi_g^b - (r_N - \rho_g^b) \sin \phi_t \\ 0 \\ 1 \end{bmatrix} \quad (11.22)$$

In Eq. (11.22), the angular parameter of the gear dedendum profile is denoted by  $\varphi_g^b$ .

Similar to the manner in which Eqs. (11.21) and (11.22) are derived, the corresponding expressions for the position vectors of point of the pinion dedendum,  $\mathbf{r}_p^b$ , and the gear addendum,  $\mathbf{r}_g^a$ , are derived:

$$\mathbf{r}_p^b(\varphi_p^b) = \begin{bmatrix} \rho_p^b \cos \varphi_p^b - (r_N + \rho_p^b) \cos \phi_t \\ \rho_p^b \sin \varphi_p^b + (r_N + \rho_p^b) \sin \phi_t \\ 0 \\ 1 \end{bmatrix} \quad (11.23)$$

$$\mathbf{r}_g^a(\varphi_g^a) = \begin{bmatrix} \rho_g^a \cos \varphi_g^a - (r_N + \rho_g^a) \cos \phi_t \\ \rho_g^a \sin \varphi_g^a + (r_N + \rho_g^a) \sin \phi_t \\ 0 \\ 1 \end{bmatrix} \quad (11.24)$$

In Eqs. (11.23) and (11.24), the angular parameter of the pinion dedendum, and of the gear addendum are designated as  $\varphi_p^b$  and  $\varphi_g^a$ , correspondingly.

Once the tooth profiles of the gear and of the mating pinion addendum and dedendum are described analytically [see Eqs. (11.21)–(11.24)], equations for the corresponding tooth flanks  $\mathcal{S}^a$ ,  $\mathcal{S}^b$ ,  $\mathcal{S}^a$  and  $\mathcal{S}^b$  can be derived.

For simplicity, but without loss of generality, equations for the position vector of point of the gear tooth flank may be generalized, and be represented in the form of a common equation:

$$\mathbf{r}(\varphi) = \begin{bmatrix} \rho \cos \varphi + A \\ \rho \sin \varphi + B \\ 0 \\ 1 \end{bmatrix} \quad (11.25)$$

where  $\varphi$  is the angular parameter of the circular-arc profile, and the constants  $A$  and  $B$  are the values, in terms of which the coordinates of center of the corresponding point are expressed in a local reference system,  $x_{cr} y_{cr}$ .

The operator,  $\mathbf{R}_s(cr \mapsto fl)$ , of a screw motion of a circular-arc profile [see Eq. (11.25)] about the  $Z$  – axis can be represented in the form [174]:



$$\mathbf{R}s(cr \mapsto fl) = \begin{bmatrix} \cos \vartheta & -\sin \vartheta & 0 & 0 \\ \sin \vartheta & \cos \vartheta & 0 & 0 \\ 0 & 0 & 1 & p\vartheta \\ 0 & 0 & 0 & 1 \end{bmatrix} \quad (11.26)$$

where:

$\vartheta$  is the angular parameter of the helical tooth flank (either  $\mathcal{S}^a$ , or  $\mathcal{S}^b$ , or  $\mathcal{S}^a$ , or  $\mathcal{S}^b$ ),  
 $p$  is the reduced pitch of the corresponding helical tooth flank.

Considered together, Eqs. (11.25) and (11.26) result in an expression for the position vector of point,  $\mathbf{r}^fl$ , of the tooth flank (either  $\mathcal{S}^a$ , or  $\mathcal{S}^b$ , or  $\mathcal{S}^a$ , or  $\mathcal{S}^b$ ) in *Novikov/conformal gearing*:

$$\mathbf{r}^fl(\varphi, \vartheta) = \mathbf{R}s(cr \mapsto fl) \cdot \mathbf{r}(\varphi) \quad (11.27)$$

In expanded form, an expression for the position vector  $\mathbf{r}^fl$  can be represented as:

$$\mathbf{r}^fl(\varphi, \vartheta) = \begin{bmatrix} (\rho \cos \varphi + A) \cos \vartheta - (\rho \sin \varphi + B) \sin \vartheta \\ (\rho \cos \varphi + A) \sin \vartheta + (\rho \sin \varphi + B) \cos \vartheta \\ p\vartheta \\ 1 \end{bmatrix} \quad (11.28)$$

The derived equation [see Eq. (11.28)] for the position vector,  $\mathbf{r}^fl$ , makes possible further calculation of the unit tangent vectors at a surface point of interest, the unit normal vector at point of the tooth flank, and the first and the second fundamental forms of the tooth flank.

It should be stressed here one more time that in *Novikov/conformal gearing*, the tooth flanks of the gear,  $\mathcal{G}$ , and of the pinion,  $\mathcal{P}$ , interact with one another only at point(s) of culmination. The rest portions of the tooth profiles do not interact with one another (and, moreover, they are *not* conjugate to one another).

### 11.2.10 CONFIGURATION OF INTERACTING TOOTH FLANKS AT POINT OF CULMINATION

Consider a section of a conformal gear pair by a transverse plane as shown in Figure 11.24. The driving pinion, of a left-hand helix, is rotating with an angular velocity,  $\omega_p$ , about its axis of rotation,  $O_p$ , in the clockwise direction. The mating gear is rotating with an angular velocity,  $\omega_g$ , about its axis of rotation,  $O_g$ . The point of contact,  $K_{bf}$ , *pseudo-travels* in the direction at right angles to and out the plane of Figure 11.24. The pinion and the gear have operating pitch radii,  $r_p$  and  $r_g = u \cdot r_p$ , correspondingly, where  $u$  is the gear ratio in the gear pair. The basic condition according to which the angular velocity ratio,  $u_\omega$ , is equal to the gear ratio,  $u$ , requires that the common normal at point of contact between the tooth flanks passes through the pitch point,  $P$ . The angle,  $\phi_t$ , is the transverse pressure angle in the gear pair. With the teeth of involute form, this condition is maintained, as the gears rotate with the teeth in contact. With the circular-arc teeth, however, the condition occurs at only one instant in any one transverse plane as the pitch circles roll together. Immediately before, and immediately after the configuration shown in Figure 11.24, there is no contact in that particular transverse plane between the teeth shown. *French* proposed [40] referring to the instantaneous contact of profiles in a transverse section as to the *culminating condition*.

When the gears are loaded, then, due to the elastic deformation of the gear materials, the contact point spreads over a certain area of contact, which results in a finite contact period.

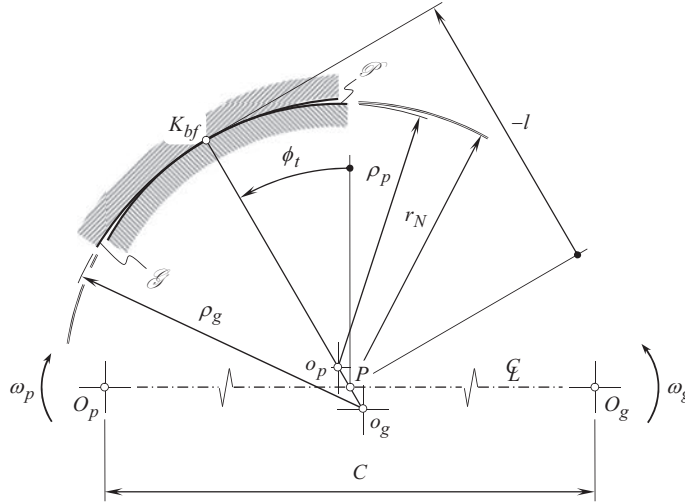


**FIGURE 11.24** The design parameters of *Novikov/conformal* gear pair that influence the contact geometry of the tooth flanks  $\mathcal{G}$  and  $\mathcal{P}$ .

The contact lines (namely, the traces of contact point,  $K$ ) on the gear tooth flank,  $\mathcal{G}$ , and on the pinion tooth flank,  $\mathcal{P}$ , are helices of opposite hands. If the screw parameter,  $p_p$ , of the pinion tooth flank (namely, the reduced pitch of the pinion),  $\mathcal{P}$ , is given, then for the calculation of the screw parameter,  $p_g$ , of the gear tooth flank  $\mathcal{G}$  (namely, of the reduced pitch of the gear) the expression  $p_g = p_p / u$  can be used. This means that *Novikov/conformal* helical gears, which are in point contact, will transform a rotation with a constant angular velocity ratio if their screw parameters,  $p_g$  and  $p_p$ , are related as follows:

$$\frac{p_g}{p_p} = \frac{\phi_g}{\phi_p} \quad (11.29)$$

In Eq. (11.29),

$$p_g = r_g \tan \lambda_g \quad (11.30)$$

where  $\lambda_g$  is the lead angle, and  $r_g$  is the pitch radius of the gear.

Similarly,

$$p_p = r_p \tan \lambda_p \quad (11.31)$$

where  $\lambda_p$  is the lead angle and  $r_p$  is the pitch radius of the pinion.

### 11.2.11 DESIGN OF *NOVIKOV/CONFORMAL* GEAR PAIR

Consider calculation of the design parameters of a *Novikov/conformal* gear pair with a circular-arc tooth profile following that proposed by Prof. *M.L. Novikov* [101]. The approach disclosed in this section of the book can be enhanced to *Novikov/conformal* gearing of the tooth profile of other geometries in a transverse section of the gear pair.

For the calculation of the design parameters of a *Novikov/conformal* gearing, the center-distance,  $C$ , and the gear ratio,  $u = \omega_p / \omega_g$ , in the gear pair are required to be specified.

The radii of the pitch circles of a gear,  $R_g$ , and of a mating pinion,  $R_p$ , can be expressed in terms of the center-distance,  $C$ , and the tooth ratio,  $u$ . The following equations:

$$R_g = C \cdot \frac{u}{1+u} \quad (11.32)$$

$$R_p = C \cdot \frac{1}{1+u} \quad (11.33)$$

are used for this purpose.

The distance,  $l$ , at which the *pseudo-path of contact*,  $P_{pc}$  is apart from the pitch point,  $P$ , is required to be specified as well as the transverse pressure angle,  $\phi_t$ , in the gear mesh.

According to Dr. *M.L. Novikov*, the displacement,<sup>26</sup>  $l$ , is the principal design parameter in *Novikov/conformal gearing*. Many of the design parameters in *Novikov/conformal gearing* can be expressed in terms of the displacement,  $l = KP$ .

For the calculation of the radii of curvature of the tooth profile of the gear,  $r_g$ , and of the mating pinion,  $r_p$ , the following empirical formulas are used:

$$r_g = l \cdot (1 + k_{rg}) \quad (11.34)$$

$$r_p = l \cdot (1 + k_{rp}) \quad (11.35)$$

The actual value of the factor,  $k_{rp}$ , should fulfill the inequality  $k_{rp} \geq 0$ . However, it is practical to set the factor,  $k_{rp}$ , equal to zero; then the equality  $r_p = l$  is observed. The factor,  $k_{rg}$ , is halls in the range of  $k_{rg} = 0.03 \dots 0.10$ .

The radius of the outside circle of the pinion,  $R_{o,p}$ , is calculated from the following formula:

$$R_{o,p} = R_p + (1 - k_{po}) \cdot l \quad (11.36)$$

The addendum factor,  $k_{po}$ , of the pinion depends on:

- a. the actual value of the pressure angle,  $\phi_t$
- d. the absolute dimensions of the gear pair
- e. the accuracy of machining of the gears, and
- f. conditions of lubrication

It is common practice to set the pinion addendum factor,  $k_{po}$ , from the following range:

$$k_{po} = 0.1 \div 0.2 \quad (11.37)$$

The radius of the root circle of the pinion,  $R_{f,p}$ , is calculated from the equation:

$$R_{f,p} = R_p - a_g - \delta \quad (11.38)$$

In Eq. (11.38), the following are designated:

$a_g$  is the tooth dedendum of the mating gear [ $a_g = (0.1 \dots 0.2) \cdot l$ ].

$\delta$  is the radial clearance in the gear pair ( $\delta = l \cdot k_{po}$ ).

<sup>26</sup> Recall that the equality  $l = r_N$  is observed here.

It is proven to be practical to set the fillet radius,  $\rho_p$ , in the range  $\rho_p = 0.3 \cdot l$ .

The radius of the root circle of the gear,  $R_{f.g}$ , is given as follows:

$$R_{f.g} = C - R_{o.p} \quad (11.39)$$

The radius of the outer circle of the gear,  $R_{o.g}$ , is calculated from the expression:

$$R_{o.g} = R_g + a_g \quad (11.40)$$

The corner of the gear tooth addendum needs to be rounded with a radius,  $\rho_g$ , the actual value of which is less than the fillet radius,  $\rho_p$ , of the pinion ( $\rho_g < \rho_p$ ).

The following relations among the design parameters of a *Novikov/conformal gearing* are recommended by Prof. *M.L. Novikov* in Ref. [101]:  $r_p = l$ ,  $r_g \leq 1.10 \cdot r_p$ ,  $\rho_p = 0.3 \cdot l$ ,  $m_t / l = 0.8$ ,  $t_p / t_g = 1.5$ ,  $\phi_t = 30^\circ$ ,  $\lambda = 60 \dots 80^\circ$  ( $\psi = 10 \dots 30^\circ$ ), and circular pitch of the teeth  $p = t_g + t_p + B$ , where backlash  $B = 0.2 \dots 0.4$  mm.

The effective face-width,  $F_{pa}$ , in the gear pair is given by:

$$F_{pa} = (1.1 \div 1.2) \cdot p \cdot \tan \lambda \quad (11.41)$$

For a preliminary analysis of *Novikov/conformal gearing*, the following empirical expression returns a practical value for the displacement,  $l$ :

$$l = (0.05 \div 0.20) \cdot R_p \quad (11.42)$$

The quality of parallel-axes *Novikov/conformal gearing* strongly depends on the following three design parameters:

1. the displacement,  $l$ ,
2. the transverse pressure angle,  $\phi_t$ , and
3. the lead angle,  $\lambda$ .

The application of *Novikov/conformal gearing* (of  $N_{by}$  – mesh of *Novikov/conformal gearing*, in particular) featuring geometries of the tooth profiles known so far, makes possible an increase of the contact strength of the gear teeth up to  $2.0 \div 2.1$  times, and the bending strength up to  $1.3 \div 1.5$  times, compared to involute helical gearing. The friction losses are up to  $2.0 \div 2.5$  less, and the tooth wear is  $3 \div 4$  times less in *Novikov/conformal gearing* [66]. All these application data are obtained for *Novikov/conformal gearing* with tooth surface hardness up to *HB 350*. *Novikov/conformal gearing* with harder tooth flanks are not thoroughly investigated yet.

Application of *Novikov/conformal gearing* makes possible (in average) up to 1.3 times the weight reduction of the gear boxes.

A uniform rotation of the shafts in *Novikov/conformal gearing* is attained only due to face overlap of the gear teeth. Geometrically, meshing of gear teeth in a transverse cross-section is instantaneous.

The non-functional portions of the tooth flanks are not conjugate to each other. Moreover, they are not envelopes to one another.

The results of this discussion give more freedom to the gear designer to make the gear teeth stronger.

An example of *Novikov/conformal gearing* gear pair is illustrated in Figure 10.25. This is a gear pair manufactured by *Westland Helicopter, Ltd.*, and implemented in the design of the gear transmission, shown in Figure 11.26 [3].

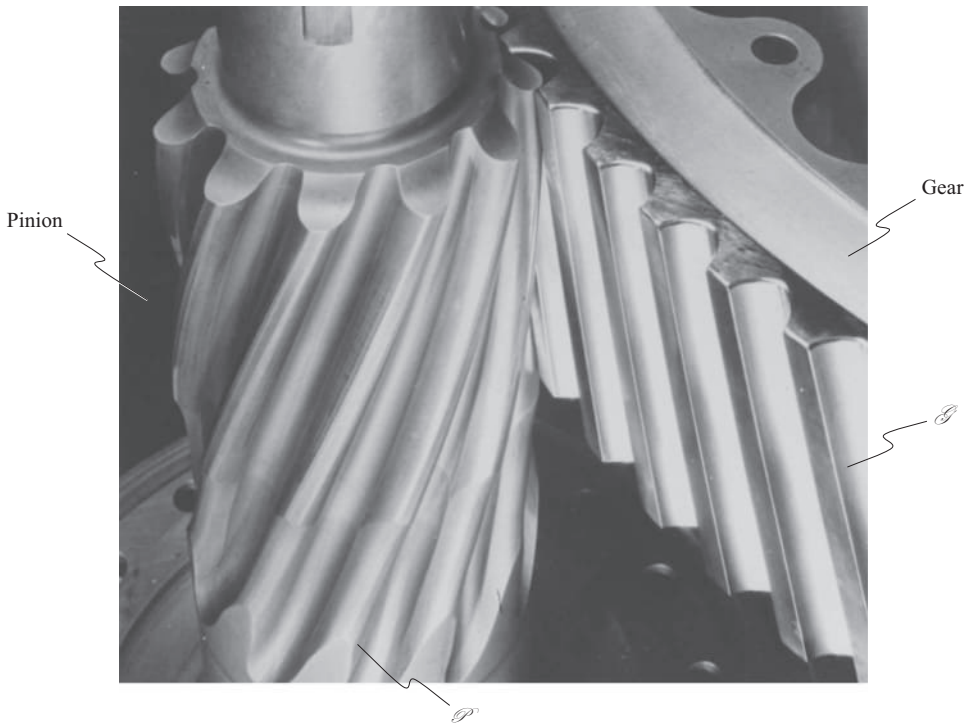


**FIGURE 11.25** Close-up of a conformal gear pair (*Novikov gear pair*) manufactured by *Westland Helicopter, Ltd.* (Adapted from: Dyson, A., Evans, H.P., and Snidle, R.W., 1986, “*Wildhaber-Novikov Circular Arc Gears: Geometry and Kinematics*,” *Proceedings of the Royal Society London A* 403: 313–340.) [33].



**FIGURE 11.26** Gearbox manufactured by *Westland Helicopters, Ltd.* (Adapted from: Astridge, D. G. et al., “*Tribology of High Conformity Gears*,” *Institution of Mechanical Engineers*, 1987, pp. 819–825.) [3].

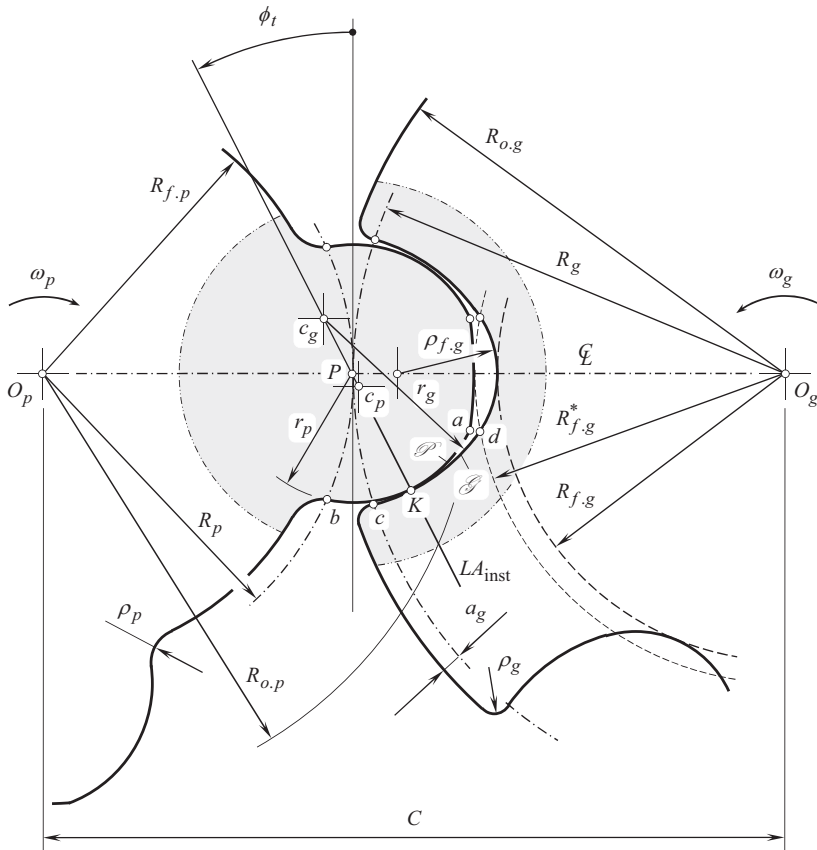


FIGURE 11.27 The kinematics, and the tooth flank geometry in parallel-axes *Novikov/conformal* gearing.

### 11.2.12 ELEMENTS OF KINEMATICS AND GEOMETRY OF *NOVIKOV/CONFORMAL* GEARING

The kinematics and the geometry in *Novikov/conformal* gearing differ from that in involute gearing as well as from gearing of other gear systems.

Referring to Figure 11.27, consider a conformal gear pair that is composed of a driving pinion and a driven gear.

The gear is rotated about the axis,  $O_g$ , and the mating pinion is rotated about the axis,  $O_p$ . The axes of rotations,  $O_g$  and  $O_p$ , are at a center-distance,  $C$ , from one another. The rotation of the gear,  $\omega_g$ , and that of the pinion,  $\omega_p$ , are synchronized with one another.

The pitch circle of the gear is of a radius,  $R_g$ , and the pitch circle of the pinion is of a radius,  $R_p$ , correspondingly. These pitch circles are in tangency to one another. The point of tangency of the pitch circles is the pitch point,  $P$ , in the gear pair. An instantaneous line of action,  $LA_{inst}$ , is a straight line through the pitch point,  $P$ . The instantaneous line of action,  $LA_{inst}$ , forms a transverse pressure angle,  $\phi_t$ , in relation to the perpendicular to the centerline,  $\ell$ .

The contact point,  $K$ , between the tooth flanks of a gear,  $\mathcal{G}$ , and of a mating pinion,  $\mathcal{P}$ , is situated within the straight line,  $LA_{inst}$ . The farther the contact point,  $K$ , is situated from the pitch point,  $P$ , the more freedom this provides to the gear designer in selection of the radii of curvature of the tooth profiles. At that same time, the farther the contact point,  $K$ , is situated from the pitch point,  $P$ , the higher the losses caused by the friction between the tooth flanks,  $\mathcal{G}$  and  $\mathcal{P}$ , and the higher the wear of the tooth flanks. Finally, the actual location of the contact point,  $K$ , is a trade-off between the two aforementioned factors.

Further, let's assume that the pinion is stationary and the gear performs an instantaneous rotation in relation to the pinion. The axis,  $P_{in}$ , of the instantaneous rotation,  $\omega_{pl}$ , is the straight line through the pitch point,  $P$ . In parallel-axes gearing, the axis of the instantaneous rotation,  $P_{in}$ , is parallel to the axes,  $O_g$  and  $O_p$ , of the rotations,  $\omega_g$  and  $\omega_p$ . When the pinion is viewed motionless, the contact point,  $K$ , traces a boundary circle (namely, the *Novikov boundary circle*) of a radius,  $r_N$ , centered at the pitch point,  $P$ .

The pinion tooth profile,  $\mathcal{P}$ , can either align with an arc of the *boundary N – circle* of a radius,  $r_N$ , or it can be relieved inside the bodily side of the pinion tooth. As a consequence, the actual location of the center of curvature,  $c_p$ , of the convex pinion tooth profile,  $\mathcal{P}$ , within the straight line,  $L_{inst}$ , is limited to just the straight-line segment  $PK$ .

On the other hand, the situation of the center of curvature,  $c_g$ , of the concave gear tooth profile,  $\mathcal{G}$ , within the instantaneous line of action,  $LA_{inst}$ , is limited to the open interval  $P; \infty$ . Theoretically, the pitch point,  $P$ , can be included into this interval for  $K$ . However, this is completely impractical, and actually the center of curvature,  $c_g$ , is situated beyond the pitch point,  $P$ . Hence, the radius of curvature,  $r_p$ , of the convex the pinion tooth profile,  $\mathcal{P}$ , is smaller compared to the radius of curvature,  $r_g$ , of the concave the gear tooth profile,  $\mathcal{G}$ , (i.e., the inequality  $r_p < r_g$  is observed).

It should be mentioned here that there are no physical constraints to design a gear pair that has a convex gear tooth profile and concave the pinion tooth profile. However, this is less practical.

Both the pinion and the gear are helical. The helices are of opposite hand, namely, one of them is right-handed, and the other one is left-handed. Because the gears are helical and are of opposite hand, the point of contact *pseudo-travels* axially. In this pseudo-motion, a *pseudo-path of contact*,  $P_{pc}$ , is generated. The *pseudo-path of contact*,  $P_{pc}$ , is parallel to the axis of instantaneous rotation,  $P_{in}$ . Therefore, all the points of the *pseudo-path of contact*,  $P_{pc}$ , are at the same radial position on both gear and pinion teeth,  $\mathcal{G}$  and  $\mathcal{P}$ . It is therefore fundamental to the operation of the gears that contact occurs nominally at a point, and the point of contact *pseudo-travels* axially across the full face-width of the gears during the rotation. It should be stated as a condition of operation of *Novikov/conformal gearing* that for a given profile, the tooth surfaces should not interact before or after culmination when rotated at angular speeds that are in the gear ratio.

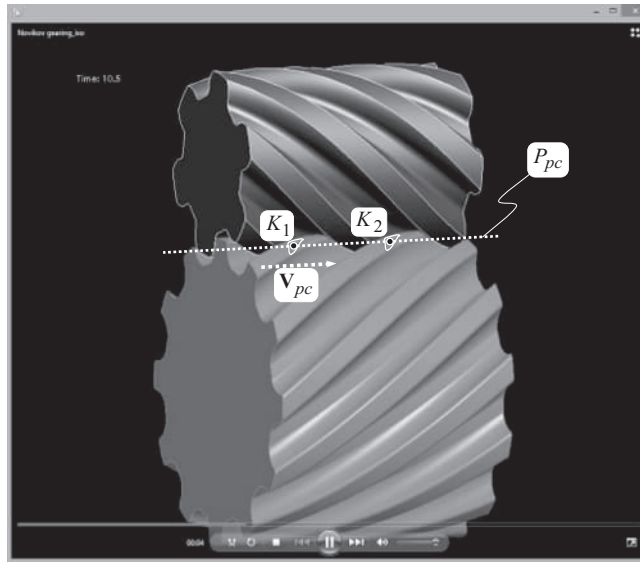
In a transverse section of the gear pair, the contact point,  $K$ , is *motionless*. [To be more exact, in the transverse section of the gear pair, the contact point,  $K$ , travels along the instantaneous line of action,  $LA_{inst}$ . However, the length,  $l_{pc}$ , of this path is zero ( $l_{pc} = 0$ ). Due to this, an illusion is created that in a transverse section of the gear pair, the contact point,  $K$ , is *motionless*. Such a *motion* of the contact point,  $K$ , along the instantaneous line of action,  $LA_{inst}$ , can be referred to as a *zero-motion*]. For parallel-axes configuration, the *pseudo-path of contact*,  $P_{pc}$ , is a straight line through the point of culmination,  $K$ . The *pseudo-path of contact*,  $P_{pc}$ , is parallel to the axes of rotation,  $O_g$  and  $O_p$ , of the gear and the mating pinion, as illustrated in Figure 11.27.

The *pseudo-motion* of the contact point,  $K$ , along the axis of the instantaneous rotation,  $P_{in}$ , in the gear pair, and the *zero-motion* of that same point,  $K$ , in a transverse section of the gear pair is illustrated in Figure 11.28.

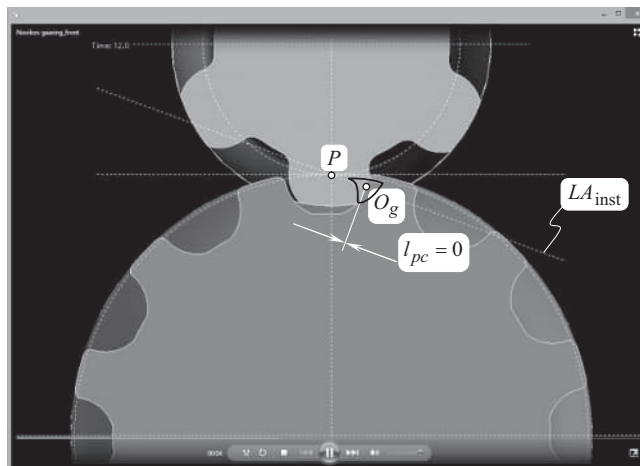
### 11.2.13 LINE OF ACTION AND PATH OF CONTACT IN NOVIKOV/CONFORMAL GEARING

A parallel-axes gear pair is schematically shown in Figure 11.29. The gear and the mating pinion rotate about their axes of rotation,  $O_g$  and  $O_p$ , with angular velocities  $\omega_g$  and  $\omega_p$ , correspondingly. The base diameter of the gear is designated as  $d_{b,g}$ , and the base diameter of the pinion is designated as  $d_{b,p}$ . Outside diameters of the gear and of the pinion are designated as  $d_{o,g}$  and  $d_{o,p}$ , correspondingly. In alignment to the *equivalent pulley-and-belt transmission*, the line of action,  $LA$ , between the tooth flanks,  $\mathcal{G}$  and  $\mathcal{P}$ , of the gear and the mating pinion is tangent to both, namely, it is tangent to the base circle of the gear, and it is tangent to the base circle of the pinion. Points of tangency are labeled as  $N_g$  and  $N_p$ , correspondingly.





(a)



(b)

**FIGURE 11.28** As the gears rotate, contact patch in *parallel-axes Novikov gearing*: (a) *pseudo-travels* in the direction of the axis of instantaneous rotation,  $P_{in}$ , in the gear pair, and (b) is stationary in a transverse section of the gear pair.

The line of action,  $LA$ , intersects the centerline,  $\Phi$ , at the pitch point,  $P$ . (The center-distance,  $C$ , is a straight-line segment of the centerline,  $\Phi$ ).

Points of intersection,  $P_g$  and  $P_p$ , of the line of action,  $LA$ , by the circles of the diameters,  $d_{o,g}$  and  $d_{o,p}$ , are the extreme points of the zone of action,  $Z_{pa}$  [and of the line of action,  $LA$ , as the inequality  $P_g P_p = Z_{pa}$  is valid).

A perpendicular through the pitch point,  $P$ , to the centerline,  $\Phi$ , forms the transverse pressure angle,  $\phi_t$ , with the line of action,  $LA$ .

When the gears rotate, the transverse pressure angle,  $\phi_t$ , is of a constant value at every instant of time, namely, it is of a constant value for all configurations of the gear and the pinion in their



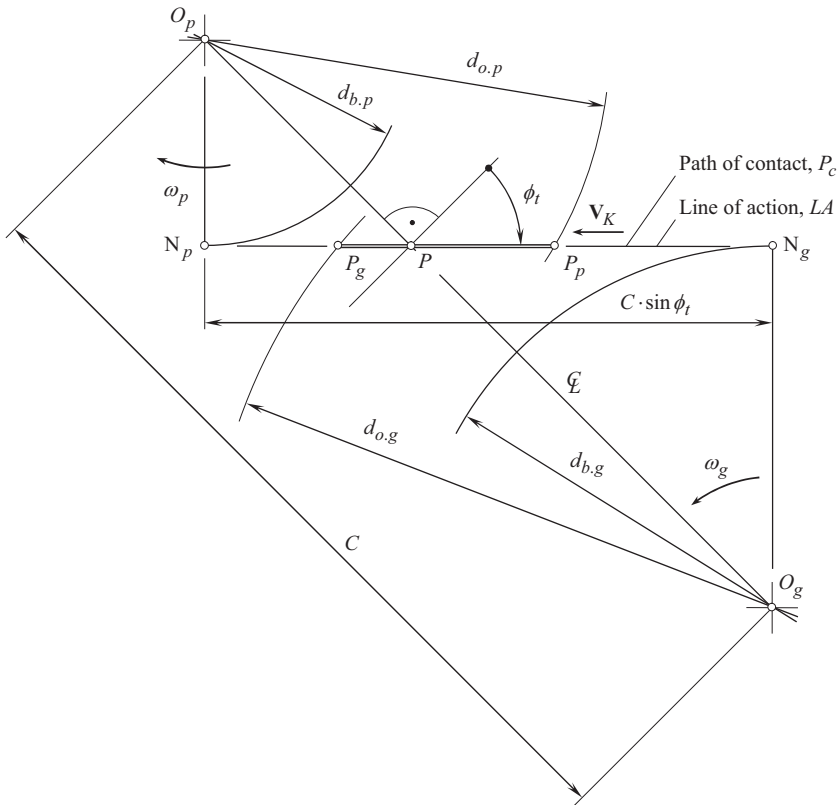


**FIGURE 11.29** In parallel-axes involute gearing, the line of action,  $LA$ , and the path of contact,  $P_c$ , align to one another.

relation to one another. Therefore, when the gears rotate, the contact point,  $K$ , between the tooth flanks  $\mathcal{G}$  and  $\mathcal{P}$  travels along the straight path of contact,  $P_c$ , and the path of contact is aligned with the line of action,  $LA$ . In parallel-axes gearing, the involute tooth profile is unique from this standpoint. Gears with tooth profiles of other geometries are not capable of transmitting a rotary motion smoothly. Only involute gearing features a straight path of contact that is aligned with the line of action. In gearing of other systems, a difference needs to be distinguished: which of the lines is the line of action,  $LA$ , and which of them is the path of contact,  $P_c$ .

Cycloid gearing is a perfect example to illustrate a difference between the line of action,  $LA$ , and the path of contact,  $P_c$ . In cycloid gearing, the path of contact,  $P_c$ , is a planar curve that is entirely situated in section of the gear pair by a transverse plane. At every point of the path of contact, an instantaneous line of action,  $LA_{\text{inst}}$ , can be constructed. An instantaneous line of action,  $LA_{\text{inst}}$ , is a straight line that is tangent to the path of contact,  $P_c$ .

As in *Novikov/conformal gearing* the length of the zone of action,  $Z_{pa}$ , is zero ( $Z_{pa} = 0$ ), the length,  $l_{la}$ , of the active portion of the line of action,  $LA$ , also is zero ( $l_{la} = 0$ ). The length,  $l_{pc}$ , of the path of contact,  $P_c$ , also is zero because of that same reason.

#### 11.2.14 CONTACT RATIO IN PARALLEL-AXES NOVIKOV/CONFORMAL GEAR PAIR

There are many similarities between the contact ratio in involute parallel-axes involute gearing, and in *Novikov/conformal gearing*. To transmit smoothly a uniform input rotary motion from a driving shaft to a driven shaft, at least one pair of teeth must be engaged in mesh at every instant of time.

The actual value of the contact ratio,  $\bar{m}$ , in helical parallel-axes gearing, is calculated from the formula [see Eq. (10.27)]:

$$\bar{m} = \frac{Z_{pa} + F_{pa} \tan \psi_b}{p_{b.op}} \quad (11.43)$$

As the length of the zone of action,  $Z_{pa}$ , in *Novikov/conformal gearing*, is zero ( $Z_{pa} = 0$ ), the contact ratio,  $\bar{m}$ , is calculated from the expression:

$$\bar{m} = \frac{F_{pa} \tan \psi_b}{p_{b.op}} \quad (11.44)$$

No face advance is possible in *Novikov/conformal gearing*.

### 11.2.15 TOOTH PROFILE SLIDING IN *NOVIKOV/CONFORMAL GEARING*

A permissible location of the point of culmination in *Novikov/conformal gearing* can be affected by the tooth profile sliding.

In *Novikov/conformal parallel-axes gearing* the point of culmination is located within the plane of action,  $PA$ . A portion of the plane of action,  $PA$ , where the culminating point,  $K$ , is situated, is limited by the line of intersection of the plane of action by the outer diameter,  $d_{o.g}$ , of the gear, and that (from the opposite side of the  $PA$ ),  $d_{o.p}$ , of the pinion. The gear and pinion teeth must be designed so as to ensure the location of the point of culmination within this interval.

Geometrically, the point of culmination,  $K$ , can be situated between the points of tangency,  $N_g$  and  $N_p$ , of the plane of action,  $PA$ , with two base cylinders of diameters,  $d_{b.g}$  and  $d_{b.p}$ , as illustrated in Figure 11.30.

There is a trade-off between the contact stress, and the sliding between the tooth flanks when determining a favorable situation of the culminating point. The smaller the radius of the *boundary N – circle* (i.e., when  $r_N \rightarrow 0$ ), the smaller the sliding between the tooth flanks; however, the contact

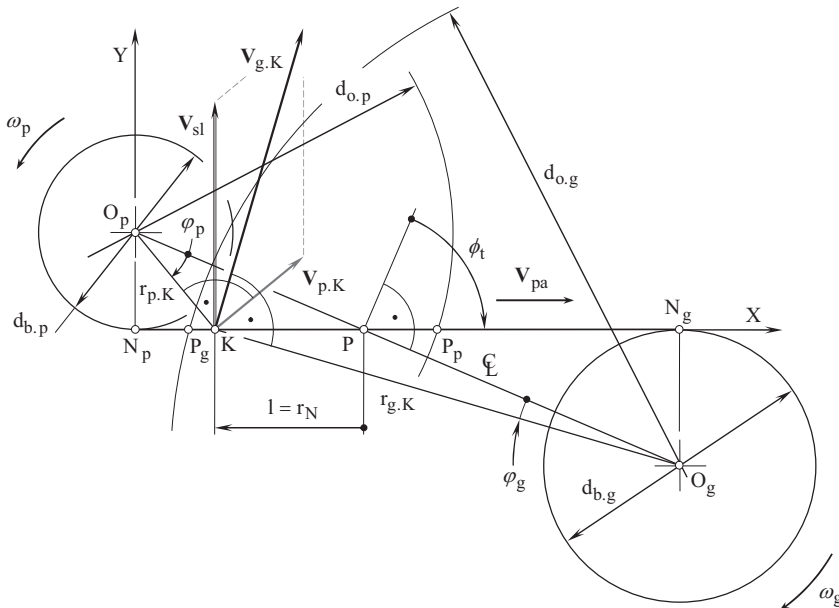


FIGURE 11.30 Tooth profile sliding in parallel-axes *Novikov/conformal gearing*.

stress in such a scenario increases, as the allowed values for the radii of tooth profile curvature of the gear and the mating pinion decrease ( $\rho_g \rightarrow 0$ ,  $\rho_p \rightarrow 0$ ). The larger the radius of the *boundary N – circle*, the smaller the contact stress; however, the sliding of the tooth flanks is larger in this later case. Theoretically, a zero radius of the *boundary N – circle* ( $r_N = 0$ ) is the smallest possible radius of this circle, and  $r_N = N_g P$  is the largest possible radius of the *boundary N – circle*. However, the permissible interval for the radius,  $r_N$ , of the *boundary N – circle* is narrowed to the straight-line segment,  $P_g P_p$ , by the outer diameters of the gear and the mating pinion,  $d_{o,g}$  and  $d_{o,p}$ , correspondingly. Therefore, either the value,  $PP_g$ , or the value,  $PP_p$ , is the largest possible radius of the *boundary N – circle*.

To make a correct decision regarding the appropriate value of radius,  $r_N$ , of the *boundary N – circle*, both the contact stress and the sliding between the tooth flanks have to be taken into account.

For the calculation of the contact stress, the radii of curvature of a gear and of a mating pinion tooth profiles strongly correlate to the radius,  $r_N$ , of the *boundary N – circle*. A certain freedom is available for the gear designer in choosing the actual value of the radius  $r_N$ .

The sliding between the tooth profile depends on the distance of the point of culmination,  $K$ , from the axis of instantaneous rotation of the gear and of the pinion. The radius,  $r_{p,K}$ , of the circle within which the culminating point is situated when rotating about the pinion axis of rotation,  $O_p$ , is calculated from the following expression:

$$r_{p,K} = \sqrt{0.5d_p^2 + 2r_N^2 + 2d_p r_N \cos \phi_t} \quad (11.45)$$

A similar formula:

$$r_{g,K} = \sqrt{0.5d_g^2 + 2r_N^2 + 2d_g r_N \cos \phi_t} \quad (11.46)$$

is used for the calculation of the radius,  $r_{g,K}$ , of the circle within which the culminating point is located when the gear pair is rotating about the gear axis of rotation,  $O_g$ .

For further analysis, it is convenient to express the sliding velocity in *Novikov/conformal gearing* in terms of the radius,  $r_N$ , of the *boundary Novikov circle*.

Consider a triangle  $\triangle KPO_p$  in Figure 11.30. The angle,  $\varphi_p$ , in the triangle  $\triangle KPO_p$  is determined using the cosine law:

$$\varphi_p = \cos^{-1} \left( \frac{r_{p,K}^2 + r_p^2 - r_N^2}{2r_{p,K} r_p} \right) \quad (11.47)$$

In Eq. (11.47), the pitch radius of the pinion is designated as  $r_p$ .

An expression similar to Eq. (11.47), can be derived for the calculation of the corresponding angle,  $\varphi_g$ , in the gear. A simpler approach for the calculation of the actual value of the angle  $\varphi_g$  is based on the ratio  $\varphi_p / \varphi_g = u$ , where  $u$  is the gear ratio of the gear pair, that is,  $\varphi_g = \varphi_p / u$ .

With that said, the linear velocity vector,  $\mathbf{V}_{p,K}$ , of the contact point,  $K$ , in its rotation with the pinion equals to:

$$\mathbf{V}_{p,K} = \omega_p r_{p,K} [\mathbf{i} \cdot \sin(\phi_t - \varphi_p) + \mathbf{j} \cdot \cos(\phi_t - \varphi_p)] \quad (11.48)$$

Similarly, the linear velocity vector  $\mathbf{V}_{g,K}$  of the contact point,  $K$ , in its rotation with the gear can be represented in the form:

$$\mathbf{V}_{g,K} = u^{-1} \omega_p r_{g,K} [\mathbf{i} \cdot \sin(\phi_t + \varphi_p / u) + \mathbf{j} \cdot \cos(\phi_t + \varphi_p / u)] \quad (11.49)$$

The sliding velocity vector,  $\mathbf{V}_{sl}$ , in *Novikov/conformal gearing* is calculated from the formula:

$$\mathbf{V}_{sl} = \mathbf{V}_{g.K} - \mathbf{V}_{p.K} \quad (11.50)$$

In parallel-axes gearing, the sliding velocity vector,  $\mathbf{V}_{sl}$ , is always perpendicular to the plane of action,  $PA$ .

For the specification of profile sliding between the tooth flanks,  $\mathcal{G}$  and  $\mathcal{P}$ , of a gear and of a mating pinion, a unitless parameter is used. This parameter is commonly referred to as *specific sliding*, and is denoted by  $\gamma$ . Two different parameters,  $\gamma$ , are distinguished.

**First**, the slide/roll ratio for the tooth flank,  $\mathcal{G}$ , of the gear (the *specific sliding of the first kind*):

$$\gamma_g = \frac{V_{sl.g}^m - V_{sl.p}^m}{V_{sl.g}^m} \quad (11.51)$$

**Second**, the slide/roll ratio for the tooth flank,  $\mathcal{P}$ , of the mating pinion (the *specific sliding of the second kind*):

$$\gamma_p = \frac{V_{sl.p}^m - V_{sl.g}^m}{V_{sl.p}^m} \quad (11.52)$$

In involute gearing, the specific sliding,  $\gamma$ , is of a positive value on the addendum portions of the tooth flanks. The parameter,  $\gamma$ , does not exceed 1. At the pitch point,  $P$ , it is equal to zero, and it is equal to 1 at the base circle of the mating gear.

The specific sliding on the dedendum portion of the tooth flanks in involute gearing is of a negative value. It is equal to zero at the pitch point,  $P$ , and it is approaching minus infinity at the base circle.

The parameters  $V_{sl.g}^m$  and  $V_{sl.p}^m$ , that have to be entered into Eqs. (11.51) and (11.52), are already available from Eqs. (11.48) and (11.49), correspondingly:

$$V_{sl.g}^m = u^{-1} \omega_p r_{g.K} \cos(\phi_t + \varphi_p / u) \quad (11.53)$$

$$V_{sl.p}^m = \omega_p r_{p.K} \cos(\phi_t - \varphi_p) \quad (11.54)$$

Commonly, the specific sliding,  $\gamma$ , is plotted along the line of action, as depicted in Figure 11.31. Only the region,  $Z_{pa}$ , within the path of contact comes into effect when investigating the engagement of the gear teeth. In the case of parallel-axes *Novikov/conformal gearing*, the length of action is zero, that is, the equality  $Z_{pa} = 0$  is valid.

The sliding is of a constant value in *Novikov/conformal gearing* as well as in *high-conformal gearing*; the specific sliding for the gear,  $\gamma_g$ , and that of the pinion,  $\gamma_p$ , are also of constant values [174]. This has to be taken into account, as commonly, in involute gearing, the sliding is different at different points of the tooth profile, and the specific sliding,  $\gamma_g$  and  $\gamma_p$ , are of a constant value.

### 11.2.16 NOVIKOV/CONFORMAL GEARING WITH TWO PSEUDO-PATHS OF CONTACT

A design of *Novikov/conformal gearing* that features two *pseudo-paths of contact* is possible. Such a possibility immediately follows from the analysis of the schematic shown in Figure 11.15.

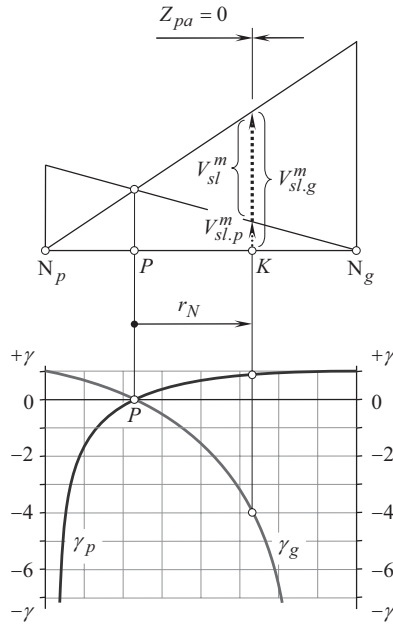


**FIGURE 11.31** Specific sliding,  $\gamma$ , in a parallel-axes *Novikov/conformal* gear pair.

A possibility of design of *Novikov/conformal* gear pair with two contact points,  $K'$  and  $K''$ , inspired *R.V. Fed'akin* to propose a design of *Novikov/conformal* gearing of two paths of contact instead [38,125], instead of a single *pseudo-path of contact*,  $P_{pc}$ , as in the original *Novikov gear system*. The invention by *R.V. Fed'akin* [38,125], is schematically illustrated in Figure 11.32. Two *pseudo-paths of contact*,  $P_{pc,bf}$  and  $P_{pc,by}$ , are the straight lines parallel to the axis of instantaneous rotation,  $P_{ln}$ , of the gears. The *pseudo-paths of contact*,  $P_{pc,bf}$  and  $P_{pc,by}$ , pass through the contact points,  $K_{by}$  and  $K_{bf}$ . They are at distances,  $+l$  and  $-l$ , from the pitch point,  $P$ , correspondingly.<sup>27</sup> As conformal gears are helical, the contact points,  $K_{by}$  and  $K_{bf}$ , are displaced in axial direction in relation to one another at a distance,  $\Delta Z$ . This distance is calculated from the formula:

$$\Delta Z = 2 \frac{l}{\tan \psi} \quad (11.55)$$

The axial displacement of the contact points results in a smoother rotation of the driven shaft in the conformal gear pair.

The average number of contact points between the gear and the pinion tooth flanks is doubled in *Novikov/conformal* gear pair of this design.

A gear for the gear system of two pseudo-paths of contact,  $P_{pc,bf}$  and  $P_{pc,by}$ , is shown in Figure 11.33.

When designing *Novikov/conformal* gearing, the gear designer is free to select a favorable smooth curve to shape the inactive portions of tooth profile of the gear and the mating pinion. An arc of the curve has to be entirely located within the interior of the *boundary N – circle* for the tooth addendum, and a corresponding arc of the dedendum must be entirely located within the exterior of the *boundary N – circle* of a radius  $r_N$ .

<sup>27</sup> The distances,  $+l$  and  $-l$ , can be set of different magnitudes,  $+l_1$  and  $-l_2$ , (where the inequality  $|+l_1| \neq |-l_2|$  is valid). This is a proven way to increase the bending strength of the gear teeth.

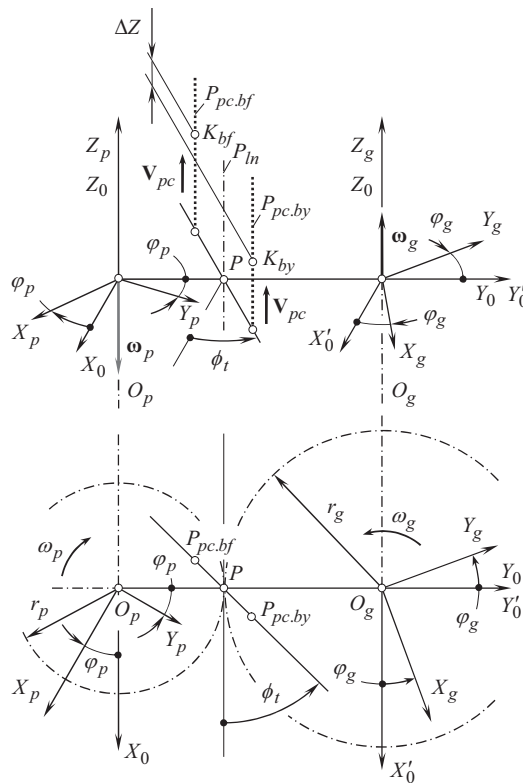


**FIGURE 11.32** Concept of conformal gear system with two pseudo-paths of contact, as proposed by R.V. Fed'akin. (Adapted from: Fed'akin, R.V., *Investigation of Strength of Circular-Arc Gear Teeth*, Ph.D. Thesis, Moscow, Zhukovskiy Aviation Engineering Academy, 1955.) [38], and by R.V. Fed'akin and V.A. Chesnokov. (Adapted from: Pat. No. 182,462, (USSR), *Gearing with Point System of Meshing and Having Multiple Paths of Contact*./R.V. Fed'akin and V.A. Chesnokov, National Cl. 47h, 6, Filed: November 20, 1963, published in B.I. No. 7, 1966.) [125].



**FIGURE 11.33** A gear for the gear system of two *pseudo-paths of contact*,  $P_{pc.bf}$  and  $P_{pc.by}$ .

### 11.2.17 LOCAL AND GLOBAL CONTACT GEOMETRY OF INTERACTING TOOTH FLANKS

The tooth flank of a gear, and that of a mating pinion in *Novikov/conformal* gear pair are assumed to be smooth regular surfaces. The tooth flanks share a common point, which, in fact, is a point of culmination.

Representation of local patches of two interacting tooth flanks,  $\mathcal{G}$  and  $\mathcal{P}$ , in the form of a surface of relative curvature is practical and extensively used kind of surface representation. Analytical description of contact geometry of the interacting tooth flanks is the main purpose of such an approach. Approximation of this kind is perfect in the differential vicinity of the point of contact. It also covers a greater area around the point of contact of the surfaces in cases when the radii of relative curvature are large enough, and significantly exceed the size of the patch of contact. Under such conditions, the contact geometry of the tooth flanks of the gear,  $\mathcal{G}$ , and the pinion,  $\mathcal{P}$ , can be perfectly described by the so-called *ellipse of contact*. The *ellipse of contact* is a three-dimensional (3D) curve whose projection onto the tangent plane through the point of contact of the surfaces resembles an ellipse. For a more accurate approximation of the contact geometry of tooth flanks of a gear,  $\mathcal{G}$ , and of a mating pinion,  $\mathcal{P}$ , in a conformal gear pair, other methods are used (see Appendix E).

Studies of the area of contact and the shape of contact area are commonly based on the assumption that the difference between the profile radii of the tooth flanks,  $\mathcal{G}$  and  $\mathcal{P}$ , is equal to zero.

In the differential vicinity of the point of contact of the tooth flanks,  $\mathcal{G}$  and  $\mathcal{P}$ , the patch of contact is bounded by an ellipse-like curve, that is, this curve can be expressed in terms of second order. However, the radii of relative curvature in the case under consideration are small enough. This is because a convex local patch of the tooth addendum interacts with a saddle-like local patch of the tooth dedendum. The high degree of conformity of the contacting tooth flanks,  $\mathcal{G}$  and  $\mathcal{P}$ , results in small radii of relative curvature. A conclusion can be immediately drawn up from the fact that the outside the differential vicinity of the point of contact, the boundary curve of the patch of contact between the tooth flanks,  $\mathcal{G}$  and  $\mathcal{P}$ , should differ from what is observed in the differential vicinity of the point of contact when the radii of relative curvature are small. This statement is proven analytically.<sup>28</sup>

In a greater area around point of contact of the tooth flanks in high-conformal gears, the terms of the third and of the higher orders rapidly become important compared with the second-order terms, and they give rise to *banana-shaped* gap contours and to the region of potential interference. It is found that a third-order approximation is quite useful in that it gives an analytical expression for the gap, which remains a good approximation of the sufficient distance away from the point of contact so as to provide a good description of these unusual features.

The qualitative results of the investigation of the contact area in *Novikov/conformal* gears are illustrated in Figure 11.34. In Figure 11.34, the shape of the tooth profiles, the shapes and configurations of the contact lines, and the shape of the contact areas, and the directions of their motion, are illustrated for various kinds of *Novikov/conformal* gear pairs.

In Figure 11.34a, an example of  $N_{bf}$  – kind *Novikov/conformal* gear pair is shown. *Novikov/conformal* gears of this design feature one *pseudo-path of contact*,  $P_{pc,bf}$  that is a straight line parallel to the axis of instantaneous rotation of the gears. The *pseudo-path of contact*,  $P_{pc,bf}$ , passes through the contact point,  $K_{bf}$ . The pinion features a concave tooth profile. The pinion is driving the gear with a convex tooth profile. The contact area between the tooth flanks,  $\mathcal{G}$  and  $\mathcal{P}$ , of the gear and of the pinion is bounded by a *banana-like* contour. The wider side of the contact area faces toward the bottom of the gear tooth.

An example of  $N_{by}$  – kind of *Novikov/conformal* gear pair is illustrated in Figure 11.34b. *Novikov/conformal* gears of this design also feature a *pseudo-path of contact*,  $P_{pc,by}$ , that is a straight line

<sup>28</sup> It should be pointed out here that because the teeth of gears in *Novikov/conformal* gearing conform to each other so closely, then the conventional *Hertzian* second-order equation may no longer be adequate.

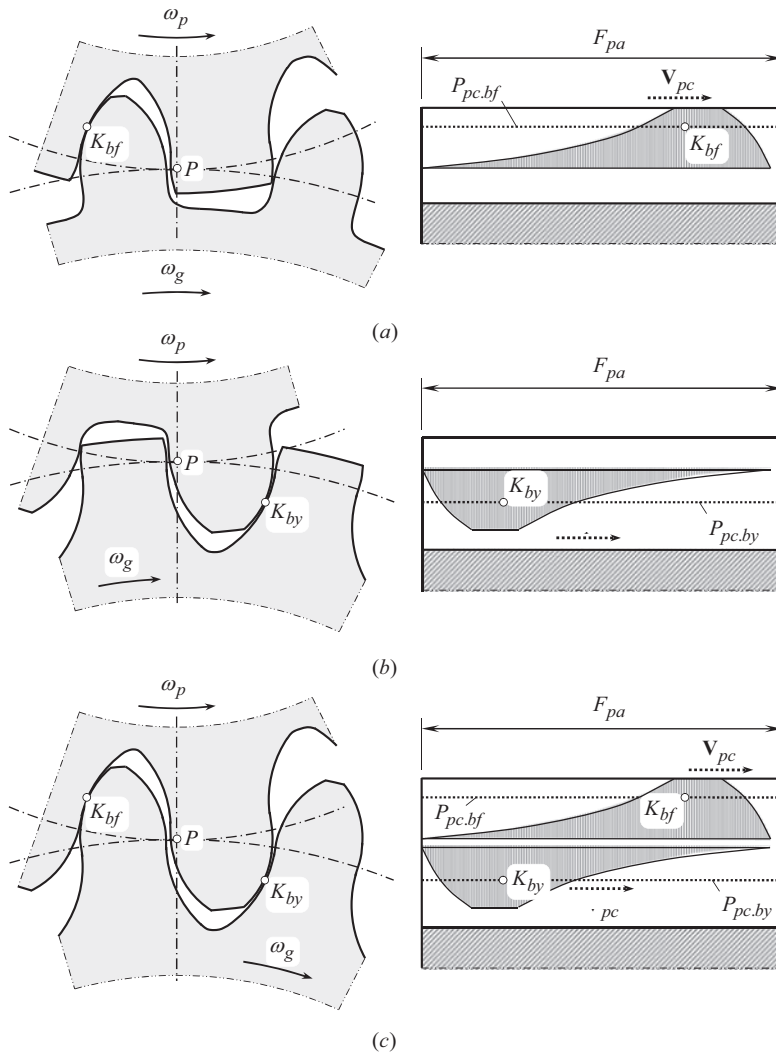


**FIGURE 11.34** Contact patches between the tooth flanks in Novikov/conformal gear pairs: (a) meshing before the pitch point,  $P$ , (b) meshing beyond the pitch point,  $P$ , (c) simultaneous meshing before and beyond the pitch point,  $P$ .

parallel to the axis of instantaneous rotation of the gears. The *pseudo-path of contact*,  $P_{pc,by}$ , passes through the contact point,  $K_{by}$ . The pinion features a convex tooth profile. The pinion is driving the gear with a concave tooth profile. The contact area between tooth flanks,  $\mathcal{S}$  and  $\mathcal{P}$ , of the gear and the pinion is bounded by a *banana-like* contour. The wider side of the contact area faces toward the top land of the gear tooth.

The most extensively used design of Novikov/conformal gears features two *pseudo-paths of contact*,  $P_{pc,bf}$  and  $P_{pc,by}$  (see Figure 11.34c). These *pseudo-paths of contact* are two straight lines parallel to the axis of instantaneous rotation of the gears. The *pseudo-path of contact*,  $P_{pc,bf}$ , passes through the contact point,  $K_{bf}$ , and the *pseudo-path of contact*,  $P_{pc,by}$ , passes through the contact point,  $K_{by}$ . The gear is driven by the pinion. The convex addendum of the gear tooth profile interacts with the concave dedendum of the pinion tooth profile, and the concave dedendum of the gear tooth profile interacts with the convex addendum of the pinion tooth profile. There are two contact areas between the tooth flanks of the gear,  $\mathcal{S}$ , and the pinion,  $\mathcal{P}$ , in this particular case. Both of them are



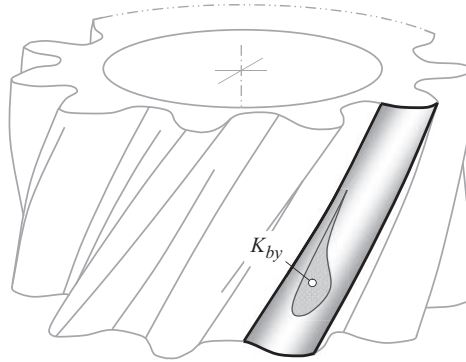


**FIGURE 11.35** An example of an experimentally obtained contact pattern between the tooth flanks of a gear,  $\mathcal{G}$ , and a mating pinion,  $\mathcal{P}$ , in a *Novikov/conformal gearing*. (Adapted from: Krasnoschokov, N.N., Fed'akin, R.V., and Chesnoschokov, V.A., *Theory of Novikov Gearing*, Moscow: Nauka, 1976.) [66].

bounded by *banana-like* contours. The wider sides of the contact areas face toward each other, and both face toward the axis of instantaneous rotation of the gears.

The shape and size of the contact area between the tooth flanks of the gear and the pinion are of importance in the stress analysis of conformal gears.

*Novikov/conformal* gears that have various values of the design parameters, namely, various values of the transverse profile angle,  $\phi_t$ , the pitch helix angle,  $\psi_g$ , the displacement,  $l$  (or  $r_N$ ), and the mismatch of the radii of profile curvature,  $\Delta r$ , were profoundly investigated [66,70]. For the experiments, an experimental rig with a closed load loop was used.

Before the experiments began, every conformal gear pair underwent rotation for a run-in period of time. Then the gears were cleaned of the remains of the lubricant and were treated with a solution of copper sulfate. Finally, the tooth flanks were coated with a layer of silver just a few micrometers thick. Electrolytic technology was used for this purpose. After the gears got prepared for testing, they were placed back in the rig in the same position in relation to each other.

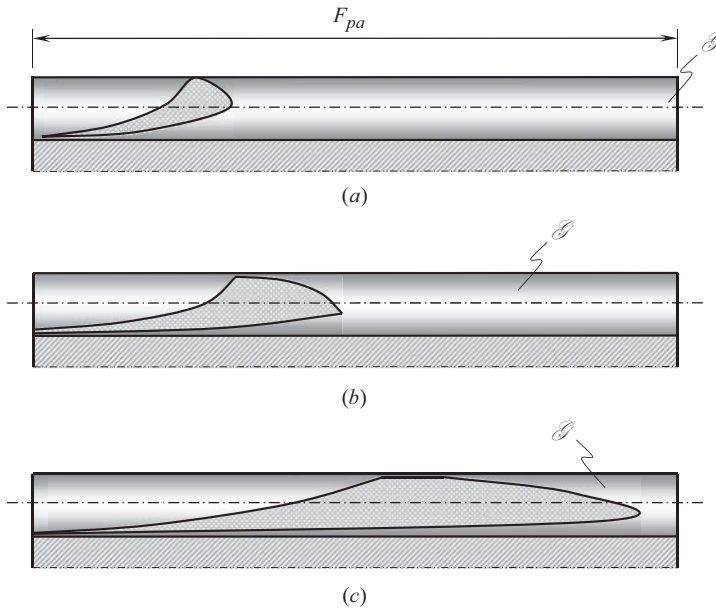
The experiments were carried out under a light torque, which was applied to one gear of the gear pair. The other gear remained stationary. Angular vibrations were applied to one of the gears. The angular magnitude of the vibrations was in the range  $\Delta\varphi \leq 15'$ . An increase in the size of the contact area did not exceed 5%.

Figure 11.35 is a reproduction of the photograph of a *Novikov/conformal* gear pair that has one *pseudo-path of contact*,  $P_{pc,by}$ , and a pitch helix angle  $\psi_g = 30^\circ$ . The *banana-like* contact area is clearly seen in Figure 11.35.

A reduction in the pitch helix angle results in a corresponding increase of the length of the contact area. Examples of various shapes of the contact area in conformal gear pairs that have different pitch helix angles are schematically depicted in Figure 11.36.

The results of research studies similar to the discussed aforementioned ones, align with those obtained by other researchers [2,226], and others.

In comparison to *Novikov/conformal gears*, a helical involute gear pair is schematically depicted in Figure 11.37. The active portion of the line of action,  $LA$ , in the transverse section of the gear pair is a straight-line segment,  $LL$ , through the pitch point,  $P$ . The active portion of the line of action is terminated by points  $L$  and  $L$ . The line of contact,  $LC$ , is a straight-line segment that is entirely located within the tooth flank of the gear. Under an applied load, the straight-line segment,  $LC$ , spreads over a narrow strip, which is the contact area between the interacting tooth flanks of the gear and of the mating pinion. It should be stressed here that the conditions of contact of the involute tooth flanks are not favorable because both the contacting surfaces are convex, and the contact area is narrow and smaller compared to that in conformal gears.



**FIGURE 11.36** The shape of the contact area between the tooth flanks in *Novikov/conformal* gear pair that has pitch helix angles: (a)  $\psi = 30^\circ$ , (b)  $\psi = 20^\circ$ , and (c)  $\psi = 10^\circ$ .

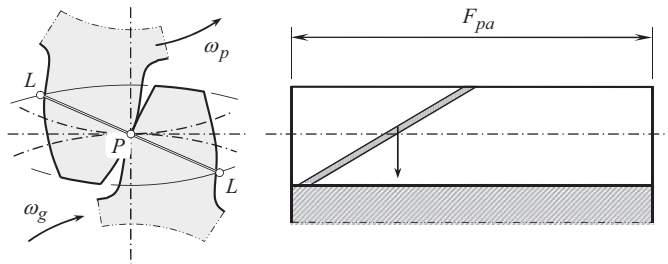


**FIGURE 11.37** Contact area between tooth flanks in a helical involute gear pair.

In addition to the favorable conditions of contact, *Novikov/conformal gears* enable better conditions for lubrication. When the gears rotate, the tooth flanks of the gear and of the mating pinion roll over each other without sliding (or almost without sliding). The speed of the rolling of the contact point in the rolling motion significantly exceeds the linear speed of rotation of the gears. Hence, the oil film thickness is larger, and the conditions of lubrication are significantly better.

### 11.2.18 THE POWER DENSITY IN *NOVIKOV/CONFORMAL* GEARING

Later on, it became clear that the use of *Novikov/conformal* gear pairs helps to increase the so-called, *power density* in the gear pair, that is, *Novikov/conformal* gearing is capable of transmitting a higher power through a smaller volume occupied by the gear pair.

The main goal for the development of *Novikov/conformal gearing*, and later on of *high-conformal gearing* (further,  $H_c$  – gearing, for simplicity) is to increase the power density transmitted in gearsets.

*Novikov/conformal gearing* features *convex-to-concave contact* of the tooth flanks of the gear and of the mating pinion. This particular kind of contact of the tooth flanks enables an increase in

the contact strength of the gear and of the pinion teeth. It is known that *convex-to-concave contact* of machine elements is always stronger compared to their *convex-to-convex contact*. Because of this, numerous attempts were made in the past to design gears with *convex-to-concave contact* of the tooth flanks of the gear and the mating pinion.

### 11.3 HIGH-CONFORMAL GEARING

The power being transmitted by a gear pair is one of the most important parameters for the evaluation of how well, or how badly a particular gear pair has been designed and manufactured. Gear pairs of various designs are capable of transmitting different maximum values of torque and rotation, that is, different amount of power. For the purpose to compare the efficiency of gear pairs of different designs, a parameter, the so-called *power density*<sup>29</sup> is used. An increase by all possible means of the power density in a gear pair is an important consideration in the future developments of the theory of gearing as well as in the manufacture and application of gears.

The performance of conformal gear pairs is strongly correlated to the degree of conformity to each other of a gear tooth flank,  $\mathcal{G}$ , and of a mating pinion tooth flank,  $\mathcal{P}$ , at every point of their contact. The more conformal are the tooth flanks,  $\mathcal{G}$  and  $\mathcal{P}$ , at points of their contact, the better the performance of the conformal gear pair, and vice versa.

#### 11.3.1 CONTACT GEOMETRY IN *HIGH-CONFORMAL GEARING*

General consideration of conformal gearing allows a preliminary conclusion that substitution of *convex-to-convex contact* of tooth flanks of a gear and a mating pinion (as it is observed in external involute gearing) by their *convex-to-concave contact* (as it is observed in *Novikov/conformal gearing*) allows an increase of contact strength of the gear teeth. Favorable conditions of contact of the tooth flanks of a gear and a mating pinion are the main anticipated advantages of *Novikov/conformal gear pair* over traditional *involute gearing*. It can be assumed that the higher the degree of conformity, the higher the load-carrying capacity of the contacting tooth flanks,  $\mathcal{G}$  and  $\mathcal{P}$ , and vice versa. This immediately entails a corresponding increase in the power density in the gear pair. The power density is of critical importance for the user of the gears. Therefore, minimum possible mismatch in the curvature of the teeth of a gear and a mating pinion is desirable.

In reality, the tooth flanks of a gear and of a mating pinion in a *Novikov/conformal gear pair* are displaced from their desirable positions. The undesirable displacements are mainly because of the manufacturing errors, and mechanical deflections of the gear teeth, of the shafts, and of the housing, that inevitably occur under the applied load, because of the thermal extensions of the components and so forth. *Novikov/conformal gearing* is sensitive to the tooth flank displacements.

To accommodate for such displacements, certain degree of mismatch in the curvature of a gear and of a mating pinion tooth is required. Small mismatches are not capable of accommodating for the linear and the angular displacements of the gear teeth. However, as the mismatch increases, the contact stresses also increase. High contact stress may lead to various forms of surface failures such as heavy wear, pitting, or scuffing damage. Therefore, a minimum degree of mismatch in the curvature of the teeth of a gear and of a mating pinion is required to be determined in order to make a *Novikov/conformal gearing* workable. Otherwise, one of two scenarios may be observed:

**First**, the gear pair is capable of absorbing the inevitable displacements of the tooth flanks, but the degree of conformity of the contacting tooth flanks is insufficient for the high load-carrying capacity of the gear pair

<sup>29</sup>The *power density* is defined as the ratio of power being transmitting by a gear pair to the volume occupied by the gear pair. It is customary to define the *power density* as the ratio of power being transmitting by a gear pair to the weight of the gear pair. In this second case, the *power density* is also referred to as the *power-to-weight ratio*.

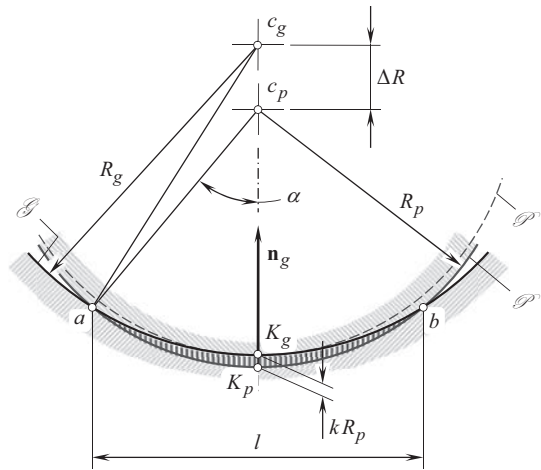


**FIGURE 11.38** Section of tooth flanks,  $\mathcal{G}$  and  $\mathcal{P}$ , of a Novikov/conformal gear pair by a plane through contact point: The plane is perpendicular to the trace of contact point across the tooth flanks,  $\mathcal{G}$  and  $\mathcal{P}$ .

**Second**, the gear pair features a sufficient degree of conformity of the tooth flanks but is not capable of accommodating the tooth flanks displacements.

In both cases, the gear pair has no chance of being successfully used in practice. In the best-case scenario, the gear pair is capable of absorbing the inevitable displacements of the tooth flanks, and, at the same time, it features at least the minimum degree of conformity of the tooth flanks of the gear and the mating pinion.

For better understanding of the *trade-off* between the load-carrying capacity of conformal gearing, and between its capabilities being reasonably insensitive with respect to the tooth flank displacements, it is instructive to discuss the following simplified schematic.

At every instant of time, the tooth flanks in a Novikov/conformal gear pair contact each other at least at one point. When the gears rotate, the point of contact traces a line over each of the two interacting tooth flanks,  $\mathcal{G}$  and  $\mathcal{P}$ . In reality, these lines are helices of opposite hands, and of equal axial pitch. As a result, at every contact point,  $K$ , the contact line of the gear,  $CL_g$ , and the contact line of the pinion,  $CL_p$ , share the common tangential straight line,  $\mathbf{t}_{CL}$ .

Let's consider a section of the tooth flanks,  $\mathcal{G}$  and  $\mathcal{P}$ , by a plane through the contact point,  $K$ . The plane is constructed so as to be perpendicular to the common tangential straight line,  $\mathbf{t}_{CL}$ . The constructed section of the tooth flanks is schematically shown in Figure 11.38.

The section of the gear tooth flank is labeled  $\mathcal{G}$ . Within the differential vicinity of the point of contact, the radius of curvature of the curve,  $\mathcal{G}$ , is labeled  $R_g$ . The radius,  $R_g$ , is of a negative value ( $R_g < 0$ ), as the tooth profile is concave.

The section of the pinion tooth flank before the load is applied is labeled  $\mathcal{P}^*$ . That same section,  $\mathcal{P}^*$ , is labeled  $\mathcal{P}$  after the load is applied, and the pinion tooth flank is slightly penetrated into the gear tooth flank. It is assumed here that within the differential vicinity of the point of contact, the radii of curvature of the curves,  $\mathcal{P}^*$  and  $\mathcal{P}$ , are of the same value,  $R_p$ . The radius of curvature is of a positive value ( $R_p > 0$ ), as the pinion tooth profile is convex.

In the initial position of the tooth profiles,  $\mathcal{G}$  and  $\mathcal{G}$ , the contact point is labeled  $K_g$ . After the load is applied and the tooth flanks interfere into each other, the contact point is labeled  $K_p$ .

The tooth profiles,  $\mathcal{G}$  and  $\mathcal{G}$ , intersect each other at two points,  $a$  and  $b$ . The distance,  $l$ , somehow correlates with the actual value of degree of conformity of the tooth profiles of the radii  $R_g$  and  $R_p$ . The greater the distance,  $l$ , the higher the degree of conformity of the tooth flanks, and vice versa.

The distance,  $l$ , between points  $a$  and  $b$  can be expressed in terms of the radii of curvature,  $R_g$  and  $R_p$ , and the displacement,  $k$ :

$$l = 2 R_p \sin \alpha \quad (11.56)$$

For the calculation the angle  $\alpha(R_g, R_p, k)$ , the following formula is derived:

$$\alpha = \cos^{-1} \left( \frac{R_p^2 - R_g^2 + (R_p + R_g - k R_p)^2}{2 R_p (R_p + R_g - k R_p)} \right) \quad (11.57)$$

Derivation of Eq. (11.57) is based on the law of cosines.

The angle  $\alpha$  in Eq. (11.56) depends on the actual values of the radii of curvature,  $R_g$  and  $R_p$ , as well as on the displacement  $k$ , as it follows from Eq. (11.57).

For the convenience of the further analysis of the plane section (see Figure 11.38), all the design parameters in Eq. (11.57) are normalized by the pinion radius  $R_p$ . The normalized design parameters are designated as follows:

$$\frac{R_p}{R_p} = 1 \quad (11.58)$$

$$\frac{R_g}{R_p} = K \quad (11.59)$$

$$\frac{k R_p}{R_p} = k \quad (11.60)$$

The angle  $\alpha$  can be expressed in terms of the normalized design parameters as:

$$\alpha = \cos^{-1} \left( \frac{1 - K^2 + (1 + K - k)^2}{2(1 + K - k)} \right) \quad (11.61)$$

The function  $l = l(k, K)$  is valid for both, the *convex-to-convex* as well as to *convex-to-concave* contacts of tooth flanks of the gear,  $\mathcal{G}$ , and the pinion,  $\mathcal{P}$ . For conformal gearing, *convex-to-concave* contact of tooth flanks is of interest.

In Figure 11.39, a three-dimensional plot of the function  $l = l(k, K)$  is shown. This plot is constructed for *convex-to-concave* contacts of tooth flanks of the gear,  $\mathcal{G}$ , and the pinion,  $\mathcal{P}$ .

The performed analysis of the 3D-plot allows the following conclusions.

Sections of the surface  $l = l(k, K)$  by the set of planes  $k_i = \text{Const}$  (see Figure 11.39) are represented by curves that feature asymptotes. For a particular curve,  $k_i = \text{Const}$ , shown in Figure 11.39 in the bold line, the axis  $\delta_{\text{cnf}}$  and the straight line  $\delta_{\text{cnf}} = 1$  are these asymptotes.

The greatest possible degree of mismatch in the curvature of the teeth of a gear and a mating pinion corresponds to an infinite value of the parameter  $K \rightarrow -\infty$ . An interval of variation in the parameter  $K$  (that starts from  $-\infty$  and goes up to approximately  $K = -2$ ) can conveniently accommodate for any desirable displacement of the tooth flanks,  $\mathcal{G}$  and  $\mathcal{P}$ , from their correct location. However, within the interval  $-\infty < K < -2$  of variation of the parameter  $K$ , an increase in the degree of conformity of the tooth profiles,  $\mathcal{G}$  and  $\mathcal{P}$ , is negligibly small. Within this interval of variation of the parameter  $K$ , the load-carrying capacity of a conformal gear pair remains approximately in the same range. Therefore, the use of just the *convex-to-concave contact* of tooth flanks of the gear and of the pinion gives limited improvement to the load-carrying capacity of the gear pair. For the *convex-to-concave contact*, an additional requirement needs to be met in order to significantly improve the load-carrying capacity of a conformal gear pair.

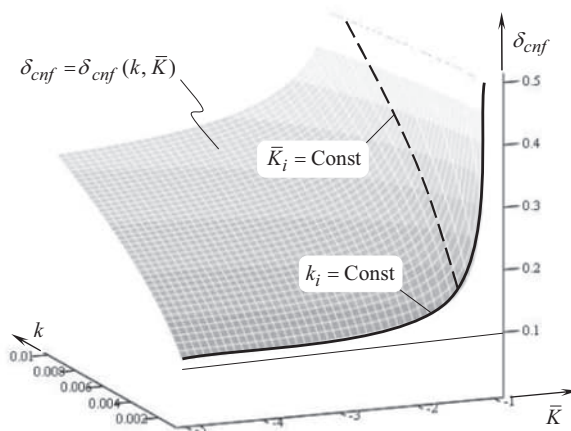


**FIGURE 11.39** Three-dimensional plot of the function  $\delta_{cnf} = \delta_{cnf}(k, \bar{K})$  constructed for *convex-to-concave* contact of the tooth flanks of a gear,  $\mathcal{G}$ , and of a mating pinion,  $\mathcal{P}$ , in *Novikov/conformal* gear pair.

On the other hand, even a small alteration in the actual value of the parameter  $K$  within the interval  $-2 < K < -1$  results in a significant increase in the degree of conformity of the tooth profiles,  $\mathcal{G}$  and  $\mathcal{P}$ . This immediately entails a corresponding increase in the load-carrying capacity of the gear pair.

### 11.3.2 HIGH-CONFORMAL PARALLEL-AXES GEARING

High-conformal gears feature *convex-to-concave contact* of tooth flanks of a gear and of a mating pinion similar to that in *Novikov-conformal gearing*.<sup>30</sup> In addition, the degree of conformity at point of contact of tooth flanks of a gear and of a pinion in *high-conformal gearing* exceeds certain critical value of the parameter  $K$ , namely, it exceeds the threshold.

In the aforementioned example (see Figure 11.39), the value of the parameter  $K$  (i.e., the value of  $K \approx -2$ ) can be referred to as a critical value (the threshold) for the parameter  $K$ , namely, it can be referred to as  $K_{cr}$ . This allows one to distinguish between *Novikov-conformal gearing* (for which  $-\infty < K < K_{cr}$ ), and *high-conformal gearing* (for which  $K_{cr} \leq K < -1$ ). Because of the favorable conditions of contact between the tooth flanks, high-conformal gears allow a higher power density when transmitting power through the gear pair.

<sup>30</sup> The concept of *Novikov gearing* was not completely understood by the majority of gear experts in the years immediately following the Prof. *M.L. Novikov* invention. Lack of information on the new gear system was the root cause for this. Later on, after the concept of *Novikov gearing* was properly disclosed and made available for use by western engineers, the principal differences between *Novikov gearing* [123] and *Wildhaber gearing* [101] retained not clear to the majority of gear experts all around the world. The essence of *Novikov gearing* is disclosed in the USSR patent [123], as well, as in Prof. *M.L. Novikov* doctoral thesis [68], and monograph [91], whereas the essence of *Wildhaber gearing* is disclosed in the U.S. patent [101]. A comparison of the principal features of the *Novikov gear system* claimed in Prof. *M.L. Novikov* patent [123] and shortly after discussed in Prof. *M.L. Novikov* doctoral thesis [68,91], and the principal features of *Wildhaber gear system* claimed in the patent [101], makes it easy to distinguish between the two. Unfortunately, the beginners and less experienced gear specialists often make no difference between *Novikov gear system* [123] and the *Wildhaber gear system* [101]. Many of them still loosely refer to *Novikov gearing* as to *W-N gearing*. The term *W-N gearing* is completely incorrect.



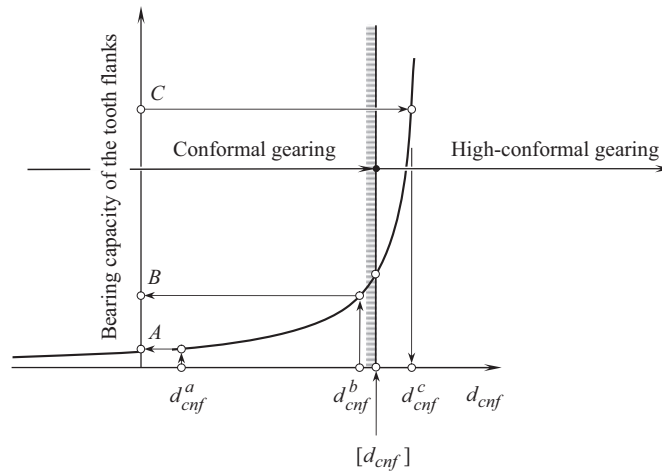


**FIGURE 11.40** Impact of the degree of conformity,  $\delta_{cnf}$ , at current point of contact of the gear tooth flank,  $\mathcal{G}$ , and of the pinion tooth flank,  $\mathcal{P}$ , onto the bearing capacity of the tooth flanks.

Without going into details of this analysis, it is clear that high-conformal gears require tighter tolerances for any displacements of the tooth flanks of a gear,  $\mathcal{G}$ , and of a mating pinion,  $\mathcal{P}$ , from their desirable location and orientation. This relates not just to the tolerances for the manufacturing errors, but to any and all displacements caused by thermal extension of the gearset, elastic deflection under operating load, and so forth. Otherwise, there could be no future for a high-conformal gear system. It also should be clear to the reader that there exist certain constraints on the maximum displacements under which *high-conformal gearing* is physically possible. If the actual values of the displacements are too large, no *high-conformal gearing* is possible at all.

The areas of existence of *conformal*, and of *high-conformal gearing*, are schematically illustrated in Figure 11.40.

The performed analysis of the 3D plot, shown in Figure 11.39, can be extended, although the extension is a bit aside from the mainstream of the subject of this book.

Consider sections of the surface  $l = l(k, K)$  by the set of planes  $K_i = \text{Const}$  (see Figure 11.39). An example of such a section is shown by the bold dashed line. For *high-conformal* gears, the parameter,  $K_i$ , for these lines falls into the interval  $K_{cr} \leq K_i < -1$ . The permissible degree of mismatch in the curvature of the teeth in *high-conformal* gears is smaller compared to that in conformal gears. Without going into the details of this analysis, it is important to point out here that the tooth profiles in high-conformal gears feature *convex-to-concave contact*, and the degree of mismatch in the curvature is small. Small degree of mismatch in the curvature allows the conclusion that the well-known *Hertz formula* is not applicable for the calculation of contact stress in high-conformal gears.

**First**, the *Hertz formula* for the calculation of contact stress was derived [48] under an assumption that the dimensions of the contact patch between two contacting surfaces are significantly smaller in comparison to the corresponding radii of curvature of the surface of relative curvature. This requirement is violated by the aforementioned features in *high-conformal* gears: A small degree of mismatch in the curvature of the teeth profiles in *high-conformal* gears results in that the size of the contact patch becomes comparable with the corresponding radii of curvature of the surface of relative curvature, which is not allowed.

**Second**, the *Hertz formula* for the calculation of contact stress was derived [48] for the cases of contact of two bodies of a simple geometry. Sphere-to-plane, sphere-to-sphere, and cylinder-to-plane are good examples of part shapes in relation to which the *Hertz formula* is valid.

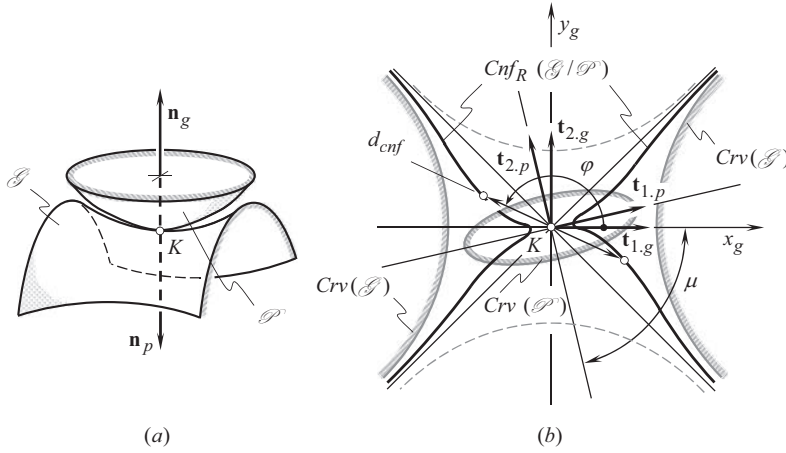


**FIGURE 11.41** Example of the indicatrix of conformity,  $Cnf_R(\mathcal{G}/\mathcal{P})$ , at point of contact of tooth flanks,  $\mathcal{G}$  and  $\mathcal{P}$ , of a gear and of a mating pinion: (a) local patches of the tooth flanks,  $\mathcal{G}$  and  $\mathcal{P}$ , in contact, and (b) the indicatrix of conformity,  $Cnf_R(\mathcal{G}/\mathcal{P})$ , at point of contact,  $K$ , of the local patches of the surfaces  $\mathcal{G}$  and  $\mathcal{P}$ .

Generally speaking, to make the *Hertz formula* valid, the alignment of the principal directions of the contacting surface is a must. At point of contact, the unit tangent vectors of the principal directions of the gear tooth flank are denoted by  $\mathbf{t}_{1.g}$  and  $\mathbf{t}_{2.g}$ . Similarly, at the same point the unit tangent vectors of the principal directions of the pinion tooth flank are denoted by  $\mathbf{t}_{1.p}$  and  $\mathbf{t}_{2.p}$ . The *Hertz formula* is valid in either of the following cases:

- $\mathbf{t}_{1.g}$  is aligned with  $\mathbf{t}_{1.p}$ , and  $\mathbf{t}_{2.g}$  is aligned with  $\mathbf{t}_{2.p}$ , or
- $\mathbf{t}_{1.g}$  is aligned with  $\mathbf{t}_{2.p}$ , and  $\mathbf{t}_{2.g}$  is aligned with  $\mathbf{t}_{1.p}$

The greater the misalignment of the principal directions, the greater the deviation in the calculated values of contact stress from their actual values, and vice versa.

The functional portions of the tooth flanks in *high-conformal gearing* are surfaces that feature complex geometry. For these surfaces, the requirement of alignment of the principal directions  $\mathbf{t}_{1.g}$ ,  $\mathbf{t}_{2.g}$  and  $\mathbf{t}_{1.p}$ ,  $\mathbf{t}_{2.p}$  is not fulfilled. This is the second reason why the *Hertz formula* is not valid for the calculation of contact stress between the tooth flanks in *high-conformal gearing*.

*Indicatrix of conformity* [either of the kind  $Cnf_R(\mathcal{G}/\mathcal{P})$ , or of the kind  $Cnf_k(\mathcal{G}/\mathcal{P})$ ], can be used for the analytical description of contact geometry of the interacting tooth flanks,  $\mathcal{G}$  and  $\mathcal{P}$ , in a gear pair (see Appendix E). These characteristic curves can be also used to construct the contour of the contact patch between two gears in *high-conformal gearing*. An example of the indicatrix of conformity,  $Cnf_R(\mathcal{G}/\mathcal{P})$ , at point of contact of tooth flanks,  $\mathcal{G}$  and  $\mathcal{P}$ , of a gear and of a mating pinion is shown in Figure 11.41. This characteristic curve is helpful when solving contact stress problem in *high-conformal gearing*.

Based on the aforementioned discussion, *high-conformal gearing* can be characterized by the following features, each of which is important and, moreover, all of them are sufficient to refer to this gear system as to *high-conformal gearing*:

- The transverse contact ratio is identical to zero ( $m_p \equiv 0$ )
- The total contact ratio,  $m_t$ , is equal to the face contact ratio,  $m_F$ , and is greater than one ( $\bar{m} = m_t = m_F > 1$ )
- The tooth profile of one member of the gear pair is convex, whereas that of the mating gear is of a concave geometry



- The convex tooth profile of one member of the gear pair is entirely located within the interior of the *boundary N – circle*, whereas the concave tooth profile of the other member of the gear pair is entirely located within the exterior of the *boundary N – circle*
- The difference between the magnitudes of the radii of curvature of the concave tooth profile and of the convex tooth profile in the gear pair is equal to, or smaller than a specified threshold for the degree of conformity, beyond which the higher degree of conformity of the interacting tooth profiles contributes much to the bearing capacity of the gear pair

*Novikov/conformal gearing* and *high-conformal gearing* share the first four features. *High-conformal gearing* differs from *Novikov/conformal gearing* only due to the latter of the aforementioned features. The difference between the radii of curvature is required to make the gear pair capable of accommodating the tooth flanks displacements due to the manufacturing errors, the deflections under the operating load, and the deflections due to heat extension as well as all the displacements.

The following should be noticed when comparing *high-conformal gearing* (as well as *Novikov/conformal gearing*) with *involute gearing*:

- The proposed by *L. Euler*, spur *involute gearing* features a transverse contact ratio,  $m_p$ , greater than one ( $m_p > 1$ ), a zero face contact ratio ( $m_F = 0$ ), and the total contact ratio,  $m_t$ , equal to the transverse contact ratio ( $m_t = m_p > 1$ ). Later on, the concept of spur involute gearing was enhanced to include the concept of helical involute gearing that features a face contact ratio greater than zero ( $m_F > 0$ ), and a total contact ratio  $\bar{m} = m_t = m_p + m_F > 1$ . [*involute (Euler) gearing* (or just *Eu – gearing*, for simplicity):  $m_p > 1$  and  $m_F = 0$  ],
- *Novikov/conformal gearing* features a zero transverse contact ratio ( $m_p \equiv 0$ ), a face contact ratio greater than one ( $m_F > 1$ ), and the total contact ratio,  $m_t$ , equal to the face contact ratio ( $\bar{m} = m_t = m_F > 1$ ). Later on, the concept of *Novikov/conformal gearing* was enhanced to include the concept of *high-conformal gearing* that, in addition, features a degree of conformity at point of contact of the interacting tooth flanks of a gear and a mating pinion equal to, or larger than a predetermined threshold [*Novikov gearing*:  $m_p \equiv 0$  and  $m_F > 1$ ].

As all possible combinations of the values of the transverse contact ratio,  $m_p$ , and the face contact ratio,  $m_F$ , are covered by either *involute (Euler) gearing*, or by *Novikov gearing*, it can be concluded from that that no new gear system can be developed based on various combinations of the contact ratios.<sup>31</sup>

The term *high-conformal gearing* differs from the term *Novikov/conformal gearing*. *Novikov/conformal gearing* features a *convex-to-concave contact* of the tooth flanks of the gear and of the pinion, and a particular configuration of the tooth flanks in relation to the line of action, under which the transverse contact ration of a gear pair is identical to zero ( $m_p \equiv 0$ ) and the face contact ratio is always greater than one ( $m_F > 1$ ). *high-conformal gearing* features, in addition, a certain pre-specified degree of conformity at point of contact,  $K$ , of the tooth flanks  $\mathcal{S}$  and  $\mathcal{P}$ . The minimum diameter,  $d_{cnf}^{\min}$ , of the indicatrix of conformity,  $Cnf(\mathcal{S}/\mathcal{P})$ , at point of contact,  $K$ , of the tooth flanks,  $\mathcal{S}$  and  $\mathcal{P}$ , can be used as a quantitative measure of the degree of conformity of the interacting tooth flanks. The degree of conformity of the tooth flanks of the gear,  $\mathcal{S}$ , and of the mating pinion,

<sup>31</sup> It is evident that the *Helical Gearing* proposed by *E. Wildhaber* does not meet the requirements of *Euler gearing*, nor does it meet the requirements of *Novikov gearing*. The widely adopted terminology *Wildhaber-Novikov gearing* clearly indicates poor understanding of the kinematics and the geometry of both gear systems, namely, of *Novikov gearing*, and of *Helical Gearing* (proposed by *E. Wildhaber*). It is important to eliminate the incorrect terminology from use among proficient gear experts. The invention by Prof. *M.L. Novikov* must be referred to as *Novikov gearing*, and *Wildhaber gearing* must be referred to as *Wildhaber gearing* (or just the *Helical Gearing*, as it was proposed by *E. Wildhaber*). There must be no place to incorrect terminology like *Wildhaber-Novikov gearing* or *W-N gearing*.

$\mathcal{P}$ , exceeds a threshold beyond which a significant increase in the bearing capacity of the interacting tooth flanks is observed. Schematically, this property of *high-conformal gearing* is illustrated in Figure 11.40.

For a certain degree of conformity,  $d_{cnf}^a$ , at point of contact of the tooth flanks,  $\mathcal{S}$  and  $\mathcal{P}$ , the bearing capacity of the tooth flanks can be evaluated by a number,  $A$ . If the degree of conformity of the tooth flanks is increased from  $d_{cnf}^a$  to a value of  $d_{cnf}^b$ , an insignificant increase in the bearing capacity of the tooth flanks from a number  $A$  to a number  $B$  occurs. The increase in the bearing capacity is insignificant in the case under consideration, as both the degrees of conformity,  $d_{cnf}^a$  and  $d_{cnf}^b$ , are smaller compared to the threshold  $[d_{cnf}]$ , beyond which a significant increase in the bearing capacity of the tooth flanks,  $\mathcal{S}$  and  $\mathcal{P}$ , occurs.

Let us assume that the degree of conformity,  $d_{cnf}^c$ , is greater than the threshold,  $[d_{cnf}]$ . When the inequality  $d_{cnf}^c > [d_{cnf}]$  is valid, the bearing capacity of the tooth flanks of the gear,  $\mathcal{S}$ , and the pinion,  $\mathcal{P}$ , grows fast.

In *high-conformal gearing*, the inequality  $d_{cnf}^c \geq [d_{cnf}]$  is always observed.

### 11.3.3 ON THE ACCURACY REQUIREMENTS FOR HIGH-CONFORMAL PARALLEL-AXES GEARING

As it was discussed in the previous sections of the book, at point of contact of the tooth flanks, *high-conformal gearing* features a degree of conformity,  $d_{cnf}$ , that exceeds a certain critical value of the degree of conformity,  $[d_{cnf}]$ , namely, it exceeds a threshold for the degree of conformity ( $d_{cnf} \geq [d_{cnf}]$ ). This condition can be attained if the tolerances for the accuracy of the gear and of the pinion, along with the tolerance for the accuracy of the gear's configuration, are tightened.

In reality, none of the design parameters of a gear pair can be kept with a zero deviation: all of the design parameters of a gear pair fall into a corresponding tolerance band for accuracy. For practical needs, it is important to estimate the influence of variation of the actual values of the design parameters on the performance of a *high-conformal gearing* gear pair.

In a *high-conformal* gear pair, the linear displacements of the gear and the pinion in relation to one another can be expressed in terms of the three components along the axes of a *Cartesian* reference system. The reference system can be associated with the gear pair so as to minimize the total number of the components to be considered when calculating the design parameters of the gear and the pinion. If one of the axes is parallel to the axis of instantaneous rotation,  $P_{ln}$ , and another one is pointed along the centerline,  $\mathfrak{t}$ , then the total linear displacement of the gear and the pinion in relation to one another is equal to the actual value of variation,  $\Delta C$ , of the center-distance,  $C$ .

In Figure 11.42 (see the upper portion of Figure 11.42), a geometrically accurate *high-conformal* gear pair is schematically shown. Here, the center-distance is equal to a certain value,  $C$ . In reality, because of the manufacturing errors, and due to the other reasons, the actual value of the center-distance,  $C^*$ , differs from  $C$  (see the lower portion of Figure 11.42). The alteration of the center-distance inevitably entails the corresponding changes to the diameters,  $d_{g.pc}$  and  $d_{p.pc}$ . The distance,  $r_N$ , of the pseudo-path of contact,  $P_{pc}$ , from the axis of instantaneous rotation,  $P_{ln}$  (in Figure 11.42, the axis of instantaneous rotation,  $P_{ln}$ , is projected into the pitch point,  $P$ ), can be expressed in terms of the diameters,  $d_{g.pc}$  and  $d_{p.pc}$ . The actual values of the diameters,  $d_{g.pc}$  and  $d_{p.pc}$ , are labeled as  $d_{g.pc}^*$  and  $d_{p.pc}^*$ , correspondingly.

The operating transverse pressure angle also alters from its nominal value,  $\phi_t$ , to the actual value,  $\phi_t^*$ .

The changes to the center-distance as well as to the transverse pressure angle, need to be considered when designing *high-conformal gear pair*.

In the lower portion of Figure 11.42:

$$\frac{PO_p^*}{PO_g^*} = \frac{d_{b,p}}{d_{b,g}} \quad (11.62)$$

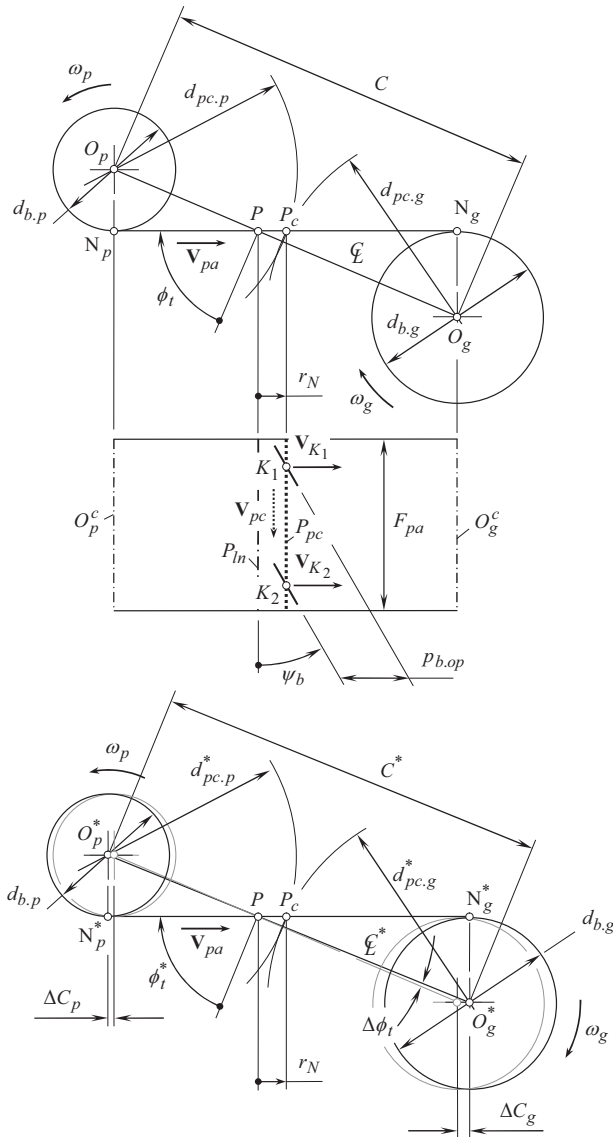


**FIGURE 11.42** Variation of the center-distance,  $C$ , and the operating transverse pressure angle,  $\phi_t$ , in real parallel-axes *high-conformal* gearing.

and

$$PO_g^* + PO_p^* = C^* \quad (11.63)$$

From these equations, the following expressions can be derived for the calculation of the parameters  $PO_g^*$  and  $PO_p^*$ :

$$PO_g^* = C^* \frac{d_{b,g}}{d_{b,g} + d_{b,p}} \quad (11.64)$$

$$PO_p^* = C^* \frac{d_{b,p}}{d_{b,g} + d_{b,p}} \quad (11.65)$$

Commonly, the actual value of the center-distance,  $C^*$ , is not known. However, the tolerance,  $[\Delta C]$ , for the accuracy of the center-distance is known. Therefore, in the calculations, the actual center-distance,  $C^*$ , is substituted with the sum  $C^* = C + [\Delta C]$ . It should be noticed here that the tolerance  $[\Delta C]$  is a signed value. With that said, Eqs. (11.64) and (11.65) cast into:

$$PO_g^* = (C + [\Delta C]) \cdot \frac{d_{b,g}}{d_{b,g} + d_{b,p}} \quad (11.66)$$

$$PO_p^* = (C + [\Delta C]) \cdot \frac{d_{b,p}}{d_{b,g} + d_{b,p}} \quad (11.67)$$

The calculated values of the parameters,  $PO_g^*$  and  $PO_p^*$ , yield the formula for the calculation of the operating transverse pressure angle,  $\phi_t^*$ :

$$\phi_t^* = \sin^{-1} \frac{d_{b,g}}{PO_g^*} = \sin^{-1} \frac{d_{b,p}}{PO_p^*} \quad (11.68)$$

Equation (11.68) yields the calculation of the design parameters,  $PN_g^*$  and  $PN_p^*$ :

$$PN_g^* = (C + \Delta C) \cdot \frac{d_{b,g}}{d_{b,g} + d_{b,p}} \cos \phi_t^* \quad (11.69)$$

$$PN_p^* = (C + \Delta C) \cdot \frac{d_{b,p}}{d_{b,g} + d_{b,p}} \cos \phi_t^* \quad (11.70)$$

Once the operating transverse pressure angle, and the design parameters,  $PN_g^*$  and  $PN_p^*$ , are known, then the diameters,  $d_{pc,g}^*$  and  $d_{pc,p}^*$ , can be calculated from the equations:

$$d_{pc,g}^* = \sqrt{d_{b,g}^2 + 4 \cdot (PN_g^* - r_N)^2} \quad (11.71)$$

$$d_{pc,p}^* = \sqrt{d_{b,p}^2 + 4 \cdot (PN_p^* + r_N)^2} \quad (11.72)$$

A change in the length of the center-distance,  $C$ , results in that that the tooth flanks,  $\mathcal{G}$  and  $\mathcal{P}$ , of the gear and the pinion interact with one another not at involute tooth points within each of them, instead, they contact at points within the tooth profiles that are originally designed with the intent to not be involved into the transmission of the rotation. Fundamental laws of gearing are inevitably violated in such a scenario. Hence, even properly designed and manufactured gears cannot be engaged in a proper mesh, and cannot perform properly.

As an example, consider the influence of variation of the center-distance alteration,  $\Delta C$ , onto the required change of radii of curvature of the gear and the pinion tooth profiles.

Figure 11.43 illustrates a portion of a concave gear tooth profile,  $\mathcal{S}^*$ , in a local vicinity of the *involute tooth point*. The *involute tooth point* coincides in Figure 11.43 with the projection of the pseudo-path of contact,  $P_{pc}$ , in the gear pair onto the plane of the drawing of Figure 11.43. The tooth profile,  $\mathcal{S}^*$ , corresponds to a case when the actual center-distance,  $C^*$ , is greater than the desirable center-distance,  $C$ , and the difference equals  $\Delta C$ . For the comparison, the original concave gear tooth profile,  $\mathcal{S}$ , constructed for zero displacement of the gears, is also shown in Figure 11.43.

As the actual linear displacement is commonly unknown, the tolerance,  $[\Delta C]$ , for this displacement is considered instead.



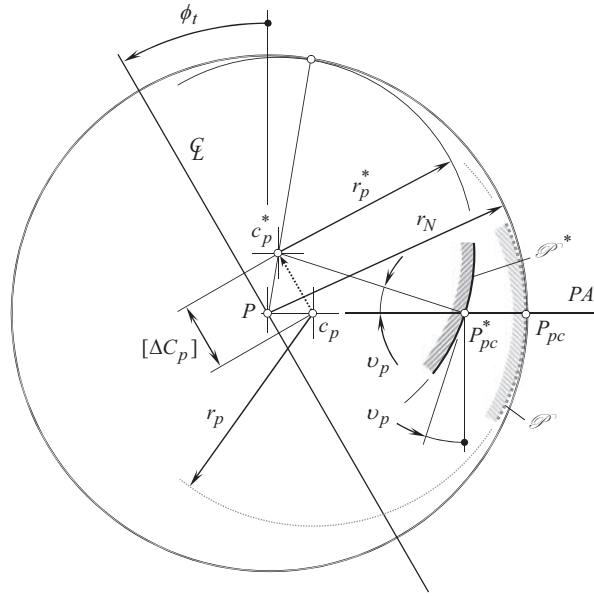


**FIGURE 11.44** Configuration of the convex pinion tooth profile,  $\mathcal{P}^*$ , in a *high-conformal* gear pair with an altered,  $[\Delta C]$ , center-distance,  $C$ .

It is clear now that the inequality  $r_g^* > r_g$  is valid.

The original concave gear tooth profile,  $\mathcal{S}$ , intersects the plane of action,  $PA$ , at a right angle. This is because the *involute tooth point* of the gear and the *involute tooth point* of the pinion make contact at culmination. Due to this, all three fundamental laws of gearing are met when the displacement is zero ( $[\Delta C] = 0$ ).

The concave gear tooth profile,  $\mathcal{S}^*$ , intersects the plane of action,  $PA$ , at a certain angle. The angle between the perpendicular to the plane of action,  $PA$ , and the tangent to the profile  $\mathcal{S}^*$  is designated as  $\nu_p$ . The smaller the angle,  $\nu_p$ , the better.<sup>32</sup>

An equation, similar to Eq. (11.76), can be derived for the convex pinion tooth profile,  $\mathcal{S}^*$ , (see Figure 11.44):

$$r_p^* = r_p - \sqrt{[\Delta C_p]^2 + (c_p P)^2 - 2[\Delta C_p](c_p P) \sin \phi_t} \quad (11.77)$$

The degree of conformity,  $d_{cnf}^{\min}$ , in the real *high-conformal gearing* needs to be calculated taken into account Eqs. (5.21) and (5.22). The calculated value of the minimum diameter,  $d_{cnf}^{\min}$ , is then compared with the threshold,  $[d_{cnf}^{\min}]$ . If the inequality  $d_{cnf}^{\min} < [d_{cnf}^{\min}]$  is observed, then the gearing can be referred to as *high-conformal gearing*. Otherwise, when the inequality  $d_{cnf}^{\min} > [d_{cnf}^{\min}]$  is valid, the gearing represents an example of conformal gear pair, and not *high-conformal gearing*.

<sup>32</sup> In involute gearing, when the center-distance alters, the contact point between the tooth flanks of a gear and of a mating pinion travels along the involute tooth profiles. Because the tooth profiles are of involute geometry, this makes involute gearing insensitive to the variation of the center-distance. In *Novikov/conformal gearing*, as well as in *high-conformal gearing*, the involute tooth profiles are truncated to the *involute tooth point*. When the center-distance changes, the contact point between the tooth flanks of the gear and the pinion travels along the tooth profiles that are designed so as to not to be engaged in gear mesh. The later makes both, *Novikov/conformal* and *high-conformal gearing* sensitive to the variation of the center-distance.

When the linear displacement,  $[\Delta C]$ , can take place in both directions, that is,  $[\Delta C^+]$  and  $[\Delta C^-]$ , the analysis is required to be performed for the both values of the displacements,  $[\Delta C^+]$  and  $[\Delta C^-]$ .

In geometrically accurate *high-conformal gearing* (as well as in conformal – *Novikov/conformal gearing*), that is, when the displacement,  $[\Delta C]$ , is zero, then both the angles,  $\nu_g$  and  $\nu_p$ , are zero, and the resultant angle,  $\nu$ , is also of a zero value. In this scenario, all three fundamental laws of gearing can be fulfilled. All possible efforts need to be undertaken to minimize the actual values of the angle  $\nu = \nu_g + \nu_p$ . For example, gearing with a larger radius of the *boundary N – circle*, are less sensitive to the axes misalignment.

Similarly, to the linear displacements of the gears in *high-conformal gearing*, the angular displacements can also be taken into account when designing a gear pair. For this analysis, the parallel-axes *high-conformal* gear pair needs to be considered as a crossed-axes gear pair having  $[\Delta C]$  as the center-distance, and having  $[\Delta \Sigma]$  as the crossed-axes angle [66,70]. Both the design parameters,  $[\Delta C]$  and  $[\Delta \Sigma]$ , are signed values. This particular problem is bulkier compared to the just considered case.

The discussion in this section of the book also indirectly confirms that neither profile modification, nor the longitudinal modification, are permissible for *Novikov/conformal gearing* as well as for *high-conformal gearing*.

## 11.4 ON THE IMPOSSIBILITY OF GENERATING-FINISHING OF GEARS FOR NOVIKOV/CONFORMAL GEARING AND HIGH-CONFORMAL GEARING

It is convenient to begin the discussion of machinability of gears for *Novikov/conformal gearing* as well as for *high-conformal gearing* in generating (continuous-indexing) machining processes, that is, in gear hobbing operation, gear shaping process, worm grinding, shaving operation, and so forth, with the analysis of mesh of the gear to be machined and the gear cutting tool to be used on this particular operation.

### 11.4.1 PECULIARITIES OF THE GEAR-MACHINING MESH

The mesh of a gear to be machined by means of the gear cutting tool is commonly referred to as the *gear-machining mesh*. When machining gears for *Novikov/conformal gearing*, as well as for *high-conformal gearing*, three groups of parameters are required to be synchronizes with one another so as to fulfill all three fundamental laws of gearing [174]. They are as follows:

- a. the design parameters of a gear to be machined
- b. the parameters of the kinematics of the gear-machining process, and
- c. the design parameters of the gear cutting tool to be applied

It is shown earlier (see Figure 11.12) that both *Novikov/conformal gearing* and *high-conformal gearing*, represent a kind of involute gearing. In involute gearing, the line of action,  $LA$ , is a straight line through the pitch point,  $P$ , in the gear pair. This line forms a transverse pressure angle,  $\phi_t$ , with a perpendicular to the centerline,  $\Phi$ . The path of contact,  $P_c$ , in involute gearing aligns with the line of action,  $LA$ . It is instructive to note here that involute gearing is the only kind of parallel-axes gearing for which the path of contact,  $P_c$ , is aligned with the line of action,  $LA$ . Fulfillment of this condition makes involute tooth profiles conjugate to one another. No other shapes of the gear teeth allow for the path of contact,  $P_c$ , be congruent to the line of action,  $LA$ . No other shapes of the gear teeth are conjugate to one another – gear teeth of other geometries can be enveloping to one another, but they can not be conjugate to one another (in gear pairs with conjugate tooth profiles, the tooth profiles are enveloping to each other, but not vice versa: gear pairs with enveloping tooth profiles are not mandatorily conjugate to one another). Therefore, involute gearing is a unique gearing from this perspective.



### 11.4.2 INEVITABLE VIOLATION OF THE FUNDAMENTAL LAWS OF GEARING IN THE GEAR-MACHINING MESH

When either *Novikov/conformal gearing*, or *high-conformal gearing* operates, the only point of the gear tooth profile, namely, the *involute tooth point* of the gear interacts with the corresponding *involute tooth point* of the mating pinion. The rest of the tooth profiles of both of the gear and of the pinion are not functional, and do not interact with one another. Moreover, the not-functional portions of the gear and of the pinion tooth profiles are *not* conjugate to one another. Because of this, certain additional freedom is given to the gear designer when designing not-functional portions of the gear and the pinion tooth profiles. *Convex-to-concave contact* of two properly configured circular-arc tooth profile is the one that is attractive for such an application.

When *machining* gears for *Novikov/conformal gearing*, and for *high-conformal* gear pairs, not *point contact* between the tooth flanks is required to be maintained in the *gear-machining mesh*, like it is observed in mesh of the tooth flanks,  $\mathcal{S}$  and  $\mathcal{P}$ , of a gear and a mating pinion in *Novikov/conformal gearing*, and *high-conformal* gear pair. Instead, *line contact* between the tooth flanks of the gear,  $\mathcal{S}$ , and of the gear cutting tool,  $\mathcal{T}$ , is required to be maintained in the *gear-machining mesh*. This means that the tooth profiles,  $\mathcal{S}$  and  $\mathcal{T}$ , must be conjugate to one another when machining gears for *Novikov/conformal gearing*, and *high-conformal gearing*.

The required line contact between the tooth flanks of a gear,  $\mathcal{S}$ , and of the gear cutting tool,  $\mathcal{T}$ , in the *gear-machining mesh* causes huge difference in meshing compared to that when *Novikov/conformal gearing*, and *high-conformal gearing* operate.

When a gear either for *Novikov/conformal gearing*, or for *high-conformal* gear pair spins in a *gear-machining mesh* (see Figure 11.45), the gear tooth flank,  $\mathcal{S}$ , and the machining surface,  $\mathcal{T}$ , of the gear cutting tool, contact each other along a line (not at point!!), that is, they make contact along the characteristic line,  $\mathcal{C}$ . The characteristic line,  $\mathcal{C}$ , is a spatial 3D curve that intersects the plane of drawing in Figure 11.45 at current contact point,  $K_i$ . The instantaneous line of action,  $LA_{inst}$ , at every contact point,  $K_i$ , is pointed along the unit normal vector,  $\mathbf{n}_i$  (see Figure 11.46), and, therefore, it is tangent at  $K_i$  to the path of contact,  $P_c$ . The tangent to the path of contact,  $P_c$ , at  $K_i$  is the

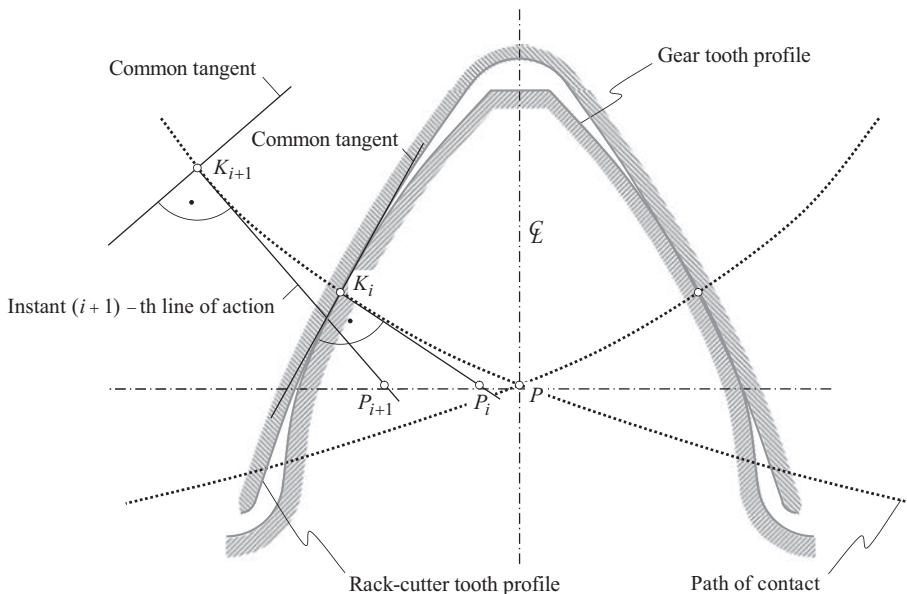


**FIGURE 11.45** Instantaneous lines of action,  $LA_{inst}$ , and paths of contact,  $P_c$ , in generating (continuous-indexing) machining processes of gears for *conformal* and *high-conformal* gearing.



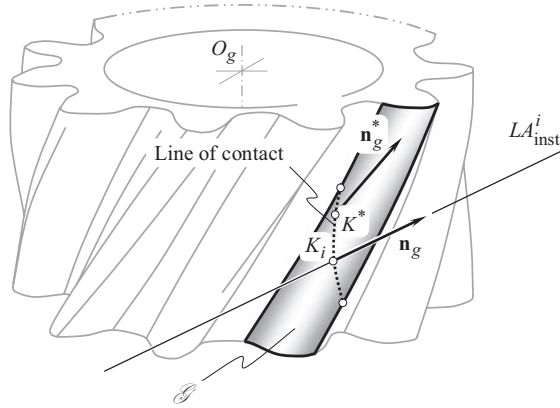


**FIGURE 11.46** Orientation of the unit normal vectors,  $\mathbf{n}_g$  and  $\mathbf{n}_g^*$ , to the gear tooth flank,  $\mathcal{G}$ , at different points,  $K_i$  and  $K^*$ , within the line of contact,  $LC$ , in generating (continuous-indexing) machining processes of gears for *conformal* and *high-conformal* gearing.

instantaneous line of action,  $LA_{inst}$ . The instantaneous line of action,  $LA_{inst}$ , intersects the centerline,  $\Phi$ , at a current pitch point  $P_i$ . The instantaneous pitch point,  $P_i$ , subdivides the center-distance,  $C$ , onto two portions,  $O_g P_i$  and  $O_T P_i$ , (i.e.,  $C = O_g P_i + O_T P_i$ ). The instantaneous ratio,  $O_g P_i / O_T P_i$ , is reciprocal to the instantaneous angular velocity ratio in the gear-machining mesh, namely:

$$\frac{O_g P_i}{O_T P_i} = \frac{\omega_{\mathcal{T}}}{\omega_g} \quad (11.78)$$

where  $\omega_g$  and  $\omega_{\mathcal{T}}$  are the rotations of the gear and the gear cutting tool, correspondingly.

When machining a gear, point,  $K_i$ , within the line of contact, travels along certain path of contact,  $P_c$ . The instantaneous line of action intersects the centerline,  $\Phi$ , at different pitch points,  $P_i$ . This means, that when the gear and the gear cutting tool rotate in a *gear-machining mesh*, the rotation of the gear can be uniform, while the rotation of the gear cutting tool inevitable is not-uniform. The latter is impossible, for example, because there could be two contact points,  $K_i$  and  $K_{i+1}$  at that same instant of time, and, as the consequence, two instantaneous pitch points,  $P_i$  and  $P_{i+1}$ . A rigid body, namely, the gear cutting tool, cannot spin at two different angular velocities simultaneously.

Another evidence of impossibility of machining/finishing of gears for *Novikov/conformal gearing*, and *high-conformal gearing* in generating (continuous-indexing) machining processes is as follows.

Assume that a gear is sliced by planes perpendicular to the gear axis,  $O_g$ , on an infinite number of slices. As gears for both for *Novikov/conformal gearing* and for *high-conformal gearing*, are always helical, each slice is turned about the gear axis,  $O_g$ , through certain angle to form a continuous helix. Hence, contact point within each slice is shifted in relation to each other along the path of contact. This immediately results in that there is an instantaneous pitch point,  $P_i$ , for every slice. The orientation of the unit normal vectors,  $\mathbf{n}_g$  and  $\mathbf{n}_g^*$ , to the gear tooth flank,  $\mathcal{G}$ , at different points,  $K_i$  and  $K^*$  (see Figure 11.46), within the instantaneous line of contact,  $LC$ , in generating (continuous-indexing) machining processes of gears for *Novikov/conformal gearing*, and *high-conformal gearing*, is different. The instantaneous lines of action,  $LA_{inst}^i$ , are pointed along the corresponding perpendicular to the gear tooth flank,  $\mathcal{G}$ .

Once the necessity of a plurality of the pitch points in the *gear-machining mesh* becomes evident, then machining/finishing of a gear for *Novikov/conformal gearing*, and for *high-conformal gearing* in a generating (continuous-indexing) gear-machining process gets impossible.

It could be thought that when the functional portion of the path of contact in the *gear-machining mesh* is close enough to a straight line, the gear as well as the pinion tooth flanks,  $\mathcal{G}$  and  $\mathcal{P}$ , can be generated within the tolerance band for the accuracy of the tooth profile. This is correct in general consideration, but is not practical because of the following. The geometry of the path of contact in the *gear-machining mesh* is strongly correlated to the geometry of the tooth flank of the gear to be machined. The radii of curvature of the gear tooth flank,  $\mathcal{G}$ , and of the pinion,  $\mathcal{P}$ , are close to the radius,  $r_N$ , of the *boundary N – circle*. The geometry of the *boundary N – circle* is different from that of the involute curve. As a result, the path of contact for a gear tooth profile with a limited mismatch from the *boundary N – circle* is different from that of a straight path of contact that occurs in the involute tooth profiles. Therefore, only wide tolerance band for the gear tooth profile accuracy makes possible an approximation of the actual path of contact in the gear-machining process by a straight-line segment. Wide tolerances for the gear tooth profile accuracy are not applicable for conformal and, especially for high-conformal gearing.

Once the entire profile of the gear teeth in *Novikov/conformal gearing* (including the non-functional portions of the gear teeth) is of non-involute geometry, this means that the profiles of this geometry cannot be machined/finished in generating (continuous-indexing) methods.<sup>33</sup> Therefore, neither gear hobs, nor shaper cutters, as well as nor worm grinding wheels, can be used for machining/finishing gears for *Novikov/conformal gearing*. Tooth profiles of the gear and of the mating pinion in *Novikov/conformal gearing* cannot be generated by the so-called *basic rack*. The so-called *basic rack* does not exist in case of *Novikov/conformal gearing*. Association of the so-called *basic rack* with gears for *Novikov/conformal gearing* is a huge mistake committed by many representatives of the gear community.

Violation of three fundamental laws of gearing, namely:

- a. of the law of contact, that is analytically expressed by the *Shishkov equation of contact*,  $\mathbf{n} \cdot \mathbf{V}_\Sigma = 0$
- b. of the conjugate action law for the interacting tooth flanks that can be expressed analytically by the *equation of conjugacy*,  $\mathbf{p}_m \times \mathbf{V}_m \cdot \mathbf{n}_g = 0$  (Prof. S.P. Radzevich, 2017 [174]), and
- c. of the law of equal base pitch of a gear, and that of a mating pinion, to an operating base pitch of the gear pair (Prof. S.P. Radzevich, 2008 [174]),

in this case is the main reason for such the infeasibility.

Despite of the entire gear/pinion tooth profile for *Novikov/conformal* as well as for *high-conformal gearing* cannot be finish-generated, the advantage can be taken from the fact that these two kinds of gearing feature point contact of the tooth flanks when operating. Hence, there is no need to accurately finish the entire tooth profile – it is sufficient to accurately finish only local portion of it that is located around the contact point,  $K$ . The gear finishing tool has to be designed so as to retain a favorable relation between tooth curvatures only at the *involute tooth point*, that is, at contact point,  $K$ .

### 11.4.3 ON THE INCONSISTENCY IN TOOTH PROFILE CURVATURES

The inconsistency in the tooth profile curvatures is another reason for why gears for *Novikov/conformal gearing* and for *high-conformal gearing* cannot be finish-generated. The origin of such the inconsistency can be traced back to the monograph by Prof. V.N. Kudriavtsev [68], and later on, it was repeated in dozens of publications by Prof. F.L. Litvin, in all standards on *Novikov/conformal gearing*, and so forth.

<sup>33</sup>It should be mentioned here that the first pair of *Novikov gears* made out of aluminum alloy (a pre-prototype) had been cut on April 25, 1954 by means of a disk-type mill cutter [1,2]. Fifteen gear pairs for testing purposes had been machined in summer of 1954 by means of a disk-type mill cutter [1,2].

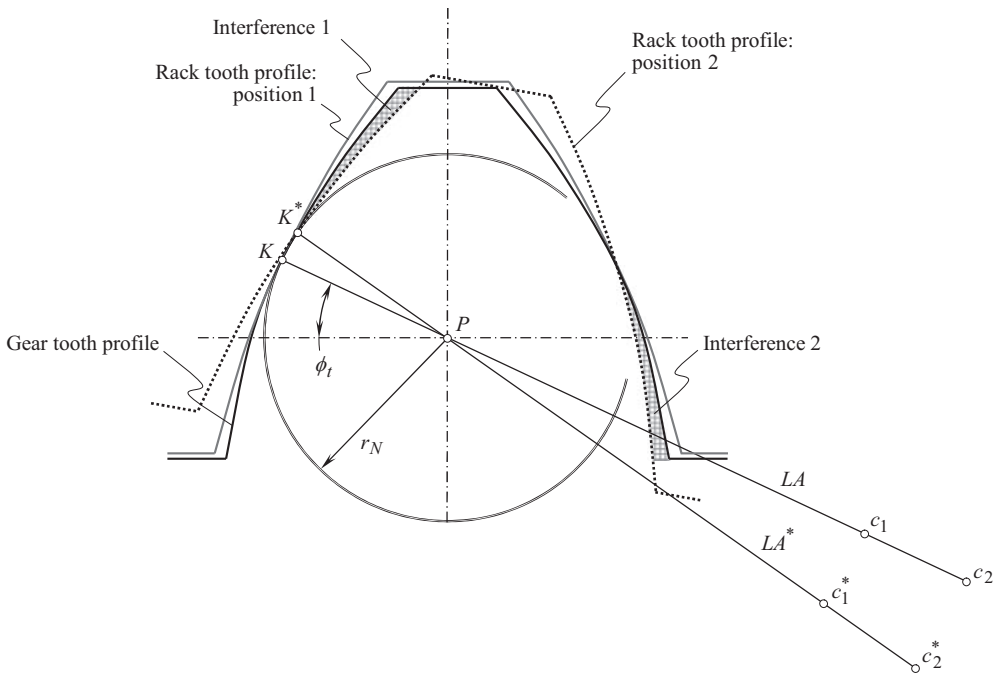


**FIGURE 11.47** Inconsistency in tooth profile curvatures in generating gears for *Novikov/conformal* and for *high-conformal gearing* by means of the basic rack: pitch point,  $P$ , is the center of instantaneous rotation.

Two consequent configurations of the gear rack in relation to the gear tooth are shown in Figure 11.47. In the initial configuration of all of the tooth profiles, all the elements of interest in the gear-machining mesh are labeled by letters with no asterisk. In another configuration, the basis rack is turned about the axis of instantaneous rotation through certain angle. In this new configuration, an asterisk is added to the labels of all the design parameters of the gear rack.

As the center of curvature,  $c_1$ , of the gear tooth profile is situated improperly in relation to the *boundary N – circle*, interference between the gear teeth, and the rack teeth is observed when the rack is turned in relation to the gear about the center of instantaneous rotation,  $P$ . No interference of this kind is permissible when finishing gears for *Novikov/conformal gearing* and *high-conformal gearing*. This is one more proof of impossibility of finishing gears for *Novikov/conformal gearing* and *high-conformal gearing* in gear generating (continuous-indexing) process.

# Section II-B

---

## Geometrically Accurate Gearing *Intersected-Axes Gear Pairs*

Gear pairs those used for transmission of a rotary motion between two shafts that intersect each other at certain angle are referred to as *intersected-axes gear pairs*<sup>1</sup> (or just  $I_a$  – *gearing*, for simplicity). The geometry of straight bevel gears has been investigated by numerous authors. Prof. *E. Buckingham* [20], Prof. *N.I. Kolchin* [82], and others, have contributed much to the investigation of approximate intersected-axes gearing.

Referring to Figure 2.16, the second stratum in the classification of possible kinds of gear vector diagrams is comprised of gear vector diagrams for intersected-axes gear pairs.

An appropriate gear vector diagram can be associated with any, and all particular designs of intersected-axes gear pair. The use of gear vector diagrams, together with the developed classification of their possible kinds (see Figure 2.16), allows for a comprehensive analysis of gearing of this kind. All possible kinds of intersected-axes gear pairs are incorporated into the analysis, and none of them can be missed, if the analysis follows the classification illustrated in Figure 2.16.

---

<sup>1</sup> Other terminology with regard to intersected-axes gear pairs can be found in the literature. Some authors loosely refer to gears of this particular kind as to *conical gear pairs*, *spherical gear pairs*, and so forth. This is true, as gear mesh in intersected-axes gears can be easily described as mesh on a sphere. However, not only intersected-axes gear pairs feature meshing on a sphere. As it is discussed below in this book, meshing in crossed-axes gear pairs can also be easily described on a sphere. Hence, the sphere of meshing is not a sufficient (a unique) indicator to refer to intersected-axes gearsets as to *spherical gear pairs*. *Intersected-axes gear pair* is the most appropriate terminology with respect to gears of this design.



# Taylor & Francis

Taylor & Francis Group

<http://taylorandfrancis.com>

## 12 Geometrically Accurate Intersected-Axes Gear Pairs

Intersected-axes gears have been used in practice for centuries. Numerous designs of intersected-axes gears can be found in *Leonardo da Vinci's* famous book *The Madrid Codices* [23]. When a motion is transmitted between shafts whose axes intersect, some form of bevel gear is applied. Although bevel gears are often made for a shaft angle of  $90^\circ$  (see Figure 12.1), they can be produced for almost any shaft angle.

The discussion on intersected-axes gears begins from the consideration of the earliest designs of this particular kind of gear pair.

## 12.1 EARLIEST DESIGNS OF INTERSECTED-AXES GEAR PAIRS

The intersected-axes gear pairs of the earliest known designs indicate strong constraints imposed by the gear technology available at that time for the production of gears. This is elaborated in the following text.

An example of intersected-axes gear pair is depicted in Figure 12.2. The gear pair is composed of a face pin-tooth gear and a lantern pinion. The pin-tooth face gear has a tooth that consists of formed pins. The pinion consists of a plurality of cylindrical pins equally spaced in a circle that is concentric with the axis of rotation of the pinion. These pins are mounted on flanges.

The axis of rotation of the gear,  $O_g$ , and that of the mating pinion,  $O_p$ , intersect at the right angle. The ratio of rotation of the gear,  $\omega_g$ , and that of the pinion,  $\omega_p$ , is reciprocal to the ratio of the pin number in the gear,  $N_g$ , and in the mating pinion,  $N_p$  (the equality  $\omega_p/\omega_g = N_g/N_p$  is valid).

The rotation vectors,  $\omega_g$  and  $\omega_p$ , are pointed along the axes of rotation,  $O_g$  and  $O_p$ , of the gear and of the pinion, correspondingly. The vectors,  $\omega_g$  and  $\omega_p$ , are a kind of sliding vectors. For convenience, they are applied at the point of intersection of the axes of rotations,  $O_g$  and  $O_p$ ; however, this is not a must: each of these two vectors can be applied at any point within the corresponding axis of

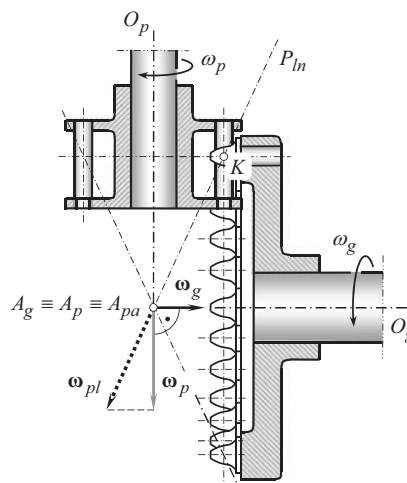


**FIGURE 12.1** Orthogonal intersected-axes gear pair.

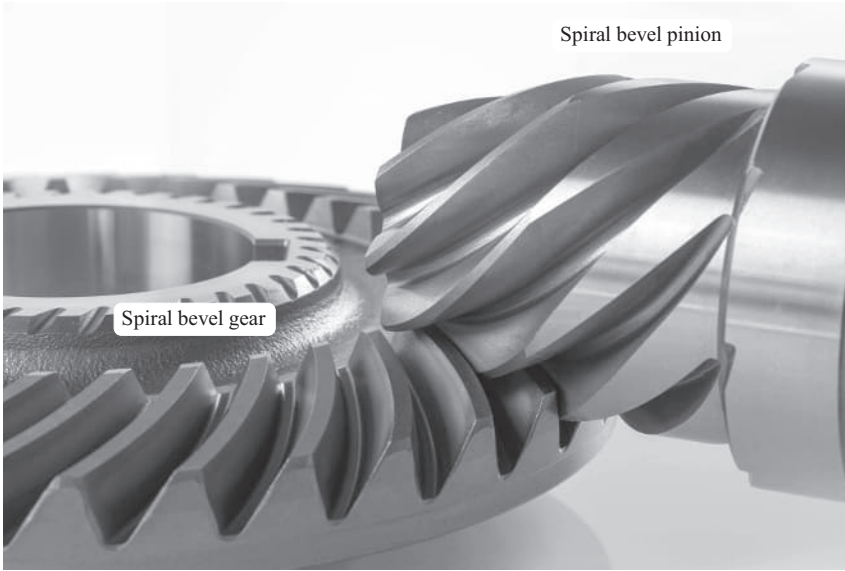


**FIGURE 12.2** Intersected-axes gear pair composed of a pin-tooth face gear and a lantern pinion.

rotation (the rotation vector  $\omega_g$  can be applied at any point of the gear axis of rotation,  $O_g$ , while the rotation vector  $\omega_p$  can be applied at any point of the pinion axis of rotation,  $O_p$ ).

The vector of instantaneous rotation,  $\omega_{pl}$ , (namely, the vector of instantaneous rotation of the pinion in relation to the gear), is pointed along the axis of instantaneous rotation,  $P_{ln}$ . The rotation vector,  $\omega_{pl}$ , equals:

$$\omega_{pl} = \omega_p - \omega_g \quad (12.1)$$

The intersected-axes gears, shown in Figure 12.2, are used to transmit a rotary motion from a driving shaft to a driven shaft when the input rotation is slow. The load-carrying capacity of a drive of such a design is very low because only point contact is observed between the mating pins or teeth [20]. The functional surfaces of the pins are convex. The radius of curvature of the pins is relatively small. Such contacts of the pins result in a low-bearing capacity of the gears (see Figure 12.2).

In the present-day industry, bevel gears illustrated in Figure 12.1 are the main type of gearing used to transmit a rotary motion between two shafts that intersect one another.

## 12.2 KINEMATICS OF INTERSECTED-AXES GEARING

Transmission and transformation of a rotary motion from a driving shaft to a driven shaft is the main purpose of intersected-axes gearing of all designs. Both the input rotation and the output rotation can be easily represented by means of a pair of corresponding rotation vectors,  $\omega_g$  and  $\omega_p$ . The variety of all possible kinds of intersected-axes gear pairs is limited to the total number of possible combinations of the rotation vectors,  $\omega_g$  and  $\omega_p$ , namely, of the rotation vectors:

1. of various magnitudes, and
2. of different shaft angles,  $\Sigma$  [recall that the shaft angle,  $\Sigma$ , is defined as the angle that is formed by the rotation vectors,  $\omega_g$  and  $\omega_p$ , namely,  $\Sigma = \angle(\omega_g, \omega_p)$ ].

The total number of gear vector diagrams of different kinds for the intersected-axes gearing is limited just to three kinds of gear vector diagrams when the actual configuration of the rotation vectors,

$\omega_g$  and  $\omega_p$ , of a gear and of a mating pinion in relation to the vector of instantaneous rotation,  $\omega_{pl}$ , is taken into account. These gear vector diagrams are plotted in Figure 12.3.

The gear vector diagram, shown in Figure 12.3a, features an obtuse angle,  $\Sigma_g$ , between the rotation vector,  $\omega_g$ , of the gear, and between the vector of instantaneous rotation,  $\omega_{pl}$ . The angle,  $\Sigma_g$ , is commonly referred to as the *gear cone angle*. The gear cone angle,  $\Sigma_g$ , can be expressed in terms of the shaft angle,  $\Sigma$ , and of the magnitudes,  $\omega_g$  and  $\omega_p$ , of the rotation vectors,  $\omega_g$  and  $\omega_p$ .

Referring to Figure 12.4, in the depicted parallelogram the sides  $\omega_g$  and  $\omega_p$  form an intersected-axes angle,  $\Sigma$ , at the triangle vertex,  $A_{pa}$ . All the sides in the triangle can be normalized by  $\omega_p$ . With that said,

- the length of the side  $\omega_g$  alters to  $\omega_g/\omega_p = u$ ,
- the length of the side  $\omega_p$  alters to  $\omega_p/\omega_p = 1$ , and
- the length of the side  $\omega_{pl}$  alters to  $\omega_{pl}/\omega_p$ .

According to the law of cosine, the length of the side  $\omega_{pl}$  alters to  $\omega_{pl}/\omega_p$ , and equals:

$$\frac{\omega_{pl}}{\omega_p} = \sqrt{1 + u^2 - 2u \cos \Sigma} \quad (12.2)$$

As depicted Figure 12.4 triangle, the sides  $\omega_p$  and  $\omega_{pl}$  form a pinion cone angle,  $\Sigma_p$ , at a triangle vertex,  $A_{pa}$ . Again, all the sides of this second triangle can be normalized by  $\omega_p$ . Then, according to the law of sines, the pinion cone angle,  $\Sigma_p$ , can be calculated from the expression:

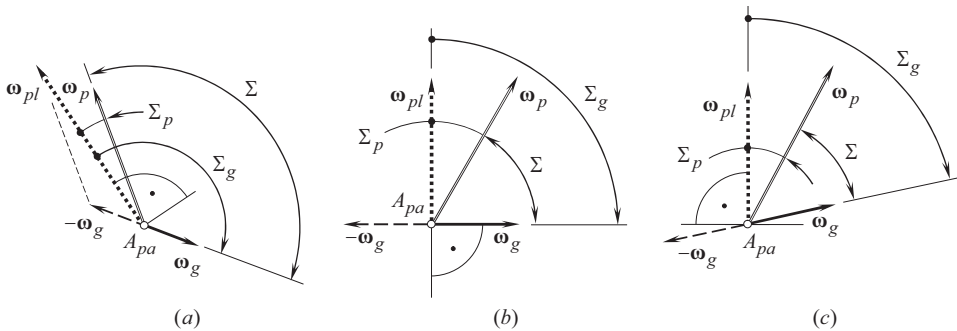


**FIGURE 12.3** Total number of possible kinds of gear vector diagrams for intersected-axes gear pairs is limited just to their three kinds: (a) external  $I_a$  – gear pair, (b) *pinion gear-to-round rack*  $I_a$  – gear pair, and (c) internal  $I_a$  – gear pair.

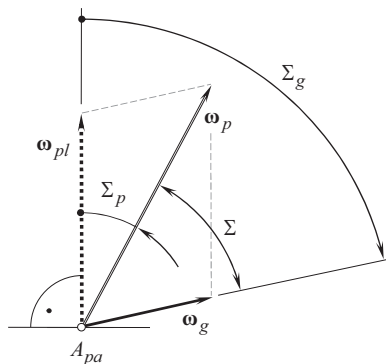


**FIGURE 12.4** The *gear cone angle*,  $\Sigma_g$ , and the *pinion cone angle*,  $\Sigma_p$ , in intersected-axes gear pair.



$$\sin \Sigma_p = \frac{\omega_{pl}}{\omega_p} \sin \Sigma \quad (12.3)$$

Equation (12.3) yields a formula for the calculation of the pinion cone angle,  $\Sigma_p$ :

$$\Sigma_p = \sin^{-1} \frac{\sin \Sigma}{\sqrt{1+u^2-2u \cos \Sigma}} \quad (12.4)$$

Ultimately, an equation for the calculation of the gear cone angle,  $\Sigma_g$ , can also be derived:

$$\Sigma_g = \Sigma + \sin^{-1} \frac{\sin \Sigma}{\sqrt{1+u^2-2u \cos \Sigma}} \quad (12.5)$$

For a shaft angle of  $90^\circ$ , Eqs. (12.4) and (12.5) reduce to:

$$\Sigma_p = \sin^{-1} \frac{1}{\sqrt{1+u^2}} \quad (12.6)$$

$$\Sigma_g = \Sigma + \sin^{-1} \frac{1}{\sqrt{1+u^2}} \quad (12.7)$$

correspondingly.

Gear vector diagram corresponds to external intersected-axes gear pair (Figure 12.3a).

For an external intersected-axes gear pair of this particular kind (namely, when  $\Sigma > 90^\circ$ ), the relation  $\Sigma_g = \angle(\omega_g, \omega_{pl}) > 90^\circ$  is valid. An equivalent expression is valid for the relation  $\Sigma_g = \angle(\omega_g, \omega_{pl}) > 90^\circ$ :

$$\omega_g \cdot (\omega_p - \omega_g) < 0 \quad (12.8)$$

or

$$\frac{\omega_g \cdot (\omega_p - \omega_g)}{|\omega_g| \cdot |\omega_p - \omega_g|} = -1 \quad (12.9)$$

Examples of gear vector diagrams constructed for external intersected-axes gearsets that feature various configurations of the rotation vectors of a gear,  $\omega_g$ , and of a mating pinion,  $\omega_p$ , (and, thus, they feature different shaft angles,  $\Sigma$ ) are depicted in Figure 12.5. As shown in Figure 12.5, examples reveal that a particular configuration of rotation vector of the gear,  $\omega_g$ , in relation to the vector of instantaneous rotation,  $\omega_{pl}$ , is critical for the determination whether or not a gear pair is external, while the relative configuration of the rotation vectors,  $\omega_g$  and  $\omega_p$ , is of secondary importance.

The performed analysis of the gear vector diagrams for intersected-axes gearing (see Figure 12.3) reveals that the rotation vectors,  $\omega_g$  and  $\omega_p$ , of a gear and of a mating pinion are not parallel to the vector of instantaneous rotation,  $\omega_{pl}$ . Therefore, sliding of tooth flanks of a gear,  $\mathcal{S}$ , and of a mating pinion,  $\mathcal{P}$ , in the lengthwise direction of the gear tooth become inevitable in intersected-axes gearing of all kinds. The sliding is caused by the projections of the rotation vectors,  $\omega_g$  and  $\omega_p$ , onto a perpendicular to the vector of instantaneous rotation,  $\omega_{pl}$ .

In a particular case, rotation vector of the gear,  $\omega_g$ , can be orthogonal to the vector of instantaneous rotation,  $\omega_{pl}$  [that is,  $\Sigma_g = \angle(\omega_g, \omega_{pl}) = 90^\circ$ ]. An equivalent expression is valid for this formula:  $\omega_g \cdot (\omega_p - \omega_g) = 0$

$$(12.10)$$

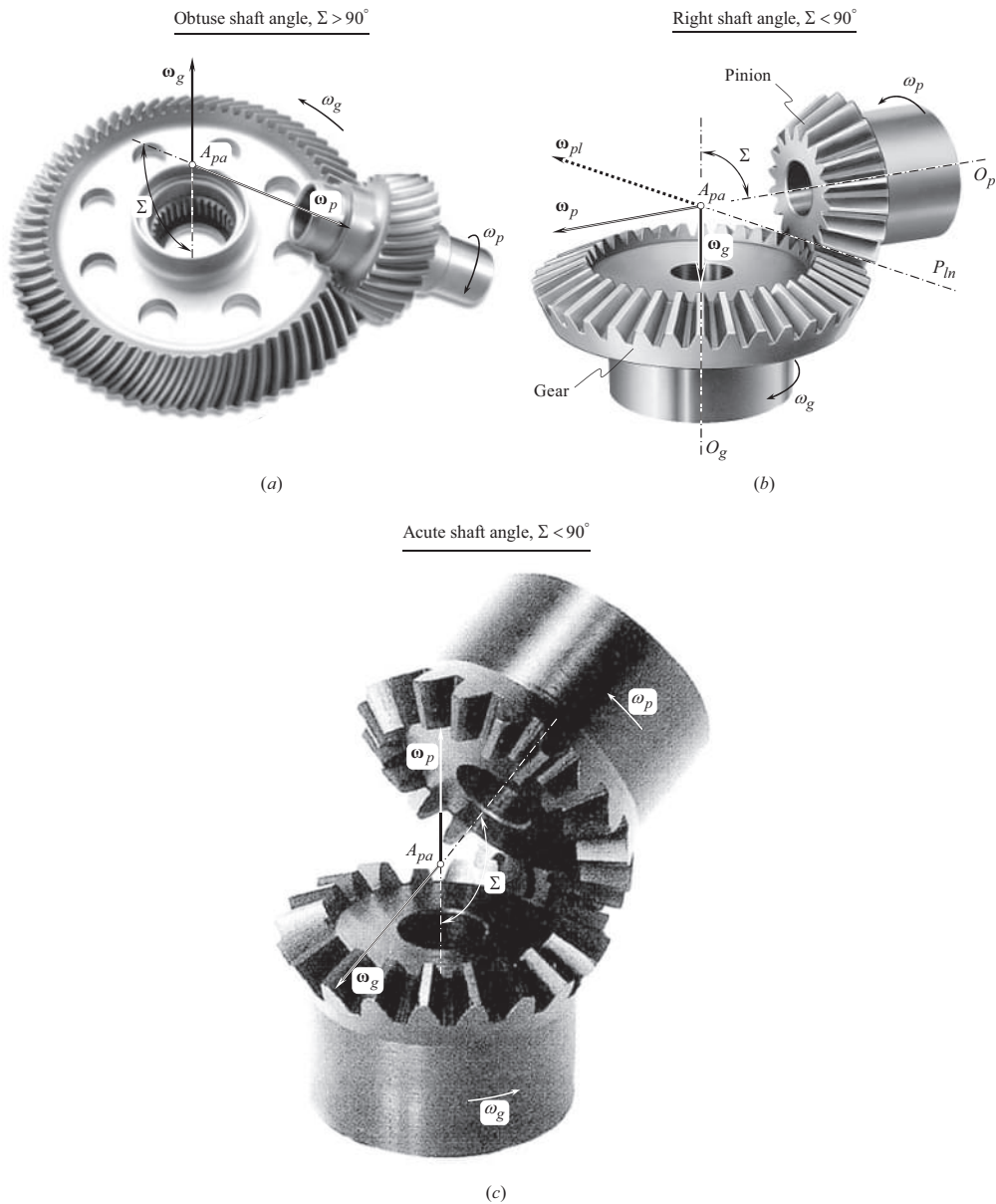


**FIGURE 12.5** External intersected-axes gear pairs that feature different configurations of the rotation vector of the gear,  $\omega_g$ , and that,  $\omega_p$ , of the mating pinion: gear pairs with (a) an obtuse shaft angle,  $\Sigma > 90^\circ$ , (b) a right shaft angle,  $\Sigma = 90^\circ$ , and (c) acute shaft angle,  $\Sigma < 90^\circ$ .

or

$$\frac{\omega_g \cdot (\omega_p - \omega_g)}{|\omega_g| \cdot |\omega_p - \omega_g|} = 0 \quad (12.11)$$

The gear vector diagram for this kind of gearsets is schematically shown in Figure 12.3b.

Ultimately, an intersected-axes gear pair may feature an acute gear cone angle,  $\Sigma_g$ , between the rotation vector,  $\omega_g$ , of a gear and between the vector of instantaneous rotation,  $\omega_{pl}$ , as schematically

illustrated in Figure 12.3c. For a gear pair of this particular kind, the relation  $\Sigma_g = \angle(\omega_g, \omega_{pl}) < 90^\circ$  is observed. An equivalent expression is valid for this configuration of the rotation vectors  $\omega_g$  and  $\omega_{pl}$ :

$$\omega_g \cdot (\omega_p - \omega_g) > 0 \quad (12.12)$$

or

$$\frac{\omega_g \cdot (\omega_p - \omega_g)}{|\omega_g| \cdot |\omega_p - \omega_g|} = +1 \quad (12.13)$$

Vector diagrams of the kind (see Figure 12.3c) correspond to internal intersected-axes gear pairs.

Internal intersected-axes gear pairs (see Figure 12.6a) are used in the design of nutation drives (see Figure 12.6b) as well as in other applications.

The analytically expressed conditions [see Eqs. (12.8)–(12.10)] along with Eq. (12.12) are summarized in Table 12.1.

Any and all intersected-axes gearsets fulfill one of three expressions outlined in Table 12.1.

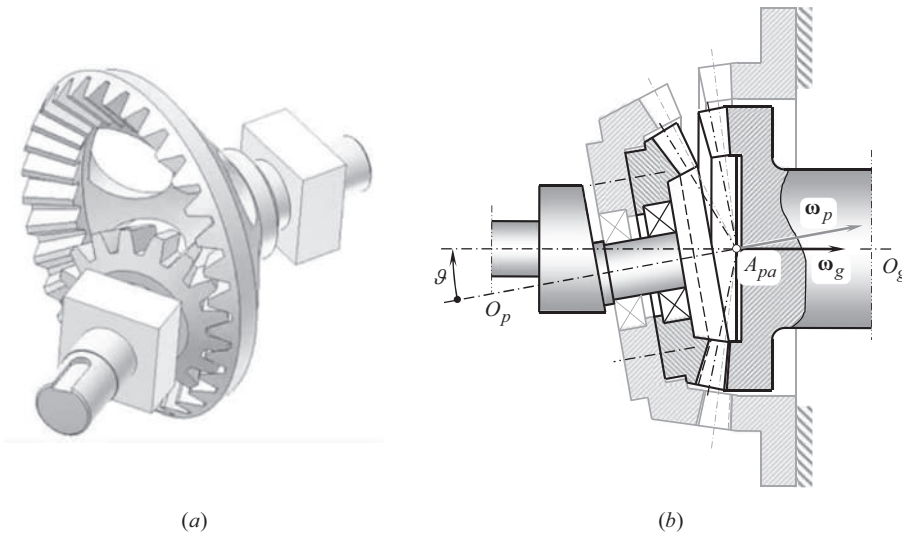


**FIGURE 12.6** Internal intersected-axes gearset: (a) close-up and (b) example of implementation in the design of a nutation drive.

**TABLE 12.1**

**Analytical Criteria of Kind of Intersected-Axes Gearing**

Kind of Intersected-Axes Gearing	Analytical Criterion [ $C = 0$ , and $\Sigma \neq 0$ ]
External intersected-axes gearset	$\omega_g \cdot (\omega_p - \omega_g) < 0$
Rack-type intersected-axes gearset	$\omega_g \cdot (\omega_p - \omega_g) = 0$
Internal intersected-axes gearset	$\omega_g \cdot (\omega_p - \omega_g) > 0$

In a particular case, the centerlines of the driving shaft and of the driven shaft intersect each other at a right angle (i.e.,  $\Sigma = 90^\circ$ ). This particular case is the most common in the present-day practice. Intersected-axes gear pairs of this kind are referred to as *orthogonal intersected-axes gear pairs*. An example of gear vector diagram for orthogonal intersected-axes gear pair is schematically shown in Figure 12.7. In this particular kind of gearing, the cross product of the rotation vectors,  $\omega_g$  and  $\omega_p$ , of a gear and of a mating pinion is always equal to zero (i.e.,  $\omega_g \times \omega_p = 0$ ).

An orthogonal intersected-axes gear pair may feature equal tooth number of a gear,  $N_g$ , and that of a mating pinion,  $N_p$ . When the mating gears are equal in size, and the shafts are positioned at  $\Sigma = 90^\circ$  to each other, the gear pair is referred to as a *miter intersected-axes gear pair*. The vector diagram for a miter gears is shown in Figure 12.8. Miter gears meet not only the requirement  $\omega_g \times \omega_p = 0$ , they also feature the rotation vectors,  $\omega_g$  and  $\omega_p$ , of equal magnitudes (i.e.,  $\omega_g = \omega_p$ ).

In a reduced case, spatial gear pair of the kind 1.2 (see Figure 2.16) transforms into the *pinion-to-rack gear pair* of the kind 1.2.2. Furthermore, a conventional *pinion-to-rack gear pair* (see 1.2.2.1 in the classification Figure 2.16) can be viewed as a reduced case of an intersected-axes gear pair of the kind 1.2.2. The similarity and the differences among gear pairs of different kinds are clearly indicated in the numbering of vector diagrams of every particular case.

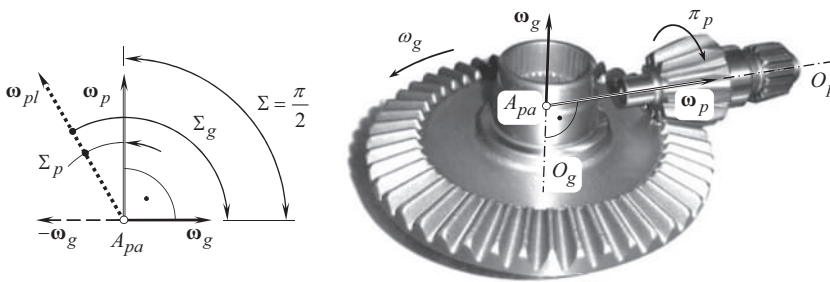


FIGURE 12.7 Gear vector diagram of an orthogonal intersected-axes gear pair.

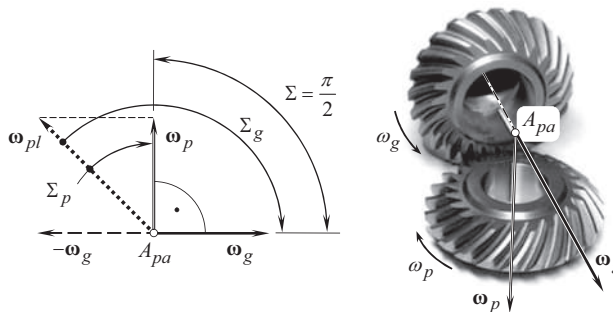


FIGURE 12.8 Gear vector diagram of a miter gear pair.

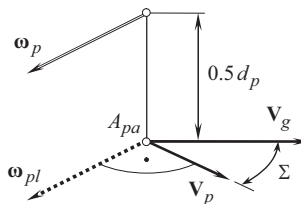


FIGURE 12.9 Gear vector diagram for a round rack-to-bevel-gear pair.

An example of vector diagram for gears of the kind 1.2.2 is shown in Figure 12.9.

It is important to point out here that gears of the kind shown in Figure 12.9 represent that same third stratum in the classification (see Figure 2.16), as the gear pairs of the kind shown in Figure 12.3. However, the gear pairs of these two different kinds represent different branches of the classification (see Figure 2.16).

### 12.3 BASE CONES IN INTERSECTED-AXES GEARSETS

The concept of base cones in intersected-axes gearing is an important consideration, as it leads directly to the concept of *equivalent pulley-and-belt transmission* in intersected-axes gearing.

Despite that to the best of the author's knowledge, it is not known yet who has to be credited with the concept of the *equivalent pulley-and-belt transmission* of a gear pair in parallel-axes gearing, this issue with respect to intersected-axes gearing is a bit more clear. It was *George B. Grant* who was the first to introduce (1887) the concept of the base cone in intersected-axes gearing [99]. He considered the base cone of a gear, and a plane, tangent to the base cone. It was not realized at that time that, by nature, the tangent plane is the plane of action. Moreover, only one base cone, and NOT two base cones in interacting bevel gears were considered by *G.B. Grant*. Later on (~2008), the concept of the *equivalent pulley-and-belt transmission* of a gear pair in intersected-axes gearing was proposed by Prof. *S.P. Radzevich* [218]. Two base cones in tangency with the plane of action were considered by Prof. *S.P. Radzevich* [218]. This concept is schematically illustrated in Figure 12.10.

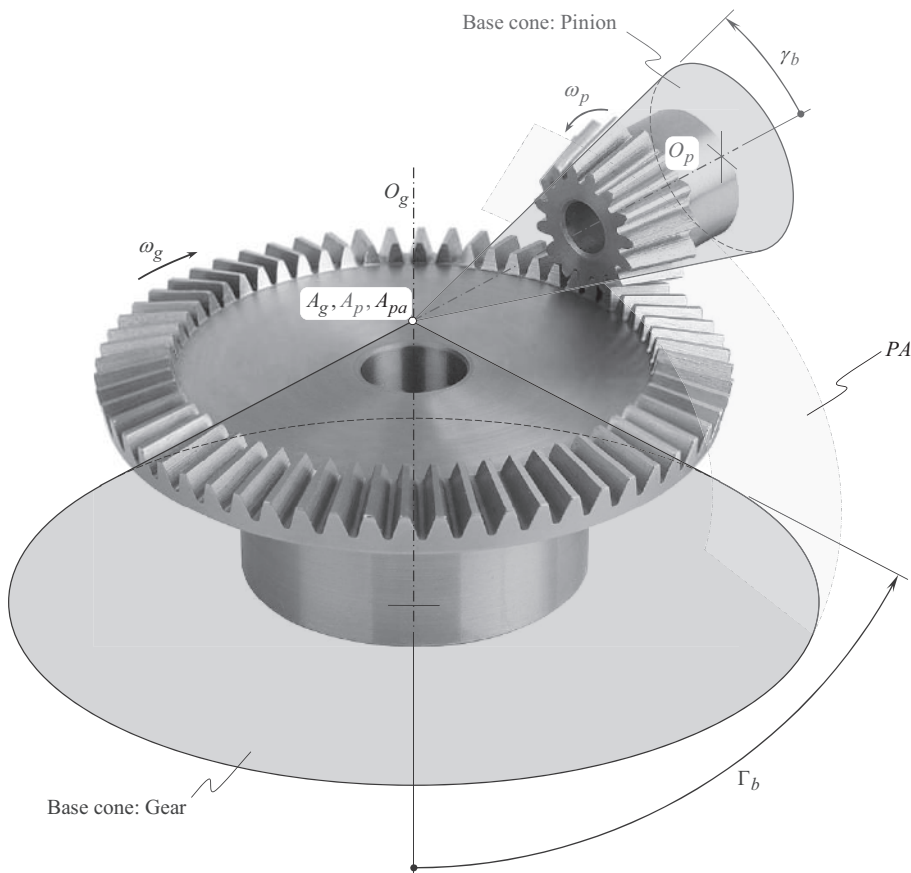


**FIGURE 12.10** On the concept of *equivalent pulley-and-belt transmission* in intersected-axes gearing. (After Prof. *S.P. Radzevich*, ~2008.)

A straight bevel gear is depicted in Figure 12.10 as an example. When bevel gears operate, the gear spins,  $\omega_g$ , about its axis of rotation,  $O_g$ . The mating pinion spins,  $\omega_p$ , about its axis of rotation,  $O_p$ . The axes of rotation,  $O_g$  and  $O_p$ , intersect one another, and the point of intersection coincides with the plane-of-action apex,  $A_{pa}$  – this is a must for the perfect performance of bevel gearing.

A base cone is associated with the gear. The gear base cone apex,  $A_g$ , is located within the gear axis of rotation,  $O_g$ . Another base cone is associated with the pinion. The pinion base cone apex,  $A_p$ , is located within the pinion axis of rotation,  $O_p$ . The gear and the pinion must be configured in relation to each other so as to ensure the apexes,  $A_g$  and  $A_p$ , snap together with the plane-of-action apex,  $A_{pa}$  – this is must. The plane of action,  $PA$ , is a plane through the plane-of-action apex,  $A_{pa}$ , that is tangential to the base cones of the gear and of the mating pinion.

Geometrically accurate intersected-axes gearsets are capable of transmitting smoothly a uniform input rotary motion from a driving shaft to a driven shaft. From this perspective, geometrically accurate intersected-axes gear pairs resemble the earlier discussed geometrically accurate parallel-axes gear pairs [see the schematic depicted in Figure 10.37]. The similarity between the gears of these two kinds can be extended further. Therefore, for convenience, it makes sense to consider geometrically accurate intersected-axes gearing in comparison with the geometrically accurate parallel-axes gearing, as parallel-axes gearing is investigated much more profoundly, and, meshing of the tooth flanks of a gear and of a mating pinion in parallel-axes gearing is easier to understand by the beginners.

For the convenience of the further analysis, the shown in Figure 12.3 gear vector diagram of an intersected-axis gear pair, the principal planes (see Figure 3.8), the plane of action,  $PA$  (see Figure 3.14), along with the design parameters of the gearset, all together are shown in Figure 12.11. The plane of action,  $PA$ , and the pitch plane,  $PP$ , are the two planes through the axis of instantaneous rotation,  $P_{ln}$ .

Geometrically accurate parallel-axes gear pair features two base cylinders, as shown in Figure 10.37. A uniform rotation of the base cylinders allows for the interpretation of parallel-axes gearing as a corresponding *equivalent pulley-and-belt transmission*. This is also valid with respect to geometrically accurate intersected-axes gear pairs. Two base cones can be associated

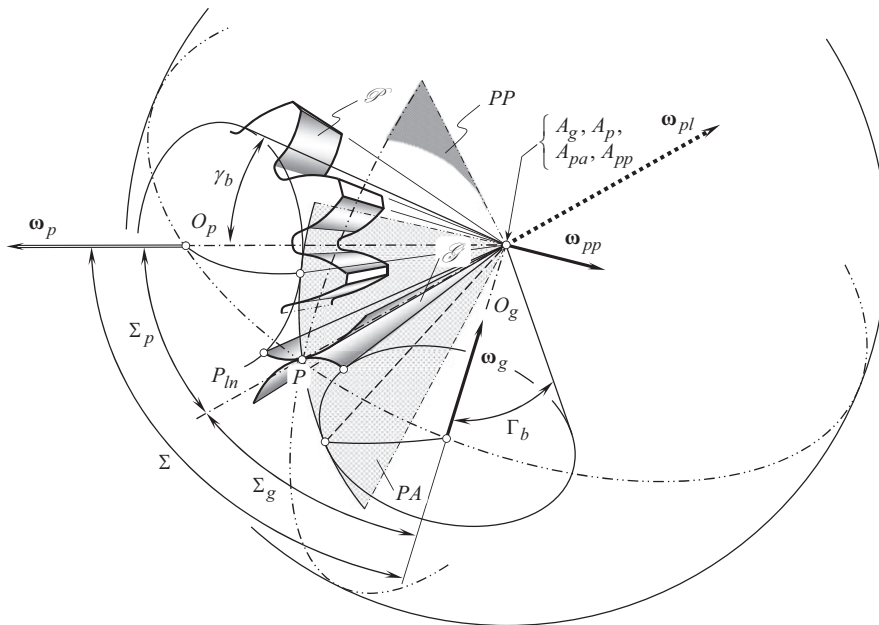


**FIGURE 12.11** Configuration of the main planes and the principal vectors in intersected-axes gear pair.

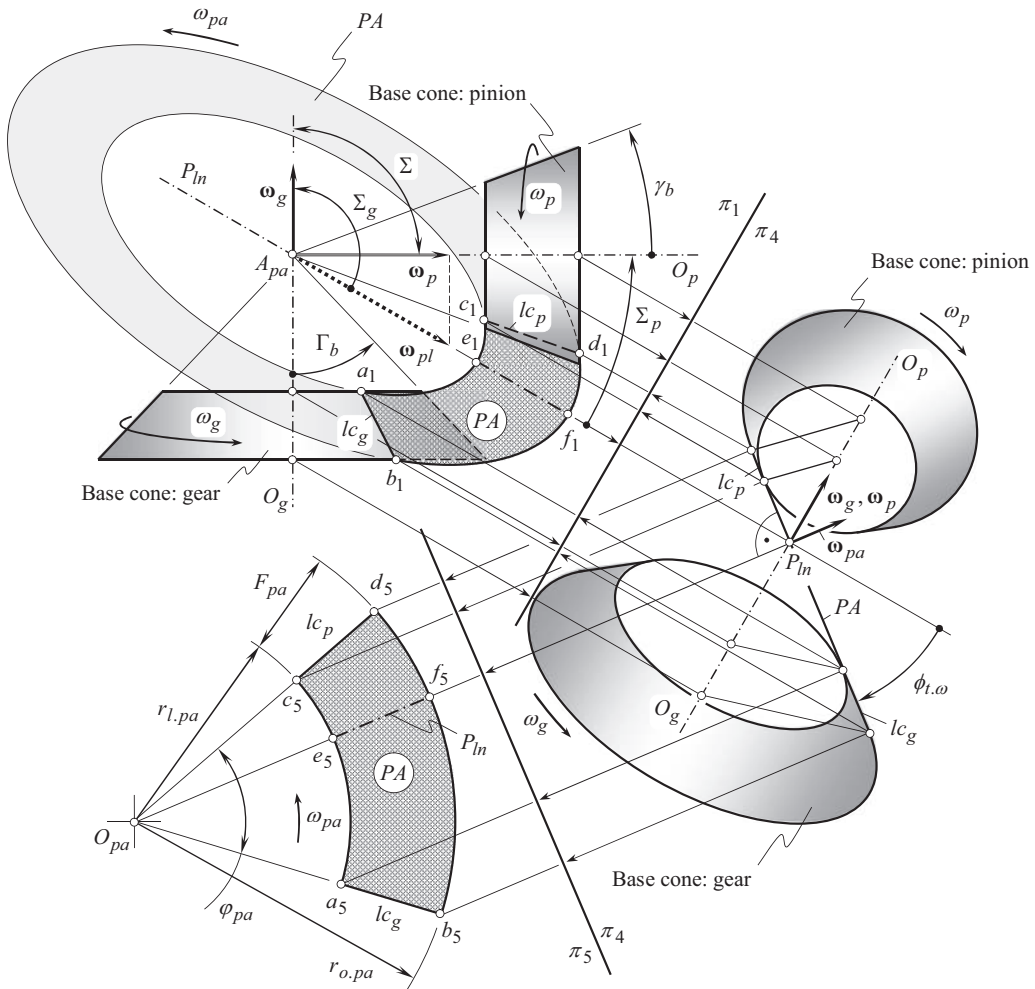


FIGURE 12.12 Base cones, and the plane of action, PA, in orthogonal intersected-axes gear pair.

with a gear as well as with a mating pinion of any and all designs. This concept is schematically illustrated in Figure 12.12. An orthogonal intersected-axes gear pair is selected here solely for illustrative purposes. Similar results of the analysis can be obtained if an intersected-axis gear pair either with an obtuse,  $\Sigma > 90^\circ$ , or with an acute,  $\Sigma < 90^\circ$ , shaft angle is selected for this purpose (without going into details of the analysis, it should be stated here that the same approach is applicable with respect to angular bevel gears that have a shaft angle,  $\Sigma \neq 90^\circ$ ).

As shown in Figure 12.12 schematic is built up on the premise of the rotation vectors,  $\omega_g$  and  $\omega_p$ , of a gear and of a mating pinion. The gear and the pinion rotate about their axes,  $O_g$  and  $O_p$ , correspondingly. The rotation vectors,  $\omega_g$  and  $\omega_p$ , allow for the construction of the vector,  $\omega_{pl}$ , of instantaneous rotation. The axis of the instantaneous rotation,  $P_{ln}$ , is aligned with rotation vector,  $\omega_{pl}$ .

The gear ratio,  $u$ , in intersected-axes gear pair can be expressed in terms of the cone angles,  $\Sigma_g$  and  $\Sigma_p$ , of the gear and of the mating pinion:

$$u = \frac{\omega_p}{\omega_g} = \frac{\cos \Sigma_g}{\cos \Sigma_p} \quad (12.14)$$

A few more equations can be used for the calculation of the gear ratio,  $u$ , in intersected-axes gearing.



From the formula for the calculation of the gear cone angle,  $\Sigma_g$ :

$$\tan \Sigma_g = \frac{\sin \Sigma}{\frac{1}{u} + \cos \Sigma} \quad (12.15)$$

The gear ratio,  $u$ , in intersected-axes, gear pair is calculated as:

$$u = \left( \frac{\sin \Sigma}{\tan \Sigma_g} - \cos \gamma \right)^{-1} = \frac{\tan \Sigma_g}{\sin \Sigma - \cos \Sigma \tan \Sigma_g} \quad (12.16)$$

Similarly, from the formula for the calculation of the pinion cone angle,  $\Sigma_p$ :

$$\tan \Sigma_p = \frac{\sin \Sigma}{u + \cos \Sigma} \quad (12.17)$$

The gear ratio,  $u$ , in intersected-axes gear pair is calculated as:

$$u = \frac{\sin \Sigma}{\tan \Sigma_p} - \cos \Sigma = \frac{\sin \Sigma - \cos \Sigma \tan \Sigma_p}{\tan \Sigma_p} \quad (12.18)$$

In orthogonal intersected-axes gear pair ( $\Sigma = 90^\circ$ ), Eqs. (12.16) and (12.18) reduce to:

$$u = \tan \Sigma_g \quad (12.19)$$

and

$$u = \tan^{-1} \Sigma_p \quad (12.20)$$

correspondingly.

The plane of action,  $PA$ , is a plane through the axis of instantaneous rotation,  $P_{ln}$ . The plane,  $PA$ , is tangent to both base cones, namely, it is tangent to the base cone of the gear, and to the base cone of the mating pinion. The plane of action,  $PA$ , forms a transverse pressure angle,  $\phi_{t,\omega}$ , with a perpendicular to the plane through the rotation vectors,  $\omega_g$  and  $\omega_p$ . The transverse pressure angle,  $\phi_{t,\omega}$ , is measured in a plane that is perpendicular to the vector of instantaneous rotation,  $\omega_{pl}$ .

The left upper portion of the schematic depicted in Figure 12.12 is plotted within the plane of projections,  $\pi_1$ . Two other planes of projections,  $\pi_2$  and  $\pi_3$ , of a standard set of the planes of projections,  $\pi_1\pi_2\pi_3$ , are not used in this particular analysis. Instead, two auxiliary planes of projections, namely, the planes,  $\pi_4$  and  $\pi_5$ , are used in this analysis. The axis of projections,  $\pi_1/\pi_4$ , is constructed so as to be perpendicular to the axis of instantaneous rotation,  $P_{ln}$ . The axis of projections,  $\pi_4/\pi_5$ , is constructed so as to be parallel to the trace of the plane of action,  $PA$ , within the plane of projections  $\pi_4$ .

The plane of action can be construed as a flexible zero thickness film that is free to unwrap from and wrap on the base cones of the gear and of the mating pinion. The zero thickness film is not allowed for any bending about an axis perpendicular to the plane,  $PA$ , itself. Under a uniform rotation of the gears, the motion of the plane of action,  $PA$ , is a pure rotation about the axis  $O_{pa}$ . The rotation vector,  $\omega_{pa}$ , is pointed along the axis,  $O_{pa}$ , and is perpendicular to the plane of action.

In intersected-axes gear pairs, the plane of action,  $PA$ , can be construed as a round cone with a  $90^\circ$  cone angle.

The rotation vectors,  $\omega_g$ ,  $\omega_p$ , and  $\omega_{pa}$ , are synchronized with one another so as to fulfil the equalities:

$$u_{p/pa} = \sin \gamma_b \quad (12.21)$$



$$u_{pa/g} = \frac{1}{\sin \Gamma_b} \quad (12.22)$$

$$u_{p/g} = u_{p/pa} \cdot u_{pa/g} = \frac{\sin \gamma_b}{\sin \Gamma_b} \quad (12.23)$$

As the rotations  $\omega_g$ ,  $\omega_p$ , and  $\omega_{pa}$ , are synchronized with one another, the actual values of the base cone angles,  $\Gamma_b$ , of a gear, and,  $\gamma_b$ , of a mating pinion, can be calculated from the following expressions:

$$\Gamma_b = \sin^{-1} \frac{\omega_g}{\omega_{pa}} \quad (12.24)$$

$$\gamma_b = \sin^{-1} \frac{\omega_p}{\omega_{pa}} \quad (12.25)$$

From this equation, an expression:

$$\omega_g \sin \gamma_b = \omega_p \sin \Gamma_b \quad (12.26)$$

can be derived.

In intersected-axes gear pairs, the base cone angles,  $\Gamma_b$  and  $\gamma_b$ , vary within the intervals  $0^\circ < \Gamma_b < 180^\circ$  and  $0^\circ < \gamma_b < 180^\circ$ , correspondingly. So, here and below, all the equations are valid for external, rack-type, and for internal gearsets. Formally, the base cone angles,  $\Gamma_b$  and  $\gamma_b$ , can be considered in narrower intervals, namely, within the intervals  $0^\circ < \Gamma_b < 90^\circ$  and  $0^\circ < \gamma_b < 90^\circ$ , correspondingly. Under such a scenario, the following inequalities are valid for intersected-axes gear pairs of various designs:

- The base cone angles, both, are of positive values ( $\Gamma_b > 0^\circ$  and  $\gamma_b > 0^\circ$ ) in external gear pairs
- The base cone angle of a gear is equal to a right angle ( $\Gamma_b = 90^\circ$ ), and that of a mating pinion is of a positive value and  $\gamma_b > 0^\circ$  in rack-type gear pairs
- The base cone angle of a gear is of negative value ( $\Gamma_b < 0^\circ$ ), and that of a mating pinion is of a positive value ( $\gamma_b > 0^\circ$ ) in internal gear pairs

It is instructive to note here that the actual value only of a gear base cone angle,  $\Gamma_b$ , can be of up to  $\Gamma_b = 90^\circ$ , and not a pinion base cone angle,  $\gamma_b$ . This is because the gear tooth count,  $N_g$ , by convention is greater than the mating pinion tooth count,  $N_p$ , and, thus, the gear base cone angle,  $\Gamma_b$ , is greater than pinion base cone angle,  $\gamma_b$  (i.e., inequality  $\Gamma_b \geq \gamma_b$  is valid).

The face width of the plane of action,  $F_{pa}$ , or, in other words, the working/effective/functional portion of the plane of action,  $PA$ , is situated in between two circles of radii,  $r_{o,pa}$  and  $r_{l,pa}$ . The total portion of the plane of action spans within a central angle,  $\varphi_{pa}$ . The angle,  $\varphi_{pa}$ , is measured in between the lines of contact,  $lc_g$  and  $lc_p$ , of the plane of action,  $PA$ , with each of the two base cones.

**Conclusion 12.1.** *Geometrically accurate intersected-axes gear pairs are those gear pairs capable of transmitting an input uniform rotary motion with a constant angular velocity ratio (smoothly).*

*Intersected-axes gear pairs for which neither equivalent base cones nor the plane of action,  $PA$ , can be constructed, are referred to as approximate intersected-axes gear pairs. The tooth flanks of approximate intersected-axes gear pairs feature geometry for which no equivalent pulley-and-belt transmission can be designed to replace the gear pair.*

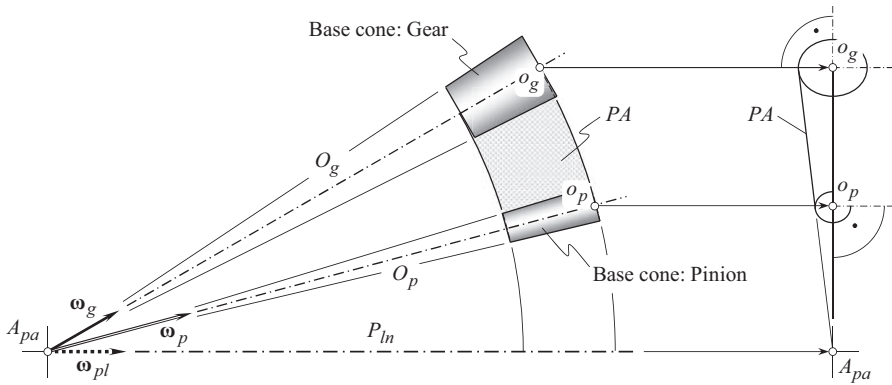


**FIGURE 12.13** Base kinematics of rotationally positive external intersected-axes gear pair: schematic of external gear-to-pinion mesh with a large transverse pressure angle,  $\phi_{\omega, t}$ .

**Conclusion 12.2.** *Approximate intersected-axes gear pairs are those gear pairs that are not capable of transmitting an input uniform rotation with a constant angular velocity ratio (smoothly).*

*Almost all the bevel gears produced in the present-day industry are the gears for approximate intersected-axes gear pairs. No angular base pitch can be specified in approximate gearsets.*

Similar to the discussion in Chapter 6, parallel-axes gearsets with a large transverse pressure angle,  $\phi_t$ , (see Figures 6.8 and 6.10), intersected-axes gear pairs with a large transverse pressure angle,  $\phi_{\omega, t}$ , can be designed, as well. The discussion on gearing of this particular kind is limited here just to a brief analysis of the base kinematics of rotationally positive external intersected-axes gear pair. Illustrated in Figure 12.13, an external gear-to-pinion mesh with a large transverse pressure angle,  $\phi_{\omega, t}$ , is considered here just for illustrative purposes. Gearsets of this design got no comprehensive investigation yet.

### 12.3.1 PATH OF CONTACT, AND INSTANTANEOUS LINE OF ACTION

The path of contact and the line of action in geometrically accurate intersected-axes gearing can be defined similarly to that they are defined in parallel-axes gearing.

Consider a plane of action,  $PA$ , in intersected-axes gear pair, as illustrated in Figure 12.14. When the gears rotate, the plane of action spins about the plane-of-action apex,  $A_{pa}$ , with an angular velocity,  $\omega_{pa}$ .

In an arbitrary configuration of the gears, arbitrary point,  $m_i$ , is chosen within the instantaneous line of contact,  $LC_{inst}$ . When the plane of action,  $PA$ , rotates, the line of contact,  $LC_{inst}$ , travels together with the plane of action. In this motion, each point,  $m_i$ , within the line of contact,  $LC_{inst}$ , traces a circular arc of a corresponding radius,  $r_{y, pa}$ . The arc, by nature, is a path of contact,  $P_c$ , in intersected-axes gear pair. All the paths of contact are planar curves each of which is situated within the plane of action,  $PA$ . A family of all the paths of contact,  $P_c$ , can be viewed as the plane of action,  $PA$ .

Neither the geometry nor the configuration of the desirable line of contact,  $LC_{des}$ , in relation to the plane of action,  $PA$ , are allowed to be altered when the tooth flank of a particular gear,  $\mathcal{G}$ , and of its mating pinion,  $\mathcal{P}$ , are generated. This feature is important for the gear cutting tool designer, for the gear inspection purposes, and so forth.

At arbitrary point,  $m_i$ , a straight line tangent to the corresponding path of contact,  $P_c$ , can be constructed. By nature, the straight line is an instantaneous line of action,  $LA_{inst}$ , through point of

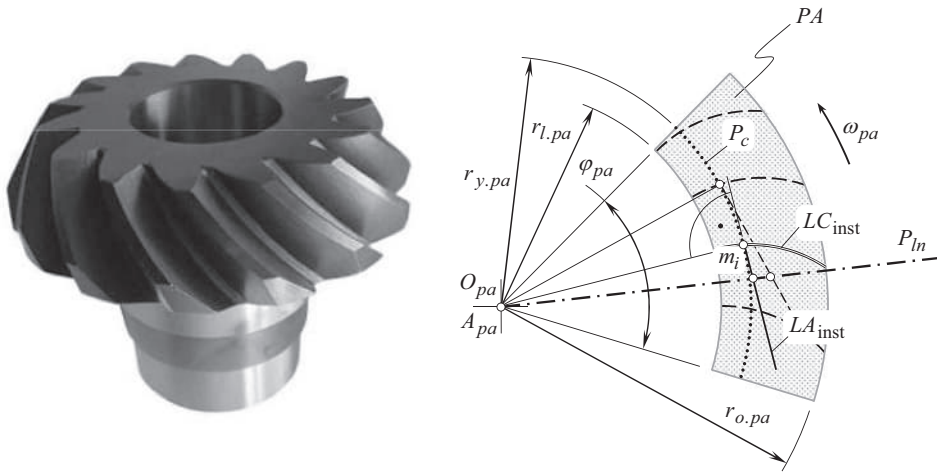


**FIGURE 12.14** Path of contact,  $P_c$ , and instantaneous line of action,  $LA_{inst}$ , in geometrically accurate intersected-axes gearing.

interest,  $m_i$ . All the instantaneous lines of action are situated within the plane of action,  $PA$ , and all of them intersect the axis of instantaneous rotation,  $P_{ln}$ , at corresponding point. If all the instantaneous lines of action,  $LA_{inst}$ , through all the points of the line of contact,  $LC$ , always intersect the axis of instantaneous rotation,  $P_{ln}$  (for any and all angular configurations of the gear and of the mating pinion), then all the centers of curvature of a gear/pinion tooth flank are located within the axis of instantaneous rotation,  $P_{ln}$ . In this way, fulfillment of the conjugate action law for the interacting tooth flanks,  $\mathcal{F}$  and  $\mathcal{P}$ , of a gear and a mating pinion in intersected-axes gearing, is ensured.

Every path of contact,  $P_c$ , can be viewed as an envelope to a family of consecutive positions of the instantaneous lines of action,  $LA_{inst}$ , when the gears rotate.

### 12.3.2 OPERATING BASE PITCH CALCULATION

By definition, the *operating base pitch*,  $\varphi_{b.op}$ , in intersected-axes gear pair (or just *OBP*, for simplicity), is an angle formed by straight lines that originate at the *plane-of-action apex*,  $A_{pa}$ , and pass through the corresponding points within two consequent desirable lines of contact,  $LC_{des}^i$  and  $LC_{des}^{i+1}$ . As the operating base pitch is an angular parameter, it is reasonable to refer to it as to *operating angular base pitch*,  $\varphi_{b.op}$ . The *operating angular base pitch*,  $\varphi_{b.op}$ , is measured within the plane of action,  $PA$ , of the gear pair. This is a calculated design parameter, and, thus, its actual value cannot be measured directly.

IIIIConsider an arbitrary intersected-axes gearset. The gear/pinion can be intersected by an arbitrary plane perpendicular to the gear/pinion center line,  $O_g$  (or  $O_p$ ). A circle of a radius  $r_{b.g}$  (or  $r_{b.p}$ ) is a line of intersection of the base cone of the gear/pinion by the normal plane. A circular arc of the length  $2\pi r_{b.g}/N_g$  (or  $2\pi r_{b.p}/N_p$ ) in the gear/pinion equals to a corresponding circular arc,  $\varphi_{b.op}$ , in the plane of action,  $PA$ . Therefore, the operating angular base pitch in an intersected-axes gear pair can be calculated from one of two formulas:

$$\varphi_{b.op} = \frac{2\pi}{N_g} \cdot \frac{r_{b.g}}{r_{pa}} \quad (12.27)$$

$$\varphi_{b.op} = \frac{2\pi}{N_p} \cdot \frac{r_{b.p}}{r_{pa}} \quad (12.28)$$

The calculated value of the operating angular base pitch,  $\phi_{b.op}$  [see Eqs. (12.27) and (12.28)], in intersected-axes gearset makes possible calculation of the operating base pitches,  $\phi_{b.g}$  and  $\phi_{b.p}$ , of a gear, and of a mating pinion. The base pitches,  $\phi_{b.g}$  and  $\phi_{b.p}$ , are calculated from the expression:

$$\phi_{b.op} = 2\pi N_g \sin \Gamma_b \quad (12.29)$$

or as:

$$\phi_{b.op} = 2\pi N_p \sin \gamma_b \quad (12.30)$$

When the gears rotate, a gear/pinion circle of a radius  $r_{b.g}$  (or  $r_{b.p}$ ) rolls with no sliding over a circle of a corresponding plane of action radius  $r_{pa}$ .

## 12.4 TOOTH FLANKS IN GEAR FOR GEOMETRICALLY ACCURATE INTERSECTED-AXES GEARSET

The conjugate tooth flanks of a gear and of a mating pinion in intersected-axes gearset are in line contact with one another.<sup>1</sup> The line of contact is entirely situated within the plane of action,  $PA$ . As the gears rotate, the line of contact travels in relation to the gear, to the pinion as well as to the gears housing. The tooth flank of the gear,  $\mathcal{G}$ , can be viewed as a locus of consecutive positions of the line of contact,  $LC$ , in its motion in relation to a reference system associated with the gear. Similarly, the tooth flank of the pinion,  $\mathcal{P}$ , can be viewed as a locus of consecutive positions of that same line of contact,  $LC$ , in its motion in relation to a reference system associated with the pinion. Ultimately, the locus of consecutive positions of that same line of contact,  $LC$ , in its motion in relation to a stationary reference system associated with the gear housing, represents the surface of action,  $S_a$ . In geometrically accurate intersected-axes gear pair, the surface of action,  $S_a$ , and the plane of action,  $PA$ , are congruent to one another (as long as the transverse pressure angle,  $\phi_{\omega.t}$ , is of a constant value along the line of contact,  $LC$ ). However, if a geometrically accurate intersected-axes gear pair features the transverse pressure angle of a different value,  $\phi_{t.\omega}$ , at different points of the line of contact,  $LC$ , the surface of action,  $S_a$ , deviates from the plane of action,  $PA$ .

Therefore, once a line of contact,  $LC$ , is specified, the kinematics of an intersected-axes gearing (see Figure 12.12) can be employed for the derivation of an analytical expression for the position vector of point of tooth flank of a gear,  $\mathcal{G}$ , and that of its mating pinion,  $\mathcal{P}$ . For this purpose, several reference systems are required to be introduced.

### 12.4.1 APPLIED COORDINATE SYSTEMS AND LINEAR TRANSFORMATIONS

Intersected-axes gearing is discussed below using for this purpose numerous coordinate systems, each of which is convenient for a particular application, and not for the analytical description of the entire gearset. Solely for convenience, in addition to the set of main reference systems (see Chapter 3), numerous auxiliary (intermediate) reference systems are also introduced below.

#### 12.4.1.1 Main Reference Systems

Main reference systems, which are discussed below, are introduced in compliance with the approach disclosed in Chapter 3: *Principal Planes and Principal Reference Systems Associated with Gear Pair*.

**First**, a *Cartesian* coordinate system,  $X_g Y_g Z_g$ , is associated with the gear, as shown in Figure 12.15.

**Second**, a *Cartesian* coordinate system,  $X_p Y_p Z_p$ , is associated with the pinion (see Figure 12.15).

<sup>1</sup> The considered below in Chapter 19  $S_{pr}$ -gearing with point contact between the tooth flanks,  $\mathcal{G}$  and  $\mathcal{P}$ , is the only exclusion from this rule.

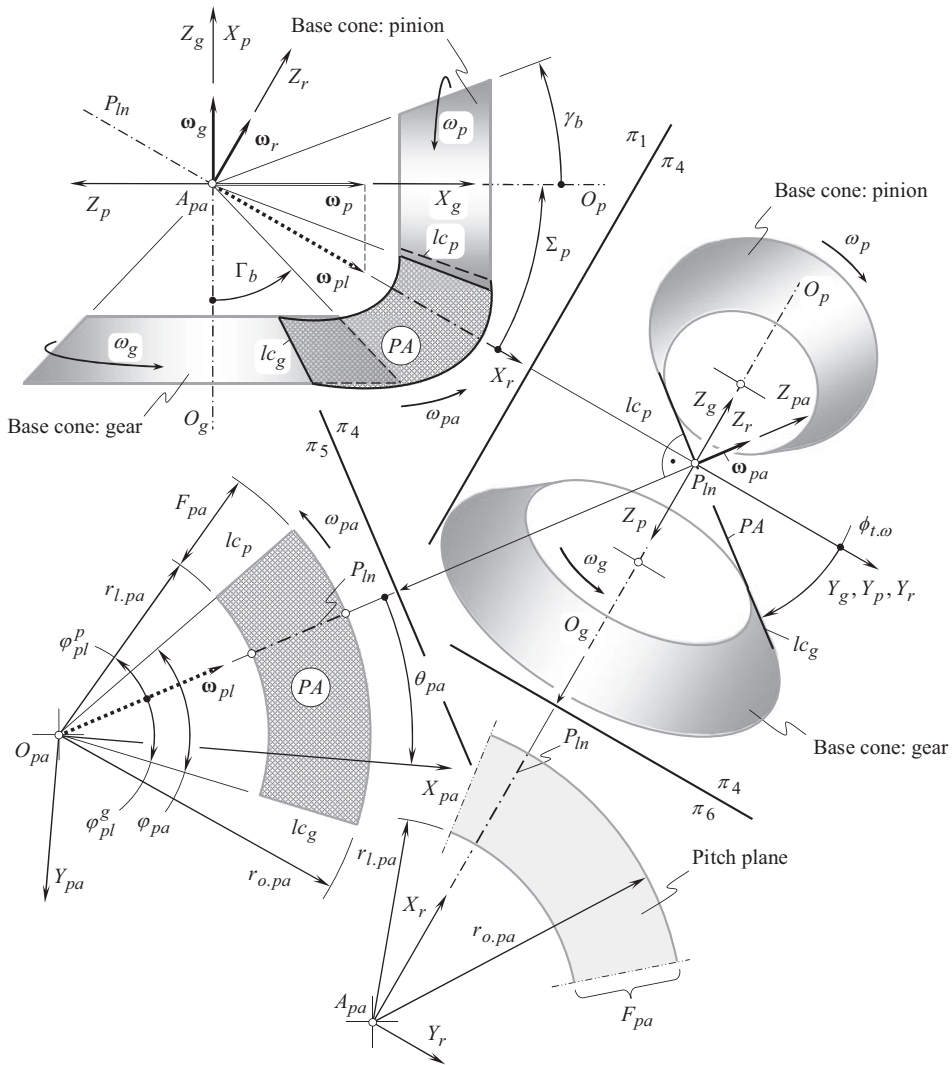


**FIGURE 12.15** Reference systems that are used for the derivation of analytical expressions for a gear tooth flank,  $\mathcal{S}$ , and its mating pinion tooth flank,  $\mathcal{P}$ , in intersected-axes gearset.

**Third**, a *Cartesian* coordinate system,  $X_r Y_r Z_r$ , is associated with the auxiliary round rack (of the crown gear, in other words) that is engaged in mesh simultaneously with both, with the gear and with its mating pinion.

**Fourth**, a *Cartesian* coordinate system,  $X_{pa} Y_{pa} Z_{pa}$ , is associated with the plane of action,  $PA$ .

**Fifth**, a stationary *Cartesian* coordinate system,  $X_h Y_h Z_h$ , is associated with the gear housing.

A few more auxiliary reference systems are used below as well.

The origin of the coordinate system  $X_r Y_r Z_r$  coincides with the plane-of-action apex,  $A_{pa}$ . The orientation of the coordinate system,  $X_r Y_r Z_r$ , is defined by the rotation vectors  $\omega_g$ ,  $\omega_p$ , and  $\omega_{pl}$ . The  $X_r$  – axis is aligned with the vector,  $\omega_{pl}$ , of instantaneous rotation. The axis  $Y_r$  aligns with the vector defined by cross product  $\omega_p \times \omega_g$ . Ultimately, the  $Z_r$  – axis is pointed along the vector that is defined by the triple vector product  $\omega_p \times \omega_g \times \omega_{pl}$ .

The coordinate system,  $X_{pa} Y_{pa} Z_{pa}$ , shares the origin with the reference system,  $X_r Y_r Z_r$ . The axis,  $X_{pa}$ , is located within the plane of action,  $PA$ . It forms an angle,  $\theta_{pa}$ , with the vector of instantaneous rotation,  $\omega_{pl}$ . The  $Y_{pa}$  – axis is also located within the plane of action,  $PA$ , and is perpendicular to

the  $X_{pa}$  – axis (here  $\theta_{pa} = \omega_{pa} \cdot t$ , and time is denoted here by  $t$ ). Finally, the axis  $Z_{pa}$  complements the axes  $X_{pa}$  and  $Y_{pa}$  to the left-hand oriented *Cartesian* coordinate system  $X_{pa}Y_{pa}Z_{pa}$ .

The coordinate system  $X_{pa}Y_{pa}Z_{pa}$  is convenient to be used for the specification of a line of contact,  $LC$ , between the gear tooth flank,  $\mathcal{S}$ , and of the pinion tooth flank,  $\mathcal{P}$ , similar to that that has been done with respect to parallel-axes gear pairs (see Figure 6.12 for more details). Then, the analytical representation of the current position of the traveling line of contact,  $LC$ , in the reference systems,  $X_gY_gZ_g$  and  $X_pY_pZ_p$ , will return an analytical expression for the tooth flanks,  $\mathcal{S}$  and  $\mathcal{P}$ , of the gear and of the pinion. Similarly, an analytical representation of a current position of the traveling line of contact,  $LC$ , in the motionless reference system,  $X_hY_hZ_h$ , will return an equation for the surface of action (usually, this is a *plane* of action).

### 12.4.1.2 Operators of Rolling

For the derivation of an equation of the gear tooth flank,  $\mathcal{S}$ , an operator  $\mathbf{Rs}(PA \mapsto \mathcal{S})$  of the resultant coordinate system transformation is required to be derived. The operator,  $\mathbf{Rs}(PA \mapsto \mathcal{S})$ , can be expressed in terms of:

- The operator of rotation,  $\mathbf{Rt}(pa \mapsto pa_0)$ , of the coordinate system  $X_{pa}Y_{pa}Z_{pa}$  about the  $Z_{pa}$  – axis through an angle,  $\theta_{pa}$ . When the axis  $X_{pa}$  is aligned to the rotation vector  $\omega_{pl}$ , then the reference system  $X_{pa}Y_{pa}Z_{pa}$  occupies a particular configuration  $X_{pa}^0Y_{pa}^0Z_{pa}^0$  (the coordinate system  $X_{pa}^0Y_{pa}^0Z_{pa}^0$  is not depicted in Figure 12.15). The operator  $\mathbf{Rt}(pa \mapsto pa_0)$  can be expressed in matrix form as:

$$\mathbf{Rt}(pa \mapsto pa_0) = \begin{bmatrix} \cos \theta_{pa} & 0 & -\sin \theta_{pa} & 0 \\ 0 & 1 & 0 & 0 \\ \sin \theta_{pa} & 0 & \cos \theta_{pa} & 0 \\ 0 & 0 & 0 & 1 \end{bmatrix} \quad (12.31)$$

- The operator of rotation,  $\mathbf{Rt}(pa_0 \mapsto r)$ , of the coordinate system  $X_{pa}^0Y_{pa}^0Z_{pa}^0$  about the vector of instantaneous rotation,  $\omega_{pl}$  (through the transverse profile angle,  $\phi_{t,\omega}$ , that is measured within a plane that is perpendicular to the rotation vector,  $\omega_{pl}$ ):

$$\mathbf{Rt}(pa_0 \mapsto r) = \begin{bmatrix} 1 & 0 & 0 & 0 \\ 0 & \cos \phi_{t,\omega} & -\sin \phi_{t,\omega} & 0 \\ 0 & \sin \phi_{t,\omega} & \cos \phi_{t,\omega} & 0 \\ 0 & 0 & 0 & 1 \end{bmatrix} \quad (12.32)$$

- The operator of rotation,  $\mathbf{Rt}(r \mapsto g)$ , of the coordinate system  $X_rY_rZ_r$  about the  $Y_r$  – axis through the angle  $\angle(\omega_r, \omega_p)$ . Note that the angle  $\angle(\omega_r, \omega_p)$  is equal to the angle  $\angle(\omega_p, \omega_{pl}) = \Sigma_p$ . The operator of rotation,  $\mathbf{Rt}(r \mapsto g)$ , can be represented in the form:

$$\mathbf{Rt}(r \mapsto g) = \begin{bmatrix} \cos \Sigma_p & 0 & \sin \Sigma_p & 0 \\ 0 & 1 & 0 & 0 \\ -\sin \Sigma_p & 0 & \cos \Sigma_p & 0 \\ 0 & 0 & 0 & 1 \end{bmatrix} \quad (12.33)$$

The operator,  $\mathbf{Rs}(PA \mapsto \mathcal{S})$ , of the resultant coordinate system transformation is equal to the product:

$$\mathbf{Rs}(PA \mapsto \mathcal{S}) = \mathbf{Rt}(r \mapsto g) \cdot \mathbf{Rt}(pa_0 \mapsto r) \cdot \mathbf{Rt}(pa \mapsto pa_0) \quad (12.34)$$

This operator,  $\mathbf{Rs}(PA \mapsto \mathcal{S})$ , allows for matrix representation in the form:

$$\mathbf{Rs}(PA \mapsto \mathcal{S}) =$$

$$\begin{bmatrix} \cos \Sigma_p \cos \theta_{pa} + \sin \Sigma_p \cos \phi_{t,\omega} \sin \theta_{pa} & \sin \Sigma_p \sin \phi_{t,\omega} & \sin \Sigma_p \cos \phi_{t,\omega} \cos \theta_{pa} - \cos \Sigma_p \sin \theta_{pa} & 0 \\ -\sin \phi_{t,\omega} \sin \theta_{pa} & \cos \phi_{t,\omega} & -\sin \phi_{t,\omega} \cos \theta_{pa} & 0 \\ \cos \Sigma_p \cos \phi_{t,\omega} \sin \theta_{pa} - \sin \Sigma_p \cos \theta_{pa} & \cos \Sigma_p \sin \phi_{t,\omega} & \sin \Sigma_p \sin \theta_{pa} + \cos \Sigma_p \cos \phi_{t,\omega} \cos \theta_{pa} & 0 \\ 0 & 0 & 0 & 1 \end{bmatrix} \quad (12.35)$$

The operator,  $\mathbf{Rs}(PA \mapsto \mathcal{P})$ , of the resultant coordinate system transformation, namely, the operator of transition from the coordinate system  $X_{pa}Y_{pa}Z_{pa}$ , associated with the plane of action,  $PA$ , to the coordinate system,  $X_pY_pZ_p$ , associated with the pinion, is equal to the product:

$$\mathbf{Rs}(PA \mapsto \mathcal{P}) = \mathbf{Rt}(r \mapsto p) \cdot \mathbf{Rt}(pa_0 \mapsto r) \cdot \mathbf{Rt}(pa \mapsto pa_0) \quad (12.36)$$

Here, the operator of rotation,  $\mathbf{Rt}(r \mapsto p)$ , can be derived in a manner, similar to that an expression for the operator  $\mathbf{Rt}(r \mapsto g)$  [see Eq. (12.33)] is derived. The similarity allows for the following expression for the operator of rotation,  $\mathbf{Rt}(r \mapsto p)$ :

$$\mathbf{Rt}(r \mapsto p) = \begin{bmatrix} \cos \Sigma_g & 0 & \sin \Sigma_g & 0 \\ 0 & 1 & 0 & 0 \\ -\sin \Sigma_g & 0 & \cos \Sigma_g & 0 \\ 0 & 0 & 0 & 1 \end{bmatrix} \quad (12.37)$$

After being substituted into Eq. (12.36), Eq. (12.37) together with Eqs. (12.31) and (12.32) returns an expression for the operator of the resultant coordinate system transformation,  $\mathbf{Rs}(PA \mapsto \mathcal{P})$ :

$$\mathbf{Rs}(PA \mapsto \mathcal{P}) =$$

$$\begin{bmatrix} \cos \Sigma_g \cos \theta_{pa} + \sin \Sigma_g \cos \phi_{t,\omega} \sin \theta_{pa} & \sin \Sigma_g \sin \phi_{t,\omega} & \sin \Sigma_g \cos \phi_{t,\omega} \cos \theta_{pa} - \cos \Sigma_g \sin \theta_{pa} & 0 \\ -\sin \phi_{t,\omega} \sin \theta_{pa} & \cos \phi_{t,\omega} & -\sin \phi_{t,\omega} \cos \theta_{pa} & 0 \\ \cos \Sigma_g \cos \phi_{t,\omega} \sin \theta_{pa} - \sin \Sigma_g \cos \theta_{pa} & \cos \Sigma_g \sin \phi_{t,\omega} & \sin \Sigma_g \sin \theta_{pa} + \cos \Sigma_g \cos \phi_{t,\omega} \cos \theta_{pa} & 0 \\ 0 & 0 & 0 & 1 \end{bmatrix} \quad (12.38)$$

The operators,  $\mathbf{Rs}(PA \mapsto \mathcal{S})$  and  $\mathbf{Rs}(PA \mapsto \mathcal{P})$ , of the resultant coordinate system transformations are a kind of operators of rolling. As operators of linear transformation of this kind are extensively used in the theory of gearing, for the analysis of intersected-axes gears, in particular, special designations, namely,  $\mathbf{Ri}(PA \mapsto \mathcal{S})$ , and,  $\mathbf{Ri}(PA \mapsto \mathcal{P})$ , are assigned to each of them:

$$\mathbf{Rs}(PA \mapsto \mathcal{S}) = \mathbf{Ri}(PA \mapsto \mathcal{S}) \quad (12.39)$$

$$\mathbf{Rs}(PA \mapsto \mathcal{P}) = \mathbf{Ri}(PA \mapsto \mathcal{P}) \quad (12.40)$$

As the operators of rolling,  $\mathbf{Ri}(PA \mapsto \mathcal{S})$  and  $\mathbf{Ri}(PA \mapsto \mathcal{P})$ , are known, the operator of rolling,  $\mathbf{Ri}(\mathcal{P} \mapsto \mathcal{S})$ , of the pinion over the gear can be calculated as:

$$\mathbf{Ri}(\mathcal{P} \mapsto \mathcal{S}) = \mathbf{Ri}(PA \mapsto \mathcal{S}) \cdot \mathbf{Ri}^{-1}(PA \mapsto \mathcal{P}) \quad (12.41)$$



Similarly, the operator of rolling,  $\mathbf{Ri}(\mathcal{S} \mapsto \mathcal{P})$ , of the gear over the pinion can be calculated either as reciprocal to the operator,  $\mathbf{Ri}(\mathcal{P} \mapsto \mathcal{S})$ , or an expression:

$$\mathbf{Ri}(\mathcal{S} \mapsto \mathcal{P}) = \mathbf{Ri}^{-1}(\mathcal{P} \mapsto \mathcal{S}) = \mathbf{Ri}(PA \mapsto \mathcal{P}) \cdot \mathbf{Ri}^{-1}(PA \mapsto \mathcal{S}) \quad (12.42)$$

can be used for the calculation of the operator of rolling  $\mathbf{Ri}(\mathcal{S} \mapsto \mathcal{P})$ .

### 12.4.1.3 Operators of Linear Transformations Associated with the Gear Housing

A stationary reference system,  $X_h Y_h Z_h$ , is associated with the housing of a gear pair. The choice of the coordinate system,  $X_h Y_h Z_h$ , depends solely on the user's convenience. In a particular case, either the stationary *Cartesian* coordinate system,  $X_g^0 Y_g^0 Z_g^0$ , or the stationary *Cartesian* coordinate system,  $X_p^0 Y_p^0 Z_p^0$ , can be used for this purpose.

The coordinate system,  $X_g^0 Y_g^0 Z_g^0$ , shares a common  $Z_g$  – axis with the coordinate system  $X_g Y_g Z_g$  associated with the gear. The coordinate system,  $X_g Y_g Z_g$ , is turned in relation to the motionless coordinate system,  $X_g^0 Y_g^0 Z_g^0$ , through an angle,  $\varphi_g$ . Similarly, the reference system,  $X_p^0 Y_p^0 Z_p^0$ , shares a common  $Z_p$  – axis with the coordinate system,  $X_p Y_p Z_p$ , associated with the pinion. The coordinate system,  $X_p Y_p Z_p$ , is turned in relation to the motionless coordinate system,  $X_p^0 Y_p^0 Z_p^0$ , through an angle,  $\varphi_p$ . It is of importance to note here that the rotation angles,  $\varphi_g$  and  $\varphi_p$ , correspond to one another according to an expression  $\varphi_p = u \varphi_g$ , and  $u$  designates the tooth ratio of the gear pair.

For external intersected-axes gearset, the rotation angles,  $\varphi_g$  and  $\varphi_p$ , are of opposite sign.

The rotation of the reference system,  $X_g Y_g Z_g$ , about the  $Z_g$  – axis through an angle,  $\varphi_g$ , is analytically described by the operator of rotation,  $\mathbf{Rt}(\mathcal{S} \mapsto h)$ . This operator is expressed in the form:

$$\mathbf{Rt}(\mathcal{S} \mapsto h) = \begin{bmatrix} \cos \varphi_g & \sin \varphi_g & 0 & 0 \\ -\sin \varphi_g & \cos \varphi_g & 0 & 0 \\ 0 & 0 & 1 & 0 \\ 0 & 0 & 0 & 1 \end{bmatrix} \quad (12.43)$$

Equation (12.43) allows for an expression for the operator of the resultant coordinate system transformation, namely, for the operator of transition,  $\mathbf{Rs}(pa \mapsto h)$ , from the coordinate system,  $X_{pa} Y_{pa} Z_{pa}$ , associated with the plane of action, to the stationary coordinate system,  $X_h Y_h Z_h$ . This operator is represented as the product:

$$\mathbf{Rs}(pa \mapsto h) = \mathbf{Rt}(\mathcal{S} \mapsto h) \cdot \mathbf{Ri}(PA \mapsto \mathcal{S}) \quad (12.44)$$

or in matrix form:

$$\mathbf{Rs}(pa \mapsto h) =$$

$$\begin{bmatrix} \cos \varphi_g (\cos \Sigma_p \cos \theta_{pa} + \sin \Sigma_p \cos \phi_{t,\omega} \sin \theta_{pa}) - \sin \varphi_g \sin \phi_{t,\omega} \sin \theta_{pa} & \sin \varphi_g \cos \phi_{t,\omega} + \sin \Sigma_p \cos \varphi_g \sin \phi_{t,\omega} \\ -\sin \varphi_g (\cos \Sigma_p \cos \theta_{pa} + \sin \Sigma_p \cos \phi_{t,\omega} \sin \theta_{pa}) - \cos \varphi_g \sin \phi_{t,\omega} \sin \theta_{pa} & \cos \varphi_g \cos \phi_{t,\omega} - \sin \Sigma_p \sin \varphi_g \sin \phi_{t,\omega} \\ \cos \Sigma_p \cos \phi_{t,\omega} \sin \theta_{pa} - \sin \Sigma_p \cos \theta_{pa} & \cos \Sigma_p \sin \phi_{t,\omega} \\ 0 & 0 \\ -\cos \varphi_g (\cos \Sigma_p \sin \theta_{pa} - \sin \Sigma_p \cos \phi_{t,\omega} \cos \theta_{pa}) - \sin \varphi_g \sin \phi_{t,\omega} \cos \theta_{pa} & 0 \\ -\sin \varphi_g (\cos \Sigma_p \sin \theta_{pa} - \sin \Sigma_p \cos \phi_{t,\omega} \cos \theta_{pa}) - \sin \varphi_g \sin \phi_{t,\omega} \cos \theta_{pa} & 0 \\ \sin \Sigma_p \sin \theta_{pa} + \cos \Sigma_p \cos \phi_{t,\omega} \cos \theta_{pa} & 0 \\ 0 & 1 \end{bmatrix} \quad (12.45)$$



The rotation of the reference system,  $X_p Y_p Z_p$ , about the  $Z_p$  – axis through an angle,  $\varphi_p = -u\varphi_g$ , is analytically described by the operator of rotation,  $\mathbf{Rt}(\mathcal{P} \mapsto h_p)$ . This operator can be expressed in the form:

$$\mathbf{Rt}(\mathcal{P} \mapsto h_p) = \begin{bmatrix} \cos \varphi_p & \sin \varphi_p & 0 & 0 \\ -\sin \varphi_p & \cos \varphi_p & 0 & 0 \\ 0 & 0 & 1 & 0 \\ 0 & 0 & 0 & 1 \end{bmatrix} \quad (12.46)$$

Equation (12.46) yields an expression for the operator of the resultant coordinate system transformation, namely, for the operator of transition,  $\mathbf{Rs}(pa \mapsto h_p)$ , from the coordinate system,  $X_{pa} Y_{pa} Z_{pa}$ , associated with the plane of action, to the stationary coordinate system,  $X_{h,p} Y_{h,p} Z_{h,p}$ . This operator can be represented as the product:

$$\mathbf{Rs}(pa \mapsto h_p) = \mathbf{Rt}(\mathcal{S} \mapsto h) \cdot \mathbf{Ri}(PA \mapsto \mathcal{S}) \quad (12.47)$$

or in matrix form:

$$\mathbf{Rs}(pa \mapsto h_p) = \begin{bmatrix} \cos \varphi_p (\cos \Sigma_g \cos \theta_{pa} + \sin \Sigma_g \cos \phi_{t,\omega} \sin \theta_{pa}) - \sin \varphi_p \sin \phi_{t,\omega} \sin \theta_{pa} & \sin \varphi_p \cos \phi_{t,\omega} + \sin \Sigma_p \cos \varphi_p \sin \phi_{t,\omega} \\ -\sin \varphi_p (\cos \Sigma_g \cos \theta_{pa} + \sin \Sigma_g \cos \phi_{t,\omega} \sin \theta_{pa}) - \cos \varphi_p \sin \phi_{t,\omega} \sin \theta_{pa} & \cos \varphi_p \cos \phi_{t,\omega} - \sin \Sigma_p \sin \varphi_p \sin \phi_{t,\omega} \\ \cos \Sigma_g \cos \phi_{t,\omega} \sin \theta_{pa} - \sin \Sigma_g \cos \theta_{pa} & \cos \Sigma_p \sin \phi_{t,\omega} \\ 0 & 0 \\ -\cos \varphi_p (\cos \Sigma_g \sin \theta_{pa} - \sin \Sigma_g \cos \phi_{t,\omega} \cos \theta_{pa}) - \sin \varphi_p \sin \phi_{t,\omega} \cos \theta_{pa} & 0 \\ -\sin \varphi_p (\cos \Sigma_g \sin \theta_{pa} - \sin \Sigma_g \cos \phi_{t,\omega} \cos \theta_{pa}) - \sin \varphi_p \sin \phi_{t,\omega} \cos \theta_{pa} & 0 \\ \sin \Sigma_g \sin \theta_{pa} + \cos \Sigma_g \cos \phi_{t,\omega} \cos \theta_{pa} & 0 \\ 0 & 1 \end{bmatrix} \quad (12.48)$$

Both the reference systems, namely, the coordinate systems,  $X_h Y_h Z_h$  and  $X_{h,p} Y_{h,p} Z_{h,p}$ , are stationary reference systems associated with the housing of the gear pair. The relation between these two coordinate systems is analytically described by the expression:

$$\mathbf{Rs}(h_p \mapsto h) = \mathbf{Rs}(pa \mapsto h) \cdot \mathbf{Rs}^{-1}(pa \mapsto h_p) \quad (12.49)$$

The derived equations for the operators of the coordinate system transformations make yield to express any and all geometrical parameters (a) of the gear, (b) of the pinion, and (c) of the gear-to-pinion mesh, in a common reference system.

## 12.4.2 TOOTH FLANK OF A GEAR IN INTERSECTED-AXES GEAR PAIR

The tooth flank of a bevel gear allows for interpretation as a locus of consecutive positions of the line of contact,  $LC$ , when the plane of action,  $PA$ , is either wrapping onto or unwrapping from the base cone of the gear, and is unwrapping from, or wrapping onto the base cone of the pinion.<sup>2</sup> In

<sup>2</sup> The proposed approach of generation of a gear/pinion tooth flank in intersected-axes gearing can be referred to as *describing approach* for the gear/pinion tooth flank generation. It is important to stress here that generation of an involute curve (a) by point, namely, in describing method and (b) by a straight line, namely, in generating method, can be equivalent to one another only in a case of parallel-axes gearing, and is not valid neither in a case of *intersected-axes*, nor in a case of *crossed-axes* gearings. Only approximate gear/pinion tooth flanks can be generated by a straight line in the latter two cases of tooth flank generation.

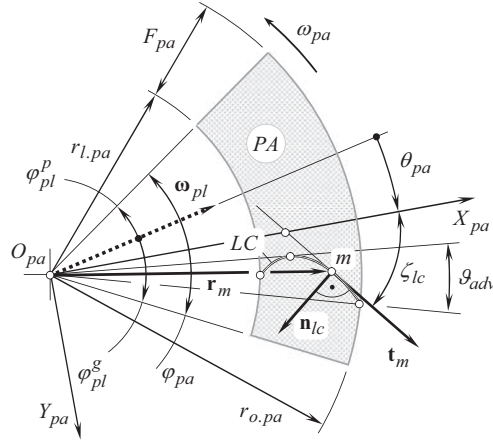


**FIGURE 12.16** General case of a desirable line of contact,  $LC$ , between a gear tooth flank,  $\mathcal{S}$ , and its mating pinion tooth flank,  $\mathcal{P}$ , in intersected-axes gearset. (Important note: the line of contact,  $LC$ , is constructed *prior* to the tooth flanks,  $\mathcal{S}$  and  $\mathcal{P}$ , are constructed.)

order to derive an expression for a gear/pinion tooth flank, the line of contact is required to be represented in a reference system associated with the gear.

Any planar curve of a reasonable geometry can be employed as the desirable line of contact,  $LC$ , in a gearset. Details on a favorable geometry of the desirable line of contact,  $LC$ , in an intersected-axes gear pair are required to be considered in detail separately.

The shape of the line of contact depends on the geometry of tooth flanks of a gear,  $\mathcal{S}$ , and that of a mating pinion,  $\mathcal{P}$  (in the lengthwise direction, in particular). Under any circumstances (with no exclusions), the line of contact,  $LC$ , is entirely situated within the coordinate plane,  $X_{pa}Y_{pa}$ , of the reference system,  $X_{pa}Y_{pa}Z_{pa}$ , associated with the plane of action, as schematically illustrated in Figure 12.16.

In general, the position vector of point,  $\mathbf{r}_{lc}$ , of the line of contact,  $LC$ , can be analytically described by an expression in matrix form:

$$\mathbf{r}_{lc}(v) = \begin{bmatrix} X_{lc}(v) \\ Y_{lc}(v) \\ 0 \\ 1 \end{bmatrix} \quad (12.50)$$

Depending on the geometry of a chosen line of contact,  $LC$ , a gear tooth flank of a complex geometry can be generated. As an example, Figure 12.17 illustrates a bevel gear that features the line of contact,  $LC$ , shaped in a form of a sine function.

In order to represent (12.50) of the position vector of point,  $\mathbf{r}_{lc}$ , of the line of contact,  $LC$ , in the reference system,  $X_gY_gZ_g$ , associated with the gear, the operator of the resultant coordinate system transformation,  $\mathbf{Rs}(PA \mapsto \mathcal{S})$ , is employed:

$$\mathbf{r}_g(v, \theta_{pa}) = \mathbf{r}_{lc}^g(v, \theta_{pa}) = \mathbf{Rs}(PA \mapsto \mathcal{S}) \cdot \mathbf{r}_{lc}(v) \quad (12.51)$$

When the axis,  $X_{pa}$ , is pointed along one of the sides of the face advance angle,  $\vartheta_{adv}$ , the actual value of the central angle,  $\theta_{pa}$ , falls into the range of (see Figure 12.16):

$$\varphi_{pl}^p + \vartheta_{adv} \leq \theta_{pa} \leq \varphi_{pl}^g - \vartheta_{adv} \quad (12.52)$$



**FIGURE 12.17** Bevel gear with tooth flanks generated by means of sine function as the line of contact,  $LC$ .

Here, the angles  $\varphi_{pl}^s$  and  $\varphi_{pl}^p$  are of the opposite signs. Otherwise, the angles that  $X_{pa}$  – axis forms with the sides of the face advance angle,  $\vartheta_{adv}$ , are required to be taken into consideration.

Substituting the position vector,  $\mathbf{r}_{lc}$  [see Eq. (12.50)] and the operator of the resultant coordinate system transformation,  $\mathbf{R}_s(PA \mapsto \mathcal{S})$  [see Eq. (12.35)], into Eq. (12.51), one can derive an expression for the position vector of point,  $\mathbf{r}_g$ , of the gear tooth flank,  $\mathcal{S}$ :

$$\mathbf{r}_g(v, \theta_{pa}) = \begin{bmatrix} (\cos \Sigma_p \cos \theta_{pa} + \sin \Sigma_p \cos \phi_{t,\omega} \sin \theta_{pa}) \cdot X(v) + \sin \Sigma_p \sin \phi_{t,\omega} \cdot Y(v) \\ -X(v) \sin \phi_{t,\omega} \sin \theta_{pa} + Y(v) \cos \phi_{t,\omega} \\ -(\sin \Sigma_p \cos \theta_{pa} - \cos \Sigma_p \cos \phi_{t,\omega} \sin \theta_{pa}) \cdot X(v) + \cos \Sigma_p \sin \phi_{t,\omega} \cdot Y(v) \\ 1 \end{bmatrix} \quad (12.53)$$

In a particular case, when the line of contact,  $LC$ , is a straight line segment, as shown in Figure 12.18, the position vector of point,  $\mathbf{r}_{lc}$ , of the line of contact,  $LC$ , is equal to the sum:

$$\mathbf{r}_{lc} = \mathbf{r}_{lc}^0 + \mathbf{r}_{lc}^\lambda \quad (12.54)$$

Here, in Eq. (12.54), the vector  $\mathbf{r}_{lc}^0$  is of a constant length,  $\mathbf{r}_{lc}^0 = \mathbf{i} \cdot r_{lc}^0$ , where  $r_{lc}^0 = |\mathbf{r}_{lc}^0|$ . Another component, namely, the vector,  $\mathbf{r}_{lc}^\lambda$ , can be represented in the form:

$$\mathbf{r}_{lc}^\lambda(\lambda) = \mathbf{i} \cdot \lambda \cos \zeta_{cl} + \mathbf{j} \cdot \lambda \sin \zeta_{cl} \quad (12.55)$$

where:

$\lambda$  – is the length of the vector  $\mathbf{r}_{lc}^\lambda$ .

$\zeta_{cl}$  – is the angle of inclination of the line of contact,  $LC$ , in relation to the  $X_{pa}$  – axis of the coordinate system  $X_{pa}Y_{pa}Z_{pa}$  (see Figure 12.18).



An expression for the position vector of point,  $\mathbf{r}_g$ , of the tooth flank of a straight bevel gear can be defined as the product:

$$\mathbf{r}_g(X_{pa}, \theta_{pa}) = \mathbf{Rs}(PA \mapsto \mathcal{S}) \cdot \mathbf{r}_{lc}(X_{pa}) \quad (12.60)$$

where the operator  $\mathbf{Rs}(PA \mapsto \mathcal{S})$  of the resultant coordinate system transformation is given by Eq. (12.35).

It is important to stress here that the expression for the position vector of point,  $\mathbf{r}_g$ , of a gear tooth flank,  $\mathcal{S}$  as well as a similar expression for the position vector of point,  $\mathbf{r}_p$ , of a mating pinion tooth flank,  $\mathcal{P}$ , are derived on the premise that both, the tooth flanks,  $\mathcal{S}$  and  $\mathcal{P}$ , are generated by means of the line of contact,<sup>3</sup>  $LC$ , that travels together with the plane of action,  $PA$ , and not as an envelope to a family of consecutive positions of the tooth flank of an auxiliary generating rack,  $\mathcal{R}$ . In this way, the necessity of implementation of elements of the theory of enveloping surfaces is eliminated, and, thus, derivation of the required equation becomes significantly easier.

Equation (12.60) allows for an expanded form of the expression for the position vector of point,  $\mathbf{r}_g$ , of the straight bevel gear tooth flank:

$$\mathbf{r}_g(X_{pa}, \theta_{pa}) = \begin{bmatrix} X_{pa}(\cos \Sigma_p \cos \theta_{pa} + \sin \Sigma_p \cos \phi_{t,\omega} \sin \theta_{pa}) \\ -X_{pa} \sin \phi_{t,\omega} \sin \theta_{pa} \\ -X_{pa}(\sin \Sigma_p \cos \theta_{pa} - \cos \Sigma_p \cos \phi_{t,\omega} \sin \theta_{pa}) \\ 1 \end{bmatrix} \quad (12.61)$$

Gears that have tooth flanks [see Eq. (12.61)] are often referred to as *involute bevel gears*. However, it is preferred to refer to gears of this particular design as to *geometrically accurate gears for intersected-axes gearsets*.

Gears for intersected-axes gear pairs that have tooth flank geometry of the just discussed geometry are analogous to parallel-axes involute gears. Under certain conditions, Eq. (12.61) can be reduced to Eq. (7.15). Only those gears for intersected-axes gear pairs that feature tooth flank geometry in compliance with Eq. (12.61) are capable of transmitting an input uniform rotation smoothly.

An analytical expression for the line of contact,  $LC$ , yields the calculation of the important design parameters of intersected-axes gearset. Expressions for:

1. the unit normal vector,  $\mathbf{n}_g$ , at point of interest of the gear tooth flank,  $\mathcal{S}$
2. the unit normal vector,  $\mathbf{n}_p$ , at point of interest of the pinion tooth flank,  $\mathcal{P}$ , and
3. the unit normal vector,  $\mathbf{n}_r$ , at point of interest of the tooth flank of the auxiliary generating round rack,  $\mathcal{R}$  (of the round basic rack),

can be derived based on the unit normal vector,  $\mathbf{n}_{lc}$ , to the line of contact,  $LC$ , which is constructed within the plane of action,  $PA$ . For this purpose, an equation for the unit normal vector,  $\mathbf{n}_{lc}$ , has to be considered together with the corresponding operator of the coordinate system transformations. The unit normal vector,  $\mathbf{n}_{lc}$ , is perpendicular to a planar curve. In a general form, the formulas for the unit normal vectors  $\mathbf{n}_g$ ,  $\mathbf{n}_p$ , and  $\mathbf{n}_r$ , can be expressed as:

$$\mathbf{n}_g(X_{pa}, \theta_{pa}) = \mathbf{Rs}(PA \mapsto \mathcal{S}) \cdot \mathbf{n}_{lc}(X_{pa}) \quad (12.62)$$

$$\mathbf{n}_p(X_{pa}, \theta_{pa}) = \mathbf{Rs}(PA \mapsto \mathcal{P}) \cdot \mathbf{n}_{lc}(X_{pa}) \quad (12.63)$$

<sup>3</sup> It is instructive to point out here, that the line of contact,  $LC$ , between the tooth flanks,  $\mathcal{S}$  and  $\mathcal{P}$ , is the first to be determined when designing an intersected-axes gearset. The tooth flanks of a gear,  $\mathcal{S}$ , and a mating pinion,  $\mathcal{P}$ , are determined on later stages (by means of the earlier constructed line of contact,  $LC$ ).

$$\mathbf{n}_r(X_{pa}, \theta_{pa}) = \mathbf{Rs}(PA \mapsto \mathcal{R}) \cdot \mathbf{n}_{lc}(X_{pa}) \quad (12.64)$$

The following conclusion can be drawn up from the above-performed analysis:

**Conclusion 12.3.** *In intersected-axes gearing with a constant pressure angle, transmission of an input uniform rotary motion from a driving shaft to a driven shaft is possible if and only if the plane of action is a plane through the axis of instantaneous rotation.*

Equation (12.53) as well as Eqs. (12.58) and (12.61) allow for the calculation of the unit normal vector,  $\mathbf{n}_g$ , to the gear tooth flank,  $\mathcal{S}$ , at any point of interest within the tooth surface,  $\mathcal{S}$ . The unit normal vector,  $\mathbf{n}_g$ , and a straight line pointed along the unit vector,  $\mathbf{n}_g$ , are used for the calculation of the deviations of an actual gear tooth flank from the tooth flank of the geometrically accurate gear.

Knowing the position vector,  $\mathbf{r}_g(v, \theta_{pa})$ , of point of interest within the gear tooth flank,  $\mathcal{S}$ , the unit normal vector,  $\mathbf{n}_g$ , is calculated as:

$$\mathbf{n}_g(v, \theta_{pa}) = \frac{\frac{\partial \mathbf{r}_g}{\partial v} \times \frac{\partial \mathbf{r}_g}{\partial \theta_{pa}}}{\left| \frac{\partial \mathbf{r}_g}{\partial v} \times \frac{\partial \mathbf{r}_g}{\partial \theta_{pa}} \right|} (v, \theta_{pa}) \quad (12.65)$$

Calculation of the derivatives  $\frac{\partial \mathbf{r}_g}{\partial v}$  and  $\frac{\partial \mathbf{r}_g}{\partial \theta_{pa}}$  from Eq. (12.53) followed by the formula transformation [see Eq. (12.65)] is a drilling procedure. The procedure of calculation of the unit normal vector,  $\mathbf{n}_g$ , can be significantly simplified if the vector  $\mathbf{n}_g$  as well as a straight line pointed along the vector,  $\mathbf{n}_g$ , are determined in the reference system  $X_{pa}Y_{pa}Z_{pa}$ , associated with the plane of action (in this reference system, the unit normal vector,  $\mathbf{n}_g$ , is identical to the unit normal vector,  $\mathbf{n}_{lc}$ , to the line of contact,  $LC$ ). Afterward, implementation of the operator,  $\mathbf{Rs}(PA \mapsto \mathcal{S})$ , of the resultant coordinate system transformation [see Eq. (12.35)] allows for the representation of both the unit normal vector,  $\mathbf{n}_{lc}$ , and the straight line along it, in the coordinate system  $X_gY_gZ_g$  associated with the gear.

Referring to Figure 12.16, the position vector,  $\mathbf{r}_m$ , of point of the line of contact,  $LC$ , can be given by an expression in vector notation:

$$\mathbf{r}_m = \mathbf{i} \cdot X_m + \mathbf{j} \cdot Y_m \quad (12.66)$$

In Eq. (12.66), the *Cartesian* coordinates of point of interest,  $m$ , are denoted by  $X_m$  and  $Y_m$ , correspondingly.

The unit tangent vector,  $\mathbf{t}_m$ , at point  $m$  can be expressed in the form:

$$\mathbf{t}_m = \mathbf{i} \cdot \cos \zeta_{cl} + \mathbf{j} \cdot \sin \zeta_{cl} \quad (12.67)$$

Consider a case when the line of contact,  $LC$ , is represented in an explicit form as  $Y_{cl} = Y_{cl}(X_{cl})$ . Inclination of the unit tangent vector,  $\mathbf{t}_m$ , in relation to the  $X_g$  – axis [see Eq. (12.67)] at point of interest,  $m$ , is specified by an angle,  $\zeta_{cl}$ :

$$\zeta_{cl} = \tan^{-1} \left( \frac{\partial Y_{cl}(X_{cl})}{\partial X_{cl}} \right) \quad (12.68)$$

Once the unit tangent vector,  $\mathbf{t}_m$  [see Eq. (12.67)], is known, an expression for the unit normal vector,  $\mathbf{n}_{lc}$ , can be represented in vector form:

$$\mathbf{n}_{lc} = -\mathbf{i} \cdot \sin \zeta_{cl} + \mathbf{j} \cdot \cos \zeta_{cl} \quad (12.69)$$

Ultimately, the implementation of Eqs. (12.66)–(12.69) allows to express the position vector of point,  $\mathbf{r}_{n,lc}$ , of a straight line through point of interest,  $m$ , along the unit vector,  $\mathbf{n}_{lc}$ :

$$\mathbf{r}_{n,lc} = \mathbf{r}_m + \lambda_n \mathbf{n}_{lc} \quad (12.70)$$

or in matrix representation as:

$$\mathbf{r}_{n,lc} = \begin{bmatrix} X_m - \lambda_n \sin \zeta_{lc} \\ Y_m + \lambda_n \cos \zeta_{lc} \\ 0 \\ 1 \end{bmatrix} \quad (12.71)$$

In Eq. (12.70),  $\lambda_n$  is the distance of point of interest,  $m$ , from the end of the position vector,  $\mathbf{r}_m$ .

In the reference system  $X_g Y_g Z_g$ , an expression for the unit normal vector,  $\mathbf{n}_g$ , to the gear tooth flank,  $\mathcal{S}$ , can be derived from the equation:

$$\mathbf{n}_g = \mathbf{Rs}(PA \mapsto \mathcal{S}) \cdot \mathbf{n}_{lc} \quad (12.72)$$

Similarly, an expression for the position vector of point,  $\mathbf{r}_{n,lc}$ , in the reference system  $X_g Y_g Z_g$ , can be derived from the equation:

$$\mathbf{r}_{n,lc}^g = \mathbf{Rs}(PA \mapsto \mathcal{S}) \cdot \mathbf{r}_{n,lc} \quad (12.73)$$

Finally, Eq. (12.73) and the operator of the resultant coordinate system transformation,  $\mathbf{Rs}(PA \mapsto \mathcal{S})$  [see Eq. (12.35)], yield an equation:

$$\mathbf{r}_{n,lc}^g(\lambda) = \begin{bmatrix} (\cos \Sigma_p \cos \theta_{pa} + \sin \Sigma_p \cos \phi_{t,\omega} \sin \theta_{pa}) \cdot (X_m - \lambda \sin \zeta_{lc}) + \sin \Sigma_p \sin \phi_{t,\omega} (Y_m + \lambda \cos \zeta_{lc}) \\ -\sin \phi_{t,\omega} \sin \theta_{pa} \cdot (X_m - \lambda \sin \zeta_{lc}) + \cos \phi_{t,\omega} (Y_m + \lambda \cos \zeta_{lc}) \\ -(\sin \Sigma_p \cos \theta_{pa} + \cos \Sigma_p \cos \phi_{t,\omega} \sin \theta_{pa}) \cdot (X_m - \lambda \sin \zeta_{lc}) + \cos \Sigma_p \sin \phi_{t,\omega} (Y_m + \lambda \cos \zeta_{lc}) \\ 1 \end{bmatrix} \quad (12.74)$$

for the position vector of point,  $\mathbf{r}_{n,lc}^g$ , of the tooth flank of the gear,  $\mathcal{S}$ , that features an arbitrary shape in the lengthwise direction.

The discussed approach can be used to develop a CAD model of a geometrically accurate gear, and its tooth flanks of all possible designs. As an example, a CAD model of a tooth of a geometrically accurate spiral bevel gear for intersected-axes gearset is shown in Figure 12.19.

When a pair of conjugate tooth flanks,  $\mathcal{S}$  and  $\mathcal{P}$ , is generated by means of a desirable line of contact,  $LC_{des}$ , an originally specified geometry of  $LC_{des}$  does not alter when the gears rotate. The desirable line of contact,  $LC_{des}$ , is a *rigid* planar curve that is entirely located within the plane of action,  $PA$ . The initially specified configuration of the  $LC_{des}$  in relation to the plane of action,  $PA$ , is retained.

Tooth flank geometry in a geometrically accurate straight bevel gear is schematically illustrated in Figure 12.20. It is evident from the analysis of the schematic shown in Figure 12.20 that the gear tooth flank,  $\mathcal{S}$ , cannot be generated by a straight-sided crown rack commonly used in the design and production of straight bevel gears. All the gears, those designed and finish-cut on the premise of a

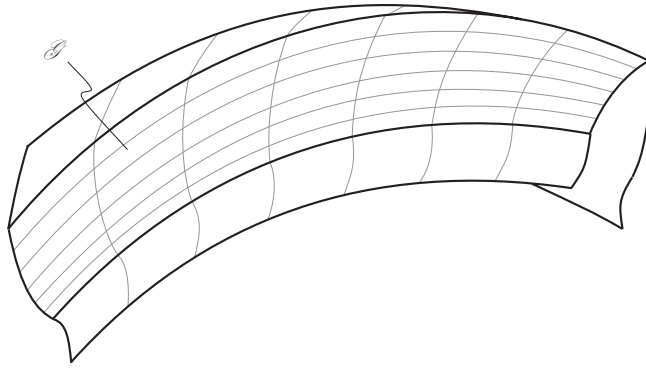


**FIGURE 12.19** CAD model of a tooth of a geometrically accurate gear for intersected-axes gearset.

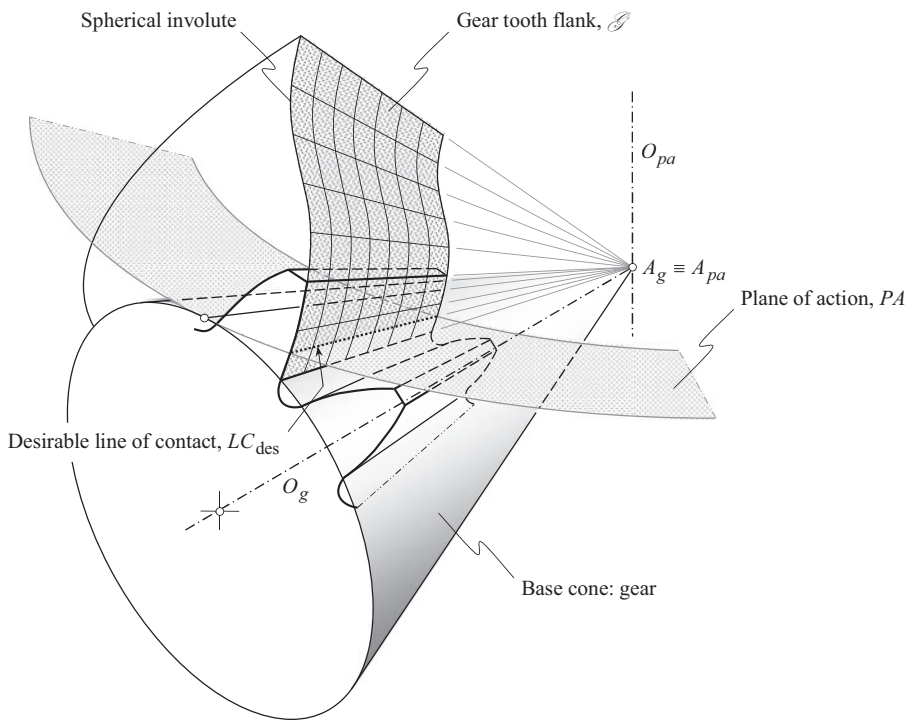


**FIGURE 12.20** Tooth flank,  $\mathcal{S}$ , of a geometrically accurate straight bevel gear.

straight-sided crown rack (see Figure 12.21) are approximate gears, and under no circumstances, they can be geometrically accurate.

When the tooth flanks,  $\mathcal{S}$  and  $\mathcal{P}$ , of a gear and of a mating pinion for an intersected-axes gear pair are generated by means of the cutter head, envelopes to corresponding families of generating surfaces of the gear cutting tool exist, however, these envelopes are not conjugate to one another, as the conjugate action law (the second fundamental law of gearing) is violated when a bevel gear is finish-generated by means of a straight-sided crown rack.

Once an equation of a gear tooth flank is derived, then a variation of the tooth flank geometry can be investigated, that is, normal curvature of the gear tooth flank can be calculated at an arbitrary point of interest, variation of the tooth profile angle, and helix angle can be determined, special



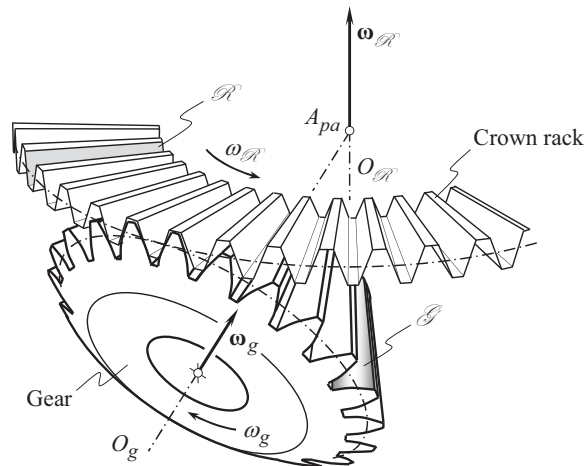


**FIGURE 12.21** Only approximate straight bevel gears can be generated by means of the straight-sided crown rack.

point of meshing can be investigated, and so forth [similar to that in parallel-axes gears (see Figure 10.45)].

An equation of a spherical involute tooth profile in intersected-axes gearing can be derived on the premise of Eq. (12.74) under an assumption that the coordinates  $X_m$ ,  $Y_m$ , and  $Z_m$ , of point of interest,  $m$ , fulfil the requirement:

$$\sqrt{X_m^2 + Y_m^2 + Z_m^2} = R_{sph} \quad (12.75)$$

where  $R_{sph}$  is the radius of a sphere on which the spherical involute tooth profile is constructed.

For a spherical involute (in  $I_a$  – gearing), a function “ $\text{inv}(\phi_{t,\omega})$ ” that is similar to that in  $P_a$  – gearing, can be determined.

In a manner, similar to that just discussed, the unit normal vector,  $\mathbf{n}_g$ , to a gear tooth flank,  $\mathcal{G}$ , as well as the position vector of point,  $\mathbf{r}_{n,lc}^g$ , of a straight line through point of interest,  $m$ , in the direction of  $\mathbf{n}_g$  can be calculated for the line of contact,  $LC$ , of any reasonable geometry. An arc of a circle, an arc of a spiral curve, a straight line segment, and so forth, are good examples of the line of contact,  $LC$ , between gears in an intersected-axes gearset.

Formulas analogous to the above-discussed equations are valid for a pinion tooth flank,  $\mathcal{P}$ , as well.

The constructed tooth flanks,  $\mathcal{G}$  and  $\mathcal{P}$ , of a gear, and of a mating pinion meet all three necessary, and sufficient fundamental laws of gearing that all geometrically accurate intersected-axes gearsets has to meet, namely, they fulfil:

- The law of contact [that can be analytically expressed by *Shishkov equation of contact*,  $\mathbf{n}_g \cdot \mathbf{V}_\Sigma = 0$ ]
- The conjugate action law (at every instant of time, an instantaneous line of action,  $LA_{\text{inst}}$ , has to be located within the plane of action,  $PA$ , and must intersect the axis of instantaneous rotation,  $P_{\text{in}}$ , of the gear pair (Prof. S.P. Radzevich, ~2008)
- The law equal angular base pitches of a gear, and that of a mating pinion, to the operating base pitch of the gear pair,  $\phi_{b,g} = \phi_{b,op}$ , and  $\phi_{b,p} = \phi_{b,op}$  (Prof. S.P. Radzevich, ~2008). Another (equivalent) form,  $\phi_{b,g} = \phi_{b,op} = \phi_{b,p}$ , of representation of these two equations,  $\phi_{b,g} = \phi_{b,op}$ , and  $\phi_{b,p} = \phi_{b,op}$ , is also known

The just listed fundamental laws that geometrically accurate intersected-axes gearing of all designs have to meet and have to be verified in the order they are listed above. For instance, there is no sense to verify the law of equal angular base pitches if the law of contact violated.

The derived equations for the gear tooth flank,  $\mathcal{S}$ , as well as for the pinion tooth flank,  $\mathcal{P}$ , can be used to construct the reference surfaces (datum surfaces) when designing, and when machining/finishing gears for geometrically accurate intersected-axes gearsets. Surfaces of this kind are equivalent to screw involute surface extensively used as a reference surface for parallel-axes involute gear pairs.

### 12.4.3 PATH OF CONTACT POINT

In geometrically accurate intersected-axes gearing certain correlation is observed between the path of contact point (namely, a point within the line of contact,  $LC$ ), and between a section of a gear tooth by a sphere centering at the plane-of-action point,  $A_{pa}$ . A path of contact point is considered in a reference system associated with the plane of action. That same curve, namely, the path of contact point, considered in a reference system associated with the gear, represents a curve that is entirely situated within the gear tooth flank,  $\mathcal{S}$ .

In the analysis of a path of contact point, represented immediately below, the following set of reference systems is associated with the plane of action, and with the gear.

The reference system,  $X_{pa}Y_{pa}Z_{pa}$ , is associated with the plane of action,  $PA$ , as shown in Figure 12.22. The axis  $Z_{pa}$  is pointed along the axis of rotation,  $O_{pa}$ , of the plane of action. When the gears rotate the plane of action reference system,  $X_{pa}Y_{pa}Z_{pa}$ , is rotated together with the gears. In an arbitrary orientation of the plane of action, the corresponding reference system is designated as  $X_{pa}^\phi Y_{pa}^\phi Z_{pa}^\phi$ . The reference system  $X_{pa}^\phi Y_{pa}^\phi Z_{pa}^\phi$  is turned about the axis  $Z_{pa}$  through an angle,  $\phi_{pa}$ .

The reference system,  $X_gY_gZ_g$ , is associated with the gear (see Figure 12.22). The axis  $Z_g$  is pointed along the axis of rotation,  $O_g$ , of the gear. When the gears rotate the gear reference system,  $X_gY_gZ_g$ , is rotated together with the gears. In an arbitrary orientation of the gear, the corresponding reference system is designated as  $X_g^\phi Y_g^\phi Z_g^\phi$ . The reference system  $X_g^\phi Y_g^\phi Z_g^\phi$  is turned about the axis  $Z_g$  through an angle,  $\phi_g$ .

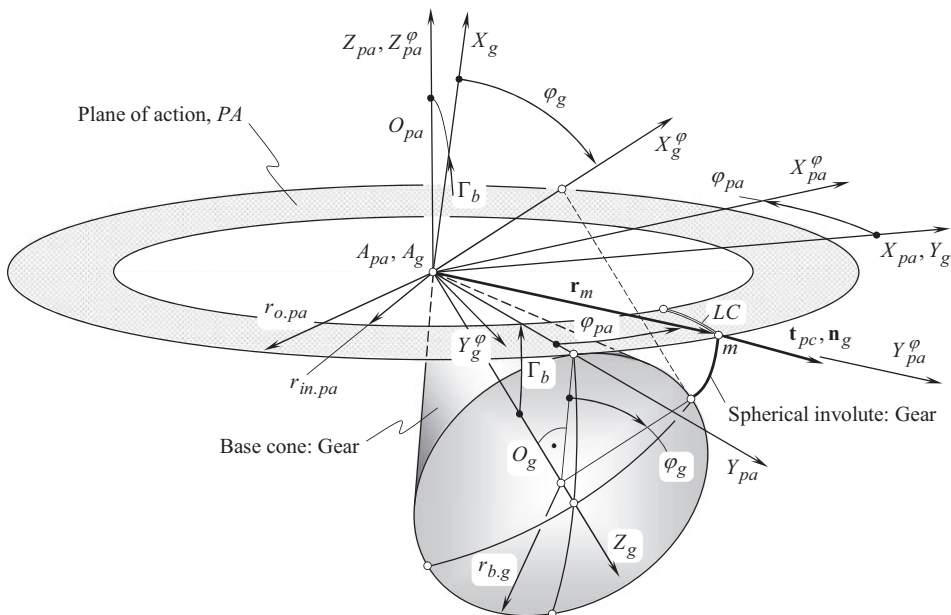


FIGURE 12.22 Path of contact point.

The angles of rotation,  $\varphi_{pa}$  and  $\varphi_g$ , correlate to one another according to the formula:  $\varphi_{pa} = u \varphi_g$ , where  $u_\omega$  is the angular velocity ratio of the pair *plane-of-action-to-gear*.

In the initial configuration of the reference systems  $X_{pa}Y_{pa}Z_{pa}$  and  $X_gY_gZ_g$ , the latter can be considered as turned in relation to the first one through the gear base-cone-angle,  $\Gamma_b$  (see Figure 12.22).

Once a set of reference systems is established, then analysis of the kinematics and the geometry of an intersected-axes gearset can be performed.

Consider point of interest,  $m$ , that is situated within the plane of action,  $PA$ , at a distance  $r_{o.pa}$  from the plane-of-action point,  $A_{pa}$  (generally speaking, this could be an arbitrary distance,  $r_{y.pa}$ ). The active portion of the plane of action is located in between two concentric circles of radii  $r_{o.pa}$  and  $r_{in.pa}$ . Here,  $r_{o.pa}$  is the radius of the outer circle of the plane of action, and  $r_{in.pa}$  is the radius of the inner circle of the plane of action. The effective face-width in the gearset equals to  $F_{pa} = r_{o.pa} - r_{in.pa}$ .

The position vector of point of interest,  $m$ , is designated as  $\mathbf{r}_m$ . In the reference system,  $X_{pa}^\varphi Y_{pa}^\varphi Z_{pa}^\varphi$ , the vector  $\mathbf{r}_m$  is specified by an equation:

$$\mathbf{r}_m = \begin{bmatrix} 0 \\ r_{o.pa} \\ 0 \\ 1 \end{bmatrix}_{X_{pa}^\varphi Y_{pa}^\varphi Z_{pa}^\varphi} \quad (12.76)$$

For the transition from the reference system,  $X_{pa}^\varphi Y_{pa}^\varphi Z_{pa}^\varphi$ , to the reference system,  $X_g^\varphi Y_g^\varphi Z_g^\varphi$ , an operator of the resultant coordinate systems transformation,  $\mathbf{Rs}(PA^\varphi \mapsto G^\varphi)$ , is required to be derived. The operator of the linear transformation,  $\mathbf{Rs}(PA^\varphi \mapsto G^\varphi)$ , can be calculated from the expression:

$$\mathbf{Rs}(PA^\varphi \mapsto G^\varphi) = \mathbf{Rt}(\varphi_g, Z_g) \cdot \mathbf{Rt}[(\Gamma_b + 90^\circ), X_{pa}] \cdot \mathbf{Rt}(\varphi_{pa}, X_{pa}^\varphi) \quad (12.77)$$

Here,  $\mathbf{Rt}(\varphi_g, Z_g)$  is the operator of the transition from the coordinate system  $X_{pa}^\varphi Y_{pa}^\varphi Z_{pa}^\varphi$  to the coordinate system  $X_{pa}Y_{pa}Z_{pa}$ ;  $\mathbf{Rt}[(\Gamma_b + 90^\circ), X_{pa}]$  is the operator of the transition from the coordinate system  $X_{pa}Y_{pa}Z_{pa}$  to the coordinate system  $X_gY_gZ_g$ ; and  $\mathbf{Rt}(\varphi_{pa}, X_{pa}^\varphi)$  is the operator of the transition from the coordinate system  $X_gY_gZ_g$  to the coordinate system  $X_g^\varphi Y_g^\varphi Z_g^\varphi$  (see Appendix D for the operators of linear transformations).

Considered together, Eqs. (12.76) and (12.77) yield an expression for the position vector of point,  $\mathbf{r}_{sph}$ , of the spherical involute of the gear:

$$\mathbf{r}_{sph} = \mathbf{Rs}(PA^\varphi \mapsto G^\varphi) \cdot \mathbf{r}_m \quad (12.78)$$

The vector,  $\mathbf{r}_{sph}$ , is the position vector of point of interest,  $m$ , expressed in the gear reference system  $X_g^\varphi Y_g^\varphi Z_g^\varphi$  (remember that the position vector of that same point of interest,  $m$ , expressed in the plane-of-action reference system  $X_{pa}^\varphi Y_{pa}^\varphi Z_{pa}^\varphi$  is designated as  $\mathbf{r}_m$ ).

Equation (12.78) is valid for all points of the line of contact,  $LC$ , of the gearset.

An example of the path of contact,  $P_c$ , is illustrated in Figure 12.23. As it follows from the analysis of modeling in Figure 12.23, no octoid profile is generated in rolling of the base cone over the plane of action,  $PA$ .

At every point of the path of point of interest,  $m$ , the instantaneous line of action,  $LA_{inst}$  (a straight line through the point of interest,  $m$ ), is tangential to the path of point,  $m$ . Therefore, the tangent vector,  $\mathbf{t}_m$ , to the path of point,  $m$ , is pointed along the unit normal vector,  $\mathbf{n}_g$ , to the gear tooth flank,  $\mathcal{S}$ . This is one more evidence of that no octoid gearing is possible, as this inevitably entails the violation of the second fundamental law of gearing.

An analysis similar to that just performed can also be performed with respect to the mating pinion.

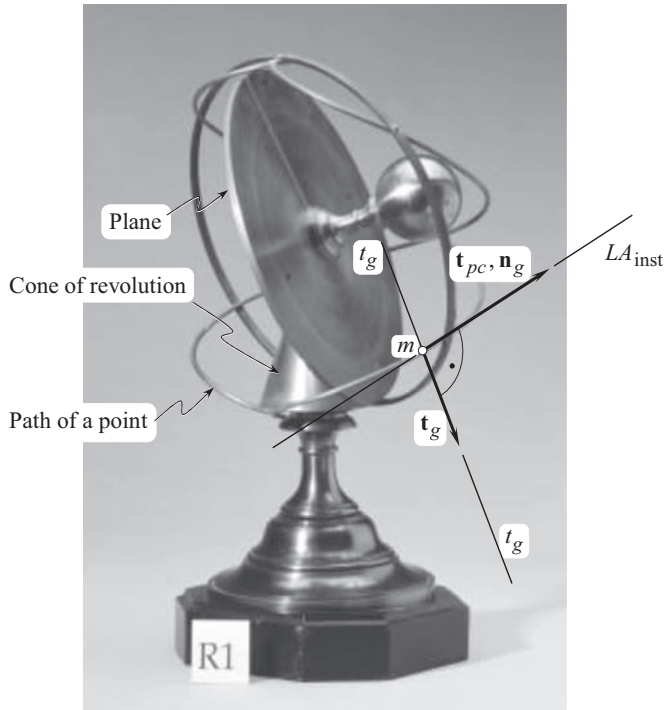


**FIGURE 12.23** Demonstration of rolling of a cone of revolution over a plane – no octoid profile is generated in such a relative motion of the base cone and the plane of action.

#### 12.4.4 INTERSECTED-AXES GEARING WITH VARIABLE PRESSURE ANGLE

The formulated above set of three fundamental laws of gearing is helpful to realize the key features of design of intersected-axes gearing with variable (within the active portion of the face width,  $F_{pa}$ ) transverse pressure angle,  $\phi_{t,\omega} = \text{var}$ . In a gearset of such a design, the transverse pressure angle,  $\phi_{t,\omega}$ , can be of a different value at different transverse sections of the gearset by a sphere that centers at the plane-of-action apex,  $A_{pa}$ . However, when the gears rotate, the actual value of the transverse pressure angle,  $\phi_{t,\omega}$ , is remained of a constant value at every transverse section of the gearset by a corresponding sphere. The possibility of variation of the transverse pressure angle,  $\phi_{t,\omega}$ , is necessary when solving the problem of synthesizing an intersected-axes gear pair with favorable design parameters, namely, of an intersected-axes gearset with desirable performance.

In a geometrically accurate gear pair the transverse pressure angle,  $\phi_t$ , is assumed to be of a constant value within a line of contact,  $LC$  (at every contact point). Certain imperfections in approximate gear pairs can be balanced/neutralized by a corresponding variation of the transverse pressure angle,  $\phi_t$ , along the line of contact,  $LC$ .

The plane of action,  $PA$ , can be subdivided onto an infinite number of infinitesimally narrow,  $dr_{pa}$ , round strips. All the round strips are centered at the plane-of-action apex,  $A_{pa}$ , and all of them pass through the axis of instantaneous rotation,  $P_m$ . The transverse pressure angle,  $\phi_{t,\omega}$ , can be set of an optimum value for each of the strips. In this way, the transverse pressure angle,  $\phi_{t,\omega}$ , is involved in the synthesizing process of the gear pair with favorable performance. In this manner, the plane of action,  $PA$ , in conventional bevel gear design, is replaced with the surface of action,  $SA$ , of a corresponding geometry. Surface of action,  $SA$ , is a kind of ruled surfaces.

Gears with a variable pressure angle,  $\phi_{t,\omega}$ , can be machined on a multi-axis NC machine.

## 12.5 ANALYTICAL REPRESENTATION OF CONJUGATE ACTION LAW IN INTERSECTED-AXES GEARING

Conjugacy is a specific property of tooth flanks of a gear,  $\mathcal{G}$ , and of its mating pinion,  $\mathcal{P}$ . Only surfaces that roll over one another can feature this unique property. Due to this property, in rolling motion of a gear and of a pinion over one another, the tooth flanks,  $\mathcal{G}$  and  $\mathcal{P}$ , can be viewed as a kind of *reversibly enveloping surfaces* (or just  $R_e$  – surfaces, for simplicity) [155]. When a gear and a mating pinion rotate uniformly, the gear tooth flank,  $\mathcal{G}$ , can be viewed as an envelope to a family of consecutive positions of the mating pinion tooth flank,  $\mathcal{P}$ . Generated this way, the gear tooth flank,  $\mathcal{G}$ , can be used to generate the mating pinion tooth flank. If the tooth flanks,  $\mathcal{G}$  and  $\mathcal{P}$ , are conjugate, then the original pinion tooth flank,  $\mathcal{P}$ , and the pinion tooth flank,  $\mathcal{P}_g$ , generated by the gear tooth flank,  $\mathcal{G}$ , are identical to one another (i.e., the tooth flanks are congruent to one another,  $\mathcal{P}_g \equiv \mathcal{P}$ ).

Tooth flanks not of an arbitrary geometry can be referred to as the *conjugate surfaces*, or, the same, *reversibly enveloping surfaces* [155].

In order to possess the property of conjugacy, a criterion to be fulfilled by two tooth flanks,  $\mathcal{G}$  and  $\mathcal{P}$ , can be established. Moreover, this criterion needs to be expressed analytically.

When a gear,  $\mathcal{G}$ , and a mating pinion,  $\mathcal{P}$ , tooth flanks interact with one another, straight lines that align to common perpendiculars,  $\mathbf{n}_g$ , through points within a current line of contact,  $LC$ , must always intersect the axis of instantaneous rotation,  $P_{ln}$  (see Figure 12.24). The conjugate action law

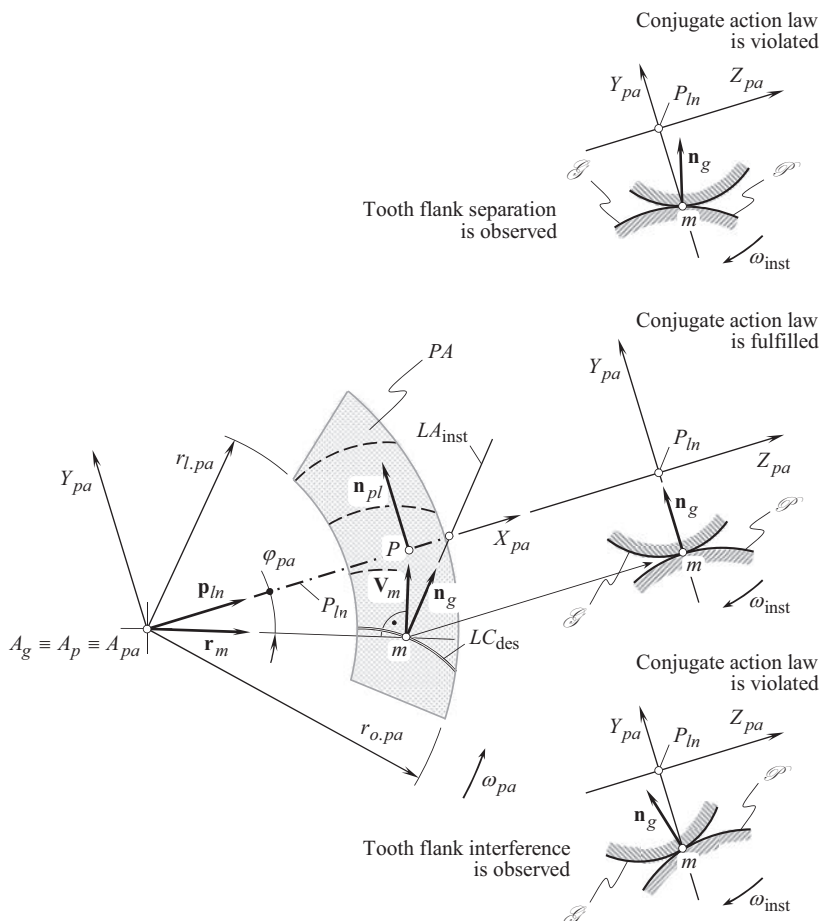


FIGURE 12.24 Fulfilment and violation of the conjugate action law in intersected-axes gearset.

must be met at all points of a desirable line of contact,  $LC_{des}$ , between the interacting tooth flanks,  $\mathcal{S}$  and  $\mathcal{R}$ . This is a key requirement to be fulfilled by conjugate tooth flanks,  $\mathcal{S}$  and  $\mathcal{P}$ , when the gears rotate.

At arbitrary point,  $m$ , within a desirable line of contact,  $LC_{des}$ , an instantaneous line of action,  $LA_{inst}$ , forms an angle with the axis of instantaneous rotation,  $P_{ln}$ . At every instant of time, every instantaneous line of action,  $LA_{inst}$ , intersects the axis of instantaneous rotation,  $P_{ln}$ , at a point – this is a must for conjugate surfaces.

A component of the instantaneous motion that is parallel to the axis of instantaneous rotation,  $P_{ln}$ , does not affect the conjugate action between the interacting tooth flanks,  $\mathcal{S}$  and  $\mathcal{P}$ . Therefore, this component of the relative motion is not considered here.

Another component of the relative motion is pointed along a straight line through point,  $P$ , that is located within the axis of instantaneous rotation,  $P_{ln}$ . The conjugate action between the interacting tooth flanks,  $\mathcal{S}$  and  $\mathcal{P}$ , is considered for this component of the relative motion.

In Figure 12.24, three vectors,  $\mathbf{p}_m$ ,  $\mathbf{V}_m$ , and  $\mathbf{n}_g$ , are constructed.

Two of three vectors, namely,  $\mathbf{p}_m$  and  $\mathbf{V}_m$ , are situated within the plane of action,  $PA$ .

The unit vector,  $\mathbf{p}_m$ , is pointed along the axis of instantaneous rotation,  $P_{ln}$ . Therefore, in the plane-of-action *Cartesian* coordinate system,  $X_{pa}Y_{pa}Z_{pa}$ , it can be analytically described by an expression:

$$\mathbf{p}_m = \mathbf{i} \quad (12.79)$$

The velocity vector,  $\mathbf{V}_m$ , is pointed along an instantaneous line of action,  $LA_{inst}$ . In the plane-of-action *Cartesian* coordinate system,  $X_{pa}Y_{pa}Z_{pa}$ , this unit vector can be analytically described as:

$$\mathbf{r}_m = \mathbf{i} \sin \varphi_{pa} + \mathbf{j} \cos \varphi_{pa} \quad (12.80)$$

The third unit vector,  $\mathbf{n}_g$ , is perpendicular to the gear tooth flank,  $\mathcal{S}$ . Therefore, it can be calculated from the equation:

$$\mathbf{n}_g = \frac{\frac{\partial \mathbf{r}_g}{\partial U_g} \times \frac{\partial \mathbf{r}_g}{\partial V_g}}{\left| \frac{\partial \mathbf{r}_g}{\partial U_g} \times \frac{\partial \mathbf{r}_g}{\partial V_g} \right|} \quad (12.81)$$

where

$\mathbf{r}_g$  is the position vector of point of the gear tooth flank,  $\mathcal{S}$ .

$U_g$  and  $V_g$  are the curvilinear (the *Gaussian*) coordinates of point of the gear tooth flank,  $\mathcal{S}$ .

The unit vector,  $\mathbf{n}_{pl}$ , is perpendicular to the axis of instantaneous rotation,  $P_{ln}$ . This vector is entirely located within the plane of action,  $PA$ , and is perpendicular to the axis of instantaneous rotation,  $P_{ln}$ . Therefore, in the plane-of-action *Cartesian* coordinate system,  $X_{pa}Y_{pa}Z_{pa}$ , it can be analytically represented in a form:

$$\mathbf{n}_{pl} = \mathbf{j} \quad (12.82)$$

A gear,  $\mathcal{S}$ , and its mating pinion,  $\mathcal{P}$ , tooth flanks are conjugate, if a straight line along the unit normal vector,  $\mathbf{n}_g$ , at every point of the line of contact,  $LC$ , intersects the axis of instantaneous rotation,  $P_{ln}$ . To meet this requirement, the unit normal vectors,  $\mathbf{n}_{pl}$  and  $\mathbf{n}_g$ , must compose a set of two coplanar vectors, and they must not be perpendicular to one another (here, the unit normal vector that is

pointed along the axis of instantaneous rotation,  $P_{ln}$ , is designated as  $\mathbf{n}_{pl}$ . Evidently, this vector is entirely located within the plane of action,  $PA$ ).

When a gear,  $\mathcal{G}$ , and its mating pinion,  $\mathcal{P}$ , tooth flanks are conjugate to one another, then the three vectors,  $\mathbf{p}_{ln}$ ,  $\mathbf{V}_m$ , and  $\mathbf{n}_g$ , are coplanar. The triple scalar product,  $\mathbf{p}_{ln} \times \mathbf{V}_m \cdot \mathbf{n}_g$ , of three coplanar vectors,  $\mathbf{p}_{ln}$ ,  $\mathbf{V}_m$ , and  $\mathbf{n}_g$ , is always zero, and, therefore, the equality:

$$\mathbf{p}_{ln} \times \mathbf{V}_m \cdot \mathbf{n}_g = 0 \quad (12.83)$$

is valid. The triple scalar product,  $\mathbf{p}_{ln} \times \mathbf{V}_m \cdot \mathbf{n}_g$ , can be represented in a form of a determinant:

$$\mathbf{p}_{ln} \times \mathbf{V}_m \cdot \mathbf{n}_g = \begin{vmatrix} X_{pl} & Y_{pl} & Z_{pl} \\ V_{m.x} & V_{m.y} & V_{m.z} \\ X_g & Y_g & Z_g \end{vmatrix} = 0 \quad (12.84)$$

In addition to Eq. (12.84), the condition:

$$\mathbf{n}_{pl} \cdot \mathbf{n}_g \neq 0 \quad (12.85)$$

is also required to be fulfilled. The parallelism of the directions specified by the unit normal vectors,  $\mathbf{n}_{pl}$  and  $\mathbf{n}_g$ , is eliminated by Eq. (12.85). No transmission of a rotary motion by means of gear teeth is possible when the unit normal vector,  $\mathbf{n}_g$ , is parallel to the axis of instantaneous rotation,  $P_{ln}$ .

An expression:

$$\mathbf{p}_{ln} \times \mathbf{n}_g \neq 0 \quad (12.86)$$

is an alternative form of representation of the condition specified by Eq. (12.85).

A gear,  $\mathcal{G}$ , and a mating pinion,  $\mathcal{P}$ , tooth flanks are said to be conjugate if and only if the conditions, those specified by Eq. (12.83) [or Eq. (12.84)] and Eq. (12.85) [or Eq. (12.86)], are fulfilled for any and all points within the line of contact,  $LC$ , for any possible configurations of the gear and the pinion in relation to one another:

$$\begin{cases} \mathbf{p}_{ln} \times \mathbf{V}_m \cdot \mathbf{n}_g = 0 \\ \mathbf{p}_{ln} \times \mathbf{n}_g \neq 0 \end{cases} \quad (12.87)$$

Equations (12.87) analytically describes the condition of conjugacy of a gear,  $\mathcal{G}$ , and of a mating pinion,  $\mathcal{P}$ , tooth flanks. If the condition [see Eqs. (12.87)] is violated (see Figure 12.24), the gear,  $\mathcal{G}$ , and the mating pinion,  $\mathcal{P}$ , tooth flanks do not conjugate to one another.

That same approach can be employed for designing hobs, and face-hobs for hobbing conical/bevel gears for intersected-axes gearsets.

## 12.6 FAVORABLE TOOTH PROPORTIONS IN INTERSECTED-AXES GEARS

The gear and its mating pinion in an intersected-axes gear pair feature a plurality of teeth. The teeth are evenly spaced circumferentially. General form of the equation of a gear tooth flank [see Eq. (12.53)] as well as Eqs. (12.58) and (12.61) of particular cases of the gear tooth flank, is necessary but is not sufficient for the specification of the tooth shape neither of the gear nor of the pinion. The gear tooth flank,  $\mathcal{G}$ , that is specified by Eq. (12.53), has to be properly located in relation (a) to the tooth flank of the opposite side of the gear tooth as well as (b) to the tooth flanks of the rest of the gear teeth.



The desirable tooth proportions in intersected-axes gearing can be established in a manner similar to that earlier established for parallel-axes gearings. Following this concept, consider a base cone of a gear in an intersected-axes gear pair. Base cones along with the configuration of the rotation vectors  $\omega_g$ ,  $\omega_p$ , and  $\omega_{pl}$  are of critical importance for the determination of the corresponding reference surfaces.

### 12.6.1 ANGULAR BASE PITCH

Three kinds of angular base pitches are distinguished in intersected-axes gearing. They are:

- a. the operating angular base pitch of a gear pair
- b. the gear angular base pitch, and
- c. the mating pinion angular base pitch

The concept of operating angular base pitch is related to a *gear-to-pinion mesh* in intersected-axes gearing. The operating angular base pitch,  $\phi_{b.op}$ , is an equivalent of the operating base pitch in parallel-axes gearing. Similar to parallel-axes gearing, the operating angular base pitch,  $\phi_{b.op}$ , is specified as the angular distance between every two adjacent lines of contact,  $LC$ . This angular distance is measured within the plane of action,  $PA$ .

#### Definition 12.1

The operating angular base pitch in intersected-axes gearing is an angular distance between tooth flanks of two adjacent lines of contact of a gear and of a mating pinion, that is measured in the plane of action.

The *operating angular base pitch* is a calculated design parameter of the gearset, and it cannot be directly measured in a gear pair.

The angular base pitch of a gear,  $\phi_{b.g}$  (also  $BP - gear$ , or just  $BP_g$ , for simplicity), and the angular base pitch of a mating pinion (also  $BP - pinion$ , or just  $BP_p$ , for simplicity) are measured within the plane of action. The angular base pitch of a gear and of its mating pinion, both, can be measured directly, and separately, in the gear, and in the pinion. The angular base pitch of a gear,  $\phi_{b.g}$ , as well as the angular base pitch of a mating pinion,  $\phi_{b.p}$ , is measured as an angle between the actual lines of intersection of the gear/pinion tooth flanks,  $\mathcal{S}$  and/or  $\mathcal{P}$ , of two neighboring teeth by a plane tangent to the base cone of the gear, and that of the mating pinion. One of the lines of intersection of the tooth flanks,  $\mathcal{S}$  and  $\mathcal{P}$ , by the tangent plane may be situated either outside of the outer diameter, or inside the root diameter of the gear/pinion. It is required to ensure that along the line of intersection, the gear/pinion tooth flank,  $\mathcal{S}$  and/or  $\mathcal{P}$ , is perpendicular to the plane of action,  $PA$ . Otherwise, no angular gear/pinion base pitch exists in the gear pair.

In order to proceed with the analysis of the angular base pitch of a gear,  $\phi_{b.g}$ , it is instructive to recall the following well-known property of two cones that share a common apex, and a common generatrix. The cones spin about their axes of rotation with no slippage. If radii of the bottom circles of the first and of the second cones are designated as  $r_1$  and  $r_2$ , then the following equality is valid:

$$r_1 \cdot \phi_1 = r_2 \cdot \phi_2 \quad (12.88)$$

where  $\phi_1$  and  $\phi_2$  are the angles which the cones are turned through.

In intersected-axes gearing, a gear and the plane of action share a common apex, and a common generatrix. Both spin about their axis of rotation with no slippage. In the consideration below, the base cone of the gear is designated below as  $\Gamma_b$ , and the base cone of the plane of action,  $PA$ , equals to a right angle ( $\Gamma_{pa} = 90^\circ$ ).



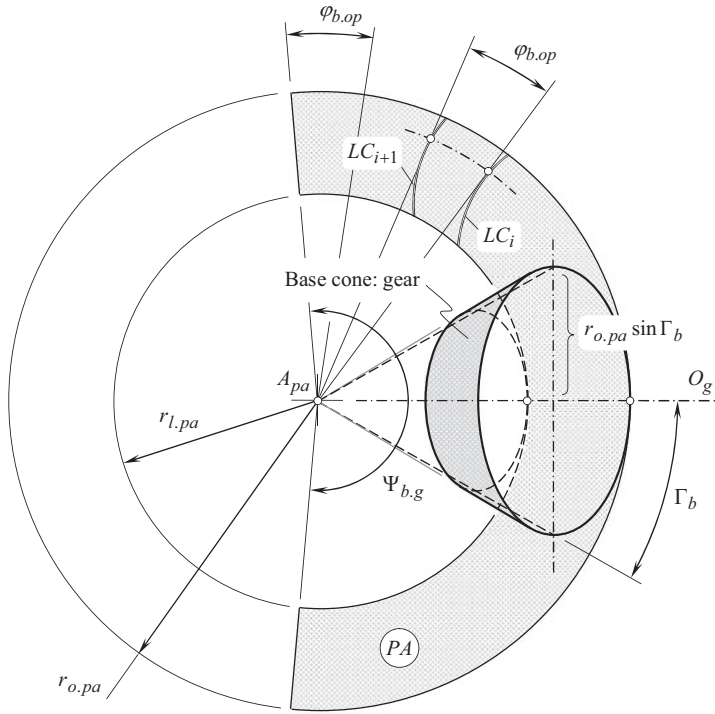


**FIGURE 12.25** On the definition of the term *angular base pitch in gear*,  $\varphi_{b,g}$ , in gear for intersected-axes gearset.

Consider a plane of action,  $PA$ , in an intersected-axes gear pair, as schematically illustrated in Figure 12.25. A pair of adjacent lines of contact,  $LC_i$  and  $LC_{i+1}$ , are at an angular distance,  $\varphi_{b,op}$ , from one another.

In order to fulfil the third fundamental law of gearing, the angular base pitch in a gear,  $\varphi_{b,g}$ , must be equal to the operating angular base pitch,  $\varphi_{b,op}$ , in intersected-axes gearing (an equality  $\varphi_{b,g} = \varphi_{b,op}$  has to be fulfilled in geometrically accurate gearset).

When the gears rotate, the base cone of the gear rolls with no slippage over the plane of action,  $PA$ .

Consider point within the base cone surface of the gear. The point is remote from the plane-of-action apex,  $A_{pa}$ , at a distance,  $r_{o,pa}$ . The arc distance:

$$\tilde{L}_{b,g} = 2\pi r_{o,pa} \sin \Gamma_b \quad (12.89)$$

is covered by the point per each revolution of the gear.

Within the plane of action,  $PA$ , a circular arc of the length  $\tilde{L}_{b,g}$  spans over a central angle,  $\Psi_{b,g}$ . The actual value of the angle,  $\Psi_{b,g}$ , is calculated from the equation:

$$\Psi_{b,g} = 360^\circ \sin \Gamma_b \quad (12.90)$$

For a gear of  $N_g$  teeth, a portion,  $\varphi_{b,g}$ , of the central angle,  $\Psi_{b,g}$ , per the gear tooth equals:

$$\varphi_{b,g} = \frac{\Psi_{b,g}}{N_g} = \frac{360^\circ}{N_g} \sin \Gamma_b \quad (12.91)$$

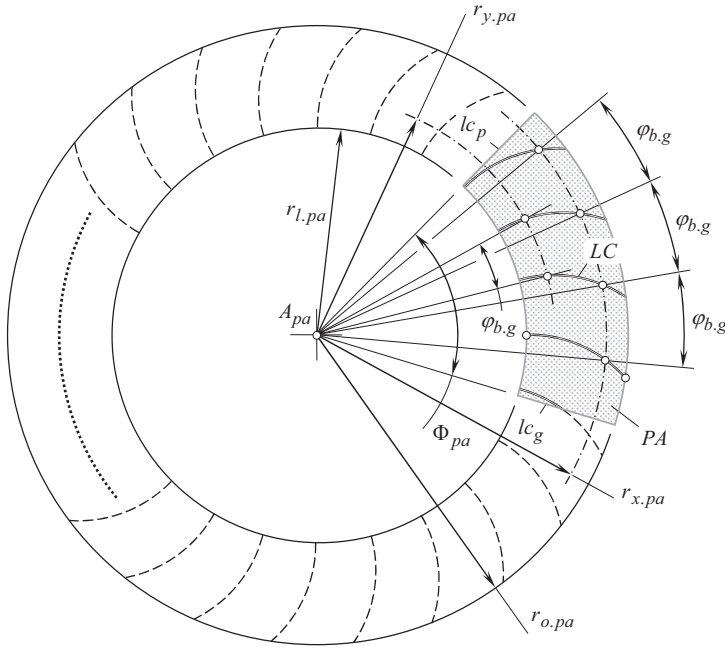


**FIGURE 12.26** The angular base pitch,  $\varphi_{b.g}$ , in a gear for intersected-axes gearing is of a constant value for all the teeth as well as within the face width of the gear.

The angle,  $\varphi_{b.g}$ , in intersected-axes gearing is an equivalent to the base pitch,  $p_b$ , in a gear in parallel-axes gearing. This is the reason for, what the angle,  $\varphi_{b.g}$ , is referred to as the *operating angular base pitch* in intersected-axes gearing.

As illustrated in Figure 12.26, the angular base pitch,  $\varphi_{b.g}$ , in a given geometrically accurate gear is remained of the same value within the face width,  $F_{pa}$ , of a gear ( $\varphi_{b.p} = \text{const}$ ), that is, it is of a constant value for any and all circles of radii  $r_{x.pa}$ ,  $r_{y.pa}$ , and so forth. The *angular length of contact* is designated in Figure 12.26 as  $\Phi_{pa}$ . The angular length,  $\Phi_{pa}$ , in intersected-axes gearing is an equivalent of the length of contact,  $Z_{pa}$ , in parallel-axes gearing.

It is the right point to stress here the correct manner to refer to the design parameter  $\varphi_{b.g}$  (as well as to the design parameter  $\varphi_{b.p}$ ). The *angular base pitch,  $\varphi_{b.g}$ , in bevel gear for intersected-axes gear pair* is the correct way to refer to the design parameter  $\varphi_{b.g}$ . In this way the design parameter  $\varphi_{b.g}$  can be easily distinguished from that in a bevel gear for crossed-axes gear pair, and, thus, and a comparison of angular base pitches in  $I_a$  – gearing, and that in  $C_a$  – gearing can be avoided. The tooth flank geometry in bevel gears for  $I_a$  – gearing, and that for  $C_a$  – gearing, are completely different from one another.

In geometrically accurate intersected-axes gearing, the angular base pitch in a gear,  $\varphi_{b.g}$ , and that,  $\varphi_{b.p}$ , in a mating pinion, both, are equal to the operating angular base pitch,  $\varphi_{b.op}$ , in the gear pair:

$$\begin{cases} \varphi_{b.g} = \varphi_{b.op} \\ \varphi_{b.p} = \varphi_{b.op} \end{cases} \quad (12.92)$$

or (for simplicity)

$$\varphi_{b.g} = \varphi_{b.p} = \varphi_{b.op} \quad (12.93)$$

All the angles  $\varphi_{b,g}$ ,  $\varphi_{b,p}$ , and  $\varphi_{b,op}$ , share a common apex that is coincident with the plane-of-action apex,  $A_{pa}$ .

It should be noted there that the tooth number,  $N_{pa}$ , within an imaginary plane of action,  $PA$ , is not mandatorily equal to an integer number. It can be expressed by a number with fractions, as well.

The angular base pitch can be expressed in terms of linear dimensions. The latter makes sense when the linear dimensions are easier to be measured.

Only *conjugate* gear tooth flanks feature the angular base pitch. The angular base pitch can not be identified for non-conjugate gear and pinion tooth flanks, as in such a case the plane of action can not be perpendicular to both adjacent tooth flanks of the gear at that same time.

A variation of the actual value of base pitch in the gear (as well as in the pinion) can be used as a measure of variation of geometry and configuration of a line of intersection of a single tooth flank (either of  $\mathcal{S}$ , or of  $\mathcal{P}$ ), and its deviation from the desirable line of contact,  $LC_{des}$ , when the gear (or the pinion) spins about its axis of rotation. This can be used in the investigation of noise excitation by an intersected-axes gearset.

The proposed concept of the operating angular base pitch in intersected-axes gear pair possesses a significant potential for the improvement of traditional methods of finish-cut gears.

All the bevel gears for intersected-axes gearing that are finish-cut by means of conventional methods of gear generating are approximate gears, as the condition specified by Eq. (12.92) is violated. However, the accuracy of bevel gears produced in the present-day industry can be improved if the set-up parameters of the gear finishing operation are determined based on the minimization of variation  $\Delta\varphi_{b,g} = (\varphi_{b,op} - \tilde{\varphi}_{b,g}) \mapsto 0$  and  $\Delta\varphi_{b,p} = (\varphi_{b,op} - \tilde{\varphi}_{b,p}) \mapsto 0$  of the approximate angular base pitches of the bevel gear,  $\Delta\varphi_{b,g}$ , and of the bevel pinion,  $\Delta\varphi_{b,p}$  [a well-known problem of minimization of the functions  $\Delta\varphi_{b,g} \mapsto \min$  and  $\Delta\varphi_{b,p} \mapsto \min$ ]. The set-up parameters under which the deviations,  $\Delta\varphi_{b,g}$  and  $\Delta\varphi_{b,p}$ , are of the smallest values can be determined. For this purpose, a CAD model of the gear is used.

By means of the proposed concept of the angular base pitches of a bevel gear,  $\varphi_{b,g}$ , and that of a bevel pinion,  $\varphi_{b,p}$ , the accuracy of the inspection of the gear, and of the pinion, can be improved. For this purpose, the angular distances between the lines of intersection of the adjacent tooth flanks by the plane of action,  $PA$ , are required to be inspected, and compared to the desirable line of contact,  $LC_{des}$ , in the gear pair.

## 12.6.2 TRANSVERSE PRESSURE ANGLE

The transverse pressure angle,  $\phi_{t,\omega}$ , is the angle that the plane of action,  $PA$ , forms with the plane that is perpendicular to the plane through the axes of rotation,  $O_g$  and  $O_p$ , of the gear and of the mating pinion. According to Figure 3.7, this is a normal plane (namely, this is the  $N_{in}$  – plane). The transverse pressure angle,  $\phi_{t,\omega}$ , is measured within a plane that is perpendicular to the axis of instantaneous rotation,  $P_{in}$  (or, the same, that is perpendicular to the vector of instantaneous rotation,  $\omega_{pl}$ , that is, similar to that, as in parallel-axes gearing). This plane is tangent to the transverse section of the intersected-axes gear pair. The transverse section in the intersected-axes gear pair is a sphere centered at the plane-of-action apex,  $A_{pa}$ , that passes through point of interest within the axis of instantaneous rotation,  $P_{in}$ .

Referring to Figure 12.12 (as well as to Figure 12.15), the transverse pressure angle,  $\phi_{t,\omega}$ , can be defined as the angle that is formed by the plane of action,  $PA$ , and by a perpendicular,  $\mathbf{n}_{pa}$ , to the plane through the axes of rotations,  $O_g$  and  $O_p$  (namely, the  $N_{in}$  – plane), of the gear and the pinion.

### Definition 12.2

Transverse pressure angle in intersected-axes gearset is said to be the angle that is formed by the plane of action, and by a perpendicular,  $\mathbf{n}_{pa}$ , to the plane through the axes of rotation of the gear and of the pinion ( $N_{in}$  – plane).

The transverse pressure angle,  $\phi_{t,\omega}$ , can be an independent design parameter in an intersected-axes gear pair. Then, the base cone angle of the gear,  $\Gamma_b$ , and that of the mating pinion,  $\gamma_b$ , can be expressed in terms of the pressure angle,  $\phi_{t,\omega}$ . Otherwise, the transverse pressure angle,  $\phi_{t,\omega}$ , can be expressed in terms of the base cone angles,  $\Gamma_b$  and  $\gamma_b$ .

The plane of action,  $PA$ , is tangent to the base cone of the gear, as schematically illustrated in Figure 12.26. Therefore, the angle that the plane of action forms with the gear axis of rotation,  $O_g$ , is equal to the base cone angle,  $\Gamma_b$ . Once the angle between the plane of action,  $PA$ , and the gear axis of rotation,  $O_g$ , is known (namely, the angle  $\Gamma_b$ ), then the unit normal vector,  $\mathbf{n}_{pa}$ , to the plane of action,  $PA$ , and the axis,  $O_g$ , form an angle of  $(90^\circ - \Gamma_b)$ .

In the reference system,  $X_r Y_r Z_r$ , the direction of the aforementioned unit normal vector,  $\mathbf{n}_{pa}$ , is analytically expressed by the equation:

$$\mathbf{n}_{pa} = \mathbf{j}_r \sin \phi_{t,\omega} + \mathbf{k}_r \cos \phi_{t,\omega} \quad (12.94)$$

In order to express the base cone angle of the gear,  $\Gamma_b$ , in terms of the transverse pressure angle,  $\phi_{t,\omega}$ , or, conversely, to express the transverse pressure angle,  $\phi_{t,\omega}$ , in terms of the base cone angle of the gear,  $\Gamma_b$ , all the design parameters of the gear pair have to be represented in a common reference system. For this purpose, the use of the *Cartesian* coordinate system  $X_g Y_g Z_g$  associated with the gear is proven to be convenient. To follow this way, the unit normal vector,  $\mathbf{n}_{pa}$ , is required to be represented in the reference system  $X_g Y_g Z_g$ .

The reference systems,  $X_g Y_g Z_g$  and  $X_r Y_r Z_r$ , are turned about the  $Y_r$  – axis in relation to one another through the pinion cone angle,  $\Sigma_p$ . The transition from the coordinate system,  $X_r Y_r Z_r$ , to the coordinate system,  $X_g Y_g Z_g$ , is analytically described by the operator of rotation,  $\mathbf{Rt}(r \mapsto g)$  [see Eq. (12.33)]. With that said, the direction of the unit normal vector,  $\mathbf{n}_{pa}^g$ , in the coordinate system,  $X_g Y_g Z_g$ , can be analytically described by an expression:

$$\mathbf{n}_{pa}^g = \mathbf{Rt}(r \mapsto g) \cdot \mathbf{n}_{pa} \quad (12.95)$$

Equations (12.33)–(12.95) yield the following expression for the unit normal vector,  $\mathbf{n}_{pa}^g$ :

$$\mathbf{n}_{pa}^g = \begin{bmatrix} \cos \Sigma_p & 0 & \sin \Sigma_p & 0 \\ 0 & 1 & 0 & 0 \\ -\sin \Sigma_p & 0 & \cos \Sigma_p & 0 \\ 0 & 0 & 0 & 1 \end{bmatrix} \cdot \begin{bmatrix} 0 \\ \sin \phi_{t,\omega} \\ \cos \phi_{t,\omega} \\ 1 \end{bmatrix} = \begin{bmatrix} \sin \Sigma_p \cos \phi_{t,\omega} \\ \sin \phi_{t,\omega} \\ \cos \Sigma_p \cos \phi_{t,\omega} \\ 1 \end{bmatrix} \quad (12.96)$$

As the unit vector along the  $O_g$  – axis is equal to  $\mathbf{k}$ , the angle  $\angle(\mathbf{n}_{pa}, \mathbf{k})$  can be calculated as:

$$\angle(\mathbf{n}_{pa}, \mathbf{k}) = \Gamma_b = \cos^{-1}[\mathbf{n}_{pa} \cdot \mathbf{k}] \quad (12.97)$$

that can also be represented in the form:

$$\Gamma_b = \tan^{-1} \left( -\frac{\sqrt{\sin^2 \Sigma_p - \cos^2 \Sigma_p \sin^2 \phi_{t,\omega}}}{\cos \Sigma_p \cos \phi_{t,\omega}} \right) \quad (12.98)$$

The transverse pressure angle,  $\phi_{t,\omega}$ , can be expressed in terms of the base cone angle,  $\Gamma_b$ , of the gear:

$$\phi_{t,\omega} = \cos^{-1} \left( \frac{\cos \Sigma_p}{\cos \Gamma_b} \right) \quad (12.99)$$

An equation similar to Eq. (12.98) is valid for the base cone angle of the pinion:

$$\gamma_b = \tan^{-1} \left( -\frac{\sqrt{\sin^2 \Sigma_g - \cos^2 \Sigma_g \sin^2 \phi_{t,\omega}}}{\cos \Sigma_g \cos \phi_{t,\omega}} \right) \quad (12.100)$$

The transverse pressure angle,  $\phi_{t,\omega}$ , can also be expressed in terms of the base cone angle,  $\gamma_b$ , of the pinion:

$$\phi_{t,\omega} = \cos^{-1} \left( \frac{\cos \Sigma_g}{\cos \gamma_b} \right) \quad (12.101)$$

Both the cone angles, namely,  $\Sigma_g$  and  $\Sigma_p$ , can be expressed in terms of the rotations of the gear,  $\omega_g$ , the pinion,  $\omega_p$ , and the angle  $\Sigma$  between the rotation vectors,  $\omega_g$  and  $\omega_p$ .

When the transverse pressure angle,  $\phi_{t,\omega}$ , is specified, the base cone angle of a gear,  $\Gamma_b$ , as well as the base cone angle of its mating pinion,  $\gamma_b$ , both can be expressed in terms of the pressure angle,  $\phi_{t,\omega}$ , of the pitch cone angle of the gear,  $\Gamma$ , and of the pitch cone angle of the pinion,  $\gamma$ .

As the plane of action,  $PA$ , is tangent to the base cones of the gear, and of the mating pinion, the plane of action,  $PA$ , forms a transverse pressure angle,  $\phi_{t,\omega}$ , with the pitch plane,  $PP$  (see Figure 12.27). An angle that the plane of action,  $PA$ , forms with the axis of rotation of the gear,  $O_g$ ,

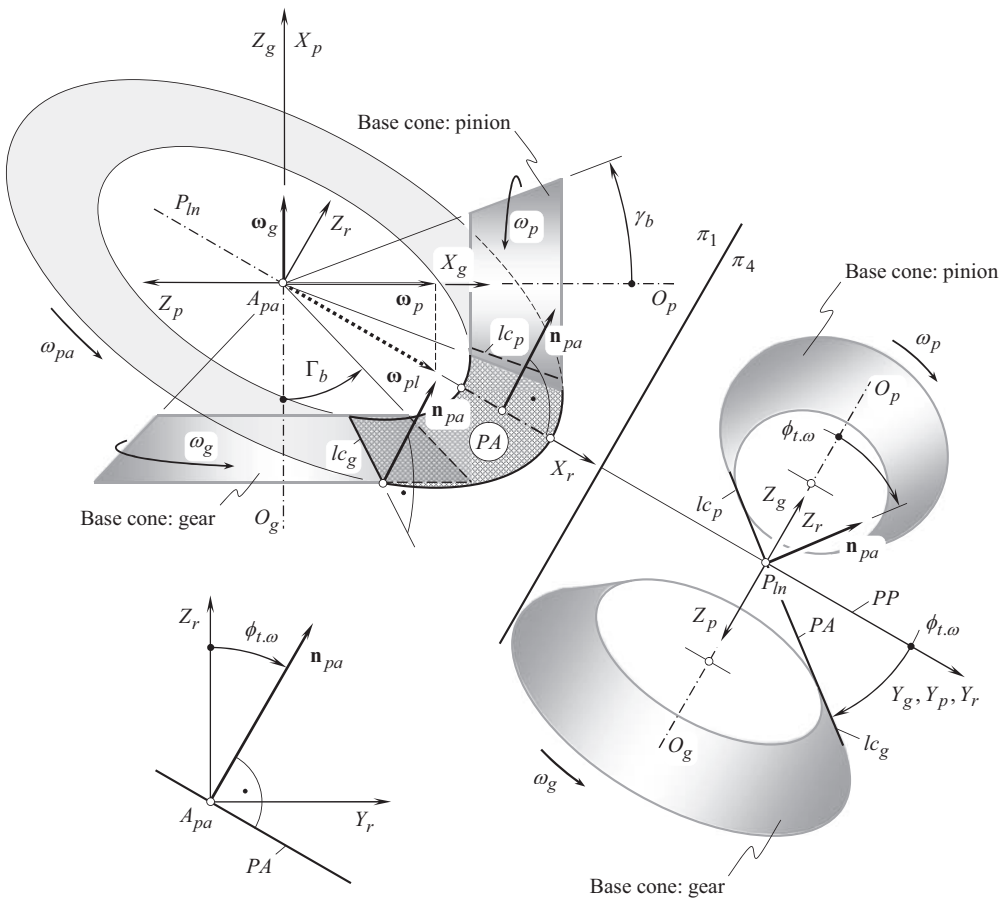


**FIGURE 12.27** Specification of configuration of the plane of action,  $PA$ , in relation to the base cones of a gear and of a mating pinion in intersected-axes gear pair.

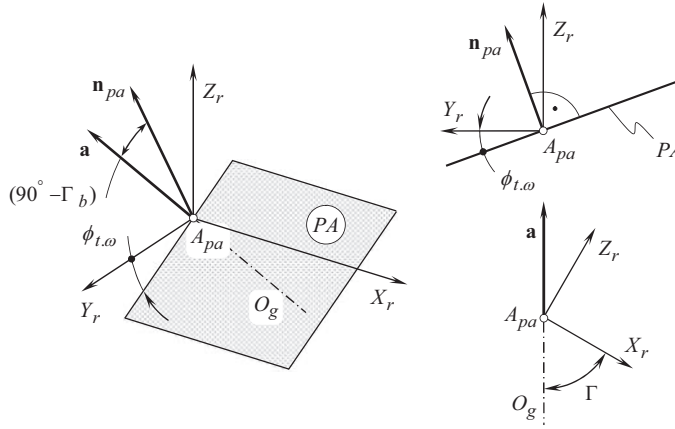


**FIGURE 12.28** Relation between the pitch cone angle,  $\Gamma$ , and the base cone angle,  $\Gamma_b$ , in intersected-axes gearing.

is equal to the base cone angle of the gear,  $\Gamma_b$ . Therefore, the unit normal vector,  $\mathbf{n}_{pa}$ , to the plane of action,  $PA$ , and the axis of rotation,  $O_g$ , form an angle  $(90^\circ - \Gamma_b)$ .

The unit normal vector,  $\mathbf{n}_{pa}$ , to the plane of action,  $PA$ , is specified by Eq. (12.94). Referring to Figure 12.28, the unit vector,  $\mathbf{a}$ , along the axis of rotation of the gear,  $O_g$ , can be analytically expressed as:

$$\mathbf{a} = -\mathbf{i} \cos \Gamma + \mathbf{k}_r \sin \Gamma \quad (12.102)$$

Once the angle  $\angle(\mathbf{n}_{pa}, \mathbf{a}) = (90^\circ - \Gamma_b)$  is determined, the base cone angle of the gear can be calculated from the formula:

$$\Gamma_b = \tan^{-1} \left( \frac{|\mathbf{n}_{pa} \times \mathbf{a}|}{\mathbf{n}_{pa} \cdot \mathbf{a}} \right) \quad (12.103)$$

The following expression for the calculation of the base cone angle,  $\Gamma_b$ , of a gear:

$$\Gamma_b = \tan^{-1} \left( \frac{\sqrt{\cos^2 \Gamma + \sin^2 \Gamma \cos^2 \phi_{t,\omega}}}{\sin \Gamma \sin \phi_{t,\omega}} \right) \quad (12.104)$$

is derived after substituting the vectors,  $\mathbf{n}_{pa}$  [from Eq. (12.94)], and,  $\mathbf{a}$  [from Eq. (12.102)], into Eq. (12.103).

A similar expression:

$$\gamma_b = \tan^{-1} \left( \frac{\sqrt{\cos^2 \gamma + \sin^2 \gamma \cos^2 \phi_{t,\omega}}}{\sin \gamma \sin \phi_{t,\omega}} \right) \quad (12.105)$$

is valid for the calculation of the base cone angle,  $\gamma_b$ , of a mating pinion.

In a particular case when the pitch-cone-angle of a gear,  $\Gamma$ , is set up equal to a right angle ( $\Gamma = 90^\circ$ ), the pitch cone becomes a flat surface, and the resulting gear is often called *crown gear*. A crown gear is a bevel gear with a planar pitch surface. The position vector of point of a crown gear is specified by Eq. (12.61) under an assumption that the equality  $\Gamma = 90^\circ$  is valid.





instantaneous rotation,  $P_{ln}$ . Evidently, the rotation vector of the pitch plane,  $\omega_{pp}$ , is perpendicular to the vector of instantaneous rotation,  $\omega_{pl}$ . Due to lack of space, the latter is not shown in Figure 12.29.

The pitch plane,  $PP$ , of the *auxiliary basic generating rack* is tangent to both, to the pitch cone of a gear, and the pitch cone of a mating pinion.

The outer radius,  $r_{o,pp}$ , of the working portion of the pitch plane,  $PP$ , is equal to the cone distance of the gear pair, while the inner radius,  $r_{l,pp}$ , is smaller than  $r_{o,pp}$  by the face width,  $F_{pp}$ . [The radii,  $r_{o,pp}$  and  $r_{l,pp}$ , of the effective portion of the pitch plane,  $PP$ , are equal to the corresponding radii,  $r_{o,pa}$  and  $r_{l,pa}$ , of the plane of action,  $PA$ , that is, the equalities  $r_{o,pp} = r_{o,pa}$  and  $r_{l,pp} = r_{l,pa}$  are valid].

The working portion of the pitch plane is also bounded by two straight-line segments. The straight line segments are, by nature, the lines of intersection of the pitch plane,  $PP$ , by the outer cone of the gear, and by the outer cone of the pinion, correspondingly. Ultimately, the working portion of the pitch plane,  $PP$ , is bounded by two circular arcs of the radii  $r_{o,pp}$  and  $r_{l,pp}$ , and by two straight line segments  $b'd'$  and  $b''d''$ .

The length of the circular arc  $\cup b'ab''$  is equal to the circumference of the circle at the larger end of the gear:

$$\cup b'ab'' = 2\pi r_{o,pp} \sin \Gamma \quad (12.106)$$

Referring to Figure 12.30, in a gear of  $N_g$  teeth, the angular pitch of the gear,  $\varphi_{N,g}$ , is calculated from the formula:

$$\varphi_{N,g} = \frac{360^\circ \cdot \cup b'ab''}{\pi d_{o,pp} N_g} = \frac{360^\circ}{N_g} \cdot \sin \Gamma \quad (12.107)$$

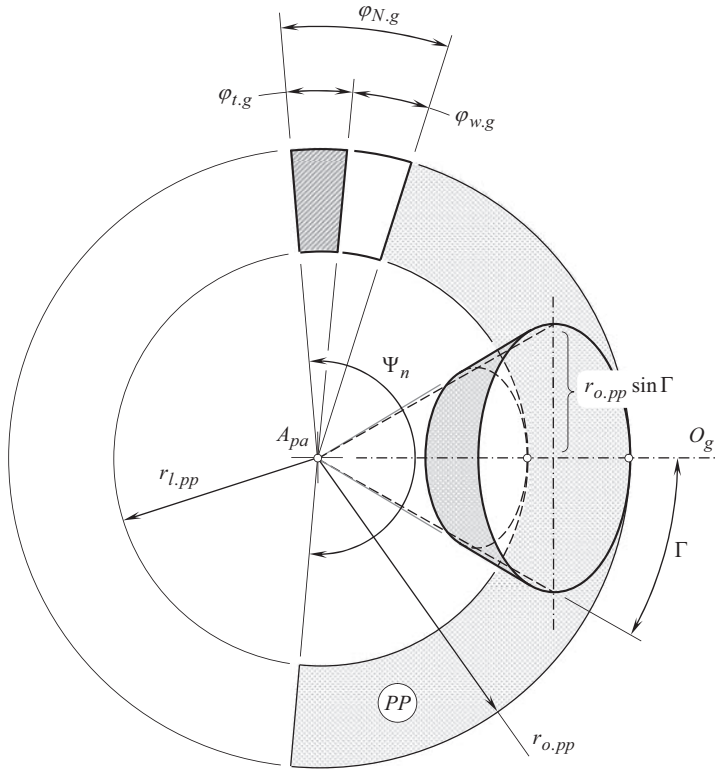


**FIGURE 12.30** On the definition of the terms, the *angular pitch*,  $\varphi_{N,g}$ , the *angular tooth thickness*,  $\varphi_{t,g}$ , and the *angular space width*,  $\varphi_{w,g}$ , in a gear for geometrically accurate intersected-axes gearset.



In Eq. (12.107), the outer diameter,  $d_{o,pp}$ , of the pitch plane is equal  $d_{o,pp} = 2r_{o,pp}$ .

The angular pitch,  $\varphi_{n,g}$ , for a bevel gear is an equivalent to the pitch,  $p$ , for a cylindrical parallel-axes gear.

The expression [see Eq. (12.107)] for the calculation of the angular pitch of the gear,  $\varphi_{N,g}$ , along with the expression [see Eq. (12.91)] for the calculation of the base angular pitch of the gear,  $\varphi_{b,g}$ , make possible an expression for the angular base pitch,  $\varphi_{b,g}$ , in terms of angular pitch,  $\varphi_{N,g}$ . For this purpose, Eqs. (12.91) and (12.107) are represented in the form:

$$N_g = \frac{360^\circ}{\varphi_{b,g}} \cdot \sin \Gamma_b \quad (12.108)$$

$$N_g = \frac{360^\circ}{\varphi_{n,g}} \cdot \sin \Gamma \quad (12.109)$$

correspondingly.

As the left sides of Eqs. (12.91) and (12.107) are equal to each other, the equality:

$$\frac{360^\circ}{\varphi_{b,g}} \cdot \sin \Gamma_b = \frac{360^\circ}{\varphi_{N,g}} \cdot \sin \Gamma \quad (12.110)$$

is valid.

The expression:

$$\varphi_b = \varphi_{N,g} \frac{\sin \Gamma_b}{\sin \Gamma} \quad (12.111)$$

immediately follows from Eq. (12.100).

Depending on the actual value of the angular pitch,  $\varphi_{N,g}$ , the so-called *low tooth count* intersected-axes gears (the *LTC – intersected-axes gears*) are recognized. A *low tooth count* intersected-axes gear features the angular pitch,  $\varphi_{n,g}$ , of a larger value compared to that in a gear with a large tooth count. Use of the base cone angle of a gear,  $\Gamma_b$  (and of a pinion,  $\gamma_b$ ), and the start-of-active-profile cone angle of the gear,  $\Gamma_{sap}$  (and of a pinion,  $\gamma_{sap}$ ), makes possible a numerical criterion to distinguish the low-tooth-count intersected-axes gear:

$$\Gamma_b > \Gamma_{sap} \quad (12.112)$$

A similar inequality:

$$\gamma_b > \gamma_{sap} \quad (12.113)$$

is valid with respect to a low-tooth-count intersected-axes pinion.

Similar to low-tooth-count gears with parallel-axes of rotation of a gear and of a mating pinion (see Section 7.3.2), Eq. (12.113) can be evolved to  $\gamma_b > k_{lrc} \cdot \gamma_{sap}$ , where the factor  $k_{lrc}$  equals  $k_{lrc} \cong (0.50 \div 0.75)$ .

In low-tooth-count intersected-axes gears, the variation of the most of principal design parameters of the tooth flanks compared to that in gears with a larger tooth count is more significant.

#### 12.6.4 ANGULAR TOOTH THICKNESS, AND ANGULAR SPACE WIDTH

The angular tooth thickness and the angular space width in intersected-axes gearing are equivalent to the tooth thickness, and to the space width in parallel-axes gearing. Both the tooth thickness and the space width are measured either within the pitch cone of the gear, or, the same, within the pitch plane,  $PP$ , of the corresponding round rack of the gear pair.

**Definition 12.4**

Angular tooth thickness in intersected-axes gearing is said to be the angular distance between the opposite tooth flanks of the gear tooth measured within the pitch plane.

**Definition 12.5**

Angular space width in intersected-axes gearing is said to be the angular distance between the opposite tooth flanks of a space between adjacent gear tooth measured within the pitch plane.

In the tight mesh of gears in an intersected-axes gear pair, the angular tooth thickness,  $\varphi_{t,g}$ , and the angular space width,  $\varphi_{w,g}$ , of a bevel gear, together form the angular pitch of the gear,  $\varphi_{N,g}$ :

$$\varphi_{t,g} + \varphi_{w,g} = \varphi_{N,g} \quad (12.114)$$

In reality, a backlash between a gear tooth flank,  $\mathcal{S}$ , and its mating pinion tooth flank,  $\mathcal{P}$ , is required to compensate for the gears heat extension, and so forth. Therefore, a backlash,  $\varphi_{B,n}$ , for a bevel gear is required to be incorporated into Eq. (12.114). Under any circumstances, the equality:

$$\varphi_{B,n} = \varphi_{w,g} - \varphi_{t,g} \quad (12.115)$$

is required to be valid.

As a gear tooth is commonly stronger compared to that of a mating pinion, it is reasonable to set the angular tooth thickness of the gear equal:

$$\varphi_{t,g} = \frac{\varphi_{N,g}}{2} - \varphi_{B,n} \quad (12.116)$$

Therefore, the angular space width of that same gear can be calculated from the equation:

$$\varphi_{w,g} = \frac{\varphi_{N,g}}{2} \quad (12.117)$$

Similar formulas:

$$\varphi_{t,p} = \frac{\varphi_{N,p}}{2} \quad (12.118)$$

$$\varphi_{w,p} = \frac{\varphi_{N,p}}{2} \quad (12.119)$$

are valid with respect to the bevel pinion.

In Eqs. (12.118) and (12.119), the angular pitch of the pinion,  $\varphi_{N,p}$ , is equal to  $\varphi_{N,p} = \varphi_{N,g}$ . It can also be calculated from the expression:

$$\varphi_{N,p} = \frac{\cup b'ab''}{N_p} = \frac{\pi d_{o,pp}}{N_p} \cdot \sin \gamma \quad (12.120)$$

Other possibilities to distribute the angular pitch,  $\varphi_{N,g}$ , among the three components  $\varphi_{t,g}$ ,  $\varphi_{w,g}$ , and  $\varphi_{B,n}$ , are permissible for a particular application of intersected-axes gearing.

**12.6.5 ANGULAR BACKLASH**

Backlash means a space between non-interacting tooth flanks of a bevel gear and of a pinion, or a difference in width of the gear tooth and of the pinion space. The backlash is necessary to achieve

correct operation of the gears to let the gears mesh without binding and/or excessive backlash, and to provide space for film of lubricating oil between the teeth. This prevents overheating and tooth damage.

Bevel gears are designed and manufactured so as to provide a specific amount of backlash when correctly assembled together. The actual amount of backlash varies with the size of the tooth and operating conditions.

In the present-day practice of gear production, unless otherwise specified, the minimum amount of total backlash of a pair of bevel gears is measured at the tightest point of mesh with a dial indicator on a bevel gear testing machine. Unless other specified, backlash is assumed to be normal backlash<sup>4</sup> and cannot be measured in the plane of rotation. But excessive backlash or play, if great enough, can cause a sudden impulse or shock load in starting or reversing that may cause serious tooth damage. Excessive or insufficient backlash can also result in noise, excessive wear and damage.

### Definition 12.6

Effective angular backlash,  $\varphi_{B.pa}$ , in geometrically accurate intersected-axes gearing is said to be the angular distance between non-interacting tooth flanks of a driving member, and of the tooth-space flank of the driven member in a gear pair, measured within the pitch plane.

Consider a virtual crown gear that is engaged in correct mesh with a gear. This crown gear can be referred to as a *crown gear/gear*, or simply as  $CG_g$ . The outer diameter of the crown gear is labeled as  $r_{o.pp}$ , the inner diameter is labeled as  $r_{i.pp}$ , and the pitch diameter is labeled as  $r_{pp}$ . The face width,  $F_{pp}$ , of the crown gear is equal to  $F_{pp} = r_{o.pp} - r_{i.pp}$ . The central angle  $\Psi_{pp}$  spans over the active portion of the crown gear,  $CG_g$ . The axis of rotation of the *crown gear/gear*,  $CG_g$ , is labeled as  $O_{pp}$ . Here, the subscript “ $pp$ ” indicates that the corresponding parameter relates to the pitch plane,  $PP$ .

The angular tooth thickness,  $\varphi_{t.g}$ , and the angular space width,  $\varphi_{w.g}$ , in a gear are measured within the pitch plane,  $PP$ , of the *crown gear/gear*,  $CG_g$ , as shown in Figure 12.31 (A similar schematic is valid for crossed-axes gearing as well). The angular pitch of the gear tooth in Figure 12.31 is labeled as  $\varphi_{x.g}$ .

Similarly, a virtual crown gear that is engaged in the correct mesh with the pinion, can be considered. This crown gear can be referred to as a *crown gear/pinion*, or simply as  $CG_p$ . The angular tooth thickness,  $\varphi_{t.p}$ , and the angular space width,  $\varphi_{w.p}$ , of a gear is measured within the pitch plane,  $PP$ , of the *crown gear/pinion*,  $CG_p$ , (not shown in Figure 12.31). The angular pitch of the pinion tooth is labeled as  $\varphi_{x.p}$  (not shown in Figure 12.31).

The angular pitch of the gear,  $\varphi_{x.g}$ , and that,  $\varphi_{x.p}$ , of the mating pinion are equal, namely, the equality  $\varphi_{x.g} = \varphi_{x.p} = \varphi_x$  is valid. Therefore, in further discussion, the designations,  $\varphi_{x.g}$  and  $\varphi_{x.p}$ , for these angular pitches are replaced with the designation  $\varphi_x$ .

When the crown gear,  $CG_g$ , and the crown gear,  $CG_p$ , are engaged in mesh, they are free to turn about the  $O_{pp}$  – axis in relation to one another through a certain angle,  $\varphi_B$ . The angle,  $\varphi_B$ , is referred to as the *angular backlash*. The *angular backlash*,  $\varphi_B$ , is calculated as:

$$\varphi_B = \varphi_{w.g} - \varphi_{t.p} \quad (12.121)$$

or as:

$$\varphi_B = \varphi_{w.p} - \varphi_{t.g} \quad (12.122)$$

<sup>4</sup> A straight line along which the so-called **normal backlash** is specified, can NOT be perpendicular to both, to the gear tooth flank,  $\mathcal{S}$ , and the pinion tooth flank,  $\mathcal{P}$ , at the same time.

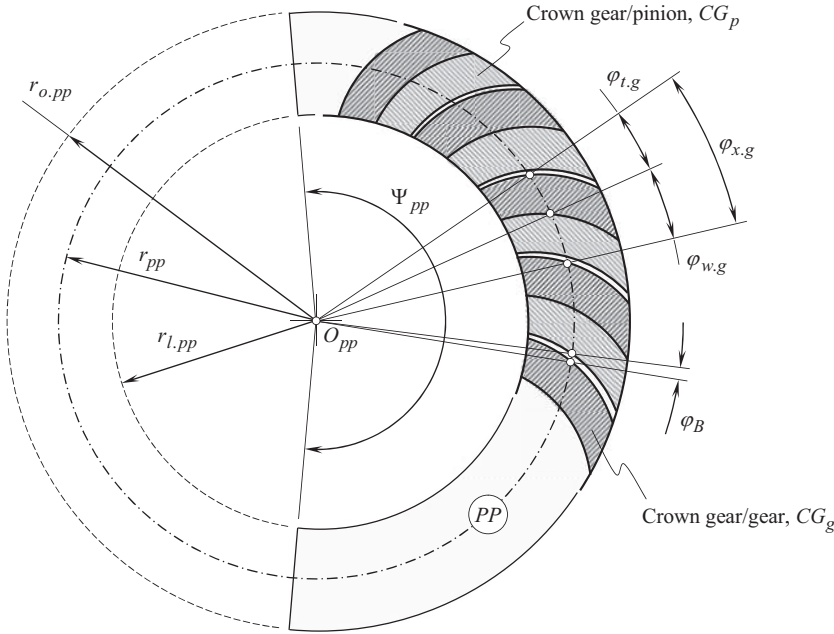


**FIGURE 12.31** On definition of the terms: (a) the *angular tooth thickness*,  $\varphi_t$ , (b) the *angular space width*,  $\varphi_w$ , and (c) the *angular backlash*,  $\varphi_B$ , in intersected-axes gearing (by means of  $CG_g - \text{to} -CG_p$  mesh).

Special instrumentation is required to be used in order to perform direct measurement of the design parameters in a gear ( $\varphi_{t,g}$ ,  $\varphi_{w,g}$ , and  $\varphi_{x,g}$ ), and in a mating pinion ( $\varphi_{t,p}$ ,  $\varphi_{w,p}$ , and  $\varphi_{x,p}$ ). Then either Eqs. (12.121) or (12.122) is used for the calculation of the angular backlash,  $\varphi_B$ .

In a bevel gear pair, the backlash is measured at a configuration of a gear and of a pinion when *two pairs of teeth are engaged in mesh*.

If the backlash does not fall within the recommended limits, no corrections to the mounting distance are allowed to adjust the backlash [178]. If possible, the tooth thickness can be corrected (reduced) by additional machining. For strength calculations, the normal backlash can be expressed in terms of the backlash in the plane of rotation.

There is a trade-off when setting an actual value of backlash: the backlash must be large enough for operating of the gear pair, and it must be small enough when reversing the rotation.

**Conclusion 12.4.** *Backlash in intersected-axes gearing is said to be an “angular” parameter and not a “linear” parameter. Backlash is measured within the pitch plane of the gear pair.*

Conventional technic can be adapted when inspecting the effective angular backlash,  $\varphi_{B,pa}$ , in geometrically accurate intersected-axes gearing (see Figure 12.32). For a certain reading,  $DTI_{\text{reading}}$ , taken from the dial-type indicator, the angular backlash,  $\varphi_{B,pa}$ , is calculated as:

$$\varphi_{B,pa} \cong \frac{DTI_{\text{reading}}}{r_{pa,B}}, \text{ rad} \quad (12.123)$$

where  $r_{pa,B}$  is the distance from the plane-of-action apex,  $A_{pa}$ , to the section at which the dial-type indicator is installed.

The effective angular backlash,  $\varphi_{B,pa}$ , is smaller compared to the angular backlash,  $\varphi_{B,n}$ , measured within the pitch plane,  $PP$ .

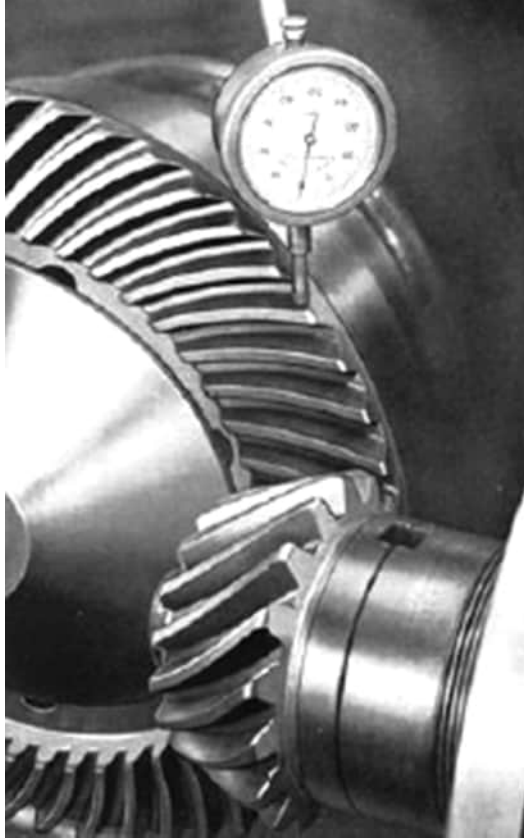


**FIGURE 12.32** Angular backlash,  $\phi_{B.pa}$ , can be calculated based on the measurement of a linear value of the backlash in compliance with the adopted practice.

#### 12.6.6 GEAR TOOTH-LINE AND GEAR SPACE-LINE IN INTERSECTED-AXES GEARS

The terms *gear tooth-line* and *gear space-line* are used in the practice of gear design, and of gear manufacture. These terms are associated mainly with gears that feature helical teeth, circular-arc teeth (in the lengthwise direction of the gear teeth), cycloid teeth, and so forth. However, these terms can be used in association with gears that feature straight teeth, for example, when the deviations of the gear teeth in their lengthwise direction are considered.

The determined values of the angular tooth thickness in a gear,  $\phi_{t.g}$  (see Eq. (12.116), and in a mating pinion,  $\phi_{t.p}$  (see Eq. (12.118) as well as the angular space widths in a gear,  $\phi_{w.g}$  (see Eq. (12.117), and in a mating pinion,  $\phi_{w.p}$  (see Eq. (12.119) make possible determination of the term *gear tooth-line*,  $G_{tl}$ , and the term *gear space-line*,  $G_{sl}$  in gears with symmetric, as well, with asymmetric tooth profile.

The construction of a *gear tooth-line*, and, similarly, of a *gear space-line*, is illustrated in Figure 12.33.

In gears with a symmetric tooth profile, the *tooth-line* can be defined as a line traced within the pitch plane of the mating crown gear (or within any other plane perpendicular to the axis of rotation,  $O_{pp}$ , of the pitch plane,  $PP$ ) by the middle point,  $c_{tl}$ , of the tooth profile. The middle point,  $c_{tl}$ , can be specified either as the point of intersection of the angular tooth thickness by the corresponding circle of a radius,  $r_{y.pp}$ , or as the point of intersection of the pitch plane,  $PP$ , by the gear tooth profile centerline,  $C_{tl}$ .

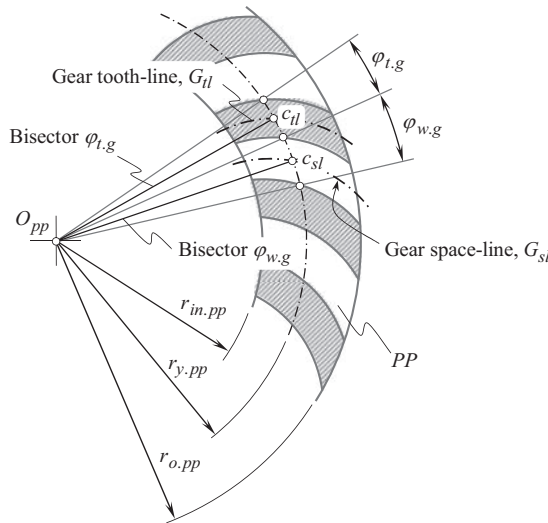


**FIGURE 12.33** On the definition of the terms the *gear tooth-line*,  $G_{tl}$ , and the *gear space-line*,  $G_{sl}$ , in gears for intersected-axes gear pairs (a similar construction is valid also for crossed-axes gear pairs).

The following definition can be drawn up from the above discussion:

#### Definition 12.7

In intersected-axes gearing, the *gear tooth-line*,  $G_{tl}$ , is a planar curve that can be viewed as a locus of middle points of the crown-rack tooth profile within the pitch plane of the crown rack (or by any other plane perpendicular to the axis of rotation of the pitch plane constructed within the gear tooth height).

A similar definition is valid with respect to the term *gear space-line*:

#### Definition 12.8

In intersected-axes gearing, the *gear space-line*,  $G_{sl}$ , is a planar curve that can be viewed as a locus of middle-points of the crown-rack tooth-space profile within the pitch plane of the crown rack (or within any other plane perpendicular to the axis of rotation of the pitch plane constructed within the gear tooth height).

These definitions are also valid with respect to gears that are used in the design of crossed-axes gears having symmetric tooth profile.

Determination of the current situation of the middle point,  $c_{tl}$ , within the tooth profile of the crown rack is simple. As an example, Figure 12.34a illustrates the determination of the point,  $c_{tl}$ , for a crown-rack tooth profile of transverse pressure angle,  $\phi_t$ , equal to  $\phi_t = 20^\circ$ . The middle point,  $c_{tl}$ , is shown here as the intersection of the tooth profile centerline,  $C_{tl}$  (the centerline,  $C_{tl}|_{20^\circ}$ , in this particular case), with the pitch plane,  $PP$ . Any point (within the pitch plane tooth height) with the centerline,  $C_{tl}|_{20^\circ}$ , can be taken as a middle-point,  $c_{tl}$ .

A similar construction in Figure 12.34,b illustrates the determination of the point,  $c_{tl}$ , in a crown-rack tooth profile of transverse pressure angle,  $\phi_t$ , equal to  $\phi_t = 28^\circ$ . Again, the middle point,  $c_{tl}$ , is shown here as an intersection of the tooth profile centerline,  $C_{tl}$  (the centerline,  $C_{tl}|_{28^\circ}$ , in this particular case), with the pitch plane,  $PP$ . Any point (within the pitch plane tooth height) with the centerline,  $C_{tl}|_{28^\circ}$ , can be taken as a middle point,  $c_{tl}$ .

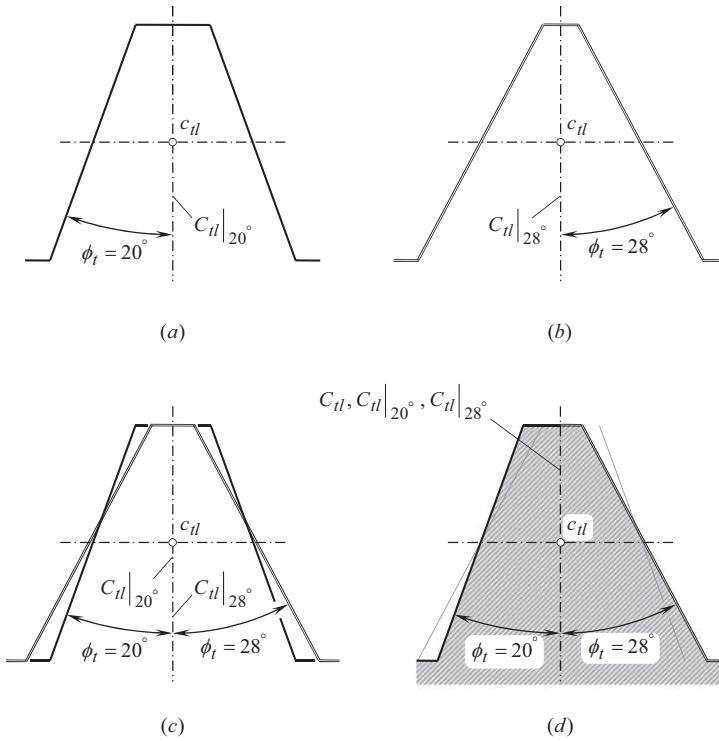


**FIGURE 12.34** On the definition of the term *gear tooth-line*,  $G_{tl}$ , in gears with asymmetric tooth profile for intersected-axes gear pairs (a similar construction is valid also for crossed-axes gear pairs) (a) symmetric tooth profile,  $\phi_t = 20^\circ$ , (b) symmetric tooth profile,  $\phi_t = 28^\circ$ , (c) tooth profiles  $\phi_t = 20^\circ$  and  $\phi_t = 28^\circ$  overlap each other, and (d) asymmetric tooth profile ( $\phi_t = 20^\circ$  and  $\phi_t = 28^\circ$ ).

In both cases, the tooth profile of the crown rack is symmetric with respect to the centerline,  $C_{tl}$ .

To construct the middle-point,  $c_{tl}$ , for an asymmetric tooth profile, two symmetric tooth profiles (with  $\phi_t = 20^\circ$  and  $\phi_t = 28^\circ$  transverse profile angles) are shown in Figure 12.34,c overlapped so as to share the centerline,  $C_{tl}$  ( $C_{tl} = C_{tl}|_{20^\circ} = C_{tl}|_{28^\circ}$ ), and having that same tooth height. Any point within the centerline,  $C_{tl}$ , can be taken as middle point,  $c_{tl}$ . As an example, an asymmetric tooth profile is shown in Figure 12.34,d. This tooth profile is constructed as a combination of two halves of the crown racks tooth profiles (with  $\phi_t = 20^\circ$  and  $\phi_t = 28^\circ$  transverse profile angles). Again, any point within the centerline,  $C_{tl}$ , can be taken here as middle point,  $c_{tl}$ .

A similar analysis can be performed on the definition of the term *gear space-line*,  $G_{sl}$ , in gears with asymmetric tooth profile for intersected-axes gear pairs (valid also for crossed-axes gear pairs), as illustrated in Figure 12.35.

This analysis pertains also to gears that are used in the design of crossed-axes gears with asymmetric tooth profile.

### 12.6.7 ANGULAR ADDENDUM AND ANGULAR DEDENDUM

The angular tooth addendum in intersected-axes gearing is specified by the angular distance between the pitch cone of the gear, and the gear top-land cone (the outer cone) of the gear.

#### Definition 12.9

Angular tooth addendum in intersected-axes gearing is said to be the angular distance between the pitch cone, and the outer cone of the gear measured in the axial section of the gear.

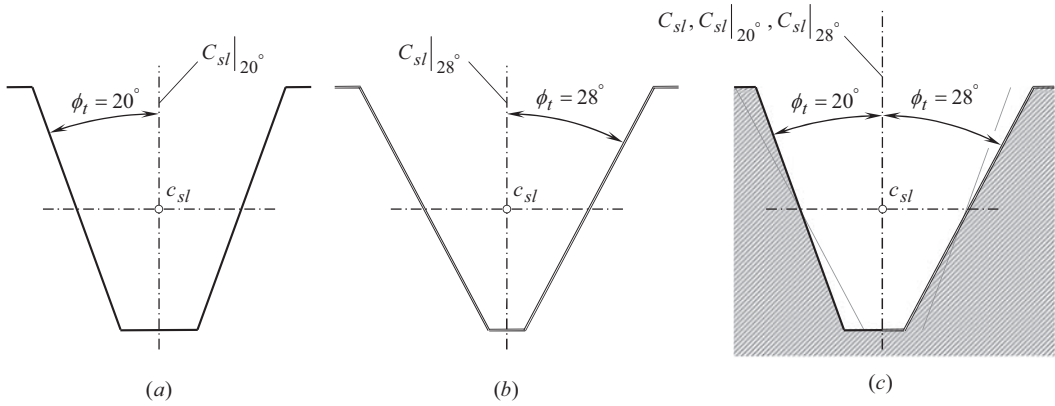


**FIGURE 12.35** On the definition of the term *gear space-line*,  $G_{sl}$ , in gears with asymmetric tooth profile for intersected-axes gear pairs (a similar construction is valid also for crossed-axes gear pairs) (a) symmetric space profile,  $\phi_t = 20^\circ$ , (b) symmetric space profile,  $\phi_t = 28^\circ$ , (c) asymmetric space profile ( $\phi_t = 20^\circ$  and  $\phi_t = 28^\circ$ ).

Similarly, the angular dedendum in intersected-axes gearing is specified by the angular distance between the pitch cone of the gear and the gear bottom-land cone (the inner cone) of the gear.

### Definition 12.10

Angular tooth dedendum in intersected-axes gearing is said to be the angular distance between the pitch cone and the inner cone of the gear measured in the axial section of the gear.

Taken together, the angular addendum,  $\Gamma_a$ , and the angular dedendum,  $\Gamma_d$ , of the gear tooth, specify the angular tooth height,  $\Gamma_h$ , of the gear (see Figure 12.29):

$$\Gamma_h = \Gamma_a + \Gamma_d \quad (12.124)$$

For standard bevel gears, the tooth height in a bevel gear is set equal to module,  $m$ . This makes possible to calculate the angular addendum,  $\Gamma_a$ , of the gear from the expression:

$$\Gamma_a = \sin^{-1} \left( \frac{m}{r_{o,pp}} \right) \quad (12.125)$$

In such a scenario, the angle,  $\Gamma_a$ , can be viewed as the *angular module*,  $\Gamma_m$  in a gear pair.

Similarly, the *angular module*,  $\gamma_m$  can be expressed in terms of the design parameters of a bevel pinion.

The dedendum of a standard bevel gear is greater, compared to the addendum at a clearance,  $c$ . Therefore, the angular dedendum,  $\Gamma_d$ , of the gear is calculated as follows:

$$\Gamma_d = \sin^{-1} \left( \frac{m + c}{r_{o,pp}} \right) \quad (12.126)$$

The difference,  $\Gamma_c$ , between the angles,  $\Gamma_d$  and  $\Gamma_a$ , is viewed as the *angular clearance*,  $\Gamma_c$  in a gear pair:

$$\Gamma_c = \Gamma_d - \Gamma_a \quad (12.127)$$



Formulas, similar to those aforementioned:

$$\gamma_a = \sin^{-1} \left( \frac{m}{r_{o,pp}} \right) \quad (12.128)$$

$$\gamma_d = \sin^{-1} \left( \frac{m+c}{r_{o,pp}} \right) \quad (12.129)$$

$$\gamma_h = \gamma_a + \gamma_d \quad (12.130)$$

are valid for the calculation of the angular addendum,  $\gamma_a$ , the angular dedendum,  $\gamma_d$ , as well as the angular tooth height,  $\gamma_h$ , in a standard bevel pinion (see Figure 12.29).

Similarly, the *angular clearance*,  $c_\gamma$ , is expressed in terms of the design parameters of a bevel pinion as:

$$\gamma_c = \gamma_d - \gamma_a \quad (12.131)$$

The aforementioned design parameters of intersected-axes gearing correlate to the corresponding design parameters in parallel-axes gearing. This correlation between the design parameters is summarized in Table 12.2.

**TABLE 12.2**

**Design Parameters in Intersected-Axes Gears and Corresponding to them  
Design Parameters in Parallel-Axes Gears**

Design Parameters of Intersected-Axes Gears		Design Parameters of Parallel-Axes Gears	
Term	Designation	Term	Designation
Tooth number	$N_g, N_p$	Tooth number	$N_g, N_p$
Pitch cone angle (gear)	$\Gamma$	Pitch diameter	$d_g, d_p$
Pitch cone angle (pinion)	$\gamma$		
Base pitch angle (gear)	$\Gamma_b$	Base pitch	$p_b$
Base pitch angle (pinion)	$\gamma_b$		
Outer cone angle (gear)	$\Gamma_o$	Outer diameter	$d_{o,g}, d_{o,p}$
Outer cone angle (pinion)	$\gamma_o$		
Root cone (gear)	$\Gamma_f$	Root diameter	$d_{f,g}, d_{f,p}$
Root cone (pinion)	$\gamma_f$		
Transverse pressure angle	$\phi_{t,\omega}$	Transverse pressure angle	$\phi_t$
Angular pitch	$\phi_n$	Normal circular pitch	$p_n$
Base pitch angle	$\phi_b$	Base pitch	$p_b$
Angular tooth thickness	$\phi_t$	Tooth thickness	$t$
Angular space width	$\phi_w$	Space width	$w$
Angular backlash <sup>a</sup>	$\phi_B$	Backlash	$B$
Angular addendum (gear)	$\Gamma_a$	Addendum	$a$
Angular addendum (pinion)	$\gamma_a$		
Angular dedendum (gear)	$\Gamma_b$	Dedendum	$b$
Angular dedendum (pinion)	$\gamma_b$		
Angular clearance	$\Gamma_c, \gamma_c$	Clearance	$c$
Angular module	$\Gamma_m, \gamma_m$	Module	$m$

<sup>a</sup> The expressions  $\phi_n = \phi_t + \phi_w$  and  $\phi_w - \phi_t = \phi_B$  are always valid.

### 12.6.8 SPECIFICATION OF DESIGN PARAMETERS IN INTERSECTED-AXES GEARING

The design parameters of intersected-axes gearset that are convenient for investigation and analysis of gears are not always those convenient in gear design and gear manufacturing practice.

The main design parameters in an intersected-axes gearing and elements of the gear tooth are schematically shown in Figure 12.36.

Additional terms and design parameters in intersected-axes gearing are defined in Figure 12.37. Note that a constant clearance is maintained by making the elements of the face cone parallel to the elements of the root cone of the mating gear. This explains the reason why the face cone apex is not coincident with the pitch-cone apex in Figure 12.37. This permits a larger fillet at the small end of the tooth that would otherwise be possible.

It is an established practice to specify the design parameters of tooth profile in intersected-axes gearing at the larger end of the gear teeth.

The addendum and the dedendum of a bevel gear are specified on the so-called the *back cone* (however, this is not a must). The straight generating line of the back cone is perpendicular to the corresponding straight generating line of the pitch cone. The angular addendum,  $\Gamma_a$ , and the angular dedendum,  $\Gamma_d$ , are calculated from the following equations:

$$\Gamma_a = \tan^{-1} \left( \frac{2a \sin \Gamma}{m N_g} \right) \quad (12.132)$$

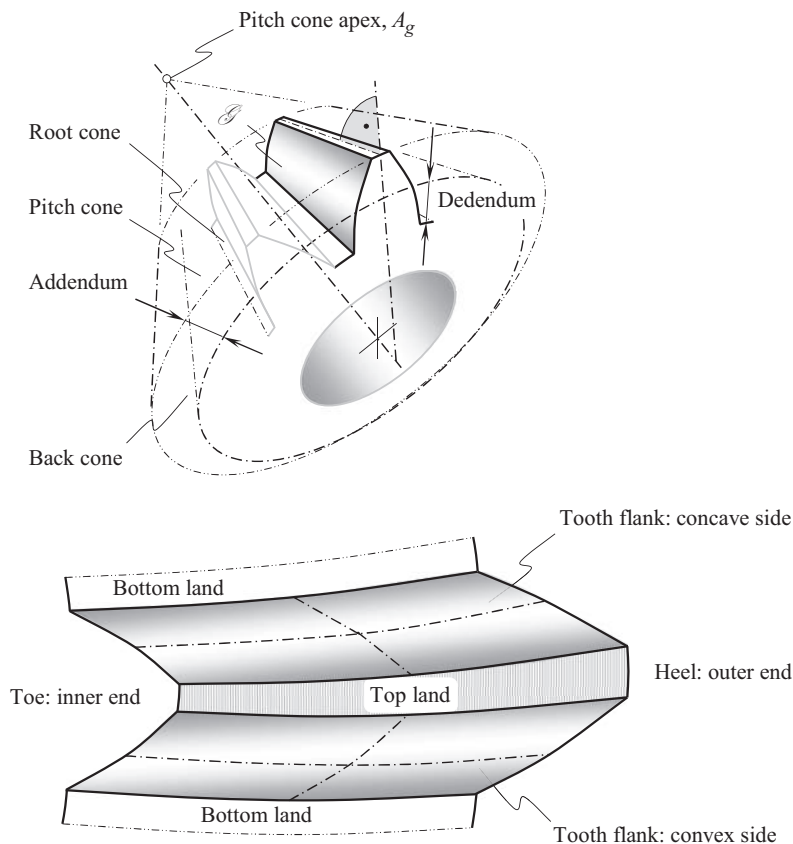
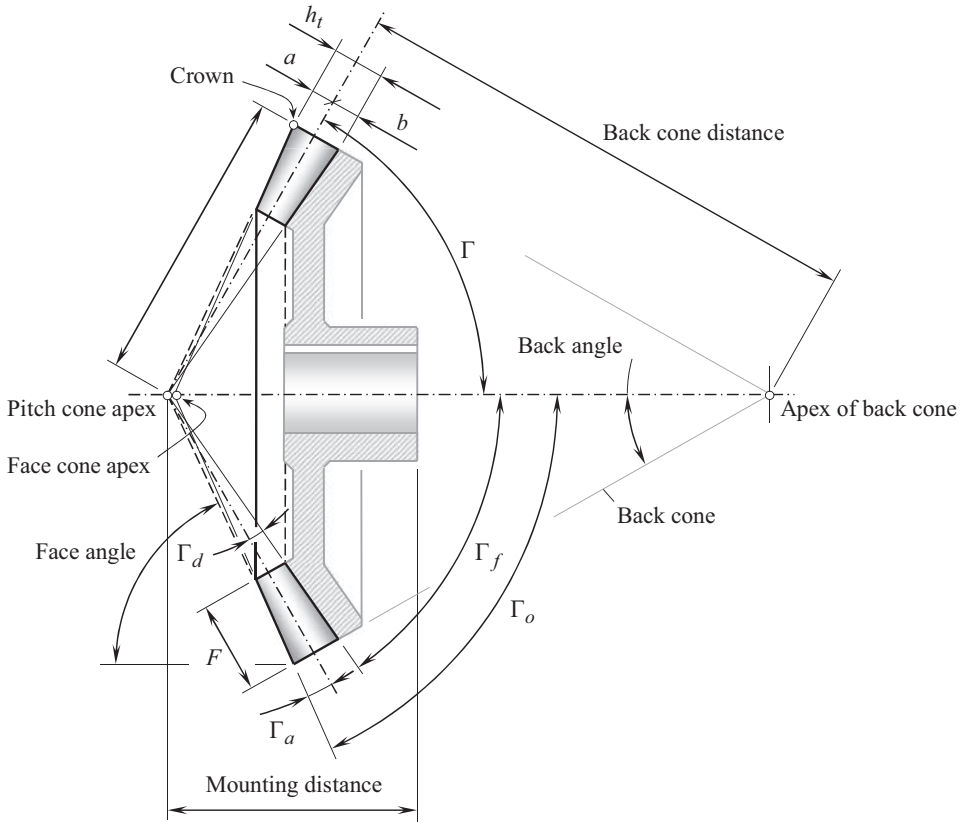


FIGURE 12.36 Main design parameters in intersected-axes gear, and elements of the gear tooth.



**FIGURE 12.37** Additional design parameters in intersected-axes gearing.

$$\Gamma_d = \tan^{-1} \left( \frac{2b \sin \Gamma}{m N_g} \right) \quad (12.133)$$

For standard gears, those for which the equalities  $a = m$  and  $b = (1.2 \div 1.3)m$  are valid (here the module of the gear is denoted by  $m$ ), Eqs. (12.132) and (12.133) are reduced to:

$$\Gamma_a = \tan^{-1} \left( \frac{2 \sin \Gamma}{N_g} \right) \quad (12.134)$$

$$\Gamma_d = \tan^{-1} \left[ \frac{(2.4 \div 2.6) \sin \Gamma}{N_g} \right] \quad (12.135)$$

Equations, similar to Eqs. (12.134) and (12.135), are valid for bevel pinion as well.

Practically, most of the straight-tooth bevel gears manufactured today use the  $\phi_{t,\omega} = 20^\circ$  profile angle.

Various types of bevel gears used in the present-day industry in the design of intersected-axes gearsets are illustrated in Figure 12.38.

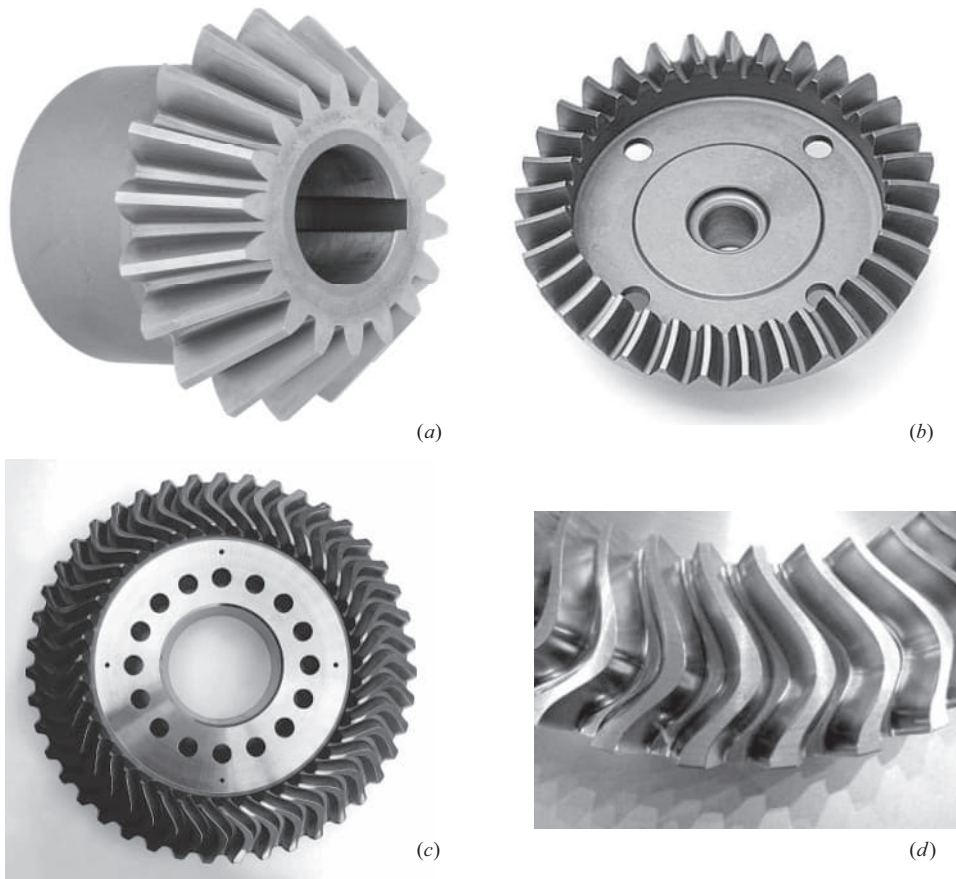


**FIGURE 12.38** Various kinds of bevel gears are used in the present-day industry in the design of intersected-axes gearsets: (a) straight bevel gear, (b) spiral bevel gear, (c) S-shaped bevel gear, and (d) teeth of the S-shaped bevel gear.

## 12.7 TREDGOLD APPROXIMATION

Mesh of gears in intersected-axes gearing occurs on a sphere<sup>5</sup> of a certain radius, similar to meshing of gears in parallel-axes gearing that is observed within a plane perpendicular to the axes of rotations of the gears. Projecting of bevel gear tooth on the surface of a sphere would indeed be a difficult and time-consuming task. Fortunately, a kind of approximation is known that reduces this task to that of ordinary spur gear. This method is called the *Tredgold's approximation*, and as long as the gear has eight or more teeth, it is accurate enough for most practical purposes (see page 88 in Ref. [46], and others). It is in almost universal use, and the terminology of bevel gear tooth has evolved around it. Moreover, the method of *Tredgold's approximation* can further be enhanced to crossed-axes gearing as well.

<sup>5</sup> Interpretation of mesh of intersected-axes gearing as mesh of gears on a sphere loosely leads to wrong terminology: intersected-axes gears sometimes are loosely referred to as *spherical gears*. This term is incorrect because mesh in crossed-axes gearing (see below) occurs also on a sphere. If such a practice is adopted, intersected-axes gears cannot be distinguished from crossed-axes gears as long, as gear pairs of both kinds are referred to as *spherical gears*. The aforementioned ambiguity caused by the term *spherical gears* can be avoided by using terms such as *intersected-axes gears* (or  $I_a$  –gearing, for simplicity), and *crossed-axes gears* (or just  $C_a$  –gearing, for simplicity). These terms are adopted in this book instead of incorrect term *spherical gears*.

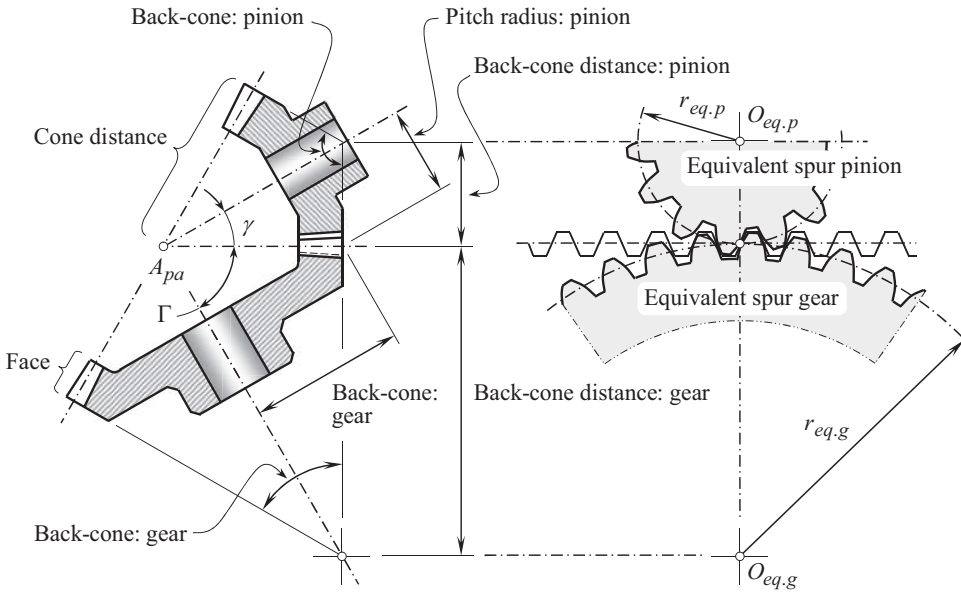


FIGURE 12.39 *Tredgold approximation in intersected-axes gearing.*

In using *Tredgold's* method, a *back cone* is formed of elements that are perpendicular to the elements of the pitch cone at the large end of the gear teeth. This is shown in Figure 12.39. The length of a back cone element is called the *back-cone radius*. Now an equivalent spur gear is constructed, whose pitch radius,  $r_{eq}$ , is equal to the back cone radius. Thus, from a pair of bevel gears, we can obtain, using *Tredgold's approximation*, a pair of equivalent spur gears, which are then used to define the tooth profiles; they can also be used to determine the tooth action and the contact conditions exactly as for ordinary spur gears, and the results will correspond closely to those for the bevel gears. From the geometry of Figure 12.39, the equivalent pitch radii are:

$$r_{eq.g} = \frac{r_g}{\cos \Gamma} \quad (12.136)$$

and

$$r_{eq.p} = \frac{r_p}{\cos \gamma} \quad (12.137)$$

The number of tooth in the equivalent spur gear equals:

$$N_{eq} = \frac{2\pi r_{eq}}{p} \quad (12.138)$$

where  $p$  is the circular pitch of the bevel gear measured at the large end of the teeth.

In the usual case, the equivalent spur gears will not have an integral number of teeth.

It should be pointed out here that the approximation that is proposed by *Tredgold*<sup>6</sup> for intersected-axes gearing can be evolved to crossed-axes gearing as well.

<sup>6</sup> Thomas Tredgold (August 22, 1788–January 28, 1829) – an English engineer, known for his early work on railroad construction.

## 12.8 PRINCIPAL FEATURES OF GEOMETRICALLY ACCURATE *NOVIKOV/CONFORMAL* AND *HIGH-CONFORMAL* INTERSECTED-AXES GEARING

*Novikov/conformal* and *high-conformal* intersected-axes gearing can be used to transmit a rotary motion from a driving shaft to a driven shaft that intersects each other at a certain angle. So far, *Novikov/conformal* and *high-conformal* intersected-axes gears got no extensive application in the industry. This is mainly because they are not profoundly investigated yet.

Geometrically accurate *Novikov/conformal/high-conformal* intersected-axes gearsets feature many similarities with geometrically accurate intersected-axes gearsets of conventional design, namely, with gearing that feature line contact between a gear and a mating pinion tooth flanks. Because of this, there is no need to consider separately, for example, kinematics of the instantaneous motion in *Novikov/conformal/high-conformal* intersected-axes gearing, as it is already discussed to the best possible extent in a corresponding section devoted to geometrically accurate intersected-axes gearing of conventional design.

Base cones of a gear and of a mating pinion is another example of similarities between *Novikov/conformal/high-conformal* intersected-axes gearing and between geometrically accurate intersected-axes gearing of conventional design.

Sliding between the tooth flanks of a gear and of a mating pinion in intersected-axes *Novikov/conformal/high-conformal* gearing can be viewed as a reduced case of that in geometrically accurate intersected-axes gearing of conventional design.

A few more similarities can be mentioned here. These similarities and a few others are omitted from the further analysis.

Below, the reader's attention is focused mainly on the key features of geometrically accurate *Novikov/conformal/high-conformal* intersected-axes gear pairs.

### 12.8.1 PATH OF CONTACT IN *NOVIKOV CONFORMAL/HIGH-CONFORMAL* INTERSECTED-AXES GEARING

When the gears rotate, the path of contact in a *Novikov conformal/high-conformal* intersected-axes gear pair is a trace of contact point within the transverse section of the gearset. For better understanding of the kinematics, and the geometry of *Novikov conformal/high-conformal* gearing, the use of the *equivalent pulley-and-belt transmission* of intersected-axes gear pair is helpful.

Refer to Figure 12.40 for details on the path of contact in *Novikov conformal/high-conformal* intersected-axes gearing.

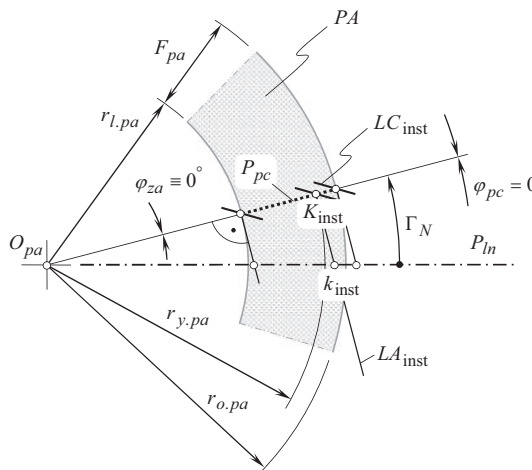


**FIGURE 12.40** Path of contact,  $\varphi_{pc} = 0^\circ$ , and pseudo-path of contact,  $P_{pc}$ , in intersected-axes *Novikov conformal/high-conformal* gear pair.

The design parameters such as: the outer radius,  $r_{o,pa}$ , of the plane of action, the inner radius,  $r_{i,pa}$ , of the plane of action, and the effective width,  $F_{pa}$ , of the plane of action,  $PA$ , in intersected-axes *Novikov conformal/high-conformal gear pair* are identical to that in intersected-axes gear pair of conventional design. The zone of action in intersected-axes *Novikov conformal/high-conformal gear* is shrunk to a straight line, as the angular width of the zone of action,  $ZA$ , is zero ( $\varphi_{za} = 0^\circ$ ). This straight line forms an angle,  $\Gamma_N$ , with the axis of instantaneous rotation,  $P_{in}$ . In intersected-axes *Novikov conformal/high-conformal gearing*, the cone with the cone angle  $\Gamma_N$  is an equivalent of the *boundary N – circle* in parallel-axes gearing.

As the gears rotate, the tooth flanks,  $\mathcal{G}$  and  $\mathcal{P}$ , of a gear and of a mating pinion make instantaneous contact at point,  $K_{inst}$ . The instantaneous line of action,  $LA_{inst}$ , is a straight line through  $K_{inst}$ . The line,  $LA_{inst}$ , is entirely located within the plane of action,  $PA$ . The instantaneous line of action,  $LA_{inst}$ , is perpendicular to the radius,  $A_{pa}K_{inst}$ , and intersects the axis of instantaneous rotation,  $P_{in}$ , at corresponding point,  $k_{inst}$ . As the angular width of the zone of action is zero ( $\varphi_{za} = 0^\circ$ ), the angular length,  $\varphi_{pc}$ , of the path of contact,  $P_c$ , is zero ( $\varphi_{pc} = 0^\circ$ ), the length,  $l_{pc}$ , of the path of contact,  $P_c$ , is also of a zero value ( $l_{pc} = 0$ ). The path of contact,  $P_c$ , is the zero-length straight-line segment of the strait instant line of action,  $LA_{inst}$ . The path of contact,  $P_c$ , is entirely located in the transverse section of the gear pair. Physically, the path of contact,  $P_c$ , is truncated to the contact point,  $K$ , but it still features a direction – the path of contact,  $P_c$ , is pointed along the instant line of action,  $LA_{inst}$ .

The instantaneous line of contact,  $LC_{inst}$ , is a zero-length straight line segment through point,  $K_{inst}$ , that is entirely located within the plane of action,  $PA$ , and is tangent to the gear helix at  $K_{inst}$ .

For different configurations of a gear, and of a mating pinion, the instantaneous contact point,  $K_{inst}$ , occupies different locations along a straight line, that is referred to as the *pseudo-path of contact*,  $P_{pc}$ . *Pseudo* is due to contact point,  $K_{inst}$ , does not travel along the straight line,  $P_{pc}$ : the rotation with the plane of action is the only motion that contact point,  $K_{inst}$ , performs. The pseudo-path of contact is a pseudo-trace of contact point that can be imagined when the gears rotate. Usually, the pseudo-path of contact,  $P_{pc}$ , is considered in a stationary reference system associated with the gear housing.

This issue is discussed in the book by the author in detail [157].

## 12.8.2 BOUNDARY CONE

When the gears rotate, a motion of the pinion in relation to the mating gear can be viewed as instantaneous rotation about the axis of instantaneous rotation,  $P_{in}$ . A boundary *N – circle* is traced up by contact point,  $K$ , in such a relative motion. In theory, the actual value of the radius,  $r_N$ , of the boundary *N – circle* is a trade-off between a desirable high contact strength of the gear tooth, and low friction between the tooth flanks of the gear,  $\mathcal{G}$ , and that of the pinion,  $\mathcal{P}$ . In practice, run-out of the gear and of the pinion as well as the displacements of other types of the tooth flanks,  $\mathcal{G}$  and  $\mathcal{P}$ , in relation to their desirable position, are required to be taken into account.

As the relative motion of a gear and of a mating pinion is an instantaneous rotation,  $\omega_{pl}$ , about the axis of instantaneous rotation,  $P_{in}$ , the plane perpendicular to the vector of instantaneous rotation,  $\omega_{pl}$ , at arbitrary point within the axis,  $P_{in}$ , can be constructed, and the relative motion of the gears can be investigated within the normal plane (as illustrated in Figure 12.41).

Within the normal plane, a boundary *N – circle* of a radius,  $r_N$ , is constructed. The boundary *N – circle* is centered at point of intersection of the axis of instantaneous rotation,  $P_{in}$ , by the normal plane. The radius,  $r_N$ , of the boundary *N – circle* equals to a desirable displacement,  $l$ , of the contact point,  $K$  [either in a positive direction to the position of the point,  $K_{by}$ , or in a negative direction to the position of the point,  $K_{bf}$ ], from the axis of instantaneous rotation,  $P_{in}$ , along the instantaneous line of action,  $LA_{inst}$ . The actual value of the displacement,  $l$  (either of a positive value,  $+l$ , or of a negative value,  $-l$ ), is a trade-off between the contact strength of the gear tooth, and the sliding between the tooth flanks of the gear and the mating pinion,  $\mathcal{G}$  and  $\mathcal{P}$ , in relation to one another. The



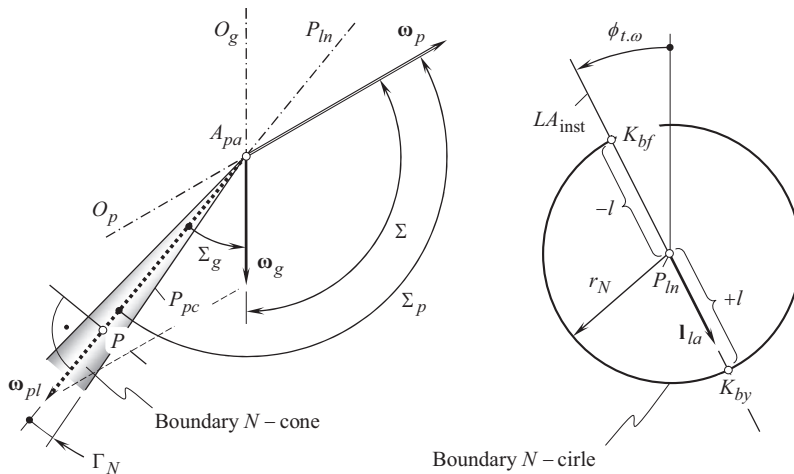


**FIGURE 12.41** Configuration of the boundary The boundary  $N$  – cone cone in Novikov conformal/high-conformal intersected-axes gear pair.

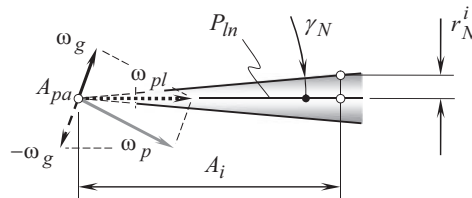


**FIGURE 12.42** Boundary cone angle,  $\gamma_N$ , in Novikov conformal/high-conformal intersected-axes gearing.

larger the distance,  $l$ , the higher the contact strength of the gear tooth, and the higher the sliding between the tooth flanks, and vice versa: the smaller the distance,  $l$ , the lower the contact strength of the gear tooth and the lower sliding between the tooth flanks.

Under the assumptions: (a) zero deviation of the displacement,  $l$ , from its desirable value (namely,  $\Delta l = 0$ ), and (b) the manufacturing errors are zero, the contact point,  $K$ , is located at the point of intersection of the boundary  $N$  – circle by the instantaneous line of action,  $LA_{inst}$ . At any point within the axis of instantaneous rotation,  $P_{ln}$ , a boundary  $N$  – circle of a certain radius,  $r_N^i$ , can be constructed, and an instantaneous line of action,  $LA_{inst}$ , can be constructed as well. The transverse pressure angle,  $\phi_{t,\omega}^i$ , is not mandatorily of the same value at all normal transverse sections of the axis,  $P_{ln}$ . The instantaneous line of action,  $LA_{inst}$ , is a line through the axis of instantaneous rotation,  $P_{ln}$ . No kinematical and/or geometrical constraints in intersected-axes Novikov conformal/high-conformal gearing are violated in such a scenario.

It is practical to retain the transverse pressure angle,  $\phi_{t,\omega}^i$ , of a certain constant value,  $\phi_{t,\omega}$ , within the active portion of the face,  $F_{pa}$ , of the gear pair. Moreover, as a normal section through point within the axis of instantaneous rotation,  $P_{ln}$ , approaches the plane-of-action apex,  $A_{pa}$ , the radius,  $r_N^i$ , of the boundary  $N$  – circle becomes smaller, correspondingly.

Consider a straight line,  $P_{pc}$ , through contact point,  $K$ , between the tooth flanks,  $\mathcal{F}$  and  $\mathcal{P}$ , of the gear and of the pinion, and through the common plane-of-action apex,  $A_{pa}$ , as illustrated in Figure 12.40. The pseudo-path of contact,  $P_{pc}$ , forms a boundary cone angle,  $\Gamma_N$ , with the axis of instantaneous rotation,  $P_{ln}$ . The boundary cone angle,  $\Gamma_N$ , (see Figure 12.42) can be expressed in terms (a) of the radius,  $r_N^i$ , of the boundary  $N$  – circle at point of interest within the axis of



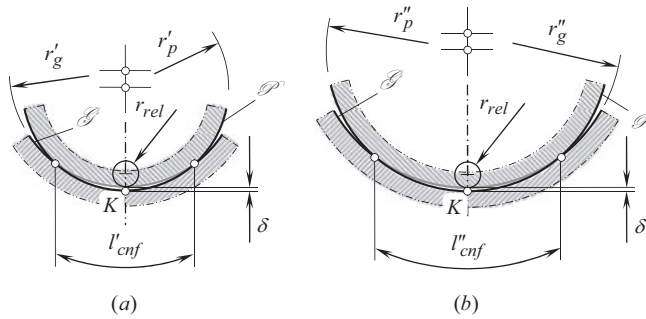


**FIGURE 12.43** Impact of the magnitude of radii of curvature of a gear tooth flank,  $\mathcal{G}$ , and of a mating pinion tooth flank,  $\mathcal{P}$ , onto the bearing capacity in gear pairs with equal radius of relative curvature,  $r_{rel}$ .

instantaneous rotation,  $P_{ln}$ , and (b) of the cone distance,  $A_i$ , of that point of interest from the plane-of-action apex,  $A_{pa}$ :

$$\Gamma_N = \tan^{-1} \left( \frac{r_N^i}{A_i} \right) \quad (12.139)$$

When rotating about the axis of instantaneous rotation,  $P_{ln}$ , a cone of revolution is generated by the straight line,  $P_{pc}$ . This cone of revolution is referred to as the *boundary N – cone* in intersected-axes *Novikov conformal/high-conformal* gearing. The following definition can be formulated based on this discussion:

### Definition 12.11

Boundary Novikov cone (or just boundary *N – cone*, for simplicity) in intersected-axes Novikov conformal/high-conformal gearing is said to be a cone of revolution generated by the pseudo-path of contact,  $P_{pc}$ , in its rotary motion about the axis of instantaneous rotation,  $P_{ln}$ .

The convex tooth flank of one member of a gear pair (primarily of the pinion,  $\mathcal{P}$ ) has to be entirely located within the interior of the boundary *N – cone*. The concave tooth flank of another member (primarily of the gear,  $\mathcal{G}$ ) of the gear pair has to be entirely located outside the interior of the boundary *N – cone*.<sup>7</sup> This requirement is of critical importance for intersected-axes *Novikov conformal/high-conformal* gearing. In a more general case, not a boundary *N – cone* should be considered, but a boundary *N – surface* of revolution should be considered instead. However, conformal and high-conformal gearsets of such design are far from being practical in the present-day industry. This is the chief reason for gearsets of this particular design are not considered here more in detail.

### 12.8.3 BEARING CAPACITY OF HIGH-CONFORMAL GEARING

The influence of an increase in radius,  $r_N$ , of the boundary *N – circle* onto a rise of contact strength in high-conformal gearing is schematically illustrated in Figure 12.43. Here, normal sections of the tooth flanks of a gear and a mating pinion for two high-conformal gear pairs are shown. The radii of relative curvature,  $r_{rel}$ , in both normal sections are equal to one another.

In the first case, shown in Figure 12.43a, the radius of curvature of the gear tooth profile,  $\mathcal{G}$ , is denoted by  $r'_g$ , while the radius of curvature of the pinion tooth profile,  $\mathcal{P}$ , within that same normal

<sup>7</sup> The concept of the *boundary N – cone* was not known in the time of Prof. *M.L. Novikov*. This is a newly (circa ~2008) introduced by Dr. *S.P. Radzevich* concept in intersected-axes *Novikov conformal/high-conformal* gearing.

plane is denoted by  $r'_p$ . The radius of relative curvature,  $r_{rel}$ , of the interacting tooth flanks is equal to  $r_{rel} = -r'_g - r'_p$  (as it is adopted in this book, the radii of curvature are signed values: convex profiles feature radii of curvature of positive values, while concave profiles feature radii of curvature of negative values). When a load is applied at contact point,  $K$ , the tooth flanks,  $\mathcal{G}$  and  $\mathcal{P}$ , approach to each other at a certain distance. This distance is designated as  $\delta$ . Under the applied load, the contact point spreads over a certain area of contact. The width of the contact area within the normal plane section in this particular case is designated as  $l'_{cnf}$ .

In the second case, shown in Figure 12.43b, the radius of curvature of the gear tooth profile,  $\mathcal{G}$ , is denoted by  $r''_g$ , while the radius of curvature of the pinion tooth profile,  $\mathcal{P}$ , within that same plane is denoted by  $r''_p$ . It should be stressed here that the inequalities  $|r''_g| > |r'_g|$  and  $r''_p > r'_p$  take place in this consideration. The radius of relative curvature,  $r_{rel}$ , of the interacting tooth flanks is equal  $r_{rel} = -r''_g - r''_p$ . Let us assume that when a load is applied at contact point,  $K$ , the tooth flanks,  $\mathcal{G}$  and  $\mathcal{P}$ , approach each other at the same distance  $\delta$ , as in the case illustrated in Figure 12.43a. Under the applied load, the contact point spreads over a certain area of contact. The width of the contact area within the normal plane section in this particular case is designated as  $l''_{cnf}$ .

An in-detail analysis is unnecessary in order to make it evident that the arc,  $l''_{cnf}$ , is larger compared to the arc,  $l'_{cnf}$ . As the inequality  $l''_{cnf} > l'_{cnf}$  is observed, it becomes evident that the bearing capacity of a high-conformal intersected-axes gearing depends not only on the relative curvature,  $r_{rel}$ , of the contacting tooth flanks, but it also depends on the magnitudes of the radii of curvature of the tooth flanks,  $\mathcal{G}$  and  $\mathcal{P}$ , at point of their contact. The larger the magnitudes of the radii,  $r_g$  and  $r_p$ , of a normal curvature of the interacting tooth flanks,  $\mathcal{G}$  and  $\mathcal{P}$ , the greater the load capacity of the high-conformal intersected-axes gearing, and vice versa. Ultimately, the following conclusion becomes valid:

**Conclusion 12.5.** *High-conformal gearing with larger magnitudes of the radii of the normal curvature of the interacting tooth flanks feature a higher load-carrying capacity, and vice versa.*

It is the right point to recall here that magnitudes of the radii,  $r_g$  and  $r_p$ , of normal curvature of the interacting tooth flanks,  $\mathcal{G}$  and  $\mathcal{P}$ , strictly correlate to the radius,  $r_N$ , of the boundary circle in the cross-section of the tooth flanks through the corresponding pitch point. Therefore, high-conformal gearing with a larger radius,  $r_N$ , of the boundary  $N$  – circle features a higher load capacity.

## 12.9 DESIGN PARAMETERS IN NOVIKOV CONFORMAL/HIGH-CONFORMAL INTERSECTED-AXES GEARSETS

The rotation vectors of a gear,  $\omega_g$ , and its mating pinion,  $\omega_p$ , should be given prior to beginning designing a high-conformal intersected-axes gear pair. Once the rotation vectors,  $\omega_g$  and  $\omega_p$ , are specified, the vector,  $\omega_{pt}$ , of instantaneous rotation as well as the shaft angle,  $\Sigma$ , can be determined. The axes of rotations,  $O_g$ ,  $O_p$ , and  $P_m$ , are the straight lines pointed along the rotation vectors,  $\omega_g$ ,  $\omega_p$ , and  $\omega_{pt}$ , correspondingly. The known configuration of the axes of rotation,  $O_g$ ,  $O_p$ , and  $P_m$ , makes possible the determination of the tooth ratio,  $u$ , and the pitch cone angles of the gear,  $\Gamma$ , and the pinion,  $\gamma$  [157,218]:

$$\Gamma = -\tan^{-1} \left( \frac{\sin \Sigma}{\omega_p / \omega_g + \cos \Sigma} \right) \quad (12.140)$$

$$\gamma = \tan^{-1} \left( \frac{\sin \Sigma}{\omega_g / \omega_p + \cos \Sigma} \right) \quad (12.141)$$

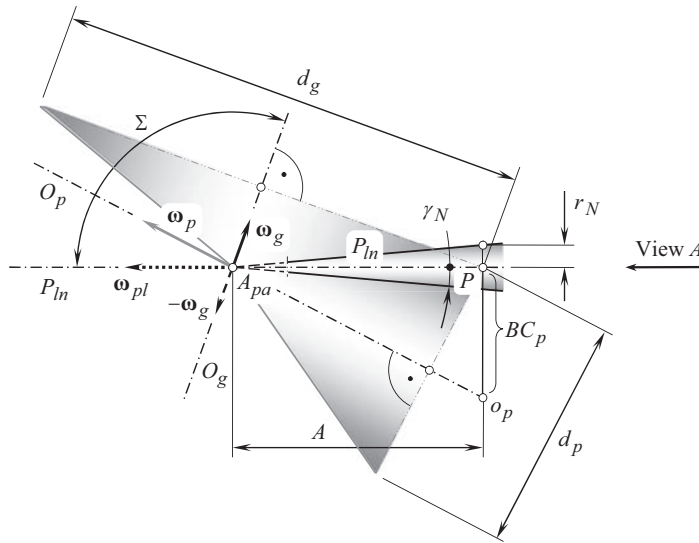


**FIGURE 12.44** Configuration of the normal reference plane in relation to the axis of instantaneous rotation,  $P_{ln}$ , and to the pitch cones of a gear and a mating pinion in *Novikov conformal/high-conformal* intersected-axes gearing.

The design parameters in a high-conformal intersected-axes gear pair can be specified based, to a great extent, on those of parallel-axes gearing. From this perspective, the vector of instantaneous rotation,  $\omega_{pl}$ , and the axis of instantaneous rotation,  $P_{ln}$ , are of critical importance. As the instantaneous motion of the pinion in relation to the mating gear is interpreted as instantaneous rotation about the axis,  $P_{ln}$ , the design parameters in a high-conformal intersected-axes gear pair can be specified within a reference plane through the pitch point,  $P$ . The pitch point,  $P$ , is at a cone distance,  $A$ , from the apex  $A_{pa}$ . The reference plane is perpendicular to the axis of instantaneous rotation,  $P_{ln}$ , as depicted in Figure 12.44.

The calculated values of the pitch cone angles,  $\Gamma$  and  $\gamma$ , along with the given cone distance,  $A$ , yield the calculation of the pitch diameter of the gear,  $d_g$ , and that of the pinion,  $d_p$ :

$$d_g = 2A \cos \Gamma \quad (12.142)$$

$$d_p = 2A \cos \gamma \quad (12.143)$$

The back cone distance of the gear,  $BC_g$ , as well as the back cone distance of the pinion,  $BC_p$ , are calculated in a manner similar to that above:

$$BC_g = 2A \sin \Gamma \quad (12.144)$$

$$BC_p = 2A \sin \gamma \quad (12.145)$$

After the normal reference plane is constructed, the tooth profile parameters of the gear and of the pinion can be specified.

Referring to Figure 12.45, two points, namely,  $o_g$  and  $o_p$ , by nature, are the points of intersection of the axes,  $O_g$  and  $O_p$ , by a reference plane normal to the axis of instantaneous rotation,  $P_{ln}$ . The points,  $o_g$  and  $o_p$ , are at a distance  $c_n = (BC_g + BC_p)$  from one another. Two circles of radii,  $BC_g$  and  $BC_p$ , that have the points  $o_g$  and  $o_p$  as the centers are constructed. The circles share a common point, which is the pitch point  $P$ .

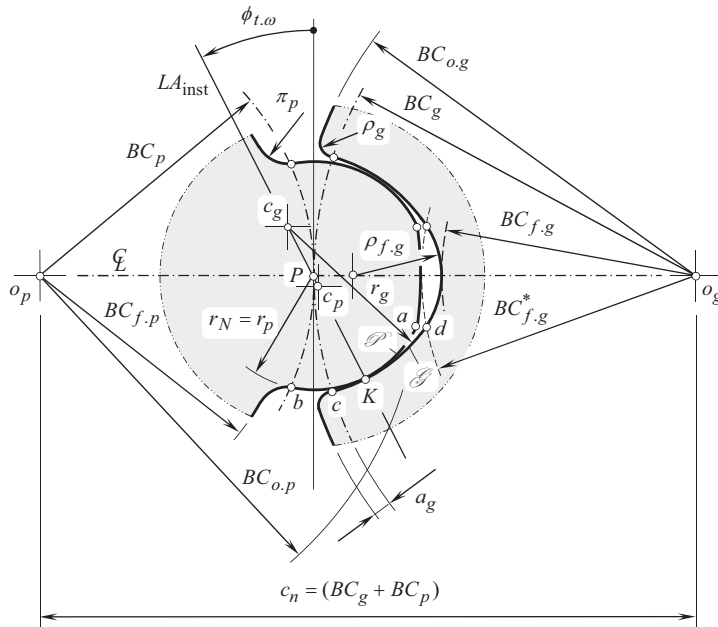


**FIGURE 12.45** Geometry of *high-conformal* intersected-axes gear pair within the reference plane perpendicular to the axis of instantaneous rotation,  $P_{in}$  (the axis,  $P_{in}$ , goes through the pitch point,  $P$ , perpendicular to the plane of drawing in Figure 12.45).

An instantaneous line of action,  $LA_{inst}$ , within the normal reference plane is the line through the pitch point,  $P$ . The line,  $LA_{inst}$ , forms a transverse pressure angle,  $\phi_{t,\omega}$ , with the perpendicular to the centerline,  $\mathcal{L}$ . The contact point,  $K$ , of the tooth flanks of the gear and of the mating pinion is a point that is situated within the instantaneous line of action,  $LA_{inst}$ . The further the contact point,  $K$ , is situated from the pitch point,  $P$ , the more freedom in selecting the radii of curvature of the tooth profiles is available for the gear designer. At the same time, the further the contact point,  $K$ , is located from the pitch point,  $P$ , the higher the friction losses (the friction occurs between the tooth flanks) and the higher wear of the tooth flanks of the gear and the pinion. Ultimately, the actual location of the contact point,  $K$ , is a kind of trade-off between the two aforementioned factors.

Let us assume that the pinion is stationary and that the gear performs an instantaneous rotation in relation to the pinion. The axis,  $P_{in}$ , of the instantaneous rotation,  $\omega_{pl}$ , is the straight line through the pitch point,  $P$ . The axis of instantaneous rotation,  $P_{in}$ , is located within the plane through the axes,  $o_g$  and  $o_p$ , and it passes through the apex,  $A_{pa}$ . When the pinion is motionless, the contact point,  $K$ , traces a boundary circle of radius,  $r_N$ , centered at  $P$ .

The pinion tooth profile,  $\mathcal{P}$ , can either align with the circular arc of the boundary circle,  $r_N$ , or it can be relieved into the bodily side of the pinion tooth. As a consequence, the location of the center of curvature,  $c_p$ , of the convex pinion tooth profile,  $\mathcal{P}$ , within the instantaneous line of action,  $LA_{inst}$ , is limited to the straight-line segment,  $PK$ . The pitch point is included in the interval  $[P, K)$ , as it is shown in Figure 12.45, while the contact point,  $K$ , is not. The designation  $[P, K)$  shows that the interval for  $c_p$  is open from the side of the contact point,  $K$ , and this interval is closed from the side of the pitch point,  $P$ .

On the other hand, the actual location of the center of curvature,  $c_g$ , of the concave gear tooth profile,  $\mathcal{G}$ , within the instantaneous line of action,  $LA_{inst}$ , is limited to the open interval  $P \rightarrow \infty$ . Theoretically, the pitch point,  $P$ , can be included in that interval for  $K$ . However, this is completely impractical, and the center of curvature  $c_g$  is actually located beyond the pitch point  $P$ . Therefore, the radius of curvature,  $r_p$ , of the convex the pinion tooth profile,  $\mathcal{P}$ , is smaller than that,  $r_g$ , of the concave the gear tooth profile,  $\mathcal{G}$ , (the inequality  $r_p < r_g$  is always observed).

Both the gear tooth and the pinion tooth are helical with helices of the opposite hand. Spur high-conformal gearing is not permissible by nature. Because both the gear and the pinion are helical with the helices of the opposite hand, the point of contact pseudo-travels along the pseudo-path of contact,  $P_{pc}$ . It is therefore fundamental to the operating of the high-conformal gears that contact occurs nominally at point, and that the point of contact pseudo-travels across the full face-width of the gears when the gears rotate. It is clearly a condition of operation that in a given profile the tooth surfaces should not interfere before, or after culmination when rotated at angular speeds that are in the gear ratio.

The transverses contact ratio,  $m_p$ , in a high-conformal gear pair is of a zero value ( $m_p \equiv 0$ ). The face contact ratio,  $m_F$ , of the gear pair is always greater than one ( $m_F > 1$ ). The total contact ratio,  $\bar{m}$ , is equal to the face contact ratio,  $m_F$ , that is, the identity  $\bar{m} \equiv m_F$  is valid in intersected-axes high-conformal gearing.

When a rotary motion is transmitted from a driving shaft to a driven shaft, contact point,  $K$ , pseudo-travels along the pseudo-path of contact,  $P_{pc}$  (and the length of the travel distance within the transverse section of the gear pair is zero), that is, within the normal reference plane. This is because  $m_p \equiv 0$  and  $m_F > 1$ , as already mentioned.

For the calculation of the design parameters in a high-conformal gear pair, the center distance,  $c_n$ , and the tooth ratio,  $u = \omega_p / \omega_g$ , in the gear pair are required to be given.

The back cone distance of the gear,  $BC_g$ , and that of the pinion,  $BC_p$ , can be expressed in terms of the center-distance,  $c_n$ , and the tooth ratio,  $u$ , as:

$$BC_g = c_n \cdot \frac{u}{1+u} \quad (12.146)$$

$$BC_p = c_n \cdot \frac{1}{1+u} \quad (12.147)$$

A distance,  $l$ , at which the pseudo-path of contact,  $P_{pc}$ , is remote from the pitch point,  $P$ , has to be known, as well as the transverse pressure angle,  $\phi_{t,\omega}$ , has to be known.

The displacement,  $l$ , is the principal design parameter in a high-conformal gear pair. In terms of the displacement,  $l$ , many of the design parameters of a high-conformal gear pair can be expressed ( $l = KP = r_N$ ).

For the calculation of the radii of curvature,  $r_g$  and  $r_p$ , of the tooth profiles of the gear and the mating pinion, correspondingly, the formulas

$$r_g = l \cdot (1 + k_{rg}) \quad (12.148)$$

$$r_p = l \cdot (1 + k_{rp}) \quad (12.149)$$

are used.

The actual value of the factor,  $k_{rp}$ , fulfils the inequality  $k_{rp} \geq 0$ . However, as the factor,  $k_{rp}$ , is often set equal to zero, the equality  $r_p = l$  is observed. The factor,  $k_{rg}$ , is set in the range of  $k_{rg} = 0.03 \dots 0.10$ .

The radius of the outer back cone distance of the pinion,  $BC_{o,p}$ , is calculated from the formula

$$BC_{o,p} = BC_p + (1 - k_{po}) \cdot l \quad (12.150)$$

The addendum factor,  $k_{po}$ , of the pinion depends on the actual value of the pressure angle,  $\phi_{t,\omega}$ , absolute dimensions of the gear pair, accuracy of machining, and conditions of lubrication. Commonly, the pinion addendum factor,  $k_{po}$ , is set in the range of:

$$k_{po} = 0.1 \div 0.2 \quad (12.151)$$

The root back cone distance of the pinion,  $BC_{f,p}$ , is calculated from the equation:

$$BC_{f,p} = BC_p - a_g - \delta \quad (12.152)$$

where

$a_g$  is the dedendum of the mating gear [ $a_g = (0.1 \dots 0.2) \cdot l$ ].  
 $\delta$  is the radial clearance in the gear pair ( $\delta = l \cdot k_{po}$ ).

It is practical to set the fillet radius,  $\rho_p$ , in the range of  $\rho_p = 0.3 \cdot l$ .

The root back cone distance of the gear,  $BC_{f,g}$ , is equal to:

$$BC_{f,g} = c_n - BC_{o,p} \quad (12.153)$$

The radius of the outer back cone distance of the gear,  $BC_{o,g}$ , is calculated from the expression

$$BC_{o,g} = BC_g + a_g \quad (12.154)$$

The corner of the gear tooth addendum should be rounded with a radius,  $\rho_g$ , which has to be less than fillet radius,  $\rho_p$ , of the pinion ( $\rho_g < \rho_p$ ).

The following relations among the design parameters in a high-conformal gear pair are proven to be practical:  $r_p = l$ ,  $r_g \leq 1.10 \cdot r_p$ ,  $\rho_p = 0.3 \cdot l$ ,  $m_n / l = 0.8$ ,  $t_p / t_g = 1.5$ ,  $\phi_{t,\omega} = 30^\circ$ ,  $\lambda = 60 \dots 80^\circ$  ( $\psi = 10 \dots 30^\circ$ ), and circular pitch of tooth  $p = t_g + t_p + B$ , where backlash  $B = 0.2 \dots 0.4$  mm.

For the design parameters,  $l$ ,  $p$ ,  $t_g$ ,  $t_p$ ,  $m_n$ , and  $B$ , a set of equivalent angular values can be calculated (see Table 12.3).

The effective face width of the gear pair is calculated from the expression:

$$F_{pa} = (1.1 \div 1.2) \cdot p \cdot \tan \lambda \quad (12.155)$$

For a preliminary analysis of high-conformal gearing, an empirical expression:

$$l = (0.05 \div 0.20) \cdot BC_p \quad (12.156)$$

returns a reasonable value for the displacement  $l$  (i.e., for the radius  $r_N$ ).

The functional face width and the axial pitch of a high-conformal gear pair depend on each other.

Consider a case when at a uniform rotation of the gear and of the pinion, the contact point,  $K$ , pseudo-travels along the pseudo-path of contact,  $P_{pc}$ , at a certain constant liner speed. As the transverse contact ratio is zero ( $m_p = 0$ ), and the total contact ratio,  $\bar{m}$ , is equal to the face contact ratio,  $m_F$ , the axial pitch,  $p_{cl,g}$ , of the helix on the gear tooth flank,  $\mathcal{G}$ , can be calculated from the formula:

$$p_{cl,g} = \frac{F_{pa}}{\bar{m}} \cdot \cos \Gamma \quad (12.157)$$

A similar expression:

$$p_{cl,p} = \frac{F_{pa}}{\bar{m}} \cdot \cos \gamma \quad (12.158)$$

is valid with respect to the axial pitch,  $p_{cl,p}$ , of the helix on the pinion tooth flank,  $\mathcal{P}$ .

The quality of high-conformal gearing strongly depends mainly on the following design parameters:  $l$ ,  $\phi_{t,\omega}$  and  $\lambda$ .

The tooth flanks,  $\mathcal{G}$  and  $\mathcal{P}$ , interact with one another only at a culminating point,  $K$ , that pseudo-travels along the pseudo-path of contact,  $P_{pc}$ .

The concept of high-conformal tooth flanks,  $\mathcal{G}$  and  $\mathcal{P}$ , is applicable also with respect to geometrically accurate intersected-axes gearing, namely, it is applicable to lengthwise tooth profiles of the interacting tooth flanks,  $\mathcal{G}$  and  $\mathcal{P}$ , and not with respect to transverse section of the teeth only.

**TABLE 12.3**  
**Design Parameters in Novikov Conformal/High-Conformal**  
**Intersected-Axis Gearing**

Design Parameter	Symbol	Equation
Angular displacement	$\varphi_l$	$\varphi_l = \tan^{-1} \left( \frac{l}{A} \right)$
Angular module	$\varphi_{m,n}$	$\varphi_{m,n} = \tan^{-1} \left( \frac{m_n}{A} \right)$
Angular pitch	$p_\varphi$	$p_\varphi = \tan^{-1} \left( \frac{p}{A} \right)$
Angular tooth thickness, gear	$\varphi_{t,g}$	$\varphi_{t,g} = \tan^{-1} \left( \frac{t_g}{A} \right)$
Angular tooth thickness, pinion	$\varphi_{t,p}$	$\varphi_{t,p} = \tan^{-1} \left( \frac{t_p}{A} \right)$
Angular space width, gear	$\varphi_{w,g}$	$\varphi_{w,g} = \tan^{-1} \left( \frac{w_g}{A} \right)$
Angular space width, pinion	$\varphi_{w,p}$	$\varphi_{w,p} = \tan^{-1} \left( \frac{w_p}{A} \right)$
Angular backlash	$\varphi_B$	$\varphi_B = \tan^{-1} \left( \frac{B}{A} \right)$
Angular addendum, gear	$\varphi_{a,g}$	$\varphi_{a,g} = \tan^{-1} \left( \frac{a_g}{A} \right)$
Angular addendum, pinion	$\varphi_{a,p}$	$\varphi_{a,p} = \tan^{-1} \left( \frac{a_p}{A} \right)$
Angular dedendum, gear	$\varphi_{d,g}$	$\varphi_{d,g} = \tan^{-1} \left( \frac{b_g}{A} \right)$
Angular dedendum, pinion	$\varphi_{d,p}$	$\varphi_{d,p} = \tan^{-1} \left( \frac{b_p}{A} \right)$

The designations:  $a_g$ ,  $b_g$  and  $a_p$ ,  $b_p$  relate to the addendum and dedendum of the gear and the pinion, respectively. These design parameters are measured within the normal reference plane of the high-conformal intersected-axis gear pair.

In geometrically accurate intersected-axes gearing with line contact of the teeth, a desirable line of contact,  $LC_{des}$ , of a zero length, that is, when the length  $l_{LC} = 0$  can be assumed. The rest of the tooth flanks,  $\mathcal{P}$  and  $\mathcal{S}$ , of a gear and of a mating pinion are relieved. The line of contact of a zero length (contact point,  $K$ ) traces the paths of contact,  $P_c$ , on each of the tooth flanks,  $\mathcal{S}$  and  $\mathcal{P}$ . The gear and the mating pinion teeth are relieved in their lengthwise direction in order to eliminate the not-working portions of the tooth flanks,  $\mathcal{S}$  and  $\mathcal{P}$ , from interaction with one another. Maximum possible degree of conformity of the tooth flanks,  $\mathcal{S}$  and  $\mathcal{P}$ , in their lengthwise direction is retained. As a reasonable approximation, the radii of curvature of the lines of intersections of the tooth flanks by the pitch plane,  $PP$  can be considered instead of the section by the plane of action,  $PA$ , (*Meusnier's* theorem). This can be viewed as a kind of the gear tooth flank lengthwise modification.

Point contact between the tooth flanks,  $\mathcal{S}$  and  $\mathcal{P}$  (as  $l_{LC} = 0$ ), gives an opportunity to design gear pairs with conformal/high-conformal contact in the lengthwise direction of the gear teeth (certain similarity with *Novikov/conformal/high-conformal gearing* with favorable contact in the transverse section of the gear teeth).



# 13 Interaction of Tooth Flanks in Geometrically Accurate Intersected-Axes Gearing

A rotation and torque in intersected-axes gearing are transmitted due to the interaction between tooth flanks of a gear and of a mating pinion.

A typical design of intersected-axes gearset is shown in Figure 13.1, as an example. Intersected centerlines of the gear and the pinion shafts is the fundamental feature of intersected-axes gearing. This fundamental feature is reflected even in the name of gearing of this particular kind: *intersected-axes gearing*.<sup>1</sup> Despite the fundamental difference, intersected-axes gearing features many similarities with other kinds of gearing, with parallel-axes gearing in particular. From this perspective, the interaction of tooth flanks in geometrically accurate intersected-axes gearing is discussed in the following section.

## 13.1 KINEMATIC AND GEOMETRIC ELEMENTS OF INTERACTION IN GEOMETRICALLY ACCURATE INTERSECTED-AXES GEARSET

*Equivalent pulley-and-belt transmission* that is analogous of geometrically accurate intersected-axes gear pair is a convenient and a powerful tool to investigate and to analyze the transmission of an input uniform rotary motion by means of intersected-axes gearing.

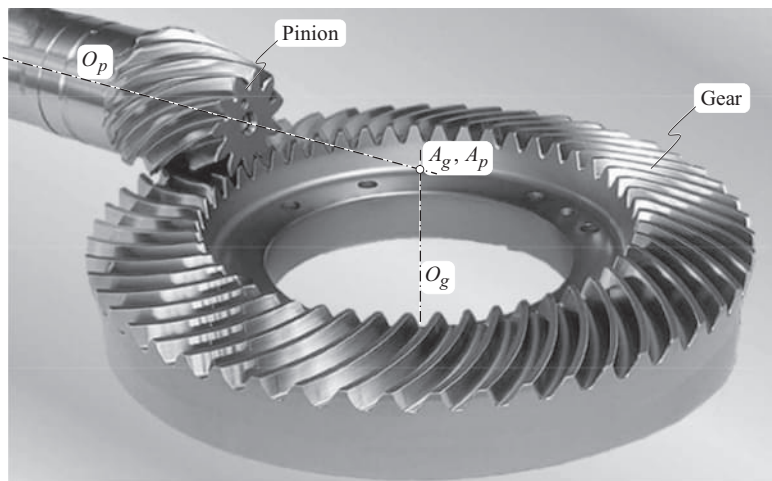


**FIGURE 13.1** Intersected-axis gearset (the center-distance is of a zero value,  $C = 0$ ).

<sup>1</sup> Because of the center-distance is of a zero value, intersected-axes gearsets can also be referred to as *zero-center-distance gearing*.



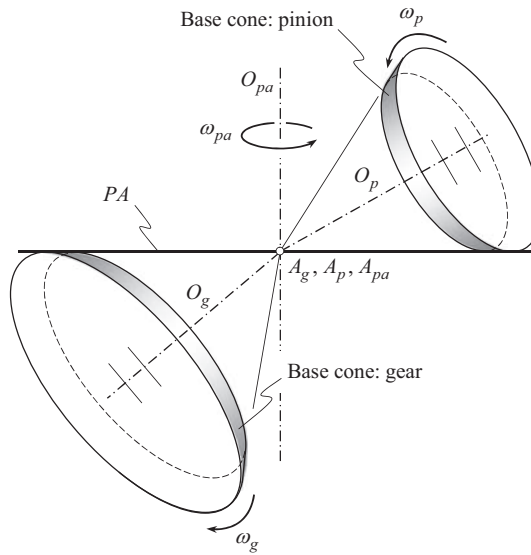


FIGURE 13.2 *Equivalent pulley-and-belt transmission* for intersected-axes gear pair.

### 13.1.1 EQUIVALENT PULLEY-AND-BELT TRANSMISSION FOR INTERSECTED-AXES GEARSET

Similar to parallel-axes gearing, *equivalent pulley-and-belt transmission* can be constructed for intersected-axes gear pair. As illustrated in Figure 13.2, the base cone of a driving pinion, the base cone of a driven gear, and the plane of action,  $PA$ , comprise the *equivalent pulley-and-belt transmission* constructed for an intersected-axes gear pair. The plane of action,  $PA$ , is viewed as a zero-thickness film that is capable of transmitting a rotary motion, that is, it is free to wrap onto the base cone of the driving member, and unwrap from the base cone of the driven member of the intersected-axes gear pair. The zero-thickness film is not allowed to be bent about an axis perpendicular the plane of action,  $PA$ .

Three rotations, namely, the rotations of the base cone of a driving pinion,  $\omega_p$ , of the base cone of a driven gear,  $\omega_g$ , and of the plane of action,  $\omega_{pa}$ , are synchronized with one another so as to eliminate sliding between the interacting surfaces of the base cones and the plane of action,  $PA$ . In the *equivalent pulley-and-belt transmission*, the driving base cone of the pinion pulls the driven base cone of the gear. In reality, the driving base cone of the pinion pushes the driven base cone of the gear.

When the base cone of the driving member rotates, it pulls the plane of action, and the latter pulls the driven member of the *equivalent pulley-and-belt transmission* constructed for the intersected-axes gear pair.

### 13.1.2 PATH OF CONTACT

When a pair of intersected-axes gears rotate, the line of contact,  $LC$ , travels together with the plane of action,  $PA$ . Every point of the line of contact,  $LC$ , traces a corresponding path of contact,  $P_c$ . As the plane of action,  $PA$ , performs a rotary motion about the plane-of-action apex,  $A_{pa}$ , then (in a stationary reference system associated with the gear pair housing), every path of contact,  $P_c$ , is shaped in the form of a circular-arc segment, each of which centered at the plane-of-action apex,  $A_{pa}$ . Therefore, in intersected-axes gearing each path of contact,  $P_c$ , is a planar curve (a circular-arc segment) that is entirely located within the plane of action,  $PA$ . An instantaneous line of action,  $LA_{inst}$ , is a straight line that is tangent to the path of contact,  $P_c$ , at every point of the  $P_c$ .

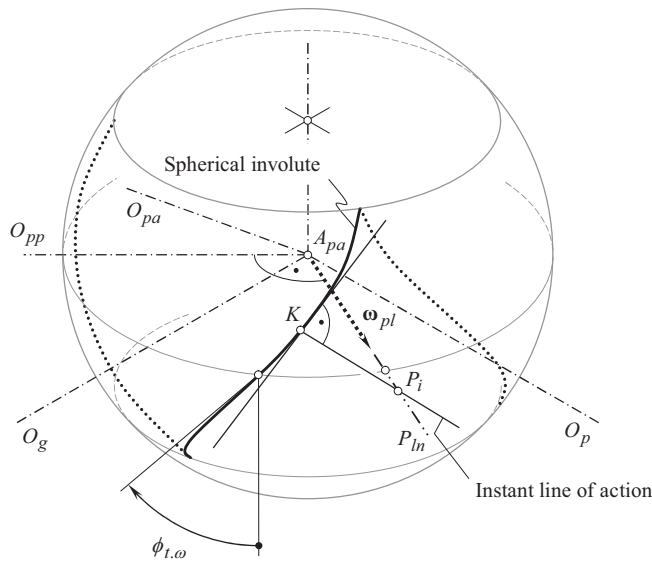


**FIGURE 13.3** Trace of contact point in intersected-axes gear pair.

In a reference system associated with the gear, contact point traces a spherical involute on the gear tooth flank,  $\mathcal{G}$  (see Figure 13.3). Similarly, in a reference system associated with the pinion, contact point traces a spherical involute on the pinion tooth flank,  $\mathcal{P}$ . This fact was clearly realized at the end of the nineteenth century (see Figures 30.39 and 30.40).

A family of paths of contact forms a surface. This surface is referred to as the *path-of-contact surface*,  $P_{cs}$ . It is evident that in intersected-axes gear pairs with a constant transverse pressure angle ( $\phi_{t,\omega} = \text{const}$ ) the path-of-contact surface,  $P_{cs}$ , is congruent to the plane of action,  $PA$ .

Consider an intersected-axes gear pair with the transverse pressure angle,  $\phi_{t,\omega}$ , variable within the effective face width,  $F_{pa}$ , of the gear pair (i.e., a case when  $\phi_{t,\omega} = \text{var}$ ). In the case under consideration, the path-of-contact surface,  $P_{cs}$ , is represented by a continuous set of the circular-arc paths of contact,  $P_c$ , that are located in different infinitesimally narrow portions of the plane of action with a different transverse pressure angle,  $\phi_{t,\omega}$ , each. The radius of a current circular-arc path of contact,  $P_c$ , can be viewed as a function of the distance of point on the pitch line,  $P_{ln}$ , from the plane-of-action-apex,  $A_{pa}$  ( $A_g, A_p$ ). The path-of-contact surface,  $P_{cs}$ , is a continuous screw surface generated by the circular arcs of a variable radius.

### 13.1.3 ZONE (FIELD) OF ACTION IN INTERSECTED-AXES GEARING

It is also convenient to employ the *equivalent pulley-and-belt transmission* for the analysis of the field (zone) of action in intersected-axes gearing.

A bevel gear and a mating pinion interact with one another only within a portion of the plane of action,  $PA$ , and not within the entire plane of action,  $PA$ . This portion of the plane of action is commonly referred to as the *zone (field) of action*,  $ZA$ . In intersected-axes gearing, the field (zone) of action is bounded by the lines of intersection of the plane of action by four boundary lines.

A circular arc of an outer radius,  $r_{o,pa}$ , and a circular arc of a limit radius,  $r_{l,pa}$ , both centered at the plane-of-action apex,  $A_{pa}$ , are the first two boundary lines of the field (zone) of action. The face width,  $F_{pa}$ , of the field (zone) of action,  $ZA$ , is calculated as (see Figure 13.4):

$$F_{pa} = r_{o,pa} - r_{l,pa} \quad (13.1)$$

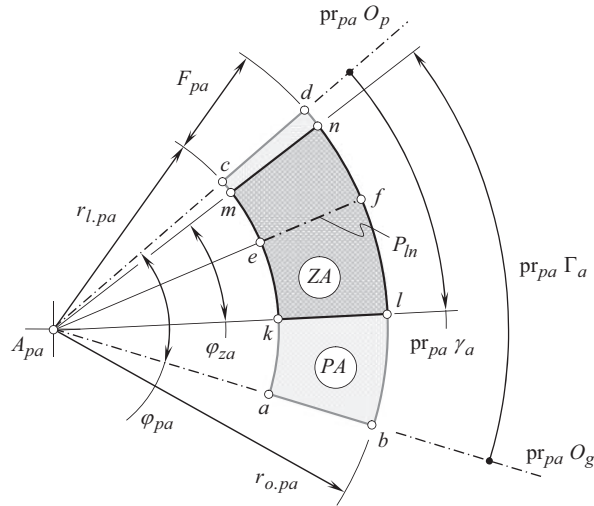


FIGURE 13.4 Zone of action, ZA, in intersected-axes gear pair.

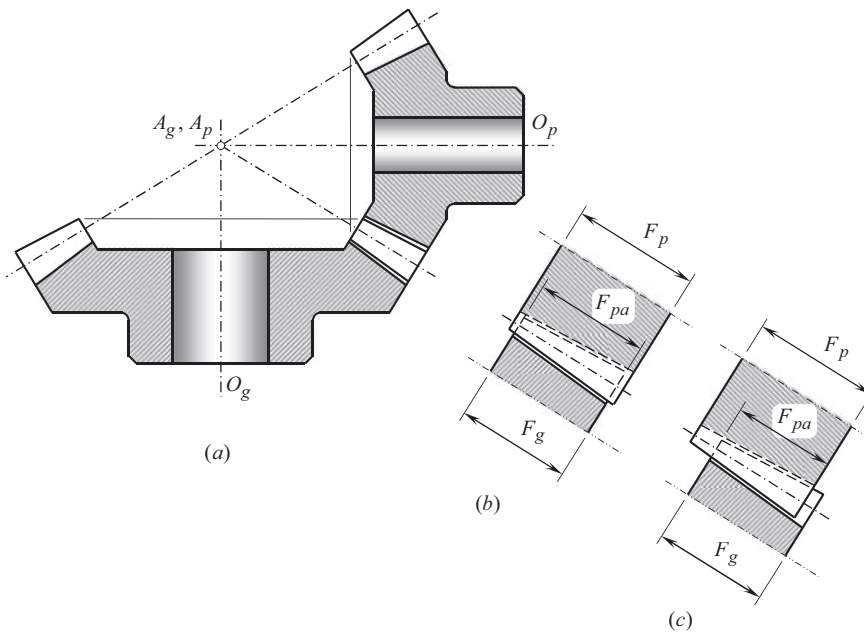


FIGURE 13.5 Schematic of an intersected-axes gear pair (a), and an effective face width,  $F_{pa}$ , in (b) properly, and (c) improperly aligned gears.

In intersected-axes gearing, the face width,  $F_{pa}$ , of the field (zone) of action, ZA, equals to the width within which the tooth flanks,  $\mathcal{S}$  and  $\mathcal{P}$ , of a gear and of a mating pinion overlap one another, as illustrated in Figure 13.5.

Two straight lines of intersection,  $kl$  and  $mn$ , of the plane of action, PA, by the outer cones of the gear, and that of the pinion, are the second two boundary lines of the field (zone) of action (see Figure 13.4).

Constructed in Figure 13.4, the angle  $\varphi_{za}$  between the straight lines  $kl$  and  $mn$  is referred to as the *angular width of zone of action*. The angular width,  $\varphi_{za}$ , of zone of action, ZA, can be expressed in terms of the design parameters of the gear and of the mating pinion as:

$$\varphi_{za} = \text{pr}_{pa}\Gamma_a + \text{pr}_{pa}\gamma_a - \varphi_{pa} \quad (13.2)$$

where

$\Gamma_a$  is the outer cone angle of the gear

$\gamma_a$  is the outer cone angle of the pinion

$\varphi_{pa}$  is the projection onto the plane of action, PA, of the intersected-axes angle,  $\Sigma$ , that is,

$$\varphi_{pa} = \text{pr}_{pa}\Sigma$$

For reference purposes, the lines of tangency,  $cd$  and  $ab$ , of the base cones of the gear and of the mating pinion with the plane of action are shown in Figure 13.4. These straight tangent lines form an angle,  $\varphi_{pa}$ , that is referred to as the *total angular width of plane of action*.

Another approach can be used for the determination of the angular width of the zone of action,  $\varphi_{za}$ .

Shown in Figure 13.4 zone of action, ZA, is of a simplest possible geometry. In reality, geometry of the zone of action can be more complex. An example of intersected-axes gear pair that features a zone of action, ZA, of a more complex geometry is illustrated in Figure 13.6.

The geometry of the actual zone of action is a critical consideration when calculating the contact ratio in an intersected-axes gear pair, especially in a low tooth count intersected-axes gearset.

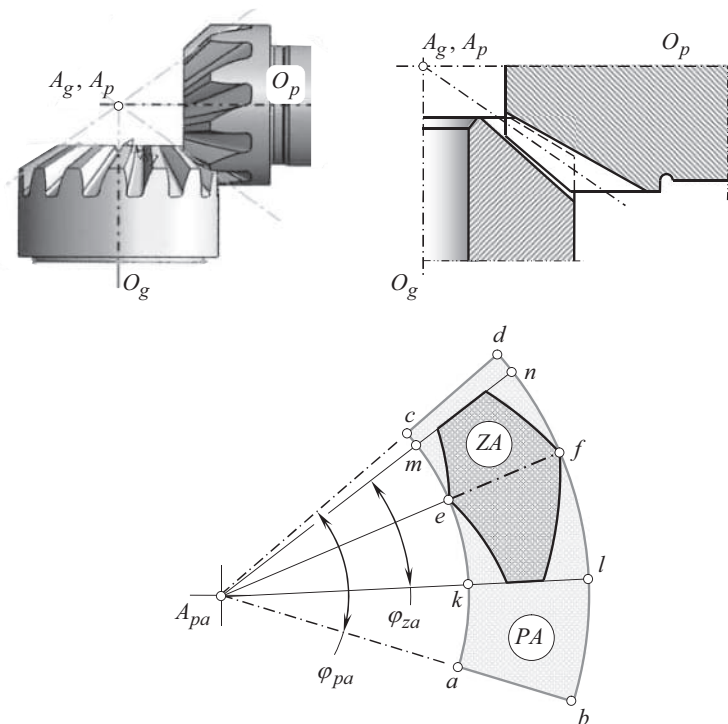


**FIGURE 13.6** Zone of action, ZA, of a complex geometry in intersected-axes gearset.

### 13.2 TRANSMISSION OF UNIFORM ROTARY MOTION IN INTERSECTED-AXES GEARING

Tooth flanks in a gear for intersected-axes gear pair can be viewed as a series of cam surfaces that act against similar surfaces of the mating gear to impart a driving motion. In order to transmit a uniform input rotation smoothly to the output shaft, three fundamental laws of gearing have to be fulfilled (see Chapter 4 for details).

The first fundamental law of gearing (the law of contact, in other words) is commonly analytically described by *Shishkov equation of contact*,  $\mathbf{n} \cdot \mathbf{V}_\Sigma = 0$ . Usually, this condition is fulfilled in all geometrically accurate intersected-axes gear pairs.

To meet the second fundamental law of gearing, interacting tooth flanks of a gear,  $\mathcal{S}$ , and of a mating pinion,  $\mathcal{P}$ , must be conjugate to one another. With respect to intersected-axes gearing, this law of gearing is discussed in detail and is analytically described in Chapter 12 (see Chapter 4).

As two (or even more) pairs of teeth make contact at the same time, fulfillment of an additional law of gearing caused by multiple interacting tooth surfaces in gears is required.

The third fundamental law of gearing that is discussed below in this section of the book, is the law that requires equality of the angular base pitches of a gear, and of a mating pinion to the operating angular base pitch of the gear pair. Here, the discussion is limited to geometrically accurate intersected-axes gearing, as no base pitch can be specified in approximate gears for intersected-axes gearsets.

A plane of action,  $PA$ , of an intersected-axes gear pair is shown in Figure 13.7a. The plane of action is intersected by a cylinder of revolution of an arbitrary radius,  $r_{y.pa}$ , having the plane-of-action centerline,  $O_{pa}$ , as the axis of its rotation. As the angular operating base pitch,  $\varphi_{b.pa}$ , of a gear pair is of a constant value, then three lengths

$$l_{b.pa} = r_{y.pa} \cdot \varphi_{b.pa} \quad (13.3)$$

$$l_{b.g} = r_{y.pa} \cdot \varphi_{b.g} \quad (13.4)$$

$$l_{b.p} = r_{y.pa} \cdot \varphi_{b.p} \quad (13.5)$$

of the circular arcs also are of constant values, that is, in this particular analysis the angular base pitches  $\varphi_{b.pa}$ ,  $\varphi_{b.g}$ , and  $\varphi_{b.p}$  can be replaced with straight-line segments of the corresponding lengths  $l_{b.pa}$ ,  $l_{b.g}$ , and  $l_{b.p}$ . Once the lengths,  $l_{b.g} = l_{b.pa}$  and  $l_{b.p} = l_{b.pa}$ , are equal, then the angular base pitches  $\varphi_{b.g} = \varphi_{b.pa}$ , and  $\varphi_{b.p} = \varphi_{b.pa}$ , are equal as well.

The unfolded section,  $A-A$ , of the gear tooth flanks,  $\mathcal{S}$ , by the cylinder of revolution is shown in Figure 13.7b, the unfolded section of the pinion tooth flanks,  $\mathcal{P}$ , by the cylinder of revolution is shown in Figure 13.7c, and the unfolded section of the intersected-axes gear pair by the cylinder of revolution is shown in Figure 13.7d. Here and below only local patches of the gear tooth flanks,  $\mathcal{S}$ , are considered, as the gear tooth flanks themselves are not constructed yet. Therefore, only small portions of the tooth flanks,  $\mathcal{S}$ , are depicted in Figure 13.7b. All these portions of the tooth flanks of a gear are located in the differential vicinity of points of intersection,  $K_g$ , of the tooth flanks,  $\mathcal{S}$ , by the path of contact,  $P_c$ . Each tooth flank,  $\mathcal{S}$ , is perpendicular to the path of contact,  $P_c$ , at points  $K_g$ . All the points  $K_g$  are evenly spaced along the path of contact. The distance between each pair of neighboring points,  $K_g$ , is equal to the angular base pitch,  $\varphi_{b.g}$ , of the gear.

A similar analysis can be performed with respect to the pinion tooth flanks,  $\mathcal{P}$ , as shown in Figure 13.7c. All these portions of the tooth flanks of the pinion are located in the differential vicinity of points of intersection,  $K_p$ , of the tooth flanks,  $\mathcal{P}$ , by the path of contact,  $P_c$ . Each of the pinion tooth flank,  $\mathcal{P}$ , is perpendicular to the path of contact,  $P_c$ , at points  $K_p$ . All the points  $K_p$  are evenly spaced along the path of contact. The distance between each pair of neighboring points,  $K_p$ , is equal to angular base pitch of the pinion,  $\varphi_{b.p}$ .

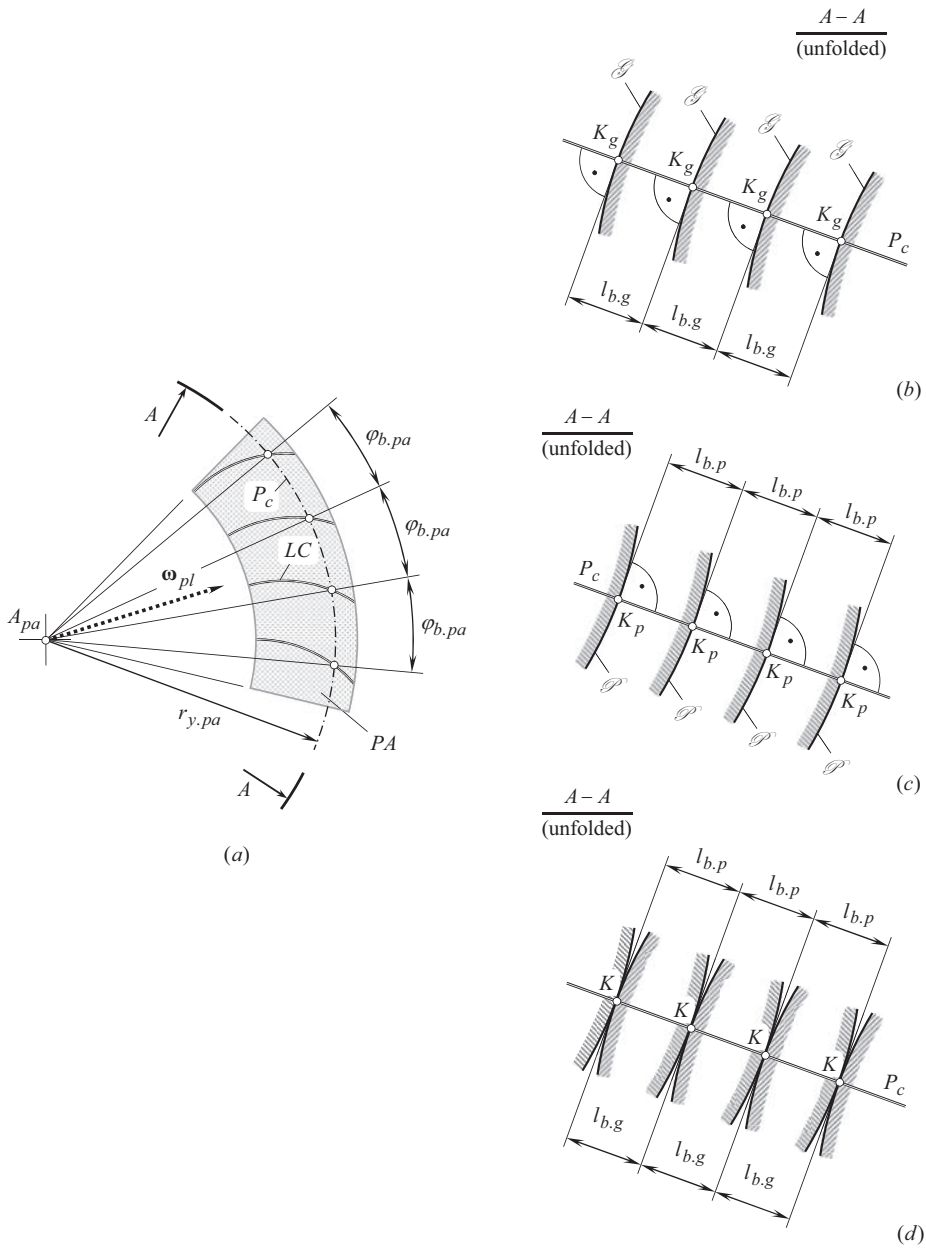


**FIGURE 13.7** On the law of equal base pitches in geometrically accurate intersected-axes gear pair: (a) plane of action,  $PA$ , and the unfolded section  $A-A$ , (b) of a gear, (c) of a mating pinion, and (d) of the gear pair.

When equality of the angular base pitches of a gear,  $\varphi_{b,g}$ , and that of a mating pinion,  $\varphi_{b,p}$ , to operating angular base pitch of the gear pair,  $\varphi_{b,op}$ , is observed, that is, when the identities,  $\varphi_{b,g} \equiv \varphi_{b,op}$  and  $\varphi_{b,p} \equiv \varphi_{b,op}$ , are valid, then the gear and the pinion can be engaged in mesh as illustrated in Figure 13.7d. Each gear point,  $K_g$ , coincides with corresponding pinion point,  $K_p$ . Due to this, the gear and the pinion points,  $K_g$  and  $K_p$ , further are designated as contact point,  $K$ .

As it follows from the analysis in Figure 13.7d, it is not a must to keep all the angular base pitches of a gear,  $\varphi_{b,g}$ , equal to one another, as well as to keep all the angular base pitches of a mating

pinion,  $\varphi_{b,p}$ , also equal to one another. It is critical to keep equal a gear angular base pitch, and a mating pinion angular base pitch to the corresponding operating angular base pitch of the gear pair for each pair of teeth engaged in mesh. Physically this is possible, but it is limited only to gearing that feature the gear ratio equal to an integer number (i.e., to 1, 2, 3, and so forth). Such a design of gearing is impractical and is not considered in this book.

When base pitches of a gear and its mating pinion are not equal to one another ( $\varphi_{b,g} \neq \varphi_{b,p}$ ), for example, the gear base pitch,  $\varphi_{b,g}$ , is smaller compared to the mating pinion base pitch,  $\varphi_{b,p}$ , and, thus, the inequality  $\varphi_{b,g} < \varphi_{b,p}$  is valid, as illustrated in Figure 13.8a, only one pair of teeth is engaged in mesh. A gap between the rest pairs of teeth of the gear,  $\mathcal{G}$ , and of the pinion,  $\mathcal{P}$ , is inevitably observed. No gaps of this sort are permissible in geometrically accurate intersected-axes gearing.

In another example illustrated in Figure 13.8, the gear angular base pitch,  $\varphi_{b,g}$ , is greater compared to the mating pinion angular base pitch,  $\varphi_{b,p}$ , and the inequality  $\varphi_{b,g} > \varphi_{b,p}$  is valid (see Figure 13.8b), again only one pair of teeth is engaged in mesh. A gap between the rest pairs of teeth in the gear,  $\mathcal{G}$ , and in the pinion,  $\mathcal{P}$ , is inevitably observed. No gaps of this sort are permissible in geometrically accurate intersected-axes gearing.

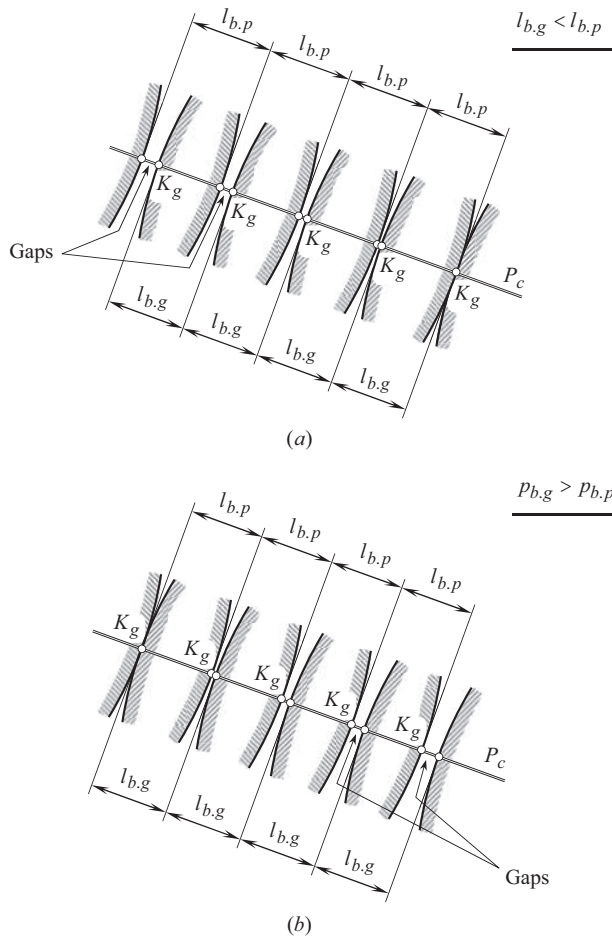


**FIGURE 13.8** Examples of violation of the law of equal angular base pitches in intersected-axes gearing: (a) the angular base pitch of a gear,  $\varphi_{b,g}$ , is smaller compared to the angular base pitch,  $\varphi_{b,p}$ , of a mating pinion ( $\varphi_{b,g} < \varphi_{b,p}$ ), and (b) the angular base pitch of a gear,  $\varphi_{b,g}$ , is larger compared to the angular base pitch,  $\varphi_{b,p}$ , of a mating pinion ( $\varphi_{b,g} > \varphi_{b,p}$ ); in both cases gaps between tooth flanks,  $\mathcal{G}$  and  $\mathcal{P}$ , are inevitably observed.



In this second example (see Figure 13.8b), the distribution of the gaps is inverse to that shown in Figure 13.8a. This is because the gear and the mating pinion are rigid bodies that physically cannot interfere into one another.

Therefore, a uniform rotation can be smoothly transmitted by means of intersected-axes gear pair if the following equalities are valid at every instant of time:

$$\varphi_{b,g} \equiv \varphi_{b,op} \quad (13.6)$$

$$\varphi_{b,p} \equiv \varphi_{b,op} \quad (13.7)$$

With that said, the third fundamental law of gearing to be fulfilled in geometrically accurate intersected-axes gear pair can be formulated in the following manner:

**The third fundamental law of gearing (in intersected-axes gearing):** *In intersected-axes gearing, in order to transmit a uniform rotary motion from a driving shaft to a driven shaft by means of gear teeth, angular base pitch of a gear, and that of a mating pinion have to be equal to the operating base pitch of the gear pair at every instant of time.*

If a discussion is limited just to intersected-axes gearing, the concept of the *angular base pitch* is applicable only to gear tooth flanks, those generated as a locus of corresponding spherical involutes. No *angular base pitch* can be specified for gears with other tooth flank geometries, such as spiral bevel gears of conventional design, and so forth. Therefore, when angular base pitches in a gear and that in a mating pinion are equal to the operating angular base pitch of the gear pair (i.e., when the identities,  $\varphi_{b,g} \equiv \varphi_{b,op}$ , and  $\varphi_{b,p} \equiv \varphi_{b,op}$  are valid), the conjugate action law is always fulfilled in the mesh of the tooth flanks,  $\mathcal{G}$  and  $\mathcal{P}$ .

The equality of angular base pitches of a gear and that of a mating pinion to the operating angular base pitch in an intersected-axes gear pair is the third fundamental law of gearing all geometrically accurate intersected-axes gearing has to fulfill.

### 13.3 CONTACT RATIO IN INTERSECTED-AXES GEARING

The contact ratio, in general, is the number of angular base pitches through which a tooth surface rotates from the beginning to the end of contact. It is important to stress here that no methods for calculation of contact ratio in intersected-axes gear pairs were known till the monograph by the Author [174] was published (~2008). Only various approximate evaluations of the contact ratio in intersected-axes gearing were available in the public domain till 2008.

For the determination of contact ratio in intersected-axes gear pair, the earlier gained experience on that with respect to parallel-axes gearing (see Section 10.4.2) is helpful. This experience is employed below.

Similar to parallel-axes gearing, contact ratio,  $\bar{m}_{ia}$ , in intersected-axes gearset can be viewed as summa of two components. One of the components is commonly referred to as the transverse contact ratio (or profile contact ratio),  $m_{ia,p}$ , and the other one is referred to as face contact ratio,  $m_{ia,F}$ :

$$\bar{m}_{ia} = m_{ia,p} + m_{ia,F} \quad (13.8)$$

Despite the terms *transverse contact ratio* and *face contact ratio* are obsolete, and are out of date, the discussion on contact ratio in intersected-axes gearing begins with the analysis of these components of the *total contact ratio*. Such an approach makes easier the transition from the obsolete terminology like the terms *transverse contact ratio* and *face contact ratio* are, to the recommended term *total contact ratio*.



### 13.3.1 TRANSVERSE CONTACT RATIO

Transverse contact ratio,  $m_{ia,p}$ , in an intersected-axes gear pair is a component of the total contact ratio that is determined within a transverse section of meshing gears. (Recall that a sphere that is centering at the plane-of-action apex,  $A_{pa}$ , is a transverse section in intersected-axes gear pair). The transverse contact ratio can also be referred to as the *profile contact ratio*.

Duration of contact of a gear tooth flank,  $\mathcal{G}$ , and of a mating pinion tooth flank,  $\mathcal{P}$ , in a particular transverse section of a gear by a sphere is specified by the angular width of the zone of action,  $\varphi_{za}$ , in an intersected-axes gear pair. The angular width of the zone of action,  $\varphi_{za}$ , is measured within the plane of action,  $PA$ . [The angle,  $\varphi_{za}$ , is an equivalent of the length of contact,  $Z_{pa}$ , in parallel-axes gearing].

The transverse contact ratio,  $m_{ia,p}$ , in an intersected-axes gear pair is determined as a ratio of the *angular length of contact*,  $\varphi_{za}$ , to the *operating base pitch angle*,  $\varphi_{b,op}$ :

$$m_{ia,p} = \frac{\varphi_{za}}{\varphi_{b,op}} \quad (13.9)$$

Here, in Eq. (13.9), the transverse contact ratio,  $m_{ia,p}$ , is expressed in terms of two design parameters, namely, of the *angular length of contact*,  $\varphi_{za}$ , and of the *operating base pitch angle*,  $\varphi_{b,op}$ .

The first of two design parameters,  $\varphi_{za}$ , is calculated in the following manner.

Tooth flank of a gear,  $\mathcal{G}$ , and tooth flank of a mating pinion,  $\mathcal{P}$ , are engaged in mesh within the angle of contact,  $\varphi_{za}$ . The design parameter  $\varphi_{za}$  is also referred to as *angular length of contact*.

Referring to Figure 13.9, the angular width of the zone of action,  $\varphi_{za}$ , can be specified as follows:

$$\varphi_{za} = (\varphi_{za,g} + \varphi_{za,p}) - \varphi_{pa} \quad (13.10)$$

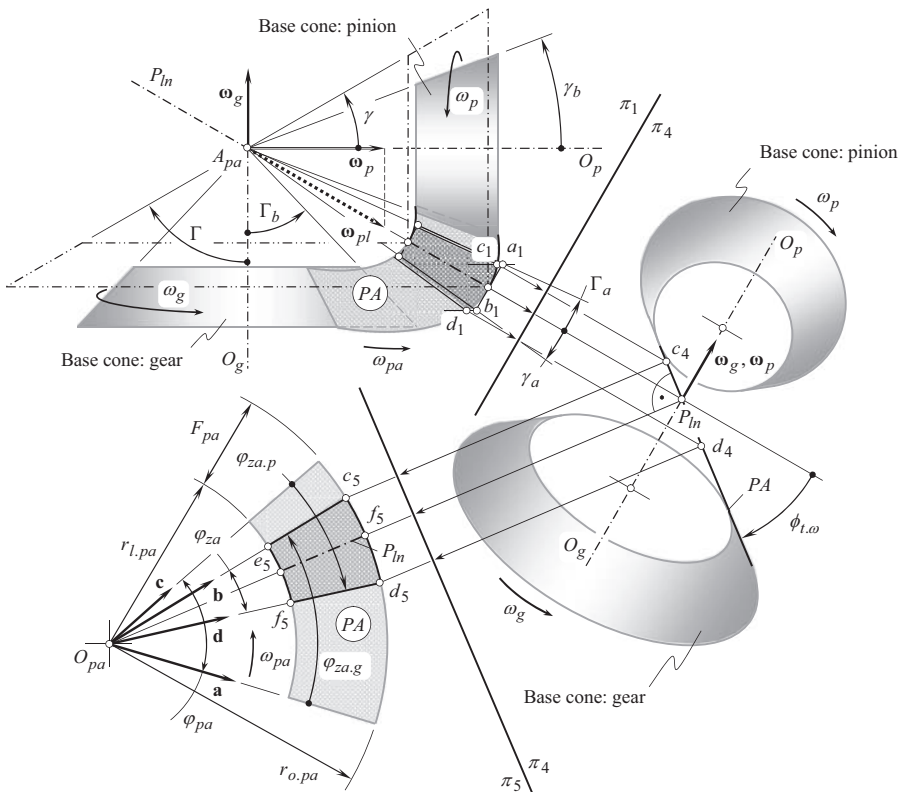


FIGURE 13.9 Angular width,  $\varphi_{za}$ , of the zone of action, ZA.

The actual value of the angular width of the zone of action,  $\varphi_{za}$ , depends on two angles. A portion of the angular width of the zone of action,  $\varphi_{za}$ , contributed by the gear is denoted by  $\varphi_{za.g}$ . Correspondingly, a portion of the angular width of the zone of action,  $\varphi_{za}$ , contributed by the pinion is designated as  $\varphi_{za.p}$ .

The second of two design parameters, namely, the operating base pitch angle,  $\varphi_{b.op}$  (or the base pitch angle of the gear,  $\varphi_{b.g}$ , or of the pinion,  $\varphi_{b.p}$ ), in an intersected-axes gear pair is specified either by Eq. (12.27) or by Eq. (12.28):

$$\varphi_{b.op} = \frac{2\pi}{N_g} \cdot \frac{r_{b.g}}{r_{pa}} = \frac{2\pi}{N_p} \cdot \frac{r_{b.p}}{r_{pa}} \quad (13.11)$$

The derived Eqs. (13.10) and (13.11) are then substituted into Eq. (13.9). In this way, an actual value of the transverse contact ratio,  $m_{ta.p}$ , is calculated for a particular application of intersected-axes gearing.

For the calculation of the components  $\varphi_{za.g}$  and  $\varphi_{za.p}$  in Eq. (13.10), the following approach is employed.

Refer to Figure 13.10 for the calculation of the component  $\varphi_{za.g}$  of the angular width of the zone of action  $\varphi_{za}$ .

A unit vector,  $\mathbf{a}$ , is constructed so as to pass through the origin of the *Cartesian* reference system,  $X_g Y_g Z_g$ , associated with the gear. The vector,  $\mathbf{a}$ , is pointed along the straight line of tangency of the base cone of the gear, and of the plane of action,  $PA$ . In the coordinate system,  $X_g Y_g Z_g$ , the vector,  $\mathbf{a}$ , can be analytically described by an expression:

$$\mathbf{a} = \mathbf{j} \cdot \sin \Gamma_b + \mathbf{k} \cdot \cos \Gamma_b \quad (13.12)$$

where  $\Gamma_b$  is the base cone angle of the gear.

A unit vector,  $\mathbf{b}$ , through the origin of the coordinate system,  $X_g Y_g Z_g$ , is pointed along the straight line of intersection of the outer cone of the gear by the plane of action,  $PA$ . In order to compose an expression for the vector  $\mathbf{b}$ , the following trick can be utilized.

The projection of the vector  $\mathbf{b}$  onto the  $Z_g$  - axis equals to  $\text{Pr}_z \mathbf{b} = \cos \Gamma_o$  (see Figure 13.10). Here, the outer cone angle of the gear is designated as  $\Gamma_o$ . The projection,  $\text{Pr}_z \mathbf{b}$ , immediately yields the calculation of the projection  $\text{Pr}_y \mathbf{b}$  of the vector,  $\mathbf{b}$ , onto the  $Y_g$  - axis. This projection equals to

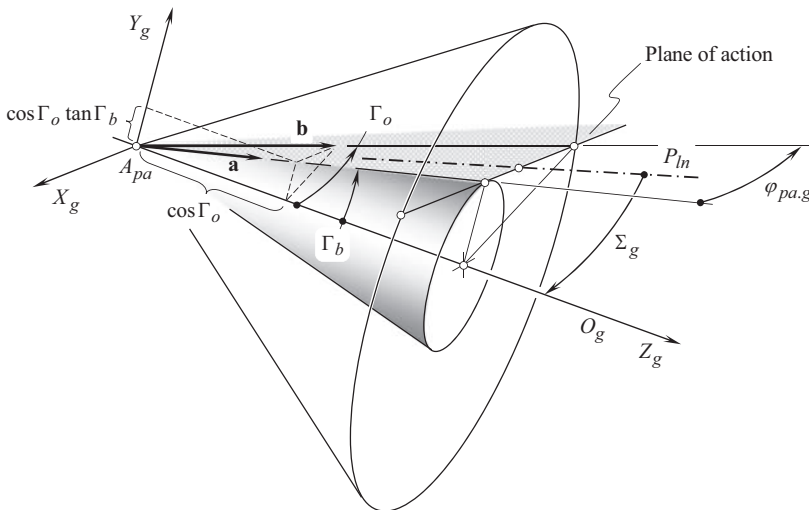


FIGURE 13.10 A schematic for the calculation of the angle,  $\varphi_{pa.g}$ .

$\text{Pr}_y \mathbf{b} = \cos \Gamma_o \tan \Gamma_b$ . Having calculated the projections  $\text{Pr}_y \mathbf{b}$  and  $\text{Pr}_z \mathbf{b}$  in the particular case under consideration, the projection  $\text{Pr}_x \mathbf{b}$  of the vector  $\mathbf{b}$  onto the  $X_g$  – axis is calculated from the equation:

$$\text{Pr}_x \mathbf{b} = \sqrt{1 - \cos^2 \Gamma_o - \cos^2 \Gamma_o \tan^2 \Gamma_b} \quad (13.13)$$

The latter expression can be represented in the form:

$$\text{Pr}_x \mathbf{b} = \sqrt{\sin^2 \Gamma_o - \cos^2 \Gamma_o \tan^2 \Gamma_b} \quad (13.14)$$

Ultimately, the unit vector,  $\mathbf{b}$ , can be analytically expressed as:

$$\mathbf{b} = \mathbf{i} \cdot \sqrt{\sin^2 \Gamma_o - \cos^2 \Gamma_o \tan^2 \Gamma_b} + \mathbf{j} \cdot \cos \Gamma_o \tan \Gamma_b + \mathbf{k} \cdot \cos \Gamma_o \quad (13.15)$$

Having the unit vectors  $\mathbf{a}$  and  $\mathbf{b}$ , an expression:

$$\varphi_{za.g} = \tan^{-1} \left( \frac{|\mathbf{a} \times \mathbf{b}|}{\mathbf{a} \cdot \mathbf{b}} \right) \quad (13.16)$$

can be used for the calculation of the angle  $\varphi_{pa.g}$ .

After it has been expended, Eq. (13.16) allows for a formula:

$$\varphi_{za.g} = \tan^{-1} \left( \sqrt{\sin^2 \Gamma_o + [1 - (\sin \Gamma_b \tan \Gamma_b + \cos \Gamma_b)^2]} \cdot \frac{\cos \Gamma_b}{\cos \Gamma_o} \right) \quad (13.17)$$

for the calculation of the angle  $\varphi_{za.g}$ .

An equation:

$$\varphi_{za.p} = \tan^{-1} \left( \sqrt{\sin^2 \gamma_o + [1 - (\sin \gamma_b \tan \gamma_b + \cos \gamma_b)^2]} \cdot \frac{\cos \gamma_b}{\cos \gamma_o} \right) \quad (13.18)$$

similar to Eq. (13.17), is derived for the calculation of the angle  $\varphi_{za.p}$ . Unit vectors  $\mathbf{c}$  and  $\mathbf{d}$  (see Figure 13.9) are used for this purpose.

Here, in Eq. (13.18):

$\gamma_o$  is the outer cone angle of the pinion.

$\gamma_b$  is the base cone angle of the pinion.

Equations (13.11) and (13.18) are further substituted into Eq. (13.10). In this way, the transverse contact ration for an intersected-axes gearing is calculated as:

$$m_{ia.p} = \frac{\tan^{-1} \left( \sqrt{\sin^2 \Gamma_o + [1 - (\sin \Gamma_b \tan \Gamma_b + \cos \Gamma_b)^2]} \cdot \frac{\cos \Gamma_b}{\cos \Gamma_o} \right)}{\varphi_b} - \frac{\tan^{-1} \left( \sqrt{\sin^2 \gamma_o + [1 - (\sin \gamma_b \tan \gamma_b + \cos \gamma_b)^2]} \cdot \frac{\cos \gamma_b}{\cos \gamma_o} \right) - \varphi_{pa}}{\varphi_b} \quad (13.19)$$

This bulky equation [see Eq. (13.19)] can be significantly reduced in (a) orthogonal intersected-axes gear pairs, (b) face gear drives, and so forth.

### 13.3.2 FACE CONTACT RATIO

The face contact ratio,  $m_{ia,F}$ , for an intersected-axes gear pair is defined as the ratio:

$$m_{ia.F} = \frac{2 \cdot \vartheta_{adv}}{\varphi_{b.op}} \quad (13.20)$$

of the face advance angle,  $\vartheta_{adv}$  (Figures 13.11 and 13.12), to the operating base pitch angle,  $\varphi_{b,op}$ , of the gear pair.

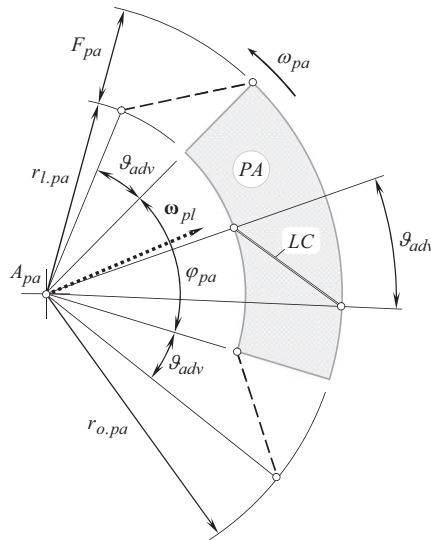


**FIGURE 13.11** On the definition of the advance angle,  $\vartheta_{adv}$  (angular advance,  $\vartheta_{adv}$ ), in geometrically accurate intersected-axes gearing.

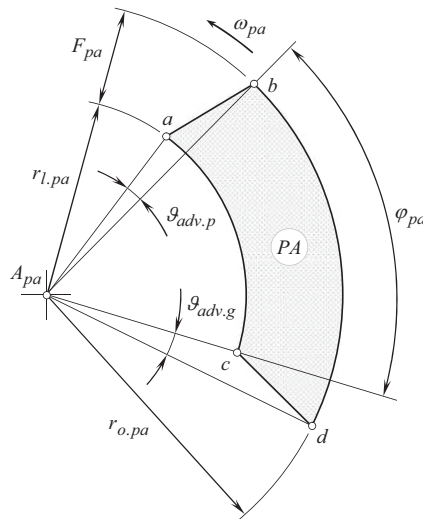


**FIGURE 13.12** On the definition of the gear advance angle,  $\vartheta_{adv.g}$  (the angular advance,  $\vartheta_{adv.g}$ ), and the pinion advance angle,  $\vartheta_{adv.p}$  (the angular advance,  $\vartheta_{adv.p}$ ), in geometrically accurate intersected-axes gearing;  $ab$  and  $cd$  are the lines of intersection of the plane of action,  $PA$ , by the outer surfaces of the gear and the pinion correspondingly.

A more in-detail example on construction of the face advance angle,  $\vartheta_{adv}$  (angular advance,  $\vartheta_{adv}$ ), in geometrically accurate intersected gearing is illustrated in Figure 13.11.

The actual value of the face advance angle,  $\vartheta_{adv}$ , depends on the geometry of the line of contact,  $LC$ , and its configuration within the plane of action,  $PA$ , in a particular design of intersected-axis gearset.

In a more general case, the outer surfaces of a gear, and that of a mating pinion could be shaped in a form of surfaces of revolution that intersect the plane of action along lines: either along the straight-line segments,  $ab$  and  $cd$ , as illustrated in Figure 13.12, or along planar curves. Such a modification to the outer surfaces of a gear, and of a mating pinion in intersected-axes gear pair results in an additional the gear face advanced angle,  $\vartheta_{adv.g}$ , and of the pinion advanced angle,  $\vartheta_{adv.p}$ . The face advanced angles,  $\vartheta_{adv.g}$  and  $\vartheta_{adv.p}$ , are signed values, and they have to be taken into account when calculating the face contact ratio,  $m_{ia.F}$ , in intersected-axes gearing.

### 13.3.3 TOTAL CONTACT RATIO

Having the components,  $m_{ia.p}$  and  $m_{ia.F}$ , calculated [see Eqs. (13.19) and (13.20), correspondingly], the total contact ratio,  $\bar{m}_{ia}$ , in geometrically accurate intersected-axes gearing can be expressed by an expression:

$$\bar{m}_{ia} = \frac{\varphi_{za} + 2 \cdot \vartheta_{adv}}{\varphi_{b.op}} \quad (13.21)$$

or in a form:

$$\bar{m}_{ia} = \frac{\varphi_{za} + 2 \cdot \vartheta_{adv} + \vartheta_{adv.g} + \vartheta_{adv.p}}{\varphi_{b.op}} \quad (13.22)$$

in a more general case of intersected-axes gearing.

This equation is valid for all kinds of intersected-axes gearing.

Contact ratio in intersected-axes gearing,  $\bar{m}_{ia}$ , is always greater than one ( $\bar{m}_{ia} \geq 1$ ). For spur gearing that has a zero-face-advance-angle,  $\vartheta_{adv}$ , the contact ratio is  $\bar{m}_{ia} = m_{ia.p} \geq 1$ , as the equality  $m_{ia.F} = 0$  is valid in this particular case of gearing. Conversely, in *Novikov/conformal* and in *high-conformal* intersected-axes gearing, the equality  $m_{ia.F} = 0$  is valid. Therefore, in *Novikov/conformal* and in *high-conformal* gear pair the contact ratio meets the inequality  $\bar{m}_{ia} = m_{ia.F} \geq 1$ .

The above consideration on contact ratio is also valid with respect to internal gears used in the design of intersected-axes gear pairs. Despite internal intersected-axes gears are not extensively used in the industry, dies for net forging of external bevel gears, electrodes for EDM, and so forth can be calculated by means of the results discussed in this section of the book.

As it follows from Eq. (13.8), contact ratio,  $\bar{m}_{ia}$ , in intersected-axes gearset can be viewed as summa of two components, namely, of the transverse contact ratio (or profile contact ratio),  $m_{ia.p}$ , and of the face contact ratio,  $m_{ia.F}$ . However, such a representation is not a must and can be viewed as an obsolete one. The total contact ratio,  $\bar{m}_{ia}$  is recommended to be used instead of the components  $m_{ia.p}$  and  $m_{ia.F}$ .

## 13.4 CONTACT MOTION CHARACTERISTICS IN INTERSECTED-AXES GEARING

Originally, there are only two motions in an intersected-axes<sup>2</sup> gearing. They are a rotation of the input shaft, and a corresponding rotation of the output shaft. These two rotary motions,  $\omega_g$  and  $\omega_p$ ,

<sup>2</sup> The discussion in Section 13.4 “Contact Motion Characteristics” is valid for both, for intersected-axes gearing with line contact between tooth flanks  $\mathcal{G}$  and  $\mathcal{P}$  of a gear and of a mating pinion, correspondingly, as well, as for *Novikov/conformal* and *high-conformal* intersected-axes gearing.

cause a few other motions, both rotational and translational, that are observed when the gears rotate. Some of these motions result in sliding of the tooth flanks,  $\mathcal{G}$  and  $\mathcal{P}$ , when the gears rotate.

When transmitting motion by means of intersected-axis gearing, rolling and sliding between the interacting tooth flanks of two mating gears take place simultaneously. Rolling and sliding occur at any point of contact within the active portion of the line of contact. Points within the axis of instantaneous rotation,  $P_m$ , are the exception: pure rolling and no sliding is occurred in points within the axis of instantaneous rotation,  $P_m$ . Investigation and analysis of sliding and rolling conditions in a gear pair is of importance from an engineering perspective. It enables, for example, determining and reducing friction losses between mating gears.

On the one hand, sliding motion between the tooth flanks,  $\mathcal{G}$  and  $\mathcal{P}$ , can entail an extensive surface wear of the gear teeth. Thus, sliding motion is required to be reduced (or even eliminated) in order to improve performance of the gear pair. From another hand, sliding motion can significantly affect conditions of lubrication in a gear pair. Therefore, in order to improve performance of the gear pair, sliding motion has to be optimized. The later means that the gears have to be designed so as to provide the most favorable conditions of lubrication of the tooth flanks,  $\mathcal{G}$  and  $\mathcal{P}$ . With that said, the necessity of in-depth understanding of conditions of sliding between the tooth flanks,  $\mathcal{G}$  and  $\mathcal{P}$ , becomes clear.

### 13.4.1 SLIDING IN GEOMETRICALLY ACCURATE INTERSECTED-AXES GEARING

A portion of the relative motion of a gear and of a mating pinion cause pure rolling of the pitch cones of the interaction gears, while another portion of the relative motion results in sliding of the tooth flanks of the gear,  $\mathcal{G}$ , and the mating pinion,  $\mathcal{P}$ . For better understanding of the nature of sliding in geometrically accurate intersected-axes gearing, use of the analysis that is based on descriptive geometry is recommended.

#### 13.4.1.1 Descriptive Geometry-Based Solution to the Problem of Determination of Sliding in Geometrically Accurate Intersected-Axes Gearing

Descriptive geometry-based approach can be used to determine the sliding conditions in intersected-axes gearing. This approach is illustrated in Figure 2.9. After a zero center-distance,  $C$ , been entered, the approach becomes valid for intersected-axes gearing. Then, the linear velocity vectors of sliding,  $\mathbf{V}_g^{sl}$  and  $\mathbf{V}_p^{sl}$ , of the gear and of the mating pinion teeth, correspondingly, can be determined on the premise of the rotation vectors of sliding,  $\boldsymbol{\omega}_g^{sl}$  and  $\boldsymbol{\omega}_p^{sl}$ . Another approach for the determination of sliding velocity vectors in intersected-axes gearset is discussed immediately below.

For the analysis of contact motion characteristics in an intersected-axes gear pair, base cone of a gear, and base cone of a mating pinion, along with the plane of action,  $PA$ , are depicted in Figure 13.13. Arbitrary point,  $m$ , within the line of contact,  $LC$ , is rotated,  $\boldsymbol{\omega}_g$ , together with the gear. The linear velocity vector,  $\mathbf{V}_g$ , is of a length:

$$V_g = |\mathbf{V}_g| = \omega_g \cdot r_{y,g} \quad (13.23)$$

where  $r_{y,g}$  is the distance of point,  $m$ , from the gear axis of rotation,  $O_g$ .

That same point,  $m$ , within the line of contact,  $LC$ , rotates,  $\boldsymbol{\omega}_p$ , together with the pinion. The linear velocity vector,  $\mathbf{V}_p$ , is of a length:

$$V_p = |\mathbf{V}_p| = \omega_p \cdot r_{y,p} \quad (13.24)$$

where  $r_{y,p}$  is the distance of point,  $m$ , from the pinion axis of rotation,  $O_p$ .

The actual configurations of the linear velocity vectors,  $\mathbf{V}_g$  and  $\mathbf{V}_p$ , depend on the angular configuration of the gear and the pinion.

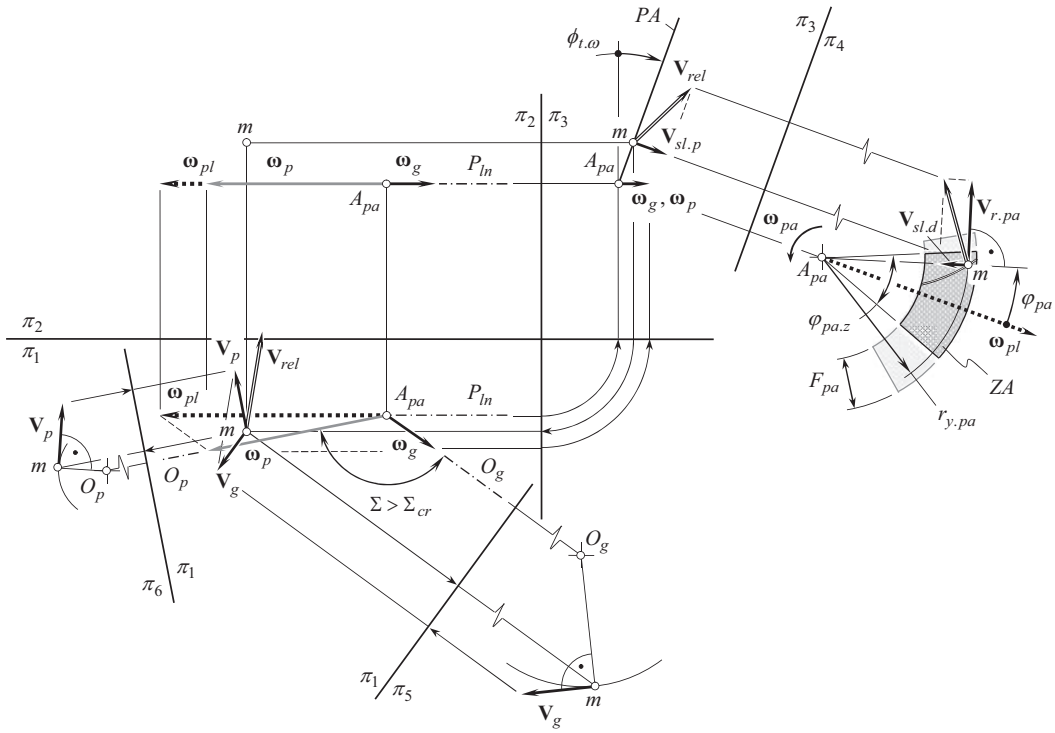


FIGURE 13.13 Sliding between tooth flanks in intersected-axes gearing.

The difference  $(\mathbf{V}_g - \mathbf{V}_p)$  is referred to as the linear velocity vector,  $\mathbf{V}_{rel}$ , of the instantaneous motion of the pinion tooth flank relative to the gear tooth flank:

$$\mathbf{V}_{rel} = \mathbf{V}_g - \mathbf{V}_p \quad (13.25)$$

Sliding of the tooth flanks,  $\mathcal{G}$  and  $\mathcal{P}$ , of the gear and of the mating pinion is caused by the linear velocity vector,  $\mathbf{V}_{rel}$ .

The sliding velocity vector can be determined graphically by implementing for this purpose of the methods developed in descriptive geometry. An example of such a construction is illustrated in Figure 13.13.

Aiming at the construction of sliding velocity vector, a reference system  $\pi_1\pi_2\pi_3$  of two orthogonal planes of projection,  $\pi_1$ ,  $\pi_2$ , and  $\pi_3$ , is employed (see Figure 13.13). Following a convention, adopted in descriptive geometry, the subscript “1” is assigned to projections onto the plane  $\pi_1$  of all the points, lines, and so forth. Similarly, the subscript “2” is assigned to projections onto the plane  $\pi_2$  of all of those same points, lines, and so forth.

The location and orientation of a pair of the rotation vectors,  $\omega_g$  and  $\omega_p$ , within the reference system  $\pi_1\pi_2$  can be arbitrary. However, solely for convenience, the rotation vectors,  $\omega_g$  and  $\omega_p$ , are depicted in the reference system  $\pi_1\pi_2$  parallel to the horizontal plane of projection  $\pi_1$ . In this scenario, the intersected-axes angle,  $\Sigma$ , is projected onto plane  $\pi_1$  with no distortion. The plane-of-action apex point is denoted as  $A_{pa}$ .

The principle of inversion of rotations is used for the construction of the instantaneous rotation vector,  $\omega_{pl}$ , namely, of the vector of rotation of the pinion about axis of instantaneous rotation,  $P_{ln}$ .

Immediately upon the rotation vector  $\omega_{pl}$  is determined, the axis of projections  $\pi_1/\pi_2$  can be constructed so as to keep it parallel to the vector of instantaneous rotation,  $\omega_{pl}$ . Such a configuration of the axis  $\pi_1/\pi_2$  is not mandatory, and its configuration can be arbitrary. Convenience is the

only reason for selecting this particular orientation for the axis of projections  $\pi_1/\pi_2$  in relation to the rotation vector,  $\omega_{pl}$ .

Within the plane of projections,  $\pi_3$ , the plane of action,  $PA$ , is a projective plane. In this plane of projections, the plane of action is described as a straight line,  $PA$ , through the plane-of-action apex,  $A_{pa}$ . The trace,  $PA$ , forms the transverse pressure angle,  $\phi_{t,\omega}$ , with the vertical connecting lines.

An additional plane of projections,  $\pi_4$ , is constructed so as to have the axis,  $\pi_3/\pi_4$ , parallel to the trace  $PA$  in the plane of projections,  $\pi_3$ . Due to that, the zone of action,  $ZA$ , is projected onto the plane  $\pi_4$  with no distortions.

Arbitrary point,  $m$ , is located within the line of contact,  $LC$ . This point is at a distance,  $r_{y,pa}$ , from the plane-of-action apex,  $A_{pa}$ . The linear velocity vectors of sliding are constructed for point  $m$ . The construction performed for point,  $m$ , can be also performed for any and all points within the zone of action,  $ZA$ .

The projections of point,  $m$ , onto the rest of the planes of projections, that is, onto the planes of projections  $\pi_1$ ,  $\pi_2$ ,  $\pi_3$ , and others, are constructed in compliance to standard procedures established in descriptive geometry.

The linear velocity vector,  $\mathbf{V}_g$ , of point  $m$  that is rotated together with the gear, is constructed in the auxiliary plane of projections,  $\pi_5$  (see Figure 13.13). The axis of projections,  $\pi_1/\pi_5$ , is perpendicular to the angular velocity vector,  $\omega_g$ , of the gear. The linear velocity vector,  $\mathbf{V}_g$ , is projected onto the plane of projections,  $\pi_5$ , with no distortions.

The linear velocity vector,  $\mathbf{V}_p$ , of point  $m$  that is rotated together with the pinion, is constructed in the auxiliary plane of projections,  $\pi_6$  Figure 13.13. The axis of projections,  $\pi_1/\pi_6$ , is perpendicular to the angular velocity vector,  $\omega_p$ , of the pinion. The linear velocity vector,  $\mathbf{V}_p$ , is projected onto the plane of projections,  $\pi_6$ , with no distortions.

The liner velocity vector,  $\mathbf{V}_{rel}$ , of the relative motion of the tooth flanks,  $\mathcal{G}$  and  $\mathcal{P}$ , at point  $m$  is constructed in the plane of projections,  $\pi_1$  (see Figure 13.13). For this purpose, projections of the linear velocity vectors  $\mathbf{V}_g$  and  $\mathbf{V}_p$  in the plane of projections,  $\pi_1$ , are constructed. Then, the projections of the liner velocity vector,  $\mathbf{V}_{rel}$ , of the relative motion onto the rest planes of projections, namely, onto the planes of projections  $\pi_2$ ,  $\pi_3$ , and  $\pi_4$ , are constructed in compliance to standard procedures established in descriptive geometry.<sup>3</sup>

Once the liner velocity vector,  $\mathbf{V}_{rel}$ , of relative motion of the tooth flanks,  $\mathcal{G}$  and  $\mathcal{P}$ , at point  $m$  is constructed (see Figure 13.13), then this vector is projected onto three perpendicular directions through point  $m$ .

The first direction is located within the plane of action,  $PA$ , and is pointed perpendicular to the straight-line segment,  $mA_{pa}$ . The projection of the liner velocity vector,  $\mathbf{V}_{rel}$ , onto this direction is labeled as  $\mathbf{V}_{r,pa}$ , as this component of the liner velocity vector,  $\mathbf{V}_{rel}$ , causes pure rotation of the plane of action,  $PA$ , about its axis of rotation,  $O_{pa}$ , and pure rotation of the gears as well. The magnitude of the linear velocity vector,  $\mathbf{V}_{r,pa}$ , depends on the rotation,  $\omega_{pa}$ , of the plane of action,  $PA$ , and on the distance,  $r_{y,pa}$ , of point of interest,  $m$ , from the plane-of-action apex,  $A_{pa}$ :

$$\mathbf{V}_{r,pa} = \omega_{pa} r_{y,pa} \quad (13.26)$$

The second direction is pointed perpendicular to the plane of action,  $PA$ . The projection of the liner velocity vector,  $\mathbf{V}_{rel}$ , onto this direction is labeled as  $\mathbf{V}_{sl,p}$ , as this component of the liner velocity vector,  $\mathbf{V}_{rel}$ , causes pure profile sliding of the gear tooth flanks,  $\mathcal{G}$  and  $\mathcal{P}$ .

The third direction is within the plane of action,  $PA$ , and is pointed along the straight-line segment,  $mA_{pa}$ . The projection of the liner velocity vector,  $\mathbf{V}_{rel}$ , onto this direction is labeled as  $\mathbf{V}_{sl,d}$ , as this component of the liner velocity vector,  $\mathbf{V}_{rel}$ , causes *drag* sliding action. In straight bevel gears, the component,  $\mathbf{V}_{sl,d}$ , causes sliding,  $\mathbf{V}_{sl,l}$ , in the lengthwise direction of the gear teeth. In more

<sup>3</sup> Note that not all the construction lines are shown in Figure 13.13, and some of them are removed from the finalized schematic.



general cases of intersected-axes gears, for instance, in cases of skew bevel gears, spiral bevel gears, and so forth, the sliding in the lengthwise direction at current point,  $m$ , of the gear teeth is tangent to the line of contact of the gear/pinion tooth flanks, and is of magnitude (see Figure 13.13):

$$V_{sl,l} = \frac{V_{sl,d}}{\cos \varphi_m} \quad (13.27)$$

Here is designated:

$V_{sl,l}$  is the magnitude of the linear velocity vector,  $\mathbf{V}_{sl,l}$ , of sliding in the lengthwise direction of the gear teeth

$V_{sl,d}$  is the magnitude of the linear velocity vector,  $\mathbf{V}_{sl,d}$ , of *drag* sliding

$\varphi_m$  is the actual value of the spiral angle at point,  $m$ , within the line of contact,  $LC$ , of the gear and pinion teeth

As it follows from the analysis of Eq. (13.27), the sliding in the lengthwise direction of the gear teeth depends on the actual value of the spiral angle at point,  $m$ , within the line of contact,  $LC$ , of the gear and pinion teeth. This means that the linear velocity vector,  $\mathbf{V}_{sl,l}$ , of sliding in the lengthwise direction of the gear teeth varies along the line of contact,  $LC$ , of the gear and pinion teeth.

It should be realized from this analysis that sliding of tooth flanks of a gear,  $\mathcal{G}$ , and of a mating pinion,  $\mathcal{P}$ , in the lengthwise direction of the gear tooth is inevitable in intersected-axes gearing of all kinds. The sliding is caused by the projections of the rotation vectors,  $\boldsymbol{\omega}_g$  and  $\boldsymbol{\omega}_p$ , onto a perpendicular to the vector of instantaneous rotation,  $\boldsymbol{\omega}_{pl}$ .

Figure 13.14 along with Eq. (13.27), both provide a good opportunity for gear researchers to perform a qualitative analysis of sliding conditions in intersected-axes gearing.<sup>4</sup> Here, in Figure 13.14, an *equivalent pulley-and-belt transmission* constructed for intersected-axes gearset is shown. The base cones of a gear and that of a mating pinion work as pulleys. A rotary motion from a driving gear to a driven gear is transmitted by means of round belt labeled as *plane of action*. A desirable line of contact,  $LC_{des}$  (not shown in Figure 13.14) is entirely situated within the plane of action,  $PA$ . The tooth flank of a gear,  $\mathcal{G}$ , is generated by the  $LC_{des}$  in its motion relative to a reference system, which the gear tooth flank will be associated with. Similarly, the pinion tooth flank,  $\mathcal{P}$ , is generated by that same line of contact,  $LC_{des}$ , in its motion relative to a reference system, which the pinion tooth flank will be associated with.

The magnitude of the linear velocity vector of profile sliding,  $\mathbf{V}_{sl,p}$  (see Figure 13.13), depends on the actual distance of point of interest,  $m$ , from the axis of instantaneous rotation,  $P_{ln}$ . The larger the distance, the larger the magnitude of the linear velocity vector of profile sliding,  $\mathbf{V}_{sl,p}$ , and vice versa. Profile sliding is of a zero value when point  $m$  is situated within the axis of instantaneous rotation,  $P_{ln}$ . Therefore, the pure rolling of the tooth flanks,  $\mathcal{G}$  and  $\mathcal{P}$ , of a gear and a mating pinion occurs at points of the axis of instantaneous rotation,  $P_{ln}$ .

Constructed at all points of the zone of action,  $ZA$ , the linear velocity vectors of profile sliding,  $\mathbf{V}_{sl,p}$ , form a field of profile sliding in an intersected-axes gear pair, as illustrated in Figure 13.15. The linear velocity vectors of profile sliding through points along the line of contact,  $LC$ , indicate the profile sliding of the tooth flanks,  $\mathcal{G}$  and  $\mathcal{P}$ , for a particular angular configuration of the gear and of the mating pinion (not shown in Figure 13.15). The entire field of profile sliding, as well as the linear velocity vectors of profile sliding through points along the line of contact,  $LC$ , both can be transferred to and constructed on either the tooth flank of the gear,  $\mathcal{G}$ , or on the tooth flank of the mating pinion,  $\mathcal{P}$ .

<sup>4</sup> Note that not all the construction lines are shown in Figure 13.14, and some of them are removed from the finalized schematic.

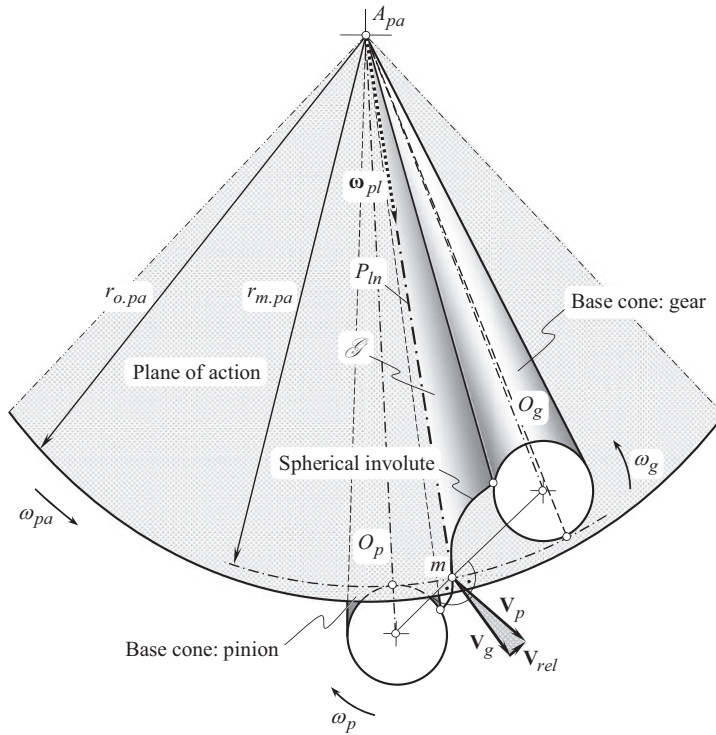


FIGURE 13.14 Contact motion characteristics in intersected-axes gearset.

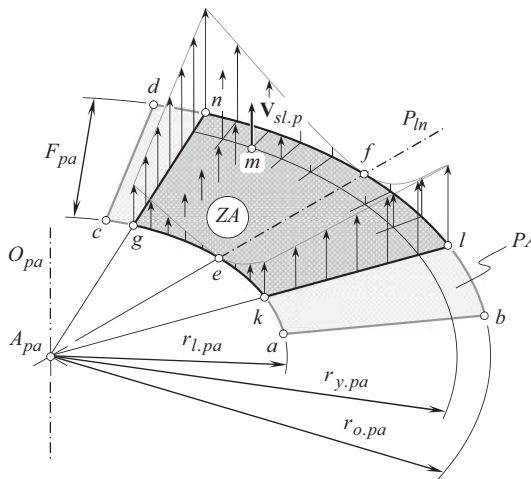
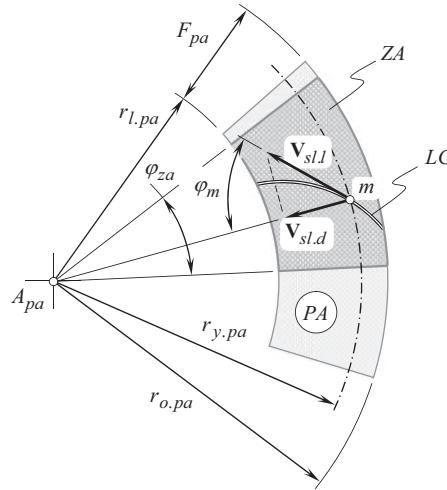


FIGURE 13.15 Field of linear velocities of profile sliding,  $\mathbf{V}_{sl,p}$ , in intersected-axes gearset.

Similarly, the magnitude of the linear velocity vector of *drag sliding*,  $\mathbf{V}_{sl,d}$ , depends on the actual value of the angular distance,  $\varphi_{m.pa}$ , of point of interest,  $m$ , from the axis of instantaneous rotation,  $P_{ln}$  (see Figure 13.16). The larger the angular distance,  $\varphi_{m.pa}$ , the larger the magnitude of the linear velocity vector of *drag sliding*,  $\mathbf{V}_{sl,d}$ , and vice versa. This is due to the linear velocity vector of the *drag sliding*,  $\mathbf{V}_{sl,d}$ , equals to a projection onto the axis of instantaneous rotation,  $P_{ln}$ , of the liner velocity vector,  $\mathbf{V}_{rel}$ , of the relative motion of the tooth flanks,  $\mathcal{G}$  and  $\mathcal{P}$ , of a gear and a mating pinion.



**FIGURE 13.16** On the definition of the linear velocity vector,  $\mathbf{V}_{sl,l}$ , of sliding in the lengthwise direction of the gear tooth.

In intersected-axes gearing, *drag sliding* is observed at all points of contact of tooth flanks,  $\mathcal{G}$  and  $\mathcal{P}$ , of a gear and a mating pinion.

Constructed at all points of the zone of action, ZA, the linear velocity vectors of *drag sliding*,  $\mathbf{V}_{sl,d}$ , form a field of *drag sliding* in an intersected-axes gear pair. The distribution of the linear velocity vectors of *drag sliding* is similar in much to that shown in Figure 13.15 for the linear velocity vectors of profile sliding,  $\mathbf{V}_{sl,p}$ . The linear velocity vectors of *drag sliding* through points along the line of contact, LC, indicate the *drag sliding* of the tooth flanks,  $\mathcal{G}$  and  $\mathcal{P}$ , for a particular angular configuration of the gear and of the mating pinion.

Total sliding of the tooth flanks,  $\mathcal{G}$  and  $\mathcal{P}$ , in an intersected-axes gear pair is specified by the linear velocity vector,  $\mathbf{V}_{sl,\Sigma}$ , of total sliding:

$$\mathbf{V}_{sl,\Sigma} = \mathbf{V}_{sl,p} + \mathbf{V}_{sl,l} \quad (13.28)$$

As the functions of the linear velocity vectors of sliding,  $\mathbf{V}_{sl,p}$  and  $\mathbf{V}_{sl,l}$ , depend on the parameters of kinematics of a gear pair, and of the design parameters of a gear, and a mating pinion, non-linearly, then the superposition of the vectors,  $\mathbf{V}_{sl,p}$  and  $\mathbf{V}_{sl,l}$  as in Eq. (13.28), is valid only in cases when linearization of the functions is permissible. This means that the linear velocity vectors,  $\mathbf{V}_{sl,p}$  and  $\mathbf{V}_{sl,l}$ , depend on parameters of kinematics of a gear pair, and of the design parameters of a gear, and of a mating pinion either linearly, or nearly linearly.<sup>5</sup>

#### 13.4.1.2 Analytical Solution to the Problem of Determination of Sliding in Geometrically Accurate Intersected-Axes Gearing

The performed descriptive geometry-based solution to the problem of determination of sliding in geometrically accurate intersected-axes gearing is helpful for better understanding of the nature of the problem under consideration. This solution to the problem also returns a rough estimate of sliding conditions that occur in intersected-axes gearing. The discussed graphical solution to the problem is also useful for the development of an analytical solution to that same problem.

<sup>5</sup> Another descriptive geometry-based solution to the problem of determination of sliding in geometrically accurate intersected-axes gearing with application to high-conformal gearing is discussed in Ref. [157]. The applied approach can be used for solving the problem under consideration not only in high-conformal gearing, but in geometrically-accurate intersected-axes gearing in a more general sense.

Again, in order to solve the problem analytically, it is necessary to derive equations for the linear velocity vectors,  $\mathbf{V}_{m,g}$  and  $\mathbf{V}_{m,p}$ , of point of interest,  $m$ , and to represent the derived expressions in a common reference system. A stationary *Cartesian* coordinate system,  $X_{pa.s}Y_{pa.s}Z_{pa.s}$ , associated with the plane of action,  $PA$ , in the intersected-axes gear pair is especially convenient for solving the problem of this sort.

For the development of an analytical solution to the problem under consideration, operators of linear transformations are extensively used below. The chief reason why the operators of linear transformations are employed for the derivation of all the necessary equations is as follows.

It is convenient to derive an expression for each of the linear velocity vectors,  $\mathbf{V}_{m,g}$  and  $\mathbf{V}_{m,p}$ , in a specific reference system and then to represent the derived equation in a reference system that is convenient to perform the further analysis. For instance, it is convenient to determine the linear velocity vector,  $\mathbf{V}_{m,g}$ , in a coordinate system associated with the gear. Similarly, it is convenient to determine the linear velocity vector,  $\mathbf{V}_{m,p}$ , in a coordinate system associated with the pinion. Later on, the derived expressions for both the vectors,  $\mathbf{V}_{m,g}$  and  $\mathbf{V}_{m,p}$ , can be represented in a common reference system. The operators of linear transformations, namely, the operators of translation, and the operators of rotation, along and about the coordinate axes are very helpful for this purpose.

Relative motion of a driving member, of a driven member in a gear pair, as well as of the plane of action, form the foundation on which the corresponding operators of the coordinate system transformations can be derived. When a gear pair is operated, the driving member, the driven member, and the plane of action, are rotated in a timely manner, that is, the rotations,  $\omega_g$ ,  $\omega_p$  and  $\omega_{pa}$ , are synchronized with one another.

As the rotations  $\omega_g$ ,  $\omega_p$ , and  $\omega_{pa}$ , are synchronized with one another, the angles of rotation,  $\varphi_{pa}$  and  $\varphi_g$ , of the plane of action, and of the gear, can be expressed in terms of the angle of rotation,  $\varphi_p$ , of the driving pinion, as:

$$\varphi_{pa} = \frac{\varphi_p}{\sin \gamma_b} \quad (13.29)$$

$$\varphi_{pa} = \frac{\varphi_g}{\sin \Gamma_b} \quad (13.30)$$

From these equations, an expression:

$$\varphi_g = \varphi_p \frac{\sin \Gamma_b}{\sin \gamma_b} \quad (13.31)$$

is derived.

Here, in Eqs. (13.29)–(13.31), the base cone angles of a gear, and that of a mating pinion are designated as  $\Gamma_b$  and  $\gamma_b$ , correspondingly.

The relative motion of the members in a gear pair, along with the applied coordinate systems, is schematically shown in Figure 13.17.

Assume, that in an intersected-axes gear pair a pinion is the driving member, and a mating gear is a driven member. To derive a formula for the operator,  $\mathbf{R}_{s_{la}}(p \rightarrow pa)$ , of transition from the coordinate system,  $X_pY_pZ_p$ , associated with the driving pinion, to the coordinate system,  $X_{pa}Y_{pa}Z_{pa}$ , associated with the plane of action,  $PA$ , consider a rotation of a driving pinion<sup>6</sup> (see Figure 13.17).

The stationary reference system,  $X_{p.s}Y_{p.s}Z_{p.s}$ , is associated with the gear housing. In the initial position, the axes of the pinion coordinate system,  $X_pY_pZ_p$ , align to the corresponding axes of the stationary coordinate system,  $X_{p.s}Y_{p.s}Z_{p.s}$ . When the pinion is rotated about the axis,  $O_p$ , through

<sup>6</sup> Not all particular coordinate system transformations here are illustrated with a corresponding schematic. The interested reader is referred to Appendix D for details in this regard.

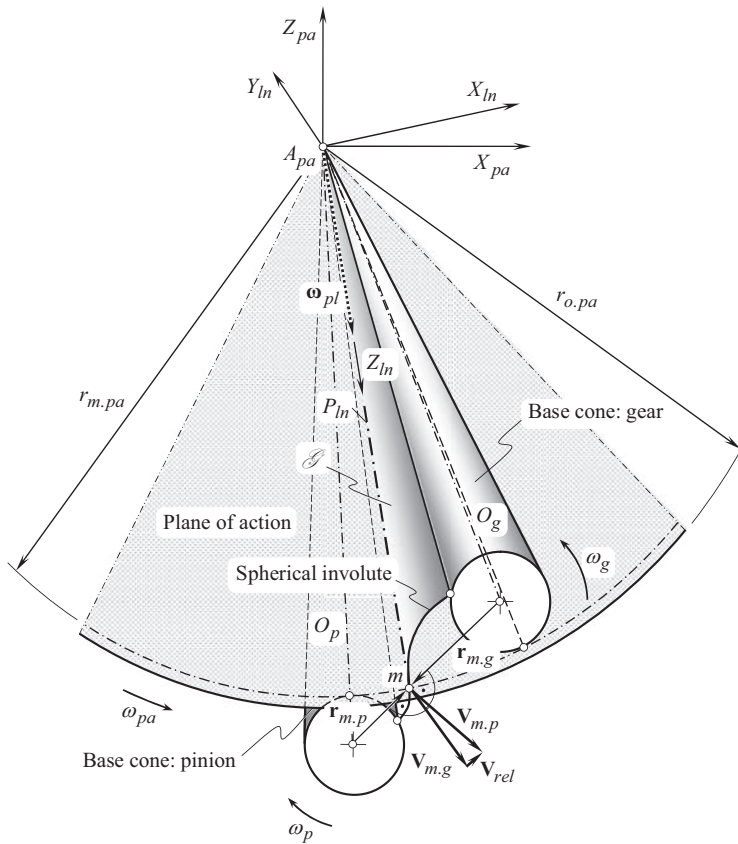


FIGURE 13.17 Reference systems associated with an intersected-axes gear pair.

an angle,  $\varphi_p$ , the reference system,  $X_p Y_p Z_p$ , is rotated together with the pinion. The transition from the pinion reference system,  $X_p Y_p Z_p$ , to the stationary reference system,  $X_{p.s} Y_{p.s} Z_{p.s}$ , is analytically described by the operator of rotation,  $\mathbf{Rt}(Z_s, \varphi_p)$ , of the reference system,  $X_p Y_p Z_p$ , through the angle,  $\varphi_p$ , about the axis,  $O_p$ , in the counter-clockwise direction.<sup>7</sup> In matrix form, this operator can be represented as:

$$\mathbf{Rt}(Z_s, \varphi_p) = \begin{bmatrix} \cos \varphi_p & -\sin \varphi_p & 0 & 0 \\ \sin \varphi_p & \cos \varphi_p & 0 & 0 \\ 0 & 0 & 1 & 0 \\ 0 & 0 & 0 & 1 \end{bmatrix} \quad (13.32)$$

The coordinate system transformation that is analytically described by the operator of rotation,  $\mathbf{Rt}(Z_s, \varphi_p)$ , is followed by the rotation of the reference system,  $X_{p.s} Y_{p.s} Z_{p.s}$ , through the base cone angle,  $\gamma_b$ , of the pinion about the axis  $Y_{p.s}$ , in the counter-clockwise direction. The rotation of this sort is analytically described by the operator of rotation,  $\mathbf{Rt}(Y_{p.s}, \gamma_b)$ . In matrix form, this operator can be represented as:

<sup>7</sup> Here and below, the direction of rotation of a coordinate system about a coordinate axis is determined looking from the arrowhead of the coordinate axis about which the rotation is performed.

$$\mathbf{Rt}(Y_{p.s}, \gamma_b) = \begin{bmatrix} \cos \gamma_b & 0 & -\sin \gamma_b & 0 \\ 0 & 1 & 0 & 0 \\ \sin \gamma_b & 0 & \cos \gamma_b & 0 \\ 0 & 0 & 0 & 1 \end{bmatrix} \quad (13.33)$$

After completion of the rotation of the coordinate system,  $X_{p.s}Y_{p.s}Z_{p.s}$ , about the axis,  $Y_{p.s}$ , through the base cone angle,  $\gamma_b$ , the coordinate system,  $X_{p.s}Y_{p.s}Z_{p.s}$ , occupies a position that is labeled as  $X_{1.s}Y_{1.s}Z_{1.s}$ . The axes of the coordinate system,  $X_{1.s}Y_{1.s}Z_{1.s}$ , and of the stationary coordinate system,  $X_{2.s}Y_{2.s}Z_{2.s}$ , associated with the plane of action,  $PA$ , need to be properly aligned to one another (the reference system,  $X_{1.s}Y_{1.s}Z_{1.s}$ , is not shown in Figure 13.17). To get the axes aligned, an additional rotation of the reference system,  $X_{1.s}Y_{1.s}Z_{1.s}$ , about the axis,  $Z_{p.s}$ , through a right angle have to be performed. An operator,  $\mathbf{Rt}(Z_{p.s}, 90^\circ)$ , of linear transformation that analytically describes this additional rotation can be represented as:

$$\mathbf{Rt}(Z_{p.s}, 90^\circ) = \begin{bmatrix} 0 & 1 & 0 & 0 \\ -1 & 0 & 0 & 0 \\ 0 & 0 & 1 & 0 \\ 0 & 0 & 0 & 1 \end{bmatrix} \quad (13.34)$$

After being turned about the axis,  $Z_{p.s}$ , through a right angle, the coordinate system in the new position is designated as  $X_{2.s}Y_{2.s}Z_{2.s}$ .

The next transition is performed from the coordinate system,  $X_{2.s}Y_{2.s}Z_{2.s}$ , to the stationary coordinate system,  $X_{pa.s}Y_{pa.s}Z_{pa.s}$ , associated with the plane of action,  $PA$ . Refer to Figure 13.17 for details on this linear transformation. For the analytical description of the rotation of the reference system,  $X_{2.s}Y_{2.s}Z_{2.s}$ , in the counter-clockwise direction about the axis  $Z_{2.s}$  through an angle,  $\sigma_p$ , the operator of rotation,  $\mathbf{Rt}(Z_{2.s}, \sigma_p)$ , is employed. In matrix form, this operator is represented as:

$$\mathbf{Rt}(Z_{2.s}, \sigma_p) = \begin{bmatrix} \cos \sigma_p & \sin \sigma_p & 0 & 0 \\ -\sin \sigma_p & \cos \sigma_p & 0 & 0 \\ 0 & 0 & 1 & 0 \\ 0 & 0 & 0 & 1 \end{bmatrix} \quad (13.35)$$

Here, the projection of the pinion cone angle,  $\Sigma_p$ , onto the plane of action,  $PA$ , is designated as  $\sigma_p$  (i.e., the equality  $\text{Pr}_{pa} \Sigma_p = \sigma_p$  is valid). Referring to Figure 13.10, it can be shown that the angle,  $\sigma_p$ , can be calculated as:

$$\sigma_p = \cos^{-1} \left( \frac{\cos \Sigma_p}{\cos \gamma_b} \right) \quad (13.36)$$

where  $\gamma_b$  is base cone angle of the pinion.

Finally, the transition is performed from the stationary coordinate system,  $X_{pa.s}Y_{pa.s}Z_{pa.s}$ , associated with the plane of action, to the coordinate system,  $X_{pa}Y_{pa}Z_{pa}$ , that is rotated together with the plane of action,  $PA$ . The operator of rotation,  $\mathbf{Rt}(Z_{pa.s}, \varphi_{pa})$ , is employed for the analytical description of the rotation of the reference system,  $X_{pa.s}Y_{pa.s}Z_{pa.s}$ , in the clockwise direction about the axis  $Z_{pa.s}$  through an angle,  $\varphi_{pa}$ . In matrix form, this operator can be represented as:

$$\mathbf{Rt}(Z_{2.s}, \varphi_{pa}) = \begin{bmatrix} \cos \varphi_{pa} & -\sin \varphi_{pa} & 0 & 0 \\ \sin \varphi_{pa} & \cos \varphi_{pa} & 0 & 0 \\ 0 & 0 & 1 & 0 \\ 0 & 0 & 0 & 1 \end{bmatrix} \quad (13.37)$$

The angle of rotation,  $\varphi_{pa}$ , of the plane of action,  $PA$ , can be expressed in terms of the angle of rotation,  $\varphi_p$ , of the pinion [see Eq. (13.29)].

For the analytical description of the resultant coordinate system transformation, namely, for the transition from the reference system,  $X_p Y_p Z_p$ , associated with the rotated pinion, to the reference system,  $X_{pa} Y_{pa} Z_{pa}$ , associated with the rotated plane of action,  $PA$ , the operator,  $\mathbf{Rs}_{la}(p \rightarrow pa)$ , of the resultant coordinate system is employed. The operator  $\mathbf{Rs}_{la}(p \rightarrow pa)$  can be expressed in terms of the operators of the elementary linear transformations as:

$$\mathbf{Rs}_{la}(p \rightarrow pa) = \mathbf{Rt}(Z_{2.s}, \varphi_{pa}) \cdot \mathbf{Rt}(Z_{2.s}, \sigma_p) \cdot \mathbf{Rt}(Z_{p.s}, 90^\circ) \cdot \mathbf{Rt}(Y_{p.s}, \gamma_b) \cdot \mathbf{Rt}(Z_s, \varphi_p) \quad (13.38)$$

Note that the order of the multipliers in Eq. (13.38) is not allowed to be altered.

For the inverse coordinate system transformation, namely, for the analytical description of the transition from the reference system,  $X_{pa} Y_{pa} Z_{pa}$ , associated with the rotated plane of action,  $PA$ , to the reference system,  $X_p Y_p Z_p$ , associated with the rotated pinion, the operator,  $\mathbf{Rs}_{la}(pa \rightarrow p)$ , of the inverse coordinate system transformation is employed. The operator,  $\mathbf{Rs}_{la}(pa \rightarrow p)$ , of this linear transformation can be expressed in terms of the operator,  $\mathbf{Rs}_{la}(p \rightarrow pa)$ , of the direct coordinate system transformation as:

$$\mathbf{Rs}_{la}(pa \rightarrow p) = \mathbf{Rs}_{la}^{-1}(p \rightarrow pa) \quad (13.39)$$

The operators,  $\mathbf{Rs}_{la}(p \rightarrow pa)$  and  $\mathbf{Rs}_{la}(pa \rightarrow p)$ , are not presented here in an expended form, as both of them are bulky.

In the reference system,  $X_p Y_p Z_p$ , associated with the rotated pinion, the linear velocity vector,  $\mathbf{V}_{m,p}$ , of point of interest,  $m$ , is analytically described by a column matrix:

$$\mathbf{V}_{m,p}|_p = \begin{bmatrix} -r_{b,p} \sin \varphi_p \\ r_{b,p} \cos \varphi_p \\ 0 \\ 1 \end{bmatrix} \quad (13.40)$$

Then, the operator of the resultant coordinate system transformation,  $\mathbf{Rs}_{la}(p \rightarrow pa)$ , is used to represent that same linear velocity vector,  $\mathbf{V}_{m,p}$ , in the coordinate system,  $X_{pa} Y_{pa} Z_{pa}$ , associated with the rotated plane of action,  $PA$ :

$$\mathbf{V}_{m,p}|_{pa} = \mathbf{Rs}_{la}(p \rightarrow pa) \cdot \begin{bmatrix} -r_{b,p} \sin \varphi_p \\ r_{b,p} \cos \varphi_p \\ 0 \\ 1 \end{bmatrix} \quad (13.41)$$

A formula for the operator,  $\mathbf{Rs}_{la}(pa \rightarrow g)$ , of the resultant coordinate system transformation, that is, for the analytical description of the transition from the reference system,  $X_{pa} Y_{pa} Z_{pa}$ , associated with the rotated plane of action,  $PA$ , to the reference system,  $X_g Y_g Z_g$ , associated with the rotated gear, can be derived similar to that Eq. (13.38) is derived for the calculation of the operator of linear transformation,  $\mathbf{Rs}_{la}(p \rightarrow pa)$ . The operators,  $\mathbf{Rt}(Z_s, \varphi_g)$ ,  $\mathbf{Rt}(Y_{g.s}, \Gamma_b)$ ,  $\mathbf{Rt}(Z_{g.s}, 90^\circ)$ ,  $\mathbf{Rt}(Z_{3.s}, \sigma_g)$ , and  $\mathbf{Rt}(Z_{3.s}, \varphi_{pa})$ , of the elementary linear transformations are employed in this case (see Figure 13.17). The above listed operators of linear transformations are composed similar to that the operators of the linear transformations [i.e.,  $\mathbf{Rt}(Z_s, \varphi_p)$ , Eq. (13.32);  $\mathbf{Rt}(Y_{p.s}, \gamma_b)$ , Eq. (13.33);  $\mathbf{Rt}(Z_{p.s}, 90^\circ)$ , Eq. (13.34);  $\mathbf{Rt}(Z_{2.s}, \sigma_p)$ , Eq. (13.35); and  $\mathbf{Rt}(Z_{2.s}, \varphi_{pa})$ , Eq. (13.37)] are composed. Ultimately:



$$\mathbf{Rt}(Z_s, \varphi_g) = \begin{bmatrix} \cos \varphi_g & \sin \varphi_g & 0 & 0 \\ -\sin \varphi_g & \cos \varphi_g & 0 & 0 \\ 0 & 0 & 1 & 0 \\ 0 & 0 & 0 & 1 \end{bmatrix} \quad (13.42)$$

$$\mathbf{Rt}(Y_{g,s}, \Gamma_b) = \begin{bmatrix} \cos \Gamma_b & 0 & \sin \Gamma_b & 0 \\ 0 & 1 & 0 & 0 \\ -\sin \Gamma_b & 0 & \cos \Gamma_b & 0 \\ 0 & 0 & 0 & 1 \end{bmatrix} \quad (13.43)$$

$$\mathbf{Rt}(Z_{g,s}, 90^\circ) = \begin{bmatrix} 0 & 1 & 0 & 0 \\ -1 & 0 & 0 & 0 \\ 0 & 0 & 1 & 0 \\ 0 & 0 & 0 & 1 \end{bmatrix} \quad (13.44)$$

$$\mathbf{Rt}(Z_{3,s}, \sigma_g) = \begin{bmatrix} \cos \sigma_g & -\sin \sigma_g & 0 & 0 \\ \sin \sigma_g & \cos \sigma_g & 0 & 0 \\ 0 & 0 & 1 & 0 \\ 0 & 0 & 0 & 1 \end{bmatrix} \quad (13.45)$$

$$\mathbf{Rt}(Z_{3,s}, \varphi_{pa}) = \begin{bmatrix} \cos \varphi_{pa} & \sin \varphi_{pa} & 0 & 0 \\ -\sin \varphi_{pa} & \cos \varphi_{pa} & 0 & 0 \\ 0 & 0 & 1 & 0 \\ 0 & 0 & 0 & 1 \end{bmatrix} \quad (13.46)$$

Here, the projection of the gear cone angle,  $\Sigma_g$ , onto the plane of action,  $PA$ , is designated as  $\sigma_g$  (therefore, the equality  $\text{Pr}_{pa} \Sigma_g = \sigma_g$  is valid). Referring to Figure 13.10, it can be shown that the angle,  $\sigma_g$ , can be calculated the following equation:

$$\sigma_g = \cos^{-1} \left( \frac{\cos \Sigma_g}{\cos \Gamma_b} \right) \quad (13.47)$$

where  $\Gamma_b$  is the base cone angle of the gear.

For the analytical description of the resultant coordinate system transformation, namely, for the transition from the reference system,  $X_g Y_g Z_g$ , associated with the rotated pinion, to the reference system,  $X_{pa} Y_{pa} Z_{pa}$ , associated with the rotated plane of action,  $PA$ , the operator,  $\mathbf{Rs}_{la}(g \rightarrow pa)$ , of the resultant coordinate system is employed. This operator is expressed below in terms of the operators of the elementary linear transformations as:

$$\mathbf{Rs}_{la}(g \rightarrow pa) = \mathbf{Rt}(Z_{3,s}, \varphi_{pa}) \cdot \mathbf{Rt}(Z_{3,s}, \sigma_g) \cdot \mathbf{Rt}(Z_{g,s}, 90^\circ) \cdot \mathbf{Rt}(Y_{g,s}, \Gamma_b) \cdot \mathbf{Rt}(Z_s, \varphi_g) \quad (13.48)$$

Note that the order of the multipliers in Eq. (13.38) is not allowed to be altered.

In the reference system,  $X_g Y_g Z_g$ , associated with the rotated gear, the linear velocity vector,  $\mathbf{V}_{m,g}$ , of point of interest,  $m$ , can be analytically described by a column matrix as:



$$\mathbf{V}_{m.g}|_g = \begin{bmatrix} -r_{b.g} \sin \varphi_g \\ r_{b.g} \cos \varphi_g \\ 0 \\ 1 \end{bmatrix} \quad (13.49)$$

Then the operator of the resultant coordinate system transformation,  $\mathbf{Rs}_{la}(g \rightarrow pa)$ , is used to represent that same linear velocity vector,  $\mathbf{V}_{m.g}$ , in the coordinate system,  $X_{pa}Y_{pa}Z_{pa}$ , associated with the rotated plane of action,  $PA$ :

$$\mathbf{V}_{m.g}|_{pa} = \mathbf{Rs}_{la}(g \rightarrow pa) \cdot \begin{bmatrix} -r_{b.g} \sin \varphi_g \\ r_{b.g} \cos \varphi_g \\ 0 \\ 1 \end{bmatrix} \quad (13.50)$$

Consider relative motion of point within the line of contact of the tooth flanks,  $\mathcal{S}$  and  $\mathcal{P}$ , of a gear, and of a mating pinion in an intersected-axes gear pair.

The vector of relative motion,  $\mathbf{V}_{rel}$ , of point of interest,  $m$ , equals to the difference:

$$\mathbf{V}_{rel} = \mathbf{V}_{m.p}|_{pa} - \mathbf{V}_{m.g}|_{pa} \quad (13.51)$$

where both the linear velocity vectors,  $\mathbf{V}_{m.g}$  and  $\mathbf{V}_{m.p}$ , are represented in a common reference system,  $X_{pa}Y_{pa}Z_{pa}$ , associated with the rotated plane of action,  $PA$ .

In the expended form, the vector of the relative motion,  $\mathbf{V}_{rel}$ , can be represented in matrix form:

$$\mathbf{V}_{rel}|_{pa} = \begin{bmatrix} V_{x.rel} \\ V_{y.rel} \\ V_{z.rel} \\ 1 \end{bmatrix} \quad (13.52)$$

The projection,  $V_{y.rel}$ , of the linear velocity vector,  $\mathbf{V}_{rel}$ , onto the coordinate axis,  $Y_{pa}$ , causes pure rolling of the gear and the mating pinion tooth flanks,  $\mathcal{S}$  and  $\mathcal{P}$ , over each other. Therefore, this component of the linear velocity vector,  $\mathbf{V}_{rel}$ , is labeled below as  $\mathbf{V}_{rol}$ .

The projection,  $V_{z.rel}$ , of the linear velocity vector,  $\mathbf{V}_{rel}$ , onto the axis,  $Z_{pa}$ , causes profile sliding of the gear and the mating pinion tooth flanks,  $\mathcal{S}$  and  $\mathcal{P}$ . Therefore, this component of the linear velocity vector,  $\mathbf{V}_{rel}$ , is labeled below as  $\mathbf{V}_{sl.p}$ .

The projection,  $V_{x.rel}$ , of the linear velocity vector,  $\mathbf{V}_{rel}$ , onto the axis,  $X_{pa}$ , causes *drag sliding* of the gear and the mating pinion tooth flanks,  $\mathcal{S}$  and  $\mathcal{P}$ . Therefore, this component of the linear velocity vector,  $\mathbf{V}_{rel}$ , is labeled below as  $\mathbf{V}_{sl.d}$ .

The total sliding,  $\mathbf{V}_{sl}$ , is calculated as the sum:

$$\mathbf{V}_{sl} = \mathbf{V}_{sl.p} + \mathbf{V}_{sl.d} \quad (13.53)$$

At different points within the zone of action,  $ZA$ , each of the linear velocity vectors, namely, the vectors  $\mathbf{V}_{sl}$ ,  $\mathbf{V}_{sl.p}$ , and  $\mathbf{V}_{sl.d}$ , varies.

A computer code for the calculation of all the components,  $\mathbf{V}_{rol}$ ,  $\mathbf{V}_{sl.p}$ , and  $\mathbf{V}_{sl.d}$ , of the linear velocity vector,  $\mathbf{V}_{rel}$ , can be developed on the premise of the equations derived above in this section of the book. Ultimately, the distribution of the components,  $\mathbf{V}_{rol}$ ,  $\mathbf{V}_{sl.p}$ , and  $\mathbf{V}_{sl.d}$ , within the zone of action,  $ZA$ , in an intersected-axes gear pair can be interpreted graphically.

### 13.4.1.3 Specific Sliding in Geometrically Accurate Intersected-Axes Gearing

For the specification of sliding between tooth flanks,  $\mathcal{S}$  and  $\mathcal{P}$ , of a gear and of a mating pinion in intersected-axes gear pair, a unitless parameter can be used, similar to that a unitless parameter is used in parallel-axes gearing. This sliding parameter can be also referred to as *specific sliding*, as it is common with respect to parallel-axes gearing, and is denoted by  $\gamma_{\Sigma}$ . An actual value of specific sliding does not depend on a rotation of the input/output shafts and depends only on the design parameters of the gear and of the mating pinion. The latter is important when optimizing the design parameters of intersected-axes gear pairs.

Two different parameters,  $\gamma_{\Sigma}$ , are distinguished.

**First**, the slide/roll ratio for the tooth flank,  $\mathcal{S}$ , of the gear:

$$\gamma_{\Sigma.g} = \frac{V_{sl.g}^m - V_{sl.p}^m}{V_{sl.g}^m} \quad (13.54)$$

**Second**, the slide/roll ratio for the tooth flank,  $\mathcal{P}$ , of the pinion:

$$\gamma_{\Sigma.p} = \frac{V_{sl.p}^m - V_{sl.g}^m}{V_{sl.p}^m} \quad (13.55)$$

The sliding velocities,  $V_{sl.g}^m$  and  $V_{sl.p}^m$ , in Eqs. (13.54) and (13.55) are calculated as explained immediately below.

In the reference system,  $X_{pa}Y_{pa}Z_{pa}$ , associated with the rotated plane of action,  $PA$ , the linear velocity vector,  $\mathbf{V}_{m.g}|_{pa}$  [see Eq. (13.50)], can be represented in the form:

$$\mathbf{V}_{m.g}|_{pa} = \begin{bmatrix} V_{x.m.g} \\ V_{y.m.g} \\ V_{z.m.g} \\ 1 \end{bmatrix} \quad (13.56)$$

The component,  $V_{z.m.g}$ , contributes to the profile sliding, and the component,  $V_{x.m.g}$ , contributes to the *drag sliding* in intersected-axes gear pair (the component,  $V_{y.m.g}$ , contributes to pure rolling of the tooth flanks,  $\mathcal{S}$  and  $\mathcal{P}$ ). The sliding velocity,  $V_{sl.g}^m$  [see Eqs. (13.54) and (13.55)], can be expressed in terms of the velocities,  $V_{x.m.g}$  and  $V_{z.m.g}$ , as:

$$V_{sl.g}^m = \sqrt{V_{x.m.g}^2 + V_{z.m.g}^2} \quad (13.57)$$

Similarly, in the reference system,  $X_{pa}Y_{pa}Z_{pa}$ , associated with the rotated plane of action,  $PA$ , the linear velocity vector,  $\mathbf{V}_{m.p}|_{pa}$  [see Eq. (13.41)], can be represented in the form:

$$\mathbf{V}_{m.p}|_{pa} = \begin{bmatrix} V_{x.m.p} \\ V_{y.m.p} \\ V_{z.m.p} \\ 1 \end{bmatrix} \quad (13.58)$$

The component,  $V_{z.m.p}$ , contributes to the profile sliding, and the component,  $V_{x.m.p}$ , contributes to the *drag sliding* in intersected-axes gear pair (the component,  $V_{y.m.p}$ , contributes to pure rolling of the tooth flanks,  $\mathcal{S}$  and  $\mathcal{P}$ ). The sliding velocity,  $V_{sl.p}^m$  [see Eqs. (13.54) and (13.55)], can be expressed in terms of the velocities,  $V_{x.m.p}$  and  $V_{z.m.p}$ , as:

$$V_{sl.p}^m = \sqrt{V_{x.m.p}^2 + V_{z.m.p}^2} \quad (13.59)$$

The sliding velocities,  $V_{sl.g}^m$  and  $V_{sl.p}^m$  [see Eqs. (13.57) and (13.59)], are entered into Eqs. (13.54) and (13.55) to calculate the specific roll/slide ratios,  $\gamma_{\Sigma.g}$  and  $\gamma_{\Sigma.p}$ , in intersected-axes gearing.

The specific sliding,  $\gamma_{\Sigma}$ , is of a positive value on the addendum portions of the tooth flanks. The parameter,  $\gamma_{\Sigma}$ , does not exceed 1. At points within the axis of instantaneous rotation,  $P_m$ , it is equal to zero, and it is equal to 1 at the base cone of the mating gear.

The specific sliding on the dedendum portion of the tooth flanks is of a negative value. It is equal to zero at points within the axis of instantaneous rotation,  $P_m$ , and it is approaching minus infinity at the base cone.

The specific rolling/sliding ratios,  $\gamma_{\Sigma.g}$  and  $\gamma_{\Sigma.p}$ , are plotted within the zone of action, ZA, as only the region, ZA, of the plane of action comes into effect when investigating the engagement of the gear teeth.

#### 13.4.1.4 Features of Specific Sliding in Geometrically Accurate Intersected-Axes Gearing

Sliding conditions in geometrically accurate intersected-axes gearing differ from that in parallel-axes gearing. *Drag sliding* in  $I_a$  – gearing is the main reason for this difference. Therefore, in addition to the specific slide/roll ratios,  $\gamma_{\Sigma.g}$  and  $\gamma_{\Sigma.p}$  [see Eqs. (13.54) and (13.55)], two more characteristics can be introduced to specify specific sliding in intersected-axes gear pairs.

Specific profile slide/roll ratios,  $\gamma_{p.g}$  and  $\gamma_{p.p}$ , are the first of two additional characteristics. These two ratios are specified as:

$$\gamma_{p.g} = \frac{V_{z.m.g} - V_{z.m.p}}{V_{z.m.g}} \quad (13.60)$$

$$\gamma_{p.p} = \frac{V_{z.m.p} - V_{z.m.g}}{V_{z.m.p}} \quad (13.61)$$

Specific *drag* slide/roll ratios,  $\gamma_{d.g}$  and  $\gamma_{d.p}$ , are the second of two additional characteristics. These two ratios are specified as:

$$\gamma_{d.g} = \frac{V_{x.m.g} - V_{x.m.p}}{V_{x.m.g}} \quad (13.62)$$

$$\gamma_{d.p} = \frac{V_{x.m.p} - V_{x.m.g}}{V_{x.m.p}} \quad (13.63)$$

Specific profile slide/roll ratios,  $\gamma_{p.g}$  and  $\gamma_{p.p}$ , and specific drag slide/roll ratios,  $\gamma_{d.g}$  and  $\gamma_{d.p}$ , are helpful for more in-detail analysis of sliding conditions in intersected-axes gearing.

It should be mentioned here that gears with a low tooth count are more vulnerable to sliding between the tooth flanks,  $\mathcal{S}$  and  $\mathcal{P}$ , of a gear and of a mating pinion in intersected-axes gear pairs. They are also more sensitive to the variation of the slide/roll conditions within the zone of action, ZA.

The performed analysis of sliding conditions in external intersected-axes gearing can be extended to internal intersected-axes gearing, as well as to intersected-axes gearing with a crown gear.

### 13.5 ELEMENTS OF DYNAMICS OF GEOMETRICALLY ACCURATE INTERSECTED-AXES GEARING

In intersected-axes gearset, the input shaft and the output shaft are loaded by an input torque, and by an output torque, correspondingly. As the gears interact with each other, a force of the interaction is exerted from the driving member of the gear pair. An actual value of the force of interaction in intersected-axes gearing, as well as the components of this force, depend on the input torque, and on the design parameters of the gear and of the mating pinion. Considering an input torque, and an

input rotation of constant values (i.e., no acceleration/deceleration is taken into account in the performed below analysis), it is required to determine the forces that act between a gear and a mating pinion tooth flanks in an intersected-axes gear pair.<sup>8</sup>

### 13.5.1 PRINCIPAL ASSUMPTION ADOPTED IN LOAD ANALYSIS OF GEOMETRICALLY ACCURATE INTERSECTED-AXES GEARING

When an intersected-axes gear pair operates, the tooth flanks,  $\mathcal{F}$  and  $\mathcal{P}$ , of the gear and of the pinion interact with one another at points within the line(s) of contact,  $LC$ . The line(s) of contact is/are entirely located within the plane of action,  $PA$ . This makes possible a conclusion that the force of interaction between the tooth flanks,  $\mathcal{F}$  and  $\mathcal{P}$ , acts along a straight line that is also entirely located within the plane of action,  $PA$ .

As the line along which the force acts is located within the plane of action,  $PA$ , then the following assumption seems to be reasonable in load analysis of geometrically accurate intersected-axes gearing.

Referring to Figure 13.18, consider base cones of a gear and of a mating pinion, along with the plane of action,  $PA$ . The gear rotates,  $\omega_g$ , about its axis of rotation,  $O_g$ , and the pinion rotates,  $\omega_p$ , about its axis of rotation,  $O_p$ , as schematically illustrated in Figure 13.18a. The plane of action,  $PA$ , is in tangency to both the base cones. The plane of action,  $PA$ , rotates,  $\omega_{pa}$ , about its axis of rotation,  $O_{pa}$  (the axis,  $O_{pa}$ , that is not shown in Figure 13.18a, is a straight line through the plane-of-action apex,  $A_{pa}$ , and that is pointed perpendicular to the plane of action,  $PA$ ) that passes through the plane-of-action apex,  $A_{pa}$ . It is instructive to point out here that in contrast to the *equivalent pulley-and-belt transmission*, in which the belt *pools* the driven member, in a real gear pair the driving gear *pushes* the driven member. In this way the actual direction of the rotation,  $\omega_{pa}$ , is specified in Figure 13.18a.

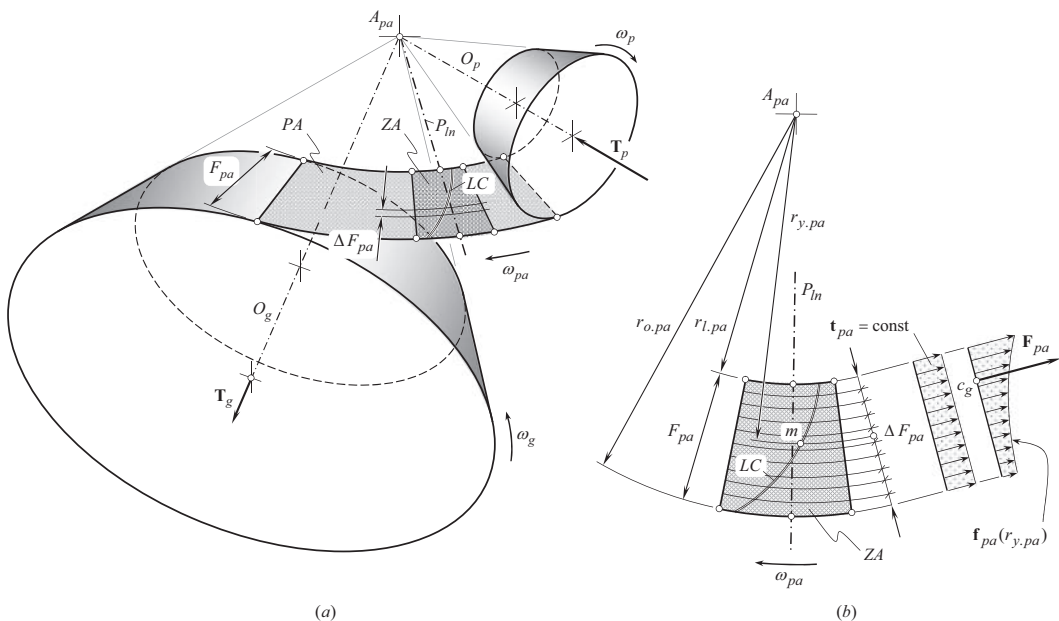


**FIGURE 13.18** Forces that act in geometrically-accurate intersected-axes gear pair: (a) schematic of a geometrically-accurate intersected-axes gear pair; and (b) a distribution of the elementary torque,  $t_{pa}$ , and of the tangential force,  $f_{pa}$ , within the active portion of the face-width,  $F_{pa}$ .

<sup>8</sup> Friction forces are incorporated into the load analysis on the later stages of this analysis.

The rotations,  $\omega_g$ ,  $\omega_p$ , and  $\omega_{pa}$ , are synchronized with one another in compliance with Eqs. (12.24)–(12.26):

$$\frac{\omega_g}{\omega_{pa}} = \sin \Gamma_b \quad (13.64)$$

$$\frac{\omega_p}{\omega_{pa}} = \sin \gamma_b \quad (13.65)$$

$$\frac{\omega_g}{\omega_p} = \frac{\sin \Gamma_b}{\sin \gamma_b} \quad (13.66)$$

The input torque,  $\mathbf{T}_p$ , is applied to the pinion shaft, and the output torque,  $\mathbf{T}_g$ , is applied to the gear shaft. The torque,  $\mathbf{T}_{pa}$ , is an *imaginary* parameter. This torque is applied to the rotated plane of action,  $PA$ . The magnitudes,  $T_g$ ,  $T_p$ , and  $T_{pa}$ , of the torques,  $\mathbf{T}_g$ ,  $\mathbf{T}_p$ , and  $\mathbf{T}_{pa}$ , correspond to one another inversely to that the rotations,  $\omega_g$ ,  $\omega_p$ , and  $\omega_{pa}$ , are synchronized with one another, that is:

$$\frac{T_g}{T_{pa}} = \frac{1}{\sin \Gamma_b} \quad (13.67)$$

$$\frac{T_p}{T_{pa}} = \frac{1}{\sin \gamma_b} \quad (13.68)$$

$$\frac{T_g}{T_p} = \frac{\sin \gamma_b}{\sin \Gamma_b} \quad (13.69)$$

Interaction between the gear tooth flank,  $\mathcal{G}$ , and of a mating pinion tooth flank,  $\mathcal{P}$ , occurs only within the zone of action,  $ZA$ , which, in fact, is a portion of the plane of action,  $PA$ . The width of the zone of action,  $F_{pa}$ , is calculated as the difference (see Figure 13.18b):

$$F_{pa} = r_{o.pa} - r_{l.pa} \quad (13.70)$$

between the outer,  $r_{o.pa}$ , and the inner,  $r_{l.pa}$ , radii of the plane of action,  $PA$ .

The interaction between the tooth flanks,  $\mathcal{G}$  and  $\mathcal{P}$ , is observed only at points of a line(s) of contact,  $LC$  (or portions of the lines of contact), those located only within the zone of action,  $ZA$ . It is common that there are one or two (and not more than three) lines of contact (or portions of the lines of contact) within the zone of action,  $ZA$ , at the same time. In intersected-axes gear pairs of special designs, the total number of the lines of contact can be greater than three.

A gear and a mating pinion can be sliced onto a large number of slices,  $N_{sl}$ , (on an infinite number of slices) each of which is perpendicular to the gear axis of rotation,  $O_g$ , and to the pinion axis of rotation,  $O_p$ , correspondingly. It is convenient to illustrate the slicing of a gear pair using the plane of action,  $PA$ , for this purpose. The thickness of the slices is designated as  $\Delta F_{pa}$ . It can be calculated as:

$$\Delta F_{pa} = \frac{F_{pa}}{N_{sl}} \quad (13.71)$$

In the best-case scenario, the number of the slices approaches an infinity ( $N_{sl} \rightarrow \infty$ ), and the slice thickness approaches to zero ( $\Delta F_{pa} \rightarrow 0$ ). In this latter case, the slice thickness is denoted by  $dF_{pa}$ . It is assumed here and below that torques transmitted by each of the slices are equal to one another. Considering the plane-of-action torque,  $\mathbf{T}_{pa}$ , the following expression:

$$\mathbf{t}_{pa} = \frac{\mathbf{T}_{pa}}{F_{pa}} = \text{const} \quad (13.72)$$

is derived for the calculation of the plane-of-action elementary torque  $\mathbf{t}_{pa}$ .

Equation is similar to Eq. (13.72):

$$\mathbf{t}_g = \frac{\mathbf{T}_g}{F_{pa}} = \text{const} \quad (13.73)$$

$$\mathbf{t}_p = \frac{\mathbf{T}_p}{F_{pa}} = \text{const} \quad (13.74)$$

are valid with respect to the elementary torque,  $\mathbf{t}_g$ , of the gear, as well as to the elementary torque,  $\mathbf{t}_p$ , of the mating pinion.

As the torque per unit length,  $\mathbf{t}_{pa}$ , is of a constant value, and the equality,  $\mathbf{t}_{pa}F_{pa} = \mathbf{T}_{pa}$ , is valid, then the actual value of the plane-of-action torque,  $\mathbf{T}_{pa}$ , is proportional to the shadowed area in Figure 13.18b.

Equal torque share among the slices is graphically illustrated in Figure 13.18b.

The above discussion makes the following assumption reasonable that is referred to as the *principal assumption* in dynamics of intersected-axes gearing:

### Principal Assumption 13.1

In intersected-axes gear pair, the torque per unit length,  $\mathbf{t}_{pa}$ , of the face width is equally shared in the axial direction among an infinite number of infinitesimally thin slices, each of which is perpendicular to the axis of rotation either of the gear, or of the pinion, or of the axis of instantaneous rotation.

A similar assumption has been made with respect to parallel-axes gear pairs (see Chapter 10).

When gears in an intersected-axes gear pair spin, an elementary tangential force that is transmitted by each slice, alters within the face width,  $F_{pa}$ . This means that when the rotation angle,  $\varphi_{pa}$ , alters from  $\varphi_{pa}^0$  to  $\varphi_{pa}^i$ , the elementary tangential force,  $\mathbf{t}_g$ , alters: (a) its direction, as  $\varphi_{pa}^i - \varphi_{pa}^0 \neq 0$ , as well as (b) its magnitude,  $t_g$ , ( $t_g^i < t_g^0$ , or, more generally,  $t_g^{i-1} < t_g^i < t_g^{i+1}$ ) – the latter is because of the variation of the arm:  $r_{b.g}^i > r_{b.g}^0$ .

When the angle,  $\varphi_{pa}^i$ , equals to zero ( $\varphi_{pa}^i = 0$ ), the elementary force,  $\mathbf{t}_g^0$ , is exactly equal to the tangential force. When the angle,  $\varphi_{pa}^i$ , is not equal to zero ( $\varphi_{pa}^i \neq 0$ ), an axial component is also generated by the elementary force,  $\mathbf{t}_g^i$ . There also exists a component of the fourth,  $\mathbf{t}_g^i$ , toward the gear axis of rotation,  $O_g$ , as well as a component along the gear axis of rotation,  $O_g$ . The bearings withhold these components of the resultant force.

The arm,  $\text{arm}^0$ , at  $\varphi_{pa}^i = 0$  equals to  $\text{arm}^0 = R_{pa}^i \sin \gamma_{b.g}$ ; an interval for the angle,  $\varphi_{pa}$ , can be expressed in terms of the dimensions of the active portion of the plane of action,  $PA$ .

The arm,  $\text{arm}^i$ , at  $\varphi_{pa}^i \neq 0$  equals to  $\text{arm}^i = (A_{pa}A_1) \sin \gamma_{b.g}$ , where  $A_{pa}A_1 = R_{pa}^i / \cos \varphi_{pa}^i$ ; ultimately:

$$\text{arm}^i = \frac{R_{pa}^i \sin \gamma_{b.g}}{\cos \varphi_{pa}^i} \quad (13.75)$$

This brief analysis needs to be taken into account when performing calculations that pertain to the vibration generation, and noise excitation in intersected-axes gear pairs.

### 13.5.2 FORCES OF INTERACTION IN GEOMETRICALLY ACCURATE INTERSECTED-AXES GEARING

The forces that act in a geometrically accurate intersected-axes gear pair are considered below in different reference systems. The analysis begins with a load applied within the plane of action,  $PA$ . Then, the analysis enhanced to the forces that act on the bearings, gear housing, and so forth.

### 13.5.2.1 Resultant Force Acting in Geometrically Accurate Intersected-Axes Gearing

The plane-of-action tangential force,  $\mathbf{F}_{pa}$ , is created by the plane-of-action torque,  $\mathbf{T}_{pa}$ . The tangential force per unit length,  $\mathbf{f}_{pa}$ , can be expressed in terms of the torque per unit length,  $\mathbf{t}_{pa}$ , and the distance,  $r_{y.pa}$ , of a particular slice from the plane-of-action point,  $A_{pa}$ :

$$\mathbf{f}_{pa} = \frac{\mathbf{t}_{pa}}{r_{y.pa}} \quad (13.76)$$

It is instructive to point out here that the tangential force per unit length,  $\mathbf{f}_{pa}$ , is a function of the distance,  $r_{y.pa}$ , of point of interest,  $m$ , from the plane-of-action point,  $A_{pa}$ , that is:

$$\mathbf{f}_{pa} = \mathbf{f}_{pa}(r_{y.pa}) \quad (13.77)$$

The distribution of the tangential force per unit length,  $\mathbf{f}_{pa}(r_{y.pa})$ , in the radial direction of the plane of action is shown in Figure 13.18b.

Having the tangential force per unit length,  $\mathbf{f}_{pa}$ , determined [see Eq. (13.76)], the resultant tangential forth,  $\mathbf{F}_{pa}$ , is calculated from:

$$\mathbf{F}_{pa} = F_{pa} \cdot \mathbf{f}_{pa} + \mathbf{t}_{pa} \int_{r_{l.pa}}^{r_{o.pa}} \frac{1}{r_{y.pa}} dr_{y.pa} = F_{pa} \cdot \mathbf{f}_{pa} + \mathbf{t}_{pa} \cdot (\ln |r_{o.pa}| - \ln |r_{l.pa}|) \quad (13.78)$$

$$\mathbf{F}_{pa} = F_{pa} \cdot \mathbf{f}_{pa} + \mathbf{t}_{pa} \cdot \ln \left| \frac{r_{o.pa}}{r_{l.pa}} \right| \quad (13.79)$$

Equations similar to Eq. (13.79):

$$\mathbf{F}_g = F_{pa} \cdot \mathbf{f}_g + \mathbf{t}_g \cdot \ln \left| \frac{r_{o.pa}}{r_{l.pa}} \right| \quad (13.80)$$

$$\mathbf{F}_p = F_{pa} \cdot \mathbf{f}_p + \mathbf{t}_p \cdot \ln \left| \frac{r_{o.pa}}{r_{l.pa}} \right| \quad (13.81)$$

are valid with respect to the gear, as well as to the mating pinion.

The resultant forth,  $\mathbf{F}_{pa}$ , is applied at point,  $c_g$ , of the line of contact,  $LC$ , that is remote from the plane-of-action apex,  $A_{pa}$ , at a distance,  $r_{cg}$  (see Figure 13.18b).

Transmission of a rotation from a driving shaft to a driven shaft is due to the tangential forth,  $\mathbf{F}_{pa}$ .

When the gears rotate, the friction is occurred between the gear tooth flank,  $\mathcal{S}$ , and the pinion tooth flank,  $\mathcal{P}$ . The friction between the compressed gear and the pinion tooth flanks is due to the sliding that occurs between tooth flanks,  $\mathcal{S}$  and  $\mathcal{P}$ . As it is already shown above (see the previous section of the book), two types of sliding are distinguished in intersected-axes gear pairs. The profile sliding is the first kind of sliding, and the *drag sliding* is the second kind of sliding in intersected-axes gearing. Therefore, friction forces of two types are required to be recognized, namely, the profile friction force,  $\mathbf{F}_{pr}$ , and the friction force in the lengthwise direction,  $\mathbf{F}_{dr}$ . These friction forces contribute to the resultant force of the interaction,  $\mathbf{F}_{\Sigma}$ , between the gear tooth flank,  $\mathcal{S}$ , and the pinion tooth flank,  $\mathcal{P}$ :

$$\mathbf{F}_{\Sigma} = \mathbf{F}_{pa} + \mathbf{F}_{pr} + \mathbf{F}_{dr} \quad (13.82)$$

The component,  $\mathbf{F}_{pa}$ , is specified by Eq. (13.79).

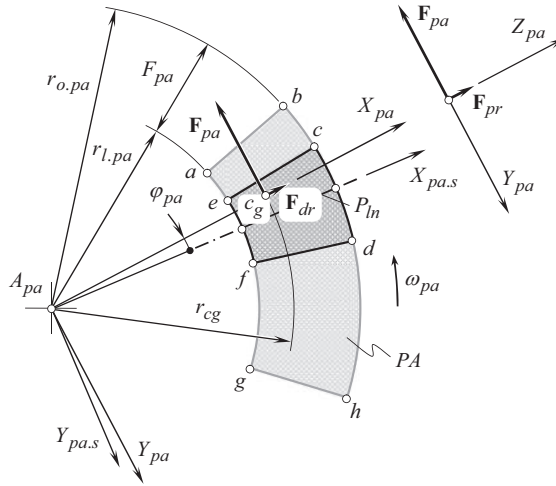


FIGURE 13.19 Tangential force,  $\mathbf{F}_{pa}$ , and friction forces,  $\mathbf{F}_{pr}$  and  $\mathbf{F}_{dr}$ , that act in intersected-axes gear pair.

In the reference system,  $X_{pa}Y_{pa}Z_{pa}$ , associated with the rotated plane of action,  $PA$ , the profile friction force,  $\mathbf{F}_{pr}$ , is pointed along the coordinate axis  $Z_{pa}$ , as illustrated in Figure 13.19. The actual value of this component equals:

$$\mathbf{F}_{pr} = \mu_{pr} \cdot \mathbf{F}_{pa} \quad (13.83)$$

Here,  $\mu_{pr}$  designates the coefficient of friction in profile sliding of the gear,  $\mathcal{G}$ , and of the pinion,  $\mathcal{P}$ , tooth flanks.

In that same reference system,  $X_{pa}Y_{pa}Z_{pa}$ , the friction force in the lengthwise direction,  $\mathbf{F}_{dr}$ , is pointed along the axis coordinate  $X_{pa}$ . The actual value of this component equals (see Figure 13.19):

$$\mathbf{F}_{dr} = \mu_{dr} \cdot \mathbf{F}_{pa} \quad (13.84)$$

The coefficient of friction in *drag sliding* of the gear,  $\mathcal{G}$ , and the pinion,  $\mathcal{P}$ , tooth flanks is denoted by  $\mu_{dr}$ .

The coefficients of friction,  $\mu_{pr}$  and  $\mu_{dr}$ , can be of different values, as the normal curvatures of the gear and the pinion tooth flanks,  $\mathcal{G}$  and  $\mathcal{P}$ , at point of interest are significantly different in the transverse, and in the lengthwise directions of the tooth flanks  $\mathcal{G}$  and  $\mathcal{P}$ . Moreover, the conditions of profile sliding, and of *drag sliding* are also different. However, when performing a preliminary analysis, the coefficients of friction,  $\mu_{pr}$  and  $\mu_{dr}$ , can be considered equal to one another ( $\mu_{pr} = \mu_{dr}$ ).

Total friction force,  $\mathbf{F}_{fr,\Sigma}$ , in geometrically accurate intersected-axes gearing is calculated as:

$$\mathbf{F}_{fr,\Sigma} = \mathbf{F}_{pr} + \mathbf{F}_{dr} \quad (13.85)$$

The friction forces,  $\mathbf{F}_{pr}$  and  $\mathbf{F}_{dr}$ , in an intersected-axes gear pair are negligibly small, and, thus, commonly, they are not taken into account when calculating the design parameters of a gear transmission. Moreover, the friction forces,  $\mathbf{F}_{pr}$  and  $\mathbf{F}_{dr}$ , do not affect the uniformity of the output rotation in a gear pair, as both,  $\mathbf{F}_{pr}$  and  $\mathbf{F}_{dr}$ , are entirely located within a plane that is perpendicular to the plane of action,  $PA$  (and that is tangent to the gear,  $\mathcal{G}$ , and to the pinion,  $\mathcal{P}$ , tooth flanks at point of interest,  $m$ ). Only the component of the resultant force of the interaction,  $\mathbf{F}_{\Sigma}$ , that is pointed along the common perpendicular to the tooth flanks,  $\mathcal{G}$  and  $\mathcal{P}$ , causes a rotation of the driven gear in an intersected-axes gear pair.



Different components of the resultant tangential force,  $\mathbf{F}_{pa}$ , of interaction between the tooth flanks,  $\mathcal{S}$  and  $\mathcal{P}$ , of a gear and of a mating pinion, along with the forces  $\mathbf{F}_g$  and  $\mathbf{F}_p$  [see Eqs. (13.80) and (13.81)] that act on the gear and of the mating pinion, are entered into equations for the calculation of the bending and contact strength of the gear and the pinion teeth, the bearings, the housing, the shafts, and so forth.

The forces that act on the gear have to be expressed in a stationary coordinate system,  $X_{g,s}Y_{g,s}Z_{g,s}$ , associated with the motionless gear (i.e., associated with the gear pair housing). The operator,  $\mathbf{Rs}_{la}(pa \rightarrow g_s)$ , of the resultant coordinate system transformation can be used for this purpose. The operator,  $\mathbf{Rs}_{la}(pa \rightarrow g_s)$ , can be represented as a product of the operators,  $\mathbf{Rt}(Y_{g,s}, \Gamma_b)$ ,  $\mathbf{Rt}(Z_{g,s}, 90^\circ)$ ,  $\mathbf{Rt}(Z_{g,s}, \sigma_g)$ , and  $\mathbf{Rt}(Z_{3,s}, \varphi_{pa})$ , of the elementary linear transformations as:

$$\mathbf{Rs}_{la}(pa \rightarrow g_s) = \mathbf{Rt}(Y_{g,s}, \Gamma_b) \cdot \mathbf{Rt}(Z_{g,s}, 90^\circ) \cdot \mathbf{Rt}(Z_{3,s}, \sigma_g) \cdot \mathbf{Rt}(Z_{3,s}, \varphi_{pa}) \quad (13.86)$$

After the resultant tangential force,  $\mathbf{F}_{pa}$  [see Eq. (13.79)], of interaction between the tooth flanks,  $\mathcal{S}$  and  $\mathcal{P}$ , has been pre-multiplied by the operator,  $\mathbf{Rs}_{la}(pa \rightarrow g_s)$ , of the linear transformation, the resultant force,  $\mathbf{F}_{g,s}$ , that acts over the gear, can be represented in the form of a column matrix:

$$\mathbf{F}_{g,s} = \mathbf{Rs}_{la}(pa \rightarrow g_s) \cdot \mathbf{F}_{pa} = \begin{bmatrix} F_{x,g,s} \\ F_{y,g,s} \\ F_{z,g,s} \\ 1 \end{bmatrix} \quad (13.87)$$

Referring to Figure 13.20, the components  $F_{x,g,s}$ ,  $F_{y,g,s}$ , and  $F_{z,g,s}$ , of the resultant force,  $\mathbf{F}_{g,s}$ , in Eq. (13.87) are equal to the separating force,  $F_{g,sep}$ , the tangential force,  $F_{g,tg}$ , and to the axial thrust,  $F_{g,ax}$ , correspondingly, that is, the equalities  $F_{x,g,s} = F_{g,sep}$ ,  $F_{y,g,s} = F_{g,tg}$ , and  $F_{z,g,s} = F_{g,ax}$ , are valid. The forces,  $\mathbf{F}_{g,sep}$ ,  $\mathbf{F}_{g,tg}$ , and  $\mathbf{F}_{g,ax}$ , are entered into the equations for the calculation of the design parameters of a gearbox.

### 13.5.2.2 Forces Acting on Gear and Pinion in Geometrically Accurate Intersected-Axes Gearing

In the reference system,  $X_{pa}Y_{pa}Z_{pa}$ , associated with the rotated plane of action,  $PA$ , an orientation of the force,  $\mathbf{F}_{pa}$  [that is specified by Eq. (13.79)], or of the resultant force,  $\mathbf{F}_\Sigma$  [that is specified by Eq. (13.82)], does not alter when the gears rotate. However, the configuration of the coordinate system,  $X_{pa}Y_{pa}Z_{pa}$ , in relation to a motionless reference system associated with the gear pair

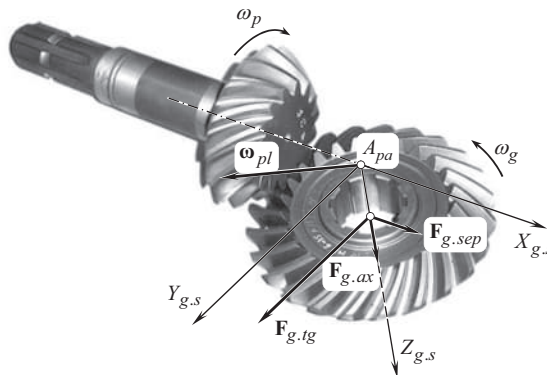


FIGURE 13.20 Forces that act on the gear in geometrically accurate intersected-axes gear pair.

housing alters when the gears rotate. Therefore, in a stationary coordinate system,  $X_{g.s}Y_{g.s}Z_{g.s}$ , associated with the motionless gear, Eq. (13.87) has to be rewritten in a form:

$$\mathbf{F}_{g.s}(\varphi_g) = \begin{bmatrix} F_{g.sep}(\varphi_g) \\ F_{g.tg}(\varphi_g) \\ F_{g.ax}(\varphi_g) \\ 1 \end{bmatrix} \quad (13.88)$$

As it follows from the analysis of Eq. (13.88), the resultant force,  $\mathbf{F}_{g.s}$ , as well as all three components,  $\mathbf{F}_{g.sep}$ ,  $\mathbf{F}_{g.tg}$ , and  $\mathbf{F}_{g.ax}$ , that act over the gear, depend on the actual value of the angle of rotation of the gear, that is, all of them are functions the angle,  $\varphi_g$ , of rotation of the gear:

$$\mathbf{F}_{g.s} = \mathbf{F}_{g.s}(\varphi_g) \quad (13.89)$$

$$\mathbf{F}_{g.sep} = \mathbf{F}_{g.sep}(\varphi_g) \quad (13.90)$$

$$\mathbf{F}_{g.tg} = \mathbf{F}_{g.tg}(\varphi_g) \quad (13.91)$$

$$\mathbf{F}_{g.ax} = \mathbf{F}_{g.ax}(\varphi_g) \quad (13.92)$$

The resultant force,  $\mathbf{F}_{g.s}(\varphi_g)$ , and the components,  $\mathbf{F}_{g.sep}(\varphi_g)$ ,  $\mathbf{F}_{g.tg}(\varphi_g)$ , and  $\mathbf{F}_{g.ax}(\varphi_g)$ , that depend on the angular parameter,  $\varphi_g$ , are an additional source of vibration generation, and noise excitation in intersected-axes gearing. When the gears rotate, point of intersection of the axis of instantaneous rotation,  $P_{ln}$ , and the instantaneous line of action,  $LA_{inst}$ , migrates along the axis of instantaneous rotation,  $P_{ln}$ . It is desirable to minimize the distance covered in this migration. In this way, the noise excitation in the gear pair is reduced.

The variation of the forces has to be minimized in order to minimize the vibration generation, and the noise excitation when an intersected-axes gear pair operates.

The variation of direction of the resultant force,  $\mathbf{F}_{g.s}(\varphi_g)$ , of the interaction of tooth flanks,  $\mathcal{S}$  and  $\mathcal{P}$ , of a gear and of a mating pinion is illustrated in Figure 13.21. For an arbitrary configuration of the line of contact,  $LC$ , between the tooth flanks,  $\mathcal{S}$  and  $\mathcal{P}$ , the coordinates of point,  $c_g$ , at which the resultant force,  $\mathbf{F}_{g.s}$ , is applied, can be determined. The component,  $\mathbf{F}_{g.ax}$ , is parallel to the axis of rotation,  $O_g$ , of the gear. The component,  $\mathbf{F}_{g.sep}$ , is perpendicular to the axis of rotation,  $O_g$ , of the gear. The magnitude,  $F_{g.sep}^*$ , of the shown in Figure 13.21 the force vector,  $\mathbf{F}_{g.sep}^*$ , equals to  $F_{g.sep}^* = F_{g.sep} / \sin \phi_{t,\omega}$ , where  $\phi_{t,\omega}$  is the transverse pressure angle in the intersected-axes gear pair. (The separating force vector,  $\mathbf{F}_{g.sep}$ , is entirely located in the normal  $N_{ln}$  – plane. In the case under consideration, the  $N_{ln}$  – plane is the plane through the axes of rotation,  $O_g$  and  $O_p$ , of the gear and of the mating pinion, correspondingly). As it follows from the analysis of the schematic depicted in Figure 13.21, for any configuration of the line of contact,  $LC$ , for which the point,  $c_g$ , is located within the zone of action,  $ZA$ , the forces,  $\mathbf{F}_{g.ax}$  and  $\mathbf{F}_{g.sep}$ , never equal to zero. Thus, the reaction forces,  $\mathbf{F}_{g.ax}^{rct}$  and  $\mathbf{F}_{g.sep}^{rct}$ , also are of non-zero values. As the forces,  $\mathbf{F}_{g.ax}^{rct}$  and  $\mathbf{F}_{g.sep}^{rct}$ , fluctuate when the gears rotate [see Eqs. (13.90) and (13.92)], an excessive vibration generation, and noise excitation can be observed when an intersected-axes gear pair operates. The variation of the forces,  $\mathbf{F}_{g.ax}^{rct}$  and  $\mathbf{F}_{g.sep}^{rct}$ , does not depend on the geometry of the line of contact,  $LC$ . This discussion is also valid in cases when multiple lines of contact, as well as multiple portions of the lines of contact, are observed in a gear pair of a particular design, as the fluctuation of the forces,  $\mathbf{F}_{g.ax}^{rct}$  and  $\mathbf{F}_{g.sep}^{rct}$ , are inevitable in perfect intersected-axes gear pairs.

An analysis similar to that above can be performed with respect to loading of the pinion in a geometrically accurate intersected-axes gear pair.

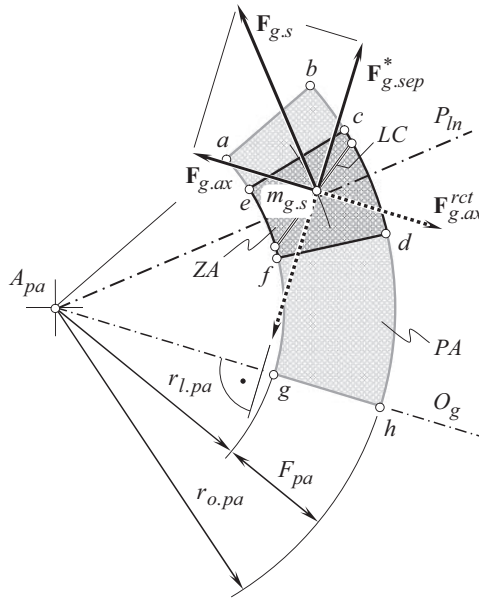


**FIGURE 13.21** Axial thrust,  $\mathbf{F}_{g.ax}(\varphi_g)$ , and separating force,  $\mathbf{F}_{g.sep}(\varphi_g)$ , as the components of the resultant force,  $\mathbf{F}_{g.s}(\varphi_g)$ , of interaction of tooth flanks,  $\mathcal{S}$  and  $\mathcal{P}$ , of a gear and of a mating pinion in geometrically accurate intersected-axes gear pair.

As it follows from the analysis of Eq. (13.88), the resultant force,  $\mathbf{F}_{p.s}$ , as well as all three components,  $\mathbf{F}_{p.sep}$ ,  $\mathbf{F}_{p.tg}$ , and  $\mathbf{F}_{p.ax}$ , that act over the pinion, depend on the angle of rotation of the pinion, namely, all of them are functions the angle,  $\varphi_p$ , of rotation of the pinion:

$$\mathbf{F}_{p.s} = \mathbf{F}_{p.s}(\varphi_p) \quad (13.93)$$

$$\mathbf{F}_{p.sep} = \mathbf{F}_{p.sep}(\varphi_p) \quad (13.94)$$

$$\mathbf{F}_{p.tg} = \mathbf{F}_{p.tg}(\varphi_p) \quad (13.95)$$

$$\mathbf{F}_{p.ax} = \mathbf{F}_{p.ax}(\varphi_p) \quad (13.96)$$

The resultant force,  $\mathbf{F}_{p.s}(\varphi_p)$ , and the components,  $\mathbf{F}_{p.sep}(\varphi_p)$ ,  $\mathbf{F}_{p.tg}(\varphi_p)$ , and  $\mathbf{F}_{p.ax}(\varphi_p)$ , that depend on the angular parameter,  $\varphi_p$ , represent an additional source of vibration generation, and noise excitation in intersected-axes gearing. When the gears rotate, point of intersection of the axis of instantaneous rotation,  $P_{ln}$ , and the instantaneous line of action,  $LA_{inst}$ , migrate. It is desirable to minimize the distance covered in this migration. In this way, the noise excitation in the gear pair goes down.

For any configuration of the line of contact,  $LC$ , at which the point,  $c_g$ , is located within the zone of action,  $ZA$ , the forces,  $\mathbf{F}_{p.ax}$  and  $\mathbf{F}_{p.sep}$ , never equal to zero. Thus, the reaction forces,  $\mathbf{F}_{p.ax}^{ret}$  and  $\mathbf{F}_{p.sep}^{ret}$ , also are of non-zero values. As the forces,  $\mathbf{F}_{p.ax}^{ret}$  and  $\mathbf{F}_{p.sep}^{ret}$ , fluctuate when the gears rotate, an excessive vibration generation, and noise excitation can be observed when an intersected-axes gear pair operates. The variation of the forces,  $\mathbf{F}_{p.ax}^{ret}$  and  $\mathbf{F}_{p.sep}^{ret}$ , does not depend on the geometry of the line of contact,  $LC$ .

This discussion is also valid in cases when multiple lines of contact, as well as multiple portions of the lines of contact, are observed in a gear pair of a particular design, as the fluctuation of the forces,  $\mathbf{F}_{p.ax}^{ret}$  and  $\mathbf{F}_{p.sep}^{ret}$ , is inevitable in perfect intersected-axes gear pairs.

### 13.5.2.3 Normal Force Acting on gear in Geometrically Accurate Intersected-Axes Gearing

For the calculations of gear teeth for contact strength, as well as for bending strength, a component,  $\mathbf{F}_{g,n}$ , of the resultant force,  $\mathbf{F}_{g,s}$ , is entered into the corresponding equations for the calculations. This component is commonly referred to as the *normal force*,  $\mathbf{F}_{g,n}$ . The vector of normal load,  $\mathbf{F}_{g,n}$ , is located within the plane of action,  $PA$ , and is perpendicular to the line of contact,  $LC$ , at point,  $c_g$ , at which the normal load is applied. The magnitude,  $F_{g,n}$ , of the normal force,  $\mathbf{F}_{g,n}$ , can be calculated as:

$$F_{g,n} = F_{g,s} \cos \psi_g \quad (13.97)$$

where  $\psi_g$  is the spiral angle of the gear tooth at point,  $c_g$ .

The vector of normal force per unit length,  $\mathbf{f}_{g,n}$ , is also entirely located within the plane of action,  $PA$ . The normal force per unit length,  $\mathbf{f}_{g,n}$ , depends on the geometry of a particular line of contact. At every point of the line of contact,  $LC$ , the applied normal load per unit length,  $\mathbf{f}_{g,n}$ , is perpendicular to the line of contact at that point.

In straight bevel gearing, the normal force per unit length,  $\mathbf{f}_{g,n}$ , is distributed similarly in much to that shown in Figure 13.18b for the force per unit length,  $\mathbf{f}_{pa}(r_{y,pa})$ . In skew bevel gearing, the normal force per unit length,  $\mathbf{f}_{g,n}$ , is distributed similar to that in straight bevel gearing – all the elementary forces are perpendicular to the line of contact,  $LC$ . The distribution of the normal force per unit length,  $\mathbf{f}_{g,n}$ , in spiral bevel gearing with a circular-arc line of contact,  $LC$ , of a radius,  $R_{lc}$ , is illustrated in Figure 13.22. In this case, all the elementary forces are pointed along the radius,  $R_{lc}$ , to the corresponding point,  $m$ , within the line of contact,  $LC$ .

In a more general case of geometrically accurate intersected-axes gearing, in face-hobbed bevel gears in particular, the following approach can be used to determine the distribution of the normal force per unit length along the line of contact,  $LC$ .

**First**, the unit normal vector,  $\mathbf{n}_{lc}$ , is constructed at every point of the line of contact,  $LC$ .

**Second**, the distribution of the normal load per unit length,  $\mathbf{f}_{g,n}$ , is constructed as a product of the unit vector,  $\mathbf{n}_{lc}$ , times the function of the distribution of the magnitude,  $f_{g,n}$ , of the normal load per unit length, that is,  $\mathbf{f}_{g,n} = f_{g,n} \cdot \mathbf{n}_{lc}$ .

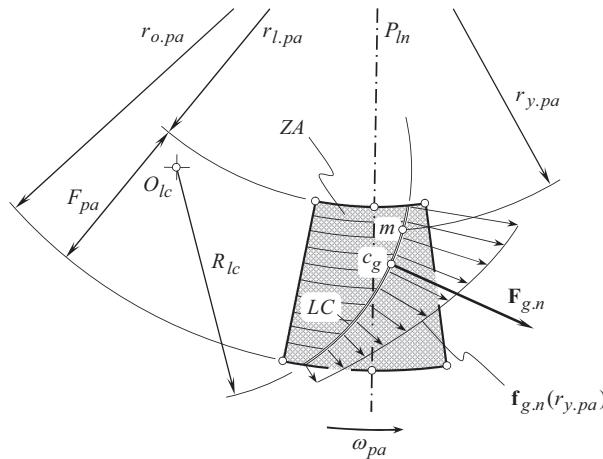


**FIGURE 13.22** The normal force,  $\mathbf{F}_{g,n}$ , and normal force per unit length,  $\mathbf{f}_{g,n}$ , acting in geometrically accurate intersected-axes gear pair.

When two, or more lines of contact (or portions of the lines of contact),  $LC_i$ , are observed, then the position vector,  $\mathbf{r}_{cg,\Sigma}$ , of the point,  $c_{g,\Sigma}$ , at which the resultant load,  $\mathbf{F}_{g,n,\Sigma}$ , is applied can be calculated as:

$$\mathbf{r}_{cg,\Sigma} = \frac{\sum_i l_{lc,i} \cdot \mathbf{r}_{cg,i}}{\sum_i l_{lc,i}} \quad (13.98)$$

where:

$i$  is the number of a line of contact (or a portion of a line of contact),  $LC_i$

$l_{lc,i}$  is the length of a line of contact (or a portion of a line of contact),  $LC_i$

$\mathbf{r}_{cg,i}$  is the position vector of a point,  $c_{g,i}$ , of a line of contact (or a portion of a line of contact),  $LC_i$

$\sum_i l_{lc,i}$  is the total length,  $TLLC$ , of all the lines of contact,  $l_{lc,i}$

The performed analysis of the forces that act in external intersected-axes gearing can also be enhanced to internal intersected-axes gearing, as well as to *pinion-gear-to-rack mesh*, as the latter is a reduced case of external intersected-axes gearing.

### 13.6 TESTING OF GEOMETRICALLY ACCURATE SPIRAL BEVEL GEARS: CONTACT PATTERN

*CAD* model of a right-angle spiral bevel gear pair was developed in compliance with the proposed method of designing bevel gears for geometrically accurate intersected-axes gear pairs. The accuracy of the developed *CAD* model has been verified by comparing the sections of the tooth flanks,  $\mathcal{S}$  and  $\mathcal{P}$ , by a plane tangent to the base cone of the gear (and of the pinion). In all cases the interacting tooth flanks,  $\mathcal{S}$  and  $\mathcal{P}$ , of the gear and of the mating pinion make line contact with each other.

#### 13.6.1 TESTING CONDITIONS

A few sets of geometrically accurate spiral bevel gears are manufactured for testing purposes [184–186]. Five-axes NC machine was used to cut the tooth flanks of the gear and of the mating pinion.

The developed *CAD* models were used for rapid prototyping, and for the converting to a *G*-code for cutting bevel gears of the proposed design<sup>9</sup> on a five-axes *NC* machine (see Figure 13.23).



**FIGURE 13.23** Spiral bevel gear and mating pinion cut on a 5-axis *NC* machine.

<sup>9</sup> Patent pending.

When cutting the gears, the radius of curvature,  $R_{lc}$ , of the desirable line of contact,  $LC_{des}$ , is set equal to both, to the convex and to the concave tooth flanks,  $\mathcal{S}$  and  $\mathcal{P}$ , of the gear and the pinion,  $R_{lc} = 200$  mm. The tolerances for the tooth flanks accuracy are of the same magnitude  $\delta$ , and of the opposite sign, that is, the radius  $R_{lc}$  is set equal to  $200_{-\delta}^0$  for the convex tooth flanks  $\mathcal{S}$  and  $\mathcal{P}$ , and it is set equal to  $200_{\delta}^0$  for the concave tooth flanks.

The accuracy of the machined spiral bevel gears was verified by means of the laser scanning of the machined tooth flanks with the consequent comparison of the scanned data with the corresponding points generated by the *CAD* model. The actual tooth flanks of the gear and of the pinion deviate from the desirable tooth flanks,  $\mathcal{S}$  and  $\mathcal{P}$ , less than 0.01 mm.

Before running the contact pattern test, the contact geometry of the bevel gears of the developed design was investigated in comparison to that of the similar gear set cut using *Gleason* method of gear generating. The comparison is performed based on the developed *CAD* models.

### 13.6.2 PREDICTING CONTACT GEOMETRY IN GEOMETRICALLY ACCURATE SPIRAL BEVEL GEARING

When a bevel gear tooth flank is generated following *Gleason* method of gear generating, the contact patch (see Figure 13.24) is of non-uniform width that is evident from the analysis of contact

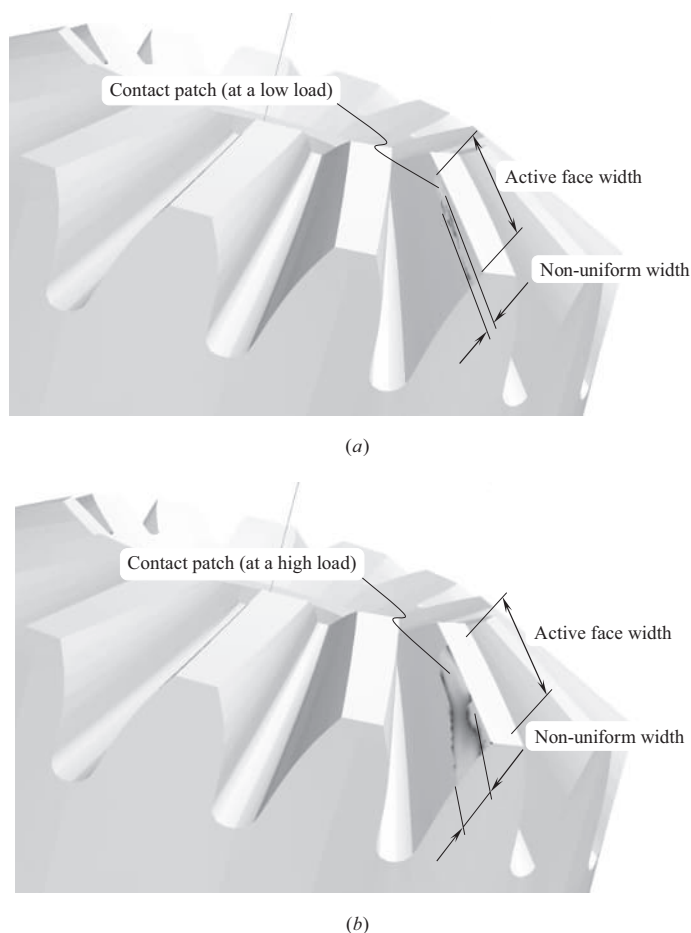


**FIGURE 13.24** Contact patch under (a) a low, and (b) a high load in gears cut by *Gleason* method.

patches at a low load (see Figure 13.24a) as well as at a high load (see Figure 13.24b). The contact patches are considered only within the active face width, that is, where the tooth flanks,  $\mathcal{G}$  and  $\mathcal{P}$ , overlap one another.

These two types of contact patch convince us that geometrically the gear and the pinion tooth flanks make contact at a distinct point, and not along a desirable line of contact. Because of the point contact, contact stresses in the vicinity of the contact points are always of an increased value.

Point contact between the tooth flanks of bevel gears cut by *Gleason* method is the consequence of the violation of the second and the third fundamental laws of geometrically accurate bevel gear tooth flank generation. The violation of the second and the third fundamental laws occurs because the geometry of the tooth flank of the imaginary crown rack that is generated by the cutting edges of the face mill cutter deviates from that of the desirable imaginary crown rack. In gears with a large tooth count, these deviations are usually small and often they can be ignored. In gears with a few teeth, the deviations become much larger and cannot be ignored, especially in cases of precision bevel gears.

In geometrically accurate spiral bevel gears, the contact patch is of a uniform width (see Figure 13.25). Therefore, the gear and the pinion tooth flanks make line contact with each other

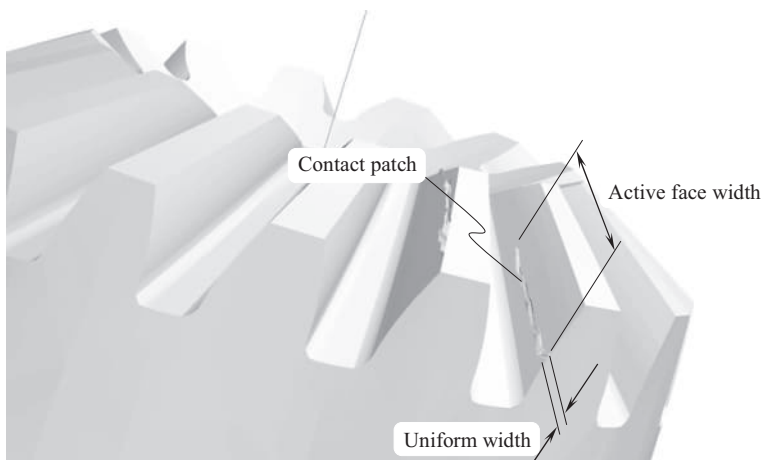


**FIGURE 13.25** Contact patch in geometrically accurate spiral bevel gears.

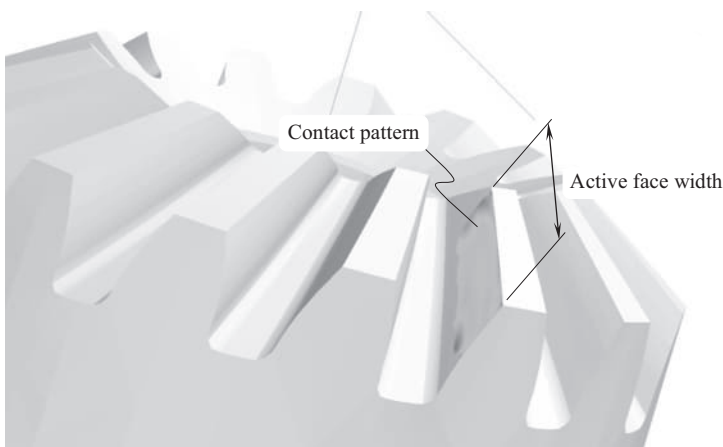


**FIGURE 13.26** The anticipated contact pattern in geometrically accurate intersected-axes gearing.



and not point contact. The line contact between the tooth flanks,  $\mathcal{S}$  and  $\mathcal{P}$ , is observed due to all three fundamental laws of gearing are fulfilled in geometrically accurate spiral bevel gearing. Line contact between the tooth flanks,  $\mathcal{S}$  and  $\mathcal{P}$ , results in a uniform loading of the bearing surfaces,  $\mathcal{S}$  and  $\mathcal{P}$ , and in the corresponding reduction of the contact stresses.

When the gear and the pinion tooth flanks are in line contact, it is anticipated that the contact pattern spreads over the entire tooth flank of the gear and the pinion, as shown in Figure 13.26.

The actual contact pattern in the machined gears (see Figure 13.23) spreads over the entire tooth flank of the gear and the pinion, as shown in Figure 13.27 (and as it was predicted in Figure 13.26). This type of the contact pattern is the most favorable, as it makes possible even loading of all portions of the gear and the pinion tooth flanks.

The tooth flanks of the gear and of the mating pinion are always in line contact with one another, as all three fundamental laws of gearing are fulfilled in the discussed design of spiral bevel gears. Line contact between the tooth flanks is favorable, as it allows for a reduction of contact stress. The power density can be increased; the noise excitation can be reduced as well as the performance of the gear pair in whole can be significantly improved.

Geometrically accurate intersected-axes gear pairs can operate at high rotations. Therefore, gearing of this kind can be used as a first stage in a gear train, where rotations are higher, but the applied torque is lower. The applied forces are lower when the torque is lower. Ultimately, bearings of a simpler design can be used in an intersected-axes gear pair that operate at lower loads. This is a significant advantage of geometrically accurate intersected-axes gearing.

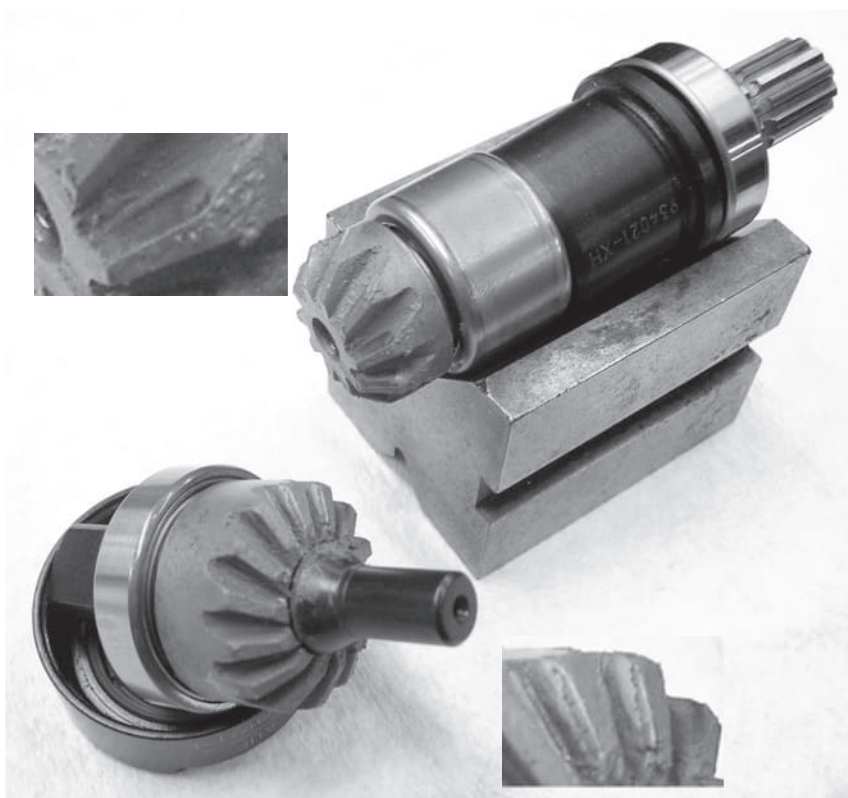


**FIGURE 13.27** The actual contact pattern in geometrically accurate spiral bevel gears.





# Taylor & Francis

Taylor & Francis Group

<http://taylorandfrancis.com>

# Section II-C

---

## Geometrically Accurate Gears

### Crossed-Axes Gearing

Gear pairs used to transmit rotation between two shafts that cross their axes of rotation are referred to as *crossed-axes gear pairs*, or simply, as  $C_a$  – *gearing*. Crossed-axes gearing of numerous designs is extensively used in the present-day industry. All of them are approximate gearing, as they feature a variable angular velocity ratio,  $u = \omega_{\text{input}} / \omega_{\text{output}} = \text{var}$ . This is amazing, but only approximate  $C_a$  – gears are investigated so far. This is mainly because the gears for approximate intersected-axes gear pairs are easier in production on the available gear generators, using for this purpose gear cutting tools available on the market. Lots of attempts were undertaken in the past to develop the theory of approximate crossed-axes gearing. Baxter [6,7], Dooner [28], Dudas, [29], Dusev and Vasil'yev [31], Dyson [32], Klingelberg [9,58], Krenzer [67], Litvin [74], Litvin and Fuentes [76], Lopato et al [78], Phillips [130], Pismanik [131], Shevel'ova [196], Shtipelman [201], Wang and Ghosh [219], Wildhaber [220], Wu and Luo [224], Zak [228], Zhuravl'ov and Iofis [230], are among those who have contributed to the theory of approximate crossed-axes gearing. This theory is still not developed yet. Moreover, it is not possible even to predict when such a theory would be developed by the gear scientists.

On the other hand, numerous attempts targeting at the improvement of crossed-axes gear-sets were undertaken in the gear industry. All of these attempts (Stadtfeld [208,209], and others – see the *Bibliography* section of the book) are based on a primitive *trial-and-error* approach (instead of a scientific approach). This approach is not applicable in such a sophisticated and science-consuming field of mechanical engineering as gear engineering is.

No geometrically accurate crossed-axes gearing (with the desirable tooth flank geometry) are investigated so far, as the gearing of this particular design has been developed only in recent years (Prof. *S.P. Radzevich*, ~2008).

Geometrically accurate crossed-axes gearing is discussed below in this section of the book.

Referring to Figure 2.16, crossed-axes gear pairs comprise the first stratum of the classification of possible kinds of gear vector diagrams.

Crossed-axes gear pair of every design can be specified by a corresponding gear vector diagram. The use of the gear vector diagrams along with the developed classification of possible kinds of gear vector diagrams (see Figure 2.16) makes possible a comprehensive analysis of gearing of this particular kind. All possible kinds of crossed-axes gear pairs are incorporated into the analysis, and none of them is missed if the consideration is based on the proposed classification of gear vector diagrams (see Figure 2.16).

---

# 14 Geometrically Accurate Crossed-Axes Gear Pairs

## *R-Gearing*

Early designs of crossed-axes gears can be found in the 1493 *Leonardo da Vinci's* famous book titled *The Madrid Codices* [23].

When a motion is transmitted between two shafts whose axes cross, some form of bevel-like gear is applied, as illustrated in Figure 14.1. Although gears of this kind are often made for a shaft angle of  $90^\circ$ , they can be produced for almost any shaft angle.

Crossed-axes gears have an extensive application in the present-day industry. The use of a crossed-axes gear-set in the design of the automobile differential is illustrated in Figure 14.2.

### 14.1 KINEMATICS OF CROSSED-AXES GEARING

Transmission and transformation of a rotary motion from a driving shaft to a driven shaft is the main purpose of the application of crossed-axes gear-sets. Both the input rotation and the output rotation can be easily represented by corresponding rotation vectors,  $\omega_g$  and  $\omega_p$ . The rotation vectors,  $\omega_g$  and  $\omega_p$ , are pointed along two straight lines, which cross one another. The closest distance of approach between the lines of action of the rotation vectors,  $\omega_g$  and  $\omega_p$ , is denoted by  $C$ . This distance is commonly referred to as *center-distance*,  $C$ . It is convenient to refer to Figures 2.9 and 2.10 when investigating geometrically accurate crossed-axes gearing.

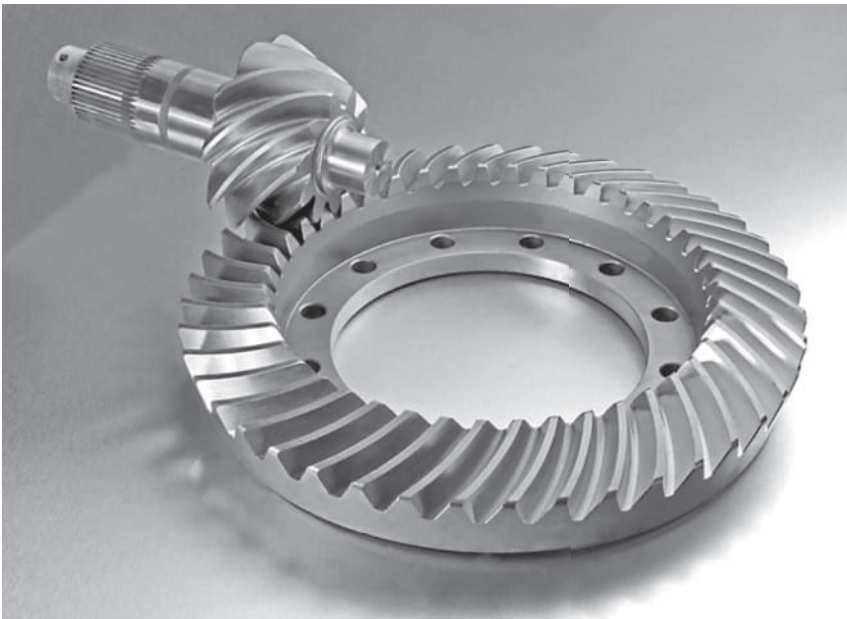


**FIGURE 14.1** Crossed-axes gear pair.

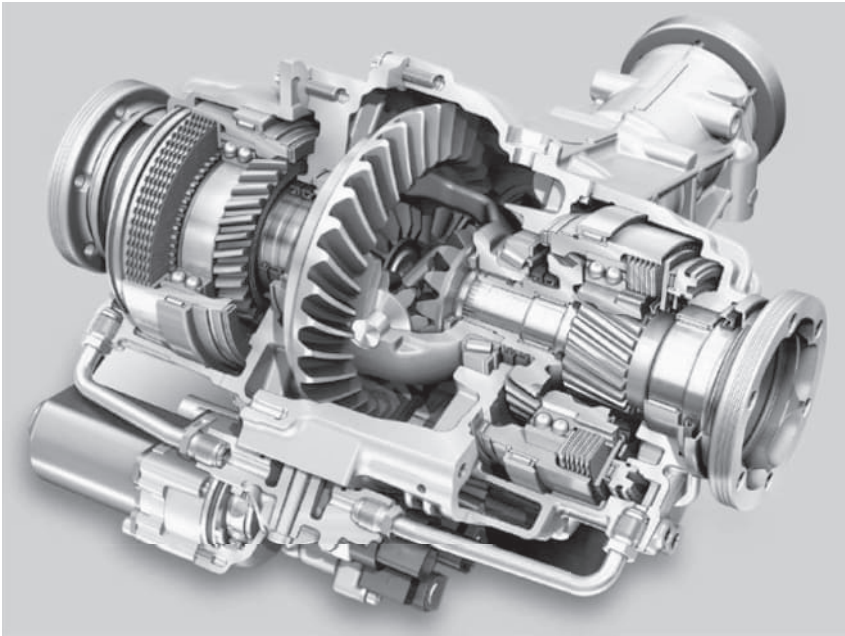


**FIGURE 14.2** Crossed-axes gear-set in the design of automobile differential.

The variety of all possible kinds of gear vector diagrams of crossed-axes gear pairs are limited to the total number of possible combinations of the rotation vectors,  $\omega_g$  and  $\omega_p$ , (a) of various magnitudes and (b) of various values of the shaft angle,  $\Sigma$  [reminder: the shaft angle,  $\Sigma$ , is specified as the angle formed by a rotation vector,  $\omega_g$ , of a gear and a rotation vector,  $\omega_p$ , of a mating pinion, that is,  $\Sigma = \angle(\omega_g, \omega_p)$ ].

The total number of gear vector diagrams of crossed-axes gear pairs of different kinds is limited just to three diagrams when the actual configuration of the rotation vectors,  $\omega_g$  and  $\omega_p$ , of a gear and of a mating pinion in relation to the vector of instantaneous rotation,  $\omega_{pl}$ , is taken into account. These gear vector diagrams are depicted in Figure 14.3. Therefore, crossed-axes gear pairs only of three different types are possible.

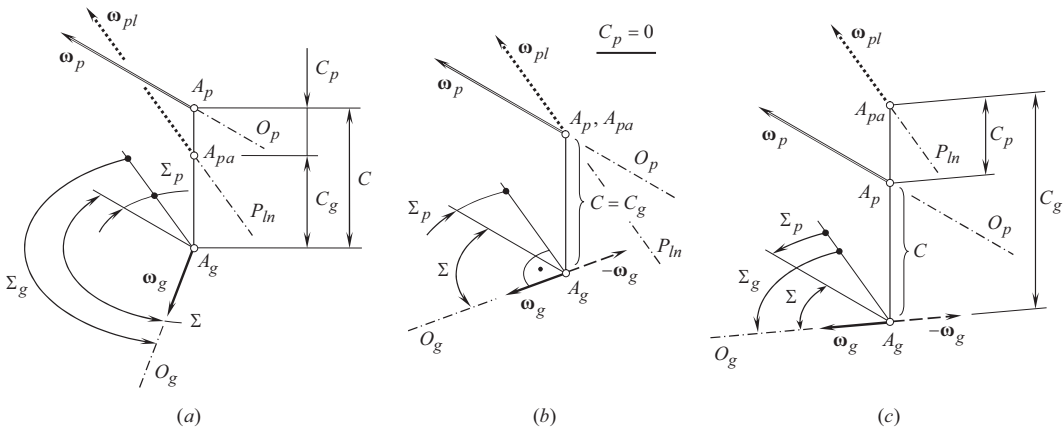


**FIGURE 14.3** The total number of possible kinds of gear vector diagrams for crossed-axes gear pairs is limited just to three diagrams: (a) for internal, (b) for rack-type, and (c) for external gear pairs.

The gear vector diagram shown in Figure 14.3a features an obtuse gear angle,  $\Sigma_g$ , between the rotation vector,  $\omega_g$ , of the gear, and the vector of instantaneous rotation,  $\omega_{pl}$ . The gear angle,  $\Sigma_g$ , can be expressed in terms of the shaft angle,  $\Sigma$ , and of the magnitudes,  $\omega_g$  and  $\omega_p$ , of the rotation vectors,  $\omega_g$  and  $\omega_p$ :

$$\Sigma_g = \tan^{-1} \left( \frac{\sin \Sigma}{\omega_p / \omega_g + \cos \Sigma} \right) \quad (14.1)$$

For a shaft angle of  $90^\circ$ , Eq. (14.1) reduces to:

$$\Sigma_g = \tan^{-1} \left( \frac{\omega_g}{\omega_p} \right) \quad (14.2)$$

The formulae for the calculation of the pinion angle,  $\Sigma_p$ , are similar to Eqs. (14.1) and (14.2):

$$\Sigma_p = \tan^{-1} \left( \frac{\sin \Sigma}{\omega_g / \omega_p + \cos \Sigma} \right) \quad (14.3)$$

and for a right shaft angle reduces to:

$$\Sigma_p = \tan^{-1} \left( \frac{\omega_p}{\omega_g} \right) \quad (14.4)$$

For a gear pair of this particular type (when  $\Sigma > 90^\circ$ ), the relation  $\Sigma_g = \angle(\omega_g, \omega_{pl}) > 90^\circ$  is valid. This relation can be represented in an equivalent form as:

$$\omega_g \cdot (\omega_p - \omega_g) < 0 \quad (14.5)$$

or as:

$$\frac{\omega_g \cdot (\omega_p - \omega_g)}{|\omega_g| \cdot |\omega_p - \omega_g|} = -1 \quad (14.6)$$

The center-distance,  $C$ , can be interpreted as summa of the gear center-distance,  $C_g$ , and the pinion center-distance,  $C_p$  (see Figure 14.4):

$$C = C_g + C_p \quad (14.7)$$

The gear pair center-distance,  $C$ , is the closest distance of approach of the gear axis of rotation,  $O_g$ , and the pinion axis of rotation,  $O_p$  (i.e.,  $O_g/O_p$ ); the gear center-distance,  $C_g$ , is the closest distance of approach of the gear axis of rotation,  $O_g$ , and the axis of instantaneous rotation,  $P_{ln}$  (i.e.,  $O_g/P_{ln}$ ); the pinion center-distance,  $C_p$ , is the closest distance of approach of the pinion axis of rotation,  $O_p$ , and the axis of instantaneous rotation,  $P_{ln}$  (i.e.,  $O_p/P_{ln}$ ).

In external crossed-axes gearing of all kinds, both the center-distances,  $C_g$  and  $C_p$ , are of positive values (i.e.,  $C_g > 0$ ,  $C_p > 0$ ).

The earlier-derived formulas [see Eqs. (2.61) and (2.62)]:

$$C_g = \frac{1 + \omega_p - \omega_g}{1 + \omega_p} \cdot C \quad (14.8)$$

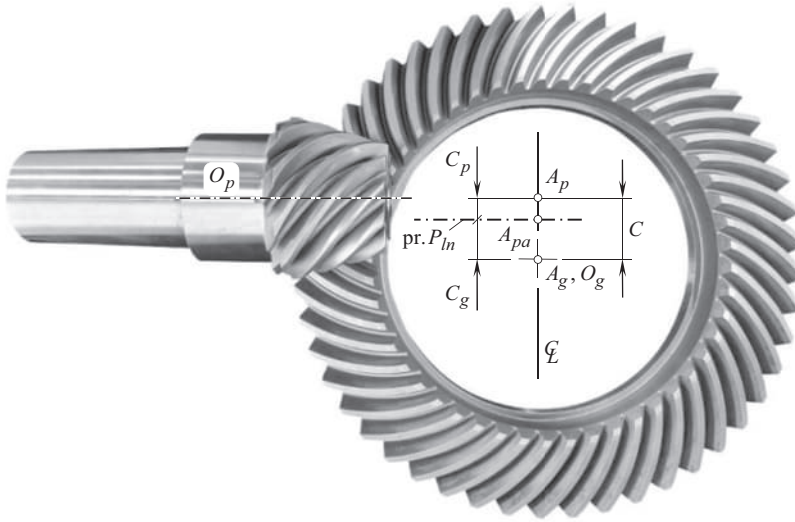


**FIGURE 14.4** The gear center-distance,  $C_g$ , the pinion center-distance,  $C_p$ , and the gear pair center-distance,  $C$ , in crossed-axes gearing.

$$C_p = \frac{1 + \omega_g - \omega_p}{1 + \omega_g} \cdot C \quad (14.9)$$

can be used for the calculation of the actual values of the center-distances,  $C_g$  and  $C_p$ , of the gear and of the mating pinion, correspondingly.

The gear ratio,  $u$ , in  $C_a$  – gearing can be expressed either in terms of the cone angles,  $\Sigma_g$  and  $\Sigma_p$ , or in terms of the distances,  $C_g$  and  $C_p$ . In this second case, consider an equality of the ratio  $C_g/C_p$  NOT to the ratio  $\omega_p/\omega_g$ , instead, to the ratio of projections of the rotation vectors,  $\omega_g$  and  $\omega_p$ , onto the pitch-line plane ( $P_{ln}$  – plane), – the plane through the centerline,  $\mathfrak{L}$ , and through the vector of instantaneous rotation,  $\omega_{pl}$ :  $C_g/C_p = |pr.\omega_p|/|pr.\omega_g|$ , or:

$$\frac{C_g}{C_p} = \frac{|\omega_p| \cdot \cos \Sigma_p}{|\omega_g| \cdot \cos \Sigma_g} \quad (14.10)$$

The gear vector diagram (see Figure 14.3a) corresponds to external crossed-axes gearing.

The configuration of rotation vector of a gear,  $\omega_g$ , in relation to the vector of instantaneous rotation,  $\omega_{pl}$ , is critical for the determination of whether or not a gear pair is external, while the relative configuration of the rotation vectors,  $\omega_g$  and  $\omega_p$ , is of secondary importance in this regard.

In a particular case, rotation vector of the gear,  $\omega_g$ , can be pointed orthogonal to the vector of instantaneous rotation,  $\omega_{pl}$ . In this case, an inequality is,  $\Sigma_g = \angle(\omega_g, \omega_{pl}) = 90^\circ$  is valid. Two equivalent forms of this property of crossed-axes gear-set:

$$\omega_g \cdot (\omega_p - \omega_g) = 0 \quad (14.11)$$

and

$$\frac{\omega_g \cdot (\omega_p - \omega_g)}{|\omega_g| \cdot |\omega_p - \omega_g|} = 1 \quad (14.12)$$

**TABLE 14.1**  
**Analytical Criteria of Kind of Crossed-Axes Gearing**

Kind of Intersected-Axes Gearing	Analytical Criterion [ $C \neq 0$ , and $\Sigma \neq 0$ ]
External crossed-axes gear pair	$\omega_g \cdot (\omega_p - \omega_g) < 0$
Rack-type crossed-axes gear pair	$\omega_g \cdot (\omega_p - \omega_g) = 0$
Internal crossed-axes gear pair	$\omega_g \cdot (\omega_p - \omega_g) > 0$

are valid.<sup>1</sup>

Crossed-axes gear pairs for which the condition  $\omega_g \perp \omega_{pl}$  is fulfilled, feature the center-distances,  $C_g$  and  $C_p$ , of the values:  $C_g = 0$ , and  $C_p = C$ , correspondingly (the equality  $C = C_g + C_p$  is still valid).

The gear vector diagram for gear drives of this particular kind is schematically depicted in Figure 14.3b. The gear vector diagram that corresponds to a crossed-axes gear pair is composed of a round rack (or of a face gear, in other words) and a conical pinion. Crossed-axes gearing of this design resembles the aforementioned *pinion-to-rack gearing* in the case of the parallel axes of the gear and the mating pinion.

Ultimately, a crossed-axes gear pair may feature an acute gear angle,  $\Sigma_g$ , between the rotation vector,  $\omega_g$ , of the gear and the vector of instantaneous rotation,  $\omega_{pl}$  (see Figure 14.3c). For this particular kind of gear pair, the inequality  $\Sigma_g = \angle(\omega_g, \omega_{pl}) < 90^\circ$  is valid. The latter expression can be represented in the following two forms:

$$\omega_g \cdot (\omega_p - \omega_g) > 0 \quad (14.13)$$

and

$$\frac{\omega_g \cdot (\omega_p - \omega_g)}{|\omega_g| \cdot |\omega_p - \omega_g|} = +1 \quad (14.14)$$

Crossed-axes gear pairs for which the condition  $\omega_g \perp \omega_{pl}$  is fulfilled, feature the center-distances,  $C_g$  and  $C_p$ , of the values  $C_g < 0$ , and  $C_p > 0$  (the equality  $C = C_g + C_p$  is still valid).

A gear vector diagram of the kind (see Figure 14.3c) corresponds to internal crossed-axes gearing.

The analytically expressed conditions [see Eqs. (14.5)–(14.11)] along with Eq. (14.13) are summarized in Table 14.1.

Any and all crossed-axes gear pairs meet one of three expressions listed in Table 14.1.

In particular cases, the centerlines of the driving shaft and of the driven shaft cross each other at a right angle (namely,  $\Sigma = 90^\circ$ ). This particular case is the most common in practice. Crossed-axes gear pairs of this kind are referred to as *orthogonal crossed-axes gear pairs*. For gearing of this particular kind, cross product of rotation vectors of the gear,  $\omega_g$ , and the pinion,  $\omega_p$ , is always equal to zero ( $\omega_g \times \omega_p = 0$ ).

An orthogonal crossed-axes gear pair may feature the tooth count of the gear,  $N_g$ , and the pinion,  $N_p$ , equal to one another (i.e.,  $N_g = N_p$ ). Crossed-axes gearing of this particular kind fulfills the requirement  $\omega_g \times \omega_p = 0$ . It is evident that the magnitudes,  $\omega_g$  and  $\omega_p$ , of the rotation vectors,  $\omega_g$  and  $\omega_p$ , in this case, are equal ( $\omega_g = \omega_p$ ). Gears of this particular kind resemble *miter gears*, which are a kind of orthogonal intersected-axes gearing with  $\omega_g = \omega_p$ .

<sup>1</sup> While a rotation vector,  $\omega_g$ , can be perpendicular to the vector of instantaneous rotation,  $\omega_{pl} = (\omega_p - \omega_g)$ , the perpendicularity of a rotation vector of the pinion,  $\omega_p$ , to the vector of instantaneous rotation,  $\omega_{pl}$ , is not considered here, as the magnitude,  $\omega_p$ , of the rotation vector,  $\omega_p$ , is smaller compared to the magnitude,  $\omega_g$ , of the rotation vector,  $\omega_g$ , that is, the inequality,  $\omega_p < \omega_g$ , is always observed. A reduced gear vector diagram ( $\omega_p = \omega_g$ ) can also be incorporated into this discussion.



## 14.2 PRESSURE ANGLE IN CROSSED-AXES GEARING

Pressure angle is an important design parameter in gearing of all kinds, and in crossed-axes gearing, in particular. The performance of a crossed-axes gear-set strongly depends on the actual value of the transverse pressure angle. Accurate specification of the transverse pressure angle is vital when designing crossed-axes gear-sets. This problem becomes even more vital in high power density gear transmissions.

### 14.2.1 CROSSED-AXES GEARING WITH TRANSVERSE PRESSURE ANGLE OF A CONSTANT VALUE

Crossed-axes gear pairs feature a transverse section that is shaped in the form of a sphere centered at the plane-of-action apex,  $A_{pa}$ . Transverse pressure angle,  $\phi_{t,\omega}$ , is specified in the following way.

**First**, a plane,  $C_{ln}^*$ , through point of interest,  $m$ , parallel to the centerline plane,  $C_{ln}$ , is constructed as illustrated in Figure 14.5. Point of interest,  $m$ , is situated within the portion of the axis of instantaneous rotation,  $P_{ln}$ , that is located within the face width,  $F_{ap}$ . The plane,  $C_{ln}^*$ , intersects the axis of rotation of the gear,  $O_g$ , and that,  $O_p$ , of the mating pinion at points,  $a$  and  $b$ . The straight line  $ab$  is entirely located within the plane,  $C_{ln}^*$ .

**Second**, a straight line through point,  $m$ , perpendicular to the straight-line segment,  $ab$ , is constructed. This perpendicular is located within the plane,  $C_{ln}^*$ .

The actual value of the transverse pressure angle,  $\phi_{t,\omega}$ , is measured within the plane,  $C_{ln}^*$ , between the aforementioned perpendicular, and between the pitch-line plane as shown in Figure 14.5. Note, that the pitch-line plane, and the plane of action,  $PA$ , are congruent to one another (i.e.,  $P_{ln} - \text{plane} \equiv \text{plane of action, } PA$ ).

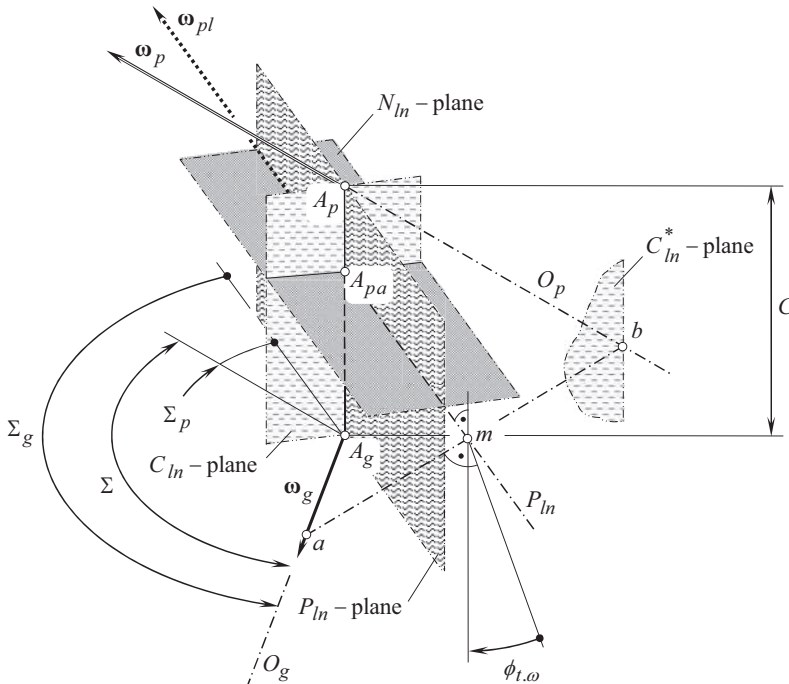


FIGURE 14.5 Transverse pressure angle,  $\phi_{t,\omega}$ , in crossed-axes gear pair.

### 14.2.2 CROSSED-AXES GEARING WITH TRANSVERSE PRESSURE ANGLE OF A VARIABLE VALUE

When the actual value of the transverse pressure angle,  $\phi_{t,\omega}$ , alters within the effective face width,  $F_{pa}$ , the *path-of-contact surface*, *PCS*. The path-of-contact surface can be viewed as a continuous set of the circular-arc paths of contact,  $P_c$ , at different transverse pressure angle,  $\phi_{t,\omega}$ . The radius of a current circular-arc path of contact is a *linear* function of the distance of point of interest within the axis of instantaneous rotation,  $P_{ln}$ , from the plane-of-action-apex,  $A_{pa}$ . The path-of-contact surface, *PCS*, is a continuous screw surface generated by the circular arcs of different radii.

As the inclination of the straight-line segment,  $ab$ , depends on the position of point of interest,  $m$ , the actual value of the transverse pressure angle,  $\phi_{t,\omega}$ , varies along the axis of instantaneous rotation,  $P_{ln}$ . For gears with a large tooth count this variation is negligibly small (the larger the tooth count of the gear, the smaller the variation of the transverse pressure angle,  $\phi_{t,\omega}$ , and vice versa). For gears with a low tooth count (*LTC* – gears), this variation can be significant and is not permissible to be ignored.

However, the entire tooth flank of a gear,  $\mathcal{G}$ , and that of a mating pinion,  $\mathcal{P}$ , in both cases are constructed from the corresponding base cones with constant base cone angles,  $\Gamma_b$  and  $\gamma_b$ . This means that despite the transverse pressure angle,  $\phi_{t,\omega}$ , varies within the face width of the gear-set, the gear ratio is remained of a constant value.

The formulated above set of three fundamental laws of gearing is helpful to realize a possibility of  $C_a$  – gearing with a variable within the active portion of the face width,  $F_{pa}$ , transverse pressure angle,  $\phi_{t,\omega} = \text{var}$ . The possibility of variation of the transverse pressure angle,  $\phi_{t,\omega}$ , is necessary when solving the problem of synthesizing a crossed-axes gear pair with favorable design parameters, that is, of a crossed-axes gear pair with the best attainable performance.

The plane of action,  $PA$ , can be subdivided onto an infinite number of infinitesimally narrow,  $dr_{pa}$ , round strips. The distance between points,  $m_{i-1}$ , and  $m_i$ , as well as that between points,  $m_i$  and  $m_{i+1}$ , equals to  $dr_{pa}$ , as illustrated in Figure 14.6. All the strips are through the axis of instantaneous

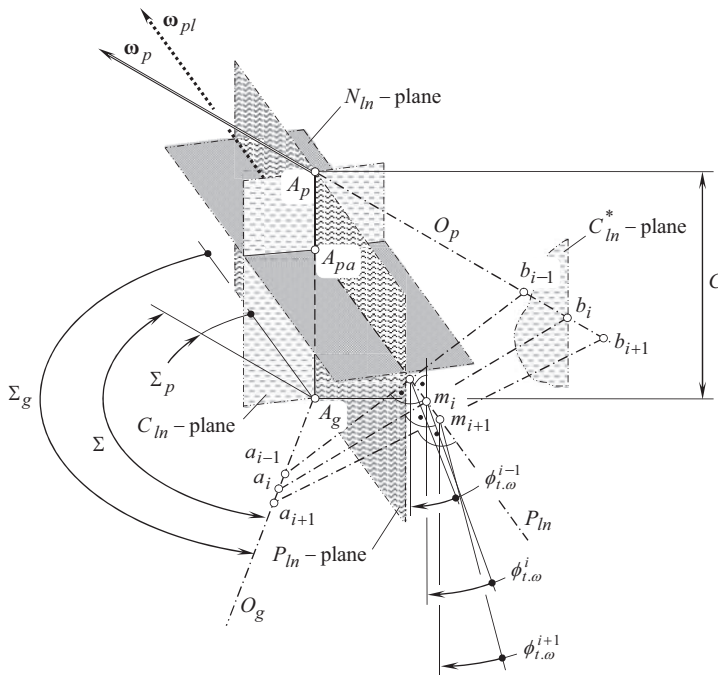


**FIGURE 14.6** Transverse pressure angles,  $\phi_{t,\omega}$ , of various values,  $\phi_{t,\omega}^{i-1}$ ,  $\phi_{t,\omega}^i$ , and  $\phi_{t,\omega}^{i+1}$ , in crossed-axes gear pair.

rotation,  $P_{ln}$ . The transverse pressure angle,  $\phi_{t,\omega}$ , can be set of a favorable value for each of the strips, that is, in this way the transverse pressure angle,  $\phi_{t,\omega}$ , is involved in the synthesizing process of the favorable gear pair. In this scenario, the plane of action,  $PA$ , is replaced by the family of narrow strips, that form a surface of action,  $SA$ . The surface of action,  $SA$ , is a kind of ruled surfaces each straight line of which is a straight line through the axes of instantaneous rotation,  $P_{ln}$ . At every point of the surfaces of action,  $SA$ , the transverse pressure angle,  $\phi_{t,\omega}$ , can be set to the most favorable value.

In this case, the entire tooth flank of a gear,  $\mathcal{S}$ , and that of a mating pinion,  $\mathcal{P}$ , are constructed from an infinite number of base cones with different base cone angles,  $\Gamma_b$  and  $\gamma_b$ , in each round strip of the surface of action,  $SA$ .

Gears with a variable pressure angle,  $\phi_{t,\omega}$ , can be cut on a multi-axis NC machine.

### 14.3 BASE CONES IN CROSSED-AXES GEAR PAIR

Geometrically accurate crossed-axes gear pairs are capable of transmitting a rotary motion smoothly. For gearing of this kind, the angular velocity ratio is of a constant value,  $\omega_p/\omega_g = \text{const}$ . From this perspective, geometrically accurate crossed-axes gear pairs resemble the earlier discussed geometrically accurate parallel-axes gear pairs and geometrically accurate crossed-axes gear pairs. This similarity can be extended further, namely, crossed-axes gearing of an appropriate design can also transmit a uniform rotation from a driving shaft to a driven shaft.

It should be noted here that in crossed-axes of rotation,  $O_g$  and  $O_p$ , of the driving shaft and the driven shaft, there is no freedom in choosing a configuration of the axis of instantaneous rotation,  $P_{ln}$ , in relation to the rotation vectors  $\omega_g$  and  $\omega_p$ . Once the rotation vectors,  $\omega_g$  and  $\omega_p$ , and their configuration relative to one another are specified, the actual configuration of the axis of instantaneous rotation,  $P_{ln}$ , can be expressed in terms of the rotations  $\omega_g$  and  $\omega_p$ , and of the center-distance,  $C$ .

Recall that geometrically accurate parallel-axes gear pairs feature two base cylinders (see Figure 10.37). Smooth rotation of the base cylinders allows for interpretation of parallel-axes gear-set as a corresponding *equivalent pulley-and-belt transmission*. Then, two base cones are associated with a gear and with a mating pinion in intersected-axes gearing (see Figure 12.12). Smooth rotation of the base cones can be viewed as an *equivalent pulley-and-belt transmission* with the belt in the form of a round belt. The concept of the *equivalent pulley-and-belt transmission* can be enhanced further to geometrically accurate crossed-axes gearing. For the first time ever, the concept of the *equivalent pulley-and-belt transmission* in crossed-axes gearing was proposed (~2008) by Prof. S.P. Radzevich [174]. Two base cones in tangency with the plane of action were considered here [174].

A base is associated with a gear, and another base cone is associated with a mating pinion of any and all crossed-axes gear pairs. This concept is schematically illustrated in Figure 14.7. The axis of rotation of the gear,  $O_g$ , and the axis of rotation of the mating pinion,  $O_p$ , cross each other at a shaft angle,  $\Sigma$ . The closest distance of approach of the axes of rotations,  $O_g$  and  $O_p$ , is denoted by  $C$ . An orthogonal crossed-axes gear pair is shown here solely for illustrative purposes. Without going into details of the analysis, it should be stated here that that same approach is applicable with respect to angular bevel gears those with a shaft angle  $\Sigma \neq 90^\circ$ , namely, either obtuse or acute shaft angle  $\Sigma$ .

The schematic shown in Figure 14.7 is constructed on the premise of the rotation vectors,  $\omega_g$  and  $\omega_p$ , of a gear and of a mating pinion. The gear and the pinion rotate about their axes,  $O_g$  and  $O_p$ , correspondingly. The rotation vectors,  $\omega_g$  and  $\omega_p$ , allow for the construction of the vector,  $\omega_{pl}$ , of instantaneous rotation. The rotation vector,  $\omega_{pl}$ , meets the requirement  $\omega_{pl} = \omega_p - \omega_g$ . The axis of instantaneous rotation,  $P_{ln}$ , is aligned with the vector of instantaneous rotation,  $\omega_{pl}$ .

The vector of instantaneous rotation,  $\omega_{pl}$ , is the vector through the plane-of-action apex,  $A_{pa}$ . The latter is located within the centerline,  $\mathfrak{L}$ . Points of intersection of the centerline,  $\mathfrak{L}$ , by the axes of rotations,  $O_g$  and  $O_p$ , are labeled as  $A_g$  and  $A_p$ . The point  $A_g$  is the point of intersection of the

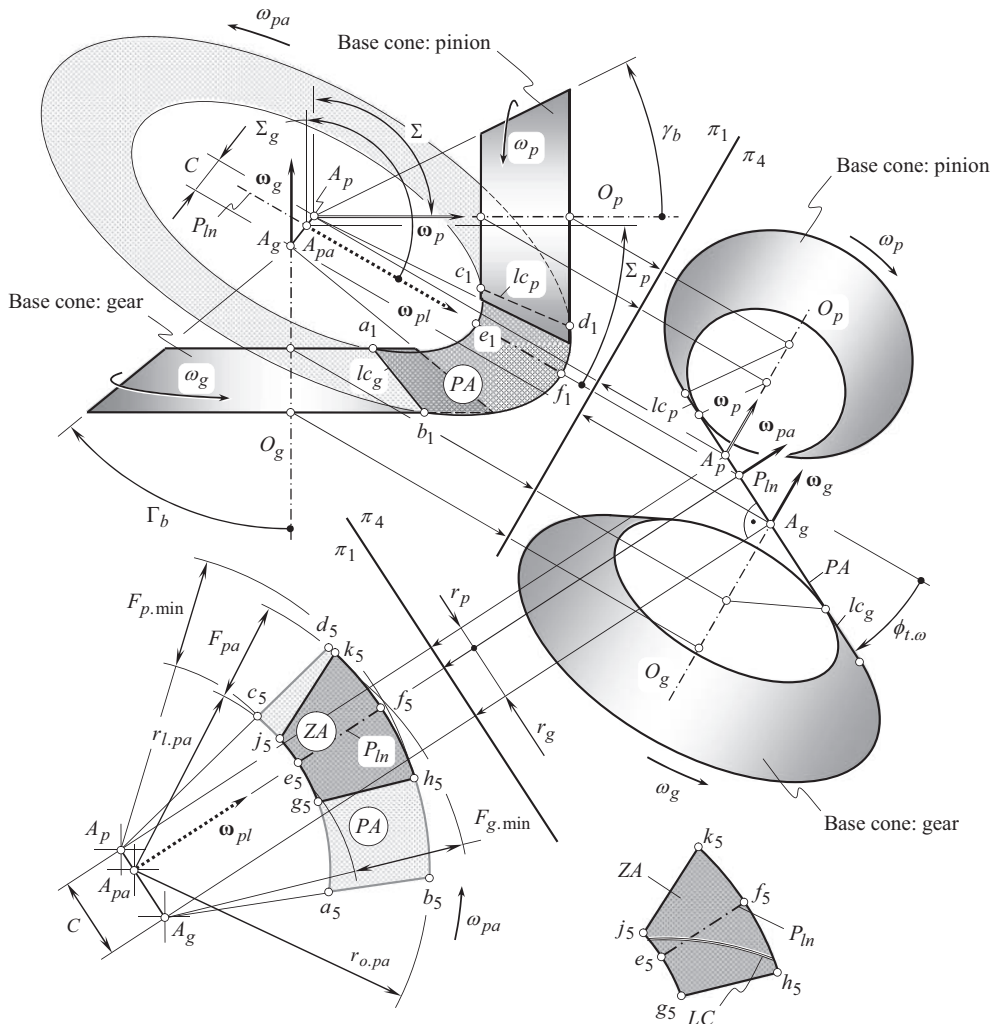


**FIGURE 14.7** The base cones, the plane of action, PA, and the zone of action, ZA, in orthogonal crossed-axes gear pair.

centerline,  $\mathfrak{L}$ , and the gear axis of rotation,  $O_g$ . The point  $A_p$ , is the point of intersection of the centerline,  $\mathfrak{L}$ , and the pinion axis of rotation,  $O_p$ .

The point  $A_{pa}$  is at a gear center-distance,  $C_g$ , from the axis of rotation,  $O_g$ , of the gear. At that same time, the point  $A_{pa}$  is at a pinion center-distance,  $C_p$ , from the axis of rotation,  $O_p$ , of the pinion. The following expression:

$$C_g + C_p = C \quad (14.15)$$

is valid. Here, in Eq. (14.15), the distances  $C_g$  and  $C_p$  are signed values. The distances  $C_g$  and  $C_p$  are of positive values ( $C_g > 0$ ,  $C_p > 0$ ) when point,  $A_{pa}$ , is located within the center-distance,  $C$ . When point,  $A_{pa}$ , is located outside the center-distance,  $C$ , the gear center-distance,  $C_g$ , is of a negative value ( $C_g < 0$ ), while the pinion center-distance,  $C_p$ , remains of a positive value ( $C_p > 0$ ).

Use of Eq. (2.21):

$$\frac{C_g}{C_p} = \frac{\omega_p^{rl}}{\omega_g^{rl}} \quad (14.16)$$

makes possible to calculate the distances,  $C_g$  and  $C_p$  [see Eqs. (2.62) and (2.63)]:

$$C_g = \frac{1 + \omega_p - \omega_g}{1 + \omega_p} \cdot C \quad (14.17)$$

and

$$C_p = \frac{1 + \omega_g - \omega_p}{1 + \omega_g} \cdot C \quad (14.18)$$

For a pair of rotation vectors,  $\omega_g$  and  $\omega_p$ , the ratio  $\tan \Sigma_g / \tan \Sigma_p$  is calculated [see Eq. (2.34)] from the formula<sup>2</sup>:

$$\frac{C_p}{C_g} = \frac{\tan \Sigma_g}{\tan \Sigma_p} \quad (14.19)$$

The plane of action,  $PA$ , is a plane through the axis of instantaneous rotation,  $P_{ln}$ . The plane of action,  $PA$ , is in tangency with both base cones, namely, with the base cone of a gear, and with the base cone of a mating pinion. Due to that, the plane of action,  $PA$ , forms a certain transverse pressure angle,  $\phi_{t,\omega}$ , in relation to a perpendicular to a plane associated with the axis of instantaneous rotation,  $P_{ln}$ . The perpendicular is constructed to the plane that passes through the vector of instantaneous rotation,  $\omega_{pl}$ , and through the centerline,  $\mathfrak{L}$ . The pressure angle,  $\phi_{t,\omega}$ , is measured within a plane that is perpendicular to the axis of instantaneous rotation,  $P_{ln}$ .

The portion of the schematic plotted in the left upper corner in Figure 14.7 is constructed within the plane of projections,  $\pi_1$ . Two other planes of projections,  $\pi_2$  and  $\pi_3$ , of the standard set of planes of projections,  $\pi_1\pi_2\pi_3$ , are not used in this particular analysis. Therefore, these planes,  $\pi_2$  and  $\pi_3$ , are not shown in Figure 14.7. Instead, two auxiliary planes of projections, namely, the planes of projections,  $\pi_4$  and  $\pi_5$ , are used. The axis of projections,  $\pi_1/\pi_4$ , is constructed so as to be perpendicular to the axis of instantaneous rotation,  $P_{ln}$ . The axis of projections,  $\pi_4/\pi_5$ , is constructed so as to be parallel to the trace of the plane of action,  $PA$ , within the plane of projections,  $\pi_4$ . The plane of action,  $PA$ , is projected with no distortions onto the plane of projections  $\pi_4$ .

The plane of action can be viewed as a flexible zero thickness film. The film is free to wrap onto or unwrap from the base cones of a gear and of a mating pinion. The plane of action,  $PA$ , is not allowed to be bent about an axis perpendicular to the plane,  $PA$ , itself. Under a uniform rotation of the gears, the plane of action,  $PA$ , spins about the axis,  $O_{pa}$ . The rotation vector,  $\omega_{pa}$ , is pointed along the axis,  $O_{pa}$ .

As the axis of instantaneous rotation,  $P_{ln}$ , and the axes of rotation of the gear,  $O_g$ , and of the pinion,  $O_p$ , cross one another. No pure rolling of the base cones of the gear, and of the mating pinion over the plane of action,  $PA$ , is observed, but rolling together with sliding of the  $PA$  over the base cones is observed instead.

In crossed-axes gearing, the plane of action,  $PA$ , can be viewed as a round cone that has a cone angle of  $90^\circ$ . As the  $\sin 90^\circ = 1$ , the magnitude,  $\omega_{pa}$ , of the rotation vector,  $\omega_{pa}$ , is calculated from the formula:

<sup>2</sup> Note that the center-distances,  $C_g$  and  $C_p$ , are measured along the center-line,  $\mathfrak{L}$ , and not in two different planes perpendicular to the axes of rotation,  $O_g$  and  $O_p$ , of a gear and of a mating pinion.

$$\omega_{pa} = \frac{\omega_g}{\sin \Gamma_b} = \frac{\omega_p}{\sin \gamma_b} \quad (14.20)$$

where

$\omega_g$  is the angular velocity of rotation of the gear.

$\omega_p$  is the angular velocity of rotation of the pinion.

$\Gamma_b$  is the base cone angle of the gear.

$\gamma_b$  is the base cone angle of the pinion.

Equation (14.20) yields a formula for the angular velocity ratio,  $u$ , in crossed-axes gearing:

$$u = \frac{\omega_p}{\omega_g} = \frac{\sin \gamma_b}{\sin \Gamma_b} = \frac{C_g}{C_p} \quad (14.21)$$

In crossed-axes gear pairs, actual values of the base cone angles,  $\Gamma_b$  and  $\gamma_b$ , fall into the ranges of  $0^\circ < \Gamma_b < 180^\circ$  and  $0^\circ < \gamma_b < (180^\circ - \Gamma_b)$ , correspondingly. Thus, all the equations here and below are valid for:

1. external crossed-axes gear pairs
2. rack-type crossed-axes gear pairs, and
3. internal crossed-axes gear pairs.

Formally, the base cone angles,  $\Gamma_b$  and  $\gamma_b$ , can be considered in the narrower intervals, namely, within the intervals  $0^\circ < \Gamma_b < 90^\circ$  and  $0^\circ < \gamma_b < 90^\circ$ , correspondingly. Under such a scenario, the following three inequalities are valid for different types of crossed-axes gear pairs:

1. The base cone angles are of positive values ( $\Gamma_b > 0^\circ$  and  $\gamma_b > 0^\circ$ ) in external gearing
2. The base cone angle of the gear is equal to a right angle ( $\Gamma_b = 90^\circ$ , while  $\gamma_b > 0^\circ$ ) for rack-type gear pairs
3. The base cone angle of the gear is of a negative value ( $\Gamma_b < 0^\circ$ , while  $\gamma_b > 0^\circ$ ) in internal crossed-axes gearing

A desirable working portion, or, in other words, *functional portion of the plane of action*,  $PA$ , can be constructed in the following way.

Consider a straight-line segment,  $ef$ , within the axis of instantaneous rotation,  $P_{in}$  (see Figure 14.7). When the gears rotate, the straight-line segment,  $ef$ , travels together with the plane of action,  $PA$ . Point,  $f$ , traces a circular arc of a radius,  $r_{o,pa}$ , while point,  $e$ , traces a circular arc of a radius,  $r_{l,pa}$ . The face width of the plane of action,  $F_{pa}$ , or, in other words, working (functional) portion of the plane of action, is located in between two circles of the radii,  $r_{o,pa}$  and  $r_{l,pa}$ . In order to have the desirable face width of the plane of action,  $F_{pa}$ , the face width of the gear,  $F_g$ , and the face width of the pinion,  $F_p$ , should be of larger values, as shown in Figure 14.7. The appropriate radii of the outer circles,  $r_{o,g}$  and  $r_{o,p}$ , as well as of the inner circles,  $r_{l,g}$  and  $r_{l,p}$ , have to be of values under which both, the face width of the gear,  $F_g$ , and the face width of the pinion,  $F_p$ , overlap the face width,  $F_{pa}$  (the radii,  $r_{o,g}$ ,  $r_{o,p}$ ,  $r_{l,g}$ , and  $r_{l,p}$ , are not labeled in Figure 14.7 because of lack of space). The radii,  $r_{o,g}$  and  $r_{l,g}$ , are centered at the gear apex,  $A_g$ , while the radii,  $r_{o,p}$  and  $r_{l,p}$ , are centered at the pinion apex  $A_p$ . The inequalities,  $F_g > F_{pa}$ , and  $F_p > F_{pa}$ , are always valid because the apexes,  $A_g$  and  $A_p$ , are not coincident to one another, and, thus, sliding in the direction of the axis of instantaneous rotation,  $P_{in}$ , is inevitable in crossed-axes gearing.

The straight-line segments,  $lc_g$  and  $lc_p$ , are pointed along the corresponding lines of contact between the plane of action,  $PA$ , and between the base cones of the gear and of the mating pinion.



The line segments,  $gh$  and  $lk$ , are the lines of intersection of the plane of action,  $PA$ , by the outer cones of the gear and that of the mating pinion. The zone of action,  $ZA$ , is bounded by the two circular arcs,  $hk$  and  $gj$ , and by the two straight line segments,  $hg$  and  $kj$ .

When the gears rotate, the entire effective face width of the gear pair,  $F_{pa}$ , has to be overlapped by the gear face width,  $F_g$ , and by the pinion face width,  $F_p$ . Therefore, the minimal gear face width,  $F_{g,min}$ , equals to the difference between the gear radii,  $r_{o,g}$  and  $r_{l,g}$ , that are centered at the gear apex,  $A_g$  (i.e.,  $F_{g,min} = r_{o,g} - r_{l,g}$ ). Similarly, the minimal pinion face width,  $F_{p,min}$ , equals to the difference between the gear radii,  $r_{o,p}$  and  $r_{l,p}$ , that are centered at the pinion apex,  $A_p$  (i.e.,  $F_{p,min} = r_{o,p} - r_{l,p}$ ).

A crossed-axes gear-set with associated base cones of the gear and of the mating pinion, and the plane of action,  $PA$ , is shown in Figure 14.8.

In reality, crossed-axes gear pairs can be composed of a gear and of a mating pinion with tooth flank geometry, for which base cones cannot be constructed. In such a case, the plane of action,  $PA$ , cannot be constructed, as well. Crossed-axes gear pairs of this kind are referred to as *approximate crossed-axes gear pairs*. No *equivalent pulley-and-belt transmission* can be constructed for approximate crossed-axes gear pairs.

**Conclusion 14.1.** *Geometrically accurate crossed-axes gear pairs are those capable of transmitting smoothly an input uniform rotary motion from a driving shaft to a driven shaft.*

**Conclusion 14.2.** *Approximate crossed-axes gear pairs are those not capable of transmitting smoothly an input uniform rotary motion from a driving shaft to a driven shaft.*

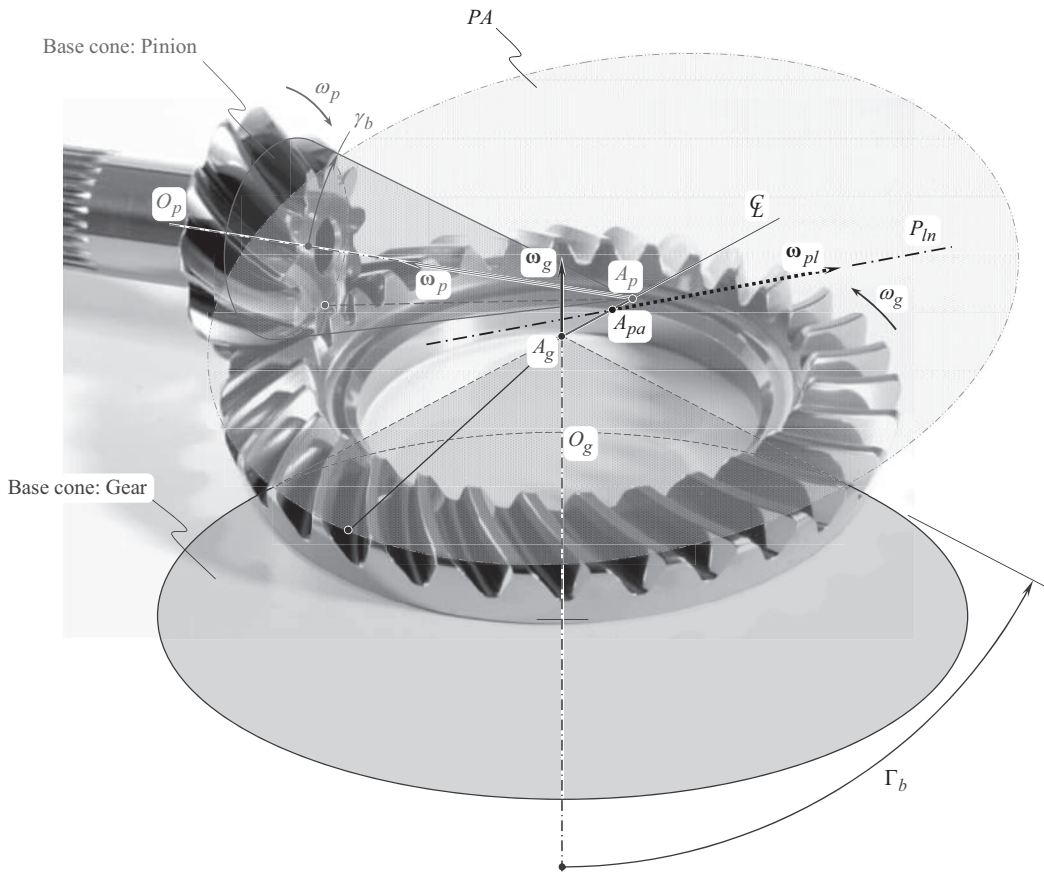


**FIGURE 14.8** Crossed-axes gear-set with associated base cones of the gear, of the mating pinion, and the plane of action,  $PA$ .

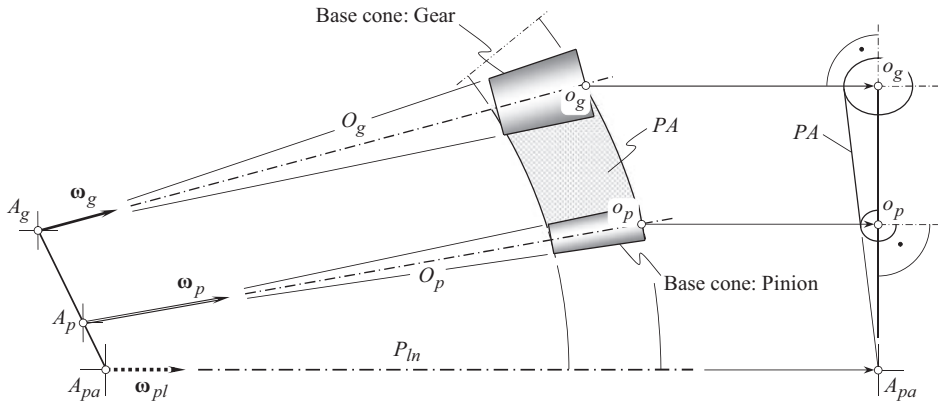


**FIGURE 14.9** Base kinematics of rotationally positive external crossed-axes gear pair: schematic of external gear-to-pinion mesh with a large transverse pressure angle,  $\phi_{\omega.t}$ .

Approximate crossed-axes gear pairs are not capable of transmitting an input rotation smoothly. However, approximate gearing is extensively used in practice, as it is much easier in production. Therefore, approximate crossed-axes gear pairs are used in cases when tolerances for the accuracy of rotation are not tight, that is, they are used in cases of low rotation, reasonable constraints on noise excitation, and so forth.

Similar to the earlier discussed gear pairs with a large transverse pressure angle,  $\phi_{\omega.t}$ :

- a. parallel-axes gear-sets (see Figures 6.8 and 6.10 in Chapter 6) and
- b. intersected-axes gear pairs (see Figure 12.13 in Chapter 12.)

Crossed-axes gear pairs with a large transverse pressure angle,  $\phi_{\omega.t}$ , are also possible. The discussion of gearing of this particular kind is limited here just to stress on the possibility of rotationally positive external intersected-axes gear pair (see Figure 14.9). Gear-sets of this design are not comprehensively investigated yet.

#### 14.4 TOOTH FLANK OF A GEAR IN GEOMETRICALLY ACCURATE CROSSED-AXES GEAR

Conjugate tooth flanks of a gear and of its mating pinion in a crossed-axes gear pair are always in line contact with one another. As the gears rotate, the line of contact travels with respect to:

- a. the gear
- b. the pinion
- c. the gear housing

Tooth flank of a gear,  $\mathcal{G}$ , can be construed as a locus of consecutive positions of the line of contact,  $LC$ , in its motion in relation to a reference system associated with the gear. Similarly, tooth flank of a pinion,  $\mathcal{P}$ , can be viewed as a locus of consecutive positions of that same line of contact,  $LC$ , in its motion in relation to a reference system associated with the pinion. Ultimately, a locus of consecutive positions of that same line of contact,  $LC$ , in its motion in relation to a stationary reference system associated with the gearing housing represents the surface of action. Therefore, once the line of contact is specified, the kinematics of a crossed-axes gearing (see Figure 14.7) can be employed for the derivation of an analytical representation of the tooth flank of a gear,  $\mathcal{G}$ , and of a mating pinion,  $\mathcal{P}$ . For this purpose, several reference systems are required to be introduced.



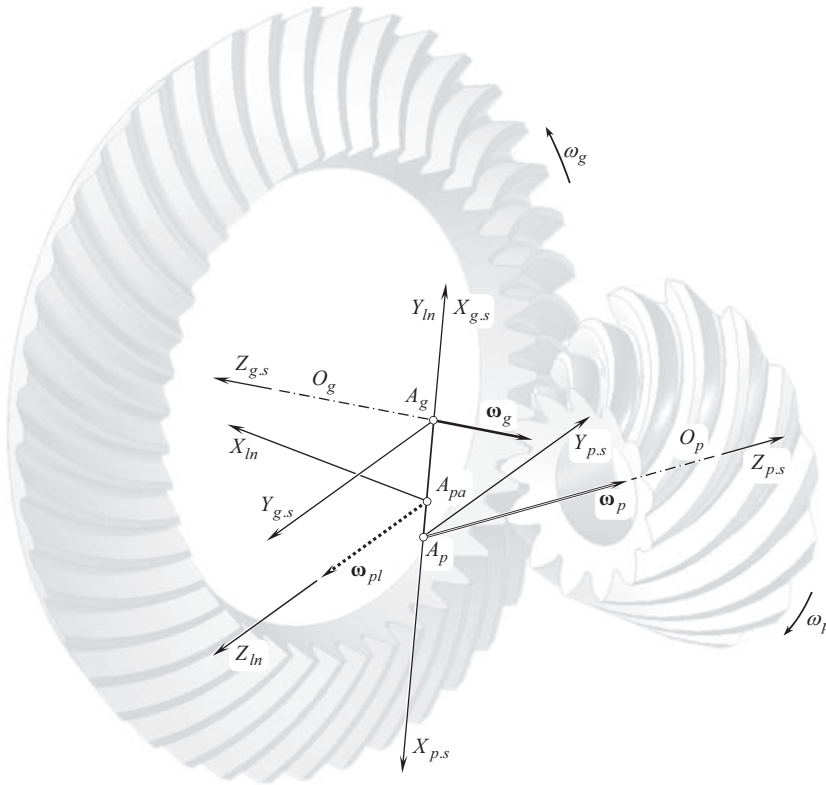


**FIGURE 14.10** A set of stationary reference systems,  $X_h Y_h Z_h$ ,  $X_{g.s} Y_{g.s} Z_{g.s}$ , and  $X_{p.s} Y_{p.s} Z_{p.s}$ , associated with intersected-axes gearing.

#### 14.4.1 APPLIED COORDINATE SYSTEMS AND LINEAR TRANSFORMATIONS

For convenience, several reference systems are introduced. They are associated with the gear, the pinion, the housing, and so forth, as illustrated in Figure 14.10. Here, a motionless reference system,  $X_h Y_h Z_h$ , of the gear pair, and two stationary reference systems,  $X_{g.s} Y_{g.s} Z_{g.s}$  and  $X_{p.s} Y_{p.s} Z_{p.s}$ , of a gear, and of its mating pinion are shown. A few auxiliary coordinate systems are also used when necessary.

##### 14.4.1.1 Main Reference Systems

**First**, a *Cartesian* coordinate system,  $X_g Y_g Z_g$ , is associated with the gear, as shown in Figure 14.11.

**Second**, a *Cartesian* coordinate system,  $X_p Y_p Z_p$ , is associated with the pinion (see Figure 14.11).

**Third**, a *Cartesian* coordinate system,  $X_r Y_r Z_r$ , is associated with the auxiliary round rack, that is engaged in mesh simultaneously with both, namely, with the gear, and with the mating pinion.

**Fourth**, a *Cartesian* coordinate system,  $X_{pa} Y_{pa} Z_{pa}$ , is associated with the plane of action,  $PA$ .

**Fifth**, a stationary *Cartesian* coordinate system,  $X_h Y_h Z_h$ , is associated with the gearing housing. A few more auxiliary reference systems are used below as well.

The origin of the coordinate system,  $X_r Y_r Z_r$ , coincides with the plane-of-action apex,  $A_{pa}$ . The orientation of the coordinate system,  $X_r Y_r Z_r$ , is determined by the rotation vectors,  $\omega_g$ ,  $\omega_p$ , and  $\omega_{pl}$ . The axis  $X_r$  is aligned with the vector,  $\omega_{pl}$ , of instantaneous rotation. The axis  $Y_r$  aligns with the vector defined by the cross product  $\omega_p \times \omega_g$  of the rotation vectors of the gear and of the pinion. Ultimately,

the  $Z_r$  – axis is pointed along the vector that is determined by the triple vector product,  $\boldsymbol{\omega}_p \times \boldsymbol{\omega}_g \times \boldsymbol{\omega}_{pl}$ , of the rotation vectors of the gear, of the pinion, and of the vector of instantaneous rotation.

The coordinate system,  $X_{pa}Y_{pa}Z_{pa}$ , shares the origin with the reference system,  $X_rY_rZ_r$ . The axis,  $X_{pa}$ , is located within the plane of action,  $PA$ , and forms an angle,  $\theta_{pa}$ , with the vector,  $\boldsymbol{\omega}_{pl}$ , of the instantaneous rotation. The  $Y_{pa}$  – axis is also located within the plane of action,  $PA$ , and is perpendicular to the  $X_{pa}$  – axis (here  $\theta_{pa} = \boldsymbol{\omega}_{pa} \cdot t$ , and time is denoted by  $t$ ). Finally, the axis  $Z_{pa}$  complements the axes,  $X_{pa}$  and  $Y_{pa}$ , to the left-hand-oriented *Cartesian* coordinate system,  $X_{pa}Y_{pa}Z_{pa}$ .

It is convenient to specify a line of contact,  $LC$ , between a gear tooth flank,  $\mathcal{G}$ , and a mating pinion tooth flank,  $\mathcal{P}$ , in the coordinate system,  $X_{pa}Y_{pa}Z_{pa}$ , similar to that that has been done with respect to parallel-axes gear pairs (see Figure 6.12 for more details). Then, the current position of the moving line of contact,  $LC$ , represented in the reference systems,  $X_gY_gZ_g$  and  $X_pY_pZ_p$ , will return analytical expressions for the position vectors of points,  $\mathbf{r}_g$  and  $\mathbf{r}_p$ , of tooth flanks,  $\mathcal{G}$  and  $\mathcal{P}$ , of the gear and of the mating pinion, correspondingly. Similarly, the representation of the current position of the moving line of contact,  $LC$ , in the motionless reference system,  $X_hY_hZ_h$ , will return an equation for the position vector of point,  $\mathbf{r}_{sa}$ , for the surface of action in crossed-axes gearing.

#### 14.4.1.2 Operators of Rolling/Sliding

Many similarities between the coordinate system transformations are employed in crossed-axes gearing, and between those used in intersected-axes gearing (see Section 12.4.1).

For the derivation of an equation for the position vector of point,  $\mathbf{r}_g$ , of the gear tooth flank,  $\mathcal{G}$ , an operator,  $\mathbf{Rs}(PA \mapsto \mathcal{G})$ , of the resultant coordinate system transformation is required to be composed. The operator,  $\mathbf{Rs}(PA \mapsto \mathcal{G})$ , can be expressed in terms of the following operators of elementary linear transformations:

1. The operator of rotation,  $\mathbf{Rt}(pa \mapsto pa_0)$ , of the coordinate system,  $X_{pa}Y_{pa}Z_{pa}$ , about the  $Z_{pa}$  – axis through an angle,  $\theta_{pa}$ . When the axis,  $X_{pa}$ , is aligned to the vector of instantaneous rotation,  $\boldsymbol{\omega}_{pl}$ , the reference system,  $X_{pa}Y_{pa}Z_{pa}$ , occupies a particular configuration,  $X_{pa}^0Y_{pa}^0Z_{pa}^0$  (the coordinate system,  $X_{pa}^0Y_{pa}^0Z_{pa}^0$ , is not shown in Figure 14.11). The operator,  $\mathbf{Rt}(pa \mapsto pa_0)$ , can be expressed in matrix form:

$$\mathbf{Rt}(pa \mapsto pa_0) = \begin{bmatrix} \cos\theta_{pa} & 0 & -\sin\theta_{pa} & 0 \\ 0 & 1 & 0 & 0 \\ \sin\theta_{pa} & 0 & \cos\theta_{pa} & 0 \\ 0 & 0 & 0 & 1 \end{bmatrix} \quad (14.22)$$

2. The operator of the translation,  $\mathbf{Tr}(-r_g, Y_g)$ , of the reference system,  $X_{pa}^0Y_{pa}^0Z_{pa}^0$ , at a distance,  $-r_g$ , along the centerline,  $P_{a,g}O_{pa}$ , to a position of the coordinate system,  $X_g^0Y_g^0Z_g^0$ :

$$\mathbf{Tr}(-r_g, Y_g) = \begin{bmatrix} 1 & 0 & 0 & 0 \\ 0 & 1 & 0 & -r_g \\ 0 & 0 & 1 & 0 \\ 0 & 0 & 0 & 1 \end{bmatrix} \quad (14.23)$$

3. The operator of rotation,  $\mathbf{Rt}(pa_0 \mapsto r)$ , of the coordinate system,  $X_g^0Y_g^0Z_g^0$ , about the vector of instantaneous rotation,  $\boldsymbol{\omega}_{pl}$ , through the transverse pressure angle,  $\phi_{t,\omega}$  (the transverse pressure angle,  $\phi_{t,\omega}$ , is measured within a plane that is perpendicular to the vector,  $\boldsymbol{\omega}_{pl}$ ):

$$\mathbf{Rt}(pa_0 \mapsto r) = \begin{bmatrix} 1 & 0 & 0 & 0 \\ 0 & \cos\phi_{t,\omega} & -\sin\phi_{t,\omega} & 0 \\ 0 & \sin\phi_{t,\omega} & \cos\phi_{t,\omega} & 0 \\ 0 & 0 & 0 & 1 \end{bmatrix} \quad (14.24)$$

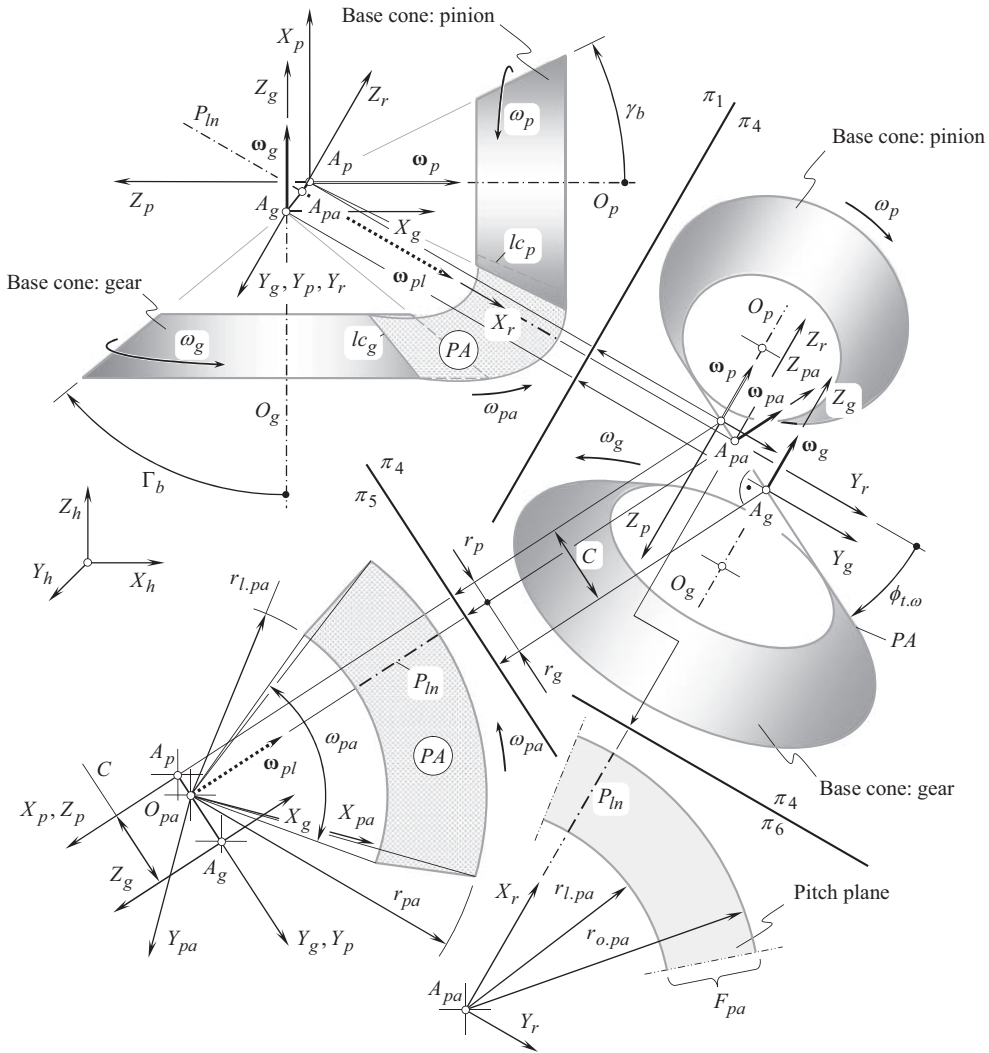


**FIGURE 14.11** Reference systems that are employed for the derivation of an analytical expression for a gear tooth flank,  $\mathcal{S}$ , and a pinion tooth flank,  $\mathcal{P}$ , in a crossed-axes gear pair.

4. The operator of rotation,  $\mathbf{Rt}(r \mapsto g)$ , of the coordinate system,  $X_r Y_r Z_r$ , about the  $Y_r$  – axis through an angle,  $\angle(\omega_r, \omega_p)$ . Note, that the angle  $\angle(\omega_r, \omega_p)$  is equal to the angle  $\angle(\omega_p, \omega_{pl}) = \Sigma_p$ . The operator of rotation,  $\mathbf{Rt}(r \mapsto g)$ , can be represented in the form:

$$\mathbf{Rt}(r \mapsto g) = \begin{bmatrix} \cos \Sigma_p & 0 & \sin \Sigma_p & 0 \\ 0 & 1 & 0 & 0 \\ -\sin \Sigma_p & 0 & \cos \Sigma_p & 0 \\ 0 & 0 & 0 & 1 \end{bmatrix} \quad (14.25)$$

III The operator,  $\mathbf{Rs}(PA \mapsto \mathcal{S})$ , of the resultant coordinate system transformation is equal to the product:

$$\mathbf{Rs}(PA \mapsto \mathcal{S}) = \mathbf{Rt}(r \mapsto g) \cdot \mathbf{Rt}(pa_0 \mapsto r) \cdot \mathbf{Tr}(-r_{w.g}, Y_g) \cdot \mathbf{Rt}(pa \mapsto pa_0) \quad (14.26)$$

This operator allows for matrix representation in an expanded form:

$$\mathbf{Rs}(PA \mapsto \mathcal{S}) = \begin{bmatrix} \cos \Sigma_p \cos \theta_{pa} + \sin \Sigma_p \cos \phi_{t,\omega} \sin \theta_{pa} & \sin \Sigma_p \sin \phi_{t,\omega} & & & \\ & -\sin \phi_{t,\omega} \sin \theta_{pa} & & \cos \phi_{t,\omega} & \\ \cos \Sigma_p \cos \phi_{t,\omega} \sin \theta_{pa} - \sin \Sigma_p \cos \theta_{pa} & \cos \Sigma_p \sin \phi_{t,\omega} & & & \\ & 0 & & 0 & \\ \sin \Sigma_p \cos \phi_{t,\omega} \cos \theta_{pa} - \cos \Sigma_p \sin \theta_{pa} & -r_g \sin \Sigma_p \sin \phi_{t,\omega} & & & \\ & -\sin \phi_{t,\omega} \cos \theta_{pa} & & -r_g \cos \phi_{t,\omega} & \\ \sin \Sigma_p \sin \theta_{pa} + \cos \Sigma_p \cos \phi_{t,\omega} \cos \theta_{pa} & -r_g \cos \Sigma_p \sin \phi_{t,\omega} & & & \\ & 0 & & 1 & \end{bmatrix} \quad (14.27)$$

The operator,  $\mathbf{Rs}(PA \mapsto \mathcal{P})$ , of the resultant coordinate system transformation, namely, the operator of the transition from the coordinate system,  $X_{pa}Y_{pa}Z_{pa}$ , associated with the plane of action,  $PA$ , to the coordinate system,  $X_pY_pZ_p$ , associated with the pinion, is equal to the product:

$$\mathbf{Rs}(PA \mapsto \mathcal{P}) = \mathbf{Rt}(r \mapsto p) \cdot \mathbf{Rt}(pa_0 \mapsto r) \cdot \mathbf{Tr}(r_p, Y_p) \cdot \mathbf{Rt}(pa \mapsto pa_0) \quad (14.28)$$

The operator of rotation,  $\mathbf{Rt}(r \mapsto p)$ , can be derived in a manner similar to that the operator of rotation,  $\mathbf{Rt}(r \mapsto g)$  [see Eq. (14.25)] is derived. The similarity allows for the following expression for the operator of rotation,  $\mathbf{Rt}(r \mapsto p)$ :

$$\mathbf{Rt}(r \mapsto p) = \begin{bmatrix} \cos \Sigma_g & 0 & \sin \Sigma_g & 0 \\ 0 & 1 & 0 & 0 \\ -\sin \Sigma_g & 0 & \cos \Sigma_g & 0 \\ 0 & 0 & 0 & 1 \end{bmatrix} \quad (14.29)$$

After Eq. (14.29) together with the Eqs. (14.22) and (14.24) are substituted into Eq. (14.28), this returns an expression for the operator,  $\mathbf{Rs}(PA \mapsto \mathcal{P})$ , of the resultant coordinate system transformation:

$$\mathbf{Rs}(PA \mapsto \mathcal{P}) = \begin{bmatrix} \cos \Sigma_g \cos \theta_{pa} + \sin \Sigma_g \cos \phi_{t,\omega} \sin \theta_{pa} & \sin \Sigma_g \sin \phi_{t,\omega} & & & \\ & -\sin \phi_{t,\omega} \sin \theta_{pa} & & \cos \phi_{t,\omega} & \\ \cos \Sigma_g \cos \phi_{t,\omega} \sin \theta_{pa} - \sin \Sigma_g \cos \theta_{pa} & \cos \Sigma_g \sin \phi_{t,\omega} & & & \\ & 0 & & 0 & \\ \sin \Sigma_g \cos \phi_{t,\omega} \cos \theta_{pa} - \cos \Sigma_g \sin \theta_{pa} & r_p \sin \Sigma_g \sin \phi_{t,\omega} & & & \\ & -\sin \phi_{t,\omega} \cos \theta_{pa} & & r_p \cos \phi_{t,\omega} & \\ \sin \Sigma_g \sin \theta_{pa} + \cos \Sigma_g \cos \phi_{t,\omega} \cos \theta_{pa} & r_p \cos \Sigma_g \sin \phi_{t,\omega} & & & \\ & 0 & & 1 & \end{bmatrix} \quad (14.30)$$

The operators,  $\mathbf{Rs}(PA \mapsto \mathcal{S})$  and  $\mathbf{Rs}(PA \mapsto \mathcal{P})$ , of linear transformations are kind of the *operators of rolling/sliding*. The transformation of rolling/sliding is extensively used in the theory of gearing, to investigate crossed-axes gearing in particular. With that said, it makes sense to introduce a special designation for the operators  $\mathbf{Rs}(PA \mapsto \mathcal{S})$  and  $\mathbf{Rs}(PA \mapsto \mathcal{P})$ ; for convenience, the operators of the linear transformations,  $\mathbf{Rs}(PA \mapsto \mathcal{S})$  and  $\mathbf{Rs}(PA \mapsto \mathcal{P})$ , can be designated as:

$$\mathbf{Rs}(PA \mapsto \mathcal{S}) = \mathbf{Rc}(PA \mapsto \mathcal{S}) \quad (14.31)$$

$$\mathbf{Rs}(PA \mapsto \mathcal{P}) = \mathbf{Rc}(PA \mapsto \mathcal{P}) \quad (14.32)$$

As the operators of rolling/sliding,  $\mathbf{Rc}(PA \mapsto \mathcal{S})$  and  $\mathbf{Rc}(PA \mapsto \mathcal{P})$ , are known, the operator of rolling,  $\mathbf{Rc}(\mathcal{P} \mapsto \mathcal{S})$ , of the pinion over the gear can be calculated from the formula:

$$\mathbf{Rc}(\mathcal{P} \mapsto \mathcal{S}) = \mathbf{Rc}(PA \mapsto \mathcal{S}) \cdot \mathbf{Rc}^{-1}(PA \mapsto \mathcal{P}) \quad (14.33)$$

Similarly, the operator of rolling,  $\mathbf{Rc}(\mathcal{S} \mapsto \mathcal{P})$ , of the gear over the pinion can be calculated either as reciprocal to the operator,  $\mathbf{Rc}(\mathcal{P} \mapsto \mathcal{S})$ , or the expression:

$$\mathbf{Rc}(\mathcal{S} \mapsto \mathcal{P}) = \mathbf{Rc}^{-1}(\mathcal{P} \mapsto \mathcal{S}) = \mathbf{Rc}(PA \mapsto \mathcal{P}) \cdot \mathbf{Rc}^{-1}(PA \mapsto \mathcal{S}) \quad (14.34)$$

can be employed for the calculation of the operator of rolling,  $\mathbf{Rc}(\mathcal{S} \mapsto \mathcal{P})$ .

#### 14.4.1.3 Operators Associated with Gear Housing

A stationary reference system,  $X_h Y_h Z_h$ , is associated with the housing of the gear pair. The choice of the coordinate system,  $X_h Y_h Z_h$ , depends mainly on the convenience of the user. In a particular case, either the stationary *Cartesian* coordinate system,  $X_g^0 Y_g^0 Z_g^0$ , or the stationary *Cartesian* coordinate system,  $X_p^0 Y_p^0 Z_p^0$ , can be employed for this purpose.

The coordinate system,  $X_g^0 Y_g^0 Z_g^0$ , shares a common  $Z_g$  – axis with the coordinate system,  $X_g Y_g Z_g$ , associated with the gear. The coordinate system,  $X_g Y_g Z_g$ , is turned in relation to the motionless coordinate system,  $X_g^0 Y_g^0 Z_g^0$ , through a certain angle,  $\varphi_g$ .

Similarly, the reference system,  $X_p^0 Y_p^0 Z_p^0$ , shares a common  $Z_p$  – axis with the coordinate system,  $X_p Y_p Z_p$ , associated with the pinion. The coordinate system,  $X_p Y_p Z_p$ , is turned in relation to the motionless coordinate system,  $X_p^0 Y_p^0 Z_p^0$ , through an angle,  $\varphi_p$ .

It is important to note here that the rotation angles,  $\varphi_g$  and  $\varphi_p$ , correspond to one another to fulfill the relation  $\varphi_p = u \varphi_g$ , and  $u$  designates the angular velocity ratio in the gear pair. For crossed-axes gearing, the following expression for  $u$ :

$$u = \frac{\omega_p^{rl}}{\omega_g^{rl}} = \frac{\omega_p \cos \Sigma_p}{\omega_g \cos \Sigma_g} \quad (14.35)$$

is valid.

Here, in Eq. (14.35), the rolling components of the rotations,  $\omega_g$  and  $\omega_p$ , are designated as  $\omega_g^{rl}$  and  $\omega_p^{rl}$ , correspondingly, and the gear and the pinion cone angles,  $\Sigma_g$  and  $\Sigma_p$ , are calculated from Eqs. (2.65) to (2.66):

$$\Sigma_g = \frac{1 - \omega_g + \omega_p}{1 + \omega_p} \Sigma \quad (14.36)$$

$$\Sigma_p = \frac{1 + \omega_g - \omega_p}{1 + \omega_g} \Sigma \quad (14.37)$$

and  $\Sigma$  is the angle between the rotation vectors of the gear,  $\omega_g$ , and the pinion,  $\omega_p$ .

For external crossed-axes gear pairs, the rotation angles,  $\varphi_g$  and  $\varphi_p$ , are of opposite sign, while for internal crossed-axes gearing the rotation angles,  $\varphi_g$  and  $\varphi_p$ , are of the same sign.

The rotation of the reference system,  $X_g Y_g Z_g$ , about the  $Z_g$  – axis through an angle,  $\varphi_g$ , is analytically described by the operator of rotation,  $\mathbf{Rt}(\mathcal{S} \mapsto h)$ . The operator of this linear transformation can be expressed in matrix form:

$$\mathbf{Rt}(\mathcal{S} \mapsto h) = \begin{bmatrix} \cos \varphi_g & \sin \varphi_g & 0 & 0 \\ -\sin \varphi_g & \cos \varphi_g & 0 & 0 \\ 0 & 0 & 1 & 0 \\ 0 & 0 & 0 & 1 \end{bmatrix} \quad (14.38)$$

Equation (14.38) makes possible an expression for the operator of the resultant coordinate system transformation, namely, for the operator of the transition,  $\mathbf{Rs}(pa \mapsto h)$ , from the coordinate system,  $X_{pa}Y_{pa}Z_{pa}$ , associated with the plane of action,  $PA$ , to the stationary coordinate system,  $X_hY_hZ_h$ . This operator of linear transformation can be represented as the product:

$$\mathbf{Rs}(pa \mapsto h) = \mathbf{Rt}(\mathcal{S} \mapsto h) \cdot \mathbf{Rc}(PA \mapsto \mathcal{S}) \quad (14.39)$$

Equation (14.39) is not represented here in expanded form, as it is too bulky.

The rotation of the reference system,  $X_pY_pZ_p$ , about the  $Z_p$ -axis through an angle,  $\varphi_p = -u\varphi_g$ , can be analytically described by the operator of rotation,  $\mathbf{Rt}(\mathcal{P} \mapsto h_p)$ . This operator can be expressed in the form:

$$\mathbf{Rt}(\mathcal{P} \mapsto h_p) = \begin{bmatrix} \cos \varphi_p & \sin \varphi_p & 0 & 0 \\ -\sin \varphi_p & \cos \varphi_p & 0 & 0 \\ 0 & 0 & 1 & 0 \\ 0 & 0 & 0 & 1 \end{bmatrix} \quad (14.40)$$

Equation (14.40) yields an expression for the operator of the resultant coordinate system transformation, namely, for the operator of transition  $\mathbf{Rs}(pa \mapsto h_p)$  from the coordinate system,  $X_{pa}Y_{pa}Z_{pa}$ , associated with the plane of action,  $PA$ , to the stationary coordinate system,  $X_{h,p}Y_{h,p}Z_{h,p}$ . This operator can be represented as the product:

$$\mathbf{Rs}(pa \mapsto h_p) = \mathbf{Rt}(\mathcal{S} \mapsto h) \cdot \mathbf{Rc}(PA \mapsto \mathcal{S}) \quad (14.41)$$

Equation (14.41) is not represented here in expanded form as it is too bulky.

Both the reference systems, namely, the coordinate systems,  $X_hY_hZ_h$  and  $X_{h,p}Y_{h,p}Z_{h,p}$ , are stationary reference systems that are somehow associated with the housing of the gear pair. The relation between these two coordinate systems is analytically described by the expression:

$$\mathbf{Rs}(h_p \mapsto h) = \mathbf{Rs}(pa \mapsto h) \cdot \mathbf{Rs}^{-1}(pa \mapsto h_p) \quad (14.42)$$

The expressions that are derived above for the operators of the coordinate system transformations make possible to derive expressions of any and all geometrical features (a) of a gear, (b) of a mating pinion, and (c) of the gear-to-pinion mesh in a common reference system.

#### 14.4.2 GEAR TOOTH FLANK IN CROSSED-AXES GEARING

The tooth flank of a gear in a crossed-axes gearing allows for its interpretation as a locus of consecutive positions of the line of contact,  $LC$ , when the plane of action,  $PA$ , is either wrapping onto or unwrapping from the base cone of the gear. For this purpose, the line of contact in its current configuration should be represented in a reference system associated with the gear.

Any planar curve of a reasonable geometry can be employed as line of contact between interacting tooth flanks in a crossed-axes gear pair. The actual geometry of tooth flanks of a gear,  $\mathcal{G}$ , and of a mating pinion,  $\mathcal{P}$ , depends on the actual shape of the line of contact. Under any circumstances,

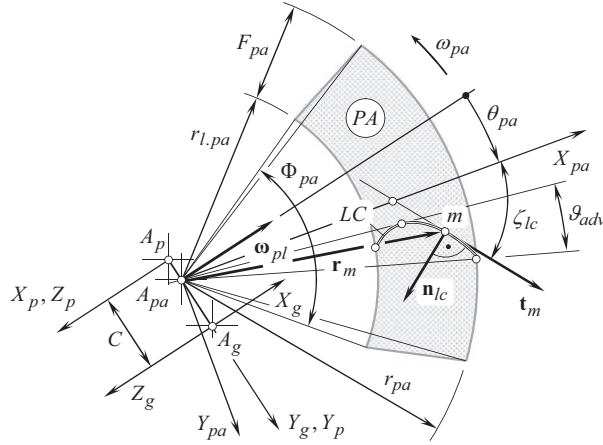


**FIGURE 14.12** Line of contact,  $LC$ , between a gear tooth flank,  $\mathcal{S}$ , and a mating pinion tooth flank,  $\mathcal{P}$ , in crossed-axes gear pair: features of the geometry.

the line of contact,  $LC$ , has to be entirely located within the coordinate plane,  $X_{pa}Y_{pa}$ , of the reference system,  $X_{pa}Y_{pa}Z_{pa}$ , associated with the plane of action,  $PA$ , as schematically illustrated in Figure 14.12.

In general, the position vector of point,  $\mathbf{r}_{lc}$ , of the line of contact,  $LC$ , can be analytically described by an expression in matrix form:

$$\mathbf{r}_{lc}(v) = \begin{bmatrix} X_{lc}(v) \\ Y_{lc}(v) \\ 0 \\ 1 \end{bmatrix} \quad (14.43)$$

To represent Eq. (14.43) for the position vector of point,  $\mathbf{r}_{lc}$ , of the line of contact,  $LC$ , in the reference system,  $X_g Y_g Z_g$ , the operator of the resultant coordinate system transformation,  $\mathbf{Rs}(PA \mapsto \mathcal{S})$ , is employed. This makes the following expression possible:

$$\mathbf{r}_g(v, \theta_{pa}) = \mathbf{r}_{lc}^g(v, \theta_{pa}) = \mathbf{Rs}(PA \mapsto \mathcal{S}) \cdot \mathbf{r}_{lc}(v) \quad (14.44)$$

for the position vector of point,  $\mathbf{r}_g$ , of the gear tooth flank,  $\mathcal{S}$ .

When the axis,  $X_{pa}$ , is pointed along one side of the face advance angle,  $\vartheta_{adv}$ , then the central angle,  $\theta_{pa}$ , is measured within the domain  $\varphi_{pl}^p + \vartheta_{adv} \leq \theta_{pa} \leq \varphi_{pl}^g - \vartheta_{adv}$  (see Figure 14.11). Here, the angles,  $\varphi_{pl}^g$  and  $\varphi_{pl}^p$ , are of opposite sign. Otherwise, the angles, that the  $X_{pa}$  – axis forms with the sides of the face advance angle,  $\vartheta_{adv}$ , have to be taken into consideration.

Substitution  $\mathbf{r}_{lc}$  [Eq. (14.43)] and  $\mathbf{Rs}(PA \mapsto \mathcal{S})$  [see Eq. (14.27)] into Eq. (14.44), yields an expression for the calculation of the position vector of point,  $\mathbf{r}_g$ , of the gear tooth flank,  $\mathcal{S}$ :

$$\mathbf{r}_g(v, \theta_{pa}) = \begin{bmatrix} (\cos \Sigma_p \cos \theta_{pa} + \sin \Sigma_p \cos \phi_{t,\omega} \sin \theta_{pa}) \cdot X(v) + \sin \Sigma_p \sin \phi_{t,\omega} \cdot Y(v) + r_p \sin \Sigma_p \sin \phi_{t,\omega} \\ -X(v) \sin \phi_{t,\omega} \sin \theta_{pa} + Y(v) \cos \phi_{t,\omega} + r_p \cos \phi_{t,\omega} \\ -(\sin \Sigma_p \cos \theta_{pa} - \cos \Sigma_p \cos \phi_{t,\omega} \sin \theta_{pa}) \cdot X(v) + \cos \Sigma_p \sin \phi_{t,\omega} \cdot Y(v) + r_p \cos \Sigma_p \sin \phi_{t,\omega} \\ 1 \end{bmatrix} \quad (14.45)$$



A line of intersection of the gear tooth flank [see Eq. (14.45)] by a sphere of certain radius centered at the plane-of-action apex,  $A_{pa}$ , is referred to a *spherical involute*,  $\text{inv}_{\text{sph}}(\phi_{t.o})$ . Equation of this curve can be derived from Eq. (14.45) if a radius,  $r_{\text{sph}}$ , of the sphere is entered into this equation.

A comparison of the expression [see Eq. (14.45)] for the position vector of point,  $\mathbf{r}_g(v, \theta_{pa})$ , of a gear tooth flank,  $\mathcal{S}$ , for crossed-axes gearing with that for intersected-axes gearing [see Eq. (12.53)] reveals that they are different. Due to inevitable axial sliding, the desirable geometries of the tooth flanks [see Eqs. (14.45) and (12.53)] are not identical. Therefore, the gears that are designed and manufactured for intersected-axes gear pairs, and the gears that are designed and manufactured for crossed-axes pairs, can *not* be interchangeable. The gears of these two different kinds cannot comprise a geometrically accurate gear pair, as they can *not* be engaged in correct mesh. The engagement, if it is possible, can be of approximate kind only.

Similar to parallel-axes gearing (see Figure 6.12), as well as to intersected-axes gearing (see Figure 12.16), the lines of contact of various geometries can be used to generate tooth flanks of a gear and of a mating pinion in crossed-axes gearing. A few examples are illustrated in Figure 14.13.

Three apexes are distinguished in geometrically accurate crossed-axes gear pairs. They are: (a) the plane-of-action apex,  $A_{pa}$ , (b) the gear-base-cone apex,  $A_g$ , and (c) the pinion-base-cone apex,  $A_p$ . (Note: in geometrically accurate intersected-axes, gear pairs all three apexes,  $A_{pa}$ ,  $A_g$ , and  $A_p$ , are coincident with one another. Therefore, in a geometrically accurate straight bevel gear pair, the line of contact,  $LC$ , is a straight line through the apex,  $A_{pa}$ ,  $A_g$ ,  $A_p$ ). In the case of crossed-axes gears, it is not clear which of the apexes,  $A_{pa}$ ,  $A_g$ , and  $A_p$ , has to be used to design a geometrically accurate straight gear pair.

In a particular case, tooth flank of a gear, and that of a mating pinion in a crossed-axes gear pair can be designed so as to retain a straight line of contact,  $LC_{\text{strait}}$ , between the tooth flanks,  $\mathcal{S}$  and  $\mathcal{P}$ , aligned with a straight line through the plane-of-action apex,  $A_{pa}$ . This is schematically illustrated in Figure 14.13a. The gears, the tooth flanks,  $\mathcal{S}$  and  $\mathcal{P}$ , of which are generated by means of the line of contact,  $LC_{\text{strait}}$ , are referred to as the *pseudo-straight-tooth crossed-axes gears* regardless of the tooth flanks,  $\mathcal{S}$  and  $\mathcal{P}$ , of this particular kind of gearing are curved surfaces. The term *pseudo-straight crossed-axes gears* reflects that the tooth flanks,  $\mathcal{S}$  and  $\mathcal{P}$ , are generated by a straight line through the plane-of-action apex,  $A_{pa}$ . When the gears rotate, at a certain instant of time the line of contact, in addition, is aligned with the axis of instantaneous rotation,  $P_{ln}$ .

Straight-line segments that have other configurations within the plane of action,  $PA$ , also are of interest from the perspective of the tooth flank generation when machining gears. In a particular case, tooth flank of a gear, and that of a mating pinion in a geometrically accurate crossed-axes gear pair can be designed so as to retain the line of contact,  $LC_{\text{spur.g}}$ , between the interacting tooth flanks,  $\mathcal{S}$  and  $\mathcal{P}$ , aligned with a straight line through the gear apex,  $A_g$ , and pointed perpendicular to the centerline,  $\mathfrak{L}$  (reminder: The centerline,  $\mathfrak{L}$ , is a straight line through the apexes  $A_g$  and  $A_p$ ). This design is schematically depicted in Figure 14.13b. When the gear rotates, the straight line along the,  $LC_{\text{spur.g}}$ , always intersects a circle of the radius  $r_{lc.g} = A_{pa}A_g$ . Both the gear tooth flank,  $\mathcal{S}$ , and the tooth flank,  $\mathcal{P}$ , of the mating pinion generated by means of the line of contact,  $LC_{\text{spur.g}}$ , of such a configuration are not the tooth flanks of a *straight* bevel gears: they are curved surfaces. Gearing of this particular design is referred to as *pseudo-straight-tooth-gear crossed-axes gearing*.

Similarly, tooth flanks of a gear and of a mating pinion in a crossed-axes gear pair can be designed so as to retain the line of contact,  $LC_{\text{spur.p}}$ , between the interacting tooth flanks,  $\mathcal{S}$  and  $\mathcal{P}$ , aligned with a straight line through the pinion apex,  $A_p$ , and pointed perpendicular to the centerline,  $\mathfrak{L}$ . This design is schematically illustrated in Figure 14.13c. When the gear rotates, the straight line along the,  $LC_{\text{spur.p}}$ , always intersects a circle of the radius  $r_{lc.p} = A_{pa}A_p$ . Both the gear tooth flank,  $\mathcal{S}$ , and the tooth flank,  $\mathcal{P}$ , of the mating pinion generated by means of the line of contact,  $LC_{\text{spur.p}}$ , of such a configuration are not the tooth flanks of a *straight* bevel gears: they are curved surfaces. Gearing of this particular design is referred to as *pseudo-straight-tooth-pinion crossed-axes gearing*.

Ultimately, an arbitrary straight line,  $LC_{\text{helical}}$ , within the plane of action,  $PA$ , can be employed to generate tooth flanks of a gear and that of a mating pinion in a crossed-axes gear pair. The straight



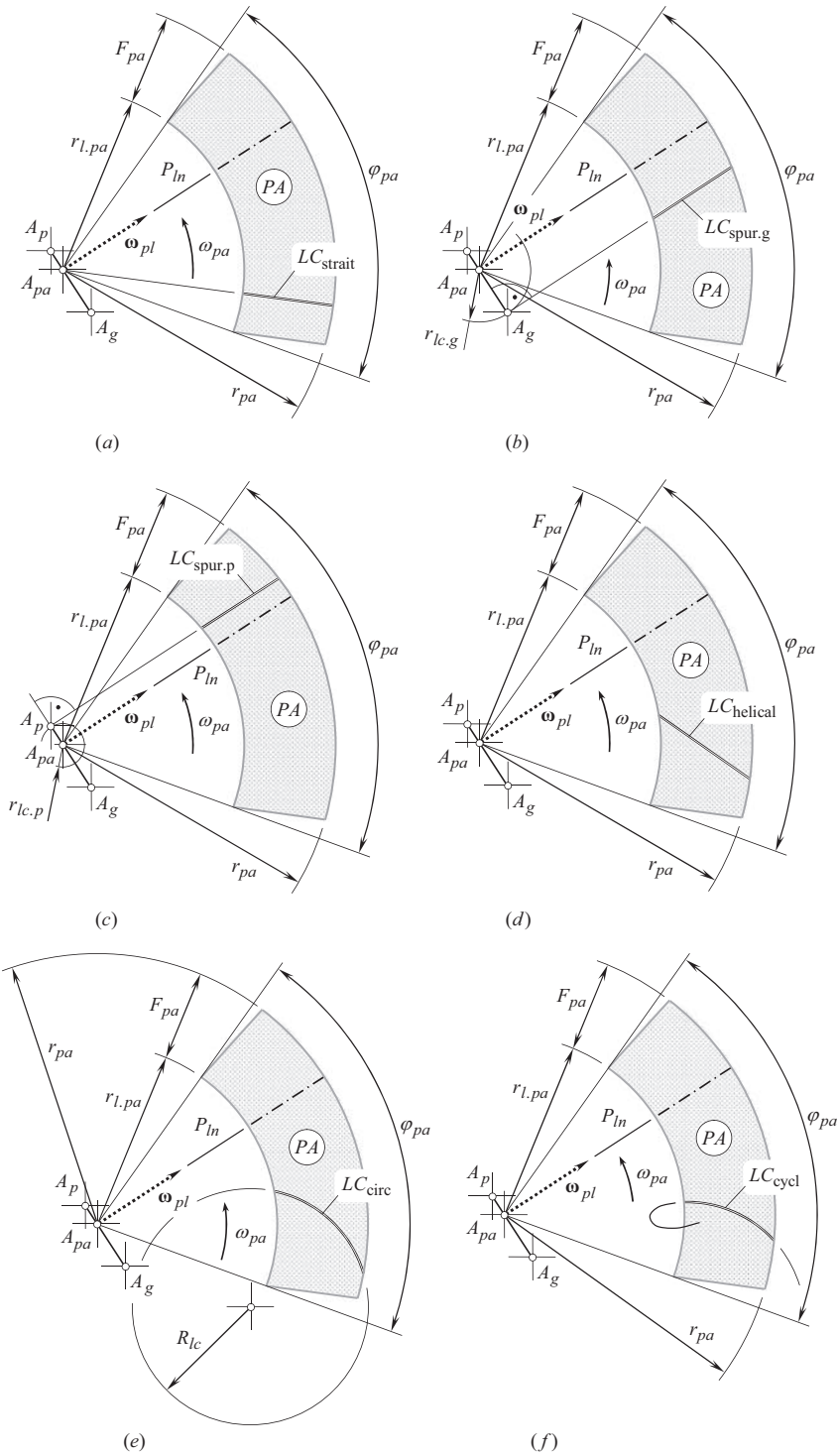


**FIGURE 14.13** Examples of possible geometries of the line of contact,  $LC$ , between a gear tooth flank,  $\mathcal{G}$ , and a mating pinion tooth flank,  $\mathcal{P}$ , in geometrically accurate crossed-axes gear pair: (a) *pseudo-straight crossed-axes gears*, (b) *straight-gear crossed-axes gears*, (c) *straight-pinion crossed-axes gears*, (d) *helical crossed-axes gears*, (e) *spiral crossed-axes gears*, and (f) *cycloid crossed-axes gears*.

line of contact,  $LC_{\text{helical}}$ , passes neither through the plane-of-action apex,  $A_{pa}$ , nor through the gear apex,  $A_g$ , nor through the pinion apex,  $A_p$ . The configuration of the line of contact for this particular kind of crossed-axes gear-set is illustrated in Figure 14.13d. In this scenario, the tooth flanks,  $\mathcal{S}$  and  $\mathcal{P}$ , of the gear and the pinion are screw surfaces.

Ultimately, one can conclude from that that no geometrically accurate crossed-axes straight bevel gearing is feasible at all.

Not only straight lines can be used for the purpose of generation of tooth flanks of a gear and of a mating pinion in crossed-axes gearing.

Figure 14.13e illustrates a case when a circular arc of certain radius,  $R_{lc}$ , is used to generate tooth flanks of a gear and of a mating pinion in crossed-axes gearing. The arc is centered at point within the plane of action,  $PA$ , and it is entirely located within the plane,  $PA$ . The tooth flanks,  $\mathcal{S}$  and  $\mathcal{P}$ , for geometrically accurate spiral bevel gears are generated in this way.

One more example of a planar line of contact,  $LC_{\text{cycl}}$ , between the gear tooth flank,  $\mathcal{S}$ , and the pinion tooth flank,  $\mathcal{P}$ , is depicted in Figure 14.13f. The line of contact,  $LC_{\text{cycl}}$ , is entirely located within the plane of action,  $PA$ . In this way, geometrically accurate cycloid bevel gears are generated.

Planar curves of other geometries also can be employed for designing gear teeth in their length-wise direction. Involute of a circle, epicycloid, hypocycloid, and so forth, are reasonable candidates for this purpose.

The main advantage of a straight line (see Figure 14.13a–d), of a circular arc (see Figure 14.13e), and of an arc of a cycloid curve (see Figure (14.13f) is due to these lines are easy to be reproduced kinematically on a machine tool when machining gears. Planar curves of other geometries that could be kinematically generated on a machine tool can also be implemented to generate tooth flanks of a gear and of a mating pinion in a crossed-axes gear pair. The convenience of generation of the line of contact,  $LC$ , is of critical importance in this regard. A case of an arbitrary planar line of contact,  $LC$ , is discussed above (see Figure 14.12).

The approach employed above for the derivation of an expression for the position vector of point of the tooth flank generated by means of an arbitrary planar curve [see Eq. (14.45)] can be used to derive an equation for the position vector of point of tooth flanks,  $\mathcal{S}$  and  $\mathcal{P}$ , generated by means of planar curves those shown in Figure 14.14.

It is appropriate time to stress here the importance of the geometry of the line of contact,  $LC$ , to solve the problem of synthesizing a crossed-axes gear pair with favorable properties. The geometry of the line of contact,  $LC$ , is a powerful tool to take control over the geometry of contact of tooth flanks of a gear,  $\mathcal{S}$ , and of a mating pinion,  $\mathcal{P}$ . This means that the contact geometry of the tooth

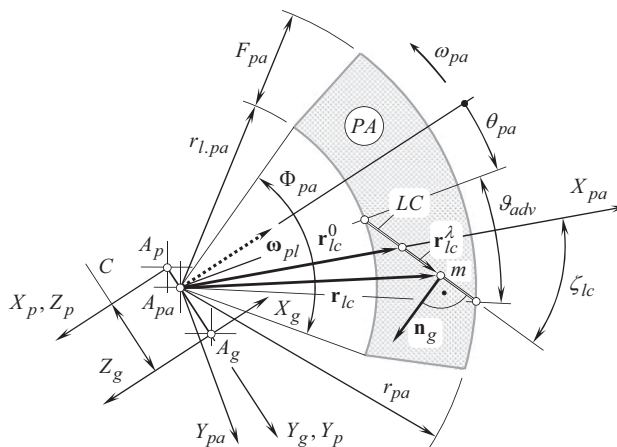


**FIGURE 14.14** The line of contact,  $LC$ , between tooth flank,  $\mathcal{S}$ , of a gear, and that of a mating pinion,  $\mathcal{P}$ , in a skew-tooth crossed-axes gear-set.

flanks,  $\mathcal{S}$  and  $\mathcal{P}$  (see Appendix E), is the key for the determination of the most favorable geometry of the line of contact,  $LC$ , for any particular case of crossed-axes gearing.

In a particular case of straight line of contact (see Figure 14.14), the position vector,  $\mathbf{r}_{lc}$ , of point of the line of contact,  $LC$ , can be represented as the sum:

$$\mathbf{r}_{lc} = \mathbf{r}_{lc}^0 + \mathbf{r}_{lc}^\lambda \quad (14.46)$$

In Eq. (14.46), the vector  $\mathbf{r}_{lc}^0$  is of a constant length,  $\mathbf{r}_{lc}^0 = \mathbf{i} \cdot r_{lc}^0$ , where  $r_{lc}^0 = |\mathbf{r}_{lc}^0|$ . Another component of the position vector of a point,  $\mathbf{r}_{lc}$ , namely, the vector  $\mathbf{r}_{lc}^\lambda$ , can be represented in the form:

$$\mathbf{r}_{lc}^\lambda(\lambda) = \mathbf{i} \cdot \lambda \cos \zeta_{cl} + \mathbf{j} \cdot \lambda \sin \zeta_{cl} \quad (14.47)$$

where

$\lambda$  – is the magnitude of the vector  $\mathbf{r}_{lc}^\lambda$

$\zeta_{cl}$  – is the angle of inclination of the line of contact,  $LC$ , in relation to the  $X_{pa}$  – axis of the coordinate system  $X_{pa}Y_{pa}Z_{pa}$  (see Figure 14.14)

Ultimately, the position vector,  $\mathbf{r}_{lc}$ , of point of the line of contact,  $LC$ , allows for representation in the form of a column matrix:

$$\mathbf{r}_{lc}(\lambda) = \begin{bmatrix} r_{lc}^0 + \lambda \cos \zeta_{cl} \\ \lambda \sin \zeta_{cl} \\ 0 \\ 1 \end{bmatrix} \quad (14.48)$$

Equation (14.48) considered together with the operator,  $\mathbf{Rs}(PA \mapsto \mathcal{S})$  [see Eq. (14.27)], of the resultant coordinate system transformation, makes possible calculation of the position vector,  $\mathbf{r}_g$ , of point of the tooth flank of a bevel gear that features an inclined line of contact:

$$\mathbf{r}_g(v, \theta_{pa}) = \mathbf{r}_{lc}^g(\lambda, \theta_{pa}) = \mathbf{Rs}(PA \mapsto \mathcal{S}) \cdot \mathbf{r}_{lc}(\lambda) \quad (14.49)$$

An expanded form of the expression for the calculation of the position vector,  $\mathbf{r}_{lc}^g$ , of point of the gear tooth flank can be derived after substituting the position vector,  $\mathbf{r}_{lc}$  [see Eq. (14.48)], and the operator of the resultant coordinate system transformation,  $\mathbf{Rs}(PA \mapsto \mathcal{S})$  [see Eq. (14.27)], into Eq. (14.49):

$$\mathbf{r}_g(\lambda, \theta_{pa}) = \begin{bmatrix} (\cos \Sigma_p \cos \theta_{pa} + \sin \Sigma_p \cos \phi_{t,\omega} \sin \theta_{pa}) \cdot (r_{lc}^0 + \lambda \cos \zeta_{lc}) + \lambda \sin \Sigma_p \sin \phi_{t,\omega} \sin \zeta_{lc} \\ - r_g \sin \Sigma_p \sin \phi_{t,\omega} (\lambda \cos \phi_{t,\omega} \sin \zeta_{lc} - \sin \phi_{t,\omega} \sin \theta_{pa}) \cdot (r_{lc}^0 + \lambda \cos \zeta_{lc}) - r_g \cos \phi_{t,\omega} \\ - (\sin \Sigma_p \cos \theta_{pa} - \cos \Sigma_p \cos \phi_{t,\omega} \sin \theta_{pa}) \cdot (r_{lc}^0 + \lambda \cos \zeta_{lc}) \\ + \lambda \cos \Sigma_p \sin \phi_{t,\omega} \sin \zeta_{lc} - r_g \cos \Sigma_p \sin \phi_{t,\omega} \\ 1 \end{bmatrix} \quad (14.50)$$

It gets clear from a comparison of Eqs. (14.50) and (12.53) that the tooth flanks of skew conical gears for a crossed-axes gear pair, and the tooth flanks of skew gears for an intersected-axes gear pair are the surfaces of different geometry. Therefore, gears that are designed and produced for crossed-axes gearing, cannot be replaced by gears that are designed and produced for intersected-axes gearing,

and vice versa. The difference between the gears gets more significant in the design of low-tooth-count gears.

In a particular case, the line of contact,  $LC$ , is aligned with the  $X_{pa}$  – axis of the *Cartesian* coordinate system  $X_{pa}Y_{pa}Z_{pa}$ . This makes possible representation the position vector,  $\mathbf{r}_{lc}$ , of point of the line of contact,  $LC$ , in the form of a column matrix:

$$\mathbf{r}_{lc}(X_{pa}) = \begin{bmatrix} X_{pa} \\ 0 \\ 0 \\ 1 \end{bmatrix} \quad (14.51)$$

An expression for the position vector,  $\mathbf{r}_g$ , of point of the tooth flank of that geometry can be determined as the product:

$$\mathbf{r}_g(X_{pa}, \theta_{pa}) = \mathbf{Rs}(PA \mapsto \mathcal{S}) \cdot \mathbf{r}_{lc}(X_{pa}) \quad (14.52)$$

where the operator,  $\mathbf{Rs}(PA \mapsto \mathcal{S})$ , of the resultant coordinate system transformation is given by Eq. (14.27).

Equation (14.52) allows for an expanded form of the expression for the position vector,  $\mathbf{r}_g$ , of point of the tooth flank of that geometry:

$$\mathbf{r}_g(X_{pa}, \theta_{pa}) = \begin{bmatrix} X_{pa}(\cos \Sigma_p \cos \theta_{pa} + \sin \Sigma_p \cos \phi_{t,\omega} \sin \theta_{pa}) - r_g \sin \Sigma_p \sin \phi_{t,\omega} \\ -X_{pa} \sin \phi_{t,\omega} \sin \theta_{pa} - r_g \cos \phi_{t,\omega} \\ -X_{pa}(\sin \Sigma_p \cos \theta_{pa} - \cos \Sigma_p \cos \phi_{t,\omega} \sin \theta_{pa}) - r_g \cos \Sigma_p \sin \phi_{t,\omega} \\ 1 \end{bmatrix} \quad (14.53)$$

Expressions for (a) the unit normal vector,  $\mathbf{n}_g$ , at point of the gear tooth flank,  $\mathcal{S}$ ; (b) the unit normal vector,  $\mathbf{n}_p$ , at point of the pinion tooth flank,  $\mathcal{P}$ ; and (c) the unit normal vector,  $\mathbf{n}_r$ , at point of the tooth flank of the auxiliary generating round rack,  $\mathcal{R}$ , can be derived based on the unit normal vector,  $\mathbf{n}_{lc}$ , at point of the line of contact,  $LC$ , which is constructed within the plane of action,  $PA$ . For this purpose, the unit normal vector,  $\mathbf{n}_{lc}$ , is required to be considered together with the corresponding operators of the coordinate system transformations. The vector,  $\mathbf{n}_{lc}$ , by nature, is perpendicular to a planar curve. Thus, this perpendicular is entirely located within the plane where the line of contact,  $LC$ , is located.

A conical gear of a crossed-axes gear pair can be engaged in mesh with a corresponding *round rack*,  $\mathcal{R}$  (or with a *crown gear*,  $\mathcal{R}$ , in other terminology). The geometry of tooth flanks of the round rack can be determined in a manner similar to that of the geometry of tooth flanks of the gear tooth flank,  $\mathcal{S}$ , was determined. The only difference is that the gear cone angle,  $\Sigma_g$ , namely, the angle formed by the rotation vectors,  $\boldsymbol{\omega}_p$  and  $\boldsymbol{\omega}_g$ , is equal to a right angle ( $\Sigma_g = 90^\circ$ ).

Equation (14.45), as well as Eqs. (14.50) and (14.53), allow for the calculation of the unit normal vector,  $\mathbf{n}_g$ , at point of the gear tooth flank,  $\mathcal{S}$ , of every particular design of crossed-axes gears. The unit normal vector,  $\mathbf{n}_g$ , and the straight line pointed along the vector,  $\mathbf{n}_g$ , are used to calculate deviations of the machined gear tooth flank from the tooth flank of the desired geometry.

Having known the position vector,  $\mathbf{r}_g(v, \theta_{pa})$ , of point of the gear tooth flank,  $\mathcal{S}$ , the unit normal vector,  $\mathbf{n}_g$ , can be calculated from the following well-known formula:

$$\mathbf{n}_g(v, \theta_{pa}) = \frac{\frac{\partial \mathbf{r}_g}{\partial v} \times \frac{\partial \mathbf{r}_g}{\partial \theta_{pa}}}{\left| \frac{\partial \mathbf{r}_g}{\partial v} \times \frac{\partial \mathbf{r}_g}{\partial \theta_{pa}} \right|} (v, \theta_{pa}) \quad (14.54)$$

Calculation of the derivatives  $\frac{\partial \mathbf{r}_g}{\partial v}$  and  $\frac{\partial \mathbf{r}_g}{\partial \theta_{pa}}$  from Eq. (14.45), followed by the formulas of linear transformation [see Eq. (14.54)] is a drilling procedure. Calculation of the unit normal vector,  $\mathbf{n}_g$ , can be significantly simplified if the vector,  $\mathbf{n}_g$ , as well as the straight line pointed along the vector,  $\mathbf{n}_g$ , are determined in the reference system  $X_{pa}Y_{pa}Z_{pa}$  (in this reference system, the unit normal vector,  $\mathbf{n}_g$ , is identical to the unit normal vector,  $\mathbf{n}_{lc}$ , to the line of contact,  $LC$ ). Afterward, the use of the operator,  $\mathbf{Rs}(PA \mapsto \mathcal{S})$ , of the resultant coordinate system transformation [see Eq. (14.27)] allows for the representation of both of the unit normal vector,  $\mathbf{n}_{lc}$ , and the straight line along,  $\mathbf{n}_{lc}$ , in the coordinate system,  $X_gY_gZ_g$ , associated with the gear.

Referring to Figure 14.12, the position vector,  $\mathbf{r}_m$ , of point of the line of contact,  $LC$ , can be specified by an expression of the form:

$$\mathbf{r}_m = \mathbf{i} \cdot X_m + \mathbf{j} \cdot Y_m \quad (14.55)$$

In Eq. (14.55), the *Cartesian* coordinates of point of interest,  $m$ , are denoted by  $X_m$  and  $Y_m$ , correspondingly.

The unit tangent vector,  $\mathbf{t}_m$ , at point of interest  $m$  can be expressed by equation:

$$\mathbf{t}_m = \mathbf{i} \cdot \cos \zeta_{cl} + \mathbf{j} \cdot \sin \zeta_{cl} \quad (14.56)$$

The inclination of the unit tangent vector,  $\mathbf{t}_m$ , in relation to the  $X_g$  – axis [see Eq. (14.56)] is specified by the angle,  $\zeta_{cl}$ . The actual value of the angle,  $\zeta_{cl}$ , can be calculated from the formula:

$$\zeta_{cl} = \tan^{-1} \left( \frac{\partial Y_{cl}(X_{cl})}{\partial X_{cl}} \right) \quad (14.57)$$

when the line of contact,  $LC$ , is represented in an explicit form as  $Y_{cl} = Y_{cl}(X_{cl})$ .

Once Eq. (14.56) is known, an expression for the calculation of the unit normal vector,  $\mathbf{n}_{lc}$ , can be represented in vector form as:

$$\mathbf{n}_{lc} = -\mathbf{i} \cdot \sin \zeta_{cl} + \mathbf{j} \cdot \cos \zeta_{cl} \quad (14.58)$$

Ultimately, the use of Eqs. (14.55)–(14.48) makes the possible derivation of an expression for the position vector of a point,  $\mathbf{r}_{n,lc}$ , of a straight line through the point  $m$  along the unit normal vector,  $\mathbf{n}_{lc}$ :

$$\mathbf{r}_{n,lc} = \mathbf{r}_m + \lambda_n \mathbf{n}_{lc} \quad (14.59)$$

or in matrix representation:

$$\mathbf{r}_{n,lc} = \begin{bmatrix} X_m - \lambda_n \sin \zeta_{lc} \\ Y_m + \lambda_n \cos \zeta_{lc} \\ 0 \\ 1 \end{bmatrix} \quad (14.60)$$

In Eqs. (14.59) and (14.60), the distance of point  $m$  from the end of the position vector,  $\mathbf{r}_m$ , is denoted by  $\lambda_n$ .

In the reference system,  $X_gY_gZ_g$ , an expression for the unit normal vector,  $\mathbf{n}_g$ , to the gear tooth flank,  $\mathcal{S}$ , can be derived from the equation:

$$\mathbf{n}_g = \mathbf{Rs}(PA \mapsto \mathcal{S}) \cdot \mathbf{n}_{lc} \quad (14.61)$$

Similarly, an expression for the position vector,  $\mathbf{r}_{n,lc}$ , of point in the reference system,  $X_g Y_g Z_g$ , can be derived from the equation:

$$\mathbf{r}_{n,lc}^g = \mathbf{Rs}(PA \mapsto \mathcal{S}) \cdot \mathbf{r}_{n,lc} \quad (14.62)$$

Finally, Eq. (14.62) and the operator  $\mathbf{Rs}(PA \mapsto \mathcal{S})$  of the linear transformation [see Eq. (14.27)] allow for an equation:

$$\mathbf{r}_{n,lc}^g(\lambda) = \begin{bmatrix} (\cos \Sigma_p \cos \theta_{pa} + \sin \Sigma_p \cos \phi_{t,\omega} \sin \theta_{pa}) \cdot (X_m - \lambda \sin \zeta_{lc}) \\ + \sin \Sigma_p \sin \phi_{t,\omega} (Y_m + \lambda \cos \zeta_{lc}) + r_g \sin \Sigma_p \sin \phi_{t,\omega} \\ - \sin \phi_{t,\omega} \sin \theta_{pa} \cdot (X_m - \lambda \sin \zeta_{lc}) + \cos \phi_{t,\omega} (Y_m + \lambda \cos \zeta_{lc}) + r_g \cos \phi_{t,\omega} \\ - (\sin \Sigma_p \cos \theta_{pa} + \cos \Sigma_p \cos \phi_{t,\omega} \sin \theta_{pa}) \cdot (X_m - \lambda \sin \zeta_{lc}) \\ + \cos \Sigma_p \sin \phi_{t,\omega} (Y_m + \lambda \cos \zeta_{lc}) + r_g \cos \Sigma_p \sin \phi_{t,\omega} \\ 1 \end{bmatrix} \quad (14.63)$$

Similarly, the unit normal vector  $\mathbf{n}_g$  at point of the gear tooth flank,  $\mathcal{S}$ , as well as the position vector,  $\mathbf{r}_{n,lc}^g$ , of point of a straight line through the point  $m$  in the direction of  $\mathbf{n}_g$  can be calculated for a line of contact,  $LC$ , of any reasonable geometry.

Formulas, similar to those above can be derived for a pinion tooth flank,  $\mathcal{P}$ , in a crossed-axes gear pair.

The aforementioned approach for the determination of the geometry of a gear tooth flank,  $\mathcal{S}$ , and of a pinion tooth flank,  $\mathcal{P}$ , is based on the generation of the tooth flanks in the form of a family of consecutive positions of the line of contact,  $LC$ , that travels together with the plane of action,  $PA$ . This approach does not require the specification of the tooth flanks in the form of enveloping surfaces to a family of consecutive positions of the generating basic rack. This means that the proposed method for the generation of tooth flanks,  $\mathcal{S}$  and  $\mathcal{P}$ , does not require the implementation of elements of the theory of enveloping surfaces. This is a significant advantage of the disclosed method over the conventional method for generation tooth flank,  $\mathcal{S}$ , of the gear, and tooth flank,  $\mathcal{P}$ , of the pinion in crossed-axes gearing.

For the correct generation of the tooth flanks,  $\mathcal{S}$  and  $\mathcal{P}$ , in gears for intersected-axes gearing, it is a must that the plane of action,  $PA$ , passes through a fixed line known as the *axis of instantaneous rotation*,  $P_{in}$ . The same requirement is a must with respect to crossed-axes gearing.

The derived equations for the gear tooth flank,  $\mathcal{S}$ , as well as for the pinion tooth flank,  $\mathcal{P}$ , can be used as reference surfaces (datum surfaces) when designing, machining, and inspecting gears for crossed-axes gearing that have line contact between tooth flanks,  $\mathcal{S}$  and  $\mathcal{P}$ , of the gear and of the pinion. Surfaces of this kind are equivalent to screw involute surfaces extensively used for parallel-axes gear pairs.

Crossed-axes gearing that has tooth flanks of the proposed geometry (which is generated by the line of contact,  $LC$ , traveling together with the plane of action,  $PA$ ) is the most general kind of gearing that features *line contact* between the tooth flanks,  $\mathcal{S}$  and  $\mathcal{P}$ . In a particular case, when the center-distance is reduced to zero ( $C = 0$ ), the crossed-axes gearing of the proposed geometry simplifies to intersected-axes gearing that has line contact between the tooth flanks. Under another scenario, namely, when the crossed-axes angle is equal either 0, or  $\pi$ , the crossed-axes gearing of the proposed geometry simplifies to parallel-axes gearing that features line contact between the tooth flanks (namely, to parallel-axes involute gearing, *Eu* – gearing).

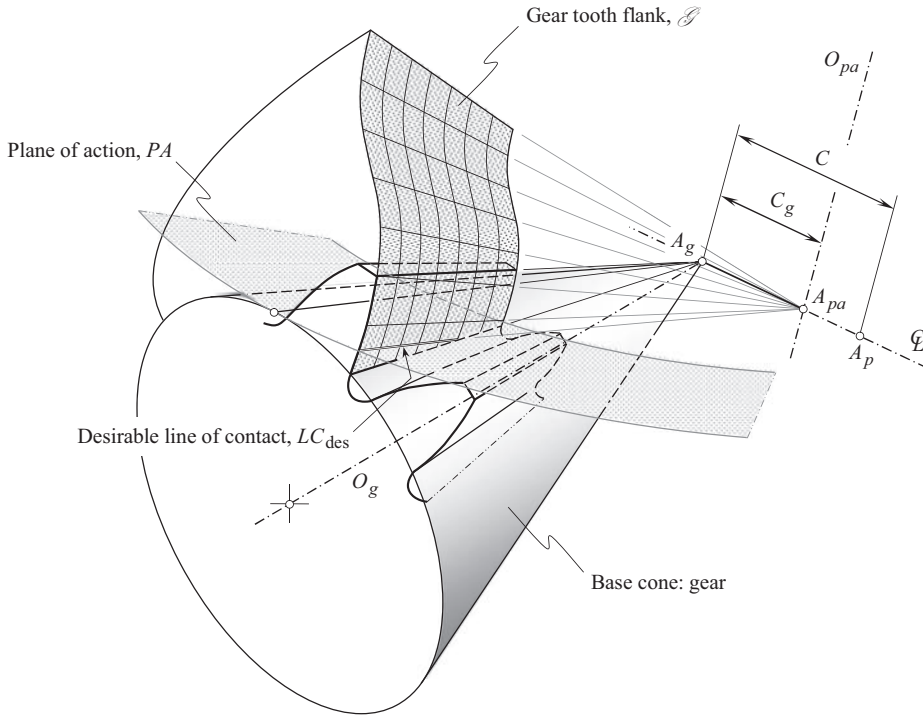


**FIGURE 14.15** Generation of tooth flank,  $\mathcal{S}$ , in geometrically accurate gear for crossed-axes gear-set.

The desirable geometry of contact between the tooth flanks of a gear and of a mating pinion in gearing<sup>3</sup> with line contact between the tooth flanks,  $\mathcal{S}$  and  $\mathcal{P}$ , can be specified on the stage of analysis of the shape and configuration of the line of contact,  $LC$ , within the plane of action,  $PA$ . The indicatrix of conformity,  $Cnf_R(\mathcal{S}/\mathcal{P})$ , at point of contact between the tooth flanks,  $\mathcal{S}$  and  $\mathcal{P}$ , can be expressed in terms of the shape and configuration of the desirable line of contact. Ultimately, those parameters of the shape and of the configuration of the line of contact are selected, under which the minimum diameter of the indicatrix of conformity,  $Cnf_R(\mathcal{S}/\mathcal{P})$ , is as small as possible. This could be the start point for solving the problem of synthesizing favorable crossed-axes gear-sets for a particular application.

When a pair of conjugate tooth flanks,  $\mathcal{S}$  and  $\mathcal{P}$ , is generated by means of a desirable line of contact,  $LC_{des}$ , an original geometry of the line of contact,  $LC_{des}$ , does not alter when the gears rotate. The desirable line of contact,  $LC_{des}$ , is a *rigid* planar curve that is entirely located within the plane of action,  $PA$ . The initially specified configuration of the  $LC_{des}$  in relation to the plane of action,  $PA$ , is remained the same.

Schematic of generation of the tooth flank of a gear for geometrically accurate crossed-axes gear-set is shown in Figure 14.15.

A spiral bevel pinion for a crossed-axes gear pair, and a spiral bevel gear are pictured in Figures 14.16 and 14.17, correspondingly.

The crossed-axes gearing, for which tooth flanks of the gear and of the pinion are generated as loci of consecutive positions of the line of contact,  $LC$ , that travels together with the plane of action,  $PA$ , is a novel kind of gearing. This novel kind of gearing ensures line contact between the tooth flanks of the gear and of the mating pinion. This gearing is referred to as the *R-gearing*.

<sup>3</sup> Crossed-axes gearing with line contact in between the tooth flanks,  $\mathcal{S}$  and  $\mathcal{P}$ , is commonly referred to as *R-gearing* (proposed by Prof. S.P. Radzevich, ~2008).





**FIGURE 14.16** Spiral bevel pinion for geometrically accurate crossed-axes gear pair.



**FIGURE 14.17** Spiral bevel gear for geometrically accurate crossed-axes gear pair.

Proposed (circa 2008) by the author of this book, *R – gearing* is the only kind of crossed-axes gears that features line contact between tooth flanks,  $\mathcal{G}$  and  $\mathcal{P}$ , of a gear and of a mating pinion.<sup>4</sup>

The tooth flanks of a gear and of a mating pinion in *R – gearing* do not allow for *sliding over itself*. Tooth flanks,  $\mathcal{G}$  and  $\mathcal{P}$ , of this particular kind of gearing cannot be formed using generating

<sup>4</sup> Many efforts have been undertaken in the past by Dr. J. Fillips [130] targeting at the development of a spatial gearing that features line contact in between the tooth flanks of a gear and of a mating pinion. In the design of spatial gearing proposed by Dr. J. Fillips (2003), both tooth flanks of the gear and of the pinion are generated by a plane that travels in relation to the axis of rotation,  $O_g$ , of the gear,  $\mathcal{G}$ , and to the axis of rotation,  $O_p$ , of the pinion,  $\mathcal{P}$  (when the pinion tooth flank,  $\mathcal{P}$ , is generated). In *R – gearing*, neither the tooth flank of a gear, nor of a mating pinion, are capable of being generated by a plane. Therefore, it should be concluded from that that in the spatial gearing proposed by Dr. J. Fillips, the tooth flanks of the mating gears are always in point contact, and they never make line contact. Research in this regard carried out later on by Dr. H. Stachel [205–207] and a few others, and targeting at the determination of a special combination of the design parameters of the gearing under which the tooth flanks make line contact – should be qualified as a mistake. No line contact in between tooth flanks of a gear and of a mating pinion is possible in the design of crossed-axes gearing proposed by Dr. H. Stachel [205–207], and a few others.



method of part surface generation by means of straight-sided auxiliary rack. However, describing the method of part surface generation perfectly fits this purpose.

## 14.5 FULFILLMENT OF CONJUGATE ACTION LAW IN *R – GEARING*

Conjugacy is a specific property of tooth flanks of a gear,  $\mathcal{G}$ , and of a mating pinion,  $\mathcal{P}$ . Only surfaces that roll over one another can feature this unique property. Due to this property, in the rolling motion of a gear and of a pinion over one another, the tooth flanks,  $\mathcal{G}$  and  $\mathcal{P}$ , can be viewed as a kind of *reversibly enveloping surfaces* (or just  *$R_e$  – surfaces*, for simplicity) [155].

The *Conjugate Action Law* (the second fundamental law of gearing) in its general form (including, but not limited to crossed-axes gearing<sup>5</sup>) was discovered (~2008) by Prof. *S.P. Radzevich* [174].

In crossed-axes gearing, when a gear and a mating pinion rotate steadily, the gear tooth flank,  $\mathcal{G}$ , can be viewed as an envelope to a family of consecutive positions of the mating pinion tooth flank,  $\mathcal{P}$ . Generated this way, the gear tooth flank,  $\mathcal{G}$ , can be used to generate the mating pinion tooth flank. If the tooth flanks,  $\mathcal{G}$  and  $\mathcal{P}$ , are conjugate, then the original pinion tooth flank,  $\mathcal{P}$ , and the pinion tooth flank,  $\mathcal{P}_g$ , generated by the gear tooth flank,  $\mathcal{G}$ , are identical to one another ( $\mathcal{P}_g \equiv \mathcal{P}$ ). Such an identity is observed not always.

Tooth flanks not of many geometries can be referred to as *conjugate surfaces*, or, the same, *reversibly enveloping surfaces* [155].

In order to be referred to as *conjugate*, a criterion to be fulfilled by two conjugate tooth flanks,  $\mathcal{G}$  and  $\mathcal{P}$ , in a crossed-axes gear pair can be expressed analytically.

When a gear,  $\mathcal{G}$ , and a mating pinion,  $\mathcal{P}$ , tooth flanks interact with one another, straight lines that align to common perpendiculars,  $\mathbf{n}_g$ , through points within a current line of contact,  $LC$ , must always intersect the axis of instantaneous rotation,  $P_{in}$ . The conjugate action law must be fulfilled at all points of the (desirable) line of contact,  $LC_{des}$ , between the interacting tooth flanks,  $\mathcal{G}$  and  $\mathcal{P}$ . This requirement is the key requirement to be fulfilled by two conjugate tooth flanks,  $\mathcal{G}$  and  $\mathcal{P}$ , when crossed-axes gears rotate.

At arbitrary point,  $m$ , within a desirable line of contact,  $LC_{des}$ , an instantaneous line of action,  $LA_{inst}$ , forms an angle with the axis of instantaneous rotation,  $P_{in}$ . At every instant of time every instantaneous line of action,  $LA_{inst}$ , intersects the axis of instantaneous rotation,  $P_{in}$ , of a gear, and of a mating pinion tooth flanks,  $\mathcal{G}$  and  $\mathcal{P}$ , which is a must for conjugate tooth flanks.

A component of the instantaneous motion that is pointed parallel to the axis of instantaneous rotation,  $P_{in}$ , does not affect the conjugate action between the interacting tooth flanks,  $\mathcal{G}$  and  $\mathcal{P}$ . Therefore, this component of the relative motion is eliminated from further analysis.

The other component of the relative motion is pointed along a straight line through the pitch point,  $P$ , that is located within the axis of instantaneous rotation,  $P_{in}$ . The conjugate action between the interacting tooth flanks,  $\mathcal{G}$  and  $\mathcal{P}$ , is considered for this component of the relative motion.

Three vectors,  $\mathbf{p}_{in}$ ,  $\mathbf{V}_m$ , and  $\mathbf{n}_g$ , are constructed, as shown in Figure 14.18.

Two of the vectors,  $\mathbf{p}_{in}$  and  $\mathbf{V}_m$ , are always located within the plane of action,  $PA$ .

The unit vector,  $\mathbf{p}_{in}$ , is pointed along the axis of instantaneous rotation,  $P_{in}$ . Therefore, in the *Cartesian* coordinate system,  $X_{pa}Y_{pa}Z_{pa}$ , associated with the plane-of-action, this vector can be analytically represented in a form:

$$\mathbf{p}_{in} = \mathbf{i} \quad (14.64)$$

<sup>5</sup> If no constraints are imposed onto a relative motion of two interacting surfaces, a conjugate surface can be determined for any smooth regular surface. In the theory of gearing, only a pair of rotations, or a rotational motion, and translational motion, are considered. With such a constraint onto the relative motion (rotations and translations), a conjugate surface can be defined not for every smooth regular surface. This means that the actual number of surfaces suitable for gear tooth flanks is limited.

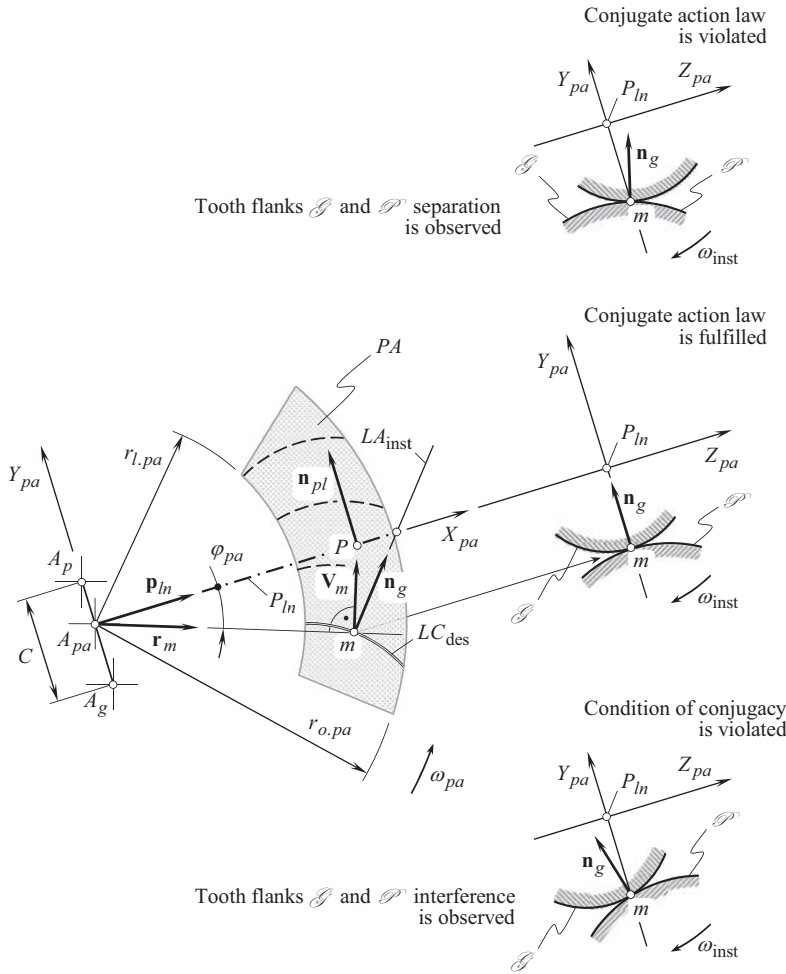


**FIGURE 14.18** Examples of fulfillment, and of violation, of the conjugate action law in crossed-axes gearing.

The velocity vector,  $\mathbf{V}_m$ , is pointed along an instantaneous line of action,  $LA_{inst}$ , through point of interest,  $m$ . In the plane-of-action *Cartesian* coordinate system,  $X_{pa}Y_{pa}Z_{pa}$ , the velocity vector,  $\mathbf{V}_m$ , can be analytically described as:

$$\mathbf{V}_m = \mathbf{i} \cdot V_m \sin \varphi_{pa} + \mathbf{j} \cdot V_m \cos \varphi_{pa} \quad (14.65)$$

The magnitude,  $V_m$ , of the linear velocity vector,  $\mathbf{V}_m$ , is omitted from the further analysis, as it does not affect the direction of the vector,  $\mathbf{V}_m$ .

The third unit vector,  $\mathbf{n}_g$ , is perpendicular to the *actual* tooth flank,  $\mathcal{G}$ , of the gear. Therefore, it can be calculated from the equation:

$$\mathbf{n}_g = \frac{\frac{\partial \mathbf{r}_g}{\partial U_g} \times \frac{\partial \mathbf{r}_g}{\partial V_g}}{\left| \frac{\partial \mathbf{r}_g}{\partial U_g} \times \frac{\partial \mathbf{r}_g}{\partial V_g} \right|} \quad (14.66)$$

where

$\mathbf{r}_g$  is the position vector of point of a gear tooth flank,  $\mathcal{S}$ .

$U_g$  and  $V_g$  are the curvilinear coordinates (the *Gaussian* coordinates) of point of a gear tooth flank,  $\mathcal{S}$ .

The unit vector,  $\mathbf{n}_{pl}$ , is entirely located within the plane of action,  $PA$ , and is perpendicular to the axis of instantaneous rotation,  $P_{ln}$ . Therefore, in the plane-of-action *Cartesian* coordinate system,  $X_{pa}Y_{pa}Z_{pa}$ , this vector can be analytically represented in a form:

$$\mathbf{n}_{pl} = \mathbf{j} \quad (14.67)$$

A gear,  $\mathcal{S}$ , and a mating pinion,  $\mathcal{P}$ , tooth flanks are conjugate, if a straight line along the unit normal vector,  $\mathbf{n}_g$ , intersects the axis of instantaneous rotation,  $P_{ln}$ , at any and all points of the line of contact,  $LC$ . In order to fulfill this requirement, the unit normal vectors,  $\mathbf{n}_{pl}$  and  $\mathbf{n}_g$ , must be coplanar (here, the unit normal vector to the axis of instantaneous rotation,  $P_{ln}$ , is designated as  $\mathbf{n}_{pl}$ . This vector is entirely located within the plane of action,  $PA$ ).

When a gear,  $\mathcal{S}$ , and a mating pinion,  $\mathcal{P}$ , tooth flanks are conjugate, then all three unit vectors,  $\mathbf{p}_{ln}$ ,  $\mathbf{V}_m$ , and  $\mathbf{n}_g$ , are coplanar. To be coplanar, the triple scalar product,  $\mathbf{p}_{ln} \times \mathbf{V}_m \cdot \mathbf{n}_g$ , of the unit vectors,  $\mathbf{p}_{ln}$ ,  $\mathbf{V}_m$ , and  $\mathbf{n}_g$ , must be equal to zero. Thus, the equality:

$$\mathbf{p}_{ln} \times \mathbf{V}_m \cdot \mathbf{n}_g = 0 \quad (14.68)$$

Must be valid. The triple scalar product,  $\mathbf{p}_{ln} \times \mathbf{V}_m \cdot \mathbf{n}_g$ , can be represented in form of a determinant:

$$\mathbf{p}_{ln} \times \mathbf{V}_m \cdot \mathbf{n}_g = \begin{vmatrix} X_{pl} & Y_{pl} & Z_{pl} \\ V_{x,m} & V_{y,m} & V_{z,m} \\ X_g & Y_g & Z_g \end{vmatrix} = 0 \quad (14.69)$$

In addition to Eq. (14.69), the condition:

$$\mathbf{n}_{pl} \cdot \mathbf{n}_g \neq 1 \quad (14.70)$$

must also be fulfilled. The parallelism of the directions specified by the unit normal vectors,  $\mathbf{n}_{pl}$  and  $\mathbf{n}_g$ , is eliminated by this condition. No rotation transmission by means of gears is possible when the unit normal vector,  $\mathbf{n}_g$ , is parallel to the axis of instantaneous rotation,  $P_{ln}$ .

An expression:

$$\mathbf{p}_{ln} \times \mathbf{n}_g = 0 \quad (14.71)$$

is an alternative form of representation of the condition, specified by Eq. (14.70).

A gear,  $\mathcal{S}$ , and a mating pinion,  $\mathcal{P}$ , tooth flanks are said to be conjugate if and only if the conditions, those specified by Eq. (14.68) [or Eq. (14.69)] and Eq. (14.70) [or Eq. (14.71)], are fulfilled for any and all points within the line of contact,  $LC$ , for any possible configurations of the gear and the pinion in relation to one another.

$$\begin{cases} \mathbf{p}_{ln} \times \mathbf{V}_m \cdot \mathbf{n}_g = 0 \\ \mathbf{p}_{ln} \times \mathbf{n}_g \neq 0 \end{cases} \quad (14.72)$$

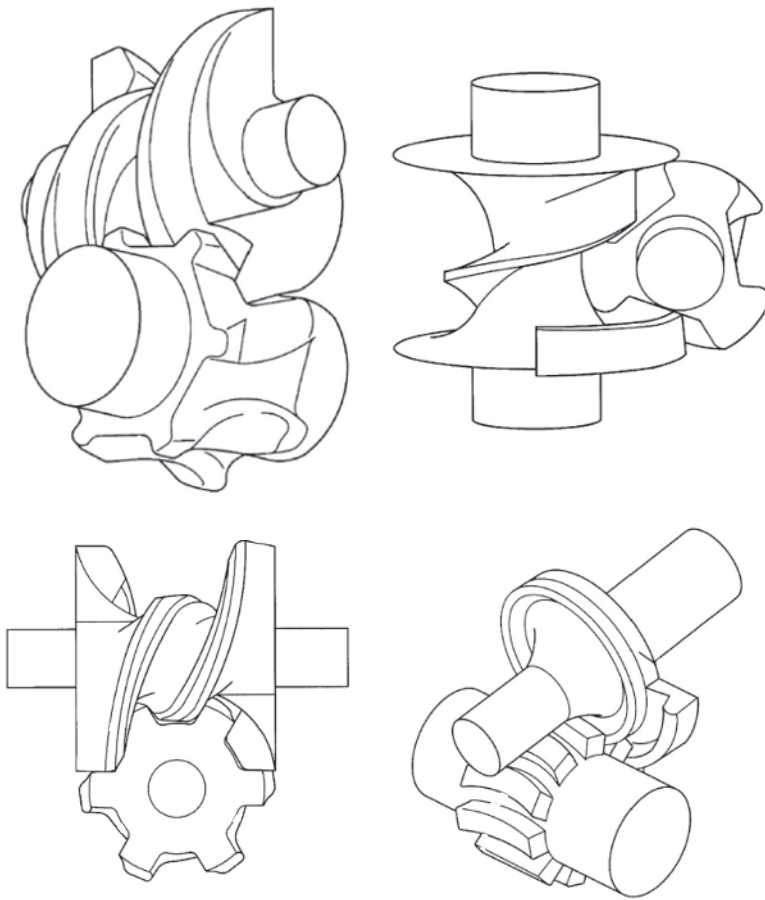


**FIGURE 14.19** Incorrect tooth profiles in crossed-axes gearing. (After Y. Fleytman: Pat. No. 6,148,683 (USA). *Worm/Worm Gear Transmission*, Y. Fleytman, Int. Cl.<sup>7</sup> **F16H 1/16**, Filed: April 12, 1999, Patented: November 21, 2000.)

When the gears rotate, conjugate action law for a gear,  $\mathcal{G}$ , and for a mating pinion,  $\mathcal{P}$ , tooth flanks is analytically described by Eq. (14.72).

Tooth profiles in *worm/worm gear transmission* are targeted at the illustration of extremely poor understanding of the scientific theory of gearing by the gear engineers from the industry (Figure 14.19). Lots of troubles to the industry<sup>6</sup> was caused by the ignorance of the conjugate action law in crossed-axes gearing (the second fundamental law of gearing).

## 14.6 DESIRABLE TOOTH PROPORTIONS IN CROSSED-AXES GEAR PAIR

A gear and a mating pinion in a crossed-axes gear pair have a plurality of teeth. The teeth are evenly spaced circumferentially. The general form of equation of a gear tooth flank [see Eq. (14.45)], as well as Eqs. (14.50) and (14.53), of the gear tooth flank,  $\mathcal{G}$ , are convenient for research purposes. However, these equations are not sufficient for the specification of the tooth shape either of a gear or of a mating pinion for engineering purposes. In the latter case, the gear tooth flank,  $\mathcal{G}$ , should be properly located in relation to the tooth flank of the opposite side of the gear tooth, as well as in relation to the tooth flanks of the rest of the gear teeth.

<sup>6</sup> New Venture Gear, Syracuse, NY (late 1990th–early 2000th).

The desirable tooth proportions in crossed-axes gearing can be established in a way similar to that the desirable tooth proportions are established in parallel-axes gearing, as well as they are established in intersected-axes gearing. Following this approach, let us begin from the operating angular base pitch in a crossed-axes gear pair.

### 14.6.1 OPERATING ANGULAR BASE PITCH

The angular distance between two adjacent desirable lines of contact,  $LC_{des}^i$  and  $LC_{des}^{i+1}$ , of a gear, and of a mating pinion tooth flanks,  $\mathcal{S}$  and  $\mathcal{P}$ , in a crossed-axes gear pair is specified by the *operating angular base pitch*,  $\varphi_{b,op}$  in the gear pair<sup>7</sup>. The *operating angular base pitch*,  $\varphi_{b,op}$  is a design parameter of critical importance for the crossed-axes gear-set.

In a crossed-axes gear pair, the operating angular base pitch is an equivalent of the operating base pitch in a parallel-axes gearing, and of the operating angular base pitch in an intersected-axes gearing. Based on these similarities, the angular distance between every two consequent tooth profiles within the plane of action,  $PA$ , is specified by the *operating angular base pitch* in the gear pair.

#### Definition 14.1

Operating base pitch,  $\varphi_{b,op}$ , in crossed-axes gearing is the angular distance between every two adjacent desirable lines of contact,  $LC_{des}^i$  and  $LC_{des}^{i+1}$ ; the angle,  $\varphi_{b,op}$ , is measured within the plane of action,  $PA$ , and is centered at the plane-of-action apex,  $A_{pa}$ .

In certain sense, *operating angular base pitch* in a crossed-axes gear pair is an equivalent of the angular module,  $\gamma_m$ , in the gear pair.

Consider a gear and the plane of action,  $PA$ , as schematically illustrated in Figure 14.20. When the gears rotate, the base cone of the gear rolls over the plane of action,  $PA$ .

Consider the point within the surface of the base cone of the gear. The point is remote from the base cone apex,  $A_g$ , at a distance  $r_{o,pa}$ . The arc distance:

$$\check{L}_{b,g} = 2\pi r_{o,pa} \sin \Gamma_b \quad (14.73)$$

is covered by the point per each rotation of the gear.

Within the plane of action,  $PA$ , a circular arc of the length  $\check{L}_{b,g}$  spans over a central angle,  $\Psi_{b,g}$ . The value of the central angle,  $\Psi_{b,g}$ , is calculated from the formula:

$$\Psi_{b,g} = 360^\circ \sin \Gamma_b \quad (14.74)$$

For a gear of  $N_g$  teeth, a portion,  $\varphi_{b,op}$ , of the central angle,  $\Psi_{b,g}$ , per gear tooth is equal<sup>8</sup>:

$$\varphi_{b,op} = \frac{\Psi_{b,g}}{N_g} = \frac{360^\circ}{N_g} \sin \Gamma_b \quad (14.75)$$

The angle,  $\varphi_{b,op}$ , in crossed-axes gearing is equivalent to the operating base pitch,  $p_{b,op}$ , in parallel-axes gearing. Due to this fact, the angle,  $\varphi_{b,op}$ , is referred to as the *operating angular base pitch* in a crossed-axes gear pair.

As illustrated in Figure 14.21, for a specified gear, the *operating angular base pitch*,  $\varphi_{b,op}$ , remains the same for any and all circles of radii  $r_{x,pa}$ ,  $r_{y,pa}$ , and so forth, within the face width,  $F_{pa}$ ,

<sup>7</sup> The concept of *operating base pitch* in a gear pair for the first time ever was introduced (~2008) by Prof. S.P. Radzevich [174]. The third fundamental law of gearing (angular base pitch of a gear, and that of a mating pinion, must be equal to operating angular base pitch in the gear pair) for the first time ever was introduced (~2008) by Prof. S.P. Radzevich [174].

<sup>8</sup> Angular normal module,  $m_{\gamma,pa}$ , is an equivalent to the angular base pitch,  $\varphi_{b,op}$ , as:  $m_{\gamma,pa} = \frac{360^\circ}{N_{pa}} = \frac{2\pi}{N_{pa}}$ .

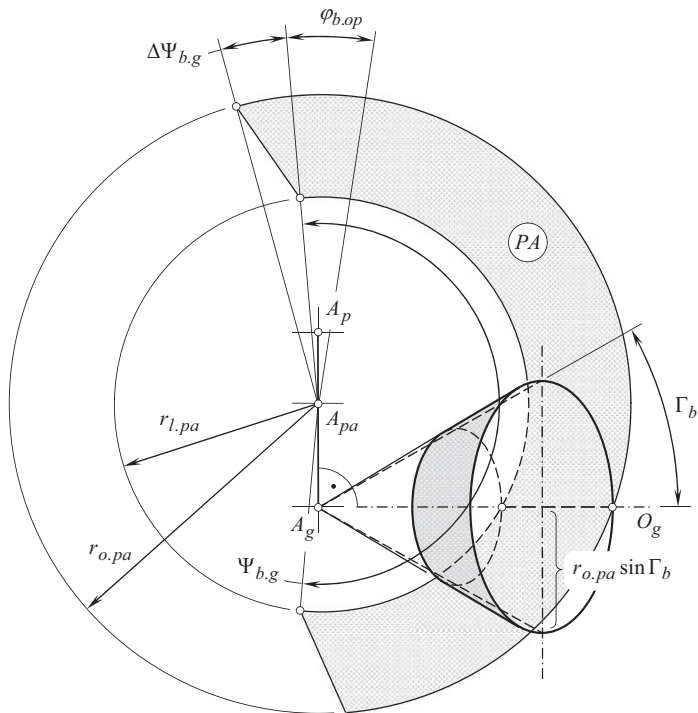


FIGURE 14.20 Definition of the term *operating angular base pitch*,  $\varphi_{b,op}$ , in crossed-axes gearing.

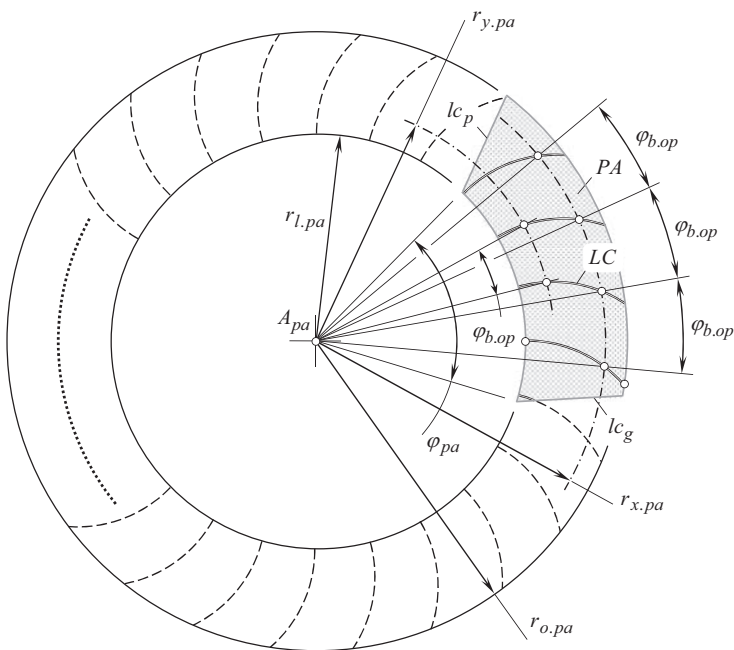


FIGURE 14.21 The *operating angular base pitch*,  $\varphi_{b,op}$ , in crossed-axes gear-set is of a constant value for all the teeth, as well as within the face width of the gear.

of the gear ( $\varphi_{b.op} = \text{const}$ ). This is of critical importance for the proper operation of geometrically accurate crossed-axes gear pairs.

It should be noted here that the tooth count,  $N_{pa}$ , within the imaginary plane of action,  $PA$ , is not mandatorily expressed by an integer number. It can be expressed by a number with fractions, as well.

The *operating angular base pitch*,  $\varphi_b$ , can be expressed in terms of linear dimensions. The latter makes sense in cases when the linear dimensions are easier to be measured.

The *operating angular base pitch*,  $\varphi_{b.op}$ , is specified within the plane of action,  $PA$ , of the gear pair. The operating angular base pitch is a calculated design parameter in a crossed-axes gear pair, that is, no direct measurement of this design parameter is possible.

The angular base pitch in a gear,  $\varphi_{b.g}$  (as well as that in a mating pinion,  $\varphi_{b.p}$ ), is specified within a plane tangent to the base cone of the gear. The gear angular base pitch can be measured directly in the gear, and in the pinion, separately. The angular base pitch is measured as an angle between the actual lines of intersection of the gear and of the mating pinion tooth flanks,  $\mathcal{S}$  and/or  $\mathcal{P}$ , of two adjacent teeth. One of the lines of intersection of the gear and of the pinion tooth flanks,  $\mathcal{S}$  and/or  $\mathcal{P}$ , by the plane of action,  $PA$ , may be located either outside of the outer cone or inside the root cone, of the gear or of the pinion.

A variation of the actual value of the angular base pitch in a gear (and in a mating pinion) can be measured as the variation of the configuration, and the geometry of the line of intersection of a single tooth flank,  $\mathcal{S}$ , (or a single tooth flank  $\mathcal{P}$ ) when the gear (or the pinion) turns about its axis of rotation.

The apex for the measurement of a gear (and a mating pinion) angular base pitch,  $\varphi_{b.g}$  (and  $\varphi_{b.p}$ ), in crossed-axes gearing coincides with the plane-of-action apex,  $A_{pa}$ , and not with the gear-base-cone apex,  $A_g$  (and the pinion-base-cone apex,  $A_p$ ).

The operating angular base pitch can be determined following the routine that is outlined immediately below:

1. Consider rolling of the base cone of the gear (of the pinion) over the plane of action,  $PA$ .  
The base cone contacts the plane of action along a straight line
2. When rolling, sliding between the base cone, and the plane of action along the line of contact is observed, however, the angular velocity ratio is not affected by the sliding
3. The sliding is observed along the axis of instantaneous rotation,  $P_{in}$
4. No sliding is observed in the direction perpendicular to the axis of instantaneous rotation,  $P_{in}$ , namely, in the tangential direction to the base cones
5. Consider the roll angle of a value  $2\pi/N_g$  (or  $2\pi/N_p$ , in the case of pinion)
6. When the base cone of the gear (of the pinion) turns about its axis through an angle  $2\pi/N_g$  (or  $2\pi/N_p$ ), the base cone turns about the plane-of-action apex,  $A_{pa}$ , through the operating base pitch angle,  $\varphi_{b.op}$
7. Once the angle of rotation of the gear (of the pinion) is known –  $2\pi/N_g$  (or  $2\pi/N_p$ ), then the equation:

$$u = \frac{C_g}{C_p} = \frac{\tan \Sigma_g}{\tan \Sigma_p} \quad (14.76)$$

is used when calculating the *operating angular base pitch*,  $\varphi_{b.op}$ .

The *operating angular base pitch*,  $\varphi_{b.op}$ , can be specified for any and all crossed-axes gear pairs, while the angular base pitches,  $\varphi_{b.g}$  and  $\varphi_{b.p}$ , of a gear and of its mating pinion can be specified only for geometrically accurate gears, that is, in conjugate tooth flanks,  $\mathcal{S}$  and  $\mathcal{P}$ , and not for tooth flanks of an arbitrary geometry.



The *operating angular base pitch*,  $\phi_{b.op}$ , can be calculated from the following formula:

$$\phi_{b.op} = \frac{2\pi}{N_g} \sin \Gamma_b = \frac{2\pi}{N_p} \sin \gamma_b \quad (14.77)$$

$$\frac{N_g}{N_p} = u \quad (14.78)$$

$$N_g = u \cdot N_p \quad (14.79)$$

$$\phi_{b.op} = \frac{2\pi}{u \cdot N_p} \sin \Gamma_b = \frac{2\pi}{N_p} \sin \gamma_b \quad (14.80)$$

The *operating angular base pitch*,  $\phi_{b.op}$ , can be construed as a vector associated with the gear pair,  $\vec{\phi}_{b.op}$ , with the gear,  $\vec{\phi}_{b.g}$ , and with the mating pinion,  $\vec{\phi}_{b.p}$ . The vectors  $\vec{\phi}_{b.op}$ ,  $\vec{\phi}_{b.g}$ , and  $\vec{\phi}_{b.p}$ , are pointed along the axes of rotation:

- $O_{pa}$ , of the plane of action,  $PA$
- $O_g$ , of the gear
- $O_p$ , of the pinion

correspondingly.

The magnitude of each of the vectors,  $\vec{\phi}_{b.op}$ ,  $\vec{\phi}_{b.g}$ , and  $\vec{\phi}_{b.p}$ , is proportional to the corresponding angular base pitch.

In crossed-axes gearing,

- the vector,  $\vec{\phi}_{b.op}$ , is applied at the plane-of-action-apex,  $A_{pa}$ , and is pointed along the axis  $O_{pa}$
- the vector,  $\vec{\phi}_{b.g}$ , is a vector of the length,  $|\vec{\phi}_{b.g}|$ , and is applied perpendicular to a plane that is tangent to the base cone of the gear; the line along which the vector  $\vec{\phi}_{b.g}$  acts, is at a distance,  $C_g$ , from the plane-of-action-apex,  $A_{pa}$ , measured along the perpendicular to the axis  $O_{pa}$
- the vector,  $\vec{\phi}_{b.p}$ , is a vector of the length,  $|\vec{\phi}_{b.p}|$ , and is applied perpendicular to a plane that is tangent to the base cone of the pinion; the line along which the vector  $\vec{\phi}_{b.p}$  acts, is at a distance,  $C_p$ , from the plane-of-action-apex,  $A_{pa}$ , measured along the perpendicular to the axis  $O_{pa}$

The corresponding tolerances,  $\Delta\vec{\phi}_{b.op}$ ,  $\Delta\vec{\phi}_{b.g}$ , and  $\Delta\vec{\phi}_{b.p}$ , in vector notation can be assigned to each of the angular base pitches:  $\vec{\phi}_{b.op}$ ,  $\vec{\phi}_{b.g}$ , and  $\vec{\phi}_{b.p}$ .

An important conclusion can be drawn up from this discussion.

Despite the angular base pitches,  $\phi_{b.g}$ ,  $\phi_{b.p}$ , and  $\phi_{b.op}$ , in crossed-axes gearing, and in intersected-axes gearing may be equal to one another, bevel gears for  $C_a$  – gearing, and that for  $I_a$  – gearing, must be named differently. This is due to the geometry of tooth flanks,  $\mathcal{I}$  and  $\mathcal{P}$ , in  $C_a$  – gearing is different from that in  $I_a$  – gearing. Thus, bevel gears, those designed and manufactured for geometrically accurate crossed-axes gearing, are not allowed to be replaced with bevel gears, those designed and manufactured for geometrically accurate intersected-axes gearing, and vice versa. The first can be referred to as *bevel gears for crossed-axes gearing*, while the others can be referred to as *bevel gears for intersected-axes gearing*.

A possible immediate way to apply the concept of angular base pitches,  $\phi_{b.g}$ ,  $\phi_{b.p}$ , and  $\phi_{b.op}$ , is targeted at an improvement of cutting/finishing of bevel gears for crossed-axes gear-sets. The set-up



parameters of the gear cutting/finishing operation can be optimized based on the minimization of variation of the angular *base pitch*. For this purpose, the angular distance between the lines of intersection of the adjacent tooth flanks by the plane of action,  $PA$ , is inspected for various angular configurations of the plane of action in relation to the gear to be inspected. The set-up parameters of favorable values correspond to the minimum variation of these deviations. For this purpose, a CAD model of the gear to be inspected is helpful.

### 14.6.2 LOW-TOOTH-COUNT CROSSED-AXES GEARS

Depending on the actual value of the angular pitch,  $\phi_b$ , the *low-tooth-count* crossed-axes gears (or *LTC* crossed-axes gears, for simplicity) are distinguished. The *low-tooth-count* crossed-axes gears feature an angular pitch,  $\phi_b$ , of a larger value compared to that in gears with a large tooth count. Use of the base cone angle of a gear,  $\Gamma_b$  (and of a pinion,  $\gamma_b$ ), and the start-of-active-profile cone angle of the gear,  $\Gamma_{sap}$  (of a pinion,  $\gamma_{sap}$ ), make possible a numerical criterion to distinguish low-tooth-count crossed-axes gear from the gears of other designs. The following inequality is valid for *low-tooth-count* crossed-axes gears:

$$\Gamma_b > \Gamma_{sap} \quad (14.81)$$

A similar inequality:

$$\gamma_b > \gamma_{sap} \quad (14.82)$$

is valid with respect to a low-tooth-count crossed-axes pinion.

Low-tooth-count crossed-axes gears feature a more significant variation of the most of principal design parameters of the tooth flanks compared to that in gears with a larger tooth count.

### 14.6.3 TRANSVERSE PRESSURE ANGLE

Transverse pressure angle,  $\phi_{t,\omega}$ , is specified in a plane that is perpendicular to the axis of instantaneous rotation,  $P_{ln}$  (or, the same, it is measured within a plane that is perpendicular to the vector of instantaneous rotation,  $\omega_{pl}$ ). Referring to Figure 14.7 (as well as to Figure 14.11), the transverse pressure angle,  $\phi_{t,\omega}$ , is the angle between a perpendicular to the plane of action,  $PA$ , and a perpendicular to the plane (a) through the vector of instantaneous rotation,  $\omega_{pl}$ , and (b) the line along the closest distance of approach of the axes of rotations,  $O_g$  and  $O_p$ , of the gear and the pinion [recall that this plane is referred to as centerline plane,  $C_{ln}$  (see Chapter 3)].

#### Definition 14.2

The transverse pressure angle in crossed-axes gear pair is the angle between a perpendicular to the plane of action, and a perpendicular to the centerline plane. The transverse pressure angle is measured within a plane that is perpendicular to the axis of instantaneous rotation.

The transverse pressure angle,  $\phi_{t,\omega}$ , can be construed as an independent design parameter in a crossed-axes gear pair. Then, the base cone angles of the gear,  $\Gamma_b$ , and that of the pinion,  $\gamma_b$ , are expressed in terms of the transverse pressure angle  $\phi_{t,\omega}$ . Otherwise, the transverse pressure angle,  $\phi_{t,\omega}$ , can be expressed in terms of the base cone angles,  $\Gamma_b$  and  $\gamma_b$ .

The plane of action,  $PA$ , is tangential to the base cone of the gear, as schematically illustrated in Figure 14.22. Therefore, the angle that the plane of action,  $PA$ , forms with the gear axis of rotation,  $O_g$ , is equal to the base cone angle,  $\Gamma_b$ . Once the angle between the plane of action,  $PA$ , and the axis,  $O_g$ , is known (this angle equals  $\Gamma_b$ ), the angle that the unit normal vector,  $\mathbf{n}_{pa}$ , to the plane of action,  $PA$ , forms with the gear axis of rotation,  $O_g$ , is equal to  $(90^\circ - \Gamma_b)$ .

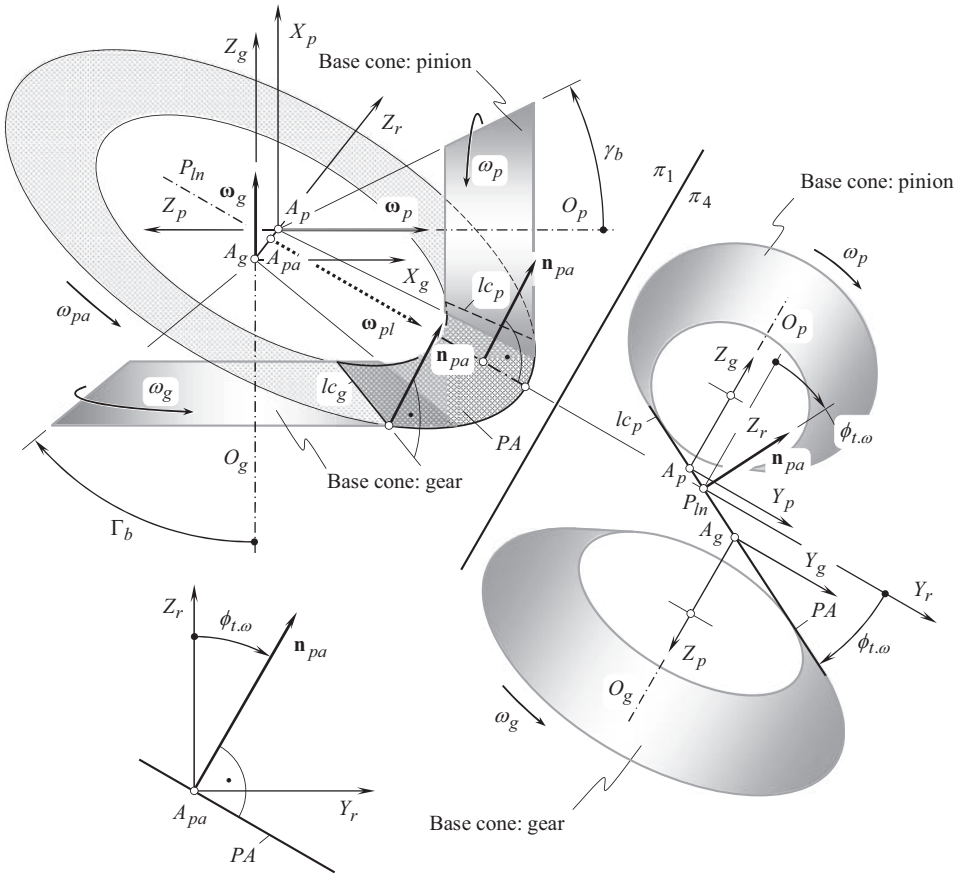


**FIGURE 14.22** Specification of the configuration of the plane of action,  $PA$ , relative to the base cone of a gear in crossed-axes gear pair.

In the *Cartesian* reference system,  $X_r Y_r Z_r$ , the direction of the aforementioned unit normal vector,  $\mathbf{n}_{pa}$ , is analytically expressed by the equation:

$$\mathbf{n}_{pa} = \mathbf{j}_r \sin \phi_{t,\omega} + \mathbf{k}_r \cos \phi_{t,\omega} \quad (14.83)$$

To express the base cone angle of the gear,  $\Gamma_b$ , in terms of the transverse pressure angle,  $\phi_{t,\omega}$ , or, conversely, to express the transverse pressure angle,  $\phi_{t,\omega}$ , in terms of the base cone angle of the gear,  $\Gamma_b$ , all the design parameters should be represented in a common reference system. Use the *Cartesian* coordinate system,  $X_g Y_g Z_g$ , associated with the gear, is convenient for the purpose of calculation of the base cone angle. To do that, the unit normal vector,  $\mathbf{n}_{pa}$ , should be represented in the reference system,  $X_g Y_g Z_g$ .

The reference systems,  $X_g Y_g Z_g$  and  $X_r Y_r Z_r$ , are turned in relation to one another about the  $Y_r$  – axis through the pinion angle  $\Sigma_p$ . Transition from the coordinate system,  $X_r Y_r Z_r$ , to the coordinate system,  $X_g Y_g Z_g$ , is analytically described by the operator of rotation,  $\mathbf{Rt}(r \mapsto g)$  [see Eq. (14.25)]. With that said, in the coordinate system,  $X_g Y_g Z_g$ , the direction of the unit normal vector,  $\mathbf{n}_{pa}$ , can be analytically described by the expression:

$$\mathbf{n}_{pa}^g = \mathbf{Rt}(r \mapsto g) \cdot \mathbf{n}_{pa} \quad (14.84)$$

Equations (14.25), (14.83), and (14.84) allow for an expression for the unit vector  $\mathbf{n}_{pa}^g$ :

$$\mathbf{n}_{pa}^g = \begin{bmatrix} \cos \Sigma_p & 0 & \sin \Sigma_p & 0 \\ 0 & 1 & 0 & 0 \\ -\sin \Sigma_p & 0 & \cos \Sigma_p & 0 \\ 0 & 0 & 0 & 1 \end{bmatrix} \cdot \begin{bmatrix} 0 \\ \sin \phi_{t,\omega} \\ \cos \phi_{t,\omega} \\ 1 \end{bmatrix} = \begin{bmatrix} \sin \Sigma_p \cos \phi_{t,\omega} \\ \sin \phi_{t,\omega} \\ \cos \Sigma_p \cos \phi_{t,\omega} \\ 1 \end{bmatrix} \quad (14.85)$$

As the unit vector along the  $O_g -$  axis is equal to  $-\mathbf{k}$ , the angle  $\angle(\mathbf{n}_{pa}^g, -\mathbf{k})$  can be calculated from the formula:

$$\angle(\mathbf{n}_{pa}^g, -\mathbf{k}) = \Gamma_b = \cos^{-1}[\mathbf{n}_{pa}^g \cdot (-\mathbf{k})] \quad (14.86)$$

This formula can also be represented in the form:

$$\Gamma_b = \tan^{-1} \left( -\frac{\sqrt{\sin^2 \Sigma_p - \cos^2 \Sigma_p \sin^2 \phi_{t,\omega}}}{\cos \Sigma_p \cos \phi_{t,\omega}} \right) \quad (14.87)$$

The transverse pressure angle,  $\phi_{t,\omega}$ , can be expressed in terms of the base cone angle,  $\Gamma_b$ , of the gear:

$$\phi_{t,\omega} = \cos^{-1} \left( \frac{\cos \Sigma_p}{\cos \Gamma_b} \right) \quad (14.88)$$

An equation similar to Eq. (14.87) is valid for the base cone angle of the pinion:

$$\gamma_b = \tan^{-1} \left( -\frac{\sqrt{\sin^2 \Sigma_g - \cos^2 \Sigma_g \sin^2 \phi_{t,\omega}}}{\cos \Sigma_g \cos \phi_{t,\omega}} \right) \quad (14.89)$$

The transverse pressure angle,  $\phi_{t,\omega}$ , can also be expressed in terms of the base cone angle,  $\gamma_b$ , of the pinion:

$$\phi_{t,\omega} = \cos^{-1} \left( \frac{\cos \Sigma_g}{\cos \gamma_b} \right) \quad (14.90)$$

Both the cone angles, namely, the angles  $\Sigma_g$  and  $\Sigma_p$ , can be expressed in terms of the rotations of the gear,  $\omega_g$ , and the pinion,  $\omega_p$ , and the angle,  $\Sigma$ , formed by the rotation vectors,  $\omega_g$  and  $\omega_p$  [see Eqs. (14.1) and (14.2)].

When the transverse pressure angle,  $\phi_{t,\omega}$ , is given, the base cone angle of a gear,  $\Gamma_b$ , as well as the base cone angle of a mating pinion,  $\gamma_b$ , both, can be expressed in terms of the transverse pressure angle,  $\phi_{t,\omega}$ , of the pitch cone angle of the gear,  $\Gamma$ , and pinion,  $\gamma$ .

As the plane of action,  $PA$ , is tangential to the base cones of the gear and the pinion, this plane forms the transverse pressure angle,  $\phi_{t,\omega}$ , with the pitch plane,  $PP$  (see Figure 14.22). An angle that the plane of action,  $PA$ , forms with the axis of rotation of the gear,  $O_g$ , is equal to the base cone angle of the gear,  $\Gamma_b$ . Therefore, the unit normal vector,  $\mathbf{n}_{pa}$ , to the plane of action,  $PA$ , and the axis of rotation,  $O_g$ , make an angle  $(90^\circ - \Gamma_b)$ .

The unit normal vector,  $\mathbf{n}_{pa}$ , to the plane of action,  $PA$ , is specified by the Eq. (14.83). Referring to Figure 14.23, the unit vector,  $\mathbf{a}$ , along the axis of rotation of the gear,  $O_g$ , can be analytically expressed as:

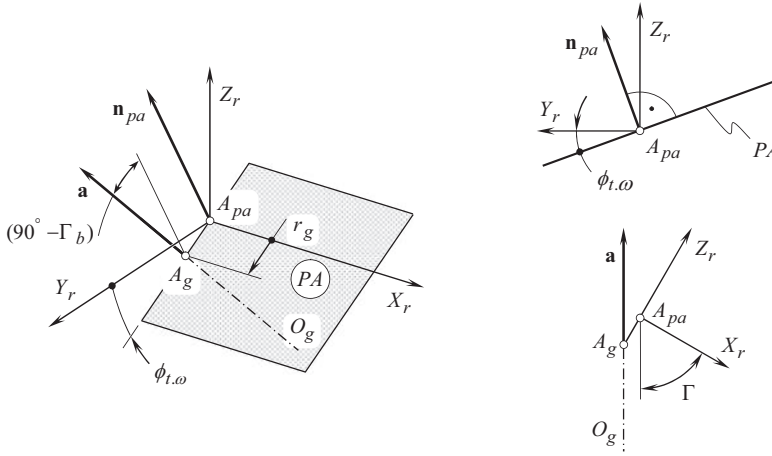


**FIGURE 14.23** Relationship between the pitch cone angle,  $\Gamma$ , and the base cone angle,  $\Gamma_b$ , in a gear for crossed-axes gearing.

$$\mathbf{a} = -\mathbf{i} \cdot r_g \cos \Gamma + \mathbf{k}_r \cdot \sin \Gamma \quad (14.91)$$

Once the equality  $\angle(\mathbf{n}_{pa}, \mathbf{a}) = (90^\circ - \Gamma_b)$  is valid, the base cone angle of the gear can be calculated from the formula:

$$\Gamma_b = \tan^{-1} \left( \frac{|\mathbf{n}_{pa} \times \mathbf{a}|}{\mathbf{n}_{pa} \cdot \mathbf{a}} \right) \quad (14.92)$$

The following expression for the calculation of the base cone angle,  $\Gamma_b$ , in a gear:

$$\Gamma_b = \tan^{-1} \left( \frac{\sqrt{\cos^2 \Gamma + \sin^2 \Gamma \cos^2 \phi_{t,\omega}}}{\sin \Gamma \sin \phi_{t,\omega}} \right) \quad (14.93)$$

is derived after substituting the vectors,  $\mathbf{n}_{pa}$  [from Eq. (14.83)], and,  $\mathbf{a}$  [from Eq. (14.91)], into Eq. (14.92).

A similar expression:

$$\gamma_b = \tan^{-1} \left( \frac{\sqrt{\cos^2 \gamma + \sin^2 \gamma \cos^2 \phi_{t,\omega}}}{\sin \gamma \sin \phi_{t,\omega}} \right) \quad (14.94)$$

is valid for the calculation of the base cone angle,  $\gamma_b$ , in a pinion.

In a particular case, when the pitch cone angle in a gear,  $\Gamma$ , is set equal to a right angle ( $\Gamma = 90^\circ$ ), the pitch cone becomes a flat surface and the resulting gear is commonly called a *crown gear*. So, a crown gear is a bevel gear with a planar pitch surface. The position vector of the point of a crown gear is specified by Eq. (14.53) under the assumption that the equality  $\Gamma = 90^\circ$  is valid.

The base cone angle of a crown gear,  $\Gamma_b$ , equals  $\Gamma_b = 90^\circ - \phi_{t,\omega}$ .

The back cone in a crown gear is degenerated to a round cylinder. The crown gear is an equivalent of the basic rack in spur and helical gears.

For an internal gearing, the value of the base cone angle,  $\Gamma_b$ , (a) either falls into the interval  $(90^\circ - \phi_{t,\omega}) < \Gamma_b < 90^\circ$ , or (b) it is equal to a right angle ( $\Gamma_b = 90^\circ$ ), or (c) its value is within the

interval  $90^\circ < \Gamma_b < 180^\circ$ . This makes possible to distinguish internal crossed-axes gear of three different types, and in this way to represent the classification of types of gear vector diagrams (see Figure 2.16) more in detail.

#### 14.6.4 ANGULAR PITCH

The angular distance between two adjacent tooth flanks measured within the pitch plane in a crossed-axes gear pair is specified by the angular pitch. The angular pitch<sup>9</sup> is centered at the pitch-plane-apex,  $A_{pp}$ .

##### Definition 14.3

The angular pitch in crossed-axes gear pair is an angular distance between two adjacent tooth flanks of the gear measured within the pitch plane.

Consider a crossed-axes gear pair, as schematically illustrated in Figure 14.24. An *auxiliary round rack* is associated with the gear pair. This auxiliary rack, or, in other words, the *round basic rack*, is an equivalent of the corresponding auxiliary rack, associated with a parallel-axes gear pair. A similar round basic rack is also used in intersected-axes gearing (see Figure 12.29).

When the gears rotate, the auxiliary round rack rotates together with the gears. The rotation of the round basic rack is synchronized with the rotations of the gear and of the pinion. The rotation vector,  $\omega_{pp}$ , of the round rack (of the pitch plane,  $PP$ ) is located within the plane that is parallel to the rotation vectors of the gear,  $\omega_g$ , and of the pinion,  $\omega_p$ . The rotation vector,  $\omega_{pp}$ , is a vector through the plane-of-action apex,  $A_{pa}$ , and is pointed perpendicular to the axis of instantaneous rotation,  $P_{in}$ . Evidently, the rotation vector,  $\omega_{pp}$ , is perpendicular to the vector of instantaneous rotation,  $\omega_{pl}$ . Due to lack of space, the latter is not shown in Figure 14.24.

The outer radius,  $r_{o,pp}$ , of the working portion of the pitch plane is equal to the cone distance of the gear pair, while the inner radius,  $r_{l,pp}$ , is smaller than  $r_{o,pp}$  by the face width,  $F_{pp}$ , of the pitch plane.

An equation for the calculation of the angular pitch of the gear,  $\varphi_{n,g}$ , in a crossed-axes gearing can be derived similarly to that an equation for the calculation of angular pitch of the gear,  $\varphi_{n,g}$ , in intersected-axes gears [see Eq. (12.91)] is derived:

$$\varphi_{n,g} = \frac{360^\circ}{N_g} \cdot \frac{\sin \Gamma}{\cos \Sigma_g} \quad (14.95)$$

In Eq. (14.95), the diameter,  $d_{o,pp}$ , equals  $d_{o,pp} = 2r_{o,pp}$ .

The difference between Eqs. (12.107) and (14.95) is due to that the rolling component,  $\omega_g^{rl}$ , of the rotation vector of the gear,  $\omega_g$ , is taken into account. The sliding component,  $\omega_g^{sl}$ , does not cause rolling motion.

The expression [see Eq. (14.95)] for the calculation of the angular pitch in the gear,  $\varphi_{n,g}$ , along with the expression [see Eq. (14.75)] for the calculation of the base angular pitch in the gear,  $\varphi_b$ , make possible an expression:

$$\varphi_b = \varphi_{n,g} \frac{\sin \Gamma_b}{\sin \Gamma} \quad (14.96)$$

for the angular base pitch,  $\varphi_b$ , in terms of the angular pitch,  $\varphi_{n,g}$ .

<sup>9</sup> Angular module,  $m_{\gamma,pp}$ , is an equivalent to the angular pitch,  $\varphi_{pp}$ , as:  $m_{\gamma,pp} = \frac{360^\circ}{N_{pp}} = \frac{2\pi}{N_{pp}}$ .

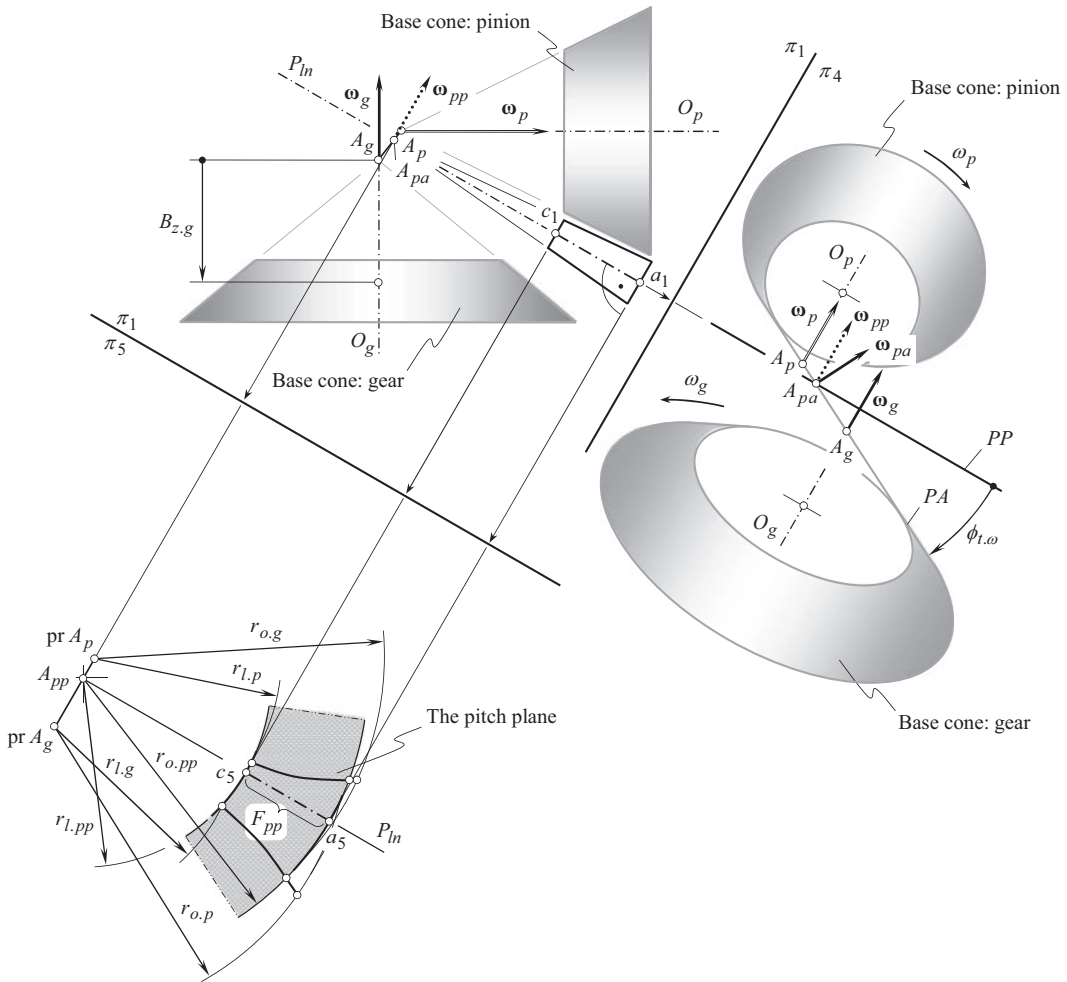


**FIGURE 14.24** Pitch surfaces in orthogonal crossed-axes gear pair (here, points  $pr A_g$  and  $pr A_p$  are the projections of the gear,  $A_g$ , and of the pinion,  $A_p$ , base cone apexes, correspondingly, onto the pitch-plane,  $PP$ ).

In geometrically accurate crossed-axes gearing, the angular base pitch in the gear,  $\phi_{b,g}$ , is equal to the angular base pitch in the pinion,  $\phi_{b,p}$ , and both of them are equal to the operating base pitch,  $\phi_{b,op}$ , in the gear pair.

#### 14.6.5 ANGULAR TOOTH THICKNESS, AND ANGULAR SPACE WIDTH, IN THE ROUND BASIC RACK

The angular tooth thickness and the angular space width in round basic rack in a crossed-axes gear pair are the equivalents to the tooth thickness, and the space width in parallel-axes gears. Both the tooth thickness and the space width are measured within the pitch plane,  $PP$ , of the corresponding round rack of the gear pair.

#### Definition 14.4

Angular tooth thickness in crossed-axes gear pair is the angular distance between opposite tooth flanks of the gear tooth measured within the pitch plane.



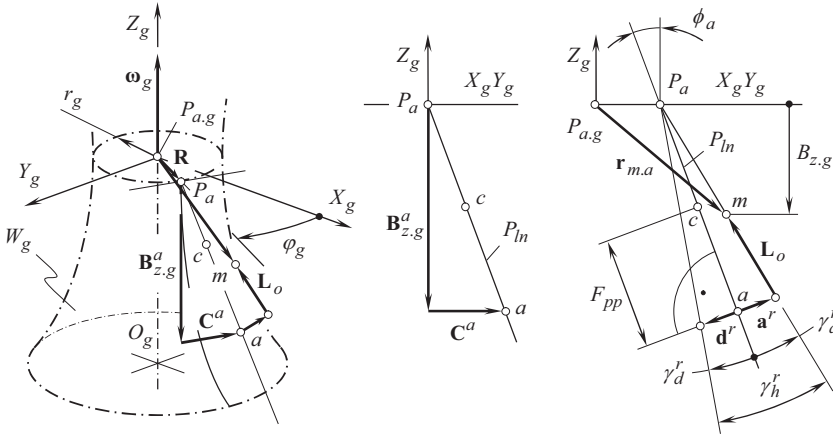


FIGURE 14.26 Generation of the outer surface of a gear for crossed-axes gearing.

$$\mathbf{R} = \mathbf{i} \cdot r_g \cos \phi_g + \mathbf{j} \cdot r_g \sin \phi_g \quad (14.100)$$

$$\mathbf{B}_{z,g} = \mathbf{k} B_{z,g} \quad (14.101)$$

$$\mathbf{C} = -\mathbf{i} B_{z,g} \tan \Sigma_g \sin \phi_g + \mathbf{j} B_{z,g} \tan \Sigma_g \cos \phi_g \quad (14.102)$$

The *Gaussian parameters*,  $\phi_g$  and  $B_{z,g}$ , of the pitch surface,  $W_g$ , are schematically shown in Figures 14.25 and 14.26.

Equations (14.99)–(14.102) yield an expression for the position vector of point,  $\mathbf{w}_g$ , of the pitch surface,  $W_g$ , in terms of the *Gaussian parameters*,  $\phi_g$  and  $B_{z,g}$ :

$$\mathbf{w}_g(\phi_g, B_{z,g}) = \begin{bmatrix} r_g \cos \phi_g - B_{z,g} \tan \Sigma_g \sin \phi_g \\ r_g \sin \phi_g + B_{z,g} \tan \Sigma_g \cos \phi_g \\ B_{z,g} \\ 1 \end{bmatrix} \quad (14.103)$$

The pitch surface,  $W_g$ , is shaped in the form of a surface of revolution, that is commonly referred to as the *hyperboloid of one sheet*.

The pitch surface,  $W_g$  [see Eq. (14.103)], is convenient to employ as a reference surface.

An equation:

$$\mathbf{w}_p(\phi_p, B_{z,p}) = \begin{bmatrix} r_p \cos \phi_p + B_{z,p} \tan \Sigma_p \sin \phi_p \\ r_p \sin \phi_p - B_{z,p} \tan \Sigma_p \cos \phi_p \\ B_{z,p} \\ 1 \end{bmatrix} \quad (14.104)$$

similar to Eq. (14.103) can be derived for the position vector of point,  $\mathbf{w}_p$ , of the pitch surface,  $W_p$ , of the mating pinion for a crossed-axes gear pair.

The *angular tooth addendum*, as well as the *angular tooth dedendum*, in gears for crossed-axes gear pair can be specified in relation to the round basic rack of the gear pair. This allows for two more definitions to be introduced:



**Definition 14.6**

The angular tooth addendum,  $\gamma'_a$ , in crossed-axes gear pair is the angular distance between the pitch plane and the outer cone of the round basic rack of the gear pair.

Similar to this, the angular dedendum in a crossed-axes gearing is specified in terms of the pitch plane of the gear and the gear bottom-land cone (inner cone of the gear).

**Definition 14.7**

The angular tooth dedendum,  $\gamma'_d$ , in crossed-axes gear pair is the angular distance between the pitch plane and the inner cone of the round basic rack of the gear pair.

For the specification of both of the angular tooth addendum and the angular tooth dedendum in gears for a crossed-axes gear pair, the use of expressions for the outer surface (the top-land-surface) of the gear, and of the inner surface (the bottom-land surface) of the gear is convenient.

An analytical expression for the position vector of point,  $\mathbf{r}_{m.a}$ , of the outer surface in the gear for crossed-axes gearing can be derived using vector approach.

Referring to Figure 14.26, and using the pitch surface,  $W_g$ , as the reference surface, the position vector,  $\mathbf{r}_{m.a}$ , of point of the *top-land-surface* in the gear for a crossed-axes gearing can be represented as the vector summa:

$$\mathbf{r}_{m.a} = \mathbf{w}_p + \mathbf{a}^r + \mathbf{L}_o \quad (14.105)$$

The vector,  $\mathbf{w}_p$ , is specified by Eq. (14.103).

The tooth addendum at the periphery of the round basic rack is specified by the vector,  $\mathbf{a}^r$ . The vector,  $\mathbf{a}^r$ , is perpendicular to the pitch surface,  $W_g$ , and the magnitude of the vector,  $\mathbf{a}^r$ , equals to the tooth dedendum at the point  $a$ . The vector,  $\mathbf{a}^r$ , can be expressed in terms of design parameters of the gear:

$$\mathbf{a}^r = -\mathbf{i} a^r \cos \Sigma_g \cos \varphi_g - \mathbf{j} a^r \cos \Sigma_g \sin \varphi_g + \mathbf{k} a^r \sin \Sigma_g \quad (14.106)$$

In Eq. (14.106), the magnitude of the vector,  $\mathbf{a}^r$ , is denoted by  $a^r$ , ( $a^r = |\mathbf{a}^r|$ ).

The vector,  $\mathbf{L}_o$ , is pointed along a straight generating line of the outer surface of the gear. The distance of point of interest,  $m$ , from the periphery of the round basic rack is equal to the magnitude of the vector,  $\mathbf{L}_o$  ( $L_o = |\mathbf{L}_o|$ ). For the calculation of the vector,  $\mathbf{L}_o$ , the following expression:

$$\mathbf{L}_o = \mathbf{i} L_o \cos(\Sigma_g + \gamma'_a) \cos \varphi_g + \mathbf{j} L_o \cos(\Sigma_g + \gamma'_a) \sin \varphi_g + \mathbf{k} [B_{z.g}^a - a^r \sin \Sigma_g - L_o \sin(\Sigma_g + \gamma'_a)] \quad (14.107)$$

is derived.

In Eq. (14.107), the length of the vector,  $\mathbf{L}_o$ , is designated as  $L_o$ , ( $L_o = |\mathbf{L}_o|$ ). The distance,  $L_o$ , can be calculated from the formula:

$$L_o = \frac{B_{z.g}^a - a^r \sin \Sigma_g - B_{z.g}}{\cos(\Sigma_g + \gamma'_a)} \quad (14.108)$$

$$L_o = \frac{B_{z.g}^a - a^r \sin \Sigma_g - B_{z.g}}{\cos(\Sigma_g + \gamma'_a)} \quad (14.109)$$

Having calculated the vectors,  $\mathbf{w}_p$ ,  $\mathbf{a}^r$  and  $\mathbf{L}_o$ , [see Eqs. (14.103), (14.104), and (14.108)], the position vector,  $\mathbf{r}_{m.a}$ , of point of the *top-land-surface* in the gear for a crossed-axes gearing can be analytically described by a matrix equation in the form:

$$\mathbf{r}_{m.a}(\varphi_g, L_o) = \begin{bmatrix} r_g \cos \varphi_g - B_{z.g} \tan \Sigma_g \sin \varphi_g - a^r \cos \Sigma_g \cos \varphi_g + L_o \cos(\Sigma_g + \gamma_a^r) \cos \varphi_g \\ r_g \sin \varphi_g + B_{z.g} \tan \Sigma_g \cos \varphi_g - a^r \cos \Sigma_g \sin \varphi_g + L_o \cos(\Sigma_g + \gamma_a^r) \sin \varphi_g \\ B_{z.g} + a^r \sin \Sigma_g + B_{z.g}^a - a^r \sin \Sigma_g - L_o \sin(\Sigma_g + \gamma_a^r) \\ 1 \end{bmatrix} \quad (14.110)$$

Referring to Figure 14.26 and using the pitch surface,  $W_g$ , as the reference surface, the position vector,  $\mathbf{r}_{m.d}$ , of point of the *bottom-land surface* of the gear in a crossed-axes gearing can be represented as a vector summa:

$$\mathbf{r}_{m.a} = \mathbf{w}_p - \mathbf{d}^r + \mathbf{L}_o \quad (14.111)$$

The vector,  $\mathbf{w}_p$ , is specified by Eq. (14.103).

The tooth dedendum at the periphery of the round basic rack is specified by the vector,  $\mathbf{d}^r$ . The vector,  $\mathbf{d}^r$ , is perpendicular to the pitch surface,  $W_g$ , and the magnitude of this vector equals to the tooth dedendum at the point  $a$ . The vector,  $\mathbf{d}^r$ , can be expressed in terms of the design parameters of the gear:

$$\mathbf{d}^r = \mathbf{i} d^r \cos \Sigma_g \cos \varphi_g + \mathbf{j} d^r \cos \Sigma_g \sin \varphi_g - \mathbf{k} d^r \sin \Sigma_g \quad (14.112)$$

In Eq. (14.112), the magnitude of the vector,  $\mathbf{d}^r$ , is designated as  $d^r$ , ( $d^r = |\mathbf{d}^r|$ ).

Ultimately, Eq. (14.107) can be used for the calculation of the vector,  $\mathbf{L}_o$ .

Having calculated the vectors,  $\mathbf{w}_p$ ,  $\mathbf{d}^r$  and  $\mathbf{L}_o$  [see Eqs. (14.10), (14.112), and (14.108)], the position vector of point,  $\mathbf{r}_{m.d}$ , of the *bottom-land surface* of the gear in a crossed-axes gearing is analytically described by a matrix equation in the form:

$$\mathbf{r}_{m.d}(\varphi_g, L_o) = \begin{bmatrix} r_g \cos \varphi_g - B_{z.g} \tan \Sigma_g \sin \varphi_g + d^r \cos \Sigma_g \cos \varphi_g + L_o \cos(\Sigma_g + \gamma_a^r) \cos \varphi_g \\ r_g \sin \varphi_g + B_{z.g} \tan \Sigma_g \cos \varphi_g + d^r \cos \Sigma_g \sin \varphi_g + L_o \cos(\Sigma_g + \gamma_a^r) \sin \varphi_g \\ B_{z.g} - d^r \sin \Sigma_g + B_{z.g}^a - a^r \sin \Sigma_g - L_o \sin(\Sigma_g + \gamma_a^r) \\ 1 \end{bmatrix} \quad (14.113)$$

In a similar manner, corresponding expressions for the *top-land-surface*, and the *bottom-land surface*, in a pinion for a crossed-axes gear pair can be derived, as well.

Once the *top-land-surface* and the *bottom-land surface* in a gear are described analytically [see Eqs. (14.110) and (14.113)], they can be approximated by corresponding cone surfaces. This is practical from the manufacturing standpoint. In most cases, the apexes of the *top-land-surface* and the *bottom-land surface* are displaced in the axial direction of the gear at a certain distance. The displacement,  $\Delta A$ , depends on the kind of approximation of the hyperboloid of one sheet by a cone surface.

Its right point to stress here that the aforementioned approximation is not a must, and both the gear and the pinion can be manufactured with these surfaces shaped in the form of hyperboloid of one sheet.

The angular addendum,  $\Gamma_a$ , and the angular dedendum,  $\Gamma_d$ , of the gear tooth together specify the angular tooth height,  $\Gamma_h$ , of the gear (see Figure 14.27) in crossed-axes gearing:

$$\Gamma_h = \Gamma_a + \Gamma_d \quad (14.114)$$

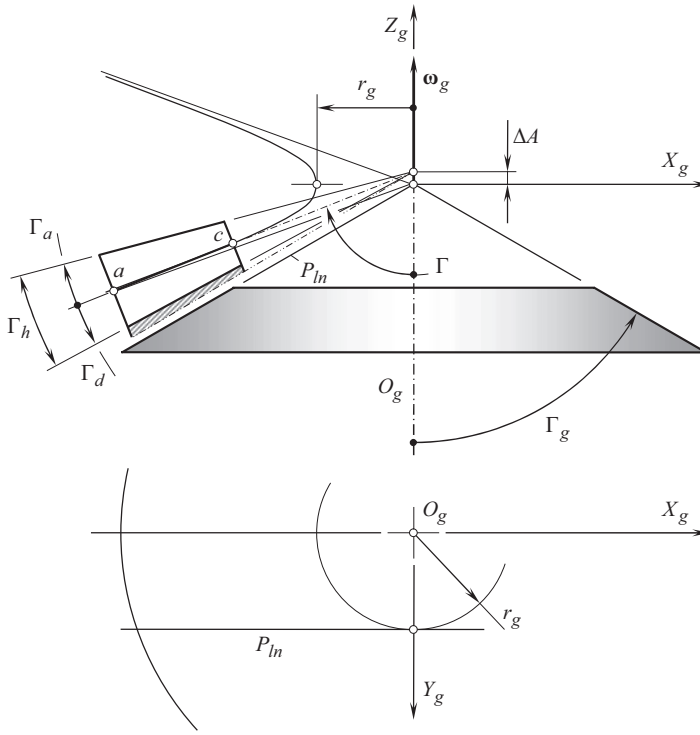


**FIGURE 14.27** Specification of the tooth addendum, and tooth dedendum, of a gear in intersected-axes gearing.

For standard gears, the tooth height of a round basic rack is set equal to module,  $m$ . This makes possible calculation the gear angular addendum,  $\Gamma_a$ :

$$\Gamma_a = \sin^{-1} \left( \frac{m}{r_{o,pp}} \right) \quad (14.115)$$

The dedendum of a standard gear is greater than the addendum at the clearance,  $c$ . Therefore, the angular dedendum,  $\Gamma_d$ , of the gear can be calculated as follows:

$$\Gamma_d = \sin^{-1} \left( \frac{m + c}{r_{o,pp}} \right) \quad (14.116)$$

Formulae similar to those aforementioned:

$$\gamma_a = \sin^{-1} \left( \frac{m}{r_{o,pp}} \right) \quad (14.117)$$

$$\gamma_d = \sin^{-1} \left( \frac{m + c}{r_{o,pp}} \right) \quad (14.118)$$

$$\gamma_h = \gamma_a + \gamma_d \quad (14.119)$$

**TABLE 14.2****Design Parameters of Crossed-Axes Gears and Their Corresponding Design Parameters of Parallel-Axes Gears**

Design Parameters of Crossed-Axes Gearing		Design Parameters of Parallel-Axes Gearing	
Term	Designation	Term	Designation
Tooth number	$N_g, N_p$	Tooth number	$N_g, N_p$
Pitch cone angle (gear)	$\Gamma$	Pitch diameter	$d_g, d_p$
Pitch cone angle (pinion)	$\gamma$	Base pitch	$p_b$
Base pitch angle (gear)	$\Gamma_b$	Outer diameter	$d_{o,g}, d_{o,p}$
Base pitch angle (pinion)	$\gamma_b$	Root diameter	$d_{f,g}, d_{f,p}$
Outer cone angle (gear)	$\Gamma_o$	Normal profile angle	$\phi_n$
Outer cone angle (pinion)	$\gamma_o$	Normal circular pitch	$p_n$
Root cone (gear)	$\Gamma_f$	Base pitch	$p_b$
Root cone (pinion)	$\gamma_f$	Tooth thickness	$t$
Normal profile angle	$\phi_n$	Space width	$w$
Angular pitch	$\phi_n$	Backlash	$B$
Base pitch angle	$\phi_b$	Addendum	$a$
Angular tooth thickness	$\phi_t$	Dedendum	$b$
Angular space width	$\phi_w$		
Angular backlash <sup>a</sup>	$\phi_B$		
Angular addendum (gear)	$\Gamma_a$		
Angular addendum (pinion)	$\gamma_a$		
Angular dedendum (gear)	$\Gamma_b$		
Angular dedendum (pinion)	$\gamma_b$		

<sup>a</sup> The expressions  $\phi_n = \phi_t + \phi_w$  and  $\phi_w - \phi_t = \phi_B$  are always valid.

are valid for the calculation of the angular addendum,  $\gamma_a$ , angular dedendum,  $\gamma_d$ , and angular tooth height,  $\gamma_h$ , in a standard pinion (see Figure 14.27) for a crossed-axes gear pair.

The angular clearance,  $\gamma_c$ , is calculated as:

$$\gamma_c = \sin^{-1} \left( \frac{c}{r_{o,pp}} \right) \quad (14.120)$$

The aforementioned design parameters in gears, and of crossed-axes gear pairs, correlate to the corresponding design parameters of parallel-axes gears. The correlation between the design parameters is outlined in Table 14.2.

#### 14.6.7 SPECIFICATION OF THE DESIGN PARAMETERS IN CROSSED-AXES GEARING

The design parameters of crossed-axes gears that are convenient for the investigation and analysis are not always identical to those used in gear design, and in gear manufacturing practice.

Crossed-axes gearing has not been profoundly investigated yet. In the meantime, many of the design parameters of the crossed-axes gear-sets can be determined only approximately, based on empirical formulas, and on accumulated experience. Experience that is accumulated in designing of intersected-axes gearing is helpful, and it can be enhanced in the area of designing crossed-axes gear pairs, as the *top-land-surface* and the *bottom-land surface* in a gear for crossed-axes gearing can be approximated by cone surfaces. Therefore, the main design parameters in crossed-axes

gearing can be determined in a manner similar to that already discussed for intersected-axes gear. This is schematically illustrated in Figures 12.36 and 12.37.

The addendum, and the dedendum, of a gear in a gear for a crossed-axes gear pair are specified on the so-called *back cone* surface. The straight generating line of the back cone is perpendicular to corresponding straight generating line of the pitch cone. The angular addendum,  $\Gamma_a$ , and angular dedendum,  $\Gamma_d$ , can be calculated from the equations:

$$\Gamma_a = \tan^{-1} \left( \frac{2a \sin \Gamma}{m N_g} \right) \quad (14.121)$$

$$\Gamma_d = \tan^{-1} \left( \frac{2b \sin \Gamma}{m N_g} \right) \quad (14.122)$$

For standard gears [for which  $a = m$  and  $b = (1.2 \div 1.3)m$ , here the module of the gear is denoted by  $m$ ] Eqs. (14.121) and (14.122) are reduced to:

$$\Gamma_a = \tan^{-1} \left( \frac{2 \sin \Gamma}{N_g} \right) \quad (14.123)$$

$$\Gamma_d = \tan^{-1} \left[ \frac{(2.4 \div 2.6) \sin \Gamma}{N_g} \right] \quad (14.124)$$

Equations similar to the above Eqs. (14.123)–(14.124) are valid also for a bevel pinion.

It is instructive to point out here that once one of the three elements listed immediately below:

- The path of contact
- The gear tooth flank geometry
- The mating pinion tooth flank geometry

is known, then the two others are predetermined by the known one. Only geometrically accurate gears feature this unique property. Moreover, this property is irrelevant to approximate crossed-axes gearing of all designs.

Geometrically accurate crossed-axes gear pairs can operate at high RPM, as they feature equal angular base pitches: the gear angular base pitch,  $\varphi_{b.g}$ , and the mating pinion angular base pitch,  $\varphi_{b.p}$ , both, are equal to operating angular base pitch,  $\varphi_{b.op}$ , of the gear pair (i.e., the following two equalities,  $\varphi_{b.g} = \varphi_{b.op}$  and  $\varphi_{b.p} = \varphi_{b.op}$ , are valid in geometrically accurate crossed-axes gear-sets). Therefore, gearing of this kind can be used in first stages in gear trains, where forces and torque are low.

## 14.7 BACKLASH IN CROSSED-AXES GEARING

Gears for crossed-axes gear pairs are designed and manufactured so as to provide a specific amount of backlash – that is, the space between mating gear teeth, or the difference in width of the gear tooth and pinion tooth to let the gears mesh without binding and to provide space for a film of lubricating oil between the teeth. This prevents overheating and tooth damage. The backlash is necessary for proper operation of the gear pair.

To optimize the performance of gears in crossed-axes gearing, the gears must be positioned together so, that they run smoothly without binding and/or excessive backlash. In the present-day practice of gear production, unless otherwise specified, the minimum amount of total backlash of a pair of gears in crossed-axes gearing is measured at the tightest point of mesh with a dial

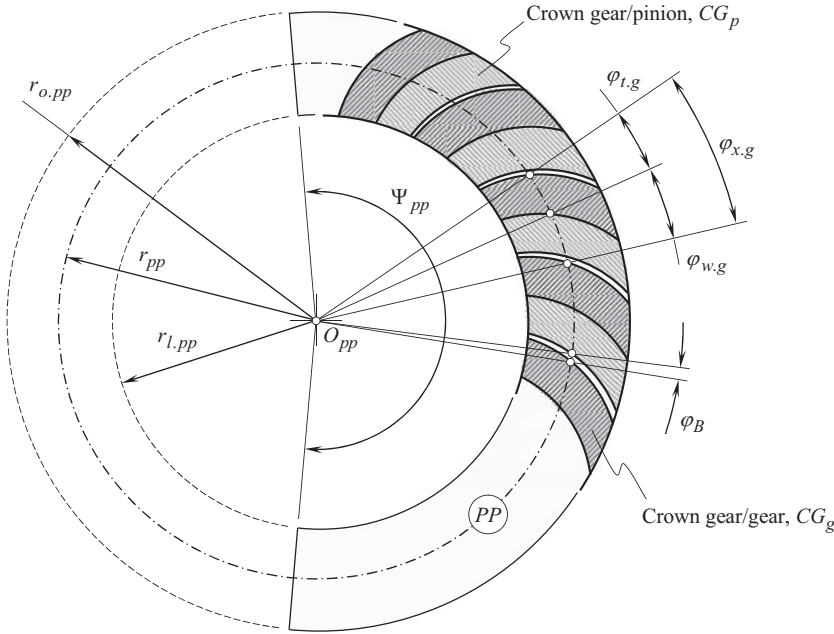


**FIGURE 14.28** On the definition of the terms: (a) the *angular tooth thickness*,  $\phi_t$ , (b) the *angular space width*,  $\phi_w$ , and (c) the *angular backlash*,  $\phi_B$ , in crossed-axes gearing by means of  $CG_g -$  to  $-CG_p$  mesh.

indicator on a bevel gear testing machine. Unless other specified, backlash is assumed to be normal backlash,<sup>10</sup> and cannot be measured in the plane of rotation. Backlash is necessary to achieve correct operation of the gears and varies with the size of the tooth and operating conditions. Gears for crossed-axes gear-sets are cut to have a definite amount of backlash when correctly assembled together. But excessive backlash, or play, if great enough, can cause a sudden impulse, or shock load in starting, or reversing that may cause serious tooth damage. Excessive, or insufficient backlash can also result in noise, excessive wear and damage.

Numerous inconsistencies are observed in the definition and interpretation of backlash in crossed-axes gearing. To avoid these inconsistencies in the definition of backlash, the backlash in crossed-axes gearing can be defined in the following way.

Consider a phantom crown gear that is engaged in correct mesh with the gear. This crown gear is referred to as a *crown gear/gear*, or simply as  $CG_g$ . The outer diameter of the crown gear is labeled as  $r_{o.pp}$ , the inner diameter is labeled as  $r_{l.pp}$ , and the pitch diameter is labeled as  $r_{pp}$ . The face width,  $F_{pp}$ , of the crown gear is equal to  $F_{pp} = r_{o.pp} - r_{l.pp}$ . The central angle  $\Psi_{pp}$  spans over the active portion of the crown gear,  $CG_g$ . The axis of rotation of the crown gear,  $CG_g$ , is labeled as  $O_{pp}$ . Here, the subscript “pp” indicates that the design parameters correspond to the pitch plane,  $PP$ .

The angular tooth thickness,  $\phi_{t.g}$ , and the angular space width,  $\phi_{w.g}$ , in a gear is measured within the pitch plane,  $PP$ , of the *crown gear/gear*,  $CG_g$ , as shown in Figure 14.28. The angular pitch of the gear teeth in Figure 14.28 is labeled as  $\phi_{x.g}$ .

Similarly, consider a phantom crown gear that is engaged in correct mesh with the pinion. This crown gear is referred to as a *crown gear/pinion*, or simply as  $CG_p$ . The angular tooth thickness,  $\phi_{t.p}$ , and the angular space width,  $\phi_{w.p}$ , of a gear is measured within the pitch plane,  $PP$ , of the *crown gear/pinion*,  $CG_p$ , (not shown in Figure 14.28). The angular pitch of the pinion teeth is labeled as  $\phi_{x.p}$  (not shown in Figure 14.28).

<sup>10</sup> A straight line along which the so-called **normal backlash** is measured can NOT be perpendicular to both, to the gear tooth flank,  $\mathcal{S}$ , and to the pinion tooth flank,  $\mathcal{P}$ , at the same time.

The angular pitches of the gear,  $\varphi_{x,g}$ , and that of the pinion,  $\varphi_{x,p}$ , are equal to one another, that is, the equality  $\varphi_{x,g} = \varphi_{x,p} = \varphi_x$ . Therefore, in the further discussion the designations for these angular pitches,  $\varphi_{x,g}$  and  $\varphi_{x,p}$ , are replaced with  $\varphi_x$ .

### Definition 14.8

Effective angular backlash,  $\varphi_{B,pa}$ , in geometrically accurate crossed-axes gearing is said to be an angular distance between the non-interacting tooth flank of a driving member, and the tooth-space flank of the driven member in a gear pair; effective angular backlash,  $\varphi_{B,pa}$ , is measured within the plane of action.

When the crown gear,  $CG_g$ , and the crown gear,  $CG_p$ , are engaged in mesh, they are free to turn about the  $O_{pp}$  – axis in relation to one another through certain angle,  $\varphi_B$ . The angle,  $\varphi_B$ , is referred to as the *angular backlash*. The *angular backlash*,  $\varphi_B$ , is calculated as:

$$\varphi_B = \varphi_{w,g} - \varphi_{t,p} \quad (14.125)$$

or as:

$$\varphi_B = \varphi_{w,p} - \varphi_{t,g} \quad (14.126)$$

**Conclusion 14.3.** *Backlash in crossed-axes gearing is an angular parameter, and not a linear parameter.*

Novel instrumentation can be developed for the direct inspection of the design parameters in a gear ( $\varphi_{t,g}$ ,  $\varphi_{w,g}$ , and  $\varphi_{x,g}$ ), and in a mating pinion ( $\varphi_{t,p}$ ,  $\varphi_{w,p}$ , and  $\varphi_{x,p}$ ). Then, either Eqs. (14.125) or (14.126) can be used for the calculation of the angular backlash,  $\varphi_B$ .

In a crossed-axes gear pair, the backlash is measured at a configuration of a gear and a mating pinion when *two pairs of teeth are engaged in mesh*.

If the backlash does not fall within the recommended limits, no corrections to the mounting distance are permissible to adjust for the backlash. If possible, the tooth thickness can be corrected (reduced) by additional machining.

There is a trade of when setting an actual value of backlash: the backlash must be large enough for operating of the gear pair, and it must be small enough when reversing the rotation.

## 14.8 POSSIBLE ANALOGY OF TREDGOLD APPROXIMATION FOR CROSSED-AXES GEARING

Meshing of crossed-axes gears is observed on a sphere of certain radius, similar to meshing of parallel-axes gears that is observed within a plane perpendicular to the axes of rotations of the mating gears. The sphere is centered at the plane-of-action apex,  $A_{pa}$ , within the instantaneous axis of rotation,  $P_{in}$ . At that same time, the sphere is centered at point within the centerline,  $\mathfrak{L}$ , between the axis of rotation of the gear,  $O_g$ , and of the pinion,  $O_p$ . *Tredgold method* can be evolved, and can be adjusted for the purposes of crossed-axes gearing.

By using the *Tredgold method*, a *back cone* is formed of elements that are perpendicular to the axis of instantaneous rotation,  $P_{in}$ , at the large end of the teeth. The length of a back cone element is called the *back-cone radius*. Now an equivalent spur gear is constructed, whose pitch radius,  $r_{eq}$ , is equal to the back cone radius. Thus, from a pair of crossed-axes gears we can obtain a pair of equivalent spur gears using the approximation, which are then used to define the tooth profiles; they can also be used to determine the tooth action and the contact conditions exactly, as for ordinary spur gears, and the results will correspond closely to those for the crossed gears. The equivalent pitch radii are:

$$r_{eq.g} = \frac{r_g}{\cos \Gamma} \quad (14.127)$$

and

$$r_{eq.p} = \frac{r_p}{\cos \gamma} \quad (14.128)$$

The tooth number in the equivalent spur gear is:

$$N_{eq} = \frac{2\pi r_{eq}}{p} \quad (14.129)$$

where  $p$  is the circular pitch of the crossed-axes gear that is measured at the large end of the tooth. In reality, the equivalent spur gears will not have an integral number of teeth.

## 14.9 MAIN FEATURES OF GEOMETRICALLY ACCURATE *NOVIKOV/CONFORMAL* AND *HIGH-CONFORMAL* CROSSED-AXES GEARING

*Novikov/conformal* and *high-conformal* crossed-axes gearing can be used for transmitting a rotary motion from a driving shaft to a driven shaft that crosses each other at an angle. Gears of this kind are capable of transmitting a uniform rotation from a driving shaft to a driven shaft. So far, *Novikov/conformal* and *high-conformal* crossed-axes gears got no application in the industry. This is chiefly because they are not profoundly investigated yet. Very limited research is carried out so far in this particular kind of gearing. A few papers by Dr. *Roslivker* [192,193] are to be mentioned in this regard.

There are many similarities between geometrically accurate crossed-axes *Novikov/conformal* and *high-conformal* gearing and gearing of conventional design, that is, that feature line contact between a gear and a mating pinion tooth flank. Because of this, there is no need to consider separately, for example, kinematics of the instantaneous motion in *Novikov/conformal* and *high-conformal* crossed-axes gearing, as it is identical to that that is already discussed in detail in a corresponding section devoted to perfect crossed-axes gearing of conventional design (*R* – gearing).

Base cones of a gear and of its mating pinion is the other example of the similarities between *Novikov/conformal* and *high-conformal* crossed-axes gearing, and between geometrically accurate crossed-axes gearing of conventional design.

Sliding between the tooth flanks of a gear and of a mating pinion in crossed-axes *Novikov/conformal* and *high-conformal* gearing can be viewed as a reduced case of that in geometrically accurate crossed-axes gearing of conventional design.

A few more similarities could be mentioned in this regard. These similarities, as well as a few others are omitted from the further analysis.

Below, the reader's attention is focused mainly on the key features of geometrically accurate *Novikov/conformal* and *high-conformal* crossed-axes gear pairs.

### 14.9.1 PATH OF CONTACT IN *NOVIKOV/CONFORMAL* AND *HIGH-CONFORMAL* CROSSED-AXES GEARING

The path of contact in a *Novikov/conformal* and *high-conformal* gear pair is a trace of contact point when the gears rotate. It is common practice to consider the path of contact,  $P_c$ , in a stationary reference system associated with the gear housing.

As the relative motion of the gear and of the mating pinion is an instant rotation,  $\omega_{pl}$ , about the axis of instantaneous rotation,  $P_m$ , a plane perpendicular to the rotation vector,  $\omega_{pl}$ , at an arbitrary



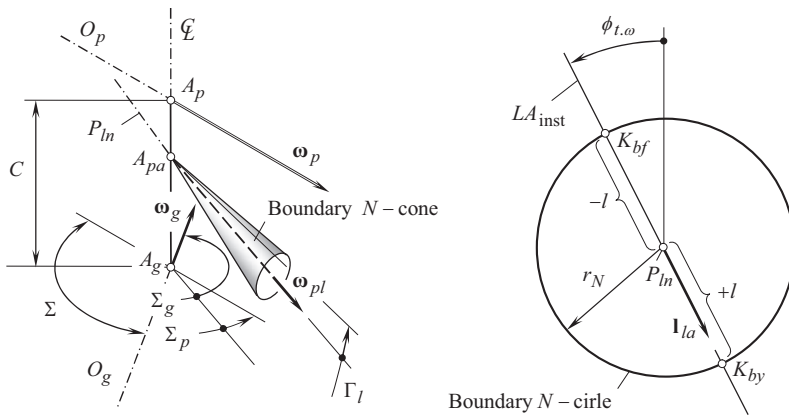


**FIGURE 14.29** Configuration of the boundary  $N$  – cone in *Novikov/conformal* and *high-conformal* crossed-axes gearing.

point  $P$  within  $P_{ln}$  can be constructed. The relative motion of the gear and the pinion can be investigated within the normal plane (see Figure 14.29).

Within the normal plane, a boundary  $N$  – circle is constructed. The center of the boundary  $N$  – circle is coincident with the point of intersection of the axis of instantaneous rotation,  $P_{ln}$ , by the normal plane. The radius,  $r_N$ , of the boundary  $N$  – circle is equal to a desirable displacement,  $l$ , of the contact point,  $K$ , from the pitch point along the instantaneous line of action,  $LA_{inst}$ . The displacements of both of a positive value,  $+l$ , and of a negative value,  $-l$ , are permissible. Therefore, two contact points,  $K_{by}$  and  $K_{bf}$ , are potentially possible.

The magnitude of the desirable displacement,  $l$ , is a trade-off between the contact strength of the gear tooth, and sliding between the tooth flanks,  $\mathcal{S}$  and  $\mathcal{P}$ , of the gear and of the pinion in relation to one another. The larger the displacement,  $l$ , the higher the contact strength of the gear tooth, and the higher the sliding between the tooth flanks. The smaller the distance,  $l$ , the lower the contact strength of the gear teeth and the lower the sliding between the tooth flanks.

#### 14.9.2 BOUNDARY $N$ – CONE IN NOVIKOV/CONFORMAL, AND HIGH-CONFORMAL CROSSED-AXES GEARING

A *boundary  $N$  – cone* in crossed-axes *Novikov/conformal*, and in *high-conformal* gearing, can be constructed in a way similar to that a *boundary  $N$  – cone* in *Novikov/conformal*, and *high-conformal* intersected-axes gearing was constructed.

When the gears rotate, a motion of the pinion in relation to the gear can be construed as instant rotation about the axis of instantaneous rotation,  $P_{ln}$ . A boundary  $N$  – circle is traced up by the contact point,  $K$ , in such a relative motion. In theory, the radius,  $r_N$ , of the boundary  $N$  – circle is a trade-off between the desirable high contact strength of the interacting tooth flanks, and low friction between the teeth flanks of the gear,  $\mathcal{S}$ , and the pinion,  $\mathcal{P}$ . In reality, a run-out of the gear and of the pinion should be taken into account.

Under an assumption:  $\Delta l = 0$ , and zero manufacturing errors, contact point,  $K$ , is located at the point of intersection of the boundary  $N$  – circle by the instantaneous line of action,  $LA_{inst}$ . At any point within the axis of instantaneous rotation,  $P_{ln}$ , a boundary  $N$  – circle of certain radius,  $r_N^i$ , can be constructed, and a line of action,  $L_{inst}^i$ , can be constructed, as well. The transverse pressure angle,  $\phi_{t,\omega}^i$ , is not mandatorily of that same value at all normal sections of the axis,  $P_{ln}$ . The instantaneous line of action,  $LA_{inst}$ , is a line through point within the pitch line,  $P_{ln}$ . The path of contact,  $P_c$ , is a zero-length straight-line segment that is aligned with the instantaneous line of action,  $L_{inst}^i$ . No kinematic and/or geometric constraints are violated in the analysis under such a consideration.

In practice, it is reasonable to retain the pressure angle,  $\phi_{t,\omega}^i$ , of certain constant value,  $\phi_{t,\omega}$ , within the active portion of the face width of the gear pair. Moreover, as a normal section through point within the axis,  $P_{ln}$ , approaches the plane-of-action apex,  $A_{pa}$ , the radius  $r_N^i$  of the boundary  $N$  – circle gets smaller. In this way, the pseudo-path of contact,  $P_{pc}$ , is the straight line through all the contact points,  $K^i$ . The pseudo-path of contact,  $P_{pc}$ , passes through the plane-of-action apex,  $A_{pa}$ . When the pseudo-path of contact,  $P_{pc}$ , is rotated about the axis of instantaneous rotation, the boundary  $N$  – cone is generated as a locus of consecutive positions of the pseudo-path of contact,  $P_{pc}$ , in its rotation about the axis,  $P_{ln}$ .

### Definition 14.9

The boundary  $N$  – cone in crossed-axes Novikov/conformal, and high-conformal gearing, is said to be a cone of revolution that is generated by rotation of the pseudo-path of contact,  $P_{pc}$ , about the axis of instantaneous rotation,  $P_{ln}$ .

The apex of the boundary  $N$  – cone coincides with the plane-of-action apex,  $A_{pa}$ .

It is natural to assume that the concave tooth flank (primarily, of the gear,  $\mathcal{G}$ ) is located within the exterior of the boundary  $N$  – cone, while the convex tooth flank (primarily, of the pinion,  $\mathcal{P}$ ) is located within the interior of the boundary  $N$  – cone. However, as the plane-of-action apex,  $A_{pa}$ , is not coincident neither with the gear-base-cone apex,  $A_g$ , nor with the pinion-base-cone apex,  $A_p$ , the boundary  $N$  – cone is not the only constraint onto the geometry of tooth flanks,  $\mathcal{G}$  and  $\mathcal{P}$ . The envelope to a family of consecutive positions of the boundary  $N$  – cone in its instantaneous screw motion is used for this purpose instead. For the gear tooth flank, the constraint is generated when the boundary  $N$  – cone is rotated about the gear axis of rotation,  $O_g$ . Similarly, for the pinion tooth flank, the constraint is generated when the boundary  $N$  – cone is rotated about the pinion axis of rotation,  $O_p$ . Ultimately, the convex tooth flank of one member of the gear pair must be entirely located with the interior of the corresponding enveloping surface, while the concave tooth flank of another member of the gear pair must be entirely located outside the interior of the corresponding enveloping surface.

The boundary cone angle,  $\Gamma_l$ , (see Figure 14.30), can be specified in terms (a) of the radius,  $r_N^i$ , of the boundary  $N$  – circle at an arbitrary point within the axis of instantaneous rotation,  $P_{ln}$ , and (b) of the cone distance,  $A_i$ , of that point from the apex,  $A_{pa}$  :

$$\Gamma_l = \tan^{-1} \left( \frac{r_N^i}{A_i} \right) \quad (14.130)$$

In general, a boundary  $N$  – surface, and not a boundary  $N$  – cone should be considered.

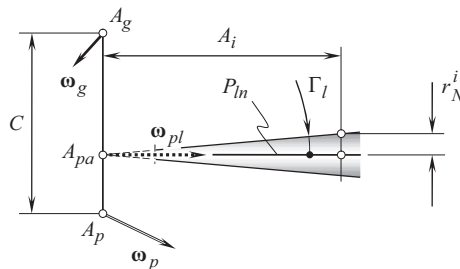


**FIGURE 14.30** Boundary  $N$  – cone angle, and cone angle,  $\Gamma_l$ , in Novikov/conformal, and high-conformal crossed-axes gearing.

### 14.9.3 BEARING CAPACITY OF CROSSED-AXES *NOVIKOV/CONFORMAL*, AND *HIGH-CONFORMAL* GEARING

The influence of an increase in radius,  $r_N$ , of the boundary  $N$  – circle on the rise of contact strength in a crossed-axes *Novikov/conformal*, and *high-conformal* gear pair, resembles in much that for the cases of parallel-axes, and intersected-axes *Novikov/conformal*, and *high-conformal* gearing.

The aforementioned conclusion on the bearing capacity of intersected-axes *Novikov/conformal*, and *high-conformal* gearing is also valid with respect to the bearing capacity of crossed-axes *Novikov/conformal*, and *high-conformal* gearing.

The bearing capacity of *Novikov/conformal*, and *high-conformal* crossed-axes gearing depends not only on the relative curvature,  $r_{rel}$ , of the interacting tooth flanks, but it also depends on the magnitudes of the radii of curvature of the tooth flanks,  $\mathcal{S}$  and  $\mathcal{P}$ , at point of their contact. The larger the magnitudes of the radii,  $r_g$  and  $r_p$ , of the normal curvature of the interacting tooth flanks,  $\mathcal{S}$  and  $\mathcal{P}$ , the larger the load capacity of the conformal/high-conformal crossed-axes gearing and vice versa.<sup>11</sup> In other words:

#### Statement 14.1

Novikov/conformal, and high-conformal crossed-axes gearing with larger magnitudes of radii of curvature of the tooth flanks feature higher load-carrying capacity.

As it can be concluded from Statement 14.1 [156], *Novikov/conformal*, and *high-conformal* crossed-axes gearing with a larger radius,  $r_N$ , of the boundary  $N$  – circle feature higher load-carrying capacity.

### 14.10 DESIGN PARAMETERS OF *NOVIKOV/CONFORMAL*, AND *HIGH-CONFORMAL* CROSSED-AXES GEARING

The designing of a *Novikov/conformal*, and *high-conformal* crossed-axes gear pair begins with the determination of the rotation vectors of the gear,  $\omega_g$ , and that of the pinion,  $\omega_p$ , in certain reference system. Once the rotation vectors,  $\omega_g$  and  $\omega_p$ , are known, the vector of instantaneous rotation,  $\omega_{pl}$ , as well as the shaft angle,  $\Sigma$ , can be determined. The axes of rotation,  $O_g$ ,  $O_p$ , and  $P_{ln}$ , are the straight lines pointed along the rotation vectors  $\omega_g$ ,  $\omega_p$  and  $\omega_{pl}$ , correspondingly. Then, the known configuration of the axes of rotations,  $O_g$ ,  $O_p$ , and  $P_{ln}$ , yields for the determination of the angular velocity ratio,  $u$ , and the pitch cone angles,  $\Gamma$ , of the gear and that,  $\gamma$ , of the pinion:

$$\Gamma = -\tan^{-1} \left( \frac{\sin \Sigma}{\omega_p / \omega_g + \cos \Sigma} \right) \quad (14.131)$$

$$\gamma = \tan^{-1} \left( \frac{\sin \Sigma}{\omega_g / \omega_p + \cos \Sigma} \right) \quad (14.132)$$

The design parameters in a *Novikov/conformal*, and *high-conformal* crossed-axes gear pair can be specified based, to a great extent, on that for *Novikov/conformal*, and *high-conformal* intersected-axes gears. From this perspective, the vector of instantaneous rotation,  $\omega_{pl}$ , and the axis of instantaneous rotation,  $P_{ln}$ , are of critical importance. As the instantaneous motion of a pinion in relation to the mating gear is interpreted as instant rotation about the axis,  $P_{ln}$ , the design parameters in

<sup>11</sup> It is right point to remind here that the magnitudes of the radii,  $r_g$  and  $r_p$ , of curvature of the interacting tooth flanks,  $\mathcal{S}$  and  $\mathcal{P}$ , strictly correlate to the radius,  $r_N$ , of the boundary circle in the section of the tooth flanks by a plane through the corresponding point within the axis of instantaneous rotation,  $P_{ln}$ .

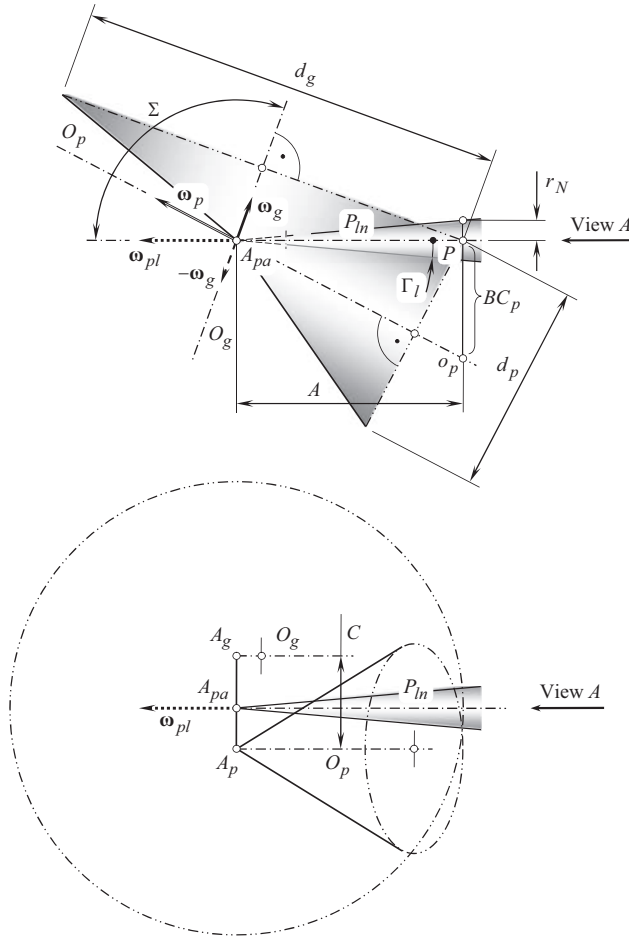


**FIGURE 14.31** Configuration of a normal reference plane in relation to the axis of instantaneous rotation,  $P_{in}$ , and the base cones of the gear and the pinion in *Novikov/conformal*, and *high-conformal* crossed-axes gear pair.

*Novikov/conformal*, and *high-conformal* crossed-axes gear pair can be specified within a reference plane through the pitch point,  $P$ . The pitch point,  $P$ , is at a cone distance,  $A$ , from the plane-of-action apex  $A_{pa}$ . The reference plane is perpendicular to the axis of instantaneous rotation,  $P_{in}$ , as schematically depicted in Figure 14.31.

The calculated values of the pitch cone angles,  $\Gamma$  and  $\gamma$ , along with the given cone distance,  $A$ , yield for the calculation of the pitch diameter of the gear,  $d_g$ , and that of the mating pinion,  $d_p$ :

$$d_g = 2A \cos \Gamma \quad (14.133)$$

$$d_p = 2A \cos \gamma \quad (14.134)$$

The back cone distance of the gear,  $BC_g$ , as well as the back cone distance of the pinion,  $BC_p$ , are calculated similarly:

$$BC_g = 2A \sin \Gamma \quad (14.135)$$

$$BC_p = 2A \sin \gamma \quad (14.136)$$

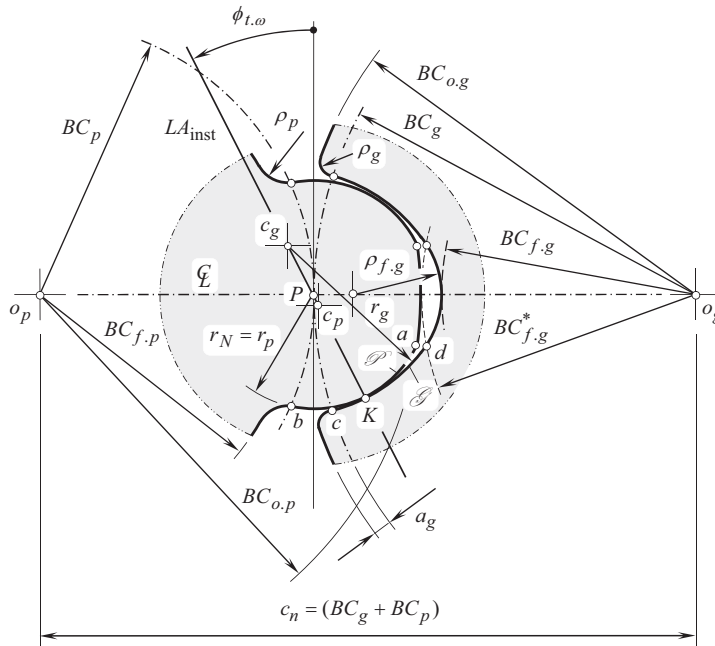


**FIGURE 14.32** Geometry of *Novikov/conformal* and *high-conformal* crossed-axes gear pair within the reference plane perpendicular to the axis of instantaneous rotation,  $P_{ln}$ .

Once the normal reference plane is constructed, the tooth profile parameters in the gear and in the mating pinion can be specified within this reference plane.

Referring to Figure 14.32, two points, namely,  $o_g$  and  $o_p$ , are, by nature, the points of intersection of the axes of rotation,  $O_g$  and  $O_p$ , by the normal reference plane. The points are at the distance  $c_n = (BC_g + BC_p)$  from one another. Two circles of radii,  $BC_g$  and  $BC_p$ , are centered at the points,  $o_g$  and  $o_p$ . The circles share a common point, which, in fact, is the pitch point  $P$ .

A straight instantaneous line of action,  $LA_{inst}$ , within the normal reference plane is the line through the pitch point,  $P$ . The instantaneous line of action,  $LA_{inst}$ , forms certain transverse pressure angle,  $\phi_{t,\omega}$ , with the perpendicular to the centerline,  $\mathcal{L}$ . The contact point,  $K$ , between the tooth flanks of the gear,  $\mathcal{G}$ , and of the mating pinion,  $\mathcal{P}$ , is point within the straight line  $LA_{inst}$ . The further the contact point,  $K$ , is located from the pitch point,  $P$ , the more freedom has the gear designer in selecting the radii of curvature of the tooth flanks. At that same time, the further the contact point,  $K$ , is located from the pitch point,  $P$ , the higher the losses due to friction between the tooth flanks, and the wear of the tooth flanks of the gear and the mating pinion. Ultimately, the favorable location of the contact point,  $K$ , is a trade-off between these two factors.

Let us assume that the pinion is stationary, and the gear performs the instant rotation in relation to the pinion. The axis,  $P_{ln}$ , of the instant rotation,  $\omega_{pl}$ , is a straight line through the pitch point,  $P$ . The axis of instantaneous rotation,  $P_{ln}$ , goes through the apex,  $A_{pa}$ . When the pinion is motionless, contact point,  $K$ , traces a boundary circle of a radius,  $r_N$ , centered at  $P$ .

In the section by a normal plane, the pinion tooth profile,  $\mathcal{P}$ , can either align with a circular arc of the boundary circle,  $r_N$ , or it can be relieved into the bodily side of the pinion tooth. As a consequence, the actual location of the center of curvature,  $c_p$ , of the convex pinion tooth profile,  $\mathcal{P}$ , within the straight line of action,  $LA_{inst}$ , is limited to the straight-line segment,  $PK$ . The pitch point is included in the interval,  $[P, K)$ , as shown in Figure 14.32, while the contact point,  $K$ , is not.

On the other hand, the actual location of the center of curvature,  $c_g$ , of the concave gear tooth profile,  $\mathcal{G}$ , within the straight line of action,  $LA_{inst}$ , is limited to the open interval  $P \rightarrow \infty$ . Theoretically,

the pitch point,  $P$ , can be included in that interval for,  $K$ . However, the latter is completely impractical, and actually the center of curvature,  $c_g$ , is located beyond the pitch point,  $P$ . Due to this fact, the radius of curvature,  $r_p$ , of the convex pinion tooth profile,  $\mathcal{P}$ , is smaller than that,  $r_g$ , of the concave gear tooth profile,  $\mathcal{G}$ , (the inequality  $r_p < r_g$  is always observed).

Both the pinion teeth and the gear teeth are helical and of the opposite hand. No spur *Novikov/conformal* and *high-conformal* gearing is feasible by nature. It is fundamental to the operating of the gears that contact occurs nominally at point, and that the length,  $l_{pc}$ , of the path of contact,  $P_c$ , in every transverse section of the gear pair is zero, that is,  $l_{pc} = 0$ . It is clearly a condition of operation that in a given profile the tooth surfaces should not interfere before or after culmination when rotated at angular speeds that are in the gear ratio. Because both the gear and the mating pinion teeth are helical and of the opposite hand, an illusion is created that the point of contact is traveling across the full face width of the gears during rotation, which is incorrect. The so-called *pseudo-path of contact*,  $P_{pc}$ , and not the *path of contact*,  $P_c$ , is created in such a motion.

The transverses contact ratio,  $m_p$ , in a *Novikov/conformal*, and *high-conformal* crossed-axes gear pair is zero ( $m_p \equiv 0$ ) – this is because the equality  $l_{pc} = 0$  is valid. The face contact ratio,  $m_F$ , is equal to the total contact ratio,  $\bar{m}$  (or  $m_t$ ), of the gear pair, and is always greater than one ( $\bar{m} = m_F = m_t > 1$ ).

To calculate the design parameters in a *Novikov/conformal* and *high-conformal* crossed-axes gear pair, the center-distance,  $c_n$ , and the tooth ratio,  $u = \omega_p/\omega_g$ , in the gear pair have to be specified.

The back cone distance of the gear,  $BC_g$ , and that,  $BC_p$ , of the pinion, can be expressed in terms of the center-distance,  $c_n$ , and of the tooth ratio,  $u$ :

$$BC_g = c_n \cdot \frac{u}{1+u} \quad (14.137)$$

$$BC_p = c_n \cdot \frac{1}{1+u} \quad (14.138)$$

The displacement,  $l$ , at which the pseudo-path of contact,  $P_{pc}$ , is remote from the pitch point,  $P$ , must be known, as well as the transverse pressure angle,  $\phi_{t,\omega}$ , in the gear pair.

The displacement,  $l$ , is the principal design parameter in a *Novikov/conformal* and *high-conformal* crossed-axes gear pair. Many of the design parameters in the *Novikov/conformal* and *high-conformal* gear pair can be expressed in terms of displacement ( $l = KP$ ).

For the calculation of the radii of curvature,  $r_g$  and  $r_p$ , of tooth profiles of the gear and of the mating pinion, respectively, the formulas:

$$r_g = l \cdot (1 + k_{rg}) \quad (14.139)$$

$$r_p = l \cdot (1 + k_{rp}) \quad (14.140)$$

are employed.

The actual value of the factor,  $k_{rp}$ , must fulfill an inequality  $k_{rp} \geq 0$ . However, when the factor,  $k_{rp}$ , can be set equal to zero, the equality  $r_p = l$  is observed. The factor,  $k_{rg}$ , is within the range  $k_{rg} = 0.03 \dots 0.10$ .

The radius of the outer back cone distance of the pinion,  $BC_{o,p}$ , is calculated from the formula

$$BC_{o,p} = BC_p + (1 - k_{po}) \cdot l \quad (14.141)$$

The addendum factor,  $k_{po}$ , of the pinion depends on: (a) the transverse pressure angle,  $\phi_{t,\omega}$ , (b) absolute dimensions of the gear pair, (c) the accuracy of machining, and (d) the conditions of lubrication. The pinion addendum factor,  $k_{po}$ , falls into the range

$$k_{po} = 0.1 \div 0.2 \quad (14.142)$$

The root back cone distance of the pinion,  $BC_{f.p}$ , is calculated from the equation

$$BC_{f.p} = BC_p - a_g - \delta \quad (14.143)$$

where

$a_g$  is the dedendum of the mating gear [ $a_g = (0.1 \dots 0.2) \cdot l$ ].

$\delta$  is the radial clearance in the gear pair ( $\delta = l \cdot k_{po}$ ).

It is proven to be practical to set the fillet radius,  $\rho_p$ , in the range of  $\rho_p = 0.3 \cdot l$ .

The root back cone distance of the gear,  $BC_{f.g}$ , equals to:

$$BC_{f.g} = c_n - BC_{o.p} \quad (14.144)$$

The radius of the outer back cone distance of the gear,  $BC_{o.g}$ , is calculated from the expression:

$$BC_{o.g} = BC_g + a_g \quad (14.145)$$

The corner of the gear tooth addendum should be rounded with the radius,  $\rho_g$ , which is less than the fillet radius,  $\rho_p$ , of the pinion ( $\rho_g < \rho_p$ ).

The following relations among the design parameters in *Novikov/conformal* and *high-conformal* crossed-axes gear pair are proven to be practical (as the first approximation):

$$r_p = l, \quad (14.146)$$

$$r_g \leq 1.10 \cdot r_p, \quad (14.147)$$

$$\rho_p = 0.3 \cdot l, \quad (14.148)$$

$$m_n/l = 0.8, \quad (14.149)$$

$$t_p/t_g = 1.5, \quad (14.150)$$

$$\phi_{t,\omega} = 30^\circ, \quad (14.151)$$

$$\lambda = 60 \dots 80^\circ (\psi = 10 \dots 30^\circ), \quad (14.152)$$

circular pitch of teeth  $p = t_g + t_p + B$ , where the backlash is in the range of  $B = 0.2 \dots 0.4$  mm.

For the design parameters  $l$ ,  $p$ ,  $t_g$ ,  $t_p$ ,  $m_n$  and  $B$ , the corresponding angular values can be calculated (see Table 14.3).

The effective face width of the gear pair is calculated as follows:

$$F_{pa} = (1.1 \div 1.2) \cdot p \cdot \tan \lambda \quad (14.153)$$

For the preliminary analysis of *Novikov/conformal*, and *high-conformal* crossed-axes gearing, an empirical expression:

$$l = (0.05 \div 0.20) \cdot BC_p \quad (14.154)$$

returns the value for the displacement,  $l$ , which could be practical.

The functional face width, and the axial pitch in a *Novikov/conformal*, and *high-conformal* gear pair depend on each other.

TABLE 14.3

**Design Parameters in *Novikov/Conformal*, and *High-Conformal* Crossed-Axes Gearing**

The Design Parameter	Symbol	Equation
Angular displacement	$\varphi_l$	$\varphi_l = \tan^{-1} \left( \frac{l}{A} \right)$
Angular module	$\varphi_{m,n}$	$\varphi_{m,n} = \tan^{-1} \left( \frac{m_n}{A} \right)$
Angular pitch	$p_\varphi$	$p_\varphi = \tan^{-1} \left( \frac{p}{A} \right)$
Angular tooth thickness (gear)	$\varphi_{t,g}$	$\varphi_{t,g} = \tan^{-1} \left( \frac{t_g}{A} \right)$
Angular tooth thickness (pinion)	$\varphi_{t,p}$	$\varphi_{t,p} = \tan^{-1} \left( \frac{t_p}{A} \right)$
Angular space width (gear)	$\varphi_{w,g}$	$\varphi_{w,g} = \tan^{-1} \left( \frac{w_g}{A} \right)$
Angular space width (pinion)	$\varphi_{w,p}$	$\varphi_{w,p} = \tan^{-1} \left( \frac{w_p}{A} \right)$
Angular backlash	$\varphi_B$	$\varphi_B = \tan^{-1} \left( \frac{B}{A} \right)$
Angular addendum (gear)	$\varphi_{a,g}$	$\varphi_{a,g} = \tan^{-1} \left( \frac{a_g}{A} \right)$
Angular addendum (pinion)	$\varphi_{a,p}$	$\varphi_{a,p} = \tan^{-1} \left( \frac{a_p}{A} \right)$
Angular dedendum (gear)	$\varphi_{d,g}$	$\varphi_{d,g} = \tan^{-1} \left( \frac{b_g}{A} \right)$
Angular dedendum (pinion)	$\varphi_{d,p}$	$\varphi_{d,p} = \tan^{-1} \left( \frac{b_p}{A} \right)$

*Note:* The following designations:  $a_g$ ,  $b_g$ , and,  $a_p$ ,  $b_p$ , relate to addendum, and to dedendum of the gear and of the pinion respectively. These design parameters are measured within the normal reference plane in the *Novikov/conformal* and *high-conformal* crossed-axes gear pair.

Consider a case of uniform rotation of the gear and the mating pinion. Because the transverse contact ratio is zero ( $m_p = 0$ ), and the total contact ratio,  $\bar{m}$  (or  $m_t$ ), equals to the face contact ratio,  $m_F$ , the axial pitch  $p_{cl,g}$  of the helix on the gear tooth flank,  $\mathcal{S}$ , is calculated from the formula:

$$p_{cl,g} = \frac{F_{pa}}{m_t} \cdot \cos \Gamma \quad (14.155)$$

A similar expression:

$$p_{cl,p} = \frac{F_{pa}}{m_t} \cdot \cos \gamma \quad (14.156)$$

is valid with respect to the axial pitch,  $p_{cl,p}$ , of the helix on the pinion tooth flank,  $\mathcal{P}$ .

The quality of *Novikov/conformal*, and *high-conformal* gearing strongly depends, first of all, on the following design parameters:  $l$ ,  $\phi_{t,\omega}$ , and  $\lambda$ .



Tooth flanks of the gear,  $\mathcal{G}$ , and of the mating pinion,  $\mathcal{P}$ , in *Novikov/conformal*, and *high-conformal* crossed-axes gearing are not conjugate surfaces, moreover, they are not envelopes to one another.

*Novikov/conformal* and *high-conformal* crossed-axes gearing is not been profoundly investigated yet. Gearing of this kind has received only episodic application, as no practical guide to the design of this gearing has been developed yet.

When designing *Novikov/conformal*, and *high-conformal* crossed-axes gear pairs, it is desirable to accommodate the actual values of the design parameters for the potential linear displacements, as well as for the potential angular displacements of the gears from their nominal configuration. Under an arbitrary combination of the elementary displacements (linear, and angular), contact point alters its location within the transverse section so as to retain the gear-set being conformal/high-conformal. The condition of high conformity has to be met at all locations of contact point, that is, under any and all displacements of the gear and its mating pinion from their desirable configuration.

---

# 15 Interaction of Gears in Geometrically Accurate Crossed-Axes Gearing

Centerlines of the gear shafts that cross one another at crossed-axes angle of certain value is the key feature of crossed-axes gearing. This feature is reflected even in the name of gearing of this type: *crossed-axes gearing*. Despite the fundamental difference, crossed-axes gearing feature many similarities with gearing of other types, namely, with parallel-axes gearing as well as with intersected-axes gearing. The interaction of tooth flanks of gears in geometrically accurate crossed-axes gearing is discussed below in this chapter from the perspective of similarity among different types of gearsets.

## 15.1 INTERACTION BETWEEN TOOTH FLANKS IN GEOMETRICALLY ACCURATE CROSSED-AXES GEARING

An *equivalent pulley-and-belt transmission* of crossed-axes gear pair is a handy and powerful mean to investigate and to analyze the transmission of a uniform rotary motion by means of crossed-axes gear-sets.

### 15.1.1 EQUIVALENT PULLEY-AND-BELT TRANSMISSION OF CROSSED-AXES GEAR PAIR

Similar to parallel-axes gearing as well as to intersected-axes gearing, an *equivalent pulley-and-belt transmission* can be constructed for a crossed-axes gear pair. As illustrated in Figure 13.7: (a) a base cone of a driving pinion, (b) a base cone of a driven gear, and (c) the plane of action,  $PA$ , all three together comprise an *equivalent pulley-and-belt transmission* of the crossed-axes gear pair. The plane of action,  $PA$ , is viewed as a zero-thickness film that is capable of transmitting a rotary motion. The zero-thickness film is free to wrap onto the base cone of the driving member, and unwrap from the base cone of the driven member of the crossed-axes gear pair. The zero-thickness film cannot be bended about an axis perpendicular the plane of action,  $PA$ .

Three rotary motions, namely, a rotation of base cone of a driving pinion,  $\omega_p$ , a rotation of base cone of a driven gear,  $\omega_g$ , and a rotation of the plane of action,  $\omega_{pa}$ , are synchronized with one another so as to avoid sliding in between the interacting surfaces of the base cones, and of the plane of action,  $PA$ , in the tangential direction of the base cones. In the *equivalent pulley-and-belt transmission* of a crossed-axes gear pair, a driving base cone of the pinion *pulls* a driven base cone of the gear. Note: in reality, a tooth flank of the driving pinion *pushes* a tooth flank of the driven gear.

In the *equivalent pulley-and-belt transmission* of a crossed-axes gear pair, the plane of action is pulled by the rotating base cone of the driving member, and the driven member of the *equivalent pulley-and-belt transmission* is pulled by the plane of action.

It is handy to investigate the path of contact in crossed-axes gearing by means of the *equivalent pulley-and-belt transmission* of the crossed-axes gear pair.

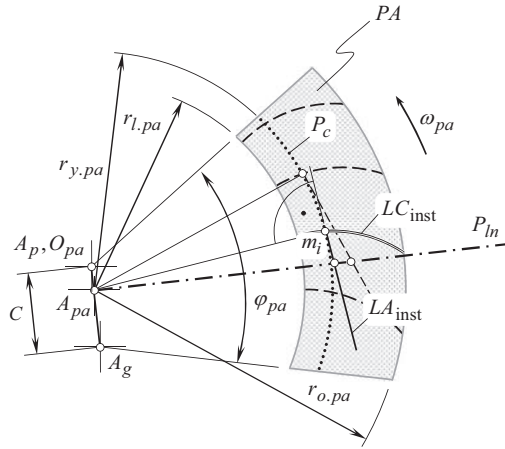


**FIGURE 15.1** Path of contact,  $P_c$ , and instantaneous line of action,  $LA_{inst}$ , in geometrically accurate crossed-axes gearing.

### 15.1.2 PATH OF CONTACT, AND INSTANTANEOUS LINE OF ACTION

The path of contact and the line of action in geometrically accurate crossed-axes gearing can be defined in a manner similar to that they are defined in parallel-axes gearing.

Consider a plane of action,  $PA$ , in crossed-axes gear pair, as illustrated in Figure 15.1. When the gears rotate, the plane of action spins about the plane-of-action apex,  $A_{pa}$ , with certain angular velocity,  $\omega_{pa}$ . The angular velocity,  $\omega_{pa}$ , is synchronized with the rotations of the gear,  $\omega_g$ , and of the pinion,  $\omega_p$ .

In an arbitrary configuration of the gears in relation to one another, arbitrary point,  $m_i$ , is chosen within the instantaneous line of contact,  $LC_{inst}$ . When the gears rotate, the line of contact,  $LC_{inst}$ , in between the tooth flanks,  $\mathcal{S}$  and  $\mathcal{P}$ , of the gear, and of the mating pinion, travels together with the plane of action. In this motion, every point,  $m_i$ , within the instantaneous line of contact,  $LC_{inst}$ , traces a circular arc of a corresponding radius,  $r_{y.pa}$ . The arc, by nature, is a path of contact,  $P_c$ , in crossed-axes gear pair. As the plane of action,  $PA$ , rotates about the plane-of-action apex,  $A_{pa}$ , every path of contact,  $P_c$ , is shaped in the form of a circular arc segment, each of which is centered at the plane-of-action apex,  $A_{pa}$ . This statement is valid when the rotary motion of the plane of action,  $PA$ , is considered in a stationary reference system associated with the gear pair housing. Therefore, in crossed-axes gearing, each path of contact,  $P_c$ , is a planar curve (a circular arc segment) that is entirely located within the plane of action,  $PA$ . An instantaneous line of action,  $LA_{inst}$ , is a straight line that is tangent to the path of contact,  $P_c$ , at point of interest within the path of contact.

Neither the geometry nor the configuration of the desirable line of contact,  $LC_{des}$ , in relation to the plane of action,  $PA$ , are allowed to be altered when generating tooth flank of a particular gear,  $\mathcal{S}$ , and of its mating pinion,  $\mathcal{P}$ . This feature is important for the gear cutting tool designer, for gear inspection purposes, and so forth.

At arbitrary point,  $m_i$ , a straight-line tangent to the corresponding path of contact,  $P_c$ , can be constructed. In nature, the straight line is an instantaneous line of action,  $LA_{inst}$ , through point of interest,  $m_i$ . All the instantaneous lines of action are situated within the plane of action,  $PA$ , and all of them intersect the axis of instantaneous rotation,  $P_{ln}$ , at a corresponding point. If all the instantaneous lines of action,  $LA_{inst}$ , through all the points of the line of contact,  $LC$ , always intersect the axis of instantaneous rotation,  $P_{ln}$  (for any and all angular configurations of the gear and of the mating pinion), then all the centers of curvature of a gear/pinion tooth flank are located within the axis of instantaneous rotation,  $P_{ln}$ . In this way, the conjugate action law in crossed-axes gearing is fulfilled.

Every path of contact,  $P_c$ , can be viewed as an envelope to a family of consecutive positions of the instantaneous lines of action,  $LA_{inst}$ , when the gears rotate.

In a reference system associated with the gear, contact point traces a spherical involute on the gear tooth flank,  $\mathcal{G}$ . Similarly, in a reference system associated with the pinion, contact point traces a spherical involute on the pinion tooth flank,  $\mathcal{P}$ .

A family of paths of contact forms a surface. This surface is referred to as the *path-of-contact surface*,  $P_{cs}$ . It is evident that in crossed-axes gear pairs with a constant transverse pressure angle ( $\phi_{t,\omega} = \text{const}$ ) the path-of-contact surface,  $P_{cs}$ , is congruent to the plane of action,  $PA$ .

Consider a crossed-axes gear pair that features transverse pressure angle,  $\phi_{t,\omega}$ , actual value of which is variable within the effective face width,  $F_{pa}$ , of the gear pair [that is, a case when the transverse pressure angle,  $\phi_{t,\omega}$ , varies ( $\phi_{t,\omega} = \text{var}$ ) along the line of contact,  $LC$ ]. In such a scenario, the *path-of-contact surface*,  $P_{cs}$ , is represented by a continuous set of circular-arc paths of contact,  $P_c$ , each of which is located in a corresponding infinitesimally narrow portion of the plane of action. Each path of contact,  $P_c$ , features different value of the transverse pressure angles,  $\phi_{t,\omega}$ . The radius of a current circular-arc path of contact,  $P_c$ , can be viewed as a function of the distance of point on the axis of instantaneous rotation,  $P_{in}$ , from the plane-of-action-apex,  $A_{pa}$ . The *path-of-contact surface*,  $P_{cs}$ , is a continuous (screw) surface generated by the circular arcs of different radii.

### 15.1.3 ZONE OF ACTION (FIELD OF ACTION) IN CROSSED-AXES GEARING

It is also handy to use the *equivalent pulley-and-belt transmission* for the investigation of the field (zone) of action in crossed-axes gearing.

A gear and a mating pinion interact with one another only within a portion of the plane of action,  $PA$ . This portion of the plane of action is commonly referred to as the *field (zone) of action*,  $ZA$ . In crossed-axes gearing, the field of action (zone of action) is bounded by four boundary lines, which all are entirely located in the plane of action,  $PA$ .

A circular arc of the outer radius,  $r_{o,pa}$ , and a circular arc of the limit radius,  $r_{l,pa}$ , both, that are centered at the plane-of-action apex,  $A_{pa}$ , are the two boundary lines of the field of action (zone of action). The face width,  $F_{pa}$ , of the field of action (zone of action),  $ZA$ , is calculated as:

$$F_{pa} = r_{o,pa} - r_{l,pa} \quad (15.1)$$

In crossed-axes gearing, face width,  $F_{pa}$ , of the field of action (zone of action),  $ZA$ , equals to the width within which the tooth flanks,  $\mathcal{G}$  and  $\mathcal{P}$ , of a gear and of a mating pinion overlap one another.

Two lines of intersection,  $kl$  and  $mn$ , of the plane of action,  $PA$ , by outer cone of the gear, and that of the mating pinion, are the other two boundary lines of the of action (zone of action), as illustrated in Figure 15.2. When the apexes of the outer cones in the gear, and in the mating pinion, are coincident with the corresponding base cone apexes, the field of action is bounded by two straight-line segments, namely, by the lines of intersection of the outer cones of the gear and of the pinion by the plane of action,  $PA$ . Commonly, the lines,  $kl$  and  $mn$ , are slightly convex. It is handy to replace these two curves by two straight line segments,  $kl$  and  $mn$ .

Constructed in Figure 15.2, the angle  $\varphi_{zas}$  that is formed by the lines  $kl$  and  $mn$ , is referred to as the *angular width of zone of action*. The angular width,  $\varphi_{zas}$ , of the zone of action,  $ZA$ , can be expressed in terms of the design parameters of a gear, and of a mating pinion. For reference purposes, the lines of tangency,  $cd$  and  $ab$ , of the base cones of the gear, and of the mating pinion with the plane of action are shown in Figure 15.2. These straight tangent lines form an angle,  $\varphi_{pa}$ , that is referred to as the *total angular width of plane of action*.

Another approach can be used for the determination of the angular width of the zone of action,  $\varphi_{pa,zs}$ .

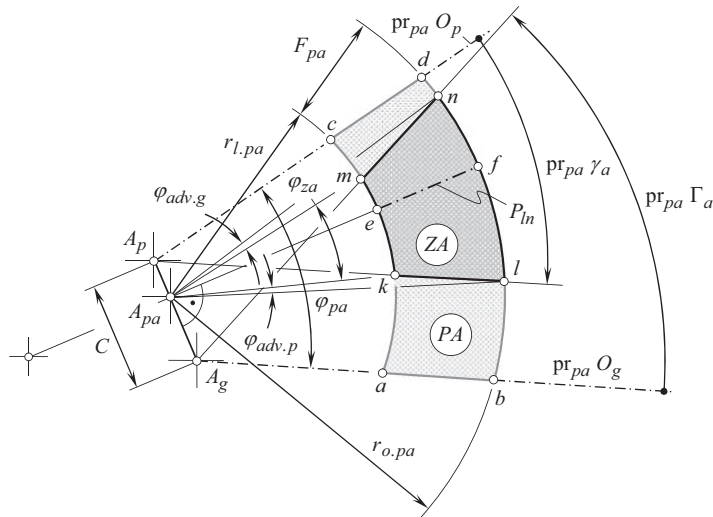


FIGURE 15.2 Field of action (zone of action), ZA, in crossed-axes gearing.

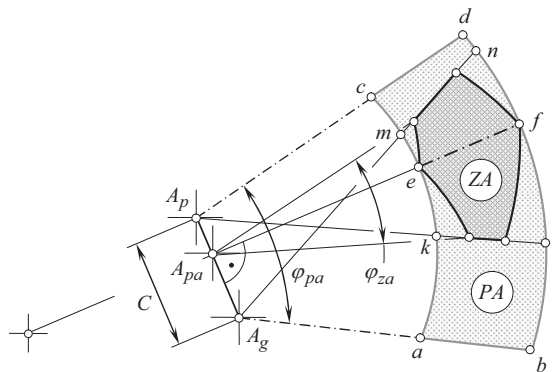


FIGURE 15.3 An example of zone of action, ZA, of a complex geometry in crossed-axes gear pair.

The zone of action, ZA, is of a simplest possible geometry (Figure 15.2). In reality, the zone of action can be of a more complex geometry. An example of crossed-axes gear pair that features zone of action, ZA, of a more complex geometry is illustrated in Figure 15.3.

In crossed-axes gearing (in worm gearing in particular), the zone of action, ZA, is not mandatorily shaped in a form of a round strip. Depending on the actual shape of the outer surfaces of both the gears in mesh, the zone of action can be bounded by lines of a more complex geometry.

The lines of contact of the plane of action, PA, with the base cones are remained the same – both of them are straight line segments.

The geometry of the actual zone of action, ZA, is a critical consideration when calculating the contact ratio in a crossed-axes gear pair.

## 15.2 TRANSMISSION OF UNIFORM ROTARY MOTION BY MEANS OF CROSSED-AXES GEARING

Tooth flanks in a gear for a crossed-axes gear pair can be viewed as a series of cam surfaces that act against similar surfaces of the mating gear to impart a driving motion. In order to transmit smoothly,

a uniform input rotation to the output shaft, three fundamental laws of gearing are required to be fulfilled.

**First**, the law of contact (i.e., analytically described by *Shishkov equation of contact*,  $\mathbf{n} \cdot \mathbf{V}_\Sigma = 0$ ) between two interacting tooth flanks,  $\mathcal{S}$  and  $\mathcal{P}$ , of a gear and of a mating pinion (the first fundamental law of gearing) has to be fulfilled when transmitting a uniform rotary motion by means of crossed-axes gearing.

**Second**, the interacting tooth flanks,  $\mathcal{S}$  and  $\mathcal{P}$ , of a gear, and of a mating pinion have to be conjugate to one another at any and all angular configurations of the gear, and of the mating pinion when the gears rotate. This means that the common perpendicular through any and all points within the line of contact intersect the axis of instantaneous rotation,  $P_{ln}$  in the gear pair (the second fundamental law of gearing).

**Third**, an angular base pitch of a gear, and that of a mating pinion, both, must be equal to operating angular base pitch of the gear pair (the third fundamental law of gearing). This requirement is because two (or even more) pairs of teeth make contact at the same time. Fulfillment of the additional condition caused by multiple interacting tooth surfaces in gears is necessary. Here, the discussion is limited to geometrically accurate crossed-axes gearing.

*Note:* Operating angular base pitch,  $\varphi_{b,op}$ , is a calculated design parameter that can be determined for crossed-axes gear pairs of any and all designs, namely, for geometrically accurate, as well as for approximate crossed-axes gearing. A gear angular base pitch,  $\varphi_{b,g}$ , and a mating pinion angular base pitch,  $\varphi_{b,p}$ , can be determined only for geometrically accurate gear and pinion – no approximate gear and pinion feature such a design parameter as the *gear angular base pitch*,  $\varphi_{b,g}$  (and the *pinion angular base pitch*,  $\varphi_{b,p}$ ).

A plane of action,  $PA$ , in a crossed-axes gear pair is shown in Figure 15.4a. The plane of action is intersected by a cylinder of revolution of an arbitrary radius,  $r_{y.pa}$ , having the plane-of-action centerline,  $O_{pa}$ , as the axis of its rotation. As the operating angular base pitch,  $\varphi_{b,pa}$ , of a gear pair is of a constant value, then the lengths:

$$l_{b,pa} = r_{y.pa} \cdot \varphi_{b,pa} \quad (15.2)$$

$$l_{b,g} = r_{y.pa} \cdot \varphi_{b,g} \quad (15.3)$$

$$l_{b,p} = r_{y.pa} \cdot \varphi_{b,p} \quad (15.4)$$

of the circular arcs also are of constant values, that is, in this particular analysis the angular base pitches  $\varphi_{b,pa}$ ,  $\varphi_{b,g}$ , and  $\varphi_{b,p}$  can be replaced with the lengths  $l_{b,pa}$ ,  $l_{b,g}$ , and  $l_{b,p}$  of the corresponding circular arcs. Once the lengths are equal ( $l_{b,g} = l_{b,pa}$  and  $l_{b,p} = l_{b,pa}$ ), then angular base pitches are also equal ( $\varphi_{b,g} = \varphi_{b,pa}$ , and  $\varphi_{b,p} = \varphi_{b,pa}$ ).

The unfolded section,  $A - A$ , of the gear tooth flanks,  $\mathcal{S}$ , by the cylinder of revolution is shown in Figure 15.4b; the unfolded section of the pinion tooth flanks,  $\mathcal{P}$ , by the cylinder of revolution is shown in Figure 15.4c; and the unfolded section of the gear crossed-axes gear pair by the cylinder of revolution is shown in Figure 15.4d.

Here and below, only local patches of the gear tooth flanks,  $\mathcal{S}$ , are considered. The gear tooth flanks themselves are not defined yet. Therefore, only small portions of the tooth flanks,  $\mathcal{S}$ , are depicted in Figure 15.4b. All these portions of the tooth flanks of a gear are located in the differential vicinity of points of intersection,  $K_g$ , of the tooth flanks,  $\mathcal{S}$ , by the path of contact,  $P_c$ . Each tooth flank,  $\mathcal{S}$ , is perpendicular to the path of contact,  $P_c$ , at points  $K_g$ . All the points  $K_g$  are evenly spaced within the path of contact. The distance between each pair of neighboring points,  $K_g$ , is equal to the angular base pitch,  $\varphi_{b,g}$ , of the gear.

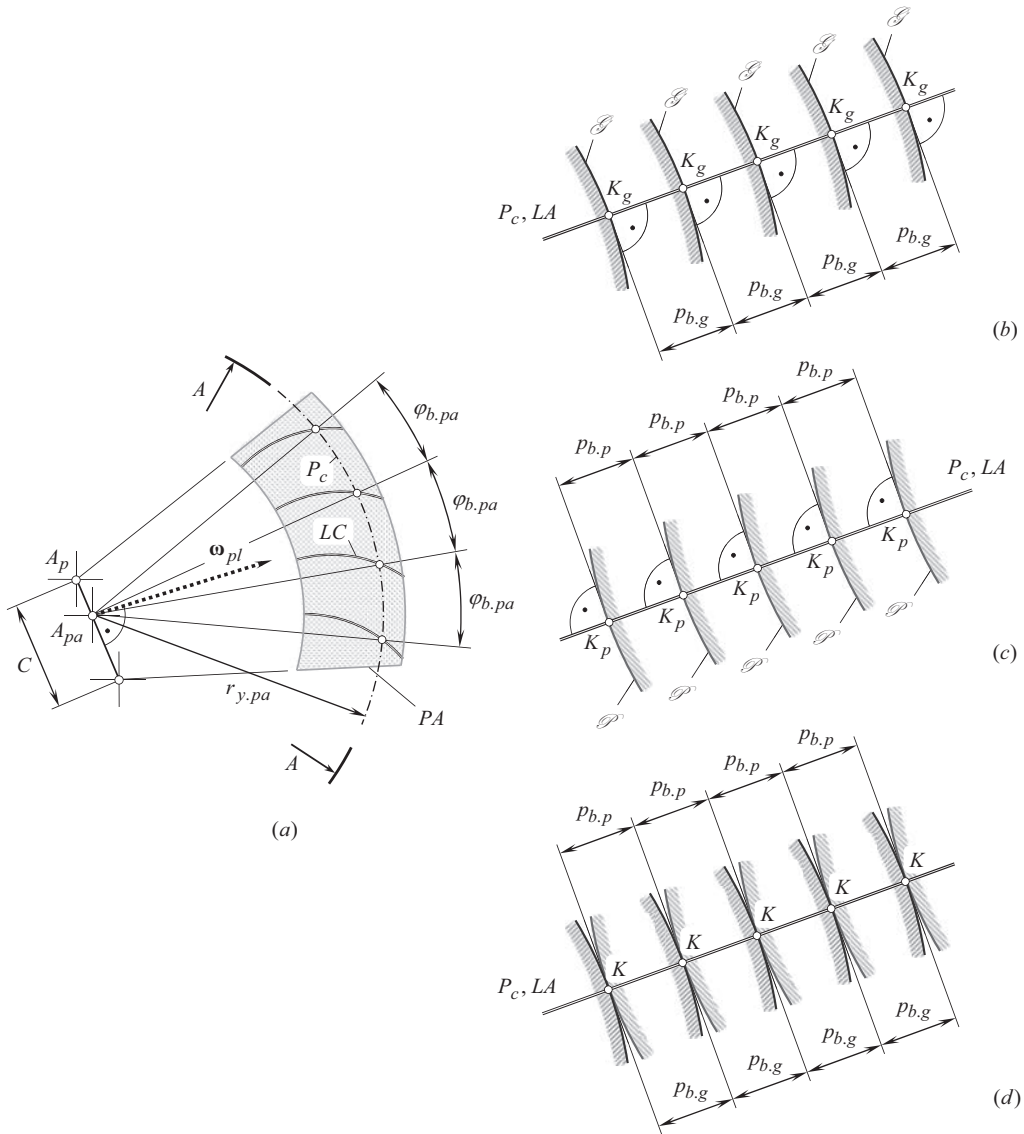


**FIGURE 15.4** On the concept of equal base pitches in geometrically accurate crossed-axes gear pair: (a) plane of action,  $PA$ , and the unfolded section  $A-A$ , (b) of a gear, (c) of a mating pinion, and (d) of the gear pair.

An analysis similar to that above can be performed with respect to the pinion tooth flanks,  $\mathcal{P}$ , as shown in Figure 15.4c. All these portions of the tooth flanks of the pinion are located in the differential vicinity of points of intersection,  $K_p$ , of the tooth flanks,  $\mathcal{P}$ , by the path of contact,  $P_c$ . Each of the pinion tooth flanks,  $\mathcal{P}$ , is perpendicular to the path of contact,  $P_c$ , at points  $K_p$ . All the points  $K_p$  are evenly spaced within the path of contact. The distance between each pair of neighboring points,  $K_p$ , is equal to angular base pitch of the pinion,  $\varphi_{b.p}$ .

When the angular base pitches of a gear,  $\varphi_{b.g}$ , and of a mating pinion,  $\varphi_{b.p}$ , are equal to operating angular base pitch of the gear pair,  $\varphi_{b.op}$ , that is, when the identities,  $\varphi_{b.g} \equiv \varphi_{b.op}$  and  $\varphi_{b.p} \equiv \varphi_{b.op}$ , are valid, then the gear, and the pinion can be engaged in mesh as illustrated in Figure 15.4d. Each gear point,  $K_g$ , coincides with corresponding pinion point,  $K_p$ . Due to this, the gear and the pinion points,  $K_g$  and  $K_p$ , further are designated as contact point,  $K$ .



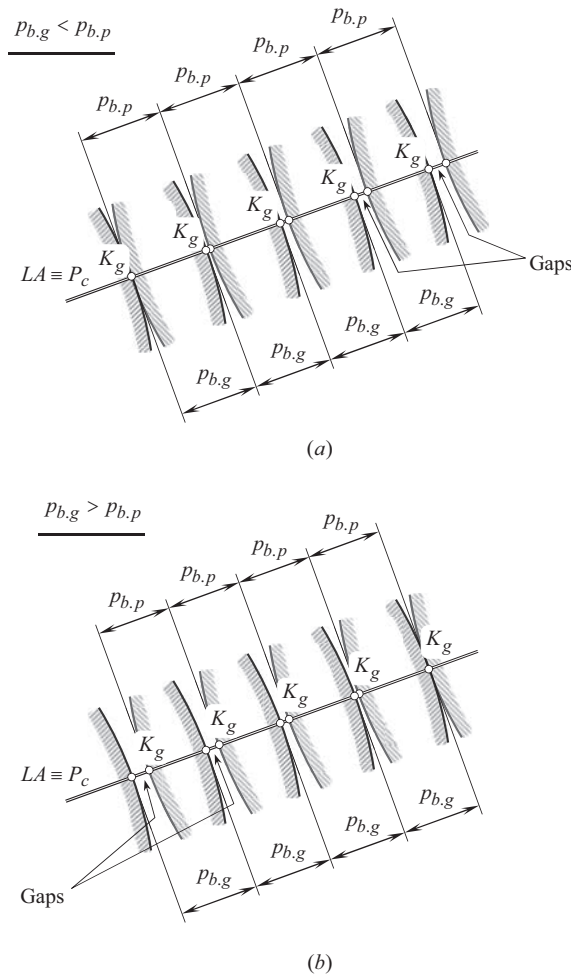


**FIGURE 15.5** Examples of violation of the third fundamental law of gearing in crossed-axes gearing: (a) the angular base pitch of a gear,  $\varphi_{b,g}$ , is smaller compared to that,  $\varphi_{b,p}$ , of a mating pinion ( $\varphi_{b,g} < \varphi_{b,p}$ ), and (b) the angular base pitch of a gear,  $\varphi_{b,g}$ , is larger compared to that,  $\varphi_{b,p}$ , of a mating pinion ( $\varphi_{b,g} > \varphi_{b,p}$ ); in both cases gaps between the tooth flanks,  $\mathcal{G}$  and  $\mathcal{P}$ , are observed.

As it follows from the analysis of Figure 15.4d, it is not a must to retain all the angular base pitches of a gear,  $\varphi_{b,g}$ , equal to one another as well as to retain all the angular base pitches of a mating pinion,  $\varphi_{b,p}$ , also equal to one another. It is critical to keep equality of a gear angular base pitch, and of a mating pinion angular base pitch, to a corresponding operating angular base pitch of the gear pair for each pair of teeth engaged in mesh. Physically this is possible, but is limited to the gear ratio in the gear pair to integer numbers, that is, to 1, 2, 3, and so forth. Such a design of gearing is impractical and is not considered in this Book.

When base pitches of a gear, and of a mating pinion are not equal to one another ( $\varphi_{b,g} \neq \varphi_{b,p}$ ), for example, the gear base pitch,  $\varphi_{b,g}$ , is smaller compared to the mating pinion base pitch,  $\varphi_{b,p}$ , and the inequality  $\varphi_{b,g} < \varphi_{b,p}$  is valid, as shown in Figure 15.5a, only one pair of teeth is always engaged in mesh. A gap between the rest pairs of teeth of the gear,  $\mathcal{G}$ , and of the pinion,  $\mathcal{P}$ , is always observed. No gaps of this sort are permissible in geometrically accurate crossed-axes gearing.

In another example, illustrated in Figure 15.5, the gear angular base pitch,  $\varphi_{b,g}$ , is greater compared to the mating pinion angular base pitch,  $\varphi_{b,p}$ , and, thus, an inequality  $\varphi_{b,g} > \varphi_{b,p}$  is valid, as



shown in Figure 15.5b. Again, only one pair of teeth is always engaged in mesh in this scenario. A gap between the rest pairs of teeth of the gear,  $\mathcal{G}$ , and of the pinion,  $\mathcal{P}$ , is always observed. No gaps of this sort are permissible in geometrically accurate crossed-axes gearing.

In this second example (see Figure 15.5b), the distribution of the gaps is inverse to that shown in Figure 15.5a. This is because the gear and the mating pinion are rigid bodies that physically cannot interfere into one another.

Therefore, a uniform rotary motion can be smoothly transmitted by means of a crossed-axes gear pair if the following identities are valid at all contact points at every instant of time:

$$\varphi_{b,g} \equiv \varphi_{b,op} \quad (15.5)$$

$$\varphi_{b,p} \equiv \varphi_{b,op} \quad (15.6)$$

With that said, the third fundamental law of gearing to be fulfilled in geometrically accurate crossed-axes gear pair can be formulated in the following manner:

**The third fundamental law of gearing (in crossed-axes gearing):** *In crossed-axes gearing, in order to transmit a uniform rotary motion from a driving shaft to a driven shaft by means of gear teeth, angular base pitch of a gear, and that of a mating pinion must be equal to operating base pitch of the gear pair at all contact points and at every instant of time.*

Only *conjugate* gear tooth flanks feature base pitch. Base pitch cannot be specified for non-conjugate gear tooth flanks. Therefore, only conjugate tooth flanks of a gear, and of a mating pinion can fulfill the *third fundamental law of gearing (in crossed-axes gearing)*.

If a discussion is limited just to crossed-axes gearing, the concept of the *angular base pitch* is applicable only to gear tooth flanks, those generated as a locus of corresponding spherical involutes. No *angular base pitch* can be specified for gears with other tooth flank geometries, such as spiral bevel gears of conventional design (generated by the straight-sided crown basic rack), and so forth. Therefore, when angular base pitches in a gear, and in a mating pinion, are equal to operating angular base pitch of the gear pair (i.e., when the identities,  $\varphi_{b,g} \equiv \varphi_{b,op}$ , and  $\varphi_{b,p} \equiv \varphi_{b,op}$ , are valid), the third fundamental law of gearing is always fulfilled.

When the angular base pitch of a gear, and that of a mating pinion, both, are equal to operating angular base pitch in the crossed-axes gear pair, the third fundamental law of gearing is fulfilled.

### 15.3 CONTACT RATIO IN CROSSED-AXES GEARING

The contact ratio, in general, is the number of angular base pitches through which a tooth surface rotates from the beginning to the end of contact.

The contact ratio,  $\bar{m}$ , in a crossed-axes gear pair can be also defined as the ratio of the total angular width,  $\Phi_{za}$ , of the zone of action,  $ZA$ , to the operating angular base pitch,  $\varphi_{b,op}$  :

$$\bar{m} = \frac{\Phi_{za}}{\varphi_{b,op}} \quad (15.7)$$

Referring to Figure 15.6, the total angular width,  $\Phi_{za}$ , of the zone of action,  $ZA$ , can be specified as follows:

$$\Phi_{za} = \varphi_{za} + \varphi_{adv,g} + \varphi_{adv,p} \quad (15.8)$$

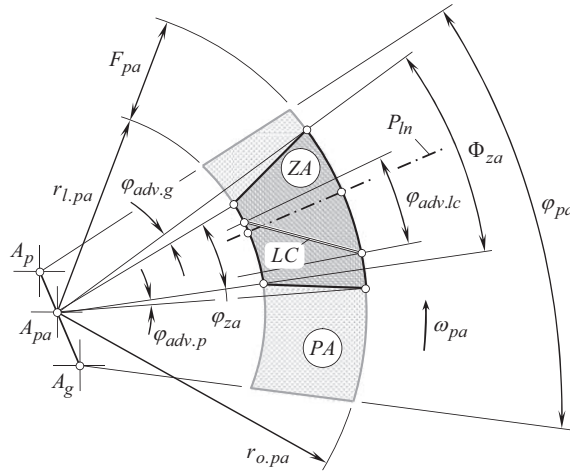


**FIGURE 15.6** Angular width,  $\Phi_{zs}$ , of the zone of action, ZA, in crossed-axes gear pair.

All the angles,  $\varphi_{zs}$ ,  $\varphi_{adv.g}$ , and  $\varphi_{adv.p}$ , are shown in Figure 15.6. [It is important to stress here on similarities in calculation of contact ratio in crossed-axes gearing, and the earlier discussed (see Section 13.3). In order to avoid ambiguities, a superscript “ca” can be appended to all the parameters in Eq. (15.8):  $\Phi_{zs}^{ca}$ ,  $\varphi_{zs}^{ca}$ ,  $\varphi_{adv.g}^{ca}$ , and  $\varphi_{adv.p}^{ca}$ . Similarly, a superscript “ia” can be appended to all the parameters in Eq. (13.22) and others for an appropriate calculations in intersected-axes gearing:  $\varphi_{zs}^{ia}$ ,  $\varphi_{adv.g}^{ia}$ ,  $\varphi_{adv.p}^{ia}$ , as well as to others].

Equation (15.8) is an equivalent of the corresponding formulas for the calculation of the total contact ratio,  $\bar{m}$ , in parallel-axes gearing (see Section 10.4), and to the formula for the calculation of the total contact ratio,  $\bar{m}$ , in intersected-axes gearing (see Section 13.3). This equation is valid for crossed-axes gearing of all designs.

Two specific advance angles,  $\varphi_{adv.g}$  and  $\varphi_{adv.p}$ , are encountered when calculating the contact ratio,  $\bar{m}$ , in crossed-axes gearing (see Figure 15.5). These advance angles are due to the center-distance,  $C$ , is not of a zero value ( $C \neq 0$ ). One of two advance angle,  $\varphi_{adv.g}$ , is at the entering side of the gear tooth, and the other one,  $\varphi_{adv.p}$ , is at the exiting side of the gear tooth.

The contact ratio,  $\bar{m}$ , can be viewed as a sum of two components (this is an obsolete practice):

$$\bar{m} = m_p + m_F \quad (15.9)$$

Despite the terms *transverse contact ratio* and *face contact ratio* are obsolete and are out of date, the discussion on contact ratio in crossed-axes gearing begins with the analysis of these components of the *total contact ratio*. This makes easier the transition from the obsolete terminology like *transverse contact ratio* and *face contact ratio* to the recommended term *total contact ratio*.

One of the components is referred to as the *transverse contact ratio*,  $m_p$ , and other one as the *face contact ratio*,  $m_F$ . Such a differentiation is not a must, as the total contact ratio,  $\bar{m}$ , can be calculated with no calculation of the components  $m_p$  and  $m_F$ .

**Transverse contact ratio.** The transverse contact ratio,  $m_p$ , in a crossed-axes gear pair is the contact ratio that is determined within a transverse section of meshing gears. (Recall that a sphere that is centering at the plane-of-action apex,  $A_{pa}$ , is a transverse section in crossed-axes gear pair). The transverse contact ratio can also be referred to as *profile contact ratio*.

The transverse contact ratio,  $m_p$ , in a crossed-axes gear pair is defined as the ratio of the angular width,  $\varphi_{za}$ , of the zone of action, ZA, to the operating base pitch angle,  $\varphi_{b.op}$ , in a gear pair:

$$m_p = \frac{\varphi_{za}}{\varphi_{b.op}} \quad (15.10)$$

Duration of contact of a gear tooth flank,  $\mathcal{G}$ , and of a mating pinion tooth flank,  $\mathcal{P}$ , in a particular transverse section of a crossed-axes gear pair is specified by the angular width of the zone of action,  $\varphi_{za}$ . The angular width of the zone of action,  $\varphi_{za}$ , is measured within the plane of action,  $PA$ , and spans over a circular arc of full face width,  $F_{pa}$ . [The angle,  $\varphi_{za}$ , is an equivalent of the length of contact,  $Z_{pa}$ , in parallel-axes gearing].

The tooth flank of a gear,  $\mathcal{G}$ , and the tooth flank of a mating pinion,  $\mathcal{P}$ , are engaged in mesh within the angular width of the zone of action,  $\varphi_{za}$ .

**Face contact ratio.** The face contact ratio,  $m_F$ , in crossed-axes gear pair can be defined as a ratio of the advance angle,  $\vartheta_{adv}$ , to the angular operating base pitch,  $\varphi_{b.op}$ :

$$m_F = \frac{\vartheta_{adv}}{\varphi_{b.op}} \quad (15.11)$$

Referring to Figure 15.6, the advance angle,  $\vartheta_{adv}$ , is specified as follows:

$$\vartheta_{adv} = \varphi_{adv.g} + \varphi_{adv.p} + \varphi_{adv.lc} \quad (15.12)$$

All the angles,  $\varphi_{adv.g}$ ,  $\varphi_{adv.p}$ , and  $\varphi_{adv.lc}$ , are shown in Figure 15.6.

The actual value of the face advance angle,  $\vartheta_{adv}$ , depends on the geometry of the line of contact,  $LC$ , and its configuration within the plane of action,  $PA$ , in a particular design of crossed-axes gear pair.

The ratio,  $\bar{m}$ , is always greater than one ( $\bar{m} \geq 1$ ). For gearing that features a zero face advance angle,  $\vartheta_{adv}$ , the contact ratio,  $\bar{m} = m_p \geq 1$ , as the equality,  $m_F = 0$ , is valid in this particular case. Conversely, in high-conformal gears, the equality,  $m_p = 0$ , is valid. Therefore, the contact ratio in a high-conformal gear pair is calculated based on the equality  $\bar{m} = m_F \geq 1$ .

Commonly, total contact ratio,  $\bar{m}$ , is higher in gear transmissions with a higher the input rotation. A higher accuracy of the gears is required in gear transmissions with a higher the input rotation, and a higher contact ratio,  $\bar{m}$ . In the high-power-density gear transmissions, high contact ratio is desirable, as this is a load sharing factor that increases the number of pairs of teeth that make contact simultaneously.

The above discussion is valid with respect to internal gears used in the design of crossed-axes gear pairs. Besides internal crossed-axes gearing is not extensively used in the industry, dies for net forging of external bevel gears, electrodes for EDM, and so forth can be calculated by means of the results discussed in this section of the book.

## 15.4 CONTACT MOTION CHARACTERISTICS IN CROSSED-AXES GEARING

Two main motions are observed in crossed-axes<sup>1</sup> gearing. They are as follows: a rotation of the input shaft, and a corresponding rotation of the output shaft. These two rotational motions,  $\omega_g$  and  $\omega_p$ , of a gear and of a mating pinion cause several other motions. Some of these motions result in sliding of tooth flanks,  $\mathcal{G}$  and  $\mathcal{P}$ , of a gear and of a mating pinion.

<sup>1</sup> This discussion is relevant to both to crossed-axes gearing with line contact in between tooth flanks of a gear and of a mating pinion,  $\mathcal{G}$  and  $\mathcal{P}$ , as well as to *Novikov/conformal gearing* and *high-conformal* crossed-axes gearings.

Rolling and sliding take place simultaneously between the tooth flanks of two mating gears when transmitting a rotary motion by means of crossed-axes gearing. Rolling and sliding occur at any point of contact within the active portion of the line of contact. Rolling and sliding occurred in crossed-axes gearing even at points within the axis of instantaneous rotation,  $P_{in}$ . Investigation and analysis of sliding and rolling conditions in a gear pair is of importance from an engineering perspective. It enables, for example, determining and reducing friction losses between the interacting tooth flanks in mating crossed-axes gears.

On the one hand, sliding motion between the tooth flanks,  $\mathcal{S}$  and  $\mathcal{P}$ , can entail an extensive surface wear of the gear teeth. Thus, sliding motion has to be reduced (or even eliminated) in order to improve the performance of the gear pair. On the other hand, sliding motion can significantly affect conditions of lubrication in a gear pair. Therefore, in order to improve the performance of the gear pair, sliding motion has to be optimized. The latter means that the gears have to be designed so as to provide the most favorable conditions of lubrication of the tooth flanks,  $\mathcal{S}$  and  $\mathcal{P}$ . With that said, the necessity of understanding of conditions of sliding between the tooth flanks,  $\mathcal{S}$  and  $\mathcal{P}$ , becomes clear.

#### 15.4.1 SLIDING IN GEOMETRICALLY ACCURATE CROSSED-AXES GEARING

Not many efforts were undertaken to this end to investigate sliding in crossed-axes gearing. Only a few publications deserve to be mentioned in this regard. The publications by Dusev [30], Dusev and Vasil'yev [31], Klingelnberg [9,58], Korostel'ev [64], and a few others are among them. Publications, those available in the public domain, reflect the results of investigation only of approximate crossed-axes gearing.

A portion of the relative motion of a gear and of a mating pinion cause rolling of the pitch surfaces of the interacting gears, while another portion of the relative motion results in sliding of the tooth flanks of the gear,  $\mathcal{S}$ , and the mating pinion,  $\mathcal{P}$ . For better understanding of the nature of sliding, an in-detail investigation of the teeth sliding in geometrically accurate crossed-axes gearing is required to be undertaken. This analysis can be performed either using descriptive-geometry based methods or using analytical methods of the analysis. Below preference is given to analytical investigation of sliding in geometrically accurate crossed-axes gearing.<sup>2</sup>

#### 15.4.2 ANALYTICAL SOLUTION TO THE PROBLEM OF DETERMINATION OF SLIDING VELOCITY IN GEOMETRICALLY ACCURATE CROSSED-AXES GEARING

There are numerous similarities between geometrically accurate crossed-axes gearing, and between geometrically accurate intersected-axes gearing. From the perspective of the analysis in this section of the book, it is critical to turn the readers' attention to sliding between tooth flanks,  $\mathcal{S}$  and  $\mathcal{P}$ , of a gear, and of a mating pinion, considered in a local reference system associated with the plane of action,  $PA$ . Considered locally, the sliding between the tooth flanks in both cases, that is, in crossed-axes gearing, and in intersected-axes gearing, is similar. The differences in the analysis appear when a configuration of the axes of rotation,  $O_g$  and  $O_p$ , of the gear and the pinion in crossed-axes gearing is taken into account, as this configuration differs from that in intersected-axes gearing. To accommodate for the different configuration of the axes of rotation,  $O_g$  and  $O_p$ , of the gear and of the mating pinion in crossed-axes gearing, and that in intersected-axes gearing, the operators of the resultant linear transformations,  $\mathbf{Rs}_{la}(p \rightarrow pa)$  and  $\mathbf{Rs}_{Ca}(p \rightarrow pa)$ , in a case of intersected-axes gearing [see Eq. (13.38)], and in a case of crossed-axes gearing (this operator of linear transformation is derived below in this section of the book), are different.

<sup>2</sup> A descriptive-geometry-based solution to the problem of determining the sliding velocity in crossed-axes gearing is not discussed here because too large in size illustrations are required for this purpose; the latter is inconvenient to be published in the book,

In order to solve the problem of determination of sliding velocity in geometrically accurate crossed-axes gearing, it is necessary to derive equations for the linear velocity vectors,  $\mathbf{V}_{m,g}$  and  $\mathbf{V}_{m,p}$ , of point of interest,  $m$ , within the line of contact,  $LC$ , between the tooth flanks,  $\mathcal{G}$  and  $\mathcal{P}$ , and to represent the derived expressions in a common reference system. A stationary *Cartesian* coordinate system,  $X_{pa,s}Y_{pa,s}Z_{pa,s}$ , associated with the plane of action,  $PA$ , in the crossed-axes gear pair is especially handy for solving the problem of determining the sliding velocity in geometrically accurate  $C_a$  – gearing.

For the derivation of an analytical solution to the problem under consideration, the operators of linear transformations are extensively used below. The chief reason for why the operators of linear transformations are used for the derivation of all the necessary equations is as follows. It is convenient to derive an analytical expression for each of the linear velocity vectors,  $\mathbf{V}_{m,g}$  and  $\mathbf{V}_{m,p}$ , in a specific reference system, and then to represent the derived equations in a common reference system that is convenient to perform the further analysis. For instance, it is convenient to determine the linear velocity vector,  $\mathbf{V}_{m,g}$ , in a coordinate system associated with the gear. Similarly, it is convenient to determine the linear velocity vector,  $\mathbf{V}_{m,p}$ , in a coordinate system associated with the pinion. Later on, the derived equations for both the vectors,  $\mathbf{V}_{m,g}$  and  $\mathbf{V}_{m,p}$ , can be represented in a common reference system. The use of the operators of linear transformations, namely, the operators of translation, and of the operators of rotation, along and about the coordinate axes is proven to be very helpful for this purpose.

Relative motion of a driving member, of a driven member in a gear pair, as well as of the plane of action, form the foundation, on which the corresponding operators of the coordinate system transformations can be derived. When a gear pair operates, the driving member, the driven member, and the plane of action, all are rotated in a timely manner, that is, the rotations,  $\omega_g$ ,  $\omega_p$  and  $\omega_{pa}$ , are synchronized with one another.

Numerous similarities between the earlier discussed derivation of the equation for the sliding velocity vector in intersected-axes gearing (see Chapter 13) and those between sliding velocity vector in crossed-axes gearing are also employed below.

A stationary *Cartesian* reference system,  $X_{p,s}Y_{p,s}Z_{p,s}$ , is associated with the gear housing. Another *Cartesian* reference system,  $X_pY_pZ_p$ , is associated with the pinion. At the beginning, the axes of the pinion coordinate system,  $X_pY_pZ_p$ , align to the corresponding axes of the stationary coordinate system,  $X_{p,s}Y_{p,s}Z_{p,s}$ . When the pinion is rotated about the axis,  $O_p$ , through a certain angle,  $\varphi_p$ , the reference system,  $X_pY_pZ_p$ , is rotated together with the pinion.

The transition from the pinion reference system,  $X_pY_pZ_p$ , to the stationary reference system,  $X_{p,s}Y_{p,s}Z_{p,s}$ , is analytically described by the operator of rotation,  $\mathbf{Rt}(Z_s, \varphi_p)$ , of the reference system,  $X_pY_pZ_p$ , through the angle,  $\varphi_p$ , about the axis,  $O_p$ , in the counter-clockwise direction.<sup>3</sup> In matrix form, this operator is represented as:

$$\mathbf{Rt}(Z_s, \varphi_p) = \begin{bmatrix} \cos \varphi_p & -\sin \varphi_p & 0 & 0 \\ \sin \varphi_p & \cos \varphi_p & 0 & 0 \\ 0 & 0 & 1 & 0 \\ 0 & 0 & 0 & 1 \end{bmatrix} \quad (15.13)$$

The coordinate system transformation that is analytically described by the operator of rotation,  $\mathbf{Rt}(Z_s, \varphi_p)$ , is followed by the rotation of the reference system,  $X_{p,s}Y_{p,s}Z_{p,s}$ , through the base cone angle,  $\gamma_b$ , of the pinion about the axis  $Y_{p,s}$ , in the counter-clockwise direction. The rotation of this

<sup>3</sup> Here and below, the direction of rotation of a coordinate system about a coordinate axis is determined looking from the arrowhead of the coordinate axis about which the rotation is performed.

sort is analytically described by the operator of rotation,  $\mathbf{Rt}(Y_{p.s}, \gamma_b)$ . In matrix form, this operator is represented as:

$$\mathbf{Rt}(Y_{p.s}, \gamma_b) = \begin{bmatrix} \cos \gamma_b & 0 & -\sin \gamma_b & 0 \\ 0 & 1 & 0 & 0 \\ \sin \gamma_b & 0 & \cos \gamma_b & 0 \\ 0 & 0 & 0 & 1 \end{bmatrix} \quad (15.14)$$

After the rotation of the coordinate system,  $X_{p.s}Y_{p.s}Z_{p.s}$ , about the axis,  $Y_{p.s}$ , through the base cone angle,  $\gamma_b$ , is completed, the coordinate system,  $X_{p.s}Y_{p.s}Z_{p.s}$ , occupies the position that is labeled as  $X_{1.s}Y_{1.s}Z_{1.s}$ . The axes of the coordinate system,  $X_{1.s}Y_{1.s}Z_{1.s}$ , and of the stationary coordinate system,  $X_{2.s}Y_{2.s}Z_{2.s}$ , associated with the plane of action,  $PA$ , have to be properly aligned with each other. To get the axes aligned, an additional rotation of the reference system,  $X_{1.s}Y_{1.s}Z_{1.s}$ , about the axis,  $Z_{p.s}$ , through a right angle must be performed. An operator,  $\mathbf{Rt}(Z_{p.s}, 90^\circ)$ , of linear transformation that analytically describes this additional rotation can be represented in matrix form:

$$\mathbf{Rt}(Z_{p.s}, 90^\circ) = \begin{bmatrix} 0 & 1 & 0 & 0 \\ -1 & 0 & 0 & 0 \\ 0 & 0 & 1 & 0 \\ 0 & 0 & 0 & 1 \end{bmatrix} \quad (15.15)$$

After been turned about the axis,  $Z_{p.s}$ , through a right angle, the coordinate system is designated as  $X_{2.s}Y_{2.s}Z_{2.s}$ .

Then, as the pinion base cone apex,  $A_p$ , is not coincident with the plane-of-action apex,  $A_{pa}$ , the origin of the reference system,  $X_{2.s}Y_{2.s}Z_{2.s}$ , has to be translated from the pinion apex  $A_p$  to the plane-of-action apex  $A_{pa}$ . This linear transformation is analytically described by an operator of transition:

$$\mathbf{Tr}(Y_{p.s}, -r_p) = \begin{bmatrix} 1 & 0 & 0 & 0 \\ 0 & 1 & 0 & -r_p \\ 0 & 0 & 1 & 0 \\ 0 & 0 & 0 & 1 \end{bmatrix} \quad (15.16)$$

The next linear transition is performed from the coordinate system,  $X_{2.s}Y_{2.s}Z_{2.s}$ , to the stationary coordinate system,  $X_{pa.s}Y_{pa.s}Z_{pa.s}$ , associated with the plane of action,  $PA$ . For the analytical description of the rotation of the reference system,  $X_{2.s}Y_{2.s}Z_{2.s}$ , in the counter-clockwise direction about the axis  $Z_{2.s}$  through an angle,  $\sigma_p$ , the operator of rotation,  $\mathbf{Rt}(Z_{2.s}, \sigma_p)$ , is used. In matrix form, this operator can be represented as:

$$\mathbf{Rt}(Z_{2.s}, \sigma_p) = \begin{bmatrix} \cos \sigma_p & \sin \sigma_p & 0 & 0 \\ -\sin \sigma_p & \cos \sigma_p & 0 & 0 \\ 0 & 0 & 1 & 0 \\ 0 & 0 & 0 & 1 \end{bmatrix} \quad (15.17)$$

Here, the projection of the pinion cone angle,  $\Sigma_p$ , onto the plane of action,  $PA$ , is designated as  $\sigma_p$  (i.e., the equality  $\text{Pr}_{pa} \Sigma_p = \sigma_p$  is valid). It can be shown that the angle,  $\sigma_p$ , can be calculated as:

$$\sigma_p = \cos^{-1} \left( \frac{\cos \Sigma_p}{\cos \gamma_b} \right) \quad (15.18)$$

where  $\gamma_b$  is the base cone angle of the pinion.

Finally, the transition is performed from the stationary coordinate system,  $X_{pa.s}Y_{pa.s}Z_{pa.s}$ , associated with the plane of action, to the coordinate system,  $X_{pa}Y_{pa}Z_{pa}$ , that is rotated together with the plane of action,  $PA$ . For the analytical description of the rotation of the reference system,  $X_{pa.s}Y_{pa.s}Z_{pa.s}$ , in the clockwise direction about the axis  $Z_{pa.s}$  through an angle,  $\varphi_{pa}$ , the operator of rotation,  $\mathbf{Rt}(Z_{pa.s}, \varphi_{pa})$ , is used. In matrix form, this operator can be represented as:

$$\mathbf{Rt}(Z_{2.s}, \varphi_{pa}) = \begin{bmatrix} \cos \varphi_{pa} & -\sin \varphi_{pa} & 0 & 0 \\ \sin \varphi_{pa} & \cos \varphi_{pa} & 0 & 0 \\ 0 & 0 & 1 & 0 \\ 0 & 0 & 0 & 1 \end{bmatrix} \quad (15.19)$$

The angle of rotation,  $\varphi_{pa}$ , of the plane of action,  $PA$ , can be expressed in terms of the angle of rotation,  $\varphi_p$ , of the pinion.

For the analytical description of the resultant coordinate system transformation, namely, for the transition from the reference system,  $X_pY_pZ_p$ , associated with the rotated pinion, to the reference system,  $X_{pa}Y_{pa}Z_{pa}$ , associated with the rotated plane of action,  $PA$ , the operator,  $\mathbf{Rs}_{Ca}(p \rightarrow pa)$ , of the resultant coordinate system is used. This operator can be expressed in terms of the operators of the elementary linear transformations as<sup>4</sup>:

$$\begin{aligned} \mathbf{Rs}_{Ca}(p \rightarrow pa) = & \mathbf{Rt}(Z_{2.s}, \varphi_{pa}) \cdot \mathbf{Rt}(Z_{2.s}, \sigma_p) \cdot \mathbf{Tr}(Y_{p.s}, -r_p) \\ & \cdot \mathbf{Rt}(Z_{p.s}, 90^\circ) \cdot \mathbf{Rt}(Y_{p.s}, \gamma_b) \cdot \mathbf{Rt}(Z_s, \varphi_p) \end{aligned} \quad (15.20)$$

Note that the order of the multipliers in Eq. (15.20) is not allowed to be altered.

For the inverse coordinate system transformation, that is, for the analytical description of transition from the reference system,  $X_{pa}Y_{pa}Z_{pa}$ , associated with the rotated plane of action,  $PA$ , to the reference system,  $X_pY_pZ_p$ , associated with the rotated pinion, the operator,  $\mathbf{Rs}_{Ca}(pa \rightarrow p)$ , of the inverse coordinate system transformation is used. The operator,  $\mathbf{Rs}_{Ca}(pa \rightarrow p)$ , of this linear transformation can be expressed in terms of the operator,  $\mathbf{Rs}_{Ca}(p \rightarrow pa)$ , of the direct coordinate system transformation as:

$$\mathbf{Rs}_{Ca}(pa \rightarrow p) = \mathbf{Rs}_{Ca}^{-1}(p \rightarrow pa) \quad (15.21)$$

The operators,  $\mathbf{Rs}_{Ca}(p \rightarrow pa)$  and  $\mathbf{Rs}_{Ca}(pa \rightarrow p)$ , are not presented here in an expanded form, as both of them are bulky.

In the reference system,  $X_pY_pZ_p$ , associated with the rotated pinion, the linear velocity vector,  $\mathbf{V}_{m,p}$ , of point of interest,  $m$ , is analytically described by a column matrix:

$$\mathbf{V}_{m,p}|_p = \begin{bmatrix} -r_{b,p} \sin \varphi_p \\ r_{b,p} \cos \varphi_p \\ 0 \\ 1 \end{bmatrix} \quad (15.22)$$

Then the operator of the resultant coordinate system transformation,  $\mathbf{Rs}_{Ca}(p \rightarrow pa)$ , is used to represent that same linear velocity vector,  $\mathbf{V}_{m,p}$ , in the coordinate system,  $X_{pa}Y_{pa}Z_{pa}$ , associated with the rotated plane of action,  $PA$ :

<sup>4</sup> It is important to stress here on the difference between the operator of the resultant coordinate system transformation,  $\mathbf{Rs}_{Ca}(p \rightarrow pa)$ , in case of crossed-axes gearing, and the similar operator of the resultant coordinate system transformation,  $\mathbf{Rs}_{Ia}(p \rightarrow pa)$ , in case of intersected-axes gearing [see Eq. (13.38)].

$$\mathbf{V}_{m.p}|_{pa} = \mathbf{R}s_{Ca}(p \rightarrow pa) \cdot \begin{bmatrix} -r_{b.p} \sin \varphi_p \\ r_{b.p} \cos \varphi_p \\ 0 \\ 1 \end{bmatrix} \quad (15.23)$$

A formula for the operator,  $\mathbf{R}s_{Ca}(pa \rightarrow g)$ , of the resultant coordinate system transformation, namely, for the analytical description of the transition from the reference system,  $X_{pa}Y_{pa}Z_{pa}$ , associated with the rotated plane of action,  $PA$ , to the reference system,  $X_gY_gZ_g$ , associated with the rotated gear, can be derived similar to that Eq. (15.20), is derived for the calculation of the operator of linear transformation,  $\mathbf{R}s_{Ca}(p \rightarrow pa)$ . The operators,  $\mathbf{Rt}(Z_s, \varphi_g)$ ,  $\mathbf{Rt}(Y_{g.s}, \Gamma_b)$ ,  $\mathbf{Tr}(Y_{p.s}, r_g)$ ,  $\mathbf{Rt}(Z_{g.s}, 90^\circ)$ ,  $\mathbf{Rt}(Z_{3.s}, \sigma_g)$ , and  $\mathbf{Rt}(Z_{3.s}, \varphi_{pa})$ , of the elementary linear transformations are used in this case. The above listed operators of linear transformations are composed similar to that the operators of the linear transformations [i.e.,  $\mathbf{Rt}(Z_s, \varphi_p)$ , Eq. (15.13);  $\mathbf{Rt}(Y_{p.s}, \gamma_b)$ , Eq. (15.14);  $\mathbf{Tr}(Y_{p.s}, r_g)$ , Eq. (15.16);  $\mathbf{Rt}(Z_{p.s}, 90^\circ)$ , Eq. (15.15);  $\mathbf{Rt}(Z_{2.s}, \sigma_p)$ , Eq. (15.17); and  $\mathbf{Rt}(Z_{2.s}, \varphi_{pa})$ , Eq. (15.19)] are composed:

$$\mathbf{Rt}(Z_s, \varphi_g) = \begin{bmatrix} \cos \varphi_g & \sin \varphi_g & 0 & 0 \\ -\sin \varphi_g & \cos \varphi_g & 0 & 0 \\ 0 & 0 & 1 & 0 \\ 0 & 0 & 0 & 1 \end{bmatrix} \quad (15.24)$$

$$\mathbf{Rt}(Y_{g.s}, \Gamma_b) = \begin{bmatrix} \cos \Gamma_b & 0 & \sin \Gamma_b & 0 \\ 0 & 1 & 0 & 0 \\ -\sin \Gamma_b & 0 & \cos \Gamma_b & 0 \\ 0 & 0 & 0 & 1 \end{bmatrix} \quad (15.25)$$

$$\mathbf{Rt}(Z_{g.s}, 90^\circ) = \begin{bmatrix} 0 & 1 & 0 & 0 \\ -1 & 0 & 0 & 0 \\ 0 & 0 & 1 & 0 \\ 0 & 0 & 0 & 1 \end{bmatrix} \quad (15.26)$$

$$\mathbf{Tr}(Y_{g.s}, r_g) = \begin{bmatrix} 1 & 0 & 0 & 0 \\ 0 & 1 & 0 & r_g \\ 0 & 0 & 1 & 0 \\ 0 & 0 & 0 & 1 \end{bmatrix} \quad (15.27)$$

$$\mathbf{Rt}(Z_{3.s}, \sigma_g) = \begin{bmatrix} \cos \sigma_g & -\sin \sigma_g & 0 & 0 \\ \sin \sigma_g & \cos \sigma_g & 0 & 0 \\ 0 & 0 & 1 & 0 \\ 0 & 0 & 0 & 1 \end{bmatrix} \quad (15.28)$$

$$\mathbf{Rt}(Z_{3.s}, \varphi_{pa}) = \begin{bmatrix} \cos \varphi_{pa} & \sin \varphi_{pa} & 0 & 0 \\ -\sin \varphi_{pa} & \cos \varphi_{pa} & 0 & 0 \\ 0 & 0 & 1 & 0 \\ 0 & 0 & 0 & 1 \end{bmatrix} \quad (15.29)$$



Here, the projection of the gear cone angle,  $\Sigma_g$ , onto the plane of action,  $PA$ , is designated as  $\sigma_g$  (i.e., the equality  $\text{Pr}_{pa} \Sigma_g = \sigma_g$  is valid). It can be shown that the angle,  $\sigma_g$ , can be calculated the following equation:

$$\sigma_g = \cos^{-1} \left( \frac{\cos \Sigma_g}{\cos \Gamma_b} \right) \quad (15.30)$$

where  $\Gamma_b$  is the base cone angle of the gear.

For the analytical description of the resultant coordinate system transformation, namely, for the transition from the reference system,  $X_g Y_g Z_g$ , associated with the rotated pinion, to the reference system,  $X_{pa} Y_{pa} Z_{pa}$ , associated with the rotated plane of action,  $PA$ , the operator,  $\mathbf{Rs}_{Ca}(g \rightarrow pa)$ , of the resultant coordinate system is employed. This operator can be expressed in terms of the operators of the elementary linear transformations:

$$\begin{aligned} \mathbf{Rs}_{Ca}(g \rightarrow pa) = & \mathbf{Rt}(Z_{3.s}, \varphi_{pa}) \cdot \mathbf{Tr}(Y_{g.s}, r_g) \cdot \mathbf{Rt}(Z_{3.s}, \sigma_g) \\ & \cdot \mathbf{Rt}(Z_{g.s}, 90^\circ) \cdot \mathbf{Rt}(Y_{g.s}, \Gamma_b) \cdot \mathbf{Rt}(Z_s, \varphi_g) \end{aligned} \quad (15.31)$$

Note that the order of the multipliers in Eq. (15.31) is not allowed to be altered.

In the reference system,  $X_g Y_g Z_g$ , associated with the rotated gear the linear velocity vector,  $\mathbf{V}_{m.g}$ , of point of interest,  $m$ , can be analytically described by a column matrix:

$$\mathbf{V}_{m.g} \Big|_g = \begin{bmatrix} -r_{b.g} \sin \varphi_g \\ r_{b.g} \cos \varphi_g \\ 0 \\ 1 \end{bmatrix} \quad (15.32)$$

Then the operator of the resultant coordinate system transformation,  $\mathbf{Rs}_{Ca}(g \rightarrow pa)$ , is employed to represent that same linear velocity vector,  $\mathbf{V}_{m.g}$ , in the coordinate system,  $X_{pa} Y_{pa} Z_{pa}$ , associated with the rotated plane of action,  $PA$ :

$$\mathbf{V}_{m.g} \Big|_{pa} = \mathbf{Rs}_{Ca}(g \rightarrow pa) \cdot \begin{bmatrix} -r_{b.g} \sin \varphi_g \\ r_{b.g} \cos \varphi_g \\ 0 \\ 1 \end{bmatrix} \quad (15.33)$$

Consider the relative motion of point within the line of contact of the tooth flanks,  $\mathcal{S}$  and  $\mathcal{P}$ , of a gear, and of a mating pinion in a crossed-axes gear pair.

The vector,  $\mathbf{V}_{rel}$ , of the relative motion of point of interest,  $m$ , within the line of contact,  $LC$ , between the tooth flanks,  $\mathcal{S}$  and  $\mathcal{P}$ , of a gear, and of a mating pinion in a crossed-axes gear pair equals to the difference:

$$\mathbf{V}_{rel} = \mathbf{V}_{m.p} \Big|_{pa} - \mathbf{V}_{m.g} \Big|_{pa} \quad (15.34)$$

where both the linear velocity vectors,  $\mathbf{V}_{m.g}$  and  $\mathbf{V}_{m.p}$ , are represented in a common reference system,  $X_{pa} Y_{pa} Z_{pa}$ , associated with the rotated plane of action,  $PA$ .

These velocities,  $\mathbf{V}_{m.g}$  and  $\mathbf{V}_{m.p}$ , decisively affect the lubrication and friction parameters on the mating flanks and, hence, influence the load capacity and efficiency of the bevel gear set.

In the expanded form, the vector of the relative motion,  $\mathbf{V}_{rel}$ , can be represented in matrix form as:

$$\mathbf{V}_{rel}|_{pa} = \begin{bmatrix} V_{x,rel} \\ V_{y,rel} \\ V_{z,rel} \\ 1 \end{bmatrix} \quad (15.35)$$

The projection,  $V_{y,rel}$ , of the linear velocity vector,  $\mathbf{V}_{rel}$ , onto the axis,  $Y_{pa}$ , causes pure rolling of the gear and the mating pinion tooth flanks,  $\mathcal{G}$  and  $\mathcal{P}$ , over each other. Therefore, this component of the linear velocity vector,  $\mathbf{V}_{rel}$ , is labeled below as  $\mathbf{V}_{rol}$ .

The projection,  $V_{z,rel}$ , of the linear velocity vector,  $\mathbf{V}_{rel}$ , onto the axis,  $Z_{pa}$ , causes profile sliding of the gear and the mating pinion tooth flanks,  $\mathcal{G}$  and  $\mathcal{P}$ . Therefore, this component of the linear velocity vector,  $\mathbf{V}_{rel}$ , is labeled below as  $\mathbf{V}_{sl.p}$ .

The projection,  $V_{x,rel}$ , of the linear velocity vector,  $\mathbf{V}_{rel}$ , onto the axis,  $X_{pa}$ , causes *drag* sliding of the gear and the mating pinion tooth flanks,  $\mathcal{G}$  and  $\mathcal{P}$ . Because of this, this component of the linear velocity vector,  $\mathbf{V}_{rel}$ , is labeled below as  $\mathbf{V}_{sl.d}$ .

Total sliding,  $\mathbf{V}_{sl}$ , in crossed-axes gearing can be calculated as the sum:

$$\mathbf{V}_{sl} = \mathbf{V}_{sl.p} + \mathbf{V}_{sl.d} \quad (15.36)$$

At different points within the zone of action,  $ZA$ , each of the components of the linear velocity vectors, namely, the vectors  $\mathbf{V}_{sl}$ ,  $\mathbf{V}_{sl.p}$ , and  $\mathbf{V}_{sl.d}$ , vary.

A computer code for the calculation of all the components,  $\mathbf{V}_{rol}$ ,  $\mathbf{V}_{sl.p}$ , and  $\mathbf{V}_{sl.d}$ , of the linear velocity vector,  $\mathbf{V}_{rel}$ , can be developed on the premise of the equations derived above in this section of the book. Ultimately, the distribution of the components,  $\mathbf{V}_{rol}$ ,  $\mathbf{V}_{sl.p}$ , and  $\mathbf{V}_{sl.d}$ , within the zone of action,  $ZA$ , in a crossed-axes gear pair can be interpreted graphically.

### 15.4.3 SPECIFIC SLIDING IN GEOMETRICALLY ACCURATE CROSSED-AXES GEARING

For the specification of sliding between tooth flanks,  $\mathcal{G}$  and  $\mathcal{P}$ , of a gear and of a mating pinion in crossed-axes gear pair, a dimensionless parameter can be used [similar to that in parallel-axes gearing (see Chapter 10), as well as in intersected-axes gearing (see Chapter 13)]. This sliding parameter can also be referred to as *specific sliding*, as it is common with respect to parallel-axes gearing, and intersected-axes gearing. Specific sliding is denoted by  $\gamma_{\Sigma}$ . An actual value of specific sliding does not depend on a rotation of the input/output shafts, and depends only on the design parameters of a gear and of a mating pinion. The latter is important when optimizing the design parameters of gears in crossed-axes gear pairs.

Two different parameters,  $\gamma_{\Sigma}$ , are distinguished.

**First**, the slide/roll ratio for tooth flank,  $\mathcal{G}$ , of a gear that is calculated from a formula:

$$\gamma_{\Sigma.g} = \frac{V_{sl.g}^m - V_{sl.p}^m}{V_{sl.g}^m} \quad (15.37)$$

**Second**, the slide/roll ratio for tooth flank,  $\mathcal{P}$ , of a pinion that is calculated from a formula:

$$\gamma_{\Sigma.p} = \frac{V_{sl.p}^m - V_{sl.g}^m}{V_{sl.p}^m} \quad (15.38)$$

The calculation of the sliding velocities,  $V_{sl.g}^m$  and  $V_{sl.p}^m$ , in Eqs. (15.37) and (15.38) is discussed immediately below.

In the reference system,  $X_{pa}Y_{pa}Z_{pa}$ , associated with the rotated plane of action,  $PA$ , the linear velocity vector,  $\mathbf{V}_{m.g}|_{pa}$  [see Eq. (15.33)], can be represented in the form:

$$\mathbf{V}_{m.g}|_{pa} = \begin{bmatrix} V_{x.m.g} \\ V_{y.m.g} \\ V_{z.m.g} \\ 1 \end{bmatrix} \quad (15.39)$$

In a crossed-axes gear pair, the component,  $V_{z.m.g}$ , contributes to the profile sliding, and the component,  $V_{x.m.g}$ , contributes to the drag sliding (the component,  $V_{y.m.g}$ , contributes to pure rolling of the tooth flanks,  $\mathcal{S}$  and  $\mathcal{P}$ ). The sliding velocity,  $V_{sl.g}^m$  [see Eqs. (15.37) and (15.38)], can be expressed in terms of the velocities,  $V_{x.m.g}$  and  $V_{z.m.g}$ , as:

$$V_{sl.g}^m = \sqrt{V_{x.m.g}^2 + V_{z.m.g}^2} \quad (15.40)$$

Similarly, in the reference system,  $X_{pa}Y_{pa}Z_{pa}$ , associated with the rotated plane of action,  $PA$ , the linear velocity vector,  $\mathbf{V}_{m.p}|_{pa}$ , can be represented in the form:

$$\mathbf{V}_{m.p}|_{pa} = \begin{bmatrix} V_{x.m.p} \\ V_{y.m.p} \\ V_{z.m.p} \\ 1 \end{bmatrix} \quad (15.41)$$

In a crossed-axes gear pair, the component,  $V_{z.m.p}$ , contributes to the profile sliding, and the component,  $V_{x.m.p}$ , contributes to sliding in the lengthwise direction of the gear tooth (the component,  $V_{y.m.p}$ , contributes to pure rolling of the tooth flanks,  $\mathcal{S}$  and  $\mathcal{P}$ ). The sliding velocity,  $V_{sl.p}^m$ , can be expressed in terms of the velocities,  $V_{x.m.p}$  and  $V_{z.m.p}$ , as:

$$V_{sl.p}^m = \sqrt{V_{x.m.p}^2 + V_{z.m.p}^2} \quad (15.42)$$

The sliding velocities,  $V_{sl.g}^m$  and  $V_{sl.p}^m$  [see Eqs. (15.40) and (15.42)], entered into the expressions:

$$\gamma_{\Sigma.g} = \frac{V_{sl.g}^m - V_{sl.p}^m}{V_{sl.g}^m} \quad (15.43)$$

$$\gamma_{\Sigma.p} = \frac{V_{sl.p}^m - V_{sl.g}^m}{V_{sl.p}^m} \quad (15.44)$$

to calculate the specific roll/slide ratios,  $\gamma_{\Sigma.g}$  and  $\gamma_{\Sigma.p}$ , in crossed-axes gearings.

The specific sliding,  $\gamma_{\Sigma}$ , is of a positive value on the addendum portions of the tooth flanks. The parameter,  $\gamma_{\Sigma}$ , does not exceed 1. At points within the axis of instantaneous rotation,  $P_{ln}$ , specific sliding,  $\gamma_{\Sigma}$ , is equal to zero, and it is equal to 1 at the base cone of the mating gear.

The specific sliding on the dedendum portion of the tooth flanks is of a negative value. It is equal to zero at points within the axis of instantaneous rotation,  $P_{ln}$ , and it approaches a minus infinity at the base cone.

The specific rolling/sliding ratios,  $\gamma_{\Sigma.g}$  and  $\gamma_{\Sigma.p}$ , can be plotted within the zone of action,  $ZA$ , as only the region,  $ZA$ , of the plane of action comes into effect when investigating the engagement of the gear teeth.

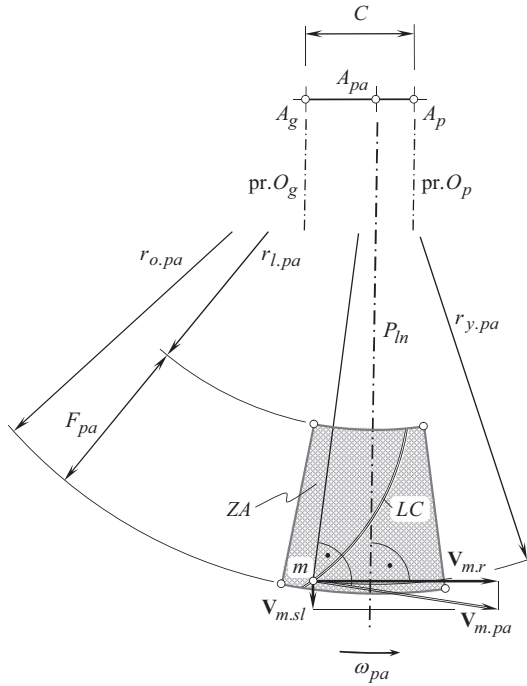


FIGURE 15.7 Origination of axial sliding in geometrically accurate crossed-axes gear pair.

#### 15.4.4 FEATURES OF SPECIFIC SLIDING IN GEOMETRICALLY ACCURATE CROSSED-AXES GEARING

The interaction of tooth flanks,  $\mathcal{S}$  and  $\mathcal{P}$ , in geometrically accurate crossed-axes gearing features sliding in the lengthwise direction of gear teeth (see Figure 15.7). Therefore, in addition to the specific roll/sliding ratios,  $\gamma_{\Sigma.g}$  and  $\gamma_{\Sigma.p}$  [see Eqs. (15.43) and (15.44)], two more characteristics are required to be introduced to specify specific sliding in crossed-axes gear pairs.

Specific profile roll/slide ratios,  $\gamma_{p.g}$  and  $\gamma_{p.p}$ , are the first additional characteristics. These two ratios are specified as:

$$\gamma_{p.g} = \frac{V_{z.m.g} - V_{z.m.p}}{V_{z.m.g}} \quad (15.45)$$

$$\gamma_{p.p} = \frac{V_{z.m.p} - V_{z.m.g}}{V_{z.m.p}} \quad (15.46)$$

Specific roll/slide ratios,  $\gamma_{d.g}$  and  $\gamma_{d.p}$ , for the sliding in the lengthwise direction of the gear teeth are the second additional characteristics. These two ratios are specified as:

$$\gamma_{d.g} = \frac{V_{x.m.g} - V_{x.m.p}}{V_{x.m.g}} \quad (15.47)$$

$$\gamma_{d.p} = \frac{V_{x.m.p} - V_{x.m.g}}{V_{x.m.p}} \quad (15.48)$$

Specific profile roll/slide ratios,  $\gamma_{p.g}$  and  $\gamma_{p.p}$ , and specific drag roll/slide ratios,  $\gamma_{d.g}$  and  $\gamma_{d.p}$ , are helpful for more in-detail analysis of sliding conditions in crossed-axes gearings.

It is right point to turn the readers' attention here that gears with a low tooth count are more vulnerable to sliding between the tooth flanks,  $\mathcal{S}$  and  $\mathcal{P}$ , of a gear and a mating pinion in crossed-axes gear pairs. They are also more sensitive to the variation of the roll/slide conditions within the zone of action,  $ZA$ .

The performed analysis of sliding conditions in external crossed-axes gearing can be extended to internal crossed-axes as well as to crossed-axes gearing with a crown gear.

The disclosed approach for the calculation of the sliding parameters in geometrically accurate crossed-axes gearing is also applicable for calculation the sliding parameters in *Novikov/conformal*, and in *high-conformal gearing*. The main feature in the latter case is that the angular face width in a gear pair is zero.

## 15.5 ELEMENTS OF DYNAMICS OF GEOMETRICALLY ACCURATE CROSSED-AXES GEARING

In a crossed-axes gear pair, the input shaft and the output shaft are loaded by an input torque and output torque, correspondingly. As the gears interact with one another, a force of the interaction is exerted from the driving member of the gear pair. An actual value of the force of interaction in crossed-axes gearing, as well as the components of this force, depend on the input torque, and on the design parameters of the gear and of the mating pinion. Considering an input torque, and an input rotation of constant values (namely, no acceleration/deceleration is taken into account in the performed below analysis), it is necessary to determine the forces that act between a gear and a mating pinion in a crossed-axes gear pair.<sup>5</sup>

### 15.5.1 PRINCIPAL ASSUMPTION ADOPTED IN THE LOAD ANALYSIS OF GEOMETRICALLY ACCURATE CROSSED-AXES GEARING

When a crossed-axes gear pair operates, the tooth flanks,  $\mathcal{S}$  and  $\mathcal{P}$ , of the gear and of the pinion interact with one another at points within the line(s) of contact,  $LC$ . The line(s) of contact is entirely located within the plane of action,  $PA$ . This makes possible a conclusion that the force of interaction between the tooth flanks,  $\mathcal{S}$  and  $\mathcal{P}$ , acts along a straight line that is also located within the plane of action,  $PA$ .

As the line of action of the force is entirely located within the plane of action,  $PA$ , then the following assumption seems to be reasonable in the load analysis of geometrically accurate crossed-axes gearing.

Referring to Figure 15.8, consider base cones of a gear and of a mating pinion, along with the plane of action. The gear is rotated,  $\omega_g$ , about its axis of rotation,  $O_g$ , and the pinion is rotated,  $\omega_p$ , about its axis of rotation,  $O_p$ , as schematically illustrated in Figure 15.8. The plane of action,  $PA$ , is in tangency to both the base cones. The plane of action,  $PA$ , rotates,  $\omega_{pa}$ , about its axis of rotation (not shown in Figure 15.8) that passes through the *plane-of-action apex*,  $A_{pa}$ , and is pointed perpendicular to the plane of action. It is instructive to point out here that in contrast to the *equivalent pulley-and-belt transmission*, where the belt *pulls* the driven member, in reality, in a gear pair, the driving gear *pushes* the driven member in a crossed-axes gearing. In this way, the direction of the rotation,  $\omega_{pa}$ , is specified in Figure 15.8.

The rotations,  $\omega_g$ ,  $\omega_p$ , and  $\omega_{pa}$ , are synchronized with one another so as to fulfill the equations:

$$\frac{\omega_g}{\omega_{pa}} = \sin \Gamma_b \quad (15.49)$$

$$\frac{\omega_p}{\omega_{pa}} = \sin \gamma_b \quad (15.50)$$

<sup>5</sup> Friction forces are incorporated into consideration on the later stages of the load analysis.

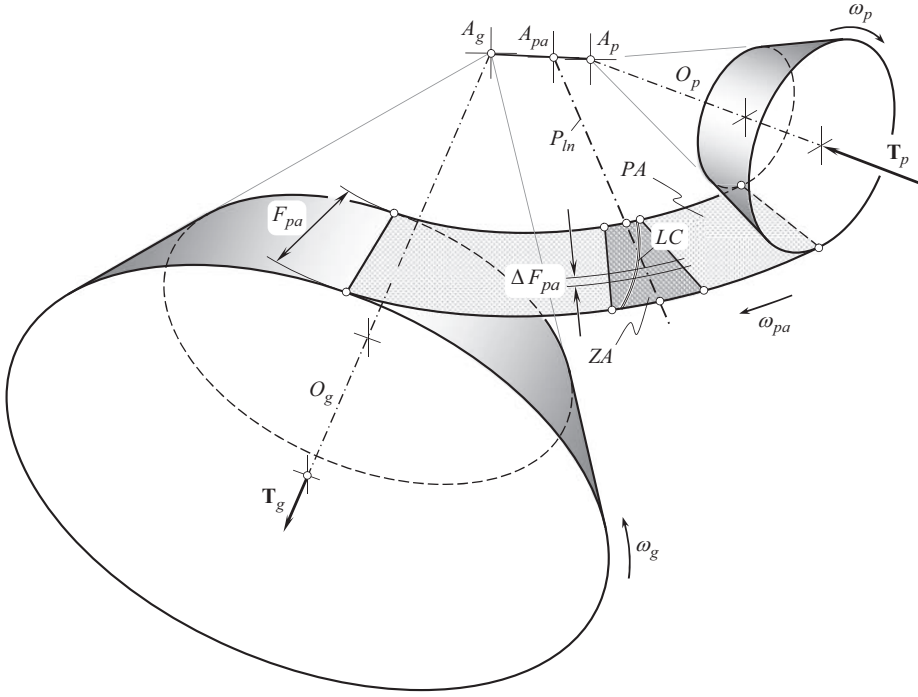


**FIGURE 15.8** On the calculation of the forces acting in geometrically accurate crossed-axes gear pair.

$$\frac{\omega_g}{\omega_p} = \frac{\sin \Gamma_b}{\sin \gamma_b} \quad (15.51)$$

The input torque,  $\mathbf{T}_p$ , is applied to the pinion shaft, and the output torque,  $\mathbf{T}_g$ , is applied to the gear shaft. The torque,  $\mathbf{T}_{pa}$ , is a *virtual* parameter. This torque is applied to the rotated plane of action,  $PA$ . The ratios of the magnitudes,  $T_g$ ,  $T_p$ , and  $T_{pa}$ , of the torques,  $\mathbf{T}_g$ ,  $\mathbf{T}_p$ , and  $\mathbf{T}_{pa}$ , are inverse to the corresponding ratios of the rotations,  $\omega_g$ ,  $\omega_p$ , and  $\omega_{pa}$  :

$$\frac{T_g}{T_{pa}} = \frac{1}{\sin \Gamma_b} \quad (15.52)$$

$$\frac{T_p}{T_{pa}} = \frac{1}{\sin \gamma_b} \quad (15.53)$$

$$\frac{T_g}{T_p} = \frac{\sin \gamma_b}{\sin \Gamma_b} \quad (15.54)$$

Interaction between a gear tooth flank,  $\mathcal{G}$ , and of a mating pinion tooth flank,  $\mathcal{P}$ , occurs only within the zone of action,  $ZA$ . Width of the zone of action is designated as  $F_{pa}$ . Width of the zone of action is,  $F_{pa}$ , is calculated as the difference (see Figure 15.9):

$$F_{pa} = r_{o,pa} - r_{l,pa} \quad (15.55)$$

between the outer,  $r_{o,pa}$ , and the inner,  $r_{l,pa}$ , radii of the plane of action,  $PA$ .



$$\mathbf{t}_p = \frac{\mathbf{T}_p}{F_{pa}} = \text{const} \quad (15.59)$$

are valid with respect to the gear as well as to the mating pinion.

As the torque per unit length,  $\mathbf{t}_{pa}$ , is of a constant value, and the equality,  $\mathbf{t}_{pa}F_{pa} = \mathbf{T}_{pa}$ , is valid, then the actual value of the plane-of-action torque,  $\mathbf{T}_{pa}$  (lumped torque), is proportional to the shadowed area in Figure 15.7.

Equal torque share among the slices is graphically illustrated in Figure 15.7.

In order to transmit a given power, it is always desirable to design and to implement gearboxes of the smallest possible size. From this perspective, the active portion of the line of contact,  $LC$ , should begin from the plane-of-action apex,  $A_{pa}$ . Evidently, the line of contact of such a geometry is far from to be practical, as the maximum contact and bending strength of the gear teeth is restricted by physical properties of a material the gear and the mating pinion are made of.

Calculation of the design parameters of the favorable portion of the line of contact is based on the assumption that the power being transmitting by a gear pair is equally shared within active portion of the gear pair face width. With that said, under the torque of a constant value, the smaller diameter of a gear/pinion, the large force and vice versa. Therefore, a practical value of the smallest possible diameter of the gear/pinion is limited by the yield contact and bending stress in the gear tooth.

The above discussion makes reasonable the following assumption that is referred to as *fundamental assumption* in dynamics of crossed-axes gearing:

### Assumption 15.1

In a crossed-axes gear pair, the torque per unit length,  $\mathbf{t}_{pa}$ , is equally shared in the radial direction among an infinite number of infinitesimally narrow slices, each of which is perpendicular to the axis of rotation either of the plane of action, or of the gear, or of the pinion.

A similar assumption has been made with respect to parallel-axes gear pairs (see Chapter 9) as well as with respect to intersected-axes gearing (see Chapter 14).

## 15.5.2 FORCES OF INTERACTION IN GEOMETRICALLY ACCURATE CROSSED-AXES GEARING

The forces that act in a geometrically accurate crossed-axes gear pair are considered below in different reference systems. The analysis begins with the load applied within the plane of action,  $PA$ . Then, the analysis enhanced to the forces that act on the bearings, on the gear housing, and so forth.

**Resultant force acting in geometrically accurate crossed-axes gearing.** In the plane-of-action,  $PA$ , the torque,  $\mathbf{T}_{pa}$ , creates the plane-of-action tangential force,  $\mathbf{F}_{pa}$ . The tangential force per unit length,  $\mathbf{f}_{pa}$ , can be expressed in terms of the torque per unit length,  $\mathbf{t}_{pa}$ , and the distance,  $r_{y.pa}$ , of a particular slice from the plane-of-action point,  $A_{pa}$ , as:

$$\mathbf{f}_{pa} = \frac{\mathbf{t}_{pa}}{r_{y.pa}} \quad (15.60)$$

It is instructive to point out here that the tangential force per unit length,  $\mathbf{f}_{pa}$ , is a function of the distance,  $r_{y.pa}$ , of point of interest,  $m$ , from the plane-of-action point,  $A_{pa}$ , that is:

$$\mathbf{f}_{pa} = \mathbf{f}_{pa}(r_{y.pa}) \quad (15.61)$$

The distribution of the tangential force per unit length,  $\mathbf{f}_{pa}(r_{y.pa})$ , in the radial direction of the plane of action is shown in Figure 15.9.



Having the tangential force per unite length,  $\mathbf{f}_{pa}$ , determined [see Eq. (15.60)], the resultant tangential forth,  $\mathbf{F}_{pa}$ , is calculated from the expression:

$$\mathbf{F}_{pa} = F_{pa} \cdot \mathbf{f}_{pa} + \mathbf{t}_{pa} \int_{r_{l,pa}}^{r_{o,pa}} \frac{1}{r_{y,pa}} dr_{y,pa} = F_{pa} \cdot \mathbf{f}_{pa} + \mathbf{t}_{pa} \cdot (\ln |r_{o,pa}| - \ln |r_{l,pa}|) \quad (15.62)$$

$$\mathbf{F}_{pa} = F_{pa} \cdot \mathbf{f}_{pa} + \mathbf{t}_{pa} \cdot \ln \left| \frac{r_{o,pa}}{r_{l,pa}} \right| \quad (15.63)$$

Equations similar to the Eq. (15.49), that is:

$$\mathbf{F}_g = F_{pa} \cdot \mathbf{f}_g + \mathbf{t}_g \cdot \ln \left| \frac{r_{o,pa}}{r_{l,pa}} \right| \quad (15.64)$$

$$\mathbf{F}_p = F_{pa} \cdot \mathbf{f}_p + \mathbf{t}_p \cdot \ln \left| \frac{r_{o,pa}}{r_{l,pa}} \right| \quad (15.65)$$

are valid with respect to the gear as well as to the mating pinion.

The resultant (lumped) forth,  $\mathbf{F}_{pa}$ , is applied at point,  $c_g$ , within the line of contact,  $LC$ , that is remote from the plane-of-action apex,  $A_{pa}$ , at a distance,  $r_{cg}$  (see Figure 15.9).

Transmission of a rotation from a driving shaft to a driven shaft is due to the tangential forth,  $\mathbf{F}_{pa}$ , that acts between the tooth flanks,  $\mathcal{S}$  and  $\mathcal{P}$ , in crossed-axes gearing.

When the gears rotate, friction is observed between a gear tooth flank,  $\mathcal{S}$ , and a mating pinion tooth flank,  $\mathcal{P}$ . The friction between the compressed gear and pinion tooth flanks,  $\mathcal{S}$  and  $\mathcal{P}$ , is due to the sliding that occurs between the tooth flanks,  $\mathcal{S}$  and  $\mathcal{P}$ . As it is already shown above (see the previous section of the book), two types of sliding are distinguished in crossed-axes gear pairs. The profile sliding is the first kind, and the sliding in the lengthwise direction of the gear teeth is the second kind of sliding in crossed-axes gearings. Therefore, friction forces of two types have to be recognized, namely: the profile friction force,  $\mathbf{F}_{pr}$ , and the friction force in the lengthwise direction,  $\mathbf{F}_{dr}$ . These friction forces contribute to the resultant force of the interaction,  $\mathbf{F}_{\Sigma}$ , between the gear tooth flank,  $\mathcal{S}$ , and the mating pinion tooth flank,  $\mathcal{P}$ :

$$\mathbf{F}_{\Sigma} = \mathbf{F}_{pa} + \mathbf{F}_{pr} + \mathbf{F}_{dr} \quad (15.66)$$

The component,  $\mathbf{F}_{pa}$ , is specified by Eq. (15.63).

In the reference system,  $X_{pa}Y_{pa}Z_{pa}$ , associated with the rotated plane of action,  $PA$ , the profile (transverse) friction force,  $\mathbf{F}_{pr}$ , is pointed along the axis  $Z_{pa}$ , as illustrated in Figure 15.10. The actual value of this force equals:

$$\mathbf{F}_{pr} = \mu_{pr} \cdot \mathbf{F}_{pa} \quad (15.67)$$

Here,  $\mu_{pr}$  designates the coefficient of friction in profile sliding of the gear,  $\mathcal{S}$ , and of the pinion,  $\mathcal{P}$ , tooth flanks.

In that same reference system,  $X_{pa}Y_{pa}Z_{pa}$ , the friction force in the lengthwise direction,  $\mathbf{F}_{dr}$ , is pointed along the axis  $X_{pa}$ . The actual value of this component equals (see Figure 15.10):

$$\mathbf{F}_{dr} = \mu_{dr} \cdot \mathbf{F}_{pa} \quad (15.68)$$

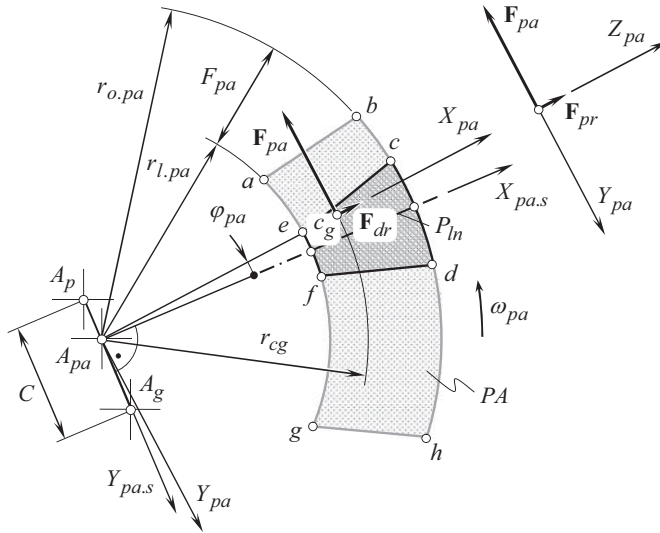


FIGURE 15.10 Tangential force,  $\mathbf{F}_{pa}$ , and friction forces,  $\mathbf{F}_{pr}$  and  $\mathbf{F}_{dr}$ , in crossed-axes gear pair.

The coefficient of friction in *drag* sliding of the gear,  $\mathcal{G}$ , and of the pinion,  $\mathcal{P}$ , tooth flanks is denoted by  $\mu_{dr}$ .

The coefficients of friction,  $\mu_{pr}$  and  $\mu_{dr}$ , can be of different values, as the normal curvatures of the gear and of the pinion tooth flanks,  $\mathcal{G}$  and  $\mathcal{P}$ , at point of interest are significantly different in the transverse, and in the lengthwise directions of the tooth flanks  $\mathcal{G}$  and  $\mathcal{P}$ . Moreover, the conditions of profile (transverse) sliding, and that in the lengthwise direction of the gear teeth, are also different. However, when performing preliminary analysis, the coefficients of friction,  $\mu_{pr}$  and  $\mu_{dr}$ , can be considered equal to one another ( $\mu_{pr} = \mu_{dr}$ ).

The total friction force (lumped force),  $\mathbf{F}_{fr.\Sigma}$ , in geometrically accurate crossed-axes gearing is calculated as:

$$\mathbf{F}_{fr.\Sigma} = \mathbf{F}_{pr} + \mathbf{F}_{dr} \quad (15.69)$$

The friction forces,  $\mathbf{F}_{pr}$  and  $\mathbf{F}_{dr}$ , in a crossed-axes gear pair are negligibly small, and, thus, commonly they are not taken into account when calculating the design parameters of a gear transmission. Moreover, the friction forces,  $\mathbf{F}_{pr}$  and  $\mathbf{F}_{dr}$ , do not affect the uniformity of the output rotation in a gear pair, as both,  $\mathbf{F}_{pr}$  and  $\mathbf{F}_{dr}$ , act along the straight lines that are entirely located within a plane that is perpendicular to the plane of action,  $PA$  (and that is tangent to the gear,  $\mathcal{G}$ , and the pinion,  $\mathcal{P}$ , tooth flanks at point of interest,  $m$ ). Only the component of the resultant force of interaction,  $\mathbf{F}_{\Sigma}$ , that is pointed along the common perpendicular to the tooth flanks,  $\mathcal{G}$  and  $\mathcal{P}$ , causes a rotation of the driven gear in a crossed-axes gear pair.

Different components of the resultant tangential force,  $\mathbf{F}_{pa}$ , of interaction between the tooth flanks,  $\mathcal{G}$  and  $\mathcal{P}$ , of a gear and of a mating pinion, along with the forces  $\mathbf{F}_g$  and  $\mathbf{F}_p$  [see Eqs. (15.64) and (15.65)] that act on the gear and the pinion, are entered into equations for the calculation of the bending, and of the contact strength of the gear and of the pinion teeth, the bearings, the housing, the shafts, and so forth.

The forces that act on the gear, have to be expressed in a stationary coordinate system,  $X_{g.s}Y_{g.s}Z_{g.s}$ , associated with the motionless gear (i.e., associated with the gear pair housing). The operator,  $\mathbf{R}_{sCa}(pa \rightarrow g_s)$ , of the resultant coordinate system transformation is used for this purpose. The

operator,  $\mathbf{Rs}_{Ca}(pa \rightarrow g_s)$ , can be represented as a product of the operators,  $\mathbf{Rt}(Y_{g,s}, \Gamma_b)$ ,  $\mathbf{Rt}(Z_{g,s}, 90^\circ)$ ,  $\mathbf{Rt}(Z_{g,s}, \sigma_g)$ ,  $\mathbf{Tr}(Y_{3,s}, r_g)$ , and  $\mathbf{Rt}(Z_{3,s}, \varphi_{pa})$ , of the elementary linear transformations as:

$$\mathbf{Rs}_{Ca}(pa \rightarrow g_s) = \mathbf{Rt}(Y_{g,s}, \Gamma_b) \cdot \mathbf{Rt}(Z_{g,s}, 90^\circ) \cdot \mathbf{Rt}(Z_{3,s}, \sigma_g) \cdot \mathbf{Tr}(Y_{3,s}, r_g) \cdot \mathbf{Rt}(Z_{3,s}, \varphi_{pa}) \quad (15.70)$$

After the resultant tangential force,  $\mathbf{F}_{pa}$  [see Eq. (15.63)], of interaction between the tooth flanks,  $\mathcal{S}$  and  $\mathcal{P}$ , of a gear and of a mating pinion, has been pre-multiplied by the operator,  $\mathbf{Rs}_{Ca}(pa \rightarrow g_s)$ , of the linear transformation, the resultant force,  $\mathbf{F}_{g,s}$ , that acts over the gear can be represented in the form of a column matrix:

$$\mathbf{F}_{g,s} = \mathbf{Rs}(pa \rightarrow g_s) \cdot \mathbf{F}_{pa} = \begin{bmatrix} F_{x,g,s} \\ F_{y,g,s} \\ F_{z,g,s} \\ 1 \end{bmatrix} \quad (15.71)$$

The components  $F_{x,g,s}$ ,  $F_{y,g,s}$ , and  $F_{z,g,s}$ , of the resultant force,  $\mathbf{F}_{g,s}$ , in Eq. (15.71) are equal to the separating force,  $F_{g,sep}$ , the tangential force,  $F_{g,tg}$ , and the axial thrust,  $F_{g,ax}$ , correspondingly, that is, the equalities  $F_{x,g,s} = F_{g,sep}$ ,  $F_{y,g,s} = F_{g,tg}$ , and  $F_{z,g,s} = F_{g,ax}$ , are valid. The forces,  $\mathbf{F}_{g,sep}$ ,  $\mathbf{F}_{g,tg}$ , and  $\mathbf{F}_{g,ax}$ , are entered into the equations for the calculation of the design parameters of a gearbox.

***Forces acting on the gear and the pinion in geometrically accurate crossed-axes gearing.***

In a reference system,  $X_{pa}Y_{pa}Z_{pa}$ , associated with the rotated plane of action,  $PA$ , an orientation of the force,  $\mathbf{F}_{pa}$  [namely, of the force specified by Eq. (15.63)], or of the resultant force,  $\mathbf{F}_\Sigma$  [that is specified by Eq. (15.66)], does not alter when the gears rotate. However, the configuration of the coordinate system,  $X_{pa}Y_{pa}Z_{pa}$ , in relation to a motionless reference system associated with the gear pair housing alters when the gears rotate. Therefore, in a stationary coordinate system,  $X_{g,s}Y_{g,s}Z_{g,s}$ , associated with the motionless gear, Eq. (15.71) has to be rewritten in a form as:

$$\mathbf{F}_{g,s}(\varphi_g) = \begin{bmatrix} F_{g,sep}(\varphi_g) \\ F_{g,tg}(\varphi_g) \\ F_{g,ax}(\varphi_g) \\ 1 \end{bmatrix} \quad (15.72)$$

As it follows from the analysis of Eq. (15.72), the resultant lumped force,  $\mathbf{F}_{g,s}$ , as well as all three components,  $\mathbf{F}_{g,sep}$ ,  $\mathbf{F}_{g,tg}$ , and  $\mathbf{F}_{g,ax}$ , that act over the gear, depend on the angle of rotation of the gear, that is, all of them are functions the angle,  $\varphi_g$ , of rotation of the gear:

$$\mathbf{F}_{g,s} = \mathbf{F}_{g,s}(\varphi_g) \quad (15.73)$$

$$\mathbf{F}_{g,sep} = \mathbf{F}_{g,sep}(\varphi_g) \quad (15.74)$$

$$\mathbf{F}_{g,tg} = \mathbf{F}_{g,tg}(\varphi_g) \quad (15.75)$$

$$\mathbf{F}_{g,ax} = \mathbf{F}_{g,ax}(\varphi_g) \quad (15.76)$$

The lumped force,  $\mathbf{F}_{g.s.}(\phi_g)$ , and the components,  $\mathbf{F}_{g.sep}(\phi_g)$ ,  $\mathbf{F}_{g.lg}(\phi_g)$ , and  $\mathbf{F}_{g.ax}(\phi_g)$ , that depend on the angular parameter,  $\phi_g$ , are an additional source of vibration generation, and noise excitation in crossed-axes gearing. When the gears rotate, point of intersection of the axis of instantaneous rotation,  $P_{ln}$ , and the instantaneous line of action,  $LA_{inst}$ , are not allowed to migrate along the axis of instantaneous rotation,  $P_{ln}$ , or, at least, the distance covered in this migration has to be the shortest possible. It is desirable to design gears so as to minimize the travel distance along the axis of instantaneous rotation.

The variation of the direction of the (resultant) lumped force,  $\mathbf{F}_{g,s}(\phi_g)$ , of interaction of tooth flanks,  $\mathcal{S}$  and  $\mathcal{P}$ , of a gear and of a mating pinion is illustrated in Figure 15.11. For an arbitrary configuration of the line of contact,  $LC$ , between the tooth flanks,  $\mathcal{S}$  and  $\mathcal{P}$ , the coordinates of point,  $c_g$ , at which the resultant force,  $\mathbf{F}_{g,s}$ , is applied, can be determined. The component,  $\mathbf{F}_{g,ax}$ , is parallel to the gear axis of rotation,  $O_g$ . The component,  $\mathbf{F}_{g,sep}$ , is perpendicular to the gear axis of rotation,  $O_g$ . The magnitude,  $F_{g,sep}^*$ , of the shown in Figure 15.12 the force vector,  $\mathbf{F}_{g,sep}^*$ , equals to  $F_{g,sep}^* = F_{g,sep} / \sin \phi_{t,\omega}$ , where  $\phi_{t,\omega}$  is the transverse pressure angle in the crossed-axes gear pair. (The separating force vector,  $\mathbf{F}_{g,sep}$ , is entirely located in the normal  $N_{in}$  – plane. The normal plane (the  $N_{in}$  – plane: see Chapter 3) is the plane through the plane-of-action-apex,  $A_{pa}$ , perpendicular to the center-line,  $\Phi$ , in the gear pair. As it follows from the analysis of the schematic shown in Figure 15.12, at any configuration of the line of contact,  $LC$ , for which the point,  $c_g$ , is located within the zone of action,  $ZA$ , the forces,  $\mathbf{F}_{g,ax}$  and  $\mathbf{F}_{g,sep}$ , never equals to zero. Thus, the reaction forces,  $\mathbf{F}_{g,ax}^{rect}$  and  $\mathbf{F}_{g,sep}^{rect}$ , also are of non-zero values. As the forces,  $\mathbf{F}_{g,ax}^{rect}$  and  $\mathbf{F}_{g,sep}^{rect}$ , fluctuate when the gears rotate [see Eqs (15.74) and (15.76)], an excessive vibration generation, and noise excitation can be observed when a crossed-axes gear pair operates. The variation of the forces,  $\mathbf{F}_{g,ax}^{rect}$  and  $\mathbf{F}_{g,sep}^{rect}$ , does not depend on the geometry of the line of contact,  $LC$ . This discussion is also valid in cases, when multiple lines of contact as well as multiple portions of the lines of contact, are observed in a gear pair of a particular design, as the forces,  $\mathbf{F}_{g,ax}^{rect}$  and  $\mathbf{F}_{g,sep}^{rect}$ , fluctuate when the gears rotate. Fluctuation of the forces,  $\mathbf{F}_{g,ax}^{rect}$  and  $\mathbf{F}_{g,sep}^{rect}$ , is inevitable in geometrically accurate crossed-axes gear pairs.

An analysis, similar to the aforementioned one can be performed with respect to loading of the pinion in a geometrically accurate crossed-axes gear pair.

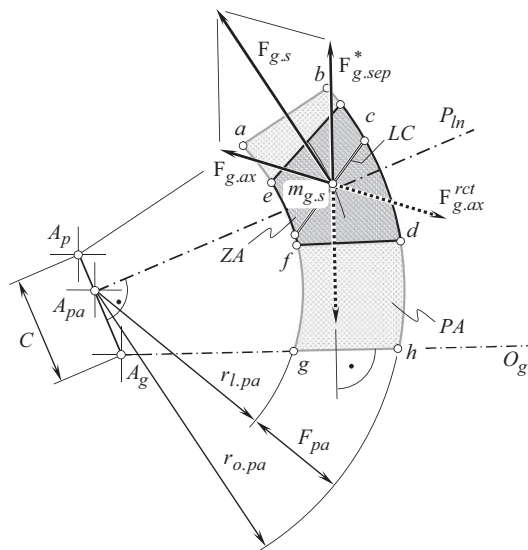


**FIGURE 15.11** The axial thrust,  $\mathbf{F}_{g,at}(\varphi_g)$ , and the separating force,  $\mathbf{F}_{g,sep}(\varphi_g)$ , as the components of the resultant (lumped) force,  $\mathbf{F}_{g,s}(\varphi_g)$ , of interaction of the tooth flanks,  $\mathcal{S}$  and  $\mathcal{P}$ , of a gear, and of a mating pinion in geometrically accurate crossed-axes gear pair.

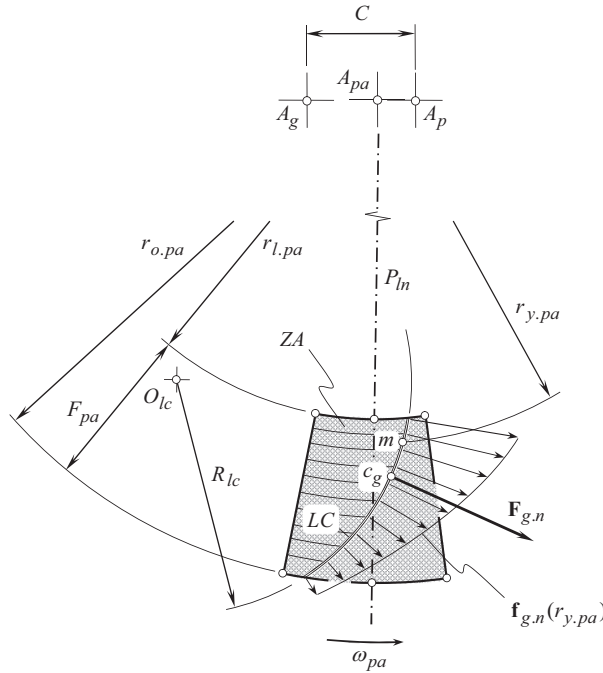


**FIGURE 15.12** Lumped normal force,  $\mathbf{F}_{g,n}$ , and normal force per unit length,  $\mathbf{f}_{g,n}$ , acting in geometrically accurate crossed-axes gear pair.

As it follows from the analysis of Eq. (15.72), the resultant lumped force,  $\mathbf{F}_{p,s}$ , as well as all three components,  $\mathbf{F}_{p.sep}$ ,  $\mathbf{F}_{p.tg}$ , and  $\mathbf{F}_{p.ax}$ , that act over the pinion, depend on the angle of rotation of the pinion, that is, all of them are functions the angle,  $\varphi_p$ , of rotation of the pinion:

$$\mathbf{F}_{p,s} = \mathbf{F}_{p,s}(\varphi_p) \quad (15.77)$$

$$\mathbf{F}_{p.sep} = \mathbf{F}_{p.sep}(\varphi_p) \quad (15.78)$$

$$\mathbf{F}_{p.tg} = \mathbf{F}_{p.tg}(\varphi_p) \quad (15.79)$$

$$\mathbf{F}_{p.ax} = \mathbf{F}_{p.ax}(\varphi_p) \quad (15.80)$$

The lumped force,  $\mathbf{F}_{p,s}(\varphi_p)$ , and the components,  $\mathbf{F}_{p.sep}(\varphi_p)$ ,  $\mathbf{F}_{p.tg}(\varphi_p)$ , and  $\mathbf{F}_{p.ax}(\varphi_p)$ , that depend on the angular parameter,  $\varphi_p$ , are an additional source of vibration generation, and noise excitation in crossed-axes gearing. When the gears rotate, no migration of point of intersection of the axis of instantaneous rotation,  $P_{ln}$ , as well as of the instantaneous line of action,  $LA_{inst}$ , along the axis of instantaneous rotation,  $P_{ln}$ , is allowed (or, at least, the distance covered in this migration has to be the shortest possible). It is desirable to design gears so as to minimize the travel distance along the axis of instantaneous rotation.

For any configuration of the line of contact,  $LC$ , when the point,  $c_g$ , is located within the zone of action,  $ZA$ , the forces,  $\mathbf{F}_{p.ax}$  and  $\mathbf{F}_{p.sep}$ , never equal to zero. Thus, the reaction forces,  $\mathbf{F}_{p.ax}^{ret}$  and  $\mathbf{F}_{p.sep}^{ret}$ , also are of non-zero values. As the forces,  $\mathbf{F}_{p.ax}^{ret}$  and  $\mathbf{F}_{p.sep}^{ret}$ , fluctuate when the gears rotate, an excessive vibration generation, and noise excitation are commonly observed when a crossed-axes gear pair operates. The variation of the forces,  $\mathbf{F}_{p.ax}^{ret}$  and  $\mathbf{F}_{p.sep}^{ret}$ , does not depend on the geometry of the line of contact,  $LC$ . This discussion is also valid with respect to the cases when multiple lines

of contact, as well as multiple portions of the lines of contact, are observed in a gear pair of a particular design, as the fluctuation of the forces,  $\mathbf{F}_{p.ax}^{rct}$  and  $\mathbf{F}_{p.sep}^{rct}$ , is inevitable in geometrically accurate crossed-axes gear pairs.

**Normal force acting on the gear in geometrically accurate crossed-axes gearing.** For the calculations of gear teeth for contact strength, as well as for contact strength analysis, a component,  $\mathbf{F}_{g,n}$ , of the resultant forth,  $\mathbf{F}_{g,s}$ , is entered into the corresponding equations for the calculations. This component is commonly referred to as the *normal force*,  $\mathbf{F}_{g,n}$ . The vector of normal load,  $\mathbf{F}_{g,n}$ , is located within the plane of action,  $PA$ , and is perpendicular to the line of contact,  $LC$ , at point,  $c_g$ , at which the normal load is applied. The magnitude,  $F_{g,n}$ , of the normal force,  $\mathbf{F}_{g,n}$ , is calculated from the expression:

$$F_{g,n} = F_{g,s} \cos \psi_g \quad (15.81)$$

where  $\psi_g$  is the actual value of the spiral angle of the gear teeth at point,  $c_g$ .

The normal force per unit length,  $\mathbf{f}_{g,n}$ , is also entirely located within the plane of action,  $PA$ . The normal force per unit length,  $\mathbf{f}_{g,n}$ , depends on the geometry of a particular line of contact. At every point of the line of contact,  $LC$ , the applied normal load per unit length,  $\mathbf{f}_{g,n}$ , is perpendicular to the line of contact at that point.

In straight bevel gearing, the normal force per unit length,  $\mathbf{f}_{g,n}$ , is distributed similar in much to that shown in Figure 15.9 for the force per unit length,  $\mathbf{f}_{pa}(r_{y.pa})$ . In skew crossed-axes gearing the normal force per unit length,  $\mathbf{f}_{g,n}$ , is distributed similar to that in straight bevel gearing – all the elementary forces are perpendicular to the line of contact,  $LC$ . The distribution of the normal force per unit length,  $\mathbf{f}_{g,n}$ , in spiral bevel gearing with a circular-arc line of contact,  $LC$ , of a radius,  $R_{lc}$ , is illustrated in Figure 15.12. In this particular case, all the elementary forces are pointed along the radius,  $R_{lc}$ , to the corresponding point,  $m$ , within the line of contact,  $LC$ .

In a more general case of geometrically accurate crossed-axes gearing, in face-hobbed bevel gears in particular, the following approach can be used to determine the distribution of the normal force per unit length along the line of contact,  $LC$ .

**First**, the unit normal vector,  $\mathbf{n}_{lc}$ , is constructed at every point of the line of contact,  $LC$ .

**Second**, the distribution of the normal load per unit length,  $\mathbf{f}_{g,n}$ , is constructed as a product of the unit vector,  $\mathbf{n}_{lc}$ , by the function of the distribution of the magnitude,  $f_{g,n}$ , of the normal load per unit length, that is,  $\mathbf{f}_{g,n} = f_{g,n} \cdot \mathbf{n}_{lc}$ .

When two or more lines of contact (or portions of the lines of contact),  $LC_i$ , are observed, then position vector,  $\mathbf{r}_{cg,\Sigma}$ , of the point,  $c_{g,\Sigma}$ , at which the resultant load,  $\mathbf{F}_{g,n,\Sigma}$ , is applied, can be calculated from the formula:

$$\mathbf{r}_{cg,\Sigma} = \frac{\sum_i l_{lc,i} \cdot \mathbf{r}_{cg,i}}{\sum_i l_{lc,i}} \quad (15.82)$$

where

$i$  is the number of a line of contact (or a portion of a line of contact),  $LC_i$ .

$l_{lc,i}$  is the length of a line of contact (or a portion of a line of contact),  $LC_i$ .

$\mathbf{r}_{cg,i}$  is the position vector of a point,  $c_{g,i}$ , of a line of contact (or a portion of a line of contact),  $LC_i$ .

$\sum_i l_{lc,i}$  is the total length,  $TLLC$ , of all the lines of contact,  $l_{lc,i}$ .

The variation of the direction of the resultant lumped force of the interaction of the tooth flanks,  $\mathcal{F}$  and  $\mathcal{P}$ , can be minimized by means of selecting proper geometry of the desirable line of contact,  $LC_{des}$ . When the gears rotate, point of intersection of the axis of instantaneous rotation,  $P_{lm}$ , and the line along the resultant force of interaction of the tooth flanks,  $\mathcal{F}$  and  $\mathcal{P}$ , are not allowed to migrate along the  $P_{lm}$ , or, at least, the distance of this migration has to be minimized. In this way, the vibration generation, and noise excitation can be minimized.

The performed analysis of the forces that act in external crossed-axes gearing can be enhanced to internal crossed-axes gearing, as well as to *pinion-gear-to-rack mesh*, as the latter is a reduced case of external crossed-axes gearing.

The disclosed approach for the calculation of the elements of dynamics in geometrically accurate crossed-axes gearing is also applicable for calculation of the elements of dynamics in *Novikov/conformal* and in *high-conformal gearing*. The main feature here is that the angular face width in a gear pair is of a zero value.

---

# 16 Geometrically Accurate Worm-Gearing

## *Peculiarities of Kinematics and Geometry<sup>1</sup>*

Worm-gearing is a particular kind of crossed-axes gearing that features a low tooth count of a pinion, and a high gear ratio of the gearset.

Commonly, in gearboxes of conventional design, the worm is the driving component, while the worm-gear is a driven component in the gear pair (see Figure 16.1). This is because worm-gearing is a kind of self-locking gearing. Worm-gearing is capable of transmitting an input rotary motion only in one direction: from a worm to a mating worm-gear, and not in both directions. Not self-locking worm-gear pair is also known; however, gearing of this design have limited application in the present-day industry.

### 16.1 WORM-GEARING: ACCOMPLISHMENTS FROM THE ANCIENT TIMES TILL NOW

High gear ratio is one of the main features of worm-gearing. Gears of this design are extensively used in cases when high reduction of the input rotation is required. High sliding velocities between the worm threads, and the tooth flanks of the worm-gear is a huge disadvantage of worm-gearing of all designs.

#### 16.1.1 EARLY DESIGNS OF WORM-GEARING

Worm-gearing is used by skilled handicrafts for centuries. Examples of primitive worm-gear pairs are depicted in Figure 16.2.

It is likely the shown in Figure 16.2a worm-gearing with cylindrical worm was the first to be invented by the old-time handicrafts. Later on, this design of worm-gearing was followed by

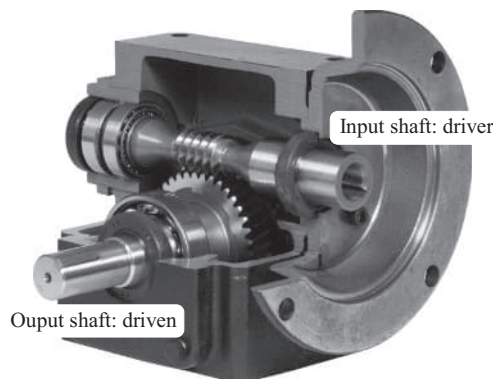


**FIGURE 16.1** Worm gearbox: cylindrical worm in mesh with helical gear.



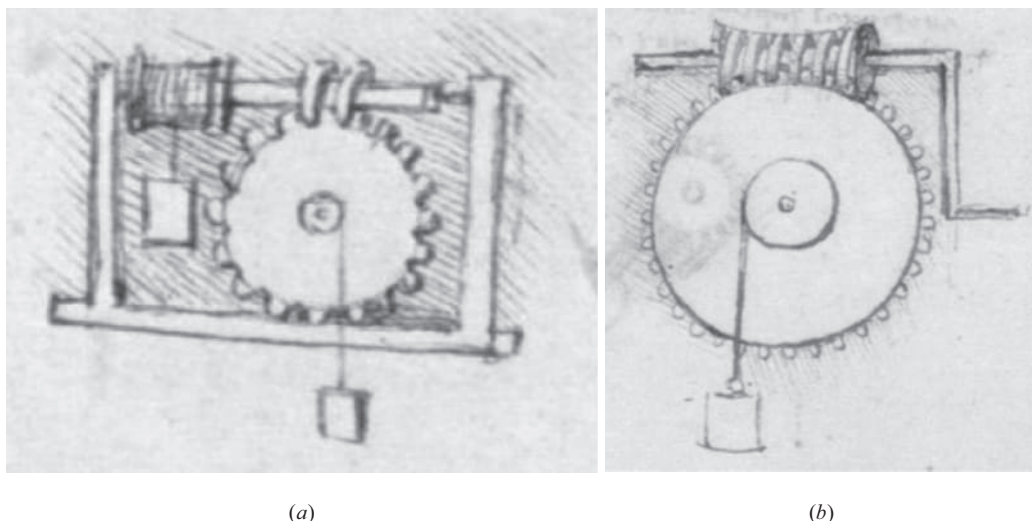


**FIGURE 16.2** Primitive ancient worm gearsets (a) with cylindrical worm and (b) with enveloping worm. (Adapted from the 1493 book by *Leonardo da Vinci* [23].)

invention of double-enveloping worm-gearing. A worm-gear pair with enveloping worm is shown Figure 16.2b.

Both shown in Figure 16.2 examples of worm-gearing are excerpted from the 1493 book by *Leonardo da Vinci* [23]. It makes sense to assume that these two designs of worm-gearing are known at least since 1493, or even from the earlier time.

*Hooke's gearing* is another example of worm-gearing of old style.<sup>2</sup>

In 1666, *Robert Hooke* demonstrated to the Royal Society a model of screw gearing that operate on parallel axes of rotation recently invented by him. Gearing of this design was described by him in *Lectiones Cutlerianae* (1674). Later on, gearing of this design was re-invented by *White*.<sup>3</sup> This gearing is also known as *White gearing*. It may be worth recalling what *White gearing* is all about.

In *White gearing* (see Figure 16.3; this illustration is excerpted from a *R. Bricard* book, 1927, [13]), one wheel has the motionless axis of rotation  $X$  and the other wheel has the motionless axis of rotation  $X^*$ . Two virtual revolute cylinders with axes  $X$  and  $X^*$  keep in touch along the straight line  $Y$ . The rotation about the axis  $X$  can be transmitted to the  $X^*$  axis through a relative rolling motion of the virtual cylinders along  $Y$ . Hence, one can synthesize gear teeth that are in point contact on the line  $Y$ . In the example of Figure 16.3, one wheel is a screw with a triangular tooth profile and the other one is a screw with a square tooth profile. The tooth contact takes place at the point  $G = G^*$  belonging to the line  $Y$ . The trajectory of  $G$  with respect to the wheel of axis  $X$  is a helix drawn on the cylinder of axis  $X$  as well, as the trajectory of  $G^*$  with respect to the wheel of axis  $X^*$ . One has to notice that, in *White gearing*, the tooth contact is the common point of two curves lying on the rolling virtual cylinders. When the gears rotate, contact point pseudo-travels along the axis  $Y$ , and

<sup>1</sup> Except of *involute worm-to-helical involute gear* (either spur or helical involute gear), all the rest designs of worm gearing are approximate by nature. Therefore, worm gearing can be also considered in the book section on approximate gearing. *Involute worm-to-helical involute gear* is the only possible kind of geometrically-accurate gearing.

<sup>2</sup> In the 1958 monograph [91], Dr. *M.L. Novikov* mentioned *Hooke's gearing* when developing a new system of gearing. The developed system of gearing was later named *Novikov gearing* in his honor.

<sup>3</sup> It is known that *R. Hooke* once has ordered a microscope to Mr. *Christopher White* of London. It makes sense to assume that Mr. *White* whose name is assigned to *White gearing*, and just mentioned Mr. *Christopher White* of London, is that same person.

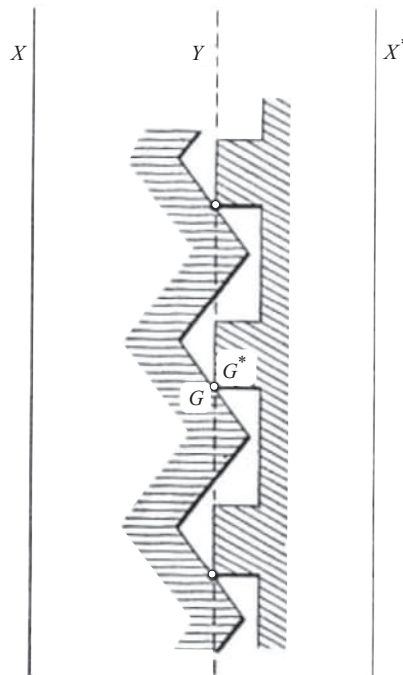


FIGURE 16.3 Sketch of *White gearing* as depicted in a *R. Bricard* (1927) book [13].

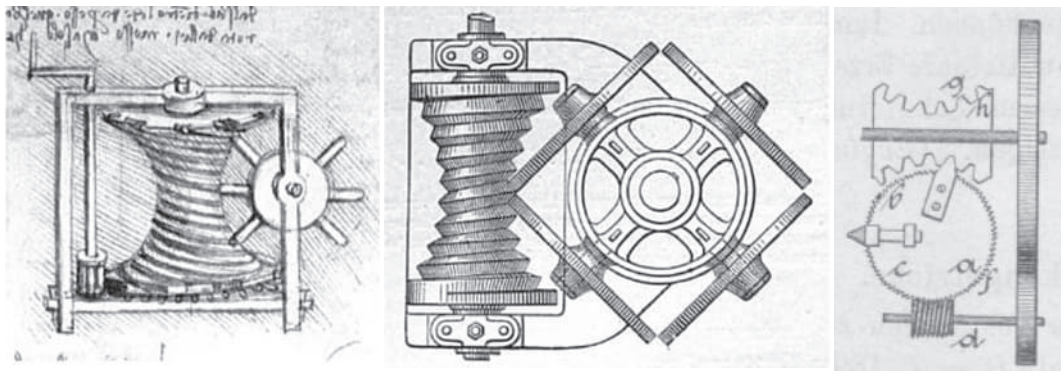
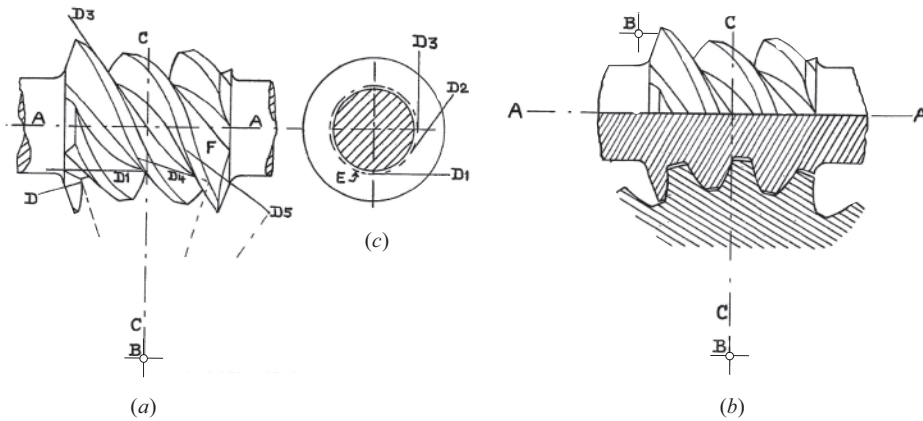


FIGURE 16.4 *Hindley's double-enveloping worm gearing* (~1739).

the axis  $Y$  is the pseudo-path of contact,  $P_{pc}$ , in *White gearing*. (see Ref. [157] for more in-detail discussion on the pseudo-path of contact,  $P_{pc}$ , in gearing). A linear velocity of the actual instantaneous motion of contact point is always along a straight line that intersects the axis of instantaneous rotation of two meshing gears.

*White gearing* can be viewed as a reduced case of worm-gearing when the crossed-axes angle,  $\Sigma$ , equals either to  $\Sigma = 180^\circ$  (in a case of external gearing), or to  $\Sigma = 0^\circ$  (in a case of internal gearing).

Double-enveloping worm gearing is known since the time of *Leonardo da Vinci*, or even earlier (see Figure 16.4).



**FIGURE 16.5** Worm gearing by *F.J. Bostock and S. Bramley-Moore* (1922) [97]: (a) is an elevation of a worm constructed according to and embodying the proposed design, (b) is a similar elevation of the worm partly in section and of a portion of a worm thread in mesh therewith, the latter being in section taken midway across the width of the teeth, and (c) is an end elevation of the worm.

Shown in Figure 16.4 a worm-gear pair is the *Hindley* type of worm-gearing (or, in other terminology, worm-gearing with the hourglass worm, or globoidal gearing). The *Hindley* worm-gearing was first used in *Hindley's* dividing engine. The first true circular dividing engine was constructed around 1739, probably by *Henry Hindley*,<sup>4</sup> a clockmaker. This was reported to the Royal Society by *John Smeaton* in 1785. The *Hindley* worm-gearing was, by the inventor, considered superior to worm-gearing of the ordinary type, in wearing quality. This advantage is not thoroughly investigated yet.

A design of conformal worm-gearing was proposed (~1922) by *F.J. Bostock* and *S. Bramley-Moore* [97]. Shown in Figure 16.5 conformal worm-gearing comprises an improved construction or formation of the thread or threads of the worm or the shape thereof and that of its mating worm wheel, and has for its object the removal or reduction of interface met between worm and wheel in the ordinary globoidal type of gear, and the obtaining of a more perfect contact between the thread of the worm and the teeth of the worm wheel, these closely conforming to each other, together with an increased load carrying capacity between the two gears.

The threads of the globoidal worm are generated by a straight line in the manner described in Figure 16.5. In, or near to a plane *CC* containing the worm wheel axis *B* and at right angles to the worm axis *A* a circle *E* is selected. This circle represents the diameter of the worm at the base of the thread, or a smaller, or larger diameter as the case may be. The straight lines such as *D*<sup>1</sup>, *D*<sup>2</sup>, or *D*<sup>3</sup>, originate from this circle *E* contained in said plane. These straight lines are lying at a constant angle to lines parallel to the axis of the worm, and tangential to a cylinder of the same diameter as the circle *E* and containing the circle *E*. One side of the globoidal worm thread *F* is generated by swinging, in a circular path, at a predetermined speed, any suitable one of these lines about a given center, such as the center of a worm wheel, or adjacent thereto the line passing through progressive positions such as *D*, *D*<sup>i</sup>, *D*<sup>4</sup>, and *D*<sup>5</sup>, at the same time causing the worm to rotate at a relative predetermined speed. It will, of course, be understood that the line chosen must lie on that side of the worm adjacent to the given center. In a similar manner, the opposite side of the thread may be generated by selecting a similar tangential straight line but pointing in the opposite direction, and

<sup>84</sup> Henry Hindley (1701–1771) was an eighteenth-century clockmaker, watchmaker, and maker of scientific instruments. He invented a screw-cutting lathe, a fusee-cutting engine, and an improved wheel-cutting engine, and made one of the first dividing engines, for the construction of accurately-graduated arcs on scientific instruments, as well, as numerous devices of other design.



**FIGURE 16.6** Worm gear pair, composed of a cylindrical worm and of a helical involute gear – geometrically accurate worm gear pair with point contact of the interacting functional surfaces.

by swinging this line in a circular path about the given center in the same manner as that previously described.

A worm made according to the design of worm-gearing under consideration may have a number of longitudinal gashes cut through its threads for the purpose of providing cutting faces, after which the sides of the threads may be relieved so, as to enable the worm to be used as a cutting tool for generating the teeth of conjugate worm wheels, made according to the invention, can be carried out on worm wheel generating machines in *common use*.

Numerous other early designs of worm-gearing are known.

It can be shown that not all fundamental laws of gearing are fulfilled in the early designs of worm-gearing. Therefore, worm-gearing of the considered designs (see Figures 16.2–16.5), as well as others, extensively used in the present-day industry, can not be referred to as geometrically accurate gearing, as worm-gearing of these designs are approximate.

### 16.1.2 WORM-GEARING OF CONVENTIONAL DESIGNS

In a simple case, worm-gear pair is composed of a cylindrical worm and of a helical involute gear, as illustrated in Figure 16.6. In worm-gearing of this design, point contact between the tooth flanks of the worm-gear,  $\mathcal{S}$ , and the worm threads,  $\mathcal{P}$ , occurs. Illustrated in Figure 16.7a, contact geometry of the interacting surfaces,  $\mathcal{S}$  and  $\mathcal{P}$ , is far from to be favorable. Because of this, the load carrying capacity of worm-gearing of the design shown in Figure 16.6, is limited.

The load-carrying capacity of two interacting functional surfaces can be increased if the surfaces,  $\mathcal{S}$  and  $\mathcal{P}$ , are designed so, as to be more conformal to one another at contact point. In worm-gearing, the use of enveloping worm-gear makes possible a significant improvement to contact geometry of the tooth flanks,  $\mathcal{S}$  and  $\mathcal{P}$ . Illustrated in Figure 16.7b schematic gives an insight on how two interacting surfaces,  $\mathcal{S}$  and  $\mathcal{P}$ , can be designed more conformal to one another. In the case under consideration, the worm-gear tooth flank is an envelope to a mating worm threads. The radius,  $r_{ax.g}$ , of the line of intersection of the gear tooth flank by the axial plane through the centerline,  $\mathfrak{t}$ , is comparable to the worm radius,  $R_w$ . The difference,  $\Delta R$ , between the magnitudes, of the radii  $r_{ax.g}$  and  $R_w$  ( $\Delta R = r_{ax.g} - R_w$ ), is of a reasonably small value. The smaller the difference,  $\Delta R$ , the higher the load carrying capacity is anticipated, and vice versa. However, a smaller difference,  $\Delta R$ , required

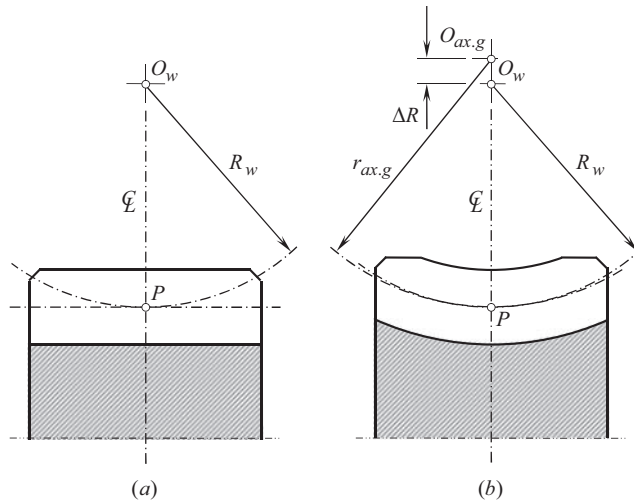


**FIGURE 16.7** Section of a worm-gear by an axial plane through the centerline,  $\mathcal{L}$ ; the worm is in mesh: (a) with involute gear (either spur or helical involute gear) and (b) with enveloping worm-gear.

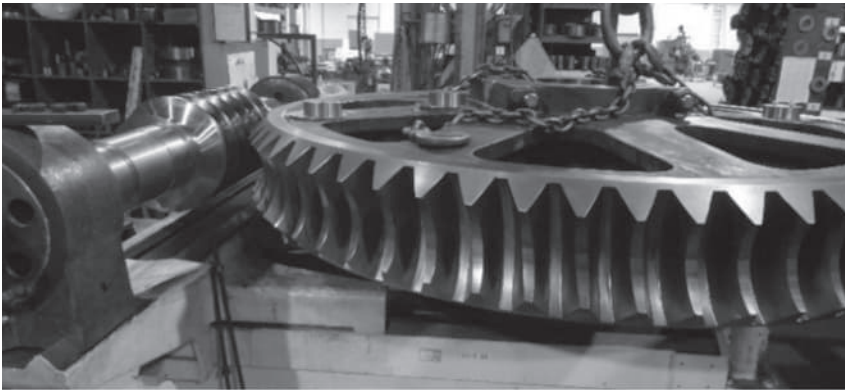


**FIGURE 16.8** Single-enveloping worm gear pair – approximate worm gear pair.

the tighter tolerances on the accuracy of machining of the components of the worm-gearset, and of assembling of the components in the gear housing.

Such a design of worm-gear pair is illustrated in Figure 16.8. Gearing is commonly referred to as *single-enveloping worm-gearing* (Figure 16.8). Two kinds of *Single-enveloping worm-gearing* are recognized. They can be either with a single-start worm or with a multiple-start cylindrical worm.

It should be reminded here that in gearing (in a general sense), and in worm-gearing in particular, only base-pitch-preserving alterations to geometry of the tooth flanks,  $\mathcal{S}$  and  $\mathcal{P}$ , are permissible. This requirement is violated in single-enveloping worm-gearing.

Three different kinds of cylindrical worms are commonly used in the design of single-enveloping worm-gear pairs. These three kinds of worms feature a specific geometry of threads (of thread-spaces) in sections of the worm by a plane. Depending on the actual configuration of the plane section in relation to the worm thread (or to the worm thread-space) the following worms are distinguished (see Figure 16.9):

- *Archimedean worm* – the straight-sided plane section either of the worm thread, or of the worm thread-space in a plane through the axis of rotation,  $O_w$ , of the worm



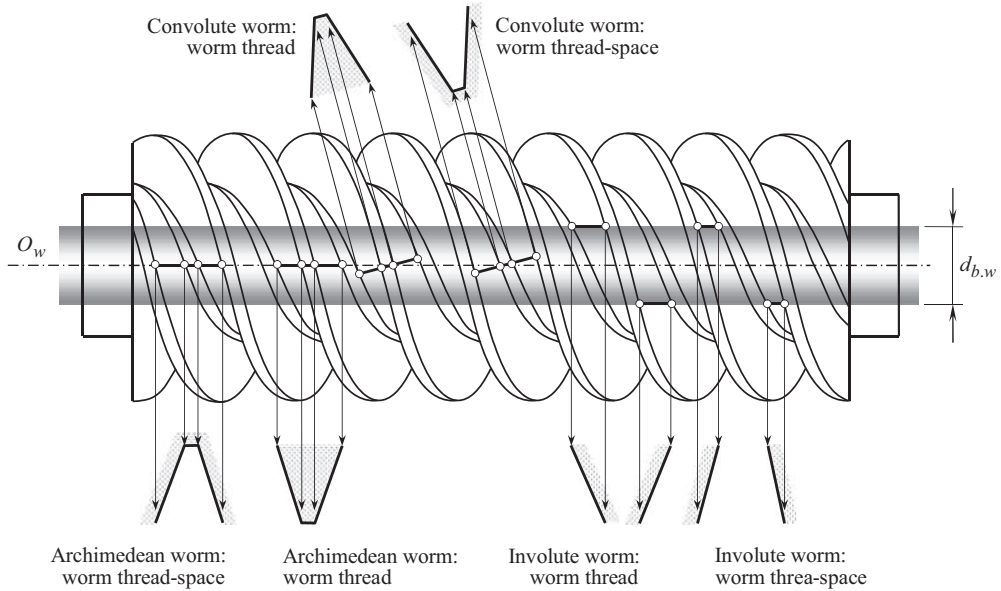


**FIGURE 16.9** Three kinds of cylindrical worms used in design of worm gearing: *Archimedean worm*, *convolute worm*, and *involute worm*.

- *Convolute worm* – the straight-sided plane section is perpendicular either to the thread line, or to the thread-space line. The thread line (the thread-space line) here is a helix on the pitch cylinder of the worm that passes either through the center of the tooth thickness, or through the center of the tooth-space width
- *Involute worm* – the straight-sided plane sections are tangential from the opposite sides to the worm base cylinder of a diameter,  $d_{b,w}$ . The straight sides of the thread profile (of the thread-space width) form a base helix angle,  $\psi_{b,w}$ , with the perpendicular to the axis of rotation of the worm,  $O_w$ , or (the same) they form a base lead angle,  $\lambda_{b,w}$ , with the axis of rotation of the worm,  $O_w$ .

The shown in Figure 16.9 worms can be either single-start worms, or they can be multiple-start worms.

The design of these worms is simple, as both, the worm thread, as well, as the worm thread-space, feature straight-side profiles. Ease in production is the main reason for the above listed cylindrical worms are extensively used in the present-day industry.

Only worm-gear sets that are composed of an involute worm in mesh with a helical involute gear are geometrically accurate. All the rest designs of worm-gearsets with cylindrical worm are approximate worm-gearsets, as they do not meet all three fundamental laws of gearing.

In addition to cylindrical worms, shown in Figure 16.9, conical worms (including, but not limited to conical involute worms), as well, as worms with other geometry of the threads are also occasionally used in the design of single-enveloping worm-gearsets.

Surfaces of *Archimedean worms*, *convolute worms*, and *involute worms*, are used as reference surfaces when designing hobs for cutting worm-gears.

Another type of worm-gears, whose pitch surface is gained by a rotating arc, which fits the part closest to the worm pitch circle around the worm shaft in central section is recognized (see Figure 16.10). Worm-gearing of this design is commonly referred to as *double-enveloping worm-gearing*. The teeth have straight-line profile in central section as illustrated in Figure 16.10. This type of worm-gear meshes near the central section. It is often loosely claimed that in *double-enveloping*

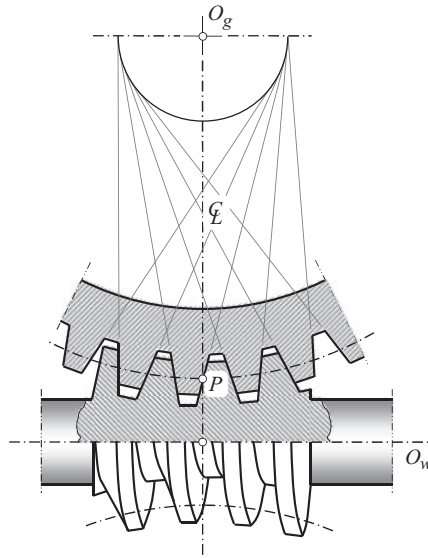


**FIGURE 16.10** *Hindley worm gearing of modern design – approximate worm gear pair.*

*worm-gearing* all the threads of the worm and the teeth of the worm-gear are constantly in line contact. This statement is incorrect, as not all three fundamental laws of gearing are fulfilled in *double-enveloping worm-gearing*. Thus, no line contact between the worm threads, and the worm-gear tooth flanks is possible at all. Only one contact (and not a plurality of contacts) between the worm threads and the worm-gear tooth flanks is observed at every instant of time. Therefore, even after the absolutely precise assembling of the gearset (that is, after the assembling with zero deviations), gearing of this design (see Figure 16.10) is not capable of increasing the load capability<sup>5</sup> of worm-gearing of the design. That same conclusion is valid with respect to *Hindley worm-gearing* (see Figure 16.4).

It is right point to briefly outline here the contribution of *Samuel I. Cone* of the USA to the field of *double-enveloping worm-gearing*.

An invention disclosure titled *Precision Worm-gearing* was filed by *S.I. Cone* to the US Patent and Trade Mark Office in 1925 [102]. The object of the invention is to form the members of a system of worm-gearing with surfaces, which may be easily generated so that both the worm and worm-gear will be generated to a high degree of precision.

A side elevation partly in section and partly in diagram of the precision worm-gearing is shown in Figure 16.11.

The numeral 1 indicates a worm-gear mounted to rotate on its center axis 2 and having circumferential teeth 3 at its outer edge for intermeshing with a thread 4 formed on the worm 5. This worm 5 is formed as an integral part of its shaft 6 and the thread 4 may be generated from a blank formed on this shaft. The side surface 7 of each tooth 3 and the corresponding side surface of the thread 4 are generate at an acute angle to the opposite side surface 8 of each tooth, and the surface 7 is given a greater slope than the surface 8.

As shown in Figure 16.11, lines forming a continuation of the surfaces 7, are all tangent to the circle 9. Lines forming continuations of the surface 8, all pass either through the axis 2, or on the

<sup>5</sup> In reality, an increased load capability in gearing of the design shown in Figure 16.10 is achieved after run-in period of time after the intentional geometry of the tooth flanks and of the threads of the worm is replaced with certain modified geometry. The modified geometry of the tooth flanks and of the threads of the worm is closer to that in geometrically accurate worm-gearing.

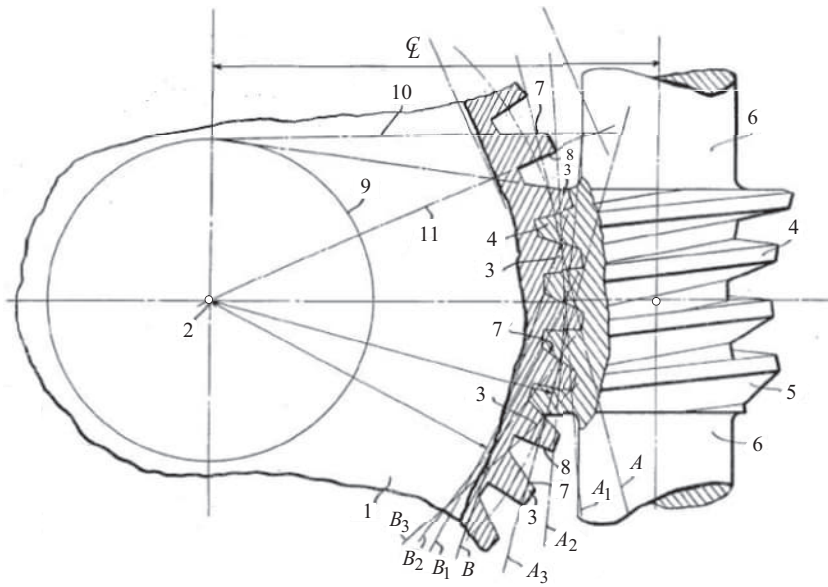


**FIGURE 16.11** Precision double-enveloping worm-gearing by S.I. Cone. (Exerted from: Pat. 1,683,163 (USA). *Precision Worm Gearing*, S.I. Cone, Filed: June 27, 1925, Patented: September 4, 1928, [102].)

opposite side of the axis 2, from the respective lines extending from the surfaces 7. In other words, the line 10 forming a continuation of the side 7 is tangent to the circle 9, whereas the line 11 forming a continuation of the side surface 8 either passes directly through the axis 2, or on the opposite side of the axis from the line 10. This permits these side surfaces being generated of different slopes relative to each other so that the pressure angle of the principal driving side of each tooth may be increased to enable the teeth to transmit a greater load, or to provide an increased strength and driving power for the teeth when the worm-gear is rotating in one direction than when rotating in the opposite direction.

As shown in the drawing (see Figure 16.11), the worm 5 is of the *Hindley* screw-type so that its thread is intermeshed with the teeth of the worm-gear throughout its entire length. The inner and the outer surfaces of the teeth 3, on the worm-gear, are properly generated and grooved out to receive the worm and so that this worm and its thread 4 will fit closely into the gear and intermesh with its thread so, as to form a driving connection between this worm and worm-gear throughout the length of contact. The cross-sectional shape of the side surface of the thread 4 is similar to the shape of the teeth 3 on the worm-gear 1, so that these parts will properly intermesh.

The lines  $A$ ,  $A_1$ ,  $A_2$ , and  $A_3$ , are all tangent to the pitch circle, or at right angles to the sides 8, and represent the lines of pressure when the sides 8 of the teeth are under pressure.

The lines  $B$ ,  $B_1$ ,  $B_2$ , and  $B_3$ , intersect the pitch circle, and are the lines of pressure when the sides 7 of the teeth are under pressure. Thus, it will be seen by varying the slope of the sides of the teeth, greater or less power may be transmitted in either direction of rotation as may be desired.

As an example, Figure 16.12 illustrates a modern design of double-enveloping worm-gear pair with multiple-start worm.

Numerous other designs of *double-enveloping worm-gearing* were developed in the recent decades, including, but not limited to those discussed in Refs. [105,114,116,118], and others. It is likely the 1962 monograph [228] is the first attempt to summarize the accomplishments in the field of design and analysis of *double-enveloping worm-gearing*.

The research and development in the field of production, and especially in the field of finishing of worm threads and of tooth flanks in double-enveloping worm-gearing, began at that same time



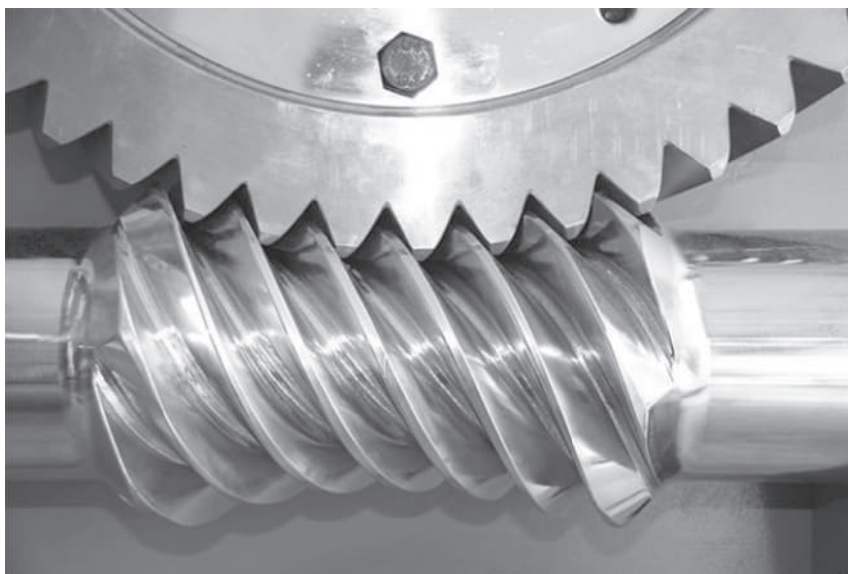


**FIGURE 16.12** Double-enveloping worm-gear pair with multiple-start worm.

when the first worm-gearing of this kind was proposed. It is known that Dr. *Lorenz* of Germany had invented (~1891) methods to generate the worm and the gear of the double-enveloping worm-gear drive and that he had received two patents for this work in 1891.

The *Cone's* invention of the precision worm-gearing [102] was followed by the novel method of generating worm-gearing [103], also proposed by *S.I. Cone*. Later on, a novel design of globoidal worm for cutting worm-gears for *double-enveloping worm-gearing* was developed [107]. The first attempt to outline the foundations of production of globoidal gearing (this is another term for *double-enveloping worm-gearing*) was undertaken by *Diker, Ya.I., Sagin, L.I.* [26].

Summarizing this brief discussion on *double-enveloping worm-gearing*, it is important to stress here on the following. It is often loosely claimed that the load carrying capacity in double-enveloping worm-gear pairs is greater compared to that in single-enveloping gearsets. It is also often loosely claimed that if the insufficient load carrying capacity in double-enveloping worm-gearing is observed, the insufficient accuracy of assembling is the root cause for that. Actually, violation of the fundamental laws of gearing is the root cause for the low load carrying capacity of a double-enveloping worm-gearing. It is common practice to try to hide the absence of improvement in load carrying capacity claiming insufficient accuracy of a worm-gearset, insufficient accuracy of assembling of the component, and the displacements of the worm and the worm-gear in relation to one another under operating load. This is of secondary importance, as violation of the fundamental laws of gearing is the root cause for insufficient load carrying capacity in a worm-gear pair.

Double-enveloping worm-gearing of all known designs represent perfect examples of situation when common sense does not help searching for correct, geometrically accurate designs of worm-gearing. Instead, it distracts the gear experts and misleads them. Double-enveloping worm-gearing is a sophisticated mechanism, and in addition to common sense, the gear theory is required to be involved when designing, and when manufacturing gear pairs of this particular kind.

In conventional worm-gear pair (see Figure 16.8), the tooth count of the pinion (which is called the *worm*) falls into the range of one to three. Worm-gear pairs with a larger number of starts,<sup>6</sup> namely, with four starts and more, are also used in the nowadays industry (see Figure 16.13).

<sup>6</sup> In worm-gearing, the term *number of threads* is often used in place of the term *number of starts*, which is incorrect. The *number of starts* in worm-gearing is a term equivalent to the term *number of teeth* in gearing of other kinds.

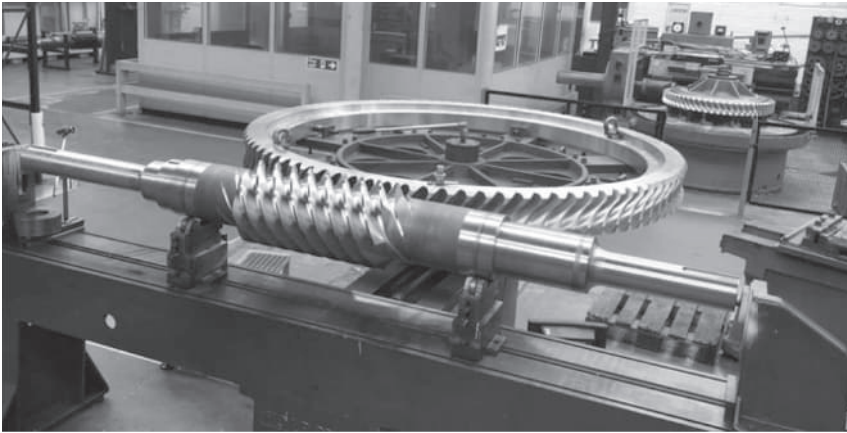


**FIGURE 16.13** Worm-gear pair with multiple-start worm.

When the number of starts of a worm equals to two, or it is larger than two, the worm is referred to as a *multiple-start worm*.

Commonly, the crossed-axes angle,  $\Sigma$ , in worm-gearing equals to a right angle (see Figure 16.8), however,  $\Sigma = 90^\circ$  is not a constraint. Worm-gearing with either an acute,  $\Sigma < 90^\circ$ , or with an obtuse,  $\Sigma > 90^\circ$ , crossed-axes angles are used in practice, as well.

### 16.1.3 SPIROID GEARING

Gear pairs that feature mesh of a worm with a crown gear are used in the industry. Worm-gear pairs of this type are an equivalent of the *rack-gear-to-pinion* gear pair in parallel-axes gearing. *Spiroid* gearing is one of numerous examples of worm-gear pair with a crown worm-gear and a conical worm.

The *Spiroid* gearing is originated from the 1954 U.S. patent on speed-reduction gearing [108]. This invention relates to speed-reduction gearing and aims at providing a skew-axes gearing of large speed-reduction ratio, which can be easily adjusted.

Gearing in which a worm engages teeth on the face of a crown gear has been proposed earlier, but in order to obtain sufficient tooth engagement in such gearing to transfer substantial power, it has heretofore been considered necessary to give the worm some peculiar form which makes it difficult and expensive to produce. Thus, in some instance, the worm has had an excessively large taper, while in others the surface, or the thread of the worm has had peculiarities, which make it expensive to produce, and in most such gearing a high reduction ratio has not been obtained.

The proposed design of reduction gearing (see Figure 16.14) [108] consists of a conical worm having only a slight taper, and having a thread of uniform cross-sectional shape and uniform lead, and a beveled gear having teeth with side faces which engage the thread of the worm throughout substantially their entire areas. The gearing, therefore, has a large power-transmitting capacity in comparison with its size. Heretofore, it has not been thought possible to obtain adequate tooth engagement in a gearing of this type; but it has been discovered that the portion of the side faces of the teeth of the gear which may be made to engage the thread of the worm depends upon the lead of the worm, so that by giving the lead a critical value hereinafter defined the tooth engagement is made nearly complete.

The conical worm may easily be produced on conventional machinery owing to its gradual taper and the uniformity of its thread. At the same time, such machinery may be used to produce a hob having the same form as the worm. This hob is used to generate the teeth on the gear by known methods. This operation would ordinarily generate the fillets and undercut surfaces on the gear,

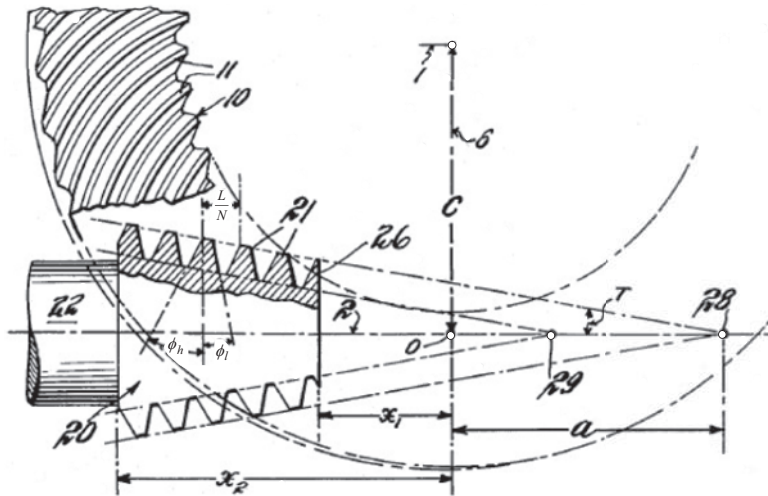


FIGURE 16.14 Concept of Spiroid gearing.

which would not contact with the thread of the worm in the operation of the gearing and would thus give it a low power transmitting ability. In accordance with the invention [108], however, fillets and undercut surfaces in the teeth of the gear are avoided by giving the lead of the worm a critical relationship to the speed reduction ratio of the gearing.

The gearing illustrated in Figure 16.14, consists of a gear 10 having teeth 11 on one of its side faces and a conical worm 20 having a thread or threads 21 engaging these teeth. The axes of the gear and worm are in skew relation, that is to say, they are non-parallel and non-intersecting.

The position of the worm with respect to the gear may most easily be specified by reference to the line 6 which is perpendicular both to the axis 2 of the worm and to the axis 1 of the gear, and to the point of intersection, *O*, of this line with the worm axis. The worm is located wholly at one side of the common perpendicular 6 with its smaller end 26 close enough to line 6 to place the apex 28 of a conical surface containing an outer surface of the thread 21 and the apex 29 of a conical surface containing the bottom surface of its thread 21 at the opposite side of this line. In a gearing in which the axes of the worm and gear are perpendicular, the common perpendicular to the axes lies in a plane, which is coincident with the gear axis and extends normal to the worm axis, and in this case the worm is located on one side of this plane and the apices 28, 29 on the other side of this plane.

To specify accurately the position of the worm with respect to the gear, the following dimensions (see Figure 16.14) may be used.

- The distance, *C*, between the axis of the worm and the axis of the gear measured along the common perpendicular to the two axes, which is less than *R*, the outer radius of the gear
- The angle, *E*, formed by the axis of the worm and axis of the gear measured from the worm axis in a plane parallel to both axes. This angle should be between  $45^\circ$  and  $135^\circ$ , and in many cases may most conveniently be made  $90^\circ$
- The distance, *x*<sub>1</sub>, from the smaller end of the worm to the point, *O*, of the common perpendicular, 6
- The distance, *x*<sub>2</sub>, from the larger end of the worm to the point, *O*, of the common perpendicular, 6
- The distance, *a*, from the point, *O*, of the common perpendicular, 6, to the apex of the conical surface containing the outer surface of the thread of the worm.

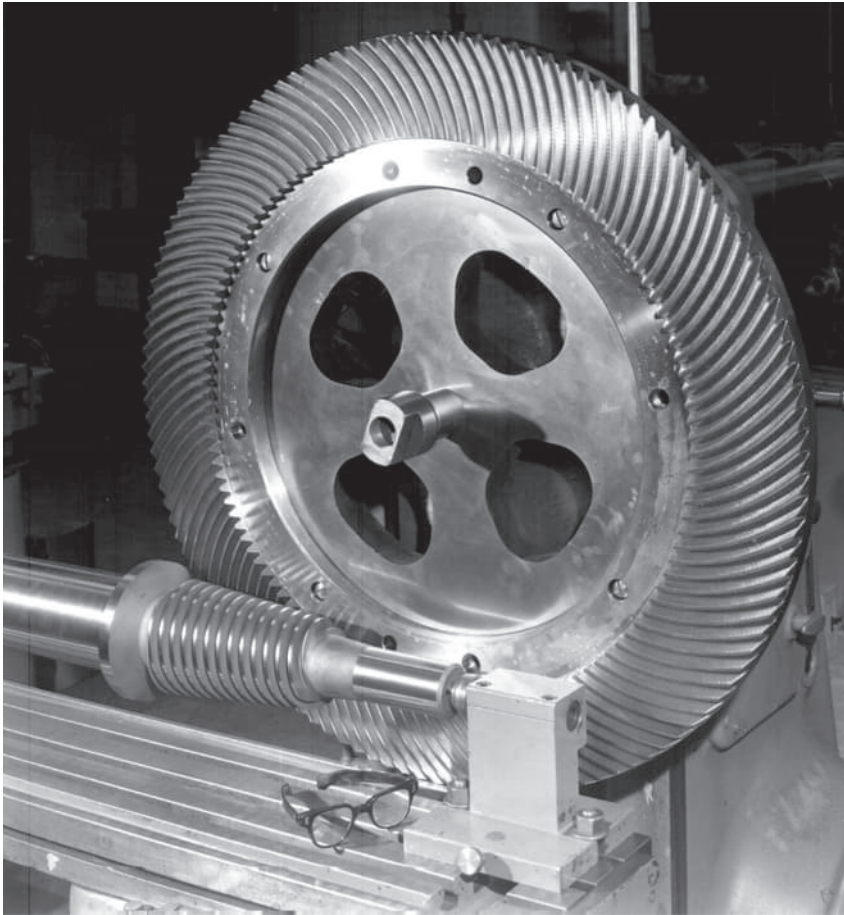


**FIGURE 16.15** *Spiroid* gear pair: Worm gear pair with a crown worm gear and a conical worm.

The form of the worm 29 is the frustrum of a cone of moderate, as distinguished from abrupt, taper. The taper angle of the worm, that is, the angle,  $T$ , between its side and its axis, is small. The thread 21 of the worm 20 is of uniform lead,  $L$ , and uniform cross-sectional shape and height. For multiple-start worms, the axial pitch, or distance between adjacent threads, is equal to the lead divided by the number of threads, or  $L/N$ , as shown in the drawing. In the particular worm illustrated, the thread 21 is a triple thread so that the axial pitch is  $L/3$ .

The cross-sectional shape of the thread is determined by the pressure angle,  $\phi_h$ , on the high side of the thread, that is, the side facing the larger end of the worm, and the pressure angle,  $\phi_l$ , on the low side of the thread, that is, the side facing the smaller end of the worm.

The concept of *Spiroid* gearing was further evolved in the U.S. Patents [109–111], and others.

A closeup of *Spiroid* gearing is depicted in Figure 16.15.

It was mistakenly claimed by the inventor of the speed-reduction gearing [108] that gearing of this kind features the higher power density due to an increased contact ratio. This is a mistake, as contact ratio in *Spiroid* gearing only slightly exceeds that in worm-gearing of conventional design. This statement can be proved based on three fundamental laws of gearing. This violation becomes evident from Figure 16.16. It is clear from the analysis of this illustration that the contact pattern does not cover the entire face width of the gear. Therefore, there is no reason to anticipate a significant increase in the power density in *Spiroid* gearing due to an increased contact ratio.

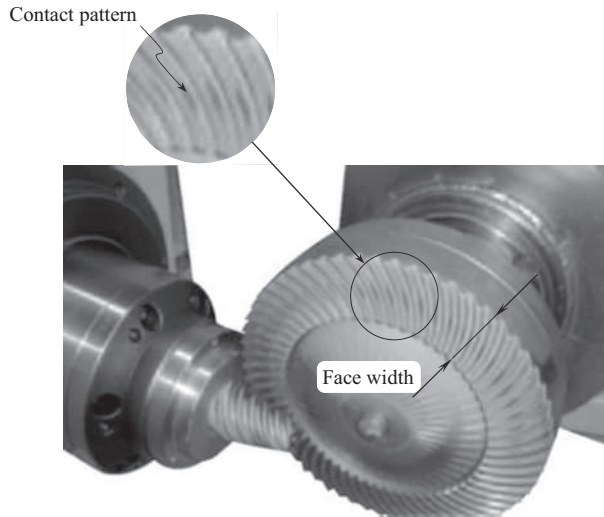


**FIGURE 16.16** In *Spiroid* gearing, the contact patterns are localized at the middle of the face width of the gear, and do not overlap the entire its face width (therefore, the contact ratio in *Spiroid* gearing is not of an increased value).

There should be another reason for the increased power density in *Spiroid* gearing, if any, but not due to an increased contact ratio.

In *Spiroid* gearing, not all three fundamental laws of gearing are fulfilled. Therefore, *Spiroid* gearing is a kind of approximate gearing, and not a kind of geometrically accurate gearing.

#### 16.1.4 HELICON GEARING

Eventually, a skew-axis gearing with a cylindrical worm was invented – as early, as in 1957 *O.E. Saari* has proposed the so-called *Helicon* gearing [113]. The object of this invention is to provide a skew-axis gearing having a cylindrical pinion of constant lead in which the teeth are asymmetrical (see Figure 16.17).

Referring now in greater particularity to the drawings in Figure 16.17, there will be seen a skew-axis gearing comprising a worm or pinion 12 and a face-gear 14. The pinion 12 is mounted on a shaft 16, and the face-gear 14 is mounted on a shaft 18. The pinion 12 is cylindrical, and the shafts 16 and 18 are located at right angles to one another, but do not intersect, or more specifically, the axes of the gears do not intersect, since the diameters of the shafts could be great enough to cause a partial intersection of the projections of the shafts. The axis of the pinion 12 is offset from the centerline of the gear 14. In general, the lower the reduction ratio, the closer the position of the pinion to the centerline of the gear, and in any event the pinion is never displaced an exceedingly great distance from the centerline. The pinion is close to the hypoid position.

The pinion is the primary member in the sense that all calculations are applied to it, and in this connection, the pitch of the teeth or threads is calculated similar to that in Ref. [108]. In this instance, the formula is:

$$L = \frac{2\pi C}{K - \frac{x}{y}} \quad (16.1)$$

In this formula:

$L$  is the lead.

$K$  is the speed ratio.



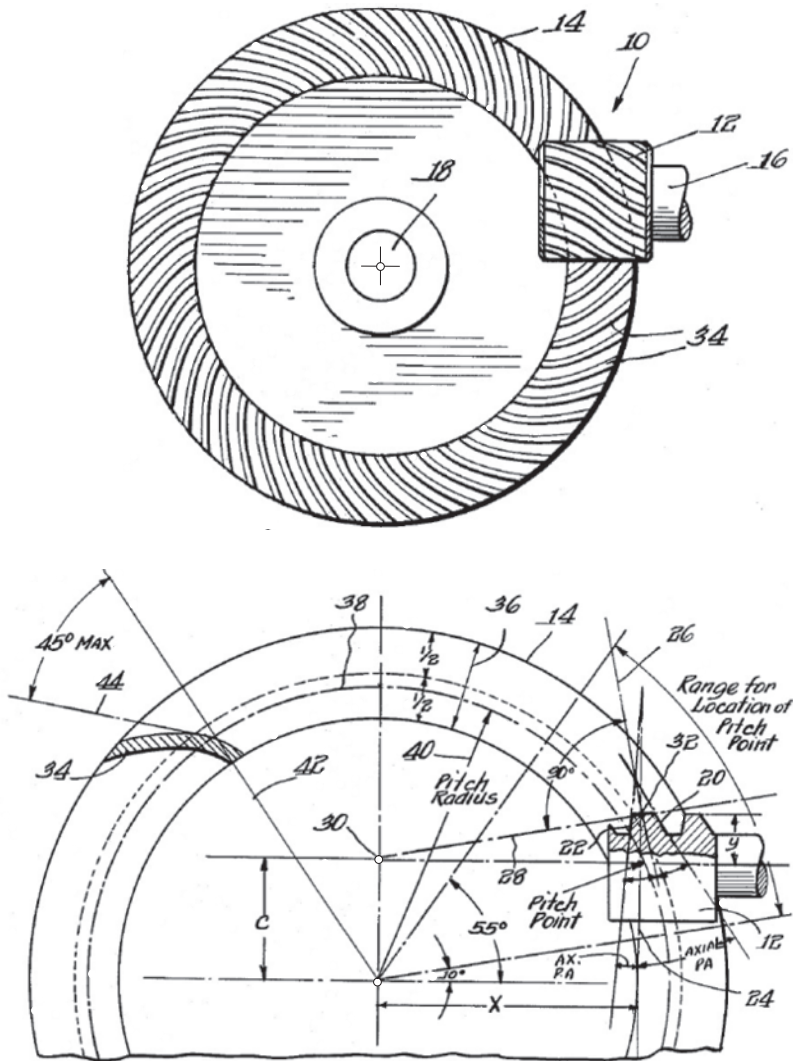


**FIGURE 16.17** Concept of *Helicon* gearing.

$C$  is the distance from the centerline of the gear (parallel to the axis of the pinion) out to the pitch point of the gear, as is note in Figure 16.17.

$x$  is the horizontal dimension from the center of the gear out to the pitch point of the gear along the axis of the pinion.

$y$  is the radius of the pinion.

The pinion is cylindrical, and the teeth are of a constant lead. However, the profile of the teeth is asymmetrical. There is a low-pressure angle on one side, and a high-pressure angle on the other side. Specifically, the high-pressure angle is on the driving side, as indicated at 20, while the low-pressure angle is on the reverse side, as indicated at 22. The low pressure angle is selected between zero and  $20^\circ$ , while the high pressure angle is selected from  $20^\circ$  to  $40^\circ$ . It will be observed that the two pressure angles are taken with respect to a line 24, which is perpendicular to the axis of the pinion. However, the total included angle is substantially symmetrical relative to a line indicated

at 26, and here in after designated at the limit pressure angle line. It will be observed that the limit pressure angle line is perpendicular to a line 28 which extends from the intersection 30 of the projected axis of the pinion 12 with a plane lying in the axis of the gear and perpendicular to the axis of the pinion, to the intersection 32 of the limit pressure angle line 26 with the circumference of the pinion 12. It will be understood that the intersecting point 32 lies on an axial plane of the pinion taken perpendicular to the axis of the gear.

Line 28 represents the line joining the pitch point and the intersection point 30 of the pinion axes of rotation with the common perpendicular between the axes. It is possible to show, by a rather involved mathematical analysis, that a helicoidal pinion having a lead determined by Eq. (16.1), and having an axial profile section perpendicular to this line 28 would have tooth action analogous to zero pressure angle in conventional parallel-axes gearing. Pinion teeth having pressure angle symmetrical to this limit angle, and differing from it by a substantial amount, will tend to have similar tooth action on both sides.

The teeth of the gear 14 are indicated at 34, and the face with of the gear teeth is indicated by the line 36. The pitch line 38, having the pitch radius 40, is always on the inner half of the gear face, whereby the pitch point is on the inner half of the gear face and at the outside diameter of the pinion. It was found desirable that pitch line 38 should always be on the inner half of the gear face to assure maximum conjugate action of the pinion teeth and the gear teeth. From the nature of the pinion and gear teeth here disclosed, maximum tooth contact will only occur when the pitch radius 40 is less than the radius of the midpoint of the gear face. Generally speaking, the lower the speed ratio of the gear [ $K$  in Eq. (16.1)], the more drastic is the deleterious effect on conjugate action of gear and pinion teeth of the non-location of the pitch line on the inner half of the gear face. If, for example, the pitch radius 40 is on the outer half of the gear face, undesirable fillets will occur in proportion to the speed ratio of the teeth. As will be observed from Eq. (16.1) with other factors fixed, the higher the speed ratio ( $K$ ) of the gearing, the less practical effect the dimensions  $x/y$  have on the resultant gear and pinion action. However, it is true that in all cases that the values for  $x$  and  $y$  in Eq. (16.1) and is initially determined by the pitch line 38 (and particularly at the lower speed ratios,  $K$ ), will have an influence on the amount of active tooth surfaces. The range for location of the pitch point is from  $10^\circ$  to  $55^\circ$  above the centerline of the gear parallel to the axis of the pinion, as illustrated in Figure 16.17.

It will be observed in Figure 16.17 that the teeth of the gear in axis view are of concave, convex configuration. Furthermore, when the pinion is turned to rotate the gear in the convex direction of the gear teeth, the radially inner ends of the gear teeth lead the radially outer ends thereof.

It may be stated that the combination of offset center position, ratio, and pinion and gear diameters must not result in a spiral angle on the gear which exceeds  $45^\circ$ , this angle being between a radius 42, and the line 44 passing through the intersection of the radius 42 and the pitch circle 38, and tangent to the gear tooth 34 at that point.

Present-day designs of *Helicon* gearing are illustrated in Figure 16.18.

The line contact, from tip to root of the teeth, is always present in a plurality of teeth.<sup>7</sup> Thus, there is a continuous motion with no discontinuities, and the gearing is quite strong. The gears can be assembled for zero backlash operation, and this is important in many applications.

Not all fundamental laws of gearing are fulfilled in *Helicon* gearing. Therefore, *Helicon* gearing is a kind of approximate gearing, and not a kind of geometrically accurate gearing.

### 16.1.5 INTERNAL WORM-GEARING

Most of worm-gearing represent external gearing. Potentially, internal mesh between a worm and an internal gearing is possible. Examples are shown in Figure 16.19. Internal worm-gearing is not profoundly investigated yet.

<sup>7</sup> This statement by Mr. O.E. Saari is incorrect. **No line contact is possible** in gearing shown in Figure 16.17, as *Helicon* gearing is a kind of approximate gearing, and not a kind of geometrically accurate gearing.

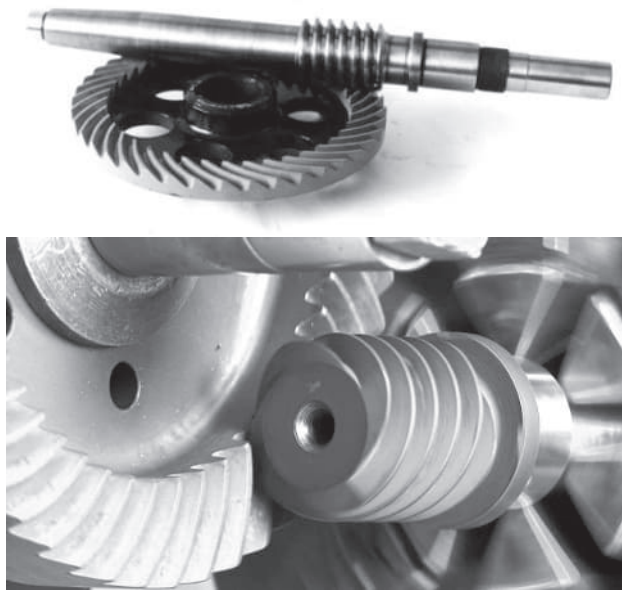


**FIGURE 16.18** *Helicon gear pair: Worm-gear pair with a crown worm gear and a cylindrical worm.*



**FIGURE 16.19** Internal worm-gear pairs.

When designing internal worm-gearing, fulfillment of three fundamental laws of gearing is a must. Otherwise, only approximate, and not geometrically accurate internal worm-gearing can be designed.

### 16.1.6 WORM-GEARING WITH ROLLING ELEMENTS

A variety of worm-gearing with rolling elements is developed in the industry. Figure 16.20 illustrates a possible design where an hourglass worm is engaged in mesh with a worm-gear with rolling elements. Fulfillment of all three fundamental laws of gearing is also a must when designing worm-gearing of such a design. Otherwise, only approximate, and not geometrically accurate worm-gearing with rolling elements can be designed.

Only one roller makes contact with the worm threads at every instant of time when the internal worm gearset (see Figure 16.20) operates.



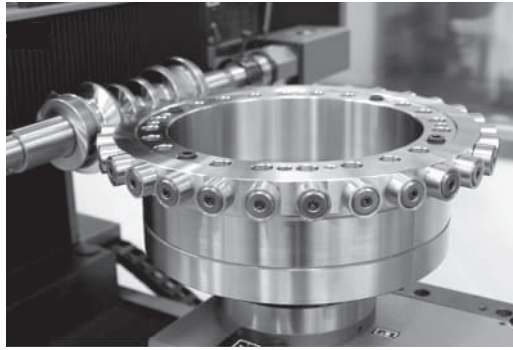


**FIGURE 16.20** Single-enveloping worm-gearing with rolling elements.

## 16.2 FUNDAMENTALS OF WORM-GEARING WITH LINE CONTACT BETWEEN WORM THREADS AND WORM-GEAR TOOTH FLANKS

Worm-gearing of all known designs feature point contact between worm threads and tooth flanks of a mating worm-gear. The line contact between the worm threads,  $\mathcal{P}$ , and the mating worm-gear tooth flanks,  $\mathcal{S}$ , is possible only in geometrically accurate worm-gear pairs. With respect to worm gearing, an involute worm in mesh with a helical involute gear is the only exclusion, as point-contact worm gearing of this particular design is geometrically accurate. Fundamentals of geometrically accurate worm-gearing with line contact between the worm threads and the worm-gear tooth flanks are briefly outlined below in this section of the book. It is right point to stress here that a line of contact is always a planar curve of a reasonable geometry, that is, a line of contact is *not* mandatorily a straight line.

The higher bearing capacity, and the higher power density, are the main two advantages of geometrically accurate line-contact worm-gearing over worm-gearing of other known designs. These two features along with a few others are due to the worm threads,  $\mathcal{P}$ , and the worm-gear tooth flanks,  $\mathcal{S}$ , make line contact with one another, and, thus, they have an increased area of contact between the interacting functional surfaces of the worm and of the worm-gear.

### 16.2.1 KINEMATICS OF GEOMETRICALLY ACCURATE WORM-GEARING

Geometrically accurate worm-gearing is a particular kind of crossed-axes gearing. Therefore, the kinematics of geometrically accurate worm-gearing is similar in much to that in the earlier discussed geometrically accurate crossed-axes gearing. The difference is chiefly to a higher gear ratio in worm-gearing compared to that in crossed-axes gearing of other designs. Once the rotation vectors of a worm-gear,  $\omega_g$ , and that of a mating worm,  $\omega_p$ , are specified, the rest of the elements of the corresponding gear vector diagram, namely, the pitch-line plane ( $P_{in}$  – plane), the centerline-plane ( $C_{in}$  – plane), the normal plane ( $N_{in}$  – plane), the plane of action,  $PA$ , the base cones, and so forth, can be constructed identically to that these elements are constructed for a crossed-axes gear pair of conventional design.

### 16.2.2 BASE CONES IN GEOMETRICALLY ACCURATE WORM-GEARING

The base cones in a geometrically accurate worm-gear pair can be viewed as envelope surfaces to a family of consecutive positions of the plane of action,  $PA$ , when the plane of action is rotated either about the worm-gear axis of rotation,  $O_g$  (forming in this way the gear base cone), or about the worm axis of rotation,  $O_p$  (forming in this way the pinion base cone). In external worm-gearing, the base cones are in permanent tangency to the plane of action from the opposite sides of the  $PA$ .

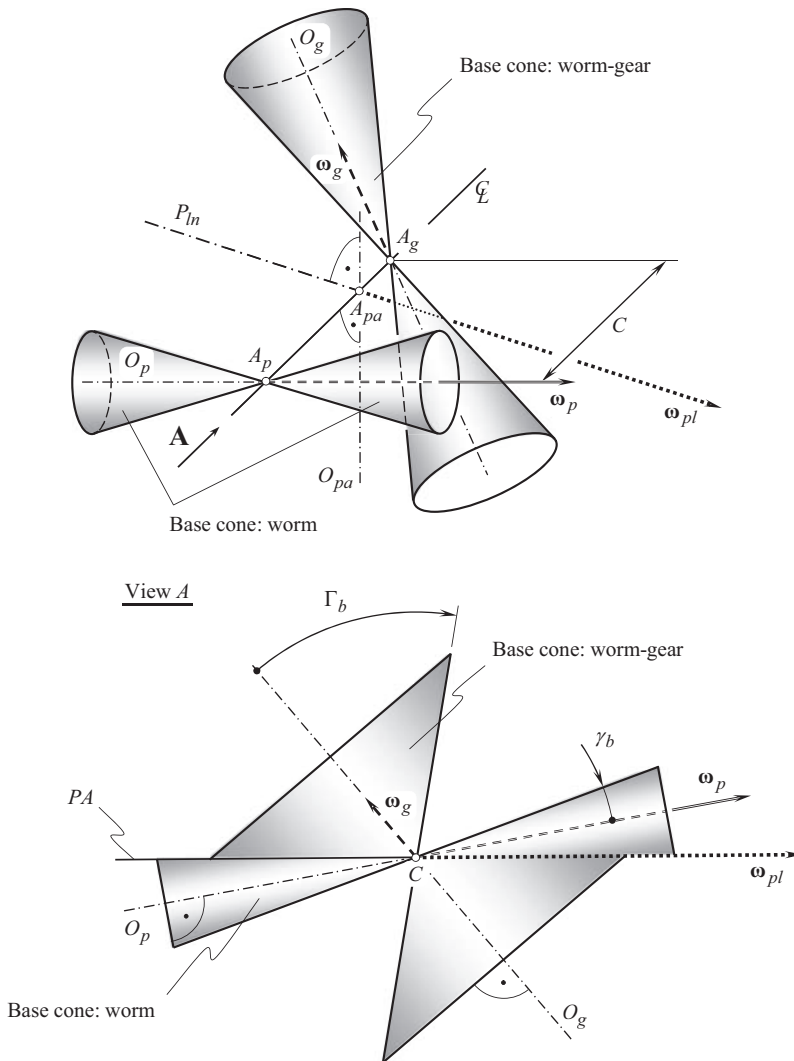


**FIGURE 16.21** Configuration of the rotation vectors,  $\omega_g$ ,  $\omega_p$ , and  $\omega_{pl}$ , and base cones, in geometrically accurate worm gear pair.

An example of possible configuration of the rotation vectors,  $\omega_g$ ,  $\omega_p$ , and  $\omega_{pl}$ , and of the base cones is illustrated in Figure 16.21. A more in-detail information on the configuration of the plane of action,  $PA$ , and base cones in geometrically accurate worm-gear pair is shown in Figure 16.22. The plane of action,  $PA$ , is shaped in the form of a portion of plane bounded by a circle centered at the plane-of-action apex,  $A_{pa}$ . The radius of the outer circle is designated as  $r_{o.pa}$ . The inner radius,  $r_{l.pa}$ , of the plane of action is zero ( $r_{l.pa} = 0$ ). Therefore, the effective width,  $F_{pa}$ , of the plane of action,  $PA$ , equals to the outer radius of the plane of action, that is, the equality,  $F_{pa} = r_{o.pa}$ , is valid.

Worm-gearing with line contact between the worm threads,  $\mathcal{P}$ , and the worm-gear tooth flanks,  $\mathcal{S}$ , features two base cones of the worm, and two base cones of the worm-gear.

The worm-gear is split into two portions by a plane through the centerline,  $\mathfrak{L}$ , perpendicular to the worm-gear axis of rotation,  $O_g$ . The tooth flanks,  $\mathcal{S}$ , of one of two portions of the worm-gear are generated from one of the base cones. The tooth flanks,  $\mathcal{S}$ , of the other of two portions of the worm-gear are generated from the other base cone.

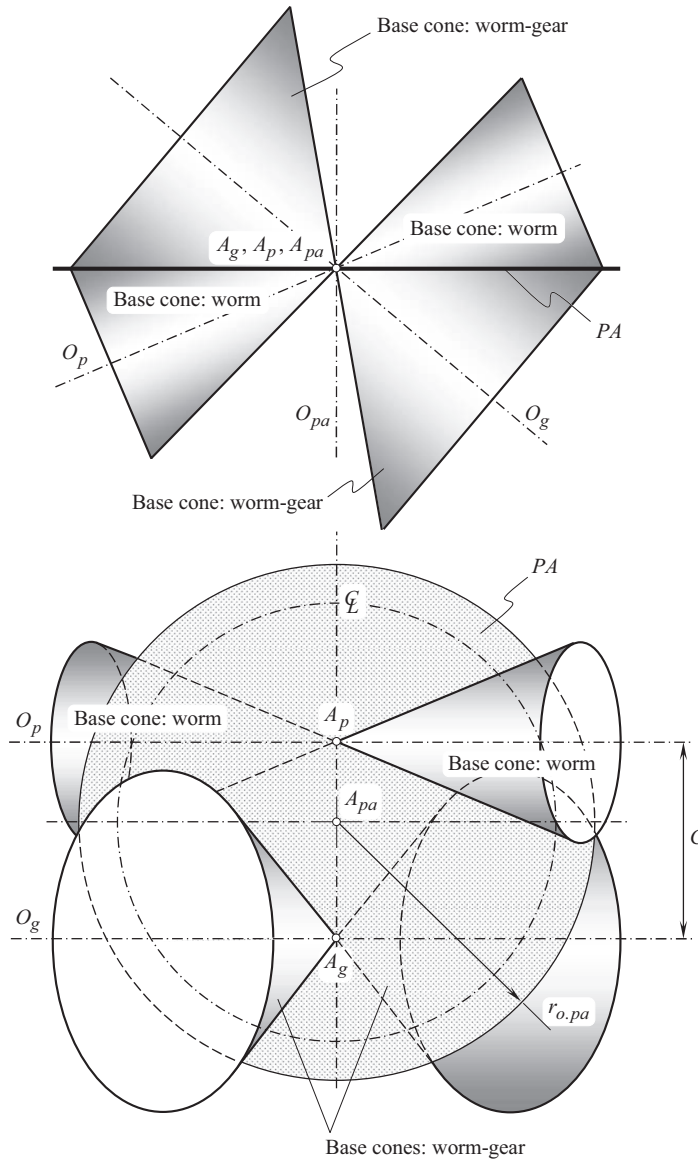


**FIGURE 16.22** Configuration of the plane of action,  $PA$ , and base cones, in geometrically accurate worm gear pair.

A similar is true with respect to the worm. The worm is split onto two portions by a plane through the centerline,  $\mathcal{L}$ , perpendicular to the worm axis of rotation,  $O_p$ . The worm threads,  $\mathcal{P}$ , of one of two portions of the worm are generated from one of the base cones. The worm threads,  $\mathcal{P}$ , of the other of two portions of the worm are generated from the other base cone.

As the kinematics in geometrically accurate worm-gearing, the plane of action, and the base cones, are similar to that in crossed-axes gearing of other designs, therefore, all the equations, those derived above for geometrically accurate crossed-axes gearing, are valid with respect to geometrically accurate worm-gearing.

Geometrically accurate worm-gear pairs of all designs can be designed using the approach adopted for design of  $R$ -gearing. Actually, only in this later case geometrically accurate gear pairs feature line contact between the functional surfaces  $\mathcal{S}$  and  $\mathcal{P}$ .

### 16.2.3 PECULIARITIES OF SLIDING IN PLANE-OF-ACTION APEX IN GEOMETRICALLY ACCURATE WORM-GEARING

Sliding between tooth flanks,  $\mathcal{S}$ , of a worm-gear, and between threads,  $\mathcal{P}$ , of a mating worm in geometrically accurate worm-gearing follows that same rule, as those established above with respect to crossed-axes gearing in a more general sense (see Chapter 15.). The sliding in the vicinity of the plane-of-action apex,  $A_{pa}$ , is the main feature of worm-gearing from this perspective. This is due to that in the vicinity of the plane-of-action apex,  $A_{pa}$ , radii of the base cones of the worm-gear and the worm are of a zero value.

As the inner radius of the plane of action,  $PA$ , in the plane-of-action apex,  $A_{pa}$ , is of a zero value ( $r_{l.pa} = 0$ ), no rolling ( $\omega_g^r = 0, \omega_p^r = 0$ ), and only axial sliding ( $\omega_g^{sl} \neq 0, \omega_p^{sl} \neq 0$ ) is observed in worm-gearing in the vicinity of the plane-of-action apex,  $A_{pa}$ , (see Figure 2.9 in Chapter 2). Therefore, unfavorable conditions of interaction between the tooth flanks,  $\mathcal{S}$ , of a worm-gear, and between threads,  $\mathcal{P}$ , of a mating worm, are observed in the vicinity of the plane-of-action apex,  $A_{pa}$ .

Not many efforts have been undertaken to this end to investigate the sliding conditions in the vicinity of the plane-of-action apex,  $A_{pa}$ , in worm-gearing. A paper by Korostel'ov [64] is one of just a few illustrative examples in this regard.

No rolling motion can be added to the contact area in the vicinity of the apex,  $A_{pa}$ , where the velocity of the rolling motion is either zero, or it is of a negligibly small value. Therefore, the area that features unfavorable conditions of interaction between tooth flanks,  $\mathcal{S}$ , of a worm-gear, and between threads,  $\mathcal{P}$ , of a mating worm is required to be eliminated from contact when the worm gear pair operates.

The parameters of the favorable, and unfavorable area in the interior of which the conditions of interaction between the tooth flanks,  $\mathcal{S}$ , of a worm-gear, and between threads,  $\mathcal{P}$ , of a mating worm can be specified in terms of the ratio  $\omega_p^{sl}/\omega_p^r$ . Within the plane of action,  $PA$ , a smallest possible area around the plane-of action apex,  $A_{pa}$ , in the interior of which conditions of interaction are unfavorable can be determined. The corresponding areas on tooth flanks,  $\mathcal{S}$ , of the worm-gear can be relieved to eliminate them from the interaction with threads,  $\mathcal{P}$ , of the mating worm.

## 16.3 CRITERION TO DISTINGUISH WORM FROM GEAR

Necessity of increasing the power density in gear transmissions is one of the main trends of evolution of the gear design, and of the worm-gearing design in particular. Because of this, gears with a low tooth count (the so-called *low-tooth-count gears*, or *LTC – gears*, for simplicity) are extensively used in the design of modern machinery. From the other hand, evolution of worm gearing tends to get more extensive applications of worm gearset with multiple-start worms.

A number of starts in a worm, and a number of teeth in a pinion are equivalent to one another. Because of that both are denoted by  $N_p$ .

Depending on a particular application, the number of starts in a worm falls into the interval  $N_p = 1 \div 5$ . Sometimes the number of starts can exceed this number ( $N_p > 5$ ). Similarly, depending on a particular application, the number of teeth in a low-tooth-count gear can be as small as  $N_p = 3$ . Sometimes the number of teeth can be even smaller ( $N_p < 3$ ). With that said, it is important to establish a quantitative criterion to distinguish a *worm* from a *low-tooth-count gear*. Use of a plane of action,  $PA$ , a zone of action,  $ZA$ , and a tooth contact ratio,  $\bar{m}$ , can be helpful when solving this particular gear problem.

One may conclude from that that eventually tooth number in gears will get smaller, while the number of starts in worm gearset will become greater. Eventually it could happen that the tooth count in a gear, and the number of starts in a worm, will get equal to one another. The difference between a *low-tooth-count gear* and a *multiple-start worm* is getting blurry. A natural question arises in this regard: *How a gear with a small number of teeth, and a multiple-start worm, can be distinguished from one another?*



**FIGURE 16.23** An example of gear element for which a criterion to distinguish *worm* from *low-tooth-count gear* is required.

The said is illustrated in Figure 16.23: Only a highly skilled and experienced gear expert can for sure identify whether the shown gear element is a multiple-start worm, or this is a *LTC* – gear. The design, calculation, manufacture, inspection, and application, of multiple-start worms, and of low-tooth-count gears are not identical to one another. Therefore, in some cases it could be critical to precisely specify the actual kind of a gear component. The necessity of a criterion to distinguish a multiple-start worm from a low-tooth-count gear is clarified by an example of a gear element shown in Figure 16.23.

A first known attempt to derive a criterion to distinguish a *multiple-start worm* from a helical *low-tooth-count gear* was undertaken by the author at around ~2008 [174]. This was an approximation to what is proposed below in this section of the book.

Commonly, there is the only line of contact,  $LC$ , of a full length between tooth flanks of a gear,  $\mathcal{G}$ , and its mating pinion,  $\mathcal{P}$ . If the base helix angle,  $\psi_b$ , is large enough, two lines of contact,  $LC_i$  and  $LC_{i+1}$ , can be observed within a tooth flank.

In a particular case, only one point of the exiting desirable line of contact,  $LC_i$ , and only one point of the entering line of contact,  $LC_{i+1}$ , are observed. This can be employed for the development of a criterion to distinguish a *multiple-start worm* from a helical *low-tooth-count gear*. Gearsets that can feature (at a certain angular configuration of the gear and of the pinion) two lines of contact within a common tooth flank a referred to as *multiple-start worm*, and gearing that at no angular configuration of the gear and the pinion features two (or more) desirable lines of contact within a common tooth flank a referred to as *low-tooth-count gear*.

It is handy to begin the discussion on the criterion to distinguish a *multiple-start worm* from a helical *low-tooth-count gear* from the design features of involute helical gear. This discussion is schematically illustrated in Figure 16.24.

Base diameter,  $d_{b,g}$ , in a helical involute gear, base helix angle,  $\psi_{b,g}$ , and the gear face width,  $F_g$ , are taken into account in the analysis immediately below.

The base helix lead,  $L_{b,g}$ , can be expressed in terms of the design parameters  $d_{b,g}$  and  $\psi_{b,g}$  :

$$L_{b,g} = \frac{\pi d_{b,g}}{\tan \psi_{b,g}} \quad (16.2)$$

As the actual value of the lead in a helical involute gear is of the same value regardless of the diameter of a cylinder at which the lead is calculated, the base helix lead,  $L_{b,g}$ , and that measured on pitch cylinder,  $L$ , are identical to one another, therefore Eq. (16.2) can be represented in the form:

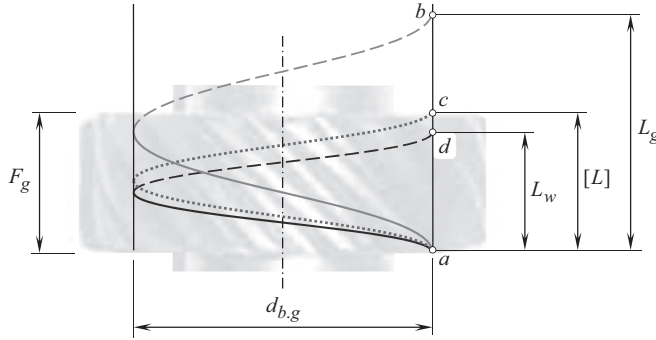


**FIGURE 16.24** Correlation between a gear element lead,  $L$ , and face width,  $F_g$ : lead in a worm  $L_w < F_g$ , lead in a helical gear  $L_g > F_g$ , and a critical lead value,  $[L]$ , when  $[L] = F_g$ .

$$L = \frac{\pi d_{b,g}}{\tan \psi_{b,g}} \quad (16.3)$$

A correlation between the lead,  $L$ , and the face width,  $F_g$ , can be employed as a criterion to distinguish a *multiple-start worm* from a **helical low-tooth-count gear**.

It is assumed here and below, that if one  $360^\circ$  – thread (in a helical gear element) spans over the pinion face width,  $F_g$ , (in this case the inequality  $L \geq F_g$  is valid), this gear element is referred to as *low-tooth-count gear*. Otherwise, the gear element is referred to as helical *multiple-start worm*.

With that said, a gear element for which an inequality ( $L < F_g$ ) is valid:

$$\frac{\pi d_{b,g}}{\tan \psi_{b,g}} < F_g \quad (16.4)$$

is referred to as *multiple-start worm*. Otherwise, when an inequality ( $L \geq F_g$ ) is valid:

$$\frac{\pi d_{b,g}}{\tan \psi_{b,g}} \geq F_g \quad (16.5)$$

The gear element is referred to as *low-tooth-count gear*.

It is important to stress here that the desirable line of contact,  $LC_{des}$ , has to be entirely located within the zone of action,  $ZA$ . To meet this requirement, a projection,  $F_{lc}$  (where  $F_{lc} = L \cdot \sin \psi_{b,g}$ ), of the desirable line of contact,  $LC_{des}$ , onto the transverse plane must be longer compared to perimeter of the base circle, that is, in helical involute gearing, an inequality:

$$F_{lc} \geq \pi d_{b,g} \quad (16.6)$$

must be fulfilled in order to refer the gear element as to *multiple-start worm*.

Once the concept of the criterion to distinguish a *multiple-start worm* from a helical *low-tooth-count gear* is clear with respect to helical involute gear, this concept can be evolved to the most general case of gearing, namely, to the case of crossed-axes gear pair.

A plurality of desirable lines of contact,  $LC_{des}$ , of various geometries are used in design of crossed-axes gearing. Moreover, a variety of configurations of the line of contact,  $LC_{des}$ , are known. Figure 16.25 illustrates examples of the geometries and configurations of the desirable line of contact,  $LC_{des}$ , in relation to the plane of action,  $PA$ , in a crossed-axes gear pair. [It is important to stress here that a gear base-cone-apex,  $A_g$ , coincides with the plane-of-action apex,  $A_{pa}$ , in intersected-axes



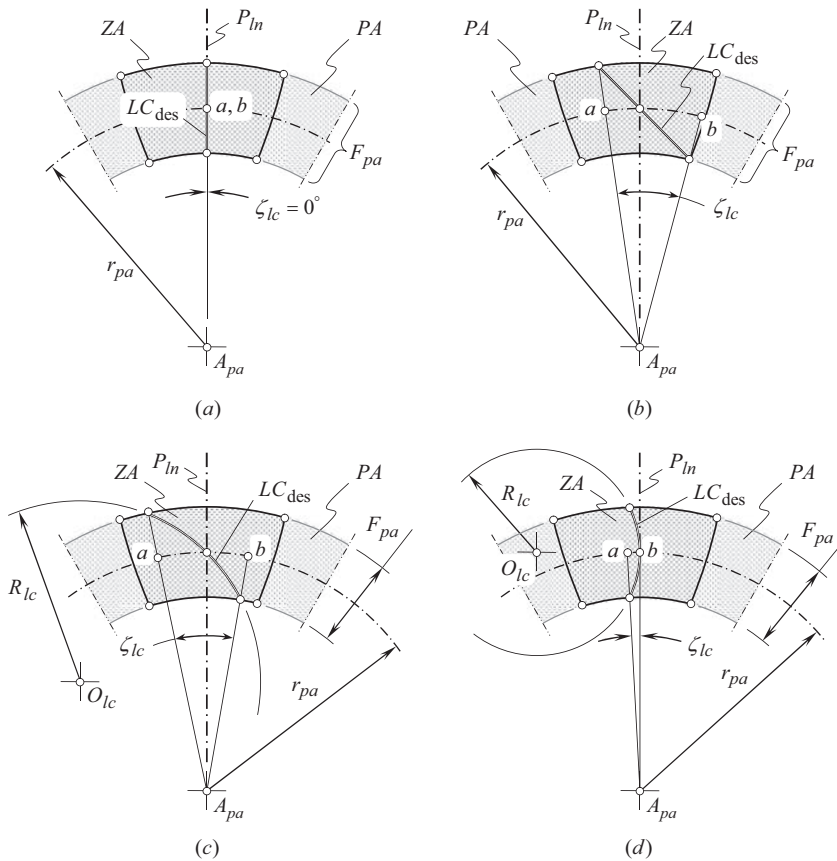


**FIGURE 16.25** Line-of-contact-span angle,  $\zeta_{lc}$ , in gearing with desirable lines of contact,  $LC_{des}$ , of various geometries: (a) straight  $LC_{des}$  (zero helix angle), (b) straight  $LC_{des}$  (skew), (c) circular-arc spiral  $LC_{des}$ , and (d) circular-arc spiral  $LC_{des}$  (zero helix angle).

gearing (when the identity,  $A_g \equiv A_{pa}$ , is valid), and a pinion base-cone-apex,  $A_g$ , is displaced from the plane-of-action apex,  $A_{pa}$ , in crossed-axes gearing (when the identity,  $A_g \neq A_{pa}$ , is observed)].

A desirable line of contact,  $LC_{des}$ , that is shaped in form of a straight line through the plane-of-action apex,  $A_{pa}$ , is shown in Figure 16.25a. The line of contact,  $LC_{des}$ , overlaps the effective face width,  $F_{pa}$ , in a gear pair, and is entirely located within the zone of action,  $ZA$ . The line-of-contact span angle,  $\zeta_{lc}$ , is of a zero value in the case under consideration ( $\zeta_{lc} = 0^\circ$ ).

In a bevel gear with skew teeth, a desirable line of contact,  $LC_{des}$ , is shaped in form of a straight line that crosses the plane-of-action axis of rotation,  $O_{pa}$ . In Figure 16.25b, the axis of rotation,  $O_{pa}$ , is a straight line through the plane-of-action apex,  $A_{pa}$ , and that is perpendicular to the plane of drawing. The line of contact,  $LC_{des}$ , overlaps the effective face width,  $F_{pa}$ , and is entirely located within the zone of action,  $ZA$ . The line-of-contact span angle,  $\zeta_{lc}$ , is of a certain value ( $\zeta_{lc} > 0^\circ$ ).

In a spiral bevel gear, a desirable line of contact,  $LC_{des}$  (see Figure 16.25c), is shaped in form of a circular-arc segment of a certain radius,  $R_{lc}$ . The line of contact,  $LC_{des}$ , overlaps the effective face width,  $F_{pa}$ , and is entirely located within the zone of action,  $ZA$ . The line-of-contact span angle,  $\zeta_{lc}$ , is of a certain value ( $\zeta_{lc} > 0^\circ$ ).

A desirable line of contact,  $LC_{des}$ , in the form of a circular-arc segment of a certain radius,  $R_{lc}$ , can be configured so as to be tangent to radial direction of the bevel gear (see Figure 16.25d). The line of contact,  $LC_{des}$ , overlaps the effective face width,  $F_{pa}$ , and is entirely located within the zone of action,  $ZA$ . The line-of-contact span angle,  $\zeta_{lc}$ , is of a certain value ( $\zeta_{lc} > 0^\circ$ ).

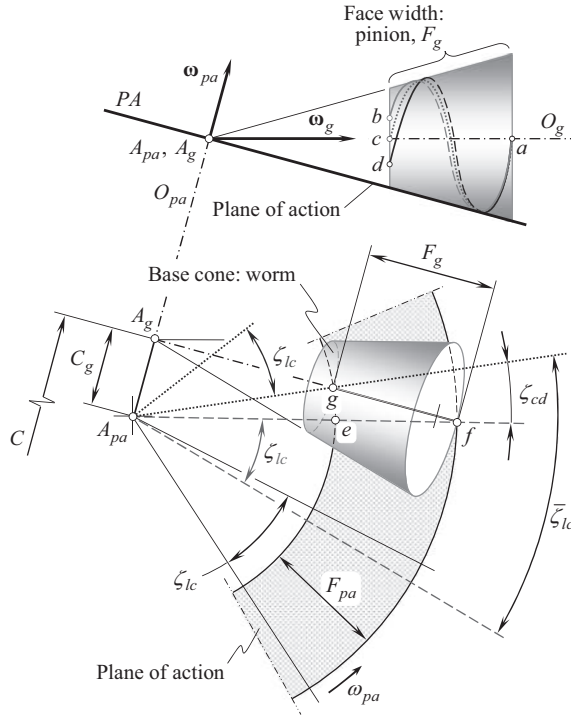


**FIGURE 16.26** Desirable line of contact,  $LC_{des}$ , wrapped over the base cone of the gear element.

In all the cases shown in Figure 16.25, the line of contact,  $LC_{des}$ , spans over the face width,  $F_{pa}$ , and is entirely located within the active portion of the plane of action,  $PA$ , at list at one instant of time. The line-of-contact-span angle,  $\zeta_{lc}$ , is important for further discussion.

As in crossed-axes gearing (see Figure 16.26), the gear apex,  $A_g$ , is displaced in relation to the plane-of-action apex,  $A_{pa}$ , at a gear center-distance,  $C_g$ . The gear axis of rotation,  $O_g$ , does not intersect the plane-of-action axis of rotation,  $O_{pa}$ . The gear center-distance,  $C_g$ , is the closest distance of approach of the crossing axes  $O_{pa}$  and  $C_g$ .

In crossed-axes gearing, the actual value of the line-of-contact-span angle,  $\bar{\zeta}_{lc}$ , is greater than that in intersected-axes gearing at a certain angle,  $\zeta_{cd}$ , caused by the displacement through the gear center-distance,  $C_g$ . The gear center-distance,  $C_g$ , is a portion of the center-distance,  $C$ , of the gear pair.

The determination of the actual value of the angle,  $\zeta_{cd}$ , is outlined immediately below.

Consider a triangle  $\triangle A_{pa}A_gf$ . This triangle is constructed in the plane of action,  $PA$ . In the triangle,  $\triangle A_{pa}A_gf$ , the side  $A_{pa}f = r_{o.pa}$  – is the outer radius of the plane of action,  $PA$ , and the side  $A_gf = r_{o.g}$  – is the outer radius of the base cone of the gear.

The actual value of the angle  $\angle fA_{pa}g$  in the triangle  $\triangle fA_{pa}g$  equals to the component,  $\zeta_{cd}$ , contributed to the total angle,  $\bar{\zeta}_{lc}$ , by the displacement,  $C_g$ , and is calculated from a formula:

$$\angle fA_{pa}g = \frac{r_{o.pa}^2 + r_{f.pa}^2 - F_g^2}{2 \cdot r_{o.pa} \cdot r_{f.pa}} \quad (16.7)$$

where  $r_{o.pa}$  and  $r_{f.pa}$  are the outer and the inner radii of the plane of action,  $PA$ . These design parameters are known from the gearset layout.

In the triangle,  $\triangle A_{ap}A_gf$ , the length of the side  $A_gf = \sqrt{(A_{ap}f)^2 - C_g^2} = \sqrt{r_{o.ap}^2 - C_g^2}$ .

In the triangle,  $\triangle A_{ap}A_gg$ , the length of the side  $A_gg = \sqrt{(A_{ap}g)^2 - C_g^2} = \sqrt{r_{f.ap}^2 - C_g^2}$ .



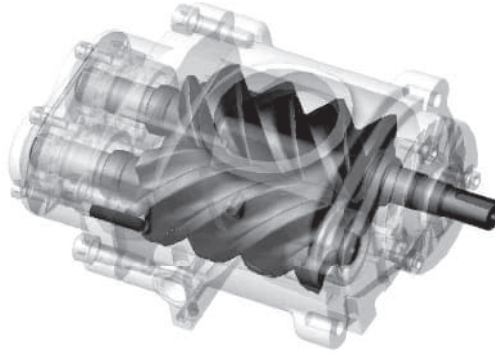


**FIGURE 16.27** Two parallel-axes multiple-start worms in the design of screw compressor working chamber.

Having the lengths of the straight-line segments  $A_g f$  and  $A_g g$  calculated, the actual value of the gear face width,  $F_g$ , is calculated from the formula:

$$F_g = fg = fA_g - gA_g = \sqrt{r_{o.ap}^2 - C_g^2} - \sqrt{r_{f.ap}^2 - C_g^2} \quad (16.8)$$

Ultimately, the total angle,  $\bar{\zeta}_{lc}$ , equals to the summa:

$$\bar{\zeta}_{lc} = \zeta_{lc} + \zeta_{cd} \quad (16.9)$$

Having the angle,  $\bar{\zeta}_{lc}$ , determined, one can proceed with the determination of the actual value of the gear base cone angle,  $\gamma_b$ .

The actual value of the base cone angle,  $\gamma_b$ , of the gear having the outer cone distance  $r_{o.g} = fA_g$ , and the face width  $F_g$ , equals:

$$\gamma_b = \frac{\bar{\zeta}_{lc}}{2\pi} \quad (16.10)$$

A gear element that features the base cone angle  $\gamma_b > \bar{\zeta}_{lc}/2\pi$ , is referred to as *low-tooth-count gear*. Otherwise, when  $\gamma_b \leq \bar{\zeta}_{lc}/2\pi$ , a gear element is referred to as *multiple-start worm*. For the calculations, the base cone angle,  $\gamma_b$ , can be expressed with the design parameters of the gear element – this is a routine procedure.

By convention, a so-called *worm factor*,  $k_w$ , can be taken into account ( $0 < k_w < 1$ ). In this latter case, the two expressions:  $\gamma_b > \bar{\zeta}_{lc}/2\pi$  and  $\gamma_b \leq \bar{\zeta}_{lc}/2\pi$ , are substituted with equivalent expressions:  $\gamma_b > k_w \cdot \bar{\zeta}_{lc}/2\pi$  and  $\gamma_b \leq k_w \cdot \bar{\zeta}_{lc}/2\pi$ . The actual value of the *worm factor*,  $k_w$ , can be determined based on the experience accumulated in the gear industry.

Shown in Figure 16.27 two parallel-axes worms in the design of screw compressor working chamber meet the definition. Therefore, both the components are referred to as *multiple-start worms* despite the axes of rotation of the worms are parallel to one another.

## 16.4 ANALYSIS OF DESIGN OF WORM-GEAR-DRIVE [PAT. NO. 257,246, USSR, 1968]

The disclosed in this chapter of the book theory of geometrically accurate worm gearing provides good opportunity to demonstrate the importance of the *Scientific Theory of Gearing* to those who are involved in the design and analysis of worm gearing.

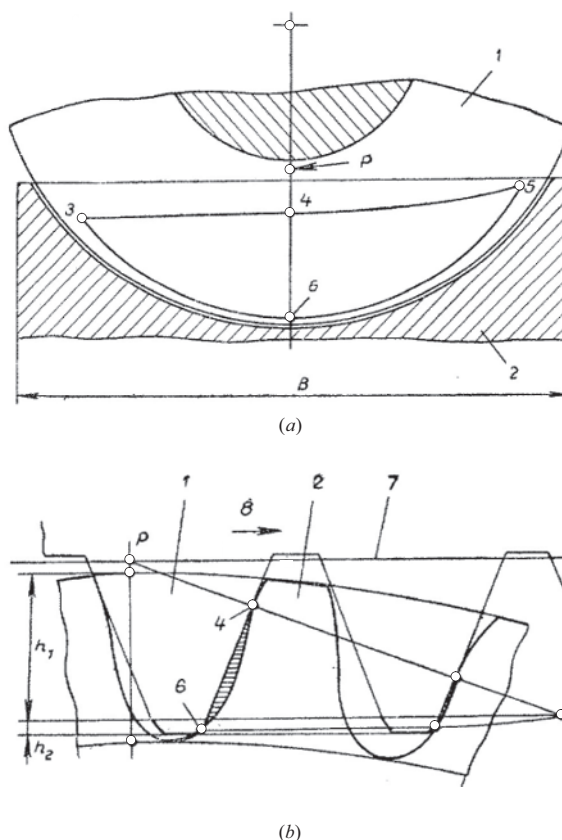


**FIGURE 16.28** A worm-gear drive proposed by Prof. *L.V. Korostel'ov* as early as in 1968 [126]: (a) a worm engaged in mesh with a worm-gear, and (b) a volume with a lubricant locked in between the worm threads and the tooth flanks of the worm-gear.

A worm-gear drive according to USSR Pat. No. 257,246 [126] is used here as an illustrative example. The invention [126] is chosen just because it is convenient to demonstrate the capabilities of the disclosed *Scientific Theory of Gearing*. It is also instructive to realize that poor understanding of the theory of gearing has resulted in numerous engineering mistakes, committed by the followers of Prof. *L.V. Korostel'ov* (see, for example, [72], as well, as numerous other patents granted to these researchers).

A complex geometry of double-enveloping worm-gear drives, along with specific conditions of lubrication, and formation of the worm-gear tooth surface, inspired many researchers to develop analytical aspects of meshing of the worm and the worm-gear tooth surface. It is likely Prof. *N.I. Kolchin* of the USSR was the first [63] to suppose a possibility of closed spaces being formed in meshing area between the surfaces of worm threads and worm-gear teeth. The research of gearing of a similar design was undertaken later on by Dr. *P.S. Zak* [229]. A few novel designs of worm-gearing were proposed. At least one of them deserves to be discussed a bit more in detail.

As early as in 1968, Prof. *L.V. Korostel'ov* of the Soviet Union invented a worm-gear drive that feature (as claimed) unique conditions of lubrication of the interacting tooth flanks of the worm-gear and the worm threads [126]. According to the invention (see Figure 16.28):

“Tooth flanks of the worm-gear and threads of the worm make line contact with one another at every instant of time. In axial section of the worm thread surface, profile of the worm threads is composed of two segments. One of the segments is either a straight-line segment, or it is a segment of a smooth

curve with a large radius of curvature. This portion of the thread profile is tangential to another segment, which is shaped either in the form of a circular arc, or in the form of a smooth curve with small deviations from the circular arc. This second portion of the thread profile corresponds to the addendum. The face width of the worm-gear exceeds width of the zone of action. No undercut is allowed to the worm-gear tooth profile. Pitch point in the worm-gear drive is shifted toward the worm axis of rotation and is located outside the outer diameter of the worm-gear.

In this case, the line of contact between the worm-gear tooth flanks and the worm threads is shaped in the form of a closed contour. The lubricant is trapped in the area within the line of contact bounded by worm-gear teeth flanks and worm threads. The lubricant becomes the third body, by means of which the torque is transmitted from the worm shaft to the worm-gear shaft.

Contact stress is reduced due to the evenly distributed contact load within the interior of the line of contact.

A worm-gear drive features an increased efficiency, as the interacting surfaces of the worm-gear and of the worm interact through a lubricant, which is squeezed out of the contact area, as the worm rotates; as a result, the trapped volume of the lubricant becomes smaller.

The proposed design of a worm-gear drive is illustrated in Figure 16.28. In Figure 16.28a, a section of the worm-gear drive by a plane perpendicular to the worm axis of rotation is schematically depicted. Similarly, a section of the worm-gear drive by a plane perpendicular to the worm-gear axis of rotation is depicted in Figure 16.28b.

The worm-gear drive is composed of a worm (1 in Figure 16.28) and the worm-gear (2 in the figure).

The line 3-4-5-6-3 represents a projection onto the plane of Figure 16.28a of the closed line of contact. The axial profile of the worm is composed of two portions. The first portion has a height,  $h_1$ , shaped in the form of a straight-line segment (or a smooth curve that has a large radius of curvature). The second portion has a height,  $h_2$ , shaped in the form of a circular arc (or a smooth curve that has a reasonably small deviation from the circular arc profile). The two portions of the worm thread profile are in tangency with each other.

The tooth profile the worm-gear (2 in Figure 16.28) is conjugate to the thread profile of the worm (the element 1 in Figure 16.28). Such profiles of the worm and the worm-gear make it possible to trap the lubricant in the hatched volume.

Pitch point,  $P$ , in the worm-gear drive is shifted toward the worm axis of rotation, and is situated outside the outer diameter of the worm-gear in order to reduce the volume of lubricant. In this case, the zone of engagement is located outside the pitch cylinder of the worm. The pitch line (denoted 7 in Figure 16.28) is a straight line through the pitch point,  $P$ .

When the worm is rotated, thread profiles are traveling in the direction of the arrow denoted by 8 in Figure 16.28. The volume of the trapped lubricant becomes smaller. The lubricant under such conditions is squeezed out of the line of contact."

Unfortunately, the worm-gearing according to the invention [126] is not workable at all.

**First**, there is no freedom in selecting tooth profiles in a mating worm-gear pair. Any and all alterations to the worm thread profile, and to the worm-gear tooth profile, are restricted by the necessity to meet all three fundamental laws of gearing – these laws of gearing must be fulfilled at any and all circumstances: Only base-pitch-preserving alterations to the tooth profile are permissible, and this is a must.

**Second**, as it follows from the analysis of Figure 16.29, neither the tooth flanks of a worm-gear nor the threads of a mating worm, can be generated by a closed line of contact that is entirely located within the plane of action. This is clearly illustrated by a simple example in parallel-axes gearing (see Figure 16.29a), as well, as in the most general example in crossed-axes gearing (see Figure 16.29b) – worm-gearing is a particular case of gearing with crossing axes of rotation of the worm, and of the worm-gear.

Note that the numbers 3, 4, 5, and 6, in Figure 16.29 correspond to that same numbers in Figure 16.28.

**Third**, no shrinkage of the desirable line of contact,  $LC_{des}$ , can be anticipated when the gears rotate. Moreover, it is not possible to retain the volume with lubricant isolated from the environment, as the desirable line of contact,  $LC_{des}$ , is entirely located in the plane of action,  $PA$ , and this is a must.

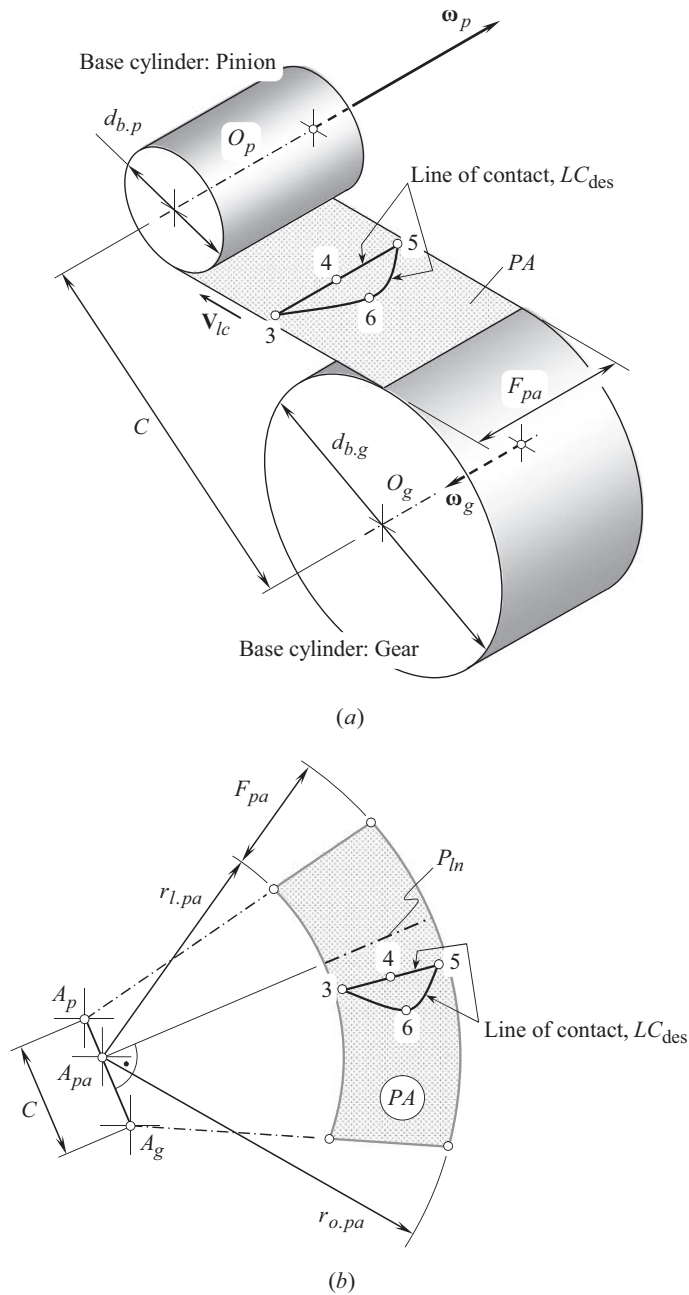


**FIGURE 16.29** On impossibility of generation of worm thread profile, and of worm-gear tooth profile, by means of a desirable line of contact in the form of a close planar curve: (a) in parallel-axes gearing and (b) in crossed-axes gearing (a worm-gear pair).

Violation of the fundamental laws of gearing is the root cause for the committed mistake [126]. The worm-gear drive shown in Figure 16.28 [126] represents an engineering mistake. This mistake is caused by the lack of knowledge in the theory of gearing. Lots of similar mistakes were committed by the followers of Prof. *L.V. Korostel'ov* [72].

In the present-day theory and practice of gearing, the number of examples that prove the importance to follow the recommendations derived from the *Scientific Theory of Gearing* is endless.



# Taylor & Francis

Taylor & Francis Group

<http://taylorandfrancis.com>

# *Part III*

---

## *Real Gears*

### *Kinematics, Geometry, and Application*

All gears and gear pairs discussed in the previous sections of the book do not exist physically. They are a kind of idealization. However, idealization of this kind is helpful for in-depth understanding of the gear tooth flank geometry, the kinematics of tooth flanks meshing, as well, as gear operation in general. Although there are many similarities between the two, real gears differ from geometrically accurate gearing for many reasons.

Real gearing, which consists of some aspects of application of gears, including, but not limited to, gear trains, planetary gearing, and so on, along with a novel concept for the calculation of the contact and bending strength of gear teeth, especially the teeth of gears featuring low tooth count (the so-called *low-tooth-count gears*, or just *LTC – gears* for simplicity), are covered in this part of the book.

All the sections deal with gears that feature linear and angular displacements of a gear, and of a mating pinion in relation to their nominal configurations. The nature of the displacements is of secondary importance at this point of this analysis. This could be either manufacturing errors, or deflections under operating load, or thermal distortions, and so forth.

Part IV of the book consists of a single Chapter 17. A room for a few more chapters is intentionally left as this part of the book has a potential for growth in the future.



# Taylor & Francis

Taylor & Francis Group

<http://taylorandfrancis.com>

---

# 17 Geometrically Accurate Real Gearing

## $S_{pr}$ – Gear System

Geometrically accurate real gears feature tooth flank geometry that is determined so as to provide the gears with the ability to be *insensitive* to any and all displacements of reasonable values of the tooth flanks from their nominal disposition. Having tooth flank geometries of this kind, the displacements are simply absorbed due to the specific shape of the tooth flanks. This makes it possible to reduce the accuracy requirements to the gear, to keep the accuracy tolerances in a wider range, and, thus, to use less accurate and cheaper gears instead of more precise and costly ones. Considered below in this chapter  $S_{pr}$  – gear system (or just  $S_{pr}$  – gearing, for simplicity) is developed aiming at accommodation for the tooth flanks displacements from their desirable location and orientation, which are caused by the manufacturing errors, by the operating loading as well as for the displacements of other nature.

### 17.1 PRELIMINARY CONSIDERATIONS

In order to derive equations for tooth flanks in geometrically accurate real gears, it is necessary to have an in-depth understanding of all root causes of high sensitivity of gearing to tooth flanks displacements under operating loads, and so forth.

#### 17.1.1 ROOT CAUSES FOR REAL GEARS DIFFER FROM GEOMETRICALLY ACCURATE GEARS

The design parameters of a geometrically accurate gear pair are exactly equal to their desirable (calculated) values. In reality, however, gear pairs undergo bending under operating load. Overheating may result in a heat distortion of the gears, shafts, and housing. The shafts of a gear, and of a mating pinion are displaced from their desirable positions because of manufacturing and mounting errors, as well, as because of the housing flexibility, and so forth. Finally, it can be concluded that under operating load, and when manufacturing errors occur, the initial configuration of the rotation vectors of a gear and of a mating pinion tends to get changed.

Shown in Figure 17.1 example illustrates parallel axes of rotation of two gears in an ideal case (see Figure 17.1a) and the misaligned axes of rotation of each gear under operating load (see Figure 17.1b). It should be noted here that the neutral and initially straight centerline of the shafts in Figure 17.1a becomes a spatial three-dimensional (3D), curved centerline under the load applied (see Figure 17.1b). This is one of the numerous root causes of the displacements of tooth flanks,  $\mathcal{S}$  and  $\mathcal{P}$ , of a gear, and of a mating pinion from their nominal location and orientation.

The displacements of the shaft bearings from their nominal configuration caused by the manufacturing errors, and the deflections under the load should be recognized as the potential root cause in gearing axes displacement. Larger displacements result in larger axes displacements and vice versa. Gearing that feature longer shafts are more sensitive to the displacements of this kind. However, the stiffness of longer shafts is lower than that of short ones. For a particular case, a favorable combination of the allowed bearing displacements and the shaft length can be determined aiming minimization of the gear's displacements. This issue could be of critical importance for the high-power-density gearboxes, for which the shafts should be of the shortest possible length. The shorter the shafts, the tighter the tolerances on the bearing's displacements.



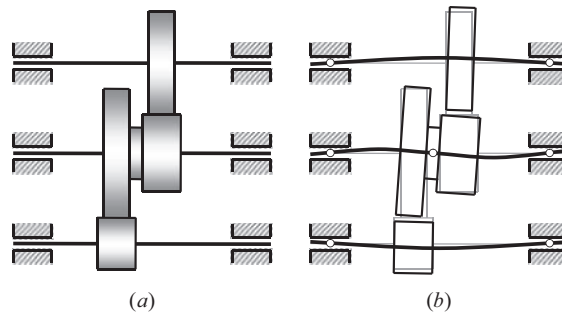


**FIGURE 17.1** An example of the root-cause for the axes displacement in parallel-axes gearing: (a) correct alignment of gear axes, and (b) gear axes are misaligned under operating load.

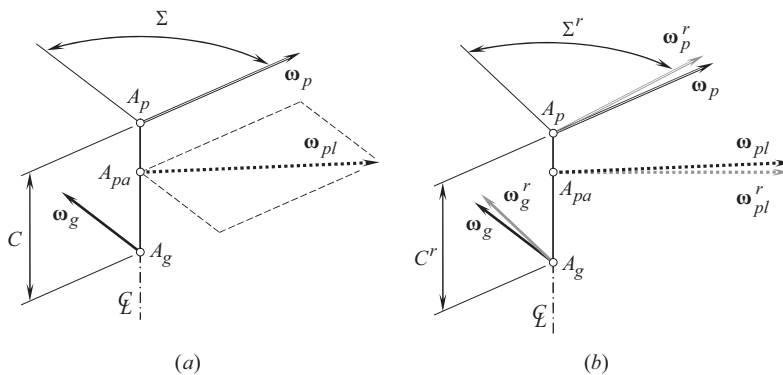


**FIGURE 17.2** Gear vector diagrams for (a) crossed-axes gear pair with zero axes displacements, and (b) corresponding real (loaded) crossed-axes gear pair with displaced axes of rotation of the gear and the mating pinion.

It is clear from the aforementioned brief consideration that in reality the axes of rotation of gears in a gearset are displaced from their desirable position. The actual root causes for the gear axes displacements are not the aim of the analysis below and, therefore, in this text, it is often omitted. In this book, the root causes for the axis displacement are not investigated; instead, the actual values of the displacements are taken into account. The actual configuration of the gear axes of rotation in relation to their desirable configuration is of critical importance and is investigated here to the best possible extent. The use of gear vector diagrams is convenient to run such an analysis.

Sown in Figure 17.2a, the gear vector diagram is constructed for an arbitrary geometrically accurate crossed-axes gear pair. The gear vector diagram is composed of a rotation vector of the gear,  $\omega_g$ , and of a rotation vector of the pinion,  $\omega_p$ . The closest distance of approach of the lines of action of the rotation vectors,  $\omega_g$  and  $\omega_p$ , is designated as  $C$ . An angle,  $\Sigma = \angle(\omega_g, \omega_p)$ , is formed by the rotation vectors,  $\omega_g$  and  $\omega_p$ . The angle,  $\Sigma$ , is the crossed-axes angle in the gear pair. The vector of instant rotation,  $\omega_{pl}$ , is constructed so as to fulfill the condition  $\omega_{pl} = \omega_p - \omega_g$ . The rotation vector,  $\omega_{pl}$ , is a vector through the *plane-of-action apex*,  $A_{pa}$ . This point is located within the centerline,  $\Phi$ , between the lines of action of the rotation vectors,  $\omega_g$  and  $\omega_p$ . The location of the apex,  $A_{pa}$ , within the centerline,  $\Phi$ , depends on the actual values of the magnitudes,  $\omega_g$  and  $\omega_p$ , of the rotation vectors,  $\omega_g$  and  $\omega_p$ .

In reality, the gear vector diagram for that same gear pair (see Figure 17.2b) differs from that constructed for the geometrically accurate gearing (see Figure 17.2a). The actual configuration of



**First**, a left-hand-oriented *Cartesian* coordinate system,  $X_g Y_g Z_g$ , is associated with the gear.

The  $Z_g$  – axis of this reference system is aligned with the rotation vector,  $\omega_g$ , of the gear.

The axis is pointed in the same direction as the rotation vector,  $\omega_g$ .

**Second**, a left-hand-oriented *Cartesian* coordinate system,  $X_p Y_p Z_p$ , is associated with the pinion. The axis  $Z_p$  of the reference system,  $X_p Y_p Z_p$ , is aligned with the rotation vector,  $\omega_p$ , of the pinion. The axis is pointed along the rotation vector,  $\omega_p$ .

**Third**, a stationary left-hand-oriented *Cartesian* coordinate system,  $X_{gp} Y_{gp} Z_{gp}$ , is associated with the gear pair.

The origin of the reference system,  $X_{gp} Y_{gp} Z_{gp}$ , is placed into the plane-of-action apex,  $A_{pa}$ , within the centerline,  $\Phi$ .

The axis  $Z_{gp}$  of the coordinate system,  $X_{gp} Y_{gp} Z_{gp}$ , is aligned with the vector of instantaneous rotation,  $\omega_{pl}$ . This axis is pointed in the same direction as the rotation vector,  $\omega_{pl}$ , is pointed. The axis  $X_{gp}$  is along the centerline,  $\Phi$ . This axis is pointed from the origin toward the gear reference system,  $X_g Y_g Z_g$ . Finally, the  $Y_{gp}$  – axis complements the first two axes to the left-hand-oriented *Cartesian* coordinate system,  $X_{gp} Y_{gp} Z_{gp}$ .

The axes,  $X_g$  and  $X_p$ , of the corresponding reference systems,  $X_g Y_g Z_g$  and  $X_p Y_p Z_p$ , are aligned with the centerline,  $\Phi$ . These axes ( $X_g$  and  $X_p$ ) are pointed in the same direction as the axis  $X_{gp}$ .

The constructed reference systems  $X_g Y_g Z_g$ ,  $X_p Y_p Z_p$ , and  $X_{gp} Y_{gp} Z_{gp}$ , by nature, represent a set of principal reference systems associated with the gear pair (see Chapter 3).

Immediately after the construction of the reference systems is completed, the corresponding operators of the coordinate systems transformation have to be composed. Following the routing practice (see Appendix D), the operator,  $\mathbf{Rs}(g \mapsto gp)$ , of transition from the coordinates system,  $X_g Y_g Z_g$ , associated with the gear, to the motionless coordinate system,  $X_{gp} Y_{gp} Z_{gp}$ , can be composed. Similarly, the operator  $\mathbf{Rs}(p \mapsto gp)$  of transition from the coordinate system,  $X_p Y_p Z_p$ , associated with the pinion, to the stationary coordinate system,  $X_{gp} Y_{gp} Z_{gp}$ , can be composed. The use of the operators of the resultant coordinate system transformations,  $\mathbf{Rs}(g \mapsto gp)$  and  $\mathbf{Rs}(p \mapsto gp)$ , makes possible representation of the gear axis of rotation,  $O_g^r$ , and the pinion axis of rotation,  $O_p^r$ , in the common reference system,  $X_{gp} Y_{gp} Z_{gp}$ , which is associated with the vector of instant rotation,  $\omega_{pl}$ , and the centerline,  $\Phi$ .

If necessary, the operators  $\mathbf{Rs}(g \mapsto gp)$  and  $\mathbf{Rs}(p \mapsto gp)$  can also be used for direct transition from the gear reference system,  $X_g Y_g Z_g$ , to the pinion reference system,  $X_p Y_p Z_p$  :

$$\mathbf{Rs}(g \mapsto p) = \mathbf{Rs}^{-1}(p \mapsto gp) \cdot \mathbf{Rs}(g \mapsto gp) \quad (17.1)$$

or in the inverse direction,

$$\mathbf{Rs}(p \mapsto g) = \mathbf{Rs}^{-1}(g \mapsto p) = \mathbf{Rs}^{-1}(g \mapsto gp) \cdot \mathbf{Rs}(p \mapsto gp) \quad (17.2)$$

The use of the operators of coordinate system transformations is helpful in solving the problem under consideration.

### 17.1.3 DISPLACEMENTS OF GEAR AXIS OF ROTATION FROM ITS DESIRABLE CONFIGURATION

Once the principal reference systems are constructed, the resultant deviation of a gear axis of rotation in real gearing from its desirable configuration can be expressed in terms of six elementary displacements, namely, in terms of three linear, and three angular displacements.

The elementary linear displacements,  $\delta_{gx}$ ,  $\delta_{gy}$ , and  $\delta_{gz}$ , are along the corresponding axes of the reference system  $X_g Y_g Z_g$  associated with the gear (see Figure 17.4a). The elementary linear displacements,  $\delta_{gx}$ ,  $\delta_{gy}$ , and  $\delta_{gz}$ , are of positive values if measured in the positive direction of the

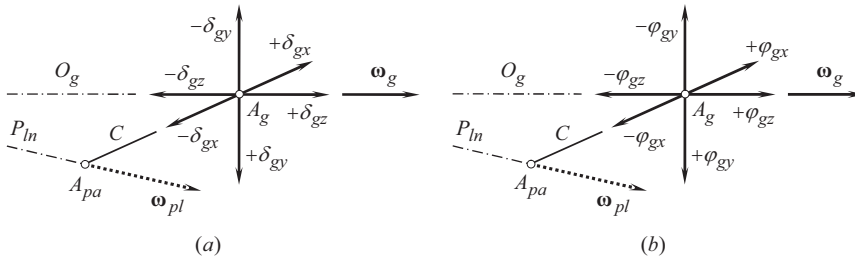


**FIGURE 17.4** Elementary displacements of gear axis of rotation,  $O_g$ , in relation to the vector of instant,  $\omega_{pl}$ : (a) linear displacements, and (b) angular displacements.

corresponding coordinate axis, and they are of negative value if measured in the corresponding opposite direction. The resultant linear displacement,  $\delta_g$ , of the gear axis of rotation,  $O_g$ , equals to a superposition of the displacements  $\delta_{gx}$ ,  $\delta_{gy}$ , and  $\delta_{gz}$ , and, thus, it can be expressed in terms of the elementary linear displacements by the following column matrix:

$$[\tilde{\delta}_g] = \mathbf{i}\delta_{gx} + \mathbf{j}\delta_{gy} + \mathbf{k}\delta_{gz} = \begin{bmatrix} \delta_{gx} \\ \delta_{gy} \\ \delta_{gz} \\ 1 \end{bmatrix} \quad (17.3)$$

The elementary angular displacements,  $\phi_{gx}$ ,  $\phi_{gy}$ , and  $\phi_{gz}$ , are about the corresponding axes of the reference system  $X_gY_gZ_g$  associated with the gear (see Figure 17.4b). The elementary angular displacements,  $\phi_{gx}$ ,  $\phi_{gy}$ , and  $\phi_{gz}$ , are of positive value if the corresponding rotation vector of the elementary displacement is pointed in the positive direction of the corresponding coordinate axis. The elementary angular displacements,  $\phi_{gx}$ ,  $\phi_{gy}$ , and  $\phi_{gz}$ , are of negative value if the elementary rotation vector of the elementary displacement is pointed in the opposite direction. However, the resultant angular displacement,  $[\tilde{\phi}_g]$ , of the gear axis of rotation,  $O_g$ , equals to a superposition of the displacements  $\phi_{gx}$ ,  $\phi_{gy}$ , and  $\phi_{gz}$ , and, thus, it can not be expressed in vector form as:

$$[\tilde{\phi}_g] \neq \mathbf{i}\phi_{gx} + \mathbf{j}\phi_{gy} + \mathbf{k}\phi_{gz} \quad (17.4)$$

as rotations are not vectors by nature.

The following approach is adopted below to calculate the resultant angular displacement,  $[\tilde{\phi}_g]$ , of the gear axis of rotation,  $O_g$ , in real gearing from its configuration in geometrically accurate gearing,  $O_g^r$ .

A unit vector,  $\mathbf{a}_g$ , is pointed along the gear axis of rotation,  $O_g$ . The vector,  $\mathbf{a}_g$ , can be expressed in terms of the axial vector,  $\mathbf{A}_g$ , of the gear, as shown in Figure 2.29 (see Chapter 2):

$$\mathbf{a}_g = \frac{\mathbf{A}_g}{|\mathbf{A}_g|} \quad (17.5)$$

The unit vector,  $\mathbf{a}_g$ , is pointed along the axis,  $Z_g$ , of the reference system,  $X_gY_gZ_g$ , associated with the geometrically accurate gear pair. Therefore:

$$\mathbf{a}_g = \mathbf{k}_g \quad (17.6)$$

After been displaced through the angle,  $[\vec{\varphi}_g]$ , the unit vector,  $\mathbf{a}_g^r$ , in the real gear pair equals to:

$$\mathbf{a}_g^r = \mathbf{Rs}(p_{rf} \rightarrow r_{eal}) \cdot \mathbf{a}_g \quad (17.7)$$

The resultant angular displacement,  $[\vec{\varphi}_g]$ , of the gear axis of rotation,  $O_g$ , can be expressed as:

$$\varphi_g = \tan^{-1} \frac{\mathbf{a}_g \cdot \mathbf{a}_g^r}{|\mathbf{a}_g \times \mathbf{a}_g^r|} \quad (17.8)$$

The operator,  $\mathbf{Rs}(p_{rf} \rightarrow r_{eal})$ , of the resultant coordinate system transformation in Eq. (17.7) is calculated as the product:

$$\mathbf{Rs}(p_{rf} \rightarrow r_{eal}) = \mathbf{Rt}(\varphi_{gz}, \hat{Z}_g) \cdot \mathbf{Rt}(\varphi_{gy}, \tilde{Y}_g) \cdot \mathbf{Rt}(\varphi_{gx}, X_g) \quad (17.9)$$

The operator,  $\mathbf{Rt}(\varphi_{gx}, X_g)$ , of the elementary coordinate system transformation can be analytically described in matrix form:

$$\mathbf{Rt}(\varphi_{gx}, X_g) = \begin{bmatrix} 1 & 0 & 0 & 0 \\ 0 & \cos \varphi_{gx} & -\sin \varphi_{gx} & 0 \\ 0 & \sin \varphi_{gx} & \cos \varphi_{gx} & 0 \\ 0 & 0 & 0 & 1 \end{bmatrix} \quad (17.10)$$

In this case, it is reasonable to take an advantage of the fact that all the angular displacements,  $\varphi_{gx}$ ,  $\varphi_{gy}$ , and  $\varphi_{gz}$ , are of small values. Taking into account that for angles of a small value, an equality  $\sin \varphi_{gx} \cong \tan \varphi_{gx} \cong \varphi_{gx}$  is valid (here, the angle,  $\varphi_{gx}$ , is expressed in radians), Eq. (17.10) is reduced to:

$$\mathbf{Rt}(\varphi_{gx}, X_g) = \begin{bmatrix} 1 & 0 & 0 & 0 \\ 0 & \sqrt{1 - \varphi_{gx}^2} & -\varphi_{gx} & 0 \\ 0 & \varphi_{gx} & \sqrt{1 - \varphi_{gx}^2} & 0 \\ 0 & 0 & 0 & 1 \end{bmatrix} \quad (17.11)$$

The operator,  $\mathbf{Rt}(\varphi_{gy}, \tilde{Y}_g)$ , of the elementary coordinate system transformation can be analytically described in matrix form as:

$$\mathbf{Rt}(\varphi_{gy}, \tilde{Y}_g) = \begin{bmatrix} \sqrt{1 - \tilde{\varphi}_{gy}^2} & 0 & -\tilde{\varphi}_{gy} & 0 \\ 0 & 1 & 0 & 0 \\ \tilde{\varphi}_{gy} & 0 & \sqrt{1 - \tilde{\varphi}_{gy}^2} & 0 \\ 0 & 0 & 0 & 1 \end{bmatrix} \quad (17.12)$$

Because the axis,  $\tilde{Y}_g$ , of the intermediate reference system,  $\tilde{X}_g \tilde{Y}_g \tilde{Z}_g$ , does not align with the coordinate axis,  $Y_g$ , of the original reference system,  $X_g Y_g Z_g$ , the angular displacements,  $\tilde{\varphi}_{gy}$  and  $\varphi_{gy}$ , are not equal to one another (i.e., the inequality,  $\tilde{\varphi}_{gy} \neq \varphi_{gy}$ , is valid). However, the angular displacements,  $\tilde{\varphi}_{gy}$ , can be expressed in terms of the angular displacements,  $\varphi_{gx}$  and  $\varphi_{gy}$ .

The operator,  $\mathbf{Rt}(\varphi_{gz}, \hat{Z}_g)$ , of the elementary coordinate system transformation can be expressed in matrix form:

$$\mathbf{Rt}(\varphi_{gz}, \hat{Z}_g) = \begin{bmatrix} \sqrt{1-\hat{\varphi}_{gz}^2} & -\hat{\varphi}_{gz} & 0 & 0 \\ \hat{\varphi}_{gz} & \sqrt{1-\hat{\varphi}_{gz}^2} & 0 & 0 \\ 0 & 0 & 1 & 0 \\ 0 & 0 & 0 & 1 \end{bmatrix} \quad (17.13)$$

Because the axis,  $\hat{Z}_g$ , of the intermediate reference system,  $\hat{X}_g\hat{Y}_g\hat{Z}_g$ , does not align with the coordinate axis,  $Z_g$ , of the original reference system,  $X_gY_gZ_g$ , the angular displacements,  $\tilde{\varphi}_{gz}$  and  $\varphi_{gz}$ , are not equal to one another (namely, the inequality,  $\tilde{\varphi}_{gz} \neq \varphi_{gz}$ , is valid). However, the angular displacements,  $\tilde{\varphi}_{gz}$ , can be expressed in terms of the angular displacements,  $\varphi_{gx}$ ,  $\varphi_{gy}$ , and  $\varphi_{gz}$ .

In a particular case(s), certain elementary displacement,  $\delta_{gx}$ ,  $\delta_{gy}$ ,  $\delta_{gz}$ , and  $\varphi_{gx}$ ,  $\varphi_{gy}$ ,  $\varphi_{gz}$ , do not affect the accuracy of the gear pair. For example, in a parallel-axes gearing, an axial linear displacement of a gear and of a mating pinion in relation to one another, as well as an angular displacement of a gear and of a mating pinion about the axes of their rotation, do not affect the accuracy of the gear pair. Such elementary displacements have to be eliminated from the further analysis.

The resultant displacement of the axis of rotation,  $O_p^r$ , of a mating pinion in real gearing from its desirable configuration,  $O_p$ , can also be expressed in terms of six displacements, namely, of three linear displacements, and three angular displacements, similar to that of the displacement of the gear axis of rotation:

$$[\tilde{\delta}_p] = \mathbf{i}\delta_{px} + \mathbf{j}\delta_{py} + \mathbf{k}\delta_{pz} = \begin{bmatrix} \delta_{px} \\ \delta_{py} \\ \delta_{pz} \\ 1 \end{bmatrix} \quad (17.14)$$

$$\varphi_p = \tan^{-1} \frac{\mathbf{a}_p \cdot \mathbf{a}_p^r}{|\mathbf{a}_p \times \mathbf{a}_p^r|} \quad (17.15)$$

where the unit vectors,  $\mathbf{a}_p$  and  $\mathbf{a}_p^r$ , are along the pinion axis of rotation,  $O_p$ , in a geometrically accurate gearing, and along the axis of rotation,  $O_p^r$ , in the corresponding real gearing.

It should be pointed out here that although the configuration of the rotation vectors,  $\omega_g^r$ ,  $\omega_p^r$ , and  $\omega_{pl}^r$ , in real gearing is different from those ( $\omega_g$ ,  $\omega_{pl}$ , and  $\omega_p$ ) in geometrically accurate gears, the tooth ratio of the gear pair ( $u = \omega_p/\omega_g$ ) remains the same. Therefore, the actual configuration of the rotation vectors,  $\omega_g^r$  and  $\omega_{pl}^r$ , as well as of the actual configuration of the rotation vectors,  $\omega_p^r$  and  $\omega_{pl}^r$ , correlate with each other so as to keep the tooth ratio of a constant value ( $u = \text{const}$ ).

It can be shown that the aforementioned correlation between pairs of the rotation vectors ( $\omega_g$ ,  $\omega_{pl}$  and  $\omega_p$ ,  $\omega_{pl}$ ) in geometrically accurate gearing, and between pairs of rotation vectors ( $\omega_g^r$ ,  $\omega_{pl}^r$  and  $\omega_p^r$ ,  $\omega_{pl}^r$ ) in real gearing, due to the equality  $u = \text{const}$ , result in negligibly small deviations of the vector of instant rotation,  $\omega_{pl}^r$ , from its desirable configuration, which is specified by the vector of instant rotation,  $\omega_{pl}$ . Thus, it can be assumed that when the location and orientation of the rotation vectors,  $\omega_g$  and  $\omega_p$ , change to,  $\omega_g^r$  and  $\omega_p^r$ , the initial location and orientation of the rotation vector,  $\omega_{pl}$ , remain the same<sup>2</sup> ( $\omega_{pl} \approx \omega_{pl}^r$ ).

<sup>2</sup> When the *relative motion* motion of a gear and of a mating pinion is considered, the rotation vector,  $\omega_{pl}^r$ , can be ignored.

The actual values of neither the elementary linear displacements ( $\delta_{gx}$ ,  $\delta_{gy}$ ,  $\delta_{gz}$  and  $\delta_{px}$ ,  $\delta_{py}$ ,  $\delta_{pz}$ ), nor of the elementary angular displacements ( $\varphi_{gx}$ ,  $\varphi_{gy}$ ,  $\varphi_{gz}$  and  $\varphi_{px}$ ,  $\varphi_{py}$ ,  $\varphi_{pz}$ ), are known. This is the first reason why the elementary displacements are inconvenient to be treated mathematically. The second reason is that a real gear pair has to be capable of accommodating the elementary displacements of *various* actual values, from the smallest possible to the largest permissible.

Both the issues can be easily resolved if the elementary displacements are replaced by the corresponding tolerances on their accuracy. In this chapter, the *tolerance* is understood in the sense of the largest permissible displacement. The tolerance for a linear displacement,  $\delta_{gx}$ , is designated as  $\{\delta_{gx}\}$ . The linear displacement,  $\delta_{gx}$ , and its corresponding tolerance,  $\{\delta_{gx}\}$ , relate to each other in the following manner:  $\delta_{gx} \leq \{\delta_{gx}\}$ . Similarly, the angular displacement,  $\varphi_{gx}$ , and its corresponding tolerance,  $\{\varphi_{gx}\}$ , relate to each other in the following manner:  $\varphi_{gx} \leq \{\varphi_{gx}\}$ . The same relation is valid with respect to the rest of the elementary displacements, both linear and angular.

For the tolerances, equations similar to Eqs. (17.3)–(17.15) are valid. For the gear axis of rotation, an equation for the elementary linear displacement can be represented in the following form:

$$[\{\vec{\delta}_g\}] = \mathbf{i}\{\delta_{gx}\} + \mathbf{j}\{\delta_{gy}\} + \mathbf{k}\{\delta_{gz}\} = \begin{bmatrix} \{\delta_{gx}\} \\ \{\delta_{gy}\} \\ \{\delta_{gz}\} \\ 1 \end{bmatrix} \quad (17.16)$$

For the angular displacement,  $\{\varphi_g\}$ , Eq. (17.8) still valid:

$$\{\varphi_g\} = \tan^{-1} \frac{\mathbf{a}_g \cdot \mathbf{a}_g^r}{|\mathbf{a}_g \times \mathbf{a}_g^r|} \quad (17.17)$$

except of the unit vectors,  $\mathbf{a}_g$  and  $\mathbf{a}_g^r$ , along the gear axes of rotation,  $O_g$  and  $O_g^r$ , have to be expressed in terms of the angular tolerances,  $\{\varphi_{gx}\}$ ,  $\{\varphi_{gy}\}$ , and  $\{\varphi_{gz}\}$ .

Similarly, for the pinion axis of rotation, the following equations are valid:

$$[\{\vec{\delta}_p\}] = \mathbf{i}\{\delta_{px}\} + \mathbf{j}\{\delta_{py}\} + \mathbf{k}\{\delta_{pz}\} = \begin{bmatrix} \{\delta_{px}\} \\ \{\delta_{py}\} \\ \{\delta_{pz}\} \\ 1 \end{bmatrix} \quad (17.18)$$

$$\{\varphi_p\} = \tan^{-1} \frac{\mathbf{a}_p \cdot \mathbf{a}_p^r}{|\mathbf{a}_p \times \mathbf{a}_p^r|} \quad (17.19)$$

where the unit vectors,  $\mathbf{a}_p$  and  $\mathbf{a}_p^r$ , along the pinion axes of rotation,  $O_p$  and  $O_p^r$ , have to be expressed in terms of the angular tolerances,  $\{\varphi_{px}\}$ ,  $\{\varphi_{py}\}$ , and  $\{\varphi_{pz}\}$ .

Ultimately, the tolerance for the total linear elementary displacement,  $\{\vec{\delta}_\Sigma\}$ , of the gear and of the pinion in real gearing is calculated as the vector summa:

$$\{\vec{\delta}_\Sigma\} = \{\vec{\delta}_g\} + \{\vec{\delta}_p\} \quad (17.20)$$

Similarly, the tolerance for the total angular displacement,  $\{\varphi_\Sigma\}$ , of the gear and the pinion in real gearing is calculated from the expression:

$$\{\varphi_\Sigma\} = \tan^{-1} \frac{\mathbf{a}_g^r \cdot \mathbf{a}_p^r}{|\mathbf{a}_g^r \times \mathbf{a}_p^r|} \quad (17.21)$$

Here, the elementary linear displacements,  $[\delta_g]$  and  $[\delta_p]$ , as well as the corresponding tolerances,  $[\{\delta_g\}]$  and  $[\{\delta_p\}]$ , for the linear displacements are treated as vectors. This is true with respect to all the linear displacements and the corresponding tolerances for these displacements. The similar is not valid with respect to the angular displacements,  $[\varphi_g]$  and  $[\varphi_p]$ , as well as for the corresponding tolerances,  $[\{\varphi_g\}]$  and  $[\{\varphi_p\}]$ , for the angular displacements. This is because the angular displacements,  $[\varphi_g]$  and  $[\varphi_p]$ , and the angular tolerances,  $[\{\varphi_g\}]$  and  $[\{\varphi_p\}]$ , are not vectors by nature, and they are not obeying the superposition law. Therefore, certain care is required when treating the rotations as vectors.

It should be pointed out here that not all of the aforementioned elementary displacements, both linear displacements ( $[\delta_g]$  and  $[\delta_p]$ ), and angular displacements ( $[\varphi_g]$  and  $[\varphi_p]$ ), are of critical importance for a particular configuration of the axes of rotation of a gear and of a mating pinion. This makes it possible to reduce the total number of the elementary displacements (or the total number of the tolerances,  $[\{\delta_g\}]$ ,  $[\{\delta_p\}]$ , and  $[\{\varphi_g\}]$ ,  $[\{\varphi_p\}]$ , for the elementary displacements,  $[\delta_g]$ ,  $[\delta_p]$  and  $[\varphi_g]$ ,  $[\varphi_p]$ , correspondingly) to be taken into account at a particular analysis.

For example, only two elementary displacements of six in total are of critical importance in parallel-axes gearing. The intersected-axes angular deviation,  $\theta_{ins}$ , is one of them, and the crossed-axes angular deviation,  $\theta_{crs}$ , is the other one. The impact of the rest of elementary displacements on the performance of a parallel-axes gear pair is negligibly small and, in many cases, it can be omitted from the analysis. The tolerances for the elementary displacements,  $\theta_{ins}$  and  $\theta_{crs}$ , are designated as  $\{\theta_{ins}\}$  and  $\{\theta_{crs}\}$  respectively ( $\theta_{ins} \leq \{\theta_{ins}\}$ ,  $\theta_{crs} \leq \{\theta_{crs}\}$ ).

#### 17.1.4 CLOSEST DISTANCE OF APPROACH BETWEEN GEAR AND MATING PINION AXES OF ROTATION

The elementary displacements alter the initial relative orientation of a gear, and of a mating pinion in a real gear pair. The actual location of the closest distance of approach (of the centerline) between the gear axis of rotation,  $O_g$ , and the pinion axis of rotation,  $O_p$ , alters in particular. Changes to the configuration of the axes,  $O_g$  and  $O_p$ , significantly depend on the actual kind of mounting of the gear and the mating pinion.

As illustrated in Figure 17.5a, even in the simplest case of parallel-axes gear pair, when the distances to the bearings on the left side,  $l_l$ , and at the right side,  $l_r$ , are equal to one another ( $l_l = l_r$ ), the shape of the neutral centerlines of the gear and of the mating pinion shafts (see Figure 17.5b) differs from that (see Figure 17.5d) when the distances to the bearings at the left side,  $l_l$ , and at the right side,  $l_r$ , are not equal to one another ( $l_l \neq l_r$ ), as illustrated in Figure 17.5c. Moreover, in the second case, certain inclination at an angle,  $\Delta\Sigma$ , between the gear and the mating pinion is observed.<sup>3</sup> The real gearing, *deformed* under operating load, can be substituted with an equivalent *displaced* gearing.

An example of an overhung bevel pinion is shown in Figure 17.6. The pinion is rotated about the axis,  $O_p$ . The pinion shaft is subject to bending under the separating load,  $P_{sep}$ . Due to the applied load,  $P_{sep}$ , the neutral centerline of the pinion shaft is getting curved. A straight line,  $O_p^r$ , tangential to the curved centerline at point,  $f$ , (here the point,  $f$ , is chosen at the middle of the face width of the pinion) is referred to as the actual axis of rotation of the pinion,  $O_p^r$ , in real gearing. Point of intersection of the centerline,  $O_p$ , by the straight tangent line,  $O_p^r$ , is equivalent to the plane-of-action apex,  $A_{pa}$ , in the real gearing.<sup>4</sup> The centerlines,  $O_p^r$  and  $O_p$ , form an acute angle,  $\Delta\Sigma$ .

A similar actual axis of rotation,  $O_g^r$ , can be determined for the mating gear. Finally, the closest distance of approach,  $C^r$ , between the axes of rotation,  $O_g^r$  and  $O_p^r$ , of the gear and of the mating pinion, can be expressed in terms of the design parameters of the gear pair, and of the applied load,  $P_{sep}$ .

<sup>3</sup> More accurately, the neutral centerline of a gear and a pinion shaft are spatial curves.

<sup>4</sup> More accurately, the neutral centerline of the pinion shaft is a spatial curve, and the plane-of-action apex,  $A_{pa}$ , is located within the centerline,  $\Phi$ .



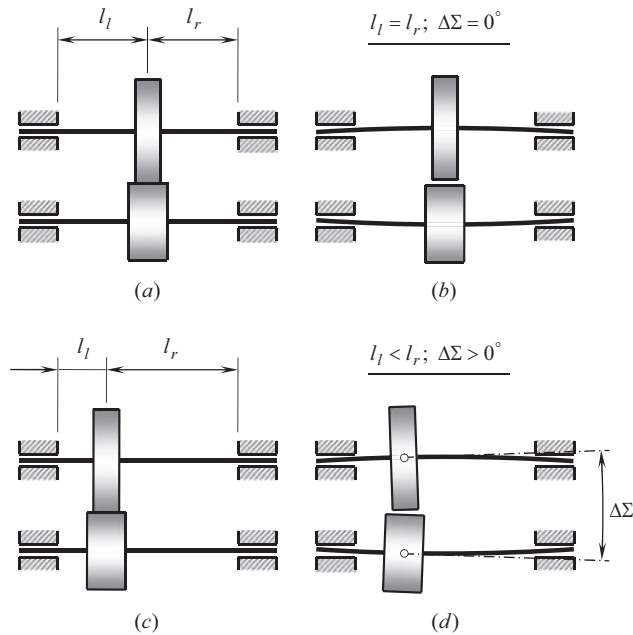


**FIGURE 17.5** Design features and shaft deflections in real parallel-axes gearing: (a) symmetrical gear pair,  $l_l = l_r$ , and (b) gear and pinion shaft deflections in (a); (c) asymmetrical gear pair,  $l_l \neq l_r$ , and (d) gear and pinion shaft deflections in (c).

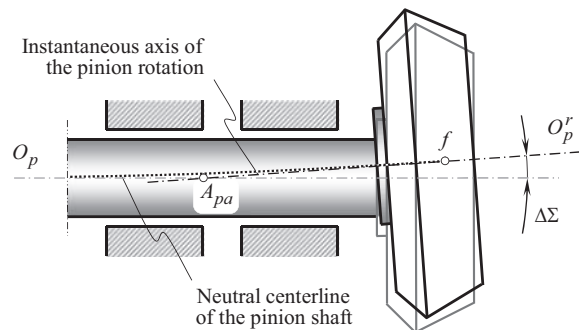


**FIGURE 17.6** Overhung bevel pinion shaft deflection under operating load.

The centerline,  $\Phi$ , between the axes of rotation,  $O_g^r$  and  $O_p^r$ , is located at a certain distance from the point,  $f$ . Denoted by  $l_{CDA}$ , this distance is referred to as the *closest distance of approach* between the gear, and the pinion axes,  $O_g^r$  and  $O_p^r$ , correspondingly. The actual value of the remote distance,  $l_{CDA}$ , strongly depends on the deflection of the pinion shaft. In order to perform further analysis, either the actual remote distance,  $l_{CDA}$ , or a tolerance for the value of this distance,  $\{l_{CDA}\}$ , is required to be known.

The shafts of straddle-mounted gears are less subject to deflections under an applied load. Examples are illustrated in Figure 17.7 with parallel-axes gearing. The angular displacements,  $\theta_{ins}$  and  $\theta_{crs}$ , depend on both, on the linear displacements of bearings at the shaft ends  $A$ ,  $B$ ,  $C$  and  $D$ , and on the actual configuration of the bearings in relation to the gears themselves. The remote distance,  $l_{CDA}$ , of the centerline in relation to the middle of a gear face width strongly depends on the actual values of the design parameters  $l_A^i$ ,  $l_B^i$ ,  $l_C^i$  and  $l_D^i$  of the gearbox (here  $i = 1, 2, 3, 4$ . These numbers 1, 2, 3, and 4 relate to the schematics (a), (b), (c), and (d) in Figure 17.7).

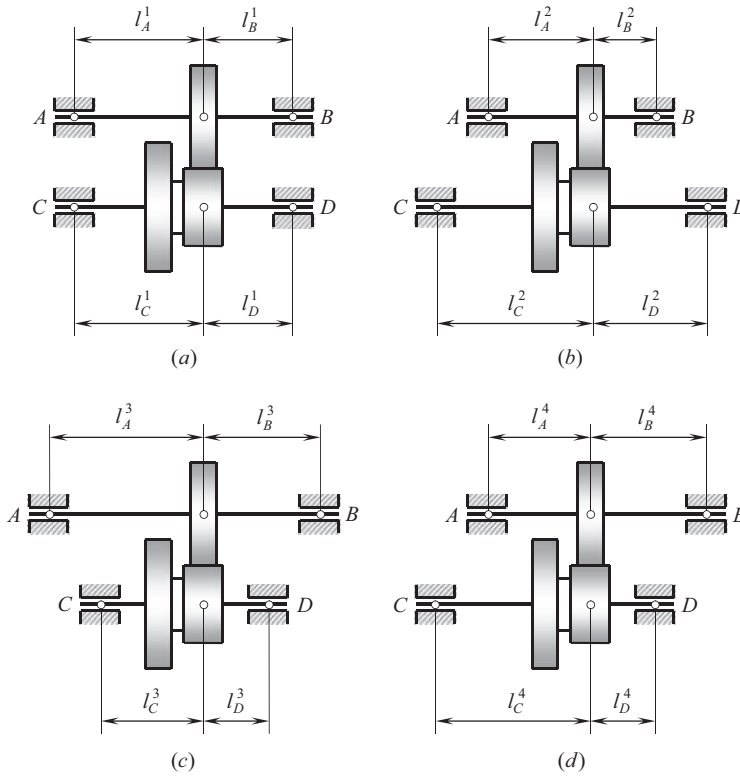


**FIGURE 17.7** Various possible configurations of straddle-mounted parallel-axes gearing: (a) both the shafts are of equal length, and are configured symmetrically in relation to one another, (b) the pinion shaft is longer compared to the gear shaft, and the shafts are configured symmetrically in relation to one another, (c) the pinion shaft is shorter compared to the gear shaft, and the shafts are configured symmetrically in relation to one another, and (d) the shafts of equal length are axially shifted in relation to one another – an example of asymmetric configuration of the shafts.

The actual values of design parameters of the tooth flank geometry in geometrically accurate real gears depend on the location of the centerline,  $c'$ , in relation to the tooth flanks of a gear,  $\mathcal{G}$ , and a mating pinion,  $\mathcal{P}$ . It is desirable to design a gearset so as to ensure the centerline, passing through the middle of the active face width of the gear pair. In this particular case, the tooth flanks are symmetrical in the lengthwise direction, which makes the assembling of the gearboxes easier. Otherwise, when gear and pinion teeth are asymmetrical, it is necessary to distinguish two ends of a gear (of a mating pinion) from each other.

The aforementioned recommendation is valid with respect to intersected-axes gearing as well as with respect to crossed-axes gearing.

As an example, consider a straddle-mounted shaft of a worm in worm gearing, as shown in Figure 17.8. The configuration of the axis of rotation,  $O_w$ , of the worm can be specified in terms of the coordinates of the shaft bearings,  $A$  and  $B$ , given in a stationary (motionless) reference system,  $X_s Y_s Z_s$ . Thus, the position vectors,  $\mathbf{r}_A$  and  $\mathbf{r}_B$ , of the points,  $A$  and  $B$ , within the axis of rotation,  $O_w$ , are known. The position vector of point of the gear axis of rotation,  $O_w$ , is designated as  $\mathbf{r}_{Ow}$ . As points within the axis  $O_w$  are considered, the following expression is valid:

$$(\mathbf{r}_{Ow} - \mathbf{r}_A) \times (\mathbf{r}_B - \mathbf{r}_A) = 0 \quad (17.22)$$

This expression casts into an equation for the position vector  $\mathbf{r}_{Ow}$ :

$$\mathbf{r}_{Ow}(\lambda^*) = \mathbf{r}_A + \lambda^* (\mathbf{r}_B - \mathbf{r}_A) \quad (17.23)$$

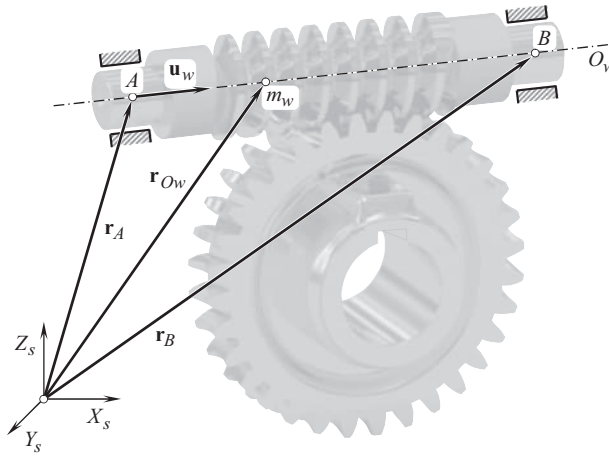


**FIGURE 17.8** A schematic of actual configuration of straddle-mounted worm shaft.

The difference,  $(\mathbf{r}_B - \mathbf{r}_A)$ , can be expressed in terms of the unit vector,  $\mathbf{u}_w$ , pointed along the axis of rotation,  $O_w$ , of the worm:

$$(\mathbf{r}_B - \mathbf{r}_A) = \lambda^{**} \mathbf{u}_w \quad (17.24)$$

This yields a simplified equation for the position vector,  $\mathbf{r}_{Ow}$ :

$$\mathbf{r}_{Ow}(\lambda) = \mathbf{r}_A + \lambda \mathbf{u}_w \quad (17.25)$$

where the equality,  $\lambda = \lambda^* \cdot \lambda^{**}$ , is valid.

An ideal configuration of the axis of rotation of the gear,  $O_w$ , is described by Eq. (17.23). In real gearing, the bearings,  $A$  and  $B$ , are displaced from their desirable positions. The vectors,  $\delta_A$  and  $\delta_B$ , of the actual displacements are usually not known. However, the tolerances,  $\{\delta_A\}$  and  $\{\delta_B\}$ , for the displacements,  $\delta_A$  and  $\delta_B$ , are commonly assigned by the gear designer, and, therefore, they are considered as known parameters of the gear set. Taking into account the tolerances  $\{\delta_A\}$  and  $\{\delta_B\}$ , an expression for the position vector of a point,  $\mathbf{r}_{Ow}^r$ , for real configuration of the axis of rotation,  $O_w^r$ , of the gear can be expressed in the following form:

$$\mathbf{r}_{Ow}^r(\lambda_w^r) = \mathbf{r}_A + \{\delta_A\} + \lambda_w^r[(\mathbf{r}_B + \{\delta_B\}) - (\mathbf{r}_A + \{\delta_A\})] \quad (17.26)$$

In Eq. (17.26), the parameter of the axis of rotation,  $O_w^r$ , is designated as  $\lambda_w^r$ .

An equation similar to Eq. (17.26) can be derived for the position vector of a point,  $\mathbf{r}_{Og}^r$ , for real configuration of the axis of rotation,  $O_g^r$ , of the mating worm gear:

$$\mathbf{r}_{Og}^r(\lambda_g^r) = \mathbf{r}_C + \{\delta_C\} + \lambda_g^r[(\mathbf{r}_D + \{\delta_D\}) - (\mathbf{r}_C + \{\delta_C\})] \quad (17.27)$$

In Eq. (17.27), an ideal configuration of the bearings,  $C$  and  $D$ , of the worm gear is specified by position vectors,  $\mathbf{r}_C$  and  $\mathbf{r}_D$ . The tolerances for the actual displacements,  $\delta_C$  and  $\delta_D$ , of the bearings,  $C$  and  $D$ , are denoted by  $\{\delta_C\}$  and  $\{\delta_D\}$ , correspondingly. The parameter of the axis of rotation,  $O_g^r$ , is designated as  $\lambda_g^r$ .

Once the expressions for the position vectors,  $\mathbf{r}_{Ow}^r$  and  $\mathbf{r}_{Og}^r$ , are derived [see Eqs. (17.26) and (17.27)], the closest distance of approach between the axes of rotation,  $O_w^r$  and  $O_g^r$ , in the real gear

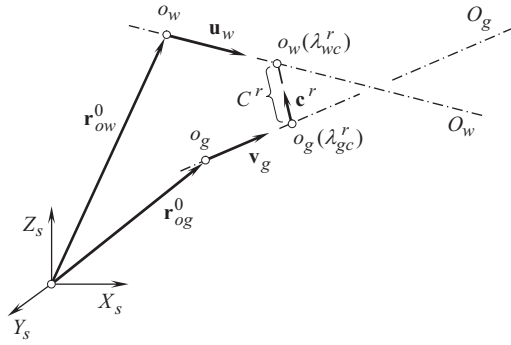


**FIGURE 17.9** Calculation of the resultant displacement along the center-distance for geometrically accurate real parallel-axes gearing.

pair can be determined. For this purpose, it is convenient to represent Eq. (17.26) in the following form:

$$\mathbf{r}_{O_w}^r(\lambda_w^r) = \mathbf{r}_{ow}^0 + \lambda_w^r \mathbf{u}_w \quad (17.28)$$

Similarly, Eq. (17.27) can be rewritten in the following form:

$$\mathbf{r}_{O_g}^r(\lambda_g^r) = \mathbf{r}_{og}^0 + \lambda_g^r \mathbf{v}_g \quad (17.29)$$

The center-distance between the axes of rotation,  $O_w^r$  and  $O_g^r$ , is designated as  $C^r$  (as shown in Figure 17.9). In the general case of crossed-axes gearing, the center-distance,  $C^r$ , is a function of the form:

$$C^r = C^r(C, \Sigma, \{\delta\}, \{\phi\}), \quad (17.30)$$

where  $\{\delta\}$ , and  $\{\phi\}$  are the tolerances for the resultant linear displacement, and the angular displacement, correspondingly. These tolerances can be expressed in terms of the tolerances for the elementary linear displacements, that is,  $\{\delta\} = \{\delta_w\} + \{\delta_g\}$ , and in terms of tolerances for elementary angular displacements, that is,  $\{\phi\} = \{\phi\}(\{\phi_w\}, \{\phi_g\})$ . The unit vector aligned with the center-distance,  $C^r$ , is denoted by  $\mathbf{c}^r$ .

The distance,  $\mathbf{d}$ , between two arbitrary points in the axes  $O_w^r$  and  $O_g^r$  can be calculated from the following equation:

$$\mathbf{d}(\lambda_w^r, \lambda_g^r) = \mathbf{r}_{O_w}^r(\lambda_w^r) - \mathbf{r}_{O_g}^r(\lambda_g^r) \quad (17.31)$$

It is necessary to determine the distance,  $\mathbf{d}(\lambda_w^r, \lambda_g^r)$ , which has a minimum length for all  $\lambda_w^r$  and  $\lambda_g^r$ . This distance corresponds to the closest distance of approach,  $C^r$ , between the gear axis of rotation,  $O_w^r$ , and the pinion axis of rotation,  $O_g^r$ , (i.e.,  $|\mathbf{d}^{\min}| = c^r$ ).

The two axes of rotation,  $O_w^r$  and  $O_g^r$ , are closest to one another at unique points, namely, at points  $o_w(\lambda_{wc}^r)$  and  $o_g(\lambda_{gc}^r)$ , for which the distance  $\mathbf{d}(\lambda_w^r, \lambda_g^r)$  attains its minimum length. The subscript “c” indicates here that a corresponding parameter is relevant to the center-distance. Also, if the axes,  $O_w^r$  and  $O_g^r$ , are not parallel (which is a trivial case), then the straight line segment,  $\mathbf{d}(\lambda_w^r, \lambda_g^r) = \mathbf{r}_{ow} - \mathbf{r}_{og}$ , joining the closest points,  $o_w(\lambda_{wc}^r)$  and  $o_g(\lambda_{gc}^r)$ , is uniquely perpendicular to both axes at the same time. No other straight-line segment between the axes,  $O_w^r$  and  $O_g^r$ , possess this property. The vector,

$\mathbf{d}_c = \mathbf{d}_c(\lambda_{gc}^r, \lambda_{pc}^r)$ , is uniquely perpendicular to the line direction vectors,  $\mathbf{u}_w$  and  $\mathbf{v}_g$ . According to this statement, the vector,  $\mathbf{d}_c$ , fulfills the following two equations simultaneously:

$$\mathbf{u}_w \cdot \mathbf{d}_c = 0 \quad (17.32)$$

$$\mathbf{v}_g \cdot \mathbf{d}_c = 0 \quad (17.33)$$

These two equations can be solved by substituting:

$$\mathbf{d}_c = \mathbf{r}_{ow}(\lambda_{wc}^r) - \mathbf{r}_{og}(\lambda_{gc}^r) = \mathbf{d}_0 + \lambda_{wc}^r \mathbf{u}_w - \lambda_{gc}^r \mathbf{v}_g \quad (17.34)$$

into each one of them to get simultaneous linear equations:

$$(\mathbf{u}_w \cdot \mathbf{u}_w) \lambda_{wc}^r - (\mathbf{u}_w \cdot \mathbf{v}_g) \lambda_{gc}^r = -\mathbf{u}_w \cdot \mathbf{d}_0 \quad (17.35)$$

$$(\mathbf{v}_g \cdot \mathbf{u}_w) \lambda_{wc}^r - (\mathbf{v}_g \cdot \mathbf{v}_g) \lambda_{gc}^r = -\mathbf{v}_g \cdot \mathbf{d}_0 \quad (17.36)$$

In Eqs. (17.34)–(17.36),  $\mathbf{d}_0 = \mathbf{r}_{ow}^0 - \mathbf{r}_{og}^0$  is the distance between two known points; in our case, it is the distance between the points,  $o_w$  and  $o_g$ .

Then, from  $\mathbf{u}_w \cdot \mathbf{u}_w = a$ ,  $\mathbf{u}_w \cdot \mathbf{v}_g = b$ ,  $\mathbf{v}_g \cdot \mathbf{v}_g = c$ ,  $\mathbf{u}_w \cdot \mathbf{d}_0 = d$ , and  $\mathbf{v}_g \cdot \mathbf{d}_0 = e$ , the solution to Eqs. (17.35)–(17.36) with respect to,  $\lambda_{wc}^r$  and  $\lambda_{gc}^r$ , can be represented as follows:

$$\lambda_{wc}^r = \frac{be - cd}{ac - b^2} \quad (17.37)$$

$$\lambda_{gc}^r = \frac{ae - bd}{ac - b^2} \quad (17.38)$$

In these equations, the denominator  $ac - b^2$  is nonzero. Note, that the following expression is always nonnegative:

$$ac - b^2 = |\mathbf{u}_w|^2 |\mathbf{v}_g|^2 - (|\mathbf{u}_w| |\mathbf{v}_g| \cos \theta)^2 = (|\mathbf{u}_w| |\mathbf{v}_g| \sin \theta)^2 \geq 0 \quad (17.39)$$

When the equality  $ac - b^2 = 0$  is valid, the two equations are dependent, the two axes,  $O_w^r$  and  $O_g^r$ , are parallel to one another, and the distance between the axes is of a constant value. We can solve for this parallel distance of separation by fixing the value of one parameter and using either equation to solve the other. Selecting  $\lambda_{wc}^r = 0$ , we get  $\lambda_{gc}^r = d/b = e/c$ .

Once the solution for  $\lambda_{wc}^r$  and  $\lambda_{gc}^r$  [see Eqs. (17.37) and (17.38)] is determined, the coordinates of the two points,  $o_w(\lambda_{wc}^r)$  and  $o_g(\lambda_{gc}^r)$ , are determined, as well. The axes of rotation,  $O_w^r$  and  $O_g^r$ , are closest to one another at these two points,  $o_w(\lambda_{wc}^r)$  and  $o_g(\lambda_{gc}^r)$ . Then the distance between these points is given as follows:

$$C^r(C, \Sigma, \{\delta\}, \{\phi\}) = |\mathbf{d}^{\min}| = \left| (\mathbf{r}_{ow}^0 - \mathbf{r}_{og}^0) + \frac{(be - cd)\mathbf{u}_w - (ae - bd)\mathbf{v}_g}{ac - b^2} \right| \quad (17.40)$$

In the general case of crossed-axes gearing, the crossed-axes angle,  $\Sigma^r$ , between the axes of rotation,  $O_g^r$  and  $O_p^r$ , is a function of the form  $\Sigma^r = \Sigma^r(C, \Sigma, \{\delta\}, \{\phi\})$ . It can be calculated from the following expression:

$$\Sigma^r(C, \Sigma, \{\delta\}, \{\phi\}) = \tan^{-1} \left( \frac{|\mathbf{u}_w \times \mathbf{v}_g|}{\mathbf{u}_w \cdot \mathbf{v}_g} \right) \quad (17.41)$$

The derived Eq. (17.41) is valid for gears of all kinds, not for worm gearing only.

For the convenience of calculation of the distance,  $l_{CDA}$ , points,  $o_w$  and  $o_g$ , can be chosen at the middle of face width of a gear, and a mating pinion respectively.<sup>5</sup>

As it follows from the analysis of Figures 17.4 and 17.9, the actual configuration of the axes of rotation,  $O_g$  and  $O_p$ , in crossed-axes gearing in relation to one another, can be specified in terms just of two parameters, namely, (a) of the center-distance,  $C$ , and (b) of the crossed-axes angle,  $\Sigma$ . Equations for both reduced cases of gearing, namely, intersected-axes gearing as well as parallel-axes gearing, can be derived from the most general case of crossed-axes gearing:

1. if the center-distance is of a zero value ( $C = 0$ ),  $C_a$  – gearing reduces to intersected-axes gearing
2. if the crossed-axes angle is either of a zero value ( $\Sigma = 0^\circ$ ), or equals  $\Sigma = \pm 180^\circ$ ,  $C_a$  – gearing reduces to parallel-axes gearing.

In particular, the specification of crossed-axes gearing in terms of the design parameters  $C$  and  $\Sigma$  is helpful when the coordinate system transformations are necessary to be performed (see the operators,  $\mathbf{Cp}_x(a_x, \varphi_x)$ , of coupled linear transformations). Note that the operators of coupled linear transformations,  $\mathbf{Cp}_x(a_x, \varphi_x)$ , are invariant with respect to the order of the elementary transformations, namely, of the translation ( $a_x$ ), and of the rotation ( $\varphi_x$ ).

## 17.2 TOOTH FLANK GEOMETRY IN GEOMETRICALLY ACCURATE REAL GEARING: $S_{pr}$ – GEAR SYSTEM

One of the major differences between real gearing and a corresponding geometrically accurate gearing is that in the former, the configuration of the axes of rotation of a gear, and of a mating pinion is different from that in the latter. This is because the configuration of the axes of rotation of the gear and of the mating pinion in geometrically accurate gearing is exactly specified, whereas in real gearing, the configuration depends on the deviation of the actual configuration of the axes of rotation from the desired configuration, and is indefinite in much. Although the deviation of the actual configuration of the axes of rotation from the desirable configuration in real gearing can be expressed in terms of the linear and of angular displacements, the actual values of both the linear displacements, and the angular displacements, are not known. However, the actual displacements can be substituted with the corresponding tolerances for the accuracy for the axes displacements.

The desirable tooth flank geometry in real gearing is determined on the premises of equality of angular base pitch of a gear, and that of a mating pinion, to an operating angular base pitch of the gear pair. The equality of angular base pitches ( $\varphi_{b,g} = \varphi_{b,op}$ , and  $\varphi_{b,p} = \varphi_{b,op}$ ) is a fundamental requirement in designing geometrically accurate real gearing.<sup>6</sup>

The equality of angular base pitches has to be complemented with that for the following distances:

- From the gear base-cone-apex,  $A_g$ , to the middle of the effective face width,  $F_{pa}$
- From the pinion base-cone-apex,  $A_p$ , to the middle of the effective face width,  $F_{pa}$
- From the plane-of-action-apex,  $A_{pa}$ , to the middle of the effective face width,  $F_{pa}$

All these distances correlate to one another. The correlation can be expressed in terms of the design parameters of the gear pair.

<sup>5</sup> CAD/CAM tools and FEA can be used to evaluate the anticipated displacements and deformations in a gear drive under an operating load.

<sup>6</sup> All three fundamental laws of gearing, namely: (a) the law of contact of the tooth flanks, (b) the conjugate action law, and (c) the law of equal angular base pitches, have to be fulfilled within the effective face width,  $F_{pa}$ , of a geometrically-accurate gear pair. In a case, the face widths of a gear,  $F_g$ , and that of a mating pinion,  $F_p$ , do not overlap one another, the effective face width,  $F_{pa}$ , is either of a zero value or of a negative value ( $F_{pa} \leq 0$ ). Neither of two is permissible for gearing, as no physical contact in between the tooth flanks,  $\mathcal{G}$  and  $\mathcal{P}$ , is observed in this case.

All three apexes:  $A_g$ ,  $A_p$ , and  $A_{pa}$  are always located within a common straight line, namely, they are located within the centerline,  $\Phi$ .

As it is shown below in this chapter, in desirable real gearing (in  $S_{pr}$  – gear system), tooth flank of one member of a gear pair rolls over tooth flank of a mating member, similar to that in geometrically accurate gearing of conventional design. In this way, a uniform rotation from the driving shaft is transmitted to the driven shaft smoothly with zero transmission error. The tooth flank of a gear,  $\mathcal{G}$ , and the tooth flank of the mating pinion,  $\mathcal{P}$ , make point contact at every instant of time. At every contact point,  $K$ , degree of conformity of the tooth flanks,  $\mathcal{G}$  and  $\mathcal{P}$ , of the gear and the pinion is of the highest attainable value. The path of contact point on the both tooth flanks,  $\mathcal{G}$  and  $\mathcal{P}$ , is a spatial curve. The location of the path of contact within the tooth flanks,  $\mathcal{G}$  and  $\mathcal{P}$ , depends on the actual values of displacements of the axes of rotation,  $O_g^r$  and  $O_p^r$ , of the gear and the pinion from their desirable configuration. The larger the axes displacement, the more the path of contact is displaced toward one of the ends of the gear pair. However, under no circumstances the path of contact intersects any of the ends of the gear and the pinion. This is due to the tooth flank geometry is determined so as to accommodate for the maximum permissible axle's displacement (that does not exceed the specified tolerance for the axes displacement).

In theory, three different types of geometrically accurate gearing are distinguished:

1. Parallel-axes gearing ( $P_a$  – gearing)
2. Intersected-axes gearing ( $I_a$  – gearing)
3. Crossed-axes gearing ( $C_a$  – gearing)

In reality, because of the axes displacement (i.e., inevitable), neither parallel-axes gearing, nor intersected-axes gearing is possible physically. Gearing of any and all designs is a kind of crossed-axes gearing. Therefore, the discussion below is focused primarily on crossed-axes gearing.

## 17.2.1 TOOTH FLANK GEOMETRY IN GEOMETRICALLY ACCURATE REAL GEARING

In gears for  $S_{pr}$  – gear system, the tooth flanks geometry is derived so as to ensure smooth transmission of a uniform rotation from a driving shaft to a driven shaft when the axes are displaced. Taken in a whole, tooth flanks,  $\mathcal{G}$  and  $\mathcal{P}$ , of a gear, and of a mating pinion are neither enveloping, nor conjugate to one another. However, because of point contact between the tooth flanks,  $\mathcal{G}$  and  $\mathcal{P}$ , at every instant of time (a) a straight line along the contact perpendicular,  $\mathbf{n}_g$ , always intersects the axis of instantaneous rotation,  $P_{in}$ , and (b) instant values of angular base pitches of a gear and a mating pinion, both, are equal to instant value of operating base pitch of the gear pair.

For convenience, particular reference systems are preferred to be used when deriving equations of a gear,  $\mathcal{G}$ , and of a mating pinion,  $\mathcal{P}$ , tooth flanks, correspondingly.

### 17.2.1.1 The Adopted Concept for Tooth Flank Generation of Gears for $S_{pr}$ – Gear System

In all cases, geometrically accurate real gear pairs subject to similar inaccuracies, as gearing of other designs. Because of the manufacturing errors, inaccuracies in the mounting distance, the deflections under applied loads, and so forth, the tooth flanks of geometrically accurate real gears are displaced from their desirable location, and their actual orientation is different from the desirable orientation. Geometrically accurate real gearing has to be designed so as to make gearing of this type insensitive to tooth flanks displacement regardless of the actual nature of these displacements.

Tooth flanks in geometrically accurate real gearing are generated by a line of contact,<sup>7</sup>  $LC$ , that is specified under an assumption that all the displacements, both the linear displacements and the

<sup>7</sup> It should be stressed from the very beginning that as the contact ratio in a gear pair is always greater than one, no alterations to the geometry of the line of contact,  $LC$ , are permissible when the gears operate. Once the geometry of the line of contact is specified for a certain pair of the gear teeth, this geometry should remain the same when the gears rotate. Otherwise, angular base pitches of a gear and that of a mating pinion in the gear pair cannot be maintained equal to operating angular base pitch of the gear pair.

angular displacements, are of a zero value. Specified this way, the tooth flank in a gear for  $S_{pr}$  – gear system is identical to that in the discussed above  $R$  – gearing (see Chapter 14). Then, an impact of the displacements onto the geometry of a gear, and of a mating pinion tooth flanks in  $S_{pr}$  – gearing is incorporated.

For this purpose, when the gears rotate, the line of contact,  $LC$ , is considered as rotated together with the plane of action,  $PA$ . Current configuration of the line of contact in relation to the plane of action is remained the same. However, the configurations of the line of contact in relation to the reference systems,  $X_gY_gZ_g$  and  $X_pY_pZ_p$ , associated with the gear and with the mating pinion, depend on the actual values of axes displacement in the gear pair. The axes displacement in the gear pair is kept within the pre-specified tolerances for the accuracy of the axes displacements.

All possible configurations of the plane of action,  $PA$ , in relation to the reference systems,  $X_gY_gZ_g$  and  $X_pY_pZ_p$ , are taken into account. The plane of action,  $PA$ , is rotated about the axis,  $O_{pa}$ , under all possible values of the deviations, both linear and angular, in terms of which the axes displacement is expressed. All possible configurations of the line of contact,  $LC$ , in relation to the reference systems,  $X_gY_gZ_g$  and  $X_pY_pZ_p$ , are considered in this way. Ultimately, a gear tooth flank,  $\mathcal{G}$ , is generated in a reference system,  $X_gY_gZ_g$ , associated with the gear, as a locus of the line of contact,  $LC$ . Similarly, a mating pinion tooth flank,  $\mathcal{P}$ , is generated in a reference system,  $X_pY_pZ_p$ , associated with the pinion, as a locus of that same line of contact,  $LC$ . Regardless of that tooth flanks,  $\mathcal{G}$  and  $\mathcal{P}$ , of a gear, and of a mating pinion are generated by that same line of contact,  $LC$ , the tooth flanks,  $\mathcal{G}$  and  $\mathcal{P}$ , in  $S_{pr}$  – gearing are always in point contact with one another. Degree of conformity at point of contact between the tooth flanks,  $\mathcal{G}$  and  $\mathcal{P}$ , in  $S_{pr}$  – gearing is always the highest possible.

The concept, adopted for the tooth flank generation of gears in  $S_{pr}$  – gear system, can be viewed in another manner.

Consider the plane of action,  $PA$ , for example, in a geometrically accurate parallel-axes gear pair as schematically illustrated in Figure 17.10. Here,  $F_{pa}$ , is the effective face width of the gear pair. Construct a desirable line of contact,  $LC_{des}$ , in the nominal configuration of the axes of rotation,  $O_g$  and  $O_p$ , of a gear and a mating pinion. After that, two extremal configurations of the desirable line of contact,  $LC_{des}$ , are constructed. One of them is for the maximal positive, and another one is for the extremal negative deviation of the desirable line of contact,  $LC_{des}$ , from its nominal configuration. All three desirable lines of contact are located within the plane of action,  $PA$ .

The plane of action,  $PA$ , can be sliced on an infinite number of slices, each of which is perpendicular to the axis of instantaneous rotation,  $P_{ln}$ , of the gear. The width of each elementary slice is designated as  $\Delta F_{pa}$ .

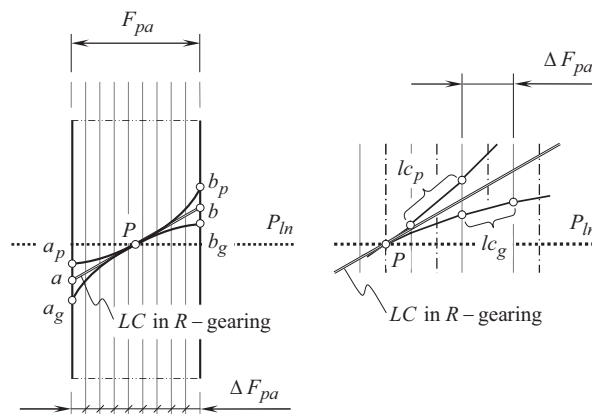


FIGURE 17.10 On the adopted concept for tooth flank generation in gears for  $S_{pr}$  – gear system.



For the slices,  $\Delta F_{pa}$ , at both ends of the face width,  $F_{pa}$ , the elementary lines of contact,  $lc_g$  and  $lc_p$ , for the gear and for the mating pinion, are constructed so as for a geometrically accurate crossed-axes gear pair having the maximal linear,  $\{\delta_g\}$  and  $\{\delta_p\}$ , and angular,  $\{\varphi_g\}$  and  $\{\varphi_p\}$ , displacements of the gear axis of rotation,  $O_g$ , and that,  $O_p$ , of the pinion from their nominal configurations in relation to the plane of action,  $PA$  [see Eqs. (17.16) and (17.17) for the calculation of the displacements,  $\{\delta_g\}$  and  $\{\varphi_g\}$ , and Eqs. (17.18) and (17.19) for the calculation of the displacements,  $\{\delta_p\}$  and  $\{\varphi_p\}$ ]. The displacements,  $\{\delta_g\}$  and  $\{\varphi_g\}$ , by nature, are the tolerances for the accuracy of the elementary displacements,  $[\delta_g]$  and  $[\varphi_g]$ , correspondingly.

For the slice,  $\Delta F_{pa}$ , at the middle of the face width,  $F_{pa}$ , the elementary lines of contact,  $lc_g$  and  $lc_p$ , are constructed so, as for a geometrically accurate crossed-axes gear pair having zero linear,  $\{\delta_g\}$  and  $\{\delta_p\}$ , and angular,  $\{\varphi_g\}$  and  $\{\varphi_p\}$ , displacements of the gear axis of rotation,  $O_g$ , and that,  $O_p$ , of the pinion from their nominal configuration in relation to the plane of action,  $PA$ .

For the rest of the slices,  $\Delta F_{pa}$ , in between the middle slice, and the slices at the both ends of the face width,  $F_{pa}$ , the elementary lines of contact,  $lc_g$  and  $lc_p$ , are constructed so, as for a geometrically accurate crossed-axes gear pair having intermediate values of the linear,  $\{\delta_g\}$  and  $\{\delta_p\}$ , and the angular,  $\{\varphi_g\}$  and  $\{\varphi_p\}$ , displacements of the gear axis of rotation,  $O_g$ , and that,  $O_p$ , of the pinion from their nominal configuration in relation to the plane of action,  $PA$ .

It is right point to stress here that instantaneous location of the plane-of-action apex,  $A_{pa}$ , as well as the instantaneous configuration of the base cone apexes,  $A_g$  and  $A_p$ , of a gear and of a mating pinion, is different for different slices. The central point,  $P$ , is remained stationary. There is certain freedom for the gear designer to choose functions of the distribution of the elementary displacements,  $[\delta_g]$ ,  $[\varphi_g]$ , and  $[\delta_p]$ ,  $[\varphi_p]$ , within the face width,  $F_{pa}$ .

Two planar curves,  $a_g Pb_g$  and  $a_p Pb_p$ , are the envelopes to the family of the elementary lines of contact,  $lc_g$  and  $lc_p$ . When the parameters of the axes displacements in  $S_{pr}$  – gearing alter, the curves,  $a_g Pb_g$  and  $a_p Pb_p$ , roll one over another. This rolling motion of the curves,  $a_g Pb_g$  and  $a_p Pb_p$ , is strictly correlated with the alteration in the axes alignment.

The tooth flanks,  $\mathcal{S}$  and  $\mathcal{P}$ , of a gear, and of a mating pinion in  $S_{pr}$  – gearing are generated by these two curves,  $a_g Pc_g$  and  $a_p Pc_p$ . One of the tooth flanks,  $\mathcal{S}$ , is constructed in the gear reference system,  $X_g Y_g Z_g$ , and another one,  $\mathcal{P}$ , is constructed in the pinion reference system,  $X_p Y_p Z_p$ .

### 17.2.1.2 Preferred Reference Systems

Prior to derive an equation for the gear tooth flank,  $\mathcal{S}$ , and for its mating pinion tooth flank,  $\mathcal{P}$ , a tolerance,  $\{C\}$ , for the center-distance,  $C$ , a tolerance,  $\{\Sigma\}$ , for the crossed-axes angle,  $\Sigma$ , and a tolerance,  $\{A\}$ , for the axial location of the gear in the direction of the gear axial vector,  $A_g$  (see Figure 2.29 in Chapter 2) are required to be specified.

The actual value of the center-distance,  $C$ , falls into the interval:

$$C - \{C_-\} \leq C \leq C + \{C^+\} \quad (17.42)$$

where  $\{C^+\}$  is the upper, and  $\{C_-\}$  is the lower maximum permissible deviations of the center-distance,  $C$ .

The actual value of the crossed-axes angle,  $\Sigma$ , falls into the interval:

$$\Sigma - \{\Sigma_-\} \leq \Sigma \leq \Sigma + \{\Sigma^+\} \quad (17.43)$$

where  $\{\Sigma^+\}$  is the upper, and  $\{\Sigma_-\}$  is the lower maximum allowed deviations of the crossed-axes angle,  $\Sigma$ .

The actual value of the axial distance,  $A$ , falls into the interval:

$$A - \{A_-\} \leq A \leq A + \{A^+\} \quad (17.44)$$

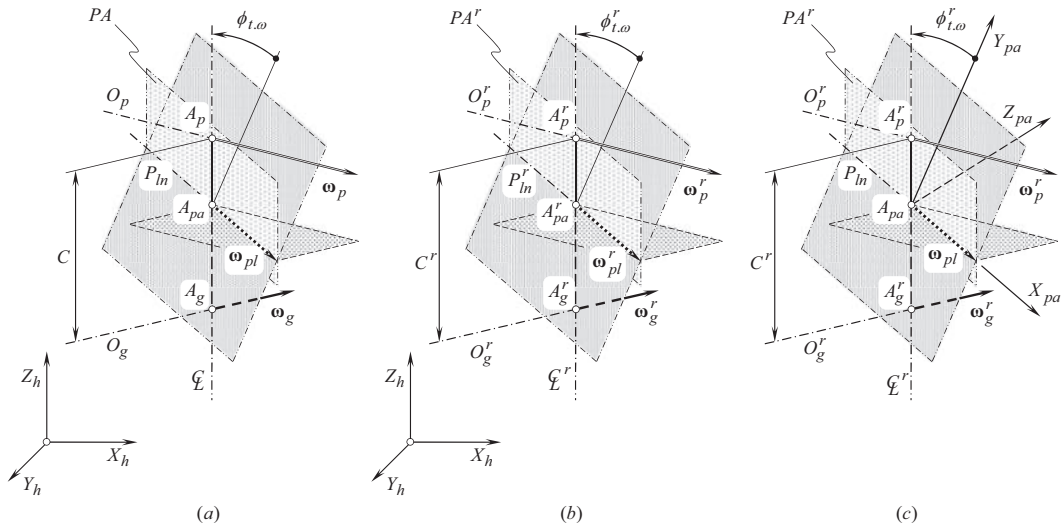


**FIGURE 17.11** Gear vector diagrams constructed for crossed-axes gear pairs: (a) geometrically accurate gear pair, (b) geometrically accurate real gear pair (in a motionless reference system associated with the gear pair housing), and (c) geometrically accurate real gear pair (in a reference system associated with the plane of action,  $PA$ ).

where  $\{A^+\}$  is the upper, and  $\{A_-\}$  is the lower maximum allowed deviations in the direction of the gear axial vector,  $\mathbf{A}_g$ .

A convenient reference system can be determined in a few steps illustrated in Figure 17.11.

**First**, for a nominal configuration of the rotation vectors in  $S_{pr}$  – gearing, all the elements of the corresponding vector diagram are predetermined by configuration of the rotation vectors,  $\omega_g$  and  $\omega_p$ , as illustrated in Figure 17.11a. The gear vector diagram can be constructed in an arbitrary reference system, in a reference system,  $X_h Y_h Z_h$ , associated with the housing of the gear pair, in particular.

**Second**, in a geometrically accurate real gear pair, all the elements of the gear vector diagram are displaced from their nominal location and orientation, as shown in Figure 17.11b. None of the angular velocity vectors in a geometrically accurate real gear pair,  $\omega_g^r$ ,  $\omega_p^r$ , and  $\omega_{pl}^r$ , align with the corresponding angular velocity vectors,  $\omega_g$ ,  $\omega_p$ , and  $\omega_{pl}$ , constructed for their nominal configuration. Moreover, the gear base-cone-apex,  $A_g^r$ , the pinion base-cone-apex,  $A_p^r$ , and the plane-of-action apex,  $A_{pa}^r$ , all of them are displaced from their nominal positions, labeled as  $A_g$ ,  $A_p$ , and  $A_{pa}$ . Ultimately, the center-distance,  $C^r$ , the crossed-axes angle,  $\Sigma^r$ , and the pressure angle,  $\phi_{t,\omega}^r$ , in a geometrically accurate real gear pair differ from that,  $C$ ,  $\Sigma$ , and  $\phi_{t,\omega}$ , in the gear vector diagram constructed for their nominal configuration. Permissible deviations of all the displacements in a geometrically accurate real gear pair in relation to their nominal values are limited by:

- the tolerance,  $\{C\}$ , for the accuracy of the center-distance,  $C$
- the tolerance,  $\{\Sigma\}$ , for the accuracy of the crossed-axes angle,  $\Sigma$
- the tolerance,  $\{A\}$ , for the accuracy of the gear axial distance,  $A$

The displacements could be more visible in a case, when both the gear vector diagrams in Figures 17.11a and b constructed together so as to overlap one another. However, as the displacements are of small values, the overlapped vector diagrams are not shown in Figure 17.11.

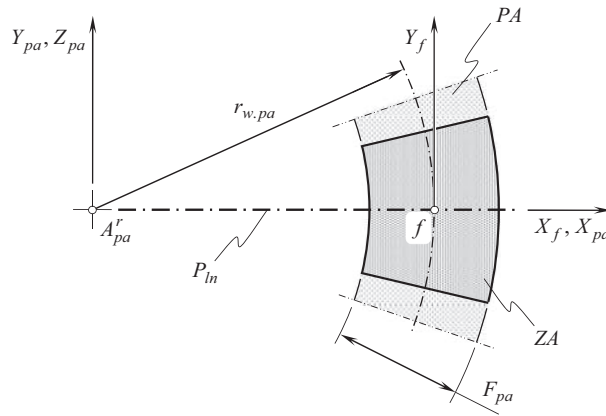


**FIGURE 17.12** The *Cartesian* reference system,  $X_f Y_f Z_f$ , associated with the plane of action,  $PA$ , and originated at the middle point,  $f$ , of the effective face width,  $F_{pa}$ .

*Third*, a reference system,  $X_{pa} Y_{pa} Z_{pa}$ , can be associated with the plane of action,  $PA$ . This reference system is originated at the plane-of-action apex,  $A_{pa}$ , and the axis,  $X_{pa}$ , is pointed along the vector of instantaneous rotation,  $\omega_{pl}$ , as illustrated in Figure 17.11c. In this case, an advantage can be taken from the fact that the configurations of the following elements of the gear vector diagram, namely, (a) of the plane-of-action apex,  $A_{pa}$ , (b) of the vector of instantaneous rotation,  $\omega_{pl}$ , and (c) of the centerline,  $\Phi$ , are not affected by the manufacturing errors, as well as by the displacements caused by other reasons. Ultimately, in the case under consideration, the plane of action,  $PA$ , becomes stationary.

*Fourth*, it is assumed below that when a gear displaces from its nominal position and orientation, position of the middle point,  $f$ , of the effective face width,  $F_{pa}$ , do not altered within the axis of instantaneous rotation,  $P_{ln}$ , and is remained the same. This point can be chosen as the origin of a *Cartesian* reference system,  $X_f Y_f Z_f$ , associated with the plane of action,  $PA$ , as illustrated in Figure 17.12. The reference system,  $X_f Y_f Z_f$ , is shifted along the axis,  $X_{pa}$ , with respect to the reference system,  $X_{pa} Y_{pa} Z_{pa}$ , at a distance,  $r_{w.pa}$ , and turned about this axis through the transverse pressure angle,  $\phi_{t.\omega}$ .

The reference system,  $X_f Y_f Z_f$ , is adopted below as a motionless reference system. It does not alter its configuration with respect to the gear housing when the gear displaces from its nominal location and orientation, caused by the manufacturing errors, under an operating load, because of the heat extension of the gear housing as well as of the rest of components of the gear transmission, and so forth.

### 17.2.1.3 Derivation of Equation of Tooth Flank in $S_{pr}$ – Gearing

One of two equivalent approaches can be employed for the analytical description of tooth flank in  $S_{pr}$  – gearing.

One of these approaches utilizes the property of the base surfaces, while another one is based on desirable variation of configuration of the plane of action in relation to the gear axis of rotation.

In the *first approach*, a family of base cones of a gear, and of a mating pinion with different cone angles, and different configurations in relation to one another, is constructed. The variation corresponds to different tooth flank displacements under the operating load when the applied load varies. All these base cones can be viewed as instantaneous base cones of the gear, and of the pinion in  $S_{pr}$  – gearing. Two envelopes to two families of instantaneous base cones represent base surfaces

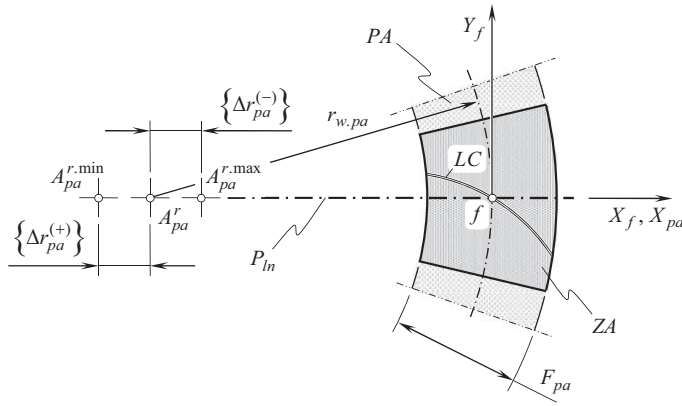


**FIGURE 17.13** Line of contact,  $LC$ , between interacting tooth flanks,  $\mathcal{S}$  and  $\mathcal{P}$ , and the tolerances,  $\{\Delta r_{pa}^{(-)}\}$  and  $\{\Delta r_{pa}^{(+)}\}$ , for the accuracy of the distance,  $r_{pa}$ .

of the gear, and that of the mating pinion in  $S_{pr}$  – gearing. Both of the base surfaces are surfaces of revolution. When base diameters are mentioned below, these means diameters of the base circles of intersection of the base surfaces by the corresponding transverse planes. The first approach is not considered in detail here.

In the *second approach*, the tooth flanks of a gear, and of a mating pinion in  $S_{pr}$  – gearing, both, are generated by a line of contact,  $LC$ , between the tooth flanks,  $\mathcal{S}$  and  $\mathcal{P}$ . Regardless of the tooth flanks not generated yet, a desirable line of contact can be constructed at this point. The line of contact,  $LC$ , is a planar curve that is entirely located within the plane of action,  $PA$ . When generating the tooth flanks, the desirable line of contact travels together with the plane of action,  $PA$ .

In the reference system,  $X_f Y_f Z_f$ , associated with the plane of action,  $PA$ , the position vector of point,  $\mathbf{r}_{lc}^{pa}$ , of a line of contact,  $LC$ , is analytically described in matrix form as:

$$\mathbf{r}_{lc}^{pa}(r_{pa}) = \begin{bmatrix} X_{lc}^{pa}(r_{pa}) \\ Y_{lc}^{pa}(r_{pa}) \\ 0 \\ 1 \end{bmatrix} \quad (17.45)$$

Here, in Eq. (17.45),  $r_{pa}$  designates a current value of the distance at which point,  $f$ , is remote from a current plane-of-action apex,  $A_{pa}^{r.cur}$ . For a specified gear pair, the distance,  $r_{pa}$ , is within the interval:

$$r_{w.pa} - \{\Delta r_{pa}^{(-)}\} \leq r_{pa} \leq r_{w.pa} + \{\Delta r_{pa}^{(+)}\} \quad (17.46)$$

The tolerances,  $\{\Delta r_{pa}^{(-)}\}$  and  $\{\Delta r_{pa}^{(+)}\}$ , for the accuracy of the distance,  $r_{pa}$ , are shown in Figure 17.13.

Considered in the reference system,  $X_f Y_f Z_f$ , the line of contact,  $LC$ , is remained stationary when the distance,  $r_{pa}$ , alters from its minimum value,  $r_{w.pa} - \{\Delta r_{pa}^{(-)}\}$ , to its maximum value,  $r_{w.pa} + \{\Delta r_{pa}^{(+)}\}$ . However, current location of the plane-of-action apex,  $A_{pa}^{r.cur}$ , travels within the interval specified by Eq. (17.46), that is, it travels between the extremal locations,  $A_{pa}^{r.min}$  and  $A_{pa}^{r.max}$ . An operator,  $\mathbf{Rs}(f \mapsto pa)$ , of the resultant coordinate system transformation can be used for the

analytical description of the transition from the *Cartesian* coordinate system,  $X_f Y_f Z_f$ , to the reference system,  $X_{pa} Y_{pa} Z_{pa}$ , associated with the plane of action,  $PA$ :

$$\mathbf{Rs}(f \mapsto pa) = \begin{bmatrix} 1 & 0 & 0 & 0 \\ 0 & \cos \phi_{t,\omega} & \sin \phi_{t,\omega} & 0 \\ 0 & -\sin \phi_{t,\omega} & \cos \phi_{t,\omega} & -r_{pa} \\ 0 & 0 & 0 & 1 \end{bmatrix} \quad (17.47)$$

It is of critical importance to stress here that the operator,  $\mathbf{Rs}(f \rightarrow pa)$ , is a function of a current value of the distance,  $r_{pa}$ .

Further, the operator,  $\mathbf{Rs}(PA \mapsto \mathcal{S})$ , of the resultant coordinate system transformation can be used for the analytical description of the transition from the *Cartesian* coordinate system,  $X_{pa} Y_{pa} Z_{pa}$ , associated with the plane of action,  $PA$ , to the *Cartesian* coordinate system,  $X_g Y_g Z_g$ , associated with the gear. Again, in the case of  $S_{pr}$  – gearing, the operator,  $\mathbf{Rs}(PA \mapsto \mathcal{S})$ , is a function of a current value of the distance,  $r_{pa}$ .

With that said, for the analytical description of the transition from the *Cartesian* coordinate system,  $X_f Y_f Z_f$ , to the coordinate system,  $X_g Y_g Z_g$ , associated with the gear, the operator,  $\mathbf{Rs}(f \mapsto \mathcal{S})$ , of the resultant coordinate system transformation can be used. The operator,  $\mathbf{Rs}(f \mapsto \mathcal{S})$ , is calculated as the product:

$$\begin{aligned} \mathbf{Rs}(f \mapsto \mathcal{S}) &= \mathbf{Rs}(PA \mapsto \mathcal{S}) \cdot \mathbf{Rs}(f \rightarrow pa) = \\ &= \mathbf{Rt}(r \mapsto g) \cdot \mathbf{Rt}(pa_0 \mapsto r) \cdot \mathbf{Tr}(-r_{w,g}, Y_g) \cdot \mathbf{Rt}(pa \mapsto pa_0) \cdot \mathbf{Rs}(f \rightarrow pa) \end{aligned} \quad (17.48)$$

Once the operators,  $\mathbf{Rs}(f \rightarrow pa)$  and  $\mathbf{Rs}(PA \mapsto \mathcal{S})$ , are functions of current value of the distance,  $r_{pa}$ , the operator,  $\mathbf{Rs}(f \mapsto \mathcal{S})$ , is also a function of this design parameter of the gear pair. Below this function is expressed in terms of the parameter,  $X_f|_{A_{pa}^{\text{inst}}}$ , which is the  $X$  – coordinate of the plane-of-action apex,  $A_{pa}^{\text{inst}}$ .

For the analytical description of a gear tooth flank,  $\mathcal{S}$ , in  $S_{pr}$  – gearing, an equation is used:

$$\mathbf{r}_g^r(r_{pa}, \varphi_p, X_f|_{A_{pa}^{\text{inst}}}) = \mathbf{Rs}(f \mapsto \mathcal{G}) \cdot \mathbf{r}_{lc}^{pa}(r_{pa}) \quad (17.49)$$

The gear tooth flank,  $\mathcal{S}$ , in  $S_{pr}$  – gearing is a surface of three independent parameters. An instantaneous value of the radius,  $r_{pa}$ , of point of the line of contact,  $LC$ , is the first of three parameters. An instantaneous value of the angle,  $\varphi_p$ , through which the input shaft is turned about the pinion axis of rotation,  $O_p$ , is the second parameter [the operator,  $\mathbf{Rs}(f \mapsto \mathcal{S})$ , of the resultant coordinate system transformation is a function of the angle,  $\varphi_p$ ], while the coordinate,  $X_f|_{A_{pa}^{\text{inst}}}$ , of the instantaneous plane-of-action apex,  $A_{pa}^{\text{inst}}$ , is the third of three design parameters.

Similarly, for the analytical description of a pinion tooth flank,  $\mathcal{P}$ , a corresponding equation is derived<sup>8</sup>:

$$\mathbf{r}_p^r(r_{pa}, \varphi_p, X_f|_{A_{pa}^{\text{inst}}}) = \mathbf{Rs}(f \mapsto \mathcal{P}) \cdot \mathbf{r}_{lc}^{pa}(r_{pa}) \quad (17.50)$$

<sup>8</sup> Another approach for the derivation of equations for the position vectors of point,  $\mathbf{r}_g$  and  $\mathbf{r}_p$ , of a gear,  $\mathcal{S}$ , and a mating pinion,  $\mathcal{P}$ , tooth flanks in  $S_{pr}$  – gearing is disclosed on page 427 through page 435 in the first edition (2012) of this book [174].

Here, the operator,  $\mathbf{Rs}(f \mapsto \mathcal{P})$ , of the transition from the reference system,  $X_f Y_f Z_f$ , associated with the plane of action,  $PA$ , to the coordinate system,  $X_p Y_p Z_p$ , associated with the pinion, is calculated as a product:

$$\begin{aligned} \mathbf{Rs}(f \mapsto \mathcal{P}) &= \mathbf{Rs}(PA \mapsto \mathcal{P}) \cdot \mathbf{Rs}(f \rightarrow pa) = \\ &= \mathbf{Rt}(r \mapsto p) \cdot \mathbf{Rt}(pa_0 \mapsto r) \cdot \mathbf{Tr}(r_p, Y_p) \cdot \mathbf{Rt}(pa \mapsto pa_0) \cdot \mathbf{Rs}(f \rightarrow pa) \end{aligned} \quad (17.51)$$

The pinion tooth flank,  $\mathcal{P}$ , in  $S_{pr}$  – *gearing* also is a surface of three independent parameters. An instantaneous value of the radius,  $r_{pa}$ , of point of the line of contact,  $LC$ , is the first of three parameters. An instantaneous value of the angle,  $\varphi_p$ , through which the input shaft is turned about the pinion axis of rotation,  $O_p$ , is the second parameter [the operator,  $\mathbf{Rs}(f \mapsto \mathcal{P})$ , of the resultant coordinate system transformation is a function of the angle,  $\varphi_p$ ], while the coordinate,  $X_f|_{A_{pa}^{\text{inst}}}$ , of the instantaneous plane-of-action apex,  $A_{pa}^{\text{inst}}$ , is the third of three parameters.

Three independent parameters,  $r_{pa}$ ,  $\varphi_p$ , and  $X_f|_{A_{pa}^{\text{inst}}}$ , are excessive for the determination of a surface, in both cases, namely, for a gear tooth flank,  $\mathcal{G}$ , as well as for a mating pinion tooth flank,  $\mathcal{P}$ , as a surface is a space of two dimensions. To resolve the issue, an advantage can be taken from the available plurality of independent parameters by setting a favorable functional correlation between two of them, namely, between the parameters,  $\varphi_p$  and  $X_f|_{A_{pa}^{\text{inst}}}$ . The function  $X_f|_{A_{pa}^{\text{inst}}} = X_f|_{A_{pa}^{\text{inst}}}(\varphi_p)$  has to be of a kind that guaranteed the tooth flanks,  $\mathcal{G}$  and  $\mathcal{P}$ , been smooth regular surfaces. Once two of three independent parameters somehow correlate to one another, then the tooth flanks,  $\mathcal{G}$  and  $\mathcal{P}$  turns to be functions of two independent parameters. Below, in this chapter, an example of such a functional correlation,  $X_f|_{A_{pa}^{\text{inst}}} = X_f|_{A_{pa}^{\text{inst}}}(\varphi_p)$ , between two of three independent parameters is considered.

The operator of the resultant coordinate system transformation,  $\mathbf{Rs}(PA \mapsto \mathcal{P})$ , namely, the operator of the transition from the reference system,  $X_{pa} Y_{pa} Z_{pa}$ , associated with the plane of action,  $PA$ , to the *Cartesian* coordinate system,  $X_p Y_p Z_p$ , associated with the pinion, is required to be composed.

The operator of the resultant coordinate system transformation,  $\mathbf{Rs}(f \mapsto \mathcal{P})$ , as well as the operators,  $\mathbf{Rs}(f \rightarrow pa)$  and  $\mathbf{Rs}(PA \mapsto \mathcal{P})$ , are functions of current value of the distance,  $r_{pa}$ .

The distance,  $r_{pa}$ , can be expressed in terms of the elementary linear displacements,  $\delta_{gx}$ ,  $\delta_{gy}$ , and  $\delta_{gz}$ , and the elementary angular displacements,  $\varphi_{gx}$ ,  $\varphi_{gy}$ , and  $\varphi_{gz}$ , of a gear, together with the elementary linear displacements  $\delta_{px}$ ,  $\delta_{py}$ , and  $\delta_{pz}$ , and the elementary angular displacements,  $\varphi_{px}$ ,  $\varphi_{py}$ , and  $\varphi_{pz}$ , of a mating pinion.

The disclosed approach for the generating a gear,  $\mathcal{G}$ , and a mating pinion,  $\mathcal{P}$ , tooth flanks can be qualitatively summarized in the following way. Consider that the plane-of-action apex,  $A_{pa}^{r, \text{cur}}$ , at its initial location coincides with the point,  $A_{pa}^{r, \text{min}}$ . For such a configuration of the axes of rotation,  $O_g$  and  $O_p$ , of a gear, and of a mating pinion the tooth flanks,  $\mathcal{G}_{\text{min}}$  and  $\mathcal{P}_{\text{min}}$ , in  $R$  – *gearing* can be generated as disclosed above (see Chapter 14). Then the apex,  $A_{pa}^{r, \text{cur}}$ , is displaced toward the plane-of-action apex,  $A_{pa}^{r, \text{max}}$ , at a reasonably small distance (or at an infinitesimally short distance). As the operators of the resultant coordinate systems transformation are functions of current value of the distance,  $r_{pa}$ , the initial configuration of the axes of rotation,  $O_g$  and  $O_p$ , is altered under such a displacement.  $R$  – *gearing* with a novel set of the design parameters can be generated for a new configuration of the axes of rotation,  $O_g$  and  $O_p$ . Gradually shifting the apex,  $A_{pa}^{r, \text{max}}$ , toward the plane-of-action apex,  $A_{pa}^{r, \text{max}}$ , a set of tooth flanks,  $\mathcal{G}_{\text{cur}}$  and  $\mathcal{P}_{\text{cur}}$ , of different  $R$  – *gearing* can be generated. Finally, when the plane-of-action apex,  $A_{pa}^{r, \text{cur}}$ , at its current location coincides with the point,  $A_{pa}^{r, \text{max}}$ , the tooth flanks,  $\mathcal{G}_{\text{max}}$  and  $\mathcal{P}_{\text{max}}$ , are generated.

The tooth flanks of a gear in  $S_{pr}$  – *gearing* are the envelopes to all the intermediate gear tooth flanks,  $\mathcal{G}_{\text{min}}$ ,  $\mathcal{G}_{\text{cur}}$ , ..., and  $\mathcal{G}_{\text{max}}$ . Similarly, the tooth flanks of a pinion in  $S_{pr}$  – *gearing* are the envelopes to all the intermediate pinion tooth flanks,  $\mathcal{P}_{\text{min}}$ ,  $\mathcal{P}_{\text{cur}}$ , ..., and  $\mathcal{P}_{\text{max}}$ . Under any and all



permissible configurations of the axes of rotation,  $O_g$  and  $O_p$ , of a gear, and of a mating pinion, the interacting tooth flanks of a gear, and of a mating pinion in  $S_{pr}$  – *gearing* make point contact with one another.

An in-detail analysis of Eq. (17.49) for the position vector of point,  $\mathbf{r}_g^r$ , of a tooth flank,  $\mathcal{S}_r$  in  $S_{pr}$  – *gearing*, as well as a similar Eq. (17.50) for the position vector of point,  $\mathbf{r}_p^r$ , of a mating pinion tooth flank,  $\mathcal{P}_r$  in  $S_{pr}$  – *gearing*, reveal that alterations (in comparison to geometrically accurate gearing) should be made to the tooth flanks of both members engaged in mesh. It is not allowed to keep one of the members with the original geometrically accurate geometry of the tooth flanks, and to compensate for the required changes the mating member of the gear pair. Making changes to the geometry of the tooth flanks of both members of the gear pair is necessary because in  $S_{pr}$  – *gearing* the geometry of the tooth flanks,  $\mathcal{S}_r$  and  $\mathcal{P}_r$ , is predetermined by a given configuration of the rotation vectors,  $\boldsymbol{\omega}_g$  and  $\boldsymbol{\omega}_p$ , of the gear and the pinion.

The tooth flanks of a gear, and of a mating pinion in  $S_{pr}$  – *gearing*, are always in point contact. However, the degree of conformity<sup>9</sup> of the interacting tooth flanks of the gear, and of the mating pinion is always of the highest possible value.

The derived equations [see Eqs. (17.49) and (17.50)] for the tooth flanks,  $\mathcal{S}$  and  $\mathcal{P}$ , of a gear, and of a mating pinion in  $S_{pr}$  – *gearing* can be used for both for design of a gear and of a mating pinion tooth flanks, as well as reference surfaces for inspection of a gear, and of a mating pinion tooth flanks. Implementation of the proposed geometry of tooth flanks in  $S_{pr}$  – *gearing* as a datum surface for the purposes of gear inspection and for measuring the deviations of an approximate gear due to *design* errors, as well as *manufacturing* errors, is an additional advantage of this novel kind of gearing.

The geometry of tooth flanks in  $S_{pr}$  – *gearing* is the target when designing real gears. Later on, the most favorable tooth flank geometry can be approximated by surfaces that are convenient for machining/finishing of gears.

The tooth flank in  $S_{pr}$  – *gearing* is also used as the *reference surface* for any and all desirable tooth flank modifications. Once the desirable tooth flank of a gear, and of a mating pinion in  $S_{pr}$  – *gearing* is specified in terms of the linear and angular displacement, of the design parameters of the gear set, and so forth, then it can be approximated by a corresponding surface that is convenient for machining. This returns a practical kind of gear tooth flank modification: not a profile modification, and not a lead modification, but a modification of the entire tooth flank of a gear and of a mating pinion.

It is instructive to stress here on the important difference between *conjugate* tooth surfaces,  $\mathcal{S}$  and  $\mathcal{P}$ , in  $S_{pr}$  – *gearing*, and that in gearing of other types: parallel-axes gearing, intersected-axes gearing, as well as crossed-axes gearing. In the later cases tooth flanks,  $\mathcal{S}$  and  $\mathcal{P}$ , of a gear and of a mating pinion are conjugate<sup>10</sup> to one another, and are in line contact with each other. In  $S_{pr}$  – *gearing*, the conjugate action law is also fulfilled; however, the tooth flanks,  $\mathcal{S}$  and  $\mathcal{P}$ , make *point contact* (and not *line contact*) with one another. It is proposed to refer to the conjugacy of this sort as to *conjugacy of higher order* of the tooth flanks,  $\mathcal{S}$  and  $\mathcal{P}$ , of a gear and of a mating pinion.  $S_{pr}$  – *conjugate tooth flank* is another potentially possible term for tooth flanks in  $S_{pr}$  – *gearing*.

<sup>9</sup> A high degree of conformity at a point of contact of the tooth flanks,  $\mathcal{S}$  and  $\mathcal{P}$ , of a gear, and of a mating pinion in  $S_{pr}$  – *gearing* is of critical importance, as the contact strength of the gear, and of the mating pinion tooth flanks strongly depends on the degree of conformity: the higher the degree of conformity, the higher the contact strength of the interacting teeth, and vice versa.

<sup>10</sup> It is right point to note here that the term *conjugate surface* is often used incorrectly. Commonly, a surface that is an envelope to a family of another surface that travels in space, is referred to as *conjugate surfaces* – this a mistake, as fulfillment of the enveloping condition,  $\mathbf{n}_e \cdot \mathbf{V}_e = 0$ , is necessary but not sufficient to generate conjugate surfaces. Therefore, the term *reversibly-enveloping surfaces* (or just  $R_e$  – surfaces, for simplicity) [155] can be considered as an alternative to the term *conjugate surface* in all three types of gearing, that is, in parallel-axes gearing, intersected-axes gearing, and crossed-axes gearing.

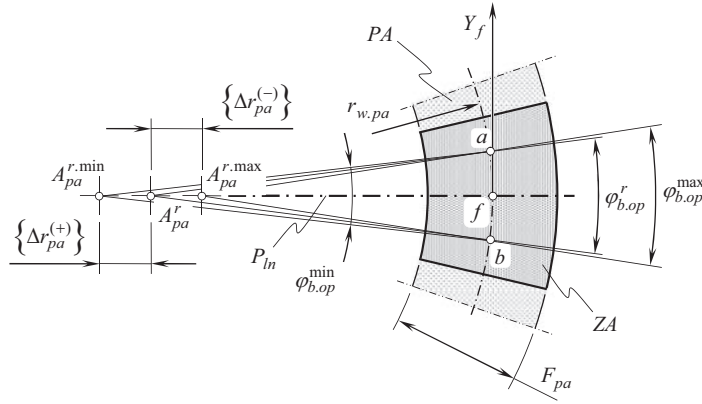


FIGURE 17.14 Operating base pitches of different values,  $\varphi_{b.op}^{min}$ ,  $\varphi_{b.op}^r$ , and  $\varphi_{b.op}^{max}$ , in  $S_{pr}$ -gearing.

#### 17.2.1.4 Angular Base Pitch in $S_{pr}$ -Gearing

In  $S_{pr}$ -gearing, at every instant of time, the angular base pitch of a gear,  $\varphi_{b.g}^{inst}$ , and that of a mating pinion,  $\varphi_{b.p}^{inst}$ , both, are equal to an instant value of the angular operating base pitch,  $\varphi_{b.op}^{inst}$ , of the gear pair<sup>11</sup> (this means that the equalities,<sup>12</sup>  $\varphi_{b.g}^{inst} = \varphi_{b.op}^{inst}$  and  $\varphi_{b.p}^{inst} = \varphi_{b.op}^{inst}$ , are valid). These two equalities have to be fulfilled within the effective face width,  $F_{pa}$ , of a gear pair. Only under such conditions, a pure rotation can be transmitted from a driving shaft to a driven shaft by means of  $S_{pr}$ -gearing.

The actual value of the instantaneous angular base pitches in  $S_{pr}$ -gearing varies depending on the actual configuration of the rotation vectors,  $\omega_g$  and  $\omega_p$ . Current configuration of the rotation vectors,  $\omega_g$  and  $\omega_p$ , varies either in time as a function of the gear pair loading, or it varies for different gear pairs of the same design. Current deviations of the rotation vectors,  $\omega_g$  and  $\omega_p$ , from their desirable configuration are not known. However, the corresponding tolerances,  $\{\Delta\varphi_{b.g}^{inst}\}$ ,  $\{\Delta\varphi_{b.p}^{inst}\}$ , and  $\{\Delta\varphi_{b.op}^{inst}\}$ , for the accuracy of configuration of the rotation vectors,  $\omega_g$  and  $\omega_p$ , can be set up. Further, the tolerances,  $\{\Delta\varphi_{b.g}^{inst}\}$ ,  $\{\Delta\varphi_{b.p}^{inst}\}$ , and  $\{\Delta\varphi_{b.op}^{inst}\}$ , the actual values of which are known, are handled, instead of the deviations,  $\Delta\varphi_{b.g}^{inst}$ ,  $\Delta\varphi_{b.p}^{inst}$ , and  $\Delta\varphi_{b.op}^{inst}$ , the actual values of which are unknown.<sup>13</sup>

Shown in Figure 17.14, is an operating angular base pitch,  $\varphi_{b.op}^r$ , constructed for a nominal configuration of the rotation vectors,  $\omega_g$  and  $\omega_p$ , in an  $S_{pr}$ -gearing. The plane-of-action pitch circle of a radius,  $r_{w.pa}$ , is intersected by the sides of the angle,  $\varphi_{b.op}^r$ , at points,  $a$  and  $b$ , namely,  $a$  and  $b$ , are at an angular distance,  $\varphi_{b.op}^r$ , from one another. One of the three design parameters,  $\varphi_{b.op}^r$ ,  $r_{w.pa}$ , and  $\widehat{ab}$ , can be expressed in terms of the rest two. Moreover, the linear distance,  $ab$ , also can be calculated:

$$ab = 2r_{w.pa} \sin \frac{\varphi_{b.op}^r}{2} \quad (17.52)$$

<sup>11</sup> In  $S_{pr}$ -gearing, the law of contact ( $\mathbf{n}_g \cdot \mathbf{V}_\Sigma = 0$ ), and the conjugate action law are fulfilled, as the tooth flanks,  $\mathcal{S}$  and  $\mathcal{P}$ , both, are generated by means of a desirable line of contact,  $LC$ . The line of contact is entirely located within an instantaneous plane of action,  $PA$ , and travels with this plane of action,  $PA$ .

<sup>12</sup> Reminder: The necessity of consideration of the concept of operating base pitch is because of the following. When a gear, and a mating pinion in an  $S_{pr}$ -gear pair are disengaged from mesh, the angular base pitches,  $\varphi_{b.g}$  and  $\varphi_{b.p}$ , of the both are remained of the same value. However, the gears cannot be engaged in proper mesh with one another when an actual configuration of the gear axes of rotation,  $O_g$  and  $O_p$ , is out of the interval that is specified for a particular  $S_{pr}$ -gear pair. This is because the actual value of the operating angular base pitch alters, as it depends on the actual configuration of the gear, and of the pinion in relation to each other, including the location in relation of the centerline.

<sup>13</sup>  $S_{pr}$ -gear system is developed so, as to accommodate for variable operating angular base pitch caused by variation of the displacements and deflections of the shafts, housing, gear and pinion teeth, and so forth, under variable operating load.



For a gear pair with the displaced tooth flanks,  $\mathcal{S}$  and  $\mathcal{P}$ , the actual values of the design parameters,  $\phi_{b.op}$  and  $r_{pa}^{inst}$ , alter, while the linear distance,  $ab$ , is remained of that same value ( $ab = \text{const}$ ). For a specified value of the distance,  $\Delta r_{pa}^{inst}$ , the current value of the angular operating base pitch,  $\phi_{b.op}^{inst}$ , is calculated as:

$$\phi_{b.op}^{inst} = 2 \sin^{-1} \frac{ab}{2(r_{w.pa} + \Delta r_{pa}^{inst})} \quad (17.53)$$

Here, in Eq. (17.53), the distance,  $\Delta r_{pa}^{inst}$ , is a signed value.

In  $S_{pr}$  – *gearing*, a gear and a mating pinion feature a *range* of base pitches, and not a fixed base pitch of a certain value. The *range* of the base pitches makes the gear pair capable of accommodating for a specified range of permissible values of the axes displacement.

The values,  $\phi_{b.op}^{\min}$  and  $\phi_{b.op}^{\max}$ , are the minimum, and the maximum values of the angular operating base pitch,  $\phi_{b.op}^{inst}$ , correspondingly, calculated from Eq. (17.53). The maximum *negative* deviation, and the maximum *positive* deviation of the angular operating base pitch,  $\phi_{b.op}^{inst}$ , from its nominal value,  $\phi_{b.op}$ , are designated as  $\Delta\phi_{b.op}^{\min}$  and  $\Delta\phi_{b.op}^{\max}$ , correspondingly. The extremal deviations,  $\Delta\phi_{b.op}^{\min}$  and  $\Delta\phi_{b.op}^{\max}$ , form an interval for permissible variation:

$$\phi_{b.op}^r - \Delta\phi_{b.op}^{\min} \leq \phi_{b.op}^{inst} \leq \phi_{b.op}^r + \Delta\phi_{b.op}^{\max} \quad (17.54)$$

of the operating base pitch,  $\phi_{b.op}^{inst}$ , in a gear pair.

The intervals of permissible variation of the angular base pitches of a gear,  $\phi_{b.g}^{inst}$ , and a mating pinion,  $\phi_{b.p}^{inst}$ , in  $S_{pr}$  – *gearing* are identical to the permissible variation of the operating angular base pitch,  $\phi_{b.op}^{inst}$ , of the gear pair [see Eq. (17.54)]. No transmission error is observed once the base pitches of a gear and its mating pinion are equal to one another, and both of them are equal to a current value of the operating base pitch of the gear pair. Ultimately,  $S_{pr}$  – gears are capable of transmitting a uniform rotary motion from a driving shaft to a driven shaft smoothly with no vibration generation and no noise excitation.

In a particular case, when the axes of rotation of a gear and of a mating pinion are exactly parallel to one another, the base cones reduce to corresponding base cylinders. Because of this, the angular operating base pitch,  $\phi_{b.op}^{inst}$ , approaches a zero (i.e.,  $\phi_{b.op}^{inst} \rightarrow 0^\circ$ ), and the corresponding radius,  $r_{pa}^{inst}$ , approaches an infinity, that is,  $r_{pa}^{inst} = (r_{w.pa} + \Delta r_{pa}^{inst}) \rightarrow \infty$ , as well as the axial distance,  $A$ , approaches an infinity ( $A \rightarrow \infty$ ). Therefore, when determining an actual value of the angular operating base pitch,  $\phi_{b.op}^{inst}$ , an indefiniteness of the sort  $0 \cdot \infty$  is observed (as an equality,  $p_b = \phi_b \cdot R_{pa}$ , is valid). The *L'Hôpital's rule* can be used<sup>14</sup> to resolve such indefinites. Also, in this particular case (i.e., in a case when an actual configuration of the rotation vectors,  $\omega_g$  and  $\omega_p$ , corresponds to that in geometrically accurate parallel-axes gear pair), the instantaneous angular operating base pitch of a gear pair,  $\phi_{b.op}^{inst}$  (a design parameter that is measured in angular units), can be replaced with the instantaneous operating base pitch of a gear pair,  $p_{b.op}^{inst}$  (a design parameter that is measured in linear units):  $p_{b.op}^{inst} = r_{pa}^{inst} \cdot \phi_{b.op}^{inst}$ . Other known technics for resolving the indefiniteness of a sort,  $0 \cdot \infty$ , can also be used.

The actual value of the operating angular base pitch,  $\phi_{b.op}^{inst}$ , depends on the deviation,  $\Delta\Sigma$ , of the crossed-axes angle,  $\Sigma$ , in a real gear pair, and it does not depend on the actual values of the deviations,  $\Delta C$ , and  $\Delta A$ , in the center-distance,  $C$ , and the length of the axial vector,  $\mathbf{A}$ . The geometry of the traces of contact point,  $K$ , on the gear,  $\mathcal{S}$ , and the mating pinion,  $\mathcal{P}$ , tooth flanks, as well as the parameters of the actual portion of the active tooth flanks,  $\mathcal{S}$  and  $\mathcal{P}$ , depend on the actual values of the deviations,  $\Delta C$ , and  $\Delta A$ .

<sup>14</sup> Guillaume François Antoine, *Marquis de l'Hôpital* (1661 – February 2, 1704), a French mathematician.

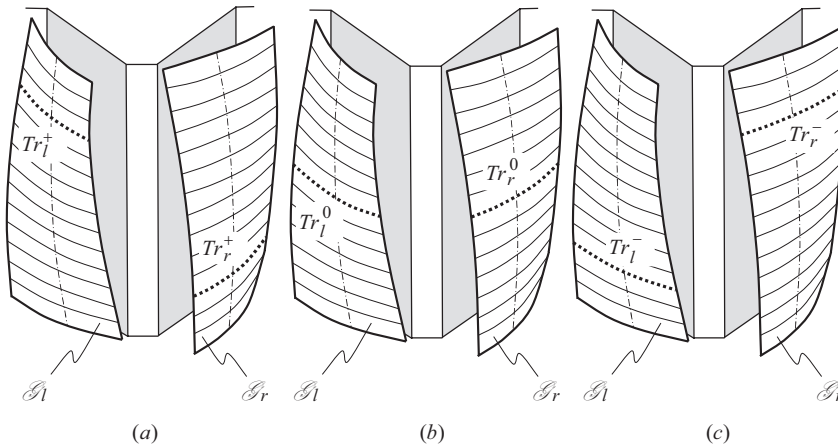


**FIGURE 17.15** Traces,  $Tr$ , of contact point on tooth flanks,  $\mathcal{G}$  and  $\mathcal{P}$ , of  $S_{pr}$  – gear depending on an actual value of the axes displacement: (a) positive axes displacement, (b) zero axes displacement, and (c) negative axes displacement.

#### 17.2.1.5 Features of Interaction of Tooth Flanks in $S_{pr}$ – Gearing

A few features of interaction of tooth flanks,  $\mathcal{G}$  and  $\mathcal{P}$ , of a gear and of a mating pinion, correspondingly, are briefly discussed immediately below. The readers' attention is focused here on the path of contact point over the tooth flanks,  $\mathcal{G}$  and  $\mathcal{P}$ , and on the features of geometry of contact between the tooth flanks,  $\mathcal{G}$  and  $\mathcal{P}$ .

*Trace of contact point on tooth flanks.* For example, the location and orientation of the trace of contact point,  $Tr$ , within tooth flank of a spur  $S_{pr}$  – gearing is schematically shown in Figure 17.15. In a case of zero axes displacement, the trace of contact point on the left flank,  $Tr_l^0$ , of the gear tooth, as well as on the right flank,  $Tr_r^0$ , of the gear tooth pass through the middle of the face of the gear (see Figure 17.15b). In a case when positive axes displacement is observed, the trace of contact point for the left side,  $Tr_l^+$ , and the right side,  $Tr_r^+$ , of the gear tooth are displaced oppositely toward the ends of the gear, as schematically illustrated in Figure 17.15a. Similarly, negative axes displacement results in the trace of contact point for the left,  $Tr_l^-$ , and for the right,  $Tr_r^-$ , sides of the gear tooth being displaced oppositely toward the opposite ends of the gear as illustrated in Figure 17.15c. The shown in Figure 17.15 schematics pertain to  $S_{pr}$  – gearing that features constant in time values of all the displacements. When the displacements alter in time, then the paths of contact of a more complex geometry are observed.

*Features of the contact geometry between the tooth flanks.* When geometrically accurate parallel-axes gears rotate, the plane of action is unwrapping from one base cylinder and is wrapping onto the other base cylinder of mating gears as it is schematically shown in Figure 10.37 (see Chapter 10). This schematic is valid as long as the axes of rotations of the gear,  $O_g$ , and its mating pinion,  $O_p$ , are parallel to one another. In reality, the axes of rotation,  $O_g^r$  and  $O_p^r$ , of a gear, and of a mating pinion are not parallel to each other. At every instant of time, the axes of rotation,  $O_g^r$  and  $O_p^r$ , cross one another at a certain crossed-axes angle instead. The actual value of the crossed-axes angle depends on current values of the parameters of the axes displacement. Therefore, for desirable parallel-axes real gearing a schematic based on crossing rotation vectors,  $\omega_g^r$  and  $\omega_p^r$ , of the gear and of the pinion should be applied, instead of that for parallel-axes gearing.

Because of the axes displacement, the parallel-axes gearing is actually a kind of crossed-axes gearing that features a distance of closest approach of the axes of rotation of a gear and of a mating pinion, as well as a crossed-axes angle. In reality, the closest distance of approach of the axes is approximately equal to the distance between parallel axes of the gear and the pinion, and the actual value of the crossed-axes angle is close to either  $180^\circ$  (in external gearing) or  $0^\circ$  (in internal gearing).

In any case, the line contact in a geometrically accurate gear pair is substituted by point contact in its corresponding  $S_{pr}$  – gearing. The degree of conformity of the tooth flanks of the gear,  $\mathcal{G}_r$ , and the pinion,  $\mathcal{P}_r$ , at every point of their contact is of the maximum possible degree. The tooth flanks of gears of no other systems of gearing feature the degree of conformity as high, as gears in  $S_{pr}$  – gearing do. The latter is of critical importance from the standpoint of reduction of contact stress, as well as of an increase in the wear resistance of the interacting tooth flanks of the gear and the mating pinion.

Tooth flanks in gears for  $S_{pr}$  – gearing always make point contact. The actual location and configuration of the path of contact point,  $P_c$ , depends on the actual value of the axes displacement. As the tooth flanks of a gear,  $\mathcal{G}_r$ , and a mating pinion,  $\mathcal{P}_r$ , are always in point contact with one another, they do not envelope each other. However, under any reasonable axes displacement, instant base pitch,  $\varphi_{b,g}^{\text{inst}}$ , of a gear and that,  $\varphi_{b,p}^{\text{inst}}$ , of a mating pinion, both, are equal to instantaneous operating base pitch,  $\varphi_{b,op}^{\text{inst}}$ , of the gear pair:

$$\varphi_{b,g}^{\text{inst}} = \varphi_{b,op}^{\text{inst}} \quad (17.55)$$

$$\varphi_{b,p}^{\text{inst}} = \varphi_{b,op}^{\text{inst}} \quad (17.56)$$

The determined geometry of tooth flanks in  $S_{pr}$  – gearing is derived to accommodate for all three components of linear displacements, and all three components of angular displacements of the gear and the pinion axes of rotation. This makes  $S_{pr}$  – gearing insensitive to the axes displacement within their reasonable range. The proposed gear system (namely,  $S_{pr}$  – gearing) is the only possible kind of self-adjustable gearing. Gearing of no other design is capable of accommodating for the axes displacement.

The concept of the *path-of-contact surface*,  $P_{cs}$ , can be easily enhanced to  $S_{pr}$  – gearing: the *path-of-contact surface*,  $P_{cs}$ , is a continuous set of the circular-arc paths of contact,  $P_c$ , at different transverse pressure angle,  $\phi_{t,\omega}$ . The radius of a current circular-arc path of contact is a *non-linear* function of the distance of point on the pitch line,  $P_m$ , from the plane-of-action-apex,  $A_{pa}$  ( $\neq A_g \neq A_p$ ). The *path-of-contact surface*,  $P_{cs}$ , is a continuous screw surface of variable transverse pressure angle,  $\phi_{t,\omega}$ , and variable angular base pitch (along the axis of instantaneous rotation,  $P_{ln}$ ).

## 17.2.2 POSSIBLE IMPROVEMENT IN SPECIFICATION OF TOOTH FLANK GEOMETRY IN $S_{pr}$ – GEARING

Linear and angular displacements of tooth flank of a gear and that of a mating pinion,  $\mathcal{G}$  and  $\mathcal{P}$ , those caused by the elastic deformation of the gear body under the applied load, can be incorporated into consideration on further steps of the analysis. It is assumed here that the gear body is deformed elastically under the applied load, while the elastic deformation of the tooth flank itself is negligibly small, and, thus, it can be ignored. In the other scenario, alteration of the tooth flank geometry under the applied load can also be taken into account.

In order to incorporate the gear tooth flank elastic deformation into the design of  $S_{pr}$  – gearing:

1. It is assumed in this analysis that the tooth flank geometry under operating load is remained the same, as before the operating load is applied – the tooth flank just turns through certain angle(s)

2. Under operating load, the gear tooth profile gets more curvature. Therefore, it can be considered as developed from a base circle of a smaller diameter, compared to that in the original involute tooth profile. In this way, the design parameters of the gear, namely, the base diameter, can be entered into the equation of indicatrix of conformity,  $Cnf_R(\mathcal{S}|\mathcal{P})$ , at point of contact of the tooth flanks,  $\mathcal{S}$  and  $\mathcal{P}$ , of a gear, and of a mating pinion. This is critical to synthesizing of favorable gearing utilizing for this purpose the properties of the indicatrix of conformity. Similarly, helix angle of the gear tooth flank, as well as other design parameters, can be involved into the synthesizing of gears of favorable design.

In both of these scenarios, the displacements of the tooth flanks,  $\mathcal{S}$  and  $\mathcal{P}$ , under operating load are considered, instead of displacements of just the axes of the gear and of the mating pinion.

### 17.3 REDUNDANT PARAMETER ELIMINATION

In real gearing, the tooth flank of a gear, and that of a mating pinion, both can be viewed as a kind of smooth regular surface. A surface is a two-dimensional space, and, thus, can be analytically expressed in terms of two parameters. As shown earlier (see Section 17.2.1.3), position vector of point,  $\mathbf{r}_g^r$ , of a gear tooth flank,  $\mathcal{S}_r$ , as well as position vector of point,  $\mathbf{r}_p^r$ , of a pinion tooth flank,  $\mathcal{P}_r$ , are expressed in terms of three parameters, that is, of  $r_{pa}$ ,  $\varphi_p$ , and  $X_f$  [see Eqs. (17.49) and (17.50)]. An excessive independent parameter in the equations for position vectors of a point,  $\mathbf{r}_g^r$  and  $\mathbf{r}_p^r$ , can be used to develop favorable designs of a gear,  $\mathcal{S}_r$ , and of a mating pinion,  $\mathcal{P}_r$ , tooth flanks in  $S_{pr}$  – gearing.

There is certain freedom in varying of actual values of the design parameters of tooth flanks of a gear,  $\mathcal{S}_r$ , and of a pinion,  $\mathcal{P}_r$ , within the intervals  $-0.5F_{pa} \leq f_{pa} \leq 0$  and  $0 \leq f_{pa} \leq +0.5F_{pa}$ . It is reasonable to assume that a zero axes displacement occurs at a midpoint of the effective face width,  $F_{pa}$ . Transition from a zero axes displacement at the midpoint to a maximum axes displacement at one end of the gear, and to a maximum axes displacement at the opposite end of the gear, follows a certain function. Thus, a synchronization with each other of the permissible linear and angular displacements in  $S_{pr}$  – gearing is permissible.

#### 17.3.1 POSSIBLE CORRELATION BETWEEN DISPLACEMENTS IN $S_{pr}$ – GEARING

Consider an  $S_{pr}$  – gear pair. The gear axis of rotation,  $O_g$ , and the pinion axis of rotation,  $O_p$ , are two crossing straight lines. These straight lines at a center-distance,  $C$ , and cross each other at a crossed-axes angle,  $\Sigma$ . Thus, a relative configuration of the axes  $O_g$ , and  $O_p$ , can be specified just by two parameters, that is, by a center-distance,  $C$ , and by a crossed-axes angle,  $\Sigma$ .

The tolerance bend,  $\Delta\Sigma^+$  and  $\Delta\Sigma_-$ , for the crossed-axes angle,  $\Sigma$ , as well as the tolerance bend,  $\Delta C^+$  and  $\Delta C_-$ , for the center-distance,  $C$ , are specified.

A desirable line of contact,  $LC_{des}$ , between the tooth flanks,  $\mathcal{S}$  and  $\mathcal{P}$ , is specified in a reference system  $X_{pa}Y_{pa}Z_{pa}$ , associated with the plane of action,  $PA$ . Two other reference systems,  $X_{hg}Y_{hg}Z_{hg}$  and  $X_{hp}Y_{hp}Z_{hp}$ , are associated with the gear housing: the first of them,  $X_{hg}Y_{hg}Z_{hg}$ , is the stationary reference system of the gear, and the second one,  $X_{hp}Y_{hp}Z_{hp}$ , is the stationary reference system of the pinion.

The plane of action,  $PA$ , is assumed motionless. Therefore, when the linear,  $\Delta C$ , and the angular,  $\Delta\Sigma$ , deviations occur, this result in alteration of the configuration of the reference systems  $X_{hg}Y_{hg}Z_{hg}$  and  $X_{hp}Y_{hp}Z_{hp}$  in relation to the stationary reference system,  $X_{pa}Y_{pa}Z_{pa}$ .

Gear ratio,  $u$ , in crossed-axes gear pair is calculated from the equation {page 336, Eq. (12.14) in Ref. [174]}:

$$u = \frac{\omega_{input}}{\omega_{output}} = \frac{\omega_p}{\omega_g} = \frac{r_{w.g}}{r_{w.p}} = \frac{C_g}{C_p} = \frac{\sin \Sigma_g}{\sin \Sigma_p} \quad (17.57)$$

[Here, in Eq. (17.57), the two following equalities are valid:  $C_g + C_p = C$ , and  $\Sigma_g + \Sigma_p = \Sigma$ ].

Under any and all values of the linear displacement,  $\Delta C$ , and the angular,  $\Delta \Sigma$ , displacement, the gear ratio,  $u$ , in the gear pair is remained the same: the gear ratio,  $u$ , in crossed-axes gear pair is independent of the actual values of the linear and the angular displacements,  $\Delta C$  and  $\Delta \Sigma$ , correspondingly.

The transition from the plane-of-action reference system,  $X_{pa}Y_{pa}Z_{pa}$ , to the gear housing reference system,  $X_{hg}Y_{hg}Z_{hg}$ , can be specified so as to have an increment of alteration of the displacements (both a linear displacement,  $\delta C$ , and an angular displacement,  $\delta \Sigma$ ) that are smaller for a larger actual value of the displacements. For example, the following multipliers can be used to accommodate for a desirable distribution of the linear and angular displacements, correspondingly:

$$f_{\Delta C}(\Delta C) = \left( 1 - \frac{\Delta C}{[\Delta C]} \right) \quad (17.58)$$

$$f_{\Delta \Sigma}(\Delta \Sigma) = \left( 1 - \frac{\Delta \Sigma}{[\Delta \Sigma]} \right) \quad (17.59)$$

Here, the maximum permissible values for the displacements,  $\Delta C$ , and  $\Delta \Sigma$ , are designated as  $[\Delta C]$  and  $[\Delta \Sigma]$ , correspondingly.

Instead of the expressions [see Eqs. (17.58) and (17.59)], other relevant functions can be used for this purpose. A normal distribution function is of a particular interest in this regard, and it can be used to derive corresponding functions to be used instead of the functions Eqs. (17.58) and (17.59).

The gear ratio,  $u$ , depends on the actual value of the linear displacement [see Eq. (17.57)] as:

$$u = \frac{C_g + \Delta C_g}{C_p + \Delta C_p} \quad (17.60)$$

Here, the components  $\Delta C_g$  and  $\Delta C_p$  of the total linear displacement,  $\Delta C$ , meet the requirement:

$$\Delta C_g + \Delta C_p = \Delta C \quad (17.61)$$

Equation (17.60) yields a formula for the calculation of the gear linear displacement,  $\Delta C_g$ :

$$\Delta C_g = u(C_p + \Delta C_p) - C_g \quad (17.62)$$

After Eq. (17.61) is taken into account, Eq. (17.60) casts into the expression:

$$\Delta C_g = \frac{u(C_p + \Delta C) - C_g}{(u + 1)C_g} \quad (17.63)$$

Similarly, Eq. (17.60) yields a formula for the calculation of the gear linear displacement,  $\Delta C_p$ :

$$\Delta C_p = \frac{C_g + \Delta C_g - uC_p}{u} \quad (17.64)$$

After Eq. (17.61) is taken into account, Eq. (17.64) casts into the expression:

$$\Delta C_p = \frac{C_g + \Delta C - (u - 1)C_p}{u} \quad (17.65)$$

The component  $\Delta C_p$  can be also calculated as the difference  $\Delta C_p = \Delta C - \Delta C_g$ .

The components,  $\Delta C_g$  and  $\Delta C_p$ , of the total linear displacement,  $\Delta C$ , are entered into the matrices of the translations when performing the transition from the plane-of-action reference system,  $X_{pa}Y_{pa}Z_{pa}$ , to the gear housing, and the pinion-housing reference systems,  $X_{hg}Y_{hg}Z_{hg}$  and  $X_{hp}Y_{hp}Z_{hp}$ , correspondingly.

In terms of components,  $\Delta \Sigma_g$  and  $\Delta \Sigma_p$ , the total angular displacement,  $\Delta \Sigma$ , the gear ratio,  $u$ , can be described by an expression:

$$u = \frac{\sin(\Sigma_g + \Delta \Sigma_g)}{\sin(\Sigma_p + \Delta \Sigma_p)} \quad (17.66)$$

Here, the components  $\Delta \Sigma_g$  and  $\Delta \Sigma_p$  of the total angular displacement,  $\Delta \Sigma$ , meet the requirement:

$$\Sigma_g + \Sigma_p = \Sigma \quad (17.67)$$

Equation (17.66) yields a formula for the calculation of the gear linear displacement,  $\Delta \Sigma_g$ :

$$\Delta \Sigma_g = \sin^{-1}[u \sin(\Sigma_p + \Delta \Sigma_p)] - \Sigma_g \quad (17.68)$$

The values,  $\Delta C \cdot f_{\Delta C}$  and  $\Delta \Sigma_g \cdot f_{\Delta \Sigma}$ , to be entered into the matrices of the coordinate system transformations.

The functions,  $f_{\Delta C}$  and  $f_{\Delta \Sigma}$ , make possible eliminating of an excessive degree of freedom in the analytical description of the desirable line of contact,  $LC_{des}$ .

A similar consideration is valid with respect to the transition from a plane-of-action reference system  $X_{pa}Y_{pa}Z_{pa}$  to a pinion-housing reference system  $X_{hp}Y_{hp}Z_{hp}$ .

### 17.3.2 ACCOUNT FOR THE NORMAL DISTRIBUTION OF MANUFACTURING ERRORS ONTO THE GEOMETRY OF TOOTH FLANKS

Use of the *Gauss'* (normal) distribution of the manufacturing errors sounds attractive from this perspective. The instantaneous values of the design parameters,  $r_{pa}$  and  $X_f$ , in  $S_{pr} - gearing$  may correlate to one another so as to follow the *Gauss'* distribution. When a gear, and a mating pinion in  $S_{pr} - gearing$ , both, are designed this way, for the smaller instantaneous values of the axes displacement (probability of which is higher), contact point is mainly located in the vicinity of the midpoint of the effective face width,  $F_{pa}$ . For the larger instantaneous values of the axes displacement (probability of which is lower), contact point is mainly located at the ends of the effective face width,  $F_{pa}$ .

As manufacturing errors perfectly follow the normal distribution, implementation of the *Gauss'* distribution formula for the derivation of an equation for position vectors of point,  $\mathbf{r}_g^r$  and  $\mathbf{r}_p^r$ , for tooth flanks,  $\mathcal{S}_g$  and  $\mathcal{S}_p$ , becomes reasonable (see Figure 17.16):

$$\varphi_{\mu, \sigma}(X) = \frac{1}{\sqrt{2\pi\sigma^2}} e^{-\frac{(X-\mu)^2}{2\sigma^2}} \quad (17.69)$$

In Eq. (17.69), the parameter  $\mu$  is the mean (location of the peak), and  $\sigma^2$  variance (the measure of the width) of the distribution.

It is reasonable to assume that actual values of the design parameters,  $r_{pa}$  and  $X_f$ , correlate to one another following the *Gauss'* distribution formula [see Eq. (17.69)]:

$$\frac{\partial X_f}{\partial r_{pa}}(r_{pa}) = \frac{1}{\sqrt{2\pi\sigma^2}} e^{-\frac{(r_{pa}-r_{w,pa})^2}{2\sigma^2}} \quad (17.70)$$

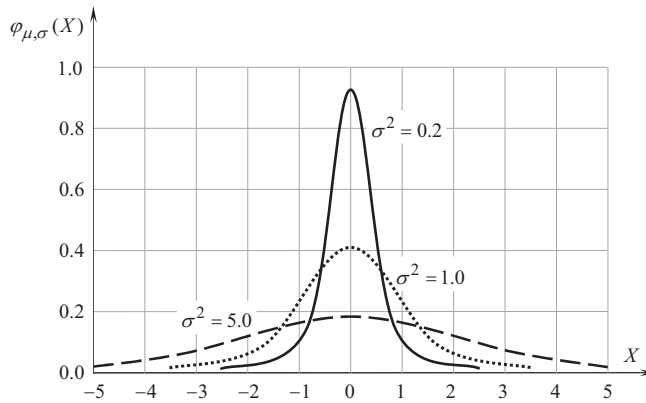


FIGURE 17.16 Probability density function ( $\mu = 0$ ).

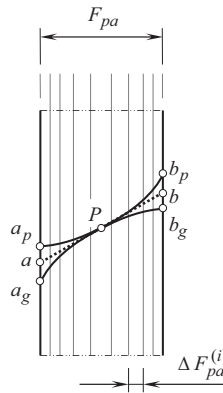


FIGURE 17.17 On account for the normal distribution of manufacturing errors onto the geometry of gear tooth flanks in  $S_{pr}$  – gearing.

The generation of the tooth flank of a gear,  $\mathcal{S}_r$  and that of its mating pinion,  $\mathcal{P}_r$  in  $S_{pr}$  – gearing, generated in accordance to Eq. (17.70), could be of practical importance, as the manufacturing errors, as well as the errors and displacements of other nature, follow the *Gauss*' distribution formula with high accuracy.

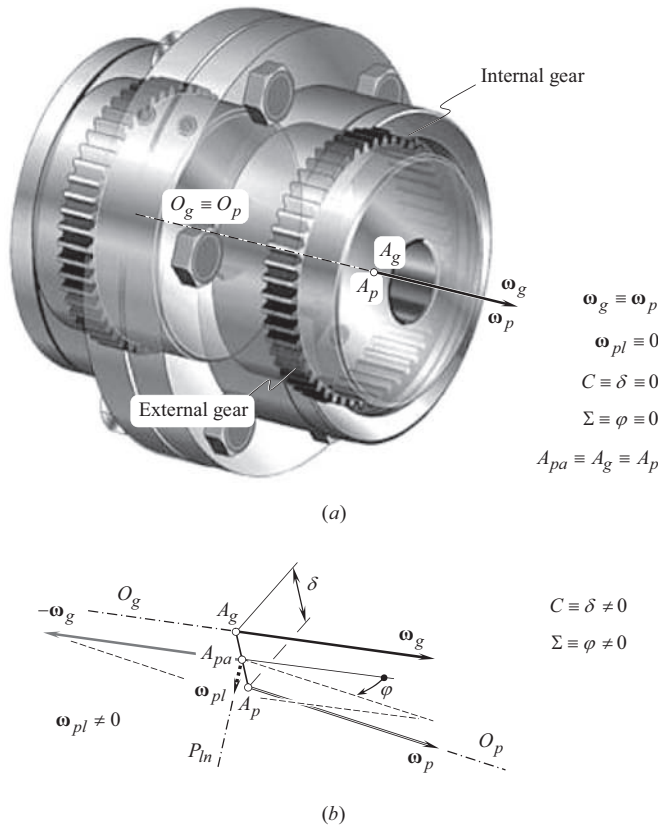
Once one of the design parameters,  $r_{pa}$  and  $X_f$ , in  $S_{pr}$  – gearing is expressed in terms another one, namely, a function,  $X_f = X_f(r_{pa})$ , is established, then position vectors of point,  $\mathbf{r}_g^r$  and  $\mathbf{r}_p^r$ , of tooth flank of a gear,  $\mathcal{S}_r$ , and its mating pinion,  $\mathcal{P}_r$ , are expressed in terms of two (and not of three) design parameters, as required for any and all smooth regular surfaces.

Figure 17.17 is helpful for better understanding of the normal distribution of manufacturing errors onto the geometry of tooth flanks of a gear, and of a mating pinion in  $S_{pr}$  – gearing. In Figure 17.10, all the slices are of equal thickness,  $\Delta F_{pa}$ . In the case illustrated in Figure 17.17, thickness,  $\Delta F_{pa}^{(i)}$ , of each  $i$  – th slice strictly follows the *Gauss*' distribution.

## 17.4 POSSIBILITY OF IMPLEMENTATION OF THE CONCEPT OF $S_{pr}$ – GEARING IN DESIGN OF GEAR COUPLING

Gear coupling (see Figure 17.18) can be viewed as been composed of two internal gear pairs featuring tooth ratio,  $u = 1$ . A gear mesh of this particular type can be viewed as degenerate case of parallel-axes gearing. In a gear coupling, one spur gear is connected to a driving shaft, and the other





**FIGURE 17.18** Implementation of the concept of  $S_{pr}$  – gearing in the design of gear coupling (a) close-up of gear coupling, and (b) gear vector diagram, constructed for gear coupling.

spur gear is connected to a driven shaft. Both spur gears interact either with a common internal spur gear or with two individual internal spur gears that share common body of the gear.

When the linear and the angular displacements of the axes of rotation of the input shaft, and of the output shaft are of zero values, tooth profile in a gear coupling is out of importance (from the standpoint of gear meshing), and it can be of an arbitrary reasonable geometry. However, gear couplings are used in cases when the linear and the angular displacements of the axes of rotation of the input shaft, and of the output shaft are of nonzero values. If the linear and the angular displacements are taken into account, the tooth flank geometry becomes of critical importance, as the gear coupling becomes a gear pair. In this scenario, interacting tooth flanks of the gears in the coupling interact with one another identically to that, the tooth flanks in crossed-axes gearing interact. For gear couplings that operate at high rotations, the geometry of the tooth flanks has to be determined based on the concept of  $S_{pr}$  – gearing.

In an ideal case, when no axes displacement occurs, the rotation vector,  $\omega_g$ , of the internal gear in a gear coupling is identical to the rotation vector,  $\omega_p$ , of the external gear in the gear coupling ( $\omega_g \equiv \omega_p$ ). As illustrated in Figure 17.18a, the crossed-axes angle is zero ( $\Sigma = 0$ ), and the closest distance of approach,  $C$ , between the gear axis, of rotation  $O_g$ , and the pinion axis of rotation,  $O_p$ , is also zero ( $C \equiv 0$ ). The gear apex,  $A_g$ , and the pinion apex,  $A_p$ , are snapped together into a common point,  $A_{pa}$ . In such a scenario, the gear coupling designer is free to select any reasonable tooth flank geometry for the gear and the pinion. In this particular case, the tooth flank geometry does not affect vibration generation and noise excitation in the gear coupling.



In reality, the axes of rotation,  $O_g$  and  $O_p$ , of the internal and external gears, respectively, do not align to one another. A certain linear displacement,  $\delta$ , and an angular displacement,  $\varphi$ , are inevitable (see Figure 17.18b). With that said, the gear coupling can be interpreted as a crossed-axes gear pair that has a center-distance,  $C = \delta$ , and a crossed-axes angle  $\Sigma = \varphi$ . The rotation vector,  $\omega_g$ , of the internal gear no longer aligns with the rotation vector,  $\omega_p$ , of the external gear. Therefore, certain rotation of the external gear in relation to the internal gear is observed. This relative rotation can be expressed in terms of the vector of instant rotation,  $\omega_{pl} = \omega_p - \omega_g$ . If the rotation,  $\omega_{pl}$ , is observed ( $\omega_{pl} \neq 0$ ), then it makes sense to implement the concept of  $S_{pr}$  – gearing in the design of internal, and of external gears of a gear coupling in order to avoid vibration generation and noise excitation when the gear coupling is operating at high rotations.

A gear coupling designed utilizing the concept of  $S_{pr}$  – gearing can feature only one external gear, and only one internal gear (instead of two external and two internal gears in the design, shown in Figure 17.18a). This means that with  $S_{pr}$  – gearing, it is sufficient to have only two components to make the gear coupling operating properly.

## 17.5 POSSIBILITY OF IMPLEMENTATION OF THE CONCEPT OF $S_{pr}$ – GEARING IN POINT CONTACT GEAR SYSTEMS

Gear systems that feature point contact between tooth flanks of a gear, and of a mating pinion, and high-conformal gears in particular, are more sensitive to the axes displacement. Therefore, point contact gearing require tighter tolerances for the actual configuration of the axis of rotation of a gear in relation to the axis of rotation of a mating pinion. It is of interest to investigate whether or not the disclosed approach for the generation of tooth flanks of desirable real gearing, namely, of  $S_{pr}$  – gearing, can be enhanced to point contact gearing of other designs.

The profile contact ratio,  $m_p$ , for any  $S_{pr}$  – gearing design is greater than zero ( $m_p > 0$ ). For spur  $S_{pr}$  – gearing, the inequality  $m_p = \bar{m} > 1$  is always observed. For helical  $S_{pr}$  – gearing, the inequality  $\bar{m} = m_p + m_F > 1$  is valid. Here, the face contact ratio is designated as  $m_F$  and the total contact ratio is denoted by  $\bar{m}$ . High-conformal gears of all kinds feature  $m_p = 0$  and  $\bar{m} = m_F > 1$ .

The generation of tooth flanks for desirable real high-conformal gears is based on the principle of generation of tooth flanks for geometrically accurate crossed-axes high-conformal gears. Two of the most unfavorable cases should be considered here.

**First**, the boundary  $N^p$  – circle is constructed for the midpoint of the effective face width,  $F_{pa}$ , of the gear. For the construction, the original configuration of the rotation vectors,  $\omega_g$ ,  $\omega_p$  and  $\omega_{pl}$ , is used. This set of the rotation vectors is complemented by zero tolerance vector,  $\{\varphi\}$ , for the angular displacement, and minimum tolerance vector,  $\{\delta\}$ , for the linear displacement. For such a configuration of the rotation vectors, the limit radius,  $r_N^p$ , is derived. The radius of curvature of the convex tooth profile does not exceed  $r_N^p$  (see Figure 17.19).

**Second**, the boundary  $N^g$  – circle is constructed for both ends of the gear. For the construction, the original configuration of the rotation vectors,  $\omega_g$ ,  $\omega_p$  and  $\omega_{pl}$ , is used. This set of the rotation vectors is complemented by the maximum tolerance vector,  $\{\varphi\}$ , for the angular displacement, and by the maximum tolerance vector,  $\{\delta\}$ , for the linear displacement. For such a configuration of the rotation vectors, the limit radius,  $r_N^g$ , is derived. The radius of curvature of the concave tooth profile exceeds the value of  $r_N^g$  (see Figure 17.19).

A performed analysis of Figure 17.19 makes possible a conclusion. In gearing that has line contact between tooth flanks of a gear and of a mating pinion, the line contact can be substituted with point contact in order to make the gearing insensitive to the axes displacement. The gear designer sacrifices the line contact for point contact. In gearing that feature point contact, there is nothing to

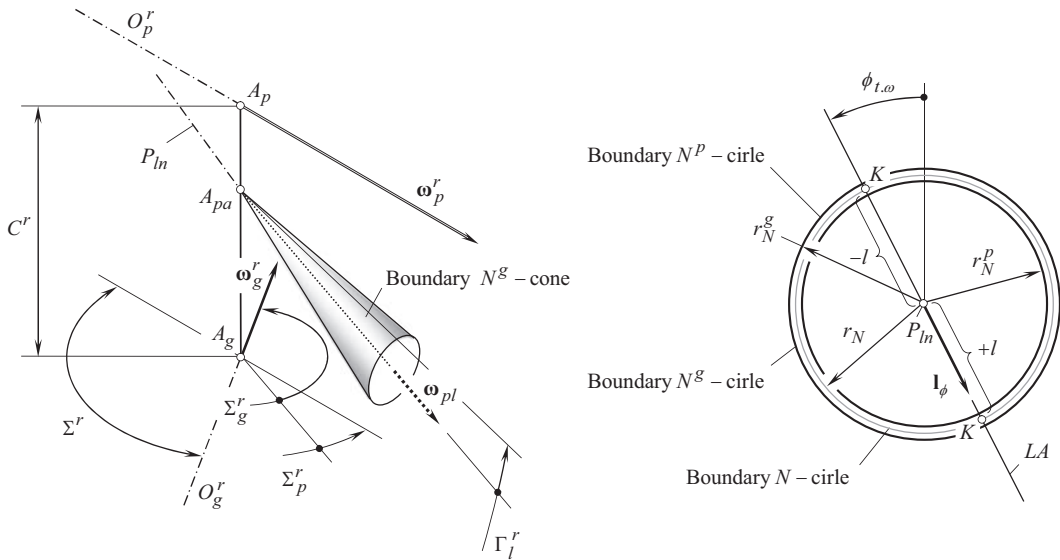


**FIGURE 17.19** Configuration of the boundary  $N$  – cone for desirable high-conformal real crossed-axes gear pair.

sacrifice – the gear and the mating pinion tooth flanks are already in point contact. This makes possible a conclusion: *No changes to the tooth flank geometry are permissible in gearing that feature point contact between the tooth flanks.*

## 17.6 CORRELATION AMONG THE GEAR SYSTEMS OF DIFFERENT KINDS

The geometrically accurate and desirable real gear systems discussed to this end, correlate to each other in a way illustrated in Table 17.1.

All types of gear pairs fall into three groups. These groups are as follows:

1. Geometrically accurate gear pairs
2. Geometrically accurate real gear pairs
3. Real (approximate) gear pairs

Equality of base pitch (angular base pitch) of a gear, and that of its mating pinion, to operating base pitch of the gear pair is the main feature of *geometrically accurate gearing*. Tooth flanks of a gear, and of a mating pinion in geometrically accurate gearing always make line contact with one another.

Geometrically accurate gears are capable of transmitting a smooth rotation from a driving shaft to a driven shaft.

*Geometrically accurate real gearing* (or  $S_{pr}$  – gearing) features certain variation in the base pitch (angular base pitch). For every gear and pinion, an interval of variation of angular base pitches can be specified. The geometry of the tooth flanks of a gear, and of a mating pinion in desirable real gearing is determined so as to ensure equality of angular base pitch of a gear, and that of its mating pinion, to the operating angular base pitch of the gear pair under any reasonable displacements of the tooth flanks in relation to each other. Tooth flanks of a gear and its mating pinion in  $S_{pr}$  – gearing always make point contact with one another. ||||The coordinates of contact point at every instant of time are predictable, and can be calculated. Tooth flanks in  $S_{pr}$  – gearing feature the maximum possible degree of conformity of the interacting tooth flanks at every point of their contact.

TABLE 17.1

**Desirable Geometries for Tooth Flanks of Gear Pairs with  $m_p > 0$  (Correlation among Gear Systems of Different Kinds)**

Configuration of the Axes of Rotation	Geometrically Accurate Gear Pairs	Geometrically Accurate Real Gear Pairs	Real (Approximate) Gearing
Parallel-axes gearing ( $P_a$ – gearing)	Involute of a circle tooth profile <sup>a</sup> used in spur, helical, herring-bone, and double-helical gears. ( $p_{b,g} \equiv p_{b,p}$ )	Parallel-axes $S_{pr}$ – gearing <sup>c</sup> used in spur, helical, herring-bone, double-helical, cycloidal gears as well as any other geometries in the lengthwise direction of the gear teeth. ( $\varphi_{b,g} = \varphi_{b,op}$ , $\varphi_{b,p} = \varphi_{b,op}$ )	Gears with a non-involute tooth profile, circular-arc tooth flank geometry in the lengthwise direction of the gear tooth cut by milling cutter, and so forth. ( $p_{b,g} \neq p_{b,op}$ , $p_{b,p} \neq p_{b,op}$ )
Intersected-axes gearing ( $I_a$ – gearing)	Involute flank developed from a base cone of the gear <sup>b</sup> used in straight tooth bevel gears. ( $\varphi_{b,g} = \varphi_{b,p}$ )	Intersected-axes $S_{pr}$ – gearing <sup>c</sup> used in bevel, skew bevel, spiral bevel gears as well as in any other geometries in the lengthwise direction of the gear teeth. ( $\varphi_{b,g} = \varphi_{b,op}$ , $\varphi_{b,p} = \varphi_{b,op}$ )	Bevel gears, spiral bevel gears, and so forth, cut on gear generators with a cutting tool with a nonzero profile angle ( $\phi_c > 0^\circ$ ). ( $\varphi_{b,g} \neq \varphi_{b,op}$ , $\varphi_{b,p} \neq \varphi_{b,op}$ )
Crossed-axes gearing ( $C_a$ – gearing)	Crossed-axes $R$ – gearing <sup>c</sup> used for various tooth flank geometries in the lengthwise direction of the gear teeth. ( $\varphi_{b,g} = \varphi_{b,p}$ )	Crossed-axes $S_{pr}$ – gearing <sup>c</sup> used in hypoid, worm gears, and so forth. ( $\varphi_{b,g} = \varphi_{b,op}$ , $\varphi_{b,p} = \varphi_{b,op}$ )	Hypoid gearing; <i>Spiroid</i> gearing; double enveloping worm gears, $ZA$ –, $ZC$ –, $ZN$ – worm gearing; and so forth. ( $\varphi_{b,g} \neq \varphi_{b,op}$ , $\varphi_{b,p} \neq \varphi_{b,op}$ )

<sup>a</sup> Proposed by *Leonhard Euler* in 1760.

<sup>b</sup> Was known to *George Grant* (see U.S. Pat. No. 407.437 of July 23, 1889; this patent is granted to him for a gear cutting machine). However, it should be stressed here that the concept of the *angular base pitch* was not known to *G. Grant*. The concept of the *angular base pitch* was introduced later by Dr. *S.P. Radzevich*.

<sup>c</sup> Proposed by Dr. *S.P. Radzevich* in around 2008.

*Real (approximate) gearing* features tooth flank geometry of a gear and of a pinion that deviates from the geometry in geometrically accurate gearing, as well as in  $S_{pr}$  – gearing. Real (approximate) gears are not capable of transmitting a smooth rotation from a driving shaft to a driven shaft.

Gear vector diagrams for all possible types of geometrically accurate gear pairs are classified in Figure 2.16. For every gear vector diagram, a corresponding gear pair can be designed. For a specified configuration of the rotation vectors of the gear,  $\omega_g$ , and of the pinion,  $\omega_p$ , and for a given rotation and torque on the input shaft, a unique desirable gear pair can be synthesized.

Similar (see Chapter 2, Figure 2.16), a classification of gear vector diagrams can be developed for the case of desirable real gearing, namely, for  $S_{pr}$  – gearing. Again, for a specified configuration of the rotation vectors of the gear,  $\omega_g$ , and the pinion,  $\omega_p$ , and for a given rotation and torque on the input shaft, a unique desirable gear pair can be synthesized. In this latter case, permissible displacement of the gear and the pinion has to be specified.

Finally, no classification of real (approximate) gearing can be developed as number of possible kinds of gears of this kind is endless (however, certain exclusions are permissible). For a specified configuration of the rotation vectors of the gear,  $\omega_g$ , and the pinion,  $\omega_p$ , multiple real (approximate) gear pair can be designed.

The discussion in this chapter of the book is summarized as follows:

- Root causes for real gears differ from geometrically accurate gears are identified. For the convenience of the analysis, different reference systems are used, and transition from one of the coordinate systems to another one is analytically described by the corresponding operators of the coordinate system transformation
- Displacements of a gear axis of rotation from its desirable configuration are discussed, and are described analytically. For this purpose, the closest distance of approach between axes of rotation of a gear and of a mating pinion is determined
- Tooth flank geometry in geometrically accurate real gearing is determined. The gearing of the proposed design is referred to as the  $S_{pr}$  – gearing. For this purpose, the adopted concept for tooth flank generation is formulated, and preferred reference systems are identified. Equations for the position vectors of a point,  $\mathbf{r}_g$  and  $\mathbf{r}_p$ , of a gear tooth flank,  $\mathcal{S}_g$ , and that of a mating pinion tooth flank,  $\mathcal{P}_p$ , are derived. Angular base pitch in  $S_{pr}$  – gearing is specified, and features of interaction of the tooth flanks are discussed
- It is shown that the concept of  $S_{pr}$  – gearing cannot be applied to gear systems that feature point contact between tooth flanks: in conformal gearing (namely, in *Novikov gearing*), as well as in high-conformal gearing
- Correlation among gear systems of various kinds is outlined.

An in-depth understanding of the kinematics, of the geometry, and of the interaction between the tooth flanks can help to identify appropriate areas of application of geometrically accurate *gearing with point contact between the tooth flanks of a gear and a mating pinion*.



# Taylor & Francis

Taylor & Francis Group

<http://taylorandfrancis.com>

# Part IV

---

## $C\Sigma u$ – Variable Gearing

Gear pairs, those discussed in the previous chapters of the book, feature the fundamental design parameters: the center distance,  $C$ , the crossed-axes angle,  $\Sigma$ , and the angular velocity ratio,  $u$ , of certain constant values. Gearing of this kind is referred to as the  $C\Sigma u$  – constant gearing. Gear pairs with the design parameters  $C$ ,  $\Sigma$ , and  $u$ , of constant values are extensively used in the present-day practice.

Along with  $C\Sigma u$  – constant gear pairs, gear pairs with variable in time fundamental design parameters: the center distance,  $C = C(t)$ , the crossed-axes angle,  $\Sigma = \Sigma(t)$ , and the angular velocity ratio,  $u = u(t)$ , are also known for a long time (here time is denoted as “ $t$ ”). Either one, or two, or even three design parameters in a gear pair ( $C$ ,  $\Sigma$ , and  $u$ ), may be variable in time. Here and below, the time “ $t$ ” can be substituted with a current value of the angle of rotation,  $\phi_{\text{driving}}$ , of the driving gear.

In contrast to  $C\Sigma u$  – constant gearing, gearing that features all three fundamental design parameters variable, are referred to as the  $C\Sigma u$  – variable gearing<sup>1</sup>. Further,  $C\Sigma u$  – variable gearing is referred to just as  $C\Sigma u$  – var gearing, for simplicity. Possible kinds and potential capabilities of  $C\Sigma u$  – var gearing, are briefly discussed below in this section of the book.

Despite all the kinds of gear pairs (parallel-axes gear pairs, intersected-axes gear pairs, and crossed-axes gear pairs) being covered by the term  $C\Sigma u$  – var gearing, the discussion below is focused, but not entirely limited to, non-circular gears. Mainly, this is due to the lack of knowledge and experience on  $C\Sigma u$  – var gearing of other kinds.

This chapter is the author’s to illustrate the potential capabilities of  $C\Sigma u$  – var gearing. Features of the kinematics, and of the geometry of tooth flanks of a gear and of a mating pinion are briefly outlined in this chapter. A novel concept to design geometrically accurate non-circular gear pairs is disclosed (and, in this way, the inconsistencies of the known approach to design and manufacturing non-circular gears are illustrated).

Part V of the book consists of a single Chapter 17 is titled “ $C\Sigma u$  – Variable Gears: Kinematics, Geometry, and Novel Concept to Design Geometrically-Accurate Gears.” Every particular kind of  $C\Sigma u$  – var gear pairs deserves to be considered in a separate chapter. A room for more chapters is intentionally left here, as  $C\Sigma u$  – var gearing has a huge potential for growth in the future.

---

<sup>1</sup> The term *Variable-Kinematic-Parameters Gearing* (or just *VKP – gearing*, for simplicity) was considered as an alternative to the term  $C\Sigma u$  – variable gearing. The preference is given to the term  $C\Sigma u$  – variable gearing, or just to the term  $C\Sigma u$  – var gearing, for simplicity.



# Taylor & Francis

Taylor & Francis Group

<http://taylorandfrancis.com>

---

# 18 $C\Sigma u$ -var Gears

## *Kinematics, Geometry, and Novel Concept to Design Geometrically Accurate Gears*

The concept of non-circular gears<sup>1</sup> originates from the precursors of engineering thought. Gears of such a design were sketched by *Leonardo da Vinci*. In the present-day industry, they found their application in many mechanical devices. Two examples are depicted in Figure 18.1. In the past, lots of efforts to investigate non-circular gears were undertaken by *Franz Reuleaux*.

Not too much is done to this end in the field of  $C\Sigma u$ -var gearing. Research by *C.-F. Chen* and *C.-B. Tsay* (2004) on elliptical gearing with circular-arc teeth is among just a few to be mentioned in this regard [19]. The recent accomplishments in the field are summarized in Ref. [77]. This book in much is a refinement of the earlier published book on the topic [78]. A contribution to the field by Prof. *D.B. Dooner* [28] also needs to be mentioned here.

The present-day literature pertaining to the design and manufacture of  $C\Sigma u$ -var gears are much less developed than that on gearing of other design.

It is often noted on the lack of correct methods of generation of non-circular gears, where the efforts are mainly focused on the methods that are based on the meshing of generating tools with master gears.

The use of the known methods of generation of tooth flanks in non-circular gears return sufficient results as long as no tight tolerances on the accuracy of the output rotation are imposed: non-circular gears are used in the design of toys, and so forth. No sufficient output can be received if these methods are used to the gears applied in the design of precise mechanisms.

The salient theme of this section of the book is to develop a general theory of geometrically accurate  $C\Sigma u$ -var gearing, gearing that is capable of smoothly transmitting power (motion and torque) from a driving shaft to a driven shaft. The end result is a novel approach in the theory of meshing of  $C\Sigma u$ -var gears. This approach has to be valid for:

- a. external gear pairs
- b. internal gear pairs, as well as to
- c. gear-to-rack gear pairs

Such a gear theory is briefly outlined below in this chapter of the book. The discussion is focused on  $C\Sigma u$ -var gearing, as non-circular gearing can be viewed as a reduces case of  $C\Sigma u$ -var gearing.

---

<sup>1</sup> It is instructive to note here that it is common practice to define the term *gear* as "... a rotating *circular* machine part having cut teeth." Therefore, certain contradiction is observed when combining the words *gear* and *non-circular* together. No contradiction is observed when the term  $C\Sigma u$ -var gearing is used instead. Moreover,  $C\Sigma u$ -vargearing can be composed of circular gears as well (A gear pair that is composed of two eccentric spur gears is a good example in this regard).



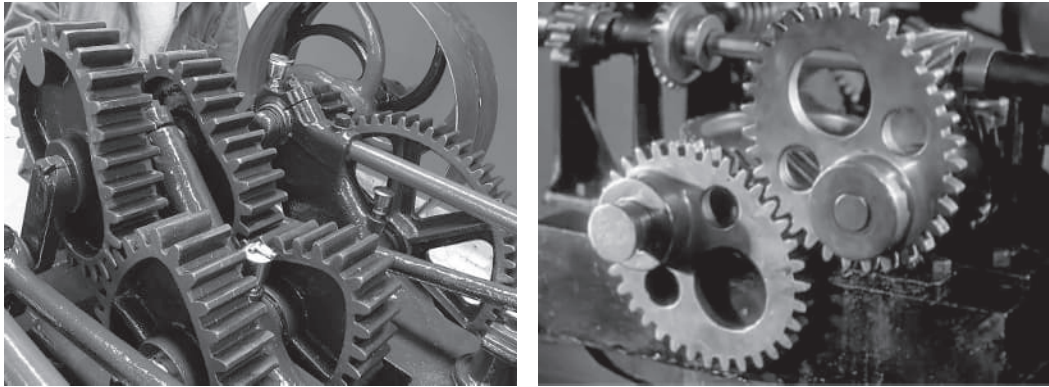


FIGURE 18.1 Examples of application of non-circular gearing.

### 18.1 PREAMBLE: PERMISSIBLE VARIATION OF DESIGN PARAMETERS IN EQUIVALENT PULLEY-AND-BELT TRANSMISSION

*Equivalent Pulley-and-Belt Transmission* is an effective mean to perform the analysis of permissible variation of the design parameters in a gear pair.

Let's begin the discussion from the analysis of the influence of the actual values of the diameters,  $d_1$  and  $d_2$ , of two pulleys on the actual value of the transverse angle,  $\phi_t$ .

For an arbitrary configuration of the pulleys, a corresponding geometrically accurate parallel-axes gear pair can be designed. This is possible because of the following.

**First**, each of the pulleys of diameters  $d_1$  and  $d_2$  can be construed as envelopes to a family of consecutive positions of a line along the straight-line segment,  $ab$ . As it is shown below in the further analysis, a line along the straight-line segment,  $ab$ , is by nature, the line of action,  $LA$ , in the corresponding gear pair. The pulley can be construed as an envelope to a family of consecutive positions of the line of action,  $LA$ , in their motion in relation to a reference associated with the pulley.

**Second**, consider an arbitrary point within the straight portion  $ab$  of the belt. When the *equivalent pulley-and-belt transmission* operates, point traces in a motionless reference system a corresponding path of contact,  $P_c$ . Evidently that in parallel-axes gearing, the path of contact,  $P_c$ , is a straight line that is aligned to the line of action,  $LA$ . This makes it possible to interpret the path of contact,  $P_c$ , as an envelope (i.e., a reduced case of envelope) to a family of the instantaneous lines of action,  $LA$ , when the pulleys rotate.

Another scenario is observed when a rotary motion from a driving shaft to a driven shaft is transmitted by means of two pulleys diameters of which,  $d_1$  and  $d_2$ , are time-dependent, that is, certain functions  $d_1 = d_1(t)$  and  $d_2 = d_2(t)$  are valid. [This feature can also be interpreted as  $d_1 = d_1(\varphi_1)$  and  $d_2 = d_2(\varphi_1)$ , where  $\varphi_1$  and  $\varphi_2$  are the angles of rotation of the pulleys of diameters  $d_1$  and  $d_2$ , and  $\varphi_2 = \varphi_1 \cdot (d_2/d_1)$ ]. Shown in Figure 18.2, schematic corresponds to a case when the belt (the line of action,  $LA$ ) travels back and forth along the centerline,  $\Phi$ . No gear pair equivalent to the *equivalent pulley-and-belt transmission* (see Figure 18.2) can be designed.

Let us assume that the transverse angle  $\phi_t$  is of a constant value ( $\phi_t = \text{const}$ ), while the pitch point,  $P$ , is migrating within the line of centers,  $\Phi$ , depending on the current value of the rotation angle,  $\varphi_p$ , of the pinion (or, the same, of the rotation angle,  $\varphi_g$ , of the gear), as schematically illustrated in Figure 18.2. In such a scenario, for any instantaneous position of the line of action,  $LA_i$ , instantaneous radii of the pulleys,  $r_{b,g}^{(i)}$  and  $r_{b,p}^{(i)}$  (i.e., the base circles, for the gear and the pinion) can

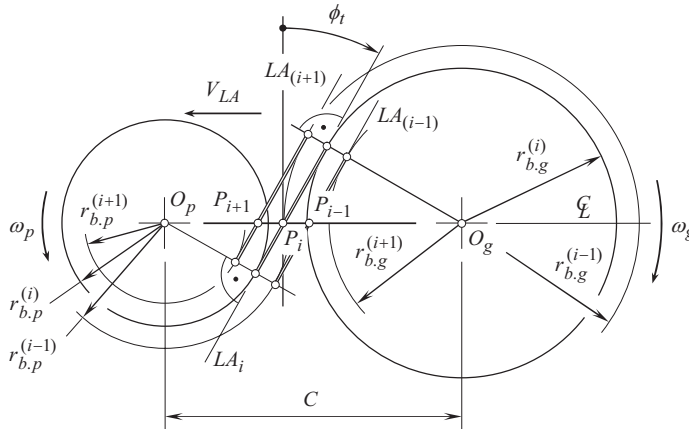


**FIGURE 18.2** Infeasibility of transmitting a rotary motion when the line of action,  $LA_i$ , travels back and forth along the centerline,  $\Phi$ :  $\phi_t = \text{const}$ ,  $r_{b,g} = r_{b,g}(\varphi_g)$ ,  $r_{b,p} = r_{b,p}(\varphi_g)$ .

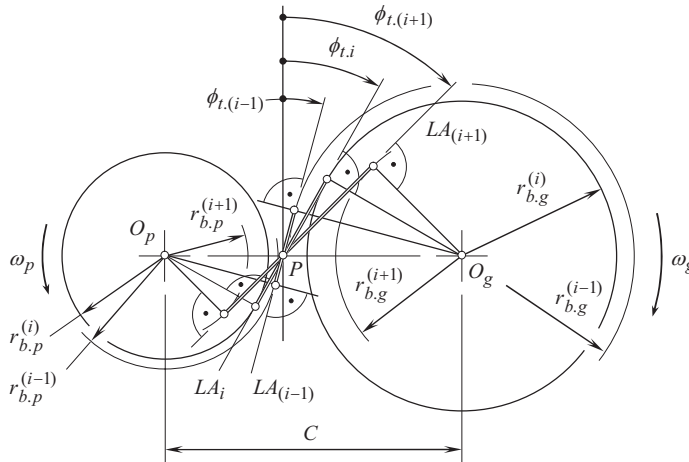


**FIGURE 18.3** Infeasibility of a geometrically accurate parallel-axes gear pair with a constant angular velocity ratio and continuously altering transverse pressure angle [ $\phi_t = \phi_t(\varphi_g)$ ,  $r_{b,g} = r_{b,g}(\varphi_g)$ , and  $r_{b,p} = r_{b,p}(\varphi_g)$ ].

be constructed. The profile of the transverse section of the pulleys (namely, of the profile of the base curve for the gearing) can be specified in terms of the instantaneous lines of action  $LA_{(i-1)}$ ,  $LA_i$ , and  $LA_{(i+1)}$ , and of the radii  $r_{b,p}^{(i-1)}$ ,  $r_{b,p}^{(i)}$ , and  $r_{b,p}^{(i+1)}$  [and  $r_{b,g}^{(i-1)}$ ,  $r_{b,g}^{(i)}$ , and  $r_{b,g}^{(i+1)}$ ] of the instantaneous base circles. Such a profile does not exist as no envelope curve can be constructed to a family of circles of different radii, and with a common center. No path of contact,  $P_c$ , is possible in the case under consideration. Ultimately, no gear tooth profile that is capable of transmitting a rotary motion from a driving shaft to a driven shaft (no gearing equivalent to the *pulley-and-belt transmission*, shown in Figure 18.2) is feasible at all. The considered translation of the instantaneous line of action along the centerline,  $\Phi$ , is not permissible.

A scenario when an instantaneous line of action,  $LA_{\text{inst}}$ , turns about the pitch point,  $P$ , when the gears rotate, is illustrated in Figure 18.3. Shown in Figure 18.3 situation is similar to that just considered in Figure 18.2. When the pulleys rotate, the angle formed by the belt and a by perpendicular to the centerline (the pressure angle,  $\phi_t$ , in other words) is continuously altering, and the line of action,  $LA$ , always is a straight line through the pitch point,  $P$ . Once the transverse pressure angle

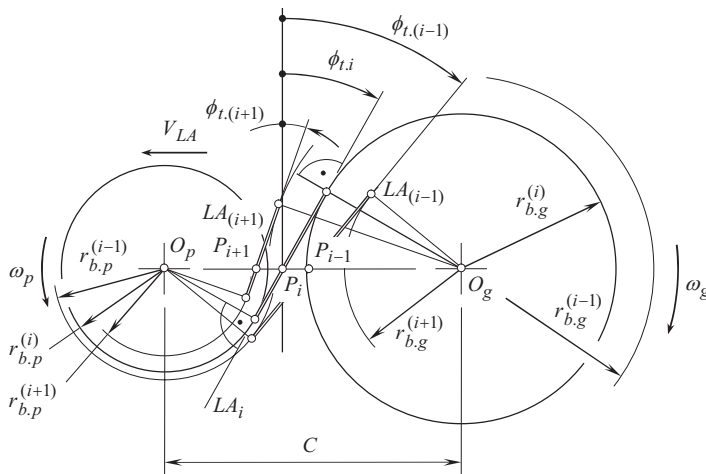


**FIGURE 18.4** Possibility of transmitting a rotary motion when an instantaneous line of action travels back and forth along the centerline,  $\Phi$ , and turns about the pitch point,  $P$ :  $\phi_t = \text{Const}$ ,  $r_{b,g} = r_{b,g}(\varphi_g)$ ,  $r_{b,p} = r_{b,p}(\varphi_p)$ .

is continuously altered, then at every instant of time an instantaneous line of action,  $LA_{\text{inst}}$ , can be constructed. Considered in a stationary reference system, no envelope to the family of consecutive positions of the instantaneous lines of action,  $LA_{\text{inst}}$ , can be constructed. This means that no path of contact,  $P_c$ . Ultimately, no gear tooth profile that is capable of transmitting a rotary motion from a driving shaft to a driven shaft can be generated at all. No pure rotation of the instantaneous line of action,  $LA_i$ , about the pitch point,  $P$ , is permissible in geometrically accurate parallel-axes gearing.

However, when both the motions, namely, a rotation of the instantaneous line of action,  $LA_{\text{inst}}$ , about the pitch point,  $P$ , and a translation of the instantaneous line of action,  $LA_{\text{inst}}$ , along the centerline,  $\Phi$ , are performed simultaneously, gear teeth of a complex geometry can be generated (see Figure 18.4). In the case under consideration, the path of contact,  $P_c$ , is a planar curve that is an envelope to the family of the instantaneous lines of action,  $LA_i$ . Angular velocity ratio,  $u$ , in Figure 18.4 is time-dependent, that is, an equality  $u = u(t)$  is valid [or  $u = u(\varphi_1)$ ].

The just mentioned path of contact,  $P_c$ , (a planar curve that is an envelope to the family of the instantaneous lines of action,  $LA_i$ ), is shown in Figure 18.5. The path of contact,  $P_c$ , is traced by contact point,  $K$ . At every point of the path of contact,  $P_c$ , a corresponding *instantaneous line of action*,  $LA_{\text{inst}}$ , can be constructed. All the instantaneous lines of action,  $LA_i$ , are tangent to the path of contact,  $P_c$ , at the corresponding point.

Arbitrary contact point within the path of contact,  $P_c$ , is labeled as  $K^i$ . When a gear, and a mating pinion, make contact at point  $K^i$ , the instantaneous line of action,  $LA_{\text{inst}}^i$ , is in tangency to the path of contact,  $P_c$ , at  $K^i$ . This is because the force exerted from the driving pinion is pointed along the common perpendicular to the interacting tooth flanks,  $\mathcal{S}$  and  $\mathcal{P}$ , considered in a transverse section of the gear pair, or, the same, the force is pointed along a straight-line tangent at contact point  $K^i$  to the path of contact,<sup>2</sup>  $P_c$ . [Friction forces are not involved yet into the analysis at this point].

Gears of the just considered kind allow for variation of the tangential component of the resultant force of interaction of the teeth in a gear pair.<sup>3</sup>

<sup>2</sup> It is right point to stress here that in non-spur gear pairs it is incorrect to interpret the line of action,  $LA$ , as a straight line perpendicular to the tooth flanks,  $\mathcal{S}$  and  $\mathcal{P}$ , of a gear, and of a mating pinion at contact point,  $K$ . The line of action,  $LA$ , should be considered as a line within the transverse section plane that, in the case of  $P_a$ -gearing, is perpendicular to the axes of rotation,  $O_g$  and  $O_p$ , of the gear and the pinion.

<sup>3</sup> This concept is used, for example, in the design of a gear pair for fluctuating limited slip automobile differentials (see: U.S. Pat. No. 8,070,640, *Fluctuating Gear Ratio Limited Slip Differential*, S.P. Radzevich, Date: December 6, 2011, Filed: March 12, 2009, Int. Cl. F16H 48/06, F16H 48/20, F16H 57/08, F16H 57/17, U.S. Cl. 475/230, [122]).

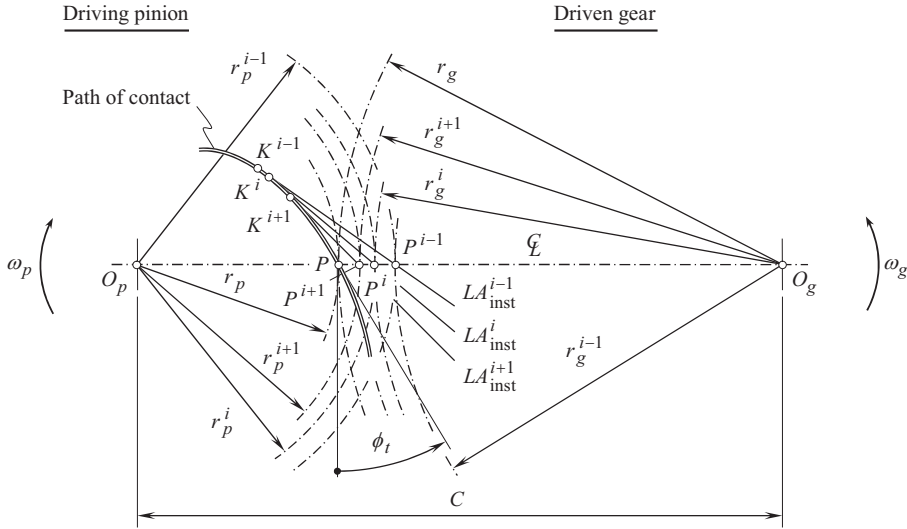


**FIGURE 18.5** Schematic of a parallel-axes gearing that features a curved path of contact,  $P_c$ .

The schematics, shown in Figures 18.4 and 18.5, are useful for the investigation and the development of non-circular gearing that features variable angular velocity ratio,  $u = u(t)$ .

## 18.2 FUNDAMENTALS OF GEOMETRICALLY ACCURATE CΣu-var GEARING

Non-circular gear pairs are designed and manufactured solely with the goal to transmit a power (motion and torque) from a driving gear to a driven gear with a pre-specified function of the angular velocity ratio, namely,  $u = u(\varphi_{\text{input}})$ . Gear pairs of this particular kind can be viewed either as *u-variable gear pairs* (or *CΣ-constant gear pairs*) where either an equality,  $\Sigma = 0^\circ$ , or an equality,  $\Sigma = 180^\circ$ , is valid.

As an example, gear vector diagram constructed for parallel-axes non-circular gearing is shown in Figure 18.6.

Having the gear vector diagram constructed, a CΣu-var gear pair has to be designed so, as to strictly comply with three fundamental laws of gearing. This means that in geometrically accurate CΣu-var gear pair at every instant of time (namely, for any and all possible angular configurations of a gear and of a mating pinion), the following three requirements are fulfilled:

1. the law of contact of the interacting tooth flanks,  $\mathcal{S}$  and  $\mathcal{P}$ , of a gear and of a mating pinion is fulfilled, and the equality,  $\mathbf{n}_g \cdot \mathbf{v}_\Sigma = 0$ , is valid
2. the conjugate action law for the interacting tooth flanks,  $\mathcal{S}$  and  $\mathcal{P}$ , is valid – at every instant of time, the common perpendicular,  $\mathbf{n}_g$ , is pointed along a straight line through pitch point,  $P$ , in its current location in relation to the axes,  $O_g$  and  $O_p$ , of the gear and the mating pinion
3. instantaneous values of the angular base pitches of a gear and of a mating pinion have to be equal to the corresponding instantaneous value of the operating base pitch in the gear pair

If all three fundamental laws of gearing are fulfilled when designing a CΣu-var gear pair, then the actual value of angular velocity ratio:

$$u(\varphi_{\text{input}}) = \frac{\omega_p}{\omega_g(\varphi_{\text{input}})} \quad (18.1)$$

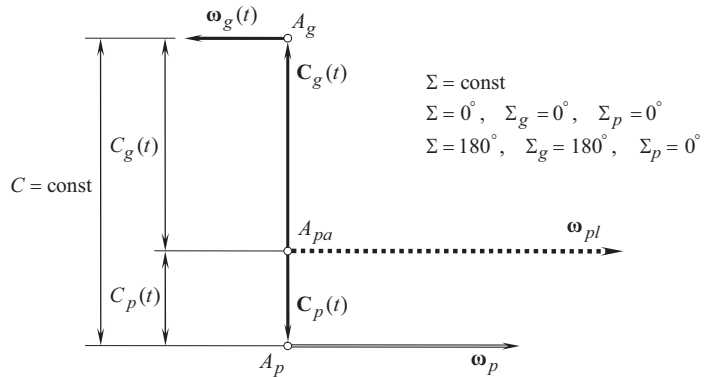


**FIGURE 18.6** Gear vector diagram constructed for an external non-circular gear pair:  $u$  – variable gear pair (the crossed-axes angle,  $\Sigma$ , is of a constant value,  $\Sigma = \text{const}$ , and can be equal either  $\Sigma = 0^\circ$  or  $\Sigma = 180^\circ$ ).

exactly corresponds to a predesigned function, a uniform input rotation is transmitted smoothly, and no fluctuation in the output rotation occurs. This can be adopted as a definition of the term *geometrically accurate  $C\Sigma u$  – var gear pair*.

### 18.3 CLASSIFICATION OF GEAR VECTOR DIAGRAMS OF $C\Sigma u$ – var GEAR PAIR

$C\Sigma u$  – var gearing can be construed as the most general kind of gearing. Varying each of the principal design parameters:  $C = C(t)$ ,  $\Sigma = \Sigma(t)$ , and  $u = u(t)$  (individually, or in any and all possible combinations), gearing of all known kinds, namely,  $P_a$  – gearing,  $I_a$  – gearing, and  $C_a$  – gearing, can be obtained [here  $t$  is time; an angle,  $\varphi_{\text{input}}$ , through which the input shaft is turned about its axis of rotation, may be employed as an alternative parameter in terms of which the actual values of the principal design parameters,  $C = C(\varphi_{\text{input}})$ ,  $\Sigma = \Sigma(\varphi_{\text{input}})$ , and  $u = u(\varphi_{\text{input}})$ , can be expressed].

When the gears rotate, the principal design parameters may vary either independently from one another or their alterations can be synchronized with one another. In this way, different reduced designs of  $C\Sigma u$  – var gear pairs are obtained.

A possibility of classification of gear vector diagrams begins with that constructed for the most general kind of  $C\Sigma u$  – var gearing. A gear vector diagram of this kind is shown in Figure 18.7. The gear vector diagram in Figure 18.7 features all three fundamental design parameters,  $C$ ,  $\Sigma$ , and  $u$ , variable.

The gear vector diagrams of  $C\Sigma u$  – gear pairs kind can be classified on the premise of the features of mobility of gearing of a corresponding design (see Figure 18.8). Four stratum are distinguished in the classification.

The gear vector diagrams of  $C\Sigma u$  – var gearing with all three principal design parameters,  $C$ ,  $\Sigma$ , and  $u$ , variable, comprise the first stratum I of the classification. Here, the principal design parameters,  $C$ ,  $\Sigma$ , and  $u$ , are varying independently from one another. A plurality of designs of  $C\Sigma u$  – var gearing, which feature various combinations of depending principal design parameters [ $\Sigma = \Sigma(C)$ ,  $u = u(C)$ ;  $C = C(\Sigma)$ ,  $u = u(\Sigma)$ ;  $C = C(u)$ ,  $\Sigma = \Sigma(u)$ ,  $C = C(\Sigma, u)$ ,  $\Sigma = \Sigma(C, u)$ , and  $u = u(C, \Sigma)$ ], can be construed as reduced cases of  $C\Sigma u$  – var gearing.

The second stratum II of the classification is comprised by the diagrams of  $C\Sigma u$  – var gearing with two of three principal design parameters variable. They are represented with  $C\Sigma$  – var gear

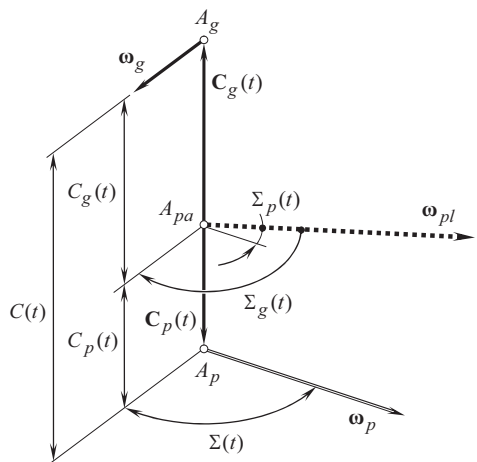


FIGURE 18.7 Gear vector diagram with three variable fundamental design parameters: of a  $C\Sigma u$ -gear pair.

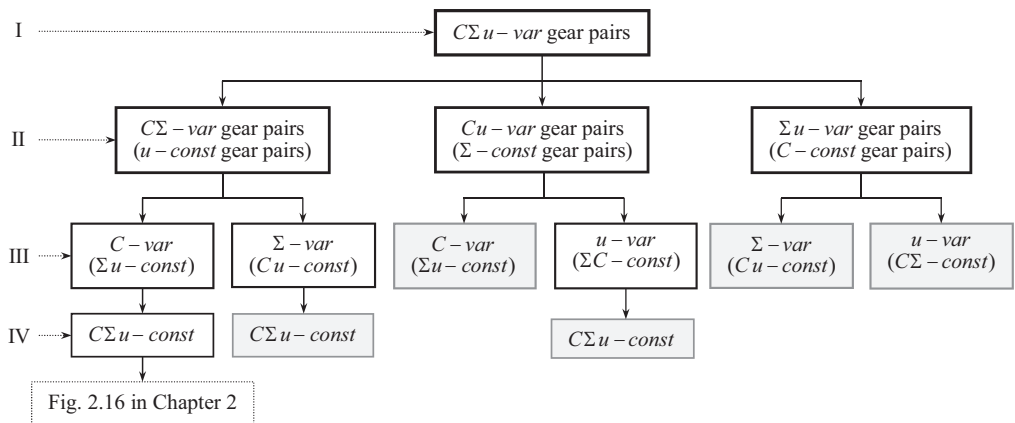
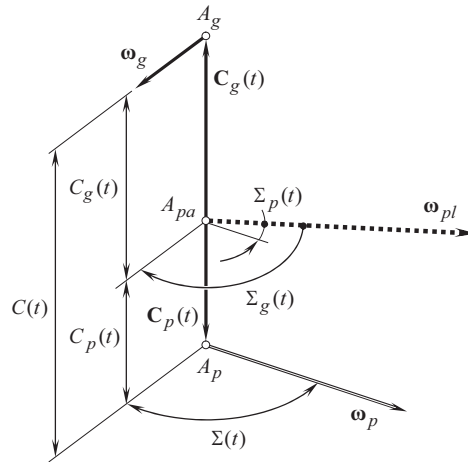


FIGURE 18.8 Four stratum of the classification of gear vector diagrams for  $C\Sigma u$ -var gearing.

pairs,  $Cu$ -var gear pairs, and  $\Sigma u$ -var gear pairs. The gear vector diagrams of these kinds can also be referred to as  $u$ -const gear pairs,  $\Sigma$ -const gear pairs, and  $C$ -const gear pairs, correspondingly.

The third stratum III of the classification is composed of the gear vector diagrams of  $C\Sigma u$ -var gearing that feature a single principal design parameters variable. There are only three kinds of gear vector diagrams of the kind under consideration. They are as follows:  $C$ -var gear pairs,  $\Sigma$ -var gear pairs, and  $u$ -var gear pairs. The gear vector diagrams of these kinds can also be referred to as  $\Sigma u$ -const gear pairs,  $Cu$ -const gear pairs, and  $\Sigma u$ -const gear pairs, correspondingly. The alternative possibilities of deriving each of these three kinds of gear vector diagrams in z8\_Figure 2A.31 are shadowed.

Finally, the fourth stratum IV of the classification is composed of the gear vector diagrams of  $C\Sigma u$ -var gearing that feature no principal design parameters variable. The gear vector diagram of this kind is represented with the only one, namely, with a gear vector diagram for  $C\Sigma u$ -const gear pairs. There are numerous ways, in which the gear vector diagram for  $C\Sigma u$ -const gear pairs can be derived. The alternative possibilities of deriving the gear vector diagram for  $C\Sigma u$ -const gear pairs are not shown in Figure 18.8.



**FIGURE 18.9** Gear vector diagram of gear pairs with three variable fundamental design parameters: of a  $C\Sigma u$  – var gear pair.

With that said, various types of gear vector diagrams of gear pairs with variable fundamental design parameters are distinguished:

- I.1. Gear vector diagrams of gear pairs with three variable fundamental design parameters (see Figure 18.9):
  - I.1.1. Rotary-negative  $C\Sigma u$  – variable gear pairs (see #1.1 in Figure 2.16)
  - I.1.2. Rotary-zero  $C\Sigma u$  – variable gear pairs (see #1.2 in Figure 2.16)
  - I.1.3. Rotary-positive  $C\Sigma u$  – variable gear pairs (see #1.3 in Figure 2.16)
- II.2. Gear vector diagrams of gear pairs with two variable fundamental design parameters (see Figure 18.10):
  - II.2.1. Rotary-negative  $\Sigma u$  – variable gear pairs:  $C = \text{const} \neq 0$  (see #1.1 in Figure 2.16)
  - II.2.2. Rotary-negative  $Cu$  – variable gear pairs:  $\Sigma = \text{const} \neq 0$  (see #1.1 in Figure 2.16)
  - II.2.3. Rotary-negative  $C\Sigma$  – variable gear pairs:  $u = \text{const}$  (see #1.1 in Figure 2.16)
  - II.2.4. Rotary-zero  $\Sigma u$  – variable gear pairs:  $C = \text{const} \neq 0$  (see #1.2 in Figure 2.16)
  - II.2.5. Rotary-zero  $Cu$  – variable gear pairs:  $\Sigma = \text{const} \neq 0$  (see #1.2 in Figure 2.16)
  - II.2.6. Rotary-zero  $C\Sigma$  – variable gear pairs:  $u = \text{const}$  (see #1.2 in Figure 2.16)
  - II.2.7. Rotary-positive  $\Sigma u$  – variable gear pairs:  $C = \text{const} \neq 0$  (see #1.3 in Figure 2.16)
  - II.2.8. Rotary-positive  $Cu$  – variable gear pairs:  $\Sigma = \text{const} \neq 0$  (see #1.3 in Figure 2.16)
  - II.2.9. Rotary-positive  $C\Sigma$  – variable gear pairs:  $u = \text{const}$  (see #1.3 in Figure 2.16)
- II.3. Gear vector diagrams of gear pairs with two variable fundamental design parameters (see Figure 18.11):
  - II.3.1. Rotary-negative  $\Sigma u$  – variable gear pairs:  $C = 0$  (see #1.1.1 in Figure 2.16)
  - II.3.2. Rotary-zero  $\Sigma u$  – variable gear pairs:  $C = 0$  (see #1.2.1 in Figure 2.16)
  - II.3.3. Rotary-positive  $\Sigma u$  – variable gear pairs:  $C = 0$  (see #1.3.1 in Figure 2.16)
- I.4. Gear vector diagrams of gear pairs with two variable fundamental design parameters (see Figure 18.12):
  - I.4.1. Rotary-negative  $Cu$  – variable gear pairs:  $\Sigma = 0^\circ$  (see #1.1.2 in Figure 2.16)
  - I.4.2. Rotary-zero  $Cu$  – variable gear pairs:  $\Sigma = \text{const} \neq 0^\circ$  (see #1.2.2 in Figure 2.16)
  - I.4.3. Rotary-positive  $Cu$  – variable gear pairs:  $\Sigma = 180^\circ$  (see #1.3.2 in Figure 2.16)
- III.5. Gear vector diagrams with one variable fundamental design parameter (see Figure 18.13):
  - III.5.1. Rotary-negative  $C$  – variable gear pairs:  $\Sigma = \text{const}$ ,  $u = \text{const}$  (see #1.1 in Figure 2.16)
  - III.5.2. Rotary-negative  $\Sigma$  – variable gear pairs:  $C = \text{const}$ ,  $u = \text{const}$  (see #1.1 in Figure 2.16)



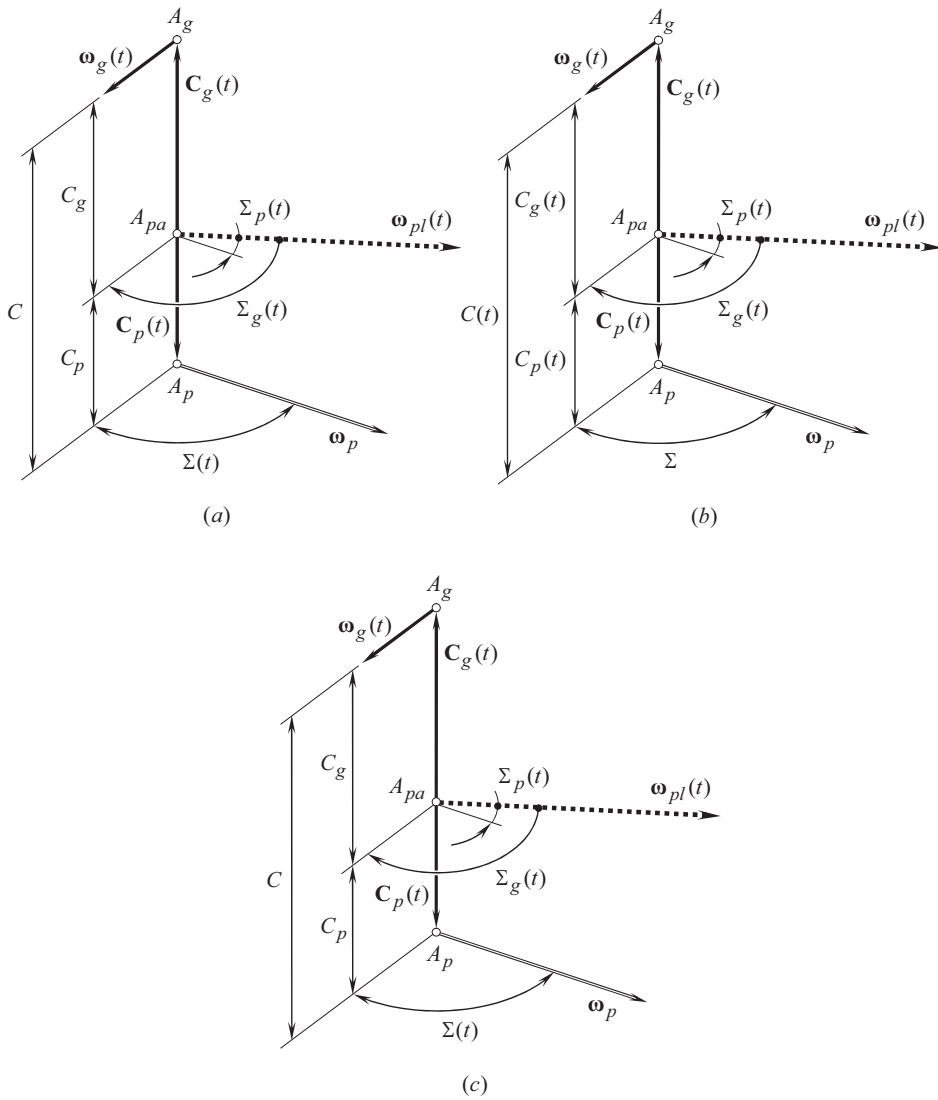


**FIGURE 18.10** Gear vector diagrams of gear pairs with two variable fundamental design parameters: of (a)  $\Sigma u$ -var gear pair (or  $C$ -const gear pair); (b)  $Cu$ -var gear pair (or  $\Sigma$ -const gear pair); and (c)  $\Sigma C$ -var gear pair (or  $u$ -const gear pair).

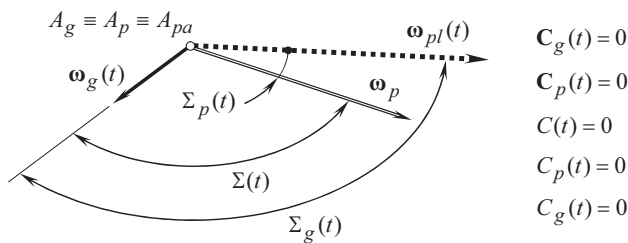


**FIGURE 18.11** Gear vector diagrams of gear pairs with two variable fundamental design parameters: of  $\Sigma u$ -variable gear pair (or  $C$ -constant gear pair,  $C = 0$ ).



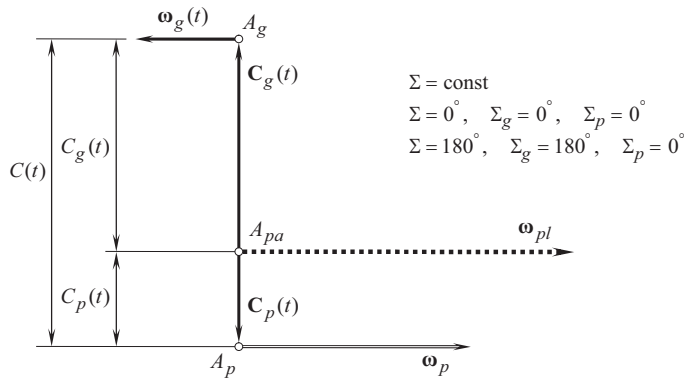


**FIGURE 18.12** Gear vector diagram of gear pairs with three variable fundamental design parameters: of a  $Cu$  – variable gear pair (the crossed-axes angle,  $\Sigma$ , is of a constant value,  $\Sigma = \text{const}$ , and can be equal either  $\Sigma = 0^\circ$  or  $\Sigma = 180^\circ$ ).

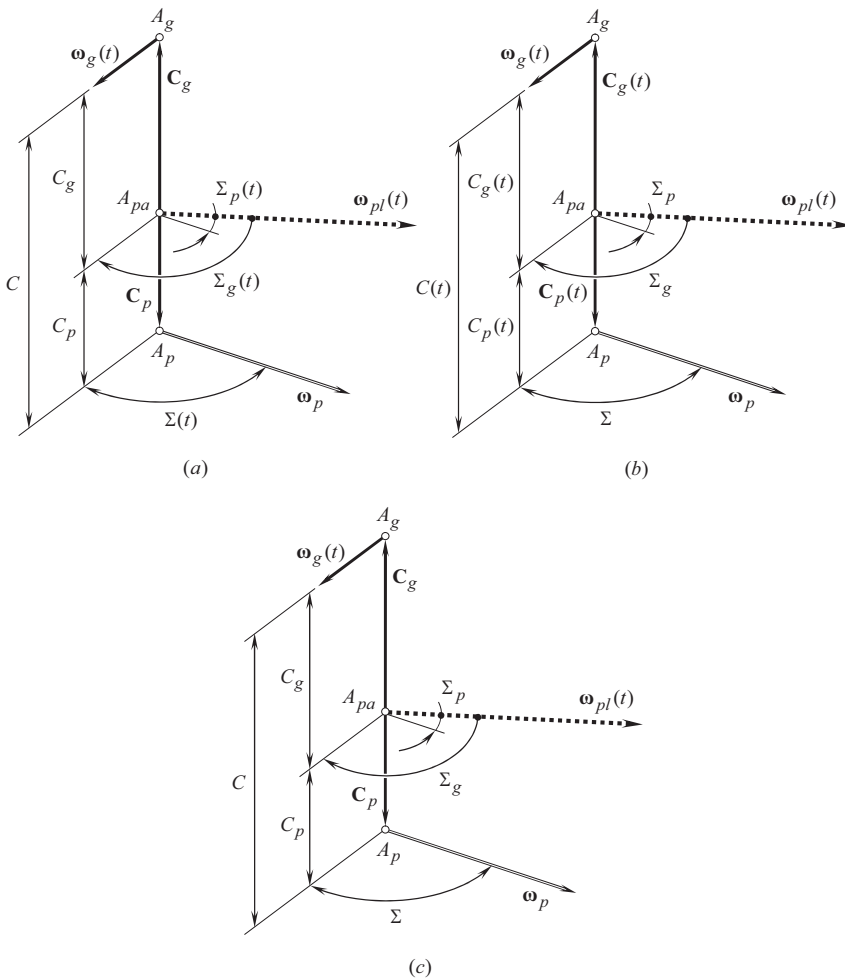


**FIGURE 18.13** Gear vector diagram of gear pairs with one variable fundamental design parameter: of (a)  $\Sigma$  – variable gear pair (or  $C, u$  – constant gear pair); (b)  $C$  – variable gear pair (or  $\Sigma, u$  – constant gear pair); and (c)  $u$  – variable gear pair (or  $\Sigma, C$  – constant gear pair) – not feasible.

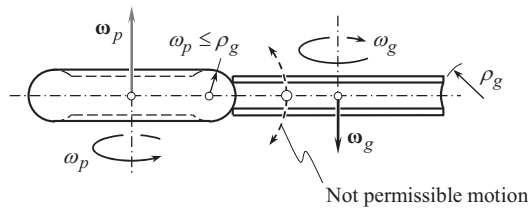


**FIGURE 18.14** Toroidal gears for transmitting a rotary motion between parallel shafts.

- III.5.3. Rotary-negative  $u$  – variable gear pairs:  $C = \text{const}$ ,  $\Sigma = \text{const}$  (see #1.1 in Figure 2.16)
- III.5.4. Rotary-zero  $C$  – variable gear pairs:  $\Sigma = \text{const}$ ,  $u = \text{const}$  (see #1.2 in Figure 2.16)
- III.5.5. Rotary-zero  $\Sigma$  – variable gear pairs:  $C = \text{const}$ ,  $u = \text{const}$  (see #1.2 in Figure 2.16)
- III.5.6. Rotary-zero  $u$  – variable gear pairs:  $C = \text{const}$ ,  $\Sigma = \text{const}$  (see #1.2 in Figure 2.16)
- III.5.7. Rotary-positive  $C$  – variable gear pairs:  $\Sigma = \text{const}$ ,  $u = \text{const}$  (see #1.3 in Figure 2.16)
- III.5.8. Rotary-positive  $\Sigma$  – variable gear pairs:  $C = \text{const}$ ,  $u = \text{const}$  (see #1.3 in Figure 2.16)
- III.5.9. Rotary-positive  $u$  – variable gear pairs:  $C = \text{const}$ ,  $\Sigma = \text{const}$  (see #1.3 in Figure 2.16)
- VI.6. Gear vector diagrams with zero variable fundamental design parameter (see Figure 2.16).

In  $C\Sigma u$  – variable gear pairs of any and all designs the design parameters:  $C$ ,  $\Sigma$ , and  $u$ , must be compatible, for example,  $\Sigma$  – var gearing is possible only in  $I_a$  – axes gearing; no  $\Sigma$  – var gearing is possible in  $C_a$  – axes gearing, and, moreover, in  $P_a$  – axes gearing.

Gear vector diagrams of gear pairs with one variable fundamental design parameter that can be derived from the gear vector diagrams of the types #1.1.1, #1.1.2, #1.2.1, #1.2.2, #1.3.1, #1.3.2, and others, are covered by those gear vector diagrams derived from the gear vector diagrams of the types #1.1, #1.2, and #1.3 above.

A few more simplifications can be done to the proposed list of the gear vector diagrams.

**An example of non-possible  $C\Sigma u$  – var gear pair:** Toroidal gear pair is often considered as an example of a gear pair that allows for variation of the shaft angle,  $\Sigma$ , in the gear pair. Gearing of this design is schematically illustrated in Figure 18.14. The radius of the gear outer contour,  $\rho_g$ , is equal to, or exceeds the corresponding radius,  $\rho_p$ , of the pinion outer contour ( $\rho_g \geq \rho_p$ ). Gear pairs with a toroidal generic shape allow for axial adjustment of the gear, and of the pinion in relation to one another. When the inequality  $\rho_g > \rho_p$  is observed, the gear pair features a tooth flank geometry that can be viewed as equivalent modification in the lengthwise direction of the gear tooth.

It is often loosely claimed that toroidal gear pairs have an additional degree of freedom, meaning that the gear can spin relative to the pinion in both directions shown by means of the dashed arrow. This is not correct, as this, the so-called *motion* is not permissible at all (see below comments to Figure 18.27).

Gear vector diagrams of all possible kinds of  $C\Sigma u$  – var gear pairs can be classified, as illustrated in Figure 18.15.

Orthogonal gear pairs have a certain advantage over the gear pairs that feature the crossed-axes angle,  $\Sigma = \text{const} \big|_{\neq 90^\circ}$ . There are only two possible kinds of gear vector diagrams of orthogonal  $Cu$  – var (or  $\Sigma$  – const). Both of them are illustrated in Figure 18.16. Shown in Figure 18.16, a gear vector diagram corresponds to external orthogonal  $Cu$  – var gearing, and that shown in Figure 18.16b gear vector diagram corresponds to internal orthogonal  $Cu$  – var gearing. No orthogonal  $Cu$  – var gearing with flat gear (with the gear cone angle  $\Sigma_g = 90^\circ$ ) is possible at all.

It is critical to point out here that the total number of the gear vector diagrams listed above is not an infinite, but, instead, it is limited to a reasonably small number of the gear vector diagrams

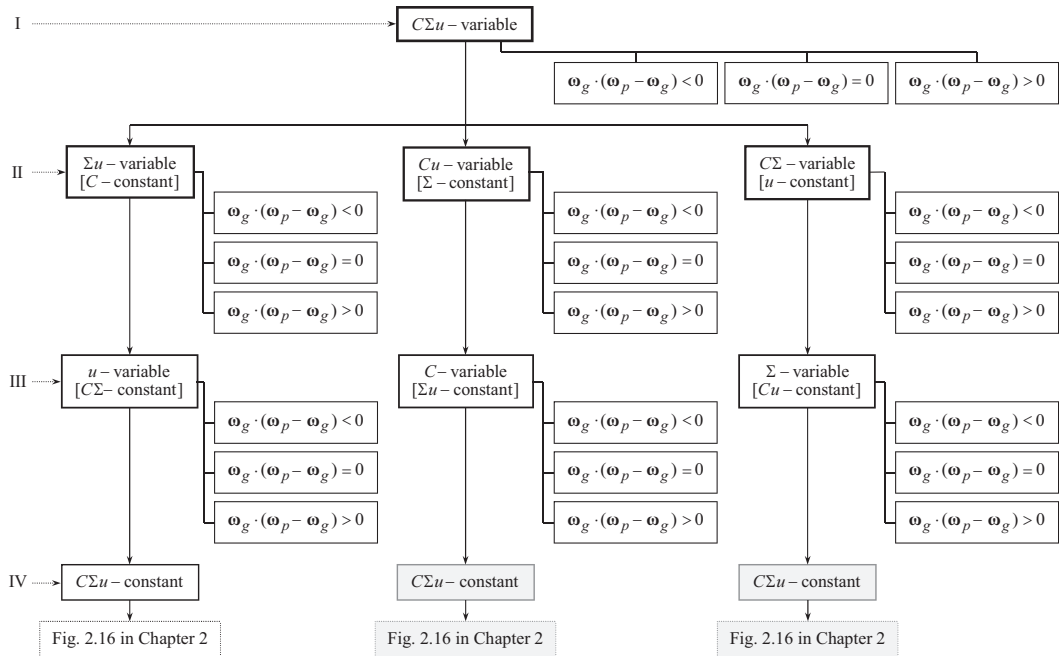


**FIGURE 18.15** Classification of possible kinds of gear vector diagrams of  $C\Sigma u$ -var gear pairs.

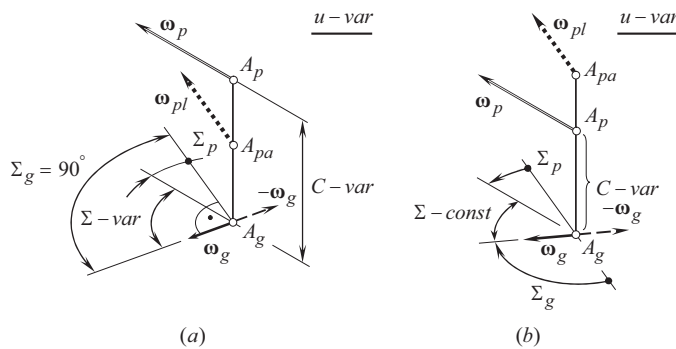


**FIGURE 18.16** Gear vector diagrams of orthogonal  $Cu$ -var (or  $\Sigma$ -const) gear pairs: (a) external mesh of the gear teeth, and (b) internal mesh of the gear teeth.

(gear vector diagrams of no other type are feasible). This means that each one of them can be investigated to the best possible extent aiming at application to design gear pairs.

Every gear vector diagram in the classification (see Figure 18.15) has to be investigated regarding whether or not a corresponding gear vector diagram is suitable to design on its premise a gear pair for a particular application.

In  $C\Sigma u$ -var gear pairs of all possible types, at every instant of time, for any and all possible configurations of a gear and its mating pinion, an instantaneous value of the base pitch of a gear, and that of a mating pinion, both have to be equal to instantaneous value of operating base pitch of the gear pair – this is a must.

$C\Sigma u$ -var gear pairs of all possible types (i.e., those listed above) is a challenging subject to be investigated in the future.

$C\Sigma u$ -var gearing can be construed as the most general kind of gearing. Varying each of the principal design parameters  $C = C(t)$ ,  $\Sigma = \Sigma(t)$ , and  $u = u(t)$  (individually, or in any and all possible combinations), gearing of all possible kinds can be derived.

CΣu-var gear pairs feature a huge potential for researchers. This chapter is just an illustration of the capabilities of CΣu-var gearing. Each particular kind of CΣu-var gear pair deserves to be discussed in a separate chapter.

## 18.4 TOOTH FLANK GENERATION IN GEOMETRICALLY ACCURATE CΣu-var GEARING

The generation of tooth flanks of a gear and of a mating pinion in geometrically accurate CΣu-var gear pair is executed on the premise of the gear vector diagram and strictly follows to all three fundamental laws of gearing.

Instead of the equalities  $\varphi_{b,g} = \varphi_{b.op}$ , and  $\varphi_{b,p} = \varphi_{b.op}$ , in CΣu-const gearing, in, CΣu-var gearing, equality of the following functions must be observed:

$$\begin{aligned}\varphi_{b,g}(C) &= \varphi_{b.op}(C), \varphi_{b,g}(\Sigma) = \varphi_{b.op}(\Sigma), \varphi_{b,g}(u) = \varphi_{b.op}(u), \\ \varphi_{b,g}(C, \Sigma) &= \varphi_{b.op}(C, \Sigma), \varphi_{b,g}(\Sigma, u) = \varphi_{b.op}(\Sigma, u), \varphi_{b,g}(C, u) = \varphi_{b.op}(C, u), \text{ and} \\ \varphi_{b,g}(C, \Sigma, u) &= \varphi_{b.op}(C, \Sigma, u).\end{aligned}$$

Similar equalities must be valid with respect to a mating pinion:

$$\begin{aligned}\varphi_{b,p}(C) &= \varphi_{b.op}(C), \varphi_{b,p}(\Sigma) = \varphi_{b.op}(\Sigma), \varphi_{b,p}(u) = \varphi_{b.op}(u), \\ \varphi_{b,p}(C, \Sigma) &= \varphi_{b.op}(C, \Sigma), \varphi_{b,p}(\Sigma, u) = \varphi_{b.op}(\Sigma, u), \varphi_{b,p}(C, u) = \varphi_{b.op}(C, u), \text{ and} \\ \varphi_{b,p}(C, \Sigma, u) &= \varphi_{b.op}(C, \Sigma, u).\end{aligned}$$

The principal features of the generation of tooth flanks in geometrically accurate CΣu-var gearing are briefly outlined below. In parallel, the readers' attention here is pointed on the weaknesses of the commonly adopted practice of generation of tooth flanks in non-circular gearing.

The principle of generation of tooth flanks,  $\mathcal{S}$  and  $\mathcal{P}$ , of a gear and of a mating pinion by means of a desirable line of contact,  $LC_{des}$ , that is associated with the plane of action,  $PA$ , can be enhanced to the generation of the tooth flanks of gears for CΣu-var gearing.

In parallel-axes gearing ( $P_a$ -gearing): an *instantaneous* location ( $r_g$ ,  $r_p$ , and  $P$ ), and an instantaneous orientation (given either by the transverse pressure angle,  $\phi_t$ , or by the base diameters,  $d_{b,g}$ , and  $d_{b,p}$ , of the gears), and the instant speed,  $V/\omega$ , of the plane of action,  $PA$ , are specified. At every instant of time the plane of action,  $PA$ , is unwrapping from one of the base cylinders and is wrapping onto another base cylinder (here, the base cylinders are not a kind of cylinders of revolution – these are cylinders in a more general sense). The current values of the base diameter, as well as the current location of the pitch pint,  $P$ , depend on the angle of rotation of the driving gear (see Figure 18.17).

At an arbitrary contact point,  $K$ , within the active portion of the line of action,  $LA$ , the actual value of the transverse pressure angle,  $\phi_{t,\Sigma}$ , can be represented as the algebraic summa,  $\phi_{t,\Sigma} = \phi_{t,g} + \phi_{t,pl}$ , of the transverse profile,  $\phi_{t,g}$ , of the gear tooth, and the *profile angle*,  $\phi_{t,pl}$ , of the pitch curve (due to the pitch curve is NOT a circle).

In order to make possible a desirable migration of the pitch pint,  $P$ , within a pre-specified interval,  $P_{max}P_{min}$ , a corresponding alteration to the current value of the transverse pressure angle,  $\phi_{t,\Sigma}$ , is necessary (in a particular case, the gear profile angle,  $\phi_{t,g}$ , can be of a constant value, and the desirable alteration can be achieved by means of variation of the pitch line profile angle,  $\phi_{t,pl}$ ).

The construction of the gear/pinion tooth profile angle can be started, for example, from the pitch point,  $P$ .

Under such an assumption, contact point,  $K$ , should travel from its original position in both directions ( $\pm\omega_p$ ) along the instantaneous line of action,  $LA_{inst}$ .

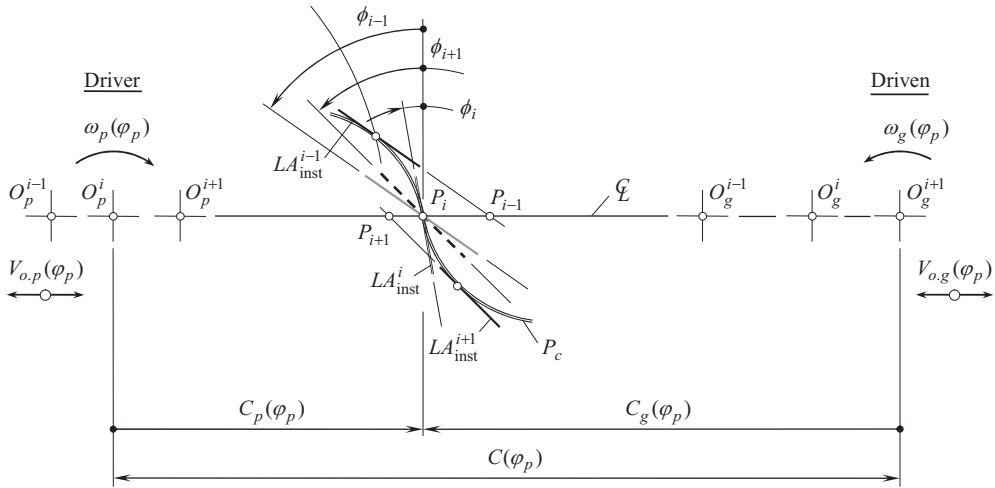


FIGURE 18.17 Generation of tooth flanks,  $\mathcal{S}$  and  $\mathcal{P}$ , in parallel-axes gear pair with non-circular gears.

For all the configurations of contact point,  $K$ , along the path of contact,  $P_c$  (not yet known curve), an instantaneous line of action,  $LA_{inst}$ , the instantaneous base diameters (or the base radii),  $d_{b,g}^{inst}$  and  $d_{b,p}^{inst}$ , can be constructed. This gives a possibility of creating an instantaneous tooth profile, and further, a tooth profile of a current gear/pinion tooth.

In a stationary reference system, the actual path of contact,  $P_c$  (a smooth curve), can be constructed as an envelope to a family of consecutive positions of the instantaneous lines of action,  $LA_{inst}$ .

The so-called *pitch lines* of a gear and a mating pinion, for example, in the case of  $\phi_{t,g} = \text{const}$ , and  $\phi_{t,pl} = \phi_{t,pl}(\varphi_p)$ , are viewed as the two loci of instantaneous pitch points,  $P_i$ , considered in the references systems,  $X_g Y_g Z_g$  and  $X_p Y_p Z_p$ , associated with the gear, and with the pinion, correspondingly. The outside profile and the SAP profile<sup>4</sup> of the gear and that of the pinion are the equidistant profiles at the distances “+”  $m$  (module), and “−”  $1.25m$  in relation to the pitch lines of the mating gears.

The desirable line of contact,  $LC_{des}$ , is retained of that same geometry. Moreover, a given configuration of the desirable line of contact,  $LC_{des}$ , in relation to the plane of action,  $PA$ , is also not altered.

Consider a parallel-axes non-circular gear pair that features a variable center-distance,<sup>5</sup>  $C(\varphi_p)$ . Here, the angle of rotation of the driver (of the pinion) is designated as  $\varphi_p$ . The gears rotate about their axes of rotation,  $O_g$  and  $O_p$ , with the variable in time rotations,  $\omega_g(\varphi_p)$  and  $\omega_p(\varphi_p)$ , correspondingly. A functionality:

$$\omega_g(\varphi_p) = \omega_p \cdot u^{-1}(\varphi_p) \quad (18.2)$$

is observed.

Here, the instantaneous angular velocity ratio is designated as  $u(\varphi_p)$ :

$$u_{inst}(\varphi_p) = \frac{\omega_{inst}^{input}(\varphi_p)}{\omega_{inst}^{output}(\varphi_p)} \quad (18.3)$$

When the gears rotate, the center-distance,  $C(\varphi_p)$ , varies [due to the velocities  $V_{o,p}(\varphi_p)$  and  $V_{o,g}(\varphi_p)$  are of non-zero values] in the range of:

$$C_{min} \leq C(\varphi_p) \leq C_{max} \quad (18.4)$$

<sup>4</sup> The SAP point stands for *start-of-active-profile point* of a gear tooth. SAP profile is a set of SAP –points at various angular configurations of the gears that rotate.

<sup>5</sup> A case of non-circular gear pair with a constant center distance,  $C = \text{const}$ , can be viewed as a reduced case of non-circular gear pair that features a variable center distance,  $C(\varphi_p)$ .

The instantaneous pitch point,  $P_i$ , that corresponds to the input rotation angle  $\varphi_p = \varphi_p^i$ , is considered motionless. The gear center-distance,  $C_g$  (between an instantaneous location of the gear axis of rotation,  $O_g$ , and the pitch point,  $P_i$ ), and the pinion center-distance,  $C_p$  (between an instantaneous location of the pinion axis of rotation,  $O_p$ , and the pitch point,  $P_i$ ), both are variable in time, namely,  $C_g = C_g(\varphi_p)$  and  $C_p = C_p(\varphi_p)$ .

The instantaneous line of action,  $LA_{\text{inst}}$ , is a straight-line segment that forms an instantaneous transverse pressure angle,  $\phi_{\text{inst}}$ , in relation to a perpendicular to the centerline,  $\mathfrak{L}$ , through the instantaneous pitch point,  $P_i$ . As the pitch point,  $P_i$ , is motionless, then, when the gears rotate, the axes of rotation,  $O_g$  and  $O_p$ , travel back and forth along the centerline,  $\mathfrak{L}$  [due to the velocities  $V_{o,p}(\varphi_p)$  and  $V_{o,g}(\varphi_p)$  are of non-zero values]. The configurations  $O_g^{i-1}$ ,  $O_g^i$ ,  $O_g^{i+1}$ , and  $O_p^{i-1}$ ,  $O_p^i$ ,  $O_p^{i+1}$  of the centers of rotations represent examples of the current locations of the gear axis of rotation,  $O_g$ , and of the pinion axis of rotation,  $O_p$ , correspondingly.

For current configuration of the gears, it is assumed that both the instantaneous center-distance,  $C_{\text{inst}}$ , and the instantaneous transverse pressure angle,  $\phi_{\text{inst}}$ , as well as the instantaneous pitch radii  $C_g(\varphi_p)$  and  $C_p(\varphi_p)$ , are specified. The angles  $\phi_{i-1}$ ,  $\phi_i$ , and  $\phi_{i+1}$ , represent the instantaneous transverse pressure angle,  $\phi_{\text{inst}}$ , at different configurations of the gears that rotate. When the gears rotate, the instantaneous line of action,  $LA_{\text{inst}}$ , occupies different locations and orientations relative to the centerline,  $\mathfrak{L}$ , and to the instantaneous pitch point,  $P_{i-1}$ ,  $P_i$ , and  $P_{i+1}$ . The instantaneous lines of action  $LA_{\text{inst}}^{i-1}$ ,  $LA_{\text{inst}}^i$ , and  $LA_{\text{inst}}^{i+1}$ , are straight lines through the corresponding instantaneous pitch point  $P_{i-1}$ ,  $P_i$ ,  $P_{i+1}$ , and so forth. The lines of action  $LA_{\text{inst}}^{i-1}$ ,  $LA_{\text{inst}}^i$ , and  $LA_{\text{inst}}^{i+1}$ , represent the instantaneous lines of action,  $LA_{\text{inst}}$ , at different configurations of the gears that rotate. When the gears rotate, the path of contact,  $P_c$ , is generated as an envelope to a family of consecutive positions of the instantaneous lines of action,  $LA_{\text{inst}}$ , that is, of the family of straight lines.

The path of contact,  $P_c$ , is considered in a stationary reference system,  $X_h Y_h Z_h$ , associated with the gear housing. In parallel-axes non-circular gearing, the path of contact,  $P_c$ , is a planar curve that is entirely located within a plane perpendicular to the axes of rotation,  $O_g$  and  $O_p$ .

Aiming at generating of the base curves in non-circular gears: (a) the pitch point is considered traveling up and down along the centerline,  $\mathfrak{L}$ , and (b) the transverse pressure angle is considered altering accordingly. The base curve of the gear,  $BC_g$ , is an envelope to a family of consecutive positions of the instantaneous line of action,  $LA_{\text{inst}}$ , when the gears rotate. The base curve of the gear,  $BC_g$ , is considered in a reference system,  $X_g Y_g Z_g$ , associated with the gear. Similarly, the base curve of the pinion,  $BC_p$ , is an envelope to a family of consecutive positions of the instantaneous line of action,  $LA_{\text{inst}}$ , when the gears rotate. The base curve of the pinion,  $BC_p$ , is considered in a reference system,  $X_p Y_p Z_p$ , associated with the pinion.<sup>6</sup>

The gear tooth profile,  $\mathcal{S}$ , is the trace of contact point,  $K$ , when the gears rotate. The gear tooth profile is specified in the reference system,  $X_g Y_g Z_g$ , associated with the gear. Similarly, the pinion tooth profile,  $\mathcal{P}$ , is the trace of contact point,  $K$ , when the gears rotate. The pinion tooth profile is specified in the reference system,  $X_p Y_p Z_p$ , associated with the pinion.

For generation of the tooth flanks,  $\mathcal{S}$  and  $\mathcal{P}$ , of a gear, and of a mating pinion, a line of contact,  $LC_{\text{des}}$ , is used. The line of contact,  $LC$ , is entirely located within the plane of action,  $PA$ , and travels together with the plane of action (see Figure 6.12 and others). In contrast to gears of other kinds, only *pseudo-straight crossed-axes gears* can be used in the design of CΣu-var gear pairs (see Figure 14.13a). This is a kind of spur gears, tooth flanks of which are generated by means of a straight line that at a certain instant of time is aligned with axis of instantaneous rotation,  $P_{lm}$ . No other tooth flank geometries are permissible as the contact ratio in CΣu-var gearing is always greater than one.

The desirable rotation of the driven shaft can be expressed in terms of instantaneous configurations of the instantaneous line of action. Then, the desirable tooth profiles have to interact with one another along the same instantaneous line of action,  $LA_{\text{inst}}$ , that is tangent to the base curves at the corresponding instant of time.

<sup>6</sup> The base curves,  $BC_g$  and  $BC_p$ , are directors of the two base cylinders, each of which is associated with a gear, and with a mating pinion. The base cylinders are cylinders in general sense of this term, and are not mandatorily cylinders of revolution.

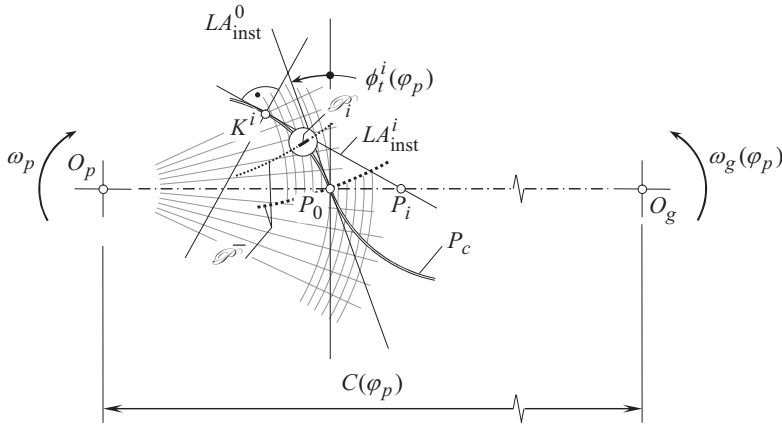


**FIGURE 18.18** Generation of infinitesimally short portion,  $\mathcal{P}_i$ , of tooth flank,  $\mathcal{P}$ , in parallel-axes gear pair with non-circular gears.

Instantaneous pitch circles of diameters,  $d_g^{\text{inst}}$  and  $d_p^{\text{inst}}$ , correspondingly, pass through the instantaneous pitch point,  $P_{\text{inst}}$ , and they are centered at the corresponding instantaneous centers of rotations,<sup>7</sup>  $O_g^{\text{inst}}$  and  $O_p^{\text{inst}}$ .

A local segment of a gear tooth flank,  $\mathcal{L}$ , and that of a mating pinion tooth flank,  $\mathcal{P}$ , can be specified in terms of instantaneous contact point,  $K$ , and the corresponding centers of rotations,  $O_g^{\text{inst}}$  and  $O_p^{\text{inst}}$ .

All the instantaneous lines of action,  $LA_{\text{inst}}$ , that is,  $LA_{\text{inst}}^{i-1}$ ,  $LA_{\text{inst}}^i$ ,  $LA_{\text{inst}}^{i+1}$ , and so forth, have to intersect the centerline,  $\Phi$ . None of the instantaneous lines of action,  $LA_{\text{inst}}$ , are allowed to pass either through the instantaneous axis of rotation,  $O_g^{\text{inst}}$ , of the gear, or through the instantaneous axis of rotation,  $O_p^{\text{inst}}$ , of the pinion.

The curved line segment of the path of contact,  $P_c$ , that corresponds to the input rotation, under which the center-distance increases from the minimal value of,  $C_{\text{min}}$ , to the maximal value of,  $C_{\text{max}}$ , and then back forth, from the maximal value of,  $C_{\text{max}}$ , to the minimal value of,  $C_{\text{min}}$ , that is, through the input rotation angle per lobe, (the active portion of the path of contact,  $P_c$ ) is divided on a certain number of arc segments, the total number of which equals to the tooth count per lobe, as illustrated in Figure 18.18. All the arc segments of the active portion of the path of contact,  $P_c$ , overlap one another. This is an equivalent of the contact ratio in conventional parallel-axes involute gearing. The tooth flank of the gear, and of the mating pinion, both, are generated by contact point that travels within a corresponding arc segment of the active portion of the path of contact,  $P_c$ .

Aiming at derivation of analytical description of a gear tooth flank, a reference system  $X_{pa}Y_{pa}Z_{pa}$  is associated with the plane of action. Another reference system,  $X_gY_gZ_g$ , is associated with the gear and is rotated with the gear. An operator of the resultant coordinate system transformation,  $\mathbf{Rs}(pa \mapsto g)$ , namely, the operator of the transition from plane-of-action reference system  $X_{pa}Y_{pa}Z_{pa}$  to the gear reference system  $X_gY_gZ_g$  can be composed following the routing outlined in Appendix D.

In a reference system  $X_{pa}Y_{pa}Z_{pa}$ , the position vector,  $\mathbf{r}_{lc}$ , of point of the line of contact,  $LC$ , can be represented by a vector equation in a form  $\mathbf{r}_{lc} = \mathbf{r}_{lc}(\varphi_{pa})$ .

The position vector of point,  $\mathbf{r}_g$ , of the gear tooth flank,  $\mathcal{L}$ , can be expressed by an equation:

$$\mathbf{r}_g = \mathbf{Rs}(pa \mapsto g) \cdot \mathbf{r}_{lc} \quad (18.5)$$

<sup>7</sup> In the present-day practice, it is common to construct pitch lines associated with the gear and with the mating pinion as an equivalent of the pitch circles in conventional parallel-axes gearing. The pitch lines are also commonly referred to as *centrodes*. By definition, *centrodes* are the two lines in contact that roll over one another with no sliding in between them. In non-circular gear pairs, the pitch lines/centrodes cannot roll over one another *with no sliding* in between them. The pitch lines of a gear, and that of a mating pinion, are useless as they are neither conjugate, nor enveloping to one another, which is a must when the gears must rotate smoothly.



As all the fundamental design parameters of the gear in a geometrically accurate  $C\Sigma u$ -var gearing can be expressed as corresponding functions of the angle,  $\varphi_{\text{input}}$ , of the input rotation [that is, as the functions  $C = C(\varphi_{\text{input}})$ ,  $\Sigma = \Sigma(\varphi_{\text{input}})$ , and  $u = u(\varphi_{\text{input}})$ ], then the operator,  $\mathbf{Rs}(pa \mapsto g)$ , of the resultant coordinate system transformation is also a function of the angle  $\varphi_{\text{input}}$ , that is, the equality:

$$\mathbf{Rs}(pa \mapsto g) = \mathbf{Rs}(pa \mapsto g) \Big|_{(\varphi_{\text{input}})} \quad (18.6)$$

is valid. Ultimately, the position vector of point,  $\mathbf{r}_g$ , of the gear tooth flank,  $\mathcal{G}$ , can be expressed in the form of matrix equation:

$$\mathbf{r}_g(\varphi_{\text{input}}, \varphi_{pa}) = \mathbf{Rs}(pa \mapsto g) \Big|_{(\varphi_{\text{input}})} \cdot \mathbf{r}_{lc}(\varphi_{pa}) \quad (18.7)$$

The parameters  $\varphi_{\text{input}}$  and  $\varphi_{pa}$  are the two *Gaussian parameters* of the gear tooth flank,  $\mathcal{G}$ .

Aiming at derivation of analytical description of a pinion tooth flank, one more reference system,  $X_p Y_p Z_p$ , is associated with the pinion, and is rotated together with the pinion. An operator of the resultant coordinate system transformation,  $\mathbf{Rs}(pa \mapsto p)$ , namely, the operator of the transition from plane-of-action reference system  $X_{pa} Y_{pa} Z_{pa}$  to the pinion reference system  $X_p Y_p Z_p$  can be derived following the routing outlined in Appendix D. The position vector of point,  $\mathbf{r}_p$ , of the pinion tooth flank,  $\mathcal{P}$ , can be expressed by an equation:

$$\mathbf{r}_p = \mathbf{Rs}(pa \mapsto p) \cdot \mathbf{r}_{lc} \quad (18.8)$$

Again, as all the fundamental design parameters of the pinion in a geometrically accurate  $C\Sigma u$ -var gearing can be expressed as corresponding functions of the angle,  $\varphi_{\text{input}}$ , of the input rotation [that is, as the functions  $C = C(\varphi_{\text{input}})$ ,  $\Sigma = \Sigma(\varphi_{\text{input}})$ , and  $u = u(\varphi_{\text{input}})$ ], then the operator,  $\mathbf{Rs}(pa \mapsto p)$ , of the resultant coordinate system transformation is also a function of the angle  $\varphi_{\text{input}}$ , that is, the equality:

$$\mathbf{Rs}(pa \mapsto p) = \mathbf{Rs}(pa \mapsto p) \Big|_{(\varphi_{\text{input}})} \quad (18.9)$$

is valid. Ultimately, the position vector of point,  $\mathbf{r}_p$ , of the pinion tooth flank,  $\mathcal{P}$ , can be expressed in the form of matrix equation:

$$\mathbf{r}_p(\varphi_{\text{input}}, \varphi_{pa}) = \mathbf{Rs}(pa \mapsto p) \Big|_{(\varphi_{\text{input}})} \cdot \mathbf{r}_{lc}(\varphi_{pa}) \quad (18.10)$$

The parameters  $\varphi_{\text{input}}$  and  $\varphi_{pa}$  are the two *Gaussian parameters* of the pinion tooth flank,  $\mathcal{P}$ .

A gear tooth flank,  $\mathcal{G}$ , and a mating pinion tooth flank,  $\mathcal{P}$ , meet all three fundamental laws of gearing. Taking into account specifics of the kinematics, and the geometry of the tooth flanks, the conjugate action law in  $C\Sigma u$ -var gearing is fulfilled regardless of the actual configuration of instantaneous lines of action alter when the gears rotate. That same is valid with respect to equality of angular base pitch of a gear and that of a mating pinion to operating base pitch of the  $C\Sigma u$ -var gear pair.

No helical gears can be used in the design of geometrically accurate  $C\Sigma u$ -var gearing; only *pseudo-straight crossed-axes gears* can be used in such applications.

There is no need to construct a *pitch curve*. Moreover, existence of *pitch curve* is more than questionable, as they do not exist at all. The latter, that is, the pitch curve is meaningless, and a kind of nonsense in  $C\Sigma u$ -var gearing. The *pitch curves* for each lobe of a gear, and of a mating pinion have to be conjugated to one another. Otherwise, if two curves that are associated with the gear and with the mating pinion cannot be served as the *pitch curves* for the gear and the pinion.

End-points of the arc segments of the active portion of the path of contact,  $P_c$ , are located within the corresponding outer curve (top-lands), and the root curve (bottom-lands) of the gear and the mating pinion correspondingly.



### 18.5 A KEY MISTAKE IN KNOWN METHODS OF MACHINING GEARS FOR GEOMETRICALLY ACCURATE $C\Sigma$ -var GEARING

In present-day industry, gear generators are used to machine gears for  $C\Sigma$ -var gear pairs. Tooth flanks of a gear, and that of a mating pinion, in this case, are generated as envelopes to the families of consecutive position of cutting edges of the gear cutting tool. Shown in Figure 18.19, gear shaping process is commonly used for machining non-circular gears for parallel-axes gearing. This is illustrated in Figure 18.20, where hobbing operation of a gear for non-circular gear pair is depicted. Gear generator of a special design is used in the operation. Shown in Figure 18.21, non-circular gears as well as non-circular gears of other designs (see Figure 18.22) can be hobbled by standard hobs.



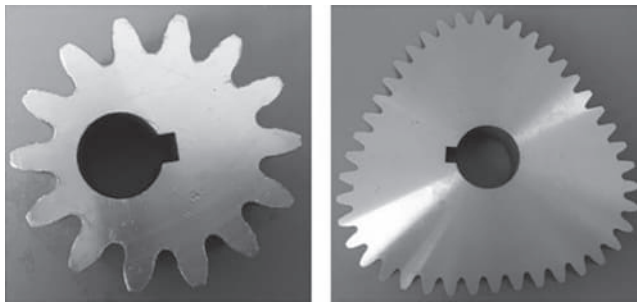
FIGURE 18.19 Shaping a non-circular gear by the gear shaper.



FIGURE 18.20 Hobbing a non-circular gear for non-circular gear pair.



**FIGURE 18.21** Elliptical gear for non-circular gear pair.



**FIGURE 18.22** Non-circular gears for parallel-axes gear pairs.

Only approximate gears for non-circular gear pairs can be cut this way. This is because of the fundamental laws of gearing, namely:

1. the law of contact
2. the conjugate action law, and
3. the law of equal base pitches of a gear to be cut, and of the hob, both, to operating base pitch in the gear hobbing process)

all the gear meshes must comply with, are violated in the gear machining mesh.

## 18.6 EXAMPLES OF APPLICATION OF CΣu-var GEARING

Application of CΣu-var gearing in the industry is illustrated below by a few examples.

A relatively simply example of CΣu-var gearing is illustrated in Figure 18.23. The gear drive features CΣu-var gearing in its design. The gears operate on parallel-axes of rotation of a gear and a mating pinion.

A schematic of Σ-var gear pair (or, the same, of Cu-const gearing) is shown in Figure 18.24. According to the invention, a pair of bevel gears includes a plurality of gear teeth and grooves radially disposed in the surface thereof from the summit thereof, respectively, so, as to be in gearing relationship from each other at a variable angle for use in various types of machines, machine tools, control machines, testing machines, medical machines, robots, toys, and like as a driving force transmitter.



**FIGURE 18.23** Gear drive with  $Cu - var$  gearing that operates on parallel-axes of rotation of a gear, and of a mating pinion.

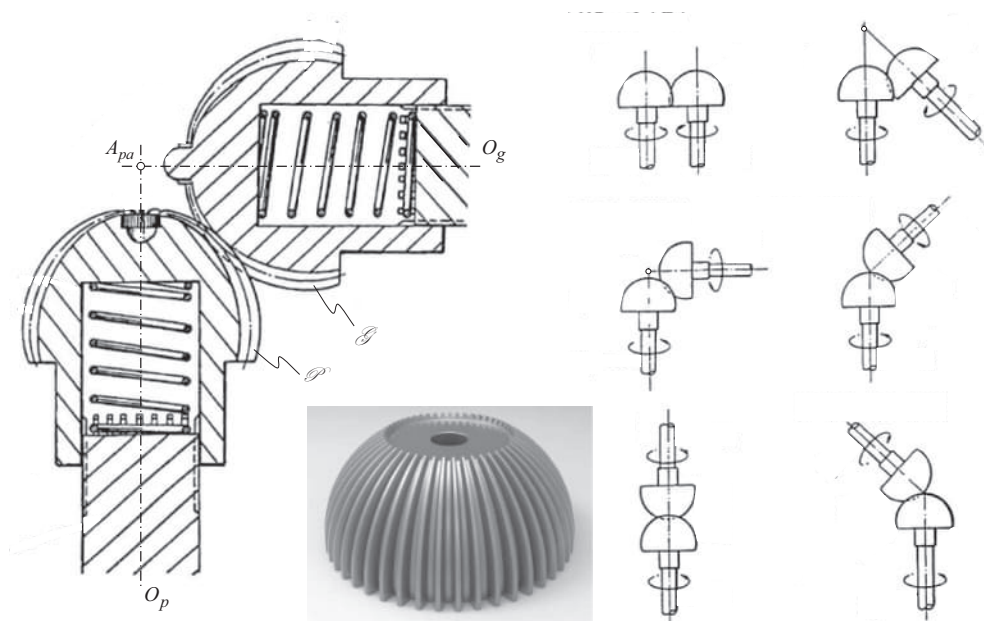


**FIGURE 18.24** A schematic of  $\Sigma - var$  gear pair (or  $Cu - const$  gearing). (After Park, D.K.: Pat. USA 5,129,275, Pair of Semi-Spherical Bevel Gears, Int. Cl. **F16H 1/20**, F16H 1/12, Filed: Oct. 3, 1990, Patented: Jul. 14, 1992.)

As the  $\Sigma - var$  gear pair (see Figure 18.24) is comprised of approximate gears, two axial springs are used to accommodate for inaccuracies in the tooth flanks,  $\mathcal{S}$  and  $\mathcal{P}$ , of a gear and a mating pinion.

No angular base pitch physically exists in  $C\Sigma u -$  gearing. Instead, the, so-called, *virtual angular base pitch* can be introduced.

### Definition 18.1

Virtual angular base pitch in a gear (and that in a pinion as well as an operating base pitch in the gear pair) is the angular base pitch of a corresponding virtual gear.

## 18.7 POSSIBILITY OF IMPLEMENTATION OF THE CONCEPT OF $S_{pr}$ -GEARING IN DESIGN OF $\Sigma$ -var GEARING

In order to derive equation of a gear tooth flank,  $G$ , the approach earlier used for the derivation of the gear/pinion tooth flank in  $S_{pr}$ -gearing can be used. Doing this, one can express the angular displacements of a gear and of a mating pinion in terms of the plane-of-action-apex,  $A_{pa}$ , displacement along the axis of instant rotation,  $P_{in}$ .

$\Sigma$ -var gear pair are investigated since the beginning of 1960s [204], or even earlier. They can be used in the design of *constant-velocity joints* (or just *CV*-joints, for simplicity). Robot arms is another area of potential application of the  $S_{pr}$ -gearing.

In the example shown in Figure 18.25, a bevel gear coupling is composed of three bevel gears. The use of  $S_{pr}$ -gear system makes possible a replacement of a gear joint having three bevel gears, with a gear joint having two  $S_{pr}$  gears, as illustrated in Figure 18.26.

Schematic of an  $\Sigma$ -var spur gear pair is illustrated in Figure 18.27.

The rotation vectors,  $\omega_g$  and  $\omega_p$ , of a gear, and of a mating pinion form a crossed-axes angle,  $\Sigma$ , that varies in time, that is,  $\Sigma = \Sigma(t)$ . The gear is rotated about its axis of rotation,  $O_g$ , with an angular velocity,  $\omega_g$ . The mating pinion is rotated about its axis of rotation,  $O_p$ , with an angular velocity,  $\omega_p$ . The axes of rotations,  $O_g$  and  $O_p$ , intersect the centerline,  $\Phi$ , through the plane-of-action apex,  $A_{pa}^{inst}$ .

In order to perform the complementary instantaneous rotation,  $\omega_{rol}$ , the gear and the pinion roll over one another. For this purpose, the gear and the pinion rotate with angular velocities,  $\omega_{rol,g}$  and  $\omega_{rol,p}$ , correspondingly, about the centers,  $o_g$  and  $o_p$ . The midpoint,  $f$ , of the face width,  $F_{pa}$ , in the gear pair is located within a straight line through the  $o_g$  and  $o_p$ .

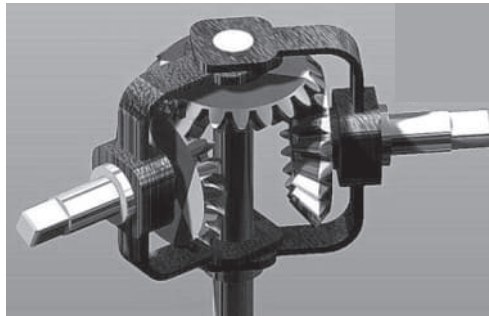


FIGURE 18.25 Bevel gear coupling.

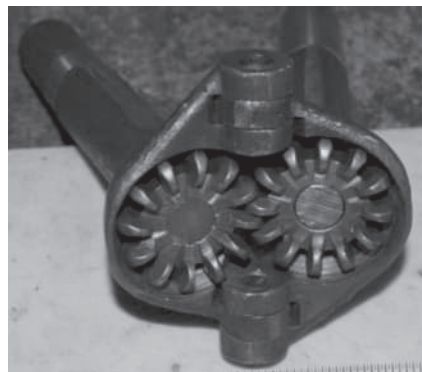
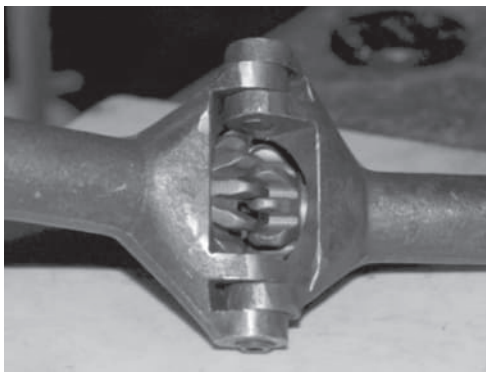


FIGURE 18.26 Gear joint composed of two gears.

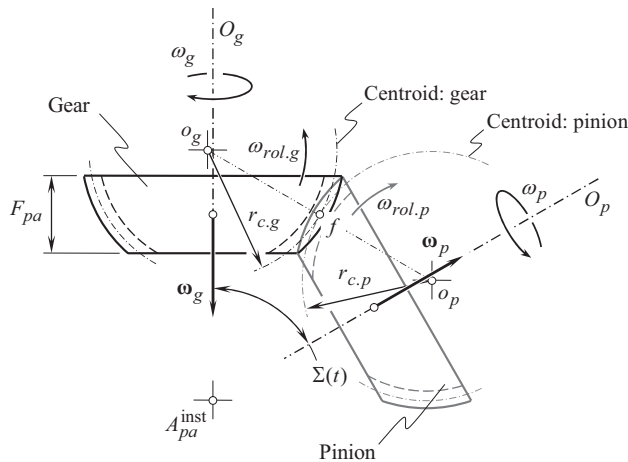


FIGURE 18.27 Schematic of geometrically accurate spur  $\Sigma$ -var gear pair.

When performing these rotations, the circular arc of a radius,  $r_{c.g}$ , associated with the gear, rolls over the circular arc of a radius,  $r_{c.p}$ , associated with the pinion. The circular arcs are centered at the centers,  $o_g$  and  $o_p$ . The circular arcs of the radii,  $r_{c.g}$  and  $r_{c.p}$ , are the centroids in the rolling motion of the gear and the pinion in their rolling motion. As the rolling motions,  $\omega_{rol.g}$  and  $\omega_{rol.p}$ , progress, the actual value of the intersected-axes angle,  $\Sigma(t)$ , varies.

The variation of the crossed-axes angle,  $\Sigma(t)$ , is illustrated in Figure 18.28.

As the rolling motions,  $\omega_{rol.g}$  and  $\omega_{rol.p}$ , progress, the actual value of the intersected-axes angle,  $\Sigma(t)$ , can be reduced, as illustrated in Figure 18.28a, or it can be increased in relation to the nominal configuration (see Figure 18.27) of a gear and of a mating pinion, as shown in Figure 18.28b.

Shown in Figure 18.28  $\Sigma$ -var gear pair is capable of transmitting a uniform input rotation smoothly from a driving shaft to a driven shaft. This is due to the tooth flanks,  $\mathcal{S}$  and  $\mathcal{P}$ , of the gear and of its mating pinion: (a) make proper contact with one another ( $\mathbf{n} \cdot \mathbf{v}_\Sigma = 0$ ), (b) are conjugate to one another, and (c) at every instant of time, angular base pitch of a gear,  $\varphi_{b.g}$ , equals to the operating angular base pitch of the gear pair,  $\varphi_{b.op}$ , and angular base pitch of a mating pinion,  $\varphi_{b.p}$ , also equals to the operating angular base pitch of the gear pair,  $\varphi_{b.op}$ , that is, the equalities,  $\varphi_{b.g} = \varphi_{b.op}$  and  $\varphi_{b.p} = \varphi_{b.op}$ , are valid.

*Constant-velocity joints* (or just *CV-joints*, for simplicity) is a potential area of application of  $\Sigma$ -var gearing in the automotive industry. Universal *R.H. Rzeppa* constant-velocity joint (see Figure 18.29) can be replaced by  $\Sigma$ -var gearing similar to that shown in Figure 18.21.

The main reason for such a replacement is as follows. *Rzeppa* constant-velocity joint (see Figure 18.29) is not capable of transmitting an input rotation smoothly. Due to features inherited from *Rzeppa* constant-velocity joint, the output rotation is not uniform; instead, it is a superposition of a uniform rotation and an oscillation of the output shaft. A potentially possible replacement of *Rzeppa* constant-velocity joint with  $\Sigma$ -var gearing ensures a uniform rotation of the output shaft under any and all angles between the shafts within the operating range of this angle. In this way, gear vibration and noise excitation are drastically reduced (or they are even eliminated).

$\Sigma$ -var gearing features an additional mobility – a rotation about the centerline,  $\mathfrak{L}$ . None of the two rest kinds of gearing, namely, *C-var* gearing and *u-var* gearing, feature additional mobilities.





**FIGURE 18.29** Universal *R.H. Rzeppa* constant-velocity joint is a potential candidate to be replaced by  $\Sigma$ –*var* gear pair.



# *Part V*

---

## *On Synthesizing of Favorable Geometrically Accurate Gear Pairs*

The main purpose of the application of gears is to transmit and to transform power (a rotation, and torque) for a specified configuration of the axes of rotation of a gear and of a mating pinion, a given gear ratio, and so forth.

Geometrically accurate gears of all kinds, that operate on parallel-axes, intersected-axes, and crossed-axes, can be designed now based on the theoretical approach outlined in the previous chapters of the book. Of course, it is always desirable to design, to produce, and to use gear pairs with the most favorable performance. Designing gears that feature a desirable performance is a challenging problem for gear designers.

A gear pair with the most favorable set of design parameters can be synthesized – the developed theory of gearing is capable of solving problems of this sort. For synthesizing a favorable gear pair, an appropriate criterion is required. Contact and bending strength of the gear teeth, wear resistance of the gear tooth flanks, condition of lubrication of the interacting tooth surfaces, efficient *EHD*-lubrication (elasto-hydro-dynamic lubrication), and so forth, can be used to develop a criterion in compliance to which a gear pair can be synthesized. It is the right point to turn the readers' attention here that all the above-listed requirements, that the synthesized gear pair has to comply with, depend on the conditions of contact between the interacting tooth flanks,  $\mathcal{S}$  and  $\mathcal{P}$ , of a gear and of a mating pinion.

A single chapter, titled “Features of Contact Geometry,” comprises this section of the book. This chapter aims at outlining a novel approach for the analytical description of the contact geometry of the interacting tooth flanks,  $\mathcal{S}$  and  $\mathcal{P}$ , of a gear, and of a mating pinion, and to illustrate in this way the possibility of synthesizing geometrically accurate gear pairs with a favorable performance using for this purpose a possible minimum of the input information.

Part VI of the book consists of Chapter 19. A room for a few more chapters is left as this part of the book has a potential for growth in the future.





# Taylor & Francis

Taylor & Francis Group

<http://taylorandfrancis.com>

---

# 19 Features of Contact Geometry

Investigation of contact geometry of curves and surfaces can be traced back to the eighteenth century. In considerable detail, the study of the contact of curves and surfaces has been undertaken by J.L. Lagrange<sup>1</sup> in his *Theorié des Fonctions Analytiques* (1797) [71], and A.L. Cauchy<sup>2</sup> in his *Leçons sur les Applications du Calcul Infinitésimal á la Geometrie* (1826) [18]. Later, in the twentieth century, an investigation in the realm of contact geometry of curves and surfaces has been undertaken by J. Favard<sup>3</sup> in his *Course de Géométrie Différentielle Locale* (1957) [37]. A few more names of the researchers who have contributed to the subject are to be mentioned.

## 19.1 ON THE MEANING OF THE TERM *SYNTHESIS OF FAVORABLE GEAR PAIR*

A gear pair is composed of two mating gears mounted in a gear housing.<sup>4</sup> Although other designs are feasible, it is common practice to mount the mating gears on shafts.

The purpose of a gear pair is twofold:

1. The use of a gear pair makes possible the transmission of power (i.e., a rotation and torque) from an input shaft to an output shaft.
2. Transformation always occurs when the power is transmitted. Either the direction/orientation or just rotation of the output motion is altered when a motion is transmitted by a gear pair.

In the present-day design practice, a gear pair can be either given or the designer is free to select a gear pair. In the first case, the design of an actual gear pair goes through a routine procedure that is well established in the industry. In the second case, the designer has an opportunity to synthesize a gear pair with favorable performance.

It is important to stress here the principal difference between the concept of *synthesis of a favorable gear pair* and between *optimization of a gear pair*.

The term *optimization of a gear pair* means the determination of an optimal (in a certain pre-specified sense) set of design parameters of an object/process whose structure is known; the structure does not undergo any changes in the object/process procedure of optimization. Optimization targets the determination (e.g., calculation) of a set of input parameters under which a given criterion of the optimization can be achieved. The structure of the object/process after optimization remains the same as before optimization.

The said is illustrated by the following.

In the case of optimization of a gear pair design, a circular arc can be pre-specified as a desirable line of contact,  $LC_{des}$ , in a gear pair. A solution to the problem of optimization returns an optimal value of the radius,  $[R_{lc}]_{opt}$ , of the desirable line of contact,  $LC_{des}$ , and an optimal configuration of the desirable line of contact,  $LC_{des}$ , in relation to the plane of action,  $PA$ .

---

<sup>1</sup> Joseph-Louis Lagrange (January 25, 1736–April 10, 1813) – an Italian born [born *Giuseppe Lodovico (Luigi) Lagrangia*] famous French mathematician and mechanician.

<sup>2</sup> Augustin-Louis Cauchy (August 21, 1789–May 23, 1857) – a famous French mathematician.

<sup>3</sup> Jean Favard (August 28, 1902–January 21, 1965) – a French mathematician.

<sup>4</sup> In contrast to a gear pair, harmonic drive is composed of more than two components; it is composed of a stator-gear, a flexible gear, and a wave generator. All the components are vital for the design and operation of harmonic drive. In this book, harmonic drive is not viewed as a gear pair and, therefore, harmonic drives are not considered.

In the case of synthesis of favorable line of contact, no constraints on the line geometry are imposed. Ultimately, it could happen that the line of contact is not a circular arc at all, but, instead, this is a curve of completely different geometry.

Crossed-axes gear pairs are convenient to illustrate the difference between *synthesis* and *optimization*.

Consider a procedure of synthesizing of a crossed-axes gear pair with a variable transverse profile angle,  $\phi_{t,\omega}$ , across the effective portion of the face width,  $F_{pa}$ . No input information is available about a desirable line of contact,  $LC_{des}$ , in this case. All the parameters of the geometry of the desirable line of contact,  $LC_{des}$ , are derived as the output of the synthesizing process. Such a problem cannot be solved in the process of optimization, when a *structure* of the desirable line of contact,  $LC_{des}$ , has to be pre-specified. More examples in this regard can be provided.

The term *synthesis of favorable gear pair* means the determining of both a desirable structure and a desirable set (in certain sense) of parameters of an object/process. In the procedure of synthesizing, the structure of the object/process is not predetermined. Moreover, usually, the structure of the object/process is unknown. The desirable structure of the object/process must be determined simultaneously with the parameters that ensure its desired functioning.

The synthesized object/process is always, in certain sense, the best of all possible ones, whereas the optimized object/process could be the best among others of that same structure, but not the best of all possible, which is not the same.

Despite numerous attempts have been made to this end to solve the problem of synthesizing a gear pair with desirable properties, the problem still remains unsolved. It is still unsolved on the kinematic/geometric level, and, moreover, it is not yet solved on a higher level. Physical phenomena (those observed when a gear pair operates) must be incorporated into the higher-level synthesis.

With respect to gear pairs, the synthesis begins with given motion requirements and proceeds to determining the type and design parameters of a desirable gear pair.

The development of the best possible design of a gear pair that is capable of transmitting and/or transforming a rotary motion from a driving shaft to the driven shaft is the main goal of *synthesis of a favorable gear pair*. Therefore, for a given configuration of the input shaft, and the output shaft, the problem of synthesizing a favorable gear pair can be solved if:

- A rotation of an input shaft, and a rotation of an output shaft are specified
- Torque applied to an input shaft is known

In the case of synthesizing a gear pair design, the geometry of a desirable line of contact,  $LC_{des}$ , is not pre-specified. A solution to the problem of synthesizing a gear pair design returns a desirable line of contact,  $LC_{des}$ , of a novel favorable geometry, as well as the best possible configuration of the desirable line of contact,  $LC_{des}$ , in relation to the plane of action,  $PA$ . Then, the calculated  $LC_{des}$  can be approximated either by a circular arc or by an arc of other appropriate geometry.

In general case, two rotations about skew axes have to be specified. One of the rotations is a rotation of the input shaft, whereas the other one is a rotation of the output shaft. An input torque is known. It is required to determine the set of the design parameters of a desirable gear pair for transmitting a steady rotation from the input shaft to the output shaft.

Here, the term *favorable gear pair* should be specified in engineering terms.<sup>5</sup>

<sup>5</sup> This interpretation of the problem of *synthesis of favorable gear pair* significantly differs from that which is commonly understood by the term *synthesizing gear pair*. In order to distinguish the proposed interpretation of the problem from what is known from other sources, this interpretation of the problem of *synthesis of favorable gear pair* can be referred to as  $S_{pr}$  – *synthesis of desirable gear pair*.

## 19.2 DUPIN INDICATRIX

Prior to discussing the problem of *synthesis favorable gear pair*, it is helpful to refresh the readers' memory of what the term *Dupin indicatrix* stands for.

At any point of a smooth regular gear tooth flank,  $\mathcal{F}$  (as well as at any point of a smooth regular pinion tooth flank,  $\mathcal{P}$ ), a corresponding *Dupin indicatrix* can be constructed. *Dupin indicatrix*,  $Dup(\mathcal{F})$ , at point of a gear tooth flank,  $\mathcal{F}$  is a planar characteristic curve of the second order. It is used for graphical interpretation of the distribution of normal curvatures of a surface in differential vicinity of a surface point.

*Dupin indicatrix* at point of a gear,  $\mathcal{F}$ , tooth flank is of critical importance in the theory of gearing, especially when synthesizing a gear pair with the most favorable performance. Generation of this planar characteristic curve is illustrated in a diagram shown in Figure 19.1.

A unit normal vector,  $\mathbf{n}_g$ , to a gear tooth flank,  $\mathcal{F}$ , at an arbitrary point,  $m$ , is constructed. Consider a plane,  $W$ , through a unit normal vector,  $\mathbf{n}_g$ , that is rotated about the vector  $\mathbf{n}_g$ . When rotating, the plane occupies consecutive positions  $W_1, W_2, W_3$ , and others. Radii of normal curvature of the line of intersection of the gear tooth flank,  $\mathcal{F}$ , by the normal planes  $W_1, W_2, W_3$ , are equal  $R_{g,1}, R_{g,2}, R_{g,3}$ , and so forth. The tooth flank,  $\mathcal{F}$ , is intersected by a plane  $Q$ . The plane  $Q$  is perpendicular to the unit normal vector,  $\mathbf{n}_g$ . This plane is at a certain small distance,  $\delta$ , from the point  $m$ . When the distance,  $\delta$ , approaches zero ( $\delta \rightarrow 0$ ), and when the scale of the line of intersection of the gear tooth flank,  $\mathcal{F}$ , by the plane,  $Q$ , approaches an infinity, then the line of intersection of the gear tooth flank,  $\mathcal{F}$ , by the plane,  $Q$ , approaches the planar characteristic curve that is commonly referred to as *Dupin indicatrix*,  $Dup(\mathcal{F})$  at point of a smooth regular gear tooth flank,  $\mathcal{F}$ .

An equation for the *Dupin indicatrix*,  $Dup(\mathcal{F})$ , can be represented in the form:

$$k_{1,g} x_g^2 + k_{2,g} y_g^2 = 1 \quad (19.1)$$

Here, the principal curvatures at point of a gear tooth flank,  $\mathcal{F}$ , are designated as  $k_{1,g}$  and  $k_{2,g}$ , correspondingly.

Equation (19.1) describes a particular case of *Dupin indicatrix*, which is represented in *Darboux frame*.

The interested reader may wish to go to Appendix E for details on *Dupin indicatrix*,  $Dup(\mathcal{F})$  and  $Dup(\mathcal{P})$ , at point of a gear,  $\mathcal{F}$ , and a mating pinion,  $\mathcal{P}$ , tooth flanks.

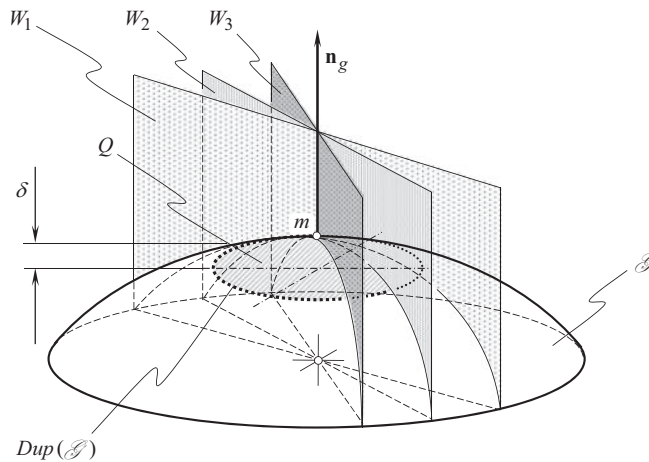


FIGURE 19.1 *Dupin indicatrix* at point of smooth regular gear tooth flank,  $\mathcal{F}$ .

### 19.3 INDICATRIX OF CONFORMITY AT POINT OF CONTACT OF A GEAR AND A MATING PINION TOOTH FLANKS

A quantitative measure of degree of conformity at point of contact of a gear tooth flank,  $\mathcal{G}$ , and a mating pinion tooth flank,  $\mathcal{P}$ , is concisely outlined immediately below.

Quantitatively, degree of conformity at point of contact of a surface  $\mathcal{P}$  to another surface  $\mathcal{G}$  can be expressed in terms of the difference between the corresponding radii of the normal curvature of the contacting surfaces. The discussed quantitative measure of the degree of conformity of two tooth flanks,  $\mathcal{G}$  and  $\mathcal{P}$ , is based on the implementation of *Dupin indicatrices*,  $Dup(\mathcal{G})$  and  $Dup(\mathcal{P})$ , constructed at point of contact of the tooth flanks,  $\mathcal{G}$  and  $\mathcal{P}$ .

*Dupin indicatrix*,  $Dup(\mathcal{G})$ , indicates the distribution of the radii of normal curvature at point of a gear tooth flank,  $\mathcal{G}$ , as it had been shown, for example, for a concave elliptic patch of the tooth flank,  $\mathcal{G}$  (see Figure 19.2).

Derived for the first time in the late 1970s [127,128], the equation of the indicatrix of conformity  $Cnf_R(\mathcal{G}/\mathcal{P})$  at point of contact of a gear tooth flank,  $\mathcal{G}$ , and a mating pinion tooth flank,  $\mathcal{P}$ , is postulated of the following structure<sup>6</sup>:

$$Cnf_R(\mathcal{G}/\mathcal{P}) \Rightarrow r_{cnf}(\varphi, \mu) = r_g(\varphi) \operatorname{sgn} R_g(\varphi) + r_p(\varphi, \mu) \operatorname{sgn} R_p(\varphi, \mu) \quad (19.2)$$

The actual location of a point  $a_\varphi$  of the *Dupin indicatrix*,  $Dup(\mathcal{G})$ , constructed at point of the gear tooth flank,  $\mathcal{G}$ , is specified by the position vector  $r_p(\varphi)$ . The actual location of a point  $b_\varphi$  of the *Dupin indicatrix*,  $Dup(\mathcal{P})$ , constructed at point of pinion tooth flank,  $\mathcal{P}$ , is specified by the position vector  $r_p(\varphi, \mu)$ . With that said, the actual location of point  $c_\varphi$  (see Figure 19.2) of the indicatrix of conformity  $Cnf_R(\mathcal{G}/\mathcal{P})$  at point of contact  $K$  of the tooth flanks,  $\mathcal{G}$  and  $\mathcal{P}$ , is specified by the position

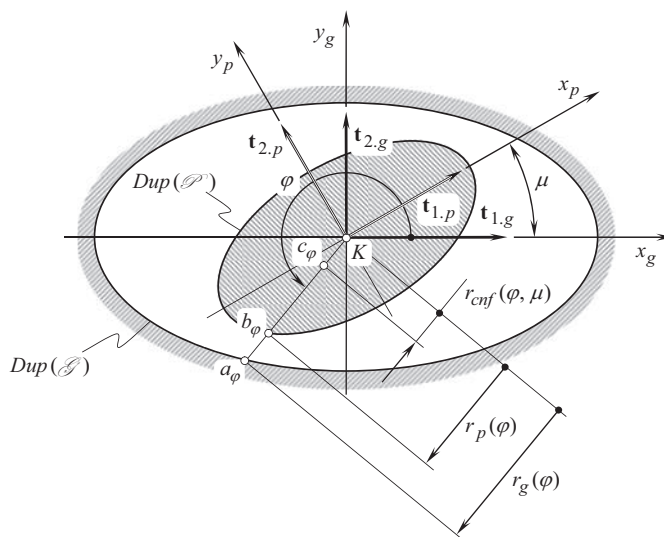


**FIGURE 19.2** To the derivation of equation of indicatrix of conformity,  $Cnf_R(\mathcal{G}/\mathcal{P})$ , at point of contact,  $K$ , of a gear tooth flank,  $\mathcal{G}$ , and of a mating pinion tooth flank,  $\mathcal{P}$ .

<sup>6</sup> Equation of this characteristic curve is known from:

- Pat. No.1249787, USSR, *A Method of Sculptured Part Surface Machining on a Multi-Axis NC Machine*, S.P. Radzevich, B23C 3/16, Filed: December 27, 1984, [127], and (in hidden form) from:
- Pat. No.1185749, USSR, *A Method of Sculptured Part Surface Machining on a Multi-Axis NC Machine*, S.P. Radzevich, B23C 3/16, Filed: October 24, 1983, [128].

vector  $r_{cnf}(\varphi, \mu)$ . Therefore, the equality  $r_{cnf}(\varphi, \mu) = Kc_\varphi$  is observed, and the length of the straight-line segment  $Kc_\varphi$  is equal to the distance  $a_\varphi b_\varphi$  (i.e.,  $Kc_\varphi = a_\varphi b_\varphi$ ).

Here, in Eq. (19.2) is designated:

$r_g = \sqrt{R_g}$  is the position vector of point of the *Dupin indicatrix*, of the gear tooth flank,  $\mathcal{G}$ , constructed at point of contact,  $K$ , with a mating pinion tooth flank,  $\mathcal{P}$ .

$R_g$  is the radius of normal curvature of the gear tooth flank,  $\mathcal{G}$ , constructed at point of contact,  $K$ , with a mating pinion tooth flank,  $\mathcal{P}$ .

$r_p = \sqrt{R_p}$  is the position vector of point of the *Dupin indicatrix* of the pinion tooth flank,  $\mathcal{P}$ , constructed at point of contact,  $K$ , with a mating gear tooth flank,  $\mathcal{G}$ .

$R_p$  is the radius of normal curvature of the pinion tooth flank,  $\mathcal{P}$ , at point of contact,  $K$ , with mating gear tooth flank,  $\mathcal{G}$ .

The maximal and the minimal degree of conformity at point of contact of tooth flanks,  $\mathcal{G}$  and  $\mathcal{P}$ , as well as the orientation of the normal plane within which the maximal, and the minimal degree of conformity are specified, can be calculated from the indicatrix of conformity,  $Cnf_R(\mathcal{G}|\mathcal{P})$ , constructed at that same point of contact.

The interested reader may wish to go to Appendix E for details on the indicatrix of conformity,  $Cnf_R(\mathcal{G}|\mathcal{P})$ , at point of contact of a gear tooth flank,  $\mathcal{G}$ , and a mating pinion tooth flank,  $\mathcal{P}$ .

## 19.4 CONCEPT OF SYNTHESIZING OF FAVORABLE GEOMETRICALLY ACCURATE GEAR PAIR

As the contact geometry at point of contact between tooth flanks of a gear and a mating pinion,  $\mathcal{G}$  and  $\mathcal{P}$ , can be precisely described analytically by means of the indicatrix of conformity,  $Cnf_R(\mathcal{G}|\mathcal{P})$ , then this planar characteristic curve can be utilized for solving the problem of synthesizing favorable geometrically accurate gear pairs.

At contact point,  $K$ , within a desirable line of contact,  $LC_{des}$ , between a saddle-like gear tooth flank,  $\mathcal{G}$ , and a convex mating pinion tooth flank,  $\mathcal{P}$ , the indicatrix of conformity,  $Cnf_R(\mathcal{G}|\mathcal{P})$  is constructed, as illustrated in Figure 19.3. Equation of the indicatrix of conformity returns the following information about the interacting tooth flanks,  $\mathcal{G}$  and  $\mathcal{P}$ , at contact point,  $K$  (see Figure 19.4):

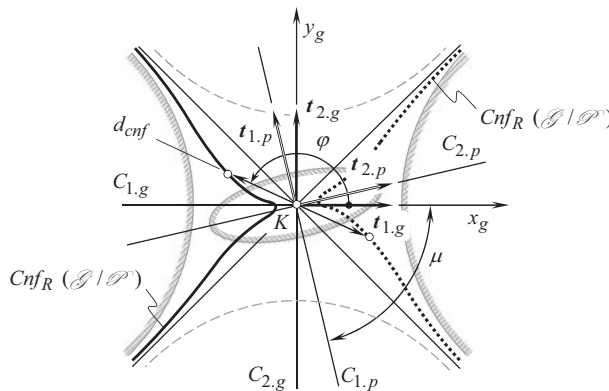


**FIGURE 19.3** Indicatrix of conformity,  $Cnf_R(\mathcal{G}|\mathcal{P})$ , at point of contact,  $K$ , of a smooth regular saddle-like gear tooth flank,  $\mathcal{G}$ , and a mating pinion convex tooth flank,  $\mathcal{P}$  (the tooth flanks,  $\mathcal{G}$  and  $\mathcal{P}$ , are in the first order of tangency).

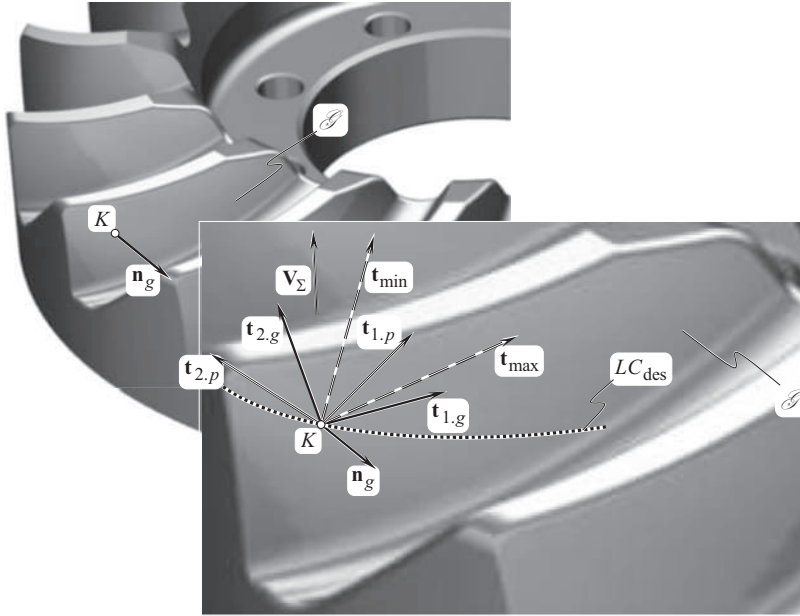


**FIGURE 19.4** Contact geometry at point,  $K$ , of contact between the teeth flanks,  $\mathcal{S}$  and  $\mathcal{P}$ , of a gear and a mating pinion.

- Configuration of the principal directions,  $\mathbf{t}_{1.g}$  and  $\mathbf{t}_{2.g}$ , on the gear tooth flank,  $\mathcal{S}$ , in relation to the linear velocity vector,  $\mathbf{V}_\Sigma$ , of their instant relative motion
- The principal radii of curvature,  $R_{1.g}$  and  $R_{2.g}$ , in the sections of the gear tooth flank,  $\mathcal{S}$ , by the first,  $C_{1.g}$ , and by the second,  $C_{2.g}$ , principal planes
- Configuration of the principal directions,  $\mathbf{t}_{1.p}$  and  $\mathbf{t}_{2.p}$ , on the pinion tooth flank,  $\mathcal{P}$ , in relation to the linear velocity vector,  $\mathbf{V}_\Sigma$ , of their instant relative motion
- The principal radii of curvature,  $R_{1.p}$  and  $R_{2.p}$ , in the sections of the pinion tooth flank,  $\mathcal{P}$ , by the first,  $C_{1.p}$ , and by the second,  $C_{2.p}$ , principal planes
- The angle,  $\mu$ , of local relative orientation of the tooth flanks,  $\mathcal{S}$  and  $\mathcal{P}$ , in relation to one another
- A current,  $d_{cnf}$  (and the minimum,  $d_{cnf}^{\min} = 0$ ), diameters of the indicatrix of conformity,  $Cnf_R(\mathcal{S} \setminus \mathcal{P})$
- A direction of the maximal,  $\mathbf{t}_{\max}$ , and the minimal,  $\mathbf{t}_{\min}$ , degree of conformity of the tooth flanks at a point within the line of their contact,  $LC_{des}$

All the output data are expressed in terms of design parameters of the gear pair and in terms of parameters of the kinematics of the relative motion of the gear and the mating pinion (all these parameters are considered variable at this point).

The active portion of the axis of instantaneous rotation,  $P_{ln}$ , can be divided into certain number,  $n_{ln}$ , of straight-line segments of a length,  $a_{ln}$ . The actual value of the transverse pressure angle,  $\phi_{t,\omega}$ , can be different at each straight-line segments of the length,  $a_{ln}$ . For each portion,  $a_{ln}$ , a corresponding narrow plane of action,  $PA_a$ , can be constructed. When the number,  $n_{ln}$ , approaches an infinity ( $N_{ln} \rightarrow \infty$ ), and the length,  $a_{ln}$ , approaches zero ( $a_{ln} \rightarrow 0$ ), then a smooth ruled surface of action,  $SA$ , can be constructed.<sup>7</sup> Such a permissible alteration of the transverse pressure angle,  $\phi_{t,\omega}$ , can be incorporated into the process of synthesizing of *synthesis of a favorable gear pair*.

<sup>7</sup> Continuous and smooth alteration of both the parameters,  $n_{ln}$  and  $a_{ln}$ , is assumed in this consideration.



A desirable parameter,  $P_s$ , the extremum of which is required to be attained when synthesizing the gear pair, has to be expressed in terms of the radius,  $r_{cnf}$ , of the indicatrix of conformity,  $P_s = P_s(r_{cnf})$ .

A solution to the set of equations:

$$\frac{\partial P_s}{\partial \varphi}(\varphi, \mu, R_g, R_p, \dots) = 0 \quad (19.3)$$

$$\frac{\partial P_s}{\partial \mu}(\varphi, \mu, R_g, R_p, \dots) = 0 \quad (19.4)$$

$$\frac{\partial P_s}{\partial R_g}(\varphi, \mu, R_g, R_p, \dots) = 0 \quad (19.5)$$

$$\frac{\partial P_s}{\partial R_p}(\varphi, \mu, R_g, R_p, \dots) = 0 \quad (19.6)$$

along with the derivatives with respect to the other design parameters of a gear pair, returns a set of the design parameters of the gear pair, and the parameters of the kinematics of the relative motion of the gear and the pinion. Where appropriate, the solution to the set of Eqs. (19.3)–(19.6) has to comply with permissible intervals for the design parameters, for example, for the transverse pressure angle,  $5^\circ \leq \phi_{t,\omega} \leq 35^\circ$ , pitch helix angle,  $-40^\circ \leq \psi \leq 40^\circ$ , and so forth.

The following conclusions from the discussion in this section of the book are briefly outlined immediately below:

- The problem of synthesizing geometrically accurate gear pairs with favorable performance is a challenging (but a solvable) problem; this problem can be solved analytically
- Implementation of an analytical description of contact geometry of tooth flanks of a gear and of a mating pinion is a promising approach to solve the problem of synthesizing of geometrically accurate gear pairs with favorable performance
- It is proposed to develop a solution to the problem of synthesizing of geometrically accurate gear pairs with favorable performance on the premise of indicatrix of conformity,  $Cnf_R(\mathcal{S}/\mathcal{P})$ , constructed at point of contact between the tooth flanks,  $\mathcal{S}$  and  $\mathcal{P}$ , of a gear and of a mating pinion (at point within a desirable line of their contact,  $LC_{des}$ )
- A gear pair of any possible kind, namely, parallel-axes gear pairs, intersected-axes gear pairs, crossed-axes gear pairs, as well as  $S_{pr}$  – gearings, can be synthesized using the disclosed approach

The proposed method of synthesizing a geometrically accurate gear pair with favorable performance needs to be evolved into engineering practice, and get convenient for practical implementation, for example, in the development of corresponding software.





# Taylor & Francis

Taylor & Francis Group

<http://taylorandfrancis.com>

# *Part VI*

---

## *Real Gears and Their Application*

This section of the book is composed of Chapters 20–29. These chapters deal with numerous areas of application of gears and all kinds of gear pairs. The consideration is mostly (but not only) focused on illustration of novel results in the theory of gearing outlined in this book.



# Taylor & Francis

Taylor & Francis Group

<http://taylorandfrancis.com>

---

# 20 Generic Gear Surfaces

Various designs of gears can be used to transmit and to transform a rotary motion from a driving shaft to a driven shaft. An actual gear pair design depends much on the configuration of two rotation vectors associated with an input shaft, and with an output shaft of the gear pair. Skew axes helical gears, worm gearing, and others are used to transmit and to transform a rotary motion from an input shaft to an output shaft, whose axes cross each other at crossed-axes angle of a specified value.

A generic gear surface is associated with a gear of any and all designs. Here and below, *generic gear surface* – is associated with a gear surface (commonly, a surface of revolution), which is used as the pitch surface when machining the gear on a gear generator.

Gears that feature various generic surfaces can be used to transmit and to transform a given rotary motion. This makes possible a conclusion that the vector diagram of a gear pair is necessary but not sufficient to identify the actual type of gearing. In this regard, the generic gear surfaces, of which a gear pair is composed, are of importance. Further development of a classification of possible types of gear pairs becomes possible if the generic gear surface is incorporated into the consideration. An orderly classification of gear pairs, and a classification of gears themselves, is a desirable prior to begin to study of gears in general. The development of scientific classification of gear pairs is a challenging problem. In general engineering practice, names have been given to most of the numerous types of gear members and gear combinations. However, these names, although generally accepted and used, are sometimes indefinite and ambiguous. In some cases, it is hard to find a sufficient number of names to distinguish between variants, which deserve some recognition of their individuality; in others, the same gear operating in different ways may have different names. The problem of classification, moreover, yields different results according to the direction from which it is approached. By treating gears according to the character of their teeth, one system of grouping emerges; by considering the relative position of the shafts they connect, another system is possible; from the point of view of the real nature of tooth action, a third grouping is possible.

In this chapter, an attempt to classify gear pairs based on their associated gear vector diagrams is undertaken.

## 20.1 ORIGINATION OF GENERIC GEAR SURFACE

Gears used in the design of various machines and mechanisms are somehow machined on machine tools. Present days' machine tools, especially numerical control machines (NC), are capable of performing any desirable motion of the cutting tool in relation to the workpiece. This makes it possible to machine a gear that has any desirable tooth flank geometry. Using any desirable motion of the cutting tool in relation to the work-gear is not a common practice in machining gears, especially machining gears in high-volume production industries.

The motions performed by the gear cutting tool in relation to the work-gear are represented either by a translation, or by a rotation, or by a combination of translations and rotations [151,152,155]. This is because translational motion and rotational motion are the two elementary motions that can be easily performed on a machine tool. If a relative motion of a gear cutting tool is limited either to a translation, or a rotation, or a combination of a few translations and rotations, then all possible types of gears and gear pairs can be identified, and consequently investigated.

Let us proceed with consideration of possible generic surfaces of gears machined on conventional machine tools used in gear manufacturing practice.

## 20.2 EXAMPLES OF GEAR PAIRS COMPOSED OF GEARS WITH GENERIC GEAR SURFACES VARIOUS GEOMETRIES

Various designs of gears can be developed for the purpose of connecting parallel shafts.

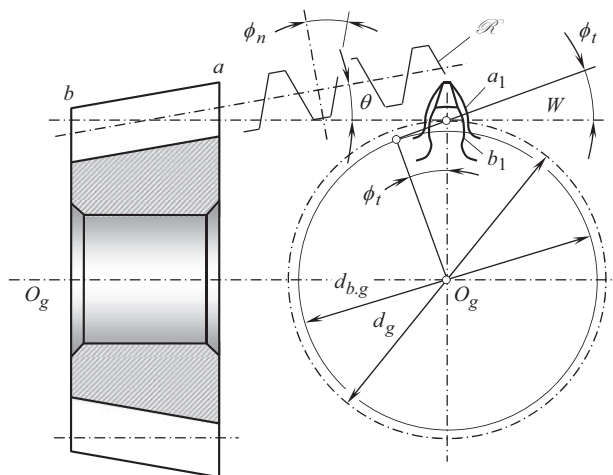
In spur and helical involute gears, teeth are generated from a basic rack whose pitch plane rolls over the pitch cylinder of the gear; further, the teeth of the basic rack are symmetrical with respect to the pitch plane, or they have, in the case of corrected gears, a plane of symmetry parallel to the pitch plane [82,83].

There is a possible departure from these conditions which leads to a type of gear that has valuable but little-explored possibilities; this type is given the name, for want of a better one, *conical involute gears*. The principle underlying generation and action of gears of this type may be approached in the following way.

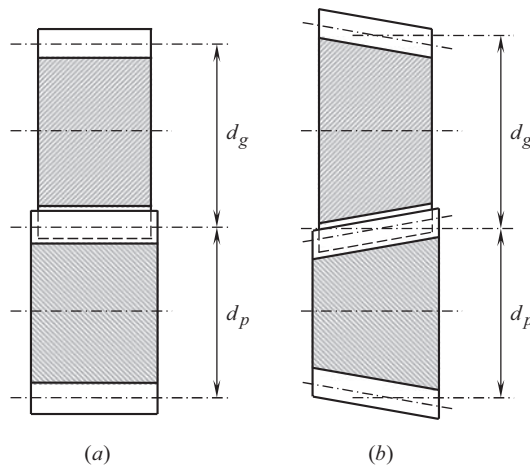
Suppose that a spur gear is generated by the rack planning process, which is carried out in the usual way except that the direction of reciprocation of the rack cutter, instead of being parallel to the axis of the gear, is inclined as shown in Figure 20.1. Since the work-gear is rolled in the same way as for a normal spur gear, it still has a pitch cylinder that rolls with the real pitch plane, represented by  $W$ , of the basic rack,  $\mathcal{R}$ , although the plane of symmetry of the teeth of the basic rack is now inclined at an angle,  $\theta$ , to the axis of the work-gear. Moreover, on all transverse planes, such as  $a$ ,  $b$ , the inclination of the profiles of the rack teeth is the same and is equal to  $\phi_n$ , whereas the intersection of the pitch plane,  $W$ , with any basic rack tooth gives a straight line representing a tooth spiral on the developed pitch cylinder. Hence, the teeth generated by the basic rack,  $\mathcal{R}$ , are involute helicoids. On sections such as  $a$  and  $b$ , the profiles,  $a_1$  and  $b_1$ , are involutes to the same base circle of diameter  $d_{b,g}$  and really represent the profiles of spur gears with different degrees of correction.

Figure 20.2a shows a pair of cylindrical gears of pitch diameters,  $d_g$  and  $d_p$ , connecting parallel shafts. The same shafts might be connected, with the same result, by a pair of conical involute gears shown in Figure 20.2b. The pitch diameters,  $d_g$  and  $d_p$ , are the diameters of the pitch cylinders when the gears are rolled with the inclined basic rack,  $\mathcal{R}$ , and the only condition is that the pitch cone angle,  $\theta$ , must be the same for both gears. If the teeth are also generated with a spiral, the spiral angles of generation,  $\psi_g$  and  $\psi_p$ , must be equal and opposite.

In comparison with the conventional cylindrical gear pair shown in Figure 20.2a, a conical involute gear pair (see Figure 20.2b) has the same pitch diameter of the gear,  $d_g$ , and the pinion,  $d_p$ .



**FIGURE 20.1** Generation of *conical involute gear* [82]. (After: Merritt, H.E., *Gear Engineering*, London: Putman Publishing, 1971, 489 p.)



**FIGURE 20.2** Derivation and example of application of *conical involute gear* [82]: (a) conventional cylindrical gear pair, and (b) conical involute gear pair. (After: Merritt, H.E., *Gear Engineering*, London: Putman Publishing, 1971, 489 p.)

Neither the pitch surfaces nor the axodes of the gear pair (see Figure 20.2b) feature conical surfaces. A conical surface is the generic gear surface of conical involute gears.

In this and other applications described below in this chapter, the angular velocity ratio is (theoretically) constant and independent of the axial position of either gear within the practical limits. Axial adjustment of either gear relative to the other will, however, alter the backlash, and may in fact provide a useful means of doing this [82,83].

A few more examples to this end can be found in Ref. [12]. Internal gear pairs similar to the aforementioned ones (see Figure 20.2) can also be designed.

The discussed example makes clear the difference between the generic gear surface and between the pitch surface as well as between the corresponding axodes. The cone in a *conical involute gear* (see Figure 20.2) is not equivalent neither to axode nor to pitch surface. *Generic gear surface* is an independent entity in gearing.

It must be stressed here that an approach that is based on the elements of vector algebra can be implemented for the analytical description of the generic gear surface in all practical cases. Vector representation of generic gear surfaces is convenient for many reasons, which are discussed immediately below in Section 20.3.

### 20.3 EVALUATION OF THE TOTAL NUMBER OF POSSIBLE GENERIC GEAR SURFACES

Once all possible types of gear design are limited just to those gears, for which generic gear surfaces are generated either by a straight-line segment, or by a circular arc, the following two actions are possible:

1. Identification of all possible types of gears
2. Development of a classification of possible types of generic gear surfaces

The classification of possible types of generic gear surfaces is important for the purpose of designing gear pairs that feature the most favorable performance in every particular application.

### 20.3.1 POSSIBLE PROFILES OF GENERIC GEAR SURFACE CONSTRUCTED IN AXIAL SECTION OF GEAR

Referring to Figure 20.3, consider generic gear surface designed for a crossed-axes gear pair.

If no constraints are imposed, the ideal generic gear surface can be viewed as the locus of consecutive positions of the axis of instantaneous rotation,  $P_{ln}$ , when the axis is rotated about the gear axis,  $O_g$ . In this way, the generic gear surface is shaped in the form of a hyperboloid of revolution of one sheet. Two hyperbolas appear in the section of this surface by a plane through the gear axis of rotation,  $O_g$ .

An analytical expression for the description of the generic gear surface can be derived in the following way.

Consider a generic gear surface that is referred to a *Cartesian* coordinate system,  $X_g^a Y_g^a Z_g^a$ , as shown in Figure 20.3. The position vector,  $\mathbf{r}_g^a$ , of arbitrary point,  $m$ , of the generic gear surface can be represented as summa of two components, namely, as:

$$\mathbf{r}_g^a = \mathbf{R}_g^a + \mathbf{L}_g^a \quad (20.1)$$

In the reference system,  $X_g^a Y_g^a Z_g^a$ , one of the components,  $\mathbf{R}_g^a$  (see Figure 20.3), is analytically represented as:

$$\mathbf{R}_g^a = \mathbf{i} \cdot \tilde{r}_g \cos \phi_g^a + \mathbf{j} \cdot \tilde{r}_g \sin \phi_g^a \quad (20.2)$$

where

$\tilde{r}_g$  is the radius of throat of the generic gear surface (the radius,  $\tilde{r}_g$ , is measured in the coordinate plane,  $X_g^a Y_g^a$ ).

$\phi_g^a$  is the angular parameter of the generic gear surface.

For the analytical description of another component,  $\mathbf{L}_g^a$ , of the position vector,  $\mathbf{r}_g^a$ , the following expression is used:

$$\mathbf{L}_g^a = -\mathbf{i} \cdot z_g^a \tan \Sigma_g \sin \phi_g^a + \mathbf{j} \cdot z_g^a \tan \Sigma_g \cos \phi_g^a + \mathbf{k} \cdot z_g^a \quad (20.3)$$

The angular parameter,  $\phi_g^a$ , is the first *Gauss'* parameter of the generic gear surface.

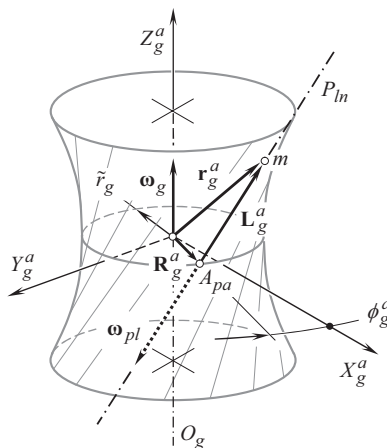


FIGURE 20.3 Analytical description of generic gear surface.

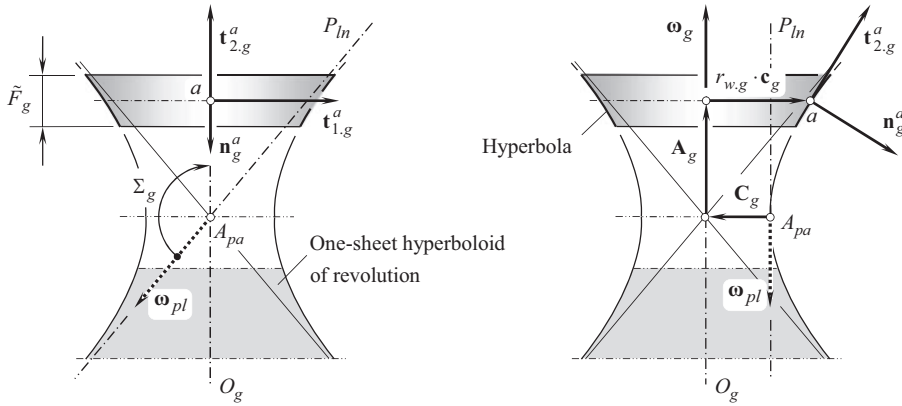


FIGURE 20.4 *Darboux trihedron*,  $\mathbf{n}_g^a \mathbf{t}_{1,g}^a \mathbf{t}_{2,g}^a$ , associated with the desirable generic gear surface.

Equations (20.2) and (20.3) yield an expression:

$$\mathbf{r}_g^a(\phi_g^a, z_g^a) = \begin{bmatrix} \tilde{r}_g \cos \phi_g^a - z_g^a \tan \Sigma_g \sin \phi_g^a \\ \tilde{r}_g \sin \phi_g^a + z_g^a \tan \Sigma_g \cos \phi_g^a \\ z_g^a \\ 1 \end{bmatrix} \quad (20.4)$$

for the position vector,  $\mathbf{r}_g^a$ , of an arbitrary point,  $m$ , of the generic gear surface.

In Eq. (20.4), another *Gauss'* parameter of the generic gear surface is denoted by  $z_g^a$ , and  $\Sigma_g$  designates the angle that the rotation vector of the gear,  $\omega_g$ , makes with the vector,  $\omega_{pl}$  of instant rotation [ $\Sigma_g = \angle(\omega_g, \omega_{pl})$ ].

The rotation vector of the gear,  $\omega_g$ , is pointed along the gear axis of rotation,  $O_g$ . The vector,  $\omega_g$ , is applied at the throat of the generic gear surface. The vector of instant rotation,  $\omega_{pl}$ , is pointed along the axis of instantaneous rotation,  $P_{ln}$ . This vector is applied at the plane-of-action apex,  $A_{pa}$ .

The face width of the gear is denoted by  $\tilde{F}_g$ . The location of the middle section of the generic gear surface is specified by the vectors  $\mathbf{C}_g$ ,  $\mathbf{A}_g$ , and  $r_{w,g} \cdot \mathbf{c}_g$ , as illustrated in Figure 20.4.

A local reference system is associated with the generic gear surface. This reference system is originated at point,  $a$ , within the axial profile of the generic gear surface. The origin,  $a$ , is at the middle of the width,  $\tilde{F}_g$ . In the particular case under consideration, the *Darboux*<sup>1</sup> *trihedron* is used as the reference system. Three unit vectors, namely, the unit normal vector,  $\mathbf{n}_g^a$ , the unit tangent vector,  $\mathbf{t}_{1,g}^a$ , of the first principal direction, and the unit tangent vector,  $\mathbf{t}_{2,g}^a$ , of the second principal direction, comprise the *Darboux trihedron* at point of interest within the generic gear surface.

The vector,  $\mathbf{n}_g^a$ , is a unit normal vector to the generic gear surface at point  $a$ . An equation:

$$\mathbf{n}_g^a = \mathbf{u}_g \cdot \mathbf{v}_g \quad (20.5)$$

can be used for the calculation of the unit normal vector,  $\mathbf{n}_g^a$ .

In Eq. (20.5), the unit tangent vector to the generic gear surface at point  $a$  are designated as  $\mathbf{u}_g$  and  $\mathbf{v}_g$ . The unit vectors,  $\mathbf{u}_g$  and  $\mathbf{v}_g$ , are dimensionless. They are given as follows:

$$\mathbf{u}_g = \frac{\mathbf{U}_g}{|\mathbf{U}_g|} \quad (20.6)$$

<sup>1</sup> Jean-Gaston Darboux (August 14, 1842–February 23, 1917), a French mathematician.



$$\mathbf{v}_g = \frac{\mathbf{V}_g}{|\mathbf{V}_g|} \quad (20.7)$$

correspondingly.

In Eqs. (20.6) and (20.7), the tangent vectors,  $\mathbf{U}_g$  and  $\mathbf{V}_g$ , are given by the expressions  $\mathbf{U}_g = \partial \mathbf{r}_g^s / \partial U_g$  and  $\mathbf{V}_g = \partial \mathbf{r}_g^s / \partial V_g$ , correspondingly, and the vector,  $\mathbf{r}_g^s$ , is the position vector of point of the generic gear surface. The *Gauss'* parameters of the generic gear surface are denoted by  $U_g$  and  $V_g$ .

The unit normal vector,  $\mathbf{n}_g$ , is a dimensionless parameter as it is expressed in terms of the dimensionless unit tangent vectors,  $\mathbf{u}_g$  and  $\mathbf{v}_g$  [see Eq. (20.5)].

Labeling of principal directions depends upon the curvature of the generic gear surface. The principal direction that features a greater curvature,  $k_{1,g}^a$ , (and, thus, a smaller radius of curvature,  $R_{1,g}^a$ ) is labeled as  $\mathbf{t}_{1,g}^a$ . The principal direction that features a smaller curvature,  $k_{2,g}^a$ , (and, thus, a greater radius of curvature,  $R_{2,g}^a$ ) is labeled as  $\mathbf{t}_{2,g}^a$  [151,152,155] (here, the curvatures,  $k_{1,g}^a$  and  $k_{2,g}^a$  as well as the corresponding radii of curvature,  $R_{1,g}^a$  and  $R_{2,g}^a$ , are signed values. They are positive in the case of convex section of the generic gear surface by a normal plane, and they are negative when the section is concave). As equality  $R_1 = k_1^{-1}$  is valid by definition, the inequalities,  $k_{1,g}^a > k_{2,g}^a$  and  $R_{1,g}^a < R_{2,g}^a$ , are always valid.<sup>2</sup> In umbilical points on a surface, when all the radii of normal curvature are of a constant value ( $R_g^a = \text{const}$ ), the *Darboux trihedron* does not exist. In this reduced case, a limit case of the *Darboux trihedron* when  $R_{1,g}^a$  approaches infinity (i.e.,  $R_{1,g}^a \rightarrow \infty$ ) is used instead of the trihedron,  $\mathbf{n}_g^a \mathbf{t}_{1,g}^a \mathbf{t}_{2,g}^a$ .

The unit tangent vectors,  $\mathbf{t}_{1,g}^a$  and  $\mathbf{t}_{2,g}^a$ , are the principal vectors at point within the generic gear surface. The first, and the second principal directions of the gear generic surface are specified by the tangent vectors,  $\mathbf{t}_{1,g}^a$  and  $\mathbf{t}_{2,g}^a$ . The vector,  $\mathbf{t}_{1,g}^a$ , is tangential to the section of the generic gear surface by a transverse plane through the point,  $a$ , as this section is convex. The first principal direction is specified by the unit tangent vector,  $\mathbf{t}_{1,g}^a$ . The vector,  $\mathbf{t}_{2,g}^a$ , is tangential to the section of the generic surface by the axial plane through the point,  $a$ , as this section is concave. The second principal direction is specified by the unit tangent vector,  $\mathbf{t}_{2,g}^a$ .

The unit tangent vectors,  $\mathbf{t}_{1,g}^a$  and  $\mathbf{t}_{2,g}^a$ , are specified by the expressions:

$$\mathbf{t}_{1,g}^a = \frac{\mathbf{T}_{1,g}^a}{|\mathbf{T}_{1,g}^a|} \quad (20.8)$$

$$\mathbf{t}_{2,g}^a = \frac{\mathbf{T}_{2,g}^a}{|\mathbf{T}_{2,g}^a|} \quad (20.9)$$

where  $\mathbf{T}_{1,g}^a$  and  $\mathbf{T}_{2,g}^a$  are the vectors of the first, and of the second principal directions of the generic gear surface. Known methods [153,159], are used for the calculation of the unit tangent vectors,  $\mathbf{t}_{1,g}^a$  and  $\mathbf{t}_{2,g}^a$ .

Once the unit vectors,  $\mathbf{n}_g^a$ ,  $\mathbf{t}_{1,g}^a$  and  $\mathbf{t}_{2,g}^a$ , are mutually orthogonal, and two of them (i.e.,  $\mathbf{t}_{1,g}^a$  and  $\mathbf{t}_{2,g}^a$ ) are pointed along the principal directions on the generic gear surface, they comprise a trihedron that is commonly referred to as *Darboux trihedron*.

As shown in Figure 20.4, the generic gear surface has a favorable geometry as it is generated by the axis,  $P_{ln}$ , when the axis is given a rotation about the gear axis of rotation,  $O_g$ . Unfortunately, a

<sup>2</sup> Remember that the algebraic values of the radii of principal curvatures,  $R_{1,g}^a$  and  $R_{2,g}^a$ , relate to each other as  $R_{2,g}^a > R_{1,g}^a$ . In the case of umbilical points, all radii of normal curvature are equal. As a result, the principal directions,  $\mathbf{t}_{1,g}^a$  and  $\mathbf{t}_{2,g}^a$  (and, consequently, the principal radii of curvature,  $R_{1,g}^a$  and  $R_{2,g}^a$ ), are not identified for umbilical points on a generic gear surface.



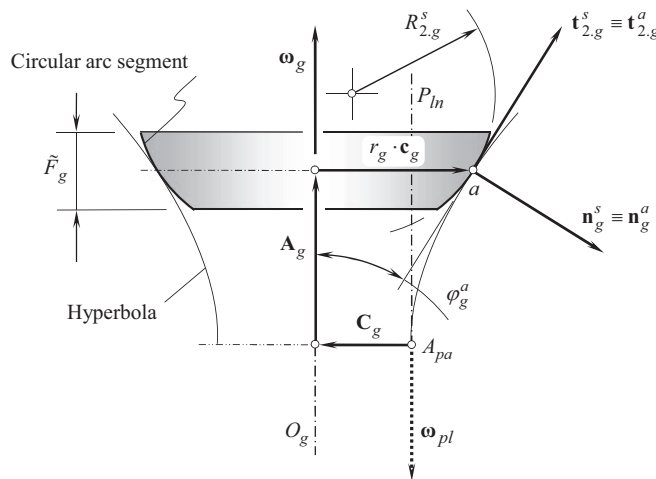


**FIGURE 20.6** Axial profile of the generic surface of a gear approximated by a convex circular arc tangential at point,  $a$ , to hyperbola.

Consider generic gear surface that is machined by a gear cutting tool. The gear cutting tool rotates relative to the work-gear. Again, no physical constraints are imposed on machining of the gear this way.

Two different methods of cutting the gear can be distinguished in this regard.

**First**, the parameters of the rotary motion of the cutting tool are so assigned, as to make the trajectory of the rotary motion of the gear cutting tool tangential at point  $a$  to the hyperbola, as schematically illustrated in Figure 20.6. In the case under consideration, the desirable hyperbolic profile of the generic gear surface is replaced with a circular arc segment that is tangential to the hyperbola at  $a$ . The approximation of the hyperbolic arc segment by the circular arc segment results in a positive curvature of the axial cross section of the generic gear surface. The direction at which the normal curvature is greater is labeled as  $\mathbf{t}_{1,g}^s$ . The normal curvature in this direction is labeled as  $k_{1,g}^s$ . The direction at which the normal curvature is of smaller value is labeled as  $\mathbf{t}_{2,g}^s$ . The normal curvature in this direction is labeled as  $k_{2,g}^s$ . Ultimately, either the two identities  $\mathbf{t}_{1,g}^s \equiv \mathbf{t}_{1,g}^a$  and  $\mathbf{t}_{2,g}^s \equiv \mathbf{t}_{2,g}^a$  (as depicted in Figure 20.6), or the inverse identities,  $\mathbf{t}_{1,g}^s \equiv \mathbf{t}_{2,g}^a$  and  $\mathbf{t}_{2,g}^s \equiv \mathbf{t}_{1,g}^a$ , are valid. In this way, the generic gear surface is affected by the kinematics of the gear-machining process. Consequently, the kinematics affects the labeling of the unit vectors of which the *Darboux trihedron* is composed.

Because the circular arc axial profile is tangential at point  $a$  to the hyperbola, no alterations to the orientation of the axial profile are observed. As a result, the *Darboux trihedron*,  $\mathbf{n}_g^s \mathbf{t}_{1,g}^s \mathbf{t}_{2,g}^s$ , associated with the approximated generic gear surface is identical to that,  $\mathbf{n}_g^a \mathbf{t}_{1,g}^a \mathbf{t}_{2,g}^a$ , associated with the desired generic gear surface.

**Second**, the parameters of the rotary motion are so assigned to cutting tool, as to make the trajectory of the rotary motion of the gear cutting tool tangential at point  $a$  to the hyperbola, as schematically illustrated in Figure 20.7. In this scenario, the desirable hyperbolic profile of the generic gear surface is replaced with a circular arc segment that is tangential to the hyperbola at point  $a$ . The approximation of the hyperbolic arc segment by the circular arc segment results in a negative curvature of the axial cross section of the generic gear surface. The identities  $\mathbf{t}_{1,g}^s \equiv \mathbf{t}_{2,g}^a$  and  $\mathbf{t}_{2,g}^s \equiv \mathbf{t}_{1,g}^a$  are valid in the case under consideration, as illustrated in Figure 20.7.



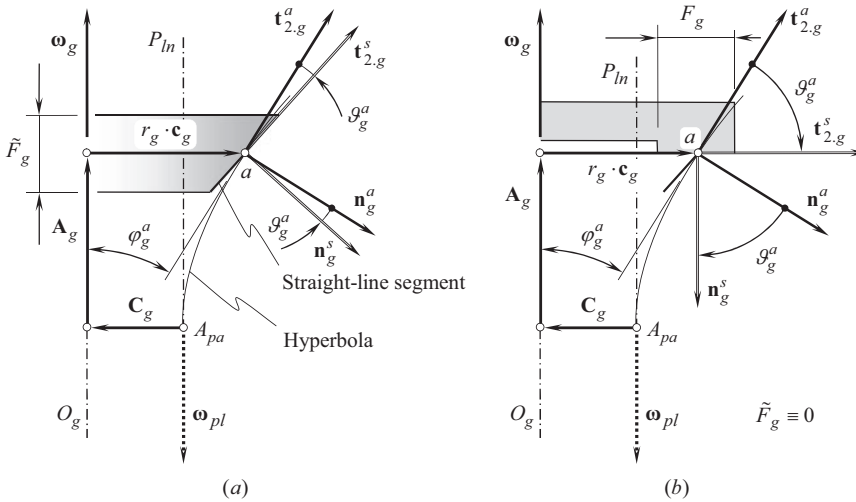


**FIGURE 20.9** Axial profile of generic gear surface in the form of a straight-line segment tilted at point,  $a$ , of the hyperbola at certain negative angle,  $\vartheta_g^s$ , in relation to the unit normal vector,  $\mathbf{n}_g^a$ : (a) conical gear, and (b) face gear.

direction, is considered to be of positive value. The orientation of the *Darboux trihedron*,  $\mathbf{n}_g^s \mathbf{t}_{1.g}^s \mathbf{t}_{2.g}^s$ , of the actual generic gear surface in relation to the *Darboux trihedron*,  $\mathbf{n}_g^a \mathbf{t}_{1.g}^a \mathbf{t}_{2.g}^a$ , of the desirable generic gear surface is specified by the angle,  $\vartheta_g^s$ . The trihedron,  $\mathbf{n}_g^s \mathbf{t}_{1.g}^s \mathbf{t}_{2.g}^s$ , is turned about the unit vector,  $\mathbf{t}_{1.g}^a$ , in a counterclockwise direction through the angle,  $\vartheta_g^s$  (see Figure 20.8a).

The actual value of the angle,  $\vartheta_g^s$ , falls into the interval  $0^\circ < \vartheta_g^s < \varphi_g^a + 90^\circ$ . In a particular case, the value of the angle,  $\vartheta_g^s$ , can be chosen as equal to the angle,  $\varphi_g^a$ , at which the tangent to the hyperbola is tilted relative to the gear axis of rotation,  $O_g$ , as shown in Figure 20.8b. A cylindrical gear for a crossed-axes gear pair is machined under such conditions.

Similarly, the straight-line segment of an actual axial profile of the generic gear surface can be tilted at an angle,  $\vartheta_g^s$ , in the opposite direction as schematically shown in Figure 20.9. The angle,  $\vartheta_g^s$ , in this case is of a negative value. The trihedron,  $\mathbf{n}_g^s \mathbf{t}_{1.g}^s \mathbf{t}_{2.g}^s$ , is turned about unit vector,  $\mathbf{t}_{1.g}^a$ , in a clockwise direction through angle,  $\vartheta_g^s$  (see Figure 20.9a).

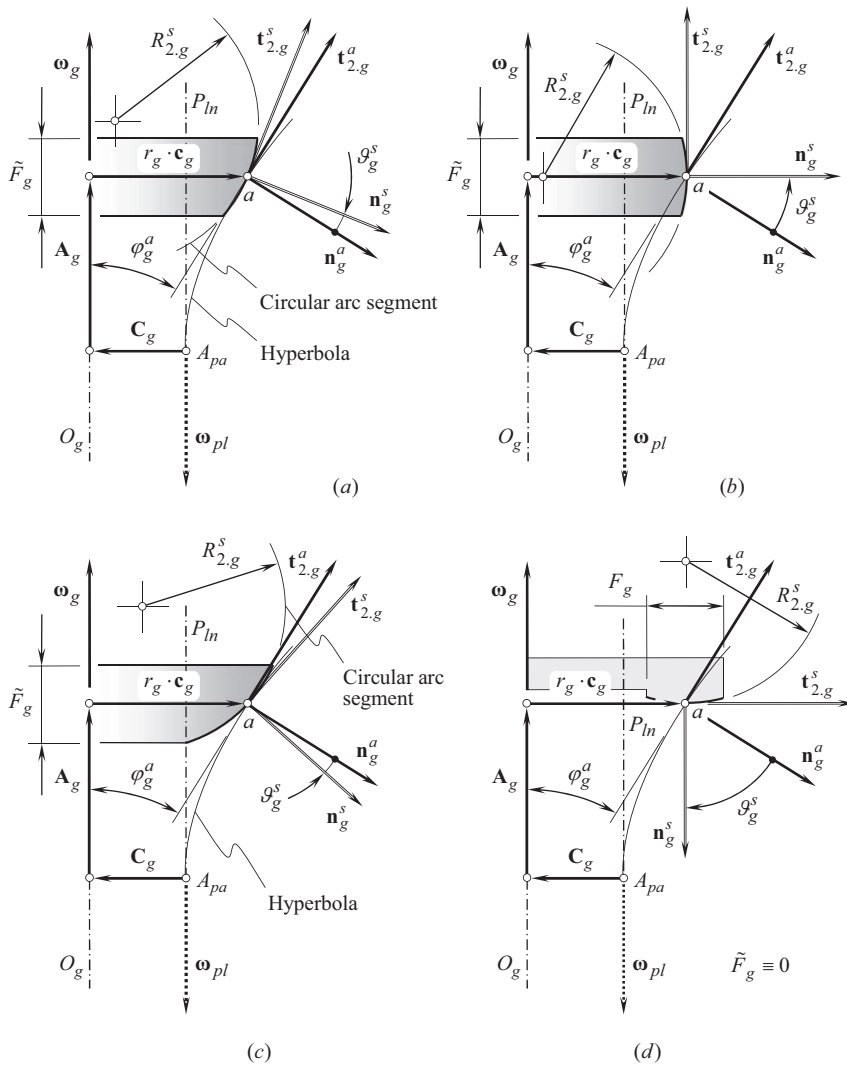
The actual value of the angle,  $\vartheta_g^s$ , falls into the interval  $-(\varphi_g^a + 90^\circ) < \vartheta_g^s < 0^\circ$ . In a particular case, the actual value of the angle  $\vartheta_g^s$  can be chosen equal to  $\vartheta_g^s = 90^\circ - \varphi_g^a$ . Under such a scenario, the straight-line segment is perpendicular to the gear axis of rotation,  $O_g$ , as shown in Figure 20.9b. A face gear for a spatial gear pair can be machined in this case.

Gears that feature the axial profile of generic gear surface in a form of straight-line segments tilted at a certain angle,  $\vartheta_g^s$ , (see Figures 20.8 and 20.9) are used in the design of special purpose gear trains.

Similar to gears that have an inclined straight-line profile (see Figures 20.8 and 20.9), circular arc axial profile of generic gear surfaces can also be tilted at either a positive or at a negative angle,  $\vartheta_g^s$ , relative to the unit normal vector,  $\mathbf{n}_g^a$ , to the desirable generic gear surface.

The results of the analysis for convex circular arc axial profiles inclined at an angle,  $\vartheta_g^s$ , in relation to the unit normal vector,  $\mathbf{n}_g^a$ , at point,  $a$ , to the hyperbola are illustrated in Figure 20.10.

When the angle,  $\vartheta_g^s$ , is of a positive value (see Figure 20.10a), the *Darboux trihedron*,  $\mathbf{n}_g^s \mathbf{t}_{1.g}^s \mathbf{t}_{2.g}^s$ , of the actual generic gear surface in relation to the *Darboux trihedron*,  $\mathbf{n}_g^a \mathbf{t}_{1.g}^a \mathbf{t}_{2.g}^a$ , of the desirable generic gear surface is turned about the unit vector,  $\mathbf{t}_{1.g}^a$ , in a counterclockwise direction through an angle,  $\vartheta_g^s$ . The actual value of the angle,  $\vartheta_g^s$ , falls into the interval  $0^\circ < \vartheta_g^s < \varphi_g^a + 90^\circ$ . In a particular case, the actual value of the angle,  $\vartheta_g^s$ , can be chosen equal to the angle,  $\varphi_g^a$ , at which the tangent to



the hyperbola is tilted relative to the gear axis of rotation,  $O_g$ , as shown in Figure 20.10b. A torus-like gear for a spatial gear pair is machined under such conditions. The outer portion of the torus serves in this case as the generic gear surface.

When the angle,  $\vartheta_g^s$ , is of a negative value (see Figure 20.10c), the *Darboux trihedron*,  $\mathbf{n}_g^s \mathbf{t}_{1,g}^s \mathbf{t}_{2,g}^s$ , of the actual generic gear surface in relation to the *Darboux trihedron*,  $\mathbf{n}_g^a \mathbf{t}_{1,g}^a \mathbf{t}_{2,g}^a$ , of the desirable generic gear surface is turned about the unit vector,  $\mathbf{t}_{1,g}^a$ , in a clockwise direction through the angle,  $\vartheta_g^s$ . The actual value of the angle,  $\vartheta_g^s$ , falls into the interval  $-(\varphi_g^a + 90^\circ) < \vartheta_g^s < 0^\circ$ . In a particular case, the actual value of the angle,  $\vartheta_g^s$ , can be equal to  $\vartheta_g^s = 90^\circ - \varphi_g^a$ , at which the tangent to the hyperbola is tilted relative to the gear axis of rotation,  $O_g$ , as shown in Figure 20.10d. A torus-like face gear for a spatial gear pair is machined under such conditions.

The results of the analysis for a concave circular arc axial profile that is inclined at a certain angle,  $\vartheta_g^s$ , in relation to the unit normal vector,  $\mathbf{n}_g^a$ , at the point,  $a$ , to the hyperbola are illustrated in Figure 20.11.



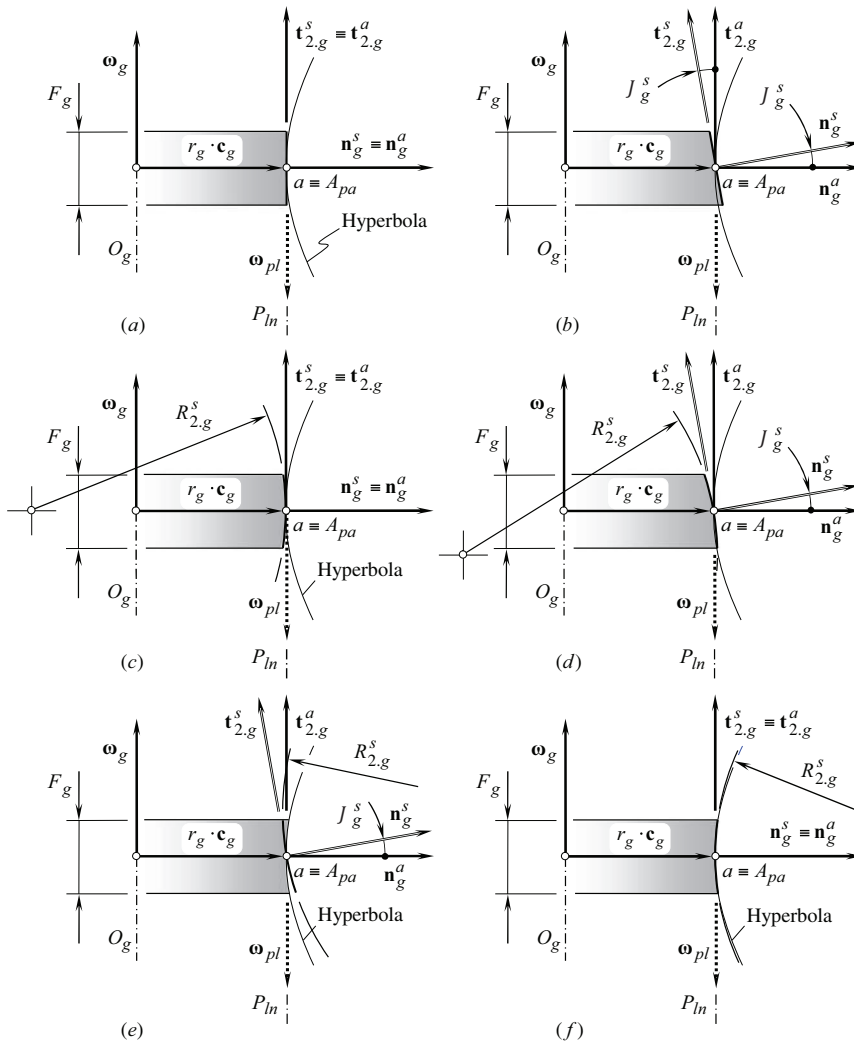


**FIGURE 20.12** Generic gear surfaces of the geometries that feature zero axial vectors ( $\mathbf{A}_g = 0$ ). (a) *straight-to-convex (tangent) contact*; (b) *straight-to-convex (inclined) contact*; (c) *convex-to-convex (tangent) contact*; (d) *convex-to-convex (inclined) contact*; (e) *convex-to-concave (inclined) contact*, and (f) *straight-to-concave (tangent) contact*.

a particular case, the value of the angle,  $\vartheta_g^s$ , can be set  $\vartheta_g^s = 90^\circ - \varphi_g^a$ , at which the tangent to the hyperbola is tilted relative to the gear axis of rotation,  $O_g$ , as shown in Figure 20.11d. A torus-like face gear for a spatial gear pair is machined under such conditions.

In addition to the possible generic gear surfaces shown in Figures 20.4–20.11, a few more generic gear surfaces can be derived under the assumption that the axial vector,  $\mathbf{A}_g$ , is equal to zero (i.e.,  $\mathbf{A}_g = 0$ ). Examples of such generic gear surfaces are schematically illustrated in Figure 20.12.

The total number of generic gear surfaces in this case is limited to six different kinds of generic gear surfaces.

**First**, a straight-line segment can be either tangential to the hyperbola at point,  $a$  (see Figure 20.12a), or it can be inclined to the hyperbola at an angle,  $\vartheta_g^s$  (see Figure 20.12b). From the perspective of gear design, it makes no difference whether the angle,  $\vartheta_g^s$ , is of a positive, or of a negative value.



**Second**, the convex circular arc profile also can be either tangential to the hyperbola at point  $a$  (see Figure 20.12c), or it can be inclined to the hyperbola at an angle,  $\vartheta_g^s$  (see Figure 20.12d). From the perspective of gear design, it makes no difference whether the angle,  $\vartheta_g^s$ , is of a positive, or of a negative value.

**Third**, this statement is also true with respect to a concave circular arc profile, which also can be either tangential to the hyperbola at point,  $a$  (see Figure 20.12e), or it can be inclined to it at a certain angle,  $\vartheta_g^s$  (see Figure 20.12f).

An intermediate conclusion can be drawn up from this discussion: the total number of possible generic gear surfaces of the considered geometry is a finite value, and it is limited to 27 generic gear surfaces. The profiles of the generic gear surfaces are constructed in the axial section of the gears. In addition to the ideal generic gear surfaces (see Figure 20.4), generic gear surfaces of three more geometries can be drawn up from each of Figures 20.5–20.7. Then, the analysis of Figures 20.8 and 20.9 returns four generic gear surfaces: two of them feature an arbitrary angle,  $\vartheta_g^s$ , and two more feature a specific value of the angle,  $\vartheta_g^s$ , that is, either  $\vartheta_g^s = \varphi_g^a$  in the first case, or  $\vartheta_g^s = 90^\circ - \varphi_g^a$  in the second case. Similarly, four generic gear surfaces can be drawn from the analysis of Figures 20.10 and 20.11. Three more generic gear surfaces of face gears can be obtained similar to that illustrated in Figures 20.9b, 20.10d, and 20.11d. The geometry of generic gear surfaces of these types is evident; therefore, it is not illustrated in the figures. Ultimately, nine more generic gear surfaces are drawn up from Figure 20.12.

As all the possible generic gear surfaces are counted, there exists an opportunity to investigate all possible designs of gears machined on conventional machine tools as well as on gear generators of conventional design.

### 20.3.2 PROFILE OF GENERIC GEAR SURFACE CONSTRUCTED IN SECTION BY PLANE AT AN ANGLE TO GEAR AXIS

Possible generic gear surfaces discussed earlier in this book are constructed in the section of the gear by a plane through the gear axis of rotation. More opportunities in this regard appear in the plane sections at an angle to the gear axis of rotation are involved in the analysis. A plane at an angle to the gear axis is referred to as the *inclined section* of the gear.

The axial section of a gear by a plane is a convenient reference for the specification of the configuration of an inclined section of the gear.

The section of a gear by axial plane is specified by a plane through the gear axis of rotation,  $O_g$ . An equivalent specification of an axial section of the approximate gear can be given in terms of the unit tangent vectors,  $\mathbf{t}_{1,g}^a$  and  $\mathbf{t}_{2,g}^a$ , of the principal directions on the desirable generic gear surface, as illustrated in Figure 20.13a.

It is convenient to specify an inclined plane section of a gear in terms of the unit tangent vectors,  $\mathbf{t}_{1,g}^s$  and  $\mathbf{t}_{2,g}^s$ , of the principal directions on the actual generic gear surface. The inclined section is a plane through the unit tangent vectors,  $\mathbf{t}_{1,g}^s$  and  $\mathbf{t}_{2,g}^s$ .

At point,  $a$ , configuration of the *Darboux trihedron*,  $\mathbf{n}_g^s \mathbf{t}_{1,g}^s \mathbf{t}_{2,g}^s$ , of the actual generic gear surface with respect to the *Darboux trihedron*,  $\mathbf{n}_g^a \mathbf{t}_{1,g}^a \mathbf{t}_{2,g}^a$ , of the desirable generic gear surface can be specified by an angle,  $\nu_g^s$ . The trihedron  $\mathbf{n}_g^s \mathbf{t}_{1,g}^s \mathbf{t}_{2,g}^s$  is turned about the common unit normal vector,  $\mathbf{n}_g^a \equiv \mathbf{n}_g^s$ , through the angle,  $\nu_g^s$ , in the clockwise direction looking from the end of the vector,  $\mathbf{n}_g^a$  (see Figure 20.13a). In a particular case, when the equality  $\nu_g^s = 0^\circ$  is valid, an inclined plane section reduces to the aforementioned axial plane section. When the angle,  $\nu_g^s$ , is not equal to zero ( $\nu_g^s \neq 0^\circ$ ), three different cases can be distinguished. Before proceeding with this matter, it is necessary to point out here the following observation: As the unit normal vector,  $\mathbf{n}_g^a$ , in general case is not perpendicular to the gear axis of rotation,  $O_g$  [the angle between the vector,  $\mathbf{n}_g^a$ , and the gear axis,  $O_g$ , is given by  $\angle(\mathbf{n}_g^a, O_g) = 90^\circ - \varphi_g^a$ ], the projection,  $\theta_g^s$ , of the angle,  $\nu_g^s$ , onto the plane through the

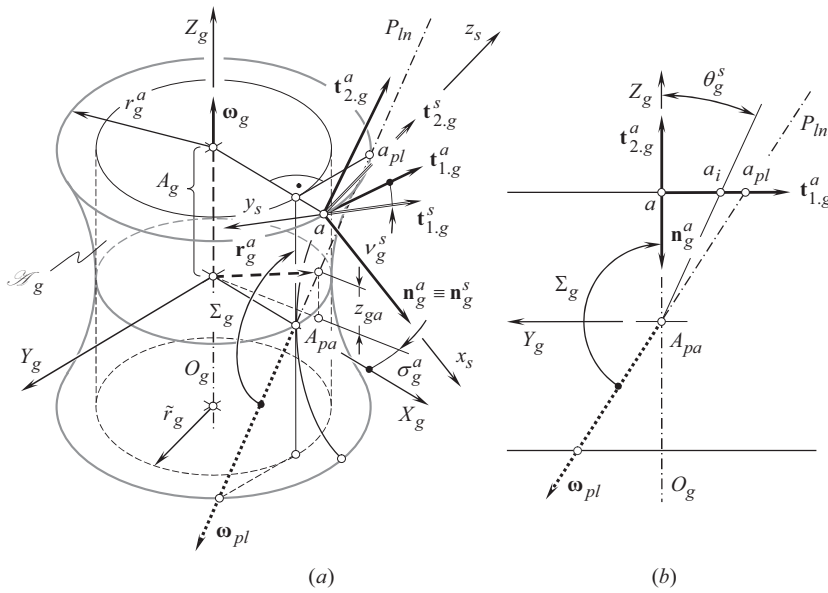


**FIGURE 20.13** Possible configurations of characteristic section of a generic gear surface by plane: (a) close-up of the generic gear surface, and (b) the vectors through arbitrary point,  $a$ .

gear axis of rotation,  $O_g$ , perpendicular to the axial plane section is not equal to the angle,  $\nu_g^s$ , itself ( $\theta_g^s \neq \nu_g^s$ ). However, the angles,  $\nu_g^s$  and  $\theta_g^s$ , correlate with each other. The correlation is of importance in further discussion, and it can be established in the following way.

The angle,  $\theta_g^s$ , can be defined as the angle that is formed by the unit tangent vector,  $\mathbf{t}_{2,g}^s$ , and the gear axis of rotation,  $O_g$ . In a local reference system,  $x_s, y_s, z_s$ , whose axes are pointed along the unit vectors,  $\mathbf{n}_g^s$ ,  $-\mathbf{t}_{1,g}^s$ , and  $\mathbf{t}_{2,g}^s$ , the unit tangent vector,  $\mathbf{t}_{2,g}^s$ , can be expressed as  $\mathbf{t}_{2,g}^s = \mathbf{k}_s$ . The directions of axes of this reference system are specified by the *Darboux trihedron*,  $\mathbf{n}_g^s, \mathbf{t}_{1,g}^s, \mathbf{t}_{2,g}^s$ , as shown in Figure 20.12. In the *Cartesian* coordinate system,  $X_g, Y_g, Z_g$ , associated with the gear, the direction of the gear axis,  $O_g$ , can be specified by the unit vector,  $\mathbf{k}_g$ . In order to calculate the value of the angle,  $\theta_g^s$ , both the vectors,  $\mathbf{t}_{2,g}^s$  and  $\mathbf{k}_g$ , have to be represented in a common reference system. Let us represent the vector,  $\mathbf{t}_{2,g}^s$ , in the coordinate system,  $X_g, Y_g, Z_g$ . For this purpose, a local coordinate system,  $x_s, y_s, z_s$ , that originates at point  $a$  is used. The unit tangent vector together with the coordinate system,  $x_s, y_s, z_s$ , have to be turned about the axis,  $x_s$  [about the unit normal vector  $\mathbf{n}_g^s (\equiv \mathbf{n}_g^a)$ ] through the angle,  $\nu_g^s$ . The operator of rotation,  $\mathbf{Rt}(\nu_g^s, \mathbf{n}_g^a)$ , is used for the analytical description of this coordinate system transformation:

$$\mathbf{Rt}(\nu_g^s, \mathbf{n}_g^a) = \begin{bmatrix} 1 & 0 & 0 & 0 \\ 0 & \cos \nu_g^s & \sin \nu_g^s & 0 \\ 0 & -\sin \nu_g^s & \cos \nu_g^s & 0 \\ 0 & 0 & 0 & 1 \end{bmatrix} \quad (20.11)$$

In this new position of the local reference system,  $x_s, y_s, z_s$ , the unit vectors,  $\mathbf{n}_g^s$ ,  $\mathbf{t}_{1,g}^s$ , and  $\mathbf{t}_{2,g}^s$ , align with corresponding unit vectors of the *Darboux trihedron*,  $\mathbf{n}_g^a, \mathbf{t}_{1,g}^a, \mathbf{t}_{2,g}^a$ .

Then, the *Darboux trihedron*,  $\mathbf{n}_g^a, \mathbf{t}_{1,g}^a, \mathbf{t}_{2,g}^a$ , is turned about the  $y_s$  - axis [about the unit tangent vector,  $\mathbf{t}_{1,g}^a$ ] through the angle,  $\varphi_g^a$  (see Figure 20.5). The operator of the rotation,  $\mathbf{Rt}(\varphi_g^a, \mathbf{t}_{1,g}^a)$ , is used for the analytical description of this coordinate system transformation:

$$\mathbf{Rt}(\varphi_g^a, \mathbf{t}_{1.g}^a) = \begin{bmatrix} \cos \varphi_g^a & 0 & -\sin \varphi_g^a & 0 \\ 0 & 1 & 0 & 0 \\ \sin \varphi_g^a & 0 & \cos \varphi_g^a & 0 \\ 0 & 0 & 0 & 1 \end{bmatrix} \quad (20.12)$$

The operator,  $\mathbf{Rs}(s \mapsto g)$ , of the resultant coordinate system transformation is calculated as the product of the operators of rotation,  $\mathbf{Rt}(\nu_g^s, \mathbf{n}_g^a)$  and  $\mathbf{Rt}(\varphi_g^a, \mathbf{t}_{1.g}^a)$ :

$$\mathbf{Rs}(s \mapsto g) = \mathbf{Rt}(\varphi_g^a, \mathbf{t}_{1.g}^a) \cdot \mathbf{Rt}(\nu_g^s, \mathbf{n}_g^a) \quad (20.13)$$

It should be noted here that the order of multipliers in Eq. (20.13) is of importance, and it cannot be altered.

Once the operator  $\mathbf{Rs}(s \mapsto g)$  of the resultant coordinate system transformation is calculated, the expression:

$$\mathbf{t}_{2.g}^{s(g)} = \mathbf{Rs}(s \mapsto g) \cdot \mathbf{t}_{2.g}^s \quad (20.14)$$

can be used for the analytical description of the unit tangent vector,  $\mathbf{t}_{2.g}^s$ , in the reference system,  $X_g Y_g Z_g$ .

Use of the expression for the unit tangent vector,  $\mathbf{t}_{2.g}^{s(g)}$  [see Eq. (20.14)], makes possible calculation of the actual value of the angle  $\theta_g^s$ :

$$\theta_g^s = \tan^{-1} \left( \frac{|\mathbf{t}_{2.g}^{s(g)} \times \mathbf{k}_g|}{\mathbf{t}_{2.g}^{s(g)} \cdot \mathbf{k}_g} \right) \quad (20.15)$$

Equations (20.12)–(20.15) allow for derivation of an expression:

$$\theta_g^s = \cos^{-1} [\cos \varphi_g^a \cdot \cos \nu_g^s] \quad (20.16)$$

for calculation of the angle,  $\theta_g^s$ .

When the angle,  $\nu_g^s$ , is equal:

$$\nu_g^s = \cos^{-1} \left[ \frac{\cos \Sigma_g}{\cos \varphi_g^a} \right] \quad (20.17)$$

the unit tangent vector,  $\mathbf{t}_{2.g}^s$ , is aligned with the axis of instantaneous rotation,  $P_{ln}$ . The actual value of the angle,  $\theta_g^s$  (see Figure 20.13b) in this particular case is equal to  $\Sigma_g$ .

Four different configurations of the inclined plane section of a gear are distinguished depending on the actual value of the angle,  $\theta_g^s$ .

**First**, the angle,  $\theta_g^s$ , can be equal to zero. When the equality  $\theta_g^s = 0^\circ$  is valid, the inclined plane section is reduced to the axial plane section of the gear.

**Second**, the actual value of the angle  $\theta_g^s$  falls into the interval  $0^\circ < \theta_g^s < 180^\circ - \Sigma_g$ . For convenience, the difference  $(180^\circ - \Sigma_g)$  is denoted as  $[\theta_g^s]$ . It can be shown that rotation of the inclined plane section about the  $x_s$  – axis through an angle,  $\nu_g^s$ , is equivalent to its rotation about the centerline through a corresponding angle,  $\theta_g^s$ . This is because the perfect generic gear surface is a surface of revolution. Every surface of revolution allows for sliding over itself. Therefore, the parameters of rotation of an inclined plane section about the centerline can be expressed in terms of the parameters of rotation of the same inclined plane

section about the unit normal vector,  $\mathbf{n}_g^a \equiv \mathbf{n}_g^s$ , and vice versa. Under such an interpretation, point  $a$  is not considered; point,  $a_i$ , can be considered instead (see Figure 20.13b).

**Third**, the actual value of the angle,  $\theta_g^s$ , can be set equal to its critical value,  $[\theta_g^s]$ . When the equality  $\theta_g^s = [\theta_g^s]$  is observed, the unit tangent vector,  $\mathbf{t}_{2,g}^{s(g)}$ , is aligned with the vector of instant rotation,  $\boldsymbol{\omega}_{pl}$ . In this particular case, point  $a$  is not considered; point  $a_{pl}$  is considered instead (see Figure 20.13b).

**Fourth**, the actual value of the angle,  $\theta_g^s$ , can exceed its critical value,  $[\theta_g^s]$ , and, thus, the inequality  $\theta_g^s > [\theta_g^s]$  is valid. Corresponding point,  $a_j$  (not shown in Figure 20.13b), in this particular case is located beyond the point,  $a_{pl}$ .

Taking into account that the first case ( $\theta_g^s = 0^\circ$ ) returns 26 possible generic gear surfaces, one of which is the perfect generic gear surface, the total number of possible generic gear surfaces is limited to just 105. Some of the generic gear surfaces resemble each other. However, even for generic gear surfaces with a similar appearance, the conditions of generation of tooth flanks could be different. Therefore, all of the generic gear surfaces should be carefully investigated individually from the perspective of their application to the gear design.

The following three important conclusions can be drawn up from this discussion:

1. The total number of possible generic gear surfaces is not infinite, but it is a finite number. This means that it is possible to count and investigate all possible designs of gears machined on conventional gear generators
2. Gears with any of the generic gear surfaces are convenient for machining, as only rotations and translations are required to reproduce the required motion of the gear cutting tool in relation to the work-gear
3. An appropriate area of application can be specified for all the gears briefly discussed in this section of the book

The above discussion is helpful to systemize possible geometries of generic gear surfaces.

## 20.4 POSSIBILITY OF CLASSIFICATION OF GEAR PAIRS

Once the total number of possible generic gear surfaces is limited to just 105, it is possible to combine the surfaces by two, and in this way to obtain all possible kinds of gear pairs. It can be proved that the total number of such combinations does not exceed  $105^2$ . Not all of the combinations are possible physically. For example, no parallel-axes gear pair can be designed using two generic gear surfaces with concave axial profiles. Because interference of the generic gear surfaces in this case is inevitable, gear pair of this particular type cannot be designed. A few examples of possible and impossible combinations of gears by two are schematically shown in Figure 20.14. A gear with a convex axial profile, and a pinion with a straight axial profile comprise a possible combination of gears. A gear pair of this type can exist physically (see Figure 20.14a). In contrast, a gear with a concave axial profile and a pinion with a straight axial profile of generic gear surface do not comprise a possible combination of gears. A gear pair of this type cannot exist physically (see Figure 20.14b). A similar behavior is observed with a gear and a pinion that have convex and concave axial profiles, correspondingly, as illustrated in Figure 20.14c and d. In order to come up with a possible combination of gears comprising a gear pair, the magnitude of the radius of curvature of the concave profile,  $R_p$ , should exceed the radius of curvature,  $R_g$ , as shown in Figure 20.14c. Otherwise, when the inequality  $R_p < R_g$  is observed, a gear pair of this geometry becomes infeasible (see Figure 20.14d). More examples to this end can be provided.

It can be assumed from this simple example that the total number of possible gear pairs is significantly less than  $105^2$ .

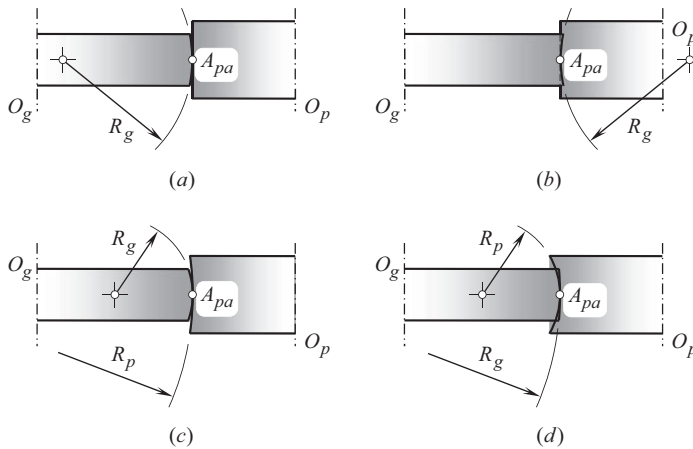


**FIGURE 20.14** Combinations of two generic gear surfaces: (a) and (c) possible, and (b) and (d) impossible combinations.

In order to evaluate the maximum number of possible kinds of gear pairs, it is useful to recall that 105 possible types of the generic surfaces are composed of one desirable generic surface, 26 generic surfaces with a convex axial profile, 26 generic surfaces with a straight axial profile, and 26 generic surfaces with a concave axial profile.

Generic gear surfaces that feature convex axial profile can be properly combined with all 105 generic surfaces of the pinion. Therefore, the total number of combinations of this particular type is limited to  $26 \cdot 105 = 2730$  combinations.

Generic gear surfaces featuring straight axial profile can be properly combined with all 70 generic surfaces of the pinion. Therefore, the total number of combinations of this particular type is limited to  $26 \cdot 70 = 1820$  combinations.

Finally, generic gear surfaces featuring concave axial profile can be properly combined with all 35 generic surfaces of the pinion. Therefore, the total number of combinations of this particular type is limited to  $26 \cdot 35 = 910$  combinations.

Because the numbers 2730, 1820, and 910, are finite numbers, the total number of possible combinations of generic gear surfaces is also a finite number. This number does not exceed 5460 combinations. Evidently, not all of these combinations exist physically. After an in-detail investigation of all the possible combinations is carried out, it becomes clear that the total number of practical types of gear pairs is significantly under the precalculated number of 5460 combinations.

The total number of possible types of gear pairs to be determined should be considered together with the possible types of vector diagrams of gear pairs (see Chapter 2, Figure 2.16). All the possible types of gear pairs can be investigated. This is because the total number of possible types of gear pairs is equal to a finite number, and not an infinite number.

The use of the aforementioned technique makes it possible to investigate all possible types of gear pairs. No gear pair can be missed under such an investigation. Novel designs of gear pairs can be discovered as the output of such an investigation.

## 20.5 EXAMPLES OF IMPLEMENTATION OF CLASSIFICATION OF GEAR PAIRS

Once the number of possible combinations of generic gear surfaces by two is found to be finite, it is possible to consider individually every possible combination of the generic surfaces by two, and to identify an appropriate area of application for each particular combination. A few illustrative examples in this regard are considered in this section.

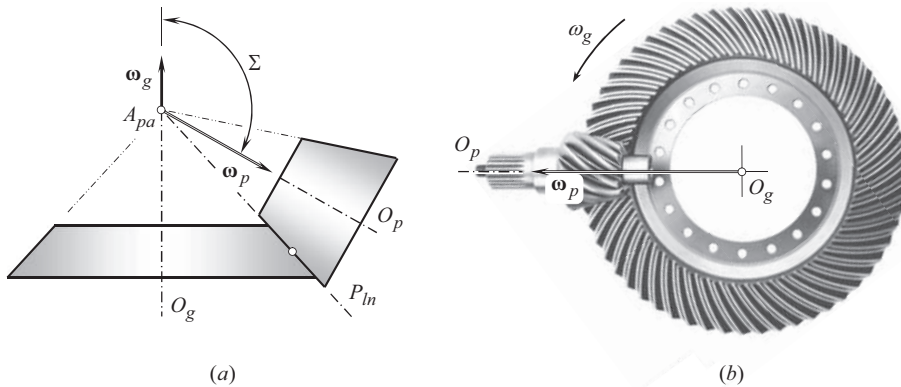


**FIGURE 20.15** (a) interacting generic gear surfaces, (b) a corresponding intersected-axes gear pair.

The desirable generic gear surfaces of gear pairs whose axes of rotation of the gear and the pinion intersect are represented with two cones that have a common apex. The perfect generic gear surfaces for the case of an external gear pair are schematically shown in Figure 20.15a. The generic gear surfaces contact each other along a straight line that is aligned with the axis of instantaneous rotation,  $P_{ln}$ . The axis of rotation of the gear,  $O_g$ , the axis of rotation of the pinion,  $O_p$ , and the axis of instantaneous rotation,  $P_{ln}$ , intersect at common point, which is coincident with the apexes  $A_g$ ,  $A_p$ , and  $A_{pa}$ .

In Figure 20.15, a trivial case of interaction of generic gear surfaces in gear pairs is shown. Many types of external conical gear pairs can be designed on the premise of this particular combination of generic gear surfaces. One of many possible examples is illustrated in Figure 20.15b.

Internal gear pairs as well as rack-type gear pairs whose axes of rotation of a gear and a mating pinion intersect, also feature the desirable generic gear surfaces, which are shaped in the form of cones. The apexes of the cones are snapped together. For internal gear pairs, a generic gear surface is represented with a surface of an internal cone of revolution, as depicted in Figure 20.16a. The generic gear surface of the pinion is represented with a surface of an external cone of revolution.

In a particular case, the pitch angle of a gear reaches  $90^\circ$ . In such a scenario, the gear degenerates into a flat gear, as schematically shown in Figure 20.16b. A gear of this kind is commonly referred to as a *round rack* (or as *crown gear*, in other terminology). The apex of the round rack is always snapped together with the apex of the pinion.

Gear pairs designed on the basis of perfect generic gear surfaces, as schematically shown in Figure 20.16, have limited application in practice. Lack of comprehensive investigation of the generic gear surfaces of these kinds is the key reason for this.

A gear and a pinion can be designed and machined in such a way that the actual generic gear surfaces of each of them differ from the desirable geometry. In cases like these, the apex of the gear or the pinion, or both, is off the axis of instantaneous rotation,  $P_{ln}$ .

Two examples of generic gear surfaces of external intersected-axes gear pairs are shown in Figure 20.17.

A gear pair may feature generic surfaces shaped in the form of external cones of revolution. When cone angles of the cones of revolution differ from the cone angle for the desirable generic gear surfaces, as illustrated in Figure 20.17a, the apex of the gear is off the axis of instantaneous rotation,  $P_{ln}$ . Ultimately, a conical gear pair can be designed on the basis of the actual generic gear surfaces of this kind. Gear pairs of this kind do not have extensive application in the present-day practice.

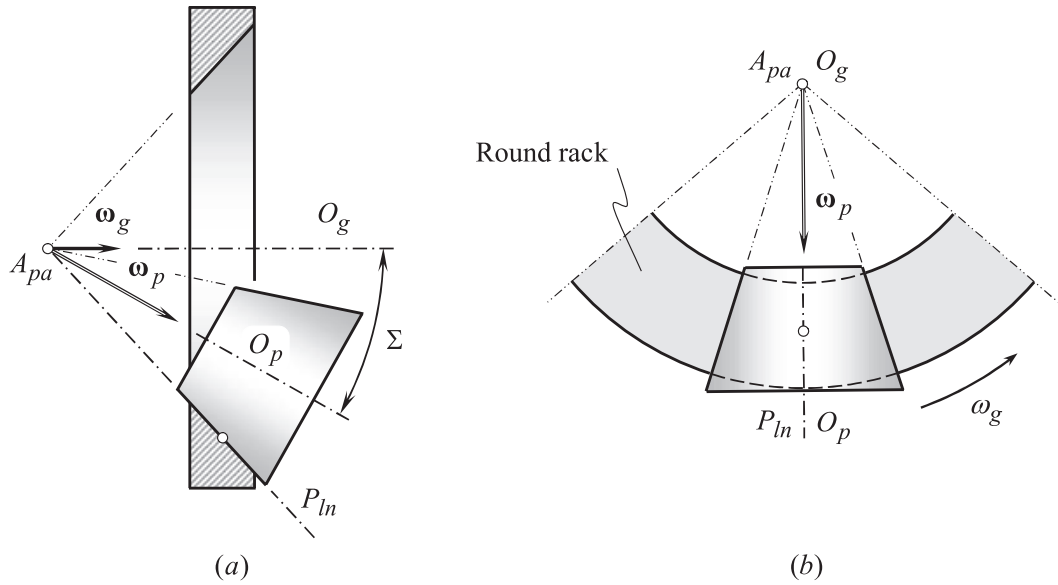


**FIGURE 20.16** Desirable generic surfaces in gear pairs with intersecting axes of rotation of gear and pinion: (a) internal gear pair, and (b) rack-type gear pair (crown gearing).

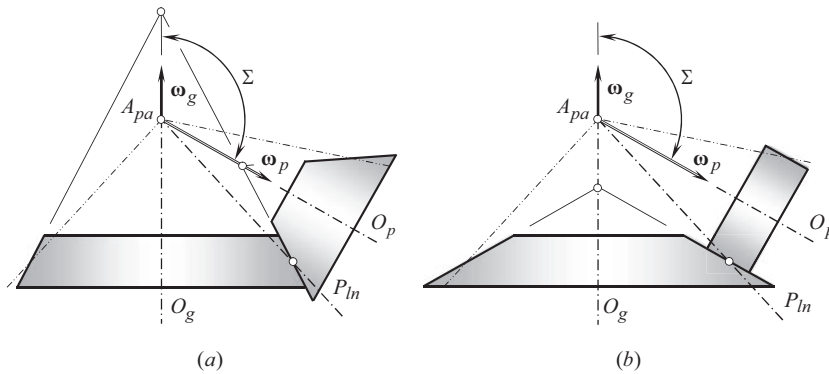


**FIGURE 20.17** (a) the gear, and the pinion cone apexes,  $A_g$  and  $A_p$ , are situated within the interior of the corresponding the gear and pinion cones, and (b) the gear, and the pinion cone apexes,  $A_g$  and  $A_p$ , are situated within the exterior of the corresponding the gear and pinion cones.

In a particular case, a gear pair can be designed in such a way that the generating straight line segment of the actual generic gear surface of the pinion is parallel to the pinion axis of rotation,  $O_p$  (see Figure 20.17b). In such a scenario, the actual generic gear surface of the pinion is not a cone of revolution; it is shaped in the form of a virtual revolute cylinder instead. Gear pairs composed of an external conical gear and a mating cylindrical pinion are used, for example, in the design of helicopter transmissions; they also have numerous other applications.

In both cases, shown in Figure 20.17 gears, are referred to as *external crown gears*.

A gear pair can be designed and machined in such a way that the actual generic gear surface of the gear is shaped in the form of an internal cone of revolution (see Figure 20.18). Many similarities can be found between external (see Figure 20.17) and internal gear pairs of these two kinds. Again, in a particular case, the actual generic gear surface of the pinion is not a cone of revolution, but is shaped in the form of a cylinder of revolution instead. Gear pairs composed of internal conical gear



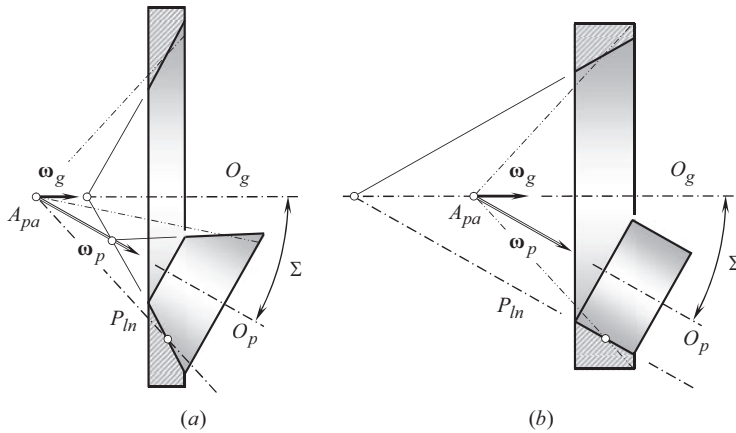


**FIGURE 20.18** (a) the gear, and the pinion cone apexes,  $A_g$  and  $A_p$ , are situated within the interior of the corresponding the gear and pinion cones, and (b) the gear, and the pinion cone apexes,  $A_g$  and  $A_p$ , are situated within the exterior of the corresponding gear and pinion cones.

and a mating cylindrical pinion have limited application in the industry. Gear pairs of this kind are not profoundly investigated yet, and their area of potential application has not been properly identified so far.

In both cases shown in Figure 20.18, gears are referred to as *internal crown gear*.

Ultimately, the generic cone of a gear in a gear pair that has intersecting axes of rotation of the gear and of the pinion can be degenerated into plane that is rotated about the gear axis of rotation,  $O_g$ . Two examples of generic gear surfaces of this type are schematically shown in Figure 20.19a and b. In a particular case, when the pitch radius of the gear approaches infinity, the gear is transformed into a straight rack (see Figure 20.19c). Gear pairs of this kind have not been profoundly investigated yet, and their area of potential application has not been properly identified so far.

In all cases illustrated in Figure 20.19, the gear is referred to as *rack-type crown gear*. Rack-type gear pairs have the following two features: (a) the pitch plane of the gear is the plane through the centerline, and (b) the apex of the pitch cone of the pinion is located within the centerline.

## 20.6 AUXILIARY GENERATING RACKS OF POSSIBLE GEOMETRIES

The discussion on generic gear surfaces can be ended with a brief consideration of gearing designed and machined on the premise of real generic gear surfaces.

Skew-axes gearing that is composed of two helical involute gears, is a perfect example of gearing that features generic gear surfaces of a gear and a mating pinion in a form of cylinders of revolution. Skew-axes gearing is used to drive the engine camshaft, as illustrated in Figure 20.20.

In gearing of this design, the axis of rotation of the gear, and the axis of rotation of the mating pinion are crossed at a crossed-axes angle. The crossed-axes angle can be either acute, or it can be obtuse, or equal to a right angle. In the particular example under consideration, the axes of rotation of the gear and the pinion are crossed at a right angle. The axes of rotation of the gear and that of the mating pinion are apart from one another at a center distance. Commonly, the pinion is the driving member of the gear pair, while the gear is the driven member of the gear pair. Skew-axes gearing is an example of gearing that features generic gear surfaces of both in a form of cylinders of revolution.

Worm gearing composed of an involute worm that is engaged in mesh with an involute gear (either a spur involute gear or a helical involute gear) is another example of gearing that features generic gear surfaces of a gear and a mating pinion in a form of cylinders of revolution. A schematic of gearing composed of a cylindrical involute worm that is engaged in mesh with a cylindrical



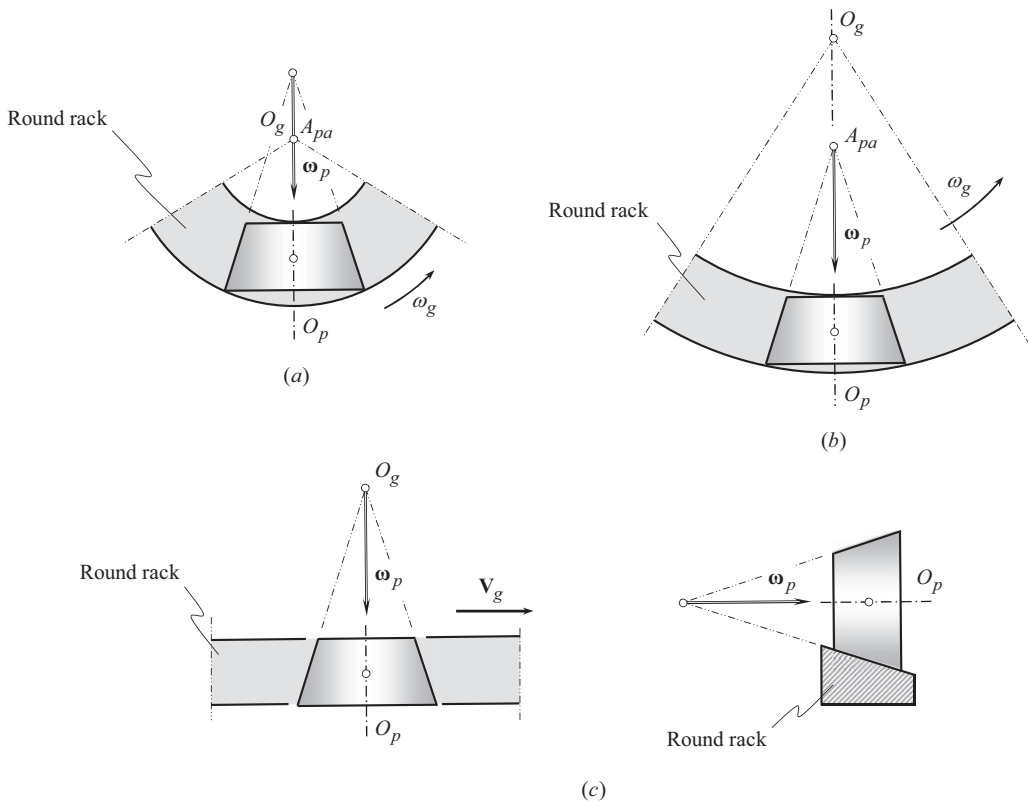


**FIGURE 20.19** (a) the gear axis of rotation,  $O_g$ , is through the plane-of-action apex,  $A_{pa}$ , (b) the pinion cone apex,  $A_p$ , is situated within the exterior of the gear cone, and (c) the gear cone is reduced to a plane.



**FIGURE 20.20** Skew-axes gearing is used to drive the engine camshaft.

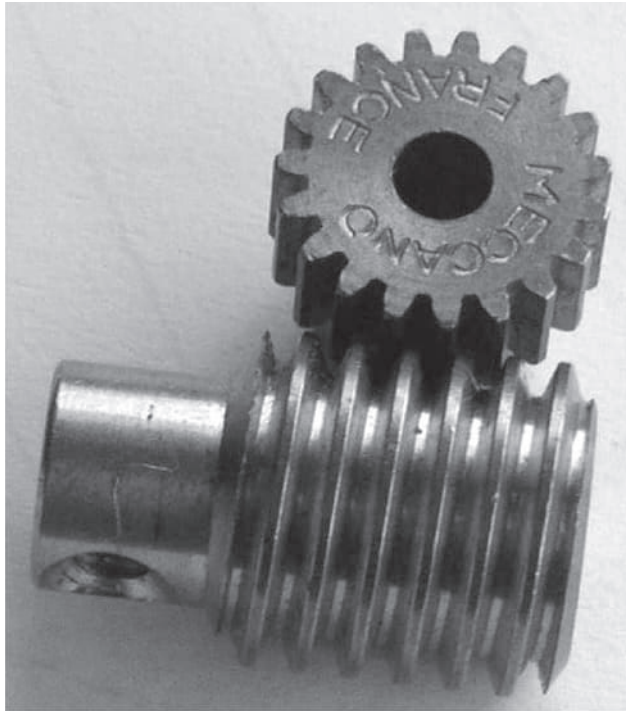


**FIGURE 20.21** Example of gear pair composed of cylindrical involute worm and helical involute gear.

involute helical gear is illustrated in Figure 20.21. Worm gearing of this type does not need in a more in detail discussion, as it is similar in much to skew-axis gearing shown in Figure 20.20.

The tooth flanks of gears in skew-axes involute gearing (see Figure 20.20), and in worm involute gearing (see Figure 20.21) are generated in accordance with the first *Olivier principle* of generation of envelope surfaces.

Once the tooth flanks of the gear and the pinion are generated in accordance with the first *Olivier principle* of surfaces generation, the geometry of the generating (auxiliary) surface needs to be investigated more in detail.

A gear tooth flank,  $\mathcal{S}$ , as well as a mating pinion tooth flank,  $\mathcal{P}$ , in a geometrically accurate crossed-axes gearing of this particular design can be interpreted as envelopes to families of consecutive positions of the auxiliary generating rack,  $\mathcal{R}$ , in its motion relative to a reference system associated with the gear and the pinion correspondingly. A straight generating rack,  $\mathcal{R}$ , is commonly used for this purpose. However, auxiliary racks of other geometries can be used for the generation of tooth flanks of the gear,  $\mathcal{S}$ , and the pinion,  $\mathcal{P}$ , as well. Feasible motions of the auxiliary generating surface,  $\mathcal{R}$ , in relation to the reference system,  $X_g Y_g Z_g$ , associated with the gear strongly depend on the geometry of the actual surface,  $\mathcal{R}$ .

In the simplest case, the virtual auxiliary rack is shaped in the form of a straight rack,  $\mathcal{R}$ , that features a symmetrical tooth profile, as depicted in Figure 20.22a. In the case of straight rack,  $\mathcal{R}$ , the equality,  $C_{r,p} = \infty$ , is valid. A straight auxiliary rack that has an asymmetrical tooth profile is also known. A rack of this particular type is schematically shown in Figure 20.22b.

An auxiliary generating rack,  $\mathcal{R}$ , can be shaped in the form of a round rack,  $\mathcal{R}$ , with an involute tooth profile. Round racks of convex, and of concave types are possible, as shown in Figure 20.22c and d correspondingly. The radius of the pitch cylinder,  $R_{r,p}$ , of the auxiliary rack,  $\mathcal{R}$ , is negative ( $R_{r,p} < 0$ ) in the first case (see Figure 20.22c), and it is positive ( $R_{r,p} > 0$ ) in the second case (see Figure 20.22d).

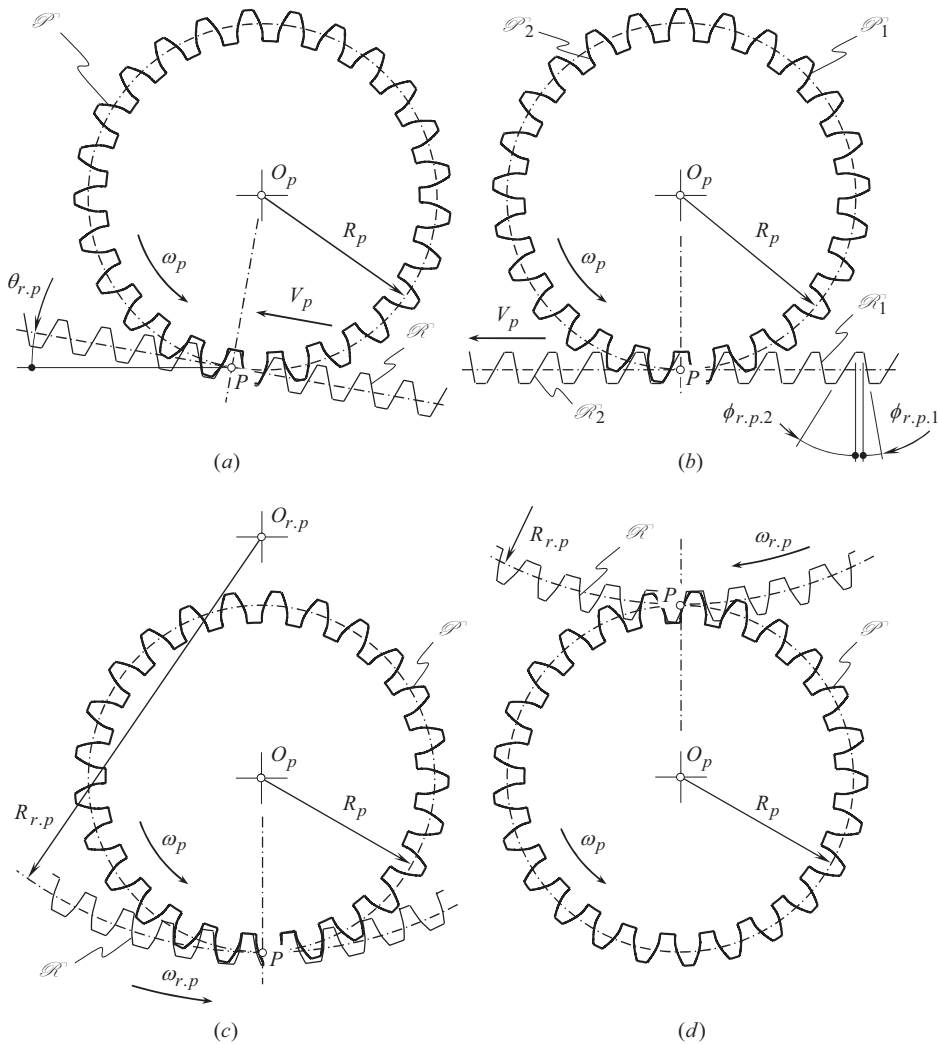


**FIGURE 20.22** Examples of possible types of auxiliary generating surfaces,  $\mathcal{R}$ : (a) straight inclined rack,  $\mathcal{R}$ , (b) straight rack,  $\mathcal{R}$ , with asymmetrical tooth profile, (c) concave round rack,  $\mathcal{R}$ , and (d) convex round rack,  $\mathcal{R}$ .

The round rack,  $\mathcal{R}$ , performs a rotation,  $\omega_{r,p}$ , about an axis of rotation,  $O_{r,p}$ , of the rack,  $\mathcal{R}$ . Superposition of the rotation of the round rack,  $\omega_{r,p}$ , with the rotation of the gear,  $\omega_g$ , results in a complex relative motion of the auxiliary rack,  $\mathcal{R}$ , about the axis of rotation,  $O_g$ , of the gear. The resultant motion,  $\omega_{scr} = \omega_p + \omega_{r,p}$ , is possible when the rotations,  $\omega_{r,p}$  and  $\omega_g$ , are synchronized with each other.

Consider an auxiliary straight rack,  $\mathcal{R}$ , of symmetrical tooth profile as it is shown in Figure 20.22a. Let us assume, that the rack,  $\mathcal{R}$ , performs a straight motion in a direction that is parallel to the pitch plane of the auxiliary rack. The straight motion of the auxiliary generating rack,  $\mathcal{R}$ , is superimposed with a rotation,  $\omega_g$ , of the gear. The resultant screw motion of the rack,  $\mathcal{R}$ , about the axis of rotation,  $O_g$ , of the gear is possible in this particular case. The tooth flank of the gear,  $\mathcal{S}$ , is generated as an envelope to a family of consecutive positions of the auxiliary rack,  $\mathcal{R}$ , that performs the screw motion with the gear axis,  $O_g$ , as the axis of the screw motion. Accordingly, the pinion tooth flank,  $\mathcal{P}$ , is generated as an envelope to a family of consecutive positions of the auxiliary rack,  $\mathcal{R}$ , that performs the screw motion with the pinion axis,  $O_p$ , as the axis of the screw motion.

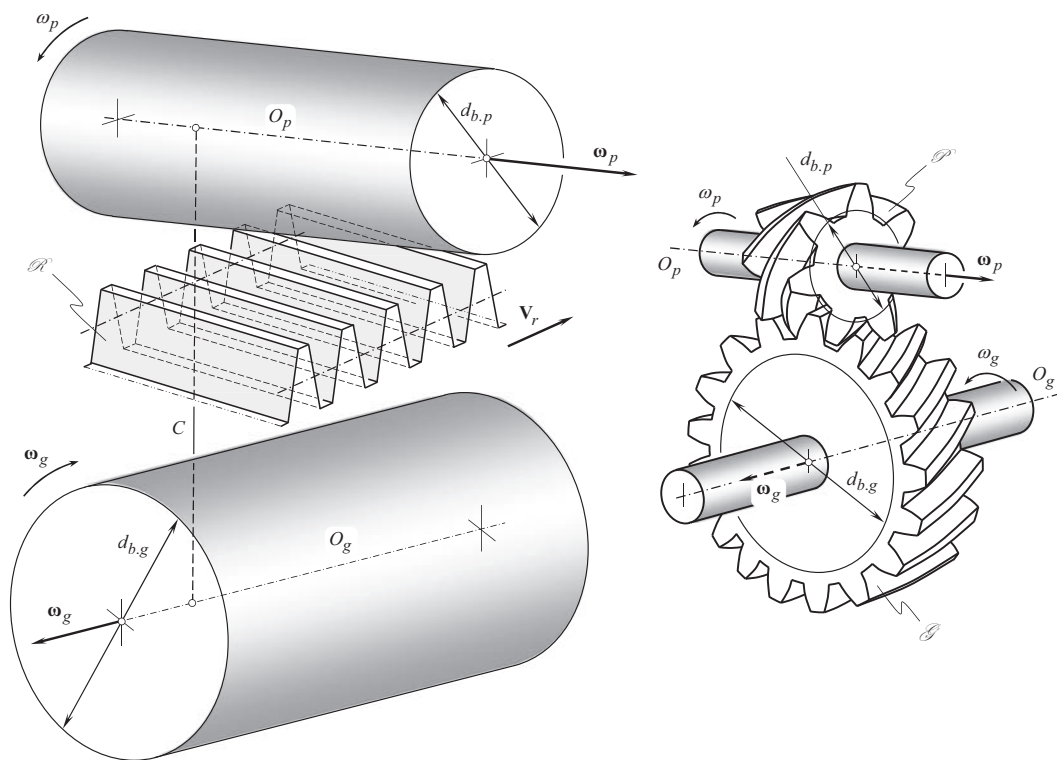


**FIGURE 20.23** Generation of tooth flanks,  $\mathcal{F}$  and  $\mathcal{P}$ , of geometrically accurate crossed-axes gears by means of straight auxiliary rack,  $\mathcal{R}$ .

The tooth flanks of a gear,  $\mathcal{F}$ , and that of a mating pinion,  $\mathcal{P}$ , generated in this way, belong to a skew-axes helical gearing (see Figure 20.23). Skew-axes gears are used in practice to transmit a rotation from a driving shaft to a driven shaft, whose axes of rotation cross one another. The use of gearing of this particular type makes sense only when the power density to be transmitted is reasonably low. This is mostly because the gear and the pinion tooth flanks are in point contact. The bearing capacity of gearing that features point contact of the tooth flanks is relatively low.<sup>4</sup>

A characteristic line,  $\mathcal{E}_{r,g}$ , in the *gear-to-rack mesh* ( $\mathcal{F}$ -to- $\mathcal{R}$  – mesh), is a straight line. The straight line,  $\mathcal{E}_{r,g}$ , is located within the lateral tooth surface of the auxiliary rack,  $\mathcal{R}$  (see Figure 20.24a). The characteristic line,  $\mathcal{E}_{r,g}$ , is tangential to the base helix of the gear. Similarly, a characteristic line,  $\mathcal{E}_{r,p}$ , in the *pinion-to-rack mesh* ( $\mathcal{P}$ -to- $\mathcal{R}$  – mesh) is also a straight line. This straight line,  $\mathcal{E}_{r,p}$ , is located within the lateral tooth surface of the auxiliary rack,  $\mathcal{R}$ . The characteristic line,  $\mathcal{E}_{r,p}$ , is tangential to the base helix of the pinion.

The characteristic lines,  $\mathcal{E}_{r,g}$  and  $\mathcal{E}_{r,p}$ , intersect each other at certain point, as schematically shown in Figure 20.24a and b. The point of intersection, by nature, is point of contact,  $K$ , of the tooth flanks,  $\mathcal{F}$  and  $\mathcal{P}$ , of the gear and the pinion at a current instant of time. As the straight lines,

<sup>4</sup> As there are no many examples of geometrically accurate gearing of the kind under consideration, and the gearing of this type is poorly investigated, it is right point to mention here about the so-called *helipoid gearing* [see: Wu, L.-L., Liu, C.-C., Tsay, C.-B., “Mathematical Model and Surface Deviation of Helipoid Gears Cut by Shaper Cutter,” *ASME J Mechanical Design*, Volume 125, Issue 2, June 2003, pp. 351–355]. *Helipoid gearing* can be viewed as an approximate *point-contact gearing*, as the base pitches of the shaper cutter is not equal to the operating angular base pitch of a helipoid gear pair [225].

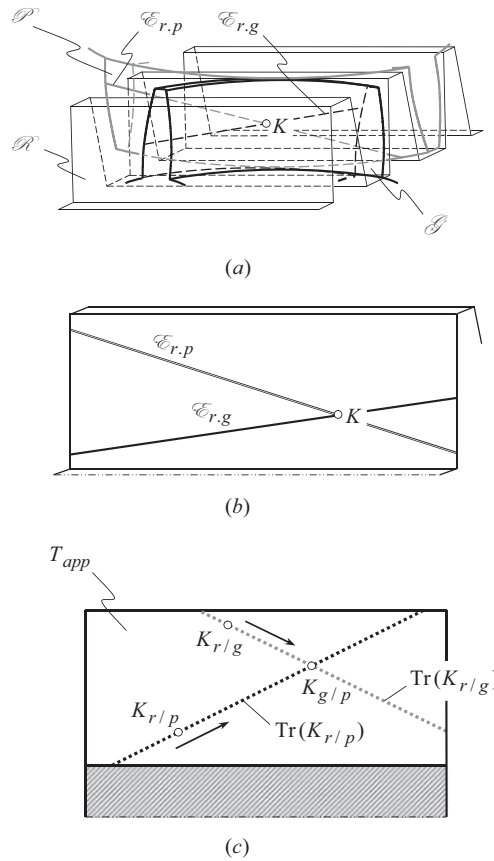


**FIGURE 20.24** Characteristic line,  $\mathcal{E}_{r,g}$ , in gear-to-rack mesh ( $\mathcal{S}$ -to- $\mathcal{R}$ -mesh), and characteristic line,  $\mathcal{E}_{r,p}$ , in pinion-to-rack mesh ( $\mathcal{P}$ -to- $\mathcal{R}$ -mesh) intersect each other at point of contact,  $K$ , of tooth flanks,  $\mathcal{S}$  and  $\mathcal{R}$  : (a) close-up, (b) intersection of the characteristics,  $\mathcal{E}_{r,g}$  and  $\mathcal{E}_{r,p}$ , at contact point,  $K$ , and (c) traces of contact,  $\text{Tr}(K_{r/g})$  and  $\text{Tr}(K_{r/p})$ , of contact points,  $K_{r/g}$  and  $K_{r/p}$ , on the auxiliary rack tooth flank,  $T_{app}$ .

$\mathcal{E}_{r,g}$  and  $\mathcal{E}_{r,p}$ , intersect one another at a distinct point, the tooth flanks,  $\mathcal{S}$  and  $\mathcal{P}$ , of the gear and the pinion are always in point contact.<sup>5</sup>

Similar to skew-axes helical gearing, a gear pair composed of a helical involute gear that is engaged in mesh with an involute worm can be designed as well. Two options are available in this particular case.

**First**, when the axis of rotation of the worm is parallel to the pitch plane of the auxiliary rack,  $\mathcal{R}$ , a worm of cylindrical type is generated by the rack,  $\mathcal{R}$ , as schematically shown in Figure 20.25. Gearing of this type is geometrically accurate; however, the power density being transmitted is low as the tooth flanks of the gear and threads of the worm are not in line contact, but rather in point contact instead. Worm gear pairs of this design have limited applications in the industry.

<sup>5</sup> It is likely only crossed-axes gearing is of interest when designing geometrically accurate *point-contact gearing*, as only in this case the characteristic lines,  $\mathcal{E}_{gr}$  and  $\mathcal{E}_{pr}$ , intersect one another. In crossed-axes gearing, as well as in parallel-axes gearing, the characteristic lines,  $\mathcal{E}_{gr}$  and  $\mathcal{E}_{pr}$ , do not intersect one another, and, therefore, no geometrically accurate *point-contact gearing* can be designed neither in a cases of  $I_a$  – axis gearing, nor in a case of  $P_a$  – axis gearing.

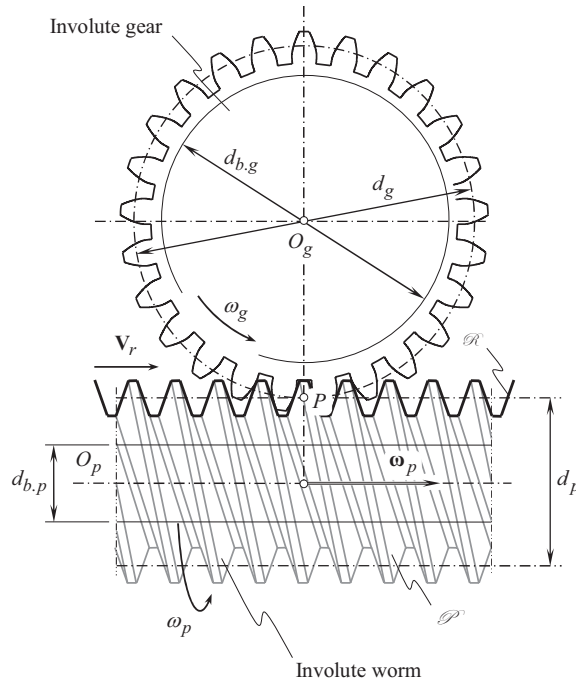


**FIGURE 20.25** Geometrically accurate crossed-axes worm gearing composed of helical involute gear and cylindrical involute worm.

In a manner just discussed, an internal cylindrical worm can be generated.

**Second**, when the axis of rotation of a worm is at an angle,  $\theta_p$ , in relation to the pitch plane of the auxiliary rack,  $\mathcal{R}$ , a worm of conical type is generated by the rack,  $\mathcal{R}$ , as schematically shown in Figure 20.26. Gearing of this type is also geometrically accurate; however, the power density being transmitted is low, as tooth flanks of the gear and threads of the worm are not in line contact, but rather in point contact instead.

In a manner just discussed, an internal conical worm can be generated.

One more example of implementation of geometrically accurate crossed-axes gearing with point contact of the tooth flanks of the gear,  $\mathcal{G}$ , and the pinion,  $\mathcal{P}$ , is illustrated in Figure 20.27.

Auxiliary racks of other geometries can be used for generating of the tooth flanks of gear and pinion for geometrically accurate intersected-axes gearing with point contact between tooth flanks of a gear and a mating pinion. As an example, Figure 20.28 illustrates possible types of external worms, the threads of which are generated by means of a convex round auxiliary rack,  $\mathcal{R}$ , (see Figure 20.28a), and by means of a concave round auxiliary rack,  $\mathcal{R}$  (see Figure 20.28b).

*General spatial involute gearing*, to the best possible extent, is investigated by Dr. J. Phillips [130], is a perfect example of *point-contact gearing*.

Internal worms, as well as internal gears for geometrically accurate crossed-axes gearing with point contact between the tooth flanks,  $\mathcal{G}$  and  $\mathcal{P}$ , are possible, as well. However, because of high sliding velocity between the tooth flanks, gear meshes of these kinds are of interest mainly for designing gear cutting tool [151,152], and not for gearing itself.

So far, geometrically accurate *point-contact gearing* is poorly investigated. There is much room for extensive research in this particular area of gearing.

Based on the developed classification of vector diagrams of gear pairs along with the concept of generic gear surfaces, all known gear drives can be developed. For example, advanced gear drives

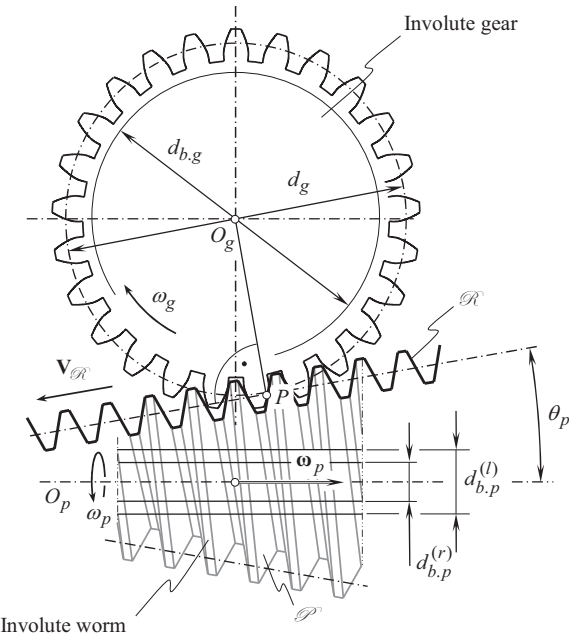


**FIGURE 20.26** Geometrically accurate crossed-axes worm gearing composed of helical involute gear and conical involute worm.

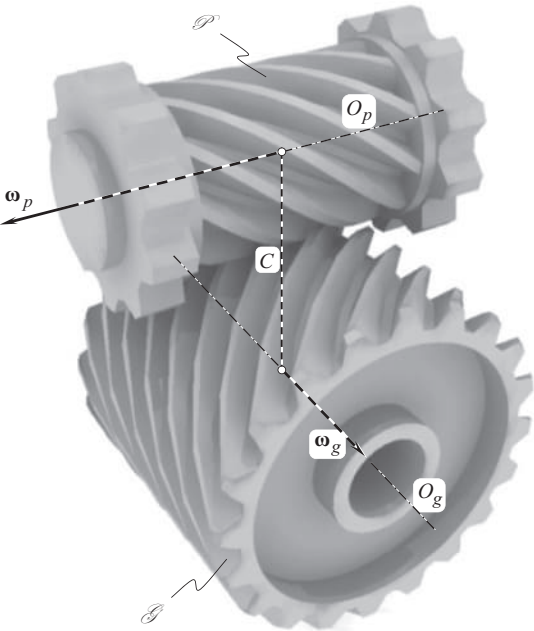


**FIGURE 20.27** External geometrically accurate crossed-axes gear set with point contact of tooth flanks of gear,  $\mathcal{G}$ , and that of pinion,  $\mathcal{P}$ .



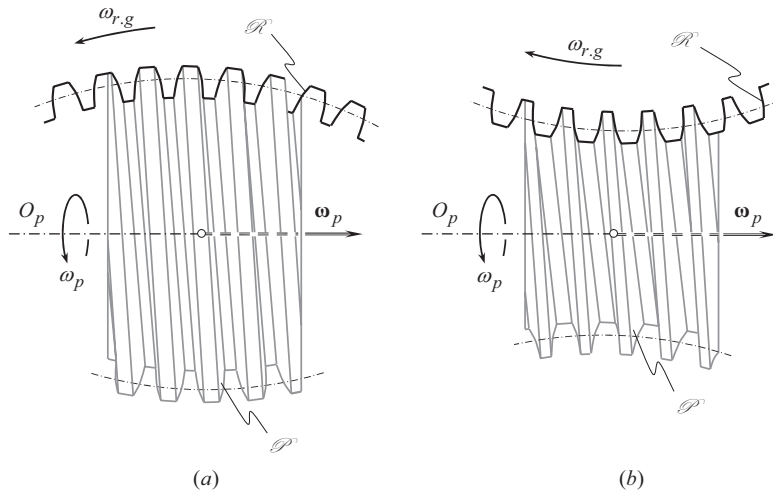


**FIGURE 20.28** External worms generated by means of (a) convex, and, (b) concave auxiliary generating rack,  $\mathcal{R}$ .

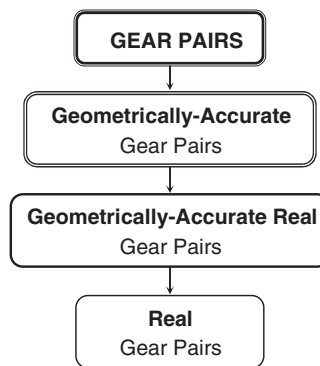


**FIGURE 20.29** Generalized classification of possible kinds of gear pairs.

such as *Spiroid* gearing [108], *Helicon* gearing [113], as well as others, can be developed using the proposed approach. Moreover, many novel gearings can be developed using the proposed approach.

The use of the discussed approach makes it possible to cover all known designs of gear pairs, as well as all novel, potentially possible designs of gear pairs, many of which have potential areas of implementation still to be identified. As the approach is based on the broad application of vector representation of gear pairs, the use of axodes and operating pitch surfaces becomes useless at all. However, pitch surfaces relevant to the corresponding gear-machining process are still useful.

The discussion on classification can be ended with a generalized classification of possible gear pairs, which is schematically depicted in Figure 20.29.

Based on the classification of possible types of vector diagrams (see Chapter 2, Figure 2.16), certain number of gear pairs can be developed for vector diagram of each kind. The gear pairs differ from one another by the geometry of tooth flanks in the lengthwise direction. All these gear pairs are referred to as *geometrically accurate gear pairs*, as they are capable of transmitting a uniform rotation of an input shaft to an output shaft smoothly.

Taking into account possible displacements of the tooth flanks of a gear and a mating pinion, a certain number of  $S_{pr}$  – gear pairs can be developed. The total number of possible  $S_{pr}$  – gear pairs



is equal to the number of ideal gear pairs. Gear pairs of this kind can also be referred to as *desirable real gear pairs*.

Ultimately, a certain number of *real gear pairs* can be developed based on a corresponding desirable gear pair. The total number of real gear pairs significantly exceeds the total number of desirable real gear pairs.

The discussion in this chapter illustrates the possibility of the development of a scientific classification of all possible kinds of gearing. It is clear now that the classification can be represented in detail based on the results of the analysis discussed in this book.

---

# 21 Approximate Real Gearing

Approximate real gears are known for a long while. Amazingly, but most of the efforts of the gear experts all around the world so far are focused not on improvements in design, and methods of production geometrically accurate gears (or real geometrically accurate gears). Instead, all the efforts are focused on improvements in design, and methods of production of approximate real gears. This is true with respect to:

- Parallel-axes gearing with modified tooth flanks of a gear and that of a mating pinion
- Intersected-axes gearing, either with gears that feature modified tooth flanks of a gear and that of a mating pinion or without modification of the tooth flanks
- Crossed-axes gearing, either with gears that feature modified tooth flanks of a gear and that of a mating pinion or without modification of the tooth flanks

Easier methods and means for manufacturing approximate real gears are the main reason for their extensive application in the present-day industry. Gears for parallel-axes gearing can be produced accurately with very small deviations of the desirable tooth flanks from a true involute profile.<sup>1</sup> In cases of intersected-axes, and crossed-axes gearing, the situation is not as clear, as in the case of gears for parallel-axes gearing.

Methods of manufacturing gears for intersected-axes gearing as well as for crossed-axes approximate real gearing are based on a design of the gear cutting tool for machining gear teeth. Tooth flanks,  $\mathcal{S}_{r.app}$  and  $\mathcal{P}_{r.app}$ , of a gear and of a mating pinion are generated as envelope surfaces to corresponding families of consecutive positions of the generating surface,  $T$ , of the gear cutting tool in its motion in relation to a reference system, which a machined gear is associated with. As a result, only the law of contact,  $\mathbf{n}_g \cdot \mathbf{v}_\Sigma = 0$ , is fulfilled in approximate real gearing, as the gear and the pinion tooth flanks,  $\mathcal{S}_{r.app}$  and  $\mathcal{P}_{r.app}$ , are enveloping to one another. The conjugate action law is violated in approximate real gearing. Moreover, the law of equal base pitches of a gear and that of a mating pinion to the operating base pitch of the gear pair<sup>2</sup> is also violated in approximate real gearing.

Gear cutting tools for machining approximate real gears, as well as the methods of machining gears of this particular type, are discussed in detail in the monograph [152] by Prof. *S.P. Radzevich*. The consideration in this monograph is limited to discussion of examples of real approximate gearing that illustrate violation of:

- The second fundamental law of gearing (a gear,  $\mathcal{S}_{r.app}$ , and a mating pinion,  $\mathcal{P}_{r.app}$ , tooth flanks are not conjugate to one another),

---

<sup>1</sup> Gears with a large tooth count for parallel-axes gearing that operate at low rotation are commonly designed and manufactured with a straight tooth profile, instead of true involute tooth profile. Parallel-axes approximate real gearing of this particular kind are permissible as the deviation of the straight-line tooth profile from the true involute profile in case of gears with a large tooth count are negligibly small, and often they can be ignored.

<sup>2</sup> It is instructive to stress here that in both, in intersected-axes real gearing, as well, as in crossed-axes approximate real gearing, only operating angular base pitch of a gear pair,  $\varphi_{b.op}$ , can be specified. Neither angular base pitch of a gear,  $\varphi_{b.g}$ , nor angular base pitch of a mating pinion,  $\varphi_{b.p}$ , can be specified in intersected-axes real gearing, and in crossed-axes approximate real gearing, as the plane of action,  $PA$ , in these cases intersects the tooth flanks,  $\mathcal{S}_{r.app}$  and  $\mathcal{P}_{r.app}$ , along the lines, at points of which common perpendiculars to the tooth flanks do not lie in a common plane. Thus, no common normal plane can be constructed in intersected-axes as well as in crossed-axes approximate real gearing. As the angular base pitches,  $\varphi_{b.g}$  and  $\varphi_{b.p}$ , do not exist, the equalities,  $\varphi_{b.g} = \varphi_{b.op}$  and  $\varphi_{b.p} = \varphi_{b.op}$ , cannot be fulfilled in intersected-axes as well as in crossed-axes approximate real gearing.

- The third fundamental law of gearing: angular base pitches of a gear and that of a mating pinion must be equal to the operating angular base pitch of the gear pair ( $\varphi_{b,g} = \varphi_{b,op}$  and  $\varphi_{b,p} = \varphi_{b,op}$ ).

Because of the low accuracy of real approximate gears, their application is limited to the transmission of relatively low rotations of the input and output shafts. Primarily, gears with a large tooth count are used in the design of transmissions of this particular kind.

## 21.1 APPROXIMATE REAL PARALLEL-AXES GEARING

It has been well known since the times of *Leonhard Euler* (1707–1783) that only gears with involute tooth profiles are capable of transmitting a uniform rotation from a driving shaft to a driven shaft. Gears that have tooth profiles of other geometries, those different from involute tooth profiles, are not capable of transmitting rotation smoothly.

Non-involute gearing is viewed as an example of real approximate parallel-axes gearing (see Table 17.1). Pin gears, gears of cycloid tooth profiles, lobe profiles in the design of *Roots blowers*, and so forth, represent perfect examples of approximate real parallel-axes gearing. In all the aforementioned cases, as well as in numerous other cases, the tooth flanks,  $\mathcal{S}_{r,app}$  and  $\mathcal{P}_{r,app}$ , of a gear and that of a mating pinion do not conjugate to one another, and the law of equal base pitches cannot be fulfilled, as the base pitches of a gear and of a mating pinion do not exist at all.

An example of approximate real parallel-axes gearing to be considered immediately below is related to parallel-axes gears cut either by the face-mill cutter or by the face hob.

As schematically illustrated in Figure 21.1 [152], the tooth flanks of a gear are generated by two face-mill cutters. In this method, the face-mill cutters rotate with an angular velocity,  $\omega_c$ , about their axes, and travel straight forward with a velocity,  $V_c$ , tangentially to the gear pitch circle. The rotation,  $\omega_g$ , and the translation,  $V_c$ , of the gear blank are synchronized with one another in a timely manner.

The axes of rotation of the face-mill cutters intersect each other at an angle,  $2 \cdot \theta_{c2}$ . The actual value of the angle  $\theta_{c2}$  falls into the interval  $0^\circ \leq \theta_{c2} \leq \phi_n$  (in a particular case of gear machining, the axes of rotation of the cutting tools can be parallel to each other). The angle  $\phi_n$  is the normal profile angle.

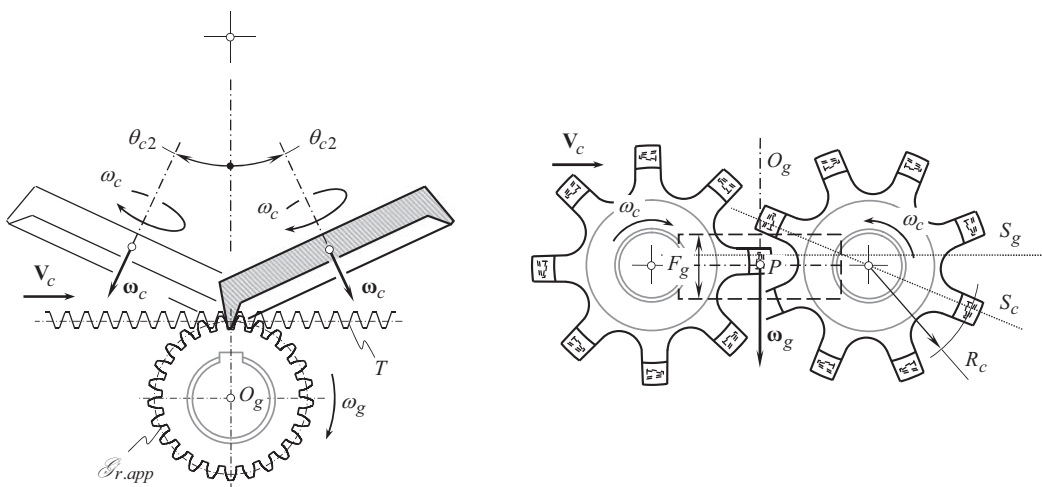


**FIGURE 21.1** Generation of tooth flanks,  $\mathcal{S}_{r,app}$ , of real approximate gear by two tilted face-mill cutters. (Adopted from: Radzevich, S.P., *Gear Cutting Tools: Science and Engineering*, 2nd Edition, CRC Press, Boca Raton, FL, 2017, 606 pages) [152].

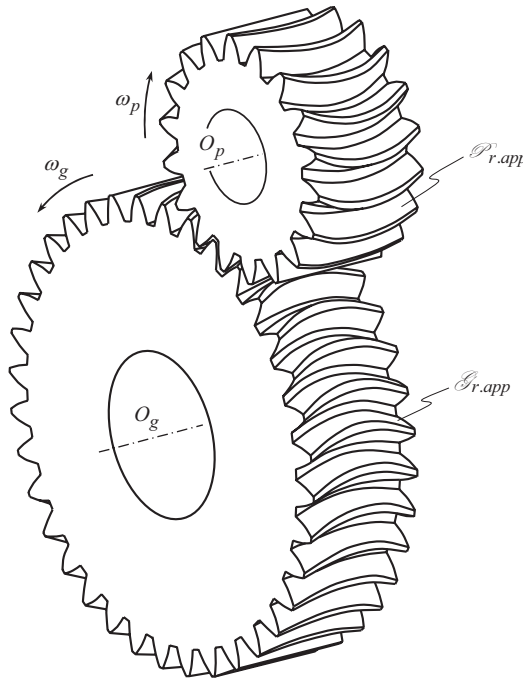


**FIGURE 21.2** Gear pair of circular arc tooth in the lengthwise direction: example of real approximate parallel-axes gearing.

A parallel-axes approximate real gear pair with arc-shaped teeth in their lengthwise direction is shown in Figure 21.2.

In all sections,  $S_g$ , perpendicular to the gear axis of rotation,  $O_g$ , the machined gear must have base pitch,  $p_{b,g}$ , of a constant value. For this purpose, in all the sections by the planes,  $S_g$ , the face-mill cutters have to have the same base pitch,  $p_{b,c}$  (that is, an equality  $p_{b,g} = p_{b,c}$  must be valid). However, the base pitch of the face-mill cutter,  $p_{b,c}$ , is not of a constant value in the sections by the planes,  $S_g$ ; instead, it is of a constant value in the sections by the axial planes,  $S_c$ . The sections,  $S_c$ , pass through the axis of rotation of the face-mill cutter. In general, the planes, denoted by,  $S_g$  and  $S_c$ , are not congruent to one another, except in one particular configuration. Therefore, the cut gear has different values of the base pitch,  $p_{b,g}$ , in different sections by the planes,  $S_g$ . As a result, gears generated in accordance with the method illustrated in Figure 21.1, are approximate real parallel-axes gears. The larger the face width,  $F_g$ , of the gear, the larger the deviations in its base pitch,  $p_{b,g}$ , from the desirable value. Similarly, the smaller the radius,  $R_c$ , of the face-mill cutter, the larger the deviations of the base pitch of the gear,  $p_{b,g}$ , from the desirable value, and vice versa.

More examples of approximate real parallel-axes gearing are known. In all cases, gears are referred to as *approximate real gears* mainly because either the tooth profile of the gear is not of involute geometry, or the tooth flanks are improperly generated in the lengthwise direction of the gear.

An example of the application of parallel-axes approximate real gears that have circular arc teeth in their lengthwise direction is illustrated in Figure 21.3.

## 21.2 APPROXIMATE REAL INTERSECTED-AXES GEARING

The application of approximate real intersected-axes gearing can be traced back to the times when the first intersected-axes pin gears were used. Since then, many significant improvements to the geometry of the interacting tooth surfaces of gears of this type have been made.

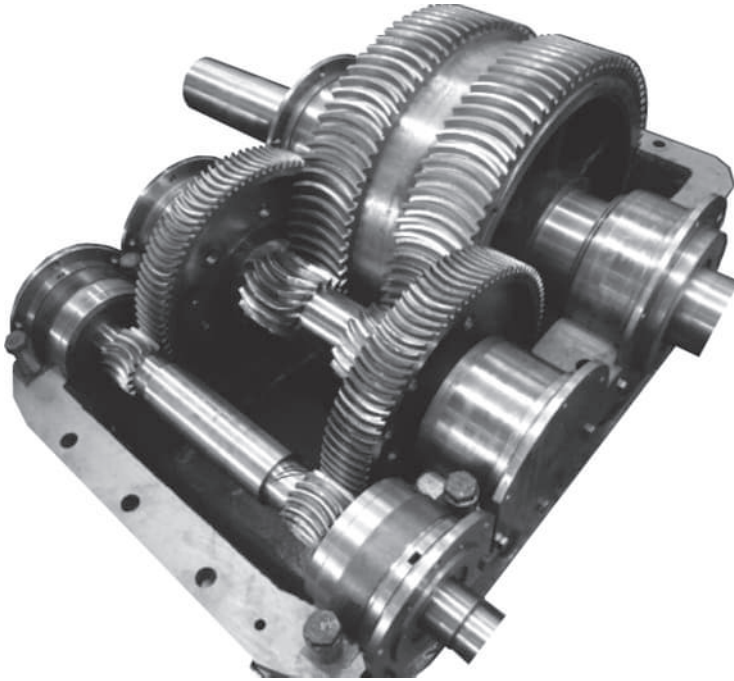


**FIGURE 21.3** Example of application of parallel-axes approximate real gears of circular arc teeth in the lengthwise direction of the gear.

### 21.2.1 ROOT CAUSES FOR INACCURACIES IN REAL INTERSECTED-AXES GEARS

Approximate real intersected-axes gears (see Table 17.1) are extensively used in the present-day industry, as in most cases, they sufficiently meet the requirements for their performance and production. Intersected-axes gearing of this type will be in use for a long while in applications with a low input/output rotation, with a low power density as well as with relatively low vibration generation and noise excitation requirements. The latter requirement is mainly due to the shape, location, and orientation of the contact pattern between the tooth flanks of the mating gears.

There are two main reasons to be noted for designing, production, and application of approximate real intersected-axes gears in the present-day industry.

**First**, the tooth flank geometry of geometrically accurate real intersected-axes gearing,  $\mathcal{G}_r$ , is not considered when determining the geometry of the generating surface,  $T$ , of the gear cutting tool for machining gears for approximate real intersected-axes gearing. Instead, for the users' convenience, the desirable generating surface,  $T$ , of the gear cutting tool is commonly replaced by a surface,  $T_{app}$ , of a simpler geometry. Such a substitution of the desirable generating surface,  $T$ , of the gear cutting tool with a chosen (approximate) surface,  $T_{app}$ , is equivalent to the replacement of a straight-sided generating rack for machining involute parallel-axes gears with a generating rack of another geometry. Evidently, the replacement entails the deviation of the machined tooth flanks from the desirable tooth flanks of the gear and of the pinion. The deviation of the actual gear tooth flank,  $\mathbf{G}_{r,app}$ , from the desirable tooth flank,  $\mathbf{G}_r$ , is associated with the deviation of the surface,  $T_r$ , from the surface  $T$ , that is inevitable in this case. As a result, real intersected-axes gearing is approximate one almost in all practical cases of implementation. The approximate gears are not capable of transmitting rotary motion smoothly.

**Second**, for transmitting a uniform rotation from a driving shaft to a driven shaft, intersected-axes gears that have various generic gear surfaces are used. The actual kind of the generic surface of a gear depends on an adopted method of gear cutting. Because of this, the machined tooth flanks,  $\mathcal{S}_{r.app}$  and  $\mathcal{S}_{r.app}$ , are neither conjugate to one another, nor of equal angular base pitches (the angular base pitches are not specified in bevel gears for approximate intersected-axes gearing). Thus, gearing of these kinds is not capable of transmitting rotary motion smoothly. This is one more reason why gears for approximate intersected-axes gearing are referred to as the *approximate real intersected-axes gears*.

The smaller the deviations of the actual generating surface,  $T_{app}$ , of a gear cutting tool of a specified design from the desirable generating surface,  $T$ , of the gear cutting tool, the smaller the deviation of the actually machined gear tooth flank,  $\mathcal{S}_{r.app}$ , from the desirable tooth flank,  $\mathcal{S}_r$ , and vice versa. The smaller the deviation of the tooth flank,  $\mathcal{S}_{r.app}$ , from the desirable tooth flank,  $\mathcal{S}_r$ , the smoother rotation can be transmitted from a driving shaft to a driven shaft.

It should be pointed out here that because approximate real intersected-axes gears are a kind of approximation to corresponding geometrically accurate real intersected-axes gears, the latter should be used as a datum surface when determining the accuracy of the former, that is, when measuring both the *design deviations* and the *manufacturing errors*. The geometry of the geometrically accurate real intersected-axes gears is required to be known for inspection purposes.

## 21.2.2 APPROXIMATE REAL INTERSECTED-AXES GEARS

Gears of various geometries in the lengthwise direction of the gear teeth are used to transmit a rotation between two shafts with intersected axes of rotation of a gear, and of a mating pinion. Straight tooth bevel gears, skew tooth bevel gears, spiral bevel gears (those cut by a face-mill cutter as well as cut by a face hob), straight teeth face gears, helical teeth face gears, and others can be mentioned as examples of approximate real intersected-axes gears.

### 21.2.2.1 Straight Tooth Bevel Gears

Depending on manufacturing methods used in gear production, multiple types of straight tooth bevel gears are recognized.

A straight tooth bevel gear cut in continuous-indexing method of gear generation is shown in Figure 21.4. A straight-sided generating round rack,  $T_{app}$ , is used for the generation of the gear tooth flanks,  $\mathcal{S}_{r.app}$ . The generating rack,  $T_{app}$ , is used as an approximate generating surface of the gear cutting tool. The tooth flanks of the rack are shaped in the form of planes.



**FIGURE 21.4** Straight bevel gear cut in continuous-indexing method of gear generation.

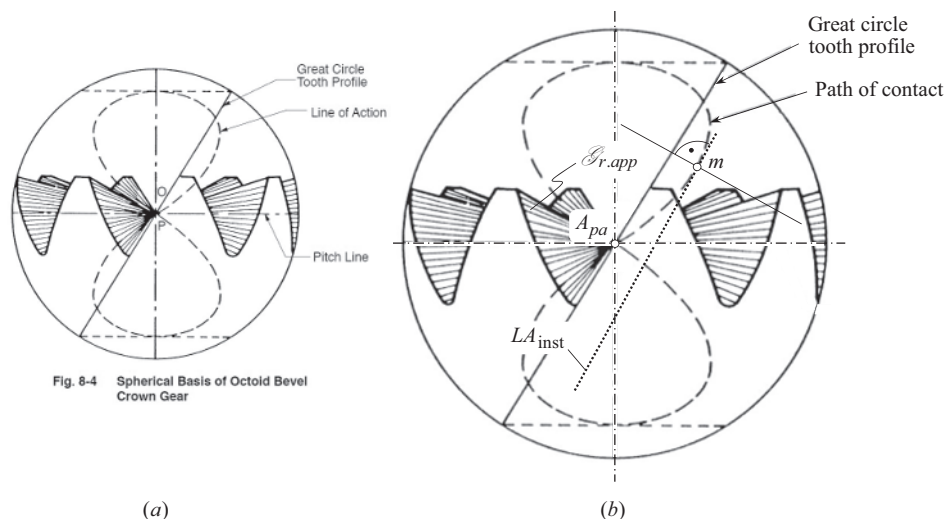


**FIGURE 21.5** The difference between the *path of contact*,  $P_c$ , and the *instantaneous line of action*,  $LA_{inst}$  in approximate real intersected-axes gearing: (a) original commonly adopted image, and (b) modified and updated image.

In the gear machining process, both a work gear and the generating round rack are continuously rotated about their axes of rotation at uniform angular velocities. The desirable tooth flank,  $T$ , of the virtual generating rack has to be shaped in the form of an involute surface developed from the base cone of the gear cutting tool. Only in this case, the generating rack,  $T$ , and the cut gear,  $\mathcal{G}_r$ , are capable of transmitting a uniform rotary motion smoothly with a constant angular velocity ratio.

The actual tooth flank,  $T_{app}$ , of the virtual generating rack (a plane) differs from the desirable tooth flank,  $T$  (an involute surface). In reality, the tooth flank of the generating rack (a plane,  $T_{app}$ ) and the tooth flank of the machined gear,  $\mathcal{G}_{r,app}$ , do not conjugate with one another. Moreover, the angular base pitch can be specified neither to the actual generating rack,  $T_{app}$ , nor for the tooth flank,  $\mathcal{G}_{r,app}$ , of the machined gear. Therefore, the mandatory condition to be met  $\varphi_{b,g} = \varphi_{b,c}$ , cannot be even discussed, as the angular base pitches,  $\varphi_{b,c}$ , and  $\varphi_{b,g}$ , of the gear and of the generating rack cannot be even specified.

As a result, a gear pair composed of a gear and a pinion both cut in the continuous-indexing method of gear generation is not capable of transmitting a uniform rotation smoothly. Gears of this type can be used only in low-rotation applications. At higher rotations, gears of this kind produce an excessive vibration and are subject to noise excitation.

All bevel gear generators operate on the so-called *octoid gear system*, and not on the involute, as is generally supposed. In the *octoid gear system*, a crown gear with plane tooth flanks is used to generate a gear,  $\mathcal{G}_{r,app}$ , and a mating pinion,  $\mathcal{P}_{r,app}$ , tooth flanks. The path of contact,  $P_c$  (loosely called the *line of action*, from which the tooth derives its name, is the peculiar *figure eight* curve, which is at right angles to the tooth curves of the crown line and tangential to the polar circles, to which the great circle crown odontoids are also tangential as shown in Figure 21.5a.

The cutting edge of the tool being is straight, and no change is required while it is in motion, except in its position, and that is accomplished by giving it a motion in such a direction that its corner moves in the radial line of the corner of the bottom of the tooth space.

The *octoid gear system*, together with the ingenious machine for planning it, was invented by *Hugo Bilgram*.<sup>3</sup> Following *George Grant*<sup>4</sup>: “This tooth owes its existence to the fact that it is the

<sup>3</sup> Hugo Bilgram (January 13, 1847–August 27, 1932), a famous American (German born) gear engineer.

<sup>4</sup> George Grant (December 21, 1849–August 16, 1917), a famous American gear engineer.





**FIGURE 21.6** Forged straight bevel gear.

only known tooth, and probably the only possible tooth, that can be practically formed by the molding planning process.”

As illustrated in Figure 21.5b, in *octoid gear system*, the trace of contact point, namely, the path of contact,  $P_c$ , is supposed to be a spatial curve. At arbitrary point,  $m$ , within the path of contact,  $P_c$ , a straight tangent line can be constructed. By nature, this straight tangent line is the instantaneous line of action,  $LA_{inst}$ . In order to generate conjugate tooth flanks,  $\mathcal{S}_r$  and  $\mathcal{S}_r$ , of a gear and that of a mating pinion, at any and all configurations of the gear and the mating pinion, the instantaneous line of action,  $LA_{inst}$ , has to intersect the axis of instantaneous rotation,  $P_{ln}$ , in the gear pair. In Figure 21.5b, the instantaneous line of action,  $LA_{inst}$ , has to pass through the plane-of-action apex,  $A_{pa}$ . It does not go through the plane-of-action apex,  $A_{pa}$ . Because of this, the tooth flank,  $T_{app}$ , of the generating rack, and the tooth flank,  $\mathcal{S}_{r,app}$ , of the machined bevel gear do not conjugate with one another. Thus, bevel gears of this particular kind are not capable of transmitting an input uniform rotary motion smoothly.

Manufacturing errors can be the root cause of the low accuracy of the gears in intersected-axes gear pairs. Such a problem arises, for example, in the high-volume production of forged gears.

Forged straight tooth bevel gears (see Figure 21.6) are used in not critical applications. Gears of this type can be manufactured with any desirable geometry of tooth flanks, as the geometry of the gear tooth flank entirely depends on the geometry of dies used in the production process of forged gears. Practically, however, forged straight bevel gears feature the same geometry of the tooth flanks, as that for cut straight bevel gears (see Figure 21.4). Therefore, in addition to the manufacturing errors, violation of the conjugate action law, along with non-existence of the angular base pitches,  $\phi_{b,g}$  and  $\phi_{b,p}$ , in a gear and that in a mating pinion are observed.

An important advantage of forging technology over gear cutting is due to this technology allows the production of straight bevel gears that have a web at the inner end of the gear tooth (see Figure 21.7), or at the outer end, or both. Gear teeth that have a web are stronger and are capable of transmitting larger torque.

### 21.2.2.2 Spiral Bevel Gears

Bevel gears for approximate real intersected-axes gear pairs can be designed so as to have curved teeth in their lengthwise direction. Three major types of curved teeth are used in the present-day industry:

- spiral bevel gears cut by face-mill cutters
- bevel gears that have teeth shaped in the form of circle cycloids, cut by face hobs
- bevel gears that have teeth shaped in the form of circle involute in their lengthwise direction, which is cut by conical hobs.

A face-milled spiral bevel gear is depicted in Figure 21.8. Fine-pitch and medium-pitch bevel gears are produced using face-milled process.





**FIGURE 21.7** Net forged straight bevel gear.



**FIGURE 21.8** Face-milled spiral bevel gear.

The tooth flanks,  $\mathcal{S}_{r.app}$  and  $\mathcal{P}_{r.app}$ , of bevel gears of this particular type are generated by means of a straight-sided generating round racks that feature the teeth shaped in the form of circular arcs in their lengthwise direction. In the gear machining process, both the work gear and the generating round rack are continuously rotating about their axes of rotation at uniform angular velocities.

Because the geometry of the actual generating rack,  $T_{app}$ , differs from that of a geometrically accurate generating rack,  $T$ , the tooth flanks,  $\mathcal{S}_{r.app}$  and  $\mathcal{P}_{r.app}$ , of a gear and its mating pinion are not conjugate to one another, and the requirement of equal angular base pitches is not met, as the angular base pitches do not exist in approximate gearing. As a result, spiral bevel gears transmit a rotation with a certain transmission error, which is inevitable. The actual value of the transmission error can be precalculated based on the set of design parameters of the spiral bevel gear, and the cutting-head used to machine the gear. Transmission errors of this particular kind are inevitable when spiral bevel gears are used to transmit a rotation between two shafts that intersect one another.



**FIGURE 21.9** Large size coarse-pitch spiral bevel gear.

Large size coarse-pitch spiral bevel gears, for example, the one shown in Figure 21.9, is commonly machined on multi-axis numerically controlled (NC) machines. End-type mill cutters are used in this process. This makes it possible to machine gear tooth flanks of any desirable geometry. However, in practice, the tooth flanks of large size coarse-pitch spiral bevel gears are designed so, as to have the tooth flank geometry similar to that of small-, and medium-pitch spiral bevel gears. The tooth flanks,  $\mathcal{S}_{r,app}$  and  $\mathcal{P}_{r,app}$ , of a gear and that of a mating pinion are not conjugate to one another. Moreover, the requirement of equal angular base pitches is not met, as the angular base pitches do not exist in bevel gears manufactured this way.

Bevel gears having the teeth shaped in the form of cycloid of a circle (gears, cut by face hobs), and bevel gears that have teeth shaped in the form of involute of a circle in their lengthwise direction (those, cut by conical hobs, the so-called *Paloid system*) have many similarities with conventional spiral bevel gears. In particular, the tooth flanks,  $\mathcal{S}_{r,app}$  and  $\mathcal{P}_{r,app}$ , of a gear and of a mating pinion cut this way, are not conjugate to one another, and the requirement of equal angular base pitches is not met. Therefore, bevel gears of this particular kind transmit a uniform rotation with certain transmission error, the actual value of which can be expressed in terms of the set of design parameters of the spiral bevel gear, and the cutting tool used to machine the gear.

Noise excitation always occurs when high rotations are transmitted by approximate spiral bevel gears. Improper location and orientation of the contact pattern is another bottleneck for bevel gears that have curved teeth in their lengthwise direction.

### 21.2.2.3 Face Gears

Face gearing (or *pseudo-bevel gearing* in other terminology) is also used to transmit a rotary motion between two shafts, the axes of which intersect one another. A face gear set consists of a face gear in combination with a spur, helical, or conical pinion. The shaft angle is commonly equal to  $90^\circ$ . However, face gear sets can be designed so, as to have other values of the shaft angle.



**FIGURE 21.10** Forged face gear.

A face gear has a planar pitch surface and a planar root surface, both of which are perpendicular to the axis of rotation of the gear (Figure 21.10).

The spur pinion is commonly a duplicate of the shaper cutter used to cut the face gear, except, of course, for the additional clearance at the tips of the cutter teeth. The face width of the teeth on the face gear has to be made quite short; otherwise, the top land will become pointed at the larger diameter of the gear.

Possible types of gears used to transmit a rotary motion between shafts whose axes of rotation intersect are not limited to the aforementioned ones. Many novel types of gearing can be designed based on various combinations of generic shapes of gears (see Chapter 20). Gearing composed of internal bevel gears is included as well.

### 21.2.3 GENERATION OF TOOTH FLANKS OF GEARS FOR INTERSECTED-AXES GEARING

The approximate generating surface of a gear cutting tool,  $T_{app}$ , is reproduced by the cutting edges of the cutting tool when machining straight bevel gears. The tooth flank of an approximate generating surface,  $T_{app}$ , is shaped in the form of plane surface in the cases of machining, both straight bevel gears of conventional design and straight bevel gears with offset teeth.

The straight cutting edge of the gear cutting tool is the simplest shape of the cutting edge to be used for the purpose of reproduction of the plane,  $T_{app}$ . The straight motion of the cutting edge is the easiest motion to be reproduced. The straight motion is performed in a direction parallel to the plane,  $T_{app}$ .

#### 21.2.3.1 Generation of Tooth Flanks of Straight Bevel Gears

Reciprocation of the straight cutting edge,  $CE$ , toward the axis of rotation,  $O_c$ , of the generation surface,  $T_{app}$ , as shown in Figure 21.11, is the most practical way of reproducing the approximate generating surface,  $T_{app}$ , of the gear cutting tool.<sup>5</sup> In such a scenario, the plane,  $T_{app}$ , is reproduced as the loci of consecutive positions of the straight cutting edge,  $CE$ , when it is reciprocating toward the axis,  $O_c$ , of rotation,  $\omega_c$ .

Principles governing the generation of bevel gears are analogous to those governing the generation of spur and helical gears, with the difference that whereas spur and helical gears are generated by tools, which represent the teeth of the basic rack, cutters used for bevel gear generation represent

<sup>5</sup> Other directions of the reciprocating motion,  $\mathbf{V}_{cut}$ , are also theoretically possible. Commonly, they are less practical in the present-day industry.

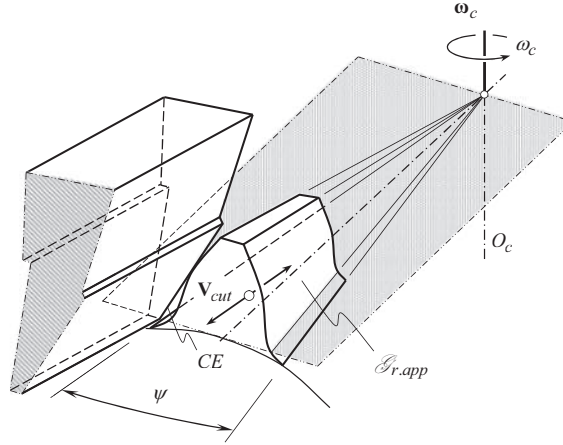


**FIGURE 21.11** Generation of the plane,  $T_{app}$ , by straight cutting edge,  $CE$ , moving toward the axis of rotation,  $O_c$ , of the gear cutting tool.

the teeth of the straight-sided basic crown wheel. The straight-sided base crown wheel is commonly called the *generating surface of the gear cutting tool*. The motions that result in the generation of gears are therefore those of rolling pitch cones instead of rolling pitch cylinders.

The cutters themselves must be given a form and a motion, which cause them to sweep out the surface of the basic crown wheel,  $T_{app}$ . The work gear is then given, relative to the cutters, the rolling motion, which the finished gear would have when engaging with the crown wheel that the cutters represent. Two distinct cases arise:

1. Each of a pair of gears (both of which are to be generated) is an envelope to the same side of the surface of the virtual crown wheel (which must therefore be symmetrical)
2. Mating gears are envelope to opposite sides of the same basic crown wheel

The first case finds application to the cutting of bevel gears that have straight (and *uncorrected*) teeth and the second in the cutting of spiral bevel gears. Considering the generation of either pair of gears individually, however, both cases reduce to the same thing, the only difference being in the setting of the cutters.

Figure 21.12 illustrates the process diagrammatically for the case of straight bevel gears. Two cutters that have straight-side cutting edges,  $CE$ , are arranged to reciprocate with a velocity,  $\mathbf{V}_{cut}$ , along the radial lines, sweeping out the surfaces,  $T_{app}$ , of the teeth of the virtual crown wheel that has its center at  $O_c$ . The cutting edge,  $CE$ , is understood as the line of intersection of the rake surface,  $R_s$ , and of the clearance surface,  $C_s$ , of the gear cutting tool.

The position vector of point,  $\mathbf{r}_{Ta}$ , of the lateral plane,  $T_{app}$ , of the generating surface of the gear cutting tool can be expressed in terms of two *Gauss'* parameters,  $u$  and  $\theta$  :

$$\mathbf{r}_{Ta}(u, \theta) = \begin{bmatrix} u \cos \theta \\ 0 \\ u \sin \theta \\ 1 \end{bmatrix} \quad (21.1)$$

In order to derive an equation for the family of lateral planes,  $T_{app}$ , when the generating surface of the gear cutting tool rolls over the pitch cone of the gear to be cut, two operators of the coordinate system transformation have to be derived.

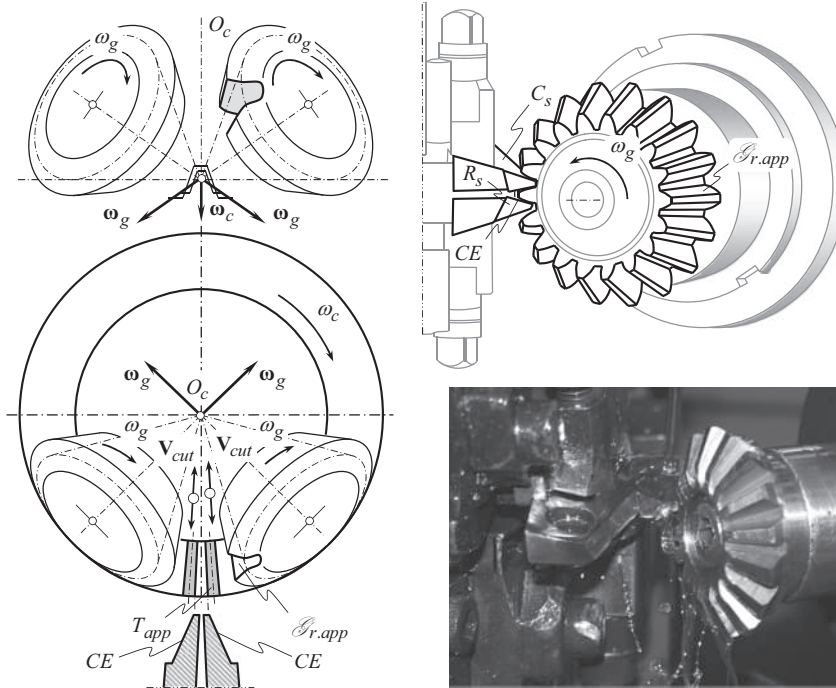


FIGURE 21.12 Diagrammatic representation of straight bevel gear generation.

The first one,  $\mathbf{Rt}(\phi, Z_t)$ , is the operator of rotation through the pressure angle,  $\phi$ . This rotation is performed about the  $Z_t$  – axis of a *Cartesian* coordinate system,  $X_t Y_t Z_t$ , which is associated with the tooth flank,  $T_{app}$ , of the generating surface of the gear cutting tool. The operator,  $\mathbf{Rt}(\phi, Z_t)$ , can be represented in matrix form as follows:

$$\mathbf{Rt}(\phi, Z_t) = \begin{bmatrix} \cos \phi & \sin \phi & 0 & 0 \\ -\sin \phi & \cos \phi & 0 & 0 \\ 0 & 0 & 1 & 0 \\ 0 & 0 & 0 & 1 \end{bmatrix} \quad (21.2)$$

The second operator,  $\mathbf{Rt}(\psi, X_T)$ , is the operator of rotation through a current angle  $\psi$ . This rotation is performed about the  $X_T$  – axis of a *Cartesian* coordinate system,  $X_T Y_T Z_T$ , which is associated with the generating surface,  $T_{app}$ , of the gear cutting tool. The following expression:

$$\mathbf{Rt}(\psi, X_T) = \begin{bmatrix} 1 & 0 & 0 & 0 \\ 0 & \cos \psi & \sin \psi & 0 \\ 0 & -\sin \psi & \cos \psi & 0 \\ 0 & 0 & 0 & 1 \end{bmatrix} \quad (21.3)$$

is derived for the operator,  $\mathbf{Rt}(\psi, X_T)$ , of the coordinate system transformation.

The operator of the resultant coordinate system transformation,  $\mathbf{Rs}(t \mapsto T)$ , namely, the operator of the transition from the reference system,  $X_t Y_t Z_t$ , to the reference system,  $X_T Y_T Z_T$ , can be expressed in the form of a dot product:

$$\mathbf{Rs}(t \mapsto T) = \mathbf{Rt}(\psi, X_T) \cdot \mathbf{Rt}(\phi, Z_t) \quad (21.4)$$

This allows the following expression for the operator of the resultant coordinate system transformation:

$$\mathbf{Rs}(t \mapsto T) = \begin{bmatrix} \cos \phi & \sin \phi & 0 & 0 \\ -\sin \phi \cos \psi & \cos \phi \cos \psi & \sin \psi & 0 \\ \sin \phi \sin \psi & -\cos \phi \sin \psi & \cos \psi & 0 \\ 0 & 0 & 0 & 1 \end{bmatrix} \quad (21.5)$$

The position vector of point,  $\mathbf{r}_{Tf}$ , of the family of lateral planes,  $T_{app}$ , when the generating surface of the gear cutting tool rolls over the pitch cone of the gear to be cut, can be analytically represented in the following form:

$$\mathbf{r}_{Tf}(u, \theta, \psi) = \mathbf{Rs}(t \mapsto T) \cdot \mathbf{r}_{Ta}(u, \theta) \quad (21.6)$$

where the subscript “ $Tf$ ” refers to the family of lateral planes  $T_{app}$ .

Equation (21.6) casts into equation:

$$\mathbf{r}_{Tf}(u, \theta, \psi) = \begin{bmatrix} u \cos \phi \cos \theta \\ u(-\sin \phi \cos \theta \cos \psi + \sin \theta \sin \psi) \\ u(\sin \phi \cos \theta \sin \psi + \sin \theta \cos \psi) \\ 1 \end{bmatrix} \quad (21.7)$$

In the reference system  $X_t Y_t Z_t$ , the unit normal vector to the plane,  $T_{app}$ , is pointed along the  $Y_t$  – axis. Therefore, in the reference system,  $X_T Y_T Z_T$ , it can be analytically described as follows:

$$\mathbf{n}_T(\phi, \psi) = \begin{bmatrix} \sin \phi \\ \cos \phi \cos \psi \\ -\cos \phi \sin \psi \\ 0 \end{bmatrix} \quad (21.8)$$

Once the expressions for the position vector,  $\mathbf{r}_{Tf}$  [see Eq. (21.7)], as well as for the unit normal vector,  $\mathbf{n}_T$ , [see Eq. (21.8)], are derived, the *Shishkov equation of contact*,  $\mathbf{n}_g \cdot \mathbf{V}_\Sigma = 0$ , can be represented in the form:

$$\cot \theta - \frac{\sin \phi \sin \psi + \tan \delta_k \cos \phi}{\cos \psi} = 0 \quad (21.9)$$

In Eq. (21.9), the angle  $\delta_k$  is used to specify the velocity vector,  $\mathbf{V}_\Sigma$ .

Equation (21.9) is used to express the angle,  $\psi$ , in terms of the parameters,  $\phi$ ,  $\theta$ ,  $\psi$ , and  $\delta_k$ . Then the derived expression for the angle,  $\psi$ , is substituted into Eq. (21.7). The position vector of point,  $\mathbf{r}_g = \mathbf{r}_g(u, \theta)$ , of the gear tooth flank,  $\mathcal{S}_{r,app}$ , can be obtained after the angular parameter,  $\psi$ , is eliminated from Eq. (21.7).

The tooth flank,  $T_{app}$ , of the generating surface of the gear cutting tool, and the flank,  $\mathcal{S}_{r,app}$ , of the generated straight tooth bevel gear, do not conjugate with one another. The bevel gears generated using this method, are not capable of transmitting an input uniform rotation smoothly. The area of application of straight tooth bevel gears is restricted to low-rotation applications.

The work gear is arranged with its axis,  $O_g$ , passing through the axis,  $O_c$ , and its pitch cone in contact with the pitch plane of the crown wheel,  $T_{app}$ . It is then given a rotation,  $\omega_g$ , about its own



axis, together with a rotation of the axis bodily about the axis,  $O_c$ , of the crown wheel,  $T_{app}$ , which are so related that the pitch cone of the work-gear rolls over the pitch plane of the crown wheel. It passes through the zone where the cutters operate; therefore, material is removed and the result is a generated tooth flank,  $\mathcal{S}_a$ . The generated tooth flank,  $\mathcal{S}_a$ , is not conjugate with the tooth flank of the basic crown wheel. It may be observed that in practice the component motions are rearranged as a matter of convenience, the work gear and the cutter head each with only rotational motion about their respective axes.

When cutting straight bevel gears, especially those that have low tooth count, the problem of tooth undercutting becomes critical. This issue is discussed in the monograph by Prof. *S.P. Radzevich* [152].

### 21.2.3.2 Generation of Tooth Flanks of Spiral Bevel Gears

Spiral bevel gears are cut by face-mill cutters. The rotation vector,  $\omega_{cut}$ , of the face-mill cutter is pointed in such a direction that it is configured parallel to the axis of rotation,  $O_c$ , of the generating surface of the cutting tool, as shown in Figure 21.13. In this way, bevel gears that have spiral teeth with a certain spiral angle,  $\psi_g$ , are produced. Although suitable spiral angles lie in the range of  $\psi_g = 15^\circ \dots 35^\circ$ , they are usually chosen in the range of  $\psi_g = 30^\circ \dots 35^\circ$  to provide adequate overlap, and it is normal practice to make spiral bevel gears with about 35% overlap.

When machining a spiral bevel gear, the cutter rotates about its axis with a certain angular velocity,  $\omega_{cut}$ . The work gear and the generating surface,  $T_{app}$ , roll over each other. For this purpose, rotations of the work-gear,  $\omega_g$ , and of the generating surface of the gear cutting tool,  $\omega_c$ , are synchronized with each other in a timely manner.

In the method of generating curved tooth bevel gears, the tooth spirals take the form of circular arcs. Straight-sided cutting tools represent the flanks of the basic crown wheel teeth and the combined motions of the generating cutter and the work-gear sweep out the surface of the virtual crown wheel teeth (round rack teeth). The generation of the tooth profiles is obtained by giving the work gear a rolling motion relative to the cutter, similar to what the finished gear would have when engaging with the crown wheel.

The tool holder is rotated to cause a cutting action while the work gear slowly rotates with the tool holder. The rotation of the work gear in relation to the tool holder causes a generating action to

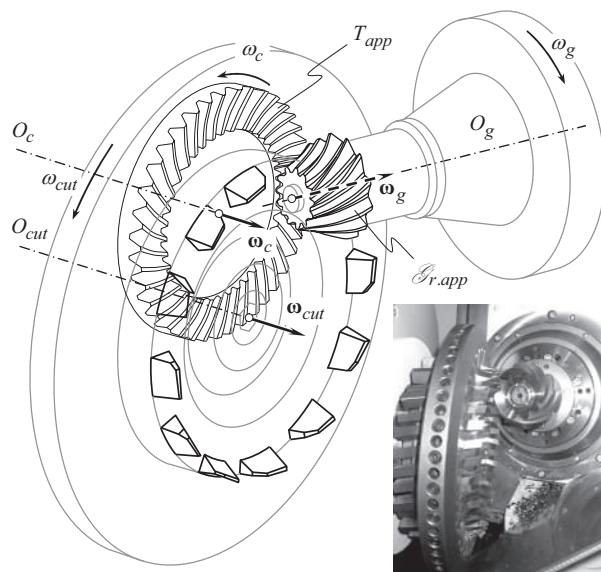


FIGURE 21.13 Representation of the generating surface,  $T_{app}$ , of the face-mill cutter.

occur. After one tooth space is finished, the machine goes through an indexing motion to bring the cutter into the next tooth slot.

Pinions are cut as the reverse of wheels in so far, as they are assumed to engage with the opposite side of the basic crown wheel surface. In practice, the axes of the generating cutter and the work gear are not inclined at the theoretical angle; the axes are arranged to accommodate the tapering depth of the tooth and also to provide deflection allowance in the tooth spirals.

During the operation, the cutter is given a rotation speed and feed rate suitable for the material of the work gear and it is fed to the full depth required while the cutter and the work-gear roll together. A copious supply of cutting oil is fed to the cutting zone to act as lubricant and coolant. It is normal to expect a minimum of 100 gears to be cut between cutter sharpenings. As soon, as a tooth space is completed, the work gear and the cutter roll out of engagement, the work gear is indexed to the next tooth space, and the cutting process continues.

Teeth are usually rough cut and finish cut as two separate operations, and if the quantities are sufficiently large it is normal to carry out rough cutting on one machine and retain the second machine solely for finishing. Wheels being rough cut may be produced without tooth generation and refinement is deferred until the finish cutting operation. Pinions are invariably fully generated, and if they are intended to be run with form cut wheels the full shape is applied to the pinion profiles only.

Gears that demand high quality are always provided with fully generated teeth on both the wheel and pinion.

In order to machine a bevel gear that has a prescribed spiral angle,  $\psi_g$ , at the central point,  $C$ , the setup parameters of the cutting tool should fulfill the values that are calculated from the formulae (see Figure 21.14):

$$H = L - R_c \cdot \sin \psi_g \quad (21.10)$$

$$V = R_c \cdot \cos \psi_g \quad (21.11)$$

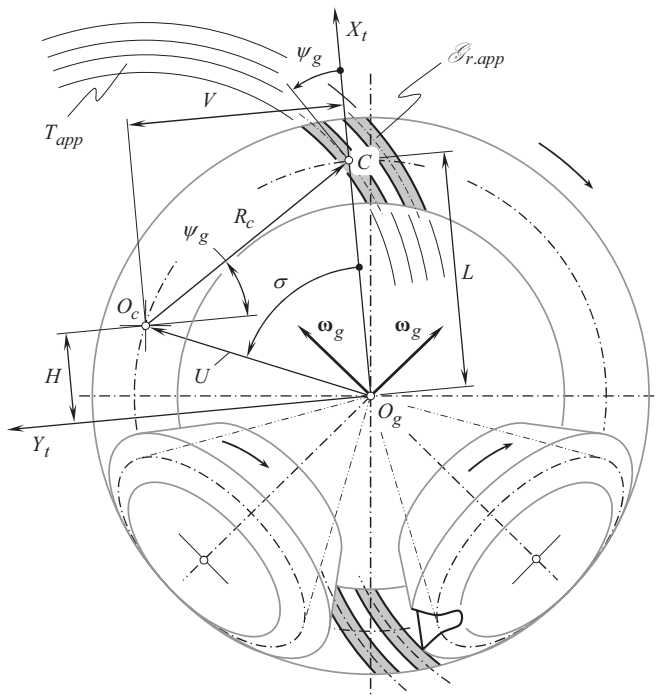
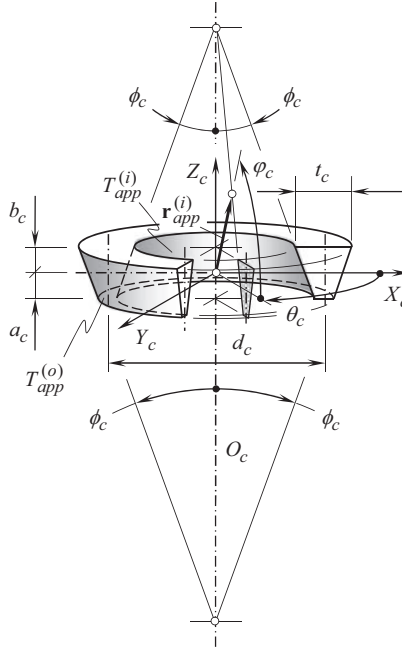


FIGURE 21.14 Diagrammatic arrangement of spiral bevel gear generation.





**FIGURE 21.15** Design parameters of the generating surface,  $T_{app}$ , of the face-mill cutter.

Bevel gear generators are often designed so that they require setup parameters expressed in polar coordinates. The polar angle,  $\sigma$ , and the offset distance  $OP = U$  can be calculated from the expressions:

$$U = \sqrt{H^2 + V^2} \quad (21.12)$$

$$\sigma = \tan^{-1} \left( \frac{V}{H} \right) \quad (21.13)$$

In a rolling motion, the coordinates  $H$  and  $V$  change their value. However, the radial offset,  $U$ , remains constant when the polar angle,  $\sigma$ , varies.

For machining of bevel gears with circular arc teeth, the generating surface of the cutting tool is chosen in the form of two cones of revolution that have a common axis of rotation (see Figure 21.15). The equation of the generating surface,  $T_{app}$ , can be derived from Figure 21.15.

The position vector of point,  $\mathbf{r}_{app}^{(i)}$ , for the inner portion,  $T_{app}^{(i)}$ , of the generating surface can be expressed in the form:

$$\mathbf{r}_{app}^{(i)}(\varphi_c, \theta_c) = \frac{(d_c - t_c)}{2} \cdot \begin{bmatrix} \cos \varphi_c \cdot \cos \theta_c \\ \cos \varphi_c \cdot \sin \theta_c \\ \sin \varphi_c \\ 1 \end{bmatrix} \cdot \frac{\cos \phi_c}{\cos(\varphi_c - \phi_c)} \quad (21.14)$$

Similarly, for the outer portion,  $T_{app}^{(o)}$ , of the generating surface for the position vector of point,  $\mathbf{r}_{app}^{(o)}$ , the following formula can be derived:

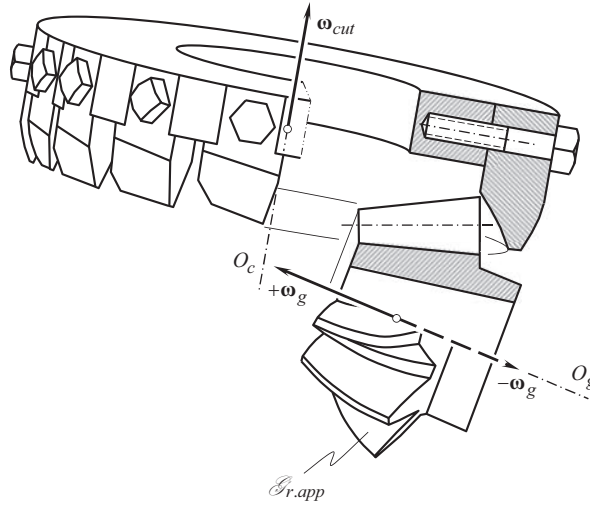


**FIGURE 21.16** Rolling motion of the face-mill cutter when cutting spiral bevel gear.

$$\mathbf{r}_{app}^{(o)}(\varphi_c, \theta_c) = \frac{(d_c + t_c)}{2} \cdot \begin{bmatrix} \cos \varphi_c \cdot \cos \theta_c \\ \cos \varphi_c \cdot \sin \theta_c \\ -\sin \varphi_c \\ 1 \end{bmatrix} \cdot \frac{\cos \phi_c}{\cos(\varphi_c - \phi_c)} \quad (21.15)$$

The lateral cutting edges,  $CE$ , of the face-mill cutter are located within the surfaces  $T_{app}^{(i)}$  and  $T_{app}^{(o)}$  [Eqs. (21.14) and (21.15)]. In this way, straight-sided cutting tools represent the flanks of the basic crown wheel teeth.

The rolling motion of the face-mill cutter in relation to the work gear (see Figure 21.16) is the same as in the case of cutting straight tooth bevel gears [see Eq. (21.5)]. Therefore, the position vector of point,  $\mathbf{r}_{app.f}^{(o)}$ , of a family of surfaces,  $T_{app}^{(o)}$ , in the rolling motion of the face-mill cutter can be calculated as the dot product of the position vector of point,  $\mathbf{r}_{app}^{(o)}$  [see Eq. (21.15)] by the operator of the resultant coordinate system transformation,  $\mathbf{Rs}(t \mapsto T)$  [see Eq. (21.5)]:

$$\mathbf{r}_{app.f}^{(o)}(\varphi_c, \theta_c, \psi) = \mathbf{Rs}(t \mapsto T) \cdot \mathbf{r}_{app}^{(o)}(\varphi_c, \theta_c) \quad (21.16)$$

The enveloping parameter,  $\psi$ , can be eliminated from Eq. (21.16). For this purpose, Eq. (21.16) is considered together with the *Shishkov equation of contact*,  $\mathbf{n}_g \cdot \mathbf{V}_\Sigma = 0$ . Ultimately, this returns an equation for tooth flank,  $\mathcal{S}_{r.app}$ , of the spiral bevel gear cut by a face-mill cutter.

Spiral bevel gears cut by face-mill cutters that have straight-sided tooth profiles are not capable of transmitting a uniform input rotation smoothly. They are subject to noise excitation when the rotation exceeds a certain limit value. This is because in the gear machining mesh the gear tooth flank,  $\mathcal{S}_{r.app}$ , and the generating surface tooth flank,  $T_{app}$ , are not conjugate to one another, and both of them do not feature the angular base pitches at all. Therefore, the law of equal operating base pitches of a gear and that of a mating pinion to operating angular base pitch of the gear pair is not fulfilled. The latter is not permissible.

When cutting spiral bevel gears, especially when cutting low-tooth-count gears, the problem of tooth undercutting becomes critical. This issue is discussed in detail in the monograph by Prof. *S.P. Radzevich* [152].

### 21.2.3.3 Tooth Flanks of Bevel Gears Cut Using Continuous-Indexing Method of Gear Machining

Two continuous-indexing methods of cutting bevel gears are used in the present-day industry:

1. Face hobbing of bevel gears: Bevel gears that have teeth shaped in the form of a cycloid in their lengthwise direction are cut by this method.
2. Hobbing of gears in *Paloid system* by means of conical hobs: Using this method, bevel gear teeth are shaped in the form of an involute curve in their lengthwise direction.

In both cases, generating surface of the gear cutting tool,  $T_{app}$ , features a straight-sided tooth profile. The tooth flanks,  $\mathcal{S}_{r,app}$ , of the gear to be machined are generated as envelopes to the corresponding families of consecutive positions of the generating surface,  $T_{app}$ , when the pitch cone that is associated with the gear cutting tool rolls with no slippage over the pitch cone of the work gear. Except for the rolling motion, tooth flanks generation by the continuous-indexing method of machining of bevel gears is similar to that by the indexing methods of bevel gear machining. This makes it possible to conclude immediately that bevel gears that have curvilinear teeth in their lengthwise direction cut by face hobs with straight-sided tooth profile, as well as gears cut in *Paloid system*, are not capable of transmitting a smooth input rotation from a driving shaft to a driven shaft. They are subject to noise excitation when the rotation exceeds a certain threshold. This is because in the gear machining mesh the gear tooth flank,  $\mathcal{S}_{r,app}$ , and the generating surface tooth flank,  $T_{app}$ , do not conjugate with one another, and both of them do not feature the angular base pitches. Therefore, the mandatory condition of equal operating base pitches of a gear and of a mating pinion to the operating angular base pitch of the gear pair is not fulfilled.

When cutting bevel gears with curvilinear teeth, especially when cutting low-tooth-count gears, the problem of tooth undercutting becomes critical. This issue is discussed in detail in the monograph by Prof. *S.P. Radzevich* [152].

### 21.2.4 EXAMPLES OF APPROXIMATE REAL INTERSECTED-AXES GEAR PAIRS

Various designs of approximate real intersected-axes gears are used to transmit and to transform a uniform rotation from a driving shaft to a driven shaft. For low-rotation applications, forged approximate real intersected-axes gear pairs are used. An example of a gear pair of this type composed of a straight bevel gear and pinion is illustrated in Figure 21.17.

Gear pairs of a bit higher accuracy are composed of cut straight bevel gears (see Figure 21.18). Commonly, the planing method of gear cutting is used to produce gears for these purposes.

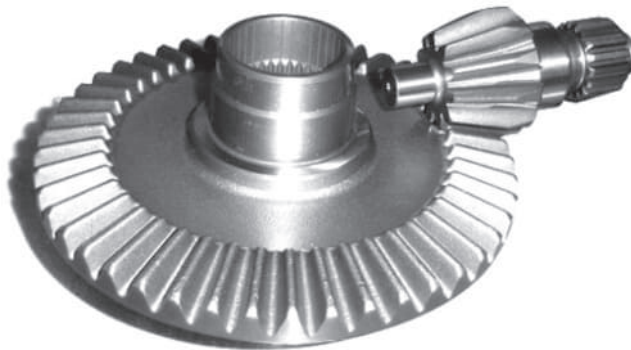


**FIGURE 21.17** Approximate real intersected-axes gear pair composed of forged straight bevel gear and pinion.



**FIGURE 21.18** Approximate real intersected-axes gear pair composed of cut planed bevel gear and pinion.



**FIGURE 21.19** Approximate real intersected-axes gear pair that features a small shaft angle.

For certain applications, approximate real intersected-axes gearing those features shaft angles of a small value, are used. An example is illustrated in Figure 21.19.

In the past, approximate real intersected-axes gear pairs composed of cast herring-bone gear and pinion were used (see Figure 21.20). Because of the poor accuracy of cast gears, gearing of this type is used in noncritical applications featuring low rotation of the input and output shafts.

Spiral bevel gear pairs with curvilinear teeth are the most extensively used design of gears. Examples of orthogonal spiral bevel gear pairs that have tooth ratio  $u = 1$  (miter gears), and  $u > 1$  are illustrated in Figure 21.21. It is not mandatory that the axes of rotation of a gear and of the mating pinion in a spiral bevel gear pair are orthogonal to each other. An example of non-orthogonal spiral bevel gear pair is shown in Figure 21.22.

Spiral bevel gear pairs are extensively used in automobile applications (see Figure 21.23). For special applications, large size spiral bevel gears are used (see Figure 21.24).

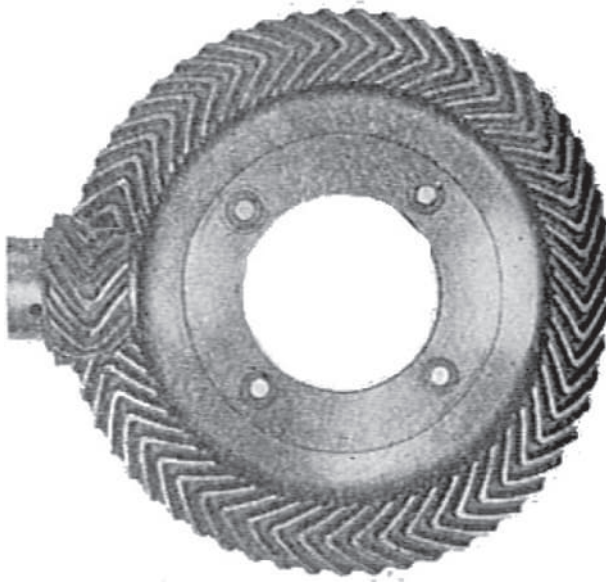


**FIGURE 21.20** Approximate real intersected-axes gear pair composed of cast herring-bone gear and pinion.

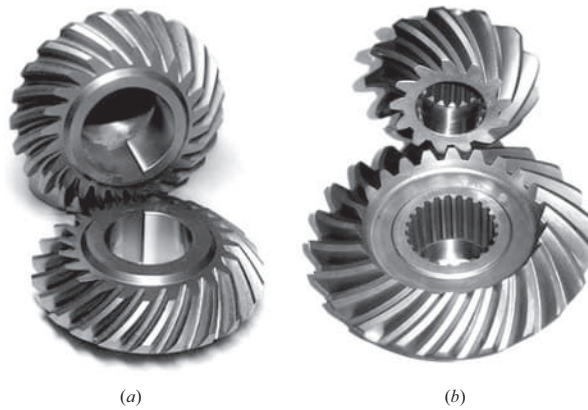


**FIGURE 21.21** Examples of approximate real crossed-axes gear pairs: orthogonal spiral bevel gear pairs that have tooth ratio (a)  $u = 1$  (miter gears), and (b)  $u > 1$ .



**FIGURE 21.22** Non-orthogonal spiral bevel gear pair.



**FIGURE 21.23** Spiral bevel gear pair for automobile application.

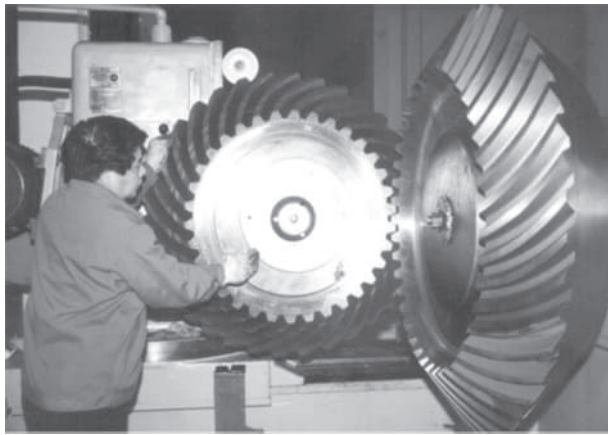


**FIGURE 21.24** Large size spiral bevel gear pair.

Both orthogonal and non-orthogonal spiral bevel gears cut by gear cutting tool that is designed on the premise of a straight-sided generating round rack are examples of approximate real intersected-axes gearing.

Face gears represent another approximate real intersected-axes gearing.

A spur involute pinion can be engaged in mesh with a face gear that has an appropriate geometry of the tooth flanks, as depicted in Figure 21.25. A gear pair of this kind is insensitive to the axial displacements of the pinion. Moreover, that same pinion can be engaged in mesh with a face gear as well as with straight bevel gears that have different number of teeth, and pitch cone angles, including mesh with a spur gear (see Figure 21.26).

Similarly, face gearing can be composed of a helical involute pinion and of a face gear that has an appropriate geometry of tooth flanks, as shown in Figure 21.27.

In face gearing, the gear tooth flank,  $\mathcal{S}_{r.app}$ , and the pinion flank,  $\mathcal{P}_{r.app}$ , are not conjugate to one another, and both of them do not feature the angular base pitches. Therefore, the mandatory law of equal angular base pitches of a gear and that of a mating pinion to the operating angular base pitch of the gear pair is not fulfilled. This is mainly because of two reasons:

1. The tooth flanks of the face gear and of the mating pinion are generated by straight-sided racks: that is, a round rack for the side gear, and a straight rack for the mating pinion. Because of this, tooth flanks of the face gear and of the mating pinion make point contact. This limits the power capacity of face gear drives



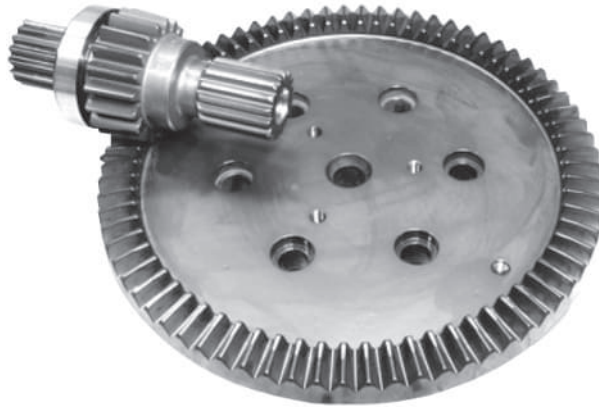


**FIGURE 21.25** Example of spur face gear pair.

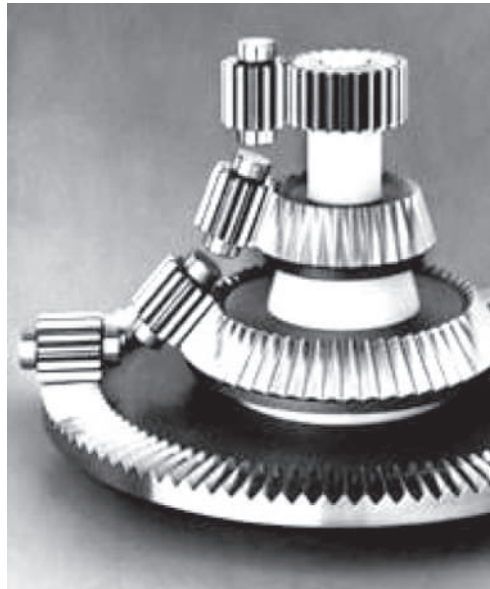


**FIGURE 21.26** Meshing of spur pinion with straight bevel gears of different pitch cone angles.

2. The tooth flanks of the face gear and the mating pinion are generated on the premise of the base surfaces, different from the surfaces in mesh of the face gear and the pinion.

Therefore, face gearing is not capable of transmitting an input uniform rotation smoothly without vibration and noise excitation. These disadvantages of face gearing become more severe when the tooth number of the face gear and the mating pinion is getting smaller.

### 21.3 APPROXIMATE REAL CROSSED-AXES GEARING

Crossed-axes gear pairs represent a group of approximate real crossed-axes gearing (see Chapter 17, Table 17.1). Manufacturing processes used in the production of gears for crossed-axes gear pairs are much the same, as those used in the production of gears for approximate real intersected-axes

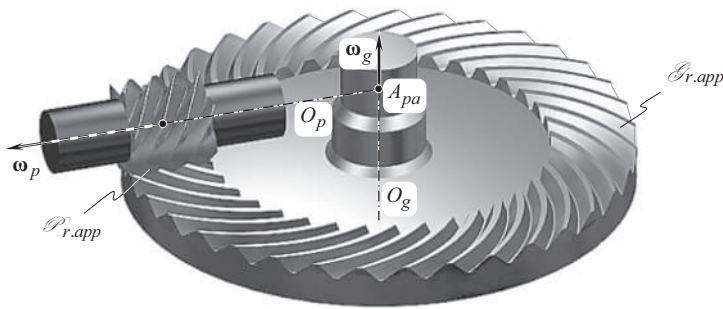


**FIGURE 21.27** Approximate real intersected-axes gearing composed of face gear and helical involute pinion.

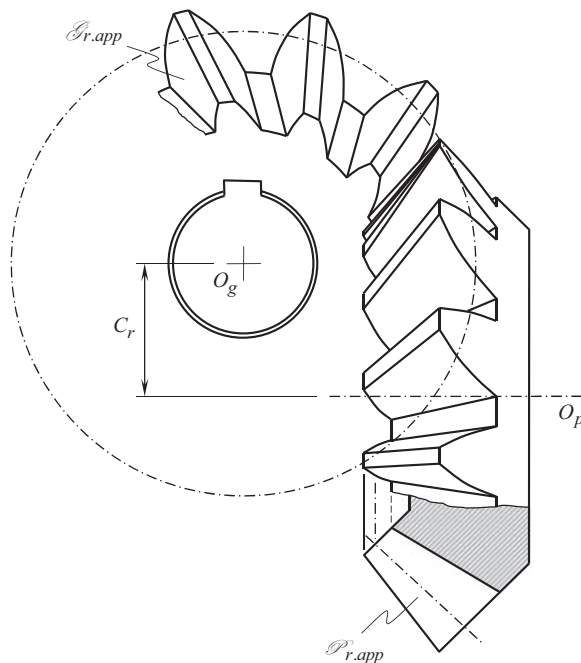


**FIGURE 21.28** Crossed-axes gear pair composed of skew tooth gear and pinion.

gearing. The tooth flanks of a gear and that of a mating pinion, are commonly generated with gear cutting tools that have a straight-sided generating rack.

The non-zero axis offset,  $C_r$ , is a principal design parameter of the gear pair that allows to differ crossed-axes gearing from intersected-axes gearing (see Figure 21.28).

Gears that have either skew teeth (as shown in Figure 21.28), or circular arc teeth (as shown in Figure 21.29), are used in the design of crossed-axes gear pairs. Commonly, the axes of rotation of a gear and of a mating pinion in crossed-axes gear pairs used in the present-day industry, cross at the right angle. Crossed-axes gears of this kind are referred to as the *orthogonal crossed-axes gearing*. In special applications, crossed-axes gears that have non-orthogonal axes of rotation, are also used (see Figure 21.30).

It is often loosely claimed that the concept of *octoid gearing* can be enhanced to crossed-axes gearing (similar to that shown in Figure 21.5), and a conical gear of a crossed-axes gear pair can be





**FIGURE 21.29** Crossed-axes gear pair composed of circular arc bevel gear and pinion.



**FIGURE 21.30** Non-orthogonal crossed-axes gear pair.

engaged in mesh with a corresponding *round rack*,  $\mathcal{R}$ . The round rack (of the crown gear, in other words) has an *octoid profile*<sup>6</sup> (see Figure 21.5). In geometrically accurate crossed-axes gearing (see Figure 21.31), the gear tooth profile is viewed as an involute curve constructed on a sphere of a corresponding diameter. The tooth profile always features point of inflection. Evidently, this is not an *octoid*. The tooth profile,  $ABC$ , of the right side of the tooth profile initially is given in a reference system  $X_r^{(r)}Y_r^{(r)}Z_r^{(r)}$ . Similarly, the tooth profile,  $AD$ , of the opposite side (the left side) is specified in a *Cartesian* coordinate system  $X_g^{(l)}Y_g^{(l)}Z_g^{(l)}$ . The coordinate systems  $X_r^{(r)}Y_r^{(r)}Z_r^{(r)}$  and  $X_r^{(l)}Y_r^{(l)}Z_r^{(l)}$  are turned in relation to one another about the  $Z_r$  – axis through the tooth thickness angle,  $\phi_t$ , of the generating rack,  $\mathcal{R}$ .

No crossed-axes gear pair with the so-called *octoid profile* is capable of transmitting a smooth rotation from a driving shaft to a driven shaft (at a uniform angular velocity of rotation of both the gear and the pinion).

Approximate real crossed-axes gear pairs composed of a face gear and a mating cylindrical pinion (either a spur pinion, as shown in Figure 21.32, or a helical pinion, as shown in Figure 21.33), are used in special applications.

<sup>6</sup> Physically, *octoid tooth profile* is not permissible in crossed-axes gearing, as it inevitably leads to violation of the conjugate action law.

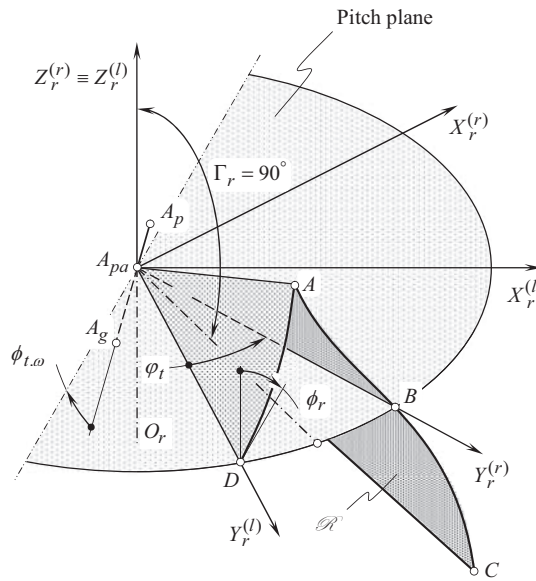


**FIGURE 21.31** Geometry of tooth flank of basic rack,  $\mathcal{R}$ , in geometrically accurate crossed-axes gear pair.



**FIGURE 21.32** Face gear pair that features offset axes of rotation of face gear and spur pinion.

Violation of the conjugate action law in the mesh of the tooth flanks,  $\mathcal{G}_{r.app}$  and  $\mathcal{P}_{r.app}$ , of a gear and that of a mating pinion, along with indefinite angular base pitches of the gear and that of the pinion, are the main reasons why real crossed-axes gearing of the discussed kind can be only approximate. Crossed-axes gears of this kind are not capable of transmitting an input uniform rotary motion smoothly from a driving shaft to a driven shaft.

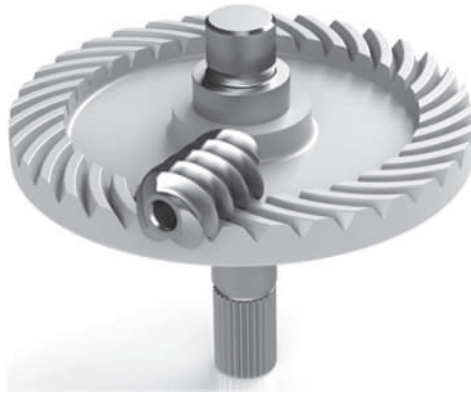


**FIGURE 21.33** Face gear pair that features offset axes of rotation of face gear and helical pinion.

## 21.4 WORM GEARING

Worm gearing represents a separate group of real crossed-axes gear pair (see Chapter 17, Table 17.1).

It makes sense to begin the discussion on worm gearing from consideration of the similarities between worm gearing, and crossed-axes gearing that is composed of helical involute gears.

Consider a crossed-axes gear pair that is composed of two helical involute gears (see Chapter 20, Figure 20.27), and a worm gearing that is composed of an involute gear and an involute worm shown in Figure 21.34. The number of teeth of the pinion is the only difference between these two types of gearing, which are shown in Figures 20.27 and 21.34, correspondingly. The worm gear can be either spur or helical. Worm gear pair features either a single start, or a multiple-start worm. However, the number of starts of the worm,  $N_w$ , is less than the tooth number of a pinion,  $N_p$ , in a crossed-axes gear pair that is composed of two helical involute gears ( $N_w < N_p$ ).

Both the power capacity of the worm-gear drive and the power density transmitted by the worm gear pair are limited by point contact between the interacting tooth flanks of a worm gear,  $\mathcal{S}_{r.app}$ , and the threads of the worm,  $\mathcal{P}_{r.app}$ .

In the worm gearing of the design under consideration, the conjugate action law in mesh of the tooth flanks of a worm gear,  $\mathcal{S}_{r.app}$ , and threads of the worm,  $\mathcal{P}_{r.app}$ , is fulfilled. It is also can be shown that at every instant of time the angular base pitch of the worm gear,  $\varphi_{b.g}$ , as well as

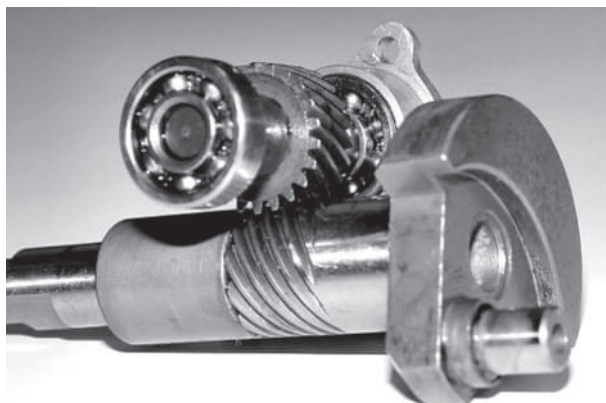


**FIGURE 21.34** Worm gear pair that is composed of involute helical gear and involute worm.

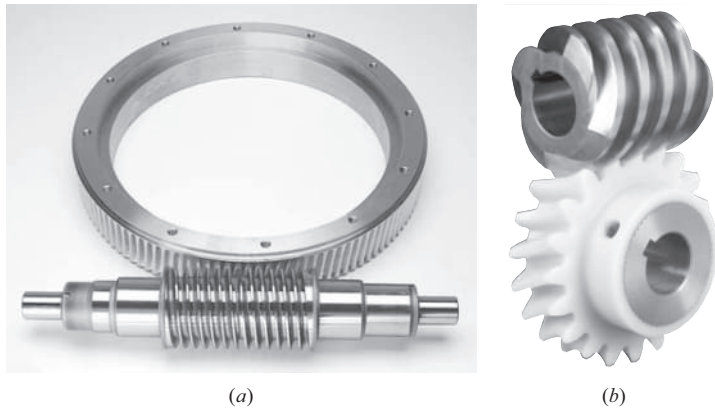


**FIGURE 21.35** Examples of worm gearing featuring cylindrical worm: (a) single-start worm and (b) four-starts worm.

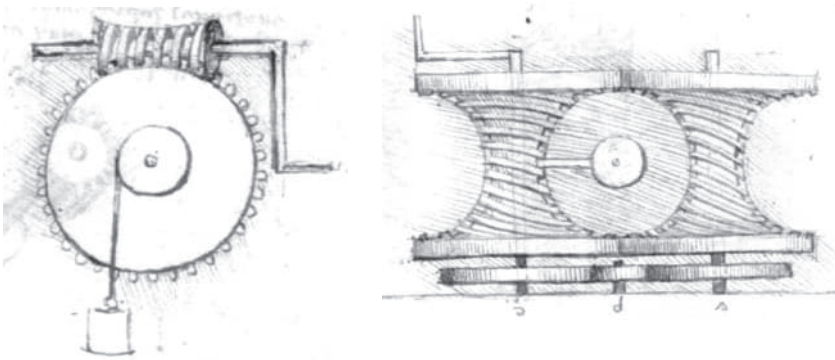


**FIGURE 21.36** Double-enveloping worm gearing from the 1493 book by Leonardo da Vinci, *The Madrid Codices*, Volume 1, Facsimile Edition of *Codex Madrid 1*, original Spanish title: *Tratado de Estatica y Mecanica en Italiano*, McGraw Hill Book Company, 1974.

the angular base pitch of the worm,  $\phi_{b,p}$ , are equal to operating base pitch,  $\phi_{b,op}$ , of the gear pair. Therefore, involute worm gearing is capable of transmitting a rotary motion smoothly.

Instead of involute worm, a worm of another design is often used in the present-day practice. An involute worm can be replaced either with an *Archimedean worm*, or a convolute worm, or a worm of other design. Such a replacement is required mainly due to manufacturing issues. Worms of designs that are easy in production, can be used to replace the desirable involute worm.

By targeting an increase of power density being transmitted through gearbox, worm gearing of single-enveloping type was developed. Worm gearing of this type features a cylindrical worm. The worm can be either a single-start worm, as illustrated in Figure 21.35a, or a multiple-start worm, for example, a four-start worm as shown in Figure 21.35b.

Designing double-enveloping worm gearing is the next step to be undertaken in order to improve the power density transmitted by the worm drive. Actually, this worm gearing has been known since the time of *da Vinci* (see Figure 21.36) [23], or even earlier. However, no discussion on worm thread geometry can be found in the book by *da Vinci* [23].

Significant improvements to the design of double-enveloping worm gearing have been done by *F.W. Lorenz*, and by *S.I. Cone*. The invention of the double-enveloping worm-gear drive (see Figure 21.37) is an interesting story centering on two individuals, *Lorenz* and *Cone*.

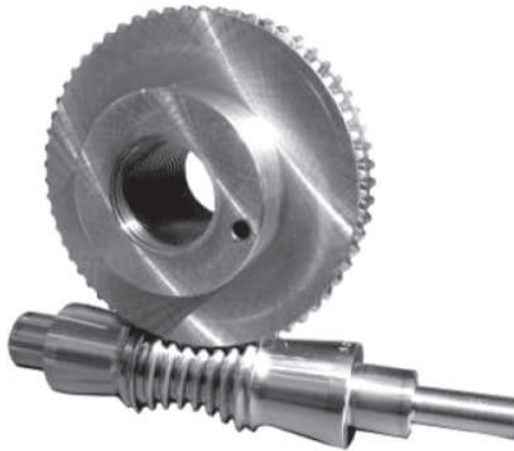


**FIGURE 21.37** Double-enveloping worm-gear drive.

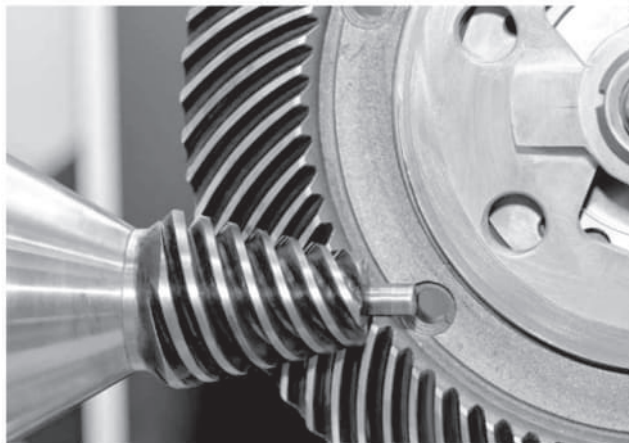


**FIGURE 21.38** *Spiroid Gearing* (1957) by *Oliver Saari* is an example of approximate gearing [111].

Invented by *Oliver Saari* (1954) *Spiroid Gearing* [108,111,113,152], is another example of improvements to the design of approximate worm gearing (see Figure 21.38). *Spiroid Gearing* is composed of a conical worm in mesh with a face gear. *Oliver Saari* is also credited with the invention of *Helicon Gearing* [113] – a novel kind of worm gearing that is composed of a cylindrical worm in mesh with a face gear.

Worm-gear drives of all known designs (except for the worm-gear drive composed of an involute gear and an involute worm) are *approximate* worm-gear drives. This is because the geometries of worm-gear teeth as well as the geometries of worm threads differ from the desirable geometries. Therefore, tooth flanks of a worm gear and threads of a mating worm do not conjugate with one another. Moreover, no angular base pitch can be specified in the design of a worm gear and of a worm. Therefore, the fundamental law of gearing all (with no exclusions) gear pairs have to comply with (namely,  $\phi_{b,g} = \phi_{b,op}$ , and  $\phi_{b,p} = \phi_{b,op}$ ) is not fulfilled. Because of this, real worm gearing can only be approximate. They are not capable of transmitting a smooth rotation from a driving shaft to a driven shaft. In order to eliminate the root cause of vibration generation and noise excitation, worm-gear tooth flanks, as well as mating worm threads should be developed from the base cones,





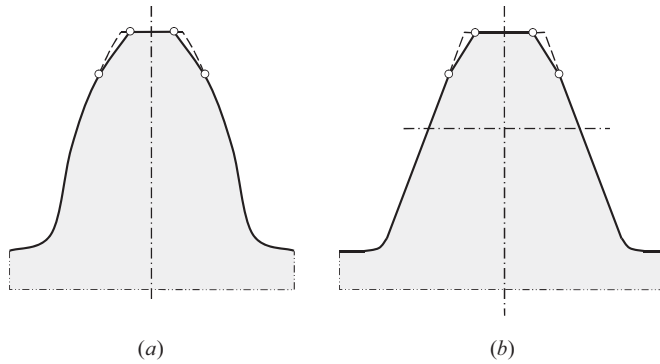


**FIGURE 21.40** Concept of tooth addendum modification: (a) modified tooth addendum of involute gear, and (b) that of basic rack.

### 21.5.1 BRIEF HISTORICAL OVERVIEW ON GEAR TOOTH FLANK MODIFICATION

The idea of gear tooth flank modification can be traced back to the first half of the twenty's century. *Walker, H.* [218] was among the first to point out the importance of tooth flank corrections for spur gears. Extensive research into the profile and longitudinal corrections on involute gear has been undertaken by *H. Sigg* [202] in 1965.

The concept of a gear tooth addendum modification is illustrated in Figure 21.40.

Initially, tooth flank modification targeted the accommodation for gear tooth deflection under operating load. Since the time of *H. Walker* [218], the key problem in gear tooth flank modification was how to get the precise deflections, including load tooth elastic deformations and shaft deflections, and how to get the load evenly distributed along the contact lines.

Eventually, the concept of spur gear tooth flank modification was applied to helical gears.

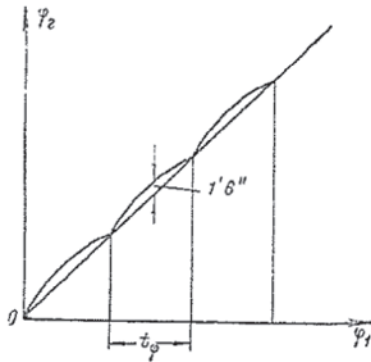
In addition to the modification of gear tooth addendum, modification of gear tooth dedendum, crown modification, and topological modification of gear tooth flanks were proposed.

Extensive research into the gear tooth flank modification was carried out by Dr. *N.I. Kolchin* of the USSR. The results of this research are discussed in his monograph [62]. The influence of the axes misalignment on the smoothness of the rotation of the driven shaft was investigated. Some of the results obtained by Dr. *N.I. Kolchin* are illustrated in Figure 21.41. Numerical examples provided by Dr. *N.I. Kolchin* reveal that transmission errors in the range of 1'6" (see Figure 21.41a) as well as deviations of the gear ratio in the range of 0.442% (see Figure 21.41b) are realistic values, which cannot be ignored when designing transmission gear drives for critical applications.

### 21.5.2 REQUIREMENTS TO DESIGN PARAMETERS OF MODIFIED PORTIONS OF TOOTH FLANKS

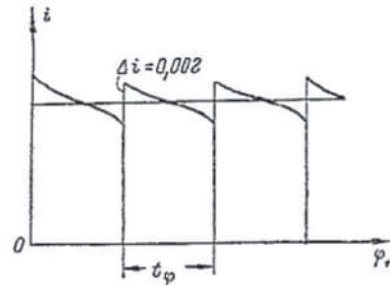
The design parameters of modified portions of tooth flanks of a gear and that of a mating pinion must be determined so, as to minimize the deviation of the real tooth flank from the geometrically accurate tooth flank. Geometrically accurate tooth flank of an involute gear (see Figure 21.42) is used as a datum surface when designing gears with a modified tooth flank geometry. Under any circumstances, the difference between the base pitches of modified portions of the interacting surfaces of a gear and of a mating pinion should be as small, as possible. In the best-case scenario, base pitch,  $\phi_{b,g}^m$ , of the modified portion of the gear tooth flank has to be equal to base pitch,  $\phi_{b,p}^m$ , of the modified portion of the mating pinion tooth flank.

The modification of tooth flanks of gears of all types should be considered as an approximation of the corresponding  $S_{pr}$  – gearing by the corresponding modified tooth flank. The smaller the deviations of the modified tooth flank from tooth flank of the corresponding  $S_{pr}$  – gearing, the better. Once the geometry of the tooth flank of an  $S_{pr}$  – gearing is determined, the design parameters of



Фиг. 119. График зависимости угла поворота ведомой шестерни в зависимости от угла поворота ведущей.

(a)



Фиг. 118. График изменения передаточного числа в зависимости от угла поворота ведущей шестерни.

(b)

**FIGURE 21.41** (a) Angle of rotation,  $\varphi_2$ , of driven shaft versus angle of rotation,  $\varphi_1$ , of driving shaft and (b) gear ratio,  $i$ , versus angle of rotation,  $\varphi_1$ , of driving shaft. {From Figure 119 on page 191, and Figure 118 on page 189 in N.I. Kolchin, 1949. *Analytical Calculation of Planar and Spatial Gearing*, Moscow, Mashgiz [62].}

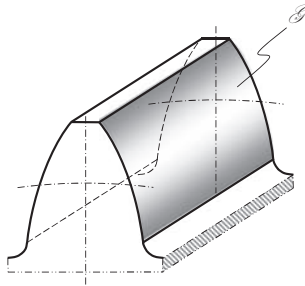


**FIGURE 21.42** Involute gear tooth flank,  $\mathcal{S}$ , as a datum surface.

any and all types of tooth flank modification can be derived targeting at a reasonable adjustment of an existing tooth flank geometry, which bridges it as close, as possible to the tooth flank geometry of the corresponding  $S_{pr}$  – gear. The geometry of tooth flanks in  $S_{pr}$  – gearing is the target at all possible tooth flank modifications.

Evidently, tooth flanks not of one member of the gear pair have to be modified. Instead, tooth flanks of both mating gears should be modified maintaining equality of the angular base pitches ( $\varphi_{b.g} = \varphi_{b.op}$ , and  $\varphi_{b.p} = \varphi_{b.op}$ ). This requirement is a must for proper designing of a gear pair.

The best-known method so far for tooth flanks modification (Maki, 1998) [120] took into account variations of torque being transmitting by a gear drive. However, even in this case the proposed method of tooth flank modification should be considered as a kind of approximation to the tooth flank of corresponding  $S_{pr}$  – gearing by smooth regular tooth flanks, the design parameters of which can be expressed in terms of the applied load.

The following conclusion can be drawn up based on the discussion in this section of the book:

Almost all kinds of gears those manufactured in the present-day industry, are a kind of approximate real gearing. In the meantime, no geometrically accurate intersected-axes as well as geometrically accurate crossed-axes gears are commonly used. The conjugate action law is not fulfilled when the gears are designed, manufactured, and used in the industry. Moreover, intersected-axes and crossed-axes approximate real gears do not feature such an important design parameter as the



*angular base pitch.* Because of this, the required condition of equality of angular base pitches of a gear and that of a mating pinion, both to the operating angular base pitch of the gear pair can not be fulfilled in intersected-axes and crossed-axes approximate real gears of conventional design. In certain cases (e.g., straight bevel gears cut by disk-type mill cutters) even condition of contact ( $\mathbf{n}_g \cdot \mathbf{v}_\Sigma = 0$ ) between the tooth flanks,  $\mathcal{S}_{r.app}$  and  $\mathcal{P}_{r.app}$ , is also violated.

Lack of knowledge in the kinematics and the geometry of geometrically accurate intersected-axes, and crossed-axes gearing is the root cause for insufficient accuracy of gears of these particular types.

### 21.5.3 KINDS OF TOOTH FLANK MODIFICATIONS

Tooth flank modifications are desirable alterations to the tooth flank face compared with the desirable geometry shown in Figure 21.42. Superimposing the nominal modifications on the main geometry produces the nominal tooth flank. The modifications can be defined in characteristic profiles of the tooth flank or in relation to the flank face. Modification depths are always given in the transverse section and normal to the involute of the main geometry.

#### 21.5.3.1 Tooth Flank Modifications Which Restrict the Usable Flank

Modification of tooth flank geometry is extensively used in the present-day industry to improve the performance first of all of parallel-axes gear pairs. Numerous kinds of tooth flank geometry are developed to this end. *Trial-and-error method* is the main tool when doing such an analysis.

*Pre-finish flank undercut:* Pre-finish (root) relief is an intentionally generated, undercut (that is, using a protuberance tool) of the transverse profile of a tooth flank in the area of the root. The magnitude of the relief,  $q_{Fs}$ , is the greatest distance between the root rounding and the involute imagined as extended to the base circle (see Figure 21.43a). Below this, the datum is a line from the involute origin to the gear center.

*Tip corner chamfering, tip corner rounding:* Tip corner chamfering and tip corner rounding are reliefs of the transverse profile which restrict the usable area of the tooth flank. Tip corner chamfering is the chamfer arising through the removal of the tip corner. In the case of tip corner rounding, this corner is radiused in the normal plane. The radial height,  $h_k$ , and the residual tooth thickness at the tip,  $s_{ak}$ , are given as the dimensions of this modification (see Figure 21.43a), and are different for chamfering and rounding.

#### 21.5.3.2 Transverse Profile Modifications

In the following,  $L_{AE}$  is used<sup>7</sup> to define the roll length for compatibility with ISO 1328-1. The length,  $L_{AE}$ , is an equivalent to length of path of contact,  $g_a$ .

*Tip and root relief:* Tip and root reliefs (see Figure 21.43b) are the continuously increasing reliefs of the transverse profile of the main geometry from defined points in each case (diameter, length of roll, roll angle) in the direction of the tip or root (mostly involute).

*Transverse profile slope modification,  $C_{H\alpha}$ :* This is similar defined as or tip or root relief, except that  $C_{H\alpha}$  extends over the whole width of the face (see Figure 21.43c).

*Profile crowning (barreling),  $C_\alpha$ :* Profile crowning is the continuously increasing relief of the transverse profile from a common defined point of the main geometry (diameter, length of roll, roll angle) in the direction of the tip and root of the gear teeth (see Figure 21.43d).

Profile crowning is generally defined with respect to the center of the length of roll of the usable flank and has a parabolic form passing through the points defined by  $C_\alpha$ .

<sup>7</sup> DIN ISO 21771:2014-08, Gears – Cylindrical Involute Gears and Gear Pairs: Concepts and Geometry (ISO 21771:2007), English translation of DIN ISO 21771:2014-08.

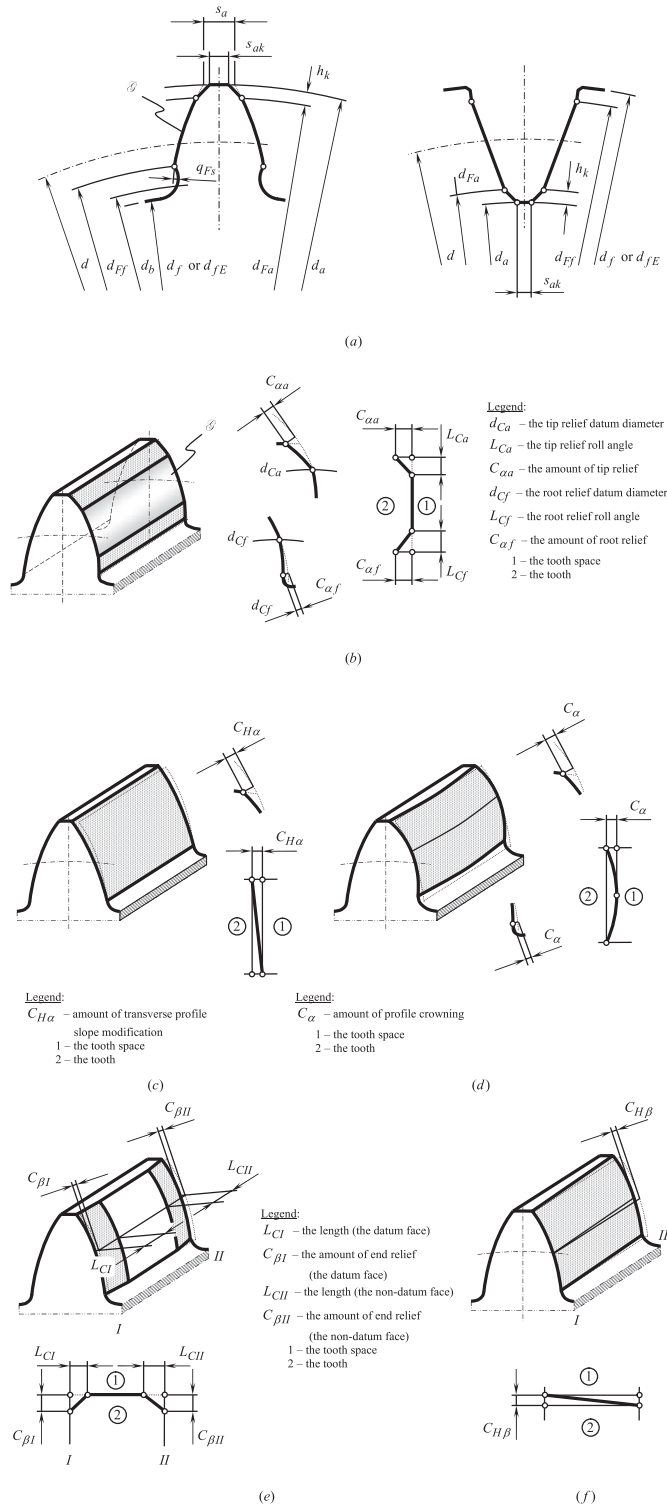


**FIGURE 21.43** Kinds of tooth flank modification of involute gear for parallel-axes gearing: (a) spur cylindrical gear with undercut and tip chamfering, (b) tip and root relief, (c) transverse profile slope modification, (d) profile crowning, (e) flank line end relief, and (f) flank line slope modification.

### 21.5.3.3 Flank Line (Helix) Modifications

Modification of flank line of a gear teeth gives the gear designer an additional opportunity to improve the performance of a gear pair.

*Flank line end relief:* Flank line end reliefs (see Figure 21.43e) are continuously increasing reliefs of the flanks line from defined points of the mail geometry in each case in the direction of the datum faces (linear or parabolic).

*Flank line (helix) slope modification,  $C_{H\beta}$ :* This is similarly defined as for end relief, but  $L_{CI}$  or  $L_{CH}$  extends across the whole face width (see Figure 21.43f). It is not necessarily linear.

*Flank line (helix) crowning,  $C_\beta$ :* Flank line crowning (see Figure 21.43a) is the continuously increasing relief of the flank line from a common defined point of the main geometry, symmetrically in the direction of both ends of the tooth (arc-shaped or parabolic).

### 21.5.3.4 Flank Face Modifications

More complex alterations to the gear tooth flank geometry are also used in practice. Examples can be readily found in the production of gears for low noise gear pairs.

*Topographical modifications:* The desirable deviation from the unmodified involute helicoid (see Figure 21.44b) is determined in relation to each point of intersection on a grid laid over the tooth flank of the main geometry.

*Triangular end relief:* Triangular end reliefs are continuously increased reliefs of the tooth flanks generally perpendicular to the generators of the main geometry (along the lines of contact) from a defined roll angle in the direction of the start or end of roll on the tooth flanks. See Figure 21.44c for details.

*Flank twist:* Twist is an effect on a flank described as a rotation of the transverse profile along a helix. There is a distinction between the twist of the transverse profile,  $S_\alpha$ , and of the flank line,  $S_\beta$ . If not otherwise defined, it changes linearly to form the beginning to the end of the usable flank. The sign of the flank twist is very important. Right-handed twist is commonly considered as a positive twist. Accordingly, left-handed twist is commonly considered as a positive twist (see Figure 21.44d for details).

When designing gears with modified tooth flanks, an advantage can be taken from implementation for this purpose of the concept, which  $S_{pr}$  – gearing is based on.

## 21.5.4 DESCRIPTION OF MODIFICATIONS BY FUNCTIONS

Modifications of the profile can be given as functions of the diameter,  $d_{Ca}$  (or  $d_{Cf}$ ), or the corresponding roll distances or angles, and modifications of the flanks lines as functions of the axial distance from the start of the usable face width in the direction of the non-datum face. The combination of both functional relationships describes the modification of the whole flank surface.

Graphically, it is usual to show tooth surface modifications as deviations from the exact involute helicoid with respect to roll length for radial deviations (as in Figure 21.43b) and position across the tooth width for axial deviations (as in Figure 21.43e).

The interested reader may wish to go to [59] for more details on gear tooth flank modification.

## 21.5.5 ON THE MOST FAVORABLE MODIFICATION OF GEAR TOOTH FLANKS

Modification of gear tooth flank results in that that modified gear inevitably becomes approximate gear – even originally geometrically accurate gear after a modification of its tooth flanks is accomplished, becomes approximate gear. So, what is the necessity to modify gear tooth flanks? The answer to this question is simple: despite tooth flanks modification, *properly modified gears*

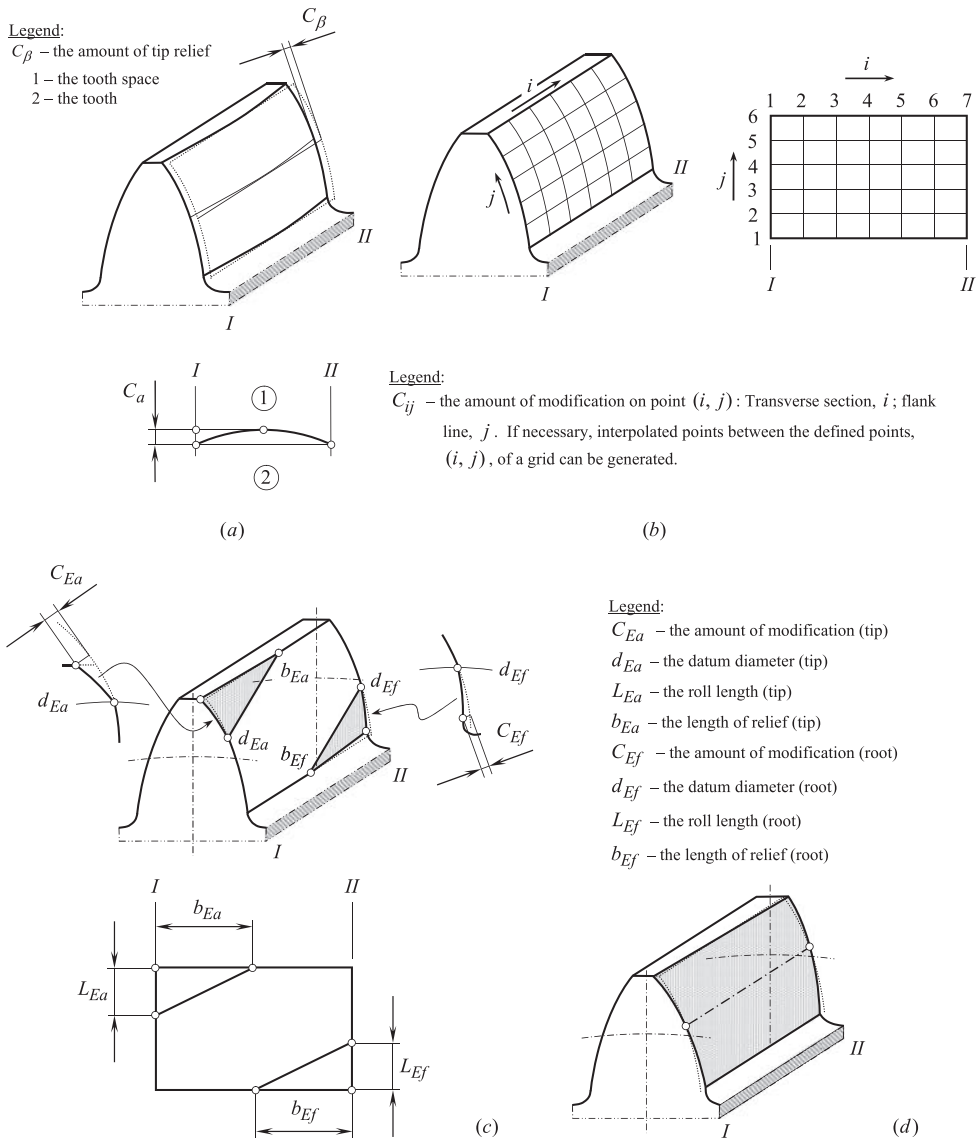


**FIGURE 21.44** Involute gear tooth flank modifications: (a) flank line crowning, (b) topographical/topological modification, (c) triangular end relief, and (d) flank twist.

(a) are less sensitive to the axes misalignment under operating load, and (b) are easier in production compare to geometrically accurate gears, which are insensitive to the axis's misalignment due to features of their tooth flank geometry.

A plurality of kinds of gear tooth flank modification is known (up to 30 kinds in total, or so) in the present-day gear design practice. Which one of them is recommended to use for a particular application? (No reliable recommendation can be given in this regard so far!!). What to do in cases when the applied load alters in time, and, therefore, the design parameters of the modified tooth flank geometry have to accommodate to this variation?

The present-day situation with gear tooth flank modification resembles the situation with the so-called *perpetual motion machine*, which the humanity was facing with a few centuries ago.

Hundreds of claims have been made in the past (just a few centuries ago) stating that:

- a. *perpetual motion machine* is invented
- b. *perpetual motion machine* is designed
- c. *perpetual motion machine* is manufactured
- d. *perpetual motion machine* is tested; and, finally, that
- e. *perpetual motion machine* is already ready to be used in the industry

Where we are now? Do we have any example of the application of *perpetual motion machine*? No, we still haven't!! Do we have a chance to get the problem of *perpetual motion machine* solved in the future? No, we have no such a chance. Ultimately, is there a reason for continuing wasting efforts and funds trying to solve an engineering problem that has NO solution at all due to the natural constraints? Per the author's opinion, there is no such a reason. However certain enthusiastic gear guys are free to continue exercising this particular problem.

Let's go back to the problem of gear tooth flank modification: there is no chance to get the problem solved using this purpose *trial-and-error* method, as this approach is endless, and can be affordable only to those who have an access to an infinite resource of funds, and no time limitations. Three fundamental laws of gearing are ignored when known methods of tooth flank modification are used in the present-day practice.

In order to get the problem under consideration solved, it is reasonable to take into account the principal features of geometry of tooth flanks in  $S_{pr}$  – gearing, namely of a gearing that is (a) geometrically accurate, and (b) is insensitive to the misalignment of gear axes under operating load, due to manufacturing errors, heat extension, and so forth. All three fundamental laws of gearing are fulfilled in  $S_{pr}$  – gearing.

The proposed concept of gear tooth flank modification is outlined immediately below:

1. For a specified application, an  $S_{pr}$  – gear pair is designed
2. The designed gear tooth flank is approximated by a surface patch of geometry that is easy to be machined (when  $S_{pr}$  – gears are approximated, the approximate equality of the angular base pitches is retained. This is the rule for the gear designer to follow with)
3. The determined geometry of the approximated tooth flank is further used as the modified tooth flank of the gear and the mating pinion

Gearing with the aforementioned modification of tooth flanks features the angular base pitches ( $\varphi_{b,g}$ ,  $\varphi_{b,p}$ , and  $\varphi_{b,op}$ ) of almost equal values ( $\varphi_{b,g} \cong \varphi_{b,op}$  and  $\varphi_{b,p} \cong \varphi_{b,op}$ ). Gears modified this way can be correctly engineered, which is important. In the meantime, the use of gears with tooth flank modification (based on approximation of  $S_{pr}$  – gear tooth flanks) is the only way to get solved the problem of the most favorable modification of gear tooth flanks.

The total number of surface patch geometries that are easy in machining is limited. Therefore, the total number of possible tooth flank modifications is also limited (and is too far from to be endless).

It is common in real gearing that driving convex tooth flank interacts with convex driven tooth flank. Point contact of between the tooth flanks,  $\mathcal{S}$  and  $\mathcal{P}$ , is a kind of *conformal contact* (that is, the contact is conformal in the lengthwise direction of the gear tooth). Regardless of the actual kind of gearing ( $P_a$  – gearing,  $I_a$  – gearing, or  $C_a$  – gearing), gear pairs that feature *conformal contact* can be evolved to *high-conformal contact* between the tooth flanks,  $\mathcal{S}$  and  $\mathcal{P}$ . For this purpose, a gear tooth flank,  $\mathcal{S}$ , and a mating pinion tooth flank,  $\mathcal{P}$ , can be generated by two different planar curves,  $lc_g$  and  $lc_p$ , correspondingly. Both the planar curves,  $lc_g$  and  $lc_p$ , are entirely located within the plane of action,  $PA$ , and are in tangency to one another at contact point,  $K$ . The curves,  $lc_g$  and  $lc_p$ , are rigidly associated with the plane of action,  $PA$ . Curvatures of the curves,  $lc_g$  and  $lc_p$ , at the contact point,  $K$ , are determined so, as to accommodate for the linear and angular displacements of the gear axes of rotation, and to minimize the contact stress at  $K$  (minimal deviations of the curves,  $lc_g$  and  $lc_p$ , from the  $LC_{des}$  in the corresponding  $R$  – gearing). Gearing of this kind features point contact of the tooth flanks,  $\mathcal{S}$  and  $\mathcal{P}$ , and due to that is less sensitive to the axis misalignment.

---

# 22 Local Geometry of Interacting Gear Tooth Flanks

Interacting tooth flanks of a gear and that of a mating pinion are of complex geometry. Investigation of local geometry of mating gear tooth flanks is a challenging problem. An advantage can be taken from the fact that by nature only small local patches interact with one another – these patches are located in the local vicinity of contact point of tooth flanks. Due to this, there is no need to involve in the analysis of the entire interacting tooth flanks. It is sufficient to consider only corresponding local patches in the differential vicinity of the contact point of the interacting tooth flanks. The local surface patches are of much simpler geometry. Moreover, local surface approximation by surfaces of the second order is permissible for this purpose.

Local geometry of interacting gear tooth flanks is considered below in the following order (according to gear types):

1. Local geometry of interacting gear tooth flanks in parallel-axes gearing
2. Local geometry of interacting gear tooth flanks in intersected-axes gearing
3. Local geometry of interacting gear tooth flanks in crossed-axes gearing

## 22.1 LOCAL GEOMETRY OF INTERACTING TOOTH FLANKS IN PARALLEL-AXES GEARING

The below discussion on the interaction of tooth flanks in parallel-axes gearing begins with the external mesh of a gear and its mating pinion. Then, the obtained results of the analysis are enhanced to the case of the internal mesh of a gear and its mating pinion.

### 22.1.1 KINEMATICS OF INTERACTION OF GEAR TOOTH FLANKS

The interaction of tooth flanks of a gear and a mating pinion in parallel-axes gearing is diagrammatically illustrated in Figure 22.1. The plane of action,  $PA$ , is tangent to base cylinders of the gear and the mating pinion. The base cylinder of the gear is of a diameter  $d_{b,g}$ , and the base cylinder of the pinion is of a diameter,  $d_{b,p}$ .

The rotation vector of the gear,  $\omega_g$ , and that of the mating pinion,  $\omega_p$ , are pointed oppositely to one another. The magnitudes,  $\omega_g$  and  $\omega_p$ , of the rotation vectors,  $\omega_g$  and  $\omega_p$ , are in inverse proportion to the diameters of the base cylinders. The rotation vectors,  $\omega_g$  and  $\omega_p$ , are at a certain center distance,  $C$ , apart from one another.

A straight line of contact,  $LC$ , of the gear and the mating pinion teeth is entirely located within the plane of action. The line of contact forms a base helix angle,  $\psi_b$ , with the axis of rotation of the gear,  $O_g$ , and that same helix angle,  $\psi_b$ , with the axis of rotation,  $O_p$ , of the pinion (because of lack of space, the base helix angle,  $\psi_b$ , is not shown in Figure 22.1). In spur gearing, the base helix angle equals to zero ( $\psi_b = 0^\circ$ ).

The plane of action,  $PA$ , can be construed as a zero-thickness film. When the gears rotate, the film unwraps from the driving pinion base cylinder of a diameter,  $d_{b,p}$ , and it wraps onto the driven gear base cylinder of a diameter,  $d_{b,g}$ . In the case of gear increasers, the film unwraps from the

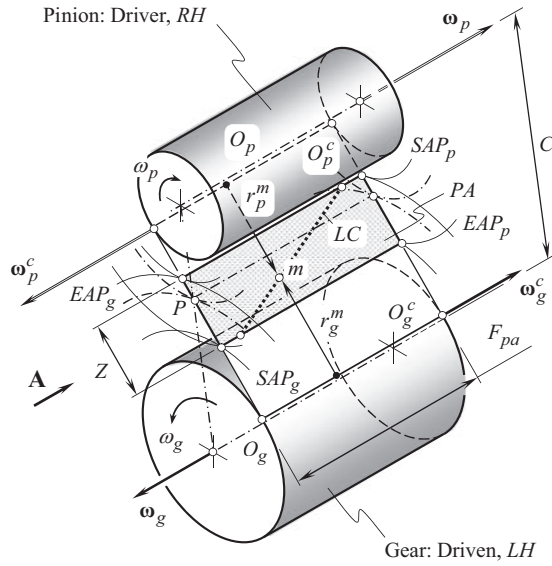


**FIGURE 22.1** Determination of the parameters of desirable local geometry of interacting gear,  $\mathcal{S}$ , and mating pinion,  $\mathcal{P}$ , tooth flanks of in parallel-axes gearing.

driving gear base cylinder of a diameter,  $d_{b,g}$ , and it wraps onto the driven pinion base cylinder of a diameter,  $d_{b,p}$ .

The line of contact,  $LC$ , travels together with the plane of action,  $PA$ , in relation to the reference systems associated with the gear, and with the pinion. Arbitrary point,  $m$ , within the line of contact,  $LC$ , traces an involute profile of the gear tooth in a reference system associated with the gear. Point,  $m$ , also traces another involute profile of the pinion tooth in a reference system associated with the pinion.

The motion of the line of contact,  $LC$ , in relation to the base cylinders can be construed as an instant rotation about a straight line of tangency between the base cylinder and the plane of action,  $PA$ . In Figure 22.1, the axis of the instant rotation of the line of contact,  $LC$ , in relation to the gear is designated as  $O_g^c$ . The vector of instant rotation is designated as  $\omega_g^c$ . Similarly, the axis of instant rotation of the line of contact,  $LC$ , in relation to the pinion is designated as  $O_p^c$ . The vector of the instant rotation is designated as  $\omega_p^c$ .

Ultimately, the instantaneous kinematics of parallel-axes gearing is specified in terms of two rotations,  $\omega_g^c$  and  $\omega_p^c$ , of the line of contact,  $LC$ , about the axes of instantaneous rotations,  $O_g^c$  and  $O_p^c$ .

### 22.1.2 LOCAL GEOMETRY OF INTERACTING TOOTH FLANKS

The local geometry of interacting tooth flanks of a gear and its mating pinion are explained in Figure 22.1. At every instant of time, the gear tooth flank,  $\mathcal{S}$ , is generated by the line of contact,  $LC$ , in its rotation,  $\omega_g^c$ , about the axis of instantaneous rotation,  $O_g^c$ . Similarly, the pinion tooth flank,  $\mathcal{P}$ , is generated by that same line of contact,  $LC$ , in its rotation,  $\omega_p^c$ , about the axis of instantaneous rotation,  $O_p^c$ .

Two surfaces that are generated by the line of contact in its rotations about the instantaneous axes of rotation,  $O_g^c$  and  $O_p^c$ , can be used as the surfaces, which model the actual tooth flanks of the gear and the pinion.

As an example, consider the line of contact,  $LC$ , in the form of a straight-line segment that forms the base helix angle,  $\psi_b$ , with the axes,  $O_g^c$  and  $O_p^c$ , of instant rotations,  $\omega_g^c$  and  $\omega_p^c$ .



In parallel-axes gearing, the axes,  $O_g^c$  and  $O_p^c$ , of instant rotations ( $\omega_g^c$  and  $\omega_p^c$ ) are parallel to one another. In the instant rotation,  $\omega_g^c$ , a cone of revolution is generated by the line of contact,  $LC$ . The axis of the cone of revolution is aligned with the axis of instantaneous rotation,  $O_g^c$ , as shown in Figure 22.2. The cone angle of the cone of revolution is equal to  $2\psi_b$ .

Similarly, in the instantaneous rotation,  $\omega_p^c$ , a cone of revolution is generated by the line of contact,  $LC$ . The axis of the cone of revolution is aligned with the axis,  $O_p^c$ , of instantaneous rotation. The line of contact,  $LC$ , is the line of tangency of the cones (see Figure 22.2). The cone angle of the cone of revolution also equals to,  $2\psi_b$ .

The modeling cone of the gear, and that of the mating pinion, are tangent to each other. The line of tangency of the modeling cones of revolution is aligned with the line of contact,  $LC$ , in the gear pair (see Figure 22.2).

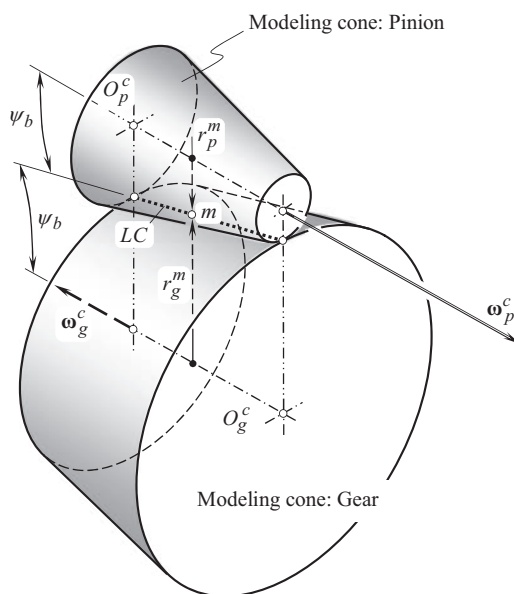
In spur gears, the line of contact,  $LC$ , is parallel to the axes of rotation of the gear,  $O_g$ , and the pinion,  $O_p$ . In this particular case, the modeling cones of revolution reduce to corresponding modeling cylinders of revolution.

If either a circular arc, an arc of a cycloid, or an arc of an arbitrary planar curve is used to generate a gear and a mating pinion tooth flanks,  $\mathcal{G}$  and  $\mathcal{P}$ , as illustrated in Figure 22.3, then, locally, in the differential vicinity of point of interest,  $m$ , the line of contact,  $LC$ , can be represented by a straight line segment,  $ab$ , that is tangent to the line of contact,  $LC$ , at  $m$ . Therefore, in the case under consideration, the gear and the pinion tooth flanks can be *locally* represented by the surfaces of the corresponding truncated cones.

The schematic depicted in Figure 22.1 is convenient for the investigation of gear drives composed of spur and helical gears as well as of gears that have either a circular-arc or cycloidal longitudinal tooth shape. It is also applicable for the analysis of parallel-axes gearing with the gear teeth of other geometries in the lengthwise direction.

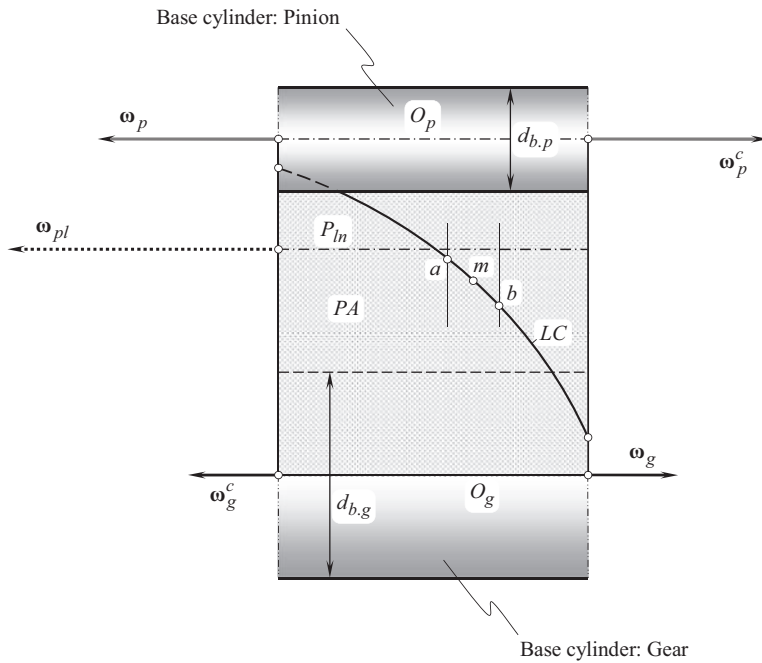
View A of Figure 22.1 is convenient for the analysis of the design features of parallel-axes gear drives.

Figure 22.4 gives a clear understanding of:



**FIGURE 22.2** Modeling cones of gear tooth flank,  $\mathcal{G}$ , and mating pinion tooth flank,  $\mathcal{P}$ , in external parallel-axes gearing.





**FIGURE 22.3** Determination of the parameters of desirable local geometry of interacting tooth flanks of gear,  $\mathcal{S}$ , and of pinion,  $\mathcal{P}$ , generated by curved line of contact,  $LC$ .

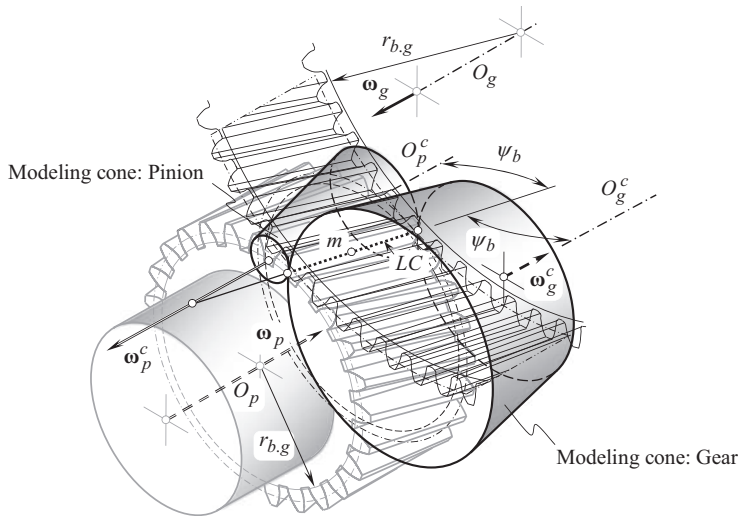


**FIGURE 22.4** Configuration of modeling cones in relation to a gear and a mating pinion in helical parallel-axes gearing.

1. How the modeling cones are configured in relation to the interacting tooth flanks,  $\mathcal{S}$  and  $\mathcal{P}$ , of a gear and a mating pinion;
2. How the axes,  $O_g^c$  and  $O_p^c$ , of instant rotations are configured in relation to the axes of rotation,  $O_g$  and  $O_p$ , of the gear and the pinion; and
3. How the vectors of instant rotations,  $\omega_g^c$  and  $\omega_p^c$ , are configured in relation to the rotation vectors,  $\omega_g$  and  $\omega_p$ , of the gear and the pinion rotations [166].

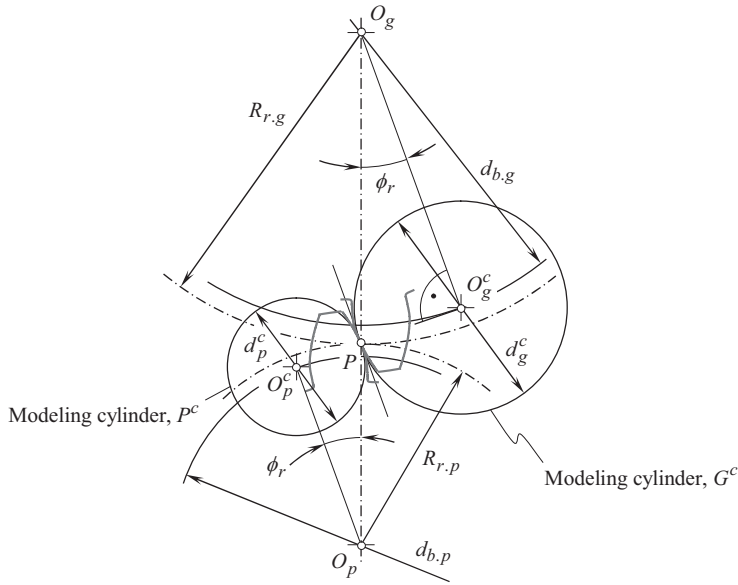


**FIGURE 22.5** Configuration of modeling cylinders,  $G^c$  and  $P^c$ , in relation to interacting tooth flanks,  $\mathcal{S}$  and  $\mathcal{P}$ , in spur gear and mating pinion.

In a particular case of spur gears, configuration of the modeling cylinders,  $G^c$  and  $P^c$ , in relation to a gear tooth flank,  $\mathcal{S}$ , and a mating pinion tooth flank,  $\mathcal{P}$ , is diagrammatically shown in Figure 22.5.

In internal helical involute gearing, the modeling cone of the ring gear,  $G^c$ , is shaped in the form of an internal truncated cone of revolution, as shown in Figure 22.6.

It should be pointed out here on how the radii of curvature of the modeling cones,  $G^c$  and  $P^c$ , in internal gearing differ from those in external gearing. Modeling cones make clear that when a point travels along the line of contact from left to right, radii of curvature of both modeling cones get

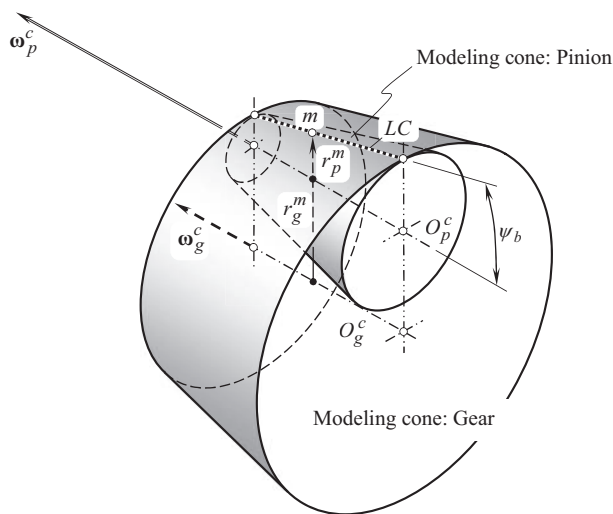


**FIGURE 22.6** Modeling cones,  $G^c$  and  $P^c$ , of gear tooth flank and mating pinion tooth flank in internal helical parallel-axes gearing.

larger (Figure 22.6). Thus, in this scenario, the relative curvature of the modeling cones in internal gearing alters slightly within the line of contact. In external gearing (see Figure 22.2), in contrast, when a point travels along the line of contact from left to right, radius of curvature of the modeling cone in the gear gets larger, while that for the pinion gets smaller. This results in an extensive change of relative curvature of the modeling cones in external gearing within active portion of the line of contact,  $LC$ .

The aforementioned can be summarized in the form of two significant advantages of internal parallel-axes gearing over external parallel-axes gearing:

1. Contact of a convex tooth flank of a pinion with a concave tooth flank of a mating gear in internal gearing is more favorable compared to contact of two convex tooth flanks of a gear and a mating pinion in external gearing
2. Alteration of relative curvature within the active portion of the line of contact in internal parallel-axes gear pair is more favorable compared to that in external parallel-axes gearing

Arbitrary point,  $m$ , within the line of contact,  $LC$ , is at a certain distance,  $r_g^m$ , from the axis of instant rotation about the gear, and it is at a distance,  $r_p^m$ , from the axis of instant rotation about the pinion. Both the axes,  $O_g^c$  and  $O_p^c$ , of instant rotations,  $\omega_g^c$  and  $\omega_p^c$ , naturally, are the lines of tangency between the plane of action,  $PA$ , and the base cylinders of the gear and the pinion.

The distances,  $r_g^m$  and  $r_p^m$ , can be expressed in terms of the base diameters,  $d_{b.g}$  and  $d_{b.p}$ , of the gear and the pinion, and in terms of the distances,  $r_{m.g}$  and  $r_{m.p}$ , of arbitrary point,  $m$ , from the axis of rotation of the gear,  $O_g$ , and from the axis of rotation of the pinion,  $O_p$ , correspondingly. For the calculation, the following formulae are used:

$$r_g^m = \sqrt{0.25 d_{m.g}^2 - r_{b.g}^2} \quad (22.1)$$

$$r_p^m = \sqrt{0.25 d_{m.p}^2 - r_{b.p}^2} \quad (22.2)$$

Calculated from Eqs. (22.1) to (22.2)], the actual values of the radii,  $r_g^m$  and  $r_p^m$ , are used further to calculate the normal radii of curvature of the modeling cones. *Mensnier formula* is used for this purpose. The normal radii of curvature, in nature, are the first principal radii of curvature at point of the tooth flanks (the second principal radii of curvature are of a zero value). A distance,  $C^c$ , between the axes of rotation of the modeling cones,  $O_g^c$  and  $O_p^c$ , equals to:

$$C^c = C \sin \phi_t \quad (22.3)$$

The height,  $h^c$ , of the both truncated cones can be calculated from the equation:

$$h^c = L_{lc} \cos \psi_b \quad (22.4)$$

where  $L_{lc}$  is the length of the line of contact,  $LC$ .

Modeling cones in low-tooth-count gears are represented with a full cone of revolution, and not with a truncated cone. The apex of the cone of revolution is within the surface of the base cylinder of the gear.

## 22.2 LOCAL GEOMETRY OF INTERACTING TOOTH FLANKS IN INTERSECTED-AXES GEARING

External intersected-axes gearing is chosen for the analysis of the interaction of tooth flanks in intersected-axes gearing. Then, the results of the analysis obtained for external gearing can be enhanced to intersected-axes gearing of other designs as well.

### 22.2.1 KINEMATICS OF INTERACTION OF TOOTH FLANKS

The interaction of tooth flanks in intersected-axes gearing is schematically illustrated in Figure 22.7. The gear rotates about its axis of rotation,  $O_g$ , at a uniform angular velocity,  $\omega_g$ . The rotation vector of the gear is designated as  $\omega_g$ . The mating pinion rotates about its axis of rotation,  $O_p$ , at a uniform angular velocity,  $\omega_p$ . The rotation vector of the pinion is designated as  $\omega_p$ . The vector of instantaneous rotation,  $\omega_{pl}$ , of the gear and the pinion is located within the plane through the rotation vectors,  $\omega_g$  and  $\omega_p$ . The rotation vector,  $\omega_{pl}$ , passes through the point of intersection,  $A_{pa}$ , of straight lines along the rotation vectors,  $\omega_g$  and  $\omega_p$ . The axis of instantaneous rotation,  $P_{ln}$ , is aligned with the vector,  $\omega_{pl}$ .

The plane of action,  $PA$ , is a plane through the vector of instantaneous rotation,  $\omega_{pl}$ , of the pinion in relation to the gear. It forms an angle in relation to the plane through the rotation vectors,  $\omega_g$  and  $\omega_p$ . This angle equals to  $(90^\circ - \phi_{\omega,t})$ , where  $\phi_{\omega,t}$  denotes the transverse pressure angle measured within a plane that is perpendicular to the axis of instantaneous rotation,  $P_{ln}$ . The plane of action,  $PA$ , is in tangency to base cones of the gear and the pinion. The base cone of the gear is designated as  $\Gamma_b$ , and that of the pinion is designated as  $\gamma_b$ .

When the gear pair operates, the plane of action rotates about the axis perpendicular to the plane of action,  $PA$ . The rotation vector of the plane of action is designated as  $\omega_{pa}$ .

The magnitudes of the rotation vectors,  $\omega_g$ ,  $\omega_p$ , and  $\omega_{pa}$ , are synchronized with one another:

$$u_{p/pa} = \sin \gamma \quad (22.5)$$

$$u_{pa/g} = \frac{1}{\sin \Gamma} \quad (22.6)$$

$$\mu_{pu/g} = \frac{\sin \gamma}{\sin \Gamma} \quad (22.7)$$

The plane of action,  $PA$ , can be viewed as a portion of a round strip of zero thickness film. This strip is absolutely flexible in a single direction, and when the gear pair operates, the round strip of zero thickness film is free to unwrapped from one of the base cones (from the base cone of the driving

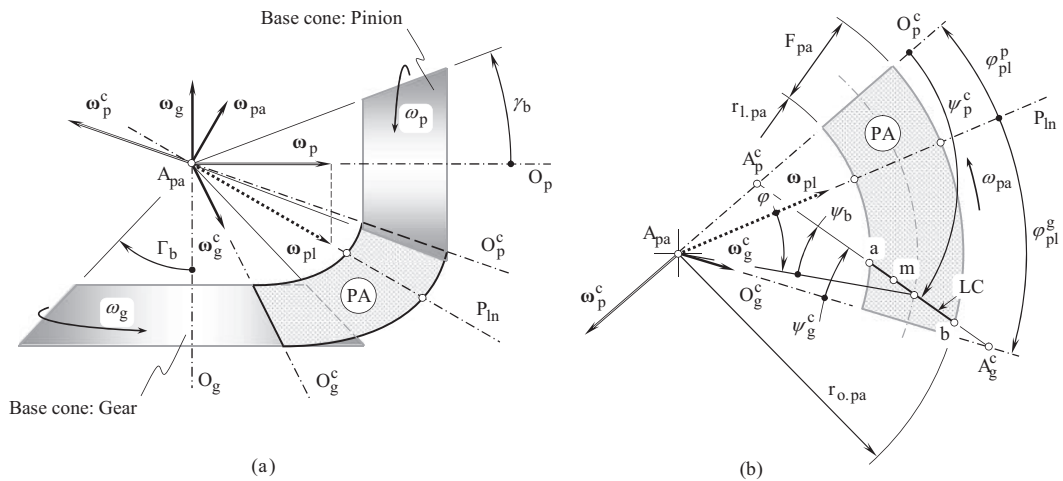


**FIGURE 22.7** Determination of the parameters of desirable local geometry of interacting tooth flanks of gear,  $\mathcal{S}$ , and mating pinion,  $\mathcal{P}$ , in intersected-axes gearing: (a) the base cones and the plane of action, and (b) desirable line of contact,  $LC$ , within the plane of action.

member), and it is free to wrap onto another base cone (onto the base cone of the driven member of the gear pair). The plane of action,  $PA$ , is absolutely rigid in the rest of the directions.

A straight desirable line of contact,<sup>1</sup>  $LC$ , between the tooth flanks of the gear and the pinion is located within the plane of action,  $PA$ . The line of contact is at a base helix angle,  $\psi_b$ , in relation to the axis of instantaneous rotation,  $P_m$ . In straight tooth bevel gears, the base helix angle equals to zero ( $\psi_b = 0^\circ$ ).

When the plane of action,  $PA$ , rotates ( $\omega_{pa}$ ), the line of contact,  $LC$ , travels together with the plane of action. In such a motion in relation to a reference system associated with the gear, the gear tooth flank,  $\mathcal{G}$ , is generated. The gear tooth flank,  $\mathcal{G}$ , can be construed as a locus of consecutive positions of the line of contact,  $LC$ , represented in that reference system (associated with the gear). Similarly, in such a motion in relation to a reference system associated with the pinion, the pinion tooth flank,  $\mathcal{P}$ , is generated. The pinion tooth flank,  $\mathcal{P}$ , can be interpreted as the locus of consecutive positions of the line of contact,  $LC$ , represented in that reference system (associated with the pinion).

A point of interest,  $m$ , taken within the desirable line of contact,  $LC$ , traces an arc of a conical involute on the gear tooth flank,  $\mathcal{G}$ . That same point,  $m$ , traces a corresponding arc of a conical involute on the pinion tooth flank,  $\mathcal{P}$ . These two involute curves are conjugate to each other, as both of them are generated by common point,  $m$ , that is located within the plane of action – the instant line of action,  $LA_{\text{inst}}$ , always intersects the axis of instantaneous rotation,  $P_m$ , in the gear pair.

The motion of the desirable line of contact,  $LC$ , in relation to the base cones can be interpreted as an instant rotation about a straight line of tangency (a) between the base cone of the gear, and the plane of action, and (b) between the base cone of the pinion, and the plane of action. In Figure 22.7, the axis of instant rotation of the desirable line of contact,  $LC$ , in relation to the base cone of the gear is designated as  $O_g^c$ . The vector of the instant rotation is designated as  $\omega_g^c$ . Similarly, the axis of instant rotation of the line of contact,  $LC$ , in relation to the base cone of the pinion is designated as  $O_p^c$ . The vector of the instant rotation is designated as  $\omega_p^c$ .

It should be pointed out here that all the rotation vectors,  $\omega_g^c$ ,  $\omega_p^c$ ,  $\omega_{pl}$ , and  $\omega_{pa}$ , are the vectors through a common point. In intersected-axes gearing, by nature, this point is the plane-of-action apex,  $A_{pa}$ .

Ultimately, the instantaneous kinematics of intersected-axes gearing is specified by two rotations,  $\omega_g^c$  and  $\omega_p^c$ , of the desirable line of contact,  $LC$ , about the axes of instantaneous rotations,  $O_g^c$  and  $O_p^c$ .

## 22.2.2 LOCAL GEOMETRY OF INTERACTING TOOTH FLANKS

Generating of local geometry of interacting tooth flanks of a gear and, a mating pinion is illustrated in Figure 22.7. At every instant of time, tooth flanks of the gear,  $\mathcal{G}$ , and those of the pinion,  $\mathcal{P}$ , are generated by the desirable line of contact,  $LC$ , that is rigidly associated with the plane of action,  $PA$ , and travels together with the plane of action.

Two surfaces generated by the desirable line of contact in its rotations about the axes of instantaneous rotation,  $O_g^c$  and  $O_p^c$ , can be employed as the surfaces that model the actual tooth flanks of the gear, and the pinion at every instant of time. It is evident that the geometry of the modeling surfaces is simpler compared to that of the actual gear and pinion. Further analysis, for example, calculation of contact stress in gearing, is significantly simplified due to the actual tooth flanks,  $\mathcal{G}$  and  $\mathcal{P}$ , can be replaced with the modeling surfaces.

The desirable line of contact,  $LC$ , in a form of a straight-line segment can be used as an example for the generation of the modeling surfaces. The desirable line of contact,  $LC$ , is at a base helix angle,  $\psi_b$ , in relation to the axis of instantaneous rotation.

<sup>1</sup> Reminder: the tooth flanks,  $\mathcal{G}$  and  $\mathcal{P}$ , of a gear and a mating pinion are not generated yet. Therefore, only desirable line of contact,  $LC_{\text{des}}$ , can be discussed, as the actual line of contact does not exist at this step of the analysis.

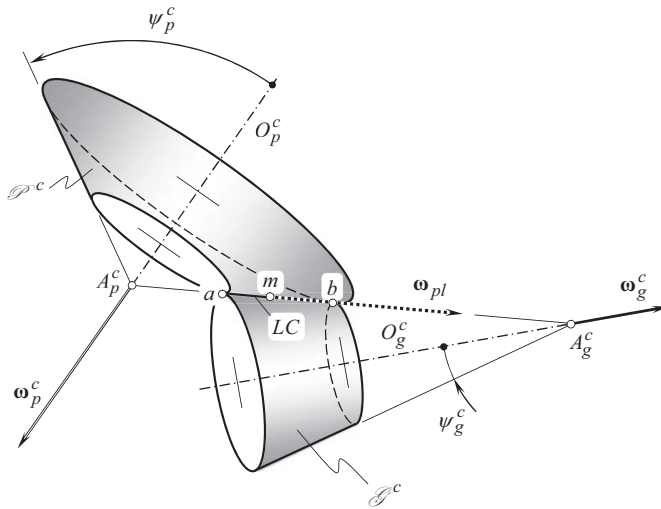


**FIGURE 22.8** Modeling cones,  $\mathcal{P}$  and  $\mathcal{P}_g$ , of gear tooth flank,  $\mathcal{F}$ , and mating pinion tooth flank,  $\mathcal{F}_g$ , in external intersected-axes gearing.

In the instant rotation,  $\omega_g^c$ , a cone of revolution is generated by the rotating line of contact,  $LC$ . The axis of instant rotation,  $O_g^c$ , is the axis of the modeling cone of revolution (see Figure 22.8). The cone angle of the cone of revolution is designated as  $\psi_g^c$ . Similarly, in the instant rotation,  $\omega_p^c$ , another cone of revolution is generated by the rotating line of contact,  $LC$ . The axis of instant rotation,  $O_p^c$ , is the axis of this modeling cone of revolution (see Figure 22.8). The cone angle of the cone of revolution is designated as  $\psi_p^c$ . The cone angles,  $\psi_g^c$  and  $\psi_p^c$ , can be expressed in terms of the base cone angle,  $\psi_b$ , and the angles that specify the current angular location of the line of contact,  $LC$ , within the plane of action,  $PA$ .

In straight bevel gears, the cone angle of the modeling cones equals to the base helix angle,  $\psi_b$ .

If either a circular arc, or an arc of a cycloid, or, finally, an arc of an arbitrary planar curve, is used as the desirable line of contact for the generation of the gear and the pinion tooth flank, then, *locally*, in the differential vicinity of point within the desirable line of contact, the line  $LC$  can be represented by a straight line segment that is tangent to the desirable line of contact,  $LC$ . Therefore, in this particular case, the gear and the pinion tooth flanks can be locally represented by surfaces of truncated cones.

Schematic is convenient for the investigation of gear drives composed of straight bevel gears, spiral bevel gears, as well as gears that have a cycloid longitudinal tooth shape (Figure 22.7). It is always applicable for the analysis of intersected-axes gearing with other geometries in the lengthwise direction of the gear teeth.

For internal intersected-axes gearing, the modeling cone of a gear is shaped in a form of an internal cone of revolution (as shown in Figure 22.9), similar to that diagrammatically illustrated in Figure 22.6.

It is instructive to point out here a manner in which radii of curvature of the modeling cones in internal gearing are altered along the line of contact in comparison to that in external gearing. An analysis of the modeling cones geometry reveals that when a point travels along the line of contact from one end to the opposite end of the modeling cones, the radii of curvature of both modeling cones get either larger or smaller. Thus, the relative curvature of the modeling cones in internal intersected-axes gearing within the line of contact alters insignificantly.

The aforementioned can be summarized in the form of two important advantages of internal gearing over external gearing:

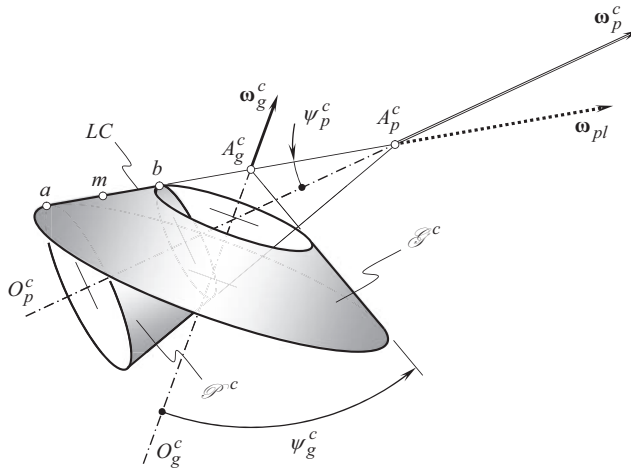


**FIGURE 22.9** Modeling cones,  $\mathcal{S}$  and  $\mathcal{P}$ , of gear tooth flank,  $\mathcal{S}$ , and mating pinion tooth flank,  $\mathcal{P}$ , in internal intersected-axes gearing.

- Contact of convex tooth flank of a pinion with concave tooth flank of a gear in internal gearing is more favorable compared to contact of two convex tooth flanks in external gearing
- Alteration of relative curvature within the line of contact in internal gearing is preferable to that in external gearing.

The dimensions of the modeling cones in external, as well as in internal intersected-axes gearing (the radii of curvature, the cone angle, and so forth), as well as the configuration of the modeling cones in relation to one another, can be expressed in terms of the design parameters of the gear pair to be modeled.

## 22.3 LOCAL GEOMETRY OF INTERACTING TOOTH FLANKS IN CROSSED-AXES GEARING

External crossed-axes gearing can be used as an example for the analysis of the interaction of tooth flanks in crossed-axes gearing. Then, the results of the analysis obtained for external gearing can be enhanced to other types of crossed-axes gearing, as well.

### 22.3.1 KINEMATICS OF INTERACTION OF TOOTH FLANKS

A schematic of interaction of tooth flanks of a gear,  $\mathcal{S}$ , and of a mating pinion,  $\mathcal{P}$ , in crossed-axes gearing is depicted in Figure 22.10. The gear rotates about its axis of rotation,  $O_g$ , at a uniform angular velocity,  $\omega_g$ . The rotation vector of the gear is designated as  $\omega_g$ . The mating pinion rotates about its axis of rotation,  $O_p$ , at a uniform angular velocity,  $\omega_p$ . The rotation vector of the pinion is designated as,  $\omega_p$ . The vector of instant rotation,  $\omega_{pl}$ , of the gear and of the pinion can be specified in terms of the rotation vectors,  $\omega_g$  and  $\omega_p$ , namely,  $\omega_{pl} = \omega_p - \omega_g$ . The rotation vector,  $\omega_{pl}$ , passes through the point,  $A_{pa}$ , within the center-line,  $\mathfrak{L}$ , for the straight lines along the rotation vectors,  $\omega_g$  and  $\omega_p$ . The axis of instant rotation,  $P_{ln}$ , is aligned with the rotation vector,  $\omega_{pl}$ .

The plane of action,  $PA$ , is a plane through the vector of instant rotation,  $\omega_{pl}$ , of the pinion in relation to the gear. The plane of action,  $PA$ , forms an angle with the plane perpendicular to the center-line,  $\mathfrak{L}$ . This angle equals to  $(90^\circ - \phi_{t,\omega})$ , where  $\phi_{t,\omega}$  denotes the transverse pressure angle measured within a plane that is perpendicular to the axis of instant rotation,  $P_{ln}$ . The plane of action

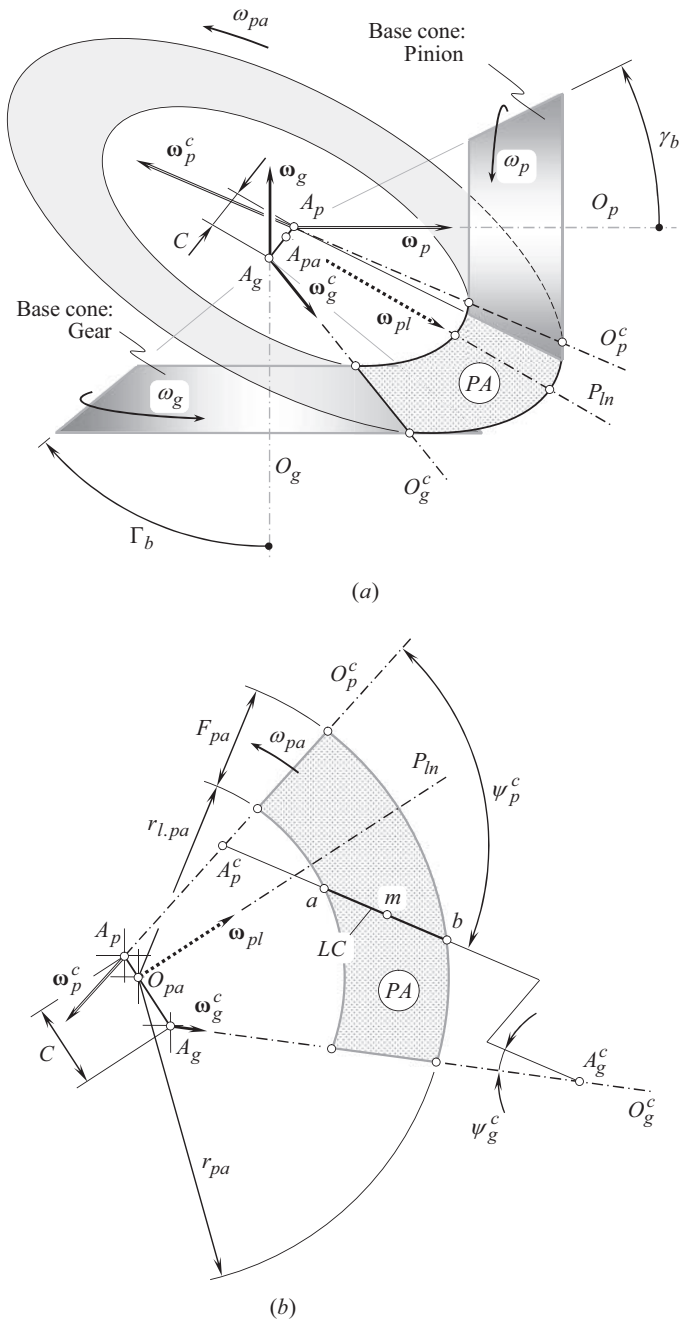


**FIGURE 22.10** Determination of parameters of desirable local geometry of interacting tooth flanks of gear,  $\mathcal{S}$ , and mating pinion,  $\mathcal{P}$ , in crossed-axes gearing: (a) base cones and plane of action, and (b) desirable line of contact,  $LC$ , within the plane of action.

is in tangency with the base cones of a gear and a mating pinion. The base cone of the gear is designated as  $\Gamma_b$ , and the base cone of the pinion is designated as  $\gamma_b$ .

When the gears rotate, the plane of action rotates about the axis,  $O_{pa}$ , that is pointed perpendicular to  $PA$ . The rotation vector of the plane of action is designated as  $\omega_{pa}$ .



The magnitudes of the rotation vectors,  $\omega_g$ ,  $\omega_p$ , and  $\omega_{pa}$ , are synchronized with one another:

$$u_{p/pa} = \sin \gamma \quad (22.8)$$

$$u_{palg} = \frac{1}{\sin \Gamma} \quad (22.9)$$

$$u_{palg} = \frac{\sin \gamma}{\sin \Gamma} \quad (22.10)$$

where  $\Gamma$  and  $\gamma$  are the pitch cone angles of the gear and the pinion, correspondingly ( $\Gamma = \Sigma_g$ , and  $\gamma = \Sigma_p$ ).

The synchronization of the rotations makes it possible to construe the plane of action,  $PA$ , as a portion of a round strip of zero thickness film. This strip is absolutely flexible in a single direction, and when the gear pair operates, the round strip of zero thickness film is free to unwrap from one of the base cones and is free to wrap over the other base cone.

A straight desirable line of contact,  $LC$ , between the tooth flanks of a gear and a mating pinion is located within the plane of action,  $PA$ . The desirable line of contact is at a base helix angle,  $\psi_b$ , in relation to the axis of instant rotation,  $P_{ln}$ .

When the plane of action,  $PA$ , rotates ( $\omega_{pa}$ ), the desirable line of contact,  $LC$ , travels together with the plane of action. In such a motion in relation to a reference system associated with the gear, the gear tooth flank,  $\mathcal{S}$ , is generated. The gear tooth flank,  $\mathcal{S}$ , can be viewed as a locus of consecutive positions of the desirable line of contact,  $LC$ , represented in that reference system. Similarly, in a motion in relation to a reference system associated with the pinion, the pinion tooth flank,  $\mathcal{P}$ , is generated. The pinion tooth flank,  $\mathcal{P}$ , can be construed as a locus of successive positions of the desirable line of contact,  $LC$ , represented in that reference system.

A point of interest,  $m$ , within the desirable line of contact,  $LC$ , traces a curve that is entirely located on the gear tooth flank,  $\mathcal{S}$ . That same point,  $m$ , traces the corresponding curve that is entirely located on the pinion tooth flank,  $\mathcal{P}$ . These two spatial curves are conjugate to each other, as both of them are generated by a common point that is located within the line of contact – the instant line of action,  $LA_{inst}$ , always intersects the axis of instant rotation,  $P_{ln}$ .

The motion of the desirable line of contact,  $LC$ , in relation to the base cones can be interpreted as the instant rotation about a straight line of tangency between the base cone of the gear and the plane of action, and between the base cone of the pinion and the plane of action, correspondingly. In Figure 22.10, the axis of instant rotation of the line of contact,  $LC$ , in relation to the base cone of the gear is designated as  $O_g^c$ . The vector of the instant rotation is designated as  $\omega_g^c$ . Similarly, the axis of instant rotation of the line of contact,  $LC$ , in relation to the base cone of the pinion is designated as  $O_p^c$ . The vector of the instant rotation is designated as  $\omega_p^c$ .

It is important to point out here that all the rotation vectors,  $\omega_g^c$ ,  $\omega_p^c$ ,  $\omega_{pl}$ , and  $\omega_{pa}$ , are not the vectors through a common point,  $A_{pa}$ , namely, through the plane-of-action apex,  $A_{pa}$ . This causes sliding of the modeling cones along the line of their contact with the plane of action,  $PA$ . Non-coincidence of the apexes  $A_g^c$ ,  $A_p^c$ , and  $A_{pa}$  is the root cause of so-called *axial sliding* in crossed-axes gearing.

Ultimately, the instantaneous kinematics of crossed-axes gearing is specified by two rotations,  $\omega_g^c$  and  $\omega_p^c$ , of the line of contact,  $LC$ , about the axes,  $O_g^c$  and  $O_p^c$ , of instant rotations,  $\omega_g^c$  and  $\omega_p^c$ , along with relative sliding of the modeling cones along the common generating line.

### 22.3.2 LOCAL GEOMETRY OF INTERACTING TOOTH FLANKS

Generating of local geometry of interacting tooth flanks of a gear, and a mating pinion in crossed-axes gearing is illustrated in Figure 22.10. At every instant of time, tooth flank of the gear,  $\mathcal{S}$ , and

that of the pinion,  $\mathcal{P}$ , are generated by the line of contact,  $LC$ , that travels together with the plane of action,  $PA$ .

Two surfaces generated by a desirable line of contact in its rotations about the axes of instant rotation,  $O_g^c$  and  $O_p^c$ , can be employed as the surfaces that model the actual tooth flanks of a gear and a mating pinion at every instant of time.

The line of contact,  $LC$ , in the form of a straight-line segment can be used as an example for generating the modeling surfaces. The line of contact,  $LC$ , forms the base helix angle,  $\psi_b$ , with the axis of instant rotation.

In the instant rotation,  $\omega_g^c$ , a cone of revolution is generated by the rotating line of contact,  $LC$ . The axis of instantaneous rotation,  $O_g^c$ , is the axis of the modeling cone of revolution (see Figure 22.11). The cone angle of the cone of revolution is designated as  $\psi_g^c$ . Similarly, in the instant rotation,  $\omega_p^c$ , another cone of revolution is generated by that same rotating line of contact,  $LC$ . The axis of instant rotation,  $O_p^c$ , is the axis of this modeling cone of revolution (see Figure 22.11). The cone angle of the cone of revolution is designated as  $\psi_p^c$ . The cone angles,  $\psi_g^c$  and  $\psi_p^c$ , can be expressed in terms of the base cone angle,  $\psi_b$ , and the angles that specify current angular configuration of the line of contact,  $LC$ , within the plane of action,  $PA$ .

If either a circular arc, or an arc of a cycloid, or finally, an arc of an arbitrary planar curve is used as the line of contact for the generation of a gear and a mating pinion tooth flank, then *locally*, in the differential vicinity of point of interest, the line of contact,  $LC$ , is represented by a straight-line segment that is tangential to the actual line of contact,  $LC$ . Therefore, in this particular case, the gear and the pinion teeth flanks can be locally represented by the surfaces of truncated cones.

The schematic shown in Figure 22.11 is convenient for the investigation of gear drives composed of gears with various tooth shapes in the lengthwise direction. It is also applicable for the analysis of crossed-axes gears that have other geometries in the lengthwise direction of the gear teeth.

For internal crossed-axes gearing, the modeling cone of the gear is shaped in the form of an internal cone of revolution similar to that diagrammatically illustrated in Figure 22.6 for parallel-axes gearing, and in Figure 22.9 for intersected-axes gearing.

The following two statements are valid for crossed-axes gearing:

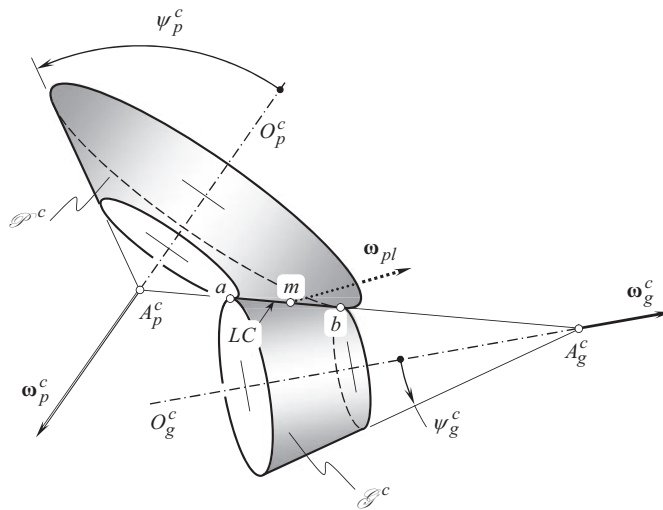


**FIGURE 22.11** Modeling cones,  $\mathcal{G}^c$  and  $\mathcal{P}^c$ , of gear tooth flank,  $\mathcal{G}$ , and mating pinion tooth flank,  $\mathcal{P}$ , in external crossed-axes gearing.

- Contact of convex tooth flank of a pinion with concave tooth flank of a gear in internal gearing is more favorable compared to contact of two convex tooth flanks of the gear and the pinion in external gearing
- Alteration of relative curvature within the line of contact in internal gearing is more preferable to that in external gearing

These two statements are equivalent to the above-formulated statements that are valid for parallel-axes gearing and intersected-axes gearing.

The dimensions of the modeling cones in external, and in internal crossed-axes gearing (the radii of curvature, the cone angle, and so forth), as well as the configuration of the modeling cones in relation to each other, can be expressed in terms of the design parameters of a gear pair to be modeled.

## 22.4 LOCAL GEOMETRY OF INTERACTING TOOTH FLANKS IN *NOVIKOV/CONFORMAL* AND IN *HIGH-CONFORMAL* GEARING<sup>2</sup>

*Novikov/conformal*, and *high-conformal* gearing can be interpreted as a particular case of involute gearing when the actual height of the field of action approaches zero and, consequently, the profile contact ratio gets equal to zero. There are many similarities between *Novikov/conformal*, and *high-conformal* gearing, and between the aforementioned kinds of gearing.

### 22.4.1 KINEMATICS OF INTERACTING TOOTH FLANKS

A parallel-axes *Novikov/conformal*, and *high-conformal* gear pair is considered as an example for the analysis of kinematics of interacting tooth flanks in *Novikov/conformal*, and *high-conformal* gears.

Consider two rotation vectors,  $\omega_g$  and  $\omega_p$ , of a gear and a mating pinion. The rotation vectors are parallel to each other, and are apart from one another at a center distance,  $C$ .

In high-conformal gearing, two base cylinders of diameters,  $d_{b,g}$  and  $d_{b,p}$ , can be constructed for a given pair of the rotation vectors,  $\omega_g$  and  $\omega_p$ , of the gear and that of the pinion when the pressure angle is known. The plane of action,  $PA$ , is in tangency with both of the base cylinders, as schematically depicted in Figure 22.12.

The base cylinders in a *Novikov/conformal*, and *high-conformal* gear pair are useful for interpretation of a gear pair in terms of *equivalent pulley-and-belt transmission*. A rotation from the driving shaft is transmitted to the driven shaft by the force acting within the plane of action. This makes it reasonable to consider the interaction of the tooth flanks of the gear and the pinion in a plane of action. Due to this, the tooth profiles of the gear and of the pinion in the section by the plane of action are of critical importance for the evaluation of the power capacity of a high-conformal gear drive.

The vector of instant rotation of the plane of action in relation to the gear is designated as  $\omega_g^c$ . This rotation vector is pointed along the line of tangency between the plane of action and the gear base cylinder of a diameter,  $d_{b,g}$ . Similarly, the vector of instant rotation of the plane of action in relation to the pinion is designated as  $\omega_p^c$ . This rotation vector is pointed along the line of tangency between the plane of action and the pinion base cylinder of a diameter,  $d_{b,p}$ .

The plane of action,  $PA$ , and a plane through the axis of rotation of the gear,  $O_g$ , and through the axis of rotation of the pinion,  $O_p$ , intersect one another. The straight line of intersection of the aforementioned planes is the *pitch line*,  $P_{in}$  (or, in other terms, the *axis of instantaneous rotation*,  $P_{in}$ ).

The height,  $Z_{pa}$ , of the field of action in a *Novikov/conformal*, and *high-conformal* gear pair equals zero ( $Z_{pa} = 0$ ).

<sup>2</sup> It is instructive to stress here one more time on that that conformal gearing, as well, as high-conformal gearing, can be viewed as a reduced case of involute gearing (see Chapter 11 for details).

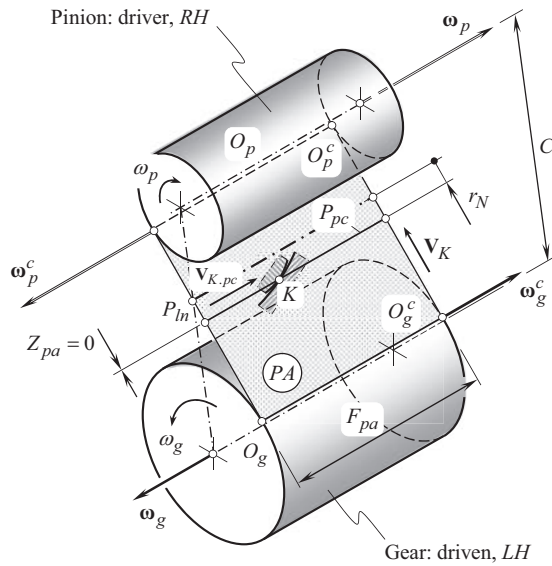


**FIGURE 22.12** Determination of the parameters of desirable local geometry of interacting tooth flanks,  $\mathcal{S}$  and  $\mathcal{P}$ , of gear and mating pinion in parallel-axes *Novikov/conformal*, and *high-conformal* gearing.

The path of contact,  $P_c$ , in *Novikov/conformal*, and *high-conformal* gearing is always of a zero length, as the length of the active portion of the line of action is zero, ( $Z_{pa} = 0$ ). However, the plurality of zero-length paths of contact,  $P_c$ , forms the so-called *pseudo-path of contact*,  $P_{pc}$ .

The pseudo-path of contact,  $P_{pc}$ , is parallel to the pitch line,  $P_{ln}$ , and is located at a distance,  $r_N$ , from the axis of instant rotation,  $P_{ln}$ . When a gear pair operates, the point of contact,  $K$ , of the tooth flanks travels together with the plane of action with a linear velocity,  $\mathbf{V}_K$ . The actual length of trajectory of this travel is zero. However, visually it looks like the point of contact,  $K$ , pseudo-travels,  $\mathbf{V}_{K,pc}$ , along the pseudo-path of contact,  $P_{pc}$ .

Since the height of the field of action in a *Novikov/conformal*, and *high-conformal* gearing is always equals zero ( $Z_{pa} = 0$ ), this makes it possible to design the gear and the pinion tooth flanks so, as to maintain convex-to-concave kind of their contact.

*Novikov/conformal*, and *high-conformal* gears allow for interpretation in terms of involute gears.

At the beginning, let us consider a straight line,  $LC$ , within the plane of action,  $PA$ , that forms a base helix angle,  $\psi_b$ , with both the rotation vectors,  $\omega_g$  and  $\omega_p$ . When the gears operate, the line of contact travels together with the plane of action from the position labeled as  $LC_1$ , to a new position labeled as  $LC_2$  (see Figure 22.13a). As long, as the line,  $LC$ , is a straight line, that travels ( $\mathbf{V}_{pa}$ ) with the plane of action,  $PA$ , this motion is equivalent to traveling of the straight line,  $LC$ , along the pitch line,  $P_{ln}$ , (see Figure 22.13b). The speed of this motion is designated as  $\mathbf{V}_{ax}$ . It is clear that the magnitudes,  $V_{pa}$  and  $V_{ax}$ , of the velocity vectors,  $\mathbf{V}_{pa}$  and  $\mathbf{V}_{ax}$ , correlate with one another in accordance to the formula  $V_{ax} = V_{pa} / \tan \psi_b$ .

The following analogy is useful in particular case under consideration.

A cylinder of revolution can be generated when the pseudo-path of contact,  $P_{pc}$ , is rotated about the axis of rotation,  $O_g$ , of the gear. The line of intersection of the gear tooth flank by the cylinder is a helix. The contact point,  $K$ , can be construed as the point of intersection of the aforementioned cylinder by the plane of action,  $PA$ . A similar consideration is valid with respect to the pinion. When the gears operate, the helix rotates. Due to this, the contact point,  $K$ , pseudo-travels along the pseudo-path of contact,  $P_{pc}$ .

When the height,  $Z_{pa}$ , of the field of action gets smaller, as illustrated in Figure 22.13b, the pseudo-motion of the straight line segment in the axial direction becomes more evident. In the limit

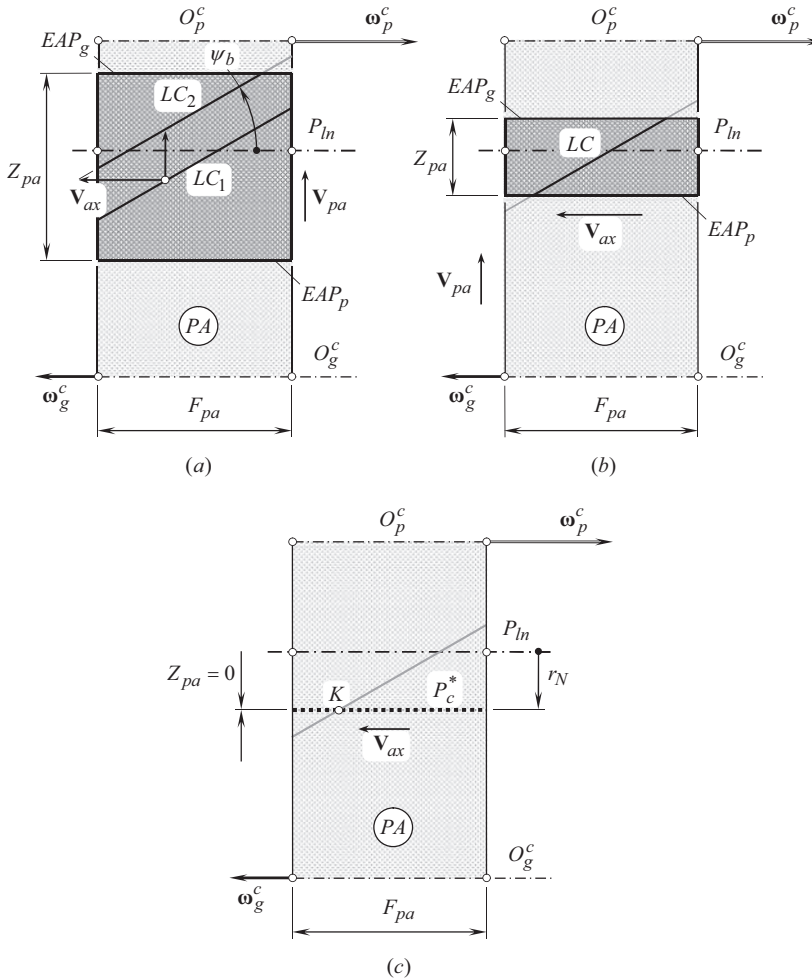


**FIGURE 22.13** Traveling of the line of contact,  $LC$ , in parallel-axes gearing: (a) high-transverse-contact-ratio gear pair, (b) regular transverse contact ratio gear pair, and (c) *Novikov/conformal*, and *high-conformal* gearing.

case ( $Z_{pa} = 0$ ), only axial motion,  $V_{ax}$ , of the  $LC$  remains. When the equality  $Z_{pa} = 0$  is observed (see Figure 22.13c), the straight line segment,  $LC$ , is of a zero length; however, the inclination angle,  $\psi_b$ , is preserved. Due to this, the base pitch,  $p_b$ , can be calculated for any and all *Novikov/conformal*, and *high-conformal* gear pairs. This is identical to the calculation for a corresponding involute gearing, and can be done in the following manner:

- The axial pitch,  $p_x$ , in a *Novikov/conformal*, and *high-conformal* gear is calculated from the formula:

$$p_x = \frac{\pi d_g}{N_g \tan \psi} \quad (22.11)$$

- The base helix angle,  $\psi_b$ , in a *Novikov/conformal*, and *high-conformal* gearing equals:

$$\psi_b = \tan^{-1}(\tan \psi \tan \phi_t) \quad (22.12)$$

- With the axial pitch,  $p_x$ , and the base helix angle,  $\psi_b$ , known, the base pitch,  $p_b$ , in a parallel-axes *Novikov/conformal*, and *high-conformal gearing* is calculated from the expression:

$$p_b = p_x \sin \psi_b \quad (22.13)$$

In Eqs. (22.11)–(22.13):

- $d_g$  is the pitch diameter in a *Novikov/conformal*, and *high-conformal gear*.
- $N_g$  is the tooth count in a *Novikov/conformal*, and *high-conformal gear*.
- $\phi_t$  is the transverse pressure angle.

Calculations similar to the aforementioned are also valid with respect to a *Novikov/conformal*, and *high-conformal* pinion.

The aforementioned consideration is true not only for external parallel-axes *Novikov/conformal*, and *high-conformal gears*, but for external *Novikov/conformal*, and *high-conformal gears* of all other kinds (intersected-axes gearing, crossed-axes gearing), as well as for internal gearing.

## 22.4.2 GEOMETRY OF INTERACTING TOOTH FLANKS

The tooth flank of a gear and that of a mating pinion in a *Novikov/conformal*, and *high-conformal* gear pair make point contact at every instant of time, as the involute tooth profiles of the gear and of the pinion are reduced to the so-called *involute tooth points*. Due to this, the geometry of the interacting tooth flanks is *local* by nature. Before and beyond the involute tooth point, tooth flank of the gear and that of the mating pinion are not conjugate to each other.

Taking advantage of this, local patches of the gear tooth flank, as well as of the pinion tooth flank, are designed so, as to make the highest possible bearing capacity of the gear pair. Because of this, a convex shape is given to tooth profiles in the transverse section of one member of the gear pair, and a corresponding concave shape is given to tooth profiles of another member of the gear pair.

Consider a *Novikov/conformal*, and *high-conformal* gear pair diagrammatically shown in Figure 22.14. The rotation vector,  $\omega_g$ , of the gear, and the rotation vector,  $\omega_p$ , of the pinion are pointed along the corresponding axes of rotation,  $O_g$  and  $O_p$ . When the gears rotate, contact point,  $K$ , *pseudo-travels* along the pseudo-path of contact,  $P_{pc}$ . Point on the gear tooth that makes contact with the pinion tooth is labeled as  $K_g$ . Accordingly, point on the pinion tooth that makes contact with the gear tooth is labeled as  $K_p$ . At certain instant of time, these points,  $K_g$  and  $K_p$ , coincide with one another. In such a position, they are labeled as c common contact point,  $K$ .

As the point,  $K_g$ , is located within the concave tooth profile of the gear, the local surface patch in the differential vicinity of the point,  $K_g$ , is of saddle type. Three unit vectors are associated with the point,  $K_g$ . They are  $\mathbf{u}_g$ ,  $\mathbf{v}_g$ , and  $\mathbf{n}_g$ . The unit vector,  $\mathbf{u}_g$ , is tangential to  $U_g$  – coordinate line on the gear tooth surface,  $\mathcal{S}$ . The unit vector,  $\mathbf{v}_g$ , is tangential to  $V_g$  – coordinate line on the gear tooth surface,  $\mathcal{S}$ . Ultimately, the unit vector,  $\mathbf{n}_g$ , is perpendicular at  $K_g$  to the gear tooth flank,  $\mathcal{S}$ . The vectors,  $\mathbf{u}_g$  and  $\mathbf{v}_g$ , are equal  $\mathbf{u}_g = \mathbf{U}_g / |\mathbf{U}_g|$  and  $\mathbf{v}_g = \mathbf{V}_g / |\mathbf{V}_g|$ , correspondingly. At point of gear tooth flank,  $\mathcal{S}$ , specified by the position vector of a point  $\mathbf{r}_g = \mathbf{r}_g(U_g, V_g)$ , the vectors,  $\mathbf{U}_g$  and  $\mathbf{V}_g$ , are calculated from the formulas  $\mathbf{U}_g = \partial \mathbf{r}_g / \partial U_g$  and  $\mathbf{V}_g = \partial \mathbf{r}_g / \partial V_g$ , where  $U_g$  and  $V_g$  represent curvilinear (*Gaussian*) coordinate lines on the gear tooth surface,  $\mathcal{S}$ .

The normal unit vector,  $\mathbf{n}_g$ , is pointed outward of the bodily side to the void side of the gear tooth, as illustrated in Figure 22.14. The normal unit vector,  $\mathbf{n}_g$ , equals  $\mathbf{n}_g = \mathbf{u}_g \times \mathbf{v}_g$ . In a particular case, an inverse cross product  $\mathbf{n}_g = \mathbf{v}_g \times \mathbf{u}_g$  is used for the calculation of the unit normal vector,  $\mathbf{n}_g$ . This depends on which of the two of the curvilinear coordinate lines is labeled as the  $U_g$  – coordinate line, and which one is labeled as the  $V_g$  – coordinate line.



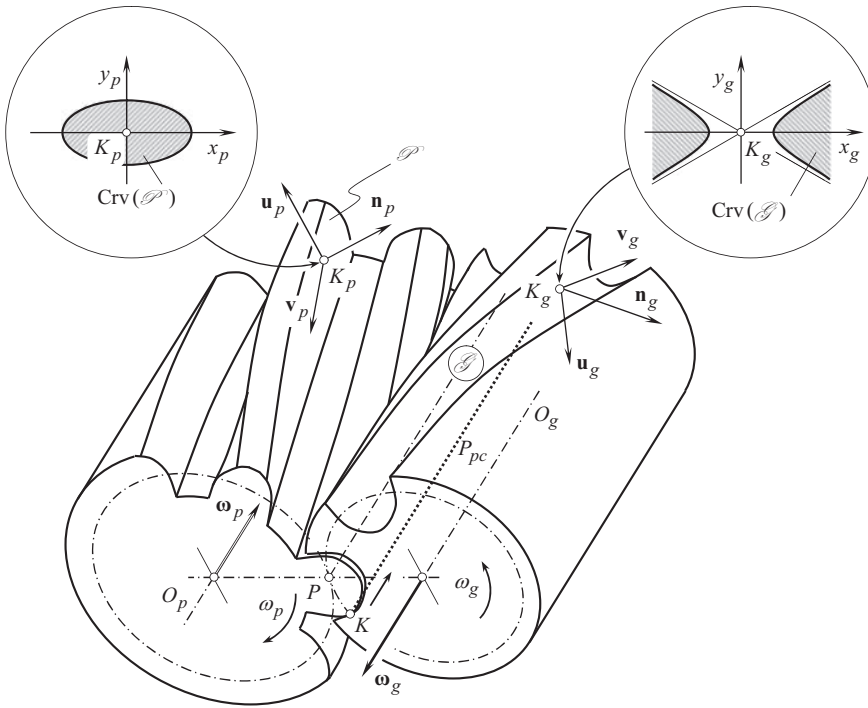


**FIGURE 22.14** Configuration of local reference systems,  $x_g y_g z_g$  and  $x_p y_p z_p$ , in relation to tooth flanks,  $\mathcal{S}$  and  $\mathcal{P}$ , of gear and mating pinion in *Novikov/conformal*, and *high-conformal* gear pair.

The unit vectors  $\mathbf{u}_g$ ,  $\mathbf{v}_g$ , and  $\mathbf{n}_g$ , are used to construct a local *Cartesian* coordinate system,  $x_g y_g z_g$ . When the unit vectors,  $\mathbf{u}_g$  and  $\mathbf{v}_g$ , are aligned with the principal directions,  $\mathbf{t}_{1,g}$  and  $\mathbf{t}_{2,g}$ , on the surface,  $\mathcal{S}$ , the axes  $x_g$ ,  $y_g$ , and  $z_g$ , align with the corresponding unit vectors,  $\mathbf{u}_g$ ,  $\mathbf{v}_g$ , and  $\mathbf{n}_g$ . For other configurations of the unit vectors,  $\mathbf{u}_g$ ,  $\mathbf{v}_g$ , and  $\mathbf{n}_g$ , a known technique can be used to construct the local *Cartesian* coordinate system,  $x_g y_g z_g$  [153].

The unit vectors,  $\mathbf{u}_p$ ,  $\mathbf{v}_p$ , and  $\mathbf{n}_p$ , on the pinion tooth flank,  $\mathcal{P}$ , at point,  $K_p$ , are constructed in a manner similar to that the set of unit vectors,  $\mathbf{u}_g$ ,  $\mathbf{v}_g$ , and  $\mathbf{n}_g$ , for the gear tooth surface,  $\mathcal{S}$ , is constructed.

The local geometry of the tooth flanks,  $\mathcal{S}$  and  $\mathcal{P}$ , in the differential vicinity of corresponding points,  $K_g$  and  $K_p$ , is expressed in terms of the *curvature indicatrices*,  $\text{Crv}(\mathcal{S})$  and  $\text{Crv}(\mathcal{P})$ , which are constructed at point,  $K_g$ , on the tooth flank,  $\mathcal{S}$ , and at point,  $K_p$ , on the tooth flank,  $\mathcal{P}$ . It should be pointed out here that the curvature indicatrix represents a portion of the tangent plane bounded by the corresponding *Dupin indicatrix* at that same point of the tooth flank. This means that the curvature indicatrix,  $\text{Crv}(\mathcal{S})$ , is a portion of the tangent plane bounded by the *Dupin indicatrix*,  $\text{Dup}(\mathcal{S})$ , and the curvature indicatrix  $\text{Crv}(\mathcal{P})$ , is a portion of the tangent plane bounded by the *Dupin indicatrix*,  $\text{Dup}(\mathcal{P})$ .

Curvature indicatrices are a convenient tool in engineering geometry of surfaces, and are extensively used for the analytical description of the local geometry of a smooth regular surface in the differential vicinity of point within the surface. Implementation of curvature indicatrices makes it clear whether a surface local patch is convex, or concave, whether a surface local patch is quasi-convex or quasi-concave, and so on [137,148,153,172].

The curvature indicatrix,  $\text{Crv}(\mathcal{S})$ , at point  $K_g$  on the local surface,  $\mathcal{S}$ , patch is represented by two portions of the tangent plane bounded by arcs of a hyperbola,  $\text{Dup}(\mathcal{S})$ . A decision whether a saddle-like local patch of a surface,  $\mathcal{S}$ , is quasi-convex, or it is quasi-concave, is made based on

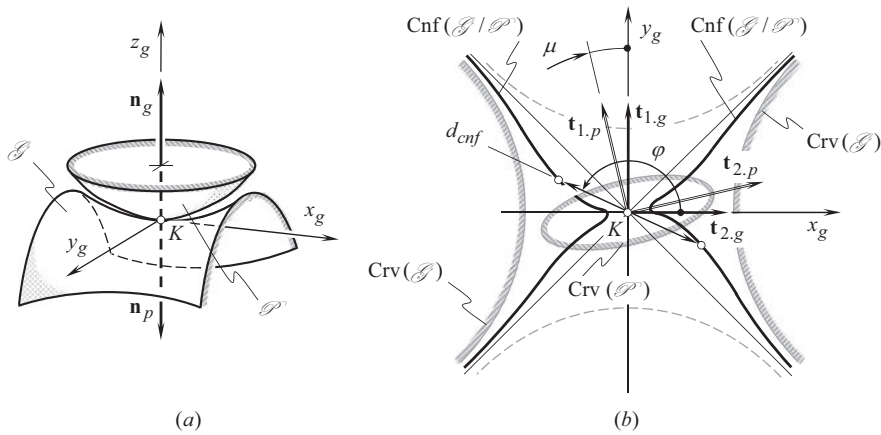


**FIGURE 22.15** Configuration of local patches of tooth flanks of gear,  $\mathcal{S}$ , and mating pinion,  $\mathcal{P}$ , and corresponding indicatrix of conformity,  $\text{Cnf}(\mathcal{S}/\mathcal{P})$ , at contact point,  $K$ , of two smooth regular tooth flanks,  $\mathcal{S}$  and  $\mathcal{P}$ : (a) schematic of surfaces contact, and (b) corresponding indicatrix of conformity,  $\text{Cnf}(\mathcal{S}/\mathcal{P})$ .

evaluation of the mean curvature,  $\mathcal{M}_g$ , and of the *Gaussian* curvature,  $\mathcal{S}_g$ , at a given surface point  $K_g$ . *Gaussian* curvature at point within a surface local patch of saddle kind is always of a negative value ( $\mathcal{S}_g < 0$ ). Mean curvature at point within a surface local patch of saddle kind can be either of a positive value, or of a negative value. Saddle-like local surface patches for which the inequality  $\mathcal{M}_g > 0$  is fulfilled, are referred to as *quasi-convex* local surface patches. Saddle-like local surface patches for which the inequality  $\mathcal{M}_g < 0$  is valid, are referred to as *quasi-concave* local surface patches.

The curvature indicatrix,  $\text{Crv}(\mathcal{P})$ , at point,  $K_p$ , within the local surface,  $\mathcal{P}$ , patch is represented by a portion of the tangent plane bounded by an ellipse,  $\text{Dup}(\mathcal{S})$ . As the tooth profile is convex, for a local surface patch of elliptical, kind the curvature indicatrix,  $\text{Crv}(\mathcal{P})$ , is located inside the corresponding *Dupin indicatrix*,  $\text{Dup}(\mathcal{P})$ . Otherwise, in the case of a concave surface patch, the curvature indicatrix is located outside the *Dupin indicatrix*.

At an instant of time when the points,  $K_g$  and  $K_p$ , get coincident, the local patches of the tooth flanks,  $\mathcal{S}$  and  $\mathcal{P}$ , make contact at a distinct point,  $K$ , as schematically illustrated in Figure 22.15a. For the purpose of the analysis, both the surfaces,  $\mathcal{S}$  and  $\mathcal{P}$ , are required to be represented in a common reference system. The left-hand-oriented *Cartesian* coordinate system,  $x_g y_g z_g$ , is used for this purpose.

For the case under consideration, the indicatrix of conformity,<sup>3</sup>  $\text{Cnf}(\mathcal{S}/\mathcal{P})$ , of the tooth surfaces,  $\mathcal{S}$  and  $\mathcal{P}$ , at the contact point  $K$  is constructed.<sup>4</sup> This characteristic curve (see Figure 22.15b) indicates that the contacting tooth flanks,  $\mathcal{S}$  and  $\mathcal{P}$ , are turned in relation to one another at an angle,  $\mu$ , of the surfaces local relative orientation. The angle of local orientation,  $\mu$ , is measured between the corresponding principal directions on the contacting surfaces at contact point,  $K$ , namely, between the first principal directions,  $\mathbf{t}_{1,g}$  and  $\mathbf{t}_{1,p}$ , or (the same) between the second principal directions,  $\mathbf{t}_{2,g}$  and  $\mathbf{t}_{2,p}$ . The higher the degree of conformity at point of contact of the tooth flanks,  $\mathcal{S}$  and  $\mathcal{P}$ , the smaller the minimum diameter,  $d_{cnf}^{\min}$ , of the indicatrix of conformity,  $\text{Cnf}(\mathcal{S}/\mathcal{P})$ , and vice versa.

<sup>3</sup> The concept of the indicatrix of conformity at point of contact of two smooth regular surfaces was proposed by the author in the late 1970s, early 1980s. It has been disclosed in two publications [127] and [128]. Later on, this concept got an extensive application in many projects and publications, including, but not limited to [148,153,172], as well, as in many others.

<sup>4</sup> For completeness of the analysis, the curvature indicatrices,  $\text{Crv}(\mathcal{S})$  and  $\text{Crv}(\mathcal{P})$ , at point of the tooth flanks,  $\mathcal{S}$  and  $\mathcal{P}$ , are indicated in Figure 22.15, as well.



The considered in this chapter local geometry of contact of a gear,  $\mathcal{G}$ , and a mating pinion,  $\mathcal{P}$ , tooth flanks can be used to investigate:

- The contact strength of the gear teeth
- The conditions of lubrication of the interacting tooth flanks,  $\mathcal{G}$  and  $\mathcal{P}$
- Gear tooth flanks wear, and so forth

The area of application of the results attained in local geometry of tooth flanks,  $\mathcal{G}$  and  $\mathcal{P}$ , of a gear and a mating pinion, is a useful tool in the scientific theory of gearing.

---

# 23 Strength of Gear Teeth

Strength of gear teeth is an important consideration. When a pair of gears operate, the stresses in gear teeth as well as in the gear body are caused by the operating load. Quantitatively, the stresses in the gear teeth are illustrated in Figure 23.1.

Contact strength and bending strength of gear teeth are the two most important indicators of performance of a gear pair. New accomplishments in the theory of gearing are helpful in the development of gear pairs with better performance. All types of gear tooth failure depend on contact stress, as well as on bending stress in the gear teeth.

The results of the research derived from the disclosed *Theory of Gearing* have a tremendous potential. They can be applied for solving a plurality of problems targeting improvement of the power density, lowering vibration generation and noise excitation, and so forth. A few areas of implementation of the developed *Theory of Gearing* are discussed below as examples. Much room becomes available for researchers and engineers in this field of mechanical engineering in this regard.

## 23.1 CONTACT STRENGTH OF GEAR TOOTH IN LOW-TOOTH-COUNT GEARING<sup>1</sup>

Today's involute gears carry far more power with greater reliability than was once thought possible. Improvements in the material and lubrication and more precise manufacture, which is made possible by modern equipment, are mainly responsible for this. Still, the search for greater strength goes on, as indicated by continuing test programs at many laboratories. As further progress from these standard approaches becomes increasingly difficult, it is worthwhile to look into better load distribution in parallel-axes gears.

Gears fail by pitting and wear as well as by tooth breakage. For the prediction of gear-tooth strength and calculating stresses within the gear-tooth body, an adequate load distribution model is required.

As discussed in Chapter 2, the results of the analysis of the instantaneous kinematics of relative motion of interacting tooth flanks of a gear, and a mating pinion,  $\mathcal{G}$  and  $\mathcal{P}$ , correspondingly, as well as those pertaining to the local geometry of the tooth flanks, are of critical importance in many practical applications. The calculation of the contact strength of gear tooth is one of the examples of potential areas of application of the aforementioned results of the research.

The contact strength of gear tooth depends on two factors:

1. The geometry of interacting tooth flanks in the differential vicinity of contact point and
2. The applied normal load at contact point

Once the local geometry of interacting tooth flanks of a gear and a mating pinion is determined, and the applied normal force is specified, the contact stress can be calculated following the routing technique.

---

<sup>1</sup> Considered in this section of the book, *low tooth count gears* can be viewed as a more general case compared to gears with a larger tooth count. The results of the calculation of contact strength obtained for low-tooth-count gears are valid for gears with a larger tooth count as well, and not vice versa.

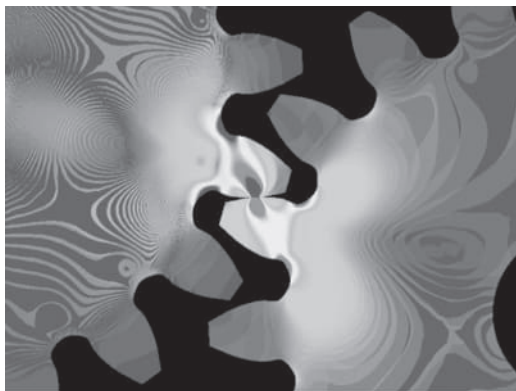


**FIGURE 23.1** Stresses in gear teeth under operating load.

An accurate model of load distribution within the line of tooth contact for gears, especially for gears that have low tooth count,<sup>2</sup> is discussed below. Gears with a low tooth count are commonly referred to as *low-tooth-count gears* (or just as *LTC – gears*, for simplicity).

### 23.1.1 ADOPTED PRINCIPAL ASSUMPTIONS

Several assumptions are adopted for the development of a load distribution model. First, it is assumed that mating gears are precise and their axes of rotation are properly aligned to each other. This assumption pertains to all kinds of gearing, namely, to parallel-axes gearing, intersected-axes gearing, and crossed-axes gearing.

It is reasonable to begin the discussion on the adopted assumptions with the assumptions made by the founder of contact mechanics of materials, the German physicist *Heinrich Hertz*.<sup>3</sup>

#### 23.1.1.1 Comments on Analytical Description of Local Geometry of Contacting Surfaces Loaded by Normal Force: *Hertz Proportional Assumption*

The investigation of the geometry of interacting surfaces under applied normal load can be traced back to the fundamental research undertaken by *H. Hertz* on the contact of solid elastic bodies [48].

Between 1886 and 1889, *Hertz* published two articles on what became known as the field of contact mechanics of materials. His work basically summarizes how two axisymmetric objects placed in contact behave under loading. The developed theory is based on *Hertz* observation of elliptical *Newton* rings formed by placing a glass sphere upon a lens; this led him to assume that the pressure exerted by the sphere follows an elliptical distribution.

The interaction of an elastic sphere and a plane is diagrammatically illustrated in Figure 23.2a. The initial contact of the sphere of a radius,  $R_{\text{sphere}}$ , and of the plane can be assumed at point,  $K$ . After a normal load,  $F_n$ , is applied, the contact point,  $K$ , spreads to a round contact patch of a radius,  $r_{pc}$ , as schematically illustrated in Figure 23.2b.

**Important notice:** Later on, contact of surfaces of *simple geometry* (*Hertz*) has been incorrectly adopted to cases of contact of surfaces with *complex geometries*.

It is of critical importance to stress here on two features of the theory developed by *Hertz*.

<sup>2</sup> Roughly, gears that feature the root diameter smaller than the base diameter are referred to as *low-tooth-count gears*. In a narrower sense, *low-tooth-count gears* are those having 15 teeth and a fewer. This definition can be enhanced to the cases of intersected-axes gearing, and of crossed-axes gearing, as well.

It should be stressed here that the results of the research obtained for *LTC – gears*, still valid for gears for which the root diameter is greater than the base diameter ( $d_{f,g} > d_{b,g}$ ).

<sup>3</sup> Heinrich Rudolf Hertz (February 22, 1857–January 1, 1894), a famous German physicist.

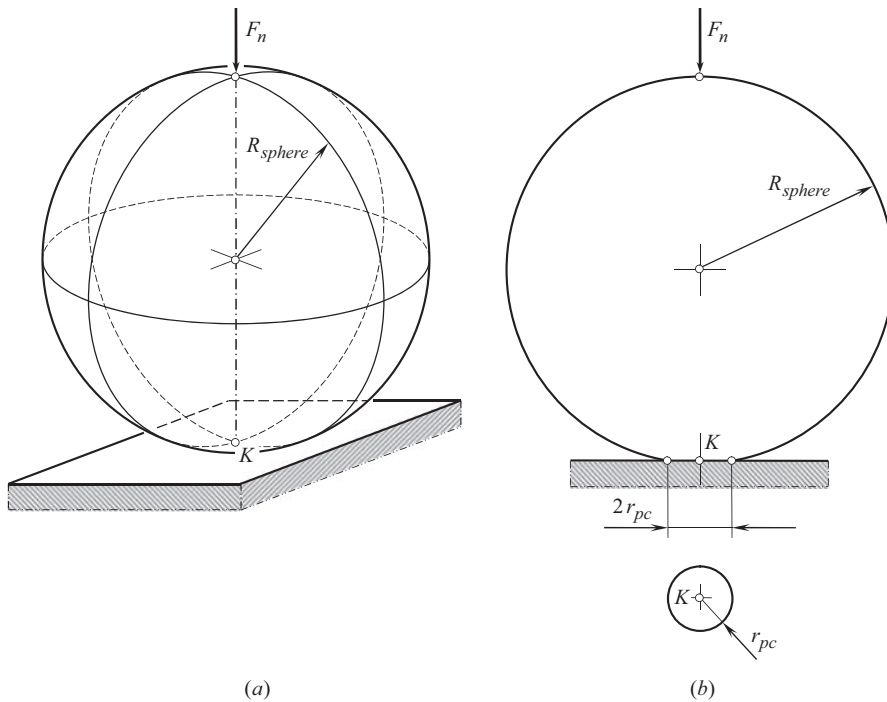


**FIGURE 23.2** Interaction of a sphere of a radius,  $R_{sphere}$ , and of a plane under a normal load,  $F_n$  : (a) geometrical model, and (b) account for elastic deformation of the sphere.

**First**, the developed theory is based on the assumption that the radius,  $r_{pc}$ , of the *contact patch* (or radius of the *bearing contact*) is much smaller compared to a radius of the sphere,  $R_{sphere}$ . The theory returns reasonable results of the calculation of contact stress if a radius,  $r_{pc}$ , is 10 (or more) times smaller than a radius of the sphere,  $R_{sphere}$ . If the inequality  $R_{sphere} \gg r_{pc}$  is not fulfilled, then the *Hertz* theory is not valid. This feature of the *Hertz* theory is often ignored, which is not correct.

### Assumption 23.1

Dimensions of the bearing contact are much smaller in comparison to the corresponding radii of curvature of the contacting elastic bodies.

The following conclusion can be immediately made from this statement: Special care is required to be undertaken when applying *Hertz* theory for the calculation of contact stress in cases of contact of elastic bodies bounded by *convex*, and by *concave* surfaces, as in this particular case the inequality  $R_{sphere} \gg r_{pc}$  is commonly violated.

**Second**, the interaction of elastic bodies bounded by surfaces only of simple geometries was considered by *H. Hertz*. A plane, spheres of various radii, and so forth were used in the research carried out by *Hertz*. It should be pointed out here that for the surfaces of such simple geometries, the principal directions at contact point,  $K$ , are either not identified (as it is observed in a sphere and in a plane) or they are congruent to one another. For the surfaces of simple geometries, the concept of the surface of relative curvature is valid. The concept of the surface of relative curvature is not valid for the surface of complex geometry in contact.

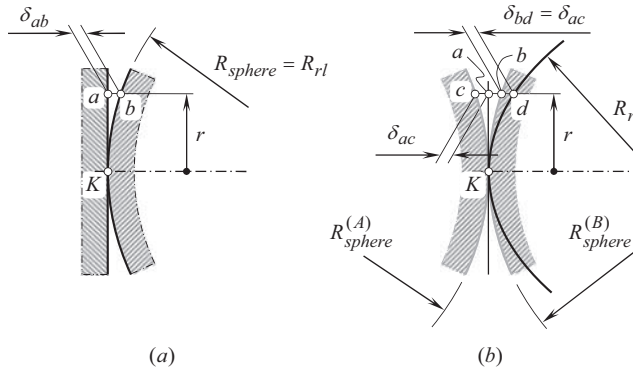


**FIGURE 23.3** Definition of relative curvature,  $R_{rl}$ , at contact point,  $K$ , of two smooth regular surfaces, 1 and 2 in cases of contact: (a) sphere-to-plane, and (b) convex sphere-to-sphere.

In the simplest case of contact of a plane and a sphere (see Figure 23.3a), an actual value of a radius of the sphere,  $R_{sphere}$ , is sufficient for an analytical description of contact geometry of the *sphere-to-plane* contact. No radius of relative curvature,  $R_{rl}$ , is necessary in this simplest case of the surfaces contact, as two radii,  $R_{sphere}$  and  $R_{rl}$ , are identical to one another ( $R_{sphere} \equiv R_{rl}$ ). The results of the analytical description of the contact geometry of a *sphere-to-plane* contact can be enhanced to suit similar problems when two bodies with more complex geometries come in contact, for example, the contact of two spheres of different radii. For this purpose, the radius of relative curvature can be taken into consideration. In the case of contact depicted in Figure 23.3a, two points,  $a$  and  $b$ , are taken at a reasonably short distance,  $r$ , from a straight line through the contact point,  $K$ . The straight line is perpendicular to the plane. Points  $a$  and  $b$  are at a distance,  $\delta_{ab}$ , from one another.

When two spheres,  $A$  and  $B$ , of radii,  $R_{sphere}^{(A)}$  and  $R_{sphere}^{(B)}$ , correspondingly (see Figure 23.3b), make contact with one another, two points,  $c$  and  $d$ , are taken into consideration. These two points are equivalent to points,  $a$  and  $b$ , in the aforementioned case of contact of a sphere, and a plane. The distance,  $\delta_{cd}$  (see Figure 23.3b), between points,  $c$  and  $d$ , significantly exceeds the distance,  $\delta_{ab}$ . For the spheres,  $A$  and  $B$ , a surface of relative curvature is designed so as to ensure equality of the distances,  $\delta_{ad}$  (see Figure 23.3b) and  $\delta_{ab}$ , as shown in Figure 23.3a. Radius of curvature of the surface of relative curvature is designated as  $R_{rl}$ . If the equality  $\delta_{ad} = \delta_{ab}$  is fulfilled, then the problem of contact of two spheres of radii,  $R_{sphere}^{(A)}$  and  $R_{sphere}^{(B)}$  (see Figure 23.3b) can be substituted with the equivalent problem of contact of a plane and a sphere (see Figure 23.3a).

In order to construct a surface of relative curvature, the following manipulations with the radii of curvatures are performed.

The contact geometry of two spheres of arbitrary radii can be expressed in terms of curvature of a sphere of relative curvature. For a sphere of a radius,  $R_{sphere}$ , its curvature is expressed by a parameter that is inverse to the radius of the sphere, namely,  $k_{sphere} = R_{sphere}^{-1}$ .

In order to accommodate the obtained results in the case of contact of two elastic bodies bounded by two spheres,  $A$  and  $B$ , a concept of the surface of relative curvature is introduced. At any normal section through contact point,  $K$ , of the bodies bounded by two spheres of the radii,  $R_{sphere}^{(A)}$  and  $R_{sphere}^{(B)}$  (with the normal curvatures,  $k_A$  and  $k_B$ , correspondingly), the normal curvature,  $k_r$ , of the surface of relative curvature is calculated from the following formula:

$$k_r = k_A + k_B \quad (23.1)$$

This formula is derived under an assumption that the deviation,  $\delta_{ad}$ , of the surface of relative curvature from the plane in the case depicted in Figure 23.3b, is equal to the deviation,  $\delta_{ab}$ , of the sphere from the plane, as illustrated in Figure 23.3a. The equality,  $\delta_{ad} = \delta_{ab}$ , is fulfilled when the

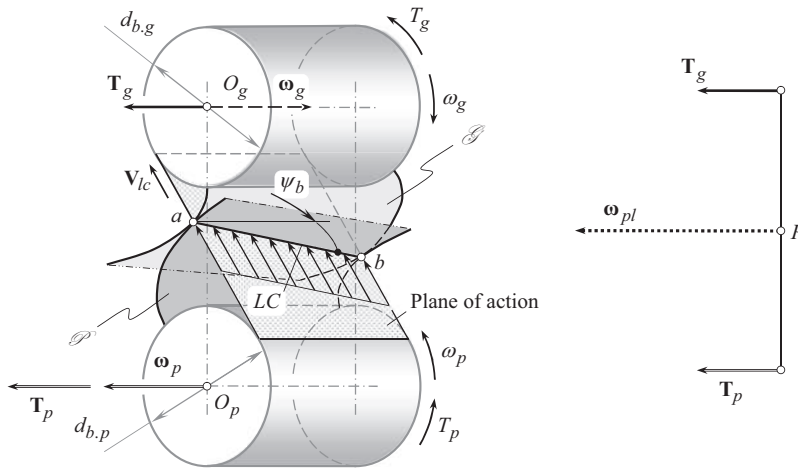


**FIGURE 23.4** Torque vectors,  $\mathbf{T}_g$  and  $\mathbf{T}_p$ , associated with gear and mating pinion.

deviations,  $\delta_{bd}$  and  $\delta_{ac}$ , are equal ( $\delta_{bd} = \delta_{ac}$ ). Such an equality ( $\delta_{ad} = \delta_{ab}$ ) is reasonable if and only if the inequality  $R_{sphere} \gg r_{pc}$  is valid. Otherwise, the application of the *Hertz* theory is invalid.

The contact of elastic bodies bounded by surfaces of more complex geometries was not investigated by *Hertz*.

Once this discussion is understood, one can proceed with the further analysis and with the calculation of contact strength of gear teeth.

### 23.1.1.2 Assumption of Even Torque Share

For the purpose of analysis as well as for the purpose of design of power gearing, the use of vectors commonly is convenient.

Power transmitted through a gear pair can be represented in terms of two parameters, namely, in terms of:

1. Rotation vectors,  $\omega_g$  and  $\omega_p$ , of driving, and of driven shafts, correspondingly, and
2. Torques,  $\mathbf{T}_g$  and  $\mathbf{T}_p$ , applied to the driving, and to the driven shafts, correspondingly, as shown in Figure 23.4.

Interaction of tooth flanks of a gear, and of a mating pinion occurs under applied load. The applied load is represented by normal force, and by friction force. Forces of the interaction between the gear and pinion teeth act within the plane of action, *PA*. As the plane of action is in tangency with both base cylinders, the tangential load is distributed evenly along the line of contact, *LC*, that passes through points, *a* and *b*.

Actual values of the forces of interaction are necessary for performing strength and stress analysis of gears. The required forces can be expressed in terms of torques acting on the input and on the output shafts and in terms of the design parameters of the gears. Ultimately, contact stresses as well as bending stresses can be calculated for a given gear pair.

The following assumption is adopted in the analysis below:

### Assumption 23.2

In geometrically accurate gearing, a torque being transmitted through a pair of gears from a driving shaft to a driven shaft is distributed evenly within the active face width of the interacting gears.

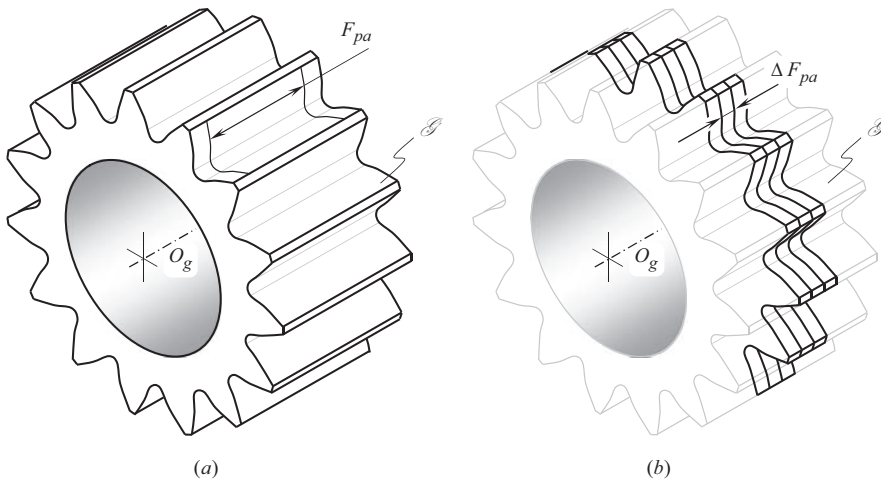


**FIGURE 23.5** Torque share within the active face width,  $F_{pa}$ , in gear pair: (a) effective face width,  $F_{pa}$ , and (b) slicing of a gear.

The active face width,  $F_{pa}$ , means either the effective face width (the overlapped portion of face widths of the gear and the pinion), or a portion of the effective face width within the lengths of the line of contact at a given instant of time.

The correctness of the assumption immediately follows from equilibrium analysis of each gear in the gear pair, which considers them as solid bodies, and an equilibrium analysis of each slice of the mating gears by transverse planes.

Consider a gear with a certain active face width,  $F_{pa}$  (see Figure 23.5a). The gear can be sliced by planes perpendicular to the gear axis of rotation,  $O_g$ , into multiple slices. Each slice is of a,  $\Delta F_{pa}$  thickness (see Figure 23.5b). The thickness,  $\Delta F_{pa}$ , can approach zero when the number of slices,  $n_s$ , approaches an infinity. In the limit case ( $\Delta F_{pa} \rightarrow 0$  when  $n_s \rightarrow \infty$ ), the thickness of slices is designated as  $dF_{pa}$ . In compliance with the aforementioned assumption, equal torque is transmitted by each slice.

For the slices featuring two (or more) portions of lines of contact, the equality of torques acting on the neighboring slices is maintained; however, the forces become twice as smaller. This is because within a slice the torque is evenly shared between two (or more) portions of the line of contact within the slice.

It should be stressed here that the torque is shared evenly within the effective face width and not within the line(s) of contact.

The adopted Assumption 23.2 makes possible the development of an accurate load model of gear teeth. This concept can be expended to gearing with intersected-axes as well as to gearing that has crossing axes of rotation of the gears.

### 23.1.2 PRINCIPAL FEATURES OF *LOW-TOOTH-COUNT GEARS*

This section of the chapter focuses on the development of a load distribution model in involute gears of a low tooth count (*LTC* – gearing, in other words).

Low-tooth-count gears feature a rapidly diminishing radius of curvature of the involute curve in the vicinity of the base circle. At the base circle, the radius of curvature becomes zero. The contact stresses (*Hertz stresses*) between gear teeth become larger as the radii of curvature become smaller; in fact, at the base circle, the stress is theoretically infinite.<sup>4</sup> Hence, involute gears should never be

<sup>4</sup> Contact stress on the base cylinder of the gear is infinite by the adopted Assumption 23.2. For this kind of tooth profile points, *Hertz* formula for the calculation of contact stresses is not valid.



designed for contact at, or near the base circle. Good design can usually minimize this drawback of the involute geometry; nevertheless, in many highly optimized designs, especially designs that have a small number of teeth, contact stress is still the principal limitation on load capacity.

A basic geometric fact of great significance for the consideration is that given a fixed center distance and speed ratio, any one of the curves (pinion tooth profile, gear tooth profile, and path of contact) completely determines the other two.<sup>5</sup> Thus, it is possible to find mathematical relationships between tooth curvatures from given properties of the path of contact.

For an involute system, the path of contact is a straight line, and the relative curvature for each of its mating gears near its base circle approaches infinity. Since a large relative curvature indicates a high probability of surface failure, one can readily understand that an involute gear is weak near its base circle. The weakness problem of involute gears is emphasized even more when one considers that for involute gears that have relatively few teeth (less than about 16), the teeth are undercut near their base circle.

A pair of spur or helical gears in mesh makes line contact, and the curvature of the mating surfaces at points along the lines of contact differs according to the relative dimensions of the gear concerned and varies with each phase of contact. In external gears, contact is *convex-to-convex*, whereas for internal gears, it is *convex-to-concave*. It is commonly supposed that the nature of teeth contact is analogous to that of two cylinders, the diameters of which are dependent on the conditions prevailing at any given point of contact on the line of action. Such an assumption is valid only for gears with a large number of teeth. Gears that have a low tooth count have to be modeled by corresponding cones of revolution.

### 23.1.3 ANALYTICAL MODEL FOR CALCULATION CONTACT STRESS

The corresponding radii of normal curvature,  $\rho_{n,g}$ , of the gear tooth flank, and that,  $\rho_{n,p}$ , of the pinion tooth flank, are measured within the plane that is perpendicular to the line of contact. At the point of intersection within the line of contact,  $LC$ , the radii of normal curvature,  $\rho_{n,g}$  and  $\rho_{n,p}$ , are equal to the lengths of the straight-line segments connecting the line of contact and the axis of rotation of the corresponding equivalent cones.

The straight-line generators of the cone surfaces,  $C_g$  and  $C_p$ , align with the corresponding straight-line generators,  $E_g$  and  $E_p$ , of the involute screw surfaces,  $\mathcal{S}$  and  $\mathcal{P}$ , of the gear, and the pinion, correspondingly. The normal curvatures of the cone surfaces,  $C_g$  and  $C_p$ , are equal to the corresponding normal curvatures of the tooth flanks,  $\mathcal{S}$  and  $\mathcal{P}$ . Along the straight-line generators, the cones of revolution,  $C_g$  and  $C_p$ , are identical to the corresponding tooth surfaces,  $\mathcal{S}$  and  $\mathcal{P}$ , up to members of the second order. Thus, the implementation of the  $DG/K$ -based<sup>6</sup> method of surface generation for the derivation of equations for the calculation of geometry of the cones of revolution,  $C_g$  and  $C_p$ , makes sense.

The equivalent cones of revolution,  $C_g$  and  $C_p$ , are loaded by the distributed load,  $f_N$ , which is pointed perpendicular to the line of contact of the equivalent cones. Under the distributed load,  $f_N$ , the equivalent cones of revolution,  $C_g$  and  $C_p$ , are rotated about their axis, as illustrated in Figure 23.6. The rotations of the equivalent cones are designated as,  $\omega_g^c$  and  $\omega_p^c$ , correspondingly.

<sup>5</sup> It should be stressed here that this statement is valid only for involute gears and is invalid in gears with other tooth flank geometries.

<sup>6</sup> The  $DG/K$ -based method of surface generation is based on fundamental results obtained in the differential geometry of surfaces, and on kinematics of multi-parametric motion of a rigid body in  $E3$  space. This method is developed by the author and is disclosed in: Radzevich, S.P., *Differential-Geometric Method of Surface Generation*, DrSc thesis. Tula, Tula Polytechnic Institute, 1991, 300p, [148]. The interested reader is referred to the monograph: Radzevich, S.P., *Kinematic Geometry of Surface Machining*, CRC Press, Boca Raton, Florida, 2007, 536p. Second edition: Radzevich, S.P., *Generation of Surfaces: Kinematic Geometry of Surface Machining*, CRC Press, Boca Raton, Florida, 2014, 738 pages [152].



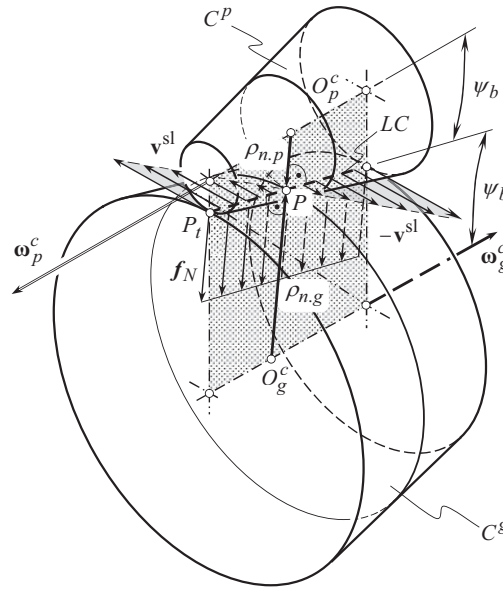


FIGURE 23.6 Interaction of modeling cones of revolution under load.

Denoted by  $\mathbf{V}^{\text{sl}}$ , the relative sliding of the cone surfaces  $C_g$  and  $C_p$  is observed under such rotation of the equivalent cones.

As it follows from this discussion, the total length of the line of contact is an important consideration for tooth failure analysis in *LTC* – gearing. The longer the total line of contact,  $LC_\Sigma$ , the lower the load per unit length of the line of contact, and vice versa.

The distribution of the tangential load,  $f_t$ , within the line of contact,  $LC$ , is linear. Moreover, the distributed load,  $f_t$ , is of a constant value. The normal component of the distributed load,  $f_N$ , can be expressed in terms of the tangential load,  $f_t$ , and of the base helix angle  $\psi_b$  as:

$$f_N = f_t \cos \psi_b \quad (23.2)$$

For further analysis, both the equivalent cones of revolution,  $C_g$  and  $C_p$ , can be sliced into an infinite number of infinitely thin,  $dL_c$ , cylinders as shown in Figure 23.7. The axis of rotation of the infinitesimally thin cylinders of the gear,  $O_g^c$ , and that of the pinion,  $O_p^c$ , are within the plane of action, and they are parallel to the line-to-tooth contact. The radii of the cylinders are equal to the first principal radii of curvature of the screw involute tooth flanks,  $\mathcal{S}$  and  $\mathcal{P}$ , or, the same, they are equal to the first principal radii of curvature of the equivalent cones of revolution,  $C_g$  and  $C_p$ . For calculation of the normal radii of curvature of the gear,  $\rho_{n,g}$ , and that of the pinion,  $\rho_{n,p}$ , the use of the *Meusnier equation* is helpful [148,153].

It should be mentioned here that in the case of large tooth counts, the modeling cones degenerate to corresponding modeling cylinders. This load distribution model is illustrated in Figure 23.8. Local substitution of screw involute surfaces with the infinitesimally thin cylinders is applicable for both gears that have a low number of teeth and gears with a regular teeth number. In cases of large tooth counts, the gear teeth are loaded as schematically illustrated in Figure 23.9.

The proposed load distribution model is used in the computer code for the computation of the distribution of contact stresses within the path of contact. An example of the results of the computation of the distribution of maximal contact stresses within the path of contact is shown in Figure 23.10.

In Figure 23.10, zones A and C are the zones where the *Hertz* assumption is not valid. Thus, *Hertz* formula is valid only for points within the zone, B, where Assumption 23.1 is fulfilled.

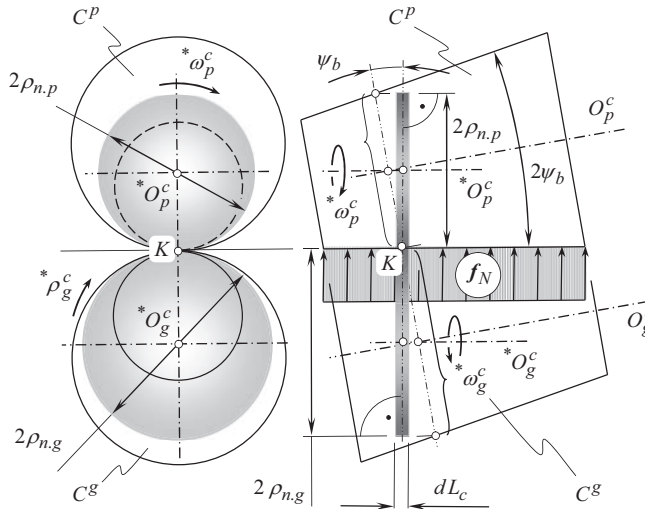


**FIGURE 23.7** Local substitution of equivalent cones of revolution,  $C^g$  and  $C^p$ , with the infinitesimally thin,  $dL_c$ , cylinders.

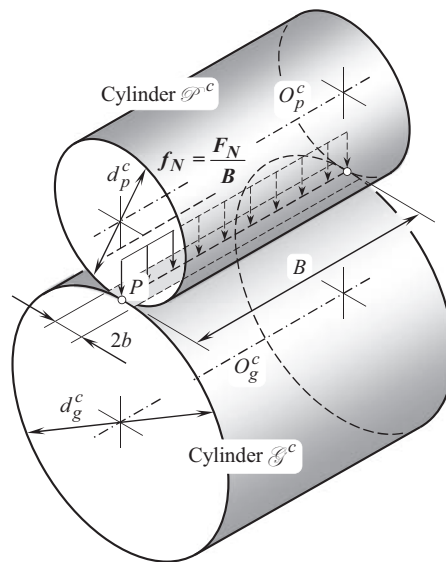


**FIGURE 23.8** Local approximation of screw involute tooth flanks,  $\mathcal{G}$  and  $\mathcal{P}$ , with equivalent cylinders of revolution,  $\mathcal{G}^c$  and  $\mathcal{P}^c$ .

The distribution curve,  $\sigma_c^{\max}(z)$ , is of asymmetric geometry. The point at which the minimum contact stresses,  $(\sigma_c^{\max})_{\min}$ , are observed is shifted from the pinion toward the gear at a certain distance,  $\Delta Z_{lr}$ . This point is at a distance,  $\Delta Z_p$ , from the pitch point,  $P$ . The shift,  $\Delta Z_{lr}$ , is caused by the normal force per unit length of the path of contact,  $f_N(z)$ , which varies within the path of contact. For conventional gear drives, this variation of the component,  $f_N(z)$ , is negligibly small. Therefore, for conventional gear drives the shift  $\Delta Z_{lr} \approx 0$ .

For a gear drive of a low number of teeth, the distribution of the maximum contact stresses within the line of contact,  $LC$ , is illustrated in Figure 23.11.



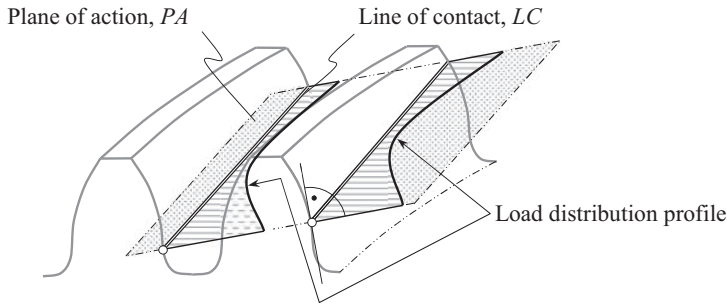


**FIGURE 23.11** Distribution of *Hertz* contact stress within line of contact, *LC*, in *low-tooth-count* gearing.

Similarly, the model of contact loads of parallel-axes gear drives can be constructed for cases of intersected-axes gearing as well as of crossed-axes gears.

#### 23.1.4 FORMULA FOR CALCULATION *HERTZ* CONTACT STRESS

The pitting resistant formula is based on *Hertz contact stress equation* for cylinders with parallel axes (see Figure 23.9). The load applied to the cylinder is the load normal to the tooth flank, and the length of contact is the minimum total length of lines of contact in the contact zone of the gear set. The radii of the cylinders are the radii of curvature of the teeth at the point of contact for the mating pair of gears. Depending on the face gear ratio of the gear set, this point can be the mean diameter of the pinion or the lowest point of single-tooth contact on the pinion. Additional rating factors are also added to the basic equation to adjust the stress due to factors peculiar to gearing. Starting with the general *Hertz equation*:

$$s_c = \frac{2W}{\pi bL} \quad (23.3)$$

$$b = \sqrt{\frac{2W}{\pi L} \cdot \frac{\frac{1-\mu_1^2}{E_1} + \frac{1-\mu_2^2}{E_2}}{\frac{1}{d_1} + \frac{1}{d_2}}} \quad (23.4)$$

where

$s_c$  is the maximum stress of parallel-axis cylinders.

$W$  is the contact load normal to the cylinders.

$b$  is the semi-width of contact between cylinders, in.

$L$  is the length of contact between cylinders, in.

$\mu_1, \mu_2$  is the *Poisson's ratio* of material of cylinders 1 and 2.

$E_1, E_2$  modulus of elasticity of material of cylinders 1 and 2.

$d_1, d_2$  diameter of cylinders 1 and 2.

#### 23.1.5 SPECIFIC PRESSURE FACTOR

Specific pressure factor,  $\gamma$ , is of critical importance when performing calculation of gear teeth on contact strength. By definition, the specific pressure factor equals to:

$$\gamma = \frac{m}{\rho_{rel}} \quad (23.5)$$

where the module is designated as  $m$ , and relative curvature is denoted by  $\rho_{rel}$ .

It is convenient to represent Eq. (23.5) in the form:

$$\gamma = \frac{mC}{\rho_g(C/\cos\phi_t - \rho_g)\cos\phi_t} \quad (23.6)$$

Here the center distance is designated as  $C$ , the transverse pressure angle is denoted by  $\phi_t$ , and radius of curvature of the gear is designated as  $\rho_g$ .

### 23.1.6 COMBINED COMPRESSIVE-SHEAR STRESS IN LOW-TOOTH-COUNT GEARING

The following stress is present in the region of contact band: In the center of the band, there is a point of maximal compressive stress. Directly underneath this point, there is a maximal subsurface shear stress. Approximately, the depth to the point of maximum shear stress is a little less than one-third the width of the band of contact.

The gear-tooth surfaces move across each other with a combination of rolling and sliding motions. The sliding motion plus friction tends to cause additional surface stresses. Just ahead of the band of contact, there is a narrow band of compression. Just behind the band of contact, there is a narrow region of tensile stresses. A bit of metal on the surface of a gear tooth goes through a cycle of compression and tension each time a mating gear tooth passes over it. There may also be rupturing of the metal due to subsurface shear stresses.

In general, the interaction between the gear- and the pinion tooth surfaces in low-tooth-count gearing can be considered as rolling and sliding of elastically dissimilar cylinders. For further analysis, the aforementioned model of tooth loading (see Figure 23.6) can be implemented. For this purpose, the zone of contact of the surfaces,  $\mathcal{S}$  and  $\mathcal{P}$ , (see Figure 23.12a) is considered as contact of two cylinders loaded by a normal force,  $W_N$ , and a shear force,  $Q$ . It is assumed that the shear force,  $Q$ , is sufficient to cause sliding of the contacting surfaces.

Shear traction, whether arising from sliding friction or other sources, causes a vertical displacement of the surface of the components [51]. However, since the shear traction distribution is mutual, the  $y$ -direction displacements will also be the same if the materials are the same. Hence, the integral equation reduces, as the influence of the shear and direct tractions may be treated separately, and

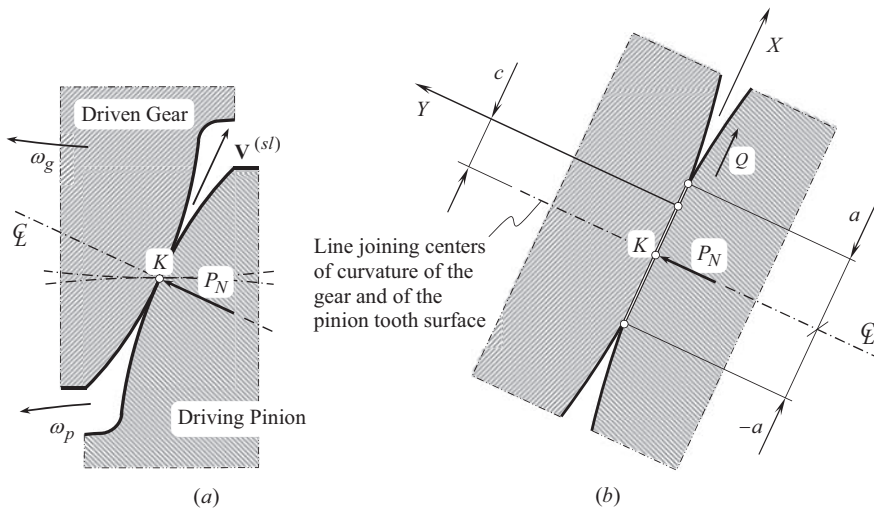


**FIGURE 23.12** Contact of two cylinders loaded by normal load,  $P_N$ , and shear force,  $Q$ , which is sufficient to cause sliding: (a) schematic of loading by normal force,  $P_N$ , and (b) shear force,  $Q$ .

such problems are said to be uncoupled. The effect of sliding of two cylinders is to induce a shear traction distribution that is limited everywhere by friction, that is, if the *Coulomb* friction law is assumed, which indicates that the friction force is proportional to the normal force and independent of speed, we have:

$$\frac{|q(x)|}{f} = -p(x) = p_0 \sqrt{1 - (x/a)^2} \quad (23.7)$$

where  $f$  designates the coefficient of friction.

However, if the contacting bodies are dissimilar there is a coupling effect. It must still be true that the shear stress is everywhere limited by friction, that is:

$$q(x) = -f \cdot p(x) \quad (23.8)$$

We do not expect the contact patch to be positioned on the line joining the centers of the cylinders:

$$\frac{1}{\pi} \int_{-a}^a \frac{p(\xi) \cdot d\xi}{x - \xi} + \beta \cdot f \cdot p(x) = \frac{-k(x - c)}{A} \quad (23.9)$$

This is a *Cauchy* singular integral equation of the second kind, which can be solved directly.

The tangential offset,  $c$ , is found from the consistent condition:

$$\int_{-a}^a \frac{(x - c) \cdot dx}{(a - x)^m (a + x)^{1-m}} \quad (23.10)$$

These equations can be more convenient treated if rewritten as follows [53]:

$$p_0 = \frac{P \cdot \sin(m\pi)}{2 \cdot \pi \cdot a \cdot m \cdot (1 - m)} \quad (23.11)$$

$$a^2 = \frac{P \cdot A}{2 \cdot \pi \cdot m \cdot (1 - m) \cdot k} \quad (23.12)$$

$$\frac{p(s) \cdot a}{P} = -\frac{\sin(m\pi)}{2 \cdot \pi \cdot m \cdot (1 - m)} \cdot (1 - s)^m (1 + s)^{1-m} \quad (23.13)$$

The aforementioned equations are expressed in terms of the parameters of the contact zone shown in Figure 23.12.

In practice, the actual value of parameter  $|\beta|$  rarely exceeds  $|\beta| = 0.4$  and, hence, if the maximal value of  $f$  is about  $f = 0.6$  then  $m$  lies in the range  $m = 0.46 \div 0.54$ . The difference from *Hertz'* solution to the problem is therefore small and confident to the very near surface.

Using the aforementioned equations, a computer code is worked out for the computation of both contact stresses, and the combined compression and shear stresses ( $C/S$  – stresses). A qualitative example of the analysis is shown in Figure 23.13. Here, the distribution of the combined  $C/S$  – stresses across the band of contact is depicted. Figure 23.13 reveals that due to the gear-tooth sliding, the stress distribution curve assumes an asymmetrical shape.

The use of the discussed method also yields computation of just contact stresses. For this purpose, it is required to enter into the aforementioned equations the load  $Q = 0$ . The results of such

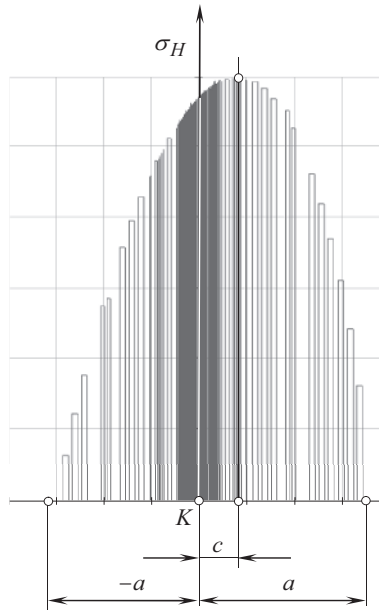


**FIGURE 23.13** Qualitative example of combined compression and shear stresses ( $C/S$  – stresses) distribution across band of contact.

computations perfectly correlate with the results of computations obtained using the method of computation of contact stresses (in accordance with the *Hertz'* approach).

The performed preliminary analysis indicates that the difference between the combined  $C/S$  – stresses and between contact stresses for a conventional gear drive in most cases is negligibly small. However, for *LTC* – gearing shear stresses could add significantly to the resultant  $C/S$  – stresses. The performed computations show that the difference between the combined  $C/S$  – stresses and between contact stresses reaches up to 15%. This result indicates that for *LTC* – gearing, shear stresses should be taken into consideration.

## 23.2 BENDING STRENGTH OF GEAR TEETH

The strength of gear teeth and bending strength, in particular, are of critical importance for all power gear trains. Gear teeth must be strong enough to withhold the applied loads. In order to design gears properly, it is necessary to know how stress in the gear tooth body can be calculated. The calculation of the bending strength of a gear tooth is a very challenging engineering problem.

### 23.2.1 COMMENTS ON *LEWIS' FORMULA*

Many attempts have been undertaken to develop a practical method to calculate the bending stress in a gear tooth loaded by torque that is being transmitted by the gear pair. Almost all attempts fall into one of two categories.

The first is based on the application of conventional equations that are developed in the *Strength of Materials*. *Lewis'* formula is the best-known way to make calculations of this sort.

The second is based on the application of the finite element method (*FEM*).

Without going into details of the implementation of *FEM* software for the computation of bending stress in a gear tooth, let us briefly outline the main reason why the conventional equations developed in *Strength of Materials* are not valid for the calculation of bending stress in a gear tooth.

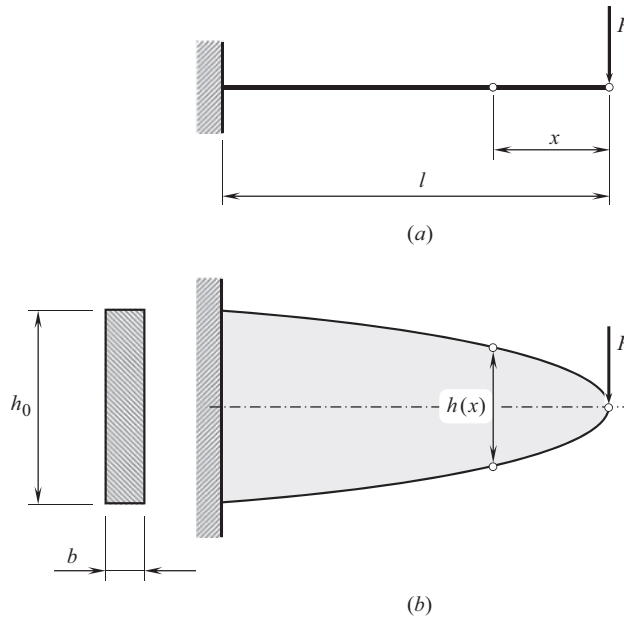


**FIGURE 23.14** Geometry of equally strong cantilever beam: (a) schematic of a cantilever beam, and (b) parabolic shape of lengthwise section of the rectangular cantilever beam.

As most of the equations are derived for engineering purposes, conventional formulas for the calculation of bending stress in a cantilever beam are derived under the *Saint Venant's Principle*.<sup>7</sup>

Some comments on the calculation of bending stress in gear teeth are briefly outlined in the section that follows immediately below.

### 23.2.1.1 Cantilever Beam of Equal Strength

There are many similarities between the loading of a gear tooth and loading of a cantilever beam. These similarities inspired gear engineers to implement the results developed for a cantilever beam for the calculation of the bending strength of a gear tooth.

Consider a cantilever beam of a certain length,  $l$ , that is loaded by a bending force,  $P$ . A schematic of this loading is illustrated in Figure 23.14a.

Let us assume that the beam is of equal bending strength. For cantilever beams of this particular kind, the maximum bending stress,  $\sigma_{\max}$ , at every cross-section is equal to the yield stress,  $[\sigma]$  :

$$\sigma_{\max} = \frac{|M(x)|}{W(x)} = [\sigma] \quad (23.14)$$

where

$M(x)$  is the applied torque [  $M(x) = Px$  ].

$P$  is the load applied at the end of the cantilever beam.

$x$  is the distance from the end of the cantilever beam to point of interest within length,  $l$ , of the beam.

<sup>7</sup> *Saint-Venant's Principle*, named after the French elasticity theorist Adhémar Jean Claude Barré de Saint-Venant, can be stated as saying that: "... the difference between the effects of two different but statically equivalent loads become very small at sufficiently large distances from load." Occasionally, *Saint-Venant's Principle* is also called *Saint-Venant's Assumption*.



$W(x)$  is the section module of the cross-sectional area at the distance  $x$  from the end of the cantilever beam.

An equation for the calculation of the dimensions of a cross-section of the equal strength beam immediately follows from Eq. (23.14):

$$W(x) = \frac{M(x)}{[\sigma]} \quad (23.15)$$

It is assumed here that the cantilever beam is of a rectangular cross-section. The width,  $b$ , of the cross-section is constant within the length,  $l$ , of the cantilever beam. The height,  $h$ , of the cantilever beam is variable,  $h = h(x)$ , within the length,  $l$ , of the cantilever beam.

With that said, Eq. (23.15) can be rewritten in the form:

$$W(x) = \frac{bh^2(x)}{6} \quad (23.16)$$

In the case under consideration, the equality  $|M(x)| = Px$  is valid. Therefore,

$$\frac{bh^2(x)}{6} = \frac{Px}{[\sigma]} \quad (23.17)$$

Equation (23.17) casts into an expression for  $h(x)$ :

$$h(x) = \sqrt{\frac{6P}{b[\sigma]}} \cdot \sqrt{x} \quad (23.18)$$

This equation can also be represented in an equivalent form:

$$x = \frac{b[\sigma]}{6P} \cdot h_x^2 \quad (23.19)$$

As follows from Eq. (23.18), the height,  $h(x)$ , of the equal strength cantilever beam follows a parabolic function (see Figure 23.14b). It should be mentioned here that for the calculation of maximum height,  $h_0$ , the following formula can be used:

$$h_0 = \sqrt{\frac{6P}{b[\sigma]}} \cdot \sqrt{l} \quad (23.20)$$

The derived Eq. (23.19) for an equal strength cantilever beam is used for the calculation of the bending strength of a gear tooth.

### 23.2.1.2 *Lewis' Formula for the Calculation of Bending Strength of Gear Teeth*

Being concerned with the necessity of performing the calculation of the bending stress of a gear tooth, in the late 1890, *W. Lewis* proposed [73] a corresponding formula. To derive the formula, *Lewis* inscribed a parabola into the gear tooth shape (see Figure 23.15) and then calculated stress in the gear teeth for the cantilever beam for the inscribed parabolic shape instead of calculating the actual the gear tooth shape.

In the worst-case scenario of gear tooth loading, the force,  $F$ , is applied at the tooth tip, namely, at point  $a$ . At point  $a$  the force,  $F$ , can be resolved into two components. The tangential component of the force,  $F$ , is labeled as  $P$ . This component can be expressed in terms of the force,  $F$ , and the

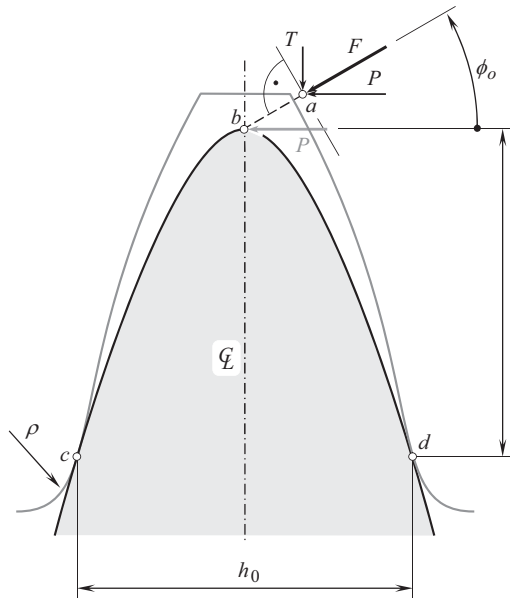


**FIGURE 23.15** Parabola inscribed into gear tooth shape.

transverse pressure angle,  $\phi_o$ , measured at a major diameter of the gear:  $P = F \cos \phi_o$ . The radial component,  $T$ , can be calculated from the expression  $T = F \sin \phi_o$ .

The line, along which the applied force,  $F$ , acts, intersects the centerline,  $\mathfrak{C}$ , of the gear tooth shape at certain point,  $b$ . The component,  $P$ , of the force,  $F$ , is applied at this point,  $b$ .

Then, a parabola is inscribed into the gear tooth shape. The apex of the parabola is located at point,  $b$ . The parabola makes tangency with the gear tooth shape at certain points,  $c$  and  $d$ . Once points,  $b$ ,  $c$  and  $d$ , are determined, the dimensions,  $h_0$  and  $l$ , are considered known design parameters.

The use of the inscribed parabola makes it possible to calculate the bending stress for a cantilever beam of known geometry and design parameters, instead of calculating the stress for an indefinite case with unknown parameters,  $h_0$  and  $l$ , for the original shape of the gear tooth. The maximum stress is equal to:

$$\sigma_{\max} = \frac{|M(x)|}{W(x)} \quad (23.21)$$

Calculations are performed for an equivalent cantilever beam, as shown in Figure 23.16. The applied distributed load is  $p = P/F_g$ , where face width of the gear is denoted by  $F_g$ . It should be pointed out here that such a schematic for the loading of the gear tooth is not equivalent to the actual loading of the gear tooth. For example, the radial component,  $T$ , is not incorporated into the diagram of the gear tooth loading shown in Figure 23.16. Ignoring the load,  $T$ , is not allowed when accurate calculations need to be performed.

However, the root cause of poor accuracy of the calculations is that when the *Saint Venant's*<sup>8</sup> *Principle* (1855) is taken into account, the *Hooke's* law is violated in the loading model that is used for derivation of *Lewis' formula*. This is illustrated in Figure 23.17.

<sup>8</sup> Adhémar Jean Claude Barré de Saint-Venant (August 23, 1797 – January 6, 1886), a French mathematician and mechanician. Saint-Venant, A. J. C. B., “Memoire sur la Torsion des Prismes,” *Mémoires Présentés Par D Divers Savants*, 14, 1855, pp. 233–560.

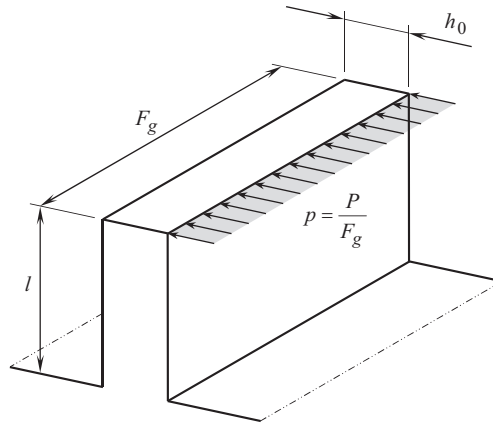


FIGURE 23.16 Equivalent cantilever beam used as a replacement for the actual shape of gear tooth.

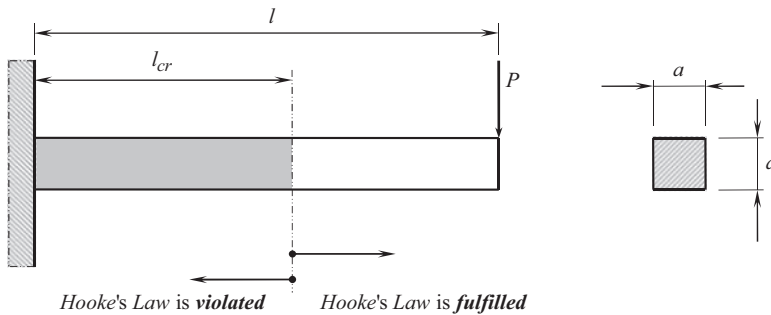


FIGURE 23.17 On explanation of *Saint Venant's Principle*.

In Figure 23.17, a cantilever beam is shown. The cantilever beam is loaded by a bending force,  $P$ . The distribution of the actual stress in the cantilever beam under the applied load strongly depends on the clamping of the beam, any changes in its shape and dimensions, and so forth. The calculated stress within the body of the cantilever beam correlates with the actual stress at a distance from the place of clamping that exceeds three to five (and not less than one) characteristic dimension, namely, the maximal dimensions of cross-section of the cantilever beam. For example, cantilever beam has squared cross-section of size  $a \times a$  (Figure 23.17). The influence of clamping on the distribution of stress is negligibly small and can be ignored at a certain critical distance,  $l_{cr} = (3 \dots 5)a$ . Within the length  $0 \leq l \leq l_{cr}$ , *Hooke's Law* is violated. This makes it impossible to have an accurate calculation of stress using elementary formulas derived from strength of materials.

With respect to gear teeth, the length,  $l_{cr}$ , should exceed  $l_{cr} = (3 \dots 5)F_g$ , [or at least  $l_{cr} = F_g$ ], where  $F_g$  designates the face width of the gear.

The discussion on the correctness of implementation of *Saint Venant's Principle* to the calculation of bending stress in gear teeth can also be illustrated by the following example.

The so-called effect of the stress concentration is due to the effect of *Saint Venant's Principle*. The stress concentration is observed in the cross-sections at which the shape, and dimensions of a specimen are changed. The larger the changes in the shape, and dimensions, the higher the raise of stress levels.

The distribution of bending stress within the body of a cantilever beam is illustrated in Figure 23.18.

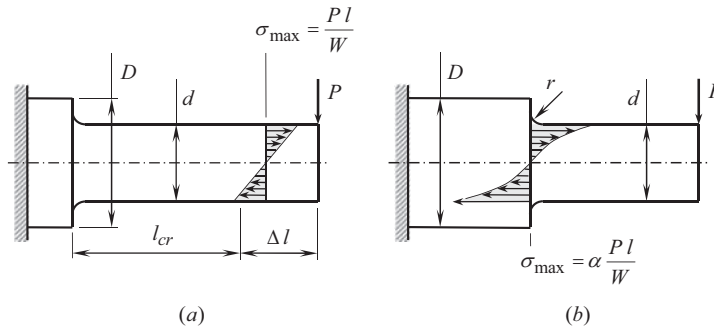


**FIGURE 23.18** Distribution of stress within the body of cantilever beam in case (a) with no effect of *Saint Venant's principle* and (b) with an effect of *Saint Venant's principle*.

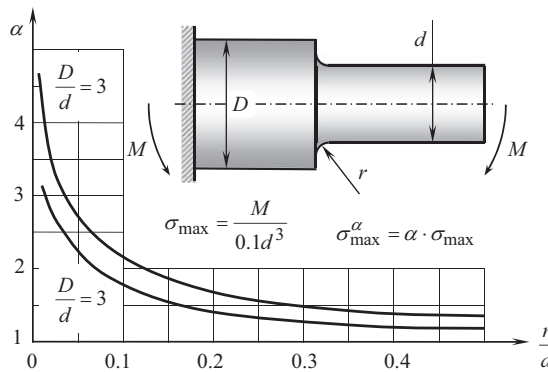


**FIGURE 23.19** Impact of stress raiser onto maximum stress within the body of cantilever beam.

No stress increase is observed in a cross-section for which there is no effect of *Saint Venant's Principle*. An example of such a cross-section is depicted in Figure 23.18a. This cross-section is located beyond the critical length,  $l_{cr}$ . Therefore, the bending stress for this cross-section can be calculated from Eq. (23.21).

In a cross-section that is closer to the place where the change of shape is observed (see Figure 23.18b), for calculation of bending stress, the following expression can be used:

$$\sigma_{\max}^{\alpha} = \alpha \sigma_{\max} \quad (23.22)$$

In Eq. (23.22), the theoretical coefficient of stress concentration is designated as  $\alpha$ .

The value of the coefficient,  $\alpha$ , depends on the ratio of the diameters,  $D$  and  $d$ , of the neighboring portions of the specimen, as well as on the radius,  $r$ , of the blend. Methods that are developed in the theory of elasticity are used for the calculation of the stress concentration factor,  $r$ .

An example of the function,  $\alpha = \alpha\left(r, \frac{d}{D}\right)$ , is illustrated in Figure 23.19. This example reveals that the use of mathematical expressions developed in the elementary strength of materials is not capable of returning accurate value for the bending stress.

The shape of a gear tooth is of a complex geometry. No elementary formulas from the strength of materials are capable of returning results of the calculations, which properly correlate with the actual bending stress within the tooth body of a gear.

No sufficient analytical solution to the problem is proposed yet.

### 23.3 EFFECTIVE LENGTH OF LINE OF CONTACT

The main purpose of power gears is to transmit torque from the input shaft to the output shaft of the gear pair. Transmission of torque from the driving pinion to the driven gear is observed when the gear teeth interact with one another. The interacting tooth flanks of the geometrically accurate gear and the mating pinion are in line contact. Physically, the power is transmitted through a narrow strip of the teeth surfaces contact. This strip is along the line(s) of contact,  $LC$ , between the gear tooth flank,  $\mathcal{G}$ , and the mating pinion tooth flank,  $\mathcal{P}$ . The longer the line of contact,  $LC$ , the more power can be transmitted by the gear pair. This clearly shows the importance of the longer line of contact between the tooth flanks of a gear and a mating pinion.

The length of the line of contact is a critical consideration for the designer of a gear pair. Three different types of the lengths of the line of contact,  $LC$ , are considered:

1. the maximum length of a single line of contact,  $l_{LC}$
2. the total length of the lines of contact,  $l_{LC}^t$ , and
3. the effective length of the lines of contact,  $l_{LC}^e$ .

Let us begin the discussion from the simplest case of the length of a single line of contact.

#### 23.3.1 LENGTH OF SINGLE LINE OF CONTACT IN PARALLEL-AXES GEARING

The length,  $l_{LC}$ , of a single line of contact can be expressed in terms of the design parameters of a gear and a mating pinion.

In spur gears, the maximum length of a single line of contact,  $l_{LC}$ , is always equal to the effective face width,  $F_{pa}$ , of the gear pair. The equality  $l_{LC} = F_{pa}$  is illustrated in Figure 23.20a. Here, the *effective face width* is understood in sense of the lengths of the gear face width,  $F_g$ , and the pinion face width,  $F_p$ , which overlap one another. The tooth flanks of the gear,  $\mathcal{G}$ , and the mating pinion,  $\mathcal{P}$ , contact one another within the entire effective face width  $F_{pa}$ .

In case of gears that have relatively small base helix angle,  $\psi_b$ , namely, when the inequality:

$$\psi_b \leq \tan^{-1} \left( \frac{Z}{F^e} \right) \quad (23.23)$$

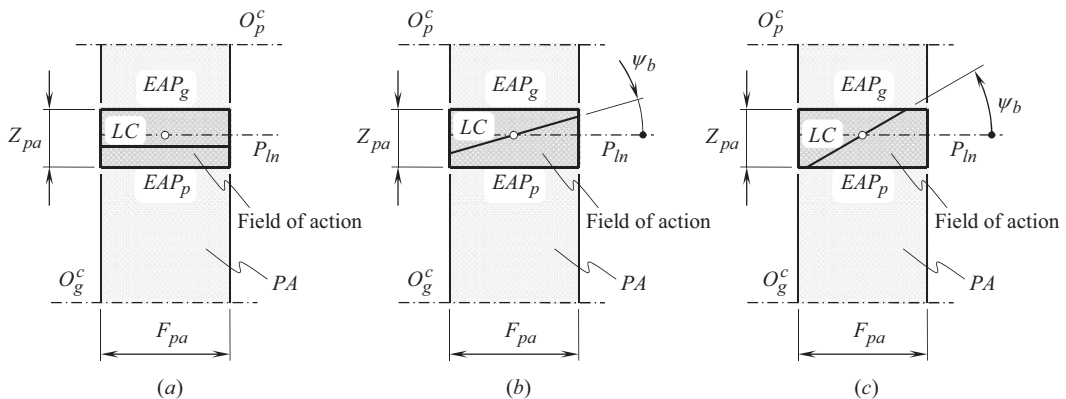


**FIGURE 23.20** Maximum length of single line of contact,  $LC$ , (a) in spur gears, (b) in helical gears with  $\psi_b \leq \tan^{-1} \left( \frac{Z}{F_{pa}} \right)$ , and (c) in helical gears with  $\psi_b \geq \tan^{-1} \left( \frac{Z}{F_{pa}} \right)$ .

is valid, the maximum length of a single line of contact,  $l_{LC}$ , can be calculated from the expression:

$$l_{LC} = \frac{F^e}{\cos \psi_b} \quad (23.24)$$

This case is illustrated in Figure 23.20b.

When the base helix,  $\psi_b$ , exceeds the value given by Eq. (23.23):

$$\psi_b \geq \tan^{-1} \left( \frac{Z}{F^e} \right) \quad (23.25)$$

the equation:

$$l_{LC} = \frac{Z}{\sin \psi_b} \quad (23.26)$$

can be used for the calculation of the maximum length of a single line of contact,  $l_{LC}$ . This case is diagrammatically shown in Figure 23.20c.

Consider an external parallel-axes gearing that is schematically illustrated in Figure 23.20. The axis of rotation,  $O_g$ , of the gear, and the axis of rotation,  $O_p$ , of the mating pinion are at a center distance,  $C$ . The radius of the base cylinder of the gear is designated as  $r_{b,g}$ , and the radius of the base cylinder of the pinion is labeled as  $r_{b,p}$ . The plane of action,  $PA$ , is in tangency to both the base cylinders. The lines of the tangency,  $O_g^c$  and  $O_p^c$ , are, by nature, the axes of rotation of the modeling cones of the gear tooth flank,  $\mathcal{S}$ , and of the pinion tooth flank,  $\mathcal{P}$ .

The plane of action,  $PA$ , is intersected by the gear outer cylinder of a radius,  $r_{b,g}$ . The line of intersection is labeled as  $EAP_g$ , which stands for the *end of the active profile* of the gear teeth. Similarly, the plane of action,  $PA$ , is intersected by the pinion outer cylinder of radius,  $r_{b,p}$ . The line of intersection is labeled as  $EAP_p$ , which stands for the *end of the active profile* of the pinion teeth. A portion of the plane of action that is located in between the lines  $EAP_g$  and  $EAP_p$  is referred to as the *field of action*. Commonly (but not always), the width,  $Z_{pa}$ , of the field of action,  $FA$ , is shorter compared to that of the plane of action,  $PA$ .

Referring to Figure 23.21, the maximum length,  $l_{LC}$ , of a single line of contact is calculated from the equation:

$$l_{LC} = \frac{Z_{pa}}{\sin \psi_b} \quad (23.27)$$

where the base helix angle is designated as  $\psi_b$ .

The width,  $Z_{pa}$ , of the field of action,  $FA$ , can be expressed in terms (a) of the radius of curvature,  $\rho_g$ , of the gear involute tooth profile, and the radius of curvature,  $\rho_p$ , of the pinion involute tooth profile at the corresponding major diameter,  $d_{o,g}$  and  $d_{o,p}$ , (b) of the center distance,  $C$ , and (c) of the transverse pressure angle,  $\phi_t$ , as:

$$Z_{pa} = (\rho_g + \rho_p) - C \sin \phi_t \quad (23.28)$$

In Eq. (23.28), the radii of curvature,  $\rho_g$  and  $\rho_p$ , are calculated from the following formulas:

$$\rho_g = \sqrt{r_{o,g}^2 - r_{b,g}^2} \quad (23.29)$$

$$\rho_p = \sqrt{r_{o,p}^2 - r_{b,p}^2} \quad (23.30)$$



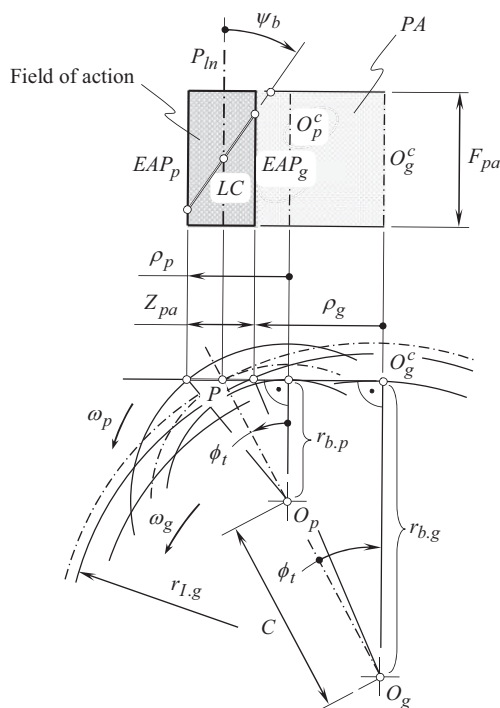


**FIGURE 23.22** Line of contact,  $LC$ , in internal parallel-axes involute gearing.

As noted previously, the maximum length of single line of contact depends on the configuration of two lines,  $EAP_g$  and  $EAP_p$ , within the plane of action. This means that changes to the shape as well as to the configuration of these two lines entail corresponding changes to the maximum length of a single line of contact,  $l_{LC}$ .

As an example, consider a parallel-axes gear pair composed of two helical involute gears that have the outside surface of the gear teeth shaped in the form of a cone of revolution.<sup>9</sup> The gear pair is schematically illustrated in Figure 23.23. The plane of action,  $PA$ , is still tangent to the base cylinders. Therefore, the borders  $EAP_g$  and  $EAP_p$  of the field of action,  $FA$ , are shaped in the form of two segments of hyperbola. For a gear pair with the base helix angle of a value,  $\psi_b$ , the maximum length of the single line of contact is equal to a certain value,  $l_{LC}$ . However, if the gear pair is designed so as to have a base helix angle of that same value but of opposite sign (i.e., of the opposite hand of the helix), this immediately allows for a significant increase in the maximum length of the single line of contact [from  $l_{LC}^{(+)}$  to  $l_{LC}^{(-)}$ ]. The gear pair that has a longer line of contact,  $LC$ , is capable of transmitting a higher power and features a higher power density. The latter is of critical importance for many applications.

Another example that illustrates the impact of alterations to the design of a gear tooth flank on the maximum length,  $l_{LC}$ , of a single line of contact,  $LC$ , is illustrated in Figure 23.24.

The portions of tooth flanks of a gear that are close to the edges at both ends of the gear face are weaker compared to those within the interior of the tooth flanks. In order to avoid teeth brakeage, it is often recommended to relieve the tooth flanks at both ends of the gear face. Similar relief is often made at the edges close to the top land of the gear teeth. For pinions that have lower tooth counts, the radius of curvature of the tooth flanks at points close to the bottomland is commonly small. It is often desirable to eliminate these portions of the tooth flanks from interaction with conjugate tooth

<sup>9</sup> Parallel-axes gearing of this particular kind is considered more in detail in Chapter 8 (see Figures 8.1-8.6, for example).



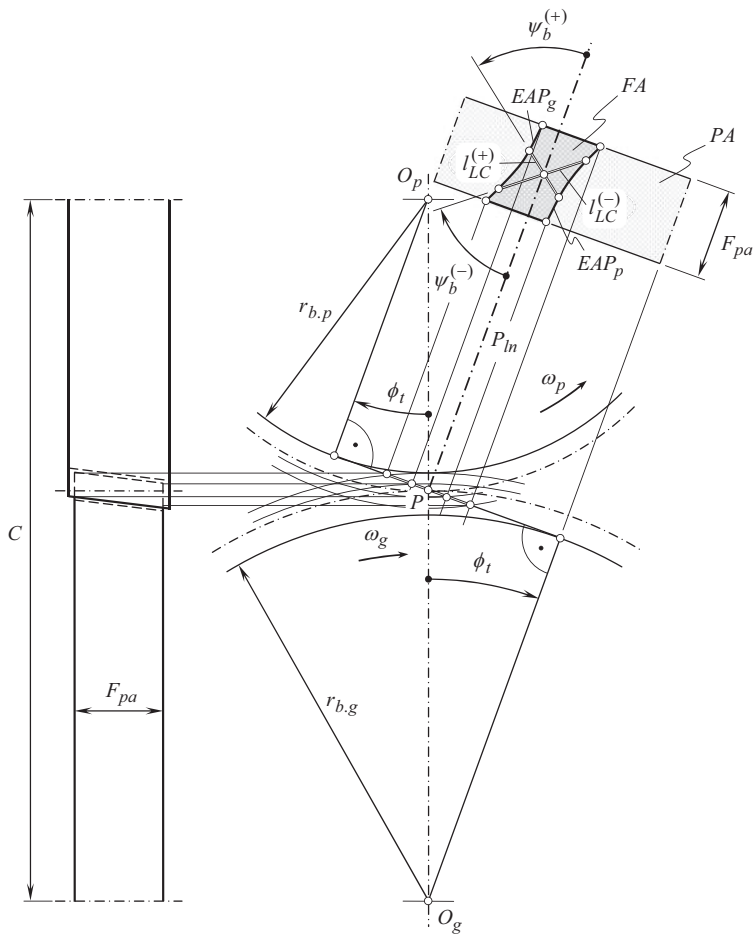


**FIGURE 23.23** Impact of the geometry of boundary curves,  $EAP_g$  and  $EAP_p$ , onto maximum length of single line of contact,  $LC$ .

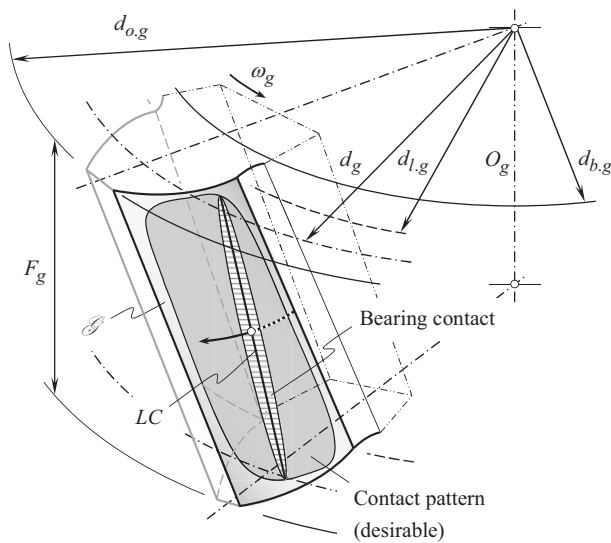


**FIGURE 23.24** An example of desirable contact pattern on tooth flanks of involute gear.

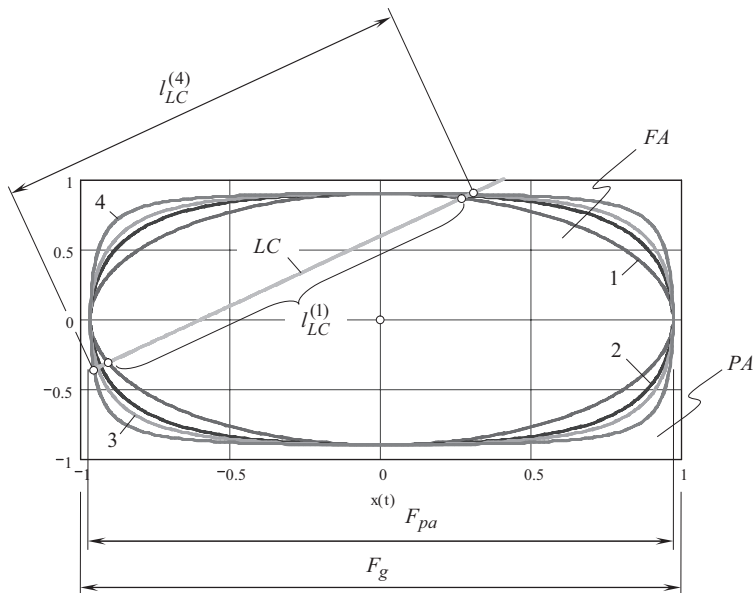


**FIGURE 23.25** The maximum length,  $l_{LC}^{(i)}$ , of single line of contact,  $LC$ , vs. design parameters of relief of tooth flank edges.

flanks of the mating gear. Tip relieving of the mating gear teeth allows for the elimination of this area of the pinion tooth flank from the interaction with the mating gear tooth. Ultimately, the desirable contact pattern is shaped in the form of a close loop, as schematically depicted in Figure 23.24.

Under an applied load, the contact line,  $LC$ , spreads to a form of a narrow, ellipse-like bearing contact area. When the bearing contact area travels across the gear tooth flank, a corresponding contact pattern is covered by the bearing contact area.

With that said, relieving the gear tooth flanks, as shown in Figure 23.24, entails corresponding changes to the geometry and parameters of the field of action. Schematically, these changes are illustrated in Figure 23.25. Depending on the design parameters of the tooth flank relief, the fields of action of different geometries 1, 2, 3, 4, and so forth, are obtained. The maximum length,  $l_{LC}$ , of a single line of contact,  $LC$ , depends on the actual shape and the design parameters of the boundary of the field of action. In the first field of action, the maximum length,  $l_{LC}^{(1)}$ , of a single line of contact,  $LC$ , is smaller compared to that in the second,  $l_{LC}^{(2)}$ , third,  $l_{LC}^{(3)}$ , and fourth,  $l_{LC}^{(4)}$ , cases (the lengths,  $l_{LC}^{(2)}$  and  $l_{LC}^{(3)}$ , are not shown in Figure 23.25).

Again, the longer the single line of contact, the better, as it makes possible a corresponding reduction in the contact load acting on the gear and the pinion teeth.

### 23.3.2 EFFECTIVE LENGTH OF LINES OF CONTACT IN PARALLEL-AXES GEARING

When a gear pair operates, the line of contact,  $LC$ , under the operating load spreads to a narrow strip of bearing contact, which is commonly shaped in the form of a long ellipse-like curve. The longer axis of the ellipse-like curve is equal to the length of a single line of contact. The length of the shorter axis depends on (a) the radii of curvature of the gear tooth flank, and the pinion tooth flank, (b) the elastic properties of a material that the gear and the pinion are made of, and (c) the applied load. For a given gear pair that transmits the torque of a specified value, the contact stress varies in time. The contact stress at a current instant of time depends on the angular orientation of the pinion in relation to the gear. This means that the maximum contact stress is observed at certain instant of time, or, in other words, at a certain angular configuration of the pinion in relation to the gear.

### 23.3.2.1 Effective Length of Lines of Contact in Spur Parallel-Axes Gearing

Again, let us consider the effective length of lines of contact for a case of a parallel-axes spur gear.

When a gear pair operates, either one or two pairs of teeth are in contact at a certain instant of time (in high contact ratio gearing, the number of pairs of teeth in contact simultaneously equals to two, and it could be even higher).

When the only pair of teeth makes contact, all the power is transmitted through a single bearing contact. This case is schematically illustrated in Figure 23.26. The contact stress depends only on the current location of the line of contact,  $LC$ , within the field of action,  $FA$ . The closer the line of contact is located to the bottomland of the pinion (i.e., closer to the  $EAP_g$  in Figure 23.26), the higher the contact stress is developed (see Figure 23.10 for details). When the line of contact is close to the bottomland of the gear (closer to the  $EAP_p$  in Figure 23.26), the contact stress also increases. However, this rise in stress is not that significant, as the relative curvature at the bottomland of the gear is a bit greater than the relative curvature at the bottomland of the pinion (see Figure 23.10).

The contact ratio in a gear pair is always greater than one. Therefore, at certain instant of time (for a certain angular configuration of the pinion in relation to the gear), the gear and the pinion teeth contact one another not along a single line of contact, but along two lines of contact, instead. This is in part due to the fact that when the gears rotate, the line of contact,  $LC$ , travels within the field of action,  $FA$ , with a certain linear velocity,  $V_{LC}$ . Diagrammatically, this case is illustrated in Figure 23.27. The lines of contact are labeled as  $LC_1$  and  $LC_2$ . They are at a distance from one another, and this distance equals to base pitch,  $p_b$ , of the gear pair.

As two lines of contact are observed, the applied load is equally shared between the lines  $LC_1$  and  $LC_2$ .

The contact stress depends only on the current location of the lines of contact,  $LC_1$  and  $LC_2$ , within the field of action,  $FA$ . The closer the line of contact,  $LC_1$ , is located to the bottomland of the pinion (closer to the  $EAP_g$  in Figure 23.27), the higher the contact stress is observed (see Figure 23.10 for details). When the line of contact,  $LC_2$ , is close to the bottomland of the gear (closer to the  $EAP_p$  in Figure 23.27), the contact stress also increases. However, this rise is not that significant, as the relative curvature at the bottomland of the gear is greater than the relative curvature at the bottomland of the pinion (see Figure 23.10).

In cases of two or more lines of contact, the total length,  $l'_{LC}$ , of the lines of contact,  $LC_i$ , is doubled (tripled, quadrupled, etc.). This makes it possible to have a corresponding reduction of contact stress, as the applied load is shared along a longer (total) line of contact, which is evident. However, a length of line of contact that should be used for the calculation of contact stress is not equal to the total length,  $l'_{LC}$ , of the lines of contact. For this purpose, an effective length,  $l^e_{LC}$ , of the lines of contact should be entered into an expression for the calculation of contact stress.

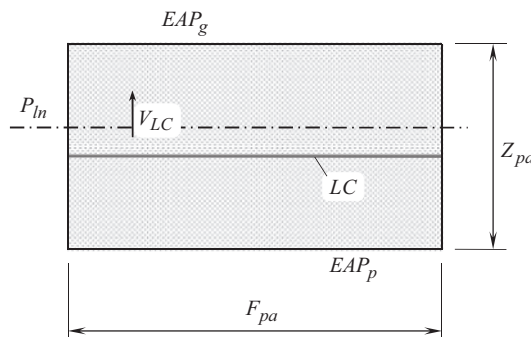


**FIGURE 23.26** Configuration of the line of contact,  $LC$ , in spur parallel-axes gearing at an instant of time that corresponds to contact of one pair of teeth of the gear, and of the pinion.

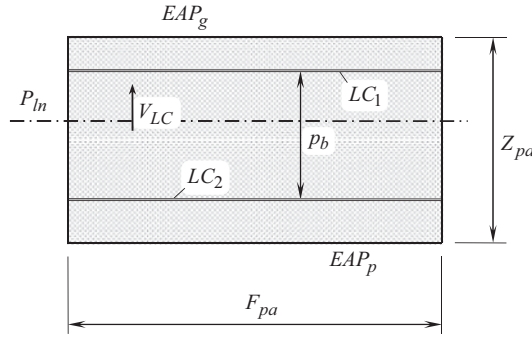


**FIGURE 23.27** Configuration of two lines of contact,  $LC_1$  and  $LC_2$ , in spur parallel-axes gearing at an instant of time that corresponds to contact of two pairs of teeth of gear, and pinion.

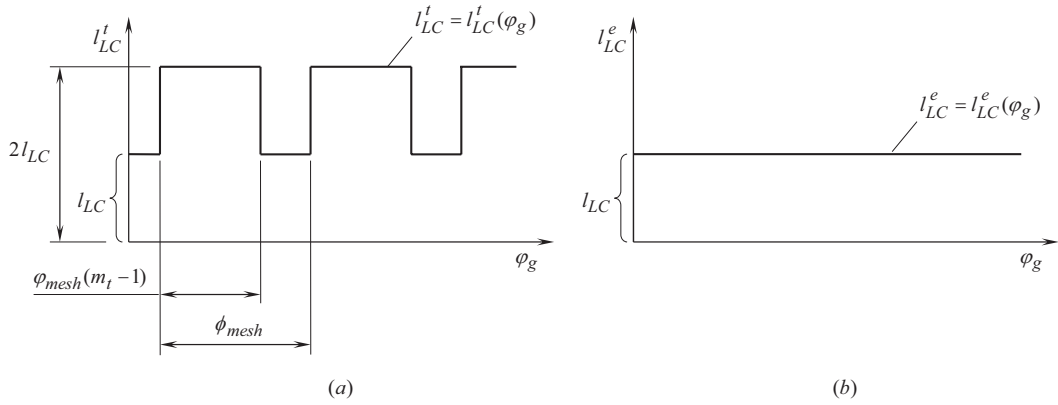


**FIGURE 23.28** Examples of functions (a)  $l_{LC}^t = l_{LC}^t(\phi_g)$ , and (b)  $l_{LC}^e = l_{LC}^e(\phi_g)$  for parallel-axis gearing with contact ratio in the range of  $1 \leq m_t < 2$ .

When two or more lines of contact are observed, the total length,  $l_{LC}^t$ , of the lines of contact,  $LC_i$ , can be expressed by the following formula:

$$l_{LC}^t = l_{LC} \cdot [\text{trunc}(m_t) + 1] \quad (23.35)$$

In Eq. (23.35), the **trunc**( $m_t$ ) function returns a number truncated to an integer portion of contact ratio,  $m_t$ .

For gearing that has a contact ratio in the range of  $1 \leq m_t < 2$ , **trunc**( $m_t$ ) = 1. Similarly, for gears with contact ratio in the range of  $2 \leq m_t < 3$ , **trunc**( $m_t$ ) = 2, etc.

However, along with an increase in the length of the line of contact, a corresponding reduction of the applied load per unit length is observed. Therefore, for the calculation of maximum contact stress, the applied load per unit length should be divided by **trunc**( $m_t$ ). Ultimately, this returns an effective length,  $l_{LC}^e$ , of the lines of contact,  $LC_i$ , for the case of spur gearing:

$$l_{LC}^e = \frac{l_{LC}}{\text{trunc}(m_t)} \quad (23.36)$$

Figure 23.28a illustrates an example of the function,  $l_{LC}^t = l_{LC}^t(\phi_g)$ , for parallel-axes gearing with a contact ratio in the range of  $1 \leq m_t < 2$ . A similar example of the function,  $l_{LC}^e = l_{LC}^e(\phi_g)$ , for

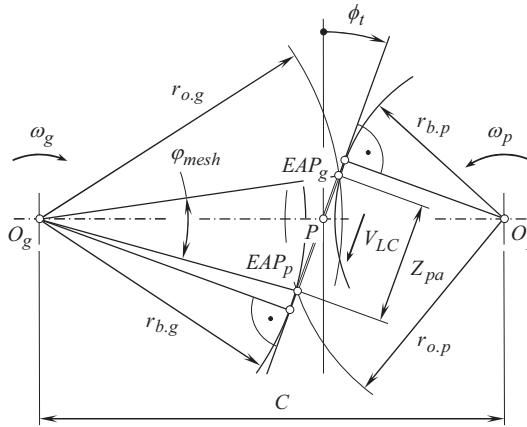


FIGURE 23.29 Specification of the angle,  $\phi_{mesh}$ , in Figure 23.28.

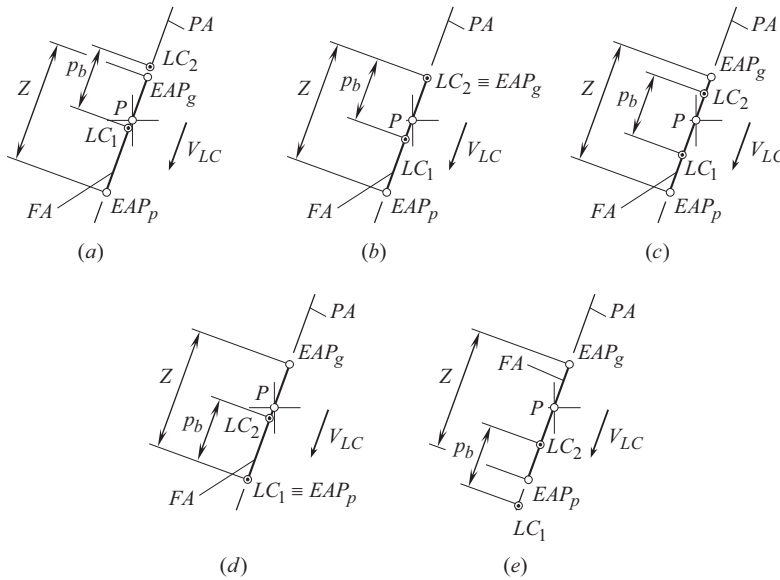


FIGURE 23.30 Progression of two lines of contact,  $LC_1$  and  $LC_2$ , through field of action,  $FA$ : (a) single line of contact,  $LC_1$ ; (b) the second line of contact,  $LC_2$ , is entering the gear  $EAP_g$  – line; (c) the zone of double-line of contact,  $LC_1$  and  $LC_2$ ; (d) a configuration of the mating gears when the first line of contact,  $LC_1$ , is aligned with the pinion  $EAP_p$  – line; and (e) single line of contact,  $LC_2$ .

parallel-axes gearing with contact ratio in that same range of  $1 \leq m_t < 2$  is shown in Figure 23.28b. Shown in Figure 23.28a, the angle  $\phi_{mesh}$  is specified in Figure 23.29.

For spur gearing with a specified contact ratio, the actual value of the effective length of the line of contact,  $l_{LC}^e$ , is predetermined by the contact ratio,  $m_t$ .

It is necessary to calculate the contact stress for the gear and the pinion configuration, at which the length of the effective line of contact,  $l_{LC}^e$ , is the minimum ( $l_{LC}^e \mapsto \min$ ). In the case of spur parallel-axes gearing, this particular problem reduces to a determination of an instant of time of single-line-of-contact engagement, when the line of contact occupies the closest possible location in relation to the bottomland of the pinion.

Consider the progression of two lines of contact,  $LC_1$  and  $LC_2$ , through the field of action,  $FA$ , as diagrammatically illustrated in Figure 23.30.

At a certain instant of time, the gear tooth flank,  $\mathcal{S}$ , and the mating pinion tooth flank,  $\mathcal{P}$ , contact one another along just one line of contact,  $LC_1$ . This relative configuration of the gear and the pinion is schematically illustrated in Figure 23.30a. The second potential line of contact,  $LC_2$ , is at a distance,  $p_b$ , from the first line of contact,  $LC_1$ . The second line of contact,  $LC_2$ , is located within the plane of action,  $PA$ , but not within the field of action,  $FA$ .

When the gears rotate, the lines of contact  $LC_1$  and  $LC_2$  travel within the plane of action. The speed of this motion is denoted by  $V_{LC}$ . At an instant of time, the second line of contact,  $LC_2$ , reaches the line  $EAP_g$ . Starting from this instant of time, two lines of contact,  $LC_1$  and  $LC_2$ , are observed (see Figure 23.30b). In this particular configuration of the gear and the pinion, the distance from the line of contact  $LC_2$  to the bottomland of the pinion is the closest possible.

While the rotation progresses, both the lines of contact continue traveling within the field of action and occupy a location as shown in Figure 23.30c.

At the final stage of double-line-of-contact mesh (see Figure 23.30d), the first line of contact,  $LC_1$ , occupies a position within the field of action at which it is closest to the bottomland of the gear. For this configuration, the line of contact,  $LC_1$ , is aligned with the line  $EAP_p$ .

Under further rotation of the gears, the gear tooth flanks,  $\mathcal{S}$ , and the mating pinion tooth flanks,  $\mathcal{P}$ , again contact one another along just one line of contact,  $LC_2$  (see Figure 23.30e). The first line of contact is located outside the field of action,  $FA$ .

As it is clear from the aforesaid consideration, the calculation of contact stress should be performed for a relative orientation of the gear, and the mating pinion, for which the first line of contact,  $LC_1$ , aligns with the line  $EAP_g$ . This particular configuration of the gear and the pinion is the most critical from the contact stress standpoint.

### 23.3.2.2 Effective Length of Lines of Contact in Helical Parallel-Axes Gearing

The effective length of the lines of contact is of critical importance for the calculation of contact stress in helical involute gearing as well as in all other kinds of gearing.

The field of action for an involute helical parallel-axes gearing is schematically depicted in Figure 23.31. The configuration corresponds to a case when three lines of contact  $LC_1$ ,  $LC_2$ , and  $LC_3$  are observed (Figure 23.31). The lines of contact,  $LC_i$  (here the number of a line of contact is denoted by  $i$ ;  $i = 1, 2, 3, \dots$ , is an integer number), are parallel to one other, and are apart from one another at a distance that is equal to the normal base pitch,  $p_{b,n}$ . The relative configuration of the lines of contact,  $LC_i$ , can be expressed either in terms of the transverse base pitch,  $p_{b,t}$ , or in terms of the axial base pitch,  $p_{b,x}$ . This is due to the fact that the following relations are valid (see Figure 23.31):

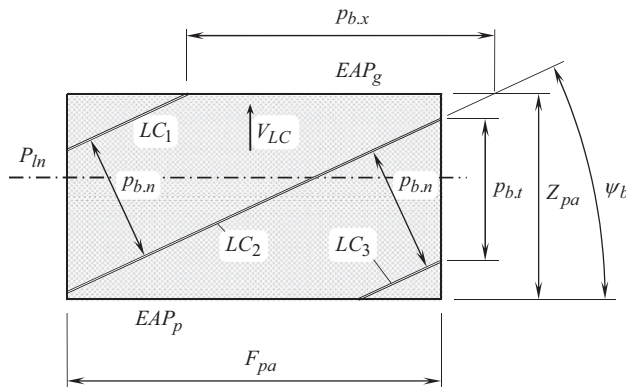


**FIGURE 23.31** Configuration of two lines of contact,  $LC_1$ ,  $LC_2$ , and  $LC_3$  in helical parallel-axes gearing at an instant of time that corresponds to contact of three pairs of teeth of mating gears.



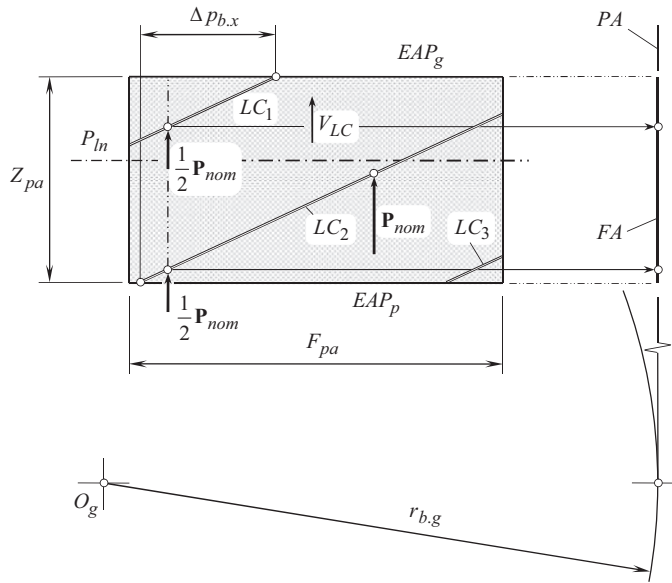


FIGURE 23.33 Load share between two lines of contact,  $LC_1$  and  $LC_2$ , in parallel-axes gearing.

When the gears rotate, all the lines of contact,  $l_{LC}^{(i)}$ , travel together with the plane of action,  $PA$ . Let us assume that the lines of contact travel from positions labeled as  $LC_1$ ,  $LC_2$ , and  $LC_3$ , to the corresponding positions designated as  $LC_1^*$ ,  $LC_2^*$ , and  $LC_3^*$ . In the new positions, the lines of contact are of lengths  $l_{LC}^{(1)*}$ ,  $l_{LC}^{(2)*}$ , and  $l_{LC}^{(3)*}$ , correspondingly.

The active portions of the lines of contact are located within the field of action,  $FA$ . When the lines of contact,  $l_{LC}^{(i)}$ , travel at a certain distance,  $\Delta p_r$ , the length of each line of contact changes from  $l_{LC}^{(i)}$  to  $l_{LC}^{(i)*}$ . Consequently, the total length,  $l_{LC}^t$ , of the lines of contact also changes.

The effective length of the lines of contact,  $l_{LC}^e$ , is used for the calculation of contact stress. Referring to Figure 23.33, consider a field of action,  $FA$ , with three lines of contact  $LC_1$ ,  $LC_2$  and  $LC_3$ .

The gear pair can be sliced by numerous planes perpendicular to the axis of rotation of the gear. Certain planes intersect just one line of contact (the line of contact  $LC_2$  in Figure 23.33). Other section planes within the length,  $\Delta p_x$ , intersect two lines of contact (the lines of contact  $LC_1$  and  $LC_2$  in Figure 23.33). Within portions of the field of action, where two (or more) lines of contact overlap one another ( $\Delta p_x$ ), the torque being transmitted is shared equally between the lines of contact. Thus, the nominal load,  $P_{nom}$ , in a section with one line of contact is equally shared between two lines of contact in a section with two lines of contact (see Figure 23.33). Due to this, the effective length of the lines of contact,  $l_{LC}^e$ , is shorter compared to that for total length,  $l_{LC}^t$ , of lines of contact. As the length,  $l_{LC}^e$ , is shorter compared to the length,  $l_{LC}^t$ , the calculated value of contact stress is higher.

It can be shown that for helical gears, the effective length of the lines of contact,  $l_{LC}^e$ , depends on the actual value of the angle of rotation of the gear,  $\varphi_g$ :

$$l_{LC}^e = l_{LC}^e(\varphi_g) \quad (23.42)$$

The effective length of the lines of contact,  $l_{LC}^e$ , can be calculated in the following way.

Different portions of the lines of contact can be distinguished. First, some portions of the lines of contact do not overlap with one other. Portions of the line of contact of this particular kind can be designated as  $LC_{0,o}^{(i)}$ . Then, a certain number of portions of the lines of contact can overlap with one another just once. Portions of this kind are designated as  $LC_{1,o}^{(i)}$ . Similarly, a certain number of



portions of the lines of contact can overlap with one another twice. Portions of this kind are designated as  $LC_{2,o}^{(i)}$  and so on.

With that said, the effective length of lines of contact,  $l_{LC}^e$ , is equal to the total length of the portions,  $LC_{0,o}^{(i)}$ , times 1, plus the total length of the portions,  $LC_{1,o}^{(i)}$ , times 0.5, plus the total length of the portions,  $LC_{2,o}^{(i)}$ , times 1/3 and so forth.

Corresponding computer codes can be developed for the calculation of effective length of lines of contact,  $l_{LC}^e$ .

The aforesaid reveals that it is a wrong way to perform the calculation of contact stress based just on the contact ratios in the gear pair. The same value of the contact ratios for spur gearing and helical gearing is not equivalent to one another. The difference becomes clear from the analysis shown in Figure 23.34. The bearing capacities of spur and helical gearing with the same contact ratio can significantly differ from one another.

The critical scenario when contact stress is maximum, corresponds to the case when the effective length of the lines of contact,  $l_{LC}^e$ , is minimal, and the contact point is located at the start of the active profile of the pinion. In this case, both the loading and the geometry of contact are unfavorable. However, it could happen that the case of unfavorable loading of the gear teeth and the case of unfavorable geometry of contact occur under different angular configurations of the gear and the pinion. Under such a scenario, it is necessary to investigate the contact stress within the angle that spans from an angle of the most unfavorable loading of the gearing to the angle of the most unfavorable geometry of contact of gear teeth of the gearing.

For certain applications, modeling of a gear tooth flank and of a mating pinion tooth flank by two surfaces of revolution can be performed.

The above-discussed approach can be enhanced to the area of intersected-axes gearing and to crossed-axes gearing. In both these cases, the plane of action should be considered in the form of a round strip tangent to base cones of the gear and the pinion. The field of action in this analysis is a portion of the plane of action.

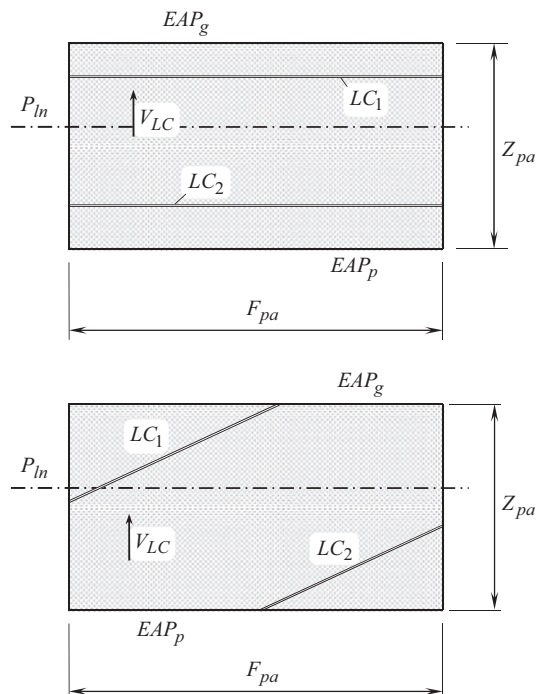


**FIGURE 23.34** Different bearing capacities of spur and helical gearing with equal contact ratios.

### 23.4 LOADING OF GEAR TEETH

When a gear pair operates, the gear tooth flanks and the pinion tooth flanks are loaded by force acting from a driving component against the driven component. In reduction gears, the pinion drives, while the gear is driven. In increasing gears, the gear drives, and the pinion is driven.

The torque is transmitted from a driving shaft to a driven shaft generates the force of interaction of the gear and the mating pinion teeth. This force acts within the plane of action,  $PA$ , which, in parallel-axes gearing, is tangential to the base cylinders of the gear and the pinion (see Figure 23.35). It is assumed here that no friction between the interacting tooth flanks,  $\mathcal{F}$  and  $\mathcal{P}$ , of the gear and its mating pinion is observed. This force is withheld by the entire active face width of the gear,  $F_{pa}$ . The load per unit length of the face width,  $\mathbf{p}_F^t$ , can be expressed in terms of the torque on the driving shaft,  $\mathbf{T}_p$ , the base diameter of the pinion,  $d_{b,p}$ , and the effective face width,  $F_{pa}$ :

$$p_F^t = 2 \frac{T_p}{d_{b,p} F_{pa}} \quad (23.43)$$

where the equalities  $p_F^t = |\mathbf{p}_F^t|$ , and  $T_p = |\mathbf{T}_p|$  are observed.

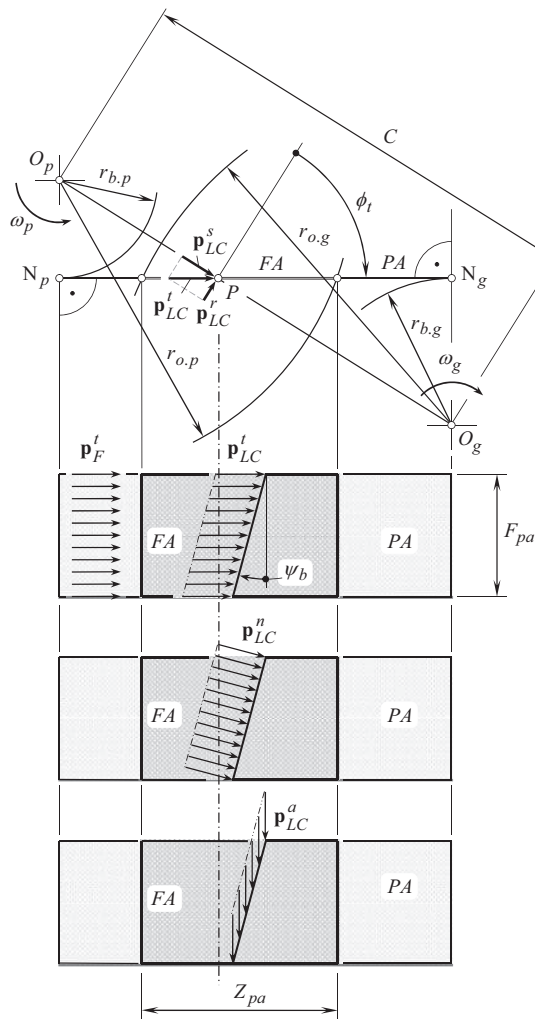


**FIGURE 23.35** Components of distributed force (force per unit length) of interaction of a gear tooth flank,  $\mathcal{F}$ , and a mating pinion tooth flank,  $\mathcal{P}$ , in helical parallel-axes gear pair.

The load,  $\mathbf{p}'_{LC}$ , is evenly distributed within the line of contact,  $LC$  (consider a simplified case when the entire power is transmitted through a load-bearing contact along a single line of contact,  $LC$ ). The load per unit length of the effective length of lines of contact,  $\mathbf{p}'_{LC}$ , can be expressed in terms of the torque on the driving shaft,  $T_p$ , the base diameter of the pinion,  $d_{b,p}$ , and the length,  $l_{LC}^e$ , of the line of contact:

$$p'_{LC} = |\mathbf{p}'_{LC}| = 2 \frac{T_p}{d_{b,p} l_{LC}^e} \quad (23.44)$$

The effective length of the lines of contact,  $l_{LC}^e$ , should be entered into Eq. (23.15) for the calculation of the load,  $\mathbf{p}'_{LC}$ , per unit length of the line of contact. In cases of single line of contact, the effective length of the lines of contact,  $l_{LC}^e$ , is equal to the length of the line of contact,  $l_{LC}$ .

The load per unit length of the line of contact,  $\mathbf{p}^n_{LC}$ , that causes contact stress, is perpendicular to the gear tooth flank. This load can be expressed in terms of the load  $\mathbf{p}'_{LC}$ , and the base helix angle,  $\psi_b$ :

$$p^n_{LC} = |\mathbf{p}^n_{LC}| = 2 \frac{T_p}{d_{b,p} l_{LC}^e} \cos \psi_b \quad (23.45)$$

Ultimately, an expression for the calculation of one more load that acts within the plane of action can be derived from Figure 23.35. This load,  $\mathbf{p}^a_{LC}$ , acts in the axial direction of the gears:

$$p^a_{LC} = |\mathbf{p}^a_{LC}| = 2 \frac{T_p}{d_{b,p} l_{LC}^e} \sin \psi_b \quad (23.46)$$

The separating load per unit length of the line of contact,  $\mathbf{p}^s_{LC}$ , acts within the plane through the axes of rotation of the gear,  $O_g$ , and that of the pinion,  $O_p$ . This load is calculated from the expression:

$$p^s_{LC} = |\mathbf{p}^s_{LC}| = 2 \frac{T_p}{d_{b,p} l_{LC}^e} \sin \phi_t \quad (23.47)$$

The component,  $\mathbf{p}^r_{LC}$ , acts in the direction perpendicular to the plane through the axes,  $O_g$  and  $O_p$ . For the calculation of this component, an expression is derived:

$$p^r_{LC} = |\mathbf{p}^r_{LC}| = 2 \frac{T_p}{d_{b,p} l_{LC}^e} \cos \phi_t \quad (23.48)$$

Equations (23.43)–(23.48) are valid for parallel-axes gearing of all kinds: spur, helical, herringbone, circular-arc gearing, and so forth. These equations can be enhanced to the cases of real gearing that have a point contact between the gear and the mating pinion tooth flanks.

The components  $\mathbf{p}'_{LC}$ ,  $\mathbf{p}^n_{LC}$ ,  $\mathbf{p}^a_{LC}$ ,  $\mathbf{p}^s_{LC}$ , and  $\mathbf{p}^r_{LC}$  in Eqs. (23.44)–(23.48) are expressed in terms of the base diameter of the pinion,  $d_{b,p}$ , and the base helix angle,  $\psi_b$ . For the needs of engineering calculations, it is preferable to express all these components in terms of design parameters of the pinion.

The base diameter of the pinion is calculated from the formula:

$$d_{b,p} = d_p \cos \phi_{t,p} \quad (23.49)$$

The transverse profile angle,  $\phi_t$ , can be expressed in terms of the normal pressure angle,  $\phi_n$ , and the pitch helix angle,  $\psi$ :

$$\tan \phi_t = \frac{\tan \phi_n}{\cos \psi} \quad (23.50)$$

The last two equations allow for the following expression for the calculation of the pinion base diameter:

$$d_{b,p} = d_p \cdot \sqrt{1 - \sin^2 \phi_n \sin^2 \psi} \quad (23.51)$$

Then, the base helix angle,  $\psi_b$ , can be expressed in terms of the pitch helix angle,  $\psi$ , and the normal pressure angle,  $\phi_n$ :

$$\psi_b = \sin^{-1}(\cos \phi_n \sin \psi) \quad (23.52)$$

After substituting these expressions for  $d_{b,p}$  and for  $\psi_b$  into Eqs. (23.44)–(23.48), the equations cast into:

$$p_{LC}^t = 2 \frac{T_p}{d_{b,p} l_{LC}^e} \quad (23.53)$$

$$p_{LC}^n = 2 \frac{T_p}{d_{b,p} l_{LC}^e} \sqrt{1 - \cos^2 \phi_n \sin^2 \psi} \quad (23.54)$$

$$p_{LC}^a = 2 \frac{T_p}{d_{b,p} l_{LC}^e} \cos \phi_n \sin \psi \quad (23.55)$$

$$p_{LC}^s = 2 \frac{T_p}{d_{b,p} l_{LC}^e} \cdot \frac{\tan \phi_n}{\sqrt{\cos^2 \psi + \tan^2 \phi_n}} \quad (23.56)$$

$$p_{LC}^r = 2 \frac{T_p}{d_{b,p} l_{LC}^e} \cdot \frac{\cos \psi}{\sqrt{\cos^2 \psi + \tan^2 \phi_n}} \quad (23.57)$$

Equations (23.53)–(23.57) return average values of the gear teeth loading. They are valid for gears that have a relatively large tooth count.

For gears that have large tooth counts, the variation of actual values of the design parameters of the gear, and the pinion tooth flanks within the tooth height, is negligibly small and, thus, it can be ignored. For low-tooth-count gearing, the variation of the actual values of the design parameters of the gear and the pinion tooth flanks cannot be ignored as this variation causes significant alterations to the geometry of the tooth flanks. Therefore, it is necessary to put into account a variation of the gear teeth loading within the tooth height. For this purpose, the diameter,  $d_{y,p}$ , of location of the current point of interest,  $m$ , within the line of contact should be considered as a variable parameter. Then, the helix angle,  $\psi_y$ , on a cylinder of a diameter,  $d_{y,p}$ , is calculated from:

$$\psi_y(d_{y,p}) = \tan^{-1} \left( \frac{d_{y,p}}{d_{b,p}} \tan \psi \right) \quad (23.58)$$

Equation:

$$d_{b,p}(d_{y,p}) = d_{y,p} \sqrt{1 - \sin^2 \phi_n \sin^2 \psi} \quad (23.59)$$

for the base diameter,  $d_{b,p}$ , and Eq. (23.58) for the helix angle,  $\psi_y$ , make the possible derivation of a set of equations for the calculation of loading for low-tooth-count gearing:

$$p_{LC}^t = 2 \frac{T_p}{d_{b,p} l_{LC}^e} \quad (23.60)$$

$$p_{LC}^n(d_{y,p}) = 2 \frac{T_p \sqrt{1 - \cos^2 \phi_n \sin^2 \psi(d_{y,p})}}{d_{y,p} \sqrt{1 - \sin^2 \phi_n \sin^2 \psi} l_{LC}^e} \quad (23.61)$$

$$p_{LC}^a(d_{y,p}) = 2 \frac{T_p \cos \phi_n \sin \psi(d_{y,p})}{d_{y,p} l_{LC}^e \sqrt{1 - \sin^2 \phi_n \sin^2 \psi}} \quad (23.62)$$

$$p_{LC}^s(d_{y,p}) = 2 \frac{T_p \tan \phi_n}{d_{y,p} l_{LC}^e \sqrt{(1 - \sin^2 \phi_n \sin^2 \psi) \cdot [\cos^2 \psi(d_{y,p}) + \tan^2 \phi_n]}} \quad (23.63)$$

$$p_{LC}^r(d_{y,p}) = 2 \frac{T_p \cos \psi}{d_{y,p} l_{LC}^e \sqrt{(1 - \sin^2 \phi_n \sin^2 \psi) \cdot [\cos^2 \psi(d_{y,p}) + \tan^2 \phi_n]}} \quad (23.64)$$

It is necessary to stress here that for the calculation of gear tooth strength, the component  $\mathbf{p}_{LC}^n$  is the most critical.

The performed analysis is of critical importance for the purposes of calculation of gear tooth loading when performing contact stress and strength calculations as well as bending strength and stress calculations.

This analysis can be enhanced to gearing of other kinds, namely, to intersected-axes gearing as well as to crossed-axes gearing.

## 23.5 METHOD FOR SIMULATION OF INTERACTION OF GEAR AND MATING PINION TOOTH FLANKS

A method for simulation of the interaction of a gear and a mating pinion tooth flanks is developed based on the method<sup>10</sup> proposed by Prof. *S.P. Radzevich* for experimental simulation of machining of sculptured part surfaces on a multi-axis NC machine [129,137,159]. The method of simulation is illustrated in Figure 23.36.

As an example of the implementation of the method of simulation, consider a gear tooth flank,  $\mathcal{G}$  (see Figure 23.36a), that interacts with the pinion tooth flank,  $\mathcal{P}$  (not shown in Figure 23.36a).

The method of simulation of the interaction of a gear, and of a mating pinion tooth flanks,  $\mathcal{G}$  and  $\mathcal{P}$ , is carried out with equivalent models,  $\mathcal{G}^m$ , of the gear tooth flank, and the pinion tooth flank,  $\mathcal{P}^m$  (see Figure 23.36b).

At point of contact of the tooth flanks,  $\mathcal{G}$  and  $\mathcal{P}$ , the local topology of the surfaces,  $\mathcal{G}^m$  and  $\mathcal{P}^m$ , can be uniquely specified by two parameters, namely, by the mean curvature,  $\bar{M}_{g(p)}$ , and by the Gaussian curvature,  $\bar{G}_{g(p)}$ . As there are only two parameters of the local geometry, the variety of kinds of modeling surfaces,  $\mathcal{G}^m$  and  $\mathcal{P}^m$ , is limited [148,153].

The surface,  $\mathcal{G}^m$ , as well as the surface,  $\mathcal{P}^m$ , is a quadric surface. Both the surfaces,  $\mathcal{G}^m$  and  $\mathcal{P}^m$ , make tangency at point,  $K$ . The local geometry of tangency of the surfaces,  $\mathcal{G}^m$  and  $\mathcal{P}^m$ , is identical to that of the gear tooth flank,  $\mathcal{G}$ , and the pinion tooth flank,  $\mathcal{P}$ , correspondingly. Due to this, the unit tangent vectors  $\mathbf{t}_{1,g}^m$  and  $\mathbf{t}_{2,g}^m$  of the principal directions on the quadric surface,  $\mathcal{G}^m$ , align with the corresponding unit tangent vectors,  $\mathbf{t}_{1,g}$  and  $\mathbf{t}_{2,g}$ , of the gear tooth flank,  $\mathcal{G}$ . Moreover, the principal radii of curvature,  $R_{1,g}^m$  and  $R_{2,g}^m$ , of the quadric surface,  $\mathcal{G}^m$ , at every contact point,  $K$ , are equal

<sup>10</sup> Pat. №1449246 (USSR). *A Method of Experimental Simulation of Machining a Sculptured Part Surface on a Multi-Axis NC Machine.* /S.P. Radzevich. Filed: February 17, 1987, Int. Cl. B 23 C, 3/16.

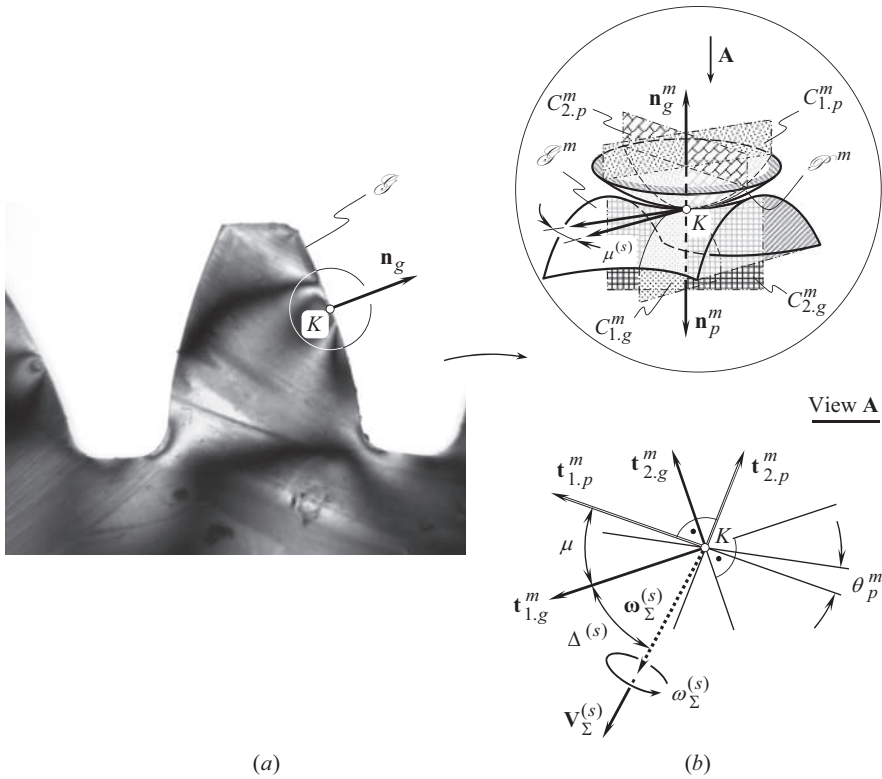


**FIGURE 23.36** Schematic of the method for simulation of interaction of a gear tooth flank,  $\mathcal{S}$ , and a mating pinion tooth flank,  $\mathcal{P}$ : (a) stress distribution in a gear tooth, and (b) elements of contact geometry of the tooth flanks  $\mathcal{S}$  and  $\mathcal{P}$ .

to the corresponding principal radii of curvature,  $R_{1,g}$  and  $R_{2,g}$ , of the gear tooth flank,  $\mathcal{S}$  (i.e., the identities  $R_{1,g}^m \equiv R_{1,g}$  and  $R_{2,g}^m \equiv R_{2,g}$  are observed). Due to this, *Euler's* formula yields a conclusion that in the differential vicinity of contact point,  $K$ , the surfaces,  $\mathcal{S}^m$  and  $\mathcal{S}$ , are locally congruent to one another up to the members of the second order.

A similar conclusion is valid with respect to the quadric surface,  $\mathcal{P}^m$ , that is used for the local simulation of the pinion tooth flank,  $\mathcal{P}$ . At point of contact,  $K$ , the unit tangent vectors,  $\mathbf{t}_{1,p}^m$  and  $\mathbf{t}_{2,p}^m$ , of the principal directions on the quadric surface,  $\mathcal{P}^m$ , align with the corresponding unit vectors,  $\mathbf{t}_{1,p}$  and  $\mathbf{t}_{2,p}$ , of the pinion tooth flank,  $\mathcal{P}$ . The principal radii of curvature,  $R_{1,p}^m$  and  $R_{2,p}^m$ , of the quadric surface,  $\mathcal{P}^m$ , are also equal to the corresponding principal radii of curvature,  $R_{1,p}$  and  $R_{2,p}$ , of the surface,  $\mathcal{P}$  (i.e., the identities  $R_{1,p}^m \equiv R_{1,p}$  and  $R_{2,p}^m \equiv R_{2,p}$  are observed). Therefore, in the differential vicinity of every contact point  $K$ , the surfaces,  $\mathcal{P}^m$  and  $\mathcal{P}$ , are locally congruent to each other up to the members of the second order.

For the orthogonally  $(U_g, V_g)$  – parameterized gear tooth flank,  $\mathcal{S}$ , the ratio  $\partial U_g / \partial V_g$  determines the value of  $\tan \xi_g$ . Here, the angle that the unit vectors,  $\mathbf{t}_{1,g}$  and  $\mathbf{t}_{2,g}$ , of the principal directions form with the coordinate  $U_g$  – and  $V_g$  – lines on the gear tooth flank,  $\mathcal{S}$ , is designated as angle,  $\xi_g$ . Usually, parameterization of the surface,  $\mathcal{S}$ , is not orthogonal. In such a case, the actual value of the angle  $\tan \xi_g$  (not shown in Figure 23.36b) can be calculated from the formula [148,153]:

$$\sin \xi_g = \frac{\partial V_g}{\partial U_g} \left[ \left( \frac{\partial V_g}{\partial U_g} \right)^2 - 2 \frac{\partial V_g}{\partial U_g} \cos \omega_g + 1 \right]^{-\frac{1}{2}} \quad (23.65)$$

For the orthogonally  $(U_p, V_p)$ – parameterized pinion tooth flank,  $\mathcal{P}$ , the ratio  $\partial U_p / \partial V_p$  determines the value of  $\tan \xi_p$ . Here the angle that the unit vectors,  $\mathbf{t}_{1,p}$  and  $\mathbf{t}_{2,p}$ , of the principal directions form with the coordinate  $U_p$ – and  $V_p$ – lines on the pinion tooth flank,  $\mathcal{P}$ , is designated as angle,  $\xi_p$ . Usually, parameterization of the pinion tooth surface,  $\mathcal{P}$ , is not orthogonal. In such a case, angle  $\tan \xi_p$  (not shown in Figure 23.36b) can be calculated from the formula [148,153]:

$$\sin \xi_p = \frac{\partial V_p}{\partial U_p} \left[ \left( \frac{\partial V_p}{\partial U_p} \right)^2 - 2 \frac{\partial V_p}{\partial U_p} \cos \omega_p + 1 \right]^{-\frac{1}{2}} \quad (23.66)$$

The quadric surfaces,  $\mathcal{S}^m$  and  $\mathcal{P}^m$ , are turned about the unit normal vector,  $\mathbf{n}_g^m$ , relative to each other through an angle,  $\mu^s$ . The angle,  $\mu^s$ , is the angle of the local relative orientation of the modeling surfaces,  $\mathcal{S}^m$  and  $\mathcal{P}^m$ . The angle,  $\mu^s$ , is identical to the angle,  $\mu$ , of the local relative orientation of the actual gear and pinion tooth surfaces,  $\mathcal{S}$  and  $\mathcal{P}$  [that is,  $\mu^s \equiv \mu$ ]. Angle  $\mu$  is the angle that makes the first,  $\mathbf{t}_{1,g}$  and  $\mathbf{t}_{1,p}$ , (or, the same, the second  $\mathbf{t}_{2,g}$  and  $\mathbf{t}_{2,p}$ ) principal directions at point of contact of the tooth flanks,  $\mathcal{S}$  and  $\mathcal{P}$ , [148,153]:

$$\mu^{(s)} \equiv \mu = \tan^{-1} \frac{|\mathbf{t}_{1,g} \times \mathbf{t}_{1,p}|}{\mathbf{t}_{1,g} \cdot \mathbf{t}_{1,p}} \equiv \tan^{-1} \frac{|\mathbf{t}_{2,g} \times \mathbf{t}_{2,p}|}{\mathbf{t}_{2,g} \cdot \mathbf{t}_{2,p}} \quad (23.67)$$

The local relative orientation of the quadric surfaces,  $\mathcal{S}^m$  and  $\mathcal{P}^m$ , in the differential vicinity of contact point,  $K$ , is identical to the local relative orientation of the actual tooth surfaces,  $\mathcal{S}$  and  $\mathcal{P}$ .

The trajectory of point of interest,  $m$ , within the line of contact,  $LC$ , relative to the gear tooth flank,  $\mathcal{S}$ , can be represented as a vector sum of the motions that the surfaces,  $\mathcal{S}$  and  $\mathcal{P}$ , perform in the mesh.

When simulating the meshing of a gear and its mating pinion tooth flanks, the quadric surfaces,  $\mathcal{S}^m$  and  $\mathcal{P}^m$ , perform the relative motion with respect to one another.

The instant relative motion of the tooth flanks,  $\mathcal{S}$  and  $\mathcal{P}$ , in mesh can be represented as an instant screw motion. Therefore, when simulating the mesh, in addition to the resultant linear motion,  $\mathbf{V}_\Sigma^s$ , the modeling quadric surfaces,  $\mathcal{S}^m$  and  $\mathcal{P}^m$ , perform rotation with the resultant angular velocity,  $\boldsymbol{\omega}_\Sigma^s$ .

When simulating, the resultant relative motion,  $\mathbf{V}_\Sigma^s$ , of the modeling surfaces,  $\mathcal{S}^m$  and  $\mathcal{P}^m$ , is identical to that,  $\mathbf{V}_\Sigma$ , of the actual gear tooth flank,  $\mathcal{S}$ , and the pinion tooth flank,  $\mathcal{P}$  [that is,  $\mathbf{V}_\Sigma^s \equiv \mathbf{V}_\Sigma$ ]. For this purpose, the angle,  $\Delta^s$ , that the vector,  $\mathbf{V}_\Sigma^s$ , forms with the unit tangent vector,  $\mathbf{t}_{1,g}^m$ , of the first principal direction on the quadric surface,  $\mathcal{S}^m$ , is kept identical to the similar angle,  $\Delta$ , that the vector,  $\mathbf{V}_\Sigma$ , forms with the unit tangent vector,  $\mathbf{t}_{1,g}$ , of the first principal direction on the gear tooth flank,  $\mathcal{S}$  (i.e.,  $\Delta^s \equiv \Delta$ ).

The instant relative screw motion of the modeling quadric surfaces,  $\mathcal{S}^m$  and  $\mathcal{P}^m$ , is identical to that of the gear tooth flank,  $\mathcal{S}$ , and the pinion tooth flank,  $\mathcal{P}$ .

At every contact point,  $K$ , implementation of the method of experimental simulation (see Figure 23.36) ensures local identity to one other of all geometric and kinematic parameters of a gear mesh to be modeled [129]:

- Of the quadric surface,  $\mathcal{S}^m$ , and the actual gear tooth flank surface,  $\mathcal{S}$
- Of the quadric surface,  $\mathcal{P}^m$ , and the actual pinion tooth flank,  $\mathcal{P}$
- Relative local orientation of the quadric surfaces,  $\mathcal{S}^m$  and  $\mathcal{P}^m$ , and the relative local orientation of the actual teeth flanks,  $\mathcal{S}$  and  $\mathcal{P}$
- The instant relative motion while simulating and the instant relative motion in mesh (i.e., the kinematics of meshing remains the same).

Shown in Figure 23.37, the indicatrix of conformity,  $Cnf(\mathcal{S} / \mathcal{P})$ , at point of contact of the gear tooth flank,  $\mathcal{S}$ , and the pinion tooth flank,  $\mathcal{P}$ , and the indicatrix of conformity  $Cnf(\mathcal{S}^m / \mathcal{P}^m)$  for the models,  $\mathcal{S}^m$  and  $\mathcal{P}^m$ , are identical to one another.

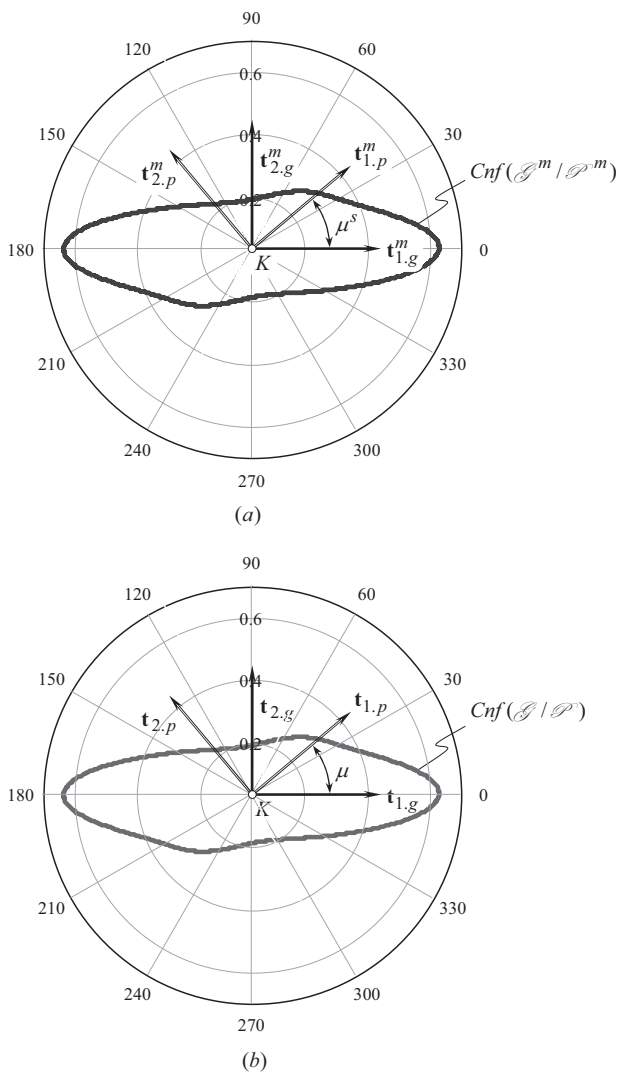


**FIGURE 23.37** Indicatrix of conformity,  $Cnf(\mathcal{S}^m / \mathcal{P}^m)$ , at point of contact of modeling surfaces,  $\mathcal{S}^m$  and  $\mathcal{P}^m$  (a), is identical to indicatrix of conformity,  $Cnf(\mathcal{S} / \mathcal{P})$ , at corresponding point of contact of a gear tooth flank,  $\mathcal{S}$ , and a mating pinion tooth flank,  $\mathcal{P}$  (b), [ $Cnf(\mathcal{S}^m / \mathcal{P}^m) \equiv Cnf(\mathcal{S} / \mathcal{P})$ ].

Ultimately, this results in high accuracy of the method of simulation of the interaction of a gear tooth flank and a mating pinion tooth flank.

When simulating the engagement of a gear and a mating pinion, it is preferred to perform continuous relative motions of the modeling quadrics,  $\mathcal{S}^m$  and  $\mathcal{P}^m$ , instead of their instant relative motions. Implementation of continuous motions leads to a significant simplification of the procedure of simulation. In order to perform the desirable continuous relative motion of the modeling quadrics,  $\mathcal{S}^m$  and  $\mathcal{P}^m$ , the use of the surfaces that allow for sliding *over themselves* is helpful. A screw surface of a constant pitch,  $p = \text{Const}$ , is the most general kind of the surfaces,  $\mathcal{S}^m$  and  $\mathcal{P}^m$ , that allow for sliding *over themselves*.

When a screw surface travels along and rotates about its axis with that same parameter of the screw motion as the instantaneous screw parameter of the screw surface itself, the envelope surface to a family of consecutive positions of the screw surface is congruent to the screw surface itself. Particular cases of surfaces that allow for sliding *over themselves* [surfaces of revolution (for which



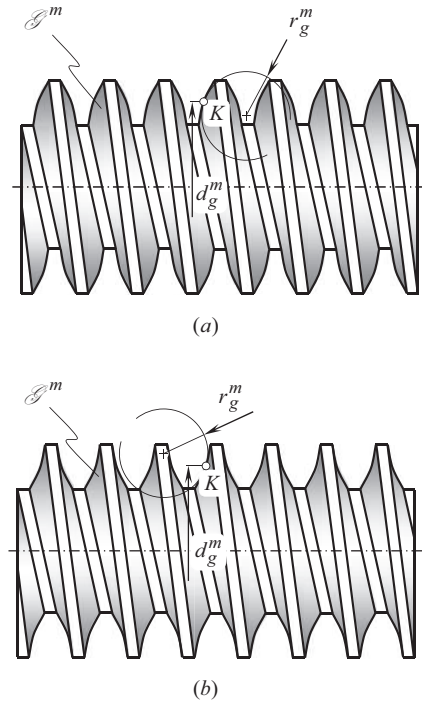


**FIGURE 23.38** An external screw with convex (a) and saddle-like (b) local patches of quadric surface,  $\mathcal{S}^m$ , for experimental simulation of interaction of a gear tooth flank,  $\mathcal{S}$ , and a mating pinion tooth flank,  $\mathcal{S}$ . Parts (a) and (b) are discussed in the text.

$p = 0$ ), surfaces of translation (for which  $p = \infty$ ) are considered in Refs [148] and [153]. Cylinders of revolution, spherical surfaces, and the plane represent examples of the simplest and completely degenerated surfaces that allow for sliding *over themselves*.

For the simulation of gear engagement, it is convenient to use a screw with external surface,  $\mathcal{S}^m$ , and either a convex or a concave thread profile (see Figure 23.38). The application of such a screw enables the simulation of both convex and saddle-like local patches of given teeth flanks,  $\mathcal{S}$ .

For simulation of concave, and saddle-like local patches of a given pinion tooth flank,  $\mathcal{S}$ , a screw with an internal surface,  $\mathcal{S}^m$ , and either convex or concave thread profile can be used (see Figure 23.39).

In both cases (see Figures 23.38 and 23.39), the screw might be either single-, or multi-threaded, as well as a single-, or multi-started. Surfaces of revolution ( $p = 0$ ) and surfaces of translation ( $p = \infty$ ) can also be used for simulation in reduced cases.

In order to provide the required parameters of the topology of the modeling surface,  $\mathcal{S}^m$ , that is, the parameters  $R_{1,g}^m \equiv R_{1,g}$ ,  $R_{2,g}^m \equiv R_{2,g}$ , the required radii of principal curvature of the surface,  $\mathcal{S}^m$ , namely, the parameters  $R_{1,p}^m \equiv R_{1,p}$ ,  $R_{2,p}^m \equiv R_{2,p}$ , and their local relative orientation, that is, the angle,  $\mu^s \equiv \mu$ , of the local relative orientation of the modeling surfaces,  $\mathcal{S}^m$  and  $\mathcal{S}$ , the parameters  $d_g^m$ , and  $r_g^m$  of the design of the screw have to be properly calculated. For this purpose, *Meusnier formula* and the *Euler formula* are used.

*Meusnier formula* establishes the correspondence between a radius of normal curvature,  $R_g$ , at point of a modeling surface,  $\mathcal{S}$  (or a modeling surface  $\mathcal{P}$ ), through a certain direction,  $\mathbf{t}_g$ , on the surface, and between the radius of curvature,  $R_g^\vartheta$ , of the surface,  $\mathcal{S}$  (or a surface  $\mathcal{P}$ ), through that same direction,  $\mathbf{t}_g$ , on the surface, which is inclined to the normal plane section at a known angle,  $\vartheta_g$ . Commonly, the *Meusnier formula* is represented in the following form:

$$R_g^\vartheta = R_g \cdot \cos \vartheta_g \quad (23.68)$$

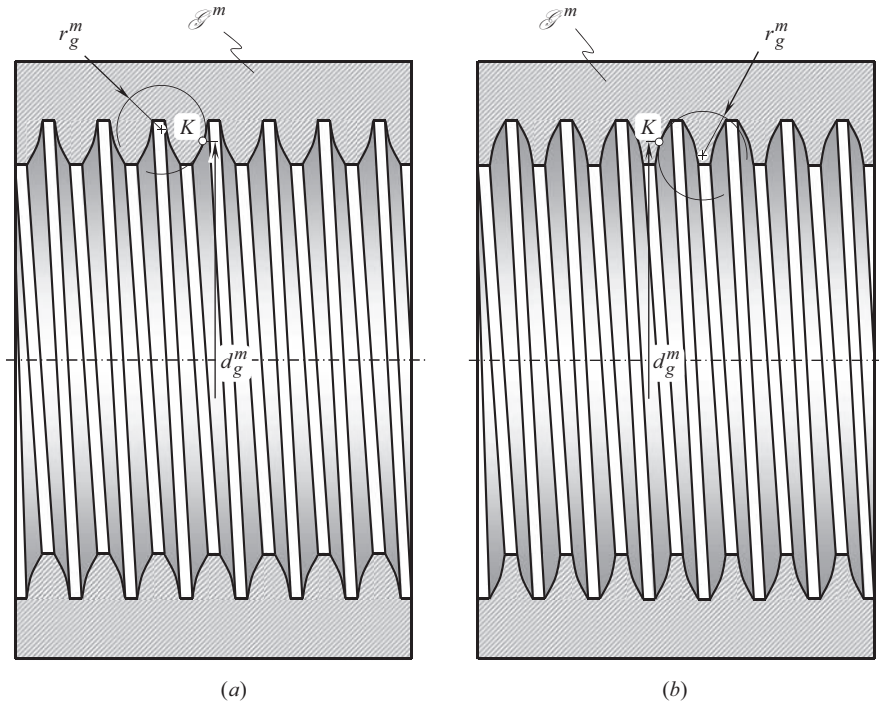


**FIGURE 23.39** An internal screw with convex (a) and saddle-like (b) local patches of quadric surface,  $\mathcal{S}^m$ , for experimental simulation of interaction of a gear tooth flank,  $\mathcal{S}$ , and the mating pinion tooth flank,  $\mathcal{P}$ . Parts (a) and (b) are discussed in the text.

Equation (23.69):

$$k_g = k_{1,g} \cos^2 \varphi + k_{2,g} \sin^2 \varphi \quad (23.69)$$

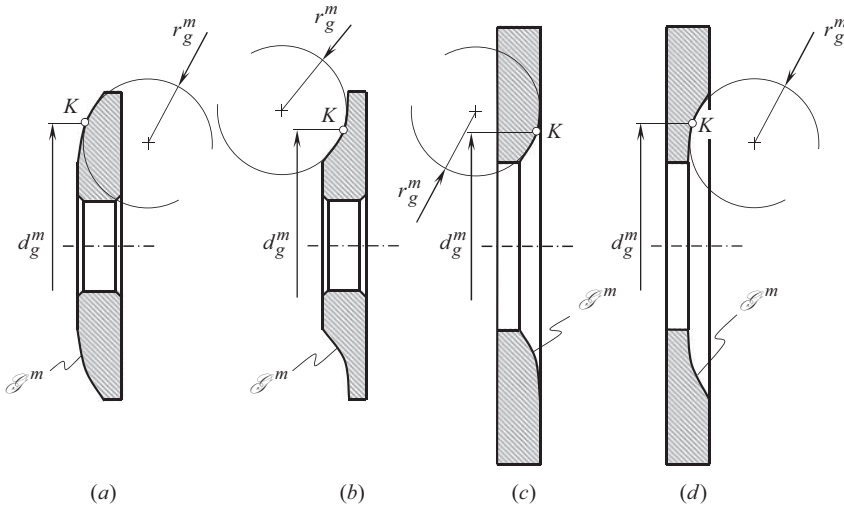
represents a conventional form of the *Euler formula*.

For the purposes of simulation, it is much more convenient to model the surface,  $\mathcal{P}^m$ , with an external, or internal surface of revolution that has either a convex, or a concave axial profile (see Figure 23.40). The same formulas can be used for the calculation of the parameters  $d_p^m$ , and  $r_p^m$  of design of the cutting tool in order to provide the identities  $R_{1,p}^m \equiv R_{1,p}$ , and  $R_{2,p}^m \equiv R_{2,p}$ .

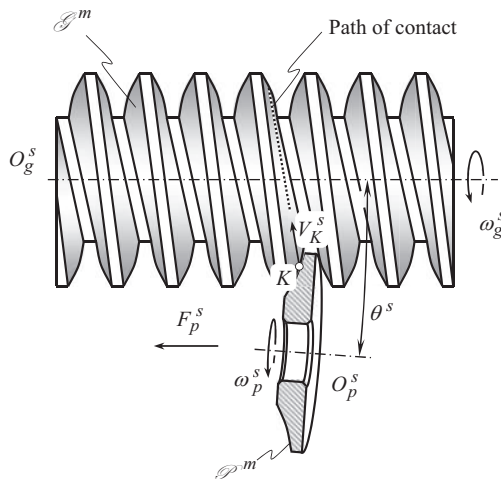
The implementation of the screw surfaces,  $\mathcal{S}^m$  (see Figures 23.38 and 23.39), and the surfaces of revolution (see Figure 23.40) allows one to attain the desirable kind of local geometry of the simulating surfaces,  $\mathcal{S}$  and  $\mathcal{P}$ .

Figure 23.41 illustrates the schematic of an example of the implementation of the disclosed method of simulation [129]. In a particular case (see Figure 23.41), the interaction of a convex local patch of the gear tooth flank,  $\mathcal{S}$ , with the saddle-like local patch of the pinion tooth flank,  $\mathcal{P}$ , is simulated with the external worm with a convex profile of threads that is interacting with the specimen with a concave axial profile. The design parameters of the worm as well as the design parameters of the specimen are pre-calculated in tight correlation with the corresponding design parameters of the actual gear tooth surface,  $\mathcal{S}$ , and the actual pinion tooth surface,  $\mathcal{P}$ , of the tool. The rotation of the worm and the specimen are timed in order to keep the resultant motion of the modeling surfaces,  $\mathcal{S}^m$  and  $\mathcal{P}^m$ , identical to the relative motion of the surfaces in the gear pair to be simulated.

In the case when either one or both modeling quadric surfaces,  $\mathcal{S}^m$  and  $\mathcal{P}^m$ , allow for sliding *over themselves*, manufacturing of the specimens for the simulation is simplified. At the same time,



**FIGURE 23.40** External (a), (b), and internal (c), (d) surfaces of revolution with (a) convex, (b) and (c) saddle-like, and (d) concave local patches of quadric surface,  $\mathcal{P}^m$ , for experimental simulation of engagement of a gear tooth flank,  $\mathcal{S}$ , and a mating pinion tooth flank,  $\mathcal{P}$ . Parts (a) through (d) are discussed in the text.



**FIGURE 23.41** Schematic of simulation of interaction of a convex local patch of a gear tooth flank,  $\mathcal{S}$ , with the saddle-like local patch of the mating pinion tooth flank,  $\mathcal{P}$ .

use of the modeling quadric surfaces,  $\mathcal{S}^m$  and  $\mathcal{P}^m$ , that allow for sliding *over themselves*, results in the possibility of two instantaneous relative motions of the surfaces,  $\mathcal{S}^m$  and  $\mathcal{P}^m$ , to be substituted with the continuous motion of their surfaces. The latter is much more convenient for simulation and enables more precise and more reliable experiment results. Ultimately, this allows for an accurate simulation of interaction of a gear tooth flank,  $\mathcal{S}$ , and a mating pinion tooth flank,  $\mathcal{P}$ .

The discussed method of simulation can also be used in stress analysis, in solving lubrication problems, and so forth.

Numerous examples of how the contact between two tooth flanks,  $\mathcal{S}$  and  $\mathcal{P}$ , of a complex geometry can be substituted with equivalent contact of surface of significantly simpler geometry are discussed in this section of the book. This makes clear an importance of the discussion in Chapter 22.

---

# 24 *SPTS* – Split Power Transmission Systems

The conventional gear drive, for example, a parallel-axes gear drive, suits most purposes well and is the most economical method of reducing speeds and increasing torques, or vice versa. The approach starts running into problems when size and weight are critical, or when wheels start becoming too large for easy manufacture. If we consider torques of the order of 1 MN·m that are needed for 6,000 kW at 60 rpm, we can estimate the wheel size for a 5–1 m final reduction. The standard rule of thumb allows us about 100 N·mm<sup>-1</sup> per mm module; so, assuming 20 mm module gives a wheel face width of about 450 mm and diameter of 2.25 m. This is not a problem, but if the torque increases, we rapidly reach the point where sizes are too large for manufacture and satisfactory heat treatment, especially as the required thickness of the carburized case also increases [203]. The solution is to split the power between two pinions so that loadings per unit face width remain the same, but the torque is doubled. A further stage in this approach is to split the power among four pinions to give a roughly quadruple increase in torque without significant increase in size. This fits well if there is a double turbine power drive, which is often required for reliability [203].

An epicyclic gearing system is particularly well suited for achieving a high-reduction ratio in a relatively small, power-dense package.

A close-up of a planetary gear set with five planetary pinions is depicted in Figure 24.1a. A cut-away view of a planetary gearbox is shown in Figure 24.1b. Planetary gearboxes can be of a very huge size as in electric-wind-power gear transmissions (see Figure 24.2), and of a very high level of complexity (see Figure 24.3), and Figure 24.4 (A planetary gear set with multiple planetary pinions in every path of power flow from a driving member to a driven member).

Bevel gears can be used in the design of *split power transmission systems* (or just *SPTS*, simplicity). As an example, a planetary gear set composed of straight bevel gears is shown in Figure 24.5, and a bevel gear set in the design of a split power transmission system with six power paths is illustrated in Figure 24.6. More examples in this regard can be provided.

The basic principles of epicyclic gearing are well established, and historically, the epicyclic gear has been used for almost as long as the simpler form of gear, which comprises a single pinion and wheel. An epicyclic gear consists of three co-axial torque-carrying members, which, quite arbitrary, can be an input, output, or stationary reaction members:

1. A *sun gear*,<sup>1</sup> which has external teeth
2. An annulus gear, which is a ring that has teeth on its inner surface
3. A planetary carrier, which supports the bearing spindles of a number of identical planetary pinions that have external teeth.

Planetary pinions are engaged in mesh with both the sun gear and the annulus.

As with any type of power transmission system, the engineer is faced with many analytical challenges during the design phase to ensure a highly reliable power train is obtained. In the case of an epicyclic gearing system, this challenge is particularly difficult due to the complex interaction of revolving and rotation components as they transmit power.

As no set of gears can ever be made to absolute precision, each of the individual gear teeth will have geometrical variations. *To achieve the gains desired with power splitting, it is absolutely*

---

<sup>1</sup> Quite often the motionless member of a planetary gear-set is considered *sun gear*.

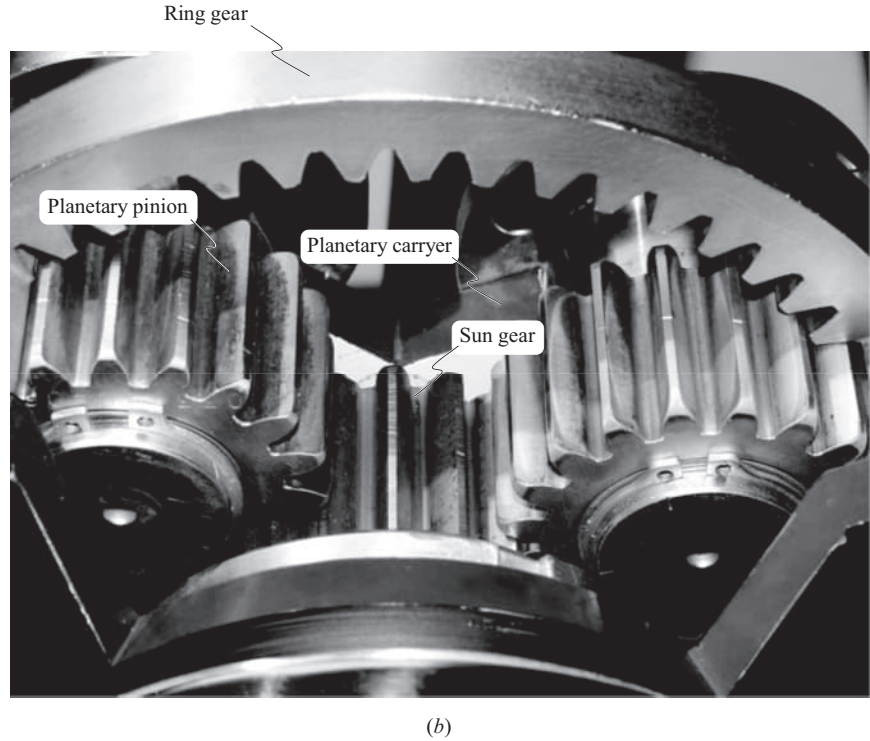
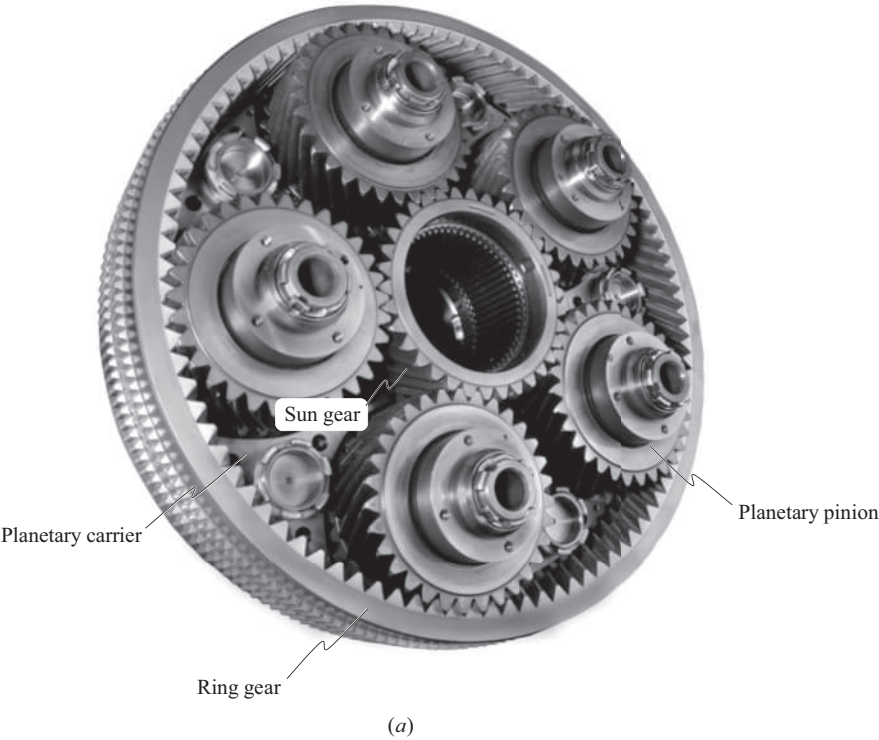
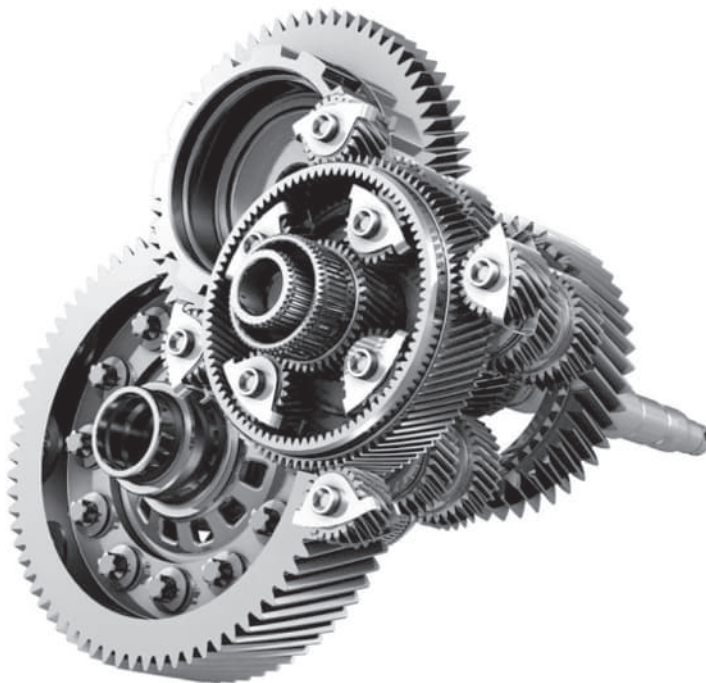


FIGURE 24.1 Close-up view (a), and cutaway view (b), of a planetary gear drive.





**FIGURE 24.2** A huge size planetary gear set for electric-wind-power transmission.



**FIGURE 24.3** A split power transmission system (SPTS) of a high level of complexity.

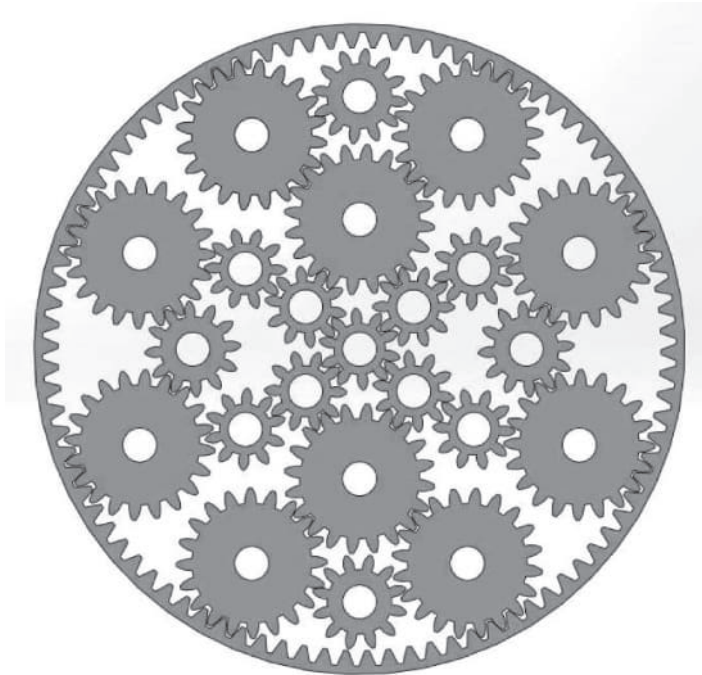


**FIGURE 24.4** A planetary gear set with multiple planetary pinions in every path of power flow.



**FIGURE 24.5** A planetary gear set that is composed of straight bevel gears.

*essential that equal power flows through each mesh in parallel.* As manufacturing tolerances, eccentricities, casing distortions, as well as displacements under operating load, are inevitable, equal power sharing is needed to be ensured by certain means.

Manufacturing errors as well as deflections of the components are the root causes for excessive mobility in a split gear drive. Excessive mobility makes equal torque sharing among all the power paths in the split gear drive impossible.

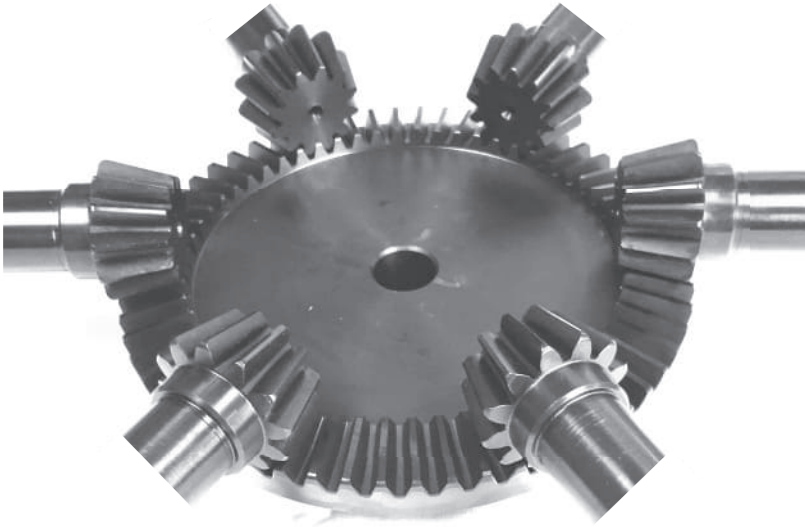


**FIGURE 24.6** Bevel gears in the design of a split power transmission system, *SPTS*, with six power paths.

## 24.1 ROOT CAUSE FOR UNEQUAL TORQUE SHARING IN A SPLIT TORQUE TRANSMISSION

Gear drives with torque sharing mesh multiple gears simultaneously so that there are errors in machining and assembly, deflections under a load, and so forth, which can cause load imbalances between them. Such load imbalances reduce transmission efficiency and durability, so high-precision manufacturing and uniform load distribution mechanisms are required.

Displacements of gears due to manufacturing errors and so on result in disengagement out of mesh in each power flow except of one of the gears, which has a minimal displacement.

As an example, Figure 24.7 shows a planetary gearbox that has three planetary pinions. It can be assumed that the axes of the sun gear,  $O_{sg}$ , the ring gear,  $O_{rg}$ , and the planetary carrier,  $O_c$ , are aligned to one another. Due to the manufacturing errors, a deviation of the actual configuration of the planetary pinion axes of rotation from their desirable locations is always observed.

A radial displacement,  $\delta r_c$ , and an angular displacement,  $\delta \varphi_c$ , are the two major contributors to the resultant displacement of the planetary pinion axis of rotation from its desirable configuration,  $O_p$ , to the actual configuration,  $O_p^*$ . (Intersected-axes and crossed-axes configurations are not considered in this example). Ultimately, the displacements,  $\delta r_c$ ,  $\delta \varphi_c$ , and others can be identified as the root cause for the low power density of the gearbox: When the ring gear is engaged in mesh with all the planetary pinions at plurality of points,  $K_{rg,p}$ , the sun gear is engaged in mesh with the planetary pinion only at one point,  $K_{sg,p}$ , and at other similar locations the sun gear is disengaged from mesh with the rest of the planetary pinions.

In order to achieve the higher power density (or, in other words, to achieve the higher *power-to-weight ratio*), all the pinions should be engaged in mesh, and all of them should be loaded equally. Split power gear drives feature excessive mobility of its members. The highest possible power density can be attained if the mobility of the gear drive is equal to one. Load equalizing means of various designs are used to minimize the mobility of a gear drive and to make it equal to one [174,187].



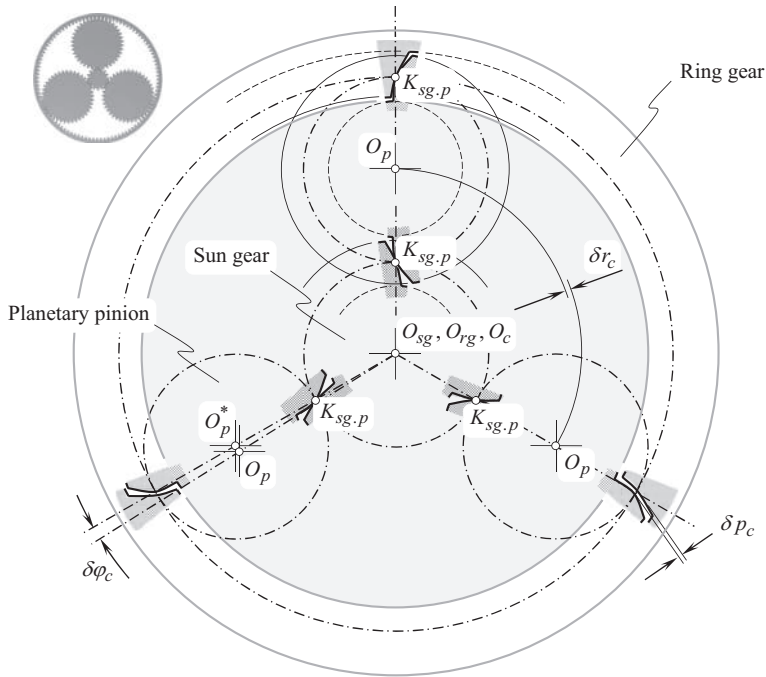


**FIGURE 24.7** Deviation of the actual configuration of the planetary pinion axis of rotation,  $O_p^*$ , from its desirable configuration,  $O_p$ .

## 24.2 MOBILITY OF SPLIT POWER TRANSMISSION SYSTEMS

The mobility of a split power transmission system can be calculated based on the principles used to determine the mobility of mechanisms of other designs. A structural formula is used for this purpose. The structural formula is based on *classes of kinematic pairs*.

A class of kinematic pair is defined as the number of constraints imposed by a given kinematic pair. The constraints of a kinematic pair are, thus, the constraints on a linear displacement along a given axis, or an angular displacement about the same axis.

The necessity of transmission of force in a kinematic pair between its links is implied by a linear displacement, whereas the necessity of transmitting a torque between the links in the kinematic pair is implied by an angular displacement. Therefore, the notion of *kinematic constraint* in a structure has as counterparts the notions of *transmitted forces* or *transmitted torques* in dynamics.

Let the total number of movable links in a mechanism be designated as  $n$ . The mechanism is said to have  $6n$  degrees of freedom (each link itself is free to move along three axes of an orthogonal *Cartesian* coordinate system and to rotate about the same axes). In order to determine mobility of this mechanism, the total number of degrees of freedom ( $6n$ ) should be deducted by constraints imposed by the kinematic pairs.

The number,  $p_i$ , of kinematic pairs of the  $i$ -th class, or order imposes  $i p_i$  constraints in total.

Thus, all the kinematic pair impose  $\sum_{i=1}^{i=5} i p_i$  constraints. However, not all the constraints should be

subtracted from  $6n$ . This is because redundant constraints duplicate other constraints without reducing the mobility of the mechanism. Let us denote the total number of redundant constraints by  $q$ . The mobility,  $w$ , of a mechanism can be calculated from the following formula<sup>2</sup>:

<sup>2</sup> Commonly, this formula is called either *Chebyshev-Grübler-Kutzbach criterion* or *Kutzbach criterion for the mobility*.

$$w = 6n - \left( \sum_{i=1}^{i=5} i p_i - q \right) \quad (24.1)$$

In a slightly different form, this formula has been proposed by Prof. A.P. Malishev.<sup>3</sup>

Ultimately, Eq. (24.1) yields an expression for  $q$ :

$$q = w - 6n + \sum_{i=1}^{i=5} i p_i \quad (24.2)$$

In expanded form, Eq. (24.2) is given as follows:

$$q = w - 6n + 5p_1 + 4p_2 + 3p_3 + 2p_4 + p_5 \quad (24.3)$$

*Malishev equation* can also be derived based on expressions used for the evaluation of both external and internal loads (within kinematic pairs) acting in a mechanism.

In a statically determined mechanism, the number of equations of equilibrium of the links is sufficient for the evaluation of the loads. In mechanisms with redundant constraints, they have to be complemented by the equations of deformation of the links, housing, and so forth. The number of the aforementioned equations is equal to the number of redundant constraints.

For planar mechanisms, the *Malishev equation* reduces to:

$$w = 3n + 2p_1 + p_2 \quad (24.4)$$

Equation (24.4) is commonly referred to as *Chebishov formula*.

Although Eq. (24.4) is derived for the case of planar mechanisms, it is also valid for certain cases of spatial mechanisms featuring kinematical pairs only of classes  $p_1$  and  $p_2$ .

### 24.3 POWER DENSITY OF GEAR TRANSMISSION SYSTEMS

The *power density* of a gear transmission system is an important consideration. The higher the *power density*, the more advanced is a gear transmission system of a particular design. The aerospace industry, the automotive industry, as well as many other industries, are targeting designing gear transmissions that feature the highest possible power density.

Conventionally, the term the *power density* is defined either as a ratio of a power being transmitted by a gear transmission to a volume occupied by the gear transmission or as a ratio of a power being transmitted by a gear transmission to the gear transmission weight. In the second case, the term *power-to-weight ratio* is commonly employed. Sometimes the term *specific power* is used as well.<sup>4</sup>

The power being transmitting by a gear pair is always known. There is uncertainty when determining the volume occupied by a gear transmission. The weight of a gear transmission can be easily determined. Therefore, the definition of the term *power density*,  $P_d$  as a ratio of a power being transmitted by a gear transmission to the gear transmission weight is preferred. In this book, the term *power density* is viewed as the *power-to-weight ratio*:

$$P_d = \frac{P}{W} \quad (24.5)$$

where the power being transmitted by a gear transmission is designated as  $P$ , and the gear transmission weight is denoted by  $W$ .

<sup>3</sup> This formula sometimes is also called *Somov-Malishev formula*.

<sup>4</sup> The terms *volume power density* and *volume specific power* are also occasionally used.

The power,  $P$ , being transmitted by a gear transmission, is always of a non-zero value,  $P \geq 0$ . The weight,  $W$ , of a gear transmission is always of a positive value,  $W > 0$ . Therefore, the *power density*,  $P_d$  is always of a non-zero value:

$$P_d \geq \frac{\geq 0}{> 0} = \geq 0 \quad (24.6)$$

In a reference system *power-to-power density-to weight* (or just  $P$ - $P_d$ - $W$  – reference system,” for simplicity) points correspond to various designs of gear transmissions, including known and unknown designs of gear transmissions. In this way, a cloud of points is formed in the  $P$ - $P_d$ - $W$  – reference system. From the top, the cloud of points is bounded by a surface,  $P_d^{\max}$ . Similarly, from the bottom, the cloud of points can be bounded by a surface,  $P_d^{\min}$ . Such a 3D plot can be useful for the gear designer, for example, to analyze trends in the gear transmission industry, and so forth.

When two, or more gear transmissions of different designs that transmit equal torque (or almost equal torque), and equal rotation (or almost equal rotation), the criterion the *power density*,  $P_d$ , perfectly works for comparison purposes. If two or more gear transmissions of different designs transmit significantly different torques, and significantly different rotations, another criterion needs to be proposed to compare the gear transmissions. It is realized here that with that same power being transmitted, design of a *Low Rotation and High Torque* gear pair, and design of a *High Rotation and Low Torque* gear pair, are significantly different.

The criterion to be developed must be expressed in terms of the torques as well as of the rotations to be transmitted.

## 24.4 EPICYCLIC GEAR DRIVES

*Epicyclic gear drive* is another term often used for *planetary gear drive*. Pedantically, the term *planetary gear* is used to describe all such gears, whereas the more commonly used *epicyclic gear* is correct only for a stationary annulus; if the planet carrier is stationary, it is a star gear. When a gear is used in an infinitely variable drive as a method of adding speeds, all three members (sun, annulus, and planet carrier) are rotating.

In epicyclic gear drives, the axes of rotation of the planetary pinions are installed in a component commonly referred to as a *carrier*. Usually, there are three, or more planetary pinions, which are engaged in mesh with the central sun gear. The planetary pinions rotate about the sun gear.

While being engaged in mesh with the sun gear, all the planetary pinions are also engaged in mesh with an internal gear. The last is commonly referred to as a *ring gear*.

The number of planetary pinions in a planetary gear drive depends on the required gear ratio. The higher the required gear ratio, the smaller the number of the planetary gears, and vice versa. This is because a higher contact ratio requires implementation of the planetary pinions of a larger size and, thus, due to lack of room, the feasible number of planetary pinions is restricted. In common practice, a correlation between the total gear ratio,  $u$ , and the permissible number of the planetary pinions is established as follows:

Total Gear Ratio ( $u$ )	Permissible Number of Planetary Pinions
12.0	3
5.2	4
3.4	5
2.7	6
2.2	7
2.0	8

The power share among the planetary pinions makes possible a more compact gear drive design. In other words, planetary gear drives are capable of the *higher power density*<sup>5</sup> compared to that in gear drives of other designs. This advantage becomes more evident in cases where very high torques are transmitted at medium and low rotations.

In planetary gear drives, manufacturing errors can never be reduced to zero. High manufacturing accuracy is required. Thus, it is necessary to specify the maximum allowed geometric variations, which are often defined as the difference between the maximum and minimum allowed backlashes of a gear mesh. (Reminder: Zero backlashes in all the gear meshes is the goal).

As the torque grows, the deflections of the planet gear teeth, planet pins, and sun and ring gear teeth engaged with that planet also grow. When the sum of those deflections closes the gap of any given planet, the planet begins to share the load, although not equally. Load sharing is proportional to the displacement of each planet's center of rotation from its original position. Planets that are not yet loaded will (obviously) not displace.

As the displacement of planetary pinion grows, the gaps of other planets close, and they begin to share load in proportion to the displacement of each, again unequally.

Some methods utilized in practice to improve the load sharing are listed as follows:

- High accuracy of all members
- Increased precision of carrier elements that locate planetary pinions
- Matching planet gear sets by tooth thickness
- Improving tooth alignment of compound planetary pinions by using matched sets of planetary pinions (compound epicyclics only)
- Oil film thickness variation due to changes in oil flow and loads in journal bearings
- Allowing radial float of one, or more elements
- Elastic deformation of the ring, or sun gear, or both
- Reducing tooth stiffness
- Elastic deformation of planetary pinion shafts
- Elastic deformation of planetary pinion carrier
- Eccentric planetary pinion shafts with a load-responsive rotation device
- Load-sensitive displacement of a journal-bearing oil film
- Load-sensitive consumption of planetary pinion shaft material when utilized as a journal bearing
- Improved gear and shaft alignment
- Reduced shaft runout
- Improved bearing quality and alignment (true position of bearing location in carrier)
- Improved assembly (location) of carrier, if the carrier is split axially
- Improved compliance of components (gears, shafts, bearings, and housing)
- Improved dynamics (operating speed vs. resonant frequencies)

Additional factors can affect bearing capabilities, because as designs are scaled up, mesh forces and, hence, bearing loads tend to rise proportionally to the size squared, whereas the capacity of rolling bearings rises more slowly and the permitted speeds decrease.

Planetary pinions are very inaccessible and very highly loaded, so they present the most difficult problems in cooling. For high-power gears, it is normal to have the planet carrier stationary as this makes introducing the large quantities of cooling oil required much easier.

These and other methods attempt to reduce load imbalance by either reducing position variation due to manufacturing allowances or allowing the movement of elements in response to a load imbalance.

---

<sup>5</sup> Or, in other words, the *higher power-to-weight ratio*. In general, these two terms, namely, *power density* and *power-to-weight ratio* are different. However, in certain cases, they can be equivalent to one another.

## 24.5 STRUCTURAL FORMULA FOR PLANETARY GEAR DRIVES

Planetary gear drives feature the following properties:

- Each of them is composed of a certain number of *elementary planetary gear drives* (see Figure 24.8). The elementary gear drives cannot be subdivided into more elementary consistent mechanisms
- The carrier (the member  $h$ ) of any elementary gear drive either has a stationary in space axis of rotation, or it is motionless
- The angular velocities of the three main members, namely, of  $a$ ,  $b$ , and  $h$ , correlate to one another in accordance with the following formula:

$$i^h = \frac{\omega_a - \omega_h}{\omega_b - \omega_h} \quad (24.7)$$

The members of a planetary gear drive that have motionless axes of rotation are referred to as the *main members*. The total number of main members in a planetary gear drive is designated as  $n_0$ .

The number of degrees of freedom in a planetary gear drive can be calculated from Eq. (24.4).

Assuming in Eq. (24.4)  $p_1 = n$ , one can obtain the following equation [69]:

$$w = n - p_2 \quad (24.8)$$

In planetary gear drives, the equality  $n = n_0 + k$  is valid (here  $k$  is the number of planetary pinions).

The number of higher kinematic pairs is equal to the number  $p_z$  of meshes, that is,  $p_z = 2k$ . These result in a formula for calculating the total number of degrees of freedom in a planetary gear drive:

$$w = n_0 - k \quad (24.9)$$

It can be shown that the total number of unbalanced degrees of freedom for a planetary gear drive can be calculated as:

$$w_{unbalanced} = k - 1 \quad (24.10)$$

The problem of evenly loading planetary pinions can be interpreted as a particular case of the more general problem of self-alignment of mechanisms [187].

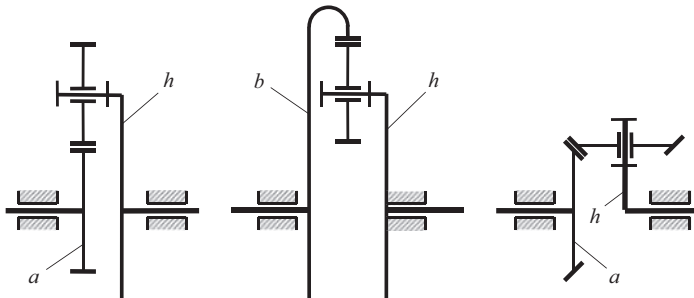


FIGURE 24.8 Elementary planetary gear drives.

## 24.6 CORRESPONDENCE AMONG ANGULAR VELOCITIES OF ALL THE MEMBERS IN PLANETARY GEAR DRIVE

To symbols that relate to rotations of a member of a planetary gear drive, a corresponding subscript is added. For example, the angular velocity of a member,  $b$ , is denoted by  $\omega_b$ .

The gear ratio is the ratio of angular velocities of the rotating members. The gear ratio is designated as  $u$ . Two subscripts are added to  $u$ , which are related to the rotating members. The first subscript is that of angular velocity in the numerator, whereas the second subscript is that in the denominator. For example, for members  $a$  and  $b$ :

$$u_{ab} = \frac{\omega_a}{\omega_b} \quad (24.11)$$

$$u_{ba} = \frac{\omega_b}{\omega_a} \quad (24.12)$$

In the case of parallel-axes of rotations, the gear ratio is positive if the rotations are in the same direction (this can be clearly shown by means of a corresponding vector diagram). Otherwise, when the rotations are in opposite directions, the tooth ratio is of a negative value.

In addition, a superscript can be used in certain cases. The superscript indicates a member in relation to which the rotations are considered. For example, if members  $A$ ,  $B$ , and  $C$  are rotating with angular velocities  $\omega_A$ ,  $\omega_B$ , and  $\omega_C$ , correspondingly, then the rotations of the members  $A$  and  $B$  in relation to the member  $C$  are equal to  $(\omega_A - \omega_C)$  and  $(\omega_B - \omega_C)$ , that is,

$$\frac{(\omega_A - \omega_C)}{(\omega_B - \omega_C)} = u_{AB}^C \quad (24.13)$$

Similarly, for a planetary gear drive:

$$\frac{(\omega_a - \omega_c)}{(\omega_b - \omega_c)} = u_{ab}^c \quad (24.14)$$

If one of the central gears is stationary, a superscript indicates the stationary member. For example, if a central gear  $b$  is motionless, then:

$$\frac{\omega_a}{\omega_h} = u_{ah}^b \quad (24.15)$$

or

$$\frac{\omega_h}{\omega_a} = u_{ha}^b = \frac{1}{u_{ah}^b} \quad (24.16)$$

The tooth ratio,  $u_{ah}^b$ , for central gears when the carrier is motionless is commonly referred to as a *tooth ratio with motionless carrier*.

Conventional rules are used for the calculation of the tooth ratio:

$$u_{ah}^b = \frac{\omega_a}{\omega_b} = \pm \frac{(r_w)_b}{(r_w)_a} = \pm \frac{z_b}{z_a} \quad (24.17)$$

Other forms of representation of Eqs. (24.11)–(24.17) are known as well.

## 24.7 FORMULATING THE PROBLEM OF EQUAL LOAD SHARING IN PLANETARY GEAR DRIVES: STATE-OF-THE-ART

Numerous designs of planetary gear drives are developed in the present-day industry. This section of the book reviews briefly some of the conceptual achievements in solving the problem of equal load sharing in planetary gear drives.

### 24.7.1 ORDINARY PLANETARY GEAR DRIVES

Ordinary planetary gear drives enable the achievement of a substantial reduction of the dimensions and weight of the gear drive, particularly, when the number of planetary pinions is large enough. However, this is true only under the condition when the *transmitted load is equally shared among all the planetary pinions*. This requires the implementation of equalizing means, which are incorporated into the design of the gear drive. Whether a design of the equalizing mechanism is appropriate, or not can be checked by counting the number of redundant constraints. The appropriate equalizing mechanism should be statically determined. For this purpose, conventional expressions derived from planar mechanisms can be used.

The equalizing mechanism of the simplest design is the one that has two planetary pinions (see Figure 24.9). The carrier is made floating [187]. It is connected to the driven shaft by two arms. The arms are parallel to the line connecting the centers of the planetary pinions. Parallelism of the lines should be ensured as the radial displacement of the center of a planetary pinion does not influence the movement of other members, whereas a tangential displacement does. This displacement should be permitted by the equalizing mechanism.

With two planetary pinions, the equalizing mechanism should not be mounted on the sun gear, or on the supporting or ring gear. Otherwise, the aforementioned direction of the arms will not be attained.

The mobility of the planetary gear drive in the case under consideration is equal to two ( $w = 2$ ). The second mobility is brought by the rotation of the carrier about both the pairs  $III_4$  and  $III_4$  in Figure 24.9. This mobility is harmful. It should be eliminated by the implementation of corresponding abutments. With  $n = 7$ ,  $p_v = 4$ ,  $p_{iii} = 4$ , and  $p_{ii} = 4$ ,

$$q = 2 - 6 \cdot 7 + 5 \cdot 4 + 3 \cdot 4 + 2 \cdot 4 = 0 \quad (24.18)$$

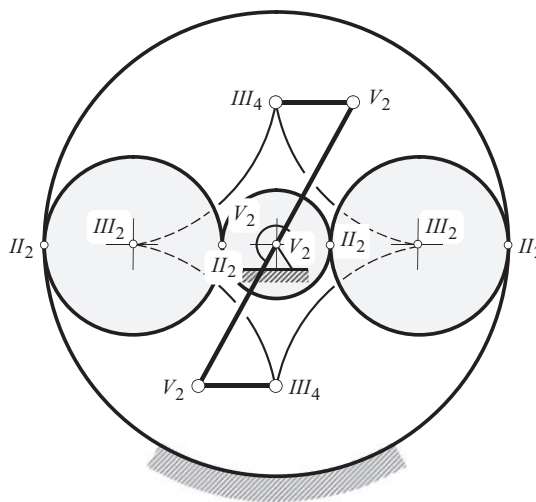


**FIGURE 24.9** Equalizing mechanism in the design of a planetary gear drive that features two planetary pinions.



The discussed approach is applicable for both planetary gearboxes of conventional design, that is, with spur and helical gears, as well as planetary gearboxes with bevel gears (see Figure 24.5) as well.

Numerous alternative approaches are known that aim an almost equal load sharing among the planetary pinions by means of eliminating the excessive mobility of the gear drive.

### 24.7.2 PLANETARY GEAR DRIVES WITH FLEXIBLE PINS

The application of gearboxes with flexible pins is based on the proposed 1969–1970 ideas of the British inventor *Ray Hicks* [49]. In 1964, *Hicks* developed a method of providing load sharing between the planetary pinions of an epicyclic gearbox, the flexible pin, which has been applied to a large variety of industrial, aerospace, and marine gearboxes from 1964 onwards.

Epicyclic gear systems have typically been equipped with straddle-mounted planetary pinions with pins supported on the input and output sides of the carrier. The torsional windup of the carrier, position accuracy of the pins, machining tolerances of the planetary gear system components, and bearings clearances can all contribute to poor load sharing among the planetary pinions as well as misaligned gear contacts in the deflected state. The double-cantilevered flexible pin concept to achieve better load sharing and gear contact patterns among a multiplicity of planetary pinions has been used to improve reliability in advanced gear drives for many years. This has resulted in consequence in a compliant epicyclic system that improves power density in the gear length direction because the probability of achieving a properly centered gear contact is increased.

In the traditional epicyclic gearing system, where the distance between planetary pinion centerlines is specified by the design to be within a fixed range, it is widely recognized that the load sharing is not equal among the planetary gear meshes. Similarly, stress is distributed variably at mesh points. Load sharing and stress distribution at each mesh point are heavily influenced by global design configuration, backlash tolerance, component design tolerances, manufacturing accuracy, component deflection, and thermal distortion. The earlier discussed Figure 24.7 shows in an exaggerated form that contact is made at the mesh point  $K_{sg,p}$  of the planetary pinion before any contact is made at the mesh points of the other planets (it is assumed that the ring gear makes contact with all the pinions at points  $K_{rg,p}$ ). In a rigid system, this condition imposes unbalanced loading among the planetary pinions.

The use of flexible pin eliminates the need for straddle mounting and thereby enables the maximum possible number of planetary pinions to be used subject to tip-to-tip clearance for any particular gear ratio. The number of planetary pinions varies with the ratio between the annulus and sun gear tooth numbers.

Load sharing is achieved by ensuring that deflection of the planetary pinion spindle under its normal load is considerably greater than the manufacturing errors that cause maldistribution, that is, if one planetary pinion tends to take more load than the others, it will deflect until the others take their share.

The original *Hicks* invention is shown in Figure 24.10 as a fragmentary and diagrammatic part-sectional elevation of an epicyclic gear with flexure, greatly enlarged for illustration. Referring to Figure 24.10, which illustrates the invention diagrammatically, the epicyclic gear broadly comprises a sun wheel 10, an annulus gear ring 11, and a plurality of planetary pinions 12, which mesh with both sun and annulus. The planets are supported on spindles 13 fast with a carrier 14. The effect of the gear depends upon whether the sun, annulus, or carrier is the input or output, and which of these three is fixed either permanently, or optionally. In any event, the center 15 of the planet teeth, measured axially, is at an equal distance from the points 16 and 17, which lie in planes contacting the point of emergence of spindle 13 from the carrier and the planet, respectively. Thus, the couples will be equal, as previously explained.

Similarly, the planet does not skew when misaligned; rather, it deflects the shaft (see Figure 24.10) until each planet is equally loaded; the annular gap 18 permits this. (It is understood that, in practice, the deflection involved is relatively slight.)

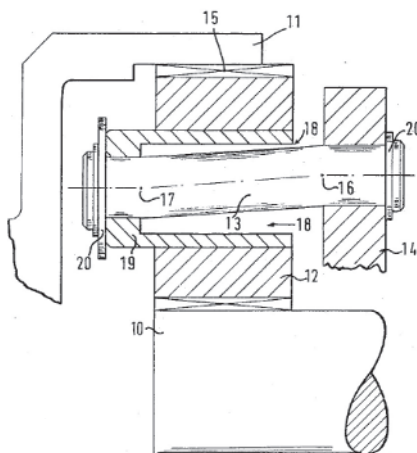


**FIGURE 24.10** A fragmentary and diagrammatic part-sectional elevation of an epicyclic gear with flexure grossly exaggerated. (After *R.J. Hicks*, US Pat. 3.303.713, 1965.)

The planet 12 may seat directly on spindle 13, or, as shown in Figure 24.10, may seat and be journaled on a sleeve 19 that provides the gap. In this case, the sleeve is fast with the spindle. The spindle is a press, or shrink-fit in the carrier 14 and possibly in the sleeve 19, but a system of c-clips 20 is also used as a precaution against damage through fit relaxation.

The use of flexible pins eliminates the need for straddle mounting and so allows the maximum possible number of planetary pinions to be used, subject to tip-to-tip clearance for any particular gear ratio. The number of planetary pinions varies with the ratio between the annulus and sun gear tooth numbers.

Load sharing is achieved by ensuring that deflection of the planetary pinion spindle under its normal load is considerably greater than the manufacturing errors that cause misallocation. Put another way, if one planetary pinion tends to take more load than the others, it will deflect until the others assume their share.

Figure 24.11a shows a typical planet gear supported by a planet spindle mounted on a flexible pin cantilevered from a simple carrier plate. The two ends of the pin are fitted to the carrier plate and the spindle, whereas the latter is counterbored to allow the pin to deflect freely.

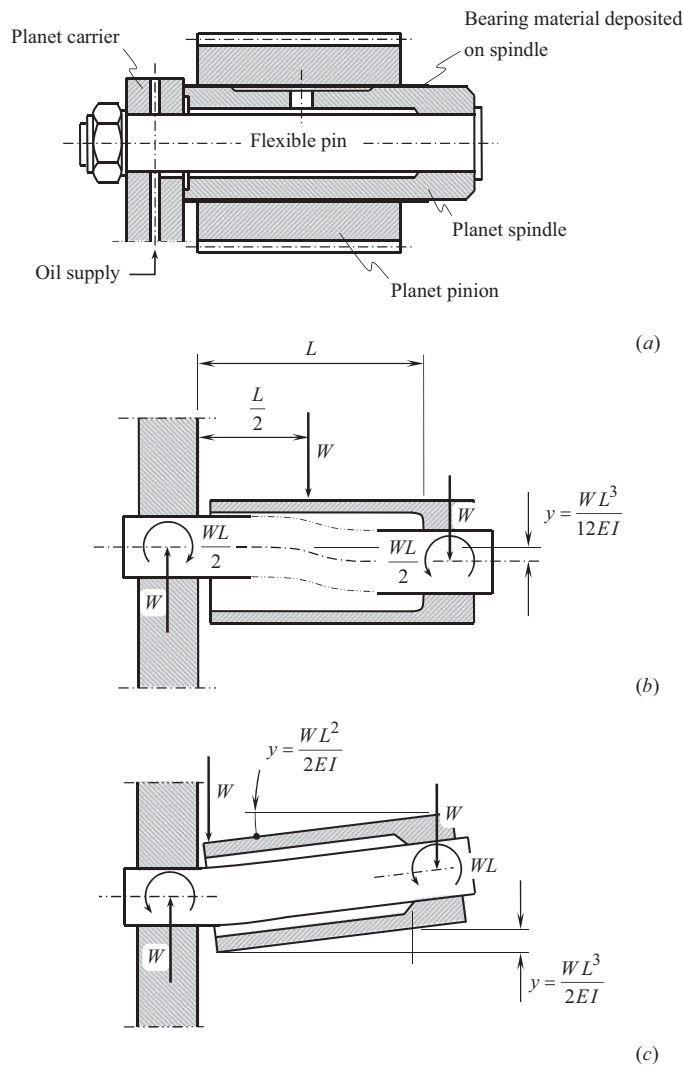
Figure 24.11b shows that a uniform tooth load, where the centroid is symmetrical with the teeth length of the flexible pin, exerts equal and opposite moments on the built-in ends so that they remain parallel during deflection.

Figure 24.11c shows that a point load concentrated on either end of the tooth face produces a relative angular deflection of that end, with respect to the other, which is six times the finite deflection that occurs when it is loaded at the center.

The deflections shown are theoretical values, which assume that the built-in portions of the pin at either end are supported so rigidly that they have zero slopes. However, static tests have shown that elastic deflections in the joints between the spindle and the carrier plane give complementary finite slopes such that the effective flexibility of the pin is more than doubled without affecting the parallel movement of the spindle.

With the proportions shown, the relative rigidity of the spindle is such that its own cantilever deflection in terms of the total is so small that it has virtually no effect on tooth load distribution. If a thinner planet spindle is used with significant flexibility, it is possible to compensate for this by reducing the length of the counterbore.

An important feature of the design is that because the planet spindle and flexible pin are co-axial, it is capable of deflection about two axes, which makes it virtually self-aligning. This means that



**FIGURE 24.11** Compact orbital gear's flexible pin: (a) planet pinion rotates on a flexibly mounted spindle, (b) planet spindle is loaded at center, and (c) planet spindle loaded at end.  $W$  is applied load,  $L$  is the length of the flex-pin, and  $E$  is the *Young's* modulus of elasticity. (After Hicks, R.J., 1969–70, *Proceedings of the Institution of Mechanical Engineers* 184, Pt. 30: 85–94 [49].)

the pin is influenced by radial as well as tangential tooth loads, and it is able to compensate helix errors of different magnitudes, or sense at the sun and annulus mesh points. It is therefore capable of compensating torsional deflection of the sun gear, which takes place in gearboxes of large tooth ratio. If the resultant load of the sun and annulus mesh points is not in the same plane as the mid-point of the unsupported portion of the flexible pin, there are two restoring effects:

1. The offset tangential load tips the spindle in the tangential plane in a manner that tends to offset the respective load points an equal amount to either side of the mid-point of the pin,
2. The radial couple resulting from the offset radial loads tilts the spindle in the radial plane until the residual couple is reduced to an amount compatible with the angular flexibility of the spindle assembly.

In short, there is a complex movement in two planes as the spindle takes up a position of minimum strain energy. This complex movement is in fact beneficial since it promotes a slight crowing effect as a result of the skewed, or non-parallel-axes.

If, on the other hand, the planetary pinion is cross-cornered so that the resultant tangential load is in the same plane, as the mid-point of the pin, there is still a radial tilting couple to provide a restoring action.

When a gearbox has a rotating planet carrier, additional radial loads and deflections are imposed on the flexible pin assembly due to the centrifugal weights of the planetary pinion, the spindle, and pin.

The flexible pin eliminates the need for straddle mounting and, therefore, enables the maximum possible number of planetary pinions to be used subject to tip-to-tip clearance for any particular epicyclic ratio. Load sharing is achieved by ensuring that deflection of the planet spindle under its normal load is considerably greater than the manufacturing errors which cause maldistribution, that is, if one planet tends to take more load than the others, it will deflect until the others take their share.

To put it simply, the flexible pin is designed to use high deflections to provide uniform tooth loads between planetary pinions and across sun-to-planet and planet-to-annulus tooth face widths. An added benefit of producing equal loads across the tooth contact face widths is the occurrence of equal loading along the planetary pinion bearings, which is the most critical element of a high-capacity low-speed epicyclic gear.

Conversely, the industrial design of epicyclic gear requires high carrier rigidity relative to the gear tooth stiffness, which is impractical and leads to maldistribution of load across the teeth and bearing, leading to premature failure.

Because a supporting shaft of the planet gear is of a flexible double cantilever construction (flexible pin system), a planetary pinion that receives more load moves in parallel due to sagging of the pinion, so that all the planetary pinions receive equal load. Consequently, an excellent equal sharing effect is shown in such cases and the whole system is of a smaller size.

Due to the flexible pin system, the shock-absorbing effect for torque variation of a prime mover or a load is expected.

If the load is distributed evenly among the teeth faces, it is the same as when a concentrated load is applied to the center; the pins flex as double cantilever beams, and parallelism relative to other planetary pinions is not lost. If there is any error in relative positioning between flexible pins, due to errors in machining, or assembly, the planetary pinion positioned here receives more load than the others and the flexible pin supporting that gear flexes further to absorb the error. Thus, the uniform load distribution mechanism keeps load distribution even.

If an eccentric load is applied to the left end of a tooth face, the flexible pin flexes as shown in Figure 24.11c and the load on the right side of the tooth face increases, mitigating the eccentric distribution of the load across the width of the tooth. The effect of gear tooth trace errors, gear casing deformation, misalignment, and other problems can be absorbed and mitigated.

However, for just about all equipment types, economics dictate the need for increased power density and improved reliability. A common approach is an attempt to build in more planets, thereby reducing forces and stresses at each mesh point. But as planets are added so is uncertainty about just how much power each planet is transmitting.

Instead of fixing the angular positions of the planetary pinions, the flexible pins were designed so that they deflect independently in a circumferential direction, which ultimately helps equalize the force distribution among the planets while transmitting torque at various levels. This feature is henceforth referred to as *torsional compliancy*.

Torsional compliancy is achieved by applying the double-cantilevered-beam design that is illustrated in Figure 24.7. Simply stated, when two tangential forces are applied to the flex-pin pinion, the angular deflection caused by the bending of the pin cantilevered from a carrier wall can be offset in the opposite direction by the angular deflection caused by bending of the sleeve cantilevered

from the other end of the pin. If sections of the pin and the sleeve are carefully designed with that goal in mind, deflection at each gear contact follows a circumferential translation, which means the axis of the gear contact does not tip from side-to-side angular positioning inaccuracy nor lead from torsional windup of the carrier.

Flexible pins have been designed into various types of equipment and the designs have typically included assembly of separable components including gears, pins, mounting sleeves, backing plates, cap-screws, and various types of rolling element bearing races and bushings.

Such a design achieves the objective of creating a torsionally compliant system. In addition, since gears are less prone to be tipped off axis because the single-sided planetary carrier can no longer wind up, it can be argued that gear contacts have a much higher probability of remaining centered at all meshes. It follows then that the flexible pin permits the designer to specify narrower gears and still avoid stress concentration at the ends of the face. Power density is therefore improved in the axial direction.

An elastic deformation of the flex-pin allows for overcoming manufacturing errors, displacements under operating load, and so forth. The elastic deformation must be large enough to accommodate manufacturing errors, and such, yet not exceed a particular given value. When zero torque is applied to the driving member of the planetary gearbox, no force is exerted from the flex-pin and no deformation of the flex-pin is observed. When the maximum torque is applied, maximum force is exerted from the flex-pin and maximum deformation of the flex-pin occurs. Because only elastic deformations of the flex-pin are considered valid (see *Young's Law*), the loaded diagram is represented by a linear function (see Figure 24.12). Huge displacements  $y$  of the flex-pin are necessary to attain the operating load that acts against the flex-pin. It is best to keep the displacements  $y$  as small as possible; however, they need to be sufficient to address the manufacturing errors, and such.

A substantial improvement can be realized if one takes advantage of modern bearing technology and advances the entire design to the next level, which is full integration of the gear with the outer races of the bearings and full integration of the sleeve with the inner races of the bearings. This advancement is the *integral flex-pin bearing* and it is illustrated in Figure 24.13. This approach to design and construction of the flexible pin arrangement provides increased opportunity to add the power density to an epicyclic gear drive in the axial and radial directions. The beam strength of the sleeve and gear are increased from the integration of bearing components allowing downsizing, especially in the radial direction.

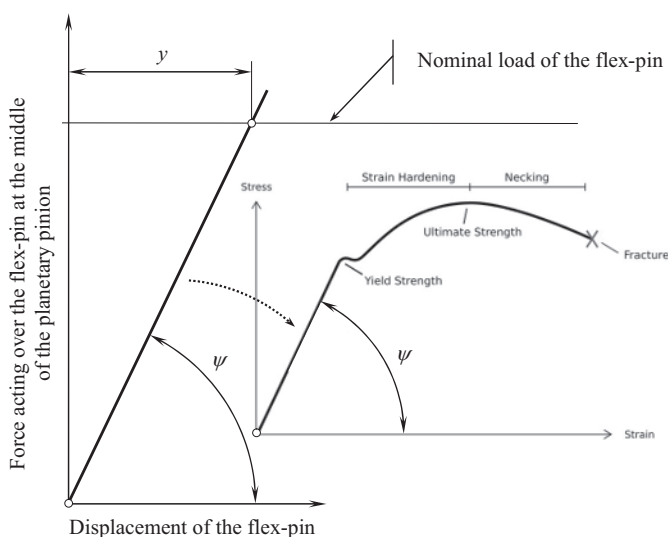
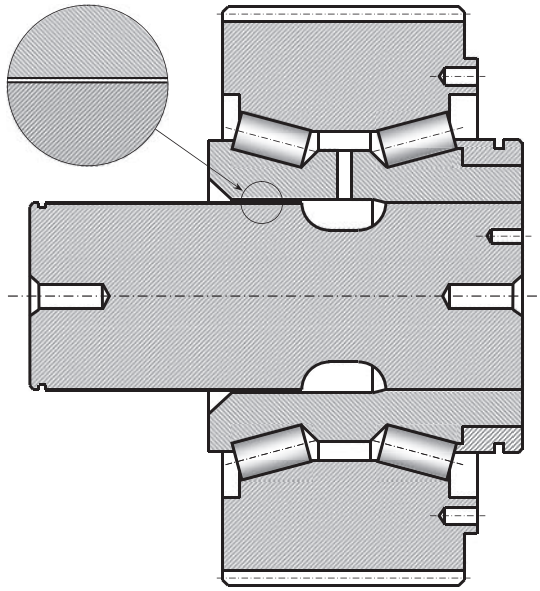


FIGURE 24.12 Stress-strain diagram for the flex-pin (US Pat. 3.303.713, 1965.)



**FIGURE 24.13** Cross-sectional view of an integrated flex-pin bearing.

Numerous other designs of planetary gear drives are based on the application of the concept of flexible pins for the purpose of equalizing load sharing among pinions.

The performed in this section of the book overview of known designs of gear trains with split of power flow reveals the complexity of equal power share in gear trains of this specific kind.

The flex-pin concept was presented here in order to make a correct comparison of this concept with the concept of elastic load-sharing device.

## 24.8 ALTERNATIVE APPROACH FOR EQUAL TORQUE SHARING IN SPLIT POWER TRANSMISSION

Elimination (or at least substantial reduction) of the total number of redundant constraints is a straightforward way of equalizing load sharing in planetary gear drives as well as in gear drives of other designs that also feature split power. Simpler methods for reasonably equal torque sharing in multi-flow gear trains have been developed as well. Neither an increase in the complexity of the design of the gear train nor significant weight increase of the gearbox occurs when these methods of load equalizing are applied.

The basic problem in all epicyclic gearing is ensuring equal load sharing among the multitude of mesh points. For example, the *Stoeckicht* system (circa 1940) solves this problem by making the annulus ring flexible while allowing it and the sun gear to float without bearings so that they are supported by their respective mesh points.

Alternatively, designers have applied a number of novel designs with various levels of success to build epicyclic gearing systems that help to distribute load among the planetary pinions more evenly, thereby increasing the power density. In general, such improvements use components in the gear train that are elastically compliant and are intended to compensate for clearance variations without imparting any negative operating characteristics, including:

- Flexible ring gears have been applied, but the effectiveness of this approach is not universal because radial deflections of the ring gear are not sufficient to compensate for clearance (backlash) variations present at the various mesh points



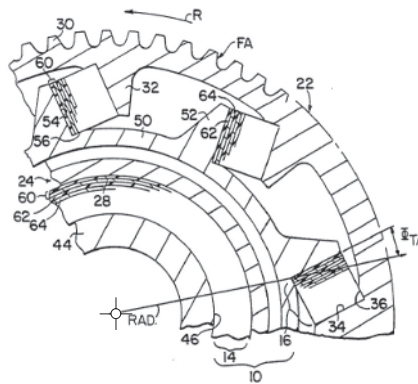


**FIGURE 24.14** The concept of the elastomeric load-sharing device. (Adapted from: U.S. Pat. No. 5,113,713, “Elastomeric Load Sharing Device,” /C.J. Isabelle, J.G. Kish, R.A. Stone, Int. Cl.<sup>5</sup> F16H 55/18, U.S. Cl. **74/410**, 74/411, 74/440, Filed: February 11, 1991, Date of Patent: May 19, 1992 [119].)

- Floating ring gear system (used in some off-highway applications)
- Floating sun gear
- Floating planet carrier
- Double-helical gear with floating members
- Floating planetary pinion, also called flexible pin, or abbreviated to *flex-pin*

In the rest of sections of this chapter, the application of elastic absorbers of manufacturing errors in the design of split power transmission systems is discussed. The focus is particularly on various designs of planetary gear drives, which present perfect examples of gear trains with split torque.

### 24.8.1 PLANETARY GEAR DRIVE WITH ELASTOMERIC LOAD-SHARING DEVICE

Application of elastomeric load-sharing device in the design of split power transmission systems is illustrated in Figure 24.14. The core (the essence) of the invention is briefly outlined below.

There are three major objectives of this invention. To provide a simplified load-sharing device that provides substantially equal torque distribution between the load paths of a split power transmission system is one of them. To provide a load-sharing device that reduces the weight and complexity of a split power transmission system is the other objective. Yet another object of the present invention is to provide a load-sharing device that enhances the overall reliability of a split power transmission system.

An elastomeric load-sharing device,<sup>6</sup> interposed in combination between a driven gear and a central drive shaft to facilitate balanced torque distribution in split power transmission systems, includes a cylindrical elastomeric bearing and a plurality of elastomeric bearing pads. The elastomeric bearing and bearing pads comprise one, or more layers, each layer including elastomer having a metal backing strip secured thereto. The elastomeric bearing is configured to have a high radial stiffness and a low torsional stiffness and is operative to radially center the driven gear and to minimize torque transfer through the elastomeric bearing. The bearing pads are configured to have a low radial and torsional stiffness and a high axial stiffness and are operative to compressively transmit torque from the driven gear to the drive shaft. The elastomeric load-sharing device has spring rates that compensate for mechanical deviations in the gear train assembly to provide balanced torque distribution between complementary load paths of split power transmission systems.

<sup>6</sup> U.S. Pat. No. 5,113,713, “Elastomeric Load Sharing Device,” /C.J. Isabelle, J.G. Kish, R.A. Stone, Int. Cl.<sup>5</sup> F16H 55/18, U.S. Cl. **74/410**, 74/411, 74/440, Filed: February 11, 1991, Date of Patent: May 19, 1992, [119].



The angular tilt of the bearing pads with respect to a radial line is generally between about  $10^\circ$  and about  $20^\circ$ .

An elastomeric material with excellent high-temperature properties and resistance to gearbox and hydraulic oils is used in the design of the elastomeric load-sharing device. A metal backing strip is secured to said elastomeric material.

Elastomeric bearing pads are sufficiently compliant to accommodate a predetermined circumferential displacement to facilitate balanced torque distribution.

An elastomeric torsional isolator can be preloaded<sup>7</sup> by a compressive load. Compressive preloading of the elastomeric torsional isolator provides a high normal force between the upper and the lower rims and the spur gear for frictionally transmitted torque across the elastomeric torsional isolator from the spur gear to the annular flange gear.

Split power designs can offer significant advantages over the traditional planetary designs for helicopter transmissions. However, it has two unique properties, gap and phase differences, which result in the risk of unequal load sharing. Various methods have been proposed to eliminate the effect of gap and promote load sharing to a certain extent.

## 24.8.2 ELASTIC LOAD-SHARING DEVICE

In order to make a split power transmission system near-insensitive to manufacturing errors as well as to the displacements of other nature, elastic load-sharing devices (*ELSD*) can be used. When designing a multi-flow gear train, many considerations should be taken into account.

### 24.8.2.1 Elastic Properties of Elastic Load-Sharing Device

The capability of an elastic load-sharing device to accommodate for manufacturing errors strongly depends on spring characteristics. The following types of spring characteristics are known. They are listed immediately below (as illustrated in Figure 24.15):

1. progressive
2. linear
3. degressive
4. substantially constant
5. progressive with knee

For implementation in the design of split power transmission system, the material with the spring characteristics: substantially constant (4), and degressive (3), are preferred. However, for most of the materials used in the production of gears and gear units, the relationship between the applied load and the displacement caused by the load is linear (2).

Significant improvement in the load-carrying capacity of a gear train with split power can be attained by improvement in the design of the preloaded elastic load-sharing device.<sup>8</sup>

A deformation of the elastic load-sharing device allows to accommodate for manufacturing errors, displacements under operating load, and so forth. The elastic deformation must be large enough to accommodate manufacturing errors, and such, yet not exceed a particular given value. When zero torque is applied to the driving member of the planetary gearbox, no force is exerted

<sup>7</sup> The necessity of a preloading of the elastomeric torsional isolator is just mentioned in the text body of the patent, and it is NOT listed among the claims of the invention. Moreover, the preload is not specified, and, per the invention, it could be either of a negligibly small value or of an extremely high value: both cases are impractical. Only a specific preloading is useful, and can be helpful to attain the objective of the invention. Considering the thickness of the elastomeric torsional isolator, no sufficient preloading of the elastomeric torsional isolator is physically possible – a large elastic deformation of the elastomeric torsional isolator is required.

<sup>8</sup> The concept of the preload elastic absorber (*PEA*) has been proposed by the author as early, as in 2000 while with *New Venture Gear, Inc.*, Syracuse, NY, USA.

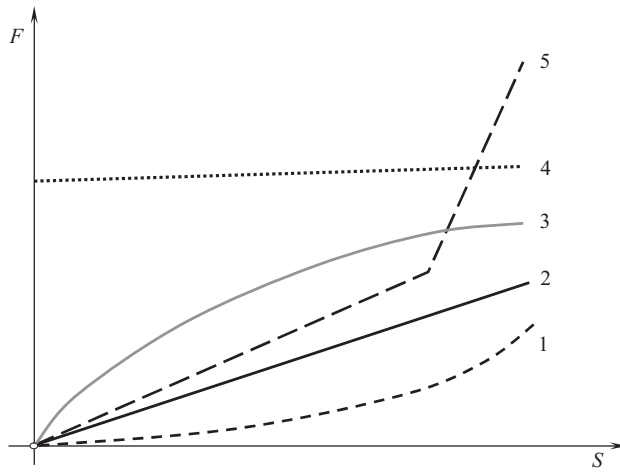


**FIGURE 24.15** Spring characteristics: (1) progressive, (2) linear, (3) degressive, (4) substantially constant, (5) progressive with knee.

from the elastic component and no deformation of the elastic component is observed. When the maximum torque is applied, maximum force is exerted from the elastic component and maximum deformation of the elastic component occurs. Because only elastic deformations of the elastic component are considered valid (see *Young's Law*), the loaded diagram is represented by a linear function (see Figure 24.12). Huge displacements  $y$  of the elastic component are necessary to attain the operating load that acts against the elastic component. It is best to keep the displacements  $y$  as small as possible; however, they need to be sufficient to address the manufacturing errors, and such.

The flex-pin concept was presented here in order to make a correct comparison of this concept with the concept of elastic load-sharing devices.<sup>9</sup>

If the preloaded elastic load-sharing device is loaded by a pre-calculated value of the load, the actual displacement of the pinions does not exceed the allowed displacement tolerance.

Consider a planetary gearbox for which the permissible range of variation of load share among the planetary pinions is equal to  $\pm OR_l$  (see Figure 24.16, upper left). The operating range of the elastic deformation,  $OR_d$ , of the elastic load-sharing device needs to be a smallest possible; however, it must also be large enough to allow for accommodation of the manufacturing errors, and the planetary pinions displacement under operating load. The two ranges  $\pm OR_l$  and  $OR_d$  specify a rectangle. In Figure 24.16, a diagonal of this rectangle forms an angle,  $\psi$ , with the horizontal axis *displacement*. The desirable stiffness,  $c$ , of the elastic load-sharing device must be equal to (or less than):

$$c \leq \tan \psi \quad (24.19)$$

Once the stiffness,  $c$ , is determined, a straight line through the origin of the coordinate system *applied load – displacement* can then be traced. This line forms the angle  $\psi$  with the horizontal axis *displacement*. Point of interception of the constructed straight line and the straight line of the nominal (operating) load,  $NL_{op}$ , specifies the desirable pre-deformation of the elastic load-sharing device (see Figure 24.16).

<sup>9</sup> The term **load sharing device** is used here and below, and not the more general term *power sharing device* because the applied load, and not the transmitted power (or rotation) is used to keep control over the actual configuration of the components in the split power transmission system.

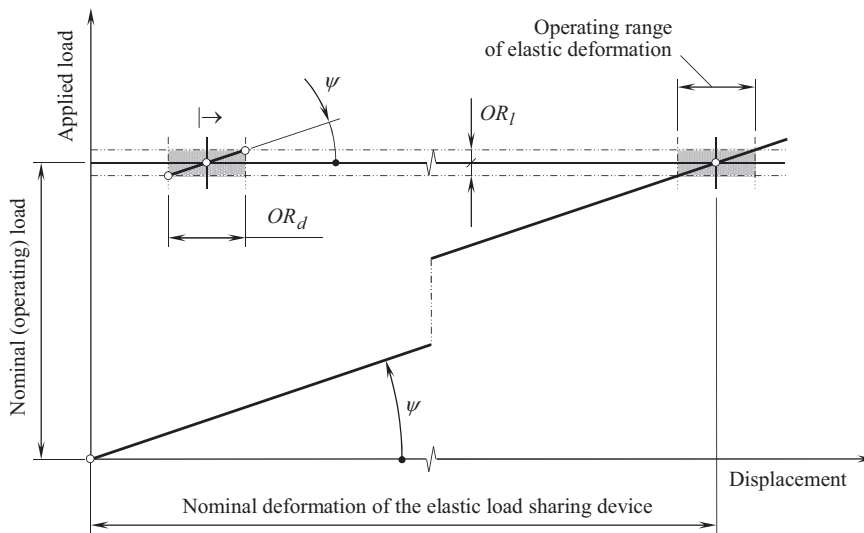


**FIGURE 24.16** Determination of the principal design parameters of the elastic load sharing device. (After Prof. S.P. Radzevich, circa 2000, *New Venture Gear*, Syracuse, NY.)

The elastic load-sharing device in (a) in a non-deformed stage, (b) in preloaded stage, and (c) fully loaded stage is shown in Figure 24.17.

The pre-deformation,  $PD_{ea}$ , of the elastic load-sharing device is calculated as:

$$PD_{ea} = (NL_{op} - OR_l) \cdot \cot \psi \quad (24.20)$$

Calculation of the design parameters of the elastic load-sharing device is based on two parameters, namely, on the design parameters  $\pm OR_l$  and  $OR_d$ .

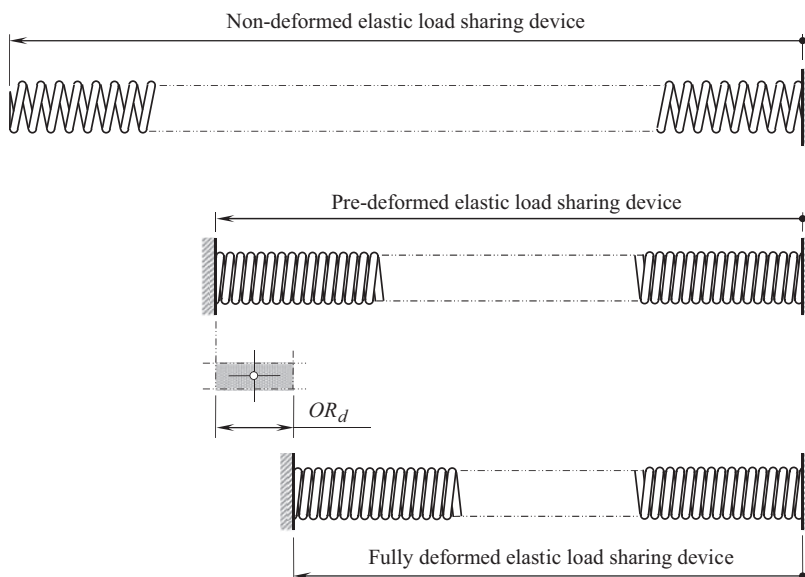


**FIGURE 24.17** Elastic load-sharing device: non-deformed, pre-deformed, and fully deformed. (After Prof. S.P. Radzevich, circa 2000, *New Venture Gear*, Syracuse, NY.)

If the preloaded elastic absorber is loaded by a pre-calculated value, the actual displacements of the pinions do not exceed the prescribed tolerance for the displacement of the pinions. Practically, this can be done, for example, in the manner discussed immediately below.

#### 24.8.2.2 Examples of Implementation of Elastic Load-Sharing Device

In some transmission systems, and in particular helicopter transmission systems, there is a need to split the power (torque) developed by the engine system so that two, or more load paths are provided for transfer of power to an output member. Such split power configurations reduce the tooth loading of the gear train assemblies comprising the respective load paths while concomitantly providing redundant paths for torque transmission. Should one gear assembly, that is, load path, become inoperative, torque will be transmitted through the remaining gear assembly, thereby ensuring the continued operation of the transmission system.

An example of the application of an elastic load-sharing device in the design of a planetary gearbox is discussed below however, it also can be used in any other design of split power transmission system).

Because of split power, planetary gearboxes can feature significantly higher power density compared to that in gear transmissions of traditional design. This is true when the torque being transmitted is equally shared among all the planetary pinions. To attain the highest possible power density (that is strongly desirable!!), the accuracy requirements for machining the components of the planetary gearbox are high, and the tolerances for the accuracy of the components of the gearbox are tight enough. The tighter the tolerances, the higher the production costs, and vice versa.

Epicyclic gear systems have typically been equipped with straddle-mounted planetary pinions with pins supported on the input and output sides of the carrier. The torsional wind up of the carrier, position accuracy of the pins, machining tolerances of the planetary gear system components, and bearings clearances, all can contribute to poor load sharing among the planet pinions as well as misaligned gear contacts in the deflected state. In the epicyclic gearing system of traditional design – that is, where the distance between planetary pinion centerlines is specified by the design to be within a fixed range – it is widely recognized that load sharing is not evenly distributed among planetary gear meshes. Furthermore, stress, too, is distributed invariably at mesh points. Load sharing and stress distribution at each mesh point are heavily influenced by global design configuration; component design tolerances; manufacturing accuracy; component deflection; and thermal distortion (see Figure 24.7).

Consider a planetary gearbox for which the permissible range of variation of load sharing among the planetary pinions is equal to  $\pm OR_l$  (see Figure 24.16). The operating range of the deformation,  $OR_d$ , of the elastic load-sharing device has to be a smallest possible.

The concept of application of the elastic load-sharing device is illustrated in Figure 24.18, where a schematic of a possible design of a planetary gearbox with almost equal load sharing among the planetary pinions is shown. The sun gear and the ring gear are mounted in the gear housing. The gear housing is stationary. A few planetary pinions (1 through 5 in Figure 24.18) are evenly distributed in the space formed by the sun gear and the ring gear. When the sun gear rotates, the torque and rotation are transmitted to the ring gear by means of the planetary pinions.

The ring gear is mounted to have a possibility to turn about its axis through an angle of a small size. In the particular case under consideration, the elastic load-sharing devices are placed in between the gear housing and the ring gear. Therefore, the ring gear and the gear housing interact with one another through the elastic load-sharing device.

Various designs of the elastic load-sharing device can be used in the design of the planetary gearbox. Shown in Figure 24.19, this can be *rectangular* springs, one or a few round springs of conventional design, a piece of elastic material with appropriate properties, and so forth.

There can be either one or several elastic load-sharing devices. Depending on an available room, the elastic load-sharing devices can be mounted from one, or from both ends of the gear set. Also, in case of necessity, the elastic load-sharing devices can be mounted from around the gear set and from both ends of the gear set.

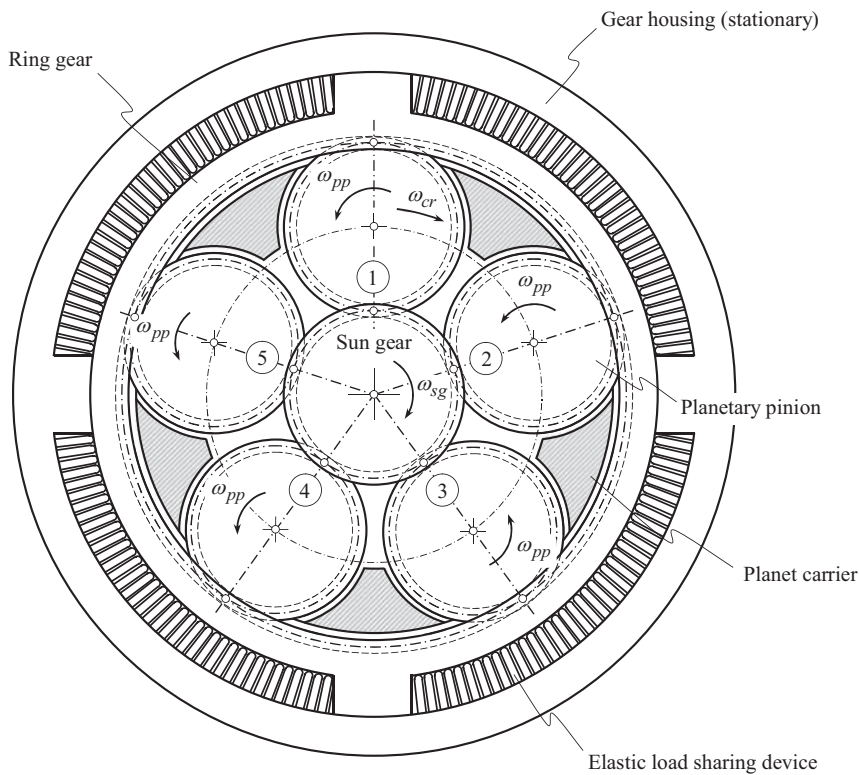


**FIGURE 24.18** Springs as elastic load-sharing device in the design of a planetary gearbox with almost equal load sharing among the planetary pinions.

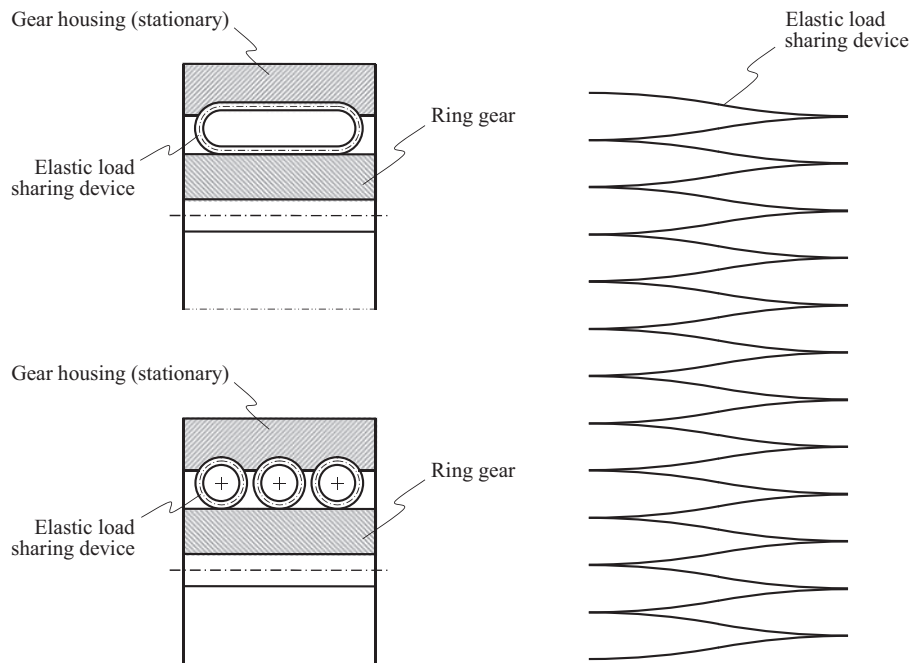


**FIGURE 24.19** Various designs of elastic load-sharing devices.

When the power (that is, a rotation and torque) is transmitted, at the beginning only one planetary pinion is engaged in tight mesh with both the sun gear and the ring gear. The rest of the planetary pinions are either under-loaded, or they can be even idle. When the applied load ramps up, the ring gear slightly turns about its axis in relation to the gear housing. Because there are two pitch points for each of the planetary pinions (one of them is in mesh with the sun gear, and another one is in mesh with the ring gear), the second planetary pinion is engaged in mesh with the ring gear, and so forth, up to a configuration when all the planetary pinions are engaged in mesh with the ring gear. The difference in load sharing among all the planetary pinions is small and is always within a pre-specified interval, for example, within the interval  $\pm 5\%$ .

Assume that a split power transmission system (a planetary gearbox) consists of  $n_{pp}$  planetary pinions (and a corresponding number of the *elastic load-sharing device*). Maximum torque being transmitting equals to  $T_{\max}$ . The design parameter of the *elastic load-sharing device*,  $OR_d$ , is specified. A permissible deviation of the torque been transmitted by the split torque transmission, from the given torque specified for the transmission must not exceed certain value,  $t_{\text{var}}$ , %.

More in detail this is illustrated in Figure 24.20. Commonly, all the planetary pinions are loaded randomly as shown in Figure 24.20a. When the split power transmission system operates, the pinion with the largest displacement is the first to get interact with the *elastic load-sharing device*. As this pinion interacts with the ring gear and with the sun gear at the same time, it pushes the *elastic load-sharing device*. However, no additional planetary pinion is engaged if the exerted torque is less than torque per one planetary pinion

$$t_p = \frac{T_{\text{nom}} - NL_{op}}{n_{pp}} \quad (24.21)$$

or:

$$t_p = \frac{T_{\text{nom}} - 0.5 \cdot NL_{op}}{n_{pp}} \quad (24.22)$$

Once the inequality:

$$t_p > \frac{T_{\text{nom}} - NL_{op}}{n_{pp}} \quad (24.23)$$

is observed, then a next planetary pinion gets engaged in interaction with the ring gear shortly. Since certain time, two planetary pinions push the ring gear, and in this way engage in mesh one more planetary pinion. Then, the next planetary pinion gets engaged in the interaction with the ring gear

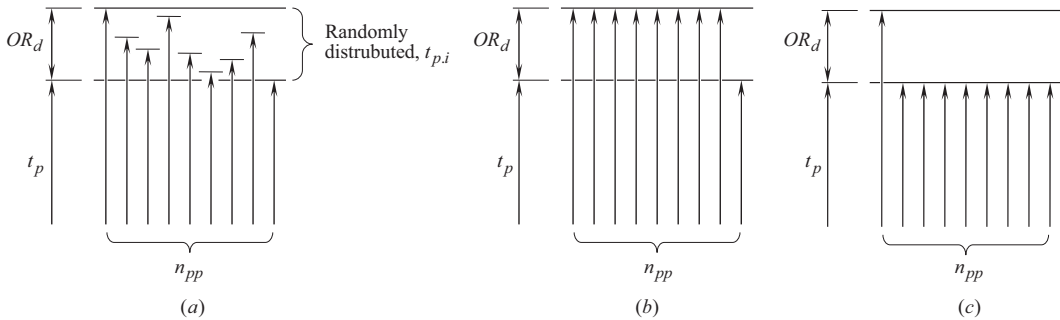


**FIGURE 24.20** Kinds of loading of the planetary pinions when an elastic load-sharing device is used: (a) randomly loaded planetary pinions, (b) maximal, and (c) minimal load capacity of the gear set.

shortly, and so forth until all the planetary pinions are engaged in the correct mesh with the ring gear.

In the best-case scenario, all the planetary pinions are fully loaded except of one of the planetary pinions that is loaded to the minimum level (see Figure 24.20b). The load capacity of the planetary gear set is maximal in this case. Finally, in the worst-case scenario, all the planetary pinions are loaded to the minimal level except of one of the planetary pinions that is loaded to the maximum level (see Figure 24.20c). The load capacity of the planetary gear set is minimal in this case.

The use of the schematic for determining the required preloading of the elastic load-sharing device (see Figure 24.16) is illustrated in Figure 24.17.

An advantage of the preloaded elastic load-sharing device over the non-loaded elastic component in the design of a planetary gearbox is illustrated in Figure 24.21. Preloading of the elastic load-sharing device along with a reduced slope of the characteristic curve together make possible an accurate adjustment of the split power transmission system to a load variation in the gear transmission.

In the worst-case scenario of load sharing among the planetary pinions in a split power transmission system, only one of  $n_{pp}$  planetary pinions is loaded the most heavily, while the rest of the planetary pinions withhold the lowest permissible torque. Remember that all the loads per planetary pinion are within the allowed band of variation,  $k$ .

The calculations reveal that in the worst-case scenario for a planetary gearbox – eight planetary pinions ( $n_{pp} = 8$ ), and the allowed variation of the load per planet pinion  $k = 0.1$  – the deviation of the transmitted load from the desirable value does not exceed 8.75%. Thus, for a planetary gear drive with three planetary pinions ( $n_{pp} = 3$ ), and the allowed variation of the load per planet pinion  $k = 0.05$ , deviation of the transmitted load from the desired value does not exceed 3.33%. The actual deviations are less than those calculated for the worst-case scenario.

The planetary gearbox with the elastic load-sharing device of the proposed design is reversible, that is, a rotation can be transmitted in both directions of rotation of the input shaft. No radial load is exerted when the elastic load-sharing device of the proposed design is used.

If the preloaded elastic load-sharing device is loaded by torque of a pre-calculated value, the actual displacement of the pinions does not exceed the allowed displacement tolerance.

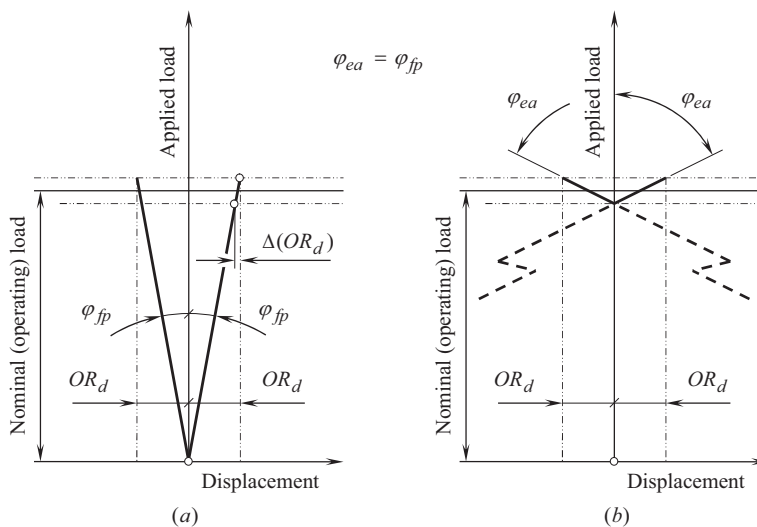


**FIGURE 24.21** Comparison of the load vs. displacement diagrams for the flex-pin approach (a) and for the elastic load-sharing device (b).



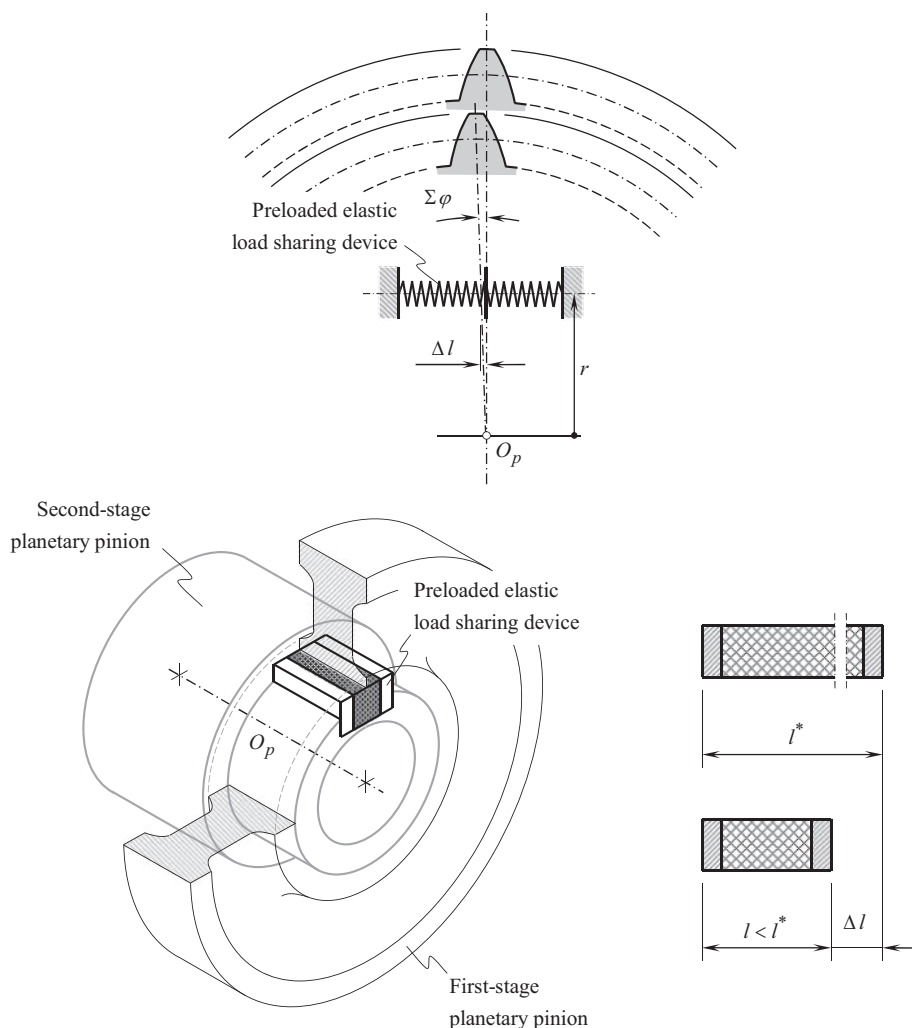


**FIGURE 24.22** Application of a preloaded elastic absorber of manufacturing errors in the design of a cluster planet pinion. (As proposed by Prof. S.P. Radzevich around 2000, *New Venture Gear*, Syracuse, NY.)

Another example of application of the elastic load-sharing device in the design of a two-stage planetary reducer is shown in Figure 24.22. The preloaded elastic load-sharing device is placed here in between the first-stage planetary pinion and the second-stage planetary pinion.<sup>10</sup>

In a two-stage planetary reducer, the preloaded elastic load-sharing device can be mounted in between the first-stage planetary pinion and the second-stage planetary pinion<sup>11</sup> (see Figures 24.21 and 24.22). It is common practice to hob both the planetary pinions of the cluster planetary pinion. For this purpose, it is preferred to assemble the cluster planetary pinion of two planetary pinions. However, note that proper phasing of the pieces in relation to one another while assembling the cluster planetary pinion is critical; mis-phasing errors with planetary pinions can be catastrophic. The preloaded elastic load-sharing device is installed between the two planetary pinions of the cluster planetary pinion (see Figures 24.21 and 24.22).

<sup>10</sup>Radzevich, S.P., *A Planetary Reducer*, Invention disclosure, filed to *New Venture Gear, Inc.*, Patent Office (Syracuse, NY) on October 30, 2001, patent pending.

<sup>11</sup>Radzevich, S.P., *A Planetary Reducer*, Invention disclosure, filed to *New Venture Gear, Inc.*, Patent Office (Syracuse, NY) on October 30, 2001, patent pending.

For equal power sharing among the planetary pinions, the misphasing  $\Delta\phi$  must be zero. As the misphasing  $\Delta\phi$  cannot be eliminated, it must be absorbed. For this purpose, it is possible to introduce an additional degree of freedom for one of the planetary pinions in relation to another and, in this way, to make the planetary pinions self-aligning. Self-alignment of the planetary pinions can be ensured by the implementation of the preloaded elastic load-sharing device. An angular displacement,  $\Delta\phi$ , to be absorbed by the elastic absorber can be eliminated when the linear displacement,  $\Delta l$ , is equal to:

$$\Delta l = \Delta\phi \cdot r \cdot \frac{\pi}{180^\circ} \quad (24.24)$$

In Eq. (24.24), the radial location of the preloaded elastic absorber is specified by the distance  $r$ . Deformation,  $\Delta l$ , of an elastic body under load usually (but not necessarily) relates to the applied load,  $T$ , linearly, or (at least) almost linearly,  $\Delta = c \cdot T$  ( $c$  is a proportionality factor equal to the rigidity of the preloaded elastic absorber). In such a case, the angle  $\phi$  can be calculated from the formula:

$$\phi = \tan^{-1}(c) \quad (24.25)$$

In general case, when  $c \neq \text{const}$ , the current value of  $c$  is equal to  $c = \frac{dT}{d(\Delta l)}$ .

The variation interval for the applied load should be known for the calculation of the design parameter of the preloaded elastic load-sharing device.

Another example of the application of the preloaded elastic load-sharing device in the design of a cluster pinion gear<sup>12</sup> is shown in Figure 24.23.

In the example under consideration, the first-stage planetary pinion is assembled with the second-stage planetary pinion.

The preloaded elastic load-sharing device must be elastic to accommodate for the misphasing error, and it should be rigid enough to transmit power from the first-stage planetary pinion to the second-stage planetary pinion.

The elastic load-sharing device is composed of two plates made of steel separated from each other by, for example, either elastomer or a spring of a conventional design.

The preloaded elastic load-sharing device is capable of accommodating a large misphasing error. The profiles  $AB$  and  $CD$  function as a cam mechanism, which allows the planets to adjust themselves in their proper relative orientation. Both profiles, that is,  $AB$  and  $CD$ , have to be determined in such a way as to incorporate friction; the inclination of the profiles must exceed the angle of friction.

Gear transmission with split power flow<sup>13</sup> features a preloaded elastic load-sharing device, which is composed of two round springs (see Figure 24.24). The round springs are preloaded in opposite directions.

The elastic load-sharing device in Figure 24.24 operates in a way similar to the aforementioned elastic absorbers operate.

Note: It should be stressed here that the elastic load-sharing device can be applied in the design of split power transmission systems (including, but not limited to, planetary gearboxes) of any and all types and sizes: small, medium, and large size.

The advantage of the elastic load-sharing device over the flex-pin concept is clearly illustrated in Figure 24.21. When the flex-pin concept is used, only a small fraction,  $\Delta(OR_d)$ , is used to overcome

<sup>12</sup>Radzevich, S.P., *A Gear Train*, Invention disclosure, filed to *New Venture Gear*, Inc. Patent Office (Syracuse, NY) on November 30, 2001, patent pending.

<sup>13</sup>Radzevich, S.P., *A Gear Transmission*, Invention disclosure, filed to *New Venture Gear*, Inc. Patent Office (Syracuse, NY) on December 30, 2001, patent pending.

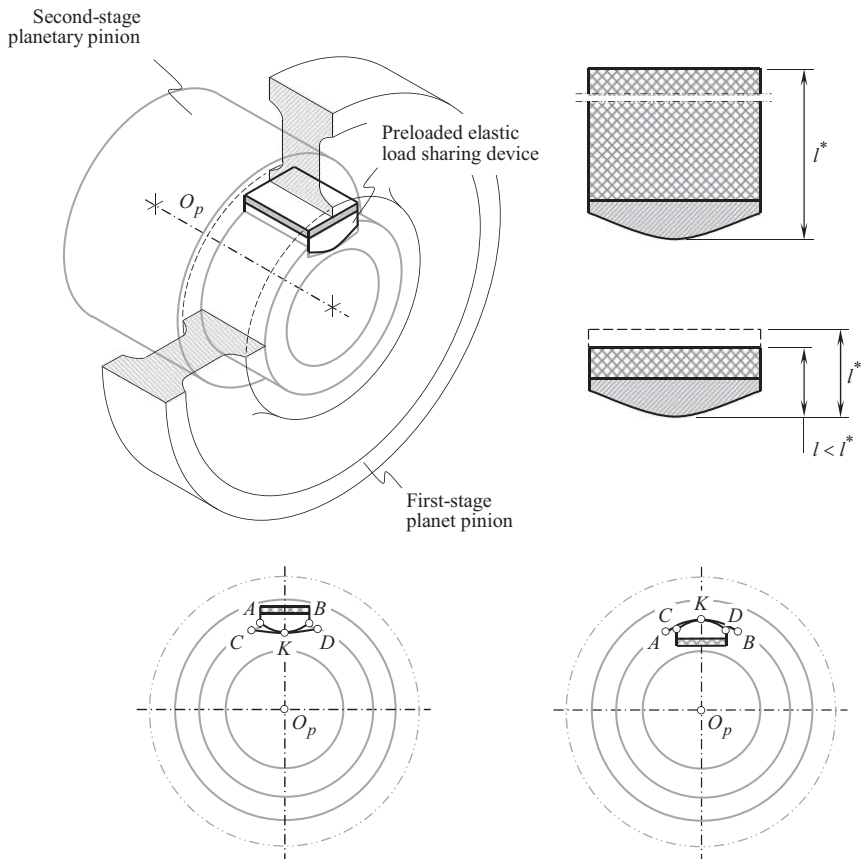


**FIGURE 24.23** A cluster pinion gear with a preloaded elastic load-sharing device. (As proposed by Prof. S.P. Radzevich around 2000, *New Venture Gear*, Syracuse, NY.)

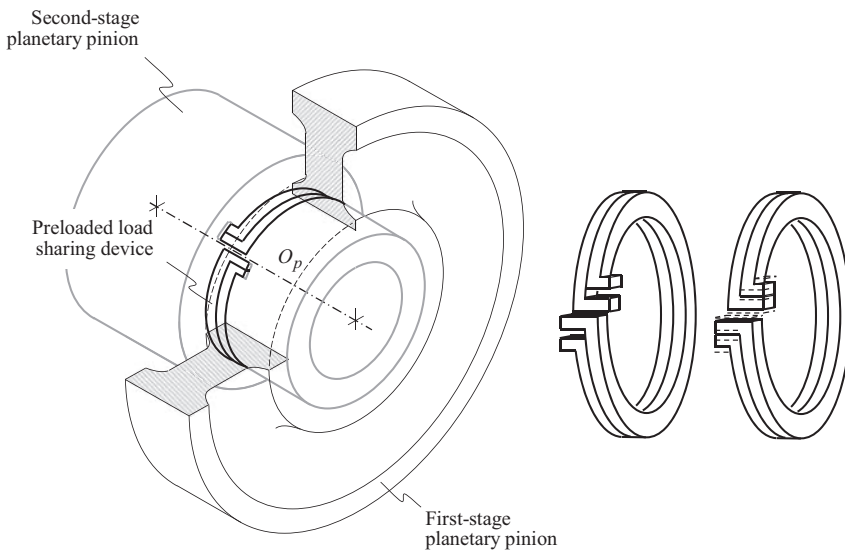


**FIGURE 24.24** An example of implementation of an elastic load-sharing device in the design of a split power transmission system. (As proposed by Prof. S.P. Radzevich around 2000.)

the unfavorable displacement of the planetary pinions under operating load (see Figure 24.21a). This is because the flex-pins are not preloaded and, therefore, the stiffness angle  $\varphi_{fp}$  is relatively small. When the concept of the elastic load-sharing device is used, the entire  $OR_d$  is used to accommodate for the unfavorable displacement of planetary pinions under operating load (see Figure 24.21b). As such, the stiffness angle,  $\varphi_{ea}$ , is significant. Typically, the inequality  $\varphi_{ea} \gg \varphi_{fp}$  is always observed. This advantage of the elastic load-sharing device is significant in that it enables higher power density for transmission through the planetary gearbox. Evidently, the presented concept of the elastic load-sharing device can be used for the improvement of power density in split power transmission systems of a variety of designs.

Numerous other examples of the implementation of the preloaded elastic load-sharing device are also known.

Use of the concept of elastic load-sharing device allows a significant improvement in power density being transmitted through the planetary gearbox. The elastic load-sharing devices can be applied in the design of split torque transmission systems of any type.

## 24.9 MAIN FEATURES OF SPLIT POWER TRANSMISSION SYSTEMS WITH PRELOADED ELASTIC LOAD-SHARING DEVICES

There is a variety of forms of application of the concept of *preloaded elastic load-sharing devices*. Application of all of them makes possible a significant increase in the power density.

In the design of a split power transmission system, for example, in a planetary gearbox, the following are true:

- All the planetary pinions are preloaded with the torque,  $t_p$ , which is equal to  $t_p = T_{nom}/n_{pp}$ , where  $T_{nom}$  denotes the total torque transmitted by the gearbox, and  $n_{pp}$  denotes the number of planetary pinions
- Elastic deformation of the load-sharing device under preloading should be at a precalculated value. Further elastic deformation of the elastic load-sharing device (within the displacements corresponding to the manufacturing errors to be absorbed) does not significantly affect the loading of the planetary pinions
- With the application of the preloaded elastic load-sharing devices, no tight tolerances are required on many dimensions
- With a preloaded elastic load-sharing device, the axes of rotation of all the planetary pinions are not deflected (as with flexible pins) and they remain straight and parallel to each other under the load.

The lower the stiffness of the elastic load-sharing device, the lower the difference in operating loading of each of the planetary pinions.

Split power transmission systems are briefly discussed in this section of the book. The problem of equal (or almost equal) load sharing among all the paths of power flow (among all the planetary pinions) is addressed. The root cause of uneven load sharing is outlined. Numerous approaches to equalize the load sharing among the planetary pinions in a planetary gearbox are reported.

In addition, the elastomeric torsional isolators are located at an angle  $10^\circ$ – $20^\circ$  to a radial direction of the gear train – a radial direction for the elastomeric torsional isolator is preferred. One more feature: the split power transmission system (U.S. Pat. No. 5,113,713) is not reversible.

---

# 25 Vector Approach in Kinematic and Dynamic Analysis of Complex Gear Transmission Systems

The application of the earlier discussed rotation vectors of a gear and its mating pinion, in gear vector diagrams in particular (see Chapter 2), can be enhanced and can be used for the kinematic and dynamic analysis of complex gear transmission systems, as well as to designing complex gear transmission systems with desirable performance.

The principal steps of the vector approach for kinematic and dynamic analysis of complex gear transmission systems are briefly outlined below. The disclosed method is applicable for the analysis of all kinds of complex gear systems with parallel-axes of rotation of the gears and pinions, including, but not limited to single-stage and multi-stage planetary gear systems in particular. The gear vector diagram for intersected-axes gear pair is constructed. The disclosed approach can be enhanced to crossed-axes gear pairs as well.

## 25.1 POSSIBLE KINDS OF GRAPHICAL REPRESENTATION OF ROTATING GEAR

Different ways can be employed aiming at graphical representation of a rotating gear. An image of a rotating gear (see Figure 25.1a) can be used in certain applications. A rotating gear can be depicted by means of its axis of rotation,  $O_g$ , and a circular arc with an arrow at its one end (see Figure 25.1b). The arrow indicates the direction of the rotation of the gear. The axis of rotation,  $O_g$ , and an arrowed circular arc can be complemented with a corresponding rotation vector,  $\omega_g$  (see Figure 25.1c) [Reminder: Rotation is not a vector by nature; therefore, special care is required to be undertaken in order to treat rotations as vectors]. The rotation vector,  $\omega_g$ , is pointed along the gear axis of rotation,  $O_g$ , and is applied at an arbitrary point within the gear axis, as the rotation vector,  $\omega_g$ , is a kind of sliding vectors. The *right-hand rule* can be used for the determination of the direction of the rotation vector,  $\omega_g$ . The rotation vector,  $\omega_g$ , of a gear itself is sufficient to specify a rotating gear (see Figure 25.1d).

A consideration similar to that discussed above is valid with respect to a gear that is rotated in the opposite direction. The latter is illustrated in Figure 25.1e–g.

For the purposes of kinematic and dynamic analysis of complex gear transmission systems, vector representation of a rotating gear (see Figure 25.1d and g) is advantageous over other possible kinds of graphical representation of a rotating gear. Therefore, in the analysis below, a rotating gear (see Figure 25.2a) is depicted by means of the rotation vector,  $\omega_g$ , as illustrated in Figure 25.2b.

In addition to the rotation vector,  $\omega_g$ , a complementary torque vector,  $T_g$ , can be assigned. The torque vector,  $T_g$ , is pointed along the gear axis of rotation,  $O_g$ . The torque vector,  $T_g$ , is applied at an arbitrary point within the gear axis, as the torque vector,  $T_g$ , is a kind of sliding vectors. It is convenient to apply the torque vector,  $T_g$ , at point at which the rotation vector,  $\omega_g$ , is applied.

Two different cases of the torque vector,  $T_g$ , are distinguished.

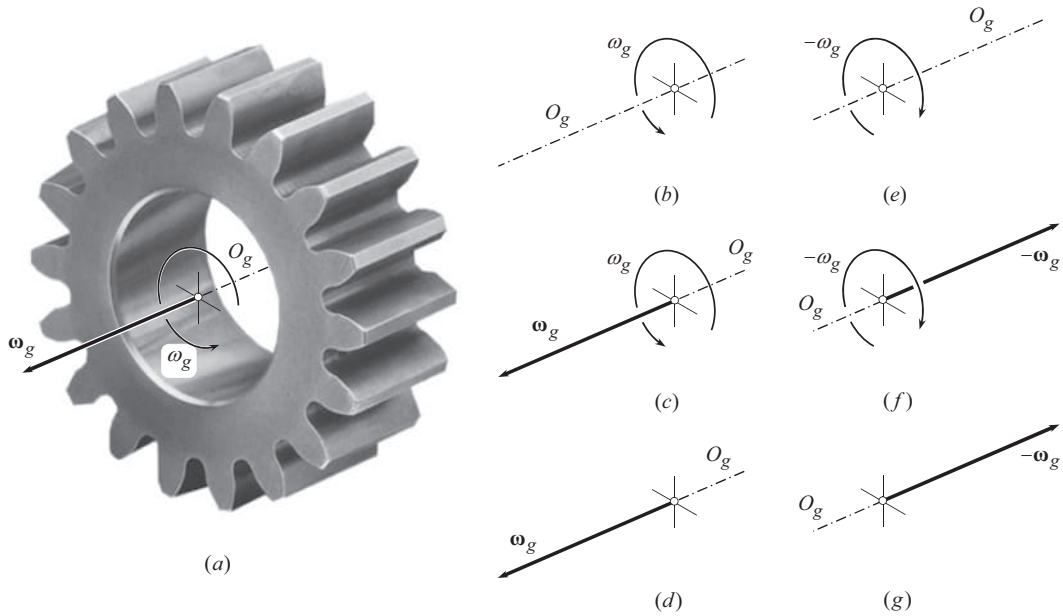


**FIGURE 25.1** Possible kinds of graphical representation of a rotating gear: (a) rotating gear, (b) direction of rotation of a gear, (c) direction of rotation of a gear, and rotation vector of a gear, (d) rotation vector of a gear, (e)–(g) are equivalents for oppositely directed cases in (b)–(d).

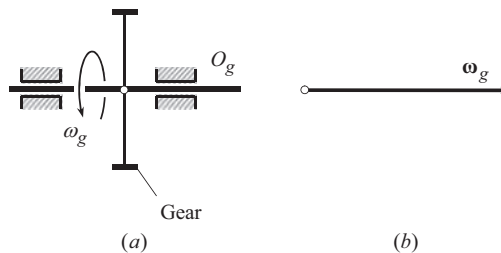


**FIGURE 25.2** Schematic of a rotating,  $\omega_g$ , gear (a), and a corresponding rotation vector,  $\omega_g$ , associated with the gear (b).

**First**, for a driving gear in a gear pair shown in Figure 25.3a, the torque vector,  $\mathbf{T}_g$ , is pointed at the direction, at which the rotation vector,  $\omega_g$ , is pointed to (see Figure 25.3b).

**Second**, for a driven gear in a gear pair shown in Figure 25.4a, the torque vector,  $\mathbf{T}_g$ , is pointed at the direction, at which that is opposite to the rotation vector,  $\omega_g$ , is pointed to (see Figure 25.4b).

Therefore, in a driving gear, the rotation vector,  $\omega_g$ , and the torque vector,  $\mathbf{T}_g$ , are always of the same direction, and in a driven gear, the rotation vector,  $\omega_g$ , and the torque vector,  $\mathbf{T}_g$ , are always of the opposite direction to each other. An illustrative example of this rule is illustrated in Figure 25.5 where an elementary gear drive is schematically shown. The gear pair is composed of gears 1 and 2. Gear 1 is rotating about the axis  $O_I$ . Accordingly, gear 2 is rotating about the axis  $O_{II}$ . Gear 1 is the driving component of the gear pair, while gear 2 is driven. The rotation vector  $\omega_1$ , and the input torque vector,  $\mathbf{T}_1$ , in the driving gear 1, are pointed in the same direction. For an external gear pair,

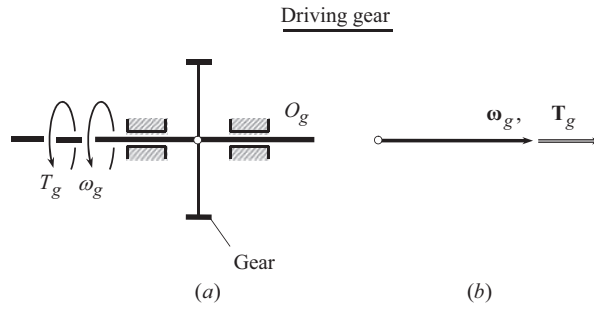


**FIGURE 25.3** Schematic of a rotating,  $\omega_g$ , gear with the applied input torque,  $T_g$  (a), and the corresponding rotation vector,  $\omega_g$ , and input torque vector,  $T_g$ , associated with the *driving* gear (b).

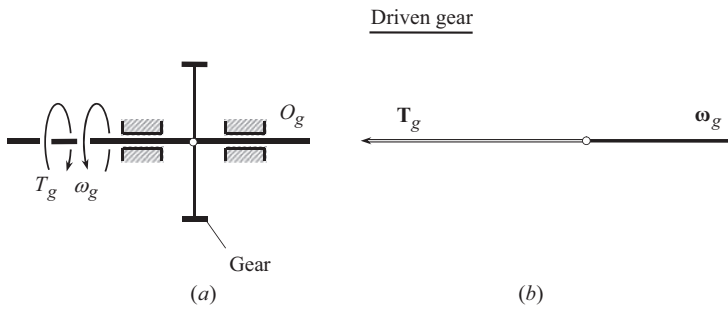


**FIGURE 25.4** Schematic of a rotating,  $\omega_g$ , gear with the applied input torque,  $T_g$  (a), and the corresponding rotation vector,  $\omega_g$ , and input torque vector,  $T_g$ , associated with the *driven* gear (b).

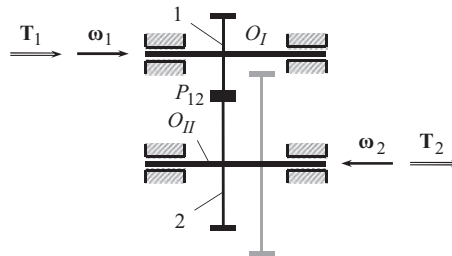


**FIGURE 25.5** Rotation vectors,  $\omega_1$  and  $\omega_2$ , and torque vectors,  $T_1$  and  $T_2$ , at the input shaft 1, and at the output shaft 2 of a gear pair.

the rotation vector  $\omega_2$  of the driven gear 2, is pointed oppositely to the rotation vector  $\omega_1$ . For an internal gear pair, the rotation vectors  $\omega_1$  and  $\omega_2$  are pointed in the same direction.

The output torque vector,  $T_2$  (the torque vector at the driven gear 2), is pointed oppositely to the rotation vector  $\omega_2$  of the second gear.

The above consideration can be construed as a kind of qualitative analysis of kinematics and of dynamics of a gear pair with parallel-axes of rotation of the gear and its mating pinion.

## 25.2 VECTOR DIAGRAMS OF COMPLEX GEAR TRANSMISSION SYSTEMS

Once the concept of the gear rotation vectors,  $\omega$ , and torque vectors,  $T$ , is understood, this allows to proceed with the analysis of kinematics and of dynamics of a gear pair, and perform the analysis in terms of the vectors,  $\omega$  and  $T$ , for every elementary gear pair.



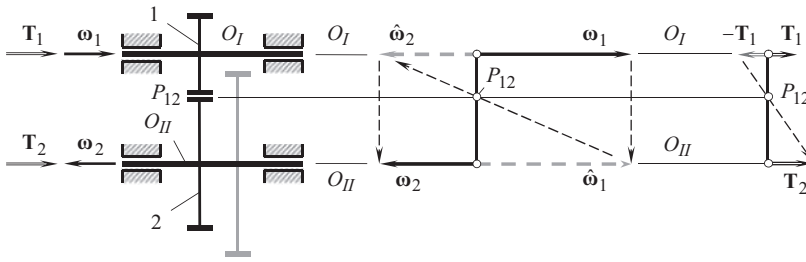


FIGURE 25.6 Elements of quantitative kinematic and dynamic analysis of an external gear pair.

For the kinematic and dynamic analysis of complex gear transmission systems, vector representation of rotations of a driving gear, and of a driven gear in a gear pair, as well as vector representation of torque vectors of the driving, and the driven gears in a gear pair, is convenient to be used.

A quantitative kinematic and dynamic analysis of an external gear pair is illustrated in Figure 25.6.

The driving gear 1 is rotated about its axis *I* with an angular velocity  $\omega_1$ . The rotation vector  $\omega_1$  of the driving gear 1 in Figure 25.6 is pointed along the axis *I*. The applied torque vector,  $\mathbf{T}_1$ , is pointed also along the gear axis of rotation, *I*. The input vectors,  $\omega_1$  and  $\mathbf{T}_1$ , are one-sided to one another.

The driving gear 1 is engaged in mesh with a driven gear 2.  $P_{12}$  is the pitch point of the gear 1-to-gear 2 mesh.

The driven gear 2 is rotated about its axis *II* with a certain angular velocity  $\omega_2$ . The rotation vector  $\omega_2$  of the driven gear is pointed along the axis *II*. The magnitude,  $\omega_2$ , of the rotation vector,  $\omega_2$ , is to be determined. The output torque vector,  $\mathbf{T}_2$ , is pointed also along the gear axis of rotation, *II*. The magnitude,  $T_2$ , of the torque vector,  $\mathbf{T}_2$ , is to be determined. In external gearing, the output vectors,  $\omega_2$  and  $\mathbf{T}_2$ , are reciprocal to one another.

A straight line through the origin of the rotation vector  $\omega_1$  is constructed in Figure 25.6. Every point within this straight line features zero rotation. Therefore, the constructed straight line is referred to as the *reference line*. Evidently, the pitch point  $P_{12}$  is located within the reference line. The actual location of the pitch point  $P_{12}$  in the vector diagram of the gear pair is defined as the intersection of the horizontal straight line through the pitch point  $P_{12}$  in the kinematic scheme of the gear pair (see the left-hand portion of Figure 25.6) by the reference line (see the right-hand portion of Figure 25.6).

The rotation vector,  $\omega_2$ , of the driven gear, and the output torque vector,  $\mathbf{T}_2$ , are constructed so, as to meet the conventional requirements external gearing obeys:

$$\omega_1 \cdot r_1 = \omega_2 \cdot r_2 \quad (25.1)$$

Here, in Eq. (25.1),  $r_1$  and  $r_2$  designate the radii of pitch circles of the driving gear 1, and of the driven gear 2, correspondingly ( $r_1 + r_2 = C$ , and  $C$  is center-distance between the axes  $O_I$  and  $O_{II}$ ).

As the ratios  $\omega_1/\omega_2$  and  $r_1/r_2$  are reciprocal to one another, two auxiliary rotation vectors,  $\hat{\omega}_1$  and  $\hat{\omega}_2$ , are used to construct the rotation vector,  $\omega_2$ . The rotation vector,  $\hat{\omega}_1$ , is pointed along the driven gear axis of rotation,  $O_{II}$ , and the rotation vector,  $\hat{\omega}_2$ , is pointed along the driving gear axis of rotation,  $O_I$ . The magnitude of the auxiliary rotation vector,  $\hat{\omega}_1$ , is equal to the magnitude of the rotation vector,  $\omega_1$ , that is, the equality  $|\hat{\omega}_1| = |\omega_1|$  is valid. The use of Eq. (25.1) allows for a construction (see Figure 25.6), by means of which the magnitude of the output rotation vector,  $\omega_2$ , is determined.

There is no need to use an auxiliary torque vector,  $\hat{\mathbf{T}}_2$ , to construct the output torque vector,  $\mathbf{T}_2$ , as the ratios  $|\mathbf{T}_1|/|\mathbf{T}_2|$  and  $r_1/r_2$  are one-sided to one another (see Figure 25.6). The determination of

the output torque vector,  $\mathbf{T}_2$ , becomes clear from the schematic shown in Figure 25.6 (at the right-hand side).

More complex gear drives can also be investigated using the approach outlined above. As an example, Figure 25.7 illustrates a gear transmission system composed of several gear pairs. The gear drive consists of two external gear pairs 1–2 and 3–4, and one internal gear pair 5–6. The gears rotate about the axes  $O_I$ ,  $O_{II}$ ,  $O_{III}$ , and  $O_{IV}$ . Points  $P_{12}$ ,  $P_{34}$ , and  $P_{56}$  are the pitch points in the gear pairs 1–2 and 3–4, and 5–6, correspondingly. The rotation,  $\omega_1$ , of the driving gear, and the input torque,  $\mathbf{T}_1$ , are given. It is necessary to determine the rest of the rotation vectors  $\omega_2$ ,  $\omega_3$ ,  $\omega_4$ ,  $\omega_5$ , and  $\omega_6$ , and torques  $\mathbf{T}_2$ ,  $\mathbf{T}_3$ ,  $\mathbf{T}_4$ ,  $\mathbf{T}_5$ , and  $\mathbf{T}_6$ .

The discussed approach (see Figure 25.6) is consequently used for each of the gear pairs 1–2 and 3–4, and 5–6 in Figure 25.7. The results of the kinematic and dynamic analysis of the gear drive are presented in Figure 25.7. It is of importance to stress here that in an internal gear pair the directions of the rotation vectors,  $\omega_5$  and  $\omega_6$ , are the same, that is, in an internal gear pair, the direction of rotation of the driven gear in comparison with the rotation of the driving gear remains the same.

The kinematic and dynamic analysis of a planetary gearbox can be performed in a similar manner.

In Figure 25.8, a schematic of a planetary gearbox, and the results of its kinematic analysis are shown. In this design, the central sun-gear 1 is a driving component, and the carrier is the driven component of the gearbox. The ring-gear 4 is stationary. The sun-gear 1 is rotated about its axis  $O_I$ . The rotation of the sun-gear is the input rotation,  $\omega_1$ . The sun-gear 1 is engaged in mesh with the planet gear 2 that is a part of the cluster planet gear 2/3.  $P_{12}$  is the pitch point of sun-gear-to-planet gear 1 mesh. The cluster planet gear 2/3 is rotated by the carrier about the axis  $O_{II}$ . The carrier is rotated about its axis,  $O_{cr}$ . The planet gear 3 is engaged in mesh with the stationary ring-gear, 4.  $P_{34}$  is the pitch point of sun-gear\_1-to-planet gear mesh.

When constructing the gear vector diagram for the rotation vectors, the axes of rotation,  $O_I$  and  $O_{II}$ , as well as the pitch points,  $P_{12}$  and  $P_{34}$ , are constructed within the reference line. When the input rotation vector,  $\omega_1$ , is given, the set of points  $O_I$ ,  $O_{II}$ ,  $P_{12}$ , and  $P_{34}$ , is the key to construct the vector diagram for the rotation vectors  $\omega_1$ ,  $\omega_2$ ,  $\omega_3$ ,  $\omega_4$ , and  $\omega_{cr}$  (see Figure 25.8).

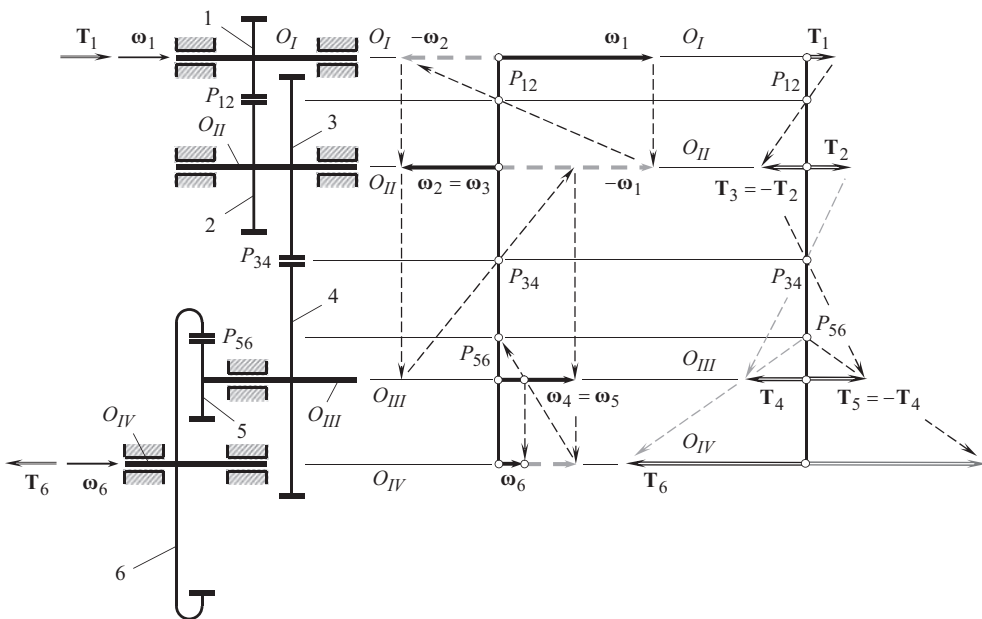


**FIGURE 25.7** Results of kinematic and dynamic analysis, performed for a complex gear transmission shown at left.

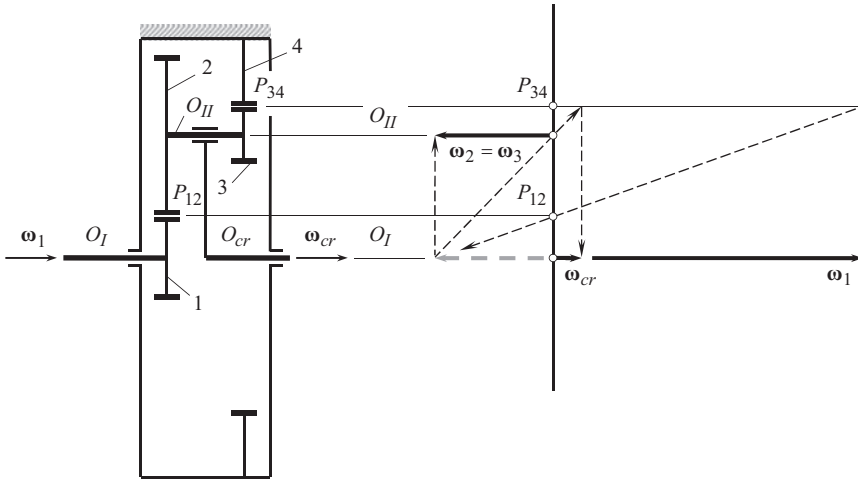


FIGURE 25.8 Results of kinematic analysis performed for a planetary gearbox shown at left.

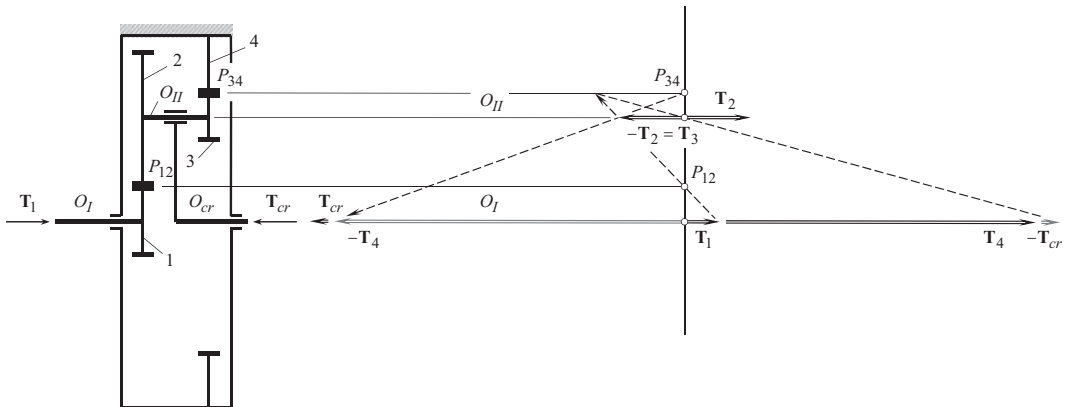


FIGURE 25.9 Results of dynamic analysis performed for a planetary gearbox shown at left.

Similarly, the dynamic analysis of the planetary gearbox can be performed. The input torque,  $\mathbf{T}_1$ , and the set of points  $O_I$ ,  $O_{II}$ ,  $P_{12}$ , and  $P_{34}$  within the reference line is the key to construct the vector diagram for the torque vectors  $\mathbf{T}_1$ ,  $\mathbf{T}_2$ ,  $\mathbf{T}_3$ ,  $\mathbf{T}_4$ , and  $\mathbf{T}_{cr}$  (see Figure 25.9).

The discussed approach can also be used for the kinematic and dynamic analysis of multi-stage (2 and more stages) planetary gearboxes.

### 25.3 FEATURES OF VECTOR DIAGRAMS OF COMPLEX GEAR TRANSMISSION SYSTEMS WITH INTERSECTED-AXES AND CROSSED-AXES GEAR PAIRS

Gear vector diagrams are developed in this book for gear pairs of all possible kinds, namely, for parallel-axes, intersected-axes, as well as crossed-axes gear pairs. As it is already discussed earlier, the vector diagrams are constructed based on the rotation vectors of a driving gear, and a driven gear. For a complex gear transmission system, a corresponding vector diagram can be constructed based on the vector diagrams of gear pairs that comprise this gear system. The vector diagrams of this sort are constructed based on the rotation vector of the driving gear and the design parameters of the gear train: the rotation vector of the driven gear is the output of this analysis. Such a feature

of the vector diagrams is already discussed in this section of the book with respect to parallel-axes gearings. Now, intersected-axes and crossed-axes gearing need to be involved in the analysis of complex gear transmission systems.

### 25.3.1 ELEMENTARY GEAR VECTOR DIAGRAM OF INTERSECTED-AXES GEAR PAIR

External and internal intersected-axes gear pairs are schematically shown in Figure 25.10.

Construction of the gear vector diagram for an external elementary intersected-axes gear pair is schematically illustrated in Figure 25.11. Two bevel gears are engaged in mesh with one another. The input gear 1 is uniformly rotated about its axis  $I$  with an angular velocity  $\omega_{in}$ . The input rotation of the driving gear 1 is also depicted by the rotation vector,  $\omega_{in}$ . The rotation vector,  $\omega_{in}$ , is pointed along the gear axis of rotation,  $I$ . The output gear 2 is uniformly rotated about its axis  $II$  with an angular velocity  $\omega_{out}$ . The output rotation of the driven gear 2 is also depicted by the rotation vector,  $\omega_{out}$ . The rotation vector,  $\omega_{out}$ , is pointed along the gear axis of rotation,  $II$ . In the particular example under consideration, the axes  $I$  and  $II$  of the rotations form a right angle. The pitch cone angle of the driven gear is labeled as  $\Gamma$ . The plane-of-action apex of the intersected-axes gear pair, point of intersection of the axes  $I$  and  $II$ , is labeled as  $A_{pa}^{12}$ .

In this example, it is necessary to determine the output rotation vector,  $\omega_{out}$ , considering the input rotation vector,  $\omega_{in}$ , and the design parameters of the intersected-axes gear pair known.

In order to construct the rotation vector,  $\omega_{out}$ , a rotation vector,  $-\omega_{in}$ , is constructed. The rotation vector,  $-\omega_{in}$ , is originated at the plane-of-action apex,  $A_{pa}^{12}$ . Then a circular arc of a radius  $|\omega_{out}|$  that

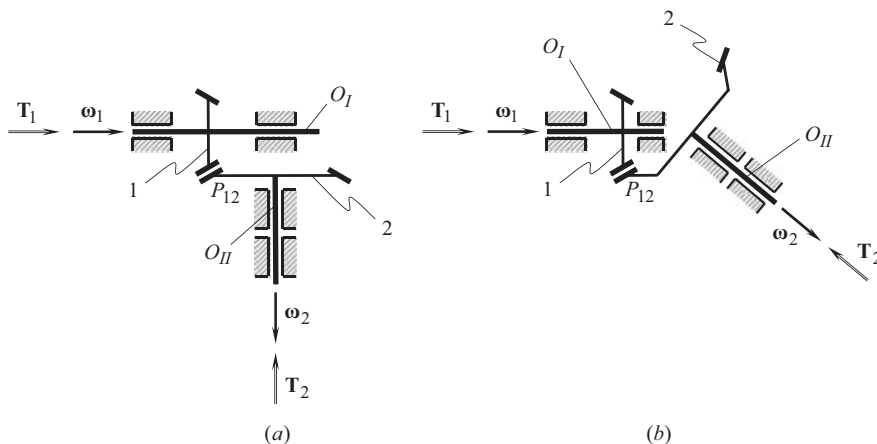


FIGURE 25.10 Schematic of (a) external, and (b) of internal intersected-axes gear pairs.

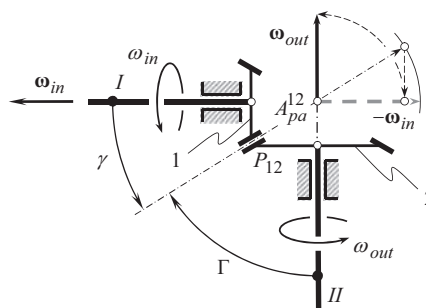
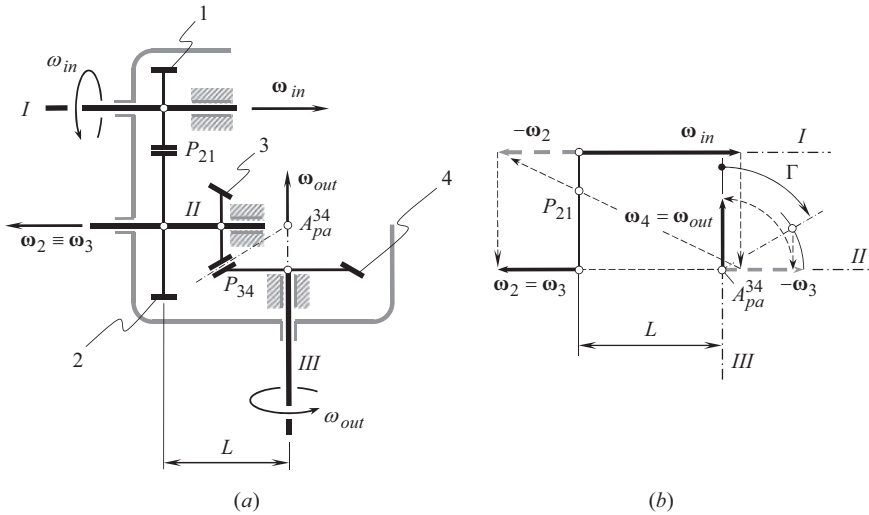


FIGURE 25.11 Gear vector diagram of an external intersected-axes gear pair.



**FIGURE 25.12** The vector diagram of a gear transmission system that consists of a bevel gear pair: (a) schematic of the gearbox, and (b) the vector diagram for the rotations.

is centered at  $A_{pa}^{12}$  is constructed. Point of intersection of the circular arc with the generating straight line of the pitch cone of the gear is projected onto the horizontal line. Then, this point is transferred to the vertical straight line as shown in Figure 25.11 by an arrowed circular arc segment. Ultimately, the output rotation vector,  $\omega_{out}$ , is constructed. The performed analysis is based on the definition of the gear ratio,  $u$ , in intersected-axes gear pair:

$$u = \frac{\sin \gamma}{\sin \Gamma} \quad (25.2)$$

where  $\gamma$  is the pitch cone angle of the driving gear.

The obtained results of the analysis can be used for the kinematic analysis of a complex gear pair schematically shown in Figure 25.12a. The gearbox is composed of a parallel-axes gear pair and an intersected-axes gear pair. The plane-of-action apex,  $A_{pa}^{12}$ , in Figure 25.12a is at a distance,  $L$ , from the driven gear 2. The kinematic analysis of the parallel-axes gear is similar to that shown in Figure 25.6. The kinematic analysis of the intersected-axes gear is similar to that shown in Figure 25.12. Here, the distance,  $L$ , can be scaled. The further dynamic analysis of the complex gear pair (see Figure 25.12) is a routine procedure.

The discussed approach can be used for the purpose of the kinematic and dynamic analysis of complex gear transmission systems composed of parallel-axes and intersected-axes gear pairs.

### 25.3.2 ELEMENTARY GEAR VECTOR DIAGRAM OF CROSSED-AXES GEAR PAIR

Two projections of a vector diagram can be constructed for a crossed-axes gear pair. A vector diagram of  $P_a$  – gearing is used to construct one of the projections (namely, the projection onto a plane perpendicular to the centerline,  $\Phi$ , namely, onto the  $N_{in}$  – plane). A vector diagram of  $I_a$  – gearing is used to construct the other projection (namely, the projection onto the  $P_{in}$  – plane).

Prior to constructing the elementary gear vector diagrams of a crossed-axes gear pair, it is instructive to note that the gear ratio in crossed-axes gear pair can be specified either as a ratio of the pitch radii,  $r_g$  and  $r_p$ , of the gear and the pinion, or as a ratio of sines of the cone angles of the gear and the pinion,  $\Sigma_g$  and  $\Sigma_p$ , correspondingly.

In the first case, when the gear ratio equals  $u = r_g/r_p$ , the analysis is performed within the pitch-line plane (see Figure 3.4). This analysis is similar to that illustrated in Figure 25.6. The projections of the input and output rotation vectors,  $\text{pr}_{pln} \boldsymbol{\omega}_{in}$  and  $\text{pr}_{pln} \boldsymbol{\omega}_{out}$ , onto the  $P_{ln}$  – plane are considered instead of the actual rotation vectors  $\boldsymbol{\omega}_{in}$  and  $\boldsymbol{\omega}_{out}$ . The rest of the steps are similar to those shown in Figure 25.62. In addition to the kinematic analysis, the dynamic analysis can be performed as well.

In the second case, when the gear ratio equals  $u = \sin \Sigma_p / \sin \Sigma_g$ , the analysis is performed within the normal plane (see Figure 3.4). This analysis is similar to that illustrated in Figure 25.11. The projections of the input and output rotation vectors,  $\boldsymbol{\omega}_{in}$  and  $\boldsymbol{\omega}_{out}$ , onto the  $N_{ln}$  – plane are considered (these projections are identical to the actual rotation vectors  $\boldsymbol{\omega}_{in}$  and  $\boldsymbol{\omega}_{out}$ ). The gear, and the pinion cone angles,  $\Sigma_g$  and  $\Sigma_p$ , are equal to the pitch cone angles,  $\Gamma$  and  $\gamma$  correspondingly. The rest of the steps are similar to those shown in Figure 25.11. In addition to the kinematic analysis, the dynamic analysis can be performed as well.

The concept of vector diagrams can be enhanced to rotations with acceleration/deceleration. This is of particular importance in dynamic analysis of gear drives, calculation of forces, and so forth. The velocities of rolling and sliding of the interacting tooth flanks of a gear and its mating pinion can also be determined by means of vector diagrams.

The discussion in this chapter can be summarized as follows. Vector diagram is an efficient tool for investigation gear pairs, as well as complex gear transmission systems. The vector diagrams of gear transmission systems are convenient in the cases, when the diagram can be plotted as a 2D graph. In cases of 3D, the vector diagrams are less convenient, and there is no evidence (in the public domain) of their application (practicality).

This tool (the vector diagrams) is convenient if 2D schematics are valid. 3D plots can be constructed, but they are less convenient.



# Taylor & Francis

Taylor & Francis Group

<http://taylorandfrancis.com>



---

# 26 Gear Ratio of Multistage Gear Transmission System

The gear ratio in a gear pair, as discussed in Chapter 2, is uniquely determined by the rotation vectors of the input shaft (commonly of the pinion,  $\omega_p$ ) and of the output shaft (commonly of the gear,  $\omega_g$ ). A multistage gear transmission system is composed of two, or more gear pairs. The gear ratio of a whole multistage gear transmission system can also be specified in terms of the rotation vectors of the input shaft,  $\omega_{in}$ , and of the output shaft,  $\omega_{out}$ .

An example of a simple two-stage gear transmission system composed of helical gears is shown in Figure 26.1. Gear transmission systems of this kind are typical for industrial applications. A multistage gear transmission system that has three to five stages is common for industrial gearboxes as well as for other applications. More complex gear trains (more than five stages in total) are used as well.

A gear transmission system of another design is illustrated in Figure 26.2. This is a complex multistage gear transmission system capable of a changeable gear ratio between the input, and the output shafts. The actual value of the gear ratio of the gear train (see Figure 26.2) depends on which of the gear pairs is engaged in mesh.

A gear transmission system can be composed either of gear pairs of the same kind (i.e., all the gear pairs in the gear transmission system are cylindrical parallel-axes gear pairs), or they can be composed of gear pairs of different kind. For example, a gear transmission system can be composed either of (a) bevel and cylindrical gear pairs or (b) a worm gear pair, and a cylindrical gear pair, or

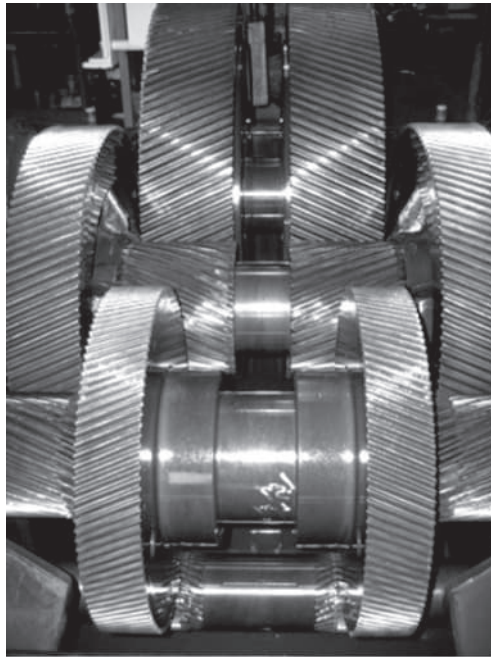


**FIGURE 26.1** A two-stage gear transmission system with split power (SPTS) composed of helical gears. Note: the power flow is split at each stage.

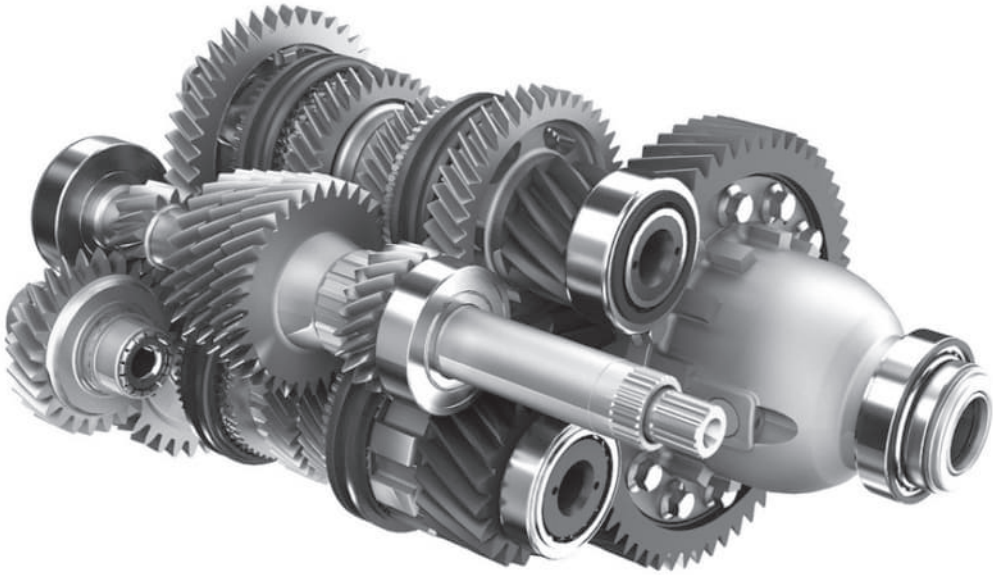


**FIGURE 26.2** A complex multistage gear transmission system.

(c) a hypoid gear pair and a cylindrical gear pair, and so forth. In the first case, the entire gear ratio is evenly distributed among all the stages of the gear transmission system. In the rest of the cases, an additional investigation is necessary to be undertaken, as losses of power in gear pairs of different kinds are also different, regardless of certain correlations among the range of the losses.

In a gear transmission system with a favorable performance, the gear ratio of each gear pair should correlate to one another. If the gear ratio in a gear pair is too small, then a larger number of gear pairs are required to provide the required gear ratio in the whole gear transmission system. If the gear ratio in a gear pair is excessive, then larger losses of the power being transmitted are observed. Neither the first nor the second is desirable. A multistage gear transmission system of a favorable design must have a reasonable number of stages, and the gear ratio in each stage must be as close to the favorable value, as possible. Otherwise, the design parameters of the whole gear transmission system can be too far from the optimal values of them.

## 26.1 PRINCIPAL KINEMATIC RELATIONSHIPS IN MULTISTAGE GEAR TRANSMISSION SYSTEM

Two different kinds of multistage gear transmission systems are distinguished below in this section of the book.

In gear transmission systems of the first kind, all the gear pairs are engaged in mesh simultaneously. The total gear ratio of the gear transmission system of this kind is of a constant value. The gear ratio cannot be changed. Gear transmission systems of this kind are used in applications when both (a) the given input rotation and (b) the desirable output rotation are of constant values.

In gear transmission systems of the second kind, only one gear on each shaft is engaged in mesh with a gear on another shaft. The total gear ratio of the gear transmission system of this kind can be changed. The actual value of the gear ratio depends on which of the gears on each shaft is engaged in mesh with a mating gear on another shaft. Gear transmission systems of this kind are used in applications when the given input rotation is of a constant value, while several desirable rotations of the output shaft are required.

Multistage gear transmission systems of the second kind represent gearing of a more general kind. Therefore, it makes sense to begin the discussion from gear drives of the second kind. The obtained results can then be reduced to simpler cases of multistage gear drives of the first kind.

A multistage gear transmission system should provide a gradation of rotations of the output shaft in a geometrical series with a selected progression ratio and a given maximum,  $\omega_{out}^{\max}$  (or  $n_{out}^{\max}$ ), and minimum,  $\omega_{out}^{\min}$  (or  $n_{out}^{\min}$ ), speeds. Methods for solving problems of this sort are based on kinematic calculations [39].

Any regularity in the series of rotational speeds,  $\omega_{out}^i$ , is the result of a similar regularity in the series of tooth ratios,  $u^j$ , in the multistage gear transmission system.

In cases when rotational speeds of the output shaft are obtained by means of gear pairs of the only kind, namely, by making engagements between sets of simple gear pairs arranged on two shafts, any series of rotational speeds of the output shaft can be achieved by selecting a corresponding series of tooth ratios for the gear pairs.

However, in cases when different rotational speeds are obtained by consecutive engagement of gear pairs, only a geometrical series of the rotational speeds can be set up. This method of speed changing requires a minimum number of gear pairs to ensure the required number of rotations of the output shaft as well as the required range of rotations of the output shaft.

### 26.1.1 RANGE RATIO OF SPEED VARIATION OF GEAR TRANSMISSION SYSTEM

The total gear ratio,  $u_{gd}$ , of a multistage gear transmission system is equal to the product of gear ratios of all the gear pairs that comprise the gear transmission system:

$$u_{gd} = \prod_{i=1}^n u_{gd}^i \quad (26.1)$$

In Eq. (26.1), the superscript “ $j$ ” is assigned to a current gear pair ( $j = 1, 2, \dots, n$  is an integer number), and the total number of the gear pairs in the multistage gear transmission system is denoted by  $n$ .

Equation (26.1) is valid for the calculation of the maximum total gear ratio,  $u_{gd}^{\max}$ , in the range, as well, as for the calculation of the minimum total gear ratio,  $u_{gd}^{\min}$ .

Following Eq. (26.1), the range ratio of the gear transmission system can be calculated from the formula:

$$R_{gd} = \frac{n^{\max}}{n^{\min}} = \frac{u_{gd}^{\max}}{u_{gd}^{\min}} = \prod_{j=1}^n R_{gd}^j \quad (26.2)$$

where  $R_{gd}^j = \frac{u_j^{\max}}{u_j^{\min}}$  is the range of gear ratios for each gear pair.

### 26.1.2 CHARACTERISTICS OF TRANSMISSION GROUP

The progression ratio of a series of gear ratios in a transmission group can be expressed in the following form:

$$\varphi_n = \varphi^x \quad (26.3)$$

where the exponent “ $x$ ” is referred to as *characteristic of the group*.

The characteristic of a group is equal to the number of speed steps for the whole complex of transmission groups kinematically preceding a given group.

The general setup equation for group transmission can be written as:

$$u_1 : u_2 : u_3 : \dots : u_n = 1 : \varphi^x : \varphi^{2x} : \dots : \varphi^{(n-1)x} \quad (26.4)$$

Equation (26.4) can be used for finding out the ratios of all the transmissions in a group in cases when the ratio  $u$  of one transmission is known.

## 26.2 ANALYTICAL METHOD FOR DETERMINING TRANSMISSION RATIOS

All standard rotational speed series are covered by the finest series, for which  $\varphi = 1.06$ . The standard gear ratio of any gear transmission system in the gearbox, in general, can be expressed as:

$$u_{st} = 1.06^{\pm E} \quad (26.5)$$

where  $E$  is an integer number.

The values  $\varphi = 1.26$  and  $\varphi = 1.41$  are other examples of practical values for the parameter  $\varphi$ .

Many calculations of the kinematics of multistage gear transmission system can be simplified if all the gear ratios are expressed in terms of progression ratio,  $\varphi$ , of the series of the rotational speeds of the output shaft being designed.

The minimum gear ratio is commonly limited to  $u_{\min} = 0.25$ . The maximum gear ratio for spur gearing is equal to  $u_{\max} = 2.0$  and  $u_{\max} = 2.5$  for helical gearing. These recommended values, for  $u_{\min}$  and for  $u_{\max}$ , make possible avoiding excessively large diameters of the driven gear, and a consequent increase in the overall radial dimensions of the gearbox. The aforementioned values of the gear ratio allow for the minimization of power losses in the gearbox.

Thus, the limit maximum range ratio in a two-shaft transmission group is equal to:

$$R^{\max} = \frac{u_{\max}}{u_{\min}} = 8 \quad (26.6)$$

Again, this value for  $R^{\max}$  is a reasonable recommendation.

## 26.3 ROTATIONAL SPEED CHART

Rotational speed charts are used to determine the actual values of gear ratio for all the gearing in the gearbox, and to determine the rotational speed of all shafts. This can be done on the premise of the kinematic diagram of gearbox. Each shaft of the gearbox is depicted by a vertical straight line in the chart. Horizontal straight lines are spaced at equal intervals. The intervals are proportional to the value of  $\log \varphi$ . They are labeled with all the rotational speeds of the corresponding shaft within the limits from the minimum to the maximum rotational speed.

A gear pair that is engaged in mesh at a definite speed of the driving shaft,  $I$ , and the driven shaft,  $II$ , is shown in the chart by rays connecting the points of the shaft lines representing this speed, as schematically illustrated in Figure 26.3.

The gear ratio is expressed in the form  $\varphi^m$ , where  $m$  is the number of intervals between the horizontal lines spanned by the corresponding ray.

If the rotational speeds are written from the bottom to the top in the increasing order of magnitude, for a speed (increase) gear pair, that is, for  $u > 1$ , and  $m > 0$ , the ray is inclined upward (in the direction from the driving shaft to the driven shaft). In the cases of reduction gear pairs, that is, when  $u < 1$ , and  $m < 0$ , the ray is inclined downward. For a gear pair for which  $u = 1$ , the exponent  $m = 0$  and the ray are horizontal. Thus, for the transmission engaged in the mesh at  $n^I = n_7$  and  $n^{II} = n_{10}$ , the ray is inclined upward and spans three intervals so that the gear ratio is:

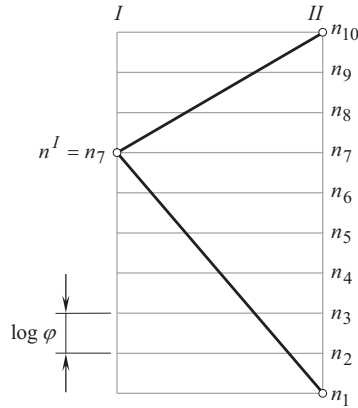


**FIGURE 26.3** An example of rotational speed chart for a gear pair ( $\varphi = 1.26$ ).

$$u^{III} = \frac{n_{10}}{n_7} = \varphi^3 \quad (26.7)$$

In the gear pair engaged in mesh at  $n^I = n_7$  and  $n^{II} = n_1$ , the ray spans six intervals, and is inclined downward. Thus, the gear ratio, in this case, is equal to:

$$u^{III} = \frac{n_1}{n_7} = \frac{1}{\varphi^6} \quad (26.8)$$

The speed chart, shown in Figure 26.3, is constructed for the progression ratio,  $\varphi = 1.26 (= \sqrt[3]{2})$ .

The analytical method for kinematic calculations is employed for research purposes as well, as for tentative calculations in studying various possible versions of the gearbox.

## 26.4 BROKEN GEOMETRIC SERIES

Academician A. Gadolin<sup>1</sup> proposed the geometric series of spindle rotational speeds for machine tools on the basis of equal probability of operation at all spindle speed steps within the whole range of variation. To adopt a spindle drive mainly for the machining of medium-size work (in terms of the capacity of the given machine tool), and taking into consideration a possibility of handing over work, near to limiting sizes (maximum and minimum), for machining in machine tools of adjacent sizes in the same size range, a broken geometric series is employed with a progression ratio  $\varphi_1$  for the middle speeds, and with  $\varphi_2 > \varphi_1^2$  for the extreme speed steps in the range of speed variation. This reduces the total number of speed steps and the number of gear pairs (in comparison to normal uniform structure). It also simplifies the construction and makes it possible to increase the range ratio of the spindle drive without changing the limiting gear ratios and without introducing a multiplier device [39].

The concept is illustrated with an example that is diagrammatically shown in Figure 26.4.

The multistage gear transmission system is in wide use in the automotive industry and in many other industries. Usually, the total gear ratio,  $u_\Sigma$ , in the multistage gear transmission system is distributed equally among all the stages; that is, the gear ratio,  $u_1$ , in the first stage of the multistage gear train is equal to the gear ratio,  $u_2$  in the second stage ( $u_1 = u_2$ ). The gear ratio,  $u_2$ , of the second

<sup>1</sup> Axel Wilhelm Gadolin (June 12, 1828–December 15, 1982), a Finnish-born Russian mechanician.

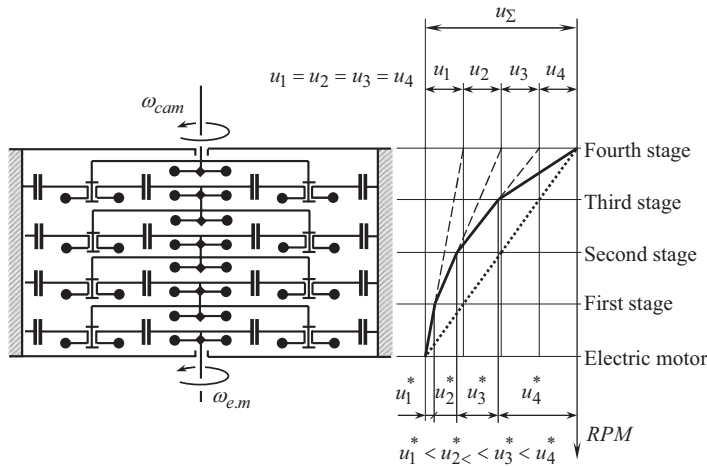


**FIGURE 26.4** Multistage gear transmission system with properly distributed gear ratios. (Prof. Radzevich, S.P., circa 2000.)

stage is equal to the gear ratio,  $u_3$ , of the third stage ( $u_2 = u_3$ ), and so on ( $\dots = u_{i-1} = u_i = u_{i+1} = \dots$ ). Equal distribution of the resultant gear ratio,  $u_\Sigma$ , among all the stages of multistage gear transmission system causes high power losses when the gear train operates.

In order to reduce losses of power in the multistage gear transmission system, it is desirable to distribute the resultant gear ratio,  $u_\Sigma$ , unequally. The gear ratio,  $u_1^*$ , in the first stage of the multistage gear train must be the smallest one. The gear ratio,  $u_2^*$ , of the second stage of the multistage gear train must exceed the gear ratio,  $u_1^*$ , of the first stage and has to be smaller than the gear ratio,  $u_3^*$ , of the third stage, and so on.

Figure 26.4 illustrates how the resultant gear ratio,  $u_\Sigma$ , has to be distributed among all the stages of the multistage gear transmission system.

## 26.5 MINIMUM NUMBER OF GEAR PAIRS

The total number of gear pairs in the groups:

$$S_p = p_a + p_b + p_c + \dots + p_r \quad (26.9)$$

that are required to obtain a specified number of speed steps  $z = p_a p_b p_c \dots p_r$  is minimum if:

$$p_a = p_b = p_c = \dots = p_r = \sqrt[m]{z} = p \quad (26.10)$$

It can be shown that when the number of transmission groups,  $m$ , is not specified, the minimum number of transmissions can be obtained under the condition that either  $p = 2$  or  $p = 3$ . Thus, it proves expedient to have either two or three transmissions in each group and, since  $2 + 2 = 2 \times 2 = 4$ ,  $p = 4$  as well.

These are actually the numbers of transmission that are employed for gearing with sliding cluster gears, when the number of gears is twice the number of transmissions. This condition does not hold true for interchangeable gears, where the same pair of gears can be interchanged.

The application of broken geometrical series considerably reduces the required number of transmissions.

## 26.6 DETERMINING TOOTH NUMBER OF GEARS OF GROUP TRANSMISSIONS

In cases where center distance is maintained at constant value, all the gears of a group are of the same module,

$$N_{\Sigma} = N_g^j + N_p^j = \text{const} \quad (26.11)$$

where:

$N_{\Sigma}$  is the sum of tooth numbers of the meshing gears.

$N_g^j$  and  $N_p^j$  are the tooth numbers, correspondingly, of driven and of driving gears.

$j$  is the integer number ( $j = 1, 2, 3, \dots, p$ ).

By definition,

$$u_j = \frac{N_g^j}{N_p^j} \quad (26.12)$$

Combining these two equations, one can obtain:

$$N_p^j = \frac{u_j}{u_j + 1} N_{\Sigma} \quad (26.13)$$

$$N_g^j = \frac{1}{u_j + 1} N_{\Sigma} \quad (26.14)$$

When the sum of the tooth numbers of the meshing gears,  $N_{\Sigma}$ , is given, Eqs. (26.13) and (26.14) can be used for the calculation of the tooth numbers of all the gears in the group. The method of the least common multiplier is commonly used for such a purpose.

In cases when  $u_j = \frac{N_g^j}{N_p^j} = \frac{a_j}{b_j}$ , where  $a_j$  and  $b_j$  are mutually prime numbers, Eqs. (26.13) and (26.14) can be rewritten in the form

$$N_p^j = \frac{a_j}{a_j + b_j} N_{\Sigma} \quad (26.15)$$

$$N_g^j = \frac{b_j}{a_j + b_j} N_{\Sigma} \quad (26.16)$$

Hence, when the tooth numbers of driven and driving gears,  $N_g^j$  and  $N_p^j$ , are integer numbers, the sum of the tooth numbers of the meshing gears,  $N_{\Sigma}$ , should be a multiplier of the sum  $a_j + b_j$ .

Gear vector diagrams can be implemented for solving the problem of the calculation of favorable gear ratios for multistage gear transmission systems. Implementation of the gear vector diagrams also sounds promising for solving gear-related kinematic problems of other sorts, as well. Gear trains with favorable performance can be *synthesized* by means of vector diagrams of gear pairs.

Gear ratio of a multistage gear transmission systems is a poorly investigated part in the theory of gearing. More efforts are required to be undertaken in the future to get things clear.





# Taylor & Francis

Taylor & Francis Group

<http://taylorandfrancis.com>

---

# 27 Gear Accuracy

Accuracy of gear teeth is an important consideration when designing, and when manufacturing gears. Even perfectly designed gears feature manufacturing errors of certain values, and, therefore, the actual tooth flanks,  $\mathcal{S}_r$  and  $\mathcal{P}_r$ , of a gear, and of a mating pinion deviate from their desirable geometries,  $\mathcal{S}$  and  $\mathcal{P}$ . For inspection purposes, tooth flanks,  $\mathcal{S}$  and  $\mathcal{P}$ , of geometrically accurate gears are used as the datum surfaces. Otherwise, no reliable results of the inspection can be obtained. In the present-day practice of inspection of gears for parallel-axes gearing either involute tooth profile or the screw involute surface is used as the datum surface – and this is correct. However, for inspection of gears for intersected-axes gearing as well as for crossed-axes gearing, no geometrically accurate tooth flanks,  $\mathcal{S}$  and  $\mathcal{P}$ , are used as the datum surfaces. Instead, approximate surfaces are used for inspection purposes, which is incorrect, especially in cases when gears with low tooth count are inspected.

Modern CMMs and GMMs (i.e., computer measuring machines and gear measuring machines, correspondingly) are capable of taking measurements when inspecting the accuracy of a surface of arbitrary geometry. When inspecting the accuracy of gears, features of the tooth flank geometry can be taken into account. The latter is helpful to simplify the method of the inspection, to improve the accuracy of the inspection, and to make the results of the inspection reliable.

In this section of the book, the readers' attention is focused mainly on the features of the tooth flanks,  $\mathcal{S}$  and  $\mathcal{P}$ , geometry that can be taken into account when developing methods of and means for inspection of the accuracy of real gears.

## 27.1 INSPECTION OF GEARS FOR PARALLEL-AXES GEAR PAIRS

Geometrically accurate gears for parallel-axes gear pairs are shaped in a form of a screw involute surface,  $\mathcal{S}$ . The screw involute surface is reduced to a surface of the involute cylinder in the case of spur gears. A close-up of a helical involute gear is shown in Figure 7.9. Here, in Figure 27.1, important features of the geometry of the screw involute surface,  $\mathcal{S}$ , are discussed.

### 27.1.1 CONCEPT OF INSPECTION OF INVOLUTE GEAR TOOTH PROFILE

A conventional method of inspection of the accuracy of involute gear tooth profile is based on the kinematic properties of the involute of a circle. The method is illustrated in Figure 27.2. For the inspection purpose, the axis of the stylus of the indicator of dial type is set tangential to the base cylinder of a base radius,  $r_{b,g}$ , of the involute gear to be inspected. Then the gear and the dial-type indicator are given relative motion so as to make the axis of the indicator of dial-type rolling with no slippage over the base circle of a radius,  $r_{b,g}$ . The required relative motion can be obtained as a superposition of a rotation,  $\omega_g$ , of the gear about its axis of rotation,  $O_g$ , and a translation either of the gear, or of the stylus, along the stylus axis, as it is shown in Figure 27.2. The gear travels straight with a linear velocity,  $V_g$ . The rotation, and the translation, velocities,  $\omega_g$  and  $V_g$ , are synchronized with one another so as to ensure rolling with no slippage of the stylus axis over the base circle. If the stylus travels straight then the direction of the translation,  $V_s$ , is reciprocal to the translation of the gear,  $V_g$ .

In the relative motion, the stylus point traces a true involute profile in a reference system associated with the gear. When inspecting an involute gear, the stylus follows the gear tooth profile. If the arrow of the dial-type indicator does not change its angular position, that is, the readings are *zero*, this means that the gear tooth profile is of a high accuracy (with zero deviation from the true

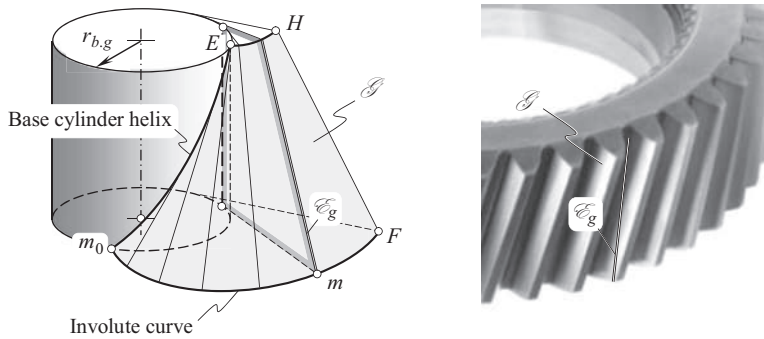


**FIGURE 27.1** Features of the geometry of tooth flank,  $\mathcal{S}$ , of a helical involute gear.

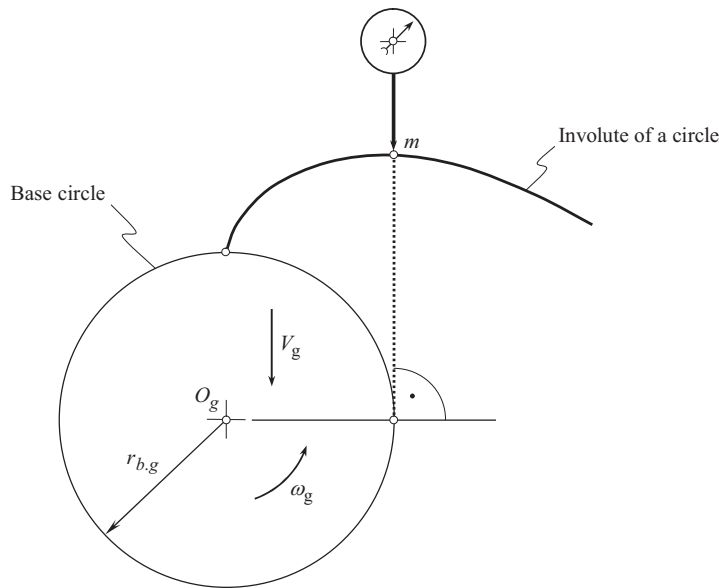


**FIGURE 27.2** Schematic of a method of inspection of accuracy of involute gear tooth profile.

involute profile). If the arrow of the dial-type indicator changes its position, that is, readings are *non-zero*, this means that the gear tooth profile deviates from the true involute profile. In this second case, a decision has to be made whether the deviations are reasonably small and all of them are within the tolerance band for the specified gear, or the deviations of the involute tooth profile are unacceptably large, and the gear is machined not in compliance to the blueprint.

After the accuracy of the involute tooth profile is inspected, then the accuracy of the helix angle is inspected. Common methods of and means for the inspection of the accuracy of the helix angle are used in this case.

The features of the involute gear tooth flank geometry are used in another method for the inspection of the accuracy of involute gear tooth flanks. The concept of the method is briefly discussed immediately below.

In a normal section of a screw involute surface by a plane, the line of intersection is a straight line. This means that a screw involute surface can be generated by a straight line,  $\mathcal{E}_g$ , that performs a corresponding screw motion about the axis of the screw involute surface. In such a motion, the straight line,  $\mathcal{E}_g$ , is tangent to the base helix of the screw involute surface (see Figure 27.1).

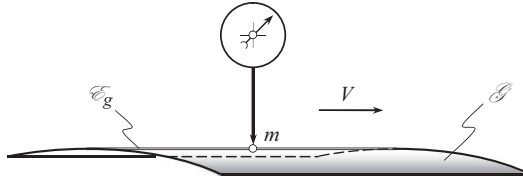


**FIGURE 27.3** Schematic of a method of inspection of the accuracy of involute gear tooth flank.

The concept of the method of inspection of an involute gear tooth flank is illustrated in Figure 27.3. The straight line,  $\mathcal{E}_g$ , is entirely situated on the screw involute surface,  $\mathcal{S}$ . The stylus of the dial-type indicator is traced along the straight generator,  $\mathcal{E}_g$ , of the gear tooth flank,  $\mathcal{S}$ . [This straight line,  $\mathcal{E}_g$ , is also shown in Figure 27.1]. In the case of geometrically accurate screw involute surface,  $\mathcal{S}$ , the readings of the dial-type indicator are zero. If the actual gear tooth flank deviates from the geometrically accurate screw involute surface,  $\mathcal{S}$ , the readings of the dial-type indicator are of non-zero value. The smaller the readings of the dial-type indicator, the smaller the deviations of the actual gear tooth flank from the geometrically accurate screw involute surface,  $\mathcal{S}$ . After the straightness and a proper configuration of one straight line on the gear tooth flank is complete, the gear is indexed, and the straightness and a proper configuration of the other straight line on the gear tooth flank are performed. The meaning of the term *indexed* in this particular case becomes clear from Figure 7.8.

### 27.1.2 SPAN MEASUREMENT

One more method of inspection of involute gears is based on the following consideration.

The normal sectional view of the auxiliary generating rack,  $\mathcal{R}_g$  (of the basic rack, in other words), is depicted in Figure 27.4 with respect to the helical involute gear. An elementary trigonometrical analysis immediately returns an equation:

$$W_k = d_{b,g} \frac{\tan \phi_t}{\sin \psi_{b,g}} \quad (27.1)$$

for the span measurement,  $W_k$ .

In Eq. (27.1):

$d_{b,g}$  is the base diameter of the helical gear.

$\phi_t$  is the transverse profile angle at the pitch diameter of the gear.

$\psi_{b,g}$  is the base helix angle of the gear.

The base tangent length is the distance between two parallel planes tangential to two opposite tooth flanks, that is, a left-hand flank, and a right-hand flank. It is an indirect measure of tooth thickness. This makes use of the property of the involute, that the points of intersection of a tangent to the base circle with a right- and left-hand involute flank are equidistant irrespective of the position of the tangent. In the case of the opposed involutes forming a tooth, this constant distance is the transverse base tooth thickness,  $s_b$ , and is equal to the length of the arc between the origins of the involutes on the base circle, as illustrated in Figure 27.5.

The involute helicoid flanks on a helical tooth have the same properties. The parallel planes tangential to the tooth flanks are at an angle,  $\psi_{b,g}$ , to the axis of rotation of the gear, and the distance between them is  $s_{bm}$ . In practice, the measurement has to be carried out over tooth flanks spanning a number,  $k$ , of teeth instead of a single tooth as shown in Figure 27.6. The number  $k$  depends on the tooth geometry, namely, on the pressure angle, the number of teeth, and the addendum modification coefficient.

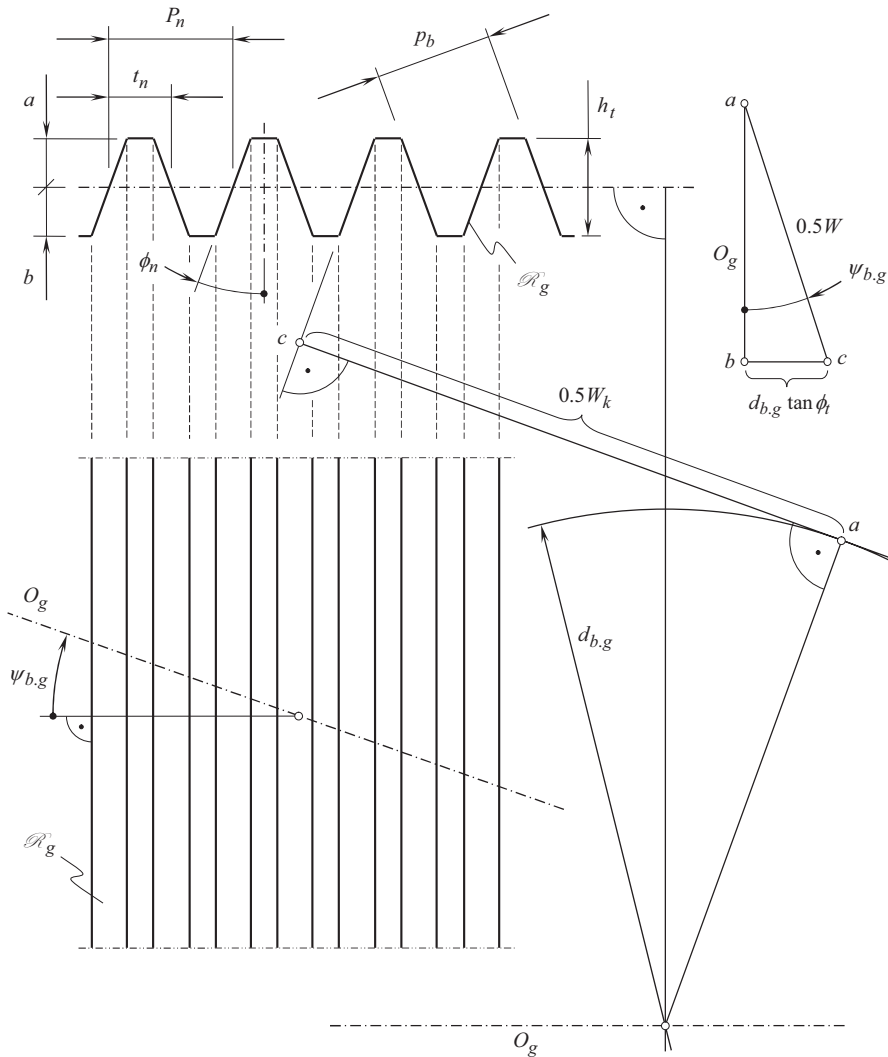


FIGURE 27.4 Calculation of the span measurement,  $W_k$ , in a helical involute gear.

The base tangent length,  $W_k$ , (subscript  $k$  after  $W$  specifies the number of teeth between the flanks measured), on spur, or helical gears is composed of the normal base tooth thickness,  $s_b$ , and a number of normal base pitches,  $p_b$ . The number of teeth included in the measurement should be chosen so that there is some latitude in the position in which the measuring instrument can be applied to the flanks.

This characteristic is also true for helical gears.

Calculation of the base tangent length,  $W_k$ :

1. The tooth thickness measured along the arc of the reference cylinder on the spur and helical gears is:

$$S_n = m \left( \frac{\pi}{2} + 2x \tan \phi \right) \quad (27.2)$$

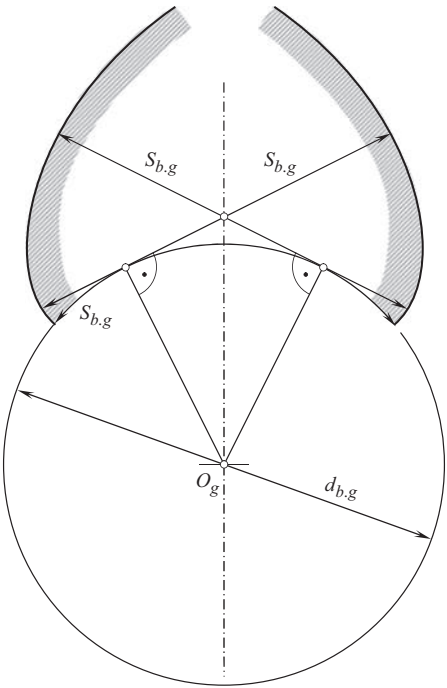


FIGURE 27.5 Equidistant base thickness of an involute gear tooth.

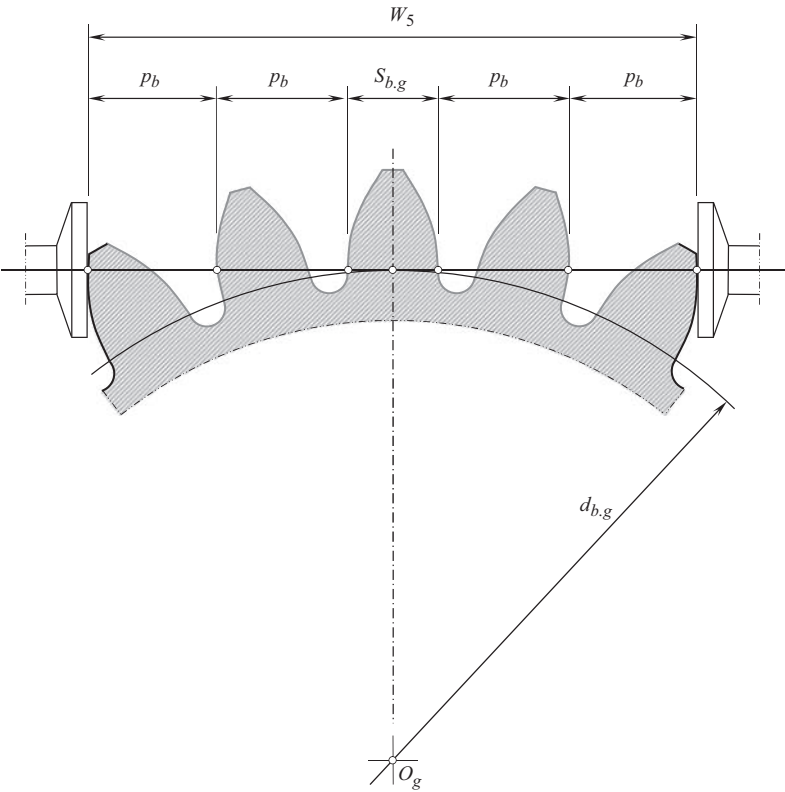


FIGURE 27.6 Base tangent length,  $W_k$ , on a spur gear.

2. The base tooth thickness measured along the arc of the base cylinder is on:

**spur gears:**

$$s_b = N m \cos \phi \left( \frac{S_n}{N m} + \text{inv } \phi \right) \quad (27.3)$$

**helical gears:**

$$s_b = N m \cos \phi \left( \frac{S_n}{N m} + \text{inv } \phi_t \right) \quad (27.4)$$

The theoretical base tangent length (without taking into account any tolerances) for gears without backlash then becomes on:

**spur gears:**

$$W_k = s_b + (k - 1)p_b \quad (27.5)$$

**helical gears:**

$$W_k = s_{bn} + (k - 1)p_b \quad (27.6)$$

The combined formula for the base tangent length,  $W_k$ , is therefore as follows:

$$W_k = m[(k - 0.5)\pi \cos \phi + N \text{inv } \phi_t \cos \phi + 2x \sin \phi] \quad (27.7)$$

The number of teeth,  $k$ , can be calculated from the following formulas:

$$k = \frac{S_x - W_1}{\pi m \cos \phi} + 1 \quad (27.8)$$

[rounded off the calculated value from Eq. (27.8) to the nearest integer number]:

$$S_x = \frac{d_b \tan \phi_x}{\cos \psi_b} \quad (27.9)$$

$$\cos \phi_x = \frac{d_b}{d_o - 2m} \quad (27.10)$$

$$W_1 = m \left( \frac{\pi}{2} \cos \phi + N \text{inv } \phi_t \cos \phi + 2x \sin \phi \right) \quad (27.11)$$

The above formulae apply to external spur and helical gears and also to the tooth space profile of internal spur and helical gears, although the base tangent length on such gears only has a largely theoretical significance.

On internal gears, the tooth thickness is measured by taking measurements between balls.

On external gears, the *actual base tangent length*,  $AW_k$ , is less than the theoretical dimension,  $W_k$ , for zero backlash by the amount of the normal backlash allowance,  $\Delta j_n$ . On internal gears, the base tangent length is increased by the amount of the backlash allowance. Therefore, the base tangent length is equal:



on external gears:

$$AW_k = W_k - \Delta j_n \quad (27.12)$$

on internal gears:

$$AW_k = W_k + \Delta j_n \quad (27.13)$$

Tooth thickness of a gear can also be inspected based on the discussed features (see Figure 27.4) of the geometry of an involute helical gear. Two approaches are used for determining the tooth thickness of an involute gear. One of them is based on span measurement over two or more gear teeth. The other one is based on measurement over balls/pins.

When the span measurement,  $W_k$ , over two or more gear teeth are given, for the calculation of circular tooth thickness,  $t_n$ , of the helical gear, the following approach can be used.

The dimension,  $W_t$ , in the transverse section that corresponds to the span measurement,  $W_k$ , of the helical gear (see Figure 27.7) and is calculated from the formula:

$$W_t = \frac{W_k}{\cos \psi_b} = W_k \frac{\sin \phi_t}{\sin \phi_n} \quad (27.14)$$

The calculated value of the dimension,  $W_t$ , allows for the calculation of transverse circular tooth thickness,  $t_t$ , at pitch diameter of the gear:

$$t_t = d \left( \frac{M_t}{d_b} - \frac{\pi N_s}{N_g} - \text{inv} \phi_t \right) \quad (27.15)$$

Here,  $N_s$  is the number of tooth spaces.

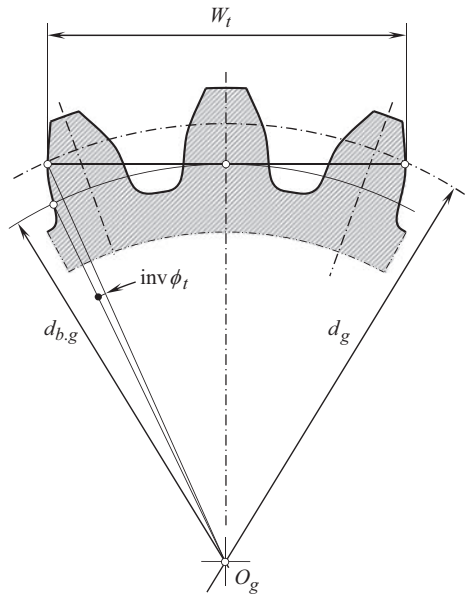


FIGURE 27.7 Span measurement,  $W_t$ , over two or more teeth in transverse section of a helical gear.

Ultimately, for the calculation of normal circular tooth thickness,  $t_n$ , the formula:

$$t_n = t_t \cos \psi \quad (27.16)$$

is used.

The number of teeth in a span is calculated from the approximate formula:

$$k = \frac{N_g}{\cos^3 \psi} \cdot \frac{\phi_t}{180^\circ} + 0.5 \quad (27.17)$$

Here  $\psi$  is the pitch helix angle of the gear.

Following another approach, either balls or pins are used for the measurement of the tooth thickness of a spur gear. For the measurement of a helical gear tooth thickness, balls are commonly used.

When the dimension over two balls or pins is given, the following approach is used for the calculation of the circular tooth thickness,  $t_n$ , of the helical gear.

For the calculations, the normal width of space between teeth is used as an input parameter. The normal space width,  $w_n$ , is equal to  $w_n = p_n - t_n$ .

The measurements are performed using balls of certain standard diameter. For a given gear, the approximate diameter of the ball is approximately equal:

$$d_{ball} \cong 1.728/P_n \quad (27.18)$$

Then, the calculated value of the diameter,  $d_{ball}$ , is rounded to the nearest standard value.

The transverse profile angle,  $\phi_m$ , to the center of the ball/pin is calculated from the equation:

$$\text{inv } \phi_m = \text{inv } \phi_t + \frac{d_{ball} - w_n \cos \phi_n}{N_g \cos \phi_n} P_n \quad (27.19)$$

With the input parameters,  $w_n$ ,  $d_{ball}$  and  $\phi_m$ , calculated, the dimension over two balls,  $D_{Me}$ , for a gear with an even tooth number is calculated from the formula:

$$D_{Me} = \frac{d_{b.g}}{\cos \phi_m} + d_{ball} \quad (27.20)$$

For gears with an odd number of teeth, the dimension over two balls is equal to:

$$D_{Me} = \frac{d_{b.g} \cos(90^\circ / N_g)}{\cos \phi_m} + d_{ball} \quad (27.21)$$

The same formulas are used for the measurement of a spur gear. The only difference is that the transverse profile angle,  $\phi_t$ , and the normal profile angle,  $\phi_n$ , in Eq. (27.19), are equal to each other.

### 27.1.3 CONSTANT CHORD TOOTH THICKNESS

Two opposite tooth profiles are simultaneously generated by a straight-sided generating rack,  $\mathcal{R}$ . In this scenario, a design parameter that relates to two involute tooth profiles in a transverse section of the gear is distinguished. This is the so-called *constant chord tooth thickness*.

Refer to Figure 27.8 in order to determine the *constant chord tooth thickness*.

Here, in Figure 27.8, a transverse section of a helical involute gear is shown. This schematic is also valid for spur gear. In Figure 27.8, point  $C$  is the point of intersection of the line of symmetry of the involute tooth by the pitch circle of a radius  $r_g$ . Two straight lines,  $AC$  and  $BC$ , through point



The height above constant chord in transverse section of external helical gear:

$$CF = CD \cdot \sin \phi_t; CF = [r_{b,g} \cdot (\phi_t + \text{inv} \phi_t) - r_g \cdot \sin \phi_t] \cdot \sin \phi_t \quad (27.31)$$

$$h_{cc} = r_{o,g} - r_g - [r_{b,g} \cdot (\phi_t + \text{inv} \phi_t) - r_g \cdot \sin \phi_t] \cdot \sin \phi_t \quad (27.32)$$

The design parameters  $t_{cc}$  and  $h_{cc}$  can be directly measured in a gear.

#### 27.1.4 TOOTH THICKNESS MEASUREMENT IN INTERNAL GEAR

For the calculation of tooth thickness in an internal gear, measurement between two pins, or balls is used. Balls are used for measuring both spur and helical gears, while pins are used for measuring spur gears only.

The required dimension between two balls can be calculated in the following way.

Normal space width,  $w_n$ , ball diameter,  $d_{ball}$ , and transverse profile angle,  $\phi_m$ , to the center of the ball are used as the input parameters for the calculations. The normal space width is calculated from the equation:

$$w_n = p_n - t_n \quad (27.33)$$

The approximate ball diameter is equal to  $d_{ball} \cong 1.44/P$ . The calculated value of the diameter,  $d_{ball}$ , is rounded then to the nearest standard value.

Transverse profile angle,  $\phi_m$ , to the center of the ball can be calculated from the equation:

$$\text{inv} \phi_m = \text{inv} \phi_t - \frac{d_{ball} - w_n \cos \phi_n}{N_g \cos \phi_n} P_n \quad (27.34)$$

For gears with an even number of teeth, the dimension between two balls,  $D_{Mi}$ , can be expressed by:

$$D_{Mi} = \frac{d_{b,g}}{\cos \phi_m} - d_{ball} \quad (27.35)$$

For gears with odd tooth count, the dimension between two balls ( $D_{Mi}$ ) can be expressed by:

$$D_{Mi} = \frac{d_{b,g} \cos(90^\circ / N_g)}{\cos \phi_m} - d_{ball} \quad (27.36)$$

Those same formulas are used for the measurements of a spur gear. The only difference is that the transverse profile angle,  $\phi_m$ , and the normal profile angle,  $\phi_n$ , in Eq. (27.34), are equal to each other.

## 27.2 INSPECTION OF GEARS FOR INTERSECTED-AXES GEAR PAIRS

The present-day practice of inspection gears for intersected-axes gear pairs is poor and inconsistent. The approximate datum surface is used for inspection purposes. This is the main reason for the inconsistencies in the gear inspection. The actual datum surface significantly deviates from the desirable datum surface, as it is generated as an envelope to a family of consecutive positions of the crown straight-sided rack in its motion in relation to the gear being inspected. Especially this becomes clear when gears with a low tooth count are inspected – in this case, the inconsistency of the known method for the inspection gears becomes more evident. As the actual datum surface itself

deviates from the desirable geometrically accurate datum surface, the output of the gear inspection cannot be accurate by nature.

For the inspection of gears for intersected-axes gear pairs the methods of and means for the inspection that are based on the features of the tooth flanks geometry can be developed.

### 27.2.1 CONCEPT OF INSPECTION OF BEVEL GEAR TOOTH PROFILE

For the inspection of bevel gears, a novel method is proposed. The determination of how much an actual tooth flank of a bevel gear deviates from the nominal (desirable) tooth flank geometry is the main goal of the gear inspection. The smaller the deviation, the more accurate bevel gear is and vice versa.

Selection of a proper reference surface for the inspection of bevel gears for intersected-axes gearing is of critical importance, especially in cases of inspection bevel gears with a low tooth count (with 12 teeth and a fewer).

In the present-day practice, a tooth flank of a crown gear is used as a reference surface. The tooth flank of a crown gear is simulated by the cutting edges of the gear cutting tool when machining the gear. When the pitch plane of a crown gear rolls with no sliding over the pitch cone of the bevel gear being inspected, the tooth flank of the bevel gear is generated as an envelope to a family of consecutive positions of the tooth flank of the crown gear. In the present-day practice, this envelope surface serves as the reference surface when inspecting bevel gears. This is a wrong practice to use the envelope to a family of crown surfaces as the datum surfaces for inspection purposes.

Similarly, the tooth flank of a crown gear is simulated by the corresponding motions of the stylus when inspecting the gear. When inspecting a bevel gear, the pitch plane of a crown gear rolls with no sliding over the pitch cone of the bevel gear being inspected. The anticipated tooth flank of the bevel gear is generated as an envelope to a family of consecutive positions of the tooth flank of the crown gear.

In known methods of inspection of bevel gears for intersected-axes gearing, the stylus travels over the tooth flank to be inspected so as to be all the time at the kinematically generated anticipated tooth flank of the bevel gear. Tooth flank of an actual gear being inspecting deviates from the tooth flank of the desirable geometry. These deviations cause the corresponding displacements of the stylus. Such a practice of inspection of a tooth flank of a bevel gear is poor.

An improper datum surface is one of the main disadvantages of known methods of inspection of bevel gears for intersected-axes gearing. Because of this, the results of the measurements do not correctly reflect the actual accuracy of the bevel gear. Ultimately, accurate gears can be recognized as of poor accuracy, and inversely, poor quality gears can be mistakenly recognized as accurate gears.

The use of the proper datum surface is one of the possible ways to improve the accuracy of the inspection of gears for intersected-axes gear pairs.

To proceed with the development of the method of inspection of bevel gears for intersected-axes gearing, a base cone of the gear to be inspected, and the plane of action has to be constructed.

When inspecting a bevel gear (see Figure 27.9), a certain relative motion of the gear to be inspected and the plane of action is performed. The gear is rotated about its axis of rotation,  $O_g$ . The plane of action,  $PA$ , is rotated about its axis of rotation,  $O_{pa}$ . The rotations,  $\omega_g$  and  $\omega_{pa}$ , are synchronized with one another.

When inspecting a bevel gear tooth profile (see Figure 27.10), the rotations,  $\omega_g$  and  $\omega_{pa}$ , are synchronized so as to keep the stylus at current point,  $m$ , on the desirable bevel gear tooth flank. The point,  $m$ , is within the plane of action,  $PA$ . The line  $a$ , along which the deviation is measured, is within the plane of action,  $PA$ , and it is perpendicular to the bevel gear tooth flank at the point,  $m$ . The stylus tip is motionless in relation to the plane of action,  $PA$ , when inspecting the profile error of the bevel gear tooth flank.



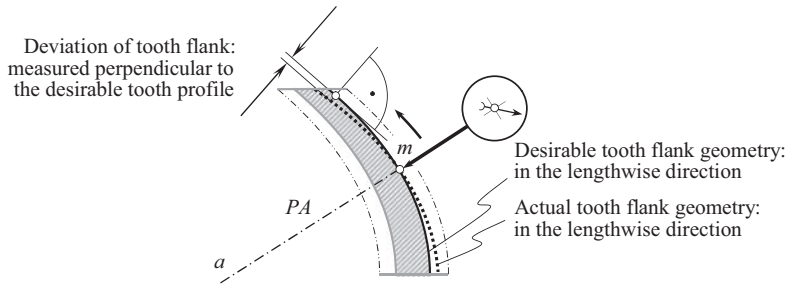


FIGURE 27.11 Inspection of accuracy in the lengthwise direction of a gear for intersected-axes gear pair.

### 27.3.1 CONCEPT OF INSPECTION OF GEAR TOOTH PROFILE

When inspecting a gear for intersected-axes gear pair (see Figure 27.12), the relative motion of the gear to be inspected and the plane of action are performed. The gear is rotated about its axis of rotation,  $O_g$ . The plane of action,  $PA$ , is rotated about its axis of rotation,  $O_{pa}$ . The rotations,  $\omega_g$  and  $\omega_{pa}$ , are synchronized with one another.

Inspection of a gear tooth profile in a gear for crossed-axes gear pair is similar to that of a gear for intersected-axes gear pair. When inspecting a gear tooth profile (see Figure 27.10), the rotations,  $\omega_g$  and  $\omega_{pa}$ , are synchronized so as to keep the stylus at current point  $m$  on the desirable bevel gear tooth flank. The axes,  $O_g$  and  $O_{pa}$ , are at a certain distance,  $C_g$ , from one another when inspecting crossed-gears. The rotations,  $\omega_g$  and  $\omega_{pa}$ , are synchronized with one another so as to keep the stylus at a current point  $m$  on the desired bevel gear tooth flank.

Point,  $m$ , is within the plane of action,  $PA$ . The line,  $a$ , along which the deviation is measured, is within the plane of action,  $PA$ , and it is perpendicular to the gear tooth flank at point,  $m$ . The stylus tip is motionless in relation to the plane of action,  $PA$ , when inspecting the profile error of the bevel gear tooth flank.

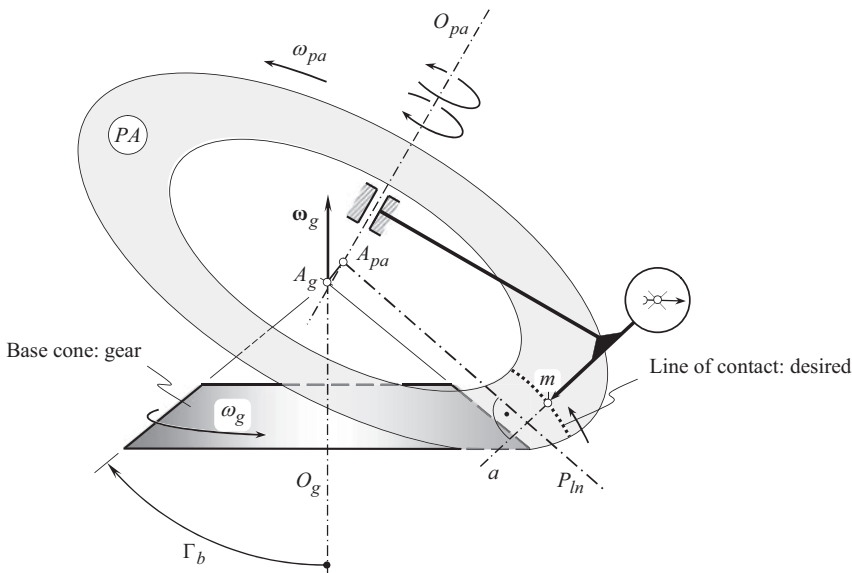
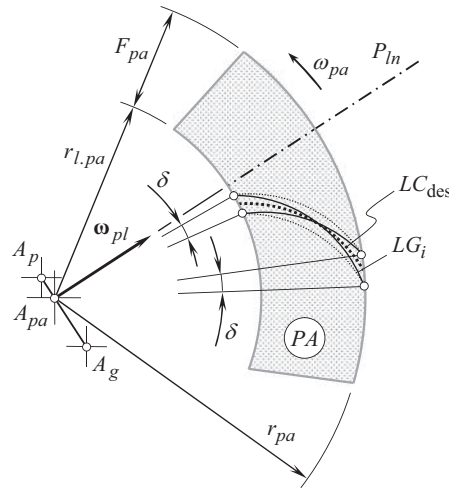


FIGURE 27.12 Kinematics of a method of inspection gears for crossed-axes gear pair.





**FIGURE 27.13** Deviation of tooth flank of actual gear from tooth flank,  $\mathcal{S}$ , of a corresponding geometrically accurate gear.

### 27.3.2 CONCEPT OF INSPECTION OF GEAR IN LENGTHWISE DIRECTION OF GEAR TEETH

When inspecting tooth flank geometry of a gear in the lengthwise direction of the gear tooth (see Figure 27.11), the stylus tip travels along the line of intersection of the desirable tooth flank by the plane of action,  $PA$ . At current point,  $m$ , the line,  $a$ , along which the deviation is measured, is situated within the plane of action,  $PA$ , and it is perpendicular to the bevel gear tooth flank at this point,  $m$ .

In the course of inspection of a gear for real crossed-axes gear pair, tooth flank of the gear,  $\mathcal{S}$ , is intersected by the plane of action,  $PA$ , along a line of intersection. In Figure 27.13, the line of intersection through an arbitrary point within the tooth flank is labeled as  $LG_i$ . When the gear is rotated simultaneously with the plane of action,  $PA$ , the geometry of the line of intersection,  $LG_i$ , of the gear to be inspected alters. A plurality of the lines of intersection,  $LG_i$ , on the actual gear tooth flank, those generated during the meshing cycle of a pair of teeth, is located within a bend of an angular width,  $\delta$ , in the plane of action,  $PA$ . The angular deviation,  $\delta_i$ , at a current configuration of the gear in relation to the plane of action,  $PA$ , can be physically measured in a gear/pinion. Current value of the angular deviation,  $\delta_i$ , can be also calculated.

In a similar manner, the variation of the angular base pitch in a gear can be inspected.

## 27.4 MOUNTING DISTANCE: ACCURACY OF AXIAL LOCATION OF GEARS IN THE GEAR HOUSING

The performance of intersected-axes and of crossed-axes gear pairs strongly depends on the accuracy of the axial location of the gears – on the accuracy of the mounting distance. Precision gearing is especially sensitive to the accuracy of mounting of gears in the gear housing.

Mounting distance in gears for intersected-axes gear pairs, as well as for crossed-axes gear pairs, is a design parameter that cannot be inspected directly, as the base cone apex of the gear does not exist physically. This is the root cause of the significant inconveniences when inspecting the accuracy of mounting distance. Therefore, indirect methods for the inspection of the accuracy of the mounting distance are used in practice.

### 27.4.1 ON THE CORRELATION BETWEEN THE TOOTH FLANK GEOMETRY AND THE MOUNTING DISTANCE

The mounting distance is a vital design parameter for intersected-axes gearings, as well as for crossed-axes gearings. The specification, inspection, and tolerancing of the mounting distance are challenging to understand by many practical gear engineers.

To make things clear, it is necessary to outline to the best possible extent what the term *mounting distance* stands for. As an example, consider tooth flank of a straight bevel gear<sup>1</sup> as illustrated in the simplified model, shown in Figure 27.14. The tooth flank of the gear,  $\mathcal{S}$ , can be construed as a family of straight lines through each point of the gear tooth profile and the gear tooth flank apex,  $A_{fg}$  (the gear tooth flank apex,  $A_{fg}$ , is an equivalent to the gear base cone apex,  $A_{bg}$ ). Only the gear tooth flank apex,  $A_{fg}$ , should be used for the specification and inspection of the mounting distance,  $MD$ . Commonly, the outer cone apex of the gear,  $A_{og.1}$ , is inward in relation to the gear tooth flank apex,  $A_{fg}$ , as shown for the straight generating line 1 in Figure 27.14. However, this is not a must as the gear outer cone apex,  $A_{og.2}$ , can be located either outward, or the gear outer cone apex,  $A_{og.3}$ , can be located inward in relation to the apex  $A_{og.1}$ , as it is illustrated in Figure 27.14 for the straight generating lines 2 and 3 of the outer cone of the gear. The actual location of the gear outer cone apex (either  $A_{og.1}$ , or  $A_{og.2}$ , or  $A_{og.3}$ ) does not affect the conditions of meshing of the gear,  $\mathcal{S}$ , and the pinion,  $\mathcal{P}$ , tooth flanks. The conditions of meshing of the gear,  $\mathcal{S}$ , and the pinion,  $\mathcal{P}$ , tooth flanks depend only on the actual location of the gear/pinion tooth flank apex,  $A_{fg}$ . Therefore, the tolerance for the mounting distance (the mounting distance is measured in relation to the gear tooth flank apex,  $A_{fg}$ ) is tight, while the configuration of the apex of the outer cone of the gear,  $A_{og}$ , is a free dimension with no specified tolerance.

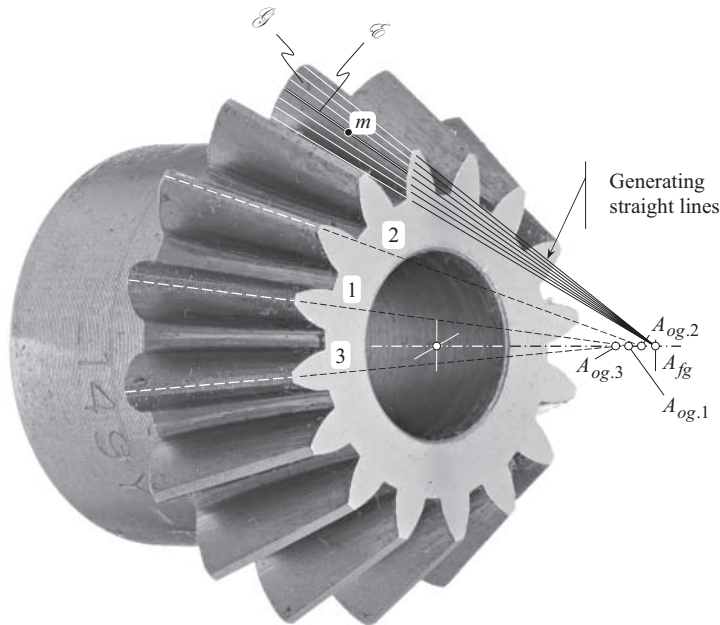


**FIGURE 27.14** A simplified model that is used in the derivation of the definition of the term *tooth flank apex*,  $A_{fg}$ , in intersected-axes gearing, and in crossed-axes gearing.

<sup>1</sup> This concept can be easily extended to bevel gears of any and all other designs.

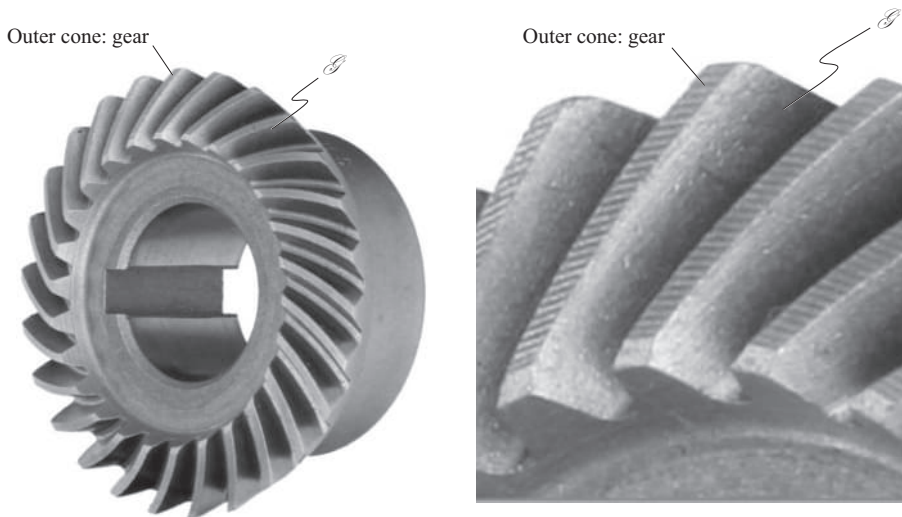


**FIGURE 27.15** Outer cone surface of a gear for intersected-axes gear pair can be used as a datum surface for inspection of the mounting distance if the cone surface is finished-cut in one setup with the gear tooth flank,  $\mathcal{S}$  (a similar is valid with respect to crossed-axes gear pair).

Depending on the accuracy of the setup parameters when cutting straight bevel gears, the axial position of the tooth flank,  $\mathcal{S}$ , can be changed. After being assembled, the gear tooth flank apex,  $A_{fg}$ , must be coincident with the centerlines in the gearbox housing. Therefore, the *mounting distance* of a gear is the distance from the gear tooth flank apex,  $A_{fg}$ , to the common reference surface of the gear. A similar definition is valid with respect to the mounting distance of a pinion.

Then, the crown is not geometrically associated with the gear tooth flank,  $\mathcal{S}$ . The performed analysis of Figure 27.15 reveals that depending on the accuracy of the setup parameters when machining straight bevel gears, the axial position of the tooth flank,  $\mathcal{S}$ , and the gear tooth flank apex,  $A_{fg}$ , can be variable.

A gear tooth flank in intersected-axes, as well as in crossed-axes gearing, must be correctly specified in relation to the common reference surface. For this purpose, arbitrary point,  $m$ , either within the tooth flank or within an extension of this surface can be used. The tooth flank apex,  $A_{fg}$  (see Figure 27.14), is convenient to be used for this purpose. It is a wrong practice to use the wedge,  $E$ , and the dimension,  $F$  (see Figure 27.15), to specify the mounting distance in  $I_a$ –,  $C_a$  – gearing.

Direct measurements of the mounting distance<sup>2</sup> are necessary. This can be done, for example, by means of laser scanning of the machined tooth flank, and creating a CAD model of the actual tooth flanks on the premise of that. Comparison of two CAD models, that is, of the desirable and of the actual tooth flanks, returns an exact number of the mounting distance in a machined gear for  $I_a$ –,  $C_a$  – gearing. Simpler methods of and means for the direct inspection of the actual mounting distance in intersected-axes and crossed-axes gearings can be developed.

Reliable methods for the calculation of the tolerances for the mounting distance in intersected-axes, as well as crossed-axes gearings, need to be developed. Tooth flank of a gear can be used for

<sup>2</sup> **Important:** In addition to the mounting distance, in  $C_a$  – gearing, one more design parameter must be inspected. This is an angle that a gear/pinion axis of rotation forms with the centerline,  $\Phi$ . A tolerance for this angle needs to be specified, and the actual deviation of the angle from required value of it needs to be inspected. An appropriate tolerance for the center distance is also required.

the inspection of the accuracy of the mounting distance. The problem in question can be resolved if an alternative equivalent surface can be used for the inspection. The outer cone surface of a gear to be inspected can be used for the inspection of accuracy of the mounting distance if this surface is finish-cut in one setup with finish machining of the tooth flanks of the gear. This can be done either if the full profile cutters are used in the design of the cutter-heads, or additional one, or two cutters are mounted on the cutter-head of the conventional design.

Inspection of the mounting distance, and of the contact pattern, are the two main approaches for the inspection of the correctness of the axial location of the gears in intersected-axes, and crossed-axes gear pairs.

## 27.4.2 MOUNTING DISTANCE IN INTERSECTED-AXES GEARING

To operate properly, gears in intersected-axes gear pairs must be properly configured in relation to one another [178].

At the beginning, let's clarify what the term *mounting distance* stands for.

**First**, and the most critical, by means of mounting distances the location of tooth flanks in the axial direction of a gear and a mating pinion are specified in relation to the centerlines in the gear housing. Apex point of a tooth flank of the gear,  $A_{fg}$ , and the pinion,  $A_{fp}$ , must coincide with the point of intersection of the centerlines in the gear housing in  $I_a$  – gearing. The pitch plane apex is commonly designated as  $A_{pp}$ , and the plane of action apex is commonly designated as  $A_{pa}$ . These two conditions can be expressed as follows:

$$A_{fg} \equiv A_{pp} \equiv A_{pa} \text{ and } A_{fp} \equiv A_{pp} \equiv A_{pa}$$

**Second**, the pitch cone apex of a gear,  $A_g$ , (and of a mating pinion,  $A_p$ ) must coincide with the apex point of a tooth flank of the gear,  $A_{fg}$ , and the pinion,  $A_{fp}$ . These two conditions can be expressed as follows:  $A_g \equiv A_{fg}$  and  $A_p \equiv A_{fp}$

**Third**, the base cone apex of a gear,  $A_{bg}$ , (and of a mating pinion,  $A_{bp}$ ) must coincide with the apex point of a tooth flank of the gear,  $A_{fg}$ , and the pinion,  $A_{fp}$ . These two conditions can be expressed as follows:  $A_{bg} \equiv A_{fg}$  and  $A_{bp} \equiv A_{fp}$

**Fourth**, there are two outer cones. One of them is of the gear and another one is of the mating pinion. There are also two root cones. Again, one of them is of the gear and another one is of the mating pinion. Neither outer cones nor root cones directly affect the actual value of the mounting distance. However, these cones need to be mentioned here, as in the present-day practice outer cones are commonly used when determining the mounting distance.

### 27.4.2.1 Relative Disposition of Base Cones in Intersected-Axes Gearing

A straight bevel gear pair is depicted in Figure 27.16 as an example. When a bevel gear pair operates, the gear spins,  $\omega_g$ , about its axis of rotation,  $O_g$ . The mating pinion spins,  $\omega_p$ , about its axis of rotation,  $O_p$ . The axes of rotation,  $O_g$  and  $O_p$ , intersect one another, and the point of intersection coincides with the plane-of-action apex,  $A_{pa}$  (the plane of action,  $PA$ , is not shown in Figure 27.16) – this is a must for the perfect performance of bevel gearing.

A base cone is associated with the gear. The gear base cone apex,  $A_g$ , is located within the gear axis of rotation,  $O_g$ . Another base cone is associated with the pinion. The pinion base cone apex,  $A_p$ , is located within the pinion axis of rotation axis,  $O_p$ . The gear, and the pinion, must be configured in relation to each other so as to ensure the apexes  $A_g$  and  $A_p$  snapped together with the plane-of-action apex,  $A_{pa}$  – this is a must [178]. Neither axial displacement of the gear, no axial displacement of the pinion, is allowed from the position shown in Figure 27.16. The plane of action,  $PA$ , is a plane through the plane-of-action apex,  $A_{pa}$ , that is in tangency to the base cones of the gear and the mating pinion.



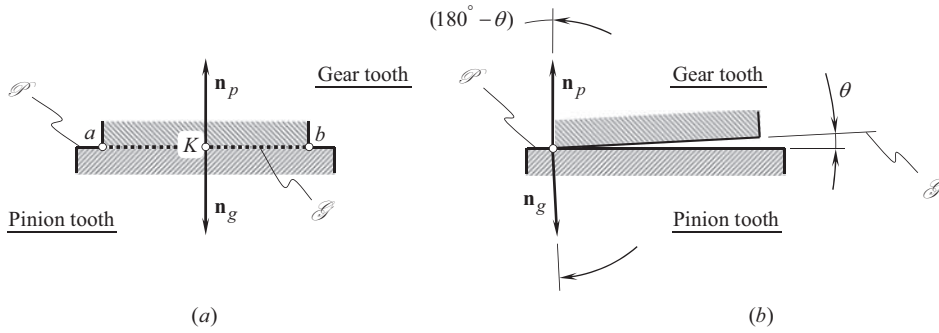


**FIGURE 27.17** Unit normal vectors,  $\mathbf{n}_g$  and  $\mathbf{n}_p$ , to tooth flanks,  $\mathcal{G}$  and  $\mathcal{P}$ , of a gear and of a mating pinion in cases of correct (a), and incorrect (b) configuration of the mating gears. The unit normal vectors,  $\mathbf{n}_g$  and  $\mathbf{n}_p$ , are not within the plane of action,  $PA$ . Instead, these unit vectors are located in a plane of action, constructed for the misaligned gears.

apex,  $A_{pa}$ , as the apex,  $A_g^*$ , is displaced axially in relation to  $A_{pa}$  at a distance  $\epsilon_g$ . (Here, we are not going into details of analysis of the gap between the gear base cone and the plane of action). In a case, depicted in Figure 27.18b, the outward displacement,  $\epsilon_g$ , is of a positive value. An inward displacement is of a negative value (not shown in Figure 27.18b).

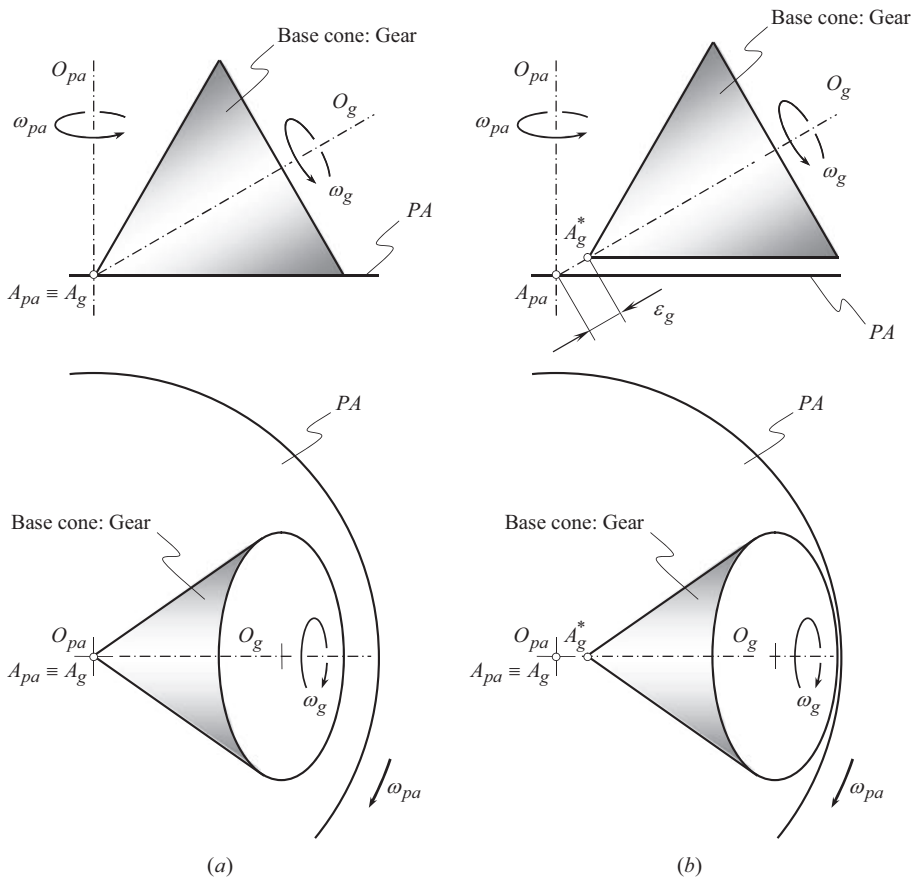


**FIGURE 27.18** Disposition of base cone of a gear in relation to the plane of action,  $PA$ , in (a) geometrically accurate and (b) misaligned intersected-axes gear pair.



The performed analysis in Figure 27.18 allows to proceed with the derivation of an equation for the calculation of the tolerance for the accuracy of the mounting distance in intersected-axes gear pair.

#### 27.4.2.4 Mounting of Gears in Intersected-Axes Gear Housing

Theoretically, in an intersected-axes gear pair, a gear base cone apex,  $A_g$ , a mating pinion base cone apex,  $A_p$ , and the plane-of-action apex,  $A_{pa}$ , must be snapped together, as schematically illustrated in Figure 27.19a. In reality, in order to transmit power, gears need to be supported. For this purpose, a gear housing (see Figure 27.19b) is used. The gear housing features a corresponding number of bores that are used to support gear shafts in the housing. A centerline of a bore for the gear shaft is labeled as  $O_{hg}$ . Correspondingly, a centerline of a bore for the pinion shaft is designated by  $O_{hp}$ . The centerlines,  $O_{hg}$  and  $O_{hp}$ , intersect at point  $A_h$ . Strong constraints on configuration of the gear and its mating pinion in the gear housing are imposed by this point,  $A_h$ . The center-distance,  $O_{hg}O_{hp}$ , between the centerlines,  $O_{hg}$  and  $O_{hp}$ , must be as short, as possible ( $O_{hg}O_{hp} \rightarrow 0$ ). Deviation in the angular configuration of the centerlines also must be the smallest possible.

The gear must be configured in the gear housing so as to keep the gear axis of rotation,  $O_g$ , aligned with the axis,  $O_{hg}$ , in the gear housing (i.e.,  $O_g \equiv O_{hg}$ ), as illustrated in Figure 27.19c. The gear base cone apex,  $A_g$ , must be coincident with the point,  $A_h$ , of intersection of the centerlines,  $O_{hg}$  and  $O_{hp}$  (i.e.,  $A_g \equiv A_h$ ). Then, the rest of the important components, namely, the bearings, shims,

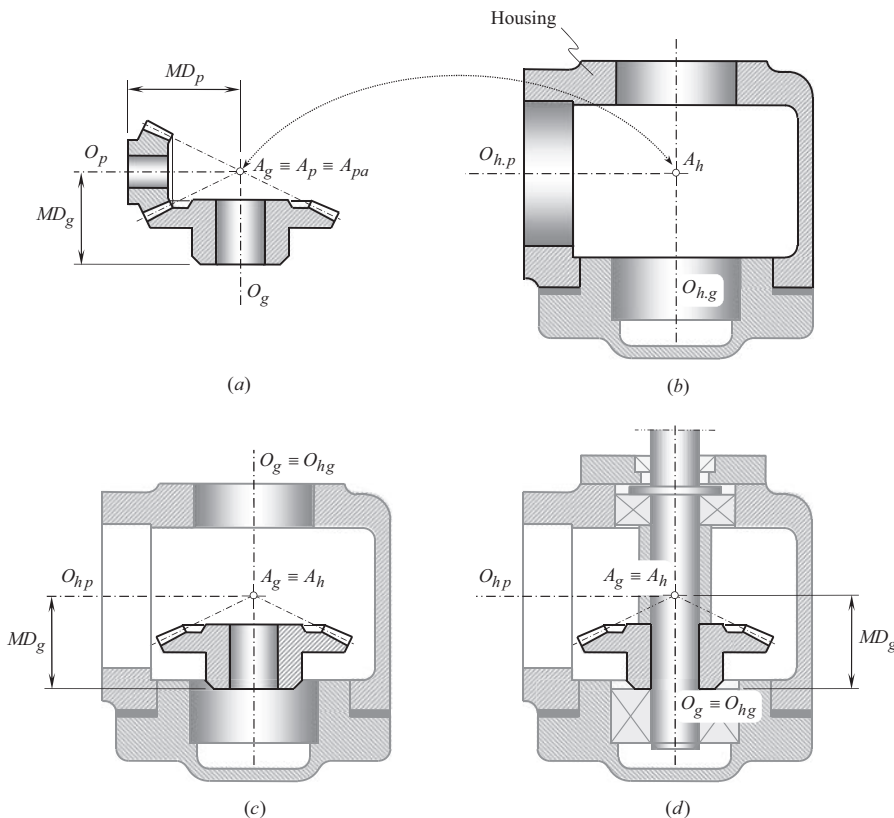


**FIGURE 27.19** Intersected-axes gearing; mounting of bevel gears in the gear housing: (a) a desirable configuration of two mating bevel gears; (b) intersecting axes of two bores in the gear housing; (c) the desirable position of the bevel gear in the gear housing; (d) the design of the components that are used for the gear mounting; (e) the desirable position of the bevel pinion in the gear housing; (f) the design of the components that are used for the pinion mounting; and (g) the final configuration of two bevel gears mounted in the gear housing.

(Continued)



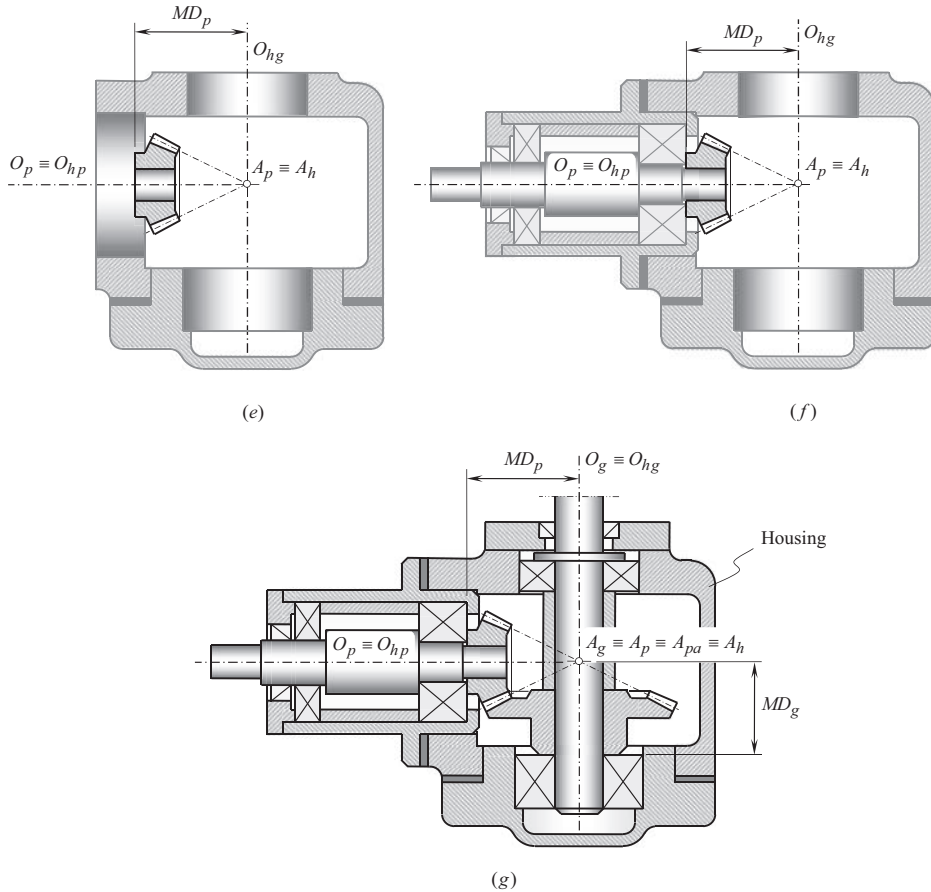


**FIGURE 27.19 (CONTINUED)** Intersected-axes gearing: mounting of bevel gears in the gear housing: (a) a desirable configuration of two mating bevel gears; (b) intersecting axes of two bores in the gear housing; (c) the desirable position of the bevel gear in the gear housing; (d) the design of the components that are used for the gear mounting; (e) the desirable position of the bevel pinion in the gear housing; (f) the design of the components that are used for the pinion mounting; and (g) the final configuration of two bevel gears mounted in the gear housing.

fasteners, and so forth, must be put together so as to keep the gear mounting distance,  $MD_g$ , to the blueprint. The gear mounting distance,  $MD_g$  is measured between the gear back face, and the corresponding gear housing face, as shown in Figure 27.19d.

Similarly, the pinion must be configured in the gear housing so as to keep the pinion axis of rotation,  $O_p$ , aligned with the axis,  $O_{hp}$  (i.e.,  $O_p \equiv O_{hp}$ ), in the gear housing, as illustrated in Figure 27.19e. The pinion base cone apex,  $A_p$ , must be coincident with the point,  $A_h$ , of the intersection of the centerlines,  $O_{hg}$  and  $O_{hp}$  (i.e.,  $A_p \equiv A_h$ ). Then, the rest of the important components, namely, the bearings, shims, fasteners, and so forth, must be put together so as to keep the pinion mounting distance,  $MD_p$ , to the blueprint. The pinion mounting distance,  $MD_p$  is measured between the pinion back face, and the corresponding gear housing face, as shown in Figure 27.19f.

Finally, once the gear and the pinion are properly mounted in the gear housing, their axes are aligned to the centerlines of the corresponding bores in the gear housing (i.e.,  $O_g \equiv O_{hg}$ , and  $O_p \equiv O_{hp}$ ), and the apexes,  $A_g$ ,  $A_p$ , and  $A_{pa}$ , all of them are snapped together with the point of intersection,  $A_h$ , of the centerlines,  $O_{hg}$  and  $O_{hp}$ , in the gear housing, as schematically illustrated in Figure 27.19g.

An important conclusion can be drawn up from the above discussion: NO axial shift of the gears from the point of intersection,  $A_h$ , of the centerlines,  $O_{hg}$  and  $O_{hp}$ , in the gear housing, is permissible

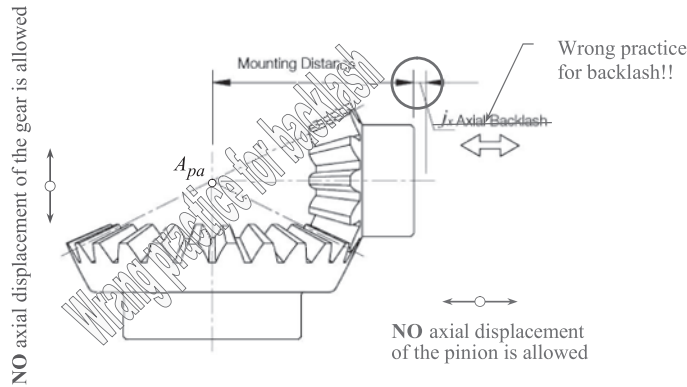


**FIGURE 27.20** Wrong practice to adjust for the backlash in intersected-axes gearing by means of *inward-outward* axial shift of the gears: NO axial shift of the gears from the point of intersection,  $A_h$ , of the centerlines,  $O_{hg}$  and  $O_{hp}$ , in the gear housing, is allowed in  $I_a$  – axes gearing, as well as in  $C_a$  – gearing [the similar is valid with respect to crossed-axes gearing].

in intersected-axes, gearing (see Figure 27.20). It is a wrong practice to adjust for the backlash in intersected-axes gearing by means of *inward-outward* axial shift of the gears.

#### 27.4.2.5 Tolerance for the Accuracy of the Mounting Distance in Intersected-Axes Gearing

Consider intersection of two teeth in contact by the plane of action,  $PA$ , as illustrated in Figure 27.21a. These teeth contact one another along a straight-line segment  $ab$ . (Here, for simplicity, but without loss of generality, a pair of geometrically accurate straight bevel gears is considered). Configuration of the gears in Figure 27.21a corresponds to a case when the centerline of the gear tooth in a section by the pitch plane is aligned with the axis of instant rotation,  $P_{ln}$ , in the gear pair.

Under any circumstances, edge contact between the gear and the pinion teeth has to be avoided. That is why, in order to keep the actual value of the angle  $\theta$  within a very tight tolerance for the accuracy of this parameter, the tolerances for the accuracy of the rest of the design parameters, on which the axes misalignment depends, have to be set very tight.

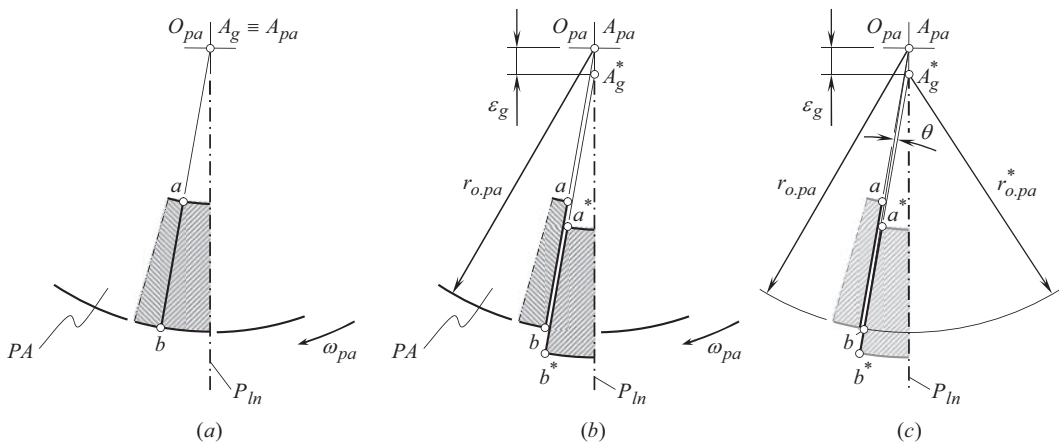


**FIGURE 27.21** Section of two interacting teeth by the plane of action,  $PA$ : (a) zero mounting distance error, (b) mounting distance error of a certain value,  $\epsilon_g$ , and (c) schematic for the derivation of the formula for the calculation of tolerance for the accuracy of the mounting distance in intersected-axes gearing.

As solely the gear mesh is considered, only the unit normal vectors  $\mathbf{n}_g$  and  $\mathbf{n}_p$  are taken into account, while the unit normal perpendiculars to the gear, and the pinion faces are ignored.

Moreover, no edge roundness, chamfers, etc. are considered in this analysis.

A case of outward displaced gear is illustrated in Figure 27.21b. As a result of the displacement, a gap between the teeth is observed. This gap is shown by two straight-line segments,  $ab$  and  $a^*b^*$ , each of which is entirely located on the tooth flanks,  $\mathcal{G}$  and  $\mathcal{P}$ , of the two interacting teeth.

A schematic for the derivation of a formula for the calculation of a tolerance for the accuracy of the mounting distance is depicted in Figure 27.21c. It should be stressed from the very beginning that point  $b$  within the straight-line segment  $ab$  is the closest point to the straight-line segment  $a^*b^*$ . Therefore, an angle,  $\theta_g$ , through which the plane of action,  $PA$ , has to be turned about the axis of rotation  $O_{pa}$  depends on the actual distance of point  $b$  to the straight-line segment  $a^*b^*$ .

Assume that the gear is motionless, and the plane of action,  $PA$ , turns about its axis of rotation,  $O_{pa}$ , through an angle at which point,  $b$ , touches the straight-line segment,  $A_g^*b^*$ . Then, consider a triangle,  $\Delta A_{pa}A_g^*b$ . In this triangle,  $A_{pa}b = r_{o,pa}$ ,  $A_{pa}A_g^* = \varepsilon_g$ , and  $A_g^*b = r_{o,pa}^*$ .

Law of cosine is used for the determination of the actual value of the angle,  $\theta_g$ :

$$\varepsilon_g^2 = r_{o,ap}^2 + (r_{o,pa}^*)^2 - 2 \cdot r_{o,ap} \cdot r_{o,pa}^* \cdot \cos \theta_g \quad (27.37)$$

Then, either the actual value of the angle,  $\theta_g$ , can be expressed in terms of the mounting distance error,  $\varepsilon_g$ , and the design parameters of the gear pair, or a maximum permissible value of the displacement,  $\varepsilon_g$ , can be expressed in terms of the maximum permissible value of the angle  $\theta_g$ , and the design parameters of the gear pair:

$$\varepsilon_g = \sqrt{r_{o,ap}^2 + (r_{o,pa}^*)^2 - 2 \cdot r_{o,ap} \cdot r_{o,pa}^* \cdot \cos \theta_g} \leq [\varepsilon_g] \quad (27.38)$$

Here,  $[\varepsilon_g]$  is the tolerance for the accuracy of the gear mounting distance,  $\varepsilon_g$ .

$$\theta_g = \cos^{-1} \left[ \frac{r_{o,ap}^2 + (r_{o,pa}^*)^2 - \varepsilon_g^2}{2 \cdot r_{o,ap} \cdot r_{o,pa}^*} \right] \leq [\theta_g] \quad (27.39)$$

Here,  $[\theta_g]$  is the tolerance for the accuracy of the gear angle,  $\theta_g$ .

It can be shown (see Figure 27.21c) that the equality:

$$r_{o,pa}^* \cong \frac{r_{o,pa} - \varepsilon_g}{\cos \varphi_{pa}} \quad (27.40)$$

is valid.

When the pinion is fully aligned, the equalities  $\varepsilon = \varepsilon_g$  and  $\theta = \theta_g$ , and Eqs. (27.38) and (27.39) can be used for the calculation of tolerance on the mounting distance in the intersected-axes gear pair.

An analysis similar to that above can be performed for a mating bevel pinion:

$$\varepsilon_p = \sqrt{r_{o,ap}^2 + (r_{o,pa}^*)^2 - 2 \cdot r_{o,ap} \cdot r_{o,pa}^* \cdot \cos \theta_p} \leq [\varepsilon_p] \quad (27.41)$$

$$\theta_p = \cos^{-1} \left[ \frac{r_{o,ap}^2 + (r_{o,pa}^*)^2 - \varepsilon_p^2}{2 \cdot r_{o,ap} \cdot r_{o,pa}^*} \right] \leq [\theta_p] \quad (27.42)$$

Here,  $[\varepsilon_p]$  is the tolerance for the accuracy of the pinion mounting distance,  $\varepsilon_p$ ; and  $[\theta_p]$  is the tolerance for the accuracy of the gear angle,  $\theta_p$ .

Further, when the gear is fully aligned, the equalities  $\varepsilon = \varepsilon_p$  and  $\theta = \theta_p$ , and Eqs. (27.41) and (27.42) can be used for the calculation of tolerance on the mounting distance in the intersected-axes gear pair.

Finally, in a more general case, a bevel gear and a mating bevel pinion, both, are misaligned. In such a scenario, either the actual value of the angle  $\theta$  can be expressed in terms of the mounting distance errors,  $\varepsilon_g$  and  $\varepsilon_p$ , and the design parameters of the gear pair, or a maximum permissible value of the displacements,  $\varepsilon_g$  and  $\varepsilon_p$ , can be expressed in terms of the maximum permissible value of the angle  $\theta$ , and the design parameters of the gear pair.

The angle  $\theta$  is the angle that is formed by two perpendiculars,  $\mathbf{n}_g$  and  $\mathbf{n}_p$  [that is,  $\theta = \angle(\mathbf{n}_g, \mathbf{n}_p)$ ], constructed at point within the edge contact of a gear,  $\mathcal{G}$ , and a mating pinion,  $\mathcal{P}$ , tooth flanks, correspondingly:  $\mathbf{n}_g$  is the unit normal vector to the gear tooth flank,  $\mathcal{G}$ , and  $\mathbf{n}_p$  the unit normal vector to the pinion tooth flank,  $\mathcal{P}$ .

For the determination of the tolerances,  $[\varepsilon_g]$  and  $[\varepsilon_p]$ , for the accuracy of the permissible axial displacements,  $\varepsilon_g$  and  $\varepsilon_p$ , of the gear and the mating pinion, either one of the tolerances (either the tolerance  $[\varepsilon_g]$ , or the tolerance  $[\varepsilon_p]$ ), or a ratio of the tolerances,  $[\varepsilon_g] / [\varepsilon_p]$ , has to be pre-specified.

The performed analysis reveals that the actual value of the angle,  $\theta$ , alters when the gears rotate. The maximum value of the angle,  $\theta$ , is observed at the very beginning of meshing of two gear teeth. As the rotation proceeds, the angle,  $\theta$ , reduces to its minimum value. A minimum value of the angle,  $\theta$ , is observed within a plane through the axis of instant rotation,  $P_m$ , oriented perpendicular to the plane of action,  $PA$ . Further, the angle,  $\theta$ , increases to its maximum value at the very end of meshing of two gear teeth.

A more in detail analysis is not presented here as the equations are bulky.

In addition to the discussed approach, another approach for the calculation of tolerance for the accuracy of the mounting distance in intersected-axes gearing is developed.

When the displacements  $\varepsilon_g$  (or the displacement  $\varepsilon_p$ ) are of a negative value, this results in the edge contact occurring at the opposite face of the gear.

### 27.4.3 MOUNTING DISTANCE IN CROSSED-AXES GEARING

In a precision crossed-axes gear pair (see Figure 27.22), the mounting distance is commonly inspected at nominal operating load, and the preloaded bearings [177].

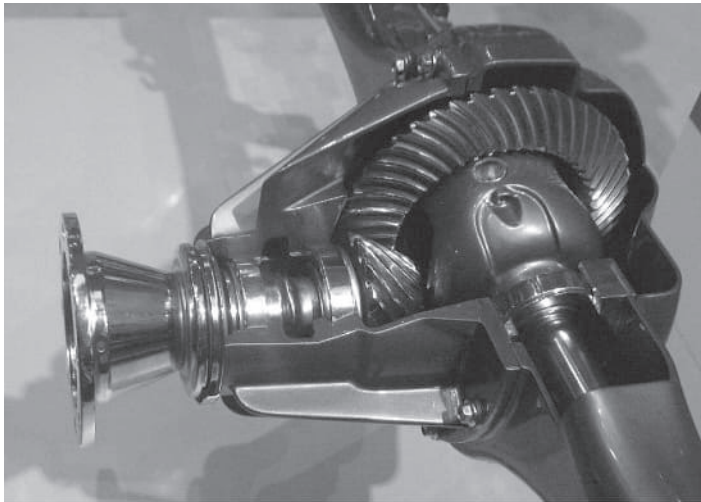


FIGURE 27.22 Crossed-axes gearing in the design of automobile differential.

### 27.4.3.1 Relative Disposition of Base Cones in Crossed-Axes Gearing

A crossed-axes gear pair that is composed of two spiral bevel gears is shown in Figure 27.23 as an example. When a crossed-axes gearing operates, the gear spins,  $\omega_g$ , about its axis of rotation,  $O_g$ . The mating pinion spins,  $\omega_p$ , about its axis of rotation,  $O_p$ . The axes of rotation,  $O_g$  and  $O_p$ , cross one another. The closest distance of approach of the axes of rotation,  $O_g$  and  $O_p$ , is designated as,  $C$ . The center-distance,  $C$ , is a straight-line segment of the centerline,  $\mathfrak{C}$ . The axes of rotation,  $O_g$  and  $O_p$ , form a crossed-axes angle,  $\Sigma$ . The angle,  $\Sigma$ , is formed by two rotation vectors,  $\omega_g$  and  $\omega_p$  [that is, by definition  $\Sigma = \angle(\omega_g, \omega_p)$ ].

The axis of rotation of the gear,  $O_g$ , is perpendicular to the centerline,  $\mathfrak{C}$ , and intersects the centerline at the gear base cone apex,  $A_g$  (see Figure 27.23). Similarly, the axis of rotation of the pinion,  $O_p$ , is also perpendicular to the centerline,  $\mathfrak{C}$ , and intersects the centerline at the pinion base cone apex,  $A_p$ . The length of the straight-line segment,  $A_gA_p$ , equals to the center-distance,  $C$ , that is, an equality  $A_gA_p = C$  is valid.

The center-distance,  $C$ , is subdivided by a point,  $A_{pa}$ , onto two straight-line segments,  $A_gA_{pa}$  and  $A_pA_{pa}$ . The ratio  $A_gA_{pa} / A_pA_{pa}$  equals to the gear ratio in the intersected-axes gear pair ( $A_gA_{pa} / A_pA_{pa} = u$ ). Point,  $A_{pa}$ , is the plane-of-action apex,  $A_{pa}$ .

The axis of instantaneous rotation,  $P_{ln}$ , is a straight line through the plane-of-action apex,  $A_{pa}$ , perpendicular to the centerline,  $\mathfrak{C}$ . The axis,  $P_{ln}$ , forms the angles,  $\Sigma_g$  and  $\Sigma_p$ , with the axes of rotation,  $O_g$  and  $O_p$ , correspondingly. The actual value of each of the angles,  $\Sigma_g$  and  $\Sigma_p$ , can be expressed in terms of the gear ratio,  $u$ , in the crossed-axes gear pair [174].

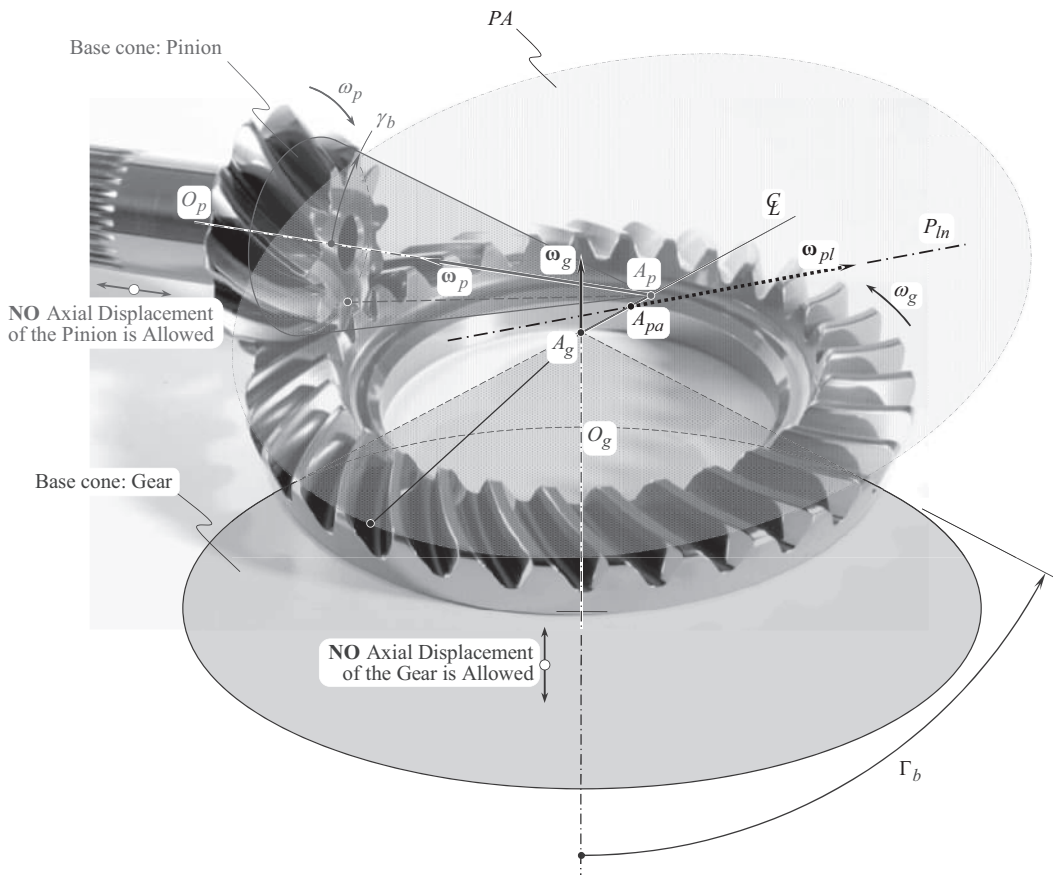


FIGURE 27.23 Crossed-axes gearing with associated base cones of a gear and that of a mating pinion.

A base cone is associated with the gear. The gear base cone apex,  $A_g$ , is located within the centerline,  $\mathfrak{L}$ . Another base cone is associated with the pinion. The pinion base cone apex,  $A_p$ , is also located within the centerline,  $\mathfrak{L}$ . The base cones of the gear and the mating pinion are in tangency with the plane of action in the gear pair – this is a must for geometrically accurate crossed-axes gearing [174].

Neither axial displacement of the gear nor axial displacement of the pinion, from the position shown in Figure 27.23 is permissible. Otherwise, edge contact between the gear and the mating pinion tooth flanks (see Figure 27.17) becomes inevitable.

#### 27.4.3.2 Disposition of Base Cone of a Gear in Relation to the Plane of Action in Crossed-Axes Gearing

In crossed-axes gearing, the interaction of tooth flanks,  $\mathcal{S}$  and  $\mathcal{P}$ , of a gear and of a mating pinion occurs within the plane of action,  $PA$ . Therefore, it makes sense to consider the disposition of base cone of a gear in relation to the plane of action. Later on, the results of the analysis obtained in this way can be applied to the disposition of base cone of a mating pinion in relation to the gear housing.

In a geometrically accurate crossed-axes gear pair the axis of rotation of a gear,  $O_g$ , and that,  $O_{pa}$ , of the plane of action,  $PA$ , are crossed, as illustrated in Figure 27.24a. The base cone apex of the gear,  $A_g$ , and the plane-of-action apex,  $A_{pa}$ , are at the gear center-distance,  $C_g$ , apart from one another. A rotation of the gear is designated as  $\omega_g$ , and a rotation of the plane of action is designated

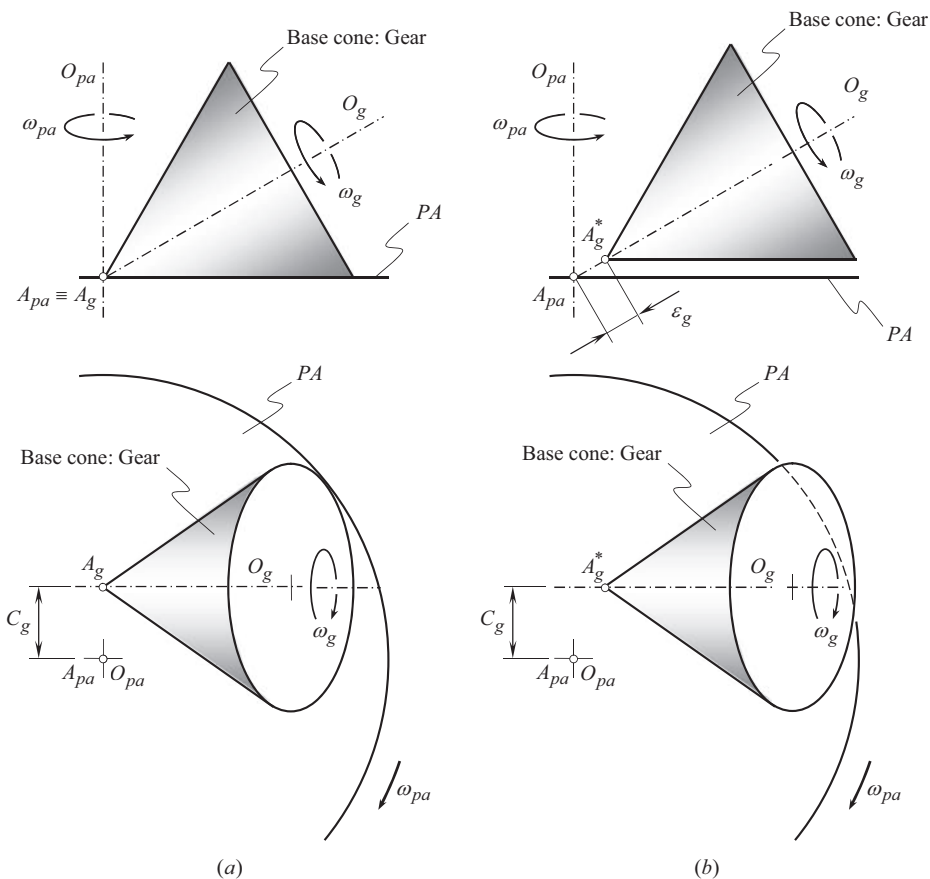


**FIGURE 27.24** Disposition of base cone of a gear in relation to the plane of action,  $PA$ , in (a) geometrically accurate and (b) misaligned crossed-axes gear pair.



as  $\omega_{pa}$ , correspondingly. Sliding between the base cone of the gear, and the plane of action only along the axis,  $P_{ln}$ , is observed when the gears rotate – no sliding is a direction perpendicular to the axis,  $P_{ln}$ , is observed.

In reality, an error,  $\varepsilon_g$ , in the mounting distance of the gear is always observed. The latter is shown in Figure 27.24b. In such a scenario, the gear base cone apex,  $A_g^*$ , does not coincide with the point,  $A_{h,g}$ , as  $A_g^*$  is displaced axially in relation to  $A_{h,g}$  at a distance  $\varepsilon_g$ . In a case, shown in Figure 27.24b, the outward displacement,  $\varepsilon_g$ , is of a positive value. An inward displacement is of a negative value (not shown in Figure 27.24b).

This discussion yields to proceed with the derivation of an equation for the calculation of the tolerance for the accuracy of the mounting distance in a crossed-axes gear pair.

### 27.4.3.3 Mounting of Gears in Crossed-Axes Gear Housing

To operate properly, gears in crossed-axes gearing have to be properly configured in relation to one another. The mounting distance is a key design parameter that helps keep gears properly configured and is the most important design parameter for ensuring the correct operation of a gear pair. The mounting distance can be specified as the distance from a locating surface on the back of one gear (most commonly a bearing seat) to the gear base cone apex,  $A_g$ .

Theoretically, in a crossed-axes gear pair, a gear base cone apex,  $A_g$ , a mating pinion base cone apex,  $A_p$ , and the plane-of-action apex,  $A_{pa}$ , have to be located within the centerline,  $\mathfrak{L}$ , at distances,  $A_g A_{pa}$  and  $A_p A_{pa}$ , as schematically illustrated in Figure 27.25.

In reality, in order to transmit power, gears need to be supported. A gear housing is used for this purpose. The gear housing features a corresponding number of bores that are used to support gear shafts in the housing. A centerline of a bore for the gear shaft is labeled as  $O_{h,g}$ . Correspondingly, a centerline of a bore for the pinion shaft is designated by  $O_{h,p}$ . The centerline,  $O_{h,g}$ , intersects the centerline,  $\mathfrak{L}$ , at point,  $A_{h,g}$ . Correspondingly, the centerline,  $O_{h,p}$ , intersects the centerline,  $\mathfrak{L}$ , at point,  $A_{h,p}$ . Strong constraints on the configuration of the gear and its mating pinion in the gear housing are imposed by the required position of points,  $A_{h,g}$  and  $A_{h,p}$ .

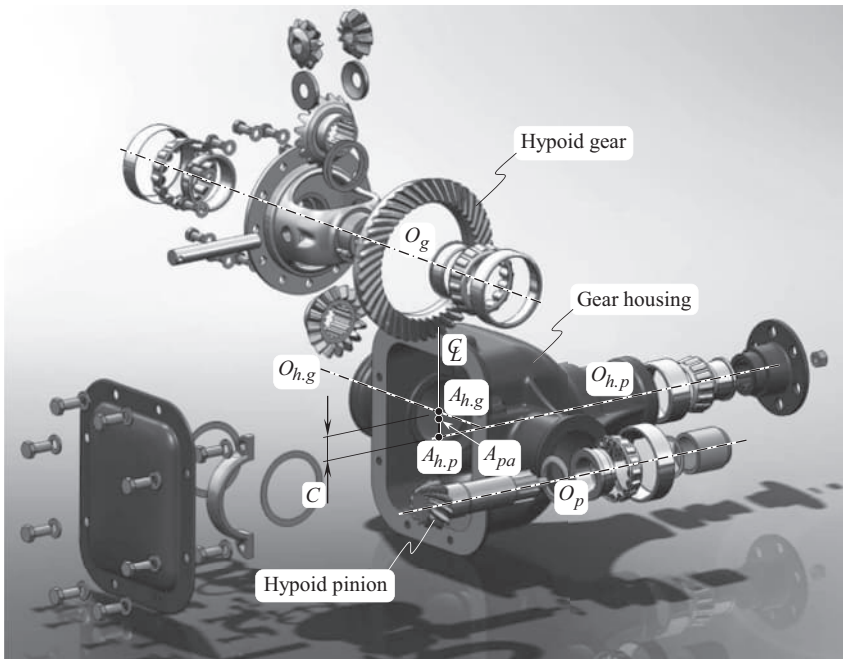


FIGURE 27.25 Mounting bevel gears in the gear housing.



The gear has to be configured in the gear housing so as to keep the gear axis of rotation,  $O_g$ , aligned with the axis,  $O_{h,g}$ , in the gear housing (i.e.,  $O_g \equiv O_{h,g}$ ). The gear base cone apex,  $A_g$ , has to be coincident with the point,  $A_{h,g}$ , of the intersection of the centerlines,  $O_{h,g}$  and  $\Phi$  (i.e.,  $A_g \equiv A_{h,g}$ ). Then, the rest of the important components, namely, the bearings, shims, fasteners, and so forth, must be put together so as to keep the gear mounting distance,  $MD_g$ , to the blueprint. The gear mounting distance,  $MD_g$  is measured between the gear back face, and the gear base cone apex,  $A_g$ .

Similarly, the pinion must be configured in the gear housing so as to keep the pinion axis of rotation,  $O_p$ , aligned with the axis,  $O_{h,p}$  (i.e.,  $O_p \equiv O_{h,p}$ ), in the gear housing. The pinion base cone apex,  $A_p$ , has to be coincident with the point,  $A_{h,p}$ , of the intersection of the centerlines,  $O_{h,p}$  and  $\Phi$  (i.e.,  $A_p \equiv A_{h,p}$ ). Then, the rest of the important components, that is, the bearings, shims, fasteners, and so forth, are put together so as to keep the pinion mounting distance,  $MD_p$ , to the blueprint. The pinion mounting distance,  $MD_p$  is measured between the pinion back face, and the gear base cone apex,  $A_p$ .

After the pinion is in position, the tapered roller bearings of the gear assembly are preloaded; at the same time the gear assembly is placed axially in the housing (see Figure 27.25).

Finally, once the gear and the pinion are properly mounted in the gear housing, their axes are aligned to the centerlines of the corresponding bores in the gear housing (i.e.,  $O_g \equiv O_{h,g}$ , and  $O_p \equiv O_{h,p}$ ), and the apexes,  $A_g$  and  $A_p$ , are snapped together with the corresponding points,  $A_{h,g}$  and  $A_{h,p}$ , as schematically illustrated in Figure 27.25.

An important conclusion can be drawn up from the above discussion (see Figures 27.23 and 27.25):

*Intermediate conclusion: In crossed-axes gearing, NO axial displacements of the gears from the position when the base cone apexes,  $A_g$  and  $A_p$ , of a gear and a mating pinion coincide with the points of intersection,  $A_{h,g}$  and  $A_{h,p}$ , of the centerlines,  $O_{h,g}$  and  $O_{h,p}$  in the gear housing by the centerline  $\Phi$ , are permissible.*

Therefore, it is a wrong practice to adjust for the backlash in crossed-axes gearing by means of *inward/outward* axial displacement of the gears. NO axial displacements of the gears from their nominal configuration are allowed.

In precision crossed-axes gearing, it is recommended to inspect the mounting distance at nominal operating load and the preloaded bearings. A tolerance for the accuracy of the mounting distance is tight.

#### 27.4.3.4 Tolerance for the Accuracy of the Mounting Distance in Crossed-Axes Gearing

Consider two teeth in contact intersected by the plane of action,  $PA$ , as illustrated in Figure 27.26a. The teeth contact one another along a straight-line segment  $ab$ . (Here, for simplicity, but without loss of generality, a pair of geometrically accurate straight bevel gears is considered).

A case of outward displaced gear is illustrated in Figure 27.26b. As a result of the displacement, a gap between the teeth is observed. This gap is shown by two straight-line segments,  $ab$  and  $a^*b^*$ , each of which is entirely located on the tooth flanks,  $\mathcal{S}$  and  $\mathcal{P}$ , of the two interacting teeth.

A schematic for the derivation of a formula for the calculation of a tolerance for the accuracy of the mounting distance is depicted in Figure 27.26c. It should be stressed here that point  $b$  within the straight-line segment  $ab$  is the closest point to the straight-line segment  $a^*b^*$ . Therefore, an angle,  $\theta_g$ , through which the plane of action,  $PA$ , has to be turned about the axis of rotation  $O_{pa}$  depends on the actual distance of point  $b$  to the straight-line segment  $a^*b^*$ .

Assume that the gear is motionless, and the plane of action,  $PA$ , turns about its axis of rotation,  $O_{pa}$ , through an angle at which point,  $b$ , touches the straight-line segment,  $A_g^*b^*$ . Then, consider a triangle,  $\Delta A_{pa}A_g^*b$ . In this triangle,  $A_{pa}b = r_{o,pa}$ ,  $A_{pa}A_g^* = \sqrt{C^2 + \varepsilon_g^2}$ , and  $A_g^*b = r_{o,pa}^*$ .

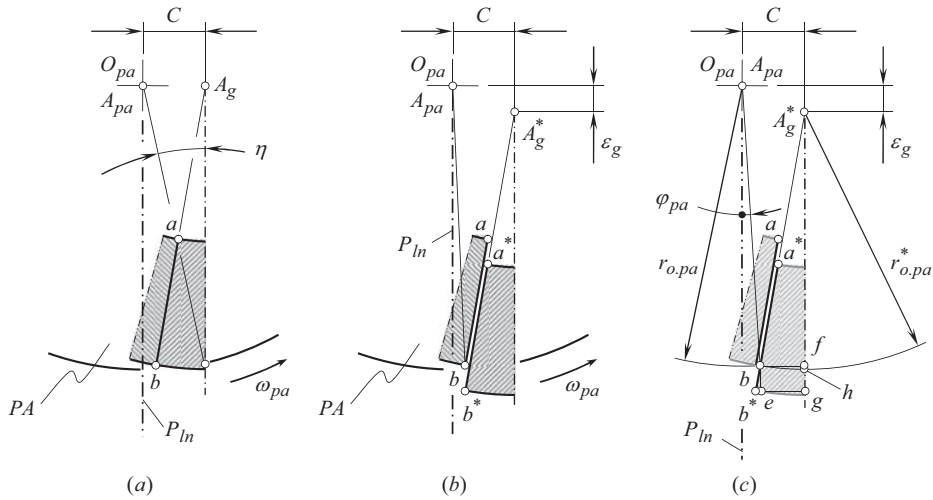


**FIGURE 27.26** Section of two interacting teeth by the plane of action,  $PA$ : (a) zero mounting distance error, (b) mounting distance error of a certain value,  $\varepsilon_g$ , and (c) schematic for the derivation of the formula for the calculation of a tolerance for the accuracy of the mounting distance in crossed-axes gearing.

Law of cosine can be used for the determination of the actual value of the angle,  $\theta_g$ :

$$\varepsilon_g^2 = r_{o,ap}^2 + (r_{o,pa}^*)^2 - 2 \cdot r_{o,ap} \cdot r_{o,pa}^* \cdot \cos \theta_g - C^2 \quad (27.43)$$

Then, either the actual value of the angle,  $\theta_g$ , can be expressed in terms of the mounting distance error,  $\varepsilon_g$ , and the design parameters of the gear pair, or a maximum permissible value of the displacement,  $\varepsilon_g$ , can be expressed in terms of the maximum permissible value of the angle  $\theta_g$ , and the design parameters of the gear pair:

$$\varepsilon_g = \sqrt{r_{o,ap}^2 + (r_{o,pa}^*)^2 - 2 \cdot r_{o,ap} \cdot r_{o,pa}^* \cdot \cos \theta_g - C^2} \leq [\varepsilon_g] \quad (27.44)$$

Here,  $[\varepsilon_g]$  is the tolerance for the accuracy of the gear mounting distance,  $\varepsilon_g$ .

$$\theta_g = \cos^{-1} \left[ \frac{r_{o,ap}^2 + (r_{o,pa}^*)^2 - \varepsilon_g^2 - C^2}{2 \cdot r_{o,ap} \cdot r_{o,pa}^*} \right] \leq [\theta_g] \quad (27.45)$$

Here,  $[\theta_g]$  is the tolerance for the accuracy of the gear angle,  $\theta_g$ .

It can be shown (see Figure 27.26c) that the equality:

$$r_{o,pa}^* \cong \frac{r_{o,pa} - \varepsilon_g}{\cos \varphi_{pa}} \quad (27.46)$$

is valid.

When the pinion is fully aligned, the equalities  $\varepsilon = \varepsilon_g$  and  $\theta = \theta_g$ , and Eqs. (27.44) and (27.45) can be used for the calculation of tolerance on the mounting distance in the crossed-axes gear pair.

An analysis similar to that above can be performed for a mating bevel pinion:

$$\varepsilon_p = \sqrt{r_{o,ap}^2 + (r_{o,pa}^*)^2 - 2 \cdot r_{o,ap} \cdot r_{o,pa}^* \cdot \cos \theta_p - C^2} \leq [\varepsilon_p] \quad (27.47)$$

$$\theta_p = \cos^{-1} \left[ \frac{r_{o,ap}^2 + (r_{o,pa}^*)^2 - \varepsilon_p^2 - C^2}{2 \cdot r_{o,ap} \cdot r_{o,pa}^*} \right] \leq [\theta_p] \quad (27.48)$$

Here,  $[\varepsilon_p]$  is the tolerance for the accuracy of the pinion mounting distance,  $\varepsilon_p$ ; and  $[\theta_p]$  is the tolerance for the accuracy of the gear angle,  $\theta_p$ .

Further, when the gear is aligned, the equalities  $\varepsilon = \varepsilon_p$  and  $\theta = \theta_p$ , and Eqs. (27.47) and (27.48) are used for the calculation of tolerance on the mounting distance in the crossed-axes gear pair.

Finally, in a more general case, a bevel gear and a mating bevel pinion, both, are misaligned. Under such a scenario, either the actual value of the angle  $\theta$  can be expressed in terms of the mounting distance errors,  $\varepsilon_g$  and  $\varepsilon_p$ , and the design parameters of the gear pair, or a maximum permissible value of the displacements,  $\varepsilon_g$  and  $\varepsilon_p$ , can be expressed in terms of the maximum permissible value of the angle  $\theta$ , and the design parameters of the gear pair.

The angle  $\theta$  is formed by two perpendiculars,  $\mathbf{n}_g$  and  $\mathbf{n}_p$  [that is,  $\theta = \angle(\mathbf{n}_g, \mathbf{n}_p)$ ], constructed at point of edge contact of a gear,  $\mathcal{G}$ , and a mating pinion,  $\mathcal{P}$ , tooth flanks, correspondingly:  $\mathbf{n}_g$  is the unit normal vector to the gear tooth flank,  $\mathcal{G}$ , and  $\mathbf{n}_p$  the unit normal vector to the pinion tooth flank,  $\mathcal{P}$ .

For the determination of the tolerances,  $[\varepsilon_g]$  and  $[\varepsilon_p]$ , for the accuracy of the permissible axial displacements,  $\varepsilon_g$  and  $\varepsilon_p$ , of the gear and the mating pinion, either one of the tolerances (either the tolerance  $[\varepsilon_g]$ , or the tolerance  $[\varepsilon_p]$ ), or a ratio of the tolerances,  $[\varepsilon_g]/[\varepsilon_p]$ , has to be pre-specified.

The performed analysis reveals that the actual value of the angle,  $\theta$ , alters when the gears rotate. The maximum value of the angle,  $\theta$ , is observed at the very beginning of meshing of two gear teeth. As the rotation proceeds, the angle,  $\theta$ , reduces to its minimum value. A minimum value of the angle,  $\theta$ , is observed within a plane through the axis of instant rotation,  $P_m$ , perpendicular to the plane of action,  $PA$ . Further, the angle,  $\theta$ , increases to its maximum value at the very end of meshing of two gear teeth.<sup>3</sup>

When the displacements  $\varepsilon_g$  (or the displacement  $\varepsilon_p$ ) are of a negative value, this results in the edge contact occurring at the opposite face of the gear.

## 27.5 CONTACT PATTERN

Gears in intersected-axes gear pairs, and in crossed-axes gear pairs, must be assembled in a specific way to ensure smooth running and a favorable load distribution between gears. Even a small axes misalignment in intersected-axes gearing (of about three angular minutes or so) results in a severe contact pattern change. The contact area should cover the entire flank surface (without edge contact concentration) if the nominal load rating is reached. An offset error of  $\pm 50$  micrometers leads to a contact pattern change of about the same magnitude.

To attain the goal (to ensure smooth running and a favorable load distribution between gears), a contact pattern between the interacting tooth flanks of a gear and a mating pinion is commonly used.

It is the right point to mention here that a proper shape along with a desirable location and orientation of the contact pattern in a gear pair is the priority number one from the standpoint of the actual value of the mounting distance.

The contact pattern is a critical attribute of any and all bevel/hypoid gear design. An example of contact pattern is depicted in Figure 27.27. For this purpose, the gear teeth are covered by a stain and roll over one another in tight mesh, as illustrated in Figure 27.28.

<sup>3</sup> A more in-detail analysis is not presented here as the equations are bulky.

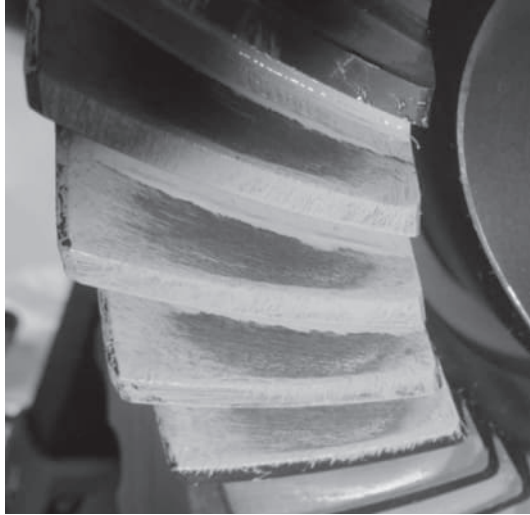


**FIGURE 27.27** An example of acceptable shape and configuration of contact pattern under a low load.



**FIGURE 27.28** Two gears with the teeth covered by stain, roll over each other in tight mesh to get a favorable shape, size, and configuration of the contact pattern.

Simply stated, the contact pattern is the area in which the gear teeth come in contact as they engage and disengage during their rotation. When a gear is installed in a gearbox and is powering the designated application, there are varying degrees of pressure – or load – on the gear teeth. These pressures are influenced by box deflections, bearing movement and temperature changes. When the

gear teeth are subjected to these variables, the contact pattern will change. There is a general rule of thumb stating that the heavier the load, the larger the contact pattern and vice versa. For a gear to perform properly under operating load, the contact pattern must be of a certain shape and at a certain location. Typically, an ideal tooth contact pattern under load should encompass the bulk of the tooth surface while avoiding any contact with the edges of the tooth flank. So far, the contact pattern is more a *qualitative* rather than a *quantitative* indicator of a gear pair quality.

The permissible variation in contact pattern location, orientation, and shape, can be used to calculate the tolerances for design parameters of a gear pair.<sup>4</sup> Unfortunately, in the present-day gear practice, contact pattern is a qualitative, and not quantitative measure of the gear pair quality.

Instead of the contact pattern analysis, the teeth flank geometry along with the actual value of the mounting distance should be measured. No contact pattern analysis is necessary if the gears for intersected-axes, and/or crossed-axes gear pairs are machined, and assembled according to the properly designed blueprint.

## 27.6 PERMISSIBLE ALTERATION TO BEVEL GEAR TOOTH FLANK GEOMETRY

As a gear and a mating pinion tooth interact with one another only within the plane of action,  $PA$ , the geometry of the tooth flanks,  $\mathcal{S}$  and  $\mathcal{P}$ , of a gear and a mating pinion allows for a slight modification (a few examples are illustrated in Figure 27.29) aiming to avoid the edge contact in gearing. The modification is allowed only for lines of intersection of the tooth flanks,  $\mathcal{S}$  and  $\mathcal{P}$ , by the plane of action. Only under such a scenario angular base pitch,  $\varphi_{b,g}$ , of a gear equals to operating angular base pitch,  $\varphi_{b,op}$ , of the gear pair (i.e., the equality  $\varphi_{b,g} \equiv \varphi_{b,op}$  is observed); and similarly, angular base pitch,  $\varphi_{b,p}$ , of a mating pinion equals to operating angular base pitch,  $\varphi_{b,op}$ , of the gear pair (i.e., the equality  $\varphi_{b,p} \equiv \varphi_{b,op}$  is also observed).

No violation of the equalities  $\varphi_{b,g} \equiv \varphi_{b,op}$  and  $\varphi_{b,p} \equiv \varphi_{b,op}$  is permissible in precision gears for intersected-axes gearing as well as in crossed-axes gearing.

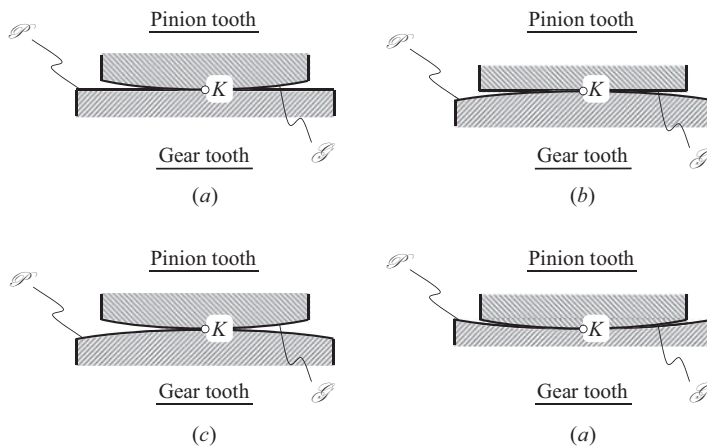


**FIGURE 27.29** Possible kinds of modification of tooth flanks,  $\mathcal{S}$  and  $\mathcal{P}$ , of a gear and a mating pinion in a section by the plane of action,  $PA$ : (a) straight gear-to-convex pinion, (b) convex gear-to-straight pinion, (c) convex gear-to-convex pinion, and (d) concave gear-to-convex pinion.

<sup>4</sup> In much, the contact pattern is a subjective (and not objective) parameter. Neither the dimensions and orientation nor the tolerances for the dimensions and orientation of the contact pattern can be assigned (and be directly measured on the shop floor). The contact pattern is an insufficiently engineered parameter of quality of a gear pair. The contact pattern is NOT measurable, that is, it can NOT be reliably measured by means commonly available on the shop floor. It is desirable to substitute the contact pattern with another reliably measurable design parameter of a gear pair. The mounting distance is a promising candidate for this purpose.

---

# 28 Gear Noise and Vibration

Noise and vibration excitation are two annoying problems. These problems have been exacerbated due to the continuous reduction in sounds from other systems' noise exciters, such as engines and so forth. All of them are theoretically preventable. Unfortunately, gear noise prevention methods can be costly, both in terms of equipment and labor. The reduction of gear noise/vibration excitation is a complex and challenging engineering problem. It is likely the 2003 book by *J.D. Smith* [203] is the only attempt so far, in which the problem of noise excitation is discussed from the most general point of view.

## 28.1 ROOT CAUSES FOR VIBRATION GENERATION AND NOISE EXCITATION

Many factors, such as transmission error, tooth impacts, mesh stiffness variation, force axial shuttling, friction, air, and lubricant entrapment, cause gear noise and vibration. Only factors that cause noise and vibration in the gear mesh are considered in this chapter.

It is reasonable to begin the analysis of root causes for vibration generation and noise excitation starting from consideration of geometrically accurate gear pairs. Later on, the obtained results of the analysis can be enhanced toward approximate gear pairs.

### 28.1.1 ROOT CAUSE FOR VIBRATION GENERATION AND NOISE EXCITATION IN GEOMETRICALLY ACCURATE GEARING

Geometrically accurate gear pairs of all kinds: parallel-axes, intersected-axes, and crossed-axes gear pairs met all three fundamental laws of gearing that gearing of all designs has to fulfill. These laws of gearing are as follows (see Chapter 4):

- *The law of contact* (or, in other words, *the first fundamental law of gearing*) of the interacting tooth flanks,  $\mathcal{S}$  and  $\mathcal{P}$ , of a gear and a mating pinion. This law of gearing is commonly analytically expressed by *Shishkov equation of contact*,  $\mathbf{n}_g \cdot \mathbf{V}_\Sigma = 0$
- *The conjugate action law* (or, in other words, *the second fundamental law of gearing*) for the interacting tooth flanks,  $\mathcal{S}$  and  $\mathcal{P}$ , of a gear and a mating pinion – at every point within the line of contact the unit normal vector,  $\mathbf{n}_g$ , of a common perpendicular is pointed along a straight line that intersects the axis of instantaneous rotation,  $P_m$ , in the gear pair
- *The equal base pitches law* (or, in other words, *the third fundamental law of gearing*): To comply with this law of gearing, angular base pitch of a gear,  $\varphi_{b,g}$ , and angular base pitch of a mating pinion,  $\varphi_{b,p}$ , both, must be equal to operating angular base pitch of the gear pair,  $\varphi_{b,op}$ . This means that the equalities  $\varphi_{b,g} = \varphi_{b,op}$  and  $\varphi_{b,p} = \varphi_{b,op}$  must be valid for any and all configurations of a gear and a mating pinion in relation to each other when the gears rotate

In geometrically accurate gear pairs, all three fundamental laws of gearing are fulfilled. Therefore, it seems from the first glimpse that there is no reason for vibration generation and noise excitation in geometrically accurate gear pairs. Unfortunately, this is not correct.

In (a) parallel-axes helical gearing, (b) intersected-axes gearing, and in (c) crossed-axes gearing, variation of the *axial* component and the *radial* component of the resultant force of the interaction between a gear and a mating pinion tooth flanks is observed. Therefore, even in the case of geometrically accurate gearing [see items (a) through (b)], noise excitation, and vibration generation become inevitable.



In geometrically accurate intersected-axes, and in crossed-axes gear pairs, the forces that act in the gear mesh vary in time. This is true first of all with respect to the axial component as well as to the radial component of the resultant force. The tangential component that causes transmission of the rotation also contributes to vibration and noise generation. However, this contribution is not that significant compared to the contribution by the axial, and the radial components.

The variation in time of the axial component of the resultant force as well as the radial component of the resultant force, both are transmitted to the gear housing, and so forth.

### 28.1.2 ROOT CAUSE FOR VIBRATION GENERATION AND NOISE EXCITATION IN APPROXIMATE GEAR PAIRS

In approximate gearing of all designs, at least one of three fundamental laws of gearing is violated.

#### 28.1.2.1 Violation of the Law of Contact

In compliance with the law of contact between tooth flanks,  $\mathcal{S}$  and  $\mathcal{P}$ , of a gear and a mating pinion, a common perpendicular,  $\mathbf{n}_g$ , to the interacting tooth flanks,  $\mathcal{S}$  and  $\mathcal{P}$ , is always orthogonal to the linear velocity vector,  $\mathbf{V}_\Sigma$ , of the resultant relative motion of the tooth flanks. Analytically, this law of gearing is described by *Shishkov equation of contact*,  $\mathbf{n}_g \cdot \mathbf{V}_\Sigma = 0$ .

The law of contact is commonly violated in cases of the so-called *edge contact* of the interacting tooth flanks,  $\mathcal{S}$  and  $\mathcal{P}$ , of a gear and a mating pinion [see Figure 27.17 in Chapter 27].

The law of contact is fulfilled in most cases of approximate gearing, as a gear,  $\mathcal{S}$ , and a mating pinion,  $\mathcal{P}$ , tooth flanks in approximate gearing are smooth surfaces having appropriate principal radii of curvature. Commonly, fulfillment of the law of contact causes no problem when designing geometrically accurate gears. However, this could be a challenging problem when designing approximate gears.

#### 28.1.2.2 Violation of the Conjugate Action Law

In approximate gearing, the conjugate action law is violated almost always.

Referring to Figure 28.1, consider the interaction between two local patches of a gear and of a mating pinion tooth profile,  $\mathcal{S}$  and  $\mathcal{P}$ . The local patches are located within the differential vicinity of contact point,  $K$ .

In a case of geometrically accurate gearing (see Figure 28.1a), a gear and a mating pinion rotate,  $\omega_g$  and  $\omega_p$ , about their axes of rotation,  $O_g$  and  $O_p$ . The axes,  $O_g$  and  $O_p$ , are at a center-distance,  $C$ , from one another. The pitch point,  $P$ , is located within the centerline,  $\mathfrak{k}$ . The ratio,  $r_g/r_p$ , of the distances,  $r_g$  and  $r_p$ , of the pitch point,  $P$ , from the axes of rotation,  $O_g$  and  $O_p$ , is reciprocal to the ratio,  $\omega_p/\omega_g$ , of the rotations of the gear and the mating pinion. Remember, that, by nature, the distances,  $r_g$  and  $r_p$ , are the gear center-distance,  $C_g$ , and the pinion center-distance,  $C_p$ , correspondingly (and, thus, the equalities  $r_g = C_g$  and  $r_p = C_p$  are valid).

The line of action,  $LA$ , is a straight line through the pitch point,  $P$ . The line of action,  $LA$ , forms a transverse pressure angle,  $\phi_t$ , with a perpendicular to the centerline,  $\mathfrak{k}$ , through the pitch point,  $P$ .

When the gears rotate, the contact point,  $K$ , travels along the line of action,  $LA$ , with a linear velocity,  $V_K$ . The tooth flanks,  $\mathcal{S}$  and  $\mathcal{P}$ , slide over one another. The linear velocity of the sliding is labeled  $V_{sl}$ .

When the gear is considered stationary, the instant motion of a gear and a mating pinion in relation to one another can be viewed as an instant rotation,  $\omega_{p/g}$ , of the pinion in relation to the gear about the pitch point,  $P$ . Otherwise, when the pinion is considered stationary, the instant motion of a gear and a mating pinion in relation to one another can be viewed as an instant rotation,  $\omega_{g/p}$ , of the gear in relation to the pinion about the pitch point,  $P$ .

It is critical to stress here that in Figure 28.1a, the common perpendicular vector,  $\mathbf{n}_g$ , is pointed along the line of action,  $LA$ . This reveals that the gear and the mating pinion tooth profiles,  $\mathcal{S}$  and



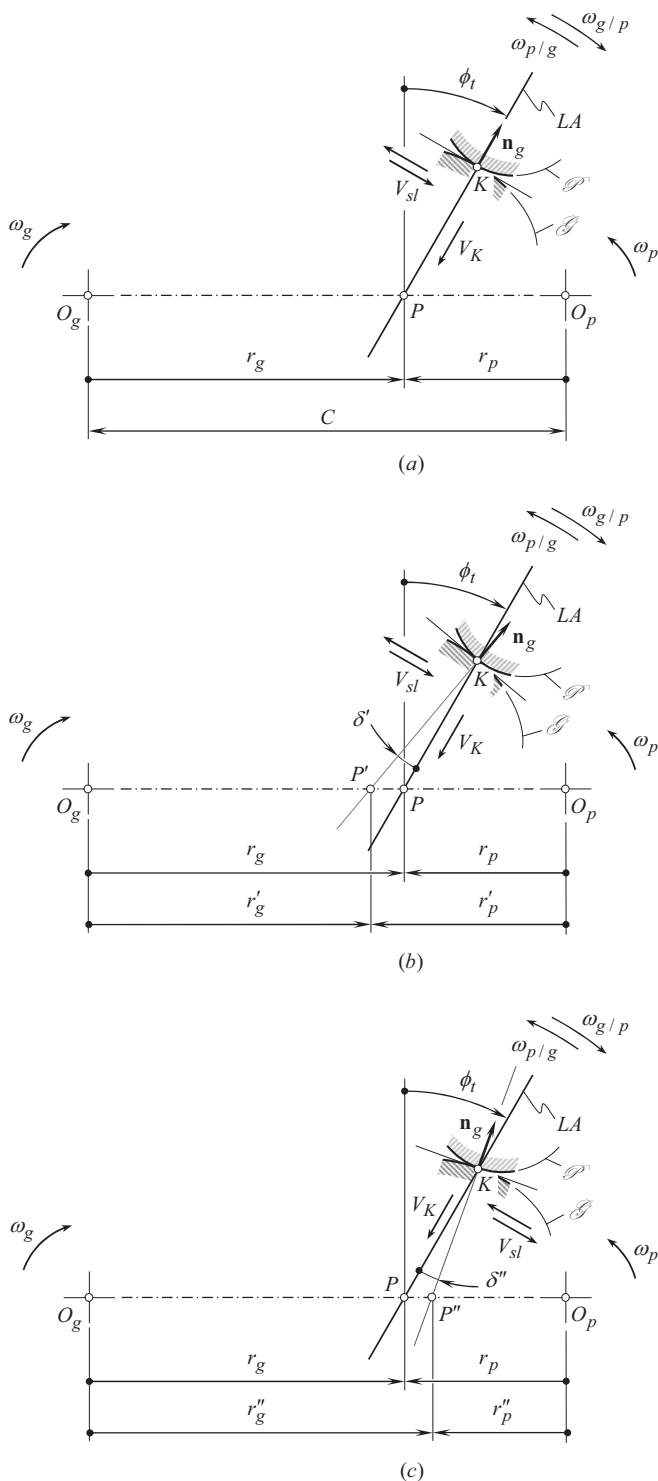


**FIGURE 28.1** Fulfillment and violation of the conjugate action law: (a) the conjugate action law is fulfilled, (b) the conjugate action law is violated: the tooth flanks,  $\mathcal{S}$  and  $\mathcal{P}$ , are turned clockwise through an angle,  $\delta'$ , and (c) the conjugate action law is violated: the tooth flanks,  $\mathcal{S}$  and  $\mathcal{P}$ , are turned counter-clockwise through an angle,  $\delta''$ .

$\mathcal{P}$ , are designed properly, and the conjugate action law for the interacting tooth profiles,  $\mathcal{G}$  and  $\mathcal{P}$ , is fulfilled.

Let's proceed to the analysis of the case shown in Figure 28.1b. In the case in question, the gear and the mating pinion tooth profiles,  $\mathcal{G}$  and  $\mathcal{P}$ , are designed so that the common perpendicular vector,  $\mathbf{n}_g$ , is turned about the contact point,  $K$ , clockwise through an angle,  $\delta'$ . A straight line along the unit vector,  $\mathbf{n}_g$ , intersects the centerline,  $\mathfrak{k}$ , at point,  $P'$  (which, by nature, is an instantaneous pitch point). The ratio,  $r'_g/r'_p$ , of the distances,  $r'_g$  and  $r'_p$ , of the instantaneous pitch point,  $P'$ , from the axes of rotation,  $O_g$  and  $O_p$ , is not reciprocal to the ratio,  $\omega_p/\omega_g$ , of the rotations of the gear and the mating pinion. Instead, the ratio,  $r'_g/r'_p$ , is reciprocal to the ratio,  $\omega_p/\omega'_g$ , of the actual instant rotations of the gear and the mating pinion. The gears tend to rotate about the instantaneous pitch point,  $P'$ , and not about the desirable pitch point,  $P$ . None of the instant rotations (neither,  $\omega_{p/g}$ , nor,  $\omega_{g/p}$ ) is feasible. This reveals that the gear and the mating pinion tooth profiles,  $\mathcal{G}$  and  $\mathcal{P}$ , are designed improperly, and the conjugate action law for the interacting tooth profiles,  $\mathcal{G}$  and  $\mathcal{P}$ , is violated.

Finally, let's analyze the case shown in Figure 28.1c. Here, the gear and the mating pinion tooth profiles,  $\mathcal{G}$  and  $\mathcal{P}$ , are designed so that the common perpendicular vector,  $\mathbf{n}_g$ , is turned about the contact point,  $K$ , counter-clockwise through an angle,  $\delta''$ . A straight line along the unit vector,  $\mathbf{n}_g$ , intersects the centerline,  $\mathfrak{k}$ , at point,  $P''$  (which, by nature, is an instantaneous pitch point). The ratio,  $r''_g/r''_p$ , of the distances,  $r''_g$  and  $r''_p$ , of the instantaneous pitch point,  $P''$ , from the axes of rotation,  $O_g$  and  $O_p$ , is not reciprocal to the ratio,  $\omega_p/\omega_g$ , of the rotations of the gear and the mating pinion. Instead, the ratio,  $r''_g/r''_p$ , is reciprocal to the ratio,  $\omega_p/\omega''_g$ , of the actual instant rotations of the gear and the mating pinion. The gears tend to rotate about the instantaneous pitch point,  $P'$ , and not about the desirable pitch point,  $P$ . None of the instantaneous rotations (neither,  $\omega_{p/g}$ , nor,  $\omega_{g/p}$ ) is permissible. This reveals that the gear and the mating pinion tooth profiles,  $\mathcal{G}$  and  $\mathcal{P}$ , are designed improperly, and the conjugate action law for the interacting tooth profiles,  $\mathcal{G}$  and  $\mathcal{P}$ , is violated.

As the line that is pointed along the unit normal vector,  $\mathbf{n}_g$ , of a common perpendicular does not go through the pitch point,  $P$ , The actual instantaneous pitch point,  $P$ , migrates ( $P'$  and  $P''$ ) up and down along the centerline,  $\mathfrak{k}$ . Therefore, the vibration generation, and noise excitation, both, increase when the gears operate.

When friction between a gear tooth flank,  $\mathcal{G}$ , and a mating pinion tooth flank,  $\mathcal{P}$ , is taken into account, the friction forces alter the actual direction of a straight line along which the resultant force of the interaction is pointed, as illustrated in Figure 28.2. The normal forces,  $\mathbf{F}_{t,1}$  and  $\mathbf{F}_{t,2}$ , are pointed along the line of action,  $LA$ . The line of action,  $LA$ , is a straight line through the pitch point,  $P$ . The vectors of friction forces,  $\mathbf{F}_{f,1}$  and  $\mathbf{F}_{f,2}$ , are entirely located within the common tangent plane, and they are perpendicular to the corresponding normal forces,  $\mathbf{F}_{t,1}$  and  $\mathbf{F}_{t,2}$ . As the inequalities  $\mathbf{F}_{f,1} \neq 0$  and  $\mathbf{F}_{f,2} \neq 0$  are valid, then the resultant force of interaction,  $\mathbf{F}_\Sigma$ , does not align with the line of action,  $LA$ , or with the instantaneous line of action,  $LA_{\text{inst}}$ . As the resultant force,  $\mathbf{F}_\Sigma$ , is no longer pointed along a line through the pitch point,  $P$ , an instantaneous pitch point,  $P_{\text{inst}}$ , is created.

The resultant force is pointed along a straight line that is not through the pitch point,  $P$ . The latter along with the variation of the normal forces,  $\mathbf{F}_{t,1}$  and  $\mathbf{F}_{t,2}$ , and friction forces  $\mathbf{F}_{f,1}$  and  $\mathbf{F}_{f,2}$ , depending on an actual configuration of the gear and the pinion in relation to one another (see Figure 28.2) are potential root causes of an excessive noise excitation. Better lubrication of the gear pair is a potential solution to this problem: the better lubrication, the lower noise excitation and vice versa. When performing the analysis, the process of vibration generation, and noise excitation, can be expressed in terms of the torques,  $\mathbf{T}_{f,1}$  and  $\mathbf{T}_{f,2}$ , created by the friction forces,  $\mathbf{F}_{f,1}$  and  $\mathbf{F}_{f,2}$ , as well as in terms of the resultant torque,  $\mathbf{T}_{f,\Sigma}$ , that is created by the resultant friction force,  $\mathbf{F}_{f,\Sigma} = \mathbf{F}_{f,1} + \mathbf{F}_{f,2}$ .

### 28.1.2.3 Violation of the Equality of Base Pitches

In approximate gearing, either base pitch of a gear or base pitch of a mating pinion, or both of them, are not equal to operating base pitch in the gear pair. Moreover, often the base pitch either of a gear, or of a mating pinion, or of both, cannot be specified at all. The operating base pitch of a gear pair is not a measurable design parameter – this design parameter can be either calculated, or it can be measured indirectly.

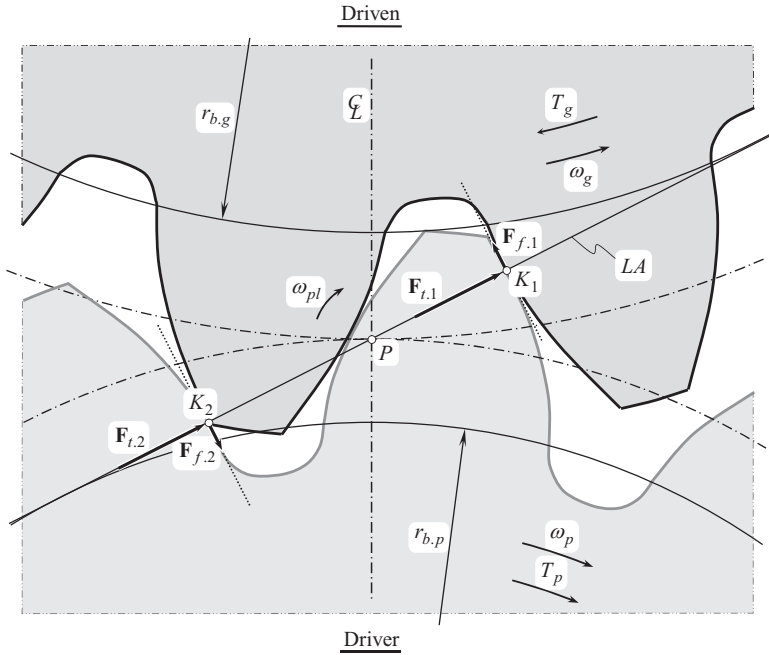


**FIGURE 28.2** Direction of the resultant force,  $\mathbf{F}_{\Sigma}$ , in a gear mesh can be affected by the friction forces,  $\mathbf{F}_{f,1}$  and  $\mathbf{F}_{f,2}$ .

The base pitch variation is a root cause for the vibration generation and for an excessive noise excitation. The parameters of noise excitation can be expressed in terms of the variation of the base pitch when the gears rotate. Thus, the noise frequency must correlate to the base pitch variation.

The base pitch variation is caused by one of the following factors (or by a combination of these factors), namely:

- The deviation of the gear tooth flank geometry in relation to the desirable geometry
- A displacement (both linear displacement, and angular displacement) of the gear tooth flank in relation to the axis of rotation of the gear/pinion (of the gear/pinion body)
- The axes misalignment

The actual value of the base pitch variation can be expressed in terms of these three elementary components.

The deviations of the tooth flank geometry from its desirable geometry as well as the displacements of the tooth flanks from their desirable location and orientation are measured from the nominal tooth flank geometry, the location and orientation specified by the gear blueprint. In this scenario, base pitches of the gear, of the mating pinion, and the operating base pitch are equal to that specified by the gear pair blueprint.

Without loss of generality, consider a simplified example to illustrate the approach employed for the analysis of the base pitch deviations, and their impact on the noise excitation in a gear pair. A parallel-axes helical gear pair is diagrammatically depicted in Figure 28.3. The gear pair features a zero axes misalignment. The gear and the pinion are rotated about their axes of rotation,  $O_g$  and  $O_p$ , correspondingly. The angular velocities,  $\omega_g$  and  $\omega_p$ , are synchronized with one another so, as to keep the ratio valid:

$$\frac{\omega_p}{\omega_g} = \frac{N_g}{N_p} \quad (28.1)$$

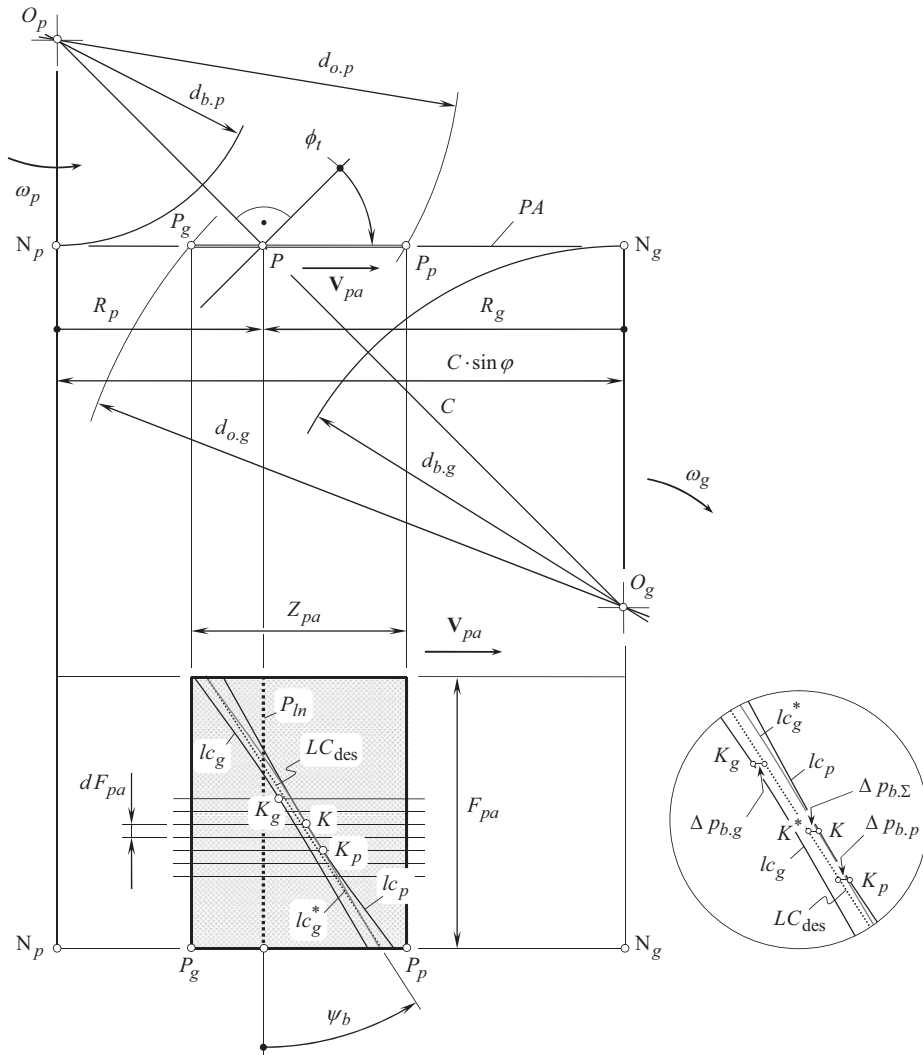


**FIGURE 28.3** Details of the concept used for the analysis of the deviations: of the base pitch,  $\Delta p_{b,g}$ , in a gear, of the base pitch,  $\Delta p_{b,p}$ , in a mating pinion, and the operating base pitch,  $\Delta p_{b,\Sigma}$ , in a gear pair.

Here, in Eq. (28.1), the tooth numbers of the gear and the pinion are designated as  $N_g$  and  $N_p$ , correspondingly.

The axes of rotation,  $O_g$  and  $O_p$ , of the gear and the pinion are at a center-distance,  $C$ , apart from one another. The transverse pressure angle is denoted by  $\phi_t$ .

The plane of action,  $PA$ , is tangent from opposite sides to the base cylinders of diameters,  $d_{b,g}$  and  $d_{b,p}$ , of the gear and the pinion, correspondingly. The width of the zone of action,  $ZA$ , equals to the effective face width,  $F_{pa}$ , and the length is equal to the length of the active portion of the zone of action,  $Z_{pa}$ . The desirable line of contact,  $LC_{des}$ , forms a base helix angle,  $\phi_t$ , with the axis of instantaneous rotation,  $P_{ln}$ . The tooth flanks,  $\mathcal{S}$  and  $\mathcal{P}$ , of the geometrically accurate gears are intersected by the plane of action,  $PA$ , along the desirable line of contact,  $LC_{des}$ .

The tooth flanks,  $\mathcal{S}_a$  and  $\mathcal{P}_a$ , of the actual gear and its mating pinion deviate from their desirable geometries,  $\mathcal{S}$  and  $\mathcal{P}$ . Therefore, the gear tooth flank,  $\mathcal{S}_a$ , is intersected by the plane of action,  $PA$ , along the gear line of contact,  $lc_g$ . The line of intersection,  $lc_g$ , does not align with the desirable line of contact,  $LC_{des}$ . Similarly, the pinion tooth flank,  $\mathcal{P}_a$ , is intersected by the plane of action,  $PA$ ,

along the pinion *line of contact*,  $lc_p$ . The line of intersection,  $lc_p$ , also does not align with the desirable line of contact,  $LC_{des}$ . Evidently, the lines of intersection,  $lc_g$  and  $lc_p$ , do not align with the desirable line of contact,  $LC_{des}$ .

The plane of action,  $PA$ , is sliced by an infinite number of planes, all of which are perpendicular to the axis of instantaneous rotation,  $P_{in}$ . The planes are at an infinitesimally short distance,  $dF_{pas}$ , from one another. Within every slice, the gear line of contact,  $lc_g$ , deviates from the desirable line of contact,  $LC_{des}$ , at a distance,  $\Delta p_{b,g}$ . At point,  $K_g$ , the deviation,  $\Delta p_{b,g}$ , is of a minimal value. Similarly, within every slice, the pinion line of contact,  $lc_p$ , deviates from the desirable line of contact,  $LC_{des}$ , at a distance,  $\Delta p_{b,p}$ . At point,  $K_p$ , the deviation,  $\Delta p_{b,p}$ , is of a minimal value. In fact, the deviations,  $\Delta p_{b,g}$  and  $\Delta p_{b,p}$ , are equal to the deviations of the linear base pitches,  $p_{b,g}$  and  $p_{b,p}$ , of the gear and the mating pinion from the operating linear base pitch,  $p_{b,op}$ , of the gear pair. As it is clear from the above discussion, the base pitch deviations are caused by the deviations in tooth flank geometries,  $\mathcal{S}_g$  and  $\mathcal{P}_g$ , of the gear and the mating pinion from their desirable geometries,  $\mathcal{S}$  and  $\mathcal{P}$ .

Theoretically, the tooth flanks,  $\mathcal{S}$  and  $\mathcal{P}$ , are at certain distance from one another, but in reality, they contact each other at point, as both the driving pinion and the driven gear are loaded by the operating torque. As the gears are loaded, there is no gap between the gear line of contact,  $lc_g$ , and the pinion line of contact,  $lc_p$ . The gear line of contact,  $lc_g$ , travels toward the pinion line of contact,  $lc_p$ . In a shifted position, the line,  $lc_g$ , is labeled as  $lc_g^*$ . These two lines of contact have a common point, that is, they share contact point,  $K$ . The distance covered by the pinion line of contact,  $lc_p$ , to get in contact with the gear line of contact,  $lc_g$ , depends on the actual values of the deviations,  $\Delta p_{b,g}$  and  $\Delta p_{b,p}$ . By nature, this distance is the operating base pitch error. In a case when minimal deviations are observed in a common slice, the total deviation of the base pitches,  $\Delta p_{b,\Sigma}$ , is equal to the sum of the instantaneous deviations,<sup>1</sup>  $\Delta p_{b,g}$  and  $\Delta p_{b,p}$ :

$$\Delta p_{b,\Sigma} = \Delta p_{b,g} + \Delta p_{b,p} \quad (28.2)$$

Commonly, the minimal deviations,  $\Delta p_{b,g}$  and  $\Delta p_{b,p}$ , are observed in different slices, and not in a common slice. Therefore, the total deviation of the base pitches,  $\Delta p_{b,\Sigma}$ , is calculated as:

$$\Delta p_{b,\Sigma} = a(\varphi_p) \cdot \Delta p_{b,g} + b(\varphi_p) \cdot \Delta p_{b,p} \quad (28.3)$$

Here, in Eq. (28.3), the multipliers,  $a(\varphi_p)$  and  $b(\varphi_p)$ , are functions of the angular configuration of the input shaft, namely, of the angular configuration of the pinion.

The instantaneous value of the total deviation of the base pitch,  $\Delta p_{b,\Sigma}$ , falls into the interval:

$$\Delta p_{b,g} - b\Delta p_{b,p} \leq \Delta p_{b,\Sigma} \leq \Delta p_{b,g} + b\Delta p_{b,p} \quad (28.4)$$

This idea of relative displacement (in micrometers) is the cause of a force variation, and hence vibration is unusual since traditionally an external force such as an out-of-balance rotating component, or vibration of the supporting ground is excited to produce a vibration. In gearing, the relative displacement between the mating gears generates forces between the teeth and the subsequent vibrations through the system.

Once the deviations of the base pitch are measured in both, in the gear, and in the mating pinion, then each of the components of the total deviation of the base pitch,  $\Delta p_{b,\Sigma}$ , can be corrected so, as to keep the base pitches,  $p_{b,g}$  and  $p_{b,p}$ , equal to the operating base pitch,  $p_{b,op}$ . This is important, as it makes clear how many deviations in the tooth flank geometry in a gear, and that in a mating pinion, contribute to the total deviation in the base pitch. Moreover, it becomes clear which one of

<sup>1</sup> The instantaneous values of the deviations,  $\Delta p_{b,g}$  and  $\Delta p_{b,p}$ , commonly are not known. However, the calculations can be performed for the tolerances,  $[\Delta p_{b,g}]$  and  $[\Delta p_{b,p}]$ , for the accuracy of the corresponding deviations.

the components, either the gear or the pinion, needs more improvement to reduce the operating base pitch variation.

Here and below, it is assumed that the total deviation of the base pitches,  $\Delta p_{b,\Sigma}$ , is specified at every instant of time.<sup>2</sup> Moreover, for convenience of the analysis below, it is also assumed that the deviation,  $\Delta p_{b,\Sigma}$ , is always observed in that same slice, and the contact point,  $K$ , does not migrate within the face of the gear pair.

The simplified in such a way model of parallel-axes gear pair is used below for the purpose to demonstrate one of the root causes of vibration generation and noise excitation in approximate gear pairs.

The variation in the current value of the base pitch causes a corresponding transmission error,  $\Delta\varphi = \Delta\varphi(\varphi_p)$ .

When approximate gears of any and all designs are used, no gear noise problem can be solved by means of sources based on the theory of gearing in its current stage of development (gear noise and gear vibration are challenging problems that motivate the further development of the scientific theory of gearing). Noisy gears have to be *isolated* from the environment, but they will still produce noise.

## 28.2 TRANSMISSION ERROR

Gear noise is caused, to a great extent, by the dynamic phenomena in tooth meshing. It can be characterized by transmission error, which is the root cause for vibration generation and for noise excitation.

A brief discussion immediately below is helpful for better understanding of the nature of transmission error.

### 28.2.1 ON THE NATURE OF TRANSMISSION ERROR

For simplicity but without loss of generality, transmission error in a gear pair may be illustrated by means of a wheel that rolls over a surface, as illustrated in Figure 28.4 [173].

When a perfect wheel rolls over a perfect flat surface (see Figure 28.4a) with no slippage, the relative motion of the wheel may be viewed as a superposition of a rotation,  $\omega$ , and a translation,  $V$ . This case corresponds to meshing of two geometrically accurate gears. No sources for noise excitation are observed under such a scenario, as this is a trivial case of rolling a circle over a plane.

In another scenario, a perfect wheel rolls over a rough surface as diagrammatically shown in Figure 28.4b. The relative motion of the wheel may be viewed as a superposition of a rotation,  $\omega$ , and a translation,  $V$ , and a certain additional motion. This case corresponds to meshing of an approximate gear with a geometrically accurate pinion. As the gear is imperfect, an additional motion,  $V_{\text{noise}}$ , that causes the noise excitation, becomes inevitable. The transmission error is designated here as  $\Delta\varphi_g$ , because it is caused by the imperfect gear. It is evident that the gear (and NOT the pinion) needs to be improved in order to reduce/eliminate the transmission error and to reduce noise excitation in the gear pair.

In another scenario, a rough wheel rolls over a perfect plane surface as schematically shown in Figure 28.4c. The relative motion of the wheel may be viewed as a superposition of a rotation,  $\omega$ , and a translation,  $V$ , and a certain additional motion. This case corresponds to meshing of a geometrically accurate gear with an approximate pinion. As the pinion is imperfect, an additional motion,  $V_{\text{noise}}$ , that causes the noise excitation, becomes inevitable. The transmission error is designated here

<sup>2</sup> It is realized here that the actual values of the deviations,  $\delta p_{b,g}$  and  $\delta p_{b,p}$ , are never known. However, corresponding tolerances,  $[\delta p_{b,g}]$  and  $[\delta p_{b,p}]$ , can be set for the accuracy of each of the deviations. Often, it is more convenient solving problems using the tolerances for the accuracy of the deviations, rather than the actual values of the deviations.

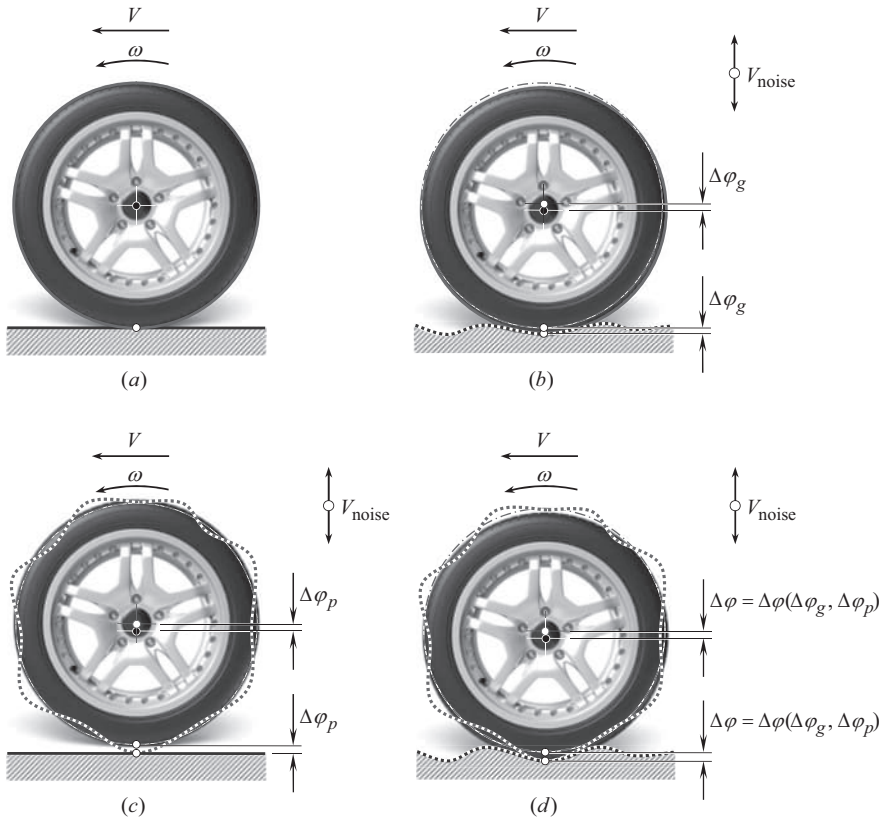


**FIGURE 28.4** Analogs of the contributions to the transmission error,  $\Delta\phi$ , in cases of meshing: (a) of perfect gear-to perfect pinion, (b) of perfect gear-to real pinion, (c) of real gear-to perfect pinion, and (d) of real gear-to real pinion.

as  $\Delta\phi_p$ , because it is caused by the imperfect pinion. It is evident that the pinion (and NOT the gear) needs to be improved in order to reduce/eliminate the transmission error and to reduce noise excitation in the gear pair.

Finally, a rough wheel rolls over a rough surface as schematically shown in Figure 28.4d. The relative motion of the wheel may be viewed as a superposition of a rotation,  $\omega$ , and a translation,  $V$ , and a certain additional motion. This case corresponds to the meshing of an approximate gear with an approximate pinion. As both, the gear and the pinion, are imperfect, an additional motion,  $V_{\text{noise}}$ , that causes the noise excitation, becomes inevitable. The transmission error is designated here as  $\Delta\phi$ , because it is caused by the imperfect gear and an imperfect pinion together. The transmission error,  $\Delta\phi$ , in this case, is a function of the components  $\Delta\phi_g$  and  $\Delta\phi_p$ , that is,  $\Delta\phi = \Delta\phi(\Delta\phi_g, \Delta\phi_p)$ . In order to reduce/eliminate the noise excitation when the gear pair operates, it is necessary to know how much each of the components,  $\Delta\phi_g$  and  $\Delta\phi_p$ , contributes to the transmission error,  $\Delta\phi$ . Unfortunately, the actual values of the components,  $\Delta\phi_g$  and  $\Delta\phi_p$ , commonly are not known. Therefore, the problem of reduction of gear noise in gear pairs of this kind turns to an indefinite one. Thus, the measured values of the transmission error cannot be used for the improvement neither of the gear nor of the pinion.

Fortunately, the actual values of the components,  $\Delta\phi_g$  and  $\Delta\phi_p$ , as well as of the transmission error,  $\Delta\phi$ , can be expressed in terms of variation of base pitches of both of a gear and a mating pinion.

Another approach can be utilized for the explanation of transmission error in gearing.



Consider a gear pair composed of a geometrically accurate gear that is engaged in mesh with an inaccurate gear. The driving gear is rotated uniformly. Regardless of which of the two gears is a driving one (either the geometrically accurate gear, or the inaccurate gear), the driven gear is rotated with certain fluctuation, that is, the driven gear is rotated unsteadily.

Assume, a rotation vector,  $\omega_g$ , of the inaccurate gear in the gear pair is specified for a case that this gear also is geometrically accurate. In reality (for the imperfect gear), the rotation vector of the gear is designated as,  $\omega_{g\Delta}$ . The transmission error in gearing can be expressed in terms of the rotation vector  $\Delta\omega_g = \omega_g - \omega_{g\Delta}$ .

### 28.2.2 DETERMINATION OF TRANSMISSION ERROR

Transmission error is the most important factor in the generation of gear noise. Transmission error is the error between the gear teeth. It can be defined in the following way: Imagine that the input gear is being driven at an absolutely uniform angular velocity. It is hoped that the output gear is rotating at a uniform angular velocity as well. Any variation from this uniform velocity gives a variation from the *correct position* of the output, and this is the *transmission error*, which will subsequently generate vibration and noise excitation. More formally:

#### Definition 28.1

Transmission error is the difference between the angular position that the output shaft of a drive would occupy if the drive were perfect and the actual position of the output.

In practical terms, the successive angular positions of the output, where the output should be, can be taken. These can be subtracted from the measured output positions to give the *error* in position. Measurements are made by measuring angular displacements, so the answers appear initially in units of seconds of arc [203].

By definition:

$$TE(t) = r_{b,g}\theta_g(t) - r_{b,p}\theta_p(t) \quad (28.5)$$

where  $r_{b,g}$  and  $r_{b,p}$  are the base pitch radii, and the angles,  $\theta_g(t)$  and  $\theta_p(t)$ , are the angles of rotation of the gear and the mating pinion, correspondingly.

When no transmission error occurs, and the input shaft rotates steadily [ $\omega_p(t) = \text{const}$ ], the output shaft also rotates steadily [ $\omega_g^{des}(t) = \text{const}$ ], as schematically illustrated in Figure 28.5a. Under the influence of transmission error, the output shaft does not rotate steadily [ $\omega_g(t) \neq \text{const}$ ]. The period of oscillation of the output shaft is designated as  $C_m$ .

Transmission error for an ideal gear train is almost a linear function of time. It can be represented in the form of a function  $\varphi_g = (N_g/N_p) \cdot \varphi_p$ . Here,  $N_g$  and  $N_p$  are the number of teeth of the gear and the pinion, and  $\varphi_g$  and  $\varphi_p$  are the rotation angles of the gear and the pinion. Due to the axis misalignment, the transmission function becomes piecewise almost linear with the period of the cycle of meshing,  $C_m$ , of a pair of teeth. Due to the jump of the angular velocity at the junction of cycles (see Figure 28.5a) [175], the acceleration approaches an infinitely large value. This causes vibration generation and noise excitation.

A desirable gear transmission function,  $\varphi_g^{des}(\varphi_p) = a \cdot \varphi_p$ , is a linear function of the angle of rotation of the input shaft,  $\varphi_p$ . Here is the factor  $a = \tan(u_t)$ . The actual gear transmission function,  $\varphi_g = \varphi_g(\varphi_p)$ , can be represented in the form of a piecewise function, as shown in Figure 28.5b.

A uniform rotation of the driving pinion, cannot be transmitted by the gear pair smoothly to the driven gear if the total deviation of the base pitch,  $\Delta p_{b,\Sigma}$ , is not of a zero value ( $\Delta p_{b,\Sigma} \neq 0$ ). The base pitch error,  $\Delta p_{b,\Sigma}$ , causes a transmission error,  $\Delta\varphi$ . The transmission error,  $\Delta\varphi$ , can be expressed in terms of the total deviation of the base pitch,  $\Delta p_{b,\Sigma}$ .

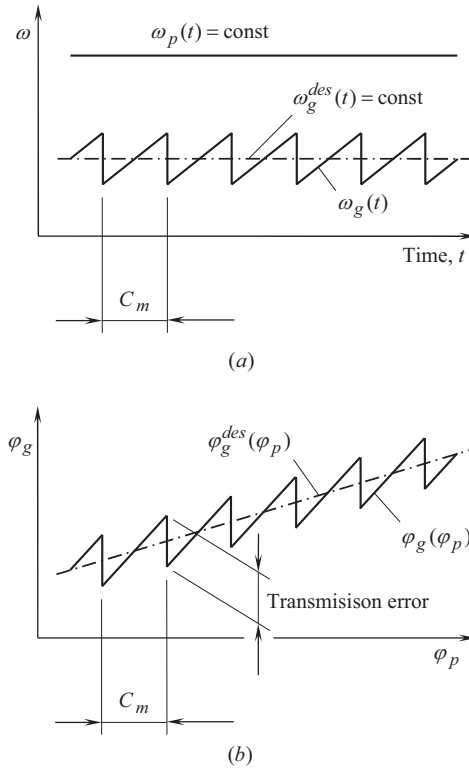


**FIGURE 28.5** Rotation of a driver,  $\omega_p(t)$ , and desirable,  $\omega_g^{des}(t)$ , and real,  $\omega_g(t)$ , rotations of the driven functions vs. time,  $t$  (a), and desirable,  $\varphi_g^{des}(\varphi_p)$ , and real,  $\varphi_g(\varphi_p)$ , transmission functions (b), (After Prof. S.P. Radzevich [175].)

Refer to Figure 28.6 to express an instantaneous value of the transmission error,  $\Delta\varphi$ , in terms of the total deviation of the base pitch,  $\Delta p_{b,\Sigma}$ .

In the case of geometrically accurate parallel-axes gear pair, contact point,  $K$ , occupies a certain position within the line of action,  $LA$ . For a specified value of the angle of rotation of the gear,  $\varphi_g$ , the distance,  $PK$ , traveled by the contact point together with the plane of action,  $PA$ , can be determined from the  $\Delta PKO_g$ :

$$PK = r_g \frac{\sin \varphi_g}{\cos(\varphi_g - \phi_t)} \quad (28.6)$$

where:

$r_g$  is the radius of the pitch circle of the gear.

$\phi_t$  is the transverse pressure angle in the gear pair.

To derive Eq. (28.6), the sine rule was applied to the  $\Delta PKO_g$ .

In reality, because the base pitch error is not equal to zero, the gears make contact not at point,  $K$ , but they contact one another at point,  $K^*$ , instead. The distance between the points,  $K$  and  $K^*$ , equals to the total deviation of the base pitch,  $\Delta p_{b,\Sigma}$ , that is, an equality  $KK^* = \Delta p_{b,\Sigma}$  is valid. The deviation,  $\Delta p_{b,\Sigma}$ , is calculated from Eq. (28.3).

An additional rotation through an angle,  $\Delta\varphi$ , is caused by the deviation of  $\Delta p_{b,\Sigma}$ . By nature, this additional rotation is equal to the instantaneous value of the transmission error.

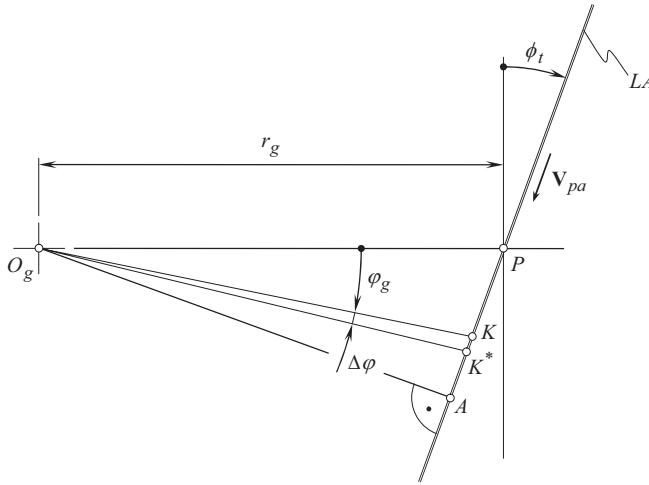


**FIGURE 28.6** A schematic for the calculation of the instantaneous value of the transmission error,  $\Delta\phi$ , in parallel-axes gear pair.

In order to determine the angle,  $\Delta\phi$ , it is necessary to determine the distance,  $K^*O_g$ . This distance can be determined from the  $\Delta PK^*O_g$ :

$$K^*O_g = r_g \sqrt{1 + \frac{\sin^2 \phi_g}{\cos^2(\phi_g - \phi_t)} - 2 \frac{\sin \phi_g}{\cos(\phi_g - \phi_t)} \sin \phi_t} \quad (28.7)$$

To derive the Eq. (28.7), the cosine rule was applied to the  $\Delta PK^*O_g$ .

Then, the rule of sine is applied to the  $\Delta PK^*O_g$ :

$$\sin(\phi_g + \Delta\phi) = \frac{r_g \sin \phi_g + \Delta p_{b,\Sigma} \cos(\phi_g - \phi_t)}{K^*O_g \cos(\phi_g - \phi_t)} \cos \phi_t \quad (28.8)$$

Ultimately, the angle,  $\Delta\phi$ , equals to:

$$\Delta\phi = \sin^{-1}(a) - \phi_g \quad (28.9)$$

For the determination of the distance,  $KO_g$ , another approach can be used. It can be written from the  $\Delta APO_g$  that:

$$O_g A = r_g \cos \phi_t \quad (28.10)$$

$$AP = r_g \sin \phi_t \quad (28.11)$$

and then from the  $\Delta AKO_g$  :

$$AK = r_g \left( \sin \phi_t - \frac{\sin \phi_g}{\sin(\phi_g - \phi_t)} \right) \quad (28.12)$$

Equations (28.10)–(28.12) yield an expression for the calculation of the distance,  $KO_g$ :

$$KO_g = r_g \sqrt{\frac{[\cos(\varphi_g - \phi_t) - 2 \sin \phi_t \sin \varphi_g] \cos(\varphi_g - \phi_t)}{\cos(\varphi_g - \phi_t)}} \quad (28.13)$$

The determined distance,  $KO_g$  [see Eq. (28.13)], is used for the derivation of Eq. (28.9).

The approach, applied for the derivation of Eq. (28.9), can also be used for the calculation of the components,  $\Delta\varphi_g$  and  $\Delta\varphi_p$ , of the transmission error,  $\Delta\varphi$ . The components,  $\Delta\varphi_g$  and  $\Delta\varphi_p$ , are contributed by the gear and the pinion, correspondingly.

Another approach can be used for the derivation of Eq. (28.9). The transmission error,  $\Delta\varphi$ , can be expressed in terms of the total deviation of the base pitch,  $\Delta p_{b,\Sigma}$ , and of base diameters of a gear and a mating pinion in a gear pair.

As the driving pinion rotates uniformly, and the distance,  $KK^*$ , is specified, then this distance is equivalent to an additional rotation of the driving pinion through an angle,  $\Delta\varphi_p$ :

$$\Delta\varphi_p = \frac{KK^*}{r_{b,p}} \quad (28.14)$$

Taking into account that  $\Delta\varphi_g = \Delta\varphi_p/u$  (here  $u$  is the gear ratio of the gear pair), Eq. (28.14) immediately returns an expression for the angular deviation,  $\Delta\varphi$ :

$$\Delta\varphi = \Delta\varphi_p = \frac{\Delta p_{b,\Sigma}}{u \cdot r_{b,p}} \quad (28.15)$$

In this case, there is no need to determine the deviation,  $\Delta\varphi$ , using the rule of sine for this purpose.

The rotation of the gear through an angle,  $\Delta\varphi$ , causes an additional rotation of the gear. This additional rotation can be represented by the rotation vector,  $\omega_{bpv}(\varphi_g)$ . The rotation vector,  $\omega_{bpv}(\varphi_g)$ , is referred to as the *base pitch variation rotation*,  $\omega_{bpv}(\varphi_g)$ .

The resultant rotation vector of the gear:

$$\omega_{\Sigma}(\varphi_g) = \omega_g + \omega_{bpv}(\varphi_g) \quad (28.16)$$

The transmission error is an integral parameter of the accuracy of the gear pair. When only transmission error is specified, it is not clear what has to be done with the gears in order to keep the base pitches equal, that is, whether a gear or a mating pinion has to be corrected, and to what extent.

It seems ridiculous that 1 mm module (25DP) gear less than an inch in diameter will have roughly the same transmission error as a 25 mm module (1DP) gear of 3 m diameter of the same quality, but this is surprisingly close to what happens in practice. This unexpected constant size of errors is liable to cause problems in the future with the current trend toward *micromechanics*. If a gear tooth is only 20  $\mu\text{m}$  tall, the base pitch is about 20  $\mu\text{m}$ , but errors of 2  $\mu\text{m}$  in pitch, or profile are still likely with corresponding transmission errors so that a speed variation of 10% becomes possible.

### 28.2.3 BASE PITCH VARIATION OF ROTATION VECTOR

When a geometrically accurate gear is rotated in mesh with an inaccurate gear, the rotation vector,  $\omega_{bpv}(\varphi_g)$ , is considered. The rotation vector,  $\omega_{bpv}(\varphi_g)$ , is referred to as the *base pitch variation of*

rotation,  $\omega_{bpv}(\varphi_g)$ . This rotation vector influences both, the magnitude, and the configuration of the vector of instant rotation,  $\omega_{pl}$ . Ultimately, the operating base pitch,  $\varphi_{b.op}$ , varies, that is, the equality  $\varphi_{b.op} = \varphi_{b.op}(t)$  is valid. Consequently, the geometrically accurate gear in mesh becomes also inaccurate, as the gear base pitch,  $\varphi_{b.g}$  (a constant value), cannot be equal to a variable value  $\varphi_{b.op} = \varphi_{b.op}(t)$ : namely, an inequality  $\varphi_{b.op} \neq \varphi_{b.op}(t)$  is observed. In such a mesh, the geometrically accurate gear is no longer a perfect one.

The variation in the configuration of the vector of instantaneous rotation,  $\omega_{pl}$ , can be illustrated by a corresponding vector diagram. In the vector diagram, the vector,  $\omega_{\Sigma}(\varphi_g)$ , of total rotation of a gear equals to:

$$\omega_{\Sigma}(\varphi_g) = \omega_g + \omega_{bpv}(\varphi_g) \quad (28.17)$$

### 28.3 VARIATION OF AXIAL AND RADIAL FORCES

Unfortunately, transmission error is not the only cause for vibration generation and noise excitation in gear transmission systems. A variation of the instantaneous (equivalent) force, namely, of its magnitude, coordinates of a point where the force is applied (especially in gears that feature a low tooth count), and the orientation, are the root causes for the vibration generation and the noise excitation. The variation of the loading is transmitted to the housing that works like panels, and so forth.

Helical gears, for example, are subjected to variation of the force between the gears. They are sensitive to the force variation in particular.

Consider a gear pair that has a nominal contact ratio of  $m_t$ . At a particular instant of time, the lengths of the theoretical lines of contact get the two extreme positions schematically depicted in Figure 28.7.

These show the plane of action for the worst case with a correct face width of an axial pitch and a small helix angle. In the case under consideration, any end relief effects or tip relief effects are ignored. A constant loading along the contact line is assumed. Practical teeth tend to give slightly larger effects.

The extreme position of the center of action of the resultant force is determined by taking moments about one end and is approximately  $[(m_t - 1)^2 + 1] / 2m_t$  from one end. This has a minimum when the total contact ratio,  $m_t$ , is equal to  $\sqrt{2}$  and the center of force oscillates about 0.086 of the face widths on either side of the center of the face.

There is a corresponding radial force variation at the bearing housings of the order of 8% of the mean value when the gears are well supported by close shafts or less if the supporting shafts are long [203].

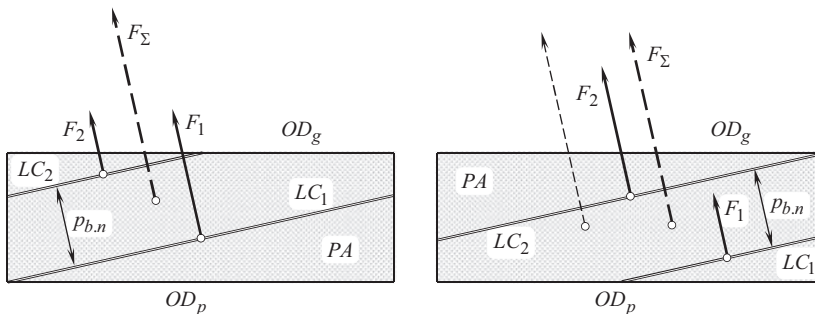


**FIGURE 28.7** Extreme positions of the lines of contact,  $LC$ , in the plane of action,  $PA$ , showing how the forces at the centers of each section of the line of contact give a resultant force whose position varies.

## 28.4 ALTERNATIVE CAUSES OF NOISE EXCITATION IN GEAR PAIR

Transmission error is not the only cause for vibration generation and noise excitation. Contact ratio and variation of point at which the resultant load is applied (especially in gears with a low tooth count) are the alternative causes for vibration generation and noise excitation. The said result in variation of load that is transmitted from the gear mesh to the housing. In the case under consideration elements of the housing work like panels generating noise.

### 28.4.1 INFLUENCE OF CONTACT RATIO

The influence of contact ratio onto the gear transmission function,  $\varphi_g = \varphi_g(\varphi_p)$ , is more, or less clear as long, as the consideration relates to an elementary gear drive (that is, to a gear-to-pinion mesh) with a contact ratio exactly equal to  $u_t = 1$ . However, in reality, the contact ratio always is greater than one ( $u_t > 1$ ). Because of this, during certain periods of meshing, not one but more pairs of teeth are engaged in mesh simultaneously. In general, the piecewise linear functions of transmission errors for distinct pairs of contacting teeth do not coincide with each other. The cycle of meshing,  $c_m^{(i)}$ , for the  $i$ -th pair of teeth is shifted in relation to the previous/consequent cycle of meshing,  $c_m^{(i\pm 1)}$ , in the direction of  $\varphi_g$ -axis at a certain distance,  $\Delta C_m$ . The actual value of the shift,  $\Delta C_m$ , depends on the actual value of contact ratio,  $u_t$ . The transmission functions,  $Tr_f^{(i)}$  and  $Tr_f^{(i\pm 1)}$ , make it possible to compose the resultant transmission function,  $Tr_f^{(\Sigma)}$ , for the elementary gear drive that has a total contact ratio  $u_t > 1$ . In the same way, the resultant transmission function,  $Tr_f^{(\Sigma)}$ , can be composed for any actual value of contact ratio that exceeds  $u_t > 2$  [175].

Figure 28.8 shows that for the case when the contact ratio is greater than one,  $u_t > 1$ , the resultant transmission function,  $Tr_f^{(\Sigma)}$ , significantly differs from that for the case when the equality,  $u_t = 1$ , is valid. The situation gets more severe when there are no common multipliers in the gear and the pinion tooth number,  $N_g$  and  $N_p$  [175].

The impact of transmission error onto noise excitation is commonly considered from the geometrical and kinematic points of view. No tooth flank wear is incorporated into the analysis.

The most reliable way to reduce noise excitation is to ensure equality of the operating base pitch of a gear to the operating base pitch of a mating pinion, and both of them keep equal to operating base pitch of the gear pair. Once the base pitches are equal to one another, the gear mesh generates no (or almost no) vibration and produces no noise excitation.

### 28.4.2 INFLUENCE OF LOCATION OF THE POINT AT WHICH THE RESULTANT LOAD IS APPLIED

There is no variation neither of the equivalent (resultant) tangential force, nor of the equivalent (resultant) axial force in a gear pair. Only variation of coordinates of point (at which the resultant force is applied) is observed. This variation is an additional root cause of noise excitation in gearing.

Migration of point at which the resultant load is applied can cause an excessive noise excitation even in geometrically accurate gearing.

When a gear rotates,  $\omega_g$ , the plane of action,  $PA$ , travels straight,  $\mathbf{V}_{pa}$  (see Figure 28.9) [170]. The arm,  $\mathbf{R}_{cg}$ , of the resultant (or the equivalent) force,  $\mathbf{F}_t$ , with respect to the bearing support is remained the same and equals:

$$|\mathbf{R}_{cg}| = \sqrt{r_{b,g}^2 + a^2} \quad (28.18)$$

where:

$r_{b,g}$  is the base radius of the gear.

$a$  is the distance of the gear from the bearing support (see Figure 28.9).

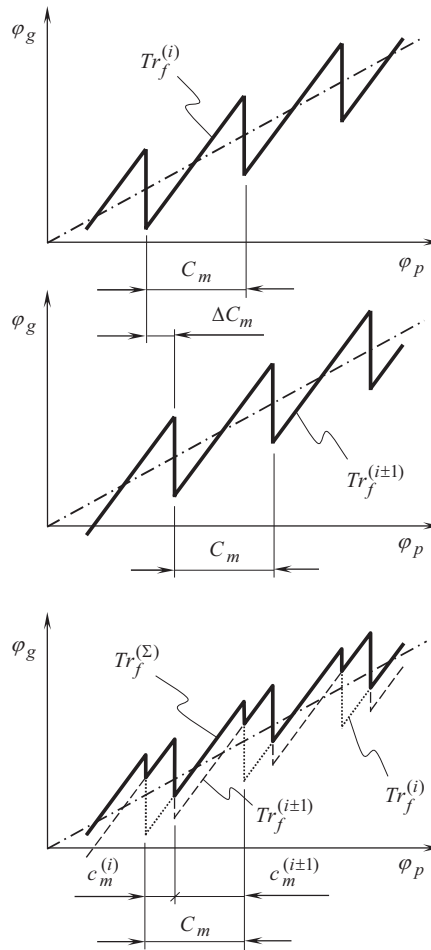


**FIGURE 28.8** Transmission function as a superposition of a linear function,  $\varphi_g^{des}(\varphi_p)$ , and piecewise linear functions for the case when total contact ratio  $m_t > 1$ . (Adopted from: Radzevich S.P., 2006. *International Journal of Vehicle Noise and Vibration* 2(4):283–91. [175]).

Point,  $c_g$ , does not migrate in the axial direction of the gear. Therefore, the force,  $\mathbf{F}_t$ , creates a bending moment of a constant value with respect to the bearing support. Thus, no variation of the deflection of the shafts, of the gear housing, and so forth, is observed in the case under consideration. Spur gears create no additional source for noise excitation.

A more general case of contact between tooth flanks,  $\mathcal{S}$  and  $\mathcal{P}$ , of a gear and a mating pinion is observed in geometrically accurate *helical*  $P_a$  – axes gearing.

When the gears rotate, commonly either two, or three lines of contact,  $LC_i$ , are observed in geometrically accurate helical  $P_a$  – axes gearing. It is convenient to distinguish in two different cases helical gearing, namely:

- when all the lines of contact,  $LC_i$ , are of a full length, and
- when one or more line(s) of contact is of a reduced length.

An equivalent load is applied at point  $c_g$ . When the gears rotate, point  $c_g$  migrates within the plane of action,  $PA$ . The migration of point  $c_g$  with a linear velocity,  $\mathbf{V}_{c_g}$ , in the axial direction of the gear pair results in a corresponding alteration of the arm,  $\mathbf{R}_{c_g}$ , of the resultant force,  $\mathbf{F}_t$ , in relation to



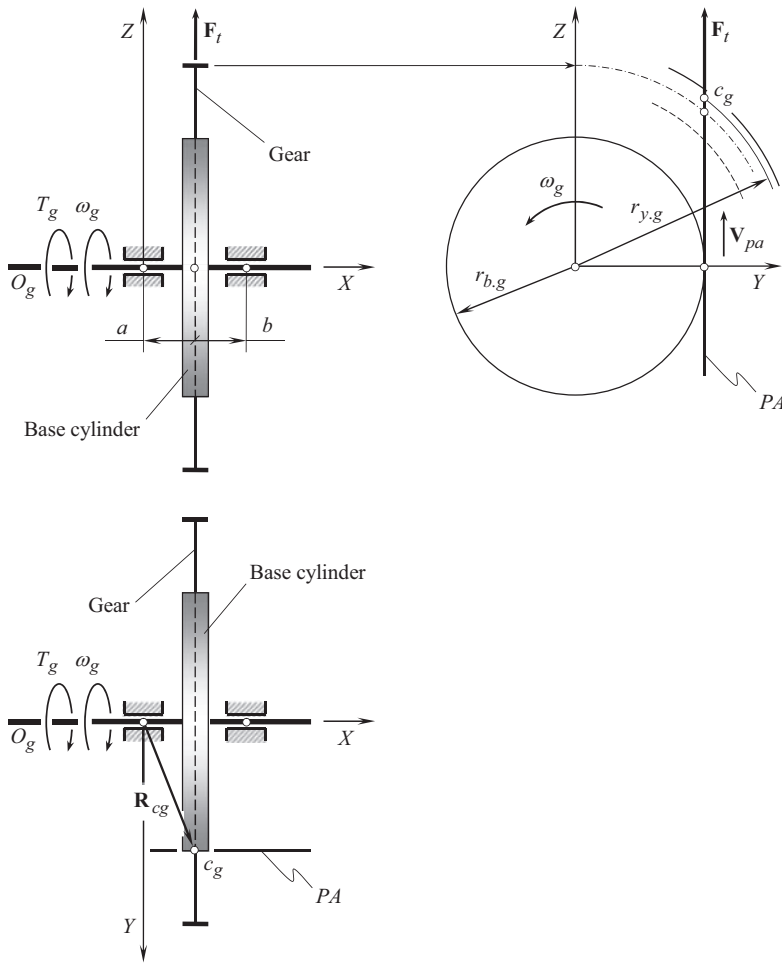


FIGURE 28.9 Bending torque in geometrically accurate spur parallel-axes gearing.

the bearing support of the gear shaft as schematically illustrated in Figure 28.10. When point  $c_g$  migrates between points  $c_g^*$  and  $c_g^{**}$ , the arm  $|\mathbf{R}_{cg}|$  of the resultant force,  $\mathbf{F}_t$ , changes in the range of:

$$|\mathbf{R}_{cg}^*| \leq |\mathbf{R}_{cg}| \leq |\mathbf{R}_{cg}^{**}| \quad (28.19)$$

A variation of magnitude,  $|\Delta \mathbf{R}_{cg}|$ , of the arm,  $\mathbf{R}_{cg}$ , results in a variable in time torque that bends the gear shaft, and deforms the gear housing, and can cause an extensive unfavorable vibration of the gear housing, and an extensive noise excitation.

When point  $c_g$  migrates between points  $c_g^*$  and  $c_g^{**}$ , the arm  $|\mathbf{R}_{cg}|$  of the resultant force,  $\mathbf{F}_t$ , alters in the range of  $|\mathbf{R}_{cg}^*| \leq |\mathbf{R}_{cg}| \leq |\mathbf{R}_{cg}^{**}|$  (see Figure 28.10).

A variation of magnitude,  $|\Delta \mathbf{R}_{cg}|$ , of the arm,  $\mathbf{R}_{cg}$ , results in a variable in time torque that bends the gear shaft, and deforms the gear housing, and can cause an extensive unfavorable vibration of the gear housing, and an extensive noise excitation.

The disclosed approach for the determining of loads acting in every pair of teeth in geometrically accurate spur and helical parallel-axes gearing can be enhanced to gear pairs with lines of contact of arbitrary geometry, that is, to gear pairs with lines of contact in the form of arcs of a circle, of a spiral curve, and so forth. Generally speaking, for this purpose the plane-of-action face width,  $F_{pa}$ , is

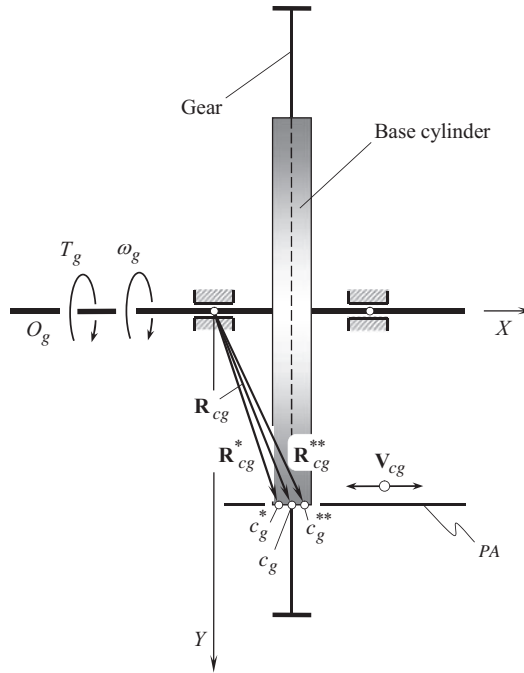


**FIGURE 28.10** Variation of bending torque in helical parallel-axes gearing.

subdivided into several segments within each of them either zero, or one, or two, and so forth, lines of contact occur. In a case of line of contact in a form of a planar curve, the corresponding portion of plane-of-action face width,  $F_{pa}$ , is sliced onto an infinite number of infinitesimally narrow slices. Portion of a line(s) of contact within each infinitesimally narrow slice is considered a straight-line segment. In such a manner loads in geometrically accurate parallel-axes gear pairs with the lines of contact of an arbitrary geometry can be determined.

Variation of the gear loading along with a variation of point at which the resultant load is applied is the root cause for an excessive noise excitation in geometrically accurate parallel-axes gearing. This results in a corresponding variation of the deformation of the gear shafts, of the gear housing, and so forth. Ultimately, geometrically accurate parallel-axes gearing produces noise. Noise of this kind is also referred to as the *gear noise*; however, noise of this kind is produced not by the gear mesh, but by other components of the gear mechanism instead: by the shafts, by bearings, as well as by the gear housing, and so forth (all of this stuff vibrates due to variation of the resultant force in gear mesh). This source of noise has to be considered as a *gear noise*, as control over the level of the noise can be achieved by proper selection of design parameters of the gears: profile angle, contact (total) ratio, helix angle, and so forth.

## 28.5 ON A POSSIBILITY OF PREDICTION OF GEAR NOISE EXCITATION

The problem of analytical prediction of noise excitation in a gear pair falls into three levels/iterations (parallel-axes gearing is considered below solely as an example for all three iterations):

- **The first level of iteration** – The geometry and configuration of a desirable line of contact,  $LC_{des}$ , is specified within the plane of action,  $PA$ . When the gears rotate, the transverse pressure angle,  $\phi_t$ , in the gear pair is retained of a constant value. Because of variation of the tooth flank geometry of a gear,  $\mathcal{G}$ , and that of a mating pinion,  $\mathcal{P}$ , the lines of intersection,

$LC_g$  and  $LC_p$ , of the tooth flanks,  $\mathcal{G}$  and  $\mathcal{P}$ , by the plane of action,  $PA$ , differ from the desirable line of contact,  $LC_{des}$ . The lines,  $LC_g$  and  $LC_{des}$ , and the lines  $LC_p$  and  $LC_{des}$ , make contact at points,  $K_g$  and  $K_p$ , correspondingly. As considered in this section of the book, a gap exists between the lines of intersection,  $LC_g$  and  $LC_p$ . The gap equals to the closest distance of approach between the lines of intersection,  $LC_g$  and  $LC_p$ , and, by nature, it is equal to the variation of the base pitch in a gear,  $\Delta p_{b,g}$ , and in the mating pinion,  $\Delta p_{b,p}$ , that is, the gap equals to the algebraic summa ( $\Delta p_{b,g} + \Delta p_{b,p}$ ).

Physically, the gap does not exist as the gears transmit a load. Zero gap is observed between the gear,  $\mathcal{G}$ , and the mating pinion,  $\mathcal{P}$ , tooth flanks when the gears transmit power.

As the input shaft rotates uniformly (with a constant angular velocity,  $\omega_p$ ), the driven shaft must make an additional turn through an angle,  $\Delta \phi_g$ , to bridge the gap. The angle,  $\Delta \phi_g$ , can be expressed in terms of the distance,  $\Delta p_{b,g} + \Delta p_{b,p}$ , and in terms of the parameters of configuration of the lines of intersection,  $LC_g$  and  $LC_p$ , by the plane of action,  $PA$ .

The variation,  $\Delta p_{b,g} + \Delta p_{b,p}$ , of the base pitch is the root cause for an excessive noise excitation in a gear pair. An analysis like that above can be performed for intersected-axes gear pairs as well as for crossed-axes gear pairs.

**Conclusion 28.1.** *The deviations, those measured within the plane of action,  $PA$ , contribute the most to the variation of the base pitch as well as to the transmission error.*

- **The second level of iteration** – It is assumed in the first level of iteration that the condition of conjugacy of the transverse sections of a gear and a mating pinion is fulfilled for all points within the line of intersection,  $LC_g$ , and for all the corresponding points within the line of intersection,  $LC_p$ . For more accurate calculations, points at which the conjugate action law is fulfilled for the gear and for the mating pinion transverse tooth profiles should be considered within spatial curves, both, for the gear, and for the pinion.

As the input shaft rotates uniformly (with a constant angular velocity,  $\omega_p$ ), the driven shaft must make an additional turn through an angle,  $\Delta \phi_g$ , to bridge the gap. The angle,  $\Delta \phi_g$ , can be expressed in terms of the distance,  $(\Delta p_{b,g} + \Delta p_{b,p})$ , and in terms of the parameters of configuration of the lines of intersection,  $LC_g$  and  $LC_p$ , by the plane of action,  $PA$ .

The variation,  $(\Delta p_{b,g} + \Delta p_{b,p})$ , of the base pitch is the root cause for an excessive noise excitation in a gear pair. An analysis like that above can be performed for intersected-axes gear pairs as well as for crossed-axes gear pairs.

**Conclusion 28.2.** *The deviations, measured perpendicular to the plane of action,  $PA$ , contribute less to the variation of the base pitch as well as to the transmission error (projections onto the plane of action,  $PA$ ).*

- **The third level of iteration** – Finally, as the desirable line of contact,  $LC_{des}$ , travels together with the plane of action,  $PA$ , the actual value of the transverse pressure angle,  $\phi_t$ , could vary depending on the actual angular configuration of the gear and the pinion in relation to one another.

As the input shaft rotates uniformly (with a constant angular velocity,  $\omega_p$ ), the driven shaft must make an additional turn through an angle,  $\Delta \phi_g$ , to bridge the gap. The angle,  $\Delta \phi_g$ , can be expressed in terms of the distance,  $\Delta p_{b,g} + \Delta p_{b,p}$ , and in terms of the parameters of configuration of the lines of intersection,  $LC_g$  and  $LC_p$ , by the plane of action,  $PA$ .

The variation,  $\Delta p_{b,g} + \Delta p_{b,p}$ , of the base pitch is the root cause for an excessive noise excitation in a gear pair. An analysis like that above can be performed for intersected-axes gear pairs as well as for crossed-axes gear pairs.

**Conclusion 28.3.** *The deviations, measured perpendicular to the plane of action,  $PA$ , contribute less to the variation of the base pitch as well as to the transmission error (projections onto the plane of action,  $PA$ ).*

Once the importance of equality of the base pitches onto the vibration generation and noise excitation is realized, then other sources of gear noise can be taken into account.

---

# 29 Design Peculiarities of Geometrically Accurate and Almost Geometrically Accurate Gears

This chapter deals with geometrically accurate and almost geometrically accurate gear pairs. Manufacture of gears for geometrically accurate and almost geometrically accurate gear pairs is almost the same as that for conventional gear pairs. Finishing a gear and a mating pinion tooth flanks is the only principal feature in the production of gears for geometrically accurate, and almost geometrically accurate gearing, from that for conventional gearing. Below in this chapter, a few examples of finishing gears for crossed-axes geometrically accurate and almost geometrically accurate gearings are discussed.

## 29.1 DESIGN PECULIARITIES OF GEARS FOR $R$ – GEARING

In order to develop a crossed-axes gearing with the desirable properties, the kinematics of  $C_a$  – gearing has to be thoroughly investigated. It is shown that tooth flanks of the gear and of the mating pinion can be generated as a locus of the desirable lines of their contact considered in corresponding reference systems associated with the gear, and with the pinion, correspondingly. Crossed-axes gearing of the proposed design<sup>1</sup> is referred to as  $R$  – gearing.  $R$  – gearing is the only kind of crossed-axes gearing with line contact between the tooth flanks of a gear and of a mating pinion. Parallel-axes involute gearing (*L. Euler*, 1760) and intersected-axes gearing with spherical involute tooth flank geometry (*G. Grant*, 1889) represent the reduced cases of  $R$  – gearing. The shaft angle is either zero or equal  $\Sigma = 180^\circ$  in the first case. In the second case, the center-distance is zero. The capability to transmit an input rotation smoothly along with a high-power-density are the two principal advantages of  $R$  – gearing over gearing of other gear systems.

### 29.1.1 ESSENCE OF KINEMATICS IN CROSSED-AXES GEARING

The kinematics and the geometry of geometrically accurate crossed-axes gearing (or just  $C_a$  – gearing, for simplicity) with line contact between the tooth flanks of the gear,  $\mathcal{G}$ , and of the mating pinion,  $\mathcal{P}$ , are discussed immediately below.

Transmission and transformation of a rotation from a driving shaft to a driven shaft is the main purpose of the implementation of crossed-axes gears. Both the input rotation and the output rotation can be easily represented by corresponding rotation vectors,<sup>2</sup>  $\boldsymbol{\omega}_g$  and  $\boldsymbol{\omega}_p$ , as shown in Figure 29.1. The rotation vectors,  $\boldsymbol{\omega}_g$  and  $\boldsymbol{\omega}_p$ , are pointed along the gear, and the pinion centerlines,  $O_g$  and  $O_p$ , correspondingly.

---

<sup>1</sup> Patent pending.

<sup>2</sup> It is instructive to note here that, by nature, rotations are not vectors. Therefore, a special care is needed to be undertaken when treating rotations as vectors.



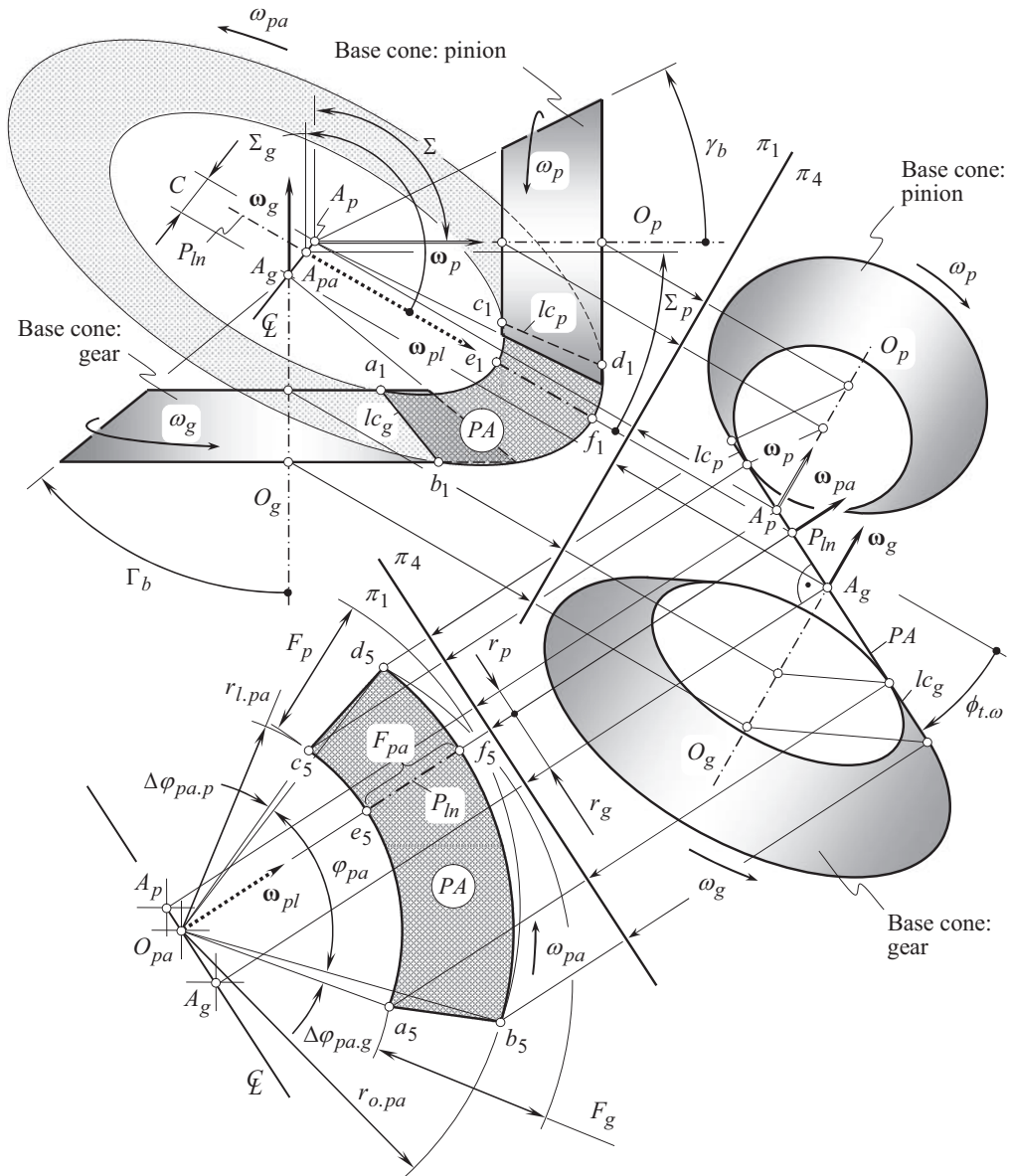


FIGURE 29.2 Base cones and the plane of action,  $PA$ , in an orthogonal crossed-axes gear pair.

The plane of action,  $PA$ , is in tangency with the base cones of the gear, and that of the pinion. Due to that, the plane of action,  $PA$ , forms a transverse pressure angle,  $\phi_{t,\omega}$ , with the  $P_{ln}$  – plane. The pressure angle,  $\phi_{t,\omega}$ , is measured within the  $C_{ln}$  – plane.

The plane of action can be viewed as a flexible zero thickness film. The film is free to wrap onto, and unwrap from the base cones of the gear, and of the pinion, correspondingly. The plane of action,  $PA$ , is not allowed to be bent about an axis perpendicular to the plane,  $PA$ .

As the axis of instantaneous rotation,  $P_{ln}$ , and the axes of rotations of the gear,  $O_g$ , and the pinion,  $O_p$ , cross one another. Pure rolling of base cones of the gear and that of the pinion over the pitch plane,  $PA$ , is not observed. Instead, rolling together with sliding of plane of action over the base cones occurs.



### 29.1.3 TOOTH FLANKS IN GEOMETRICALLY ACCURATE CROSSED-AXES GEARS

Conjugate tooth flanks<sup>3</sup> of a gear and of a mating pinion in a crossed-axes gear pair are in line contact with one another. As the gears rotate, the line of contact travels in relation to several reference systems. These reference systems are associated:

- a. with the gear
- b. with the pinion, and
- c. with the housing.

Tooth flank of the gear,  $\mathcal{G}$ , can be construed as a locus of consecutive positions of the desirable line of contact,  $LC_{des}$ , in its motion in relation to the reference system,  $X_gY_gZ_g$ , associated with the gear. Similarly, tooth flank of the pinion,  $\mathcal{P}$ , can be represented as a locus of consecutive positions of that same line of contact,  $LC_{des}$ , in its motion in relation to the reference system,  $X_pY_pZ_p$ , associated with the pinion. Ultimately, a locus of consecutive positions of that same line of contact,  $LC_{des}$ , in its motion in relation to a stationary reference system associated with the gear housing,  $X_hY_hZ_h$ , represents the plane of action (or, more generally, the *surface of action*). Therefore, once the line of contact is specified, the kinematics of crossed-axes gearing (see Figure 29.2) can be employed for the derivation of an analytical representation of the tooth flanks of the gear,  $\mathcal{G}$ , and its mating pinion,  $\mathcal{P}$ . For this purpose, several auxiliary reference systems are commonly used. A *Cartesian* coordinate system,  $X_rY_rZ_r$ , associated with the plane of action (see Figure 29.3), is one of the auxiliary reference systems.

In a local *Cartesian* reference system,  $x_{lc}y_{lc}z_{lc}$ , associated with the plane of action,  $PA$ , and centered at the center,  $O_{lc}$ , of the circular arc of a radius  $R_{lc}$ , the position vector,  $\mathbf{r}_{des}^{(lc)}$ , of point of the desirable line of contact,  $LC_{des}$ , is analytically described by an expression in the form (see Figure 29.4):

$$\mathbf{r}_{des}^{(lc)}(\varphi_{lc}) = \begin{bmatrix} R_{lc} \cos \varphi_{lc} \\ R_{lc} \sin \varphi_{lc} \\ 0 \\ 1 \end{bmatrix} \quad (29.4)$$

where  $\varphi_{lc}$  is the angular parameter of the desirable line of contact,  $LC_{des}$ .

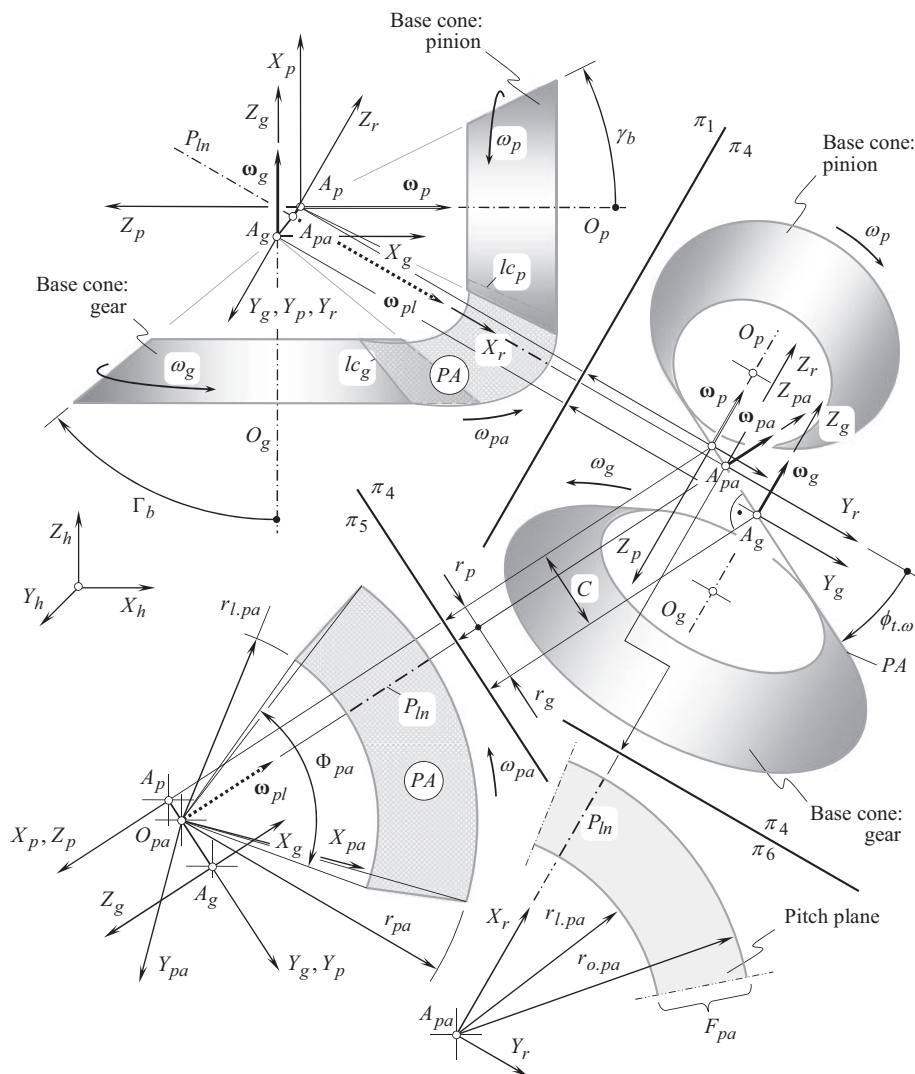
In the reference system  $X_{pa}Y_{pa}Z_{pa}$ , the position vector,  $\mathbf{r}_{des}^{(pa)}$ , of point of the desirable line of contact,  $LC_{des}$ , is analytically described by an equation:

$$\mathbf{r}_{des}^{(pa)}(\varphi_{lc}) = \underbrace{\mathbf{Tr}[(r_{w.pa} - R_{lc} \sin \psi_{lc}), X] \cdot \mathbf{Tr}(R_{lc} \cos \psi_{lc}, Y)}_{\mathbf{Rs}(lc \mapsto pa)} \cdot \mathbf{r}_{des}^{(lc)}(\varphi_{lc}) \quad (29.5)$$

where  $\mathbf{Tr}[(r_{w.pa} - R_{lc} \sin \psi_{lc}), X]$  and  $\mathbf{Tr}(R_{lc} \cos \psi_{lc}, Y)$  are the elementary operators of the translations along the coordinate axes  $X$  and  $Y$ , correspondingly. Well-known formulae (see Appendix D) are used for the calculation of these operators. The interested reader may wish to exercise on his/her own composing the operators of translation, as well as the operators of rotation,  $\mathbf{Rt}(\varphi \mapsto X)$ , used below.  $\mathbf{Rs}(lc \mapsto pa)$  is the operator of the resultant coordinate system transformation, namely, the operator of transition from  $x_{lc}y_{lc}z_{lc}$  to  $X_{pa}Y_{pa}Z_{pa}$ .

Ultimately, it can be shown that in the reference system,  $X_{pa}Y_{pa}Z_{pa}$ , associated with the plane of action, an expression for the position vector,  $\mathbf{r}_{des}^{(pa)}$ , of point can be written in matrix form:

<sup>3</sup> *Reversibly-enveloping surfaces* (or just  $R_e$ –surfaces, for simplicity) is the other term for conjugate tooth flanks [The term *reversibly-enveloping surfaces* was proposed by Prof. S.P. Radzevich (2013)].


$$\mathbf{r}_{des}^{(pa)}(\varphi_{lc}) = \mathbf{R}\mathbf{s}(lc \mapsto pa) \cdot \mathbf{r}_{des}^{(lc)}(\varphi_{lc}) = \begin{bmatrix} R_{lc} \cos \varphi_{lc} + r_{w,pa} + R_{lc} \sin \psi_{lc} \\ R_{lc} \sin \varphi_{lc} - R_{lc} \cos \psi_{lc} \\ 0 \\ 1 \end{bmatrix} \quad (29.6)$$

When the gears rotate, the desirable line of contact,  $LC_{des}$ , travels with respect to a reference system  $X_gY_gZ_g$  associated with the gear. Simultaneously,  $LC_{des}$  travels with respect to a reference system,  $X_pY_pZ_p$ , associated with the pinion. Therefore, the gear tooth flank,  $\mathcal{F}$ , can be viewed as a locus of consecutive positions of the line of contact,  $LC_{des}$ , considered in the reference system  $X_gY_gZ_g$ . Similarly, the pinion tooth flank,  $\mathcal{P}$ , can be viewed as a locus of consecutive positions of the line of contact,  $LC_{des}$ , considered in the reference system  $X_pY_pZ_p$ . To derive equations for the position vectors of point of the gear tooth flank,  $\mathbf{r}_g$ , and the pinion tooth flank,  $\mathbf{r}_p$ , the operators,  $\mathbf{Rs}(pa \mapsto g)$

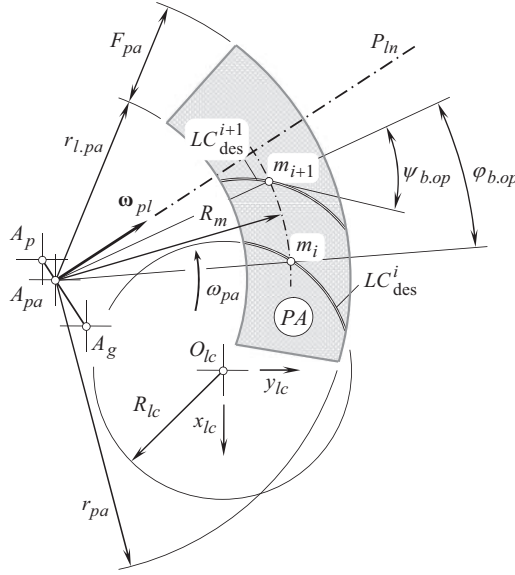


**FIGURE 29.4** Configuration of the desirable line of contact,  $LC_{des}$ , in the form of an arc of a circle within the plane of action,  $PA$ , in a crossed-axes gear pair.

and  $\mathbf{Rs}(pa \mapsto p)$ , of transition from the reference system  $X_{pa}Y_{pa}Z_{pa}$  to the reference systems  $X_gY_gZ_g$  and  $X_pY_pZ_p$  are used:

$$\mathbf{r}_g(\varphi_{lc}, \varphi_g) = \mathbf{Rs}(pa \mapsto g) \cdot \mathbf{r}_{des}^{(lc)}(\varphi_{lc}) \quad (29.7)$$

$$\mathbf{r}_p(\varphi_{lc}, \varphi_p) = \mathbf{Rs}(pa \mapsto p) \cdot \mathbf{r}_{des}^{(lc)}(\varphi_{lc}) \quad (29.8)$$

The operator of the resultant coordinate system transformation  $\mathbf{Rs}(pa \mapsto g)$  is a function of the angle of rotation,  $\varphi_g$ , of the gear, and of the angular parameter  $\varphi_{lc}$ . The angles  $\varphi_g$  and  $\varphi_{lc}$  are the *Gaussian coordinates* of point of the gear tooth flank,  $\mathcal{S}$ . The operator of the resultant coordinate system transformation  $\mathbf{Rs}(pa \mapsto p)$  is a function of the angle of rotation of the pinion,  $\varphi_p$ , and of the angular parameter  $\varphi_{lc}$ . The angles  $\varphi_p$  and  $\varphi_{lc}$  are the *Gaussian coordinates* of point of the pinion tooth flank,  $\mathcal{P}$ .

Paths of contact,  $P_c$ , are the circular arcs through points of the desirable line of contact,  $LC_{des}$ . All the paths of contact are situated within the plane of action,  $PA$ , and are centered at the plane-of-action apex,  $A_{pa}$ . It can be construed that paths of contact lie on spheres<sup>4</sup> all of which are centered at the plane-of-action apex,  $A_{pa}$ .

At every instant of time, the instantaneous line of action,  $LA_{inst}$ , is a straight line tangent to the path of contact at corresponding to its point. All the instantaneous lines of action intersect the axis of instant rotation,  $P_{ln}$ . In this way, fulfillment of the conjugate action law is ensured.

The discussed approach for the determination of the geometry of the gear tooth flank,  $\mathcal{S}$ , and the pinion tooth flank,  $\mathcal{P}$ , is based on the generation of tooth flanks in the form of a family of consecutive positions of the line of contact,  $LC$ , that travels together with the plane of action,  $PA$ .

<sup>4</sup> Because the paths of contact in crossed-axes gearing lie on spheres, crossed-axes gearing can be loosely called as *spherical gearing*. This causes a confusion because engagement in mesh in intersected-axes gearings is also observed on spheres. Therefore, the terms *intersected-axes gearing* and *crossed-axes gearing* are preferred rather than ambiguous term *spherical gearing*.

This approach does not require the specification of the tooth flanks in the form of envelopes to corresponding families of consecutive positions of the generating basic rack. This means that the proposed method for the generation of the tooth flanks,  $\mathcal{S}$  and  $\mathcal{P}$ , does not require the implementation of the elements of the theory of enveloping surfaces. This is a significant advantage of the disclosed method of generation of tooth flank,  $\mathcal{S}$ , of the gear, and tooth flank,  $\mathcal{P}$ , of the pinion in crossed-axes gearing over the conventional methods.

The derived equations for the gear tooth flank,  $\mathcal{S}$ , as well as for the pinion tooth flank,  $\mathcal{P}$ , can be used as reference surfaces (datum surfaces) when (a) designing, (b) machining, and (c) inspecting gears for crossed-axes gearing that feature line contact between tooth flanks,  $\mathcal{S}$  and  $\mathcal{P}$ , of the gear and its mating pinion. They are constructed on the premise of describing (and not enveloping) the principle of surface generation.

Crossed-axes gearing that has tooth flanks of the proposed geometry is the most general kind of gearing that features *line contact* between the tooth flanks,  $\mathcal{S}$  and  $\mathcal{P}$ . In a particular case, when the center-distance is reduced to zero ( $C = 0$ ),  $C_a$  – gearing of the proposed geometry simplifies to  $I_a$  – gearing that has line contact between the tooth flanks,  $\mathcal{S}$  and  $\mathcal{P}$ . In another scenario, namely, when the crossed-axes angle is equal either 0 or  $\pi$ ,  $C_a$  – gearing of the proposed geometry simplifies to  $P_a$  – gearing that features line contact of the tooth flanks.

The desirable geometry of contact of tooth flanks of a gear and a pinion,  $\mathcal{S}$  and  $\mathcal{P}$ , in  $R$  – gearing can be specified when analyzing the shape and configuration of the line of contact,  $LC$ , within the plane of action,  $PA$ . The indicatrix of conformity,  $Cnf_R(\mathcal{S}/\mathcal{P})$ , at point of contact of the tooth flanks,  $\mathcal{S}$  and  $\mathcal{P}$  (see Appendix E), can be expressed in terms of the shape and configuration of the line of contact. Ultimately, those parameters of the shape and configuration of the line of contact are selected, under which the minimum diameter of the indicatrix of conformity,  $Cnf_R(\mathcal{S}/\mathcal{P})$ , is the smallest possible.

## 29.2 PERMISSIBLE SIMPLIFICATION: DESIGN PECULIARITIES OF GEARS FOR $R_{sp}$ –GEARING

A novel design<sup>5</sup> of precision gearing that is insensitive to the axes misalignment (as well as to other sources of the linear, and angular displacements of tooth flanks,  $\mathcal{S}$  and  $\mathcal{P}$ , from their desired configuration) is disclosed immediately below.

For the derivation of an equation for the position vector of point of the tooth flanks,  $\mathcal{S}$  and  $\mathcal{P}$ , an equation of the line of contact,  $LC$ , is used. Initially, this equation is commonly given in a reference system,  $X_{lc}Y_{lc}Z_{lc}$ , associated with the plane of action,  $PA$ . In order to convert the equation of the line of contact,  $LC$ , to a corresponding equation of the gear tooth flank,  $\mathcal{S}$ , as well as to a corresponding equation of the pinion tooth flank,  $\mathcal{P}$ , operators of coordinate system transformation are used. To compose the required operators of the coordinate system transformation,  $\mathbf{Rs}(LC \rightarrow \mathcal{S})$  and  $\mathbf{Rs}(LC \rightarrow \mathcal{P})$ , the schematic depicted in Figure 29.5 is helpful.

Then, the position vector  $\mathbf{r}_g$  of point of the gear tooth flank,  $\mathcal{S}$ , is expressed by the equation:

$$\mathbf{r}_g = \mathbf{Rs}(LC \rightarrow \mathcal{S}) \cdot \mathbf{r}_{lc} \quad (29.9)$$

Similarly, position vector  $\mathbf{r}_p$  of point of the pinion tooth flank,  $\mathcal{P}$ , is expressed by the equation:

$$\mathbf{r}_p = \mathbf{Rs}(LC \rightarrow \mathcal{P}) \cdot \mathbf{r}_{lc} \quad (29.10)$$

<sup>5</sup>  $R_{sp}$ –Gearing Insensitive to Axes Misalignment and other Displacement and Methods of Producing Gears./ S.P. Radzevich, International Application Number PCT/US 038753, International Filing Date: May 20, 2014, International Publication Number 2014/189903 A1, Int. Pat. Classification F16H 1/26 (2006.01), Priority Data: 13/900,946, May 23, 2013, 34 pages.

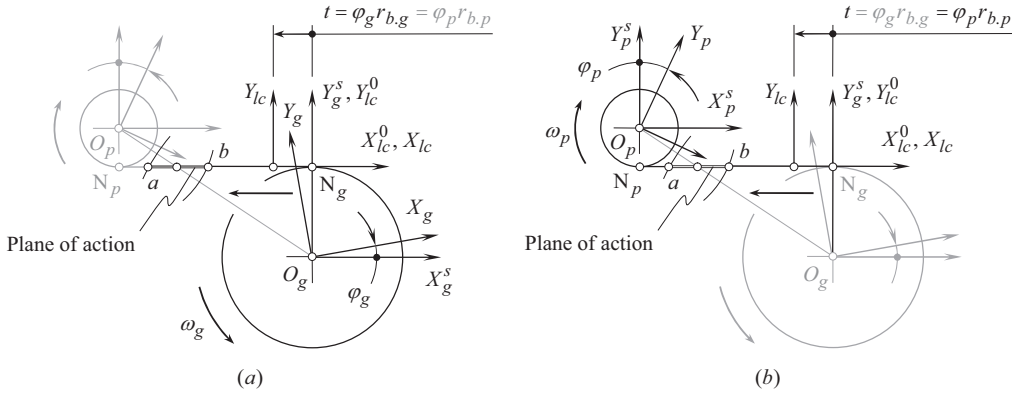


FIGURE 29.5 Applied reference systems: (a) associated with the gear, and (b) associated with the pinion.

Composing of operators of the coordinate system transformation is a routine procedure (see Appendix D).

The matrices  $\mathbf{Rs}(LC \rightarrow \mathcal{F})$  and  $\mathbf{Rs}(LC \rightarrow \mathcal{P})$  of the resultant coordinate system transformation are composed as product of certain number of the operators  $\mathbf{Tr}(a_x, X)$ ,  $\mathbf{Tr}(a_y, Y)$ ,  $\mathbf{Tr}(a_z, Z)$ , and  $\mathbf{Rt}(\phi_x, X)$ ,  $\mathbf{Rt}(\phi_y, Y)$ ,  $\mathbf{Rt}(\phi_z, Z)$  of elementary coordinate system transformation.

For the analytical description of the translation along the coordinate axes, the operators of translation  $\mathbf{Tr}(a_x, X)$ ,  $\mathbf{Tr}(a_y, Y)$ , and  $\mathbf{Tr}(a_z, Z)$ , are used. The operators yield matrix representations in the following form:

$$\mathbf{Tr}(a_x, X) = \begin{bmatrix} 1 & 0 & 0 & a_x \\ 0 & 1 & 0 & 0 \\ 0 & 0 & 1 & 0 \\ 0 & 0 & 0 & 1 \end{bmatrix} \quad (29.11)$$

$$\mathbf{Tr}(a_y, Y) = \begin{bmatrix} 1 & 0 & 0 & 0 \\ 0 & 1 & 0 & a_y \\ 0 & 0 & 1 & 0 \\ 0 & 0 & 0 & 1 \end{bmatrix} \quad (29.12)$$

$$\mathbf{Tr}(a_z, Z) = \begin{bmatrix} 1 & 0 & 0 & 0 \\ 0 & 1 & 0 & 0 \\ 0 & 0 & 1 & a_z \\ 0 & 0 & 0 & 1 \end{bmatrix} \quad (29.13)$$

in which  $a_x$ ,  $a_y$ , and  $a_z$ , are signed values that denote distances of translations along corresponding axes.

For the analytical description of the rotation about the coordinate axes, the operators of rotation  $\mathbf{Rt}(\phi_x, X)$ ,  $\mathbf{Rt}(\phi_y, Y)$ , and  $\mathbf{Rt}(\phi_z, Z)$ , are used. The operators yield representation in the form of the homogenous matrices:

$$\mathbf{Rt}(\phi_x, X) = \begin{bmatrix} 1 & 0 & 0 & 0 \\ 0 & \cos \phi_x & \sin \phi_x & 0 \\ 0 & -\sin \phi_x & \cos \phi_x & 0 \\ 0 & 0 & 0 & 1 \end{bmatrix} \quad (29.14)$$

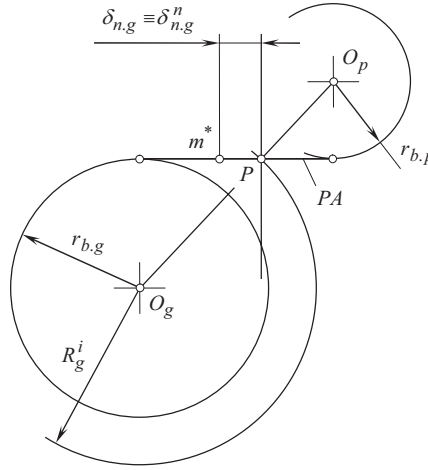


**FIGURE 29.6** The deviation,  $\delta_{n,g}$ , is measured within the plane of action,  $PA$ .

$$\mathbf{Rt}(\varphi_y, Y) = \begin{bmatrix} \cos \varphi_y & 0 & -\sin \varphi_y & 0 \\ 0 & 1 & 0 & 0 \\ \sin \varphi_y & 0 & \cos \varphi_y & 0 \\ 0 & 0 & 0 & 1 \end{bmatrix} \quad (29.15)$$

$$\mathbf{Rt}(\varphi_z, Z) = \begin{bmatrix} \cos \varphi_z & \sin \varphi_z & 0 & 0 \\ -\sin \varphi_z & \cos \varphi_z & 0 & 0 \\ 0 & 0 & 1 & 0 \\ 0 & 0 & 0 & 1 \end{bmatrix} \quad (29.16)$$

Here,  $\varphi_x$ ,  $\varphi_y$ , and  $\varphi_z$ , are signed values that denote the angles of rotation about a corresponding axis:  $\varphi_x$  is an angle of rotation around the  $X$  – axis (pitch);  $\varphi_y$  is an angle of rotation around the  $Y$  – axis (roll), and  $\varphi_z$  is an angle of rotation around the  $Z$  – axis (yaw). Further details on the coordinate system transformations are not discussed, but are well within the skill level of one of ordinary skills in the art.

Manufacturing errors and elastic deformation of the shafts, of the housing, of the bearings, and so forth, are the main contributors to the resultant linear and angular displacements of the tooth flanks  $\mathcal{S}$  and  $\mathcal{P}$  in real parallel-axes gearing. Gearing of the proposed design is capable of accommodating all of these displacements.

Let's consider an impact of the resultant linear/angular displacements of the tooth flanks  $\mathcal{S}$  and  $\mathcal{P}$  in real parallel-axes-gearing onto the actual deviation of the base pitch from the nominal value of it. The resultant displacement can be decomposed onto two components. One of the components is within the plane of action,  $PA$ , while another component is in the direction orthogonal to  $PA$ .

Refer to Figure 29.6. This diagram illustrates the case when the deviation,  $\delta_{n,g}$ , is within the plane of action,  $PA$ . Due to this displacement,  $\delta_{n,g}$ , the resultant displacement,  $\delta_{n,g}^n$ , in the direction perpendicular to the tooth profile is identical to  $\delta_{n,g}$ , and the identity  $\delta_{n,g}^n \equiv \delta_{n,g}$  is valid.

From another hand (see Figure 29.7), a deviation of that same value,  $\delta_{\tau,g}$ , but in the direction tangential to the gear/pinion tooth flank, results in a much smaller deviation  $\delta_{\tau,g}^n$  :

$$\delta_{\tau,g}^n = r_\delta - \sqrt{r_\delta^2 - \delta_{\tau,g}^2} \quad (29.17)$$

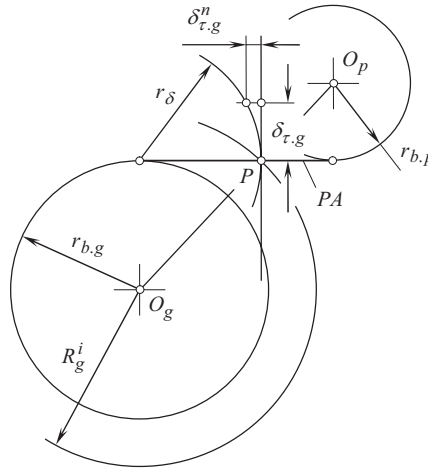


**FIGURE 29.7** The deviation,  $\delta_{\tau,g}$ , is measured in the direction tangential to the gear/pinion tooth flank.

This means that the component,  $\delta_{n,g}$ , that is measured in the direction within the plane of action,  $PA$ , is the major contributor to the actual variation of the base pitch.

In gearing of the proposed design (in the  $R_{sp}$  – gearing) the negligibly small component  $\delta_{\tau,g}^n$  [see Eq. (29.17)] of the resultant deviation is omitted. As a consequence, the proposed  $R_{sp}$  – gearing features several advantages over known designs of gearing.

The geometry of tooth flanks of a gear and of a mating pinion in  $R_{sp}$  – gearing is capable of accommodating for various values of the axis misalignment. In this way, base pitch of the gear is always equal to operating base pitch,  $\phi_b^{op}$ , of the gear pair. Similarly, base pitch of the pinion is always equal to the operating base pitch,  $\phi_b^{op}$ , of the gear pair. Ultimately, base pitches of the gear, and of the mating pinion are *always* equal to one another, as well as they are equal to operating base pitch of the gear pair.

The geometry of the line of contact is not limited to straight line segments, circular arc segments, and cycloid arc segments. Any planar curve that is entirely located within the plane of action can be employed as a desirable line of contact. The actual geometry of the line of contact may be chosen based on manufacturing preferences, for example, a line of contact that ensures a low-cost manufacturing technique may be utilized.

Any planar curve that is entirely located within the plane of action may be utilized for the purpose of producing a worm gear set with a reduced noise and vibration characteristic, and an increased loading capacity.



---

# 30 A Brief Overview on Evolution of the *Scientific Theory of Gearing*<sup>1</sup>

Gears are the means by which the power is transferred from source to application. Gears and gear transmissions have been used since the earliest times, and they are still extensively used in the modern industry. Gearing and geared transmissions drive the machines of modern industry. Gears move the wheels and propellers that transport us over the sea, on land, and in the air. Transmission and transformation of rotation from an input shaft to an output shaft is the main purpose of gearing of all kinds. A sizeable section of industry and commerce in today's world depends on gearing for its economy, production, and livelihood. No doubt gearing of all kinds will be extensively used for a long while in the future.

The art and science of gearing have their roots before the Common Era. Practical men were able by various empirical means to get gears adequate for their needs, at least until the early nineteenth century, when the mathematician's work was translated into practical language. Purely empirical solutions for the form of gear teeth can only be accounted for by the fact that gears operate at *low speeds* and under *small loads*. Yet many engineers and researchers continue to delve into the areas where improvements are necessary, seeking to quantify, establish, and codify methods to make gears meet the ever-widening needs of advancing technology. It should be stressed here that the scientific theory of gearing is the only reliable foundation to design, production, and application of gears and geared mechanisms.

Two different considerations when the state-of-the-art of gearing is discussed have to be distinguished. Gear design, and gear manufacture, that are based on the common sense of smart handicrafts is one of them. An engineering approach that is based on scientific accomplishments in the theory of gearing is the other one.

Besides gears and gear transmissions are investigated for a long while, the present-day knowledge of the gear theory is poor and is completely insufficient. Not too much is contributed to the theory of gearing since the time of *Leonhard Euler* (since the middle of the eighteenth century) who is recognized as the founder of the scientific theory of gearing.

It should be stated here that by the beginning of the twenty-first century (by the year of ~2010) scientific theory of gearing has not been developed at all.

Taking into account the incompleteness and the inconsistency of the present-day knowledge on the theory of gearing, an in-depth investigation into the gear kinematics, and the gear geometry has been undertaken by the author. Most of the results of the research that has been carried out are discussed in the earlier editions [174] of this book, as well as in numerous scientific papers, and conference proceedings. Fundamentals of the scientific theory of gearing are based on the key accomplishments in the kinematics of gearing, and the geometry of the gear tooth flanks. With that said, it makes sense to begin the discussion with a brief overview of the evolution of the scientific theory of gearing, bearing in

---

<sup>1</sup> This chapter of the book is organized in the following manner. At the beginning, a brief overview of the pre-*Eulerian* period of the gear art is done. Then, the fundamental accomplishments in the *scientific* theory of gearing are identified, and a name of the corresponding key contributor(s) is associated (where possible) with each of the fundamental accomplishments. As the overall number of the *fundamental* accomplishments in the scientific theory of gearing is limited to a few names, the overall number of the fundamental contributors to the *scientific* theory of gearing is also limited. Irrespective of many other researchers (not mentioned in this section of the book) have also contributed a lot to the field of gearing, they are not regarded as the *fundamental contributors* to the *scientific* theory of gearing, as their contribution to the gear art is not fundamental by nature.

mind the kinematics of gearing, and the gear tooth flank geometry. This will help us to identify what is already done in the field to this end, where we are now, and what has to be done in the future.

Such an analysis is required in order to associate every and all fundamental accomplishments in the scientific theory of gearing with the right names of gear researchers, those who have to be credited with the corresponding accomplishment.<sup>2</sup> A contribution to the theory of gearing of each of the potential contributor should be determined only by what he or she specifically contributed to the science, but NOT by the fact that he or she worked a lot in this area, and have authored/co-authored books and scientific papers. Unfortunately, in the meantime, not all the achievements in the field of gearing can be attributed with right names of the corresponding gear researchers.

Several significant achievements in the theory of gearing cannot be credited to the right persons, as their names are not known. For example, the names of the contributors for: (a) *equivalent pulley-and-belt transmission*, (b) condition of equal base pitches in gearing, are not known. A few more achievements in this regard can be mentioned. It is desirable to get the right names identified.

The just mentioned, as well as some other accomplishments, are vital to the scientific theory of gearing.<sup>3</sup>

In order to cover all the key gear theoreticians and to miss none of them, the following approach is adopted below.

**First**, all (with no exclusions) the fundamental accomplishments in the scientific theory of gearing are listed in a chronological order.

**Second**, a right name of the gear researcher is associated (where possible) with each of the fundamental accomplishments. For example, *Leonhard Euler* (and none of the others) is credited with the application of the involute of a circle for the gear tooth profile, as he was the first to prove that the involute tooth profile fits the best the needs of the gear tooth geometry, regardless of the involute of a circle was known<sup>4</sup> long before *Euler* has made his discovery in 1760.

In addition to that, it is necessary to stress the readers' attention on a few huge mistakes committed in the past by the gear researchers when investigating gears. This will help us to better understand the theory, and to properly value those scientists who contributed much to the scientific theory of gearing. The aforementioned mistakes can be referred to as the *key mistakes* in the theory of gearing. Following such an approach, it becomes possible to separate the names of the principal contributors to the scientific theory of gearing from the names of those who contributed less to the subject, and, moreover, from the names of those who committed mistakes that significantly affected the evolution of the theory of gearing.

The results of the research carried out by the author, and a few papers he has authored earlier [135,145,164], are extensively used when writing this section of the book. Other sources [22,217,223], and others, those available in the public domain, are used as well. The consideration begins with the ancient gear designs that are created only due to the common sense of smart handicrafts and ends with the modern scientific theory of gearing.

Tons of sources (monographs, scientific papers, conference proceedings, patents on inventions, and so forth) were investigated by the author in order to make possible the representation of the principal accomplishments in the scientific theory of gearing in a chronological order. A limited number of the most important sources were selected for more in-detail analysis. These sources are summarized in Table 30.1. The reported analysis is based primarily on the results of the research listed in Table 30.1.

<sup>2</sup> *The beginning of wisdom is to call things by their right names* – a Chinese proverb.

<sup>3</sup> Those, who don't know their own history, have no chance for success in the future.

<sup>4</sup> *Philippe de la Hire* is the first who invented and analytically described (1696) the involute of a circle. Later on (in the eighteenth century), *Leonhard Euler* has proved that involute curve best fits the gear tooth profile in parallel-axes gearing.

**TABLE 30.1****Main Contributions to the Gear Science**

No.	Year	The Name of the Key Contributor*	Source of Information
1.	1493	da Vinci, Leonardo	da Vinci, Leonardo, <i>The Madrid Codices</i> , Volume 1, 1493, Facsimile Edition of <i>Codex Madrid 1</i> , original Spanish title: <i>Tratado de Estatica y Mechanica en Italiano</i> , McGraw Hill Book Company, 1974.
2.	1754	Euler, L.	Euler, L., <i>De Optissima Figura Rotatum Dentibus Tribuenda. Supplementum de Figura Dentium Rotatum</i> , Novi Commentarii Academial Petropolitanae, 1754/55, 1765.
3.	1841	Willis, R.	Willis, R., <i>Principles of Mechanisms, Designed for the Use of Students in the Universities and for Engineering Students Generally</i> , London, John W. Parker, West Stand, Cambridge: J. & J.J. Deighton, 1841, 446p. Willis, R., "On the Teeth of Wheels," Trans. Civ. Eng., Vol. II, 1838.
4.	1842	Olivier, T.	Olivier, T., <i>Théorie Géométrique des Engrenages destinés</i> , Bachelier, Paris 1842, 132 pages. [in French].
5.	1861	Reuleaux, F.	Reuleaux, F., <i>The Constructor, a Hand-Book of Machine Design</i> by F. Reuleaux, Authorized translation, complete and unabridged from the 4 <sup>th</sup> enl. German ed. By Henry Harrison Suplee. Philadelphia, H.H. Suplee, 1893. -312p. [First German edition published in 1861 with title: Der Constructeur. Ein Handbuch zum Gebrauch beim Maschinen-Entwerfen].
6.	1863	Gibbs, J.W.	Gibbs, J.W., <i>On the Form of the Teeth of Wheels in Spur Gearing</i> , Doctoral Dissertation, Yale University, New Haven, Conn., 1863.
7.	1886	Gochman, H.I.	Gochman, H.I., <i>Theory of Gearing Generalized and Developed Analytically</i> , Odessa, 1886, 229 pages. [In Russian].
8.	1887	Grant, G.B.	U.S. Pat. No. 407.437. <i>Machine for Planing Gear Teeth</i> . /G.B. Grant, Filed: January 14, 1887 (serial No. 224,382), Patent issued: July 23, 1889. Grant, G.B., <i>A Treatise on Gear Wheels</i> , 11 <sup>th</sup> edition, Philadelphia Gear Works, Inc., Philadelphia, 1906, 105 p.
9.	1912	Flanders, R.E.	Flanders, R.E., <i>Bevel Gearing</i> , 4 <sup>th</sup> Edition, Machinery's Reference Series, Number 37, The Industrial Press, 1912, 48 pages.
10.	1917	Oberg, E.	Oberg, E., <i>Spur and Bevel Gearing</i> , The Industrial Press, New York, 1917, 274p.
11.	1935	Dicker, Ya.I.	Dicker, Ya.I., <i>Involute Gearing</i> , Moscow, Orgametal, 1935, 220 pages. [In Russian]. Dicker, Ya.I., <i>Internal Gearing: Spur and Helical</i> , Moscow, Orgametal, 1938, 138 pages. [In Russian].
12.	1936	Cormac, P.	Cormac, P., <i>A Treatise on Screws and Worm Gear, Their Mills and Hobs</i> , London, Chapman & Hall, Ltd., 1936, 138p.
13.	1948	Fraifeld, I.A.	Fraifeld, I.A., <i>Continuously Indexing Cutting Tools</i> , Moscow, Mashgiz, 1948, 252 pages. [In Russian].
14.	1948	Shishkov, V.A.	Shishkov, V.A., "Elements of Kinematics of Generating and Conjugating in Gearing," in: <i>Theory and Calculation of Gears</i> , Vol. 6, Leningrad: LONITOMASH, 1948. [In Russian]. Shishkov, V.A., <i>Generation of Surfaces in Continuously Indexing Methods of Machining</i> , Moscow, Mashgiz, 1951, 152 pages. [In Russian].
15.	1948	Wildhaber, E.	Wildhaber, E., <i>Foundations of Meshing of Bevel and Hypoid Gearings</i> , Translated and comments by Eng. A.V. Slepak, Moscow, Mashgiz, 1948, 176 pages. [In Russian]. – This book is available in no other languages.
16.	1949	Kolchin, N.I.	Kolchin, N.I., <i>Analytical Calculation of Planar and Spatial Gearings</i> , Moscow-Leningrad, Mashgiz, 1949, 210 pages. [In Russian].
17.	1949	Buckingham, E.	Buckingham, E., <i>Analytical Mechanics of Gears</i> , Dover Publications, Inc., New York, 1988, 546p. (The 1 <sup>st</sup> print – 1949).
18.	1950	Davidov, Ya.S.	Davidov, Ya.S., <i>Non-Involute Gearing</i> , Moscow, Mashgiz, 1950, 179 pages. [In Russian].

(Continued)

**TABLE 30.1 (Continued)**  
**Main Contributions to the Gear Science**

No.	Year	The Name of the Key Contributor*	Source of Information
19.	1953	Nikolayev, A.F.	Nikolayev, A.F., <i>Kinematical Foundations of the Theory of Spatial Gearing</i> , Doctoral Thesis, Moscow, STANKIN, 1953. [In Russian].
20.	1955	Novikov, M.L.	Novikov, M.L., <i>Fundamental Issues of Geometrical Theory of Point Gear Meshing for Application in Powerful Gear Transmissions</i> , Doctoral Thesis, Moscow, Military Aviation Academy, 1955. [In Russian]. Novikov, M.L., <i>Gearing and Cam Mechanisms with Point System of Meshing</i> , Pat. No. 10913 (USSR), Cl. 47, 6. Filed: April 19, 1956. [In Russian]. Novikov, M.L., <i>Gearing with New Type of Meshing</i> , Moscow, Military Aviation Academy, 1958, 186 pages. [In Russian].
21.	1959	Kudr' avtsev, V.N.	Kudr' avtsev, V.N., <i>Calculation and Design of Novikov Gearing</i> , Leningrad, Military Aviation Academy, 1959, 78 pages. [In Russian].
22.	1960	Buckingham, E., Ryffel, H.H.	Buckingham, E., Ryffel, H.H., <i>Design of Worm and Spiral Gears: A Manual for the Design and Manufacture of All-Redress-Action Worm and Spiral Gear Drives</i> , The Industrial Press, New York, 1960, 450p.
23.	1960	Litvin, F.L.	Litvin, F.L., <i>Non-Circular Gears</i> , 2 <sup>nd</sup> edition, Moscow-Leningrad, Mashgiz, 1956, 311 pages. [In Russian]. (1 <sup>st</sup> edition: 1950, 218 pages). [In Russian]. Litvin, F.L., <i>Theory of Gearing</i> , 2 <sup>nd</sup> edition, Moscow, Nauka, 1968, 584 pages. (1 <sup>st</sup> edition: 1960). [In Russian]. Litvin, F.L., <i>Theory of Gearing</i> , NASA Reference Publication 1212, AVSCOM Technical Report, 88-C-035, 1989, 470p. Litvin, F.L., <i>Gear Geometry and Applied Theory</i> , Prentice Hall, Englewood Cliffs, NJ, 1994, 724p. Litvin, F.L., Fuentes, A., <i>Gear Geometry and Applied Theory</i> , 2 <sup>nd</sup> Edition, Cambridge University Press, Cambridge, UK, 2004, 800p.
24.	1961	Saari, O.E.	Saari, O.E., <i>Analytical Theory of Gear Tooth Surfaces</i> , Illinois Institute of Technology, 1961, 114 pages.
25.	1961	Baxter, M. L., Jr.	Baxter, M.L., Jr., "Basic Geometry and Tooth Contact of Hypoid Gears," <i>Industrial Mathematic</i> , Vol. 11, No. 2, pp. 19–42, 1961. Baxter, Meriwether L. Jr., "Basic Theory of Gear-Tooth Action and Generation." This is the opening chapter of <i>Gear Handbook</i> , 1 <sup>st</sup> Edition, Editor Darle Dudley, McGraw Hill, New York 1962.
26.	1964	Korostel'ev, L.V.	Korostel'ev, L.V., <i>Geometrical and Kinematical Indicators of Bearing Capacity of Spatial Gearing</i> , Doctoral Thesis, Moscow, Stankin, 1964, 48 pages. [In Russian].
27.	1968	Dus'ev, I.I. and Vasilyev, V.M.	Dus'ev, I.I. and Vasilyev, V.M., <i>Analytical Theory of Spatial Gearing and its Implementation to Hypoid Gearing</i> , Rostov-on-Don, Book Publishers, 1968, 148 pages. [In Russian]. Dus'ev, I.I., <i>Analytical Theory of Spatial Gearing and its Implementation to Hypoid Gearing</i> , Rostov-on-Don, Doctoral Thesis, Novocherkassk, Novocherkassk Polytechnic Institute, 1970. [In Russian].
28.	1968	Lashn'ev, S.I.	Lashn'ev, S.I., <i>Fundamentals of the Theory of Surface Generation by Means of Disk-Type, Rack-Type and Worm-Type Cutting Tools</i> , Doctoral Thesis, Tula, Tula Polytechnic Institute, 1968, 268 pages. [In Russian]. Lashn'ev, S.I., <i>Generation of Gear Tooth Flanks by Means of Rack-Type and Worm-Type Cutting Tools</i> , Moscow, Mashinostroyeniye, 1971, 216 pages. [In Russian].
29.	1969	Gavrilenko, V.A.	Gavrilenko, V.A., <i>Fundamentals of Theory of Involute Gearing</i> , Moscow, Mashinostroyeniye, 1969, 432 pages. [In Russian].
30.	1969	Chasovnikov, L.D.	Chasovnikov, L.D., <i>Gearing</i> , Moscow, Mashinostroyeniye, 1969, 486 pages. [In Russian].

(Continued)

**TABLE 30.1 (Continued)****Main Contributions to the Gear Science**

No.	Year	The Name of the Key Contributor*	Source of Information
31.	1969	Dyson, A.	Dyson, A., <i>A General Theory of the Kinematics and Geometry of Gears in Three Dimensions</i> , Clarendon Press, Oxford, 1969, 141p.
32.	1969	Timofeyev, B.P.	Timofeyev, B.P., <i>Synthesis and Analysis of Spiral Bevel Gearing</i> , Doctoral Thesis, Leningrad, Leningrad Polytechnic Institute, 1969. [In Russian].
33.	1971	Merritt, H.E.	Merritt, H.E., <i>Gear Engineering</i> , Putman Publishing, London, New York, Toronto, 1971, 489p.
34.	1972	Yerikhov, M.L.	Yerichov, M.L., <i>Principles of Systematization, Methods of Analysis, and Problems of Synthesis of Schematics of Gearing</i> , Doctoral Thesis, Khabarovsk, Khabarovsk Polytechnic Institute, 1972, 373 pages. [In Russian].
35.	1972	Pismanik, K.M.	Pismanik, K.M., <i>Theoretical Foundations of Tooth Flank Generation in Bevel and Hypoid Gearing</i> , Doctoral Thesis, Saratov, Saratov Polytechnic Institute, 1972, 408 pages. [In Russian]. Pismanik, K.M., <i>Hypoid Gearing</i> , Moscow, Mashinostroyeniye, 1964, 27 pages. [In Russian].
36.	1974	Sakharov, G.N.	Sakharov, G.N., <i>Theoretical Issues of Continuously Indexing Cutting Tools</i> , Doctoral Thesis, Moscow, STANKIN, 1974, 320 pages. [In Russian]. Sakharov, G.N., <i>Continuously Indexing Cutting Tools</i> , Moscow, Mashinostroyeniye, 1983, 232 pages. [In Russian].
37.	1976	Gul'ayev, K.I.	Gul'ayev, K.I., <i>Theoretical Foundations of Synthesis and Finishing of Bevel Gearings</i> , Doctoral Thesis, Leningrad, 1976. [In Russian].
38.	1977	Lopato, G.A., Segal', M.G.	Lopato, G.A., Kabatov, N.F., Segal', M.G., <i>Spiral Bevel and Hypoid Gearing</i> , 2 <sup>nd</sup> Edition, Moscow, Mashinostroyeniye, 1977, 423 pages. [In Russian].
39.	1978	Shtipelman, B.A.	Shtipelman, B.A., <i>Design and Manufacture of Hypoid Gears</i> , John Wiley & Sons, New York, 1978, 394p.
40.	1979	Henriot, G.	Henriot, G., <i>Traité Théorique et Pratique des Engrenages: Théorie et Technologie</i> , Vol. 1, 6 <sup>th</sup> Edition, Bordas, Paris, 1979, 662 pages.
41.	1980	Schulz, V.V.	Schulz, V.V., <i>Geometrical Optimization of Worn Kinematical Pairs</i> , Doctoral Thesis, Kiev, 1980, 32 pages. [In Russian].
42.	1985	Goldfarb, V.I.	Goldfarb, V.I., <i>Fundamentals of the Theory of Automated Geometrical Analysis and Synthesis of Generalized Type of Worm Gearing</i> , Doctoral Thesis, Izhevsk, Izhevsk Mechanical Institute, 1985, 432 pages. [In Russian].
43.	1987	Colbourne, J. R.	Colbourne, J. R., <i>The geometry of involute gears</i> , New York, Springer-Verlag, 1987, 532 p.
44.	1987	Lagutin, S.A.	Lagutin, S.A., "Meshing Space and its Elements," <i>Mashinovedeniye</i> , №4, 1987, pp. 69–75.
45.	1989	Sizrantsev, V.N.	Sizrantsev, V.N., <i>Synthesis of Cylindrical Gearing with Localized Contact</i> , Doctoral Thesis, Kurgan, Kurgan Polytechnic Institute, 1989, 428 pages. [In Russian].
46.	1989	Xuezhu Dong	Xuezhu Dong, <i>Theoretical Foundation of Gear Meshing</i> . China Machine Press, Beijing, 1989. [In Chinese]. Xuezhu Dong, <i>Design and Modification of Hourglass Worm Drives</i> , China Machine Press, Beijing, 2004. [In Chinese].
47.	1992	Wu, D.R. and Luo, J.S.	Wu, D.R., Luo, J.S., <i>A Geometric Theory of Conjugate Tooth Surfaces</i> , World Scientific Publishing, River Edge, NJ, 1992, 192p.
48.	1994	Shishov, V.P.	Shishov, V.P., <i>Theory, Mathematical Foundations, and Synthesis of High Power Density Gearings for Industrial Transportation</i> , Doctoral Thesis, East Ukrainian State University, Lugansk, 1994, 580 pages. [In Russian].
49.	1994	Wang, X.C.	Wang, X.C., Ghosh, S.K., <i>Advanced Theories of Hypoid Gears</i> , Studies in Applied Mechanics, Vol. 36, Elsevier, Amsterdam, 1994, 341p.

(Continued)

**TABLE 30.1 (Continued)**  
**Main Contributions to the Gear Science**

No.	Year	The Name of the Key Contributor*	Source of Information
50.	1995	Vulgakov, E.B.	Vulgakov, E.B., <i>Theory of Involute Gearing</i> , Moscow, Mashinostroyeniye, 1995, 320 pages. [In Russian].
51.	1995	Dooner, D.B.	Dooner, D.B., <i>Kinematic Geometry of Gearing</i> , 2 <sup>nd</sup> Ed., John Wiley & Sons, Inc., New York, 2012, 512 p. (1 <sup>st</sup> edition: Dooner, D.B., Seireg, A.A., <i>The Kinematic Geometry of Gearing. A Concurrent Engineering Approach</i> , John Wiley & Sons, Inc., NY, 1995, 450p.).
52.	1999	Sheveleva, G.I.	Sheveleva, G.I., <i>Theory of Surface Generation and of Contact of Moving Bodies</i> , Moscow, STANKIN, 1999, 494 pages. [In Russian].
53.	1999	Silich, A.A.	Silich, A.A., <i>Development of Geometrical Theory of Novikov Gearing and Generation of their Tooth Flanks</i> , Doctoral Thesis, Kurgan, Kurgan Polytechnic Institute, 1999, 534 pages. [In Russian].
54.	2000	Dudas, I.	Dudas, I., <i>The Theory and Practice of Worm Gear Drives</i> , London, Penton Press, 2000, 314p.
55.	2003	Phillips, J.	Phillips, J., <i>General Spatial Involute Gearing</i> , Springer, Berlin Heidelberg, 2003, 498 p.
56.	2005	Pavlov, A.I.	Pavlov, A.I., <i>Modern Theory of Gearing</i> , Kharkov, Kharkov National Automotive State University, 2005, 100 pages. [In Russian]. Pavlov, A.I., <i>Synthesis of High Loaded Gearing on the Basis of Linear Gear Meshes with Convex-to-Concave Contact of Tooth Flanks</i> , Doctoral Thesis, East Ukrainian State University, Lugansk, 2009, 42 pages. [In Russian].
57.	2007	Krenzer, T.	Krenzer, T., <i>The Bevel Gear</i> , Published October 1, 2007, 252 pages.
58.	2008	Radzevich, S.P.	Radzevich, S.P., <i>Theory of Gearing: Kinematics, Geometry, and Synthesis</i> , CRC Press, Boca Raton, Florida, 2012, 743 pages. Radzevich, S.P., <i>Gear Cutting Tools: Fundamentals of Design and Computation</i> , Boca Raton Florida, 2010, 754 pages. Radzevich, S.P., <i>Geometry of Surfaces: A Practical Guide for Mechanical Engineers</i> , Wiley, 2013, 264 pages. Radzevich, S.P., <i>Generation of Surfaces: Kinematic Geometry of Surface Machining</i> , CRC Press, Boca Raton, Florida, 2014, 738 pages. Radzevich, S.P., <i>High-Conformal Gearing: Kinematics and Geometry</i> , CRC Press, Boca Raton, Florida, 2015, 368 pages. Radzevich, S.P., <i>Fundamentals of Surface Generation, Monograph</i> , Kiev, Rastan, 2001, 592p. (In Russian). Radzevich, S.P., <i>Differential-Geometric Method of Surface Generation</i> , Dr. Sci. Thesis, Tula, Tula Polytechnic Institute, 1991, 300 pages.
59.	2009	Xuntang, W.	Xuntang, W., <i>Principle of Gearing</i> , Xi'an Jiaotong University, Xi'an, 2009. [In Chinese].
60.	2011	Tsukanov, O.N.	Tsukanov, O.N., <i>Fundamentals of Synthesis of Non-Involute Gearings in Generalized Parameters</i> , Chel'abinsk, South-Ural State University Publishers, 2011, 140 pages. [In Russian].
61.	2013	Stadtfeld, H.J.	Stadtfeld, H.J., <i>Gleason Kegelradtechnologie: Ingenieurwissenschaftliche Grundlagen und modernste Herstellungsverfahren für Winkelgetriebe</i> , Renningen, Expert-Verlag, 2013, 491p. Stadtfeld, H.J., <i>Gleason Bevel Gear Technology: The Science of Gear Engineering and Modern Manufacturing Methods for Angular Transmissions</i> , The GLEASON Works, Rochester, New York, 2014, 491p.

\* The accomplishments in the field of geometrical blocking contours of involute gear: Groman, M.B., "Selection of Gear Tooth Profile Correction," *Bulletin of Mechanical Engineering*, 1955, No. 2, pp. 3–13. Groman, M.B., "On Geometrical Blocking Contours of Involute Gear," *Bulletin of Mechanical Engineering*, 1952, No. 12, pp. 12–17. As well, as numerous others, less important accomplishments, are not considered in detail here, and, thus, none of them are not covered neither in Table 30.1, nor in Figure 30.55.



### 30.1 PRELIMINARY REMARKS

Scientific theory of gearing is the foundation for gear design, for production, inspection, and application of gears. In the beginning, it makes sense to clarify the meaning of the term *scientific theory of gearing*.

As it is understood from the text below, a *scientific theory* has to be based on a few postulates (on the input information), which the entire theory can be derived from. A fewer the total number of the postulates (of the input information), the more powerful scientific theory can be derived on such a basis, and vice versa. In the case of the *scientific theory of gearing*, the minimum required input information is limited to:

- a. a disposition of an input shaft relative to an output shaft
- b. an input rotation
- c. an input torque, and
- d. an output rotation (or an output torque)

An entire analytical description of gearing, that is, of the kinematics, and the geometry of a gear pair, of elements of gear dynamics, and so forth, can be derived from the clauses (a)–(d).

All the results in the scientific theory of gearing are interconnected with one another. Any additional information on gearing (if any is available) can also be incorporated into the analysis. No collection of more or less independent accomplishments in the theory can be referred to as a *scientific theory of gearing*. With that said, it is clear now that all the earlier developed so-called *theories of gearing* [proposed by *Th. Olivier* (1842) [95], *Ch. Gochman* (1886) [44], *F. Litvin* and *A. Fuentes* (2004) [76], *D. Dooner* (2012) [28], as well as numerous others] cannot be referred to as *scientific theories of gearing*, as they represent just a collection of scientific/engineering results that are independent of one another, are not interconnected with one another, and do not form a theory.

Despite gears and geared transmissions having been investigated for a long while, the present-day knowledge of the gear theory is completely insufficient. Moreover, the author is doubtful that all the principal accomplishments in the theory of gearing are known to all the gear researchers, those who are actively involved in the research in the field.

### 30.2 THREE MAIN PERIODS IN THE EVOLUTION OF THE GEAR ART AND GEAR SCIENCE

Gears are used to transmit and to transform a rotation from an input shaft to an output shaft. Depending on a particular application, gearing has to meet certain additional requirements. High accuracy of transmission of rotation, high power density,<sup>5</sup> and so forth are among them.

The development and investigation of gearing with a constant angular velocity ratio<sup>6</sup> (namely, gearing for which the equality  $\omega_p/\omega_g = \text{const}$  is valid) is one of the main goals of the scientific theory of gearing. Gearing with a constant angular velocity ratio (or gearing with a pre-specified function of the angular velocity ratio) is commonly called *geometrically accurate gearing*, or (some time) as *ideal gearing*, or just as *perfect gearing*, for simplicity. More generally, the design of gearing with a prescribed function of the angular velocity ratio is also covered by the scientific theory of gearing.

The evolution of gearing from the earliest times to nowadays is concisely discussed here with the emphasis on the *theory of gearing*, as this is vital to understand the foundations of gearing. The consideration is mainly focused on the kinematics of gear pairs, the geometry of interacting tooth

<sup>5</sup> The term *power density* is commonly used as an equivalent to the term *power-to-weight ratio*. Increasing the power density of a gearbox is often a design engineer's primary goal.

<sup>6</sup> In a more general sense, namely, when non-circular gears are taken into account, the use of *geometrically accurate gearing* makes possible an exact function of the pre-specified angular velocity ratio.



flanks, as well as on some other kinematic and geometric aspects of gears and gear pairs.<sup>7</sup> Not many scientists can be credited with the fundamental contributions to the field of gearing – only a few of them, those who was the first to discover and contribute to the theory of gearing a result that is of fundamental nature.

As it was earlier (circa 2012) proposed by the author [174], the evolution of the theory of gearing falls into three periods, namely:

- a. pre-*Eulerian* period of the gear art
- b. the time when the fundamental contribution by *L. Euler* has been done (this is the origin of the scientific theory of gearing)
- c. post-*Eulerian* period of the evolution of the theory of gearing

The principal accomplishments in the scientific theory of gearing are considered below in a chronological order in alignment with the just mentioned three periods of evolution. It is assumed that all (or, at least, almost all) principal accomplishments are covered in this text.

### 30.2.1 PRE-EULERIAN PERIOD OF EVOLUTION OF THE GEAR ART

The use of gear technology can be traced back to the fourth century BC in Greece and in China, although there is some indirect evidence that they existed even earlier than that [217]. According to Coy, J.J., et al. [22], the earliest written descriptions of gears are said to have been made by *Aristotle* in the fourth century BC. It has been pointed out that the passage attributed by some to *Aristotle*, in *Mechanical Problems of Aristotle* (ca. 280 BC), was actually from the writings of his school. In the passage in question, there was no mention of gear teeth on the parallel wheels, and they may just as well have been smooth wheels in frictional contact. Therefore, the attribution of gearing to *Aristotle* is most likely incorrect.

Gears appear in works connected to *Hero of Alexandria*, in Roman Egypt circa AD 50, but can be traced back to the mechanics of the Alexandrian school in the third century BC Ptolemaic Egypt, and were greatly developed by the Greek polymath *Archimedes* (287–212 BC).

The real beginning of gearing was *probably* with *Archimedes*, who in about 250 BC invented the endless screw turning a toothed wheel, which was used in engines of war. *Archimedes* also used gears to simulate astronomical ratios. The *Archimedean* were early forms of the wagon mileage indicator (odometer) and the surveying instrument. These devices were *probably* based on *thought* experiments of *Heron of Alexandria* (ca. 60 AD), who wrote on theoretical mechanics and the basic elements of mechanisms.

Because of the force-multiplying properties of gears, early engineers used them for hoisting heavy loads such as building materials. The mechanical advantage of gears was also used for ship anchor hoists and catapult pre-tensioning. Gears were used in wind and water wheel machinery for decreasing or increasing the provided rotational speed for application to pumps and other powered machines. An early gear arrangement was used to power textile machinery. The rotational speed of water or horse-drawn wheel was typically too slow to use, so a set of wooden gears needed to be used to increase the speed to a usable level.

Judging from the history books is one thing. Finding hard evidence of actual gears is another.<sup>8</sup> The biggest problem in finding archeological evidence of gears is that early gear materials were not built to last. Gears manufactured at this time were probably made of bronze. When bronze tools and mechanical pieces broke, they were simply melted down and refashioned into something else.

<sup>7</sup> The evolution of the geared mechanisms is out of the scope of this book.

<sup>8</sup> Some researchers claim that early examples of gears dated from the fourth century B.C. in China (Zhan Guo times – late East Shou dynasty), which have been preserved at the Luoyang Museum of Henan Province, China.

The oldest surviving relic in Europe containing gears is the *Antikythera mechanism*,<sup>9</sup> named for the Greek island near which the mechanism was discovered in a sunken ship in 1900. The Antikythera mechanism is an example of a very early intricate geared device, designed to calculate astronomical positions. The mechanism is identified as a calendrical Sun and Moon computing mechanism. Its time of construction is now estimated between 150 and 100 BC. The mechanism is not only the earliest relic of gearing,<sup>10</sup> but is also an extremely complex arrangement of epicyclic differential gearing.

The *Antikythera mechanism* (see Figure 30.1) is the oldest<sup>11</sup> artifact known consisting of gears. Here, an image of the originally discovered *Antikythera mechanism* is shown in Figure 30.1a. Figure 30.1b illustrates the *Antikythera mechanism* overlapped with the image of its replica. A three-dimensional reconstruction of the *Antikythera mechanism* is depicted in Figure 30.1c. The device has more than 30 gears, although some scientists suggested as many as 72 gears, with teeth formed through equilateral triangles.

Commonly gears of early design were made out of wood with cylindrical pegs, and were often lubricated with animal fat grease. An example of old stile gears made out of wood is illustrated in Figure 30.2.

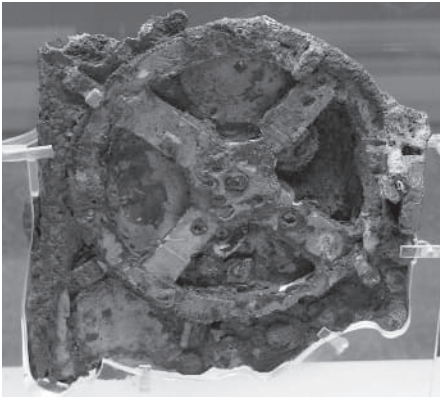
In ancient times, only transmission and transformation of a rotary motion was the main purpose of gearing. The quality of rotation of the output shaft, that is, smoothness of its rotation, was out of importance. No special care was taken of the geometry of the interacting tooth surfaces of the gears in gearing of old designs (see Figures 30.1 and 30.2). Practical men were able by various empirical means to get gears adequate for their needs, at least until the early nineteenth century, when the mathematician's work was translated into practical language. It was common practice to build pin gears made up of wood. Initially, the shape of teeth was either not important, or just flat, for example, in power transmissions like *Vitruvius'* watermills dated back to 40 BC, or a precision of contact was achieved by manual adjustment of each pair of gears in contact as for the *Antikythera mechanism*. Purely empirical solutions for the form of gear teeth can only be accounted for by the fact that gears operated at *low speeds* and under *small loads*. The gear tooth profile geometry was not considered at all, and pin-gears successfully met all the requirements of that time. No theory of gearing was necessary to design old stile gears as the rotations were low, and there were no constraints on power density of the gearing. The smart ancient craftsmen were governed only by common sense when designing and manufacturing the gears.

The art of gearing was carried through the European Dark Ages, appearing in Islamic instruments such as the geared astrolabes that were used to calculate the positions of the celestial bodies. Perhaps the art was relearned by the clock- and instrument-making artisans of fourteenth century Europe, or perhaps some crystallizing ideas and mechanisms were imported from the East after the crusades of the XI through the XIII centuries.

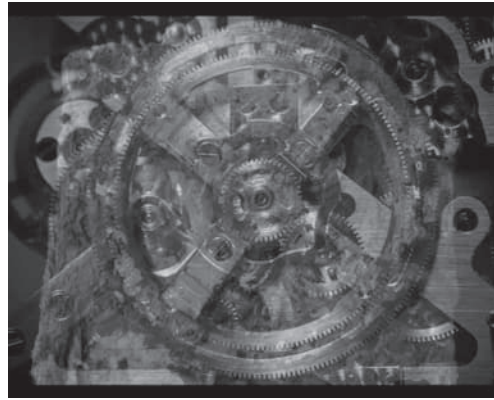
<sup>9</sup> The artifact was recovered in 1900–1901 from the Antikythera shipwreck off the Greek island of Antikythera. Its significance and complexity were not understood until decades later. Believed to have been designed and constructed by Greek scientists, the instrument has been dated either between 150 and 100 BC, or, according to a more recent view, at 205 BC. This precious example of antique genius complexity grade was so high that artefacts of a similar complexity and workmanship did not reappear for a millennium and a half, when mechanical astronomical clocks were built in Europe.

<sup>10</sup> The *South-pointing chariot* (invented in the fifth century BC) is another known device that contains gears. Unfortunately, only numerous present-day *reconstructions* (not even *replicas* !!) of the *South-pointing chariot* are known, and no original artefact is recovered yet.

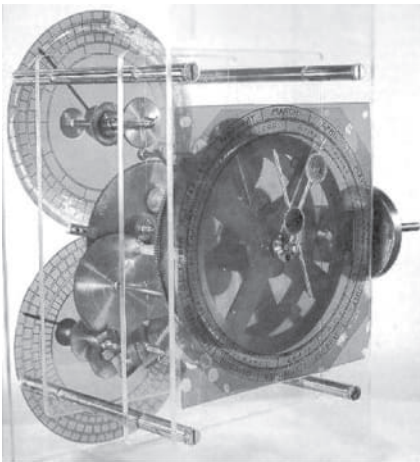
<sup>11</sup> The earliest known reference to a gear was around 50 AD; *Hero of Alexandria*, though the *Book of Song*, suggests that the south-pointing chariot may have employed differential gears as early as the reign of the Zhou Dynasty (1045–256 BC) of China (Radzevich, S.P. *Dudley's Handbook of Practical Gear Design and Manufacture*, 3rd ed., Boca Raton, FL: CRC Press, 2016, 629 pages.). However, no artefact of the south-pointing chariot is discovered so far. Only nowadays designed *reconstructions* are known. Therefore, in the meantime, it is incorrect to consider the south-pointing chariot as relic of a mechanism with gears.



(a)



(b)



(c)

**FIGURE 30.1** The *Antikythera mechanism*, (100 BC to 205 BC): (a) originally discovered artifact, (b) the *Antikythera mechanism* overlapped with the image of its replica, and (c) a three-dimensional reconstruction of the *Antikythera mechanism*.



**FIGURE 30.2** Old-style gears made out of wood.



**FIGURE 30.3** *Leonardo di ser Piero da Vinci* (1452–1519).

It appears that an English abbot of St. Alban's monastery, born *Richard of Wallingford* in 1330 AD, reinvented the epicyclic gearing concept. He applied it to an astronomical clock that he began to build and that was completed after his death.

A mechanical clock of a slightly later period was conceived by *Giovanni de Dondi* (1348–1364). Diagrams of this clock, which did not use differential gearing, appear in the sketchbooks of *Leonardo da Vinci* (1452–1519) (see Figure 30.3), who designed geared mechanisms himself.

Numerous designs of gearing appear in the famous book by *Leonardo da Vinci* (see Figure 30.4) [23]. In 1967, two of *Leonardo da Vinci's* manuscripts, lost in the National Library in Madrid since 1830, were rediscovered. One of the manuscripts, written between 1493 and 1497 and known as *Codex Madrid I* (see Figure 30.4) [23], contains 382 pages with some 1600 sketches. Included among this display of *Leonardo's* artistic skill and engineering ability are his studies of gearing. Among these are tooth profile designs and gearing arrangements that were centuries ahead of their *invention*.

Numerous other famous names have indicated their interest to gears and gear drives. *Albrecht Dürer*<sup>12</sup> (1471–1528), *Robert Hooke*<sup>13</sup> (1635–1703), and numerous others can be mentioned in this regard.

The history of modern gears started in 1525 and is associated with the name of *Albrecht Durer* [217], who is credited with the discovery of epicycloidal shape (ca. 1525).

For a long while, the most accurate gears were produced by clockmakers and instrument makers. Questions of exact tooth form, pressure angle, and strength of gear teeth did not enter into the designs of the clockmakers and instrument makers.

<sup>12</sup> Albrecht Dürer (May 21, 1471–6 April 6, 1528), a German painter, printmaker, mathematician, engraver, and theorist.

<sup>13</sup> In 1666, *R. Hooke* [Robert Hooke, (28 July [O.S.18 July] 1635–3 March 1703) was an English natural philosopher, architect, and polymath] demonstrated for *The Royal Society* a model of gearing that he has invented earlier. Later on, the gearing of this kind *Hooke* described in his 1674 book *Lectiones Cutlerianae*. The gearing of this particular kind is nowadays known as *White's gearing*. May be this is somehow associated with Mr. *Christipher White* of London who manufactured a microscope for *R. Hooke*.



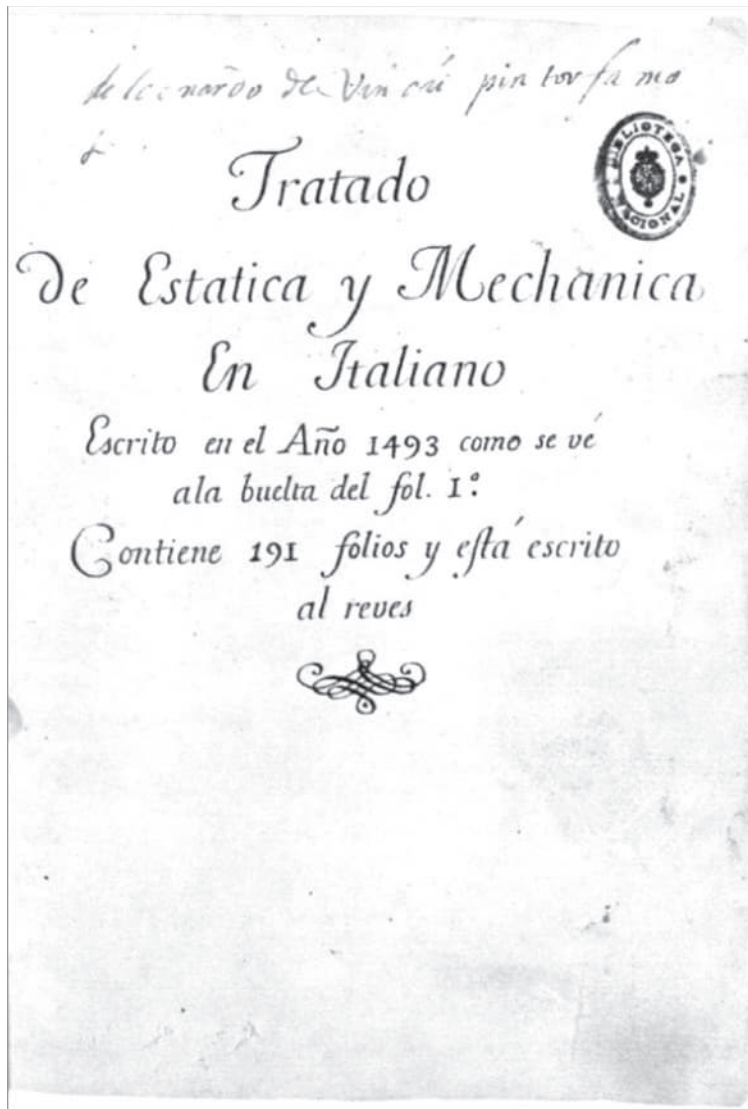


**FIGURE 30.4** Title page of the 1493 book *The Madrid Codices* by Leonardo da Vinci, [23].

The so-called *lantern gears*, having simple rectangular, or cylindrical tooth profiles, gradually were replaced with more sophisticated cycloid profiles. In the seventeenth century, the Dutch mathematician *Christiaan Huygens*<sup>14</sup> studied the circle involute in order to apply it to his first pendulum clock.

Contemporary gears for the uniform transmission of power and rotation are based much on the application of mathematical curves discovered by scientists in the XVIs and XVIIs centuries, in the design of teeth flanks. In the period 1450–1750, the mathematics of gear-tooth profiles and theories of geared mechanisms became established.

Mathematicians turned their attention to gear tooth profile only in the seventeenth century. *Girard Desargus* (1591–1661), *Philippe de La Hire* (1640–1718) [24], and *Charles Camus* (1699–1768) [16,17], are the names of the most prominent contributors to the gear science in the pre-Eulerian

<sup>14</sup> Christiaan Huygens, also spelled Huyghens (April 14, 1629–July 8, 1695), was a Dutch physicist, mathematician astronomer, and inventor,



**FIGURE 30.5** *Girard Desargues* (1591–1661).



**FIGURE 30.6** *Philippe de La Hire* (1640–1718).

period of evolution of the gear theory. They have summarized the main accomplishments in the field of gearing in the pre-*Eulerian* period of time.

In particular, the first record on the use of cyclic curves as the tooth profile of a gear is related to *Girard Desargues*<sup>15</sup> (see Figure 30.5). *Desargues*' work on gearing is known mostly from the records made by his student *Philippe de la Hire*.<sup>16</sup> A treaty on epicycloids and their usage in mechanics is discussed in his book [24]. *Philippe de la Hire* (see Figure 30.6) was the first to describe the

---

<sup>15</sup> Girard Desargues (February 21, 1591–September 1661) was a French mathematician and engineer.

<sup>16</sup> Philippe de la Hire (March 18, 1640–April 21, 1718) was a French physicist, astronomer, mathematician, and engineer.



**FIGURE 30.7** Charles Camus (1699–1768).

use of epicycloids for gears that ensured (as he loosely meant) a uniform transmission of rotation. *De la Hire* considered the involute as the best among exterior cycloids since he recognized that it is the special case in which the generating circle's radius is infinite. He also noted that the involute tooth gives the teeth of the corresponding rack as having straight sides. It took 150 years before this principle found practical application.

The first major contribution to the geometry of gear wheels came from France. *Charles Etienne Louis Camus*<sup>17</sup> (see Figure 30.7) is the first mathematician to work the theory of gear teeth into a systematic and general theory of mechanism.

*Camus* repeated much of *de La Hire*'s work, although he added many important elements of his own. He gives a detailed analysis of the teeth desirable for the combination of a spur and lantern gear. *Camus* did, however, correct *de La Hire* in that he recognized the fact of sliding of even the epicycloid teeth one upon the other and said that this phenomenon is one of the principal sources of friction and wear in gearing.

The action of engaged teeth relative to the line of centers is discussed, and he points out that the action is best when engagement takes place after the working face of the driving tooth has passed the line of centers, that is, during the receding action.

*Camus* goes on to consider the problem of the minimum number of teeth and that of the proper form for the ends of the teeth. He deals with true bevel gears and uses the rolling-cone principle for their analysis. But he considers only the case of interaction of a crown and a bevel gear.

*Camus* does not consider the involute tooth at all. Although he analyzes trains of gears, he says nothing of the form of teeth required in a series of three or more gears. This can probably be accounted for by the fact that he had only clockwork in mind. The mills of this era seldom had trains of more than two gears engaged.

As early as in 1733 *Camus* published his book [17], in which he showed that in order to get an output a uniform angular velocity from a uniform input angular velocity, it is necessary that the shapes of the two teeth are such that they can be generated like epicycloids by rolling one and the same curve on two different circles.

<sup>17</sup> Charles Étienne Louis Camus (August 25, 1699–February 2, May 4, 1768) was a French mathematician and mechanician.



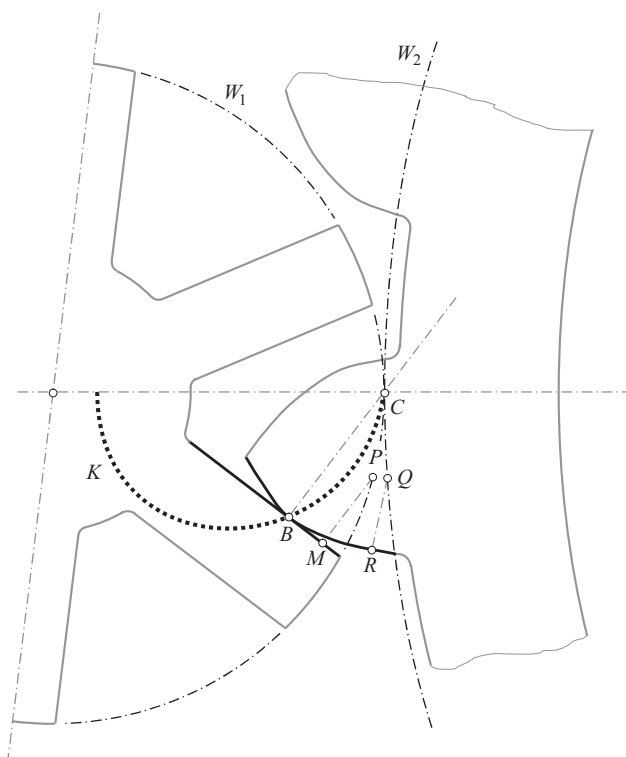


**FIGURE 30.8** Schematic of the *Camus'* principle of gearing (1733).

*Camus* was the first [17] who formulated the condition that, in his opinion, has to be fulfilled for a pair of gears to be able of transmitting rotation smoothly. According to *Camus*, the sufficient condition can be formulated as follows:

*If in a uniform rotation, power is to be transmitted via a pair of teeth, then the normal to the teeth flanks at the contact point (within the path of contact) must pass through the pitch point.*

Another formulation of that same condition by other researchers is represented in the form:

*If an auxiliary curve is rolling on the pitch circles of circular gears, any point attached to this curve traces conjugate profiles.*

This sounds similar to the fundamental theorem of gearing known nowadays – *Camus* was close to discover the *conjugate action law* for the case of parallel-axes gearing, however, he failed to make the last step [17].

The *Camus'* principle of gearing is illustrated with 1733 schematic (see Figure 30.8). In this schematic, the path of contact, namely, a curved line segment *KBC*, and the line of action at different angular configurations of the mating gears, that is, *BC*, *MP*, and *RQ*, do not align with one another.<sup>18</sup> The schematic (see Figure 30.8) reveals that *Camus* did not make a difference between the *path of contact* and between the *line of action*. *Camus* loosely assumed that the line of action, *LA*, in geometrically accurate gearing can be shaped in a form of a planar curve (as illustrated in

<sup>18</sup> It is instructive to note here that shown in Figure 30.8 schematic is a kind of mistake because of the following reasons. First, the path of contact is an envelope to a family of consecutive positions of the instantaneous line of action. Therefore, it is not permissible that the line of action, *BC*, intersects the path of contact, *KBC*. The path of contact must be in tangency with the line of action, *BC*. Second, when numerous instantaneous lines of contact are through the pitch point *C*, then no envelope curve (that is, no path of contact) can be constructed. A few more reasons for infeasibility of gearing shown in Figure 30.8 to be mentioned.

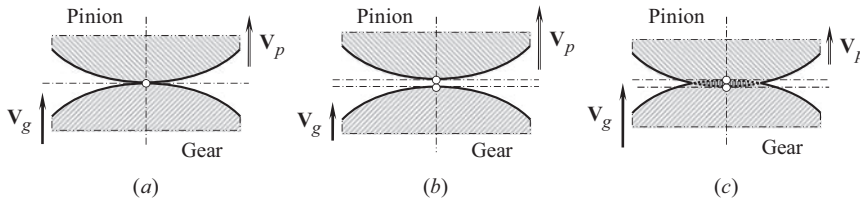


**FIGURE 30.9** Condition of contact of a gear, and of a mating pinion tooth flanks  $\mathcal{G}$  and  $\mathcal{P}$ . (a) correct contact,  $\mathbf{V}_g = \mathbf{V}_p$ , (b) separation of the tooth flanks is observed,  $\mathbf{V}_g < \mathbf{V}_p$ , and (c) interference of the tooth flanks occurs,  $\mathbf{V}_g > \mathbf{V}_p$ .

Figure 30.8). According to Figure 30.8, the interacting tooth flanks are **NOT conjugate** to each other at all!!

Despite *Camus* being close to discovering the fundamental theorem of parallel-axes gearing, he did not succeed in doing that. As it is shown below in this book, for gears that operate on parallel shafts, the only feasible case is when both the *path of contact* and the *line of action* are straight lines that align with one another, as it is observed only in involute gearing. Therefore, it is incorrect to credit *Camus* with the discovery of the *conjugate action law* in parallel-axes gearing.

Clearly, *Camus* had the basis for a theory of mechanism of gear teeth, but it was not systematically and completely worked out, as in *R. Willis* [222].

Despite the mathematicians began investigating some curves aiming their application for the purpose of gearing, no foundations in the theory of gearing have been made at that time. The results of the research undertaken by *Desargus*, *de La Hire*, and *Camus*, are very close to the origin of the scientific theory of gearing. However, these results do not form the basis of the theory, they cannot be considered the origin of the scientific theory of gearing.

The condition of contact of the interacting tooth flanks is the only contribution to the scientific theory of gearing attained in the *pre-Eulerian* period of the gear art. The initially proposed for a more general case, the condition of contact of two machine elements can be implemented with respect to gears as well. This condition is schematically illustrated in Figure 30.9. It took about a century before the method of common perpendiculars was developed by *Franz Reuleaux* in the second half of the nineteenth century on the premise of the condition of contact.

In order to fulfill the condition of contact of two interacting tooth flanks (or, in other words, in order to align with *the first fundamental law of gearing*), the contact point, both of a gear and of a mating pinion tooth flanks, must travel with equal velocities along the common perpendicular, namely, the equality  $\mathbf{V}_g \equiv \mathbf{V}_p$  has to be valid (see Figure 30.9a). In this scenario, the relative velocity is zero ( $\mathbf{V}_{rel} = 0$ ). If an inequality  $\mathbf{V}_g < \mathbf{V}_p$  is valid, the components 1 and 2 separate from one another (see Figure 30.9b), and the relative velocity is of a positive value ( $\mathbf{V}_{rel} > 0$ ). Inversely, if an inequality  $\mathbf{V}_g > \mathbf{V}_p$  is observed, the components 1 and 2 interfere with one another (see Figure 30.9c). The relative velocity is of a negative value in this scenario ( $\mathbf{V}_{rel} < 0$ ). None of these two scenarios is permissible in geometrically accurate gearing.

The condition of contact is important to the theory of gearing. Unfortunately, it is not known who should be credited with this important accomplishment. It is likely this is because the condition of contact has been discovered long before the scientist has turned their attention to the gear science.

At the time of *Charles Camus*, a well-known clockmaker *Henry Hindley*<sup>19</sup> used to work on gears. It is likely that the first true circular dividing engine was constructed by *Hindley* in around 1739. This was reported to the Royal Society by *John Smeaton* in 1785. Approximately in 1765, *Henry Hindley* invented the double-enveloping hourglass worm drive [94] illustrated in Figure 30.10. The

<sup>19</sup> Henry Hindley (1701–1771) was an eighteenth-century clockmaker, watchmaker, and maker of scientific instruments. He invented a screw-cutting lathe, a fusee-cutting engine and an improved wheel-cutting engine, and made one of the first dividing engines, for the construction of accurately graduated arcs on scientific instruments.

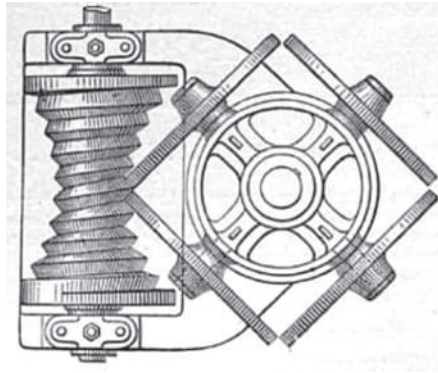


**FIGURE 30.10** Schematic of the 1765 *Henry Hindley* double-enveloping hourglass worm drive.

hourglass worm is lathed by a lathe with a straight blade. The meshing worm wheel is generated by an hourglass hob similar to the hourglass worm.

The *Hindley type of worm-gear* was first used in *Hindley's* dividing engine, and was, by the inventor, considered superior to the ordinary type, in wearing quality. Investigation has practically settled that the nature of contact between the worm thread and the teeth of the ordinary worm wheel is that of line contact, extending across the tooth on the pitch line. It was shown later on that in the *Hindley type of worm-gear* no line contact between the worm threads, and the gear tooth flanks are observed.

A few more gear researchers actively worked on gear design in this century. The names of *J. Imison*, [55], *R. Buchanan*, [14], and *G.B. Airy*, [1], deserve to be mentioned (in a chronological order) in this regard.

Accomplishments in the field of gear art and gear science, attained in the pre-*Eulerian* period of evolution of the gear art, are briefly summarized immediately below:

- Various primitive designs of wooden gearing were developed with the purpose to transmit a rotation between two shafts
- Gears that operate (a) on parallel shafts – namely, parallel-axes gearing, (b) on intersected shafts – namely, intersected-axes gearing, and (c) on crossed shaft – namely, crossed-axes gearing, were known in the pre-*Eulerian* period of evolution of the gear art
- All the early designs of gearing operate at low rotations and transmit small torques
- Per the author's opinion, the condition of contact was already known to *Camus* (1733) [13,17], or even to *Desargues*. The contact condition states that: *At every point of contact of tooth flanks of a gear,  $\mathcal{G}$  and a mating pinion,  $\mathcal{P}$ , the projection of the relative velocity vector onto the common perpendicular to the interacting tooth flanks is of a zero value*
- No tooth flank geometry was taken into account, first of all because of the absence of the necessity of doing that: Low power density wooden gears that operate at low rotations met the current customer requirements of that time. No special requirements for the smoothness of the output rotation were set at this period of time
- It became clear that the performance of a gear pair depends on a specific tooth profile of the mating gears, namely, teeth wear in gearing depends on the actual shape of a gear and a mating pinion tooth
- Mathematicians indicated an interest to a special tooth profile of a gear and a mating pinion that allows the lowest tooth flank wear. *Desargues*, *de la Hire*, and *Camus*, are the main contributors to the gear science in the pre-*Eulerian* period of time
- Epicycloid was investigated as a potential candidate that can be used to shape the gear teeth, and epicycloidal tooth flank geometry was proposed for gearing that operates on parallel shafts
- It was realized that in gearing with epicycloidal geometry of the gear teeth a rotation cannot be transmitted smoothly, that is, with a constant angular velocity ratio



**FIGURE 30.11** *Leonhard Euler (1707–1783).*

- Involute of a circle was known at that time (*de la Hire*, 1696). However, there was no understanding that this curve best meets the needs of gearing; besides the mathematicians began investigating some curves aiming their application for the purpose of gearing, and no foundations in the theory of gearing have been made in pre-*Eulerian* period of evolution of the gear science.

Whilst the fundamental principles of gearing have not changed and ancient cog-wheels served the same purposes, they have very little in common with modern gears. Ultimately, all the gearing that was common in the pre-*Eulerian* period of evolution of the gear art is far from being referred to as *geometrically accurate gearing*, as they are not capable of transmitting an input uniform rotation smoothly. Geometrically inaccurate gears (those feature variable angular velocity ratio) are still in use even in the present-day industry in cases when the rotations are low, and the transmitted power is small, as well.

It is important to stress the readers' attention here on relatively a few publications on the history of gears, partly because the gears were overlooked for centuries due to the unavailability of power engines, and therefore, the early development of the subject is not properly documented. The fact that the history of modern gears only extends over only two centuries and is tied together with the development of new manufacturing methods and the Industrial Revolution is the other reason.

### **30.2.2 THE TIME WHEN THE FUNDAMENTAL CONTRIBUTION BY *LEONHARD EULER* HAS BEEN DONE – THE ORIGIN OF THE *SCIENTIFIC THEORY OF GEARING***

The interest of mathematicians (at the beginning such as *Desargues*, *de La Hire*, and *Camus*, and later on of *Euler*) seems to have come from a desire to increase efficiency and reduce wear in mills of various types where, although the speeds were low, the load was substantial. Indirectly, these problems were associated with the quality of the transmitted rotation, namely, with the smoothness of rotation of the output shaft.

This was *Leonhard Euler*<sup>20</sup> (1707–1783), a famous scientist (born in Switzerland), to whom the origin of the scientific theory of gearing can be traced back to (see Figure 30.11). The main

<sup>20</sup>Leonhard Euler (April 15, 1707–September 18, 1783) was a pioneering Swiss mathematician and physicist.

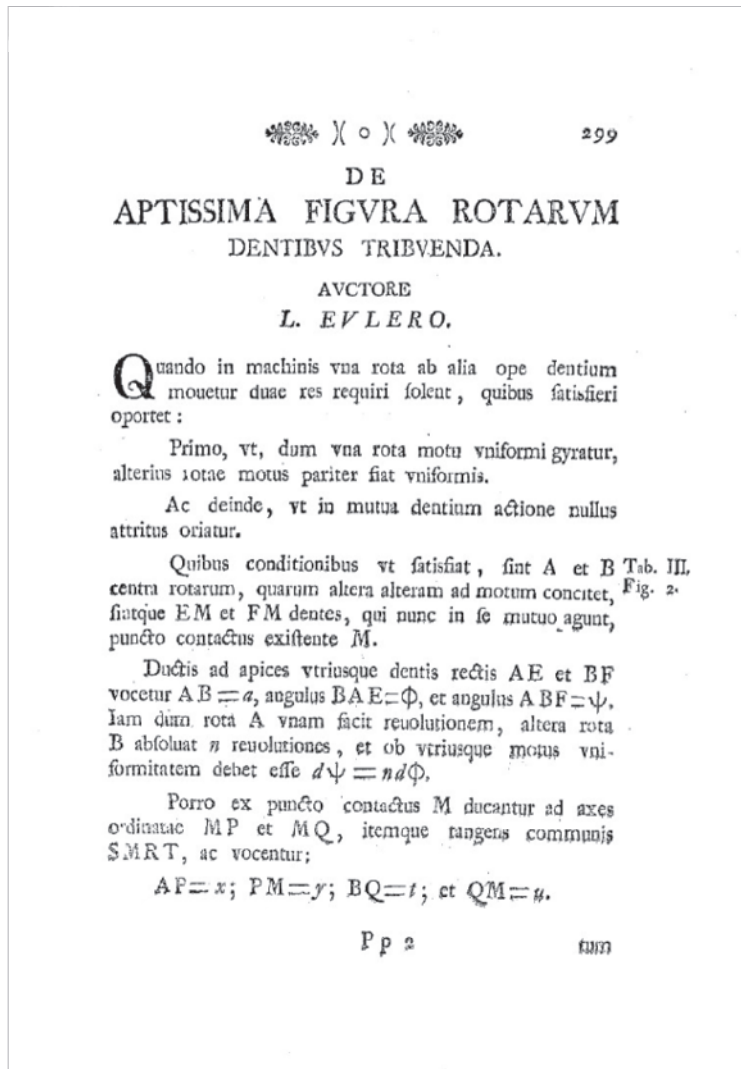


**FIGURE 30.12** Title page of the 1754–55 paper by *L. Euler*, “De Aptissima Figura Rotarum Dentibus Tribuenda,” in: *Academiae Scientiarum Imperiales Petropolitanae, Novi Commentarii*, t. V, pp. 299–316.

contribution by *L. Euler* to the scientific theory of gearing is outlined in his two papers [35] and [36]. In these articles, *Euler* has proved that the involute of a circle is the best planar curve that fits to shape a gear tooth profile in geometrically accurate parallel-axes gearing.

*Leonhard Euler* has formulated the conjugate action law for gear pairs that operate on parallel axes. Fulfillment of the conjugate action law allows a uniform speed ratio to be maintained. Since then, the fundamental design of gear geometry has not changed significantly.

### 30.2.2.1 Involute Tooth Profile for Parallel-Axes Gearing

In the *Euler*’s first paper (see Figure 30.12) on gears [35] (written in the first half of the 1750s), he proved the usefulness of the involute of a circle<sup>21</sup> to be used in the shape of gear teeth flanks, and

<sup>21</sup> *Leonhard Euler* is commonly credited with the invention of involute gear tooth profile, which the best fits the practical needs of the industry.



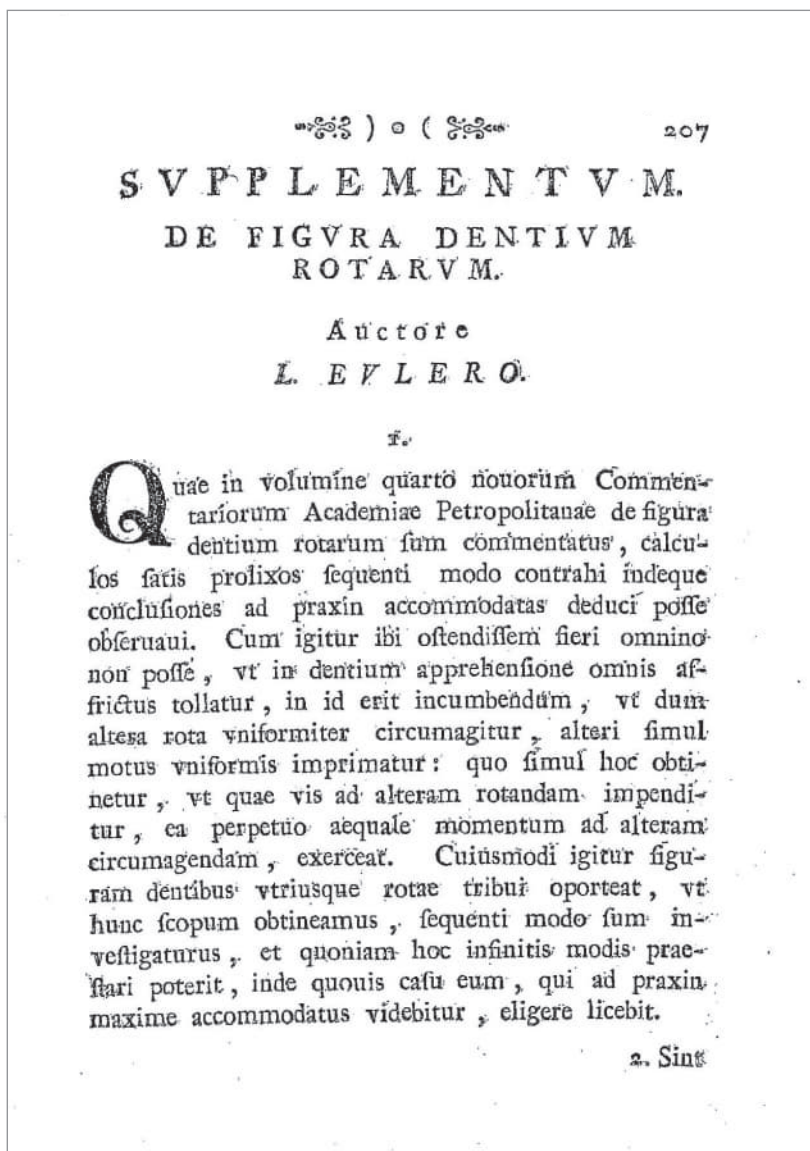


**FIGURE 30.13** Title page of the 1767 paper by L. Euler “Supplementum. De figura dentium rotarum.” In: *Novi Commentarii Academiae Scientiarum Petropolitanae* t. 11, 1767, pp. 207–231.

that in gearing, the tooth profile sliding is inevitable. As for the shape of the teeth, *Euler* in this paper did not succeed in going beyond what was already done by *Camus*. However, the second paper by *Euler* (see Figure 30.13) [36] (written presumably 10 years later) is very original. In this next paper on gearing [36], *Euler* also shows the grasp and precision of his great mathematical mind. He specifically states the conditions:

- Uniform rotary motion of both gears
- In the mutual action of the teeth *nullus atritus oriatur* (no interference between the mating teeth flanks) [however, a gap between the mating teeth flanks, that is, equality of base pitches of the mating gears is not considered yet]

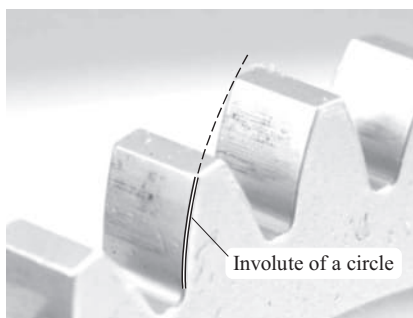


**FIGURE 30.14** Involute gear teeth.

The following conclusion can be drawn up from the discussion above:

**Conclusion 30.1.** *The scientific theory of gearing originated from two famous Euler's papers on the geometry of the ideal shape of gear teeth in parallel-axes gearing.*

*The scientific theory of gearing is tightly associated with the application of an involute of a circle to shape gear teeth in parallel-axes gearing. Although the involute of a circle was known to mathematicians long before the time, when L. Euler has carried out his research on the shape gear teeth, it was L. Euler who proposed to use the involute of a circle in the design of geometrically accurate parallel-axes gearing.*

By now, the kinematics and geometry of parallel-axes involute gearing, both, are investigated so extensively that there is no need to discuss gearing of this design here more in detail, as it is trivial, and is outlined in textbooks on machine and mechanisms science.

### 30.2.2.2 The Euler-Savary Formula

Written by *Euler*, the two papers on gear wheels [35,36] are part of a development that started essentially with the investigation of the ordinary *cycloid*: the curve described by a point on the circumference of a circle when this circle rolls without slipping on a straight line [61]. In this paper [36] *Euler* derived a formula that is equivalent to the *Euler-Savary formula*<sup>22</sup> in the present-day interpretation. It is remarkable that although *Euler* was merely studying a very specific subject, gear wheels, the *Euler-Savary*<sup>23</sup> formula belongs from a modern point of view to planar theoretical kinematics and has general validity. *Euler* in this context also discovered the so-called involute gearing, nowadays the most popular form of gearing (see Figure 30.14).

When a planar motion is considered at a particular instant of time, a modern kinematician thinks of a particular position of a moving axode in relation to a stationary axode. The point where the two curves touch each other is the *instantaneous center of rotation* (or the *pitch point*, in other terminology). Clearly, an arbitrary point *P* of the moving plane describes a curve in the stationary plane. At a particular moment under consideration, point *P* coincides with a particular point of the curve that it traces. The tangent to the curve in this particular point can be constructed easily by means of the pitch point. How about the center of curvature at this particular point? Nineteenth century kinematicians have extensively studied the relation between the points of the moving plane and the corresponding centers of curvature of their trajectories in the stationary plane. This particular relation has many properties.

<sup>22</sup>The consequences drawn up from the *Euler-Savary formula* (the *involute tooth profile*, and the *conjugate action law*) are important to the theory of gearing, while the formula itself is of less importance.

<sup>23</sup>Félix Savary (October 4, 1797–July, 15, 1841) was a French mathematician and mechanician.



The *Euler's* approach is outlined in the excellent paper by *Koetsier, T.* [61]. Refer to Figure 30.15a, where an arbitrary configuration of two interacting planar curves is shown. The stationary axode is  $\pi_1$ . The moving axode is  $\pi_2$ . The point  $O$  at which the two axodes touch each other is the instantaneous center of rotation (or pitch point) at the moment that we are considering. The  $k_2$  is a curve in the moving plane. The  $k_1$  is the envelope in the stationary plane of the set of positions in the stationary plane of  $k_2$ . In the position under consideration, the curves,  $k_1$  and  $k_2$ , touch each other at the point  $C$ . The points  $N_1$ ,  $N_2$ ,  $M_1$ , and  $M_2$  are, correspondingly, the centers of curvature of the planar curves  $k_1$ ,  $k_2$ ,  $\pi_1$ , and  $\pi_2$ , corresponding to the points  $C$  and  $O$ . Let  $\theta$  be the angle between the common tangent to the axodes and the common perpendicular at  $C$  to the curves  $k_1$  and  $k_2$ . Then the following expression is valid:

$$\left( \frac{1}{ON_1} - \frac{1}{ON_2} \right) \cdot \sin \theta = \frac{1}{OM_1} - \frac{1}{OM_2} \quad (30.1)$$

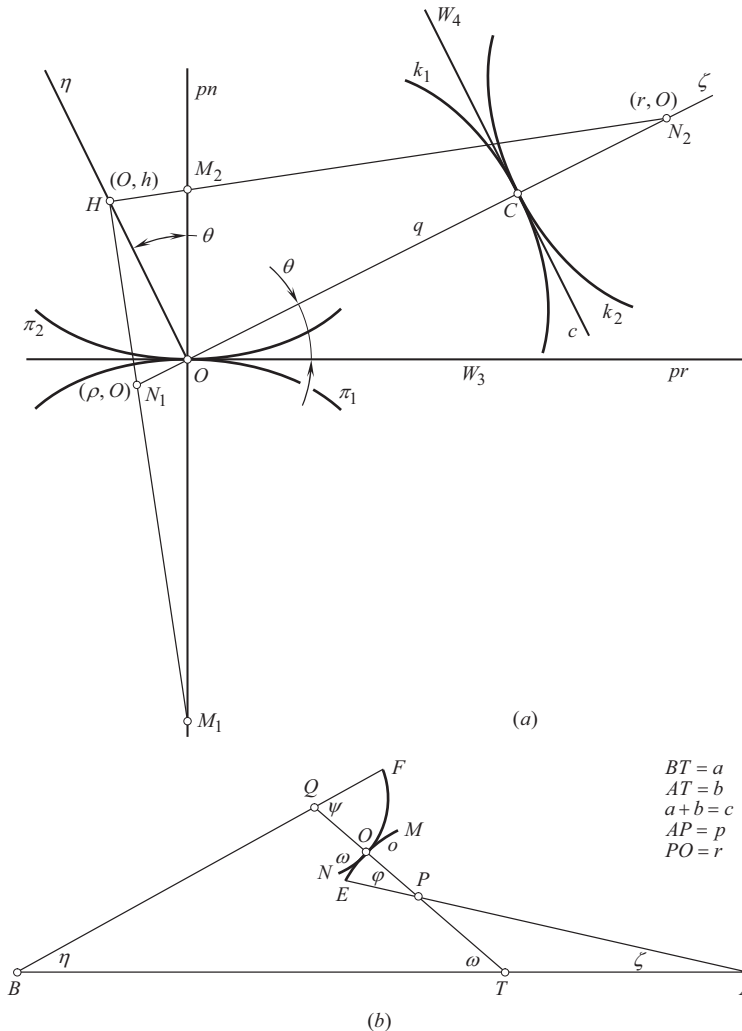


**FIGURE 30.15** The schematics used by *L. Euler* for the derivation of the involute gear tooth profile. [Adapted from: Euler, L. "Supplementum. De Figura Dentium Rotarum." *Novi Commentarii adacemiae Petropolitanae*, t. 11, 1767, pp. 207–231. (E330, *Opera omnia*, 17, pages 196–219)], [36]: (a) an arbitrary configuration of two interacting planar curves; (b) a moment,  $M_A$ , about the center  $A$  yields a moment,  $M_B$ , about the center  $B$ ; (c) derivation of Equation (30.3); (d) the moment when involute gearing has been discovered [61].

(Continued)

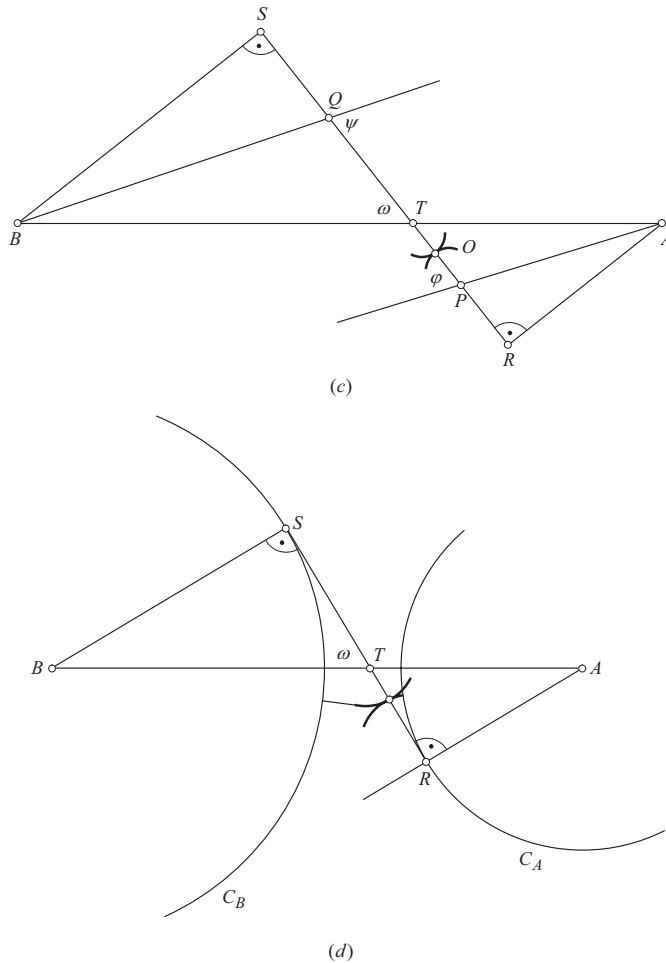


**FIGURE 30.15 (CONTINUED)** The schematics used by *L. Euler* for the derivation of the involute gear tooth profile. [Adapted from: Euler, L. “Supplementum. De Figura Dentium Rotarum.” *Novi Commentarii adademiae Petropolitanae*, t. 11, 1767, pp. 207–231. (E330, *Opera omnia*, 17, pages 196–219)], [36]: (a) an arbitrary configuration of two interacting planar curves; (b) a moment,  $M_A$ , about the center  $A$  yields a moment,  $M_B$ , about the center  $B$ ; (c) derivation of Equation (30.3); (d) *the moment when involute gearing has been discovered* [61].

This is the *Euler-Savary formula*, or theorem. The variables  $ON_1$ ,  $ON_2$ ,  $OM_1$  and  $OM_2$  correspond to the directed line segments, and are signed values. The pitch point,  $O$ , is the origin of a *Cartesian* coordinate system with  $pr$  as positive  $x$  – axis, and  $pn$  as positive  $y$  – axis. Similarly,  $O$  is also the origin of a *Cartesian* coordinate system  $O\xi\eta$  with directed line segment  $OC$  defining the positive direction of the  $\xi$  – axis. The two systems have the same orientation. As for the signs of the variables in the *Euler-Savary formula*,  $ON_i$ , is positive if moving from  $O$  to  $N_i$  is a move in the direction of the  $\xi$  – axis.  $OM_i$  is positive if moving from  $O$  to  $M_i$  is a move in the direction of the  $x$  – axis.

A modern proof of the *Euler-Savary formula* was given in 1970 by *G.R. Veldkamp* [213].

### 30.2.2.3 Leonhard Euler and the Euler-Savary Formula

In his papers on gears [35,36], *Euler* didn’t investigate general planar motion at a particular instant of time. Instead, he investigated the form of the teeth of gear wheels. The general validity of the formula that he discovered is an accidental spin-off of his research [61]. This arises because, in general, just as for first- and second-order properties, a planar motion at a particular instance can

be represented by a circle rolling without slipping on another circle. This is exactly what we are dealing with when we have planar circular gear wheels fulfilling the *Euler's* condition of a constant velocity ratio [61].

*Euler's* papers on the ideal shape of gear teeth are part of the research earlier undertaken by *Ch. Camus* [17]. *Euler* discovered an expression for the relationship that is nowadays called the *Euler-Savary formula*, a result concerning radii of curvature in instantaneous planar kinematics.

*Euler* started with Figure 30.15b. The points *A* and *B* are the centers of the two wheels. The curves, *EOM* and *FON*, are the two profiles of the teeth of the wheels. *O* is the point where the two profiles touch and the line perpendicular to the tangent in *O* cuts *AB* in the point *T*. When the gear wheels rotate, a moment  $M_A$  about the center *A* yields a moment  $M_B$  about the center *B*. It is easy to see that at the instant of time under consideration, the ratio of these two moments equals  $BT / AT$ . *Euler* argues that the condition of a constant velocity ratio implies that the ratio of these two moments must be constant, which leads to a kinematical result:

*The common normal at the point where the profiles touch each other intersects AB in a stationary point T.*

This statement by *Euler* is equivalent to what is now known as the *conjugate action law in parallel-axes gearing* [174].

From the modern point of view, point *T* is the pole of the motion of the two gear wheels with respect to each other. The axodes of the two gear wheels are two circles, one of which is centered at *A*, and another one is centered at *B*. The two circles touch one another at point, *T*. *Euler* has proved a kinematical result by means of a dynamical argument.

After making clear that the point *T* is stationary, *Euler* determined several relations between the parameters depicted in Figure 30.15b, and differentiated them. He basically considered a slight change in the position of the two profiles with respect to each other, using the fact that the common normal intersects the center-distance, *AB*, always at the stationary point *T*. After some calculations are executed, this reveals that the ratio of the angular velocities,  $d\eta / d\xi$ , is equal to the ratio  $TA/TB$ . For an arbitrary configuration of the profiles, *Euler* then derives the following expression that enabled him, in principle, to calculate the actual value of the radius of curvature  $\rho'$  of the profile *NOM* out of the parameters of profile *EOM* :

$$\rho' = c \cdot \cos \omega - r - p \cdot \cos \varphi - \frac{b^2 \cdot \cos \omega \cdot d(p \sin \varphi)}{c \cdot d(p \cdot \sin \varphi) - a^2 \cdot d\varphi \cos \omega} \quad (30.2)$$

The explanation for the parameters in Eq. (30.2) can be found in Figure 30.15b.

In a particular configuration, one can assume, without loss of generality, that the profile *EOM* is a circle and that the center of curvature of the profile *NOM* coincides with *Q*. Then, the equalities,  $dp = 0$  and  $\rho' = OQ$ , are valid. Moreover, if the foot points of the perpendiculars from, respectively *A* and *B*, on the line *PQ* (see Figure 30.15c), are designated as *R* and *S*, then it can be shown that Eq. (30.2) implies:

$$RT \cdot SQ \cdot TP + ST \cdot RT \cdot TQ = 0 \quad \text{or} \quad \frac{RT \cdot TP}{RP} + \frac{ST \cdot TQ}{SQ} = 0 \quad (30.3)$$

This is the *Euler's* version of the *Euler-Savary formula*.<sup>24</sup> It can be shown that Eq. (30.3) is equivalent to Eq. (30.1).

The *Euler-Savary formula* has an amazing interpretation. It turns out that when *p* coincides with *R*, then *Q* coincides with *S*. Naturally *Euler* considered the possibility that this is the case during the

<sup>24</sup>Félix Savary was the first to derive the *Euler-Savary formula* in its modern form. *Savary's* proof can be found in: *Leçons et cours autographiés, Notes sur les machines*, par le professeur F. Savary, Ecole Polytechnique, 1835–1836 (unpublished lecture notes; available in the Bibliothèque Nationale in Paris).

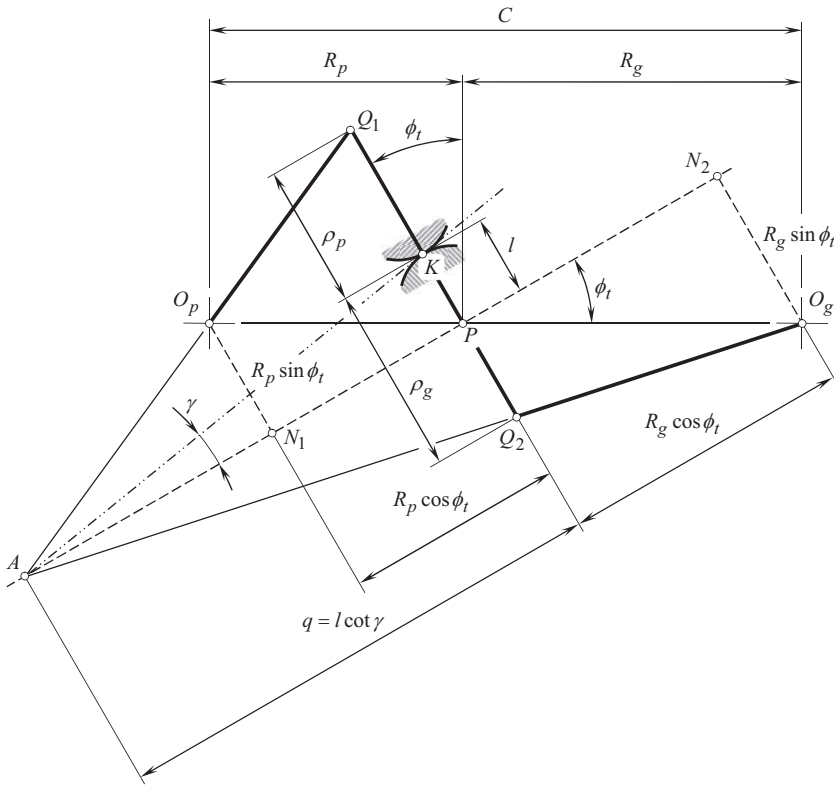


**FIGURE 30.16** Schematic of the equivalent three-bar mechanism that is used nowadays for the derivation of *Euler-Savary formula*.

entire motion. The profiles then are involutes of the circles  $C_B$  and  $C_A$  (see Figure 30.15d). *At this moment involute gearing has been discovered* [61].

In Figure 30.16, a schematic of the equivalent three-bar mechanism that is used nowadays for the derivation of *Euler-Savary formula* is shown. In particular, a formula for the calculation of an actual value of the radius of curvature,  $\rho_p$ , is derived based on the similarity of the triangles  $\triangle AQ_1P$  and  $\triangle AO_pN_1$ . A formula for the calculation of an actual value of the radius of curvature,  $\rho_g$ , is derived based on the similarity of the triangles  $\triangle AO_gN_2$  and  $\triangle AQ_2P$ .

A reduced case of the equivalent three-bar mechanism that is used nowadays for the derivation of an involute gear tooth profile is shown in Figure 30.17. The joints are located at points  $Q_1^*$  and  $Q_2^*$ , instead of points  $Q_1$  and  $Q_2$  correspondingly.

The proposed by *L. Euler* parallel-axes involute gearing with zero axes misalignment, and zero displacements deserves to be referred to as *Eulerian gearing*, or simply as  $E_u$  – gearing.<sup>25</sup>

### Definition 30.1

Eulerian gearing (or just  $E_u$  – gearing, for simplicity) is a kind of parallel-axes involute gearing that features zero axes misalignment/displacement.

<sup>25</sup> Such a terminology can be used for scientific purposes (but not only), similar to that the terms *Newtonian fluid*, *absolutely rigid body*, *absolutely black body*, and so forth, that can be easily found in the public domain.



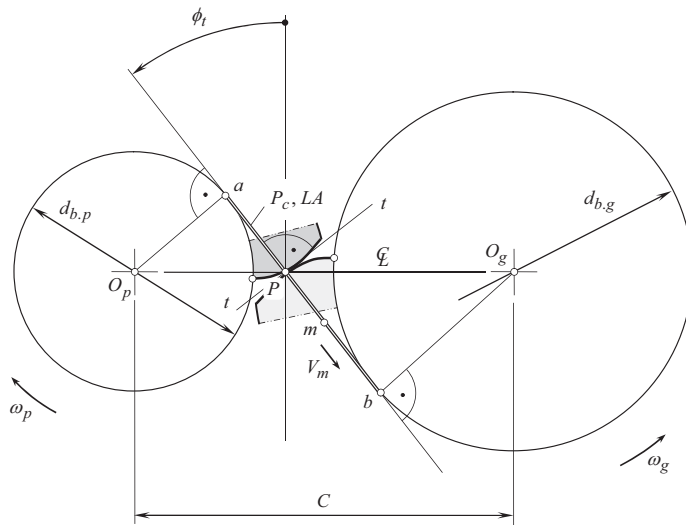


**FIGURE 30.18** Schematic of the *equivalent pulley-and-belt transmission* (for parallel-axes gearing).

*L. Euler* and *F. Savary*<sup>26</sup> together have devised an analytical method for determining the curvature centers of gear teeth flanks.

The importance of the *conjugate action law* worked out by *L. Euler* (gears designed according to this law have a steady speed ratio), became correctly realized much later.<sup>27</sup>

For over a century, the invention of the involute tooth profile was not used in practice. The Industrial Revolution in Britain in the eighteenth century saw an explosion in the use of metal gearing. The science of gear design and manufacture rapidly developed through the nineteenth century. The invention and the beginning of the application of steam and gas turbines that operate at high rotations and produce lots of power immediately turn the attention of engineers to involute gearing.

It should be stressed here that the concept of the *gear/pinion base pitch* (linear base pitch), as well as the concept of the *operating base pitch* (linear operating base pitch in the gear pair) in a parallel-axes gear pair was not known in the time of *L. Euler*.

#### 30.2.2.4 Equivalent Pulley-and-Belt Transmission

After the *conjugate action law* for parallel-axes gearing has been formulated by *L. Euler*, it can be assumed that approximately at this time the importance of the so-called *equivalent pulley-and-belt transmission* was realized. The *equivalent pulley-and-belt transmission* is a powerful means for the analysis of parallel-axes gearing.

For more in-detail analysis of the *equivalent pulley-and-belt transmission*, refer to Figure 30.18. Here, the directions of rotation of the driving and driven gears are reversed compared to that in *equivalent pulley-and-belt transmission*, as a driven pulley is *pulled* by the belt, while the driven gear is *pushed* by the driving gear.

For correctly designed tooth flanks of a gear and its mating pinion, contact point of the tooth flanks,  $\mathcal{S}$  and  $\mathcal{P}$ , traces a straight path of contact,  $P_c$ . When friction is not taken into account, a force is acting perpendicular to the common tangent plane,  $t-t$ , to the tooth flanks,  $\mathcal{S}$  and  $\mathcal{P}$ , through  $P$ . As long, as friction is not accounted, the acting force is always perpendicular to the tooth flanks,  $\mathcal{S}$

<sup>26</sup> *Félix Savary* was the first to derive the *Euler-Savary formula* in its modern form. *Savary's* proof can be found in : *Leçons et cours autographiés*, Notes sur les machines, par le professeur F. Savary, Ecole Polytechnique 1835–1836 (unpublished lecture notes; available in the Bibliothèque Nationale in Paris).

<sup>27</sup> There is no evidence on whether or not *Euler* stressed [35,36] on the difference between the line of action,  $LA$ , and the path of contact,  $P_c$ .

and  $\mathcal{P}$ , at current point of their contact. The straight line of action,  $LA$ , is aligned with the straight path of contact,  $P_c$ , that is, in geometrically accurate parallel-axes gearing the following identity  $LA \equiv P_c$  is observed at every instant of time when the gears rotate.

To the best of the author's knowledge, it is not yet known when exactly the *equivalent pulley-and-belt transmission* was proposed, and who has to be credited with the invention of this scientific tool.<sup>28</sup>

The accomplishments in the theory of gearing in the time when the fundamental contribution by *L. Euler* has been done, are briefly summarized immediately below:

- It is proven by *L. Euler* in the mid of eighteenth century that involute tooth profile feet have the best parallel-axes gearing
- The fundamental theorem of parallel-axes gearing (the *conjugate action law of parallel-axes gearing*) is known due to *Euler*, and *Savary*
- There is no evidence that a difference between the line of action,  $LA$ , and the path of contact,  $P_c$ , was realized by *Euler* and *Savary*, mainly because in cases of parallel-axes gearing these two lines align with each another
- No significant accomplishments at that time were done in the area of intersected-axes gearing as well as crossed-axes gearing

The invention of the involute tooth profile for parallel-axes gearing is one of the cornerstone accomplishments in the scientific theory of gearing. This achievement is referred to as *the origin of the scientific theory of gearing*.

Later on, during the Industrial Revolution, gear design and manufacture rapidly evolved and were properly documented.

### 30.2.3 POST-EULERIAN PERIOD OF EVOLUTION OF THE THEORY OF GEARING

The necessity of the theory of gearing for the needs of gear practitioners is realized for a long while. Since the time when *L. Euler* carried out his research on involute gearing, the scientific theory of gearing got a significant impulse. Numerous contributions to the scientific theory of gearing have been done in the post-*Eulerian* period of evolution of the gear theory. Principal accomplishments in the scientific theory of gearing are outlined below in a chronological order.

#### 30.2.3.1 Robert Willis and the Fundamental Theorem of Parallel-Axes Gearing

In the nineteenth century, a profound investigation of mechanisms in general sense has been undertaken by *Robert Willis*<sup>29</sup> (see Figure 30.19). In his 1841 book [222] titled *Principles of Mechanisms* (see Figure 30.20), *R. Willis* compiled the lectures for his students, and knowledge about gears which could be used in practice. In the book, gearing was discussed by the author to the best extent possible in his time.

Despite the *fundamental theorem of parallel-axes gearing* was already known to *L. Euler*, and to *F. Savary*, this theorem got an extensive recognition in Europe due to publication of it in the famous book by *Robert Willis* [222]. This is the reason in Europe the *fundamental theorem of parallel-axes gearing* is often referred to as the *Willis' theorem*. The latter is incorrect.

In the present days, the *fundamental theorem of gearing* is known (see Figure 30.21) mainly due to the 1841 book by *R. Willis* [222]:

<sup>28</sup> The *equivalent pulley-and-belt transmission* of a gear pair in both, in intersected-axes gearing, as well as in crossed-axes gearing, for the first time ever, was proposed (~2008) by Prof. *S.P. Radzevich* [174]. Two base cones in tangency with the plane of action were considered [174] in this analysis.

<sup>29</sup> Reverend Robert Willis (February 27, 1800–February 28, 1875), an English academic, was a professor at Cambridge.



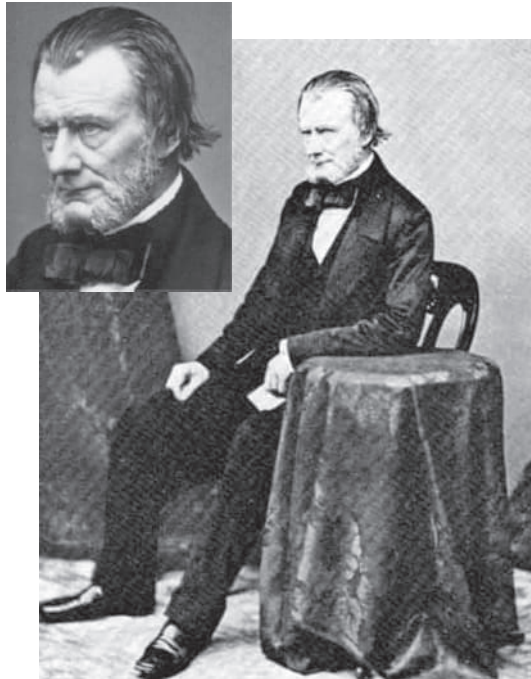


**FIGURE 30.19** Reverend Robert Willis (1800–1875).

**Fundamental theorem of parallel-axes gearing (according to R. Willis):** *The angular velocities of the two pieces are to each other inversely as the segments into which the “line of action” divides the line of centers, or inversely as the perpendiculars from centers of motion upon the line of action.*

As the theorem was known to *Euler* and to *Savary* long before *Willis*, and because *Camus* was very close to discover this theorem, nowadays the *fundamental theorem of parallel-axes gearing* is commonly referred to as *Camus-Euler-Savary fundamental theorem of gearing* (or just as to *CES – theorem of gearing*, for simplicity). It is evident that the contribution by *Camus* is also covered by the term *CES – theorem of gearing*.

As already stressed in this chapter of the book, in parallel-axes gearing, the line of action,  $LA$ , and the path of contact,  $P_a$ , represent two different straight lines that are congruent to one another. The *fundamental theorem of parallel-axes gearing* gives an insight into the importance and the necessity of how to make difference between these two lines,  $LA$  and  $P_a$ . Unfortunately, in the meantime, this difference is not realized at all by the most of gear researchers.

Generalizing *CES – theorem of gearing* to a case of crossed-axes gearing, one can come up with a conclusion (~2008, Prof. *S.P. Radzevich*), according to which:

**Fundamental theorem of gearing (general case):** *Two smooth regular surfaces, that travel in relation to one another, are referred to as “conjugate surfaces” if and only if the surfaces contact each other along a line, and a common perpendicular through every point of the line of contact intersects the axis of instantaneous rotation of the surfaces, and further.*

**Conjugate spatial curves:** *Two (spatial) curves within two smooth regular surfaces, that travel in relation to one another, are called “conjugate curves” if and only if the curves are always in contact, and a common perpendicular through contact point intersects the axis of instantaneous rotation of the surfaces.*

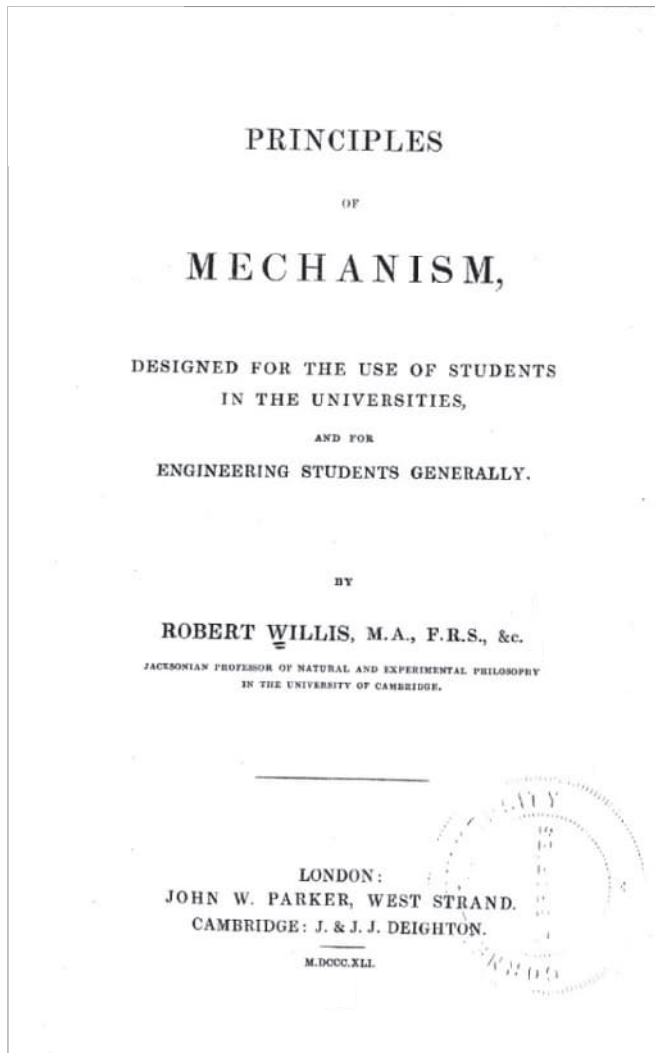


**FIGURE 30.20** Title page of the book: Willis, R., *Principles of Mechanisms, Designed for the Use of Students in the Universities and for Engineering Students Generally*, London, John W. Parker, West Stand, Cambridge: J. & J.J. Deighton, 1841, 446p.

*Reversibly enveloping surfaces* (or  $R_e$  – surfaces, for simplicity), and *reversibly enveloping curves* (or  $R_e$  – curves, for simplicity) are the other terms for conjugate surfaces, and conjugate curves [155].

### 30.2.3.2 A Mistake (1842) Committed by *Theodore Olivier*

The research in the field of theory of gearing has been significantly affected by *Theodore Olivier*<sup>30</sup> (see Figure 30.22). As early as in 1842 a monograph by *Th. Olivier* on the theory of gearing [95]

<sup>30</sup>Théodore Olivier (January 21, 1793–August 5, 1853), a French mathematician and engineer.

At the beginning of his career, Olivier was interested in a special kind of spur or bevel gear that was claimed in 1810, by an engineer named *White* whose biography is unknown, to be frictionless. Such an outcome seems to contradict Euler's work on tooth profiles. According to Olivier, who oddly misspelt *White* as *With* in 1839, see: Olivier, Th., "Recherches géométriques sur les engrenages de With," (*With* is a misspelling of *White*). (This memoir is followed by what was presented at the French Academy of Sciences on the same topic in 1825, pp. 304–316), *Journal Math. Pures et Appliquées*, **4**, 1839, pp. 281–303. Olivier, Th., "Note sur les engrenages de White," *Journal Math. Pures et Appliquées*, **5**, 1840, pp. 146–153. *White* was not a geometer and consequently was unable to prove the astonishing property of this gearing.

38. If the line of direction of the link in link-work, of the common normal to the curves in contact motion, and of the connector in wrapping motion, be severally termed the line of action, we can express the separate propositions which relate to the Velocity Ratio, by saying that the angular velocities of the two pieces are to each other inversely as the segments into which the *line of action* divides the line of centers, or inversely as the perpendiculars from the centers of motion upon the line of action.

I have confined these investigations, for the present,

**FIGURE 30.21** The fundamental theorem of parallel-axes gearing as formulated in: Willis, R., *Principles of Mechanisms, Designed For the Use of Students in the Universities and for Engineering Students Generally*, London, John W. Parker, West Stand, Cambridge: J. & J.J. Deighton, 1841, 446p.



**FIGURE 30.22** *Théodore Olivier* (1793–1853).

was published. This monograph (see Figure 30.23) is the first known monograph<sup>31</sup> ever to be titled *Geometric Theory of Gearing* (*Théorie Géométrique des Engrenages*).

In his 1842 book [95], *Th. Olivier* proposed two principles of generation of gear teeth. These principles are commonly referred to as the *first*, and the *second Olivier's principles of generation of envelope surfaces*. Later on, both these principles got an extensive usage by gear scientists. Unfortunately, *Th. Olivier* considered tooth flanks,  $\mathcal{S}$  and  $\mathcal{P}$ , of a gear and its mating pinion just as the envelope surfaces (that is insufficient), and not as conjugate surfaces.

<sup>31</sup> Therefore, it is incorrect to claim that *F. Litvin* is the author of the *first book on the theory of gearing* [Litvin, F.L., *Theory of Gearing*, Moscow, Nauka, 1960], as numerous gear experts of Russia often do.

It is likely the 1842 book by Th. Olivier (Olivier, T., *Théorie Géométrique des Engrenages destinés*, Bachelier, Paris 1842, 118 pages.) [95] is the first book ever titled as *Theory of Gearing*. This book by Th. Olivier is followed by 1852 book by E. Sang (Sang, E., *New General Theory of the Teeth of Wheels*, Edinburgh, 1852.) [194], then by 1886 master thesis by H.I. Gochman (Gochman, H.I., *Theory of Gearing Generalized and Developed Analytically*, Odessa, 1886, 229 pages.) [44], as well as by numerous others books on the topic, published later. All the books published so far under the title *Theory of Gearing* (starting from the first 1842 book by Th. Olivier [95], and ending with the latest publications in the field – by the year of ~2010) consist no scientific *theory of gearing*. These books cannot be referred to as a theory of gearing, rather they represent collections of know achievements in the field of gearing, having no ability to predict novel unknown designs of gears and gearing.

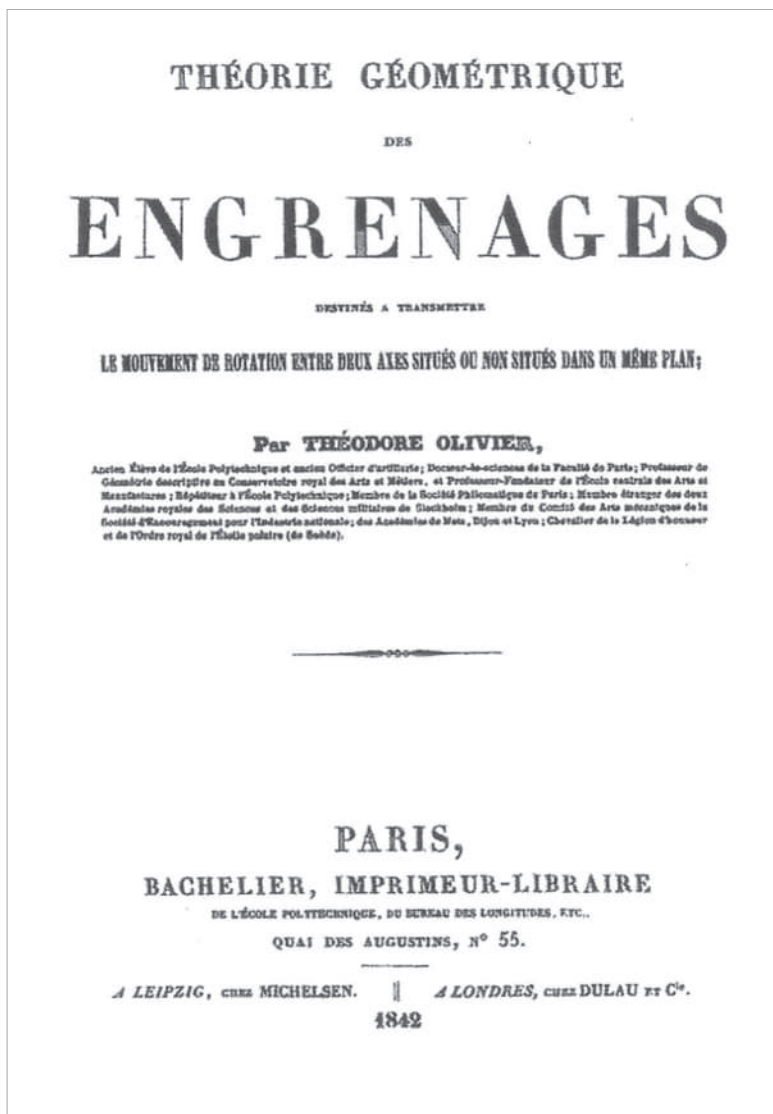


**FIGURE 30.23** Title page of the first ever monograph on gearing published by Olivier, Th., *Théorie Géométrique des Engrenages destinés*, (*Geometric Theory of Gearing*), Bachelier, Paris 1842, 118 pages.

Graphical methods developed in descriptive geometry were extensively used by *Th. Olivier* in this book [95].

In general case of gear meshing, both the principles proposed by *Th. Olivier*, are incorrect (~2008, Prof. *S.P. Radzevich*), as the condition of conjugacy of the interacting tooth flanks of a gear,  $\mathcal{G}$ , and its mating pinion,  $\mathcal{P}$ , is not taken into account (the condition of conjugacy is just ignored).

The research carried out by *Th. Olivier* significantly affected the evolution of gear science. The 1842 mistake, committed by *Th. Olivier* in the gear science, misleads the gear experts all around the world for over a century and a half. This mistake still misleading the gear experts even now. Tons of research in the gear science and gear application had no chance for success due to this mistake even before the research started.

The violation of the conjugate action law is a huge mistake committed by *Th. Olivier*.



**FIGURE 30.24** *Thomas Tredgold (1788–1829).*

Due to the mistake committed by *Th. Olivier*, no geometrically accurate gears can be designed, and only geometrically inaccurate (approximate) gears can be designed instead. There is no chance to anticipate any significant improvements if gears are designed following the *Olivier principles*. Therefore, *Th. Olivier*, cannot be considered as a co-founder of the scientific theory of gearing, as his accomplishments are a kind of mistake that has negatively affected the further development of the gear science.

### 30.2.3.3 Miscellaneous Improvements to the Gear Art

The second known monograph on the theory of gearing has been published in 1852 by *E. Sang* [194]. This book, titled as *A New General Theory of the Teeth of Wheels*, is nothing more rather than a collection of the known achievements in the field of gearing. Therefore, the contribution by *E. Sang* to the theory of gearing is at least doubtful.

Among the experts in the field of gearing in that period of time the name *Thomas Tredgold*<sup>32</sup> (see Figure 30.24) should be mentioned as well. As a gear person, he is mostly known for approximation of bevel gears (i.e., of intersected-axes gears) by cylindrical gears (i.e., by parallel-axes gears). The proposed approximation, namely, the so-called *Tradgold approximation*, significantly simplifies the calculation of bevel gearing in engineering practice.

Proposed by *A.C. Semple*<sup>33</sup> in the first half of the nineteenth century (1848), the curved tooth configuration in their lengthwise direction captured the interest of many mechanical engineers and inventors.

### 30.2.3.4 The Research Carried Out by *Chaim Gochman*

One more effort to evolve the theory of gearing was undertaken by *Chaim Gochman*<sup>34</sup> (1851–1916) in 1886 (see Figure 30.25). In his master's thesis (see Figure 30.26), he converted the results earlier obtained by *Th. Olivier* (who used primarily graphical methods for solving problems in the field of gearing) into those same results, obtained by means of the methods developed in analytical geometry [44]. As it is stated on page 7 in the research accomplished by *Ch. Gochman* [44], no new scientific results are contributed by *Gochman* to those earlier obtained by *Olivier* [95]. The interested

<sup>32</sup> Thomas Tredgold (August 22, 1788–January 28, 1829), an English engineer and author.

<sup>33</sup> U.S. Patent No. 5,647, *Rack and Pinion*, *Amzi C. Semple*, June 27, 1848.

<sup>34</sup> Chaim I. Gochman (1851–1916), was a Russian (of Jewish origin) mechanician (Novorossiysk University, Odessa, now in Ukraine).





**FIGURE 30.25** *Chaim I. Gochman (1851–1916).*

reader is referred to [164] for details on this research. (Taking into account this later conclusion, the accomplishments by *Th. Olivier*, and those by *Ch. Gochman*, below are considered together).

Like it has been done earlier by *Th. Olivier* [95], *Ch. Gochman* in his master's thesis [44] loosely considered tooth flanks of a gear and a mating pinion only as envelope surfaces to one another. The requirement of conjugacy of the mating tooth flanks was ignored, which is a huge mistake. Fulfillment of the condition of contact is sufficient only in the cases when *no* rolling motion is observed. Otherwise, this condition needs to be complemented with (a) the condition of conjugacy, and (b) the equality of a gear base pitch and its mating pinion base pitch to the operating base pitches of a gear pair [174].

It must be clearly realized that the terms *conjugate surfaces* and *envelope surfaces* are not equivalent to one another: all conjugate surfaces are enveloping to each other, but NOT vice versa – not all envelope surfaces are conjugate to one another. In detail, the mistake committed by *Th. Olivier* [95], and later repeated by *Ch. Gochman* [44], is discussed by Prof. *S.P. Radzevich* [164].

The bottom-line of this discussion is as follows: there is no chance to develop a scientific theory of gearing taking into account only the condition of contact of tooth flanks of a gear and a mating pinion, and ignoring:

- a. the condition of conjugacy of the interacting tooth flanks
- b. equality of base pitch of a gear and that of a mating pinion to operating base pitch of the gear pair, and so forth

The direction of evolution of the gear science that strictly follows the *Olivier-Gochman* approach, represents the dead end in the evolution of the theory of gearing.



**FIGURE 30.26** Title page of Master Thesis by Ch. Gochman: *Theory of Gear Teeth Engagement, Generalized and Developed by Implementation of Mathematical Analysis*, Odesa (Ukraine), 1886, 229 pages.

The condition of proper meshing in geometrically accurate gearing was understood by *Euler*, by *Savary*, and later on by *R. Willis*. The conjugate action law was ignored by *Th. Olivier*, and by ALL of the followers of this approach in the gear science (*Gochman*, *Litvin*, and others).<sup>35</sup>

### 30.2.3.5 Equality of Base Pitches in Geometrically Accurate Parallel-Axes Gearing

The interaction of tooth flanks,  $\mathcal{S}$  and  $\mathcal{P}$ , of a gear and its mating pinion to a certain extent can be construed as that in a cam mechanism, especially in cases when just one pair of teeth is engaged in mesh. It is common in gearing that two, or even more pairs of teeth are engaged in mesh at that same time. In order to make multiple engagements possible, base pitch in interacting tooth flanks,  $\mathcal{S}$

<sup>35</sup> Later on, that same mistake was committed by *Ch. Gochman* (1886), the Russian researcher of gears and gearing. This mistake is also observed in all the books by *F. Litvin* (1914–2017), *V.A. Shishkov* [197], *G.I. Shevel'eva* [196], as well as in many other books by the authors, those who adopted the *Olivier's* approach. It is likely Dr. *I.A. Fraifeld* [41] is among those, who was the most affected by the two *Olivier principles*. Generating (finish-hobbing) of gears for *Novikov gearing* is another example where ignorance of the condition of conjugacy resulted in insufficient accuracy of the machined gears.



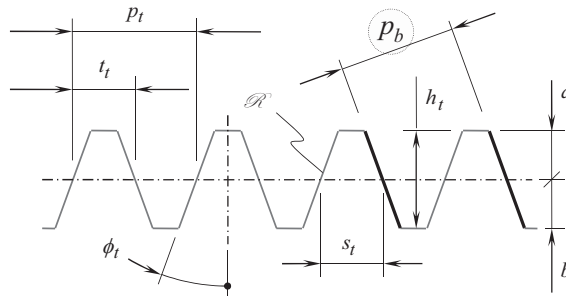


**FIGURE 30.27** Base pitch,  $p_b$ , in a basic rack,  $\mathcal{R}$ .

and  $\mathcal{P}$ , have to be equal to one another, that is, fulfillment of an equality  $p_{b,g} = p_{b,p}$  is a must in geometrically accurate parallel-axes gearing. Here,  $p_{b,g}$  and  $p_{b,p}$  are base pitches (see Figure 30.27) of a gear and a mating pinion, correspondingly. Only involute gears feature base pitch, and only involute gear pairs are capable of transmitting a uniform rotary motion smoothly from a driving shaft to a driven shaft. Gear tooth profiles of no other geometries feature these properties. Gears with non-involute tooth profile feature no base pitches. Therefore, as in non-involute gear pairs base pitches do not exist, thus, they can not be equal, and, ultimately, the gear pair is not capable of transmitting a uniform input rotation smoothly.

The condition according to which base pitches of a gear and that of a mating pinion in a geometrically accurate gear pair have to be equal to one another is an important contribution to the scientific theory of gearing. Unfortunately, no name of a gear researcher is known who was the first to come up with this significant accomplishment in the theory of gearing. Moreover, even the exact date when this accomplishment was attained also is not known. Hopefully, both the name of the gear person and the right date will be identified in the future.

### 30.2.3.6 Geometrically Accurate Worm Gearing

In 1915, *F.J. Bostock* and *Percy Brown* of *David Brown* company (both of the United Kingdom) have invented an involute worm gear drive based on the application of a screw involute surface of the worm thread. The proposed design of worm gearing features point contact of the interacting threads of the worm, and tooth flanks of the worm gear.

### 30.2.3.7 Shishkov Equation of Contact, $\mathbf{n}_g \cdot \mathbf{V}_\Sigma = 0$

The *condition of contact* of interacting tooth flanks of a gear,  $\mathcal{G}$ , and of a mating pinion,  $\mathcal{P}$ , is the first scientific result of fundamental importance that can be used in the foundation of the scientific theory of gearing. The *condition of contact* is also known as the *enveloping condition*. The contact condition states that:

**Condition of contact:** *At every point of contact of tooth flanks of a gear,  $\mathcal{G}$  and a mating pinion,  $\mathcal{P}$ , the projection of the relative velocity vector onto the common perpendicular to the interacting tooth flanks is zero.*

The condition of contact of two interacting tooth flanks in a gear pair is known for centuries. Per the author's opinion, this important condition was already known to *Camus* (1733) [17], or even to *Desargues*. Developed (1875) by *Franz Reuleaux*, the method of common perpendiculars [188,189] utilizes the condition of contact of two interacting surfaces of machine elements.

As the theory of gearing evolves, new additional requirements to the theory arose. Since the time when the gear scientists started realizing the importance of the *condition of contact*, the forms of representation of this condition were different. In particular, the condition of contact (see

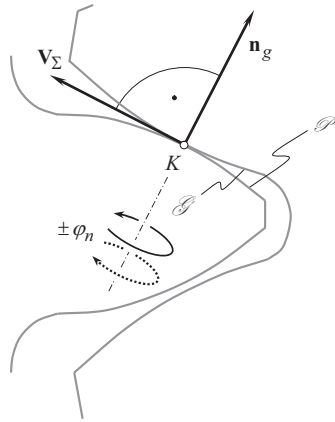


**FIGURE 30.28** Permissible instantaneous relative motions of tooth flanks,  $\mathcal{S}$  and  $\mathcal{P}$ , in gearing that is aligned with the *Law of contact* – the *first fundamental law of gearing*.

Figure 30.28) required an analytical representation. Numerous attempts were undertaken to derive an appropriate equation that reflects the proper condition of contact of a gear,  $\mathcal{S}$ , and a mating pinion,  $\mathcal{P}$ , tooth flanks.

Various forms of representation of the *condition of contact* were proposed since the time when gear scientists began realizing the importance of this condition. Without going into details of the analysis of this particular problem,<sup>36</sup> it should be stressed here that finally the condition of contact is represented in the form of a simple equation. This equation appears as the dot product of the unit vector of the common perpendicular,  $\mathbf{n}_g$ , at point of contact of the tooth flanks  $\mathcal{S}$  and  $\mathcal{P}$ , and the instantaneous linear velocity vector,  $\mathbf{V}_\Sigma$ , of the resultant relative motion of the tooth flanks,  $\mathcal{S}$  and  $\mathcal{P}$ . When the condition of contact is met, the dot product of these two vectors equals to zero:

$$\mathbf{n}_g \cdot \mathbf{V}_\Sigma = 0 \quad (30.4)$$

This was Prof. V.A. *Shishkov* (see Figure 30.29) who (in the 1940s, but not later 1948<sup>37</sup>) proposed Eq. (30.4) to analytically describe the condition of contact of two tooth flanks,  $\mathcal{S}$  and  $\mathcal{P}$ , (see Figure 30.30) [197,198].

Equation (30.4) is based on the fact that at common point(s) (points of contact, in other words), the linear velocity vector of the instant relative motion of the gear and the mating pinion,  $\mathbf{V}_\Sigma$ , and the unit vector of the common perpendicular,  $\mathbf{n}_g$ , must be perpendicular to one another.

The equation of contact in the form of dot product  $\mathbf{n}_g \cdot \mathbf{V}_\Sigma = 0$  is known as *Shishkov equation of contact* [174,197] and numerous of others. This equation can be viewed as an analytical form of representation of the *method of common perpendiculars*, earlier proposed by F. *Reuleaux*.

The *Shishkov equation of contact* is a valuable contribution to the scientific theory of gearing. Later on, in 1950<sup>th</sup>, *Shishkov equation of contact* was used by F.L. *Litvin*, Ya.S. *Davidov*, and by others. Nowadays, this equation is extensively used by many gear researchers. Unfortunately, this equation is often loosely supposed by less experienced gear experts to be an equation of conjugacy, which is not correct. The interested reader may wish to go to [197] for more details on *Shishkov equation of contact*.

<sup>36</sup>For details on the subject, the interested reader is referred to the paper: Radzevich, S.P., “Concisely on the Kinematic Method and on the History of the Equation of Contact in the Form of  $\mathbf{n}_g \cdot \mathbf{V}_\Sigma = 0$ ,” In: *Theory of Mechanisms and Machines*, 2010, No. 1. Vol. 15, pp. 42–51. <http://tmm.spbstu.ru>.

<sup>37</sup>It could happen that the equation of contact,  $\mathbf{n}_g \cdot \mathbf{V}_\Sigma = 0$ , can be found out even in earlier (before 1948) publications by Prof. V.A. *Shishkov* – in his earlier papers, PhD thesis, and so forth.



FIGURE 30.29 Professor Vasyli A. Shishkov.

### 30.2.3.8 Diagram of Screw (by Professor A.F. Nikolayev) and its Application in Gearing

The diagram of screw (or simply the *screw diagram*) was known in engineering science in the nineteenth century. In 1950, Professor A.F. Nikolayev proposed [88] to use the diagram of screw for the determination of conjugate ruled surfaces with line contact. Diagram of screw is a helpful means for the analysis and investigation of gearing with crossing axes of rotation of a gear and its mating pinion [89]. It is extensively used in the present-day practice.

### 30.2.3.9 Principal Planes, and Reference Systems Associated with Gear Pair

For a gear pair with a specified set of the design parameters, a corresponding gear vector diagram for the rotations (as well as for the torques) can be constructed. Several principal directions are associated with a gear pair [174]. These directions are defined in terms of:

- a. the rotation vector of a gear, and that of a mating pinion
- b. the instantaneous rotation vector, and
- c. the centerline.

The use of the principal directions allows for the construction of a set of principal planes, and principal reference systems associated with a gear pair. By means of the principal planes, and principal reference systems, the analysis of gearing of all kinds can be significantly simplified.

A set of principal planes is comprised of *pitch-line plane* (or just  $P_{ln}$  – *plane*, for simplicity), *centerline plane* (or just  $C_{ln}$  – *plane*, for simplicity), *normal plane* (or just  $N_{ln}$  – *plane*, for simplicity), and the plane of action,  $PA$ . These planes are shown in Figure 30.31:

*Pitch-line plane* is the plane through the axis of instantaneous rotation,  $P_{ln}$ , and the centerline,  $\Phi$ , of the gear pair

*Centerline plane* is the plane through the centerline,  $\Phi$ , of the gear pair perpendicular to the pitch line,  $P_{ln}$

*Normal plane* is the plane through the plane-of-action apex,  $A_{pa}$ , perpendicular to the centerline,  $\Phi$ , of the gear pair

*Plane of action* is the plane through the axis of instantaneous rotation,  $P_{ln}$ , at a transverse pressure angle,  $\phi_{t,\omega}$ , with respect to the centerline,  $\Phi$ , of the gear pair.



**FIGURE 30.30** Title page of the 1951 monograph by Prof. V.A. Shishkov [198].

Introduced by Prof. *S.P. Radzevich* [174], this set of planes is referred to as the *set of principal planes* associated with a gear pair.

A set of main reference systems is associated with the gear vector diagram as shown in (see Figure 30.32). The rotation vectors  $\omega_g$  and  $\omega_p$  of a gear, and that of a mating pinion are at a certain center-distance,  $C$ , and cross one another at a certain crossed-axes angle. Points  $A_g$  and  $A_p$  are points of intersection of the gear axis of rotation,  $O_g$ , and the pinion axis of rotation,  $O_p$ , correspondingly, with the centerline,  $\mathfrak{L}$ . The point  $A_g$  is referred to as the *gear base cone apex*, and the point  $A_p$  is referred to as the *pinion base cone apex*. The vector of instant rotation,  $\omega_{pl}$ , of the pinion in relation to the gear is a vector through the point  $A_{pa}$ . This point is located within the centerline,  $\mathfrak{L}$ . The point  $A_{pa}$  is referred to as the *plane-of-action apex*.

Having the set of the principal planes constructed, a set of main reference systems is introduced:

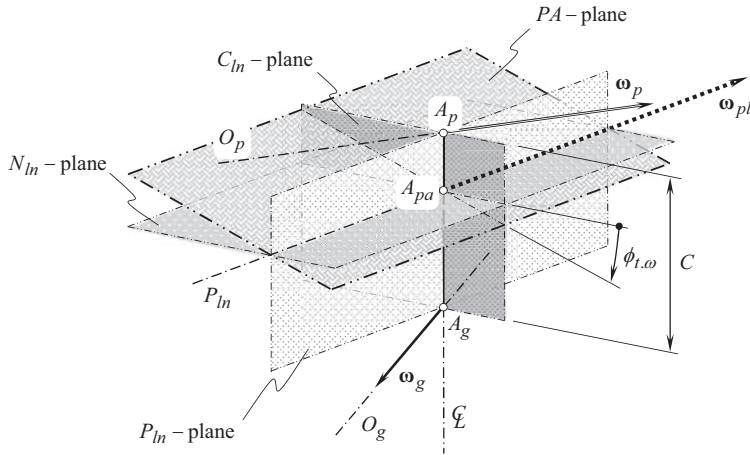


**FIGURE 30.31** Set of principal planes, associated with a gear pair: the pitch-line plane (the  $P_{in}$  – plane), the centerline plane (the  $C_{in}$  – plane), the normal plane (the  $N_{in}$  – plane), and the plane of action (the  $PA$  – plane).

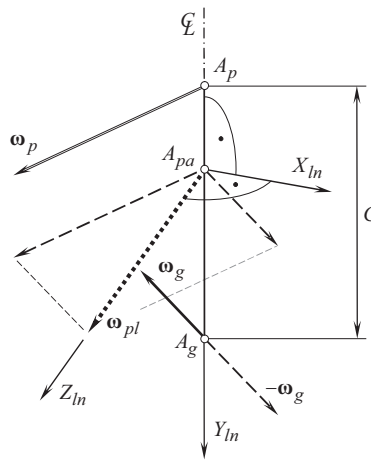


**FIGURE 30.32** Main reference system,  $X_{in}Y_{in}Z_{in}$ , associated with a gear pair.

- The main reference system,  $X_{in}Y_{in}Z_{in}$ , associated with the gear pair
- The stationary gear reference system,  $X_{g.s}Y_{g.s}Z_{g.s}$
- The gear reference system,  $X_gY_gZ_g$
- The stationary pinion reference system,  $X_{p.s}Y_{p.s}Z_{p.s}$
- The pinion reference system,  $X_pY_pZ_p$

Introduced by Prof. *S.P. Radzevich* [174], this set of reference systems is referred to as the *set of main reference systems* associated with a gear pair.

### 30.2.3.10 Contact Geometry: Indicatrix of Conformity at Point of Contact of Tooth Flanks

A challenging problem of synthesizing gear pairs with a desirable performance can be solved on the premiss of in-detail analysis of contact geometry of the interacting tooth flanks of a gear, and of its mating pinion.

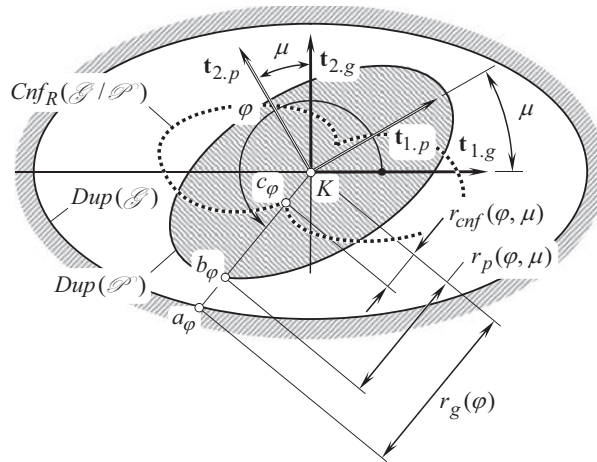


**FIGURE 30.33** On the definition of the term *indicatrix of conformity*,  $Cnf_R(\mathcal{S} \mapsto \mathcal{P})$ , at point of contact of tooth flanks,  $\mathcal{S}$  and  $\mathcal{P}$ . (After Prof. *S.P. Radzevich*, [148,174].)

In order to analytically describe the contact geometry of interacting tooth flanks,  $\mathcal{S}$  and  $\mathcal{P}$ , of a gear and its mating pinion, a planar characteristic curve was proposed by Prof. *S.P. Radzevich* in the late 1970s – early 1980s [127,128]. This characteristic curve is commonly referred to as the *indicatrix of conformity*,  $Cnf_R(\mathcal{S} \mapsto \mathcal{P})$  at point of contact of two smooth regular part surfaces in the first order of tangency. The degree of conformity at point(s) of contact of tooth flanks,  $\mathcal{S}$  and  $\mathcal{P}$ , of a gear and a mating pinion, is indicated by this curve.

The *indicatrix of conformity*,  $Cnf_R(\mathcal{S} \mapsto \mathcal{P})$  is derived on the premise of *Dupin indicatrices*,  $Dup(\mathcal{S})$  and  $Dup(\mathcal{P})$ , of the tooth flanks,  $\mathcal{S}$  and  $\mathcal{P}$ , at point of their contact.

The equation of the *indicatrix of conformity*,  $Cnf_R(\mathcal{S} \mapsto \mathcal{P})$  at a point of contact of a gear tooth flank,  $\mathcal{S}$ , and a mating pinion tooth flank,  $\mathcal{P}$ , is defined by the following structure (see Figure 30.33):

$$Cnf_R(\mathcal{S} \mapsto \mathcal{P}) \Rightarrow r_{cnf}(\varphi, \mu) = r_g(\varphi) \operatorname{sgn} R_g(\varphi) + r_p(\varphi, \mu) \operatorname{sgn} R_p(\varphi, \mu) \quad (30.5)$$

Here,

$R_g$  and  $R_p$  are the radii of normal curvature of a gear, and a mating pinion tooth flank,  
 $\left( r_g = \sqrt{R_g}, \text{ and } r_p = \sqrt{R_p} \right)$ .

$\mu$  is the angle of local relative orientation of the tooth flanks,  $\mathcal{S}$  and  $\mathcal{P}$ , at point  $K$  of their contact.

$\varphi$  is the angular parameter of the indicatrix of conformity,  $Cnf_R(\mathcal{S} \mapsto \mathcal{P})$

Indicatrix of conformity,  $Cnf_R(\mathcal{S} \mapsto \mathcal{P})$ , at a point of contact of two interacting tooth flanks,  $\mathcal{S}$  and  $\mathcal{P}$ , is vital for designing geometrically accurate gear pairs, and, especially, for solving a problem of synthesizing<sup>38</sup> the most favorable gear pair for a particular application. This characteristic curve is helpful when solving the contact strength problems, bending strength problems, the problems of lubrication of the interacting tooth flanks, and so forth.

<sup>38</sup> The claimed by *F. Litvin* [76] (as well as 1960, 1968 editions of this book) solution to the problem of *local synthesis* (what the term *local synthesis* stands for?) of gear pairs with favorable properties is still not solved yet. In the present days, this problem is still even not correctly formulated. To solve this problem, an accurate analytical description of contact geometry of a gear, and of a mating pinion interacting tooth flanks is required [indicatrix of conformity,  $Cnf_R(\mathcal{S} \mapsto \mathcal{P})$ ].

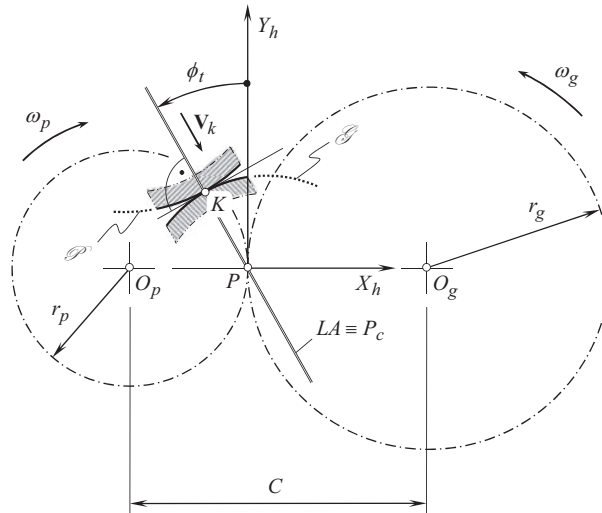


FIGURE 30.34 The line of action,  $LA$ , and the path of contact,  $P_c$ , in parallel-axes involute gearing.

### 30.2.3.11 Condition of Conjugacy of Interacting Tooth Flanks (General Case: for Gears of all Kinds)

The condition of conjugacy<sup>39</sup> of two interacting tooth flanks of a gear, and that of a mating pinion, is a bit tricky. Informally, the condition of conjugacy can be interpreted in the following manner.

Assume that the tooth profile of one member of a gear pair is given. Then, tooth profile of a mating member of the gear pair can be generated as an envelope to a family of consecutive positions of the first member in its motion in relation to the second member. Then assume that the tooth profile of the second member of a gear pair is known, and the tooth profile of the first member of the gear pair is generated as an envelope to a family of consecutive positions of the second member in its motion in relation to the first member. Then, compare the obtained tooth profiles of the first member of the gear pair with its original profile. The interacting tooth flanks are conjugate to one another if the tooth profiles of the first member of the gear pair in both cases (namely, the initially given tooth profile, and that generated by means of second member) are identical to each other. Otherwise, the interacting tooth flanks are not conjugate to one another.

The condition of conjugacy of interacting surfaces is more robust rather than the enveloping condition. All conjugate surfaces are enveloping to one another, but not vice versa – not all enveloping surfaces are conjugate.

In parallel-axes gearing, the problem of conjugacy of the tooth profiles/flanks has been solved in the eighteenth century (~1760) by *L. Euler*.

In parallel-axes involute gearing (see Figure 30.34), the line of action,  $LA$ , and the path of contact,  $P_c$ , align to each other at every point of contact,  $K$ , of the tooth flanks  $\mathcal{G}$  and  $\mathcal{P}$  of the gear, and of the pinion, correspondingly. This is possible as both the line of action,  $LA$ , and the path of contact,  $P_c$ , are straight lines through the pitch point,  $P$ , at transverse pressure angle,  $\phi_t$ , to a perpendicular to the center line. This feature of involute gearing is the root cause of confusion, as the line of contact, and the path of contact, are commonly not distinguished from one another in intersected-axes gearing, as well as in crossed-axes gearing.

To correct the mistake committed (1842) by *Th. Olivier*, and later on followed by *Ch. Gochman* (1886), as well as by many other followers, it is necessary to make difference between the line of

<sup>39</sup> Conjugate tooth profiles/surfaces are also known as *reversibly enveloping* profiles/surfaces (or just as  $R_e$  – profiles/surfaces, for simplicity) [155].



action, and the path of contact in a gear pair. The *Camus-Euler-Savary fundamental theorem of gearing* has to be fulfilled at every instant of meshing of a gear and its mating pinion. The *CES – fundamental theorem of gearing* is a valuable contribution to the scientific theory of gearing.<sup>40</sup>

At around 2008 [174], condition of conjugacy of tooth flanks,  $\mathcal{S}$  and  $\mathcal{P}$ , in intersected-axes gearing, and in crossed-axes gearing was derived by Prof. *S.P. Radzevich*. According to Prof. *S.P. Radzevich* [174], in order to be conjugate, two tooth flanks,  $\mathcal{S}$  and  $\mathcal{P}$ , must be designed so, as:

- a. to retain the instantaneous line of action,  $LA_{\text{inst}}$ , within the plane of action, and
- b. to ensure that the straight line,  $LA_{\text{inst}}$ , intersects the axis of instant rotation,  $P_{\text{in}}$ , at every angular configuration of the gears when they rotate

Later on, the condition of conjugacy of a gear,  $\mathcal{S}$ , and a mating pinion,  $\mathcal{P}$ , tooth flanks was described analytically by Prof. *S.P. Radzevich* (2017) in a form of triple scalar product  $\mathbf{p}_{\text{in}} \times \mathbf{V}_{\text{m}} \cdot \mathbf{n}_{\text{g}} = 0$  [174].

In his famous work [36], *L. Euler* proposed an equation for the involute tooth profiles of a gear and its mating pinion that are conjugate to one another. No special attention was made neither to the fulfillment of the condition of contact ( $\mathbf{n}_{\text{g}} \cdot \mathbf{V}_{\Sigma} = 0$ ) nor on that the interacting tooth flanks must be conjugated to one another. There is no evidence that *Euler* himself realized the importance of the condition of conjugacy for the interacting tooth flanks of a gear and its mating pinion. Moreover, amazingly, but even now the solution to the problem of conjugacy of the tooth flanks is not understood in all detail by most of the gear community all around the world.

The conjugate action law is of critical importance when designing gears for high-power-density gear pairs as well as of gear pairs for low-noise/noiseless transmissions.

### 30.2.3.12 Angular Base Pitches: Operating Angular Base Pitch in Gear Pair

In order to transmit a rotary motion from one shaft to another shaft, more than one pair of teeth needs to be engaged in mesh simultaneously at certain periods of time. In order to ensure two, or more pairs of teeth are engaged in mesh simultaneously, base pitches of the mating gears must be equal to one another. In the meantime, this fundamental requirement<sup>41</sup> is known only with respect to geometrically accurate parallel-axes gearing (with zero axes misalignment).

The earlier, discussed in this chapter, concept on equal linear base pitches of a gear, and of a mating pinion in geometrically accurate parallel-axes gearing is evolved (Prof. *S.P. Radzevich*, circa 2008 [174]) to the most general case of gearing, namely, to the case of crossed-axes gearing (intersected-axes gearing is viewed here as a reduced case of  $C_a$  – gearing). For this purpose, a *concept of angular operating base pitch of a gear pair*,  $\varphi_{b,op}$ , is introduced.<sup>42</sup> The gear angular base pitch,  $\varphi_{b,g}$ , as well as the mating pinion angular base pitch,  $\varphi_{b,p}$ , both must be equal to the operating base pitch,  $\varphi_{b,op}$ , of the gear pair:

$$\begin{cases} \varphi_{b,g} \equiv \varphi_{b,op} \\ \varphi_{b,p} \equiv \varphi_{b,op} \end{cases} \quad (30.6)$$

The concept of angular base pitches of a gear, and that of a mating pinion, both equal to an operating angular base pitch in the gear pair is illustrated in Figure 30.35.

The *condition for the equality of the base pitches* of two mating gears [see a set of Eq. (30.6)] is a valuable contribution to the scientific theory of gearing. This condition is used when designing precision gearing of all kinds.

<sup>40</sup> Recall that the *CES – fundamental theorem of gearing* is proven only for the case of parallel-axes gearing with zero axes misalignment.

<sup>41</sup> It is right point to mention here that the Author failed trying to identify the name of a gear researcher who should be credited with this fundamental requirement in the theory of gearing.

<sup>42</sup> The concept of *operating base pitch* in gear pair for the first time ever was introduced (~2008) by Prof. *S.P. Radzevich* [174].

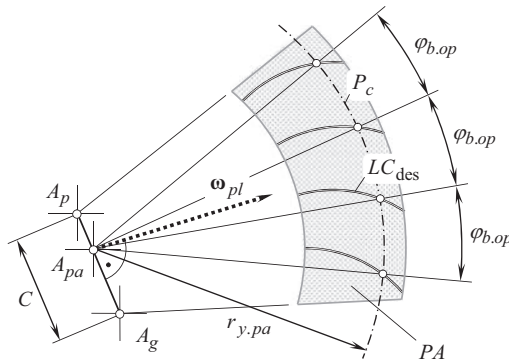


**FIGURE 30.35** On the concept of equal angular base pitches of a gear, and that of a mating pinion, both to operating angular base pitch of the gear pair. (After Prof. S.P. Radzevich [174].)

### 30.2.3.13 Crossed-Axes Gearing with Line Contact between the Tooth Flanks (*R*-Gearing)

The problem of geometrically accurate parallel-axes gearing with line contact between the tooth flanks has been solved by *L. Euler*, who proposed (circa ~1760) involute gear tooth profile. *Euler, L.* deserves involute gearing to be called as *Euler gearing* (or, in other words, as *E<sub>u</sub> – gearing*). The problem of geometrically accurate intersected-axes gearing with line contact between the tooth flanks has been solved (at least in part) by *G. Grant*, who proposed (1887) a method of generation of geometrically accurate bevel gear tooth flank. Gearing of this design is referred to as *G<sub>r</sub> – gearing*. For the first time ever, the problem of geometrically accurate crossed-axes gearing with line contact between the tooth flanks (the so-called, *R – gearing*) has been solved (~2008) by Prof. S.P. Radzevich [174]. Tooth flank  $\mathcal{S}$  of a gear (and that of a mating pinion  $\mathcal{P}$ ) in crossed-axes gearing of this design is generated by a line of contact,  $LC_{des}$ , of a desirable geometry that travels together with the plane of action,  $PA$ , when the gears rotate. The tooth flanks,  $\mathcal{S}$  and  $\mathcal{P}$ , are viewed as loci of the desirable lines of contact,  $LC_{des}$ , considered in a corresponding reference system. *R – gearing* is the only kind of crossed-axis gearing with line contact between the tooth flanks that meets all three fundamental laws of gearing.<sup>43</sup>

The interested reader is referred to [174] for more in-detail description of the principal features of design of *R – gearing*.

### 30.2.3.14 Scientific Classification of Gearing

An extensive use of vector representation of gear pairs makes possible the development of a scientific classification of gear vector diagrams (Prof. S.P. Radzevich, circa 2008 [174]). The gear vector diagrams of gear pairs with a constant value of the center-distance,  $C$ , the crossed-axes angle,  $\Sigma$ , and the gear ratio,  $u$  (the so-called *CΣu – constant gear pairs*), as well as the so-called *CΣu – variable gear pairs* (with variable values of the design parameters  $C$ ,  $\Sigma$ , and  $u$ ), are covered by the classification. The classification of the gear vector diagrams was further evolved to a scientific classification of gear pairs themselves.

### 30.2.3.15 Geometrically Accurate Real Gearing

On the premise of the recent accomplishments in the scientific theory of gearing, a novel gear system is developed by Prof. S.P. Radzevich at around ~2008 [174]. This gear system is referred to as *S<sub>pr</sub> – gearing*. Gearing of this system is insensitive to the axes misalignment caused by manufacturing

<sup>43</sup> In order to fulfil the third fundamental law of gearing, the second fundamental law of gearing must be fulfilled, as the base pitches can be defined only for conjugate tooth flanks, and not for tooth flanks of other geometries. In order to fulfil the second fundamental law of gearing, the first fundamental law of gearing must be fulfilled, as conjugate surfaces exist if and only if two interacting surfaces meet the first fundamental law of gearing.

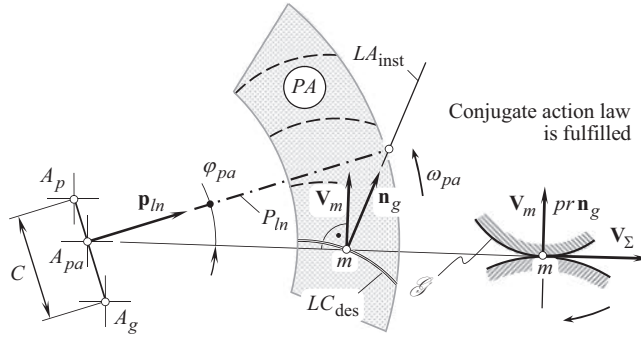


**FIGURE 30.36** On derivation of equation of conjugacy,  $\mathbf{p}_{ln} \times \mathbf{V}_m \cdot \mathbf{n}_g = 0$ , of interacting tooth flanks,  $\mathcal{S}$  and  $\mathcal{P}$ . (After Prof. S.P. Radzevich, [174]).

errors, displacements of gears under operating load, and so forth. If gears in a  $S_{pr}$  – gear pair are manufactured to the tolerances for the gear accuracy, this ensures that the gear pair is insensitive to the axes misalignment, actual values of which do not exceed the tolerances for the accuracy of the axes' misalignment. This means that the angular base pitch of the gear, and that of the mating pinion, are remained equal to an instantaneous value of the operating angular base pitch of the gear pair as long, as the actual value of the axes displacement is within the tolerance band for the deviations.

### 30.2.3.16 Generalized Equation of Conjugacy of Interacting Tooth Flanks: for Gearing of All Kinds

The condition of conjugacy (see Figure 30.36) of the interacting tooth flanks of a gear and of a mating pinion,  $\mathcal{S}$  and  $\mathcal{P}$ , provides a verbal description of the requirements to be met by two conjugate tooth flanks. In 2017, an equation of conjugacy of the tooth flanks,  $\mathcal{S}$  and  $\mathcal{P}$ , was derived by Prof. S.P. Radzevich [174]:

$$\mathbf{p}_{ln} \times \mathbf{V}_m \cdot \mathbf{n}_g = 0 \quad (30.7)$$

Here, in Figure 30.36, is designated:

$\mathbf{p}_{ln}$  is the unit vector pointed along the axis of instant rotation,  $P_{ln}$

$\mathbf{V}_m$  is the linear velocity vector of point of a desirable line of contact,  $LC_{des}$ , between the tooth flanks  $\mathcal{S}$  and  $\mathcal{P}$

$\mathbf{n}_g$  is the unit vector of a common perpendicular at point of contact of the tooth flanks  $\mathcal{S}$  and  $\mathcal{P}$ .

If the condition of conjugacy [see Eq. (30.7)] is fulfilled at every point of the desirable line of contact,  $LC_{des}$ , and at every instant of time when the gears rotate, the designed this way gear pair is capable of transmitting smoothly an input uniform rotation to the output shaft.

Accomplishments in the theory of gearing in the post-Eulerian period of evolution of the theory of gearing are briefly summarized immediately below:

- The fundamental theorem of parallel-axes gearing (namely, the *Camus-Euler-Savary fundamental theorem of gearing*) is formulated. Later on, this theorem was published in the 1841 book by Robert Willis [222], and sometimes it is loosely referred to as *Willis fundamental theorem of gearing*
- The importance of the *condition of contact* between two interacting tooth flanks (namely, the *enveloping condition*) is realized; various forms of verbal, as well as of analytical representation of this condition are known at that time

- Investigation into intersected-axes, and to crossed-axes gearing began at this time
- A huge mistake in the interpretation of the interaction between tooth flanks of mating gears has been committed by *Th. Olivier* [95] (1842), and shortly after repeated by *Ch. Gochman* [44] (1886). All the research in the field of gearing in the years since 1842 and through the recent years are significantly affected by this mistake
- Prof. V.A. *Shishkov* proposed to represent the earlier known condition of contact of interacting tooth flanks of a gear and a mating pinion in the form of equation  $\mathbf{n}_g \cdot \mathbf{V}_\Sigma = 0$ . This equation is a key equation in the kinematic method of surface generation (method of common perpendiculars by *Franz Reuleaux*). Commonly, this equation is referred to as *Shishkov equation of contact*  $\mathbf{n}_g \cdot \mathbf{V}_\Sigma = 0$
- The importance of the conjugate action law is not realized at that time, and in most cases, this law of gearing is ignored. This is a consequence of the mistake committed by *Th. Olivier* in 1842
- The requirement according to which the base pitches of a gear, and of a mating pinion, is understood only in part, and only for the simplest case of parallel-axes gearing. The concept of the operating base pitch in a gear pair is not realized at all

The *contact condition* (or, the *enveloping condition*, in other terminology) [including, but not limited to the *Shishkov equation of contact*  $\mathbf{n}_g \cdot \mathbf{V}_\Sigma = 0$ ], and the *fundamental theorem* of parallel-axes gearing can be considered as the main contribution to the scientific theory of gearing attained at this time.

Till the end of the nineteenth century, the development of the tooth flank profile shape was more or less completed for parallel-axes gearing. Since that time, involute gearing prevailed as the most advantageous shape of the gear teeth flanks.

### 30.3 OTHER CONTRIBUTIONS TO THE FIELD OF GEOMETRICALLY ACCURATE GEARING

Regardless of the unavailability of the scientific theory of gearing till the beginning of the twenty-first century, gear practitioners on their own have proposed numerous designs of geometrically accurate gearing.

#### 30.3.1 TOOTH FLANK GEOMETRY IN GEOMETRICALLY ACCURATE INTERSECTED-AXES GEARING

For over a century involute parallel-axes gearing was the only kind of geometrically accurate gearing, for which geometry of the tooth flanks (namely, the involute tooth profile) was known. The desirable geometry of tooth flanks neither in geometrically accurate intersected-axes gearing nor in geometrically accurate crossed-axes gearing was known.

This was *George Barnard Grant*<sup>44</sup> (1849–1917) (see Figure 30.37) who proposed (January 14, 1887) a correct method for the generation of tooth flanks in geometrically accurate intersected-axes gearing [99]. The use of *Grant's* invention makes it possible generation of geometrically accurate bevel gears tooth flanks. This is due to that in one of the possible applications of the invention, "... the rolling cone is increased in size until its center angle is ninety degrees, and it becomes a plane circle. Its element will form an epicycloidal surface as before, but it is now

<sup>44</sup>George Barnard Grant (December 21, 1849–August 16, 1917), he is considered one of the founders of gear-cutting industry in USA [*Grant* established a gear-cutting machine shop in Charlestown, Massachusetts. When this business expanded, he moved the workshop to Boston, expanded it and named it the *Grant Gear Works* (1877). From this extremely successful establishment evolved the *Philadelphia Gear Works* (1892), and the *Cleveland Gear Works* (*Boston Gear Works*, and *Lexington Gear Works*, are the two more companies to mention here). *George Grant* even wrote several very successful books on the subject, for example *A treatise on gear wheels; A handbook on the teeth of gears, their curves, properties and practical construction*, and so forth].



**FIGURE 30.37** *George Barnard Grant (1849–1917).*

cone with a circular base; but there are many  
 45 curves that would act as its base without al-  
 tering the principle of its operation. When  
 the rolling cone is increased in size until its  
 center angle is ninety degrees, it becomes a  
 plane circle. Its element will form an epicy-  
 50 cloidal surface as before; but it is now called  
 an “involute” surface. The involute sur-  
 face is a special case of the epicycloidal sur-  
 face, differing from it principally in the valu-  
 able feature that it will allow a variation in  
 the center distance of the shafts of spur-gears, 55  
 or in the angle between the shafts of bevel-  
 gears; without affecting the uniformity of the  
 motion transmitted.

In the figures, the gear-blank 19 is held by  
 a gear-spindle 20, that is supported by the 60  
 frame 25 and oscillated by the index-wheel  
 21. The index-wheel receives a slow feeding  
 motion by means of the pinion 22.

**FIGURE 30.38** The essentials of *G. Grant’s* invention [U.S. Pat. No. 407,437. *Machine for Planing Gear Teeth*. /G.B. Grant, Filed: January 14, 1887 (serial No. 224,382), Patented: July 23, 1889].

called an “involute” surface” (see Figure 30.38). Therefore, the bevel gear tooth flanks are generated by describing the method adopted in the case of intersected-axes gearing, that is, bevel gearing in particular. This is a significant scientific achievement by *G. Grant* in the field of scientific theory of gearing. Figure 30.39 is impressive evidence of perfect tooth flank geometry in a bevel gear, correctly realized by *G. Grant* at the end of the nineteenth century. An elementary device



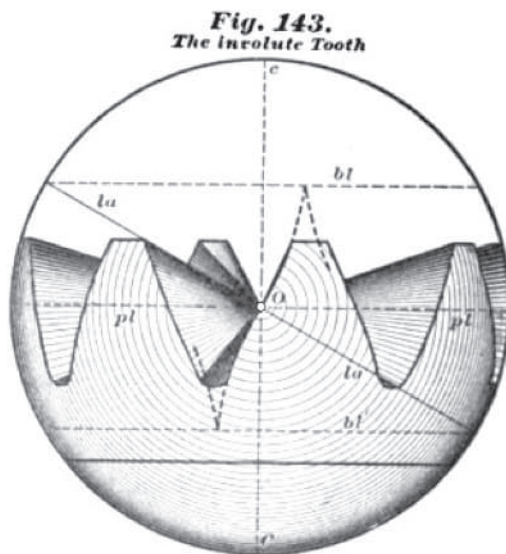


**FIGURE 30.39** The involute tooth flank in bevel gear according to *G. Grant* [see Fig. 143 in: Grant, G.B., *A Treatise on Gear Wheels*, 6<sup>th</sup> edition, Philadelphia Gear Works, Inc., Philadelphia, 1893, 105 p.].

(see Figure 30.40) was used in the past to demonstrate the principal features of meshing in a geometrically accurate bevel gear pair.<sup>45</sup>

The contribution by *G. Grant* is incomplete, as he proposed only a method for generating tooth flanks of a gear for intersected-axes gear pairs. The concept of *gear/pinion angular base pitch*, as well as the concept of the *operating angular base pitch* in an intersected-axes gear pair, was not known to *G. Grant*.

However, *G. Grant* was a gear practitioner and not a gear researcher. Per the Author's opinion, *G. Grant* underestimated his contribution to the scientific theory of gearing. (Moreover, there is no evidence that *Grant's* achievement is properly valued by nowadays gear community). In addition, in the time of *G. Grant*, there was no necessity for more accurate bevel gears compared to those produced by the gear generating method. Because of this, the invention by *G. Grant* was forgotten for over a century. Anyway, *George Grant* has to be recognized as a prominent gear expert of his time.

The *Grant's* achievement got no extensive application in the industry, as for a long while (and even nowadays) the industry is fulfilled with approximate bevel gears that are easier in production.

### 30.3.2 CONTRIBUTION BY PROF. N.I. KOLCHIN

In the mid of the twentieth century, valuable analytical research in the field of gearing (in bevel gearing in particular) has been undertaken by Prof. *A.I. Kolchin* of the USSR (see Figure 30.41) [62,63]. Prof. *A.I. Kolchin* analytically described the results discovered and known in the public domain before his book was published. However, his contribution to the theory of gearing was important as a profound mathematical analysis of gears has been started from his research [62].

<sup>45</sup> *Grant G.B.* was the first to introduce (1887) the concept of the base cone in intersected-axes gearing [99]. He considered base cone of a gear, and a plane, tangent to the base cone. It was not realized at that time that the tangent plane is, by nature, the plane of action. Moreover, only one base cone, and NOT two base cones of interacting bevel gears were considered by *G.B. Grant* [99].

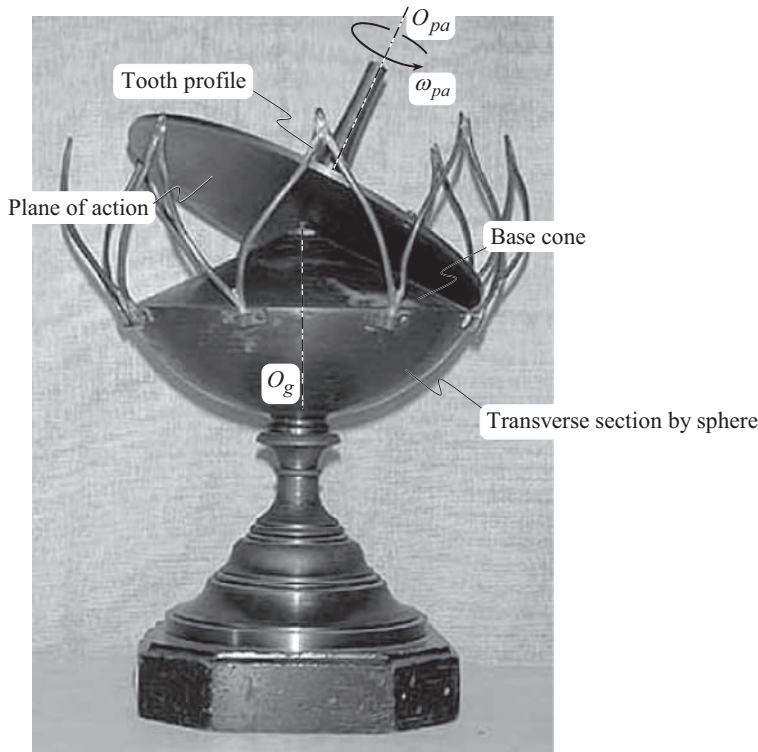


**FIGURE 30.40** Demonstration of the principal features of meshing in geometrically accurate bevel gear pair.

### 30.3.3 CONTRIBUTION BY PROF. V.L. NOVIKOV

In the late 1940s and early 1950s, an extensive research work in the field of gearing has been carried out by Prof. *M.L. Novikov*<sup>46</sup> (see Figure 30.42) in Moscow, at *Military Aviation Engineering Academy*. Ultimately, a novel design of high-performance gearing was proposed [123]. Later on, the results of the research were summarized in the doctoral thesis [90], and in the monograph [91] by Prof. *M.L. Novikov*.

The proposed design of gearing features *convex-to-concave* contact between interacting tooth flanks of a gear, and of a mating pinion.

When Prof. *M.L. Novikov* carried out his research in the field of conformal gearing, he loosely assumed that in order to transmit a uniform rotary motion from an input shaft to an output shaft, the gear teeth do not need to have special shapes, such as the involute of a circle. He meant that, if a gear is made helical then the helix itself can ensure uniform angular motion and tooth profiles can then be chosen with a view to minimizing contact stresses. This is a bit confusing; in order to transmit a rotation smoothly, mating tooth profiles must be either involute or, in a degenerate case, they can feature the *involute tooth point* geometry. The gear designer is free to design the rest of the gear, and of the mating pinion tooth profiles depending on a particular application of the gear pair.

*Novikov gearing* is a kind of helical gearing that features a zero length of the field of action, that is, the equality  $Z_a = 0$  is valid in *Novikov gearing* (this entails a zero transverse contact ratio,  $m_p = 0$ , in *Novikov gearing*). The equality of base pitch of a gear and that of a mating pinion, to

<sup>46</sup>Mikhail L. Novikov (March 25, 1915–August 19, 1957), a famous Soviet gear researcher.



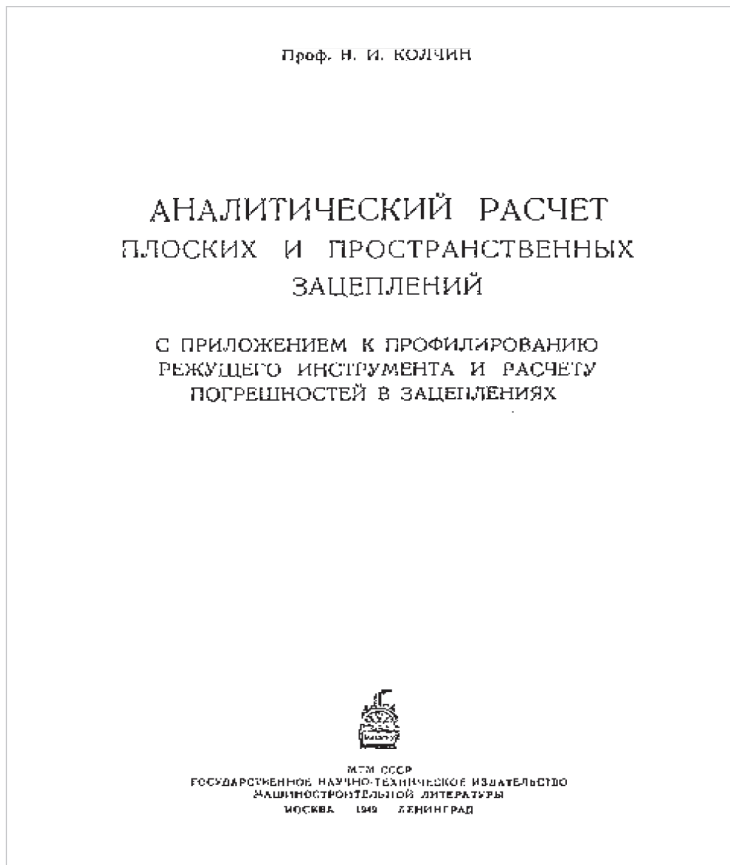


**FIGURE 30.41** Title page of the 1949 monograph by Dr. Kolchin, N.I., *Analytical Calculation of Planar and Spatial Gearing*, Moscow, Mashgiz, 1949, 210 p.



**FIGURE 30.42** Dr. Mikhail L. Novikov (1915–1957).

operating base pitch of the gear pair is the principal feature of *Novikov gearing* that distinguishes it from helical non-involute gearing of other designs.

It is customary to associate *Novikov gearing*<sup>47</sup> with the patent *Gear Pairs and Cam Mechanisms Having Point System of Meshing* [123]. Evidence can be found in scientific literature that reveals unfamiliarity of the gear community all around the world with this original publication [123] on *Novikov gearing* (see Appendix H for details). As early as in 1955, before the invention application was filed, a doctoral thesis [90] on the subject had been defended by Prof. *M.L. Novikov*. The author's familiarity with the practice of defending the doctoral thesis adopted in the former Soviet Union allows for an assumption that the concept of *Novikov gearing* had been proposed in the late 1940s. After Prof. *M.L. Novikov* was granted with the patent [123], a monograph by him (see Figure 30.43) was published [91]. The concept of *Novikov gearing* is discussed in detail in the two aforementioned valuable sources [90] and [91]. Unfortunately, none of them is quoted by the gear experts in Western countries as well as in the USA. This makes possible a conclusion that the gear experts all around the world are not familiar with these two valuable sources of information on *Novikov gearing*.

Formally, the tooth flanks have a circular arc profile. Actually, as it has been shown later by Prof. *S.P. Radzevich* [156], *Novikov conformal gearing* is a reduced kind of involute gearing in which the involute tooth profile is shrunk to a point, and the rest of the tooth profiles are shaped in the form of a circular arc. Because of this, *Novikov conformal gearing* is a kind of geometrically accurate gearing that is capable of transmitting an input steady rotation smoothly.

### 30.3.4 CONTRIBUTION BY PROF. V.A. GAVRILENKO

Extensive research in the field of gearing in the 1930s through the 1960s has been carried out by Prof. *V.A. Gavrilenko*<sup>48</sup> (see Figure 30.44). He spent decades on extensive research in the field of gearing, in the geometrical theory of involute gearing in particular. In the author's opinion, the most systematic discussion on involute gearing ever can be found in the monograph by Prof. *V.A. Gavrilenko* (see Figure 30.45) [43]. Unfortunately, the fundamental monographs by Prof. *V.A. Gavrilenko* are not known for the most of gear experts neither in Europe nor in the United States.

### 30.3.5 CONTRIBUTION BY PROF. E.B. VULGAKOV

In traditional gear design, the module  $m$  in the metric system (or diametral pitch  $DP$  in the Imperial system) is a scale factor for defining the gear tooth size.<sup>49</sup> *Vulgakov*<sup>50</sup> (see Figure 30.46) proposed to use the gear base diameter and tooth count in a gear instead of gear module (or gear diametral pitch) (see Figure 30.47).

Both the *module* and the *diametral pitch* are artificial scale factors, while the base diameter is inherited to a gear and a gear pair [216].

### 30.3.6 CONTRIBUTION BY THE OTHER GEAR THEORETICIANS

For a long time, a book by Prof. *Earl Buckingham* [15] of the United States was among just a few sources of information on the gear theory.

<sup>47</sup>The first pair of *Novikov gearing* made of aluminum alloy (a pre-prototype) was cut on April 25, 1954, by a disk-type mill cutter. For testing, 15 gear pairs were machined in the summer of 1954 by the disk-type mill cutter. Hobs for cutting gears for *Novikov gearing* were proposed later on by Professor *V.N. Kudr'avtsev* (as early as in 1956).

<sup>48</sup>Vladimir A. Gavrilenko (June 21, 1899–June 6, 1977), Doctor (Engineering) Sciences and Professor of Mechanical Engineering (Bauman State Technical University, Moscow, Russia).

<sup>49</sup>Curiously, module and diametral pitch are size dimensions, which cannot be directly measured on a gear. They are really reference values used to calculate other size dimensions which are measurable.

<sup>50</sup>Edgar B. Vulgakov (1927–2006) – Professor, Dr.(Eng.)Sci, designer of aircraft engines.

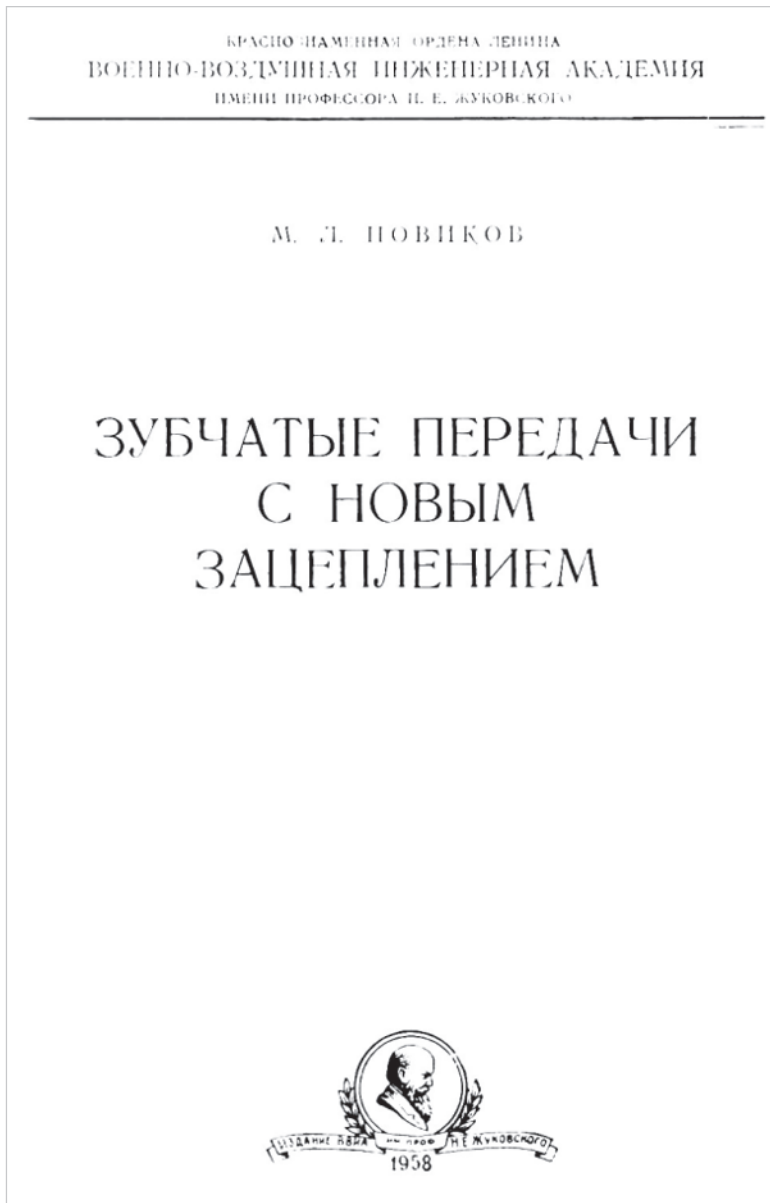


**FIGURE 30.43** Title page of *Novikov's monograph, Gearing with a Novel Kind of Meshing*, 1958 [91].

Intensive research on spatial gearing (namely, crossed-axes gearing) has been undertaken by Prof. *Hellmuth Stachel*<sup>51</sup> of Austria.

Intensive research into spatial involute gearing was undertaken by Prof. *J.R. Phillips*<sup>52</sup> [130] who is credited with a new look and in an in-depth understanding of the kinematics and the geometry of involute gearing with crossing axes of rotation of a driving gear and of a driven gear.

A few more names of the gear researchers are to be mentioned. They are Prof. *Earl Buckingham* (1887–1978) of the USA, Prof. *Chrisanf F. Ketov* (1887–1948) of Russia/USSR, Prof. *Gustav Niemann*

<sup>51</sup> Hellmuth Stachel (born October 6, 1942) – is an Austrian mathematician, a Professor of Geometry at the Technical University of Vienna, who is known due to his contributions to geometry, kinematics, and computer-aided design.

<sup>52</sup> Jack Raymond Phillips (July 18, 1923–January 11, 2009) – a famous kinematician of Australia.



**FIGURE 30.44** Professor *Vladimir A. Gavrilenko* (1899–1977).

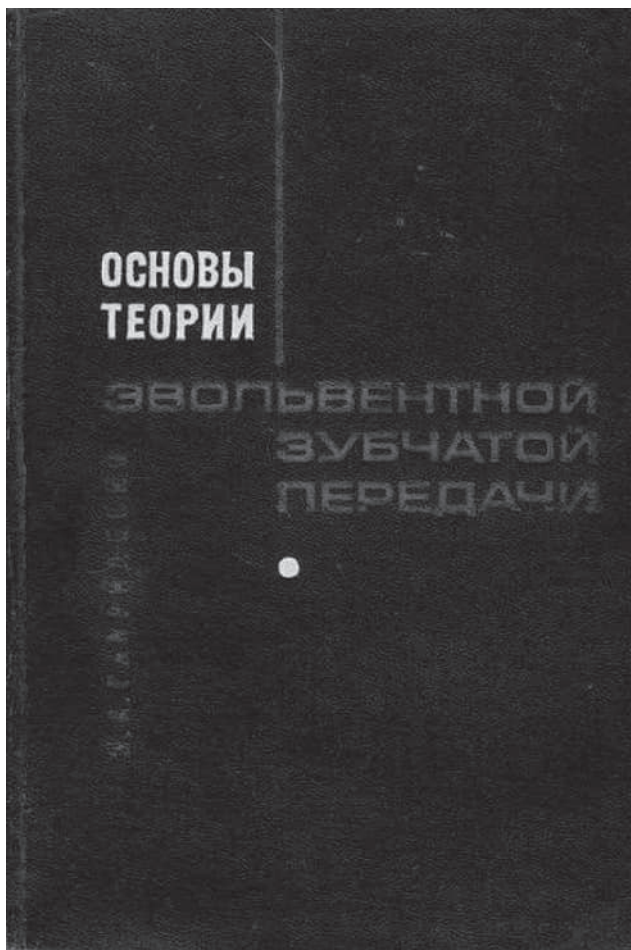


**FIGURE 30.45** Title page of the 1969 book by Professor *Vladimir A. Gavrilenko* [Gavrilenko, V.A., *Fundamentals of the Theory of Involute Gearing*, Moscow, Mashinostroyeniye, 1969, 432 pages].



**FIGURE 30.46** Prof. *Edgar B. Vulgakov* (1928–2006).

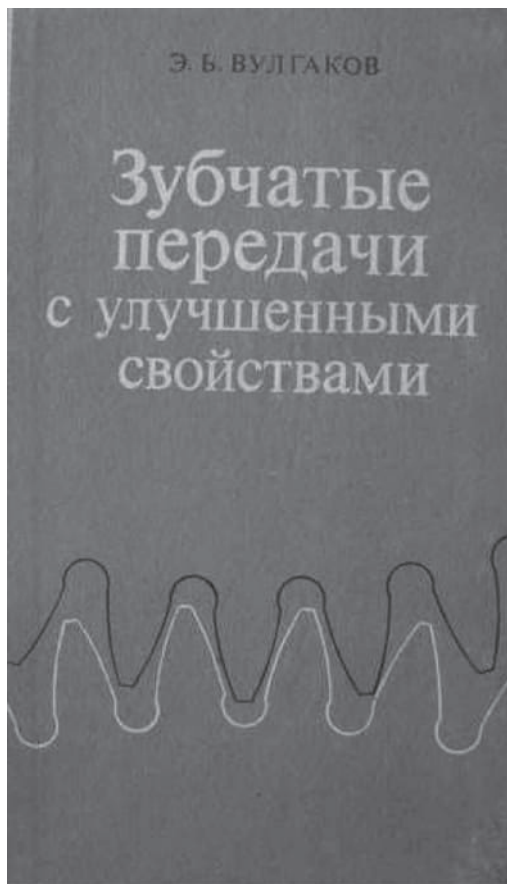


**FIGURE 30.47** Title page of the 1974 book by Professor *Edgar B. Vulgakov* [Vulgakov, E.B., *Gears with Improved Characteristics*. Moscow, Mashinostroyeniye, 1974, 264 pages].



**FIGURE 30.48** C. Walton Musser (1909–1998).

(1899–1982) of Germany, Dr. *Meriwether L. Baxter* (1914–1994) of the USA, *F.J. Bostock* of the United Kingdom, Arthur Sykes of the United Kingdom, Dr. *H.E. Merrit* of the United Kingdom, Prof. *W.A. Tuplin* of the United Kingdom, and others. Prof. *G.I. Shevel'eva* (1929–2005), Prof. *M.L. Erikhov* (1937–2002), Dr. *M.G. Segal'* (1931–2000), and Prof. *Ya.S. Davydov* (1914–2003), all four of the former USSR, have contributed a lot to the gear science.

### 30.3.7 CONTRIBUTION BY WALTON MUSSER

In the late 1950s, *Walton Musser*<sup>53</sup> (see Figure 30.48) proposed a novel kind of transmission, the so-called, *harmonic drive* (or *strain wave gearing*, in other terminology). Although this invention revolutionized the theory of *machines and mechanisms*, harmonic drive is not a gear drive in the sense considered in this monograph [a gear pair is comprised of **three** components (namely, of a gear, a mating pinion, and a housing), while a *harmonic drive* is comprised of **four** components (namely, of a wave generator that is connected to the input shaft, flex-spline, circular spline that is connected to the output shaft, and a housing)]. Another nature of transmitting the input motion is the chief reason why harmonic drives are not discussed in this monograph; this kind of transmission is out of the scope of the book.

The accomplishments in the field of gearing at this time are briefly summarized immediately below:

- A breakthrough invention in the field of intersected-axes gearing has been made by *G. Grant*. He proposed a *Machine for Planing Gear Teeth* (U.S. Pat. No. 407.437, [99] that is capable of machining geometrically accurate straight bevel gears. The geometry of straight bevel gear tooth flank (that is equivalent to the involute of a circle in cases of parallel-axes gearing) is proposed by *G. Grant* for the case of intersected-axes gearing<sup>54</sup>

<sup>53</sup> Walton Clarence Musser (April 5, 1909–June 8, 1998), a famous American inventor; he is the inventor of the *harmonic drive* (1957).

<sup>54</sup> Per the author's opinion, *G. Grant* did not realize in all details the importance of his invention. In the time of *Grant*, the industry was fulfilled with the available on the market approximate gears; no interest to precision (and more costly) bevel gears was indicated by the industry at that time.



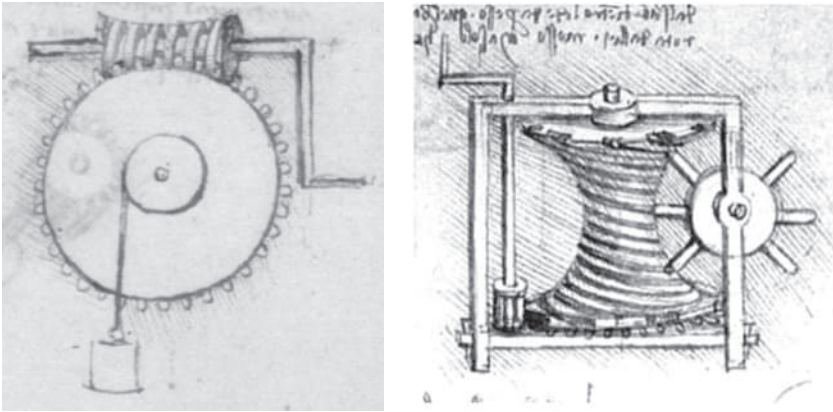


**FIGURE 30.49** Early design of double-enveloping worm gearing (adapted from: da Vinci, Leonardo, *The Madrid Codices*, Volume 1, 1493, Facsimile Edition of *Codex Madrid 1*, original Spanish title: *Tratado de Estatica y Mechanica en Italiano*, McGraw Hill Book Company, 1974. [23]).

- A novel design of conformal gearing was proposed by Prof. *M.L. Novikov* [123]. In the time of Prof. *M.L. Novikov*, the gearing of his design was the only workable design of conformal gearing among numerous designs known at that time.

*Grant's* invention [99] is an important contribution to the theory of gearing. *Novikov's* invention completely aligns with the well-developed theory of parallel-axes involute gearing, as *Novikov conformal gearing* is a reduced case of involute gearing.

### 30.4 DEVELOPMENTS IN THE FIELD OF GEOMETRICALLY INACCURATE GEARING<sup>55</sup>

To meet the immediate needs of the industry, gear engineers from the industry proposed numerous approximate designs of gearing. Initially, when the designs were proposed, it was loosely assumed that each of the designs is capable of transmitting an input uniform rotation smoothly. In numerous cases it was shown later on that, unfortunately, they do not meet all the requirements the geometrically accurate gears must meet. Thus, gears of these kinds are referred to as *geometrically inaccurate gears* or as *approximate gears*.

#### 30.4.1 SAMUEL CONE DOUBLE-ENVELOPING WORM GEARING

The first rudimentary *double-enveloping* worm gear drive was known since the time of *Leonardo da Vinci* [23] (see Figure 30.49). Present-day double-enveloping worm gearing was proposed as early as in 1891 by Dr. *Friedrich Wilhelm Lorenz*<sup>56</sup> of Germany. In his invention, Dr. *Lorenz* proposed methods to generate the worm and the gear of the double-enveloping worm-gear drive, and then he received two patents for these accomplishments. A bit later (at a round 1920) and independently a similar double-enveloping worm gearing was proposed by Mr. *Samuel Cone*<sup>57</sup> of the United States. *Wilhelm Lorenz* and *Samuel Cone* understood very well the advantages of the drives they had

<sup>55</sup> For more in-detail discussion on manufacturing of gears for approximate gearing the interested reader may wish to go to Chapter 1 “Gears: Brief Notes on the History of Methods of Machining Gears and of Design of Gear Cutting Tools” in the book: Radzevich, S.P., *Gear Cutting Tools: Science and Engineering*, CRC press, Boca Raton, Florida, 2017, 606 pages.

<sup>56</sup> Friedrich Wilhelm Lorenz (1842–1924), Doctor of Engineering, inventor, and founder of the *Lorenz Company*.

<sup>57</sup> Samuel I. Cone (1842–1924), a civilian machinist and draftsman, an American inventor of double-enveloping worm gearing.



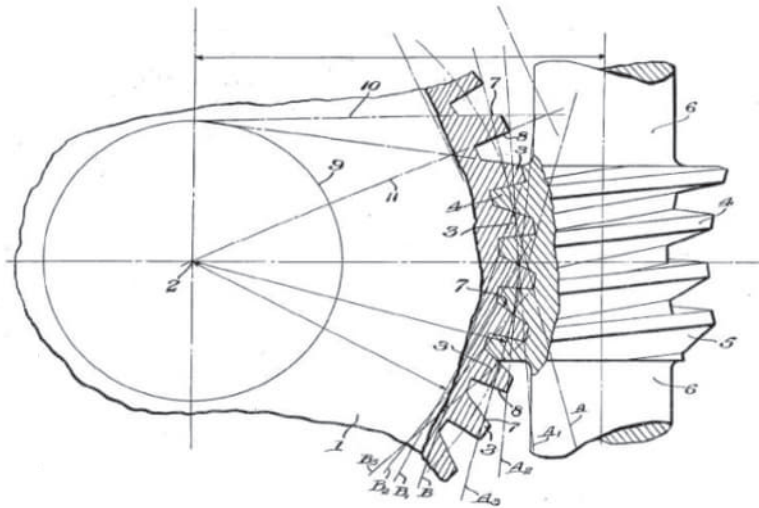


**FIGURE 30.50** Precision worm gearing by *Samuel I. Cone* (Adapted from: USA Pat. No. 1,683,163, *Precision Worm Gearing*, *S.I. Cone*, Filed: June 27, 1926, Patented: September 4, 1928).

invented, particularly, the increased load capacity due to the higher contact ratio<sup>58</sup> (as seemed in the time of Dr. *F.W. Lorenz*, Mr. *S. Cone*) in comparison with that of conventional worm-gear drives. Although the geometry of the *Lorenz* and *Cone* drives differs, both types offer this advantage.

*Samuel I. Cone* patented the applicable technology to manufacture this worm drive at the beginning of the twentieth century, [102]. This type of gear achieved an extensive application rapidly because of its advantages.

This invention is illustrated in Figure 30.50. The object of the invention is to form the members of a system of worm gearing with surfaces, which may be easily generated so that both the worm and worm gear will be generated to a high degree of precision [102]. The flanks of the worm wheel teeth may have a twisted, or warped surface correctly generated and disposed at an acute angle to each other, or they may be straight-sided spur gear, or skew teeth.

This system of gearing is particularly adapted to the transmission of power where more power is required to be transmitted in one direction of rotation than is required to be transmitted in the other directions. With this form of gearing, the desired result may be obtained without varying the power delivered to the shaft of the worm.

Double-enveloping worm gearing by *Samuel I. Cone* resembles the *Hindley worm gearing* (see Figure 16.4).

Double-enveloping worm gearing is an example of approximate gearing, as it does not meet all three fundamental laws of gearing.

### 30.4.2 APPROXIMATE (GEOMETRICALLY INACCURATE) BEVEL GEARING

The early accomplishments in the field of bevel gearing are tightly connected with the name of *William Gleason*<sup>59</sup> (see Figure 30.51). In 1874, his invention of the straight bevel gear planer for the production of bevel gears with straight teeth substantially advanced the progress of gear making.

<sup>58</sup> This is a mistake, as the contact ratio can be specified only in *geometrically accurate gearing*, and the contact ratio cannot be specified in *geometrically inaccurate gearing* or in *approximate gearing*.

<sup>59</sup> William Gleason (1836–1922), founder of *The Gleason Works*, Rochester, NY. Came in (1851) to the United States, Rochester, NY from Ireland. He was a skilled mechanics and a gifted inventor. His 1874 invention of a straight bevel gear planer for production of bevel gears substantially advance the progress of making bevel gears



**FIGURE 30.51** *William Gleason (1836–1922).*

The early part of the twentieth century was the beginning of the automotive industry, which required a broader application of bevel gears to transform rotation and power between intersected axes. In the 1920s, automotive industry designers also needed (a) a gear drive to transform motions and power between crossed axes, and (b) a lower location for the driving shaft. Gear engineers met these needs with pioneering developments directed at designing new types of gear drives and the equipment and tools to generate the gears for these drives.

The proposed designs of bevel gears in the present-day industry are examples of approximate gearing as they are developed and manufactured based on the application of the virtual straight-sided crown gear (basic crown rack). Because of this, present-day bevel gears of all kinds, namely, straight bevel gears, skew bevel gears, spiral bevel gears, as well as others, both face-milled and face-hobbed do not meet three fundamental laws of gearing.

### 30.4.3 APPROXIMATE (GEOMETRICALLY INACCURATE) CROSSED-AXES GEARING

The concept of crossed-axes gearing can be traced back to the times of *Leonardo da Vinci* [23].

The need for more accurate and quieter running gears became obvious with the advent of the automobile. Although the hypoid gear was within manufacturing capabilities by 1916, it was not used practically until 1926, when it was used in the Packard automobile. The hypoid gear made it possible to lower the drive shaft and gain more usable floor space. By 1937 almost all cars used hypoid-gearred rear axles.

The success with the design, manufacture, and application of the contemporary crossed-axes gearing is credited much to two famous gear experts, namely to *Nikola Trbojevič* (also known as *Nicholas Terbo*), and to *Ernest Wildhaber*.

*Nikola Trbojevič* (see Figure 30.52), a world-known research engineer, mathematician, and inventor, was a nephew and friend of *Nikola Tesla*. Mr. *Trbojevič*<sup>60</sup> held nearly 200 U.S. and foreign patents on inventions, principally in the field of gear design.

<sup>60</sup> Nikola John Trbojevič (May 21, 1886–December 2, 1973), also known as *Nicholas J. Terbo*, a world known research engineer, mathematician and inventor, held the basic patent for the *Hypoid Gear*.



**FIGURE 30.52** *Nikola John Trbojevich, also known as Nicholas J. Terbo (1886–1973).*

Mr. *Trbojevich*'s most notable work that brought him international recognition was the invention of the *Hypoid gear*. First published in 1923, it was a new type of spiral bevel gear employing previously unexploited mathematical techniques. The *Hypoid gear* is used on the great majority of all cars, trucks, and military vehicles today. Together with his invention of the tools and machines necessary for its manufacture, the *Hypoid gear* became an integral part of the final drive mechanism of automobiles by 1931. Its effect was immediately apparent in that the overall height of rear-drive passenger automobiles was reduced by at least four inches.

*Ernest Wildhaber*<sup>61</sup> (see Figure 30.53) is one of the most famous engineers and inventors in the field of gear manufacture and design. He is granted with 348 patents<sup>62</sup> (in total), some of which have a broad application in the gear industry mainly due to his work as an engineering consultant for *The Gleason Works*. The hypoid gear drive is of the most famous inventions by Dr. *Wildhaber*. He proposed different pressure angles for the driving and coast tooth sides of a hypoid gear, which allowed him to provide constancy of the tooth top-land.

In 1954–55, a young ITW (Illinois Tool Works, Chicago, IL, USA) engineer by the name of *Oliver Saari*<sup>63</sup> (see Figure 30.54) finalized his patent application for a novel gear technology. The gear set consists of a gear and a helical pinion, and is similar to spiral bevel gear set, except the pinion axis is moved a certain distance off the gear axis.

The proposed designs of crossed-axes gears in the present-day industry are examples of approximate gearing as they are developed and manufactured based on the application of the imaginary crown gear with straight-sided profile (basic crown rack). Because of this, present-day crossed-axes gears of all kinds, both face-milled and face-hobbed do not meet all three fundamental laws of gearing.

<sup>61</sup> Ernest Wildhaber (1893–1979), Doctor of Engineering, h.c., inventor, and consultant for *The Gleason Works*.

<sup>62</sup> The number of 348 patents came in from my personal library. According to other researchers, *Wildhaber* is granted with 279 patents.

<sup>63</sup> Oliver Saari (March 22, 1918–January 25, 2000), a well-known gear engineer of the United States, the key developer of the *Spiroid* family of gears.



**FIGURE 30.53** *Ernest Wildhaber (1893–1979).*



**FIGURE 30.54** *Oliver E. Saari (1918–2000).*

#### **30.4.4 APPROXIMATE (GEOMETRICALLY INACCURATE) CROSSED-AXES GEARING: FACE GEARING**

Face gearing can be viewed as a reduced case either of intersected-axes gearing or of crossed-axes gearing when the gear pitch cone angle (in both cases) increases to the right angle. All known designs of face gearing, both intersected-axes gearing and crossed-axes gearing, are geometrically inaccurate gearing as they do not meet all three fundamental laws of gearing. The face cutting technique used by *The Gleason Works*, *Klingelnberg-Oerlikon*, *Yutaka Seimitsu Kogyo, LTD*, to produce crossed-axes gears is based upon an *empirical* and manufacturing technology that predates the World War II.

Accomplishments in the field of gearing in that period of time can be briefly summarized as follows:

- Double-enveloping (approximate) gearing was proposed by *Wilhelm Lorenz* of Germany (1874), and a bit later (at a round 1920) by *Samuel Cone* of the United States
- Design methods for machining of approximate hypoid gearing were proposed by *Nikola Trbojevich*, and later on improved by *Ernest Wildhaber*, both of the United States
- Face gearing is extensively used in the design of *Fellow's* gear shaping machines

The most significant contributions to the field of gearing at that time related mainly to approximate gearing.

### 30.5 THEORY OF GEARING AT THE BEGINNING OF THE TWENTY-FIRST CENTURY: STATE-OF-THE-ART

It should be stated here from the very beginning that no self-consistent (or potentially self-consistent) scientific theory of gearing has been developed by the beginning of the twenty-first century (by the year of ~2010).

Among others, a self-consistent scientific theory of gearing must possess two important properties.

**First**, it must cover all known designs of gears and gearing with no exclusion.

**Second**, it must cover all (with no exclusion) unknown yet designs of gears and gearing, namely, the theory must possess the property to predict novel designs of gears and gearing.

All the books published so far under the title *Theory of Gearing* [starting from the first (1841) book by *Théodore Olivier* [95], and ending with the latest publications in the field – by the year of ~2010] consist of no scientific theory of gearing. These books can not be referred to as *theory of gearing*, rather they represent collections of known achievements in the field of gearing, having no ability to predict novel unknown designs of gears and gearing.

No doubt, a scientific theory of gearing is necessary to gear researchers as well as engineers as the theory is a powerful means for the development of novel designs of gears and gearing with prescribed performance. Such a scientific theory of gearing can be developed now. With that said, it is important to revise the earlier obtained accomplishments in the field of gearing and select those of them that can be useful in the development of the fundamental scientific theory of gearing.

### 30.6 FAVORABLE APPROXIMATE GEARING

Easier manufacture is the principal advantage of approximate gearing over geometrically accurate gearing. Due to this advantage, approximate gears will be used in the industry in the future.

A theory of favorable approximate gearing can be (and will be) developed on the premise of the scientific theory of gearing [174]. Only in such a scenario approximate gear pairs with favorable design parameters can be designed.

### 30.7 ACCOMPLISHMENTS IN THE FIELD OF NON-CIRCULAR GEARING

The most general case of non-circular gears with crossing axes of rotation is analyzed. For the analysis, a reference system, associated with gear pair in a natural way is used [the axes of the reference system are pointed along:

- a. the axis of instant rotation,  $P_{in}$
- b. the center-distance,  $\Phi$ , and
- c. perpendicular to these two directions,  $P_{in}$  and  $\Phi$ .

In the analysis, the center-distance  $C$ , the crossed-axes angle  $\Sigma$ , and the gear ratio  $u$ , are assumed variables. In particular cases, one or even two design parameters are considered of a constant value. Under such the assumption, a classification of perfect  $C\Sigma u$ -gearing is developed (Prof. S.P. Radzevich, ~2017) [174].

### 30.8 TENTATIVE CHRONOLOGY OF EVOLUTION OF THE THEORY OF GEARING

Summarizing the discussion in the previous sections of this chapter, the benchmarking achievements in the theory of gearing are diagrammatically illustrated in Figure 30.55.

The proposed chronology of evolution of the scientific theory of gearing begins with an analysis of what was done in the pre-Eulerian period of evolution of the gear art. Contributions to the field of gearing by *Desargues*, *de la Hire*, and *Camus*, comprise the pre-Eulerian period of evolution of the theory of gearing. These accomplishments are labeled by ⑩ in the chart shown in Figure 30.55.

The pre-Eulerian period of evolution of the gear art is followed by the time when the fundamental contribution to the theory of gearing has been made by *L. Euler*.

Derivation of the *Euler-Savary equation*, along with the invention of parallel-axes involute gearing<sup>64</sup> by *L. Euler* (~1760), and the fundamental theorem for parallel-axes gearing, are the benchmarking achievements, ①, in the theory of gearing. The latter is considered as the origin of the *scientific theory of gearing*.

Despite of the *fundamental theorem of parallel-axes gearing* was already known to *L. Euler* and *F. Savary*, lots of efforts to discover this theorem were undertaken by *Ch. Camus*, who was close to discover this theorem. Therefore, this theorem is referred to as *Camus-Euler-Savary fundamental theorem of gearing*. Later on, in 1841, this theorem was published in the book by *R. Willis* [222]. *Camus-Euler-Savary fundamental theorem of parallel-axes gearing* is valid only for parallel-axes gearing.

*L. Euler* and *F. Savary* (along with *Ch. Camus*) are granted with the *fundamental theorem of gearing*.

A huge mistake was committed by *Th. Olivier* (1842), who proposed his version of the theory of gearing ③ based just on the enveloping condition for the interacting tooth flanks of a gear and a mating pinion [95]. The condition of conjugacy of the tooth flanks is not taken into account by *Th. Olivier*.

A parallel line in Figure 30.55 (namely, the accomplishments, labeled by shown in dark color ②, ③, ④, ⑤, ⑥, and ⑦) corresponds to a wrong way of evolution of gearing. The mistake, committed by *Th. Olivier*, and later on (1886) repeated by *Ch. Gochman* [44], significantly influenced the further fundamental developments in the theory of gearing (see items ③ through ⑦, and others in the chart shown in Figure 30.55). Only geometrically inaccurate gears can be designed following this way. This is the dead end of the evolution of gear science.

The accomplishments in the theory of gearing, those, labeled by ④ through ⑥, are not associated with the necessity to meet the conjugate action law, are applicable in both branches, that is: (a) in the *dead end* of evolution of the gear science<sup>65</sup> (see items ④ through ⑦, in the chart), as well as (b) in the way that leads to the self-consistent scientific theory of gearing (see items ④ through ⑩, and others in the chart) [174].

No geometrically accurate intersected-axes, and crossed-axes gearing can be designed following the way ② through ⑦. No correct tooth flank modification in parallel-axes gearing is possible – only trial and error method can be used to determine the parameters of the tooth flank modification if the way ② through ⑦ is followed.

<sup>64</sup>It needs to be stressed here that *involute of a circle* itself was known long before the invention of involute gearing by *L. Euler*.

<sup>65</sup>It is right point to stress here that the *dead end* in the diagram in Figure 30.55 means that no *geometrically accurate*  $I_a$ -, and  $C_a$ -gearing are possible, no *correct* tooth flank modification in  $P_a$ -gearing is possible, trial and error method is dominated.



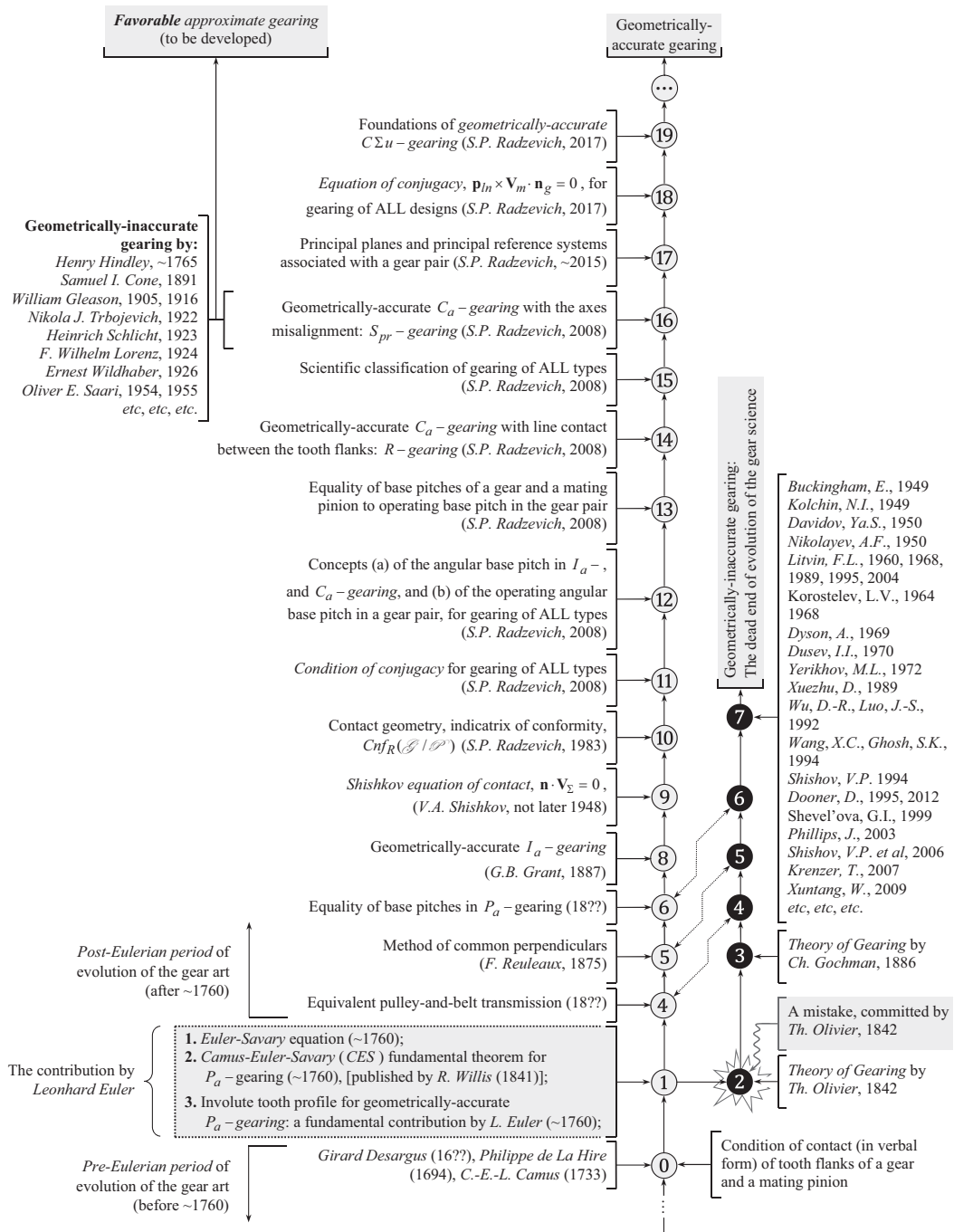


FIGURE 30.55 Tentative chronology of evolution of the scientific theory of gearing.

The condition that requires equal base pitches of a gear and its mating pinion (only in cases of parallel-axes gearing) is known for a long while (note, the *operating base pitch* in a gear pair is not known yet). Per the author's estimate, this requirement © is known since the mid of the nineteenth century. Unfortunately, in the meantime, the name of the gear scientist who should be credited with this significant accomplishment in the scientific theory of gearing is not identified yet.



Spherical involute surface in geometrically accurate bevel gearing ⑧ is known since 1887.

*Shishkov equation of contact* ⑨ deserves to be mentioned here, as the use of this equation makes possible significant simplifications of application of kinematic method of surface generation, especially in cases when both the contact perpendicular,  $\mathbf{n}_g$ , and the instantaneous linear velocity vector,  $\mathbf{V}_\Sigma$ , can be determined with no derivatives of equations of the tooth flanks,  $\mathcal{S}$  and  $\mathcal{P}$ , as well as the parameters of the kinematics of a gear pair.

Contact geometry of interacting tooth flanks,  $\mathcal{S}$  and  $\mathcal{P}$ , are investigated analytically, and an equation of the indicatrix of conformity,  $Cnf_R(\mathcal{S} / \mathcal{P})$ , at point of contact of the tooth flanks of a gear,  $\mathcal{S}$ , and a mating pinion,  $\mathcal{P}$ , is derived ⑩ [127,128,148,151], and others.

Then, the listed immediately below accomplishments were contributed by Professor *S.P. Radzevich* in around ~2008:

- condition of conjugacy (the conjugate action law) of the tooth flanks of gear pairs of all designs ⑪, including intersected-axes gear pairs, and crossed-axes gear pairs
- the concepts ⑫ of (a) *base pitch* in intersected-axes gear pairs, and crossed-axes gear pairs, along with (b) the *operating base pitch* in gear pairs of all types
- equality of base pitches of a gear and its mating pinion to the *operating base pitch* ⑬ in gear pairs of all kinds
- design of geometrically accurate crossed-axes gearing with line contact between the tooth flanks,  $\mathcal{S}$  and  $\mathcal{P}$ , namely,  $R$  – gearing ⑭
- a scientific classification ⑮ of vector diagrams of gear pairs of all kinds
- design of geometrically accurate (crossed-axes) gearing insensitive to the axle's misalignment ⑯, namely,  $S_{pr}$  – gearing
- A set of the principal planes, and the main reference systems, associated with a gear pair ⑰,

Later on:

- Equation of conjugacy  $\mathbf{p}_m \times \mathbf{V}_m \cdot \mathbf{n}_g = 0$  ⑱ of the interacting tooth flanks,  $\mathcal{S}$  and  $\mathcal{P}$ , of a gear and a mating pinion for gearing of all types is derived by Prof. *S.P. Radzevich* (~2017)
- Principal kinematics of geometrically accurate  $C\Sigma u$  – gearing ⑲

are established.

The developed design of  $S_{pr}$  – gearing ⑯ can be used as a foundation of favorable approximate gearing. Gearing of this kind can be properly engineered and can replace gears with tooth flank modifications (which are engineered properly in the meantime). The accumulated experience (*Hindley, Cone, Gleason, Trbojevich, Schlicht, Lorenz, Wildhaber, Saari*, and others) can be taken into account when developing favorable approximate gearing.

It should be realized that the chart in Figure 30.55 is tentative. More accomplishments in the scientific theory of gearing, and the corresponding gear researcher's names, can be added in the chart if a more in-detail investigation into the evolution of the scientific theory of gearing would be undertaken. Only the key (the fundamental) accomplishments in the scientific theory of gearing are included in the chart in its current form.

Generally speaking, geometrically accurate gear pairs of any kind can be designed based on the scientific theory of gearing.<sup>66</sup>

The listed accomplishments form the foundation of the *self-consistent scientific theory of gearing* (Prof. *S.P. Radzevich*, 2012, 2018).

The proposed chronology (see the chart) is open for further improvements. Constructive recommendations, comments, and concerns are welcome.

<sup>66</sup> Theory of gearing can be viewed as a kind of *map* that helps the user traveling from one point (location) to another point (location) in a most efficient way.

### 30.9 ON THE OTHER EFFORTS THAT PERTAIN TO EVOLUTION OF SCIENTIFIC THEORY OF GEARING

The author has turned his interest to the evolution of gear science over a decade ago [134,135,168].

Despite gears being extensively used in the industry of many industrially developed countries, not too much accomplishments to the theory of gearing are contributed to this end. No accomplishments to the theory of gearing came in from North America (including the USA and Canada), from Europe (including Germany, Austria, as well as the rest of the European countries), and from Asia (including, but not limited to China, Taiwan, Japan, and South Korea). In Australia, only the 2003 book by *Jack Phillips* on *General Spatial Involute Gearing* [130] deserves to be mentioned in this regard. Production of quality gears in the industry is based much on the accumulated experience, and not on the means and methods derived from the theory of gearing – empirical approach prevails here in the field. Even lead gear companies in the field of gear design and manufacture indicate poor familiarity with the latest achievements in the theory of gearing. An article [210] perfectly illustrates this statement. An in-detail analysis of this article is available in the public domain [158].

In recent years, numerous papers on the history of gearing (both in English and in Russian languages) have been authored/co-authored by *D. Babichev, N. Barmina, S. Lagutin, A. Volkov*, and others of Russia (see Bibliography section of this book). All these publications are available in the public domain. A claim on the so-called *Russian school of theory of gearing* has been aggressively made by the Authors. It should be stressed here that all these publications are focused on gearing in a more general sense, and not on the principal accomplishments in the scientific theory of gearing.

The discussion in this chapter of the book along with the results of the earlier performed retrospective analysis on the history of the evolution of the scientific theory of gearing [135,174] reveal that this aggressive claim has been made with no sufficient validity. What is actually contributed by the so-called *Russian school in the theory of gearing* to the development of the scientific theory of gearing? The author failed trying to identify any significant accomplishment to the theory of gearing actually contributed by representatives of the so-called *Russian school in the theory of gearing*: what accomplishments by the *Russian school in the theory of gearing* can be added to the chart (see Figure 30.55)? Is there something missing in this chart? What is related (or can be related) to the scientific theory of gearing and can be indicated in the chart? Are there significant accomplishments to the scientific theory of gearing (made by representatives of the so-called *Russian school of theory of gearing*) that are not taken into account (and not indicated in the chart shown in Figure 30.55)? Feel free to name them, if any! An appropriate comment will be helpful for the enhancement of our understanding of the evolution of the scientific theory of gearing.

In the published papers and monographs authored even by the leading Soviet/Russian gear researchers, there is no evidence of understanding of the kinematics and geometry of:

- a. *Novikov gearing* [that is, the representatives of the so-called *Russian school of the Theory of Gearing* have indicated/revealed poor proficiency in the field of gearing, and failed to reveal the difference between *Novikov gearing* and *Wildhaber gearing*]
- b. *Spiroid gearing*<sup>67</sup> (and geometrically accurate worm gearing in a more general sense)
- c. geometrically accurate intersected-axes, and (more generally) crossed-axes gearing
- d. geometrically accurate gears with the axes misalignment, and so forth
- e. still make no difference between enveloping surfaces and conjugate surfaces
- f. *Russian school of theory of gearing* is not capable of demonstrating that the so-called gearing<sup>68</sup> proposed by a charlatan *V.V. Stanovskoi* (<http://www.ec-gearing.ru/company.php>) is a fake (a sort of absurd)

<sup>67</sup> After about 40 (!) Ph.D. thesis, and 5 (!) Dr.Sci thesis, are defended by these people, how is it permissible to ask a question: “What do we know about spiroid gearing”? What did you do all this time?

<sup>68</sup> Amazingly, but this stupid gearing is supported by two doctors of science (Dr. *Scherbakov, N.R.*, the chairperson of *Geometry* department, and Dr. *Bubenchikov, A.M.*, the chairperson of *Theoretical Mechanics* department, both of Tomsk State University, Russia) who are granted with highest scientific degree of – the degree of Dr.Sci in mathematics and physics!!

- g. for decades [for over “50 (!) Years in the Theory and Practice of Gearing”], they carry out meaningless research on gearing with a *closed line of contact that shrinks* when the gears rotate

A few more can be mentioned in this regard.

What can be expected from the less experienced gear researchers of Russia?

Prof. *Ya.S. Davidov*, one of the Soviet *coryphaeus* in the field of gearing, in his “Memories ...” correctly compared all the Russian gear theoreticians with the *swamp* (<http://referat.znate.ru/text/index-8600.html>). The following dialog took place between Prof. *F.L. Litvin* and Prof. *Ya.S. Davidov*, when they were discussing the features of *Novikov gearing*: “In one of the conversations with me F.L. Litvin very correctly compared the work of Novikov to the rock thrown into the swamp and caused a stirring of water” (It is likely Prof. *Ya.S. Davidov* compares the gear community in the Soviet Union/Russia with a *swamp* – it makes sense). Can someone ignore this opinion of two well-known Soviet/Russian gear researchers (of Prof. *F.L. Litvin*, and Prof. *Ya.S. Davidov*), when they have compared all the Russian gear theoreticians with the *swamp*? This comparison is one more evidence of that the claim on the special so-called *Russian school of theory of gearing* is at least doubtful, if not to say more.

No special the so-called *Russian school of theory of gearing* is established so far. It is recommended to the Authors of the recent publications (*D. Babichev*, *N. Barmina*, *S. Lagutin*, *A. Volkov*, and others of Russia) to be more modest when placing a doubtful material to the public domain.

The just made conclusion has to be taken into account when the readers meet the meaningless term *Russian school of theory of gearing* (as well as similar terms introduced by Russians in recent years: *classical school of theory of gearing* and *the gold age of theory of gearing*). In the meantime, experienced readers are skeptical with that, and are commonly having a laugh when they read about the so-called *Russian school of theory of gearing* [168].

---

# 31 On the Lack of Understanding of the *Scientific Theory of Gearing* by the Majority of Gear Scientists and Engineers

The *scientific theory of gearing* outlined in this book is a new theory in the realm of gear science and arts. Despite the origin of the scientific theory of gearing can be traced back to the fundamental research carried out by *Leonhard Euler* in the eighteenth century, the rapid growth of this theory began only early twenty-first century. Through the first two decades of the twenty-first century most (but not all!!) of the key problems in the proposed theory of gearing are solved. It is the right time now to study what is already achieved in this area of mechanical engineering and to implement these results in the everyday gear practice. Unfortunately, the latest achievements in the scientific theory of gearing are ignored by the majority of the gear scientist and gear engineers. It is likely the lack of understanding of the scientific theory of gearing by the majority of the gear scientists, engineers, and practitioners is the root cause for that.

It takes time for a considerable amount of gear experts to get familiar with the theory, study it, and begin using it in everyday practice. Evidently, this cannot be done instantly.

To properly evaluate the advantages, and benefits of usage of the proposed *scientific theory of gearing*, in-depth knowledge of the theory along with a reasonably extensive experience in implementation of it in practice are necessary. Otherwise, there is no chance to evaluate the theory properly, and to get benefited from the theory. Moreover, toxic environment can be formed in the gear community due to the lack of knowledge about the proposed *scientific theory of gearing*.

Nowadays, some well-known gear experts, those who pose themselves as gear theoreticians, commit huge mistakes when trying to evaluate the theory, not being qualified to do such an evaluation.

As an illustrative example, consider a recently published article [210] in the *Gear Solutions* magazine. The author of this article has made a weak attempt to review some key accomplishments in the *scientific theory of gearing* and has demonstrated the absence of understanding of the cornerstone ideas of gear science (see Figure 31.1).

The article [210] is instructive, as it makes clear the poor knowledge of the gear experts when they make an attempt to participate in a discussion on the theoretical aspects of the gear art in a general sense of this term.

Over a year later, another article was published in *Gear Solutions* magazine [158]. The author's attention in the article [158] is focused mainly on the analysis of the principal mistakes committed in the article [210].

For a very short period, this article has appeared in the August 2020 issue of the *Gear Solutions* magazine. Shortly after the article was removed from the magazine. The August 2020 issue of the *Gear Solutions* magazine does not contain anymore the earlier published article [158]. This is nonsense, but the already published article was withdrawn from the issue of the magazine!! (Evidence of that can be found on page 6 of this issue of the *Gear Solutions* magazine – for details,

---

<sup>1</sup> The original version of the entire August 2020 issue of the *Gear Solutions* magazine (that contains the article [158]) is available upon request.

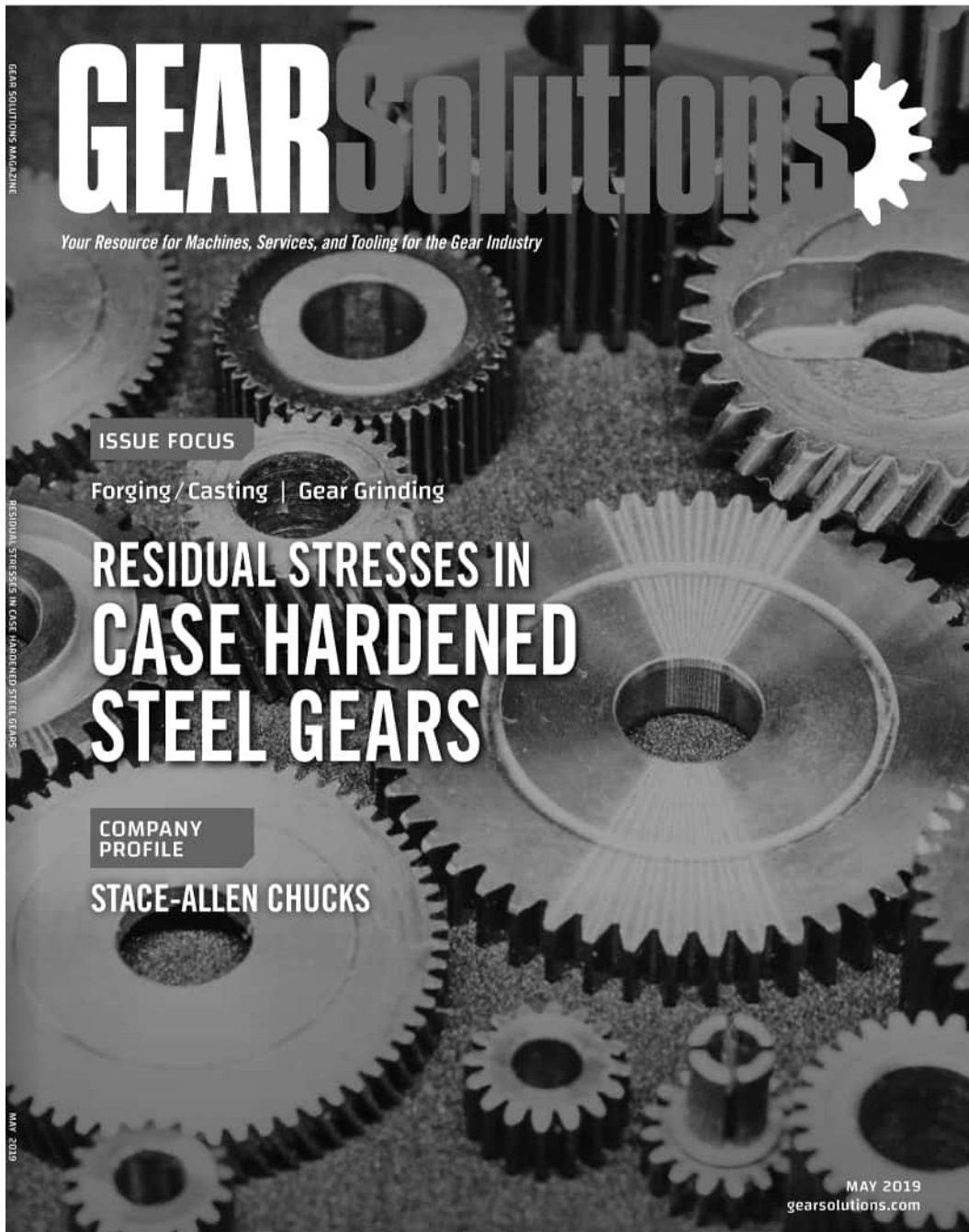


**FIGURE 31.1** Facsimile of the article: Stadtfeld, H.J., “Why are Today’s Hypoids the Perfect Crossed-Axes Gear Pairs?,” *Gear Solutions* magazine, May 2019, pages 42–50, [210].

(Continued)





**FIGURE 31.1 (CONTINUED)** Facsimile of the article: Stadtfeld, H.J., “Why are Today’s Hypoids the Perfect Crossed-Axes Gear Pairs?,” *Gear Solutions* magazine, May 2019, pages 42–50, [210].

(Continued)



## Gear scientists, gear engineers, and gear manufacturers have worked successfully for many decades on finding the optimal flank forms and the optimal non-conjugate flank surface interaction.

By Dr. HERMANN J. STADTFELD

In 1924, Ernest Wildhaber, a well-known gear scientist, invented hypoid gearing. Compared to spiral bevel gears, hypoid gears provide an offset that allows lowering of the body of rear wheel drive vehicles by 50mm or more. This is possible because the propeller shaft between engine/transmission and the driving axle is not positioned at the center of the drive axle but is lowered by the offset amount (Figure 1). This allows the vehicle designer to lower the floor of the vehicle and subsequently the entire body by the same amount. Lowering the center of gravity of a passenger car by 50mm reduces the inertia responsible for sideways rolling by more than 10 percent, which provides better vehicle handling and more active safety. The lower body also reduces the CV coefficient for air resistance, providing higher gas mileage. Less than five years after the invention of hypoid gearing, all large automotive manufacturers around the world had converted their passenger cars and trucks to hypoid drive axles with a lower vehicle body.

Ernest Wildhaber emigrated from Switzerland to the U.S. in 1919 and was hired by The Gleason Works as a gear theoretician. Wildhaber received 279 patents, many of which changed the world of gearing. The cylindrical gear tooth profile that is today called *Wildhaber-Novikov* gearing was invented by Ernest Wildhaber in 1926. Mikhail Novikov, a Russian scientist with no access to western publications, invented the same tooth profile independent from Wildhaber in 1956. The contributions of both scientists are honored today by calling this system *Wildhaber-Novikov* gears.

Ernest Wildhaber is the father of modern gear theory. His pioneering contributions have been invaluable for the development of today's gear calculation and manufacturing processes.

### NEWS ABOUT HYPOID GEARS?

A recently published article by S.P. Radzevich [1] attempts to explain that hypoid gearsets designed and manufactured today lack good performance and are not perfect but approximate. The article seemingly questions the credibility of many scientists and gear engineers who worked on the theory and its

improvement over approximately 100 years. However, reading the article carefully quickly reveals some key misperceptions and false assumptions. This write-up is meant to be a response on behalf of established gear theory and manufacturing.

In the following sections, certain statements and mathematical relationships of the published article are discussed and countering responses are presented and explained. Also, some assumptions about manufacturing and application procedures are discussed and compared to established practices today. The top-

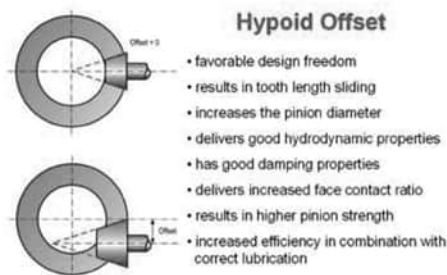


Figure 1: Features of pinion offset.

ics of this paper are structured accordingly in:

- ▶ The three fundamental laws of gearing.
- ▶ Perfect conjugacy.
- ▶ Real world applications.
- ▶ Transmission design.
- ▶ Heat treatment, lapping and grinding.

### THE THREE FUNDAMENTAL LAWS OF GEARING

The first fundamental law of gearing quoted in [1]  $\mathbf{n}_1 \cdot \mathbf{V}_2 = 0$  also implies  $|\mathbf{N}_1 \times \mathbf{R}_1| = i \cdot |\mathbf{N}_2 \times \mathbf{R}_2|$ , where  $i$  is the constant transmission ratio. The three cases in Figure 2 visualize the problem of non-constant ratio and are noncompliant with the first gearing law because of a ratio change from case to case. This problem led Leonard Euler to discover the involute tooth profile. A simplistic mathematical approach teaches that the effective radius vector  $\mathbf{R}$  remains unchanged while the contacting point between two mating flanks moves from  $\mathbf{R}_{b2}$  to  $\mathbf{R}_{b1}$  as shown to the

May 2019 43

**FIGURE 31.1 (CONTINUED)** Facsimile of the article: Stadtfeld, H.J., “Why are Today’s Hypoids the Perfect Crossed-Axes Gear Pairs?,” *Gear Solutions* magazine, May 2019, pages 42–50, [210].

(Continued)



right in Figure 3 (movement along the line of action).

The line of action in parallel axes cylindrical gearing is a straight line, connecting the two base circles. If the surface normal vectors  $N_1$  and  $N_2$  are within the line of action, then the vector product  $|N_1 \times R_1|$  remains constant during a complete mesh cycle. The consequent application of this principle leads to the construction of an involute, as shown to the right in Figure 3.

The line that forms the tooth surface elements while traveling from position "a" to "f" along the line of engagement (line of action) is always perpendicular to the line of action. This principle implies that a tool, simply with straight cutting edges as shown in Figure 4, can be used to form the complex involute profile. Figure 4 also demonstrates the principle of profile shift while maintaining the first fundamental law of gearing.

The second fundamental law of gearing, which was proposed in 2017,  $P_{10} \times V_{m1} + n_p = 0$  [1], is a redundant relationship to the first gearing law and it is limited to cylindrical gears with parallel axes and straight bevel gears without hypoid offset. In this case, it adds nothing to the first gearing law; conjugacy is already given by the relationships required in the first gearing law.

The third fundamental gearing law is quoted in [1] in two different notations. The first notation covers only the special case of ratio = 1:

$$\Phi_{b,g} = \Phi_{b,p} = \Phi_{b,op}$$

However, the first notation is incorrect for all cases with different base pitch diameters because the circular pitch and not the angular pitch has to be equal between pinion, gear, and the operating base pitch. The second notation:

$$P_{b,g} = P_{b,p} = P_{b,op}$$

is consistent with the requirement of equal circular pitch, but the article makes no mention of the different notations.

#### PERFECT CONJUGACY IN STRAIGHT BEVEL GEARSETS

Bevel gears with intersecting axes is the topic of a series of three papers published between October 2014 and January 2015 [2]. A straight bevel gearset with skew teeth was modeled, and a sample was manufactured. This publication addressed two points: the design of a gearset with low tooth count and the solution for perfect conjugacy. There is no mention in the article that the Coniflex<sup>®</sup> straight bevel gear system has been used since the 1940s for low tooth count gearsets such as differential gears.

Straight bevel gears such as Gleason Coniflex have tapered depth teeth, where the pitch cones roll on each other and the pitch apexes of pinion and gear match the crossing point of the axes. In the standard case, the face and root cone apexes match the crossing point. In such a standard Coniflex design, the base elements are also cones with cone apexes that match the crossing point of the axes. The involute development in Figure 3 can be applied to an infinite number of normal sections along the face width of a straight bevel gear which allows an involute development similar to that for cylindrical gears. The conical base elements of both members can be connected with a straight line (the line of action) in each section along the face width, whereas the plurality of all lines of action forms a plane (the plane of action).

This principle is shown in Figure 5. The two cones in Figure 5 are base cones of a straight bevel or a spiral bevel gearset. In the right two graphics, the view is directed such that the plane of action appears as a line that is tangential to the two cone-enveloping surfaces. The left side graphic in Figure 5 shows the plane of action three-dimensionally and how it connects the two base elements.

The plane of action cannot be extended beyond its tangential contacting line with the base element as shown incorrectly in

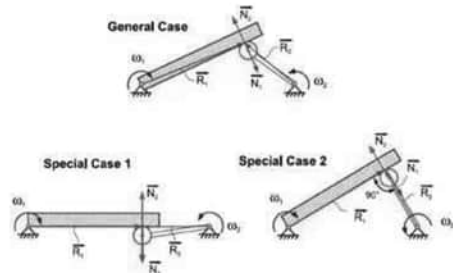


Figure 2: Three general cases of motion transmission with a bar and a crank.

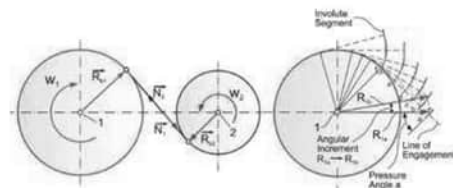


Figure 3: Line of action between base circles (left) and subsequent involute development.

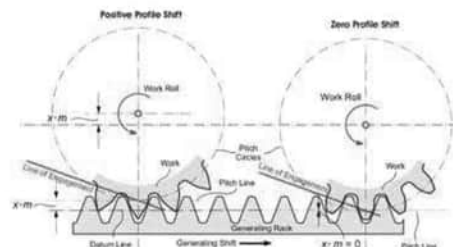


Figure 4: Generating rack with straight profile forming involute profiles.

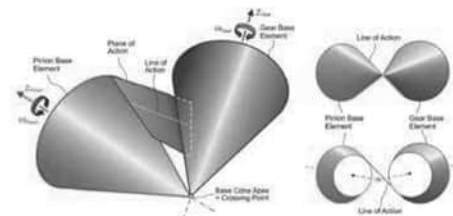


Figure 5: Conical base elements and plane of engagement.

Figure 1 in [2] and Figure 6 in [1]. The plane of action only exists where tooth engagement is possible and it is different than the generating gear plane (more specifically explained later).

There is, however, one difference from the true involute of cylin-

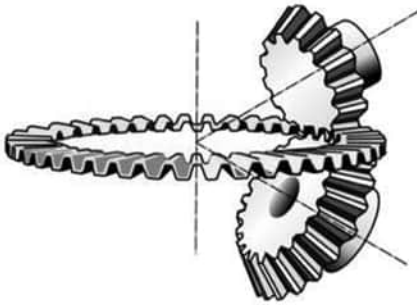


Figure 6: Ring shaped generating rack with trapezoidal profile.

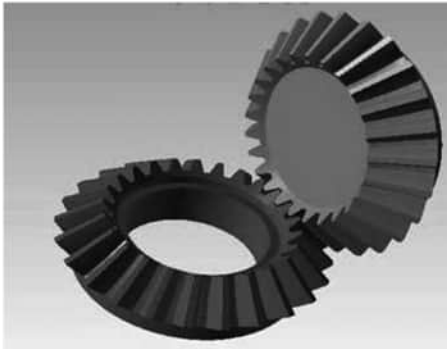


Figure 7: Solid model computer graphic of a perfectly conjugate straight bevel gearset.

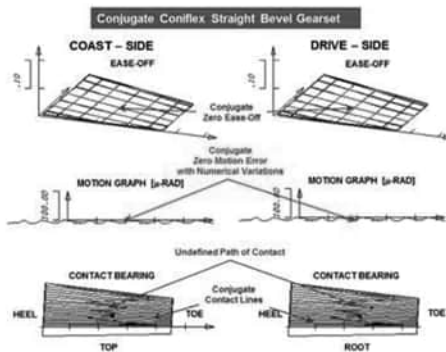


Figure 8: Tooth contact analysis of the perfectly conjugate straight bevel gearset.

dical gears. The rotation of pinion and gear does not occur in the normal plane but in the transverse plane. Because of this difference, the flank profile of straight bevel gears (and all other bevel gear types) is called Octoide. The Octoide is the analog function of an

involute, and it provides to bevel gears the same advantages as an involute provides to cylindrical gears. Those advantages are constant ratio, center distance insensitivity, and ease of manufacturing.

Like cylindrical gears, bevel gears also have a trapezoidal generating profile. The straight rack of cylindrical gears becomes a ring, as shown in Figure 6. It is required to establish certain conditions in order to make the ring rack the generating gear for a pinion and a ring gear that will mesh perfectly together with zero transmission error and line contact identical to cylindrical gears. Those conditions are postulated in the kinematic coupling requirements:

» The flank surfaces of the generating gears of the two mating bevel gears are congruent (same shape but mirror images, as given in the example of Figure 6).

» The generating gears of the two mating bevel gears require identical axes of rotation (Top and bottom side of the generating gear in Figure 6 form the same generating gear, which rotates in both cases around the same axis and therefore satisfies condition 2).

» The surface of engagement of pinion and ring gear must be identical to the surface of engagement between pinion and generating gear and also to the one between ring gear and generating gear (without detailed knowledge of the surfaces of engagement, the global condition in Figure 6 seems to satisfy this requirement).

The generating gear principle has to be understood as the ultimate vehicle to form the teeth of two mating gears. The first fundamental law of gearing is fully executed by choosing trapezoidal profiles and by applying the kinematic coupling requirements. Gears are designed and manufactured in order to mesh with each other. What better way to manufacture them by way of a generating gear? The generating gear is represented by the manufacturing machine; it forms the teeth of the gear (at the bottom in Figure 6) while meshing with this gear perfectly. If the pinion is manufactured with the same generating gear but on the opposite side (at the top in Figure 6) and if the generating gear is imagined infinitely thin, then the result is a pinion that perfectly meshes with the gear having zero motion error. It is also given, in such a case, that line contact between the pinion and gear flank surfaces exists along the entire face width. The extraordinary effort shown in [2] to calculate straight bevel gear tooth surfaces that are skew with asymmetric teeth is based on the falsely assumed conjugate requirement. The sample gear pair shown in [2] was manufactured on a machining center with a ball nose endmill in a milling operation likely taking many hours to complete. It is rather simple and straightforward to manufacture a significantly better, perfectly conjugate straight bevel gearset in only a few minutes by using the generating gear method and a standard bevel gear manufacturing machine.

An example straight bevel gearset computer model is shown in Figure 7. The solid model in Figure 7 has been generated by using standard Gleason basic settings, based on the generating gear approach and by applying a standard Coniflex® Plus cutter head as used on Phoenix bevel gear manufacturing machines. The Coniflex straight bevel gear calculation for conjugate contact has to be conducted with a dish angle of 0° and no root angle correction ( $\Delta\text{GammaM} = 0$ ). The dish angle is creating the length crowning and a  $\Delta\text{GammaM}$  creates the profile crowning. With a dish angle of 0° and a  $\Delta\text{GammaM}$  of 0° flank lead lines are straight lines and the profile is a true Octoide (involute equivalent).

A contact analysis of the gearset in Figure 7 is shown in Figure 8. The top of the figure shows the Ease-Offs of left and right flank (called coast and drive side in the graphic). The center of the figure shows the motion transmission errors of the pinion and gear flank pairs. The two bottom graphics are the representation of the tooth contact pattern. The contact pattern graphics are axial

**FIGURE 31.1 (CONTINUED)** Facsimile of the article: Stadtfeld, H.J., “Why are Today’s Hypoids the Perfect Crossed-Axes Gear Pairs?,” *Gear Solutions* magazine, May 2019, pages 42–50, [210].

(Continued)

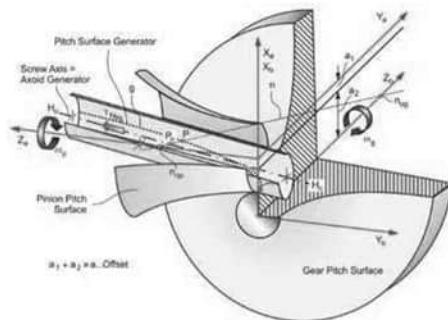


Figure 9: The correct pinion and gear pitch surfaces.

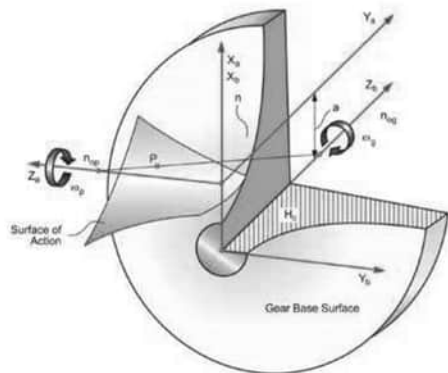


Figure 10: Surface of action connecting the gear and pinion base surfaces.

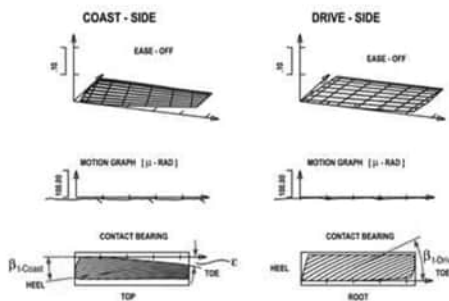


Figure 11: Ease-Offs, motion graphs, and contact lines of a real conjugate hypoid gearset.

projections of the flank surfaces and the contact lines in the same plane a two-dimensional part print would show the tooth area.

The contact analysis in Figure 8 confirms the full line contact

in each roll position (lower graphics) as well as the zero motion error (only numerical static) in the center graphic which makes this example the perfectly conjugate straight bevel gearset. In the lower graphic the path of contact was calculated as a zig-zag line which indicates an undefined contact path. This means that due to the conjugacy, every point along each contact line is a path of contact point which makes the analysis program pick random points.

The Ease-Off base plane (top graphics in Figure 8) defines the conjugate state of a flank surface pair. Because the Ease-Off graph of the calculated flank pairs matches the presentation plane (base plane) precisely, that is the proof that a conjugate and precisely rolling gearset was the input of this contact analysis calculation.

The above experiment creating a conjugate straight bevel gearset is strictly academic. Conjugacy is the basis of all gearsets manufactured in high volume on dedicated manufacturing machines. A conjugate bevel gearset cannot be used for a power transmission because manufacturing tolerances and load affected deflections as well as material expansions and deformations under high operating temperatures will result in edge contact and high load concentrations. The load concentrations already start with moderate load and cause material damage and considerable noise emission. Although conjugacy is used as a reference for each design, predetermined amounts of length and profile crowning are applied. The right amount of crowning makes a gearset quiet and gives it the required load carrying capacity. The crowning is shown in the Ease-Off graphics with the conjugate reference always being present as the Ease-Off base plane. Several Ease-Off examples of a gearset with length and profile crowning are shown in the proceedings of this paper.

## PERFECT CONJUGACY IN HYPOID GEARSETS

It begins to become more problematic for hypoid gears. In [1] the pitch elements of crossed axes hypoid gears are drawn as cones. Even though the face cones of hypoid gears and pinions are machined conical, the pitch elements are hyperboloids.

Ernest Wildhaber and Arthur Stewart described their invention of hypoid gearing in 1926 [3]. Boris Shtipelman published in 1978 the relationships and derivations required to understand hypoid gears and their hyperbolic pitch elements [4]. Figure 9 offers a graphical interpretation of the hyperbolic pitch elements and their generator. The pitch surface generator is a line which winds on the surface of a cylinder beginning at the crossing point of the axes, equal to the first contact point of the pinion and gear pitch surfaces. The pitch surface generator is developed by the connecting line between the pinion and gear pitch surfaces ( $\mathbf{n}_{op}$  -  $\mathbf{n}_{og}$ ) by shifting the connecting line along the pinion and gear axes. The connecting line ( $\mathbf{n}_{op}$  -  $\mathbf{n}_{og}$ ) is normal to the pitch elements. Point P is one point of the pitch surface generator. If the division of the vector products of the distances between the axes and point P and their respective axis direction equals the ratio i of the hypoid gearset then one point of the pitch surface generator is found with:

$$\{(\mathbf{n}_{op} \cdot \mathbf{P}) \times \mathbf{Z}_a\} / \{(\mathbf{P} \cdot \mathbf{n}_{og}) \times \mathbf{Z}_b\} = i$$

Although the pitch elements are hyperbolic and not conical, it is possible to use conical faces for the blanks of pinion and gear. If point P in Figure 9 was chosen at the center of the face width, then line ( $\mathbf{n}_{op}$  -  $\mathbf{n}_{og}$ ) can be used as a normal vector to define the face angle a blank with straight face cones if the hypoid set was manufactured by face hobbing, which implies parallel depth teeth.

Straight face cones will merely influence the top root clearance of the gearset in the range of 30 to 60 microns. Using straight face cones will not change the form of the pitch surface nor will it influence the base surface. Those functional surfaces are given by the



kinematical relationships and have to be considered when thinking about the shape of the surface of action. No plane of action can exist between two hyperbolic base elements. The correct surface of action is curved and warped, as shown in Figure 10.

The conclusion is that the second fundamental law of gearing according to [1] does not exist and is not related in any way to the conjugacy of gears (as explained and demonstrated in the following section).

#### CONJUGACY BETWEEN MESHING FLANKS

The term conjugate is used in mathematics for two or more surfaces that contact each other along a line. Since the 1970s, the term conjugate has also been employed in gear technology literature to define the "exact" gear pair which presents a triple plurality of line contact between two gear flanks during the meshing process [5].

#### DEFINITION OF THE CONJUGATE GEAR PAIR

1: The flanks contact along a line (contact line), which is only limited by the boundaries of the teeth i.e. the working area.

2: The line contact between the flanks exists within the entire area of engagement in every mesh position.

3: Line contact is maintained in the entire area of engagement if pinion and ring gear are rotated by angular increments where:  $(\text{angular pinion increment}) / (\text{angular ring gear increment}) = \text{transmission ratio}$ .

The Ease-Off is a three-dimensional graphic of the flank deviations from a conjugate pair. It is calculated by transformation of a pinion flank "into" the gear coordinate system according to the first gearing law, resulting in a virtual gear flank that is conjugate to the actual pinion flank. This conjugate gear flank will then be compared to the present gear flank, where all differences in arc length are plotted point by point in ordinate direction into the Ease-Off graphic.

If both mating bevel gears have conjugate manufacturing data, then the Ease-Off graphic has no deviations in ordinate direction. Also, if the pinion flanks and the gear flanks have spiral angle and pressure angle errors of equal amounts, the Ease-Off graphic will not show any deviation. Although the individual gears are considered incorrect in this case, they will roll conjugate with each other, which subsequently leads to an Ease-Off without any ordinate values. Figure 11 shows the analysis results of a typical conjugate hypoid gearset. The Ease-Off graphics have zero crowning magnitudes in the ordinate direction. The motion graph has, next to some numerical entrance and exit variation, zero motion error. The contact bearings show line contact within the entire working area. The coast side contact ends at a toe root undercut (section e).

Each spiral bevel and hypoid gearset with uniform tooth depth has a conjugate base design. This applies to all face hobbed and some face milled gearsets. A simple explanation of hypoid gearset conjugacy is possible with a non-generated gear that meshes with a generated pinion. For the calculation and manufacturing process, the hyperbolic pitch elements are calculated for the gear first. Then a suitable blade profile (gear cutter in Figure 12) is chosen and positioned in a face cutter head. The cutter head is positioned to create the desired spiral angle. With this procedure, a non-generated gear can be created by computer simulation and it can be manufactured with a bevel gear cutting machine [6].

A pinion cutter (see Figure 12) is positioned in a mathematical model or in a bevel gear cutting machine such that it represents one tooth of the non-generated gear by rotating around its axis. An additional simultaneous rotation around the pinion generating gear axis results in this pinion cutter becoming the generat-



**PEI Piselli Enterprises Inc.**

**SAMPUTENSILI MODEL S-750 CNC GEAR HOBBER – NEW 2007**

- 6-Axis CNC Gear Hobber, 30" Max Diameter w/ Tailstock. 2DP/12mm, 30" Face, Siemens 840D Controller.
- Very Little Use – "LIKE NEW"

**Fellows 100-12 Hydrostroke**

**A/C Marand 330S Spline Roller**

**Liebherr LC-122 CNC Gear Hobber**

**PEI Piselli Enterprises Inc.**

820 Cochran Street  
Statesville, NC 28677  
704.609.0766  
[www.pisellient.com](http://www.pisellient.com)  
rich@pisellient.com

**THE #1 SOURCE FOR YOUR USED GEAR MACHINERY — AND MORE!** 

May 2019

47

**FIGURE 31.1 (CONTINUED)** Facsimile of the article: Stadtfeld, H.J., "Why are Today's Hypoids the Perfect Crossed-Axes Gear Pairs?," *Gear Solutions* magazine, May 2019, pages 42–50, [210].

(Continued)

ing gear of a conjugate pinion. If the pinion is positioned with the same offset that was used to determine the pitch surfaces (Figure 9), then the cutter rotation around the pinion generating gear axis will form a pinion that is perfectly conjugate to the non-generated gear. The tooth contact analysis in Figure 11 has been obtained from such a non-generated hypoid gearset and therefore shows perfect conjugacy.

More complicated is the generation of a conjugate bevel or hypoid gearset with tapered depth teeth (see Figure 13). If the generating gear axes have identical axes of rotation that are perpendicular to the pitch line, the rotating cutter heads and their blades will not follow the root line of a tapered depth tooth. Tilting the cutter head in order to follow the root line would violate the first kinematic coupling requirement for teeth that are congruent to the slots of the mating member. The solution was developed in the 1940s [7].

If the cutting edges are adjusted in the cutting machine such that tooth reference profile and depth is matched at midface, and if an axial motion of the cradle is introduced that guides the blades along the tapered root line while the generating roll progresses along the face width, then the requirements of congruent teeth and slots are fulfilled with the result of perfect conjugacy.

The process configuration and kinematics in Figure 13 is called *Duplex Completing*. Today, all face-milled and ground spiral bevel and hypoid gears are manufactured with the Duplex Completing process. The axial cradle movement in this process is called *Helical Motion* and was first introduced with mechanical bevel gear machines in the late 1940s. The *Helical Motion* of the days of mechanical machines required an additional change gear box which actuated a cam that moved the sliding base during the generation process. Today's CNC controlled Phoenix® free form machines have the *Helical Motion* capability automatically by their interpolated axes movement.

#### WHY IS CONJUGACY NOT DESIRABLE FOR REAL WORLD APPLICATIONS?

In 1926, Ernest Wildhaber [3, 8] was the first to propose applying surface crowning on hypoid gears. Wildhaber acknowledged that the slightest deviations in the gear housing and in the building position, as well as deflections affected by load and heat, will cause edge contact with peak stress levels of a multiple of the allowable values the gearset had been designed for. The conjugate gearset used for the TCA in Figure 11 was repeated with realistic displacement values of 50µm offset, 50µm pinion cone and 30° of shaft angle change. The results in Figure 14 show warped and tilted Ease-Offs and severe edge contact on heel and top. This edge contact will cause noisy operation followed by pittings and tooth fracture.

The theoretically conjugate hypoid set will not fulfill any of the fundamental gearing laws in case of the smallest gearbox inaccuracies or deflections. As mentioned above, already small deflections at moderate loads lead to load concentrations on the edges of conjugate flank pairs and can cause material damage and considerable noise emission. As such, the conjugate gear pair is not suitable for any task in a power transmission.

The introduction of 80µm length crowning and 15µm profile crowning to the conjugate hypoid design delivers the analysis results shown in Figure 15. The crowning makes the gearset insensitive to expected inaccuracies in the gear housing and load and heat affected deflections. Applying the same amounts of shaft displacements then used for the TCA of the conjugate hypoid set in Figure 14 moves the mean point slightly out of the initial position (see Figure 16), but a large contact area within the tooth boundaries is still maintained.

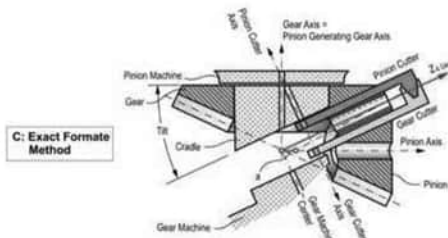


Figure 12: Generating of perfect conjugate hypoid pair.

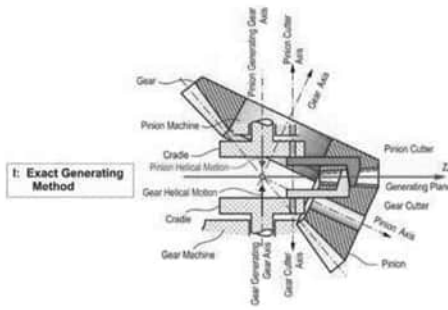


Figure 13: Generating of a conjugate tapered depth bevel gearset.

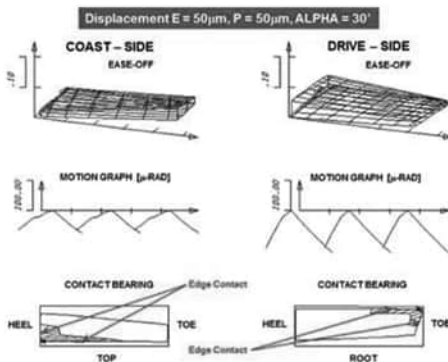


Figure 14: TCA of conjugate hypoid set from Figure 11 with shaft displacements.

It was demonstrated that the hypoid gearset with length and profile crowning in Figure 15 was developed based on a conjugate design. The first and third fundamental gearing law, mentioned in this paper, applies to the hypoid set in Figure 15 at the mean point roll position, if the load is zero. The first and third fundamental gearing law will apply in the area of contact as the load increases and the Hertzian contact spreads in contact line direction as well as in path of contact direction. This ideal condition can only be

**FIGURE 31.1 (CONTINUED)** Facsimile of the article: Stadtfeld, H.J., “Why are Today’s Hypoids the Perfect Crossed-Axes Gear Pairs?,” *Gear Solutions* magazine, May 2019, pages 42–50, [210].

(Continued)

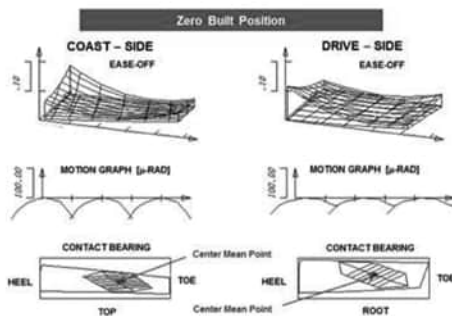


Figure 15: TCA of hypoid set from Figure 11 without any displacements.

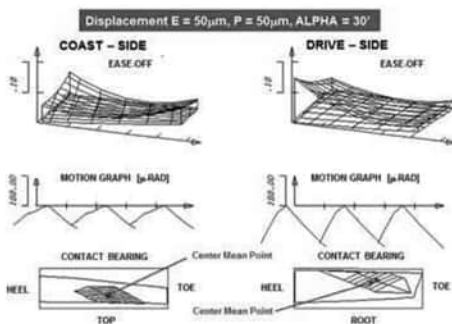


Figure 16: TCA of hypoid set from Figure 11 with added crowning and shaft displacement.

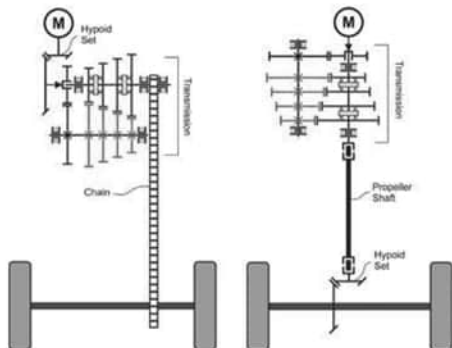


Figure 17: Hypoid gearset locations in vehicles with rear wheel drive.

achieved with correct amounts of crowning, adjusted to the operating displacements. It is interesting to mention that a hypoid gearset with crowning will fulfill the first and third fundamental gearing laws even in case of gearbox inaccuracies.

## TRANSMISSION ORIENTATIONS

The proposal in [1] to place the hypoid gearset between motor and transmission is not practical. Hypoid gears are not used as simple reducers, but their purpose is to redirect rotation and torque by a certain angle, commonly  $90^\circ$ . In case of hypoids, the second purpose of lowering the center of gravity of a vehicle body has become very important in the automotive and truck industry. The redirection of rotation and torque has to be done at the driving axle of a vehicle. The engine orientation of vehicles with a rear wheel drive is longitudinal. Because engines of cars and trucks are commonly in the front, a longitudinal oriented propeller shaft transmits the engine rotation to the rear drive axle (Figure 17, right side). The transmission, which is located between engine and propeller shaft, needs to have a gear shaft orientation identical to the direction of the engine crankshaft. The hypoid gearset redirects rotation and torque and provides the final reduction at the drive axle. The advantage of this concept is the lower torque in the complex shift or automatic transmission and the high torque only at the ring gear at the drive axle.

A concept as shown in the left side graphic in Figure 17 would require, for example, a chain connection from the transmission output to the drive axle. This solution has low efficiency, causes high noise, provides an unacceptable packaging, and is not very reliable.

## IS LAPPING AN ATTEMPT TO MAKE HYPOID GEARS CONJUGATE?

In [1, 2] it is mentioned that lapping of bevel and hypoid gearsets can be omitted if the gear geometry consists of a conjugate design. This reveals a misperception about the reason for lapping (and grinding). Lapping and grinding are hard-finishing operations. The soft manufactured bevel and hypoid gearsets have to be heat-treated, which in the most common case begins with a case carburizing of standard gear steels such as AISI 8620 or 16MnCr5. In order to give the low carbon steel a surface hardness in the 60 HRC range, a layer of carbon enrichment below the surface of 0.8 to 1.5 mm depth is placed by a diffusion process. After the carburizing a quenching in oil and an additional tempering takes place. The result is a surface hardness that is commonly close to 60 HRC and a core hardness in the 30 HRC range. Case hardening provides an ideal transition between surface and core hardness that makes gears on the surface hard and wear resistant and in the core ductile. This makes shock loads and certain small plastic deformations tolerable without failure of the gearset. One major side effect of the heat-treatment process is the distortion of the gears that is caused by the carburizing, the re-crystallization of the steel, and the quenching. In order to make a gearset after heat-treatment suitable for power transmissions, for example in cars and trucks, a hard-finishing operation is required. The hard-finishing operation eliminates the heat-treatment distortions hereby providing the flank surfaces with the correct geometry from before the heat-treatment back. In addition, hard-finishing improves the surface finish to a low roughness and waviness, which enhances the hydrodynamic lubrication and reduces noise. Grinding and skiving are the preferred hard-finishing methods, creating a defined surface form that duplicates the original designed surfaces in the single micron range.

In case of face-hobbed bevel and hypoid gearsets, grinding is not possible, because of the epicyclic flank lead function. Skiving can generate epicyclic lead functions, but is not yet accepted for the high production volumes in the automotive and truck industry. This leaves only the lapping process for the hard-finishing of face-hobbed angular gearsets. However, the face-hobbed surface texture and the relative sliding between the flanks of hypoid gears make lapping an ideal alternative. Lapping can remove the surface scale

**FIGURE 31.1 (CONTINUED)** Facsimile of the article: Stadtfeld, H.J., "Why are Today's Hypoids the Perfect Crossed-Axes Gear Pairs?," *Gear Solutions* magazine, May 2019, pages 42–50, [210].

(Continued)



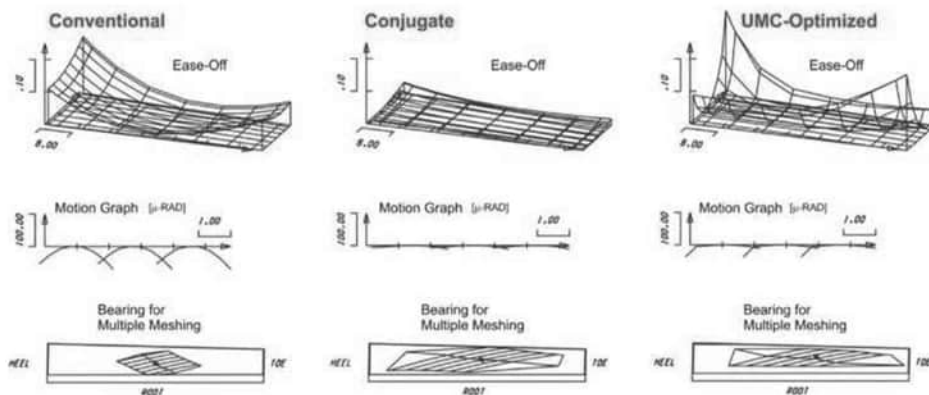


Figure 18: From conventional crowning via conjugate to UMC-optimized.

left from heat-treatment, and it re-matches two mating members by removing some runout and flank form distortions. Lapping can reduce the transmission error in many cases due to the fact that the major material removal is in the center region of the teeth where the tooth contact under light load is expected. In order for the lapping to work well, more crowning than required in the hard-finished gearset is used in the gearset design for the soft cutting. Lapping removes about 30 percent of this crowning, such that the length and profile crowning is just right after the lapping. Soft cutting of parts that are lapped after heat treatment considers a stock allowance of 0.03mm in the pinion and 0.01mm in the gear. If grinding is the hard finishing process (for face milled gearsets) then the design crowning is identical to the desired crowning after hard finishing. Between soft cutting and grinding, a uniform stock allowance of 0.10mm to 0.15mm is applied to the pinion and gear flanks.

### SUMMARY

Conjugacy between the members of straight bevel, spiral bevel, and hypoid gears was only the first step and goes back more than 100 years. Quickly, the early scientists and engineers found out that conjugacy only gives us an important basis, but not a solution for power transmissions. Angular gearsets under load experience deflections that move them away from their theoretical position by half a millimeter and more. Well-designed and manufactured bevel and hypoid gearsets today can live up to those requirements and still maintain a power density that is four times higher than it was 50 years ago.

Transmission errors of 50 to 150 micro-radian that were normal in the 1970s are in today's high-power density gearsets only between 5 and 15 micro-radian. All this was achieved by converting a global length and profile crowning (Figure 18, left) first back to conjugacy (Figure 18, center) and then into a UMC<sup>TM</sup>-optimized selective crowning, which is limited to particular regions of the

teeth as shown in the right graphic in Figure 18. It is notable that the flank center of the UMC-optimized Ease-Off is conjugate, and the transmission error is next to zero. In lapping, similar effects as in grinding are achieved by using low inertia spindles with rotational compliance and high-speed torque control (SmartLap<sup>TM</sup>).

The dream of conjugate angular gearsets turned out to be a false objective. Gear scientists, gear engineers, and gear manufacturers worked successfully for many decades on finding the optimal flank forms and the optimal non-conjugate flank surface interaction. The conjugate tooth design is today considered simple compared to a sophisticated higher order surface modulation. There is still room for improvement, but this cannot be achieved by going back to antiquated conjugate designs. »

### REFERENCES

- [1] Radzevich, S.P.; Design Features of Perfect Gears for Crossed-Axes Gear Pairs; Gear Solutions Magazine, February 2019, Pages 36 to 43.
- [2] Radzevich, S.P.; Preliminary Results of Testing of Low Tooth-Count Bevel Gears of a Novel Design, Part I, II and III, Gear Solutions Magazine, October 2014, December 2014 and January 2015.
- [3] Wildhaber, E.; Stewart, A.J.; Design, production and application of the hypoid rear axle gear; The Journal of the Society of Automotive Engineers Vol. 18, Issue 6, June 1926, Pages 575 to 589.
- [4] Shtipelman, B.; Design and Manufacture of Hypoid Gears; John Wiley & Sons, Inc., New York, 1978.
- [5] Stadtfeld, H.J.; Gleason Bevel Gear Technology; Expert Publishing, Renningen, Germany, May 2017.
- [6] Schriefer, H.; Verzahnungsgeometrie und Laufverhalten bogenverzahnter; Kegelradgetriebe Dissertation RWTH Aachen, 1983.
- [7] Wildhaber, E.; Relationships of Bevel Gears – Design for Duplex Cutting; American Machinist, October 1946.
- [8] Wildhaber, E.; Relationships of Bevel Gears -Tooth Contact; American Machinist, February 1946.

### ABOUT THE AUTHOR

Dr. Hermann J. Stadtfeld is vice president of Bevel Gear Technology at The Gleason Works.



see Figure 31.2, where the name of the authors of this article is mistakenly not removed). Scientific problems cannot be solved this way.

The article [158] is important, as numerous common mistakes committed by other gear experts are responded there. However, because the article [158] is removed from August 2020 issue of the *Gear Solutions* magazine, and, thus, it is no longer available in the public domain, facsimile of this article can be found in Figure 31.3 immediately below.

## FROM THE EDITOR



### Industry keeps adapting to the new normal

The craziness that seems to be the driving force of 2020 has affected almost every part of our lives — from the tiniest things we may take for granted to the larger health issues that keep us up at night.

As we try to make sense and adapt to what has become a new normal, *Gear Solutions* has tried to adapt as well.

Our August issue and our September issue were originally scheduled to be a springboard for the International Manufacturing Technology Show. But like so many other 2020 tradeshows, the organizers were forced to shift gears due to the coronavirus pandemic.

I must applaud IMTS for working toward making the best lemonade out of the lemons COVID-19 has thrown at us. Even though the Chicago show is officially canceled, IMTS organizers are working to take much of the tradeshow virtual. A virtual experience means no face-to-face camaraderie as with past shows, but attendees will still get the benefit of IMTS' experts and presenters. And I suspect no one is going to really miss their annual soft pretzel food run. (OK, full confession: I do love a soft pretzel.)

It is somewhat of a relief to know that technology has been an awesome tool in keeping a lot of our business going in these weird times.

With physical tradeshows on hold, please take time to see how *Gear Solutions* can also be your ally in getting your message to your customers. We offer many ways in which to remind the industry that your products and services are available.

That's good news for your audience in search of the very services and products that you can provide every day. And with the world trying to cope with economic and medical hardships, the deep reach *Gear Solutions* can provide is more important than ever.

With that in mind, I hope you find the involute gearing and gear design articles in our August issue of interest.

In a fascinating article from Christian Weber, Thomas Tobie, and Karsten Stahl — all with the University of Munich's Gear Research Centre — the authors share their insights on the rapid and precise manufacturing of special involute gears for prototype testing.

Next up, frequent contributor Stephen Radzevich discusses the most critical accomplishments in the scientific theory of gearing.

And, as always, you'll find some expert and innovative advice from our columnists. I always appreciate the wisdom and time they volunteer for the magazine.

With all that in mind, a final reminder that *Gear Solutions* is here to serve you. If you have any suggestions or would like to contribute, please contact me. I'm always looking for exciting articles to share.

Stay safe and healthy out there, and, as always, thanks for reading!



**KENNETH CARTER, editor**  
editor@gearsolutions.com  
(800) 366-2185 x204



6 gearsolutions.com

## GEARSolutions\*

David C. Cooper  
PUBLISHER

---

**EDITORIAL**

Kenneth Carter  
EDITOR

Jennifer Jacobson  
ASSOCIATE EDITOR

Joe Crowe  
CONTRIBUTING EDITOR

---

**SALES**

Dave Gomez  
NATIONAL SALES MANAGER

Tom McNulty  
REGIONAL SALES MANAGER

---

**CIRCULATION**

Teresa Cooper  
MANAGER

Jamie Willett  
ASSISTANT

---

**DESIGN**

Rick Frennea  
CREATIVE DIRECTOR

Michele Hall  
GRAPHIC DESIGNER

---

**CONTRIBUTING WRITERS**

REBECCA BRINKLEY  
E. BUDDY DAMM  
BRIAN DENGEL  
D. SCOTT MACKENZIE  
ADRIAN NOWOJSKY  
STEPHEN RADZEVICH  
KARSTEN STAHL  
THOMAS TOBIE  
CHRISTIAN WEBER

---



**PUBLISHED BY MEDIA SOLUTIONS, INC.**  
P. O. Box 1987 • Pelham, AL 35124  
(800) 366-2185 • (205) 380-1580 fax

David C. Cooper  
PRESIDENT

Teresa Cooper  
OPERATIONS

**FIGURE 31.2** Facsimile of page 6 of the August 2020 issue of the *Gear Solutions* magazine, where the marks of the removed article [158] are still available.



**FIGURE 31.3** Facsimile of the article: Radzevich, S.P., “Knowledge (of Gear Theory) is Power in the Design, Production, and Application of Gears.” Courtesy of *Gear Solutions* magazine, August 2020, pages 38–44, [158].

(Continued)

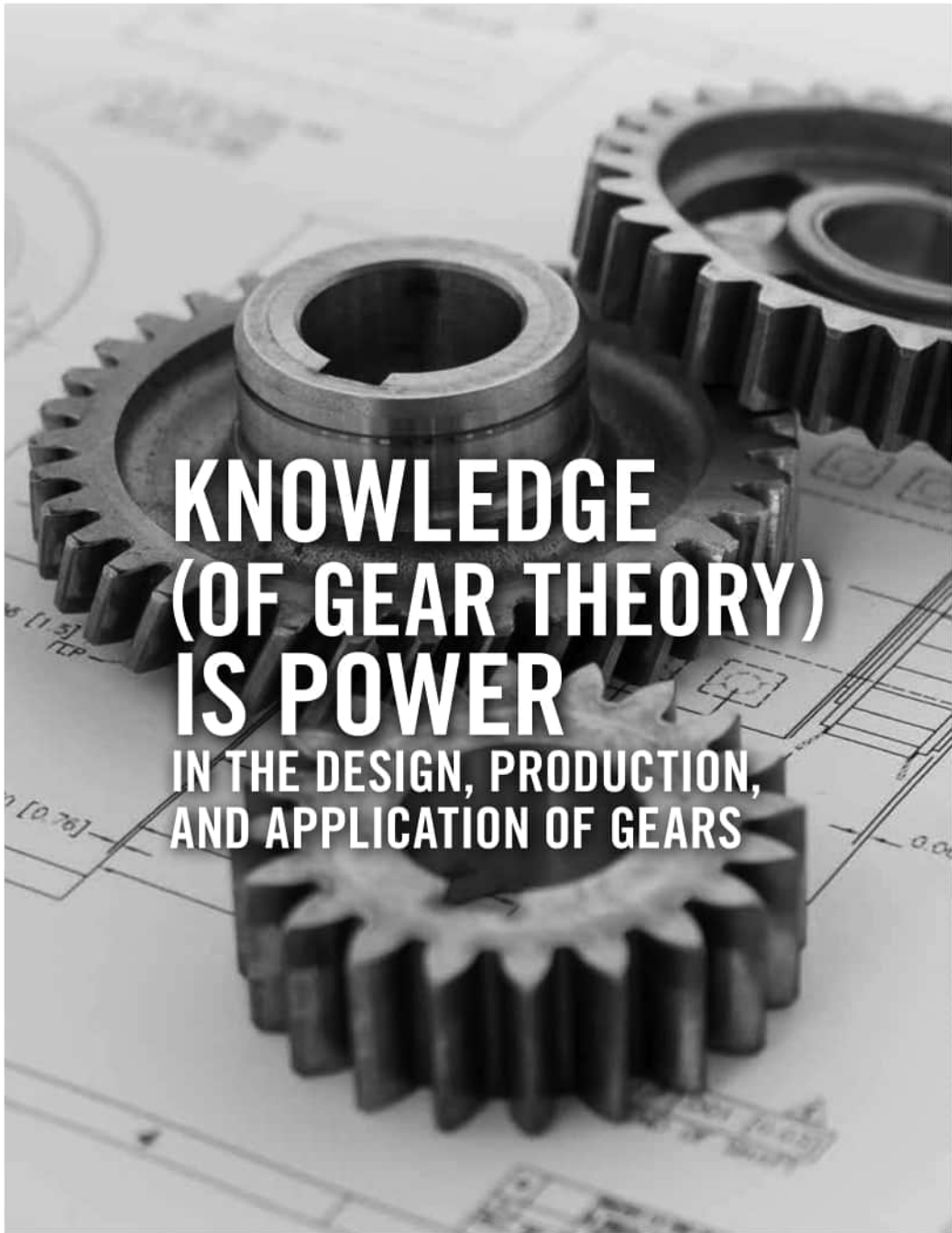


**FIGURE 31.3 (CONTINUED)** Facsimile of the article: Radzevich, S.P., “Knowledge (of Gear Theory) is Power in the Design, Production, and Application of Gears.” Courtesy of *Gear Solutions* magazine, August 2020, pages 38–44, [158].

(Continued)



## In this article, a few of the most critical accomplishments in the scientific theory of gearing will be discussed.

By STEPHEN P. RADZEVICH

**T**he now-famous equation, “knowledge is power” (“scientia potestas est”), was coined by Francis Bacon (January 22, 1561–April 9, 1626). Formulated as early as 1597, this famous equation was proven to be correct for centuries. Knowledge in any and all areas of human activity gives one a strong advantage over those less knowledgeable ones. Gearing is no exception. Knowledgeable and skilled gear engineers always have a greater chance for success doing business, rather than less knowledgeable and less skilled ones. This article is aimed at the promotion of knowledge (namely, the promotion of the “scientific theory of gearing”) to gear practitioners, and, in this way, to equip them with a means to achieving success running a business in the gear industry.

### INTRODUCTION

The necessity of scientific foundations of gearing for design and manufacturing has long been realized by gear practitioners. Gears that operate on parallel axes of rotation of a gear and a mating pinion are the first to attract attention of mathematicians and gear theoreticians. It was Leonhard Euler who, in the mid-18th century, proved that an involute tooth profile fits the best gears that operate on parallel axes of rotation of a gear and a mating pinion.

Having started his own career in gearing in 1975, the author had many opportunities to get familiar with state-of-the-art innovations in both gear design and gear production. Shortly after graduating from college, the author was faced with: (a) numerous specific problems in gearing, and (b) the absence of an adequate means to solve these problems. The decades of research in the field of gearing theory by the author has resulted in a 2018 monograph titled “Theory of Gearing: Kinematics, Geometry, and Synthesis” [10]. It definitely makes sense to the gear community to get familiar with the capabilities that the proposed theory of gearing provides gear practitioners. In this article, a few of the most critical accomplishments in the scientific theory of gearing will be briefly discussed. The author concludes many in the gear community may be unfamiliar with the key accomplishments in the scientific theory of gearing. A recently published (2019) *Gear Solutions* article [15] (and not this article only) is taken as a representative example that proves this conclusion. Unfortunately, there are plenty of publications of this sort in current journals and magazines for gear engineers and scientists. Moreover, the article [15] (as well as other similar publications) may mislead gear practitioners, offering wrong approaches in the field of gear design

and gear manufacturing. All the ambiguities in the practice of gear design and gear production should be eliminated. An old Chinese proverb, “The beginning of wisdom is to call things by their right names,” is a good place to start.

### MOTIVATION

This article was necessitated by the recently published article: Stadtfeld, H.J., “Why are Today’s Hypoids the Perfect Crossed-Axes Gear Pairs?” *Gear Solutions* magazine, May 2019, pp. 42–50 [15]. These comments pertain to the key accomplishments in the scientific theory of gearing. The comments could be confusing to inexperienced gear community members, especially those who attempt to study the gear theory on their own and apply the theory in their practical work.

Here and below in this text, the article [15], is used solely as a representative example of an improper understanding of the scientific theory of gearing by a majority of gear practitioners, including those who may call themselves “gear theoreticians.” An additional reason to reference the article [15] is that it claims to be written on behalf of established gear theory and manufacturing (see page 43 in [15]): “This write-up is meant to be a response on behalf of established gear theory and manufacturing.” No reference is provided in [15] as to whether this “established gear theory” is available to the reader in the public domain.

Recommendation to the readers of the current article: Except for section 1, the rest of the sections in this article intentionally reflect the article [15]. This is to help the reader better understand what these two articles are about, their differences, and why the approach outlined in the current article is advantageous over the approach recommended in the article [15]. When reading the current article, it is recommended to have the article [15] for comparison.

### 1 THE INTRODUCTORY SECTION: NOVIKOV GEARING (CONFORMAL GEARING)

The evolution of gear art is heavily associated with Ernest Wildhaber. No doubt, Wildhaber is a gifted inventor and a famous gear engineer. Despite that, Wildhaber has never been recognized as a gear scientist, as is loosely claimed in [15] (page 43). Because of that, Wildhaber cannot be granted with the title of “the father of modern gear theory” (see page 43 in [15]). Both these statements are incorrect: Wildhaber was NOT a gear scientist at all, and, therefore, it is incorrect to refer to him as the father of modern gear theory. Wildhaber is credited with NO key accomplishments in the scientific theory of gearing (see [10] for details). A difference between the terms “a

August 2020 **39**

**FIGURE 31.3 (CONTINUED)** Facsimile of the article: Radzevich, S.P., “Knowledge (of Gear Theory) is Power in the Design, Production, and Application of Gears.” Courtesy of *Gear Solutions* magazine, August 2020, pages 38–44, [158].

(Continued)



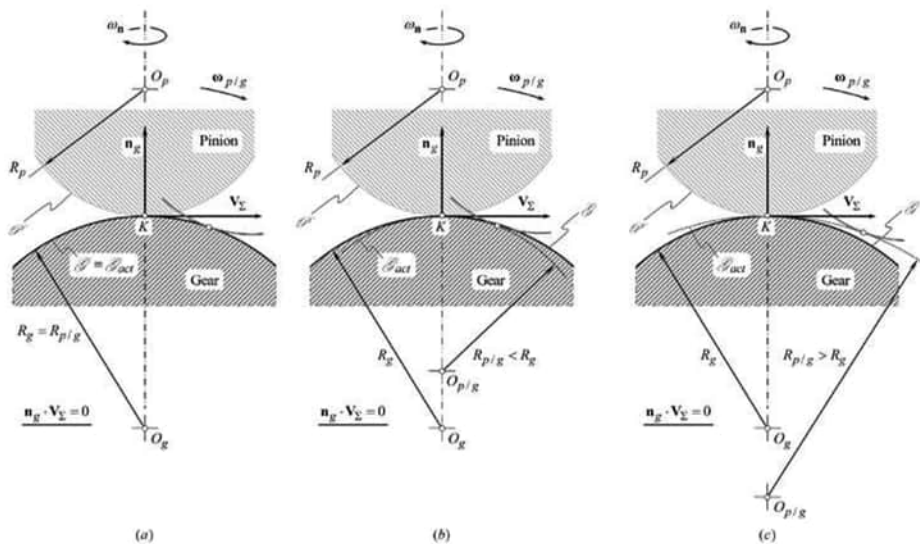


Figure 1: Examples of (a) fulfillment, and violation: (b) interference, and (c) separation, of a gear,  $\mathcal{G}$ , and its mating pinion,  $\mathcal{P}$ ; tooth flanks: the “Shishkov equation of contact,  $\mathbf{n}_g \cdot \mathbf{V}_K = 0$ ” is fulfilled in all three cases (a) through (c), while the law of conjugacy is violated in the cases (b) and (v).

gifted inventor and a famous gear engineer” and “a gear scientist” must be noted.

The earlier performed comparison of “Novikov gearing” [2], and Wildhaber “Helical gearing” [1] reveals these two gear systems are completely different, and, moreover, these gear systems are not compatible with one another [10, 7, 9]. On top of that, the term “Wildhaber-Novikov gearing” is incorrect by nature, as these two gear systems (namely, Wildhaber “Helical gearing” [1] and “Novikov gearing” [2]) cannot be combined into a common gear system (see [10, 7, 9], and others, for details). It is a huge mistake to adopt the term “Wildhaber-Novikov gearing.”

“Novikov gearing” can be viewed as a reduced case of a parallel-axes involute gear pair, while Wildhaber “Helical gearing” cannot ([3, 6] and numerous other sources).

Today’s gear professionals should know the difference between “Novikov gearing” [2] and Wildhaber “Helical gearing” [1].

## 2 NEWS ABOUT HYPOID GEARS?

The article [15] proves today’s hypoid gearsets are approximate by nature, and, thus, they are not geometrically-accurate gearsets. No alterations can be even anticipated.

Further, no attempt is taken in the article [15] to “question the credibility of the scientists and gear engineers who worked on the theory and its improvement over approximately 100 years.” No gear theory was developed during these 100 years, and no key scientific accomplishments are attained at this period of time. “Trial-and-error method” is the main — and perhaps only — tool used for “over approximately 100 years.” But this is not a theory of gearing. Instead, this is a collection of more-or-less reasonable solutions to separate gear problems. Combined together, these solutions do not form a gear theory.

40 [gearsolutions.com](http://gearsolutions.com)

## 3 THE THREE FUNDAMENTAL LAWS OF GEARING

Leonhard Euler can be credited for originating geometrically-accurate gears (even though the term “geometrically-accurate gears” was introduced much later [10]). It is proven [10] that, in order to be referred to as “geometrically-accurate,” the gears have to fulfill three fundamental laws of gearing. The fulfillment of three fundamental laws of gearing is necessary and sufficient to refer to a gearset as a “geometrically-accurate gearset.” To the best possible extent, all three fundamental laws of gearing are discussed in [10]. These laws of gearing are briefly outlined here:

The first fundamental law of gearing: “At every point of contact of tooth flanks of a gear and a mating pinion, the vector of their instantaneous relative motion has to be orthogonal to the common perpendicular at every instant of time.”

In this form, the first fundamental law of gearing is valid for gearing of all designs that operate on parallel axes, intersecting axes, and crossing axes of rotation of a gear and its mating pinion.

Numerous interpretations of the first fundamental law of gearing are known. The most practical and extensively adopted way of interpretation of the first fundamental law of gearing is to analytically describe this law of gearing in the form of the “Shishkov equation of contact,  $\mathbf{n}_g \cdot \mathbf{V}_K = 0$ .” The “Shishkov equation of contact,  $\mathbf{n}_g \cdot \mathbf{V}_K = 0$ ” is known to practically every gear engineer. Professor V.A. Shishkov was the first to express (~1948) the first fundamental law of gearing in the form of the dot product of a unit vector of a common perpendicular,  $\mathbf{n}_g$ , by the vector of the resultant linear velocity,  $\mathbf{V}_K$ , of the tooth flanks in relation to one another. Both the vectors,  $\mathbf{n}_g$  and  $\mathbf{V}_K$ , are calculated at the contact point of a gear and its mating pinion tooth flanks.

The second fundamental law of gearing is often referred to as the “conjugate action law.” When the “Shishkov equation of contact,

**FIGURE 31.3 (CONTINUED)** Facsimile of the article: Radzevich, S.P., “Knowledge (of Gear Theory) is Power in the Design, Production, and Application of Gears.” Courtesy of *Gear Solutions* magazine, August 2020, pages 38–44, [158].

(Continued)



Figure 2: Rotationally-positive external parallel-axes gear pair (Pat. No. 163857, USSR, A Helical Gearing, B.V. Shitikov, N.A. Bayazitov, Int. Cl. F06h, Filed: February 25, 1963, Published: July 22, 1964.).

$n_g \cdot V_\Sigma = 0$ " is fulfilled, the "conjugate action law" can either be fulfilled, or it can be violated. In Figure 1, an example of interaction of local patches of the tooth flanks,  $\mathcal{S}$  and  $\mathcal{P}$ , is schematically illustrated. The tooth flanks,  $\mathcal{S}$  and  $\mathcal{P}$ , make contact at point,  $K$ . The radii of curvature of the interacting tooth flanks at contact point,  $K$ , equal to  $R_g$  and  $R_p$ , correspondingly (see Figure 1a). The centers of curvature of the tooth profiles,  $\mathcal{S}$  and  $\mathcal{P}$ , are denoted by  $O_g$  and  $O_p$ , correspondingly. In the instantaneous motion of the pinion,  $\mathcal{P}$ , in relation to the gear,  $\mathcal{S}$ , the pinion performs an instantaneous rotation,  $\omega_{p/g}$ , about the point  $O_g$ . The radius of curvature of the generated actual gear tooth flank,  $\mathcal{S}_{act}$ , equals to  $R_{p/g} = R_g$ . In this scenario, the second fundamental law of gear is fulfilled, and the actual tooth flank,  $\mathcal{S}_{act}$ , is identical to the desirable gear tooth flank,  $\mathcal{S}$ , as shown in Figure 1a.

**Note:** In Figure 1a, the rotation,  $\omega_p$ , of the pinion,  $\mathcal{P}$ , in relation to the gear,  $\mathcal{S}$ , about the contact perpendicular,  $n_g$ , is not prohibited by the second fundamental law of gearing.

If the instantaneous rotation is performed either about the center  $O_{p/g}$  (when  $R_{p/g} < R_g$ , see Figure 1b), or about the center  $O_{p/g}$  (when  $R_{p/g} > R_g$ , see Figure 1c), the second fundamental law of gear is violated, and the actual tooth flank,  $\mathcal{S}_{act}$ , differs from the desirable gear tooth flank,  $\mathcal{S}$ .

**Reminder:** The first fundamental law of gearing (as well as the "Shishkov equation of contact,  $n_g \cdot V_\Sigma = 0$ ") is fulfilled in all three cases shown in Figure 1, while the second fundamental law of gearing is fulfilled only in the first case illustrated in Figure 1a. The schematic in Figure 1 is helpful for understanding the difference between the first and second fundamental laws of gearing and prevents the making of unsubstantiated conclusions in this regard.

**Important:** When the second fundamental law of gearing is fulfilled, the first fundamental law of gearing is always fulfilled, and not vice versa.

With that said, it makes sense to go back to the article [15] and compare the results illustrated in Figure 1 with a loosely made statement (see page 44 in [15]): "The second fundamental law of gearing, ... , is a redundant relationship to the first gearing law, and it is limited to cylindrical gears with parallel axes and straight bevel gears without hypoid offset. In this case, it adds nothing to the first gearing law; conjugacy is already given by the relationships required in the first gearing law." It is correct to question whether a gear practitioner has a chance for success in the design and production of today's sophisticated gear systems if he or she strictly follows the afore mentioned quote (see page 44 in [15]).

In the most general case of gearing (namely, in the case of "crossed-axes gearing", or " $C_a$  – gearing", for simplicity) the second fundamental law of gearing is formulated as:

**The second fundamental law of gearing:** "In order to smoothly transmit a uniform rotary motion from a driving shaft to a driven shaft by means of gear teeth, perpendiculars to the tooth flanks of the interacting teeth at all points of their contact must intersect the axis of instantaneous rotation in the gear pair."

In a reduced case of gears that operate on parallel axes of rotation of a gear and its mating pinion (namely, in the case of "parallel-axes gearing", or " $P_a$  – gearing", for simplicity) this fundamental law of gearing is formulated as:

**The second fundamental law of (parallel-axes) gearing:** "In parallel-axes gearing, in order to smoothly transmit a uniform rotary motion from a driving shaft to a driven shaft by means of gear teeth, perpendiculars to the tooth flanks of the teeth at all points of their contact must pass through a stationary point located on the line of centers, namely, the pitch point  $P$ ; the pitch point subdivides the center-distance reciprocal to the angular velocities of the gear and the pinion." (Robert Willis, 1841 [16])

These days, the second fundamental law of gearing (in a case of parallel-axes gearing) is commonly referred to as "Camus-Euler-Savari fundamental law of gearing" (or "fundamental law of gearing," for simplicity).

The second fundamental law of gearing is also often referred to as "conjugate action law" – and this is also correct.

The design of "Alpha Worm Gearing" (New Venture Gear, Syracuse, NY; US Pat. No. 6,148,683, Nov. 21, 2000) is a good example of the violation of the second fundamental law of gearing. Violation of the second fundamental law of gearing is the main reason for this design fail, and it has caused major financial damage to the gear industry.

The third fundamental law of gearing relates to the distribution of the gear teeth over the periphery of a gear and a mating pinion. In the most general case of gearing (in the case of crossed-axes gearing), the third fundamental law of gearing is formulated as:

**The third fundamental law of gearing:** "In order to smoothly transmit a uniform rotary motion from a driving shaft to a driven shaft by means of gear teeth, at every instant of time the angular base pitch of a gear, and that of a mating pinion, both have to be equal to the operating angular base pitch in the gear pair."

In a reduced case of "parallel-axes gearing," this fundamental law of gearing is formulated as:

**The third fundamental law of gearing (in parallel-axes gearing):** "In parallel-axes gearing, in order to smoothly transmit a uniform rotary motion from a driving shaft to a driven shaft by means of gear teeth, at every instant of time base pitch of a gear and that of a mating pinion, both must be equal to the operating base pitch in the gear pair."

**FIGURE 31.3 (CONTINUED)** Facsimile of the article: Radzevich, S.P., "Knowledge (of Gear Theory) is Power in the Design, Production, and Application of Gears." Courtesy of *Gear Solutions* magazine, August 2020, pages 38–44, [158].

(Continued)

All the geometrically-accurate gears (that is, all the precision gears — with no exception) meet all three fundamental laws of gearing — this is a must.

#### 4 PERFECT CONJUGACY IN STRAIGHT BEVEL GEARSETS

The title of the section “Perfect Conjugacy in Straight Bevel Gearsets” in the article [15] may be confusing to readers, as “conjugacy” by nature cannot be “perfect” or “imperfect.” Gearsets of all kinds are either conjugate, or they are not conjugate. The term “perfect conjugacy” could be considered analogous to saying “a bit pregnant.”

It is loosely claimed (see page 44 in [15]) that: “The plane of action cannot be extended beyond its tangential contacting line with the base element as shown incorrectly ... The plane of action exists where tooth engagement is possible.” Gearsets that feature the plane of action that extends far beyond its tangential contacting line with the base element have been known for decades. As an example, a parallel-axes gear set of this particular kind is depicted in Figure 2 [14]. Later on, this concept was evolved (~2008) by Prof. S.P. Radzevich to the cases of intersected-axes gearing, as well as to crossed-axes gearing [10].

In a set of articles [11], [12], and [13], the preliminary results of testing of low-tooth-count spiral bevel gears of a novel design are discussed. Without going into details of design and manufacture of spiral bevel gears of this design (proposed by Prof. S.P. Radzevich, ~2008, and designed using the earlier developed scientific theory of gearing [10]), it is right to stress the following:

1. As shown in Figure 3, the predicted contact patch is perfect (see Figure 7a on page 21 in [13]).

2. As shown in Figure 4, the predicted contact pattern is perfect (see Figure 9 on page 23 in [13]).

3. As shown in Figure 5, the contact pattern in the roll test is also perfect (see Figure 10 on page 23 in [13]), and it indicates excellent correlation with the predicted one.

4. No lapping was used to finish the gears.

5. No adjusting for the axial configuration of the gear and the mating pinion is required, and the gears are ready to run.

In today's production of precision gears, the use of the lapping process is inevitable. Those knowledgeable in the scientific theory of gearing can eliminate dirty and obsolete lapping processes from finishing tooth flanks of gears for precision gearsets.

Concerning the statements on page 45 in [15] that state: “The Octoid is the analog function of an involute, and it provides to bevel gears the same advantage as an involute provides to cylindrical gears. ... bevel gears have a trapezoidal generating profile. The straight rack ... becomes a ring ... as shown in Figure 6.” It has been known for a while that the tooth profile of a crown rack for generating a geometrically-accurate bevel gear has to be shaped in the form of a curve illustrated in (see Figure 6) [10], and NOT in the form of a straight-sided crown rack. Only approximate bevel gears can be generated by the just-mentioned straight-sided crown rack “shown in Figure 6” [15]. No gearing with the so-called “octoid” path of contact is possible at all: If one assumes the path of contact shaped in a form of an octoid curve, this inevitably entails violation of the second fundamental law of gearing — it is important to bear this in mind. The so-called “octoid gearing” is a mistake that often travels from one publication to another.

Concerning the statement on page 46 in [15] that states: “Conjugacy is the basis of all gearsets manufactured in high volume on dedicated manufacturing machines.” All the bevel gears manufactured in high volume on dedicated manufacturing machines are generated by means of straight-sided crown rack (shown in Figure 6, page 45 in [15]), and, thus, all of them are approximate gears.

42 gearsolutions.com

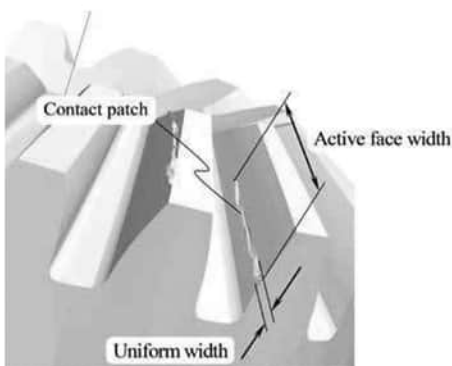


Figure 3: Predicted contact patch in geometrically-accurate intersected-axes spiral bevel gears.

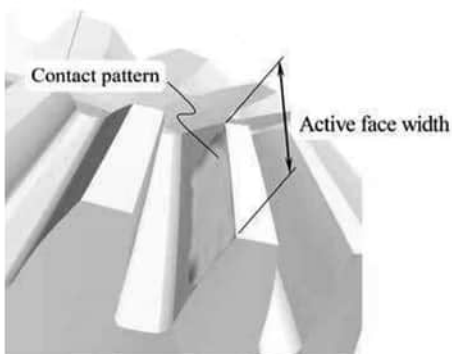


Figure 4: The predicted contact pattern in geometrically-accurate intersected-axes gearing.

Only approximate bevel gears can be generated by just mentioned straight-sided crown rack “shown in Figure 6” [15]. As the generated bevel gears are approximate, no conjugate bevel gear pairs can be composed of these gears.

Concerning the statement on page 46 in [15] that states: “Conjugate bevel gearsets cannot be used for a power transmission because manufacturing tolerances and ...” Today's gear industry is capable of manufacturing precision helical involute gears that are extensively used, for example, in the design of turbine reducers. The gear industry is NOT capable of manufacturing precision bevel gears, and this is the main reason for precision bevel gears NOT being extensively used in the industry. The bottom-line is: Precision bevel gears are NOT extensively used in the industry solely because the gear industry is not capable of producing (for a reasonable cost) these kinds of gears.

Concerning the statement on page 46 in [15] that states: “The right amount of crowning makes a gearset quiet and gives it the required load carrying capacity”. How can the “right amount” be determined for a particular bevel gear application? The desirable amount of crowning can be determined by means of a “trial and error method” — this is the only tool developed by the “established

**FIGURE 31.3 (CONTINUED)** Facsimile of the article: Radzevich, S.P., “Knowledge (of Gear Theory) is Power in the Design, Production, and Application of Gears.” Courtesy of *Gear Solutions* magazine, August 2020, pages 38–44, [158].

(Continued)





Figure 5: Contact pattern in geometrically-accurate spiral bevel gears in roll test.

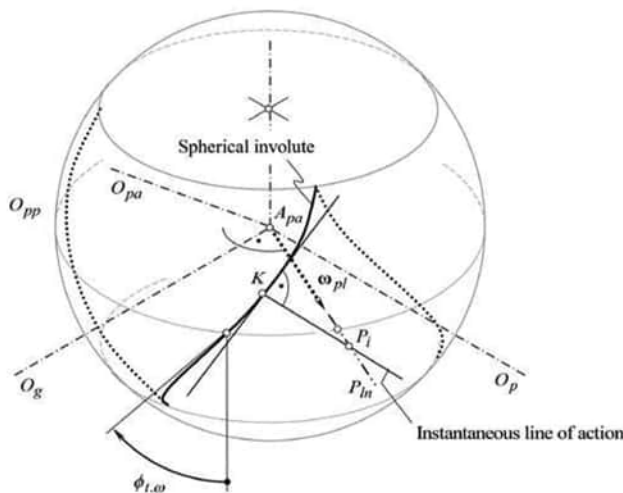


Figure 6: Trace of contact point in geometrically-accurate intersected-axes gear pair.

gear theory" in [15]. Today's scientific theory of gearing not only gives an answer to the question of how the "right amount" can be determined, but it also provides an in-detail specification of the entire modified tooth flank. Properly engineered gears (both design and production) do not need to use a "trial and error method."

## 5 PERFECT CONJUGACY IN HYPOID GEARSETS

The discussion on "perfect conjugacy in hypoid gearsets" in [15] is similar to "perfect conjugacy in straight bevel gearsets" discussed earlier (see Section 4). Again, the title of the section "Perfect

Conjugacy in Straight Bevel Gearsets" in the article [15] may be confusing to readers as "conjugacy," by nature, can neither be "perfect" nor "imperfect." Gearsets of all kinds are either conjugate, or they are not conjugate.

Concerning the statement on page 46 in [15] that states: "... the pitch elements of crossed axes hypoid gears are drawn as cones." It fails to describe one of the key features of the modern scientific theory of gearing [10]: In order to design gears for hypoid gearsets, no pitch elements are required at all. The term: "... the pitch elements are hyperboloids" is obsolete and is no longer used in the modern scientific theory of gearing [10].

Concerning the statement on page 47 in [15] that states: "No plane of action exists between two hyperbolic base elements." It is correct, as it proves there is no place for hyperboloids in the kinematics and the geometry of gears with crossing axes of rotation of a gear and its mating pinion.

Concerning the statement on page 47 in [15] that says: "The correct surface of action is curved and wrapped, as shown in Figure 10." Surface of action in hypoid gearing (as well as in gearing of all other kinds) is a plane through the axis of instantaneous rotation, or it is a plane through the common perpendiculars constructed at all points of the line of contact between the interacting tooth flanks of a gear and its mating pinion. The normal forces of interaction in gearing are commonly described

by means of vectors. A vector is a quantity possessing both magnitude and direction. Vectors are described by means of straight-line segments with a specified direction. This leaves no room for "curved surface of action."

## 5.1 CONJUGACY BETWEEN MESHING FLANKS

Concerning the statement on page 47 in [15] that says: "The term conjugate is used in mathematics for two or more surfaces that contact each other along a line. Since the 1970s, the term conjugate has also been employed in gear technology literature to define..." Line contact between two surfaces (namely, between tooth flanks of two mating gears) is not sufficient (and is not always necessary) to refer to the pair of surfaces as to "conjugate surfaces." In addition, the second fundamental law of gearing has to be fulfilled for conjugate surfaces, which is a must. Moreover, it has been discovered over the last 10 years that two surfaces (two tooth flanks) can be conjugate to one another even when they are in point contact.

## 5.2 DEFINITION OF THE CONJUGATE GEAR PAIR

Concerning the statement on page 47 in [15] that says: "... hypoid gearset conjugacy is possible with a non-generated gear that meshes with a generated pinion." This reveals a poor understanding of the term "conjugacy," as no conjugate action is possible between non-generated tooth flank and generated tooth flank.

## 6 WHY IS CONJUGACY NOT DESIRABLE FOR REAL WORLD APPLICATIONS?

Most gear engineers don't doubt whether the conjugacy of inter-

**FIGURE 31.3 (CONTINUED)** Facsimile of the article: Radzevich, S.P., "Knowledge (of Gear Theory) is Power in the Design, Production, and Application of Gears." Courtesy of *Gear Solutions* magazine, August 2020, pages 38–44, [158].

(Continued)

acting tooth flanks is desirable. Conjugacy is always desirable — especially in high-power-density transmissions and in high RPM-gearsets. Unfortunately, with no lapping process in finishing the tooth flanks, the gear industry is not capable of producing precision gears for real-world gearsets. For over a decade, a concept of crossed-axes gearsets that are insensitive to the mating gears axes displacements (both, the linear displacements, as well as the angular displacements) were introduced to the public [10]. Gears of this system are commonly referred to as “ $S_{pr}$  — gearing.” The “ $S_{pr}$  — gearing” is a kind of point contact conjugate gearing capable of absorbing all the linear and angular displacements of a gear and its mating pinion axes of rotation, as long as the actual values of these displacements are within the prespecified tolerances for the accuracy of the gearset. At the same time, the “ $S_{pr}$  — gearing” features the highest possible power density being transmitting by the gearset.

## 7 TRANSMISSION OPERATIONS

Only time will tell if it is practical “... to place the hypoid gearset between motor and transmission ...?” (see page 49 in [15]). Looking to the future, one can conclude that the vehicle powertrain is not the only potential application of gears with crossing axes of rotation of a gear and a mating pinion.

## 8 IS LAPPING AN ATTEMPT TO MAKE HYPOID GEARS CONJUGATE?

Eventually, the lapping process in the production of gears for bevel and hypoid gearsets will be eliminated [6]. The gear-grinding process is a No. 1 candidate for the future of gear-finishing operations. The sooner the key accomplishments in the scientific theory of gearing reaches gear practitioners, the sooner gear lapping will be replaced by gear grinding. This negates the statement on page 49 in [15] that says: “This reveals a misperception about the reason for lapping.”

An in-depth familiarity with the key accomplishments in the scientific theory of gearing will make it possible to eliminate the gear-lapping process and replace it with the gear-grinding process. This is a reliable evolution of the gear design practice and the gear-finishing processes in particular.

## 9 SUMMARY

It is important to note that over the last 100 years, the gear industry has failed to:

- ▶ Eliminate lapping process.
- ▶ Avoid the necessity of adjustment of bevel/hypoid gears in pairs (that makes the gears not-self-replaceable).
- ▶ Eliminate the necessity of pairing of gears that operate on intersected, as well as on crossing axes of rotation of a gear and its mating pinion.
- ▶ Solve the problem of excessive gear noise excitation and vibration generation.

## CONCLUSION

In conclusion, it is likely the gear industry could end up wasting funds and time following the direction of evolution outlined in the article [15].

- In the article [15] there is no evidence of:
- ▶ Whether the third fundamental law of gearing is understood by the author.
- ▶ The importance of the concept of the “operating base pitch” in

a gear pair is realized.

▶ The concept of a gear, of a mating pinion base pitch in intersected-axes gearing, and in crossed-axes gearing, along with the concept of the “operating base pitch” in intersected-axes, and in crossed-axes gearsets as realized by the author.

Not all the inconsistencies in [15] are addressed here — only some of the larger issues. However, a more detailed analysis (if necessary) can be undertaken. ■

## REFERENCES

- [1] Pat. USA, No. 1,601,750, Helical Gearing, /E. Wildhaber, Patented: October 5, 1926, Filed: November 2, 1923.
- [2] Pat. USSR, No. 109,113, Gear Pairs and Cam Mechanisms Having Point System of Meshing, /M.L. Novikov, National Classification 47h, 6; Filed: April 19, 1956, published in Bull. of Inventions No.10, 1957.
- [3] Radzevich, S.P., “An Examination of High-Conformal Gearing”, *Gear Solutions*, February, 2018, pages 31-39.
- [4] Radzevich, S.P., “Conjugate Action Law in Intersected-Axes Gear Pairs and in Crossed-Axes Gear Pairs”, *Gear Solutions* magazine, June 2020, pages 42-48.
- [5] Radzevich, S.P., “Design Features of Perfect Gears for Crossed-Axes Gear Pairs”, *Gear Solutions*, February, 2019, pp. 36-43.
- [6] Radzevich, S.P., *Gear Cutting Tools: Science and Engineering*, 2nd Edition, CRC Press, Boca Raton, FL, 2017, 606 pages.
- [7] Radzevich, S.P., *Dudley’s Handbook of Practical Gear Design and Manufacture*, Third Edition, CRC Press, Boca Raton, FL, 2016, 629 pages.
- [8] Radzevich, S.P., *High-Conformal Gearing: Kinematics and Geometry*, 2nd edition, Elsevier, Amsterdam, 2020, 506 pages.
- [9] Radzevich, S.P., “On the Inconsistency of the Term “Wildhaber-Novikov Gearing”; A New Look at the Concept of “Novikov Gearing””, Appendix A, pp. 487-501, in: Radzevich, S.P., (Editor), *Advances in Gear Design and Manufacture*, CRC Press, Boca Raton, Florida, 2019, 549 pages.
- [10] Radzevich, S.P., *Theory of Gearing: Kinematics, Geometry, and Synthesis*, 2nd edition, revised and expanded, CRC Press, Boca Raton, FL, 2018, 934 pages.
- [11] Radzevich, S.P., et al, “Preliminary Results of Testing of Low-Tooth-Count Bevel Gears of a Novel Design. Part 1”, *Gear Solutions*, October 2014, pp. 25-26.
- [12] Radzevich, S.P., et al, “Preliminary Results of Testing of Low-Tooth-Count Bevel Gears of a Novel Design. Part 2”, *Gear Solutions*, December 2014, pp. 20-21.
- [13] Radzevich, S.P., et al, “Preliminary Results of Testing of Low-Tooth-Count Bevel Gears of a Novel Design. Part 3”, *Gear Solutions*, January 2015, pp. 20-23.
- [14] Shitikov, B.V., Bayazitov, N.A., A Helical Gearing, Pat. No. 163857, USSR, Int. Cl. F06h, Filed: February 25, 1963, Published: July 22, 1964. [see also: Bayazitov, N.A., *Helical Gears with a New Type of Gearing*, Ph.D. Thesis, Kazan’, Kazan’ Technological & Chemical Institute, 1964.].
- [15] Stadtfeld, H.J., “Why are Today’s Hypoids the Perfect Crossed-Axes Gear Pairs?”, *Gear Solutions* magazine, May 2019, pp. 42-50.
- [16] Willis, R., *Principles of Mechanisms, Designed for the Use of Students in the Universities and for Engineering Students Generally*, London, John W. Parker, West Stand, Cambridge: J. & J.J. Deighton, 1841, 446 pages.

## ABOUT THE AUTHOR

Stephen P. Radzevich, Dr.(Eng.)Sci, can be reached at radzevich@usa.com or at (586) 292-7209.

**FIGURE 31.3 (CONTINUED)** Facsimile of the article: Radzevich, S.P., “Knowledge (of Gear Theory) is Power in the Design, Production, and Application of Gears.” Courtesy of *Gear Solutions* magazine, August 2020, pages 38–44, [158].

In this second article [158], the author's comments on all the mistakes and inconsistencies committed in the article [210], those pertaining to the gear science, are concisely outlined.

**Conclusion.** *The outlined in this book scientific theory of gearing is an efficient means for solving sophisticated problems in gear design, gear production, gear inspection, and gear application.*

Only proficient and knowledgeable gear experts are allowed to use the proposed theory of gearing. This theory is developed not for amateurs, and not for inexperienced gear experts.



# Taylor & Francis

Taylor & Francis Group

<http://taylorandfrancis.com>

---

# Appendix A

## *Elements of Vector Calculus*

The *vector*, the key to all the theory of part surface generation, is a triple real number (in most computer languages these are usually called *floating point numbers*) and is noted in a **bold** typeface, that is, **A** or **a**.

Care must be taken to differentiate between two types of vectors:

1. *Position vector* – A position vector runs from the origin of coordinate (0, 0, 0) to a point (X, Y, Z) and its length gives the distance of the point from the origin. Its components are given by (X, Y, Z). The essential concept to understand about a position vector is that it is anchored to specific coordinates (points in space). The set of points that are used to describe the shape of all part surfaces can be thought of as position vectors.
2. *Direction vector* – A direction vector differs from a position vector in that it is *not* anchored to specific coordinates. Frequently, direction vectors are used in a form where they have unit length; in this case, they are said to be *normalized*. The most common application of a direction vector in the theory of part surface generation is to specify the orientation of a surface or ray direction. For this, we use a direction vector at right angles (*normal*) and pointing away from the part surface. Such *normal* vectors are also the key in many calculations in the theory of part surface generation.

Vector calculus is a powerful tool for solving many geometrical and kinematical problems, which pertain to the design and generation of part surfaces. In this book, *vectors are understood as quantities that have magnitude and direction and obey the law of addition.*

### A.1 FUNDAMENTAL PROPERTIES OF VECTORS

The distance-and-direction interpretation suggests a powerful way to visualize a vector, and that is as a directed line segment or arrow. The length of the arrow (at some predetermined scale) represents magnitude of the vector, and the orientation of the segment and placement of the arrowhead (at one end of the segment or the other) represents its direction.

Vectors possess certain properties, the set of which is commonly interpreted as the set of fundamental properties of vectors.

#### A.1.1 ADDITION

Given two vectors **a** and **b**, their sum (**a + b**) is graphically defined by joining the tail of **b** to the head of **a**. Then, the line from the tail of **a** to the head of **b** is the sum **c = (a + b)**.

#### A.1.2 EQUALITY

Two vectors are equal when they have the same magnitude and direction. Position of the vectors is unimportant for equality.

### A.1.3 NEGATION

The vector  $-\mathbf{a}$  has the same magnitude as  $\mathbf{a}$  but opposite direction.

### A.1.4 SUBTRACTION

From the properties of *addition* and *negation*, the following  $\mathbf{a} - \mathbf{b} = \mathbf{a} + (-\mathbf{b})$  can be defined.

### A.1.5 SCALAR MULTIPLICATION

The vector  $k\mathbf{a}$  has the same direction as  $\mathbf{a}$ , with a magnitude  $k$  times that of  $\mathbf{a}$ .  $k$  is called a scalar as it changes the scale of the vector  $\mathbf{a}$ .

## A.2 MATHEMATICAL OPERATIONS OVER VECTORS

The following rules and mathematical operations can be determined from the above listed fundamental properties of vectors.

### A.2.1 COMPONENTS OF VECTORS

Let's assume that a set of three vectors  $\mathbf{a}$ ,  $\mathbf{b}$ ,  $\mathbf{c}$  and two scalars  $k$  and  $t$  are given. Then, vector addition and scalar multiplication have the following properties:

$$\mathbf{a} + \mathbf{b} = \mathbf{b} + \mathbf{a} \quad (\text{A.1})$$

$$\mathbf{a} + (\mathbf{b} + \mathbf{c}) = (\mathbf{a} + \mathbf{b}) + \mathbf{c} \quad (\text{A.2})$$

$$k(t\mathbf{a}) = kt\mathbf{a} \quad (\text{A.3})$$

$$(k+t)\mathbf{a} = k\mathbf{a} + t\mathbf{a} \quad (\text{A.4})$$

$$k(\mathbf{a} + \mathbf{b}) = k\mathbf{a} + k\mathbf{b} \quad (\text{A.5})$$

Magnitude  $a$  of a vector  $\mathbf{a}$  is:

$$a = |\mathbf{a}| = \sqrt{a_x^2 + a_y^2 + a_z^2} \quad (\text{A.6})$$

where  $a_x$ ,  $a_y$ , and  $a_z$  are the scalar components of  $\mathbf{a}$ .

A unit vector  $\bar{\mathbf{a}}$  in the direction of a vector  $\mathbf{a}$  is:

$$\bar{\mathbf{a}} = \frac{\mathbf{a}}{|\mathbf{a}|} = \frac{\mathbf{a}}{a} \quad (\text{A.7})$$

The components  $\bar{a}_x$ ,  $\bar{a}_y$ , and  $\bar{a}_z$  of a unit vector  $\bar{\mathbf{a}}$  are also the direction cosines of the vector  $\bar{\mathbf{a}}$ :

$$\cos \alpha = \bar{a}_x \quad (\text{A.8})$$

$$\cos \beta = \bar{a}_y \quad (\text{A.9})$$

$$\cos \gamma = \bar{a}_z \quad (\text{A.10})$$

It is common practice to denote the components  $\bar{a}_x$ ,  $\bar{a}_y$ , and  $\bar{a}_z$  by  $l$ ,  $m$  and  $n$  accordingly.

### A.2.2 SCALAR PRODUCT (OR DOT PRODUCT) OF TWO VECTORS

The formula:

$$\mathbf{a} \cdot \mathbf{b} = a_x b_x + a_y b_y + a_z b_z = |\mathbf{a}| |\mathbf{b}| \cos \angle(\mathbf{a}, \mathbf{b}) \quad (\text{A.11})$$

is commonly used for calculation of scalar product of two vectors  $\mathbf{a}$  and  $\mathbf{b}$ .

Equation (A.11) can also be represented in the form:

$$\mathbf{a} \cdot \mathbf{b} = [\mathbf{a}]^T \cdot [\mathbf{b}] = \begin{bmatrix} a_x & a_y & a_z \end{bmatrix} \cdot \begin{bmatrix} b_x \\ b_y \\ b_z \end{bmatrix} \quad (\text{A.12})$$

Angle  $\angle(\mathbf{a}, \mathbf{b})$  between two vectors  $\mathbf{a}$  and  $\mathbf{b}$  is calculated from:

$$\angle(\mathbf{a}, \mathbf{b}) = \cos^{-1} \left( \frac{\mathbf{a} \cdot \mathbf{b}}{|\mathbf{a}| |\mathbf{b}|} \right) \quad (\text{A.13})$$

Scalar product of two vectors  $\mathbf{a}$  and  $\mathbf{b}$  features the following properties:

$$\mathbf{a} \cdot \mathbf{a} = |\mathbf{a}|^2 \quad (\text{A.14})$$

$$\mathbf{a} \cdot \mathbf{b} = \mathbf{b} \cdot \mathbf{a} \quad (\text{A.15})$$

$$\mathbf{a} \cdot (\mathbf{b} + \mathbf{c}) = \mathbf{b} \cdot \mathbf{a} + \mathbf{b} \cdot \mathbf{c} \quad (\text{A.16})$$

$$(k\mathbf{a}) \cdot \mathbf{b} = \mathbf{a} \cdot (k\mathbf{b}) = k(\mathbf{a} \cdot \mathbf{b}) \quad (\text{A.17})$$

If  $\mathbf{a}$  is perpendicular to  $\mathbf{b}$ , then:

$$\mathbf{a} \cdot \mathbf{b} = 0 \quad (\text{A.18})$$

### A.2.3 VECTOR PRODUCT (OR CROSS PRODUCT) OF TWO VECTORS

Vector product of two vectors can be calculated from the formula:

$$\mathbf{a} \times \mathbf{b} = (a_y b_z - a_z b_y) \mathbf{i} + (a_z b_x - a_x b_z) \mathbf{j} + (a_x b_y - a_y b_x) \mathbf{k} \quad (\text{A.19})$$

Here, in Eq. (A.19),  $\mathbf{i}$ ,  $\mathbf{j}$ , and  $\mathbf{k}$  are unit vectors in the  $X$ ,  $Y$ , and  $Z$  directions of the reference system  $XYZ$ , in which the vectors  $\mathbf{a}$  and  $\mathbf{b}$  are specified.

Vector product possess the following property: in case  $\mathbf{a} \times \mathbf{b} = \mathbf{c}$ , then the vector  $\mathbf{c}$  is perpendicular to a plane through the vectors  $\mathbf{a}$  and  $\mathbf{b}$ .

Vector product of two vectors  $\mathbf{a}$  and  $\mathbf{b}$  features the following properties:

$$\mathbf{a} \times \mathbf{b} = \begin{vmatrix} \mathbf{i} & \mathbf{j} & \mathbf{k} \\ a_x & a_y & a_z \\ b_x & b_y & b_z \end{vmatrix} \quad (\text{A.20})$$



$$\mathbf{a} \times \mathbf{b} = |\mathbf{a}| |\mathbf{b}| \mathbf{n} \sin \angle(\mathbf{a}, \mathbf{b}) \quad (\text{A.21})$$

where unit normal vector to the plane through the vectors  $\mathbf{a}$  and  $\mathbf{b}$  is denoted by  $\mathbf{n}$  :

$$|\mathbf{a} \times \mathbf{b}| = |\mathbf{a}| |\mathbf{b}| \sin \angle(\mathbf{a}, \mathbf{b}) \quad (\text{A.22})$$

Coordinates of the vector product  $\mathbf{a} \times \mathbf{b}$  can also be expressed in the form:

$$|\mathbf{a} \times \mathbf{b}| = \begin{bmatrix} 0 & -a_z & a_y \\ a_z & 0 & -a_x \\ -a_y & a_x & 0 \end{bmatrix} \cdot \begin{bmatrix} b_x \\ b_y \\ b_z \end{bmatrix} = \begin{bmatrix} -a_z b_y + a_y b_z \\ -a_x b_z + a_z b_x \\ -a_y b_x + a_x b_y \end{bmatrix} \quad (\text{A.23})$$

$$\mathbf{a} \times \mathbf{b} = -\mathbf{b} \times \mathbf{a} \quad (\text{A.24})$$

$$\mathbf{a} \times (\mathbf{b} + \mathbf{c}) = \mathbf{a} \times \mathbf{b} + \mathbf{a} \times \mathbf{c} \quad (\text{A.25})$$

$$(k\mathbf{a}) \times \mathbf{b} = \mathbf{a} \times (k\mathbf{b}) = k(\mathbf{a} \times \mathbf{b}) \quad (\text{A.26})$$

$$\mathbf{i} \times \mathbf{j} = \mathbf{k}, \mathbf{j} \times \mathbf{k} = \mathbf{i}, \mathbf{k} \times \mathbf{i} = \mathbf{j} \quad (\text{A.27})$$

If  $\mathbf{a}$  is parallel to  $\mathbf{b}$ , then:

$$\mathbf{a} \times \mathbf{b} = \mathbf{0} \quad (\text{A.28})$$

#### A.2.4 TRIPLE SCALAR PRODUCT OF THREE VECTORS

The product  $(\mathbf{a} \times \mathbf{b}) \cdot \mathbf{c}$  is commonly referred to as *triple scalar product* of three vectors  $\mathbf{a}$ ,  $\mathbf{b}$ , and  $\mathbf{c}$ .

Triple scalar product of three vectors  $\mathbf{a}$ ,  $\mathbf{b}$ , and  $\mathbf{c}$  features the following properties:

$$(\mathbf{a} \times \mathbf{b}) \cdot \mathbf{c} = (\mathbf{b} \times \mathbf{c}) \cdot \mathbf{a} = (\mathbf{c} \times \mathbf{a}) \cdot \mathbf{b} \quad (\text{A.29})$$

$$(\mathbf{b} \times \mathbf{c}) \cdot \mathbf{a} = \mathbf{a} \cdot (\mathbf{b} \times \mathbf{c}) \quad (\text{A.30})$$

$$(\mathbf{a} \times \mathbf{b}) \cdot \mathbf{c} = \mathbf{a} \cdot (\mathbf{b} \times \mathbf{c}) \quad (\text{A.31})$$

$$\mathbf{a} \cdot (\mathbf{b} \times \mathbf{c}) = \begin{vmatrix} a_x & a_y & a_z \\ b_x & b_y & b_z \\ c_x & c_y & c_z \end{vmatrix} \quad (\text{A.32})$$

### A.2.5 TRIPLE VECTOR PRODUCT OF THREE VECTORS

The product  $(\mathbf{a} \times \mathbf{b}) \times \mathbf{c}$  is commonly referred to as *triple vector product* of three vectors  $\mathbf{a}$ ,  $\mathbf{b}$ , and  $\mathbf{c}$ .

The product  $(\mathbf{a} \times \mathbf{b}) \times \mathbf{c}$  can be evaluated by two vector products. However, it also can be evaluated in a more simply way by use of the identity:

$$(\mathbf{a} \times \mathbf{b}) \times \mathbf{c} = (\mathbf{a} \cdot \mathbf{c})\mathbf{b} - (\mathbf{b} \cdot \mathbf{c})\mathbf{a} \quad (\text{A.33})$$

It should be mentioned here that in general, the triple vector products  $(\mathbf{a} \times \mathbf{b}) \times \mathbf{c}$  and  $\mathbf{a} \times (\mathbf{b} \times \mathbf{c})$  are not equal:

$$(\mathbf{a} \times \mathbf{b}) \times \mathbf{c} \neq \mathbf{a} \times (\mathbf{b} \times \mathbf{c}) \quad (\text{A.34})$$

Analytical interpretation of many problems and results in the field of geometry of surfaces are getting much simpler when vector calculus is used.

### A.2.6 LAGRANGE EQUATION FOR VECTORS

For the purposes of calculation of mixed product of vectors,  $\mathbf{a}$  and  $\mathbf{b}$ , an equation:

$$(\mathbf{a} \times \mathbf{b}) \cdot (\mathbf{a} \times \mathbf{b}) = (\mathbf{a} \cdot \mathbf{a})(\mathbf{b} \cdot \mathbf{b}) - (\mathbf{a} \cdot \mathbf{b})^2 \quad (\text{A.35})$$

can be used.

Equation (A.35) is due to *Lagrange*.<sup>1</sup>

## A.3 ON THE SIMILARITY AND DIFFERENCE BETWEEN VECTORS AND MATRICES

A vector,  $\mathbf{a}$ , is commonly represented in the form:

$$\mathbf{a} = ia + jb + kc \quad (\text{A.36})$$

That same vector,  $\mathbf{a}$ , allows for matrix representation in one of the following forms:

$$\mathbf{a} = \begin{bmatrix} a \\ b \\ c \end{bmatrix} \quad (\text{A.37})$$

$$\mathbf{a} = \begin{bmatrix} a \\ b \\ c \\ 1 \end{bmatrix} \quad (\text{A.38})$$

$$\mathbf{a} = \begin{bmatrix} 1 & 0 & 0 & a \\ 0 & 1 & 0 & b \\ 0 & 0 & 1 & c \\ 0 & 0 & 0 & 1 \end{bmatrix} \quad (\text{A.39})$$

<sup>1</sup> Joseph-Louis Lagrange (January 25, 1736 – April 10, 1813), a famous French mathematician, astronomer and mechanician.

Operations over vectors in matrix representation [see the form Eq. (A.39)] is preferred as multiple coordinate system transformations are often required.

Vectors obey the commutative law, that is, the equalities,  $\mathbf{a} \times \mathbf{b} = \mathbf{b} \times \mathbf{a}$ ,  $\mathbf{a} \cdot \mathbf{b} = \mathbf{b} \cdot \mathbf{a}$ , are valid for vectors. This is not always applicable to matrices.

Two kinds of products are valid for vectors, that is, dot product ( $\mathbf{a} \cdot \mathbf{b}$ ), and cross product ( $\mathbf{a} \times \mathbf{b}$ ) of vectors, that is not valid with respect to matrices.

# Appendix B

## *Elements of Differential Geometry of Surfaces*

Discussion in this book is focused primarily on the elements of theory of gear cutting tool design.

The gear and the pinion tooth flank and their motion in space in relation to one another are analytically described in a reference system. An orthogonal *Cartesian*<sup>1</sup> reference system is a major kind of reference systems that is commonly used for this purpose. Mutually perpendicular coordinate axes of a *Cartesian* coordinate system are conventionally labeled as  $X$ ,  $Y$ , and  $Z$ .

In a *Cartesian* reference system, the axes can be oriented either in a left or in a right-handed sense. A right-handed *Cartesian* reference system is preferred, and all algorithms and formulae used in this book assume a right-handed convention.

A coordinate system provides a numerical frame of reference for the three-dimensional space in which the theory is developed. Two coordinate systems are particularly useful to us: the ubiquitous *Cartesian* ( $XYZ$ ) rectilinear system, and the spherical polar ( $r, \theta, \varphi$ ) or angular system. *Cartesian* coordinate systems are the most commonly used, but angular coordinates are often helpful as well.

### B.1 SPECIFICATION OF A GEAR TOOTH FLANK

A gear tooth flank could be uniquely determined by two independent variables. Therefore, we give a gear tooth flank  $\mathcal{S}$  (see Figure B.1), in most cases, by expressing its rectangular coordinated  $X_g, Y_g$ , and  $Z_g$ , as functions of two *Gaussian*<sup>2</sup> coordinates  $U_g$  and  $V_g$  in a certain closed interval<sup>3</sup>:

$$\mathcal{S} \Rightarrow \mathbf{r}_g = \mathbf{r}_g(U_g, V_g) = \begin{bmatrix} X_g(U_g, V_g) \\ Y_g(U_g, V_g) \\ Z_g(U_g, V_g) \\ 1 \end{bmatrix} \quad (\text{B.1})$$

$$U_{1,g} \leq U_g \leq U_{2,g}; V_{1,g} \leq V_g \leq V_{2,g}$$

where

$\mathbf{r}_g$  is the position vector of a point of the gear tooth flank,  $\mathcal{S}$ .

$U_g$  and  $V_g$  are the curvilinear coordinates (*Gaussian coordinates*) of the gear tooth flank,  $\mathcal{S}$ .

$X_g, Y_g, Z_g$  are the *Cartesian* coordinates of the point of the gear tooth flank,  $\mathcal{S}$ .

$U_{1,g}, U_{2,g}$  are the boundary values of the closed interval of the  $U_g$  – parameter.

$V_{1,g}, V_{2,g}$  are the boundary values of the closed interval of the  $V_g$  – parameter.

<sup>1</sup> René Descartes (March 31, 1596–February 11, 1650), (Latinized form: Renatus Cartesius), a French mathematician, philosopher and writer.

<sup>2</sup> Johan Carl Friedrich Gauss (April 30, 1777–February 23, 1855) – a famous German mathematician and physical scientist.

<sup>3</sup> All the equations that are valid for the gear tooth flank,  $\mathcal{S}$ , are also valid for the pinion tooth flank,  $\mathcal{S}$ .

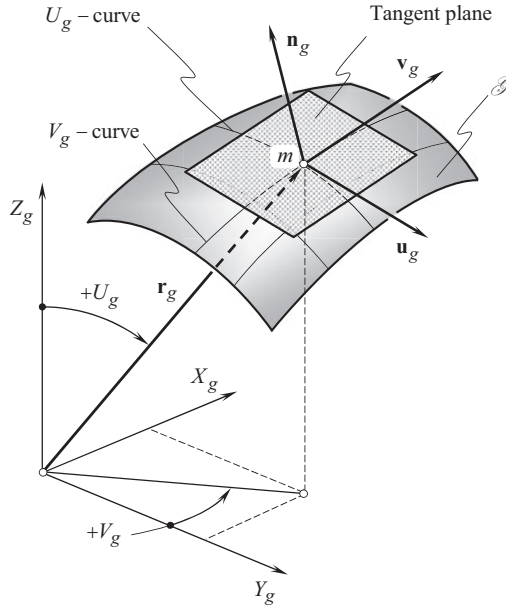


**FIGURE B.1** Principal parameters of local topology at point of gear tooth flank,  $\mathcal{S}$ .

The parameters  $U_g$  and  $V_g$  must enter into Eq. (B.1) independently, which means that the matrix:

$$\mathbf{M} = \begin{bmatrix} \frac{\partial X_g}{\partial U_g} & \frac{\partial Y_g}{\partial U_g} & \frac{\partial Z_g}{\partial U_g} \\ \frac{\partial X_g}{\partial V_g} & \frac{\partial Y_g}{\partial V_g} & \frac{\partial Z_g}{\partial V_g} \end{bmatrix} \quad (\text{B.2})$$

has a rank 2.

Positions, where the rank is 1 or 0 are singular points; when the rank at all points is 1, then Eq. (B.1) represents a curve.

Other methods of surface's specification are known as well. Specification of a gear tooth flank by

- An equation in explicit form
- An equation in implicit form, and
- A set of parametric equations

are among the most frequently used in practice methods of surfaces specification.

It is assumed here and below that any given kind of a gear tooth flank,  $\mathcal{S}$ , specification can be converted either into the vector form, or into the matrix form of its specification as it is following from Eq. (B.1).

## B.2 TANGENT VECTORS AND TANGENT PLANE; UNIT NORMAL VECTOR

The following notation is proven to be convenient in the consideration below.

The first derivatives of  $\mathbf{r}_g$  with respect to *Gaussian coordinates*  $U_g$  and  $V_g$  are designated as:

$$\frac{\partial \mathbf{r}_g}{\partial U_g} = \mathbf{U}_g \quad (\text{B.3})$$

$$\frac{\partial \mathbf{r}_p}{\partial V_p} = \mathbf{V}_p \quad (\text{B.4})$$

and for the unit tangent vectors:

$$\mathbf{u}_g = \frac{\mathbf{U}_g}{|\mathbf{U}_g|} \quad (\text{B.5})$$

$$\mathbf{v}_g = \frac{\mathbf{V}_g}{|\mathbf{V}_g|} \quad (\text{B.6})$$

correspondingly.<sup>4</sup>

Direction of the tangent line to the  $U_g$  – coordinate line through a given point  $m$  on the gear tooth flank,  $\mathcal{S}$ , is specified by the unit tangent vector  $\mathbf{u}_g$  (as well as by the tangent vector  $\mathbf{U}_g$ ). Similarly, direction of the tangent line to the  $V_g$  – coordinate line through that same point  $m$  on a gear tooth flank  $\mathcal{S}$  is specified by the unit tangent vector  $\mathbf{v}_g$  (as well as by the tangent vector  $\mathbf{V}_g$ ).

Significance of the unit tangent vectors  $\mathbf{u}_g$  and  $\mathbf{v}_g$  becomes evident from the following considerations.

**First**, unit tangent vectors  $\mathbf{u}_g$  and  $\mathbf{v}_g$  yield an equation of the tangent plane to a gear tooth flank  $\mathcal{S}$  at a specified point  $m$  :

$$\text{Tangent plane} \Rightarrow \begin{bmatrix} [\mathbf{r}_{t,p} - \mathbf{r}_g^m] \\ \mathbf{u}_g \\ \mathbf{v}_g \\ 1 \end{bmatrix} = 0 \quad (\text{B.7})$$

where

$\mathbf{r}_{t,p}$  is the position vector of a point of the tangent plane to a gear tooth flank  $\mathcal{S}$  at a specified point  $m$ .

$\mathbf{r}_g^m$  is the position vector of a point  $m$  on a gear tooth flank  $\mathcal{S}$ .

**Second**, tangent vectors yield an equation of the perpendicular  $\mathbf{N}_g$ , and of the unit normal vector  $\mathbf{n}_g$  to a gear tooth flank  $\mathcal{S}$  at a given point  $m$  :

$$\mathbf{N}_g = \mathbf{U}_g \times \mathbf{V}_g \quad (\text{B.8})$$

and

$$\mathbf{n}_g = \frac{\mathbf{N}_g}{|\mathbf{N}_g|} = \frac{\mathbf{U}_g \times \mathbf{V}_g}{|\mathbf{U}_g \times \mathbf{V}_g|} = \mathbf{u}_g \times \mathbf{v}_g \quad (\text{B.9})$$

When the order of the multipliers in Eqs. (B.8) and (B.9) is chosen properly, then the unit normal vector  $\mathbf{n}_g$  (as well as the normal vector  $\mathbf{N}_g$ ) is pointed outward of the bodily side of the surface  $\mathcal{S}$ .

<sup>4</sup> It is right point to underline here that the unit tangent vectors  $\mathbf{u}_p$  and  $\mathbf{v}_p$  are dimensionless values as it is following from Eqs. (B.5) and (B.6).

### B.3 LOCAL FRAME

Two unit tangent vectors  $\mathbf{u}_g$  and  $\mathbf{v}_g$  along with the unit normal vector  $\mathbf{n}_g$  comprise a local frame  $\mathbf{u}_g, \mathbf{v}_g, \mathbf{n}_g$  having the origin at a current point  $m$  on a gear tooth flank  $\mathcal{S}$ . Unit tangent vector  $\mathbf{u}_g$  is perpendicular to the unit normal vector  $\mathbf{n}_g$  (i.e.,  $\mathbf{u}_g \perp \mathbf{n}_g$ ), as well as unit tangent vector  $\mathbf{v}_g$  is also perpendicular to the unit normal vector  $\mathbf{n}_g$  (i.e.,  $\mathbf{v}_g \perp \mathbf{n}_g$ ). Speaking generally, the unit tangent vectors  $\mathbf{u}_g$  and  $\mathbf{v}_g$  are not perpendicular to one another, they form a certain angle  $\omega_g$ . In order to construct an orthogonal local frame, either the unit tangent vector  $\mathbf{u}_g$  in the local frame  $(\mathbf{u}_g, \mathbf{v}_g, \mathbf{n}_g)$  must be substituted with a unit tangent vector  $\mathbf{u}_g^*$ , or the unit tangent vector  $\mathbf{v}_g$  in that same local frame  $(\mathbf{u}_g, \mathbf{v}_g, \mathbf{n}_g)$  must be substituted with a unit tangent vector  $\mathbf{v}_g^*$ . For the calculation of the newly introduced unit tangent vectors  $\mathbf{u}_g^*$  and  $\mathbf{v}_g^*$  the following equations can be used:

$$\mathbf{u}_g^* = \mathbf{u}_g \times \mathbf{n}_g \quad (\text{B.10})$$

$$\mathbf{v}_g^* = \mathbf{v}_g \times \mathbf{n}_g \quad (\text{B.11})$$

It is convenient to choose that order of the multipliers in Eqs. (B.10) and (B.11), which preserves the orientation (the hand) of the original local frame  $(\mathbf{u}_g, \mathbf{v}_g, \mathbf{n}_g)$ , namely, if the original local frame  $(\mathbf{u}_g, \mathbf{v}_g, \mathbf{n}_g)$  is right-hand oriented, then the newly constructed local frame [either the local frame  $(\mathbf{u}_g^*, \mathbf{v}_g, \mathbf{n}_g)$ , or the local frame  $(\mathbf{u}_g, \mathbf{v}_g^*, \mathbf{n}_g)$ ] should also be a right-hand oriented local frame, and vice versa.

It should be pointed out here that another possibility to construct an orthogonal local frame is also available. Local frame of this kind is commonly referred to as *Darboux<sup>5</sup> frame*, and is briefly considered below in this section of the book.

Unit tangent vectors  $\mathbf{u}_g$  and  $\mathbf{v}_g$  to a surface  $\mathcal{S}$  at a point  $m$  are of critical importance when solving practical problems in the field of gearing. This statement is proven by numerous examples shown below.

### B.4 FUNDAMENTAL FORMS OF SURFACE

Consider two other important issues concerning the gear tooth flank geometry – both relate to intrinsic geometry in differential vicinity of a current surface point  $m$ .

*First fundamental form of a surface.* The first issue is the so-called the *first fundamental form*,  $\Phi_{1,g}$  of a gear tooth flank  $\mathcal{S}$ . The metric properties of a gear tooth flank  $\mathcal{S}$  are described by the first fundamental form,  $\Phi_{1,g}$ , of the surface. Usually, the first fundamental form,  $\Phi_{1,g}$ , is represented as the quadratic form:

$$\Phi_{1,g} \Rightarrow ds_g^2 = E_g dU_g^2 + 2F_g dU_g dV_g + G_g dV_g^2 \quad (\text{B.12})$$

Here, in Eq. (B.12) is designated:

$s_g$  is the linear element on a gear tooth flank  $\mathcal{S}$  ( $s_g$  is equal to the length of a segment of a certain curve on a gear tooth flank  $\mathcal{S}$ ).

$E_g, F_g, G_g$  are the fundamental magnitudes of the first order at a surface point.

Equation (B.12) for the first fundamental form,  $\Phi_{1,g}$ , is known from many advanced sources. In the theory of gearing, another form of analytical representation of the first fundamental form,  $\Phi_{1,g}$ , is proven to be useful:

<sup>5</sup> Jean Gaston Darboux (August 14, 1842–February 23, 1917), a French mathematician.



$$\Phi_{1,g} \Rightarrow ds_g^2 = \begin{bmatrix} dU_g & dV_g & 0 & 0 \end{bmatrix} \cdot \begin{bmatrix} E_g & F_g & 0 & 0 \\ F_g & G_g & 0 & 0 \\ 0 & 0 & 1 & 0 \\ 0 & 0 & 0 & 1 \end{bmatrix} \cdot \begin{bmatrix} dU_g \\ dV_g \\ 0 \\ 0 \end{bmatrix} \quad (\text{B.13})$$

This kind of analytical representation of the first fundamental form  $\Phi_{1,p}$  is proposed by Prof. *S.P. Radzevich* (~2008).

The practical advantage of Eq. (B.13) is that it can easily be incorporated into computer programs when multiple coordinate system transformations are used. The last is vital for the theory of gearing.

Fundamental magnitudes of the first order  $E_g$ ,  $F_g$ ,  $G_g$ , can be calculated from the set of the following equations:

$$E_g = \mathbf{U}_g \cdot \mathbf{U}_g \quad (\text{B.14})$$

$$F_g = \mathbf{U}_g \cdot \mathbf{V}_g \quad (\text{B.15})$$

$$G_g = \mathbf{V}_g \cdot \mathbf{V}_g \quad (\text{B.16})$$

Equations (B.14)–(B.16) can be represented in an expanded form:

$$E_g = \frac{\partial \mathbf{r}_g}{\partial U_g} \cdot \frac{\partial \mathbf{r}_g}{\partial U_g} = \frac{\partial X_g}{\partial U_g} \cdot \frac{\partial X_g}{\partial U_g} + \frac{\partial Y_g}{\partial U_g} \cdot \frac{\partial Y_g}{\partial U_g} + \frac{\partial Z_g}{\partial U_g} \cdot \frac{\partial Z_g}{\partial U_g} \quad (\text{B.17})$$

$$F_g = \frac{\partial \mathbf{r}_g}{\partial U_g} \cdot \frac{\partial \mathbf{r}_g}{\partial V_g} = \frac{\partial X_g}{\partial U_g} \cdot \frac{\partial X_g}{\partial V_g} + \frac{\partial Y_g}{\partial U_g} \cdot \frac{\partial Y_g}{\partial V_g} + \frac{\partial Z_g}{\partial U_g} \cdot \frac{\partial Z_g}{\partial V_g} \quad (\text{B.18})$$

$$G_g = \frac{\partial \mathbf{r}_g}{\partial V_g} \cdot \frac{\partial \mathbf{r}_g}{\partial V_g} = \frac{\partial X_g}{\partial V_g} \cdot \frac{\partial X_g}{\partial V_g} + \frac{\partial Y_g}{\partial V_g} \cdot \frac{\partial Y_g}{\partial V_g} + \frac{\partial Z_g}{\partial V_g} \cdot \frac{\partial Z_g}{\partial V_g} \quad (\text{B.19})$$

Fundamental magnitudes of the first order,  $E_g$ ,  $F_g$ ,  $G_g$ , are functions of the  $U_g$  – and  $V_g$  – coordinates of a point of a gear tooth flank  $\mathcal{S}$ . In general form, these relationships can be represented in the form:

$$E_g = E_g(U_g, V_g) \quad (\text{B.20})$$

$$F_g = F_g(U_g, V_g) \quad (\text{B.21})$$

$$G_g = G_g(U_g, V_g) \quad (\text{B.22})$$

It is important to point out here that fundamental magnitudes  $E_g$  and  $G_g$  are always positive (i.e.,  $E_g > 0$ ,  $G_g > 0$ ), and the fundamental magnitude  $F_g$  can equal zero ( $F_g \geq 0$ ). This results in that the first fundamental form,  $\Phi_{1,g}$  at a point of a gear tooth flank  $\mathcal{S}$ , is always positively defined ( $\Phi_{1,g} \geq 0$ ), and it cannot be of a negative value.

By use of the first fundamental form,  $\Phi_{1,g}$ , the following major parameters of geometry of a gear tooth flank  $\mathcal{S}$  can be calculated:

- a. Length of a curve-line segment on a gear tooth flank  $\mathcal{S}$
- b. Square of a gear tooth flank  $\mathcal{S}$  portion that is bounded by a closed curve on the surface,  
and
- c. Angle between any two directions on a gear tooth flank  $\mathcal{S}$ .

Length,  $s_g$ , of a curve-line segment:

$$U_g = U_g(t) \quad (\text{B.23})$$

$$V_g = V_g(t) \quad (\text{B.24})$$

on a gear tooth flank,  $\mathcal{S}$ , is given by the equation:

$$s_g = \int_{t_0}^t \sqrt{E_g \left( \frac{dU_g}{dt} \right)^2 + 2F_g \frac{dU_g}{dt} \frac{dV_g}{dt} + G_g \left( \frac{dV_g}{dt} \right)^2} dt \quad (\text{B.25})$$

$$t_0 \leq t \leq t_1$$

For calculation of square,  $\mathcal{S}_g$ , of a gear tooth flank  $\mathcal{S}$  patch  $\Sigma$ , which is bounded by a closed curve on the surface  $\mathcal{S}$ , the following equation can be used:

$$\mathcal{S}_g = \iint_{\Sigma} \sqrt{E_g G_g - F_g^2} dU_g dV_g \quad (\text{B.26})$$

Ultimately, value of the angle,  $\omega_g$ , between two given directions through a certain point  $m$  on a gear tooth flank  $\mathcal{S}$  can be calculated from one of the equations below:

$$\cos \omega_g = \frac{F_g}{\sqrt{E_g G_g}} \quad (\text{B.27})$$

$$\sin \omega_g = \frac{H_g}{\sqrt{E_g G_g}} \quad (\text{B.28})$$

$$\tan \omega_g = \frac{H_g}{F_g} \quad (\text{B.29})$$

For the calculation of the discriminant,  $H_g$ , of the first fundamental form,  $\Phi_{1,g}$ , the following equation can be used:

$$H_g = \sqrt{E_g G_g - F_g^2} \quad (\text{B.30})$$

It is assumed here that the discriminant,  $H_g$ , is always nonnegative – that is,  $H_g = +\sqrt{E_g G_g - F_g^2}$ .

The first fundamental form,  $\Phi_{1,g}$ , represents the length of a curve-line segment, and thus it is always nonnegative – that is, the inequality  $\Phi_{1,g} \geq 0$  is always valid.

The first fundamental form,  $\Phi_{1,g}$ , remains the same when the surface is banding. This is another important feature of the first fundamental form  $\Phi_{1,g}$ .

*Second fundamental form of a surface.* The *second fundamental form*,  $\Phi_{2,g}$  of a gear tooth flank  $\mathcal{S}$  is another of the two above-mentioned issues. Second fundamental form  $\Phi_{2,g}$  describes curvature of a smooth regular surface  $\mathcal{S}$ .

Consider a point  $K$  on a smooth regular part surface  $\mathcal{S}$  (see Figure B.2). Location of the point  $K$  is specified by two coordinates  $U_g$  and  $V_g$ . A line through the point  $K$  is entirely located within the surface  $\mathcal{S}$ . A nearby point  $m$  is located within the line through the point  $K$ . Location of the point  $m$  is specified by the coordinates  $U_g + dU_g$  and  $V_g + dV_g$  as it is infinitesimally close to the point  $K$ . The closest distance of approach of the point  $m$  to the tangent plane through the point  $K$  is expressed by the second fundamental form  $\Phi_{2,g}$ . Torsion of the curve  $Km$  is ignored. Therefore, the distance  $a$  is assumed equal to zero ( $a = 0$ ).

The second fundamental form,  $\Phi_{2,g}$ , describes the curvature of a smooth, regular part surface  $\mathcal{S}$ . Usually, it is represented as the quadratic form (see Figure B.2):

$$\Phi_{2,g} \Rightarrow -d\mathbf{r}_g \cdot d\mathbf{n}_g = L_g dU_g^2 + 2M_g dU_g dV_g + N_g dV_g^2 \quad (\text{B.31})$$

Equation (B.31) is known from many advanced sources.

In the theory of gearing, another analytical representation of the second fundamental form,  $\Phi_{2,g}$ , is proven to be useful:

$$\Phi_{2,g} \Rightarrow \begin{bmatrix} dU_g & dV_g & 0 & 0 \end{bmatrix} \cdot \begin{bmatrix} L_g & M_g & 0 & 0 \\ M_g & N_g & 0 & 0 \\ 0 & 0 & 1 & 0 \\ 0 & 0 & 0 & 1 \end{bmatrix} \cdot \begin{bmatrix} dU_g \\ dV_g \\ 0 \\ 0 \end{bmatrix} \quad (\text{B.32})$$

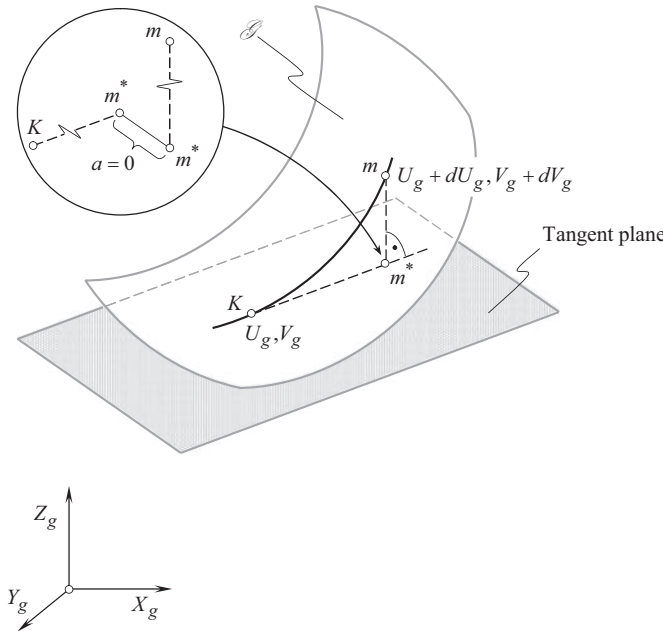


**FIGURE B.2** On the definition of the second fundamental form,  $\Phi_{2,g}$ , at point of smooth gear tooth flank,  $\mathcal{S}$

This analytical representation of the second fundamental form,  $\Phi_{2,P}$ , is proposed by Prof. *S.P. Radzevich* (~2008).

Similar to Eq. (B.13), the practical advantage of Eq. (B.32) is that it can be easily incorporated into computer programs when multiple coordinate system transformations are used. The last is vital for both for the theory of gearing.

In Eq. (B.32), the parameters  $L_g$ ,  $M_g$ ,  $N_g$  designate fundamental magnitudes of the second order.

By definition, fundamental magnitudes of the second order are equal:

$$L_g = -\mathbf{U}_g \cdot \frac{\partial \mathbf{n}_g}{\partial U_g} = \mathbf{n}_g \cdot \frac{\partial \mathbf{U}_g}{\partial U_g} \quad (\text{B.33})$$

$$M_g = -\frac{1}{2}(\mathbf{U}_g \cdot \frac{\partial \mathbf{n}_g}{\partial V_g} + \mathbf{V}_g \cdot \frac{\partial \mathbf{n}_g}{\partial U_g}) = \mathbf{n}_g \cdot \frac{\partial \mathbf{U}_g}{\partial V_g} = \mathbf{n}_g \cdot \frac{\partial \mathbf{V}_g}{\partial U_g} \quad (\text{B.34})$$

$$N_g = -\mathbf{V}_g \cdot \frac{\partial \mathbf{n}_g}{\partial V_g} = \mathbf{n}_g \cdot \frac{\partial \mathbf{V}_g}{\partial V_g} \quad (\text{B.35})$$

For the calculation of the fundamental magnitudes of the second order of a smooth regular gear tooth flank  $\mathcal{S}$  the following equations can be used:

$$L_g = \frac{\frac{\partial \mathbf{U}_g}{\partial U_g} \times \mathbf{U}_g \cdot \mathbf{V}_g}{\sqrt{E_g G_g - F_g^2}} \quad (\text{B.36})$$

$$M_g = \frac{\frac{\partial \mathbf{U}_g}{\partial V_g} \times \mathbf{U}_g \cdot \mathbf{V}_g}{\sqrt{E_g G_g - F_g^2}} = \frac{\frac{\partial \mathbf{V}_g}{\partial U_g} \times \mathbf{U}_g \cdot \mathbf{V}_g}{\sqrt{E_g G_g - F_g^2}} \quad (\text{B.37})$$

$$N_g = \frac{\frac{\partial \mathbf{V}_g}{\partial V_g} \times \mathbf{U}_g \cdot \mathbf{V}_g}{\sqrt{E_g G_g - F_g^2}} \quad (\text{B.38})$$

Equations (B.36)–(B.38) can be represented in an expanded form:

$$L_g = \frac{\begin{vmatrix} \frac{\partial^2 X_g}{\partial U_g^2} & \frac{\partial^2 Y_g}{\partial U_g^2} & \frac{\partial^2 Z_g}{\partial U_g^2} \\ \frac{\partial X_g}{\partial U_g} & \frac{\partial Y_g}{\partial U_g} & \frac{\partial Z_g}{\partial U_g} \\ \frac{\partial X_g}{\partial V_g} & \frac{\partial Y_g}{\partial V_g} & \frac{\partial Z_g}{\partial V_g} \end{vmatrix}}{\sqrt{E_g G_g - F_g^2}} \quad (\text{B.39})$$

$$M_g = \frac{\begin{vmatrix} \frac{\partial^2 X_g}{\partial U_g \partial V_g} & \frac{\partial^2 Y_g}{\partial U_g \partial V_g} & \frac{\partial^2 Z_g}{\partial U_g \partial V_g} \\ \frac{\partial X_g}{\partial U_g} & \frac{\partial Y_g}{\partial U_g} & \frac{\partial Z_g}{\partial U_g} \\ \frac{\partial X_g}{\partial V_g} & \frac{\partial Y_g}{\partial V_g} & \frac{\partial Z_g}{\partial V_g} \end{vmatrix}}{\sqrt{E_g G_g - F_g^2}} \quad (\text{B.40})$$

$$N_P = \frac{\begin{vmatrix} \frac{\partial^2 X_g}{\partial V_g^2} & \frac{\partial^2 Y_g}{\partial V_g^2} & \frac{\partial^2 Z_g}{\partial V_g^2} \\ \frac{\partial X_g}{\partial U_g} & \frac{\partial Y_g}{\partial U_g} & \frac{\partial Z_g}{\partial U_g} \\ \frac{\partial X_g}{\partial V_g} & \frac{\partial Y_g}{\partial V_g} & \frac{\partial Z_g}{\partial V_g} \end{vmatrix}}{\sqrt{E_g G_g - F_g^2}} \quad (\text{B.41})$$

Fundamental magnitudes of the second order,  $L_g$ ,  $M_g$ ,  $N_g$ , are also functions of the  $U_g$  – and  $V_g$  – coordinates of a point of a gear tooth flank  $\mathcal{S}$ . In general form, these relationships can be represented in the form:

$$L_g = L_g(U_g, V_g) \quad (\text{B.42})$$

$$M_g = M_g(U_g, V_g) \quad (\text{B.43})$$

$$N_g = N_g(U_g, V_g) \quad (\text{B.44})$$

The discriminant,  $T_g$ , of the second fundamental form,  $\Phi_{2,g}$ , can be calculated from the following equation:

$$T_g = \sqrt{L_g N_g - M_g^2} \quad (\text{B.45})$$

We now come to the theorem, which is essential justification for considering the differential geometry of surfaces in connection with the six fundamental magnitudes. It has been proven (1867) first by Bonnet,<sup>6</sup> and may be enunciated as follows:

### Theorem B.1

When six fundamental magnitudes  $E_g$ ,  $F_g$ ,  $G_g$  and  $L_g$ ,  $M_g$ ,  $N_g$  are given, and when they fulfill the Gauss characteristic equation, and the two Mainardi<sup>7</sup> -Codazzi<sup>8</sup> relations, they determine a gear tooth flank  $\mathcal{S}$  uniquely say as to its position and orientation in space.

<sup>6</sup> Pierre Ossian Bonnet (December 22, 1819–June 22, 1892), a French mathematician.

<sup>7</sup> Gaspare Mainardi (June 27, 1800–March 9, 1879) – an Italian mathematician.

<sup>8</sup> Delfino Codazzi (March 7, 1824–July 21, 1873) – an Italian mathematician.

This theorem is commonly referred to as the *main theorem in the theory of surface*, or simply as *Bonnet theorem*. According to the main theorem, two surfaces that have identical first and second fundamental forms must be either congruent or symmetrical to one another. By use of six fundamental magnitudes, all parameters of local geometry of a given part surface can be calculated.

## B.5 PRINCIPAL DIRECTIONS ON AT POINT OF GEAR TOOTH FLANK

Direction of vectors of principal directions,  $\mathbf{T}_{1,g}$  and  $\mathbf{T}_{2,g}$  at a point on a gear tooth flank  $\mathcal{S}$ , can be specified in terms of the ratio  $dU_g/dV_g$ . For the vectors of the first,  $\mathbf{T}_{1,g}$ , and for the second,  $\mathbf{T}_{2,g}$ , principal directions at a point  $m$  of a smooth, regular part surface  $\mathcal{S}$  the corresponding values of the ratio  $dU_g/dV_g$  are calculated as roots of the quadratic equation:

$$\begin{vmatrix} E_g dU_g + F_g dV_g & F_g dU_g + G_g dV_g \\ L_g dU_g + M_g dV_g & M_g dU_g + N_g dV_g \end{vmatrix} = 0 \quad (\text{B.46})$$

The first principal plane section,  $C_{1,g}$ , is perpendicular to a gear tooth flank  $\mathcal{S}$  at a current surface point  $m$ , and passes through the vector of the first principal direction  $\mathbf{T}_{1,g}$ . The second principal plane section,  $C_{2,g}$ , is orthogonal to a gear tooth flank  $\mathcal{S}$  at a current surface point  $m$ , and passes through the vector of the second principal direction  $\mathbf{T}_{2,g}$ .

The principal directions  $\mathbf{T}_{1,g}$  and  $\mathbf{T}_{2,g}$  can be identified at any and all points of a smooth, regular gear tooth flank  $\mathcal{S}$  except of umbilic points, and in flatten points of the surface. At umbilic points of a surface, as well as at flatten points, principal directions cannot be identified.

In the theory of gearing, it is often preferred to use not the vectors  $\mathbf{T}_{1,g}$  and  $\mathbf{T}_{2,g}$  of the principal directions, but, instead, to use the unit vectors  $\mathbf{t}_{1,g}$  and  $\mathbf{t}_{2,g}$  of the principal directions. The unit tangent vectors  $\mathbf{t}_{1,g}$  and  $\mathbf{t}_{2,g}$  are calculated from the equations:

$$\mathbf{t}_{1,g} = \frac{\mathbf{T}_{1,g}}{|\mathbf{T}_{1,g}|} \quad (\text{B.47})$$

$$\mathbf{t}_{2,g} = \frac{\mathbf{T}_{2,g}}{|\mathbf{T}_{2,g}|} \quad (\text{B.48})$$

correspondingly.

Unit tangent vectors  $\mathbf{t}_{1,g}$  and  $\mathbf{t}_{2,g}$  of principal directions at a point  $m$  on a gear tooth flank  $\mathcal{S}$  along with unit normal vector  $\mathbf{n}_g$  at that same point  $m$  comprise an orthogonal local frame  $(\mathbf{t}_{1,g}, \mathbf{t}_{2,g}, \mathbf{n}_g)$ . All three unit vectors,  $\mathbf{t}_{1,g}$ ,  $\mathbf{t}_{2,g}$ , and  $\mathbf{n}_g$ , are mutually perpendicular to one another. The local frame  $(\mathbf{t}_{1,g}, \mathbf{t}_{2,g}, \mathbf{n}_g)$  is commonly referred to as *Darboux frame*.

## B.6 CURVATURES AT POINT OF GEAR TOOTH FLANK

The first,  $R_{1,g}$ , and the second,  $R_{2,g}$ , principal radii of curvature at a point of a gear tooth flank  $\mathcal{S}$  are measured within the first and in the second principal plane sections,  $C_{1,g}$  and  $C_{2,g}$ , accordingly. For the calculation of values of the principal radii of curvature, the following equation is commonly used:

$$R_g^2 - \frac{E_g N_g - 2F_g M_g + G_g L_g}{T_g} R_g + \frac{H_g}{T_g} = 0 \quad (\text{B.49})$$

Remember that algebraic values of the radii of principal curvature,  $R_{1,g}$  and  $R_{2,g}$ , relate to one another as  $R_{2,g} > R_{1,g}$ . In particular cases, at umbilic points on a gear tooth flank  $\mathcal{S}$ , no principal curvatures can be identified as all normal curvatures of the tooth surface  $\mathcal{S}$  at an umbilic point are equal to one another.

Another two important parameters of local topology of a gear tooth flank  $\mathcal{S}$  are:

1. Mean curvature,  $\mathcal{M}_g$ , and
2. Intrinsic curvature (*Gaussian curvature* or *full curvature*) curvature,  $\mathcal{G}_g$ .

For the calculation of the curvatures  $\mathcal{M}_g$  and  $\mathcal{G}_g$ , the following equations are commonly used:

$$\mathcal{M}_g = \frac{k_{1,g} + k_{2,g}}{2} = \frac{E_g N_g - 2 F_g M_g + G_g L_g}{2 \cdot (E_g G_g - F_g^2)} \quad (\text{B.50})$$

$$\mathcal{G}_g = k_{1,g} \cdot k_{2,g} = \frac{L_g N_g - M_g^2}{E_g G_g - F_g^2} \quad (\text{B.51})$$

The expressions for the mean curvature  $\mathcal{M}_g$  and for the *Gaussian curvature*,  $\mathcal{G}_g$ :

$$\mathcal{M}_g = \frac{k_{1,g} + k_{2,g}}{2} \quad (\text{B.52})$$

$$\mathcal{G}_g = k_{1,g} \cdot k_{2,g} \quad (\text{B.53})$$

considered together yield a quadratic equation with respect to principal curvatures  $k_{1,g}$  and  $k_{2,g}$ :

$$k_g^2 - 2 \mathcal{M}_g k_g + \mathcal{G}_g = 0 \quad (\text{B.54})$$

The following formulae

$$k_{1,g} = \mathcal{M}_g + \sqrt{\mathcal{M}_g^2 - \mathcal{G}_g} \quad (\text{B.55})$$

$$k_{2,g} = \mathcal{M}_g - \sqrt{\mathcal{M}_g^2 - \mathcal{G}_g} \quad (\text{B.56})$$

are the solutions to Eq. (B.54).

Here, in Eqs. (B.55) and (B.56), the first principal curvature of a gear tooth flank  $\mathcal{S}$  at a current point  $m$  is designated as  $k_{1,g}$ , and  $k_{2,g}$  designates the second principal curvature of a gear tooth flank  $\mathcal{S}$  at that same point  $m$ .

The principal curvatures  $k_{1,g}$ , and  $k_{2,g}$  are the reciprocals to the corresponding principal radii of curvature  $R_{1,g}$ , and  $R_{2,g}$ :

$$k_{1,g} = \frac{1}{R_{1,g}} \quad (\text{B.57})$$

$$k_{2,g} = \frac{1}{R_{2,g}} \quad (\text{B.58})$$

The first principal curvature,  $k_{1,g}$ , is always larger than the second principal curvature,  $k_{2,g}$ , of a gear tooth flank  $\mathcal{S}$  at a current point  $m$  – that is the inequality:

$$k_{1,g} > k_{2,g} \quad (\text{B.59})$$

is always valid.



## B.7 BRIOSCHI FORMULA FOR GAUSS CURVATURE

*Gauss* curvature at surface,  $\mathcal{S}$ , point  $m$  can be expressed in terms of just three fundamental magnitudes  $E_g, F_g, G_g$ , of the first order, and their derivatives of the first, and of the second order, that is, with no application of three fundamental magnitudes  $L_g, M_g, N_g$ , of the second order. For this purpose, *Brioschi*<sup>9</sup> formula for *Gauss* curvature can be used:

$$G_g = \frac{\begin{vmatrix} -\frac{1}{2} \frac{\partial^2 E_g}{\partial V_g^2} + \frac{\partial^2 F_g}{\partial U_g \partial V_g} - \frac{1}{2} \frac{\partial^2 G_g}{\partial U_g^2} & \frac{1}{2} \frac{\partial E_g}{\partial U_g} & \frac{\partial F_g}{\partial U_g} - \frac{1}{2} \frac{\partial E_g}{\partial V_g} \\ \frac{\partial F_g}{\partial V_g} - \frac{1}{2} \frac{\partial G_g}{\partial U_g} & E_g & F_g \\ \frac{1}{2} \frac{\partial G_g}{\partial V_g} & F_g & G_g \end{vmatrix}}{(E_g G_g - F_g^2)} \quad (B.60)$$

For an orthogonally parametrization (namely, when the equality  $F_g = 0$  is valid), *Gaussian* curvature is:

$$G_g = -\frac{1}{2\sqrt{E_g G_g}} \left( \frac{\partial}{\partial U_g} \frac{\frac{\partial G_g}{\partial U_g}}{\sqrt{E_g G_g}} + \frac{\partial}{\partial V_g} \frac{\frac{\partial E_g}{\partial V_g}}{\sqrt{E_g G_g}} \right) \quad (B.61)$$

The *Brioschi* formula gives *Gaussian* curvature solely in terms of the first fundamental form, as illustrated by Eqs. (B.60) and (B.61).

Other formats of representation of the *Brioschi* formula for *Gauss* curvature are also known.

## B.8 NATURAL FORM OF SURFACE REPRESENTATION

This brief consideration of major elements of part surface geometry makes it possible the introduction of two definitions that are of critical importance for further discussion.

As it is already mentioned earlier in this section of the book, it proven by *Bonnet* that the specification of the first and the second fundamental forms determines a unique surface if the *Gauss' characteristic equation* and the *Mainardi-Codazzi relations of compatibility* are satisfied, and those two surfaces that have identical the first and the second fundamental forms are congruent.<sup>10</sup> Six fundamental magnitudes determine a surface uniquely, except as to position and orientation in space.

Specification of a surface in terms of the first and the second fundamental forms is usually called the *natural kind* of surfaces representation. In general form, this kind of part surfaces representation can be expressed by a set of two equations:

$$\begin{array}{l} \text{Natural form} \\ \text{of surface } \mathcal{S} \text{ representation} \end{array} \Rightarrow \mathcal{S} = \mathcal{S}(\Phi_{1.g}, \Phi_{2.g}) \begin{cases} \Phi_{1.g} = \Phi_{1.g}(E_g, F_g, G_g) \\ \Phi_{2.g} = \Phi_{2.g}(E_g, F_g, G_g, L_g, M_g, N_g) \end{cases} \quad (B.62)$$

<sup>9</sup> Francesco Brioschi (22 December 1824 to 13 December 1897) was an Italian mathematician.

<sup>10</sup> Two surfaces with the identical first and second fundamental forms might also be symmetrical. Refer to the literature – Koenderink, J.J., *Solid Shape*, The MIT Press, Cambridge, MA, 1990, 699 pages – on differential geometry of surfaces for details about this specific issue.

Equation (B.62) can be derived from Eq. (B.1). A given gear tooth flank  $\mathcal{S}$  can be expressed in both forms, namely, either by Eq. (B.19) or by Eq. (B.1).

## B.9 A FEW MORE USEFUL EQUATIONS

Many calculations of parameters of geometry can be significantly simplified by using the first and of the second fundamental forms of a smooth, regular part surface  $\mathcal{S}$ .

1. For the calculation of value of radius,  $R_g$ , of normal curvature within a normal plane section through a current point  $m$  on a gear tooth flank  $\mathcal{S}$  and at a given direction, the following equation can be used:

$$R_g = \frac{\Phi_{1,g}}{\Phi_{2,g}} \quad (\text{B.63})$$

2. *Euler formula* for the calculation of normal curvature,  $k_{\theta,g}$ , at a point  $m$  in a direction that is specified by the angle,  $\theta$ , can be represented as follows:

$$k_{\theta,g} = k_{1,g} \cos^2 \theta + k_{2,g} \sin^2 \theta \quad (\text{B.64})$$

Here, in Eq. (B.64),  $\theta$  is the angle that the normal plane section,  $C_g$ , makes with the first principal plane section,  $C_{1,g}$ . In other words,  $\theta = \angle(\mathbf{t}_g, \mathbf{t}_{1,g})$ ; here  $\mathbf{t}_g$  designates the unit tangent vector within the normal plane section  $C_g$ .

Equation (B.64) also is a good illustration of significant simplification of the calculations when fundamental magnitudes,  $E_g, F_g, G_g$ , of the first and  $L_g, M_g, N_g$  of the second order are used.

In order to get a profound understanding of differential geometry of surfaces, the interested reader may wish to go to advanced monographs in the field. Systematic discussion of the topic is available from many sources. The author would like to turn the reader's attention to the books by *doCarmo, Eisenhart, Stuik*, and others.

## B.10 ILLUSTRATIVE EXAMPLE

Consider an example of how an analytical representation of a surface in a *Cartesian* reference system can be converted into the natural representation of that same surface.

A *Cartesian* coordinate system  $X_g Y_g Z_g$  is associated with a gear tooth flank  $\mathcal{S}$  as it is schematically shown in Figure B.3.

Position vector of a point,  $\mathbf{r}_g$ , of the gear tooth flank  $\mathcal{S}$  can be represented as summa of three vectors:

$$\mathbf{r}_g = \mathbf{A} + \mathbf{B} + \mathbf{C} \quad (\text{B.65})$$

Each of the vectors  $\mathbf{A}$ ,  $\mathbf{B}$ , and  $\mathbf{C}$  can be expressed in terms of projections onto the axes of the reference system  $X_g Y_g Z_g$ . Then, Eq. (B.65) casts into the equation:

$$\mathbf{r}_g(U_g, V_g) = \begin{bmatrix} r_{b,g} \cos V_g + U_g \cos \tau_{b,g} \sin V_g \\ r_{b,g} \sin V_g - U_g \sin \tau_{b,g} \sin V_g \\ r_{b,g} \tan \tau_{b,g} - U_g \sin \tau_{b,g} \\ 1 \end{bmatrix} \quad (\text{B.66})$$

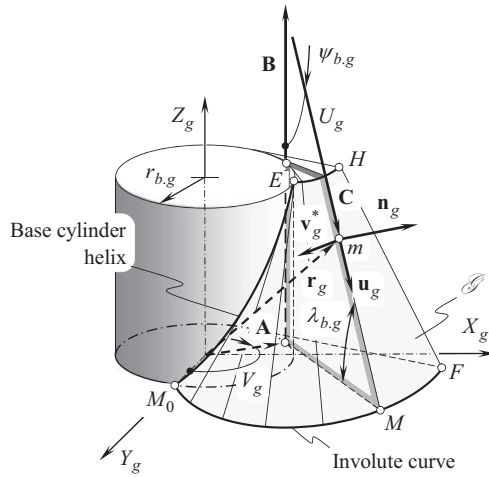


**FIGURE B.3** Derivation of the natural form of representation of gear tooth flank,  $\mathcal{S}$ .

This yields the calculation of two tangent vectors  $\mathbf{U}_g(U_g, V_g)$  and  $\mathbf{V}_g(U_g, V_g)$ , which are correspondingly equal:

$$\mathbf{U}_g(U_g, V_g) = \begin{bmatrix} \cos \tau_{b,g} \sin V_g \\ -\cos \tau_{b,g} \cos V_g \\ -\sin \tau_{b,g} \\ 0 \end{bmatrix} \quad (\text{B.67})$$

$$\mathbf{V}_g(U_g, V_g) = \begin{bmatrix} -r_{b,g} \sin V_g + U_g \cos \tau_{b,g} \cos V_g \\ r_{b,g} \cos V_g + U_g \cos \tau_{b,g} \sin V_g \\ r_{b,g} \tan \tau_{b,g} \\ 0 \end{bmatrix} \quad (\text{B.68})$$

Substituting the derived vectors  $\mathbf{U}_g$  and  $\mathbf{V}_g$  into Eq. (B.14), one can come up with formulae for the calculation of the fundamental magnitudes of the first order:

$$E_g = 1 \quad (\text{B.69})$$

$$F_g = -\frac{r_{b,g}}{\cos \tau_{b,g}} \quad (\text{B.70})$$

$$G_g = \frac{U_g^2 \cos^4 \tau_{b,g} + r_{b,g}^2}{\cos^2 \tau_{b,g}} \quad (\text{B.71})$$

These expressions can be substituted directly to Eq. (B.12) for the first fundamental form  $\Phi_{1,g}$  of the gear tooth flank,  $\mathcal{S}$ :

$$\Phi_{1,g} \Rightarrow dU_g^2 - 2 \frac{r_{b,g}}{\cos \tau_{b,g}} dU_g dV_g + \frac{U_g^2 \cos^4 \tau_{b,g} + r_{b,g}^2}{\cos^2 \tau_{b,g}} dV_g^2 \quad (\text{B.72})$$

The derived expressions for the fundamental magnitudes  $E_g$ ,  $F_g$ , and  $G_g$  [see Eqs. (B.69)–(B.71)] can also be substituted to Eq. (B.13). In this way, a corresponding matrix representation of the first fundamental form  $\Phi_{1.g}$  of the gear tooth flank,  $\mathcal{S}$ , can be calculated. The interested reader may wish to complete these formulae on his or her own.

The discriminant,  $H_g$ , of the first fundamental form of the gear tooth flank,  $\mathcal{S}$ , can be calculated from the expression:

$$H_g = U_g \cos \tau_{b.g} \quad (\text{B.73})$$

In order to derive an equation for the second fundamental form,  $\Phi_{2.g}$ , of the gear tooth flank,  $\mathcal{S}$ , the second derivatives of the position vector of a point,  $\mathbf{r}_g(U_g, V_g)$ , with respect to  $U_g$  – and  $V_g$  – parameters are necessary. The above-derived equations for the tangent vectors  $\mathbf{U}_g$  and  $\mathbf{V}_g$  [see Eqs. (B.67) and (B.68)] make it possible the following expressions for the derivatives under consideration:

$$\frac{\partial \mathbf{U}_g}{\partial U_g} = \begin{bmatrix} 0 \\ 0 \\ 0 \\ 1 \end{bmatrix} \quad (\text{B.74})$$

$$\frac{\partial \mathbf{U}_g}{\partial V_g} \equiv \frac{\partial \mathbf{V}_g}{\partial U_g} = \begin{bmatrix} \cos \tau_{b.g} \cos V_g \\ \cos \tau_{b.g} \sin V_g \\ 0 \\ 1 \end{bmatrix} \quad (\text{B.75})$$

$$\frac{\partial \mathbf{V}_g}{\partial V_g} = \begin{bmatrix} -r_{b.g} \cos V_g - U_g \cos \tau_{b.g} \sin V_g \\ -r_{b.g} \sin V_g + U_g \cos \tau_{b.g} \cos V_g \\ 0 \\ 1 \end{bmatrix} \quad (\text{B.76})$$

Further, substitute these expressions [see Eqs. (B.74)–(B.76)] into Eqs. (B.36)–(B.38). After the necessary formulae transformations are complete, then Eqs. (B.36)–(B.38) cast into the set of formulae for the calculation of the fundamental magnitudes of the second order of the gear tooth flank,  $\mathcal{S}$ . This set of formulae is as follows:

$$L_g = 0 \quad (\text{B.77})$$

$$M_g = 0 \quad (\text{B.78})$$

$$N_g = -U_g \sin \tau_{b.g} \cos \tau_{b.g} \quad (\text{B.79})$$

Further, after substituting Eqs. (B.77)–(B.79) into Eq. (B.31), an equation for the calculation of the second fundamental form of the gear tooth flank,  $\mathcal{S}$ , can be represented in the form:

$$\Phi_{2.g} \Rightarrow -d\mathbf{r}_g \cdot d\mathbf{N}_g = -U_g \sin \tau_{b.g} \cos \tau_{b.g} dV_g^2 \quad (\text{B.80})$$

Similar to Eq. (B.72), the derived expressions for the fundamental magnitudes  $L_g$ ,  $M_g$  and  $N_g$  of the second order can be substituted into Eq. (B.32) for the second fundamental form  $\Phi_{2.g}$ . In this way a corresponding matrix representation of the second fundamental form,  $\Phi_{2.g}$ , of the surface  $\mathcal{S}$  can be derived. The interested reader may wish to complete this formulae transformation on his or her own.

**TABLE B.1**  
**Fundamental Magnitudes of the First and the Second Order**  
**of Involute Gear Tooth Flank,  $\mathcal{S}$**

$E_g = 1$	$L_g = 0$
$F_g = -\frac{r_{b,g}}{\cos \tau_{b,g}}$	$M_g = 0$
$G_g = \frac{U_g^2 \cos^4 \tau_{b,g} + r_{b,g}^2}{\cos^2 \tau_{b,g}}$	$N_g = -U_g \sin \tau_{b,g} \cos \tau_{b,g}$

For the calculation of the discriminant,  $T_g$ , of the second fundamental form,  $\Phi_{2,g}$ , of the gear tooth flank,  $\mathcal{S}$ , the following expression can be used:

$$T_g = U_g \sin \tau_{b,g} \cos \tau_{b,g} \quad (\text{B.81})$$

The natural representation of the gear tooth flank,  $\mathcal{S}$ , can be expressed in terms of the derived set of six equations for the calculation of the fundamental magnitudes of the first  $E_g, F_g, G_g$  and of the second  $L_g, M_g$  and  $N_g$  (see Table B.1).

All major elements of local geometry of the gear tooth flank,  $\mathcal{S}$ , can be calculated based on the fundamental magnitudes,  $E_g, F_g, G_g$ , of the first,  $\Phi_{1,P}$ , and  $L_g, M_g, N_g$ , of the second  $\Phi_{2,g}$ , fundamental forms. Location and orientation of the gear tooth flank,  $\mathcal{S}$ , are the two parameters that remain indefinite.

Once a part surface is represented in natural form – that is, it is expressed in terms of six fundamental magnitudes of the first and of the second order – then further calculation of parameters of a gear tooth flank  $\mathcal{S}$  becomes much easier. In order to demonstrate significant simplification of the calculation of parameters of a gear tooth flank  $\mathcal{S}$ , several useful equations are presented below as examples.

# Appendix C

## Change of Surface Parameters

When designing a form cutting tool, it is often necessary to treat two or more surfaces simultaneously. For example, cutting edge of the cutting tool can be considered as the line of intersection of the generating surface  $T$  of the form cutting tool by the rake surface  $R_s$ . Equation of the cutting edge can't be derived on the premises of equations of the surfaces  $T$  and  $R_s$  as long as the initial parameterization of the surfaces is improper.

When two surfaces  $\mathbf{r}_i$  and  $\mathbf{r}_j$  are necessary been treated simultaneously, then it is required that they are not only represented in a common reference system, but the  $U_i$  – and  $V_i$  – parameters of one of the surfaces  $\mathbf{r}_i = \mathbf{r}_i(U_i, V_i)$  have to be synchronized with the corresponding  $U_j$  – and  $V_j$  – parameters of another surface  $\mathbf{r}_j = \mathbf{r}_j(U_j, V_j)$ . The procedure of changing of surface parameters is used for this purpose. The use of the procedure allows representation of one of the surfaces, for example of the surface  $\mathbf{r}_j = \mathbf{r}_j(U_j, V_j)$  in the terms of the  $U_i$  – and  $V_i$  – parameters, say as  $\mathbf{r}_j = \mathbf{r}_j(U_i, V_i)$ .

If the parameterization of a surface is transformed by the equations  $U^* = U^*(U, V)$  and  $V^* = V^*(U, V)$ , we obtain the new derivatives:

$$\frac{\partial \mathbf{r}}{\partial U^*} = \frac{\partial \mathbf{r}}{\partial U} \cdot \frac{\partial U}{\partial U^*} + \frac{\partial \mathbf{r}}{\partial V} \cdot \frac{\partial V}{\partial U^*} \quad (\text{C.1})$$

$$\frac{\partial \mathbf{r}}{\partial V^*} = \frac{\partial \mathbf{r}}{\partial U} \cdot \frac{\partial U}{\partial V^*} + \frac{\partial \mathbf{r}}{\partial V} \cdot \frac{\partial V}{\partial V^*} \quad (\text{C.2})$$

so that:

$$\mathbf{A}^* = \left[ \begin{array}{c|c} \frac{\partial \mathbf{r}}{\partial U^*} & \frac{\partial \mathbf{r}}{\partial V^*} \end{array} \right] = \mathbf{A} \cdot \mathbf{J} \quad (\text{C.3})$$

where

$$\mathbf{J} = \left[ \begin{array}{cc} \frac{\partial U}{\partial U^*} & \frac{\partial U}{\partial V^*} \\ \frac{\partial V}{\partial U^*} & \frac{\partial V}{\partial V^*} \end{array} \right] \quad (\text{C.4})$$

is called the *Jacobian matrix* of the transformation.

It can be shown that the new fundamental matrix  $\mathcal{G}^*$  is given by:

$$\mathbf{G}^* = \mathbf{A}^{*T} \mathbf{A}^* = \mathbf{J}^T \mathbf{A}^T \mathbf{A} \mathbf{J} = \mathbf{J}^T \mathbf{G} \mathbf{J} \quad (\text{C.5})$$

From this equation we see by the properties of determinants that  $|\mathbf{G}^*| = |\mathbf{J}|^2 |\mathbf{G}|$ . Using this result and Eqs. (C.1) and (C.2), we can show that the unit surface normal  $\mathbf{n}$  is invariant under the transformation, as we could expect.

The transformation of the second fundamental matrix can similarly be shown to be given by:

$$\mathbf{D}^* = \mathbf{J}^T \mathbf{D} \mathbf{J} \quad (\text{C.6})$$

by differentiating Eqs. (C.1) and (C.2) and using the invariance of  $\mathbf{n}$ . From Eqs. (C.5) and (C.6), it can be shown that the principal curvatures and directions are invariant under the transformation.

We conclude that the unit normal vector  $\mathbf{n}$  and the principal directions and curvatures are independent of the parameters used and are therefore geometric properties of the surface itself. They should be continuous if the surface is to be tangent and curvature continuous.



---

# Appendix D

## *Applied Coordinate Systems and Linear Transformations*

Consequent coordinate systems transformations can be easily described analytically with the implementation of matrices. The use of matrices for the coordinate system transformation<sup>1</sup> can be traced back to the mid of 1940s<sup>2</sup> when Dr. *S.S. Mozhayev*<sup>3</sup> began describing coordinate system transformations by means of matrices.

Below, coordinate systems transformation is briefly discussed from the standpoint of its implementation in the theory of gearing.

### D.1 COORDINATE SYSTEM TRANSFORMATION

Homogeneous coordinates utilize a mathematical trick to embed three-dimensional coordinates and transformations into a four-dimensional matrix format. As a result, inversions or combinations of linear transformations are simplified to inversions or multiplication of the corresponding matrices.

#### D.1.1 HOMOGENEOUS COORDINATE VECTORS

Instead of representing each point  $\mathbf{r}(x, y, z)$  in three-dimensional space with a single three-dimensional vector,

$$\mathbf{r} = \begin{bmatrix} x \\ y \\ z \end{bmatrix} \quad (\text{D.1})$$

homogeneous coordinates allow each point  $\mathbf{r}(x, y, z)$  to be represented by any of an infinite number of four-dimensional vectors:

$$\mathbf{r} = \begin{bmatrix} T \cdot x \\ T \cdot y \\ T \cdot z \\ T \end{bmatrix} \quad (\text{D.2})$$

---

<sup>1</sup> 1 Matrices were introduced into mathematics by *A. Cayley* in 1857. They provide a compact and flexible notation particularly useful in dealing with linear transformations, and they presented an organized method for the solution of systems of linear differential equations.

<sup>2</sup> Application of matrices for the purposes of analytical representation of coordinate system transformation should be credited to Dr. *S.S. Mozhayev* [Mozhayev, S.S., *General Theory of Cutting Tools*, Doctoral Thesis, Leningrad, Leningrad Polytechnic Institute, 1951, 295 pages]. Dr. *S.S. Mozhayev* began using matrices for this purpose in the mid of 1940s. Later on, matrix approach for coordinate system transformation has been used by *Denavit & Hartenberg*, as well as by many other researchers.

<sup>3</sup> S.S. Mozhayev – is a soviet scientist known mainly for his accomplishments in the theory of cutting tool design.

The three-dimensional vector corresponding to any four-dimensional vector can be calculated by dividing the first three elements by the fourth, and a four-dimensional vector corresponding to any three-dimensional vector can be created by simply adding a fourth element and setting it equal to one.

### D.1.2 HOMOGENEOUS COORDINATE TRANSFORMATION MATRICES OF THE DIMENSION $4 \times 4$

Homogeneous coordinate transformation matrices operate on four-dimensional homogeneous vector representations of traditional three-dimensional coordinate locations. Any three-dimensional linear transformation (translation, rotation, and so forth) can be represented by a  $4 \times 4$  homogeneous coordinate transformation matrix. Because of the redundant representation of three-space in a homogeneous coordinate system, an infinite number of different  $4 \times 4$  homogeneous coordinate transformation matrices are available to perform any given linear transformation. This redundancy can be eliminated to provide a unique representation by dividing all elements of a  $4 \times 4$  homogeneous transformation matrix by the last element (which will become equal to one). This means that a  $4 \times 4$  homogeneous transformation matrix can incorporate as many as 15 independent parameters. The generic format representation of a homogeneous transformation equation for mapping the three-dimensional coordinate  $(x_1, y_1, z_1)$  to the three-dimensional coordinate  $(x_2, y_2, z_2)$  is:

$$\begin{bmatrix} T^* \cdot x_2 \\ T^* \cdot y_2 \\ T^* \cdot z_2 \\ T^* \end{bmatrix} = \begin{bmatrix} T^* \cdot a & T^* \cdot b & T^* \cdot c & T^* \cdot d \\ T^* \cdot e & T^* \cdot f & T^* \cdot g & T^* \cdot h \\ T^* \cdot i & T^* \cdot j & T^* \cdot k & T^* \cdot m \\ T^* \cdot n & T^* \cdot p & T^* \cdot q & T^* \end{bmatrix} \cdot \begin{bmatrix} T \cdot x_2 \\ T \cdot y_2 \\ T \cdot z_2 \\ T \end{bmatrix} \quad (\text{D.3})$$

If any two matrices or vectors of this equation are known, the third matrix (or vector) can be calculated, and then the redundant  $T$  element in the solution can be eliminated by dividing all elements of the matrix by the last element.

Various transformation models can be used to constrain the form of the matrix to transformations with fewer degrees of freedom.

### D.1.3 TRANSLATIONS

Translation of a coordinate system is one of the major linear transformations used in the theory of part surface generation. Translations of the coordinate system  $X_2Y_2Z_2$  along axes of the coordinate system  $X_1Y_1Z_1$  are depicted in Figure D.1. Translations can be analytically described by the homogeneous transformation matrix of dimension  $4 \times 4$ .

For an analytical description of translation along coordinate axes, the operators of translation  $\mathbf{Tr}(a_x, X)$ ,  $\mathbf{Tr}(a_y, Y)$ , and  $\mathbf{Tr}(a_z, Z)$  are used. These operators yield matrix representation in the form:

$$\mathbf{Tr}(a_x, X) = \begin{bmatrix} 1 & 0 & 0 & a_x \\ 0 & 1 & 0 & 0 \\ 0 & 0 & 1 & 0 \\ 0 & 0 & 0 & 1 \end{bmatrix} \quad (\text{D.4})$$

$$\mathbf{Tr}(a_y, Y) = \begin{bmatrix} 1 & 0 & 0 & 0 \\ 0 & 1 & 0 & a_y \\ 0 & 0 & 1 & 0 \\ 0 & 0 & 0 & 1 \end{bmatrix} \quad (\text{D.5})$$

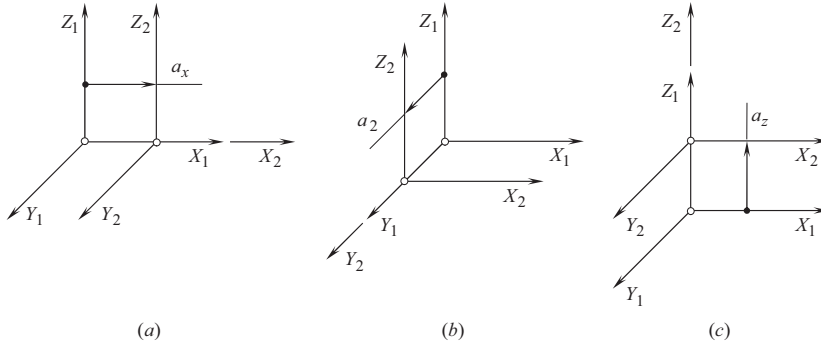


**FIGURE D.1** Analytical description of the operators of translations  $\mathbf{Tr}(a_x, X)$ ,  $\mathbf{Tr}(a_y, Y)$ ,  $\mathbf{Tr}(a_z, Z)$  along the coordinate axes of a *Cartesian* reference system  $XYZ$ : (a) a translation along the axis  $X$ ; (b) a translation along the axis  $Y$ ; and (c) a translation along the axis  $Z$ .

$$\mathbf{Tr}(a_z, Z) = \begin{bmatrix} 1 & 0 & 0 & 0 \\ 0 & 1 & 0 & 0 \\ 0 & 0 & 1 & a_z \\ 0 & 0 & 0 & 1 \end{bmatrix} \quad (\text{D.6})$$

Here, in Eqs. (D.4)–(D.6), the parameters  $a_x$ ,  $a_y$ , and  $a_z$  are signed values that denote the distance of translation along the corresponding axis.

Consider two coordinate systems,  $X_1Y_1Z_1$  and  $X_2Y_2Z_2$ , displaced along the  $X_1$  – axis at a distance  $a_x$  as schematically depicted in Figure D.1a. A point  $m$  in the reference system  $X_2Y_2Z_2$  is given by the position vector  $\mathbf{r}_2(m)$ . In the coordinate system,  $X_1Y_1Z_1$ , that same point  $m$  can be specified by the position vector  $\mathbf{r}_1(m)$ . Then the position vector  $\mathbf{r}_1(m)$  can be expressed in terms of the position vector  $\mathbf{r}_2(m)$  by the equation:

$$\mathbf{r}_1(m) = \mathbf{Tr}(a_x, X) \cdot \mathbf{r}_2(m) \quad (\text{D.7})$$

Equations similar to Eq. (D.7) are valid for the operators  $\mathbf{Tr}(a_y, Y)$ , and  $\mathbf{Tr}(a_z, Z)$  of the coordinate system transformation. The latter is schematically illustrated in Figure D.1b and c.

The use of the operators of translation  $\mathbf{Tr}(a_x, X)$ ,  $\mathbf{Tr}(a_y, Y)$ , and  $\mathbf{Tr}(a_z, Z)$  makes it possible an introduction of an operator  $\mathbf{Tr}(a, \mathbf{A})$  of a combined transformation. Suppose that point,  $p$ , on a rigid body goes through a translation describing a straight line from a point  $p_1$  to a point  $p_2$  with a change of coordinates of  $(a_x, a_y, a_z)$ . This motion of the point,  $p$ , can be analytically described with a resultant translation operator  $\mathbf{Tr}(a, \mathbf{A})$ :

$$\mathbf{Tr}(a, \mathbf{A}) = \begin{bmatrix} 1 & 0 & 0 & a_x \\ 0 & 1 & 0 & a_y \\ 0 & 0 & 1 & a_z \\ 0 & 0 & 0 & 1 \end{bmatrix} \quad (\text{D.8})$$

The operator  $\mathbf{Tr}(a, \mathbf{A})$  of the resultant coordinate system transformation can be interpreted as the operator of translation along an arbitrary axis having the vector  $\mathbf{A}$  as the direct vector.

An analytical description of the translation of the coordinate system  $X_1Y_1Z_1$  in direction of an arbitrary vector  $\mathbf{A}$  to the position of  $X_2Y_2Z_2$  can be composed from Figure D.2. The operator of translation  $\mathbf{Tr}(a, \mathbf{A})$  of that particular kind can be expressed in terms of the operators  $\mathbf{Tr}(a_x, X)$ ,  $\mathbf{Tr}(a_y, Y)$ , and  $\mathbf{Tr}(a_z, Z)$  of elementary translations:

$$\mathbf{Tr}(a, \mathbf{A}) = \mathbf{Tr}(a_z, Z) \cdot \mathbf{Tr}(a_y, Y) \cdot \mathbf{Tr}(a_x, X) \quad (\text{D.9})$$

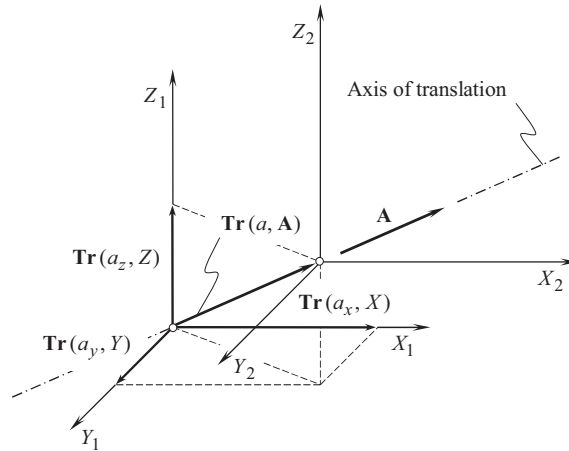


**FIGURE D.2** Analytical description of an operator,  $\mathbf{Tr}(a, \mathbf{A})$ , of translation along an arbitrary axis (vector  $\mathbf{A}$  is the direction vector of the axis).

Evidently, the axis along the vector  $\mathbf{A}$  is always the axis through the origins of both the reference systems  $X_1Y_1Z_1$  and  $X_2Y_2Z_2$ .

Any and all coordinate system transformations that do not change the orientation of a geometrical object are referred to as *orientation-preserving transformation* or *direct transformation*. Therefore, the transformation of translation is an example of a direct transformation.

#### D.1.4 ROTATION ABOUT A COORDINATE AXIS

Rotation of a coordinate system about a coordinate axis is another major linear transformation used in the theory of part surface generation. A rotation is specified by an axis of rotation and the angle of the rotation. It is a fairly simple trigonometric calculation to obtain a transformation matrix for a rotation about one of the coordinate axes.

Possible rotations of the coordinate system  $X_2Y_2Z_2$  about the axis of the coordinate system  $X_1Y_1Z_1$  are illustrated in Figure D.3.

For analytical description of rotation about a coordinate axis, the operators of rotation  $\mathbf{Rt}(\varphi_x, X_1)$ ,  $\mathbf{Rt}(\varphi_y, Y_1)$ , and  $\mathbf{Rt}(\varphi_z, Z_1)$  are used. These operators of linear transformations yield representation in the form of homogeneous matrices:

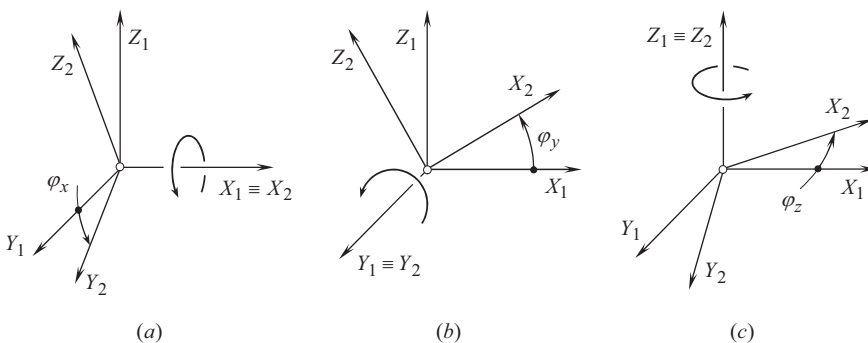


**FIGURE D.3** Analytical description of the operators of rotation  $\mathbf{Rt}(\varphi_x, X)$ ,  $\mathbf{Rt}(\varphi_y, Y)$ , and  $\mathbf{Rt}(\varphi_z, Z)$ , about the coordinate axes of a *Cartesian* reference system  $X_1Y_1Z_1$ : (a) a rotation about the axis  $X_1$ ; (b) a rotation about the axis  $Y_1$ ; and (c) a rotation about the axis  $Z_1$ .

$$\mathbf{Rt}(\varphi_x, X_1) = \begin{bmatrix} 1 & 0 & 0 & 0 \\ 0 & \cos \varphi_x & \sin \varphi_x & 0 \\ 0 & -\sin \varphi_x & \cos \varphi_x & 0 \\ 0 & 0 & 0 & 1 \end{bmatrix} \quad (\text{D.10})$$

$$\mathbf{Rt}(\varphi_y, Y_1) = \begin{bmatrix} \cos \varphi_y & 0 & \sin \varphi_y & 0 \\ 0 & 1 & 0 & 0 \\ -\sin \varphi_y & 0 & \cos \varphi_y & 0 \\ 0 & 0 & 0 & 1 \end{bmatrix} \quad (\text{D.11})$$

$$\mathbf{Rt}(\varphi_z, Z_1) = \begin{bmatrix} \cos \varphi_z & \sin \varphi_z & 0 & 0 \\ -\sin \varphi_z & \cos \varphi_z & 0 & 0 \\ 0 & 0 & 1 & 0 \\ 0 & 0 & 0 & 1 \end{bmatrix} \quad (\text{D.12})$$

Here  $\varphi_x$ ,  $\varphi_y$ , and  $\varphi_z$  are signed values that denote the corresponding angles of rotations about a corresponding coordinate axis:  $\varphi_x$  is the angle of rotation around the  $X_1$  – axis (pitch) of the *Cartesian* coordinate system  $X_1Y_1Z_1$ ;  $\varphi_y$  is the angle of rotation around the  $Y_1$  – axis (roll), and  $\varphi_z$  is the angle of rotation around the  $Z_1$  – axis (yaw) of that same *Cartesian* reference system  $X_1Y_1Z_1$ .

Rotation about a coordinate axis is illustrated in Figure D.3.

Consider two coordinate systems  $X_1Y_1Z_1$  and  $X_2Y_2Z_2$ , which are turned about  $X_1$  – axis through an angle  $\varphi_x$  as shown in Figure D.3a. In the reference system  $X_2Y_2Z_2$ , a point  $m$  is given by a position vector  $\mathbf{r}_2(m)$ . In the coordinate system  $X_1Y_1Z_1$ , that same point  $m$  can be specified by the position vector  $\mathbf{r}_1(m)$ . Then, the position vector  $\mathbf{r}_1(m)$  can be expressed in terms of the position vector  $\mathbf{r}_2(m)$  by the equation:

$$\mathbf{r}_1(m) = \mathbf{Rt}(\varphi_x, X) \cdot \mathbf{r}_2(m) \quad (\text{D.13})$$

Equations similar to the above Eq. (D.13), are also valid for other operators  $\mathbf{Rt}(\varphi_y, Y)$  and  $\mathbf{Rt}(\varphi_z, Z)$  of the coordinate system transformation. These elementary coordinate system transformations are schematically illustrated in Figure D.3b and c accordingly.

### D.1.5 ROTATION ABOUT AN ARBITRARY AXIS THROUGH THE ORIGIN

When a rotation is to be performed around an arbitrary vector based on the origin, the transformation matrix must be assembled from a combination of rotations about the *Cartesian* coordinate.

Two different approaches for the analytical description of a rotation about an arbitrary axis through the origin are discussed below.

#### D.1.5.1 Conventional Approach

Analytical description of rotation of the coordinate system  $X_1Y_1Z_1$  about an arbitrary axis through the origin to the position of a reference system  $X_2Y_2Z_2$  is illustrated in Figure D.4. It is assumed here that the rotation is performed about the axis having a vector  $\mathbf{A}_0$  as the direction vector. The operator  $\mathbf{Rt}(\varphi_A, \mathbf{A}_0)$  of rotation of that kind can be expressed in terms of the operators  $\mathbf{Rt}(\varphi_x, X)$ ,  $\mathbf{Rt}(\varphi_y, Y)$ , and  $\mathbf{Rt}(\varphi_z, Z)$  of elementary rotations:

$$\mathbf{Rt}(\varphi_A, \mathbf{A}_0) = \mathbf{Rt}(\varphi_z, Z) \cdot \mathbf{Rt}(\varphi_y, Y) \cdot \mathbf{Rt}(\varphi_x, X) \quad (\text{D.14})$$

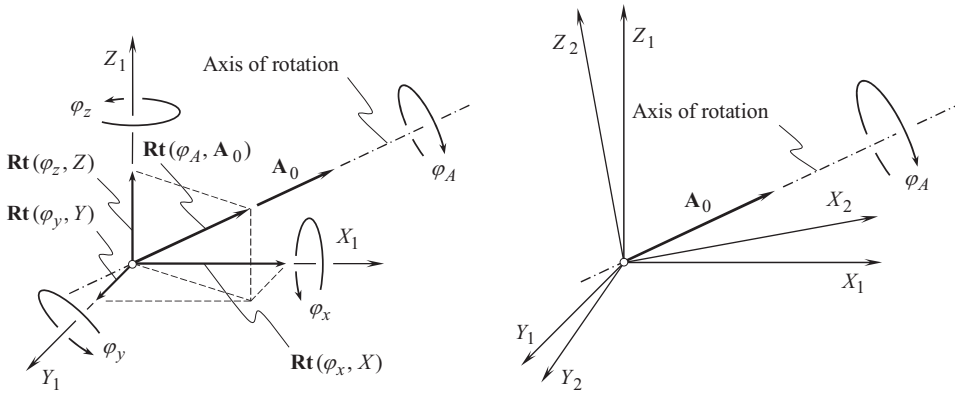


**FIGURE D.4** Analytical description of the operator  $\mathbf{Rt}(\varphi_A, \mathbf{A}_0)$  of rotation about an arbitrary axis through the origin of a *Cartesian* coordinate system  $X_1Y_1Z_1$  (the vector  $\mathbf{A}$  is the direction vector of the axis of rotation).

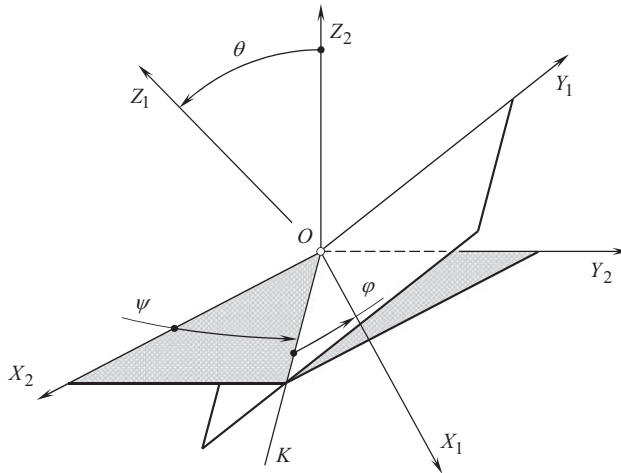


**FIGURE D.5** *Euler angles.*

Evidently, the axis of rotation (a straight line along the vector  $\mathbf{A}_0$ ) is always an axis through the origin.

The operators of translation and of rotation also yield linear transformations of other kinds as well.

### D.1.5.2 Eulerian Transformation

*Eulerian transformation* is a well-known kind of linear transformation used extensively in mechanical engineering. This kind of linear transformation is analytically described by the operator  $\mathbf{Eu}(\psi, \theta, \varphi)$  of *Eulerian*<sup>4</sup> transformation.

The operator  $\mathbf{Eu}(\psi, \theta, \varphi)$  is expressed in terms of three *Euler angles* (or *Eulerian angles*)  $\psi$ ,  $\theta$ , and  $\varphi$ . Configuration of an orthogonal *Cartesian* coordinate system  $X_1Y_1Z_1$  in relation to another orthogonal *Cartesian* coordinate system  $X_2Y_2Z_2$  is defined by the *Euler angles*  $\psi$ ,  $\theta$ , and  $\varphi$ . These angles are shown in Figure D.5.

<sup>4</sup> Leonhard Euler (April 15, 1707–September 18, 1783), a famous Swiss mathematician and physicist who spent most of his life in Russia and Germany.

The line of intersection of the coordinate plane  $X_1Y_1$  of the first reference system by the coordinate plane  $X_2Y_2$  of the second reference system is commonly referred to as *line of nodes*. In Figure D.5, the line  $OK$  is the line of nodes. It is assumed here and below that the line of nodes,  $OK$ , and the axes  $Z_1$  and  $Z_2$  form a frame of that same orientation as the reference systems  $X_1Y_1Z_1$  and  $X_2Y_2Z_2$  do.

The *Euler angle*,  $\varphi$ , is referred to as the *angle of pure rotation*. This angle is measured between the  $X_1$  – axis and the line of nodes,  $OK$ . The angle of pure rotation,  $\varphi$ , is measured within the coordinate plane  $X_1Y_1$  in the direction of the shortest rotation from the axis  $X_1$  to the axis  $Y_1$ .

The *Euler angle*,  $\theta$ , is referred to as the *angle of nutation*. The angle of nutation,  $\theta$ , is measured between the axes  $Z_1$  and  $Z_2$ . The actual value of this angle never exceeds  $180^\circ$ .

The *Euler angle*,  $\psi$ , is referred to as the *angle of precession*. The angle of precession,  $\psi$ , is measured in the coordinate plane  $X_2Y_2$ . This is the angle between the line of nodes,  $OK$ , and the  $X_2$  – axis. Direction of the shortest rotation from the axis  $X_2$  to the axis  $Y_2$  is the direction in which the angle of precession is measured.

In case, when the angle of nutation is equal either  $\theta = 0^\circ$  or  $\theta = 180^\circ$ , then the *Euler angles* are not defined.

The operator  $\mathbf{Eu}(\psi, \theta, \varphi)$  of *Eulerian transformation* allows for the following matrix representation:

$$\mathbf{Eu}(\psi, \theta, \varphi) = \begin{bmatrix} -\sin\psi \cos\theta \sin\varphi + \cos\psi \cos\varphi & \cos\psi \cos\theta \sin\varphi + \sin\psi \cos\varphi & \sin\theta \sin\varphi & 0 \\ -\sin\psi \cos\theta \cos\varphi - \cos\psi \sin\varphi & \cos\psi \cos\theta \cos\varphi - \sin\psi \cos\varphi & \sin\theta \cos\varphi & 0 \\ \sin\theta \sin\varphi & -\cos\psi \cos\theta & \cos\theta & 0 \\ 0 & 0 & 0 & 1 \end{bmatrix} \quad (\text{D.15})$$

It is important to stress here on difference between the operator  $\mathbf{Eu}(\psi, \theta, \varphi)$  of *Eulerian transformation*, and between the operator  $\mathbf{Rt}(\psi_A, \mathbf{A}_0)$  of rotation about an arbitrary axis through the origin.

The operator  $\mathbf{Rt}(\psi_A, \mathbf{A})$  of rotation about an arbitrary axis through the origin can result in that same final orientation of the coordinate system  $X_2Y_2Z_2$  in relation to the coordinate system  $X_1Y_1Z_1$  as the operator  $\mathbf{Eu}(\psi, \theta, \varphi)$  of *Eulerian transformation* does. However, the operators of linear transformations  $\mathbf{Rt}(\psi_A, \mathbf{A}_0)$  and  $\mathbf{Eu}(\psi, \theta, \varphi)$  are the operators of completely different nature. They can result in identical coordinate system transformation, but they are not equal to one another.

### D.1.6 ROTATION ABOUT AN ARBITRARY AXIS NOT THROUGH THE ORIGIN

The transformation corresponding to the rotation of an angle  $\varphi$  around an arbitrary vector not through the origin cannot readily be written in a form similar to the rotation matrices about the coordinate axes.

The desired transformation matrix is obtained by combining a sequence of elementary translation and rotation matrices. (Once a single  $4 \times 4$  matrix has been obtained representing the composite transformations, it can be used in the same way as any other transformation matrix).

Rotation of the coordinate system  $X_1Y_1Z_1$  to a configuration, which the coordinate system  $X_2Y_2Z_2$  possesses, can be performed about a corresponding axis that features an arbitrary configuration in space (see Figure D.6). The vector  $\mathbf{A}$  is the direction vector of the axis of the rotation. The axis of the rotation is not a line through the origin.

The operator of linear transformation of this particular kind  $\mathbf{Rt}(\psi_A, \mathbf{A})$  can be expressed in terms of the operator  $\mathbf{Tr}(a, \mathbf{A})$  of translation along, and of the operator  $\mathbf{Rt}(\psi_A, \mathbf{A}_0)$  of rotation about an arbitrary axis through the origin:

$$\mathbf{Rt}(\varphi_A, \mathbf{A}) = \mathbf{Tr}(-b, \mathbf{B}^*) \cdot \mathbf{Rt}(\varphi_A, \mathbf{A}_0) \cdot \mathbf{Tr}(b, \mathbf{B}) \quad (\text{D.16})$$



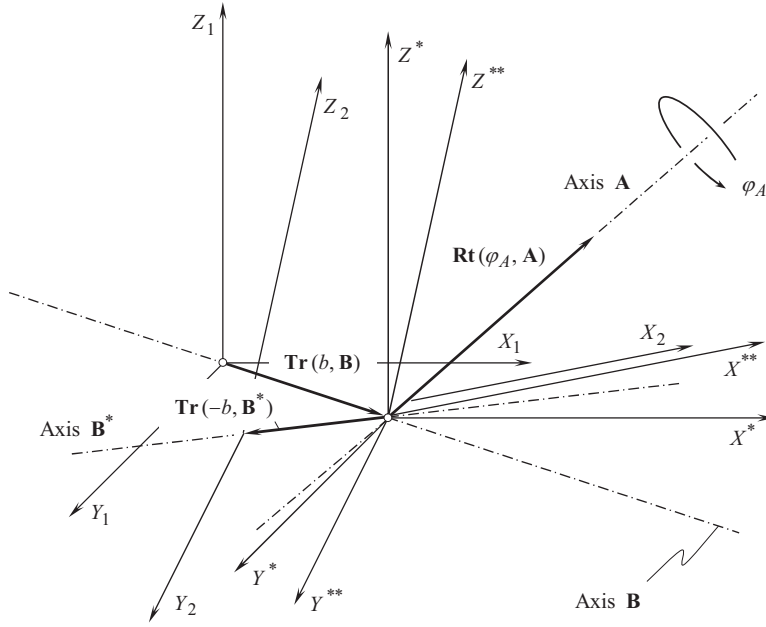


**FIGURE D.6** Analytical description of the operator,  $\mathbf{Rt}(\varphi_A, \mathbf{A})$ , of rotation about an arbitrary axis not through the origin (vector  $\mathbf{A}$  is the direction vector of the axis of rotation).

Here, in Eq. (D.16) is designated:

$\mathbf{Tr}(b, \mathbf{B})$  is the operator of translation along the shortest distance of approach of the axis of rotation and origin of the coordinate system.

$\mathbf{Tr}(-b, \mathbf{B}^*)$  is the operator of translation in the direction opposite to the translation  $\mathbf{Tr}(b, \mathbf{B})$  after the rotation  $\mathbf{Rt}(\varphi_A, \mathbf{A})$  is completed.

In order to determine the shortest distance of approach,  $B$ , of the axis of rotation (that is, the axis along the direction vector  $\mathbf{B}$ ) and origin of the coordinate system, consider the axis ( $\mathbf{B}$ ) through two given points  $\mathbf{r}_{B.1}$  and  $\mathbf{r}_{B.2}$ .

The shortest distance between a certain point  $\mathbf{r}_0$ , and the straight line through the points  $\mathbf{r}_{B.1}$  and  $\mathbf{r}_{B.2}$  can be calculated from the following formula:

$$B = \frac{|(\mathbf{r}_2 - \mathbf{r}_1) \times (\mathbf{r}_1 - \mathbf{r}_0)|}{|\mathbf{r}_2 - \mathbf{r}_1|} \quad (\text{D.17})$$

For the origin of the coordinate system, the equality  $\mathbf{r}_0 = 0$  is observed. Then,

$$B = |\mathbf{r}_1| \cdot \sin \angle[\mathbf{r}_1, (\mathbf{r}_2 - \mathbf{r}_1)] \quad (\text{D.18})$$

Matrix representation of the operators of translation  $\mathbf{Tr}(a_x, X)$ ,  $\mathbf{Tr}(a_y, Y)$ ,  $\mathbf{Tr}(a_z, Z)$  along the coordinate axes, together with the operators of rotation  $\mathbf{Rt}(\varphi_x, X)$ ,  $\mathbf{Rt}(\varphi_y, Y)$ ,  $\mathbf{Rt}(\varphi_z, Z)$  about the coordinate axes is convenient for implementation in the theory of part surface generation. Moreover, the use of the operators is the simplest possible way to analytically describe the linear transformations.

### D.1.7 RESULTANT COORDINATE SYSTEM TRANSFORMATION

The operators of translation  $\mathbf{Tr}(a_x, X)$ ,  $\mathbf{Tr}(a_y, Y)$ , and  $\mathbf{Tr}(a_z, Z)$  together with the operators of rotation  $\mathbf{Rt}(\varphi_x, X)$ ,  $\mathbf{Rt}(\varphi_y, Y)$ , and  $\mathbf{Rt}(\varphi_z, Z)$  are used for the purpose of composing the operator  $\mathbf{Rs}(1 \mapsto 2)$  of the resultant coordinate system transformation. The transition from the initial *Cartesian* reference system  $X_1Y_1Z_1$  to other *Cartesian* reference system  $X_2Y_2Z_2$  is analytically described by the operator  $\mathbf{Rs}(1 \mapsto 2)$  of the resultant coordinate system transformation.

For example, the expression:

$$\mathbf{Rs}(1 \mapsto 5) = \mathbf{Tr}(a_x, X) \cdot \mathbf{Rt}(\varphi_z, Z) \cdot \mathbf{Rt}(\varphi_x, X) \cdot \mathbf{Tr}(a_y, Y) \quad (\text{D.19})$$

indicates that the transition from the coordinate system  $X_1Y_1Z_1$  to the coordinate system  $X_5Y_5Z_5$  is executed in the following four steps (see Figure D.7):

1. translation  $\mathbf{Tr}(a_y, Y)$  followed by
2. rotation  $\mathbf{Rt}(\varphi_x, X)$ , followed by
3. second rotation  $\mathbf{Rt}(\varphi_z, Z)$ , and finally followed by the
4. translation  $\mathbf{Tr}(a_x, X)$ .

Ultimately, the equality:

$$\mathbf{r}_1(m) = \mathbf{Rs}(1 \mapsto 5) \cdot \mathbf{r}_5(m) \quad (\text{D.20})$$

is valid.

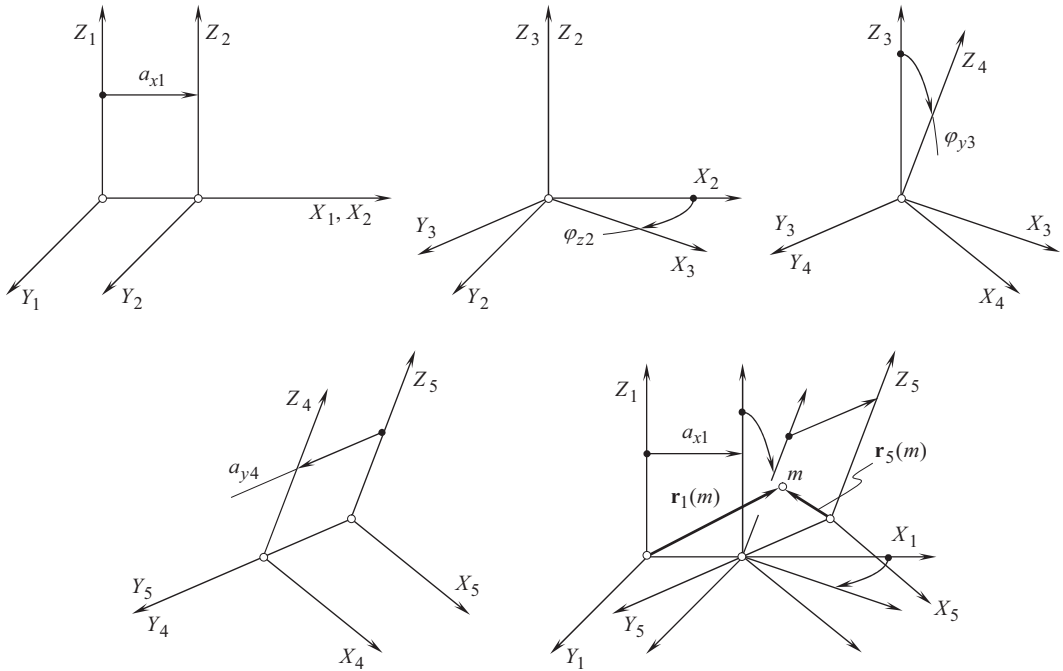


**FIGURE D.7** An example of the resultant coordinate system transformation, analytically expressed by the operator  $\mathbf{Rs}(1 \mapsto 5)$ .

When the operator  $\mathbf{Rs}(1 \mapsto t)$  of the resultant coordinate system transformation is specified, then the transition in the opposite direction can be performed by means of the operator  $\mathbf{Rs}(t \mapsto 1)$  of the inverse coordinate system transformation. The following equality can be easily proven:

$$\mathbf{Rs}(t \mapsto 1) = \mathbf{Rs}^{-1}(1 \mapsto t) \quad (\text{D.21})$$

In the above example illustrated in Figure D.7, the operator  $\mathbf{Rs}(5 \mapsto 1)$  of the inverse resultant coordinate system transformation can be expressed in terms of the operator  $\mathbf{Rs}(1 \mapsto 5)$  of the direct resultant coordinate system transformation. Following Eq. (D.21), one can come up with the equation:

$$\mathbf{Rs}(5 \mapsto 1) = \mathbf{Rs}^{-1}(1 \mapsto 5) \quad (\text{D.22})$$

It is easy to show that the operator  $\mathbf{Rs}(1 \mapsto t)$  of the resultant coordinate system transformation allows for representation in the following form:

$$\mathbf{Rs}(1 \mapsto t) = \mathbf{Tr}(a, A) \cdot \mathbf{Eu}(\psi, \theta, \varphi) \quad (\text{D.23})$$

The linear transformation  $\mathbf{Rs}(1 \mapsto t)$  [see Eq. (D.23)] can also be expressed in terms of rotation about an axis  $\mathbf{Rt}(\varphi_A, A)$ , not through the origin [see Eq. (D.16)].

## D.2 COMPLEX COORDINATE SYSTEM TRANSFORMATION

In particular cases of complex coordinate system transformations that are repeatedly used in practice, special-purpose operators of coordinate system transformation can be composed of elementary operators of translation and operators of rotation.

### D.2.1 LINEAR TRANSFORMATION DESCRIBING A SCREW MOTION ABOUT A COORDINATE AXIS

Operators for the analytical description of screw motions about an axis of the *Cartesian* coordinate system are a particular case of the operators of the resultant coordinate system transformation.

By definition (see Figure D.8), the operator  $\mathbf{Sc}_x(\varphi_x, p_x)$  of a screw motion about  $X$  – axis of the *Cartesian* coordinate system  $XYZ$  is equal to:

$$\mathbf{Sc}_x(\varphi_x, p_x) = \mathbf{Rt}(\varphi_x, X) \cdot \mathbf{Tr}(a_x, X) \quad (\text{D.24})$$

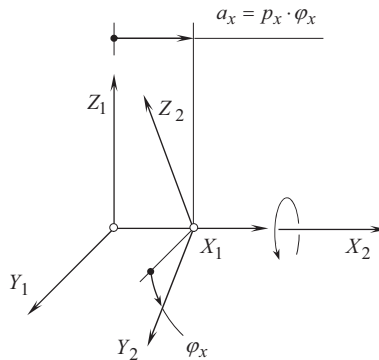


FIGURE D.8 On analytical description of the operator of screw motion,  $\mathbf{Sc}_x(\varphi_x, p_x)$ .

After substituting of the operator of translation  $\mathbf{Tr}(a_x, X)$ , and the operator of rotation  $\mathbf{Rt}(\varphi_x, X)$  [see Eq. (D.10)], Eq. (D.24) casts into the expression:

$$\mathbf{Sc}_x(\varphi_x, p_x) = \begin{bmatrix} 1 & 0 & 0 & p_x \cdot \varphi_x \\ 0 & \cos \varphi_x & \sin \varphi_x & 0 \\ 0 & -\sin \varphi_x & \cos \varphi_x & 0 \\ 0 & 0 & 0 & 1 \end{bmatrix} \quad (\text{D.25})$$

for the calculation of the operator of the screw motion  $\mathbf{Sc}_x(\varphi_x, p_x)$  about  $X$  – axis.

The operators of screw motions  $\mathbf{Sc}_y(\varphi_y, p_y)$  and  $\mathbf{Sc}_z(\varphi_z, p_z)$  about  $Y$  – and  $Z$  – axis correspondingly are defined in a way similar to that, the operator of the screw motion  $\mathbf{Sc}_x(\varphi_x, p_x)$  is defined:

$$\mathbf{Sc}_y(\varphi_y, p_y) = \mathbf{Rt}(\varphi_y, Y) \cdot \mathbf{Tr}(a_y, Y) \quad (\text{D.26})$$

$$\mathbf{Sc}_z(\varphi_z, p_z) = \mathbf{Rt}(\varphi_z, Z) \cdot \mathbf{Tr}(a_z, Z) \quad (\text{D.27})$$

Using Eqs. (D.5) and (D.6) together with Eqs. (D.11) and (D.12), one can come up with the expressions:

$$\mathbf{Sc}_y(\varphi_y, p_y) = \begin{bmatrix} \cos \varphi_y & 0 & -\sin \varphi_y & 0 \\ 0 & 1 & 0 & p_y \cdot \varphi_y \\ \sin \varphi_y & 0 & \cos \varphi_y & 0 \\ 0 & 0 & 0 & 1 \end{bmatrix} \quad (\text{D.28})$$

$$\mathbf{Sc}_z(\varphi_z, p_z) = \begin{bmatrix} \cos \varphi_z & \sin \varphi_z & 0 & 0 \\ -\sin \varphi_z & \cos \varphi_z & 0 & 0 \\ 0 & 0 & 1 & p_z \cdot \varphi_z \\ 0 & 0 & 0 & 1 \end{bmatrix} \quad (\text{D.29})$$

for the calculation of the operators of the screw motion  $\mathbf{Sc}_y(\varphi_y, p_y)$  and  $\mathbf{Sc}_z(\varphi_z, p_z)$  about  $Y$  – and  $Z$  – axis.

Screw motions about a coordinate axis as well as screw surfaces are common in the theory of part surface generation. This makes it practical to use the operators of the screw motion  $\mathbf{Sc}_x(\varphi_x, p_x)$ ,  $\mathbf{Sc}_y(\varphi_y, p_y)$ , and  $\mathbf{Sc}_z(\varphi_z, p_z)$  in the theory of part surface generation.

In case of necessity, an operator of the screw motion about an arbitrary axis either through the origin of the coordinate system or not through the origin of the coordinate system can be derived following the method similar to that used for the derivation of the operators  $\mathbf{Sc}_x(\varphi_x, p_x)$ ,  $\mathbf{Sc}_y(\varphi_y, p_y)$  and  $\mathbf{Sc}_z(\varphi_z, p_z)$ .

## D.2.2 LINEAR TRANSFORMATION DESCRIBING ROLLING MOTION OF A COORDINATE SYSTEM

One more practical combination of a rotation and of a translation is often used in the theory of part surface generation.

Consider a *Cartesian* coordinate system  $X_1Y_1Z_1$  (see Figure D.9). The coordinate system  $X_1Y_1Z_1$  is traveling in the direction of  $X_1$  – axis. Velocity of the translation is denoted by  $V$ . The coordinate system  $X_1Y_1Z_1$  is rotating about its  $Y_1$  – axis simultaneously with the translation. Speed of the rotation is denoted as  $\omega$ . Assume that the ratio  $V/\omega$  is constant. Under such a scenario, the resultant motion of the reference system  $X_1Y_1Z_1$  to its arbitrary position  $X_2Y_2Z_2$  allows interpretation in the

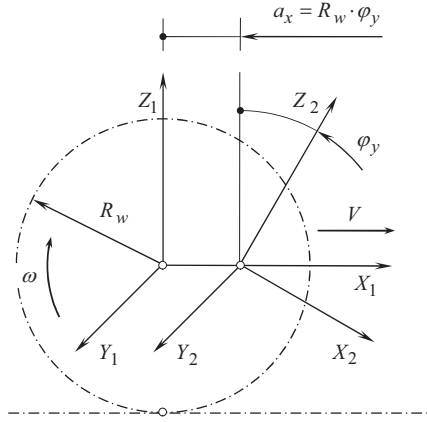


**FIGURE D.9** Illustration of transformation of rolling,  $\mathbf{Rl}_x(\varphi_y, Y)$ , of a coordinate system.

form of rolling with no sliding of a cylinder of radius  $R_w$  over the plane. The plane is parallel to the coordinate  $X_1Y_1$  – plane, and it is remote from it at the distance  $R_w$ . For the calculation of radius of the rolling cylinder, the expression  $R_w = V/\omega$  can be used.

Due to the rolling of the cylinder of a radius,  $R_w$ , over the plane is performed with no sliding, a certain correspondence between the translation and the rotation of the coordinate system is established. When the coordinate system turns through a certain angle  $\varphi_y$ , then the translation of origin of the coordinate system along  $X_1$  – axis is equal to  $a_x = \varphi_y \cdot R_w$ .

Transition from the coordinate system  $X_1Y_1Z_1$  to the coordinate system  $X_2Y_2Z_2$  can be analytically described by the operator of the resultant coordinate system transformation  $\mathbf{Rs}(1 \mapsto 2)$ . The  $\mathbf{Rs}(1 \mapsto 2)$  is equal:

$$\mathbf{Rs}(1 \mapsto 2) = \mathbf{Rt}(\varphi_y, Y_1) \cdot \mathbf{Tr}(a_x, X_1) \quad (\text{D.30})$$

Here  $\mathbf{Tr}(a_x, X_1)$  designates the operator of the translation along  $X_1$  – axis, and  $\mathbf{Rt}(\varphi_y, Y_1)$  is the operator of the rotation about  $Y_1$  – axis.

Operator of the resultant coordinate system transformation of the kind [see Eq. (D.30)] is referred to as the *operator of rolling motion over a plane*.

When the translation is performed along the  $X_1$  – axis, and the rotation is performed about the  $Y_1$  – axis, the operator of rolling is denoted as  $\mathbf{Rl}_x(\varphi_y, Y)$ . In this particular case, the equality  $\mathbf{Rl}_x(\varphi_y, Y) = \mathbf{Rs}(1 \mapsto 2)$  [see Eq. (D.30)] is valid. Based on this equality, the operator of rolling over a plane  $\mathbf{Rl}_x(\varphi_y, Y)$  can be calculated from the equation:

$$\mathbf{Rl}_x(\varphi_y, Y) = \begin{bmatrix} \cos \varphi_y & 0 & -\sin \varphi_y & a_x \cdot \cos \varphi_y \\ 0 & 1 & 0 & 0 \\ \sin \varphi_y & 0 & \cos \varphi_y & a_x \cdot \sin \varphi_y \\ 0 & 0 & 0 & 1 \end{bmatrix} \quad (\text{D.31})$$

While rotation remains about the  $Y_1$  – axis, the translation can be performed not along the  $X_1$  – axis, but along the  $Z_1$  – axis instead. For rolling of this kind, the operator of rolling is equal:

$$\mathbf{Rl}_z(\varphi_y, Y) = \begin{bmatrix} \cos \varphi_y & 0 & -\sin \varphi_y & -a_z \cdot \sin \varphi_y \\ 0 & 1 & 0 & 0 \\ \sin \varphi_y & 0 & \cos \varphi_y & a_z \cdot \cos \varphi_y \\ 0 & 0 & 0 & 1 \end{bmatrix} \quad (\text{D.32})$$

For the cases when the rotation is performed about the  $X_1$  – axis, the corresponding operators of rolling are as follows:

$$\mathbf{Rl}_y(\varphi_x, X) = \begin{bmatrix} 1 & 0 & 0 & 0 \\ 0 & \cos \varphi_x & \sin \varphi_x & a_y \cdot \cos \varphi_x \\ 0 & -\sin \varphi_x & \cos \varphi_x & -a_y \cdot \sin \varphi_x \\ 0 & 0 & 0 & 1 \end{bmatrix} \quad (\text{D.33})$$

for the case of rolling along the  $Y_1$  – axis, and

$$\mathbf{Rl}_z(\varphi_x, X) = \begin{bmatrix} 1 & 0 & 0 & 0 \\ 0 & \cos \varphi_x & \sin \varphi_x & a_z \cdot \sin \varphi_x \\ 0 & -\sin \varphi_x & \cos \varphi_x & a_z \cdot \cos \varphi_x \\ 0 & 0 & 0 & 1 \end{bmatrix} \quad (\text{D.34})$$

for the case of rolling along the  $Z_1$  – axis.

Similar expressions can be derived for the case of rotation about the  $Z_1$  – axis:

$$\mathbf{Rl}_x(\varphi_z, Z) = \begin{bmatrix} \cos \varphi_z & \sin \varphi_z & 0 & a_x \cdot \cos \varphi_z \\ -\sin \varphi_z & \cos \varphi_z & 0 & a_x \cdot \sin \varphi_z \\ 0 & 0 & 1 & 0 \\ 0 & 0 & 0 & 1 \end{bmatrix} \quad (\text{D.35})$$

$$\mathbf{Rl}_y(\varphi_z, Z) = \begin{bmatrix} \cos \varphi_z & \sin \varphi_z & 0 & a_y \cdot \sin \varphi_z \\ -\sin \varphi_z & \cos \varphi_z & 0 & a_y \cdot \cos \varphi_z \\ 0 & 0 & 1 & 0 \\ 0 & 0 & 0 & 1 \end{bmatrix} \quad (\text{D.36})$$

Use of the operators of rolling Eqs. (D.31)–(D.36) significantly simplifies the analytical description of the coordinate system transformations.

### D.2.3 LINEAR TRANSFORMATION DESCRIBING ROLLING OF TWO COORDINATE SYSTEMS

In the theory of part surface generation, combinations of two rotations about parallel axes are of particular interest.

As an example, consider two *Cartesian* coordinate systems  $X_1Y_1Z_1$  and  $X_2Y_2Z_2$  shown in Figure D.10. The coordinate systems  $X_1Y_1Z_1$  and  $X_2Y_2Z_2$  are rotated about their axes  $Z_1$  and  $Z_2$ . The axes of the rotations are parallel to each other ( $Z_1 \parallel Z_2$ ). The rotations  $\omega_1$  and  $\omega_2$  of the coordinate systems can be interpreted so that a circle of a certain radius  $R_1$  that is associated with the coordinates system  $X_1Y_1Z_1$ , is rolling with no sliding over a circle of the corresponding radius  $R_2$  that is associated with the coordinate system  $X_2Y_2Z_2$ . When the center-distance  $C$  is known, then radii,  $R_1$  and  $R_2$ , of the circles (that is, of centrodes) can be expressed in terms of the center-distance,  $C$ , and of the given rotations,  $\omega_1$  and  $\omega_2$ . For the calculations, the following formulae:

$$R_1 = C \cdot \frac{1}{1 + u} \quad (\text{D.37})$$

$$R_2 = C \cdot \frac{u}{1 + u} \quad (\text{D.38})$$

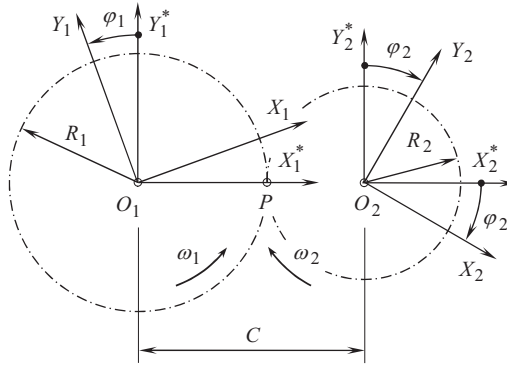


**FIGURE D.10** On derivation of the operator of rolling,  $\mathbf{Rr}_u(\varphi_1, Z_1)$ , of two coordinate systems.

can be used. Here, the ratio  $\omega_1/\omega_2$  is denoted by  $u$ .

In the initial configuration, the  $X_1$  – and  $X_2$  – axes align to each other. The  $Y_1$  – and  $Y_2$  – axes are parallel to each other. As shown in Figure D.10, the initial configuration of the coordinate systems  $X_1Y_1Z_1$  and  $X_2Y_2Z_2$  is labeled as  $X_1^*Y_1^*Z_1^*$ , and  $X_2^*Y_2^*Z_2^*$ , correspondingly.

When the coordinate system  $X_1Y_1Z_1$  turns through a certain angle  $\varphi_1$ , then the coordinate system  $X_2Y_2Z_2$  turns through the corresponding angle  $\varphi_2$ . When the angle  $\varphi_1$  is known then the corresponding angle  $\varphi_2$  is equal to  $\varphi_2 = \varphi_1/u$ .

Transition from the coordinate system  $X_2Y_2Z_2$  to the coordinate system  $X_1Y_1Z_1$  can be analytically described by the operator of the resultant coordinate system transformation  $\mathbf{Rs}(1 \mapsto 2)$ . In the case under consideration, the operator  $\mathbf{Rs}(1 \mapsto 2)$  can be expressed in terms of the operators of the elementary coordinate system transformations:

$$\mathbf{Rs}(1 \mapsto 2) = \mathbf{Rt}(\varphi_1, Z_1) \cdot \mathbf{Rt}(\varphi_1/u, Z_1) \cdot \mathbf{Tr}(-C, X_1) \quad (\text{D.39})$$

Other equivalent combinations of the operators of elementary coordinate system transformations can result in that same operator  $\mathbf{Rs}(1 \mapsto 2)$  of the resultant coordinate system transformation. The interested reader may wish to exercise on his or her own deriving the equivalent expressions for the operator  $\mathbf{Rs}(1 \mapsto 2)$ .

The operator of the resultant coordinate system transformations of the kind [see Eq. (D.39)] are referred to as the *operators of rolling motion over a cylinder*.

When rotations are performed around the  $Z_1$  – and the  $Z_2$  – axis, the operator of rolling motion over a cylinder is designated as  $\mathbf{Rr}_u(\varphi_1, Z_1)$ . In this particular case the equality  $\mathbf{Rr}_u(\varphi_1, Z_1) = \mathbf{Rs}(1 \mapsto 2)$  [see Eq. (D.39)] is valid. Based on this equality, the operator of rolling  $\mathbf{Rr}_u(\varphi_1, Z_1)$  over a cylinder can be calculated from the equation:

$$\mathbf{Rr}_u(\varphi_1, Z_1) = \begin{bmatrix} \cos\left(\varphi_1 \cdot \frac{u+1}{u}\right) & \sin\left(\varphi_1 \cdot \frac{u+1}{u}\right) & 0 & -C \\ -\sin\left(\varphi_1 \cdot \frac{u+1}{u}\right) & \cos\left(\varphi_1 \cdot \frac{u+1}{u}\right) & 0 & 0 \\ 0 & 0 & 1 & 0 \\ 0 & 0 & 0 & 1 \end{bmatrix} \quad (\text{D.40})$$

is derived.

For the inverse transformation, the inverse operator of rolling of two coordinate systems  $\mathbf{Rr}_u(\varphi_2, Z_2)$  can be used. It is equal to  $\mathbf{Rr}_u(\varphi_2, Z_2) = \mathbf{Rr}_u^{-1}(\varphi_1, Z_1)$ . In terms of the operators of



the elementary coordinate system transformations the operator  $\mathbf{Rr}_u(\varphi_2, Z_2)$  can be expressed as follows:

$$\mathbf{Rr}_u(\varphi_2, Z_2) = \mathbf{Rt}(\varphi_1/u, Z_2) \cdot \mathbf{Rt}(\varphi_1, Z_2) \cdot \mathbf{Tr}(C, X_1) \quad (\text{D.41})$$

Other equivalent combinations of the operators of elementary coordinate system transformations can result in that same operator  $\mathbf{Rr}_u(\varphi_2, Z_2)$  of the resultant coordinate system transformation. The interested reader may wish to exercise on his or her own deriving the equivalent expressions for the operator  $\mathbf{Rr}_u(\varphi_2, Z_2)$ .

For the calculation of the operator of rolling of two coordinate systems  $\mathbf{Rr}_u(\varphi_2, Z_2)$ , the equation:

$$\mathbf{Rr}_u(\varphi_2, Z_2) = \begin{bmatrix} \cos\left(\varphi_1 \cdot \frac{u+1}{u}\right) & -\sin\left(\varphi_1 \cdot \frac{u+1}{u}\right) & 0 & C \\ \sin\left(\varphi_1 \cdot \frac{u+1}{u}\right) & \cos\left(\varphi_1 \cdot \frac{u+1}{u}\right) & 0 & 0 \\ 0 & 0 & 1 & 0 \\ 0 & 0 & 0 & 1 \end{bmatrix} \quad (\text{D.42})$$

can be used.

Similar to that the expression [see Eq. (D.40)] is derived for the calculation of the operator of rolling  $\mathbf{Rr}_u(\varphi_1, Z_1)$  around the  $Z_1$  – and  $Z_2$  – axis, corresponding formulae can be derived for the calculation of the operators of rolling  $\mathbf{Rr}_u(\varphi_1, X_1)$  and  $\mathbf{Rr}_u(\varphi_1, Y_1)$  about parallel axes  $X_1$  and  $X_2$ , as well as about parallel axes  $Y_1$  and  $Y_2$ .

The use of the operators of rolling about two axes  $\mathbf{Rr}_u(\varphi_1, X_1)$ ,  $\mathbf{Rr}_u(\varphi_1, Y_1)$  and  $\mathbf{Rr}_u(\varphi_1, Z_1)$  substantially simplifies the analytical description of the coordinate system transformations.

#### D.2.4 COUPLED LINEAR TRANSFORMATION

It is the right point to notice here that a translation,  $\mathbf{Tr}(a_x, X)$ , along the  $X$  – axis of a *Cartesian* reference system,  $XYZ$ , and a rotation,  $\mathbf{Rt}(\varphi_x, X)$ , about the axis  $X$  of that same coordinate system,  $XYZ$ , obey the commutative law, that is, these two coordinate system transformations can be performed in different order equally. This means that the operators,  $\mathbf{Cp}_x(a_x, \varphi_x)$ , of coupled linear transformations are invariant with respect to the order of the elementary transformations, namely, of the translation/rotation – this is important. It makes no difference whether the translation,  $\mathbf{Tr}(a_x, X)$ , is initially performed, which is followed by the rotation,  $\mathbf{Rt}(\varphi_x, X)$ , or the rotation,  $\mathbf{Rt}(\varphi_x, X)$ , is initially performed, which is followed by the translation,  $\mathbf{Tr}(a_x, X)$ . This is because of the dot products  $\mathbf{Rt}(\varphi_x, X) \cdot \mathbf{Tr}(a_x, X)$  and  $\mathbf{Tr}(a_x, X) \cdot \mathbf{Rt}(\varphi_x, X)$  are identical to one another:

$$\mathbf{Rt}(\varphi_x, X) \cdot \mathbf{Tr}(a_x, X) \equiv \mathbf{Tr}(a_x, X) \cdot \mathbf{Rt}(\varphi_x, X) \quad (\text{D.43})$$

This means that the translation from the coordinate system  $X_1Y_1Z_1$  to the intermediate coordinate system  $X^*Y^*Z^*$  followed by the rotation from the coordinate system  $X^*Y^*Z^*$  to the finale coordinate system  $X_2Y_2Z_2$  produces the same reference  $X_2Y_2Z_2$  as in a case when the rotation from the coordinate system  $X_1Y_1Z_1$  to the intermediate coordinate system  $X^*Y^*Z^*$  followed by the translation from the coordinate system  $X^*Y^*Z^*$  to the finale coordinate system  $X_2Y_2Z_2$ .

The validity of Eq. (D.43) is illustrated in Figure D.11. The translation,  $\mathbf{Tr}(a_x, X)$ , that is followed by the rotation,  $\mathbf{Rt}(\varphi_x, X)$ , as shown in Figure D.11a, is equivalent to the rotation,  $\mathbf{Rt}(\varphi_x, X)$ , that is followed by the translation,  $\mathbf{Tr}(a_x, X)$  as shown in Figure D.11b.

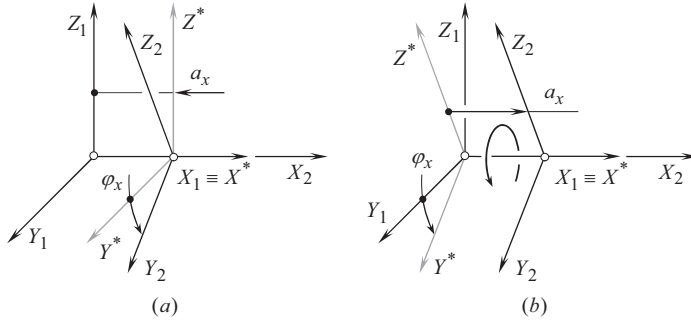


**FIGURE D.11** On the equivalency of the linear transformations  $\mathbf{Rt}(\varphi_x, X) \cdot \mathbf{Tr}(a_x, X)$  and  $\mathbf{Tr}(a_x, X) \cdot \mathbf{Rt}(\varphi_x, X)$ , that comprise the operator,  $\mathbf{Cp}_x(a_x, \varphi_x)$ , of coupled linear transformation of a *Cartesian* reference system  $XYZ$ : (a) a translation  $\mathbf{Tr}(a_x, X)$  followed by a rotation  $\mathbf{Rt}(\varphi_x, X)$ ; and (b) a rotation  $\mathbf{Rt}(\varphi_x, X)$  followed by a translation  $\mathbf{Tr}(a_x, X)$ .

Therefore, the two linear transformations,  $\mathbf{Tr}(a_x, X)$  and  $\mathbf{Rt}(\varphi_x, X)$ , can be coupled into a linear transformation:

$$\mathbf{Cp}_x(a_x, \varphi_x) = \mathbf{Rt}(\varphi_x, X) \cdot \mathbf{Tr}(a_x, X) \equiv \mathbf{Tr}(a_x, X) \cdot \mathbf{Rt}(\varphi_x, X) \quad (\text{D.44})$$

The operator of linear transformation,  $\mathbf{Cp}_x(a_x, \varphi_x)$ , can be expressed in matrix form (see Figure D.12a):

$$\mathbf{Cp}_x(a_x, \varphi_x) = \begin{bmatrix} 1 & 0 & 0 & a_x \\ 0 & \cos \varphi_x & \sin \varphi_x & 0 \\ 0 & -\sin \varphi_x & \cos \varphi_x & 0 \\ 0 & 0 & 0 & 1 \end{bmatrix} \quad (\text{D.45})$$

This expression is composed based on Eq. (D.4) for the linear transformation  $\mathbf{Tr}(a_x, X)$ , and on Eq. (D.10) that describes the linear transformation  $\mathbf{Rt}(\varphi_x, X)$ .

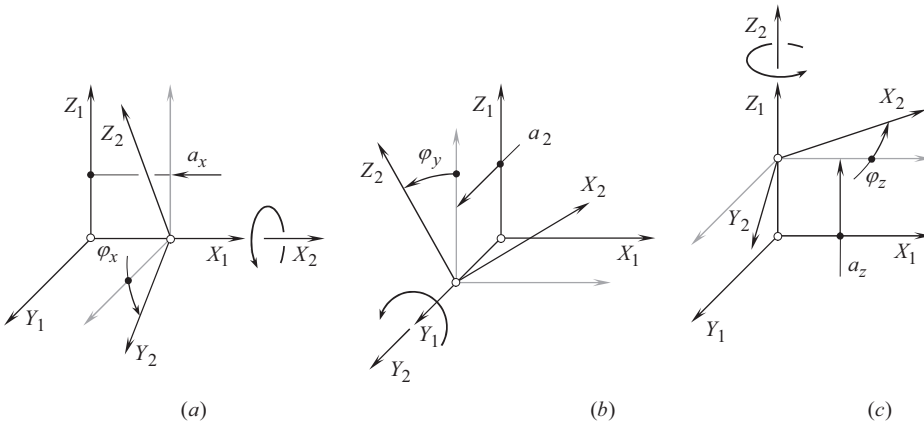


**FIGURE D.12** On the equivalency of linear transformations  $\mathbf{Rt}(\varphi_x, X) \cdot \mathbf{Tr}(a_x, X)$ ,  $\mathbf{Tr}(a_y, Y) \cdot \mathbf{Rt}(\varphi_y, Y)$ , and  $\mathbf{Tr}(a_z, Z) \cdot \mathbf{Rt}(\varphi_z, Z)$ , that comprise the operators,  $\mathbf{Cp}_x(a_x, \varphi_x)$ ,  $\mathbf{Cp}_y(a_y, \varphi_y)$ , and  $\mathbf{Cp}_z(a_z, \varphi_z)$ , of coupled linear transformation of a *Cartesian* reference system  $XYZ$ : (a) a translation  $\mathbf{Tr}(a_x, X)$  followed by a rotation  $\mathbf{Rt}(\varphi_x, X)$ ; (b) a translation  $\mathbf{Tr}(a_y, Y)$  followed by a rotation  $\mathbf{Rt}(\varphi_y, Y)$ ; and (c) a translation  $\mathbf{Tr}(a_z, Z)$  followed by a rotation  $\mathbf{Rt}(\varphi_z, Z)$ .

Two reduced cases of operator of the linear transformation,  $\mathbf{Cp}_x(a_x, \varphi_x)$ , are distinguished.

**First**, it could happen that in a particular case the component,  $a_x$ , of the translation is zero, that is  $a_x = 0$ . Under such a scenario the operator of linear transformation,  $\mathbf{Cp}_x(a_x, \varphi_x)$ , reduces to the operator of rotation,  $\mathbf{Rt}(\varphi_x, X)$ , and the equality  $\mathbf{Cp}_x(a_x, \varphi_x) = \mathbf{Rt}(\varphi_x, X)$  is observed in the case under consideration.

**Second**, it could happen that in a particular case the component,  $\varphi_x$ , of the rotation is zero, that is  $\varphi_x = 0^\circ$ . Under such a scenario the operator of linear transformation,  $\mathbf{Cp}_x(a_x, \varphi_x)$ , reduces to the operator of translation,  $\mathbf{Tr}(a_x, X)$ , and the equality  $\mathbf{Cp}_x(a_x, \varphi_x) = \mathbf{Tr}(a_x, X)$  is observed in the case under consideration.

The said is valid with respect to the translations and the rotations along and about the axes  $Y$  and  $Z$  of a *Cartesian* reference system  $XYZ$ . The corresponding coupled operators,  $\mathbf{Cp}_y(a_y, \varphi_y)$  and  $\mathbf{Cp}_z(a_z, \varphi_z)$ , for linear transformations of these kinds can also be composed (see Figure D.12b and c):

$$\mathbf{Cp}_y(a_y, \varphi_y) = \begin{bmatrix} \cos \varphi_y & 0 & \sin \varphi_y & 0 \\ 0 & 1 & 0 & a_y \\ -\sin \varphi_y & 0 & \cos \varphi_y & 0 \\ 0 & 0 & 0 & 1 \end{bmatrix} \quad (\text{D.46})$$

$$\mathbf{Cp}_z(a_z, \varphi_z) = \begin{bmatrix} \cos \varphi_z & \sin \varphi_z & 0 & 0 \\ -\sin \varphi_z & \cos \varphi_z & 0 & 0 \\ 0 & 0 & 1 & a_z \\ 0 & 0 & 0 & 1 \end{bmatrix} \quad (\text{D.47})$$

In the operators of linear transformations,  $\mathbf{Cp}_x(a_x, \varphi_x)$ ,  $\mathbf{Cp}_y(a_y, \varphi_y)$ , and  $\mathbf{Cp}_z(a_z, \varphi_z)$ , values of the translations  $a_x$ ,  $a_y$ , and  $a_z$ , as well as values of the rotations  $\varphi_x$ ,  $\varphi_y$ , and  $\varphi_z$ , are finite values (and not continuous). The linear and angular displacements do not correlate to one another in time; thus, they do not comprise a screw. They are just a kind of couples of a translation along, and a rotation about a coordinate axis of a *Cartesian* reference system.

Introduction of the operators of linear transformation,  $\mathbf{Cp}_x(a_x, \varphi_x)$ ,  $\mathbf{Cp}_y(a_y, \varphi_y)$ , and  $\mathbf{Cp}_z(a_z, \varphi_z)$ , makes the linear transformations easier as all the operators of the linear transformations become uniform.

The operators of linear transformation  $\mathbf{Cp}_x(a_x, \varphi_x)$ ,  $\mathbf{Cp}_y(a_y, \varphi_y)$ , and  $\mathbf{Cp}_z(a_z, \varphi_z)$ , do not obey the commutative law. This is because rotation is not a vector by nature. Therefore, special care should be undertaken when treating rotations as vectors – when implementing coupled operators of linear transformations in particular.

The operators of coupled linear transformations  $\mathbf{Cp}_x(a_x, \varphi_x)$ ,  $\mathbf{Cp}_y(a_y, \varphi_y)$ , and  $\mathbf{Cp}_z(a_z, \varphi_z)$ , [see Eq. (D.45) through Eq. (D.47)] can be used for the purpose of analytical description of a resultant coordinate system transformation. Under such a scenario, the operator,  $\mathbf{Rs}(1 \mapsto t)$ , of a resultant coordinate system transformation can be expressed in terms of all the operators  $\mathbf{Cp}_x(a_x, \varphi_x)$ ,  $\mathbf{Cp}_y(a_y, \varphi_y)$ , and  $\mathbf{Cp}_z(a_z, \varphi_z)$  by the following expression:

$$\mathbf{Rs}(1 \mapsto t) = \prod_{\substack{i=1 \\ j=x,y,z}}^{t-1} \mathbf{Cp}_j^i(a_j^i, \varphi_j^i) \quad (\text{D.48})$$

In Eq. (D.48), only operators of coupled linear transformations are used.

### D.2.5 AN EXAMPLE OF NON-ORTHOGONAL LINEAR TRANSFORMATION

Consider a non-orthogonal reference system  $X_1Y_1Z_1$  having certain angle  $\omega_1$  between the axes  $X_1$  and  $Y_1$ . Axis  $Z_1$  is perpendicular to the coordinate plane  $X_1Y_1$ . Another reference system  $X_2Y_2Z_2$  is

identical to the first coordinate system  $X_1Y_1Z_1$ , and is turned about  $Z_1$  – axis through a certain angle  $\varphi$ . Transition from the reference system  $X_1Y_1Z_1$  to the reference system  $X_2Y_2Z_2$  can be analytically described by the operator of linear transformation:

$$\mathbf{Rt}_\omega(1 \rightarrow 2) = \begin{bmatrix} \frac{\sin(\omega_1 + \varphi)}{\sin \omega_1} & \frac{\sin \varphi}{\sin \omega_1} & 0 & 0 \\ -\frac{\sin \varphi}{\sin \omega_1} & \frac{\sin(\omega_1 - \varphi)}{\sin \omega_1} & 0 & 0 \\ 0 & 0 & 1 & 0 \\ 0 & 0 & 0 & 1 \end{bmatrix} \quad (\text{D.49})$$

In order to distinguish the operator of rotation in the orthogonal linear transformation  $\mathbf{Rt}(1 \rightarrow 2)$  from the similar operator of rotation in a non-orthogonal linear transformation  $\mathbf{Rt}_\omega(1 \rightarrow 2)$ , the subscript “ $\omega$ ” is assigned to the last.

When  $\omega = 90^\circ$ , Eq. (D.49) casts into Eq. (D.12).

### D.2.6 CONVERSION OF A COORDINATE SYSTEM HAND

Application of matrix method of coordinate system transformation presumes that both of the reference systems “ $i$ ” and “ $(i \pm 1)$ ” are of the same hand. This means that it is assumed from the very beginning that both of them are either right-hand-, or left-hand-oriented *Cartesian* coordinate systems. In the event the coordinate systems  $i$  and  $(i \pm 1)$  are of the opposite hand, say one of them is the right-hand-oriented coordinate system while another one is a left-hand-oriented coordinate system, then one of the coordinate systems must be converted into the oppositely oriented *Cartesian* coordinate system.

For the conversion of a left-hand-oriented *Cartesian* coordinate system into a right-hand-oriented coordinate system or vice versa, the operators of reflection are commonly used.

In order to change the direction of  $X_i$  axis of the initial coordinate system  $i$  to the opposite direction (in this case in the new coordinate system  $(i \pm 1)$  the equalities  $X_{i\pm 1} = -X_i$ ,  $Y_{i\pm 1} \equiv Y_i$  and  $Z_{i\pm 1} \equiv Z_i$  are observed) the operator of reflection  $\mathbf{Rf}_x(Y_i Z_i)$  can be applied. The operator of reflection yields representation in matrix form:

$$\mathbf{Rf}_x(Y_i Z_i) = \begin{bmatrix} -1 & 0 & 0 & 0 \\ 0 & 1 & 0 & 0 \\ 0 & 0 & 1 & 0 \\ 0 & 0 & 0 & 1 \end{bmatrix} \quad (\text{D.50})$$

Similarly, implementation of the operators of reflections  $\mathbf{Rf}_y(X_i Z_i)$  and  $\mathbf{Rf}_z(X_i Y_i)$  change the directions of  $Y_i$  axis and  $Z_i$  axes onto opposite directions. The operators of reflections  $\mathbf{Rf}_y(X_i Z_i)$  and  $\mathbf{Rf}_z(X_i Y_i)$  can be expressed analytically in the form:

$$\mathbf{Rf}_y(X_i Z_i) = \begin{bmatrix} 1 & 0 & 0 & 0 \\ 0 & -1 & 0 & 0 \\ 0 & 0 & 1 & 0 \\ 0 & 0 & 0 & 1 \end{bmatrix} \quad (\text{D.51})$$

$$\mathbf{Rf}_z(X_i Y_i) = \begin{bmatrix} 1 & 0 & 0 & 0 \\ 0 & 1 & 0 & 0 \\ 0 & 0 & -1 & 0 \\ 0 & 0 & 0 & 1 \end{bmatrix} \quad (\text{D.52})$$

A linear transformation that reverses direction of the coordinate axis is an *opposite transformation*. Transformation of reflection is an example of *orientation-reversing transformation*.

### D.3 USEFUL EQUATIONS

The sequence of the successive rotations can vary depending on the intention of the researcher. Several special types of successive rotations are known, including *Eulerian transformation*, *Cardanian transformation*, two kinds of *Euler-Krylov transformations*, and so forth. The sequence of the successive rotations can be chosen from a total of 12 different combinations. Even though the *Cardanian transformation* is different from the *Eulerian transformation* in terms of the combination of the rotations, they both use a similar approach to calculate the orientation angles.

#### D.3.1 RPY-TRANSFORMATION

A series of rotations can be performed in the order *roll matrix*, ( $R$ ), by *pitch matrix* ( $P$ ), and finally by *yaw matrix*, ( $Y$ ). The linear transformation of this kind is commonly referred to as *RPY – transformation*. The resultant transformation of this kind can be represented by the homogenous coordinate transformation matrix:

$$\mathbf{RPY}(\varphi_x, \varphi_y, \varphi_z) = \begin{bmatrix} \cos \varphi_y \cos \varphi_z + \sin \varphi_x \sin \varphi_y \sin \varphi_z & \cos \varphi_y \sin \varphi_z - \sin \varphi_x \sin \varphi_y \cos \varphi_z & \cos \varphi_x \sin \varphi_y & 0 \\ -\cos \varphi_x \sin \varphi_z & \cos \varphi_x \cos \varphi_z & \sin \varphi_x & 0 \\ \sin \varphi_x \cos \varphi_y \sin \varphi_z - \sin \varphi_y \cos \varphi_z & -\sin \varphi_x \cos \varphi_y \cos \varphi_z - \cos \varphi_y \sin \varphi_z & \cos \varphi_x \cos \varphi_y & 0 \\ 0 & 0 & 0 & 1 \end{bmatrix} \quad (\text{D.53})$$

The *RPY – transformation* can be used for solving problems in the field of part surface generation.

#### D.3.2 OPERATOR OF ROTATION ABOUT AN AXIS IN SPACE

A spatial rotation operator for the rotational transformation of a point about a unit axis  $\mathbf{a}_0(\cos \alpha, \cos \beta, \cos \gamma)$  passing through the origin of the coordinate system can be described as follows, with  $\mathbf{a}_0 = \mathbf{A}_0 / |\mathbf{A}_0|$  designating the unit vector along the axis of rotation  $\mathbf{A}_0$ .

Suppose the angle of rotation of the point about  $\mathbf{a}_0$  is  $\theta$ , the *rotation operator* is expressed by:

$$\mathbf{Rt}(\theta, \mathbf{a}_0) = \begin{bmatrix} (1 - \cos \theta) \cos^2 \alpha + \cos \theta & (1 - \cos \theta) \cos \alpha \cos \beta - \sin \theta \cos \gamma \\ (1 - \cos \theta) \cos \alpha \cos \beta + \sin \theta \cos \gamma & (1 - \cos \theta) \cos^2 \beta + \cos \theta \\ (1 - \cos \theta) \cos \alpha \cos \gamma - \sin \theta \cos \beta & (1 - \cos \theta) \cos \beta \cos \gamma + \sin \theta \cos \alpha \\ 0 & 0 \\ (1 - \cos \theta) \cos \alpha \cos \gamma + \sin \theta \cos \beta & 0 \\ (1 - \cos \theta) \cos \beta \cos \gamma - \sin \theta \cos \alpha & 0 \\ (1 - \cos \theta) \cos^2 \gamma + \cos \theta & 0 \\ 0 & 1 \end{bmatrix} \quad (\text{D.54})$$

Solution to a problem in the field of part surface generation can be significantly simplified by the implementation of the rotational operator  $\mathbf{Rt}(\theta, \mathbf{a}_0)$  [see Eq. (D.54)].

### D.3.3 COMBINED LINEAR TRANSFORMATION

Suppose a point,  $p$ , on a rigid body rotates with an angular displacement,  $\theta$ , about an axis along a unit vector,  $\mathbf{a}_0$ , passing through the origin of the coordinate system at first, and then followed by a translation at a distance,  $B$ , in the direction of a unit vector,  $\mathbf{b}$ . The linear transformation of this kind can be analytically described by the homogenous matrix

$$\mathbf{Rt}(\theta_{\mathbf{a}_0}, B_{\mathbf{b}}) = \begin{bmatrix} (1 - \cos \theta) \cos^2 \alpha + \cos \theta & (1 - \cos \theta) \cos \alpha \cos \beta - \sin \theta \cos \gamma & & & \\ (1 - \cos \theta) \cos \alpha \cos \beta + \sin \theta \cos \gamma & (1 - \cos \theta) \cos^2 \beta + \cos \theta & & & \\ (1 - \cos \theta) \cos \alpha \cos \gamma - \sin \theta \cos \beta & (1 - \cos \theta) \cos \beta \cos \gamma + \sin \theta \cos \alpha & & & \\ 0 & 0 & & & \\ & (1 - \cos \theta) \cos \alpha \cos \gamma + \sin \theta \cos \beta & B \cos \alpha & & \\ & (1 - \cos \theta) \cos \beta \cos \gamma - \sin \theta \cos \alpha & B \cos \beta & & \\ & (1 - \cos \theta) \cos^2 \gamma + \cos \theta & B \cos \gamma & & \\ & 0 & 1 & & \end{bmatrix} \quad (\text{D.55})$$

More operators of particular linear transformations can be found in the literature.

## D.4 CHAINS OF CONSEQUENT LINEAR TRANSFORMATIONS AND A CLOSED LOOP OF CONSEQUENT COORDINATE SYSTEMS TRANSFORMATIONS

Consequent coordinate system transformations form chains (circuits) of linear transformations. The elementary chain of coordinate system transformation is composed of two consequent transformations. Chains of linear transformations play an important role in the theory of part surface generation.

Two different kinds of chains of consequent coordinate system transformations are distinguished.

**First**, transition from the coordinate system  $X_g Y_g Z_g$  associated with the gear tooth flank,  $\mathcal{S}$ , to the local *Cartesian* coordinate system  $x_g y_g z_g$  having the origin at a point,  $K$ , of contact of the gear tooth flank,  $\mathcal{S}$ , and of the pinion tooth flank,  $\mathcal{P}$ . This linear transformation is also made up of numerous operators of intermediate coordinate system transformations ( $X_{in} Y_{in} Z_{in}$ ). It forms a chain of direct consequent coordinate system transformations illustrated in Figure D.13a.

The local coordinate system,  $x_g y_g z_g$ , is associated with the gear tooth flank,  $\mathcal{S}$ . The operator  $\mathbf{Rs}(\mathcal{S} \rightarrow K_g)$  of the resultant coordinate system transformation for a direct chain of the linear transformations can be composed using for this purpose a certain number of the operators of translations [see Eq. (D.4) through Eq. (D.6)], and a corresponding number of the operators of rotations [see Eq. (D.10) through Eq. (D.12)].

**Second**, transition from the coordinate system,  $X_g Y_g Z_g$ , to the local *Cartesian* coordinate system,  $x_p y_p z_p$ , with the origin at a point  $K$  of contact of the tooth flanks,  $\mathcal{S}$  and  $\mathcal{P}$ . The local coordinate system,  $x_p y_p z_p$ , is associated to pinion tooth flank,  $\mathcal{P}$ . This linear transformation is also made up of numerous intermediate coordinate system transformations ( $X_j Y_j Z_j$ ), for example, transitions from the coordinate system  $X_h Y_h Z_h$  associated with gear housing, to numerous intermediate coordinate system  $X_i Y_i Z_i$ . The linear transformation of this kind forms a chain of inverse consequent coordinate system transformations shown in Figure D.13b). The operator  $\mathbf{Rs}(\mathcal{S} \rightarrow K_p)$  of the resultant coordinate system

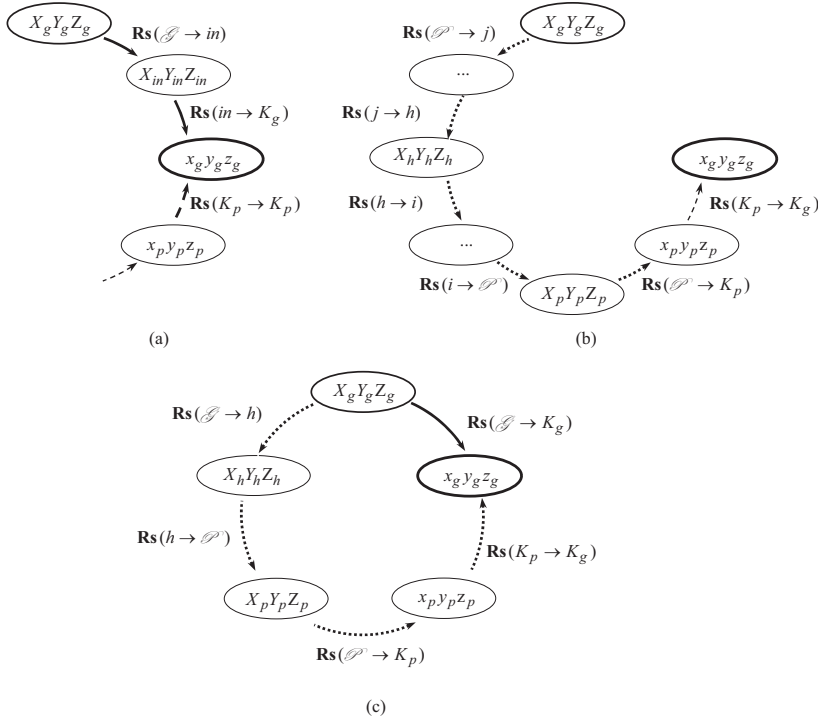


**FIGURE D.13** An example of direct chain (a), of reverse chain (b), and a closed loop (c) of consequent coordinate system transformations.

transformations for the inverse chain of transformations can be composed using for this purpose a certain number of the operators of translations [see Eq. (D.4), Eq. (D.5), and Eq. (D.6)], and a corresponding number of the operators of rotations [see Eq. (D.10) through Eq. (D.12)].

Chains of the direct and of the reverse consequent coordinate system transformations together with the operator of transition from the local coordinate system,  $x_p y_p z_p$ , to the local coordinate system,  $x_g y_g z_g$ , form a closed loop (a closed circuit) of the consequent coordinate system transformations depicted in Figure D.13c.

If a closed loop of the consequent coordinate system transformations is complete, implementation of a certain number of the operators of translations [see Eqs. (D.4)–(D.6)], and a corresponding number of the operators of rotations [see Eqs. (D.10)–(D.12)] returns a result that is identical to the input data. This means that the analytical description of a meshing process specified in the original coordinate system remains the same after the implementation of the operator of the resultant coordinate system transformations. This condition is the necessary and sufficient condition for the existence of a closed loop of consequent coordinate system transformations.

Implementation of the chains, as well as of the closed loops of consequent coordinate system transformations makes it possible consideration of the meshing process of the teeth flanks,  $\mathcal{S}$  and  $\mathcal{P}$ , in any and all of reference systems that make up the loop. Therefore, for consideration of a particular problem of part surface generation, the most convenient reference system can be chosen.

In order to complete the construction of a closed loop of a consequent coordinate system transformations, an operator of transformation from the local coordinate system,  $x_p y_p z_p$ , to the local coordinate system,  $x_g y_g z_g$ , must be composed. Usually, the local reference systems,  $x_g y_g z_g$  and  $x_p y_p z_p$ , are the kind of semi-orthogonal coordinate systems. This means that the axis,  $z_p$ , is always



orthogonal to the coordinate plane,  $x_g y_g$ , while the axes,  $x_g$  and  $y_g$ , can be either orthogonal or not orthogonal to each other. The same is valid with respect to the local coordinate system,  $x_p y_p z_p$ .

Two possible ways for performing the required transformation of the local reference systems,  $x_g y_g z_g$  and  $x_p y_p z_p$ , are considered below.

Following the first way, the operator  $\mathbf{Rt}_\omega(p \rightarrow g)$  of the linear transformation of semi-orthogonal coordinate systems (see Figure D.14) must be composed. The operator  $\mathbf{Rt}_\omega(p \rightarrow g)$  can be represented in the form of the homogenous matrix:

$$\mathbf{Rt}_\omega(p \rightarrow g) = \begin{bmatrix} \frac{\sin(\omega_p + \alpha)}{\sin \omega_p} & -\frac{\sin(\omega_g - \omega_p - \alpha)}{\sin \omega_p} & 0 & 0 \\ -\frac{\sin \alpha}{\sin \omega_p} & \frac{\sin(\omega_g - \alpha)}{\sin \omega_p} & 0 & 0 \\ 0 & 0 & -1 & 0 \\ 0 & 0 & 0 & 1 \end{bmatrix} \quad (\text{D.56})$$

Here is designated:

$\omega_g$  is the angle that makes  $U_g$  and  $V_g$  coordinate lines on the gear tooth flank,  $\mathcal{G}$ .

$\omega_p$  is the angle that makes  $U_p$  and  $V_p$  coordinate lines on the pinion tooth flank,  $\mathcal{P}$ .

$\alpha$  is the angle that makes the axes,  $x_g$  and  $x_p$ , of the local coordinate systems  $x_g y_g z_g$  and  $x_p y_p z_p$ .

The auxiliary angle  $\beta$  in Figure D.14 is equal to  $\beta = \omega_T + \alpha$ .

The inverse coordinate system transformation, that is, the transformation from the local coordinate system,  $x_g y_g z_g$ , to the local coordinate system,  $x_p y_p z_p$ , can be analytically described by the operator  $\mathbf{Rt}_\omega(g \rightarrow p)$  of the inverse coordinate system transformation. The operator  $\mathbf{Rt}_\omega(g \rightarrow p)$  can be represented in the form of the homogenous matrix:

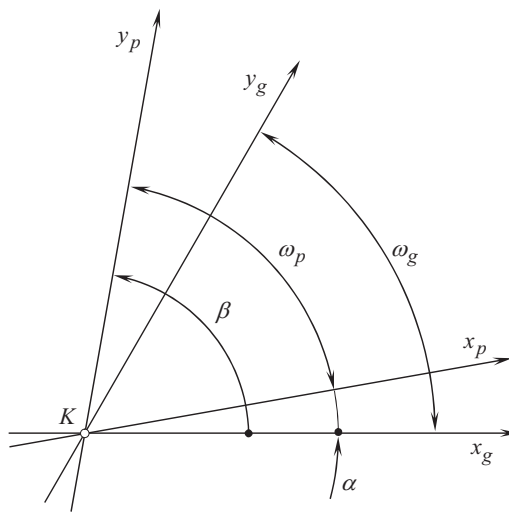


**FIGURE D.14** Local coordinate systems,  $x_g y_g z_g$  and  $x_p y_p z_p$ , with the origin at contact point,  $K$ .

$$\mathbf{Rt}_\omega(g \rightarrow p) = \begin{bmatrix} \frac{\sin(\omega_g - \alpha)}{\sin \omega_g} & \frac{\sin(\omega_g - \omega_p - \alpha)}{\sin \omega_g} & 0 & 0 \\ \frac{\sin \alpha}{\sin \omega_g} & \frac{\sin(\omega_p + \alpha)}{\sin \omega_g} & 0 & 0 \\ 0 & 0 & -1 & 0 \\ 0 & 0 & 0 & 1 \end{bmatrix} \quad (\text{D.57})$$

Following the second way of transformation of the local coordinate systems, the auxiliary orthogonal local coordinate system must be constructed.

Let's consider an approach, according to which a closed loop (a closed circuit) of the consequent coordinate system transformations can be composed.

In order to construct an orthogonal normalized basis of the coordinate system  $x_g y_g z_g$ , an intermediate coordinate system  $x_1 y_1 z_1$  is used. Axis  $x_1$  of the coordinate system  $x_1 y_1 z_1$  is pointed out along the unit vector  $\mathbf{u}_g$  that is tangent to the  $U_g$  – coordinate curve (see Figure D.15). Axis  $y_1$  is directed along vector  $\mathbf{v}_g$  that is tangent to the  $V_g$  – coordinate line on the gear tooth flank,  $\mathcal{S}$ . The axis,  $z_1$ , aligns with unit normal vector,  $\mathbf{n}_g$ , and is pointed outward the gear tooth body.

For a gear tooth flank,  $\mathcal{S}$ , having orthogonal parameterization (for which  $F_g = 0$ , and therefore  $\omega_g = \pi/2$ ), analytical description of coordinate system transformations is significantly simpler. Further simplification of the coordinate system transformation is possible when the coordinate  $U_g$  – and  $V_g$  – lines are congruent to the lines of curvature on the part surface  $\mathcal{S}$ . Under such a scenario, the local coordinate system is represented by *Darboux frame*.

In order to construct *Darboux frame*, principal directions on the gear tooth flank,  $\mathcal{S}$ , must be calculated. Determination of the unit tangent vectors,  $\mathbf{t}_{1,g}$  and  $\mathbf{t}_{2,g}$ , of the principal directions on the gear tooth flank,  $\mathcal{S}$ , is considered in Appendix B.

In the common tangent plane, the orientation of the unit vector,  $\mathbf{t}_{1,g}$ , of the first principal direction on the gear tooth flank,  $\mathcal{S}$ , can be uniquely specified by the included angle,  $\xi_{1,g}$ , that the unit vector,  $\mathbf{t}_{1,g}$ , forms with the  $U_g$  – coordinate curve. This angle depends on both, on the gear tooth flank,  $\mathcal{S}$ , geometry, and on the gear tooth flank,  $\mathcal{S}$ , parameterization. Depicted in Figure D.16, is

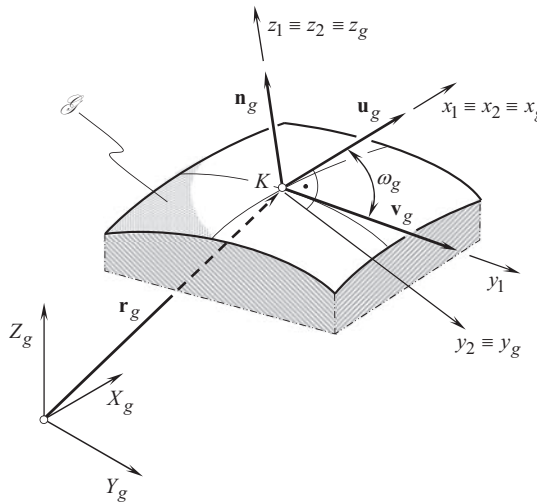
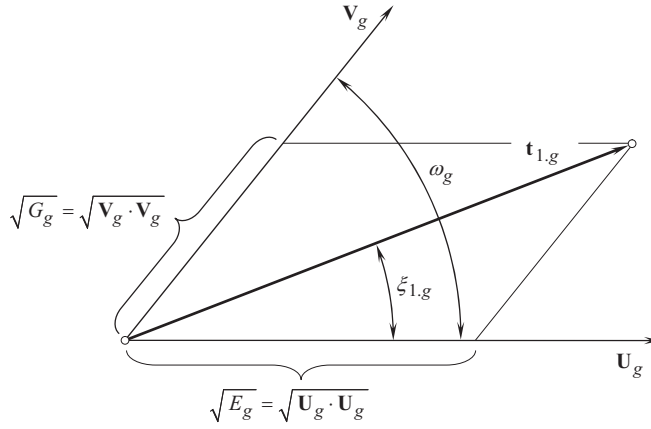


FIGURE D.15 Local coordinate system,  $x_g y_g z_g$ , associated with the gear tooth flank,  $\mathcal{S}$ .



**FIGURE D.16** Differential relationships between the tangent vectors,  $\mathbf{U}_g$  and  $\mathbf{V}_g$ , the fundamental magnitudes of the first order, the included angle,  $\xi_{1,g}$ , and the direction of the unit tangent vector,  $\mathbf{t}_{1,g}$ .

the relationship between the tangent vectors  $\mathbf{U}_g$  and  $\mathbf{V}_g$ , and the included angle  $\xi_{1,g}$ . From the law of sine's,

$$\frac{\sqrt{G_g}}{\sin \xi_{1,g}} = \frac{\sqrt{E_g}}{\sin[\pi - \xi_{1,g} - (\pi - \omega_g)]} = \frac{\sqrt{F_g}}{\sin(\omega_g - \xi_{1,g})} \quad (\text{D.58})$$

Here,  $\omega_g = \cos^{-1}(F_g / \sqrt{E_g G_g})$ .

Solving the expression above for the included angle,  $\xi_{1,g}$ , results in:

$$\xi_{1,g} = \tan^{-1} \frac{\sqrt{E_g G_g - F_g^2}}{E_g + F_g} \quad (\text{D.59})$$

Another possible way of constructing of the orthogonal local basis of the local *Cartesian* coordinate system,  $x_P y_P z_P$ , is based on the following consideration.

Consider an arbitrary non-orthogonal and not normalized basis,  $\mathbf{x}_1 \mathbf{x}_2 \mathbf{x}_3$  (see Figure D.17a). Let's construct an orthogonal and normalized basis based on the initial given basis,  $\mathbf{x}_1 \mathbf{x}_2 \mathbf{x}_3$ .

Cross product of any two of three vectors,  $\mathbf{x}_1, \mathbf{x}_2, \mathbf{x}_3$ , for example, cross product of the vectors  $\mathbf{x}_1 \times \mathbf{x}_2$ , determines a new vector,  $\mathbf{x}_4$  (see Figure D.17b). Evidently, the vector,  $\mathbf{x}_4$ , is orthogonal to the coordinate plane,  $\mathbf{x}_1 \mathbf{x}_2$ . Then, use the calculated vector,  $\mathbf{x}_4$ , and one of two original vectors,  $\mathbf{x}_1$  or  $\mathbf{x}_2$ , for instance, use the vector,  $\mathbf{x}_2$ . This yields the calculation of a new vector,  $\mathbf{x}_5 = \mathbf{x}_4 \times \mathbf{x}_2$  (see Figure D.17c). The calculated basis,  $\mathbf{x}_1 \mathbf{x}_4 \mathbf{x}_5$ , is orthogonal. In order to convert it into a normalized basis, each of the vectors,  $\mathbf{x}_1, \mathbf{x}_4$ , and  $\mathbf{x}_5$  must be divided by its magnitude:

$$\mathbf{e}_1 = \frac{\mathbf{x}_1}{|\mathbf{x}_1|} \quad (\text{D.60})$$

$$\mathbf{e}_4 = \frac{\mathbf{x}_4}{|\mathbf{x}_4|} \quad (\text{D.61})$$

$$\mathbf{e}_5 = \frac{\mathbf{x}_5}{|\mathbf{x}_5|} \quad (\text{D.62})$$

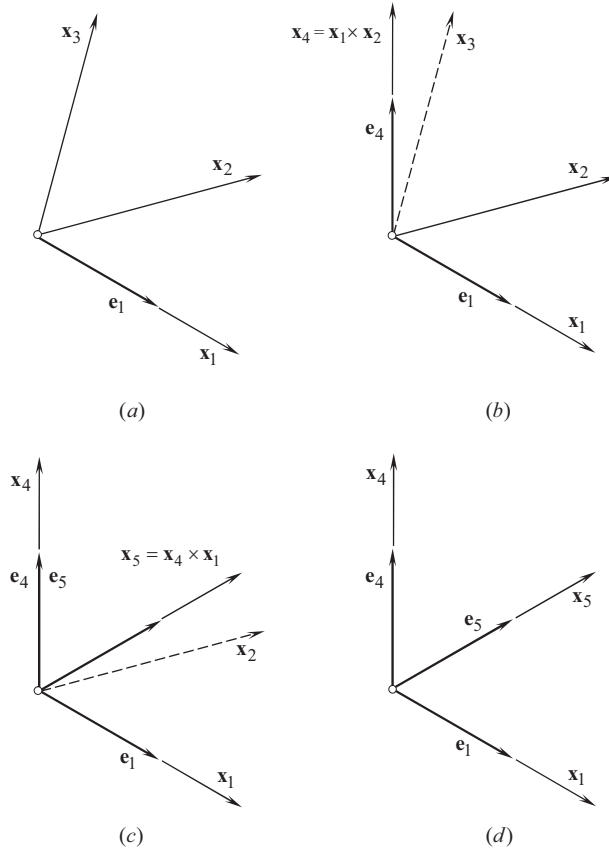


**FIGURE D.17** A normalized and orthogonally parameterized basis,  $\mathbf{e}_1\mathbf{e}_4\mathbf{e}_5$ , that is constructed from an arbitrary basis,  $\mathbf{x}_1\mathbf{x}_2\mathbf{x}_3$ : (a) configuration of the axis  $\mathbf{e}_1$  in relation to the basis  $\mathbf{x}_1\mathbf{x}_2\mathbf{x}_3$ ; (b) construct  $\mathbf{e}_4$  perpendicular to  $\mathbf{x}_1\mathbf{x}_2$ ; (c) construct  $\mathbf{x}_5 = \mathbf{x}_4 \times \mathbf{x}_1$ ; and (d) the axes of the constructed basis,  $\mathbf{x}_1\mathbf{x}_4\mathbf{x}_5$ , are aligned with the corresponding axes of the desirable basis,  $\mathbf{e}_1\mathbf{e}_4\mathbf{e}_5$ .

The resultant basis  $\mathbf{e}_1\mathbf{e}_4\mathbf{e}_5$  (see Figure D.17d) is always orthogonal, as well as it is always normalized.

In order to complete the analytical description of a closed loop of consequent coordinate system transformations, it is necessary to compose the operator  $\mathbf{Rs}(K_p \rightarrow K_g)$  of transformation from the local reference system,  $x_p y_p z_p$ , to the local reference system,  $x_g y_g z_g$  (see Figure D.13c).

In the case under consideration, the axes,  $z_g$  and  $z_p$ , align with the common unit normal vector,  $\mathbf{n}_g$ . The axis,  $z_g$ , is pointed out from the bodily side to the void side of the gear tooth flank,  $\mathcal{S}$ . The axis,  $z_p$ , is pointed oppositely. Due to that, the following equality is observed:

$$\mathbf{Rs}(K_p \rightarrow K_g) = \mathbf{Rt}(\varphi_z, z_p) \quad (\text{D.63})$$

The inverse coordinate system transformation can be analytically described by the operator:

$$\mathbf{Rs}(K_g \rightarrow K_p) = \mathbf{Rs}^{-1}(K_p \rightarrow K_g) = \mathbf{Rt}(-\varphi_z, z_p) \quad (\text{D.64})$$

Implementation of the discussed results allows for:

- representation of the gear tooth flank,  $\mathcal{S}$ , and the pinion tooth flank,  $\mathcal{P}$ , of the form cutting tool, as well as their relative motion in a common coordinate system, and

- b. consideration meshing of the gear tooth flank,  $\mathcal{S}$ , in any desired coordinate system that is a component of the chain and/or the closed loop of consequent coordinate system transformations.

Transition from one coordinate system to another coordinate system can be performed in two feasible directions, say in direct and in inverse directions.

## D.5 IMPACT OF THE COORDINATE SYSTEMS TRANSFORMATIONS ONTO FUNDAMENTAL FORMS OF THE SURFACE

Every coordinate system transformation entails a corresponding alteration to equation of the gear tooth flank,  $\mathcal{S}$ , and/or pinion tooth flank,  $\mathcal{P}$ . Because of this, it is often necessary to re-calculate coefficients of the first  $\Phi_{1,g}$  and of the second  $\Phi_{2,g}$  fundamental forms of the gear tooth flank,  $\mathcal{S}$  (as many times as the coordinate system transformation is performed). This routing and time-consuming operation can be eliminated if the operators of coordinate system transformations are used directly to the fundamental forms  $\Phi_{1,g}$  and  $\Phi_{2,g}$ .

After being calculated in an initial reference system, the fundamental magnitudes  $E_g, F_g$ , and  $G_g$  of the first,  $\Phi_{1,g}$ , and the fundamental magnitudes  $L_g, M_g$ , and  $N_g$  of the second,  $\Phi_{2,g}$ , fundamental forms can be determined in any new coordinate system using for this purpose the operators of translation, of rotation and of resultant coordinate system transformation. Transformation of such kind of the fundamental magnitudes,  $\Phi_{1,g}$  and  $\Phi_{2,g}$ , becomes possible due to the implementation of a formula, that can be found immediately below.

Let's consider a gear tooth flank,  $\mathcal{S}$ , that is given by equation  $\mathbf{r}_g = \mathbf{r}_g(U_g, V_g)$ , where  $(U_g, V_g) \in \mathcal{S}$ .

For the analysis below, it is convenient to use the equation of the first fundamental form,  $\Phi_{1,g}$ , of the gear tooth flank,  $\mathcal{S}$ , represented in matrix form:

$$[\Phi_{1,g}] = \begin{bmatrix} dU_g & dV_g & 0 & 0 \end{bmatrix} \cdot \begin{bmatrix} E_g & F_g & 0 & 0 \\ F_g & G_g & 0 & 0 \\ 0 & 0 & 1 & 0 \\ 0 & 0 & 0 & 1 \end{bmatrix} \cdot \begin{bmatrix} dU_g \\ dV_g \\ 0 \\ 0 \end{bmatrix} \quad (\text{D.65})$$

Similarly, the equation of the second fundamental form  $\Phi_{2,g}$  of the gear tooth flank,  $\mathcal{S}$ , can be given by:

$$[\Phi_{2,g}] = \begin{bmatrix} dU_g & dV_g & 0 & 0 \end{bmatrix} \cdot \begin{bmatrix} L_g & M_g & 0 & 0 \\ M_g & N_g & 0 & 0 \\ 0 & 0 & 1 & 0 \\ 0 & 0 & 0 & 1 \end{bmatrix} \cdot \begin{bmatrix} dU_g \\ dV_g \\ 0 \\ 0 \end{bmatrix} \quad (\text{D.66})$$

The coordinate system transformation that is performed by the operator of linear transformation  $\mathbf{Rs}(1 \rightarrow 2)$  transfers the equation  $\mathbf{r}_g = \mathbf{r}_g(U_g, V_g)$  of the gear tooth flank,  $\mathcal{S}$ , initially given in  $X_1Y_1Z_1$ , to the equation  $\mathbf{r}_g^* = \mathbf{r}_g^*(U_g^*, V_g^*)$  of that same gear tooth flank,  $\mathcal{S}$ , in a new coordinate system  $X_2Y_2Z_2$ . It is clear that  $\mathbf{r}_g \neq \mathbf{r}_g^*$ .

In the new coordinate system, the gear tooth flank,  $\mathcal{S}$ , is analytically described by the following expression:

$$\mathbf{r}_g^*(U_g^*, V_g^*) = \mathbf{Rs}(1 \rightarrow 2) \cdot \mathbf{r}_g(U_g, V_g) \quad (\text{D.67})$$

The operator of the resultant coordinate system transformation  $\mathbf{Rs}(1 \rightarrow 2)$  casts the column matrices of variables in Eq. (D.65) and Eq. (D.66) to the form:

$$[dU_g^* \quad dV_g^* \quad 0 \quad 0]^T = \mathbf{Rs}(1 \rightarrow 2) \cdot [dU_g \quad dV_g \quad 0 \quad 0]^T. \quad (\text{D.68})$$

Substitution of Eq. (D.68) into Eqs. (D.65) and (D.66) makes it possible the expressions for the fundamental forms,  $\Phi_{1,g}^*$  and  $\Phi_{2,g}^*$ , in the new coordinate system:

$$[\Phi_{1,g}^*] = [\mathbf{Rs}(1 \rightarrow 2) \cdot [dU_g \quad dV_g \quad 0 \quad 0]^T]^T \cdot [\Phi_{1,g}] \cdot \mathbf{Rs}(1 \rightarrow 2) \cdot [dU_g \quad dV_g \quad 0 \quad 0]^T \quad (\text{D.69})$$

$$[\Phi_{2,g}^*] = [\mathbf{Rs}(1 \rightarrow 2) \cdot [dU_g \quad dV_g \quad 0 \quad 0]^T]^T \cdot [\Phi_{2,g}] \cdot \mathbf{Rs}(1 \rightarrow 2) \cdot [dU_g \quad dV_g \quad 0 \quad 0]^T \quad (\text{D.70})$$

The following equation is valid for multiplication:

$$[\mathbf{Rs}(1 \rightarrow 2) \cdot [dU_g \quad dV_g \quad 0 \quad 0]^T]^T = \mathbf{Rs}^T(1 \rightarrow 2) \cdot [dU_g \quad dV_g \quad 0 \quad 0] \quad (\text{D.71})$$

Therefore,

$$[\Phi_{1,g}^*] = [dU_g \quad dV_g \quad 0 \quad 0]^T \cdot \left\{ \mathbf{Rs}^T(1 \rightarrow 2) \cdot [\Phi_{1,g}] \cdot \mathbf{Rs}(1 \rightarrow 2) \right\} \cdot [dU_g \quad dV_g \quad 0 \quad 0] \quad (\text{D.72})$$

$$[\Phi_{2,g}^*] = [dU_g \quad dV_g \quad 0 \quad 0]^T \cdot \left\{ \mathbf{Rs}^T(1 \rightarrow 2) \cdot [\Phi_{2,g}] \cdot \mathbf{Rs}(1 \rightarrow 2) \right\} \cdot [dU_g \quad dV_g \quad 0 \quad 0] \quad (\text{D.73})$$

It can be easily shown that the matrices  $[\Phi_{1,g}^*]$  and  $[\Phi_{2,g}^*]$  in Eqs. (D.72) and (D.73) represent quadratic forms with respect to  $dU_g$  and  $dV_g$ .

The operator of transformation  $\mathbf{Rs}(1 \rightarrow 2)$  of the gear tooth flank,  $\mathcal{S}$ , having the first,  $\Phi_{1,g}$ , and the second,  $\Phi_{2,g}$ , fundamental forms from the initial coordinate system  $X_1Y_1Z_1$  to the new coordinate system,  $X_2Y_2Z_2$ , results in that in the new coordinate system the corresponding fundamental forms are expressed in the form:

$$[\Phi_{1,g}^*] = \mathbf{Rs}^T(1 \rightarrow 2) \cdot [\Phi_{1,g}] \cdot \mathbf{Rs}(1 \rightarrow 2) \quad (\text{D.74})$$

$$[\Phi_{2,g}^*] = \mathbf{Rs}^T(1 \rightarrow 2) \cdot [\Phi_{2,g}] \cdot \mathbf{Rs}(1 \rightarrow 2) \quad (\text{D.75})$$

Equations (D.74) and (D.75) reveal that after the coordinate system transformation is completed, the first  $\Phi_{1,g}^*$  and the second  $\Phi_{2,g}^*$  fundamental forms of the gear tooth flank,  $\mathcal{S}$ , in the coordinate system  $X_2Y_2Z_2$  are expressed in terms of the first,  $\Phi_{1,g}$ , and the second,  $\Phi_{2,g}$ , fundamental forms initially represented in the coordinate system  $X_1Y_1Z_1$ . In order to do that, the corresponding fundamental form (either the form,  $\Phi_{1,g}$ , or the form,  $\Phi_{2,g}$ ) must be pre-multiplied by  $\mathbf{Rs}(1 \rightarrow 2)$  and after that it been post-multiplied by  $\mathbf{Rs}^T(1 \rightarrow 2)$ .

Implementation of Eqs. (D.74) and (D.75) significantly simplifies formulae transformations.

Equations similar to those above Eqs. (D.74) and (D.75) are valid with respect to pinion tooth flank,  $\mathcal{P}$ .

In the case of the use of the third,  $\Phi_{3,g}$ , and of the fourth,  $\Phi_{4,g}$ , fundamental forms, their coefficients can be expressed in terms of the fundamental magnitudes of the first and of the second order.



# Taylor & Francis

Taylor & Francis Group

<http://taylorandfrancis.com>



---

# Appendix E

## *Contact Geometry of a Gear and a Mating Pinion Tooth Flanks*

In the theory of gearing, the kinematics of gearing is considered as the prime element of the gear pair. Other important elements of gearing, namely:

- a. The shape and the geometry of the gear tooth flank,  $\mathcal{S}$ , and
- b. The shape and the geometry of the mating pinion tooth flank,  $\mathcal{P}$  (as well as numerous others)

are considered as the secondary elements of gearing. This does not mean that the importance of the secondary elements is lower than that of the primary element. No, this is incorrect. This means just that the most favorable parameters of the secondary elements can be expressed in terms of the parameters of the prime element. Ultimately, the entire gear pair can be synthesized on the premise just of the prime element – that is, on the premise of the desirable kinematics of the gear pair. In other words, having just the desirable kinematics of the gear pair to be designed, it is possible to synthesize the rest of the design parameters of the gear pair. Only the kinematics of gearing is used for synthesizing the best possible gear pair for transmitting the input rotation and torque.

In order to solve the problem of synthesizing the most favorable gear pair, an appropriate analytical description of contact geometry of the gear tooth flank,  $\mathcal{S}$ , and the mating pinion tooth flank,  $\mathcal{P}$ , is required. The problem of the analytical description of contact geometry between two smooth regular surfaces in the first order of tangency is a sophisticated one.

Investigation of contact geometry of curves and surfaces can be traced back to the eighteenth century. In considerable detail, the study of the contact of curves and surfaces has been undertaken by *J.L. Lagrange*<sup>1</sup> in his *Theorié des Fonctions Analytiques* (1797), and *A.L. Cauchy*<sup>2</sup> in his *Leçons sur les Applications du Calcul Infinitésimal á la Geometrie* (1826). Later on, in the twentieth century, an investigation in the realm of contact geometry of curves and surfaces has been undertaken by *J. Favard*<sup>3</sup> in his *Course de Gèomètrie Diffèrentielle Locale* (1957). A few more names of the researchers in the field are to be mentioned.

The results of the research obtained in the field of contact geometry of two smooth regular surfaces are widely used in the theory of gearing. The problem of synthesizing the most favorable gear pair can be solved on the premise of the analysis of topology of the contacting surfaces in differential vicinity of the point of their contact.

Various methods for the analytical description of contact geometry between two smooth regular surfaces are developed by now. The latest achievements in the field are discussed in plurality of papers and monograph available in the public domain.

An in-detail analysis of known methods of analytical description of the geometry of contact between two smooth regular surfaces uncovered poor capability of known methods for solving problems in the field of designing efficient gear pairs. Therefore, an accurate method for the analytical description of contact geometry between two smooth regular surfaces,  $\mathcal{S}$  and  $\mathcal{P}$ , in the first order

---

<sup>1</sup> Joseph-Louis Lagrange (January 25, 1736–April 10, 1813) – an Italian born [born Giuseppe Lodovico (Luigi) **Lagrangia**] famous French mathematician and mechanician.

<sup>2</sup> Augustin-Louis Cauchy (August 21, 1789–May 23, 1857) – a famous French mathematician.

<sup>3</sup> Jean Favard (August 28, 1902–January 21, 1965) – a French mathematician.

of tangency, which fits the needs of the theory of gearing, is necessary. Such a method is worked out in this chapter.

It is convenient to begin the discussion starting from analytical description of local relative orientation of the gear tooth flank,  $\mathcal{S}$ , and the mating pinion tooth flank,  $\mathcal{P}$ . The proposed analytical description is relevant to differential vicinity of the point of contact,  $K$ , of the tooth flanks,  $\mathcal{S}$  and  $\mathcal{P}$ .

## E.1 LOCAL RELATIVE ORIENTATION AT POINT OF CONTACT OF A GEAR AND A MATING PINION TOOTH FLANKS

When the gears rotate, a gear tooth flank,  $\mathcal{S}$ , and the mating pinion tooth flank,  $\mathcal{P}$ , are in permanent tangency with one another. The contacting surfaces,  $\mathcal{S}$  and  $\mathcal{P}$ , can be locally approximated by the corresponding quadrics as schematically illustrated in Figure E.1. The requirement to be permanently in tangency to each other imposes a kind of restrictions on the relative configuration (location and orientation) of the tooth flanks,  $\mathcal{S}$  and  $\mathcal{P}$ , and on their instantaneous relative motion.

In the theory of gearing, a quantitative measure of the relative orientation of the gear tooth flank,  $\mathcal{S}$ , and of the mating pinion tooth flank,  $\mathcal{P}$ , is established.

Relative orientation of the at a point of contact of the gear tooth flank,  $\mathcal{S}$ , and of the mating pinion tooth flank,  $\mathcal{P}$ , is specified by the angle,  $\mu$ , of local<sup>4</sup> relative orientation of the surfaces. By definition, angle  $\mu$  is equal to the angle that the unit tangent vector,  $\mathbf{t}_{1,g}$ , of the first principal direction of the gear tooth flank,  $\mathcal{S}$ , forms with the unit tangent vector,  $\mathbf{t}_{1,p}$ , of the first principal direction of the mating pinion tooth flank,  $\mathcal{P}$ . That same angle,  $\mu$ , can also be determined as the angle that makes the unit tangent vectors,  $\mathbf{t}_{2,g}$  and  $\mathbf{t}_{2,p}$ , of the second principal directions of the surfaces,  $\mathcal{S}$  and  $\mathcal{P}$ , at contact point,  $K$ . This immediately yields equations for the calculation of the angle,  $\mu$ :

$$\sin \mu = |\mathbf{t}_{1,g} \times \mathbf{t}_{1,p}| = |\mathbf{t}_{2,g} \times \mathbf{t}_{2,p}|, \quad (\text{E.1})$$

$$\cos \mu = \mathbf{t}_{1,g} \cdot \mathbf{t}_{1,p} = \mathbf{t}_{2,g} \cdot \mathbf{t}_{2,p}, \quad (\text{E.2})$$

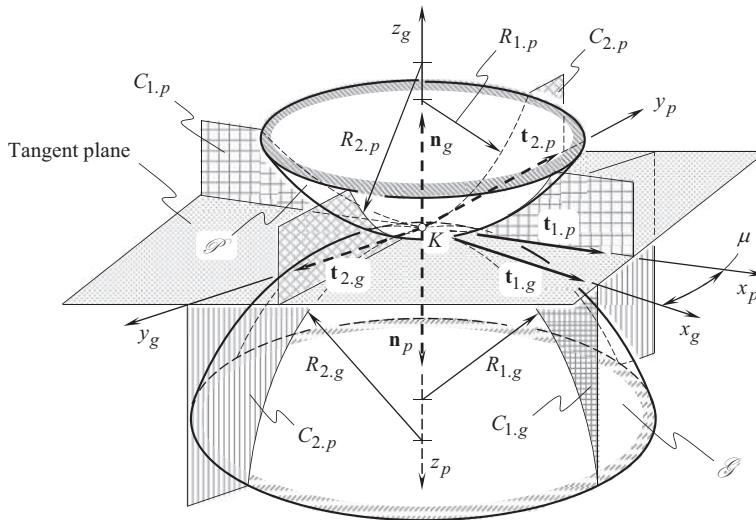


**FIGURE E.1** Local configuration of two quadrics that are tangent to a gear tooth flank  $\mathcal{S}$  and to a mating pinion tooth flank  $\mathcal{P}$  at contact point  $K$ . (After Prof. S.P. Radzevich, ~2008.)

<sup>4</sup> The surfaces orientation is local by nature, as it relates only to differential vicinity of point,  $K$ , of contact of the tooth flanks,  $\mathcal{S}$  and  $\mathcal{P}$ .

$$\tan \mu = \frac{|\mathbf{t}_{1,g} \times \mathbf{t}_{1,p}|}{\mathbf{t}_{1,g} \cdot \mathbf{t}_{1,p}} \equiv \frac{|\mathbf{t}_{2,g} \times \mathbf{t}_{2,p}|}{\mathbf{t}_{2,g} \cdot \mathbf{t}_{2,p}} \quad (\text{E.3})$$

Here is designated:

$\mathbf{t}_{1,g}, \mathbf{t}_{2,g}$  is the unit vectors of principal directions on the gear tooth flank,  $\mathcal{S}$ , measured at contact point,  $K$ .

$\mathbf{t}_{1,p}, \mathbf{t}_{2,p}$  is the unit vectors of principal directions on the mating pinion tooth flank,  $\mathcal{P}$ , at that same contact point,  $K$ , of the tooth flanks,  $\mathcal{S}$  and  $\mathcal{P}$ .

Directions of the unit tangent vectors,  $\mathbf{t}_{1,g}$  and  $\mathbf{t}_{2,g}$ , of the principal directions on the gear tooth flank,  $\mathcal{S}$  (as well as directions of the unit tangent vectors  $\mathbf{t}_{1,p}$  and  $\mathbf{t}_{2,p}$  of the principal directions on the pinion tooth flank,  $\mathcal{P}$ ) can be specified in terms of the ratio  $dU_g/dV_g$  (or in terms of the ratio  $dU_p/dV_p$  in case of the pinion tooth flank,  $\mathcal{P}$ ). The corresponding values of the ratio,  $dU_{g(p)}/dV_{g(p)}$ , are calculated as roots of the quadratic equation:

$$\begin{vmatrix} E_{g(p)} \frac{dU_{g(p)}}{dV_{g(p)}} + F_{g(p)} & F_{g(p)} \frac{dU_{g(p)}}{dV_{g(p)}} + G_{g(p)} \\ L_{g(p)} \frac{dU_{g(p)}}{dV_{g(p)}} + M_{g(p)} & M_{g(p)} \frac{dU_{g(p)}}{dV_{g(p)}} + N_{g(p)} \end{vmatrix} = 0 \quad (\text{E.4})$$

In case of point contact of the surfaces,  $\mathcal{S}$  and  $\mathcal{P}$ , an actual value of the angle,  $\mu$ , is calculated at contact point,  $K$ . If the tooth flanks,  $\mathcal{S}$  and  $\mathcal{P}$ , are in line contact, then actual value of the angle,  $\mu$ , can be calculated at every point within the line of contact.<sup>5</sup> The line of contact of the tooth flanks,  $\mathcal{S}$  and  $\mathcal{P}$ , is commonly referred to as *characteristic line*,  $\mathcal{E}$ , or just as *characteristic*,  $\mathcal{E}$ , for simplicity.

Determination of the angle,  $\mu$ , of local relative orientation of the tooth flanks,  $\mathcal{S}$  and  $\mathcal{P}$ , of a gear and a mating pinion is illustrated in Figure E.1.

In order to calculate an actual value of the angle,  $\mu$ , of local relative orientation of the tooth flanks,  $\mathcal{S}$  and  $\mathcal{P}$ , the unit vectors of the principal directions,  $\mathbf{t}_{1,g}$  and  $\mathbf{t}_{1,p}$ , are employed.

Consider tooth flanks,  $\mathcal{S}$  and  $\mathcal{P}$ , in point contact, which are represented in a common reference system. The surfaces make contact at a point,  $K$ . For further analysis, an equation of the common tangent plane to the tooth flanks,  $\mathcal{S}$  and  $\mathcal{P}$ , at the contact point,  $K$ , is necessary (see Figures E.1 and E.2).

$$(\mathbf{r}_p - \mathbf{r}_K) \cdot \mathbf{u}_g \cdot \mathbf{v}_g = 0 \quad (\text{E.5})$$

Here:

$\mathbf{r}_p$  is the position vector of a point of the common tangent plane.

$\mathbf{r}_K$  is the position vector of the contact point,  $K$ .

$\mathbf{u}_g$  and  $\mathbf{v}_g$  are unit vectors that are tangent to  $U_g$  – and  $V_g$  – coordinate lines on the gear tooth flank,  $\mathcal{S}$  at the contact point,  $K$ .

The angle  $\omega_g$  is the angle that is formed by the unit vectors,  $\mathbf{u}_g$  and  $\mathbf{v}_g$ . The actual value of the angle,  $\omega_g$ , can be calculated from one of the following equations:

<sup>5</sup> It is worthy pointing out here that in a case of line contact, relative orientation of two surfaces,  $\mathcal{S}$  and  $\mathcal{P}$ , is predetermined in *global* sense. However, actual value of the angle,  $\mu$ , of the surface *local* relative orientation at different points of the characteristic,  $\mathcal{E}$ , is different.

$$\sin \omega_g = \frac{\sqrt{E_g G_g - F_g^2}}{\sqrt{E_g G_g}} \quad (\text{E.6})$$

$$\cos \omega_g = \frac{F_g}{\sqrt{E_g G_g}} \quad (\text{E.7})$$

$$\tan \omega_g = \frac{\sqrt{E_g G_g - F_g^2}}{F_g} \quad (\text{E.8})$$

Equations similar to Eqs. (E.6)–(E.8) are also valid for the calculation of the angle,  $\omega_p$ , at a point on the pinion tooth flank,  $\mathcal{P}$ .

Tangent directions,  $\mathbf{u}_g$  and, to the  $U_g$  – and  $V_g$  – coordinate lines at a point on the gear tooth flank,  $\mathcal{G}$ , as well as tangent directions,  $\mathbf{u}_p$  and  $\mathbf{v}_p$  to the  $U_p$  – and  $V_p$  – coordinate at a point lines on the pinion tooth flank,  $\mathcal{P}$ , are specified in terms of the angles,  $\theta$  and  $\varepsilon$ . For the calculation of actual values of the angles,  $\theta$  and  $\varepsilon$ , the following equations can be used:

$$\cos \theta = \mathbf{u}_g \cdot \mathbf{u}_p \quad (\text{E.9})$$

$$\cos \varepsilon = \mathbf{v}_g \cdot \mathbf{v}_p \quad (\text{E.10})$$

The angle,  $\xi_g$ , is the angle that the first principal direction,  $\mathbf{t}_{1.g}$ , on the gear tooth surface,  $\mathcal{G}$ , forms with the unit tangent vector,  $\mathbf{u}_g$  (see Figure E.2). The equation for the calculation of an actual value of the angle,  $\xi_g$ , is derived by Prof. *S.P. Radzevich*:

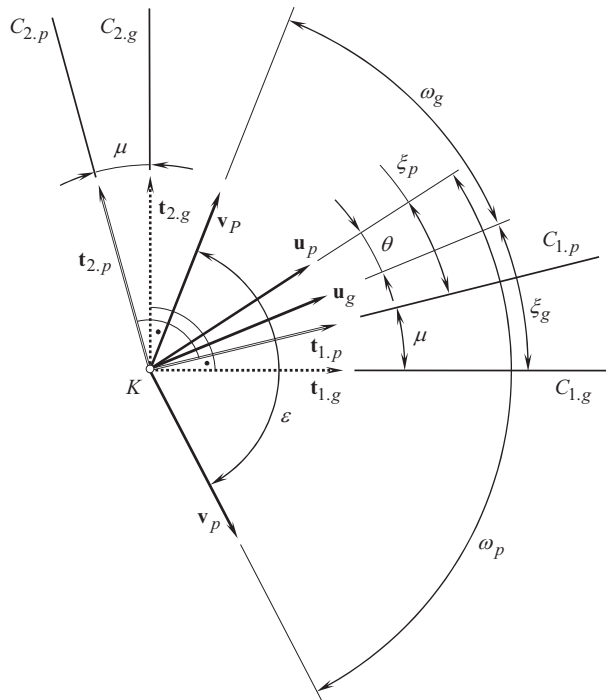


**FIGURE E.2** Local *relative* orientation at contact point of tooth flanks of a gear,  $\mathcal{G}$ , and a mating pinion,  $\mathcal{P}$ , considered in a common tangent plane.

$$\sin \xi_g = \frac{\eta_g}{\sqrt{\eta_g^2 - 2\eta_g \cos \omega_g + 1}} \sin \omega_g \quad (\text{E.11})$$

where  $\eta_g$  designates the ratio  $\eta_g = \frac{\partial U_g}{\partial V_g}$ .

In the event  $F_g = 0$ , the following equality,  $\tan \xi_g = \eta_g$ , is observed. Here, the ratio,  $\eta_g$ , is equal to the root of the quadratic equation:

$$(F_g L_g - E_g M_g) \eta_g^2 + (G_g L_g - E_g N_g) \eta_g + (G_g M_g - F_g N_g) = 0 \quad (\text{E.12})$$

which immediately follows from the equation:

$$\begin{vmatrix} E_g dU_g + F_g dV_g & F_g dU_g + G_g dV_g \\ L_g dU_g + M_g dV_g & M_g dU_g + N_g dV_g \end{vmatrix} = 0 \quad (\text{E.13})$$

The equation for the calculation of actual value of the angle,  $\xi_g$ , allows for another representation. The following chain rule,  $d\mathbf{r}_g$  can be represented in the form:

$$d\mathbf{r}_g = \mathbf{U}_g dU_g + \mathbf{V}_g dV_g \quad (\text{E.14})$$

By definition,  $\tan \xi_g = \frac{\sin \xi_g}{\cos \xi_g}$ . The functions,  $\sin \xi_g$  and  $\cos \xi_g$ , yield representation as:

$$\sin \xi_g = \frac{|\mathbf{U}_g \times d\mathbf{r}_g|}{|\mathbf{U}_g| \cdot |d\mathbf{r}_g|} \quad (\text{E.15})$$

$$\cos \xi_g = \frac{\mathbf{U}_g \cdot d\mathbf{r}_g}{|\mathbf{U}_g| \cdot |d\mathbf{r}_g|} \quad (\text{E.16})$$

The last expressions yield:

$$\tan \xi_g = \frac{\sin \xi_g}{\cos \xi_g} = \frac{|\mathbf{U}_g \times d\mathbf{r}_g|}{\mathbf{U}_g \cdot d\mathbf{r}_g} = \frac{|\mathbf{U}_g \times d\mathbf{r}_g|}{\mathbf{U}_g \cdot (\mathbf{U}_g dU_g + \mathbf{V}_g dV_g)} = \frac{|\mathbf{U}_g \times d\mathbf{r}_g| \cdot dV_g}{\mathbf{U}_g \cdot \mathbf{U}_g dU_g + \mathbf{U}_g \cdot \mathbf{V}_g dV_g} \quad (\text{E.17})$$

By definition:

$$\mathbf{U}_g \cdot \mathbf{U}_g = E_g \quad (\text{E.18})$$

$$\mathbf{U}_g \cdot \mathbf{V}_g = F_g \quad (\text{E.19})$$

$$|\mathbf{U}_g \times \mathbf{V}_g| = \sqrt{E_g G_g - F_g^2} \quad (\text{E.20})$$

Equations (E.14)–(E.20) yield the formula:

$$\tan \xi_g = \frac{\sqrt{E_g G_g - F_g^2}}{\eta_g \cdot E_g + F_g} \quad (\text{E.21})$$

for the calculation of the actual value of the angle  $\xi_g$ .

Equations similar to the above Eqs. (E.11) and (E.21) are also valid for the calculation of the actual value of the angle,  $\xi_p$ , that the first principal direction,  $\mathbf{t}_{1,p}$ , at a point on the pinion tooth flank,  $\mathcal{P}$ , forms with the unit tangent vector,  $\mathbf{u}_p$ .

The performed analysis makes possible the following equations for the calculation of the unit vectors of principal directions,  $\mathbf{t}_{1,g}$  and  $\mathbf{t}_{2,g}$ :

$$\mathbf{t}_{1,g} = \mathbf{Rt}(\xi_g, \mathbf{n}_g) \cdot \mathbf{u}_g \quad (\text{E.22})$$

$$\mathbf{t}_{2,g} = \mathbf{Rt}\left[\left(\xi_g + \frac{\pi}{2}\right), \mathbf{n}_g\right] \cdot \mathbf{u}_g \quad (\text{E.23})$$

for the gear tooth flank,  $\mathcal{G}$ , and similar equations for the calculation of the unit vectors of principal directions,  $\mathbf{t}_{1,p}$  and  $\mathbf{t}_{2,p}$ :

$$\mathbf{t}_{1,p} = \mathbf{Rt}(\xi_p, \mathbf{n}_g) \cdot \mathbf{u}_p \quad (\text{E.24})$$

$$\mathbf{t}_{2,p} = \mathbf{Rt}\left[\left(\xi_p + \frac{\pi}{2}\right), \mathbf{n}_g\right] \cdot \mathbf{u}_p \quad (\text{E.25})$$

for the pinion tooth flank,  $\mathcal{P}$ .

The operator of rotation  $\mathbf{Rt}(\varphi_A, A_0)$  through an angle  $\varphi_A$  about an axis  $A_0$  is employed for the calculation of the operators of rotation in Eqs. (E.22)–(E.25).

## E.2 THE SECOND-ORDER ANALYSIS: PLANAR CHARACTERISTIC IMAGES

For a more accurate analytical description of contact geometry of the gear tooth flank,  $\mathcal{G}$ , and the pinion tooth flank,  $\mathcal{P}$ , consideration of the second-order parameters is necessary. The second-order analysis incorporates elements of both the first order and elements of the second-order analysis. For performing the second-order analysis, familiarity with *Dupin indicatrix* is highly desirable<sup>6</sup> is a perfect start-point for consideration of the second-order analysis.

### E.2.1 PRELIMINARY REMARKS: *DUPIN INDICATRIX*

At any point of a smooth regular gear tooth flank,  $\mathcal{G}$  (as well as at any point of a smooth regular pinion tooth flank,  $\mathcal{P}$ ), a corresponding *Dupin indicatrices* can be constructed. *Dupin indicatrix*,  $Dup(\mathcal{G})$  at a point of a gear tooth flank,  $\mathcal{G}$ , as well as *Dupin indicatrix*,  $Dup(\mathcal{P})$  at a point of the pinion tooth flank,  $\mathcal{P}$ , are planar characteristic curves of the second order. They are used for graphical interpretation of the distribution of normal radii of curvature of a surface in the differential vicinity of a surface point.

*Dupin indicatrices* at a point of the tooth flank,  $\mathcal{G}$  (as well as at a point of the tooth flank,  $\mathcal{P}$ ) are of critical importance in the theory of gearing. Generation of this planar characteristic curve is illustrated in a diagram shown in Figure E.3.

A plane  $W$  through the unit normal vector,  $\mathbf{n}_g$ , to the gear tooth flank,  $\mathcal{G}$ , at a point,  $m$ , is rotating about the unit normal vector,  $\mathbf{n}_g$ . While rotating, the plane occupies consecutive positions,  $W_1$ ,  $W_2$ ,  $W_3$ , and others. The radii of the normal curvature of the line of intersection of the gear tooth flank,  $\mathcal{G}$ , by normal planes,  $W_1$ ,  $W_2$ ,  $W_3$ , are equal  $R_{g,1}$ ,  $R_{g,2}$ ,  $R_{g,3}$ , and so forth. The gear tooth flank,  $\mathcal{G}$ , is intersected by a plane,  $Q$ . The plane,  $Q$ , is orthogonal to the unit normal vector,  $\mathbf{n}_g$ . This plane is at a certain small distance,  $\delta$ , from the point,  $m$ . When the distance,  $\delta$ , approaches zero ( $\delta \rightarrow 0$ ),

<sup>6</sup> Fransua Pier Charles Dupin (October 6, 1784–January 18, 1873) – a French mathematician.

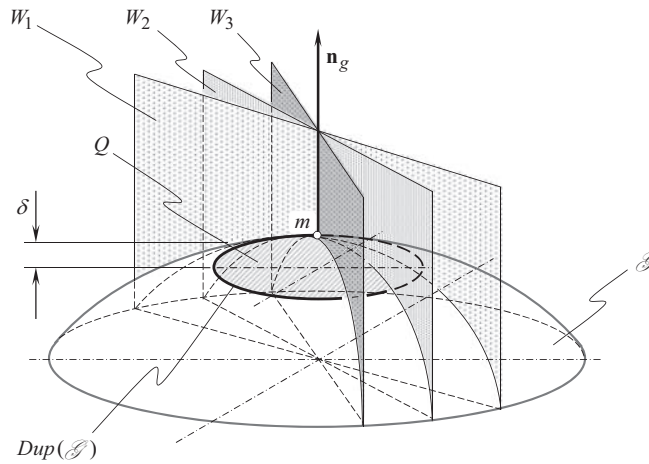


**FIGURE E.3** Dupin indicatrix at point of smooth regular gear tooth flank,  $\mathcal{S}$ .

and when the scale of the line of intersection of the gear tooth flank,  $\mathcal{S}$ , by the plane,  $Q$ , approaches infinity, then the line of intersection of the gear surface,  $\mathcal{S}$ , by the plane,  $Q$  approaches to the planar characteristic curve that is commonly referred to as *Dupin indicatrix*,  $Dup(\mathcal{S})$ .

In the differential geometry of surfaces, a surface is construed as a zero-thickness film. Because of this, *Dupin indicatrices* of the following five different types are distinguished in differential geometry of surfaces (see Figure E.4):

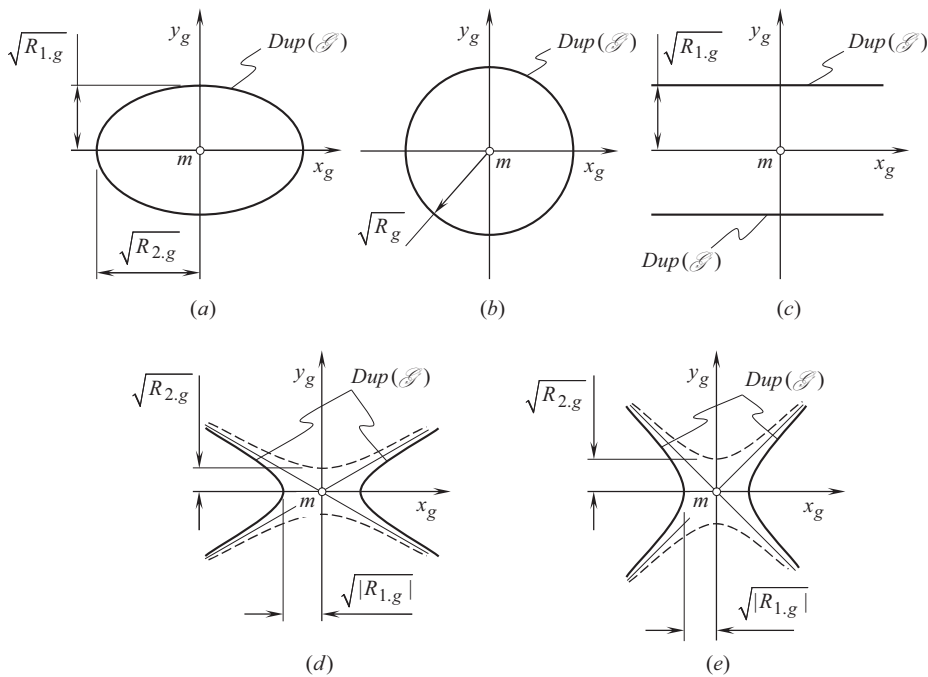


**FIGURE E.4** Five different kinds of Dupin indicatrix,  $Dup(\mathcal{S})$ , at point,  $m$ , of a smooth regular gear tooth flank that are constructed for local surface patches of: (a) elliptical kind, (b) umbilical kind, (c) parabolical kind, (d) hyperbolic kind, and (e) minimal kind.



1. elliptic (see Figure E.4a)
2. umbilic (see Figure E.4b)
3. parabolic (see Figure E.4c)
4. hyperbolic (see Figure E.4d)
5. minimal (see Figure E.4e).

*Dupin indicatrix* for a plane local surface patch doesn't exist. In the case of plane, all points of the *Dupin indicatrix* are remote to infinity.

For local surface patches having negative full curvature ( $\mathcal{S}_g < 0$ ), phantom branches (i.e., the branches that are not intersected by a plane perpendicular to the unite normal vector,  $\mathbf{n}_g$ , to the gear tooth flank,  $\mathcal{S}$ , at a point,  $m$ ) of the characteristic curve,  $Dup(\mathcal{S})$ , in Figure E.4d and e are shown in dashed lines.

An easy way to derive an equation of the characteristic curve,  $Dup(\mathcal{S})$ , is discussed immediately below.

*Euler formula:*

$$k_{1,g} \cos^2 \varphi + k_{2,g} \sin^2 \varphi = k_g \quad (\text{E.26})$$

yields representation in the form:

$$\frac{k_{1,g}}{k_g} \cos^2 \varphi + \frac{k_{2,g}}{k_g} \sin^2 \varphi = 1 \quad (\text{E.27})$$

Transition from polar coordinates to *Cartesian coordinates* can be performed using well-known formulas:

$$x_g = \rho \cos \varphi \quad (\text{E.28})$$

$$y_g = \rho \sin \varphi \quad (\text{E.29})$$

These formulas make it possible the following expressions for  $\cos^2 \varphi = x_g^2 / \rho^2$  and  $\sin^2 \varphi = y_g^2 / \rho^2$ . After substituting the last formulas into the above equation Eq. (E.27), one can come up with the equation:

$$\frac{k_{1,g}}{k_g} \cdot \frac{x_g^2}{\rho^2} + \frac{k_{2,g}}{k_g} \cdot \frac{y_g^2}{\rho^2} = 1. \quad (\text{E.30})$$

It is convenient to designate  $\rho = \sqrt{k_g^{-1}}$ . Principal curvatures  $k_{1,g}$  and  $k_{2,g}$  are the roots of the quadratic equation:

$$\begin{vmatrix} L_g - E_g k_g & M_g - F_g k_g \\ M_g - F_g k_g & N_g - G_g k_g \end{vmatrix} = 0 \quad (\text{E.31})$$

Substituting the calculated values of the principal curvatures  $k_{1,g}$  and  $k_{2,g}$  into Eq. (E.30), and after performing necessary formulae transformations, an equation<sup>7</sup> for the *Dupin indicatrix*,  $Dup(\mathcal{S})$  can be represented in the form:

<sup>7</sup> The same equation of the *Dupin indicatrix* could be derived in another way. *Coxeter* considers a pair of conics obtained by expanding an equation in *Monge's* form in a *McLaurin* series:

$$z = z(0, 0) + z_1 x + z_2 y + \frac{1}{2} (z_{11} x^2 + 2z_{12} xy + z_{22} y^2) + \dots = \frac{1}{2} (b_{11} x^2 + 2b_{12} xy + b_{22} y^2)$$

This gives the equation  $(b_{11} x^2 + 2b_{12} xy + b_{22} y^2) = \pm 1$  of the *Dupin indicatrix*.

$$k_{1,g} x_g^2 + k_{2,g} y_g^2 = 1 \quad (\text{E.32})$$

Equation (E.32) describes a particular case of the *Dupin indicatrix*, which is represented in *Darboux frame*.<sup>8</sup>

General form of equation of *Dupin indicatrix* at a point  $m$  of a gear tooth flank,  $\mathcal{S}$ , is often represented as:

$$\text{Dup}(\mathcal{S}) \Rightarrow \frac{L_g}{E_g} x_g^2 + \frac{2M_g}{\sqrt{E_g G_g}} x_g y_g + \frac{N_g}{G_g} y_g^2 = 1 \quad (\text{E.33})$$

In Eq. (E.33), the characteristic curve,  $\text{Dup}(\mathcal{S})$ , is expressed in terms of the fundamental magnitudes,  $E_g$ ,  $F_g$ , and  $G_g$  of the first,  $\Phi_{1,g}$ , and in terms of the fundamental magnitudes,  $L_g$ ,  $M_g$ , and  $N_g$  of the second order,  $\Phi_{2,g}$ , at a point of the gear tooth flank,  $\mathcal{S}$ .

### E.2.2 MATRIX REPRESENTATION OF EQUATION OF DUPIN INDICATRIX AT POINT OF A GEAR TOOTH FLANK

Like any other quadratic form, equation of *Dupin indicatrix* of the gear tooth flank,  $\mathcal{S}$ , can be represented in matrix form:

$$\text{Dup}(\mathcal{S}) \Rightarrow \begin{bmatrix} x_g & y_g & 0 & 0 \end{bmatrix} \cdot \begin{bmatrix} \frac{L_g}{E_g} & \frac{2M_g}{\sqrt{E_g G_g}} & 0 & 0 \\ \frac{2M_g}{\sqrt{E_g G_g}} & \frac{N_g}{G_g} & 0 & 0 \\ 0 & 0 & \mp 1 & 0 \\ 0 & 0 & 0 & 1 \end{bmatrix} \cdot \begin{bmatrix} x_g \\ y_g \\ 0 \\ 0 \end{bmatrix} = \pm 1 \quad (\text{E.34})$$

In *Darboux frame*, this equation reduces to:

$$\text{Dup}(\mathcal{S}) \Rightarrow \begin{bmatrix} x_g & y_g & 0 & 0 \end{bmatrix} \cdot \begin{bmatrix} L_g & M_g & 0 & 0 \\ M_g & N_g & 0 & 0 \\ 0 & 0 & \mp 1 & 0 \\ 0 & 0 & 0 & 1 \end{bmatrix} \cdot \begin{bmatrix} x_g \\ y_g \\ 0 \\ 0 \end{bmatrix} = \pm 1 \quad (\text{E.35})$$

It is convenient to implement matrix representation of equation of the *Dupin indicatrix* (see above), for instance, when investigating spatial gearings, that is, crossed-axis gearings, when multiple coordinate system transformations are required.

The equation of *Dupin indicatrix* can be represented in the form:

$$r_{\text{Dup}}(\varphi) = \sqrt{|R_g(\varphi)|} \cdot \text{sgn } \Phi_{2,g}^{-1} \quad (\text{E.36})$$

<sup>8</sup> Jean Gaston Darboux (August 13, 1842–February 23, 1917), a French mathematician.

The last equation reveals that the position vector of a point of the *Dupin indicatrix*,  $Dup(\mathcal{S})$ , in any direction is equal to the square root of the radius of curvature in that same direction.<sup>9</sup>

### E.3 DEGREE OF CONFORMITY AT POINT OF CONTACT OF A GEAR AND A MATING PINION TOOTH FLANKS (IN THE FIRST ORDER OF TANGENCY)

For an accurate analytical description of contact geometry of the gear and the mating pinion tooth flanks in the first order of tangency, a higher order analysis is necessary to be done.

The discussed below method of a higher order analysis is targeting the development of an analytical description of degree of conformity of the pinion tooth flank,  $\mathcal{P}$ , to the gear tooth flank,  $\mathcal{S}$ , at a current point,  $K$  of their contact. The higher the degree of conformity of the tooth flanks,  $\mathcal{S}$  and  $\mathcal{P}$ , the closer these surfaces are to each other in differential vicinity of the point,  $K$ . This qualitative (*intuitive*) definition of degree of conformity of two smooth regular surfaces needs in a corresponding quantitative measure.

#### E.3.1 PRELIMINARY REMARKS

Implementation of the resultant deviation,  $l_{cnf}$  (see Figure E.5), of two smooth regular surfaces in contact for the analytical description of contact geometry of two surfaces in contact is a type of straightforward solution to the problem under consideration. This approach is proven to be computational ineffective. However, the approach gives an insight into how an effective method for solving the problem under consideration can be developed.

As seen in Figure E.5, three geometrical parameters are interrelated when a deviation of a surface from the tangent plane is considered in differential vicinity of a surface point. They are:

- the measure of the deviation,  $m_g m_g^*$ , of a gear tooth flank,  $\mathcal{S}$ , from the tangent plane,  $l_{cnf}$ ,
- the distance,  $K m_g^*$ , of a current point,  $m_g$ , from the contact point,  $K$ , and
- radius of normal curvature  $R_g$  of the gear tooth flank,  $\mathcal{S}$ , at the contact point,  $K$ .

As a consequence of this relationship among the parameters,  $m_g m_g^*$ ,  $K m_g^*$ , and  $R_g$ , any one of them can be used for the purposes of quantitative evaluation of degree of conformity of the contacting tooth flanks,  $\mathcal{S}$  and  $\mathcal{P}$ , of the gear and the mating pinion. As it is following from Figure E.5:

$$m_g m_g^* = R_g - \sqrt{R_g^2 - (K m_g^*)^2} \Big|_{m_g \rightarrow K} \mapsto l_{cnf} \quad (E.37)$$

Inversely, for the radius of normal curvature,  $R_g$ , at a point of the gear tooth flank,  $\mathcal{S}$ , the following expression is valid:

$$R_g = \frac{(m_g m_g^*)^2 + (K m_g^*)^2}{2 \cdot m_g m_g^*} \quad (E.38)$$

Ultimately, one may conclude that any legitimate analytical function of normal radii of curvature,  $R_g$  and  $R_p$ , at a point of contact of the gear tooth flank,  $\mathcal{S}$ , and the pinion tooth flank,  $\mathcal{P}$ , can be used for this particular purpose.

<sup>9</sup> Similar to *Dupin indicatrix*,  $Dup(\mathcal{S})$ , a planar characteristic curve of another type can be introduced. Equation of this characteristic curve can be postulated in the form:  $r_{Dup,k}(\varphi) = \sqrt{|k_g(\varphi)|} \cdot \text{sgn } \Phi_{2,g}^{-1}$ . Application of curvature indicatrix in the form,  $r_{Dup,k}(\varphi)$ , makes possible avoiding uncertainty in cases of plane surface. For plane surface, the characteristic curve,  $Dup(\mathcal{S})$ , does not exist, while,  $r_{Dup,k}(\varphi)$ , exists. It shrinks to the point,  $m$ , on the gear tooth flank,  $\mathcal{S}$ .

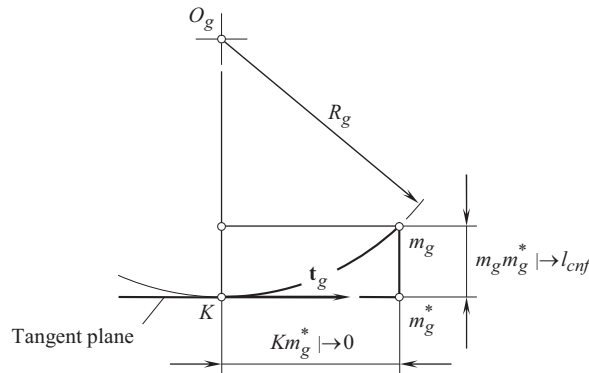


**FIGURE E.5** On transition from the resultant deviation,  $l_{cnf}$ , to indicatrix of conformity,  $Cnf (\mathcal{S} / \mathcal{P})$ , at contact point,  $K$ , between two smooth regular tooth flanks,  $\mathcal{S}$  and  $\mathcal{P}$ .

Consider two smooth regular tooth flanks,  $\mathcal{S}$  and  $\mathcal{P}$ , in the first order of tangency that make contact at a point,  $K$ . Degree of conformity of the tooth flanks,  $\mathcal{S}$  and  $\mathcal{P}$ , can be construed as a function of radii of normal curvature,  $R_g$  and  $R_p$ , of the contacting surfaces. Radii of normal curvature,  $R_g$  and  $R_p$ , of the tooth flanks,  $\mathcal{S}$  and  $\mathcal{P}$ , are taken in a common normal plane section through the point,  $K$ . For a specified radius of normal curvature,  $R_g$ , of the tooth flank,  $\mathcal{S}$ , the degree of conformity of the tooth flanks depends upon the corresponding value of radius of normal curvature,  $R_p$ , of the pinion tooth flank,  $\mathcal{P}$ .

In most cases of gear meshing, degree of conformity at a point of contact of the tooth flanks,  $\mathcal{S}$  and  $\mathcal{P}$ , is not constant and it is changing as coordinates of the contact point change. Degree of the surfaces conformity to one another depends on orientation of the normal plane section through the contact point,  $K$ , and changes as the normal plane section is turning about the common perpendicular,  $\mathbf{n}_g$ . This statement immediately follows from the above-made conclusion that degree of conformity at a point of contact of the tooth flanks,  $\mathcal{S}$  and  $\mathcal{P}$ , yields interpretation in terms of radii of normal curvature,  $R_g$  and  $R_p$ .

The change of degree of conformity of a gear tooth flank,  $\mathcal{S}$ , and a mating pinion tooth flank,  $\mathcal{P}$ , due to turning of the normal plane section about the common perpendicular,  $\mathbf{n}_g$ , is illustrated in Figure E.6. Here, in Figure E.6, just two-dimensional examples are shown, for which that same normal plane section of the gear tooth flank,  $\mathcal{S}$ , makes contact with different plane sections,  $\mathcal{P}^i$ , of the pinion tooth flank,  $\mathcal{P}$ .

In the example shown in Figure E.6a, radius of normal curvature,  $R_p^1$ , of the convex plane section,  $\mathcal{P}^1$ , of the pinion tooth flank,  $\mathcal{P}$ , is positive ( $R_p^1 > 0$ ). Convex normal plane section of the pinion tooth flank,  $\mathcal{P}$ , makes contact with the convex normal plane section ( $R_g > 0$ ) of a gear tooth flank,  $\mathcal{S}$ . The degree of conformity of the pinion tooth flank,  $\mathcal{P}$ , to the gear tooth flank,  $\mathcal{S}$ , in Figure E.6a is relatively low as both the contacting surfaces are convex.

Another example is shown in Figure E.6b. The radius of normal curvature,  $R_p^2$ , of convex plane section,  $\mathcal{P}^2$ , of the pinion tooth flank,  $\mathcal{P}$ , also is positive ( $R_p^2 > 0$ ). However, its value exceeds the value,  $R_p^1$ , of the radius of normal curvature in the first example ( $R_p^2 > R_p^1$ ). This results in that degree of conformity of the pinion tooth flank,  $\mathcal{P}$ , to the gear tooth flank,  $\mathcal{S}$  (Figure E.6b), is greater compared to that shown in Figure E.6a.

In the next example depicted in Figure E.6c, the normal plane section  $\mathcal{P}^3$  of the pinion tooth flank,  $\mathcal{P}$ , is represented with locally flatten section. Radius of normal curvature,  $R_p^3$ , of the flatten plane section,  $\mathcal{P}^3$ , approaches infinity ( $R_p^3 \rightarrow \infty$ ). Thus, the inequality,  $R_p^3 > R_p^2 > R_p^1$ , is valid. Therefore, degree of conformity of the pinion tooth flank,  $\mathcal{P}$ , to the gear tooth flank,  $\mathcal{S}$  in Figure E.6c, is also getting greater.

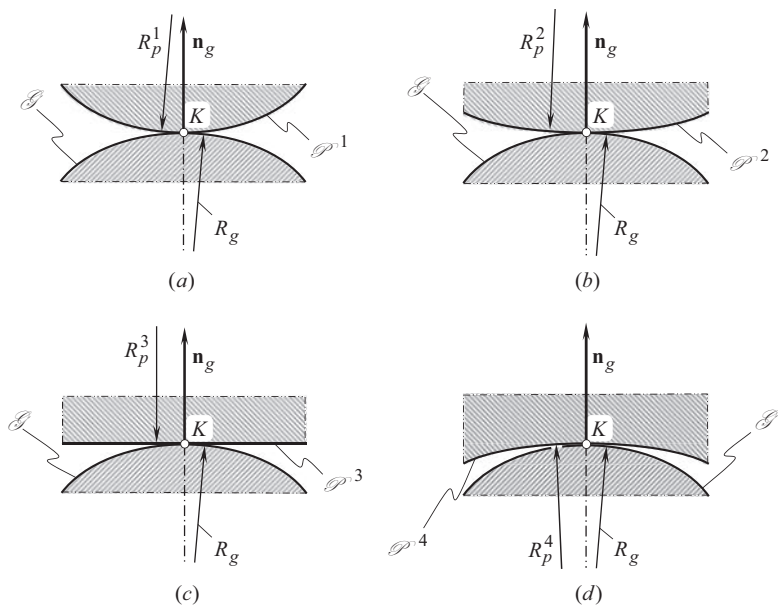


**FIGURE E.6** On analytical description of contact geometry of two smooth regular tooth flanks,  $\mathcal{S}$  and  $\mathcal{P}$ , in contact, by a plane through the common perpendicular: (a) convex-to-convex contact (low level of conformity), (b) convex-to-convex contact (higher level of conformity).

Finally, for a concave normal plane section,  $\mathcal{P}^4$ , of the pinion tooth flank,  $\mathcal{P}$ , that is illustrated in Figure E.6d, radius of normal curvature,  $R_p^4$ , is of negative value ( $R_p^4 < 0$ ). In this case, degree of conformity of the pinion tooth flank,  $\mathcal{P}$ , to the gear tooth flank,  $\mathcal{S}$ , is the greatest of four examples considered in Figure E.6.

The examples shown in Figure E.6, qualitatively illustrate what is known intuitively regarding the different degree of conformity of two smooth regular surfaces in the first order of tangency. Intuitively one can realize that in the examples shown in Figure E.6a–d, degree of conformity at a point of contact of two tooth flanks,  $\mathcal{S}$  and  $\mathcal{P}$ , is gradually increased.

A similar observation is made for a given pair of the tooth flanks,  $\mathcal{S}$  and  $\mathcal{P}$ , when different sections of the surfaces by a plane surface through the common perpendicular,  $\mathbf{n}_g$ , are considered (see Figure E.7a). When rotating the plane section about the common perpendicular,  $\mathbf{n}_g$ , it can be observed that degree of conformity of the gear and the pinion tooth flanks,  $\mathcal{S}$  and  $\mathcal{P}$ , is different in different configurations of the cross-sectional plane (see Figure E.7b).

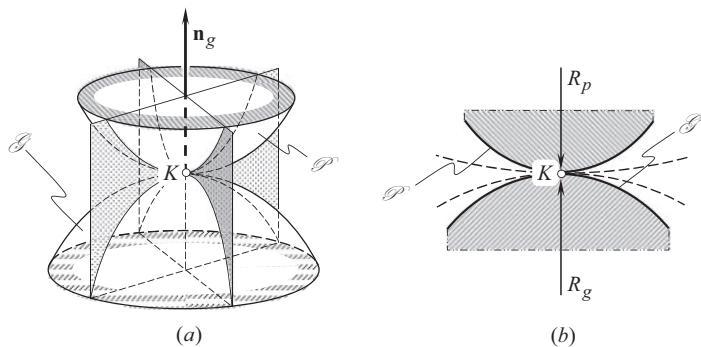


**FIGURE E.7** Sections of two smooth regular tooth flanks,  $\mathcal{S}$  and  $\mathcal{P}$ , of a gear and a mating pinion: (a) close-up, (b) section by a normal plane.

The above examples provide an intuitive understanding of what the degree of conformity at a point of contact of two smooth regular tooth flanks,  $\mathcal{S}$  and  $\mathcal{P}$ , means. The examples cannot be employed directly for the purpose to evaluate in quantities the degree of conformity at a point of contact of two smooth regular tooth flanks,  $\mathcal{S}$  and  $\mathcal{P}$ . The next necessary step to be made up is to introduce an appropriate quantitative evaluation of the degree of conformity of two smooth regular surfaces in the first order of tangency. In other words, how can a certain degree of conformity of two smooth regular surfaces being described analytically?

### E.3.2 INDICATRIX OF CONFORMITY AT POINT OF CONTACT OF TOOTH FLANKS OF A GEAR AND A MATING PINION

This section is aiming introduction of a quantitative measure of degree of conformity at a point of contact between two smooth regular surfaces. The degree of conformity at a point of contact of two tooth flanks,  $\mathcal{S}$  and  $\mathcal{P}$ , indicates how the pinion tooth flank,  $\mathcal{P}$ , is close to the gear tooth flank,  $\mathcal{S}$ , in differential vicinity of a point,  $K$ , of their contact, say how much the surface,  $\mathcal{P}$ , is *congruent* to the surface,  $\mathcal{S}$ , in differential vicinity of the contact point,  $K$ . This particular type of congruency between the contacting surfaces,  $\mathcal{S}$  and  $\mathcal{P}$ , can also be construed as the *local congruency* of the contacting surfaces.

Quantitatively, the degree of conformity at a point of contact of a smooth regular surface,  $\mathcal{P}$ , to another surface,  $\mathcal{S}$ , can be expressed in terms of the difference between the corresponding radii of normal curvature of the contacting surfaces. In order to develop a quantitative measure of the degree of conformity of the tooth flanks,  $\mathcal{S}$  and  $\mathcal{P}$ , it is convenient to implement *Dupin indicatrices*,  $Dup(\mathcal{S})$  and  $Dup(\mathcal{P})$ , constructed at a point of contact of the gear tooth flank,  $\mathcal{S}$ , and the pinion tooth flank,  $\mathcal{P}$ , correspondingly.

It is natural to assume that the smaller difference between the normal curvatures of the surfaces,  $\mathcal{S}$  and  $\mathcal{P}$ , in a common cross-section by a plane through the common normal vector,  $\mathbf{n}_g$ , results in a greater degree of conformity at a point of contact of the tooth flanks,  $\mathcal{S}$  and  $\mathcal{P}$ .

*Dupin indicatrix*,  $Dup(\mathcal{S})$  indicates the distribution of radii of normal curvature at a point of the gear tooth flank,  $\mathcal{S}$ , as it had been shown, for example, for a concave elliptic patch of the surface,  $\mathcal{S}$  (see Figure E.8). For a gear tooth flank,  $\mathcal{S}$ , equation of this characteristic curve in polar coordinates can be represented in the following form:

$$Dup(\mathcal{S}) \Rightarrow r_g(\varphi_g) = \sqrt{|R_g(\varphi_g)|} \quad (\text{E.39})$$

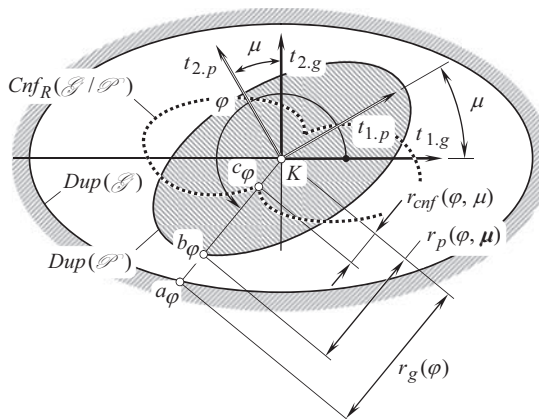


**FIGURE E.8** On the definition of the indicatrix of conformity,  $Cnf_R(\mathcal{P} \mapsto \mathcal{S})$ , at point of contact of tooth flanks,  $\mathcal{S}$  and  $\mathcal{P}$ . (After Prof. S.P. Radzevich: Radzevich, S.P., *Differential-Geometric Method of Surface Generation*, Dr.Sci. Thesis, Tula, Tula Polytechnic Institute, 1991, 300 pages.)

where

$r_g$  is the position vector of a point of the *Dupin indicatrix*,  $Dup(\mathcal{S})$  at a point of the gear tooth flank,  $\mathcal{S}$ .

$\varphi_g$  is the polar angle of the indicatrix,  $Dup(\mathcal{S})$ .

The similar is true with respect to the *Dupin indicatrix*,  $Dup(\mathcal{P})$  at a point of the pinion tooth flank,  $\mathcal{P}$ , as it had been shown, for instance, for a convex elliptical patch of the pinion tooth flank,  $\mathcal{P}$  (see Figure E.8). Equation of this characteristic curve in polar coordinates can be represented in the following form:

$$Dup(\mathcal{P}) \Rightarrow r_p(\varphi_p) = \sqrt{|R_p(\varphi_p)|} \quad (E.40)$$

where

$r_p$  is the position vector of a point of the *Dupin indicatrix*,  $Dup(\mathcal{P})$  at a point of the pinion tooth flank,  $\mathcal{P}$ .

$\varphi_p$  is the polar angle of the indicatrix,  $Dup(\mathcal{P})$ .

In the coordinate plane,  $x_g y_g$ , of the local reference system,  $x_g y_g z_g$ , the equalities,  $\varphi_g = \varphi$  and  $\varphi_p = \varphi + \mu$ , are valid. Therefore, in the coordinate plane,  $x_g y_g$ , Eqs. (E.39) and (E.40) cast into:

$$Dup(\mathcal{S}) \Rightarrow r_g(\varphi) = \sqrt{|R_g(\varphi)|} \quad (E.41)$$

$$Dup(\mathcal{P}) \Rightarrow r_p(\varphi, \mu) = \sqrt{|R_p(\varphi, \mu)|} \quad (E.42)$$

When degree of conformity at a point of contact of the to the gear tooth flank,  $\mathcal{S}$ , is greater, then the difference between the functions  $r_g(\varphi)$  and  $r_p(\varphi, \mu)$  becomes smaller and vice versa. The last makes valid the following conclusion:

**Conclusion E.1.** *The distance between the corresponding<sup>10</sup> points of the Dupin indicatrices,  $Dup(\mathcal{S})$  and  $Dup(\mathcal{P})$ , constructed at a point of contact of a gear tooth flank,  $\mathcal{S}$  and a mating pinion tooth flank,  $\mathcal{P}$ , can be employed for the purpose of indication of the degree of conformity at a point of contact of the gear tooth flank,  $\mathcal{S}$  and of the pinion tooth flank,  $\mathcal{P}$ , at the contact point,  $K$ .*

The equation of the *indicatrix of conformity*,  $Cnf_R(\mathcal{S} / \mathcal{P})$  at a point of contact of a gear tooth flank,  $\mathcal{S}$ , and a mating pinion tooth flank,  $\mathcal{P}$ , is defined by the following structure:

$$\begin{aligned} Cnf_R(\mathcal{S} / \mathcal{P}) \Rightarrow r_{cnf}(\varphi, \mu) &= \sqrt{|R_g(\varphi)|} \operatorname{sgn} R_g(\varphi) + \sqrt{|R_p(\varphi, \mu)|} \operatorname{sgn} R_p(\varphi, \mu) = \\ &= r_g(\varphi) \operatorname{sgn} R_g(\varphi) + r_p(\varphi, \mu) \operatorname{sgn} R_p(\varphi, \mu) \end{aligned} \quad (E.43)$$

Because of the location of a point,  $a_\varphi$ , of the *Dupin indicatrix*,  $Dup(\mathcal{S})$  at a point of the gear tooth flank,  $\mathcal{S}$ , is specified by the position vector,  $r_g(\varphi)$ , and the location of a point,  $b_\varphi$ , of the *Dupin indicatrix*,  $Dup(\mathcal{P})$  at a point of the pinion tooth flank,  $\mathcal{P}$ , is specified by the position vector,  $r_p(\varphi, \mu)$ , then the location of a point,  $c_\varphi$  (see Figure E.8) of the *indicatrix of conformity*,  $Cnf_R(\mathcal{S} / \mathcal{P})$

<sup>10</sup> Corresponding points of the *Dupin indicatrices*,  $Dup(\mathcal{S})$  and  $Dup(\mathcal{P})$ , share the same straight line through the contact point,  $K$ , of the tooth flanks,  $\mathcal{S}$  and  $\mathcal{P}$ , and are located at the same side of the point,  $K$ .



at a point of contact,  $K$ , of the tooth flanks,  $\mathcal{S}$  and  $\mathcal{P}$ , is specified by the position vector  $r_{cnf}(\varphi, \mu)$ . Therefore, the equality  $r_{cnf}(\varphi, \mu) = Kc_\varphi$  is observed, and the length of the straight-line segment,  $Kc_\varphi$ , is equal to the distance,  $a_\varphi b_\varphi$ .

Here, in Eq. (E.43) is designated:

$r_g = \sqrt{|R_g|}$  is the position vector of a point of *Dupin indicatrix* of the gear tooth flank,  $\mathcal{S}$ , at a point  $K$  of contact with pinion tooth flank,  $\mathcal{P}$ .  
 $r_p = \sqrt{|R_p|}$  is the position vector of a corresponding point of the *Dupin indicatrix* of the pinion tooth flank,  $\mathcal{P}$ .

Here, in Eq. (E.43), the multipliers  $\text{sgn } R_g(\varphi)$  and  $\text{sgn } R_p(\varphi, \mu)$  are assigned to each of the functions,  $r_g(\varphi) = \sqrt{|R_g(\varphi)|}$  and  $r_p(\varphi, \mu) = \sqrt{|R_p(\varphi, \mu)|}$ , accordingly just for the purpose to remain the corresponding sign of the functions, that is, to remain that same sign that the radii of normal curvature,  $R_g(\varphi)$  and  $R_p(\varphi, \mu)$ , have.

Ultimately, one can conclude that position vector,  $r_{cnf}$ , of a point of the *indicatrix of conformity*,  $Cnf_R(\mathcal{S} / \mathcal{P})$  can be expressed in terms of position vectors,  $r_g$  and  $r_p$ , of the *Dupin indicatrices*,  $Dup(\mathcal{S})$  and  $Dup(\mathcal{P})$ .

For the calculation of a current value of the radius of normal curvature,  $R_g(\varphi)$ , at point of the gear tooth flank,  $\mathcal{S}$ , the equality:

$$R_g(\varphi) = \frac{\Phi_{1,g}}{\Phi_{2,g}} \quad (\text{E.44})$$

can be used.

Similarly, for the calculation of the current value of the radius of normal curvature,  $R_p(\varphi, \mu)$ , at point of pinion tooth flank,  $\mathcal{P}$ , the equality:

$$R_p(\varphi, \mu) = \frac{\Phi_{1,p}}{\Phi_{2,p}} \quad (\text{E.45})$$

can be employed.

Use of the angle,  $\mu$ , of local relative orientation of the tooth flanks,  $\mathcal{S}$  and  $\mathcal{P}$ , indicates that the radii of normal curvature,  $R_g(\varphi)$  and  $R_p(\varphi, \mu)$ , are taken in a common normal plane section through the contact point,  $K$ .

Further, it is well-known that the inequalities,  $\Phi_{1,g} \geq 0$  and  $\Phi_{1,p} \geq 0$ , are always valid. Therefore, Eq. (E.43) can be rewritten in the following form:

$$r_{cnf} = r_g(\varphi) \text{sgn } \Phi_{2,g}^{-1} + r_p(\varphi, \mu) \text{sgn } \Phi_{2,p}^{-1} \quad (\text{E.46})$$

For the derivation of an equation of the *indicatrix of conformity*,  $Cnf_R(\mathcal{S} / \mathcal{P})$ , it is convenient to use the *Euler equation* for normal radius of curvature,  $R_g(\varphi)$ , at a point of the gear tooth flank,  $\mathcal{S}$ :

$$R_g(\varphi) = \frac{R_{1,g} \cdot R_{2,g}}{R_{1,g} \cdot \sin^2 \varphi + R_{2,g} \cdot \cos^2 \varphi} \quad (\text{E.47})$$

Here, the radii of principal curvature,  $R_{1,g}$  and  $R_{2,g}$ , are the roots of the quadratic equation:

$$\begin{vmatrix} L_g \cdot R_g - E_g & M_g \cdot R_g - F_g \\ M_g \cdot R_g - F_g & N_g \cdot R_g - G_g \end{vmatrix} = 0 \quad (\text{E.48})$$

Recall, that the inequality,  $R_{1,g} < R_{2,g}$ , is always observed.

Equations (E.47) and (E.48) allow for the expression of the radius of normal curvature,  $R_g(\varphi)$ , at a point of the gear tooth flank,  $\mathcal{G}$ , in terms of the fundamental magnitudes of the first order,  $E_g$ ,  $F_g$ , and  $G_g$ , and of the fundamental magnitudes of the second order,  $L_g$ ,  $M_g$ , and  $N_g$ .

A similar consideration is applicable for the pinion tooth flank,  $\mathcal{P}$ . Omitting routing analysis, one can conclude that the radius of normal curvature,  $R_p(\varphi, \mu)$ , of the at a point of the pinion tooth flank,  $\mathcal{P}$ , can be expressed in terms of the fundamental magnitudes of the first order,  $E_p$ ,  $F_p$ , and  $G_p$ , and of the fundamental magnitudes of the second order,  $L_p$ ,  $M_p$ , and  $N_p$ .

Finally, on the premise of the above-performed analysis, the following equation for the *indicatrix of conformity*,  $Cnf_R(\mathcal{G} \mid \mathcal{P})$  at a point of contact of the tooth flanks,  $\mathcal{G}$  and  $\mathcal{P}$ , can be derived:

$$r_{cnf}(\varphi, \mu) = \sqrt{\frac{E_g G_g}{L_g G_g \cos^2 \varphi - M_g \sqrt{E_g G_g} \sin 2\varphi + N_g E_g \sin^2 \varphi}} \operatorname{sgn} \Phi_{2,g}^{-1} + \sqrt{\frac{E_p G_p}{L_p G_p \cos^2(\varphi + \mu) - M_p \sqrt{E_p G_p} \sin 2(\varphi + \mu) + N_p E_p \sin^2(\varphi + \mu)}} \operatorname{sgn} \Phi_{2,p}^{-1} \quad (\text{E.49})$$

Equation (E.49) of the characteristic curve<sup>11</sup>  $Cnf_R(P/T)$  is known from the late 1970s.

Analysis of Eq. (E.49) reveals that the *indicatrix of conformity*,  $Cnf_R(\mathcal{G} \mid \mathcal{P})$  at a point of contact of a gear tooth flank,  $\mathcal{G}$ , and the mating pinion tooth flank,  $\mathcal{P}$ , is represented by a planar centro-symmetrical curve of the fourth order. In particular cases, this characteristic curve possesses also a property of mirror symmetry. Mirror symmetry of the indicatrix of conformity is observed, for example, when the angle,  $\mu$ , of local relative orientation of the tooth flanks,  $\mathcal{G}$  and  $\mathcal{P}$ , is equal  $\mu = \pm \pi \cdot n / 2$ , where  $n$  designates an integer number.

It is important to notice here, that even for the most general case of gearing, the position vector of a point,  $r_{cnf}(\varphi, \mu)$ , of the *indicatrix of conformity*,  $Cnf_R(\mathcal{G} \mid \mathcal{P})$  is not dependent on the fundamental magnitudes,  $F_g$  and  $F_p$ . Independence of the *indicatrix of conformity*,  $Cnf_R(\mathcal{G} \mid \mathcal{P})$  of the fundamental magnitudes,  $F_g$  and  $F_p$ , is because of the following.

Coordinate angle,  $\omega_g$ , at a point of the gear tooth flank,  $\mathcal{G}$ , can be calculated from the formula:

$$\omega_g = \arccos \frac{F_g}{\sqrt{E_g G_g}} \quad (\text{E.50})$$

It is natural that the position vector,  $r_{cnf}(\varphi, \mu)$ , of a point of the indicatrix of conformity,  $Cnf_R(\mathcal{G} \mid \mathcal{P})$ , is not a function of the coordinate angle,  $\omega_g$ . Although the position vector,  $r_{cnf}(\varphi, \mu)$ , depends on the fundamental magnitudes,  $E_g$ ,  $G_g$  and  $E_p$ ,  $G_p$ , the above analysis makes it clear why the position vector,  $r_{cnf}(\varphi, \mu)$ , does not depend upon the fundamental magnitudes  $F_g$  and  $F_p$ .

Two illustrative examples of the *indicatrix of conformity*,  $Cnf_R(\mathcal{G} \mid \mathcal{P})$  at a point of contact of a gear tooth flank,  $\mathcal{G}$ , and a mating pinion tooth flank,  $\mathcal{P}$ , are shown in Figure E.9. The first example (see Figure E.9a) relates to the cases of contact of a saddle-like local patch of the tooth surface,  $\mathcal{G}$ , and of a convex elliptic-like local patch of tooth surface,  $\mathcal{P}$ . The second one (see Figure E.9b) is for the case of contact of a convex parabolic-like local patch of the tooth surface,  $\mathcal{G}$ , and of a convex elliptic-like local patch of tooth,  $\mathcal{P}$ . For both cases (see Figure E.9), the corresponding curvature indicatrices  $Crv(\mathcal{G})$

<sup>11</sup> Equation of this characteristic curve is known from:

- Pat. No.1249787, USSR, *A Method of Sculptured Part Surface Machining on a Multi-Axis NC Machine*, S.P. Radzevich, B23C 3/16, Filed: December 27, 1984, and (in hidden form) from:
- Pat. No.1185749, USSR, *A Method of Sculptured Part Surface Machining on a Multi-Axis NC Machine*, S.P. Radzevich, B23C 3/16, Filed: October 24, 1983.

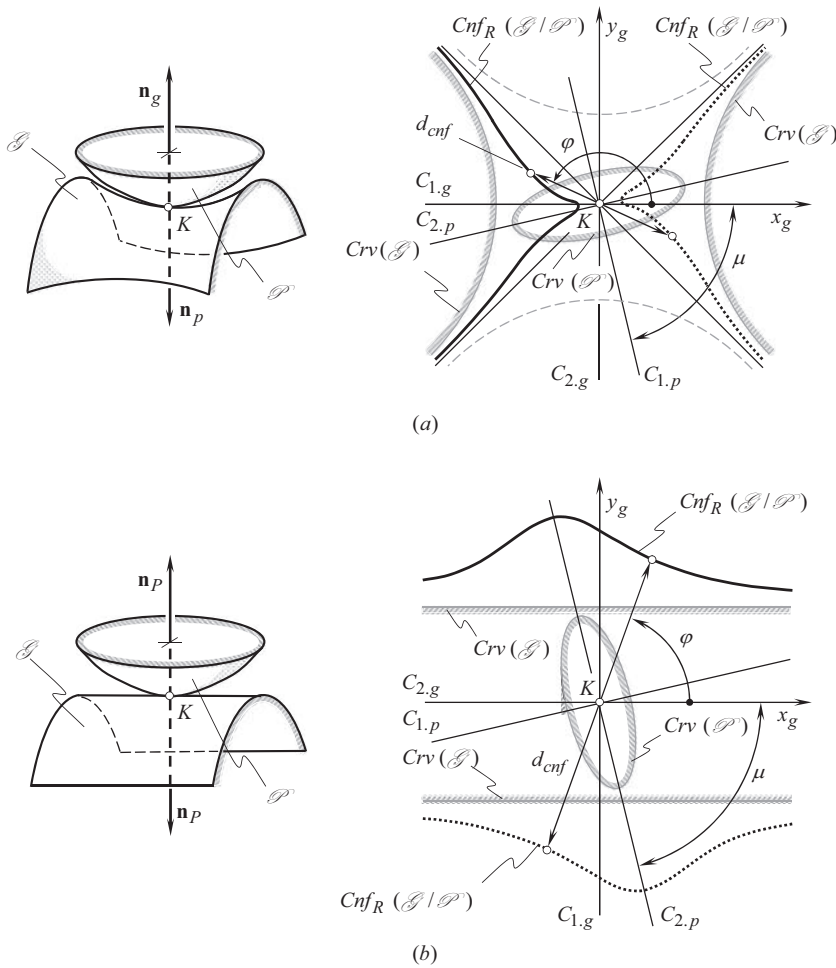


**FIGURE E.9** Examples of indicatrix of conformity,  $Cnf_R(\mathcal{S}/\mathcal{P})$ , at point of contact,  $K$ , of a smooth regular gear tooth flank,  $\mathcal{S}$ , and a mating pinion tooth flank,  $\mathcal{P}$ : (a) elliptical-to-hyperbolical contact of the surfaces; and (b) elliptical-to-parabolical contact of the surfaces.

and  $Crv(\mathcal{P})$  at the point of contact of the tooth flanks,  $\mathcal{S}$  and  $\mathcal{P}$ , are depicted in Figure E.9 as well. The imaginary (phantom) branches of the *Dupin indicatrix*,  $Dup(\mathcal{S})$  (not labeled in Figure E.9a) for the saddle-like local patch of the gear tooth flank,  $\mathcal{S}$ , are shown in a dashed line (see Figure E.9a).

A gear tooth flank,  $\mathcal{S}$ , and the pinion tooth flank,  $\mathcal{P}$ , can make contact geometrically however physical conditions of their contact could be violated. Violation of the physical condition of contact results in that the bodies those bounded by the contacting surfaces,  $\mathcal{S}$  and  $\mathcal{P}$ , interfering with one another. Implementation of the *indicatrix of conformity*,  $Cnf_R(\mathcal{S}/\mathcal{P})$  immediately uncovers the surfaces interference if there is any. Three illustrative examples of the violation of physical condition of contact are illustrated in Figure E.10. When correspondence between the radii of the normal curvature of the contacting tooth flanks,  $\mathcal{S}$  and  $\mathcal{P}$ , is inappropriate, then the *indicatrix of conformity*,  $Cnf_R(\mathcal{S}/\mathcal{P})$  either intersects itself (see Figure E.10a) or all of its diameters become negative (see Figure E.10b and c).

Another interpretation of satisfaction and violation of physical condition of contact of two smooth regular tooth flanks,  $\mathcal{S}$  and  $\mathcal{P}$ , is illustrated in Figure E.11. Condition of physical contact is fulfilled when all diameters of the *indicatrix of conformity*,  $Cnf_R(\mathcal{S}/\mathcal{P})$  are positive. In this case, the gear tooth flank,  $\mathcal{S}$ , and the mating pinion tooth flank,  $\mathcal{P}$ , may contact one another like two rigid

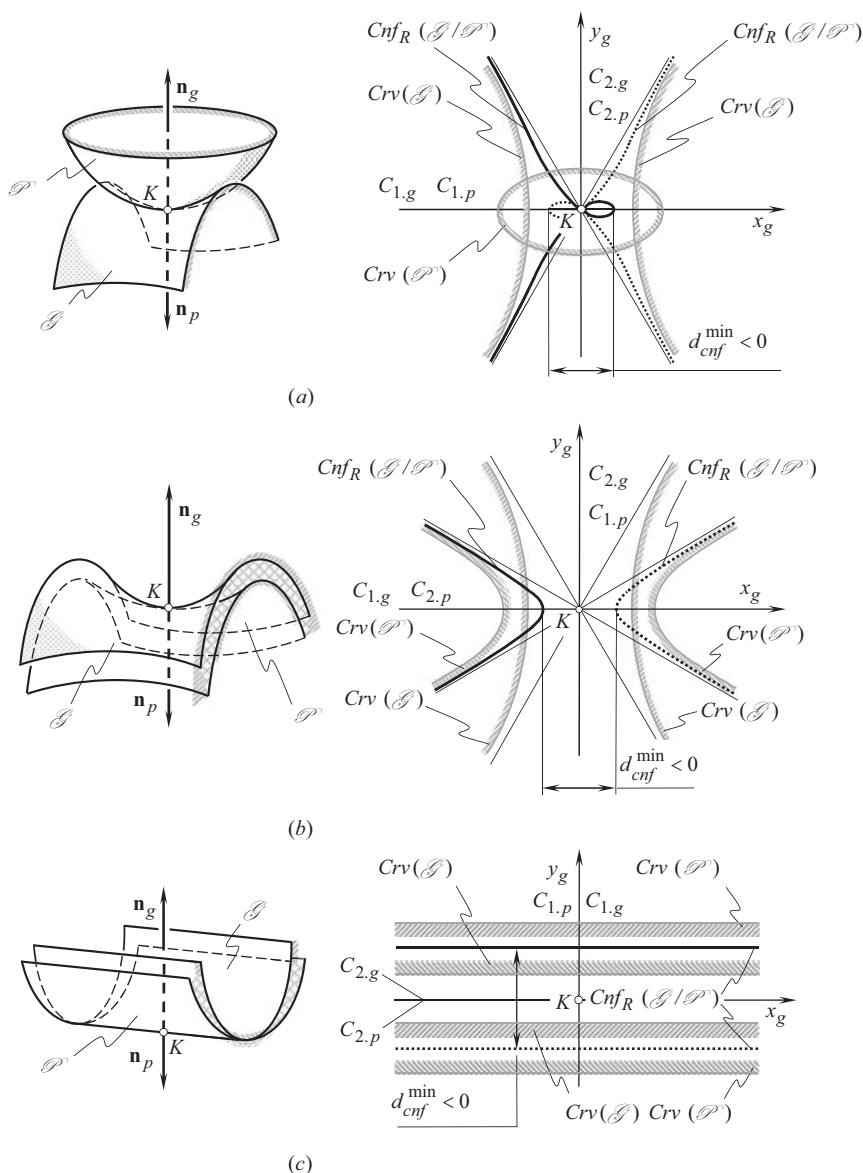


**FIGURE E.10** Examples of violation of physical condition of contact of a smooth regular gear tooth flank,  $\mathcal{S}$  and a mating pinion tooth flank,  $\mathcal{P}$ : (a) elliptical-to-hyperbolic contact of the surfaces; (b) hyperbolic-to-hyperbolic contact of the surfaces; and (c) parabolical-to-parabolical contact of the surfaces.

bodies do. An example of the *indicatrix of conformity*,  $Cnf_R(\mathcal{S}/\mathcal{P})$  for such a case is depicted in Figure E.11a. In cases when this planar characteristic curve has negative diameters as it is schematically shown in Figure E.11b, the physical contact between the tooth flanks,  $\mathcal{S}$  and  $\mathcal{P}$ , is infeasible.

The value of the current diameter<sup>12</sup>  $d_{cnf}$  of the *indicatrix of conformity*,  $Cnf_R(\mathcal{S}/\mathcal{P})$  indicates the degree of conformity to each other of the gear tooth flank,  $\mathcal{S}$ , and the mating pinion tooth flank,  $\mathcal{P}$ , in a corresponding cross-section of the surfaces by normal plane through the common

<sup>12</sup>Diameter of a symmetrical that possesses a property of central symmetry, curve can be defined as a distance between two points of the curve, measured along the corresponding straight line through the center of symmetry of the curve.

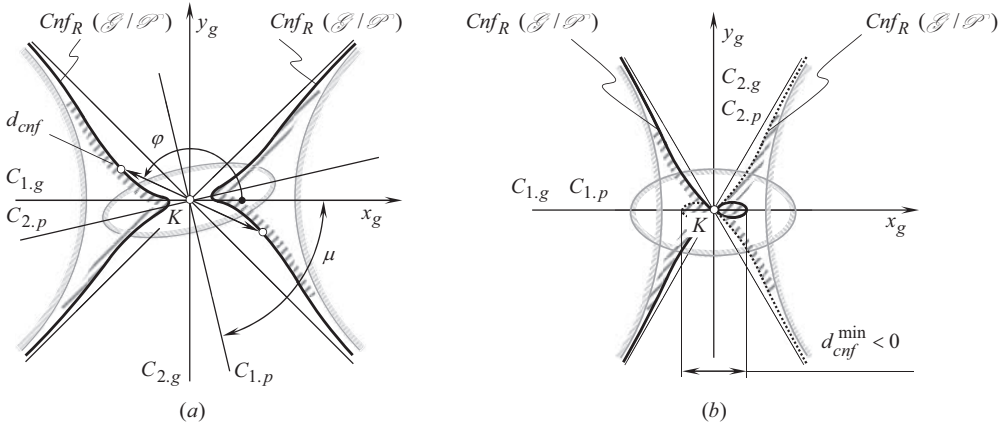


**FIGURE E.11** Another interpretation of satisfaction (a) and of violation (b) of condition of physical contact of a smooth regular gear tooth flank,  $\mathcal{S}$ , and a mating pinion tooth flank,  $\mathcal{P}$ .

perpendicular. The orientation of the normal plane section with respect to the tooth flanks,  $\mathcal{S}$  and  $\mathcal{P}$ , is specified by the corresponding central angle,  $\varphi$ .

For the orthogonally parameterized gear tooth flank,  $\mathcal{S}$ , and the mating pinion tooth flank,  $\mathcal{P}$ , equation of the *Dupin indicatrices*,  $Dup(\mathcal{S})$  and  $Dup(\mathcal{P})$ , simplifies to:

$$L_g x_g^2 + 2M_g x_g y_g + N_g y_g^2 = \pm 1 \quad (\text{E.51})$$

$$L_p x_p^2 + 2M_p x_p y_p + N_p y_p^2 = \pm 1 \quad (\text{E.52})$$

After being represented in a common reference system, the use of Eqs. (E.51) and (E.52) make possible a simplified equation of the *indicatrix of conformity*,  $Cnf_R(\mathcal{S}|\mathcal{P})$  at a point of contact of the tooth flanks,  $\mathcal{S}$  and  $\mathcal{P}$ :

$$\begin{aligned} r_{cnf}(\varphi, \mu) = & (L_g \cos^2 \varphi - M_g \sin 2\varphi + N_g \sin^2 \varphi)^{-0.5} \text{sgn } \Phi_{2,g}^{-1} + \\ & + [L_p \cos^2(\varphi + \mu) - M_p \sin 2(\varphi + \mu) + N_p \sin^2(\varphi + \mu)]^{-0.5} \text{sgn } \Phi_{p,T}^{-1} \end{aligned} \quad (\text{E.53})$$

Equation (E.53) is valid for the orthogonally parameterized tooth flanks,  $\mathcal{S}$  and  $\mathcal{P}$ .

When designing gears, a reasonable degree of conformity,  $cnf_{res}$ , at point of contact of a gear,  $\mathcal{S}$ , and a mating pinion,  $\mathcal{P}$ , tooth flanks is a trade-off between the desirable maximal degree of conformity,  $cnf_{max}$  (max bearing capacity), and a minimal permissible degree of conformity,  $cnf_{min}$  (min sensitivity to the axes misalignment), that is, the inequality  $cnf_{min} < cnf_{res} < cnf_{max}$  is observed.

### E.3.3 VECTOR, AND MATRIX REPRESENTATION OF INDICATRIX OF CONFORMITY

Equation (E.49) of the indicatrix of conformity,  $Cnf_R(\mathcal{S}|\mathcal{P})$ , at point of contact of tooth flanks of a gear, and of a mating pinion,  $\mathcal{S}$  and  $\mathcal{P}$ , yields representation in both vector and matrix forms.

Consider a unit tangent vector,  $\mathbf{t}_{cnf}(\varphi)$ , through contact point,  $K$ , in a common section of the contacting surfaces,  $\mathcal{S}$  and  $\mathcal{P}$ , by a normal plane. The unit tangent vector,  $\mathbf{t}_{cnf}(\varphi)$ , is entirely located in a common tangent plane through contact point,  $K$ . In a common normal section, radii of curvature of the tooth flanks,  $\mathcal{S}$  and  $\mathcal{P}$ , are designated as  $R_g$  and  $R_p$ , correspondingly. For convenience, the following designation is used here:  $r_g(\varphi) = \sqrt{R_g(\varphi)}$  and  $r_p(\varphi + \mu) = \sqrt{R_p(\varphi + \mu)}$ .

The position vector,  $\mathbf{r}_{cnf}$ , of point of the indicatrix of conformity at point of contact of tooth flanks,  $\mathcal{S}$  and  $\mathcal{P}$ , of a gear and a mating pinion can be expressed in terms of the parameters  $r_g$  and  $r_p$  as follows:

$$\mathbf{r}_{cnf}(\varphi + \mu) = [r_g(\varphi) - r_p(\varphi + \mu)] \cdot \mathbf{t}_{cnf}(\varphi) \quad (\text{E.54})$$

In a conventional equation for  $Cnf_R(\mathcal{S} / \mathcal{P})$ , the distance,  $r_{cnf}(\varphi)$ , can be replaced with,  $\mathbf{r}_{cnf}$ , after the corresponding expression for  $Cnf_R(\mathcal{S} / \mathcal{P})$  is multiplied by  $\mathbf{t}_{cnf}(\varphi)$ .

The unit vector,  $\mathbf{t}_{cnf}(\varphi)$ , can be expressed in terms of fundamental magnitudes of the first and the second order at a point of contact,  $K$ , of tooth flanks,  $\mathcal{S}$  and  $\mathcal{P}$ , of a gear and a mating pinion.

Matrix representation of the indicatrix of conformity,  $Cnf_R(\mathcal{S} / \mathcal{P})$ , follows immediately:

$$\mathbf{r}_{cnf}(\varphi, \mu) = \begin{bmatrix} r_{cnf}(\varphi, \mu) \cos \varphi \\ r_{cnf}(\varphi, \mu) \sin \varphi \\ 0 \\ 1 \end{bmatrix} \quad (\text{E.55})$$

Equation of the indicatrix of conformity,  $Cnf_R(\mathcal{S} / \mathcal{P})$ , in matrix form [see Eq. (E.55)] is preferred when this characteristic curve ( $Cnf_R(\mathcal{S} / \mathcal{P})$ ) is involved in a multiple coordinate system transformation.

#### E.3.4 DIRECTIONS OF EXTREMUM DEGREE OF CONFORMITY AT POINT OF CONTACT OF TOOTH FLANKS OF A GEAR AND A MATING PINION

The directions, those along which degree of conformity at a point of contact of a gear tooth flank,  $\mathcal{S}$ , and a mating pinion tooth flank,  $\mathcal{P}$ , is extremum – that is, degree of conformity reaches either maximal of its value or minimal of its value, are of prime importance for engineering applications. This issue is especially important for synthesizing a favorable gear pair.

The directions of extremal degree of conformity of the contacting smooth regular tooth flanks,  $\mathcal{S}$  and  $\mathcal{P}$ , that is, the directions pointed along the extremal diameters,  $d_{cnf}^{\min}$  and  $d_{cnf}^{\max}$ , of the *indicatrix of conformity*,  $Cnf_R(\mathcal{S} / \mathcal{P})$ , can be found from the equation of the *indicatrix of conformity*,  $Cnf_R(\mathcal{S} / \mathcal{P})$ . For the reader's convenience, the equation of this characteristic curve is transformed and is represented in the following form:

$$r_{cnf}(\varphi, \mu) = \sqrt{|r_{1,g} \cos^2 \varphi + r_{2,g} \sin^2 \varphi|} \operatorname{sgn} \Phi_{2,g}^{-1} + \sqrt{|r_{1,p} \cos^2(\varphi + \mu) + r_{2,p} \sin^2(\varphi + \mu)|} \operatorname{sgn} \Phi_{2,p}^{-1} \quad (\text{E.56})$$

Two directions within the common tangent plane are specified by the angles,  $\varphi_{\min}$  and  $\varphi_{\max}$ . These directions feature an extremum degree of conformity of the pinion tooth flank,  $\mathcal{P}$ , to the gear tooth flank,  $\mathcal{S}$ . The angles are the roots of equation:

$$\frac{\partial}{\partial \varphi} r_{cnf}(\varphi, \mu) = 0. \quad (\text{E.57})$$

It can be easily proved that in general case of contact of two smooth regular tooth flanks,  $\mathcal{S}$  and  $\mathcal{P}$ , the difference between the angles,  $\varphi_{\min}$  and  $\varphi_{\max}$ , is not equal to  $0.5\pi$ . This means that the equality

$$\varphi_{\min} - \varphi_{\max} = \pm 0.5\pi n \quad (\text{E.58})$$

is not always observed, and in most cases the relationship:

$$\varphi_{\min} - \varphi_{\max} \neq \pm 0.5\pi n \quad (\text{E.59})$$

is valid (here  $n$  is an integer number). The condition [see Eq. (E.58)]:  $\varphi_{\min} = \varphi_{\max} \pm 0.5\pi n$  is fulfilled only in cases when the angle,  $\mu$ , of local relative orientation of the contacting surfaces,  $\mathcal{S}$  and  $\mathcal{P}$ , is equal to  $\mu = \pm 0.5\pi n$ , and thus the principal directions,  $\mathbf{t}_{1,g}$  and  $\mathbf{t}_{2,g}$ , of the gear tooth flank,  $\mathcal{S}$ , and the principal directions,  $\mathbf{t}_{1,p}$  and  $\mathbf{t}_{2,p}$ , of the mating pinion tooth flank,  $\mathcal{P}$ , either aligned to each other or they are directed oppositely.

This enables one making the following statement:

### Statement E.1

In general case of contact of two smooth regular tooth flanks, the directions along which degree of conformity of the tooth flanks,  $\mathcal{S}$  and  $\mathcal{P}$ , is extremal are not orthogonal to one another. This statement is important for engineering applications. Solution to equation,  $\partial r_{\text{rel}}(\varphi) / \partial \varphi = 0$ , returns two extremal angles,  $\varphi_{\min}$  and  $\varphi_{\max} = \varphi_{\min} + 90^\circ$  [here  $r_{\text{rel}}(\varphi)$  denotes position vector of a point of *Dupin indicatrix* at point of the surface of relative curvature]. Equation (E.57) allows for two solutions,  $\varphi_{\min}^*$  and  $\varphi_{\max}^*$ . Therefore, the extremal difference:

$$\Delta\varphi_{\min} = \varphi_{\min} - \varphi_{\min}^* \quad (\text{E.60})$$

as well as the extremal difference:

$$\Delta\varphi_{\max} = \varphi_{\max} - \varphi_{\max}^* \quad (\text{E.61})$$

can be easily calculated.

In general, neither the extremal difference,  $\Delta\varphi_{\min}$ , nor the extremal difference,  $\Delta\varphi_{\max}$ , is equal to zero. They are equal to zero only in particular cases, say when the angle,  $\mu$ , of local relative orientation of the surfaces,  $\mathcal{S}$  and  $\mathcal{P}$ , fulfills the relationship  $\mu = \pm 0.5\pi n$ . Let us consider an example that illustrates Statement E.1.

### Example

As an illustrative example, let us describe analytically contact geometry of two convex parabolic patches of the contacting tooth flanks,  $\mathcal{S}$  and  $\mathcal{P}$  (see Figure E.12). The example pertains to finishing a helical involute gear by a disk-type shaving cutter. In the example under consideration, the design parameters of the gear and of the shaving cutter, along with the specified the gear and the shaving cutter configuration yield the following numerical data for the calculation. At the point,  $K$ , of the tooth flanks contact, principal curvatures of the gear tooth flank,  $\mathcal{S}$ , are equal  $k_{1,g} = 4\text{mm}^{-1}$  and  $k_{2,g} = 0$ . Principal curvatures of the mating pinion tooth flank,  $\mathcal{P}$ , are equal  $k_{1,p} = 1\text{mm}^{-1}$  and  $k_{2,p} = 0$ . The angle,  $\mu$ , of local relative orientation of the tooth flanks,  $\mathcal{S}$  and  $\mathcal{P}$ , is equal  $\mu = 45^\circ$ .

Two approaches can be implemented for the analytical description of the contact geometry of the tooth flanks,  $\mathcal{S}$  and  $\mathcal{P}$ . The first one is based on the implementation of *Dupin indicatrix* of the surface of relative curvature. The second one is based on the application of the *indicatrix of conformity*,  $Cnf_R(\mathcal{S}|\mathcal{P})$  constructed at a contact point,  $K$ , of the interacting tooth flanks,  $\mathcal{S}$  and  $\mathcal{P}$ .

The first approach. In the case under consideration, normal curvature  $K_R$  of the surface of relative curvature,  $\kappa$ , can be analytically expressed as:

$$k_R = k_{1,g} \cos^2 \varphi - k_{1,p} \cos^2 (\varphi + \mu) \quad (\text{E.62})$$

Therefore, the following equality:



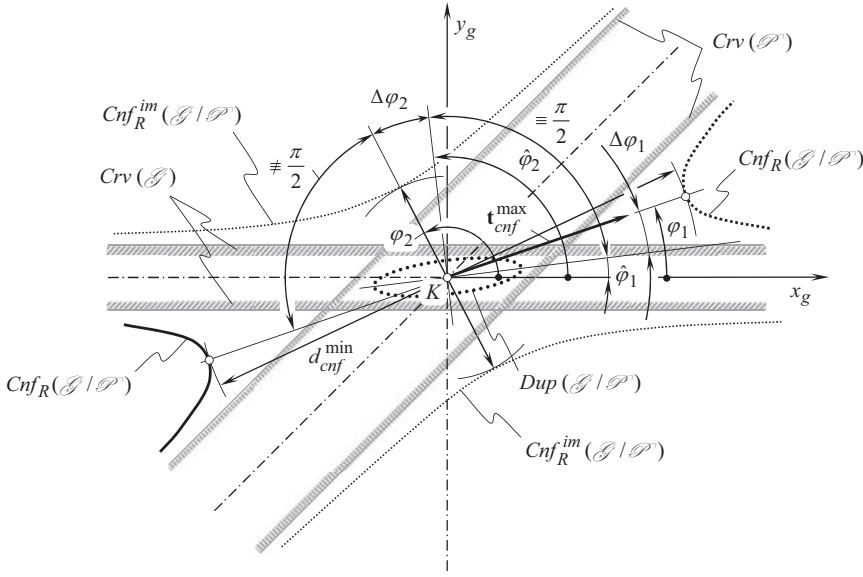


FIGURE E.12 Example: Determination of the optimum instantaneous kinematics in a gear shaving operation.

$$\frac{\partial k_R}{\partial \varphi} = -2k_{1,g} \sin \varphi \cos \varphi + 2k_{1,p} \sin(\varphi + \mu) \cos(\varphi + \mu) = 0 \quad (\text{E.63})$$

is valid for the directions of the extremum degree of conformity of the tooth flanks,  $\mathcal{S}$  and  $\mathcal{P}$ , at every point of their contact.

For the directions of the extremal degree of conformity at the point of contact of the gear tooth flank,  $\mathcal{S}$ , and the mating pinion tooth flank,  $\mathcal{P}$ , Eq. (E.63) yields calculation of the extremal values  $\varphi_{\min} = 7^\circ$  and  $\varphi_{\max} = \varphi_{\min} + 90^\circ = 97^\circ$  of the angles  $\varphi_{\min}$  and  $\varphi_{\max}$ .

The direction that is specified by the angle  $\varphi_{\min} = 7^\circ$ , indicates the direction of the minimal diameter of the *Dupin indicatrix* of the surface of relative curvature. That same direction corresponds to the maximal degree of conformity at the point of contact of the tooth flanks,  $\mathcal{S}$  and  $\mathcal{P}$ . Another direction, which is specified by the angle  $\varphi_{\max} = 97^\circ$ , indicates the direction of the minimum degree of conformity of the contacting tooth flanks,  $\mathcal{S}$  and  $\mathcal{P}$ , at that same contact point.

The second approach. For the case under consideration, the use of Eq. (E.49) of the *indicatrix of conformity*,  $Cnf_R(\mathcal{S}|\mathcal{P})$  at a point of contact of the gear tooth flank,  $\mathcal{S}$ , and the mating pinion tooth flank,  $\mathcal{P}$ , makes it possible calculation of the extremal angles  $\varphi_{\min}^* = 19^\circ$  and  $\varphi_{\max}^* = 118^\circ$ .

Imaginary branches of the *indicatrix of conformity*,  $Cnf_R^{\text{im}}(\mathcal{S}|\mathcal{P})$  at the point of contact of the tooth flanks,  $\mathcal{S}$  and  $\mathcal{P}$ , in Figure E.12 are depicted in dashed line. It is important to stress the readers' attention here onto two issues.

**First**, the extremal angles,  $\varphi_{\min}$  and  $\varphi_{\max}$ , that are calculated using the first approach, are not equal to the corresponding extremal angles,  $\varphi_{\min}^*$  and  $\varphi_{\max}^*$ , that are calculated using the second approach. The relationships,  $\varphi_{\min} \neq \varphi_{\min}^*$  and  $\varphi_{\max} \neq \varphi_{\max}^*$ , are generally observed.

**Second**, the difference,  $\Delta\varphi^*$ , between the extremal angles,  $\varphi_{\min}^*$  and  $\varphi_{\max}^*$ , is not equal to half of  $\pi$ . Therefore, the relationship,  $\varphi_{\max}^* - \varphi_{\min}^* \neq 90^\circ$ , between the extremal angles,  $\varphi_{\min}^*$  and  $\varphi_{\max}^*$ , is observed. In general case of contact of two sculptured surfaces the directions of the extremal degree of conformity of the gear tooth flank,  $\mathcal{S}$ , and the mating pinion tooth flank,  $\mathcal{P}$ , are not orthogonal to one another.

The discussed example reveals that in general cases of contact of two smooth regular tooth flanks, the *indicatrix of conformity*,  $Cnf_R(\mathcal{S}|\mathcal{P})$  can be implemented for the purpose of accurate analytical description of the contact geometry of the surfaces. The *Dupin indicatrix* of the surface of relative curvature can be implemented for this purpose only in particular cases of the surfaces,  $\mathcal{S}$  and  $\mathcal{P}$ ,

relative orientation. Application of the *Dupin indicatrix* of the surface of relative curvature enables only approximate analytical description of the geometry of contact of the surfaces. The *Dupin indicatrix* of the surface of relative curvature could be equivalent to the indicatrix of conformity only in degenerate cases of contact of the surfaces. Advantages of the indicatrix of conformity over the *Dupin indicatrix* of the surface of relative curvature are due to that this characteristic curve,  $Cnf_R(\mathcal{S}|\mathcal{P})$ , is a curve of the fourth order.

### E.3.5 IMPORTANT PROPERTIES OF INDICATRIX OF CONFORMITY $Cnf_R(\mathcal{S}|\mathcal{P})$ AT POINT OF CONTACT OF TOOTH FLANKS OF A GEAR AND A MATING PINION

The performed analysis of Eq. (E.49) of the *indicatrix of conformity*,  $Cnf_R(\mathcal{S}|\mathcal{P})$  at a point of contact of a gear tooth flank and a mating pinion tooth flank reveals that this characteristic curve possesses the following important properties.

1. *Indicatrix of conformity*,  $Cnf_R(\mathcal{S}|\mathcal{P})$  at point of contact of the tooth flanks,  $\mathcal{S}$  and  $\mathcal{P}$ , is a planar characteristic curve of the fourth order. It possesses the property of central symmetry, and, in particular cases, it also possesses the property of mirror symmetry.
2. *Indicatrix of conformity*,  $Cnf_R(\mathcal{S}|\mathcal{P})$  is closely related to the surfaces,  $\mathcal{S}$  and  $\mathcal{P}$ , second fundamental forms,  $\Phi_{2,g}$  and  $\Phi_{2,p}$ . This characteristic curve is invariant with respect to the kind of parameterization of the tooth flanks,  $\mathcal{S}$  and  $\mathcal{P}$ , but its equation does. A change in the surfaces,  $\mathcal{S}$  and  $\mathcal{P}$ , parameterization leads to that the equation of the *indicatrix of conformity*,  $Cnf_R(\mathcal{S}|\mathcal{P})$  also changes, while the shape and parameters of this characteristic curve remain unchanged.
3. The characteristic curve,  $Cnf_R(\mathcal{S}|\mathcal{P})$ , is independent of the actual value of the coordinate angle,  $\omega_g$ , that form the coordinate lines,  $U_g$  and  $V_g$ , on the gear tooth flank,  $\mathcal{S}$ . It is also independent of the actual value of the coordinate angle,  $\omega_p$ , that form the coordinate lines,  $U_p$  and  $V_p$ , on the mating pinion tooth flank,  $\mathcal{P}$ . However, parameters of the *indicatrix of conformity*,  $Cnf_R(\mathcal{S}|\mathcal{P})$  are depending upon the angle,  $\mu$ , of local relative orientation of the tooth flanks,  $\mathcal{S}$  and  $\mathcal{P}$ . Therefore, for a given pair of the tooth flanks,  $\mathcal{S}$  and  $\mathcal{P}$ , degree of conformity of the surface varies correspondingly to the variation of the angle,  $\mu$ , while the pinion tooth flank,  $\mathcal{P}$ , is spinning around the unit vector of the common perpendicular.

More properties of the *indicatrix of conformity*,  $Cnf_R(\mathcal{S}|\mathcal{P})$  at point of contact of a gear tooth flank,  $\mathcal{S}$ , and a mating pinion tooth flank,  $\mathcal{P}$ , can be outlined.

### E.3.6 CONVERSE INDICATRIX OF CONFORMITY AT POINT OF CONTACT OF TOOTH FLANKS OF A GEAR AND A MATING PINION

For the *Dupin indicatrix*,  $Dup(\mathcal{S}|\mathcal{P})$  at point of the surface of relative curvature,  $\mathcal{R}$ , there exists a corresponding inverse *Dupin indicatrix*,  $Dup_k(\mathcal{S}|\mathcal{P})$ . Similarly, for the *indicatrix of conformity*,  $Cnf_R(\mathcal{S}|\mathcal{P})$ , at a point of contact of the tooth flanks,  $\mathcal{S}$  and  $\mathcal{P}$ , there exists a corresponding *converse indicatrix of conformity*,  $Cnf_k(\mathcal{S}|\mathcal{P})$ . This characteristic curve can be expressed directly in terms of the surfaces,  $\mathcal{S}$  and  $\mathcal{P}$ , normal curvatures,  $k_g$  and  $k_p$  :

$$Cnf_k(\mathcal{S}|\mathcal{P}) \Rightarrow r_{cnf}^{cnv}(\varphi, \mu) = \sqrt{|k_g(\varphi)|} \cdot \text{sgn } \Phi_{2,g}^{-1} - \sqrt{|k_p(\varphi, \mu)|} \cdot \text{sgn } \Phi_{2,p}^{-1} \quad (\text{E.64})$$

For the derivation of an equation of the *converse indicatrix of conformity*,  $Cnf_k(\mathcal{S}|\mathcal{P})$ , the *Euler formula* for a surface normal curvature is used in the following representation:

$$k_g(\varphi) = k_{1,g} \cos^2 \varphi + k_{2,g} \sin^2 \varphi \quad (\text{E.65})$$

$$k_p(\varphi, \mu) = k_{1,p} \cos^2(\varphi + \mu) + k_{2,p} \sin^2(\varphi + \mu) \quad (\text{E.66})$$

Here in Eqs. (E.65) and (E.66), the principal curvatures of the gear tooth flank,  $\mathcal{S}$ , are designated as  $k_{1,g}$  and  $k_{2,g}$ , while  $k_{1,p}$  and  $k_{2,p}$  designate the principal curvatures of the mating pinion tooth flank,  $\mathcal{P}$ .

After substituting Eqs. (E.65) and (E.66) into Eq. (E.64), one can come up with the equation:

$$r_{cnf}^{env}(\varphi, \mu) = \sqrt{|k_{1,g} \cos^2 \varphi + k_{2,g} \sin^2 \varphi| \operatorname{sgn} \Phi_{2,g}^{-1}} - \sqrt{|k_{1,p} \cos^2(\varphi + \mu) + k_{2,p} \sin^2(\varphi + \mu)| \operatorname{sgn} \Phi_{2,p}^{-1}} \quad (\text{E.67})$$

for the *converse indicatrix of conformity*,  $Cnf_k(\mathcal{S}|\mathcal{P})$  at point of contact of the tooth flanks  $\mathcal{S}$  and  $\mathcal{P}$  in the first order of tangency.

Here, in Eq. (E.67), principal curvatures  $k_{1,g}$ ,  $k_{2,g}$  and  $k_{1,p}$ ,  $k_{2,p}$  can be expressed in terms of the corresponding fundamental magnitudes  $E_g$ ,  $F_g$ , and  $G_g$  of the first and  $L_g$ ,  $M_g$ , and  $N_g$  of the second order of the gear tooth flank  $\mathcal{S}$ , and in terms of the corresponding fundamental magnitudes  $E_p$ ,  $F_p$ , and  $G_p$  of the first and  $L_p$ ,  $M_p$ , and  $N_p$  of the second order of the mating pinion tooth flank  $\mathcal{P}$ . Following this way, Eq. (E.67) of the *converse indicatrix of conformity*,  $Cnf_k(\mathcal{S}|\mathcal{P})$  can be cast to the form that is similar to Eq. (E.49) of the ordinary *indicatrix of conformity*,  $Cnf_R(\mathcal{S}|\mathcal{P})$  at a point of contact of the tooth flanks,  $\mathcal{S}$  and  $\mathcal{P}$ .

It can be shown that similar to the *indicatrix of conformity*,  $Cnf_R(\mathcal{S}|\mathcal{P})$ , the characteristic curve  $Cnf_k(\mathcal{S}|\mathcal{P})$  also possesses the property of central symmetry. In particular cases of the surfaces contact, it also possesses the property of mirror symmetry. The directions of the extremal degree conformity of the gear tooth flank,  $\mathcal{S}$ , and the mating pinion tooth flank,  $\mathcal{P}$ , are orthogonal to one another only in degenerate cases of the surfaces contact.

Equation (E.67) of the *converse indicatrix of conformity*,  $Cnf_k(\mathcal{S}|\mathcal{P})$  is convenient for implementation when:

- a. either the gear tooth flank  $\mathcal{S}$ , or
- b. mating pinion tooth flank  $\mathcal{P}$ , or
- c. both of them

feature point(s) or line(s) of inflection. In the point(s) or (line(s)) of inflection, radii of normal curvature,  $R_{g(p)}$  of the surface,  $\mathcal{S}$  and  $\mathcal{P}$ , are equal to infinity. Points/lines of inflection cause indefiniteness when calculating the position vector,  $r_{cnf}(\varphi, \mu)$ , of a point of the characteristic curve,  $Cnf_R(\mathcal{S}|\mathcal{P})$ . Equation (E.67) of the *converse indicatrix of conformity*,  $Cnf_k(\mathcal{S}|\mathcal{P})$  is free of the disadvantages of such kind, and therefore it is recommended for practical applications.

---

# Appendix F

## *The Closest Distance of Approach of Tooth Flanks of a Gear, and a Mating Pinion*

In general, the problem of the calculation of the closest distance of approach between two smooth regular surfaces is sophisticated and challenging. As per the author's knowledge, no general solution to the problem of calculation of the closest distance of approach between two smooth regular surfaces is available in the public domain. For the purpose of calculation of the deviation,  $\delta_g$ , of the actual gear tooth flank,  $\mathcal{S}_{ac}$ , with respect to the desired (nominal) gear tooth flank,  $\mathcal{S}_{nom}$ , the problem under consideration can be reduced to the problem of computation of the closest distance of approach between two torus surfaces,  $Tr_g$  and  $Tr_p$ .

Consider a gear tooth flank,  $\mathcal{S}$ , and mating pinion tooth flank,  $\mathcal{P}$ , that initially are given in a common coordinate system,  $X_h Y_h Z_h$ , associated with the gear housing, as illustrated in Figure F.1. The tooth flanks,  $\mathcal{S}$  and  $\mathcal{P}$ , are locally approximated by portions of torus surfaces,  $Tr_g$  and  $Tr_p$ , respectively. Again, not all points of the torus surfaces,  $Tr_g$  and  $Tr_p$ , can be used for the local approximation of the gear and the pinion tooth flanks,  $\mathcal{S}$  and  $\mathcal{P}$ . Only points that are located either within the biggest meridian or within the smallest meridian of the torus surface are employed for this purpose.

The points,  $K_g$  and  $K_p^*$ , are chosen as the first guess points on the torus surfaces,  $Tr_g$  and  $Tr_p$ . For the analysis below, it is convenient to relabel the points,  $K_g$  and  $K_p^*$ , to  $g_i$  and  $p_i$  accordingly.

For a given configuration of the torus surfaces,  $Tr_g$  and  $Tr_p$ , the closest distance of approach between these surfaces can be used as a first approximation to the closest distance of approach between the original gear and the pinion tooth flanks,  $\mathcal{S}$  and  $\mathcal{P}$ .

The closest distance of approach between the torus surfaces,  $Tr_g$  and  $Tr_p$ , is measured along the common perpendicular to these surfaces. The following equations can be composed on the premises of this property of the closest distance of approach.

Unit normal vector,  $\mathbf{n}_{Tr,g}$ , to the torus surface,  $Tr_g$ , is located within a plane through the axis of rotation of the surface,  $Tr_g$ . In the coordinate system  $X_{tr,g} Y_{tr,g} Z_{tr,g}$  that is associated with the torus surface,  $Tr_p$ , the equation of a plane through the axis of rotation of the torus surface,  $Tr_g$ , can be expressed in the form:

$$[\mathbf{r}_{\tau g} - \mathbf{r}_{tr,g}^{(0)}] \times \mathbf{k}_{tr,g} \times \mathbf{R}_{tr,g} = 0 \quad (\text{F.1})$$

In Eq. (F.1) is designated:

$\mathbf{r}_{\tau g}$  is the position vector of point of the plane through the axis of rotation of the torus,  $Tr_g$ .

$\mathbf{r}_{tr,g}^{(0)}$  is the position vector of point within the plane,  $\mathbf{r}_{\tau g}$  (it is assumed below that this point coincides with the origin of the coordinate system,  $X_{tr,g} Y_{tr,g} Z_{tr,g}$ ).

$\mathbf{k}_{tr,g}$  is the unit vector of the  $Z_{tr,g}$  – axis.

Equation (F.1) is expressed in terms of the radius,  $\mathbf{R}_{tr,g}$ . This indicates that the set of all planes through the fixed  $Z_{tr,g}$  – axis forms a pencil of planes. The equation of the pencil of planes,  $\mathbf{r}_{\tau g}$ , in the common coordinate system,  $X_h Y_h Z_h$ , can be represented in the form:

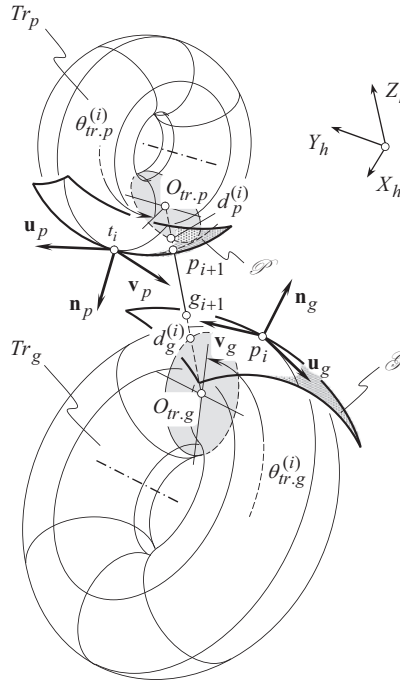


**FIGURE F.1** Calculation of the closest distance of approach between a gear tooth flank,  $\mathcal{S}$ , and a mating pinion tooth flank,  $\mathcal{P}$ .

$$\mathbf{r}_{\tau_g}(Z_{tr,g}, V_{tr,g}, \theta_{tr,g}) = \mathbf{R}\mathbf{s}(Tr_g \mapsto h) \cdot \begin{bmatrix} V_{tr,g} \cdot \cos \theta_{tr,g} \\ V_{tr,g} \cdot \sin \theta_{tr,g} \\ Z_{tr,g} \\ 1 \end{bmatrix} \quad (\text{F.2})$$

The unit normal vector,  $\mathbf{n}_{Tr,p}$ , to the torus surface,  $Tr_p$ , is located within a plane through the axis of rotation of the surface,  $Tr_p$ . In the coordinate system,  $X_{tr,p}Y_{tr,p}Z_{tr,p}$ , that is associated with the surface,  $Tr_p$ , equation of a plane through the axis of rotation of the torus surface,  $Tr_p$ , can be represented in the form:

$$[\mathbf{r}_{\tau_p} - \mathbf{r}_{tr,p}^{(0)}] \times \mathbf{k}_{tr,p} \times \mathbf{R}_{tr,p} = 0 \quad (\text{F.3})$$

Here is designated:

$\mathbf{r}_{\tau_p}$  is the position vector of point of the plane through the torus,  $Tr_p$ , axis of rotation.

$\mathbf{r}_{tr,p}^{(0)}$  is the position vector of point within the plane,  $\mathbf{r}_{\tau_p}$  (it is assumed below that this point coincides with the origin of the coordinate system,  $X_{tr,p}Y_{tr,p}Z_{tr,p}$ ).

$\mathbf{k}_{tr,p}$  is the unit vector of the  $Z_{tr,p}$  - axis.

Equation (F.3) is expressed in terms of the radius,  $\mathbf{R}_{tr,p}$ . This indicates that the set of all planes through the fixed  $Z_{tr,p}$  - axis forms a pencil of planes. The equation of this pencil of planes,  $\mathbf{r}_{\tau_p}$ , in the common coordinate system,  $X_hY_hZ_h$ , can be represented in the form:

$$\mathbf{r}_{\tau_p}(Z_{tr,p}, V_{tr,p}, \theta_{tr,p}) = \mathbf{Rs}(Tr_p \mapsto h) \cdot \begin{bmatrix} V_{tr,p} \cdot \cos \theta_{tr,p} \\ V_{tr,p} \cdot \sin \theta_{tr,p} \\ Z_{tr,p} \\ 1 \end{bmatrix} \quad (\text{F.4})$$

A straight line through the points,  $d_g^{(i)}$  and  $d_p^{(i)}$ , along which the shortest distance of approach,  $d_{gp}^{\min}$ , of the torus surfaces,  $Tr_g$  and  $Tr_p$ , is measured, is the line of intersection of the planes,  $\mathbf{r}_{\tau_g}$  and  $\mathbf{r}_{\tau_p}$ . Therefore, this line,  $d_{gp}^{\min}$ , must be aligned with both unit normal vectors,  $\mathbf{n}_{tr,g}$  and  $\mathbf{n}_{tr,p}$ .

In the coordinate system,  $X_h Y_h Z_h$ , the equation for the unit normal vector,  $\mathbf{n}_{tr,g}$ , to the torus surface,  $Tr_g$ , yields representation in matrix form:

$$\mathbf{n}_{tr,g} = \mathbf{Rs}(Tr_g \mapsto h) \cdot \begin{bmatrix} (C_{tr,g} + \cos \varphi_{tr,g}) \cdot \cos \varphi_{tr,g} \cdot \cos \theta_{tr,g} \\ (C_{tr,g} + \cos \varphi_{tr,g}) \cdot \cos \varphi_{tr,g} \cdot \sin \theta_{tr,g} \\ (C_{tr,g} + \cos \varphi_{tr,g}) \cdot \sin \varphi_{tr,g} \\ 1 \end{bmatrix} \quad (\text{F.5})$$

where  $C_{tr,g}$  designates the parameter  $C_{tr,g} = 1 - \frac{R_{2,g}}{R_{1,g}}$ .

Similarly, in the coordinate system,  $X_h Y_h Z_h$ , the equation for the unit normal vector,  $\mathbf{n}_{tr,p}$ , to the torus surface,  $Tr_p$ , yields matrix representation in the form:

$$\mathbf{n}_{tr,p} = \mathbf{Rs}(Tr_p \mapsto h) \cdot \begin{bmatrix} (C_{tr,p} + \cos \varphi_{tr,p}) \cdot \cos \varphi_{tr,p} \cdot \cos \theta_{tr,p} \\ (C_{tr,p} + \cos \varphi_{tr,p}) \cdot \cos \varphi_{tr,p} \cdot \sin \theta_{tr,p} \\ (C_{tr,p} + \cos \varphi_{tr,p}) \cdot \sin \varphi_{tr,p} \\ 1 \end{bmatrix} \quad (\text{F.6})$$

where  $C_{tr,p}$  designates the parameter  $C_{tr,p} = 1 - \frac{R_{2,p}}{R_{1,p}}$ .

Evidently, the points  $O_{tr,g}$ ,  $O_{tr,p}$ ,  $d_g^{(i)}$ , and  $d_p^{(i)}$  (see Figure F.1) are located within the straight line through the centers,  $O_{tr,g}$  and  $O_{tr,p}$ . The position vector,  $\mathbf{r}_{cd}$ , of this straight line can be calculated from the equation:

$$(\mathbf{r}_{cd} - \mathbf{r}_{cg}) \times (\mathbf{r}_{cd} - \mathbf{r}_{cp}) = 0 \quad (\text{F.7})$$

where is designated:

$\mathbf{r}_{cg}$  is the position vector of a point on the circle of a radius,  $R_{tr,g}$ .

$\mathbf{r}_{cp}$  is the position vector of a point on the circle of a radius,  $R_{tr,p}$ .

It is necessary that the straight line,  $\mathbf{r}_{cd}$ , be along the unit normal vectors,  $\mathbf{n}_{tr,g}$  and  $\mathbf{n}_{tr,p}$ , to the torus surfaces,  $Tr_g$  and  $Tr_p$ .

Considered together, Eqs. (F.2), (F.4), and (F.7), make possible calculation of the closest distance of approach between the torus surfaces,  $Tr_g$  and  $Tr_p$ . Then, the straight line,  $d_{gp}^{\min}$ , intersects the part surface,  $\mathcal{S}$ , and the generating surface,  $\mathcal{P}$ , of the form cutting tool at the points,  $g_{i+1}$  and  $p_{i+1}$ , correspondingly. The points,  $g_{i+1}$  and  $p_{i+1}$ , serve as the second guess to the closest distance of approach between the surfaces,  $\mathcal{S}$  and  $\mathcal{P}$ .

The cycle of the recursive calculations is repeated as many times, as necessary for making the deviation of the calculation of the closest distance of approach between the surfaces,  $\mathcal{S}$  and  $\mathcal{P}$ , smaller than the maximal permissible value.

There is an alternative approach for the calculation of the closest distance of approach between two torus surfaces. The direction of the unit normal vector to an offset surface to,  $Tr_g$ , is identical to the direction of the unit normal vector,  $\mathbf{n}_{tr.g}$ , to the torus surface,  $Tr_g$ . This statement is also valid for the unit normal vector  $\mathbf{n}_{tr.T}$  to the torus surface,  $Tr_p$ . This property of the unit normal vectors,  $\mathbf{n}_{tr.g}$  and  $\mathbf{n}_{tr.p}$ , can be used for the modification of the method of calculation of the closest distance of approach between two torus surfaces.

The equation of the circle of radius,  $R_{tr.g}$ , yields matrix representation:

$$\mathbf{r}_{cg}(\theta_{tr.g}) = \mathbf{Rs}(G \mapsto h) \cdot \begin{bmatrix} R_{tr.g} \cdot \cos \theta_{tr.g} \\ R_{tr.g} \cdot \sin \theta_{tr.g} \\ 0 \\ 1 \end{bmatrix} \quad (\text{F.8})$$

The equation of the circle of radius,  $R_{tr.p}$ , can be analytically described in the similar way:

$$\mathbf{r}_{cp}(\theta_{tr.p}) = \mathbf{Rs}(P \mapsto h) \cdot \begin{bmatrix} R_{tr.p} \cdot \cos \theta_{tr.p} \\ R_{tr.p} \cdot \sin \theta_{tr.p} \\ 0 \\ 1 \end{bmatrix} \quad (\text{F.9})$$

The distance,  $d_{gp}$ , between two arbitrary points on the circles,  $\mathbf{r}_{cg}(\theta_{tr.g})$  and  $\mathbf{r}_{cp}(\theta_{tr.p})$ , equals:

$$d_{gp}(\theta_{tr.g}, \theta_{tr.p}) = |\mathbf{r}_{cg}(\theta_{tr.g}) - \mathbf{r}_{cp}(\theta_{tr.p})| \quad (\text{F.10})$$

The distance,  $d_{gp}$ , is minimal for a specific (optimal) combination of the parameters,  $\theta_{tr.g}$  and  $\theta_{tr.p}$ . The favorable values of the parameters,  $\theta_{tr.g}$  and  $\theta_{tr.p}$ , can be calculated on the solution of the set of two equations:

$$\frac{\partial}{\partial \theta_{tr.g}} \mathbf{r}_{cg}(\theta_{tr.g}) = 0 \quad (\text{F.11})$$

$$\frac{\partial}{\partial \theta_{tr.p}} \mathbf{r}_{cp}(\theta_{tr.p}) = 0 \quad (\text{F.12})$$

On the solution of Eqs. (F.11) and (F.12), the optimal values,  $\theta_{tr.g}^{(opt)}$  and  $\theta_{tr.p}^{(opt)}$ , can be determined. These angels specify the direction of the closest distance of approach of the torus surfaces,  $Tr_g$  and  $Tr_p$ .

Following this method, the three-dimensional problem of calculation of the closest distance of approach of two torus surfaces is reduced to the problem of calculation of the closest distance of approach between two circles. Under a certain scenario, the last approach could possess an advantage over the previous approach.

Convergence of the disclosed algorithms for the computation of the closest distance of approach between two smooth regular surfaces is illustrated in Figure F.2. The computation procedure is convergent regardless of the actual location of the first guess points on the surfaces,  $\mathcal{S}$  and  $\mathcal{P}$ .



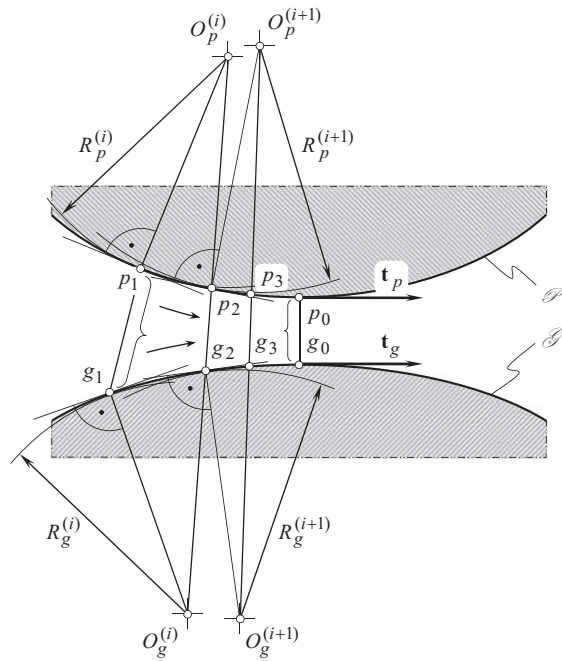


**FIGURE F.2** Convergence of the methods of calculation of the closest distance of approach of a gear tooth flank,  $\mathcal{G}$ , and a mating pinion tooth flank,  $\mathcal{P}$ .

It is instructive to draw attention here to the similarities between the disclosed iterative method for the computation of the closest distance of approach between two smooth regular surfaces, and between the *Newton-Raphson's method*, the iterative method of chords, and so forth. Many similarities can be found in this comparison.



# Taylor & Francis

Taylor & Francis Group

<http://taylorandfrancis.com>

---

# Appendix G

## *Engineering Formulae for Specification of Gear Tooth Flank*

The engineering representation of gear tooth flank can be converted into scientific representation and vice versa. For the conversion, it is convenient to use the so-called *Fundamental Gear Equations* listed in Table G.1. More useful equations can be found out from many advanced sources.

Formulae used for the conversion from English (pitch) system to metric system are summarized in Table G.2.

The formula  $P = \frac{25.4}{m}$  is used to express diametral pitch  $P$  in terms of module  $m$ . The expression:

$$m = \frac{25.4}{P} \quad (\text{G.1})$$

is used for the inverse conversion. For the correspondence between millimeters and inches, the ratio:

$$\text{Millimeters (mm)} = \frac{\text{Inches}}{.03937} = 25.4 \text{ Inches} \quad (\text{G.2})$$

$$\text{Inches} = .03937 \text{ mm} = \frac{\text{mm}}{25.4} \quad (\text{G.3})$$

is valid.

A brief analysis of the types of gears used in industry, together with the analysis of the local topology of gear tooth flanks to be machined, is necessary for the design of gear cutting tools, especially gear cutting tools for machining/finishing of precision gears.

**TABLE G.1**  
**Fundamental Gear Equations**

Name of the Parameter	Formulae
Transverse diametral pitch, $P_t$	$P_t = P_n \cos \psi$
Pitch diameter, $D$	$D = \frac{N}{P_t}$
Standard addendum, $a$	$a = \frac{1}{P_n}$
Outside diameter, $D_o$	$D_o = D + 2 \cdot a$
Transverse pressure angle, $\phi_t$	$\tan \phi_t = \frac{\tan \phi_n}{\cos \psi}$
Base diameter, $d_b$	$d_b = D \cdot \cos \phi_t$
Lead, $L$	$L = \pi \cdot D \cdot \cot \psi = \frac{\pi \cdot D}{\tan \psi}$ $L = \pi \cdot d_b \cdot \cos \psi_b$
Normal circular pitch, $p_n$	$p_n = \frac{\pi}{P_n}, p_n = \frac{\pi \cdot D \cdot \cos \psi}{N}$
Standard normal circular thickness, $t_n$	$t_n = \frac{p_n}{2}, t_n = t \cdot \cos \psi$
Axial pitch, $p_x$	$p_x = \frac{\pi}{P_n \cdot \sin \psi} = \frac{p_n}{\sin \psi} = \frac{L}{N}$
Transverse circular pitch, $p_t$	$p_t = \frac{\pi}{P_t} = \frac{p_n}{\cos \psi}$
Helix angle, when the given center-distance is standard, $\psi$	$\cos \psi = \frac{N_p + N_g}{2 \cdot p_n \cdot C}$
Operating pitch diameter (pinion), $D_{rp}$ ; with non-standard center-distance, $C$	$D_{rp} = \frac{2 \cdot C \cdot N_p}{N_p + N_g}$
Operating pressure angle, $\phi_{rt}$ ; with non-standard center-distance $C$ ,	$\sin \phi_{rt} = \frac{d_{bp} + d_{bg}}{2 \cdot C}$
Normal diametral pitch, $P_n$	$P_n = P_t \cdot \sec \psi$
Helix angle, $\psi$	$\cos \psi = \frac{N}{D \cdot P_n}, \sin \psi = \frac{\pi \cdot N}{P_n \cdot L}$
Helix angle, $\psi_y$ at any diameter, $d_y$	$\tan \psi_y = \frac{d_y}{d_1} \cdot \tan \psi_1$
Transverse circular pitch, $p_{t2}$ at any diameter, $d_y$	$p_{t2} = \frac{\pi \cdot d_y}{N}$
Involute function of pressure angle	$\text{inv} \phi = \tan \phi - \check{\phi}$

(Continued)

TABLE G.1 (Continued)  
Fundamental Gear Equations

Name of the Parameter	Formulae
Normal pressure angle, $\phi_n$	$\begin{aligned}\tan \phi_n &= \tan \phi_t \cdot \cos \psi \\ \sin \phi_n &= \sin \phi \cdot \cos \psi_b \\ \cos \phi_n &= \sin \psi_b \cdot \csc \psi\end{aligned}$
Transverse pressure angle $\phi_{ty}$ , at any diameter, $d_y$	$\cos \phi_{ty} = \frac{d_b}{d_y}$
Base helix angle, $\psi_b$	$\begin{aligned}\cos \psi_b &= \frac{\cos \psi \cdot \cos \phi_n}{\cos \phi_t} = \frac{\sin \phi_n}{\sin \phi_t} \\ \sin \psi_b &= \sin \psi \cdot \cos \phi_n \\ \tan \psi_b &= \tan \psi \cdot \cos \phi_t\end{aligned}$
Base pitch, $p_b$ (here $\rho$ designates radius of profile curvature)	$p_b = \frac{\pi \cdot d_b}{N} = \frac{\pi \cdot D \cdot \cos \phi_t}{N} = \rho \cdot \cos \phi_t$

TABLE G.2  
Formulae for the Conversion from Pitch System to Metric System

Name of the Parameter	English (in)	Metric (mm)
Pitch diameter, $D$	$D = \frac{N}{P}$	$D = m \cdot N$
Addendum, $a$	$a = \frac{1}{P}$	$a = m$
Standard outside diameter, $D_o$	$D_o = D + 2 \cdot a$	$D_o = D + 2 \cdot m$
Base diameter, $d_b$	$d_b = D \cdot \cos \phi$	
Circular pitch, $p$	$p = \frac{\pi}{P}$	$p = \pi \cdot m$
Standard circular tooth thickness, $t$	$t = \frac{p}{2}$	
Average backlash per pair, $B$	$B = \frac{.040}{P}$	$B = .040 \cdot m$



# Taylor & Francis

Taylor & Francis Group

<http://taylorandfrancis.com>

---

# Appendix H

## *On the Inadequacy of the Terms Wildhaber-Novikov Gearing, and W-N Gearing*

*Wildhaber Helical Gearing* [101], and *Novikov Gearing* [123] are briefly discussed below aiming to illustrate the inadequacy of the terms *Wildhaber-Novikov Gearing*, and *W-N Gearing*. As it follows from the discussion, helical gearing proposed by Dr. E. Wildhaber must be referred to as *Wildhaber Helical Gearing* or so. Helical gearing proposed by Dr. M. Novikov must be referred to as *Novikov Gearing* or so. The extensively used terms *Wildhaber-Novikov Gearing* and *W-N Gearing* are meaningless and are commonly used by poorly knowledgeable people.

### H.1 WILDHABER'S HELICAL GEARING

Helical gearing with circular arc tooth profile [101] targets an improved power capacity of the gear pair. The invention relates to the tooth shape of gears, which run on parallel axes, and may be applied to helical gears, such as single helical gears and double helical gears or herringbone gears.

The purpose of the invention is threefold:

1. To provide helical gearing with an improved tooth contact, so as to lessen surface stresses and wear;
2. To provide helical gearing, which is capable of rapid and accurate production, and which may be ground without difficulty, if so desired.
3. To provide accurate gearing of circular tooth profile.

The invention is illustratively exemplified in the accompanying drawings, in which, Figure H.1a is a side elevational view of the proposed gear showing parts thereof in section; Figure H.1d is a normal sectional view of Figure H.1a, taken on the lines 2-2 of the latter figure; Figure H.1g is a side elevational view of a pair of gears constructed in accordance with the invention; Figure H.1h is a sectional view taken through a pair of gears; Figure H.1b and c are sectional views of milling cutters used in the manufacture of gear of the proposed design; Figure H.1e and f are elevational views of corresponding tools of rack shape, to be used in reciprocating machines for cutting helical gears in accordance with the invention; Figure H.1k and l are side elevational views of the improved gear showing a pair of grinding wheels in different operating positions, the wheels being set to grind opposite tooth surfaces; Figure H.1m is a view of a gear taken in normal section and showing the grinding wheels in operation position; Figure H.1n is a view of a mate pinion showing the grinding wheels in operation position; Figure H.1o is a view of modified form of gear made in accordance with the invention; Figure H.1j is a sectional view taken through an internal gear and its pinion; Figure H.1i is a normal section through helical teeth of composite outline, constructed from the invention; Figure H.1p is a view of reciprocating tool of rack shape in operating position; and Figure H.1s is a view of a modified type of reciprocating tools, in position to start a cut on a herringbone gear.

Referring to the drawings, and particularly to Figure H.1a and d, 1 denotes a helical gear having teeth 2 in contact with the teeth 3 of a mating pinion 4. In order to clearly illustrate the degree of contact between the teeth of the gear and pinion, tooth 4 is shown in section in Figure H.1a.



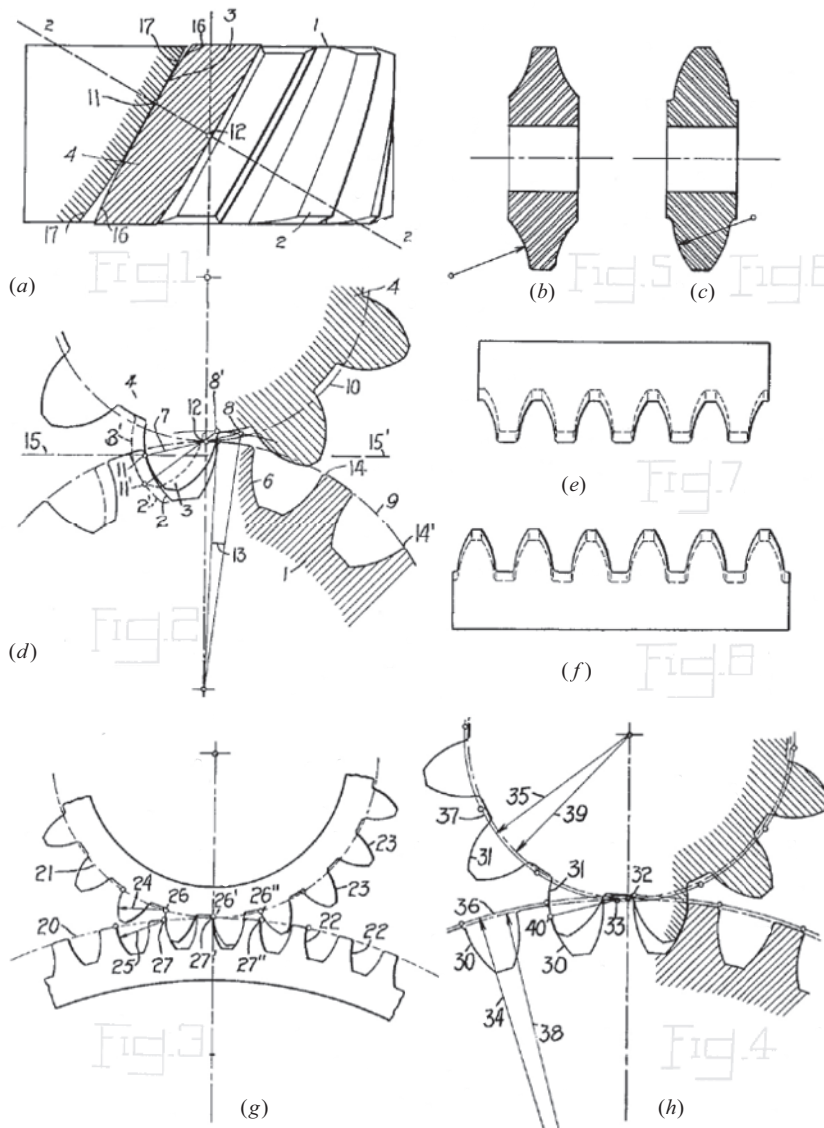


**FIGURE H.1** Helical Gearing. (After E. Wildhaber., US Patent 1,601,750, Patented: October 5, 1926, Filed: November 2, 1923).

(Continued)

It is customary to analyze helical gearing with reference to a normal section, that is, line 2-2 of Figure H.1a, line 2-2 being normal to the helix of the pitch circle. Figure H.1d illustrates the said normal section 2-2 for both pinion 4 and gear 1.

It has been assumed as an example that the tooth profiles 6 of gear 1 are circular arcs of radii 7 and centers 8, in the shown normal section. Centers 8 are situated close to the pitch circle 9 of the gear.<sup>1</sup> The corresponding teeth of pinion 4 are so shaped as to allow rolling of the pitch circles 9 and 10 on each other as well known to those skilled in the art.

<sup>1</sup> Centers 8 need to be situated along the line of action, LA, that is a must. Otherwise, the condition of contact ( $\mathbf{n} \cdot \mathbf{V}_2 = 0$ ) is violated.

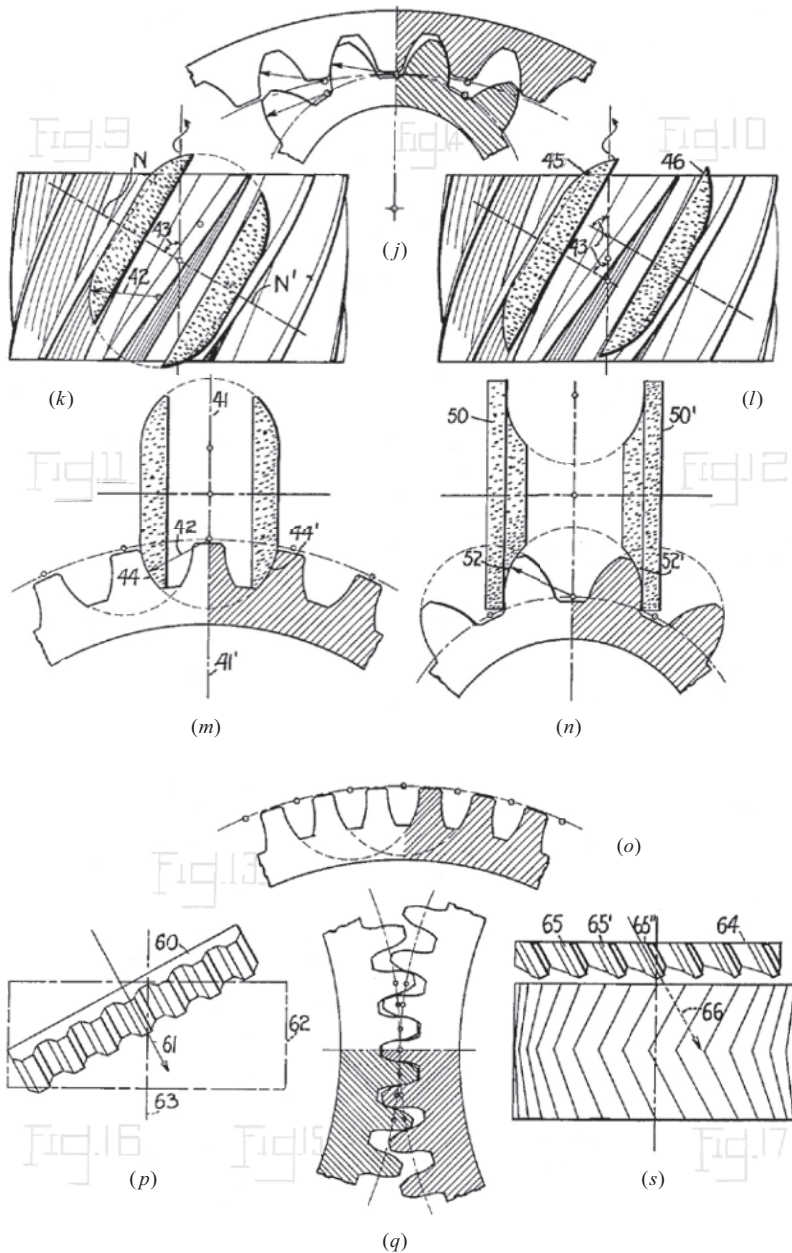


**FIGURE H.1 (CONTINUED)** (a) a side elevational view of the proposed gear showing parts thereof in section; (b) and (c) sectional views of milling cutters used in the manufacture of gear of the proposed design; (d) a normal sectional view of Figure 31.3,a; (e) and (f) elevational views of corresponding tools of rack shape, to be used in reciprocating machines for cutting helical gears in accordance with the invention; (g) a side elevational view of a pair of gears constructed in accordance with the invention; (h) a sectional view taken through a pair of gears; (j) a sectional view taken through an internal gear and its pinion; (k) side elevational view of the improved gear showing a pair of grinding wheels in different operating positions, the wheels being set to grind opposite tooth surfaces; (l) a normal section through helical teeth of composite outline, constructed from the invention; (m) a view of a gear taken in normal section and showing the grinding wheels in operation position; (n) a view of a mate pinion showing the grinding wheels in operation position; (o) a view of modified form of gear made in accordance with the invention; (p) a view of reciprocating tool of rack shape in operating position; (q) ; and (s) a view of a modified type of reciprocating tools, in position to start a cut on a herringbone gear.

When the gear tooth 2 is in the position shown, in Figure H.1a and d, and its center at 8, than it contacts with tooth 3 at point 11, which may be determined by a perpendicular to tooth 2 through point 12, point 12 being the contact point between the two pitch circles 9 and 10. The said perpendicular is, in the present case, the connecting line between point 12 and center 8 of the tooth profile.

Another position 2' of the gear tooth, and 3' of the corresponding pinion tooth are shown in dotted lines in Figure H.1d. The tooth profiles contact here at a point 11', which can be determined like point 11. It will be noted that the contact point has traveled from 11 to 11' during a small angular motion of the gears.<sup>2</sup> The contact point has passed practically over the whole active profile during a turning angle 13 of the gear, which angle corresponds to a fraction only of the normal pitch 14, 14'. The said normal pitch equals the circle pitch of the shown normal section.

In gearing now in use, however, the tooth outline and the tooth proportions are so selected, that the contact of corresponding normal profiles lasts for an angle, which, as a rule, corresponds to more than one full pitch.

In gearing according to the invention, the contact point between two normal profiles passes over the whole active profile during a turning angle, which corresponds to less than one half the normal pitch, and usually to much less than that.

Gearing designed according to the invention, allows the teeth to come into better contact with each other, inasmuch as the tooth surfaces remain much closer to each in a direction perpendicular to the contact line between two mating gears. This is illustrated by a section taken in direction of lines 15, 15' of Figure H.1d. In Figure H.1a, the lateral profile 16 of tooth 3 and profile 17 of tooth 2 of said section are shown to contact at point 11, and to remain close to each other on their whole length. The same holds true for other sections, taken parallel to sections 15, 15'.

Close contact between teeth is well known to reduce wear and to improve the efficiency of the gears.

Although a circular arc is shown as the normal tooth profile of gear 1, in Figure H.1d, it will be understood that this is not the only shape to affect the stated purpose, of increasing the speed, at which the contact point travels over the tooth profile of a normal section. As a rule, however, the shape can be approximated by a circle, whose center is close to the pitch center.

The gearing according to the present invention is strictly a gearing for helical teeth. It would not be advisable on straight teeth, on account of the explained short duration of contact between tooth profiles. This would cause intermittent action, whereas on helical gears similar parts of the teeth are always in contact, on account of the twisted nature of the tooth surfaces.

Figure H.1g may be considered as a view taken in the direction of the axes of a pair of gears. The tooth profiles are the circles in a section, which are perpendicular to the axes. The gear is provided with helical teeth, with working faces below the pitch circle 20, while the pinion teeth have working faces above the pitch circle 21 only. The working profiles 22 of the gear are concave and circular, and their centers are substantially situated on the pitch circle 20. The convex working profiles 23 of the pinion are also of circular shape. Their radii 24 are substantially the same as the radii 25 of the mate profiles. The centers 26, 26', 26'' are similarly situated on pitch circle 21. Profile centers 27, 27', 27'' of pitch circle 20, and profile centers 26, 26', 26'' of pitch circle 21 correspond to each other. They coincide during the mesh, which takes place on the whole tooth profile at once.

Figure H.1g may also be considered as a section perpendicular to the helical teeth and shows then the normal tooth profiles.

Figure H.1h shows a refinement of the preferred embodiments of the invention. It is a normal section through the helical teeth, but can also be considered as a section perpendicular to the axes. Corresponding profiles 30 and 31 are circular, as in Figure H.1g, but in this case, the radius of the concave circular profile 30 is made, a trifle larger than the radius of the convex circular profile 31.

<sup>2</sup> Once the contact point has traveled from 11 to 11' during a small angular motion of the gears, this immediately reveals that the transverse contact ratio,  $m_p$ , in the *Wildhaber's Helical Gearing* is greater than 0, that is,  $m_p > 0$ , which is not permissible.

Consequently, the profile centers 32 and 33 do not exactly coincide during the mesh. The radii 34 and 35 of the circles 36 and 37, constituted by the profile centers 32 and 33, respectively, are not accurately identical with the pitch radii 38 and 39 of the two gears. The sum of the radii 34 and 35 is a trifle larger than the sum of the pitch radii. The radii 34 and 35 are so selected so that the main tooth pressure runs about in a direction 33, 40.

The slight difference of the radii of profiles 30 and 31 facilitates the tooth contact and allows for small errors in making and assembling.

Figure H.1b and c show a pair of milling cutters for milling gear teeth. The cutter may be applied in the usual manner, their axis being inclined in correspondence with the tooth inclination, that is, with the helix angle of teeth. It will be found that the cutters to be inclined for an angle, which is a trifle smaller than the helix angle in the pitch circle, for producing most accurate results.

In Figure H.1e and f a pair of rack-shaped cutters is shown.<sup>3</sup> These cutters are for use in a reciprocating machine. The teeth of these tools are relieved inwardly, in the usual manner, as evident by the dotted lines.

The convex grinding wheels, shown in Figure H.1k, are illustrated in their operating positions, in a view which is taken perpendicular to the axis of the gear blank as well as to the axis of the grinding wheels, that is, in a view along the gear radii 41, 41' of Figure H.1m. The wheels which are to produce concave circular teeth profiles in a normal section, are of convex circular profile, its radius 42 being the same as the radius of the concave circular profile. The grinding wheels are inclined for an angle 43, which equals the helix angle of the teeth, in the pitch circle. The wheels grind along their profiles indicated in dotted lines 44 and 44', which are located in a normal section. As shown in Figure H.1k, the two grinding wheels are coaxially arranged with respect to each other.

The device shown in Figure H.1l corresponds to that shown in Figure H.1k, with the exception that the grinding wheels 45 and 46 are not coaxially arranged. Although the arrangement shown in Figure H.1k imposes certain restrictions on the tooth design, it is frequently preferred. The arrangement of Figure H.1l is advantageous when grinding wheels are not free to run out, for instance, when they must clear against a shoulder or in the case of herringbone teeth.

Referring particularly to Figure H.1m, a normal section is illustrated and taken along lines N, N' of Figure H.1k. In this view, the axis of the coaxially arranged grinding wheels is situated in the said normal section. The wheels grind along the profiles 44 and 44' of the shown normal section, while the blank performs a translator motion in the direction of its axis, and, in timed relation thereto, a turning motion about its axis. In other words, the blank is screwed past the grinding wheels.

Figure H.1n discloses a normal section through the teeth of the mating gear or pinion. Grinding wheels 50 and 50' are provided with concave circular profiles 52 and 52' with which they grind the convex gear teeth.

It will be understood that milling cutters might be used instead of the grinding wheels shown in Figure H.1k–n; also that grinding wheels of a shape shown in Figure H.1b and c might be used, if so desired.

The teeth ground according to Figure H.1k, m, and n are preferably so designed, that the centers of opposite tooth arcs 44 and 44', 52 and 52', respectively, in Figure H.1n coincide. In Figure H.1m and n, the tooth arcs of every third tooth side have a common center.

The tooth arcs of every fifth tooth side have a common center in the normal section shown in Figure H.1o.

In Figure H.1m, the common center of opposite tooth arcs of alternate teeth is situated on the centerline of the intermediate tooth. The corresponding pinion shows convex circular profiles, of which opposite tooth sides of adjacent teeth have common centers in the middle of the intermediate tooth space.

<sup>3</sup> Conformal gears cannot be cut by rack cutters, and, more generally, they cannot be machined in any gear generating process.

The normal section shown in Figure H.1j shows an internal gear and its mate pinion, constructed in accordance with the concave tooth profiles. In external gears, similarly, preference is given to providing the larger gear with concave tooth profiles.

The normal section through a pair of helical gears, shown in Figure H.1q, discloses opposite tooth profiles, the addendum being convex and the dedendum concave.

A rack-shaped planing tool is illustrated in operating position in Figure H.1p. Tools of this kind have been shown in another view in Figure H.1e and f. The reciprocatory tool 60 moves in the direction 61, at an inclination, which equals the helix angle of the teeth. Gear 62, with its axis 63, is shown in dotted and dash lines. In order to cut the proper tooth shape, gear blank 62 after every cut is slightly fed in a rolling generating motion with respect to a rack which is embodied by tool 60.

Another reciprocatory tool 64 is shown in Figure H.1s, the tool in this case being provided with stepped teeth 65, 65', 65'' which allow it to clear shoulders, and herringbone teeth. The tool moves in the direction 66 of the helical teeth, which cuts.

Other ways of producing gearing according to the invention, that is, hobbing, planing with a pinion cutter, rolling and casting, may be contemplated, but it is not deemed necessary at this time to give a detailed explanation of the mechanism used in connection therewith.

Briefly stated, the invention consists in providing helical gearing of such a profile, that the tooth contact passes rapidly over the normal profile of the teeth. This has been found to result in close contact between helical mate teeth. In a direction at right angles to the contact line, the mate teeth recede from each other only slightly and thus provide a tooth contact, which is not very far from surface contact.

It is claimed<sup>4</sup> that *Wildhaber's gearing* features a non-zero transverse contact ratio ( $m_p > 0$ ), and a non-zero face contact ratio  $m_F > 0$ . The total contact ratio,  $m_t$ , is greater than one ( $m_t \equiv m_p + m_F > 1$ ).

The *Wildhaber's gearing* (see Figure H.1) does not meet the condition of contact. The condition of conjugacy of the tooth flanks, and the condition of equality of the base pitches of the gear and the pinion to the operating base pitch are not fulfilled in this design of gearing. This immediately yields a conclusion that *Wildhaber's gearing* is not workable at all.

The invention by *Wildhaber* is explained to the best possible extent in Refs [156] and [157].

## H.2 NOVIKOV GEARING

*Novikov Gearing* [123] is an example of conformal helical gearing. For a long while, *Novikov's* patent (S.U. Patent No. 109,113 of 1956) was not available to most of the gear experts.

Known designs of gearing, those featuring point system of meshing, feature low contact strength and are not widely used in practice.

The contact strength of known designs of gearing with a line system of meshing, including the widely used involute gearing, is limited.

The proposed gearing<sup>5</sup> [123] features higher contact strength due to favorable curvatures of the interacting tooth flanks. Under equivalent contact stress, similar dimensions, and comparable remaining design parameters, greater circular forces are permissible by the proposed gearing. Lower sensitivity to manufacturing errors and to deflections under the load is the other advantage of the proposed gearing.

The proposed gearing can be designed either with parallel, intersecting, or crossing axes of rotations of the gears. External gearing as well as internal gearing of the proposed system of meshing is possible. The tooth ratio of the proposed gearing can be either of constant value or it can be variable, and time-dependent. The proposed concept of gearing can be utilized in the design of cam mechanisms.

<sup>4</sup> Wildhaber, E., *Helical Gearing*, US Patent 1,601,750, Patented: October 5, 1926, Filed: November 2, 1923.

<sup>5</sup> Pat. No. 109,113, (USSR). *Gear Pairs and Cam Mechanisms Having Point System of Meshing*. /M.L. Novikov, National Classification 47h, 6; Filed: April 19, 1956, published in Bull. of Inventions No.10, 1957.



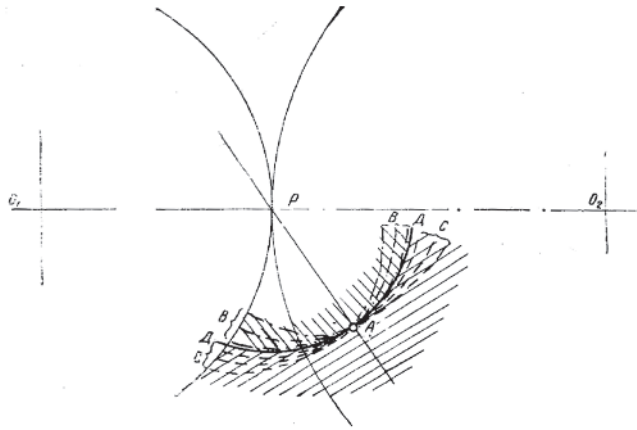


**FIGURE H.2** Helical gearing. (After Dr. M.L. Novikov, Pat. No. 109,113, (USSR). *Gear Pairs and Cam Mechanisms Having Point System of Meshing*. / National Classification 47h, 6; Filed: April 19, 1956, published in Bull. of Inventions No.10, 1957.)

In Figure H.2, possible tooth profiles in the cross-section of tooth flanks by a plane that is perpendicular to the instant axis of relative rotation through the current point of contact are illustrated.

Here, the point of intersection of the planar cross-section by the axis of instant relative rotation is denoted by  $P$ .

$O_1$  and  $O_2$  are the points of intersection of the planar cross-section by the axes of the gear and the pinion.

$A$  is the point of meshing (in its current location).

$PA$  denotes the line of action.

$\mathcal{D}A\mathcal{D}$  is the circle centered at the point  $P$  which corresponds to the limit case of the tooth profiles (in the case the profiles are aligned to each other).

Several curves,  $BAB$ , represent examples of the tooth profiles of one of the mating gears. The curves  $BAB$  are arbitrary smooth curves, which are located inside of the circular arc  $\mathcal{D}A\mathcal{D}$  (i.e., the arcs are located within the bodily side of the limit tooth flank of one of the gears). The curves  $BAB$  are located close to the circular arc  $\mathcal{D}A\mathcal{D}$  and they feature a high degree of conformity to the circular arc.

Several curves,  $CAC$ , represent examples of the tooth profiles of the second of the mating gears. The curves  $CAC$  are arbitrary smooth curves, which are located outside of the circular arc  $\mathcal{D}A\mathcal{D}$  (i.e., the arcs are located within the bodily side of the limit tooth flank of another of two gears). The curves  $CAC$  are also located close to the circular arc  $\mathcal{D}A\mathcal{D}$  and they feature a high degree of conformity to the circular arc.

The entity of the invention is disclosed below in detail.

The location and orientation either of a straight path of contact or a smooth curved path of contact are specified in space in which the location and orientation of the axes of rotations of the gear and the pinion are given. The path of contact is located reasonably close to the axis of instant relative rotation of the gears. Either constant or time-dependent (smoothly varying in time) speed of motion of the contact point along the path of contact is assigned. A coordinate system is associated with the gear, and a corresponding coordinate system is associated with the pinion. In the coordinate systems, the moving contact point traces the so-called *contact lines*.<sup>6</sup> One of the *paths*

<sup>6</sup> The *contact line* is a term used by Dr. M.L. Novikov. Actually, the contact line is the *pseudo-path of contact*.

*of contact* is associated with the gear and another one is associated with the pinion. Certain smooth regular surfaces through the *pseudo-paths of contact* can be used as the tooth flanks of the gear and the pinion. The following requirements should be fulfilled in order to the surfaces can be used as the tooth flanks:

- At every location of the contact point, the tooth flanks should have a common perpendicular, and thus, the requirements of the main theorem of meshing should be satisfied.
- The curvatures of the tooth profiles should correspond to each other.
- No tooth flank interference occurs within the working portions of the surfaces.

The proposed tooth flanks fulfill the above-listed requirements and allow for high contact strength of the gear teeth.

Consider a plane through the current contact point, which is perpendicular to the instant axis of relative rotation. Then, two circular arcs are constructed. The circular arcs are centered at points within the straight line through the pitch point and the contact point. The arcs centers are located close to the pitch point. The constructed circular arcs can be considered an example of the tooth profiles of the gear and the pinion. The tooth flanks are generated as loci of the tooth profiles constructed for all possible locations of the contact point. The working portion of one of two tooth flanks is convex, while the working portion of another tooth flank is concave (in the direction toward the axis of instant relative rotation). In a particular case, the radii of tooth profiles could be of the same magnitude and equal to the distance from the contact point to the axis of instant relative rotation. The centers of both profiles, in this particular case, are located at the axis of instant relative rotation. Under such a scenario, point meshing reduces to a special line meshing. This would require an extremely high accuracy of the center distance and independence of it from operation conditions, which is impractical. Point meshing is preferred when designing tooth profiles. A small difference between the radii of curvature of the tooth profiles is desirable. It should be kept in mind that during run-in period of time, point meshing of the gear teeth will transform to the above-mentioned *locally line* meshing of the tooth profiles. However, the theoretical point contact of the tooth flanks will be retained.

Tooth profiles can differ from the circular arcs. However, the tooth profiles of other geometries (those always passing through the contact point) should be located (for one gear) within the interior of the above-mentioned circular arc profile that centers at the point within the axis of instant relative rotation as shown in Figure H.2. For another gear, the tooth profile should be located outside the circular arc.

The law of motion of the contact point (i.e., speed of the point and its trajectory) should be chosen so as to minimize friction and wear losses. The friction and wear loss is proportional to the relative sliding velocity in the gear mesh. Therefore, it is desirable to reduce the sliding velocity as much as possible. For this purpose, the path of contact should be located not far from the axis of instant relative rotation. On the other hand, a too-close location of the path of contact to the axis of instant relative rotation is also not desirable as that reduces the contact strength of the gear tooth flanks. In addition, it is recommended to ensure favorable angles between the common perpendicular (along which the tooth flanks of one of the gears act against the tooth flank of another gear) and between the axes of rotations of the gears.

Opposite sides of tooth profiles are designed in a similar manner to that just discussed. Tooth thicknesses and angular pitch are assigned to ensure the required bending tooth strength.

The face width of the gear or the length of the gear teeth should correlate to their pitch to ensure the required value of the face contact ratio. Gear pairs can feature either one point of contact (when working portions of the tooth flank contact each other just in one point, excluding the phases of the teeth re-engagement), or they can feature multiple contact points when the tooth flanks contact each other at several points simultaneously.



For parallel axis gear pairs, it is preferred to use a straight line as the path of contact, which is parallel to the axes of rotations of the gear and the pinion. The speed of the contact point along the straight path of contact can be of constant value. In this particular case, the radii of curvature of the tooth profiles in all cross-sections by planes are equal to each other. Tooth flanks in this case are regular screw surfaces. Gears that feature tooth flanks of such geometry are easy to manufacture, and they can be cut on machine tools available on the market.

An example of parallel axis gearing with limit geometry of the tooth profiles is illustrated in Figure H.2. Point contact of the tooth flanks in this particular case is transformed to almost line contact of the tooth flanks. The curved contact line is located across the tooth profile. When axial thrust in the gear pair is strongly undesirable, herringbone gears can be used instead.

*Novikov gearing* (see Figure H.2) meets the condition of contact as well as it meets the condition of conjugacy of the tooth surfaces, and the condition of equality of the base pitches of the gear and the pinion to the operating base pitch. *Novikov gearing* is a kind of perfect gearing.<sup>7</sup> *Novikov gearing* is the only feasible type of gearing with point contact of the tooth flanks that is capable of transmitting a rotation smoothly. As it is clear now, *Novikov gearing* is a reduced type of involute gearing.

---

<sup>7</sup> It needs to be noticed here that Dr. E. Wildhaber did not recognize the difference between *Novikov gearing* and the helical gearing proposed by him [101]. This conclusion immediately follows from the Wildhaber's statement: "I may say also that it gives me satisfaction to see the original concept vindicated through the Russian reinvention and effort and through subsequent efforts and articles." This Wildhaber's statement can be found on page 949 in the paper by T. Allan [Allan, T., "Some Aspects of the Design and Performance of Wildhaber-Novikov Gearing," *Proc. Inst. Mech. Engrs, Part I*, v. 179, n. 30, 1964/1965, pp. 931–954.] (see the Communications section). Other evidences in this concern are also known.



# Taylor & Francis

Taylor & Francis Group

<http://taylorandfrancis.com>

---

# Conclusion

The principal accomplishments and new results in the gear science are briefly outlined below.

The approach used in this book for the analysis of the fundamental contributions is helpful to associate the fundamental accomplishments in the theory of gearing with the proper names of the researchers credited for these accomplishments. Then, it is also helpful to separate the names of the key contributors to the scientific theory of gearing from the names of other scientists/engineers not contributed to the fundamentals to the *Scientific Theory of Gearing*.

The total number of fundamental accomplishments in gear science is limited. Therefore, the total number of names of scientists/engineers, who really contributed to the fundamentals of the *Scientific Theory of Gearing*, is also limited.

The kinematics of a gear pair is discussed to the best possible extent. Gear vector diagrams are extensively used for this purpose. *Rotationally positive*, *rotationally negative*, and *rotationally zero*, gear pairs are introduced in this research, and an analytical criterion of all types of gear pairs is proposed.

The use of gear vector diagrams makes possible the development of a scientific classification of all possible types of the gearvector diagrams. Upon the classification was developed, a set of complementary vectors to vector diagrams of gear pairs is introduced.

Possible future developments in the theory of gearing are an important output from the analysis undertaken when carrying out this analysis.

For the convenience of the further analysis of gears and gear pairs, a set of principal planes, and a set of main reference systems, associated with a gear pair are introduced.

Then, conditions for transmitting a uniform rotary motion smoothly from a driving shaft to a driven shaft are formulated in a form of three fundamental laws of gearing. These three fundamental laws of gearing briefly can be referred to as: (a) The law of contact; (b) The conjugate action law, and (c) The law of equal base pitches of a gear, and a mating pinion, both, to operating base pitch of the gear pair.

*Shishkov equation of contact*,  $\mathbf{n} \cdot \mathbf{V}_\Sigma = 0$ , (Prof. V.A. Shishkov, late 1940s) is adopted for to analytical description of the first fundamental law of gearing.

*Equation of conjugacy*,  $\mathbf{p}_{ln} \times \mathbf{V}_m \cdot \mathbf{n}_g = 0$ , (Prof. S.P. Radzevich, 2017) is adopted for to analytical description of the second fundamental law of gearing.

A set of two *equalities*,  $\varphi_{b,g} = \varphi_{b,op}$  and  $\varphi_{b,p} = \varphi_{b,op}$ , (Prof. S.P. Radzevich, 2008) is adopted for to analytical description of the third fundamental law of gearing.

In geometrically accurate gear pairs, all three fundamental laws of gearing are met; if one (or more) fundamental law(s) of gearing is violated, no smooth transmission of a uniform rotation from an input shaft to an output shaft is possible at all.

The kinematics and geometry of parallel-axe gearing is discussed. The analysis of the kinematics, gear ratio, and a variation of the permissible transverse pressure angle, in parallel-axes gearing are covered in this discussion. Gear pairs with gear ratio in the range of,  $-\infty \leq u \leq +\infty$ , are considered.

A desirable line of contact between tooth flanks of a gear and its mating pinion, the line of action, and the path of contact in a gear pair are analyzed. The concept of the *operating base pitch* in a gear pair is introduced.

Special attention is given to the analysis of contact ratio in parallel-axes involute gearing. The contact ratio in parallel-axes involute gearing is discussed to the best possible extent. In particular, transverse contact ration in a *low-tooth-count gearing* got in detail consideration.

Sliding conditions and specific sliding between a gear and a mating pinion tooth flanks in both external and internal parallel-axes gearing are discussed in detail, along with the forces acting within the plane of action, and in a transverse section of a perfect parallel-axes involute gear pair.

On top of that, Novikov/conformal, and high-conformal parallel-axes gearings are discussed. It is shown that conformal gearing (*Novikov gearing*, in other words), and high-conformal parallel-axes gearing, represent reduced cases of parallel-axes involute gearing that features zero-length of the line of action, zero-length the path of contact, and a certain length of the pseudo-path of contact. Principal features of high-conformal gearing are outlined, and the difference between Novikov/conformal gearing, and high-conformal gearing is shown. The impossibility of finish-cutting gears for Novikov/conformal, and high-conformal gearing in generating (continuous-indexing) machining processes is illustrated in detail.

It is proven that no geometrically accurate helical gear pairs with a non-involute tooth profile [*Roots blower*, rotors for oil pumps, along with *Helical Gearing* by Dr. E. Wildhaber (US Pat. No. 1,601,750), and so forth] is possible at all.

For the analysis of intersected-axes gearing, an *equivalent pulley-and-belt transmission* is constructed. The path of contact, and the instantaneous line of action, are investigated by means of the *equivalent pulley-and-belt transmission*. Equations of the tooth flanks of gear pairs are derived.

It is shown that, by nature, most of the desirable tooth proportions in intersected-axes gear pairs are the *angular*, and not the *linear* design parameters, that is: the *angular* base pitch, the *angular* pitch, the *angular* tooth thickness, the *angular* space width, the *angular* backlash, the *angular* addendum, the *angular* dedendum, and so forth.

Geometrically accurate Novikov/conformal, and high-conformal intersected-axes gearing got particular attention. The path of contact and the pseudo-path of contact, the boundary cones, and the bearing capacity of high-conformal gearing are covered in this discussion. The design parameters of Novikov/conformal, and high-conformal intersected-axes gearing are discussed as well.

*Equivalent pulley-and-belt transmission* is employed for the analysis of the path of contact, and the zone (the field) of action in intersected-axes gearing. Conditions to transmit a uniform rotary motion by means of gear teeth in intersected-axes gearing are covered in this discussion, along with the analysis of the transverse contact ratio, the face contact ratio, and the total contact ratio. Sliding of the tooth flanks, and elements of dynamics of geometrically accurate intersected-axes gearing are investigated. Principal assumption adopted in the load analysis of geometrically accurate intersected-axes gearing is formulated.

The kinematics of crossed-axes gearing is investigated. The pressure angle and the base cones in crossed-axes gear pair are constructed. Ultimately, this yields an expression for the gear tooth flank in geometrically accurate crossed-axes gearing. Geometrically accurate crossed-axes gearing of this kind is referred to as *R – gearing*. The condition of conjugacy of tooth flanks of a gear and a mating pinion in *R – gearing* is described analytically. *R – gearing* in crossed-axes gearing is an equivalent of involute gearing in parallel-axes gearing.

It is shown that, by nature, most of the desirable tooth proportions in crossed-axes gear pairs are *angular*, and not the *linear* design parameters, that is: the *angular* base pitch, the *angular* pitch, the *angular* tooth thickness, the *angular* space width, the *angular* backlash, the *angular* addendum, the *angular* dedendum, and so forth.

Special consideration is given to the analysis of the main features of geometrically accurate Novikov/conformal, and high-conformal crossed-axes gearing. The path of contact, the pseudo-path of contact, the *boundary N-cone*, and bearing capacity of crossed-axes Novikov/conformal, and high-conformal gearing, along with the calculation of the design parameters of Novikov/conformal, and high-conformal crossed-axes gearing, are covered in this discussion.

*Equivalent pulley-and-belt transmission* is employed for the investigation of the tooth flanks in geometrically accurate crossed-axes gearing. The path of contact, and the zone (the field) of action, are investigated, and the conditions for transmitting a uniform rotary motion by means of teeth in

crossed-axes gearing are analyzed. Contact ratio in crossed-axes gearing is discussed to the best possible extent. Transverse contact ratio, face contact ratio, and total contact ratio are covered in this discussion.

Sliding, specific sliding, and the features of specific sliding, between tooth flanks are investigated, along with elements of dynamics of geometrically accurate crossed-axes gearing.

A principal assumption adopted in the load analysis of geometrically accurate crossed-axes gearing is formulated, and the forces of interaction in geometrically accurate crossed-axes gearing are analyzed.

Design peculiarities of geometrically accurate worm gearing are discussed with focus on that worm gearing with line contact between the worm threads and the worm-gear tooth flanks is a particular kind of crossed-axes gearing, considered earlier in this book. The kinematics, the base cones, and the peculiarities of sliding in the plane-of-action apex in geometrically accurate worm gearing are covered in this discussion. An analytical criterion to distinguish a worm from a helical gear with a low tooth count is proposed.

Examples of gearings with the point contact between the tooth flanks of a gear and a mating pinion is covered on the discussion of geometrically accurate gearing with point contact. This analysis is followed by the approach to generate tooth flanks in *gearing with point contact between tooth flanks of a gear and a mating pinion*.

A novel kind of crossed-axe gearing that is insensitive to the axes displacement/misalignment is proposed. The proposed design of gearing is referred to as  $S_{pr}$  – gear system. Finally, a correlation among the gear systems of various types is summarized.

A novel approach to design geometrically accurate non-circular gears is proposed.

An approach for synthesizing geometrically accurate gear pairs is proposed. The meaning of the term *synthesis of favorable gear pair* is clarified. A concept of synthesis of favorable geometrically accurate gear pair is proposed.

Generic gear shapes are analyzed to the best possible extent. The origination of the generic gear shape, and examples of gear pairs composed of gears with various generic gear shapes are covered in this discussion. The total number of possible generic gear shapes of different geometry is evaluated. A possibility of classification of gear pairs is discussed, and examples of implementation of classification of gear pairs are provided.

The local geometry of interacting tooth flanks of a gear and of a mating pinion is considered. The kinematics, and the local geometry of the interacting tooth flanks are discussed. This discussion is followed by the analysis of local geometry of the interacting tooth flanks in gearings of all kinds.

Various aspects of the gear tooth strength are analyzed. The *Hertz proportional assumption*, and the *assumption of equal torque share*, are the two key assumptions adopted in this analysis. In the analysis, the readers' attention is stressed on the importance of the *Saint-Venant principle* (or *Saint-Venant assumption*, in other words) in bending strength of gear teeth.

The gear tooth profile modification generated by means of the basic rack shift is considered. The addendum modification (profile shift), profile shift coefficient, and gear tooth flank geometry depending on the profile shift coefficient, are covered.

Root cause for unequal torque sharing in a split power transmission system (SPTS), mobility of split power transmission systems, and the *power density* of gear transmission systems are analyzed. Ultimately, a novel approach for equal torque sharing in split power transmission systems is proposed. This includes, but is not limited to the planetary gear drive with elastomeric load sharing device, and examples of implementation of elastic load sharing device. The main features of split power transmission systems with preloaded elastic load sharing devices are outlined.

Vector approach for the kinematic, and dynamic analysis of complex gear systems are briefly outlined.

A few novel methods for the inspection of gears are briefly discussed. A perfect (geometrically accurate) datum surface is used in every of the considered methods of gear inspection. These makes the methods of gear inspection more accurate, and the readings more reliable.

The kinematic, and the geometric factors that affect the noise excitation in gearing are briefly discussed. Some physical factors, like a variation of the loading in a gear pair, that allow for a kinematic/geometric interpretation are also outlined here.

Design peculiarities of geometrically accurate and almost geometrically accurate gears are discussed. Features of the design of gears for  $R$  – gearing, as well as for  $R_p$  – gearing, are considered here as examples.

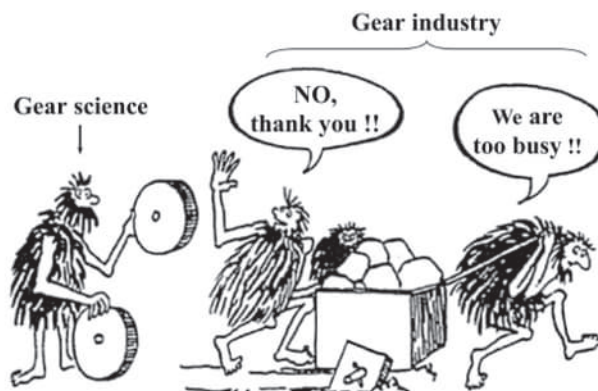
Aiming the development of the *Scientific Theory of Gearing*, this research ends with a brief scientific overview in the area of gear science and gear art. For this purpose, all the fundamental accomplishments in the field are listed in a chronological order, and a corresponding name of a scientist/engineer is assigned to each of the fundamental accomplishments. For example, *Leonhard Euler* is granted for the application of involute tooth profile in gears for parallel-axes gear pairs; *Charles Camus*, *Leonhard Euler*, and *Felix Savary*, are granted for the formulating of the main theorem of parallel-axes gearing (the so-called *CES – theorem*), and so forth. The aforementioned names of gear scientists illustrate positive contributions to the *Scientific Theory of Gearing*. There are also a few names of gear scientists, who committed huge mistakes that have negatively affected the evolution of the gear art. *Theodore Olivier*, *Chaim Gochman*, and a few more names to mention in this regard.

The reported results of the research are applicable to gearing of all kinds that are operating under various conditions (see Figure 1). Here, in Figure 1, the area where gears can be used for the transmission of a motion, is constructed. Gearing can be used for transmission of a rotation in the range of the lowest rotation,  $RPM_{min}$ , to a certain highest rotation,  $RPM_{max}$ . No rotation  $RPM$  that is either lower than  $RPM_{min}$ , or is higher than  $RPM_{max}$ , is permissible because of the physical constraints. A range for torque being transmitting is designated as,  $Trq_{min}$ , for a minimal torque, and,  $Trq_{max}$ , for a maximal torque. A highest power,  $P_{max}$ , that can be transmitted by a gear pair equals:

$$P_{max} = RPM_{max} \cdot Trq_{max}$$

Considering  $P_{max} = \text{Const}$ , a boundary hyperbola can be constructed in the reference system,  $RPM/Trq$ .

Transmission of a rotary motion from a driving shaft to a driven shaft by means of teeth in a gear pair is possible only within the shadowed interior of the contour shown in Figure 1. Areas of preferable applications of gear pairs of different types are also shown. The schematic shown in the figure below is qualitative (not a quantitative one), and intuitive.



# Notation

$A_{pa}$	– is the plane-of-action apex in a gear pair
$A_g$	– is the gear base cone apex
$A_p$	– is the pinion base cone apex
$C$	– is the closest distance of approach between a gear axis of rotation, $O_g$ , and a mating pinion axis of rotation, $O_p$ (center-distance)
$Cnf_R(\mathcal{S}/\mathcal{P})$	– is the indicatrix of conformity at a point of contact, $K$ , of a gear tooth flank, $\mathcal{S}$ , and a mating pinion tooth flank, $\mathcal{P}$
$C_{1,g}, C_{2,g}$	– is the first and the second principal plane sections of a gear tooth flank, $\mathcal{S}$
$\mathbf{Cp}_x(a_x, \varphi_x)$	– is the operator of coupled linear transformation along and about the axis, $X$
$\mathbf{Cp}_y(a_y, \varphi_y)$	– is the operator of coupled linear transformation along and about the axis, $Y$
$\mathbf{Cp}_z(a_z, \varphi_z)$	– is the operator of coupled linear transformation along and about the axis, $Z$
$C_{1,p}, C_{2,p}$	– is the first and the second principal plane sections of a mating pinion tooth flank, $\mathcal{P}$
$\mathcal{E}$	– is the characteristic line
$E_g, F_g, G_g$	– is the fundamental magnitudes of the first order of a gear tooth flank, $\mathcal{S}$
$E_p, F_p, G_p$	– is the fundamental magnitudes of the first order of a mating pinion tooth flank, $\mathcal{P}$
$\mathbf{Eu}(\psi, \theta, \varphi)$	– is the operator of the <i>Eulerian transformation</i>
$\mathcal{S}$	– is the gear tooth flank
$\mathcal{P}$	– is the pinion tooth flank
$K$	– is the point of contact between the tooth flanks, $\mathcal{S}$ and $\mathcal{P}$ (or a point within a line of contact, $LC$ , between the tooth flanks, $\mathcal{S}$ and $\mathcal{P}$ )
$LA$	– is the line of action
$LA_{inst}$	– is the instant line of action
$LC$	– is the line of contact between the tooth flanks, $\mathcal{S}$ and $\mathcal{P}$
$LC_{des}$	– is the line desired of contact between the tooth flanks, $\mathcal{S}$ and $\mathcal{P}$
$L_g, M_g, N_g$	– are the Fundamental magnitudes of the second order of a gear tooth flank, $\mathcal{S}$
$L_p, M_p, N_p$	– are the fundamental magnitudes of the second order of a mating pinion tooth flank, $\mathcal{P}$
$O_g$	– is the gear axis of rotation
$O_p$	– is the pinion axis of rotation
$PA$	– is the plane of action
$P_{in}$	– is the axis of instant rotation
$\mathbf{Rl}_x(\varphi_y, Y)$	– is the operator of rolling over a plane ( $Y$ – axis is the axis of rotation, $X$ – axis is the axis of translation)
$\mathbf{Rl}_z(\varphi_y, Y)$	– is the operator of rolling over a plane ( $Y$ – axis is the axis of rotation, $Z$ – axis is the axis of translation)
$\mathbf{Rl}_y(\varphi_x, X)$	– is the operator of rolling over a plane ( $X$ – axis is the axis of rotation, $Y$ – axis is the axis of translation)
$\mathbf{Rl}_z(\varphi_x, X)$	– is the operator of rolling over a plane ( $X$ – axis is the axis of rotation, $Z$ – axis is the axis of translation)
$\mathbf{Rl}_x(\varphi_z, Z)$	– is the operator of rolling over a plane ( $Z$ – axis is the axis of rotation, $X$ – axis is the axis of translation)
$\mathbf{Rl}_y(\varphi_z, Z)$	– is the operator of rolling over a plane ( $Z$ – axis is the axis of rotation, $Y$ – axis is the axis of translation)
$\mathbf{Rr}_u(\varphi, Z)$	– is the operator of rolling of two coordinate systems
$\mathbf{Rs}(A \mapsto B)$	– is the operator of the resultant coordinate system transformation, say from the coordinate system $A$ to the coordinate system $B$



$\mathbf{Rt}(\varphi_x, X)$	– is the operator of rotation through an angle $\varphi_x$ about $X$ – axis
$\mathbf{Rt}(\varphi_y, Y)$	– is the operator of rotation through an angle $\varphi_y$ about $Y$ – axis
$\mathbf{Rt}(\varphi_z, Z)$	– is the operator of rotation through an angle $\varphi_z$ about $Z$ – axis
$R_{1.g}, R_{2.g}$	– is the first and the second principal radii of curvature at a point of a gear tooth flank, $\mathcal{S}$
$R_{1.T}, R_{2.T}$	– is the first and the second principal radii of curvature at a point of a mating pinion tooth flank, $\mathcal{P}$
$\mathbf{Sc}_x(\varphi_x, p_x)$	– is the operator of screw motion about $X$ – axis
$\mathbf{Sc}_y(\varphi_y, p_y)$	– is the operator of screw motion about $Y$ – axis
$\mathbf{Sc}_z(\varphi_z, p_z)$	– is the operator of screw motion about $Z$ – axis
$\mathbf{Tr}(a_x, X)$	– is the operator of translation at a distance $a_x$ along $X$ – axis
$\mathbf{Tr}(a_y, Y)$	– is the operator of translation at a distance $a_y$ along $Y$ – axis
$\mathbf{Tr}(a_z, Z)$	– is the operator of translation at a distance $a_z$ along $Z$ – axis
$U_g, V_g$	– are the curvilinear ( <i>Gaussian</i> ) coordinates of a point on a gear tooth flank $\mathcal{S}$
$U_p, V_p$	– are the curvilinear ( <i>Gaussian</i> ) coordinates of a point on a mating pinion tooth flank $\mathcal{P}$
$\mathbf{U}_g, \mathbf{V}_g$	– are the tangent vectors to curvilinear coordinate lines on the work gear tooth flank $\mathcal{S}$
$\mathbf{U}_p, \mathbf{V}_p$	– are the tangent vectors to curvilinear coordinate lines on a mating pinion tooth flank, $\mathcal{P}$
$\mathbf{V}_\Sigma$	– is the vector of the resultant motion of a pinion tooth flank, $\mathcal{P}$ , in relation to a tooth flank, $\mathcal{S}$ , of a gear
$k_{1.g}, k_{2.g}$	– are the first and second principal curvatures of a gear tooth flank, $\mathcal{S}$
$k_{1.p}, k_{2.p}$	– are the first and second principal curvatures of a mating pinion tooth flank, $\mathcal{P}$
$\mathbf{n}_g$	– is the unit normal vector at point of a gear tooth flank, $\mathcal{S}$
$\mathbf{n}_p$	– is the unit normal vector at point of a mating pinion tooth flank, $\mathcal{P}$
$r_{cnf}$	– is the position vector of a point of the indicatrix of conformity, $Cnf_R(\mathcal{S} \mathcal{P})$
$\mathbf{r}_g$	– is the position vector of a point of a gear tooth flank, $\mathcal{S}$
$\mathbf{r}_p$	– is the position vector of a point of a pinion tooth flank, $\mathcal{P}$
$\mathbf{t}_{1.g}, \mathbf{t}_{2.g}$	– are the unit tangent vectors of principal directions on a gear tooth flank, $\mathcal{S}$
$\mathbf{t}_{1.p}, \mathbf{t}_{2.p}$	– are the unit tangent vectors of principal directions on a mating pinion tooth flank, $\mathcal{P}$
$\mathbf{u}_g, \mathbf{v}_g$	– are the unit tangent vectors to curvilinear coordinate lines on the work gear tooth flank, $\mathcal{S}$
$\mathbf{u}_p, \mathbf{v}_p$	– are the unit tangent vectors to curvilinear coordinate lines on a mating pinion tooth flank, $\mathcal{P}$
$x_g y_g z_g$	– is the local <i>Cartesian</i> coordinate system having origin at point of contact of the tooth flanks, $\mathcal{S}$ and $\mathcal{P}$

## GREEK SYMBOLS

$\Phi_{1.g}, \Phi_{2.g}$	– are the first and second fundamental forms of a gear tooth flank, $\mathcal{S}$
$\Phi_{1.p}, \Phi_{2.p}$	– are the first and second fundamental forms of a mating pinion tooth flank, $\mathcal{P}$
$\Sigma$	– is the crossed-axis angle
$\Sigma_g$	– is the gear cone angle
$\Sigma_p$	– is the pinion cone angle
$\varphi_{b.op}$	– is the operating base pitch of a gear pair
$\varphi_{b.g}$	– is the base pitch of a gear
$\varphi_{b.p}$	– is the base pitch of a pinion
$\phi_n$	– is the normal pressure angle of a gear tooth
$\phi_t, \phi_{t.\omega}$	– is the transfer pressure angle of a gear tooth
$\mu$	– is the angle of the tooth flanks, $\mathcal{S}$ and $\mathcal{P}$ , local relative orientation

$\omega_p$	– is the rotation of a pinion
$\omega_g$	– is the rotation of a gear
$\omega_{pl}$	– is the instant rotation of a pinion in relation to a gear

## SUBSCRIPTS

<i>cnf</i>	Conformity
max	Maximum
min	Minimum
opt	Optimal
<i>g</i>	Gear
<i>p</i>	Pinion



# Taylor & Francis

Taylor & Francis Group

<http://taylorandfrancis.com>

---

# Glossary

Here we list, alphabetically, the most commonly used terms in gearing and in gear theory. Most of newly introduced terms are also listed below.

**Active portion of the plane of action:** is a portion of the plane of action,  $PA$ , that is located within the effective face width,  $F_{pa}$ , of a gear pair, and is bounded by the lines of intersection of the  $PA$  by the outer surfaces of a gear, and that of its mating pinion. [see: *Field of action*].

**Active profile:** part of a gear tooth profile that experiences contact during the mesh cycle.

**Addendum:** in parallel-axes gearing, the addendum of a gear tooth is the radial distance from the nominal pitch circle to the top of the tooth (or, in other words, this is the portion of the gear tooth above the reference pitch surface). This concept can be enhanced to all other kinds of gears.

**Addendum angle:** in a bevel gear, this is the angle between elements of the pitch cone and the face cone.

**Addendum modification:** a displacement of nominal addendum profile in radial direction of the gear.

**Angular backlash:** it is said to be the angular distance between the non-interacting tooth flanks of a driving member, and the tooth-space flank of the driven member in a gear pair, measured within the pitch plane.

**Angular base pitch:** this is an angle measured within the plane of action; the apex of the angle is coincident to the plane-of-action apex,  $A_{pa}$ ; the sides of the angle are through the corresponding points of intersection of two adjacent teeth flanks of the gear.

**Angular pitch:** this is the angle subtended by the circular pitch, usually expressed in radians.

**Angular pitch (in intersected-axes gearing):** it is said to be an angular distance between two adjacent tooth flanks of a gear measured within the pitch plane.

**Angular space width:** is said to be the angular distance between the opposite tooth flanks of a space between adjacent gear tooth measured within the pitch plane.

**Angular tooth addendum:** in intersected-axes gearing, it is said to be the angular distance between the pitch cone, and the outer cone of the gear, measured in axial section of the gear.

**Angular tooth dedendum:** in intersected-axes gearing, it is said to be the angular distance between the pitch cone, and the inner cone of the gear, measured in axial section of the gear.

**Angular tooth thickness:** it is said to be the angular distance between the opposite tooth flanks of the gear tooth, measured within the pitch plane.

**Apex to back:** in a bevel gear, this is the distance from the apex of the pitch cone to a locating surface at the back of the gear.

**Approximate gearing:** a means of which a rotation of the driving shaft at a *uniform angular velocity* is transmitted to the corresponding rotation of the driven shaft at a **not uniform angular velocity**; the tooth flanks of the gear and that of the mating pinion in approximate gearing are not conjugate to each other (the third fundamental law of gearing can be also violated in approximate gearing).

**Arc of action:** the angular displacement of the input defined by the mesh cycle. It can also be understood as the arc on the pitch circle through which a tooth profile moves from the beginning to the end of contact with a mating tooth profile.

**Arc of approach:** the arc on the pitch circle through which a tooth profile moves from its beginning of contact with a mating tooth profile until it reaches the pitch point.

**Arc of recess:** the arc on the pitch circle through which a tooth profile moves from contact with a mating tooth profile at the pitch point until contact ends.

- Axial pitch:** in a parallel-axes gear pair,  $p_x$ , is measured in the axial direction in helical gears, and is equal to the distance between points of intersection of two adjacent desirable lines of contact,  $LC_{des}$ , by a straight line parallel to the axis of instantaneous rotation  $P_m$ .
- Axial runout:** also known as *wobble*, this is the runout of the gear in the axial direction, measured at just below the root circle; it is expressed as a *total indicator reading*.
- Axis of instant rotation:** the straight line through the plane-of-action apex along the vector of instant rotation; also referred to as the *pitch line*.
- Axodes:** a pair of ruled surfaces that roll and slide upon one another in a special way such that there is no relative sliding perpendicular to the generators of the ruled surfaces; an obsolete term with limited usage (not recommended for use in the *Theory of Gearing*).
- Back angle:** in a bevel gear, this is the angle that complements to  $90^\circ$  the angle between an element of the back cone and the vector of the gear rotation; it is usually equal to the pitch angle. [The elements of the back cone of a bevel gear extend from the outside diameter of the gear blank to its axis and are perpendicular to the elements of the pitch cone – this is another definition of the term *back angle*].
- Back cone distance:** the distance along an element of the back cone from its apex to the pitch circle.
- Backlash:** amount the tooth space of one gear exceeds the tooth width of its mating gear; or, in other words, backlash,  $B_{pp}$ , in parallel-axes gearing is the distance between a not-interacting tooth flanks of a driving member, and that of a driven member, measured within the pitch plane in the gear pair.
- Base angular pitch:** the angular distance between two adjacent lines of contact of tooth flanks of a gear and its mating pinion, measured within the plane of action of the gear pair, and the angle apex coincides with the plane-of-action apex in the gear pair.
- Base circle:** in parallel-axes gearing, the base circle is the circle from which involute tooth profiles are developed.
- Base cylinder:** of a gear (of a pinion) is a cylinder of revolution that is generated as an envelope to a family of consecutive positions of the plane of action,  $PA$ , in its rotary motion in relation to a reference system associated with the gear (the pinion) when the gears rotate.
- Base diameter:** in parallel-axes gearing, this is the diameter of the base circle of an involute gear.
- Base helix angle:** the angle of crossing of the straight generating line of a screw involute tooth surface with the gear axis of rotation.
- Base pitch:** this is the pitch, measured along the circumference of the base circle, or along the *line of action*; it is therefore the circumference of the base pitch divided by the number of teeth; it is the same if measured along the line of action because the corresponding profiles of involute gear teeth are parallel curves, and the base pitch is the constant distance between them along the common normal in the direction of rotation, which, by definition, is the line of action.
- Bottom land:** this is the surface at the bottom of a tooth space which adjoins the fillets. For full fillet teeth, there is no bottom land as such.
- Boundary Novikov circle:** or just *boundary  $N$  – circle*, for simplicity, is a circle centered at the pitch point of a parallel-axes Novikov/conformal gearing, the radius of which is equal to the distance of the contact point between the tooth flanks of a gear and that of a mating pinion from the pitch point of the gear pair; a transverse section in Novikov/conformal gearing is subdivided by this circle onto two portions – the convex tooth profile of one member of the gearing must be entirely located within the interior of the boundary  $N$  – circle, while the concave tooth profile of another member of the gearing must be entirely located within the exterior of the boundary  $N$  – circle.<sup>1</sup> To be more precise, the concept of the *boundary  $N$  – circle* should be referred to as the *boundary  $N$  – cylinder*.

<sup>1</sup> The concept of the *boundary  $N$  – circle* was introduced by Prof. S.P. Radzevich at around 2008. This concept was not known in the time of Dr. M.L. Novikov.

- Boundary Novikov cone:** or just *boundary  $N$  – cone*, for simplicity, in intersected-axes, and in crossed-axes Novikov/conformal and high-conformal gearing is said to be a cone of revolution generated by the pseudo-path of contact,  $P_{pc}$ , in its rotary motion about the axis of instant rotation,  $P_{in}$ ; this cone subdivides the space onto two portions – the convex tooth flank of one member of the gear pair must be entirely located within the interior of the *boundary  $N$  – cone*, while the concave tooth flank of another member of the gear pair must be entirely located within the exterior of the *boundary  $N$  – cone*.
- Cartesian coordinate system:** a reference system that is comprised of three mutually perpendicular straight axes through the common origin. Determination of the location of a point in *Cartesian* coordinate system is based on the distances along the coordinate axes. Commonly, the axes are labeled as  $X$ ,  $Y$ , and  $Z$ . Often, either a subscript or a superscript is added to designation of the reference system  $XYZ$ .
- Center-distance (gear):** the gear center-distance,  $C_g$ , is the closest distance of approach between a gear axis of rotation,  $O_g$ , and an axis of instantaneous rotation,  $P_{in}$ , in the gear pair,  $O_p$  (that is,  $O_g/P_{in}$ ).
- Center-distance (gear pair):** the gear pair center-distance,  $C$ , is the closest distance of approach between a gear axis of rotation,  $O_g$ , and its mating pinion axis of rotation,  $O_p$  (that is,  $O_g/O_p$ ). It is measured along the mutual perpendicular to the axes, called the *line of centers*. In particular case of crossed-axes gearing, the center-distance is often referred to as the *offset*.
- Center-distance (pinion):** the pinion center-distance,  $C_p$ , is the closest distance of approach, between a pinion axis of rotation,  $O_p$ , and an axis of instantaneous rotation,  $P_{in}$ , in the gear pair,  $O_p$ , that is,  $O_p/P_{in}$ .
- Centerline:** this is the straight line that is perpendicular to the two axes of rotation,  $O_g$  and  $O_p$ .
- Centerline plane:** is the plane (the  $C_{in} - plane$ ) through the centerline,  $\mathfrak{C}$ , of the gear pair perpendicular to the pitch-line,  $P_{in}$ .
- Centrode:** A line of intersection between axodes and their corresponding transverse planes. The term *centrode* is applicable to parallel-axes gearing; this is an obsolete term with limited usage (not recommended for use in *Theory of Gearing*).
- Characteristic line:** a limit configuration of the line of intersection of a moving surface that occupies two distinct positions when the distance between the surfaces in these positions approaches zero. In the limit case, a characteristic line aligns with the line of tangency of the moving surface and with the envelope to a family of consecutive positions of the moving surface. In other words, this is the curve of intersection of a single surface as defined by two distinct its configurations.
- Chordal addendum:** the *chordal addendum* is used for the purpose of setting a gear tooth vernier to measure the tooth thickness, which is the chord length subtended by the two flanks of a gear tooth at the nominal pitch circle. The distance from the chord to the top of the tooth is known as the *chordal addendum*.
- Chordal thickness:** the length of the chord subtended by the two flanks of a gear tooth, usually at the nominal pitch circle diameter.
- Circular pitch:** the distance between the corresponding profiles of two adjacent teeth as measured along the pitch circle. It is therefore the circumference of the pitch circle divided by the number of teeth.
- Circular tooth thickness:** the length of arc between the two flanks of a gear tooth, usually at the nominal pitch circle diameter.
- Clearance:** a measure of the amount of space that exists between the tip of one gear tooth and the tooth-space bottom of the mating gear.
- Cone distance:** in a bevel gear, the distance from the base of its cone to the cone's apex is called the *cone distance*.

- Conjugate:** a term used to describe gear tooth forms, which properly mate with each other. More generally, *conjugate* stands for reciprocally related and interchangeable, as to properties, as two points, lines, and so on. When a gear and a mating pinion tooth flanks,  $\mathcal{S}$  and  $\mathcal{P}$ , interact with one another, the common perpendicular intersects the axis of instant rotation if the tooth flanks,  $\mathcal{S}$  and  $\mathcal{P}$ , conjugate to one another, and do not intersect the axis of instant rotation if the tooth flanks,  $\mathcal{S}$  and  $\mathcal{P}$ , are not conjugate to one another.
- Contact ratio:** the measure of the average number of pairs of teeth in contact during the mesh cycle. In parallel-axes gearing, it is equal to the length of the *arc of action* divided by the *transverse base pitch*.
- Crossed-axes gearing:** the axes of rotation of a gear and its mating pinion in a gear pair of this kind (in  $C_a$  – gearing) cross each other.
- Crowned teeth:** crowned teeth are often specified for spur, helical, and straight-tooth bevel gears. They are thicker at, or near the center of the tooth face than at the ends of the teeth. The purpose of crowning is to minimize the chance of end bearing of the teeth when there is misalignment in assembly, distortion from heat treating, or deflection under load. The amount of crowning is commonly in the neighborhood of .0003” per inch of face (.0006” change in tooth thickness per inch of face). Crowned gears are examples of *approximate gears*.
- Darboux frame:** in the differential geometry of surfaces, this is a local moving *Cartesian* reference system associated with the surface. *Darboux frame* is originated at surface point. The axes of the *Darboux frame* are pointed along three unit vectors, namely, along the unit normal vector to the surface, and along two unit tangent vectors of the principal directions on the gear tooth flank.
- Dedendum:** the dedendum of a gear tooth is the radial distance from the nominal pitch circle to its root circle. In other words, this is a portion of the gear tooth below the reference pitch surface.
- Dedendum angle:** in a bevel gear, this is the angle between elements of the root cone and pitch cone.
- Degree of conformity:** a qualitative measure of how close to one another are the tooth flank of one member of a gear pair to the tooth flank of another member of the gear pair in the differential vicinity of point of their contact (or at point within the line of contact of the tooth flanks).
- Desirable line of contact:** the line of contact,  $LC_{des}$ , between tooth flanks,  $\mathcal{S}$  and  $\mathcal{P}$ , of a gear and its mating pinion; this is a planar curve that is entirely located within the plane of action,  $PA$ , and possesses desirable geometry that makes possible a favorable design and a desirable performance of the gear pair.
- Diametral pitch:** this is the number of teeth per inch of pitch diameter of a gear.
- Effective face width:** is a width of the portion of the plane of action,  $PA$ , within which a gear and its mating pinion tooth flanks,  $\mathcal{S}$  and  $\mathcal{P}$ , interact with one another; the effective face width,  $F_{pa}$ , is measured along a straight line through the plane-of-action apex,  $A_{pa}$ .
- Effective length of lines of contact:** a portion of the total length of the line(s) of contact within which the driving gear is acting against the driven gear.
- Effective radius of curvature:** a measure of the relative distance between two planar curves in tangency expressed in terms of the radius of curvature of each curve.
- Evolute:** a locus of the centers of curvature for a planar curve.
- Face width:** the length between two ends of a gear. It is equal to the teeth length of spur gearing. In helical, or herringbone gearing, it is equal to the length of the teeth multiplied by cosine of the helix angle.
- Field of action:** a portion of the plane of action bounded by two lines of intersection of outer surfaces of the gear and the pinion, and by two lines specified in terms of effective face width of the gear pair (it is also often called the *zone of action*). [see: *Active portion of the plane of action*; *Zone of action*].



**Fillet:** a part of the tooth profile below the active region.

**Fillet radius:** the radius of an arc approximating the root fillet curve.

**Gear apex:** in a crossed-axes gear pair, this is a point of intersection of the gear axis of rotation with the centerline.

**Gear pair:** gear pair is an elementary mechanism that is composed of two mating gears mounted in a housing; a *gear pair* is used to transmit and to transform a rotary motion from an input shaft to an output shaft.

**Gear ratio:** the ratio between the instantaneous displacement of the output and the input. It is also known as the *speed ratio*, which is the number of teeth in the driven member (usually the larger, or the gear) divided by the number of teeth in the driver (usually the smaller, or the pinion).

**Gear space-line:** is a planar curve,  $G_{sl}$ , generated as a locus of middle-points of the crown-rack tooth-space profile within the pitch plane of the crown rack (or within the any other plane perpendicular to the axis of rotation of the pitch plane constructed within the gear tooth height).

**Gear tooth line:** is a planar curve, generated as a locus of middle-points of the crown-rack tooth-space profile within the pitch plane of the crown rack (or within the any other plane perpendicular to the axis of rotation of the pitch plane constructed within the gear tooth height). This line is considered in the unfolded onto a plane the pitch surface of the gear. The gear tooth line is equidistant to the lines of intersection of the opposite tooth flanks of the gear tooth by the pitch plane.”

**Generalized rack-type gear pair:** a crossed-axes gearing for which the vector of instant rotation is perpendicular to the gear axis of rotation.

**Generic gear surface:** a surface of revolution generated by the pitch line (in the gear machining process) about the gear axis of rotation.

**Geometrically accurate gearing:** a parallel-axes gearing, intersected-axes gearing, and/or crossed-axes gearing that is capable of transmitting a uniform rotation of the driving shaft to a uniform rotation of the driven shaft.

**Heel:** the thickest end of a bevel gear tooth.

**Helix angle:** in helical and herringbone gears, this is the angle between the gear teeth and the axis of rotation of the gear. The orientation of the basic rack in relation to the gear axis of rotation is specified by the helix angle.

**Hunting ratio:** a particular tooth ratio of a gear pair. This term is used to describe two toothed bodies in mesh where the ratio of number of teeth cannot be reduced using a common integer. If the hunting ratio exists between two toothed bodies in mesh, each tooth of one body meshes with each tooth of the other body.

**Indicatrix of conformity:** a planar centro-symmetrical characteristic curve of the fourth order that is used for the analytical description of the geometry of contact of a gear tooth flank and a mating pinion tooth flank. In particular cases, the indicatrix of conformity also possesses the property of mirror symmetry.

**Instantaneous line of action:** is a straight line,  $LA_{inst}$ , in a transverse section of the gear pair that is pointed along the common perpendicular,  $\mathbf{n}$ , at point of contact,  $K$ , of the tooth flanks,  $\mathcal{S}$  and  $\mathcal{P}$ .

**Instantaneous pitch point:** is a point of intersection,  $P_{inst}$ , of the centerline,  $\mathfrak{t}$ , by the instantaneous line of action,  $LA_{inst}$ .

**Intersected-axes gearing:** the axes of rotation of a gear and its mating pinion in a gear pair of this kind (in  $I_a$  – gearing) intersect each other.

**Involute:** a curve traced by a point on a flexible band at it is wrapped on/unwrapped from another curve (the *evolute*).

**Lead:** the axial advance of a helix for one complete turn, as in the treads of cylindrical worms and the teeth of helical gears.

- Lead angle:** the angle between any helix and plane of rotation. It is the complement to the helix angle and used for convenience in worms and hobs. It is understood to be at the standard pitch diameter.
- Line of action:** the straight line that is tangential to the base circles of two mating gears. Its intersection with the centerline of the two base circles defines the *pitch point*; in parallel-axes gearing the *line of action*,  $LA$ , can be also specified as a straight line of intersection of the plane of action,  $PA$ , by a transverse plane in the gear pair.
- Line of contact:** a line within which a gear tooth flank,  $\mathcal{S}$ , and a mating pinion tooth flank,  $\mathcal{P}$ , share common points.
- Long-and-short addendum:** this term is used to describe modified gear teeth in which the pinion teeth are cut on an oversize blank and the gear teeth are cut on a blank that is undersize by the same amount.
- Low-tooth-count gear:** in parallel-axes gearing, a gear of a base diameter,  $d_b$ , which equals to, or greater than root diameter,  $d_{f.g}$  (for which the inequality  $d_{b.g} \geq d_{f.g}$  is valid), is referred to as the **low-tooth-count gear** (or  $LTC$  – gear, for simplicity).
- Main reference systems:** is a set of *Cartesian* coordinate systems having the coordinate axes pointed along (a) the rotation vectors of a gear,  $\omega_g$ , and its mating pinion,  $\omega_p$ ; (b) the vector of instant rotation,  $\omega_{pl}$ ; (c) the centerline,  $C$ ; and (d) the corresponding lines of intersection of the principal planes (the  $P_{in}$  – plane, the  $C_{in}$  – plane, and the  $N_{in}$  – plane,) in the gear pair.
- Master gear:** used in checking a production gear in a composite action inspection test, by rolling the master with the production gear in tight mesh (spring loaded) and measuring the variation in centers. Usually, the master gear is hardened, with ground teeth, and produced to a high degree of accuracy.
- Mesh cycle:** the time length defined as the instance that two teeth come into contact until they get separated. The mesh cycle also yields interpretation in terms of angles of rotation or in terms of the length the contact point travels through.
- Module (of a gear):** the design parameter used for specifying the size of gear teeth using *ISO* standards. The module is specified as the ratio of the pitch diameter in millimeters to the number of teeth. The module is reciprocal of diametral pitch.
- Mounting distance (in crossed-axes gearing):** this is the distance from the plane-of-action apex (namely, the crossing point of the centerline, and the axis of instant rotation of two bevel gears in mesh with each other) to a locating surface of each gear. It is used in assembling crossed-axes gearing.
- Mounting distance (in intersected-axes gearing):** this is the distance from the crossing point of the axes of two bevel gears in mesh with each other to a locating surface of each. It is used in assembling bevel gearing.
- Non-involute gearing:** in parallel-axes gearing, non-involute gearing is comprised of gears that have non-involute tooth profile. Non-involute gearing is an example of *approximate gearing*.
- Normal plane:** is the plane (the  $N_{in}$  – plane) through the plane-of-action-apex,  $A_{pas}$ , perpendicular to the centerline,  $\mathfrak{L}$ , of the gear pair.
- Normal pressure angle:** the pressure angle that is measured within a plane perpendicular to the axis of instant rotation of the gear and the pinion.
- Number of teeth, or threads:** the number, of teeth or threads contained in the whole circumference of the pitch circle.
- Operating angular base pitch (in intersected-axes gearing, and in crossed-axes gearing):** is an angular distance between tooth flanks of two adjacent lines of contact of a gear and a mating pinion, that is measured within the plane of action.

- Operating base pitch (in parallel-axes gearing):** is a linear distance between every two adjacent desirable lines of contact,  $LC_{des}^i$  and  $LC_{des}^{i\pm 1}$ , measured in a section of the plane of action by a transverse plane.
- Out-of-pitch-point-mesh gearing:** is a kind of gearing (just *OPPM* – gearing, for simplicity), in which the pinion is situated in between the pitch point and the active portion of the line of action,  $LA$ .
- Parallel-axes gearing:** the axes of rotation of a gear and its mating pinion in a gear pair of this kind (in  $P_a$  – gearing) are parallel to one another.
- Path of contact (in geometrically accurate parallel-axes gearing):** is a straight line,  $P_c$ , traced by contact point in a motionless transverse section of the gear pair.
- Path of contact surface:** is a ruled surface,  $PCS$ , generated as a locus of consecutive positions of the instantaneous lines of action,  $LA_{inst}$ .
- Pinion:** the smallest of two gears in mesh.
- Pinion apex:** in a crossed-axes gear pair, this is a point of intersection of the pinion axis of rotation with the centerline.
- Pitch:** this is a measure of tooth spacing and size.
- Pitch circle:** circle through the pitch point that is centered on the gear/pinion axis of rotation (other definitions for the *pitch circle* are also known).
- Pitch (nominal) diameter:** is the diameter of the pitch circle of a gear.
- Pitch line:** is a straight line through the pitch point that is located in a transverse plane perpendicular to the centerline (other definitions for the *pitch line* are also known).  $P_m - P_m$
- Pitch-line plane:** In a crossed-axes gear pair, this is a plane (the  $P_m$  – plane) through the centerline and through the axis of instantaneous rotation of the gear and the pinion. For intersected-axes gearing, as well as for parallel-axes gearing, the  $P_m$  – plane can be also defined as the plane through the axis of rotation of the gear and the pinion.
- Pitch point:** is a point of intersection,  $P$ , of the centerline by the line of action; *pitch point* can also be specified as the point of tangency of two pitch circles, or of the pitch circle and the pitch line (other definitions for the *pitch point* are also known).
- Pitch surfaces:** A pair of ruled surfaces that roll and slide upon one another and are used as a reference when designing direct-contact mechanisms for spatial motion. In general, pitch surfaces are different from axodes.
- Plane of action:** is the plane through the axis of instantaneous rotation,  $P_m$ , at a transverse pressure angle,  $\phi_{t,\omega}$ , that forms a transverse pressure angle,  $\phi_t$ , with the normal plane ( $N_m$  – plane).
- Plane-of-action apex:** in a crossed-axes gear pair, this is a point of intersection of the axis of instant rotation,  $P_m$ , with the centerline,  $\mathcal{L}$ .
- Point of contact:** Any point at which two tooth flanks touch each other.
- Power density:** The ratio of amount of power transmitted to the weight of the gear pair (the *power-to-weight ratio*); also known as the amount of power transmitted through unit volume of the gearbox.
- Pressure angle:** is the included angle between the line of action,  $LA$ , and the normal plane (the  $N_m$  – plane).
- Principal assumption in dynamics of gearing:** a torque per unit length,  $\mathbf{t}_{pa}$ , is equally shared in the axial direction among an infinite number of infinitesimally thin slices, each of which is perpendicular to the axis of rotation either of the gear, or of the pinion, or of the axis of instantaneous rotation.
- Principal kinematics:** a pre-specified configuration of a set of rotation vectors: of the rotation vectors,  $\omega_g$  and  $\omega_p$ , of a gear and its mating pinion, along with the vector of instant rotation,  $\omega_{pt}$ .

**Principal planes:** is a set of planes composed of the principal planes: the pitch-line plane (the  $P_{ln}$  – plane), the centerline plane (the  $C_{ln}$  – plane), and the normal plane (the  $N_{ln}$  – plane) in the gear pair.

**Profile angle:** the angle that makes a tangent to the gear tooth profile and centerline of the gear tooth.

**Pseudo-path of contact:** in Novikov/*conformal gearing*, and in *high-conformal gearing*, this is a line along which contact point *pseudo-travels*.

**Rack:** a toothed wheel whose pitch radius is infinite, pitch circle is a straight line, tooth number is infinite.

**R – gearing:** is a geometrically accurate crossed-axes gearing that features *line contact* between tooth flanks of a gear and that of a mating pinion. Crossed-axes gearing of no other kind features *line contact* between the tooth flanks.

**Rotation vector:** is a pseudo-vector pointed along an axis of rotation that has a magnitude equal to the rotation about the axis. The direction of the rotation vector depends on the direction of the rotation. Commonly, the rotation vector is designated as  $\omega$ . The magnitude of the rotation vector is commonly denoted by  $\omega$ . Therefore, the equality  $\omega = |\omega|$  is valid. The rotation vector of a gear is designated as  $\omega_g$ , the rotation vector of the mating pinion is designated as  $\omega_p$ , and the rotation vector of the plane of action is designated as  $\omega_{pa}$ .

**Runout:** is a phenomenon describing the variation in pitch surface that results from nonzero eccentricity. There is a difference between the desired location of the axis of rotation and its actual location. It is measured in the radial direction and the amount of runout is the difference between the highest and the lowest reading in 360°. For gear teeth, runout is usually checked by placing a pin in tooth spaces and rolling past a dial indicator or by rolling with a master gear.

**Shaft angle:** is the angle between the axes of two gear shafts.

**Spacing:** the term *spacing* is used as a general term to describe the accuracy with which teeth are spaced around the gear.

**Span measure:** the measurement of the distance across several teeth of gears too large to use pin measurements; the measurement is made along a line tangent to the base circle.

**Spiral angle:** is the angle between the tooth and an element of the pitch cone in a spiral bevel gear.

**Throat diameter:** is the diameter of the addendum circle at the center of the face of a cylindrical, or double-enveloping worm gear.

**Throat form radius:** is the radius of the throat of a cylindrical or double-enveloping worm gear in section by an axial plane.

**Tip radius:** is the radius between the outside and the side cutting edges of hobs and other gear cutting tools.

**Tip relief:** is an arbitrary modification of the tooth profile near the tip of the teeth to minimize or eliminate tip interference.

**Toe:** in a bevel gear, or pinion, this is the thinnest end of a tooth.

**Tolerance:** is the amount by which a specific dimension is permitted to vary. It is usually expressed as the difference between the maximum and minimum limits allowed.

**Top land:** is the width, or thickness, of a gear tooth measured at its maximum (for external gears) or minimum (for internal gears) diameter.

**Total length of the lines of contact:** means a summa of the length of all the lines of contact that occur at a specified instant of time.

**Transmission function:** is the ratio between the instantaneous position of the output and the instantaneous position of the input.

**Transverse pressure angle:** is said to be the angle between the plane of action,  $PA$ , and a perpendicular,  $\mathbf{n}_{pa}$ , to the plane through the axes of rotation of the gear and the pinion (the  $N_{ln}$  – plane).

**Undercut:** is a portion of a gear tooth profile undesirably cut out in a gear generated process.

**Vector of instant rotation:** is a pseudo-vector that is pointed along the axis of instant rotation either of a pinion in relation to the gear, or of the gear in relation to the pinion. The actual direction of this vector depends on the direction of rotation of the gear and the pinion. The rotation vector is commonly designated as  $\omega_{pl}$ .

**Whole depth:** is the distance from the top land of a gear tooth to its root.

**Winding relationship:** is a manufacturing specification between the coordinates used to parameterize the cutter and those used to parameterize the desired gear.

**Working depth:** is the depth at which gear teeth are engaged.

**Zone of action:** is the portion of the plane of action within which the tooth flanks of the gear and of the pinion interact with one another [see: *Active portion of the plane of action*; *Field of action*).



# Taylor & Francis

Taylor & Francis Group

<http://taylorandfrancis.com>

---

# References

- [1] Airy, G.B., “XVIII. On the Forms of the Teeth of Wheels,” *Transactions of the Cambridge Philosophical Society*, Vol. 2, 1827, pp. 277–286.
- [2] An’ishchenko, V.V., Koval’enko, G.D., “Investigation of Contact Stress in Novikov Gears Using Photo-Elastic Approach,” in: *NoviTheory of Gearingkov Gearing*, Vol. I, TsINTIAM, Moscow, 1964.
- [3] Astridge, D.G., Shotter, B.A., Dyson, A., Evans, H.P., Snidle, R.W., “Tribology of High Conformity Gears,” pp. 819–825 in: *IMEchE Conference on Tribology—Friction Lubrication and Wear, Fifty Years On, London*, 1987.
- [4] Ball, R.S., *A Treatise on the Theory of Screws*, Cambridge University Press, Cambridge, NY, 1998, 588p.
- [5] Ball, R.S., *The Theory of Screws*, Hodges & Foster, Dublin, 1876.
- [6] Baxter, M.L., Jr., “Basic Geometry and Tooth Contact of Hypoid Gears,” *Industrial Mathematic*, Vol. 11, No. 2, pp. 19–42, 1961.
- [7] Baxter, M.L. Jr., “Basic Theory of Gear-Tooth Action and Generation,” in: *Gear Handbook*, 1st edition, edited by D. Dudley, McGraw Hill, New York, 1962.
- [8] Bayazitov, N., *Helical Gears with a New Type of Gearing*, Ph.D. Thesis, Kazan Technological & Chemical Institute, Kazan, 1964.
- [9] *Bevel Gear: Fundamentals and Applications*, edited by J. Klingelnberg, Springer-Verlag GmbH, Berlin, Heidelberg, 2016, 328p.
- [10] Böehm, W., “Differential Geometry II,” pp. 367–383 in: *Curves and Surfaces for Computer Aided Geometric Design. A Practical Guide*, 2nd edition, Academic Press, Inc., Boston, 1990, 444p.
- [11] Bonnet, P.O., *Journal de l’École polytechnique*, Vol. xiii, p. 31, 1867.
- [12] Börner, J., Humm, K., Joachim, F., “Development of Conical Involute Gears (Beveloids) for Vehicle Transmissions,” *Gear Technology magazine*, November/December 2005, pp. 28–35.
- [13] Bricard, R., *Leçons de cinématique, Tome II*, Gauthier-Villars, Paris, 1927, 352p.
- [14] Buchanan, R., *An Essays on the Teeth of Wheels: Comprehending Principles, and their Application in Practice, to, Millwork and Other Machinery. With Numerous Figures, Revised by Peter Nicholson*. William Savage, London, 1808.
- [15] Buckingham, E., *Analytical Mechanics of Gears*, Dover Publications, Inc., New York, 1988, 546p.
- [16] Camus, Ch.E.L., *Cours de Mathématique: Elements de Mécanique Statique, Second Volume*, Durand, Paris, 1759.
- [17] Camus, C.-É.-L., “Sur la Figure des Dentes des Rouës, et des Ailes des Pignons, Pour Rendre les Horloges Plus Parfaites,” pp. 117–140 in: *History de l’Académie royale des Sciences*, Paris, 1733.
- [18] Cauchy, A.L., *Leçons sur les Applications du Calcul Infinitésimal à la Geometrie*, Imprimerie royale, Paris, 1826.
- [19] Chen, C.-F., Tsay, C.-B., “Computerized Tooth Profile Generation and Analysis of Characteristics of Elliptical Gears with Circular-Arc Teeth,” *Journal of Materials Processing Technology*, Vol. 148, 2004, pp. 226–234.
- [20] Chironis, N., “Design of Novikov Gears,” pp. 124–135 in: *Gear Design and Application*, edited by N.P. Hironis, McGraw-Hill Company, New York, 1967, 374 p.
- [21] Cormac, P., *A Treatise on Screws and Worm Gear, Their Mills and Hobs*, Chapman & Hall, Ltd., London, 1936, 138p.
- [22] Coy, J.J., Townsend, D.P., Zaretsky, E.V., *Gearing*, NASA Reference Publication 1152, AVSCOM, Technical Report 84-C-15, 1985, 76p.
- [23] da Vinci, L., *The Madrid Codices*, Volume 1, 1493, Facsimile Edition of “*Codex Madrid 1*,” original Spanish title: *Tratado de Estatica y Mechanica en Italiano*, McGraw Hill Book Company, 1974.
- [24] de la Hire, P., “Traité des Epicycloïdes, & de Leurs Usages Dans les Mechaniques,” in: *Mémoires de Mathématique et de Physique*, Impr. Royale, Paris, 1694.
- [25] Denavit, J., Hartenberg, R.S., “A Kinematics Notation for Lower-Pair Mechanisms Based on Matrices,” *ASME Journal of Applied Mechanics*, Vol. 77, 1955, pp. 215–221.
- [26] Diker, Ya.I., Sagin, L.I., *Fundamentals of Production of Globoidal Gearing*, Mashgiz, Moscow, 1960, 256p.



- [27] do Carmo, M.P., *Differential Geometry of Curves and Surfaces*, Prentice-Hall, Englewood Cliffs, NJ, 1976, 503p.
- [28] Dooner, D.B., *Kinematic Geometry of Gearing*, 2nd edition, John Wiley & Sons, Inc., New York, 2012, 512p. [First edition: Dooner, D.B., Seireg, A.A., *The Kinematic Geometry of Gearing. A Concurrent Engineering Approach*, John Wiley & Sons, Inc., NY, 1995, 450p].
- [29] Dudas, I., *The Theory and Practice of Worm Gear Drives*, Penton Press, London, 2000, 314p.
- [30] Dusev, I.I., "Sliding between Enveloping Gear Teeth Surfaces in Spatial Gearing," *Proceedings of the Universities, Mechanical Engineering*, 1968, No. 4, pp. 15–18.
- [31] Dusev, I.I., Vasilyev, V.M., *Analytical Theory of Spatial Gearings and its Application to Investigation of Hypoid Gearing*, Rostov-on-Don Book Publishers, Rostov-on-Don, 1968, 148p.
- [32] Dyson, A., *A General Theory of the Kinematics and Geometry of Gears in Three Dimensions*, Clarendon Press, Oxford, 1969, 141p.
- [33] Dyson, A., Evans, H.P., Snidle, R.W., "Wildhaber-Novikov Circular Arc Gears: Geometry and Kinematics," *Proceedings of the Royal Society of London. A. Mathematical and Physical Sciences*, Vol. 403, 1986, pp. 313–340.
- [34] Errichello, R.L., "Morphology of Micropitting," *Gear Technology*, November/December 2012, pages 74–81.
- [35] Euler, L., "De Aptissima Figura Rotarum Dentibus Tribuenda" ("On Finding the Best Shape for Gear Teeth"), pp. 299–316, in: *Academiae Scientiarum Imperiales Petropolitanae, Novi Commentarii*, 1754–55.
- [36] Euler L., "Supplementum. De Figura Dentium Rotarum," pp. 207–231 in: *Novi Commentarii adacemiae Petropolitanae 11*, 1767.
- [37] Favard, J., *Course de Géométrie Différentielle Locale*, Gauthier-Villars, Paris, 1957, viii+553p.
- [38] Fed'akin, R.V., *Investigation of Strength of Circular-Arc Gear Teeth*, Ph.D. Thesis, Zhukovskii Military Aviation Engineering Academy (MAEA), Moscow, 1955.
- [39] Fedot'onok, A.A., *Kinematic Structure of Machine Tools*, Mashinostroyeniye, Moscow, 1970, 403p.
- [40] Fisher, G. (Editor), *Mathematical Models*, Friedrich Vieweg & Sohn, Braunachweig/Wiesbaden, 1986.
- [41] Fraifeld, I.A., *Cutting Tools that Work on Principle*, Mashgiz, Moscow, 1948, 252p.
- [42] French, M.J., "Conformity of Circular-Arc Gears," *Journal of Mechanical Engineering Science*, Vol.7, No. 2, 1965, pp. 220–223.
- [43] Gavrilenko, V.A., *Fundamentals of Theory of Involute Gearing*, Mashinostroyeniye, Moscow, 1969, 432p.
- [44] Gochman, H.I., *Theory of Gearing Generalized and Developed Analytically*, Odessa (Ukraine), 1886, 229p.
- [45] Golovin, A.A., Tarabarin, V.B., *Russian Models from the Mechanisms Collection of Bauman University*, History of Mechanism and Machine Science 5, Springer, Zurich, 2008, 238p.
- [46] Grant, G.B., *A Treatise on Gear Wheels*, 6th edition, Philadelphia Gear Works, Inc., Philadelphia, 1893, 105 p.
- [47] Gray, A., "Plücker's Conoid," pp. 435–437 in: *Modern Differential Geometry of Curves and Surfaces with Mathematics*, edited by A. Gray, 2nd edition, CRC Press, Boca Raton, FL, 1997.
- [48] Hertz, H., "Über die Berührung Fester Elastischer Körper (The Contact of Solid Elastic Bodies)," *Journal für die Reine und Angewandte Mathematik (Journal for Pure and Applied Mathematics)*, Berlin, 1881, pp. 156–171; *Über die Berührung Fester Elastischer Körper und Über die Härte (The Contact of Solid Elastic Bodies and Their Harnesses)*, Berlin, 1882; Reprinted in: H.Hertz, *Gesammelte Werke (Collected Works)*, Vol. 1, pp. 155–173 and pp. 174–196, Leipzig, 1895, or the English translation: *Miscellaneous Papers*, translated by D.E. Jones and G.A. Schott), pp. 146–162, 163–183, London: McMillan and Co., Ltd., 1896.
- [49] Hicks, R.J., "Experience with Compact Orbital Gears in Service," *Proceedings of the Institution of Mechanical Engineers*, Vol. 184, Pt. 30, 1969–1970, pp. 85–94.
- [50] Hill, M., *Kinematics of Gerotors*, 2nd edition, The Peter Reilly Company, Philadelphia, 1927, 44p.
- [51] Hills, D.A., Nowell, D., Sackfield, A., *Mechanics of Elastic Contact*, Butterworth-Heinemann Ltd., Oxford, 1993, 496p.
- [52] Hills, D.A., Sackfield, A., "Sliding Contact between Dissimilar Elastic Cylinders," *Journal of Tribology*, Vol. 107, 1985, pp. 463–466.
- [53] [http://www.math.hmc.edu/faculty/gu/curves\\_and\\_surfaces/surfaces/plucker.html](http://www.math.hmc.edu/faculty/gu/curves_and_surfaces/surfaces/plucker.html).
- [54] <http://www.mathcurve.com/surfaces/plucker/plucker.shtml>.
- [55] Imison, J., *A Treatise on the Mechanical Powers*, Printed by the author, and sold by R. Jameson, London, 1787.
- [56] Jeffreys, H., *Cartesian Tensors*, University Press, Cambridge, 1961, 93p.
- [57] Kapelevich, A.L., *Asymmetric Gearing*, CRC Press, Boca Raton, FL, 2018, 287p.

- [58] *Kegelräder: Grundlagen, Anwendungen*, edited by J. Klingenberg, Springer, Heidelberg, 2008, 381p.
- [59] Klebanov, B.M., "Gear Drive Engineering," pp. 165–241 in: *Advances in Gear Design and Manufacture*, edited by S.P. Radzevich, CRC Press, Boca Raton, FL, 2019, 549p.
- [60] Koenderink, J.J., *Solid Shape*, The MIT Press, Cambridge, MA, 1990, 699p.
- [61] Koetsier, T., "Euler and Kinematics," pp. 167–194 in: *Leonhard Euler: Life, Work and Legacy*, Series: Studies in the History and Philosophy of Mathematics, Vol. 5, edited by R.E. Bradley, C.E. Sandifer, Elsevier, Amsterdam, 2007, 534p.
- [62] Kolchin, N.I., *Analytical Calculation of Planar and Spatial Gearing*, Mashgiz, Moscow, 1949, 210p.
- [63] Kolchin, N.I., "Analytical Foundations of the Differential Method of Gear Investigation," *Proceedings of the Seminar on Machine and Mechanism Theory*, Vol. XVI, No. 64, 1957, pp. 26–53 (in Russian).
- [64] Korostelev, L.V., "Kinematical Indicators of Bearing Capacity in Spatial Gearing," *Proceedings of the Universities, Mechanical Engineering*, No. 10, 1964, pp. 5–15.
- [65] Korostelev, L.V., *Peculiarities of Meshing in the Pole of Worm Gearing*, Mashinovedeniye, Moscow, 1967, 5p.
- [66] Krasnoschokov, N.N., Fed'akin, R.V., Chesnokov, V.A., *Theory of Novikov Gearing*, Nauka, Moscow, 1976, 173p.
- [67] Krenzer, T., *The Bevel Gear*, 2007, 252p.
- [68] Kudriavtsev, V.N., *Calculation and Design of Novikov Gearing*, Zhukovskii Military Aviation Engineering Academy (MAEA), Leningrad, 1959, 78p.
- [69] Kudriavtsev, V.N., et al., *Planetary Gear Drives*, Mashinostroyeniye, Leningrad, 1977, 536p.
- [70] Kul'ikov, G.V., Fed'yakin, R.V., Chesnokov, V.A., "An Investigation of Contact Strength of Novikov Gears," in: *Novikov Gearing*, Vol. II, Zhukovskii Military Aviation Engineering Academy (MAEA), Moscow, 1962.
- [71] Lagrange, J.L., *Théorie des Fonctions Analytiques*, Impr. De la République, prairial an V, Paris, 1797, 277 p.
- [72] Lagutin, S.A., Verhovsky, A., Sandler, A., "Fluid Friction Worm Gears: State of Art and Development Prospects," in: *Proceedings of the 3rd International Conference "Power Transmissions '09"*, edited by A. Mihailidis, 1–2 October 2009, Chalkidiki, Greece, 6p.
- [73] Lewis, W., "Investigation of the Strength of Gear Teeth," in: *Proc. of the Engineers Club*, Philadelphia, PA, 1893, pp. 16–23.
- [74] Litvin, F.L., *Gear Geometry and Applied Theory*, Prentice Hall, Englewood Cliffs, NJ, 1994, 724p.
- [75] Litvin, F.L., *Noncircular Gears*, Mashgiz, Moscow, 1950, 218p.
- [76] Litvin, F.L., Fuentes, A., *Gear Geometry and Applied Theory*, 2nd edition, Cambridge University Press, Cambridge, UK, 2004, 800p.
- [77] Litvin, F.L., Fuentes-Anzar, A., Gonzalez-Perez, I., Hayasaka, K., *Noncircular Gears: Design and Generation*, Cambridge University Press, New York, 2009, 204p.
- [78] Lopato, G.A., Kabatov, N.F., Segal, M.G., *Spiral Bevel and Hypoid Gearings*, 2nd edition, Mashinostroyeniye, Moscow, 1977, 423p.
- [79] Lowe, P.G., "A Note on Surface Geometry with Special Reference to Twist," *Mathematical Proceedings of the Cambridge Philosophical Society*, Vol. 87, 1980, pp. 481–487.
- [80] Lowe, P.G., *Basic Principles of Plate Theory*, Surrey University, 1982.
- [81] *MAAG Gear Book: Calculation and Practice of Gears, Gear Drives, Toothed Couplings and Synchronous Clutch Couplings*, MAAG Gear Company, Ltd., Zurich/Switzerland, 1990, 440p.
- [82] Merritt, H.E., *Gear Engineering*, Putman Publishing, London, 1971, 489p.
- [83] Michalec, G.W., *Precision Gearing: Theory and Practice*, John Wiley & Sons, Inc., New York, 1966, 620p.
- [84] Miron, R., "Observatii a Supra Unor Formule din Geometria Varietatilor Neonolome  $E_3^2$ ," *Buletinul Institutului Politehnic din Iasi*, 1958.
- [85] Mozhayev, S.S., *A Generalized Theory of Cutting Tools*, Doctoral Thesis, Leningrad, Leningrad Polytechnic Institute, 1953, 295p.
- [86] Mozhayev, S.S., *Analytical Theory of Twist Drills*, Mashgiz, Moscow, Leningrad, 1948, 136p.
- [87] Nieman, G., "Novikov Gear System and other Special Gear Systems for High Load Carrying Capacity," *VDI, Berichte*, 1961, p. 47.
- [88] Nikolayev, A.F., "A Diagram of Screw and Its Application to the Determination of Conjugate Ruled Surfaces with Line Contact," *Proceedings of Seminar on the Theory of Mechanisms and Machines, Academy of Sciences of the USSR, Institute of Machine Science*, 1950, Vol. 10, No. 37, pp. 52–106.
- [89] Nikolayev, A.F., *Kinematic Principles of the Theory of Spatial Gearing*, Doctoral Thesis, Stankin, Moscow, 1953, 48 pages.

- [90] Novikov, M.L., *Fundamentals of Geometric Theory of Gearing with Point Meshing for High Power Density Transmissions*, Doctoral Thesis, Moscow, Zhukovskii Military Aviation Engineering Academy (MAEA), 1955.
- [91] Novikov, M.L., *Gearing with a Novel Kind of Teeth Meshing*, Published by Zhukovskii Military Aviation Engineering Academy (MAEA), Moscow, 1958, 186p.
- [92] Nutbourn, A.W., "A Circle Diagram for Local Differential Geometry," in: *Mathematics of Surfaces, Conference Proceedings, Institute of Mathematics and its Application*, edited by J. Gregory, Oxford University Press, Oxford, 1986.
- [93] Nutbourn, A.W., Martin, R.R., *Differential Geometry Applied to Curve and Surface Design, Volume 1: Foundations*, Ellis Horwood Ltd. Publishers, Chichester, 1988, 282p.
- [94] Oberg, E., *Spiral and Worm Gearing*, The Industrial Press, New York; The Machinery Publishing Co., Inc., London, 1920, 274p.
- [95] Olivier, T., *Théorie Géométrique des Engrenages destinés à transmettre le mouvement de rotation entre deux axes situés ou non dans un même plan*, (Geometric Theory of Gearing), Bachelier, Paris, 1842, 118p.
- [96] Pat. No. 186,436, (GB), *Improvements in and Relating to Gear Teeth*, F.J. Bostock and S. Bramley-Moore, Filed: July 2, 1921, Patented: October 2, 1922.
- [97] Pat. No. 208,332, (GB), *Improvements in or Relating to Worm-gearing*, F.J. Bostock and S. Bramley-Moore, Filed: November 9, 1922, Patented: December 20, 1923.
- [98] Pat. No. 5,647, (USA). *Rack and Pinion*, Amzi C. Semple, June 27, 1848.
- [99] Pat. No. 407,437, (USA). *Machine for Planing Gear Teeth*./G.B. Grant, Filed: January 14, 1887 (serial No. 224,382), Patented: July 23, 1889.
- [100] Pat. No. 1,425,144, (USA). *Toothed Gearing*, /H.J. Schmick, Patented: August 8, 1922, Filed: June 30, 1921, Serial No. 481.561.
- [101] Pat. No. 1,601,750, (USA). *Helical Gearing*. /E. Wildhaber, Filed: November 2, 1923, published October 5, 1926.
- [102] Pat. No. 1,683,163, (USA). *Precision Worm Gearing*./S.I. Cone, Filed: June 27, 1925, Patented: September 4, 1928.
- [103] Pat. 1,751,540 (USA). *Method of Generating Worm Gearing*, S.I. Cone, Filed: June 27, 1925, Patented: March 25, 1930.
- [104] Pat. No. 1,816,273 (USA), *Gearing*./E. Wildhaber, Filed: June 18, 1928, patented: July 28, 1931.
- [105] Pat. 1,828,800 (USA). *Hindley Worm-gearing*, S.I. Cone, Filed: June 27, 1925, Patented: September 8, 1931.
- [106] Pat. No. 1,934,754, *Method and Means for Forming Gears*./E. Wildhaber, Filed: March 23, 1931, patented: November 14, 1933.
- [107] Pat. 2,026,215 (USA). *Globoidal Hob*, S.I. Cone, Filed: May 2, 1927, Patented: December 31, 1935.
- [108] Pat. No. 2,696,125, (USA), *Speed-Reduction Gearing*./O.E. Saari, Cl. 74-459.5, Filed: July 12, 1954.
- [109] Pat. 2,731,886 (USA). *Method of Making Speed-Reduction Gearing*, O.E. Saari, Filed: July 12, 1954, Patented: January 24, 1956.
- [110] Pat. 2,776,578 (USA). *Skew Axis Gearing and Method of Making Same*, O.E. Saari, Filed: February 18, 1954, Patented: January 8, 1957.
- [111] Pat. 2,896,467 (USA). *Skew Axis Gearing with Plane Tooth Gear*, O.E. Saari, Filed: October 1, 1957, Patented: July 28, 1959.
- [112] Pat. No. 2,906,143 (USA), *Strain Wave Gearing*, C.W. Musser, Filed: March 21, 1955, Patented: September 29, 1959.
- [113] Pat. No. 2,954,704, (USA), *Skew Axis Gearing*./O.E. Saari, Cl. 74-466, Filed: April 10, 1957, Patented: October 4, 1960.
- [114] Pat. 3,079,808 (USA). *Gear Drive with Worm-gearing*, E. Wildhaber, Filed: February 8, 1960, Patented: March 5, 1963.
- [115] Pat. 3,303,713, (USA). *Load Equalizing Means for Planetary Pinions*: Raymond J. Hicks, February 14, 1967, Filed: February 8, 1965.
- [116] Pat. 3,386,305 (USA). *Worm-gearing*, E. Wildhaber, Filed: April 28, 1966, Patented: June 4, 1968.
- [117] Pat. No. 3,786,719, (USA). *Hobbing Cutter*, /K. Kimura, and M. Ainoura, (AZUMI), 1974.
- [118] Pat. 4,047,449 (USA). *Globoid Worm-gearing and Method of Making Globoid Worm Thereof*./V.A. Popov, Int. Cl. F16 H 55/04; F16H 1/16, Filed: January 29, 1976, Patented: September 13, 1977.
- [119] Pat. No. 5,113,713 (USA), "Elastomeric Load Sharing Device," /C.J. Isabelle, J.G. Kish, R.A. Stone, Int. Cl.5 F16H 55/18, U.S. Cl. 74/410, 74/411, 74/440, Filed: February 11, 1991, Date of Patent: May 19, 1992.

- [120] Pat. No. 6,112,611, (USA), *Gear With Modified Tooth Surface and Gear Tooth Surface Modification Method*./H. Maki, Filed: May 18, 1998, Int. Cl. B23F 9/00, B23F 19/00.
- [121] Pat. No. 6,117,036 (USA), *Split Helical Planetary Assembly*, J.L. Lanzon, R. Mizon, R.C. Williams, Int. Cl. F16H 37/08, Filed: July 29, 1999, Patented: September 12, 2000.
- [122] Pat. No. 8,070,640 (USA) *Fluctuating Gear Ratio Limited Slip Differential*, S.P. Radzevich, Date: December 6, 2011, Filed: March 12, 2009, Int. Cl. F16H 48/06, F16H 48/20, F16H 57/08, F16H 57/17, U.S. Cl. 475/230.
- [123] Pat. No. 109,113, (USSR). *Gear Pairs and Cam Mechanisms Having Point System of Meshing*. /M.L. Novikov, National Classification 47h, 6; Filed: April 19, 1956, published in Bull. of Inventions No.10, 1957.
- [124] Pat. No. 163,857, USSR, *A Helical Gearing*./B.V. Shitikov, N.A. Bayazitov, Int. Cl. F06h, Filed: February 25, 1963, Published: July 22.
- [125] Pat. No. 182,462, (USSR), *Gearing Featuring Point System of Meshing and Having Multiple Lines of Action*./ R.V. Fed'akin and V.A. Chesnokov, National Cl. 47 h, 6, Filed: November 20, 1963, published in B.I. No. 7, 1966.
- [126] Pat. No. 257,246, (USSR), *A Worm-Gear Drive*./ L.V. Korostel'ov, Filed: October 25, 1968, Int. Cl. F 16h.
- [127] Pat. No. 1,185,749, (USSR), *A Method of Sculptured Surface Machining on a Multi-Axis NC Machine*./ S.P. Radzevich, Int. Cl. B23c 3/16, Filed: October 24, 1983.
- [128] Pat. No. 1,249,787, (USSR), *A Method of Sculptured Surface Machining on Multi-Axis NC Machine*./ S.P. Radzevich, Int. Cl. B23c 3/16, Filed: December 27, 1984.
- [129] Pat. No. 1,449,246 (USSR). *A Method of Experimental Simulation of Machining of a Sculptured Surface on Multi-Axis NC Machine*./S.P. Radzevich, Int. Cl. B 23 C, 3/16, Filed: February 17, 1987.
- [130] Phillips, J., *General Spatial Involute Gearing*, Springer, New York, 2003, 498p.
- [131] Pismanik, K.M., *Hypoid Gearing*, Mashinostroyeniye, Moscow, 1964, 227p.
- [132] Plücker, J., "On a New Geometry of Space," *Philosophical Transactions of the Royal Society of London*, Vol. 155, 1865, pp. 725–791.
- [133] Prudhomme, R., Lemasson, G., *Cinématique*, École Nationale Supérieure d'Arts et Métiers, École d'Ingénieurs, Paris, 1906, 1955.
- [134] Radzevich, S.P., "A Brief Overview on the Evolution of Gear Art: Design and Production of Gears, Gear Science," pp. 418–485 in: *Advances in Gear Science and Manufacture*, edited by S.P. Radzevich, CRC Press, Boca Raton, FL, 2019, 570p.
- [135] Radzevich, S.P., "A Brief Overview on the Evolution of the Scientific Theory of Gearing: A Preliminary Discussion," pp. 1035–1046 in: *Proceedings of International Conference on Gears 2015*, October 5–7, 2015, Technische Universität München (TUM), Garching (near Munich), Germany, 2015.
- [136] Radzevich, S.P., *A Method for Designing of the Optimal Form-Cutting-Tool for Machining of a Given Sculptured Surface on Multi-Axis NC Machine*. – Pat. №4242296/08 (USSR), Filed: March 31, 1987.
- [137] Radzevich, S.P., "A Novel Method for Mathematical Modeling of a Form-Cutting-Tool of the Optimum Design," *Applied Mathematical Modeling*, Vol. 31, December 2007, pp. 2639–2654.
- [138] Radzevich, S.P., "A Novel Result in the Classical Theory of Envelope Curves and Surfaces," *Bulletin of Science and Technical Development*, No. 8(156), 2020, pp. 12–21. [www.vntr.ru](http://www.vntr.ru)
- [139] Radzevich, S.P., *A Parallel-Axis Involute Gearing*, Invention disclosure PDS 10-PPD-161, submitted to Eaton Patent on February 9, 2010.
- [140] Radzevich, S.P., "A Possible Way of Evolution of Novikov Gearing," pp. 39–40 in: *Proceedings of the IX International Conference "Complex Assurance of Quality of Technological Processes & Systems"*, May 14–16, 2019, Chernihiv (Ukraine), Vol. 1, 2019.
- [141] Radzevich, S.P., "A Possibility of Application of Plücker's Conoid for Mathematical Modeling of Contact of Two Smooth Regular Surfaces in the First Order of Tangency," *Mathematical and Computer Modeling*, Vol. 42, 2004, pp. 999–1022.
- [142] Radzevich, S.P., "About Hob Idle Distance in Gear Hobbing Operation," *ASME Journal of Mechanical Design*, Vol. 124, December 2002, pp. 772–786.
- [143] Radzevich, S.P., *CAD/CAM of Sculptured Surfaces on Multi-Axis NC Machine: The DG/K-Based Approach*, M&C Publishers, San Rafael, CA, 2008, 114p.
- [144] Radzevich, S.P., *Classification of Surfaces*, Monograph, UkrNIINTI, Kiev, No. 1440-Yk88, 1988, 185p.
- [145] Radzevich, S.P., "Concisely on Kinematic Method and about History of the Equation of Contact in the Form  $\mathbf{n} \cdot \mathbf{V} = 0$ ," *Theory of Mechanisms and Machines*, Vol. 8, No. 1 (15), 2010, pp. 42–51. <http://tmm.spbstu.ru>



- [146] Radzevich, S.P., *Design and Investigation of Skiving Hobs for Finishing of Hardened Gears*, Ph.D. Thesis, Kiev Polytechnic Institute, Kiev, 1982, 298p.
- [147] Radzevich, S.P., "Design of Shaving Cutter for Plunge Shaving a Topologically Modified Involute Pinion," *ASME Journal of Mechanical Design*, Vol. 125, September 2003, pp. 632–639.
- [148] Radzevich, S.P., *Differential-Geometric Method of Surface Generation*, Dr.Sci. Thesis, Tula Polytechnic Institute, Tula, 1991, 300p.
- [149] Radzevich, S.P., *Dudley's Handbook of Practical Gear Design and Manufacture*, 3rd edition, CRC Press, Boca Raton, FL, 2016, 629p. [2nd Edition: Radzevich, S.P., *Dudley's Handbook of Practical Gear Design and Manufacture*, CRC Press, Boca Raton, FL, 2012, 896p.].
- [150] Radzevich, S.P., "Experience Gained from Reading Master's Thesis by Ch.I. Gochman "Theory of Gearing, Generalized and Evolved by Analysis"," in: *Theory of Machines and Mechanisms*, 2011, Vol. 9, No. 1, pp. 33–43. [http://tmm.spbstu.ru/17/radzevich\\_17.pdf](http://tmm.spbstu.ru/17/radzevich_17.pdf)
- [151] Radzevich, S.P., *Fundamentals of Surface Generation, Monograph*, Rastan, Kiev, 2001, 592p.
- [152] Radzevich, S.P., *Gear Cutting Tools: Science and Engineering*, 2nd edition, CRC Press, Boca Raton, FL, 2017, 606p. [1st edition: Radzevich, S.P., *Gear Cutting Tools: Fundamentals of Design and Computation*, CRC Press, Boca Raton, FL, 2010, 786p].
- [153] Radzevich, S.P., *Generation of Surfaces: Kinematic Geometry of Surface Machining*, CRC Press, Boca Raton, FL, 2014, 738p. [1st edition: Radzevich, S.P., *Kinematic Geometry of Surface Machining*, CRC Press, Boca Raton, FL, 2008, 508p.].
- [154] Radzevich, S.P., "Generating Surfaces of Worm-Type Gear Cutting Tools," pp. 64–78, in: *Advance Processes in Production Technology*, VolgPI, Volgograd, 1985.
- [155] Radzevich, S.P., *Geometry of Surfaces: A Practical Guide for Mechanical Engineers*, 2nd edition, Springer International Publishing, 2019, 466p. [1st edition: Radzevich, S.P., *Geometry of Surfaces: A Practical Guide for Mechanical Engineers*, Wiley, 2013, 264p].
- [156] Radzevich, S.P., "High-Conformal Gearing: A new look at the concept of Novikov gearing," pp. 457–470 in: *Proceedings of International Conference on Gears 2015*, October 5–7, 2015, Technische Universität München (TUM), Garching (near Munich), Germany, 2015.
- [157] Radzevich, S.P., *High-Conformal Gearing: Kinematics and Geometry*, 2nd edition, Elsevier, Amsterdam, 2020, 506p. [1st edition: Radzevich, S.P., *High-Conformal Gearing: Kinematics and Geometry*, CRC Press, Boca Raton, FL, 2015, 332 pages].
- [158] Radzevich, S.P., "Knowledge (of Gear Theory) is Power in the Design, Production, and Application of Gears," *Gear Solutions* magazine, August 2020, pp. 38–44.
- [159] Radzevich, S.P., "Mathematical Modeling of Contact of Two Surfaces in the First Order of Tangency," *Mathematical and Computer Modeling*; Vol. 39, No. 9–10, May 2004, pp. 1083–1112.
- [160] Radzevich, S.P., *Methods for Investigation of the Conditions of Contact of Surfaces, Monograph*, UkrNIINTI, Kiev, 1987, 103p.
- [161] Radzevich, S.P., "Multi-Axis Part Surface Machining on NC Machines," pp. 200–251, in: *Modeling of Systems, Calculation of Elements, Part Surface Generation, Protective Coatings, and New Equipment in Machine Building*, Vischa Shkola, Kyiv, 1989.
- [162] Radzevich, S.P., "On Analytical Description of the Geometry of Contact of Surfaces in Highest Kinematic Pairs," *Theory for Mechanisms and Machines*, Vol. 3, No. 5, 2005, pp. 3–14.
- [163] Radzevich, S.P., "On Fundamental Principles of Gear Cutting Tool Design: The DG/K-Based Approach," in: *Proceedings of International Conference on Gears*, October 4–6, 2010, Munich, Germany.
- [164] Radzevich, S.P., "On the Master Thesis: Gochman, Ch.I., Theory of Gear Teeth Engagement, Generalized and Developed by Implementation of Mathematical Analysis," *Theory of Mechanisms and Machines*, Vol. 17, No. 1, 2011, pp. 33–43. [http://tmm.spbstu.ru/01\\_2011.html](http://tmm.spbstu.ru/01_2011.html)
- [165] Radzevich, S.P., "On the Priority of Dr. M.L. Novikov in the Development of Novikov Gearing," *Theory of Mechanisms and Machines*, <http://tmm.spbstu.ru>, (in press).
- [166] Radzevich, S.P., "On Tooth Failure Analysis in Small-Teeth-Number Gearing: An Analytical Approach," 2006 Fall Technical Meeting, October 22–24, 2006, Grosvenor Resort, Orlando, FL, AGMA Paper 06FTM11 2006, 22p.
- [167] Radzevich, S.P., *Part Surface Generation on Multi-Axis NC Machines. Monograph*, Vischa Shkola, Kyiv, 1991, 192p.
- [168] Radzevich, S.P., "Principal Accomplishments in the Scientific Theory of Gearing," pp. 7–18 in: *Proceedings of the 6th International BAPT Conference "Power Transmissions 2019, 19–22.062019 Varna,"* Vol. 1: Design, Analysis, Simulation, and Optimization, Balkan Association of Power Transmissions, Varna, 2019.

- [169] Radzevich, S.P., "Possible Kinds of the Vector Diagrams of Gear Pairs," *Theory of Mechanisms and Machines*, Vol. 7, No. 2, 2009, pp. 10–18. [www.http://tmm.spbstu.ru/journal.html](http://tmm.spbstu.ru/journal.html).
- [170] Radzevich, S.P., "Root Cause for Noise Excitation in Geometrically-Accurate (Perfect) Parallel-Axes Gearing," *Gear Solutions* magazine, October 2019, pp. 36–44.
- [171] Radzevich, S.P.,  $R_{sp}$  – Gearing Insensitive to Axes Misalignment and other Displacement, and Methods of Producing Gears, International Application Number PCT/US 038753, International Filing Date: May 20, 2014, International Publication Number 2014/189903 A1, Int. Pat. Classification F16H 1/26 (2006.01), Priority Data: 13/900,946, May 23, 2013, 34p.
- [172] Radzevich, S.P., *Sculptured Surface Machining on Multi-Axis NC Machine*, Monograph, Vishcha Schola, Kiev, 1991, 192p.
- [173] Radzevich, S.P., "The Root Cause for Gear Noise Excitation," *Gear Solutions* magazine, December, 2018, pp. 24–29.
- [174] Radzevich, S.P., *Theory of Gearing: Kinematics, Geometry, and Synthesis*, 2nd edition, CRC Press, Boca Raton, FL, 2018, 934p. [1st Edition: Radzevich, S.P., *Theory of Gearing: Kinematics, Geometry, and Synthesis*, CRC Press, Boca Raton, Florida, 2012, 760 pages].
- [175] Radzevich, S.P., "Technological Methods for Noise/Vibration Reduction in Driveline/Transmission of Truck and All-Wheel-Drive Vehicles," *International Journal of Vehicle Noise and Vibration*, Vol. 2, No. 4, 2006, pp. 283–291.
- [176] Radzevich, S.P., "Three Fundamental Laws of Gearing: for Gear Design and Gear Production," pp. 21–23 in: *Proceedings of the VIII International Conference "Complex Assurance of Quality of Technological Processes & Systems"*, May 10–12, 2018, Chernihiv (Ukraine), Vol. 1, 2018.
- [177] Radzevich, S.P., "Understanding the Mounting Distance: Crossed-Axes Gearing (Hypoid Gearing)," *Gear Solutions* magazine, February 2020, pp. 38–43.
- [178] Radzevich, S.P., "Understanding the Mounting Distance: Intersected-Axes Gearing (Bevel Gearing)," *Gear Solutions* magazine, December 2019, pp. 42–47.
- [179] Radzevich, S.P., "Vector Representation of Gear Pairs. Part I," in: *Theory of Mechanisms and Machines*, Vol. 6, No. 2, 2008, pp. 74–81. [www.http://tmm.spbstu.ru/journal.html](http://tmm.spbstu.ru/journal.html).
- [180] Radzevich, S.P., "Vector Representation of Gear Pairs. Part II," in: *Theory of Mechanisms and Machines*, Vol. 7, No. 1, 2009, pp. 17–26. [www.http://tmm.spbstu.ru/journal.html](http://tmm.spbstu.ru/journal.html).
- [181] Radzevich, S.P., et al., "A Gear Set for XLocker Differential," Patent Application Publication, Pub. No.: US 2010/0323840 A1, U.S. Cl. 475/220, Filed: June 17, 2009. (Patent pending).
- [182] Radzevich, S.P., et al., "Gear Train with Split Torque," Patent Application Publication, Pub. No.: US 2010/0261568 A1, Pub. Date: October 14, 2010, Int. Cl. F16H 48/06, F16H 1/16, U.S. Cl. 475/226; 74/425, Filed: April 14, 2009. (Patent pending).
- [183] Radzevich, S.P., Goodman, E.D., Palaguta, V.A., "Tooth Surface Fundamental Forms in Gear Technology," *University of Niš, the Scientific Journal Facta Universitatis, Series: Mechanical Engineering*, Vol. 1, No. 5, 1998, pp. 515–525.
- [184] Radzevich, S.P., Irigireddy, V., Vijayakar, S.M., Stewart, J., Warner, T.P., "Preliminary Results of Testing of Low-Tooth-Count Bevel Gears of a Novel Design. Part 1," *Gear Solutions*, October 2014, pp. 25–26.
- [185] Radzevich, S.P., Irigireddy, V., Vijayakar, S.M., Stewart, J., Warner, T.P., "Preliminary Results of Testing of Low-Tooth-Count Bevel Gears of a Novel Design. Part 2," *Gear Solutions*, December 2014, pp. 20–21.
- [186] Radzevich, S.P., Irigireddy, V., Vijayakar, S.M., Stewart, J., Warner, T.P., "Preliminary Results of Testing of Low-Tooth-Count Bevel Gears of a Novel Design. Part 3," *Gear Solutions*, January 2015, pp. 20–23.
- [187] Reshetov, L.N., *Self-Aligning Mechanisms*, Translated from Russian by L.M. Sachs, Mir Publishers, Moscow, 1982, 582p. (Russian edition: Moscow, Mashinostroyeniye, 1979).
- [188] Reuleaux, F., *The Constructor, a Hand-Book of Machine Design* by F. Reuleaux, Authorized translation, complete and unabridged from the 4th enl. German ed. By Henry Harrison Suplee. Philadelphia, H.H. Suplee, 1893, 312p. [First German edition published in 1861 with title: Der Constructeur. Ein Handbuch zum Gebrauch beim Maschinen-Entwerfen].
- [189] Reuleaux, F., *The Kinematics of Machinery: Outlines of a Theory of Machines*, Translated and Edited by Alexander B. W. Kennedy, and with a New Introduction by Eugene S., Ferguson, Dover Publishers, Inc., New York, 1963, 622p. [Translated from: Reuleaux, F., *Theoretische Kinematik: Grundzüge einer Theori des Maschinenwesens*, 1875].
- [190] Rodin, P.R., *Fundamentals of Part Surface Generation in Cutting Process*, Vishcha Shkola, Kyiv, 1977, 192p.

- [191] Rosenauer, N., Willis, A.H., *Kinematics of Mechanisms*, Associated General Publications Pty Ltd., Sydney, Australia, 1953, 395p.
- [192] Roslivker, Ye.G., "Hyperboloid Novikov Gearing," pp. 87–112 in: *Novikov Gearings*, Vol. 3, Zhukovskii Military Aviation Academy Publishers, Moscow, 1964.
- [193] Roslivker, Ye.G., "Investigation of Hyperboloid and Bevel Novikov Gearing," pp. 5–85, in: *Novikov Gearings*, Vol. 3, Manufacturing Research Institute Publishers, Rostov-on-Don, 1964.
- [194] Sang, E., *A New General Theory of the Teeth of Wheels*, A&C Black, North Bridge, Edinburgh, 1852, 257p.
- [195] Savary, F., *Journal de Mathematique*, 1845.
- [196] Shevel'ova, G.I., *Theory of Surface Generation and of Contact of Moving Bodies*, MosSTANKIN, Moscow, 1999, 494p.
- [197] Shishkov, V.A., "Elements of Kinematics of Generating and Conjugating in Gearing," in: *Theory and Calculation of Gears*, Vol. 6, LONITOMASH, Leningrad, 1948, p. 123.
- [198] Shishkov, V.A., *Generation of Surfaces in Continuous-Indexing Methods of Surface Machining*, Mashgiz, Moscow, 1951, 152p.
- [199] Shishov, V.P., *Theory, Mathematical Foundations, and Synthesis of High-Power-Density Gearing for Industrial Transportation*, Doctoral Thesis, East Ukrainian State University, Luhansk, 1994, 580p (in Russian).
- [200] Shishov, V.P., Nosko, P.L., Fil', P.V., *Theoretical Foundations of Synthesis of Gearing*, East Ukrainian State University Publishers, Luhansk, 2006, 408p.
- [201] Shtipelman, B.A., *Design and Manufacture of Hypoid Gears*, John Wiley & Sons, New York, 1978, 394p.
- [202] Sigg, H., "Profile and Longitudinal Corrections on Involute Gears," AGMA 109.16, Chicago, IL, October 24–27, 1965, 25p.
- [203] Smith, J.D., *Gear Noise and Vibration*, 2nd edition, Marcel Dekker Inc., New York, 2003, 318p.
- [204] Soldatkin, Ye.P., "Gearings with Variable Angle between the Gear and Pinion Axes of Rotation," *Vestnik Mashinostroyeniya*, No. 7, 1962. [Солдаткин Е.П., "Зубчатые передачи с переменным углом между осями," *Вестник машиностроения*, 1962, №7].
- [205] Stachel, H., "Instantaneous spatial kinematics and the invariants of the axodes," in: *Proc. Ball 2000 Symposium*, Cambridge, No. 23, 2000.
- [206] Stachel, H., "On Jack Phillips' Spatial Involute Gearing," pp. 43–48 in: *Proc. 11th ICGG*, Guangzhou, P.R. China, 2004.
- [207] Stachel, H., "On Spatial Involute Gearing," pp. 27–39 in: *6th International Conference on Applied Informatics*, Eger, Hungary, January 27–31, 2004.
- [208] Stadtfeld, H.J., *Gleason Bevel Gear Technology: Basics of Gear Engineering and Modern Manufacturing Methods for Angular Transmissions*, The Gleason Works, Rochester, NY, 2014, 503p.
- [209] Stadtfeld, H.J., *Gleason Kegelradtechnologie: Ingenieurwissenschaftliche Grundlagen und modernste Herstellungsverfahren für Winkelgetriebe*, Expert-Verlag, Renningen, 2013, 491p.
- [210] Stadtfeld, H.J., "Why are Today's Hypoids the Perfect Crossed-Axes Gear Pairs?," *Gear Solutions* magazine, May 2019, pp. 42–50.
- [211] Struik, D.J., *Lectures on Classical Differential Geometry*, 2nd edition, Addison-Wesley Publishing Company Inc., Massachusetts, 1961, 232p.
- [212] Vaisman, I., "Unele Observatii Privind Suprafetele si Varietatile Neonolomne din  $S_3$  Euclidian," *Mathematica, Academia R.P.R., Filila Iasi, Studii si Cercetari Stiintifice*, Vol. 10, No. 1, p. 195.
- [213] Veldkamp, G.R., *Kinematica*, Scheltema & Holkema, Amsterdam, 1970, pp. 70–72.
- [214] Vogel, W.F., *Involutometry and Trigonometry*, Michigan Tool Company, Book Production by Denham & Co., Detroit, MI, 1945, 321p.
- [215] von Seggern, D., *CRC Standard Curves and Surfaces*, CRC Press, Boca Raton, FL, 1993, 288p.
- [216] Vulgakov, E.B., *Gears with Improved Characteristics*, Mashinostroyeniye, Moscow, 1974, 264p.
- [217] Vullo, V., *Volume 3: Gears: A Concise History*, Series: Springer Series in Solid Structural Mechanics, Vol. 12, Springer, Cham, 2020.
- [218] Walker, H., "Gear Tooth Deflection and Profile Modification," *Engineer*, Vol. 166, 1938, pp. 434–436.
- [219] Wang, X.C., Ghosh, S.K., *Advanced Theories of Hypoid Gears*, Studies in Applied Mechanics, Vol. 36, Elsevier, Amsterdam, 1994, 341p.
- [220] Wildhaber, E., *Foundations of Meshing of Bevel and Hypoid Gearing*, A collection of journal papers translated from English and comments by A.V. Slepak, Moscow, Mashgiz, 1948, 176p (in Russian).
- [221] Willis, R., "On the Teeth of Wheels," *Trans. Civ. Eng.*, Vol. II, 1838.



- [222] Willis, R., *Principles of Mechanisms, Designed for the Use of Students in the Universities and for Engineering Students Generally*, John W. Parker, London, J. & J.J. Deighton, West Stand, Cambridge, 1841, 446p.
- [223] Woodbury, R.S., *History of the Gear-Cutting. A Historical Study in Geometry and Machine*, The M.I.T. Press, Cambridge, MA, 1958, 135p.
- [224] Wu, D.R., Luo, J.S., *A Geometric Theory of Conjugate Tooth Surfaces*, World Scientific Publishing, River Edge, NJ, 1992, 192p.
- [225] Wu, L.-L., Liu, C.-C., Tsay, C.-B., "Mathematical Model and Surface Deviation of Helipoid Gears Cut by Shaper Cutter," *ASME J Mechanical Design*, Vol. 125, No. 2, June 2003, pp. 351–355.
- [226] Yakovlev, A.S., Pecheniy, V.I., "An Experimental Investigation of the Load Distribution within the Patch of Contact in Novikov Gears," in: *Reliability and Quality of Gearing*, Vol. 18-67-36, NIINFORMT'AZhMASh, Moscow, 1967.
- [227] Yerikhov, M.L., *Principles of Arrangement, Methods of Synthesis, and Issues of Analysis of Gearing*, Dr. Sci. Thesis, Khabarovsk Polytechnic Institute, Khabarovsk, 1972, 324p.
- [228] Zak, P.S., *Globoid Gearing*, MASHGIZ, Moscow, 1962, 256p.
- [229] Zak, P.S., "On Bearing Contact in Worm Gearing," *Vestnik Mashinostroyeniya*, 1968, No. 3, pp. 14–17.
- [230] Zhuravl'ov, G.A., Iofis, R.B., *Hypoid Gearing, Problems and Evolution*, Rostov State University Publishers, Rostov, 1978, 160p.



# Taylor & Francis

Taylor & Francis Group

<http://taylorandfrancis.com>

---

# Bibliography

- Abadjiev, V., Abadjieva, E., Kawasaki, H., Mouri, T., “Computer Synthesis Approaches of Hyperboloid Gear Drives with Linear Contact,” *Journal of Theoretical and Applied Mechanics*, Vol. 44, No. 3, August 2014, pp. 101–118. <https://doi.org/10.2478/jtam-2014-0013>.
- Adams, C.E., *Plastics Gearing: Selection and Application*, Marcel Dekker, Inc., New York, 1986, 384p.
- Addomine, M., Figliolini, G., Pinestri, E., “A Landmark in the History of Non-Circular Gears Design: The Mechanical Masterpiece of Dondi’s Astrarium,” *Mechanism and Machine Theory*, Vol. 122, April 2018, pp. 219–232.
- Airy, G.B., “On the Forms of the Teeth of Wheels,” *Transactions of the Cambridge Philosophical Society*, Vol. II, 1825, p. 277.
- Alexandrov, V.M., Romalis, B.L., *Contact Problems in Engineering*, Mashinostroyeniye, Moscow, 1986, 174p.
- Allan, T., “Some Aspects of the Design and Performance of Wildhaber-Novikov Gearing,” *Proceedings of the Institution of Mechanical Engineers*, Vol. 179, No. 1, June 1964, pp. 931–954.
- Apex Dynamics. *Gear History – Where do Gearboxes Originate?* <https://www.apexdyna.nl/en/news/gear-history/>.
- Asbridge, H.H., *American Machinist*, Dec. 1910, p. 1211.
- Astridge, D.G., Shotter, B.A., Dyson, A., Evans, H.P., Snidle, R.W., “Tribology of High Conformity Gears,” pp. 819–828 in: *IMEchE Conference on Tribology—Friction Lubrication and Wear, Fifty Years On, London*, Vol. 2, 1987, Mechanical Engineering Publications, London.
- Babichev, D., Lagutin, S., Barmina, N., “Review of the Russian School in the Theory and Geometry of Gearing. Part 1. Origins of the Theory of Gearing and its Golden Period of 1935–1975” in: *Proceedings of 2015 IFToMM Workshop on History of Mechanism and Machine Science*, May 26–28, 2015, St-Petersburg, Russia. <http://hmms2015.ru>
- Babichev, D., Lagutin, S., Barmina, N., “Russian School of the Theory and Geometry of Gearing: Its Origin and Golden Period (1935–1975),” *Frontiers of Mechanical Engineering*, Vol. 11, No. 1, 2016, pp. 44–59.
- Babichev, D.T., Lagutin, S.A., Barmina, N.A., “Overview of the Works of the Russian School of Theory of and the Geometry of Gearing. Part 1. Origins of the Theory of Gearing, and its Heyday Time in 1935–1975,” *Theory of Mechanisms and Machines*, Vol. 14, No. 3(31), 2016, pp. 101–134.
- Babichev, D.T., Lagutin, S.A., Barmina, N.A., “Overview of the Works of the Russian School of Theory of and the Geometry of Gearing. Part 2. Development of the Classical Theory of Gearing and Establishment of the Theory of Real Gearing in 1976–2000,” *Theory of Mechanisms and Machines*, Vol. 15, No. 3(35), 2017, pp. 86–119.
- Babichev, D.T., Lagutin, S.A., Barmina, N.A., “Russian School of the Theory and Geometry of Gearing. Part 2. Development of the Classical Theory of Gearing and Establishment of the Theory of Real Gearing in 1976–2000,” pp. 1–46 in: *New Approaches to Gear Design and Production, (Mechanisms and Machine Science, Book 81)*, edited by Goldfarb, V.I., Trubachov, E., Barmina, N., Springer, Zurich, 2020, 529p.
- Babichev, D.T., Volkov, A. E., “History of Evolution of the Theory of Gearing,” *Journal of Scientific and Technological Development*, Vol. 5, No. 93, 2015, pp. 25–42.
- Babichev, D.T., Volkov, A.E., “History of the Development of the Gears Theory,” *Bulletin of Scientific and Engineering Evaluation*, No. 5(93), 2015, pp. 25–42. <http://www.vntr.ru>
- Ball, R.S., *A Treatise on the Theory of Screws*, Cambridge University Press, Cambridge, NY, 1998, 588p.
- Ball, R.S., *The Theory of Screws*, Hodges & Foster, Dublin, 1876.
- Baozhen, L., Löwe, H., Wang, X., “A New Approach to the Theory of Gearing Using Modern Differential Geometry,” pp. 1379–1390 in: *Proceedings of the International Conference on Gears 2013, Europe invites the world, VDI-Society for Product and Process Design*, Vol. 2, Oct 7–9, 2013, Technical University of Munich (TUM), München, DE.
- Baranov, G.G., “Some Problems of the Theory Novikov Gearing for the Modified Center Distance,” *Mechanics of Machines*, Vol. 31–32, 1972, pp. 93–107 (in Russian).
- Baxter, M.L., Jr., “Basic Geometry and Tooth Contact of Hypoid Gears,” *Industrial Mathematic*, Vol. 11, No. 2, 1961, pp. 1–28.
- Bayazitov, N., *Helical Gears with a New Type of Gearing*, Ph.D. Thesis, Kazan’ Technological & Chemical Institute, Kazan’, 1964.
- Bazhin, A.A., *Gear Cutting Tools*, ONTI NKTP, Moscow, 1935, 112p.

- Belyaev, A.E., *Mechanical Drives with Ball Intermediate Bodies*, TsNTI Publishers, Tomsk, 1992, 231p.
- Bernoulli, J., *Opera Omnia*, Lausanne and Geneva, t. III, "Lect. Hospitalii," XXII, 1742, p. 454.
- Bilgram, H., U.S. Patent No. 749,683 of Jan. 12, 1904.
- Bobkov, M.N., *Theoretical Aspects of the Technology of Manufacturing Cylindrical Wheels with Circular Teeth*, DSc Thesis, 05.02.08 – Mechanical Engineering Technology, 05.03.01 – Processes of Mechanical and Physical-Technical Manufacturing, Machine Tools and Tools, Tula, Tula State University, 1998, 40 pages. <http://tekhnosfera.com/teoreticheskie-aspekty-tehnologii-izgotovleniya-tsilindricheskikh-koles-s-krugovymi-zubyami>
- Bodmer, J.G., "On the Pitch of Spur and Bevel Wheels and the Shape of the Teeth of Worm Wheels and Worms Working into Each Other," *Minutes of Proceedings of the Institution of Civil Engineers*, Vol. II, 1843, p. 32.
- Bostan, I.A., *Precession Gear Drives with Multipair Meshing*, edited by S.A. Shuvalov, Shtiintsa, Kishinev, 1991, 342p.
- Brodskiy, I.L., "Some Problems in the Theory of the Envelope of Multi-Parameter Family of Tool Surfaces," *Mashinovedenie*, Vol. 3, 1969, pp. 32–39 (in Russian).
- Brown, U.S. Patent No. 45,294 of November 29, 1864.
- Buchanan, R., *Essay on the Teeth of Wheels*, Edinburgh, 1808.
- Buchanan, R., *Practical Essays on Millwork and Other Machinery, Mechanical and Descriptive*, 3 vols, Printed by Gibson & Sanderson, for J. Taylor, Edinburgh, 1814.
- Buchanan, R., *Treatise on Millwork*, 3rd edition, London, 1841, pp. 83–172.
- Buckingham, E., *Analytical Mechanics of Gears*, Dover Publications, Inc., New York, 1988, 546p.
- Buckingham, E., *Analytical Mechanics of Gears*, New York, 1949.
- Buckingham, E., Ryffel, H.H., *Design of Worm and Spiral Gears: A Manual for the Design and Manufacture of All-Redress-Action Worm and Spiral Gear Drives*, The Industrial Press, New York, 1960, 450p.
- Camus, C.E.L., Hawkins, J.I., *A Treatise on the Teeth of Wheels, Demonstrating the Best Forms, Which Can be Given to Them for the Purpose of Machinery, Such as Mill-Work and Clock-Work, and the Art of Finding their Numbers*, Translated from the French of M. Camus, 2nd ed., carefully revised and enlarged with Details of the Present Practice of Mill-Wrights, Engine Makers, and other Mechanists, John Isaak Hawkins, James S. Hudson, London, 1837.
- Candee, A.H., *Introduction to the Kinematic Geometry of Gear Teeth*, Chilton Co., Book Division, Philadelphia, 1961, 204p.
- Cardano, G., *De Rerum Varietate*, Basel, 1557, pp. 263–372.
- Cayley, A., "A Memoir on the Theory of Matrices," *Philosophical Transactions of the Royal Society of London*, Vol. 148, 1858, pp. 17–37.
- Chasovnikov, L.D., *Gear Transmissions*, Mashinostroyeniye, Moscow, 1969, 486p.
- Chen, H.-C., Duan, Z.-Y., Liu, J., Wu, H.-J., "Research on Basic Principle on Molding-Surface Conjugation," *Mechanism and Machine Theory*, Vol. 43, No. 7, July 2008, pp. 791–811.
- Chen, Y., Zhang, G., Chen, B., Luo, W., Li, F., Chen, Y., "A Novel Enveloping Worm Pair via Employing the Conjugate Planar Internal Gear as Counterpart," *Mechanism and Machine Theory*, Vol. 67, September 2013, pp. 17–31. <https://doi.org/10.1016/j.mechmachtheory.2013.04.001>
- Chironis, N.P. (Editor), *Gear Design and Application*, McGraw-Hill, New York, 1967, 374p.
- Colbourne, J. R., *The Geometry of Involute Gears*, Springer-Verlag, New York, 1987, 532p.
- Cormac, P., *A Treatise on Screws and Worm Gear, Their Mills and Hobs*, Chapman & Hall, Ltd., London, 1936, 138p.
- Crosher, W.P., *A Gear Chronology: Significant Events and Dates Affecting Gear Development*, Book Publishers Xlibris LLC, Bloomington, 2014, 260p.
- Crosher, W.P., *A Gear Chronology: Significant Events and Dates Affecting Gear Development*, Xlibris Corporation, 2014, 260 p.
- Crosher, W.P., *Design and Application of the Worm Gear*, ASME Press, New York, 2002, 256p.
- Cusanus, N., *Opera*, Paris, Vol. II, 1451, pp. 33–59.
- da Vinci, L., The Madrid Codices, *Volume 1, Facsimile Edition of "Codex Madrid I," 1493, original Spanish title: Tratado de Estatica y Mechanica en Italiano*, McGraw Hill Book Company, 1974.
- Daryani, P.H., *The Art of Gear Fabrication*, Industrial Press, Inc., New York, 2001, 208p.
- Davidov, Ya.S., *Non-Involute Gearing*, Mashgiz, Moscow, 1950, 179p.
- Davis, J.R. (Editor), *Gear Materials, Properties, and Manufacture*, ASM Press, 2005, 339p.
- de La Hire, F., *Traité de Mécanique: ou l'on Explique Toot ce qui est Nécessaire Dans la Pratique des Arts, & les Propriétés des Corps Pesants Lesquelles ont un Plus Grand Usage Dans la Physique*, De l'Imprimerie Royale, A Paris, 1695.
- de La Hire, F., *Traité des Epicycloïdes*, Paris, 1694.

- de la Hire, P., *Mémoires de Mathématique et de Physique*, Impr. Royale, Paris, 1694.
- Denavit, J., Hartenberg, R.S., "A Kinematics Notation for Lower-Pair Mechanisms Based on Matrices," *ASME Journal of Applied Mechanics*, Vol. 77, 1955, pp. 215–221.
- Derek de Solla Price, "Gears from the Greeks. The Antikythera Mechanism: A Calendar Computer from ca. 80 B. C.," *Transactions of the American Philosophical Society*, Vol. 64, No. 7, 1974, pp. 1–70.
- Di Puccio, F., Gabiccini, M., Guiggiani, M., "Alternative formulation of the theory of gearing," *Mechanism and Machine Theory*, Vol. 40, No. 5, May 2005, pp. 613–637.
- Dong, X., *Theoretical Foundation of Gear Meshing*, China Machine Press, Beijing, 1989.
- Dooner, D., Vivet, M., Acinapura, A., Desmet, W., Mundo, D., "On the Determination of Fully Conjugate Hypoid Tooth Flanks," *Mechanism and Machine Theory*, Vol. 144, February 2020, p. 103649. <https://www.sciencedirect.com/science/article/abs/pii/S0094114X19314612>
- Dooner, D.B., "On Evolutoids and Spatial Involutoids to Define Hypoid Flank Geometry," *Mechanism and Machine Theory*, Vol. 156, February 2021, 104150. <https://doi.org/10.1016/j.mechmachtheory.2020.104150>
- Dooner, D.B., "On the Third Law of Gearing: A Study on Hypoid Gear Tooth Contact," *Mechanism and Machine Theory*, Vol. 134, April 2019, pp. 224–248.
- Dooner, D.B., Seireg, A.A., *The Kinematic Geometry of Gearing. A Concurrent Engineering Approach*, John Wiley & Sons, Inc., New York, 1995, 450p.
- Dowd, A.A., *Spiral and Worm Gearing*, Lightning Source, Inc., 2001, 288p.
- Drago, R.J., *Fundamentals of Gear Design*, Butterworths, Boston, 1988, 560p.
- Dudas, I., *The Theory and Practice of Worm Gear Drives*, Penton Press, London, 2000, 314p.
- Dudley, D.W., *Gear Handbook: The Design, Manufacture, and Application of Gears*, McGraw-Hill, New York, 1962.
- Dudley, D.W., *Handbook of Practical Gear Design*, McGraw-Hill, Inc., New York, 1984.
- Dudley, D.W., *Handbook of Practical Gear Design*, CRC Press, Boca Raton, FL, 1994, 688p.
- Dudley, D.W., *Practical Gear Design*, McGraw-Hill, New York, 1954.
- Dudley, D.W., *The Evolution of the Gear Art*, AGMA, Washington, DC, 1969, 93p.
- Dudley, D.W., *Zahnräder-Berechnung, Entwurf und Herstellung nach Amerikanischen Erfahrungen*, Springer-Verlag, Berlin, 1961.
- Dürer, A., *Underweysung der Messung mit dem Zirckel und Richtscheit*, n. p., 1525, pp. 6–17.
- Dus'ev, I.I., Vasil'yev, V.M., *An Analytical Theory of Spatial Gearing and its Application to Hypoid Gearing*, Rostov-on-Don, Book Publishers, 1968, 148p.
- Dyson, A., *A General Theory of the Kinematics and Geometry of Gears in Three Dimensions*, Clarendon Press, Oxford, 1969, 141p.
- Eberhardt, H.J., "Influence of the Automobile on Gear Cutting and Gear Cutting Machinery," in: *Meeting Am. Soc. Mech. Eng., May 26–27, 1921*, partially reprinted in: *Mechanical Engineering*, Aug. 1921.
- Euler, L., "De Aptissima Figure Rotarum Dentibus Tribuenda" ("On Finding the Best Shape for Gear Teeth"), pp. 299–316 in: *Academiae Scientiarum Imperiales Petropolitae, Novi Commentarii*, 1754–55.
- Euler, L., "De Consturctione Aptissima Molarum Alatarum," pp. 41–108 in: *Academiae Scientiarum Imperiales Petropolitae, Novi Commentarii*, Vol. IV, 1743.
- Euler, L., "De Figura Dentinum Rotarum," 1765, pp. 207–231.
- Ewert, R.H., *Gears and Gear Manufacture: The Fundamentals*, Chapman & Hall, International Thomson Publishing, 1997, 220p.
- Fairbairn, W., *Treatise of Mills and Millwork*, London, 1864.
- Fed'akin, R.V., Chesnokov, V.A., "Novikov Gearing," *Vestnik Mashinostroyeniya*, No. 4, 1958, pp. 3–11 (in Russian).
- Fed'akin, R.V., Chesnokov, V.A., *A Gear Drive*, SU Pat. 735855, Int. Cl. F 16 h 1/18, Filed: June 28, 1967.
- Fed'akin, R.V., Chesnokov, V.A., *Calculation of Novikov Gearing*, VVIA, Moscow, 1982, 114p.
- Fed'akin, R.V., *On Selection of Teeth Shape having Circular Profile*, NMS No. 13–14, VVIA, Moscow, 1957, pp. 63–94.
- Ferguson, J., *Ferguson's Lectures on Select Subjects*, New Ed., edited by D. Brewster, 2nd edition, Bell & Bradfute, Edinburgh, 1806, pp. 10–226.
- Field, J.V., Wright, M.T., "The Early History of Mathematical Gearing," *Endeavour*, Vol. 9, No. 4, 1985, pp. 198–203.
- Figliolini, G., Stachel, H., Angeles, J., "On Martin Disteli's Main Achievements in Spatial Gearing: Disteli's Diagram," in: *Proceedings of EuCoMeS, European Conference on Mechanism Science, Obergurgl (Austria)*, February 21–26, 2006, 12p.
- Figliolini, G., Stachel, H., Angeles, J., "On the Synthesis of Spatial Cycloidal Gears," *Meccanica*, Vol. 48, No. 5, 2013, pp. 1239–1249.

- Flanders, R.E., "Interchangeable Involute Gear Tooth Systems," *Journal of the American Society of Mechanical Engineers*, Dec. 1908, pp. 1501–1520.
- Flanders, R.E., *Am. Mach.*, Dec. 1910, p. 1064, and *Machinery*, Jan. 1911, p. 369, Mar. 1911, p. 569, June 1911, p. 798.
- Flanders, R.E., *Bevel Gearing*, 4th edition, Machinery's Reference Series, Number 37, The Industrial Press, 1912, 48p.
- French, M.J., "Gear Conformity and Local Capacity," *Proceedings of the Institution of Mechanical Engineers, Part I*, Vol. 180, No. 43, June 1965, pp. 1013–1024.
- Gavril'enko, V.A., *Fundamentals of Involute Gearing*, Mashinostroyeniye, Moscow, 1969, 432p.
- Gibbs, J.W., *On the Form of the Teeth of Wheels in Spur Gearing*, Doctoral Dissertation, Yale University, New Haven, Conn., 1863.
- Gochman, H.I., *Theory of Gearing Generalized and Developed Analytically*, Odessa, 1886, 229p.
- Gol'dfarb, V.I., *Fundamentals of Theory of Computer Aided Geometric Analysis and Synthesis of General Kind of Worm Gearing*, Doctoral Thesis, Moscow Aviation Institute, 1986, 48p.
- Goldfarb, V.I., "Some Exercises with Equations of Meshing: Review of Fundamental Manuscript," pp. 61–68 in: *Gears in Design, Production and Education. Mechanism and Machine Science*, edited by N. Barmina, E. Trubachev. Springer, Cham, Vol. 101, 2021. [https://doi.org/10.1007/978-3-030-73022-2\\_2](https://doi.org/10.1007/978-3-030-73022-2_2)
- Goldfarb, V.I., "What We Know About Spiroid Gearing," pp. 19–29 in: *Proceedings of the International Conference on Mechanical Transmissions*, Chongqing University, Science Press, Beijing, China, Vol. 1, 2006.
- Goldfarb, V.I., Barmina, N. (Editors), *Theory and Practice of Gearing and Transmissions: In Honor of Professor Faydor L. Litvin, (Mechanisms and Machine Science, Book 34)*, Springer, Zurich, 2016, 450p.
- Goldfarb, V.I., Trubachov, E., Barmina, N. (Editors), *Advanced Gear Engineering, (Mechanisms and Machine Science, Book 51)*, Springer, Zurich, 2018, 512p.
- Goldfarb, V.I., Trubachov, E., Barmina, N. (Editors), *New Approaches to Gear Design and Production, (Mechanisms and Machine Science, Book 81)*, Springer, Zurich, 2020, 529p.
- Golofast, L.M., Erikhov, M.L., Silich, A.A., "Investigation of machine-tool meshing when cutting Novikov gears by the hob," pp. 11–12 in: *Proceedings of 3rd All-Union Symposium on "Theory and Practice of Spatial Gearing,"* KSU, Kurgan.
- Golofast, L.M., Silich, A.A., "Investigation of Errors of Profiling of Worm Grinding Wheels (for Machining of Novikov Gears)," pp. 123–131 in: *Theory of Machines of Metallurgy and Mining Machinery*, UPI, Sverdlovsk, 1986.
- Golovin, A.A., Tarabarin, V.B., *Russian Models from the Mechanisms Collection of Bauman University, History of Mechanism and Machine Science 5*, Springer, Zurich, 2008, 238p.
- Grant, G.B., *A Treatise on Gear Wheels*, 11th edition, Philadelphia Gear Works, Inc., Philadelphia, 1906, 105p.
- Grant, G.B., *Handbook of the Teeth of Gears*, Boston, 1885.
- Grant, G.B., *Machinery*, June 1911, p. 813.
- Grant, G.B., *Odontics, or the Theory and Practice of the Teeth of Gears*, Lexington, MA, 1891.
- Gribanov, V.M., Medintseva, Y.V., Ratov, D.V., *Novikov Gears: Accuracy Problems*, Lugansk, 2010, 252p.
- Gribanov, V.M., *Theory of Hyperboloid Gears*, Volodymyr Dahl East Ukrainian National University, Lugansk, 2003, 272p (in Russian).
- Gromyko, P.N., Makaryevich, D.M., Dokonov, L.G., et al., *Precession Reducing Mechanisms of Different Dedication*, Byelorussko-Rossiiskii University Publishers, Mogilev, 2013, 273p.
- Gul'ayev, K.I., *Theoretical Foundations of Synthesis and of Finishing of Bevel Gearing*, Doctoral Thesis, Leningrad, 1976, 48 p.
- Hawkins, J.I., *Teeth of Wheels*, London, 1806.
- Herrmann, G., "Die Zahnflächen und ihre automatische Erzeugung" in: *Vr. Der V. Beförderung des Gewerbflusses im Preussen*, Berlin, 1877, p. 61.
- Hertz, H., "On Contact of Solid Elastic Bodies and on Hardness," *Journal of Mathematics*, Vol. 92, 1881, pp. 156–171.
- Hertz, H., "Über die Berührung Fester Elastischer Körper (The Contact of Solid Elastic Bodies)," *Journal für die Reine und Angewandte Mathematik (Journal for Pure and Applied Mathematic)*, Berlin, 1881, pp.156–171; *Über die Berührung Fester Elastischer Körper und Über die Härte (The Contact of Solid Elastic Bodies and Their Harnesses)*, Berlin, 1882; Reprinted in: H.Hertz, *Gesammelte Werke (Collected Works)*, Vol. 1, pp. 155–173 and pp. 174–196, Leipzig, 1895, or the English translation: *Miscellaneous Papers*, translated by D.E. Jones and G.A. Schott), pp.146–162, 163–183, London: McMillan and Co., Ltd., 1896.
- Hills, D.A., Nowell, D., Sackfield, A., *Mechanics of Elastic Contact*, Butterworth-Heinemann Ltd., Oxford, 1993, 496p.



- Hooke, R., *Lectiones Cutlerianae*, London, No.2, “Animadiversions on Helvius ‘Machina Coeledits,’” 1679, pp. 70–72 and Figs. 20 and 21 (the date of 1666 is Hooke’s).
- Howes, M.A. (Editor), *Source Book on Gear Design, Technology and Performance, A Comprehensive Collection of Outstanding Articles from the Periodical and Reference Literature*, IIT Research Institute, American Society for Metals, Metals Park, OH, 1980, 417p.  
<http://journal.hep.com.cn/fme/EN/10.1007/s11465-015-0360-z>  
<http://link.springer.com/article/10.1007/s11465-015-0360-z>  
<https://onlinelibrary.wiley.com/doi/abs/10.1002/gamm.200910005>
- Hunt, K.H., *Kinematic Geometry of Mechanisms*, Clarendon Press, Oxford, 1978, 465p.
- Imison, J., *A Treatise on the Mechanical Powers*, Printed by the author, and sold by R. Jameson, London, 1787.
- Imison, J., *Mechanical Power*, London, 1787.
- Itkis, M.Ya., *Cylindrical Novikov Gearing: Calculation of Geometric Parameters*, Local Book Publisher, Volgograd, 1973, 312p.
- Ivanov, M.N., *Harmonic Drives*, Visshaya Shkola, Moscow, 1981, 160p.
- Johann, A., Scheurle, J., “On the Generation of Conjugate Flanks for Arbitrary Gear Geometries,” *GAMM-Mitteilungen* Vol. 32, No. 1, 2009, pp. 61–79. <https://doi.org/10.1002/gamm.200910005>
- Johnson, D.C., *Gear Teeth with Circular Arc Profiles: the Novikov Gearing System*, Engineering, London, 1960. <http://trove.nla.gov.au/work/18014966>
- Johnson, D.C., *Novikov Gears (Gear Teeth with Circular Arc Profile)*, Engineering, 1959.
- Kabatov, N.F., Lopato, G.A., *Spiral Conical Gearing*, Mashinostroyeniye, Moscow, 1966.
- Kaestner, A.G., “De Dentibus Rotarum,” in: *Commentationes Societatis Regiae Scientiarum Gottingensis, Classis Mathematicae*, t. IV, pp. 3–25, and idem., “De Dentibus Rotarum,” t. 5, 1782, p. 3.
- Kaneo, Y., “Fundamental Theory of Toothed Gearing, IV,” *Proceedings of the Japan Academy*, Vol. 25, No. 3–5, 1949, pp. 133–138.
- Kapelevich, A.L., *Direct Gear Design*, 2nd edition, CRC Press, Boca Raton, 2021, 364p. [Kapelevich, A.L., *Direct Gear Design*, 1st edition, CRC Press, Boca Raton, 2013, 299p].
- Kird’ashev, Yu.N., *Closed Gearing of Differential Kind*, Mashinostroyeniye, Leningrad, 1969, 176p.
- Kirichenko, A.F., “Geometric Parameters of Novikov Cylindrical Gears with Two Points of Contact,” *J. Izvestiya VUZov, Mashinostroyeniye*, Vol. 5, 1977, pp. 30–33.
- Kirichenko, A.F., *Further Development of the Theory of Gearing for the Purposes of Power Drives*, Mashinostroyeniye, L’viv, 2003.
- Kirichenko, A.F., *Theory, Calculation, and Analysis of 3D Bending Stress of Gear Teeth*, Doctoral Thesis, Moscow, 1991, 32p.
- Kis’el’ev, S.S., *Methods for Design of Series of External Gear Drives*, ITMO-State University, St. Petersburg, 2007, 112p.
- Klingelberg, J. (Editor), *Bevel Gear: Fundamentals and Applications*, 1st edition, Springer Vieweg, Berlin, Heidelberg, 2016, 325p.
- Kolchin, N.I., *Analytical Calculation of Planar and Spatial Gearing*, Mashgiz, Moscow-Leningrad, 1949, 210p.
- Kolchin, N.I., Oparin, G.V., “Novikov Gearing with Two Lines of Meshing and Helical Canal Surfaces of Teeth,” *Izvestiya VUZov*, Vol. 8, 1968, pp. 29–32 (in Russian).
- Korostel’ev, L.V., *Geometric and Kinematic Criteria of Bearing Capacity of Spatial Gearing*, Doctoral Thesis, Moscow, Stankin, 1964, 48 pages.
- Korostelev, L.V., *Geometric and Kinematic Indicators of the Bearing Capacity of Spatial Gearing*, Dr.Sci. Thesis, Moscow, Stankin, 1964, 48p.
- Korotkin, V.I., Kharitonov, Yu.D., *Novikov Gearing*, Rostov State University Publishers, Rostov-on-Don, 1991, 208p.
- Korotkin, V.I., Onishkov, N.P., Kharitonov, Yu.D., (2007), *Novikov Gearing: Achievements and the Development*, Mashinostroyeniye-1, Moscow, 384p.
- Korotkin, V.I., Onishkov, N.P., Kharitonov, Yu.D., *Novikov Gearing: Achievements and Development*, Nova Science Publishers, Inc., New York, 2011, 249p.
- Krasnoschekov, N.N., Fed’akin, R.V., Chesnokov, V.A., *Theory of Novikov Gearing*, Nauka, Moscow, 1976, 174p.
- Krenzer, T., *The Bevel Gear*, 2007, 252p.
- Krenzer, T.J., *Tooth Contact Analysis of Spiral Bevel and Hypoid Gears Under Load*, The Gleason Works, Rochester, NY, 1981.
- Kreynes, M.A., Rozovskii, M.S., *Gear Drives (Selection of Optimal Schematic)*, Nauka, Moscow, 1972, 427p.
- Krylov, N.N., “Kinematics of Gears with a Variable Angle between the Crossed Axes,” *Proceedings of Seminar on TMM USSR Academy of Sciences*, 1965. (in Russian).



- Kudr'avtsev, V.N., *Gear Transmissions*, Mashgiz, Moscow-Leningrad, 1957, 264p.
- Kudr'avtsev, V.N., *Planetary Gear Transmissions*, 2nd Edition, Mashinostroyeniye, Leningrad, 1966, 308p.
- Kudryavtsev, V.N., "On the issue of Novikov gearing," pp. 33–44, in: *Research and Development of Novikov Gearing*, 1960 (in Russian).
- Kudr'avtsev, V.N., Derzhavets, Yu.A., Glukhar'ev, E.G., *Design and Calculation of Gear Reducers*, Mashinostroyeniye, Leningrad, 1971, 328p.
- Kudr'avtsev, V.N., et al., *Planetary Gear Transmissions, Handbook*, edited by V.N. Kudr'avtsev, Yu.N. Kird'ashev, Mashinostroyeniye, Leningrad, 1977, 536p.
- Kudr'avtsev, V.N., et al., *Strength and Reliability of Gear Transmissions, Handbook*, edited by V.N. Kudr'avtsev, Yu.A. Derzhavets, Mashinostroyeniye, Leningrad, 1977, 240p.
- Kudr'avtsev, V.N., Kuz'min, I.S., Filippenko, A.L., *Calculation and Design of Gear Reducers*, Polytechnica, St. Petersburg, 1993, 448p.
- Kutzbach, K., "Grundlagen und meure Fortschritte des Zahnradzengung," pp. 913, 1076, 1105 in: *Z.V.D.I.*, 1924.
- Lagutin, S.A., "50 Years in the Theory and Practice of Gearing," *IOP Conference: Materials Science and Engineering*, Vol. 393, 2018, p. 012001. <https://doi.org/10.1088/1757-899X/393/1/012001>.
- Lagutin, S.A., "Meshing Space and its Elements," *J. Mashinovedeniye*, Vol. 4, 1987, pp. 69–73.
- Lagutin, S., Barmina, N., "Prof. F.L. Litvin: Contribution to the Formation of the Russian School of the Theory of Gearing," pp. 19–36 in: *Theory and Practice of Gearing and Transmission*, Series: Mechanism and Machine Science 34, edited by V. Goldfarb, N. Barmina (eds.), Springer, Cham, 2016.
- Lei, B., Cheng, G., Löwe, H., Wang, X., "Remanufacturing the Pinion: An Application of a New Design Method for Spiral Bevel Gears," *Advances in Mechanical Engineering*, Vol. 6, 2014, p. 257581.
- Lei, B., Löwe, H., Feng, Y., Wang, X., "A Design Method for the Pinion of a Spiral Bevel Gear Drive Admitting Full Control on the Contact Area and the Transmission Error," in: *23rd Reliability, Stress Analysis, and Failure Prevention Conference, Boston, Massachusetts, USA, August 2–5, 2015*, 9p.
- Lei, B., Löwe, H., Wang, X., "A New Approach to the Theory of Gearing Using Modern Differential Geometry," *VDI-Berichte*, Vol. 2199, 2013, pp. 1379–1390.
- Lei, B., Löwe, H., Wang, X., Wang, Q., "The Fundamental Law of Gearing," pp. 1249–1255 in: *Proceedings of the International Gear Conference*, 27th–29th August 2018, Lyon Villeurbanne, France, 2018.
- Leibniz, G.W.F., *Societati Regiae Scientiarum, Miscellanea Berolinensia*, Berlin, Vol. I, "Tentamen Natura et Remediis Resistentiarum," 1710, p. 315.
- Lewis, E.J., *Machinery*, Apr. 1911, p. 659.
- Lewis, M.J.T., "Gearing in the Ancient World," *Endeavour*, Vol. 17, No. 3, 1993, pp. 110–115.
- Lewis, W., "Interchangeable Involute Gearing," *Proceedings of the Institution of Mechanical Engineers*, Vol. 79, No. 1, 1910, pp. 307–314.
- Lewis, W., "Investigation of the Strength of Gear Teeth," pp. 16–23 in: *Proceedings of the Engineers Club*, Philadelphia, PA, 1893.
- Liang, D., Chen, B., Gao, Y., Peng, S., and Qin, S., "Geometric and Meshing Properties of Conjugate Curves for Gear Transmission," *Mathematical Problems in Engineering*, Vol. 2014, 2014, p. 484802. <https://doi.org/10.1155/2014/484802>
- Litvin, F.L., "Applied Theory of Gearing: State of the Art," *ASME Journal of Vibration and Acoustics*, Vol. 117, No. B, 1995, pp. 128–134.
- Litvin, F.L., *Cylindrical Worm Gearing of New Kinds*, Mashgiz, Moscow, 1962, 103p.
- Litvin, F.L., *Development of Gear Technology and Theory of Gearing*, NASA Reference Publication 1406, ARL-TR-1500, 1997, 114p.
- Litvin, F.L., *Gear Geometry and Applied Theory*, Prentice Hall, Englewood Cliffs, NJ, 1994, 724p.
- Litvin, F.L., *Non-Circular Gears*, 2nd Edition, Mashgiz, Moscow-Leningrad, 1956, 311p.
- Litvin, F.L., "Toward the Investigation of Spatial Gearing with Linear Contact of Surfaces," *Proceedings of Seminar on TMM, USSR Academy of Sciences*, Vol. 49, 1953, pp. 16–55 (in Russian).
- Litvin, F.L., *Theory of Gearing*, 2nd Edition, Nauka, Moscow, 1968, 548p.
- Litvin, F.L., *Theory of Gearing*, NASA Reference Publication 1212, AVSCOM Technical Report, 88-C-035, 1989, 470p.
- Litvin, F.L., Fuentes, A., *Gear Geometry and Applied Theory*, 2nd Edition, Cambridge University Press, Cambridge, UK, 2004, 800p.
- Litvin, F.L., Fuentes-Anzar, A., Gonzalez-Perez, I., Hayasaka, K., *Noncircular Gears: Design and Generation*, Cambridge University Press, New York, 2009, 204p.
- Logue, C.H., *American Machinist*, Oct. 1907, pp. 573–575.

- Lopato, G.A., Kabatov, N.F., Segal', M.G., *Spiral Bevel and Hypoid Gearing*, 2nd Edition, Mashinostroyeniye, Moscow, 1977, 423p.
- L'ukshin, V.S., *Theory of Screw Surfaces: For the Purposes of Design of Cutting Tools*, Mashinostroyeniye, Moscow, 1968, 372p.
- Lynwander, P., *Gear Drive Systems: Design and Application*, Marcel Dekker, New York, 1983, 415p.
- Maag Gear-Wheel Company Ltd. *MAAG Gear Book. Calculation and Manufacture of Gears and Gear Drives for Designers and Works Engineers*, MAAG Gear-Wheel Company Ltd., Zurich/Switzerland, 1963, 576p.
- Maag Gear-Wheel Company Ltd. *MAAG Gear Book: Calculation and Practice of Gears, Gear Drives, Toothed Couplings and Synchronous Clutch Couplings*, MAAG Gear Company, Ltd., Zurich/Switzerland, 1990, 440p.
- Maag Gear-Wheel Company Ltd. *MAAG-Teshchenbuch*, 2nd Edition, MAAG Gear-Wheel Company Ltd., Zurich/Switzerland, 1985, 727p.
- Maddison, F., "Early Mathematical Wheelwork: Byzantine Calendrical Gearing," *Nature*, Vol. 314, 1985, pp. 316–317.
- Maitra, G.M., *Handbook of Gear Design*, 2nd Edition, Tata McGraw-Hill Publishing Company Limited, New Delhi, 2001, 534p.
- Marc, L., *Investigation of the Conformal Gear for Helicopter Power Transmission*, Boeing Co., Morton, PA, June 1964, 136p.
- Matschoss, C., *Geschichte des Zahnrades*, Berlin, 1940, p. 68.
- Merritt, H.E., *Gear Engineering*, Putman Publishing, London, New York, Toronto, 1971, 489p.
- Michalec, G.W., *Precision Gearing: Theory and Practice*, John Wiley & Sons, Inc., New York, 1966, 620p.
- Moiseyenko, D.Y., "Basic Law for the General Case of Gearing and its Geometric Interpretation," *Izvestiya VUZov*, Vol. 7, 1972, pp. 50–53 (in Russian).
- Morivaki, I., Doi, S., Iba, D., Yomenura, T., Haizumi, K., "Conjugate Tooth Profile of Circular Spline to Involute Flex Gear in Strain Wave Gearing," pp. 973–983 in: *Proceedings of International Conference on Gears 2019*, September 18–20, 2019, Technical University of Munich (TUM), Garching (near Munich), Germany, 2019.
- Mozhayev, S.S., *Analytical Theory of Twist Drills*, Moscow-Leningrad, 1948, 136p.
- Mozhayev, S.S., *Generalized Theory of Cutting Tools*, Leningrad Polytechnic Institute, Leningrad, 1951, 295p.
- Nagata, T., Shichino, H., Tamura, Y., Kawai, H., Ohta, Y., Komori, M., *Development of Optimal Tooth Flank in Spiral Gears by Contact Analysis and Measurement*, Technical paper. Komatsu Technical Report, Vol. 59, No. 166, 2013, 6p. <https://home.komatsu/en/company/tech-innovation/report/pdf/166-E01.pdf>
- Nesmelov, I.P., Goldfarb, V.I., "Non-Differential Approach to Solving the Task of Enveloping," pp. 3–10 in: *Mechanics of Machines*, Vol. 61, Nauka, Moscow, 1983.
- Nieman, G., "Novikov Gear System and Other Special Gear Systems for High Load Carrying Capacity," *VDI Berichte*, No. 47, 1961.
- Nikolayev, A.F., "A Diagram of Screw and its Application to the Determination of Conjugated Ruled Surfaces with Line Contact," *Proceedings of Seminar on the Theory of Mechanisms and Machines, Academy of Sciences of the USSR, Institute of Machine Science*, Vol. 10, No. 37, 1950, pp. 52–106.
- Nikolayev, A.F., *Kinematic Principles of the Theory of Spatial Gearing*, Doctoral Thesis, Moscow, Stankin, 1953, 48p.
- Nordex, Inc., *History of Gears*, <https://nordex.com/about/history/>.
- Novikov, M.L., *Gearing with a New Kind of Meshing*, VVIA Publishers, Moscow, 1958, 186p.
- Novikov, M.L., *Principal Considerations of Geometric Theory of Point Gearing for Power Transmissions*, Doctoral Thesis, VVIA Publishers, Moscow, 1955.
- Oberg, E., *Spur and Bevel Gearing*, The Industrial Press, New York, 1917, 274p.
- Olivier, T., *Théorie Géométrique des Engrenages destinés à transmettre le mouvement de rotation entre deux axes ou non situés dans un même plan*, Bulletin de la soc d'Encouragement etc., Vol. xxviii, 1839, p. 430.
- Olivier, T., *Théorie Géométrique des Engrenages destinés*, Bachelier, Paris, 1842, 118p.
- Onishchenko, V.P., *Prediction of Duration of Power Gearing Based on Modeling of the Teeth Wear*, Zeszyty Naukowe Politechniki Śląskiej, Mechanika, z. 131, Gliwice, 1999, 200p.
- Pappi, *Math. Col. Commandini, Bononiae*, lib. XIII, p. 461 and prop. 24, 1660, p. 480.
- Pascal, B., *Oeuvres*, La Haye, t. V, 1779, pp. 135–275.
- Pat. No. 1.601.750 (USA), *Helical Gearing*,/Ernest Wildhaber, filed: November 2, 1923.
- Pat. No. 163857, USSR, *A Helical Gearing*,/B.V. Shitikov, N.A. Bayazitov, Int. Cl. F06h, Filed: February 25, 1963, Published: July 22, 1964.
- Pavl'enko, A.V., Fed'akin, R.V., Chesnokov, V.A., *Novikov Gearing*, Technika, Kiev, 1978, 144p.

- Pavlov, A.I., *Modern Theory of Gearing*, KhNADU, Kharkov, 2005, 100p.
- Phillips, J., *General Spatial Involute Gearing*, Springer, Berlin, Heidelberg, 2003, 498p.
- Pismanik, K.M., *Hypoid Gearing*, Mashinostroyeniye, Moscow, 1964, 227p.
- Pismanik, K.M., *Theoretical Foundations of Grinding of Bevel and Hypoid Gearing*, Doctoral Thesis, Saratov Polytechnic Institute, 1972, 408p.
- Popov, A.P., *Gearing with Point Contact of the Tooth Flanks*, ATOLL, Nikolayev, 2011, 700p.
- Porvatov, N.A., Panin, G.F., *Use of Novikov Gearing in Construction and Road Building Machinery*, Defense Technical Information Center, 1973, 7p.
- Production of Gears for Jet Engines*, edited by Yu.S. Yeliseyev, Mashinostroyenie, Moscow, 2001, 493p.
- Production of Gears. Handbook*, edited by S.N. Kalashnikov, A.S. Kalashnikov et al., Mashinostroyenie, Moscow, 1990, 463p.
- Radzevich, S.P. (Editor), *Advances in Gear Science and Manufacture*, CRC Press, Boca Raton, FL, 2019, 570p.
- Radzevich, S.P., "A Brief Overview on the Evolution of Gear Art: Design and Production of Gears, Gear Science," pp. 418–485 in: *Advances in Gear Science and Manufacture*, edited by S.P. Radzevich, CRC Press, Boca Raton, FL, 2019, 570p.
- Radzevich, S.P., *A Method of Sculptured Surface Machining on Multi-Axis NC Machine.*/ Pat. No. 1,185,749, USSR, Int. Cl. B23c 3/16, Filed: October 24, 1983.
- Radzevich, S.P., *A Method of Sculptured Surface Machining on Multi-Axis NC Machine.*/ Pat. No. 1,249,787, USSR, Int. Cl. B23c 3/16, Filed: December 27, 1984.
- Radzevich, S.P., "A New Angle on Cutting Bevel Gears," *Gear Solutions*, 2010, pp. 42–47.
- Radzevich, S.P., "A Novel Method of Inspection of Gears for Crossed-Axes Gear Pairs," pp. 27–28 in: *Proceedings of the IX International Conference "Comprehensive Quality Assurance of Technological Processes and Systems – 2017"*, April 24–27, 2019, Chernihiv (Ukraine), Vol. 1, 2017, 208p.
- Radzevich, S.P., "A Possible Way of Evolution of Novikov Gearing," pp. 39–40 in: *Proceedings of the IX International Conference "Comprehensive Quality Assurance of Technological Processes and Systems – 2019"*, May 14–16, 2019, Chernihiv (Ukraine), Vol. 1, 2019.
- Радзевич, С.П., "Новый результат в классической теории огибающих кривых и поверхностей," Вестник научно-технического развития, №8(156), 2020, с. 12–21..pdf, www.vntr.ru.
- Radzevich, S.P., "An Examination of High-Conformal Gearing," *Gear Solutions*, 2018, pp. 31–39.
- Radzevich, S.P., "AGMA/ANSI/ISO Standards on Bevel and Hypoid Gears," *Gear Solutions*, September 2017, pp. 45–56.
- Radzevich, S.P., "Concisely on Kinematic Method and about History of the Equation of Contact in the Form  $\mathbf{n} \cdot \mathbf{V} = 0$ ," *Theory of Mechanisms and Machines*, No. 1 (15), 8, 2010, pp. 42–51. <http://tmm.spbstu.ru>
- Radzevich, S.P., "Conjugate Action Law in Design and Production of Precision Intersected-Axes, and Crossed-Axes Gearing," pp. 26–27 in: *Comprehensive Quality Assurance of Technological Processes and Systems – 2020, Proceedings of the X International Scientific Conference*, Vol. 1, April 29–30, 2020, Chernihiv, 2020, 273p.
- Radzevich, S.P., "Conjugate Action Law in Intersected-Axes Gear Pairs and in Crossed-Axes Gear Pairs," *Gear Solutions Magazine*, June 2020, pp. 42–48.
- Radzevich, S.P., "Design Features of Worm Gearing, Composed of Plastic and/or Powder-Metal Components," *Gear Solutions magazine*, August 2019, pp. 36–40.
- Radzevich, S.P., *Differential-Geometric Method of Surface Generation*, Dr.Sci. Thesis, Tula Polytechnic Institute, Tula, 1991, 300p.
- Radzevich, S.P., *Dudley's Handbook of Practical Gear Design and Manufacture*, 3rd edition, CRC Press, Boca Raton, FL, 2016, 629p.
- Radzevich, S.P., *Fundamentals of Surface Generation, Monograph*, Rastan, Kiev, 2001, 592p.
- Radzevich, S.P., "High-Conformal Gearing: A New Look at the Concept of Novikov Gearing," pp. 457–470 in: *Proceedings of International Conference on Gears 2015*, October 5–7, 2015, Technical University of Munich (TUM), Garching (near Munich), Germany, 2015.
- Radzevich, S.P., "High-Conforming Gearing: Kinematics and Geometry," pp. 846–857 in: *International Gear Conference 2014, Conference Proceedings*, Vol. II, Lyon Villerurbanne, France, 26–28 August, 2014.
- Radzevich, S. P. "On Fundamentals of the Scientific Theory of Gearing" pp. 165–172 in: *Power Transmissions, Proceedings of the 4th International Conference*, held at Sinaia, Romania, June 20–23, 2012, Editor: George Dobre, Assisted by Mihai Robert Vladu, Mechanism and Machine Science, Vol. 13, Springer, 2013.
- Radzevich, S.P., "On Fundamental Principles of Gear Cutting Tool Design: The DG/K-Based Approach," in: *Proceedings of International Conference on Gears*, October 4–6, 2010, Munich, Germany.

- Radzevich, S.P., "On Infeasibility of Generating of Geometrically Accurate Form Gear Teeth in Generating Methods of Gear Machining," pp. 26–27 in: *Comprehensive Quality Assurance of Technological Processes and Systems – 2020, Proceedings of the VI International Scientific Conference*, Vol. 1, April 26–29, 2016, Chernihiv, 2016, 273p.
- Radzevich, S.P., "On Infeasibility of Generating of Geometrically Accurate Form Gear Teeth in Generating Methods of Gear Machining," in: *Комплексне забезпечення якості технологічних процесів та систем – 2016*, Матеріали VI міжнародної науково-практичної конференції, 26–29 квітня 2016, Чернігів, с. 32–34.
- Radzevich, S.P., "On the Inconsistency of the Term "Wildhaber-Novikov Gearing": A New Look at the Concept of "Novikov Gearing"," pp. 487–501, in: *Advances in Gear Design and Manufacture*, edited by S.P. Radzevich, CRC Press, Boca Raton, FL, 2019, 549p.
- Radzevich, S.P., "Precision Bevel Gears with Low Tooth Count," *Gear Solutions*, September 2015, pp. 33–41.
- Radzevich, S.P., "Principal Accomplishments in the Scientific Theory of Gearing," pp. 7–18, in: *Proceedings of the 6th International BAPT Conference "Power Transmissions 2019, 19-22.062019 Varna,"* Vol. 1: Design, Analysis, Simulation, and Optimization, Balkan Association of Power Transmissions, Varna, 2019.
- Radzevich, S.P. (Editor), *Recent Advances in Gearing: Scientific Theory and Applications*, Springer, Zurich, 2021, 556p.
- Radzevich, S.P., "Three Fundamental Laws of Gearing: for Gear Design and Gear Production," pp. 21–23 in: *Proceedings of the VIII International Conference "Complex Assurance of Quality of Technological Processes & Systems,"* May 10–12, 2018, Chernihiv (Ukraine), Vol. 1, 2018.
- Radzevich, S.P., Irigireddy, V.V., *Precision Bevel Gears with Low Tooth Count*, AGMA Technical Paper 14FTM18, American Gear Manufacturers Association, 2014, 12p.
- Radzevich, S.P., [Radzevich, S.P., Irigireddy, V., Vijayakar, S.M., Stewart, J., Warner, T.P.], "Preliminary Results of Testing of Low-Tooth-Count Bevel Gears of a Novel Design. Part 1," *Gear Solutions*, October 2014, pp. 25–26.
- Radzevich, S.P., [Radzevich, S.P., Irigireddy, V., Vijayakar, S.M., Stewart, J., Warner, T.P.], "Preliminary Results of Testing of Low-Tooth-Count Bevel Gears of a Novel Design. Part 2," *Gear Solutions*, December 2014, pp. 20–21.
- Radzevich, S.P., [Radzevich, S.P., Irigireddy, V., Vijayakar, S.M., Stewart, J., Warner, T.P.], "Preliminary Results of Testing of Low-Tooth-Count Bevel Gears of a Novel Design. Part 3," *Gear Solutions*, January 2015, pp. 20–23.
- Radzevich, S.P., Storchak, M.G. (Editors), *Advances in Gear Theory and Gear Cutting Tool Design*, Springer, Zurich, 2022, 556p.
- Ramsden, J., *Description of an Engine for Dividing Mathematical Instruments*, London, 1777.
- Reuleaux, F., "Die Thomasche Rechenmaschine," *Civilingenieur*, Band VIII, Helft 3.
- Reuleaux, F., *Lehrbuch der Kinematik*, Braunschweig, 1875.
- Reuleaux, F., *The Constructor, A Hand-Book of Machine Design*, H.H. Supplee, Philadelphia, 1893, 312p.
- Roslivker, E.G., "Hyperboloid Gears with Novikov Gearing," pp. 87–112 in: *Gears with Novikov Gearing*, Vol. 3, 1964a (in Russian).
- Roslivker, E.G., "Investigation of Hyperboloid, Helical and Bevel Gears with Novikov Gearing," pp. 5–85 in: *Gears with Novikov Gearing*, Vol. 3, 1964b (in Russian).
- Rudenko, N.F., *Planetary Gearing: Theory, Application, Calculation and Design*, 3rd Edition, Mashgiz, Moscow, 1947.
- Rudenko, V.N., *Planetary and Harmonic Drives*, Mashinostroyeniye, Moscow, 1980, 148p.
- Sang, E., "Essay on the Forms of the Teeth of Wheels, Part I. Wheels with the Axes Parallel to Each Other," *Edinburgh New Philosophical Journal*, Vol. 24, 1838, p. 217.
- Sang, E., *Trans. Roy. Scot. Soc. Arts.*, 1837.
- Saribay, Z.-B., Bill, R.-C., Smith, E.-C., Rao, S.-B., "Geometry and Kinematics of Conjugate Meshing Face-Gear Pairs," *Journal of the American Helicopter Society*, Vol. 62, No. 3, July 2017, pp. 1–10.
- Schriefer, H., *Verzahnungsgeometrie und Laufverhalten Bogenverzahnter Kegelradgetriebe*, Dissertation RWTH Aachen, 1983.
- Schultz, V.V., *Geometric Optimization of Wearing Kinematic Pairs*, Doctoral Thesis, Kiev, 1980, 32p.
- Schultz, V.V., *Shape of Natural Wear of Machine Parts and Tools*, Mashinostroyeniye, Leningrad, 1990, 208p.
- Sevr'uk, V.N., *Theory of Circular-Screw Surfaces in Design of Novikov Gearing*, KhPU Publishers, Kharkov, 1972, 167p.
- Shelomov, V.B., *Properties of Structure of Planetary Gear Boxes*, Nestor, St. Petersburg, 2004, 206p.
- Sheveleva, G.I., *Design of Gearing According to Local Conditions*, Mashinostroyeniye, Moscow, 1986.



- Shevel'eva, G.I., *Theory of Surface Generation and of Contact of Moving Bodies*, STANKIN Publishers, Moscow, 1999, 494p.
- Shiskov, V.A., *Generation of Surfaces*, Mashgiz, Moscow, 1951, 152p.
- Shishov, V.P., *Theory, Mathematical Support and Synthesis of Power Gearing for the Needs of Industrial Transportation*, Doctoral Thesis, Vostochnoukrainskiy University, Lugansk, 1994, 580p.
- Shishov, V.P., Nosko, P.L., Fil', P.V., *Theoretical Foundation of Synthesis of Gearing*, Vostochnoukrainskiy University, Dal' SNU Publishers, Lugansk, 2006, 408p.
- Shishov, V.P., Nosko, P.L., Rev'akina, O.A., *Gears with Arc-Shaped Teeth: Theory, Analysis, and Synthesis*, Volodymyr Dahl East Ukrainian National University, Lugansk, 2004, 336p (in Russian).
- Shishov, V.P., Nosko, P.L., Velychko, N.I., Karpov, A.P., *Heavily-Loaded Helical Gears*, Volodymyr Dahl East Ukrainian National University, Lugansk, 2009, 240p (in Russian).
- Shotter, B.A., *The Lynx Transmission and Conformal Gearing*, SAE Paper 781041, Aerospace Meeting, Town & Country, San Diego, November 27–30, 1978, 7p.
- Shtipelman, B.A., *Design and Manufacture of Hypoid Gears*, John Wiley & Sons, New York, 1978, 394p.
- Silich, A.A., *Cylindrical Novikov Gearing*, LAP Lambert Academic Publishing, Saarbrücken, 2013, 100p.
- Silich, A.A., *Novikov Gearing: Geometric Calculation of Cylindrical Gearing*, Monograph, Tiumen', Publisher of the Tiumen' Institute of Industry, 2016, 79p.
- Silich, A.A., *The Development of a Geometric Theory of Design of Novikov Gearing, and of the Tooth Flanks Generation Process*, Doctoral Thesis, Kurgan State University, Kurgan, 1999, 534p.
- Silich, A.A., "To Geometric Analysis of Cylindrical Novikov Gears," pp. 13–26 in: *Proceedings of Symposium on "Theory of Mechanisms, Strength of Machines and Equipment,"* Kurgan, KGU, 1997.
- Simon, V.V., "Multi-Objective Optimization of Hypoid Gears to Improve Operating Characteristics," *Mechanism and Machine Theory*, Vol. 146, April 2020, p. 103727.
- Smith, J.D., *Gear Noise and Vibration*, Marcel Dekker Inc., New York, 1999.
- Smith, J.D., *Gear Noise and Vibration*, 2nd edition, Marcel Dekker Inc., New York, 2003, 318p.
- Smith, J.D., *Gears and Their Vibration, A Basic Approach to Understanding Gear Noise*, The Macmillan Press Ltd., 1983.
- Snesar'ev, G.A., *Theoretical Foundations of Series of Gear Reducers*, Doctoral Thesis, MVTU, Moscow, New York, 1980, 32 pates.
- Soldatkin, E.P., "On the Axes of Meshing in the Gears with the Variable Shaft Angle," *Izvestiya VUZov*, Vol. 12, 1974, pp. 62–65 (in Russian).
- Stachel, H., "Spatial Involute Gearing - A New Type of Skew Gears."
- Stadtfeld, H.J., *Advanced Bevel Gear Technology*, The Gleason Works, Division of Gleason Corporation, Rochester, NY, 2000, 343p.
- Stadtfeld, H.J., *Gear Encyclopedia*, The Gleason Works, Division of Gleason Corporation, Rochester, NY, 2008, 462p.
- Stadtfeld, H.J., *Gleason Bevel Gear Technology*, Expert Publishing, Renningen, Germany, May 2017.
- Stadtfeld, H.J., *Gleason Bevel Gear Technology*, The Gleason Works, Division of Gleason Corporation, Rochester, NY, 1995, 202p.
- Stadtfeld, H.J., *Gleason Bevel Gear Technology: Basics of Gear Engineering and Modern Manufacturing Methods for Angular Transmissions*, The Gleason Works, Rochester, NY, 2014, 503p.
- Stadtfeld, H.J., *Handbook of Bevel and Hypoid Gears*, R.I.T., Rochester, NY, 1993, 251p.
- Stadtfeld, H.J., *Practical Gear Engineering: Answers to Common Gear Manufacturing Questions*, Gleason Corporation, Rochester NY, 2019, 395p.
- Stribeck, R., "Berechnung der Zahnräder," in *Z.V.D.I.*, 1894, p. 1182.
- Sukhorukov, Yu.N., *Modification of Cylindrical Involute Gears. Handbook*, Technika, Kiev, 1992, 197p.
- Sushko, Yu.A., *Graphs of Gear Drives*, Mashinostroyeniye, Leningrad, 1983, 216p.
- Syzrantsev, V., Seelich, A., "Theoretical and experimental research of Novikov gear shaving," pp. 143–150 in: *Proc. Int. Conf. on Gearing, Transmissions, and Mechanical Systems*. Nottingham, 2000.
- Syzrantsev, V.N., *Synthesis of Meshing of Spur and Helical Gears with Localized Contact*, DSc Thesis, Leningrad, 1989.
- Syzrantsev, V.N., Erikhov, M. L., et al., "Novikov-Wildhaber Gearing. New Methods of Geometric Analysis, Technology of Manufacturing and Control. Experimental Studies of Load Capacity and Service Life," *J Gearing and Transmissions*, Vol. 1, 2000, pp. 29–37.
- Taiz, B.A., *Gear Accuracy and Inspection*, Mashinostroyeniye, Moscow, 1972, 368p.
- TCA: *Tooth Contact Analysis. Formulas and Calculation Procedure*, The Gleason Works, Rochester, NY, 1964.
- Tkachenko, V.A., *Design of Planetary Gear Drives*, KhGU Publishers, Kharkov, 1991, 182p.

- Tkachenko, V.A., *Planetary Gear Drives: Optimal Design*, KhAI Publishers, Kharkov, 2003, 446p.
- Townsend, D.P., *Dudley's Gear Handbook. The Design, Manufacture, and Application of Gears*. 2nd Edition, McGraw Hill, Inc., New York, 1992, 1111p.
- Tredgold, T., *Practical Essay on the Strength of Cast Iron*, London, 1822, pp. 85–86.
- UGEARS Mechanical models, *History of Gears*, Aug. 04, 2017, <https://ugears.online/blogs/news/history-of-gears>.
- Understanding Tooth Contact Analysis*, The Gleason Works, Rochester, NY, 1981.
- Valikov, E.N., Popov, A.L., “Classification of types of spatial gears”, In: *Bulletin of the Tula State University, Technical Sciences*, Issue 8, part 1, Tula, TulGU Publishing House, 2017, p. 121–126.
- Valikov, Ye.N., Popov, A.L., “Classification of Kinds of Spatial Gearing,” pp. 121–126 in: *Proceedings of Tula State University, Engineering Sciences*, Vol. 8, Part 1, Tula State University Publishers, Tula, 2017.
- Varsimashvili, RSh., “Meshing of Bevel Gears with Variable Gear Ratio,” *Journal of Izvestiya VUZov, Mashinostroenie*, Vol. 10, 1976, pp. 70–75.
- Varsimashvili, RSh., *Planetary and Differential Gears with Non-Circular Gearwheels*, Metsniereba, Tbilisi, 1987.
- Vasiliev, V.M., “Derivation of the Euler-Savary Formula for Spatial Gearing,” *Theory of Mechanisms and Machines*, 1971, Vol. 10, pp. 101–107 (in Russian).
- Verbitskiy, L.L., “The Curvature of the Mating Surfaces in Novikov Gearing,” pp. 36–61 in: *Gears with Novikov Gearing*, 1964, Vol. 3 (in Russian).
- Volkov, A.E., Babichev D.T., “History of Gearing Theory Development,” pp. 71–102 in: *25th Working Meeting of IFToMM Permanent Commission for Standardization of Terminology on MMS*, Saint-Petersburg, Russia, June 23–29, 2014.
- Volkov, A.E., Medv'ed'ev, V.I., *Computation of Spiral Bevel Gearing for Design and Manufacturing Purposes*, MGTU “Stankin,” Moscow, 2007, 151p.
- Vorontsov, B.S., *CAD/CAM System for Gear Generation*, Doctoral thesis, KPI, Kyiv, 2018, 40p.
- Vulgakov, E.B., *Theory of Involute Gearing*, Mashinostroyeniye, Moscow, 1995, 320p.
- Vullo, V., *Gears: A Concise History*, Series: Springer Series in Solid Structural Mechanics, Vol. 12, Springer, Cham, 2020.
- Vullo, V., *Gears: Geometric and Kinematic Design*, Springer Series in Solid and Structural Mechanics, Vol. 1, Springer, Cham, 2020.
- Walker, H., “Gear Tooth Deflection and Profile Modification,” *The Engineer*, Vol. 166, 1938, pp. 409–412.
- Wang Shu Ren Zhu Bian, *Concise Course of the Meshing Theory of Gearing*, University Press, 1991.
- Wang, X.C., Ghosh, S.K., *Advanced Theories of Hypoid Gears*, Studies in Applied Mechanics, Vol. 36, Elsevier, Amsterdam, 1994, 341p.
- Watson, H.J., *Modern Gear Production*, Pergamon Press, New York, 1970, 359p.
- Wells, C.F., Shotter, B.A., “The Development of “Circarc” Gearing,” *AEI Engineering*, March/April, 1962.
- White, J., *Mémoire*, Paris, 1812.
- Wildhaber, E., “Basic Relations of Bevel Gears,” *American Machinist*, Vol. 89, No. 20, September 7, 1945.
- Wildhaber, E., “Basic Relationship of Hypoid Gears – II,” *American Machinist*, Vol. 90, No. 5, February 28, 1946.
- Wildhaber, E., “Basic Relationship of Hypoid Gears – III,” *American Machinist*, Vol. 90, No. 6, March 14, 1946.
- Wildhaber, E., “Basic Relationship of Hypoid Gears,” *American Machinist*, Vol. 90, No. 4, February 14, 1946.
- Wildhaber, E., “Conjugate Tooth Surfaces,” *American Machinist*, Vol. 90, No. 13, June 20, 1946.
- Wildhaber, E., “Design for Duplex Cutting,” *American Machinist*, Vol. 90, No. 17, August 15, 1946.
- Wildhaber, E., “Gear Tooth Curvature Treated Simply,” *American Machinist*, Vol. 89, No. 18, August 30, 1945.
- Wildhaber, E., “Gear Tooth Sliding,” *American Machinist*, Vol. 90, No. 15, July 18, 1946.
- Wildhaber, E., “Relationships of Bevel Gears – Design for Duplex Cutting,” *American Machinist*, October 1946.
- Wildhaber, E., “Relationships of Bevel Gears – Tooth Contact,” *American Machinist*, February 1946.
- Wildhaber, E., “Relative Curvature Controls Gear Tooth Surface Strength,” *American Machinist*, Vol. 89, No. 21, October 11, 1945.
- Wildhaber, E., “Skew Hypoid Gears,” *American Machinist*, Vol. 90, No. 16, August 1, 1946.
- Wildhaber, E., “Special Analysis of Gear Mesh Clarifies Curvature Conditions,” *American Machinist*, Vol. 89, No. 22, October 25, 1945.
- Wildhaber, E., “Surface Curvature,” *Product Engineering*, May, 1956.
- Wildhaber, E., “Tooth Contact,” *American Machinist*, Vol. 90, No. 12, June 6, 1946.

- Wildhaber, E., *Fundamentals of Bevel and Hypoid Gearing*, Translated from English by A.V. Slepak, Mashgiz, Moscow, 1948, 176p.
- Wildhaber, E., Stewart, A.J., "Design, Production, and Application of the Hypoid Rear Axle Gear," *The Journal of the Society of Automotive Engineers*, Vol. 18, No. 6, June 1926, pp. 575–589.
- Willis, R., "On the Teeth of Wheels," *Trans. Civ. Eng.*, Vol. II, 1838.
- Willis, R., *Principles of Mechanisms, Designed for the Use of Students in the Universities and for Engineering Students Generally*, John W. Parker, London, J. & J.J. Deighton, West Stand, Cambridge, 1841, 446p.
- Winter, H. and Looman, J., "Tools for Making Helical Circular Arc Spur Gears," *VDI Berichte*, No. 47, 1961.
- Winter, H., Stölzle, K., Placzek, T., *Topological Tooth Modifications and Contact Patterns of Spur and Helical Gears*, AGMA Paper 89FTM6, AGMA, 1989, 10p.
- Woodbury, R.S., *History of the Gear-Cutting. A Historical Study in Geometry and Machine*, The M.I.T. Press, Cambridge, MA, 1958, 135p.
- Worm Gearing*, Machinery's Reference Series, Number 1, 4th edition, The Industrial Press, New York, 1910, 48p.
- Wu, D.R., Luo, J.S., *A Geometric Theory of Conjugate Tooth Surfaces*, World Scientific Publishing, River Edge, NJ, 1992, 192 (204)p.
- Wu, L.-L., Liu, C.-C., Tsay, C.-B., "Mathematical Model and Surface Deviation of Helipoid Gears Cut by Shaper Cutter," *ASME Journal of Mechanical Design*, Vol. 125, No. 2, June 2003, pp. 351–355.
- Xuntang, W., *Principle of Gearing*, Xi'an Jiaotong University, Xi'an, 2009.
- Yerikhov, M.L., *Principles of Systematization, Methods of Analysis and Problems of Synthesis of Gearing*, Doctoral Thesis, Leningrad Polytechnic Institute, 1972, 48p.
- Young, T., *Lectures on Natural Philosophy and the Mechanical Arts*, London, Vol. I, p. 175, and plate 15, 1807.
- Zablonskii, K.I., *Gearing: The Load Share in Gear Mesh*, Tekhnika, Kiev, 1977, 298p.
- Zamoruev, G.B., "Two Algorithmic Forms of the Equation of Meshing," *Izvestiya VUZov*, Vol. 10, 1977, pp. 64–68.
- Zarrouk, D., "A Vectorial Method to Derive the Equivalent Rotation of Two Successive Finite Rotations," *Mechanism and Machine Theory*, Vol. 126, August 2018, pp. 265–272.
- Zhao, Y., Wei, W., Dong, X., "Some Problems on the 2DOF Theory of Gearing," *Mechanism and Machine Theory*, Vol. 43, No. 8, August 2008, pp. 1024–1037.
- Zhaojun, Y., Hong, Z., Wang, B., Zhang, X., "New Tooth Profile Design of Spiral Bevel Gears with Spherical Involute," *International Journal of Advancements in Computing Technology (IJACT)*, Vol. 4, No. 19, October 2012, pp. 462–469.
- Zheng, F., Hua, L., Chen, D., "Generation of Noncircular Bevel Gears with Free-Form Tooth Profile and Curvilinear Tooth Lengthwise," *ASME Journal of Mechanical Design*, Vol. 138, No. 6, 2016, p. 064501.
- Zhuravl'ev, G.A., Iofis, R.B., *Hypoid Gearing: Problems and the Development*, University Press, Rostov-on-Don, 1978, 160p.
- Zhuravl'ev, V.L., *Production of Globoid Gears*, Mashinostroyeniye, Moscow, 1998, 350p.



# Index

Note: **Bold** page numbers refer to tables; *italic* page numbers refer to figures.

- accurate real gearing 605–641, **640**; *see also* real gearings
- accurate worm gearing 573–589; *see also* worm gearing
- active profile 173
- addendum 173, 192
- addendum angle 8, 420–422, 524–529, 528
- addendum modification 173, 192, 227–230, 228, 230, 233–236, 740, 740, 1105
- Analytical Calculation of Planar and Spatial Gearing* 714, **921**, 968
- angular base pitch 101, 104–106, 383–385, 399, 405–408, 422, 442–445, 444, 514–518, 515, 530
- angular pitch 253, 621, 621, 685–687, 690–693
- antikythera mechanism 927, 928
- apex 28–29, 36–37, 40, 54
- approximate real gearings; *see also* real gearings
  - bevel gears in 715–717
  - continuous-indexing processes 728
  - crossed-axes gearing 732–736, 733–736
  - developments in 711
  - examples of 728–732, 728–732
  - face gearing 719–720, 720
  - inaccuracies of 713–714
  - intersected-axes gearings 713–720
  - parallel-axes gearings 712, 712–713, 713
  - spiral bevel gears 717, 717–718, 718
  - straight tooth bevel gears 715–717, 715–717, 720–724, 721, 722
  - tooth flanks in 712, 712–713, 713
  - tooth modifications 739–746, 740, 741, 743, 745
  - undercut in 742, 743
  - worm gearing 736–739, 736–739
- archimedes 926
- arc of action 253, 254
- arc of approach 261, 262
- arc of recess 261, 262
- Aristotle 926
- automobile differentials 198, 276, **277**
- axial pitch 209, 212, 260, 321, 331, 435, 541
- axis misalignment 739, 746, 898, 918
- axis of instant rotation 92, 95, 665, 752, 754–759, 878, 880, 886, 910, 914
- axodes 39–42, 42
- back cone distance 424, 426, 432, 434, 435, 537, 539, 540
- backlash 6, 81, **191**, 270, 270, **295**, 337, 415–418
- base angular pitch 414, 522
- base circle 110, 111, 125, 129–131, 151, 153, 157, 169, 174–178, 180, 198, 224, 248
- base cones
  - in crossed-axes gearing 487–488
  - in intersected-axes gearing 378–380, 378–383, 383
  - in worm gearing 590–593, 591, 592
- base cylinder 129, 134–137, 142, 143, 158, 162, 166, 167, 185, 209, 242, 247, 250, 251, 271
- base diameter 340, 594, 625, 633, 657, 658, 752, 799–801, **1090**, **1091**
- base helix angle 80, 143, 144, 149, 163, 182, 187, 187–188, 188
- base lead angle 162–164, 188, 212, 579
- base pitches
  - in crossed-axes gearing 546–550, 548, 549
  - of gears 919, 938, 941, 944–946, 951, 954, 960–961
  - in intersected-axes gearing 384–385, 405–408, 406, 407
  - in involute gearing 104, 354, 1098
  - in Novikov gearing 305–311, 306, 307
  - in real gearings 629–631, 631
  - violation of equality of 892–896, 893
- bending torque 292, 298, 905, 906
- bevel gear coupling 665, 665
- bevel gear pairs
  - in approximate real gearings 715–720, 716–720, 975–976
  - face gearing 719–720, 720
  - in intersected-axes gearing 378, 378–383, 379, 383
  - spiral bevel gears 474–477, 474–477, 717–719, 718, 719
  - straight tooth bevel gears 50, 54, 88, 715–717, 715–717
- bottom land 161, 164, 168, 421, 423, 524, 526, 527, 529, 661
- boundary Novikov circle 307, 316, 317, 344, 430
- boundary Novikov cone 430, 534–536, 535
- calculus, elements of 1007–1012
- Camus, Charles 930–936, 932, 938, 947, 954
- Camus-Euler-Savary theorem 88–95, 89–91, 93, 94, 107, 214, 304
- Cartesian coordinate system 12, 28, 68, 69, 145, 146, 151, 154, 182, 202–206, 237, 385–387, 389, 393, 403, 409, 457, 494, 495, 498, 512, 519, 554, 608, 626, 684, 722, 764, 815, 941, 1013, 1025, 1036, 1040, 1042, 1048
- centerline plane 63, 486, 518, 590, 956, 958
- CΣu-variable gearing 645–668, 646–655, 662–668
- characteristic curve 99, 357, 673–675, 765, 834, 959, 1064–1068, 1074, 1076, 1078, 1081
- characteristic line 162, 183–185, 188, 189, 207–210, 365, 705, 706, 1061
- circular arc 5–11, 10, 20, 21, 98, 137, 149–150, 969
- circular pitch 21, **191**, 192, **194**, **195**, **1090**
- complementary torque vector 839
- complex gear transmission systems 839–847, 840–846; *see also* Gear systems
- condition of conjugacy 91, 98, 156, 307, 404, 907, 950, 952, 960–961, 963
- condition of contact 83–85, 98, 742, 934, 934, 952, 954, 955, 961, 1075, 1076
- Cone, Samuel 974, 979
- conformal gearing 301–305, 302; *see also* High-conformal gearing
  - design features of 304
  - origination of 301–303

- conformal gearing (*Cont.*)
  - potential designs of 305
  - power density 303
- conformity, degree of 1068–1071, 1069, 1070, 1078–1081, 1080
- conformity, extremum degree of 1078–1081, 1080
- conformity, indicatrix of 674, 1075, 1076, 1081–1082
- conical involute gears
  - geometry of 202–209
  - kinematics of 201–209
  - with straight teeth 209, 209
  - tooth flanks and 201, 202–209
- conjugacy, condition of 86–101, 100, 950, 952
- conjugate action 11–13, 17, 86–88, 87, 89, 91, 93, 105, 118, 155, 214, 367, 397, 398, 402, 402–404
- contact, condition of 83–85, 98, 742, 934, 934, 952, 954–955, 961, 963, 1075
- contact geometry; *see also* geometry
  - degree of conformity 1068–1077, 1069, 1070
  - Dupin indicatrix 673, 673–675
  - extremum degree of conformity 1078–1081, 1080
  - features of 671–677
  - of gear and mating pinion 1059–1064
  - indicatrix of conformity 1071–1077, 1075, 1076, 1077, 1081
  - local orientations 1060, 1060–1064, 1062
  - planar characteristics 1064–1067, 1065
  - of tooth flanks 934
- contact lines method 309
- contact motion
  - in crossed-axes gearing 450–451
  - in intersected-axes gearing 552–562, 561
  - of mating pairs 282–288
- contact ratio
  - in helical gears 246, 246–247, 247
  - in high-conformal gearing 301–324, 302, 306
  - in internal involute gearing 212–221
  - in intersected-axes gearing 445–450, 446, 447, 449
  - in noise excitation 893, 906, 907
  - in parallel-axes gearing 1103
- convex-to-concave contact 100, 301–304, 302, 351, 352, 354–358, 365, 967
- coordinate systems
  - arbitrary axis and 1035–1037
  - Cartesian system 145, 386, 1040, 1043
  - chains of linear transformations and 1050–1056, 1052, 1053, 1054, 1055
  - closed loop coordinate system 1050–1056, 1052, 1053, 1054, 1055
  - complex coordinate systems 1040–1049, 1042, 1044
  - consequent coordinate system transformations and 1050–1056, 1052, 1053, 1054, 1055
  - conversion of 1048–1049
  - coupled linear transformations 1045–1047
  - for crossed-axes gearing 385–399, 552–559
  - Eulerian transformation and 1036, 1036–1037
  - examples of 1033, 1034, 1036
  - homogeneous coordinate transformations 1031–1032
  - homogeneous coordinate vectors 1032
  - linear transformations and 1031–1057
  - local coordinate system 1052, 1053, 1053
  - non-orthogonal linear transformation and 1047–1048, 1052
  - for parallel-axes gearing 146, 282
  - for real gearings 603, 605, 607
  - rolling motion and 1041–1043, 1042
  - rolling of two systems 1043–1045, 1044
  - rotation of coordinate axis 1034, 1034–1045
  - schematics of 147
  - screw motion and 1040–1041
  - tangent vectors and 1054, 1054
  - for tooth flanks 145, 147
  - transformations and 1031–1032
  - translations and 1032–1034, 1033, 1034
  - useful equations for 1049–1050
- crossed-axes angle 26, 28, 28–30, 29, 35, 36, 43–50, 44, 48, 52, 59, 77, 312, 364, 507, 575, 583, 606, 607, 618, 622
- crossed-axes gearing
  - analytical criterion of 43, 43, 485
  - angular addendum in 524–529, 528
  - angular base pitch of, 514–518, 515, 522, 523
  - angular dedendum in 524–529, 525, 528
  - angular tooth thickness in 417, 523–524
  - approximate real gearings 732–736, 733–736
  - backlash in 530–532, 531
  - base cones in 488–493, 489, 492, 493
  - base pitches in 101–107, 102, 103
  - bearing capacity of 536
  - boundary cones in 534–535, 535
  - conjugate action law, fulfillment of 510–513, 511, 513
  - contact motion in 552–562, 561
  - contact ratio in 445–450, 446, 447
  - coordinate systems for 494–510, 496
  - crossed-axes worm gearing 707, 708
  - design parameters of 536–542, 537, 538
  - design peculiarities of 909–915
  - desirable tooth proportions in 513–530, 515, 519, 521, 523
  - diagrams of 484
  - dynamics of 562–565
  - elements of 562–565
  - examples of 40, 42, 698–701, 700, 701
  - forces acting in 562–565, 563
  - gear housing and 498–499
  - gear tooth accuracy 868–870, 869, 870
  - high-conformal crossed-axes 533–536, 534
  - kinematics of 481–485
  - linear transformations for 494–495
  - line of contact in 500, 502, 503, 912–913, 914
  - load analysis of 465–467
  - low tooth count in 518
  - nonorthogonal crossed-axes 730, 731
  - operators associated with 498–499
  - orthogonal crossed-axes 488
  - path of contact in 533–534, 534
  - perfect crossed-axes gearing 925
  - pitch surfaces in 412, 412–414, 413
  - plane of action in 518, 518, 753, 754, 755
  - possible types of 698
  - pressure angle in 486–488
  - pulley-and-belt analogy of 438, 543
  - real crossed-axes gearing 639
  - reference plane in 432, 432–434, 433
  - reference systems for 494–495, 496, 553, 912
  - rolling conditions in 387, 388, 495
  - round basic rack and 452–454
  - sliding conditions in 495–498

- spiral bevel pinion for 508, 509, 977
- tooth flanks in 493–510, 494, 496, 508, 509
- tooth proportions in 513–530, 515, 519, 521, 523
- transmission of rotation 546–550, 548, 549
- transverse pressure angle in 518–522, 519, 521
- Tredgold approximation for 532–533
- vector diagrams for 844–847
- zone of action of 439–441, 440, 441
- crown gear 33, 386, 411, 416, 418, 505, 521, 531, 562, 700, 701, 867
- curvatures of surfaces 673, 773, 1071
- Cu*-variable gear 643, 652
- cycloidal gearing 6, 143
  
- Darboux frame 673, 1022, 1053, 1067, 1114
- Darboux, Jean-Gaston 685, 1067
- Darboux trihedron 685, 685–692, 694
- Da Vinci, Leonardo **921**, 929, 929, 930
- dedendum 4–6, 9, 11, 133, 173, **181**, 189, **193**, 222, 223, **235**, 288, 301, 325, 326, 333, 336, 345, 420–423
- dedendum angle 420–422, 421
- De Dondi, Giovanni 929
- degree of conformity 1068–1077, 1069, 1070
- degree of conformity, extremum 1078–1081, 1080
- De La Hire, Philippe 920, 930–936, 931, 980
- deliberate departure 174
- Desargues, Girard 931, 931, 935, 954
- design peculiarities
  - of almost perfect gears 909–918
  - of crossed-axes gearing 912–915
  - of perfect gears 909–918
  - for real gearings 915–918
- desired line of contact 138–141, 582; *see also*
  - Line of contact
- double-helical gears 23, 23, 171, **640**
- double-tooth contact regions 267, 267
- driven shaft, rotation of 117
- Dupin indicatrix 673, 673, 1064–1067, 1065
- Dürer, Albrecht 929
  
- Elastic deformation 220, 221, 334, 632, 740, 769, 825, 917
- elastic load sharing devices 828, 829, 831, 832, 838
- elastomeric load sharing device 827, 827–828, 1105
- end chamfer 173, 261, 262
- end radius 173
- epicyclical gear drives 821
- equal base pitches 17, 18, 101–107, 102, 103, 144, 150, 214, 443, 548
- equation of contact
  - in approximate real gearings 723, 727
  - gear noise and 889–890
  - interacting tooth flanks and 68, 81, 82, 83, 88, 91
  - in intersected-axes gearing 398
  - in involute gearing 198–200, 199
  - in noninvolute gearing 9, 13
- Eulerian gearing 943
- Eulerian transformation 1036–1038, 1038
- Euler, Leonhard 107, 157, 358, 712, 919, 920, **921**, 926, 936, 936, 985
- Euler-Savary equation 95–98, 97, 322, 980
  
- face advance 260, 260–264, 261, 264
- face contact ratio 1, 80, 266, 308, 310, 311, 357, 358, 434, 445, 449–450, 551, 552
- face gearing 719–720, 720, 732, 978–979
- face of tooth 173
- face width 80, 84, 134, 151, 161, 163, 173, 180, 242–246, 245, 246
- favorable gear pair; *see also* Gear pairs
  - conformity of 674–675, 1071
  - designing 118–119, 157
  - Dupin indicatrix of 673, 673
  - meaning of 671–672
  - optimization of 671–672
  - point contact of 638–641
  - synthesis of 488, 671–673
  - tooth flanks in 767, 771, 773, 774
- field of action 253, 330, 331, 439, 545, 546, 760, 761, 787–789, 791, 794
- fillet 161, 164, 168, 173, 189, 190, 222, 223, 228
- fillet curves 173, 318
- fillet radius 190, 223, 228, 337, 435, 540
- fillet undercut 190, 190, 223
- fundamental theorem of gearing 88, 90, 933, 946, 947, 961, 963, 980
  
- Gavrilenko, Vladimir A. **922**, 969, 971
- gear apex 37, 491, 492, 501, 503, 597, 637
- gear art 919, 925–936, 951, 980
- gearbox 834, 836, 838, 843
- gear cone angle 36, 42, 69, 70, 74, 77, 373, 373, 374, 558, 655, 910
- gear coupling 53, 53, 54, 123, 124, 217–218, 218, 636–638, 637
- gear coupling design concepts 636–637, 637, 638
- gear drives
  - characteristics of 851–852
  - epicyclical gear drives 816–817, 821, 822
  - examples of 849, 850
  - gear pairs in 854
  - gear ratios of 849–855, 854
  - gear transmission systems 815–816
  - multistage gear drives 850–852
  - planetary gear drives 812–813, 818, 818, 827–828
  - power density of 815–816
  - rotational speeds 852–853, 853
  - speed variation for 851–852
  - transmission characteristics 851–852
  - transmission ratios 852
- gear housing 17, 146, 297, 385, 398, 428, 498, 554, 624, 659, 831
- gearings
  - accomplishments with 980–982
  - approximate gearings 974–979
  - art of 919–984
  - background of 919–984
  - concluding remarks on 1103–1106
  - design parameters of 646–649
  - developments in 974–979
  - explanation of 919–984
  - fundamentals of 947
  - geometrically accurate gearings 1, 2, 24, 79, 85, 86, 89, 90, 91, 95, 901–904, 905, 909, 912, 925, 936
  - glossary of terms 1111–1119
  - history of 919–984
  - ideal gearings 195
  - intersected-axes gearing 369, 371–436
  - introduction to xxvii–xxxviii

gearings (*Cont.*)

- involute gearing 113–140
- laws of 79–107
- overview of 919–982
- parallel-axes gearings 712, 712–713, 713
- post-Eulerian period of 946–964
- pre-Eulerian period of 926–946
- theory of 919–984

gearing, theory of 919–961; *see also* theory of gearing  
*Gearing with a Novel Kind of Meshing* 970

## gear noise

- causes of 889–896
- equation of contact and 889–890
- vibration and 889–896

gear pairs; *see also* specific gear pairs

- axial vectors of 55–57, 56
- bolt-and-nut pair 25–26
- definition of 25–26
- design parameters of 227, 234, 266–281, 276
- dynamic analysis of 839–847, 840–846
- elastic deformation in 268, 268
- examples of 119, 728, 728, 730, 737
- favorable gear pairs 855, 959, 1059, 1078, 1105
- formulas for 57–59
- fundamentals of 79, 81–101, 89, 90
- gear diameters 233, 235
- kinematic analysis of 839–846, 840–846
- kinematics of 25–43, 26–32
- low tooth count 1103
- in multistage gear drives 855
- parallel-axes gearing and 153–157, 154, 155
- perfect gear pairs 640, 641
- planes associated with 61–64, 62–64
- possible types of 681, 683, 709
- pulley-and-belt analogy of 86–88, 87, 646–649, 647, 648
- rack-to-rack pair 25–26
- reference systems for 61–78, 69, 70
- transmission of motion by 25–26
- types of 756
- undercut in 262–268
- vector representation of 683, 709, 839, 842, 962, 1032

## gear ratios

- of multistage gear drives 853–854, 854
- in parallel-axes gearing 124–129, 126, 248–250

## gears

- apex of 37, 68, 491–492
- base pitches of 17, 18, 21, 22, 80, 101–107, 103, 106
- complex gear systems 839, 1105
- contact geometry of 81, 98–99, 138, 335, 348, 357, 475–477
- design of 117, 197, 681, 682, 694, 697
- design peculiarities of 909–918
- distance of approach for 1083–1087
- early designs of 117
- face width 80, 84, 134, 151, 161, 163, 173, 180, 242–246, 245, 246
- gear joint 665, 665
- gear-to-pinion mesh 129, 129, 130, 131, 132, 383, 383, 405
- generic shapes of 655, 720
- low-tooth-count gear 518
- master gear 645
- mating pinion and 1059–1064

- old-style gears 928
- point contact of 638–641
- shapes of 683–694, 684, 685, 687, 688, 689
- simulating gear and pinion 802–808, 803, 805–808
- strength of 767–808
- terminology of 172–174
- tooth flanks in 712, 712–713, 713

## gear shapes

- axial sections 684–694, 687–693
- classification of 697–698, 698
- cross-section of 701, 703, 705
- examples of 682, 682–683, 683
- generic shapes 683–694, 684, 685, 687, 688, 689
- possible number of 1105

*Gear Solutions* magazine 985, 986–1005

## gear systems

- analysis of 839–847
- complex gear systems 839–847, 842, 843
- with crossed-axes gearing 844–847, 845, 846
- dynamic analysis of 839–847, 842, 843
- with intersected-axes gearing 844–847, 845, 846
- kinematic analysis of 839–847, 842, 843
- rotating gear images 839–841, 840, 841
- $S_{pr}$ -gear system 677
- vector approach for 839–847
- vector diagrams for 841–844

gear teeth; *see also* tooth flanks

- accuracy of 857–888, 858–861, 863, 865, 868, 871, 872, 874
- bending strength of 780–785
- cantilever beam and 781, 781–782, 783, 784
- contact patterns 586, 821
- engineering formulae for 1089–1091, 1090, 1091
- features of 772–773
- Hertz contact stress equation 777
- Hertz proportional assumption 768–771, 1105
- interactions of 768–771, 769–772
- Lewis's formula 780–785, 781
- line of contact in 786–791
- load analysis of 775, 799, 799–802
- mounting distance of 873–880, 876, 877
- Saint Venant's principle 781, 784, 784
- simulating gear and pinion 802–808, 803, 805–808
- specific pressure factor 777–778
- strength of 767–808
- stresses in 767–768, 768, 772–773, 780

## gear tooth line 172, 418–425, 419

gear tooth profile; *see also* Tooth flanks

- accuracy of teeth 857–888, 858–861, 863, 865, 868–872, 874, 875
- addendum modification 227–230, 228–230
- contact patterns 586, 821
- elements of 172, 173, 174
- generation of 153–157, 154
- geometrical blocking contours 236–239, 238, 239
- geometry of 603
- helix angle and 397
- involute gearing and 198
- length of 198–200, 199
- in lengthwise direction 167–171, 168–171, 714
- modifications of 227–230, 228–230
- mounting distance of 873–886, 874–885
- parallel-axes gearing and 153–157, 154, 155, 157
- profile shift coefficient 228–230, 230–233, 231, 233

- rack shift and 227–239
  - sliding angle of 451–456, 452, 455, 456
  - sliding conditions in 282–287, 282–287
  - strength of teeth 767–798
- gear-to-pinion mesh 129, 129–132, 383, 383, 405
- gear-to-rack mesh 222–225, 222–225
- gear transmission systems 815–816, 839, 841–847, 842, 849
- Generation of Surfaces in Continuous-Indexing Methods of Surface Machining* 304, **921**
- geometrical blocking contours 920
- geometrically accurate gearings 2, 79, 85, 86, 104, 117–119, 154, 302–305, 369, 586, 588, 603, 606–611, 619, 620, 628; *see also* Gearings
- Geometric Theory of Gearing (Théorie Géométrique des Engrenages)* **921**, 949, 950
- geometry
  - of conical involute gears 202–209
  - contact geometry 671–677
  - elements of 1013–1028
  - features of 671–677
  - of gear tooth profile 603
  - in high-conformal gearing 301–324, 302, 306
  - interacting tooth flanks and 68, 81, 82, 83, 88, 91
  - intersected-axes gearings 713–720
  - in involute gearing 104, 354, 1098
  - kinematics of 25–43, 26–32, 201–209
  - of surfaces 1013–1028
  - of tooth flanks 145, 147, 201, 202–209, 493–510, 494, 496, 508, 509, 712, 712–713, 713, 767, 771, 773, 774, 934
- gleason method, gear generating 475, 475
- Gleason, William 975, 976
- glossary 1111–1119
- Gochman, Chaim 83, 925, 951, 952, 953, 980, 1106
- Grant, George Barnard 88, 107, 116, 378, **921**, 964–966, 965
- helical gears
  - bending torque in 904–906, 905, 906
  - design parameters of **193–196**
  - determining angle of 187, 187–188
  - equation of 182–186
  - examples of 702, 703
  - formulas for **194–195**
  - gearbox with 23, 23
  - generating basic rack of 186–189, 186–189, 192, **193**, 210
  - helix angle 278, 281
  - involute gearing and 145, 145–146, 163, 174
  - line of contact in 786, 786
  - load distribution in 289, 289–298
  - noninvolute gearing and 18–22, 19, 20, 21
  - Novikov gearing and 1098–1101, 1099
  - parallel-axes gearing and 246, 246–247, 247
  - pitch of 193
  - tooth flanks and 241, 241–246, 246, 247
  - tooth profile angle 278, 281
  - Wildhaber-Novikov gearing and 1093–1101, 1094, 1095
  - zone of action of 253–261, 262
- helix angle 25, 143, 149, 171, 182, 186–189, 191, 192, 204
- helix modification 174
- Heron of Alexandria 926
- Hertz contact stress equation 777
- Hertz, Heinrich 768–771
- Hertz proportional assumption 768–771, 776, 777
- high-conformal crossed-axes 533–536; *see also* Crossed-axes gearing
- high-conformal gearing
  - accuracy for 359–365, 360, 362, 363
  - bearing capacity of 430, 430–431, 536
  - boundary cones in 428–430, 429
  - close-up of 338
  - continuous-indexing processes 364–368, 365, 366
  - convex-to-concave contact of 301–304, 302, 354–356, 355, 362, 363, 363, 761, 762
  - degree of conformity 355–356, 356, 357, 358–359
  - design parameters of 330, 330–331, 431–436, 432, **436**, 536–542, **541**
  - geometry in 339–340, 348–355, 349–351, 432, 433
  - kinematics of 338, 432–436, 433
  - machining processes in 364–368, 365, 366
  - origin of 301–303
  - parallel-axes gearing and 355–368
  - path of contact in 427, 427–428
  - point of culmination 309, 334–335
  - power density in 351–352
  - pseudo-path of contact 345–351, 347, 361, 427–428
  - reference plane in 536–537, 537, 538
  - tooth flanks in 316–324, 348–351, 761–765, 762–764
- high-conformal intersected-axes; *see also* Intersectedaxes gearing
- hyperboloids 39, 42, 524, 525, 527, 684, 685
- hypoid gear 55, **640**, 687, 850, 886, 976, 977
- ideal gearings 925; *see also* geometrically accurate gearings
- indicatrix of conformity 1071–1077, 1075, 1076, 1081–1082
- instant line of action; *see also* line of action
  - description of 933
  - in high-conformal gearing 339–340
  - in involute gearing 648
  - in parallel-axes gearing 647, 648, 648–649
- internal involute gearing; *see also* involute gearing
  - design parameters of 217
  - examples of 213, 215
  - gear coupling in 217–218, 218
  - sliding conditions in 282–287, 286
  - tooth thickness in 866
- intersected-axes gearing
  - analytical criterion of **376**
  - angular addendum in 420–422
  - angular backlash in 415–417, 418
  - angular base pitch of 405–408, 406, 442–445, 443, 444
  - angular dedendum in 420–422
  - angular pitch of 412–414, 413
  - approximate real gearings 713–732
  - base cones in 378–385, 380, 410, 411, 412
  - base pitches in 384–385, 405–408, 406
  - bearing capacity of 430, 430–431
  - bevel gears in 378–383, 390–399, 391, 392, 411, 414–417, 425, 715–719
  - boundary cones in 428–430, 429
  - case of, 79–80, 80f, 81f 63–64, 64, 65
  - cone angle 373, 373



intersected-axes gearing (*Cont.*)

- contact motion in 450–464, 452, 455
  - contact pattern in 474–477, 475–477
  - contact ratio in 550–552, 551
  - coordinate systems for 385–390, 456–462
  - crown gear 411–416
  - design parameters of 422, 423, 423–425, 431–436, 432, 436
  - designs of 371–378
  - dynamics of 464–474
  - early designs of 371–372
  - elements of 464–474
  - equal base pitch of 442–445, 443, 444
  - face width of 439–441, 440
  - forces acting in 464–474, 465, 469, 470, 472, 473
  - gear tooth accuracy 866–868, 868–869
  - gear tooth line in 418–419, 419
  - geometry of 432, 432–433, 433
  - high-conformal intersected-axes 427–431
  - inaccuracies of 714–715
  - kinematics of 372–378
  - linear transformations for 385–390
  - linear velocity vector in 451–456, 460–461
  - line of action in 383–384, 384
  - line of contact in 390–391, 391, 392
  - load analysis of 464–474
  - miter intersected-axes, 333–334, 335f 377, 377
  - nutating drives and 376, 376
  - operating base pitches in 384–385
  - orthogonal intersected-axes 377, 380
  - path of contact in 383–384, 427, 427–428, 438–439, 439
  - perfect gear pairs 371–436
  - pitch cone angle in 409–410, 410, 411, 412
  - plane of action in 438–443
  - pressure angle in 385, 395
  - pulley-and-belt analogy of 438–439, 439
  - reference systems for 68–72, 69, 456–470, 458
  - rolling conditions in 387–390
  - rotation vectors of 481–490, 516–518
  - round basic rack and 412–413
  - round rack-to-bevel gears 377, 377
  - sliding conditions in 451–452, 452, 456, 463–464
  - spiral bevel gears and 474, 474–477, 475, 477
  - tooth flanks in 385–399, 386, 391, 392, 437–477, 720–728, 752–756, 753, 755–756
  - tooth thickness in 414–415, 417
  - transverse pressure angle in 407, 408–411
  - Tredgold approximation 425–426, 426
  - vector diagrams for 844–847, 845, 846
  - zone of action of, 383–384, 383f, 385f 439–441, 440, 441
- involute gearing
- base diameter of 188, 188–189
  - of circle 157, 157–159
  - concept of 934, 943–944, 960, 960, 964–965
  - conical involute gears 201–212
  - contact ratio in 250–265, 261
  - design parameters of 269, 269–270
  - double-tooth contact regions in 267, 267
  - examples of 702, 703
  - external gear pair 269, 269–281
  - face contact ratio in 260, 260–261
  - gear tooth profile 153–200

- geometry and 121–151
- helical gears and 161–167, 162, 163
- internal involute gearing 212–221
- kinematics of 121–151
- line of action in 153, 154
- line of contact in 789, 790
- noninvolute gearing 1–22
- parallel-axes gearing and 121–161, 241–299, 246, 249
- path of contact in 960, 961
- pinion-gear-to-rack mesh 222, 222–225, 223
- screw involute surface 145–146, 146, 161–167, 167, 183, 183–185
- sliding angle of 282–287, 283, 288
- spur involute gears 122, 129–132, 159–167, 161, 162
- theory of 966, 967–969
- tooth flank generation 153–200
- tooth flank interaction 241–299

## kinematics

- of complex gear systems 839–847, 843
- of conical involute gears 202–212
- of crossed-axes gearing 481–485, 909–910, 910
- fundamentals of 25–59
- of gear pairs 25–59, 28, 839–847, 842, 843, 1103–1106
- geometry and 121–151, 701–710, 1103–1106
- in high-conformal gearing 338, 339, 339–340
- of intersected-axes gearing 371–378
- involute gearing and 121–151
- of multistage gear drives 849–852
- of noninvolute gearing 11–13
- of parallel-axes gearing 121–124
- of rotation vectors 27–59
- of tooth flanks 136–151, 747–748, 752–754, 756–758, 760–763
- vector approach for 839–847
- vector representation of 27–59
- of worm gearing 590

Kolchin, N. I. 921, 966

## lantern gearing 2–3, 3

laws of gearing 442–445, 550, 711, 1103

lead angle 162–163, 212, 337, 348

leading flank 172

length of action 253, 269, 345

Lewis's formula 780–781

## linear transformations

- coordinate systems and 1031–1057
- for crossed-axes gearing 494–507
- for intersected-axes gearing 385–390

linear velocity vector 90–91

line of action; *see also* geometrically accurate gearings

- description of 11–16
- instant line of action 22, 82–83
- in intersected-axes gearing 383–384, 384
- in involute gearing 136–141, 139, 281

## line of contact

- in crossed-axes gearing 202–203, 500, 502, 503, 914
- desired line of contact 138, 144, 147
- equation of contact and 98
- in gear teeth 786–792
- in helical gears 786, 787
- for intersected-axes gearing 390–391, 391, 393
- in involute gearing 136–138, 149, 149–150, 789, 790

- in parallel-axes gearing 288–298, 291, 294, 786–790, 786–798, 792–787
  - in real gearings 625, 625, 636–638, 639
  - in worm gearing 573–577
- Litvin, F. L. **922**
- local frame 1016
- Lorenz, Friedrich Wilhelm 975, 979
- low-tooth-count gear 195, 197–198, 244, 255–256, 257, 274, 593–595, 598, 767–780
- Madrid Codices, The* 371, 481, 737, **921**, 930, 974
- master gear 645; *see also* gears
- mating gear pairs; *see also* gear pairs
  - contact motion of 282–288, 284
  - contact ratio of 79–81
  - internal involute gearing 212–221
  - tooth flanks and 241–244, 247
  - tooth thickness in 866
- mating pinion; *see also* pinion
  - contact geometry of 1059–1082
  - distance of approach for 1083–1087, 1084, 1087
  - gears and 747–766
  - simulating gear and pinion 802–808, 803, 805–808
  - tooth flanks and 671–677, 676, 754–756, 960–961, 1059–1087
- Mechanical Problems of Aristotle* 926
- mesh cycle; *see also* gear pairs
- meshing point 277, 278–281, 305, 398, 1099
- mismatch 174
- mounting distance 417, 424, 532, 620, 870–886
- multistage gear drives; *see also* gear drives
  - characteristics of 851–855
  - examples of 849, 850
  - gear pairs in 854–855
  - gear ratios of 849–855, 854
  - of helical gears 849, 849
  - kinematics of 850–852
  - rotational speeds 852–853, 853
  - transmission characteristics 852
  - transmission ratios 852
- Musser, C. Walton 218, 973
- New General Theory of the Teeth of Wheels* 949, 951
- noise excitation
  - causes of 889–908
  - contact ratio in 902, 903, 904
  - load variation on 902
  - prediction of 906–908
  - vibration and 889–908
- nominal profile 173
- noncircular gears
  - design concepts 645–668
  - developments in 650–652
  - diagrams of 650, 658
  - elliptical gears 663
  - examples of 646, 662, 663
  - fundamentals of 649–650
  - gear shapers 662
  - machining processes in 662, 662–663, 663
- noninvolute gearing; *see also* involute gearing
  - helical gears and 18–22, 19, 20, 21
  - interaction with racks 14, 14–18
  - kinematics of 12, 12–16, 16
  - linear velocity vector in 11–17
  - rotation and 11–18, 12
  - spline shafts and 14, 14–17, 16
  - spur noninvolute gears 1–22
- normal plane 57, 62, 63, 64, 65, 66
- normal pressure angle 281, 800
- Novikov gearing 20–22, 302, 303, 305–318, 350, 358, 967, 969, 983, 984, 1093–1101; *see also* Wildhaber-Novikov gearing
  - concept of 307, 309
  - essence of 305–311
  - involute (Euler) gearing 358
  - tooth flanks in 307
  - tooth profiles of 305
  - transverse contact ratio 311
- Novikov, Mikhail L. 305, 698, **921–924**, 967–969
- nutaton, angle of 1037
- nutaton drives 485
- oil pumps 10, 10–11
- Olivier, Théodore 948–951, 949, 979, 1106
- operating base pitches
  - of gears 656, 938–939, 952, 961, 964, 981–984
  - in intersected-axes gearing 384–385
  - in involute gearing 242, 270–272, 313
  - in Novikov gearing 330, 330–331
  - in real gearings 629, 629–631
- parallel-axes gearing
  - approximate real gearings 712–713, 713, 714
  - arcs in 253, 253
  - base diameter of 143, 340–342
  - base pitches in 101–107
  - bending torque in 292, 292–298, 298
  - Camus-Euler-Savary theorem for 88–95
  - case of 64–65, 65
  - conformal gearing 301–368
  - contact ratio in 253, 446–448
  - coordinate systems for 145, 146, 278–281, 281
  - design parameters of 646–650
  - face advance in 261, 261
  - features of 121–135, 122, 126, 128
  - forces acting in 298, 298–299
  - gear axis displacement 613–619, 614, 617
  - gear ratio in 124–129, 248–268
  - gear tooth accuracy 857–866, 858–861, 863
  - helical gears and 246, 246–247, 247
  - high-conformal gearing 301–368
  - involute gearing and 121–161, 241–299
  - kinematics of 121–124
  - line of contact in 289–298, 296, 664–667, 786–798
  - load distribution in, 232–240, 232f 289–298, 298
  - permissible motions in 81–85, 84
  - pinion-gear-to-rack mesh 222–225, 223, 224
  - real parallel-axes gearing 614, 614–615, 617
  - reference systems for 956–959, 958
  - rotationally positive gear pair 132–134, 134
  - spur involute gears 122, 159–161
  - straddle-mounted gearing 614–616, 616
  - terminology of 172–174
  - tooth flanks in 241, 241–299, 747–752
  - transverse pressure angle variation 129, 129–135, 130, 132, 135



- path of contact
  - in crossed-axes gearing 533–534, 543–544
  - description of 933–934, 944
  - in intersected-axes gearing 383–384, 437–438, 438
  - in involute gearing 138–141, 139, 140
  - in spur involute gears 174–180
- perfect gearings
  - accurate real gearings 605–641, **640**
  - developments in 964–974
  - explanation of 925
  - parallel-axes gearing 121–135
  - perfect crossed-axes gearing 481–485
  - tooth flanks in 912–915
- perfect parallel-axes gear pairs
  - base cones in 378, 488
  - base pitches in 270–274, 272
  - bending torque in 297
  - dynamics of 464–474
  - elements of 464–474
  - forces acting in 470–472
  - gear tooth profile and 153–157, 154, 155
  - geometrical blocking contours 920
  - geometrically accurate gearings 119
  - tooth flanks and 142, 143, 146, 151
- pin gearing 2, 3
- pinion; *see also* mating pinion
  - apex of 68–72, 491, 501, 637, 699
  - contact geometry of 1059–1082
  - distance of approach for 613–619
  - gears and 159–170, 747–766, 1059–1087
  - gear-to-pinion mesh 129–132, 405, 499, 903
  - tooth flanks and 747–766, 960–961, 1059–1082
- pinion apex 37, 69, 491, 492, 501, 503, 555, 637
- pinion-gear-to-rack mesh 222–225, 222–225
- pinion reference system 75–77
- pitch circle 5, 11, 12, 20, 131, 154
- pitch diameter 180–182, 201, 206
- pitch line 34, 43, 174
- pitch-line plane 61–63, 62–65
- pitch point 4–6, 9, 88–89, 112, 129–130, 899
- pitch surfaces 172, 174, 521, 523, 524, 524
- plane of action
  - apex of 36–37, 50, 383–384, 405–406
  - in crossed-axes gearing 409–410, 410, 912–915, 913
  - in involute gearing 136–138
  - in real gearings 624, 624–628, 917, 917–918
  - in worm gearing 590–591, 592
- planes
  - associated with gear pairs 61–78
  - centerline plane 63–64, 64–68
  - normal plane 62–63, 63–66
  - pitch-line plane 61–62, 62–66
- planetary gear drives 811–812, 813–825, 818, 820, 823, 827–828, 832–837
- point of contact
  - of favorable gear pair 671–673, 674–675
- point of culmination 309, 329, 334–335, 335
- point of meshing 277, 278–281, 305, 398, 1099
- power density 301, 303, 351–352
- pressure angle
  - in crossed-axes gearing 486, 487–488, 518–522
  - description of 929
  - in intersected-axes gearing 405–408, 407
  - in involute gearing 960
  - in parallel-axes gearing 112–116, 129–130, 129–139
- Principles of Mechanisms* 89, **921**, 946, 948, 949
- profile angle 137, 158–159, 175–176, 180, 182, 187, 189, 190, 191
- profile modification 173
- profile shift, 158 173
- pseudo-path of contact 307–310, 310, 317, 336, 340, 346, 348, 349, 350, 361, 428–430, 435, 535, 575
- pulley-and-belt analogy
  - in crossed-axes gearing 543, 910
  - in intersected-axes gearing 438, 438
  - in parallel-axes gearing 86–88, 87, 109–116, 110–114
- rack 25–26, 33–34, 932, 976–977
- rack shift
  - addendum modification 227–230, 228–230, 233–236, 234, **235**, **236**
  - gear tooth modifications 227–239
  - generating 227–239
  - profile shift coefficient 230–232, 231, 233, 236–239, 237, 237–239, 239
- Radzevich, S. P. **924**, 952, 961, 962, 969, 980, 997–1004
- real gearings
  - angular base pitch in 629, 629–630
  - applications of 679–746
  - approximate real gearings 711–746, 974–979, 975–978
  - auxiliary generating surfaces 709
  - base pitches in 629, 629–630
  - bevel gear coupling 665, 665
  - constant velocity joints 665
  - coordinate systems for 607, 607–613, 609, 622–628, 623–625
  - design features of 613–619, 614–617
  - design peculiarities for 915–918, 916–918
  - gear axis displacement 608–613, 609, 617
  - gear axis distance of approach 613–619, 614–617
  - gear coupling design concepts 636–638, 637
  - gear joint 665, 665
  - geometrically accurate real gearings 605–641, **640**
  - line of contact in 625, 625–628, 638–639, 639
  - operating base pitches in 629, 629–630
  - overhung bevel pinion 613, 614
  - plane of action in 624–628, 625, 917, 917–918
  - real crossed-axes gearing 605–607, 606–607
  - reference systems for 607, 607–613, 622–628, 623–625
  - shaft deflection in 613, 614
  - $S_{pr}$ -gear system and 605–641, 915–918, 916–918
  - straddle-mounted gearing 614–615, 615, 616
  - tooth flanks in 619–641, 621, 623–625, 629, 631, 636, 637, 639, **640**
  - types of 639–641, **640**
  - vector diagrams 606
  - $\Sigma$ -var gearing 665–666, 665–668
- reference systems
  - for crossed-axes gearing 552–562, 561, 911, 913
  - for gear pairs 70, 956, 957–958, 958
  - motionless reference system 69, 69–71, 70
  - for real gearings 607, 607–613, 622–624, 623, 624
- R-gearing 481–542; *see also* crossed-axes gearing
- Richard of Wallingford* 929
- root 173
- root curve 172, 661
- roots blower 7, 7–9, 8, 10, 18–19, 19, 20, 712
- rotating gears 839–841, 840–841

- rotational speeds 852–853, 853
- rotation, transmission of
  - in crossed-axes gearing 479–480, 546–550, 548–549
  - description of 919
  - to driven shaft 79–107
  - in involute gearing 135–136, 142
  - in non-involute gearing, 11–18, 12, 14, 16, 18
  - in parallel-axes gearing 109–116, 110–114, 248, 249
- rotation vectors
  - of complex gear systems 839–847, 842, 843
  - diagrams of 28, 32, 40, 42, 44, 45–46, 49, 51–53
  - of intersected-axes gearing 371–383, 375, 385–388
  - kinematics of 27–43
- Saint Venant's principle 781, 783, 784, 1105
- Sang, E. 951
- Savary, Felix 942, 945–946, 953, 980, 1106
- scientific theory of gearing 985
- screw involute surface
  - generation of 204–205, 205
  - in involute gearing 145, 145, 161–167, 162, 163, **167**, 182–186, 183, 271, 271–273, 273
  - in parallel-axes gearing 270–272, 271, 273
- Semple, Amzi C. 951
- shaft angle 50, 371–380, 375, 481–488, 719, 729, 729
- Shevel'eva, G. I. **921**, 953
- Shishkov, V. A. 15, 83–84, 98, **921**, 953, 955–956, 964, 982
- skew-axes gearing 702, 703
- span measurement 859–864, 860, 863
- spatial gear pairs 39, 41, 42, 44, 46, 56, 377, 684–685, 684–694, 687–693; *see also* crossed-axes gearing
- spiral angle 454, 473, 571, 682, 724–725
- spiral bevel gears 474–477, 474–477, 717–719, 718, 718–719, 724–727, 724–727; *see also* bevel gear pairs
- spiral bevel pinion 503, 508–509
- split torque transmission systems
  - elastic load sharing devices 827, 827–838, 829, 830, 832–835, 837
  - elastomeric load sharing device 827, 827–828
  - epicyclical gear drives 816–817, 821–826, 822–823, 825–826, 826, 827, 831
  - examples of 811, 812, 813
  - features of 838
  - gear ratio 816–817
  - gear transmission systems 815–816
  - load sharing devices 827–838, 829, 830, 832–835, 837
  - mobility of 814–815
  - planetary gear drives 811–814, 818, 818–826, 820, 822–823, 825–826, 827–838, 829, 830, 832–835, 837
  - power density 815–816
  - preloaded elastic sharing devices 828–831, 829–830, 834–838, 835, 837
  - torque sharing in 813, 814, 826, 826–838, 827
- $S_{pr}$ -gear system 605–641, 915–916; *see also* real gearings
- spur involute gears; *see also* involute gearing
  - design parameters of **181**, **191**
  - generating basic rack of 180–182, **181**, 181
  - generating straight line of 174–180, 175–177, 179, 187–188, 187–188, 189
  - line of contact in 786, 786
  - parallel-axes gearing and 119, 123, 129, 131
  - tooth flanks and 137, 159–161, 160–161, 174–180, 175–177, 179, 182–186, 183, 241, 242–246, 242–246
  - undercut in 190, 190, 198
- spur non-involute gears 1–11, 2–4, 7–8, 10; *see also* non-involute gearing
- Stadtfeld, H.J. 986–995
- straight line, generating 174–180, 175–177, 179, 187–189, 187–189
- surfaces; *see also* screw involute surface
  - change of parameters for 1029
  - coordinate system transformations and 1056–1057
  - differential geometry of 1013–1028
  - forms of 1016–1022, 1019
  - geometry of 1013–1028
  - parameters of 1029–1030
- tangent plane 1014–1015
- tangent vectors 1014–1015, 1053–1054, 1054
- Terbo, Nicholas 976, 977
- terms, glossary of 1111–1119
- Tesla, Nikola 976
- theory of gearing; *see also* gearings; gears
  - accomplishments in twenty-first century 979, 980–982, 981
  - chronology of evolution 980–982, 981
  - concluding remarks on 1103–1106
  - contributors to 919, **921–924**
  - developments in 936–941, 936–979, 943–945, 947–960, 962, 963, 965–968, 970–978
  - evolution of 919–984
  - explanation of 919–920, **921–924**
  - introduction to xxvii–xxviii
  - origin of 936–941, 936–946, 943–945
  - overview of 919–984
- Theory of Gear Teeth Engagement 953
- tip chamfer 173
- tip circle 172
- tip diameter 172
- tip-easing modification 173
- tip radius 173
- tip relief 902
- Tip relief 791
- tolerances 356, 359–364, 360, 362–363, 475
- tooth alignment error 174
- tooth-chamfering 173
- tooth face 173
- tooth flanks; *see also* gear teeth; gear tooth profile
  - in approximate real gearings 712–713, 712–713, 716, 717, 720–728, 721–722, 724–727
  - auxiliary generating surfaces 701, 702–709, 702–710, 705–707
  - base pitches in 142, 142–144, 150, 151
  - circular-arc teeth 167–170, 168–171
  - conical involute gears and 201, 201–212
  - conjugacy between 86–101, 87, 89, 89–91, 91, 93, 94, 97, 99, 100, 402, 402–404, 960, 960–961
  - contact geometry of 671–677, 673–674, 958–960, 959, 960, 1059–1082
  - contact of 9–18, 18, 81–86, 138, 142, 142–151, 145–150, 150, 177–179, 179, 203–209, 267, 304, 398, 723, 727, 934–935, 952, 958–960, 959, 960, 1059–1082

tooth flanks (*Cont.*)

coordinate systems for 145–151, 147, 149, 202  
 in crossed-axes gearing 385–401, 386, 391–393,  
   397–399, 401, 402, 402–425, 406, 407,  
   410–413, 417–421, **422**, 423–425, 522–523,  
   543–572, 704–705, 705, 756–760, 757, 759, 910  
 curvature and 274–278, 276, **277**, 278  
 curvatures of 1022–1023  
 degree of conformity of 1068–1082, 1069, 1069–1071,  
   1075–1077, 1080  
 design features of 701–710, 702–709, 747–766  
 distance of approach for 1083–1087, 1084, 1087  
 double-tooth contact regions in 267, 267  
 Dupin indicatrix of 673, 673  
 engineering formulae for 1089, **1090–1091**  
 equation of 182–186, 183  
 examples of 1025–1028, 1026, **1028**  
 extremum degree of conformity 1068–1082,  
   1069–1071, 1075–1077, 1080  
 in favorable gear pair 671–672  
 of gear and pinion 671–677, 676, 747–766, 960,  
   960–961, 1059–1082  
 gear-to-rack mesh 705–706, 706  
 generating basic rack of 186, 187, 204  
 generation of 145–151, 146, 149, 153–186, 186,  
   **192**, 192–200, **194–196**, 204, 210, 620–624,  
   621, 623–624, 657–661, 658, 660, 701–710,  
   702–709, 720–728, 721–722, 724–727  
 geometry of 145, 145–150, 145–151, 160, 162,  
   162, 168, 168, 202, 202–209, 204, 205, 209,  
   274–278, 276, 277, 348–351, 349–351,  
   633–636, 636, **640**, 704–705, 747–766,  
   1013–1028, 1014  
 helical gears and 241, 246, 246–247, 247  
 in high-conformal gearing 316–324, 318–320, 322,  
   323, 331–334, 348–351, 349–351, 760–766,  
   761, 762, 764, 765  
 indicatrix of conformity 1071, 1071–1077, 1075,  
   1076, 1081  
 interaction of 241–299, 308–309, 309, 437–477,  
   631–632, 747–766, 768–771, 769–771, 778  
 in internal gears 866  
 in intersected-axes gearing 20–728, 385–390, 386,  
   391, 392, 393, 437–477, 752–756, 753, 755, 756  
 in involute gearing 241–299  
 kinematics of 747–748, 753–754, 756–758, 760–763  
 local orientation for 1060, 1060–1064, 1062  
 low tooth count 518, 772–773, 778–780  
 magnitudes of 1020–1025, **1024**  
 manufacturing errors in 635–636, 636  
 of mating gear pairs 241–246, 247  
 modifications of 740–741, 740–746, 743, 745  
 in parallel-axes gearing 241, 241–299, 747–752,  
   748–751  
 in perfect crossed-axes gearing 912–915  
 in perfect parallel-axes gear pairs 437–477  
 plot tooth flank 285, 285  
 point contact of 636–638  
 point of culmination 309  
 principal directions on 1022  
 in real gearings 619–620, 621, 622–641, **640**  
 schematics of 146, 147  
 separation of 82, 83, 91  
 simulating gear and pinion 802–808, 803, 805–808

sliding angle of 282, 283–288, 283–288  
 sliding conditions in 282–287, 282–287, 343, 343–345  
 spur involute gears and 137, 159–161, 160, 160–161,  
   181, 182–186, 183, 241, 242–246, 242–246  
 strength of 767–808  
 tooth thickness of 414–415, 417, 523–524, 866

## tooth helix 174

## tooth-rounding 174

## tooth spiral 174

## tooth trace 174

## top land 349, 420, 423, 526, 661, 789, 977

## trailing flank 172

## transmission

characteristics of 851–852

error in 896–902, 897, 899, 900, 902

of motion 25–26, 26

of rotation 11–18, 12, 15, 16, 18, 79–107, 109–116,  
   110–114, 135–136, 142, 248, 249, 479–480,  
   546–550, 548–549, 919, 932, 1106

split torque transmissions 809–838

transmission function 896–906, 897, 899, 900, 902,  
   904–906

transverse contact ratio 446, 446–448, 447

transverse pressure angle variation; *see also* pressure  
 angle

in crossed-axes gearing 486, 486–488, 487, 518–522,  
   519, 521

in intersected-axes gearing 407, 408–411, 410–411

in parallel-axes gearing 129–132, 129–135,  
   134–135, 135

Trbojevič, Nikola John 976–977, 977

*Treatise on Gear Wheels*, A **921**, 964, 966

tredgold approximation 425–426, 426, 532–533, 951

Tredgold, Thomas 951, 951

## undercut

in approximate real gearings 742, 743

crossed-axes gearing and 438–450

face contact ratio and 449, 449–450

in gear pairs 236–239, 237–239, 257, 261–262

spiral bevel gears and 724–727, 724–728

in spur involute gears 189–190, 190, 198

## unit normal vector

crossed-axes gearing and 394–410

high-conformal gearing and 365–366, 366

intersected-axes gearing and 394–409

tangent vectors and 1014–1015

tooth flanks and 81–101, 182–183, 204–205

## unit tangent vector

gear pairs and 55, 685–688, 694–697

gear ratios and 128

intersected-axes gearing and 394–395

relative orientation and 1060, 1060–1064, 1062

tangent plane and 1014–1015

tooth flanks and 164, 328, 334, 802–804,  
   1060–1062, 1064

unit vector 30, 55–56, 94, 164, 179, 203, 205–207,  
   211–212, 955

vector calculus, elements of 1007–1012

vector of instant rotation 31, 34–39, 35, 57–58, 121–124,  
   371–375

vectors, properties of 1007–1008

vibration causes 889–908

- Wildhaber, Ernest 976–977, 978, 979, 1093
- Wildhaber-Novikov (W-N) gearing 20, 22, 302, 311, 355, 358, 1093–1101; *see also* Novikov gearing
- Willis, Robert **921**, 946–948, 947, 948, 953
- worm gearing
- accurate worm gearing 573–601
  - analysis of 598–601, 599, 601
  - approximate real gearings 736–739, 736–739
  - base cones in 590–592, 591–592
  - conical worm gear 583, 584, 585, 590–592
  - conventional designs 577–583, 578
  - crossed-axes worm gearing 706–707, 707, 708
  - crown worm gear 583, 585
  - distinguishing 593–598, 594–598
  - double-enveloping gear 582, 582, 599, 737, 737, 738
  - early designs of 573–577
  - examples of 579, 594, 703
  - helicon gearing 586–588, 587
  - internal worm-gearing 588–589, 589
  - internal worm gears 588, 589, 589
  - kinematics of 590
  - line of contact in 590–593, 591–592
  - multiple-start worms 582, 593
  - peculiarities of 590–593, 591–592
  - plane of action in 590–593, 592
  - with rolling elements 589–590, 590
  - rotation vectors of 590–591, 591
  - single-start worm 736, 737
  - sliding conditions in 593
  - spiroid gearing 583–586, 585, 586
  - straddle-mounted gearing 615, 616
  - tooth profile of 599, 599–600
  - worm threads and 590–601, 591, 592, 594–598, 599
- zone of action
- in crossed-axes gearing 439–441, 440, 441, 446
  - in external gearing 254–255
  - face advance 260, 260–264, 261
  - of helical gears 253, 255, 256, 260–263, 260–264
  - in internal gearing 256–258, 257, 258
  - in intersected-axes gearing 439–441, 440–441
  - in involute gearing 79, 253, 255–256, 260, 263
  - in low-tooth-count gearing 255–256, 256
  - in parallel-axes gearing 250
  - in pinion gear-to-rack mesh 258–260, 259
  - preliminary remarks 250–254
  - single-tooth contact 264–265



Taylor & Francis Group  
an informa business



# Taylor & Francis eBooks

[www.taylorfrancis.com](http://www.taylorfrancis.com)

A single destination for eBooks from Taylor & Francis with increased functionality and an improved user experience to meet the needs of our customers.

90,000+ eBooks of award-winning academic content in Humanities, Social Science, Science, Technology, Engineering, and Medical written by a global network of editors and authors.

## TAYLOR & FRANCIS EBOOKS OFFERS:

A streamlined experience for our library customers

A single point of discovery for all of our eBook content

Improved search and discovery of content at both book and chapter level

## REQUEST A FREE TRIAL

[support@taylorfrancis.com](mailto:support@taylorfrancis.com)

 **Routledge**  
Taylor & Francis Group

 **CRC Press**  
Taylor & Francis Group